ANGEWANDTE CHEMIE
INTERNATIONAL EDITION
A Journal of the Gesellschaft Deutscher Chemiker
2001
40/13
Page 2363 – 2556

EDITORIAL

Minireviews, Referees, Journals, and the Future

Referees are hanging judges, not military surgeons
Kurt Tucholsky

Minireviews make their debut in this issue of *Angewandte Chemie*. We launch this new section, which is placed, and covers in many respects the ground, between *Reviews* and *Highlights*, with an article by Pierre Braunstein and Neil M. Boag on "Alkyl, Silyl, and Phosphane Ligands—Classical Ligands in Nonclassical Bonding Modes". Last year, having accepted a particularly remarkable *Communication* by H. Werner et al. on dinuclear rhodium complexes with bridging trialkylphosphane ligands, we invited Pierre Braunstein to illuminate this "rule-breaking" discovery in a *Highlight*. He immediately saw great potential in this idea and wished to include the bridging phosphane ligands in a series alongside bridging alkyl and silyl ligands. He delivered a manuscript that was too long and broad to be a *Highlight* but not comprehensive enough to be a *Review*. At the same time, at this year's meeting of the Editorial Board of *Angewandte Chemie*, there was some criticism of the *Highlights* section, in particular that the articles often had the character of a minireview and would be better labeled as such. The value of minireviews is that they not only serve modern habits (browsing, zapping) but also that they offer the flexibility to treat topics at a time, and in a suitable manner, when a review would be premature or inappropriate. In the future, in *Highlights* (five manuscript pages) particularly important new research results should be illuminated in detail and critically judged, in *Minireviews* (ten manuscript pages) current topics should be presented in a concise review style, and *Reviews* (up to 40 manuscript pages), as ever, will offer a broad range of longer articles, from very personal assessments of the productive areas of research of one protagonist to the classical review article from any area of chemistry (see also our "Notice for Authors"). Alluding to Chekhov we hope that the brevity of the *Minireviews* will make them attractive to many talented authors.

Referee's reports like the manuscripts to be reviewed can be good or bad, correct or wrong, and need to be interpreted. This is not difficult when the reports are so clearly formulated as one that Kurt Mislow sent to me, which was originally published in a slightly different form by Marshall Gates in 1954 (*J. Chem. Educ.* **1954**, *31*, 456 – 457). It is not unusual for the interpretation of a referee report by the author of the manuscript in question to be different to the interpretation given by an editor; this is particularly true when the manuscript has been rejected. As reviewers are, in contrast to the opinion of Kurt Tucholsky (a German writer from the first half of the 20th century), both hanging judges *and* military surgeons, they have a questionnaire to fill out (Figure 1), and should justify the opinions given in these responses (this is their "judicial" role) and comment on the manuscript; suggestions for improvement are more than welcome (their "surgical function"). It is not uncommon for a referee to judge a manuscript to be "important" (Question 1) and in spite of this to recommend rejection (Question 4). Another frequently occurring combination is the response "less important" coupled with the recommendation for acceptance (with or without minor or major alterations). With the exception of rare cases in which the reasons and comments of the reviewer suggest another course of action, these combinations of responses by reviewers are interpreted by the editors to lead to rejection, whereas they are often seen in a more positive light by the authors. The second case is easy to explain: *Angewandte Chemie* aims to present readers with (very) important results and manuscripts which, according to our reviewers, are less important must therefore be rejected. The first case is not so easy, there could be two reasons for the discrepancy, either the reviewer simply wishes to save the

This manuscript must either be drastically reduced or fully oxidized.
Anonymous

1)	How important do you consider the results reported?	
	very important	□ *)
	important	□ *)
	less important	□ *)
	unimportant	□ *)
2)	Do the data obtained by experiment or calculation verify the hypotheses and conclusions?	
	Yes □	No □ *)
3)	Is the length of the manuscript appropriate to its contents?	
	Yes	□ *)
	No, the manuscript is too long	□ *)
	No, the manuscript is too short	□ *)
4)	Do you recommend acceptance of the Communication?	
	Yes, without alterations	□ *)
	Yes, after minor alterations	□ *)
	Yes, but only after major alterations	□ *)
	No	□ *)
5)	If you are of the opinion that the contribution is not suitable for publication in ANGEWANDTE CHEMIE, please indicate which other journal you consider more appropriate:	

***) please give comments on the enclosed sheet.**

Figure 1. Referee questionnaire for *Angewandte Chemie*.

  1433-7851/01/4013-2365 $ 17.50+.50/0

Chemistry

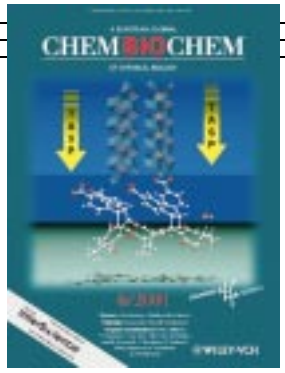

ChemBioChem

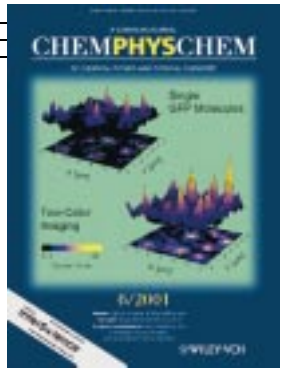

ChemPhysChem

author from the harsh judgment of less important or unimportant in sentencing the manuscript, while clearly justifying the reasons for the rejection in later comments, or alternatively thinks the core of the results to be genuinely important but judges that the research has not been performed adequately, or that the results are as yet not fully confirmed and therefore recommends rejection. Even when the division between the categories is not as clear as one would like (and occasionally results in crosses being placed between two categories) we appeal to referees to provide reports that contain as few "contradictions" as possible and to authors to understand our interpretation, which always has the interests of the readers at heart who do not wish to receive, to use the imagery of Karl Kraus (a Viennese writer of the early 20th century), any wood shavings but rather finely crafted furniture.

Academic know-it-alls can live in the belief that the important product of carpentry is the wood shavings.
Karl Kraus

Journals, especially new ones, are frequently seen as a plague and, that there are on the whole too many as opposed to too few journals is nothing new. In spite of this there is a continual flow of new journals and often for good reasons. To give a few examples, the American Chemical Society has recently launched among others *Organic Letters*, the *Journal of Combinatorial Chemistry*, *Biomacromolecules*, and *Nano Letters*; from the Royal Society of Chemistry come new journals such as *Green Chemistry*; and the Gesellschaft Deutscher Chemiker (the German Chemical Society) together with Wiley-VCH has with—in each case, various different—European partner societies, brought out, first *Chemistry—A European Journal* and last year *ChemBioChem* and *ChemPhysChem* (other new journals from Wiley-VCH are *Fuel Cells*, *Proteomics*, and *Single Molecules*). *Chemistry* is so successful—recently the 3333rd manuscript was received, the impact factor has settled around the very impressive level of 5, and in October we will celebrate the publication of the 100th issue,—that its launch no longer needs to be justified, particularly when one considers the strengthening of the European (and worldwide) chemistry journal market that has resulted. *ChemBioChem* and *ChemPhysChem* are celebrating their first birthdays (launched in July and August 2000, respectively), and although they are "hidden" at the back of *Angewandte Chemie*, have rapidly gained a high profile and have already published many excellent articles. To emphasize their independent character, we are bringing them out of their *Angewandte* hiding place immediately. From *ChemBioChem* double issue 7/8 and *ChemPhysChem* double issue 8/9 (to be published at the start and middle of August, respectively) both journals will be bound separately (also satisfying the needs of librarians), but both journals will continue to be delivered to all the subscribers of *Angewandte Chemie*.

ChemBioChem* and *ChemPhysChem help reinforce chemistry's standing as "the central science". Particularly at the boundaries with biology and physics, chemistry is not a service science providing methods and materials but rather an equal partner, to say the least.

The future belongs to *ChemBioChem* and *ChemPhysChem* but no less so to *Angewandte Chemie*. And how does its future look? With the aim of publishing excellent manuscripts from all areas of chemistry the journal has been extremely successful—and this with an accelerating growth in recent years. More authors than ever before want to publish their best work in *Angewandte Chemie*. In the first six months of 2001 around 20% more *Communications* were submitted than in the same period the previous year. The editorial staff who cannot bear to hear my favorite Wilhelm Genazino (a contemporary German writer) quote any more, have however, once again, successfully increased the throughput. This year over 5000 pages will be published, which is an average of well over 200 pages per issue. When does more cease to be better? Should *Angewandte Chemie* remain an attractive racing boat (with the eventual consequence of appearing weekly) or become a huge container ship? Which sections of the journal do you like best, or is it in fact the mixture of articles that you like? Your response to these questions and any other comments or criticisms about *Angewandte Chemie* and its future interest us greatly!

It will always be the same my dear, the impossible is the normal.
Wilhelm Genazino

Dr. Peter Gölitz

PS: Recently it has become possible for users of the electronic version of *Angewandte Chemie* (and all the other journals in Wiley InterScience) to be informed automatically of new publications in their interest areas through the service "ContentDirect".

  1433-7851/01/4013-2366 $ 17.50+.50/0

COVER PICTURE

The cover picture shows linear motor molecules in action on a silicate support. Under the spotlight, tethered threadlike polyether chains (pink) intercepted by electron-donating naphthalene units (red) doff and don electron-accepting cyclobis(paraquat-*p*-phenylene) girdles (blue). Their risque actions are revealed by the luminescence of the naphthalene units when the girdles are removed. The temporal sequence (left to right) shows the bare thread donning a girdle and then doffing it under the influence of light. The action is attentively monitored by the luminescence spectra; the intensity increases when the girdle is doffed and is quenched when it is donned. More about this process is reported by Zink, Stoddart, and co-workers on p. 2447 ff.

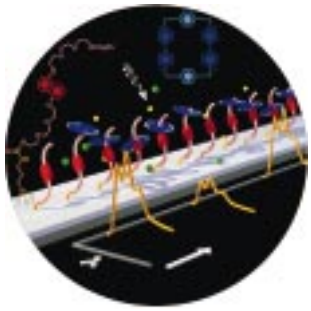

REVIEW

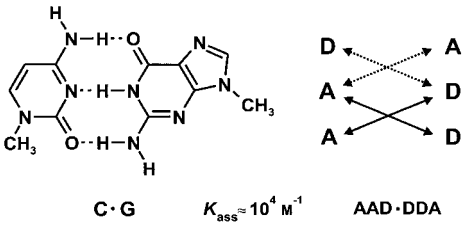

The combined strength of weak interactions at the molecular level can be used to build thermodynamically stable structures with exciting new properties. This review describes the characteristic traits of a new type of organic synthesis which uses the formation of hydrogen bonds between a H-bond donor (D) and an acceptor (A) group, such as in the AAD · DDA module 1-methylcytosine · 9-methylguanine (see scheme).

Angew. Chem. **2001**, *113*, 2446 – 2492

Keywords: hydrogen bonds · molecular recognition · noncovalent interactions · self-assembly · supramolecular chemistry

MINIREVIEW

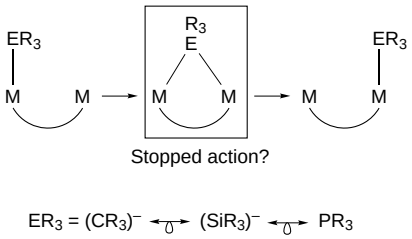

Unusual bonding modes and reactivity of familiar ligands in organometallic and coordination chemistry, such as alkyl, silyl, and phosphane ligands, have become increasingly apparent in recent years. This contribution highlights the similarities between ostensibly unrelated systems (isolobal principle; see scheme) and summarizes their relevance both to fundamental molecular chemistry and catalysis.

Angew. Chem. **2001**, *113*, 2493 – 2500

Keywords: alkyl ligands · bridging ligands · cluster compounds · dinuclear complexes · P ligands · Si ligands

HIGHLIGHTS

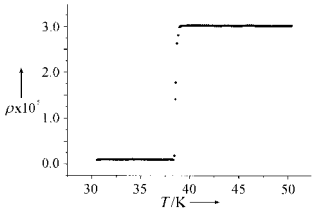

It was a sensation, when in January this year the message went around the world that magnesium diboride MgB_2, known for fifty years, becomes superconducting below the relatively moderate temperature of 39 K (see picture). The commercially available compound was simply overlooked during the search for new superconductors over the past decades.

Angew. Chem. **2001**, *113*, 2501 – 2503

Keywords: borides · magnesium · superconductivity

  1433-7851/01/4013-2367 $ 17.50+.50/0

COMMUNICATIONS

VIPs

The following communications are "Very Important Papers" in the opinion of two referees. They will be published shortly (those marked with a diamond will be published in the next issue). Short summaries of these articles can be found on the *Angewandte Chemie* homepage at the address http://www.angewandte.com

  1433-7851/01/4013-2368 $ 17.50+.50/0

Keywords: molecular machines · pseudorotaxanes · sol – gel processes · supramolecular chemistry

Keywords: chirality · helical structures · nonlinear optics · structure determination

Keywords: cobalt · magnetic properties · molybdenum · polyoxometalates · solid-state structures

  1433-7851/01/4013-2369 $ 17.50+.50/0

  1433-7851/01/4013-2370 $ 17.50+.50/0

  1433-7851/01/4013-2371 $ 17.50+.50/0

  1433-7851/01/4013-2372 $ 17.50+.50/0

  1433-7851/01/4013-2374 $ 17.50+.50/0

  1433-7851/01/4013-2375 $ 17.50+.50/0

Supporting information on the WWW (see article for access details).

* Author to whom correspondence should be addressed

  1433-7851/01/4013-2376 $ 17.50+.50/0

BOOKS

WEB SITES

SERVICE

Issue 12, 2001 was published online on June 13, 2001.

Don't forget all the Tables of Contents from 1995 onwards may be still found on the WWW under: http://www.angewandte.com

The Cooperativity Concept

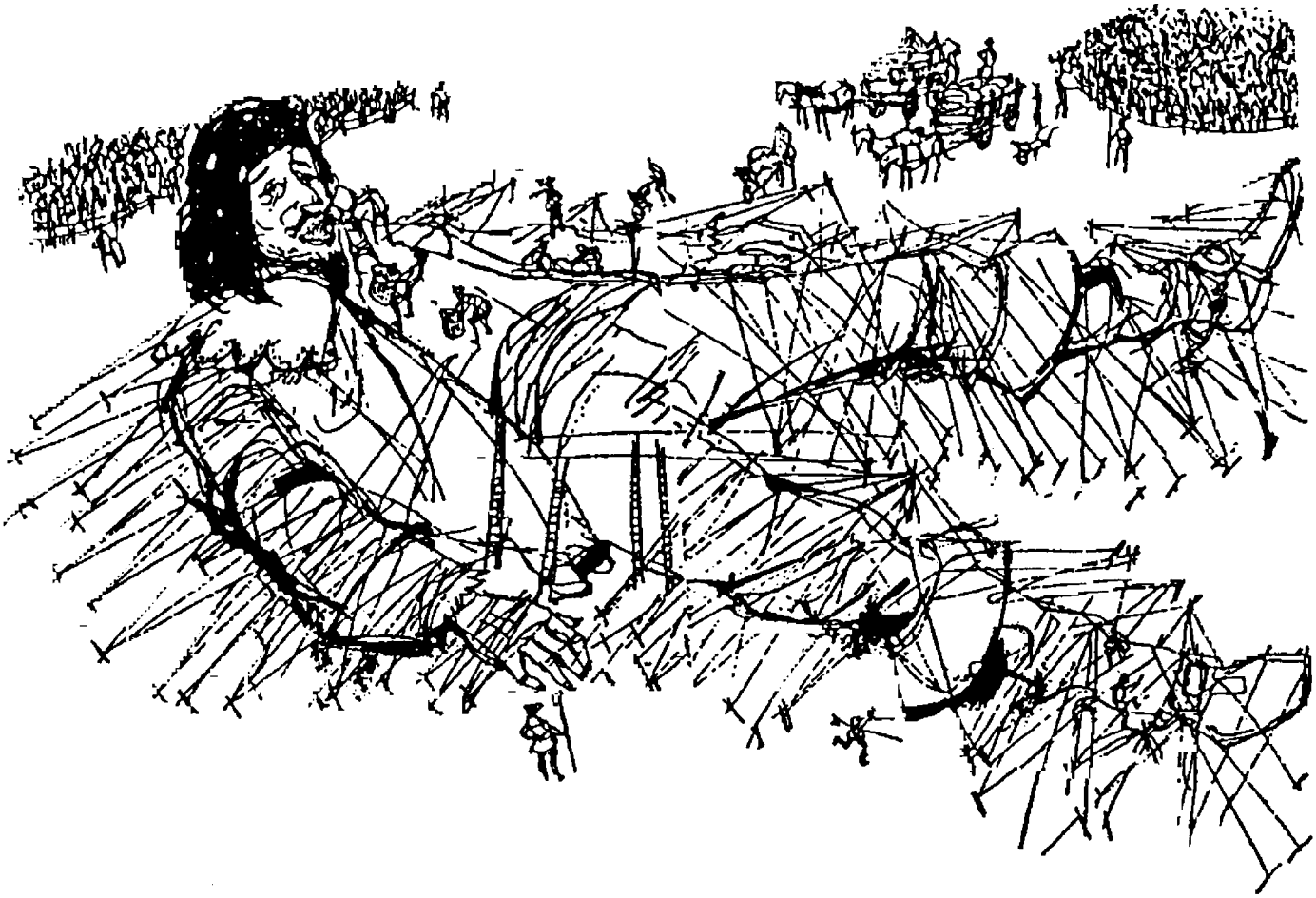

Gulliver constrained by a multitude of weak "bonds". Illustration by Ulrike Schramm in Jonathan Swift's *Gullivers Reisen*; reprinted with permission from Überreuter Verlag, Vienna.

ANGEWANDTE
CHEMIE

Noncovalent Synthesis Using Hydrogen Bonding

Leonard J. Prins, David N. Reinhoudt, and Peter Timmerman*

Hydrogen bonds are like human beings in the sense that they exhibit typical grouplike behavior. As an individual they are feeble, easy to break, and sometimes hard to detect. However, when acting together they become much stronger and lean on each other. This phenomenon, which in scientific terms is called *cooperativity*, is based on the fact that "1+1 is more than 2". By using this principle, chemists have developed a wide variety of chemically stable structures that are based on the reversible formation of multiple hydrogen bonds. More than 20 years of fundamental studies on these phenomena have gradually developed into a new discipline within the field of organic synthesis, and is nowadays called "*noncovalent* synthesis". This review describes noncovalent synthesis based on the reversible formation of multiple hydrogen bonds. Starting with a thorough description of what the "hydrogen bond" really is, it guides the reader through a variety of bimolecular and higher order assemblies and exemplifies the general principles that determine their stability. Special focus is given to reversible capsules based on hydrogen-bonding interactions that exhibit interesting encapsulation phenomena. Furthermore, the role of hydrogen-bond formation in self-replicating processes is actively discussed, and finally the review briefly summarizes the development of novel materials (nanotubes, liquid crystals, polymers, etc.) and principles (dynamic libraries) that recently have emanated from this intriguing field of research.

Keywords: hydrogen bonds · molecular recognition · noncovalent interactions · self-assembly · supramolecular chemistry

1. Hydrogen Bonding

"The discovery of the Hydrogen Bond could have won someone the Nobel Prize, but it didn't."
George A. Jeffrey, Wolfram Saenger, 1991

1.1. Introduction

Molecules can be simply regarded as a collection of atoms connected by high-energy covalent bonds (50–100 kcal mol^{-1}) that result from partial overlap between atomic (hybrid) orbitals. In chemical reactions, different molecules "interact" with each other by the stepwise breaking and making of covalent bonds. These are relatively slow processes that usually have high kinetic barriers. For more than a century organic chemists have been studying chemical reactions in a systematic way, which has ultimately led to the development of a wealth of synthetic methods. Virtually every chemical transformation can nowadays be achieved, which renders the total synthesis of structurally very complex molecules with molecular weights $\leq$1000 Da, such as taxol or brevetoxin, possible.[1–3] However, the synthesis of molecular structures with molecular weights $\geq$1000 Da through the stepwise formation of covalent bonds generates a formidable challenge. With the exception of the synthesis of polymeric structures (both synthetic and biological in origin), which uses repetitive reaction sequences, the field of covalent synthesis reaches the limit of what is synthetically achievable in terms of time requirements and yields.

1.2. Noncovalent Synthesis

Molecules can also "interact" with other molecules through weak interactions (0.1–5 kcal mol^{-1}), such as hydrogen bonding, van der Waals, or dispersive forces, which are collectively known as noncovalent interactions. Such interactions play a key role in fundamental biological processes, such as protein folding or the expression and transfer of genetic information. The universal importance of molecular recognition phenomena observed in biological systems seriously started to

[*] Dr. P. Timmerman, Ir. L. J. Prins, Prof. Dr. D. N. Reinhoudt
Laboratory of Supramolecular Chemistry and Technology
MESA$^+$ Research Institute
University of Twente
P.O. Box 217, 7500 AE Enschede (The Netherlands)
Fax: (+31) 53-4894645
E-mail: P.Timmerman@ct.utwente.nl

  1433-7851/01/4013-2383 $ 17.50+.50/0

Table 1. Characteristics of covalent and noncovalent synthesis.

	Covalent	Noncovalent
building block	atoms	molecules, ions
target	molecule	assembly
molecular weight	1 – 1000 Da	1 – 100 kDa
bond type	covalent	ionic, hydrophobic, metal coordination, hydrogen bond
bond energy	35 – 135 kcal mol^{-1}	2 – 20 kcal mol^{-1}
kinetic stability	high	low
ΔG components	$\Delta H \gg T\Delta S$	$\Delta H \approx T\Delta S$
solvent effects	secondary	primary
characteristics	–	cooperativity

fascinate synthetic chemists in the early 1970s. Inspired by the accidental discovery of the crown ethers by Charles Pedersen in 1967, the research groups of Lehn and Cram started to explore the chemistry of synthetic receptors for small charged and neutral molecules, for which they were awarded the Nobel Prize in 1987. Subsequently, these and other groups have extended this work to synthetic receptors involving hydrogen bonding and other noncovalent interactions. More than 30 years of research in this field shows that noncovalent interactions have an enormous potential for the construction of chemical structures exhibiting a high degree of structural complexity. This novel synthetic approach, also known as "noncovalent synthesis", is actively explored in a variety of chemistry subdisciplines (for the characteristics of both covalent and noncovalent syntheses see Table 1).[4] Several types of noncovalent interactions have been studied in this respect, for example, hydrophobic interactions,[5, 6] metal coordination,[7, 8] ionic interactions,[9] and hydrogen-bonding interactions. This review covers noncovalent synthetic work in which formation of hydrogen bonds is of primary importance. Since some of the work covered here has been the topic of previous reviews,[4, 10–19] we will concentrate on concepts and principles that have emerged from this area over the past decade.

1.3. The Hydrogen Bond

Weak interactions between molecules containing hydroxyl groups were already noted in 1892 by Nernst.[20] Although nameless at that time, Werner included them ten years later in his concept of "Nebenvalenz" (minor valence), which was in fact a proper description of the phenomenon of hydrogen bonding.[21] Suggestions that the hydrogen atom was the center of this weak interaction were first made in 1920 by Huggins as well as Latimer and Rodebush.[22, 23] It was not


D. N. Reinhoudt


P. Timmerman


L. Prins

David N. Reinhoudt was born in 1942 in The Netherlands. He studied Chemical Technology at the Delft University of Technology and obtained his PhD in chemistry in 1969 with H. C. Beijerman. In the period 1970 – 1975 he worked at Shell where he started the crown ether research program. In 1975 he was appointed as a part-time professor (extraordinarius) at the University of Twente, followed by the appointment as a full professor in 1978. He is the scientific director of the MESA$^+$ Research Institute. The major part of his research deals with supramolecular chemistry and (nano)technological applications, for example, in "lab-on-a-chip", electronic or optical sensor systems, catalysis, and molecular materials. He is the author of more than 650 scientific publications, patents, review articles, and books. He has been honored with the Izatt – Christensen award (1995) and the Simon Stevin Mastership (1998).

Peter Timmerman was born in Ommen, The Netherlands in 1966. He received his degree in chemistry in 1989 with G. W. Klumpp at the Free University in Amsterdam. In 1994 he obtained his PhD at the University of Twente (UT) with D. N. Reinhoudt working on the synthesis of rigid cavities by the combination of calix[4]arenes and resorcinarenes, for which he was awarded the Backer Prize. Then he moved to the Eidgenössische Technische Hochschule (ETH) in Zürich, Switzerland for a postdoctoral stay with F. N. Diederich, where he worked on the chemistry of fullerenes. In 1995 he returned to the University of Twente, where he currently holds a Docent position in the group of D. N. Reinhoudt. His current research interests center around the various aspects of self-assembly based on hydrogen bonding and ionic interactions, with a particular focus on noncovalent combinatorial synthesis.

Leonard Prins, born in 1974, studied Chemical Technology at the University of Twente, The Netherlands. He obtained his undergraduate degree in 1996 with D. N. Reinhoudt. In 1997, after spending three months in the group of R. Ungaro in Parma, Italy, he rejoined the Reinhoudt group as a graduate student. His research deals with the noncovalent synthesis of chiral hydrogen-bonded assemblies.

until 1935–6 that Bernal and Huggins proposed the actual term "hydrogen bond" (abbreviated as H-bond),[24, 25] which has become generally adopted to describe this phenomenon. Soon after, it became apparent that associations between molecules containing polar X–H bonds and nonbonding electron pairs on atom Y are generally characterized by relatively high interaction energies.[26, 27] Since then, H-bonding interactions have continued to fascinate chemists—from theoreticians to biochemists and material scientists.[28]

H-bonds connect atoms X and Y that have electronegativities larger than that of hydrogen, namely, C, N, O, F, P, S, Cl, Se, Br, and I. The XH group is generally referred to as the "proton donor" (D) and the Y atom is called the "proton acceptor" (A) group. The strength of a H-bond increases with an increase in the dipole moment of the X–H bond and the electron lone pair on atom Y. Hence, the strongest H-bonds are formed between atoms N, O, and F acting as X and Y, although C–H can also act as a donor.[29] "π" H-bonds involve an interaction between a partially positive hydrogen atom and the electrons of unsaturated double and/or triple bonds.[30]

The first theoretical models suggested that H-bonding exclusively involves an electrostatic interaction between the partially positive hydrogen atom of the donor and the lone pair of the acceptor.[31] Nowadays, it is generally accepted that H-bonding can be described neither by electrostatic theory nor by weak covalent bonding alone, but involves a complicated superposition of five individual contributions[32, 33] which are of similar magnitude:

1) electrostatic or coulomb energy (ΔE_{COU})
2) exchange repulsion (ΔE_{EX})
3) polarization energy (ΔE_{POL})
4) charge-transfer energy or covalent bonding (ΔE_{CHT})
5) dispersion forces (ΔE_{DIS}).

The surprising success of the early electrostatic models in calculating H-bond energies has been attributed mainly to an accidental cancellation of the other contributions. The conclusion of valence bond (VB) and molecular orbital (MO) theories is that H-bond energy is mainly electrostatic at long distances, but at shorter distances repulsion between the electrons of the H–X bond and the lone pair on atom Y as well as delocalization of electrons from the lone pair π orbital on the acceptor to a σ* antibonding orbital on the proton donor come into play.[34] MO calculations indicate that 0.01 to 0.03 electrons are transferred upon formation of the H-bond.

Most theories of H-bonds claim an angle dependence of the H-bond energy, with a maximum value for a linear bond.[35] Kollman and Allen proposed that the ideal geometry involves a compromise between the optimal angle for ΔE_{COU} and ΔE_{CHT}, since the other three energy contributions are virtually angle insensitive.[27] The preference for linear H-bonds was demonstrated for small-ring lactams and monocarboxylic acids.[26] The situation becomes more complicated when the acceptor has more than one lone pair or when the donor has more than one hydrogen atom capable of forming H-bonds, and can lead to the formation of three-center ("bifurcated") or four-center ("trifurcated") H-bonds.[36] These and other factors are reflected in the deviations from planarity that are often observed in crystals.

The energy of a H-bond in the gas phase is typically in the range of 2–20 kcal mol^{-1}, which is much weaker than covalent bonds, but significantly larger than dipolar or London dispersion force energies (< 2 kcal mol^{-1}). If either the donor or acceptor is charged the electronic attraction will be amplified, and consequently the H-bonds become much stronger (10–45 kcal mol^{-1}).[37, 38] The thermodynamic stabilities of H-bonded complexes in solution are very dependent on the solvent. The stabilities are usually highest in apolar solvents without H-bonding properties, such as alkanes. The stabilities are lower for solvents that can act either as a H-bond donor or acceptor by themselves, because of competitive H-bonding with the solvent. Kinetic studies by Hammes and Park revealed that H-bond formation is diffusion controlled, with the rate of dissociation being a direct measure of the relative strength.[39]

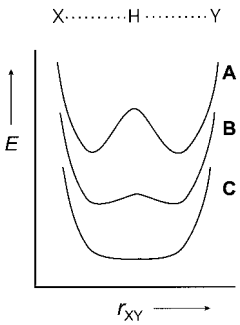

Scheme 1. Potential energy wells for three different types of hydrogen bonds: A) the double-well potential, B) the low-barrier potential, and C) the single-well potential.

H-bonds have been classified into three different types: A) weak or double-well H-bonds, B) low-barrier H-bonds (LBHBs), and C) very strong or single-well H-bonds (Scheme 1). For single-well potentials the hydrogen atom is symmetrically fixed between the two donor atoms, while for double-well potentials there are two minima in which the hydrogen atom is closer to one of the donors. The single-well potential is generally observed for short, "strong" H-bonds, namely, those in which the O···O distance is less than 2.5 Å, such as in the maleate or phthalate monoanions,[40] while double-well potentials are more common for longer H-bonds (O···O distance is approximately 2.8 Å). Recently, the existence of low-barrier H-bonds with energies between 12 and 24 kcal mol^{-1} was claimed, where the balance of the pK_a values of the donor and acceptor was suggested to be an essential feature.[41] Cleland and Kreevoy, and Frey et al. proposed the formation of such LBHBs in the transition state in enzyme-catalyzed reactions to explain the observed rate enhancements.[42, 43] In the meantime, this theory was disproven by other groups, who showed that extra stabilization of a H-bond does not occur when the difference in the pK_a values of the donor and acceptor approaches zero.[44–47]

1.4. Experimental Detection of H-Bonds

Unlike the formation of covalent bonds which involves massive shifts of electron density, the rearrangements that occur as a consequence of H-bonding are more subtle. There is a small shift of electron density from the proton acceptor to the donor, which can be taken as a characteristic for the formation of a H-bond. The effectiveness of a certain technique is dependent on whether it can measure a property that *changes* upon formation of a H-bond. This section

summarizes the most important techniques that have been used for this purpose.

1.4.1. ^{1}H NMR Spectroscopy

The electron densities at the protons involved in H-bonds are decreased, and consequently their NMR signals are shifted to lower magnetic fields.[26, 48, 49] The magnitude of the chemical shift is indicative of the strength of the H-bond. The greatest shortcoming of ^{1}H NMR spectroscopy is that no observable is directly related to the concentration of the monomer (in the fast exchange regime). Therefore, most H-bonding studies have been conducted by monitoring ^{1}H NMR shifts as a function of concentration. Regression analysis of the raw data gives *indirect* information about the strength of the H-bond. Several other approaches to deduce the existence of H-bonds are available, such as measuring hydrogen exchange rates (EXSY), ^{2}H quadrupolar splittings, and ^{1}H/^{2}H isotope shifts. Recently, scalar couplings across H-bonds between two ^{15}N spins have been observed ($^2J = 6.5$-7.0 Hz).[50] Such couplings are comparable in size to the average vicinal coupling between protons in a H-C-C-H fragment, and for the first time enable the *direct* measurement of a H-bond. Furthermore, 2D NMR techniques, such as NOESY, COSY, and TOCSY, have greatly facilitated the characterization of H-bonded assemblies with sizes approaching that of biological assemblies.

1.4.2. Vibrational Spectroscopy

The formation of H-bonds causes a large red-shift ($\geq 100\ cm^{-1}$) of the fundamental X–H stretching vibration, and occurs as a consequence of a lengthening of the X–H bond. In addition, the intensity of the new band is significantly increased, sometimes by more than an order of magnitude, and broadened. The magnitude of the red-shift correlates linearly with the H-bond strength (Badger–Bauer relation).[37] The strength of intermolecular H-bonds is directly related to the intensity of the H-bonded X–H frequency. Raman vibrational intensities are much less affected by H-bonding.

1.4.3. X-Ray and Neutron Diffraction

X-ray and neutron diffraction "see" hydrogen atoms in a different way and with different accuracy (± 0.02 and 0.001 Å, respectively), because X-ray scattering occurs by the electronic cloud of the H atom, whereas neutron scattering occurs mainly by the H nucleus.[51] Although there are a considerable number of neutron diffraction studies on H-bonded crystals, X-ray diffraction studies remain one of the most commonly applied techniques.

1.4.4. Mass Spectrometry

The detection of H-bonded structures by mass spectrometry is severely hampered by the difficulty of ionizing these structures in a nondestructive way. Several ion-labeling techniques in combination with soft ionization methods, such as electrospray ionization (ESI) and matrix-assisted laser-desorption/ionization (MALDI), have significantly improved this, as demonstrated for multi-component H-bonded assemblies of relatively high thermodynamic stability (see Sections 3 and 4).[52, 53]

1.4.5. Quantum Mechanics

Quantum chemical calculations offer a rich source of supplementary information concerning H-bonding.[37] For example, most of the experimental data on H-bonding are obtained in various solvents, whereas simulations are often carried out in isolation from the surroundings, which increases their added value. Moreover, it has proven difficult to directly extract the H-bond energies from spectroscopic data, while calculations can address the energetics directly. Growing sophistication in computer hardware and more efficient algorithms have dramatically increased the level of accuracy that can be expected from computer calculations.

1.5. The Biological Importance of H-bonds

H-bonds have an enormous impact on our daily life. Without them wooden structures would collapse, cement would crumble, oceans would vaporize, and all living things would disintegrate into random dispersions of inert matter. Moreover, the remarkable properties of H_2O, that is, its extremely high boiling point (100 °C versus -60.7 °C for H_2S), the contraction of solid H_2O on melting, and a maximum density of liquid H_2O at 3.984 °C, all rely merely on the formation of H-bonded networks.[54]

Most natural building blocks, such as carbohydrates, amino acids, and nucleic acids, offer a rich source of H-bond donors and acceptors. This most likely arises because life has evolved in an aqueous environment where interactions with water play an important role. Therefore, the existence of H-bonds has long been regarded to play a crucial role in many biogically relevant processes, such as recognition between DNA base pairs, ligand-binding to receptor sites, enzyme catalysis, and α-helix or β-sheet formation. Although it is generally accepted that such processes additionally involve ion–ion, dipole–dipole, hydrophobic, and steric interactions, the relative contributions of each interaction is still poorly understood. However, recent findings in DNA base pairing and receptor–ligand binding studies convincingly showed that the contribution of H-bonding to the overall binding energies has long been overestimated at the expense of hydrophobic interactions.[55, 56] As a matter of fact, the average energy of a neutral H-bond in solution is up to 1.5 kcal mol^{-1}, which means that H-bond formation simply cannot be the main driving force for binding processes that occur in water. H-bonds are, in fact, very important for the specificity of the structure, but do not contribute much to the overall thermodynamic stability. For example, they can play an important role in specifying a unique conformation of a protein relative to a dynamic-averaged ensemble of folded states.

The relative weakness of the H-bond is essential to processes that involve the transfer of biological information,

because in this way it can be switched on and off by energies that are within the range of thermal fluctuations at ambient temperatures.[57] On the other hand, the energy content of a single H-bond is certainly not sufficient to control the structure of biological macromolecules. Likewise, H-bonds are considered as important contributors to the selectivity in binding processes (primarily as a result of their strong directionality) which act cooperatively with other interactions to provide the necessary amount of energy for these binding processes.

2. Self-Assembly by H-Bond-Directed Dimerization

"It will be many years before our understanding of molecular structure becomes great enough to encompass in detail such substances as the proteins […]; but the attack on these substances by the methods of modern structural chemistry can be begun now, and it is my belief that this attack will ultimately be successful."

Linus Pauling, 1939

2.1. Introduction

This section describes noncovalent structures that are formed by the H-bond-directed self-assembly of two complementary components. As a consequence of their relative structural simplicity, most of these assemblies have been thoroughly characterized by using a variety of different techniques (Section 1.4). Moreover, systematic binding studies and structural modifications on these complexes have provided basic knowledge and fundamental insight into the physical parameters that govern the self-assembly process, as exemplified by the "Jorgensen model" and "Schneider's rule" (see Section 2.2). The assemblies described in this section have been classified according to synthetic motifs and motifs known from bio-recognition, such as the DNA nucleobases. The synthetic motifs have been further subdivided according to the number of H-bonds involved.

2.2. The Jorgensen Model

In 1967, Rich and co-workers systematically compared the experimental binding data available for triply H-bonded dimeric complexes in $CHCl_3$.[58] Surprisingly, they found very different stabilities for these assemblies, with values ranging from $\sim 10^2$ to $10^4 - 10^5\,\text{M}^{-1}$, which clearly proved that the number of H-bonds involved is certainly not the only important parameter.[59, 60] More than 20 years later, Jorgensen and co-workers showed that these differences in stability can be largely attributed to attractive and repulsive *secondary* interactions. Stabilization arises from electrostatic attraction between positively and negatively polarized atoms in adjacent H-bonds, whereas destabilization is likewise the result of electrostatic repulsion between two positively or negatively polarized atoms (Scheme 2). Monte Carlo and molecular dynamics simulations showed that the 1-methylcytosine · 9-methylguanine (C · G) dimer (AAD · DDA) is 10.7 kcal mol^{-1} lower in energy than the 1-methyluracil · 2,6-diaminopyridine (U · DAP) dimer (ADA · DAD array). This result is in close agreement with experimental binding data for these complexes.[61, 62] Formation of the C · G dimer involves two attractive and two repulsive secondary interactions, whereas in the U · DAP dimer all the secondary interactions are repulsive. The net difference of four repulsive interactions fully accounts for the lower stability of the U · DAP dimer when each interaction involves 2 – 3 kcal mol^{-1}. This model predicts the highest association constant for an AAA · DDD complex with exclusively four attractive secondary interactions. This was proven experimentally one year later by Murray and Zimmerman.[63]

Based on a comparison of experimental binding data for 58 different synthetic hydrogen-bonded complexes, Sartorius and Schneider derived a simple empirical rule that can be used to predict the binding strength of a given complex. They postulated that the free energy for dimerization consists only of two increments: a contribution of 1.88 kcal mol^{-1} for each H-bond and ± 0.7 kcal mol^{-1} for each attractive or repulsive secondary interaction.[64]

2.3. Synthetic Motifs

2.3.1. 1-H-Bond Modules and the Concept of Cooperativity

A large variety of organic functionalities exist that can dimerize through the formation of a single H-bond (1-H). For example, functional groups such as phenols, amines, *trans*-amides, sulfonamides, and phospoamides form homodimers, while heterodimeric assemblies are formed, for example, between pyridines and carboxylates. However, the relatively low stability of assemblies based on a single H-bond severely

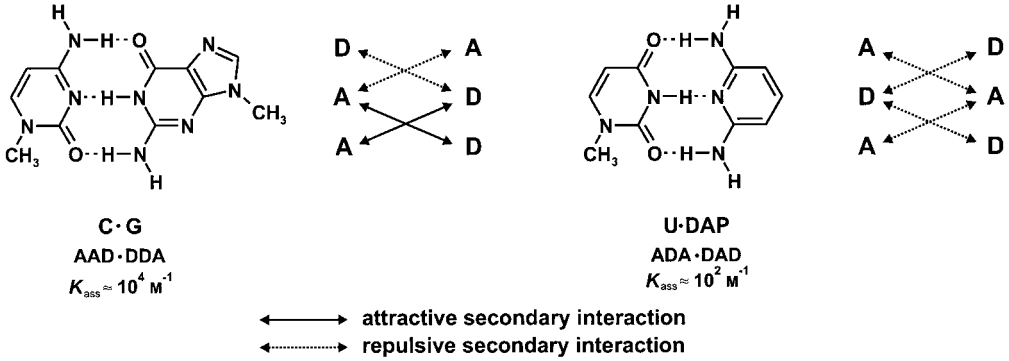

Scheme 2. Attractive and repulsive secondary interactions account for the 10.7 kcal mol^{-1} difference in thermodynamic stability for the 1-methylcytosine · 9-methylguanine (C · G) dimer and the 1-methyluracil · 2,6-diaminopyridine (U · DAP) dimer.

limits their direct utility in the noncovalent synthesis of well-defined assemblies.

Two different strategies have been applied to increase the stability of H-bonded assemblies in which *cooperativity* between individual binding sites plays a key role. In the first, individual 1-H bond recognition motifs are covalently connected to give multidentate modules that can associate through the formation of multiple H-bonds.[65] Hunter and co-workers employed this approach to create a series of so-called zipper complexes which are held together by a combination of multiple H-bonding interactions between different amide units and additional edge-to-face $\pi-\pi$ interactions in the spacer ($\mathbf{1}_2$, Scheme 3).[66, 67] The system

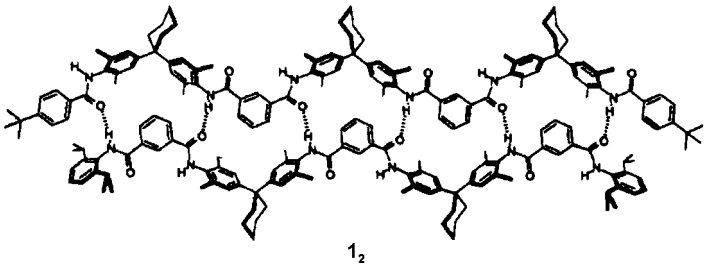

$\mathbf{1}_2$

$K_{ass} = 1.1\times10^{3}\ M^{-1}$

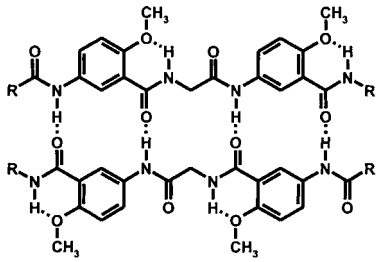

$\mathbf{2}_2$

$K_{ass} > 4.4\times10^{4}\ M^{-1}$

Scheme 3. Multidentate zipper complexes as reported by Hunter and co-workers ($\mathbf{1}_2$) and Gong and co-workers ($\mathbf{2}_2$).

clearly displays positive cooperativity ($\Delta G_{n\text{-mer}} > n\Delta G_{\text{monomer}}$) since the overall thermodynamic stability of the multidentate complexes increases exponentially with the number of connected binding sites. Similarly, Gong et al. recently described the dimerization of self-complementary oligoamides prepared from readily available starting materials such as isophthalic acid and 1,3-phenylenediamine ($\mathbf{2}_2$, Scheme 3).[68] More elaborate synthetic pathways were used to assemble a dimer held together by six H-bonds. This dimer has an association constant of about $10^9\ M^{-1}$.[69]

The second strategy involves the covalent synthesis of modules of rigid linear arrays of multiple H-bonding sites. This approach has received by far the most attention, and has recently resulted in the synthesis of self-complementary modules that dimerize through the formation of up to six H-bonds (see Section 2.3.4).

2.3.2. 2-H-Bond Modules

A variety of polar functionalities have a strong tendency to dimerize through the formation of two H-bonds. Many solid-state dimeric assemblies have been reported, for example, homodimers based on carboxylic acids,[51, 70] *cis*- and *trans*-amides,[71–75] imides,[76, 77] ureas,[70, 78] oxalamides,[79] and 10-hydroxy-10,9-borazarophenanthrenes,[80] or heterodimers based on carboxylic acids and amides,[81] 2-amido- or amino-pyridines,[82, 83] 2-amino-4-pyrimidones,[84] or dipyrrinone.[85] The relatively low enthalpic gain for the common AD · DA complexes (two repulsive secondary interactions) is not sufficient to fully compensate for the concomitant loss in entropy, which means that these complexes are usually only stable at relatively high ($>10^{-2}$ M) concentration. Sartorius and Schneider indeed predicted a K_{ass} value of about $60\ M^{-1}$ in $CHCl_3$, which is far too low to render the individual motif useful for noncovalent synthesis. A significantly higher value was obtained for the AA · DD complex formed from 2-methyl-1,8-naphthyridine and *N*,*N*′-dimethylurea ($K_{ass} \approx 6400\ M^{-1}$ in $CHCl_3$), which is virtually identical to the value calculated by Sartorius and Schneider.[64] However, Zimmerman and Murray observed much lower stabilities ($K_{ass} \approx 260\ M^{-1}$ in $CHCl_3$) for a closely related AA · DD complex.[86] Moreover, they showed that the stability of these complexes was significantly increased (about $3000\ M^{-1}$) by additional secondary interactions, which resulted in the formation of bifurcated H-bonds (AA · DDD H-bonded dimer **3**, Scheme 4).[87]

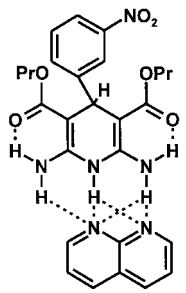

3

DDD · AA

$K_{ass} = 3\times10^{3}\ M^{-1}$

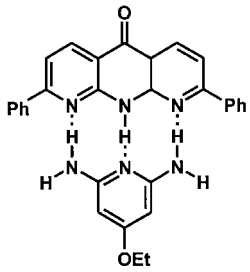

6

ADA · DAD

$K_{ass} = 78\ M^{-1}$

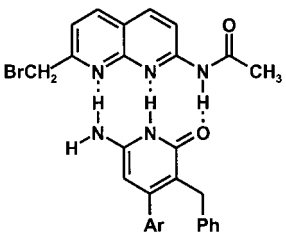

7

AAD · DDA

$K_{ass} = 1.7\times10^{4}\ M^{-1}$

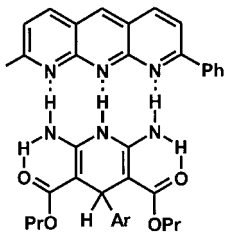

8

AAA · DDD

$K_{ass} > 10^{5}\ M^{-1}$

Scheme 4. Examples of a DDD · AA dimer stabilized by a bifurcated H-bond, and various 3-H-bonded dimers (ADA · DAD, AAD · DDA, and AAA · DDD arrays) with their corresponding stability constants.

Association constants up to 4260 M^{-1} in $CD_3CN/CDCl_3$ (5/95) were found for benzamidium guests bound to naphthyridine embedded in dendrimers of various sizes.[88]

The thermodynamic stability of noncovalent assemblies based on 2-H modules can be significantly improved by connecting multiple modules in a covalent manner, similar to that discussed for 1-H-bonded modules (Section 2.3.1). The research group of Wuest, one of the pioneers in the field of noncovalent synthesis, was among the first to exemplify this principle by utilizing the self-complementarity of the 2-pyridone recognition motif.[89, 90] The bidentate modules **4** (C_s) and **5** (C_{2v}), in which two 2-pyridone units are covalently linked by a rigid acetylene spacer, exhibit very different assembly behavior as a result of the different orientation of the pyridone moieties (Scheme 5).[75] The self-complementary

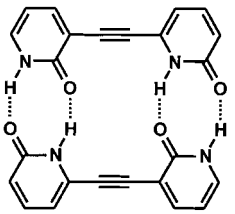

4_2

$K_{ass} > 6x10^4\ M^{-1}$

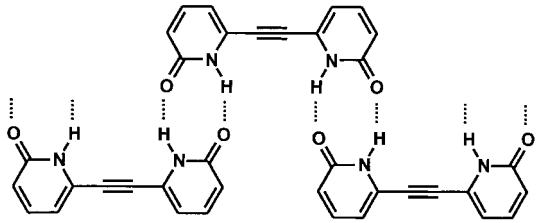

5_n

Scheme 5. Self-assembly behavior of the self-complementary (C_{2v}) and non-self-complementary (C_s) dipyridone modules **4** and **5**.

C_s isomer **4** forms very stable dimers in $CHCl_3$ ($K_{ass} >$ 60 000 M^{-1} at 25 °C), whereas the C_{2v} isomer **5** forms undefined polymeric aggregates. A more flexible analogue of **4** gave very similar results, with the difference that small amounts of (cyclo)oligomeric aggregates were observed at higher concentrations. Presumably, intramolecular H-bonding within these fexible modules preorganizes the pyridone binding sites for preferential dimerization.[91]

2.3.3. 3-H-Bond Modules

In general, 3-H-bond assembly motifs exhibit a significantly higher stability than the corresponding motifs based on two H-bonds. This feature raises their potential as a structural module for noncovalent synthesis.[92] Numerous structural variations of readily available heteroaromatics, such as pyridine[93–96] and triazine,[95, 97] have been studied in great detail. Since homodimerization is intrinsically not possible for 3-H-bond motifs, these complexes have often been designed as receptors.[98, 99] Some representative examples (**6**–**8**) with corresponding stability constants are depicted in Scheme 4. The additional H-bond in 3-H-bonded complexes contributes favorably to the overall negative enthalpy of association. However, as Jorgenson demonstrated, this stabilizing effect may be partly counterbalanced by repulsive secondary interactions that depend on the arrangement of the donor and acceptor sites in the H-bond array. Zimmerman and coworkers studied the difference in thermodynamic stability of a series of dimeric complexes with ADA · DAD, DAA · AAD, and AAA · DDD arrays with 0, 2, and 4 favorable secondary interactions, respectively, in order to test Jorgenson's hypothesis on secondary interactions.[63, 100] The stability constants were found to be of the order of 10^2, 10^3–10^4, and $> 10^5\ M^{-1}$, respectively, in $CHCl_3$, which are fully in line with Jorgenson's model.

2.3.4. Modules with Four and More H-Bonds

Recently the first synthetic modules that can dimerize through the formation of four H-bonds were described. Apart from the expected increase in stability, the even number of H-bond donors and acceptors allows self-complementarity to be introduced in these motifs. Self-complementarity provides an attractive property for applications in polymeric materials (see Section 6) or molecular capsules (see Section 4).

Meijer and co-workers were the first to describe a series of 2-ureido-4(1*H*)-pyrimidone derivatives that can dimerize through the formation of four H-bonds.[101, 102] The fact that certain types of ureidopyrimidones exist in three different tautomeric forms significantly complicates the assembly process. For example, the 6(1*H*)-pyrimidinone module **9** exists in a tautomeric equilibrium with the 4(1*H*)-pyrimidinone monomer **10** (AADD) and the pyrimidin-4-ol monomer **11** (DADA; Scheme 6). Both species are self-complementary with apparent dimerization constants of $> 10^6$ and $4.5 \times 10^5\ M^{-1}$ in $CHCl_3$, respectively. Predicted values using Schneider's rule were in very good agreement with the experimental value for the AADD dimer ($3.6 \times 10^6\ M^{-1}$ versus $> 10^6\ M^{-1}$), while a large difference was observed for the DADA dimer ($3.1 \times 10^2\ M^{-1}$ versus $> 4.5 \times 10^5\ M^{-1}$). This large discrepancy was attributed to preorganization of the H-bond array by formation of intramolecular H-bonds and the presence of a strong O–H ··· O=C H-bond in **11** instead of the weaker N–H ··· O=C H-bond as used in the calculation of Schneider. Indeed it was found that dimerization constants of structural analogues that cannot form the intramolecular H-bond show a much better agreement with Schneider's predictions.[101]

In subsequent work, two 2-ureido-4(1*H*)-pyrimidinones were covalently coupled through a *m*-xylylene spacer, which resulted in self-complementary molecules that can dimerize through the formation of eight H-bonds.[103] ^1H NMR spectroscopic and X-ray crystallographic analysis revealed the presence of three different isomers (**12_2**–**14_2**; Scheme 7). The individual dimers in isomer **12_2** (C_{2h}) and **13_2** (D_2) are both in the 2-ureido-4(1*H*)-pyrimidinone form and adopt either a *syn* or an *anti* orientation, which causes **13_2** to be chiral. In isomer

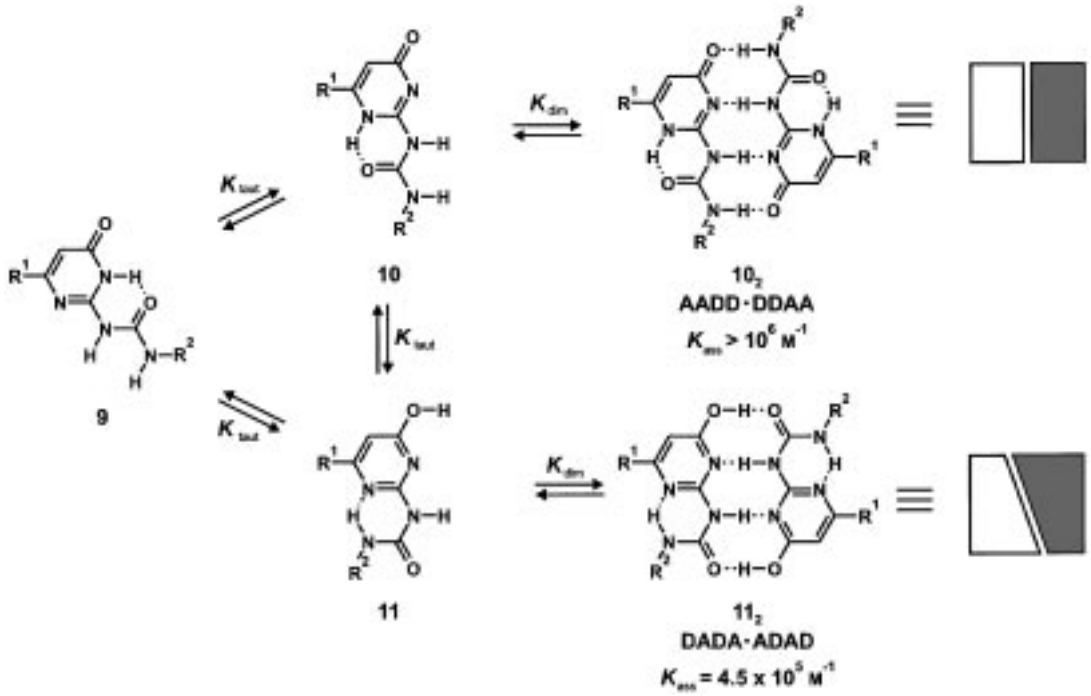

Scheme 6. Three different tautomeric forms of Meijer and co-workers' 6(1*H*)-pyrimidinones, with their corresponding dimerization equilibria.

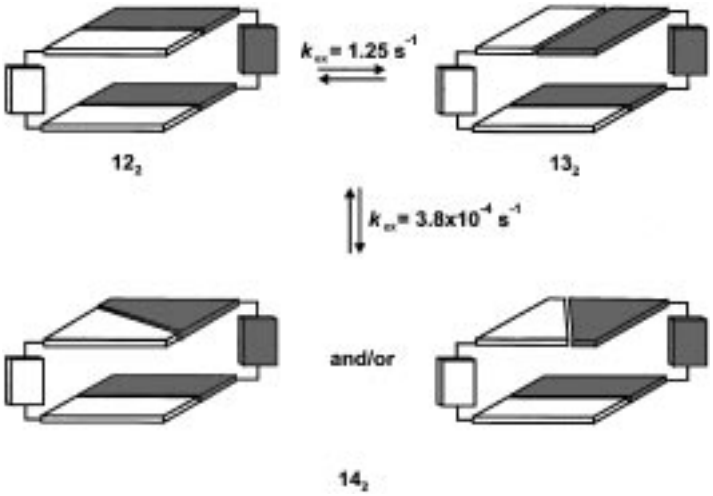

Scheme 7. Tautomerization and dimerization equilibria for dimeric duplexes based on the 4(1*H*)-pyrimidinone H-bond module.

14$_2$ (C_s) one of the dimers has tautomerized to the pyrimidin-4-ol tautomer. Interconversion of isomers **12**$_2$ and **13**$_2$ is fast ($k_{ex} = 1.25\ s^{-1}$) and occurs by dissociation of one single dimer (that is, four H-bonds). Both isomers interconvert slowly ($k_{ex} = 3.8 \times 10^{-4}\ s^{-1}$) with isomer **14**$_2$, a process that involves the tautomerization of one single dimer. The very high stability of these dimeric systems combined with their easy accessibility makes them ideal modules for the noncovalent synthesis of supramolecular polymers (see Section 6.4) Recently, de Mendoza and co-workers reported the dimerization of calix[4]arenes functionalized with two 2-ureidopyrimidin-4(1*H*)-one units.[104] Similar to the assemblies of Meijer and co-workers, different tautomeric structures were observed in the ^{1}H NMR spectrum. The complex exhibits a very high thermodynamic stability, since dissociation involves the simultaneous cleavage of eight cooperative H-bonds. For this reason, dissociation of the dimeric complex in a DMSO/$CHCl_3$ mixture only starts when the DMSO content is above 50%.

A structurally related module with an AADD H-bond array was reported by Corbin and Zimmerman.[105] In this case, analysis of the assembly process was also complicated by the presence of different tautomeric forms. In addition to this, heterodimerization of two different tautomers was observed as a result of their structural complementarity. The dimeric assemblies are highly stable in $CHCl_3$. Only a lower limit of $10^7\ M^{-1}$ could be estimated for the dimerization constant from ^{1}H NMR measurements. Davis et al. designed a compact module (AADD·DDAA) based on the squaramide unit.[106] The first heteromeric dimer involving four H-bonds (DAAD·ADDA) was reported by Lüning and Kühl.[107] The stability constant of $2000\ M^{-1}$ in $CHCl_3$ is fully in line with the expected value based on Schneider's rule. It must be noted though that the dimerization constant dropped to $16\ M^{-1}$ when bulky substituents were introduced.

Very recently, Corbin and Zimmerman reported a recognition motif (DDAADD·AADDAA) that involves six H-bonds.[108] Both monomers exist as intramolecularly H-bonded conformers which mutually unfold in solution to form a robust heterodimer with an association constant of around $5 \times 10^5\ M^{-1}$.

2.4. Motifs Inspired by Nature

Nature offers three sets of H-bonded dimers that are formed by complementary nucleobases, namely, the base pairs adenine·thymine (A·T), adenine·uracil (A·U), and guanine·cytosine (G·C). The specific interactions within these

base pairs are typically referred to as Watson – Crick type and they play a key role in the storage and decoding of genetic information. In an alternative mode, H-bonding may occur on the Hoogsteen edge. Consequently, the thermodynamic stabilities and related binding characteristics of these naturally occurring dimers have been studied extensively.[109–111] Other research groups have studied synthetic nucleotide base analogues with other H-bond patterns, such as the 6-aminopyrazin-2-one ring system,[112, 113] or transition metal complexes of synthetic or natural bases.[114, 115] These compounds have mainly received interest as potential drugs that can induce DNA mismatching. The relatively low binding constants of individual nucleotide base pairs strongly hampers their potential utility as noncovalent synthetic platforms. Sessler et al. employed the same strategy as used for synthetic motifs to develop a series of artificial dinucleotide modules with the ultimate objective of introducing sequence specifity in the self-assembly process.[116] ^{1}H NMR titrations in DMSO showed that the homodimers of the self-complementary AU dinucleotide **15**, in which the A and U nucleobases are connected through the very rigid 1,8-diethynylanthracene spacer (Scheme 8), have a dramatically improved stability

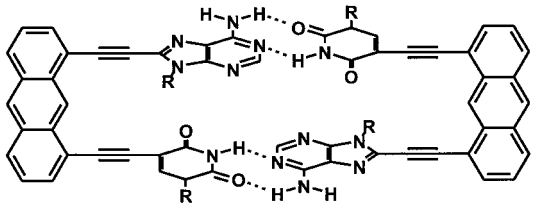

15$_2$

Scheme 8. Sessler and Wang's artificial dinucleotide complex **15**$_2$.

compared to the monomeric base pairs, whereas the use of flexible spacers hardly improves the dimer stability.[117, 118] It was also found that the presence of bulky protecting groups causes severe steric hindrance in the dimers, which leads to a significant reduction in their stability. Recently, the same research group reported a structurally very similar dinucleotide based on chemically modified guanine moieties which self-associates through the formation of eight H-bonds.[119] The corresponding homodimer was found to be stable in pure DMSO, whereas the unmodified G·G dimer, which forms only four H-bonds, is completely dissociated in DMSO/$CHCl_3$ (3/7). These results once again emphasize the importance of structural rigidity and positive cooperativity for the thermodynamic stability of noncovalent assemblies.

There is a currently growing interest in the use of DNA itself as a building block for noncovalent synthesis, as pioneered by the work of Seeman and co-workers.[120, 121] The key advantage of using DNA is the ability to specify intermolecular interactions by means of "sticky ends" technology. Short pieces of DNA, two or three turns, can be regarded as stiff building blocks, a feature essential for the formation of well-defined assemblies. Other attractive properties of DNA-based self-assembly are the readily automated synthesis, the easy modification with functional groups, and the mild conditions under which self-assembly occurs. Chen and Seeman synthesized geometrically complex structures, such as a cube[122] and a truncated octahedron,[123] fully composed of polynucleotides. Other research groups have exploited a similar approach, but used DNA only to link the components, and used synthetic molecules as branching points.[124] For example, von Kiedrowski and co-workers reported a DNA analogue of acetylene: a dimer held together by three double-stranded DNA linkages.[125]

2.5. Ion-pair-Reinforced Motifs

H-bonded assemblies in which the individual components carry opposite charges usually have increased stabilities relative to assemblies consisting of neutral components. In particular, the complexation of guanidinium cations with a variety of different anions, such as carboxylates,[126–129] sulfonates,[130] phosphates,[131, 132] and nitrates,[133] has been studied extensively. Such complexes can have association constants as high as $10^6\,\text{M}^{-1}$ in polar solvents such as DMSO. Recently, a K_{ass} value of $10^3\,\text{M}^{-1}$ in H_2O/DMSO (4/6) was reported for 2-(guanidiniocarbonyl)-1*H*-pyrrole carboxylate complexes.[134] These complexes have an increased stability relative to complexes of the guanidinium cation, because of the presence of additional H-bonds. 3-Acylaminopyridinium ions are also used instead of guanidinium ions to form tight H-bonded complexes with carboxylates.[135] Imidazolines,[136] tetrahydropyrimidines,[137] and amidines[138, 139] form very tight complexes with carboxylic acids as a result of proton transfer. Metzger and Lippert reported the dimerization of the zwitterionic 7,9-dimethylguanine, which exists as a 1:1 mixture of its neutral and cationic form at physiological pH values ($pK_a = 7.19$). The H-bond arrays of both forms are complementary, which results in the formation of a monocationic homodimer.[140] A cationic AAA·DDD complex with a K_{ass} value of $> 5 \times 10^5\,\text{M}^{-1}$ as determined from fluorescence measurements was reported by Bell and Anslyn.[141] Finally, Schneider and Wang studied a large variety of 1:1 complexes formed between tetrasubstituted porphyrins (with pyridinium, anilinium, or benzoate moieties) and negatively or positively charged ligands.[142]

3. Self-Assembly of H-bonded Multimers

"The chemist finds illustration, inspiration, and stimulation in natural processes, as well as confidence and reassurance since they are proof that such highly complex systems can indeed be achieved on the basis of molecular components."

Jean-Marie Lehn, 1995

3.1. Introduction

Nature offers many examples of self-assembled nanostructures and therefore provides a rich source of inspiration for the design of synthetic assemblies. One such example involves the multicomponent assembly of the G_4 motif found in DNA

(Scheme 9). The ends of eukaryotic chromosomes, the telomeres, are composed of simple repeating sequences in which the 5′-3′ DNA strand contains tracts of four guanine residues alternating with short tracts of A/T-rich sequences. This strand is extended to produce a 3′-overhang containing additional sequences of guanine. It has been shown that tetramerization of the guanine sequences and subsequent stacking of the tetramers is responsible for the dimerization of telomeric DNA.[143]

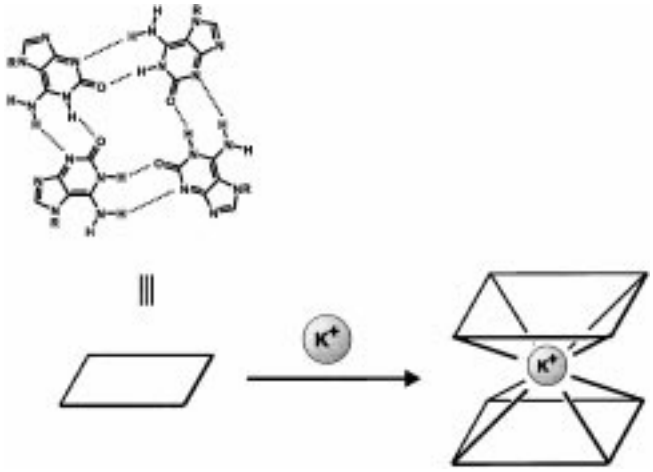

Scheme 9. Metal-induced stacking of the G-quartet.

Like guanine, synthetic molecules will only assemble into well-defined structural motifs if they are encoded with the appropiate H-bonding information and geometry. Most frequently, derivatized (hetero)aromatic molecules are used as modules, since their flat shape and rigidity optimally ensures the formation of 2D assemblies that are more easy to handle than 3D structures. The fixed geometry of aromatic six-membered rings ensures that the angle between two H-bonding sites is fixed either at 60° or 120°, which preferentially leads to trimeric or hexameric assemblies. This section reviews a number of multicomponent H-bonded assemblies that have been extensively studied with respect to their use in noncovalent synthesis.

3.2. Trimesic Acid and Isophthalic Acid Assemblies

Benzene-1,3,5-tricarboxylic acid (trimesic acid) crystallizes in a two-dimensional lattice, in which six trimesic acid units form a cyclic hexamer with an internal cavity of 14 Å (Scheme 10a).[144] X-ray studies revealed that the formation of channels, through which guest molecules can diffuse, is not observed even in the presence of guest molecules, such as *n*-tetradecane or isooctane, which can efficiently fill the channels.[145] Studies by Zimmerman and co-workers showed that the third carboxylic acid moiety is involved in non-standard H-bonding, which results in a lack of long-range ordering in the crystal. The crystallization of isophthalic acid (benzene 1,3-dicarboxylic acid) derivatives coupled through a rigid covalent linker resulted in the formation of zeolite-like channels inside the crystals.[146–148] In contrast to trimesic acid,

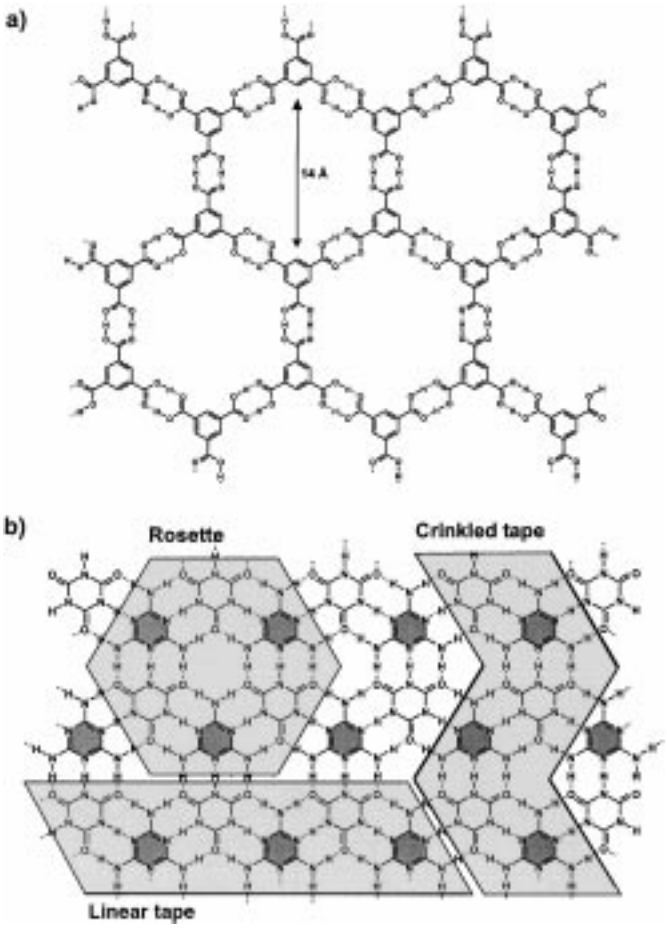

Scheme 10. Crystal lattices of trimesic acid (a) and isocyanuric acid and melamine (b).

isophthalic acid crystallizes in infinite chains.[149] The preference for the chain structure is most likely the consequence of subtle packing forces in the crystal, since 5-decylisophthalic acid selectively crystallizes as the cyclic hexamer.[150] However, a further increase in the alkyl chain length again results in the formation of infinite chains as a result of favorable interdigitation of the alkyl chains.[151, 152]

The assembly of isophthalic acid in solution has received very little attention. Although vapor-pressure osmometry (VPO) and ^{1}H NMR experiments suggest the formation of multicomponent assemblies above a concentration of 15 mM in toluene,[150, 152] quantitative data for the single hexamer have never been reported. A dendritic structure utilizing the self-assembly of cyclic hexamers based on isophthalic acid is discussed in Section 6.

3.3. Isocyanuric Acid · Melamine Assemblies

3.3.1. The Isocyanuric Acid · Melamine (CA · M) Lattice

Cyanuric acid can exist in two tautomeric forms of which the one with all protons residing on the nitrogen atoms, called isocyanuric acid (CA), is the thermodynamically most favored.[153] The three orthogonal ADA H-bonding arrays of isocyanuric acid are mutually complementary with the three

DAD arrays of melamine (M). Both compounds are rigid and the solid-state structure of the 1:1 complex of CA and M was therefore expected to be an infinite 2D lattice of alternating CA and M molecules connected through extensive H-bonds (Scheme 10b). Only recently was this prediction confirmed by X-ray crystallographic analysis.[154]

Similar to the lattice of trimesic acid (Section 3.2), three submotifs are discernible in the CA · M lattice, namely, the infinite linear and crinkled tapes, and a finite cyclic rosette motif (Scheme 10b). The research groups of Whitesides and Lehn showed that blocking one of the H-bonding arrays of both the cyanuric acid and melamine component gives either one of the submotifs.[155–157] Detailed crystallographic studies on a variety of 1:1 complexes of melamine[156] or 2,4,6-triaminopyrimidine derivatives[155] with either cyanuric or barbituric acid derivatives revealed that subtle structural changes in either the melamine or barbiturate component strongly affect the stability of the linear or crinkled tapes in an unpredictable manner.[158] Recently, Timmerman and co-workers reported the first synthesis of well-defined tapelike structures that are stable in solution.[159] They described the selective self-assembly of linear trimelamine **16** and bis(barbituric acid) derivative **17** into the [2 × 2] grid $\mathbf{16}_2 \cdot \mathbf{17}_2$ through the cooperative formation of 24 H-bonds (Scheme 11). The modular approach employed here can in principle be extended to much larger grids and provides access to well-defined oligomeric tapelike structures in solution.

Proton transfer of the highly acidic cyanurate NH proton to the relatively basic pyrimidine nitrogen atom was observed by Mascal et al. in pyrimidine – cyanurate cocrystals.[160, 161] Consequently, the tape structures, which consist of alternating

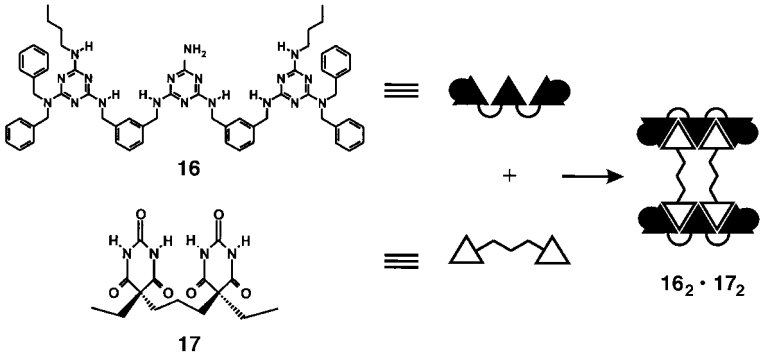

Scheme 11. Self-assembly of the tapelike structure $\mathbf{16}_2 \cdot \mathbf{17}_2$.

ADA · DAD and AAA · DDD arrays should exhibit increased stability according to Jorgenson's model of secondary interactions (see Section 2.2).

3.3.2. The Rosette Motif

The tapelike structures are less useful for the noncovalent synthesis of nanostructures in solution as a result of their undefined shape and size, as well as their limited solubility. However, the rosette motif does not suffer from these disadvantages, and consequently has been studied extensively. Whitesides and co-workers developed two different strategies to promote the selective formation of rosette assemblies: peripheral crowding and covalent preorganization. The concept of peripheral crowding can best be illustrated by comparing the crystal structures of a series of 1:1 complexes of *N*,*N*′-bis(*p*-Y-phenyl)melamine **18** and 5,5-diethylbarbituric acid (BAR) (Scheme 12).[162, 163] Linear tapes are formed

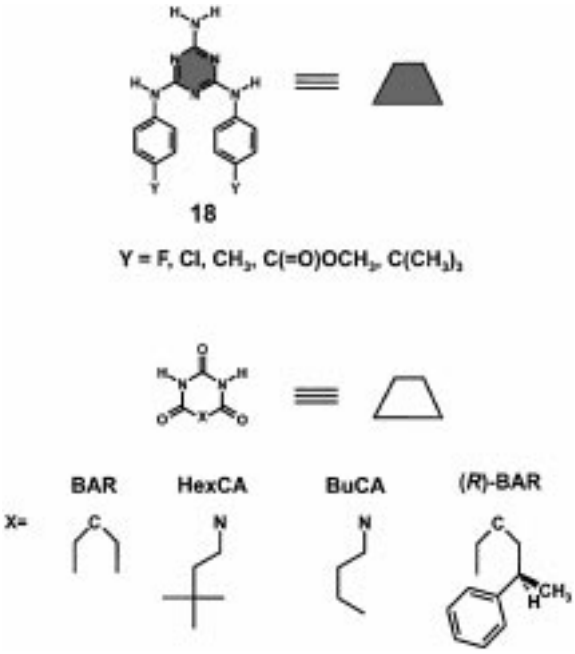

Scheme 12. Melamines **18** used by Whitesides and co-workers to study the effect of peripheral crowding and the molecular structure of frequently employed barbiturates and cyanurates.

preferentially with melamines with small substituents Y, such as F, Cl, or CH_3. Increasing the size of substituent Y, for example, $C(=O)OCH_3$, promotes the selective formation of crinkled tapes, primarily as a result of the relief of unfavorable steric interactions between the Y substituents on adjacent melamine units that are present in the corresponding linear tapes. A further increase in size, for example, when Y is $C(CH_3)_3$, finally gives exclusively the rosette structure, in which all the repulsive steric interactions are minimized relative to those in the corresponding tapelike structures.

Covalent preorganization of the melamine and cyanurate units provides an alternative way to promote the exclusive formation of rosettes. In addition to this, the resulting assembly exhibits a higher thermodynamic stability as a result of the reduced number of separate components (from six to four or even two) and consequently a larger I_{Tm} value (see Section 3.3.4).[164] The first example involves the assembly of trismelamine hub(M)$_3$ **19**, in which three melamine units are covalently preorganized through semirigid spacers ("spokes") onto a C_3-symmetrical central hub, with three equivalents of a single cyanurate or barbiturate molecule (Scheme 13a).[157, 165] A sufficient degree of rigidity in the spokes is essential since analogues lacking one of the phenylene moieties exhibit a much lower thermody-

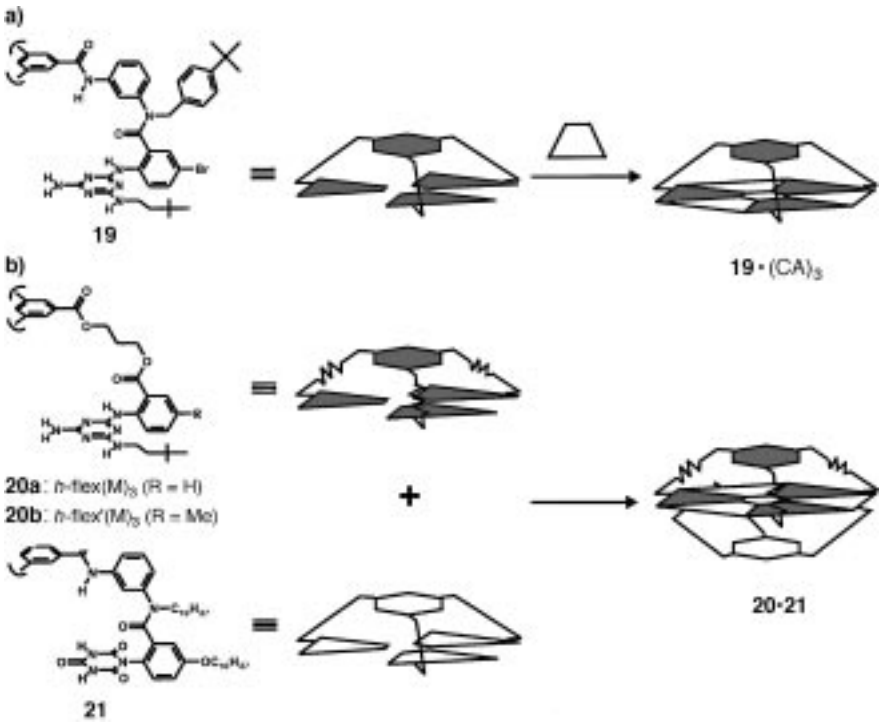

Scheme 13. Self-assembly of $\mathbf{19}\cdot(CA)_3$ (a) and $\mathbf{20}\cdot\mathbf{21}$ (b).

namic stability (for example, **20**). Moreover, complex formation was not observed at all for frameworks that do not contain any rigid element, such as a phenylene or amide moiety, in the spokes. ^{1}H NMR competition experiments clearly proved the increase in the thermodynamic stability of the preorganized rosette $\mathbf{19}\cdot(CA)_3$. This assembly was formed quantitatively upon addition of **19** to a solution of the six-component single-rosette assembly $(\mathbf{18})_3\cdot(CA)_3$. A further reduction of the number of particles consequently stabilizes the assembly even more, for example, when the three cyanurate units are covalently preorganized in a similar manner as the three melamine units.[166] The two-component assembly consisting of *h*-flex(M)$_3$ **20** and hub(CA)$_3$ **21** (1:1 ratio; Scheme 13b) is among the thermodynamically most stable assemblies synthesized which also exhibits a very high kinetic stability (see Section 3.3.6).

3.3.3. Self-Assembly of Dynamic Nanostructures

Having developed a general methodology for the exclusive formation of the rosette submotif, Whitesides and co-workers employed this motif as a module for the construction of larger assemblies, which had the potential for internal cavities.[167] The assembly of oligomelamine derivatives, such as hub(MM)$_3$ **22** (obtained by modular extension of hub(M)$_3$ **19** with three additional melamine units; Scheme 14a),[168] and six equivalents of neohexylCA (hexCA) leads to the quantitative formation of the seven-component assembly $\mathbf{22}\cdot(hexCA)_6$, which is held together by a total of 36 H-bonds. The assembly process displays positive cooperativity, since no partially formed assemblies but only the fully intact assembly $\mathbf{22}\cdot(hexCA)_6$ and free **22** are observed when less than six equivalents of neohexylCA are present. In a similar fashion the ten-component assembly $\mathbf{23}\cdot(hexCA)_9$, with three parallel rosette layers, can be assembled from hub(MMM)$_3$ **23** and nine molecules of neohexylCA (Scheme 14b). For multicomponent assemblies such as $\mathbf{23}\cdot(hexCA)_9$ it takes 48 h at room temperature before the assembly process has reached the thermodynamic equilibrium.[169]

A different approach towards noncovalent assemblies with improved stability involves the sideways connection of two rosette layers.[170] *m*-Xylylene- and furane-based linkers were found to provide sufficient preorganization of the melamine and cyanurate units while being flexible enough to adapt to local perturbations. The assembly of bis(M)$_2$ **24** or bis(CA)$_2$ **25** with two equivalents of a monomelamine or -cyanurate unit gives double rosette assemblies $\mathbf{24}_3\cdot(CA)_6$ and $\mathbf{25}_3\cdot(M)_6$, respectively, which have improved thermodynamic stability compared to single rosettes (Scheme 14c; see Section 3.3.4). However, the stability of these rosette assemblies depends critically on the peripheral crowding within the linkers and substituents. A combination of the two approaches has been used to obtain the two most stable assemblies of the rosette family, namely the five-component assembly $\mathbf{19}_2\cdot\mathbf{25}_3$ and the four-component assembly $\mathbf{22}\cdot\mathbf{25}_3$ (Scheme 14d).[168, 171]

Reinhoudt and co-workers showed that calix[4]arenes serve as excellent linkers for double-rosette assemblies.[172] Calix[4]arenes diametrically substituted with two melamine fragments at the upper rim were found to form the thermodynamically stable double rosettes $\mathbf{26}_3\cdot(BA)_6$ or $\mathbf{26}_3\cdot(CA)_6$ with a large variety of different barbiturates and cyanurates (Scheme 15).[173, 174] The conformation of the calixarene skeleton thereby plays an important role. Calix[4]arenes fixed either in the pinched cone or 1,3-*alternate* conformation perfectly preorganize the melamine units in the preferred planar orientation and consequently form stable assemblies, while assemblies based on the flexible tetramethoxycalix[4]arene skeleton are much less stable.[175] In addition to this, the calixarene module provides sufficient steric bulk to exclude the formation of tapelike structures and therefore enables the introduction of a wide variety of nonbulky functional groups. Recently, the quantitative formation of the 15-component tetrarosette assemblies $\mathbf{27a}_3\cdot(BAR)_{12}$ and $\mathbf{27b}_3\cdot(BAR)_{12}$, which consist of four parallel rosette layers that are held together by a total of 72 H-bonds, was reported by Reinhoudt and co-workers (Scheme 16).[176] The tetramelamine components **27a** and **27b** consist of two calix[4]arene dimelamine units that are covalently connected either through a rigid *m*-xylylene (**27a**) or a flexible hexyl spacer (**27b**).

3.3.4. Thermodynamic Stability

The large series of structurally related rosette assemblies available, which differ mainly in the number of H-bonds and

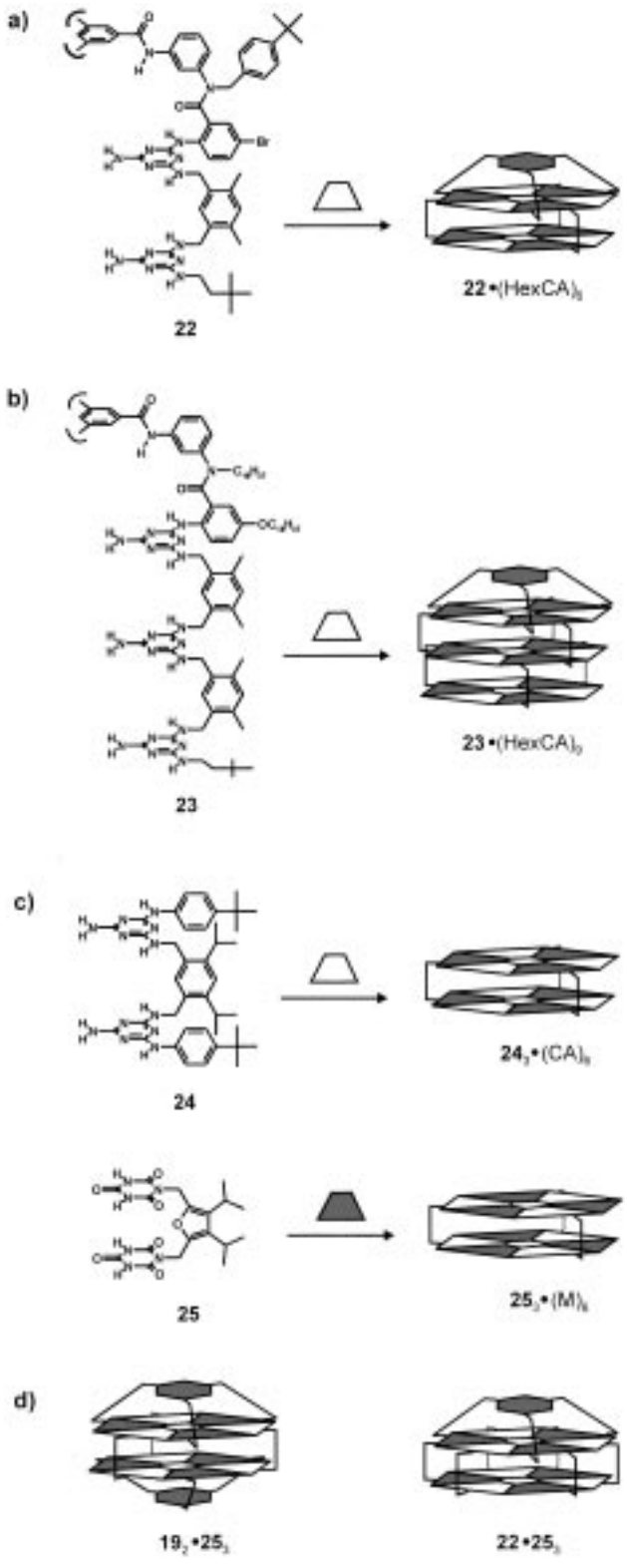

Scheme 14. Self-assembly of $\mathbf{22}\cdot(\mathrm{HexCA})_6$ (a), $\mathbf{23}\cdot(\mathrm{HexCA})_9$ (b), $\mathbf{24}_3\cdot(\mathrm{CA})_6$ and $\mathbf{25}_3\cdot(\mathrm{M})_6$ (c), and $\mathbf{19}_2\cdot\mathbf{25}_3$ and $\mathbf{22}\cdot\mathbf{25}_3$ (d).

the number of associating particles, has provided a unique opportunity to study their thermodynamic stability in a systematic way.[164] The thermodynamic stability reflects the difference in free energy ΔG between the assembly and the free components. The enthalpy term ΔH is mainly determined by the enthalpy of H-bond formation and is proportional to the number N_{HB} of H-bonds: $\Delta H = c_1 N_{HB}$. The entropy term ΔS is determined by changes in the translational, rotational, and conformational entropy, which all together are proportionally related to $N-1$, where N is the number of particles involved.[177] The entropy term is therefore written as $\Delta S = c_2(N-1)$. From this quantitative analysis it follows that $\Delta G = c_1 N_{HB} - c_2(N-1)T$. From this equation a melting point index $I_{\mathrm{Tm}} = N_{HB}/(N-1)$ was defined as a parameter that qualitatively predicts the stability of a particular H-bonded assembly. ^{1}H NMR titration experiments with polar solvents such as DMSO or methanol have been used to measure the stability in solution.[164] The χ value, that is, the amount of polar solvent at which only 50% of the assembly is present in solution, has been defined as a general indicator for the thermodynamic stability of an assembly. Comparison of the calculated (I_{Tm}) and experimentally determined stabilities (χ_{DMSO}) clearly exemplifies the predictive value of this relatively simple parameter. In principle, a thermodynamic evaluation such as this is not restricted to H-bonded rosette assemblies, but should be applicable to other noncovalent systems as well. However, it should be noted that comparison of I_{Tm} values for a series of assemblies is only meaningful when these are structurally related in terms of rigidity. For example, $\mathbf{19}\cdot(\mathrm{CA})_3$ and $\mathbf{20}\cdot(\mathrm{CA})_3$ (Scheme 13) have identical I_{Tm} values, but these values do not reflect the much lower thermodynamic stability of the latter that arises because of higher entropic costs. Similarly, replacement of the barbiturate for cyanurate units in an assembly does not change the I_{Tm} value, but is known to significantly increase the thermodynamic stability as a result of the increased H-bond strength of cyanurates.

3.3.5. Kinetic Stability

One of the major differences between covalent and noncovalent synthesis concerns the fact that the thermodynamically stable noncovalent assemblies are kinetically not inert. This marks one of the most intriguing aspects of noncovalent assemblies and provides unique opportunities to study the mechanism of assembly formation (see Section 3.3.8). However, kinetic stability measurements are often complicated by the fact that exchange occurs too fast to be followed conveniently by ^{1}H NMR spectroscopy.

The dissociation rates of H-bonded assemblies rapidly decrease with the number of H-bonds that are broken in the dissociation of a particular component. For example, the dissociation rate constant of the 1-cyclohexyluracil dimer (cleavage of two H-bonds) is of the order of $10^8 - 10^9\ \mathrm{s}^{-1}$ in $CHCl_3$ at 20 °C,[39] while a rate constant of $21\ \mathrm{s}^{-1}$ in $CDCl_3$ at 20 °C was determined for the dissociation of the BAR units from assembly $\mathbf{26b}_3\cdot(\mathrm{BAR})_6$ (cleavage of six H-bonds).[178] Furthermore, it was found that exchange rates are particularly sensitive to the polarity and H-bond character of the solvent. For example, the exchange of dimelamines **26a** and **26b** (cleavage of 12 H-bonds) in a mixture of assemblies $\mathbf{26a}_3\cdot(\mathrm{BAR})_6$ and $\mathbf{26b}_3\cdot(\mathrm{BAR})_6$ to give the heteromeric assemblies $\mathbf{26a}_2\cdot\mathbf{26b}_1\cdot(\mathrm{BAR})_6$ and $\mathbf{26a}_1\cdot\mathbf{26b}_2\cdot(\mathrm{BAR})_6$ occurs within seconds in $CDCl_3$, even at −50 °C, while it takes 2.5 hours in toluene at 25 °C to reach the thermodynamic equilibrium

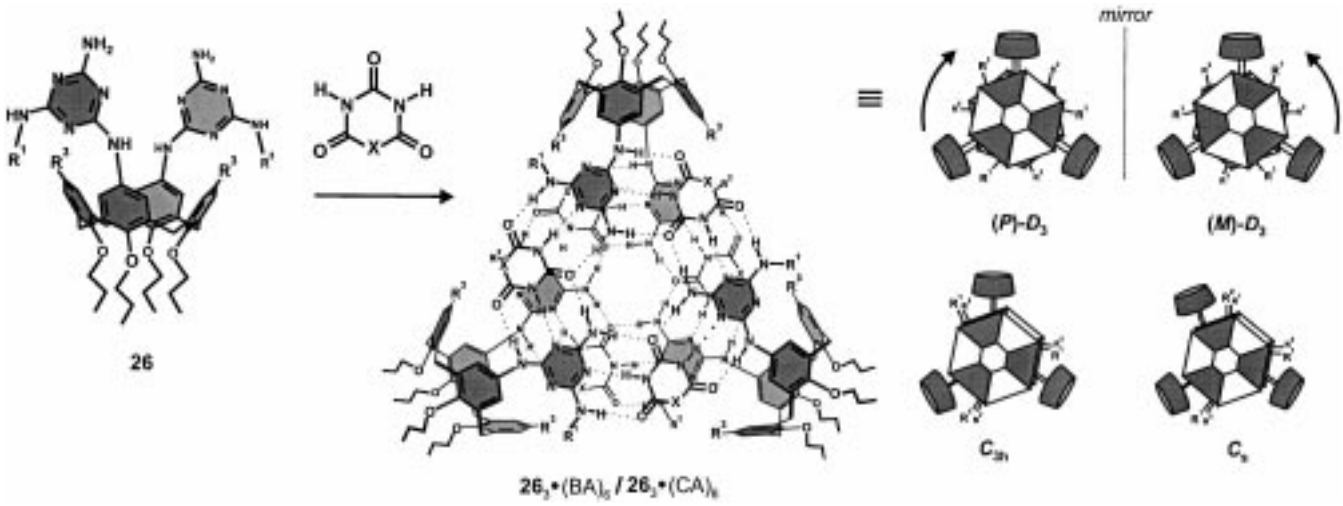

Scheme 15. Self-assembly of calix[4]arene double rosettes and the possible conformational isomers. **26a**: $R^1 = R^2 = (CH_2)_3CH_3$, $R^3 = H$; **26b**: $R^1 = R^2 = (CH_2)_3CH_3$, $R^3 = NO_2$; **26c**: $R^1 = R^2 = (R)$-$CH(C_6H_5)CH_3$, $R^3 = H$; **26d**: $R^1 = (R)$-$CH(C_6H_5)CH_3$, $R^2 = (S)$-$CH(C_6H_5)CH_3$, $R^3 = H$; **26e**: $R^1 = R^2 = (CH_2)_6CH{=}CH_2$, $R^{32} = H$.

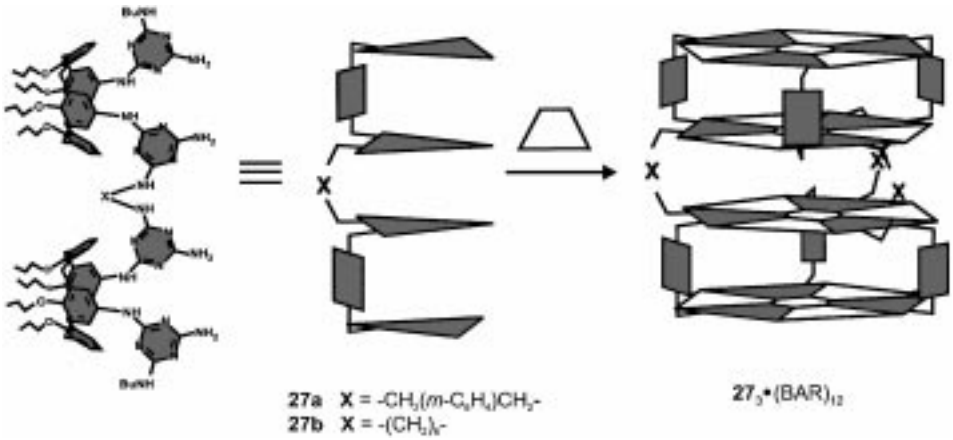

Scheme 16. Self-assembly of calix[4]arene tetrarosettes.

(Scheme 17).[179] ^{1}H NMR measurements for the related assemblies **26a**$_3 \cdot$(BuCA)$_6$ and **26b**$_3 \cdot$(BuCA)$_6$ gave a rate constant of $7.0 \times 10^{-5}\,s^{-1}$ for the dissociation of the dimelamine fragments at 70 °C in [D$_6$]benzene, which clearly reflects the very high kinetic stability of these dynamic structures.[180]

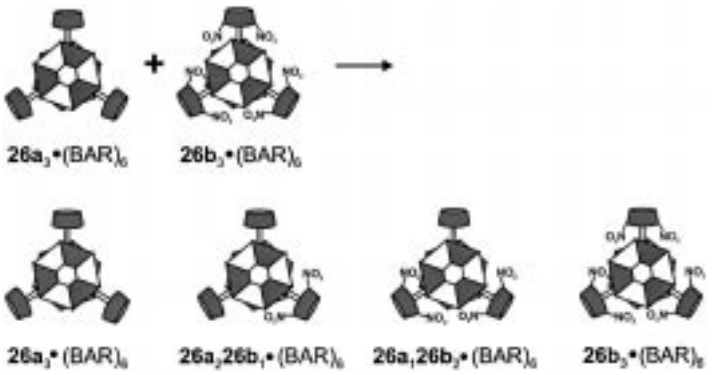

Scheme 17. Exchange of calix[4]arene dimelamines **26a** and **26b** results in the formation of heteromeric assemblies **26a**$_2 \cdot$**26b**$_1 \cdot$(BAR)$_6$ and **26a**$_1 \cdot$ **26b**$_2 \cdot$(BAR)$_6$.

Seto and Whitesides have used kinetic measurements extensively to study the exchange mechanism of assemblies with very high stability, such as **20**$\cdot$**21** (see Scheme 13).[166] Analysis of the kinetic data for the exchange of **20a** with **20b**, a closely related structural analogue, in the assembly **20a**$\cdot$**21** gave a rate constant of $5.0 \times 10^{-7}\,s^{-1}$ for the exchange. On the basis of these data a mechanism was proposed in which assembly **20a**$\cdot$**21** completely dissociates into the free components **20a** and **21** through disruption of 18 H-bonds, followed by re-assembly of **21** and **20b** into the new assembly **20b**$\cdot$**21**.

In view of the data presented here, which show that the rate of exchange of assembly components tremendously decreases with the number of disrupted H-bonds ($10^8\,s^{-1}$ for 2 H-bonds versus $5.0 \times 10^{-7}\,s^{-1}$ for 18 H-bonds), it can readily be expected that H-bond-directed self-assembly processes will become kinetically rather than thermodynamically controlled; this phenomenon is well-known for covalent and coordinative bond-forming processes.[181] Recently, Reinhoudt et al. found such a case, namely the self-assembly of 3 calix[4]arene tetramelamine and 12 CYA units into a 15-component structure, in a similar way as the assembly of double rosettes. However, it turned out that the assembly is not formed even after extensive heating in chloroform for many hours, and is most likely the result of the initial formation of kinetically stable products that resist the subsequent reassembly into the thermodynamically more stable tetrarosettes.

3.3.6. Characterization of Rosette Assemblies

A solubility test often provides qualitative information about the assembly process. In general the individual compo-

nents with polar H-bonding sites are sparingly soluble in apolar solvents, such as chloroform or toluene. Upon formation of a well-defined assembly, such as the rosette, the solubility in apolar solvents dramatically increases, since all the polar sites are utilized in strong H-bonding interactions.[171] However, when nondefined tapelike assemblies containing polar end groups are formed, the solubility is often too low and the assemblies tend to precipitate.

Structural identification of H-bonded assemblies with low kinetic stability by ^{1}H NMR spectroscopy is troublesome when free components and assemblies are in fast exchange on the NMR time scale. In this case the proton signals represent an average resonance for all the species in solution and it is therefore impossible to decide whether rosette or tape assemblies are formed.[163] In cases where slow exchange between the assembly and components occurs ^{1}H NMR data provide a wealth of information about the assembly process. The spectra of well-defined assemblies usually display very sharp signals, while the spectra are often very broad for nondefined oligomeric assemblies. The H-bonded NH protons, which resonate between $\delta = 14$ and 16, are excellent probes for studying the structure and stability (both thermodynamic and kinetic) of the assemblies. The number of NH proton signals also provides important information regarding the structural symmetry of the assembly. For example, one of the assemblies of $\mathbf{19} \cdot (CA)_3$ shows eight different signals for the NH protons of the H-bonded cyanurates, two (high intensity) for the C_3-symmetrical isomer, and six for the less symmetrical C_1 isomer (see Section 3.3.7).[182] Similar evaluations have been worked out for larger assemblies, but the huge number of possible isomers and consequently the huge number of different signals may render analysis very complicated.[183] The presence of two different signals for the barbiturate NH protons in the ^{1}H NMR spectrum of assembly $\mathbf{26}_3 \cdot (BAR)_6$ first of all reveals that both protons reside in a chemically different environment within the assembly as a result of the dissymmetric substitution of the melamine units. Moreover, it shows that the assembly is exclusively present as the D_3 isomer (see Section 3.3.7).[173]

In cases of slow exchange ^{1}H NMR titration experiments are also used to obtain information regarding the stoichiometry and cooperativity of the assembly process. For example, the spectrum of a mixture of calix[4]arene dimelamine **26a** and BAR in $CDCl_3$ shows exclusively signals for assembly $\mathbf{26a}_3 \cdot (BAR)_6$ with a 1:2 ratio of the components, while below or beyond this ratio additional signals for free **26a** or BAR are observed (Scheme 18).[172] Signals for intermediate or partially formed $\mathbf{26}_3 \cdot (BAR)_6$ are not observed at any point of the titration, which indicates that assembly $\mathbf{26}_3 \cdot (BAR)_6$ is formed in a cooperative manner.

A variety of different techniques have been used to estimate the molecular weight of H-bonded assemblies. Vapor-pressure osmometry (VPO) studies by Seto and Whitesides showed that the VPO data generally correspond very well with calculated molecular weights for assemblies with very high stability.[171] However, the results for assemblies with low thermodynamic stability are strongly dependent on the assembly concentration,[163] which severely limits the general use of this technique. The results of gel permeation chromatography (GPC) studies are also strongly dependent on the assembly stability, since assemblies with low kinetic stability tend to show severe tailing as a result of (partial) decomposition on the column.

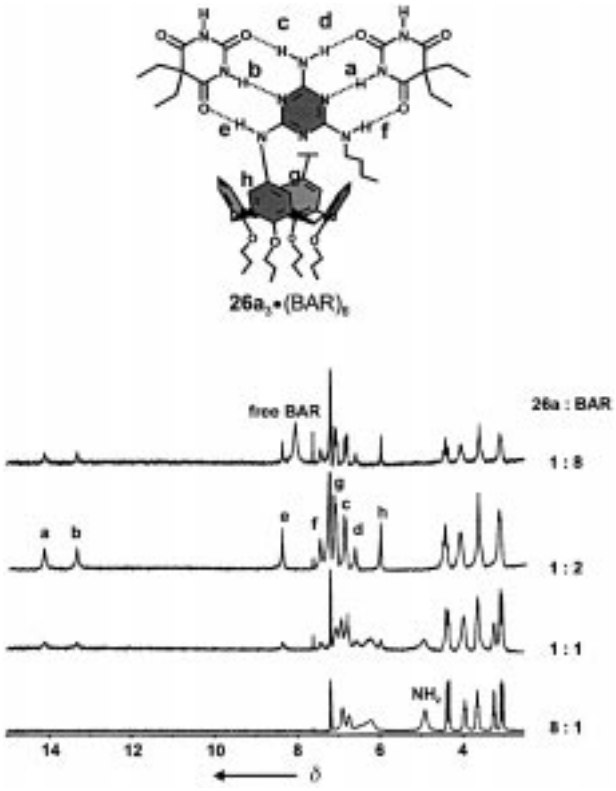

Scheme 18. NMR titration of calix[4]arene dimelamine **26a** with BAR.

Several research groups have investigated the identification of H-bonded aggregates by mass spectrometry. These studies reveal that ion-labeling techniques are usually required to observe the assemblies.[184] Lehn and co-workers reported ion-labeling electron-spray mass spectrometry (IL-ESMS) studies of single rosettes derivatized with [18]crown-6 moieties by using K^+ ions.[185] This labeling method enables the identification of intact rosette assemblies, but a significant amount of fragmented assemblies were observed as well. A very similar method was recently reported by Sessler and co-workers, who showed that H-bonded assemblies derivatized with ferrocene groups can be detected by ESMS after oxidation in air (O-ESMS).[186] Whitesides and co-workers employed a more pragmatic approach, in which ionization of the neutral assemblies occurs by labeling with Ph_4PCl.[187] Several different rosette assemblies were found to form strong complexes with chloride ions, most likely through cooperative binding to the three amide NH groups of the hub spacer. More recently, a Ag^+ labeling technique for the mass spectrometric identification of single, double, and tetrarosettes was reported by the Reinhoudt group.[53, 188] These studies show that assemblies with (aromatic) π-donor, cyano, or crown ether functionalities form strong complexes with Ag^+ ions which can be detected using MALDI-TOF MS (TOF = time-of-flight). The absence of signals for fragmented assemblies illustrates the unprecedented mildness of this technique.

Single-crystal X-ray diffraction studies have not been used very often for the structural characterization of rosette-type assemblies, because of difficulties in obtaining suitable crystals. So far, only two crystal structures of an isolated single rosette and one of a calix[4]arene-based double rosette have been reported.[162, 173, 189]

Computational simulations by Whitesides and co-workers showed that the DP parameter, that is, the average deviation from planarity, correlates well with the relative thermodynamic stabilities of a variety of hub-based single-rosette assemblies determined experimentally. Less preorganization in the spacers results in a larger deviation from planarity.[190, 191] Molecular dynamics (MD) simulations in chloroform solvent boxes revealed that one molecule of chloroform strongly stabilizes the assembly by filling the empty cavity between the hub spacer and the rosette motif. This fact could not be confirmed experimentally, most likely because of fast exchange with the bulk solvent. Similar solvent effects were also found by Reinhoudt and co-workers, who studied conformational isomerism (see Section 3.3.7) in a variety of different double-rosette assemblies using MD simulations.[174] In most cases the difference in the relative stability of the three isomers was determined by steric interactions between the components. However, it was also found that in certain cases chloroform molecules penetrated the assembly, which caused a distortion and eventually a complete destruction of the structure.

3.3.7. Regioselectivity in Noncovalent Synthesis

The products of noncovalent synthesis are often—as for covalent synthesis—not uniform as a result of tautomerism, stereoisomerism, or conformational isomerism (for an early example see Section 2.3.4). For example, assembly **19** · $(CA)_3$ is present in two conformers having either C_3 or C_1 symmetry, each of them being present as a mixture of enantiomers.[166] The observed isomerism is the result of the dissymmetrical substitution pattern of the melamine fragments. In the C_3 isomer all three melamine fragments have an identical orientation (depending on the enantiomer, either *P* (clockwise) or *M* (anticlockwise)). The orientation of one melamine fragment in the C_1 isomer is reversed, which lowers the symmetry of the assembly.

The double-rosette assemblies display a similar kind of regioisomerism and can be present in three different isomeric forms with either D_3, C_{3h}, or C_s symmetry (Scheme 15).[174] In the D_3 isomer the melamine units of each calix[4]arene adopt a staggered orientation, which causes the assembly to be chiral. The C_{3h} and C_s isomers, in which the melamine units are in an eclipsed orientation, have a plane of symmetry and are therefore achiral. The C_{3h} and C_s isomers are different in the sense that the C_s isomer lacks a C_3 axis as a result of a 180° rotation of one of the calix[4]arene moieties. In most cases one of the isomers is formed predominantly. However, small structural changes or solvent effects affect the isomer distribution in an unpredictable manner. Recently, it was shown that peripheral chiral groups in the assembly can be used to direct the regioselective formation of the isomers with D_3, C_{3h}, and C_s symmetry.[174] For example, assembly **26a**$_3$ · $(hexCA)_6$ is formed as a mixture of all three isomers in a 5:2:3 ratio as apparent from the presence of 10 different signals for the NH protons of hexCA. When the achiral butyl substituents in **26a** are replaced by (*R*)-1-phenylethyl groups, as in **26c**, the D_3 isomer is formed exclusively, as evident from the presence of only two signals for the NH protons of hexCA. The reason for the observed selectivity is that the chiral substituents have a strongly preferred orientation with respect to the rosette core which can only be adopted when the assembly is present in the D_3 form. For similar reasons, the C_{3h} and C_s isomers are formed exclusively when dimelamine **26d**, which carries one (*R*)- and one (*S*)-1-phenylethyl substituent, is used. In this case the chiral substituents can only adopt their preferred orientation when the melamine fragments assemble in the eclipsed isomeric form.

3.3.8. Stereoselectivity in Noncovalent Synthesis

Assemblies composed of achiral components express supramolecular chirality when the building blocks are arranged in an unsymmetrical fashion. Yang et al. showed that an achiral barbiturate and melamine assemble into an enantiomeric pair of supermolecules as a result of the presence of a double bond in the barbiturate component.[192] Further assembly results in the formation of mesoscopic supercoiled structures. Since the components themselves are achiral, both left- and right-handed supercoils are observed.

As mentioned before, assembly **26a**$_3$ · $(BAR)_6$ is exclusively present as the D_3 isomer, as was proven both by ^{1}H NMR spectroscopic and X-ray crystallographic analysis.[173] The assembly is chiral and consequently forms a racemic mixture of *M* and *P* enantiomers, since none of the individual components (**26a** or BAR) contains a chiral center (Scheme 15). The Reinhoudt group found that the use of chiral dimelamines or cyanurates strongly induces the helicity of the assembly, and results in the *diastereoselective* formation of assemblies with either *M* or *P* helicity, depending on the configuration of the chiral substituent (*R* or *S*) used. The asssembly process occurs with an unprecedentedly high diastereoselectivity ($de > 98\,\%$) according to ^{1}H NMR and CD measurements.[193] The assemblies exhibit a high CD intensity ($\Delta\varepsilon \approx 100\ cm^2\,m\,mol^{-1}$), in contrast to the free chiral components that are hardly CD active ($\Delta\varepsilon < 8\ cm^2\,m\,mol^{-1}$). The assembly of trismelamine **19** with optically active cyanurates also displays diastereoselectivity, but the *de* value is only 35 % in this case.[194]

Recently, the same group reported the first example of an enantiomerically pure H-bonded assembly (*M*)-**26b**$_3$ · $(BuCA)_6$ which does not contain any chiral carbon centers.[180] The enantioselective synthesis of assembly (*M*)-**26b**$_3$ · $(BuCA)_6$ is a two-step procedure that starts with the diastereoselective assembly ($de > 98\,\%$) of achiral dimelamine **26b** and enantiomerically pure barbiturate (*R*)-BAR to give exclusively (*M*)-**26b**$_3$ · $((R)\text{-BAR})_6$. In the second step, the chiral (*R*)-BAR units are quantitatively replaced by achiral BuCA units, to give assembly (*M*)-**26b**$_3$ · $(BuCA)_6$ in the enantiomerically pure form (Scheme 19). This assembly turns out to be surprisingly stable towards racemization ($E_{act} =$

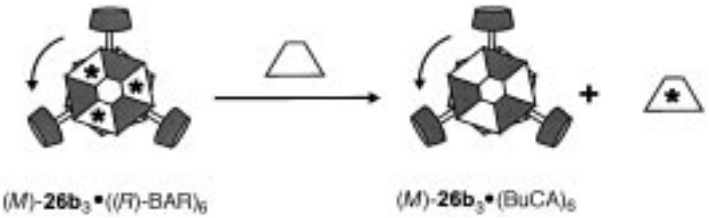

Scheme 19. Noncovalent synthesis of an enantiomerically pure H-bonded assembly.

25.3 kcal mol^{-1}), with a half-life of 4.5 days in benzene at 18 °C. Detailed kinetic studies revealed that racemization of assembly (M)-**26b**$_3 \cdot$(BuCA)$_6$ occurs by a dissociative mechanism, with a rate constant of 1.1×10^{-5} s^{-1}, in which the expelled (R)-BAR acts as a catalyst.

3.4. Miscellaneous motifs

H-bonding between simple dicarboxylic acids and diacylaminopyridines can result in a variety of structures, which subtly depend on the spacers that separate the functional groups. Initial solid-state studies by Hamilton and co-workers revealed that 1:1 complexes are formed when the spacers of both components are comparible in size. However, when the spacer of the diacid is much longer than the spacer of the diacylaminopyridine component, the molecules arrange themselves into infinite linear arrays.[82] Changing the bite angle between the two acylaminopyridine rings by using a 1,3- instead of a 1,4-functionalized phenylene unit results in the formation of a H-bonded helix with heptanedioic acid as the complementary component.[195, 196] Interestingly, when the size and conformational flexibility of the diacid substrate was restricted, the compounds assembled as the discrete $[2 \times 2]$ aggregate **28**$_2 \cdot$**29**$_2$ both in the solid state and in solution (Scheme 20).[197]

An early example of the assembly of self-complementary components involves the noncovalent cyclotrimerization of pyrido[4,3-*g*]-quinoline **30** (Scheme 20). The cyclic trimer is formed in a cooperative way through the formation of six H-bonds.[198] Both VPO and ^{1}H NMR dilution studies confirm the high stability of the assembly ($K_{ass} = 20000\,\text{M}^{-2}$ in $CDCl_3$). Phthalhydrazides exist as an equilibrium of three tautomeric forms, of which the lactim–lactam tautomer can self-assemble into a trimer through the formation of six H-bonds. This motif has been found in the crystal structure of luminol and has been used as a module for supramolecular liquid crystals (see Section 6).[199]

The groups of Lehn and Mascal both reported the assembly behavior of the self-complementary compound **31**, which is designed in such a way that it can only assemble into a cyclic hexameric motif (Scheme 20).[200, 201] These Janus-type molecules, named after the Roman doubly faced god, possess complementary AAD and DDA H-bonding arrays at an angle of 120°. Assembly studies of **31** in apolar solvents were hampered by solubility problems, but ^{1}H NMR spectroscopic and VPO measurements indicated that the desired hexamer is indeed formed in solution.[200] Moreover, X-ray crystallographic studies confirmed the presence of the cyclic hexamer in the solid state.[201] Recently, Kolotuchin and Zimmerman described the synthesis of a very similar molecule with complementary AAD and DDA H-bonding sites.[202] The increased solubility of this assembly strongly facilitated the characterization using 2D NMR techniques and size-exclusion chromatography (SEC).

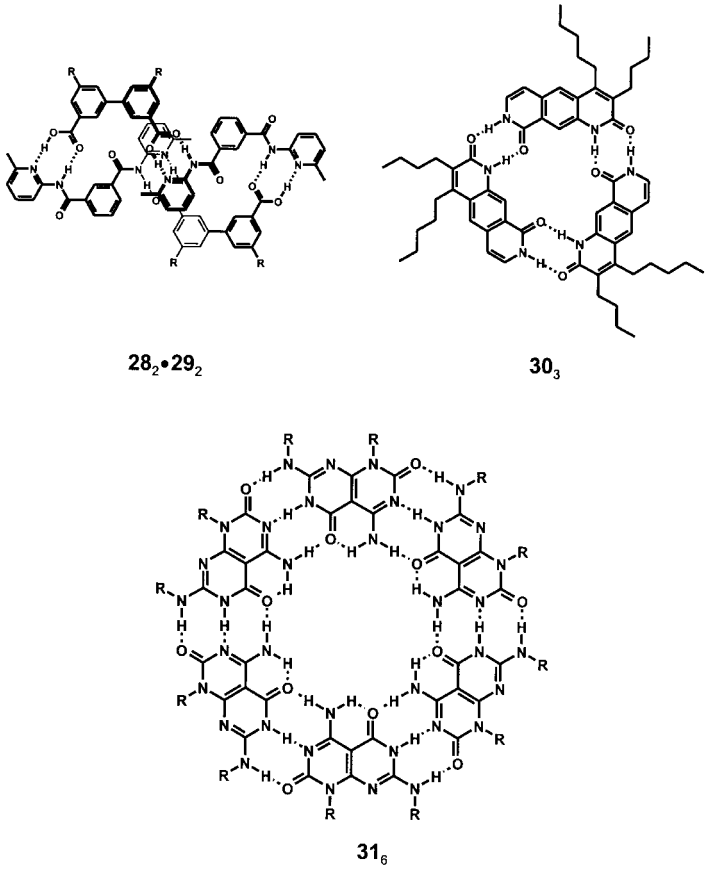

Scheme 20. Miscellaneous multimeric assemblies.

3.5. Self-Assembled Ionophores by H-Bonding

H-bonded assemblies often show interaction with ionic guest molecules, but this type of recognition has not been studied in detail, presumably since higher order aggregates are usually formed. The main contributions in this area come from the groups of Davis and Gottarelli, who studied the cation-binding properties of the well-known G-quartet and related self-assembled structures (see Scheme 9).[203, 204] Earlier studies in the 1970s and 1980s by the Pinnavaia and Laszlo groups already revealed that isolated 5′-guanosine monophosphates also form H-bonded tetramers that have a large tendency to stack.[205, 206] These studies revealed the crucial role of cations such as Na^+, K^+, and Rb^+ in stabilizing the guanosine tetramer through ion–dipole interactions with the inner carbonyl moieties.[207, 208] Furthermore, K^+ ions were shown to induce the stacking of two tetramers into an octameric structure, the exact molecular structure of which was recently confirmed by NMR spectroscopy.[208–211] The

molecular structure of the G-quartet itself has also been unraveled by NMR detection of the N−H···O=C H-bonds in the ^{13}C- and ^{15}N-labeled nucleic acid strand d(GGGTTCAGG), which forms a dimeric quadruplex containing two G-quartets.[212] The binding of monovalent metal ions could be directly detected using ^{205}Tl NMR spectrometry[213] and ESI-MS.[214] Recently, Sessler et al. reported the formation of a G-quartet even in the absence of templating metal cations. In this case, peripheral aryl moieties are presumed to stabilize the tetramer over ribbonlike structures.[215]

Both Gottarelli and Davis envisioned the potential utility of the G-quartet for the extraction of metal cations into organic media. Gottarelli et al. studied the ability of 3′,5′-didecanoyl-2′-deoxyguanosine to extract metal picrates into organic solvents. The binding selectivity of the assembly for cations decreased in the order of $K^+ > Na^+ > Cs^+$.[203] Similar results were obtained by Davis et al.[204] with self-assembled ionophores derived from isoguanosine derivatives.[216] They showed that the self-assembled ionophores act as a phase-transfer catalyst by transporting a nucleophilic counterion either from the solid or the aqueous phase.[217] The selectivity of the assembly for Cs^+ ions is comparable to the best synthetic covalent ionophores.[218] Remarkably, while exploring the properties of the Cs^+ complex Davis and co-workers found that this cation induces the formation of a duplex of pentamers, rather than a duplex of tetramers as observed for the K^+ ion.[219] Self-assembled ionophores can have significant advantages over covalent ionophores, such as calixarene crown ethers or cryptands, in terms of recovery of the host molecules from the complexes, which is an important step in the isolation of radioactive ^{137}Cs isotopes from nuclear aqueous waste. Recovery is relatively simple for noncovalent ionophores since the ion complexes can be strongly destabilized upon the addition of agents that disrupt H-bonds.

Stoddart and co-workers reported the self-assembly of H-bonded assembly **32**, which exhibits an affinity for anions (Scheme 21).[220] They found that macrocyclic polyethers form inclusion complexes of varying stoichiometries with secondary dibenzylammonium ions. The driving force for this assembly process is the formation of charged H-bonds and, occasionally, $\pi-\pi$ stacking interactions. The charged nitrogen atoms of the dibenzylammonium ions are directed towards the center of the assembly, which leads to complexation of one of the three PF_6^- counterions inside this cavity through

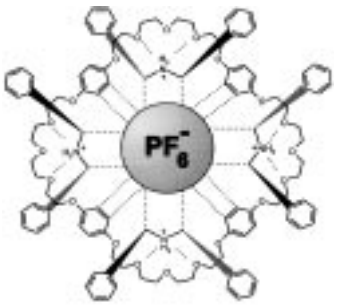

32

Scheme 21. Complexation of a PF_6^- ion in a self-assembled cavity.

C−H···F H-bond formation and Coulombic interactions. Increasing the size of the crown ether results in a more complete encapsulation of the anion.

Another example of anion-templated self-assembly by H-bonding was reported by de Mendoza and co-workers.[221] Two or more chiral guanidinium salts were covalently connected through a small spacer in such a way that the individual guanidium sites cannot interact with the same anion. Polysulfate anions were then added to induce the formation of a double-helical structure, which was confirmed. The chirality of the helix is induced as a result of the presence of chiral centers in the individual strands, which makes it possible to study the assembly process by circular dichroism. Later studies revealed that the tetraguanidinium strand interacts both in water and aqueous methanol with an oligopeptide containing anionic aspartate residues at matching positions.[222]

4. Molecular Containers by H-Bond-Directed Self-Assembly

"Simple objects with concave surfaces can be arranged in order of their increasing concavity, for example, saucers, bowls, pots, vases, and spheres. If organic compounds are to resemble such objects, provision must be made to enforce their shapes by limiting their conformational mobility. In principle, spheres can be assembled from rigid saucers by simple connecting groups. Once the concept of spherical compounds is in mind, fascinating questions about possible occupancy of their interiors seeks answers, and a new field of research is born."
Donald Cram, 1994

4.1. Introduction

Closed-surface compounds have always intrigued chemists because of their synthetic complexity and their aesthetically pleasing shape. The synthesis of dodecahedron (**33**; Scheme 22), one of the five Platonic solids and regarded as the "Mount Everest of Alicyclic Chemistry", remained elusive for more than 20 years, until Paquette et al. reported its 23-step synthesis in 1983.[223] These and other early examples mainly involved molecular cages too small to encapsulate guest molecules. In 1983, Cram proposed the synthesis of hydrocarbon sphere **34** (Scheme 22) that is large enough to accommodate simple organic compounds, inorganic ions, or gases.[224] This hypothetical molecule has formed the scientific basis for most of the synthetic work in the field of molecular encapsulation.

The first successful syntheses of molecular capsules, named carcerands and cryptophanes, were reported in 1985 by the groups of Cram and Collet.[225, 226] In general, capsules are always filled with one or more solvent molecules (DMF, EtOAc, DMSO, etc.) that act as a template during their formation. A severe drawback of carceplexes (carcerands with encapsulated guests) is that the encapsulated guest molecules are physically entrapped and can only be expelled after breakage of one or more covalent bonds. This feature

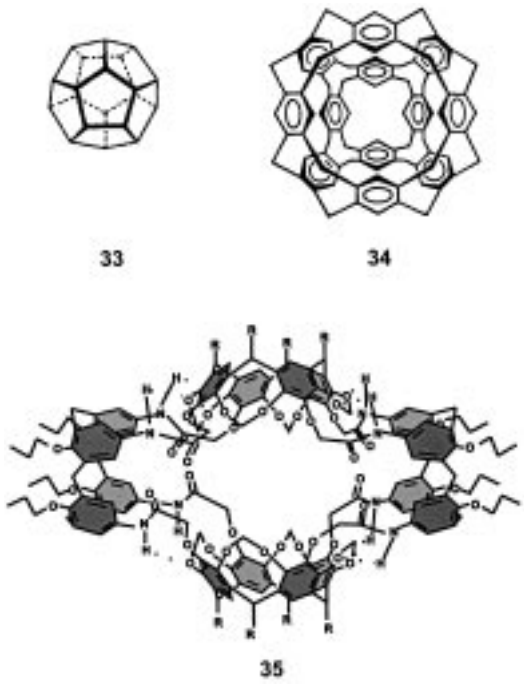

Scheme 22. Covalent cavity-containing molecules.

limits their potential application in catalysis and drug-delivery systems. Cram et al. developed new cages—named hemicarcerands—that have portals through which guest molecules can be exchanged.[227] The solvent molecule that is initially encapsulated during the synthesis is liberated at elevated temperatures to give the empty cage. Subsequently, the guest of choice enters the cavity and becomes kinetically trapped inside the hemicarcerand upon lowering the temperature.

The synthesis of rigid cavities with large internal voids, such as holand **35** (Scheme 22) becomes increasingly demanding and poses limits to what is synthetically achievable.[228] Practical limitations such as these have mainly initiated research activities on noncovalent container systems, which form in a reversible manner with concomitant self-correcting behavior. Guest encapsulation in reversible systems occurs spontaneously upon the addition of the appropriate guest molecule, provided that the host–guest complex is thermodynamically stable. Therefore, covalent synthesis remains restricted to the preparation of simple modules that are programmed for their own assembly, which makes structural modifications on the capsules far easier.

This section reviews recent achievements on the self-assembly of molecular capsules through H-bonding. The emphasis will be on novel principles and concepts that have emerged from these studies. For more detailed information the reader is referred to previous reviews on this topic.[229–233]

4.2. Structural Design of H-Bonded Capsules

Molecular design of the building blocks is an essential element in the successful formation of thermodynamically stable noncovalent capsules.[234] The individual components must be curved and complementary in size in order to form a spherical object. The simplest way to bisect a sphere is to cut it in two halves along the equator (Scheme 23a). Kim and Gokel reported the very first attempt to form a molecular box by noncovalent synthesis using H-bonding interactions.[235] 4,13-Diaza-[18]crown-6 was derivatized with two side arms terminated with adenine or thymine residues. In the proposed structure the roof and floor of the box were constituted of crown ethers, while the A-T base pairs functioned as side walls. VPO and ^{1}H NMR studies revealed some kind of aggregation, but the monomers were too flexible and consequently failed to form well-defined assemblies.[236] These findings strongly emphasize the importance of rigidity in the modules. From this perspective, macrocyclic structures such as cyclodextrins, calixarenes, resorcinarenes, and cavitands were subsequently identified as ideal for the discrete self-assembly of molecular capsules, because they are curved and rigid. Moreover, ample procedures for the selective introduction of directive functional groups have been developed over the last ten years for these molecules.

Aoyama and co-workers were the first to recognize these advantages and reported on a boxlike structure in which methyl glucoside forms a sandwich-type complex with two molecules of resorcinarene.[237] It is disputable, however, whether the ternary complex can be regarded as a true H-bonded capsule, since H-bonding does not seem to occur between the capsule halves themselves, but only between the self-assembled host and the guest.

As a direct result of the studies of Cram et al. towards the properties of carcerands, Sherman and co-workers focused their attention on the noncovalent intermediate complex preceding the formation of these covalent capsules.[238, 239] The two resorcinarene parts in this complex are held together by four charged H-bonds that are formed between the anionic phenolate and phenol groups. Böhmer and co-workers reported on a related resorcinarene dimer that is formed through eightfold H-bonding between phenolic hydroxyl groups and ester carbonyl groups.[240] Reinhoudt and co-workers reported the heterodimerization of two cavitands through fourfold pyridine–carboxylic acid interactions with an association constant of $> 10^7\,\mathrm{M}^{-1}$ in chloroform.[241]

Calix[4]arenes are part of the same class of compounds as resorcinarenes and cavitands. However, their general use as a module for H-bonded capsules is in some cases hampered by the much higher conformational flexibility of the macrocycle, which causes either a collapse of the cavity,[242–244] or the formation of undefined assemblies.[245] Only calix[4]arenes that are substituted at the upper rim with four urea moieties form the well-defined capsule $\mathbf{36}_2$ in solution (Scheme 23a).[246–248] The reason is that the urea H-bonds are directed sideways, which allows H-bonding between the two parts when the calix[4]arenes adopt the cone conformation. Recently, the larger calix[6]arenes substituted either with three carboxylic acid or three urea moieties were found to dimerize. The resulting capsules have small cavities that allow entrapment of guests such as *N*-methyl-4-picolinium iodide and solvent molecules, respectively.[249, 250]

Other H-bonded capsules constructed by this design principle include the homodimers from cyclocholates,[251]

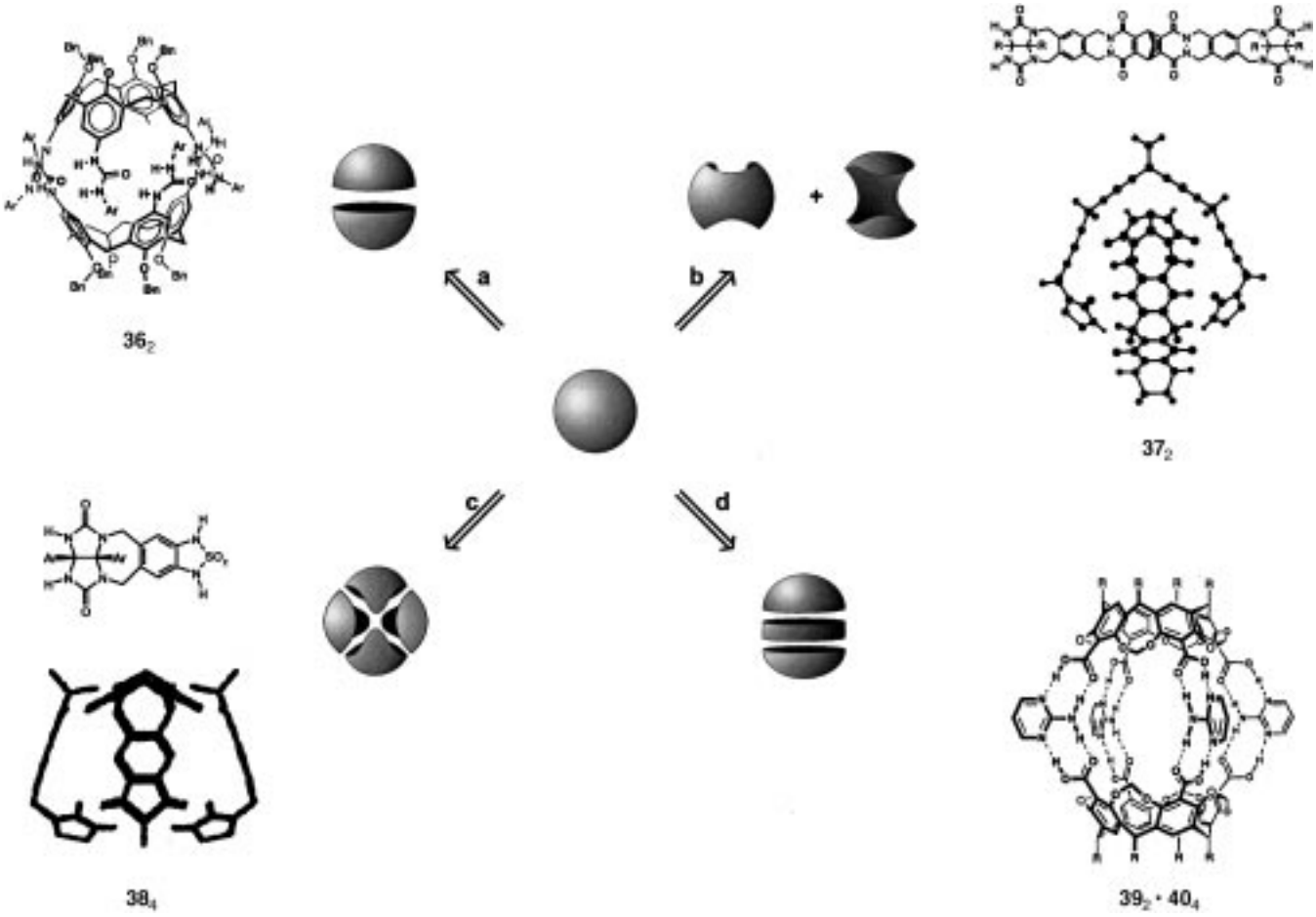

Scheme 23. Four strategies for the noncovalent synthesis of molecular containers.

cyclotriveratrylenes,[252] and a heterodimer from a complementary cyclodextrin and porphyrin.[253, 254] In other cases the formation of H-bonded capsules based on resorcinarenes was only observed in the solid state. The low thermodynamic stability of these capsules is a consequence of the relatively weak H-bonds and the fact that cocrystallized solvent molecules are part of the cage.[255–257]

Two examples of capsules with a cylindrical shape were recently reported by Rudkevich, Rebek, and co-workers.[184, 258] In one of these cases, deep-cavity cavitands with extended aromatic walls dimerize by the formation of eight bifurcated H-bonds between imide functionalities. The cylindrical shape of the capsule, with outer dimensions of roughly 1.0×1.8 nm, gives the cavity unique guest-binding properties (see Section 4.3.4).

A second class of capsules is formed from modules with D_{2d} symmetry—analogous to the way a tennis ball is formed from two identical halves (Scheme 23b). All these systems make use of the H-bonding properties of glycoluril.[259] Connecting two glycoluril moieties through a benzene spacer results in a rigid, concave monomer with C_{2v} symmetry that meets all the requirements to form a capsule on dimerization.[260] The first "molecular tennis ball" assembled in this way possesses a cavity size of 61 Å^3, which decreases to 37 Å^3 when the benzene spacer is substituted with an ethylene spacer. Much bigger capsules, such as "softball" $\mathbf{37}_2$ with a cavity size of 313 Å^3, were obtained by using larger spacers containing functionalities that form H-bonds with the glycoluril moieties (Figure 23b).[261] However, the information in these modules is not unique for dimerization to occur, since higher order aggregates were observed in the absence of suitable templates. The thermodynamic stability of these capsules was further improved upon the introduction of additional H-bonding sites in the spacer.[262] An enhanced stability can also be achieved by using multidentate modules. Assemblies such as the so-called "jelly doughnut" and phthalocyanine dimer (not shown) with C_{3v} and C_{4v} symmetry, respectively, have an increased stability as a result of the larger number of H-bonds that are formed upon capsule formation.[263, 264] The flattened cavity shape allows the encapsulation of disklike guests.

Recently, Rebek and co-workers reported an alternative capsule that is chemically related to the tennis ball structures, but is constructed by using a new design principle (Figure 23c). Capsule $\mathbf{38}_4$ is formed from four different fragments, with the driving force for assembly being H-bond formation between the sulfamide and glycoluril moieties.[265] Previously, MacGillivray and Atwood reported a molecular box constructed from six resorcinarenes, but the thermodynamic stability of this six-component capsule in solution has so far remained unclear, most likely because the presence of eight water molecules is crucial for its assembly.[266]

Yet another method for constructing molecular boxes was very recently demonstrated by Kobayashi et al. (Figure 23 d), who followed an approach used earlier by Lehn and co-workers to construct bisporphyrin cages.[267] Instead of bisecting a sphere along the equatorial plane, they cut it two times along both the "tropic of Capricorn and Cancer". Chemically, this translates into assembly $\mathbf{39}_2 \cdot \mathbf{40}_4$, in which two cavitands with four carboxylic acid groups **39** act as end-caps, and four 2-aminopyrimidine molecules **40** act as "connectors". Conceptually, this approach is very interesting, since it allows for a wide variation in size and structural diversity inside the capsule simply by varying the spacer units. MacGillivray et al. reported the crystal structure of a capsule with similar architecture obtained from cocrystallization of *C*-methylcalix[4]resorcinarene and 4,4′-bipyridine in the presence of nitrobenzene.[268]

4.3. Guest Encapsulation

Most noncovalent capsules, like their covalent counterparts, are formed only when suitable guest molecules are present to fill the interior. For instance, the glycoluril-based monomers of Morgan Conn and Rebek form nondefined aggregates in the absence of suitable guest molecules that can act as a template.[230] In this way, the addition of small amounts of guest molecules to solvents, which are themselves poor guests, can spontaneously induce the formation of well-defined capsules with the desired guest inside. Alternatively, guests that are sparingly soluble in organic media can be encapsulated by solid–liquid extractions.[240] A selection of guests that have been used in encapsulation studies is shown in Scheme 24. A special example are the supramolecular Matroschka dolls consisting of cryptates encapsulated in cavitand-based dimers.[269]

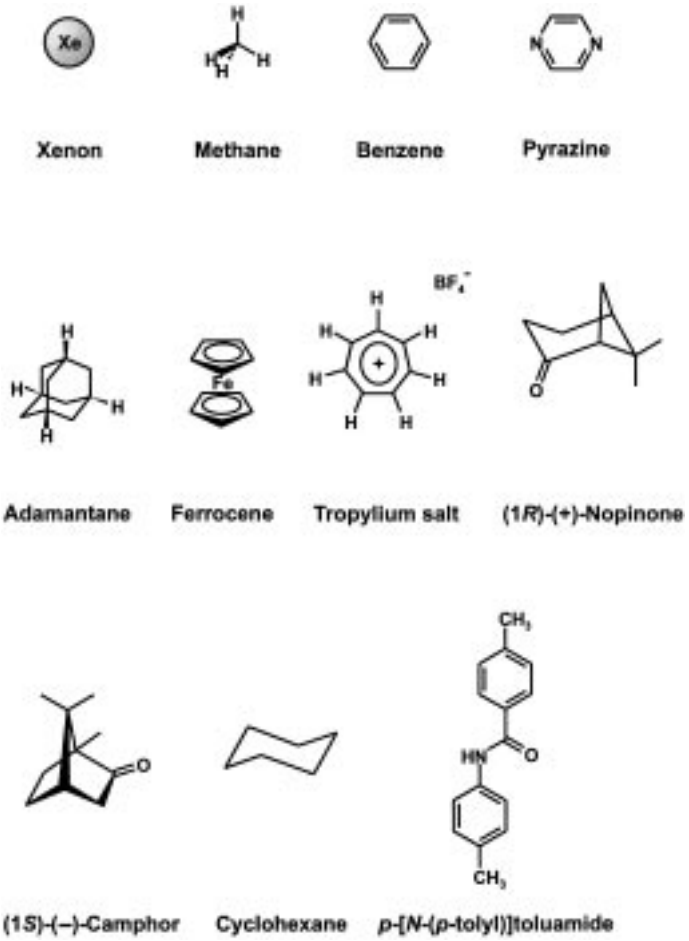

Scheme 24. Typical examples of guest molecules.

4.3.1. Characterization

NMR spectroscopy provides valuable information regarding molecular structure, guest inclusion, and the thermodynamic and kinetic parameters of the assembly process. In general, the proton signals of encapsulated guests experience upfield chemical shifts resulting from anisotropic shielding effects of the capsule. The magnitude of this chemical shift provides useful information about the orientation of the specific guest inside the capsule. Parts of the guest that are directed towards the apolar hemispheres of the capsule experience a larger anisotropic shielding than protons located in the polar equator and hence exhibit a larger chemical shift.[270, 271] Cohen and co-workers utilized pulsed-field gradient (PFG) NMR spectroscopy to show that the diffusion coefficient of encapsulated benzene in tetraureacalix[4]arene capsules is similar to the diffusion coefficient of the capsule itself, thus providing supporting evidence for its encapsulation.[272] Recently, ESI-MS was also used to characterize capsular complexes.[273, 274] The inclusion of ionic guest molecules gives charged complexes that can be readily detected by mass spectrometry. In certain cases it has been possible to identify the capsules by X-ray crystallography.[240, 255, 256, 266, 275–277] This technique, however, provides only structural information, and gives no thermodynamic or kinetic information.

4.3.2. Thermodynamics of Guest Encapsulation

Naturally, the size of the capsules poses restrictions to what kind of guest molecules can be encapsulated. Guests that are significantly larger than the cavity simply cannot fit without disrupting the structure of the capsule. On the other hand, the encapsulation of guests that are too small becomes unfavorable from an entropic point of view, since large voids remain inside the capsules. Mecozzi and Rebek studied a large collection of capsules with their guests and observed that the highest association constants are typically found for guests that fill the cavity to $55 \pm 9\,\%$.[278] This number corresponds remarkably well to the volume occupied by molecules in the liquid state. These guests have the appropiate size and shape for optimal van der Waals interactions with the cage. Deviations may occur as a result of specific functional groups on the guests, such as H-bond acceptors or donors, which cause additional stabilizing interactions. For instance, tetraureacalix[4]arene capsule $\mathbf{36}_2$ with a cavity of approximately 190 Å^3 binds a small guest, such as pyrazine, despite the fact that this guest only fills the cavity to 38 %.[247] The unexpected stability of this complex is attributed to stabilizing interactions

of the C–H bonds of pyrazine with the aromatic π surfaces of the calix[4]arenes and of the partially negative nitrogen atom with the polar H-bonded seam of the urea moieties. Pyrazine is also one of the best guests for the capsules reported by Sherman and co-workers, for which a similar evaluation holds.[279]

This study makes it clear that in most cases the driving force for the encapsulation process is strictly of enthalpic origin. A conceptual breakthrough was accomplished by Kang and Rebek, who observed that guest inclusion can also be entropically driven.[262] The thermodynamic stability of softball $\mathbf{37}_2$ with encapsulated adamantane and ferrocene derivatives was found to increase with temperature, which correlates with a positive entropy term. The positive entropy term results form the replacement of two molecules by one larger guest (Scheme 25a).

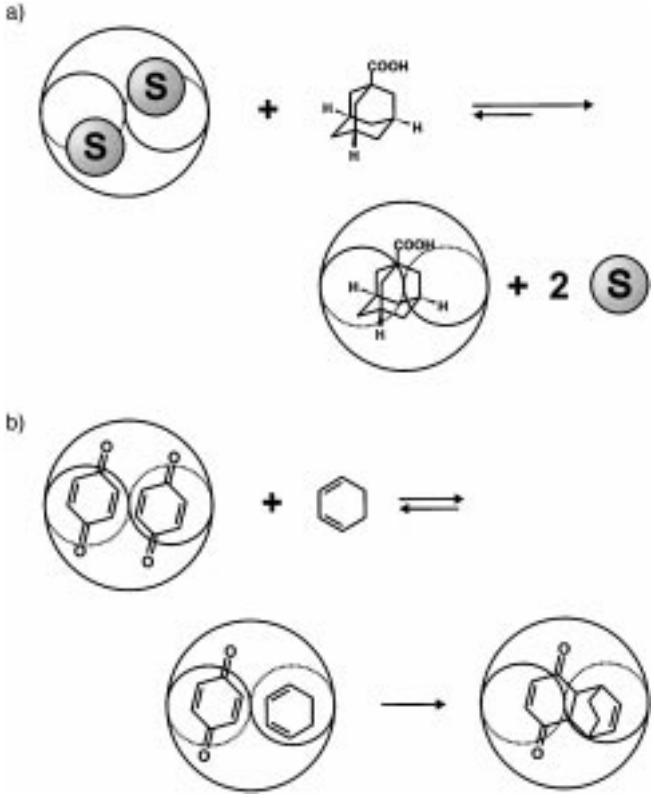

Scheme 25. a) Entropy-driven encapsulation in the softball (S = solvent molecule) and b) the softball as a mini-reactor for a Diels–Alder reaction.

4.3.3. Kinetics and Mechanism for Guest Exchange

Guest exchange in Cram's hemicarcerands occurs by an S_N1-type mechanism, which starts with the formation of an energetically highly unfavorable void that is subsequently filled with the new guest. The weak interactions that hold the H-bonded capsules together make alternative mechanisms for guest exchange possible that involve intermediates with significantly lower energies. Guest exchange may either occur through a dissociative mechanism, which involves full dissociation of the capsule, or a gating mechanism, which involves partial dissociation of the capsule, to create a portal (Scheme 26). Exchange studies by Rebek and co-workers with tennis ball complexes showed that the exchange rate for

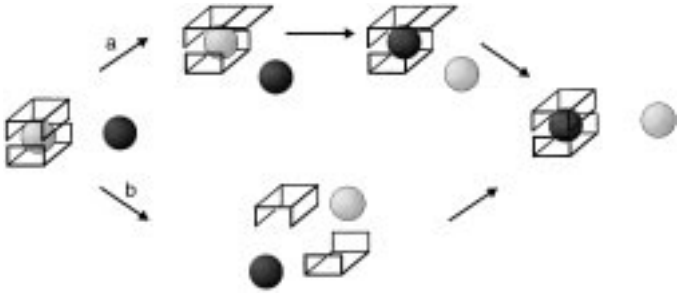

Scheme 26. Guest exchange can occur either by a gating (a) or a dissociative mechanism (b).

methane and ethane encapsulation is a factor of 5–8 higher than the observed dissociation rate of the empty capsule.[280] On the basis of these results they proposed a mechanism in which the seven-membered ring connecting the glycoluril and the aromatic spacer undergoes inversion, thus creating a portal for guests to exchange by an S_N2-type mechanism. Calculations by Houk et al. showed that the energy barrier of the rate-determining step in the gating mechanism, that is, breaking four H-bonds and ring inversion, is equally as high as that for dissociation of the capsule (30 versus 29 kcal mol^{-1}). However, the positive entropy term of about 6–12 kcal mol^{-1} for the dissociative mechanism, which is absent in the gating mechanism, renders it energetically the most favorable pathway. The discrepancy between kinetic and computational data illustrates the difficulties for a fundamental understanding of these dynamic processes.

In the case of the softball, both kinetic and computational studies indicate that the gating mechanism occurs. The eight additional H-bonds in the softball decrease the dissociation rate of the capsule to days.[281] In contrast to this, the guest-exchange process occurs within several minutes, which indicates that in this case exchange must take place through a gating mechanism. Kinetic studies support this view, since they reveal the presence of intermediate structures, which most likely correspond to a softball with one or two arms flipped over. Computational studies also support the gating mechanism, with an energy preference of 46 kcal mol^{-1} over the dissociative mechanism.[282]

Guest (benzene) exchange in tetraureacalix[4]arene dimers proceeds with a rate constant of 0.47 s^{-1}, as determined by EXSY measurements.[283] Böhmer and co-workers showed that the half-life increases from about 1 s to 60 h upon increasing the steric bulkiness of the urea units.[284] This enormous increase in kinetic stability results from a mechanical entanglement of the bulky residues which hinders "dethreading" of the monomers, similar to the process observed in rotaxanes.

4.3.4. New Physical Properties of Encapsulated Guests

The isolation of individual molecules inside molecular capsules can significantly change their chemical and physical properties. For this reason, Cram et al. characterized the interior of (hemi)carcerands as "a new phase of matter", which has unique properties that are different from the gas, liquid, or solid phase. This was most convincingly illustrated

by the successful isolation of cyclobutadiene inside a hemicarcerand. This extremely reactive molecule can normally only be isolated in an argon matrix at 8 K.[285]

Encapsulated guests in H-bonded capsules also exhibit novel physical properties as a result of the new chemical environment that they experience inside the capsule. One particular example involves the slightly increased barrier for ring inversion of cyclohexane ($\Delta\Delta G^{*} = 0.30$ kcal mol^{-1}) encapsulated inside the "jelly doughnut" assembly.[286] The energy difference is attributed to favorable C-H-π interactions that stabilize the ground-state chair conformation (D_{6h}) relative to intermediate conformations of higher energy. Similar stabilizing interactions are responsible for the constrained rotation of pyrazine inside Sherman's capsule.[270]

The cylindrical capsule recently described by Rudkevich and co-workers deserves special attention in regard to novel guest properties.[258] This capsule has an internal space of 5.7×14.7 Å that is well suited for guests with complementary shapes, such as bibenzyl and terphenyl. The relationship between the shape of the cavity and the guest becomes apparent from encapsulation studies of (*E*)- and (*Z*)-stilbene. Competition experiments reveal that the capsule has a selectivity for the *E* isomer of at least 50:1.[287] Unstable molecules, such as benzoyl peroxide, or noncovalent complexes, such as the H-bonded pyridone dimer, can be stabilized inside the capsule as well, a phenomenon that is reminiscent of the stabilization of cyclobutadiene inside Cram's carcerands. The noncovalent nature of these capsules enables an induced release of the guest molecules, for example, by the addition of polar solvents or competing guests, whereas the guests in covalent cages are kinetically trapped.[288]

4.4. Self-Assembled Capsules as Mini-Reactors

The encapsulation of two molecules inside a self-assembled cavity offers great potential with regard to catalysis. The catalytic effect results from a dramatic increase in the effective molarity of the reagents upon encapsulation. The use of molecular containers as mini-reactor vessels was first reported by Kang and Rebek following their discovery that the softball $\mathbf{37}_2$ can encapsulate two different guest molecules.[262] Subsequently, they studied the effect of the capsule on the Diels–Alder reaction between quinone and cyclohexadiene. When a mixture of the reactants was added to the capsule, only encapsulation of quinone was observed. Cyclohexadiene was apparently encapsulated also in very small, but sufficient, amounts, because the encapsulated product of the Diels–Alder reaction was formed slowly over time (Scheme 25b).[289, 290] A 200-fold rate acceleration was observed in the presence of the capsule over the control reaction. Product inhibition prevented real turnover and therefore this capsule does not truly act as a catalyst. True catalysis was subsequently observed when cyclohexadiene was replaced by the sterically more-demanding thiophene dioxide derivative. In this case the product of the Diels–Alder reaction with benzoquinone is expelled from the cavity as a result of its lowered affinity for the capsule.[291]

4.5. Chiral Capsules

Capsules display supramolecular chirality when the monomers are arranged in a dissymmetrical fashion upon formation of the assembly.[292] This phenomenon poses a new and intriguing question: do chiral capsules discriminate in the binding of chiral guest molecules? Recent work by the Rebek group reveals some of the answers. When a dissymetric spacer is used to connect two glycoluril moieties (C_s symmetry), for example, in **41**, the resulting capsule is formed as a pair of enantiomers (C_1 symmetry).[293] The inclusion of chiral guests gives rise to diastereomeric complexes, which are clearly observable by a doubling of the host and guest signals in the ^{1}H NMR spectra (Scheme 27). A maximum *de* value of 35% was observed, with a corresponding $\Delta\Delta G^{0}$ value of

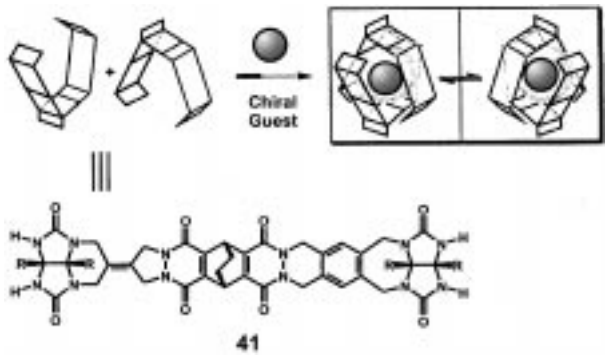

41

Scheme 27. Dissymmetrization of the monomer results in the formation of an enantiomeric pair of softballs. Encapsulation of chiral guests causes the complexes to be diastereomers.

0.4 kcal mol^{-1}. The selectivity increases with guest size as a result of increased van der Waals contacts of the guest with the capsule walls. Recent studies show that these capsules memorize the induced chirality after the chiral guest is exchanged with an achiral guest.[294] In another approach, the monomers were desymmetrized by substituting the two glycoluril moieties with different side groups.[295] Again, the capsules were formed as a pair of enantiomers, but in contrast to the previous study no diastereoselectivity was observed upon the addition of chiral guests. Apparently, diastereoselective guest encapsulation is only observed if the chiral information in the capsule is directed inwards, that is, influences the interior of the capsule.

The tetraureacalix[4]arene capsules exhibit supramolecular chirality as a result of the directionality of the H-bonded seam of the urea moieties, provided that the northern and southern hemisphere of the capsule are different. Böhmer and co-workers showed that the mixing of two symmetrical homomeric capsules spontaneously results in the formation of statistical amounts of the asymmetrical heterodimeric capsule.[248, 283] Surprisingly, Rebek and co-workers discovered that the asymmetrical heterodimer is formed exclusively when two symmetrical ureido- and sulfonylureido-functionalized calix[4]arenes were combined.[296] Subsequent studies with a variety of heterodimers with chiral α-methylbenzylamino or amino acid side chains revealed that heterodimerization was not quantitative in all cases, but the amount of heterodimer

present was sufficient to study the complexation behavior of chiral guests. Addition of (−)-nopinone to heterodimers of opposite handedness indeed gave diastereomeric complexes. However, these chiral capsules exhibit modest enantioselectivities in the binding of chiral guests (1.3:1).[297]

Carceroisomerism, the new type of isomerism resulting from two different alignments of asymmetrical guests in capsules with different hemispheres,[298] was also observed in H-bonded capsules. Chapman and Sherman found that pyrazine can adopt two different orientations inside their capsule, with an activation energy for rotation around the pseudo-C_1 axes of 18 kcal mol^{-1}. This value is almost identical to that found for the very similar covalent complex.[270] Rotation of the guest around the equatorial axes requires partial breakage of the assembly, which raises the energy barrier.

4.6. Inclusion Complexes in the Solid State

Crystal engineers aim to design solid-state structures by using functional building blocks. In this respect H-bonding interactions provide a unique tool because of their high directionality and easy synthetic access. It is beyond the scope of this review to give an exhaustive overview of all the crystal structures in which H-bonding plays an important role. However, the three examples presented here merely illustrate the potential of H-bonding in crystal engineering, especially regarding the formation of open "zeolite-like" materials.

As an extension of the study on the self-assembly of 2-pyridone dimers in solution (see Section 2.3.2) Wuest and co-workers covalently arranged four 2-pyridone moieties in a tetrahedral fashion around a central carbon atom to give multidentate modules called tectons.[299] Crystallization of this tecton from butyric acid/methanol/hexane mixtures gave diamondoid networks with large internal chambers occupied by butyric acid molecules. This very robust organic material displays zeolite-type properties in the sense that the network is sufficiently porous to permit exchange of guests.[300]

Russell and Ward made use of the H-bonding interactions between guanidinium cations and sulfonates for the construction of solid-state materials with guest-selective binding properties.[301] Initial studies addressed the question of structural diversity within the individual building blocks,[302, 303] while later work focussed on tailoring the solid-state structure to optimize guest recognition properties.[304, 305]

Aoyama and co-workers described the formation of crystals of anthracenediresorcinol derivatives, such as **42**, that are stabilized through extensive H-bonding networks (Scheme 28).[306] The cavities inside the crystals are occupied by a variety of different guest molecules, such as quinones, alkyl benzoates, aliphatic esters, and ketones, as well as nitrobenzene.[307] Moreover, the cocrystallized solvent molecules can be exchanged for a variety of other guests without destroying the crystals.[308] These organic solids can promote stereoselectivity in the Diels–Alder reaction between acrolein and cyclohexadiene, unfortunately not in a catalytic manner.[309]

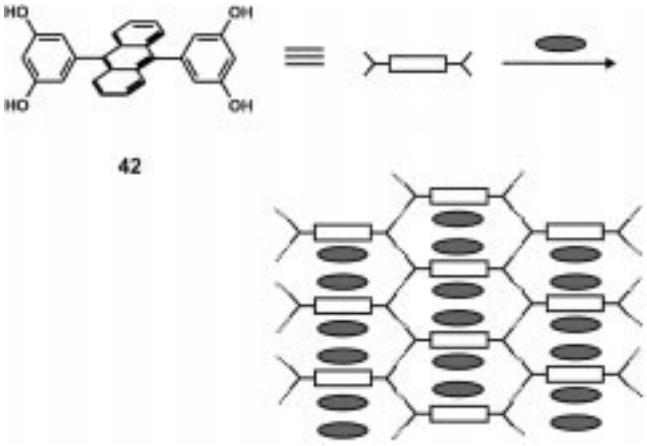

Scheme 28. Crystallization of anthracene-bis(resorcinol) derivatives, such as **42**, results in the formation of porous networks.

5. Templated Synthesis

"The use of one molecule as a template to guide and facilitate the synthesis of another […] has not hitherto been attempted in laboratory synthesis, although it seems probable that it is common in living systems. It represents a challenge which must, and surely can, be met by organic chemistry."
Alexander Todd, 1956

5.1. Introduction

Template-directed synthesis uses noncovalent interactions to enhance the rate and/or selectivity of a particular chemical reaction.[310–313] The catalytic effect can be the direct result of complex formation between (self-)complementary reactants (Scheme 29A), or can be exerted by an external template that is (self-)complementary to the reactants (Figure 29B and C). Self-replication (Scheme 29C) involves a special type of templating, in which molecules catalyze their own formation by formation of complexes with both the reactants. This type

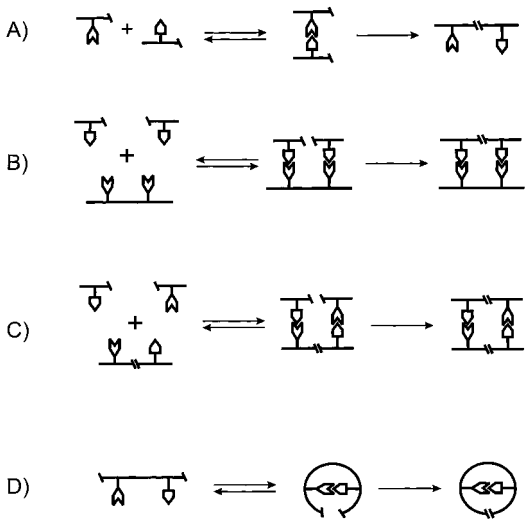

Scheme 29. Types of template effects: in bimolecular reactions (A and B), self-replicating systems (C), and macrocyclization reactions (D).

of catalysis is commonly observed in any system that bears self-complementary recognition sites, but its occurrence can be strongly attenuated by intramolecular complexation as a direct result of insufficient structural rigidity of the linker unit.[314] Finally, intramolecular template effects frequently occur in macrocyclization reactions (Scheme 29 D), and are commonly used to promote the formation of large macrocycles or mechanically interlocked systems.

The majority of template effects are positive and consequently lead to a decrease in the activation energy for the reaction. The observed effects, which are entropic in nature, are the result of a higher effective concentration of the substrates within the complex, and can be best expressed in terms of an effective molarity—the ratio of the rate constants for the templated and the nontemplated reaction.[315] In addition to this, the template can lower the energy of the transition state through stabilizing enthalpic interactions.[316] Template effects can also be negative, which means that the template increases the energy barrier for the reaction by reducing the effective concentration of the reactants.[310]

This section summarizes recent efforts in templated synthesis that involve the formation of H-bonded complexes. A special example of templated synthesis was discussed in Section 4.4, in which the binding of two reactive molecules inside a hydrogen-bonded molecular capsule was found to catalyze their chemical reaction. Since many reviews cover the early work in this field, we will mainly focus on developments during the last decade.[317–321]

5.2. Reaction of Molecules with Complementary Binding Sites

To date, there has been relatively little interest in the occurrence of internal template effects, most likely because of the overwhelming attention paid to the self-replicative effects that are usually observed in these systems (see Section 5.4). Rebek and co-workers reported a tenfold rate increase for the reaction between amine **43** and active ester **44** (8.2 mM in $CHCl_3$) to give **45**, which arises as a direct result of the formation of Watson–Crick H-bonds ($K_{ass} = 60\,M^{-1}$) between the adenine and Kemp's triacid moieties (Scheme 30).[322] Rate enhancements as large as 3500 were observed in a more elaborate system in which the flexibility of the linkers allows a much better approach of the reactive groups.[323]

Philp and co-workers studied the recognition-induced control of Diels–Alder reactions using the 2-amidopyridine · carboxylic acid motif ($K_{ass} \sim 170\,M^{-1}$; Scheme 31).[324, 325] A drastic increase in the *endo*/*exo* product selectivity ($\Delta\Delta G^0 = 21.9\,kJ\,mol^{-1}$ for the recognition-mediated reaction and $4.7\,kJ\,mol^{-1}$ for the control reaction) was observed for the reaction between **46** and **47a**, while for the reaction between **46** and **47b** the selectivity was hardly different to that of the control reaction ($\Delta\Delta G^0 = 6.2\,kJ\,mol^{-1}$ for the recognition-mediated process and $6.1\,kJ\,mol^{-1}$ for the control reaction). Selective formation of the *exo* product was observed in a structurally analogous system, and occurred most likely as the result of intramolecular H-bonding.[326] Only the formation of

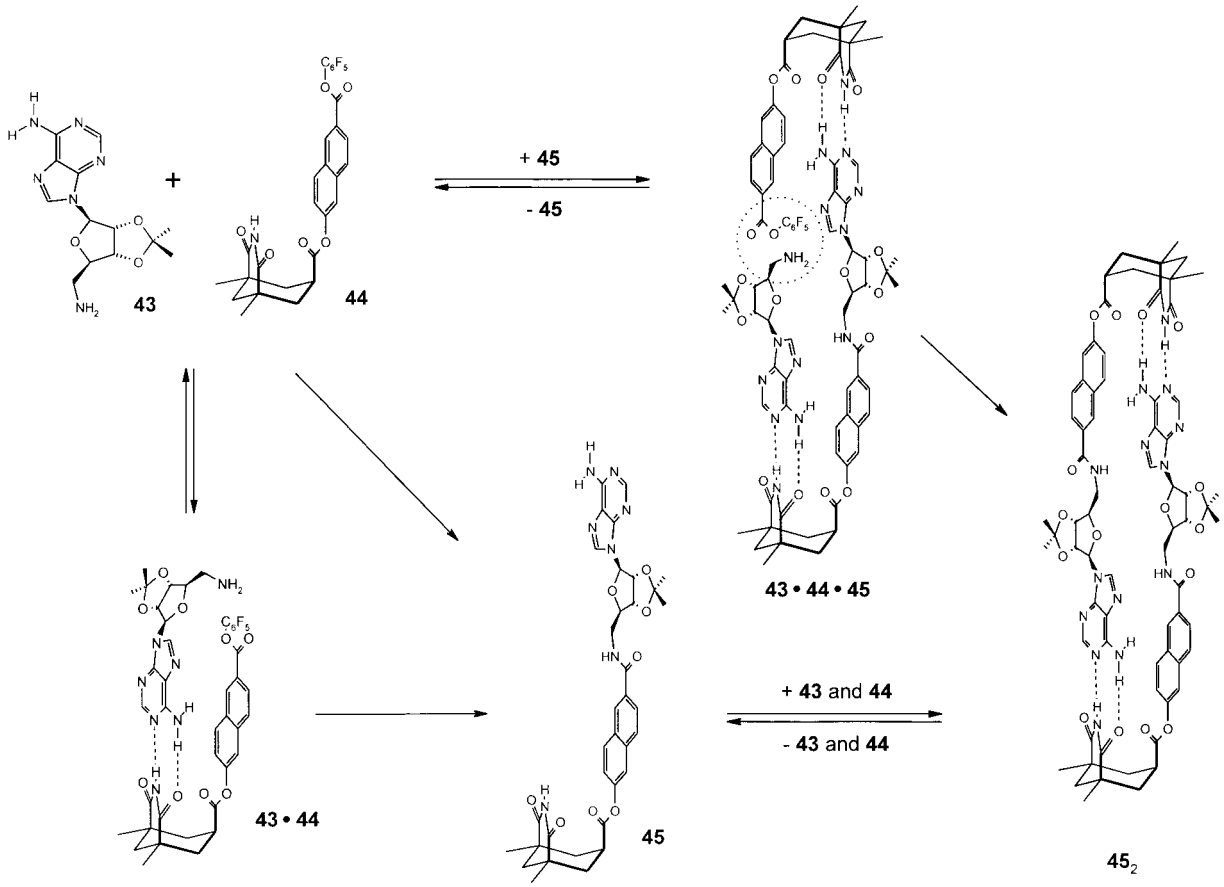

Scheme 30. Self-replication cycle for the templated synthesis of template **45**.

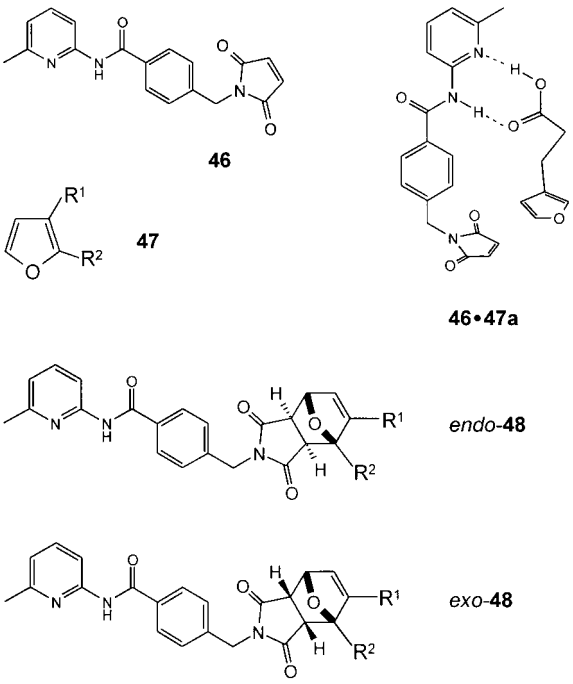

Scheme 31. Recognition-induced control of the Diels–Alder reaction between diene **47** and dienophile **46**.

endo-**48a** showed a positive template effect (kinetic effective molarity 63 mM), while for all other products the activation barrier for formation had increased as a result of the formation of H-bonds. Similar studies for a [2+3] dipolar cycloaddition reaction showed a much larger rate acceleration (kinetic effective molarity 2.16 M), although the stability of the reactive complex was much lower ($K_{ass} \approx 28\,M^{-1}$). These results clearly illustrate that the strength of the association of the reactive partners does not seem to correlate with the observed rate effects.[327]

5.3. External Template Effects

Template-directed reactions which model DNA replication have received a great deal of attention. Early work by Orgel demonstrated that the template-directed ligations of most activated nucleotides are inefficient and nonregiospecific (preference of natural 3′-5′ over unnatural 2′-5′ ligation), except for the 5′-phosphoro-2-methylimidazolides, which show relatively high efficiency and regioselectivity in the coupling reactions.[320] Moreover, it was found that pyrimidine-rich oligo- and polynucleotides efficiently act as templates for the polycondensation of activated mononucleotides, while purine-rich oligonucleotides do not.[328, 329] For example, the pentamer d(pGGCGG) was obtained in 18% yield by using d(pCCGCC) as a template. Under enzyme-free conditions the templated synthesis of an oligonucleotide 14-mer was achieved in 2% yield; the main problems were the limited regiospecificity and efficiency of the coupling reaction.[330] Significantly higher yields were obtained in coupling reactions with oligonucleotide fragments of three or more base pairs. Goodwin and Lynn reported a fourfold increase in the yield of the reversible imine formed between the trimers d(CGT)-CHO and H_2N-d(TGC) in the presence of the template hexamer d(GCAACG) at 0 °C, while at 30 °C the yield was hardly different.[331] Moreover, it was found that the selectivity for trimer H_2N-d(TGC) and tetramer H_2N-d(TTTT) in this reaction also showed a large temperature dependance (about 2:1 at 30 °C and >30:1 at 0 °C). Both findings reflect the improved stability of the ternary complex at lower temperatures.

Ross Kelly et al. described the first example of template effects in truly synthetic systems involving H-bonding.[332] The template contains two identical noncomplementary ADD recognition sites where two substrate molecules with DAA recognition sites can be bound. A sixfold rate increase was observed at reactant and template concentrations of 4.0 mM. Product inhibition was not observed in this case since the product precipitated as a salt after formation. A second template with nonidentical binding sites (DAA-ADA) turned out to be more effective, most likely because nonproductive complexes with two identical substrates are not formed in this case.[333]

Rebek and co-workers extensively studied the role of geometrical factors on the template effect in acyl transfer reactions by using the recognition of adenosines by synthetic receptors based on Kemp's triacid.[316, 334] These studies showed that rate enhancements can differ by a factor of 160 depending on the geometrical orientation of the two recognition sites. The observed differences are not solely entropic, but also seem to be the result of geometry-dependent formation of internal H-bonds that can stabilize the transition state for acylation. Another study by the same research group showed that template effects can be further improved by two orders of magnitude when additional stabilizing functionalities are incorporated.[323] Interestingly, the template can be turned "on" and "off" when a light-switchable diazobenzene spacer is used.[335] While the *E* isomer of the template has a negligable effect on the reaction rate, irradiation with light of 366 nm wavelength causes nearly a tenfold rate enhancement, which is clearly attributed to the presence of 50% of the active *Z* isomer.

Very recently, Krische and co-workers used similar template effects in the covalent casting of one-dimensional H-bonding motifs for the preparation of duplex molecular strands.[336]

5.4. Self-Replication

When Watson and Crick discovered the DNA double helix in 1953, they realized immediately that its replication involved a templated synthesis, in which a single strand of DNA acts as a template for the formation of the double strand. An autocatalytic process in which the reaction product serves as the specific catalyst for its own synthesis by recognizing and promoting coupling of the reactants is the most basic form of molecular self-replication. In fact, the realization that self-replication can be regarded as a primitive sign of a living

system has inspired many different research groups to investigate this type of catalysis in synthetic systems.[318–320, 337, 338]

5.4.1. Synthetically Modified DNA and RNA

In 1986 von Kiedrowski reported the first example of nonenzymatic self-replication in the chemical ligation of the self-complementary trinucleotides d(^{Me}CCGp) (**49**) and d(oCGG^{ClPh}) (**50**; o = hydroxyl; ClPh = 3′-(2-chlorophenyl) phosphate).[339] As expected, the addition of various amounts of the template product d(^{Me}CCGpoCGG^{ClPh}) (**51**) increased the rate of product formation according to the empirical square-root law for template autocatalysis: $d[\mathbf{51}]/dt = [\mathbf{49}][\mathbf{50}](k_a[\mathbf{51}]^{1/2} + k_b)$, where k_a and k_b are the rate constants for the autocatalytic and the noninstructed process, respectively. Sequence-variation studies of **51** showed that the self-complementary product is formed faster than any of the other sequences, which indicates that the observed autocatalysis is indeed the result of a template effect.[340] Luisi and co-workers found that the kinetics for self-replication of **51** inside vesicles are comparable to bulk-phase conditions.[341]

Autocatalytic behavior was also reported by Zielinski and Orgel for the synthesis of tetranucleotide triphosphoamidates, in which chemical ligation involves phospoamidate bond formation.[342] This work provides the first evidence for the self-replication of synthetically modified biomolecules. Parabolic growth, a characteristic of self-replicating systems that suffer from product inhibition, was observed by von Kiedrowski in a similar replicating system involving the synthesis of d(^{MTM}CCGpnCGG^{ClPh}) (MTM = 5′-*O*-methylthiomethyl; pn = 3′-5′phosphoamidate).[343] Parabolic growth is usually only observed for replicators with a high catalytic efficiency ($k_a/k_b = 300-400$). The same system even showed characteristics of information transfer and selection, though very concealed, when the template molecule was synthesized from three different components.[344]

Cross-catalytic self-replication of complementary templates proceeds with efficiencies similar to those of self-complementary replicators. In this case, the template does not catalyze its own formation, but rather a complementary template that subsequently catalyzes the original template's synthesis. Sievers and von Kiedrowski performed a study in which the two self-complementary templates d(^{MTM}CGGpnCCG^{ClPh}) (AB) and d(^{N3}CCGpnCGG^{ClPh}) (BA; N3 = 5′-azido-5′deoxy) and the two complementary templates d(^{MTM}CGGpnCGG^{ClPh}) (AA) and d(^{N3}CCGpnCCG^{ClPh}) (BB) compete in a combinatorial synthesis with four common trinucleotide precursors. This study revealed that selective stimulation of template synthesis, and thus information transfer, occurs on seeding the reactions with one of the four templates.[345, 346] One year later, Orgel and co-workers showed that RNA oligonucleotides can also template the synthesis of complementary PNA strands (and vice versa). Moreover, they showed that ligation to form chimeras proceeds efficiently both on PNA and on DNA templates. The efficiency of the ligation is primarily determined by the number of backbone bonds at the ligation site and the relative orientation of the template and substrate strands.[347] These experiments demonstrate that takeovers of this kind can occur without the loss of genetic information, which supports the idea that other genetic systems might have preceded RNA.[348]

The self-replication of duplex DNA by means of triple-helix formation was reported by Li and Nicolaou.[349] Initially, the duplex DNA strand binds two complementary single-strand DNA fragments and catalyzes their chemical ligation. Upon raising the pH the single-strand DNA is released and now can serve as a template for the synthesis of the complementary strand, thus giving a copy of the original duplex DNA. This scheme of stepwise replication has the potential of overcoming the problem of product inhibition. Recently, the surface-promoted replication and exponential amplification of DNA analogues (SPREAD) was reported.[350] The role of the solid support is to separate complementary templates which would otherwise form stable duplexes. Similar processes might also have played a role in the origin of life on Earth, since the earliest replicating systems may have proliferated by spreading on mineral surfaces.

Eschenmoser and co-workers studied the replicating behavior of pyranosyl-RNAs, synthetic analogues of the natural furanosyl-RNAs, which display exceptional base-pairing behavior as a result of their much higher rigidity.[351] It was found that the tetramer-2′-phosphate p-ribo(C_4)-2′-p (**52**) regioselectively (4′-2′) ligates to form higher oligomers **54** in the presence of template p-ribo(G_8) (**53**; Scheme 32). No ligation was observed in the absence of the template or in the presence of "wrong" templates (four mismatched pairs in the product octamer), which shows that the template effect is sequence selective. Similarly, the template p-ribo(C_8) (**55**) catalyzes the ligation of p-ribo(G_4)-2′-p (**56**) with comparable efficiency,

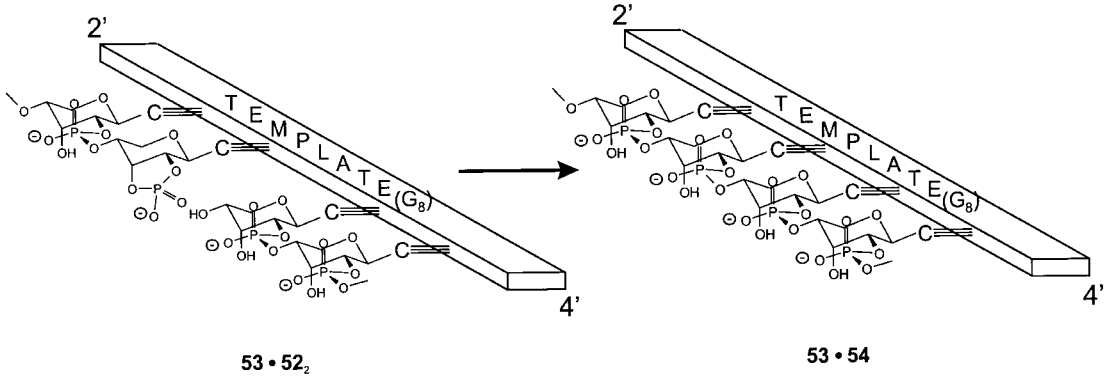

53 • 52$_2$ **53 • 54**

Scheme 32. Ligation of p-RNA tetranucleotide-2′,3′-cyclophosphate **52** on p-RNA template **53**.

which shows that the C_8 and G_8 octamers **53** and **55** can self-replicate by a double replication cycle. Further experiments showed that the template effects are highly stereoselective, namely, templates containing a single *enantio*-ribopyranosyl are not active at all.[352] The main difference to the natural furanosyl-RNAs is the remarkable absence of self-deactivation for G-rich templates in the p-RNA series.

5.4.2. Other Synthetic Systems

In living systems, single strands often act as templates during phosphate transfer reactions. Rebek and co-workers showed that self-replication also occurs in the acyl transfer reaction between adenosine amine **43** and the activated ester **44** to give the self-complementary product **45** (Scheme 30).[322] The self-replicative activity of product **45** is the result of the careful design of the molecules;[353] steric interaction between the two ribose "bulges" keeps the dimer $\mathbf{45}_2$ apart ($K_{dim} = 630\,M^{-1}$) so that it is available for the desired templation. It was found that the initial rate of this reaction at 8.2 mM increases by 40–70% upon addition of 0.2–0.5 equivalents of product **45**.[314] A similar rate effect was not observed with crippled analogues of **45**, in which one of the recognition sites was blocked. Simple "amide-catalysis" as suggested by Menger et al. cannot explain the observed rate enhancement at this low concentration.[338, 354, 355] Furthermore, Menger et al. claimed that an alternative mechanism in which recognition of only one reactant is required could also explain the observed effects.[356] However, detailed analysis of the reaction kinetics by Reinhoudt's group clearly revealed that self-replication as defined by Rebek and co-workers operates in this system.[357] Other pathways, such as the (bimolecular) pathways described by Menger et al., obscure the simple picture of the ternary complex **43**·**44**·**45** being the only explanation for the observed rate enhancement. Simulations by Reinhoudt et al. showed that reaction of **43** and **44** in the ternary complex is 6.8 times faster than for the uncatalyzed bimolecular reaction, which illustrates the efficiency of the template **45**. Sigmoidal growth was observed in a structurally optimized system in which the naphthyl spacer was replaced by a dibenzyl spacer to suppress the bimolecular reaction.[358–360]

A xanthene-based replicator that utilizes the recognition between thymine and diaminotriazine residues also shows autocatalytic behavior.[361] Crossover or recombination experiments between different replicators gives both active and inactive mutants, the activity of which entirely depends on their molecular shape.[361] Competition experiments using several different replicators revealed that the more effective replicator rapidly takes over the system's resources.[362] In a primitive way these experiments resemble mutations in nature which form the basis for biological evolution. Quite recently, Rebek and co-workers showed that the formation of hydrogen-bonded molecular capsules (Section 4) also exhibit recognition features that are characteristic of self-replication.[363]

Terfort and von Kiedrowski reported the only synthetic system that replicates in a polar solvent.[364] The system explores the relatively strong association between amidinium **57** and carboxylate **58** ($K_{ass} = 350\,M^{-1}$ in DMSO) to self-organize the reactants in the reactive termolecular complex **57**·**58**·**59** (Scheme 33). The system exhibits an autocatalytic efficiency (factor by which the template is built faster by the autocatalytic way than by the nonautocatalytic way) of $16.4\,M^{-1/2}$, which is comparable to that of the hexanucleotide **51** ($24\,M^{-1/2}$) and Rebek's system ($22\,M^{-1/2}$).

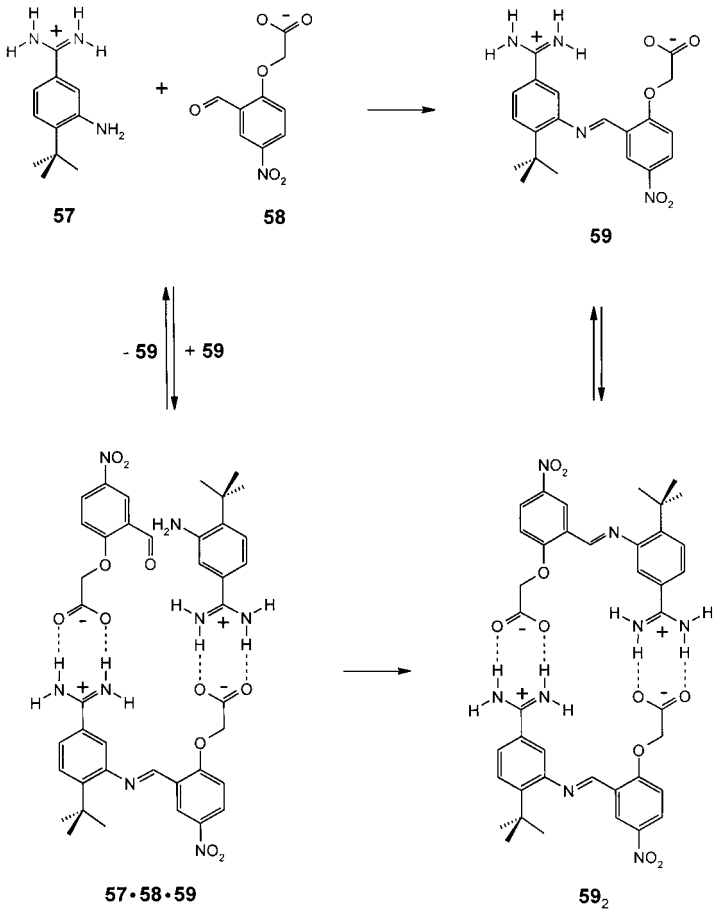

Scheme 33. Self-replication as observed in polar solvents by formation of the ternary complex **57**·**58**·**59**.

Persico and Wuest studied self-replicative effects in the copper-induced oxidative coupling of 3- and 6-ethynylpyridones.[365] A purely statistical product distribution was found, despite the fact that only one of the three products was complementary to itself. This observation prompted the authors to conclude that self-replication was not operative in their system, either because of rigidity in the system or because of strong dimerization of the template ($K_{dim} > 6.0 \times 10^4\,M^{-1}$ in $CHCl_3$). However, an alternative explanation could be that a template effect is indeed present, but that it is obscured by the fact that the two non-self-complementary products form a replication cycle because they are complementary to each other and therefore can catalyze each others formation.

Wang and Sutherland reported the first example of self-replication in a Diels–Alder reaction by utilizing the H-bond mediated recognition between 6-acylamino-2-pyridone and

2-acylamino-1,8-naphthyridine.[366] Although transition-state binding to the template is reasonably effective (effective molarity about 4 M), no attempts were made to study the effect of added template on the *endo*/*exo* product ratio.

5.5. Templated Cyclizations

5.5.1. Macrocyclization Reactions

Template effects can drastically alter the course of macrocyclization reactions and consequently promote the formation of one particular product.[367] For example, intramolecular H-bond formation is responsible for the observed template effects in amide-based macrocyclization reactions as studied by Hunter and co-workers. It was found that the reaction between isophthaloyl dichloride and diamine **60a** yields 88% of the cyclic tetramer **61a**, while higher oligomers were not found (Scheme 34).[368] In their studies of the covalent capture of noncovalent peptide ensembles Clark and Ghadiri observed template effects that result from intermolecular H-bonding.[369, 370] Olefin metathesis of homoallylglycine-bearing octapeptide dimer $\mathbf{62_2}$ smoothly yielded the corresponding covalent cyclic dimer **63** in 65% yield, whereas no product was formed in the absence of the H-bonded dimer (Scheme 35).

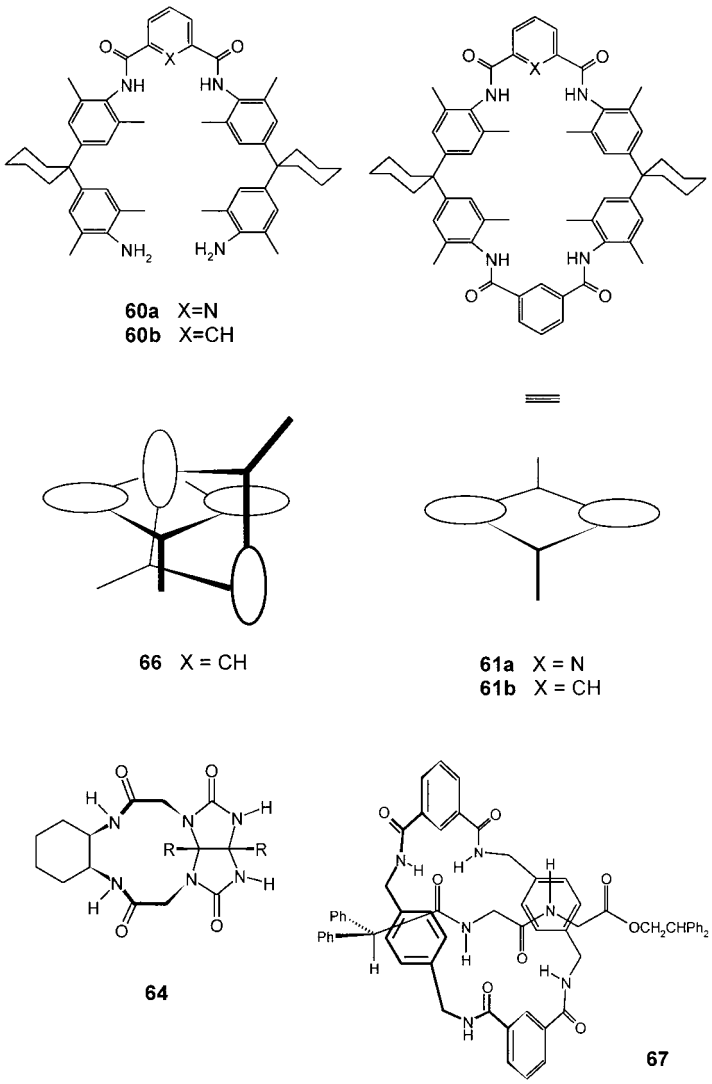

Scheme 34. Templated-directed synthesis of macrocycle **61** and **64**, catenane **66**, and peptide rotaxane **67**.

Rudkevich and Rebek reported a cyclization reaction that was templated by the product (**64**) of the reaction (Scheme 34).[363] The observed template effect strongly resembles that of the self-replicating systems as discussed in Section 5.4, but differs in the sense that in this case the product catalyzes the *intra*molecular cyclization of an intermediate (unimolecular reaction) rather than the *inter*molecular reaction between the reactants (bimolecular reaction). The template both increases the yield of the reaction (from 20 to 55%) as well as the rate (more than threefold) of its own formation. Whether the reaction exhibits true autocatalytic behavior awaits further kinetic studies.

Recently, Reinhoudt's group reported one of the most spectacular examples of templated synthesis in which H-bond formation is involved (Scheme 35). Reaction of assembly $\mathbf{26e}_3 \cdot (\mathrm{BAR})_6$, which carries 1-octenyl side chains, with Grubbs catalyst in CD_2Cl_2 resulted in the covalent linkage of the three calix[4]arene units **26e** through a threefold metathesis reaction to give the 123-membered macrocycle **65** as the corresponding hydrogen-bonded assembly $\mathbf{65} \cdot (\mathrm{BAR})_6$ in 96% yield.[371] Not a single trace of **65** was formed in the absence of BAR as a template. Moreover, the reaction turned out to be extremely sensitive to the length of the alkenyl spacer: with 1-hexenyl side chains the reaction did not give any of the desired trimer, while for 1-decenyl spacers the yield was reduced to 71% yield.

5.5.2. Catenane and Rotaxane Formation

Catenane formation involves a special type of template effect, one in which an empty macrocycle (one half of the catenane) complexes its linear precursor and subsequently templates the formation of the catenane.[372–374] The clear difference with most self-replicating systems is the nonreversibility of the dimer formation. Therefore, reversibly formed catenanes could potentially exhibit self-replicating behavior.[375]

Significant amounts of the catenated product **66** (29%) were formed in the reaction between **60b** and isophthaloyl dichloride as a direct result of the formation of strong intermolecular H-bonds between the empty macrocycle **61b** and its linear precursor (Scheme 34).[376] Very similar catenanes were reported shortly after by the group of Vögtle,[377] who extended the concept further to the synthesis of amide-linked rotaxanes by using anion complexation.[378] Later, Leigh and co-workers found similar template effects in the formation of catenanes obtained from isophthaloyl dichloride and benzylic diamines.[379, 380] Moreover, this research group reported that linear amides[381] or peptides[382] can also act as templates in the synthesis of amide-based rotaxanes such as **67** with yields as high as 62% (Scheme 34).[375] A novel class of pseudorotaxanes that were stabilized largely by H-bonding interactions between secondary dialkylammonium salts and crown ethers, was recently reported by Stoddart and co-

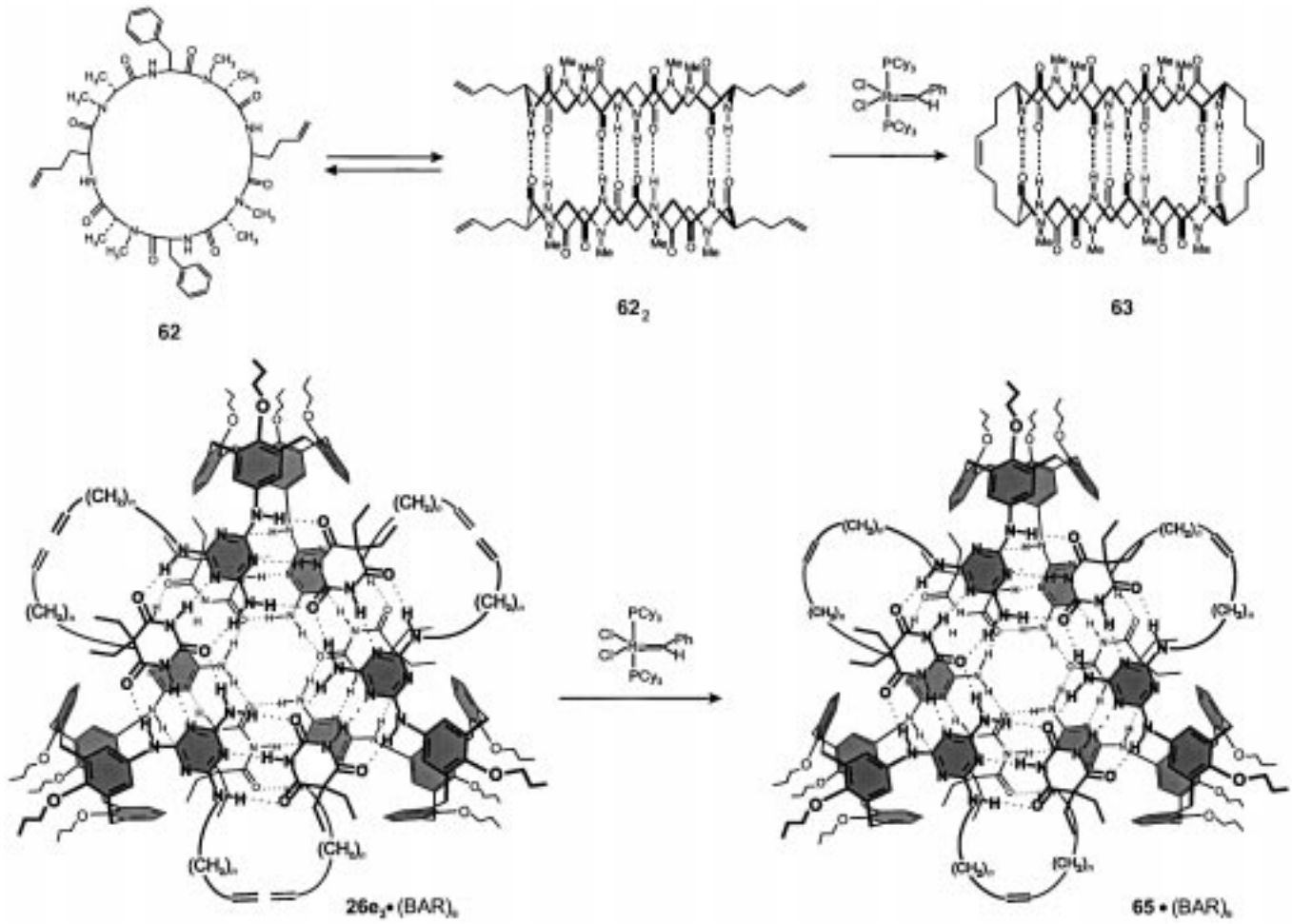

Scheme 35. Covalent capture of octapeptide dimer $\mathbf{62}_2$ and double-rosette assembly $\mathbf{26e}_3 \cdot (BAR)_6$.

workers.[383] This recognition motif was also used for the preparation of [2]rotaxanes as pH-controllable molecular shuttles.[384]

6. Properties and Applications of H-bonded Assemblies

"The most fundamental and lasting objective of synthesis is not production of new compounds, but production of new properties"
George Hammond, 1968

6.1. Introduction

A lot of work on self-assembly through H-bonding is aimed at a particular application, such as in Section 4 where H-bonded molecular capsules for guest complexation and molecular catalysis were described. This section reviews H-bonded assemblies that exhibit novel properties *as a direct result* of the H-bonding interactions. A full coverage of all the literature would certainly be beyond the scope of this review and therefore only a representative selection of important developments is given, which adequately illustrates where the field is moving.

6.2. Photo- and Redox-Active Assemblies

6.2.1. Photoactive Assemblies

The mechanism of how energy and electrons are transferred over long distances in biological systems, such as DNA or in light harvesting systems, is currently not known. H-Bonded model systems have been studied to provide fundamental insight into these processes. Hamilton and co-workers showed that the fluorescence of a dansyl moiety (dansyl = 5-dimethylaminonaphthalene-1-sulfonyl) is quenched as a result of energy transfer to a free-base porphyrin connected by six H-bonds.[385] Sessler and co-workers studied the energy transfer in 1:1 H-bonded complexes of cytosine-substituted zinc and free-base porphyrins.[386] The time-resolved fluorescence measurements of the zinc porphyrin showed bi-exponential decay profiles as a result of significant dissociation of the cytosine dimer (cleavage of only two H-bonds) under the experimental conditions. The longer lifetimes, which account for $\geq 80\,\%$ of the total fluorescence, correspond to the monomeric zinc porphyrin present. The shorter lifetimes originate from quenching of the Zn-porphyrin fluorescence by energy transfer to the free-base porphyrin. Further studies on rigid analogues utilizing the G·C base-pair motif allowed the complete elucidation of the mechanism of energy transfer.[387]

Time-resolved fluorescence meaurements showed that singlet–singlet energy transfer occurs through a Förster-type mechanism (through-space) with a rate constant of $9 \times 10^8\ s^{-1}$ and a quantum efficiency of 60%. Transient absorption measurements showed that triplet–triplet energy transfer is very slow and occurs by a Dexter-type mechanism (through bond).

Photoinduced electron transfer (ET) occurs when the energy level of the excited state of the donor is high enough to reduce the acceptor.[388] Studies on complexes based on imide · diamidopyridine interactions[389, 390] and carboxylic acid dimerization[391] revealed that H-bonded interfaces hardly pose a barrier for ET, with rates only slightly lower (about $10^{10}\ s^{-1}$) than for covalently bound structures (about $10^{11}\ s^{-1}$). High-field EPR studies of noncovalent complexes of Zn-porphyrins with either quinone or dinitrobenzene units have shown that ET pathways are stabilized by multiple H-bonding interactions.[392, 393]

6.2.2. Redox-Active Assemblies

The research groups of Yano and Rotello have extensively studied the mechanism by which flavoenzymes change the redox properties of cofactors through a combination of H-bonding, electrostatic interactions, and $\pi-\pi$ interactions.[394, 395] Flavin binds to diamidopyridine derivatives through threefold H-bonding (DAD · ADA array) with $K_{ass} = 10^2 - 10^3\ M^{-1}$ in chloroform. Cyclic voltammetry measurements revealed that the flavin radical anion is significantly stabilized upon complexation with diamidopyridine.[396] The K_{ass} value of the complex increases by a factor of 500 upon reduction of the flavin unit as a result of increased electron density at the carbonyl groups. Similar increases in binding strength upon reduction have been reported for simple imide · amidopyridine and quinone · urea dimers.[397] On the basis of this principle, a three-component molecular switch that could be controlled electrochemically was constructed (Scheme 36).[398] The system is composed of two receptor molecules (**68** and **69**) that can both form a dimeric complex with naphthalimide **70**. In the oxidized state, guest molecule **70** has a higher affinity for receptor **68** as a result of favorable stacking interactions ($K_{ass} = 1840\ M^{-1}$ for $\mathbf{68} \cdot \mathbf{70}_{ox}$ and $150\ M^{-1}$ for $\mathbf{69} \cdot \mathbf{70}_{ox}$). In the reduced state, however, the electrostatic repulsion strongly destabilizes the $\mathbf{68} \cdot \mathbf{70}_{red}$ complex, while the K_{ass} value for dimer $\mathbf{69} \cdot \mathbf{70}_{red}$ increases to $41\,000\ M^{-1}$ as a result of stronger H-bonding interactions. Consequently, guest **70** "switches" from receptor **68** to receptor **69** upon reduction.

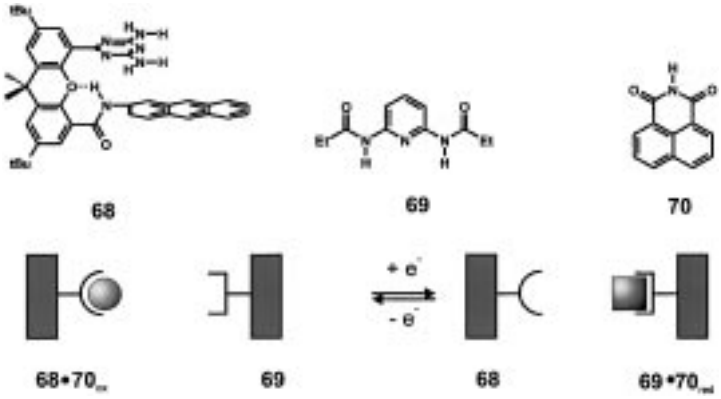

Scheme 36. A three-component electrochemically controlled switch.

6.3. Self-Assembly at Interfaces

6.3.1. Sensor Development: The Air–Water Interface

Ariga and Kunitake observed that monolayers of alkylated guanidinium at the air–water interface associate with phosphates present in the aqueous phase with a K_{ass} value of $10^6 - 10^7\ M^{-1}$.[399] This value contrasts strongly with the dimerization constant of $1.4\ M^{-1}$ in bulk water. The strong enhancement of the binding affinity is attributed to a dramatic decrease in the dielectric constant close to the hydrophobic phase. This effect offers the possibility of utilizing H-bonding interactions for molecular recognition purposes in Langmuir films at the air–water interface.[400–404] Since Langmuir monolayers are in a dynamic equilibrium, they can to some extent be regarded as a dynamic library of functionalities (see Section 6.6). Kunitake and co-workers showed that mixed monolayers displaying an ADA, a DA, and a guanidinium recognition motif selectively recognize FAD through a three-point interaction with the complementary isoalloxazine (DAD), adenosine (DA), and phosphate moieties (Scheme 37).[405] X-ray photoelectron

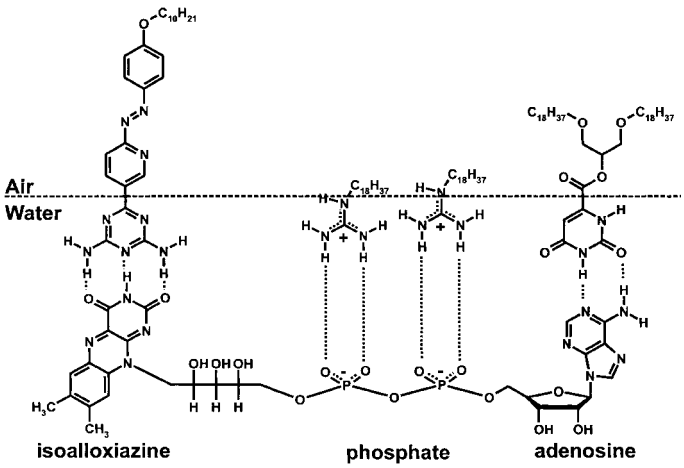

Scheme 37. Selective recognition of FAD by a mixed monolayer through a three-point interaction between complementary sites.

spectroscopic analysis of the Langmuir film transferred from an aqueous phase containing FAD revealed that one single FAD molecule was bound to the three recognition units. The same approach was applied to bind water-soluble dipeptides to monolayers of peptide-functionalized dialkyl amphiphiles. This study significantly widens the scope of this technique.[406] An interesting future development will be the use of interfacial molecular recognition to create patterns with molecular resolution in Langmuir films.

6.3.2. Nanotechnology: The Solid–Air Interface

Organic and inorganic structures of nanosize dimensions (1-100 nm) are at the focal point of current nanotechnological

developments. The controlled organization of nanoparticles into well-ordered two- and three-dimensional arrays is of crucial importance for the development of nanoelectronics. The directionality and reversibility of H-bonds make them perfectly suitable to serve as linkers between nanoparticles.[407] Mirkin et al. showed that the addition of "sticky" DNA strands to a solution of Au colloids functionalized with complementary single DNA strands resulted in the formation of well-defined 3D networks.[408] Transmission electron microscopy (TEM) studies showed close-packed assemblies of the colloids with a uniform separation of about 60 Å. Formation of the network causes a characteristic color change from red to purple as a consequence of a change in the surface plasmon resonance of Au. The color change reversed upon heating, which proved the reversibility of the network formation. In subsequent work this property was used for the colorimetric detection of polynucleotides.[409] The "melting" temperature T_m of a network formed between polynucleotide targets and Au colloids functionalized with DNA recognition elements is strongly dependent on the complementarity between the DNA strands. A mismatch of only one base pair reduces the T_m value by 5 K. The high sensitivity of the system is apparent from the detection limit of approximately 10 fmol for the unoptimized system.

Alivisatos, Schultz, and co-workers employed DNA hybridization to control the spatial position of individual nanoparticles.[410] The Au colloids were monofunctionalized with 18-base single DNA strands to prevent formation of a three-dimensional network. The addition of complementary single DNA strands containing 37 or 56 bases resulted in DNA strands containing two or three Au colloids, respectively, with the spatial position depending on the base-pair sequence (Scheme 38a). In a similar fashion, the spatial orientation of Au particles of different sizes can be controlled.[411] However, a uniform spatial separation of the particles was hampered by the relatively low rigidity of the DNA backbone. Besides DNA, biotin–streptavidin,[412] amidopyridine–imide,[413] and triazine–thymine interactions[414] have been employed for the same purpose.

The self-assembly of H-bonded structures also provides an efficient route to fabricate nanostructures on solid surfaces.[415] The research groups of Whitesides and Reinhoudt have shown that the mixing of dimelamines and dicyanurates (see Section 3.3) in a 1:1 ratio resulted in the formation of polymeric stacks of rosettes.[416, 417] Drop-casting solutions of these polymeric structures onto a graphite surface enabled the long-range ordering of the nanorods to be shown by atomic-force microscopy (AFM). Recently, Kern and co-workers showed that the self-assembly of regular patterns of 4-[*trans*-2-(pyrid-4-yl-vinyl)]benzoic acid units on a Ag(111) surface occurred as a result of strong pyridine·carboxylic acid and weak C=O···H–C H-bonding interactions (Scheme 38b).[418] Pattern formation turned out to be strongly affected by the substrate–surface interactions. Van Esch, Feringa, and co-workers employed H-bonding interactions between urea moieties to assemble fibers with regularly spaced thiophene groups, which results in a high charge mobility in these materials.[419] These fibers were shown to form highly elongated aggregates on solid substrates.[420]

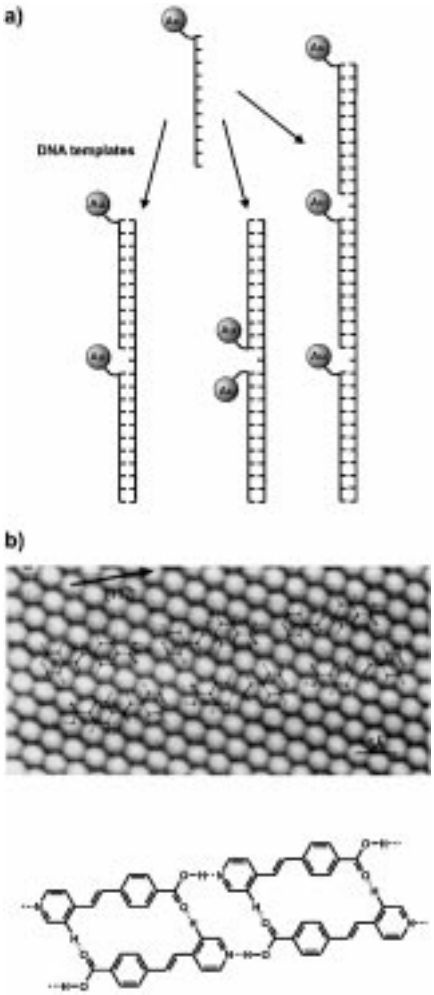

Scheme 38. a) DNA hybridization to control the spatial orientation of Au nanoparticles. b) Regular patterns of 4-[*trans*-2-(pyrid-4-ylvinyl)]benzoic acid units on an Ag(111) surface.

6.4. Macromolecular Assemblies

6.4.1. Polymers

Supramolecular polymers can be defined as polymers in which the individual subunits are connected through non-covalent interactions. Polymers of this type are expected to display novel, interesting properties, for example, liquidlike behavior upon heating or dilution. After entanglement of the individual polymer strands, dissociation of single connector units should still be possible without losing the polymeric properties. For this purpose, H-bonding interactions provide an attractive option because of their directionality, reversibility, and the possibility of controlling the strength of the interactions by altering the number of H-bonds involved. Early attempts by the groups of Griffin and Lehn were based on 1-H-bond and 3-H-bond modules, such as the carboxylic acid·pyridine motif or the uracil·2,6-diacylaminopyridine motif.[421–423] Unfortunately, the stability of these complexes was not sufficient to induce polymeric properties in solution. Similar results were obtained for macromolecular structures composed of H-bonded complexes based on melamine·barbiturate,[192, 424] pyrimidine·isocyanuric acid,[425] melamine·

imide,[426, 427] or 2,6-diaminotriazine · imide interactions.[428] Cocrystallization of compounds with complementary H-bonding sites has often led to the formation of well-defined polymeric strands, but in general the stability was too low under dynamic conditions.[155, 195, 429–433]

In order to generate polymer chains of sufficient length that exhibit true polymeric properties, the association constant of the individual H-bonding modules should be significantly higher than those of 3H-bond modules. This concept has initiated the search for novel building blocks that (self-)associate with $K_{ass} > 10^6\,M^{-1}$.[434] A breakthrough was achieved by Sijbesma, Meijer, and co-workers when they developed a quadruple H-bonded motif based on the dimerization of 2-ureido-4-pyrimidones (see Section 2.3.4).[435] It was found that ditopic monomers containing two 2-ureido-4-pyrimidone moieties that cannot interact in an intramolecular fashion spontaneously form polymers in chloroform. The number-average degree of polymerization of $P_n = 700$ at 40 mM corresponds to an average molecular weight of about 500 kDa. These H-bonded structures display the anticipated behavior of true polymers for the first time. The equilibrium is shifted in favor of the monomer units at low concentrations or elevated temperatures, which consequently causes liquidlike behavior of the polymer solution. The viscosity drops sharply when small amounts of monofunctional "stoppers" are added, which means that polymer formation is reversible. Interestingly, in situ generation of stopper molecules by photoinduced cleavage of an *o*-nitrobenzyl protecting group caused a large drop in the viscosity η_{rel} upon irradiation with light.[436] The same module has been used as end-caps of low molecular weight telechelic polymers to change their properties[437, 438] and also in three-dimensional polymer networks.[439]

Another type of H-bonded polymer was recently reported by Rebek and co-workers which employed two tetraureacalix[4]-arenes connected covalently by a rigid spacer.[440, 441] In these systems the addition of guest molecules induces the formation of polymer strands, while the H-bonded capsules serve as connector units. Recently, it was also shown that mesogeneity can be induced by incorporating long aliphatic chains.[442]

6.4.2. Dendrimers

Dendrimers are a special class of polymers with unique properties as a consequence of their uniform size and shape. There are only a few examples of using H-bonding for the self-assembly of well-defined dendritic structures of nanometer dimensions.[443, 444] Zimmerman et al. constructed dendritic wedges of different generations containing a rigid concave spacer that preorganizes two isophthalic acid moieties in a parallel fashion (Scheme 39a).[445] The self-association of these monomers through the formation of a double hexameric motif in the core resulted in the spontaneous formation of dendrimers with molecular weights up to 30 kDa. The dendritic wedges preferentially form a cyclic hexamer rather than a polymeric structure because steric repulsion between the wedges is minimized in the cycle. Molecular modeling studies showed that the structure of these assemblies is disk-shaped with a thickness of 2 nm and a diameter of 9 nm.

By using a similar approach, Reinhoudt and co-workers used the rosette motif for the self-assembly of noncovalent dendrimers.[446] In this case, metallodendrimer wedges were functionalized with a barbiturate moiety at the focal point. The addition of one equivalent of melamine resulted in the quantitative formation of dendritic structures that have a rosette moiety inside the core (Scheme 39b). The unique feature of this approach is that two orthogonal noncovalent interactions for self-assembly are employed: metal–ligand coordination (Pd–CN) in the wedges and H-bonding in the core.

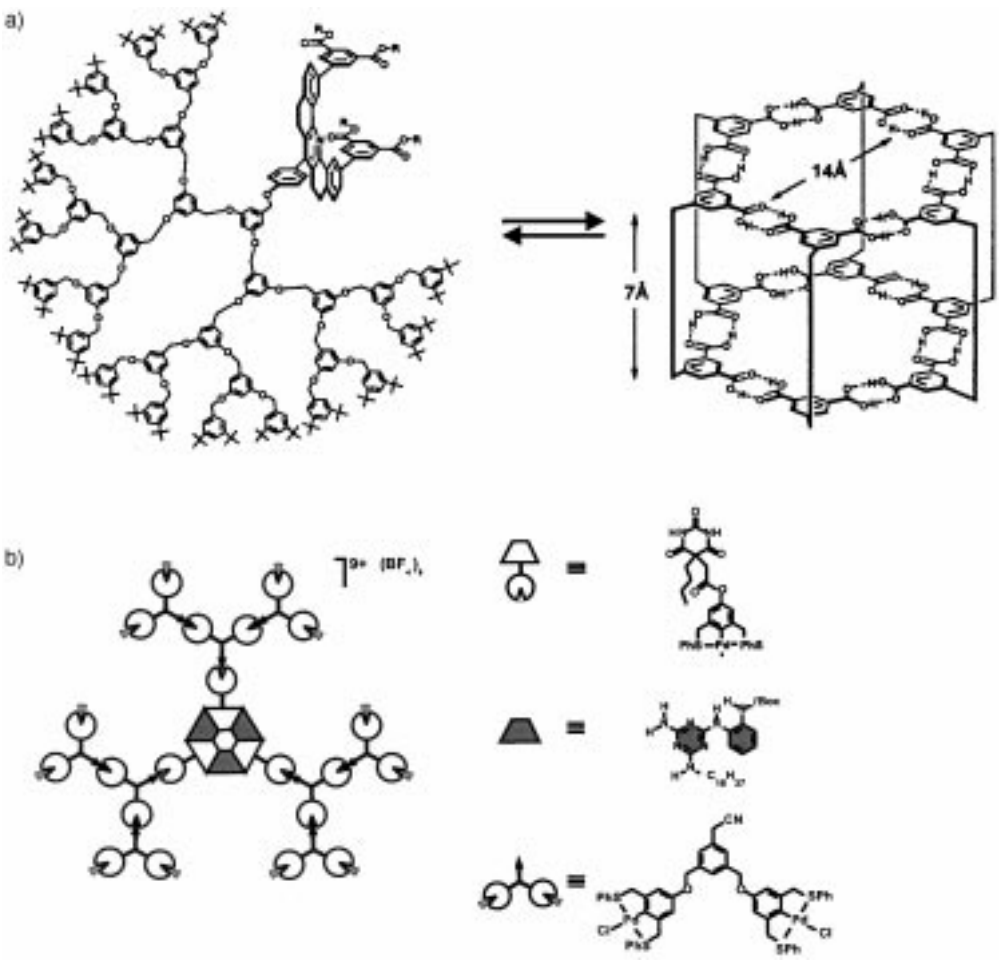

Scheme 39. Self-assembled dendrimers with H-bonded cores.

6.4.3. Self-Assembled Nanotubes

In 1974, De Santis et al. suggested that cyclic peptides composed of an even number of amino acids with alternating chirality should form tubelike stacks through backbone H-bonding.[447] However, it was not until 1993 that Ghadiri et al. reported the first assembly of organic nanotubes based on this design principle (Scheme 40 a).[448, 449] The first nanotubes were composed of eight-membered cyclic peptide **71** with the sequence (L-Gln-D-Ala-L-Glu-D-Ala)$_2$. The successful organization of these units into nanotubes relies on two issues. Firstly, the cycle is flat with all the backbone amide functionalities perpendicular to the plane of the ring, which allows orthogonal stacking through the formation of eight H-bonds. Secondly, the amino acid substituents point outwards, which creates an empty interior with an internal van der Waals diameter of roughly 7 Å.

The diameter of these nanotubes can be controlled simply by changing the number of amino acids in the cyclic peptide.[450] Not only are these structures aesthetically very appealing, they also serve as excellent transport channels in lipid bilayer membranes. Single-channel conductance measurements indicated channel activities for K^+ and Na^+ similar to naturally occurring channel-forming proteins, such as gramicidin A and amphotericin B, with rates exceeding 10^7 ions per second.[451] Nanotubes with larger internal diameters transport glucose across lipid bilayers.[452] The insertion of self-assembled nanotubes in self-assembled monolayers (SAMs) of thiols or thioethers on gold was also studied.[453] Cyclic voltammetry showed that the nanotubes act as selective ion channels, since only redox couples small enough to pass through the channels showed redox activity. The thermodynamic parameters for nanotube formation were inferred from studies on the isolated recognition motif.[454]

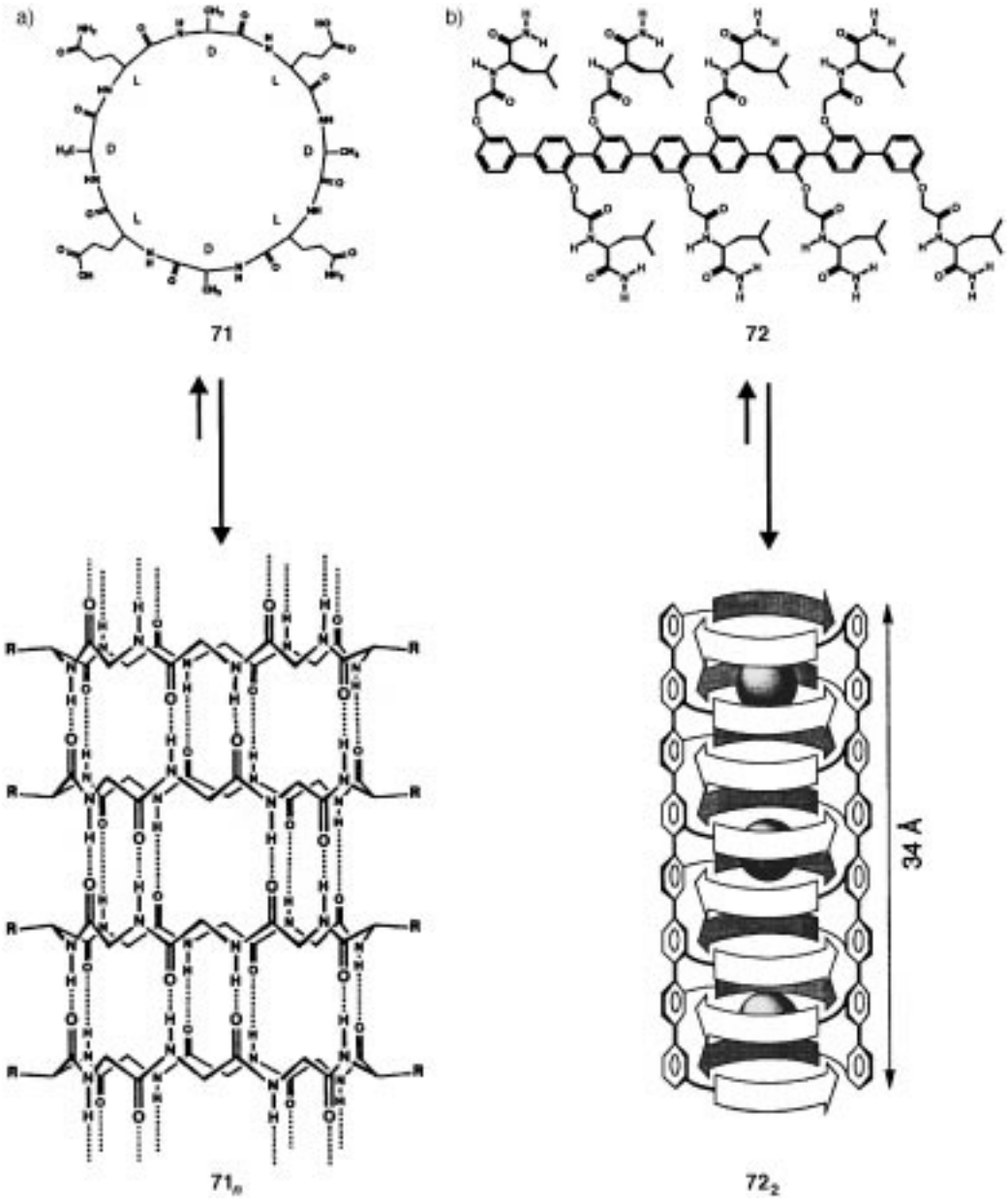

Scheme 40. Self-assembled nanotubes based on cyclic peptides (a) and oligo-anisoles (b).

Selective N-methylation of one side of the cyclic peptide only allows formation of dimeric structures. Variable temperature ^{1}H NMR studies revealed that the assembly process is enthalpy driven with $\Delta H^0_{298} = -11.0\,\mathrm{kcal\,mol^{-1}}$ and $\Delta S^0_{298} = -23.7\,\mathrm{cal\,K^{-1}\,mol^{-1}}$.

Other peptide nanotubes constructed from cysteine-based macrocyclic bisureas,[455] serine-based cyclodepsipeptides,[456] and cyclic tetramers of 3-aminobutanoic acid have been reported.[457] Recently, Matile and co-workers reported self-assembled ionophores **72** based on oligoanisoles that are functionalized with "sticky" peptide ends that self-assemble in water (Scheme 40b).[458–460] An intriguing aspect of these nanotubes is their ability to transport protons across lipid bilayers.

6.4.4. Liquid Crystalline Materials

H-bonded complexes with liquid crystalline properties can form from two different components that are not mesogenic by themselves.[461–464] H-bonding gives extended rigid aromatic mesogens, which strongly stabilize the mesophase. Kato and Fréchet used the formation of a single H-bond between pyridine and carboxylic acid to obtain a large variety of mesogenic complexes, such as 2:1 complexes between 4,4′-bipyridines and carboxylates.[465] These studies were followed by related systems based on phenol–stilbazole,[466] carboxylic acid–stilbazole,[467] phenol–pyridine,[468] alcohol–imidazole,[469] and carboxylic acid–amidopyridine interactions.[470] Liquid crystalline properties were introduced in covalent polymers by using a similar approach, for example, by the addition of stilbazole derivatives to a polyacrylate with 4-oxybenzoic acid side chains.[471]

Several examples of multicomponent assemblies that form discotic liquid crystals have been reported. X-Ray studies on fibres obtained from a guanosine 3′-phosphate gel revealed that the guanosine tetramers (see Section 3.5) are piled on top of one another, with the sugar moieties located on the periphery. Gottarelli, Spada, and co-workers showed that oligomers containing between two and six deoxyguanosine moieties form liquid crystalline phases in water at very low concentrations (2.5% w/w for d(GpG)).[472, 473] A strong stabilizing effect observed for different alkali cations in the order $K^+ > Rb^+ > Na^+ > Cs^+$ was attributed to intra- and interassembly binding to oxygen donors. Columnar aggregates were also observed for derivatives that could not form interassembly H-bonds. Other discotic liquid crystals were obtained from synthetic, disklike recognition motifs based on α-pyridone dimerization[474, 475] and lactim–lactam trimerization.[199] Meijer and co-workers showed that intramolecular H-bonding can be used to organize the core of a covalent molecule into a flat disk, which induced columnar liquid crystalline behavior.[476]

6.5. H-Bonding in Water

It is nowadays a generally accepted view that simple H-bonded complexes, such as a single A·T or C·G base pair, do not form in bulk water in the absence of additional stabilizing interactions, such as ion pairing and hydrophobic interactions.[477, 478] For example, Rebek and co-workers showed that the strength of binding of 9-ethyladenine to water-soluble derivatives of Kemp's triacid imide is correlated to the surface area of the hydrophobic group facing the binding pocket.[479] The formation of H-bonded complexes within the lipophilic core of micelles has been reported by Nowick et al.[480] Recently, Komiyama and co-workers found that poly(2-vinyl-4,6-diamino-1,3,5-triazine) (PVDAT) efficiently binds pyrimidine derivatives from aqueous solutions through the formation of complementary H-bonds,[481] as confirmed by ^{1}H NMR spectroscopy and ultrafiltration experiments.[482] The order of the binding activity (U, T > A ≫ C, G) coincides with the number of H-bonds formed between the host and guest. The corresponding monomers show virtually no activity, which indicates that the binding is predominantly the result of a polymer effect.

Recently, Meijer and co-workers described the first example of multicomponent H-bonded assemblies that are stable in water.[483] The structures form as a result of cooperative stacking and H-bonding interactions.

The formation of H-bonded complexes at the air–water interface has already been described in Section 6.3.1.

6.6. Self-Assembled Receptors: Dynamic Combinatorial Chemistry

6.6.1. Self-Assembly of Functionalities

The use of H-bonded assemblies as a molecular platform for guest recognition studies requires the introduction of compatible functional groups. The research groups of Lehn and Whitesides both showed that the presence of peripheral Zn-porphyrins is fully compatible with the formation of single-rosette assemblies.[484, 485] However, in both cases complexation of guest molecules to the apical binding site of the Zn center is prevented. Reinhoudt and co-workers constructed a bifunctional receptor that consists of a calix[4]arene binding site that is selective for Na^+ ions, and a Zn-porphyrin that is capable of binding SCN^- ions.[486] Both modules carry complementary H-bond recognition sites (DAD·ADA), and binding studies showed that the 1:1 H-bonded complex has an increased affinity for NaSCN as a direct result of H-bond formation.

Studies by Timmerman et al. on the assembly behavior of functionalized calix[4]arenes revealed that double-rosette assemblies are compatible with a large variety of functional groups, such as polar nitro and cyano groups.[173] Significant destabilization was only observed for functionalities that cause severe steric hindrance within the assembly or as a result of the formation of additional H-bonds. Guest binding does not occur in these assemblies, since the functionalities are located in between the rosette layers, an area inaccessible for guest molecules. In the next generation of receptor assemblies the binding functionalities, such as Zn-porphyrins or peptides, were located at the periphery of the assembly (Scheme 41).[487, 488] The C_3-symmetrical assembly $\mathbf{73}_3\cdot(\mathrm{BAR})_6$, which carries two circular arrays of three Zn-

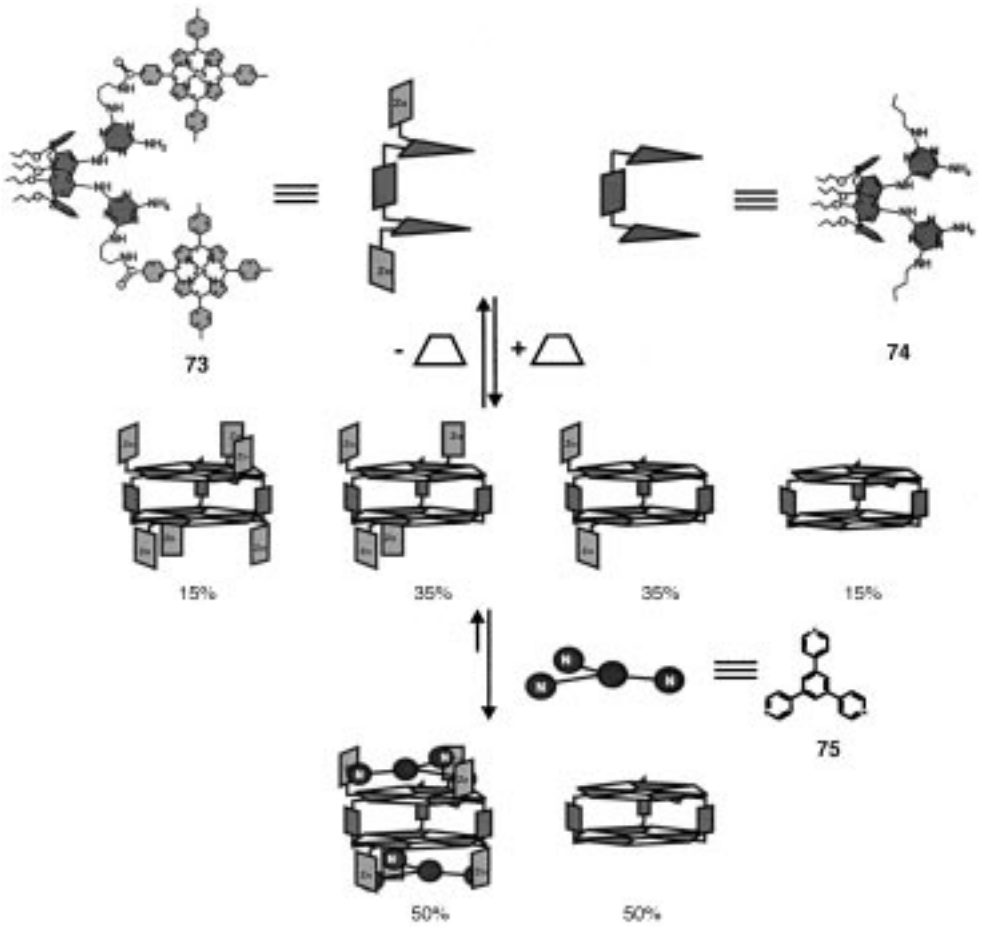

Scheme 41. Guest-templated formation of the strongest receptor in a DCL.

porphyrin units, binds strongly to the trispyridine guest **75** through threefold coordination to the Zn centers.

6.6.2. Dynamic Combinatorial Chemistry

Dynamic combinatorial libraries (DCLs) have recently attracted a great deal of attention in the rapidly growing field of combinatorial chemistry.[489–491] The interest in DCLs relies mainly on two important features. First of all, structural diversity in DCLs is generated spontaneously by mixing single components of the library under reversible conditions. Secondly, the reversible character of DCLs permits target-driven amplification of selected library members by means of thermodynamic equilibria shifting as a result of molecular recognition phenomena. The high thermodynamic stability of H-bonded assemblies combined with their usually low kinetic stability renders them very suitable for the generation of dynamic libraries.[492] Moreover, H-bonding interactions have been used extensively to induce guest-templated amplification.

The first model study on H-bonded DCLs was reported by Timmerman and co-workers.[179] This study showed that a statistical mixture (1:3:3:1) of four possible double-rosette assemblies is formed instantaneously by mixing the components in $CHCl_3$ at room temperature (see also Section 3.3.5). Recently, the same group reported a four-component DCL of receptors $\mathbf{73}_n\mathbf{74}_{3-n}\cdot(BAR)_6$ ($n=0-3$) which was obtained by mixing the homomeric assemblies $\mathbf{73}_3\cdot(BAR)_6$ and $\mathbf{74}_3\cdot(BAR)_6$ in a 1:1 ratio (Scheme 41).[487] The various members of this library all contain a different number of Zn-porphyrin units and consequently exhibit different binding affinities for the trispyridine guest **75**. Subsequent addition of **75** induced a shift of the library composition from statistical (1:3:3:1) to an almost 1:1 mixture of assemblies $\mathbf{73}_3\cdot(BAR)_6\cdot\mathbf{75}_2$ and $\mathbf{74}_3\cdot(BAR)_6$ as a direct result of the preferential binding of **75** to the all-porphyrin assembly $\mathbf{73}_3\cdot(BAR)_6$. Recently, Rebek and co-workers showed the occurrence of guest-template effects in DCLs of H-bonded capsules.[493]

H-bonding interactions have been extensively employed to drive the chemical evolution of DCLs of potential receptors. The concept was first illustrated by Eliseev and Nelen in a study on the rapid interconversion of a dicarboxylate between three isomeric forms upon irradiation with UV light.[494] From the three receptors, only the *cis*–*cis* isomer, which has the ideal geometry to complex guanidinium, shows significant retention on an affinity column loaded with immobilized arginine. Repetitive isomerization–selection cycles have been used to generate the *cis*–*cis* receptor from the mixture in 85% yield.

Huc et al. reported DCLs that are formed by the coordination of Pd^{II} ions to bipyridines (Scheme 42).[495] Bipyridine ligands **76** and **77**, with and without additional H-bonding arrays, respectively, were used to generate a library of three different complexes, only one of which displays a DAD · DAD array that is complementary to a barbituric acid derivative (ADA · ADA). Addition of this guest to the library resulted in a small, but significant, shift of the equilibrium towards the complex with the highest affinity. Similar template effects were observed recently by the same group in DCLs of conformational isomers of di- and polytopic receptors.[496]

7. Conclusions and Perspectives

"Research is not to follow known tracks, but instead to crumble into the forest in the hope that one leaves a track behind."

Noncovalent synthesis has dramatically changed the way in which chemists approach the generation of molecular structures of nanosize dimensions. Whereas molecules tradition-

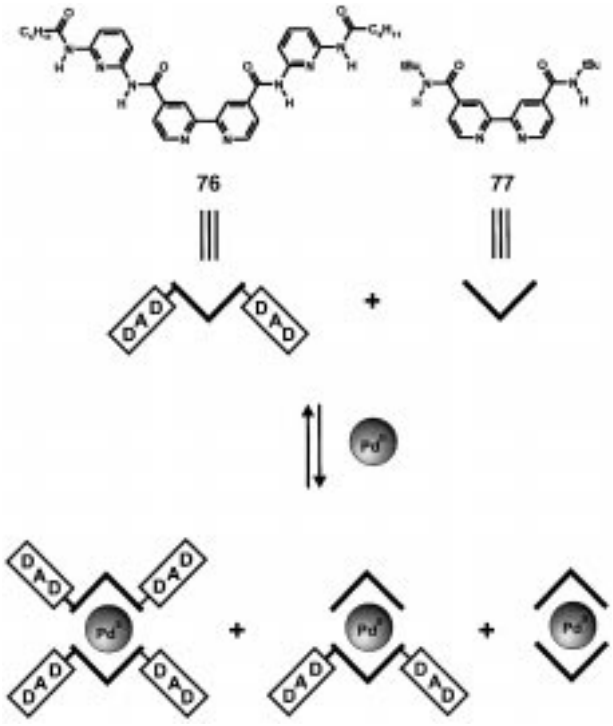

Scheme 42. A DCL based on bipyridine – Pd^{II} coordination.

ally were synthesized by the stepwise formation of covalent bonds, the use of multiple weak interactions to organize molecular components into supramolecular nanostructures is now a very attractive and fruitful alternative. In addition to this, the noncovalent assemblies display fundamentally different properties in comparison to purely covalent structures. What originally started as a curiosity has now developed into a mature field of research that will have a major impact on the way chemistry is conducted in the next decade. At the end of this review, we will give a short highlight of a number of new and promising developments that may initiate new research areas in the coming decade.

7.1. Catalyzed Noncovalent Synthesis

The majority of H-bond-directed self-assembly processes discussed in this review take place under thermodynamically controlled conditions. This means that such processes benefit from self-repairing as a direct result of the fact that the reverse process, namely, the breakdown of these assemblies, is rapid on the laboratory timescale. However, with the increase in the number of individual H-bonds that are involved in the assembly process, the rate of disassembly will rapidly decrease. Ultimately, this will lead to situations in which the self-assembly process becomes kinetically controlled and suffers from the same problems as those observed in covalent synthesis. Several examples of kinetic control in self-assembly processes have been described recently.[181, 497, 498] Whitesides and co-workers reported that the kinetic stability of multidentate complexes based on the vancomycin-D-Ala-D-Ala recognition motif can be drastically decreased by the addition of the monovalent ligand N^{α}-Ac-L-Lys-D-Ala-D-Ala.[499] In other words, the monovalent ligand "catalyzes" the intermolecular exchange process of the tripodal ligands in the complex by temporarily binding to the free binding sites of the fully or partially uncomplexed states that are formed during the exchange process.

Recently, Reinhoudt, Timmerman, and co-workers reported a similar form of catalysis in a hydrogen-bond-mediated self-assembly process.[180] It was found that the presence of free barbiturate (*R*)-BAR (Scheme 12) catalyzes the racemization of an enantiomerically pure assembly $\mathbf{26}_3 \cdot (\mathrm{BuCA})_6$ (Scheme 19) by activation of the assembly for the exchange of the melamine components. Kinetic analysis of the system revealed that about 80% of racemization occurs at 1 mM concentrations by the catalytic pathway, with a corresponding rate constant of $14.7 \times 10^{-3}\,\mathrm{M^{-1}s^{-1}}$. Other kinetically controlled self-assembly processes involving H-bonding have been identified which are subject to catalysis under certain conditions.[500] Without doubt, this type of catalysis in self-assembly processes will receive increasing interest in the near future and may ultimately determine the dimensions of nanostructures that we may be able to generate.

7.2. Combinatorial Libraries of Artificial Receptor Systems by Noncovalent Synthesis

The combinatorial philosophy, which has revolutionized the way in which covalent bond making processes are performed nowadays, is about to create a paradigm shift in noncovalent synthesis. Processes that form noncovalent bonds are ideally suited to be performed in combinatorial fashion for two reasons. First of all, such processes are clean, high-yielding, and (in most cases) take place under thermodynamic control. This means that combinatorial libraries of H-bonded assemblies are formed spontaneously upon mixing the individual components. Moreover, the resulting libraries are dynamic in nature, which means that guest-templating effects are applicable.[490–492]

At the moment, noncovalent combinatorial synthesis is still in its infancy. Initial studies are concerned with simple model systems,[179] in which strong guest-templating effects have already been observed.[487, 493] Future work in this area should therefore be directed at library characterization and lead/hit identification.[371] Once these problems have been solved, it seems beyond doubt that the combinatorial approach is going to provide the ultimate solution to the development of artificial receptor systems that mimic the binding properties of natural antibodies in terms of affinity and selectivity.[492] The high degree of control that can be achieved over chirality in noncovalent assemblies may pave the way to optically pure chiral cavities that encapsulate chiral guest molecules with high enantioselectivity, for example, for purification purposes or enantioselective catalysis inside capsules.

7.3. H-Bond-Directed Self-Assembly in Water

The majority of synthetic H-bonded assemblies are studied in apolar solvents, such as chloroform or toluene. Usually,

such structures do not assemble in water because the polar water molecules compete favorably in H-bond-forming processes and strongly destabilize the assemblies. But why then does nature provide ample examples of binding processes based on H-bonding, such as formation of the DNA duplex or substrate binding in enzyme pockets, even though such processes occur in the presence of water? The most likely answer to this question is that the formation of H-bonds in biological systems generally takes place within a hydrophobic microenvironment from which water molecules are excluded as a result of hydrophobic effects. The hydrophobic pockets are usually formed as a result of the clustering of multiple hydrophobic fragments that are in some way preorganized, either on a polymeric backbone or as a result of cooperative binding interactions. Only very recently, an example of a synthetic multicomponent H-bonded assembly that forms in an aqueous environment was reported.[483] However, it will not take long before many such structures will appear in the literature. Ultimately, a systematic study of the self-assembling properties of H-bonded assemblies that exist in water will help to unravel the underlying principles that govern self-assembling processes in this mysterious solvent.

Received: September 27, 2000 [A 432]

[1] K. C. Nicolaou, R. K. Guy, *Angew. Chem.* **1995**, *107*, 2047 – 2059; *Angew. Chem. Int. Ed. Engl.* **1995**, *34*, 2079 – 2090.
[2] J. J. Masters, J. T. Link, L. B. Snyder, W. B. Young, S. J. Danishefsky, *Angew. Chem.* **1995**, *107*, 1886 – 1888; *Angew. Chem. Int. Ed. Engl.* **1995**, *34*, 1723 – 1726.
[3] K. C. Nicolaou, *Angew. Chem.* **1996**, *108*, 644 – 664; *Angew. Chem. Int. Ed. Engl.* **1996**, *35*, 589 – 607.
[4] G. M. Whitesides, E. E. Simanek, J. P. Mathias, C. T. Seto, D. N. Chin, M. Mammen, D. M. Gordon, *Acc. Chem. Res.* **1995**, *28*, 37 – 44.
[5] W. Blokzijl, J. B. F. N. Engberts, *Angew. Chem.* **1993**, *105*, 1610 – 1644; *Angew. Chem. Int. Ed. Engl.* **1993**, *32*, 1545 – 1579.
[6] M. Rekharsky, Y. Inoue, *Chem. Rev.* **1998**, *98*, 1875 – 1917.
[7] M. Fujita, K. Ogura, *Bull. Chem. Soc. Jpn.* **1996**, *69*, 1471 – 1482.
[8] C. Piguet, G. Bernardinelli, G. Hopfgartner, *Chem. Rev.* **1997**, *97*, 2005 – 2062.
[9] M. Alamgir Hossain, H.-J. Schneider, *Chem. Eur. J.* **1999**, *5*, 1284 – 1290.
[10] M. C. Etter, *Acc. Chem. Res.* **1990**, *23*, 120 – 126.
[11] J.-M. Lehn, *Angew. Chem.* **1990**, *102*, 1347 – 1362; *Angew. Chem. Int. Ed. Engl.* **1990**, *29*, 1304 – 1319.
[12] G. M. Whitesides, J. P. Mathias, C. T. Seto, *Science* **1991**, *254*, 1312 – 1319.
[13] M. C. Etter, *J. Phys. Chem.* **1991**, *95*, 4601 – 4610.
[14] J. S. Lindsey, *New J. Chem.* **1991**, *15*, 153 – 180.
[15] D. S. Lawrence, T. Jiang, M. Levett, *Chem. Rev.* **1995**, *95*, 2229 – 2260.
[16] D. Philp, J. F. Stoddart, *Angew. Chem.* **1996**, *108*, 1242 – 1286; *Angew. Chem. Int. Ed. Engl.* **1996**, *35*, 1154 – 1194.
[17] M. M. Conn, J. Rebek, Jr., *Chem. Rev.* **1997**, *97*, 1647 – 1668.
[18] M. C. T. Fyfe, J. F. Stoddart, *Acc. Chem. Res.* **1997**, *30*, 393 – 401.
[19] R. E. Melendez, A. D. Hamilton, *Top. Curr. Chem.* **1998**, *198*, 97 – 129.
[20] W. Nernst, *Z. Phys. Chem.* **1892**, *8*, 110.
[21] A. Werner, *Liebigs Ann. Chem.* **1902**, *322*, 261.
[22] M. L. Huggins, *Angew. Chem.* **1971**, *83*, 163 – 168; *Angew. Chem. Int. Ed. Engl.* **1971**, *10*, 147 – 152, and references therein.
[23] W. M. Latimer, W. H. Rodebush, *J. Am. Chem. Soc.* **1920**, *42*, 1419 – 1433.
[24] J. D. Bernal, H. D. Megaw, *Proc. R. Soc. London A* **1935**, *151*, 384 – 420.
[25] M. L. Huggins, *J. Org. Chem.* **1936**, *1*, 407 – 456.
[26] P. Schuster, G. Zundel, C. Sandorfy, *The Hydrogen Bond: Recent Developments in Theory and Experiments*, *Vol. 1 – 3*, North-Holland, Amsterdam, **1976**.
[27] P. A. Kollman, L. A. Allen, *Chem. Rev.* **1972**, *72*, 283 – 303.
[28] Recent review: *Monatsh. Chem.* **1999**, *130* (special issue, No. 8).
[29] Y. Gu, T. Kar, S. Scheiner, *J. Am. Chem. Soc.* **1999**, *121*, 9411 – 9422.
[30] J. L. Atwood, F. Hamada, K. D. Robinson, G. W. Orr, R. L. Vincent, *Nature* **1991**, *349*, 683 – 684.
[31] L. Pauling, *Proc. Natl. Acad. Sci. USA* **1928**, *14*, 359 – 362.
[32] C. A. Coulson, U. Danielsson, *Ark. Fys.* **1954**, *8*, 205, 239 – 244.
[33] H. Tsubomura, *Bull. Chem. Soc. Jpn.* **1954**, *27*, 445 – 450.
[34] C. Fonseca Guerra, F. M. Bickelhaupt, J. G. Snijders, E. J. Baerends, *Chem. Eur. J.* **1999**, *5*, 3581 – 3594.
[35] G. C. Pimental, A. L. McClellan, *The Hydrogen Bond*, Freeman, San Francisco, **1960**.
[36] R. Taylor, O. Kennard, W. Versichel, *J. Am. Chem. Soc.* **1984**, *106*, 244 – 248.
[37] *Hydrogen Bonding: A Theoretical Perspective* (Ed.: S. Scheiner), Oxford University Press, New York, **1997**.
[38] D. A. Bell, E. V. Anslyn, *J. Org. Chem.* **1994**, *59*, 512 – 514.
[39] G. G. Hammes, A. C. Park, *J. Am. Chem. Soc.* **1968**, *90*, 4151 – 4157.
[40] C. L. Perrin, J. D. Thoburn, *J. Am. Chem. Soc.* **1992**, *114*, 8559 – 8565.
[41] F. Hibbert, J. Emsley, *Adv. Phys. Org. Chem.* **1990**, *26*, 255.
[42] W. W. Cleland, M. M. Kreevoy, *Science* **1994**, *264*, 1887 – 1890.
[43] P. A. Frey, S. A. Whitt, J. B. Tobin, *Science* **1994**, *264*, 1927 – 1930.
[44] A. Warshel, A. Papazyan, P. A. Kollman, *Science* **1995**, *269*, 102 – 104.
[45] S. Scheiner, T. Kar, *J. Am. Chem. Soc.* **1995**, *117*, 6970 – 6975.
[46] S. Shan, S. Loh, D. Herschlag, *Science* **1996**, *272*, 97 – 101.
[47] Y. Kato, L. M. Toledo, J. Rebek, Jr., *J. Am. Chem. Soc.* **1996**, *118*, 8575 – 8579.
[48] J. A. Pople, W. G. Schneider, H. J. Bernstein, *High Resolution Nuclear Magnetic Resonance*, McGraw-Hill, New York, **1959**, chap. 15.
[49] R. Konrat, M. Tollinger, G. Kontaxis, B. Kräutler, *Monatsh. Chem.* **1999**, *130*, 961 – 982.
[50] A. J. Dingley, S. Grzesiek, *J. Am. Chem. Soc.* **1998**, *120*, 8293 – 8297.
[51] C. B. Aakeroy, K. R. Seddon, *Chem. Soc. Rev.* **1993**, 397 – 407.
[52] C. A. Schalley, *Int. J. Mass Spectrom.* **2000**, *194*, 11 – 39.
[53] P. Timmerman, K. A. Jolliffe, M. Crego Calama, J.-L. Weidmann, L. J. Prins, F. Cardullo, B. H. M. Snellink-Ruel, R. Fokkens, N. M. M. Nibbering, S. Shinkai, D. N. Reinhoudt, *Chem. Eur. J.* **2000**, *6*, 4104 – 4115.
[54] D. Hadzi, W. J. Orville-Thomas, J. Tomasi, *Theoretical Treatments of Hydrogen Bonding*, Wiley, Chichester, **1997**.
[55] S. Moran, R. X. F. Ren, S. Rumney IV, E. T. Kool, *J. Am. Chem. Soc.* **1997**, *119*, 2056 – 2057.
[56] A. M. Davis, S. J. Teague, *Angew. Chem.* **1999**, *111*, 778 – 792; *Angew. Chem. Int. Ed.* **1999**, *38*, 736 – 749.
[57] G. A. Jeffrey, W. Saenger, *Hydrogen Bonding in Biological Structures*, Springer, Berlin, **1991**.
[58] Y. Kyogoku, R. C. Lord, A. Rich, *Proc. Natl. Acad. Sci. USA* **1967**, *57*, 250 – 257.
[59] Y. Kyogoku, R. C. Lord, A. Rich, *Biochim. Biophys. Acta* **1969**, *179*, 10 – 17.
[60] A. D. Hamilton, D. Van Engen, *J. Am. Chem. Soc.* **1987**, *109*, 5035 – 5036.
[61] W. L. Jorgenson, J. Pranata, *J. Am. Chem. Soc.* **1990**, *112*, 2008 – 2010.
[62] J. Pranata, S. G. Wierschke, W. L. Jorgenson, *J. Am. Chem. Soc.* **1991**, *113*, 2810 – 2819.
[63] T. J. Murray, S. C. Zimmerman, *J. Am. Chem. Soc.* **1992**, *114*, 4010 – 4011.
[64] J. Sartorius, H.-J. Schneider, *Chem. Eur. J.* **1996**, *2*, 1446 – 1452.
[65] A. Nadin, S. Derrer, R. P. McGeary, J. M. Goodman, P. R. Raithby, A. B. Holmes, *J. Am. Chem. Soc.* **1995**, *117*, 9768 – 9769.
[66] A. P. Bisson, C. A. Hunter, *Chem. Commun.* **1996**, 1723 – 1724.
[67] H. Adams, F. J. Carver, C. A. Hunter, J. C. Morales, E. M. Seward, *Angew. Chem.* **1996** , *108*, 1628 – 1631; *Angew. Chem. Int. Ed. Engl.* **1996**, *35*, 1542 – 1544.
[68] B. Gong, Y. Yan, H. Zeng, E. Skrzypczak-Jankunn, Y. W. Kim, J. Zhu, H. Ickes, *J. Am. Chem. Soc.* **1999**, *121*, 5607 – 5608.
[69] H. Zeng, R. S. Miller, R. A. Flowers II, B. Gong, *J. Am. Chem. Soc.* **2000**, *122*, 2635 – 2644.

[70] X. Zhao, Y.-L. Chang, F. Fowler, J. W. Lauher, *J. Am. Chem. Soc.* **1990**, *112*, 6627 – 6634.
[71] G. C. Hammes, H. O. Spivey, *J. Am. Chem. Soc.* **1966**, *88*, 1621 – 1625.
[72] G. C. Hammes, A. C. Park, *J. Am. Chem. Soc.* **1969**, *91*, 956 – 961.
[73] S. E. Krikorian, *J. Phys. Chem.* **1982**, *86*, 1875 – 1881.
[74] E. Gentric, J. Lauransan, C. Roussel, J. Metzger, *Nouv. J. Chim.* **1980**, *4*, 743 – 746.
[75] Y. Ducharme, J. D. Wuest, *J. Org. Chem.* **1988**, *53*, 5787 – 5789.
[76] M. C. Etter, S. M. Reutzel, *J. Am. Chem. Soc.* **1991**, *113*, 2586 – 2598.
[77] J. Hine, S. Hahn, J. Hwang, *J. Org. Chem.* **1988**, *53*, 884 – 887.
[78] M. C. Etter, Z. Urbañczyk-Lipkowska, M. Zia-Ebrahimi, T. W. Panunto, *J. Am. Chem. Soc.* **1990**, *112*, 8415 – 8426.
[79] S. Coe, J. J. Kane, T. L. Nguyen, L. M. Toledo, E. Wininger, F. W. Fowler, J. W. Lauher, *J. Am. Chem. Soc.* **1997**, *119*, 86 – 93.
[80] K. D. M. Harris, B. M. Kariuki, C. Lambropoulos, D. Philp, J. M. A. Robinson, *Tetrahedron* **1997**, *53*, 8599 – 8612.
[81] P. L. Wash, E. Maverick, J. Chiefari, D. A. Lightner, *J. Am. Chem. Soc.* **1997**, *119*, 3802 – 3806.
[82] F. Garcia-Tellado, S. J. Geib, S. Goswami, A. D. Hamilton, *J. Am. Chem. Soc.* **1991**, *113*, 9265 – 9269.
[83] D. A. Adsmond, M. C. Etter, *J. Chem. Soc. Chem. Commun.* **1990**, 589 – 591.
[84] R.-F. Liao, J. W. Lauher, F. W. Fowler, *Tetrahedron* **1996**, *52*, 3153 – 3162.
[85] S. E. Boiadjiev, D. T. Anstine, E. Maverick, D. A. Lightner, *Tetrahedron: Asymmetry* **1995**, *6*, 2253 – 2270.
[86] S. C. Zimmerman, T. J. Murray, *Tetrahedron Lett.* **1994**, *35*, 4077 – 4080.
[87] R. Taylor, O. Kennard, W. Versichel, *J. Am. Chem. Soc.* **1984**, *106*, 244 – 248.
[88] S. C. Zimmerman, Y. Wang, P. Bharathi, J. S. Moore, *J. Am. Chem. Soc.* **1998**, *120*, 2172 – 2173.
[89] M. Gallant, M. T. P. Viet, J. D. Wuest, *J. Am. Chem. Soc.* **1991**, *113*, 721 – 723.
[90] E. Boucher, M. Simard, J. D. Wuest, *J. Org. Chem.* **1995**, *60*, 1408 – 1412.
[91] M. Gallant, M. T. P. Viet, J. D. Wuest, *J. Org. Chem.* **1991**, *56*, 2284 – 2286.
[92] A. D. Burrows, C.-W. Chan, M. M. Chowdhry, J. E. McGrady, D. M. P. Mingos, *Chem. Soc. Rev.* **1995**, 329 – 339.
[93] H.-J. Schneider, R. K. Juneja, S. Simova, *Chem. Ber.* **1989**, *122*, 1211 – 1213.
[94] S. J. Geib, S. C. Hirst, C. Vicent, A. D. Hamilton, *J. Chem. Soc. Chem. Commun.* **1991**, 1283 – 1285.
[95] F. H. Beijer, R. P. Sijbesma, J. A. J. M. Vekemans, E. W. Meijer, H. Kooijman, A. L. Spek, *J. Org. Chem.* **1996**, *61*, 6371 – 6380.
[96] A. L. Moraczewski, L. A. Banszynski, A. M. From, C. E. White, B. D. Smith, *J. Org. Chem.* **1998**, *63*, 7258 – 7262.
[97] I. Willner, J. Rosengaus, S. Biali, *Tetrahedron Lett.* **1992**, *33*, 3805 – 3808.
[98] A. D. Hamilton, D. Little, *J. Chem. Soc. Chem. Commun.* **1990**, 297 – 300.
[99] T. K. Park, J. Schroeder, J. Rebek, Jr., *J. Am. Chem. Soc.* **1991**, *113*, 5125 – 5127.
[100] E. E. Fenlon, T. J. Murray, M. H. Baloga, S. C. Zimmerman, *J. Org. Chem.* **1993**, *58*, 6625 – 6628.
[101] F. H. Beijer, H. Kooijman, A. L. Spek, R. P. Sijbesma, E. W. Meijer, *Angew. Chem.* **1998**, *110*, 79 – 82; *Angew. Chem. Int. Ed.* **1998**, *37*, 75 – 78.
[102] F. H. Beijer, R. P. Sijbesma, H. Kooijman, A. L. Spek, E. W. Meijer, *J. Am. Chem. Soc.* **1998**, *120*, 6761 – 6769.
[103] B. J. B. Folmer, R. P. Sijbesma, H. Kooijman, A. L. Spek, E. W. Meijer, *J. Am. Chem. Soc.* **1999**, *121*, 9001 – 9007.
[104] J. J. González, P. Prados, J. de Mendoza, *Angew. Chem.* **1999**, *111*, 546 – 549; *Angew. Chem. Int. Ed.* **1999**, *38*, 525 – 528.
[105] P. S. Corbin, S. C. Zimmerman, *J. Am. Chem. Soc.* **1998**, *120*, 9710 – 9711.
[106] A. P. Davis, S. M. Draper, G. Dunne, P. Ashton, *Chem. Commun.* **1999**, 2265 – 2266.
[107] U. Lüning, C. Kühl, *Tetrahedron Lett.* **1998**, *39*, 5735 – 5738.
[108] P. S. Corbin, S. C. Zimmerman, *J. Am. Chem. Soc.* **2000**, *122*, 3779 – 3780.
[109] L. D. Williams, B. Chawla, B. S. Shaw, *Biopolymers* **1987**, *26*, 591 – 603.
[110] L. D. Williams, N. G. Williams, B. S. Shaw, *J. Am. Chem. Soc.* **1990**, *112*, 829 – 833.
[111] C. Roberts, R. Bandaru, C. Switzer, *J. Am. Chem. Soc.* **1997**, *119*, 4640 – 4649.
[112] J. J. Voegel, U. von Krosigk, S. A. Benner, *J. Org. Chem.* **1993**, *58*, 7542 – 7547.
[113] J. J. Voegel, S. A. Benner, *J. Am. Chem. Soc.* **1994**, *116*, 6929 – 6930.
[114] R. Faggiani, C. J. L. Lock, B. Lippert, *J. Am. Chem. Soc.* **1980**, *102*, 5418 – 5419.
[115] A. Houlton, D. M. P. Mingos, D. J. Williams, *J. Chem. Soc. Chem. Commun.* **1994**, 503 – 504.
[116] J. L. Sessler, D. Magda, H. Furuta, *J. Org. Chem.* **1992**, *57*, 818 – 826.
[117] J. L. Sessler, R. Wang, *J. Am. Chem. Soc.* **1996**, *118*, 9808 – 9809.
[118] J. L. Sessler, R. Wang, *Angew. Chem.* **1998**, *110*, 1818 – 1821; *Angew. Chem. Int. Ed.* **1998**, *37*, 1726 – 1729.
[119] J. L. Sessler, R. Wang, *J. Org. Chem.* **1998**, *63*, 4079 – 4091.
[120] C. M. Niemeyer, *Angew. Chem.* **1997**, *109*, 603 – 606; *Angew. Chem. Int. Ed. Engl.* **1997**, *36*, 585 – 587.
[121] N. C. Seeman, *Acc. Chem. Res.* **1997**, *30*, 357 – 363.
[122] J. Chen, N. C. Seeman, *Nature* **1991**, *350*, 631 – 633.
[123] Y. Zhang, N. C. Seeman, *J. Am. Chem. Soc.* **1994**, *116*, 1661.
[124] J. Shi, D. E. Bergstrom, *Angew. Chem.* **1997**, *109*, 70 – 72; *Angew. Chem. Int. Ed. Engl.* **1997**, *36*, 111 – 113.
[125] M. Scheffler, A. Dorenbeck, S. Jordan, M. Wüstefeld, G. von Kiedrowski, *Angew. Chem.* **1999**, *111*, 3514 – 3518; *Angew. Chem. Int. Ed.* **1999**, *38*, 3311 – 3315.
[126] F. P. Schmidtchen, M. Berger, *Chem. Rev.* **1997**, *97*, 1609 – 1646.
[127] C. Schmuck, *Eur. J. Org. Chem.* **1999**, 2397 – 2403.
[128] M. I. Nelen, A. V. Eliseev, *J. Chem. Soc. Perkin Trans. 2* **1997**, 1359 – 1364.
[129] B. Linton, A. D. Hamilton, *Tetrahedron* **1999**, *55*, 6027 – 6038.
[130] V. A. Russell, M. C. Etter, M. D. Ward, *J. Am. Chem. Soc.* **1994**, *116*, 1941 – 1952.
[131] R. P. Dixon, S. J. Geib, A. D. Hamilton, *J. Am. Chem. Soc.* **1992**, *114*, 365 – 366.
[132] T. Schrader, *Chem. Eur. J.* **1997**, *3*, 1537 – 1541.
[133] K. Schellhaas, H.-G. Schmalz, J. W. Bats, *Chem. Eur. J.* **1998**, *4*, 57 – 66.
[134] C. Schmuck, *Chem. Commun.* **1999**, 843 – 844.
[135] K.-S. Jeong, Y. L. Cho, *Tetrahedron Lett.* **1997**, *38*, 3279 – 3282.
[136] A. Kraft, R. Fröhlich, *Chem. Commun.* **1998**, 1085 – 1086.
[137] A. Kraft, A. Reichert, *Tetrahedron* **1999**, *55*, 3923 – 3930.
[138] O. Félix, M. W. Hosseini, A. De Cian, J. Fischer, *Angew. Chem.* **1997**, *109*, 83 – 85; *Angew. Chem. Int. Ed. Engl.* **1997**, *36*, 102 – 104.
[139] A. Kraft, *J. Chem. Soc. Perkin Trans. 1* **1999**, 705 – 714.
[140] S. Metzger, B. Lippert, *Angew. Chem.* **1996**, *108*, 1321 – 1323; *Angew. Chem. Int. Ed. Engl.* **1996**, *35*, 1228 – 1229.
[141] D. A. Bell, E. V. Anslyn, *Tetrahedron* **1995**, *51*, 7161 – 7172.
[142] H.-J. Schneider, M. Wang, *J. Org. Chem.* **1994**, *59*, 7464 – 7472.
[143] W. I. Sundquist, A. Klug, *Nature* **1989**, *342*, 825 – 829.
[144] D. J. Duchamp, R. E. Marsh, *Acta Crystallogr. Sect. B* **1969**, *25*, 5 – 19.
[145] F. H. Herbstein, M. Kapon, G. M. Reisner, *J. Inclusion Phenom.* **1987**, *5*, 211 – 214.
[146] S. V. Kolotuchin, E. E. Fenlon, S. R. Wilson, C. J. Loweth, S. C. Zimmerman, *Angew. Chem.* **1995**, *107*, 2873 – 2876; *Angew. Chem. Int. Ed. Engl.* **1995**, *34*, 2654 – 2657.
[147] S. V. Kolotuchin, P. A. Thiessen, E. E. Fenlon, S. R. Wilson, C. J. Loweth, S. C. Zimmerman, *Chem. Eur. J.* **1999**, *5*, 2537 – 2544.
[148] A. Zafar, J. Yang, S. J. Geib, A. D. Hamilton, *Tetrahedron Lett.* **1996**, *37*, 2327 – 2330.
[149] R. Alcala, S. Martinez-Carrera, *Acta Crystallogr. Sect. B* **1972**, *28*, 1671 – 1677.
[150] J. Yang, J.-L. Marendaz, S. J. Geib, A. D. Hamilton, *Tetrahedron Lett.* **1994**, *35*, 3665 – 3668.
[151] S. Valiyaveettil, V. Enkelmann, K. Müllen, *J. Chem. Soc. Chem. Commun.* **1994**, 2097 – 2098.
[152] S. Valiyaveettil, K. Müllen, *New J. Chem.* **1998**, 89 – 95.
[153] E. M. Smolin, L. Rapoport, *The Chemistry of Heterocyclic Compounds, Vol. 13*, Interscience, New York, **1959**, pp. 33 – 36.
[154] A. Ranganathan, V. R. Pedireddi, C. N. R. Rao, *J. Am. Chem. Soc.* **1999**, *121*, 1752 – 1753.

[155] J.-M. Lehn, M. Mascal, A. DeCian, J. Fischer, *J. Chem. Soc. Chem. Commun.* **1990**, 479 – 480.
[156] J. A. Zerkowski, C. T. Seto, D. A. Wierda, G. M. Whitesides, *J. Am. Chem. Soc.* **1990**, *112*, 9025 – 9026.
[157] C. T. Seto, G. M. Whitesides, *J. Am. Chem. Soc.* **1990**, *112*, 6409 – 6411.
[158] J. A. Zerkowski, J. P. Mathias, G. M. Whitesides, *J. Am. Chem. Soc.* **1994**, *116*, 4305 – 4315.
[159] P. Lipkowski, A. Bielejewska, H. Kooijman, A. L. Spek, P. Timmerman, D. N. Reinhoudt, *Chem. Commun.* **1999**, 1311 – 1312.
[160] M. Mascal, P. S. Fallon, A. S. Batsanov, B. R. Heywood, S. Champ, M. Colclough, *J. Chem. Soc. Chem. Commun.* **1995**, 805 – 806.
[161] M. Mascal, J. Hansen, P. S. Fallon, A. J. Blake, B. R. Heywood, M. H. Moore, J. P. Turkenburg, *Chem. Eur. J.* **1999**, *5*, 381 – 384.
[162] J. A. Zerkowski, C. T. Seto, G. M. Whitesides, *J. Am. Chem. Soc.* **1992**, *114*, 5473 – 5475.
[163] J. P. Mathias, E. E. Simanek, J. A. Zerkowski, C. T. Seto, G. M. Whitesides, *J. Am. Chem. Soc.* **1994**, *116*, 4316 – 4325.
[164] M. Mammen, E. E. Simanek, G. M. Whitesides, *J. Am. Chem. Soc.* **1996**, *118*, 12614 – 12623.
[165] C. T. Seto, G. M. Whitesides, *J. Am. Chem. Soc.* **1993**, *115*, 905 – 916.
[166] C. T. Seto, G. M. Whitesides, *J. Am. Chem. Soc.* **1993**, *115*, 1330 – 1340.
[167] L. Isaacs, D. N. Chin, N. Bowden, Y. Xia, G. M. Whitesides, *Perspectives in Supramolecular Chemistry*, *Vol. 4* (Ed.: D. N. Reinhoudt), Wiley, **1999**, pp. 1 – 46.
[168] J. P. Mathias, C. T. Seto, E. E. Simanek, G. M. Whitesides, *J. Am. Chem. Soc.* **1994**, *116*, 1725 – 1736.
[169] J. P. Mathias, E. E. Simanek, C. T. Seto, G. M. Whitesides, *Angew. Chem.* **1993**, *105*, 1848 – 1852; *Angew. Chem. Int. Ed. Engl.* **1993**, *32*, 1766 – 1769.
[170] J. P. Mathias, E. E. Simanek, G. M. Whitesides, *J. Am. Chem. Soc.* **1994**, *116*, 4326 – 4340.
[171] C. T. Seto, G. M. Whitesides, *J. Am. Chem. Soc.* **1991**, *113*, 712 – 713.
[172] R. H. Vreekamp, J. P. M. Van Duynhoven, M. Hubert, W. Verboom, D. N. Reinhoudt, *Angew. Chem.* **1996**, *108*, 1306 – 1309; *Angew. Chem. Int. Ed. Engl.* **1996**, *35*, 1215 – 1218.
[173] P. Timmerman, R. H. Vreekamp, R. Hulst, W. Verboom, D. N. Reinhoudt, K. Rissanen, K. A. Udachin, J. Ripmeester, *Chem. Eur. J.* **1997**, *3*, 1823 – 1832.
[174] L. J. Prins, K. A. Jolliffe, R. Hulst, P. Timmerman, D. N. Reinhoudt, *J. Am. Chem. Soc.* **2000**, *122*, 3617 – 3627.
[175] J.-L. Weidmann, K. A. Jolliffe, L. J. Prins, P. Timmerman, D. N. Reinhoudt, *J. Chem. Soc. Perkin Trans. 2* **2000**, *10*, 2077 – 2089.
[176] K. A. Jolliffe, P. Timmerman, D. N. Reinhoudt, *Angew. Chem.* **1999**, *111*, 983 – 986; *Angew. Chem. Int. Ed.* **1999**, *38*, 933 – 937.
[177] M. Mammen, E. I. Shakhnovich, J. M. Deutch, G. M. Whitesides, *J. Org. Chem.* **1998**, *63*, 3821 – 3830.
[178] P. Timmerman, R. Hulst, unpublished results.
[179] M. Crego Calama, R. Fokkens, N. M. M. Nibbering, P. Timmerman, D. N. Reinhoudt, *Chem. Commun.* **1998**, 1021 – 1022.
[180] L. J. Prins, F. de Jong, P. Timmerman, D. N. Reinhoudt, *Nature* **2000**, *408*, 181 – 184.
[181] B. Hasenkopf, J.-M. Lehn, N. Boumediene, E. Leize, A. Van Dorsselaer, *Angew. Chem.* **1998**, *110*, 3458 – 3460; *Angew. Chem. Int. Ed.* **1998**, *37*, 3265 – 3268.
[182] E. E. Simanek, M. I. M. Wazeer, J. P. Mathias, G. M. Whitesides, *J. Org. Chem.* **1994**, *59*, 4904 – 4909.
[183] D. N. Chin, E. E. Simanek, X. Li, M. I. M. Wazeer, G. M. Whitesides, *J. Org. Chem.* **1997**, *62*, 1891 – 1895.
[184] S. Ma, D. M. Rudkevich, J. Rebek, Jr., *J. Am. Chem. Soc.* **1998**, *120*, 4977 – 4981.
[185] K. C. Russell, E. Leize, A. Van Dorsselaer, J.-M. Lehn, *Angew. Chem.* **1995**, *107*, 244 – 248; *Angew. Chem. Int. Ed. Engl.* **1995**, *34*, 209 – 213.
[186] M. Scherer, J. L. Sessler, A. Gebauer, V. Lynch, *Chem. Eur. J.* **1998**, *4*, 152 – 158.
[187] X. Cheng, Q. Gao, R. D. Smith, E. E. Simanek, M. Mammen, G. M. Whitesides, *J. Org. Chem.* **1996**, *61*, 2204 – 2206.
[188] K. A. Jolliffe, M. Crego Calama, R. Fokkens, N. M. M. Nibbering, P. Timmerman, D. N. Reinhoudt, *Angew. Chem.* **1998**, *110*, 1294 – 1297; *Angew. Chem. Int. Ed.* **1998**, *37*, 1247 – 1251.
[189] Y. Wang, B. Wei, Q. Wang, *J. Crystallogr. Spectrosc. Res.* **1990**, *20*, 79.
[190] D. N. Chin, D. M. Gordon, G. M. Whitesides, *J. Am. Chem. Soc.* **1994**, *116*, 12033 – 12044.
[191] E. E. Simanek, M. Mammen, D. M. Gordon, D. N. Chin, J. P. Mathias, C. T. Seto, G. M. Whitesides, *Tetrahedron* **1995**, *51*, 607 – 619.
[192] W. Yang, X. Chai, L. Chi, X. Liu, Y. Cao, R. Lu, Y. Jiang, X. Tang, H. Fuchs, T. Li, *Chem. Eur. J.* **1999**, *5*, 1144 – 1149.
[193] L. J. Prins, J. Huskens, F. de Jong, P. Timmerman, D. N. Reinhoudt, *Nature* **1999**, *398*, 498 – 502.
[194] E. E. Simanek, S. Qiao, I. S. Choi, G. M. Whitesides, *J. Org. Chem.* **1997**, *62*, 2619 – 2621.
[195] S. J. Geib, C. Vincent, E. Fan, A. D. Hamilton, *Angew. Chem.* **1993**, *105*, 83 – 85; *Angew. Chem. Int. Ed. Engl.* **1993**, *32*, 119 – 121.
[196] C.-Y. Huang, V. Lynch, E. V. Anslyn, *Angew. Chem.* **1992**, *104*, 1259 – 1261; *Angew. Chem. Int. Ed. Engl.* **1992**, *31*, 1244 – 1246.
[197] J. Yang, E. Fan, S. J. Geib, A. D. Hamilton, *J. Am. Chem. Soc.* **1993**, *115*, 5314 – 5315.
[198] S. C. Zimmerman, B. F. Duerr, *J. Org. Chem.* **1992**, *57*, 2215 – 2217.
[199] M. Suárez, J.-M. Lehn, S. C. Zimmerman, A. Skoulios, B. Heinrich, *J. Am. Chem. Soc.* **1998**, *120*, 9526 – 9532.
[200] A. Marsh, M. Silvestri, J.-M. Lehn, *Chem. Commun.* **1996**, 1527 – 1528.
[201] M. Mascal, N. M. Hext, R. Warmuth, M. H. Moore, J. P. Turkenburg, *Angew. Chem.* **1996** , *35*, 2347 – 2350; *Angew. Chem. Int. Ed. Engl.* **1996**, *35*, 2204 – 2206.
[202] S. V. Kolotuchin, S. C. Zimmerman, *J. Am. Chem. Soc.* **1998**, *120*, 9092 – 9093.
[203] G. Gottarelli, S. Masiero, G. P. Spada, *J. Chem. Soc. Chem. Commun.* **1995**, 2555 – 2557.
[204] J. T. Davis, S. Tirumala, J. R. Jenssen, E. Radler, D. Fabris, *J. Org. Chem.* **1995**, *60*, 4167 – 4176.
[205] T. J. Pinnavaia, H. T. Miles, E. D. Becker, *J. Am. Chem. Soc.* **1975**, *97*, 7198 – 7200.
[206] C. Detellier, P. Laszlo, *J. Am. Chem. Soc.* **1980**, *102*, 1135 – 1141.
[207] T. J. Pinnavaia, C. L. Marshall, C. M. Mettler, C. L. Fisk, H. T. Miles, E. D. Becker, *J. Am. Chem. Soc.* **1978**, *100*, 3625 – 3627.
[208] M. Borzo, L. P. Detellier, A. Paris, *J. Am. Chem. Soc.* **1980**, *102*, 1124 – 1134.
[209] E. Bouhoutsos-Brown, C. L. Marshall, T. J. Pinnavaia, *J. Am. Chem. Soc.* **1982**, *104*, 6576 – 6584.
[210] J. A. Walmsley, R. G. Barr, E. Bouhoutsos-Brown, T. J. Pinnavaia, *J. Phys. Chem.* **1984**, *88*, 2599 – 2605.
[211] A. L. Marlow, E. Mezzina, G. P. Spada, S. Masiero, J. T. Davis, G. Gottarelli, *J. Org. Chem.* **1999**, *64*, 5116 – 5123.
[212] A. Liu, A. Majumdar, W. Hu, A. Kettani, E. Skripkin, D. J. Patel, *J. Am. Chem. Soc.* **2000**, *122*, 3206 – 3210.
[213] S. Basu, A. A. Szewczak, M. Cocco, S. A. Strobel, *J. Am. Chem. Soc.* **2000**, *122*, 3240 – 3241.
[214] K. Fukushima, H. Iwahashi, *Chem. Commun.* **2000**, 895 – 896.
[215] J. L. Sessler, M. Sathiosatham, K. Doerr, V. Lynch, K. A. Abboud, *Angew. Chem.* **2000**, *112*, 1356 – 1359; *Angew. Chem. Int. Ed.* **2000**, *39*, 1300 – 1303.
[216] S. Tirumala, J. T. Davis, *J. Am. Chem. Soc.* **1997**, *119*, 2769 – 2776.
[217] A. L. Marlow, J. T. Davis, *Tetrahedron Lett.* **1999**, *40*, 3539 – 3542.
[218] J. T. Davis, S. Tirumala, A. L. Marlow, *J. Am. Chem. Soc.* **1997**, *119*, 5271 – 5272.
[219] M. Cai, A. L. Marlow, J. C. Fettinger, D. Fabris, T. J. Haverlock, B. A. Moyer, J. T. Davis, *Angew. Chem.* **2000**, *112*, 1339 – 1341; *Angew. Chem. Int. Ed.* **2000**, *39*, 1283 – 1285.
[220] M. C. T. Fyfe, P. T. Glink, S. Menzer, J. F. Stoddart, A. J. P. White, D. J. Williams, *Angew. Chem.* **1997**, *109*, 2160 – 2162; *Angew. Chem. Int. Ed. Engl.* **1997**, *36*, 2068 – 2072.
[221] J. Sánchez-Quesada, C. Seel, P. Prados, J. de Mendoza, *J. Am. Chem. Soc.* **1996**, *118*, 277 – 278.
[222] T. Haack, M. W. Peczuh, X. Salvatella, J. Sánchez-Quesada, J. de Mendoza, A. D. Hamilton, E. Giralt, *J. Am. Chem. Soc.* **1999**, *121*, 11813 – 11820.
[223] L. A. Paquette, R. J. Ternansky, D. W. Balogh, G. Kentgen, *J. Am. Chem. Soc.* **1983**, *105*, 5446 – 5450.
[224] D. J. Cram, *Science* **1983**, *219*, 1177 – 1183.

[225] D. J. Cram, S. Karbach, Y. H. Kim, L. Baczynskyj, G. W. Kalleymeyn, *J. Am. Chem. Soc.* **1985**, *107*, 2575 – 2576.
[226] J. Canceill, L. Lacombe, A. Collet, *J. Am. Chem. Soc.* **1985**, *107*, 6993 – 6996.
[227] D. J. Cram, M. E. Tanner, C. B. Knobler, *J. Am. Chem. Soc.* **1991**, *113*, 7717 – 7727.
[228] P. Timmerman, W. Verboom, F. C. J. M. Van Veggel, W. P. Van Hoorn, D. N. Reinhoudt, *Angew. Chem.* **1994**, *106*, 1313 – 1316; *Angew. Chem. Int. Ed. Engl.* **1994**, *33*, 1292 – 1295.
[229] J. Rebek, Jr., *Pure Appl. Chem.* **1996**, *68*, 1261 – 1266.
[230] M. Morgan Conn, J. Rebek, Jr., *Chem. Rev.* **1997**, *97*, 1647 – 1668.
[231] J. de Mendoza, *Chem. Eur. J.* **1998**, *4*, 1373 – 1377.
[232] J. Rebek, Jr., *Acc. Chem. Res.* **1999**, *32*, 278 – 286.
[233] J. Rebek, Jr., *Chem. Commun.* **2000**, 637 – 643.
[234] L. R. MacGillivray, J. L. Atwood, *Angew. Chem.* **1999**, *111*, 1084 – 1096; *Angew. Chem. Int. Ed.* **1999**, *38*, 1018 – 1933.
[235] M. Kim, G. W. Gokel, *J. Chem. Soc. Chem. Commun.* **1987**, 1686 – 1688; Corrigendum: M. Kim, G. W. Gokel, *J. Chem. Soc. Chem. Commun*. **1990**, 948.
[236] O. F. Schall, G. W. Gokel, *J. Am. Chem. Soc.* **1994**, *116*, 6089 – 6100.
[237] Y. Kickuchi, Y. Tanaka, S. Sutarto, K. Kobayashi, H. Toi, Y. Aoyama, *J. Am. Chem. Soc.* **1992**, *114*, 10 302 – 10 306.
[238] R. G. Chapman, N. Chopra, E. D. Cochien, J. C. Sherman, *J. Am. Chem. Soc.* **1994**, *116*, 369 – 370.
[239] R. G. Chapman, J. C. Sherman, *J. Am. Chem. Soc.* **1998**, *120*, 9818 – 9826.
[240] A. Shivanyuk, E. F. Paulus, V. Böhmer, *Angew. Chem.* **1999**, *111*, 3091 – 3094; *Angew. Chem. Int. Ed.* **1999**, *38*, 2906 – 2909.
[241] I. Higler, L. Grave, E. Breuning, W. Verboom, F. de Jong, T. M. Fyles, D. N. Reinhoudt, *Eur. J. Org. Chem.* **2000**, 1727 – 1734.
[242] K. Koh, K. Araki, S. Shinkai, *Tetrahedron Lett.* **1994**, *35*, 8255 – 8258.
[243] A. Arduini, M. Fabbi, M. Mantovani, L. Mirone, A. Pochini, A. Secchi, R. Ungaro, *J. Org. Chem.* **1995**, *60*, 1454 – 1457.
[244] O. Struck, W. Verboom, W. J. J. Smeets, A. L. Spek, D. N. Reinhoudt, *J. Chem. Soc. Perkin Trans. 2* **1997**, 223 – 227.
[245] R. H. Vreekamp, W. Verboom, D. N. Reinhoudt, *J. Org. Chem.* **1996**, *61*, 4282 – 4288.
[246] K. D. Shimizu, J. Rebek, Jr., *Proc. Natl. Acad. Sci. USA* **1995**, *92*, 12 403 – 12 407.
[247] B. C. Hamann, K. D. Shimizu, J. Rebek, Jr., *Angew. Chem.* **1996**, *108*, 1425 – 1427; *Angew. Chem. Int. Ed. Engl.* **1996**, *35*, 1326 – 1329.
[248] O. Mogck, V. Böhmer, W. Vogt, *Tetrahedron* **1996**, *52*, 8489 – 8496.
[249] A. Arduini, L. Domiano, L. Ogliosi, A. Pochini, A. Secchi, R. Ungaro, *J. Org. Chem.* **1997**, *62*, 7866 – 7868.
[250] J. J. González, R. Ferdani, E. Albertini, J. M. Blasco, A. Arduini, A. Pochini, P. Prados, J. de Mendoza, *Chem. Eur. J.* **2000**, *6*, 73 – 80.
[251] R. P. Bonar-Law, J. K. M. Sanders, *Tetrahedron Lett.* **1993**, *34*, 1677 – 1680.
[252] S. B. Lee, J.-I. Hong, *Tetrahedron Lett.* **1996**, *37*, 8501 – 8504.
[253] S. Zhao, J. H. T. Luong, *J. Chem. Soc. Chem. Commun.* **1994**, 2307 – 2308.
[254] S. Zhao, J. H. T. Luong, *J. Chem. Soc. Chem. Commun.* **1995**, 663 – 664.
[255] K. Murayama, K. Aoki, *Chem. Commun.* **1998**, 607 – 608.
[256] K. N. Rose, L. Barbour, G. W. Orr, J. L. Atwood, *Chem. Commun.* **1998**, 407 – 408.
[257] A. Shivanyuk, K. Rissanen, E. Kolehmainen, *Chem. Commun.* **2000**, 1107 – 1108.
[258] T. Heinz, D. M. Rudkevich, J. Rebek, Jr., *Nature* **1998**, *394*, 764 – 766.
[259] J. W. H. Smeets, R. P. Sijbesma, L. van Dalen, A. L. Spek, W. J. J. Smeets, R. J. M. Nolte, *J. Org. Chem.* **1989**, *54*, 3710 – 3717.
[260] R. Wyler, J. de Mendoza, J. Rebek, Jr., *Angew. Chem.* **1993**, *105*, 1820 – 1822; *Angew. Chem. Int. Ed. Engl.* **1993**, *32*, 1699 – 1701.
[261] R. S. Meissner, J. Rebek, Jr., J. de Mendoza, *Science* **1995**, *270*, 1485 – 1488.
[262] J. Kang, J. Rebek, Jr., *Nature* **1996**, *382*, 239 – 241.
[263] R. M. Grotzfeld, N. Branda, J. Rebek, Jr., *Science* **1996**, *271*, 487 – 489.
[264] A. Lützen, S. D. Starnes, D. M. Rudkevich, J. Rebek, Jr., *Tetrahedron Lett.* **2000**, *41*, 3777 – 3780.
[265] T. Martín, U. Obst, J. Rebek, Jr., *Science* **1998**, *281*, 1842 – 1845.
[266] L. R. MacGillivray, J. L. Atwood, *Nature* **1997**, *389*, 469 – 472.
[267] C. M. Drain, R. Fischer, E. G. Nolen, J.-M. Lehn, *J. Chem. Soc. Chem. Commun.* **1993**, 243 – 245.
[268] L. R. MacGillivray, P. R. Diamente, J. L. Reid, J. A. Ripmeester, *Chem. Commun.* **2000**, 359 – 360.
[269] A. Lützen, A. R. Renslo, C. A. Schalley, B. M. O'Leary, J. Rebek, Jr., *J. Am. Chem. Soc.* **1999**, *121*, 7455 – 7456.
[270] R. G. Chapman, J. C. Sherman, *J. Am. Chem. Soc.* **1995**, *117*, 9081 – 9082.
[271] F. C. Tucci, D. M. Rudkevich, J. Rebek, Jr., *J. Am. Chem. Soc.* **1999**, *121*, 4928 – 4929.
[272] L. Frish, S. E. Matthews, V. Böhmer, Y. Cohen, *J. Chem. Soc. Perkin Trans. 2* **1999**, 669 – 671.
[273] C. A. Schalley, T. Martín, U. Obst, J. Rebek, Jr., *J. Am. Chem. Soc.* **1999**, *121*, 2133 – 2138.
[274] C. A. Schalley, R. K. Castellano, M. S. Brody, D. M. Rudkevich, G. Siuzdak, J. Rebek, Jr., *J. Am. Chem. Soc.* **1999**, *121*, 4568 – 4579.
[275] O. Mogck, E. F. Paulus, V. Böhmer, I. Thondorf, W. Vogt, *Chem. Commun.* **1996**, 2533 – 2534.
[276] R. G. Chapman, G. Olovsson, J. Trotter, J. C. Sherman, *J. Am. Chem. Soc.* **1998**, *120*, 6252 – 6260.
[277] K. Kobayashi, T. Shirasaka, K. Yamaguchi, S. Sakamoto, E. Horn, N. Furukawa, *Chem. Commun.* **2000**, 41 – 42.
[278] S. Mecozzi, J. Rebek, Jr., *Chem. Eur. J.* **1998**, *4*, 1016 – 1022.
[279] K. Nakamura, C. Sheu, A. E. Keating, K. N. Houk, J. C. Sherman, R. G. Chapman, W. L. Jorgenson, *J. Am. Chem. Soc.* **1997**, *119*, 4321 – 4322.
[280] T. Szabo, G. Hilmersson, J. Rebek, Jr., *J. Am. Chem. Soc.* **1998**, *120*, 6193 – 6194.
[281] J. Santamaría, T. Martín, G. Hilmersson, S. L. Craig, J. Rebek, Jr., *Proc. Natl. Acad. Sci. USA* **1999**, *96*, 8344 – 8347.
[282] X. Wang, K. N. Houk, *Org. Lett.* **1999**, *1*, 591 – 594.
[283] O. Mogck, M. Pons, V. Böhmer, W. Vogt, *J. Am. Chem. Soc.* **1997**, *119*, 5706 – 5712.
[284] M. O. Vysotsky, I. Thondorf, V. Böhmer, *Angew. Chem.* **2000**, *112*, 1309 – 1312; *Angew. Chem. Int. Ed.* **2000**, *39*, 1264 – 1267.
[285] D. J. Cram, M. E. Tanner, R. Thomas, *Angew. Chem.* **1991**, *103*, 1048 – 1051; *Angew. Chem. Int. Ed. Engl.* **1991**, *30*, 1024 – 1027.
[286] B. M. O'Leary, R. M. Grotzfeld, J. Rebek, Jr., *J. Am. Chem. Soc.* **1997**, *119*, 11 701 – 11 702.
[287] T. Heinz, D. M. Rudkevich, J. Rebek, Jr., *Angew. Chem.* **1999**, *111*, 1206 – 1209; *Angew. Chem. Int. Ed.* **1999**, *38*, 1136 – 1139.
[288] S. K. Körner, F. C. Tucci, D. M. Rudkevich, T. Heinz, J. Rebek, Jr., *Chem. Eur. J.* **2000**, *6*, 187 – 195.
[289] J. Kang, J. Rebek, Jr., *Nature* **1997**, *385*, 50 – 52.
[290] J. Kang, G. Hilmersson, J. Santamaría, J. Rebek, Jr., *J. Am. Chem. Soc.* **1998**, *120*, 3650 – 3656.
[291] J. Kang, J. Santamaría, G. Hilmersson, J. Rebek, Jr., *J. Am. Chem. Soc.* **1998**, *120*, 7389 – 7390.
[292] C. Nuckolls, F. Hof, T. Martín, J. Rebek, Jr., *J. Am. Chem. Soc.* **1999**, *121*, 10 281 – 10 285.
[293] J. Rivera, T. Martín, J. Rebek, Jr., *Science* **1998**, *279*, 1021 – 1023.
[294] J. M. Rivera, S. L. Craig, T. Martín, J. Rebek, Jr., *Angew. Chem.* **2000**, *112*, 2214 – 2216; *Angew. Chem. Int. Ed.* **2000**, *39*, 2130 – 2132.
[295] Y. Tokunaga, J. Rebek, Jr., *J. Am. Chem. Soc.* **1998**, *120*, 66 – 69.
[296] R. K. Castellano, B. H. Kim, J. Rebek, Jr., *J. Am. Chem. Soc.* **1997**, *119*, 12 671 – 12 672.
[297] R. K. Castellano, C. Nuckolls, J. Rebek, Jr., *J. Am. Chem. Soc.* **1999**, *121*, 11 156 – 11 163.
[298] P. Timmerman, W. Verboom, F. C. J. M. van Veggel, J. P. M. van Duynhoven, D. N. Reinhoudt, *Angew. Chem.* **1994**, *106*, 1313 – 1315; *Angew. Chem. Int. Ed. Engl.* **1994**, *33*, 2345 – 2348.
[299] M. Simard, D. Su, J. D. Wuest, *J. Am. Chem. Soc.* **1991**, *113*, 4696 – 4698.
[300] X. Wang, M. Simard, J. D. Wuest, *J. Am. Chem. Soc.* **1994**, *116*, 12 119 – 12 120.
[301] V. A. Russell, M. D. Ward, *Chem. Mater.* **1996**, *8*, 1654 – 1666.
[302] V. A. Russell, M. C. Etter, M. D. Ward, *Chem. Mater.* **1994**, *6*, 1206 – 1217.
[303] V. A. Russell, M. C. Etter, M. D. Ward, *J. Am. Chem. Soc.* **1994**, *116*, 1941 – 1952.
[304] V. A. Russell, C. C. Evans, W. Li, M. D. Ward, *Science* **1997**, *276*, 575 – 579.

[305] J. A. Swift, V. A. Russell, M. D. Ward, *Adv. Mater.* **1997**, *9*, 1183 – 1186.
[306] K. Endo, T. Sawaki, M. Koyanagi, K. Kobayashi, H. Masuda, Y. Aoyama, *J. Am. Chem. Soc.* **1995**, *117*, 8341 – 8352.
[307] Y. Aoyama, K. Endo, T. Anzai, Y. Yamaguchi, T. Sawaki, K. Kobayashi, N. Kanehisa, H. Hashimoto, Y. Kai, H. Masuda, *J. Am. Chem. Soc.* **1996**, *118*, 5562 – 5571.
[308] K. Endo, T. Ezuhara, M. Koyanagi, H. Masuda, Y. Aoyama, *J. Am. Chem. Soc.* **1997**, *119*, 499 – 505.
[309] K. Endo, T. Koike, T. Sawaki, O. Hayashida, H. Masuda, Y. Aoyama, *J. Am. Chem. Soc.* **1997**, *119*, 4117 – 4122.
[310] S. Anderson, H. L. Anderson, J. K. M. Sanders, *Acc. Chem. Res.* **1993**, *26*, 469 – 475.
[311] R. Hoss, F. Vögtle, *Angew. Chem.* **1994**, *106*, 389 – 398; *Angew. Chem. Int. Ed. Engl.* **1994**, *33*, 375 – 384.
[312] T. J. Hubin, A. G. Kochinski, A. L. Vance, D. H. Busch, *Advances in Supramolecular Chemistry*, *Vol. 5*, JAI, **1999**, p. 237.
[313] F. Diederich, P. J. Stang, *Template Directed Synthesis*, Wiley-VCH, Weinheim, **2000**.
[314] J. S. Nowick, Q. Feng, T. Tjivikua, P. Ballester, J. Rebek, Jr., *J. Am. Chem. Soc.* **1991**, *113*, 8831 – 8839.
[315] L. Mandolini, *Adv. Phys. Org. Chem.* **1986**, *22*, 1 – 111.
[316] I. Huc, R. J. Pieters, J. Rebek, Jr., *J. Am. Chem. Soc.* **1994**, *116*, 11 592 – 11 593.
[317] M. Famulok, J. S. Nowick, J. Rebek, Jr., *Acta Chem. Scand.* **1992**, *46*, 315.
[318] L. E. Orgel, *Nature* **1992**, *358*, 203 – 209.
[319] S. Hoffmann, *Angew. Chem.* **1992**, *103*, 1032 – 1035; *Angew. Chem. Int. Ed. Engl.* **1992**, *31*, 1013 – 1016.
[320] L. E. Orgel, *Acc. Chem. Res.* **1995**, *28*, 109 – 118.
[321] A. Robertson, A. J. Sinclair, D. Philp, *Chem. Soc. Rev.* **2000**, *29*, 141 – 152.
[322] T. Tjivikua, P. Ballester, J. Rebek, Jr., *J. Am. Chem. Soc.* **1990**, *112*, 1249 – 1250.
[323] I. Huc, R. J. Pieters, J. Rebek, Jr., *J. Am. Chem. Soc.* **1994**, *116*, 10 296 – 10 297.
[324] D. Philp, A. Robertson, *Chem. Commun.* **1998**, 879 – 880.
[325] A. Robertson, D. Philp, N. Spencer, *Tetrahedron* **1999**, *55*, 11 365 – 11 384.
[326] R. Bennes, D. Philp, N. Spencer, B. M. Kariuki, K. D. M. Harris, *Org. Lett.* **1999**, *1*, 1087 – 1090.
[327] C. A. Booth, D. Philp, *Tetrahedron Lett.* **1998**, 6987 – 6990.
[328] T. Inoue, L. E. Orgel, *Science* **1983**, *219*, 859 – 862.
[329] B. G. Bag, G. von Kiedrowski, *Pure Appl. Chem.* **1996**, *68*, 2145 – 2152 .
[330] O. L. Acevedo, L. E. Orgel, *J. Mol. Biol.* **1987**, *197*, 187 – 193.
[331] J. T. Goodwin, D. G. Lynn, *J. Am. Chem. Soc.* **1992**, *114*, 9197 – 9198.
[332] T. Ross Kelly, C. Zhao, G. J. Bridger, *J. Am. Chem. Soc.* **1989**, *111*, 3744 – 3745.
[333] T. Ross Kelly, G. J. Bridger, C. Zhao, *J. Am. Chem. Soc.* **1990**, *112*, 8024 – 8034.
[334] R. J. Pieters, I. Huc, J. Rebek, Jr., *Tetrahedron* **1995**, *51*, 485 – 498.
[335] F. Würthner, J. Rebek, Jr., *Angew. Chem.* **1995**, *107*, 503 – 505; *Angew. Chem. Int. Ed. Engl.* **1995**, *34*, 446 – 448.
[336] E. A. Archer, N. T. Goldberg, V. Lynch, M. J. Krische, *J. Am. Chem. Soc.* **2000**, *122*, 5006 – 5007.
[337] E. A. Wintner, J. Rebek, Jr., *Acta Chem. Scand.* **1996**, *50*, 469 – 485.
[338] M. M. Conn, E. A. Wintner, J. Rebek, Jr., *J. Am. Chem. Soc.* **1994**, *116*, 8823 – 8824.
[339] G. Von Kiedrowski, *Angew. Chem.* **1986**, *98*, 932 – 934; *Angew. Chem. Int. Ed. Engl.* **1986**, *25*, 932 – 935.
[340] G. von Kiedrowski, B. Wlotzka, J. Helbing, *Angew. Chem.* **1989**, *101*, 1259 – 1261; *Angew. Chem. Int. Ed. Engl.* **1989**, *28*, 1235 – 1237.
[341] C. Böhler, W. Bannwarth, P. L. Luisi, *Helv. Chim. Acta* **1993**, *76*, 2313 – 2320.
[342] W. S. Zielinski, L. E. Orgel, *Nature* **1987**, *327*, 346 – 347.
[343] G. von Kiedrowski, B. Wlotzka, J. Helbing, M. Matzen, S. Jordan, *Angew. Chem.* **1991**, *103*, 456 – 459; *Angew. Chem. Int. Ed. Engl.* **1991**, *30*, 423 – 426 .
[344] T. Achilles, G. von Kiedrowski, *Angew. Chem.* **1993**, *105*, 1225 – 1228; *Angew. Chem. Int. Ed. Engl.* **1993**, *32*, 1198 – 1201.
[345] D. Sievers, G. von Kiedrowski, *Nature* **1994**, *369*, 221 – 224.
[346] D. Sievers, G. von Kiedrowski, *Chem. Eur. J.* **1998**, *4*, 629 – 641.
[347] M. Koppitz, P. E. Nielsen, L. E. Orgel, *J. Am. Chem. Soc.* **1998**, *120*, 4563 – 4569.
[348] C. Böhler, P. E. Nielsen, L. E. Orgel, *Nature* **1995**, *376*, 578 – 581.
[349] T. Li, K. C. Nicolaou, *Nature* **1994**, *369*, 218 – 221.
[350] A. Luther, R. Brandsch, G. von Kiedrowski, *Nature* **1998**, *396*, 245 – 635.
[351] S. Pitsch, R. Krishnamurthy, M. Bolli, S. Wendeborn, A. Holzer, M. Minton, C. Lesueur, I. Schlonvogt, B. Jaun, A. Eschenmoser, *Helv. Chim. Acta* **1995**, *78*, 1621 – 1635.
[352] M. Bolli, R. Micura, S. Pitsch, A. Eschenmoser, *Helv. Chim. Acta* **1997**, *80*, 1901 – 1951.
[353] M. M. Conn, J. Rebek, Jr., *Curr. Opin. Struct. Biol.* **1994**, *4*, 629 – 635.
[354] F. M. Menger, A. V. Eliseev, N. A. Khanjin, *J. Am. Chem. Soc.* **1994**, *116*, 3613 – 3614.
[355] E. A. Wintner, B. Tsao, J. Rebek, Jr., *J. Org. Chem.* **1995**, *60*, 7997 – 8001.
[356] F. M. Menger, A. V. Eliseev, N. A. Khanjin, M. J. Sherrod, *J. Org. Chem.* **1995**, *60*, 2870 – 2878.
[357] D. N. Reinhoudt, D. M. Rudkevich, F. de Jong, *J. Am. Chem. Soc.* **1996**, *118*, 6880 – 6889.
[358] V. Rotello, J. I. Hong, J. Rebek, Jr., *J. Am. Chem. Soc.* **1991**, *113*, 9422 – 9423.
[359] M. M. Conn, E. A. Wintner, J. Rebek, Jr., *Angew. Chem.* **1994**, *33*, 1665 – 1667; *Angew. Chem. Int. Ed. Engl.* **1994**, *106*, 1577 – 1579.
[360] E. A. Wintner, M. M. Conn, J. Rebek, Jr., *J. Am. Chem. Soc.* **1994**, *116*, 8877 – 8884.
[361] Q. Feng, T. K. Park, J. Rebek, Jr., *Science* **1992**, 1179 – 1180.
[362] J. I. Hong, Q. Feng, V. Rotello, J. Rebek, Jr., *Science* **1992**, 848 – 850.
[363] D. M. Rudkevich, J. Rebek, Jr., *Angew. Chem.* **1997**, *109*, 877 – 879; *Angew. Chem. Int. Ed. Engl.* **1997**, *36*, 846 – 848.
[364] A. Terfort, G. von Kiedrowski, *Angew. Chem.* **1992**, *104*, 626 – 628; *Angew. Chem. Int. Ed. Engl.* **1992**, *31*, 654 – 656.
[365] F. Persico, J. D. Wuest, *J. Org. Chem.* **1993**, *58*, 95 – 99 .
[366] B. Wang, I. O. Sutherland, *Chem. Commun.* **1997**, 1495 – 1496.
[367] N. V. Gerbeleu, V. B. Arion, J. Burgess, *Template Synthesis of Macrocyclic Compounds*, Wiley-VCH, Weinheim, **1999**.
[368] F. J. Carver, C. A. Hunter, R. J. Shannon, *J. Chem. Soc. Chem. Commun.* **1994**, 1277 – 1280.
[369] T. D. Clark, M. R. Ghadiri, *J. Am. Chem. Soc.* **1995**, *117*, 12 364 – 12 365.
[370] T. D. Clark, K. Kobayashi, M. R. Ghadiri, *Chem. Eur. J.* **1999**, *5*, 782 – 792.
[371] F. Cardullo, M. Crego Calama, B. H. M. Snellink-Ruël, J.-L. Weidmann, A. Bielejewska, R. Fokkens, N. M. M. Nibbering, P. Timmerman, D. N. Reinhoudt, *Chem. Commun.* **2000**, 367 – 368.
[372] G. A. Breault, C. A. Hunter, P. C. Mayers, *Tetrahedron* **1999**, *55*, 5265 – 5293.
[373] F. Vögtle, T. Dünnwald, T. Schmidt, *Acc. Chem. Res.* **1996**, *29*, 451 – 460.
[374] R. Jäger, F. Vögtle, *Angew. Chem.* **1997**, *109*, 966 – 980; *Angew. Chem. Int. Ed. Engl.* **1997**, *36*, 930 – 944.
[375] T. A. Kidd, D. A. Leigh, A. J. Wilson, *J. Am. Chem. Soc.* **1999**, *121*, 1599 – 1600.
[376] C. A. Hunter, D. H. Purvis, *Angew. Chem.* **1992**, *104*, 779 – 782; *Angew. Chem. Int. Ed. Engl.* **1992**, *31*, 792 – 795.
[377] F. Vögtle, S. Meier, R. Hoss, *Angew. Chem.* **1992**, *104*, 1628 – 1630; *Angew. Chem. Int. Ed. Engl.* **1992**, *31*, 1619 – 1622.
[378] G. M. Hübner, J. Gläser, C. Seel, F. Vögtle, *Angew. Chem.* **1999**, *111*, 395 – 398; *Angew. Chem. Int. Ed.* **1999**, *38*, 383 – 386.
[379] A. G. Johnston, D. A. Leigh, R. J. Pritchard, M. D. Deegan, *Angew. Chem.* **1995**, *107*, 1324 – 1327; *Angew. Chem. Int. Ed. Engl.* **1995**, *34*, 1209 – 1212.
[380] A. G. Johnston, D. A. Leigh, L. Nezhat, J. P. Smart, M. D. Deegan, *Angew. Chem.* **1995**, *107*, 1327 – 1331; *Angew. Chem. Int. Ed. Engl.* **1995**, *34*, 1212 – 1216.
[381] A. G. Johnston, D. A. Leigh, A. Murphy, J. P. Smart, M. D. Deegan, *J. Am. Chem. Soc.* **1996**, *118*, 10 662 – 10 663.
[382] D. A. Leigh, A. Murphy, J. P. Smart, A. M. Slawin, *Angew. Chem.* **1997**, *109*, 752 – 756; *Angew. Chem. Int. Ed. Engl.* **1997**, *36*, 729 – 732.

[383] P. R. Ashton, E. J. T. Chrystal, P. T. Glink, S. Menzer, C. Schiavo, N. Spencer, J. F. Stoddart, P. A. Tasker, A. J. P. White, D. J. Williams, *Chem. Eur. J.* **1996**, *2*, 709 – 726.
[384] P. R. Ashton, R. Ballardini, V. Balzani, I. Baxter, A. Credi, M. C. T. Fyfe, M. T. Gandolfi, M. Gomez-Lopez, M.-V. Martinez-Diaz, A. Piersanti, N. Spencer, J. F. Stoddart, M. Venturi, A. J. P. White, D. J. Williams, *J. Am. Chem. Soc.* **1998**, *120*, 11 932 – 11 942.
[385] P. Tecilla, R. P. Dixon, G. Slobodkin, D. S. Alavi, D. H. Waldeck, A. D. Hamilton, *J. Am. Chem. Soc.* **1990**, *112*, 9408 – 9410.
[386] A. Harriman, D. J. Magda, J. L. Sessler, *J. Chem. Soc. Chem. Commun.* **1991**, 345 – 348.
[387] J. L. Sessler, B. Wang, A. Harriman, *J. Am. Chem. Soc.* **1995**, *117*, 704 – 714.
[388] C. J. Chang, J. D. K. Brown, M. C. Y. Chang, E. A. Baker, D. G. Nocera, *Natural and Artificial Supramolecular Systems*, *Vol. 3* (Ed.: V. Balzani), Wiley, New York, **2000**.
[389] A. Osuka, H. Shiratori, R. Yoneshima, T. Okada, S. Taniguchi, N. Mataga, *Chem. Lett.* **1995**, 913 – 914.
[390] A. Osuka, R. Yoneshima, H. Shiratori, T. Okada, S. Taniguchi, N. Mataga, *Chem. Commun.* **1998**, 1567 – 1568.
[391] C. Turró, C. K. Chang, G. E. Leroi, R. I. Cukier, D. G. Nocera, *J. Am. Chem. Soc.* **1992**, *114*, 4013 – 4015.
[392] A. Berman, E. S. Izraeli, H. Levanon, B. Wang, J. L. Sessler, *J. Am. Chem. Soc.* **1995**, *117*, 8252 – 8257.
[393] A. Berg, Z. Shuali, M. Asano-Someda, H. Levanon, M. Fuhs, K. Möbius, R. Wang, C. Brown, J. L. Sessler, *J. Am. Chem. Soc.* **1999**, *121*, 7433 – 7434.
[394] N. Tamura, K. Mitsui, T. Nabeshima, Y. Yano, *J. Chem. Soc. Perkin Trans. 2* **1994**, 2229 – 2237.
[395] A. Niemz, V. M. Rotello, *Acc. Chem. Res.* **1999**, *32*, 44 – 52.
[396] E. C. Breinlinger, A. Niemz, V. M. Rotello, *J. Am. Chem. Soc.* **1995**, *117*, 5379 – 5380.
[397] Y. Ge, R. R. Lilienthal, D. K. Smith, *J. Am. Chem. Soc.* **1996**, *118*, 3976 – 3977.
[398] R. Deans, A. Niemz, E. C. Breinlinger, V. M. Rotello, *J. Am. Chem. Soc.* **1997**, *119*, 10 863 – 10 864.
[399] K. Ariga, T. Kunitake, *Acc. Chem. Res.* **1998**, *31*, 371 – 378.
[400] H. Kitano, H. Ringsdorf, *Bull. Chem. Soc. Jpn.* **1985**, *58*, 2826 – 2828.
[401] R. Ahuja, P.-L. Caruso, K. Möbius, W. Paulus, H. Ringsdorf, G. Wildburg, *Angew. Chem.* **1993**, *105*, 1082 – 1085; *Angew. Chem. Int. Ed. Engl.* **1993**, *32*, 1033 – 1036.
[402] T. Kawahara, K. Kurihara, T. Kunitake, *Chem. Lett.* **1992**, 1839 – 1842.
[403] H. Koyano, P. Bissel, K. Yoshihara, K. Ariga, T. Kunitake, *Chem. Eur. J.* **1997**, *3*, 1077 – 1082.
[404] S. Champ, J. A. Dickinson, P. S. Fallon, B. R. Heywood, M. Mascal, *Angew. Chem.* **2000**, *112*, 2828 – 2831; *Angew. Chem. Int. Ed.* **2000**, *39*, 2716 – 2719.
[405] K. Taguchi, K. Ariga, T. Kunitake, *Chem. Lett.* **1995**, 701 – 702.
[406] J. C. MacDonald, G. M. Whitesides, *Chem. Rev.* **1994**, *94*, 2383 – 2420.
[407] J. J. Storhoff, C. A. Mirkin, *Chem. Rev.* **1999**, *99*, 1849 – 1862.
[408] C. A. Mirkin, R. L. Letsinger, R. C. Mucic, J. J. Storhoff, *Nature* **1996**, *382*, 607 – 609.
[409] R. Elghanian, J. J. Storhoff, R. C. Mucic, R. L. Letsinger, C. A. Mirkin, *Science* **1997**, *277*, 1078 – 1081.
[410] A. P. Alivisatos, K. P. Johnsson, X. Peng, T. E. Wilson, C. J. Loweth, M. P. Bruchez, Jr., P. G. Schultz, *Nature* **1996**, *382*, 609 – 611.
[411] C. J. Loweth, W. B. Caldwell, X. Peng, A. P. Alivisatos, P. G. Schultz, *Angew. Chem.* **1999**, *111*, 1925 – 1929; *Angew. Chem. Int. Ed.* **1999**, *38*, 1808 – 1812.
[412] C. M. Niemeyer, W. Bürger, J. Peplies, *Angew. Chem.* **1998**, *110*, 2391 – 2395; *Angew. Chem. Int. Ed.* **1998**, *37*, 2265 – 2268.
[413] L. Cusack, R. Rizza, A. Gorelov, D. Fitzmaurice, *Angew. Chem.* **1997**, *109*, 887 – 890; *Angew. Chem. Int. Ed. Engl.* **1997**, *36*, 848 – 851.
[414] A. K. Boal, F. Ilhan, J. E. DeRouchey, T. Thurn-Albrecht, T. P. Russell, V. M. Rotello, *Nature* **2000**, *404*, 746 – 748.
[415] Y. W. Cao, X. D. Chai, T. J. Li, J. Smith, D. Li, *Chem. Commun.* **1999**, 1605 – 1606.
[416] I. S. Choi, X. Li, E. E. Simanek, R. Akaba, G. M. Whitesides, *Chem. Mater.* **1999**, *11*, 684 – 690.
[417] H.-A. Klok, K. A. Jolliffe, C. L. Schauer, L. J. Prins, J. P. Spatz, M. Moller, P. Timmerman, D. N. Reinhoudt, *J. Am. Chem. Soc.* **1999**, *121*, 7154 – 7155.
[418] J. V. Barth, J. Weckesser, C. Cai, P. Günter, L. Bürgi, O. Jeandupeux, K. Kern, *Angew. Chem.* **2000**, *39*, 1230 – 1233; *Angew. Chem. Int. Ed.* **2000**, *39*, 1230 – 1233.
[419] F. S. Schoonbeek, J. H. van Esch, B. Wegewijs, D. B. A. Rep, M. P. de Haas, T. M. Klapwijk, R. M. Kellogg, B. L. Feringa, *Angew. Chem.* **1999**, *111*, 1486 – 1490; *Angew. Chem. Int. Ed.* **1999**, *38*, 1393 – 1397.
[420] D. B. A. Rep, R. Roelfsema, J. H. van Esch, F. S. Schoonbeek, R. M. Kellogg, B. L. Feringa, T. T. M. Palstra, T. M. Klapwijk, *Adv. Mater.* **2000**, *12*, 563 – 566.
[421] C. Fouquey, J.-M. Lehn, A.-M. Levelut, *Adv. Mater.* **1990**, *2*, 254 – 257.
[422] M. Kotera, J.-M. Lehn, J.-P. Vigneron, *J. Chem. Soc. Chem. Commun.* **1994**, 197 – 199.
[423] P. Bladon, A. C. Griffin, *Macromolecules* **1993**, *26*, 6604 – 6610.
[424] K. Hanabusa, T. Miki, Y. Taguchi, T. Koyama, H. Shirai, *J. Chem. Soc. Chem. Commun.* **1993**, 1382 – 1384.
[425] S. W. Jeong, S. Shinkai, *Nanotechnology* **1997**, *8*, 179 – 185.
[426] N. Kimizuka, T. Kawasaki, K. Hirata, T. Kunitake, *J. Am. Chem. Soc.* **1995**, *117*, 6360 – 6361.
[427] F. Würthner, C. Thalacker, A. Sautter, *Adv. Mater.* **1999**, *11*, 754 – 758.
[428] R. H. Vreekamp, W. Verboom, D. N. Reinhoudt, *Recl. Trav. Chim. Pays-Bas* **1996**, *115*, 363 – 370.
[429] J.-M. Lehn, M. Mascal, A. DeCian, J. Fischer, *J. Chem. Soc. Perkin Trans. 2* **1992**, 461 – 467.
[430] P. R. Ashton, G. R. Brown, W. Hayes, S. Menzer, D. Philp, J. F. Stoddart, D. J. Williams, *Adv. Mater.* **1996**, *8*, 564 – 567.
[431] K. C. Russell, J.-M. Lehn, N. Kyritsakas, A. DeCian, J. Fischer, *New J. Chem.* **1998**, *22*, 123 – 128.
[432] M. Mazik, D. Bläser, R. Boese, *Tetrahedron Lett.* **1999**, *40*, 4783 – 4786.
[433] T. B. Norsten, R. McDonald, N. R. Branda, *Chem. Commun.* **1999**, 719 – 720.
[434] N. Zimmerman, J. S. Moore, S. C. Zimmerman, *Chem. Ind.* **1998**, 604 – 610.
[435] R. P. Sijbesma, F. H. Beijer, L. Brunsveld, B. J. B. Folmer, J. H. K. K. Hirschberg, R. F. M. Lange, J. K. L. Lowe, E. W. Meijer, *Science* **1997**, *278*, 1601 – 1604.
[436] B. J. B. Folmer, E. Cavini, R. P. Sijbesma, E. W. Meijer, *Chem. Commun.* **1998**, 1847 – 1848.
[437] B. J. B. Folmer, R. P. Sijbesma, R. M. Versteegen, J. A. J. van der Rijt, E. W. Meijer, *Adv. Mater.* **2000**, *12*, 874 – 878.
[438] J. H. K. K. Hirschberg, F. H. Beijer, H. A. van Aert, P. C. M. M. Magusin, R. P. Sijbesma, E. W. Meijer, *Macromolecules* **1999**, *32*, 2696 – 2705.
[439] R. F. M. Lange, M. Van Gurp, E. W. Meijer, *J. Polym. Sci. Part A* **1999**, *37*, 3657 – 3670.
[440] R. K. Castellano, D. M. Rudkevich, J. Rebek, Jr., *Proc. Natl. Acad. Sci. USA* **1997**, *94*, 7132 – 7137.
[441] R. K. Castellano, J. Rebek, Jr., *J. Am. Chem. Soc.* **1998**, *120*, 3657 – 3663.
[442] R. K. Castellano, C. Nuckolls, S. H. Eichhorn, M. R. Wood, A. J. Lovinger, J. Rebek, Jr., *Angew. Chem.* **1999**, *111*, 2764 – 2768; *Angew. Chem. Int. Ed.* **1999**, *38*, 2603 – 2606.
[443] F. Zeng, S. C. Zimmerman, *Chem. Rev.* **1997**, *97*, 1681 – 1712.
[444] Y. Wang, F. Zeng, S. C. Zimmerman, *Tetrahedron Lett.* **1997**, *38*, 5459 – 5462.
[445] S. C. Zimmerman, F. Zeng, D. E. C. Reichert, S. V. Kolotuchin, *Science* **1996**, *271*, 1095 – 1098.
[446] W. T. S. Huck, R. Hulst, P. Timmerman, F. C. J. M. van Veggel, D. N. Reinhoudt, *Angew. Chem.* **1997**, *109*, 1046 – 1049; *Angew. Chem. Int. Ed. Engl.* **1997**, *36*, 1006 – 1008.
[447] P. De Santis, S. Morosetti, R. Rizzo, *Macromolecules* **1974**, *7*, 52 – 58.
[448] M. R. Ghadiri, J. R. Granja, R. A. Milligan, D. E. McRee, N. Khazanovich, *Nature* **1993**, *366*, 324 – 327.
[449] M. R. Ghadiri, *Adv. Mater.* **1995**, *7*, 675 – 677.
[450] N. Khazanovich, J. R. Granja, D. E. McRee, R. A. Milligan, M. R. Ghadiri, *J. Am. Chem. Soc.* **1994**, *116*, 6011 – 6012.
[451] M. R. Ghadiri, J. R. Granja, L. K. Bühler, *Nature* **1994**, *369*, 301 – 304.
[452] J. R. Granja, M. R. Ghadiri, *J. Am. Chem. Soc.* **1994**, *116*, 10 785 – 10 786.
[453] K. Motesharei, M. R. Ghadiri, *J. Am. Chem. Soc.* **1997**, *119*, 11 306 – 11 312.

[454] M. R. Ghadiri, K. Kobayashi, J. R. Granja, R. K. Chadha, D. E. McRee, *Angew. Chem.* **1995**, *107*, 76 – 78; *Angew. Chem. Int. Ed. Engl.* **1995**, *34*, 93 – 95.
[455] D. Ranganathan, C. Lakshmi, I. L. Karle, *J. Am. Chem. Soc.* **1999**, *121*, 6103 – 6107.
[456] D. Ranganathan, V. Haridas, R. Gilardi, I. L. Karle, *J. Am. Chem. Soc.* **1998**, *120*, 10793 – 10800.
[457] D. Seebach, J. L. Matthews, A. Meden, T. Wessels, C. Baerlocher, L. B. McCusker, *Helv. Chim. Acta* **1997**, *80*, 173 – 182.
[458] L. A. Weiss, N. Sakai, B. Ghebremariam, C. Ni, S. Matile, *J. Am. Chem. Soc.* **1997**, *119*, 12142 – 12149.
[459] N. Sakai, N. Majumdar, S. Matile, *J. Am. Chem. Soc.* **1999**, *121*, 4294 – 4295.
[460] B. Baumeister, S. Matile, *Chem. Commun.* **2000**, 913 – 914.
[461] T. Kato, J. M. J. Fréchet, *J. Am. Chem. Soc.* **1989**, *111*, 8533 – 8534.
[462] M.-J. Brienne, J. Gabard, J.-M. Lehn, I. Stibor, *J. Chem. Soc. Chem. Commun.* **1989**, 1868 – 1870.
[463] H. Takeda, Y. Sakurai, S. Takenaka, H. Miyake, T. Doi, S. Kusabayashi, *Chem. Lett.* **1989**, 1335 – 1338.
[464] C. M. Paleos, D. Tsiourvas, *Angew. Chem.* **1995**, *107*, 1839 – 1855; *Angew. Chem. Int. Ed. Engl.* **1995**, *34*, 1696 – 1711.
[465] T. Kato, *Supramol. Sci.* **1996**, *3*, 53 – 59.
[466] K. Willis, D. J. Price, H. Adams, G. Ungar, D. W. Bruce, *J. Mater. Chem.* **1995**, *5*, 2195 – 2199.
[467] K. N. Koh, K. Araki, T. Komori, S. Shinkai, *Tetrahedron Lett.* **1995**, *36*, 5191 – 5194.
[468] T. Koga, H. Ohba, A. Takase, S. Sakagami, *Chem. Lett.* **1994**, 2071 – 2074.
[469] T. Kato, T. Kawakami, *Chem. Lett.* **1997**, 211 – 212.
[470] T. Kato, Y. Kubota, M. Nakano, T. Uryu, *Chem. Lett.* **1995**, 1127 – 1128.
[471] T. Kato, J. M. J. Fréchet, *Macromolecules* **1989**, *22*, 3818 – 3819.
[472] P. Mariani, C. Mazabard, A. Garbesi, G. P. Spada, *J. Am. Chem. Soc.* **1989**, *111*, 6369 – 6373.
[473] G. Gottarelli, G. P. Spada, A. Garbesi in *Comprehensive Supramolecular Chemistry*, *Vol. 9* (Eds.: J. L. Atwood, J. E. D. Davies, D. D. MacNicol, F. Vögtle, J.-M. Lehn, J.-P. Sauvage, M. Wais Hosseini), Pergamon, Oxford, **1996**, pp. 483 – 506.
[474] R. Kleppinger, C. P. Lillya, C. Yang, *Angew. Chem.* **1995**, *107*, 1762 – 1764; *Angew. Chem. Int. Ed. Engl.* **1995**, *34*, 1637 – 1638.
[475] R. Kleppinger, C. P. Lillya, C. Yang, *J. Am. Chem. Soc.* **1997**, *119*, 4097 – 4102.
[476] A. R. A. Palmans, J. A. J. M. Vekemans, H. Fischer, R. A. Hikmet, E. W. Meijer, *Chem. Eur. J.* **1997**, *3*, 300 – 307.
[477] C. M. Paleos, D. Tsiourvas, *Adv. Mater.* **1997**, 695 – 710.
[478] R. E. Lemieux, *Acc. Chem. Res.* **1996**, *29*, 373 – 380.
[479] V. M. Rotello, E. A. Viani, G. Deslongchamps, B. A. Murray, J. Rebek, Jr., *J. Am. Chem. Soc.* **1993**, *115*, 797 – 798.
[480] J. S. Nowick, J. S. Chen, G. Noronha, *J. Am. Chem. Soc.* **1993**, *115*, 7636 – 7644.
[481] H. Asanuma, T. Ban, S. Gotoh, T. Hishiya, M. Komiyama, *Macromolecules* **1998**, *31*, 371 – 377.
[482] H. Asanuma, T. Hishiya, M. Komiyama, *Chem. Lett.* **1998**, 1087 – 1088.
[483] J. H. K. K. Hirschberg, L. Brunsveld, A. Ramzi, J. A. J. M. Vekemans, R. P. Sijbesma, E. W. Meijer, *Nature* **2000**, *407*, 167 – 170.
[484] C. M. Drain, K. C. Russell, J.-M. Lehn, *Chem. Commun.* **1996**, 337 – 338.
[485] E. E. Simanek, L. Isaacs, X. Li, C. C. C. Wang, G. M. Whitesides, *J. Org. Chem.* **1997**, *62*, 8994 – 9000.
[486] D. M. Rudkevich, A. N. Shivanyuk, Z. Brzozka, W. Verboom, D. N. Reinhoudt, *Angew. Chem.* **1995**, *107*, 2300 – 2302; *Angew. Chem. Int. Ed. Engl.* **1995**, *34*, 2124 – 2126.
[487] M. Crego Calama, P. Timmerman, D. N. Reinhoudt, *Angew. Chem.* **2000**, *112*, 771 – 774; *Angew. Chem. Int. Ed.* **2000**, *39*, 755 – 758.
[488] J. K. M. A. Kerckhoffs, M. Crego Calama, I. Luyten, P. Timmerman, D. N. Reinhoudt, *Org. Lett.* **2000**, *2*, 4121 – 4124.
[489] Y. R. de Miguel, J. K. M. Sanders, *Curr. Opin. Chem. Biol.* **1998**, *2*, 417 – 421.
[490] J.-M. Lehn, *Chem. Eur. J.* **1999**, *5*, 2455 – 2463.
[491] I. Huc, R. Nguyen, *Combin. Chem. High Throughput Screen.* **2001**, *4*, 53 – 74.
[492] P. Timmerman, D. N. Reinhoudt, *Adv. Mater.* **1999**, *11*, 71 – 74.
[493] F. Hof, C. Nuckolls, J. Rebek, Jr., *J. Am. Chem. Soc.* **2000**, *122*, 4251 – 5252.
[494] A. V. Eliseev, M. I. Nelen, *J. Am. Chem. Soc.* **1997**, *119*, 1147 – 1148.
[495] I. Huc, M. J. Krische, D. P. Funeriu, J.-M. Lehn, *Eur. J. Inorg. Chem.* **1999**, 1415 – 1420.
[496] V. Berl, I. Huc, J.-M. Lehn, A. DeCian, J. Fischer, *Eur. J. Org. Chem.* **1999**, 3089 – 3094.
[497] J. Rao, J. Lahiri, L. Isaacs, R. M. Weis, G. M. Whitesides, *Science* **1998**, *280*, 708 – 712.
[498] F. Ibukuro, T. Kusukawa, M. Fujita, *J. Am. Chem. Soc.* **1998**, *120*, 8561 – 8562.
[499] J. Rao, J. Lahiri, R. M. Weis, G. M. Whitesides, *J. Am. Chem. Soc.* **2000**, *122*, 2698 – 2710.
[500] V. Paraschiv, P. Timmerman, D. N. Reinhoudt, unpublished results (2000).

Alkyl, Silyl, and Phosphane Ligands—Classical Ligands in Nonclassical Bonding Modes

Pierre Braunstein* and Neil M. Boag

Dedicated to Professor Guy Ourisson on the occasion of his 75th birthday

Abstract: Alkyl, silyl, and phosphane ligands are amongst the most familiar and ubiquitous ligands in organometallic and coordination chemistry. The C, Si, and P donor atoms of these ligands are sp^3-hybridized and the ligands are related to each other by the isolobal analogy: $(CR_3)^-(SiR_3)^-PR_3$. Herein, we demonstrate that although a number of unusual observations concerning the reactivity and bonding of these ligands appears unrelated at first sight, they in fact provide offer an exiting and consistent picture that may form the basis for new paradigms. The characterization of stable complexes in which alkyl, silyl, and phosphane ligands behave as symmetrical bridges confirms that there is no inherent thermodynamic instability associated with these bonding situations, and, in fact, reactivity studies suggest that these ligands should be able to bridge between metal centers in reaction intermediates or transition states.

Knowledge of the nature of metal–ligand interactions is the crux in understanding the structure and the reactivity of inorganic and organometallic complexes. The bonding modes adopted by ligands in mononuclear chemistry offer few surprises now, although a complete understanding of the intimate nature of the metal–ligand interaction may require the use of high-level theoretical calculations. In dinuclear and cluster chemistry, however, a higher degree of complexity may arise due to the possibility for familiar "monodentate" ligands to adopt bridging roles between all or some of the framework metal atoms. Examples of such complexes have been isolated and provide indispensable structural models for intermediates in ligand-transfer processes, and for understanding the stereochemistry of transmetalations.[1] Critically, solution structures may vary significantly from those in the solid state;[2–4] the latter perhaps represent an intermediate in a fluxional process or reaction profile present in solution with considerable implications in homogeneous catalysis. In such cases, variable-temperature NMR spectroscopy combined with labeling studies is invaluable in probing the nature of the metal–ligand interaction.[5]

In this contribution we focus on recent chemistry dealing with three types of ligands, alkyl, silyl, and phosphane groups, which are certainly amongst the most familiar and ubiquitous ligands in organometallic and coordination chemistry. Their donor atoms, C, Si, and P, respectively, are sp^3-hybridized in all three cases and these ligands are related to each other by the isolobal analogy: $(CR_3)^- \leftrightarrow_{\circ} \rightarrow (SiR_3)^- \leftrightarrow_{\circ} \rightarrow PR_3$. A number of unusual observations concerning the reactivity and bonding of these ligands have been recently and independently reported. Although they all appear unrelated at first sight, we would like to show here that they offer an exiting and consistent picture that may form the basis for new paradigms.

1. Bridging Alkyl Ligands

There are currently more examples of bridging alkyl groups than of silyl or phosphane groups; thus, an understanding of the bridging reactivity of these latter ligands will be initially based on alkyl chemistry. Five basic bridging alkyl structural types have been described (Scheme 1), although in practice, complexes can exhibit intermediate geometries and an exact identification is often rendered problematic due the difficulties associated in accurately locating hydrogen atoms when using X-ray data.[6] In discussing the distribution of these structures,

[*] Dr. P. Braunstein
Laboratoire de Chimie de Coordination
UMR CNRS 7513
Université Louis Pasteur
4, rue Blaise Pascal, 67070 Strasbourg Cédex (France)
Fax: (+33) 390-241-322
E-mail: braunst@chimie.u-strasbg.fr

Dr. N. M. Boag
Chemistry, School of Sciences
University of Salford
Salford, M5 4WT (UK)

  1433-7851/01/4013-2427 $ 17.50+.50/0

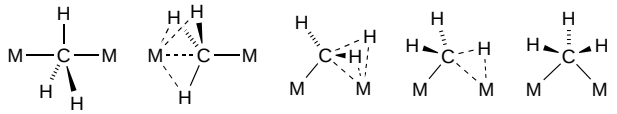

I II III IV V

Scheme 1. Possible bridging modes for a methyl group. A metal–metal interaction is possible in modes III–V.

three broad areas may be defined: main group elements, early transition metals/lanthanides, and late transition metals.

Main group elements will not be considered here although many examples are known (for leading references, see ref. [7]) especially the definitive example of a type V structure for $[Al_2(CH_3)_6]$, recently confirmed through a powder neutron diffraction study of $[Al_2(CD_3)_6]$ (**1**) at 4.5 K, which also established the staggered conformation of the bridges with respect to each other (C_{2h} molecular symmetry).[8] Although this is a common structural type for aluminum,[9] $[(C_6F_5)_3Al(\mu\text{-}CH_3)Al(C_6F_5)_3]^-$ has recently been shown to exhibit a type I structure.[10]

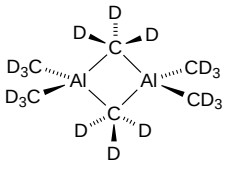

1

The commercial importance to olefin polymerization of early transition metal and lanthanide metallocenes in conjunction with increasingly sophisticated cocatalysts has led to the isolation of many examples of bridging alkyl groups on these metals. Indeed, the presence of bridging alkyl groups is fundamental to the activity of these complexes.[11] In homodinuclear complexes, only type I (e.g. **2**)[12] or V (e.g. **3**)[13] structures have been reported. The former species is

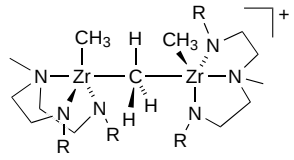

R = mesityl

2

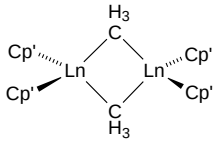

Cp' = $C_5H_4SiMe_2R$ (R = Me, *t*Bu)

3

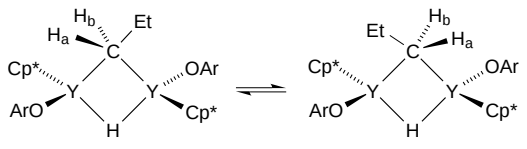

4 Ar = 2,6-tBu$_2$C$_6$H$_3$

postulated to undergo exchange of the terminal methyl groups through a $Zr(\mu\text{-}CH_3)_3Zr$ intermediate and an example of the latter, **4**, undergoes inversion at the bridging carbon atom.[14] More structural variation is observed in species involving alkyl bridging to Lewis acids with examples of every bridging type.[15]

Middle and late transition metals offer less diversity and, except in heterodinuclear complexes where the second atom is an alkali metal (e.g. $[(cod)_2Rh_2(\mu\text{-}CH_2SiMe_3)_4Li_2]$ (type III; cod = 1,5-cyclooctadiene)[16]) or lanthanide (e.g. $[(i\text{Pr}_2)\text{P}(\text{CH}_2)_2\text{P}(i\text{Pr}_2)\text{Pt}(\mu\text{-Me})_2\text{Yb}(\text{C}_5\text{Me}_5)_2]$ (type III)[17]), only exhibit structural types IV and V. There are only a few examples of symmetric bridging alkyl groups and recent ones include **5** (Cp* = C_5Me_5), which results from P–C bond activation of PMe_3 at a dimolybdenum center [Eq. (1)],[18] and $[\{CpV(\mu\text{-}NC_6H_3(i\text{Pr})_2)\}_2(\mu\text{-Me})]$ derived through reductive dimerization using MeMgCl.[19]

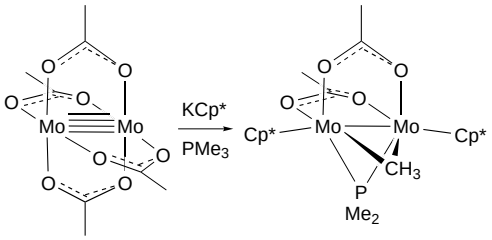

5 (1)

In most cases, however, agostic M···C···H interactions (Scheme 1, type IV) tend to prevail,[20] as, for example, in the dinuclear complex $[Cp_2Fe_2(\mu\text{-}CH_3)(\mu\text{-CO})(\mu\text{-dppm})]PF_6$[21] (dppm = bis(diphenylphosphanyl)methane) or in $[HOs_3(CO)_{10}(\mu\text{-}CH_3)]$ (**6**), the best known example of a transition metal cluster containing a semibridging alkyl ligand.[22] In these cases, tautomerism between a bridging alkyl group and a methylene hydride is always possible. Cluster **6** exists in solution as a 1:3 mixture of the methyl (**6a**) and methylene (**6b**) tautomers, whereas only the latter is present in the solid state, thus providing an excellent example of the dangers of relying solely on solid-state structures.[22c]

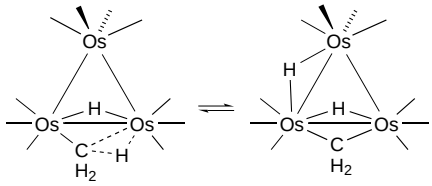

6a **6b**

These varying interactions of alkyl groups on dinuclear centers are of considerable interest for homogeneous and heterogeneous catalysis since they correspond to possible pathways for alkyl migration[23] and dynamic exchange of terminal alkyl[24] or aryl groups[25] between adjacent metals.

A triply bridging bonding mode for the methyl group is best exemplified in $(MeLi)_4$, in which it caps the faces of the Li_4 tetrahedron.[26] However, the bonding is mostly ionic in this case owing to the large difference in electronegativity between Li and C; this can be seen in the isostructural $(t\text{BuLi})_4$ with the rapid migration of *t*Bu groups between faces (or Li atoms between apices) in solution and the solid state.[27] Triply bridging methyl groups in transition metal clusters are extremely rare. There is a solitary example of a symmetrical

  1433-7851/01/4013-2428 $ 17.50+.50/0 *Angew. Chem. Int. Ed.* **2001**, *40*, No. 13

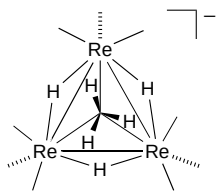

7

μ_3-CH_3 ligand, $[Re_3(\mu\text{-}H)_3(\mu_3\text{-}CH_3)(CO)_9]^-$ (**7**).[28] The methyl ligand in $[Fe_3(\mu\text{-}H)(\mu_3\text{-}CH_3)(CO)_9]$ exhibits agostic bonding, and the cluster is in equilibrium with two other tautomers, $[Fe_3(\mu\text{-}H)_2(\mu_3\text{-}CH_2)(CO)_9]$ and $[Fe_3(\mu\text{-}H)_3(\mu_3\text{-}CH)(CO)_9]$, clearly revealing the dynamic potential of such systems.[29]

The doubly and triply bridging modes of alkyl groups to transition metals, with or without an agostic component, are relevant to the incipient activation of the C–H bond at a multimetal site,[30] the modes of chemisorption of these groups on metal surfaces, and subsequent heterogeneously catalyzed reactions.[31] Reversible hydrogen elimination/addition from methyl/methylene or methylene/methylidyne groups in particular mimics reactivity found for such groups on surfaces (Scheme 2).

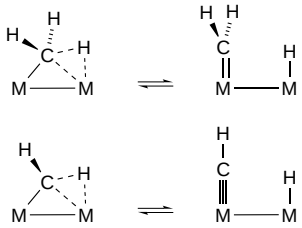

Scheme 2. Ligand transformations on surfaces.

2. *Bridging Silyl Ligands*

It is interesting now to examine the situation with the heavier silyl analogues. Transition metal silyl complexes have remained of great interest owing to their intrinsic fundamental importance, the possible comparisons they provide with their carbon homologues, and their reactivity and implications in numerous catalytic reactions of considerable (industrial) value.[32]

Until recently, complexes in which a bridging bonding mode for a silyl ligand had been established by X-ray diffraction were limited to boranes[33] and the polynuclear copper complex $[Li(thf)_4][Cu_5Cl_4\{Si(SiMe_3)_3\}_2]$.[34] However, recent studies in dirhodium chemistry have allowed full characterization of the first example in which the silyl ligand occupies a symmetrical bridging position between the metals. These complexes, $[(i\text{Pr}_3\text{P})(\text{H})\text{Rh}(\mu\text{-Cl})(\mu\text{-SiAr}_2)(\mu\text{-SiAr}_3)\text{Rh}(\text{H})(\text{P}i\text{Pr}_3)]$ (Ar = Ph, *p*-FC_6H_4), were prepared according to Equation (2) and, like bridging alkyl complexes, provide

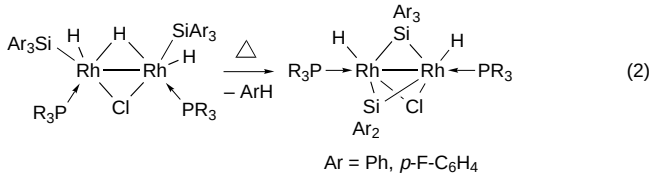

(2)

Ar = Ph, *p*-F-C_6H_4

interesting structural models of possible intermediates in ligand-migration reactions.[35] The mirror symmetry of this molecule is noteworthy. The isolation of this dirhodium complex is particularly timely since recent independent studies by different groups, including ours, have concluded that the silyl ligand can migrate intramolecularly from one metal to another in dinuclear complexes. In their studies on diruthenium complexes, Akita, Moro-oka, and co-workers[36] [Eq. (3)] and Girolami and co-workers[37] [Eq. (4)] concluded

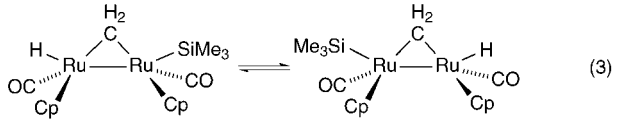

(3)

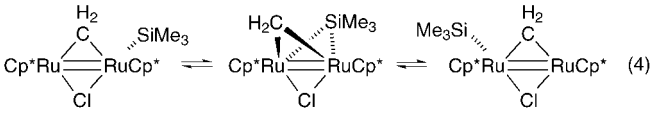

(4)

from variable-temperature NMR studies that the SiR_3 ligand could reversibly flip from one Ru center to the other; an intermediate with a μ-SiR_3 ligand was suggested, although it could not be isolated.

In our own studies on Fe–Pt complexes, we could actually isolate and structurally characterize isomeric complexes in which a silyl ligand is bound to either Fe or Pt and study the parameters that trigger this unusual isomerization (Scheme 3).[38] This reaction was shown to be intramolecular

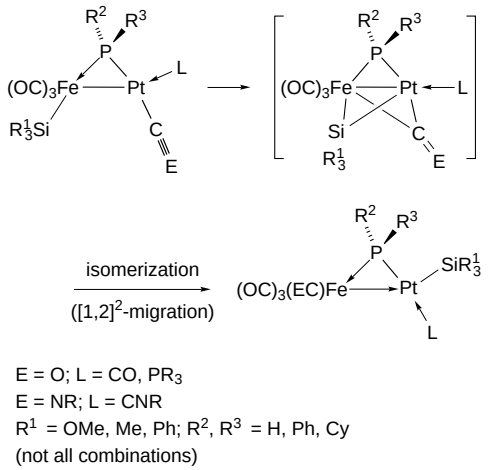

Scheme 3. Dyotropic-type concerted mechanism of silyl migration in Fe–Pt complexes.

and it may be promoted by an external nucleophile, such as CO or isonitrile. The course of the silyl group migration was found to depend on a) the steric properties of the SiR^1_3 ligand such that for a given μ-PR^2R^3 bridge ($R^2 = R^3 = Ph$) the migration rate decreases in the order $Si(OMe)_3 > SiMe_2Ph > SiMePh_2 \gg SiPh_3$, b) the phosphido bridge, for which the migration rate decreases in the order μ-$PPh_2 \gg \mu$-PHCy for a given silyl ligand ($R^1 = OMe$), and c) the external nucleophile.

We have suggested that this dyotropic-type process occurs via an intermediate containing a bridging silyl ligand.[38]

Evidently, these are still rare transformations[39] and the occurrence and intermediacy of such bonding modes are likely to be more general and occur more frequently than is so far realized. In this context, it is noteworthy that recent studies with diruthenium complexes,[36b] analogous to those of Equation (3), and with heteronuclear Mo–Re complexes[40] have shown that an $SnMe_3$ or $SnPh_3$ ligand can also reversibly migrate from one metal center to another.

With mono- or diorganosilyl ligands, the occurrence of agostic M···Si···H interactions dominates, as in **8**, and

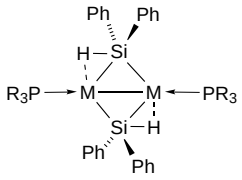

8

M = Pd, Pt

destroys the symmetry observed in the previous examples.[41] This situation is similar to those in which an alkyl ligand interacts in an unsymmetrical bridging mode, through a M–C σ bond and an agostic M···C···H three-center, two-electron bond with the adjacent metal center. Such an interaction may be considered as representing an "arrested" stage on the reaction coordinate towards full addition of the Si–H bond, a key step in, for example, the metal-catalyzed dehydrocoupling of hydrosilanes leading to silicon oligomers and polymers. In most cases (M = Pd, Pt, Fe, W, Ti), the two M(μ-η^2-HSi) units are coplanar,[42] but a dirhodium complex has been characterized in which they are almost orthogonal to each other.[43] Exchange between bridging and terminal silyl ligands and terminal and bridging hydrides has been postulated based on the fluxionality observed in some bridged diplatinum complexes (Scheme 4).[42b] This should be kept in

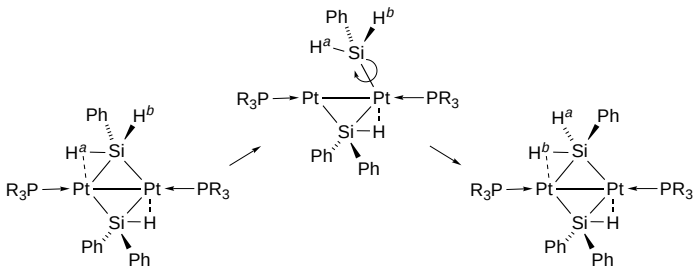

Scheme 4. Fluxionality of bridged diplatinum complexes by the exchange of bridging and terminal silyl and hydride ligands.

mind when examining the situation with phosphane ligands (see Section 3) where terminal bonding was the rule until bridging modes were suggested in reaction mechanisms and eventually structurally demonstrated. It was recently shown that the photochemical reaction of the μ-silyl complex **9** with SiH_2R_2 in a sealed tube at about 5 °C affords the μ-silane complex **10**, whereas reversion to **9** occurs under a CO atmosphere at room temperature [Eq. (5)].[44]

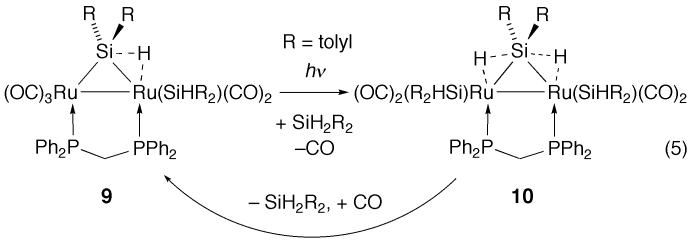

(5)

3. Bridging Phosphane Ligands

The isolobal relationship between the alkyl, silyl, and the phosphane ligand $(CR_3)^- \leftrightarrow (SiR_3)^- \leftrightarrow PR_3$ naturally leads to an examination of the bonding situation of phosphanes in dinuclear and cluster complexes. On the basis of the crystal structure determination of the first platinum–gold cluster **11**, the isolobal analogy $Au(PPh_3) \leftrightarrow H$, and theoretical consid-

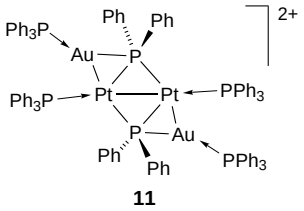

11

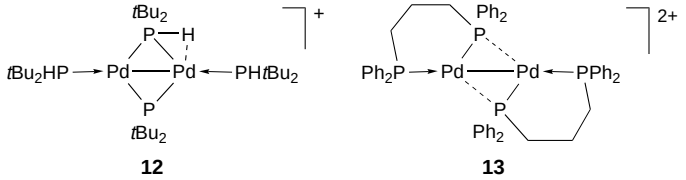

12 **13**

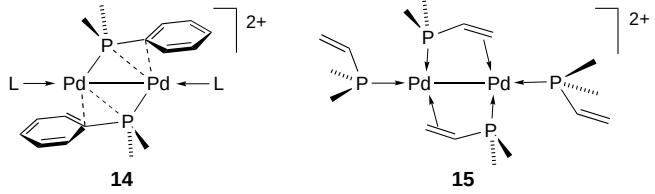

14 **15**

erations (note the striking similarity between **11** and **8** above!), the prediction was made in 1989 that a doubly bridging bonding mode for phosphane ligands should be possible.[45] However, until very recently, only examples of semibridging phosphanes had been discovered, remarkably in dipalladium chemistry. Following the isolation of **12**[46] and **13**,[47] a few more examples have been described,[48] including complexes containing arylphosphanes whose *ipso*-carbon atom participates in three-center, two-electron bonding such as in **14**.[47, 49] The role played by the P–H and P–C(aryl) σ bonds in complexes of type **12** and **14**, respectively, which provide two extra electrons in an agostic interaction, allows these phosphane ligands to be considered as formally four-electron donors to the metal centers. This is somewhat related

  1433-7851/01/4013-2430 $ 17.50+.50/0 *Angew. Chem. Int. Ed.* **2001**, *40*, No. 13

to the situation of the bridging diphenylvinylphosphane in $[\{Pd[\mu\text{-}PPh_2(CH{=}CH_2)][PPh_2(CH{=}CH_2)]\}_2]^{2+}$ (**15**).[50] In this case, however, the phosphorus atom clearly interacts with only one metal center, which leaves such systems out of the scope of the present discussion.

Until very recently, there was no characterized example of a symmetrically bridging μ_2-PR_3 ligand, although a bonding analysis of the model compound $[\{(H_3P)Cu(\mu\text{-}PPH_3)\}_2]^{2+}$ had been performed.[51] This has been very recently rectified in an elegant study in which Werner and co-workers were able to prepare the unusual dinuclear rhodium complex **16** (Scheme 5); this complex contains a PMe_3 ligand which

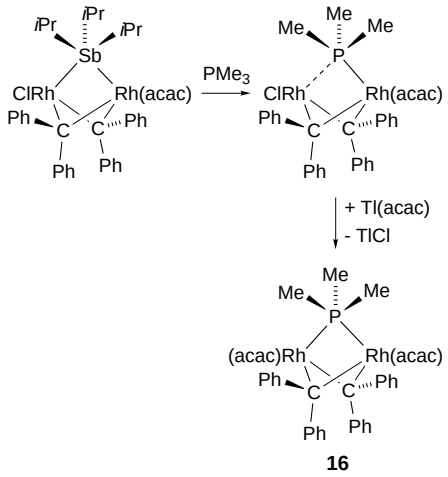

16

Scheme 5. Synthesis of the first complex with a bridging PMe_3 ligand. acac = acetylacetonate.

exhibits almost symmetric bridging between two rhodium centers (Rh–(μ-P) 2.2707(7) and 2.5700(8) Å).[52] Other dirhodium complexes with a semibridging PMe_3 ligand were also reported in this work. The ^{31}P NMR resonance signal of the μ-PMe_3 ligand in **16** is a triplet, owing to coupling with two equivalent rhodium atoms. This complex is only the second example of a symmetrical bridging situation for an ER_3 ligand in Group 15, and follows the report in 1994 of the related complexes **17** which were the first examples of bridging stibane ligands.[53a,b] The high symmetry of these molecules is reminiscent of that observed with the dinuclear complexes containing a bridging silyl ligand, and consistent with the predictions made earlier.[45] Interestingly, the stibane ligand in **17** could not be directly substituted with PMe_3 to afford **16**, although $Sbi Pr_3$ can easily be substituted by smaller stibanes, for example, $SbMe_3$ or $SbEt_3$.[53c]

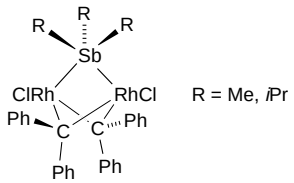

17

Shortly after complex **16** was reported, Réau, Halet, and co-workers described an elegant access to the dipalladium complex **18** with a symmetrically bridging phosphole ligand [Eq. (6)] and provided a theoretical analysis of the bonding interactions.[54] This bonding situation in a molecule of high symmetry (again!) appears remarkably stable, as a result of

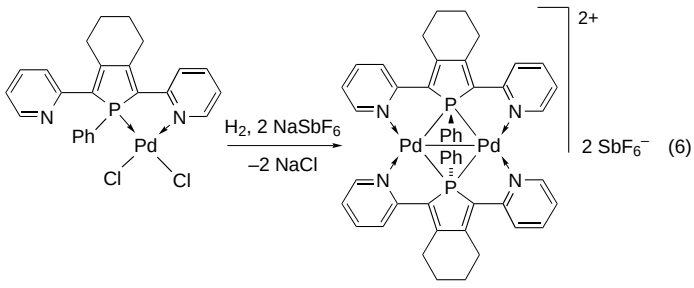

18

highly delocalized Pd–Pd and Pd–P bonding, and this complex does not react with CO or PPh_3.

Numerous examples of intramolecular, dynamic exchange of ligands between metal atoms in polynuclear and cluster complexes are known, and this is most common with CO, CNR, and NO ligands.[55] Until very recently, only one study dealt with the intramolecular nature of the rapid exchange (on the NMR time scale) of a phosphane ligand between two metal centers.[56] The isolation of complexes with bridging PR_3 ligands is therefore particularly relevant to such a phenomenon and to reactivity studies recently performed on cluster complexes that strongly suggested the possibility of intramolecular phosphane migration. Thus, it was found in the course of metal site selectivity studies in reactions of tetrahedral MCo_3 (M = Fe, Ru) carbonyl clusters that phosphane migration from one metal center to an adjacent site can easily take place. The quantitative conversion of the kinetic product $[HRuCo_3(CO)_{10}(PMe_2Ph)_2]$ (**19**; [Co-P,Co-P] isomer) of the reaction between $[HRuCo_3(CO)_{11}(PMe_2Ph)]$ and PMe_2Ph into its [Co-P,Ru-P] isomer **20** occurs upon standing in CH_2Cl_2 overnight [Eq. (7)].[57] The interconversion between the [Co-P,Ru-P] and [Co-P,Co-P] isomers **21** and **22**, which involves phosphane migration between Ru and Co has also been discussed [Eq. (8)].[58]

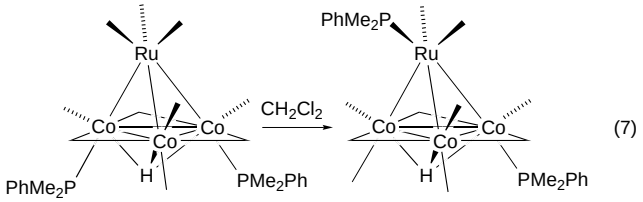

19 **20**

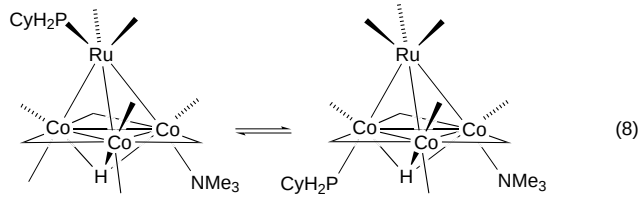

21 **22**

Variable-temperature NMR studies by Adams et al. have now suggested that the interconversion of the platinum–phosphane isomer **23** and the ruthenium–phosphane isomer

24 of the carbido cluster $[PtRu_5(CO)_{15}(PMe_2Ph)(\mu_6\text{-}C)]$ occurs by intramolecular shifts of the phosphane and carbonyl ligands between the metal atoms (Scheme 6).[59] Here again,

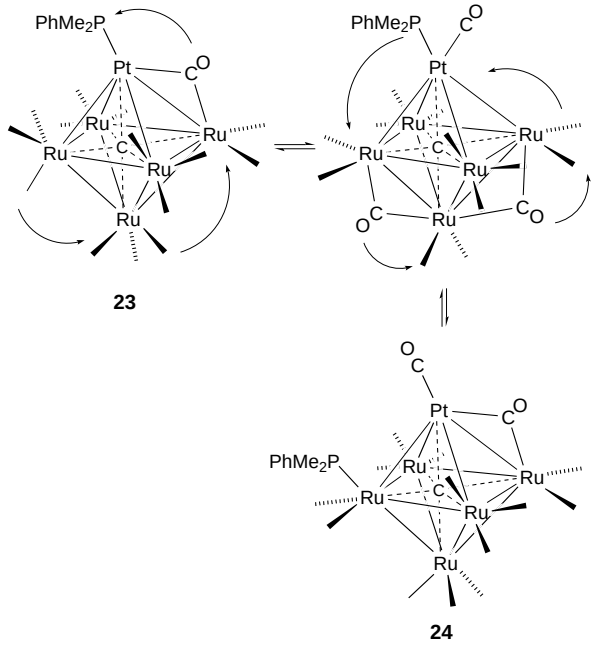

Scheme 6. Proposed mechanism for cluster isomerization by intramolecular shifts of the phosphane and carbonyl ligands between the metal atoms.

the very common and stable bridging situations for μ_2-CO and μ_3-CO ligands in carbonyl chemistry contrast with the paucity of data concerning phosphanes, although the latter are amongst the most familiar and ubiquitous ligands in the molecular chemistry of metals.

Triply bridging phosphanes should not be excluded from consideration and indeed a complex with a triply bridging phosphane ligand, the palladium cluster **25**, has been described,[60] although the situation of the atypical, strong π-acceptor μ_3-PF_3 ligand in **25** should of course be compared to that of the familiar triply bridging CO ligand, also a two-electron donor.

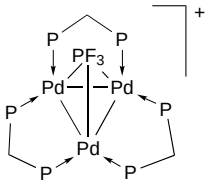

25

It is also a striking coincidence that independent reactivity studies concerning the intramolecular migration, whether reversible or not, of the isolobal silyl and phosphane ligands have appeared within such a short period of time.

4. Conclusion and Perspectives

We hope to have provided a useful framework to look at and relate novel and still rare bridging bonding modes for familiar ligands such as alkyl, silyl, and phosphane ligands in dinuclear and cluster chemistry. In addition to having an sp^3-hybridized donor atom, these ligands are mutually related by the isolobal analogy. The characterization of stable complexes in which they behave as symmetrical bridges confirms that there is no inherent thermodynamic instability associated with these bonding situations. Based on experimental observation, it is likely that a higher molecular symmetry is probably necessary for "stopping" these ligands en route from one metal to another although this "stopped intermediate" may involve agostic bonding, a situation particularly favored if the metal framework is not completely symmetrical. The structural investigations are nicely complemented by reactivity studies that suggest or in some cases even show that these ligands should indeed be able to bridge between metal centers in reaction intermediates or transition states. The consistent picture that emerges from these recent investigations strongly suggests that this phenomenon may actually be more general than originally believed and should now be fully considered in reactivity studies, including catalytic mechanisms.

[1] J. Holton, M. F. Lappert, R. Pearce, P. I. W. Yarrow, *Chem. Rev.* **1983**, *83*, 135.
[2] P. Braunstein, C. de Bellefon, S.-E. Bouaoud, D. Grandjean, J.-F. Halet, J.-Y. Saillard, *J. Am. Chem. Soc.* **1991**, *113*, 5282.
[3] P. J. Dyson in *Metal Clusters in Chemistry*, *Vol. 2* (Eds.: P. Braunstein, L. A. Oro, P. R. Raithby), Wiley-VCH, Weinheim, **1999**, p. 1028.
[4] O. Rossell, M. Seco, G. Segalés in *Metal Clusters in Chemistry*, *Vol. 2* (Eds.: P. Braunstein, L. A. Oro, P. R. Raithby), Wiley-VCH, Weinheim, **1999**, p. 1053.
[5] M. Brookhart, M. L. H. Green, L. L. Wong, *Prog. Inorg. Chem.* **1988**, *36*, 1.
[6] W. T. Klooster, R. S. Lu, R. Anwander, W. J. Evans, T. F. Koetzle, R. Bau, *Angew. Chem.* **1998**, *110*, 1326; *Angew. Chem. Int. Ed.* **1998**, *37*, 1268.
[7] W. M. Boesveld, P. B. Hitchcock, M. F. Lappert, D. S. Liu, S. Tian, *Organometallics* **2000**, *19*, 4030.
[8] G. S. McGrady, J. F. C. Turner, R. M. Ibberson, M. Prager, *Organometallics* **2000**, *19*, 4398.
[9] a) J. Klosin, G. R. Roof, E. Y. X. Chen, K. A. Abboud, *Organometallics* **2000**, *19*, 4684; b) Z. K. Yu, J. M. Wittbrodt, M. J. Heeg, H. B. Schlegel, C. H. Winter, *J. Am. Chem. Soc.* **2000**, *122*, 9338.
[10] E. Y. X. Chen, K. A. Abboud, *Organometallics* **2000**, *19*, 5541.
[11] a) K. Vanka, M. S. W. Chan, C. C. Pye, T. Ziegler, *Organometallics* **2000**, *19*, 1841; b) M. S. W. Chan, T. Ziegler, *Organometallics* **2000**, *19*, 5182.
[12] R. R. Schrock, A. L. Casado, J. T. Goodman, L. C. Liang, P. J. Bonitatebus, W. M. Davis, *Organometallics* **2000**, *19*, 5325. For a further example of a linear Zr-CH_3-Zn bridged complex characterized by X-ray diffraction, see A. P. Duncan, S. M. Mullins, J. Arnold, R. G. Bergman, *Organometallics* **2001**, *20*, 1808.
[13] H. Schumann, M. R. Keitsch, J. Demtschuk, G. A. Molander, *J. Organomet. Chem.* **1999**, *582*, 70.
[14] C. J. Schaverien, *Organometallics* **1994**, *13*, 69.
[15] a) E. Y. X. Chen, T. J. Marks, *Chem. Rev.* **2000**, *100*, 1391; b) X. J. Song, M. Thornton-Pett, M. Bochmann, *Organometallics* **1998**, *17*, 1004; c) S. Kleinhenz, K. Seppelt, *Chem. Eur. J.* **1999**, *5*, 3573.
[16] M. A. Kulzick, R. A. Andersen, E. L. Muetterties, V. W. Day, *J. Organomet. Chem.* **1987**, *336*, 221.
[17] D. J. Schwartz, G. E. Ball, R. A. Andersen, *J. Am. Chem. Soc.* **1995**, *117*, 6027.
[18] J. H. Shin, G. Parkin, *Chem. Commun.* **1998**, 1273.
[19] M. C. W. Chan, J. M. Cole, V. C. Gibson, J. A. K. Howard, *Chem. Commun.* **1997**, 2345.
[20] a) B. E. Bursten, R. H. Cayton, *Organometallics* **1986**, *5*, 1051; b) F. Ozawa, J. W. Park, P. B. Mackenzie, W. P. Schaefer, L. M. Henling, R. H. Grubbs, *J. Am. Chem. Soc.* **1989**, *111*, 1319.
[21] G. M. Dawkins, M. Green, A. G. Orpen, F. G. A. Stone, *J. Chem. Soc. Chem. Commun.* **1982**, 41.
[22] a) R. B. Calvert, J. R. Shapley, *J. Am. Chem. Soc.* **1978**, *100*, 7726; b) D. H. Hamilton, J. R. Shapley, *Organometallics* **2000**, *19*, 761; c) A. J. Schultz, J. M. Williams, R. B. Calvert, J. R. Shapley, G. D. Stucky, *Inorg. Chem.* **1978**, *18*, 319.
[23] A. Fukuoka, T. Sadashima, I. Endo, N. Ohashi, Y. Kambara, T. Sugiura, K. Miki, N. Kasai, S. Komiya, *Organometallics* **1994**, *13*, 4033.

  1433-7851/01/4013-2432 $ 17.50+.50/0

[24] J. R. Torkelson, F. H. Antwi-Nsiah, R. McDonald, M. Cowie, J. G. Pruis, K. J. Jalkanen, R. L. DeKock, *J. Am. Chem. Soc.* **1999**, *121*, 3666.

[25] X. Q. Yan, R. J. Batchelor, F. W. B. Einstein, X. H. Zhang, R. Nagelkerke, D. Sutton, *Inorg. Chem.* **1997**, *36*, 1237.

[26] E. Weiss, T. Lambertsen, B. Schubert, J. K. Cockcroft, A. Wiedenmann, *Chem. Ber.* **1990**, *123*, 79.

[27] a) R. D. Thomas, M. T. Clarke, R. M. Jensen, T. C. Young, *Organometallics* **1986**, *5*, 1851; b) G. H. Penner, Y. C. P. Chang, *Chem. Commun.* **2000**, 1803.

[28] T. Beringhelli, G. D'Alfonso, M. Panigati, F. Porta, P. Mercandelli, M. Moret, A. Sironi, *J. Am. Chem. Soc.* **1999**, *121*, 2307.

[29] T. K. Dutta, J. C. Vites, G. B. Jacobsen, T. P. Fehlner, *Organometallics* **1987**, *6*, 842.

[30] R. D. Adams, I. T. Horváth, *Prog. Inorg. Chem.* **1985**, *33*, 127.

[31] a) E. L. Muetterties, T. N. Rhodin, E. Band, C. F. Brucker, W. R. Pretzer, *Chem. Rev.* **1979**, *79*, 91; b) R. C. Baetzold, *J. Am. Chem. Soc.* **1983**, *105*, 4271; c) G. A. Somorjai, S. M. Davis, *Platinum Met. Rev.* **1983**, *27*, 54; d) *Studies in Surface Science and Catalysis, Vol. 29* (Eds.: B. C. Gates, L. Guczi, H. Knözinger), Elsevier, Amsterdam, **1986**; e) P. Braunstein, J. Rosé in *Catalysis by Di- and Polynuclear Metal Cluster Complexes* (Eds.: R. D. Adams, F. A. Cotton), Wiley-VCH, New York, **1998**, p. 443; f) G. Papoian, J. K. Nørskov, R. Hoffmann, *J. Am. Chem. Soc.* **2000**, *122*, 4129.

[32] a) B. Marciniec, *Comprehensive Handbook on Hydrosilylation*, Pergamon, Oxford, **1992**; b) P. Braunstein, M. Knorr, *J. Organomet. Chem.* **1995**, *500*, 21; c) H. K. Sharma, K. H. Pannell, *Chem. Rev.* **1995**, *95*, 1351; d) N. Auner, J. Weis, *Organosilicon Chemistry III. From Molecules to Materials*, Wiley-VCH, Weinheim, **1997**; e) F. Gauvin, J.-F. Harrod, H. G. Woo, *Adv. Organomet. Chem.* **1998**, *42*, 363; f) G. Kickelbick, U. Schubert, *Monatsh. Chem.* **1998**, *129*, 329; g) P. Braunstein, M. Knorr, C. Stern, *Coord. Chem. Rev.* **1998**, *178–180*, 903; h) H. Tobita, H. Ogino, *Adv. Organomet. Chem.* **1998**, *42*, 223; i) J. Y. Corey, J. Braddock-Wilking, *Chem. Rev.* **1999**, *99*, 175; j) I. Beletskaya, C. Moberg, *Chem. Rev.* **1999**, *99*, 3435; k) M. Suginome, Y. Ito, *Chem. Rev.* **2000**, *100*, 3221.

[33] J. C. Calabrese, L. F. Dahl, *J. Am. Chem. Soc.* **1971**, *93*, 6042.

[34] A. Heine, D. Stalke, *Angew. Chem.* **1993**, *105*, 90; *Angew. Chem. Int. Ed. Engl.* **1993**, *32*, 121.

[35] a) K. Osakada, T.-A. Koizumi, T. Yamamoto, *Angew. Chem.* **1998**, *110*, 364; *Angew. Chem. Int. Ed.* **1998**, *37*, 349; b) K. Osakada, *J. Organomet. Chem.* **2000**, *611*, 323.

[36] a) M. Akita, T. Oku, R. Hua, Y. Moro-Oka, *J. Chem. Soc. Chem. Commun.* **1993**, 1670; b) M. Akita, R. Hua, T. Oku, M. Tanaka, Y. Moro-Oka, *Organometallics* **1996**, *15*, 4162.

[37] a) W. Lin, S. R. Wilson, G. S. Girolami, *J. Am. Chem. Soc.* **1993**, *115*, 3022; b) W. Lin, S. R. Wilson, G. S. Girolami, *Organometallics* **1994**, *13*, 2309; c) Q. D. Shelby, W. Lin, G. S. Girolami, *Organometallics* **1999**, *18*, 1904.

[38] a) P. Braunstein, M. Knorr, B. Hirle, G. Reinhard, U. Schubert, *Angew. Chem.* **1992**, *104* 1641; *Angew. Chem. Int. Ed. Engl.* **1992**, *31*, 1583; b) P. Braunstein, M. Knorr, G. Reinhard, U. Schubert, T. Stährfeldt, *Chem. Eur. J.* **2000**, *6*, 4265.

[39] P. Braunstein, T. Faure, M. Knorr, *Organometallics* **1999**, *18*, 1791.

[40] E. M. López, D. Miguel, J. Pérez, V. Riera, C. Bois, Y. Jeannin, *Organometallics* **1999**, *18*, 490.

[41] Y.-J. Kim, S.-C. Lee, J.-I. Park, K. Osakada, J.-C. Choi, T. Yamamoto, *J. Chem. Soc. Dalton Trans.* **2000**, 417.

[42] a) S.-H. Choi, Z. Lin, *J. Organomet. Chem.* **2000**, *608*, 42; b) J. Braddock-Wilking, Y. Levchinsky, N. P. Rath, *Organometallics* **2000**, *19*, 5500.

[43] L. Rosenberg, M. D. Fryzuk, S. J. Rettig, *Organometallics* **1999**, *18*, 958.

[44] a) H. Hashimoto, Y. Hayashi, M. Kira, *Abstract Paper P-48, 32nd Organosilicon Symposium* (Milwaukee, WI) **1999**; b) H. Hashimoto, Y. Hayashi, M. Kira, *Abstract Paper P037, The 12th International Symposium on Organosilicon Chemistry* (Sendai, Japan) **1999**; c) I. Aratani, H. Hashimoto, C. Kabuto, M. Kira, *Abstract Paper P888, International Chemical Congress of Pacific Basin Societies* (Honolulu, HI) **2000**.

[45] R. Bender, P. Braunstein, A. Dedieu, Y. Dusausoy, *Angew. Chem.* **1989**, *101*, 931; *Angew. Chem. Int. Ed. Engl.* **1989**, *28*, 923.

[46] A. Albinati, F. Lianza, M. Pasquali, M. Sommovigo, P. Leoni, P. S. Pregosin, H. Rüegger, *Inorg. Chem.* **1991**, *30*, 4690.

[47] P. H. M. Budzelaar, P. W. N. W. van Leeuwen, C. F. Roobeek, A. G. Orpen, *Organometallics* **1992**, *11*, 23.

[48] a) P. Leoni, M. Pasquali, M. Sommovigo, F. Laschi, P. Zanello, A. Albinati, F. Lianza, P. S. Pregosin, H. Rüegger, *Organometallics* **1993**, *12*, 1702; b) P. Leoni, M. Pasquali, A. Fortunelli, G. Germano, A. Albinati, *J. Am. Chem. Soc.* **1998**, *120*, 9564; c) P. Leoni, G. Pieri, M. Pasquali, *J. Chem. Soc. Dalton Trans.* **1998**, 657.

[49] T. Murahashi, T. Otani, T. Okuno, H. Kurosawa, *Angew. Chem.* **2000**, *112*, 547; *Angew. Chem. Int. Ed.* **2000**, *39*, 537.

[50] W. L. Wilson, J. H. Nelson, N. W. Alcock, *Organometallics* **1990**, *9*, 1699.

[51] P. Alemany, S. Alvarez, *Inorg. Chem.* **1992**, *31*, 4266.

[52] T. Pechmann, C. D. Brandt, H. Werner, *Angew. Chem.* **2000**, *112*, 4069; *Angew. Chem. Int. Ed.* **2000**, *39*, 3909.

[53] a) P. Schwab, N. Mahr, J. Wolf, H. Werner, *Angew. Chem.* **1994**, *106*, 82; *Angew. Chem. Int. Ed. Engl.* **1994**, *33*, 97; b) H. Werner, *J. Organomet. Chem.* **1995**, *500*, 331; c) P. Schwab, J. Wolf, N. Mahr, P. Steinert, U. Herber, H. Werner, *Chem. Eur. J.* **2000**, *6*, 4471.

[54] M. Sauthier, B. Le Guennic, V. Deborde, L. Toupet, J.-F. Halet, R. Réau, *Angew. Chem.* **2001**, *113*, 234; *Angew. Chem. Int. Ed.* **2001**, *40*, 228.

[55] L. J. Farrugia, A. G. Orpen in *Metal Clusters in Chemistry, Vol. 2* (Eds.: P. Braunstein, L. A. Oro, P. R. Raithby), Wiley-VCH, Weinheim, **1999**, p. 1001.

[56] A. M. Bradford, G. Douglas, L. Manojlovic-Muir, K. W. Muir, R. J. Puddephatt, *Organometallics* **1990**, *9*, 409.

[57] P. Braunstein, J. Rosé, D. Toussaint, S. Jääskeläinen, M. Ahlgren, T. A. Pakkanen, J. Pursiainen, L. Toupet, D. Grandjean, *Organometallics* **1994**, *13*, 2472.

[58] S. Bouherour, P. Braunstein, J. Rosé, L. Toupet, *Organometallics* **1999**, *18*, 4908.

[59] R. D. Adams, B. Captain, W. Fu, P. J. Pellechia, *Chem. Commun.* **2000**, 937.

[60] A. L. Balch, B. J. Davies, M. M. Olmstead, *J. Am. Chem. Soc.* **1990**, *112*, 8592.

  1433-7851/01/4013-2433 $ 17.50+.50/0

Superconductivity in MgB_2 at 39 K—A Sensational and Curious Discovery

Jürgen Köhler*

Superconductivity was first observed in 1911 by Kammerlingh Onnes in mercury by cooling it with liquid helium at 4 K. Since then many metallic elements and compounds showing such a material property have been found; however, with the exception of the ceramic oxocuprate superconductors discovered in the last few years, their critical temperatures T_C all lie below 30 K. Thus it was a sensation, when Jun Akimitsu and collegues announced their discovery in January this year[1] that the metallic magnesium diboride MgB_2 becomes superconducting below the relatively moderate temperature of 39 K.[2] The interest of the authors was originally focussed on the semiconducting CaB_6, which becomes ferromagnetic on slight doping with electrons.[3] Their intention was to partially substitute Ca in this boride by the lighter homologue Mg, and it seemed evident to use MgB_2 (known since 1953)[4, 5] the boron-richest phase in the Mg/B system, as the starting material. MgB_2 is commercially available, currently costs approximately one € per gram, and is a common reactant for the syntheses of elemental boron, boranes, or transition metal borides.[6] One can imagine the astonishment of the researchers, when they discovered that a chemical which can be found in every lab cupboard becomes superconducting already at 39 K (see Figure 1).

The discovery appears especially curious if one considers that generations of scientists have undertaken great efforts for almost a century to find new superconductors with higher transition temperatures. Central to these efforts was B. T. Matthias, who has prepared, doped, and tested thousands of metallic oxides, nitrides, carbides, and also numerous borides for superconductivity.[7] Nevertheless, until the middle of the 1980s a T_C value of 23 K in Nb_3Ge[8] was the upper limit, which appeared to be unsurmountable. Because the venture of reaching higher critical temperatures appeared increasingly hopeless no public research funding was given in the USA for the search for new superconducting materials for a number of years. This all changed when fifteen years ago Bednorz and Müller[9] presented the first superconducting oxocuprate with a T_C of 40 K!, for which they received the Nobel prize for physics a year later. This initialized a tremendous search for

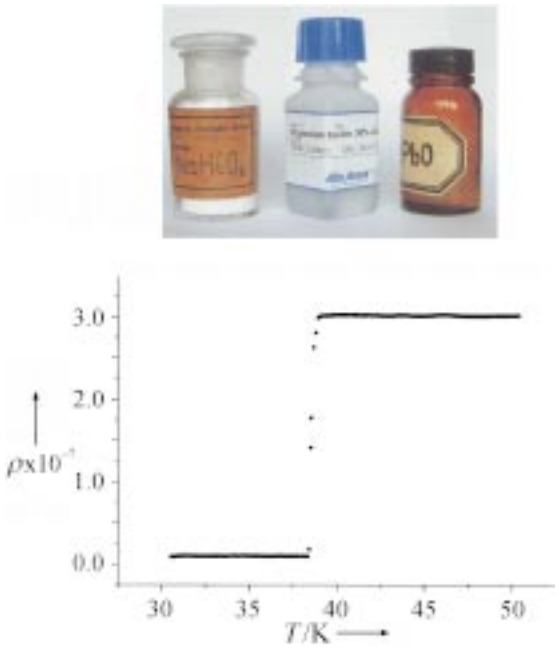

Figure 1. Temperature dependence of the electric resistance (resistivity) ρ [Ωm] (bottom) of magnesium diboride MgB_2 acquired commercially (top).

further such compounds, and has subsequently led to the discovery of the new ceramic high-temperature superconductors.[10] The best superconductor of this modern generation indeed works above 100 K, but cannot transport sufficient current for practical applications without being cooled far below its critical temperature. Conventional superconductors with higher T_C values have been found only recently, for example 33 K in $Cs_xRb_yC_{60}$,[11] 30 K in $Ba_{1-x}K_xBiO_3$,[12] and 52 K in hole-doped surfaces of C_{60} crystals.[13] MgB_2 with a transition temperature of 39 K lies in this order of magnitude and has been simply overlooked during the search for new superconductors over the past decades.

The structure of MgB_2 is hexagonal and contains sheets of B and Mg, which are alternatingly stacked along the *c* axis (Figure 2). The B atoms form a honeycomb net (6^3 net), similar to the arrangement of the C atoms in graphite, and each B atom is surrounded by three equidistant B atoms. The Mg atoms between the boron sheets lie above and below the centers of the benzene-like B_6 rings, which are two-dimensionally condensed. The B_2^{2-} sheet is isoelectronic to a C sheet

[*] Priv.-Doz. Dr. J. Köhler
Max-Planck-Institut für Festkörperforschung
Heisenbergstrasse 1, 70569 Stuttgart (Germany)
Fax: (+49) 711-689-1091
E-mail: jkoeh@simaix.mpi-stuttgart.mpg.de

  1433-7851/01/4013-2435 $ 17.50+.50/0

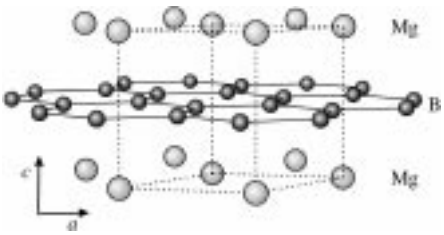

Figure 2. Crystal structure of MgB_2 together with the unit cell. The B_2^{2-} sheets are highlighted.

in graphite and also exhibits an extended π-electron sytem with sp^2-hybridized atomic orbitals at B.

What then makes the decisive difference between graphite, which does not superconduct even at lowest temperatures, and MgB_2? Through the layers of Mg^{2+} ions lying between the B_2^{2-} sheets the structure of MgB_2 is markedly more three-dimensional. According to band sructure calculations,[14] the π orbitals perpendicular to the plane (p_z) are stabilized by the Mg^{2+} ions and lowered in energy to such an extent that they lie below the p – σ orbitals. Because of this electrons from the p – σ bands are shifted to the p-π bands corresponding to a hole-doping of the p – σ bands. In other words the Fermi level crosses the p – σ bands in MgB_2, which in this case is evidently decisive for the occurrence of superconductivity. This band can be filled by substituting Mg by Al, which leads to lower T_C values when doping up to 10 %, and at higher doping leads to the complete disappearance of superconductivity.[15]

Within the BCS theory (named after the discoverers Bardeen, Cooper, and Schrieffer) the critical temperature of a superconductor can be calculated according to $T_C = \omega_{ph} \exp(-1/\lambda^*)$.[16] The phonon frequency ω_{ph} corresponds to the thermal motion of the atoms, which plays the decisive role in the electron – phonon coupling process with the constant λ^* which is relevant for the attractive interaction of two electrons with spin $= \pm ½$ to a so-called Cooper pair with $S = 0$. The boron isotope effect, which is charateristic for conventional BCS superconductivity was measured for MgB_2:[17] The T_C value for $Mg^{10}B_2$ lies approximately 1 K higher than that for $Mg^{11}B_2$. Furthermore measurements of the heat capacity[18] and results of tunneling spectroscopy investigations[19] indicate that MgB_2 is a conventional BCS superconductor with a weak-to-moderate electron – phonon coupling.

Detailed analyses of the electron – phonon coupling in MgB_2 on the basis of quantum-mechanical calculations show[20, 21] that the p – σ electrons couple very strongly to a high-frequency B–B stretching mode, whose limiting structures can be described as "benzoid" and "quinoid" (see Scheme 1). Within such a mode the degree of overlap of the π bonding changes, as does that of the p – σ bonding, whose band lies at the Fermi level. The calculated electron – phonon coupling constant results in an expected T_C value of 40 K for MgB_2. That MgB_2 can be well described by means of reliable theoretical tools is also shown by the calculation of the pressure dependence of the elastic and electronic properties of MgB_2,[22] according to which the value of T_C should decrease by -1.4 K per GPa. This value is in good agreement with the experimental value of $-1.6\ K\,GPa^{-1}$ published shortly thereafter.[23, 24] Through application of external pressure the interatomic B–B and Mg–B distances are shortened. Consequently the phonons become harder, that is ω_{ph} becomes larger, simultaneously however, the density of states at the Fermi level becomes smaller, and also the electron – phonon coupling is weakened, so that the observed decrease of the T_C value under pressure can be well explained within the BCS scenario.

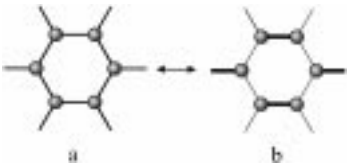

Scheme 1. Limiting structures of the phonon in a B_2^{2-} sheet in MgB_2 which is relevant for the occurrence of superconductivity: a) "benzoid" with equal B–B distances and b) "quinoid" with short (bold) and long B–B distances.

Finally the relevance of Akimitsu's discovery for possible applications is worth mentioning. Nowadays superconducting materials in the form of strong magnets are used in daily life, for example in magnetic resonance tomography in hospitals or transport based on magnetic levitation. Although MgB_2 is not the best superconductor, a great deal is expected owing to its potential for applications; it is a so-called type 2 superconductor[25] with large values for the upper critical magnetic field H_{c2}, and the critical current, at which the superconductivity disappears, is relatively high.[26] These are important quantities for applicable superconducting wires[27] or thin films,[28] which can transport large amounts of current. As MgB_2 can be used as a superconducting material slightly below its T_C value of 39 K, there is even the chance that instead of cooling with liquid helium—which is technologically demanding—it might be possible to cool with electrical aggregates.

The enormous interest in the superconductivity of MgB_2 has led to a scenario where numerous research teams have been attracted to this new topic like a gold rush, similar to what happened with the oxocuprate superconductors fifteen years ago. Within weeks after the announcement of the discovery, hundreds of publications could be found on preprint servers and a head-to-head race for establishing priorities had started. It is hoped that the lessons from the past will be learned and that not too much research capacity will be wasted and that preliminary results will not be published too hastily. The discovery by Akimitsu and co-workers, however, gives rise to expectations that variants of MgB_2 or further simple materials with even higher critical temperatures will be found which can lead to a better understanding of superconductivity and new potential applications for superconducting materials.

[1] J. Akimitsu, *Symposium on Transition Metal Oxides* (Sendai, Japan, January 10, 2001), **2001**.
[2] J. Nagamatsu, N. Nakagawa, T. Muranaka, Y. Zenitani, A. Akimitsu, *Nature* **2001**, *410*, 63.
[3] D. P. Young, D. Hall, M. E. Torelli, Z. Fisk, J. L. Sarrao, J. D. Thompson, H.-R. Ott, S. B. Oseroff, R. G. Goodrich, R. Zysler, *Nature* **1999**, *397*, 412.
[4] J. Russel, R. Hirst, F. A. Kanda, A. J. King, *Acta Crystallogr.* **1953**, *6*, 870.

  1433-7851/01/4013-2436 $ 17.50+.50/0

[5] M. Jones, R. Marsh, *J. Am. Chem. Soc.* **1954**, *76*, 1434.
[6] E. G. Killian, R. B. Kaner, *Chem. Mater.* **1996**, *8*, 333.
[7] B. T. Matthias, *Superconductivity of d- and f-Band Metals*, American Institute of Physics, New York, **1972**, p. 367.
[8] J. R. Gavaler, *Appl. Phys. Lett.* **1973**, *23*, 480.
[9] J. G. Bednorz, K. A. Müller, *Z. Phys. B* **1986**, *64*, 189.
[10] H. Takagi, *Physica C* **2000**, *341 – 348*, 3.
[11] K. Tanigaki, T. W. Ebbesen, S. Saito, J. Mizuki, J. S. Tsai, Y. Kubo, S. Kuroshima, *Nature* **1991**, *352*, 222.
[12] L. F. Schneemeyer, J. K. Thomas, T. Siegrist, B. Batlogg, L. W. Rupp, R. L. Opila, R. V. Cava, *Nature* **1988**, *332*, 814.
[13] J. H. Schön, C. Kloc, B. Batlogg, *Nature* **2000**, *408*, 549.
[14] J. M. An, W. E. Picket, *Phys. Rev. Lett.* **2001**, *86*, 4366.
[15] J. S. Slusky, N. Rogado, K. A. Regan, M. A. Hayward, P. Khalifah, T. He, K. Inumaru, S. Loureiro, M. K. Haas, H. W. Zandbergen, R. J. Cava, *Nature* **2001**, *410*, 343.
[16] J. Bardeen, L. N. Cooper, J. R. Schrieffer, *Phys. Rev.* **1957**, *108*, 1175.
[17] S. L. Bud'ko, G. Lapertot, C. Petrovic, C. E. Cunningham, N. Anderson, P. C. Canfield, *Phys. Rev. Lett.* **2001**, *86*, 1877.
[18] R. K. Kremer, B. J. Gibson, K. Ahn, cond-mat/0102432. The references given here and in the following for electronic Preprints can be retrieved at the internet address http://xxx.lanl/gov/archive/cond-mat on quoting the corresponding number.
[19] A. Sharoni, I. Fellner, O. Millo, cond-mat/0102325.
[20] J. Kortus, I. I. Mazin, K. D. Belashchenko, V. P. Antropov, L. L. Boyer, *Phys. Rev. Lett.* **2001**, *86*, 4656.
[21] Y. Kong, O. V. Dolgov, O. Jepsen, O. K. Andersen, *Phys. Rev. B* **2001**, in press, cond-mat/0102499.
[22] I. Loa, K. Syassen, *Solid State Commun.* **2001**, *118*, 279.
[23] B. Lorenz, R. L. Meng, C. W. Chu, *Phys. Rev. B* **2001**, in press, cond-mat/0102264.
[24] M. Monteverde, M. Nunez-Regueiro, N. Rogado, K. A. Regan, M. A. Hayward, T. He, S. M. Loureiro, R. J. Cava, *Science* **2001**, *292*, 75.
[25] K.-H. Müller, G. Fuchs, A. Handstein, K. Nenkov, V. N. Narozhnyi, D. Eckert, *Solid State Commun.* **2001**, *118*, 1.
[26] D. K. Finnemore, J. E. Ostenson, S. L. Bud'ko, G. Lapertot, P. C. Canfield, *Phys. Rev. Lett.* **2001**, *86*, 2420.
[27] P. C. Canfield, D. K. Finnemore, S. L. Bud'ko, J. E. Ostenson, G. Lapertot, C. E. Cunningham, C. Petrovic, *Phys. Rev. Lett.* **2001**, *86*, 2423.
[28] W. N. Kang, H.-J. Kim, E.-M. Choi, C. U. Jung, S.-I. Lee, cond-mat/0103179.

RNA Interference: A New Way to Analyze Protein Function

Ute Schepers and Thomas Kolter*

Introduction

Within the last few years a tremendous amount of work has been done to identify the genetic background of different species. Even the human genome has been sequenced. However, the data obtained create a need for additional information that will allow us to understand the determinants of biochemical, biological, and pharmacological processes. In particular, more information is needed to enable us to assign functions to the gene products, mostly proteins, encoded by the genome of a species (functional genomics). Recently, a novel technique has been described which promotes a much faster and simplified analysis of protein function. This technique uses gene-specific double-stranded RNA (dsRNA) to disrupt gene expression at the level of messenger RNA (mRNA) in tissue culture and whole organisms (Scheme 1).[1]

Function of Proteins

Researchers have been looking for methods to study the function of proteins for a long time. In the past various experimental procedures have been used but have often turned out to be very laborious and time consuming. A common method to investigate the function of proteins and other biological molecules is the knock-out experiment.

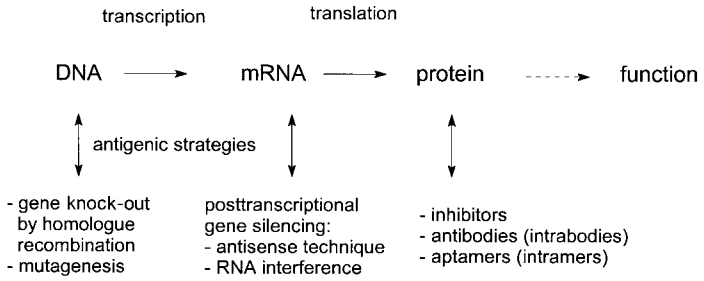

Scheme 1. Examples of methods for the disruption of protein function.

For this purpose, the phenotype of tissue cultures or organisms that lack a specific protein due to mutations or alterations is analyzed. In humans, inherited diseases were used as models for these knock-out experiments.

One of the most promising new techniques for the study of protein function seems to be the RNA interference (RNAi) method. It is based on the degradation of selected mRNA by administration of double-stranded RNA. RNAi offers strong advantages over other antigenic strategies[2] such as gene knock-out by homologue recombination, antisense oligonucleotides, or ribozymes.[3]

History

RNAi was discovered in 1995 in the nematode *Caenorhabditis elegans*, a model organism for biological experiments,[4] when researchers attempted to use the antisense RNA approach to inactivate the expression of a single gene. *C. elegans* was injected with RNA complementary to a target

[*] Dr. T. Kolter, Dr. U. Schepers
Kekulé-Institut für Organische Chemie und Biochemie der Universität
Gerhard-Domagk Strasse 1, 53121 Bonn (Germany)
Fax: (+49) 228-73-77-78
E-mail: tkolter@uni-bonn.de

  1433-7851/01/4013-2437 $ 17.50+.50/0

mRNA (antisense RNA), in order to capture this mRNA and to prevent the production of the encoded protein. Surprisingly, simultaneous injection of sense and antisense RNA was much more effective in suppression of specific gene expression than antisense RNA alone.[1] This finding was the basis for a simple method of disabling the expression of selected proteins, through the introduction of exogenous dsRNAs.

RNAi falls into the category of post-transcriptional gene silencing (PTGS). PTGS was observed in several organisms in the early 1990s and was subsequently named as "cosuppression" in plants, "quelling" in fungi, and "RNA interference" in nematodes and insects.[5, 6] It is thought to be an ancient self-defense mechanism of cells, to combat infection by RNA viruses and transposons (mobile parasitic stretches of DNA that can be inserted into the host's genome). During the process of copying themselves these viruses and transposons generate dsRNA that is recognized and degraded by the host cell. This self-defense mechanism has previously been described in a number of organisms, such as trypanosomes,[7] insects,[8, 9] plants,[10] and recently in mouse embryonic stem cells and oocytes.[11] The latter result is of considerable interest for future applications. RNAi involves this mechanism through the introduction of exogenous dsRNA. If this trigger mimics a part of the (single-stranded) host-cell mRNA sequence, the homologous mRNA will be degraded as well as the exogenous RNA.

For a long time RNAi has not been applied to mammals because these organisms were thought to have evolved a different response to RNA viruses and transposons. Extremely small amounts of dsRNA can trigger a signal cascade, part of which is the activation of dsRNA responsive protein kinase R (PKR). PKR phosphorylates and inactivates the translation factor EIF2α leading to a global suppression of protein biosynthesis and subsequently to programmed cell death (apoptosis). However, it seems that recent RNAi experiments in mouse embryonic stem cells have been successful.[11] It is possible that the interferon response has not yet developed in these early embryonic mouse cells, and there may be difficulties in using RNAi in later developmental stages. Nevertheless, there will be many efforts to develop this technique for application in differentiated mammalian cells.

Mechanism

To date, the mechanism underlying RNAi is still unclear. One current model that has been proposed is based on experiments with *C. elegans* and other species (Scheme 2). In response to substoichiometric amounts of dsRNA, levels of homologous mRNA sequences are drastically decreased within 2–3 h.[12] This degradation happens in two steps: First, exogenous dsRNA is cleaved into fragments containing 21–23 nucleotides and, second, these fragments trigger the degradation of the homologous endogenous mRNA.

Genetic screening with *C. elegans* and insects has identified some gene families required for PTGS. They encode for proteins which are assembled in complexes. These complexes contain 3′–5′ exonucleases, helicases, RNA polymerases, and RNA binding proteins. In *Drosophila* it has been recently discovered that a nuclease of the RNAse III family is involved

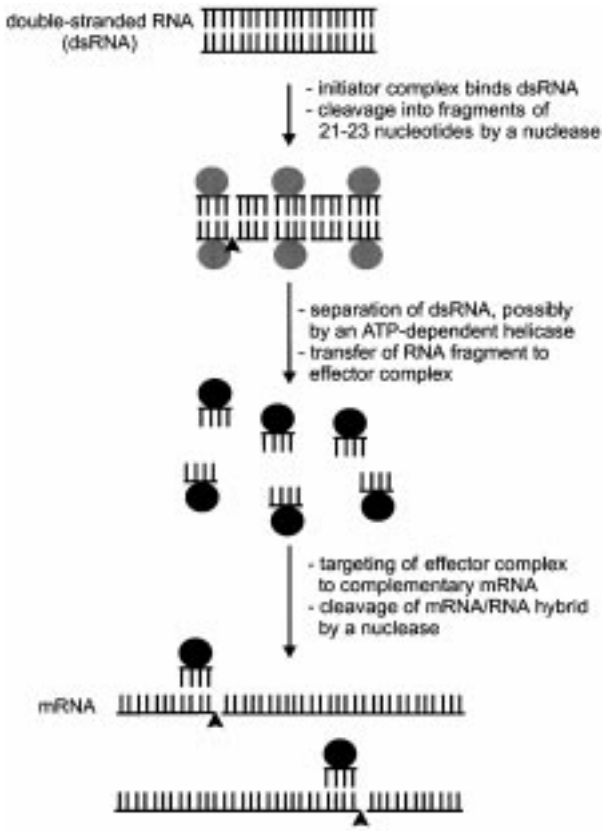

Scheme 2. Proposed mechanism of PTGS by RNAi (modified from ref. [12] after consideration of ref. [13]).

during initiation in the cleavage of dsRNA into fragments of 21–23 nucleotides.[12] The identity of this nuclease has been demonstrated in *Drosophila*.[13] It is thought, at least in *Neurospora*[14] and presumably also in *C. elegans*,[13] that these fragments of dsRNA will be amplified by dsRNA-dependent RNA polymerases to enhance the alarm signal in the cell. The newly generated fragments will be separated by an ATP-dependent helicase[12] and subsequently targeted to the complementary mRNA by RNA binding proteins. Further nucleases will be activated to degrade the newly created dsRNA derived from the fragment and the complementary mRNA.

With this mechanism, addition of exogenous dsRNA can be used to knock out a specific protein. Since RNAi is happening posttranscriptionally, the exogenous dsRNA has to be complementary to exon sequences of the gene that is to be knocked out. Double-stranded RNA sequences complementary to nontranscribed sequences, like introns and promoter regions, are ineffective.[1] Meanwhile, expression of a number of proteins with highly conserved (homologous) domains can be disrupted by addition of just one dsRNA encoding this region.[1, 8]

Application and Outlook

As with intracellular antibodies (intrabodies) or aptamers (intramers),[15] a remarkable feature of RNAi is the disruption of protein expression without manipulation of the genetic

  1433-7851/01/4013-2438 $ 17.50+.50/0

material. Compared to the generation of traditional knock-out animals by homologue recombination, the method is simple and fast.

Antisense techniques, where a 1:1 hybridization of endogenous mRNA with antisense RNA is necessary, often fail to exhibit full gene silencing, whereas the application of catalytic amounts of dsRNA promotes the complete degradation of homologous mRNA. With antisense DNA instead of antisense RNA, degradation of mRNA/DNA hybrids will be triggered by RNase H.[3]

RNAi allows the disruption of protein expression not only in tissue cultures and organisms, but also during different developmental stages of the organism. This offers a strong advantage over the competing gene knock-out method in animals, since eliminating the gene of interest is often lethal for the embryo. Although it is already possible to generate inducible and tissue-specific knock-out/transgenic animals using the Cre/loxP technique,[16] this approach is still very laborious. At present researchers are attempting to apply RNAi to mammals, which would reduce time-consuming steps like homologous recombination and site-directed mutagenesis.

An absolute requirement for RNAi is the knowledge of the nucleic acid sequence for about 200 – 1000 bases. Transient phenotypes can be created using modern transfection technology such as lipid transfer, micro-injection, gene-gun methods, or feeding to introduce dsRNA into tissue culture or organisms, as described for *C. elegans*.[1]. Thereby, simultaneous and parallel knock-out of a number of proteins offers a new way to analyze the function of either known or unknown proteins in single experiments or with high-throughput screening (*C. elegans*).[17, 18]

To generate inheritable and inducible RNAi phenotypes in tissue culture or organisms, one has to manipulate the genetic background. The resulting transgenic cell lines or organisms carry plasmids that contain a stretch of DNA encoding for about 1000 bases of the gene to be silenced in a sense and antisense orientation (inverted repeat). During transcription of the inverted repeat sequence an RNA molecule is formed that is supposed to fold back into a hairpin-like structure by intramolecular hybridization. The resulting RNA is then effectively double stranded. RNAi phenotypes can be induced in a variety of tissues as well as in different developmental stages, through the use of tissue-specific or drug-inducible promoters to express the hairpin dsRNA. Among many other advantages there is one which is of common interest. RNAi can be used to disrupt the expression of viral and parasitic proteins as a defense against pathogens. So far, it has been reported that transformation of tobacco plants with a hairpin DNA encoding a protease of the potato virus Y lead to a complete immunization against the virus.[19]

It is very impressive how many insights researchers have gained on the function of proteins using a variety of methods. Nevertheless, despite the tremendous success of knock-out or gene-silencing experiments, one has to be critical in judging data obtained in cell cultures. The absence of the appropriate multicellular surroundings or the artificial conditions can lead to discrepancies between results obtained in cell cultures and in whole organisms.[20] Even the analysis of knock-out animals can be misleading; for example, knock-out mice developed as models for severe human diseases like Tay – Sachs disease[21] or Lesch – Nyhan syndrome[20] do not show the expected phenotypes. In this respect, one also has to be concerned about the analysis of protein functions derived from RNAi experiments.

There are still plenty of mysteries concerning the mechanism and the application of RNAi but the number of researchers focussing on RNAi is growing rapidly and promises increasing developments in this field.[22]

[1] A. Fire, S. Q. Xu, M. K. Montgomery, S. A. Kostas, S. E. Driver, C. C. Mello, *Nature* **1998**, *391*, 806 – 811.
[2] K.-Y. Jen, A. M. Gewirtz, *Stem Cells* **2000**, *18*, 307 – 319.
[3] U. Galderisi, A. Cascino, A. Giordano, *J. Cell. Physiol.* **1999**, *181*, 251 – 257.
[4] S.Guo, K. J. Kemphues, *Cell* **1995**, *81*, 611 – 620.
[5] Review: R. H. A. Plasterk, R. F. Ketting, *Curr. Opin. Genet. Dev.* **2000**, *10*, 562 – 567.
[6] Review: B. L. Bass, *Cell* **2000**, *101*, 235 – 238.
[7] H. Ngo, C. Tschudi, K. Gull, E. Ullu, *Proc. Natl. Acad. Sci. USA* **1998**, 95, 14687 – 14692.
[8] J. R. Kenerdell, R. W. Carthew, *Cell* **1998**, *95*, 1017 – 1026.
[9] L. Misquitta, B. M. Paterson, *Proc. Natl. Acad. Sci. USA* **1999**, *96*, 1451 – 1456.
[10] A. J. Hamilton, D. C. Baulcombe, *Science* **1999**, *286*, 950 – 952.
[11] F. Wianny, M. Zernicka-Goetz, *Nat. Cell Biol.* **2000**, *2*, 70 – 75.
[12] P. D. Zamore, T. Tuschl, P. A. Sharp, D. P. Bartel, *Cell* **2000**, *101*, 25 – 33.
[13] E. Bernstein, A. A. Caudy, S. M. Hammond, G. J. Hammond, *Nature* **2001**, *409*, 363 – 366.
[14] C. Cognoni, G. Macino, *Nature* **1999**, *399*, 166 – 169.
[15] M. Famulok, G. Mayer, M. Blind, *Acc. Chem. Res.* **2000**, *33*, 591 – 599.
[16] A. Nagy, *Genesis* **2000**, *26*, 99 – 109.
[17] P. Gonczy, G. Echeverri, K. Oegema, A. Coulson, S. J. Jones, R. R. Copley, J. Duperon, J. Oegema, M. Brehm, E. Cassin, E. Hannak, M. Kirkham, S. Pichler, K. Flohrs, A. Goessen, S. Leidel, A. M. Alleaume, C. Martin, N. Ozlu, P. Bork, A. A. Hyman, *Nature* **2000**, *408*, 331 – 336.
[18] A. G. Fraser, R. S. Kamath, P. Zipperlen, M. Martinez-Campos, M. Sohrmann, J. Ahringer, *Nature* **2000**, *408*, 325 – 330.
[19] N. A. Smith, S. P. Singh, M.-B. Wang, P. A. Stoujesdijk, A. G. Green, P. M. Waterhouse, *Nature* **2000**, *407*, 319 – 320.
[20] T. Kolter, T. Magin, K. Sandhoff, *Traffic* **2000**, *1*, 803 – 804.
[21] T. Kolter, *Angew. Chem.* **1997**, *109*, 2044 – 2048; *Angew. Chem. Int. Ed. Engl.* **1997**, *36*, 1955 – 1959.
[22] For a recent review, see: T. Tuschl, *ChemBioChem* **2001**, *2*, 239 – 245.

  1433-7851/01/4013-2439 $ 17.50+.50/0

First Metallabenzenes and now a Stable Metallabenzyne

Warren R. Roper*

Many important examples of compounds with transition metal carbon multiple bonds can be derived, in a formal sense, by replacement of a carbon atom in an alkene or alkyne with a metal center and associated ligands. Thus in Scheme 1 we see that carbene complexes (A, or metalla-alkenes), are related to

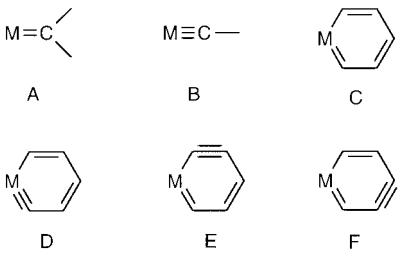

Scheme 1. Some known and unknown classes of compound with metal–carbon multiple bonds.

alkenes and that carbyne complexes (B, or metalla-alkynes) are related to alkynes. A particularly interesting example of cyclic carbene complexes are metallabenzenes (C) derived from replacement of one C–H group in benzene, the archetypal "aromatic" compound, by a metal center and associated ligands. The first example of such a compound was reported nearly twenty years ago[1] and numerous studies since then[2] have confirmed that metallabenzenes have all the attributes of conventional aromatic systems, that is: ring planarity, no bond length alternation, downfield chemical shifts for ring protons, and even in some cases that they undergo electrophilic aromatic substitution reactions.[3] Some representative examples of stable metallabenzenes are shown in Scheme 2.

The possibility of obtaining isolable metal complexes from metal replacement of a C–H group in the reactive intermediate, *o*-benzyne, as illustrated by D, E, and F (Scheme 1), at first sight seems rather fanciful. Isomer D is related to a metal carbyne complex just as metallabenzene C is related to a metal carbene complex. Structural studies of many metal carbyne complexes[4] have revealed that the angle at the carbyne carbon atom is usually near to 180° (the mean is 173°) with a few exceptional cases having angles as low as 160°. Similar angles are also found for acetylenes. Therefore, considerable ring-strain would be expected in D, just as in E and F. However, any expectation that a complex of type D would be unstable is shattered by the recent report from Jia and co-workers[5] that reaction between $[OsCl_2(PPh_3)_3]$ and trimethylsilylacetylene leads to four products the major one of which is the stable, structurally characterized, metallabenzyne complex **1**.

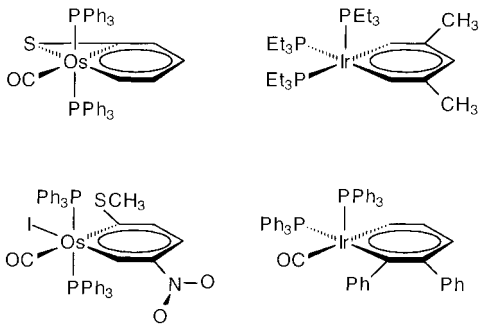

Scheme 2. Some stable metallabenzenes.

Jia and co-workers propose the sequence of steps shown in Scheme 3 to account for the formation of **1**. Initially, reaction between $[OsCl_2(PPh_3)_3]$ and trimethylsilylacetylene (in the presence of H_2O) produces the coordinatively unsaturated

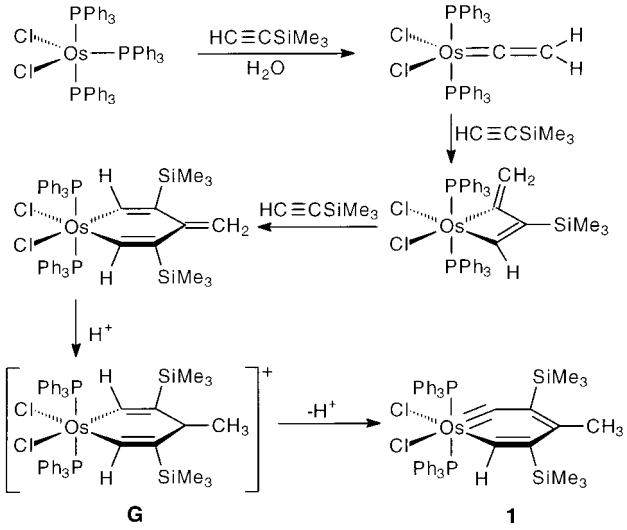

Scheme 3. Proposed route to **1**.[5]

vinylidene complex, $[Os(=C=CH_2)Cl_2(PPh_3)_2]$. This complex undergoes two successive cycloaddition reactions with further trimethylsilylacetylene to give first an osmacyclobutene and then an osmacyclohexadiene complex. The direction of each addition is probably dictated by steric factors. Protonation of the osmacyclohexadiene complex then gives **G** which is more reasonably depicted as **H** or **I** (see Scheme 4) and can be seen as a cationic osmabenzene complex. Loss of a proton from a metal-bound carbon atom then produces the observed metallabenzyne product **1**. The experimental data for **1** is convincing, the ^{13}C NMR spectrum shows signals corresponding to two metal-bound carbon atoms, one of which is carbene-like and one carbyne-like, and the X-ray crystal structure shows

[*] Prof. W. R. Roper
Department of Chemistry
The University of Auckland
Private Bag 92019, Auckland (New Zealand)
Fax: (+64) 9-373-7422
E-mail: w.roper@auckland.ac.nz

  1433-7851/01/4013-2440 $ 17.50+.50/0

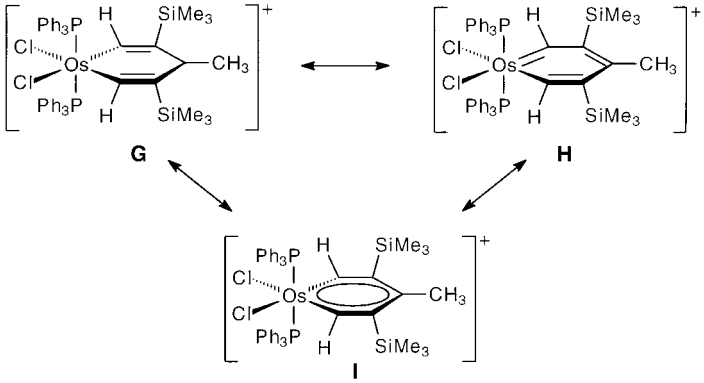

Scheme 4. Valence bond representations of the intermediate metallabenzene.

one Os–C bond of 1.815(4) Å (at the high end of observed Os≡C bonds[6]), and another Os–C bond of 1.939(5) Å (slightly shorter than observed in other osmabenzenes[3]). Other ring C–C distances are typical of regular aromatic systems. The angle at the carbyne carbon atom is 148.7(3)°, considerably larger than the angle at the other metal-bound carbon of 138.6(5)°. These very large ring angles are accommodated partly by the angle at osmium closing to 78.1(2)°.

So why is metallabenzyne **1** a stable isolable complex? The reactivity of **1** will certainly be reduced by the steric protection of the strained Os≡C bond provided by the ligands at the osmium center and the nearby trimethylsilyl group on the adjacent carbon atom. Simple protonation back to the precursor **G** (or **H**, **I**) will not be favored because the cationic osmabenzene so formed will have the acidity of what is already an acidic α-CH group enhanced. However, it may also be that the ring strain is not as great as might have been expected. The angle at the carbyne carbon atom is only 12° less than that observed in some noncyclic carbyne complexes. Metallabenzyne **1** will certainly not be unique. We must await with interest reports of the reactivity of **1**, the syntheses of other metallabenzynes, and possible interconversions of metallabenzenes and metallabenzynes. Organometallic chemistry can still provide some startling surprises!

[1] G. P. Elliott, W. R. Roper, J. M. Waters, *J. Chem. Soc. Chem. Commun.* **1982**, 811–813.

[2] a) J. R. Bleeke, *Acc. Chem. Res.* **1991**, *24*, 271–277; b) J. R. Bleeke, R. Behm, Y.-F. Xie, M. Y. Chiang, K. D. Robinson, A. M. Beatty, *Organometallics* **1997**, *16*, 606–623; c) J. R. Bleeke, R. Behm, *J. Am. Chem. Soc.* **1997**, *119*, 8503–8511; d) R. D. Gilbertson, T. J. R. Weakley, M. M. Haley, *J. Am. Chem. Soc.* **1999**, *121*, 2597–2598.

[3] C. E. F. Rickard, W. R. Roper, S. D. Woodgate, L. J. Wright, *Angew. Chem.* **2000**, *112*, 766–768; *Angew. Chem. Int. Ed.* **2000**, *39*, 750–752.

[4] a) H. P. Kim, R. J. Angelici, *Adv. Organomet. Chem.* **1987**, *27*, 51–111; b) A. Mayr, H. Hoffmeister, *Adv. Organomet. Chem.* **1991**, *32*, 227–324.

[5] T. B. Wen, Z. Y. Zhou, G. Jia, *Angew. Chem.* **2001**, *113*, 2005–2008; *Angew. Chem. Int. Ed.* **2001**, *40*, 1951–1954.

[6] G. R. Clark, C. M. Cochrane, K. Marsden, W. R. Roper, L. J. Wright, *J. Organomet. Chem.* **1986**, *315*, 211–230; G. R. Clark, N. R. Edmonds, R. A. Pauptit, W. R. Roper, J. M. Waters, A. H. Wright, *J. Organomet. Chem.* **1983**, *244*, C57–C60; L.-J. Baker, G. R. Clark, C. E. F. Rickard, W. R. Roper, S. D. Woodgate, L. J. Wright, *J. Organomet. Chem.* **1998**, *551*, 247–259; H. Werner, S. Jung, B. Weberndörfer, J. Wolf, *Eur. J. Inorg. Chem.* **1999**, 951–957; P. Crochet, A. Esteruelas, A. M. López, M.-P. Martínez, M. Oliván, E. Oñate, N. Ruiz, *Organometallics* **1998**, *17*, 4500–4509; L. M. Hodges, M. Sabat, W. D. Harman, *Inorg. Chem.* **1993**, *32*, 371–372.

  1433-7851/01/4013-2441 $ 17.50+.50/0

The sixfold connectivity of the NaCl crystal lattice is familiar to all chemists but is still rare for coordination framework polymers. Higher connectivities were previously unknown.

The diagram shows the first example of an eight-connected coordination network with CsCl-like topology.

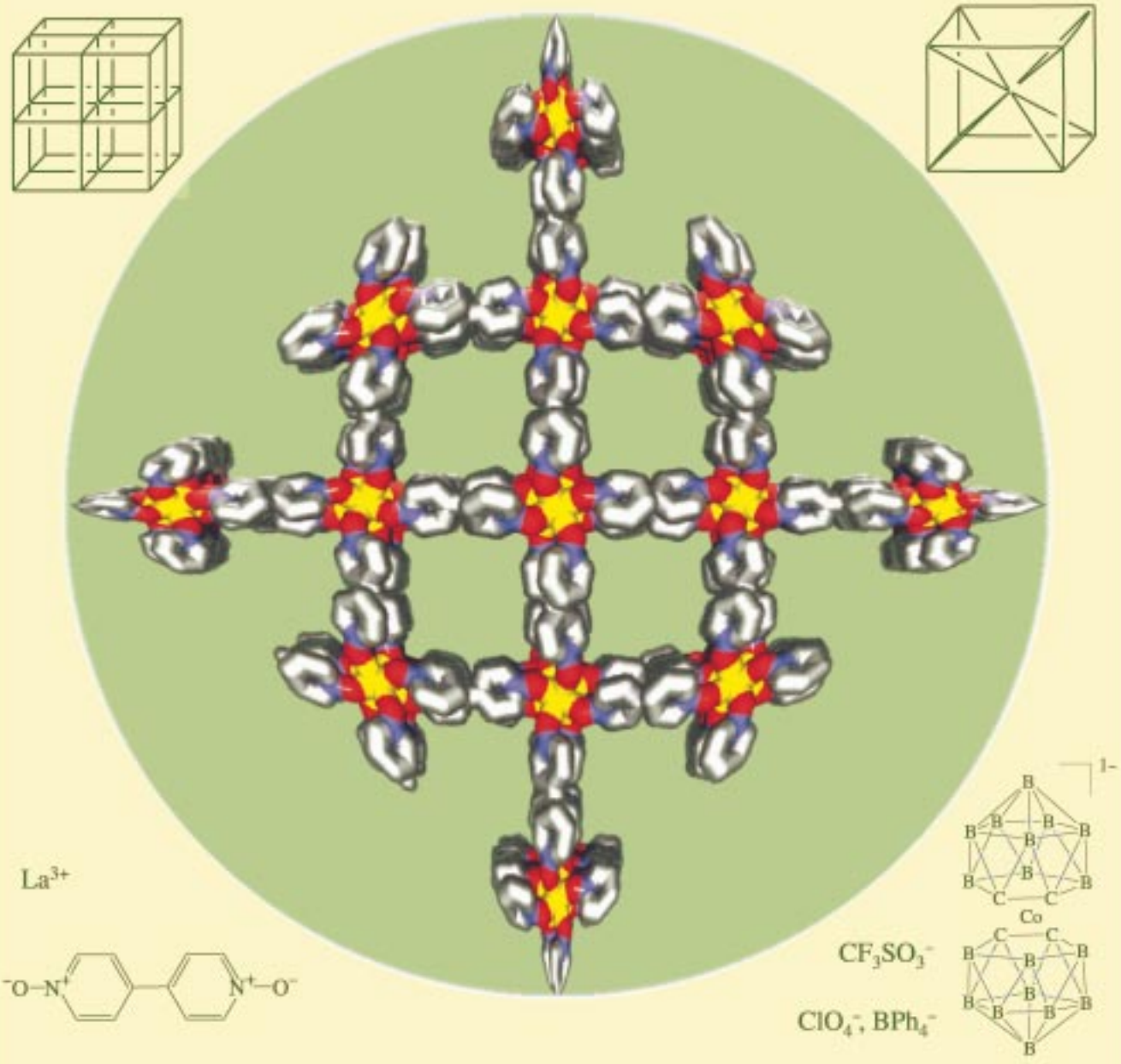

By using the ligand 4,4′-bipyridine-*N*,*N*′-dioxide to bridge La^{III} centers, coordination networks of six-, seven-, and eight-connected topologies can be constructed. What is a seven-connected framework? Find out more on the following pages.

  1433-7851/01/4013-2443 $ 17.50+.50/0

Unprecedented Seven- and Eight-Connected Lanthanide Coordination Networks**

De-Liang Long, Alexander J. Blake, Neil R. Champness,* Claire Wilson, and Martin Schröder*

The classification by Wells[1] of framework materials according to their topological structures allows a general understanding of solid-state structures. Of the structural types depicted by Wells the majority are based upon three- and four-connected topologies which are commonly found in framework materials such as zeolites and, more recently, in coordination polymers.[2] Much of this latter work has focussed on d-block metal ions using three-,[3] four-,[4] or six-connected nodes,[5] and more recently, examples of five-connected structures have been reported.[5a, 6] Three-dimensional structures with high connectivity are familiar in the form of the NaCl lattice (6:6 coordination:connectivity) or CsCl (8:8 coordination:connectivity), but examples of six-connected structures are still rare for coordination framework polymers,[5] and connectivities higher than this are unknown. Due to their limited coordination numbers, it is difficult for polymeric structures with such high topological connectivites to be generated with d-block metal ions, and even six-connected nodes are uncommon with d-block metals due to steric hindrance for most commonly used heterocyclic N-donor ligands. Despite the tendency of lanthanide ions to adopt high coordination numbers, connectivities greater than six remain unknown for lanthanide coordination polymers.[7] We recently reported a general strategy for the construction of lanthanide coordination networks using 4,4′-bipyridine-*N*,*N*′-dioxide (L) as a bridging ligand and coordinating NO_3^- ions as terminal groups to give unusual three- and four-connected networks.[8] L not only presents a suitable donor atom for lanthanide ions, but its limited steric hindrance additionally offers the potential for higher coordination numbers and homoleptic coordination spheres. Thus, in the absence of competing ligands, the reaction of La^{III} cations with L is attractive for the synthesis of highly connected framework coordination polymers. Furthermore, we anticipated that by using noncoordinating and/or bulky anions such as $CF_3SO_3^-$, BPh_4^-, and $[Co(C_2H_{11}B_9)_2]^-$, lanthanide coordination networks with unusually high connectivity topologies could be prepared. We report herein three new coordination polymers with highly unusual three-dimensional network structures **1**–**3**, which adopt eight-, seven-, and six-connected lanthanum nodes, respectively.

$[La(L)_4]\cdot(CF_3SO_3)_3\cdot 4.2\,CH_3OH$ **1**

$[La(L)_4]\cdot(BPh_4)\cdot(ClO_4)_2\cdot 2.75\,CH_3OH$ **2**

$[La(L)_4]\cdot([Co(C_2H_{11}B_9)_2])_3\cdot 0.5\,CH_3OH$ **3**

Compound **1** was obtained by mixing methanolic solutions of $La(CF_3SO_3)_3$, 2,2′-bipyridine-*N*,*N*′-dioxide, and L. Complexes **2** and **3** were prepared by mixing methanolic solutions of a lanthanum salt, the sodium salt of the desired bulky anion, and L to afford a precipitate which dissolved with concomitant formation of crystals of the desired product over several days.

Single-crystal X-ray structural determinations confirm that compounds **1**,[9], **2**,[10] and **3**[11] have polymeric structures based on networks of *homoleptic* eight-coordinate La^{III} centers linked through L. In **1** the 4,4′-bipyridine-*N*,*N*′-dioxide ligands bridge to eight different neighboring metal centres (Figure 1a) forming a three-dimensional body-centered *cubic*, CsCl-like, framework structure (Figure 2a). This is the first example of this network topology observed for coordination polymers, and represents the highest connected topology of any known coordination network. The structure can be considered as being composed of (4,4) two-dimensional nets, parallel to the (100) plane, which intersect with further perpendicular (4,4) nets, parallel to the (010) plane (see Scheme 1a). The perpendicular nets are canted at such an angle that an eight-connected structure is generated. The

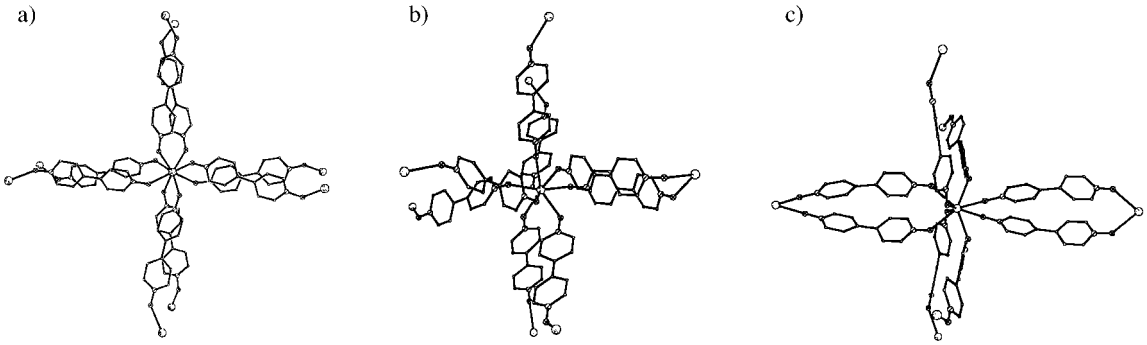

Figure 1. Views of the homoleptic eight-coordinate La^{III} centers in **1** (a), **2** (b), and **3** (c) illustrating the connections to eight, seven, and six nearest La^{III} neighbors, respectively.

[*] Dr. N. R. Champness, Prof. Dr. M. Schröder, Dr. D.-L. Long, Dr. A. J. Blake, Dr. C. Wilson
School of Chemistry, The University of Nottingham
University Park, Nottingham NG7 2RD (UK)
Fax: (+44) 115-9513563
E-mail: Neil.Champness@nottingham.ac.uk
M.Schroder@nottingham.ac.uk

[**] This work was supported by the Royal Society and the Engineering and Physical Sciences Research Council (Royal Society K. C. Wong and EPSRC postdoctoral fellowships to D.-L.L.).

  1433-7851/01/4013-2444 $ 17.50+.50/0

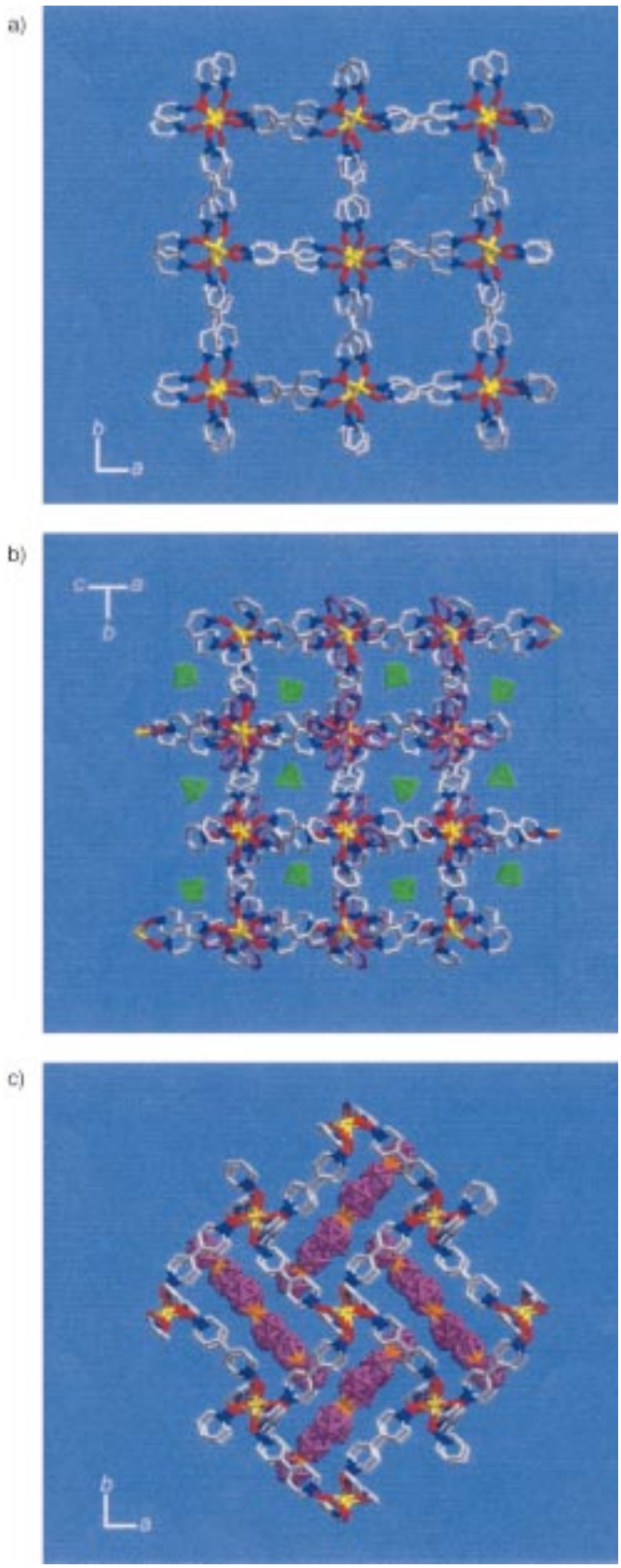

Figure 2. a) Square channels formed by the eight-connected coordination network in **1**. b) 3D structure of **2** showing cavities that accommodate BPh_4^- anions (purple) and channels accommodate ClO_4^- ions (green tetrahedrons). c) Cavities within the six-connected topology of compound **3** that accommodate the bulky $[Co(C_2H_{11}B_9)_2]^-$ ions. Methanol molecules are omitted for clarity.

framework is tetragonally distorted along the *c* axis as a result of the compressed square antiprismatic coordination geometry of the La^{III} cation, and comprises linked cuboids with dimensions of about $18 \times 18 \times 9$ Å. Channels of effective cross-section of about 9×9 Å run parallel to the *c* axis and are occupied by the $CF_3SO_3^-$ ions and MeOH solvent molecules.

The use of 2,2′-bipyridine-*N*,*N*′-dioxide in the preparation of **1** is crucial. When no 2,2′-bipyridine-*N*,*N*′-dioxide is added to the reaction of $La(CF_3SO_3)_3$ with L, a microcrystalline product is formed in only a few hours. X-ray powder diffraction studies confirm that this product adopts an unidentified phase different to that observed for **1**. The same reaction in the presence of 2,2′-bipyridine-*N*,*N*′-dioxide (La:2,2′-bipyridine-*N*,*N*′-dioxide ratio 1:1 or 1:2), produces **1**. Interestingly, the period of time prior to the first appearance of crystals increases as the La:2,2′-bipyridine-*N*,*N*′-dioxide ratio increases, while higher La:2,2′-bipyridine-*N*,*N*′-dioxide ratios (1:3 or 1:4) result in slowing of the crystallization process to such an extent that no solid can be isolated from the reaction mixture. 2,2′-Bipyridine-*N*,*N*′-dioxide reacts with La^{III} cations to form stable, highly symmetrical discrete species $[La(2,2'\text{-bipyridine-}N,N'\text{-dioxide})_4]^{3+}$, an example of cubic eight-coordination,[14] and thus, the presence of 2,2′-bipyridine-*N*,*N*′-dioxide may effect the crystal growth of **1** in two ways. First, it may decelerate the process of lanthanum coordination polymer formation by slowing the rate of reaction between La^{III} cations and L by forming intermediate La^{III}–2,2′-bipyridine-*N*,*N*′-dioxide species. Second, the highly symmetrical $[La(2,2'\text{-bipyridine-}N,N'\text{-dioxide})_4]^{3+}$ ions or related species may template the formation of the eight-coordinate geometry of the La^{III} centers observed in **1**, and thus induce the tetragonal structure observed in the final product, $\{[La(L)_4]^{3+}\}_\infty$.

Although the lanthanum centers in **2** adopt an eight-coordinate geometry, as observed in **1**, the infinite structure that is formed is quite different. Although eight bridging ligands L ligate each metal center, each La^{III} ion is bridged to *seven* nearest neighbors because a pair of ligands L form a "double-bridge" (Figure 1b). Although several bridging modes have been established for L,[15] this is the first observation of the "double-bridge" mode. The resultant three-dimensional (3D) structure can be described as consisting of (6,3) nets (parallel to the crystallographic $(10\bar{1})$ plane, the double-bridge being considered as one connection) interlinked by (4,4) nets (parallel to the crystallographic (010) plane) (Scheme 1b). Thus, the 3D structure that is formed adopts the unprecedented topology $4^{17}6^2$, which represents the first example of a seven-connected coordination network structure. The large cavities found in this structure (Figure 2b) are occupied by ClO_4^- and BPh_4^- counteranions and MeOH solvent molecules.

In **3**, each La^{III} center is ligated by eight molecules of L but is linked to only six nearest neighbors with two pairs of ligands L giving two "double-bridges" (Figure 1c). This affords a six-connected NaCl-like 3D structure (Scheme 1c). The network structure can be considered as two perpendicular (4,4) nets intersecting in a similar manner to that observed in **1**. However, in the case of **3** the (4,4) nets are not canted, in contrast to **1**, so that two "double-bridges" are common to

  1433-7851/01/4013-2445 $ 17.50+.50/0

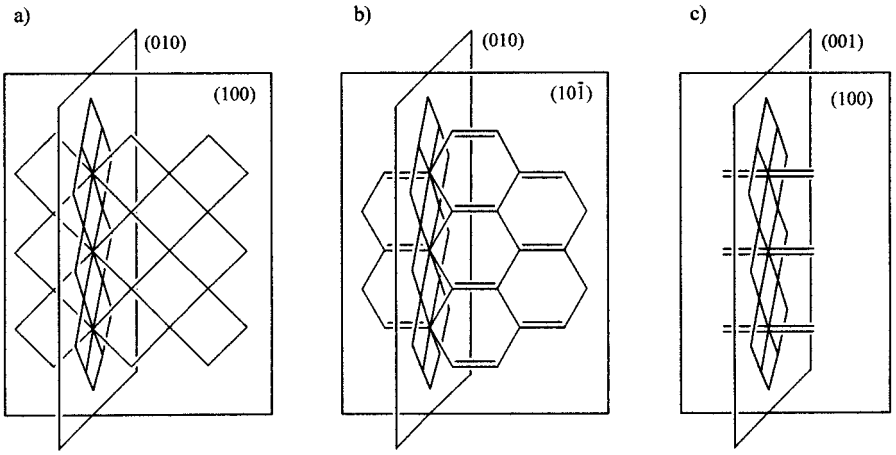

Scheme 1. Schematic representations of the topologies observed in **1** (a), **2** (b), and **3** (c) illustrating the intersecting canted (4,4) nets in **1**, (6,3) and (4,4) nets in **2** and (4,4) nets in **3**. "Double-bridges" are represented by pairs of parallel lines.

both nets to give a six-connected structure. The two "double-bridges" run parallel to the *c* axis, while the four remaining mono bridges propagate along the two diagonal directions of the *ab* face. The structure adopted is noncentrosymmetric, and the chiral cavities which are formed accommodate the $[Co(C_2H_{11}B_9)_2]^-$ ion and MeOH solvent molecules (Figure 2c).

Due to its large size, $[Co(C_2H_{11}B_9)_2]^-$ has been widely used as a counteranion in the extraction and separation of metal ions,[16a–d] but its use as a counteranion in the construction of coordination networks is extremely rare.[16e] As might be expected, our experiments indicate that this anion is preferentially crystallized upon coordination polymer formation over more commonly used anions. Thus, when either $LaCl_3$ or $La(NO_3)_3$ are used as starting materials in the presence of L and $[Co(C_2H_{11}B_9)_2]^-$, the same product, **3**, is obtained. In contrast, the reaction of $LaCl_3$ or $La(NO_3)_3$ with L in the presence of BPh_4^- ions affords different products depending on whether the nitrate or chloride is used as starting material.[17] $[Co(C_2H_{11}B_9)_2]^-$ also appears to have a significant effect in directing lanthanide coordination polymer formation, suprisingly affording the same 3D structures as **3** with either Eu^{III} or Ho^{III} ions,[18] despite the significant and usually influential contraction in cationic radius.[8]

We have confirmed that lanthanide ions can adopt high coordination numbers that can be employed for the construction of highly connected frameworks. The structures reported here are extremely unusual in that homoleptic La^{III} nodes have been used to form the first examples of eight- and seven-connected networks. The differences between the structures reported here highlight the importance of choice of anion upon framework topology, and the subtle balance between different topological structures formed by lanthanide coordination polymers. Our success in preparing the highly connected coordination frameworks of **1**–**3** confirm the potential for developing new structural families of solid-state materials using lanthanide-based coordination polymers.

Received: January 16, 2001 [Z16435]

[1] A. F. Wells, *Three-Dimensional Nets and Polyhedra*, Wiley, New York, **1977**.

[2] For recent reviews regarding the development of the inorganic crystal engineering see: a) A. Müller, H. Reuter, S. Dillinger, *Angew. Chem.* **1995**, *107*, 2505; *Angew. Chem. Int. Ed. Engl.* **1995**, *34*, 2328; b) O. M. Yaghi, H. Li, C. Davis, D. Richardson, T. L. Groy, *Acc. Chem. Res.* **1998**, *31*, 474; c) A. J. Blake, N. R. Champness, P. Hubberstey, W.-S. Li, M. A. Withersby, M. Schröder, *Coord. Chem. Rev.* **1999**, *183*, 117; d) S. R. Batten, R. Robson, *Angew. Chem.* **1998**, *110*, 1558; *Angew. Chem. Int. Ed.* **1998**, *37*, 1460; e) P. J. Hagrman, D. Hagrman, J. Zubieta, *Angew. Chem.* **1999**, *111*, 2798; *Angew. Chem. Int. Ed.* **1999**, *38*, 2638; f) M. Fujita, *Acc. Chem. Res.* **1998**, *32*, 53; g) N. R. Champness, M. Schröder, *Curr. Opin. Solid State Mater. Sci.* **1998**, *3*, 419.

[3] a) O. M. Yaghi, H. Li, T. L. Groy, *Inorg. Chem.* **1997**, *36*, 4292; b) S. Subramanian, M. J. Zaworotko, *Angew. Chem.* **1995**, *107*, 2295; *Angew. Chem. Int. Ed. Engl.* **1995**, *34*, 2127; c) H. Gudbjartson, K. Biradha, K. M. Poirier, M. J. Zaworotko, *J. Am. Chem. Soc.* **1999**, *121*, 2599; d) K. Biradha, K. V. Domasevitch, B. Moulton, C. Seward, M. J. Zaworotko, *Chem. Commun.* **1999**, 1327.

[4] See for example: a) J. A. Real, E. Andres, M. C. Munoz, M. Julve, T. Granier, A. Bousseksou, F. Varret, *Science* **1995**, *268*, 265; b) M. Fujita, Y. J. Kwon, O. Sasaki, K. Yamaguchi, K. Ogura, *J. Am. Chem. Soc.* **1995**, *117*, 7287; c) W. Lin, O. R. Evans, R.-G. Xiong, Z. Wang, *J. Am. Chem. Soc.* **1998**, *120*, 13272; d) M. Kondo, T. Yoshitomi, K. Seki, H. Matsuzaka, S. Kitagawa, *Angew. Chem.* **1997**, *109*, 1844; *Angew. Chem. Int. Ed. Engl.* **1997**, *36*, 1725; e) M. A. Withersby, A. J. Blake, N. R. Champness, P. Hubberstey, W.-S. Li, M. Schröder, *Angew. Chem.* **1997**, *109*, 2421; *Angew. Chem. Int. Ed. Engl.* **1997**, *36*, 2327. f) L. Carlucci, G. Ciani, D. M. Proserpio, *Chem. Commun.* **1999**, 449; g) S. W. Keller, S. Lopez, *J. Am. Chem. Soc.* **1999**, *121*, 6306; h) Q.-M. Wang, G.-C. Guo, T. C. W. Mak, *Chem. Commun.* **1999**, 1849; i) S. R. Batten, B. F. Hoskins, R. Robson, *Chem. Eur. J.* **2000**, *6*, 156.

[5] a) L. Carlucci, G. Ciani, D. M. Proserpio, A. Sironi, *Angew. Chem.* **1995**, *107*, 2037; *Angew. Chem. Int. Ed. Engl.* **1995**, *34*, 1895; b) P. C. M. Duncan, D. M. L. Goodgame, S. Menzer, D. J. Williams, *Chem. Commun.* **1996**, 2127; c) D. M. L. Goodgame, D. A. Grachvogel, I. Hussain, A. J. P. White, D. J. Williams, *Inorg. Chem.* **1999**, *38*, 2057; d) B. F. Hoskins, R. Robson, D. A. Slizys, *Angew. Chem.* **1997**, *109*, 2861; *Angew. Chem. Int. Ed. Engl.* **1997**, *36*, 2752.

[6] a) S. R. Batten, B. F. Hoskins, R. Robson, *New J. Chem.* **1998**, *22*, 173; b) D.-L. Long, A. J. Blake, N. R. Champness, C. Wilson, M. Schröder, *J. Am. Chem. Soc.* **2001**, *123*, 3401; c) P. D. Szuromi, *Science* **2001**, *291*, 5513.

[7] For representative examples of open-framework structures of lanthanide coordination polymers, see: a) G. A. Doyle, D. M. L. Goodgame, S. P. W. Hill, D. J. Williams, *J. Chem. Soc. Chem. Commun.* **1993**, 207; b) L. H. Carrad, D. M. L. Goodgame, S. P. W. Hill, D. J. Williams, *J. Chem. Soc. Chem. Dalton Trans.* **1993**, 1003; c) D. M. L. Goodgame, S. Menzer, A. T. Ross, D. J. Williams, *Inorg. Chim. Acta* **1996**, *251*, 141; d) D. M. L. Goodgame, S. Menzer, A. M. Smith, D. J. Williams, *Chem. Commun.* **1997**, 339; e) D. M. L. Goodgame, S. P. W. Hill, D. J. Williams, *Inorg. Chim. Acta* **1998**, *272*, 131; f) L. Ma, O. R. Evans, B. M. Foxman, W. Lin, *Inorg. Chem.* **1999**, *38*, 5837; g) T. M. Reineke, M. Eddaoudi, M. O'Keeffe, O. M. Yaghi, *Angew. Chem.* **1999**, *111*, 2712; *Angew. Chem. Int. Ed.* **1999**, *38*, 2590; h) L. Pan, X. Huang, J. Li, Y. Wu, N. Zheng, *Angew. Chem. Int. Ed.* **2000**, *39*, 527; i) T. M. Reineke, M. Eddaoudi, D. Moler, M. O'Keeffe, O. M. Yaghi, *J. Am. Chem. Soc.* **2000**, *122*, 4843; j) B.-Q. Ma, D.-S. Zhang, S. Gao, T.-Z. Jin, C.-H. Yan, G.-X. Xu, *Angew. Chem.* **2000**, *112*, 3790; *Angew. Chem. Int. Ed.* **2000**, *39*, 3644; k) T. M. Reineke, M. Eddaoudi, M. Fehr, D. Kelley, O. M. Yaghi, *J. Am. Chem. Soc.* **1999**, *121*, 1651.

[8] D.-L. Long, A. J. Blake, N. R. Champness, M. Schröder, *Chem. Commun.* **2000**, 1369.

  1433-7851/01/4013-2446 $ 17.50+.50/0

[9] a) Single-crystal X-ray experiments were performed on either a Nonius kappaCCD diffractometer (**1**) or a Bruker SMART1000 CCD diffractometer (**2**,**3**) both equipped with an Oxford Cryosystems open-flow cryostat (graphite-monochromated $Mo_{K\alpha}$ radiation, $\lambda = 0.71073$ Å). All structures were solved by direct methods[11] and all non-hydrogen atoms were located by using subsequent difference Fourier methods.[12] b) Crystals of **1** were grown by the following procedure: Lanthanum triflate hydrate (0.029 g, 5×10^{-5} mol), and 2,2′-bipyridine-*N*,*N*′-dioxide (0.010 g, 5×10^{-5} mol) were dissolved in MeOH (10 mL). After 24 h 4,4′-bipyridine-*N*,*N*′-dioxide hydrate (0.022 g, 1×10^{-4} mol) in MeOH (10 mL) was added. After about three days a crystalline product **1**, suitable for X-ray diffraction was formed. Crystal data for **1**, $C_{47.2}H_{48.8}F_9LaN_8O_{21.2}S_3$, $M_r = 1473.43$, tetragonal, $P\bar{4}c2$, $a = 25.9970(4)$, $c = 26.7847(6)$ Å, $V = 18102.3(6)$ Å^3, $T = 150(2)$ K, $Z = 12$, $\rho_{calcd} = 1.622$ Mg m^{-3}, $F(000) = 8923$, $\mu(Mo_{K\alpha}) = 0.920$ mm^{-1}. Crystal morphology: colorless block. Crystal dimensions: $0.20 \times 0.20 \times 0.11$ mm. A total of 19471 unique reflections were collected ($R_{int} = 0.325$), $\theta_{max} = 27.48°$. Semiempirical absorption correction from equivalents. Weighting scheme $w = 1/[\sigma^2(F_o^2) + (0.199P)]$, where $P = [\max(F_o^2,0) + 2F_c^2]/3$. Goodness-of-fit on F^2 was 1.025, $R1$ (for 6414 reflections with $I > 2\sigma(I)$) = 0.132, $wR2 = 0.309$. Data/parameters 19471/650. Largest difference Fourier peak and hole 2.87 and -1.15 e Å^{-3}, respectively. c) Crystallographic data (excluding structure factors) for the structures reported in this paper have been deposited with the Cambridge Crystallographic Data Centre as supplementary publication nos. CCDC-154975 (**1**), CCDC-154976 (**2**), and CCDC-154977 (**3**). Copies of the data can be obtained free of charge on application to CCDC, 12 Union Road, Cambridge CB2 1EZ, UK (fax: (+44) 1223-336-033; e-mail: deposit@ccdc.cam.ac.uk).

[10] Crystals of **2** were grown by the following procedure: Lanthanum perchlorate hydrate (0.022 g, 4×10^{-5} mol) and sodium tetraphenylborate (0.028 g, 8×10^{-5} mol) were dissolved in MeOH (15 mL). 4,4′-Bipyridine-*N*,*N*′-dioxide hydrate (0.033 g, 1.5×10^{-4} mol) in MeOH (10 mL) was added. The mixture produced a white precipitate, which transformed into pale yellow plate crystals over a period of about seven days. Crystal data for **2**, $C_{66.75}H_{63}BCl_2LaN_8O_{18.75}$, $M_r = 1497.87$, monoclinic, $P2_1/n$, $a = 13.2242(11)$, $b = 38.366(3)$, $c = 13.2515(11)$ Å, $\beta = 99.752(1)$, $V = 6626(2)$ Å^3, $T = 150(2)$ K, $Z = 4$, $\rho_{calcd} = 1.501$ Mg m^{-3}, $F(000) = 3062$, $\mu(Mo_{K\alpha}) = 0.805$ mm^{-1}. Crystal morphology: yellow triangular plate. Crystal dimensions: $0.17 \times 0.06 \times 0.04$ mm. A total of 12705 unique reflections were collected ($R_{int} = 0.095$), $\theta_{max} = 27.15°$. Semiempirical absorption correction from equivalents. Weighting scheme $w = 1/[\sigma^2(F_o^2) + (0.261P)]$, where $P = [\max(F_o^2,0) + 2F_c^2]/3$. Goodness-of-fit on F^2 was 0.902, $R1$ (for 6541 reflections with $I > 2\sigma(I)$) = 0.062, $wR2 = 0.096$. Data/parameters 12705/861. Largest difference Fourier peak and hole 1.55 and -0.99 e Å^{-3}, respectively.[9c]

[11] Crystals of **3** were grown by the following procedure: Lanthanum chloride hydrate (0.012 g, 3×10^{-5} mol) and $Na[Co(C_2H_{11}B_9)_2]$ (0.035 g, 1×10^{-4} mol) were dissolved in MeOH (10 cm^3). 4,4′-Bipyridine-*N*,*N*′-dioxide hydrate (0.033 g, 1.5×10^{-4} mol) in MeOH (10 cm^3) was added, producing a white emulsion-like precipitate, from which large yellow plate crystals grew in about three days. Crystal data for **3**, $C_{52.5}H_{100}B_{54}Co_3LaN_8O_{8.5}$, $M_r = 1878.85$, orthorhombic, $P2_12_12$, $a = 17.5705(14)$, $b = 18.571(2)$, $c = 13.3355(11)$ Å, $V = 4351.4(10)$ Å^3, $T = 150(2)$ K, $Z = 2$, $\rho_{calcd} = 1.434$ Mg m^{-3}, $F(000) = 1894$, $\mu(Mo_{K\alpha}) = 1.098$ mm^{-1}. Crystal morphology: yellow plate. Crystal dimensions: $0.34 \times 0.12 \times 0.03$ mm. A total of 10175 unique reflections were collected ($R_{int} = 0.067$), $\theta_{max} = 28.69°$. Semiempirical absorption correction from equivalents. Weighting scheme $w = 1/[\sigma^2(F_o^2) + (0.0156P)]$, where $P = [\max(F_o^2,0) + 2F_c^2]/3$. Goodness-of-fit on F^2 was 0.919, $R1$ (for 7301 reflections with $I > 2\sigma(I)$) = 0.044, $wR2 = 0.061$. Data/parameters 10175/575. Flack parameter = 0.027(12). Largest difference Fourier peak and hole 0.98 and -0.71 e Å^{-3}, respectively.[9c]

[12] SHELXS-97: G. M. Sheldrick, *Acta Crystallogr. Sect A*. **1990**, *46*, 467.

[13] G. M. Sheldrick, SHELXL-97, Universität Göttingen, Germany, **1997**.

[14] A. R. Al-Karaghouli, R. O. Day, J. S. Wood, *Inorg. Chem.* **1978**, *17*, 3702.

[15] D.-L. Long, A. J. Blake, N. R. Champness, M. Schröder, *Chem. Commun*. **2000**, 2273.

[16] For example see: a) C. Viñas, S. Gomez, J. Bertran, F. Teixidor, J.-F. Dozol, H. Rouquette, *Chem. Commun*. **1998**, 191; b) V. V. Romanovskii, D. W. Wester, *Sep. Sci. Technol*. **1999**, *34*, 2141; c) R. M. Chamberlin, K. D. Abney, *J. Radioanal. Nucl. Chem*. **1999**, *241*, 437; d) I. B. Sivaev, V. I. Bregadze, *Collect. Czech. Chem. Commun*. **1999**, *64*, 783; e) for example of sodium salt polymer of cyclotriveratrylene see: M. J. Hardie, C. L. Raston, *Angew. Chem.* **2000**, *112*, 3993; *Angew. Chem. Int. Ed*. **2000**, *39*, 3835.

[17] D.-L. Long, A. J. Blake, N. R. Champness, M. Schröder, unpublished results.

[18] For the europium analogue of **3**, elemental analysis calcd for $C_{52.5}H_{100}B_{54}Co_3EuN_8O_{8.5}$(%): C 33.33, H 5.33, N 5.92; found: C 32.75, H 5.16, N 5.78; cell dimensions: orthorhombic, $a = 17.4254(3)$, $b = 18.6346(3)$, $c = 13.2015(2)$ Å, $V = 4289.7(2)$ Å^3. For the holmium analogue of **3**, elemental analysis calcd for $C_{52.5}H_{100}B_{54}Co_3HoN_8O_{8.5}$(%): C 33.10, H 5.29, 5.88; found: C 32.76, H 5.65, N 6.05; cell dimensions: orthorhombic, $a = 17.363(7)$, $b = 18.715(5)$, $c = 13.184(5)$ Å, $V = 4284(2)$ Å^3.

Working Supramolecular Machines Trapped in Glass and Mounted on a Film Surface**

Shinye Chia, Jianguo Cao, J. Fraser Stoddart,* and Jeffrey I. Zink*

Dedicated to Professor Siegfried Hünig on the occasion of his 80th birthday

The concept of a macroscopic machine can be realized[1] in solution at a supramolecular level in complexes where the self-assembly[2] of the components can be reversed upon quelling temporarily the molecular recognition that exists between the matching components. Thus, a supramolecular machine can be defined as an assembly of two or more molecular components designed to perform mechanical-like motions with respect to each other in response to some energy supply—for example, chemical, electrochemical, or photochemical—that can be switched on and off at will. One of the most highly investigated classes of supramolecular machines[1, 3] are those based on the complexes known as pseudorotaxanes.[4] The reason for this is that the dethreading and rethreading movements of a thread through the center of a ring are reminiscent of the action of a linear motor. Numerous artificial supramolecular machines,[1] based on pseudorotaxanes,[4] exist that can be induced to undergo co-conformational change[5] by chemical,[6] electrochemical,[7] and photochemical[8–10] means. They have been demonstrated[1] to operate efficiently in solution, albeit in an incoherent manner. In order to realize the full potential of these supermolecules in a machine-shop setting, they have to be organized at interfaces[11] or deposited on surfaces[12] so that they can be made to operate in unison. Herein we describe two solid-state supramolecular machines in action: one in which the machines are trapped physically in a rigid, nanoporous, optically transparent matrix, and the other in which

[*] Prof. J. F. Stoddart, Prof. J. I. Zink, S. Chia, J. Cao
Department of Chemistry and Biochemistry
University of California, Los Angeles
405 Hilgard Avenue, Los Angeles, CA 90095-1569 (USA)
Fax: (+1) 310-206-1843
E-mail: stoddart@chem.ucla.edu, zink@chem.ucla.edu

[**] We thank the National Science Foundation and the Sandia National Laboratories for supporting this research.

one component of the machine is tethered onto the surface of a silica film.

In [2]pseudorotaxanes, which are stabilized (in part at least) by π-donor/π-acceptor interactions—for example, such as those present[8] when the naphthalenedioxy donor ring system in 1,5-bis[2-(2-hydroxyethoxy)ethoxy]naphthalene (BHEEN) is threaded through the middle of the tetracationic cyclophane, cyclobis(paraquat-*p*-phenylene) ($CBPQT^{4+}$) with its two accepting bipyridinium units—charge-transfer (CT) absorption bands are evident in the visible region of the spectrum. Excitation of these bands leads[1, 8] formally to the transfer of an electron from the donor to one of the two acceptors, thus nullifying the CT and C–H···O interactions[8] responsible for the pseudorotaxane formation in the first place. However, photochemical reduction of the bipyridinium units in $CBPQT^{4+}$ requires[1, 8] additional ingredients, such as a photosensitizer P (9-anthracenecarboxylic acid, ACA) to serve as a photoactivated reductant, and a sacrificial reagent added to prevent fast back-electron transfer. Since the emission of BHEEN is quenched when it is threaded through $CBPQT^{4+}$, the change in the emission intensity of BHEEN can be used to follow the dethreading and rethreading upon oxygenation of the solution (Scheme 1).

Our first solid-state device was prepared by condensation of a sol–gel[13] silica framework[14] around the [2]pseudorotaxane (BHEEN ⊂ $CBPQT^{4+}$), ACA (the photosensitizer), and a sacrificial reagent (ethylenediaminetetraacetate, EDTA). An aged monolithic sample (dimensions $0.8 \times 0.8 \times 3.5$ cm^3) was placed under an atmosphere of nitrogen. Light of wavelength 365 nm from a 100-W Hg lamp was used to irradiate the photosensitizer, thus reducing the $CBPQT^{4+}$ cyclophane. Molecules of BHEEN are excited by the 308-nm wavelength light from a XeCl excimer laser. The emission is monitored and used as an indicator of threading and dethreading processes. After one hour of irradiation, the initially pink sample with a charge transfer band at 520 nm becomes either clear or pale blue at the irradiated spot. The fading of the pink color indicates dissociation of the pseudorotaxane, while the appearance of the blue color comes from bipyridinium units in the cyclophane which have been reduced to radical cations. The increased emission following irradiation (Figure 1) proves that BHEEN and $CBPQT^{4+}$ have dissociated.[8] The emission intensity after 12 hours of oxidation in air decreased to its initial level as a consequence of the reformation of the pseudorotaxane. The dethreading process was roughly an order of magnitude slower in the gel than in solution, probably because of the interaction between the negatively charged pore walls of the silicate matrix and the oppositely charged tetracationic cyclophane. The spatial confinement within the nanopores could also contribute to the decrease in molecular mobility. Prolonged and localized irradiation leads to decomposition of the molecular ingredients (including the sacrificial reagent) so that the second dethreading is only 15% of that of the first under the concentration conditions of the experiment.

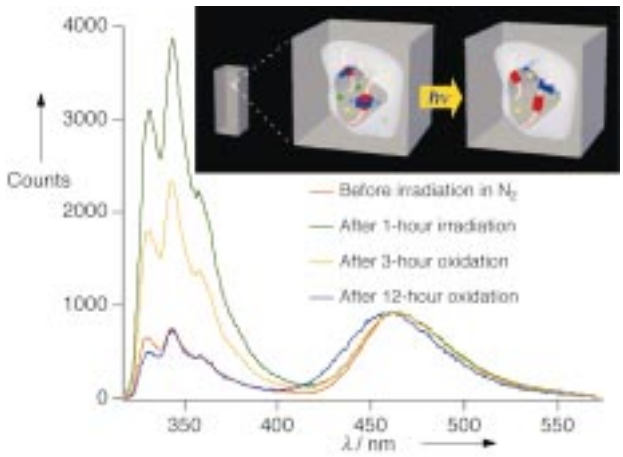

Figure 1. Illustration of a supramolecular machine in action in an interior pore of a sol–gel monolith. Shown are the emission spectra of BHEEN in the sol–gel monolith before irradiation (red), and complete (12 h, green) photoinduced reduction and dethreading of $CBPQT^{4+}$ to give free BHEEN, and following oxidation by dioxygen which diffuses through the pores and causes partial (yellow) and complete rethreading (blue). The peaks observed between 300 and 400 nm arise from BHEEN emission and that at 400 nm from the reference standard (coumarin 480). The insert shows a $0.8 \times 0.8 \times 3.5$ cm^3 transparent monolith. The magnification shows a pore (< 100 nm) containing $CBPQT^{4+}$ (blue), BHEEN (red and pink) in threaded form, together with ACA (yellow) and EDTA (green). After irradiation ($h\nu$), the pseudorotaxanes become dissociated.

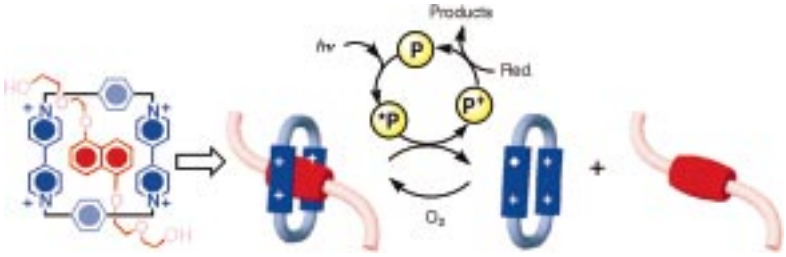

Scheme 1. Light-driven dethreading in aqueous solution of the [2]pseudorotaxane (BHEEN ⊂ $CBPQT^{4+}$) by excitation of the external photosensitizer, 9-anthracenecarboxylic acid (ACA), in the presence of a sacrificial reductant (Red. = triethanolamine). Dioxygen is used to effect rethreading. See ref. [8].

The second device we report is one involving (Figure 2) the operation of a supramolecular machine on the surface of a solid support. We reasoned that attaching the BHEEN derivative BHEEEN—which has an extra ethoxy unit in each polyether chain, one of which is terminated with a benzyl ether group[15]—onto a solid support would allow $CBPQT^{4+}$ to be captured on threading and then to be released again upon dethreading. The surfaces of the sol–gel film have silanol groups which can be treated (Scheme 2) with a suitably functionalized silicon alkoxide for subsequent molecular anchoring of the monobenzylated BHEEEN. In this investigation, we used silicon substrates that were dip-coated to give a sol–gel film of 150-nm thickness.[16] All spectra were recorded from the derivatized surface. These films were functionalized by treating the surface silanol groups with isocyanatopropyltriethoxysilane (ICPES) by using a vapor-phase reaction which is known[17] to result in the tethering of the lower boiling monomeric silane to the film.[18] The monobenzylated BHEEEN was then coupled (Scheme 2) to the isocyanate groups on the surface, which resulted in the

  1433-7851/01/4013-2448 $ 17.50+.50/0 *Angew. Chem. Int. Ed.* **2001**, *40*, No. 13

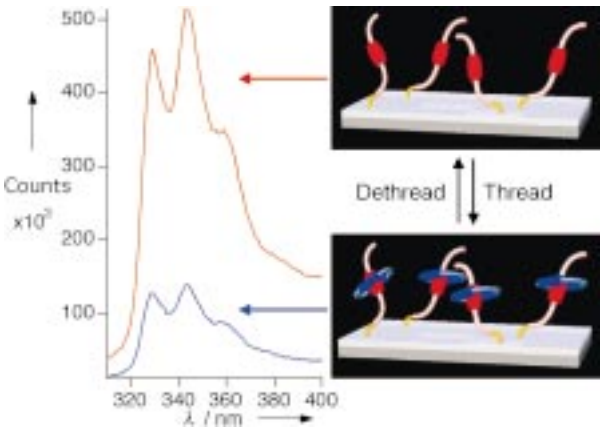

Figure 2. Illustration of the threading and dethreading of a supramolecular machine in action on a sol–gel surface. The emission spectrum (blue) arises from the small proportion of "unthreaded" monobenzylated BHEEEN after treatment of the derivatized surface with CBPQT·4Cl. The emission spectrum (red) from the surface corresponds to the increase in dethreaded monobenzylated BHEEEN following irradiation in the presence of ACA and EDTA.

formation of carbamates. The derivatized films were placed firstly in an aqueous solution of CBPQT·4Cl for two days. This immersion treatment had the effect (see T1 in Figure 3a) of reducing the emission intensity of the film at 344 nm from 100% down to 4%. The film was immersed in an aqueous solution (ca. 3.5 mL) containing ACA (ca. 30 μM) and EDTA (ca. 30 mM) and then irradiated with light of wavelength 365 nm for 2–4 hours. The observed 14% emission (see D1 in Figure 3a) is a result of the combined emission for 1) the 4% base of unthreaded units, 2) units that have been dethreaded photochemically, and 3) units that become dethreaded as a result of re-equilibration. The degree of dethreading as a result of this re-equilibration was estimated from a control experiment by soaking a separate film in water and comparing its emission intensity with that of the photochemically reduced film. Three threading and dethreading redox cycles (T1/D1–T2/D2–T3/D3; Figure 3a) are shown and the relative amounts of the photochemically induced dethreading diminish a little with each cycle. This trend could be attributed to decomposition or to the loss of the BHEEEN-containing units on prolonged irradiation and/or

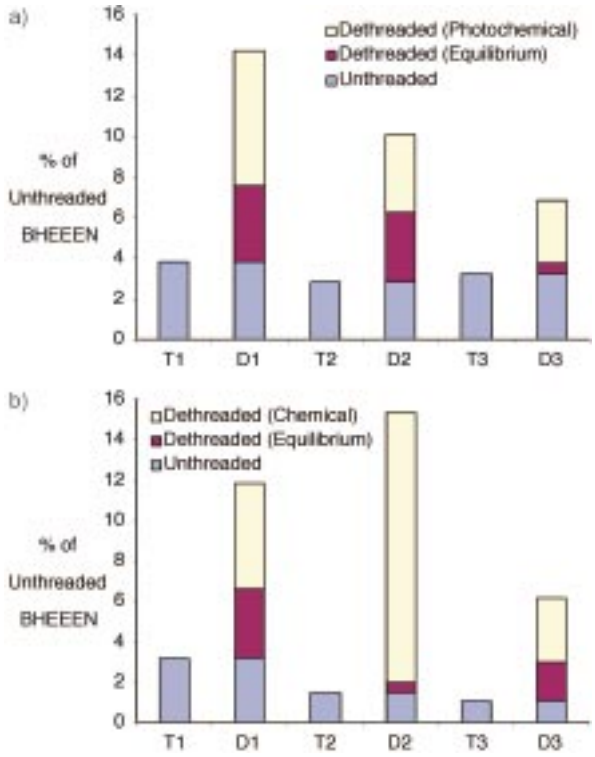

Figure 3. Histograms recording relative luminescent intensities after three sequential threading (T) and dethreading (D) cycles by supramolecular machines on a sol–gel surface. In (a) the machines are photochemically driven and in (b) they are chemically driven.

soaking. Chemical reductions with $NaBH_4$ caused (Figure 3b) dethreading of the supramolecular machines mounted on films in the same manner[19] as for the photochemical experiments.

In summary, we have trapped pseudorotaxanes in a silica monolith and mounted them on a silica film. We have also demonstrated threading and dethreading of the pseudorotaxanes in and on these solid supports. The method of attachment of machine components that we have chosen, namely, derivatization with trialkoxysilane groups, has general applicability. In principle, supramolecular machines can be attached, not only to silica, but also to oxidized silicon surfaces and many metal oxide surfaces, thus facilitating the formation of other types of superstructures and different kinds of activation, such as direct electrical reduction. The sol–gel support that we have chosen for this proof of principle also offers a lot of opportunities for fabrication. Its structure cannot only be provided in the form of macroscopic monolithic blocks or as thin films, as demonstrated here, but it can also be presented in the form of

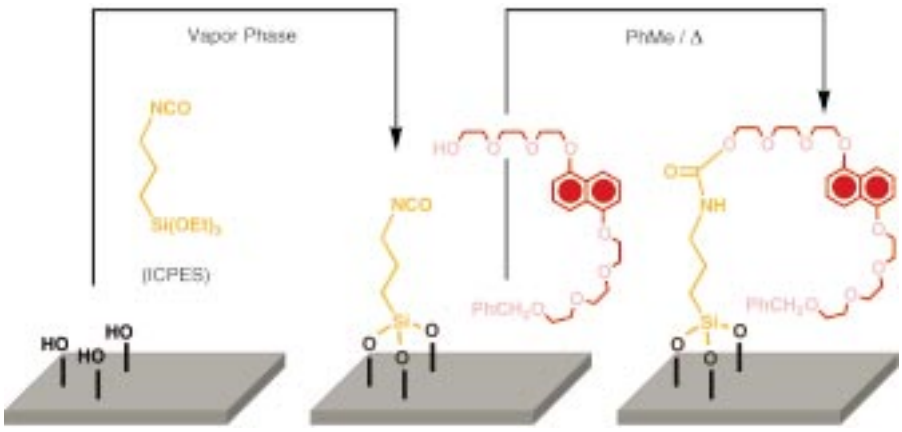

Scheme 2. The two-step procedure used to anchor monobenzylated BHEEEN onto the surface of a sol–gel film.

  1433-7851/01/4013-2449 $ 17.50+.50/0

fibres and templated porous materials with long-range order. The ability to encapsulate molecules in a synthetic framework will allow us to position the power supply, for example, a photosensitizer as the transducer, in the proximity of the machine.[20] In addition, the use of templated silica will enable ordered arrays of machines and other functional materials to be constructed.

Experimental Section

CBPQT·4 PF_6,[21] 1,5-bis[2-(2-hydroxyethoxy)ethoxy]naphthalene (BHEEN),[22] and 1,5-bis[2-(2-(2-hydroxyethoxy)ethoxy)ethoxy]naphthalene (BHEEEN)[23] were prepared as described in the literature.

The water-soluble tetracationic cyclophane CBPQT·4 Cl was obtained from its tetrakis(hexafluorophosphate) salt[21] as follows: Bu_4NCl (134 mg, 0.48 mmol) was added to a solution of CBPQT·4 PF_6 (133 mg, 0.12 mmol) in $MeNO_2$ (5 mL). The solution was stirred for 24 h at room temperature. The precipitate was filtered off and washed ($MeNO_2$) to afford CBPQT·4 Cl as a white solid (78 mg, 98 %). ^{1}H NMR (400 MHz, D_2O, 300 K): $\delta =$ 5.76 (s, 8 H), 7.53 (s, 8 H), 8.18 (d, $J = 7$ Hz, 8 H), 9.00 (d, $J = 7$ Hz, 8 H).

BHEEEN was monobenzylated as follows: BHEEEN (424 mg, 1.00 mmol) in THF (30 mL) was added to a suspension of NaH (36 mg, 1.50 mmol) in dry THF (30 mL) under Ar. The solution was stirred for 30 min at room temperature and then for a further 30 min under reflux. A solution of $PhCH_2Br$ (172 mg, 1.00 mmol) in THF (20 mL) was added dropwise during 15 min and then the reaction mixture was heated under reflux for 12 h. It was then cooled and MeOH (5 mL) was added. The solvents were removed and the oily residue was dissolved in CH_2Cl_2 (50 mL) before being washed with saturated aqueous Na_2CO_3 solution (2 × 50 mL) and H_2O (2 × 50 mL). The organic layer was dried ($MgSO_4$), filtered, and the CH_2Cl_2 was removed under vacuum. The resulting oil was subjected to column chromatography on silica gel using MeOH/EtOAc (5/95) as the eluant to afford a yellow oil of monobenzylated BHEEEN (235 mg, 46 %). ^{1}H NMR (360 MHz, $CDCl_3$, 300 K): $\delta = 2.89$ (br s, 1 H), 3.55 – 3.68 (m, 12 H), 3.72 – 3.77 (m, 4 H), 3.90 – 3.95 (m, 4 H), 4.22 (t, $J = 5$ Hz, 4 H), 4.52 (s, 2 H), 6.78 (d, $J = 8$ Hz, 2 H), 7.23 – 7.34 (m, 7 H), 7.84 – 7.87 (dd, $J = 3$, 8 Hz, 2 H); ^{13}C NMR (90 MHz, $CDCl_3$, 300 K): $\delta = 61.4$, 63.0, 67.0, 68.9, 69.2, 69.5, 70.3, 71.0, 72.3, 72.9, 105.4, 114.3, 124.8, 125.7, 126.5, 127.2, 128.0, 138.0, 154.0, 154.1; liquid secondary ion MS (LSI-MS): m/z: 515 $[M+H]^+$; elemental analysis calcd (%) for $C_{29}H_{38}O_8$ (514.26): C 67.70, H 7.39; found: C 67.18, H 7.21.

The silicate sol was prepared by stirring a mixture of tetraethylorthosilicate, EtOH, H_2O, and HCl (molar ratios: $1/4/16/8 \times 10^{-4}$) at 70 °C for 1 h. BHEEN (40 μL, 1 mM in EtOH), CBPQT·4 Cl (40 μL, 1 mM in H_2O), ACA (4 μL, 1 mM in EtOH), and EDTA (0.1 M, 0.4 mL in H_2O) were added to the silicate sol (2 mL) in distilled H_2O (1.52 mL). The mixture was allowed to gel in a sealed polystyrene cuvette (1 × 1 × 4 cm) for 1 week. The seal was punctured to allow slow evaporation of the solvent over 2 weeks, which resulted in an aged monolithic sample ($\sim 0.8 \times 0.8 \times 3.5$ cm^3).

The sol – gel silica films were prepared by dip-coating silicon substrates with the sol mixture,[16] followed by sintering. The silicon substrates were cut into 1-cm wide strips and cleaned using a H_2O_2/H_2SO_4 (1/4 by volume) solution, followed by rinsing with boiling H_2O. The films were loaded into an apparatus similar to the one described in ref. [17] and then heated to 120 °C for 1 h under a dynamic vacuum. ICPES (1 mL) and dry PhMe (20 mL) were added to the apparatus under N_2. The reaction mixture was heated under reflux for 6 h. The functionalized films were soaked in PhMe for 1 day to remove free ICPES. The monobenzylated BHEEEN was coupled to the functionalized films by heating the monobenzyl derivative (40 μL) of BHEEEN in PhMe (25 mL) for 4 h. The films were then rinsed with PhMe and H_2O, followed by soaking in H_2O for 1 day prior to carrying out any threading – dethreading experiments.

Received: March 19, 2001 [Z 16786]

[1] a) V. Balzani, A. Credi, F. M. Raymo, J. F. Stoddart, *Angew. Chem.* **2000**, *112*, 3484 – 3530; *Angew. Chem. Int. Ed.* **2000**, *39*, 3348 – 3391; b) R. Ballardini, V. Balzani, A. Credi, M. T. Gandolfi, M. Venturi, *Acc. Chem. Res.* **2001**, *34*, 445 – 455.

[2] a) J. S. Lindsey, *New J. Chem.* **1991**, *15*, 153 – 180; b) D. Philp, J. F. Stoddart, *Synlett* **1991**, 445 – 458; c) D. Philp, J. F. Stoddart, *Angew. Chem.* **1996**, *108*, 1242 – 1286; *Angew. Chem. Int. Ed. Engl.* **1996**, *35*, 1155 – 1196; d) M. C. T. Fyfe, J. F. Stoddart, *Acc. Chem. Res.* **1997**, *30*, 393 – 401; e) L. F. Lindoy, I. M. Atkinson, *Self-Assembly in Supramolecular Systems* (Ed.: J. F. Stoddart), Royal Society of Chemistry, Cambridge, **2000**.

[3] For an impressive example of a real-space observation of single-molecule (hexa-*tert*-butyldecacyclene) rotors surrounded by like molecules that form a supramolecular bearing on an atomically clean Cu(100) surface, see J. K. Gimzewski, C. Joachim, R. R. Schlitter, V. Langlais, H. Tang, I. Johannsen, *Science* **1998**, *281*, 531 – 533.

[4] Pseudorotaxanes are complexes (supermolecules) that resemble rotaxanes by virtue of being comprised of wheel-like and axle-like components, but their components are free to dissociate from each other; see P. R. Ashton, D. Philp, N. Spencer, J. F. Stoddart, *J. Chem. Soc. Chem. Commun.* **1991**, 1677 – 1679.

[5] We have advocated the use of the term co-conformation to designate the different three-dimensional spatial arrangements of the constituent parts in supramolecular systems, for example, pseudorotaxanes; see M. C. T. Fyfe, P. T. Glink, S. Menzer, J. F. Stoddart, A. J. P. White, D. J. Williams, *Angew. Chem.* **1997**, *109*, 2158 – 2160; *Angew. Chem. Int. Ed. Engl.* **1997**, *36*, 2068 – 2070.

[6] a) M. Asakawa, S. Iqbal, J. F. Stoddart, N. D. Tinker, *Angew. Chem.* **1996**, *108*, 1054 – 1056; *Angew. Chem. Int. Ed. Engl.* **1996**, *35*, 976 – 978; b) A. Credi, V. Balzani, S. J. Langford, J. F. Stoddart, *J. Am. Chem. Soc.* **1997**, *119*, 2679 – 2681; c) A. Credi, M. Montalti, V. Balzani, S. J. Langford, F. M. Raymo, J. F. Stoddart, *New J. Chem.* **1998**, *22*, 1061 – 1065; d) E. Ishow, A. Credi, V. Balzani, F. Spadola, L. Mandolini, *Chem. Eur. J.* **1999**, *5*, 984 – 989; e) V. Balzani, A. Credi, G. Mattersteig, O. A. Matthews, F. M. Raymo, J. F. Stoddart, A. J. P. White, D. J. Williams, *J. Org. Chem.* **2000**, *65*, 1924 – 1936; f) V. Balzani, P. Ceroni, A. Credi, M. Gómez-López, C. Hamers, J. F. Stoddart, R. Wolf, *New J. Chem.* **2001**, *25*, 25 – 31.

[7] a) A. Mirzoian, A. E. Kaifer, *Chem. Eur. J.* **1997**, *3*, 1052 – 1057; b) P. R. Ashton, V. Balzani, J. Becher, A. Credi, M. C. T. Fyfe, G. Mattersteig, S. Menzer, M. B. Nielsen, F. M. Raymo, J. F. Stoddart, M. Venturi, D. J. Williams, *J. Am. Chem. Soc.* **1999**, *121*, 3951 – 3957; c) V. Balzani, J. Becher, A. Credi, M. B. Nielsen, F. M. Raymo, J. F. Stoddart, A. M. Talarico, M. Venturi, *J. Org. Chem.* **2000**, *65*, 1947 – 1956; d) for a really fine account of the emerging field of supramolecular electrochemistry, see A. E. Kaifer, M. Gómez-Kaifer, *Supramolecular Electrochemistry*, Wiley-VCH, Weinheim, **1999**.

[8] a) R. Ballardini, V. Balzani, M. T. Gandolfi, L. Prodi, M. Venturi, D. Philp, H. G. Ricketts, J. F. Stoddart, *Angew. Chem.* **1993**, *105*, 1362 – 1364; *Angew. Chem. Int. Ed. Engl.* **1993**, *32*, 1301 – 1303; b) P. R. Ashton, R. Ballardini, V. Balzani, S. E. Boyd, A. Credi, M. T. Gandolfi, M. Gómez-López, S. Iqbal, D. Philp, J. A. Preece, L. Prodi, H. G. Ricketts, J. F. Stoddart, M. S. Tolley, M. Venturi, A. J. P. White, D. J. Williams, *Chem. Eur. J.* **1997**, *3*, 152 – 170.

[9] a) P. R. Ashton, R. Ballardini, V. Balzani, E. C. Constable, A. Credi, O. Kocian, S. J. Langford, J. A. Preece, L. Prodi, E. R. Schofield, N. Spencer, J. F. Stoddart, S. Wenger, *Chem. Eur. J.* **1998**, *4*, 2413 – 2422; b) P. R. Ashton, V. Balzani, O. Kocian, L. Prodi, N. Spencer, J. F. Stoddart, *J. Am. Chem. Soc.* **1998**, *120*, 11190 – 11191.

[10] a) A. C. Benniston, A. Harriman, D. Philp, J. F. Stoddart, *J. Am. Chem. Soc.* **1993**, *115*, 5298 – 5299; b) A. C. Benniston, A. Harriman, D. S. Yufit, *Angew. Chem.* **1997**, *109*, 2451 – 2454; *Angew. Chem. Int. Ed. Engl.* **1997**, *36*, 2356 – 2358; c) A. C. Benniston, A. Harriman, V. M. Lynch, *J. Am. Chem. Soc.* **1995**, *117*, 5275 – 5291; d) M. Seiler, H. Dürr, I. Willner, E. Joselevich, A. Doren, J. F. Stoddart, *J. Am. Chem. Soc.* **1994**, *116*, 3399 – 3404; e) M. Kropf, E. Joselevich, H. Dürr, I. Willner, *J. Am. Chem. Soc.* **1996**, *118*, 655 – 665; f) E. David, R. Born, E. Kaganer, E. Joselevich, H. Dürr, I. Willner, *J. Am. Chem. Soc.* **1997**, *119*, 7778 – 7790.

[11] For examples of Langmuir films of pseudorotaxanes, see a) R. C. Ahuja, P.-L. Caruso, D. Möbius, G. Wildburg, H. Ringsdorf, D. Philp, J. A. Preece, J. F. Stoddart, *Langmuir* **1993**, *9*, 1534 – 1544; b) R. C. Ahuja, P.-L. Caruso, D. Möbius, D. Philp, J. A. Preece, H. Ringsdorf, J. F. Stoddart, G. Wildburg, *Thin Solid Films* **1996**, *284/285*, 671 – 677.

  1433-7851/01/4013-2450 $ 17.50+.50/0

[12] For recent examples of supramolecular systems deposited on surfaces, see a) P. Laitenberger, C. G. Claissens, L. Kuipers, F. M. Raymo, R. E. Palmer, J. F. Stoddart, *Chem. Phys. Lett.* **1997**, *279*, 209–214; b) G. Ashkenasy, G. Kalyuzhny, J. Libman, I. Rubenstein, A. Shanzer, *Angew. Chem.* **1999**, *111*, 1333–1336; *Angew. Chem. Int. Ed.* **1999**, *38*, 1257–1261; c) M. Lahav, L. Leiserowitz, *Angew. Chem.* **1999**, *111*, 2691–2694; *Angew. Chem. Int. Ed.* **1999**, *38*, 2533–2536; d) A. Semenov, J. P. Spatz, M. Müller, J.-M. Lehn, B. Sell, D. Schubert, C. H. Weidl, U. S. Schubert, *Angew. Chem.* **1999**, *111*, 2701–2705; *Angew. Chem. Int. Ed.* **1999**, *38*, 2547–2550; e) N. Bampos, C. N. Woodburn, M. E. Welland, J. K. M. Sanders, *Angew. Chem.* **1999**, *111*, 2949–2953; *Angew. Chem. Int. Ed.* **1999**, *38*, 2780–2783; f) H. Imahori, H. Yamada, S. Ozawa, K. Ushida, Y. Sakata, *Chem. Commun.* **1999**, 1165–1166; g) D. Ryan, S. N. Rao, H. Rensmo, D. Fitzmaurice, J. A. Preece, S. Wenger, J. F. Stoddart, N. Zaccheroni, *J. Am. Chem. Soc.* **2000**, *122*, 6252–6257; h) M. Lahav, A. N. Shipway, I. Willner, M. B. Nielsen, J. F. Stoddart, *J. Electroanal. Chem.* **2000**, *482*, 217–221; i) G. Cooke, F. M. A. Duclairoir, V. M. Rotello, J. F. Stoddart, *Tetrahedron Lett.* **2000**, *41*, 8163–8166.

[13] C. J. Brinker, G. W. Scherer, *Sol–Gel Science*, Academic Press, San Diego, **1990**.

[14] A silica sol–gel provides a stable transparent matrix for encapsulating molecules physically in a macroscopic solid; see a) B. Dunn, J. I. Zink, *Chem. Mater.* **1997**, *9*, 2280–2291; b) D. Avnir, *Acc. Chem. Res.* **1995**, *28*, 328–334; c) B. Dunn, J. I. Zink, *J. Mater. Chem.* **1991**, *1*, 903–913. The sol–gel process is a synthetic technique for preparing oxide gels, glasses, and inorganic compounds at far lower temperatures than is possible by conventional synthesis. The approach is based on the hydrolysis and condensation of molecular precursors such as metal alkoxides. It has received considerable attention because it possesses a number of desirable characteristics in terms of producing materials of high purity and excellent homegeneity. Moreover, since the sol–gel approach is a solution-based method, it is readily adaptable to producing thin films and fibres as well as bulk materials. The flexible solution chemistry associated with the synthesis of sol–gels makes it possible to incorporate a large variety of organic molecules in the inorganic oxide matrix. The optical properties of the molecular dopants are then imparted upon the solid derived from the sol–gel. Hence this process gives rise to a large number of materials with interesting and unique properties. The interconnected nanopores in sol–gels are filled with liquid which can provide supramolecular machines with a local solution environment in which large molecular movements (co-conformational changes) can be performed, with the silicate framework providing the macroscopic support. The silicate matrix is also transparent to visible light and this transparency makes it possible to study a photoactivated system inside its pores.

[15] This particular BHEEEN derivative with four oxygen atoms present in each of its polyether chains is well suited to maximizing the C–H···O interactions with $CBPQT^{4+}$; see M. Asakawa, W. Dehaen, G. L'abbé, S. Menzer, J. Nouwen, F. M. Raymo, J. F. Stoddart, D. J. Williams, *J. Org. Chem.* **1996**, *61*, 9591–9595.

[16] a) M. H. Huang, H. M. Soyez, B. Dunn, J. I. Zink, *Chem. Mater.* **2000**, *12*, 231–235; b) F. Nishida, J. McKiernan, B. Dunn, J. I. Zink, C. J. Brinker, A. J. Hurd, *J. Am. Ceram. Soc.* **1995**, *78*, 1640–1648.

[17] I. Haller, *J. Am. Chem. Soc.* **1978**, *100*, 8050–8055.

[18] The derivatization of the silica surface by using monomeric ICPES is important as the first step in the anchoring of the monobenzylated BHEEEN derivative. If this derivative is treated first of all with ICPES prior to silanization, then undesired oligomers are formed on the silica surface.

[19] The derivatized films were immersed in an aqueous solution of $CBPQT\cdot 4Cl$ for two days. The residual percentage (ca. 3.4%) of unthreaded BHEEEN is shown by T1 in Figure 3b. Dethreading, was effected by immersing the film in an aqueous solution (ca. 4 mL) of $NaBH_4$ (ca. 2 nM) for 2–3 h. The resulting luminescent intensity is shown in D1 in Figure 3b. Threading and dethreading was demonstrated over three redox cycles, namely, T1/D1–T2/D2–T3/D3.

[20] Ordered arrays of molecular motors are essential to the life of a cell; see a) R. A. Cross, *Nature* **2000**, *406*, 839–840; b) T. Hasson, R. E. Cheney, *Curr. Opin. Cell Biol.* **2001**, *13*, 29–35.

[21] P.-L. Anelli, P. R. Ashton, R. Ballardini, V. Balzani, M. Delgado, M. T. Gandolfi, T. T. Goodnow, A. E. Kaifer, D. Philp, M. Pietraszkiewicz, L. Prodi, M. V. Reddington, A. M. Z. Slawin, N. Spencer, J. F. Stoddart, C. Vicent, D. J. Williams, *J. Am. Chem. Soc.* **1992**, *114*, 193–218.

[22] D. B. Amabilino, P.-L. Anelli, P. R. Ashton, G. R. Brown, E. Córdova, L. A. Godinez, W. Hayes, A. E. Kaifer, D. Philp, A. M. Z. Slawin, N. Spencer, J. F. Stoddart, M. S. Tolley, D. J. Williams, *J. Am. Chem. Soc.* **1995**, *117*, 11142–11170.

[23] P. R. Ashton, J. Huff, S. Menzer, I. W. Parsons, J. A. Preece, J. F. Stoddart, M. S. Tolley, A. J. P. White, D. J. Williams, *Chem. Eur. J.* **1996**, *2*, 31–44.

Helical Superstructures of a C_2-Symmetric Molecule Exhibiting Strong Second Harmonic Generation in the Solid-State**

P. Gangopadhyay and T. P. Radhakrishnan*

The design of molecular materials for quadratic nonlinear optical (NLO) applications involves optimization of the structure at both the molecular and the materials level.[1] Molecular design aims at the maximization of the hyperpolarizability (β) as well as the incorporation of structural features that facilitate suitable assembly in the bulk phase. The latter features include hydrogen-bonding functionalities,[2] ionic groups,[3] optimally long alkyl chains,[4] and chirality.[5, 6] Of these, only chirality ensures noncentrosymmetric organization, an essential prerequisite for the observation of quadratic NLO effects. However, even though the basic symmetry requirement is satisfied, efficient exploitation of the inherently strong molecular nonlinear response is rarely achieved at the bulk level. An exceptionally successful case is that of *N*-4-nitrophenyl-(*S*)-prolinol (NPP).[6] We previously investigated the strategic placement of stereogenic centers in push-pull quinonoid molecules to achieve enhanced second harmonic generation (SHG).[7] A logical extension of this study is that an axial chiral system having a strong β component coincident with the symmetry axis would be a promising candidate. We also envisaged that C_2-symmetric molecules could potentially form helical assemblies, the chirality of which extends over the whole molecular superstructure. Recent studies have demonstrated enhanced NLO effects arising from supramolecular chirality in polymers,[8] mesoscopic systems,[9] and Langmuir–Blodgett films.[10] Helical

[*] Dr. T. P. Radhakrishnan, P. Gangopadhyay
School of Chemistry
University of Hyderabad
Hyderabad—500046 (India)
Fax: (+91) 40-3012460
E-mail: tprsc@uohyd.ernet.in

[**] Financial support from the DST (Swarnajayanti Fellowship) and the use of the National Single Crystal Diffractometer Facility (funded by the DST at the School of Chemistry, University of Hyderabad) are gratefully acknowledged. P.G. thanks the University Grants Commission for a senior research fellowship. We thank du Pont Deutschland for a generous gift of 1,2-diaminocyclohexane.

Supporting information for this article is available on the WWW under http://www.angewandte.com or from the author.

molecules with large hyperpolarizability have been studied computationally and experimentally.[11] There has been continued interest in the design of helical assemblies of metal complexes[12] and organic molecules.[13] However, to the best of our knowledge, there has been no demonstration of strong SHG in the solid state in structurally characterized organic molecular crystals built up of helical supramolecular assemblies. We have now realized this using the C_2-symmetric *N*,*N*′-bis(4-nitrophenyl)-(1*R*,2*R*)-diaminocyclohexane (BNDC).

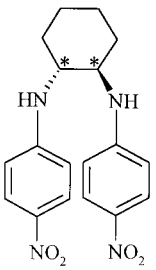

BNDC

There is a brief report of weak SHG observed in the related compound having only one 4-nitrophenyl group,[14] although no structural information is available. We have prepared the bis-substituted product by the reaction of 1,2-diaminocyclohexane with 4-fluoronitrobenzene in the presence of K_2CO_3 in DMSO. Initially we investigated the racemic material, *rac*-BNDC; interestingly it has a noncentrosymmetric crystal structure (Table 1)[15] with molecular tapes generated through intermolecular H-bonds (Figure 1), and exhibits weak SHG in a Kurtz–Perry experiment.[16] The 1*R*,2*R* enantiomer was prepared from carefully isolated, enantiomerically pure (1*R*,2*R*)-diaminocyclohexane. Crystallization of BNDC is found to be very sensitive to the solvent and growth conditions; extensive polymorphism occurs. Crystals grown from ethyl acetate, methanol, and acetone had different platelike morphologies and unit cells. Different batches of crystals from ethyl acetate alone showed two distinct, though very similar, unit cells. Microcrystalline powders of the various crystals showed SHG in the range 5–20 U. We have investigated the crystal structure of thin, long plates of BNDC grown from ethyl acetate (Table 1). They belong to the $P2_12_12_1$ space group, with one molecule in the asymmetric unit. Two types of intermolecular N–H···O interactions lead to the formation of helical assemblies with different pitches that extend along the three crystallographic axes (Figure 2). The helices oriented along the *a* and *b* axes are *M* (left-handed), whereas the one along the *c* axis is *P* (right-handed). Since the orthogonally oriented helices with different handedness do not lead to strong SHG, we explored other solvent systems for crystallization in an effort to produce a lattice structure with helical motifs of a single handedness that are oriented in one direction.

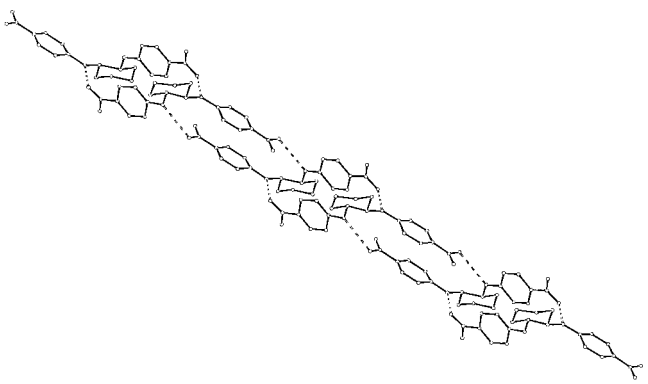

Figure 1. H-bonded tape structure in *rac*-BNDC obtained from a single-crystal X-ray analysis. The alternating molecules are enantiomers. The H-bonds are shown by broken lines.

Crystals with a distinct prismatic morphology different from the earlier cases could be grown from mixtures of ethyl acetate (ea)/hexane and pentan-3-one (diethyl ketone, dek)/hexane. Spectroscopic characterizations indicated the inclusion of solvent molecules, and hence these crystals were labeled as BNDC.ea and BNDC.dek, respectively. Freshly grown crystals show strong SHG (Table 1). However, loss of solvent is observed over a period of a few days leading to opaque crystals or powders with diminished SHG capabilities which melt at 200–204 °C. X-ray investigations showed that both crystals belong to the $C222_1$ space group and have similar cell dimensions (Table 1) and identical lattice structures. The asymmetric unit consists of a half molecule each of BNDC and the solvent; a C_2 operation generates the other halves. The BNDC molecules form *M*-helices that extend solely along the *c* axis, with disordered solvent molecules in the helical channels. Both the nitro and amino groups are involved in noncovalent interactions between the BNDC molecules, thus ruling out any strong interactions with the solvent molecules. Since no weak interactions are found either, we carried out crystallizations from pentan-2,4-dione (acetyl acetone, acac) to take advantage of the possible weak interactions between the solvent molecules and BNDC.

Table 1. Significant crystallographic data and powder SHG capability of the various crystals.[a]

	rac-BNDC	BNDC	BNDC·ea	BNDC·dek	BNDC·acac
formula of asymmetric unit	$C_{36}H_{40}N_8O_8$	$C_{18}H_{20}N_4O_4$	$C_{11}H_{14}N_2O_3$	$C_{11.5}H_{15}N_2O_{2.5}$	$C_{11.5}H_{14}N_2O_3$
space group	$P2_1$	$P2_12_12_1$	$C222_1$	$C222_1$	$C222_1$
a [Å]	10.210(4)	10.2375(19)	11.793(2)	12.084(2)	12.3650(11)
b [Å]	15.34(2)	12.827(2)	15.737(3)	15.847(3)	15.8963(10)
c [Å]	11.933(3)	13.662(9)	12.750(4)	12.935(3)	12.5817(9)
β [°]	109.43(3)	90	90	90	90
V [Å^3]	1762(3)	1794.0(13)	2366.1(10)	2477.0(9)	2473.0(3)
Z	2	4	8	8	8
no. of refl. with	$I \geq \sigma_I$ 3104	$I \geq \sigma_I$ 1813	$I \geq \sigma_I$ 1190	$I \geq 2\sigma_I$ 1287	$I \geq \sigma_I$ 1221
total no. of param.	469	235	156	150	159
$R(I \geq 2\sigma_I)$	0.0453	0.0454	0.0514	0.0689	0.0446
SHG	6 U	20 U	0.93 NPP	1.01 NPP	1.15 NPP

[a] 1 U = SHG of urea with an average particle size ≥150 μm, 1 NPP = SHG of NPP with an average particle size ≥175 μm (our calibration measurements gave 1 NPP = 115 U; reported values for NPP are in the range 50–150 U.[5, 6, 14]

  1433-7851/01/4013-2452 $ 17.50+.50/0 *Angew. Chem. Int. Ed.* **2001**, *40*, No. 13

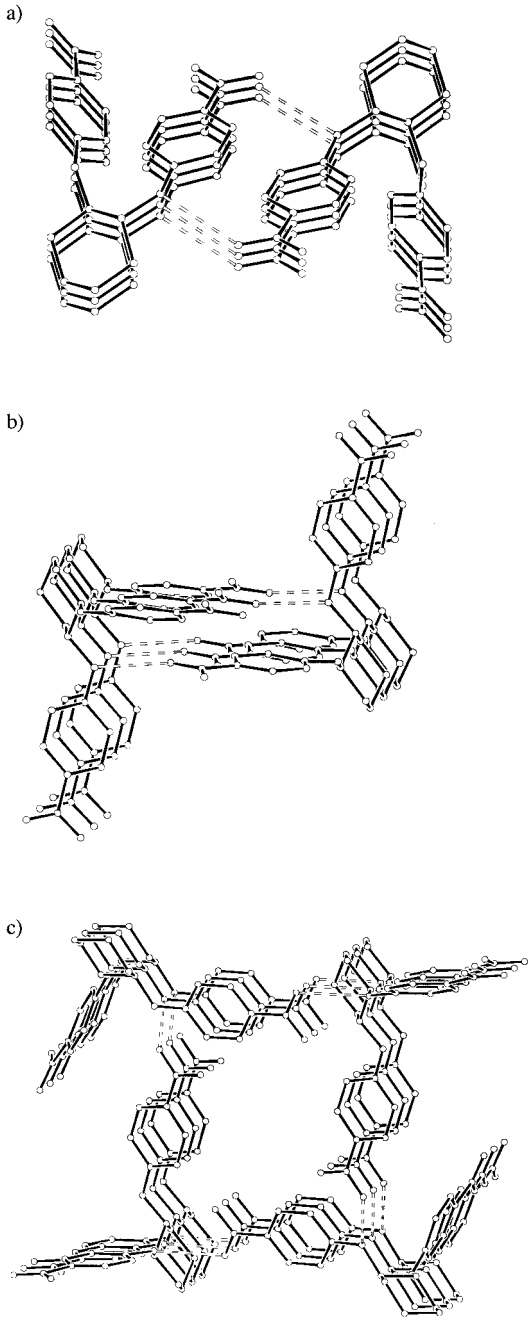

Figure 2. Helical superstructures in BNDC obtained from single-crystal X-ray analysis: view along the helical axis parallel to the *a* (a), *b* (b), and *c* axes (c). The H-bonds are shown by broken lines.

Prismatic crystals were grown by diffusion of hexane into a solution of BNDC in acetyl acetone. The BNDC.acac crystals are found to be considerably more stable than the earlier two toward solvent loss at room temperature; when heated the crystals show a shrinkage at 130–135 °C as a consequence of solvent expulsion, and then melt at 202 °C. Strong SHG, which is stable over several weeks, is observed in the crystals, and a powder study showed a phase-matchable SHG 1.15 times that of NPP (Table 1). An X-ray study once again showed a $C222_1$ space group with cell dimensions and molecular structure similar to BNDC.ea and BNDC.dek, and with an identical lattice structure. The C_2-symmetric BNDC molecules assemble into a beautiful *M*-helix extending along the *c* axis (Figure 3a, b) and with a dipolar interaction between the nitro groups of neighboring molecules. N–O bonds of adjacent molecules are oriented in an antiparallel

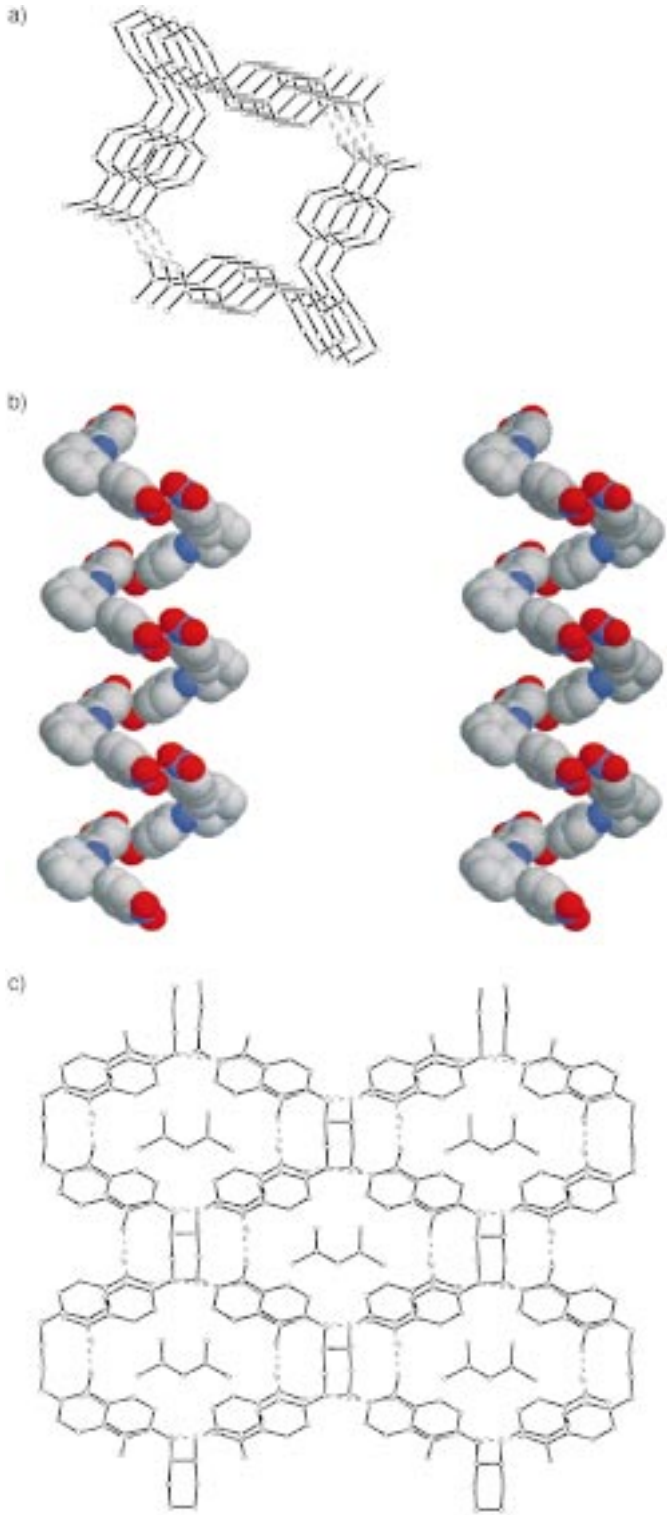

Figure 3. The helical superstructure in BNDC.acac obtained from a single-crystal X-ray analysis: a) view along the helical axis (*c* axis), and b) stereo-view perpendicular to the helical axis (space-filling representation). Solvent molecules are omitted for clarity. c) View of the packing of helical channels (projection onto the *ab* plane) including the solvent molecules. The H-bonds and interactions of the nitro groups are shown by broken lines.

  1433-7851/01/4013-2453 $ 17.50+.50/0

manner to form a gently twisted parallelogram with sides of length 1.230 Å (N–O) and 3.175 Å (nonbonded N···O), and angles of 105.1° (N-O···N) and 73.6° (O-N···O). The helical superstructures assemble to form the lattice shown in Figure 3c through formation of intermolecular H-bonds between the amino and nitro groups, with an N···O distance of 3.003 Å and an N-H···O angle of 143.9°. The two oxygen atoms of the nitro group participate in the dipolar and H-bonding interactions, respectively. The acetyl acetone solvent molecules exist in the helical channels; unlike the earlier two cases, there is no sign of disorder. The central carbon atom lies on the C_2 axis and the bond lengths clearly indicate an enol structure. Several weak H-bonding interactions are observed between the central sp^2 carbon atom of acetyl acetone and the amino nitrogen and the phenyl ring carbon atoms on the BNDC molecule in its vicinity (the shortest C···N and C···C distances are 3.733 and 3.623 Å, respectively). The oxygen atoms of acetyl acetone also show weak interactions with some of the phenyl ring carbon atoms of BNDC (the shortest C···O distances are 3.612 and 3.855 Å). The cooperative effect of these interactions appears to stabilize the solvent molecules in the helical channels.

The asymmetric unit in BNDC·acac (as well as the other two solvated ones) is the half molecule *N*-alkyl-4-nitroaniline. Taking into account its orientation with respect to the crystal axes we have used the oriented gas model[17] to estimate the effective susceptibility coefficient b_{XYZ} (notation of ref. [17]) as 0.151. This value is smaller than the theoretical limit of 0.192 for the 222 point group, but is higher than the value in the well-known NLO crystal 3-methyl-4-nitropyridine-1-oxide (POM)[18] and may be contrasted with the b_{YXX} value of 0.380 in NPP.[6] We have estimated the hyperpolarizability of the half unit of the BNDC molecule at 1.17 eV to be 23.7×10^{-30} esu by using semiempirical AM1/TDHF[19] computation on the full molecule and by assuming a vectorial addition of the contributions of the half units (calculated β tensor components show that the usual 1D model is appropriate for BNDC as well as the half unit). The $\beta_{1.17}$ value of NPP from AM1/TDHF calculations is 29.2×10^{-30} esu; the experimental value[20] is $42 \pm 9 \times 10^{-30}$ esu. In the absence of any information at the moment on the local field factors and phase-matching conditions in BNDC·acac, we assume these factors to be similar to those in NPP. The approximate ratio of the effective susceptibilities of BNDC·acac:NPP then works out to be 0.32:1, which implies a ratio of 0.1:1 between the SHGs of the powders (for details see the Supporting Information). Even if allowance is made for error margins on this estimate, the observed powder SHG of BNDC·acac which is comparable to that of NPP and is very much larger than is suggested by the ratio above. The discrepancy may be traced to one of the following effects in BNDC·acac: the modification of local field factors leading to enhanced bulk susceptibility; an optimal combination of the phase-matching conditions;[16] or the extended helical superstructure giving rise to an enhancement of the β value over that calculated for a single molecule. In view of the basic NLO chromophore being the traditional 4-nitroaniline moiety and the recent demonstrations of enhanced nonlinearity in aggregate structures,[8–10] the helical superstructure appears to be the most probable cause of the enhanced SHG in BNDC·acac. A complete resolution of this question has to await single-crystal SHG measurements for which large enough crystals are not as yet available.

The BNDC crystals illustrate the facile formation of helical supramolecular assemblies from simple building blocks. An examination of the relation between the solvent of crystallization and the superstructures formed is instructive. Crystallization from ethyl acetate resulted in the mutually orthogonal helical motifs assembled solely through the formation of H-bonds. The addition of nonpolar hexane to ethyl acetate led to the realization of dipolar interactions of the nitro group and the single helical motif. Retention of the solvent molecules is critically dependent on their capability to enter into weak noncovalent interactions with the channel walls. These observations provide a basis for further exploration of these helical architectures. The robust channel structure, which accommodates different solvent molecules, suggests the possibility of incorporating a variety of active species in a chiral environment. The strong SHG together with the thermal stability and versatility of the structural framework points to the potential of helical superstructures in the design of efficient molecular NLO materials.

Received: January 15, 2001
Revised: April 5, 2001 [Z16422]

[1] a) J. Zyss, D. S. Chemla in *Nonlinear Optical Properties of Organic Molecules and Crystals*, *Vol. 1* (Eds.: D. S. Chemla, J. Zyss), Academic Press, New York, **1989**, p. 23; b) N. J. Long, *Angew. Chem.* **1995**, *107*, 37; *Angew. Chem. Int. Ed. Engl.* **1995**, *34*, 21; c) J. Zyss, J. F. Nicoud, *Curr. Opin. Solid State Mater. Sci.* **1996**, *1*, 533.
[2] a) C. Serbutoviez, J. F. Nicoud, J. Fischer, I. Ledoux, J. Zyss, *Chem. Mater.* **1994**, *6*, 1358; b) K. Huang, D. Britton, M. C. Etter, S. R. Byrn, *J. Mater. Chem.* **1995**, *5*, 379.
[3] S. R. Marder, J. W. Perry, W. P. Schaefer, *Science* **1989**, *245*, 626.
[4] a) P. Gangopadhyay, S. Sharma, A. J. Rao, D. N. Rao, S. Cohen, I. Agranat, T. P. Radhakrishnan, *Chem. Mater.* **1999**, *11*, 466; b) P. Gangopadhyay, T. P. Radhakrishnan, *Chem. Mater.* **2000**, *12*, 3362.
[5] D. F. Eaton, *Science* **1991**, *253*, 281.
[6] J. Zyss, J. F. Nicoud, M. Coquillay, *J. Chem. Phys.* **1984**, *81*, 4160.
[7] M. Ravi, D. N. Rao, S. Cohen, I. Agranat, T. P. Radhakrishnan, *Chem. Mater.* **1997**, *9*, 830.
[8] M. Kauranen, T. Verbiest, C. Boutton, M. N. Teerenstra, K. Clays, A. J. Schouten, R. J. M. Nolte, A. Persoons, *Science* **1995**, *270*, 966.
[9] K. Clays, E. Hendrickx, T. Verbiest, A. Persoons, *Adv. Mater.* **1998**, *10*, 643.
[10] a) T. Verbiest, S. V. Elshocht, M. Kauranen, L. Hellemans, J. Snauwaert, C. Nuckolls, T. J. Katz, A. Persoons, *Science* **1998**, *282*, 913; b) S. V. Elshocht, T. Verbiest, M. Kauranen, L. Ma, H. Cheng, K. Y. Musick, L. Pu, A. Persoons, *Chem. Phys. Lett.* **1999**, *309*, 315.
[11] a) M. Panda, J. Chandrasekhar, *J. Am. Chem. Soc.* **1998**, *120*, 13517; b) H.-J. Deussen, E. Hendrickx, C. Boutton, D. Krog, K. Clays, K. Bechgaard, A. Persoons, T. Bjørnholm, *J. Am. Chem. Soc.* **1996**, *118*, 6841.
[12] a) B. F. Abrahams, S. R. Batten, H. Hamit, B. F. Hoskins, R. Robson, *Chem. Commun.* **1996**, 1313; b) C. Piguet, G. Bernardinelli, G. Hopfgartner, *Chem. Rev.* **1997**, *97*, 2005; c) H. C. Aspinall, J. F. Bickley, J. L. M. Dwyer, N. Greeves, A. Steiner, *Angew. Chem.* **2000**, *112*, 2980; *Angew. Chem. Int. Ed.* **2000**, *39*, 2858.
[13] a) T. B. Norsten, R. McDonald, N. R. Branda, *Chem. Commun.* **1999**, 719; b) J. R. Koe, M. Fujiki, M. Motonaga, H. Nakashima, *Chem. Commun.* **2000**, 389; c) J. H. K. K. Hirschberg, L. Brunsveld, A. Ramzi, J. A. J. M. Vekemans, R. P. Sijbesma, E. W. Meijer, *Nature* **2000**, *407*, 167.

  1433-7851/01/4013-2454 $ 17.50+.50/0

[14] J. F. Nicoud, R. J. Twieg in *Nonlinear Optical Properties of Organic Molecules and Crystals*, *Vol. 2* (Eds.: D. S. Chemla, J. Zyss), Academic Press, New York, **1989**, p. 221.
[15] Crystallographic data (excluding structure factors) for the structures reported in this paper have been deposited with the Cambridge Crystallographic Data Centre as supplementary publication nos. CCDC-155121 – 155125. Copies of the data can be obtained free of charge on application to CCDC, 12 Union Road, Cambridge CB2 1EZ, UK (fax: (+44) 1223-336-033; e-mail: deposit@ccdc.cam.ac.uk).
[16] S. K. Kurtz, T. T. Perry, *J. Appl. Phys.* **1968**, *39*, 3798. All the BNDC crystals are transparent yellow; powder SHG measurements were carried out using a nanosecond-pulsed Nd:YAG laser operating at 1064 nm.
[17] J. Zyss, J. L. Oudar, *Phys. Rev. A* **1982**, *26*, 2028.
[18] a) J. Zyss, D. S. Chemla, J. F. Nicoud, *J. Chem. Phys.* **1981**, *74*, 4800; b) M. Sigelle, R. Hierle, *J. Appl. Phys.* **1981**, *52*, 4199.
[19] a) M. J. S. Dewar, E. G. Zoebisch, E. F. Healy, J. J. P. Stewart, *J. Am. Chem. Soc.* **1985**, *107*, 3902; b) M. Dupuis, S. Karna, *J. Comput. Chem.* **1991**, *12*, 487; c) MOPAC93, Fujitsu Inc.
[20] M. Barzoukas, D. Josse, P. Fremaux, J. Zyss, J. F. Nicoud, J. O. Morley, *J. Opt. Soc. Am. B* **1987**, *4*, 977.

A New Family of Layered Molybdenum(V) Cobalto-Phosphates Built up of $[H_{14}(Mo_{16}O_{32})Co_{16}(PO_4)_{24}(H_2O)_{20}]^{10-}$ Wheels

Charlotte du Peloux, Anne Dolbecq, Pierre Mialane, Jérôme Marrot, Eric Rivière, and Francis Sécheresse*

Metal – oxo cluster compounds exhibit unusual topological properties, and are attractive in view of their use in various fields ranging from catalysis to medicine.[1] Self-assembly processes involving Mo^V lead to a structurally diverse family of well-defined ring-shaped nanoparticles or clusters,[2] and it has been shown recently that such compounds can be connected in several different ways to design extended solids.[3] An alternative way to this step-by-step aggregation process for the design of oxomolybdenum frameworks is the one-pot hydrothermal method. Hydrothermal synthesis of fully reduced molybdenum phosphates has thus been extensively used to prepare solid-state materials. The octahedral coordination of the metal centers combined with the tetrahedral geometry of the phosphate groups is at the origin of a large variety of structures, ranging from one-dimensional polymers to three-dimensional open frameworks.[4] Among these materials, to our knowledge, the only examples of molybdenum phosphates that incorporate first-row transition metals are based on the same building unit, namely the well-characterized $[P_4Mo_6O_{25}(OH)_3]^{3-}$ ion.[5] We describe here the synthesis, structure, and magnetic properties of the new two-dimensional cobaltomolybdenum phosphate **1**, which is constructed from unprecedented large structural groups containing sixteen Co^{II} and sixteen Mo^V ions. These groups are linked by four dicobalto bridges. The related compound **2** has been also isolated and characterized by X-ray diffraction. The structure of **2** contains the same basal units connected by four tetrahedral Co^{II} centers.

$$[(Mo_2O_4)_8(HPO_4)_{14}(PO_4)_{10}\{Co_{22}Cl_2(H_2O)_{42}\}]\cdot 28\,H_2O \quad \mathbf{1}$$

$$[(Mo_2O_4)_8(HPO_4)_{14}(PO_4)_{10}\{Co_{19}Na_4(H_2O)_{34}\}]\cdot 14\,H_2O \quad \mathbf{2}$$

Reaction of sodium molybdate with Mo metal as reducing agent, phosphoric acid, and Co^{II} chloride under hydrothermal conditions gave, for a starting pH of 2.0, red parallelepiped crystals of **1** in good yield and, for an initial pH of 3.9 and a smaller amount of Co^{II}, dark purple crystals of the related compound **2**. A single-crystal structure determination of **1**[6] revealed a two-dimensional network. The structure can be described as building groups containing sixteen molybdenum centers and four tetramers of cobalt that form a wheel with a diameter of 19 Å with overall C_{4v} symmetry (Figure 1a). Valence bond summations have been applied on all atoms to confirm the valence of the metal atoms and to locate water molecules and fourteen terminal hydroxo groups of the

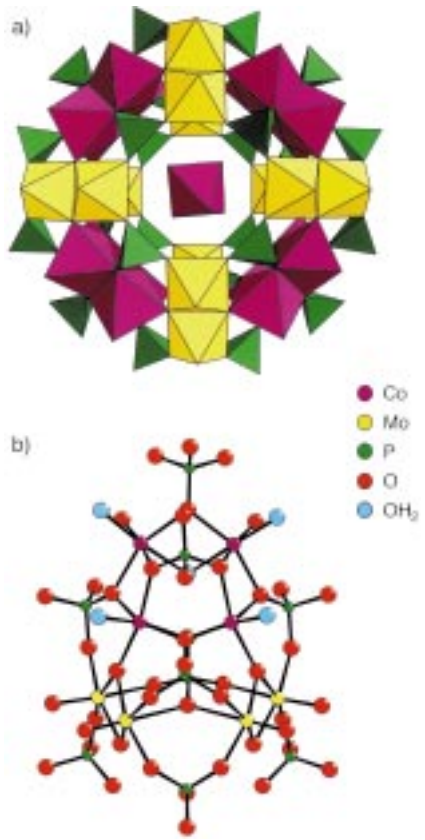

Figure 1. a) Polyhedral representation of the building unit in **1** and **2**; b) ball-and-stick side view of one quarter of the building unit showing the tetramers of Co^{II} and Mo^V.

[*] Prof. F. Sécheresse, C. du Peloux, Dr. A. Dolbecq, Dr. P. Mialane, Dr. J. Marrot
Institut Lavoisier, IREM, UMR 8637
Université de Versailles Saint-Quentin
45 Avenue des Etats-Unis, 78035 Versailles (France)
Fax: (+33) 1-39-25-43-81
E-mail: secheres@chimie.uvsq.fr
Dr. E. Rivière
Laboratoire de Chimie Inorganique, URA CNRS 420
Institut de Chimie Moléculaire d'Orsay
Université Paris-Sud
91405 Orsay (France)

  1433-7851/01/4013-2455 $ 17.50+.50/0

phosphato ligands.[7] On this basis, the wheel is anionic with the general formula $[(Mo_2O_4)_8(HPO_4)_{14}(PO_4)_{10}Co_{16}(H_2O)_{20}]^{10-}$. The arrangement of the sixteen Mo^V centers can be described as four tetramers linked together through phosphato groups, leading to an hexadecamer of Mo^V centers. Each Mo tetramer (Figure 1b) is formed by two $\{Mo_2(\mu\text{-}O)_2\}$ dimers, a common structural arrangement among Mo^V-containing compounds that results from the tendency of the Mo^V ions to form diamagnetic Mo–Mo pairs.[4] The four molybdenum atoms are bridged by three phosphato groups through a μ_3-oxygen and six μ_2-oxygen atoms. Two phosphato groups connect a tetramer of Mo centers to two tetramers of Co centers. A tetramer of cobalt centers (Figure 1b) consists of four distorted edge-shared octahedra, the metal centers forming almost a square with angles and edges in the range of 89.28–90.59° and 3.16–3.37 Å, respectively. The Co^{II} centers are bridged through six phosphato groups and a water molecule. The coordination sphere of each Co^{II} center is completed by a terminal water molecule and an oxygen atom arising from the $\{Mo_2(\mu\text{-}O)_2\}$ groups. A noteworthy feature in the structure of **1** is the presence of an isolated $[Co^{II}(H_2O)_6]^{2+}$ octahedron enclosed in the wheel (Figure 1a), the Co^{II} center is located at an inversion center. This encapsulated Co^{II} monomer is stabilized by hydrogen bonding ($d_{O\cdots O} = 2.696$–2.830 Å) between the oxygen atoms of the water molecules and μ_2-oxygen atoms of the phosphate groups surrounding the $[Co^{II}(H_2O)_6]^{2+}$ octahedron. Each wheel is connected to four other wheels by four cobalt dimers through phosphato groups (Figure 2a). While two of them are the dimeric entities $\{Co_2(H_2O)_6(\mu\text{-}PO_4)_2(PO_4)_2\}$, the two other dimers $\{Co_2(H_2O)_4(\mu\text{-}PO_4)_2(PO_4)_2(\mu\text{-}Cl)_2\}$ have been found disordered over two positions. In the latter species, the chloride ions are *trans* to the μ-phosphato ligand, and are shared with cobalt ions of the wheel. Notably, attempts to synthesize a chlorine-free analogue of **1** have been so far unsuccessful. The connection of the wheels through dimeric Co^{II} octahedra produces the layer structure depicted in Figure 2a. Finally, a $Co^{II}(H_2O)_5$ group is attached to the inorganic layer through an oxygen atom of a phosphate.

The structure of the building block of compound **2** is analogous to that for compound **1**. Nevertheless, the nature of the groups connecting the wheels are different, leading to a drastic change of the two-dimensional structure. In **2**, each wheel is connected to four other wheels by four cobalt monomers in a distorted tetrahedral environment, which imposes a nonplanar arrangement. The angle between two adjacent building groups, which was calculated considering the geometry of the $\{CoO_4\}$ linker, is 81.2(3)° (Figure 2b).

The magnetic behavior of a microcrystalline sample of compound **1** was studied in the range 2–300 K, and the result is shown in Figure 3 in the form of a plot of $\chi_M T$ versus T (where χ_M is the magnetic susceptibility per unit of **1**).[8] The curve exhibits a continuous decrease upon cooling from 300 K ($\chi_M T = 55.54\ cm^3 mol^{-1} K$, $g = 2.32$) to 2 K ($\chi_M T = 11.75\ cm^3 mol^{-1} K$). As a result of the pairing of the d^1 electrons in the Mo^V dimers, the only magnetically active species in **1** are the Co^{II} ions. As high-spin octahedral Co^{II} ions possess the orbitally degenerate ground state $^4T_{1g}$, spin-orbit coupling leads to a value of $\chi_M T$ for 22 Co^{II} ions at room

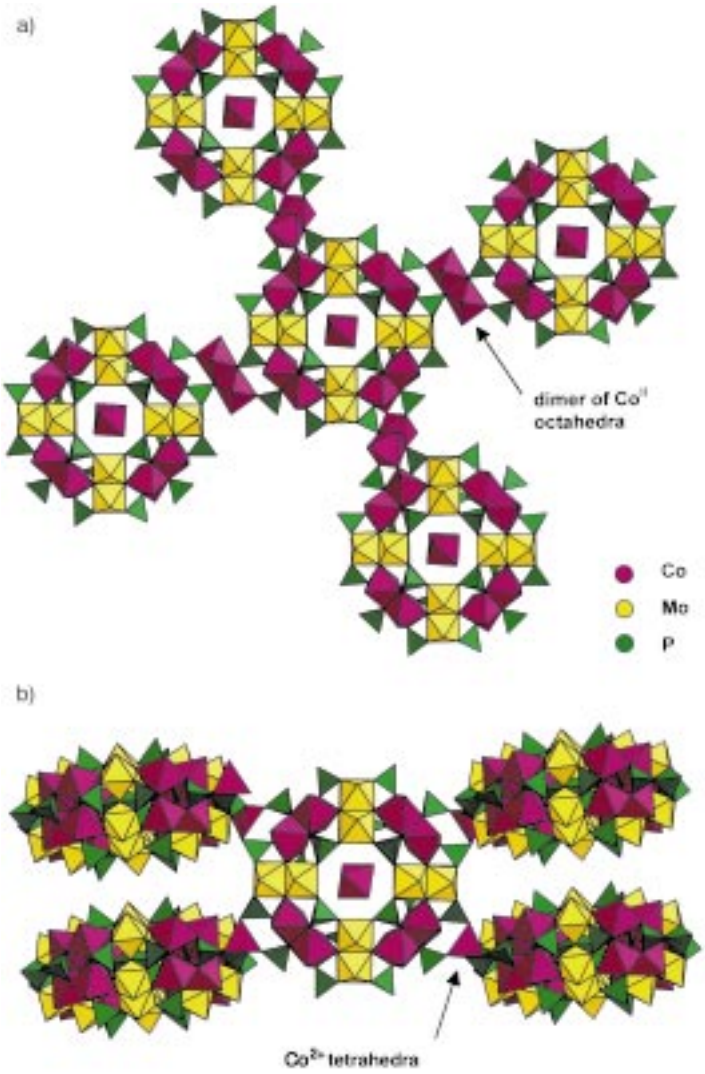

Figure 2. View of the connecting scheme between the building groups in a) **1** and b) **2**.

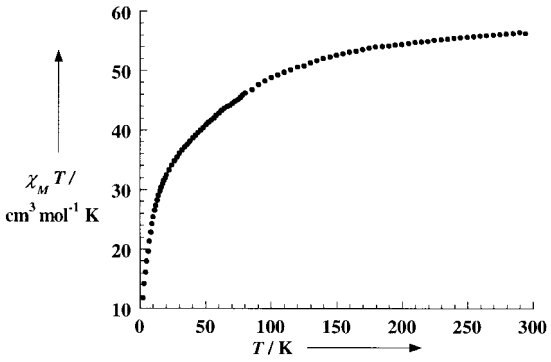

Figure 3. Plot of the dependence of $\chi_M T$ on temperature for **1**.

temperature greater than expected for the spin-only case ($\chi_M T = 41.25\ cm^3 mol^{-1} K$). Nevertheless, the low-temperature $\chi_M T$ value is significantly below the theoretical value calculated for isolated Co^{II} centers for any values of Δ/λ, where λ refers to the spin–orbit coupling parameter and Δ to the ligand-field splitting parameter.[9] This clearly indicates the presence of relatively strong antiferromagnetic Co^{II}–Co^{II}

  1433-7851/01/4013-2456 $ 17.50+.50/0

interactions. This result differs from that previously found by Casañ-Pastor et al. for the tetrameric cobalto–polyoxometalate $[Co_4O_{14}(H_2O)_2(PW_9O_{27})_2]^{10-}$,[10] which displayed ferromagnetic coupling. This difference could be tentatively explained by the fact that the Co-O-Co angles are 90° and ~100° for this compound, and range between 94.9(2)° and 108.1(2)° for **1**, leading in this case to a nonorthogonality of the magnetic orbitals through the bridging oxygen atoms. Furthermore, due to the topology of the Co_4O_{16} groups, spin frustration phenomenon must not occur for **1** due to the long distances of the diagonals of the near square formed by the cobalt centers (4.61–4.63 Å compared to 3.16–3.37 Å for the side of the near square).

In summary, novel extended magnetic solids composed of cobalt(II) and molybdenum(V) phosphates based on a new and complex structural core have been obtained and characterized crystallographically. The versatility of Co^{II} ions, which can adopt both the octahedral and tetrahedral coordination, results in two different organizations of these building groups in the solid, which are controlled by the conditions used for the hydrothermal synthesis. In preliminary experiments, we have found that replacement of Co^{II} by other transition metals of the first row can lead to compounds presenting an isostructural building block, but with an arrangement specific to the metal center and the synthetic conditions. A structural and magnetic characterization of the whole family is in progress.

Experimental Section

1: A mixture of $Na_2MoO_4\cdot 2H_2O$ (0.470 g, 1.94 mmol), Mo (0.030 g, 0.31 mmol), H_3PO_4 (8 M, 0.53 mL, 4.22 mmol), $CoCl_2\cdot 6H_2O$ (0.804 g, 3.38 mmol), and water (4 mL) was stirred, and the pH adjusted to 2.0 with HCl (1 M). The resulting suspension was sealed in a 23 mL Teflon-lined reactor which was kept at 180 °C for 70 h. Red parallelepiped crystals of **1** were isolated as a single product by filtration and washed with water (30% yield, based on total Mo). **1**: IR: $\tilde{\nu}$ = 566 (m), 588 (m), 769 (w), 920 (sh), 959 (s), 1018 (s), 1109 (s) cm^{-1}.

2: The analogous compound **2** was synthesized by a similar procedure starting from a mixture of $Na_2MoO_4\cdot 2H_2O$ (0.470 g, 1.94 mmol), Mo (0.030 g, 0.31 mmol), H_3PO_4 (8 M, 0.53 mL, 4.22 mmol), $CoCl_2\cdot 6H_2O$ (0.200 g, 0.84 mmol), and water (4 mL). Then, the pH was adjusted to 3.9. Dark purple parallepiped crystals were obtained in poor yield, mixed with an unidentified blue powder. **2**: IR: $\tilde{\nu}$ = 528 (m), 587 (m), 773 (m), 942 (sh), 970 (s), 1024 (s), 1076 (s) cm^{-1}.

Received: January 22, 2001 [Z16478]

[1] a) *Polyoxometalates: From Platonic solid to Anti-Retroviral Activity* (Eds.: M. T. Pope, A. Müller), Kluwer, Dordrecht, **1994**; b) M. T. Pope, A. Müller, *Angew. Chem.* **1991**, *103*, 56; *Angew. Chem. Int. Ed. Engl.* **1991**, *30*, 34; c) *Chem. Rev.* **1998**, *98*, 1–389, special issue on polyoxometalates (Guest ed.: C. Hill).

[2] a) Among the impressive work accomplished by Prof. Dr. Müller et al., see for example A. Müller, S. Q. N. Shah, H. Bögge, M. Schmidtmann, *Nature* **1999**, *397*, 48; A. Müller, S. K. Das, P. Kögerler, H. Bögge, M. Schmidtmann, A. X. Trautwein, V. Schünemann, E. Krickemeyer, W. Preetz, *Angew. Chem.* **2000**, *112*, 3555; *Angew. Chem. Int. Ed.* **2000**, *39*, 3413, and references therein; b) S. W. Zhang, D. Q. Liao, M. C. Shao, Y. Q. Tang, *J. Chem. Soc. Chem. Commun.* **1986**, 835; c) F. Sécheresse, E. Cadot, A. Dolbecq, *J. Solid State Chem.* **2000**, *152*, 78.

[3] a) G. Liu, Y.-G. Wei, Q. Yu, Q. Liu, S.-W. Zhang, *Inorg. Chem. Commun.* **1999**, *2*, 434; b) A. Müller, E. Krickemeyer, H. Bögge, M. Schmidtmann, F. Peters, C. Menke, J. Meyer, *Angew. Chem.* **1997**, *109*, 500; *Angew. Chem. Int. Ed. Engl.* **1997**, *36*, 484.

[4] See for a review: R. C. Haushalter, L. A. Mundi, *Chem. Mater.* **1992**, *4*, 31.

[5] a) L. A. Mundi, R. C. Haushalter, *Inorg. Chem.* **1992**, *31*, 3050; b) L. A. Mundi, R. C. Haushalter, *Inorg. Chem.* **1993**, *32*, 1579; c) P. Lightfoot, D. Masson, *Acta Crystallogr. Sect. C* **1996**, *52*, 1077; d) L. Xu, Y. Sun, E. Wang, E. Shen, Z. Liu, C. Hu, *J. Solid State Chem.* **1999**, *146*, 533.

[6] Crystal data and structure refinement for **1**: a dark red crystal (0.26 × 0.20 × 0.06 mm) was analyzed with a Siemens SMART three-circle diffractometer equipped with a CCD two-dimensional detector using $Mo_{K\alpha}$ monochromated radiation (λ = 0.71073 Å). Triclinic, space group $P\bar{1}$, a = 16.0238(5), b = 17.6267(6), c = 19.6432(7) Å, α = 109.285(1), β = 113.379(1), γ = 97.726(1)°, V = 4575.6(3) Å^3, Z = 2, ρ_{calcd} = 2.417 g cm^{-3}, $\mu(Mo_{K\alpha})$ = 3.296 mm^{-1}, $F(000)$ = 3232, 32241 reflections measured, of which 22674 were independent, 1170 refined parameters, R = 0.0522, wR_2 = 0.1541. Crystal data and structure refinement for **2**: a dark purple crystal (0.20 × 0.10 × 0.10 mm) was analyzed. Monoclinic, space group $P2_1/n$, a = 15.7711(2), b = 17.01940(10), c = 30.2699(4) Å, β = 98.539(1)°, V = 8034.8(2) Å^3, Z = 3, ρ_{calcd} = 2.677 g cm^{-3}, $\mu(Mo_{K\alpha})$ = 3.541 mm^{-1}, $F(000)$ = 6277, 54435 reflections measured, of which 20850 were independent, 1094 refined parameters, R = 0.0655, wR_2 = 0.1612. For **1** and **2**, data reduction was performed with the SAINT software. The absorption correction was based on multiple and symmetry-equivalent reflections in the data set using the SADABS program based on the method of Blessing. The structures were solved by direct methods and refined by full-matrix least-squares using the SHELX-TL package. As crystal structures show disorder in the range of water molecules, the exact formula and molecular weight have been established considering data from thermogravimetic studies. For **2**, a disorder has been found on two phosphato groups, occupying two different sites with a ratio ⅔:⅓. Further details on the crystal structure investigations may be obtained from the Fachinformationszentrum Karlsruhe, 76344 Eggenstein-Leopoldshafen, Germany (fax: (+49) 7247-808-666; e-mail: crysdata@fiz-karlsruhe.de), on quoting the depository numbers CSD-411682 (**1**) and CSD-411686 (**2**).

[7] N. E. Brese, M. O'Keeffe, *Acta Crystallogr. Sect. B* **1991**, *47*, 192. Here, a table with the ranges of valence bond summations (VBS) for oxygen atoms and bond lengths (Å) has been deposited as supplementary material.

[8] Magnetic susceptibility measurements were carried out with a Quantum Design SQUID Magnetometer with an applied field of 5000 G. The independence of the susceptibility value with regard to the applied field was checked at room temperature.

[9] O. Kahn, *Molecular Magnetism*, VCH, New York, **1993**, p. 38.

[10] a) N. Casañ-Pastor, J. Bas-Serra, E. Coronado, G. Pourroy, L. C. W. Baker, *J. Am. Chem. Soc.* **1992**, *114*, 10380–10383; b) H. Andres, J. M. Clemente-Juan, M. Aebersold, H. U. Güdel, E. Coronado, H. Büttner, G. Kearly, J. Melero, R. Burriel, *J. Am. Chem. Soc.* **1999**, *121*, 10028–10034.

The First Inorganic "Tennis Ball" Encapsulating an Anion**

Kwan Mook Kim,* Jung Su Park, Yeong-Sang Kim, Yong Ju Jun, Tae Yi Kang, Youn Soo Sohn, and Moo-Jin Jun*

A number of calixarene and glycouril derivatives are known to dimerize and encapsulate reversibly various substrates[1] such as dichloromethane, methane, cyclohexane, adamantane, and ferrocene within their cavities.[2] A notional "tennis ball"[3] coined by Rebek, Jr. came from the roughly spherical dimer of the glycouril derivative which was prepared by condensing two molecules of diphenylglycouril with durene tetrabromide. The tennis ball has the molecular interface which resembles the seam of a real ball. Hydrogen-bond acceptor and donor sites of glycouril units at the ends of the molecule play an important role in the dimerization. The name, "softball",[4] was used to describe the dimer of bigger glycouril derivatives. Inorganic artificial hosts[5–7] are of great interest because the metal can play a pivotal role in specific functions such as magnetism, catalysis, and molecular recognition. Though the strategy of metal-templated self-assembly is routinely exploited in preparing the inorganic hosts, it is generally difficult to acquire reversible characteristics of the assembly. A metal complex that assembles like the glycourils or calixarenes is desirable since the resulting self-assembled inorganic host molecules may have novel encapsulation or reaction properties. Here we report an anion encapsulating tennis-ball-like dimer which is formed by self-assembly of two metal complexes.

Bis(ethylthio)methylenepropanedioate (BETMP) is a multidentate ligand containing two sulfur atoms and two carboxylate groups. A diamineplatinum(II) moiety, [(dach)Pt^{II}] (dach = *trans*(±)-1,2-diaminocyclohexane) binds to the ligand exclusively through the two sulfur atoms.[8] In our recent crystallographic study of K_2Cu(BETMP), on the other hand, the copper(II) ion was found to be coordinated by carboxylate groups of the ligand.[9] Such different coordination properties of the ligand toward the metal ions prompted us to synthesize a new heteronuclear complex using BETMP, copper(II), and [(dach)Pt^{II}] as building units. We have successfully obtained a crystalline material with the formula {(dach)Pt(BETMP)}$_2$-Cu$(BF_4)_2$ (**1**·$(BF_4)_2$) from the concentrated aqueous solution of Cu$(BF_4)_2$ and (dach)Pt(BETMP) in a molar ratio of 1:2. The structure of **1**·$(BF_4)_2$ was elucidated by the X-ray crystallography (Figure 1).[10] Two molecules of [(dach)Pt-(BETMP)] are linked by one copper(II) ion through the carboxylate groups of the BETMP ligand from the opposite sides, and two BF_4 anions weakly interact with the copper ion.

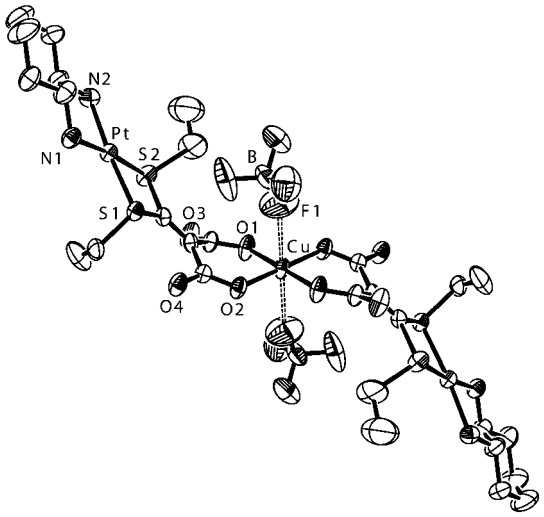

Figure 1. Structure of **1**·$(BF_4)_2$ (ORTEP drawing). Hydrogen atoms are omitted for clarity.

Compound **1** is a zwitterionic complex which has an overall +2 charge: +2 charges are located around each platinum atom and −2 charges around the copper atom. If the two Pt complexes in **1** lie in the same direction, then **1** would have concave shape similar to the glycouril compounds that form a tennis ball or softball. Compound **1** contains hydrogen-bonding acceptor (carboxylate) and donor (amine) groups; thus, the dimerization of **1** should be feasible. The tennis-ball-like dimerization of **1** would lead to a maximization of the electrostatic interaction between the opposite local charges, and indeed, **1** has been found to dimerize in methanol to form such a tennis ball.

The crystalline material **1**·$(BF_4)_2$ was dissolved in methanol, and octahedron-shaped crystals were grown from the concentrated solution. The X-ray crystallographic study[10] of the crystal revealed that it has a molecular composition of [[{(dach)Pt(BETMP)}$_2$Cu]$_2(BF_4)$]$(BF_4)_3$ (**2**·$(BF_4)_3$). The molecular structure of **2** is shown in Figure 2a, and the core of the structure is shown as a space-filling diagram in Figure 2b. The core of the structure has a nearly spherical shape whose surface is incorporated with six metal centers. The hydrogen-bonding interaction between NH of one monomer and O2 of the other (the N···O2 distance is 2.87 Å) is clearly evident in Figure 2b. This interaction is expected to be a driving force for the formation of the dimer as in the case of the tennis ball formation with the glycouril derivatives. The electrostatic interaction between ionic parts of the molecule, and the close contact (3.65 Å) of two sulfur atoms of different monomers seem to also contribute to the gathering of the two monomers. The line of contact between the two monomers resembles the seam of a tennis ball, and hydrogen bonds and sulfur close contacts could be regarded as stitches along the seam. A BF_4 anion is centered in the cavity resulting from the dimerization.

[*] Dr. K. M. Kim, Dr. Y. S. Sohn
Life Science Division
Korea Institute of Science and Technology
Seoul 130-650 (Korea)
Fax: (+82) 2-958-5089
E-mail: kkmook@kist.re.kr
Prof. M.-J. Jun, J. S. Park, Y.-S. Kim, Y. J. Jun, T. Y. Kang
Department of Chemistry
Yonsei University
Seoul 120-749 (Korea)
Fax: (+82) 2-364-7050
E-mail: mjjun@yonsei.ac.kr

[**] This work was financially supported by a Korean Research Foundation grant (No. 1997-011-D 00013).

  1433-7851/01/4013-2458 $ 17.50+.50/0

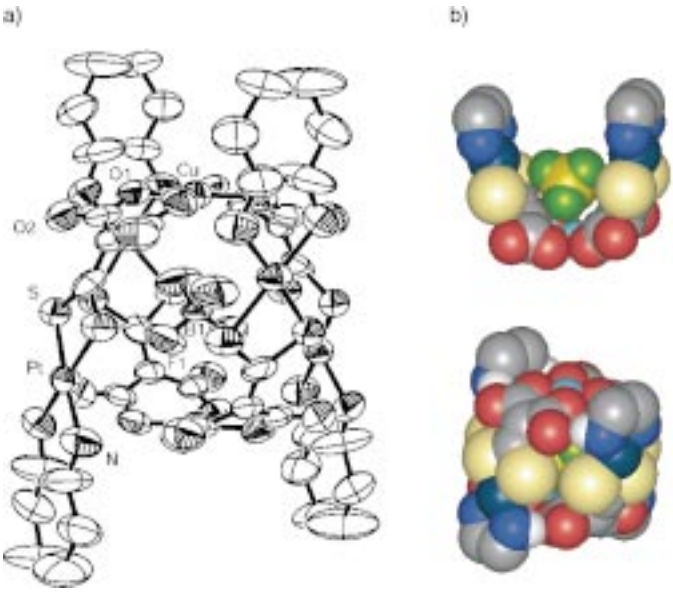

Figure 2. a) Structure of **2** (ORTEP drawing). Hydrogen atoms, three BF_4 anions outside the cavity, and ethyl groups attached to sulfur atoms are omitted for clarity. b) Space-filling diagram of the core of **2** and its interior structure; color code: C: gray; H: white; N: blue; O: red; S: yellow; F: green; B: dark yellow; Cu: sky blue; Pt: dark blue.

The distance from the boron atom to the van der Waals surface of each atom surrounding the anion lies in the range of 2.1 – 2.4 Å. The volume of the cavity calculated from the minimum distance is 39 $Å^3$, which is comparable to that of the tennis ball described by Rebek, Jr. et al.[3]

The existence of the tennis ball structure of $\mathbf{2}\cdot(BF_4)_3$ in methanol is supported by ^{19}F NMR data. The spectra recorded both in D_2O and [D_1]methanol with 2,3-tetrafluorobutane-1,4-diol as an internal standard exhibit the same signals for the free BF_4 anion and the internal standard. The ratio of the integral of the BF_4 signal of $\mathbf{2}\cdot(BF_4)_3$ to the signal of the internal standard, however, drops by approximately 25% in [D_1]methanol compared with that in D_2O. The same result was obtained when $\mathbf{1}\cdot(BF_4)_2$ was used instead of $\mathbf{2}\cdot(BF_4)_3$. Such a reduction of the BF_4 signal in [D_1]methanol implies that one BF_4 ion is encapsulated by the tennis ball in methanol; the paramagnetic copper ions make the NMR signal of this BF_4 ion undetectable.

UV/Vis spectra of $\mathbf{2}\cdot(BF_4)_3$ and $\mathbf{1}\cdot(BF_4)_2$ recorded in water and methanol at a concentration of 5 mM show a maximum absorption λ_{max} at 795 and 695 nm, respectively. It is known that the hydrated copper(II) ion shows a λ_{max} at around 800 nm[11] and copper carboxylate complexes at 680 – 720 nm;[12] therefore, it is likely that **1** (or **2**) is partly dissociated to $Cu^{II}(OH_2)_x + 2$[(dach)Pt(BETMP)] at low concentration in water.

Based on the results of ^{19}F NMR, UV/Vis, and crystallographic studies, it can be concluded that $Cu(BF_4)_2$ and two equivalents of [(dach)Pt(BETMP)] assemble to form the heterotrinuclear complex $\mathbf{1}\cdot(BF_4)_2$, and two copies of **1** assemble to form the inorganic tennis ball **2**, which encapsulates one BF_4 anion (Scheme 1). The formation of **1** can be described as copper-templated self-assembly and that of **2** as noncovalent-bond-directed self-assembly. In water, **1** begins

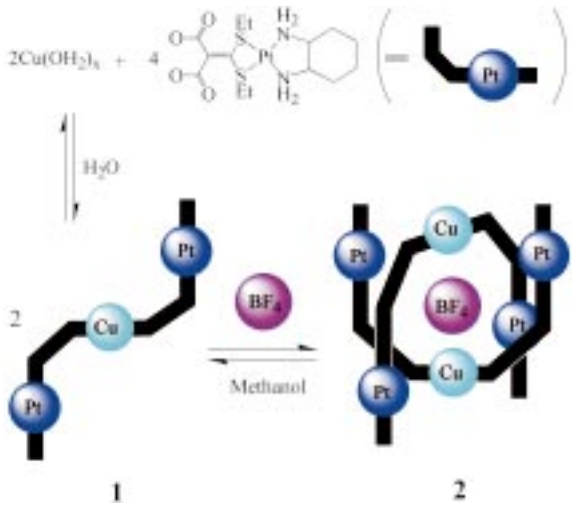

Scheme 1. The self-assembly processes leading to **1** and **2**.

to crystallize at concentrations of about ~0.1M, and significant amounts of the dissociated form exist at the lower concentration. In methanol, however, **2** is predominantly observed. The occurrence of different assembling processes observed in water and methanol can be explained by the different coordination capability and hydrogen-bonding ability of the solvents. We have also obtained very similar crystallographic and UV/Vis spectroscopic results in case of different anions such as NO_3 and ClO_4.

The tennis ball or softball structures known to date are composed of organic moieties and are formed in aprotic solvents. Compound **2** is the first example of a metal-containing tennis ball that is formed in methanol. The platinum atoms in the shell of **2** constitute an important part of the structure, whereas the copper atoms play a key role in directing the assembly of **1** in water and in the encapsulation of the anion through their interaction in methanol.

Experimental Section

Crystallization of $\mathbf{1}\cdot(BF_4)_2$: An aqueous solution (5 mL) of $Cu(BF_4)_2\cdot x H_2O$ (0.54 g, 2.3 mmol) was added to the aqueous slurry (5 mL) of [(dach)Pt(BETMP)] (2.4 g, 4.4 mmol) which was prepared by the literature method.[8] After the addition, a clear solution was obtained, from which blue, block crystals of $\mathbf{1}\cdot(BF_4)_2$ (2.45 g, 85%) were obtained in a few days.

Crystallization of $\mathbf{2}\cdot(BF_4)_3$: Compound $\mathbf{1}\cdot(BF_4)_2$ was dissolved in a minimum volume of methanol, from which blue-green octagonal crystals of $\mathbf{2}\cdot(BF_4)_3$ were isolated in 90% yield. Compound $\mathbf{2}\cdot(BF_4)_3$ could be also obtained by the addition of $Cu(BF_4)_2\cdot x H_2O$ to [(dach)Pt(BETMP)] in methanol.

Received: February 19, 2001 [Z16638]

[1] For recent reviews, see: a) J. Rebek, Jr., *Acc. Chem. Res.* **1999**, *32*, 278; b) J. de Mendoza, *Chem. Eur. J.* **1998**, *4*, 1373; c) M. M. Conn, J. Rebek, Jr., *Chem. Rev.* **1997**, *97*, 1647; d) S. Shinkai, *Tetrahedron* **1993**, *49*, 8933; e) V. Böhmer, *Angew. Chem.* **1995**, *107*, 785; *Angew. Chem. Int. Ed. Engl.* **1995**, *34*, 713.

[2] a) N. Branda, J. Wyler, J. Rebek, Jr., *Science* **1994**, *263*, 1267; b) R. S. Meissner, J. Rebek, Jr., J. de Mendoza, *Science* **1995**, *270*, 1485; c) J. Kang, J. Rebek, Jr., *Nature* **1996**, *382*, 239; d) O'Leary, R. M. Grotzfeld, J. Rebek, Jr., *J. Am. Chem. Soc.* **1997**, *119*, 11701.

  1433-7851/01/4013-2459 $ 17.50+.50/0

[3] R. Wyler, J. de Mendoza, J. Rebek, Jr., *Angew. Chem.* **1993**, *105*, 1820; *Angew. Chem. Int. Ed. Engl.* **1993**, *32*, 1699.
[4] R. Meissner, X. Garcias, S. Mecozzi, J. Rebek, Jr., *J. Am. Chem. Soc.* **1997**, *119*, 77.
[5] For recent reviews, see: a) P. J. Stang, *Chem. Eur. J.* **1998**, *4*, 19; b) B. Linton, A. D. Hamilton, *Chem. Rev.* **1997**, *97*, 1669.
[6] Metal-templated self-assembling capsules: a) O. D. Fox, J. F.-Y. Leung, J. M. Hunter, N. K. Dalley, R. G. Harrison, *Inorg. Chem.* **2000**, *39*, 783; O. D. Fox, N. K. Dalley, R. G. Harrison, *Inorg. Chem.* **1999**, *38*, 5860; b) O. D. Fox, M. G. B. Drew, E. J. S. Wilkinson, P. D. Beer, *Chem. Commun.* **2000**, 391; c) Z. Zhong, A. Ikeda, M. Ayabe, S. Shinkai, S. Sakamoto, K. Yamaguchi, *J. Org. Chem.* **2001**, *66*, 1002.
[7] Metal-containing hydrogen-bonded boxes: a) Y. Kuroda, A. Kawashima, Y. Hayashi, H. Ogoshi, *J. Am. Chem. Soc.* **1997**, *119*, 4929; b) A. Lützen, S. D. Starnes, D. M. Rudkevich, J. Rebek, Jr., *Tetrahedron Lett.* **2000**, *41*, 3777.
[8] Y. S. Sohn, K. M. Kim, S. J. Kang, O.-S. Jung, *Inorg. Chem.* **1996**, *35*, 4274.
[9] K. M. Kim, J. S. Park, Y. S. Sohn, M.-J. Jun, unpublished results.
[10] The X-ray data were collected on an Enraf-Nonius CAD4 automated diffractometer equipped with a Mo X-ray tube at room temperature. Crystal data of $\mathbf{1}\cdot(BF_4)_2$: triclinic, $P\bar{1}$ (no. 2), $Z=1$, $a=10.289(3)$, $b=11.209(2)$, $c=11.752(3)$ Å, $\alpha=96.81(2)$, $\beta=112.58(2)$, $\gamma=111.33(2)^\circ$, $V=1111.9(4)$ Å^3, $\mu=7.023$ mm^{-1}, $\rho_{calcd}=2.032$ g cm^{-3}, $R1=0.0343$, $wR2=0.0912$ for 3636 unique reflections($I>2\sigma(I)$) and 268 variables. Crystal data of $\mathbf{2}\cdot(BF_4)_3$: tetragonal, $I4_1/acd$ (no. 142), $Z=4$, $a=22.498(4)$, $c=23.16(4)$ Å, $V=11724(21)$ Å^3, $\mu=5.324$ mm^{-1}, $d_{calcd}=1.501$ g cm^{-3}, $R1=0.0733$, $wR2=0.1879$ for 1109 unique reflections($I>2\sigma(I)$) and 147 variables. The structure solution and refinement of the data were handled with the SHELXS-86 and SHELXL-97 programs. Crystallographic data (excluding structure factors) for the structures reported in this paper have been deposited with the Cambridge Crystallographic Data Centre as supplementary publication nos. CCDC-160943 ($\mathbf{1}\cdot(BF_4)_2$) and CCDC-160944 ($\mathbf{2}\cdot(BF_4)_3$). Copies of the data can be obtained free of charge on application to CCDC, 12 Union Road, Cambridge CB2 1EZ, UK (fax: (+44) 1223-336-033; e-mail: deposit@ccdc.cam.ac.uk).
[11] J. Bjerrum, C. J. Ballhausen, C. K. Jørgensen, *Acta Chem. Scand.* **1954**, *8*, 1275.
[12] D. P. Graddon, *J. Inorg. Nucl. Chem.* **1958**, *7*, 93.

Optically Active Seleninic Acids: Optical Resolution and Stability

Toshio Shimizu, Itaru Watanabe, and Nobumasa Kamigata*

Tricoordinate sulfur compounds are well known to have pyramidal structures, and many chiral tricoordinate sulfur compounds have already been isolated and clearly characterized.[1] Recently, chiral tricoordinate selenium and tellurium compounds, such as oxides,[2] onium salts,[3] ylides,[4] and imides,[5] have also been isolated, and their properties have been studied.[6–8] Chalcogenic acids are also tricoordinate and are considered to have pyramidal structures. However, no studies on optically active chalcogenic acids have been reported. There are at least two possible explanations for this: first, sulfinic acids readily undergo disproportionation[9] to give thiol sulfonates and sulfonic acids. Second, facile racemization of chalcogenic acids may occur via achiral chalcogenate anions with extrusion of a proton and/or by an intra- or intermolecular proton-transfer reaction. Seleninic acids do not disproportionate to the corresponding selenol selenonates and selenonic acids. Therefore, it may be possible to isolate optically active seleninic acids if we could suppress their racemization. We examined the optical resolution of areneseleninic acids by means of liquid chromatography on an optically active column and found that seleninic acid could be optically resolved, although the racemization was fast, especially at high concentrations, and also that bulky alkyl substituents on the benzene ring of areneseleninic acids were effective in retarding racemization. Here we describe the first optical resolution and the stability of seleninic acids.

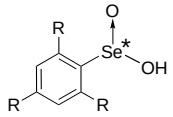

1: R = H
2: R = Me
3: R = Et
4: R = *i*Pr
5: R = *t*Bu

When the optical resolution of 2,4,6-trimethylbenzeneseleninic acid (**2**) was examined on an analytical scale by liquid chromatography on an optically active column packed with amylose carbamate derivative/silica gel (Daicel Chiralpak AS; 4.6 × 250 mm), two peaks corresponding to he enantiomers were observed on the chromatogram, whereas only one peak was observed in the case of benzeneseleninic acid (**1**), as shown in Figure 1. This result shows that

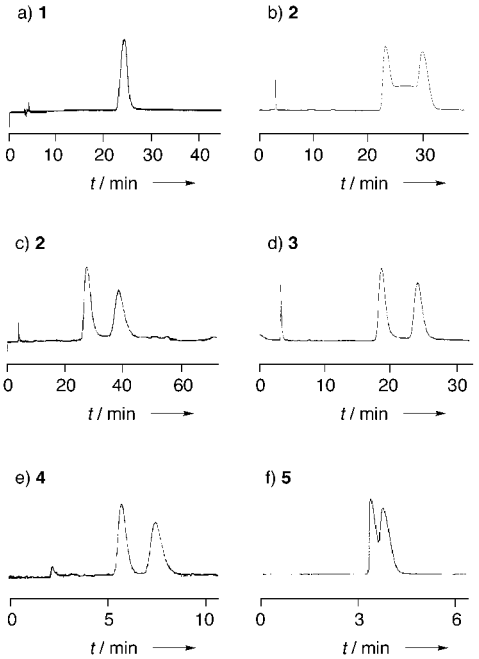

Figure 1. Chromatographic resolution of racemic seleninic acids **1**–**5** on an optically active column packed with amylose carbamate derivative/silica gel (Daicel Chiralpak AS; 4.6 × 250 mm) by HPLC on an analytical scale at 25 °C at a flow rate of 1.0 cm^3 min^{-1}. Eluent: a) hexane/2-propanol (85/15); b) hexane/2-propanol (95/5); c) hexane/2-propanol (90/10) (at 0 °C); d) hexane/2-propanol (98/2); e) hexane/2-propanol (98/2); f) hexane/2-propanol (98/2).

[*] N. Kamigata, T. Shimizu, I. Watanabe
Department of Chemistry, Graduate School of Science
Tokyo Metropolitan University
Minami-ohsawa, Hachioji, Tokyo 192-0397 (Japan)
Fax: (+81) 426-77-2525
E-mail: kamigata-nobumasa@c.metro-u.ac.jp

Supporting information for this article is available on the WWW under http://www.angewandte.com or from the author.

  1433-7851/01/4013-2460 $ 17.50+.50/0

the hydrogen atom in seleninic acid is fixed to a certain extent to one oxygen atom, at least in the case of substituted benzeneseleninic acids such as **2**. However, the unusual shape of the chromatogram of **2** at 25 °C indicated that racemization occurred on the column. When the chromatographic resolution of **2** was carried out at 0 °C, the two enantiomers could be optically resolved. Similarly, optical resolution of areneseleninic acids **3** and **4**, which have more bulky alkyl substituents on the benzene ring, was also carried out by using the same column. In these cases, satisfactory resolution was obtained even at 25 °C. These results indicate that bulky alkyl substituents on the benzene ring are useful for retarding racemization and also show that failure of the resolution in the case of **1** is due to rapid racemization in the column. However, resolution of **5**, which has the most bulky substituent, was not satisfactory, perhaps due to insufficient recognition of chirality because the bulky alkyl substituents at the *ortho* positions of the benzene ring mask the chiral selenium center of **5**.

The optical resolution of areneseleninic acids **2**–**4** was carried out by HPLC on the same type of optically active column on a preparative scale (10 mm × 250 mm). Optically pure seleninic acids (+)-**2**, (+)-**3**, and (−)-**4** were obtained as first-eluted solutions, and their optical purities were confirmed by HPLC analysis. The second-eluted portions were found to contain (−)-**2**, (−)-**3**, and (+)-**4**, with optical purities of 58, 30, and 68%, respectively. The inability to obtain optically pure seleninic acids from the latter eluates is due to tailing of the first-eluted enantiomers on a preparative scale. Since concentration of the solution by evaporation under reduced pressure yielded completely racemized seleninic acids, specific rotations were measured on the eluted solution. Concentrations were determined by comparison of the UV spectra with those of authentic racemic samples. The specific rotations of the optically active seleninic acids are summarized in Table 1. Circular dichroism spectra were also measured

Table 1. Specific rotations of optically active seleninic acids **2**–**4**.

Seleninic acid	First-eluted enantiomer *ee* [%]	$[\alpha]_{435}$	Second-eluted enantiomer *ee* [%]	$[\alpha]_{435}$
2	100	709.4 (*c* 0.01)[a]	58	−337.4 (*c* 0.01)[a]
3	100	471.4 (*c* 0.01)[b]	30	−131.9 (*c* 0.01)[b]
4	100	−493.1 (*c* 0.01)[c]	68	395.1 (*c* 0.01)[c]

[a] In hexane/2-propanol (90/10). [b] In hexane/2-propanol (98/2). [c] In hexane/2-propanol (99/1).

for the eluted solutions, and the seleninic acids with a positive specific rotation, (+)-**2**, (+)-**3**, and (+)-**4**, showed positive first Cotton effects at 283, 283, and 281 nm, and negative second Cotton effects at 229, 239, and 240 nm, respectively (Figure 2). On the other hand, (−)-**2**, (−)-**3**, and (−)-**4** showed negative first Cotton effects and positive second Cotton effects in the same regions.

The kinetics of racemization of the optically active seleninic acids were examined in the eluted solutions. The rates of racemization for optically active seleninic acids (+)-**2**, (+)-**3**, and (−)-**4** at 25 °C showed a good linear relationship with first-order rate plots under dilute conditions (Figure 3). The rate

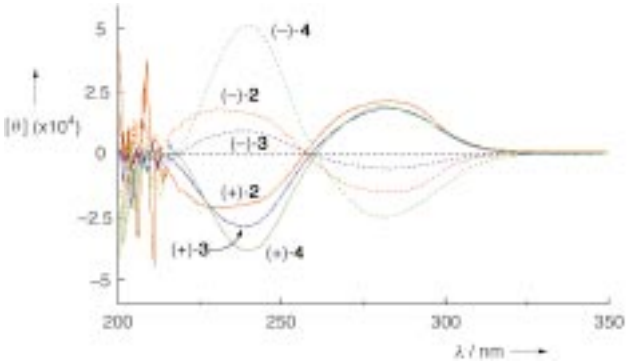

Figure 2. Circular dichroism spectra of optically active seleninic acids **2**–**4**. Solvent: **2** in hexane/2-propanol (90/10); **3** in hexane/2-propanol (98/2); **4** in hexane/2-propanol 99/1.

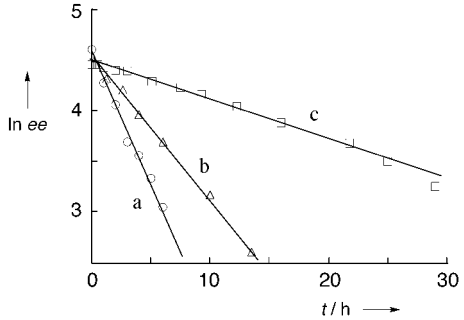

Figure 3. First-order rate plots for the racemization of optically active seleninic acids. a) (+)-**2** (1.52×10^{-4} M) in hexane/2-propanol (90/10); b) (+)-**3** (1.08×10^{-4} M) in hexane/2-propanol (98/2); c) (−)-**4** (1.09×10^{-4} M) in hexane/2-propanol (99/1).

constants for (+)-**2**, (+)-**3**, and (−)-**4** were 6.97×10^{-5}, 3.81×10^{-5}, and 1.11×10^{-5} s^{-1}, and the $t_{1/2}$ values were 2.76, 5.05, and 17.3 h, respectively. These results mean that areneseleninic acids with more bulky alkyl substituents are more stable against racemization than those with less bulky substituents, and bulky alkyl substituents on the benzene ring retard racemization of the seleninic acid. (Note, however, that the concentrations and solvent mixtures are different.) There are at least two plausible mechanisms for racemization with a first-order rate constant. One is a pathway via an achiral seleninate anion with extrusion of a proton, and the other is vertex (pyramidal) inversion. In tricoordinate sulfur compounds, vertex inversion is known to occur.[1] However, the barriers to vertex inversion for the corresponding selenium analogues are too high for such inversion to occur at room temperature.[6, 10] Therefore, racemization of the seleninic acids may proceed via the corresponding achiral seleninate anions **6** with extrusion of a proton, at least under dilute conditions. It was also found that the rate of racemization increased with increasing concentration in the case of (−)-**4** (1.46×10^{-3} M; initial $t_{1/2} = 2.06$ h), and the rate of racemization deviated from the first-order rate plot, while the half-life increased under high-dilution conditions, and the plots showed a first-order reaction (2.02×10^{-5} M; $k = 5.85 \times 10^{-6}$ s^{-1}, $t_{1/2} = 32.9$ h). These results indicate that racemization by an intermolecular proton-exchange reaction via intermolecularly associated structures also takes

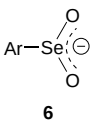

6

place at high concentrations, although the order of the reaction could not be determined. This can explain why concentration of the eluate by evaporation of the solvent caused complete racemization of the seleninic acids.

Although the mechanism of racemization is not clear, we have obtained for the first time optically pure seleninic acids from racemic mixtures by optical resolution. The absolute configurations and details of the mechanism of racemization of optically active seleninic acids are currently under investigation. Recently, benzeneseleninic acids have been commonly used in various oxidation reactions.[11] Therefore, the optically active seleninic acids are expected to act as asymmetric oxidizing reagents.

Experimental Section

Preparation of racemic seleninic acids: Racemic seleninic acids **2**–**4** were prepared by oxidation of the corresponding diselenides with ozone at $-30\,^{\circ}C$ in dichloromethane, followed by hydrolysis, in 64, 28, and 72% yields, respectively, according to the literature procedure.[12] Seleninic acid **5** was also prepared according to the literature procedure.[13] All new seleninic acids gave satisfactory spectral data and combustion analyses.

Typical procedure for optical resolution of areneseleninic acids: Racemic areneseleninic acid (50 mg) in eluent (0.3 mL) was charged to an optically active column packed with amylose carbamate derivative/silica gel (Daicel Chiralpak AS; 10×250 mm) and eluted with hexane containing 10 (for **2**), 2 (for **3**), and 1 (for **4**) vol% 2-propanol at a flow rate of $1.0\,mL\,min^{-1}$. About 15 mg of each optically active areneseleninic acid was collected as eluate from the first- and second-eluted portions, and the specific rotations and the circular dichroism spectra were recorded on the eluted solutions, the concentrations of which were determined by comparison of the UV spectra with those of authentic racemic samples. Chemical structures of the optically active seleninic acids were confirmed by mass spectrometry and ^1H NMR spectroscopy after concentration, although racemization was occurring during the concentration.

Received: March 5, 2001 [Z16721]

[1] Books: a) P. Metzner, A. Thuillier, *Sulfur Reagents in Organic Synthesis*, Academic Press, London, **1993**; b) *The Chemistry of Sulphones and Sulphoxides* (Eds.: S. Patai, A. Rappoport, C. J. M. Stirling), Wiley, New York, **1988**; c) *The Chemistry of the Sulphonium Group* (Eds.: C. J. M. Stirling, S. Patai), Wiley, New York, **1981**; d) M. Mikolajczyk, J. Drabowicz, *Top. Stereochem.* **1982**, *13*, 333.

[2] a) D. N. Jones, D. Mundy, R. D. Whitehouse, *J. Chem. Soc. Chem. Commun.* **1970**, 86; b) F. A. Davis, J. M. Billmers, O. D. Stringer, *Tetrahedron Lett.* **1983**, *24*, 3191; c) T. Shimizu, M. Kobayashi, *J. Org. Chem.* **1987**, *52*, 3399; d) T. Shimizu, K. Kikuchi, Y. Ishikawa, I. Ikemoto, M. Kobayashi, N. Kamigata, *J. Chem. Soc. Perkin Trans. 1* **1989**, 597; e) T. Shimizu, Y. Yamazaki, H. Taka, N. Kamigata, *J. Am. Chem. Soc.* **1997**, *119*, 5966; f) H. Taka, Y. Yamazaki, T. Shimizu, N. Kamigata, *J. Org. Chem.* **2000**, *65*, 2127.

[3] a) M. Kobayashi, K. Koyabu, T. Shimizu, K. Umemura, H. Matsuyama, *Chem. Lett.* **1986**, 2117; b) T. Shimizu, T. Urakubo, N. Kamigata, *J. Org. Chem.* **1996**, *61*, 8032; c) J. Zhang, S. Saito, T. Koizumi, *J. Org. Chem.* **1998**, *63*, 2117.

[4] a) N. Kamigata, Y. Nakamura, K. Kikuchi, I. Ikemoto, T. Shimizu, H. Matsuyama, *J. Chem. Soc. Perkin Trans. 1* **1992**, 1721; b) T. Takahashi, N. Kurose, S. Kawanami, A. Nojiri, Y. Arai, T. Koizumi, M. Shiro, *Chem. Lett.* **1995**, 379; c) N. Kamigata, A. Matsuhisa, H. Taka, T. Shimizu, *J. Chem. Soc. Perkin Trans. 1* **1995**, 821.

[5] a) V. P. Krasnov, V. I. Naddaka, V. I. Minkin, *Zh. Org. Khim.* **1981**, *17*, 445; b) N. Kamigata, H. Taka, A. Matsuhisa, H. Matsuyama, T. Shimizu, *J. Chem. Soc. Perkin Trans. 1* **1994**, 2257; c) T. Shimizu, N. Seki, H. Taka, N. Kamigata, *J. Org. Chem.* **1996**, *61*, 6013; d) H. Taka, T. Shimizu, F. Iwasaki, M. Yasui, N. Kamigata, *J. Org. Chem.* **1999**, *64*, 7433.

[6] Review: T. Shimizu, N. Kamigata, *Rev. Heteroatom Chem.* **1998**, *18*, 11.

[7] Reviews: a) T. Shimizu, N. Kamigata, *Org. Prep. Proced. Int.* **1997**, *29*, 603; b) N. Kamigata, T. Shimizu, *Rev. Heteroatom Chem.* **1991**, *4*, 226.

[8] Books: a) *The Chemistry of Organic Selenium and Tellurium Compounds* (Eds.: S. Patai, Z. Rappoport), Wiley, New York, **1987**; b) *Organoselenium Chemistry* (Ed.: D. Liotta), Wiley, New York, **1987**; c) C. Paulmier, *Selenium Reagents and Intermediates in Organic Synthesis*, Pergamon, Oxford, **1986**.

[9] J. L. Kice, K. W. Bowers, *J. Am. Chem. Soc.* **1962**, *84*, 605.

[10] a) T. Shimizu, A. Matsuhisa, N. Kamigata, S. Ikuta, *J. Chem. Soc. Perkin Trans. 2* **1995**, 1805; b) T. Shimizu, N. Kamigata, S. Ikuta, *J. Chem. Soc. Perkin Trans. 2* **1999**, 1469.

[11] Book: T. G. Back in *Organoselenium Chemistry* (Ed.: T. G. Back), Oxford University Press, Oxford, **1999**, p. 93.

[12] H. J. Reich, C. P. Jasperse, *J. Org. Chem.* **1988**, *53*, 2389.

[13] G. Ayrey, D. Barnard, D. T. Woodbridge, *J. Chem. Soc.* **1962**, 2089.

  1433-7851/01/4013-2462 $ 17.50+.50/0

$[\{(t\mathrm{BuC_5H_4})_2\mathrm{Nb(CO)}\}_3\mathrm{Co_9(CO)_8Te_6}\cdot 3\,\mathrm{Cr(CO)_5}]$: Unusual Stabilization of a Cubic Body-Centered Metal Telluride Cluster by Peripheral Complex Fragments**

Henri Brunner, A. Claudia Stückl, Joachim Wachter,* Robert Wanninger, and Manfred Zabel

Transition metal clusters, which contain M_8 cubes with heavy main group elements as bridging ligands, serve as simple models for solid-state structures.[1] Clusters of the type $[M_9L_8(\mu_4\text{-}E)_6]$ ($M = Ni$, Pd; $L = PPh_3$, CO, Cl; $E = GeEt$,[2] As,[3] Sb,[4] Te[5]) are characterized by an additional metal atom in the center of the cluster. The first cobalt-containing representative of the $[M_9L_8(\mu_4\text{-}E)_6]$ class of compounds is the cluster salt $[(C_5Me_5)_2Nb(CO)_2]_2[Co_9(CO)_8Te_6]$ ($[(C_5Me_5)_2Nb(CO)_2]_2$ (**1**)), which was only obtained in very low yields, so that it is impossible to further investigate its chemical properties.[6] We now report on a rational synthesis of a cluster, that is closely related to the anion $[\mathbf{1}]^{2-}$, but whose metal telluride sphere is expanded by peripheral transition metal complex fragments.

The reaction of $[Cp'_2Nb(Te_2)H]$ ($Cp' = t\mathrm{BuC_5H_4}$)[7] with two equivalents of $[Co_2(CO)_8]$ in boiling toluene gave the dark red neutral compound $[\{Cp'_2Nb(CO)\}_3Co_9(CO)_8Te_6]$ (**2**) in good yield after chromatographic work-up on silica gel. As mass spectra of **2** could not be obtained, its composition was derived from an X-ray diffraction analysis of the $Cr(CO)_5$-adduct **3** (see below) and confirmed by C, H analyses. The IR spectrum of **2** exhibits three bands at 2005, 1965, and 1915 cm^{-1} typical of terminal CO absorptions, along with the characteristic $\nu(C-H)$ frequencies of the $t\mathrm{BuC_5H_4}$ groups. The CO pattern may be explained by the presence of nonequivalent sets of Co(CO) and $Cp'_2Nb(CO)$ units.[8]

Complex **2** reacted with an excess of $[Cr(CO)_5(thf)]$ in THF solution to give the red-brown complex **3** and dark brown **4**. Both compounds were purified by column chromatography without decomposition. The composition of **3** was determined by means of X-ray crystallography and the resulting formula $[\{Cp'_2Nb(CO)\}_3Co_9(CO)_8Te_6\cdot 3\,Cr(CO)_5]$ was confirmed by C, H analyses. The dark brown compound **4** could not yet be structurally characterized, but according to its IR spectrum it contains $Cr(CO)_5$ groups, and C,H analyses are in agreement with the formula $[\{Cp'_2Nb(CO)\}Co_9(CO)_8Te_6\cdot 3\,Cr(CO)_5]$. The IR spectrum of **3** exhibits a pattern in the region of the terminal CO absorptions which may be interpreted as the sum of the bands of **2** and those of the coordinated $Cr(CO)_5$ fragments (2055 cm^{-1}). Complex **4** reveals a very similar pattern.

Inspite of intense efforts single crystals of **3** were obtained only as very thin needles, and the crystallographic study[9] suffered accordingly from the low quality of the crystals. Whereas the heavy atoms could be refined anisotropically, the identification of the solvent molecules in the crystal was problematic. The dominating structural feature of the molecule is a Co_8 cube, which contains a central cobalt atom (Figure 1). The faces of the cube are bridged by six Te ligands,

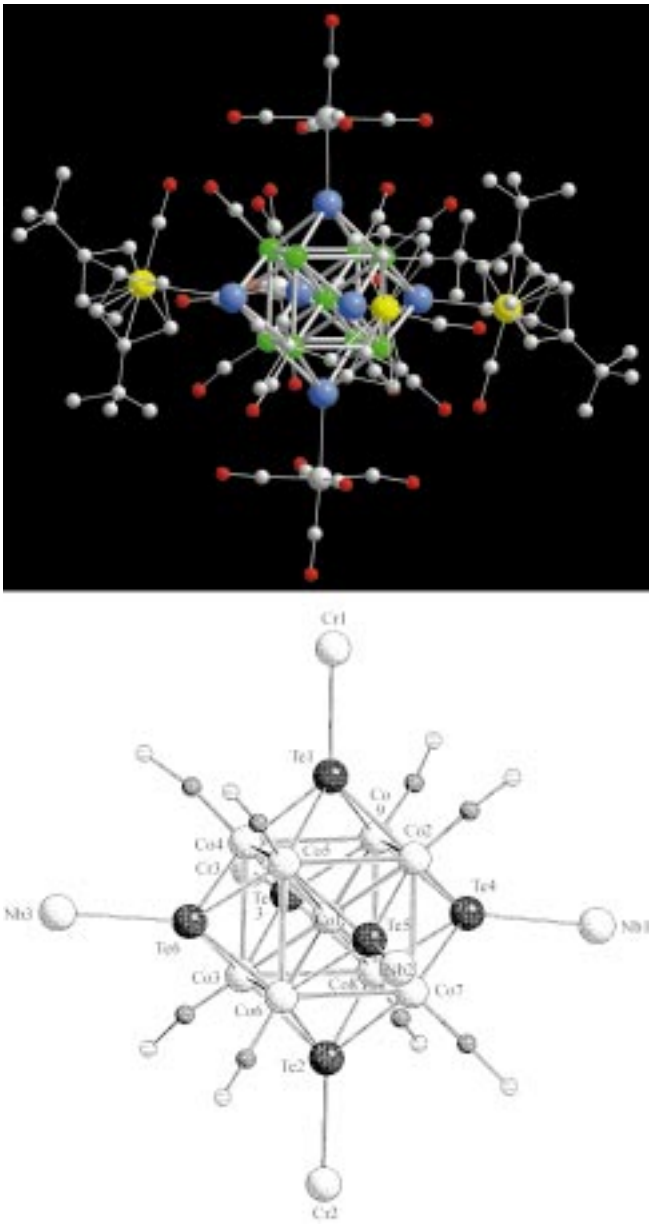

Figure 1. Structure of **3** in the crystal. Top: overview; bottom: $[Co_9(CO)_8Te_7]$ core with attached Cr and Nb atoms, which denote $Cr(CO)_5$ and $Cp'_2Nb(CO)$ fragments, respectively. Selected distances [Å] and angles [°]: Co1-Te1 2.925(4), Co1-Te2 2.912(4), Co1-Te3 2.927(3), Co1-Te4 2.956(5), Co1-Te5 2.928(3), Co1-Te6 2.940(5), Co1-Co2 2.395(5), Co1-Co3 2.408(5), Co1-Co4 2.382(6), Co1-Co5 2.394(5), Co1-Co6 2.386(4), Co1-Co7 2.381(6), Co1-Co8 2.412(5), Co2-Te1 2.488(5), Co2-Co5 2.778(9), Co2-Co9 2.741(8), Co3-Te2 2.505(5), Co4-Te1 2.479(4), Co4-Te3 2.477(4), Co4-Co5 2.754(4), Co5-Te1 2.492(3), Co6-Te2 2.475(4), Co7-Te2 2.474(3), Co8-Te2 2.489(3), Co8-Te4 2.481(4), Co9-Te1 2.490(4), Cr1-Te1 2.643(6), Cr2-Te2 2.638(5), Cr3-Te3 2.633(4), Nb1-Te4 2.860(4), Nb2-Te5 2.871(3), Nb3-Te6 2.837(4); Co3-Co1-Co5 109.5(2), Co4-Co1-Co7 179.7(2), Co5-Co1-Co6 71.0(2), Te1-Co1-Te2 179.6(2), Te1-Co1-Te4 90.3(2), Te4-Co1-Co8 53.9(2), Te5-Co2-Co1 73.0(2), Te1-Co4-Te6 113.0(2), Co4-Te1-Co5 67.3(2), Co1-Te1-Cr1 128.5(2), Co1-Te2-Cr2 176.3(2), Co1-Te5-Nb2 174.6(2), Co1-Te6-Nb3 174.2(2).

[*] Dr. J. Wachter, Prof. Dr. H. Brunner, Dr. A. C. Stückl, Dr. R. Wanninger, Dr. M. Zabel
Institut für Anorganische Chemie der Universität Regensburg
93040 Regensburg (Germany)
Fax: (+49) 941-943-4439
E-mail: Joachim.Wachter@chemie.uni-regensburg.de

[**] This work was supported by the Deutsche Forschungsgemeinschaft.

  1433-7851/01/4013-2463 $ 17.50+.50/0

to which three $Cp'_2Nb(CO)$ and three $Cr(CO)_5$ fragments are coordinated. These groups are arranged in a meridional manner with respect to the Te_6 octahedron. Inspite of the relatively low quality of the structure solution a comparison of bond parameters of **3** and $[\mathbf{1}]^{2-}$ reflects a weak, but unequivocal trend, which may be interpreted as a slight contraction of the Co_9Te_6 cube in **3**: 1) The distances of each Te bridge from the corners of the Co_8 cage in **3** are on average 0.03 Å shorter than in $[\mathbf{1}]^{2-}$, a similar trend is observed for the distances of the Te atoms from the central Co1 atom; 2) the Co–Co edges in **3** (mean 2.76(1) Å) are 0.01 Å shorter than in $[\mathbf{1}]^{2-}$, as are the distances of Co1 from the corners of the cube.

The Nb–Te distances (mean 2.856 Å) are typical of Nb–Te single bonds.[3, 10] The Cr–Te distances (mean 2.638(5) Å) are about 0.1 Å shorter than those in anionic chromium tellurides,[11] but slightly longer than those in [*cyclo*-$Te_4\{Cr(CO)_5\}_4$].[12] The contribution of the $Cr(CO)_5$ fragments in stabilizing the Co_9Te_6 cube is still a matter of speculation, but there is no doubt that they improve considerably the crystallization properties of the resulting product **3**.

Each of the three niobocenecarbonyl units in **2** and **3** acts as a 17-electron fragment, which is anchored covalently to the cluster core through the Te ligands. Complex **4**, however, contains only one of these units. Consequently, each of the Te ligands linked to Nb centers contributes five electrons to the metal valence electrons (MVE) of the cluster. The other Te ligands provide only four electrons each, whereas their lone pair of electrons may stabilize "outer" unsaturated complex fragments as realized in **3**. This results in 124 MVE ($(9\times 9$ for Co) + (8×2 for CO) + (3×5 for μ_5-Te) + (3×4 for μ_4-Te)) for the $Co_9(CO)_8Te_6$ core in **2** (and analogously in **3**). By comparison the cluster core of **4** contains 122 MVE and that of $[\mathbf{1}]^{2-}$ 123 MVE.

The observed weak contraction of the Co_9Te_6 cube, when comparing the structural parameters of $[\mathbf{1}]^{2-}$ and **3**, is qualitatively supported by density functional theory (DFT) calculations. These have been carried out on the structure model of the $Co_9(CO)_8Te_6$ cluster core bearing two- and threefold negative charge, for example $[\mathbf{1}]^{2-}$[6] and $[\mathbf{1}]^{3-}$. The MO scheme of $[\mathbf{1}]^{3-}$ is built up as following: Its HOMO, which is already known from $[\mathbf{1}]^{2-}$ to contain a high Co1-d_{z^2} orbital portion as well as significant s/p contributions of the axial Te atoms in a_{1g} symmetry, incorporates the additional valence electron of the Co_9Te_6 core. The resulting higher electron density of the $a_{1g}(d_{z^2})$ state along with the similar energetic level of the $d_{x^2-y^2}$ and d_{z^2} orbitals in $[\mathbf{1}]^{3-}$ should slightly enhance the interaction between Co1 and the six Te atoms.

The reaction of $[Cp'_2Nb(Te_2)H]$ with $[Co_2(CO)_8]$ is strongly temperature dependent. At 0 °C $[Co_4(CO)_{10}Te_2]$[13] and low quantities of $[\{Cp'_2Nb(CO)\}Co_3(CO)_6Te_2]$ are formed. The latter contains, like its peralkylated analogue,[6] a trigonal-bipyramidal $Co_3(CO)_6Te_2$ cluster to which a $Cp'_2Nb(CO)$ fragment is connected through an apical Te ligand. At higher temperature the neutral cluster **2** is formed. This is in strong contrast to the system $[(C_5Me_5)_2Nb(Te_2H)]/[Co_2(CO)_8]$, which gives rise to the formation of salts that are built up from pentagonal-prismatic $[Co_{11}(CO)_{10}Te_7]^{n-}$ ions ($n=1, 2$)[6] and $[(C_5Me_5)_2Nb(CO)_2]^+$ ions. The formation of such different cluster skeletons may be a consequence of the different structures of the employed niobocene tellurides.[7]

In contrast to the salt $[(C_5Me_5)_2Nb(CO)_2]_2$-**1**, complexes **2** and **3** are of covalent nature. Cluster **2** may be considered as a potential precursor of the hypothetical compound $[Cp'_2Nb(CO)_2]_3[Co_9(CO)_8Te_6]$, containing $[\mathbf{1}]^{3-}$ as cluster anion. Attempts to prepare this salt, starting from **2** by high-pressure carbonylation (200 bar CO, THF) of the niobocene component, gave thus far only $[Co_4(CO)_{10}Te_2]$.[13] Further experiments to synthesize the anion $[\mathbf{1}]^{3-}$ are planned, mainly to establish the presumed redox relationship with the above-mentioned $[\mathbf{1}]^{2-}$. However, the formation of the niobocene dicarbonyl cation $[Cp_2Nb(CO)_2]^+$ (Cp = Cp′, C_5Me_5), which is responsible for the charge separation in $[(C_5Me_5)_2Nb(CO)_2]_2$ (**1**), may be favored in the case of the more electron-rich C_5Me_5 ligand.

The reaction of $[Cp'_2Nb(Te_2)H]$ with $[Co_2(CO)_8]$ provides an efficient access to cubic metal-centered cobalt telluride clusters. Anchoring of peripheral complex fragments permits the realization of clusters with different charge and electron counts. Finally, the expeceted reactivity potential of **2** may extend the knowledge on the chemistry of metal telluride clusters.

Experimental Section

2: The mixture of $[Cp'_2Nb(Te_2)H]$ (550 mg, 0.930 mmol),[7] $[Co_2(CO)_8]$ (640 mg, 1.872 mmol), and toluene (100 mL) was stirred for 3 h at 110 °C. After the mixture had been cooled to room temperature, the solvent was removed and the residue dissolved in THF (15 mL). Chromatography on SiO_2 (activity II-III, column 15 cm, ∅ 3 cm) with THF gave a broad dark red band that contained **2** (630 mg, 0.241 mmol; 78 %). Recrystallization of **2** from THF/pentane (5:1) gave fine dark needles. Elemental analysis (%) calcd for $C_{65}H_{78}Co_9Nb_3O_{11}Te_6$ (2609.97): C 29.91, H 3.01; found: C 29.63, H 3.37; IR (KBr): $\tilde{\nu}$(CO) = 2005 (m), 1965 (vs), 1915 (vs) cm^{-1}.

$[\{Cp'_2Nb(CO\}_xCo_9(CO)_8Te_6\cdot 3Cr(CO)_5]$ ($x=3$: **3**; $x=1$: **4**): A solution of $[Cr(CO)_5(thf)]$ (1.45 mmol) in THF (150 mL) was added to the dark red solution of **2** (630 mg, 0.241 mmol) in THF (30 mL) and stirred in the dark for 12 h at room temperature. After evaporation of the solvent the residue was dissolved in THF (12 mL) and chromatographed on SiO_2 (column 20 cm, ∅ 5 cm). A red-brown band was eluted with THF which contained **3** (560 mg, 0.193 mmol; 68 %), whereas weakly colored bands eluted with THF/acetone (4:1) were not isolated. The dark brown complex **4** was eluted with THF/acetone (1:1) in 270 mg yield. Recrystallization of **3** from CH_2Cl_2/toluene (1:1) gave dark red crystals. **3**: Elemental analysis (%) calcd for $C_{80}H_{78}Co_9Cr_3Nb_3O_{26}Te_6$ (3186.12): C 30.16, H 2.47; found: C 30.66, H 2.66; IR (KBr): $\tilde{\nu}$(CO) = 2055 (s), 2005 (m), 1960 (vs), 1920 (vs) cm^{-1}. **4**: Elemental analysis (%) calcd for $C_{42}H_{26}Co_9Cr_3NbO_{24}Te_6$ (2677.9): C 20.52, H 1.07; found: C 21.06, H 1.68; IR (KBr): $\tilde{\nu}$(CO) = 2050 (s), 2010 (m), 1965 (vs), 1930 (vs) cm^{-1}.

Received: January 10, 2001 [Z 16398]

[1] a) R. Gautier, J.-F. Halet, J.-Y. Saillard, *Eur. J. Inorg. Chem.* **1999**, 673–678; b) R. Gautier, J.-F. Halet, J.-Y. Saillard in *Metal Clusters in Chemistry, Vol. 3* (Eds.: P. Braunstein, L. A. Oro, P. R. Raithby), Wiley-VCH, **1999**, pp. 1643–1663.

[2] J. P. Zebrowski, R. K. Hayashi, A. Bjarnason, L. F. Dahl, *J. Am. Chem. Soc.* **1992**, *114*, 3121–3125.

[3] a) D. Fenske, H. Fleischer, C. Persau, *Angew. Chem.* **1989**, *101*, 1740–1742; *Angew. Chem. Int. Ed. Engl.* **1989**, *28*, 1665–1667; b) D. Fenske, J. Ohmer, K. Merzweiler, *Angew. Chem.* **1988**, *100*, 1572–1573; *Angew. Chem. Int. Ed. Engl.* **1988**, *27*, 1512–1513.

[4] D. Fenske, C. Persau, *Z. Anorg. Allg. Chem.* **1991**, *593*, 61–68.

[5] J. G. Brennan, T. Siegrist, S. M. Stuczinski, M. L. Steigerwald, *J. Am. Chem. Soc.* **1989**, *111*, 9240–9241.

  1433-7851/01/4013-2464 $ 17.50+.50/0

[6] H. Brunner, D. Lucas, T. Monzon, Y. Mugnier, B. Nuber, B. Stubenhofer, A. C. Stückl, J. Wachter, R. Wanninger, M. Zabel, *Chem. Eur. J.* **2000**, *6*, 493 – 530.
[7] R. Wanninger, PhD Thesis, Universität Regensburg, **2000**, pp. 33 – 47.
[8] $[(MeC_5H_4)_2Nb(CO)Cl]$: $\tilde{\nu}(CO) = 1910\ cm^{-1}$ (A. Fakhr, Y. Mugnier, R. Broussier, B. Gautheron, E. Laviron, *J. Organomet. Chem.* **1983**, *255*, C8 – C10).
[9] Crystal structure analysis of **3**: dark red crystals, $0.20 \times 0.08 \times 0.06$ mm, monoclinic, $P2_1/c$, $a = 15.471(2)$, $b = 29.281(1)$, $c = 26.472(2)$ Å, $\beta = 103.64(1)^\circ$, $V = 11\,653(2)$ Å^3, $Z = 4$, $\rho_{calcd} = 1.938\ g\,cm^{-3}$, $\theta = 1.86 – 25.15^\circ$, $\mu = 3.329\ mm^{-1}$, 32 866 measured reflections, 16 178 independent reflections ($R_{int} = 0.122$), 3384 observed reflections ($I > 2\sigma(I)$), 614 refined parameters, $R1 = 0.0593$, $wR2 = 0.0912$, max./min. residual electron density $0.701/-0.558\ e\,Å^{-3}$. Data were collected on a STOE-IPDS diffractometer ($Mo_{K\alpha}$ radiation) at 173 K. The structure was solved by direct methods using SIR97 and refined against F^2 (SHELXL-97) with all reflections. Refinement with anisotropic temperature factors was only possible for the heavy atoms. Remaining, still important residual electron densities from the difference Fourier analyses could not be refined. Voids at $x, y, z = 0.5, 0.0, 0.5$ and $x, y, z = 0.5, 0.5, 0.0$ were localized with the program SQUEEZE.[14] Each of them has a volume of 1281 Å^3 and contains 48 and 49 electrons, respectively. These numbers correspond roughly to toluene molecules, however, the volume of the voids is too high for only one such molecule. The portion of these electrons at the calculated structure factors was considered by Fourier back transformation and was subtracted from the observed structure factors. The final refinement was carried out with these data. Crystallographic data (excluding structure factors) for the structure reported in this paper have been deposited with the Cambridge Crystallographic Data Centre as supplementary publication no. CCDC-155021. Copies of the data can be obtained free of charge on application to CCDC, 12 Union Road, Cambridge CB2 1EZ, UK (fax: (+44) 1223-336-033; e-mail: deposit@ccdc.cam.ac.uk).
[10] a) W. Tremel, *J. Chem. Soc. Chem. Commun.* **1992**, 126 – 128; b) H. Kleinke, W. Tremel, *Chem. Commun.* **1999**, 1175 – 1176.
[11] a) W. A. Flomer, S. C. O'Neal, J. W. Kolis, D. Jeter, A. W. Cordes, *Inorg. Chem.* **1988**, *27*, 969 – 971; b) L. C. Roof, W. T. Pennington, J. W. Kolis, *Inorg. Chem.* **1992**, *31*, 2056 – 2064; c) S. Stauf, C. Reisner, W. Tremel, *Chem. Commun.* **1996**, 1749 – 1750.
[12] O. Blacque, H. Brunner, M. M. Kubicki, B. Nuber, B. Stubenhofer, J. Wachter, B. Wrackmeyer, *Angew. Chem.* **1997**, *109*, 361 – 362; *Angew. Chem. Int. Ed. Engl.* **1997**, *36*, 351 – 352.
[13] R. C. Ryan, L. F. Dahl, *J. Am. Chem. Soc.* **1975**, *97*, 6904 – 6906.
[14] P. van der Sluis, A. L. Spek, *Acta Crystallogr. Sect. A.* **1990**, *46*, 194.

A Very Rigid Bis-bispidine Tetraazamacrocycle and Its Unusual Copper(II) Complex**

Peter Comba,* Hans Pritzkow, and Wolfgang Schiek

Dedicated to Professor Dieter Sellmann on the occasion of his 60th birthday

Macrocyclic ligands have been used extensively to stabilize metal ions in specific oxidation and electronic states, and to tune the metal ion selectivity.[1–5] The 14-membered tetraazamacrocycle cyclam (1,4,8,11-tetraazacyclotetradecane; Scheme 1) is known to provide an ideal donor set and geometry for tetragonal coordination of copper(II) centers.

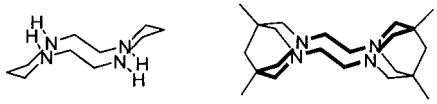

Scheme 1. The ligands cyclam and L (= **3**).

The conformational flexibility of the five- and six-membered chelate rings and the configurational flexibility of the coordinated secondary amino groups of cyclam and other tetraazamacrocyclic ligands may be reduced and, therefore, the selectivity increased by substituents at the amines or the carbon backbone or by reinforcing the backbone with rings or multiple bonds.[6–8] Several attempts have been made to decrease the flexibility of the cyclam backbone, for example, with derivatives containing one or two piperazine rings.[9, 10] The bispidine backbone (bispidine = 3,7-diazabicyclo[3.3.1]-nonane) is known to be an extremely rigid fragment, and a range of *N*,*N*′-substituted tetradentate,[11, 12] as well as C^{α},$C^{\alpha'}$-substituted tetra-,[13–18] penta-, and hexadentate ligands,[18] and their transition metal compounds have been prepared and studied. Macrocyclic cyclam derivatives with two bispidine caps are expected to be highly preorganized and extremely rigid. These ligands have no configurational flexibility; with respect to the conformation there are only two possible arrangements of the five-membered chelate rings: λ,λ and λ,δ.

Derivatives of L have been proposed and reported but neither a full characterization, including an experimental structure, nor any spectroscopically or structurally characterized metal complexes have been published.[19, 20]

Molecular models of the free ligand L and the corresponding copper(II) compound (two conformations each) are shown in Figure 1.[21–25] These indicate that, indeed, L is highly preorganized for coordination of copper(II). The only distortions are a zigzag orientation for the λ,δ conformer and a twist of the two planes defined by the two N donors and the central carbon atom of the methylene bridge of each bispidine cap for the λ,λ conformer. These distortions arise due to the

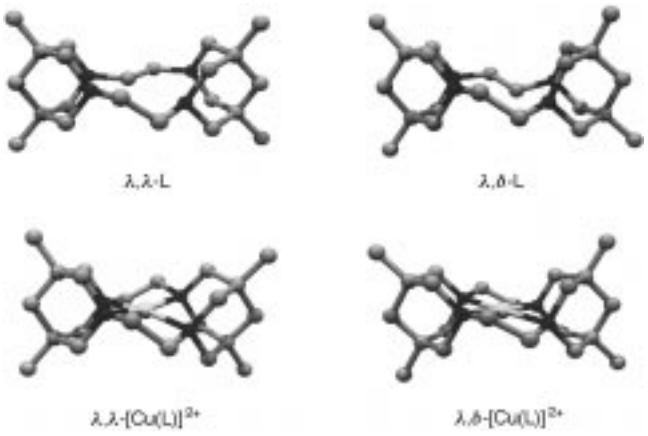

Figure 1. Computed structures of L and $[Cu(L)]^{2+}$.[21–23]

[*] Prof. Dr. P. Comba, Dr. H. Pritzkow, W. Schiek
Anorganisch-chemisches Institut der Universität Heidelberg
Im Neuenheimer Feld 270, 69120 Heidelberg (Germany)
Fax: (+49) 6221-546617
E-mail: comba@akcomba.oci.uni-heidelberg.de

[**] This work was supported by the Deutsche Forschungsgemeinschaft (DFG). Bispidine = 3,7-diazabicyclo[3.3.1]nonane.

geometry of ethylene bridges between the two caps (en-type "chelate" rings) and the repulsion of the lone pairs of electrons at the N atoms. A similar but less pronounced distortion occurs in the calculated structures of the copper(II) complexes. Moreover, the calculations indicate that, owing to repulsion by the methylene groups of the bispidine caps, the bonds to the axial donors, Cu–OH_2, are much elongated (Cu six-coordinate: ca. 2.97 Å vs. ca. 2.48 Å in $[Cu(cyclam)(OH_2)_2]^{2+}$;[26] Cu five-coordinate: ca. 2.66 Å vs. ca. 2.3 Å[27]). The Cu–N distances of about 1.98 Å[23, 28] are significantly shorter than those in $[Cu(cyclam)(OH_2)_2]^{2+}$ (ca. 2.01 Å[26]). This and the fact that tertiary amines are stronger σ donors than secondary amines[27, 29] leads to the expectation that L might produce copper(II) complexes with a very strong ligand field, especially for the four-coordinate Cu^{II} compounds (high energy shift of the $d_{x^2-y^2}$ orbital due to Cu–N bond strengthening; low energy shift of the d_{z^2} orbital due to elimination of the interaction with axial donors). Furthermore, from molecular mechanics MM calculations it appears that the reduced complex with four-coordinate Cu^{I} has a similar structure but is less stable than the oxidized Cu^{II} form shown in Figure 1 (ca. $+6$ kJ mol^{-1}, Cu^{I}–N = 2.00 Å (av)).

The d–d transitions can be obtained starting from computed structures by MM-AOM calculations (AOM = angular overlap model).[27, 29–34] The predicted transition energies for the six- and four-coordinate copper(II) complexes with L[35] are compared with experimental data and data of $[Cu(cyclam)(OH_2)_2]^{2+}$ in Table 1. These computations support the expectation that L induces extremely high ligand fields for the copper(II) center, which is in sharp contrast to preliminary data of an analogous compound of L.[19]

Table 1. Computed (MM-AOM) and experimentally determined electronic transitions of $[Cu(L)]^{2+}$ and $[Cu(L)(OH_2)_2]^{2+}$ as well as $[Cu(cyclam)]^{2+}$.[a]

Compound	$E_1(xz)$[b,c]	$E_2(yz)$[b,c]	$E_3(xy)$[b,c]	$E_4(z^2)$[b,c]
$[Cu(L)(OH_2)_2]^{2+}$ in H_2O (exp.)	23250 (430)	–[d]	–[d]	ca. 19200 (520)
λ,λ-$[Cu(L)(OH_2)_2]^{2+}$ (calcd)	23000	23380	22120	19530
λ,δ-$[Cu(L)(OH_2)_2]^{2+}$ (calcd)	23560	23640	22650	19640
$[Cu(L)]^{2+}$ in $MeNO_2$ (exp.)	25640 (390)	–[d]	–[d]	–[d]
λ,λ-$[Cu(L)]^{2+}$ (calcd)	24660	25040	23400	23580
λ,δ-$[Cu(L)]^{2+}$ (calcd)	24660	25220	23770	23770
$[Cu(cyclam)]^{2+}$ (exp.)[42]	19900 (500)	–[d]	–[d]	–[e]
$[Cu(cyclam)]^{2+}$ (calcd)[42]	19200	20020	20400	13600

[a] Similar results are obtained for $[Cu(L)(OH_2)]^{2+}$.[25, 35] [b] In cm^{-1} (nm); arbitrary assignment. [c] See ref. [27] for AOM parameters. [d] Single unresolved band. [e] Not reported.

The ligand L (= **3**) was prepared by reaction of 5,7-dimethyl-1,3-diazaadamantane and the bis(α-bromoacetamide) (**1**) of 1,5-dimethyl-3,7-diazabicyclo[3.3.1]nonane, following a general method,[36] and reduction of the resulting cyclic bis-amide **2** with diisbutylaluminum hydride (DIBAL-H; Scheme 2). Analytically pure samples of L and crystals suitable for the determination of the structure by X-ray crystallography were obtained by sublimation (see Experimental Section).[37] The structure of L is shown in Figure 2.[38] The ligand is, as predicted by the force-field calculations, highly preorganized, and the crystallized λ,δ conformer shows the expected zigzag geometry. The ligand backbone efficiently

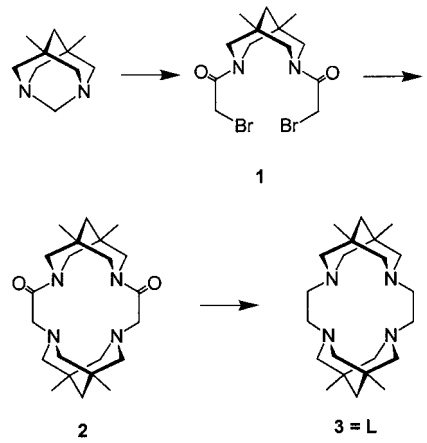

Scheme 2. Synthesis of the tetraazamacrocycle **3**.

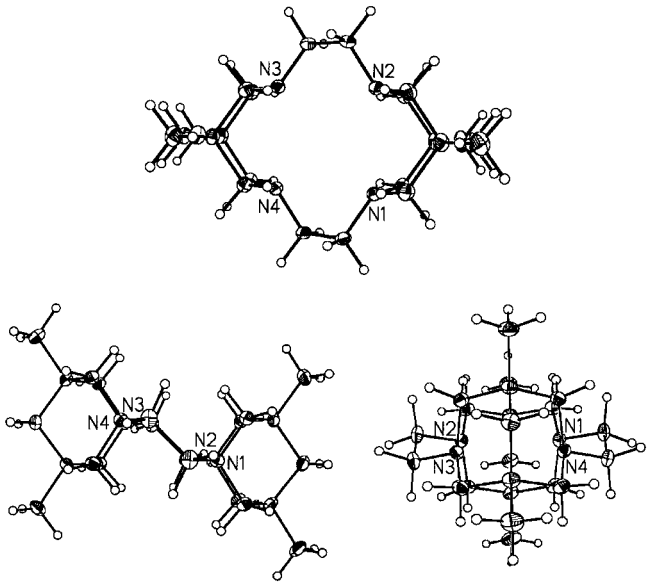

Figure 2. Structure of L (ORTEP plots[38]).

shields the cavity, and the rigidity of the structure prevents a dynamic process which could make the amine lone pairs more accessible for coordination. Therefore, the expectations are that coordination of metal ions and metal ion exchange might be processes with high activation barriers (see ref. [39, 40] for mechanistic studies of macrocycle complexation and dissociation). Furthermore, coordination of donors in the axial positions should be sterically hindered.

Copper(II) complexes were obtained by refluxing an equimolar mixture of L and $Cu(CF_3SO_3)_2$ in CH_3CN/THF. The orange perchlorate salt precipitated from a purple solution, which was obtained by ion-exchange chromatographic purification of an aqueous solution of the crude product (see Experimental Section). Because of the assumed high basicity of L,[19] water was omitted during the complexation process. Complexation experiments at room temperature in CH_3CN afforded only insoluble greenish powders with the stoichiometry Cu^{2+}:L:$CF_3SO_3^-$ = 1:1:2 (elemental analysis). This underlines the role of the high activation barrier.

  1433-7851/01/4013-2466 $ 17.50+.50/0

The electronic spectra are in good agreement with the expectations (see Table 1 and Figure 3). The four-coordinate, orange, Cu^{II} compound has the strongest ligand field for a

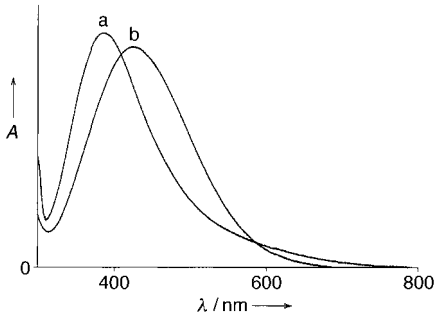

Figure 3. Electronic spectra of $[Cu(L)](ClO_4)_2$ in CH_3NO_2 (a) and in H_2O (b).

Cu^{II}–tetramine donor set observed so far.[29] In comparison with the parent $[Cu(cyclam)]^{2+}$ compound there is a shift of the maximum by 110 nm (5740 cm^{-1}, 68 kJ mol^{-1}) to lower wavelengths. This is the result of the increased nucleophilicity of the amines, a significant shortening of the Cu–N bonds, and the shielding of the axial coordination sites.[27, 29, 41, 45]

Experimental Section

A solution of bromoacetyl chloride (7.1 g, 45.1 mmol) in THF (50 mL) was added dropwise to a solution of 5,7-dimethyl-1,3-diazaadamantane (2.26 g, 14.8 mmol)[43] and $NaHCO_3$(4.2 g, 50 mmol) in THF/H_2O (120 mL; 2/1). The mixture was stirred at 0 °C for 2 h. Evaporation of THF at room temperature led to a white precipitate, which was filtered and washed with H_2O. Recrystallization from ethylacetate yielded 3,7-bis(2-bromoacetyl)-1,5-dimethyl-3,7-diazabicyclo[3.3.1]nonane (**1**) in the form of white needles (4.9 g; 83 %). Elemental analysis (%) calcd for $C_{13}H_{20}Br_2N_2O_2$ (396.12): C 39.42, H 5.09, Br 40.34, N 7.07, O 8.08; found: C 39.51, H 5.09, Br 40.38, N 7.07; ^{1}H NMR (200 MHz, $CDCl_3$, 20 °C): $\delta = 0.98$ (s, 6H; CH_3), 1.48 (s, 2H; H9), 2.45 (dd, $J = 13.9$, 2.5 Hz, 2H; H2a, H6a), 3.00 (dd, $J = 13.7$, 2.5 Hz, 2H; H4a, H8a), 3.66 (d, $J = 13.9$ Hz, 2H; H2e, H6e), 3.68 (d, $J = 11.3$ Hz, 2H; CH_2Br), 4.04 (d, $J = 11.3$ Hz, 2H; CH_2Br), 4.54 (d, $J = 13.7$ Hz, 2H; H4e, H8e); ^{13}C NMR (75 MHz, $CDCl_3$, 20 °C): $\delta = 24.1$ (CH3), 26.4 (CH_2Br), 31.1 (C1, C5), 46.7 (C9), 51.1 (C2, C8), 56.3 (C4, C6), 165.8 (CO).

A solution of **1** (5.3 g, 13.4 mmol), 5,7-dimethyl-1,3-diazaadamantane (2.2 g, 13.4 mmol), and Et_3N (5.5 mL, 40 mmol) in EtOH (650 mL) was refluxed for two days. The solvent was evaporated and the white residue washed with ice-cold water (20 mL). Filtration and drying yielded the crude macrocyclic bisamide **2** as a white powder (2.8 g, 53 %), which was used for the next step without further purification.

DIBAL-H (40 mL, 1 M solution in THF) was added to a solution of **2** (2.8 g, 7.2 mmol) in THF at −5 °C under argon. The mixture was slowly heated to 30 °C and stirred for 36 h. After addition of more DIBAL-H (20 mL) in THF, the mixture was heated to 50 °C for 2 h. Usual workup led to a yellow residue, from which pure **3** (1.3 g, 50 %) was obtained by sublimation at 100 °C and 0.1 Torr. Elemental analysis (%) calcd for $C_{22}H_{40}N_4$ (360.58): C 73.28, H 11.18, N 15.54; found: C 73.18, H 11.13, N 15.21; ^{1}H NMR (500 MHz, $CDCl_3$, 20 °C): $\delta = 0.80$ (s, 12H; CH_3), 1.24 (s, 4H; H9, H9′), 2.19 (d, $J = 10.3$ Hz, 8H; H2a, H4a, H6a, H8a, H2a′, H4a′, H6a′, H8a′), 2.56 (s, 8H; CH_2-CH_2), 2.74 (d, $J = 10.3$ Hz, 8H; H2e, H4e, H6e, H8e, H2e′, H4e′, H6e′, H8e′); ^{13}C NMR (125 MHz, $CDCl_3$, 20 °C): $\delta = 24.8$ (CH_3), 32.0 (C1, C5, C1′, C5′), 45.7 (C9, C9′), 52.4 (CH_2CH_2), 62.9 (C2, C4, C6, C8, C2′, C4′, C6′, C8′).

In an argon atmosphere, a solution of $Cu(CF_3SO_3)_2$ (2 g, 5.5 mmol) in THF/CH_3CN (50 mL; 4/1) was added dropwise to a refluxing solution of L (1.26 g, 3.5 mmol) in THF/CH_3CN (100 mL; 4/1) and the resulting solution was refluxed for 24 h. After evaporation of the solvent, the residue was dissolved in hot H_2O (500 mL), filtered and, after cooling, adsorbed onto a Sephadex SP C-25 cation exchange resin (Na^+ form). The macrocyclic complex was eluted with 0.15 M $NaClO_4$ as the first band. The orange product (0.15 g, 0.25 mmol; 7 %) precipitated upon concentration of the purple eluate to 20 mL. Elemental analysis (%) calcd for $C_{22}H_{40}N_4 \cdot Cu(ClO_4)_2$ (623.03): C 42.41, H 6.47, N 8.99; found: C 42.55, H 6.60, N 9.10.

Received: February 1, 2001 [Z 16541]

[1] G. A. E. Melson, *Coordination Chemistry of Macrocyclic Complexes*, Plenum, New York, **1982**.
[2] L. F. Lindoy, *The Chemistry of Macrocyclic Ligand Complexes*, Cambridge University Press, Cambridge, **1989**.
[3] B. Dietrich, P. Viout, J.-M. Lehn, *Macrocyclic Chemistry. Aspects of Organic, Inorganic and Supramolecular Chemistry*, VCH, Weinheim, **1993**.
[4] S. R. Cooper, *Crown Compounds: Toward Future Applications*, VCH, Weinheim, **1992**.
[5] N. V. Gerbeleu, V. B. Arion, J. Burgess, *Template Synthesis of Macrocyclic Compounds*, Wiley-VCH, Weinheim, **1999**.
[6] R. D. Hancock, G. Pattrick, P. W. Wade, G. D. Hosken, *Pure Appl. Chem.* **1993**, *65*, 473.
[7] P. Comba in *Chemistry at the Beginning of the Third Millennium* (Eds.: L. Fabbrizzi, A. Poggi), Springer, Berlin, **2000**, p. 49.
[8] P. Comba, *Coord. Chem. Rev.* **2000**, *200–202*, 217.
[9] J. Chapman, G. Ferguson, J. F. Gallagher, M. C. Jennings, D. Parker, *J. Chem. Soc. Dalton Trans.* **1992**, 345.
[10] K. P. Wainwright, *Inorg. Chem.* **1980**, *19*, 1396.
[11] G. D. Hosken, R. D. Hancock, *J. Chem. Soc. Chem. Commun.* **1994**, 1363.
[12] G. D. Hosken, C. C. Allan, J. C. A. Boeyens, R. D. Hancock, *J. Chem. Soc. Dalton Trans.* **1995**, 3705.
[13] P. Comba, B. Nuber, A. Ramlow, *J. Chem. Soc. Dalton Trans.* **1997**, 347.
[14] P. Comba, B. Kanellakopulos, C. Katsichtis, A. Lienke, H. Pritzkow, F. Rominger, *J. Chem. Soc. Dalton Trans.* **1998**, 3997.
[15] H. Börzel, P. Comba, C. Katsichtis, W. Kiefer, A. Lienke, V. Nagel, H. Pritzkow, *Chem. Eur. J.* **1999**, *5*, 1716.
[16] H. Börzel, P. Comba, K. S. Hagen, C. Katsichtis, H. Pritzkow, *Chem. Eur. J.* **2000**, *6*, 914.
[17] P. Comba, A. Lienke, *Inorg. Chem.* **2001**, submitted.
[18] P. Comba, M. Merz, M. Kerscher, H. Börzel, unpublished results.
[19] Y. Miyakawa, K. Goto, T. Inazu, *Chem. Lett.* **2000**, 620.
[20] D. S. C. Black, G. B. Deacon, M. Rose, *Tetrahedron* **1995**, *51*, 2055.
[21] P. Comba, T. W. Hambley, N. Okon, G. Lauer, MOMEC97 a molecular modeling package for inorganic compounds, CVS, e-mail: cvs@t-online.de, Heidelberg, **1997**.
[22] J. E. Bol, C. Buning, P. Comba, J. Reedijk, M. Ströhle, *J. Comput. Chem.* **1998**, *19*, 512.
[23] Structures calculated by well-tuned force fields are assumed to lead to accuracies of about ±0.01 Å (bond lengths; note that the axial bonds to copper(II) are very weak and, therefore, their predicted distances might be considerably less accurate); ±2° (valence angles), ±5° (torsion angles; symmetrical structures, that is, averages of all corresponding structural parameters).[24] Note that the validation of computed structures by the computation of molecular properties is in general an important factor for accurate predictions (e.g., the MM-AOM method).
[24] P. Comba, T. W. Hambley, *Molecular Modeling of Inorganic Compounds*, 2nd ed., Wiley-VCH, Weinheim, **2001**.
[25] The two possible conformations each of four-, five-, and six-coordinate Cu^{II} species ($[Cu(L)(OH_2)_n]^{2+}$, $n = 0, 1, 2$) were optimized; only the four-coordinate Cu^{II} complexes are shown in Figure 1. The force-field calculations use harmonic potentials, that is, the axial donors cannot dissociate, and it is not possible to deduce the relative stabilities from the strain energies of the four-, five-, and six-coordinate Cu^{II} species. For each of the three sets of structures the λ,λ conformer was more stable than the λ,δ conformer (four-coordinate: +14 kJ mol^{-1}; five-coordinate: +13 kJ mol^{-1}; six-coordinate: +8 kJ mol^{-1}).
[26] J. Emsley, M. Arif, P. A. Bates, M. A. Hursthouse, *J. Chem. Soc. Chem. Commun.* **1988**, 1387.

  1433-7851/01/4013-2467 $ 17.50+.50/0

[27] P. Comba, T. W. Hambley, M. A. Hitchman, H. Stratemeier, *Inorg. Chem.* **1995**, *34*, 3903.
[28] Cu–N (four-coordinate): 1.97 (λ,λ), 1.98 Å (δ,λ); Cu–N (five-coordinate): 1.98 (λ,λ), 1.99 Å (δ,λ); Cu–N (six-coordinate): 1.97 (λ,λ), 2.00 Å (δ,λ).
[29] P. Comba, *Coord. Chem. Rev.* **1999**, *182*, 343.
[30] P. V. Bernhardt, P. Comba, *Inorg. Chem.* **1993**, *32*, 2798.
[31] P. Comba in *Implications of Molecular and Materials Structure for New Technologies* (Eds.: J. K. A. Howard, F. H. Allen, G. P. Shields), Kluwer, Dordrecht, **1999**, p. 87.
[32] CAMMAG[33, 34] with a published parameter set[27, 31] was used for the AOM calculations.
[33] M. Gerloch, University of Cambridge, Cambridge, UK, **1991**.
[34] H. Stratemeier, M. A. Hitchman, P. Comba, P. V. Bernhardt, M. J. Riley, *Inorg. Chem.* **1991**, *30*, 4088.
[35] The five-coordinate Cu^{II} species are spectroscopically similar to the six-coordinate Cu^{II} species and not explicitely discussed here.
[36] J. S. Bradshaw, K. E. Krakowiak, R. M. Izatt, *Aza-Crown Macrocycles*, *Vol. 51*, Wiley, New York, **1993**.
[37] L ($C_{22}H_{40}N_4$): $M_r = 360.58$, monoclinic, space group $P2_1/c$, $a = 10.3548(3)$, $b = 13.5490(4)$, $c = 15.6230(4)$ Å, $\beta = 97.351(2)^\circ$, $V = 2173.8(10)$ Å^3, $Z = 4$, $\rho_{calcd} = 1.102$ g cm^{-3}, $F(000) = 800$, $\mu(Mo_{K\alpha}) = 0.07$ mm^{-1}, $\theta_{max} = 32^\circ$. $R_1 = 0.045$ ($I > 2\sigma(I)$), w$R_2 = 0.141$ (all reflections). Data collection: Bruker AXS SMART 1000 area detector, $Mo_{K\alpha}$ radiation $\lambda = 0.71073$ Å, $T = 190$ K; 7243 unique reflections. The structure was solved by direct methods and refined against F^2 on all data by full-matrix least-squares with SHELXTL 5.10,[44] non-hydrogen atoms anisotropic, hydrogen atoms located and refined isotropically. Crystallographic data (excluding structure factors) for the structure reported in this paper have been deposited with the Cambridge Crystallographic Data Centre as supplementary publication no. CCDC-155971. Copies of the data can be obtained free of charge on application to CCDC, 12 Union Road, Cambridge CB2 1EZ, UK (fax: (+44) 1223-336-033; e-mail: deposit@ccdc.cam.ac.uk).
[38] C. K. Johnson, ORTEP: A Thermal Ellipsoid Plotting Program, Oak Ridge National Laboratories, Oak Ridge, TN, **1965**.
[39] D. Cabbiness, D. W. Margerum, *J. Am. Chem. Soc.* **1970**, *92*, 2152.
[40] L. Hertli, T. A. Kaden, *Helv. Chim. Acta* **1974**, *57*, 1328.
[41] P. Comba in *Intermolecular Interactions* (Eds.: W. Gans, J. C. A. Boeyens), Plenum, New York, **1998**, p. 97.
[42] L. Fabbrizzi, M. Micheloni, P. Paoletti, *J. Chem. Soc. Dalton Trans.* **1979**, 1581.
[43] A. I. Kuznetsov, E. B. Basargin, M. Kh. Ba, A. S. Moskovin, I. V. Miroshnichenko, M. Ya. Bosnikov, *Khim. Geterotsikl. Soedin. Sb.* **1989**, 647.
[44] G. M. Sheldrick, SHELXTLV5.10, Bruker AXS, Madison, WI, **1999**.
[45] Note added in proof (May 30, 2001): while this manuscript was in press, a publication on the synthesis and structure of a ligand similar to L appeared: Y. Miyahara, K. Goto, T. Inazu, *Tetrahedron Lett.* **2001**, *42*, 3097.

Novel Amide-Based Molecular Knots: Complete Enantiomeric Separation, Chiroptical Properties, and Absolute Configuration**

Fritz Vögtle,* Annette Hünten, Erik Vogel, Sven Buschbeck, Oliver Safarowsky, Janosch Recker, Amir-Hossain Parham, Michael Knott, Walter M. Müller, Ute Müller, Yoshio Okamoto,* Takateru Kubota, Wolfgang Lindner, Eric Francotte, and Stefan Grimme*

Recently we described the first knot-shaped molecule[1] containing amide bonds.[2] We now report the syntheses of new "knotanes",[3] the first complete separation of a racemic knotane mixture, and the experimental and theoretical characterization of the compounds; we also give hints about a possible formation mechanism.

The baseline separation of the racemic trefoil knot **3aα**[2] (see Scheme 1) was achieved by high-pressure liquid chromatography (HPLC)[4] on a Chiralpak-AD-type column that is not commercially available, in which the silica gel and the chiral stationary phase are covalently bound so that the material does not "bleed out", even if lipophilic eluents are used. While, previously, eluents like hexane/ethanol (85/15) without trichloromethane resulted only in incomplete resolution (peaks with "shoulders"),[2] we were now able to

[*] Prof. Dr. F. Vögtle, Dipl.-Chem. A. Hünten, Dipl.-Chem. E. Vogel, Dipl.-Chem. S. Buschbeck, Dr. O. Safarowsky, M.Sc. J. Recker, Dr. A.-H. Parham, Dipl.-Chem. M. Knott, W. M. Müller, U. Müller
Kekulé-Institut für Organische Chemie
und Biochemie der Universität Bonn
Gerhard-Domagk-Strasse 1, 53121 Bonn (Germany)
Fax: (+49) 228-735662
E-mail: voegtle@uni-bonn.de

Prof. Dr. Y. Okamoto, T. Kubota
Nagoya University
Department of Applied Chemistry
Graduate School of Engineering
Chikusa-ku, Nagoya 464-8603 (Japan)
Fax: (+81) 52-789-3188
E-mail: okamoto@apchem.nagoya-u.ac.jp

Prof. Dr. S. Grimme
Organisch-Chemisches Institut
(Abt. Theoretische Chemie)
Westfälische Wilhelms-Universität
Corrensstrasse 40, 48149 Münster (Germany)
Fax: (+49) 251-8336515
E-mail: grimmes@uni-muenster.de

Prof. Dr. W. Lindner
Institut für Analytische Chemie
Universität Wien
Währingerstrasse 38, 1090 Wien (Austria)

Dr. E. Francotte
Novartis Pharma AG
Drug Discovery, K-122.P.25
4002 Basel (Switzerland)

[**] We would like to thank Prof. F. V. Schurig for his advice regarding the separation of the enantiomers. The results reported here were, in part, presented in Chamonix (September 2000; W.L.) and in Vienna, Tsukuba, Kopenhagen, Bordeaux, and Strasbourg (October–December 2000; F.V.).

  1433-7851/01/4013-2468 $ 17.50+.50/0

separate the enantiomers with an astonishingly large separation factor (α) of 2.14 (Figure 1, Table 1).

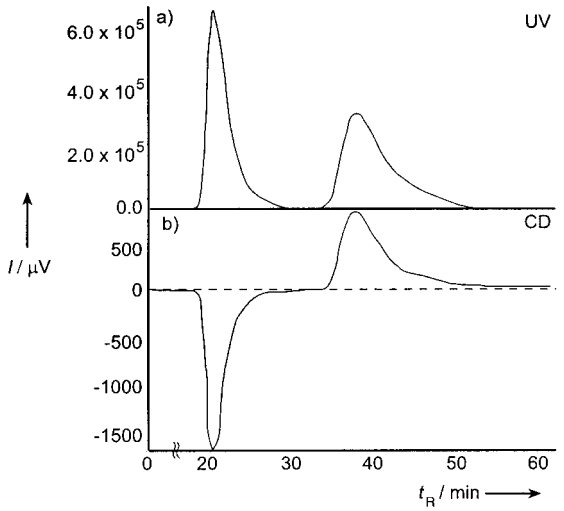

Figure 1. Separation of racemic knot **3aα** by HPLC: a) UV detection and b) circular dichroism detection of both enantiomers. Both graphs were measured at $\lambda = 280$ nm and show intensity I against retention time t_R.

The experimental circular dichroism (CD) spectra of the enantiomers of **3aα** are shown in Figure 2; the two curves a and b are mirror symmetrical and exhibit maxima at 240 nm ($\Delta\varepsilon = +100$, $-108\ mol^{-1}\,L\,cm^{-1}$), 272 nm ($\Delta\varepsilon = \pm 4\ mol^{-1}\,L\,cm^{-1}$), and 293 nm ($\Delta\varepsilon = \pm 8\ mol^{-1}\,L\,cm^{-1}$). Curves c and d in Figure 2 are theoretically calculated CD spectra of knotane **3aα** that were simulated prior to the actual experimental measurements. They were calculated with a semiempirical π-electron method (time-dependent Pariser–Parr–Pople, TDPPP),[6a] with all benzene and amide building blocks accounted for (altogether 156 π electrons, 144 atoms). The TDPPP calculation and the subsequent simulation of the CD spectrum[6b] were based once upon the crystal structure (Figure 2, curve c) and once upon a fully optimized AM1 geometry (Figure 2, curve d).[6c] Considering the simplicity of the calculation method and the complexity of the molecule, the resulting theoretical spectrum represents an astonishingly close fit to the experimentally obtained curve. The AM1-geometry method delivers a quite accurate prediction of the position and intensity of the strong band at 240 nm. The multitude of transitions of this band result mainly from the exciton-coupled $B_{a/b}$ states of the benzene/benzene-amide units. The slightly positive band at around 290 nm in the CD spectrum corresponds to the intensive shoulder in the UV spectrum ($\varepsilon = 40\,000\ mol^{-1}\,L\,cm^{-1}$), caused by the lowest transitions in the benzeneamide-units. The negative Cotton effect at 270 nm, also correctly predicted by the calculation, is due to the coupled L_b transitions. Since the sign of the two weak signals relies heavily on the applied geometry, they do not allow an assignment of the absolute configuration. In contrast, the strong band at 240 nm is stable in respect to variations in the calculations and allows the absolute configuration of the laevorotatory enantiomer at 365 nm (with a negative Cotton effect at 240 nm) to be clearly assigned as ppp.[7, 8] The strong blue shift of this band when the crystal structure is used as the basis for the TDPPP calculation is explained by a higher degree of intertwinement between the amide and the benzene units (decrease of conjugation) compared to the AM1 structure, which seems to reflect better

Table 1. Experimental data of enantiomer separation.

Compd	HPLC resin	Eluent *n*-hexane/ Cl_3CH/*i*PrOH	Flow rate [mL min^{-1}]	Selectivity factor $\alpha = k_2'/k_1'$
3aα	Chiralpak-AD-type[5]	30/20/1	0.5	2.14
3aβ	Chiralpak-AD-type[5]	30/20/1	0.5	2.14
3bα	Chiralpak-AD-type[5]	15/10/1	0.5	11.32
3cα	Chiralcel-OD-type[9]	65/30/5[a]	0.8[b]	1.34
3aα	Chiralpak-AD-type[9]	75/21/4	0.7[a]	1.60
3aγ	Chiralpak-AD-type[5]	60/40/1	0.5	1.92
3aδ	Chiralpak-AD-type[5]	60/40/2	0.5	1.78

[a] With ethanol instead of isopropylalcohol. [b] Column dimensions: 250 × 4 mm.

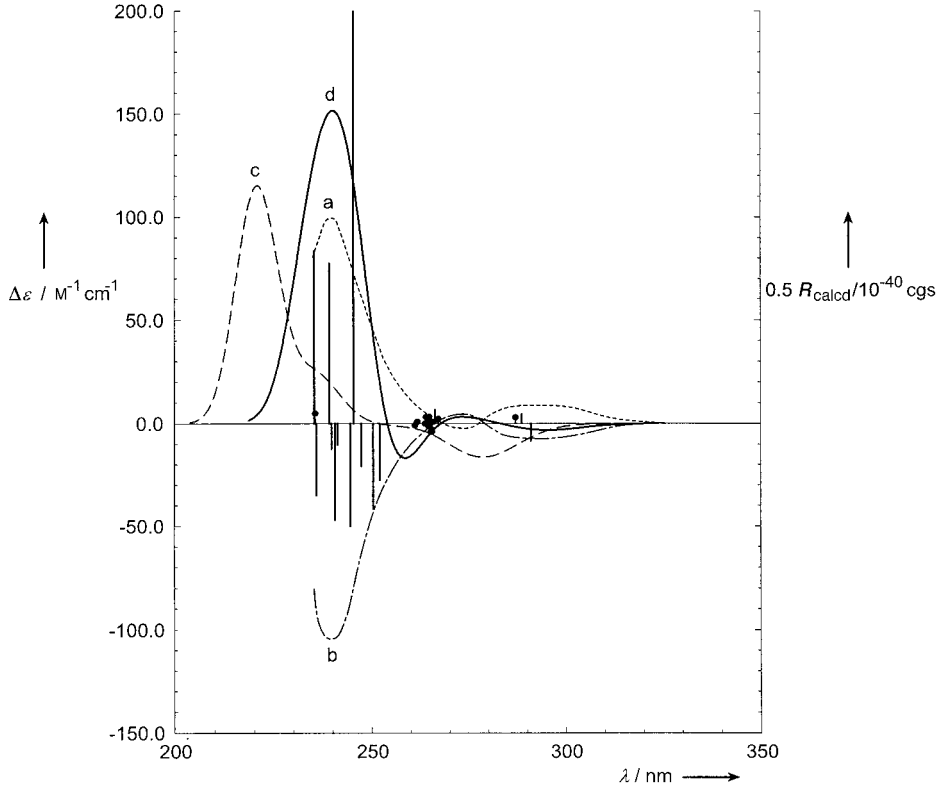

Figure 2. Experimental CD spectra of knotane **3aα**: a) (+)-enatiomer (----); b) (−)-enatiomer (– – –). Theoretical CD spectra of knotane **3aα**: c) Based on the X-ray crystal structure analysis (– – –); d) based upon the knot structure calculated with AM1 (——).

  1433-7851/01/4013-2469 $ 17.50+.50/0

the situation in solution. We know from molecular dynamic simulations (5 ps at 300 K)[6d] that the knot structure is relatively fixed by hydrogen bonds and sterically demanding substituents. This allows us to conclude that no significant differences in the theoretical simulation are to be expected due to the flexibility of the molecular knot.

The limits and possibilities of knotane formation were explored (Scheme 1). Initial attempts to synthesise the knot **3aα** from the "inverted building block" (that is, by treatment

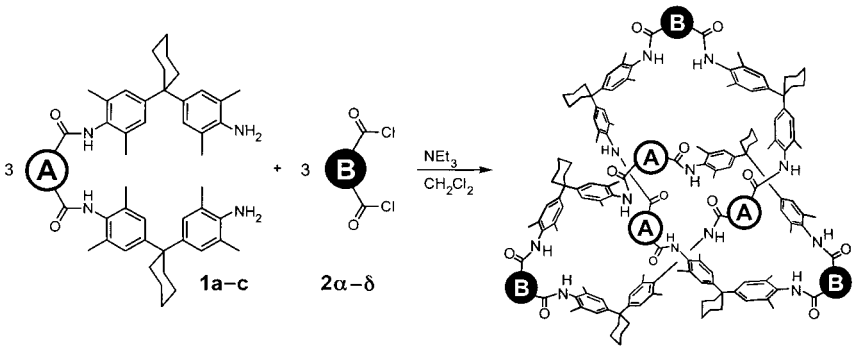

3	aα	aβ	aγ	aδ	bα	cα
A	a	a	a	a	b	c
B	α	β	γ	δ	α	α
Yield [%]	20	4	9	10	1	2

Scheme 1. New amide molecular knots **3**.

of the extended diamide with acid chloride **2α** to form building block "**1α**" (not shown) and then trimerization and cyclization with isophthalic acid dichloride failed to deliver any isolable amounts of knotane. The previously published synthesis of **3aα** proved to be quite solvent dependent: The use of dimethylformamide as the solvent instead of dichloromethane did not lead to the formation of knotane in noticeable amounts. In order to make the ^{1}H NMR signal assignment of the **3aα** knotane easier, the diamide **1a** was treated with 5-deutero-2,6-pyridine dicarboxylic acid dichloride **2β**. The enantiomers of the new knotane **3aβ** were separated under conditions similar to those for **3aα**, in order to verify the previous results. The steric bulk of a methyl group in the 5-position seems to be sufficiently small to allow a new molecular knot **3bα** to be formed from 5-methyl-isophthalic acid diamide **1b**. The racemate separation on the Chiralpak-AD column is mentioned earlier (Table 1).

The X-ray crystal structure analysis of knotane **3aα**[2] showed the existence of intramolecular hydrogen bonds between the amide protons and the pyridine nitrogen atom. This could allow a preference of conformation in an intermediate structure during the synthesis, thus allowing the knotted structure to be formed. The aim of the following reaction was to investigate whether the knot synthesis failed when the specific conformation of the intermediate structure was not allowed to form. The 3,5-pyridine building block **1c** was reacted with acid chloride **2α** to yield the knotane **3cα**. This was separated into its enantiomers on a chiral stationary phase (CSP) of the OD type,[9] in which the stationary phase forms a branched, polymeric coating on the silica and makes it, therefore, solvent resistant (Table 1). The separated peak volumes were collected from several experiments on this column and an external CD spectrometer was used to record the two mirror-symmetrical CD spectra. Similar chromatographic separation results were obtained for **3cα** with a two dimensionally branched CSP of the AD type; under the same separation conditions as above an α value of 1.6 was obtained (Table 1).

Furthermore the 2,6-pyridinedicarboxylic acid dichlorides **2γ** and **2δ**, substituted in the 4-position, were reacted with the building block **1a**. The successful syntheses yielded the knotanes **3aγ** and **3aδ**, which could be quantitatively baseline separated into their respective enatiomers (Table 1).

Summing up the results of the knotane syntheses so far, we are able to draw the following conclusions regarding the nature of the templating formation mechanism:[2, 10] No additional templating agent (external template) is used, rather all six educt molecules are reacting in an "internal templating reaction" that yields the molecular knot. A helical host loop, suggested by the crystal structure[2] of the knot **3aα** could wind itself around the guest **1a** (Figure 3). The host/guest bonding is then achieved through hydrogen bonding. The two remaining acid chlorides **2a** react with the terminal amide groups of the loop, thus forming the molecular knot **3aα**: A novel preorganization pattern.[11]

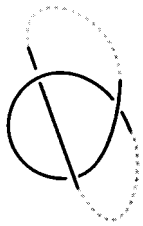

Figure 3. Postulated supramolecular template to allow formation of the molecular knot (host loop and amide host are fixed by hydrogen bonds between the CONH hydrogen atoms and the carbonyl oxygen atoms.

In spite of the complex formation mechanism, knotane synthesis can be carried out with other arene building blocks, such as thiophene rings,[12a] as well as with the introduction of other functional groups (for example, methoxy groups in **3aδ**). The cleavage of ether groups[12b] allows, for the first time, the use of molecular knots as precursors for further reactions (for example, nano particles[13]). We therefore have strong evidence to believe that topologically chiral molecular knots,[1–3] which up until now have been rather rare, will increase significantly in number in the future.

Received: December 21, 2000 [Z16314]

  1433-7851/01/4013-2470 $ 17.50+.50/0

[1] An overview on molecular knots: a) G. Schill, *Catenanes, Rotaxanes and Knots*, Academic Press, New York, **1971**; b) *Molecular Catenanes, Rotaxanes and Knots* (Eds.: J.-P. Sauvage, C. Dietrich-Buchecker), Wiley-VCH, Weinheim, **1999**; c) J.-P. Sauvage, C. Dietrich-Buchecker in *Molecular Catenanes, Rotaxanes and Knots* (Eds.: J.-P. Sauvage, C. Dietrich-Buchecker), Wiley-VCH, Weinheim, **1999**, pp. 105 – 142; d) N. C. Seeman in *Molecular Catenanes, Rotaxanes and Knots* (Eds.: J.-P. Sauvage, C. Dietrich-Buchecker), Wiley-VCH, Weinheim, **1999**, pp. 323 – 356; e) P. R. Ashton, O. A. Matthews, S. Menzer, F. M. Raymo, N. Spencer, J. F. Stoddart, D. J. Williams, *Liebigs Ann.* **1997**, 2485 – 2494; f) G. A. Breault, C. A. Hunter, P. C. Mayers, *Tetrahedron* **1999**, *55*, 5265 – 5293; g) for nomenclature and absolute configuration of chiral knots, see: C. Dietrich-Buchecker, G. Rapenne, J.-P. Sauvage, A. De Cian, J. Fischer, *Chem. Eur. J.* **1999**, *5*, 1432 – 1439.

[2] a) O. Safarowsky, M. Nieger, R. Fröhlich, F. Vögtle, *Angew. Chem.* **2000**, *112*, 1699 – 1701; *Angew. Chem. Int. Ed.* **2000**, 39, 1616 – 1618; b) P. Zurer, *Chem. Eng. News* **2000**, *78*(19), 14; c) S. Albus, *Nachr. Chem.* **2000**, *7/8*, 887.

[3] O. Safarowsky, B. Windisch, A. Mohry, F. Vögtle, *J. Prakt. Chem.* **2000**, *5*, 437 – 444.

[4] So far racemic knotane mixtures have not been separated by chromatography, instead separation has been achieved through diastereomers: "Unfortunately, this technique seemed to be inappropriate to the resolution of the knot" (ref. [1b], p. 36).

[5] N. Enomoto, S. Furukawa, Y. Ogasawara, H. Akano, Y. Kawamura, E. Yashima, Y. Okamoto, *Anal. Chem.* **1996**, *68*, 2798 – 2804.

[6] a) For the PPP-SCF method (overview: M. Scholz, H. J. Köhler, *Quantenchemie*, *Vol. 3*, Hüthig, Heidelberg, **1981**), standard parameters (J. Pancir, I. Matousek, R. Zahradnik, *Collect. Czech. Chem. Commun.* **1973**, *38*, 3039) and the Mataga – Nishimoto and Ohno – Klopman approximations (N. Mataga, K. Nishimoto, *Z. Phys. Chem. NF* **1957**, *12*, 335; K. Ohno, *Theor. Chim. Acta* **1964**, 219; G. J. Klopman, *J. Am. Chem. Soc.* **1964**, *86*, 4450) were used for the two-electron integrals ($\gamma = 1.2\gamma_{MN} - 0.2\gamma_{OK}$). Contracted cartesian Gaussian functions (STO-6G) and standard Slater exponents were used as the basis for the p atomic orbitals (pAOs). The electrical (velocity form) and magnetical dipol integrals were calculated exactly with the Löwdin-deorthogonalized ZDO basis. To describe the nonplanarity of the conjugated units, the oriented pAOs were represented by the sum of the $c_{x^*}p_x$, $c_{y^*}p_y$, and $c_{z^*}p_z$ AOs, while the coefficient $c_x - c_z$ was determined by the plane's orientation in space, as defined by its closest π neighbors. The entire program, which also includes the solution of the TDPPP equation, can be downloaded from the WWW as a fortran source code from: http://www.uni-muenster.de/Chemie/OC/research/grimme/. b) The broadening of the oscillation of each transition was simulated by summing up Gaussian curves that have been weighted based upon rotational strength, with a width of 0.2 eV at a height of e^{-1}. The theoretical $\Delta\varepsilon$ values are obtained as absolutes, that is, they can be directly compared with the experimental data. See also: S. Grimme, J. Harren, A. Sobanski, F. Vögtle, *Eur. J. Org. Chem.* **1998**, 1491 – 1509; c) AM1: M. J. S. Dewar, E. G. Zoebisch, E. F. Healy, J. J. P. Stewart, *J. Am. Chem. Soc.* **1985**, *107*, 3902 – 3909; MOPAC 6.0: J. J. P. Stewart, *QCPE Bull.* **1985**, *5*, 133; d) MMX force field: PCModel 7.0, Serena Software, Bloomington, **1999**.

[7] For nomenclature of molecular knots and their chirality, see ref. [1c], as well as D. M. Walba, *Tetrahedron* **1985**, *41*, 3161 – 3212; M. Epple, *Die Entstehung der Knotentheorie*, Vieweg, Wiesbaden, **1999**, pp. 31 – 43.

[8] In supplement to ref. [3]: The determination of the relative positions of the knot's cross-over sections is carried out as follows (Figure 4): If it is possible to project the line crossing below (broken arrow) onto the line running above (complete arrow) by a rotation of less than 180°, the cross-over section is marked by a superscript p (clockwise rotation) or m (counterclockwise rotation). To determine the direction of the arrows, they have to be moved along the graph in a clockwise motion. The molecular knots described here can therefore be characterized as 3_1^{ppp} or 3_1^{mmm}, depending on the enantiomer.

[9] a) E. Francotte, *J. Chromatogr. A* **2001**, *906*, 379 – 397; b) N. M. Maier, P. Franco, W. Lindner, *J. Chromatogr. A* **2001**, *906*, 3 – 33.

[10] a) *Templated Organic Synthesis* (Eds.: F. Diederich, P. J. Stang), Wiley-VCH, Weinheim, **2000**; b) N. V. Gerbeleu, V. B. Arion, J. Burgess, *Template Synthesis of Macrocyclic Compounds*, Wiley-VCH, Weinheim, **1999**; c) R. Hoss, F. Vögtle, *Angew. Chem.* **1994**, *106*, 389 – 398; *Angew. Chem. Int. Ed. Engl.* **1994**, *33*, 375 – 384; d) S. Anderson, H. L. Anderson, J. K. M. Sanders, *Acc. Chem. Res.* **1993**, *26*, 469 – 475.

[11] O. Safarowsky, PhD Thesis, Universität Bonn, **2000**.

[12] Preliminary results: a) M. Knott, Diploma Thesis, Universität Bonn, **2000**; b) E. Vogel, Dissertation, Universität Bonn, **2001**.

[13] Molecular knots of this type measure 4 – 5 nm across.

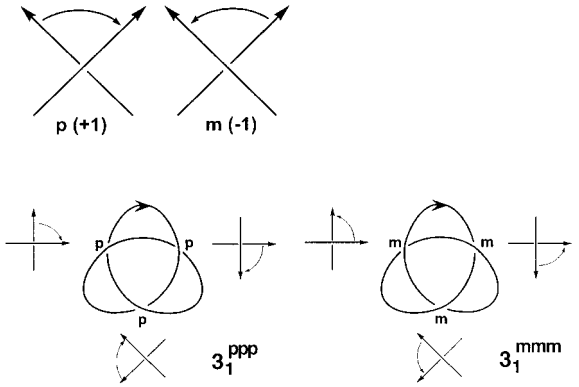

Figure 4. Determination of the chirality of knotted molecules.

Synthesis of the First 1,3,4-Triphosphole Complex**

Rainer Streubel,* Udo Schiemann, Peter G. Jones, Jörg Grunenberg, Hans-Martin Schiebel, and Dietrich Gudat*

Dedicated to Professor Manfred Regitz on the occasion of his 65th birthday

The development of phosphorus-containing 6π-arenes such as phosphinines (phosphabenzenes) is currently attracting attention because of the considerable interest from industry in novel directing ligands for catalytic processes,[1, 2] yet it still suffers from a lack of rational and efficient synthetic methods. Interesting candidates as novel ligands with 6π-electron systems besides phosphinines are phosphorus-rich hetero-

[*] Prof. Dr. R. Streubel, Dipl.-Chem. U. Schiemann, Prof. Dr. P. G. Jones
Institut für Anorganische und Analytische Chemie
der Technischen Universität Braunschweig
Postfach 3329, 38023 Braunschweig (Germany)
Fax: (+49) 531-391-5387
E-mail: r.streubel@tu-bs.de

Dr. J. Grunenberg, Dr. H.-M. Schiebel
Institut für Organische Chemie
der Technischen Universität Braunschweig
Postfach 3329, 38023 Braunschweig (Germany)

Prof. Dr. D. Gudat
Institut für Anorganische Chemie der Universität Bonn
Gerhard-Domagk-Strasse 1, 53121 Bonn (Germany)
Fax: (+49) 228-73-5327
E-mail: dgudat@uni-bonn.de

[**] This work was supported by the Deutsche Forschungsgemeinschaft and the Fonds der Chemischen Industrie. We thank Andreas Weinkauf for measuring the X-ray data.

phospholes, in which, according to theoretical studies, the replacement of CH groups by P atoms induces an increasing tendency towards planarization of the tricoordinate phosphorus center in the ring.[3, 4] A milestone in this field was the first synthesis of aromatic 1,2,4-triphosphole derivatives.[5, 6]

In the course of our systematic investigations towards the synthesis of novel heterophosphole complexes with a tricoordinate phosphorus atom and one[7] or two[8–10] further heteroatoms in the ring, we have now obtained the first 1,3,4-triphosphole complex **3** in good yield (>90% of crude product) by thermally induced, regiospecific insertion of the phosphaalkyne **2**[11] into the P–P bond of the 1*H*-diphosphirene complex **1** (Scheme 1); preliminary results will be reported, hereafter. The starting material **1** is readily available by methanolysis of **4**.[12] Formation of a regioisomer of **3** was not observed.

As a possible reaction mechanism for the formation of **3** we postulate the initial formation of a phosphanediyl **5**, which then undergoes a [2+1] cycloaddition with **2** to give the 1*H*-diphosphirene derivative **6**, which in turn undergoes a ring expansion to afford the 1,3,4-triphosphole complex **7**. A subsequent 1,3-shift

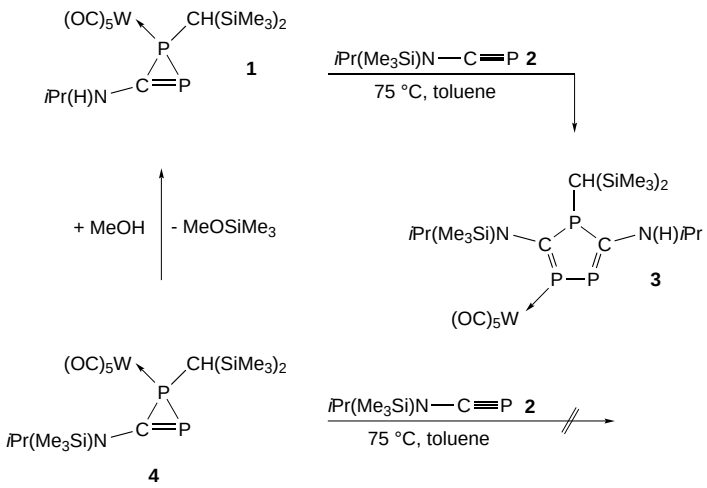

Scheme 1. Reactions of the 1*H*-diphosphirene complexes **1** and **4** with phosphaalkyne **2.**

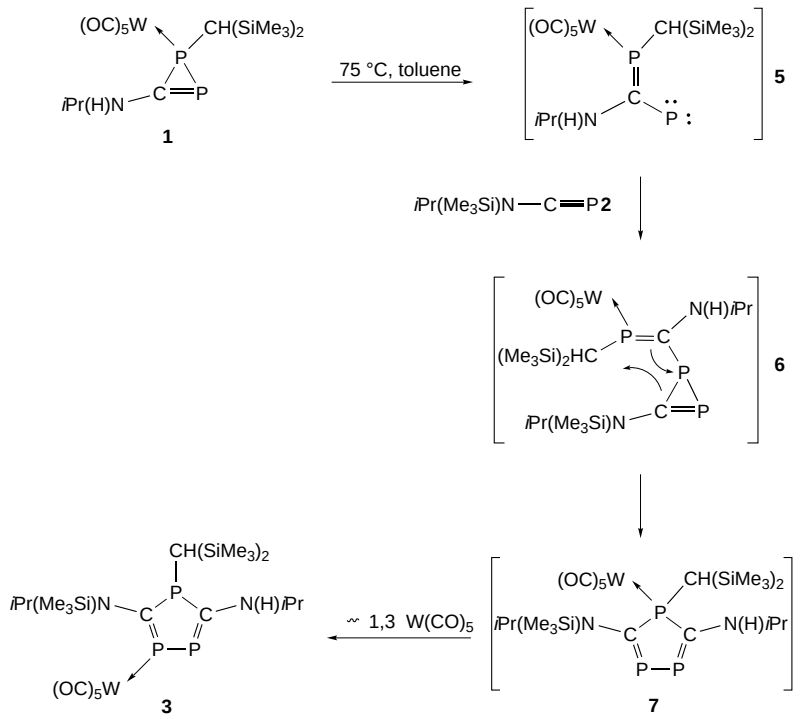

Scheme 2. Proposed reaction mechanism for the formation of the 1,3,4-triphosphole complex **3**.

of the $(CO)_5W$ fragment in **7** yields the final product **3** (Scheme 2). These hypotheses are based on former results and model considerations of the chemical behavior of reactive 1*H*-diphosphirene complexes, for which P–P[13] or P–C bond cleavage processes[14] have also been suggested as primary reaction steps. Likewise, migrations of coordinated metal complex fragments from $\sigma^3\lambda^3$- to $\sigma^2\lambda^3$-phosphorus centers have been reported repeatedly.[12, 15] Surprisingly, control experiments revealed that the 1*H*-diphosphirene complex **4** failed to react with **2** under similar conditions. Even though the lack of significant differences between the molecular structures of complexes **1** and **4** (vide infra) gave no explicit clue for a different bonding situation, we propose as the most reasonable explanation of this remarkable chemoselectivity that the activation energy required for the formation the reactive intermediate of type **5** is liable to considerable electronic substituent influences.

The constitution of complexes **1**, **3**, and **4** follows unequivocally from their NMR and MS data.[16] In addition, the molecular structures of complexes **1** (Figure 1) and **4** were determined from single-crystal X-ray diffraction studies.[17]

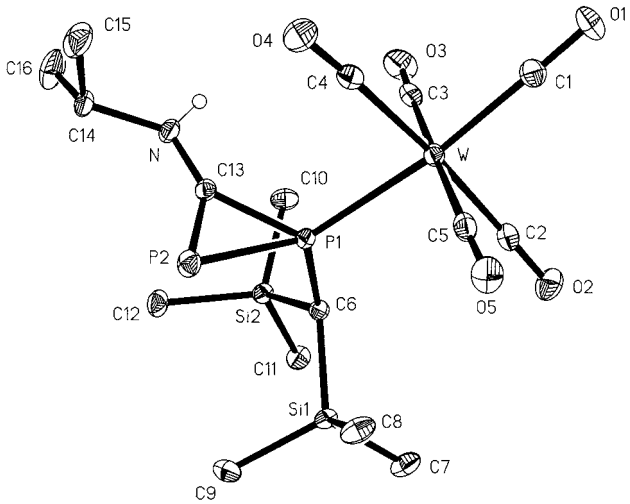

Figure 1. Molecular structure of compound **1** in the crystal (thermal ellipsoids at 30% probability level; H atoms are omitted for clarity). Selected bond lengths [pm] and angles [°]: W-P1 251.97(12), P1-C6 183.2(3), P1-C13 178.8(3), P1-P2 217.56(14), P2-C13 169.6(3), C13-N 132.7(4); P2-P1-C13 49.49(10), P2-C13-P1 77.22(13), C13-P2-P1 53.28(10), P2-C13-N 142.4(2).

  1433-7851/01/4013-2472 $ 17.50+.50/0

The individual bond lengths and angles exhibit no peculiarities and show close similarities in both complexes. The dihedral angle C14-N-C13-P2 in **1** (−173.7°) indicates an almost coplanar orientation of the amino group relative to the plane of the three-membered ring, with the bulky substituent on the nitrogen atom pointing away from the coordinated phosphorus atom. Conjugation between the P–C double bond and the lone pair of electrons at the nitrogen atom is indicated by the relatively short C–N distance. Interestingly, and in contrast to other 1*H*-diphosphirene complexes that have less sterically demanding substituents at the σ^3-phosphorus atom,[18, 19] only a single conformer of **1** is observed even in solution.

The postulated constitution of **3** was further substantiated by an X-ray diffraction study, even though an adequate final refinement of the structure proved impossible owing to severe disorder of the *i*Pr(Me$_3$Si)N group. Nevertheless, the available data provided evidence for a weakly pyramidal configuration at the σ^3-phosphorus atom[20] which points to the presence of a low inversion barrier and can be understood as a step towards aromatization of the cyclic π system.[5, 6]

The assumption of a low inversion barrier at the σ^3-phosphorus atom was corroborated by solution NMR studies. The ^{1}H NMR spectrum of **3** at 25 °C displays a broad signal for the methyl protons of the (Me$_3$Si)$_2$CH substituent, which decoalesces when the temperature is lowered, and finally splits into two equally intense singlets at −45 °C. Similar splittings were observed for the methyl protons in both *N*-isopropyl groups. The results of lineshape analyses revealed that all three exchange processes occur at the same rate and can thus be assigned to a single dynamic process whose activation parameters were determined from an Eyring plot as $\Delta H^{\neq} = 41.4 \pm 1.2$ kJ mol^{-1} and $\Delta S^{\neq} = -50 \pm 5$ eu. Based on the analysis of 2D ^{1}H ROESY spectra taken at different temperatures, the observed effects can be explained as the result of hindered rotation of the *i*Pr(Me$_3$Si)N group which at −45 °C is frozen in a notably twisted orientation relative to the ring plane.[21] Additional NMR measurements gave no evidence of further dynamically induced signal-broadening effects down to −92 °C. In summary, these findings prove that the P inversion in **3** must proceed at the same rate as or a higher rate than the rotation of the *i*Pr(Me$_3$Si)N group, and that the activation barrier for the amine rotation can thus be regarded as an upper limit for the P-inversion barrier.

To gain a better estimate of the magnitude of the P-inversion barrier in the 1,3,4-triphosphole **3**, quantum-mechanical model calculations (at the B3LYP/6-31+G(d)+ZPE level)[22, 23] were carried out. The results indicate an increase of the inversion energies for the compounds $H_2C_2P_3H$ (**8**), $H_2N(H)C_2P_3H$ (**9**), and $(H_2N)_2C_2P_3H$ (**10**) with increasing number of amino groups ($\Delta E = 25.2$ (**8**), 53.6 (**9**), 70.7 (**10**) kJ mol^{-1}). This trend is markedly reduced when one considers for **9** and **10** interconversion between conformers that represent transition states with respect to C–N bond rotation and feature a nearly orthogonal arrangment of the lone pairs of electrons on the NH_2 groups and the π orbitals in the ring, respectively ($\Delta E =$ 16.8 (**9**), 21.3 (**10**) kJ mol^{-1}). A stabilization of an appropriate conformation for the *i*Pr(Me$_3$Si)N group in **3** together with the influence of the sterically demanding (Me$_3$Si)$_2$CH substituent, which acts in favor of a planarization of the σ^3-phosphorus atom,[5] should be sufficient to decrease the P-inversion barrier to a few kJ mol^{-1}.

Fragmentation of **3** in negative-ion CI mass spectra occurs by elimination of 1,1-dimethylsilaethene and 1,1-dimethyl-1-silapropene to give first a triphospholide complex $[\{(i\text{Pr(H)N})_2C_2P_3\}^{182}W(CO)_5]^-$ (*m*/*z* 555), and further by cleavage of the W(CO)$_5$ fragment to yield the free triphospholide $[(i\text{Pr(H)N})_2C_2P_3]^-$ (*m*/*z* 233). Additional studies aimed at the realization of reductive cleavage of the exocyclic (SiMe$_3$)$_2$CH group in condensed phases and the achievement of π tuning in the 1,3,4-triphosphole ring system by transformation of the amino functions in **3** are currently in progress.

Experimental Section

1: Complex **4** (0.688 g, 1 mmol) was dissolved in *n*-pentane (10 mL), methanol (2 mL) was added at room temperature, and the solution was stirred for approximately 60 min at 30 °C; the end of the reaction was determined by ^{31}P NMR spectroscopy. The solution was evaporated in vacuum (ca. 0.1 mbar) and the solid residue was dissolved in *n*-pentane (5 mL), cooled to −25 °C, and the resulting precipitate separated from the supernatant solvent. The obtained solid was washed several times with small quantities of *n*-pentane, and dried in vacuum. Yield: 295 mg (48 %), m.p. 47 °C (decomp). Selected NMR data: ^{13}C{^{1}H} NMR (50.3 MHz, $CDCl_3$, 25 °C, ext. TMS): $\delta = 1.88$ (dd, ^3J(P,C) = 3.7, ^4J(P,C) = 4.3 Hz; Si(CH$_3$)$_3$), 2.10 (d, ^3J(P,C) = 2.2 Hz; Si(CH$_3$)$_3$), 21.5 (s; NCH*C*H$_3$), 22.0 (s; NCH*C*H$_3$), 26.9 (dd, ^1J(P,C) = 42.2, ^2J(P,C) = 10.0 Hz; PCH), 52.3 (d, ^3J(P,C) = 2.2 Hz; N*C*H(CH$_3$)$_2$), 193.3 (dd, J(P,C) = 79.1, 33.3 Hz; PPC), 197.2, (d, ^2J(P,C) = 8.2, ^1J(W,C) = 126.8 Hz; *cis*-CO), 200.4 (d, ^2J(P,C) = 30.3 Hz; *trans*-CO); ^{31}P{^{1}H} NMR (81.0 MHz, $CDCl_3$, 25 °C, ext. 85 % H_3PO_4): $\delta = -31.6$ (d, J(P,P) = 127.5 Hz), −150.6 (d, J(P,P) = 127.5, ^1J(W,P) = 264.4 Hz).

3: 1*H*-diphosphirene complex **1** (0.246 g, 0.4 mmol) was dissolved in toluene (6 mL), *N*-trimethylsilyl(isopropyl)aminophosphaethyne (0.14 g (0.80 mmol) was added, and the solution was stirred for 3 h at 75–80 °C. Completion of the reaction was determined by ^{31}P NMR control. The solution was then evaporated in vacuum (0.01 bar), the red oily residue was dissolved in *n*-pentane (3 mL), and complex **3** was crystallized at −20 °C. Complex **3** was obtained as a bright red solid after drying in vacuum. Yield: 110 mg (35 %), m.p. 108 °C (decomp). Selected NMR data: ^{13}C{^{1}H} NMR (75.4 MHz, C_7D_8, −50 °C, ext. TMS): $\delta = 6.8$ (d, J(P,C) = 2.3 Hz; CH(Si*C*H$_3$)$_3$), 7.1 (d, J(P,C) = 2.3 Hz; CH(Si*C*H$_3$)$_3$), 8.6 (s; N(SiCH$_3$)$_3$), 20.4 (dd, J(P,C) = 55.5, 7.1 Hz; (Me$_3$Si)$_2$CH), 25.6 (s; HNCH*C*H$_3$), 28.9 (s; SiNCH*C*H$_3$), 29.6 (d, J(P,C) = 3.8 Hz; SiNCH*C*H$_3$), 54.3 (d, J(P,C) = 15.3 Hz; HNCH), 61.1 (d, J(P,C) = 7.6 Hz; SiN*C*H), 186.6 (ddd, J(P,C) = 21.8, 5.9, 5.5 Hz; P^{1}C), 201.5 (dd, J(P,C) = 4.1, 3.2 Hz; *cis*-*C*O), 204.7 (dm, J(P,C) = 28.2 Hz; *trans*-*C*O), 216.3 (ddd, J(P,C) = 77.6, 28.0, 4.9 Hz; P^{2}C); ^{31}P{^{1}H} NMR (121.5 MHz, C_7D_8, −30 °C, ext. 85 % H_3PO_4): $\delta = 220.9$ (dd, J(P^1,P^2) = 422, J(P^1,P^3) = 126, J(W,P^1) = 230 Hz; P^1), 88.3 (dd, J(P^2,P^1) = 422, J(P^2,P^3) = 26, J(W,P^2) = 25 Hz; P^2), 40.4 (dd, J(P^3,P^1) = 126, J(P^3,P^2) = 26 Hz; P^3).

Received: February 2, 2001
Revised: April 24, 2001 [Z16545]

[1] a) F. Mathey, *Coord. Chem. Rev.* **1994**, *137*, 1; b) P. LeFloch, F. Mathey, *Coord. Chem. Rev.* **1998**, *179–180*, 771.

[2] a) E. J. M. Boer (Shell), World Patent Application 95/04087, **1995**; b) B. Breit, *Chem. Commun.* **1996**, 2071; c) E. J. M. Boer, I. Gilmore, F. Korndorfer, A. D. Horton, *J. Mol. Catal. A* **1998**, *128*, 155; d) B. Breit, *J. Mol. Catal. A* **1999**, *134*, 143; e) B. Breit, R. Paciello, B. Geißler, M. Röper (BASF AG), DE 19621967 A1, **1999**; f) R. Paciello, E. Zeller, B. Breit, M. Röper (BASF AG), DE 19743167 A1, **1999**.

[3] L. Nyulászi, *J. Phys. Chem.* **1996**, *100*, 6194.

  1433-7851/01/4013-2473 $ 17.50+.50/0

[4] a) L. Nyulászi, *Inorg. Chem.* **1996**, *35*, 4690; b) M. N. Glokhotsev, A. Dransfeld, P. von R. Schleyer, *J. Phys. Chem.* **1996**, *100*, 13447.

[5] F. G. N. Cloke, P. B. Hitchcock, P. Hunnable, J. F. Nixon, L. Nyulászi, E. Niecke, V. Thelen, *Angew. Chem.* **1998**, *110*, 1139; *Angew. Chem. Int. Ed.* **1998**, *37*, 1083.

[6] F. E. Hahn, L. Wittenbecher, D. Le Van, R. Fröhlich, B. Wibbeling, *Angew. Chem.* **2000**, *112*, 2393; *Angew. Chem. Int. Ed.* **2000**, *39*, 2307.

[7] 2*H*-1,2-Azaphospholes: a) R. Streubel, H. Wilkens, A. Ostrowski, C. Neumann, F. Ruthe, P. G. Jones, *Angew. Chem.* **1997**, *109*, 1549; *Angew. Chem. Int. Ed. Engl.* **1997**, *36*, 1492; b) H. Wilkens, A. Ostrowski, J. Jeske, F. Ruthe, P. G. Jones, R. Streubel, *Organometallics* **1999**, *18*, 5627.

[8] 2*H*-1,3,2-Diazaphospholes: a) H. Wilkens, F. Ruthe, P. G. Jones, R. Streubel, *Chem. Eur. J.* **1998**, *4*, 1542; b) R. Streubel, U. Schiemann, N. Hoffmann, Y. Schiemann, P. G. Jones, D. Gudat, *Organometallics* **2000**, *19*, 475.

[9] 2*H*-1,4,2-Diazaphospholes: R. Streubel, H. Wilkens, P. G. Jones, *Chem. Eur. J.* **2000**, *6*, 3997.

[10] 2*H*-1,2,3-Azadiphospholes: G. N. Cloke, P. B. Hitchcock, U. Schiemann, R. Streubel, J. F. Nixon, D. J. Wilson, *Chem. Commun.* **2000**, 1659.

[11] R. Appel, M. Poppe, *Angew. Chem.* **1989**, *101*, 70; *Angew. Chem. Int. Ed. Engl.* **1989**, *28*, 53.

[12] R. Streubel, L. Ernst, J. Jeske, P. G. Jones, *J. Chem. Soc. Chem. Commun.* **1995**, 2113.

[13] F. Mercier, L. Ricard, F. Mathey, M. Regitz, *J. Chem. Soc. Chem. Commun.* **1991**, 1305.

[14] M. Julino, M. Slany, U. Bergsträßer, F. Mercier, F. Mathey, M. Regitz, *Chem. Ber.* **1995**, *128*, 991.

[15] R. Matos, M. F. Meidine, J. F. Nixon, B. F. Trigo Passos, E. Niecke, D. Barion, *J. Organomet. Chem.* **1990**, *390*, C89.

[16] **1**: MS (EI, 70 eV, ^{182}W): *m*/*z* (%): 613 (18) $[M]^+$; **3**: MS (EI, 70 eV, 10000 resolution (10%-Tal-Def.)) *m*/*z* (%): 788.1188 ± 2 ppm (16) $[M]^+$ $C_{23}H_{43}N_2O_5P_3Si_3{}^{184}W$; negative-ion MS (CI, NH_3, ^{182}W): *m*/*z* (%): 785 (6) $[M-H]^-$, 713 (9) $[M-H-(H_3C)_2SiCH_2]^-$, 627 (78) $[M-H-(H_3C)_2SiCH_2\text{-}(H_3C)_2SiCHCH_3]^-$, 555 (69) $[\{(i\text{Pr(H)N})_2C_2P_3\}^{182}W(CO)_5]^-$.

[17] Crystal structure analysis of complex **1** ($C_{16}H_{27}NO_5P_2Si_2W$): triclinic, space group $P\bar{1}$, $a = 10.577(4)$, $b = 11.441(4)$, $c = 11.970(4)$ Å, $\alpha = 70.47(2)$, $\beta = 79.07(2)$, $\gamma = 62.66(2)^\circ$, $V = 1211.6$ Å^3, $Z = 2$, $\mu = 5.0$ mm^{-1}, $T = -130\,^\circ$C. A crystal (yellow plate, ca. $0.5 \times 0.4 \times 0.2$ mm) was mounted in perfluoropolyether at $-130\,^\circ$C on a Stoe STADI-4 diffractometer. Intensities were registered up to $2\theta_{max}$ 50° using $Mo_{K\alpha}$ radiation; 4277 reflections of a total of 5117 were independent ($R_{int} = 0.015$). After a semiempirical absorption correction (ψ scans, transmittance 0.61–0.96), the structure was solved by the heavy-atom method and refined with full-matrix least-squares methods on F^2 (program SHELXL-93, G. M. Sheldrick, Universität Göttingen). The hydrogen atom at the nitrogen center was refined free, all others with a riding model or as rigid methyl groups. The final *wR*2 based on F^2 for all data was 0.045, and the conventional $R(F)$ value was $R1 = 0.019$; 257 parameters, $S = 1.07$, max. residual electron density 0.85 e Å^{-3}. Crystallographic data (excluding structure factors) for the structure reported in this paper have been deposited with the Cambridge Crystallographic Data Centre as supplementary publication no. CCDC-160390. Copies of the data can be obtained free of charge on application to CCDC, 12 Union Road, Cambridge CB2 1EZ, UK (fax: (+44) 1223-336-033; e-mail: deposit@ccdc.cam.ac.uk). Note: The crystal structure of **4** will be published elsewhere in the near future.

[18] R. Streubel, N. H. T. Huy, L. Ricard, F. Mathey, *Phosphorus Sulfur Relat. Elem.* **1993**, *77*, 229.

[19] R. Streubel, U. Schiemann, unpublished results.

[20] Several attempts were made to determine the crystal structure of **3**; the measurement (at $-130\,^\circ$C) gave a value of 322° for the sum of bond angles at the $\sigma^3\lambda^3$-phosphorus atoms in two independent molecules which matches approximately the value found for a 3,4-bisphosphonio-1,2-diphosphole: G. Jochem, H. Nöth, A. Schmidpeter, *Chem. Ber.* **1996**, *129*, 1083.

[21] The key to the assignment of the conformation was the appearance of cross peaks that connect the protons in the *N*-*i*Pr and *N*-$SiMe_3$ groups, respectively, with *only one* of the anisochronous $CSiMe_3$ groups. This suggested a static, quasi-orthogonal orientation of the $(Me_3Si)_2CH$ and *i*Pr(Me_3Si)N groups with respect to the plane of the five-membered ring. The onset of rotation with increasing temperature led to the appearance of the missing cross peaks. Analysis of the cross peaks originating from the N(H)*i*Pr signals revealed that the amino group has either a static and coplanar orientation relative to the ring, or undergoes fast rotation.

[22] A. D. Becke, *J. Chem. Phys.* **1993**, *98*, 5648.

[23] Gaussian 98 (Revision A.6), M. J. Frisch, G. W. Trucks, H. B. Schlegel, G. E. Scuseria, M. A. Robb, J. R. Cheeseman, V. G. Zakrzewski, J. A. Montgomery, R. E. Stratmann, J. C. Burant, S. Dapprich, J. M. Millam, A. D. Daniels, K. N. Kudin, M. C. Strain, O. Farkas, J. Tomasi, V. Barone, M. Cossi, R. Cammi, B. Mennucci, C. Pomelli, C. Adamo, S. Clifford, J. Ochterski, G. A. Petersson, P. Y. Ayala, Q. Cui, K. Morokuma, D. K. Malick, A. D. Rabuck, K. Raghavachari, J. B. Foresman, J. Cioslowski, J. V. Ortiz, B. B. Stefanov, G. Liu, A. Liashenko, P. Piskorz, I. Komaromi, R. Gomperts, R. L. Martin, D. J. Fox, T. Keith, M. A. Al-Laham, C. Y. Peng, A. Nanayakkara, C. Gonzalez, M. Challacombe, P. M. W. Gill, B. G. Johnson, W. Chen, M. W. Wong, J. L. Andres, M. Head-Gordon, E. S. Replogle, J. A. Pople, Gaussian, Inc., Pittsburgh, PA, **1998** Note: The barrier which was determined here for **8** with the B3LYP/6-31+G(d)-method lies approximately 2.5 kcal mol^{-1} higher than the earlier results;[3, 4] it is known, however, that the MP2/6-31G(d)-method underestimates the P-inversion barrier by 8–12 kJ mol^{-1}.

Unexpected Splitting of ansa-Ytterboacene and ansa-Calcoacene: Formation of $[(\eta^2\text{-}C_{12}H_8)ZrCl_2(thf)_3]$ and $(Me_3Si)_2C_{12}H_8$**

Igor L. Fedushkin,* Tatyana V. Petrovskaya, Mikhail N. Bochkarev,* Sebastian Dechert, and Herbert Schumann*

Recently we reported on the synthesis of the C_2-symmetric *trans-rac*-ansa-lanthanoacenes[1] $[(\eta^5\text{-}C_{12}H_8)_2M(thf)_2]$ (M = Yb, **1**; Sm, **2**) by reductive coupling of acenaphthylene (acene) with activated metallic ytterbium or samarium.[2] The acenyl radical anions formed in the course of these redox reactions dimerize to biacenyl dianions which stereoselectively coordinate the simultaneously formed M^{2+} cations. In contrast, the

[*] Dr. I. L. Fedushkin, Prof. Dr. M. N. Bochkarev, T. V. Petrovskaya
G. A. Razuvaev Institute of Organometallic Chemistry
Russian Academy of Sciences
Tropinina 49, 603950 Nizhny Novgorod GSP-445 (Russia)
Fax: (+7) 8312-661497
E-mail: igorfed@imoc.sinn.ru

Prof. Dr. H. Schumann, Dipl.-Chem. S. Dechert
Institut für Chemie, Technische Universität Berlin
Strasse des 17. Juni 135, 10623 Berlin (Germany)
Fax: (+49) 30-3142-2168
E-mail: schumann@chem.tu-berlin.de

[**] Organometallic Compounds of the Lanthanides, Part 148. This work was supported by the Fonds der Chemischen Industrie, the Deutsche Forschungsgemeinschaft, the Alexander von Humboldt Foundation (I.L.F.), and the Russian Foundation for Basic Research (Grant No. 01-03-32631). We thank Dr. Yuri A. Kurskii and Dr. Vladimir I. Nevodchikov for assistance with recording NMR and ESR spectra. Part 147: I. L. Fedushkin, T. V. Petrovskaya, F. Girgsdies, V. I. Nevodchikov, R. Weimann, H. Schumann, M. N. Bochkarev, *Izv. Akad. Nauk Ser. Khim.* **2000**, 1897–1904; *Russ. Chem. Bull. Int. Ed.* **2000**, *49*, 1869-1876.

  1433-7851/01/4013-2474 $ 17.50+.50/0

reduction of acene with alkali metals stops with the formation of adducts of the acenyl radical anions and the respective metal cations.[3] Also naphthalene and alkali metals form radical anion/metal cation adducts, but the latter react with lanthanide halides to give lanthanide complexes that contain naphthalene dianions.[4] Considering the similarities in the reactivity of acene and naphthalene towards metals one can suggest that the ansa-lanthanoacenes **1** and **2** may disclose a combination of the chemical features of both cyclopentadienyl and naphthalene complexes, thus reacting either with retention of the ansa-ligand framework or acting as reducing agents. Here we report on the unexpected reactivity of the ytterboacene complex **1** and of the analogeous calcium complex which was prepared for the first time.

The calcoacene complex $[(\eta^5\text{-}C_{12}H_8)_2Ca(thf)_2]$ (**3**) is formed with yields of about 80% by reduction of acene with metallic calcium activated by iodine in THF. It crystallizes from THF or benzene as yellow thin plates which, unfortunately, were not suitable for an X-ray diffraction analysis. However, since the ^{1}H NMR spectrum of **3**, like that of the diamagnetic complex **1**, shows only one set of eight resonance signals for the ring protons, and since its IR spectrum is identical with those of **1** and **2**, the obvious supposition is that the molecular structure of **3** is similar to that of its structurally characterized lanthanide analogues **1** and **2**.

In the course of our investigations on catalytically active ansa-zirconocenes,[5] we studied the reactions of the ansa complexes **1** and **3** with $ZrCl_4$. The reaction of equimolar amounts of the ytterbium complex **1** and $ZrCl_4$ in THF immediately proceeds, already at ambient temperature, and dark-green crystals can be isolated from the solution. The crystal structure analysis of the product reveals that it is not the corresponding ansa-zirconoacene. In contrast to our expectation the ansa-biacenyl ligand was split, leading to the formation of $[(C_{12}H_8)ZrCl_2(thf)_3]$ (**4**) in 86% yield. The reaction of the calcoacene **3** with $ZrCl_4$ also produces compound **4**, but in lower yield.

Shapiro et al.[6] have demonstrated the successful transfer of the ansa-bisindenyl ligand framework of $[\{Ph_2C_2H_2(\eta^5\text{-}4,7\text{-}Me_2C_9H_4)_2\}Ca(thf)_2]$ from the calcium center to the iron center, whereas the reaction with $[ZrCl_4(SMe_2)_2]$ or $[ZrCl_4(thf)_2]$ produced a complex mixture of products which could not be separated and identified.

Compound **4** is extremely sensitive to air and moisture. In contrast to the ^{1}H NMR spectra of **1** and **3** which show one set of eight resonance signals for the protons of the ansa ligand, the ^{1}H NMR spectrum of **4** shows only four ring proton signals, thus indicating that the framework of the ansa-biacenyl ligand undergoes a decoupling process in the course of the transmetalation reaction. The weak ESR signal, which is obtained for solutions of **1** in THF and which is assigned to the acene radical anion $C_{12}H_8^-$ ($A_H = 0.06, 0.3, 0.54, 0.64$ mT; $g = 2.0027$), demonstrates that already in solution an equilibrium exists between complex **1**, decoupled acenyl radical anions, and divalent ytterbium cations. In the presence of $ZrCl_4$, the acenyl radical anions evidently disproportionate into neutral acenaphthylene and aromatic acenyl dianions; the latter form compound **4** under elimination of ytterbium dichloride (Scheme 1).

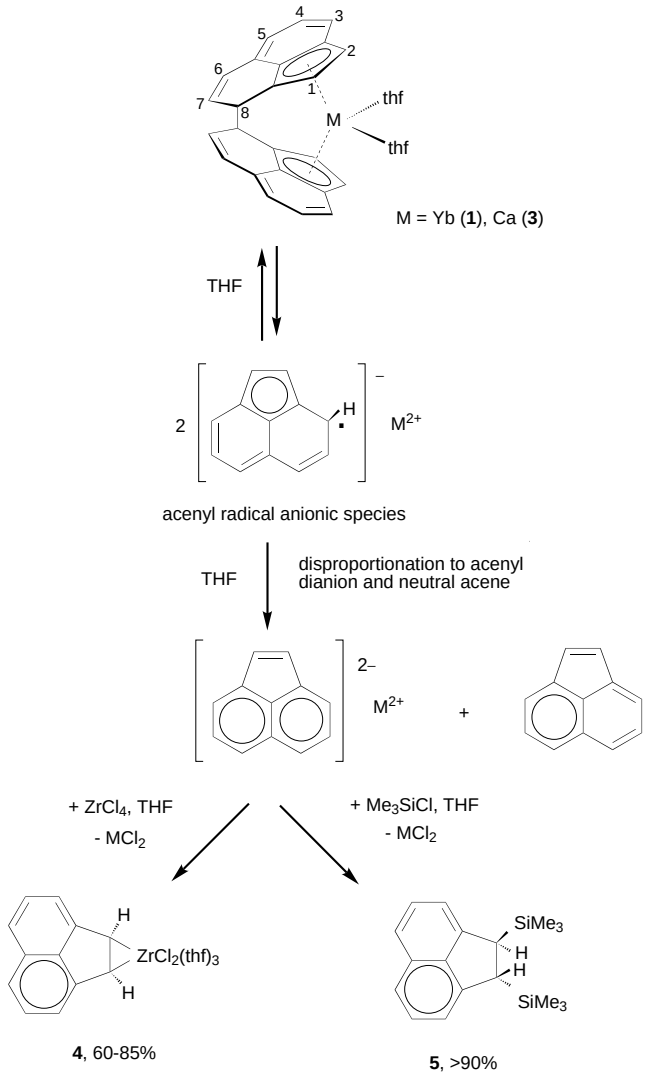

Scheme 1. Mechanism of the formation of **4** and **5**.

A similar decoupling of the ansa-biacenyl ligand takes place when **1** or **3** react with Me_3SiCl in THF; the product 1,2-bis(trimethylsilyl)-substituted acenaphthene $(Me_3Si)_2C_{12}H_8$ (**5**) is formed in more than 90% yield.

The molecular structures of **4** (Figure 1) and **5** (Figure 2) were determined by single-crystal X-ray diffraction[7] on crystals obtained from THF or hexane, respectively.

In **4** the coordination geometry around the zirconium atom is that of a slightly distorted pentagonal bipyramid in which the two Cl atoms adopt the apical positions (Cl1-Zr-Cl2 165.4°) and the three THF molecules and the acenyl ligand form the equatorial plane. The bond lengths Zr–C1 (2.270 Å), Zr–C5 (2.288 Å), and C1–C5 (1.495 Å) indicate that the Zr-C1-C5 fragment can be described as a metallacycle with a $\sigma\text{-}\eta^2$-bonding mode rather than with a $\pi\text{-}\eta^2$ coordination of the zirconium atom. Similar $\sigma\text{-}\eta^2$-bonding modes were described by Alt et al. for $[(\eta^5\text{-}C_5H_4CMe_2H)(\eta^5\text{:}\eta^2\text{-}C_5H_4CMe_2C_9H_7)Zr(PMe_3)]$[12a] and $[(\eta^5\text{-}C_5H_5)_2Zr(\eta^2\text{-}C_2H_4)\text{-}(PMe_3)]$,[12b] whereas for $[CpRh(acene)_2]$ the $\pi\text{-}\eta^2$-bonding mode is well documented.[13]

The molecular structure of compound **5** shows the two trimethylsilyl groups σ-bonded to C7 and C11. They

  1433-7851/01/4013-2475 $ 17.50+.50/0

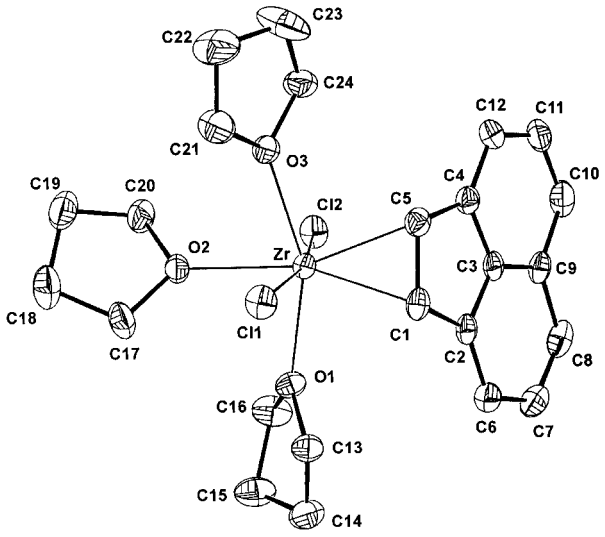

Figure 1. Molecular structure (ORTEP drawing) of **4** (thermal ellipsoids drawn at the 50% probability level). Hydrogen atoms are omitted for clarity. Relevant bond length [Å] and angles [°]: Zr-Cl1 2.4748(10), Zr-Cl2 2.4498(9), Zr-O1 2.269(2), Zr-O2 2.375(2), Zr-O3 2.292(2), Zr-C1 2.270(3), Zr-C5 2.288(4), C1-C2 1.480(5), C2-C3 1.420(5), C3-C4 1.423(5), C4-C5 1.476(5), C1-C5 1.495(5), C2-C6 1.379(5), C6-C7 1.416(5), C7-C8 1.381(5), C8-C9 1.428(5), C9-C10 1.416(5), C10-C11 1.365(6), C11-C12 1.416(6), C3-C9 1.399(5), C4-C12 1.376(5); Cl2-Zr-Cl1 165.36(3), O1-Zr-C1 84.04(11), C5-Zr-O3 83.68(11), O1-Zr-O2 78.69(8), O2-Zr-O3 77.06(9), O1-Zr-O3 155.59(9).

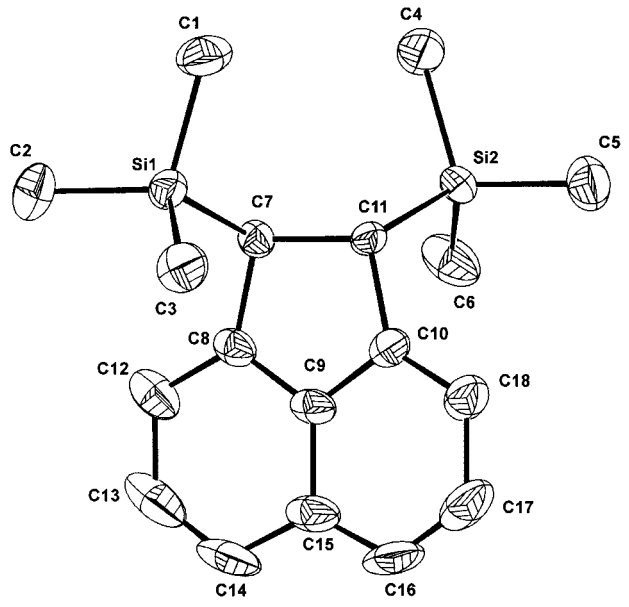

Figure 2. Molecular structure (ORTEP drawing) of **5** (thermal ellipsoids drawn at the 30% probability level). Hydrogen atoms are omitted for clarity. Relevant bond length [Å] and angles [°]: Si1-C7 1.894(4), Si2-C11 1.886(5), C7-C8 1.501(7), C8-C9 1.402(7), C9-C10 1.404(7), C10-C11 1.501(6), C7-C11 1.578(6), C8-C12 1.373(7), C12-C13 1.395(10), C13-C14 1.340(10), C14-C15 1.424(9), C10-C11 1.501(6), C7-C11 1.578(6), C8-C12 1.373(7), C12-C13 1.395(10), C13-C14 1.340(10), C14-C15 1.424(9), C15-C16 1.389(10), C16-C17 1.340(10), C17-C18 1.421(9), C10-C18 1.372(7), C9-C15 1.416(7); C11-C7-Si1 110.3(3), C7-C11-Si2 112.0(3).

are *trans*-positioned, perhaps because of steric factors. The C–C bond lengths in **5** are in the range of the corresponding bond lengths in acenaphthene.

Experimental Section

All manipulations were performed under a nitrogen atmosphere or in vacuum. Elemental analyses were obtained by using a Perkin-Elmer Series II CHNS/O 2400 Analyzer. The extreme sensitivity of **4** towards air and moisture prevented satisfying results for its elemental analysis. NMR spectra were recorded on a Bruker DPX 200 instrument, ESR spectra on a Bruker 200D-SRC spectrometer. The commercially available acenaphthylene (Aldrich; purity 75%) was further purified to 85% (10 to 15% acenaphthene as impurity) by sublimation (80°/10^{-1} Torr). The given quantities of acenaphthylene and the yields of the products are calculated on pure acenaphthylene.

3: A mixture of calcium filings (2.7 g, 67.3 mmol) and iodine (1.5 g, 5.91 mmol) was stirred in THF (50 mL) at room temperature until the color of iodine disappeared. The main part of the CaI_2 formed was extracted with refluxing THF (ca. 100 mL) leaving only a small amount (1 to 2 mmol) as reaction accelerator. Acenaphthylene (1.14 g, 5.9 mmol) in THF (25 mL) was added to the calcium metal, and the mixture was stirred for 4 h at 50 °C. Extraction of the yellow crystalline precipitate with refluxing THF followed by cooling and concentration of the extract gave **3** (1.42 g; 78%); m.p. > 140 °C (decomp); ^{1}H NMR (200 MHz, [D$_8$]THF, 20 °C, TMS): $\delta = 6.86$ (d, ^3J(H,H) = 8.2 Hz, 2H; CH, H^3), 6.60 (dd, ^3J(H,H) = 9.6, 2.0 Hz, 2H; CH, H^6), 6.39 (dd, ^3J(H,H) = 8.2, 6.4 Hz, 2H; CH, H^4), 6.31 (d, ^3J(H,H) = 3.0 Hz, 2H; CH, H^1), 6.21 (d, ^3J(H,H) = 6.4 Hz, 2H; CH, H^5), 5.98 (dd, ^3J(H,H) = 9.6, 3.4 Hz, 2H; CH, H^7), 5.58 (d, ^3J(H,H) = 3.0 Hz, 2H; CH, H^2), 4.54 (s, 2H; CH, H^8), 3.7 (m, 8H; CH_2), 1.6 (m, 8H; CH_2); IR (Nujol): $\tilde{\nu}$ = 1180 w, 1030 s, 880 s, 720 w, 795 s, 745 s, 715 s cm^{-1}; elemental analysis calcd (%) for $C_{32}H_{32}O_2Ca$ (488.68): C 78.65, H 6.60; found: C 77.81, H 6.38.

4: A mixture of **1** (1.65 g, 2.65 mmol) and $ZrCl_4$ (0.63 g, 2.7 mmol) was stirred in THF (35 mL) at 20 °C for a few minutes. Filtration and concentration of the solution in vacuum to 5 mL gave **4** (1.21 g; 86%) as dark green crystals; m. p. > 110 °C (decomp); ^{1}H NMR (200 MHz, [D$_8$]THF, 20 °C, TMS): $\delta = 6.95$ (dd, ^3J(H,H) = 8.2, 7.2 Hz, 2H; CH), 6.57 (d, ^3J(H,H) = 8.2 Hz, 2H; CH), 6.34 (d, ^3J(H,H) = 7.2 Hz, 2H; CH), 4.15 (s, 2H; CH), 3.72 (m, 12H; CH_2), 1.61 (m, 12H; CH_2); ^{13}C NMR (50.32 MHz, [D$_8$]THF, 20 °C, TMS): $\delta = 147.32$, 133.30, 127.41, 127.05, 115.34, 110.65, 87.45.

5: A mixture of **3** (2.7 g, 5.52 mmol) and Me_3SiCl (1.3 g, 11.96 mmol) in THF (15 mL) was stirred for 30 min at 20 °C and 10 min at 40 °C. The solvent was removed in vacuum and the product extracted with hexane (2 × 15 mL). Crystallization from hexane yielded **5** (1.52 g, 93%) as large colorless crystals; m. p. 121 °C; ^{1}H NMR (200 MHz, CD_2Cl_2, 20 °C, TMS): $\delta = 7.43$ (d, ^3J(H,H) = 7.8 Hz, 2H; CH), 7.35 (dd, ^3J(H,H) = 7.8, 6.6 Hz, 2H; CH), 7.06 (d, ^3J(H,H) = 6.6 Hz, 2H; CH), 2.93 (s, 2H; CH), −0.09 (s, 18H; CH_3); elemental analysis calcd (%) for $C_{18}H_{26}Si_2$ (298.58): C 72.41, H 8.78; found: C 72.25, H 8.92.

Received: February 19, 2001 [Z16635]

[1] The term ansa-metalloacenes denotes that these metallocenes are based on acenaphthylene.

[2] I. L. Fedushkin, S. Dechert, H. Schumann, *Angew. Chem.* **2001**, *113*, 584–586; *Angew. Chem. Int. Ed.* **2001**, *40*, 561–563.

[3] a) F. Gerson, B. Weidmann, *Helv. Chim. Acta* **1966**, *49*, 1873–1878; b) W. E. Rhine, J. H. Davis, G. Stucky, *J. Organomet. Chem.* **1977**, *134*, 139–149; c) H. Bock, C. Arad, C. Näther, *J. Organomet. Chem.* **1996**, *520*, 1–13.

[4] a) I. L. Fedushkin, M. N. Bochkarev, H. Schumann, L. Esser, G. Kociok-Köhn, *J. Organomet. Chem.* **1995**, *489*, 145–151; b) M. N. Bochkarev, I. L. Fedushkin, A. A. Fagin, H. Schumann, J. Demtschuk, *Chem. Commun.* **1997**, 1783–1784; c) M. N. Bochkarev, *Russ. Chem. Rev.* **2000**, *69*, 783–794.

[5] a) R. L. Halterman, D. R. Fahey, E. F. Bailly, D. W. Dockter, O. Stenzel, J. L. Shipman, M. A. Khan, S. Dechert, H. Schumann, *Organometallics* **2000**, *19*, 5464–5470; b) R. L. Halterman, H. Schumann, F. Dübner, *J. Organomet. Chem.* **2000**, *604*, 12–19.

[6] P. J. Shapiro, K. M. Kane, A. Vij, D. Stelck, G. J. Matare, R. L. Hubbard, B. Caron, *Organometallics* **1999**, *18*, 3468–3473.

[7] X-ray structure data: Siemens-SMART-CCD diffractometer, ω scans, $Mo_{K\alpha}$ radiation ($\lambda = 0.71073$ Å), graphite monochromator, $T = 173$ K

  1433-7851/01/4013-2476 $ 17.50+.50/0

(**4**), 293 K (**5**), SADABS[8] for absorption correction, structure solution with direct methods (SHELXS-97[9]), refinement against F^2 (SHELXL-97[10]) with anisotropic thermal parameters for all non-hydrogen atoms, hydrogen positions with fixed isotropic thermal parameters ($U_{iso}=0.08$ Å^2) on calculated positions. The PLATON[11] program was used for the geometric analysis of the structures. Data collection for **4**: crystal dimensions $0.42\times0.30\times0.24$ mm, orthorhombic, space group *Pbca*, $a=25.2916(7)$, $b=16.8904(5)$, $c=10.9754(3)$ Å, $V=4688.5(2)$ Å^3, $Z=8$, $\rho_{calcd}=1.503\times10^3$ kg m^{-3}, $\mu=0.720$ mm^{-1}, $F(000)=2192$, $3.2^\circ\le2\theta\le52.0^\circ$, $-31\le h\le29$, $-20\le k\le12$, $-13\le l\le13$, 29774 data collected, 4597 unique data ($R_{int}=0.0996$), 3439 data with $I>2\sigma(I)$, 271 refined parameters, GOF(F^2) = 1.110, final R indices ($R_1=\Sigma||F_o|-|F_c||/\Sigma|F_o|$, $wR_2=[\Sigma w(F_o^2-F_c^2)^2/\Sigma w(F_o^2)^2]^{1/2}$) $R_1=0.0483$, $wR_2=0.0949$, max./min. residual electron density 0.842/$-$0.829 e Å^{-3}. Data collection for **5**: crystal dimensions $0.76\times0.58\times0.42$ mm, monoclinic, space group $P2_1/c$, $a=9.1647(1)$, $b=22.9299(6)$, $c=9.3960(2)$ Å, $\beta=111.067(1)^\circ$, $V=1842.55(7)$ Å^3, $Z=4$, $\rho_{calcd}=1.076\times10^3$ kg m^{-3}, $\mu=0.183$ mm^{-1}, $F(000)=648$, $3.6^\circ\le2\le50.0^\circ$, $-10\le h\le7$, $-27\le k\le26$, $-11\le l\le11$, 11114 data collected, 3206 unique data ($R_{int}=0.1493$), 1833 data with $I>2\sigma(I)$, 187 refined parameters, GOF(F^2) = 1.045, final R indices ($R_1=\Sigma||F_o|-|F_c||/\Sigma|F_o|$, $wR_2=[\Sigma w(F_o^2-F_c^2)^2/\Sigma w(F_o^2)^2]^{1/2}$) $R_1=0.0903$, $wR_2=0.2057$, max./min. residual electron density 0.519/$-$0.445 e Å^{-3}. Crystallographic data (excluding structure factors) for the structures reported in this paper have been deposited with the Cambridge Crystallographic Data Centre as supplementary publication nos. CCDC-158204 (**4**) and CCDC-158205 (**5**). Copies of the data can be obtained free of charge on application to CCDC, 12 Union Road, Cambridge CB21EZ, UK (fax: (+44) 1223-336-033; e-mail: deposit@ccdc.cam.ac.uk).

[8] G. M. Sheldrick, Empirical Absorption Correction Program, Universität Göttingen, **1996**.

[9] G. M. Sheldrick, Program for Crystal Structure Solution, Universität Göttingen, **1990**.

[10] G. M. Sheldrick, Program for Crystal Structure Refinement, Universität Göttingen, **1997**.

[11] A. L. Spek, PLATON A Multipurpose Crystallographic Tool, University of Utrecht, **2000**.

[12] a) E. H. Licht, H. G. Alt, W. Milius, S. Abu-Orabi, *J. Organomet. Chem.* **1998**, *560*, 69–75; b) H. G. Alt, C. E. Denner, U. Thewalt, M. D. Rausch, *J. Organomet. Chem.* **1988**, *356*, C83–C85.

[13] J. Müller, C. Hirsch, K. Qiao, K. Ha, *Z. Anorg. Allg. Chem.* **1996**, *622*, 1441–1448.

A New Strategy for Synthesizing Endohedral Metallocenophanes**

Gerald Scholz, Rolf Gleiter,* and Frank Rominger

Dedicated to Professor Edgar Heilbronner on the occasion of his 80th birthday

Cyclophanes are versatile ligands and are capable of including metals, as shown in **A** and **B**. Such endohedral metallocenophanes are known mostly for five- or six-membered-ring π systems, with transition metals or main group elements. Two methods have been described for the preparation of endohedral metallocenophanes:[1] the reaction of a cyclophane with metals or metal salts, or the stepwise assembly of the bridge from a metallocene. Examples for the first strategy are the preparation of bridged titanocenes, zirconocenes ($m=4$), and ferrocenes ($m=2$) [Eq. (1)][2, 3] as well as of chromocene derivatives ($n=2$, 3) [Eq. (2)],[4] and complexes of Group III and IV metals with cyclophanes.[1, 5] In the second strategy [Eq. (3)], the tethers are built stepwise on the metallocene.[1, 6]

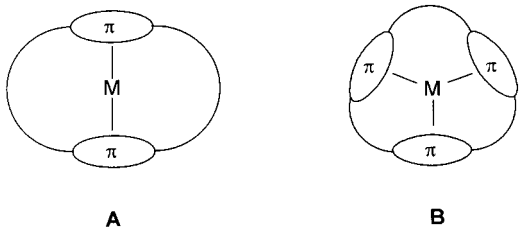

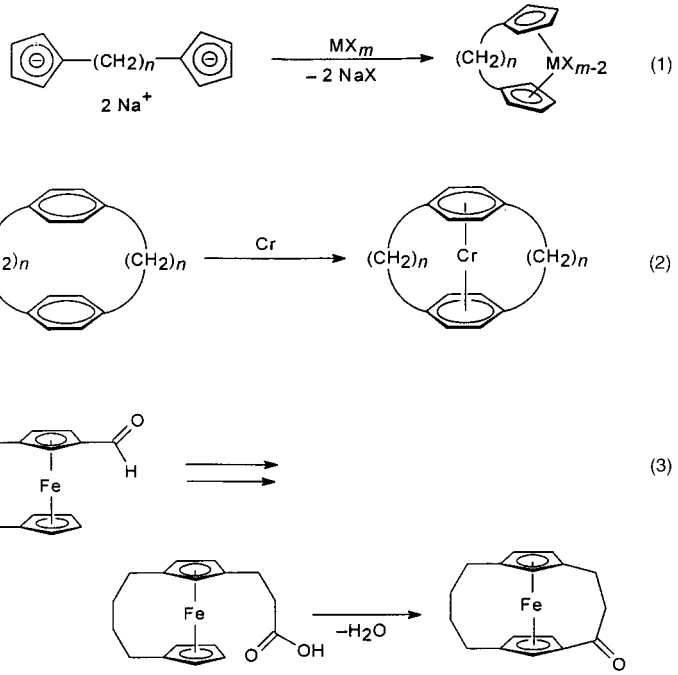

Our new protocol makes use of an intramolecular metal-catalyzed oligomerization of alkynes that are tethered to a π ligand (Scheme 1). This method is especially suited for constructing cyclobutadienes, cyclopentadienones, and benzene rings as π units, which are formed in a template reaction. We report herein the first synthesis of endohedral cobaltacyclophanes with cyclopentadienyl and cyclobutadiene rings as π units (Scheme 2 and 3). The key compounds in our protocol are the disubstituted dicarbonyl(η^5-cyclopentadienyl)cobalt derivatives **5a–c** in which two triple bonds are tethered to the Cp ring through an alkanediyl bridge. To synthesize the corresponding ligands **4a–c**, we treated 3-ethoxycyclopent-2-en-1-one (**2**)[7] with the Grignard reagents[8] derived from the ω-haloalkynes **1a–c**[9] and magnesium to yield the cyclopentenones **3a–c**. A second Grignard reaction gave the

[*] Prof. Dr. R. Gleiter, Dipl.-Chem. G. Scholz, Dr. F. Rominger
Organisch-chemisches Institut der Universität
Im Neuenheimer Feld 270, 69120 Heidelberg (Germany)
Fax: (+49) 6221-544205
E-mail: rolf.gleiter@urz.uni-heidelberg.de

[**] This work was supported by the Deutsche Forschungsgemeinschaft, the Fonds der Chemischen Industrie, and the BASF AG Ludwigshafen.

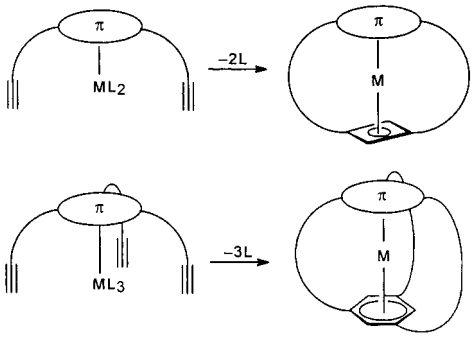

Scheme 1. General protocol for the synthesis of endohedral metallocenophanes by a template reaction.

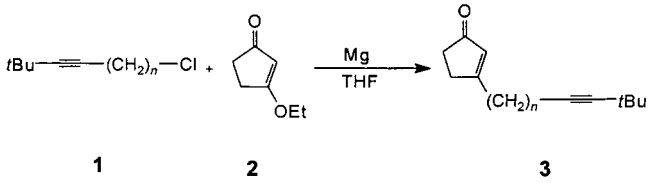

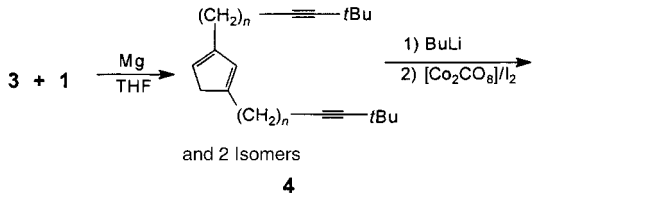

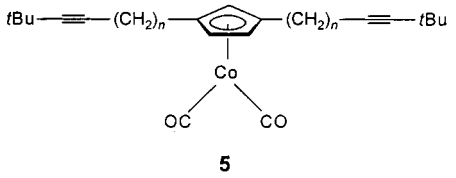

Scheme 2. Synthesis of **5**. $n = 3$ (**a**), 4 (**b**), 5 (**c**).

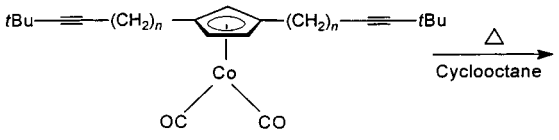

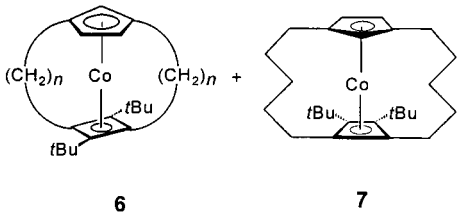

Scheme 3. Thermolysis of **5**. $n = 3$ (**a**), 4 (**b**), 5 (**c**).

cyclopentadienes **4a–c** in 25% yield over two steps. This stepwise assembly facilitates the synthesis of cyclopentadienes with chains of different length. To obtain the metallocenes **5a–c**, we followed a protocol introduced by Rausch and coworkers[10] by treating the lithium salt of **4** with an equimolar mixture of $[Co_2(CO)_8]$ and I_2 in THF (60–65% yield).[11]

The synthesis of the second π ligand was achieved by heating **5a–c** in cyclooctane at reflux (Scheme 3). Compounds **5a** and **5b** gave only one intramolecular reaction product, **6a** and **6b**, in yields of 35% and 39%, respectively. Treatment of **5c** under the same conditions gave a mixture of **6c** and **7** (1:1, 10% yield).[11] We ascribe this to the longer alkanediyl chains which allow the formation of two different metallacycles as intermediates. The composition of the **6c/7** mixture was determined by NMR spectroscopy. In the ^{1}H NMR spectrum we find three signals (1:4:1)[11] for the protons of the cyclopentadienyl rings. The *tert*-butyl groups give rise to three upfield signals (1:1:2).[11] From these observations we conclude that there is a 1:1 mixture of **6c** and **7**, which is corroborated by the ^{13}C NMR spectroscopic data of the mixture. Moreover, the data assigned to **6c** are close to those found for **6a** and **6b**.

In the case of **6a** and **6b**, we were able to isolate single crystals that allowed an X-ray diffraction study.[12] The molecular structure of **6a** in the solid state is shown in Figure 1. The planes of the two π ligands are not parallel but

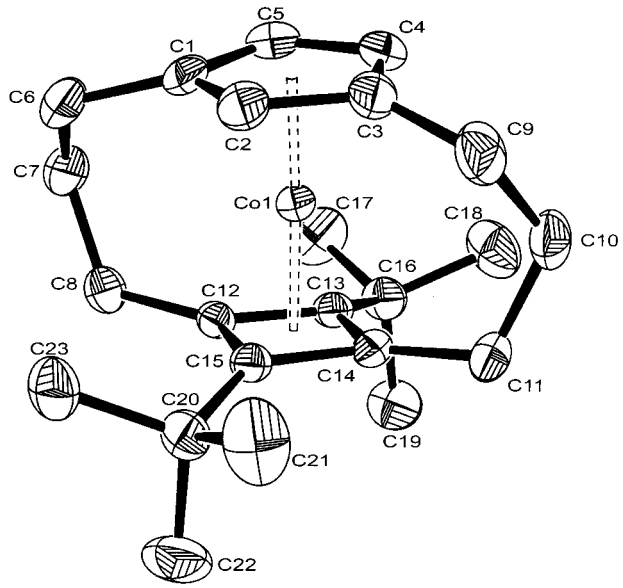

Figure 1. Structure of **6a** (ORTEP plot; thermal elipsoids at 50% probability level; H atoms have been omitted for clarity). Selected distances [Å]: C1-C2 1.441(3), C1-C5 1.424(3), C2-C3 1.443(3), C3-C4 1.420(3), C4-C5 1.420(3), C12-C13 1.482(2), C12-C15 1.463(3), C13-C14 1.476(3), C14-C15 1.469(2), Cp_c-Co 1.604(2), Co-Cbd_c 1.645(2).

slightly inclined (6°) to each other. The atoms C7 and C10 of the propanediyl bridges are bent out of the C1-C6-C8-C12 and C3-C6-C11-C14 planes (see Figure 1), respectively, to avoid eclipsed conformations. The distances between the center of the Cp ring (Cp_c) and Co (1.604 Å) and the between the center of the cyclobutadiene (Cbd) ring (Cbd_c) and Co (1.645 Å) are slightly shorter than those reported for non-tethered metallocenes (Cp_c–Co 1.660 Å, Co–Cbd_c 1.681 Å).[13] In the case of **6b**, in which both π ligands are tethered with two tetramethylene bridges, the distances between the cobalt atom and the centers of the Cp and Cbd

  1433-7851/01/4013-2478 $ 17.50+.50/0

ligands are larger than in **6a** (**6b**; Cp_c–Co 1.670 Å; Cbd_c–Co 1.692 Å) and close to those found for the parent system.[13] The new protocol reported herein for the synthesis of endohedral metallocenophanes has several advantages: it is not limited to stable cyclophanes as starting materials, and the length of the bridges and their substitution pattern on the first ligand are variable.

Received: February 9, 2001 [Z16591]

[1] Review: J. Schulz, F. Vögtle, *Top. Curr. Chem.* **1994**, *172*, 41.

[2] Reviews: R. L. Halterman in *Metallocenes: Synthesis, Reactivity, Applications*, *Vol. 1* (Eds.: A. Togni, R. L. Halterman), Wiley-VCH, Weinheim, **1998**, p. 455; R. L. Halterman, *Chem. Rev.* **1992**, *92*, 965.

[3] A. Lüttringhaus, W. Kullik, *Angew. Chem.* **1958**, *70*, 438; K. Hafner, C. Mink, H.-J. Lindner, *Angew. Chem.* **1994**, *106*, 1566; *Angew. Chem. Int. Ed. Engl.* **1994**, *33*, 1479; S. Miyake, L. M. Henling, J. E. Beslaw, *Organometallics* **1998**, *17*, 5328.

[4] C. Elschenbroich, R. Möckel, U. Zenneck, *Angew. Chem.* **1978**, *90*, 560; *Angew. Chem. Int. Ed. Engl.* **1978**, *17*, 531; A. R. Koray, M. L. Ziegler, N. E. Blank, M. W. Haenel, *Tetrahedron Lett.* **1979**, *26*, 2465.

[5] Review: H. Schmidbaur, *Angew. Chem.* **1985**, *97*, 893; *Angew. Chem. Int. Ed. Engl.* **1985**, *24*, 893; P. Jutzi, R. Krallmann, G. Wolf, B. Neumann, H. G. Stammler, *Chem. Ber.* **1991**, *124*, 2391.

[6] Review: M. Hisatome, *Rev. Heteroat. Chem.* **1992**, *6*, 142; M. Hisatome, J. Watanabe, K. Yamakawa, *Bull. Chem. Soc. Jpn.* **1994**, *67*, 280.

[7] C. Ruangstayanand, H.-J. Rimek, F. Zymalkowski, *Chem. Ber.* **1970**, *103*, 2403.

[8] K. Ishii, T. Nakano, T. Zenko, M. Kotera, M. Sakamoto, *J. Chem. Soc. Perkin Trans. 1* **1991**, 2057.

[9] The chloroalkynes were prepared analogously to those reported by J. White, C. G. Whiteley, *Synthesis* **1993**, 1141.

[10] W. P. Hart, D. W. Macomber, M. D. Rausch, *J. Am. Chem. Soc.* **1980**, *102*, 1196.

[11] Most relevant analytical data of **5**–**7**: **5a** ^{1}H NMR (500 MHz, C_6D_6): $\delta = 1.24$ (s, 18H), 1.46–1.52 (q, 4H), 2.01–2.08 (m, 8H), 4.48 (s, 2H), 4.61 (s, 1H); ^{13}C NMR (125 MHz, C_6D_6): $\delta = 18.7$ (CH_2), 27.4 (CH_2), 27.6 (C), 30.3 (CH_2), 31.6 (CH_3), 78.1 (C), 83,6 (CH), 85.6 (CH), 90.0 (C), 105.4 (C). **5b**: ^{1}H NMR (300 MHz, C_6D_6): $\delta = 1.22$ (s, 18H), 1.29–1.43 (m, 8H), 1.85–1.90 (m, 4H), 1.99–2.04 (m, 6H), 4.49 (2H), 4.61 (1H); ^{13}C NMR (75 MHz, C_6D_6): $\delta = 18.8$ (CH_2), 27.6 (C), 27.9 (CH_2), 29.1 (CH_2), 30.0 (CH_2), 31.6 (CH_3), 78.4 (C), 83.4 (CH), 85.4 (CH), 89.4 (C), 105.9 (C). **5c**: ^{1}H NMR (300 MHz, C_6D_6): $\delta = 1.12$–1.91 (m, 28H), 2.06 (m, 4H), 2.08 (m, 6H), 4.50 (s, 2H), 4.60 (s, 1H); ^{13}C NMR (75 MHz, C_6D_6): $\delta = 18.7$ (CH_2), 27.3 (C), 28.1 (CH_2), 28.5 (CH_2), 28.9 (CH_2), 30.3 (CH_2), 31.4 (CH_3), 78.5 (C), 83.2 (CH), 85.3 (CH), 89.0 (C), 105.8 (C). **6a**: yellow solid, m.p. 95 °C; ^{1}H NMR (300 MHz, C_6D_6): $\delta = 1.13$ (s, 9H), 1.22 (s, 9H), 1.58–1.75 (m, 8H), 1.94–1.98 (m, 2H), 2.29–2.35 (m, 2H), 4.63 (s, 2H), 5.33 (s, 1H); ^{13}C NMR (125 MHz, C_6D_6): $\delta = 22.7$ (CH_2), 24.3 (CH_2), 31.3 (CH_3), 32.5 (CH_3), 32.6 (C), 33.4 (C), 41.6 (CH_2), 66.4 (C), 82.2 (CH), 85.7 (CH), 91.9 (C), 94.9 (C), 100.7 (C); HR-MS (positive ions) calcd for $C_{23}H_{33}Co$: 368.1914; found: 368.1904. **6b**: yellow solid, m.p. 135 °C; ^{1}H NMR (300 MHz, C_6D_6): $\delta = 1.25$ (s, 9H), 1.30 (s, 9H), 1.51–1.72 (m, 8H), 2.13–2.17 (m, 4H), 2.25–2.33 (m, 2H), 2.62–2.69 (m, 2H), 4.84 (s, 3H); ^{13}C NMR (75 MHz, C_6D_6): $\delta = 28.3$ (CH_2), 28.5 (CH_2), 29.9 (CH_2), 31.7 (CH_2), 31.9 (CH_3), 32.0 (C), 32.9 (C), 33.1 (CH_3), 70.3 (C), 79.1 (CH), 81.4 (CH), 90.5 (C), 90.8 (C), 95.1 (C); HRMS (positive EI) calcd for $C_{25}H_{37}Co$: 396.2227; found: 396.2229. **6c** + **7**: yellow solid; ^{1}H NMR (300 MHz, C_7D_8): $\delta = 1.16$ (s, 9H), 1.17 (s, 9H), 1.26 (s, 18H), 1.73–1.30 (br, 18H), 2.03–1.75 (br, 10H), 2.73–2.21 (br, 12H), 4.48 (s, 1H), 4.72 (s, 4H), 4.89 (s, 1H); ^{13}C NMR (125 MHz, C_6D_6): $\delta = 22.5$ (CH_2), 23.6 (CH_2), 23.9 (CH_2), 24.2 (CH_2), 24.3 (CH_2), 24.9 (CH_2), 24.9 (CH_2), 25.4 (CH_2), 26.1 (CH_2), 30.2 (CH_2), 30.8 (CH_3), 31.5 (C), 31.6 (CH_3), 31.8 (C), 32.4 (C), 32.9 (CH_3), 74.0 (C), 77.0 (C), 77.2 (CH), 77.3 (CH), 79.4 (CH), 83.5 (CH), 85.7 (C), 85.8 (C), 88.3 (C), 94.6 (C), 96.7 (C); HR-MS (positive ions) calcd for $C_{27}H_{41}Co$: 424.2540; found: 424.2537.

[12] X-ray analysis of **6a**: $C_{23}H_{33}Co$, $M_r = 368.42$, monoclinic, space group $P2_1/c$, crystal dimensions: $0.36 \times 0.20 \times 0.08$ mm^3, $a = 14.0457(1)$, $b = 9.9803(1)$, $c = 14.3919(2)$ Å, $\beta = 103.97(1)^\circ$, $V = 1957.72(4)$ Å^3, $Z = 4$, $T = 200(2)$ K, $\rho_{calcd} = 1.25$ g cm^{-3}, Bruker Smart CCD, $Mo_{K\alpha}$ radiation, 19646 reflections collected, 4474 unique reflections ($R_{int} = 0.0446$), 3451 observed reflections with $I > 2\sigma(I)$, an empirical absorption correction was applied by using SADABS,[14] based on the Laue symmetry of the reciprocal space, $\mu = 0.88$ mm^{-1}, $T_{min} = 0.74$, $T_{max} = 0.94$. The structure was solved by the Patterson method and refined against F^2 with a full-matrix least-squares algorithm by using the SHELXTL (5.1) software package,[15] 223 parameters refined, $R1 = 0.034$, $wR2 = 0.073$ ($I > 2\sigma(I)$), GOF = 1.04. The maximum and minimum residual electron density is 0.28 and -0.35 e Å^{-3}, respectively. X-ray analysis of **6b**: $C_{25}H_{37}Co$, $M_r = 396.48$, orthorhombic, space group $Pna2_1$, crystal dimensions: $0.58 \times 0.42 \times 0.24$ mm^3, $a = 10.3000(1)$, $b = 13.5018(1)$, $c = 15.0996(1)$ Å, $V = 2099.88(3)$ Å^3, $Z = 4$, $T = 200(2)$ K, $\rho_{calcd} = 1.25$ g cm^{-3}, Bruker Smart CCD, $Mo_{K\alpha}$ radiation, 15308 reflections collected, 3098 unique reflections ($R_{int} = 0.0812$), 2306 observed reflections with $I > 2\sigma(I)$, an empirical absorption correction was applied by using SADABS,[14] based on the Laue symmetry of the reciprocal space, $\mu = 0.82$ mm^{-1}, $T_{min} = 0.65$, $T_{max} = 0.86$. The structure was solved by direct methods and refined against F^2 with a full-matrix least-squares algorithm by using the SHELXTL (5.1) software package,[15] 241 parameters refined, $R1 = 0.037$, $wR2 = 0.068$ ($I > 2\sigma(I)$), GOF = 0.96. The maximum and minimum residual electron density is 0.72 and -0.29 e Å^{-3}, respectively. The crystallographic data (excluding structure factors) for the structures reported herein have been deposited with the Cambridge Crystallographic Data Centre as supplementary publication no. CCDC-161078 (**6a**) and CCDC-161079 (**6b**). Copies of the data can be obtained free of charge on application to CCDC, 12 Union Road, Cambridge CB21EZ, UK (fax: (+44) 1223-336-033; e-mail: deposit@ccdc.cam.ac.uk).

[13] P. E. Riley, R. E. Davis, *J. Organomet. Chem.* **1976**, *113*, 157.

[14] G. M. Sheldrick, 1996, unpublished work based on the method described in R. H. Blessing, *Acta Crystallogr. Sect. A* **1995**, S1, S33.

[15] G. M. Sheldrick, Bruker Analytical X-ray-Division, Madison, WI, **1997**.

Low-Temperature Selective Catalytic Reduction (SCR) of NO with NH_3 by Using Mn, Cr, and Cu Oxides Supported on Hombikat TiO_2**

Panagiotis G. Smirniotis,* Donovan A. Peña, and Balu S. Uphade

Nitrogen oxides are man-made pollutants, emitted from mobile and stationary sources, that greatly contribute to the formation of smog, acid rain, and ozone. Automobiles are the primary mobile sources of NO_x emissions, while the stationary sources consist of oil and coal-fired power stations and nitric acid production plants. The direct health hazards related to NO_x are bronchitis, pneumonia, viral infections, and hay fever. Selective catalytic reduction (SCR) of NO with ammonia in the presence of oxygen [Eq. (1)] is the proven technology for

$$4\,NO + 4\,NH_3 + O_2 \longrightarrow 4\,N_2 + 6\,H_2O \quad (1)$$

[*] Prof. P. G. Smirniotis, D. A. Peña, B. S. Uphade
Chemical Engineering Department
University of Cincinnati
Cincinnati, OH 45221-0171 (USA)
Fax: (+1) 513-556-3473
E-mail: Panagiotis.Smirniotis@UC.EDU

[**] We are grateful to the Ohio Coal Development Office (OCDO), Columbus, Ohio, for financial support and for allowing us to publish the findings.

effective removal of NO_x from stationary sources.[1] A process based on V_2O_5/TiO_2[2–6] catalysts with or without the addition of either WO_3 or MoO_3 was developed and successfully commercialized for NO_x removal (catalysts for NO_x removal are known as DeNOx catalysts). The system is successful because of its high activity and resistance to SO_2 poisoning. However, the main disadvantage of this type of catalyst is that it does not work at reaction temperatures $\leq 250\,^{\circ}C$. The other disadvantages include over-oxidation of NH_3 to N_2O and NO and the oxidation of SO_2 to SO_3. There is an urgent need for the development of low-temperature SCR methods for the treatment of flue gas, especially from electric power plants, shaft furnaces, and waste incinerators. Large quantities of NO_x are generated at such sites, and the flue-gas temperature at the outlet of the heat-recovery system or smokestack is normally $\leq 150\,^{\circ}C$.

Platinum-based catalysts were found to be highly active for the reaction in Equation (1), however, the scarcity of Pt, the oxidation of NH_3 to NO_x at relatively high temperature, high cost, and rapid poisoning under stack-gas conditions have prompted worldwide efforts to develop low-cost supported metal or mixed metal oxide catalysts. Metal oxides, such as MoO_3,[7] CuO, and MnO_x,[8, 9] supported on TiO_2, Al_2O_3, or activated carbon fibers have been reported to be active for the SCR process at temperatures greater than $300\,^{\circ}C$, however, the high temperature results in poor N_2 selectivity. Recently, a highly active and SO_2 resistant activated-carbon-supported V_2O_5 catalyst was reported,[10] however, it is active only above $150\,^{\circ}C$ and also needs specific pretreatment for initial activation. Additionally, the stability of carbon-containing catalysts in O_2 is low.

Herein we show that transition metal oxides supported on Hombikat TiO_2 display substantial activity for NO reduction and also a 100% yield of N_2 at much lower reaction temperatures ($\leq 120\,^{\circ}C$, Table 1); to our knowledge, these catalytic results are the best reported so far. Of the catalysts we studied, the best results were obtained over the Mn on Hombikat TiO_2 catalyst. The catalyst characterization and activity data obtained at $100\,^{\circ}C$ and $120\,^{\circ}C$ for various transition metal oxides deposited on different supports are given in Table 1. From X-ray diffraction (XRD) studies only weak peaks arising from transition metal oxides were obtained, suggesting that the catalysts are mostly amorphous. Surprisingly the observed metal dispersion for our best catalyst was poor even on a high-surface-area support, indicating that high metal dispersion is not crucial. Noteworthy is that catalysts containing metals other than Mn, Cr, and Cu are far less active; the multivalent nature of Mn, Cr, and Cu oxides may facilitate the redox activity of the catalysts.

Consistent with the literature data,[11] our Cr/TiO_2 catalyst also produced undesired N_2O which indicates the possible presence of CrO_2, however, this phase was not detected in our XRD analysis. Ni on Hombikat TiO_2 shows no activity, which is attributed to the confined monovalent oxidation state of nickel and also the low surface concentration of nickel observed from X-ray photoemission spectroscopy (XPS). Our XPS data confirmed that the Mn/Hombikat TiO_2 system has the greatest metal oxide surface concentration (Table 1). This result suggests that more MnO_x species are available to participate in the reaction, which may explain the excellent performance of the Mn/Hombikat TiO_2 catalyst. Deconvoluted XPS spectra for Mn $2p_{3/2}$ indicate the presence of MnO_2 (642.2 eV) as the major phase and Mn_2O_3 (641.2 eV) as a minor phase along with a third phase, possibly partially undecomposed manganese nitrate (643.8 eV) resulting from the relatively low calcination temperature. The binding-energy values match well with the literature values.[12] The results suggest the possibility of redox behavior during the catalytic reaction.

A Fourier Transform infrared (FT-IR) spectroscopy study of NH_3 shows that the Brønsted:Lewis acid site ratio for the Mn/Hombikat TiO_2 system is lower than that of the other catalysts (see Table 1). In contrast, V/Hombikat TiO_2, which resembles a typical medium-temperature DeNOx catalyst, shows a large number of Brønsted ($1421\ cm^{-1}$) rather than Lewis ($1607\ cm^{-1}$) acid sites. These results clearly indicate that Lewis acidity is more important than Brønsted acidity for low-temperature SCR catalysts. The NH_3 FT-IR results are

Table 1. Catalyst characterization, activity data, and comparison with literature results involving commercial catalysts.

Support	Transition metal	Surface area [$m^2 g^{-1}$]		Metal dispersion [%]	M2p/M′2p[l]	Crystal phases[m]	Total acidity [$\mu mol\,g^{-1}$]	[n]	NO conversion (%) at	
		support	catalyst						100 °C	120 °C
TiO_2[a]	V	309	51	12.2	0.4	V_2O_5, V_2O_4	9.8	6.09	10	19
TiO_2[a]	Cr	309	143	10.4	0.6	CrO_2, Cr_2O_3	55.8	0.11	80	91
TiO_2[a]	Mn	309	204	8.9	6.0	MnO_2, Mn_2O_3	23.2	0.07	82	100
TiO_2[a]	Ni	309	163	40.4	0.1	NiO	42.7	0.11	0	4
TiO_2[a]	Cu	309	140	47.2	–	CuO, Cu_2O	12.5	0.21	56	95
TiO_2[b]	Mn	53	52	7.3	0.2	MnO_2, Mn_2O_3	15.2	0.59	67	96
TiO_2[c]	Mn	9	14	7.0	0.5	MnO_2, Mn_2O_3	1.1	0.76	38	64
SiO_2[d]	Mn	559	421	7.0	0.8	MnO_2, Mn_2O_3	5.9	0.24	57	93
γ-Al_2O_3[e]	Mn	205	180	6.8	3.4	MnO_2, Mn_2O_3	31.0	0.40	56	89
1.4% w/w V_2O_5, 9.0% w/w WO_3/TiO_2[f] (a catalyst similar to a commercial DeNOx catalyst)[f][14]								–	12[g]	98[h]
NO_xCAT920LT (a Pt based commercial catalyst)[i][15]							–	–	63[j]	91[k]

[a] Hombikat, [b] Degussa P25, [c], [d] Aldrich, [e] Puralox, M = V, Cr, Mn, Ni, Cu; M′ = Ti, Si, Al, [f] experimental conditions: catalyst weight 160 mg, p = 1 atm, flow rate $60\ cm^3\,min^{-1}$; feed He with 800 ppm each of NH_3 and NO and 1 vol% O_2, [g] at $150\,^{\circ}C$ and 98% N_2 selectivity, [h] at $300\,^{\circ}C$ and 98% N_2 selectivity, [i] experimental conditions: N_2 with 500 ppm NO, 400 ppm NH_3, and 4 vol% O_2, GHSV = 24000 h^{-1}, [j] at $180\,^{\circ}C$ and 45% N_2 selectivity, [k] at $240\,^{\circ}C$ and 35% N_2 selectivity, [l] emission intensity ratios from XPS measurements of surface elemental composition, [m] from XRD and XPS measurements, [n] ratio of Brønsted to Lewis acid centers.

  1433-7851/01/4013-2480 $ 17.50+.50/0

consistent with those reported by Busca and co-workers.[13] The NO conversion improved with increased Mn loading of the Hombikat TiO_2, and can be attributed to the increased surface concentration of Mn (determined by XPS; Table 1). 20 wt% Mn/Hombikat TiO_2 tested over a broad temperature range (80–180 °C) showed only trace amounts of N_2O (<5%) at 180 °C. In addition this catalyst showed no decrease in activity after 50 h on stream at 120 °C.

The activity of Mn-, Cr-, and Cu-loaded Hombikat TiO_2 catalysts was compared with the commercial V_2O_5/TiO_2[14] and noble metal[15] based catalysts (Table 1). Although the results on the commercial catalysts were not collected under identical experimental conditions, they do demonstrate the superior performance of our catalysts over both the commercial catalysts. High catalytic activity of our catalysts at low temperature is attributed to the redox behavior of the metal oxides, the high surface concentration of transition metal oxides, and Lewis acidity.

Any SCR catalyst intended for commercial application should be tested in the presence of water and at space velocities close to industrial scale. Our best catalyst, 20 wt% Mn/Hombikat TiO_2, showed excellent results (Figure 1) at

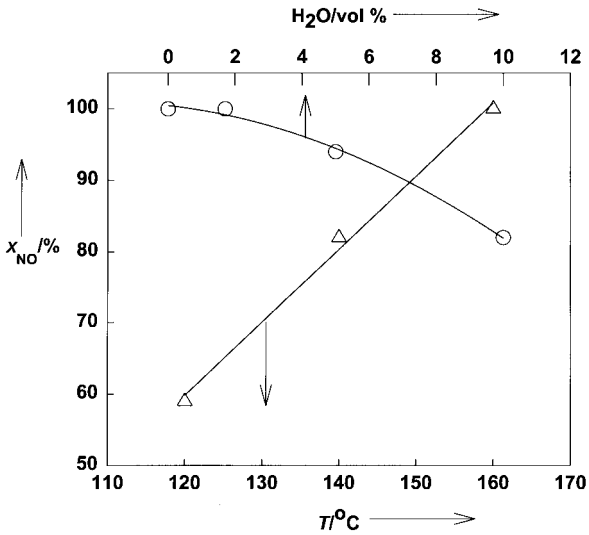

Figure 1. Influence of inlet water concentration on NO conversion in the SCR reaction over 20 wt% Mn/Hombikat TiO_2 at different temperatures, feed: NO = NH_3 = 2000 ppm, O_2 = 2 vol%, He carrier gas, H_2O = 1.7–10 vol%, catalyst = 0.1 g, total flow = 17.3 mL min^{-1}. △ = 1.7 vol% H_2O, ○ = 160 °C.

120–180 °C with inlet water concentrations as high as 10 vol%, indicating very good hydrothermal stability. Less than 3% N_2O formation was detected at 180 °C. These results are superior to those in the literature. The same catalyst was also tested in a wide gas hourly space velocity (GHSV) range (4000 h^{-1} to 64000 h^{-1}). The results (Figure 2) show an approximate 50% decrease in NO conversion at higher GHSV. However, it should be noted that we have used higher levels of NO (2000 ppm) in the feed than that found in coal-fired power plants (400–500 ppm).

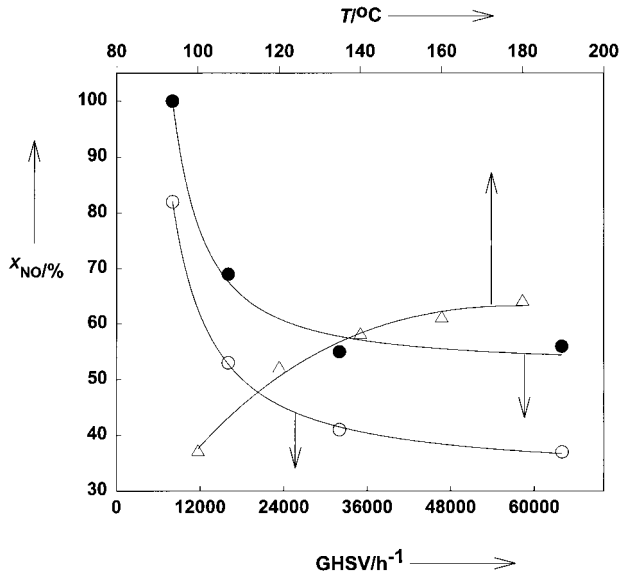

Figure 2. Influence of GHSV on NO conversion in the SCR reaction at different temperatures over 20 wt% Mn/Hombikat TiO_2 feed: NO = NH_3 = 2000 ppm, O_2 = 2 vol%, He carrier gas, catalyst = 0.1 g, total flow = 17.3 mL min^{-1}, ○ = 120 °C, ● = 140 °C, △ = 64000 h^{-1}.

In conclusion, a new highly active, time-stable, and water resistant catalyst operating at low temperature (80–180 °C) has been developed for the SCR of NO with NH_3 in excess O_2. Further studies are in progress to better understand the mechanistic aspects of our catalytic system.

Experimental Section

Transition metal oxides were deposited on various supports (Table 1) using aqueous solutions of metal nitrates. In a typical synthesis, distilled water (50 mL) was added to a 100 mL beaker containing the support (1.0 g). The mixture was heated to 70 °C under continuous stirring. A measured quantity of metal nitrate was added, and the mixture was evaporated to dryness. The paste obtained was further dried overnight at 110 °C, ground and sieved (80 mesh). Prior to the catalytic experiments, the catalysts were activated in situ by passing oxygen (4.18% in He) for 2 h at 400 °C. The SCR of NO at atmospheric pressure was carried out in a fixed-bed ceramic aluminum oxide reactor (internal diameter 6 mm) containing catalyst (0.1 g; 80 mesh). Oxygen (Wright Bros., 4.18% in He), ammonia (Matheson, 3.89% in He) and nitric oxide (Air Products, 2.0% in He) were used as received. The inlet concentrations of NO and NH_3 were 2000 ppm, whereas the O_2 concentration was 20000 ppm. The total flow of inlet gases was set at 17.3 mL min^{-1} to achieve a GHSV of 8000 h^{-1}. The reaction temperature was measured by a type K thermocouple inserted directly into the catalyst bed. The reactants and products were analyzed on-line using a mass spectrometer. Catalysts calcined at 400 °C for 2 h were used for XRD, NH_3 FT-IR, XPS and NH_3 temperature-programmed desorption (TPD).

Received: June 19, 2000
Revised: March 12, 2001 [Z15282]

[1] H. Bosch, F. Janssen, *Catal. Today* **1988**, *2*, 369–531.
[2] M. Inomata, A. Miyamoto, Y. Murakami, *J. Catal.* **1980**, *62*, 140–148.
[3] F. Janssen, F. van den Kerkhof, H. Bosch, J. R. H. Ross, *J. Phys. Chem.* **1987**, *91*, 5921–5927.
[4] J. A. Odriozola, J. Soria, G. A. Somarjai, H. Heinemann, J. F. Garcia de la Banda, M. Lopez Granados, J. C. Conesa, *J. Phys. Chem.* **1991**, *95*, 240–246.

  1433-7851/01/4013-2481 $ 17.50+.50/0

[5] S. C. Wood, *Chem. Eng. Prog.* **1994**, *90*, 32 – 38.
[6] J. A. Dumesic, N.-Y. Topsøe, H. Topsøe, T. Slabiak, *J. Catal.* **1996**, *163*, 409 – 417.
[7] M. de Boer, A. J. van Dillen, D. C. Koningsberger, F. J. J. G. Janssen, T. Koerts, J. W. Geus, *Stud. Surf. Sci. Catal.* **1992**, *72*, 133 – 145.
[8] L. Singoredjo, R. Korver, F. Kapteijn, J. Moulijn, *Appl. Catal. B* **1992**, *1*, 297 – 316.
[9] M. Yoshikawa, A. Yasutake, I. Mochida, *Appl. Catal. A* **1998**, *173*, 239 – 245.
[10] Z. Zhu, Z. Liu, S. Liu, H. Niu, *Appl. Catal. B* **1999**, *23*, L229 – L233.
[11] H. Schneider, M. Maciejewski, K. Köhler, A. Wokaun, A. Baiker, *J. Catal.* **1995**, *157*, 312 – 320.
[12] F. Kapteijn, A. D. van Langeveld, J. A. Moulijn, A. Andreïni, M. A. Vuurman, A. M. Turek, J.-M. Jehng, I. E. Wachs, *J. Catal.* **1994**, *150*, 94 – 104.
[13] J. M. G. Amores, V. S. Escribano, G. Ramis, G. Busca, *Appl. Catal. B* **1997**, *13*, 45 – 58.
[14] L. J. Alemany, L. Lietti, N. Ferlazzo, P. Forzatti, G. Busca, E. Giamello, F. Bregani, *J. Catal.* **1995**, *155*, 117 – 130.
[15] A. T. Krishnan, A. L. Boehman, *Appl. Catal. B* **1998**, *18*, 189 – 198.

Total Synthesis of Colombiasin A**

K. C. Nicolaou,* Georgios Vassilikogiannakis, Wolfgang Mägerlein, and Remo Kranich

Colombiasin A (**1**) is a novel diterpene recently isolated from a biologically active (against *Mycobacterium tuberculosis* H37Rv) extract obtained from the gorgonian octocoral, *Pseudopterogorgia elisabethae*, collected off San Andres Island, Colombia.[1] Its structure is characterized by a tetracyclic carbon framework whose periphery is decorated with four methyl groups, two carbonyl functions, two double bonds, and one hydroxy group. In addition, this unprecedented molecular architecture includes six stereogenic centers, two of which are adjacent quaternary carbon atoms. Despite the elegant spectroscopic studies that led to the structural elucidation of the colombiane skeleton, the absolute stereochemistry of colombiasin A (**1**) remains unassigned. The intrigue surrounding this natural product is heightened by a proposal suggesting elisabethin A (which was also found in *Pseudopterogorgia elisabethae*[2]) as a biogenetic precursor of **1**.[1] Here we report the total synthesis of colombiasin A (**1**) by a strategy which also delivered its C7 epimer as well as several other analogues.

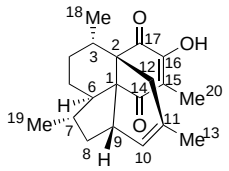

1: colombiasin A

A brief retrosynthetic analysis of colombiasin A (**1**) is presented in Scheme 1. Inspection of the target's architecture suggested quinone **A** as the cornerstone of its construction.

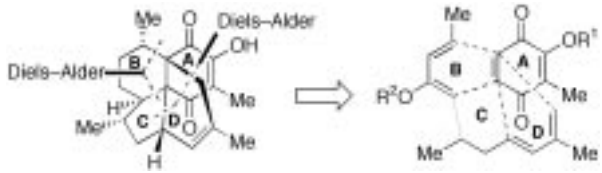

Scheme 1. Retrosynthetic analysis of colombiasin A (**1**).

Two Diels – Alder reactions, first with diene **B** (intermolecular) and then with diene **D** (intramolecular), along the sequence of elaboration, were expected to complete the polycyclic skeleton of the molecule. According to this plan, the elaboration sequence between the two cycloadditions would require both tethering of domains **B** and **D** as well as reoxidation of ring **A** to a new quinone moiety after fusion of ring **B**. To facilitate tethering of segments **B** and **D** (i.e. forming the C6–C7 bond), an oxygen-based functional group (R^2O) was temporarily incorporated into diene **B** as shown in Scheme 1. As described below, two runs of the derived strategy were necessary to reach colombiasin A (**1**).

The construction of the first key intermediate, ketone **6**, starting with the first of the projected Diels – Alder reactions is summarized in Scheme 2. Thus, reaction of diene **2** with quinone **3**[3] (obtained by *ortho*-methylation of 1,2,4-trimethoxybenzene[4] followed by oxidative demethylation[5]

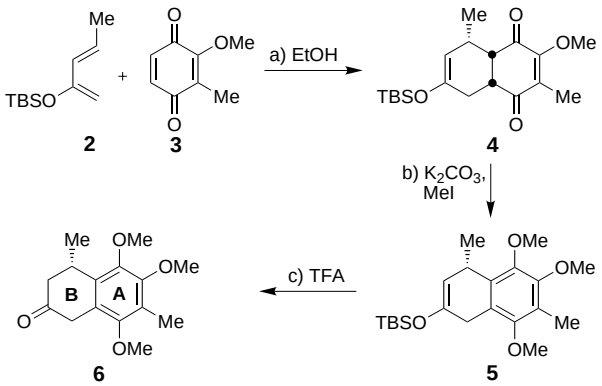

Scheme 2. Construction of **AB** ring system **6**. a) EtOH, 25 °C, 2 h, 83 %; b) K_2CO_3 (5.0 equiv), MeI (20 equiv), acetone, reflux, 48 h, 83 %; c) 2 % TFA in CH_2Cl_2, 25 °C, 2 h, 91 %. TFA = trifluoroacetic acid; TBS = *tert*-butyldimethylsilyl.

[*] Prof. Dr. K. C. Nicolaou, Dr. G. Vassilikogiannakis, Dr. W. Mägerlein, Dr. R. Kranich
Department of Chemistry and The Skaggs Institute for Chemical Biology
The Scripps Research Institute
10550 North Torrey Pines Road, La Jolla, CA 92037 (USA)
Fax: (+1) 858-784-2469
E-mail: kcn@scripps.edu
and
Department of Chemistry and Biochemistry
University of California, San Diego
9500 Gilman Drive, La Jolla, CA 92093 (USA)

[**] This work was financially supported by the National Institutes of Health (USA) and The Skaggs Institute for Chemical Biology, postdoctoral fellowships from Bayer AG (to R.K. and W.M.), and grants from Abbott, Amgen, ArrayBiopharma, Boehringer-Ingelheim, Glaxo, Hoffmann-La Roche, DuPont, Merck, Novartis, Pfizer, and Schering Plough.

  1433-7851/01/4013-2482 $ 17.50+.50/0

with AgO/HNO_3) in ethanol, at ambient temperature, resulted in the formation of the desired *endo* cycloadduct **4** as the sole product in 83% yield. The rather labile compound **4** was then masked as its aromatic derivative **5** by exposure to an excess of K_2CO_3 and MeI (83% yield) and the TBS group was then removed with TFA to afford the desired ketone **6** in 91% yield.

With the bicyclic **AB** system **6** in hand, the next objective was to introduce the requisite chain at C6 for the next planned cycloaddition reaction. After failing to accomplish this goal by direct alkylation, we next turned our attention to a sigmatropic rearrangement equivalent (structure **7**, Scheme 3) as a

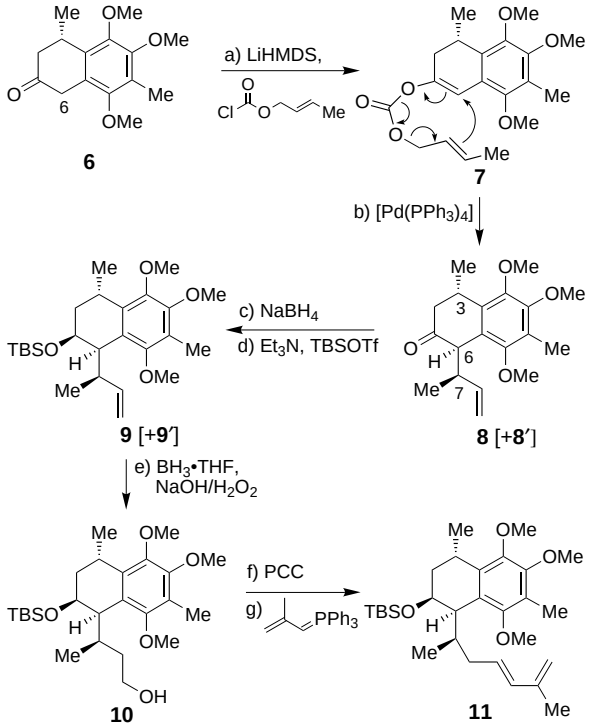

Scheme 3. Construction of intramolecular Diels–Alder precursor **11**. a) LiHMDS (1.2 equiv), THF, −78 °C, 1 h; then crotyl chloroformate (1.4 equiv), 25 °C, 30 min, 94%; b) $[Pd(PPh_3)_4]$ (0.04 equiv), THF, 25 °C, 15 min, 58% plus 24% of isomeric *E*-disubstituted olefin **8′**; c) $NaBH_4$ (3.0 equiv), MeOH, 25 °C, 30 min, 96%; d) Et_3N (2.0 equiv), TBSOTf (1.2 equiv), CH_2Cl_2, −78 °C, 1 h, 95%; e) $BH_3 \cdot THF$ (3 equiv), THF, 25 °C, 2 h; then 3 M NaOH and 30% H_2O_2, 25 °C, 1 h, 82%; f) PCC (1.5 equiv), CH_2Cl_2, 25 °C, 1.5 h, 91%; g) 2-methyl-2-propenyltriphenylphosphonium bromide (1.5 equiv), *n*BuLi (1.5 equiv), THF, 0 → 25 °C, 1 h; then aldehyde, 70 °C, 8 h, 70% plus 23% *Z* isomer. LiHMDS = lithium bis(trimethylsilyl)-amide; OTf = trifluoromethanesulfonate; PCC = pyridinium chlorochromate.

possible means to form the required C–C bond. A major issue shadowing this proposition, however, was the relative stereochemistry of the three stereogenic centers in the anticipated product, although initial molecular modeling studies appeared favorable for the required arrangement. In the event, a palladium(0)-induced intramolecular allylation[6] was employed to accomplish the desired goal. Thus, regioselective enolate formation from **6** (LiHMDS) followed by quenching with crotyl chloroformate[7] furnished the desired carbonate **7** (see Table 1) in 94% yield. Exposure of the latter compound

Table 1. Selected physical properties of compounds **7**, **16**, **18**, **23**, and **24**.[a]

7: Colorless syrup; $R_f = 0.51$ (silica gel, ethyl acetate/hexane 1/3); IR (film): $\tilde{\nu}_{max} = 2937, 1756, 1457, 1406, 1231, 1078, 966\ cm^{-1}$; ^1H NMR: $\delta = 6.50$ (d, $J = 2.9$ Hz, 1H), 5.89 (m, 1H), 5.66 (m, 1H), 4.62 (d, $J = 6.6$ Hz, 2H), 3.86 (s, 3H), 3.81 (s, 3H), 3.67 (s, 3H), 3.43 (m, 1H), 2.88 (ddd, $J = 16.9$, 7.3, 2.9 Hz, 1H), 2.18 (m, 1H), 2.16 (s, 3H), 1.76 (dd, $J = 6.6$, 0.7 Hz, 3H), 1.18 (d, $J = 7.0$ Hz, 3H); ^{13}C NMR: $\delta = 152.9, 150.9, 150.8, 148.4, 146.2, 132.8, 130.1, 124.2, 123.3, 120.9, 108.1, 69.0, 61.3, 60.7, 60.0, 32.7, 27.6, 20.6, 17.8, 9.1$; HR-MS: calcd for $C_{20}H_{26}O_6Na$ $[M+Na^+]$: 385.1621, found: 385.1612

16: Colorless glass; $R_f = 0.47$ (silica gel, ethyl acetate/hexane 1/6); IR (film): $\tilde{\nu}_{max} = 2929, 1673, 1625, 1448, 1290, 1142, 1114\ cm^{-1}$; ^1H NMR: $\delta = 5.66$ (br s, 1H), 3.87 (s, 3H), 3.15 (br m, 1H), 2.37 (br d, $J = 18.1$ Hz, 1H), 2.27 (m, 1H), 2.07 (m, 1H), 1.99 (br d, $J = 18.1$ Hz, 1H), 1.90–2.00 (m, 2H), 1.85 (s, 3H), 1.67 (m, 1H), 1.59 (m, 1H), 1.55 (br s, 3H), 1.35–1.47 (m, 2H), 1.34 (d, $J = 7.0$ Hz, 3H), 1.28 (m, 1H), 0.90 (d, $J = 7.3$ Hz, 3H); ^{13}C NMR: $\delta =$ 202.1, 198.7, 156.2, 129.7, 129.2, 125.2, 66.8, 59.7, 51.7, 43.8, 36.7, 36.6, 34.2, 34.1, 33.3, 30.7, 24.3, 22.8, 17.3, 15.7, 9.9; HR-MS: calcd for $C_{21}H_{28}O_3$ $[M+H^+]$: 329.2111, found: 329.2103

18: Colorless syrup; $R_f = 0.50$ (silica gel, ethyl acetate/hexane 1/2); IR (film): $\tilde{\nu}_{max} = 2935, 1723, 1461, 1404, 1253, 1105, 1071, 1009, 880, 837, 777\ cm^{-1}$; ^1H NMR: $\delta = 9.50$ (d, $J = 1.1$ Hz, 1H), 4.31 (m, 1H), 3.83 (s, 3H), 3.79 (s, 3H), 3.73 (s, 3H), 3.62 (br dd, $J = 6.2$, 3.3 Hz, 1H), 3.29 (m, 1H), 2.89 (m, 1H), 2.16 (s, 3H), 2.11 (m, 1H), 1.60 (dd, $J = 12.8$, 4.0 Hz, 1H), 1.24 (d, $J = 7.0$ Hz, 3H), 1.10 (d, $J = 7.0$ Hz, 3H), 0.92 (s, 9H), 0.11 (s, 6H); ^{13}C NMR: $\delta = 204.7, 152.2, 150.5, 147.2, 133.6, 125.2, 123.5, 67.6, 60.4, 60.3, 59.9, 47.9, 42.1, 35.5, 29.1, 25.9, 23.4, 18.2, 13.6, 9.5, -4.5, -4.8$; HR-MS: calcd for $C_{24}H_{40}O_5SiNa$ $[M+Na^+]$: 459.2537, found: 459.2554

23: Colorless glass; $R_f = 0.60$ (silica gel, ethyl acetate/hexane 1/1); IR (film): $\tilde{\nu}_{max} = 3488, 2930, 1672, 1628, 1446, 1294, 1115\ cm^{-1}$; ^1H NMR: $\delta = 5.67$ (br s, 1H), 3.98 (br m, 1H), 3.87 (s, 3H), 3.10 (br m, 1H), 2.38 (br d, $J = 18.4$ Hz, 1H), 2.34 (m, 2H), 2.06 (m, 1H), 1.95 (br d, $J = 18.4$ Hz, 1H), 1.93 (dd, $J =$ 5.5, 2.6 Hz, 1H), 1.86 (s, 3H), 1.74–1.83 (m, 2H), 1.65 (br s, 1H), 1.62 (m, 1H), 1.55 (br s, 3H), 1.33 (d, $J = 7.3$ Hz, 3H), 0.91 (d, $J = 7.3$ Hz, 3H); ^{13}C NMR: $\delta = 202.3, 198.5, 155.7, 131.5, 129.4, 124.9, 67.2, 63.7, 59.7, 52.7, 51.4, 41.3, 38.2, 37.0, 34.7, 33.4, 28.7, 22.7, 22.4, 17.7, 10.3$; HR-MS: calcd for $C_{21}H_{28}O_4$ $[M+H^+]$: 345.2060, found: 345.2058

24: Colorless glass; $R_f = 0.47$ (silica gel, ethyl acetate/hexane 1/6); IR (film): $\tilde{\nu}_{max} = 2925, 1675, 1629, 1453, 1268, 1139, 1108\ cm^{-1}$; ^1H NMR: $\delta = 5.66$ (br s, 1H), 3.88 (s, 3H), 3.01 (br m, 1H), 2.41 (br d, $J = 19.0$ Hz, 1H), 2.12 (m, 1H), 1.91 (br d, $J = 19.0$ Hz, 1H), 1.89 (s, 3H), 1.78–1.89 (m, 5H), 1.57 (br s, 3H), 1.32 (d, $J = 7.0$ Hz, 3H), 1.29–1.36 (m, 3H), 0.82 (d, $J = 7.0$ Hz, 3H); ^{13}C NMR: $\delta = 203.1, 198.7, 155.1, 131.5, 129.5, 123.5, 63.5, 59.8, 51.6, 48.3, 39.6, 39.0, 36.6, 34.1, 33.6, 31.9, 31.1, 22.8, 22.2, 17.8, 10.4$; HR-MS: calcd for $C_{21}H_{28}O_3$ $[M+H^+]$: 329.2111, found: 329.2105

[a] ^1H NMR: 500 MHz, $CDCl_3$; ^{13}C NMR: 125 MHz, $CDCl_3$. HR-MS: matrix-assisted laser desorption/ionization.

to catalytic amounts of $[Pd(PPh_3)_4]$ in THF at ambient temperature led to terminal olefin **8** as the major product (58% yield) accompanied by its isomeric *E*-8,9-disubstituted olefin (**8′**, 24%, not shown). Although both regioisomers (**8** and **8′**) were formed as single diastereoisomers, it was difficult at this stage to assign the relative stereochemistry. It was decided, however, to push forward, hoping for full structural elucidation upon rigidification of the structure through the anticipated second cycloaddition. Toward this end, the inseparable mixture of **8** and **8′** was stereoselectively reduced with $NaBH_4$ and the resulting mixture of β-alcohols was protected as the TBS derivatives (**9** and **9′**), a mixture which was then subjected to hydroboration–oxidation to afford two hydroxy compounds, from which pure primary alcohol **10** was isolated by flash column chromatography. Finally, the requisite diene **11** was produced by PCC-mediated oxidation of **10** followed by Wittig reaction of the resulting aldehyde with the ylide derived from 2-methyl-2-propenyltriphenylphospho-

nium bromide and *n*BuLi. Diene **11** was formed as the major product and was accompanied by smaller amounts of its *Z* stereoisomer (*E*/*Z* ≈ 3/1, 93% total yield). This lack of stereochemical exclusivity in this reaction was inconsequential, since both geometrical isomers (the *Z* having first been converted to the *E* isomer) led to the same [4+2] cycloadduct (see below).

With diene **11** secured, the stage was now set for unveiling the quinone moiety to attempt the construction of the missing part of the targeted framework. As shown in Scheme 4, when **11** was treated with AgO/HNO_3 in dioxane[5] at ambient

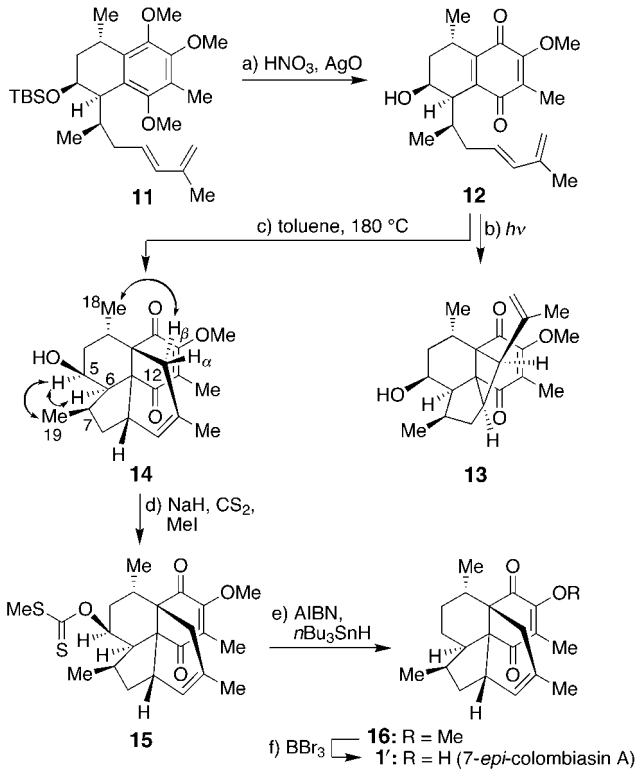

Scheme 4. Oxidation of aromatic diene **11** and synthesis of 7-*epi*-colombiasin A (**1′′**). a) Dioxane/6 M HNO_3 (10:1), 25 °C, 2 h; then AgO (5.0 equiv), 25 °C, 1 h, 27%; b) visible light, benzene, 25 °C, 15 min, 91%; c) toluene (sealed tube), in the dark, 180 °C, 5 h, 89%; d) NaH (5.0 equiv), $THF/CS_2/MeI$ (4/1/1), 50 °C, 5 h, 85%; e) AIBN (cat.), *n*Bu_3SnH (5.0 equiv), toluene, careful deoxygenation, 110 °C, 30 min, 88%; f) BBr_3, (10 equiv), CH_2Cl_2, −78 °C, 20 min, 40% plus 20% of **1′′′**. AIBN = 2,2′-azobisisobutyronitrile.

temperature, quinone **12** was obtained in only 27% yield, with the remainder of the material being converted to numerous unidentified by-products. Despite the low yield in this step, however, we were encouraged to advance forward since we hoped to then be able to at least ascertain the pending stereochemical issues of our intermediates. Interestingly, our initial attempt to thermally induce the intramolecular cycloaddition reaction within structure **12** (toluene, 120 °C, sealed tube, ordinary room light) led to the exclusive formation of the [2+2] cycloadduct **13** in 80% yield. In an effort to confirm the suspected photochemically induced [2+2] cycloaddition process, we irradiated **12** with visible light (sunlamp) in benzene at ambient temperature and, indeed, observed its fast (15 min) and clean conversion to **13** (91% yield). Furthermore, and gratifyingly, when **12** was heated in toluene at 180 °C (sealed tube) in the dark, the desired [4+2] cycloadduct **14** was obtained in 89% yield (*endo*/*exo* ≈ 9/1). Analysis of the NMR spectra of the major (*endo*) isomer **14** and comparison to those of colombiasin A (**1**)[1] revealed its stereochemical structure. Particularly suggestive of the indicated C7-*epi* stereochemistry in **14** were the observed NOEs for Me18/H12β, H5/H6, and H5/Me19 (see arrows in structure **14**, Scheme 4). Having assembled the advanced intermediate **14**, and despite the incorrect stereochemistry at C7, we decided to transverse the remaining short sequence to 7-*epi*-colombiasin A (**1′**) with two objectives in mind. First, the exercise was expected to prepare the ground for the real intermediate to follow, and second, to render the final target (7-*epi*-colombiasin A, **1′**) available for biological evaluation. The two remaining tasks before reaching **1′** were deoxygenation at C5 and deprotection of the C16 hydroxy group. The former requirement was fulfilled upon conversion of **14** to its xanthate **15**[8] (NaH, CS_2, MeI, 85% yield) followed by treatment of the latter with *n*Bu_3SnH/AIBN[9] (toluene, 110 °C, 88% yield), while the second objective was accomplished by demethylation of the resulting compound **16** (see Table 1) with BBr_3 (CH_2Cl_2, −78 °C, 40% yield). A second product obtained in the last reaction (20% yield) was identified as the isomer of **1′** in which the double bond had shifted from the C10−C11 to the adjacent C11−C12 position (compound **1′′′**). While the chromatographic and spectroscopic data for both **1′** and **1′′′** were consistent with their assigned structures, they differed from those of colombiasin A (**1**).

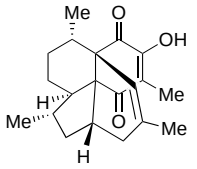

1′′: $\Delta^{11,12}$-colombiasin A

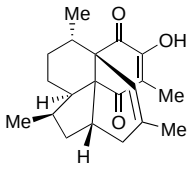

1′′′: 7-*epi*-$\Delta^{11,12}$-colombiasin A

Refocusing on the original objective of reaching colombiasin A (**1**), we returned to terminal olefin **9**, whose C7 stereocenter now required inversion prior to its further processing (see Scheme 5). This was accomplished by epimerizing the corresponding aldehyde **17** (obtained by oxidative cleavage)[10] to the correct C7 epimer **18** (NaOMe/MeOH, **17**/**18** ≈ 2/1, chromatographic separation and recycling, 97% total recovery for each cycle, see Table 1) and reolefination of the latter compound ($Ph_3P{=}CH_2$, 97% yield). The resulting terminal olefin **19** was then converted to the desired diene system **20** by the three-step procedure developed earlier for the C7 epimeric series (see Scheme 5 for details).

The oxidation of the aromatic moiety of diene **20** proved to be even more challenging than that of its epimer **11**, leading only to traces of the desired quinone under the same AgO/HNO_3 conditions.[5] At this stage, the suspicion that the diene system was interfering with the oxidation of the aromatic nucleus led us to temporarily engage it with a molecule of SO_2 as a cyclic sulfone (see Scheme 6).[11] Thus, dissolution of **20** in

  1433-7851/01/4013-2484 $ 17.50+.50/0 *Angew. Chem. Int. Ed.* **2001**, *40*, No. 13

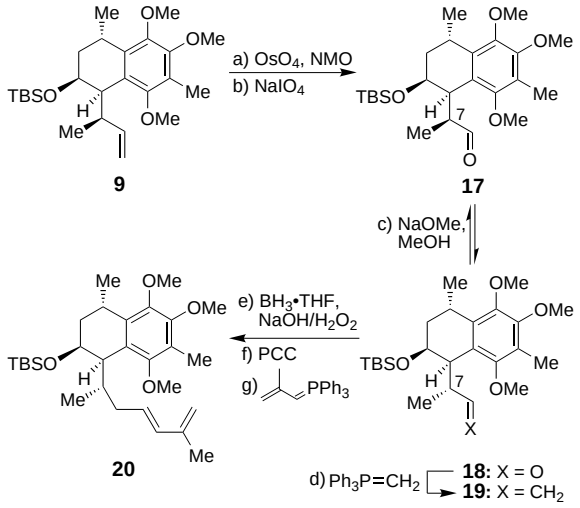

Scheme 5. Epimerization at C7 and synthesis of aromatic diene **20**. a) OsO_4 (0.05 equiv), NMO (2.0 equiv), acetone/H_2O (10/1), 25 °C, 5 h, 89 %; b) $NaIO_4$ on silica gel, CH_2Cl_2, 25 °C, 30 min, 82 %; c) NaOMe (4 equiv), MeOH/THF (2:1), 25 °C, 12 h, 30 % of **18** and 67 % of **17**; d) methyltriphenylphosphonium bromide (1.5 equiv), KO*t*Bu (1.4 equiv), THF, 25 °C, 1 h; then **18**, 25 °C, 30 min, 97 %; e) $BH_3 \cdot$THF (3 equiv), THF, 25 °C, 1 h; then 3 M NaOH and 30 % H_2O_2, 25 °C, 1 h, 87 %; f) PCC (1.5 equiv), CH_2Cl_2, 25 °C, 1 h; 95 %; g) 2-methyl-2-propenyltriphenylphosphonium bromide (1.5 equiv), *n*BuLi (1.5 equiv), THF, 0 → 25 °C, 1 h; then aldehyde, 70 °C, 8 h, 70 % plus 19 % *Z* isomer. NMO = 4-methylmorpholine *N*-oxide.

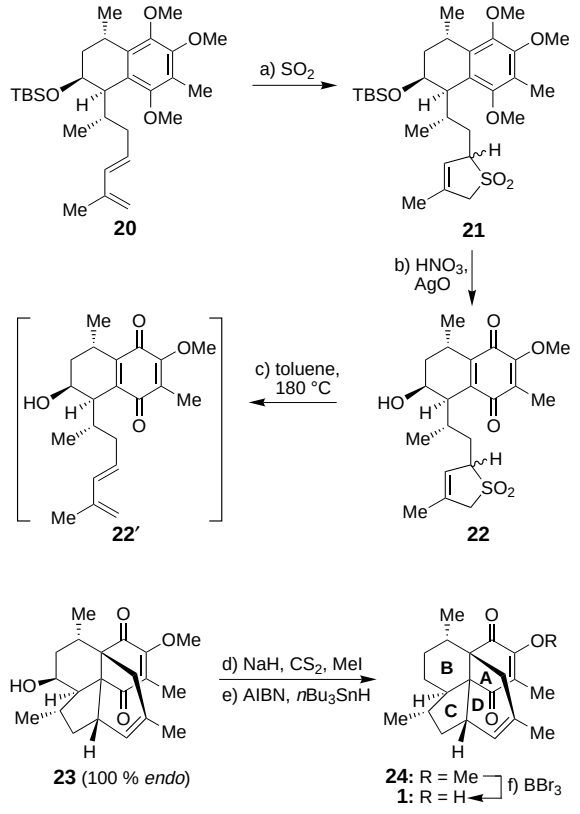

Scheme 6. Completion of the synthesis of colombiasin A (**1**). a) SO_2, sealed tube, 25 °C, 30 min, 97 %; b) dioxane/6 M HNO_3 (10/1), 25 °C, 2 h; then AgO (6.0 equiv), 25 °C, 1 h, 85 %; c) toluene (sealed tube), 180 °C, 20 min, 89 %; d) NaH (5.0 equiv), THF/CS_2/MeI (4/1/1), 50 °C, 3 h, 91 %; e) AIBN (cat.), nBu_3SnH (5.0 equiv), toluene, careful deoxygenation, 110 °C, 30 min, 88 %; f) BBr_3, (10 equiv), CH_2Cl_2, −78 °C, 30 min, 30 % plus 20 % of **1″**.

liquid SO_2 in a sealed tube at ambient temperature led to the formation of sulfone **21** in 97 % yield (≈1.2/1 mixture of diastereoisomers). Most gratifyingly, the AgO/HNO_3 oxidation of this sulfone (**21**) proceeded smoothly, furnishing the yellow quinone **22** in 85 % yield. Subsequent heating of a solution of **22** in toluene at 180 °C (in the dark, sealed tube) led to a single (*endo*) cycloadduct **23** (see Table 1) in 89 % yield, apparently through a sequence of cheletropic extrusion of SO_2, followed by [4+2] cycloaddition through the presumed intermediacy of the fleeting (under the reaction conditions) diene–quinone **22′** (see Scheme 6). Noteworthy features of this cascade sequence are not only the high-yielding oxidation of the aromatic nucleus to the corresponding quinone (**21** → **22**), but also the stereoselective manner (single isomer) in which the colombiasin A framework is formed (**22** → **23**). Finally, the extra oxygen in **23** was removed from C5 by the previously applied protocol involving xanthate formation followed by reductive cleavage of the C–O bond, leading to *O*-methyl colombiasin (**24**, see Table 1), from which colombiasin A (**1**) itself was generated upon treatment with BBr_3 (30 %) as described above for 7-*epi*-colombiasin A (**1′**). The final deprotection step was again accompanied by the formation of colombiasin A's $\Delta^{11,12}$ isomer (**1″**, 20 %). Synthetic colombiasin A (**1**) proved identical to an authentic sample[12] by the usual criteria (TLC, IR, ^{1}H and ^{13}C NMR, MS) except for the fact that it had no optical rotation, as expected based on its racemic synthesis.

To address the issue of the absolute stereochemistry and asymmetric synthesis of colombiasin A (**1**), the initial Diels–Alder reaction (**2** + **3** → **4**, Scheme 2) was carried out in the presence of a chiral catalyst ([(*S*)-BINOLTiCl$_2$],[13] toluene, −60 → −10 °C). The resulting product (**4**) was then elaborated according to Scheme 2 to ketone **6**, and the latter compound was analyzed by HPLC (R_t = 6.1 and 6.7 min for the two enantiomers, 0 → 50 % *i*PrOH in hexane over 35 min, 1.5 mL min^{-1}, CHIRALCEL OD-H chiral column), revealing an *ee* of 94 % ($[\alpha]_D^{23} = -140°$, c = 9.5 mg mL^{-1}, $CHCl_3$). Following this encouraging asymmetric induction (which was also demonstrated in the opposite sense in the presence of the other enantiomeric form of the catalyst), we anticipate both asymmetric synthesis of colombiasin A (**1**) and determination of its absolute stereochemistry.[14] The described chemistry is also expected to facilitate chemical biology studies with this new class of compounds.

Received: April 9, 2001 [Z16923]

[1] A. D. Rodríguez, C. Ramírez, *Org. Lett.* **2000**, *2*, 507–510.

[2] A. D. Rodríguez, E. González, S. D. Huang, *J. Org. Chem.* **1998**, *63*, 7083–7091.

[3] a) R. B. Woodward, F. Sondheimer, D. Taub, K. Heusler, W. M. McLamore, *J. Am. Chem. Soc.* **1952**, *74*, 4223–4251; b) S. M. Bloom, *J. Org. Chem.* **1959**, *24*, 278–280.

[4] M. C. Carreño, J. L. García Ruano, M. A. Toledo, A. Urbano, *Tetrahedron: Asymmetry* **1997**, *8*, 913–921.

[5] a) J. L. Luly, H. Rapoport, *J. Org. Chem.* **1981**, *46*, 2745–2752; b) C. D. Snyder, H. Rapoport, *J. Am. Chem. Soc.* **1972**, *94*, 227–231.

[6] a) J. Tsuji, I. Minami, I. Shimizu, *Tetrahedron Lett.* **1983**, *24*, 1793–1796; b) J. Tsuji, Y. Ohashi, I. Minami, *Tetrahedron Lett.* **1987**, *28*, 2397–2398; c) L. A. Paquette, F. Gallou, Z. Zhao, D. G. Young, J. Liu, J. Yang, D. Friedrich, *J. Am. Chem. Soc.* **2000**, *122*, 9610–9620.

[7] M. L. Falck-Pedersen, T. Benneche, K. Undheim, *Acta Chem. Scand.* **1993**, *47*, 63–67.
[8] J. D. Roberts, S. W. Sauer, *J. Am. Chem. Soc.* **1949**, *71*, 3925–3929.
[9] a) D. H. R. Barton, S. W. McCombie, *J. Chem. Soc. Perkin Trans. 1* **1975**, 1574–1585; b) D. H. R. Barton, D. Crich, A. Lobberding, S. Z. Zard, *Tetrahedron* **1986**, *42*, 2329–2338; c) for a review see: D. Crich, L. Quintero, *Chem. Rev.* **1989**, *89*, 1413–1432.
[10] Y.-L. Zhong, T. K. M. Shing, *J. Org. Chem.* **1997**, *62*, 2622–2624.
[11] S. Yamada, T. Suzuki, H. Takayama, *J. Org. Chem.* **1983**, *48*, 3483–3488.
[12] We thank Professor A. D. Rodríguez of the University of Puerto Rico for kindly providing us with an authentic sample as well as spectra of colombiasin A (**1**).
[13] a) K. Mikami, M. Terada, Y. Motoyama, T. Nakai, *Tetrahedron: Asymmetry* **1991**, *2*, 643–646; b) K. Mikami, Y. Motoyama, M. Terada, *J. Am. Chem. Soc.* **1994**, *116*, 2812–2820; c) J. D. White, Y. Choi, *Org. Lett.* **2000**, *2*, 2373–2376.
[14] Based on the chirality of the catalyst used to induce the asymmetry[13] in **4** and the rotation ($[\alpha]_D^{23} = -61°$, $c = 1\ mg\,mL^{-1}$, $CHCl_3$) of the synthetic natural product obtained from this intermediate, we tentatively assign the shown absolute stereochemistry of colombiasin A. Further studies to confirm this assignment are in progress.

Reactions of Organoselenenyl Iodides with Thiouracil Drugs: An Enzyme Mimetic Study on the Inhibition of Iodothyronine Deiodinase**

Wolf-Walther du Mont,* Govindasamy Mugesh, Cathleen Wismach, and Peter G. Jones

The monodeiodination of the prohormone thyroxine (**T4**) to the biologically active hormone 3,5,3′-triiodothyronine (**T3**) is the first step in thyroid hormone action and the type I iodothyronine deiodinase (ID-1), an enzyme containing selenocysteine in its active site, is responsible for most of this conversion [Eq. (1)].[1] ID-1 is an integral membrane

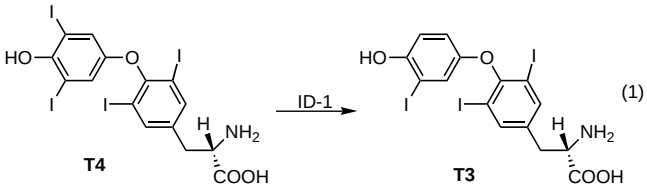

(1)

protein the highest amounts of which are found in the liver, kidney, and thyroid. The 5′-deiodination catalyzed by ID-1 is a ping-pong, bisubstrate reaction in which the selenol group of the enzyme (E-SeH) first reacts with thyroxine (**T4**) to form a enzyme selenenyl iodide (E-SeI) complex with release of deiodinated iodothyronine (**T3**). Subsequent reaction of the selenenyl iodide with an unidentified cytoplasmic thiol cofactor (possibly glutathione, GSH) releases I^- ions and regenerates the E-SeH active site (Scheme 1).[2]

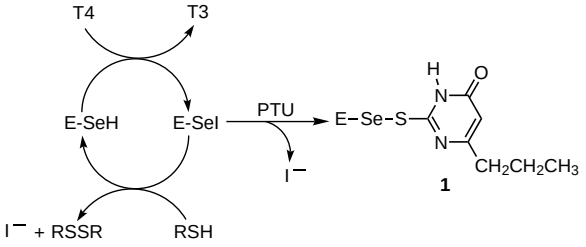

Scheme 1. Proposed mechanism for iodothyronine deiodination of thyroxin **T4** by ID-1 and the inhibition of ID-1 by PTU.

It was proposed that the drug 6-*n*-propyl-2-thiouracil (PTU), derived from thiourea, inhibits the activity of the enzyme, probably by reacting with the selenenyl iodide intermediate to form a stable selenenyl sulfide.[2] The selenenyl sulfide **1** is considered to be a dead-end product since this compound does not react with thiols under physiological conditions. Owing to this property, PTU is often used in the treatment of severely hyperthyroid (Graves disease) patients and is therefore well known as an antithyroid drug.

The formation of a mixed selenenyl sulfide adduct (**1**, Scheme 1) in the reaction of the selenenyl iodide with PTU has been proposed mainly on the basis of the following assumptions. 1) The PTU inhibition is noncompetitive with respect to thyroxine and competitive with respect to thiol cofactor, which suggests that PTU and cofactor react with the same enzyme intermediate.[1a] 2) The thiouracil derivatives are particularly reactive towards protein sulfenyl iodide (S–I) groups[1a] and presumably even more reactive towards selenenyl iodide (Se–I) groups. However, since the discovery that the ID-1 is a selenium-containing enzyme, the reactions of thiourea drugs with E-SeI and their mechanisms have never been experimentally verified. In contrast to ID-1, the other two deiodinases (ID-2 and ID-3) are insensitive to PTU.[1c] It is, therefore, still a matter of debate as to whether PTU reacts with a covalent Se–I species or if it reacts with the enzyme active site (E-SeH). Moreover, no reasons have been given for the insensitivity of ID-2 and ID-3 towards PTU.[1c] Herein, we report the first model studies on the reactivity of PTU towards selenenyl iodides as a basis for the deiodinase inhibition.

The reactions of organoselenenyl iodides as enzyme-mimetic substrates with thiourea derivatives have not been studied previously as areneselenenyl iodides such as PhSeI are themselves generally unstable and disproportionate in solution.[3a] Even the sterically hindered areneselenenyl iodides such as **2** have been found to exist in equilibrium with iodine and the corresponding diselenide in solution.[3b,c] The "non-existence" of stable binary Se–I compounds is associated with the very similar electronegativities of Se and I, that is, the lack of ionic contribution to the resonance energy in the covalent Se–I bond.[4] However, the recent observations that the

[*] Prof. Dr. W.-W. du Mont, Dr. G. Mugesh, Dipl.-Chem. C. Wismach, Prof. Dr. P. G. Jones
Institut für Anorganische und Analytische Chemie
Technische Universität Braunschweig
Postfach 3329, 38023 Braunschweig (Germany)
Fax: (+49) 531-391-5387
E-mail: w.du-mont@tu-bs.de

[**] This study was supported by the Alexander von Humboldt-Stiftung in the form of a research fellowship to G. M.

  1433-7851/01/4013-2486 $ 17.50+.50/0

covalent Se–I bond could be stabilized against dismutation (disproportionation) reactions by introducing sterically highly demanding alkyl substituents[3a,d] (**3**) or internally chelating groups[5] (e.g. **4**) have given opportunities for studying the reactivity of pure Se–I compounds.

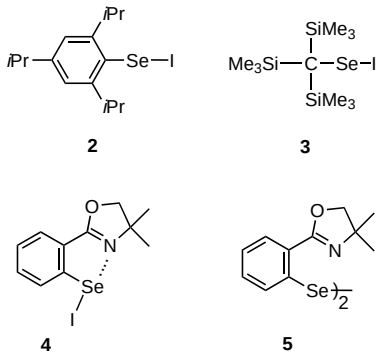

2 **3** **4** **5**

When "PhSeI" ($0.5\,Ph_2Se_2I_2$) and **2**, which are known to disproportionate to diselenide and iodine or their adducts,[3a,b] were treated independently with stoichiometric amounts of PTU or 6-methyl-2-thiouracil (MTU) in the presence of triethylamine, both the reactions afforded the corresponding diselenides, rather than the selenenyl sulfides, as the only products. This indicates that the unstable selenenyl iodides PhSeI and **2** are reduced by PTU and MTU to the corresponding diselenides (and not the PTU/MTU derivatives). These properties of PhSeI and **2** therefore resemble the inhibitory action of PTU-insensitive deiodinases.

In the absence of triethylamine, selenenyl iodide **3** reacted with PTU and MTU much more slowly than the internally chelated compound **4**. Although compound **4** reacted rapidly with PTU and MTU under similar experimental conditions, it unexpectedly afforded the diselenide **5** as the major product. This result indicates that the HI produced during the reaction may act as a catalyst for the diselenide formation. However, in the presence of triethylamine, no diselenide is formed and both **3** and **4** reacted rapidly with PTU and MTU to give the desired selenenyl sulfides **6**–**9** (Scheme 2). Since the liberated HI in both cases was trapped with triethylamine the compounds **6**–**9** could be purified conveniently by column chromatography. Remarkably, the diselenides **5**[6] and **10**[7] did not react with PTU and MTU, which indicates that the

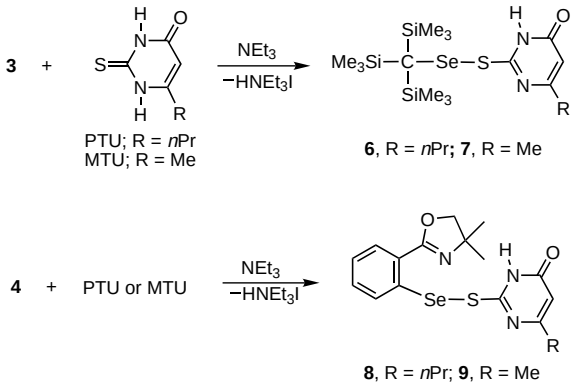

Scheme 2. Synthesis of the thiouracil derivatives.

ID-1 enzyme inhibition by PTU and MTU results from the specific reactivity of the Se–I bond towards these drugs.

The reactions of **4** with PTU and MTU were found to be faster than those of **3**, probably because of an increase in the electrophilic reactivity of selenium atom in compound **4** by Se···N interactions. Whereas the Se–I bond in compound **3** is a 2-center 2-electron (2c-2e) covalent bond, the Se–I bond in compound **4** can be considered as a result of Se···N interactions as part of a 3c-4e system. Therefore, the Se–I bond in **4** is thermodynamically stabilized (and also dismutation resistant) in isolated form and kinetically activated towards reactions with nucleophilic reagents. As suggested for the natural enzyme,[1c] the hydrogen atom attached to N1 of PTU and MTU plays an important role in the reactions. The replacement of the hydrogen atom at the N1 position by a methyl group normally produces inactive substances. For example, it has been reported that the 6-anilino-2-thiouracil **11** exhibits 85% inhibition towards human placenta deiodinase activity, but the N-methylated derivative **12** exhibits only 2% inhibition.[8] In agreement with this, the inactivity of

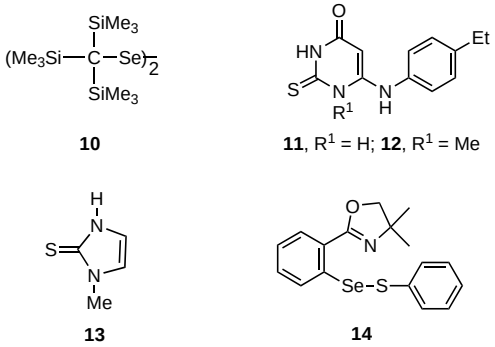

10 **11**, R^1 = H; **12**, R^1 = Me

13 **14**

methimazole (MMI) **13**, another commonly used anti-thyroid drug that inhibits thyroid peroxidase (TPO), towards ID-1 has been ascribed to the presence of a methyl substituent at the N1 position.[1a,c] We found that MMI reacts with selenenyl iodide **3**, in the presence of triethylamine, with a rate comparable to that of PTU and MTU, with deprotonation of the N3 atom.[9]

In the drug-induced deiodinase inhibition, the fast reaction between the inhibitors and selenenyl iodide intermediate (E-SeI) and the inactivity of the resulting selenenyl sulfide towards reducing agents such as GSH are the important factors that determine the potency of the drugs. In our model studies, although compounds **3** and **4** react with PTU, the stability of the resulting selenenyl sulfides **6** and **8** towards thiols differs considerably. The internally chelated compound **8** reacted rapidly with PhSH to form the selenenyl sulfide **14** (thiol exchange), whereas the sterically hindered derivative **6** was found to be unreactive towards PhSH after 24 h under identical experimental conditions. In this regard, the PTU-derivative **6** clearly differs from the MMI-derivative, which reacts readily with PhSH leading to a thiol-exchange reaction.[9]

Although the "steric protection" is much more efficient than the internal chelation in stabilizing the selenenyl sulfides

  1433-7851/01/4013-2487 $ 17.50+.50/0

against further reaction with thiols, the existence of hydrogen bonding in the PTU-derivative **6** enhances its stability towards thiols. The absence of such hydrogen bonding in the MMI-derivative may be the reason for the inactivity of MMI towards ID-1 inhibition.[9] The X-ray crystal structure of compound **6** shows that the selenium atom is considerably shielded by the $SiMe_3$ groups (Figure 1).[10] The thiouracil moiety in **6** exists in a keto form that is stabilized by intermolecular hydrogen bonding, thus forming a centrosymmetric dimer.

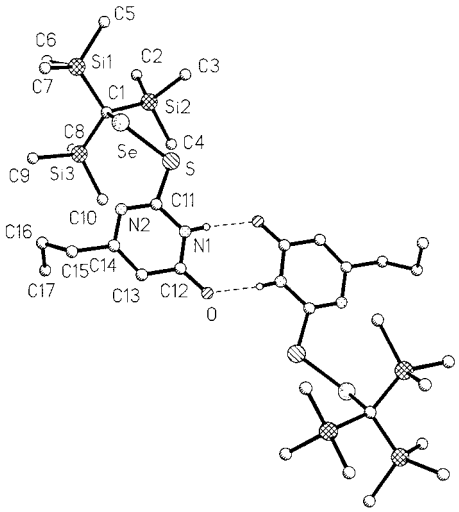

Figure 1. Molecular structure of **6** showing hydrogen bonding (only the H atom involved in hydrogen bonding is shown). Selected bond lengths [Å] and angles [°]: Se-S 2.2014(4), Se-C1 2.0043(15), S-C11 1.7681(16), C1-Si1 1.9270(15), C1-Si2 1.9130(15), C1-Si3 1.9042(16), C12-O 1.2398(18); C1-Se-S 105.91(4), C11-S-Se 103.78(5), Si1-C1-Se 99.84(7), Si2-C1-Se 110.34(7), Si3-C1-Se 108.29(7).

The higher reactivity of compound **8** with PhSH, compared with that of **6**, may also be attributed to the intramolecular Se···N interaction in compound **8**, which increases the electrophilic character of selenium center. This observation led us to investigate whether the PTU derived selenenyl sulfide **8** can be prepared from **14** which, as a result of internal chelation, should be activated towards nucleophilic attack. When pure **14**[11] was treated with PTU, we were unable to detect any **8** even after 24 h. Our observations indicate that the formation of **14** by thiol exchange from **8** with PhSH is an irreversible process.

In summary, the mechanism for the inhibition of iodothyronine deiodinase by thiourea based drugs is experimentally verified by utilizing two selenenyl iodides as enzyme-mimetic substrates (E-SeI) stabilized by steric protection or internal chelation. This model study supports the assumptions that 1) PTU does not react with the native enzyme but only with an E-SeI intermediate containing a covalent Se–I bond and 2) some basic amino acid residues such as histidine near the active center may kinetically activate the Se–I bond, or these residues may act as general bases for the abstraction of HI during the inhibition. This study also suggests that the possible disproportionation of the E-SeI intermediate to diselenides may, at least partially, account for the insensitivity of certain selenium-containing deiodinases towards thiourea drugs.

Experimental Section

General: All reactions were carried out under nitrogen using standard vacuum-line techniques.

6: NEt_3 (2 mmol) and PTU (0.17 g, 1 mmol) were added to a solution of **3** (0.44 g, 1 mmol) in toluene (20 mL). The mixture was stirred at room temperature for 10 min, and the resulting turbid solution was separated by filtration. After removal of the solvent from the filtrate, the crude product was loaded onto a silica gel (70–230 mesh) column, elution with hexane:ethylacetate (2:1) afforded **6** as the second yellow fraction which was collected and evaporated to dryness to give a yellow solid, crystallization from CH_2Cl_2:hexane to afford yellow crystals of **6** (0.41 g, yield 85%); m.p. 104 °C; ^{1}H NMR (400 MHz, C_6D_6, TMS): $\delta = 0.10$ (s, 27H), 0.58 (t, 3H), 1.37 (m, 2H), 2.02 (t, 2H), 5.80 (s, 1H), 6.97 (s, 1H); ^{13}C NMR (100.6 MHz, C_6D_6, TMS): $\delta = 1.36$, 2.93, 13.58, 21.19, 39.32, 109.45, 159.16, 163.67, 168.85; ^{77}Se NMR (38.2 MHz, C_6D_6, Me_2Se): $\delta = 506$; ^{29}Si NMR (39.8 MHz, C_6D_6, TMS): $\delta = 3.4$; CI-MS: *m/z* (%): 481 (100) [$M^+ - H$], 188, 171, 90; elemental analysis calcd (%) for $C_{17}H_{36}N_2O_2SSeSi_3$: C 42.50, H 7.50, N 5.83, S 6.67; found: C 42.93, H 7.78, N 5.48, S 6.81. Compounds **7**–**9** were synthesized by similar procedures.

Received: January 18, 2001 [Z16451]

[1] a) "Biochemistry of Deiodination": J. L. Leonard, T. J. Visser in *Thyroid Hormone Metabolism* (Ed.: G. Hennemann), Marcel Dekker, New York, **1986**, p. 189; b) M. J. Berry, L. Banu, P. R. Larsen, *Nature* **1991**, *349*, 438; c) P. R. Larsen, M. J. Berry, *Annu. Rev. Nutr.* **1995**, *15*, 323; d) J. Köhrle, *Acta Med. Austriaca* **1996**, *23*, 17; e) "Intracellular Pathways of Iodothyronine Metabolism": J. L. Leonard, J. Köhrle in *The Thyroid* (Eds.: L. E. Braverman, R. D. Utiger), Lippincott-Raven, Philadelphia, **1996**, p. 144; f) D. L. St. Germain, V. A. Galton, *Thyroid* **1997**, *7*, 655.

[2] M. J. Berry, J. D. Kieffer, J. W. Harney, P. R. Larsen, *J. Biol. Chem.* **1991**, *266*, 14155.

[3] a) W.-W. du Mont, *Main Group Chem. News* **1994**, *2*(3), 18; b) W.-W. du Mont, A. Martens von Salzen, S. Pohl, W. Saak, *Inorg. Chem.* **1990**, *29*, 4848; c) W.-W. du Mont, S. Kubiniok, K. Peters, H.-G. Schnering, *Angew. Chem.* **1987**, *99*, 820; *Angew. Chem. Int. Ed. Engl.* **1987**, *26*, 780; d) W.-W. du Mont, I. Wagner, *Chem. Ber.* **1988**, *121*, 2109.

[4] T. Klapötke, J. Passmore, *Acc. Chem. Res.* **1989**, *22*, 234.

[5] a) G. Mugesh, A. Panda, H. B. Singh, R. J. Butcher, *Chem. Eur. J.* **1999**, *5*, 1411; b) A. Panda, G. Mugesh, H. B. Singh, R. J. Butcher, *Organometallics* **1999**, *18*, 1986.

[6] G. Mugesh, A. Panda, H. B. Singh, N. S. Punekar, R. J. Butcher, *Chem. Commun.* **1998**, 2227.

[7] I. Wagner, W.-W. du Mont, S. Pohl, W. Saak, *Chem. Ber.* **1990**, *123*, 2325.

[8] T. Nogimori, C. H. Emerson, L. E. Braverman, C.-F. Wu, J. Gabino, G. E. Wright, *J. Med. Chem.* **1985**, *28*, 1692.

[9] The facile reaction of **3** with MMI/NEt_3 indicates that it is not the different reactivities of MMI and the thiourea derivatives PTU and MTU towards the E-SeI intermediate that control the different degrees of ID-1 inhibition but the difference in the reactivities of the resulting selenenyl sulfides. This is clearly connected with the fact that the MMI derived selenylsulfide does not possess any N–H and/or –N(H)C(=O)– groups for hydrogen bonding. The complete study of the reactivity of MMI towards Se–I bonds, the reactions of the resulting selenenyl sulfides with thiols, and their relevance to the natural systems will be discussed in the forthcoming full paper.

[10] Crystal data for **6** ($C_{17}H_{36}N_2OSSeSi_3$): $M_r = 479.77$, triclinic, space group $P\bar{1}$, $a = 9.2050(10)$, $b = 9.6540(10)$, $c = 14.0974(14)$ Å, $\alpha = 99.181(3)$, $\beta = 98.911(3)$, $\gamma = 91.627(3)°$, $V = 1220.0(2)$ Å^3, $Z = 2$, $\rho_{calcd} = 1.306$ Mg m^{-3}, $Mo_{K\alpha}$ radiation ($\lambda = 0.71073$ Å), $T = 153$ K; yellow prisms, crystal dimensions $0.40 \times 0.17 \times 0.07$ mm, crystals mounted in inert oil. Intensity data was collected by using the ω method in the 2θ range 5–60°. Of 20640 reflections collected on a Bruker SMART 1000 CCD diffractometer, 7049 were unique ($R_{int} = 0.0486$) and used for all calculations. After absorption correction (multiple scan) the structure was solved by direct methods. All non-hydrogen atoms were refined anisotropically on F^2 using full-matrix least-squares to give $R_1 = 0.0344$, $wR_2 = 0.0794$ ($I > 2\sigma(I)$); $R_1 = 0.0406$,

  1433-7851/01/4013-2488 $ 17.50+.50/0

$wR_2 = 0.0822$ (all data). The NH proton was refined freely, methyl H atoms as rigid, and other H atoms as a riding model. Crystallographic data (excluding structure factors) for the structure reported in this paper have been deposited with the Cambridge Crystallographic Data Centre as supplementary publication no. CCDC-154120. Copies of the data can be obtained free of charge on application to CCDC, 12 Union Road, Cambridge CB2 1EZ, UK (fax: (+44) 1223-336-033; e-mail: deposit@ccdc.cam.ac.uk).

[11] G. Mugesh, A. Panda, H. B. Singh, N. S. Punekar, R. J. Butcher, *J. Am. Chem. Soc.* **2001**, *123*, 839.

Tuning the Electronic Structure of Halidobis(*o*-imino-benzosemiquinonato)-iron(III) Complexes**

Hyungphil Chun, Thomas Weyhermüller, Eckhard Bill, and Karl Wieghardt*

Mononuclear complexes of iron(III) (d^5) containing redox-inert, closed-shell ("innocent") ligands adopt either a high-, intermediate-, or low-spin electron configuration: $S_{Fe} = 5/2$, $3/2$, or $1/2$, respectively. An increasing number of non-heme, pentacoordinate, pure intermediate-spin complexes have in recent years been characterized by X-ray crystallography, magnetic susceptibility measurements, Mössbauer, and electron paramagnetic resonance (EPR) spectroscopy.[1] Examples pertinent to this work are complexes **A**[1f] and **B**.[1d]

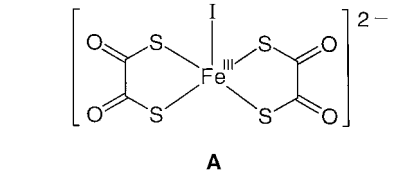

A

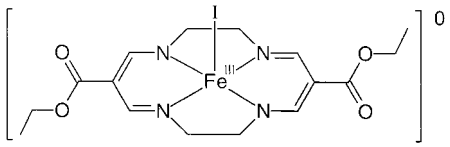

B

The binding of a Fe^{III} ion to open-shell ("noninnocent"), π-radical ligands such as phenoxyls[2a] or *o*-benzosemiquinonates[2b] inevitably induces a strong intramolecular, antiferromagnetic spin coupling between the magnetic orbitals of the π radicals and the available metal-centered, half-filled t_{2g} orbitals of the Fe^{III} ion. This gives rise to electronic ground states ranging from $S_t = 2$[2a,b] to $S_t = 0$[2c] depending on the number of coordinated radicals and the actual local spin state at the Fe^{III} ion in a given compound. *O,N*-coordinated *o*-aminophenolates have been shown to be readily oxidized by air to yield the corresponding *o*-iminobenzosemiquinonates, $(L^{ISQ})^-$.[3, 4] The octahedral complex $[Fe^{III}(L^{ISQ})_3]$ possesses an $S_t = 1$ ground state comprising a high-spin Fe^{III} ion ($S_{Fe} = 5/2$) coupled antiferromagnetically to three $(L^{ISQ})^-$ π-radical ligands.[3b]

We have now discovered that the pentacoordinate halidobis(*o*-iminosemiquinonato)iron(III) complexes **1**–**3** are readily prepared and that the local spin state of the respective Fe^{III} ion is tuned from a high-spin state in the chloro species **1** to a pure intermediate-spin state in the iodo complex **3**; in the bromo analogue **2** both spin isomers are present in the cystalline state in a 1:1 ratio. The crystal structures of **1**, **2**, and **3** have been determined with high precision by X-ray crystallography at 100 K. Figure 1 shows the structure of **3** (the structures of **1** and **2** are very similar and not shown); Table 1 summarizes selected bond lengths.

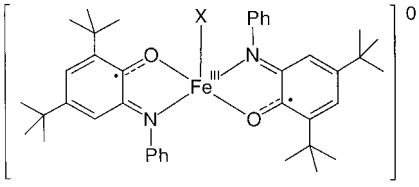

X = Cl, Br, I
trans-$[Fe(L^{ISQ})_2Cl]$ **1**
trans-$[Fe(L^{ISQ})_2Br]$ **2**
trans-$[Fe(L^{ISQ})_2I]$ **3**

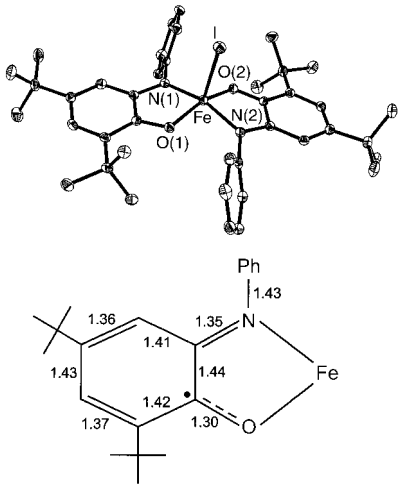

Figure 1. Structure of a neutral molecule in crystals of **3** ($S_t = 1/2$; top). The average C–C, C–O, and C–N bond lengths of the *o*-iminobenzosemiquinonate(1 –) π-radical ligand in **1**, **2**, and **3** are shown below. The estimated error is ±0.01 Å (3σ).

Table 1. Selected bond lengths [Å] in **1**, **2**, **3**, and [Fe("N_2S_2")I].[c]

	Fe–X	Fe–N(1)	Fe–N(2)	Fe–O(1)	Fe–O(2)
$[Fe^{III}(L^{ISQ})_2Cl]$ **1**	2.2203(7)	2.042(2)	2.041(2)	1.962(1)	1.964(1)
$[Fe^{III}(L^{ISQ})_2Br]$ **2**[a]	2.3665(9)	1.897(4)	1.886(4)	1.869(3)	1.877(3)
$[Fe^{III}(L^{ISQ})_2Br]$ **2**[b]	2.3694(9)	2.045(4)	2.050(4)	1.950(3)	1.953(3)
$[Fe^{III}(L^{ISQ})_2I]$ **3**	2.5912(5)	1.885(2)	1.885(2)	1.869(1)	1.881(1)
[Fe("N_2S_2")I][6]	2.5552(9)	1.842(4)	1.851(5)	2.181(2)[c]	2.188(2)[c]

[a] Molecule 1. [b] Molecule 2. [c] Fe–S bond length.

[*] Prof. Dr. K. Wieghardt, Dr. H. Chun, Dr. T. Weyhermüller, Dr. E. Bill
Max-Planck-Institut für Strahlenchemie
Stiftstrasse 34–36, 45470 Mülheim an der Ruhr (Germany)
Fax: (+49) 208-306-3952
E-mail: wieghardt@mpi-muelheim.mpg.de

[**] This work was supported by the Fonds der Chemischen Industrie. H. Chun thanks the Alexander von Humboldt Foundation for a stipend.

It is important to note that the geometrical details of the *O*,*N*-coordinated $(L^{ISQ})^-$ ligand are identical in all three structures within our small 3σ limits of ± 0.01 Å; the average C–O, C–N, and C–C bond lengths are given in Figure 1. These values are consistent with those of all other complexes of this type reported to date.[3, 4] Thus, in complexes **1**–**3** the ligand is always an *o*-iminosemiquinonate(1−) radical with $S_{rad} = ½$.[3, 4]

A comparison of the Fe–O and Fe–N distances in **1** and **3** (Table 1) reveals that the Fe^{III} ions in the neutral $[Fe^{III}(L^{ISQ})_2X]$ (X = Cl, I) molecules must possess different local spin states, since these distances are long in **1**, but significantly shorter in **3**. Compound **2** crystallizes in the triclinic space group $P\bar{1}$ with $Z = 4$, indicating that two crystallographically independent molecules of $[Fe^{III}(L^{ISQ})_2Br]$ are present in the unit cell. The Fe–N and Fe–O bond lengths of the first molecule match those in **3** and those of the second molecule are identical to those in **1**. Thus, crystals of **2** contain an 1:1 mixture of two spin isomers of $[Fe^{III}(L^{ISQ})_2Br]$. As we will show below, **1** contains a high-spin and **3** a pure intermediate-spin iron center, whereas solid **2** contains both isomers in a ratio 1:1.

Variable-temperature magnetic susceptibility measurements on solid samples of **1**, **2**, and **3** have been performed by using a SQUID magnetometer (external field 1 T). Figure 2 shows the temperature dependence of the effective

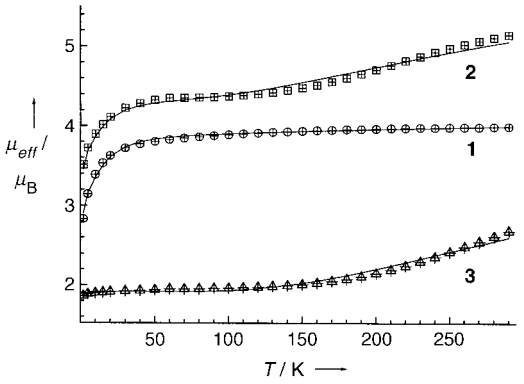

Figure 2. Temperature dependence of the effective magnetic moment μ_{eff} as calculated per *one* Fe ion for **1** and **3**, and per *two* Fe ions (double molecular weight) for **2**.

magnetic moments, where we have calculated μ_{eff} per *one* Fe ion for **1** and **3**, but per *two* Fe ions for **2**. The curve obtained for **1** is readily simulated for an $S_t = ⅜$ ground state with a zero-field splitting parameter $|D_{3/2}|$ of 18 cm^{-1} and an effective *g* value of 2.0 (fixed). The X-band EPR spectrum of a frozen CH_2Cl_2 solution of **1** at 10 K (Figure 3) displays a typical $S_t = ⅜$ signal with small rhombicity ($E/D \approx 0$).

In contrast, solid **3** displays a temperature-independent μ_{eff} of about 1.9 μ_B in the range 10–150 K; above 150 K μ_{eff} increases to 2.7 μ_B per Fe^{III} ion at 300 K. Complex **3** clearly possesses an $S_t = ½$ ground state. The temperature dependence (see Figure 2) was successfully modeled by assuming intramolecular coupling of the two radical ligands $S_{rad} = ½$ with a central intermediate-spin Fe^{III} ion, $S_{Fe} = ⅜$, by using the spin Hamiltonian $\mathcal{H} = -2JS_{rad}S_{Fe}$. A strong antiferromagnetic coupling of $J = -145(20)$ cm^{-1} is typical for such complexes.[2] In agreement with these results, the EPR spectrum of **3** in frozen CH_2Cl_2 solution at 10 K displays an axial $S_t = ½$ signal which was satisfactorily simulated with $g_\parallel = 2.189$ and $g_\perp = 2.134$ (Figure 3). These *g* values indicate that the unpaired electron in **3** resides in a metal-centered d orbital.

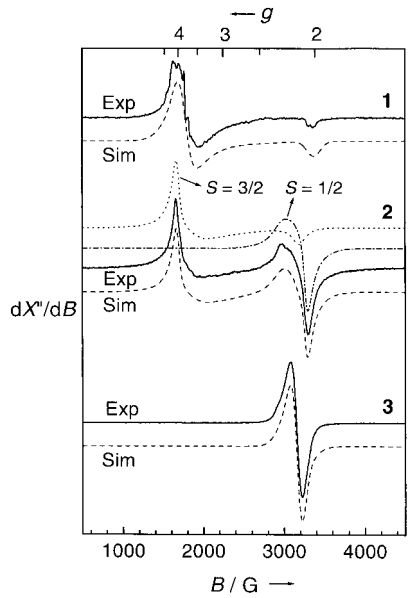

Figure 3. X-band EPR spectra of frozen CH_2Cl_2 solutions of **1**, **2**, and **3**. The dotted lines represent simulations (Sim, Table 2). Conditions: $T = 10$ K, frequency = 9.47 GHz; power = 100 μW for **1** and **2**, 50 μW for **3**; modulation amplitude = 10 G for **1** and **2**, 31 G (for **3**).

Compound **2** displays a fascinating temperature dependence of μ_{eff} which is nearly temperature independent at 4.3 μ_B in the range 50–150 K; below 50 K it decreases to 3.5 μ_B at 4 K due to zero-field splitting of the $S_t = ⅜$ component, but increases above 150 K to 5.2 μ_B at 300 K due to decoupling of the spins of the $S_t = ½$ component. The 4.3 μ_B value corresponds nicely to the expected value of 4.2 μ_B calculated for a 1:1 mixture of an $S_t = ½$ and an $S_t = ⅜$ system by using the simple relation $\mu_{eff} = (\mu_1^2 + \mu_2^2)^{1/2}$ with $\mu_1 = 1.73$ μ_B and $\mu_2 = 3.87$ μ_B. For the $S_t = ½$ component a coupling constant *J* of $-100(20)$ cm^{-1}; and for the $S_t = ⅜$ state a zero-field splitting parameter of $|D_{3/2}| = 18$ cm^{-1} was established from the fit shown in Figure 2. The EPR spectrum of **2** in frozen CH_2Cl_2 at 10 K (Figure 3) shows signals due to an $S_t = ⅜$ and an $S_t = ½$ system. The ratio of the two species *in solution* was found to be about 7:3 in the temperature range 2–35 K. The relative abundance of both spin isomers in **2** might be an arbitrary "frozen" Boltzmann distribution prevailing in fluid solution, whereas in the solid state this distribution is fixed at 1:1.

The zero-field Mössbauer spectra of solid samples of **1**, **2**, and **3** provide independent spectroscopic information on the local spin and oxidation states of the iron ions (Table 2); the spectra recorded at 80 K are shown in Figure 4. Complexes **1** and **3**[5] exhibit each a *single* quadrupole doublet where the large isomer shift for **1** indicates the presence of a high-spin Fe^{III} ion ($S_{Fe} = ⅝$), and, for **3**, the smaller value is typical for a

  1433-7851/01/4013-2490 $ 17.50+.50/0

Table 2. X-band EPR and Mössbauer parameters.

Complex	S_t[a]	g_1	g_2	g_3	δ [mm s^{-1}][b]	$\lvert\Delta E_Q\rvert$ [mm s^{-1}][c]	T [K][d]
1	3/2	3.985	3.871	2.010	0.45	1.26	80
2	3/2	4.030	3.643	2.130	0.47	1.22	80
	1/2	2.272	2.105	2.071	0.23	2.62	80
3	1/2	2.189($g_\parallel$), 2.134($g_\perp$)			0.24	2.80	80
A[1f]	3/2	ca. 4			0.30	3.5	77
B[1d]	3/2	5.38	2.70	1.74	0.18	3.56	120
[Fe("N_2S_2")I][6]	1/2	2.206	2.125	2.063	0.11	3.41	4.2
[Fe(L^{ISQ})$_3$][3b]	1				0.54	1.03	80

[a] Ground state. [b] Isomer shifts versus α-Fe at 298 K. [c] Quadrupole splitting. [d] Measurement temperature for the Mössbauer spectra.

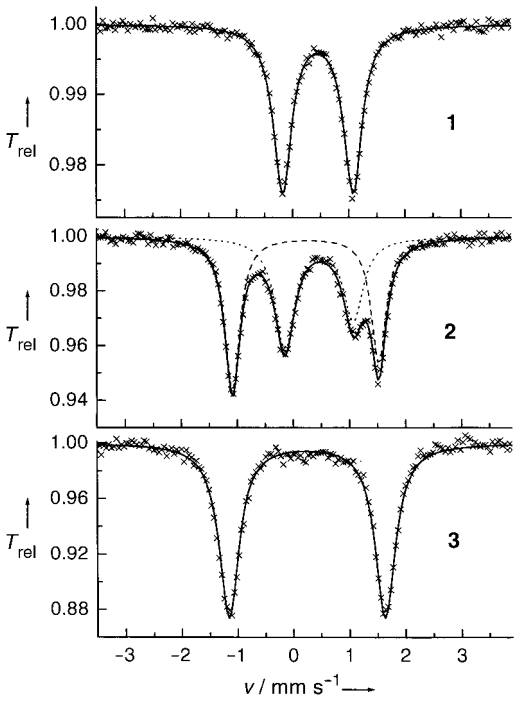

Figure 4. Zero-field Mössbauer spectra of solid samples of **1**, **2**, and **3** measured at 80 K (parameters see Table 2).

pure intermediate-spin Fe^{III} species ($S_{Fe} = 3/2$).[1] We note that the large quadrupole splitting of **1** as well as the large zero-field splitting are typical of high-spin, five-coordinate Fe^{III} complexes with some spin admixture ($S = 5/2 \leftrightarrow S = 3/2$) due to the presence of a close lying excited spin quartet state which is mixed into the $S = 5/2$ ground state. This situation is also clearly reflected in the low average value $(g_1 + g_2)/2 = 3.93$ which would be 4.0, if the spin of the central Fe^{III} ion in **1** would be purely $S = 5/2$.

Consistent with the X-ray structure analysis, the spectrum of **2** displays two distinctly different quadrupole doublets (ratio 53:47 ~ 1:1; Figure 4); the isomer shifts correspond to those of a high-spin (as in **1**) and an intermediate-spin Fe^{III} ion (as in **3**).

We have shown that in a series of isostructural complexes the local spin-state of the central Fe^{III} ion is 5/2 in **1**, 5/2 and 3/2 in **2**, and purely 3/2 in **3**. This fine-tuning is governed by the nature of the halide ion in apical position.[1a] Coupling of these Fe^{III} ions to two π-radical ligands yields the observed ground states: $S_t = 3/2$ for **1**, 3/2 and 1/2 for **2**, and 1/2 for **3**.

In the light of the above results we would like to offer an alternative description of the electronic structure of the structurally very similar complex [Fe("N_2S_2")I] reported by Sellmann et al.[6] which is shown in Figure 5. These authors

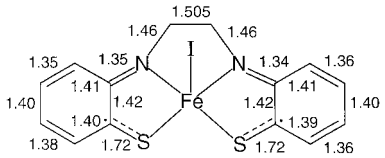

Figure 5. Schematic representation of the structure of [Fe("N_2S_2")I].[6] The bond lengths were obtained from the Cambridge Crystallographic Data Centre: no. CCDC-100299. The estimated error of the C–C, C–S, and C–N bond lengths is ± 0.02 Å (3σ).

considered the ligand 1,2-ethanediamide-*N*,*N*′-bis(2-benzenethiolate)(4 –), "N_2S_2", to be a redox-innocent, closed-shell tetraanion and, consequently, have assigned a formal oxidation state of +v to the iron center. This species possesses an $S_t = 1/2$ ground state like **3**. In our view the spectroscopic (or physical) oxidation state[7] of the central iron ion in this complex is +III. An intermediate-spin Fe^{III} ion ($S_{Fe} = 3/2$) is *N*,*S*-coordinated to two *o*-iminothionebenzosemiquinonato(1 –) π radicals ($S_{rad} = 1/2$) which couple antiferromagnetically to the t_{2g}^4 subshell of the Fe^{III} ion (d_{xy}^2, d_{xz}^1, d_{yz}^1, $d_{z^2}^1$) yielding the observed metal-centered $S_t = 1/2$ ground state ($d_{z^2}^1$) as in **3**. This proposal is supported by the following experimental data:[6] 1) The two *N*,*S*-coordinated ligand parts of "N_2S_2" display the same geometrical distortions which are reported here for the $(L^{ISQ})^-$ ligands in **3**: the C–S bonds are short (1.72 Å) and approach the length for a C=S double bond, as are the C–N bonds (1.35 Å). In addition, although not quite beyond their experimental 3σ error limits, both phenyl rings display typical quinoid-type distortions. 2) The Mössbauer parameters (see Table 2) are in excellent agreement with those reported for complexes **2**, **3**, **A**, and **B** all of which contain an intermediate-spin Fe^{III} ion. 3) The EPR spectra for [Fe("N_2S_2")I] and **3** are very similar.

Experimental Section

The ligand 2-anilino-4,6-di-*tert*-butylphenol, H[L^{AP}], has been prepared as described previously.[3]

Syntheses of complexes: The ligand H[L^{AP}] (1.5 mmol) and triethylamine (3 mmol) dissolved in methanol (20 mL) or ethanol/dichloromethane (1/1) were added the ferrous salts (1 mmol) $FeCl_2 \cdot 4H_2O$, $FeBr_2$, or FeI_2 in methanol (30 mL). Triphenylphosphane (2 mmol) was additionally added to the reaction mixtures of **2** and **3** to facilitate crystallization. The solution was heated to reflux in the presence of air for 1 h. After filtration, the solution was allowed to stand at ambient temperature for two to three days whereupon dark crystalline precipitates formed which were collected by filtration and washed with cold methanol and acetone. Yields: **1**: 0.51 g (88 %); **2**: 0.21 g (38 %); **3**: 0.39 g (67 %). Elemental analyses (%) calcd for $C_{40}H_{50}N_2O_2ClFe$: C 70.43, H 7.39, N 4.11, Cl 5.20; found: C 70.26, H 7.37, N 4.13, Cl 5.23; calcd for $C_{40}H_{50}N_2O_2BrFe$: C 66.12, H 6.94, N 3.86, Br 11.00; found: C 65.94, H 7.08, N 3.78, Br 10.90; calcd for $C_{40}H_{50}N_2O_2IFe$: C 62.10, H 6.51, N 3.62, I 16.40; found: C 61.86; H 6.42, N 3.57, I 16.26. EI mass spectra showed the correct molecular ion peak at m/z 681 for $[\mathbf{1}]^+$, 727 for $[\mathbf{2}]^+$, and 773 for $[\mathbf{3}]^+$. EPR, Mössbauer, and magnetic susceptibility equipment and procedures for simulation of data are the same as described in ref. [2a].

  1433-7851/01/4013-2491 $ 17.50+.50/0

Crystal structure analysis data for **1**: $C_{40}H_{50}N_2O_2ClFe$, $M_r = 682.12$, triclinic, $P\bar{1}$, $a = 10.738(1)$, $b = 13.195(1)$, $c = 14.061(1)$ Å, $\alpha = 75.19(1)$, $\beta = 79.71(1)$, $\gamma = 77.80(1)^\circ$, $V = 1866.1(3)$ Å^3, $Z = 2$, $\rho_{calcd} = 1.214$ Mg m^{-3}; $\mu(Mo_{K\alpha}) = 0.511$ mm^{-1}, $F(000) = 726$; 18080 reflections collected at 100(2) K; 9891 independent reflections; GOF = 0.990; $R = 0.0508$; $wR2 = 0.1059$. Crystal structure analysis data for **2**: $C_{40}H_{50}N_2O_2BrFe$, $M_r = 726.58$, triclinic, $P\bar{1}$, $a = 10.4544(9)$, $b = 14.737(1)$, $c = 24.387(2)$ Å, $\alpha = 86.88(2)$, $\beta = 84.89(2)$, $\gamma = 87.58(2)^\circ$, $V = 3734.0(5)$ Å^3, $Z = 4$, $\rho_{calcd} = 1.292$ Mg m^{-3}; $\mu(Mo_{K\alpha}) = 1.509$ mm^{-1}, $F(000) = 1524$; 29363 reflections collected at 100(2) K; 12766 independent reflections; GOF = 0.949; $R = 0.0552$; $wR2 = 0.1030$. Crystal structure data analysis for **3**: $C_{40}H_{50}N_2O_2IFe$, $M_r = 773.57$, monoclinic, $P2_1/c$, $a = 13.497(1)$, $b = 26.326(2)$, $c = 11.672(1)$ Å, $\beta = 112.99(2)^\circ$, $V = 3817.9(6)$ Å^3, $Z = 4$, $\rho_{calcd} = 1.346$ Mg m^{-3}; $\mu(Mo_{K\alpha}) = 1.238$ mm^{-1}, $F(000) = 1596$; 38047 reflections collected at 100(2) K; 12090 independent reflections; GOF = 1.007; $R = 0.039$; $wR2 = 0.072$. Crystallographic data (excluding structure factors) for the structures reported in this paper have been deposited with the Cambridge Crystallographic Data Centre as supplementary publication no. CCDC-159894 (**1**), CCDC-159895 (**2**), and CCDC-159896 (**3**). Copies of the data can be obtained free of charge on application to CCDC, 12 Union Road, Cambridge CB2 1EZ, UK (fax: (+44) 1223-336-033; e-mail: deposit@ccdc.cam.ac.uk).

Received: March 13, 2001 [Z16765]

[1] a) S. Koch, R. H. Holm, R. B. Frankel, *J. Am. Chem. Soc.* **1975**, *97*, 6714; b) D. P. Riley, D. H. Busch, *Inorg. Chem.* **1984**, *23*, 3235; c) K. L. Kostka, B. G. Fox, M. P. Hendrich, T. J. Collins, C. E. F. Rickard, L. J. Wright, E. Münck, *J. Am. Chem. Soc.* **1993**, *115*, 6746; d) H. Keutel, I. Käpplinger, E.-G. Jäger, M. Grodzicki, V. Schünemann, A. X. Trautwein, *Inorg. Chem.* **1999**, *38*, 2320; e) E.-G. Jäger, H. Keutel, *Inorg. Chem.* **1997**, *36*, 3512; f) D. Nicarchos, A. Kostikas, A. Simopoulos, D. Coucouvanis, D. Piltingsrud, R. E. Coffman, *J. Chem. Phys.* **1978**, *69*, 4411.

[2] a) M. D. Snodin, L. Ould-Moussa, U. Wallmann, S. Lecomte, V. Bachler, E. Bill, H. Hummel, T. Weyhermüller, P. Hildebrandt, K. Wieghardt, *Chem. Eur. J.* **1999**, *5*, 2554; b) R. M. Buchanan, S. L. Kessel, H. H. Downs, C. G. Pierpont, D. N. Hendrickson, *J. Am. Chem. Soc.* **1978**, *100*, 7894; c) W. O. Koch, V. Schünemann, M. Gerdan, A. X. Trautwein, H.-J. Krüger, *Chem. Eur. J.* **1998**, *4*, 1255.

[3] a) P. Chaudhuri, C. N. Verani, E. Bill, E. Bothe, T. Weyhermüller, K. Wieghardt, *J. Am. Chem. Soc.* **2001**, *123*, 2213; b) H. Chun, C. N. Verani, P. Chaudhuri, E. Bothe, E. Bill, T. Weyhermüller, K. Wieghardt, *Inorg. Chem.*, in press.

[4] C. N. Verani, S. Gallert, E. Bill, T. Weyhermüller, K. Wieghardt, P. Chaudhuri, *Chem. Commun.* **1999**, 1747.

[5] We have also recorded the Mössbauer spectrum of **3** at 298 K; a single quadrupole doublet is observed ($\delta = 0.22$ mm s^{-1}, $|\Delta E_Q| = 2.21$ mm s^{-1}). This clearly establishes that the increasing magnetic moment at temperatures > 100 K for **3** (Figure 2) is *not* due to a spin crossover $S_t = \frac{1}{2} \rightarrow S_t = \frac{3}{2}$.

[6] D. Sellmann, S. Emig, F. W. Heinemann, *Angew. Chem.* **1997**, *109*, 1808; *Angew. Chem. Int. Ed. Engl.* **1997**, *36*, 1734.

[7] C. K. Jörgensen, *Struct. Bonding (Berlin)* **1966**, *1*, 234.

Separation of Enantiomers by Extraction Based on Lipase-Catalyzed Enantiomer-Selective Fluorous-Phase Labeling**

Benno Hungerhoff, Helmut Sonnenschein, and Fritz Theil*

Lipase-mediated kinetic resolution of racemic alcohols and their esters by esterification or hydrolysis, respectively, is a well-established method for the preparation of enantiomerically pure or enriched building blocks.[1] Lipases are cheap biocatalysts; the reactions can be run with standard equipment and are highly selective in many cases. However, there is one major drawback of this type of biotransformation, which affords one of the enantiomers as an alcohol and the other one as the corresponding carboxylate: The products must be separated by chromatography. This separation step may not be a serious problem on the laboratory scale. However, on a large scale in the pharmaceutical industry, a chromatographic step might be the reason this method is not considered to be a useful access to enantiomerically pure intermediates. Until now, there has been no general solution to overcome this disadvantage.

On the other hand, remarkable progress has been made for the extractive separation of homogeneous catalysts,[2] reagents, and products[3] equipped with perfluorinated auxiliary groups. This methodology is based on partitioning between the organic and fluorous phases in order to improve the recovery of the homogeneous catalyst and the isolation of products from the reaction mixture.

From the progress made in performing reactions in fluorous media and/or improving workup procedures by the introduction of a fluorous phase,[4] the following question arises: Is it possible to apply a highly fluorinated acyl donor to a lipase-catalyzed kinetic resolution of a racemic alcohol? Such an acyl donor should promote lipase-mediated enantiomer-selective acyl transfer onto the faster-reacting enantiomer and, thereby, simultaneously label it. This labeled enantiomer with a "teflon ponytail"[2b] could then be recognized selectively by a fluorous phase, to allow the extractive separation of the fluorinated and nonfluorinated enantiomers between a fluorous and an organic solvent.

For a successful realization of this principle a suitable acyl donor is required. This reagent should be accepted by the lipase forming the reactive acyl enzyme, that subsequently reacts in an enantiomer-selective manner with a racemic alcohol. Furthermore, the transferred acyl residue should have a sufficient fluorine content to allow selective separation of the fluorinated ester from the nonfluori-

[*] Dr. F. Theil, Dr. B. Hungerhoff
ASCA GmbH
Richard-Willstätter-Strasse 12, 12489 Berlin (Germany)
Fax: (+49) 30-6392-4103
E-mail: theil@asca-berlin.de
Dr. H. Sonnenschein
Institut für Nichtklassische Chemie an der Universität Leipzig
Permoserstrasse 15, 04303 Leipzig (Germany)

[**] This work was supported by the Deutsche Forschungsgemeinschaft (grant: TH 562/3-1) and the Fonds der Chemischen Industrie.

  1433-7851/01/4013-2492 $ 17.50+.50/0

nated alcohol in an appropriate biphasic organic/fluorous system.

Esters of the structure $CF_3(CF_2)_n(CH_2)_mCOOR$ (where R = vinyl or 2,2,2-trifluoroethyl, for example) were designed as suitable irreversible or quasi-irreversible acyl donors.[1c] A spacer of one or two methylene groups ($m = 1$ or 2) should be necessary to exclude a nonselective chemical acylation of the alcohol. The commercially available alcohol **1**[5] was selected as a useful starting material for the synthesis of the ester **2**,[6] envisaged as a potential acyl donor and synthesized in high yield by the method shown in Scheme 1.

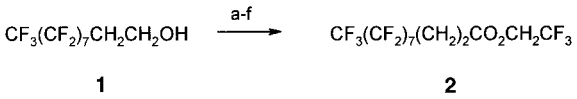

Scheme 1. Synthesis of the highly fluorinated acyl donor **2**. a) 4-$CH_3C_6H_4SO_2Cl$, b) LiBr, c) Mg, d) CO_2, e) PCl_5, f) CF_3CH_2OH, pyridine.

In order to demonstrate the feasibility of the principle, we chose 1-phenylethanol (*rac*-**3**) as the alcohol to be resolved. After screening of lipases and solvents, lipase B from *Candida antarctica* (CAL-B) in acetonitrile turned out to be a useful biocatalytic system with ester **2** as the acylating agent; the resolution of the enantiomers of *rac*-**3** into (*R*)-**4** and (*S*)-**3** proceeded with high efficacy within 19 hours (Scheme 2). The corresponding ester with one less CH_2 group ($m = 1$) was not suitable as an acyl donor.

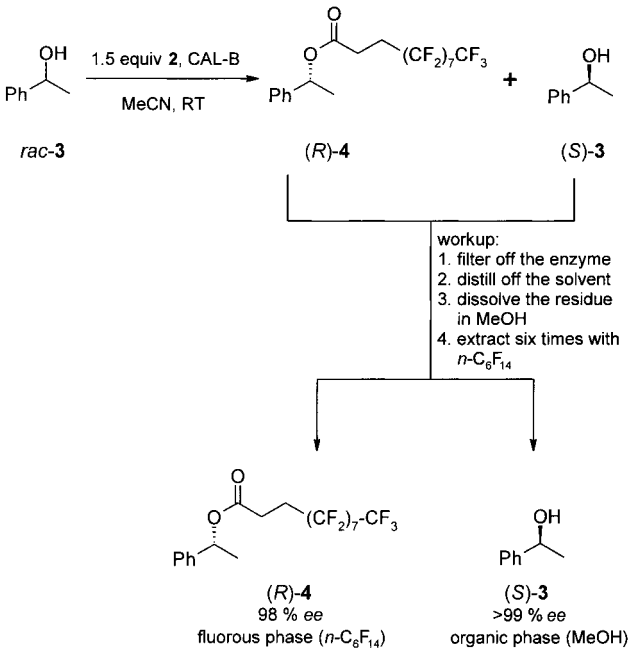

Scheme 2. Lipase-catalyzed kinetic resolution of *rac*-**3** and subsequent extractive separation of the products with a biphasic fluorous/organic solvent system.

In order to determine the yields and enantiomeric excesses (*ee*)[7] of the products, the reaction mixture was worked up conventionally with purification by flash column chromatography to yield (*R*)-**4** (46% yield, *ee* > 99%) and (*S*)-**3** (41% yield, *ee* > 99%). In comparison, the resolution of *rac*-**3** with vinyl acetate in *tert*-butyl methyl ether in the presence of *Pseudomonas* sp. lipase reached 50% conversion after 44 hours to yield the corresponding (*R*)-acetate and (*S*)-**3** with *ee* values of > 99 and 93%, respectively.[8] This demonstrates that the reactivity of perfluoroester **2** is, at least, in the same range as that of vinyl acetate.

In the next step, we looked for a suitable biphasic fluorous/organic solvent system to separate ester (*R*)-**4** from alcohol (*S*)-**3** whilst avoiding chromatography. Screening of organic solvents immiscible with *n*-perfluorohexane such as cyclohexane, toluene, THF, and methanol showed that the biphasic mixture methanol/*n*-perfluorohexane was the system of choice and allowed a very efficient separation of the compounds *rac*-**3** and *rac*-**4**, which were used as model substances. When an equimolar mixture of *rac*-**3** and *rac*-**4** was extracted at least five times with *n*-perfluorohexane, *rac*-**3** remained in the organic phase and *rac*-**4** moved into the fluorous phase. The organic phase was contaminated with less than 1% of *rac*-**4** and the fluorous phase contained less than 1% of *rac*-**3**.

After identification of the appropriate fluorous/organic biphasic system for the separation of (*R*)-**4** and (*S*)-**3**, the reaction mixture was worked up as follows (Scheme 2): The enzyme was filtered off, the solvent was removed under reduced pressure, and the products were separated by partition between methanol and *n*-perfluorohexane. This method yielded (*S*)-**3** with an *ee* value of 99% in the organic phase and (*R*)-**4** with an *ee* value of 98% in the fluorous phase, which also contained the excess of the acylating agent **2**.

Comparison of the results obtained by conventional chromatographic separation and extractive separation shows that there is almost no difference between both procedures regarding the purity and the yield of the products. After the extractive workup (*S*)-**3** was contaminated with a trace (not more than 1%) of (*R*)-**4**.[9] The *ee* value of 98% determined after saponification of (*R*)-**4** to (*R*)-**3**, represents an impurity of not more than 1% of (*S*)-**3** in the fluorous phase. In addition, saponification of the mixture of (*R*)-**4** and **2** to yield (*R*)-**3** allows the almost quantitative recovery of the fluorinated carboxylic acid in solid form as the lithium salt.

This newly developed methodology for the separation of enantiomers, which combines a lipase-catalyzed kinetic resolution with fluorous-phase labeling and separation of the products in a biphasic fluorous/organic solvent system, should also be applicable for the enantiomer-selective hydrolysis or alcoholysis of fluorous-phase labeled esters of racemic alcohols and for the enantiomer-selective alcoholysis of esters of racemic carboxylic acids with highly fluorinated alcohols.[10] We are currently investigating further applications of this newly developed strategy.

Experimental Section

A solution of *rac*-**3** (1.22 g, 10 mmol) in MeCN (65 mL) was treated with ester **2** (8.61 g, 15 mmol) and CAL-B (Chirazyme L-2, c.-f., lyo., Roche Diagnostics, Mannheim; 2.00 g). The reaction mixture was stirred at ambient temperature until the conversion reached approximately 50% (19 h). The enzyme was filtered off and the solid residue was washed with acetone (2 × 40 mL). The combined filtrates were evaporated under reduced pressure and the residue was dissolved in MeOH (25 mL). The

  1433-7851/01/4013-2493 $ 17.50+.50/0

resulting solution was extracted with n-C_6F_{14} (6×25 mL). The organic phase was concentrated to dryness to yield (*S*)-**3** (0.59 g, 48 % yield, 99 % *ee*) with approximately 1 % of (*R*)-**4**. From the fluorous phase a mixture of (*R*)-**4** (*ee* 98 %) and the excess of **2** (8.50 g) was isolated.

Saponification of (*R*)-**4**: The mixture of (*R*)-**4** and **2** was dissolved in THF and water (1/1, 40 mL) together with LiOH (0.64 g, 26.7 mmol), and the mixture was heated to reflux for 3 h. Subsequently, the reaction mixture was diluted with cyclohexane (100 mL), cooled to 0 °C, and filtered. The filter cake was washed with a mixture of cyclohexane (100 mL) and *tert*-butyl methyl ether (30 mL). The filtrate was concentrated to dryness to yield (*R*)-**3** (0.57 g, 47 %, 98 % *ee*). The remaining solid filter cake (7.35 g, 98 %) consists of the lithium salt of the perfluorinated carboxylic acid.

Received: January 25, 2001
Revised: March 12, 2001 [Z16506]

[1] a) C.-S. Chen, C.-J. Sih, *Angew. Chem.* **1989**, *101*, 711 – 724; *Angew. Chem. Int. Ed. Engl.* **1989**, *28*, 695 – 707; b) W. Boland, C. Frößl, M. Lorenz, *Synthesis* **1991**, 1049 – 1072; c) K. Faber, S. Riva, *Synthesis* **1992**, 895 – 910; d) E. Santaniello, P. Ferraboschi, P. Grisenti, *Enzyme Microb. Technol.* **1993**, *15*, 367 – 382; e) F. Theil, *Chem. Rev.* **1995**, *95*, 2203 – 2227; f) U. T. Bornscheuer, R. J. Kazlauskas, *Hydrolases in Organic Synthesis*, Wiley-VCH, Weinheim, **1999**; g) G. Carrea, S. Riva, *Angew. Chem.* **2000**, *112*, 2312 – 2341; *Angew. Chem. Int. Ed.* **2000**, *39*, 2226 – 2254.

[2] a) I. T. Horváth, J. Rábai, *Science* **1994**, *266*, 72 – 75; b) J. A. Gladysz, *Science* **1994**, *266*, 55 – 56; c) B. Cornils, *Angew. Chem.* **1997**, *109*, 2147 – 2149; *Angew. Chem. Int. Ed. Engl.* **1997**, *36*, 2057 – 2059; d) B. Betzemeier, M. Cavazini, S. Quici, P. Knochel, *Tetrahedron Lett.* **2000**, *41*, 4343 – 4346.

[3] a) D. P. Curran, M. Hoshino, *J. Org. Chem.* **1996**, *61*, 6480 – 6481; b) P. Wipf, J. T. Reeves, *Tetrahedron Lett.* **1999**, *40*, 4649 – 4652; c) S. Röver, P. Wipf, *Tetrahedron Lett.* **1999**, *40*, 5667 – 5670.

[4] a) D. P. Curran, *Angew. Chem.* **1998**, *110*, 1231 – 1255; *Angew. Chem. Int. Ed.* **1998**, *37*, 1174 – 1196; b) U. Diederichsen, *Nachr. Chem. Tech. Lab.* **1999**, *47*, 805 – 809.

[5] One can expect that the currently very high price of the alcohol (104.10 € for 50 g, Avocado/ABCR) should go down significantly if there is a need for bulk quantities.

[6] B.p. 57 °C (1×10^{-3} mbar); ^{1}H NMR (300 MHz, $CDCl_3$): $\delta = 2.52$ (tt, $^1J = 8.4$, $^2J = 8.0$ Hz, 2H), 2.76 (t, $J = 8.4$ Hz, 2H), 4.42 (q, $J = 8.4$ Hz, 2H).

[7] Before determination of the *ee* value, (*R*)-**4** was saponified to the corresponding alcohol (*R*)-**3**. The *ee* values of the enantiomeric alcohols (*R*)- and (*S*)-**3** were determined by HPLC on a Chiralcel OJ column (250×4.6 mm; eluent: *n*-heptane/*n*-propanol 95/5; flow rate: 1 mL min^{-1}; UV detection at 254 nm). The absolute configurations of the enantiomeric alcohols were assigned by comparison with commercially available authentic samples.

[8] K. Laumen, D. Breitgoff, M. P. Schneider, *J. Chem. Soc. Chem. Commun.* **1988**, 1459 – 1461.

[9] Extraction was carried out in an ordinary separation funnel. The residual 1 % of alcohol (*S*)-**3** left in the fluorous phase could either be caused by contamination of the glassware (for example, a stopcock) or by incomplete separation of the phases. However, a reextraction of the fluorous phase with methanol should remove the trace of (*S*)-**3**.

[10] We have not tested whether esterases or proteases will also accept long-chain fluoroesters.

  1433-7851/01/4013-2494 $ 17.50+.50/0

A New Type of Doubly Silylamido-Bridged Cyclopentadienyl Group 4 Metal Complexes**

Jesús Cano, Pascual Royo,* Maurizio Lanfranchi, Maria Angela Pellinghelli, and Antonio Tiripicchio

Dedicated to Professor Rafael Usón on the occasion of his 75th birthday

The isolation of metal complexes containing the η^1-amidosilyl-η^5-cyclopentadienyl ligand, which provides more acidic metal centers with a more open coordination site than the ansa-dicyclopentadienyl compounds, has proved particularly useful.[1] These structural features are responsible for their catalytic ability to copolymerize long-chain α-olefins.[2] Numerous contributions in this field have benefited from the research into the use of variously substituted ligands,[3] the characterization of the active cationic species,[4] the development of new industrial applications,[5] and the reactivity of the metal-coordinated amidosilyl moiety.[6]

Few examples of doubly bridged η^5-cyclopentadienyl-di(η^1-ligand) metal compounds have been reported.[7] We have now extended our studies in this field by synthesizing new substituted cyclopentadienyl ligands that can form more than one amidosilyl bridge, that is di(η-amidosilyl)-η^5-cyclopentadienyl ligands, and characterizing and studying the reactivity of their Group 4 metal complexes.

The di(amidosilyl)cyclopentadiene $C_5H_4[SiMe_2(NHtBu)]_2$ (**1**) was synthesized as a yellow oil from 1,1-$(SiMe_2Cl)_2C_5H_4$[8] and LiNH*t*Bu in 12 h at room temperature using THF as solvent. Selective deprotonation of the more acidic cyclopentadiene proton and only one of the amino protons of **1** by using $[Zr(NMe_2)_4]$ afforded the monosilylamido derivative **2** as a light-brown oil (Scheme 1). A C_6D_6 solution of **2** was heated to 110 °C to give the disilylamido compound **3** with evolution of $NHMe_2$. However this reaction was reversed when the mixture was cooled to room temperature, preventing the isolation of **3**. Similar deprotonation of **1** by using the tetrabenzyl compound $[Zr(CH_2Ph)_4]$, gave a mixture of the brown monosilylamido **4**, identified by ^{1}H NMR spectroscopy, and the disilylamido derivative **5** at room temperature (Scheme 1), while **5** was the unique reaction product at

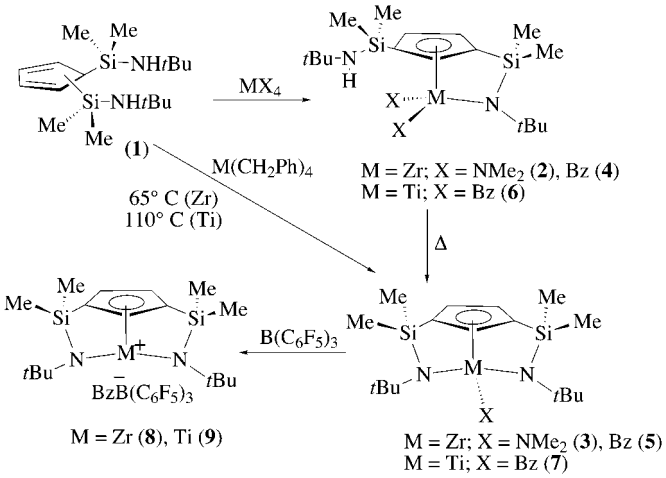

Scheme 1. Synthesis of neutral bridged η^5-cyclopentadienyl mono- and di(η-amidosilyl)titanium and -zirconium complexes and their cationic species.

temperatures higher than 65 °C. The deprotonating capacity of complex **5** facilitated the irreversible transformation of **2** into **3** by elimination of the $NHMe_2$ resulting from that transformation. A similar reaction of **1** with $[Ti(CH_2Ph)_4]$ gave the monosilylamido complex **6** as a red solid, which could only be transformed into the disilylamido derivative **7** by refluxing a solution of the compound in toluene.

All the new compounds were characterized by elemental analyses, and the ^{1}H and ^{13}C NMR spectra were consistent (see Supporting Information) with the asymmetry of the monosilylamido compounds **2**, **4**, and **6**, and with the presence of a plane of symmetry in the disilylamido compounds **3**, **5**, and **7** (Scheme 1). The chemical shifts of the *t*Bu tertiary carbon atoms were observed between $\delta = 55.8$ (**3**) and $\delta = 61.5$ (**6**) for bridged, and between $\delta = 49.6$ (**2**) and $\delta = 49.8$ (**6**) for unbridged amidosilyl groups; the $\Delta\delta$ values[9] were between 20.2 and 27.2 for bridged and between 15.7 and 16.0 for unbridged amidosilyl groups, respectively. Treatment of solutions of **5** and **7** in toluene with one equivalent of $B(C_6F_5)_3$ gave the complexes **8** and **9**, respectively (Scheme 1). The ^{1}H, ^{13}C, and ^{19}F NMR spectra of **8** and **9** in C_6D_6 were consistent with their formulation as the salts of C_s-symmetric base-free cations and the $[(CH_2Ph)B(C_6F_5)_3]^-$ ion.[10, 11]

Crystals of **9** suitable for a single-crystal X-ray structure determination were grown by cooling a saturated solution of **9** in benzene. The structure of **9** (Figure 1) shows a titanium cation with the centroid of the cyclopentadienyl ring and the two amido-N atoms occupying three positions in a pseudo-tetrahedral ligand arrangement, the fourth position being occupied by the "*meta*-C–H bond" or alternatively by a "*meta*-C atom" of the phenyl ring of the benzylborate anion. The η^5-cyclopentadienyl di(η-amidosilyl) ligand shows a strongly constrained geometry, which allows it to interact with the metal as a tridentate ligand; the C1 and C3 atoms that bear the amidosilyl arms are pyramidally distorted, as shown by the sums of the bond angles (348.0° and 348.1°, respectively). The Ti–N and the Ti–CE1 (CE1 is the Cp centroid) distances are similar to those observed in related neutral amidosilylcyclopentadienyl compounds.[3d] The Ti–C21 dis-

[*] Prof. Dr. P. Royo, J. Cano
Departamento de Química Inorgánica
Facultad de Ciencias, Universidad de Alcalá
Campus Universitario, 28871 Alcalá de Henares (Spain)
Fax: (+34) 91-8854683
E-mail: pascual.royo@uah.es
Prof. Dr. M. Lanfranchi, Prof. Dr. M. A. Pellinghelli, Prof. Dr. A. Tiripicchio
Dipartimento di Chimica Generale ed Inorganica
Chimica Analitica, Chimica Fisica
Università di Parma, Centro di Studio per la Strutturistica Diffrattometrica del CNR
Parco Area delle Scienze 17 A, 43100 Parma (Italy)

[**] We thank the Dirección General de Enseñanza Superior e Investigación Científica (DGESEIC) for financial support of this work (Project PB97-0776). J.C. thanks the CAM for a Postgraduate Fellowship.

Supporting information for this article is available on the WWW under http://www.angewandte.com or from the author.

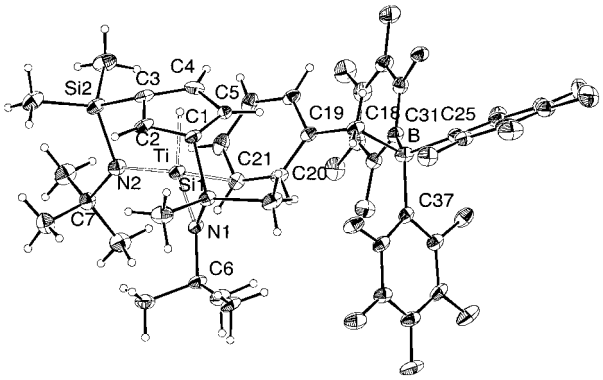

Figure 1. Molecular structure of **9** (the ellipsoids for the atoms are drawn at 30 % probability level). Selected interatomic distances [Å] and angles [°]: Ti-CE1 1.997(5), Ti-N1 1.959(4), Ti-N2 1.946(5), Ti-C21 2.447(6), Ti-M1 2.33, Ti-H21 2.30; N1-Ti-N2 126.3(2), CE1-Ti-N1 106.7(2), CE1-Ti-N2 106.6(2), CE1-Ti-M1 129.5(3), N1-Ti-M1 95.0(3), N2-Ti-M1 95.0(3); CE1 and M1 are the centroid of the Cp ring and the midpoint of the C21-H bond, respectively.

tance (Ti–C21 2.447(6) Å) is about 0.3 Å longer than that normally expected for covalent Ti–C σ bonds. The interaction with the electron pair in the C–H bond is consistent with the distances observed from Ti to H21 and to the middle of the C–H bond (M1) (Ti–H21 2.30, Ti–M1 2.33 Å). Metal–η^6-phenyl,[11, 12] metal–η^5-phenyl,[13] and metal–η^3-phenyl[14] interactions for related benzylborate anions have been reported but, as far as we are aware, there have been no reports of this type of interaction in which a single *meta*-C_{phenyl}–H bond of the benzylborate anion interacts with the empty hybrid metal orbital of a typical "three leg piano stool" coordination. Furthermore, the alternative interaction with the p orbital of the *meta*-C_{phenyl} atom similar to that found for η^1-benzene-coordinated silver compounds[15] cannot be ignored.

Compound **8** polymerizes ethylene at room temperature and pressure[16] despite being free of alkyl ligands. Immediate polymerization was observed when a teflon-valved Schlenk tube containing **8** was evacuated and filled with ethylene. The polymerization activity of compound **5** was measured by using a solution containing methylaluminoxane (MAO; 19.3 mmol) and **5** (4.2 μmol) in *n*-hexane (600 mL) at 4 atm ethylene and 70 °C. The observed activity after 15 min was 7.4×10^5 g PE (mol Zr)$^{-1}$ h^{-1} atm^{-1}. The polyethylene (PE) produced showed a very high molecular weight ($M_w = 5.4 \times 10^5$) with a polydispersity index M_w/M_n of 1.9. It was insoluble in 1,2,4-trichlorobenzene preventing its characterization by NMR spectroscopy. Compound **5** was also an active catalyst for the copolymerization of ethylene and 1-hexene. When the same experiment was carried out under the same conditions but with the prior addition of 1-hexene (10 mL), the resulting polymer ($M_w = 4.1 \times 10^5$ and $M_w/M_n = 2.2$) after 30 min contained 0.7 mol % of 1-hexene and the catalytic activity was 3.5×10^5 g polymer (mol Zr)$^{-1}$ h^{-1} atm^{-1}.

Experimental Section

Full experimental details, analytical data and NMR assignments for all compounds are provided as Supporting Information.

Representative procedure: A solution of [Ti(CH_2Ph)$_4$] (2.14 g, 5.2 mmol) in toluene (70 mL) was cooled to 0 °C, and an equimolar amount of **1** was added by syringe. The resulting yellow solution was warmed for 5 h to 65 °C. The solvent was removed under vacuum and the residue was extracted into pentane (70 mL). After filtration and removal of the solvent, complex **6** was isolated as a red solid (2.87 g, 5.2 mmol, 100 %).

A similar reaction carried out under reflux gave complex **7** (5.93 g, 12.9 mmol, 100 %) as a dark red solid.

A solution of the monobenzyl complex **7** (0.116 g, 0.25 mmol) in toluene (20 mL) was treated with B(C_6F_5)$_3$ (0.126 g, 0.25 mmol) at room temperature and the mixture was stirred for 30 min and then cooled to –35 °C. The solvent was filtered off from the resulting insoluble residues, which were then dried under vacuum to give **9** (0.13 g, 60 % yield) as an orange crystalline solid. An appropriate monocrystal of **9** was separated for study using X-ray diffraction methods.

^{1}H NMR (300 MHz, C_6D_6, 20 °C, TMS) for **6**: $\delta = 0.21$, 0.27 (2s, 2 × 3 H; Si*Me*$_2$NH*t*Bu), 0.37, 0.38 (2s, 2 × 3 H; Si*Me*$_2$N*t*Bu), 0.72 (s, 1 H; NH*t*Bu) 1.07 (s, 9 H; NH*t*Bu), 1.44 (s, 9 H; N*tBu*), 2.47, 2.55, 2.81, 2.97 (4d, $J = 10.5$ Hz, 4 × 1 H; C*H*$_2$Ph), 5.83, 6.14, 6.83 (3m, 3 × 1 H; C_5H_3), 6.87–7.20 (m, 10 H; CH_2*Ph*); ^{13}C NMR (300 MHz, C_6D_6, 20 °C, TMS): $\delta = 0.6$, 1.5 (Si*Me*$_2$NH-*t*Bu), 2.4, 2.9 (Si*Me*$_2$N*t*Bu), 33.8(NH*t*Bu), 34.3 (N*t*Bu), 49.8(NH*t*Bu$_{ipso}$), 61.5 (N*t*Bu$_{ipso}$), 79.6, 83.7 (CH_2*Ph*), 110.2, 122.8 (C_5H_{3ipso}), 122.1, 122.5, 123.0 (C_5H_3), 125.9 126.8, 126.8, 127.4, 128.5, 128.6, 128.7, 128.9, 129.8, 132.6 (C_6H_5), 149.6, 150.1 (C_6H_{5ipso}); elemental analysis for **6**: calcd: C 62.68, H 8.68, N 5.76; found: C 62.58, H 8.75, N 6.08.

^{1}H NMR (300 MHz, C_6D_6, 20 °C, TMS) for **7**: $\delta = 0.39$, 0.40 (2s, 2 × 6 H; $SiMe_2$), 1.42 (s, 18 H; N*tBu*), 2.61 (s, 2 H; C*H*$_2$Ph), 6.14 (d, 2 H; C_5H_3), 6.40 (t, 1 H; C_5H_3), 6.89 (m, 1 H; C_6H_5), 7.00 (m, 2 H; C_6H_5), 7.22 (m, 2 H; C_6H_5); ^{13}C NMR (300 MHz, C_6D_6, 20 °C, TMS):$\delta = 2.1$, 2.2 ($SiMe_2$), 35.6 (N*t*Bu), 59.3 (N*t*Bu$_{ipso}$), 69.6 (*C*H$_2$Ph), 117.7 (C_5H_{3ipso}), 121.5, 126.3 (C_5H_3), 128.5, 130.3, 132.6 (C_6H_5), 152.4 (C_6H_{5ipso}); elemental analysis for **7**: calcd: C 67.82, H 8.71, N 4.81; found: C 67.36, H 8.75, N 5.07.

^{1}H NMR (300 MHz, C_6D_6, 20 °C, TMS) for **9**: $\delta = 0.19$, 0.38 (2s, 2 × 6 H; $SiMe_2$), 1.12 (s, 18 H; N*tBu*), 3.49 (s, 2 H; BCH_2), 5.03 (m, 1 H; C_5H_3), 5.86 (m, 2 H; C_5H_3), 6.21–7.10 (m, 5 H; C_6H_5); ^{13}C NMR (300 MHz, C_6D_6, 20 °C, TMS): $\delta = 0.6$, 1.4 ($SiMe_2$), 34.6 (N*t*Bu), 59.3 (N*t*Bu$_{ipso}$), 122.1, 126.2 (C_5H_3), 126.1 (C_5H_{3ipso}), 128.3, 128.7, 132.9 (C_6H_5), 135.1, 140.1, 145.8, 150.9 (C_6F_5); ^{19}F NMR (300 MHz, C_6D_6, 20 °C, CCl_3F): $\delta = 132.1$ (m, 2 F; *o*-C_6F_5), 163.6 (m, 1 F; *p*-C_6F_5), 167.2 (m, 2 F; *m*-C_6F_5).

Crystal data of **9** ($C_{42}H_{40}BF_{15}N_2Si_2Ti$, $M_r = 972.65$): $T = 173(2)$ K, $\lambda = 1.54184$ Å; triclinic, space group $P\bar{1}$, unit cell dimensions, $a = 11.564(6)$, $b = 13.531(6)$, $c = 14.020(7)$ Å, $\alpha = 78.32(2)$, $\beta = 87.64(2)$, $\gamma = 87.01(2)°$, $V = 2144.3(18)$ Å^3; $Z = 2$; $\rho_{calcd} = 1.506$ g cm^{-3}; $\mu = 3.124$ mm^{-1}, $F(000) = 992$, crystal size $0.42 \times 0.38 \times 0.25$ mm, θ range 3.22–69.99°. Reflections collected and unique 8113, observed 4019 [$I > 2\sigma(I)$]. Full-matrix least-squares refinement on F^2,[17] 578 parameters, hydrogen atoms introduced in the geometrically calculated positions and refined riding on the parent atoms, goodness-of-fit on F^2 0.877. Final R indices [$I > 2\sigma(I)$], $R1 = 0.0665$, $wR2 = 0.1634$, R indices (all data) $R1 = 0.1349$, $wR2 = 0.2051$. Crystallographic data (excluding structure factors) for the structure reported in this paper have been deposited with the Cambridge Crystallographic Data Centre as supplementary publication no. CCDC-152472. Copies of the data can be obtained free of charge on application to CCDC, 12 Union Road, Cambridge CB2 1EZ, UK (fax: (+44) 1223-336-033; e-mail: deposit@ccdc.cam.ac.uk).

Received: January 22, 2001 [Z 16465]

[1] a) P. J. Shapiro, E. E. Bunel, W. E. Piers, J. E. Bercaw, *Synlett* **1990**, *2*, 74; b) P. J. Shapiro, E. Bunel, W. P. Schaefer, J. E. Bercaw, *Organometallics* **1990**, *9*, 867; c) J. Okuda, *Chem. Ber.* **1990**, *123*, 1649; d) P. J. Shapiro, W. E. Cotter, W. P. Schaefer, J. A. Labinger, J. E. Bercaw, *J. Am. Chem. Soc.* **1994**, *116*, 4623.

[2] a) P. C. Möhring, N. J. Coville, *J. Organomet. Chem.* **1994**, *479*, 1; b) H. H. Brintzinger, D. Fischer, R. Mülhaupt, B. Rieger, R. M. Waymouth, *Angew. Chem.* **1995**, *107*, 1255; *Angew. Chem. Int. Ed. Engl.* **1995**, *34*, 1143; (corrigendum: H. H. Brintzinger, D. Fischer, R. Mülhaupt, B. Rieger, R. M. Waymouth, *Angew. Chem.* **1995**, *107*, 1652; *Angew. Chem. Int. Ed. Engl.* **1995**, *34*, 1368); c) A. L. Mcknight, R. M. Waymouth, *Chem. Rev.* **1998**, *98*, 2587; d) W. Kaminsky, *J. Chem. Soc. Dalton Trans.* **1998**, 1413; e) G. G. Hlatky, *Coord. Chem. Rev.* **1999**, *181*, 256.

  1433-7851/01/4013-2496 $ 17.50+.50/0

[3] a) A. K. Hughes, A. Meetsma, J. H. Teuben, *Organometallics* **1993**, *12*, 1936; b) W. A. Herrmann, M. J. A. Morawietz, *J. Organomet. Chem.* **1994**, *482*, 169; c) J. Okuda, F. J. Schattenmann, S. Wocadlo, W. Massa, *Organometallics* **1995**, *14*, 789; d) D. W. Carpenetti, L. Kloppenburg, J. T. Kupec, J. L. Petersen, *Organometallics* **1996**, *15*, 1572; e) S. Ciruelos, T. Cuenca, R. Gómez, P. Gómez-Sal, A. Manzanero, P. Royo, *Organometallics* **1996**, *15*, 5577; f) R. Gómez, P. Gómez-Sal, A. Martín, A. Núñez, P. A. del Real, P. Royo, *J. Organomet. Chem.* **1998**, *564*, 93; g) B. Royo, P. Royo, L. M. Cadenas, *J. Organomet. Chem.* **1998**, *551*, 293; h) T. Eberle, T. P. Spaniol, J. Okuda, *Eur. J. Inorg. Chem*. **1998**, 237; i) L. Duda, G. Erker, R. Fröhlich, F. Zippel, *Eur. J. Inorg. Chem.* **1998**, 1153; j) D. Kunz, G. Erker, R. Fröhlich, G. Kehr, *Eur. J. Inorg. Chem.* **2000**, 409.

[4] a) M. Bochmann, *J. Chem. Soc. Dalton Trans.* **1996**, 255; b) Y.-X. Chen, P.-F. Fu, C. L. Stern, T. J. Marks, *Organometallics* **1997**, *16*, 5958; c) B. E. Bosch, G. Erker, R. Fröhlich, O. Meyer, *Organometallics* **1997**, *16*, 5449; d) Y.-X. Chen, T. J. Marks, *Organometallics* **1997**, *16*, 3649; e) A. Bertuleit, C. Fritze, G. Erker, R. Fröhlich, *Organometallics* **1997**, *16*, 2891; f) G. Lanza, I. L. Fragalà, T. J. Marks, *J. Am. Chem. Soc.* **1998**, *120*, 8257; g) F. Amor, A. Butt, K. E. Du Plooy, T. B. Spaniol, J. Okuda, *Organometallics* **1998**, *17*, 5836; h) R. Gómez, P. Gómez-Sal, P. A. del Real, P. Royo, *J. Organomet. Chem.* **1999**, *588*, 22.

[5] a) J. C. Stevens, F. J. Timmers, D. R. Wilson, G. F. Schmidt, P. N. Nickias, R. K. Rosen, G. W. Knight, S. Lai (Dow), EP 416815, **1991** [*Chem. Abstr*. **1991**, *115*, 93163]; b) J. M. Canich (Exxon), EP 420436, **1991** [*Chem. Abstr*. **1991**, *115*, 184145].

[6] a) P. Jutzi, U. Siemeling, *J. Organomet. Chem.* **1995**, *500*, 175; b) P. Jutzi, T. Redeker, *Eur. J. Inorg. Chem*. **1998**, 663; c) T. Cuenca, P. Royo, *Coord. Chem. Rev.* **1999**, *193–195*, 447; d) R. Kempe, *Angew. Chem.* **2000**, *112*, 478; *Angew. Chem. Int. Ed.* **2000**, *39*, 468; e) L. H. Gade, *Chem. Commun.* **2000**, 173.

[7] a) M. D. Fryzuk, S. S. S. H. Mao, P. B. Duval, S. J. Rettig, *Polyhedron* **1995**, *14*, 11; b) M. D. Fryzuk, L. Jafarpour, *Organometallics* **1999**, *18*, 4050; c) M. D. Fryzuk, P. B. Duval, S. S. S. H. Mao, M. J. Zaworotko, L. R. MacGillivray, *J. Am. Chem. Soc.* **1999**, *121*, 2478; d) I. L. Feduskin, S. Dachert, H. Schuman, *Organometallics* **2000**, *19*, 4066; e) P. Doufou, K. A. Abboud, J. M. Boncella, *J. Organomet. Chem.* **2000**, *603*, 213.

[8] J. M. Rozell, P. R. Jones, *Organometallics* **1985**, *4*, 2206.

[9] a) W. A. Nugent, B. L. Haymore, *Coord. Chem. Rev.* **1980**, *31*, 123; b) D. E. Wigley, *Prog. Inorg. Chem.* **1994**, *42*, 239; c) M. J. Humphries, M. L. H. Green, M. A. Leech, V. C. Gibson, M. Jolly, D. N. Williams, M. R. J. Elsegood, W. Clegg, *J. Chem. Soc. Dalton Trans.* **2000**, 4044.

[10] A. D. Horton, J. de With, *Chem. Commun.* **1996**, 1375.

[11] No phenyl coordination of the phenyl ring to the metal was observed in solution: C. Pellecchia, A. Grassi, A. Immirzi, *J. Am. Chem. Soc.* **1993**, *115*, 1160.

[12] a) M. G. Thorn, Z. C. Etheridge, P. E. Fanwick, I. P. Rothwell, *Organometallics* **1998**, *17*, 3636; b) G. Jiménez Pindado, M. Thornton-Pett, M. B. Hursthouse, S. J. Coles, M. Bochmann, *J. Chem. Soc. Dalton Trans.* **1999**, 1663; c) J. Sassmannshausen, A. K. Powell, C. E. Anson, S. Wocadlo, M. Bochmann, *J. Organomet. Chem.* **1999**, *592*, 84; d) P. J. W. Deckers, A. J. van der Linden, A. Meetsma, B. Hessen, *Eur. J. Inorg. Chem.* **2000**, 929.

[13] C. Pellecchia, A. Immirzi, A. Grassi, A. Zambelli, *Organometallics* **1993**, *12*, 4473.

[14] a) J. Scholz, M. Schlegel, K.-H. Thiele, *Chem. Ber.* **1987**, *120*, 1369; b) A. D. Horton, J. H. G. Frijns, *Angew. Chem.* **1991**, *103*, 1181; *Angew. Chem. Int. Ed. Engl.* **1991**, *30*, 1152.

[15] a) K. Shelly, D. C. Finster, Y. J. Lee, W. R. Scheidt, C. A. Reed, *J. Am. Chem. Soc.* **1985**, *107*, 5955; b) M. Laguna, M. D. Villacampa, M. Contel, J. Garrido, *Inorg. Chem.* **1998**, *37*, 133; c) A. S. Batsanov, S. P. Crabtree, J. A. K. Howard, C. W. Lehmann, M. Kilner, *J. Organomet. Chem.* **1998**, *550*, 59.

[16] P. Royo, J. Cano, M. A. Flores, EP 01500020.1 **2001**.

[17] G. M. Sheldrick, SHELXL-97, Program for the Solution and the refinement of Crystal Structures, Universität Göttingen, Germany, **1997**.

Tetrathiafulvaleno-Annelated Porphyrins**

Jan Becher,* Thomas Brimert, Jan O. Jeppesen, Jens Z. Pedersen, Roman Zubarev, Thomas Bjørnholm, Niels Reitzel, Torben R. Jensen, Kristian Kjaer, and Eric Levillain

Dedicated to Professor Michael P. Cava on the occasion of his 75th birthday

Porphyrins are of fundamental importance in biological systems and are currently in focus for applications in supramolecular[1] and materials chemistry, for which the porphyrin chromophore has been extensively modified to enhance the desired properties.[2] Langmuir–Blodgett (LB) films[3] of porphyrin derivatives have been studied because of their optical, magnetic, and electrical properties.[4] Tetrathiafulvalene (TTF) is able to exist in three different stable redox states (TTF, $TTF^{+\bullet}$, and TTF^{2+}). For this reason TTF derivatives have found widespread use[5] in materials chemistry. Since the first TTF charge-transfer complex with metallic behavior was reported[5a] a huge number of TTF radical-cation salts have been studied resulting in the discovery of organic superconductivity in some of these systems.[5a] Although there have been some attempts to combine TTF chemistry with porphyrin chemistry, the direct combination of these two major fields has so far been unsuccessful, most likely on account of the lack of an appropriate pyrrolo-TTF unit. Some of us recently developed an efficient synthesis of the parent pyrrolo[3,4-*d*]-TTF ring system using a nonclassical and simple pyrrole synthesis.[6] With this building block at hand, we decided to prepare the first examples of single molecules in which the intriguing optical and metal-ion binding properties of the

[*] Prof. J. Becher, Dr. T. Brimert, M. Sc. J. O. Jeppesen, Dr. J. Z. Pedersen, Prof. R. Zubarev
Department of Chemistry
Odense University (University of Southern Denmark)
Campusvej 55, 5230, Odense M (Denmark)
Fax: (+45) 66-15-87-80
E-mail: jbe@chem.sdu.dk

Prof. T. Bjørnholm, N. Reitzel
Nano-Science Center, Department of Chemistry
University of Copenhagen
Universitetsparken 5, 2100, Copenhagen Ø (Denmark)

Dr. T. R. Jensen, Dr. K. Kjaer
Condensed Matter Physics and Chemistry Department
Risø National Laboratory
Building 108, Post Office Box 49, 4000 Roskilde (Denmark)

Dr. E. Levillain
Ingénierie Moléculaire et Matériaux Organiques
CNRS UMR 6501, Université d'Angers, 49045 Angers (France)

[**] We gratefully acknowledge financial support from Carlsbergfondet and Bengt Lundquists Minnesfond for a post-doctoral position to T. B., the University of Odense for a Ph.D. scholarship to J. O. J. and the French Embassy Copenhagen for a travel grant to J. B. We thank HASYLAB at DESY, Hamburg for beam time at beam line BW1 and DANSYNC for financial support. The gift of Jan Skov Peterson's FORTRAN program LSQREFL is gratefully acknowledged. Finally, we thank Prof. K. S. Murray, University of Monash, Australia for helpful discussions.

Supporting information for this article is available on the WWW under http://www.angewandte.com or from the author.

porphyrin molecule have been coupled with the favorable redox properties of the TTF moiety. The direct annelation of the porphyrin core with four TTF units situated at the periphery gives a porphyrin in which the annulene π-electron system is extended by direct conjugation with TTF units.

Here, we report 1) two synthetic routes to the first tetrathiafulvaleno-annelated fully conjugated porphyrins **5a**, **b**, 2) preliminary physical characterization of these novel porphyrin systems, and 3) structural studies of the porphyrin **5a** obtained from Langmuir films.

Our approach to the porphyrins **5a**, **b** is outlined in Scheme 1 (**5a** and **5b** refer to the mixtures **5ai** and **5aii**, and **5bi** and **5bii**, respectively). Vilsmeier formylation of the pyrrolo-TTF[6b] **1** under standard conditions produced the formylpyrrolo-TTF **2** in 96% yield. Reduction of the formyl group proceeded quantitatively to give the alcohol **3**. Treatment of **3** with *p*-toluenesulfonic acid (TsOH) in EtOH (RT, 1 min) gave a dark green precipitat of **4a** in quantitative yield (Scheme 1, Route A). The plasma desorption mass spectrum (PD-MS) of this compound[7] featured a peak at $m/z = 1837.5$, which corresponds with the porphyrinogen **4a** ($M^{+\cdot} = 1839.2$). Furthermore, small peaks at $m/z = 2299.3$ and 2757.0 were observed indicating the formation of cyclic pentapyrrole ($M^{+\cdot} = 2299.0$) and cyclic hexapyrrole ($M^{+\cdot} = 2758.8$), respectively.[8] When the cyclization was carried out in benzene, precipitation of **4a** was avoided, and subsequent oxidation with 2,3-dichloro-5,6-dicyano-1,4-benzoquinone (DDQ) was performed in a one-pot reaction to afford **5a** in 89% yield (oxidation occurred spontaneously when a solution of **4a** was left standing a few days under ambient conditions). This resulted in a pitch black solid, purified by chromatography. The PD-MS of this product (Figure 1) featured a peak at

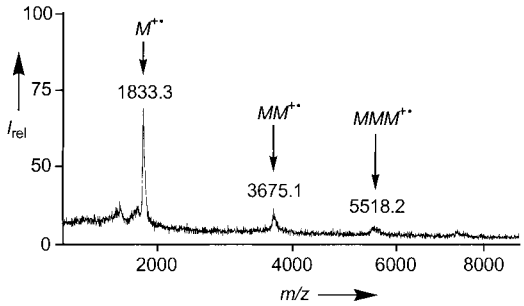

Figure 1. PD-MS spectrum of the porphyrin **5a**.

$m/z = 1833.3$, corresponding to the porphyrin **5a** ($M^{+\cdot} = 1833.1$). Stirring the pyrrolo-TTF **1** with paraformaldehyde ($(HCHO)_n$) or benzaldehyde and a catalytic amount of TsOH in THF at room temperature, produced the porphyrinogens **4a**, **b** (Scheme 1, Route B) in excellent yields (70–80%). These intermediates could be either isolated and purified by chromatography, or directly oxidized with DDQ in THF yielding **5a**, **b**, respectively.[9]

High resolution matrix-assisted laser-desorption/ionization mass spectra (MALDI-MS) of **4b**, **5a**, and **5b** showed the exact masses, $m/z = 2140.239$, 1830.076, and 2134.203, respec-

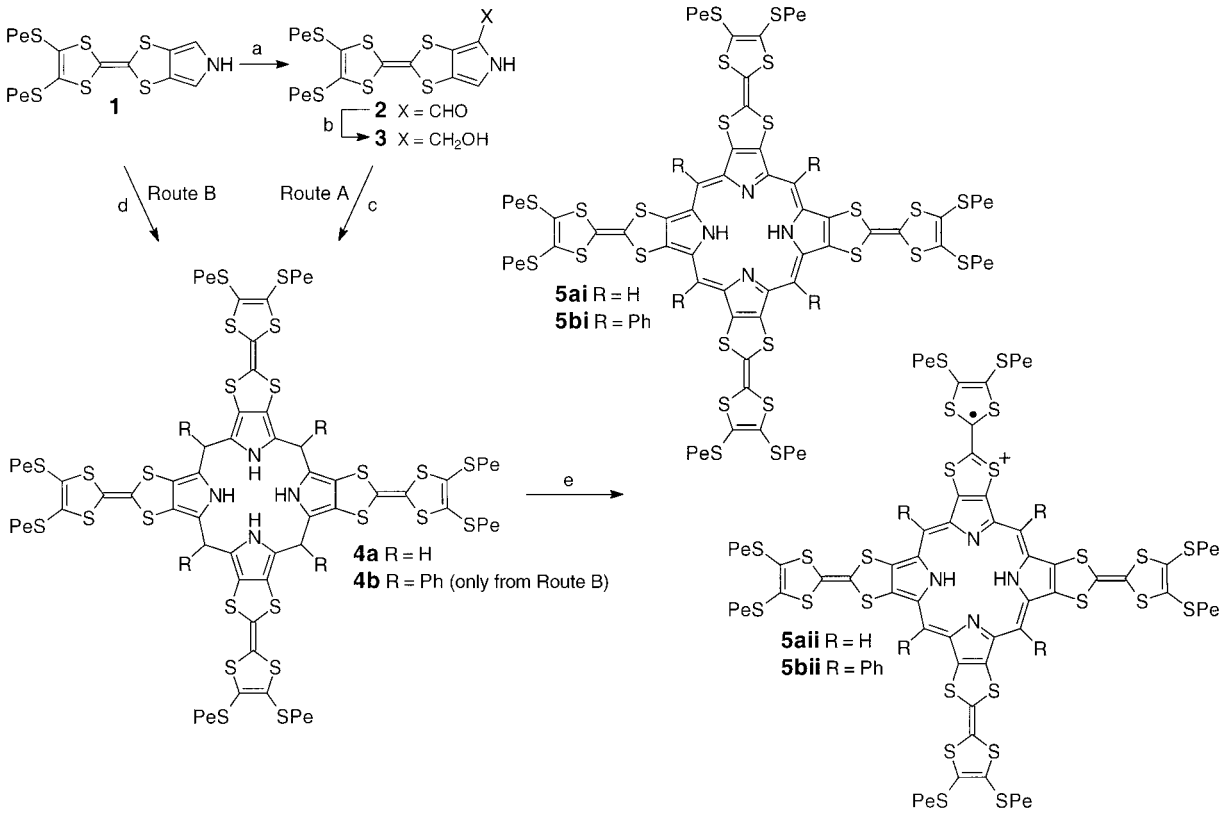

Scheme 1. Synthesis of the porphyrins **5a**, **b**: a) $DMF/POCl_3$, 96%; b) $NaBH_4$/THF, RT, quantitative; c) TsOH(cat.)/EtOH or $C_6H_6 \rightarrow$ **4a**; d) $(HCHO)_n$ or PhCHO/TsOH(cat.)/THF, RT, 18 h; e) DDQ/C_6H_6 or THF $\rightarrow$ **5a** 89% from **3**, Route A (one-pot), **5a** 48% from **1**, Route B (one-pot), **5b** 55% from **1**, Route B (one-pot). Pe = *n*-C_5H_{11}.

  1433-7851/01/4013-2498 $ 17.50+.50/0

tively, corresponding to $C_{100}H_{116}N_4S_{24}^{+\bullet}$, $C_{76}H_{94}N_4S_{24}^{+\bullet}$, and $C_{100}H_{110}N_4S_{24}^{+\bullet}$ (calcd masses $M^{+\bullet} = 2140.2492$, 1830.0770, and 2134.2022). Electron paramagnetic resonance (EPR) spectroscopy revealed strong signals, arising from radicals, as broad singlets without any detectable hyperfine structure at $g =$ 2.0084 and 2.0044 for **5a** and **5b**, respectively, either used neat or in CH_2Cl_2 solution. The linewidths and *g*-values are consistent with the presence of a TTF radical cation.[10] Quantitative EPR measurements in CH_2Cl_2 showed that the isolated product **5a** contained 19% unpaired spin,[11] indicating that compound **5a** consist of a mixture of the neutral porphyrin (**5ai**) and the radical cation porphyrin (**5aii**) in a ratio of approximately 4:1 (Scheme 1). Solution oxidation potentials (vs Ag/AgCl) obtained from cyclic voltammograms (CVs) of compound **1** recorded in CH_2Cl_2 revealed two pairs of reversible redox waves at $E^1_{1/2} = 0.48$ V and $E^2_{1/2} = 0.93$ V. The porphyrinogen **4b** gave a CV that is fully analogous with that of a nonconjugated tetra-TTF,[12] showing two pairs of reversible oxidation waves at $E^1_{1/2} = 0.49$ V and $E^2_{1/2} = 0.87$ V, whereas the porphyrins **5a** and **5b** showed CVs with reversible waves $E^1_{1/2} = 0.63$ V, $E^2_{1/2} = 1.10$ V and $E^1_{1/2} =$ 0.58 V, $E^2_{1/2} = 0.96$ V for **5a** and **5b**, respectively.[13] Thin layer cyclic voltammetry[14] (TLCV) and the deconvoluted voltammograms of both **5a** (Figure 2) and **5b** revealed that the first oxidation waves actually correspond to two one-

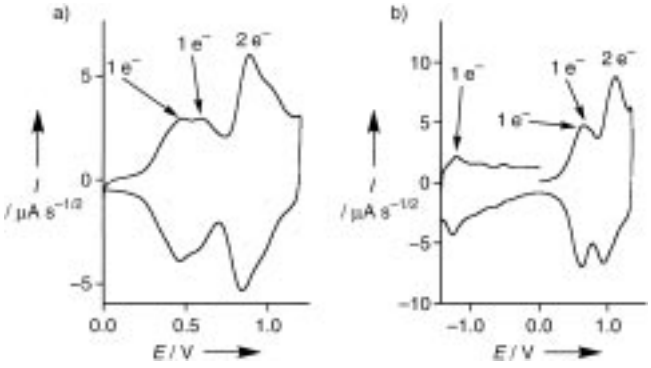

Figure 2. Deconvoluted voltammograms (vs Ag/AgCl) of a solution of **5a** (1.00 mM) in CH_2Cl_2/nBu$_4$NPF$_6$ (0.4 M) on platinum electrode; a) scan rate 0.1 V s^{-1}, b) scan rate = 0.2 V s^{-1}.[14]

electron processes with $\Delta E < 100$ mV, whereas the second wave involves a one-step two-electron process. Thus, first a radical cation is formed, which is then closely followed by the formation of a dication (probably as a biradical). Finally, a tetracation is formed. These results suggest the presence of an isolated electron-withdrawing 18 π-electron porphyrin ring system in which the pyrrolo *c*-bonds in two of the TTF units are included in the 18 π-electron ring system. Therefore, those two TTF units do not show the electrochemical characteristics of a normal TTF unit and hence only a total of four electrons are removed during oxidation of the neutral porphyrin. Furthermore, the deconvoluted voltammograms of compound **5a** (Figure 2b) and **5b** showed one reversible wave at $E_{1/2} =$ -1.3 V (1 electron), which could be assigned to the first reduction of the porphyrin ring system. The ^{1}H NMR spectra (250 MHz) of compound **5a** and **5b** recorded in $CDCl_3$ at 298 K featured only very broad peaks, which could be explained by the presence of radicals or slow tumbling resulting from aggregation in solution. Evidence for aggregation is observed in the PD-MS (Figure 1) of **5a**, which revealed small peaks at $m/z = 3675.1$ and 5518.2. These peaks can not be explained by the presence of cyclic polypyrroles of higher order. Instead, we suggest that the porphyrins aggregate together in the gas phase forming dimers ($MM^{+\bullet} =$ 3666.1) and trimers ($MMM^{+\bullet} = 5499.2$).

Information about the packing of the porphyrin **5a** at an air–water interface comes from X-ray diffraction studies of Langmuir films. Compound **5a** spreads readily from $CHCl_3$ solutions on water resulting in formation of a well-defined thin film. Compression on a Langmuir trough reveals a compression isotherm[7] with a onset in the pressure rise at a mean molecular area, mma = 50 Å^2 and a collapse at 35 Å^2 corresponding to a lateral pressure, $\pi = 40$ mN m^{-1}. X-ray diffraction[7] studies using synchrotron X-rays[15] on a Langmuir film compressed to a nominal mean molecular area of 48 Å^2 ($\pi = 5$ mN m^{-1}) reveal a broad Bragg peak (possibly split) corresponding to a repeat distance of 23–27 Å and coherence length of $\xi = 50$–60 Å indicating weak lateral order in the thin film. Model independent fits[16] to the X-ray reflectivity measured on the same film reveal an electron-density profile along the surface normal ($\rho(z)$) corresponding to a 60 Å thick film with a mean electron density relative to water $\rho/\rho_{water} = 1.18$. The rms (root mean square) film rough-

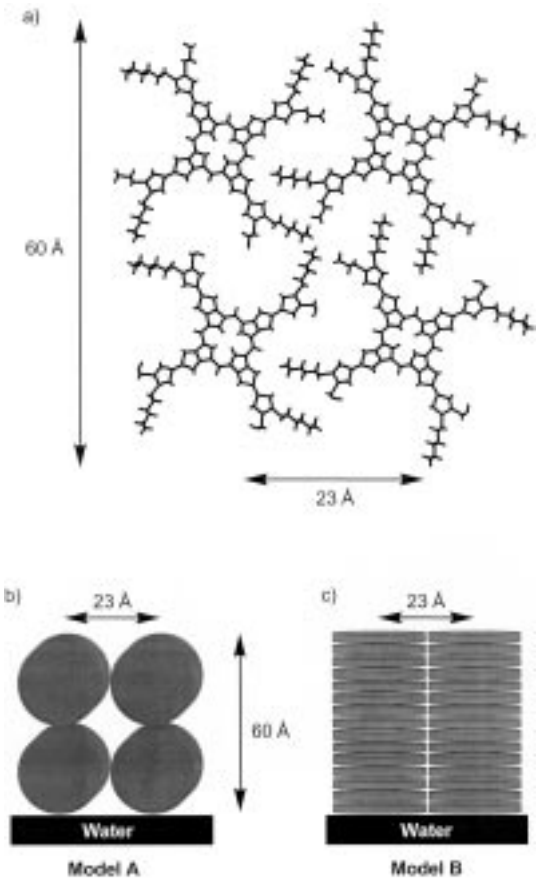

Figure 3. Proposed structure of the porphyrin **5a** deduced from X-ray diffraction studies using synchrotron X-rays on a Langmuir film of **5a**. Details are given in the text.

  1433-7851/01/4013-2499 $ 17.50+.50/0

ness $\sigma = 7$ Å towards the film – air interface. Measurements by atomic force microscopy[7] (AFM) on films transferred to mica by horizontal dipping show smooth films with occasional 50 Å deep defects. Based on this limited structural data we propose the structural model depicted in Figure 3a in which the four peripheral thioalkyl substituted TTF moieties interdigitate to fill space. The in-plane repeat distance of 23 – 27 Å agrees well to the resulting edge-to-edge close-packed arrangement (Figure 3a). Two orientations of stacks of these molecules are in accordance with the data. In one model (Model A, Figure 3b) stacks run along the water surface in two layers, in the other (Model B, Figure 3c) stacks of approximately 15 molecules run along the surface normal. The measured thickness of 60 Å corresponds roughly to the thickness of model A. Indirect information about the repeat distance along the normal to the porphyrin plane ($d_{\pi\text{-stack}}$) may be deduced by assuming a rectangular unit cell and by using the measured electron density of the film $\rho/\rho_{water} = 1.18$[17] or the area per molecule (Model A). In both cases we obtain $d_{\pi\text{-stack}} = 3.5 - 4.2$ Å, which agrees with the typical stacking distances between π-stacked TTF molecules. Diffraction studies of bulk samples could not reveal any long-range order and attempts to grow single crystals of the compounds presented here have so far failed.

Further work is aimed at complete physical characterization and understanding of these novel porphyrin ring systems, together with further functionalization and generation of mono, bis-, and tris-(tetrathiafulvaleno)-annelated porphyrins and their metal complexes.

Experimental Section

2: $POCl_3$ (0.23 g, 1.50 mmol) was added to anhydrous DMF under an atmosphere of nitrogen and stirred at room temperature for 10 min. A solution of the pyrrolo-TTF[6b] **1** (0.45 g, 1.01 mmol), dissolved in anhydrous DMF (5 mL) was added dropwise and the mixture became dark violet. The mixture was stirred for another 20 min, whereupon an aqueous solution of NaOAc (10%, 20 mL; Ac = acetyl) and H_2O (20 mL) were added. The resulting slurry was stirred for 10 min and the solid collected, redissolved in Me_2CO (100 mL) and concentrated under vacuum. The crude product was dissolved in CH_2Cl_2 (50 mL) and dried ($MgSO_4$). The solvent was removed under reduced pressure and the resulting yellow powder was subjected to column chromatography (SiO_2, EtOAc). The yellow band ($R_f = 0.5$) was collected and the solvent evaporated affording the aldehyde **2** (0.46 g, 96%) as yellow needles: M.p. 139.5 – 140.5 °C; ^{1}H NMR (CD_3SOCD_3, 250 MHz, 298 K): $\delta = 0.84$ (t, $J = 7.1$ Hz, 6H), 1.20 – 1.40 (m, 8H), 1.55 (m, 4H), 2.84 (t, $J = 7.0$ Hz, 4H), 7.25 (s, 1H), 9.51 (s, 1H), 12.44 (br s, 1H); ^{13}C NMR (CD_3SOCD_3): $\delta = 13.8$, 21.6, 28.9, 29.9, 35.4, 109.4, 118.7, 120.1, 120.8, 125.0, 126.7, 126.9, 177.6; MS (EI): m/z (%) = 475 $[M]^+$ (100); IR (KBr): $\tilde{\nu} = 1645$ cm^{-1} (C=O); elemental analysis calcd (%) for $C_{19}H_{25}NOS_6$ (475.77): C 47.97, H 5.30, N 2.94, S 40.43; found C 48.08, H 5.35, N 3.03, S 40.28.

5a (Route A, one-pot reaction): $TsOH \cdot H_2O$ (20 mg, 0.11 mmol) was added to a solution of the hydroxymethylpyrrolo-TTF **3** (0.54 g, 1.13 mmol) in C_6H_6 (20 mL). The reaction mixture was stirred at room temperature and monitored by thin layer chromatography (TLC). After approximately 3 min, all of the starting material **3** had been consumed and DDQ (0.19 g, 0.84 mmol) was added in one portion. The reaction mixture was stirred for another 30 min and the solvent removed under vacuum to afford a pitch-black residue. The crude product was purified by column chromatography (SiO_2, gradient of CH_2Cl_2/MeOH 1:0 → 19:1) affording the porphyrin **5a** (0.46 g, 89%) as a black powder: M.p. no visible melting 25 – 250 °C; ^{1}H NMR ($CDCl_3$, 250 MHz, 298 K): $\delta = 0.91$ (br s, 24H), 1.37 (br s, 32H), 1.64 (br s, 16H), 2.84 (br s, 16H); MS(PD): $m/z = 1833.3$ $[M]^+$ 3675.1 $[MM]^+$, 5518.2 $[MMM]^+$; HiResMALDI-MS: $m/z = 1830.0764$ (calcd for $C_{76}H_{94}N_4S_{24}^{+\bullet} = 1830.0770$); UV/Vis ($CH_2Cl_2$): λ_{max} (ε [M^{-1}cm^{-1}]) 297 (43000), 393 nm (33000); elemental analysis calcd (%) for $C_{76}H_{94}N_4S_{24}$ (1833.05): C 49.80, H 5.17, N 3.06; found C 50.12, H 5.43, N 3.23.

Received: January 17, 2001 [Z16440]

[1] J. N. H. Reek, A. E. Rowan, R. de Gelder, P. T. Beurskens, M. J. Crossley, S. De Feuter, F. de Scryver, R. J. M. Nolte, *Angew. Chem.* **1997**, *109*, 396 – 399; *Angew. Chem. Int. Ed. Engl.* **1997**, *36*, 361 – 363.

[2] a) K. M. Smith, *Porphyrins and Metalloporphyrins*, Elsevier, Amsterdam, **1975**; b) D. Dolphin, *The Porphyrins*, *Vol. 8*, Academic Press, New York, **1978**; c) *The Porphyrin Handbook*, *Vol. 1* (Eds.: K. M. Kadish, K. M. Smith, R. Guilard), Academic Press, San Diego, **2000**.

[3] a) M. C. Petty, *Langmuir-Blodgett Films. An Introduction*, Cambridge University Press, Cambridge, **1996**, pp. 1 – 234; b) T. Bjørnholm, T. Hassenkam, N. Reitzel, *J. Mater. Chem.* **1999**, *9*, 1975 – 1990.

[4] a) H. Chou, C.-T. Chen, K. F. Stork, P. W. Bohn, K. S. Suslick, *J. Phys. Chem.* **1994**, *98*, 383 – 385; b) E. Dalcanale in *Comprehensive Supramolecular Chemistry*, *Vol. 10* (Eds.: J. L. Atwood, J. E. D. Davies, D. D. MacNicol, F. Vögtle, D. Reinhoudt), Pergamon, Oxford, **1996**, chap. 20; c) J. B. Peng, G. A. Lawrie, G. T. Barnes, I. R. Gentle, G. J. Foran, M. J. Crossley, Z. Huang, *Langmuir* **2000**, *16*, 7051 – 7055.

[5] For TTF reviews, see a) *Organic Superconductors including Fullerenes* (Eds.: J. M. Williams, J. R. Ferraro, R. J. Thorn, K. D. Carlson, U. Geise, H. H. Wang, A. M. Kini, M.-H. Wangbo), Prentice-Hall, Engelwood Cliffs, **1992**, pp. 1 – 210; b) G. Schukat, E. Fanghänel, *Sulfur Rep.* **1996**, *18*, 1 – 294; c) M. R. Bryce, *J. Mater. Chem.* **2000**, *10*, 589 – 598; d) M. B. Nielsen, C. Lomholt, J. Becher, *Chem. Soc. Rev.* **2000**, *29*, 153 – 164.

[6] a) J. O. Jeppesen, K. Takimiya, F. Jensen, J. Becher, *Org. Lett.* **1999**, *1*, 1291 – 1294; b) J. O. Jeppesen, K. Takimiya, F. Jensen, T. Brimert, K. Nielsen, N. Thorup, J. Becher, *J. Org. Chem.* **2000**, *65*, 5794 – 5805.

[7] A PD-MS spectrum of compound **4a** and a Langmuir – Blodgett compression isotherm of the porphyrin **5a**, together with a description of the AFM and XRD measurements on **5a** are available in the Supporting Information.

[8] The formation of cyclic polypyrroles (pentamer, hexamer etc.) from condensation of pyrroles have been reported, see: J.-I. Setsune, Y. Katakami, N. Iizuna, *J. Am. Chem. Soc.* **1999**, *121*, 8957 – 8958, and refs. therein.

[9] If the pentyl groups are interchanged with methyl groups the porphyrins are virtually insoluble.

[10] F. Wudl, G. M. Smith, E. J. Hufnagel, *J. Chem. Soc. Chem. Commun.* **1970**, 1453 – 1454.

[11] The radical content was determined at room temperature through double integration of the EPR signal and comparison with aknown standard, the stable radical 2,2,6,6-tetramethyl-1-piperidine-*N*-oxyl measured under identical experimental conditions. All attempts to obtain the neutral porphyrin **5ai** exclusively by chemical reduction of the paramagnetic mixture of the neutral porphyrin **5ai** and the radical cation porphyrin **5aii**, was unsuccessful.

[12] J. Lau, J. Becher, *Synthesis* **1997**, 1015 – 1020.

[13] CV was performed using 0.89, 0.84, 1.10, and 0.75 mM solutions of **1**, **4b**, **5a**, and **5b**, respectively, in anhydrous CH_2Cl_2 with nBu$_4$NPF$_6$ (0.10 M) as supporting electrolyte and Ag/AgCl as reference electrode at a scan rate of 0.1 V s^{-1}.

[14] TLCV of **5a** (0.93 mM) + dichloronaphthoquinone (1.88 mM) + nBu$_4$NPF$_6$ (0.45 M) in deoxygenated CH_2Cl_2, platinum electrode = 0.0314 cm^2, scan rate = 5 mV s^{-1}, layer = close to 20 μm.

[15] J. Als-Nielsen, D. Jacquemain, K. Kjaer, F. Leveiller, M. Lahav, L. Leiserowitz, *Phys. Rep.* **1994**, *246*, 251 – 313.

[16] J. S. Pedersen, I. W. Hamley, *J. Appl. Crystallogr.* **1994**, *27*, 36 – 49.

[17] This value corresponds to a mass density $\rho = 1.2$ g cm$^{-3} = M_W V^{-1} N_A^{-1}$ (M_W = molecular weight, V = unit cell volume, N_A = Avogadros constant).

Bis(germavinylidene) [(Me$_3$SiN=PPh$_2$)$_2$C=Ge→Ge=C-(Ph$_2$P=NSiMe$_3$)] and 1,3-Dimetallacyclobutanes [M{μ^2-C(Ph$_2$P=NSiMe$_3$)$_2$}]$_2$ (M = Sn, Pb)**

Wing-Por Leung,* Zhong-Xia Wang, Hung-Wing Li, and Thomas C. W. Mak

Compounds containing a double bond between a Group 14 element and carbon (>M=C<; M = Si, Ge, Sn) have attracted much attention in the past 15 years, and have been the focus of several reviews.[1] By contrast, the low-valent, analogous metallavinylidenes (:M=C<) are scarce. Nevertheless, spectroscopic and theoretical studies of the transient silavinylidene [:Si=CH$_2$] and germavinylidene [:Ge=CH$_2$] have been carried out.[2–5] The low stability of these metallavinylidenes could be due to the reduced steric crowding at the low-coordinate metal center, which more readily leads to oligomerization. We report here the synthesis and structures of the first example of a stable bis(germavinylidene) as well as two novel, low-valent 1,3-dimetallacyclobutanes; the latter are believed to form by dimerization of the intermediate metallavinylidenes

The monolithium salt [CH(Ph$_2$P=NSiMe$_3$)$_2$Li(thf)] (**1**) was used as the ligand transfer reagent. It was prepared by the metalation reaction of bis(iminophosphorano)methane, CH$_2$(Ph$_2$P=NSiMe$_3$)$_2$, with *n*BuLi in THF. This lithium salt had been reported by Stephan and Ong,[6] but its structure was not well-established as X-ray quality crystals were not obtained. We have now determined the X-ray structure of **1**. The NMR spectral data of **1** are slightly different from that of the unsolvated compound reported previously.[6]

The reaction of GeCl$_2$·dioxane with two equivalents of **1** afforded bis(germavinylidene) **2** (Scheme 1). Unexpectedly **2**

[(Me$_3$SiN=PPh$_2$)$_2$C=Ge→Ge=C(Ph$_2$P=NSiMe$_3$)$_2$] **2**

was formed upon further deprotonation of **1**. Compound **1** acts both as a ligand transfer reagent and as a base for dehydrochlorination. The by-product in the reaction is presumably the neutral bis(iminophosphorano)methane. The analogous reaction of **1** with PbCl$_2$ afforded the 1,3-plumbacyclobutane [Pb{μ^2-C(Ph$_2$P=NSiMe$_3$)$_2$}]$_2$ (**3**). Metal compounds derived from monolithium salts by double deprotonation of the ligands have been reported. For example, [Pd(μ-Cl)$_2$Pt{C(PPh$_2$)$_2$}$_n$],[7] [Pt$_2${C(PH$_2$P=S)$_2$}-(MeOcod)$_2$] (MeOcod = 8-methoxycyclooct-4-ene-1-yl),[8]

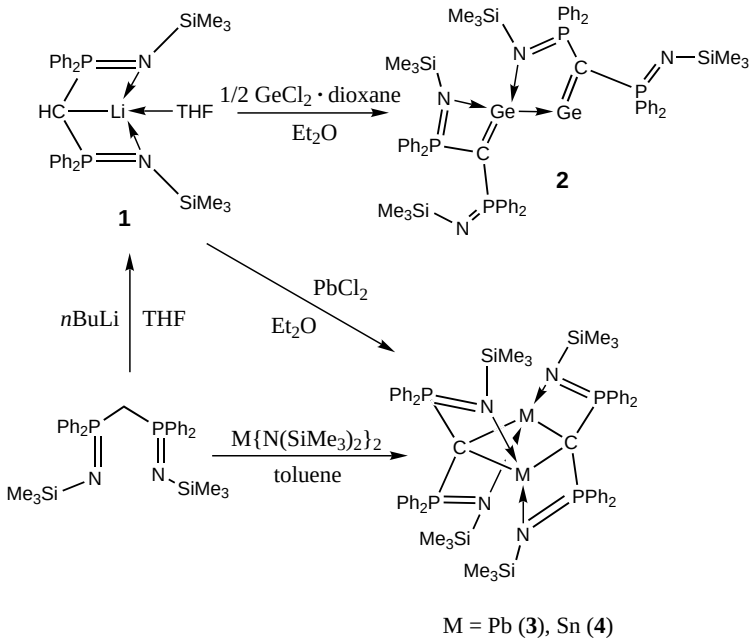

Scheme 1.

and [(AlMe$_2$)$_2${μ^2-C(Ph$_2$P=NSiMe$_3$)$_2$-κ^4C,C′N,N′}][9] result from double deprotonation of the P–CH$_2$–P backbone.

The dimetallacyclobutanes [M{μ^2-C(Ph$_2$P=NSiMe$_3$)$_2$}]$_2$ (M = Pb (**3**), Sn (**4**)) can also be prepared from the reaction of M{N(SiMe$_3$)$_2$}$_2$ with CH$_2$(Ph$_2$P=NSiMe$_3$)$_2$. Similar reactions have been reported by Cavell and co-workers in the synthesis of hafnium and samarium complexes containing M=C bonds.[10, 11] It is suggested that **3** and **4** result from the head-to-tail cyclodimerization of metallavinylidene intermediates [:M=C(Ph$_2$P=NSiMe$_3$)$_2$] (M = Pb, Sn).

Compounds **1**–**4** have been characterized by elemental analysis, NMR spectroscopy, and X-ray crystallography. The X-ray structure data for **1** and **4** will be reported elsewhere.

The molecular structure of **2** is shown in Figure 1.[12] It comprises two germavinylidenes [:Ge=C(Ph$_2$P=NSiMe$_3$)$_2$] bonded together in a head-to-head manner. The molecule is asymmetrical with two different germanium environments: Ge(1) is bonded to the methanediide carbon atom C(1′) and Ge(2), and subtended at an angle of 89.3(3)°. The four-coordinate Ge(2) is bonded to Ge(1), C(2′), and two imino nitrogen atoms from the germavinylidenes. Each germavinylidene has an additional uncoordinated imino group. The Ge–Ge bond distance of 2.483(1) Å is longer than those reported for compounds containing a Ge–Ge double bond (2.213–2.347 Å).[13] Therefore, the Ge–Ge bonding in **2** is more appropriately described as a donor–acceptor interaction, similar to that in the tin(II)–tin(II) complexes [R$^N_2$Sn→SnCl$_2$] (R^N = CH(SiMe$_3$)C$_6$H$_6$N-8) and the asymmetric distannene **5**.[14, 15] In **2**, the four-coordinate Ge(2) behaves as the donor and the two-coordinate Ge(1) behaves as a Lewis acid center. The Ge–C bond in **2** (1.905(8) and 1.908(7) Å) are much shorter than the Ge–C single bonds in some Ge^{II}–alkyl and Ge^{II}–aryl compounds (2.012–2.135 Å).[16] The structure of **2** also shows *trans* linkage of the C=Ge–Ge=C skeleton (C(1′)-Ge(1)-Ge(2) 89.3(3)°,

[*] Prof. Dr. W.-P. Leung, Dr. Z.-X. Wang, H.-W. Li, Prof. T. C. W. Mak
Department of Chemistry
The Chinese University of Hong Kong
Shatin, New Territories, Hong Kong (China)
Fax: (+852) 26035057
E-mail: kevinleung@cuhk.edu.hk

[**] We thank the Hong Kong Research Grants Council for supporting this work.

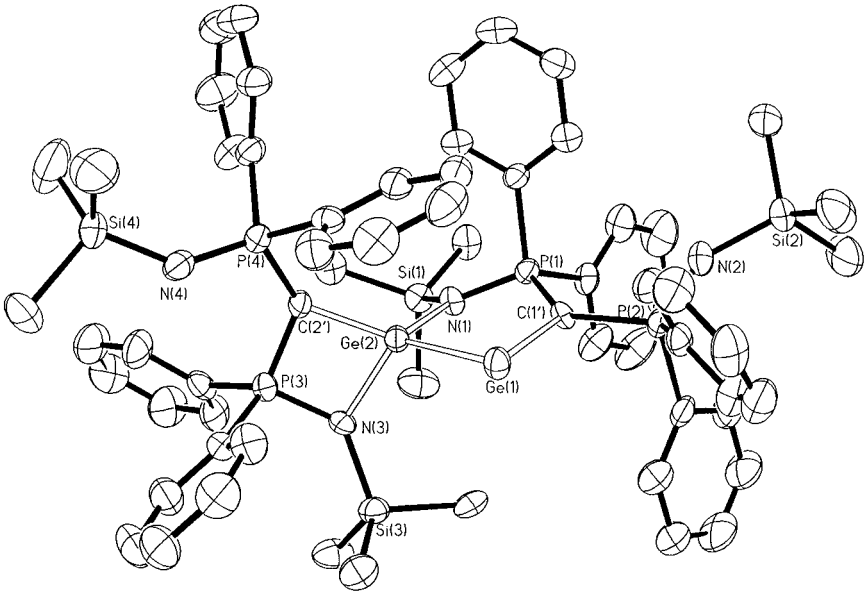

Figure 1. ORTEP drawing of **2**; hydrogen atoms are omitted for clarity. Selected bond distances [Å] and angles [°]: Ge(1)–Ge(2) 2.4827(13), Ge(1)–C(1′) 1.908(7), Ge(2)–C(2′) 1.905(8), Ge(2)–N(1) 1.971(6), Ge(2)–N(3) 1.974(6), P(1)–C(1′) 1.755(8), P(2)–C(1′) 1.754(8), P(3)–C(2′) 1.702(9), P(4)–C(2′) 1.746(8), P(1)–N(1) 1.623(7), P(2)–N(2) 1.535(8), P(3)–N(3) 1.655(7), P(4)–N(4) 1.552(8); C(1′)-Ge(1)-Ge(2) 89.3(3), C(2′)-Ge(2)-N(1) 120.1(3), C(2′)-Ge(2)-N(3) 80.4(3), N(1)-Ge(2)-N(3) 108.4(3), C(2′)-Ge(2)-Ge(1) 128.2(3), N(1)-Ge(2)-Ge(1) 100.5(2), N(3)-Ge(2)-Ge(1) 117.5(2), P(1)-C(1′)-P(2) 121.0(4), P(3)-C(2′)-P(4) 125.7(5).

C(2′)-Ge(2)-Ge(1) 128.2(3)°). The bis(germavinylidene) skeleton is twisted along the Ge–Ge axis at an angle of 43.9°.

[{1-{N(*t*Bu)C(SiMe$_3$)C(H)}-2-{N(*t*Bu)(SiMe$_3$)CC(H)}-C$_6$H$_4$}Sn → Sn{1,2-{N(*t*Bu)(SiMe$_3$)CC(H)}$_2$C$_6$H$_4$}] **5**

The ^{1}H and ^{13}C NMR spectra of **2** showed only one set of SiMe$_3$ signals, which does not correspond to the X-ray structure. This may be due to fluxional coordination of the imino nitorogen atoms at the germanium centers in solution.

The molecular structure of 1,3-dimetallacyclobutane **3** is shown in Figure 2. It consists of two metal atoms bridged by two methanediide carbon atoms, forming a 1,3-M$_2$C$_2$ four-membered ring. The two imino nitrogen atoms of the ligand coordinate to the tetrahedral metal center to form MCPN four-membered rings. These MCPN rings together with the M$_2$C$_2$ ring, as the base, form a structure framework similar to an "open box". The geometry around each of the metal centers is square pyramidal.

The average Sn–C distance of 2.376 Å in **4** is longer than that in the stannene [{(Me$_3$Si)$_2$CH}$_2$Sn=C{(B*t*Bu)$_2$C(SiMe$_3$)$_2$}] (2.025(4) Å).[16] Similarly the Pb–C bond in **3** (2.477 Å) is longer than that in the lead(II) alkyl compound [Pb{CH(SiMe$_3$)(C$_9$H$_6$N-8)}$_2$] (2.336(3) Å).[17] The metal–metal distances in dimetallacyclobutanes **3** and **4** are too long to consider the presence of bonding interactions.

Experimental Section

2: A solution of **1** (1.16 g, 1.82 mmol) in Et$_2$O (25 mL) was added to a cooled (ca. −90 °C) suspension of GeCl$_2$·dioxane (0.21 g, 0.91 mmol) in Et$_2$O with stirring. The mixture was stirred at room temperature for 18 h and then filtered. Hexane (20 mL) was added to the filtrate, and the solution concentrated to about 5 mL. After the mixture was allowed to stand for 5 d, compound **2** was obtained as red-orange crystals (0.24 g, 42%), m.p. 110–111 °C. Elemental analysis calcd (%) for C$_{62}$H$_{76}$N$_4$Ge$_2$P$_4$Si$_4$: C 59.16, H 6.09, N 4.45; found: C 58.95, H 6.30, N 4.47; ^{1}H NMR (300 MHz, C$_6$D$_6$, 25 °C, TMS): δ = 0.08 (s, 36H, SiMe$_3$), 7.00–7.08 (m, 24H, Ph), 7.73–7.80 (m, 16H, Ph); ^{13}C{^{1}H} NMR (75.47 MHz, C$_6$D$_6$, 25 °C, TMS): δ = 3.53 (SiMe$_3$), 128.10, 130.47, 131.95, 137.02 (Ph); ^{31}P{^{1}H} NMR (161.92 MHz, C$_6$D$_6$, 25 °C, 80% H$_3$PO$_4$): δ = 34.59.

3 (method 1): A mixture of CH$_2$(Ph$_2$P=NSiMe$_3$)$_2$ (1.28 g, 2.29 mmol) and Pb{N(SiMe$_3$)$_2$}$_2$ (1.23 g, 2.33 mmol) in toluene (25 mL) was stirred at room temperature for 40 h. Solvent was removed in vacuo and the residue was dissolved in Et$_2$O. After filtration, the filtrate was concentrated to about 5 mL. After the mixture was allowed to stand for 3 d, yellow crystals of **3** (1.40 g, 79.8%) were obtained, m.p. 234–237 °C. Elemental analysis calcd (%) for C$_{62}$H$_{76}$N$_4$P$_4$Pb$_2$Si$_4$: C 48.74, H 5.01, N 3.67; found: C 48.80, H 5.08, N 3.74; ^{1}H NMR (300 MHz, C$_6$D$_6$, 25 °C, TMS): δ = −0.43 (s, 36H, SiMe$_3$), 6.90–7.70 (m, 40H, Ph); ^{13}C{^{1}H} NMR (75.47 MHz, C$_6$D$_6$, 25 °C, TMS): δ = 4.18 (SiMe$_3$), 128.24, 128.50, 130.47, 131.14, 131.94, 133.15 (Ph); ^{31}P{^{1}H} NMR (161.92 MHz, C$_6$D$_6$, 25 °C, 80% H$_3$PO$_4$): δ = 5.46.

3 (method 2): A cooled solution of **1** (0.77 g, 1.21 mmol) in Et$_2$O (20 mL) was added to PbCl$_2$ (0.17 g, 0.61 mmol) with stirring. The mixture was warmed to RT and stirred for 18 h. After filtration and concentration of the filtrate, **3** obtained as yellow crystals (0.39 g, 83.6%).

4: A mixture of CH$_2$(Ph$_2$P=NSiMe$_3$)$_2$ (0.27 g, 0.49 mmol) and Sn{N(SiMe$_3$)$_2$}$_2$ (0.44 g, 1.00 mmol) in toluene (15 mL) was stirred at room temperature for 42 h. After removal of the solvent in vacuo, the residue was extracted with Et$_2$O and filtered. Hexane (20 mL) was added to the filtrate, and the solution concentrated to about 2 mL. After the mixture was allowed to stand for 3 d, yellow crystals of complex **4** (0.23 g, 70.2%) were obtained, m.p. 210–211 °C. ^{1}H NMR (300 MHz, C$_6$D$_6$, 25 °C, TMS):

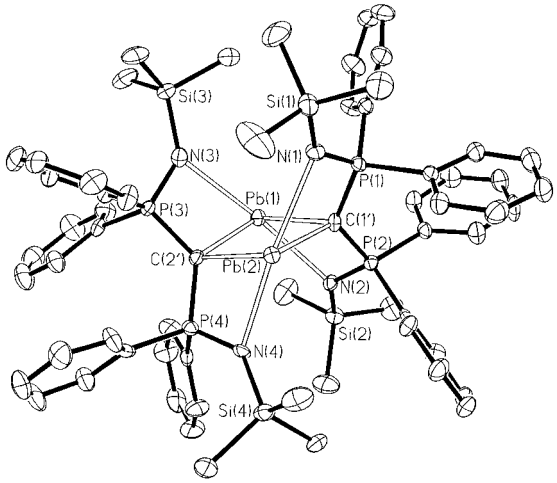

Figure 2. ORTEP drawing of **3**; hydrogen atoms are omitted for clarity. Selected bond distances [Å] and angles [°]: Pb(1)–C(2′) 2.452(7), Pb(1)–C(1′) 2.493(6), Pb(1)–N(2) 2.619(5), Pb(1)–N(3) 2.708(6), Pb(2)–C(1′) 2.451(7), Pb(2)–C(2′) 2.510(7), Pb(2)–N(4) 2.572(5), Pb(2)–N(1) 2.689(6), P(1)–N(1) 1.573(6), P(2)–N(2) 1.604(5), P(3)–N(3) 1.581(6), P(4)–N(4) 1.595(6); C(2′)-Pb(1)-C(1′) 91.6(2), C(1′)-Pb(2)-C(2′) 91.2(2), C(1′)-Pb(1)-N(2) 63.2(2), C(2′)-Pb(1)-N(2) 108.6(2), C(2′)-Pb(1)-N(3) 61.3(2), C(1′)-Pb(1)-N(3) 109.7(2), N(2)-Pb(1)-N(3) 168.45(18), C(1′)-Pb(2)-N(4) 106.2(2), C(2′)-Pb(2)-N(4) 64.21(19), C(1′)-Pb(2)-N(1) 62.4(2), C(2′)-Pb(2)-N(1) 113.1(2), N(4)-Pb(2)-N(1) 168.53(19).

  1433-7851/01/4013-2502 $ 17.50+.50/0 *Angew. Chem. Int. Ed.* **2001**, *40*, No. 13

$\delta = 0.04$ (s, 36H, $SiMe_3$), 6.92 – 7.11 (m, 24H, Ph), 7.40 – 7.74 (m, 16H, Ph); $^{13}C\{^1H\}$ NMR (75.47 MHz, C_6D_6, 25 °C, TMS): $\delta = 3.65$ ($SiMe_3$), 130.09, 132.87, 139.25, 140.44 (Ph); $^{31}P\{^1H\}$ NMR (161.92 MHz, C_6D_6, 25 °C, 80% H_3PO_4): $\delta = 12.34$.

Received: January 18, 2001
Revised: March 22, 2001 [Z16444]

[1] a) J. Escudie, H. Ranaivonjatovo, *Adv. Organomet. Chem.* **1999**, *44*, 113; b) M. Driess, H. Grützmacher, *Angew. Chem.* **1996**, *108*, 900; *Angew. Chem. Int. Ed. Engl.* **1996**, *35*, 828.
[2] H. Leclercq, I. Dubois, *J. Mol. Spectrosc.* **1979**, *76*, 39.
[3] M. Izuha, S. Yamamoto, D. Saito, *J. Chem. Phys.* **1996**, *105*, 4923.
[4] W. H. Harper, E. A. Ferrall, R. K. Hilliard, S. M. Stogner, R. S. Grev, D. J. Clouthier, *J. Am. Chem. Soc.* **1997**, *119*, 8361.
[5] S. M. Stogner, R. S. Grev, *J. Chem. Phy.* **1998**, *108*, 5458.
[6] C. M. Ong, D. W. Stephan, *J. Am. Chem. Soc.* **1999**, *121*, 2939.
[7] S. I. Al-Resayes, P. B. Hitchcock, J. F. Nixon, *J. Chem. Soc. Chem. Commun.* **1986**, 1710.
[8] J. Browning, K. R. Dixon, R. W. Hilts, *Organometallics* **1989**, *8*, 552.
[9] A. Kasani, R. McDonald, M. Ferguson, R. G. Cavell, *Organometallics* **1999**, *18*, 4241.
[10] R. P. Kamalesh Babu, R. McDonald, R. G. Cavell, *Chem. Commun.* **2000**, 481.
[11] A. Kasani, M. Ferguson, R. G. Cavell, *J. Am. Chem. Soc.* **2000**, *122*, 726.
[12] Crystal data for **2** ($C_{64}H_{81}Ge_2N_4O_{0.5}P_4Si_4$): $M = 1295.75$, crystal size $0.60 \times 0.45 \times 0.25$ mm, $a = 21.030(4)$, $b = 16.453(3)$, $c = 19.919(4)$ Å, $\alpha = 90$, $\beta = 91.62(3)$, $\gamma = 90°$, $V = 6890(2)$ Å^3, $\rho_{calcd} = 1.249$ g cm^{-3}, $\mu = 1.075$ mm^{-1}, $Z = 4$, monoclinic, space group $P2_1/c$, $\lambda = 0.71073$ Å, $T = 293(2)$ K, $2\theta_{max} = 48°$, 11179 measured reflections, 10823 independent and 5511 observed reflections ($I > 2\sigma(I)$), 697 refined parameters, $R1 = 0.0725$, $wR2 = 0.1843$, largest diff. peak and hole 0.3833 and -0.696 e Å^{-3}. Crystal data for **3** ($C_{62}H_{76}N_4P_4Pb_2Si_4$): $M = 152.89$, crystal size $0.78 \times 0.19 \times 0.17$ mm, $a = 10.4752(14)$, $b = 44.827(6)$, $c = 14.068(2)$ Å, $\alpha = 90$, $\beta = 100.796(3)$, $\gamma = 90°$, $V = 6489.0(15)$ Å^3, $\rho_{calcd} = 1.564$ g cm^{-3}, $\mu = 5.395$ mm^{-1}, $Z = 4$, monoclinic, space group $P2_1/n$, $\lambda = 0.71073$ Å, $T = 293(2)$ K, ϕ/ω scans, $2\theta_{max} = 56.22°$, 45654 measured reflections, 15684 independent and 8598 observed reflections ($I > 2\sigma(I)$), 686 refined parameters, $R1 = 0.0468$, $wR2 = 0.0804$, largest diff. peak and hole 1.356 and -1.686 e Å^{-3}. The crystal data were measured on an IP Rigaku diffractometer (for **2**) or a Brüker SMART CCD area detector (for **3**). The structures were solved by direct methods using SHELXS-97 and refined using SHELXL-97. Crystallographic data (excluding structure factors) for the structures reported in this paper have been deposited with the Cambridge Crystallographic Data Centre as supplementary publication no. CCDC-160423 and 160424. Copies of the data can be obtained free of charge on application to CCDC, 12 Union Road, Cambridge CB2 1EZ, UK (fax: (+44) 1223-336-033; e-mail: deposit@ccdc.cam.ac.uk).
[13] K. M. Baines, W. G. Stibbs, *Adv. Organomet. Chem.* **1996**, *39*, 275.
[14] W.-P. Leung, W.-H. Kwok, F. Xue, T. C. W. Mak, *J. Am. Chem. Soc.* **1997**, *119*, 1145.
[15] W.-P. Leung, H. Cheng, R.-B. Huang, Q.-C. Yang, T. C. W. Mak, *Chem. Commun.* **2000**, 451.
[16] H. J. Meyer, G. Baum, W. Massa, S. Berger, A. Berndt, *Angew. Chem.* **1987**, *99*, 559; *Angew. Chem. Int. Ed. Engl.* **1987**, *26*, 546.
[17] W.-P. Leung, W.-H. Kwok, L.-H. Weng, L. T. C. Law, Z.-Y. Zhou, T. C. W. Mak, *J. Chem. Soc. Dalton Trans.* **1997**, 4301.

A Synthetic Pore-Mediated Transmembrane Transport of Glutamic Acid**

Jorge Sánchez-Quesada, Hui Sun Kim, and M. Reza Ghadiri*

Synthetic constructs that are specifically designed to allow transport of hydrophilic substances across cell membranes are important research tools with possible applications in gene and antisense therapy, metabolite regulation, and drug delivery.[1] However, surprisingly the design of synthetic transmembrane pores from first principles has remained largely unexplored.[2, 3] Here we describe the design and functional characterization of a self-assembling transmembrane peptide nanotube channel that is capable of highly efficient transport of L-glutamic acid.

Appropriately designed cyclic peptides with an even number of hydrophobic α-amino acids with alternating D and L configurations have been previously shown to self-assemble through directed hydrogen-bonding networks into antiparallel β-sheet tubular structures in lipid bilayers forming active ion channels.[4] One attractive feature of the self-assembling peptide nanotube class of transmembrane supramolecular structures is that pore size can be tuned by the choice[5] and the number of α-amino acids employed in the cyclic peptide subunit design. In this context we have shown previously that cyclic octapeptides size-selectively transport small ions,[4, 6] whereas decapeptides can also transport small molecules such as glucose.[3]

The present system is based on eight- and ten-residue cyclic peptides **1**[4] and **2**,[3] respectively, which form transmembrane channels (Scheme 1). Inspection of space-filling models derived from X-ray structural analogues of peptide nanotubes suggests that a completely dehydrated glutamate ion in an extended conformation would barely fit inside a channel formed by the cyclic octapeptide **1** (7 Å van der Waals internal diameter) but could be easily accommodated in a transmembrane pore derived from cyclic decapeptide **2** (10 Å van der Waals internal diameter).[3] We therefore sought to examine the utility of self-assembling peptide nanotubes for size-selective transmembrane transport of glutamate ions.

Previous attenuated total reflection/Fourier transform infrared (ATR-FTIR) spectroscopic studies of the peptide **1** in lipid multibilayers indicated that the self-assembled transmembrane channel adopts an orientation of $7 \pm 1°$ relative to the average plane of membrane.[7] In analogous studies for decapeptide **2**, the peptide assembly in the lipid bilayer displayed backbone amide bands indicative of the expected

[*] Prof. M. R. Ghadiri, Dr. J. Sánchez-Quesada, Dr. H. Sun Kim
Departments of Chemistry and Molecular Biology, and
The Skaggs Institute for Chemical Biology
The Scripps Research Institute
10550 North Torrey Pines Road, La Jolla, CA 92037 (USA)
Fax: (+1) 858-784-2798
E-mail: ghadiri@scripps.edu

[**] This work is supported by a grant from the National Institutes of Health (Grant: GM52190).

Supporting information for this article is available on the WWW under http://www.angewandte.com or from the author.

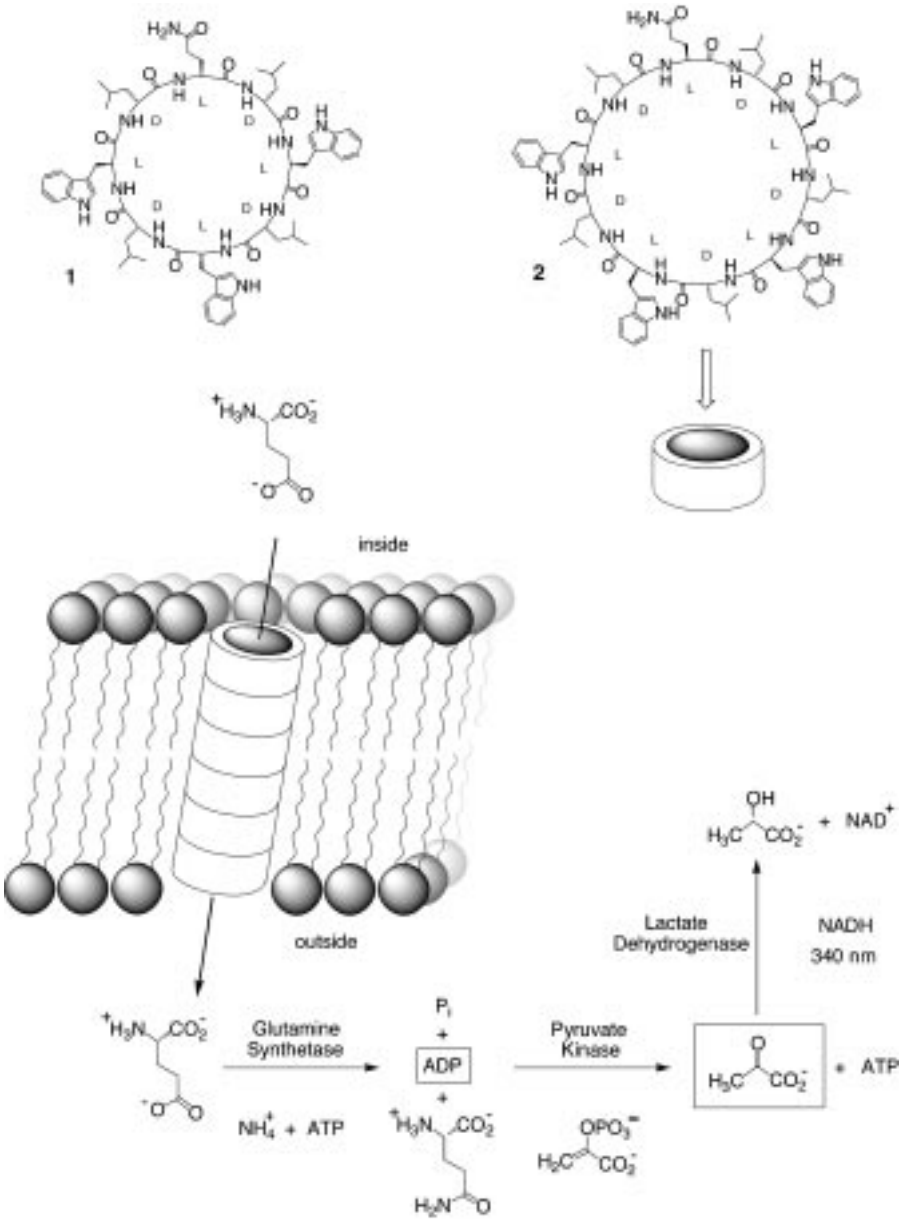

Scheme 1. Chemical structures of cyclooctapeptide **1** and cyclodecapeptide **2**, and the reaction scheme employed for the analysis of glutamic acid transport. The enzymes and cofactors reside in the extravesicular milieu, and are hydrophilic and too large to penetrate the lipid bilayer. Therefore, only the glutamic acid released upon introduction of the channel-forming peptide, can undergo the enzymatic reaction noted.

hydrogen-bonded antiparallel β-sheet tubular structure: amide I bands at 1635 (perpendicular component, strong) and 1691 cm^{-1} (parallel component, weak), an amide II band at 1539 cm^{-1}, and an amide A (N–H stretch) band at $\sim$3285 cm^{-1} (Figure 1). The longitudinal axis of the peptide channel assembly was determined to be oriented approximately perpendicular to the membrane plane, at an angle of $3 \pm 2^\circ$ from the lipid hydrocarbon chain tilt.[8] These results are consistent with the membrane-spanning orientation of the tubular assemblies required for an intrapore-mediated mode of transport.

Channel-mediated glutamic acid transport from the inside of large unilamellar vesicles to the external solvent under isotonic solution conditions was continuously monitored by an enzymatic assay operating in the extravesicular milieu (Scheme 1). This highly sensitive spectrophotometric assay couples glutamine synthetase activity with the reactions catalyzed by pyruvate kinase and lactate dehydrogenase, by monitoring NADH oxidation at 340 nm. The pyruvate kinase and lactate dehydrogenase were added in appropriate excess of the glutamine synthetase, and glutamine synthetase has a high catalytic efficiency, so the observed rate of NADH oxidation was directly proportional to the vesicular release of glutamic acid.[9]

The transport activity mediated by the ten-residue cyclic peptide ensemble **2** showed a saturation-type behavior, due to the limited peptide solubility in the lipid bilayer, and displayed an apparent rate constant of approximately 2.0 mol of glutamic acid per minute per 1.0 M cyclic peptide for vesicles containing 500 mM glutamic acid in the presence of 1.0 μM peptide **2** (Figure 2a).[10] Control fluorescence experiments using vesicle-entrapped carboxyfluorescein dye molecules indicated that the release of glutamic acid to the extravesicular milieu is not due to the rupture of the lipid vesicles. Furthermore, neither the octapeptide **1** nor gramicidin[11] (which form channels with, respectively, $\sim$7 and $\sim$2.6 Å van der Waals internal diameters) showed glutamate transport activity under similar assay conditions (Figure 2b).

We investigated the ion-channel behavior for peptides **1** and **2** by performing single-channel conductance experiments in planar lipid bilayers.[12] Conductance Λ measured at different

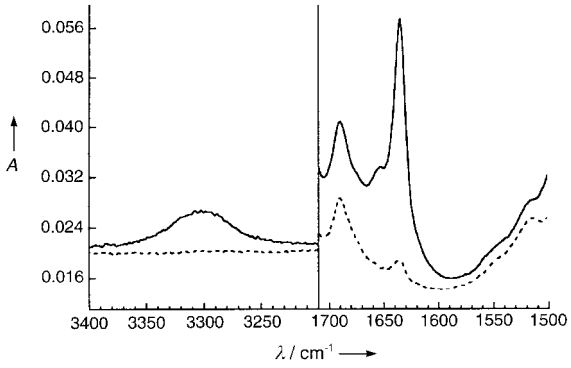

Figure 1. ATR-FTIR spectrum of the amide regions of **2** in a 1,2-myristoyl-*sn*-glycero-3-phosphatidylcholine multibilayer film. The solid and dotted lines indicate absorption of parallel and perpendicular polarized light, respectively.

  1433-7851/01/4013-2504 $ 17.50+.50/0 *Angew. Chem. Int. Ed.* **2001**, *40*, No. 13

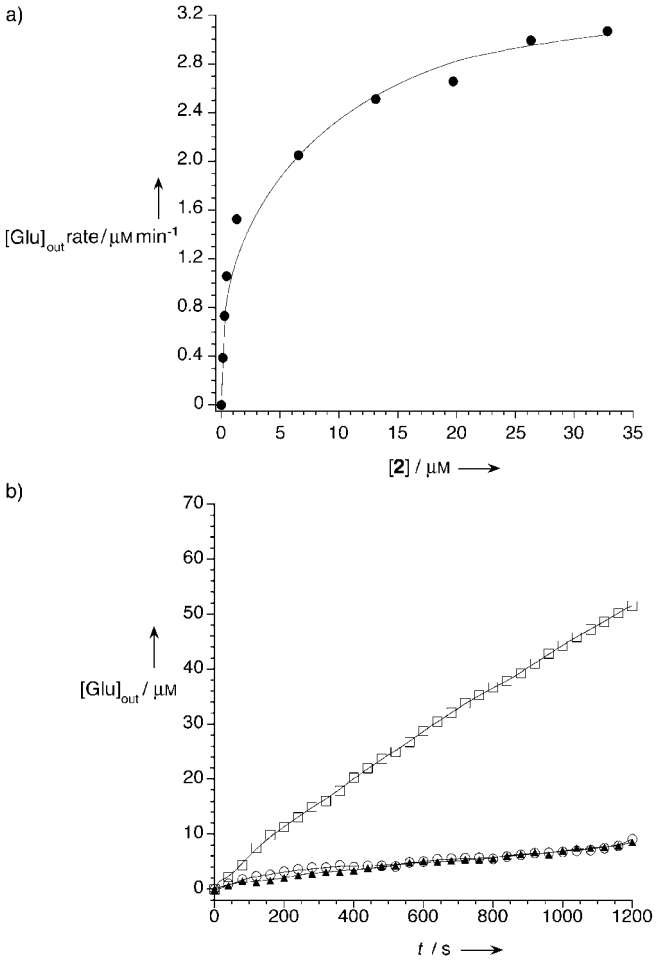

Figure 2. a) The glutamate efflux rate ($[Glu]_{out}$ rate) from vesicles is dependent on the initial concentrations of the cyclic peptide **2**; b) glutamate efflux ($[Glu]_{out}$) from vesicles over time, after the addition of 13.1 μM quantities of each the following compounds: gramicidin A (▲), octapeptide peptide **1** (○), and decapeptide **2** (□).

NaCl concentrations could be fitted to a Michaelis–Menten saturation model for both cyclopeptides ($\Lambda_{max} = 11.5 \pm 0.3$ pS, $K_M = 8.1 \pm 1.9$ mM for **1**; $\Lambda_{max} = 13.0 \pm 0.5$ pS, $K_M = 28.1 \pm 5.6$ mM for **2**; Figure 3a and b); this indicates that channel occupancy is restricted to a single ion.[13] On the other hand, whereas the open probabilities P_{open} were similar (0.25 ± 0.05 and 0.27 ± 0.04 for **1** and **2**, respectively), the mean opening times (Figure 3c and d) were longer for the octapeptide channel ($\tau = 1340 \pm 50$ ms) than for the decapeptide channel ($\tau = 168 \pm 12$ ms), as expected due to the greater conformational freedom in **2**. Reverse potential determination from experiments employing asymmetric NaCl concentrations revealed total cation selectivity for these cyclic peptide based channels, similar to that observed for gramicidin A under the same conditions (Table 1).

With these data at hand we then turned to study the behavior of these transmembrane channels when the monosodium salt of glutamic acid (NaGlu) was employed as the electrolyte. Although tabulated activity coefficients for NaGlu in bulk solutions are available,[14]

Table 1. Reversal potentials for gramicidin A (gram.), and the cyclic peptides **1** and **2** with "asymmetric" NaCl concentrations.

	c/t[a]		
	100/300	100/500	100/1000
E_r calcd [mV][b]	−24.9	−36.5	−52.8
E_r gram. [mV]	−27.9 ± 0.1	−40.4 ± 0.1	−55.4 ± 0.1
E_r **1** [mV]	−28.2 ± 0.1	−41.1 ± 0.2	−55.1 ± 0.6
E_r **2** [mV]	−26.9 ± 0.4	−40.9 ± 0.6	−54.2 ± 1.2

[a] c/t refers to the ratio of the NaCl concentrations (mM) on the cis (c) and trans (t) sides of the lipid bilayer. [b] The reverse potentials, E_r, were calculated with the GHK equation.

they are not appropriate in the present studies since the activity coefficients are expected to be altered in buffered solutions and/or by interactions of the electrolyte components with the polar lipid head groups. Therefore, we directly measured the activities of NaGlu by employing gramicidin A as a standard whose transmembrane pore diameter is known to be too small to allow glutamate transport. We measured the biionic potential for gramicidin in planar lipid bilayers separating isotonic NaCl on the cis side and NaGlu on the trans side (Figure 4, Table 2); it was then possible to calculate the activities for the NaGlu solutions with the GHK equation.[15] The biionic potential for the octapeptide **1** observed under the same conditions was comparable to that obtained with gramicidin, which indicates no glutamate

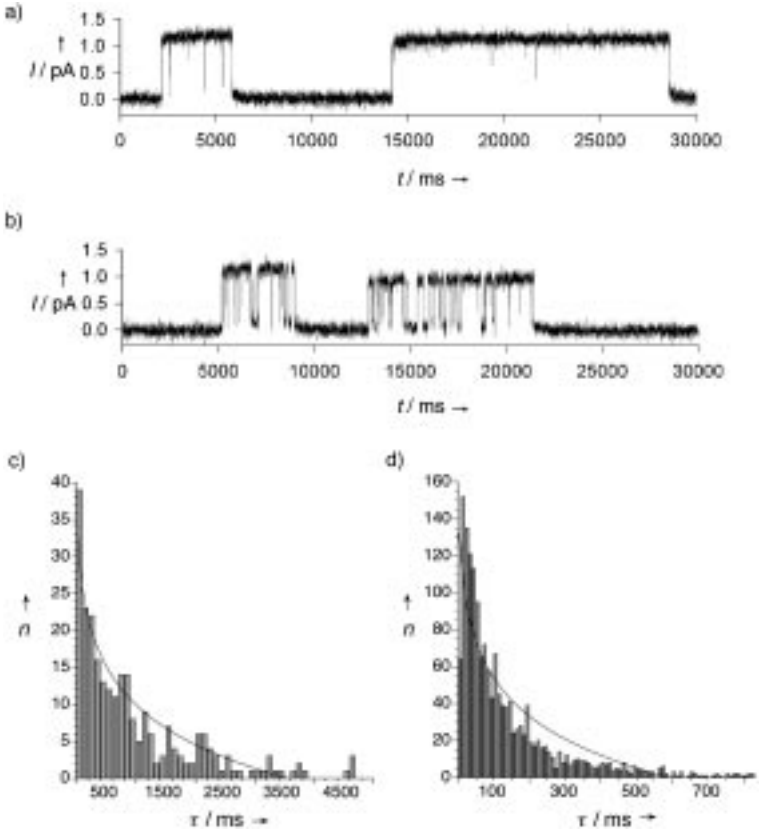

Figure 3. Traces showing 30 seconds of channel activity for a) **1** and b) **2** in 100 mM NaCl at a transmembrane holding potential of +100 mV. Signals were Bessel filtered at 5 kHz and sampled at 100 μs. Dwell time histograms for c) **1** and d) **2** obtained from traces recorded in 100 mM NaCl at a transmembrane potential of +100 mV. I = current, n = number of observations, τ = dwell time.

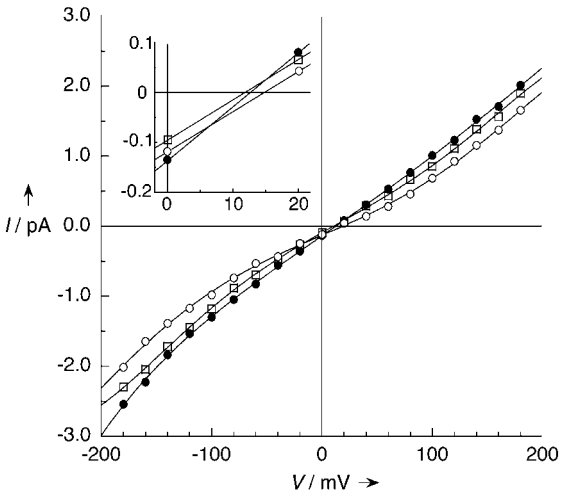

Figure 4. Current/voltage (I/V) plot for gramicidin A (●), **1** (□), and **2** (○) in lipid bilayers separating isotonic 300 mM NaCl and NaGlu on the cis and trans sides, respectively. I/V curves are averaged from 30 individual I/V experiments. The inset shows the higher reversal potential for peptide **2**.

Table 2. Reverse potentials and permeability ratios for gramicidin A (gram.), and the cyclic peptides **1** and **2** obtained for NaCl and NaGlu solutions on the cis and trans sides of the lipid bilayer, respectively.

	c/t[a]		
	100/100	300/300	1000/1000
E_r gram. [mV]	11.3 ± 0.7	12.6 ± 0.8	13.1 ± 0.7
E_r **1** [mV]	11.8 ± 0.6	11.8 ± 1.1	12.3 ± 0.9
E_r **2** [mV]	13.7 ± 0.6	14.8 ± 0.6	15.3 ± 0.5
NaGlu activity[b]	0.049 ± 0.001	0.128 ± 0.004	0.201 ± 0.006
P_{Na^+}/P_{Glu^-}[c] **2**	6.3 ± 0.7	6.5 ± 1.1	6.3 ± 0.9

[a] c/t refers to the ratio of the NaCl and NaGlu concentrations (mM) on the cis (c) and trans (t) sides of the lipid bilayer, respectively. [b] Activities for sodium glutamate (NaGlu) were calculated from the measured biionic potential with gramicidin A and the GHK equation. [c] Permeability ratios for sodium and glutamate ions with decapeptide **2** were calculated with the GHK equation. Activities for sodium glutamate solutions were taken from the experiments where gramicidin A was used as a standard.

transport with pores formed by **1** (Figure 4, Table 2). However, with **2** a higher potential needs to be applied to counteract the chemical gradient (Figure 4, Table 2) and this indicates a substantial transport of the aminoacid ($P_{Na}/P_{Glu} = 6.4 \pm 0.9$). Considering that P_{open} is about 0.27 and assuming an average of six cyclic peptides per assembly (28 Å length, enough to span a lipid bilayer), in bilayers separating 0.5 M NaGlu and NaCl at 0 V ($I = 0.19$ pA), the rate of transport can be evaluated as 2.7×10^4 mol of glutamate per second per 1.0 M cyclic peptide.

In conclusion, we have described the first example of highly efficient aminoacid transport by a de novo designed channel system. This study indicates potential utility for this class of biomaterials in biosensor applications as well as in biological settings such as size-selective molecular delivery vehicles.

Received: February 1, 2001 [Z16543]

[1] For recent reviews on colloid-based drug delivery agents, see: a) N. V. Majeti, M. N. V. Ravi Kumar, *J. Pharm. Sci.* **2000**, *3*, 234–258; b) G. M. Barat, *Pharm. Sci. Technol. Today* **2000**, *3*, 163–171. For dendrimers, see: c) H. Yoo, P. Sazani, R. L. Juliano, *Pharm. Res.* **1999**, *16*, 1799–1804; d) M. Liu, K. Kono, J. M. J. Frechet, *J. Controlled Release* **2000**, *65*, 121–131; e) L. G. Schultz, S. C. Zimmerman, *Pharm. News* **1999**, *6*, 25–29. For polymers, see: f) D. C. Bibby, N. M. Davies, I. G. Tucker, *Int. J. Pharm.* **2000**, *197*, 1–11. For liquid crystals as drug delivery agents, see: g) F. Castelli, B. Conti, D. E. Maccarrone, U. Conte, G. Puglisi, *Int. J. Pharm.* **1998**, *176*, 85–98. For recent reviews in antisense therapy and metabolite regulation, see: h) A. R. Yuen, B. I. Siki, *Front. Biosc.* **2000**, *5*, 588–593; i) S. M. Stepkowski, *Curr. Opin. Mol. Ther.* **2000**, *2*, 304–317; j) E. Uhlmann, *Curr. Opin. Drug Disc. Dev.* **2000**, *3*, 203–213; k) J. J. Schwartz, S. Zhang, *Curr. Opin. Mol. Ther.* **2000**, *2*, 162–167; l) A. A. Mountain, *Trends Biotechnol.* **2000**, *18*, 119–128.

[2] a) D. T. Bong, T. D. Clark, J. R. Granja, M. R. Ghadiri, *Angew. Chem.* **2001**, *113*, 1016–1041; *Angew. Chem. Int. Ed.* **2001**, *40*, 988–1011; b) G. J. Kirkovits, C. D. Hall, *Adv. Supramol. Chem.* **2000**, *7*, 1–47.

[3] J. R. Granja, M. R. Ghadiri, *J. Am. Chem. Soc.* **1994**, *116*, 10785–10786.

[4] M. R. Ghadiri, J. R. Granja, L. K. Buehler, *Nature* **1994**, *369*, 301–304.

[5] β-Amino acids have been successfully employed in the design of cyclic peptide-based transmembrane ion channels: T. D. Clark, L. K. Buehler, M. R. Ghadiri, *J. Am. Chem. Soc.* **1998**, *120*, 651–656.

[6] K. Motesharei, M. R. Ghadiri, *J. Am. Chem. Soc.* **1997**, *119*, 11306–11312.

[7] H. S. Kim, J. D. Hartgerink, M. R. Ghadiri, *J. Am. Chem. Soc.* **1998**, *120*, 4417–4424.

[8] With respect to the surface normal, the tilt of the peptide tube axis was $28.5 \pm 1^\circ$ and the lipid hydrocarbon chain tilt was $26 \pm 2^\circ$.

[9] D. Schomburg, M. Salzmann, D. Stephan, *Enzyme Handbook*, *Vol. 2*, Springer, Berlin, **1990**.

[10] This is an underestimation of the actual rate of transport since only a fraction of the total peptides are expected to self-assemble into transport-competent pores.

[11] O. S. Smart, J. Breed, G. R. Smith, M. S. P. Sansom, *Biophys. J.* **1997**, *72*, 1109–1126.

[12] Planar lipid bilayers from 1,2-diphytanoyl-*sn-glycero*-3-phosphocholine were prepared as described in M. Montal, P. Mueller, *Proc. Natl. Acad. Sci. USA* **1972**, *69*, 3561–3566. All electrolyte solutions employed were buffered with 3-(*N*-morpholino)propane sulfonic acid (MOPS; 5 mM; pH 7.5).

[13] Conductance was observed to decrease at high NaCl concentrations (over 1M). This is consistent with the presence of more than one ion inside the channel under those conditions, where the resulting repulsion diminishes the transport rate: W. D. Stein, *Channels, Carriers and Pumps: An Introduction to Membrane Transport*, Academic Press, San Diego, **1990**.

[14] O. D. Bonner, *J. Chem. Eng. Data* **1981**, *26*, 147–148.

[15] B. Hille, *Ionic Channels of Excitable Membranes*, Sinauer, Sunderland, **1991**.

  1433-7851/01/4013-2506 $ 17.50+.50/0

Stereoselective Hydrocyanation of Alkenyl Sulfoxides as a Method to Highly Enantiomerically Enriched Compounds with Tertiary and Quaternary Chiral Carbon Atoms**

Jose L. García Ruano,* Marta Cifuentes García, Nieves M. Laso, Ana M. Martín Castro, and Jesús H. Rodríguez Ramos*

Hydrocyanation of double bonds is an important synthetic task because it allows the direct transformation of alkenes into carboxylic acid derivatives.[1] With regard to catalytic asymmetric hydrocyanation, the results obtained so far can be considered as rather modest.[2] Thus, in the case of norbornene and norbornadiene—some of the most well studied substrates because of the rigidity conferred by the bicyclic structure[3, 4]—palladium complexes bearing the phosphane–phosphite ligand (*R*)-2-(diphenylphosphino)-1,1′-binaphthalen-2′-yl (*S*)-1,1′-binaphthalen-2,2′-diylphosphite ((*R*,*S*)-BINAPHOS) were claimed to be the most efficient chiral catalysts, although only 48% *ee* was obtained.[5] The highest enantiomeric excess ever reported for an enantioselective hydrocyanation corresponds to reactions of arylethenes catalyzed by glucose-derived bisphosphinite–Niquel complexes (the *ee* value ranged from 40 to 70%, but in the case of the 6-methoxy-2-vinylnaphthalene it increased to 91%).[6] This result was not improved by the use of chiral aryl diphosphite ligands derived from binaphthol.[7] Diastereoselective hydrocyanations of double bonds, involving the nucleophilic addition of cyanide to deactivated alkenes,[8, 9] have been occasionally carried out on chiral substrates[10] to obtain difunctionalized substrates in diastereoselective processes. The low efficiency of the above-mentioned methods indicates that finding a general method to achieve the asymmetric hydrocyanation of alkenes, and thus allow the synthesis of nitriles bearing a chiral center at α-C, still remains a challenge.

The use of the sulfinyl group as a chiral inductor in asymmetric synthesis has been widely exploited.[11] The ability of the sulfinyl oxygen atom to associate with different metals is the key for controlling the stereoselectivity of many reactions. For reactions of α-sulfinyl ketones with aluminum reagents $YAlR_2$ (Y = H,[12] alkyl,[13] CN[14]), it could be established that formation of the Al–OS bond as a preliminary step in the intramolecular transfer of the Y^- group was responsible for the high stereoselectivity. We envisioned that unsaturated sulfinyl derivatives could react with Et_2AlCN in the manner of a highly stereocontrolled intramolecular cyanide transfer. This assumption was verified for alkynyl sulfoxides.[15] Here we report that hydrocyanation of alkenyl sulfoxides with Et_2AlCN is completely stereoselective. This reaction allows the transformation of terminal alkynes into nitriles bearing tertiary or quaternary chiral centers at α-C (Scheme 1). The chemical versatility of the cyano and sulfinyl groups suggests that this is a general method for preparing any kind of chiral carbon atom that is not bonded to a heteroatom.

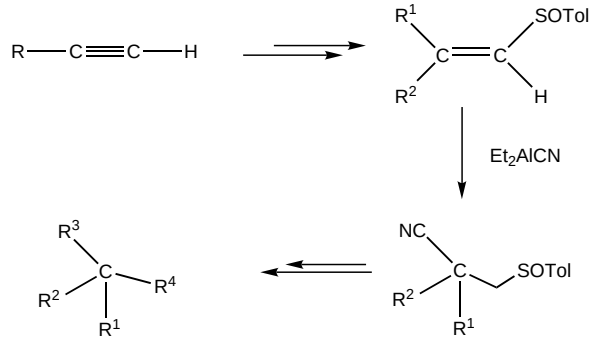

Scheme 1. General scheme for the hydrocyanation of alkenyl sulfoxides with Et_2AlCN, and further reaction of the nitriles obtained to provide compounds containing chiral centers. Tol = 4-tolyl.

The starting compounds for the asymmetric hydrocyanation were obtained from alkynyl sulfoxides **1**[15] and **2** (Scheme 2). A sequence involving sulfinylation of terminal alkynes followed by stereoselective reduction or alkylation of the alkynyl sulfoxide[16] provided vinyl sulfoxides **3** (from **1**)

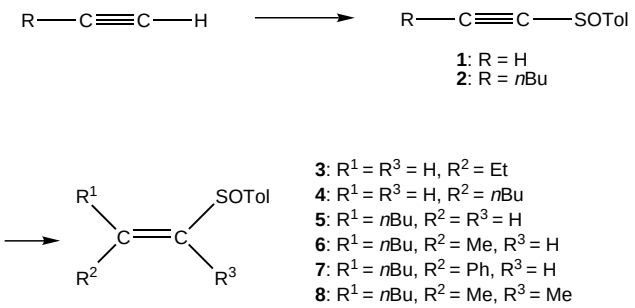

Scheme 2. Synthesis of vinyl sulfoxides **3**–**8**.

and **4**–**8** (from **2**). Capture of the intermediates from the reaction of lithium dimethyl cuprate with **2**, yielding **6**, with MeI as an electrophile allows the preparation of tetrasubstituted ethylene **8**.

The reaction of alkenyl sulfoxides **3**–**5** with Et_2AlCN in refluxing THF (15 min) solely afforded β-sulfinyl nitriles **9**–**11** in very good yields (Table 1, entries 1–5). The (*E*)-sulfoxide **4** was more reactive than the *Z* isomer **5**. The β,β'-disubstituted compound **6** exhibited lower reactivity than the monoalkylated vinylsulfoxides **3**–**5**, and required heating for two hours at reflux to afford a 96:4 mixture of **12a** and **12b**, epimers at carbon, which could not be separated (entry 6). Fortunately, the reaction was completely stereoselective at room temperature, although it required 48 h (entry 7). The

[*] Prof. J. L. García Ruano, Prof. J. H. Rodríguez Ramos, M. Cifuentes García, Dr. N. M. Laso, Dr. A. M. Martín Castro
Departamento de Química Orgánica (C-I)
Universidad Autónoma de Madrid
Cantoblanco, 28049-Madrid (Spain)
Fax: (+34) 91-3973966
E-mail: joseluis.garcia.ruano@uam.es

[**] This work was supported by the Dirección General de Investigación Científica y Técnica (grants BQU 2000-0246 and PB98-0102).

Supporting information for this article is available on the WWW under http://www.angewandte.com or from the author.

  1433-7851/01/4013-2507 $ 17.50+.50/0

Table 1. Results from the hydrocyanation of alkenyl sulfoxides with Et_2AlCN.

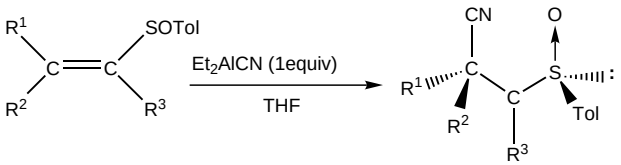

Entry	R^1	R^2	R^3	Substrate	*t*	*T* [°C][a]	Product	Yield [%]	de [%]
1	H	Et	H	**3**	15 min	65	**9**	80	> 98
2	H	*n*Bu	H	**4**	15 min	65	**10**	90	> 98
3	*n*Bu	H	H	**5**	15 min	65	**11**	75	> 98
4	H	*n*Bu	H	**4**	4 h	25	**10**	90	> 98
5	*n*Bu	H	H	**5**	24 h	25	**11**	75	> 98
6	*n*Bu	Me	H	**6**	2 h	65	**12a**/**12b**[b]	72	92
7	*n*Bu	Me	H	**6**	48 h	25	**12a**[c]	72	> 98
8	*n*Bu	Ph	H	**7**	24 h	65	**13**	82[d]	> 98
9	*n*Bu	Me	Me	**8**	48 h	65	**14**	–[e]	–

[a] The reactions were carried out at room temperature (25 °C) or in refluxing THF (66 °C). [b] Epimers **12a** and **12b** were obtained in a 96:4 mixture. [c] 10 % of vinyl sulfone was also isolated. [d] Conversion 58 % (42 % of the starting material **7** was recovered). [e] Product **14** was not formed.

presence of a phenyl group at the double bond decreased the reactivity of the alkenyl sulfoxide even more. Therefore, the transformation of **7** into **13** (isolated in 48 % yield) was not complete after heating for 24 h at reflux (42 % of unaltered **7** was recovered, entry 8). An increase in the reaction time and in the amount of reagent did not improve these results, but caused decomposition of **7**. In all these reactions the order of addition was critical for obtaining the nitriles in good yields: The alkene must be added to Et_2AlCN. Compound **8** did not evolve into sulfinyl nitrile **14**[17] after heating for 48 h at reflux (entry 9).

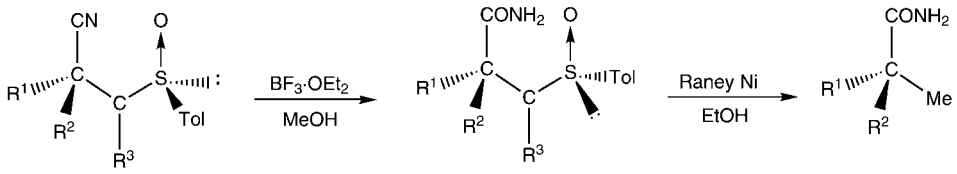

9: R^1 = H, R^2 = Et — **15** (75%) — **21** (82%)
10: R^1 = H, R^2 = *n*Bu — **16** (78%) — **22** (84%)
11: R^1 = *n*Bu, R^2 = H — **17** (70%) — **23** (80%)
12: R^1 = *n*Bu, R^2 = Me — **18** (70%)
13: R^1 = *n*Bu, R^2 = Ph — **19** (76%) — **24** (84%)

Scheme 3. Hydrolysis and subsequent reduction of nitriles **9**–**13**.

The most relevant result of all these hydrocyanation reactions is the almost complete stereoselectivity. Starting from enantiopure alkenyl sulfoxides, only one diastereoisomer of the corresponding nitrile could be detected in the crude products by 300-MHz ^{1}H NMR analysis. The desired configuration at α-C of the resulting sulfinyl nitriles could be achieved by choosing either the configuration at the sulfinylic sulfur atom or that of the double bond in the starting compound.

Hydrolysis of these nitriles with $BF_3 \cdot OEt_2$ and methanol[18] afforded sulfinyl amides **15**–**19** (Scheme 3). Product **16** gave suitable crystals that could be analyzed by X-ray diffraction,[19] thus allowing unequivocal assignment of the configuration as (2*S*,(S)*S*).[20] Accordingly, we can state that the *S* configuration induced at the chiral carbon atom in the hydrocyanation step is opposite to that of the sulfur atom in (*E*)-vinyl sulfoxide (*R*)-**4**.

The stereochemical results could be rationalized by assuming association of the aluminum atom with the sulfinyl oxygen atom prior to the intramolecular transfer of the cyanide group. In Scheme 4 are depicted the two possible chairlike transition states for such a transfer, $\mathbf{TS_B}$ being clearly more stable than $\mathbf{TS_A}$ from the point of view of sterics. This stereochemical model also explains the lower reactivity of the (*Z*)-sulfoxides with respect to the *E* isomers as a consequence

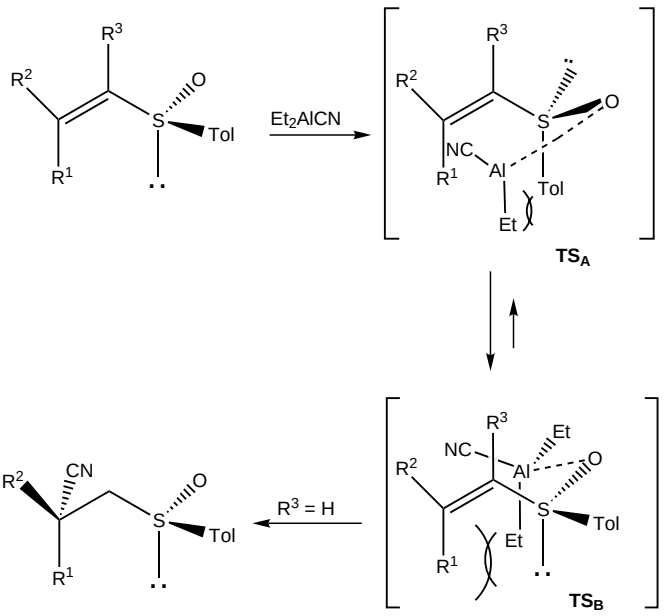

Scheme 4. Possible mechanism for the hydrocyanation of alkenyl sulfoxides.

  1433-7851/01/4013-2508 $ 17.50+.50/0

of the $(R^1/Et)_{1,3\text{-p}}$ interaction. The lower reactivity of dialkyl and alkyl aryl acrylonitriles compared to monosubstituted substrates is not unexpected considering the influence of the substituents on the electronic density at the double bond. This could also be responsible for the low reactivity of trisubstituted vinyl sulfoxide **8**, but the $(O/R^3)_{gauche}$ and $(Tol/R^3)_{gauche}$ interactions present when $R^3 \neq H$ can also be involved in the destabilization of both $\mathbf{TS_A}$ and $\mathbf{TS_B}$.

Desulfinylation of the amides **15**–**17** and **19** with Raney nickel afforded the corresponding enantiopure amides **21**–**24**, which were isolated in good yields (>70%, Scheme 3).[21]

In summary we have shown that the hydrocyanation of alkenyl sulfoxides with Et_2AlCN takes place in a completely stereoselective manner. Taking into account the chemical versatility of the cyano and sulfinyl groups, this reaction can be considered as the key step in a short sequence that allows the creation of optically pure molecules containing tertiary or quaternary chiral centers from terminal alkynes, as illustrated with the preparation of amides **21**–**24**.

Received: December 22, 2000
Revised: March 26, 2001 [Z16322]

[1] G. Helmchen, R. W. Hoffmann, J. Mulzer, E. Schaumann, *Methods Org. Chem. (Houben-Weyl)*, Vol. 21d, **1995**.
[2] M. Hodgson, D. Parker, R. J. Taylor, G. Ferguson, *Organometallics* **1988**, *7*, 1761.
[3] a) P. S. Elmes, W. R. Jackson, *J. Am. Chem. Soc.* **1979**, *101*, 6128; b) P. S. Elmes, W. R. Jackson, *Ann. N. Y. Acad. Sci.* **1980**, *333*, 225.
[4] R. Noyori, H. Takaya, *Acc. Chem. Res.* **1990**, *23*, 345.
[5] T. Horiuchi, E. Shirakawa, K. Nozaki, H. Takaya, *Tetrahedron: Asymmetry* **1997**, *8*, 57.
[6] a) T. V. RajanBabu, A. L. Casalnuovo, *J. Am. Chem. Soc.* **1992**, *114*, 6265; b) A. L. Casalnuovo, T. V. RajanBabu, T. A. Ayers, T. H. Warren, *J. Am. Chem. Soc.* **1994**, *116*, 9869.
[7] M. Yan, Q.-Y. Xu, A. S. C. Chan, *Tetrahedron: Asymmetry* **2000**, *11*, 845.
[8] W. Nagata, M. Yoshiota, *Org. React.* **1977**, *25*, 255.
[9] D. N. Piatak, P.-F. L. Tang, *Can. J. Chem.* **1987**, *65*, 1327.
[10] K. Utimoto, Y. Wakabayashi, T. Horiie, M. Inoue, Y. Shishiyama, M. Obayashi, H. Nozaki, *Tetrahedron* **1983**, *39*, 967.
[11] a) M. C. Carreño, *Chem. Rev.* **1995**, *95*, 1717; b) J. L. García Ruano, B. Cid, *Top. Curr. Chem.* **1999**, *204*, 1–126, and references therein.
[12] a) J. L. García Ruano, *Phosphorus Sulfur Silicon Relat. Elem.* **1993**, *74*, 233; b) R. Sánchez-Obregón, B. Ortiz, F. Walls, F.Yuste, J. L. García Ruano, *Tetrahedron: Asymmetry* **1999**, *10*, 947, and references therein.
[13] a) A. B. Bueno, M. C. Carreño, J. L. García Ruano, *An. Quim. Int. Ed.* **1994**, *90*, 442; b) J. L. García Ruano, C. García Paredes, *Tetrahedron Lett.* **2000**, *41*, 261.
[14] J. L. García Ruano, A. M. Martín Castro, J. H. Rodríguez, *Recent Res. Devel. Org. Chem. Part I* **2000**, *4*, 261.
[15] J. L. García Ruano, A. Esteban Gamboa, A. M. Martín Castro, J. H. Rodríguez, M. I. López Solera, *J. Org. Chem.* **1998**, *63*, 3324.
[16] H. Kosugi, M. Kitaota, K. Tagami, A. Takahashi, H. Uda, *J. Org. Chem.* **1987**, *52*, 1078.
[17] After the reaction mixture was heated for 24 h at reflux, we isolated an unexpected compound (30% yield) which has not been identified yet.
[18] These conditions promote the conversion of sulfinyl nitriles into sulfinyl amides with inversion of the configuration at sulfur (see refs. [14c, 15]) The hydrolysis of nitrile **12** with KOH in refluxing *t*BuOH (J. H. Hall, M. Gisler, *J. Org. Chem.* **1976**, *41*, 3769) afforded diastereomer **18′**, an epimer at sulfur of **18**, because under these conditions neither the configuration at carbon or at sulfur is affected.
[19] Proper crystals of compunds **9**–**13** could not be obtained.
[20] Crystallographic data (excluding structure factors) for the structure reported in this paper have been deposited with the Cambridge Crystallographic Data Centre as supplementary publication no. CCDC-154583 (**16**). Copies of the data can be obtained free of charge on application to CCDC, 12 Union Road, Cambridge CB2 1EZ, UK (fax: (+44) 1223-336-033; e-mail: deposit@ccdc.cam.ac.uk).
[21] As the optical purity of the amides could not be established by chiral shift reagents or chiral HPLC, the chemical correlation of **21** with commercially availale (*S*)-2-methylbutanoic acid was neccesary. The amides derived from (*S*)-2-methylbutanoic acid and from **21** by desulfurization exhibited a specific rotation of the same value and sign. Therefore, we can conclude that the configuration at C2 of **21** must be *S*, in complete agreement with the X-ray structure analysis.

Synthesis of a Remarkably Stable Dehydro[14]annulene**

Grant J. Palmer, Sean R. Parkin, and John E. Anthony*

Dehydroannulenes are a fascinating class of carbon-rich molecules which have been studied intensively.[1] With the development of improved synthetic methodologies, these macrocycles are now being exploited for their potential material properties. Recent applications employ such annulenes as conjugated scaffolds for nonlinear optical applications[2] and as precursors for carbon nanotube synthesis.[3] We are currently exploring the use of fused dehydroannulenes as components in conjugated ladder polymers (e.g. acynes **1** and rylynes **2**).

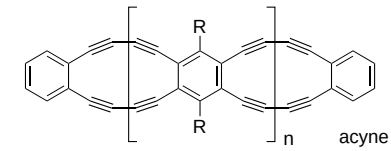

1

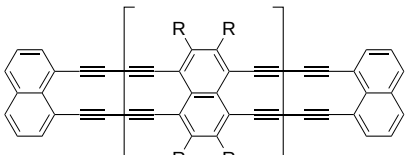

2

While the phenyldiacetylene macrocycles that comprise **1** are well-known compounds,[4] the class of dehydroannulenes that make up the backbone of **2** is poorly understood. The parent compound **3** was prepared in 1968 by Mitchell and Sondheimer, who were unable to fully characterize this new

[*] Prof. J. E. Anthony, G. J. Palmer, Dr. S. R. Parkin
Department of Chemistry
University of Kentucky
Lexington, KY, 40506-0055 (USA)
Fax: (+1) 859-323-1069
E-mail: anthony@pop.uky.edu

[**] The authors acknowledge the National Science Foundation (CHE-9875123) and the Office of Naval Research (N00014-99-1-0859) for support of this research. NMR spectroscopy facilities were enhanced by the National Science Foundation CRIF program (CHE-997841) and the Research Challenge Trust Fund of the University of Kentucky.

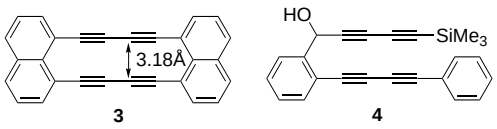

3 4

annulene because it decomposed rapidly, even in dilute solution.[5] They postulated that this instability arose from the proximity of the alkynes in the rigid macrocycle. Indeed, the high reactivity of this structural motif has been exploited in acyclic systems such as **4**, which undergo facile intramolecular cyclization to form extended aromatic structures.[6] Recently, several examples of unconjugated macrocyclic butadiynes have been shown to be stable at room temperature,[7] which has led us to revisit the chemistry of compounds based on **3**, the fundamental component of ladder polymer **2**.

If the decomposition of **3** is in fact related to the proximity of the two parallel butadiyne units (calculated distance: 3.18 Å),[8] substituents which increase the separation between these units should stabilize the macrocycle. For example, it has been shown that changes in alkyne terminus separation of as small as 0.05 Å can have a significant effect on reactions such as the Bergman cycloaromatization.[9] According to ab initio calculations, the butadiyne units in acenaphthene derivative **6** are separated by 3.25 Å (Scheme 1), an increase of 0.07 Å

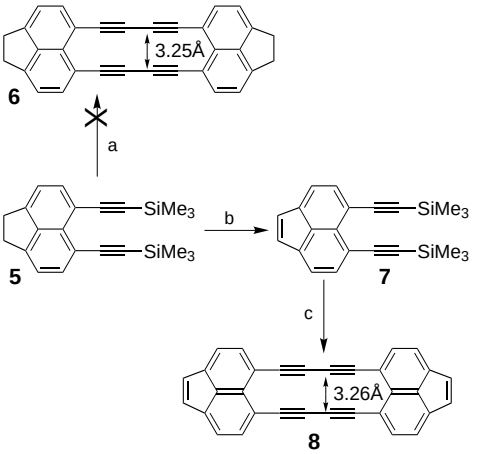

Scheme 1. Synthesis of macrocycle **8**. Reagents and conditions: a) 1. K_2CO_3 in MeOH/THF; 2. CuCl/TMEDA in CH_2Cl_2; b) DDQ (2,3-dichloro-5,6-dicyano-1,4-benzoquinone); c) 1. K_2CO_3 in MeOH/THF; 2. CuCl/TMEDA in CH_2Cl_2, 75%.

compared to **3**. Thus, 5,6-diethynylacenaphthene[10] was subjected to oxidative cyclization under high-dilution conditions. Analysis of the resulting insoluble solid by high-resolution LD-MS (laser desorption mass spectrometry) showed only small amounts of both residual starting material and a dimerized, acyclic species. Compound **6** could not be detected, presumably as a result of the rapid decomposition of the macrocycle.

Examination of the π-bond topology of **3** reveals that the perimeter of that macrocycle is not fully conjugated, unlike other stable dehydroannulenes. The acenaphthylene-derived macrocycle **8** addresses this deficiency, leading to a fully-conjugated 28 π-electron macrocycle. Although this cycle is formally antiaromatic, numerous other antiaromatic dehydroannulenes have been shown to be stable.[11] To prepare **8**, diethynylacenaphthylene **7** was synthesized by the oxidation of acenaphthene **5**. Desilylation followed by oxidative cyclization led to a brilliant orange powder, which was sparingly soluble in dichloromethane.

The UV/Vis spectrum of this new compound (Figure 1) strongly resembles that reported for **3**, with two characteristic peaks at 455 and 485 nm (**3** shows absorbances at 502 and 540 nm). This stable compound survived recrystallization

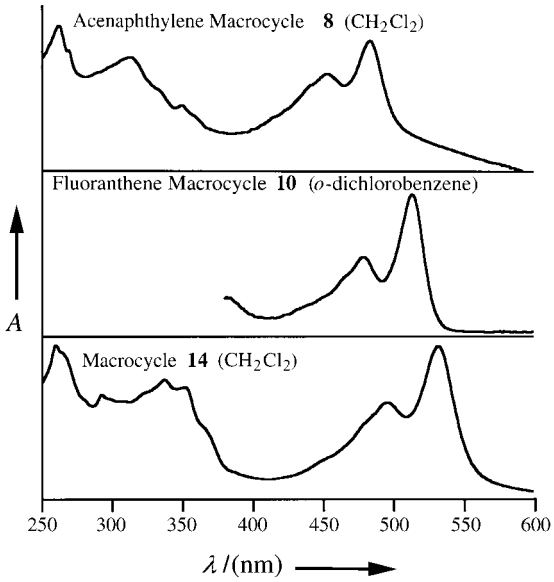

Figure 1. UV/Vis spectra of compounds **8**, **10**, and **14**.

from *o*-dichlorobenzene (180 °C) without decomposition. High-resolution mass spectrometry and ^1H NMR spectroscopy support the structural assignment for **8**. Unfortunately, this compound proved to be too insoluble for further characterization.

In an attempt to synthesize a more characterizable macrocycle, fluoranthene **9** was prepared[12] and alkynylated (Scheme 2). Desilylation followed by oxidative cyclization again led to a stable orange powder, which exhibited characteristic absorbances at 480 and 515 nm. Surprisingly, this compound was significantly less soluble than the ace-

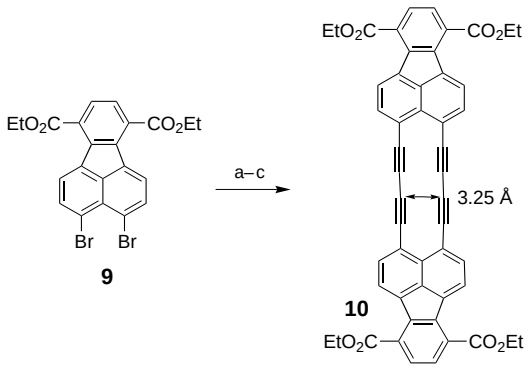

Scheme 2. Synthesis of **10**. Reagents and conditions: a) $Me_3SiCCSnBu_3$/$[(Ph_3P)_2PdCl_2]$; b) K_2CO_3 in EtOH/THF; c) CuCl/TMEDA in CH_2Cl_2.

  1433-7851/01/4013-2510 $ 17.50+.50/0

naphthylene derivative **8**. Although the high-resolution mass spectrum and UV/Vis absorption spectrum supported the assignment of macrocyclic structure **10**, a species soluble enough for more thorough characterization was still required.

A more aggressive solubilization strategy was utilized in the preparation of **14** (Scheme 3). Beginning with quinone **11**, treatment with a Grignard reagent followed by reductive

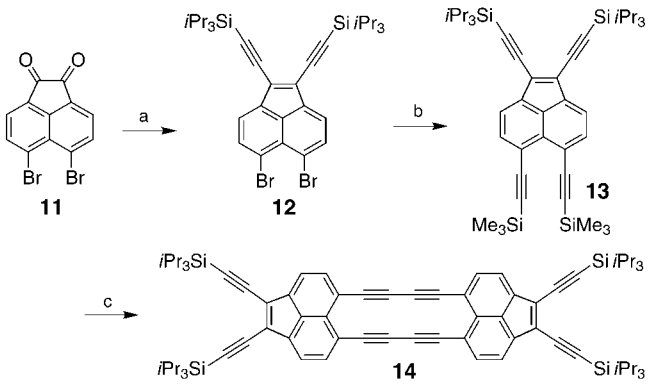

Scheme 3. Synthesis of **14**. Reagents and conditions: a) 1. iPr$_3$SiCCMgBr; 2. AcOH/SnCl$_2$, 80%; b) Me$_3$SiCCSnBu$_3$, [(Ph$_3$P)$_2$PdCl$_2$], 60%; c) 1. K$_2$CO$_3$ in MeOH/THF; 2. CuCl/TMEDA in acetone, 88%.

deoxygenation led to the very soluble enediyne **12**.[13] Alkynylation by Stille coupling[14] led to tetrayne **13**, which was selectively desilylated and oxidatively coupled to yield a deep red solution of macrocycle **14**. This soluble material shows remarkable thermal and photochemical stability. Solutions of **14** were heated at $>190\,^{\circ}$C for several hours, or left in direct sunlight for a period of several weeks, without noticeable decomposition. Examination of the ^{1}H NMR spectrum shows a slight paratropic shift of all of the aromatic protons of the macrocycle with respect to the acyclic starting material. The FTIR, ^{13}C NMR, and mass spectral analyses all support the structural assignment of **14**.

Slow evaporation of a 1,2-dichloroethane solution of compound **14** led to dark purple crystals with a golden metallic luster. The structure was determined by X-ray crystallographic analysis (Figure 2).[15] Consistent with calculations, the central carbon atoms of the two butadiyne units (C14–C1) are indeed splayed outward, separated by a distance of 3.23 Å. Even with this distortion, the butadiyne units are nearly linear, with the most extreme variation from linearity a mere 7°. As expected, the annulene backbone is planar to within 0.05 Å.

We have demonstrated that with proper functionalization, the preparation of stable naphthalene diacetylene macrocycles is possible. The distance between butadiyne units in these systems has been found to be less important to stability than conjugation. We are currently exploring the incorporation of these stabilized macrocycles into new carbon ladder polymers based on **2**.

Received: February 23, 2001 [Z16670]

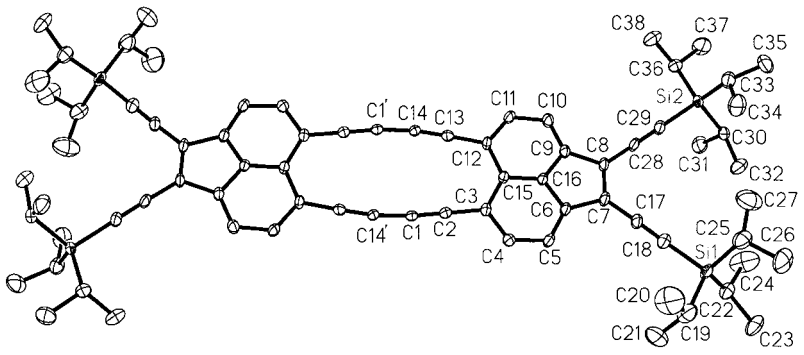

Figure 2. Molecular structure of **14** (ORTEP plot) in the crystal. Selected bond lengths [Å] and angles [°]: C1′-C14 1.371(3), C14-C13 1.201(3), C13-C12 1.430(3), C12-C15 1.441(3), C15-C3 1.439(3), C3-C2 1.428(3), C2-C1 1.202(3), C1-C14′ 1.371(3), C12-C11 1.389(3), C11-C10 1.407(3), C10-C9 1.370(3), C9-C8 1.474(3), C8-C7 1.379(3), C7-C6 1.472(3), C6-C5 1.369(3), C5-C4 1.402, C4-C3 1.398(3), C15-C16 1.394(3), C9-C16 1.411(3), C16-C6 1.413(3); C1′-C14-C13 173.6(2), C14-C13-C12 176.3(2), C13-C12-C15 121.34(19), C12-C15-C3 129.65(18), C15-C3-C2 123.26(19), C3-C2-C1 178.0(2), C2-C1-C14′ 172.7(2).

[1] a) H. Meier, *Synthesis* **1972**, 235; b) M. Nakagawa, *Pure Appl. Chem.* **1975**, *44*, 885; c) N. Huang, F. Sondheimer, *Acc. Chem. Res.* **1982**, *15*, 96; d) S. Akiyama, *Anal. Sci.* **1994**, *10*, 365; e) R. R. Tykwinski, F. Diederich, *Liebigs Ann.* **1997**, 649; f) W. J. Youngs, C. A. Tessier, J. D. Bradshaw, *Chem. Rev.* **1999**, *99*, 3153; g) M. M. Haley, J. J. Pak, S. C. Brand, *Top. Curr. Chem.* **1999**, *201*, 81.

[2] For example donor–acceptor substituted dehydroannulenes: J. J. Pak, T. J. R. Weakley, M. M. Haley, *J. Am. Chem. Soc.* **1999**, *121*, 8182.

[3] K. P. Baldwin, A. J. Matzger, D. A. Scheiman, C. A. Tessier, K. P. C. Vollhardt, W. J. Youngs, *Synlett* **1995**, 1215.

[4] a) O. M. Behr, G. Eglinton, A. R. Galbraith, R. A. Raphael, *J. Chem. Soc.* **1960**, 3614; b) U. H. F. Bunz, V. Enkelmann, *Chem. Eur. J.* **1999**, *5*, 263.

[5] R. H. Mitchell, F. Sondheimer, *Tetrahedron* **1968**, *24*, 1397.

[6] a) K. Miyawaki, R. Suzuki, T. Kawano, I. Ueda, *Tetrahedron Lett.* **1997**, *38*, 3943; b) K. Miyawaki, T. Kawano, I. Ueda, *Tetrahedron Lett.* **2000**, *41*, 1447.

[7] a) R. Gleiter, R. Merger, J. Chavez, T. Oeser, H. Irngartinger, H. Pritzkow, B. Nuber, *Eur. J. Org. Chem.* **1999**, 2841; b) F. Sondheimer, Y. Amid, R. Wolovsky, *J. Am. Chem. Soc.* **1957**, *79*, 6263.

[8] Distances reported in this paper were calculated by using ab initio HF methods in Mac Spartan Plus (version 1.1.9): Wavefunction, Inc., 18401 Von Karman Ave., Ste. 370, Irvine, CA 92612.

[9] a) K. C. Nicolaou, W.-M. Dai, *Angew. Chem.* **1991**, *103*, 1453; *Angew. Chem. Int. Ed. Engl.* **1991**, *30*, 1387; b) R. G. Bergman, *Acc. Chem. Res.* **1973**, *6*, 25.

[10] J. J. González, A. Francesch, D. J. Cárdenas, A. M. Echavarren, *J. Org. Chem.* **1998**, *63*, 2854.

[11] A. J. Matzger, K. P. C. Vollhardt, *Tetrahedron Lett.* **1998**, *39*, 6791, and references therein.

[12] L. T. Scott, P.-C. Cheng, M. M. Hashemi, M. S. Bratcher, D. T. Meyer, H. B. Warren, *J. Am. Chem. Soc.* **1997**, *119*, 10963.

[13] W. Baidossi, H. Schumann, J. Blum, *Tetrahedron* **1996**, *52*, 8349.

[14] J. K. Stille, *Angew. Chem.* **1986**, *98*, 504; *Angew. Chem. Int. Ed. Engl.* **1986**, *25*, 508.

[15] Data for the X-ray structure analysis: Crystals from 1,2-dichloroethane, $C_{76}H_{92}Si_4$ ($M_r = 1117.86$); crystal size $0.26 \times 0.20 \times 0.08$ mm^3; monoclinic, space group $I2/a$, $a = 21.717(3)$, $b = 13.8940(10)$, $c = 22.961(2)$ Å, $\beta = 101.235(10)^{\circ}$, $Z = 4$, $V = 6795.4(12)$ Å^3, $\rho_{calcd} = 1.093$ g cm^{-3}, $T = 173(1)$ K, $2\theta = 50$, 11692 reflections measured, 5980 were unique ($R_{int} = 0.0372$), and 4831 were observed ($I > 2\sigma(I)$), $Mo_{K\alpha}$ radiation ($\lambda = 0.71073$ Å), graphite monochromated, data were corrected for Lorentz and polarization effects. The structure was solved by direct methods and refined with the full-matrix, least-squares method; $R_1 = 0.0561$, $wR_2 = 0.1080$ (for 4831 reflections with

$I > 2\sigma(I)$), $R_1 = 0.0768$, $wR_2 = 0.1153$ (for all data); data-to-parameter ratio 16.52; residual electron density $+0.302/-0.260$ e Å^{-3}. Crystallographic data (excluding structure factors) for the structure reported in this paper have been deposited with the Cambridge Crystallographic Data Centre as supplementary publication no. CCDC-158650. Copies of the data can be obtained free of charge on application to CCDC, 12 Union Road, Cambridge CB21EZ, UK (fax: (+44) 1223-336-033; e-mail: deposit@ccdc.cam.ac.uk).

IR-UV Double-Resonance Photodissociation of Nitric Acid ($HONO_2$) Viewed as Molecular Information Processing**

Thomas Witte, Christine Bucher, Françoise Remacle, Detlev Proch, Karl L. Kompa, and R. D. Levine*

One route to nanoscale computing is to make single molecules that can mimic the function of conventional components of electronic logic circuits, such as switches or wires. There is therefore increasing activity in producing molecules that can conduct electrical current or can be instructed to turn it on or off when placed within a suitable support. This field of activity, sometimes known as molecular electronics[1] or molecular scale electronics,[2] is a major current research area. Now that several groups[2–4] have demonstrated that a molecule can act as a switch,[5] it is possible to begin thinking about replacing transistors by single molecules within larger digital devices. The chemical pumping of molecules in solution that induces changes that can be optically detected has also been been studied for some time[6–8] as a possible route to logic gates. More generally, the progress in supramolecular chemistry towards the construction of molecular machines[9, 10] opens up many possibilities for an induced response.

An alternative to the approach in which a molecule acts as a single switch is a scheme where the function of an entire logic circuit is performed by a single isolated molecule.[11, 12] A particular molecular coordinate, which could be a reactive one, acts as the bus for information transfer. This alternative route has the distant goal of incorporating the logic capabilities of a complete integrated circuit on a single molecule. A more modest goal is the experimental demonstration of a circuit containing several connected logic gates as a (logic) equivalent of the intramolecular dynamics of a single molecule. The experimental demonstration of such a scheme is presented herein.

A molecule in a molecular logic gate scheme[11] becomes a vehicle for information processing, where the input is optical excitation. In the experiment discussed below the resonance requirement is paramount, and an intramolecular motion is essential for the logic action. We discuss time-resolved measurements because one advantage of our gates is that they can be ultrafast, as reported for a number of other systems.[11] With our device we get the output as an optical signal. However, the recent experiments of Crim and co-workers[13] suggest that the logic of the present approach can be probed by chemical means.

A conventional logic circuit is built from connected switches. The advantage of the approach we follow is that by operating a single molecule as a logic circuit one avoids the need to connect switches. The circuit reported here is already equivalent to several switches, and this, we hope, is only the beginning. The logic gate that we describe is completely irreversible since the molecule is destroyed. This dissociation is not an essential aspect and we have discussed[11] other molecules where this need not be the case, and where the initial state can be recovered as quickly as one picosecond.

The power of organic synthesis to design molecules should not be overlooked. What one wants is a circuit that is operable over many cycles. The first step is the need to regenerate the ground state. In some systems, for example, the photoinduced keto–enol tautomerism, this requirement is inherently satisfied. In other systems, such as electrocyclic ring openings, the photoprocess generates more than one possible product, and this can be used to advantage. In essence what we look for is a prompt intramolecular response to an optical excitation. Typically, such a response involves a rotation of part of a molecule relative to another to bring about a recoupling of the electronic orbitals.

Since the 1970s great advances have been made possible by combining laser spectroscopy and reaction dynamics. The double-resonance experiment that we discuss falls into this class. The principles[14–16] are understood and the application to the $HONO_2$ system has been previously studied.[17, 18] What is new and interesting is the hitherto unknown effect determined by the order of the two ultrafast UV and IR pulses. Still, it can be asked if what we are discussing is little more than a semantic rephrasing of an experiment. What we actually do is to explore the implications of a spectroscopic experiment from a new point of view, which opens up options and possibilities that are not evident without it. It also raises new questions of principle. For the moment, however, we just want to highlight a cross-disciplinary study involving modern chemical physics and Boolean logic. We are aware that one can carry our ideas into the non-Boolean (that is, quantal) regime, but for now we will view the experiment in chemical kinetic, that is, classical, terms.

To introduce the subject we begin with the IR-UV double-resonance experiment of Crim and co-workers (Figure 1).[14, 17–19] An IR photon generates a vibrationally excited state (OH stretch overtone) of the ground electronic state of

[*] Prof. Dr. R. D. Levine
The Fritz Haber Research Center for Molecular Dynamics
The Hebrew University, Jerusalem 91904 (Israel)
Fax: (+972) 2-651-3742
E-mail: rafi@fh.huji.ac.il

Prof. Dr. R. D. Levine, T. Witte, Dr. C. Bucher, Dr. F. Remacle, Dr. D. Proch, Prof. Dr. K. L. Kompa
Max-Planck-Institute of Quantum Optics
85740 Garching (Germany)

Dr. F. Remacle
Permanent address:
Département de Chimie, B6
Université de Liège, 4000 Liège (Belgium)

[**] This work was supported by the James Franck Program for Laser-Matter Interaction.

  1433-7851/01/4013-2512 $ 17.50+.50/0

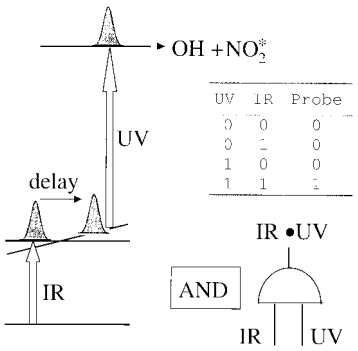

Figure 1. A schematic drawing of the IR-UV pumping scheme for a positive delay time and the corresponding AND gate. The truth table is also shown. The energy level scheme indicates that there should be a delay after the absorption of the IR pulse so that the energy can redistribute before absorption of the UV photon. Two intermediate levels are shown so as to indicate that there is an intramolecular process that takes place during the delay between the two pulses. The AND logic gate is shown as a semi-circle. The lines show the inputs and outputs using a Boolean notation so that, for example, ω_{UV} has the value 0 or 1 when a UV laser pulse is not used or is applied to the molecule, respectively. The output ($\omega_{IR}\omega_{UV}$) is detected as the fluorescence of NO_2^*. The value of the output, corrected for background as discussed in the Experimental Section, is zero unless both lasers are on.

$HONO_2$. A second, this time UV, photon takes the molecule up to the (second[20, 21]) electronically excited level from which the reactive process initiates. In principle (see Experimental Section) the UV photon does not have sufficient energy on its own to access this level. The reactive process, dissociation to $OH + NO_2^*$, results in an observable fluorescence from the electronically excited NO_2^* species. This experiment by itself is equivalent to the logic AND gate[22] (shown as a semi-circle in Figure 1), since an output signal is possible only if both input photons are "on". The truth table for this gate is also shown in Figure 1.

The dynamics for the above kind of experiment have been thoroughly discussed.[14, 17–19] The time delay after excitation with the IR photon is necessary for redistribution of the energy in the ground electronic state of HNO_3. The time scale is established by delaying the femtosecond-long UV signal. It takes about 12 ps (Figure 2) for the necessary intramolecular vibrational relaxation (IVR), as characterized by the time taken for the NO_2^* fluorescence to reach a maximum. The electronic fluorescence of NO_2^* decays on a nanoscale time scale.

An AND gate is not a universal logic gate. Several universal logic gates are known, with the most familiar being the "NotAND" gate, which is usually written as "NAND".[22] To make a "NAND" gate we also need to know when "neither photon beam is on". To build the equivalent of a NAND gate one has to monitor the depletion of ground-state HNO_3. Since this is not an easy experiment, we have followed a quite different route.

We allow the UV signal to either be delayed or ahead of the IR pulse. This process gives us a new Boolean variable, the delay time τ. When $\tau = 1$, one has the usual setup: IR signal first and UV signal delayed. But when $\tau = 0$, one has the counter-intuitive arrangement where the UV signal is applied before the IR signal. An input equivalent to $\tau = 0$ is $\bar{\tau} = 1$, where the bar denotes the negation of the Boolean variable. The choice of $\tau = 1$ or 0 is operational and is determined by the arrangement of the delay line (see insert in Figure 2).

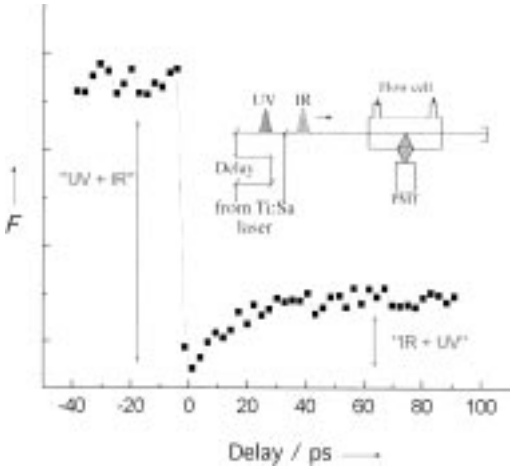

Figure 2. The (single photon) count rate for the fluorescence (F) of NO_2^* versus the delay time between the femtosecond-long IR and UV laser pulses. A positive delay time was used in the arrangement of Crim and co-workers, where the IR pulse is the first to be on, as shown in the insert (PMT = photomultiplier). A negative delay time is the counter-intuitive arrangement, where the UV pulse is first on. Note the sub-picosecond time taken for the fluorescence of NO_2^* to increase to a maximum when the delay time is negative. The count rate is corrected for the background as discussed in the Experimental Section.

The experimental results for the fluorescence of the NO_2^* species versus the physical delay time between the femtosecond-long IR and UV signals are shown in Figure 2. The right-hand side ($\tau > 0$) of the plot reproduces the experiment of Crim and co-workers.[17] The left-hand side ($\tau < 0$), however, is new and quite different. It shows that the same (to within experimental error) fluorescence signal for NO_2^* is observed for either sign of the delay time. However, for a negative delay, the time taken for the increase in the NO_2^* fluorescence signal is sub-picosecond. For a delay of one to several picoseconds, one can categorically distinguish between the variables τ and $\bar{\tau}$. We emphasize again that the distinction is not based on any difference in the character of the fluorescence spectrum, but on the sign of the delay time (provided that it is of the order of a picosecond). The experimental observation that negative and positive values of the delay time are distinguishable makes the experiment logically equivalent to the logic circuit shown in Figure 3.

The circuit shown has four gates. The lines connecting them are for visualization purpose only and indicate which variables are input to which gate. The circuit is equivalent to the dynamics of only one molecule, and by using single photon counting (as shown in Figure 2) fewer than 10^3 events are sufficient to result in a reasonable signal to noise ratio, particularly so if the distinction between τ and $\bar{\tau}$ is made around one picosecond. The elements of the circuit are: a) an AND gate, as in Figure 1, which yields the output 1 only if both photons are present; b) a NOT gate, shown as a triangle,[22] which is a simple one-input gate such that the output is 1 or 0 if the input is 0 or 1; c) an AND gate, to the

  1433-7851/01/4013-2513 $ 17.50+.50/0

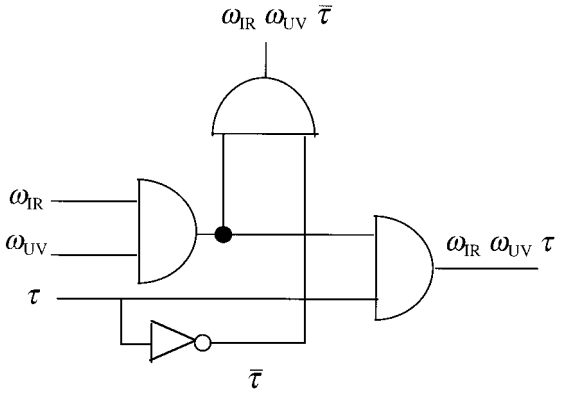

Figure 3. The logic circuit which is the equivalent of the experiment described in Figure 2 when the NO_2^* fluorescence is detected after a short time (around a picosecond). τ is the Boolean variable whose value is 1 if the delay time is experimentally set to be positive and 0 if it is negative. $\bar{\tau}$ is the logic complement of τ. The complementary variable is generated by a NOT gate (shown as a triangle). The two distinct outputs, $\omega_{IR}\omega_{UV}\tau$ and $\omega_{IR}\omega_{UV}\bar{\tau}$, are detected by experimentally gating the fluorescence count of NO_2^* to short (of the order of picoseconds) times. The gates are connected because the output of the first AND gate, the one shown in Figure 1, can be detected for either value of τ.

right of the figure, whose output is 1 only when both photons are present and the time delay is positive; and d) an AND gate whose output is 1 only when both photons are present and the time delay is negative. The circuit shown in Figure 3 is not meant to have a 1:1 correspondence with the experimental setup, it is meant to perform the same logic (compute a Boolean function) as implemented by the experiment. There are 2^{2^n} Boolean functions of n Boolean variables and the function $\omega_{IR}\omega_{UV}\bar{\tau}$ is not the logic complement of the other function $\omega_{IR}\omega_{UV}\tau$.

At the moment it cannot be established with certainty why the counter-intuitive pulse sequence works. The photochemical interpretation is that by applying the UV pulse first, one accesses a lower, quasibound electronically excited state that is dissociated by the subsequent IR pulse. The known theoretical results[20, 21] for the electronic states of HNO_3 are not inconsistent with this possibility, but one cannot rule out a photophysical route, similar to that known for STIRAP pumping,[23] where the first UV photon couples the ground state and the second electronically excited state. Experiments using better count rates are in progress for the purpose of elucidating this point.

An alternative to the route that we discuss here, and a route that allows a chemical reading of the output, is provided by the recent experiment of Crim and co-workers[13] on controlling the Cl + HNCO reaction. This experiment has a double-resonance part as discussed earlier, but the vibrationally excited ground-state HNCO molecule is given another dynamic option, namely to react with a Cl atom. In this way, the Cl atom that does not react with a vibrationally cold HNCO molecule probes the IR absorption.

We have shown how the different intramolecular dynamics of HNO_3 when excited to different states (vibrational overtone of the ground electronic state versus an excited electronic state) can be used to represent connected logic circuits. This confirms our suggestion[11] that molecular motions can be used as a bus for the purpose of information processing. We have also shown how the direction of time can be used as a logic variable.

Experimental Section

The experimental arrangement (Figure 2) was adapted from the design of Crim and co-workers.[17] The key difference is the option of a negative delay time between the femtosecond-long IR and UV pulses. The sign of the delay time is determined by the mechanical arrangement of the mirrors and is set before the lasers are switched on. This arrangement is the logic equivalent of the NOT gate. For a positive time delay, the experiment reproduces the reported results.[17] There is some signal from the UV pulse alone on both sides of the zero delay, presumably as a result of the dissociation of hot molecules. This background signal was subtracted from the count rate reported in Figure 2.

Received: December 27, 2000
Revised: March 13, 2001 [Z16363]

[1] J. M. Tour, *Acc. Chem. Res.* **2000**.
[2] M. A. Reed, J. M. Tour, *Sci. Am.* **2000**, *282*, 86.
[3] C. Joachim, J. K. Gimzewski, A. Aviram, *Nature* **2000**, *408*, 541.
[4] J. R. Heath, *Pure Appl. Chem.* **2000**, *72*, 11.
[5] C. P. Collier, G. Mattersteig, E. W. Wong, Y. Luo, K. Beverly, J. Sampaio, F. M. Raymo, J. F. Stoddart, J. R. Heath, *Science* **2000**, *289*, 1172.
[6] A. P. de Silva, H. Q. N. Gunaratne, C. P. McCoy, *J. Am. Chem. Soc.* **1997**, *119*, 7891.
[7] T. Gunnlaugsson, D. A. Mac Donail, D. Parker, *Chem. Commun.* **2000**, 93.
[8] J. J. La Clair, *Angew. Chem.* **1999**, *111*, 3231; *Angew. Chem. Int. Ed.* **1999**, *38*, 3045.
[9] V. Balzani, A. Credi, F. M. Raymo, J. F. Stoddart, *Angew. Chem.* **2000**, *112*, 3484; *Angew. Chem. Int. Ed*. **2000**, *39*, 3348.
[10] A. Credi, V. Balzani, S. J. Langford, J. F. Stoddart, *J. Am. Chem. Soc.* **1997**, *119*, 2679.
[11] K. L. Kompa, R. D. Levine, *Proc. Natl. Acad. Sci. USA* **2001**, *98*, 410.
[12] F. Remacle, E. W. Schlag, H. L. Selzle, K. L. Kompa, U. Even, R. D. Levine, *Proc. Natl. Acad. Sci. USA* **2001**, *98*, 2973.
[13] E. Woods, H. L. Berghout, C. M. Cheatum, F. F. Crim, *J. Phys. Chem. A* **2000**, *104*, 10356.
[14] F. F. Crim, *Science* **1990**, *249*, 1387.
[15] S. A. Reid, H. Reisler, *Ann. Rev. Phys. Chem.* **1996**, *47*, 495.
[16] R. N. Zare, *Science* **1998**, *279*, 1875.
[17] D. Bingemann, M. P. Gorman, A. M. King, F. F. Crim, *J. Chem. Phys.* **1997**, *107*, 661.
[18] A. Sinha, R. L. Vanderwal, F. F. Crim, *J. Chem. Phys.* **1989**, *91*, 2929.
[19] A. Sinha, R. L. Vanderwal, F. F. Crim, *J. Chem. Phys.* **1990**, *92*, 401.
[20] Y. Y. Bai, G. A. Segal, *J. Chem. Phys.* **1990**, *92*, 7479.
[21] T. L. Myers, N. R. Forde, B. Hu, D. C. Kitchen, L. J. Butler, *J. Chem. Phys.* **1997**, *107*, 5361.
[22] M. H. Lewin, *Logic Design and Computer Organization*, Addison-Wesley, Reading, **1983**.
[23] K. Bergmann, H. Theuer, B. W. Shore, *Rev. Mod. Phys.* **1998**, *70*, 1003.

  1433-7851/01/4013-2514 $ 17.50+.50/0

Oxide Addition to a Reactive Polysulfide Flux: Synthesis of $K_4Ba[Ti_6OS_{20}]$ Containing Isolated $[Ti_6OS_8(S_2)_6]^{6-}$ Clusters**

Fu Qiang Huang and James A. Ibers*

Dedicated to Professor Hans-Georg von Schnering on the occasion of his 70th birthday

A plethora of zero-dimensional chalcogenide cluster compounds are known, especially for the early transition metals.[1–3] For Group 4 and 5 metals, the stability of such clusters is often critically dependent on the presence of interstitial atoms.[4] Such interstitial atoms have been introduced adventitiously in syntheses involving solution chemistry,[2] an example being the synthesis of $[PPh_4]_2[Ti_3O(S_2)_3Cl_6]$ from the reaction of $TiCl_4$ with $S(SiMe_3)_2$ in CH_2Cl_2.[5] Introduction of interstitial atoms into solid-state clusters has progressed from the adventitious[6] to the deliberate.[3, 4, 7, 8] Almost all such solid-state syntheses involve the combination of the elements at high temperatures, often achieved by arc melting.

Since the synthesis of $K_4Ti_3S_{14}$ in 1987 by the reaction of Ti metal with a K_2S_n ($n \geq 2$) flux,[9, 10] the so-called "reactive flux method" has been used extensively to synthesize a wide variety of alkali metal (A) or Cu/metal (M)/polychalcogenide (Q_n) compounds, especially for metals from Groups 4 or 5.[9–21] The structures of many of these compounds comprise the hexagonal closest packing of one-dimensional M/Q chains, separated by A atoms.[22] The A/Group 4/Q_n structures are especially interesting, because they all contain linear M/Q chains. Although isolated two-dimensional M/Q layers and one-dimensional M/Q chains are known in solid-state binary[23–26] and ternary Group 4 metal chalcogen compounds,[15, 27] no zero-dimensional M/Q clusters have been found in A/M/Q compounds.[28]

We find that the low-temperature reactive flux method can be modified by the deliberate introduction of diverse potential interstitial species to afford zero-dimensional cluster compounds. We illustrate this with the synthesis of the solid-state cluster compound $K_4Ba[Ti_6OS_{20}]$ from a reactive flux similar to that used in the synthesis of the one-dimensional compound $K_4Ti_3S_{14}$, but augmented by the deliberate introduction of TiO_2. Specifically, this compound results in yields of approximately 70% from the reaction of K_2S_n, BaS, Ti, and TiO_2 at 823 to 873 K.

Two different crystal modifications of $K_4Ba[Ti_6OS_{20}]$ (hexagonal, space group *P6₃22* and orthorhombic, space group *Fddd*) are obtained, depending on the heating regime. Both consist of well-separated $[Ti_6OS_8(S_2)_6]^{6-}$ anionic clusters and K^+ and Ba^{2+} cations. The clusters are essentially identical in the two modifications; one such $[Ti_6OS_8(S_2)_6]^{6-}$ cluster is illustrated in Figure 1. It consists of an O-centered Ti_6 octahedron inscribed in a cube of eight S atoms with an S_2^{2-} group bonded on the outside of the cube to each Ti^{4+} center.

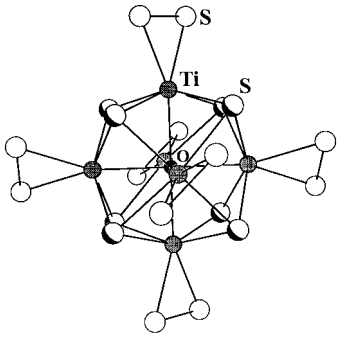

Figure 1. Structure of the $[Ti_6(O)S_8(S_2)_6]^{6-}$ cluster.

Although the idealized symmetry of $[Ti_6(O)S_8(S_2)_6]^{6-}$ could be as high as D_{3d}, it is D_3 in the hexagonal modification and D_{2h} in the orthorhombic modification. A similar core is found in the structures of $[Zr_6SS_8Cp_6]$ ($Cp = C_5H_5$)[29] and $[V_6OSe_8(PMe_3)_6]$.[29] Bond lengths within the anion are given in Table 1. These are normal. In particular, the Ti–O distances of 2.2824(5) to 2.2943(7) Å are expected for a Ti–O single bond, the S–S distances of 2.058(1) to 2.064(1) Å are expected for an S–S single bond, and the Ti···Ti distances are too long to be bonding. The absence of such bonding is consistent with the K/Ba ratio as given and the presence of Ti^{4+}.

Table 1. Selected distances for the $[Ti_6OS_8(S_2)_6]^{6-}$ clusters in $K_4Ba[Ti_6OS_{20}]$.

Space group *P6₃22*		Space group *Fddd*	
Ti–S1	2.376(1)	Ti1–S1 (×2)	2.375(1)
Ti–S2	2.370(1)	Ti1–S4 (×2)	2.4273(7)
Ti–S3	2.384(1)	Ti1–S5 (×2)	2.5285(7)
Ti–S3	2.532(1)	Ti2–S2	2.3743(8)
Ti–S3	2.536(1)	Ti2–S3	2.3786(8)
Ti–S4	2.472(1)	Ti2–S4	2.4364(8)
Ti–O	2.2890(7)	Ti2–S4	2.5701(8)
S1–S2	2.058(1)	Ti2–S5	2.3778(8)
Ti···Ti	3.235(2)	Ti2–S5	2.5375(8)
Ti···Ti (×2)	3.237(1)	Ti1–O	2.2943(7)
Ti···Ti	3.240(2)	Ti2–O	2.2824(5)
		S1–S1	2.064(1)
		S2–S3	2.0608(9)
		Ti1···Ti2 × 2	3.2241(7)
		Ti1···Ti2 × 2	3.2483(7)
		Ti2···Ti2	3.224(1)
		Ti2···Ti2	3.2318(1)

Experimental Section

Synthesis: The following reagents were used as obtained: K (Aldrich, 99.5%), BaS (Alfa, 99.7%), Ti (Aldrich, 99.7%), TiO_2 (Aldrich, 98.9+%), and S (Alfa, 99.5%). K_2S was prepared by stoichiometric reaction of the elements in liquid NH_3. Both crystal modifications of $K_4Ba[Ti_6OS_{20}]$ were prepared by the reactions of K_2S, BaS, Ti, TiO_2, and S in the molar ratio of 1:0.25:1:0.25:7. The mixtures were loaded into two carbon-coated fused-

[*] Prof. J. A. Ibers, F. Q. Huang
Department of Chemistry
Northwestern University
2145 Sheridan Road
Evanston, IL 60208-3113 (USA)
Fax: (+1) 847-491-2976
E-mail: ibers@chem.northwestern.edu

[**] This research was supported by the U.S. National Science Foundation (CHE98-19385 and DMR00-96676). This work made use of facilities supported by the MRSEC program of the National Science Foundation (DMR00-76097) at the Materials Research Center of Northwestern University.

  1433-7851/01/4013-2515 $ 17.50+.50/0

silica tubes under an argon atmosphere in a glove box. These tubes were sealed under a 10^{-4} Torr atmosphere and then placed in a computer-controlled furnace. The sample in the first tube was heated to 823 K at 1.5 K min^{-1}, kept at 823 K for three days, very slowly cooled at 4 K h^{-1} to 423 K, then cooled to room temperature to afford black hexagonal plates of the hexagonal modification in about 80% yield. The sample in the second tube was heated to 873 K at 1.5 K min^{-1}, kept at 873 K for two days, when the furnace was turned off. Black needles of the orthorhombic modification were obtained in about 70% yield. The reaction mixtures were washed free of alkali metal chalcogenides with dimethylformamide and then dried with acetone. Analysis of these crystals with an energy-dispersive X-ray (EDX)-equipped Hitachi S-4500 scanning electron microscope showed K/Ba/Ti/S approximately in the ratio 5:1:10:30; the presence of O was observed but could not be quantified.

General crystallographic details: Bruker Smart 1000 CCD diffractometer,[30] graphite-monochromatized $Mo_{K\alpha}$ radiation ($\lambda = 0.71073$ Å), $T = 153$ K. Data were collected by an ω scan of 0.3° in groups of 606, 606, and 606 frames at ϕ settings of 0°, 120°, and 240° for the hexagonal modification and in groups of 606, 606, 606, and 606 frames at ϕ settings of 0°, 90°, 180°, and 270° for the orthorhombic modification. The exposure times were 15 s frame^{-1}. Intensity data were collected with the program SMART.[30] Cell refinement and data reduction were carried out with the use of the program SAINT,[30] face-indexed absorption corrections were carried out with the program XPREP,[31] and the frame variations were further corrected with the use of the program SADABS.[30] The structures were solved with the direct methods program SHELXS and refined with the least-squares program SHELXL of the SHELXTL-PC suite of programs.[31] The final refinements included anisotropic displacement parameters and a secondary extinction correction. Crystal structure analysis of $K_4Ba[Ti_6OS_{20}]$: black hexagonal plate, $0.040 \times 0.078 \times 0.084$ mm, hexagonal, $P6_322$, $a = 9.3386(4)$, $c = 18.130(1)$ Å, $V = 1369.3(1)$ Å^3, $T = 153$ K, $Z = 2$, $\rho_{calcd} = 3.004$ g cm^{-3}, $\theta_{max.} = 28.88°$, 11 429 reflections measured, 1175 unique, 1064 observed with $I > 2\sigma(I)$, $\mu = 52.12$ cm^{-1}, min/max transmission = 0.685/0.816, $R_1 = 0.0374$, $wR_2 = 0.0895$. Black needle, $0.096 \times 0.112 \times 0.248$ mm, orthorhombic, $Fddd$, $a = 11.106(2)$, $b = 15.338(2)$, $c = 32.265(5)$ Å, $V = 5496.0(13)$ Å^3, $T = 153$ K, $Z = 8$, $\rho_{calcd} = 2.993$ g cm^{-3}, $\theta_{max.} = 28.85°$, 16 008 reflections measured, 1749 unique, 1590 observed with $I > 2\sigma(I)$, $\mu = 51.94$ cm^{-1}, min/max transmission = 0.459/0.713, $R_1 = 0.0336$, $wR_2 = 0.0894$.

Further details on the crystal structure investigations may be obtained from the Fachinformationszentrum Karlsruhe, 76344 Eggenstein-Leopoldshafen, Germany (fax: (+49) 7247-808-666; e-mail: crysdata@fiz-karlsruhe.de), on quoting the depository numbers CSD-411697 for the orthorhombic modification and CSD-411698 for the hexagonal modification.

Received: February 22, 2001 [Z16664]

[1] T. Saito, *Adv. Inorg. Chem.* **1997**, *44*, 45 – 91.
[2] T. Saito in *Early Transition Metal Clusters with π-Donor Ligands* (Ed.: M. H. Chisholm), VCH, New York, **1995**, pp. 63 – 164.
[3] J. D. Corbett, *Inorg. Chem.* **2000**, *39*, 5178 – 5191.
[4] J. D. Corbett, E. Garcia, Y.-U. K. Kwon, A. Guloy, *Pure Appl. Chem.* **1990**, *62*, 103 – 112.
[5] U. Müller, V. Krug, *Angew. Chem.* **1988**, *100*, 277; *Angew. Chem. Int. Ed. Engl.* **1988**, *27*, 293 – 294.
[6] A. Simon, *J. Solid State Chem.* **1985**, *57*, 2 – 16.
[7] J. D. Corbett, *J. Alloys Compd.* **1995**, *229*, 10 – 23.
[8] F. Rogel, J. Zhang, M. W. Payne, J. D. Corbett in *Electron Transfer in Biology and the Solid State. Inorganic Compounds with Unusual Properties*, *Vol. 226* (Eds.: M. K. Johnson, R. B. King, D. M. Kurtz, Jr., C. Kutal, M. L. Norton, R. A. Scott), American Chemical Society, Washington, DC, **1990**, pp. 369 – 402.
[9] S. A. Sunshine, D. Kang, J. A. Ibers, *J. Am. Chem. Soc.* **1987**, *109*, 6202 – 6204.
[10] S. A. Sunshine, D. Kang, J. A. Ibers, *Mater. Res. Soc. Symp. Proc.* **1987**, *97*, 391 – 396.
[11] D. Kang, J. A. Ibers, *Inorg. Chem.* **1988**, *27*, 549 – 551.
[12] P. M. Keane, J. A. Ibers, *Inorg. Chem.* **1991**, *30*, 1327 – 1329.
[13] J. A. Cody, J. A. Ibers, *Inorg. Chem.* **1994**, *33*, 2713 – 2715.
[14] M. A. Pell, J. A. Ibers, *Chem. Mater.* **1996**, *8*, 1386 – 1390.
[15] M. A. Pell, J. A. Ibers, *Chem. Ber.* **1997**, *130*, 1 – 8.
[16] D. Röhnert, C. Näther, W. Bensch, *Acta Crystallogr. Sect. C* **1997**, *53*, 165 – 167.
[17] S. Herzog, C. Näther, P. Dürichen, W. Bensch, *Z. Anorg. Allg. Chem.* **1998**, *624*, 2021 – 2024.
[18] W. Bensch, C. Näther, P. Dürichen, *Angew. Chem.* **1998**, *110*, 140 – 142; *Angew. Chem. Int. Ed.* **1998**, *37*, 133 – 135.
[19] O. Krause, C. Näther, W. Bensch, *Acta Crystallogr. Sect. C* **1999**, *55*, 1197 – 1199.
[20] S. Herzog, C. Näther, W. Bensch, *Z. Anorg. Allg. Chem.* **1999**, *625*, 969 – 974.
[21] W. Bensch, P. Dürichen, C. Näther, *Solid State Sci.* **1999**, *1*, 85 – 108.
[22] F. Q. Huang, J. A. Ibers, *Inorg. Chem.* **2001**, *40*, 865 – 869.
[23] P. Monceau, *Electronic Properties of Inorganic Quasi-One-Dimensional Compounds*, D. Reidel, Dordrecht, Netherlands, **1985**.
[24] H. Fjellvåg, A. Kjekshus, *Solid State Commun.* **1986**, *60*, 91 – 93.
[25] S. Furuseth, H. Fjellvåg, *Acta Chem. Scand.* **1991**, *45*, 694 – 697.
[26] S. Furuseth, L. Brattås, A. Kjekshus, *Acta Chem. Scand.* **1973**, *27*, 2367 – 2374.
[27] J. A. Cody, M. F. Mansuetto, M. A. Pell, S. Chien, J. A. Ibers, *J. Alloys Compd.* **1995**, *219*, 59 – 62.
[28] Note added in proof: Prof. W. Bensch has called our attention to an abstract describing the related compound $K_6TiS_{18}O$ (R. Tillinski, C. Näther, W. Bensch, *Z. Kristallogr. Suppl.* **1999**, *16*, 66).
[29] D. Fenske, A. Grissinger, M. Loos, J. Magull, *Z. Anorg. Allg. Chem.* **1991**, *598/599*, 121 – 128.
[30] SMART Version 5.054 Data Collection and SAINT-Plus Version 6.02A Data Processing Software for the SMART System, Bruker Analytical X-Ray Instruments, Inc., Madison, WI, USA, **2000**.
[31] G. M. Sheldrick, SHELXTL DOS/Windows/NT Version 5.10, Bruker Analytical X-Ray Instruments, Inc., Madison, WI, USA, **1997**.

Switching a Catalyst System from Ethene Polymerization to Ethene Trimerization with a Hemilabile Ancillary Ligand**

Patrick J. W. Deckers, Bart Hessen,* and Jan H. Teuben

The chemistry of transition metal complexes with hemilabile ancillary ligands (i.e., with multidentate ligands that have a mixture of tightly bound and substitutionally labile functionalities) is enjoying an increasing popularity.[1] These hemilabile ligands can stabilize reactive metal centers by the chelate effect, but keep the metal accessible for substrate molecules by virtue of the substitutionally labile character of one of the functionalities. Examples of such hemilabile ligands include phosphine – ether, cyclopentadienyl – alkene, and phosphine – arene ligands. In some cases, hemilabile ligands were found to influence the selectivity and stability of transition metal catalysts.[2] Here we report that the catalyst system $[(\eta^5\text{-}C_5H_4CMe_2R)TiCl_3]$/MAO (MAO = methylalumoxane) is transformed from an ethene polymerization catalyst into an ethene trimerization catalyst, producing 1-hexene, by simply changing the ligand substituent R from a methyl to a

[*] Dr. B. Hessen, P. J. W. Deckers, Prof. Dr. J. H. Teuben
Dutch Polymer Institute/Center for Catalytic Olefin Polymerization
Stratingh Institute for Chemistry and Chemical Engineering
University of Groningen
Nijenborgh 4, 9747 AG Groningen (The Netherlands)
Fax: (+31) 50-3634315
E-mail: hessen@chem.rug.nl

[**] Netherlands Institute for Catalysis Research (NIOK) publication RUG 01-04-02.

  1433-7851/01/4013-2516 $ 17.50+.50/0

phenyl group. It appears that the hemilabile behavior of the cyclopentadienyl ligand with a pendant arene group is responsible for this drastic switch in catalyst performance.

The catalyst precursors used in this study, $[(\eta^5\text{-}C_5H_4CMe_2R)TiCl_3]$ (R = Ph, **1**; 3,5-dimethylphenyl, **2**; Me, **3**), are readily obtained by reaction of 6,6-dimethylfulvene with the appropriate RLi reagent followed by reaction with $TiCl_4$, or by reaction of $TiCl_4$ with the corresponding $Me_3Si(C_5H_4CMe_2R)$ reagent.[3, 4] In previous work by us and others it has been shown that cationic dialkyl derivatives of **1** and **2** can be generated by reaction of the trimethyl complexes $[(\eta^5\text{-}C_5H_4CMe_2Ar)TiMe_3]$ with Lewis acids such as $B(C_6F_5)_3$, and that in these cationic species $[(C_5H_4CMe_2Ar)TiMe_2]^+$ the arene moiety is η^6-coordinated to the metal center. For Ar = 3,5-$Me_2C_6H_3$ this yields a relatively stable 16-electron complex that does not polymerize propene at ambient temperature and pressure.[4] For Ar = C_6H_5 the coordination is noticeably weaker, and a modest activity in propene polymerization was reported.[3]

We have now observed that activation of the trichloride **1** with 1000 equiv of the cocatalyst MAO in toluene under ethene pressure generates a catalyst that converts ethene predominantly to 1-hexene. Results of catalytic ethene conversion experiments under various conditions are listed in Table 1. The catalyst produces at ambient temperatures olefin trimerization products with high selectivity (95–98 wt% overall). These products consist of two fractions: C_6 products (>99% 1-hexene) and C_{10} products (cotrimers of ethene and 1-hexene). The C_{10} fraction consists mainly (>75%) of 5-methyl-non-1-ene. In addition, some 1-octene (1 wt%) and polyethene (PE, 1–3 wt%) is produced. The rate of production of 1-hexene increases with increasing ethene pressure, the C_6 productivity being about 550–600 kg per mole Ti, h, and bar over a range of 2–10 bar in ethene pressure. The thermal stability of the catalyst is modest, and increasing the reaction temperature decreases the overall catalyst productivity due to catalyst degradation (as seen from the decrease in the ethene uptake rate over the run period) and increases the relative amount of PE produced (see Table 1).

Table 1. Catalytic ethene conversion with the **1**/MAO catalyst system (toluene solvent, 15 μmol Ti, Al:Ti = 1000, 30 min run time).

p(ethene) [bar]	*T* [°C]	C_6 products [g] (wt%)	C_{10} products [g] (wt%)	PE [g] (wt%)	Productivity[a]
2	30	8.0 (87)	1.0 (11)	0.2 (1.6)	1066
5	30	20.9 (83)	3.5 (14)	0.5 (1.8)	2787
10	30	47.2 (86)	5.1 (9)	1.4 (2.6)	6292
5	50	12.4 (83)	1.6 (11)	0.7 (4.6)	1653
5	80	3.3 (76)	0.2 (4)	0.8 (19)	440

[a] In kg C_6 product per mole Ti and h.

The importance of the pendant arene group on the ancillary ligand for 1-hexene production can be seen by comparing the performance of the three catalyst systems **1**–**3**/MAO (Table 2). Making the pendant arene group more electron-rich by adding methyl substituents significantly diminishes the catalyst activity (but the selectivity for trimerization is retained), whereas the absence of a pendant arene group leads to the predominant formation of PE. This indicates that a) the pendant arene group is essential to obtaining selective trimerization, and that b) this catalysis is likely to involve reversible coordination of the arene moiety to the metal center. It may be noted that even for the *tert*-butylcyclopentadienyl system **3**/MAO some ethene trimerization is observed. A related observation was made recently by Pellecchia et al. in ethene polymerization with $[(\eta^5\text{-}C_5Me_5)TiMe_2]$-$[MeB(C_6F_5)_3]$ in toluene as catalyst, where the PE obtained contains a noticeable amount of *n*-butyl side groups.[5] It was suggested that the catalyst is partly converted to a species that trimerizes ethene to 1-hexene, which is then incorporated into the polymer. Our observations indicate that transient coordination of the toluene solvent to the metal center may be instrumental in this,[6] albeit less efficient than the pendant arene group in the $[(\eta^5\text{-}C_5H_4CMe_2Ar)TiCl_3]$/MAO systems as the interaction is intermolecular rather than intramolecular.

Table 2. Catalytic ethene conversion with the **1**–**3**/MAO catalyst systems (toluene solvent, 5 bar ethene, 30 °C, 15 μmol Ti, Al:Ti = 1000, 30 min run time).

Catalyst (R)	C_6 products [g] (wt%)	C_{10} products [g] (wt%)	PE [g] (wt%)	Productivity[a]
1 (Ph)	20.9 (83)	3.5 (14)	0.5 (1.8)	2787
2 (3,5-$Me_2C_6H_3$)	7.9 (93)	0.5 (5)	0.1 (1.3)	1053
3 (Me)	0.5 (17)	0.1 (4)	2.4 (76)	66

[a] In kg C_6 product per mole Ti and h.

The only family of catalysts known thus far to give highly selective ethene trimerization is based on chromium (mixtures of Cr salts with alkylaluminum compounds and added ligands, especially imidazoles, or coordinating solvents such as 1,2-dimethoxyethane).[7] Very recently, selective trimerization of higher alkenes with triazacyclohexane–chromium species was also reported.[8] The catalysis in these systems is proposed to proceed via metallacyclic intermediates, chromacyclopentanes and chromacycloheptanes, where β-H abstraction from the latter, followed by reductive elimination, leads to 1-hexene formation and a low-valent Cr species. The latter can then couple two ethene molecules to regenerate the chromacyclopentane.[9, 10] It is possible that a similar cycle is operative in the present titanium system. Several catalytic C-C coupling reactions have been reported in neutral Ti systems that involve the Ti^{IV}/Ti^{II} couple (e.g., in the bis(aryloxy)titanium compounds).[11] The question is then how the system converts from the cationic species $[(C_5H_4CMe_2Ar)TiMe_2]^+$ (generated by the reaction of the corresponding trichloride with MAO) to a cationic metallacyclopentane. A proposal for this process is shown in Scheme 1.

The initially generated species $[(C_5H_4CMe_2Ph)TiMe_2]^+$ will undergo multiple ethene insertions into the Ti–Me bonds (where during ethene capture the arene is likely to be noncoordinating) to produce bis(*n*-alkyl) compounds $[(C_5H_4CMe_2Ph)Ti(CH_2CH_2R)_2]^+$. These are in equilibrium (through β-H elimination) with hydride–olefin species. Normally, dissociation of the olefin is energetically unfavorable unless it is driven out by another incoming ligand (e.g.,

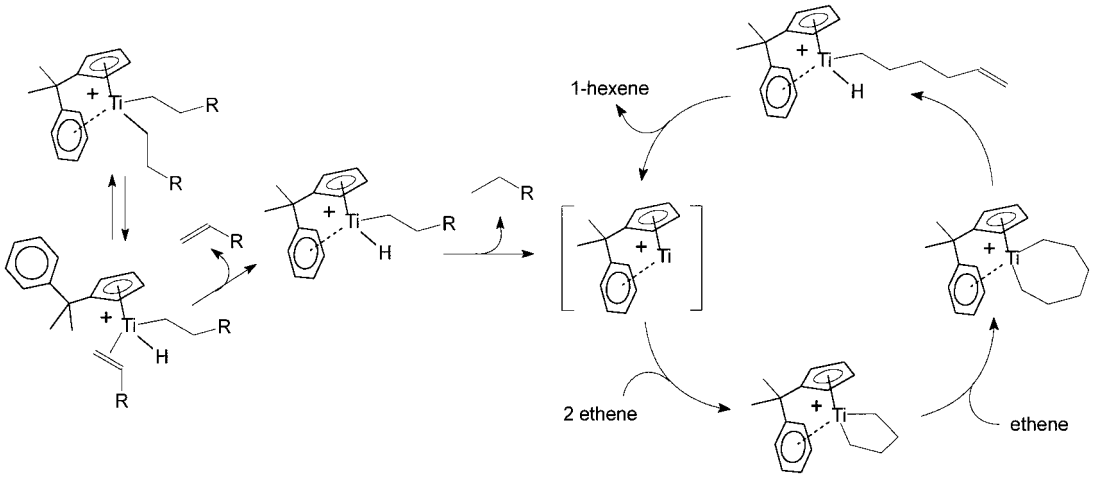

Scheme 1. Proposed reaction pathway for catalyst transformation and catalytic ethene trimerization in the system studied.

ethene, which will then rapidly insert into the M–H bond, resulting in the normal chain transfer process for catalytic ethene polymerization).[12] In the system with the pendant arene group it is possible that the alkene is driven out by the incoming arene, which will lead to a 16-electron hydride–alkyl species, $[(\eta^5,\eta^6\text{-}C_5H_4CMe_2Ph)Ti(H)(CH_2CH_2R)]^+$. Reductive elimination then releases CH_3CH_2R and forms a Ti^{II} intermediate which can capture two ethene molecules to give a cationic titanacyclopentane. This species can then perform the catalytic ethene trimerization (Scheme 1), following the pathway described above for the Cr-based catalysts.

We are presently investigating the validity of this proposal. Although we did observe that the independently generated ionic species $[(\eta^5,\eta^6\text{-}C_5H_4CMe_2Ar)TiMe_2][MeB(C_6F_5)_3]$ reacts with ethene in $[D_8]$toluene to generate 1-hexene (NMR tube experiment), we have as yet not been successful in observing and isolating the proposed cationic titanacyclopentane intermediate. Nevertheless, we feel that the present proposal is reasonable given the observations made thus far.

In conclusion, we have identified a catalyst system, $[(\eta^5\text{-}C_5H_4CMe_2R)TiCl_3]$/MAO, that, by attachment of a pendant arene group to the cyclopentadienyl ancillary ligand (R = aryl), can be transformed from an ethene polymerization catalyst to a selective ethene trimerization catalyst. Although ethene oligomerizations that produce 1-hexene in excess of the amount expected from Schultz–Flory product distributions, and ethene polymerization catalysts that produce branched polyethenes are known (e.g., for certain Ziegler-type catalyst systems),[13] to our knowledge the present system is the first highly selective ethene trimerization catalyst that is not based on chromium. The principle that a hemilabile ligand functionality can divert the metal species from one catalytic cycle into another may be applicable to other types of catalysis.

Experimental Section

All manipulations of catalyst and cocatalyst solutions were carried out under purified nitrogen atmosphere using standard glove-box and Schlenk techniques. The compounds **1**–**3** were prepared according to literature procedures.[3, 4] A toluene solution of MAO (26 wt%, Akzo Nobel Chemicals) was used as received. Toluene (Aldrich, anhydrous, 99.8%) was passed over columns of Al_2O_3 (Fluka), BASF R3–11 supported Cu oxygen scavenger, and molecular sieves (4 Å) under nitrogen atmosphere prior to use. Ethene (AGA polymer grade) was passed over BASF R3-11 supported Cu oxygen scavenger and molecular sieves (4 Å). Cyclooctane (used as internal standard) was distilled from sodium prior to use. Product analyses were performed by GC on a HP 6890 instrument equipped with a HP-1 dimethylpolysiloxane column (19095 Z-123) and by GC/MS using a HP 5973 mass-selective detector attached to a HP 6890 GC instrument.

General procedure for the catalytic ethene conversions: A stainless-steel 1-L autoclave (Medimex), fully temperature- and pressure-controlled and equipped with solvent and catalyst injection systems, was preheated in vacuo for 45 min at 100 °C. The reactor was cooled to the desired temperature, charged with 200 mL of toluene, and pressurized with ethene. After equilibrating for 15 min, the appropriate amount of MAO/toluene was injected, together with 25 mL of toluene. Subsequently, a mixture of 2.50 mL of cyclooctane (internal standard) and 1.0 mL of a 15 mM stock solution of the titanium halide complex in toluene was injected, together with 25 mL of toluene, to start the reaction. During the reaction the ethene pressure was kept constant to within 0.1 bar of the initial pressure by replenishing flow. The run was ended by adding an aliquot of ethanol, and the reactor was vented. Remaining residual MAO was destroyed by adding further ethanol, and samples of the reaction mixture were taken to analyze and quantify the soluble components by GC and GC/MS. The polymer was stirred for 1 h in acidified ethanol, repeatedly rinsed with ethanol on a glass frit, and dried in vacuo at 70 °C overnight.

Received: February 27, 2001 [Z16694]

[1] For a recent review on transition metal complexes with hemilabile ligands, see: C. S. Slone, D. A. Weinberger, C. A. Mirkin, *Prog. Inorg. Chem.* **1999**, *48*, 233–350.

[2] See for example: a) E. Lindner, B. Keppeler, H. A. Mayer, K. Gierling, R. Fawzi, M. Steinmann, *J. Organomet. Chem.* **1996**, *526*, 175–184; b) S. Mecking, W. Keim, *Organometallics* **1996**, *15*, 2650–2656; c) M. Nandi, J. Jin, T. V. RajanBabu, *J. Am. Chem. Soc.* **1999**, *121*, 9899–9900, and references therein.

[3] J. Sassmannshausen, A. K. Powell, C. E. Anson, S. Wocadlo, M. Bochmann, *J. Organomet. Chem.* **1999**, *592*, 84–94.

[4] P. J. W. Deckers, A. J. van der Linden, A. Meetsma, B. Hessen, *Eur. J. Inorg. Chem.* **2000**, 929–932.

[5] C. Pellecchia, D. Pappalardo, G.-J. Gruter, *Macromolecules* **1999**, *32*, 4491–4493.

[6] D. J. Gillis, M.-J. Tudoret, M. C. Baird, *J. Am. Chem. Soc.* **1993**, *115*, 2543–2545.

[7] a) J. R. Briggs (Union Carbide), US-A 4668838, **1987** [*Chem. Abstr.* **1987**, *107*, 178604]; b) W. K. Reagan, B. K. Conroy (Phillips Petroleum), EP 416304, **1990** [*Chem. Abstr.* **1992**, *116*, 60189]; c) M. Tamura, K. Uchida, K. Iwanaga, Y. Ito (Sumitomo Chemical), EP

  1433-7851/01/4013-2518 $ 17.50+.50/0

699648, **1995** [*Chem. Abstr.* **1996**, *124*, 344431]; d) Y. Araki, H. Nakamura, Y. Nanba, T. Okano (Mitsubishi Chemical), US-A 5856612, **1997** [*Chem. Abstr.* **1997**, *127*, 161493].
[8] R. D. Köhn, M. Haufe, G. Kociok-Köhn, S. Grimm, P. Wasserscheid, W. Keim, *Angew. Chem.* **2000**, *112*, 4519–4521; *Angew. Chem. Int. Ed.* **2000**, *39*, 4337–4339.
[9] J. R. Briggs, *J. Chem. Soc. Chem. Commun.* **1989**, 674–675.
[10] R. Emrich, O. Heinemann, P. W. Jolly, C. Krüger, G. P. J. Verhovnik, *Organometallics* **1997**, *16*, 1511–1513.
[11] a) M. G. Thorn, J. E. Hill, S. A. Waratuke, E. S. Johnson, P. E. Fanwick, I. P. Rothwell, *J. Am. Chem. Soc.* **1997**, *119*, 8630–8641; b) S. A. Waratuke, M. G. Thorn, P. E. Fanwick, A. P. Rothwell, I. P. Rothwell, *J. Am. Chem. Soc.* **1999**, *121*, 9111–9119.
[12] P. Margl, L. Deng, T. Ziegler, *J. Am. Chem. Soc.* **1999**, *121*, 154–162, and references therein.
[13] See for example: S. Murtuza, S. B. Harkins, G. S. Long, A. Sen, *J. Am. Chem. Soc.* **2000**, *122*, 1867–1872, and references therein.

An Insoluble Polymer-Bound Bis-Oxazoline Copper(II) Complex: A Highly Efficient Heterogeneous Catalyst for the Enantioselective Mukaiyama Aldol Reaction**

Simonetta Orlandi, Alessandro Mandoli, Dario Pini, and Piero Salvadori*

In recent years asymmetric catalytic procedures have been emerging as a major option for the preparation of chiral compounds in enantiomerically enriched form, especially when the catalyst system consists of readily available, cheap and nontoxic components.[1] However, the recovery of the catalyst and its reuse is often mandatory for large-scale applications. At present, one of the most promising solutions for this problem seems to be the anchoring of effective soluble systems on an insoluble matrix, ideally without any reduction of catalytic performances with respect to the homogeneous phase.[2, 3] While this strategy is well established in reduction and oxidation processes,[4, 5] few examples have been reported for C–C bond-forming reactions.[6]

In our continuing effort to develop heterogeneously catalyzed asymmetric Mukaiyama aldol reactions,[7] we became interested in bis-oxazoline (box) ligands **1**.[8] In spite of the versatility of this class of chiral auxiliaries, few supported copper box complexes have been reported to date.[9] They rely on ion exchange to anchor them to an organic or inorganic host. The application of these immobilized catalysts to asymmetric cyclopropanation and aziridination led to modest enantioselectivity, which could be related to unfavorable interactions between the metal complex and the support.[10, 11] Better results were recently reported by Evans et al. for a hetero Diels–Alder reaction with Cu^{II}–box in the presence of Florisil, although the use of a poor solvent for the metal complex was required for effective recovery of the catalyst.[12]

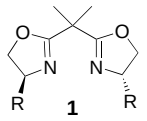

1

To develop a versatile, reusable, insoluble box ligand equivalent to the homogeneous systems **1**, the preparation of bis-oxazoline covalently bound to an inert polystyrene matrix was designed. The chiral monomer **2a** was synthesized by the route depicted in Scheme 1,[13] together with the soluble model **2b** of the supported ligand.

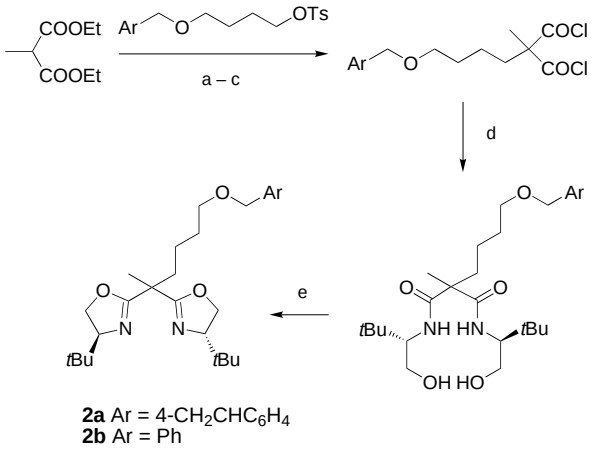

Scheme 1. a) NaH, THF, reflux, 24 h, 65–95%; b) 18 M KOH, reflux, 3 h, 82–89%; c) $(COCl)_2$, cat. DMF, CH_2Cl_2, RT, 18 h; d) (*S*)-*t*BuCH(NH_2)-CH_2OH (2 equiv), Et_3N, CH_2Cl_2, RT, 35 min; e) TsCl, Et_3N, cat. DMAP, CH_2Cl_2, RT, 27 h, 50–55% over two steps. Ts = *p*-toluenesulfonyl, DMAP = 4-dimethylaminopyridine.

The AIBN-initiated copolymerization of **2a** with styrene and divinylbenzene (DVB), in the presence of toluene as a porogen agent,[14] followed by exhaustive extraction with THF and CH_2Cl_2, afforded **3** (Scheme 2). It was characterized by IR spectroscopy ($\tilde{\nu}_{C=N} = 1655\ cm^{-1}$),[15] and its content of chiral ligand (0.31 mmol g^{-1}) was evaluated by nitrogen elemental analysis. A maximum metal uptake of 0.18 mmol g^{-1} was determined by equilibrating **3** with an excess of $Cu(OTf)_2$ in THF.

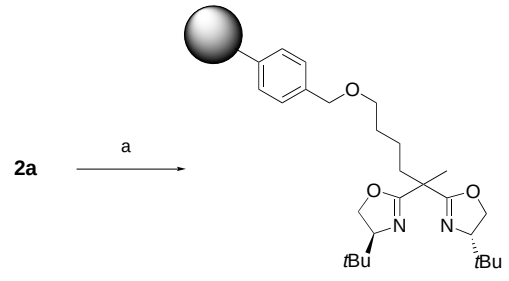

3

Scheme 2. a) Styrene, DVB (**2a**:styrene:DVB = 7:42:51), AIBN, toluene (60% v/v), 80 °C, 18 h. AIBN = azobisisobutyronitrile.

[*] Prof. P. Salvadori, M. Sc. S. Orlandi, Dr. A. Mandoli, Prof. D. Pini
Dipartimento di Chimica e Chimica Industriale, Università di Pisa
Centro di Studio del C.N.R. per le Macromolecole Stereordinate ed Otticamente Attive
Via Risorgimento 35, 56126 Pisa (Italy)
Fax: (+39) 050-918-409
E-mail: psalva@dcci.unipi.it

[**] This work was supported by MURST, Università di Pisa (National Project "Stereoselezione in Sintesi Organica, Metodologie ed Applicazioni"), and Consiglio Nazionale delle Ricerche (CNR).

  1433-7851/01/4013-2519 $ 17.50+.50/0

The supported box **3** was next used in the Cu^{II}-catalyzed Mukaiyama aldol addition of ketene thioacetal **4** to methyl pyruvate **5** [Eq. (1); TMS = trimethyl silyl]; for comparative

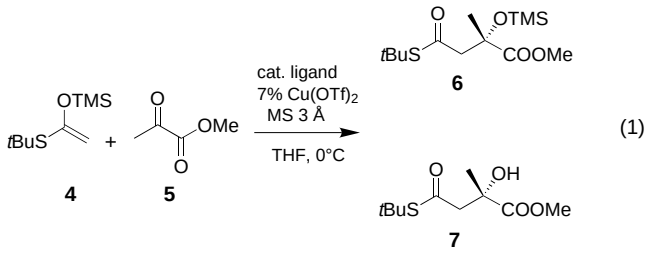

(1)

purposes, test runs with the soluble ligand **1** (R = *t*Bu) and the model compound **2b** were also carried out. The reactions were performed under standard conditions[16] with 3 Å molecular sieves (MS) as water scavengers. A slightly higher ligand-to-metal ratio was used in the case of **3** (Table 1) to compensate for the reduced ligand availability (see above). Although the heterogeneous catalyst **3** · $Cu(OTf)_2$ proved less active than the homogeneous catalysts derived from **1** (R = *t*Bu) and **2b** (entries 1 and 2), the silylated aldol **6** and its hydrolysis product **7** were formed after 1 h in high overall yield (entry 3) and with an enantiomeric excess comparable to those obtained with the soluble ligands **1** and **2b**.[17]

Table 1. Catalytic asymmetric Mukaiyama reaction.

Entry	Recycle	Ligand [mol %]	*t* [min]	**6** + **7** yield [%][a]	(*S*)-**7** *ee* [%][b]
1	–	**1** (R = *t*Bu) (7.7)	15	100	94
2	–	**2b** (7.7)	15	100	92
3	0	**3** (12.4)	60	90	90
4	1	**3**[c] (12.4)	60	85	91
5	2	**3**[c] (12.4)	60	86	89
6	3	**3**[c] (12.4)	60	81	88
7	4	**3**[c] (12.4)	60	52	91
8	5	**3**[c, d] (12.4)	60	96	89
9	6	**3**[d, e] (12.4)	120	97	93
10	7	**3**[d, e] (12.4)	240	97	93

[a] Determined by GLC and ^{1}H NMR spectroscopy with methyl-1-naphthoate as internal standard. [b] Determined by HPLC. Absolute configuration by comparison of the optical rotation and the retention time with those of an authentic sample. [c] Supported ligand from the previous run. [d] Fresh MS were added. [e] Supported copper complex from the previous run.

At the end of the reaction, the polymer-supported catalyst was quantitatively recovered by filtration, together with the MS, washed with CH_2Cl_2 and dried in vacuum. To assess the recycling effectiveness of the supported ligand, the initial amount of $Cu(OTf)_2$ in THF was added to the recovered material, any excess of metal removed by filtration, and the heterogeneous catalyst employed in a new aldol reaction. In four successive runs by this procedure, almost unchanged *ee* values were obtained together with a moderate reduction in rate (entries 4–7). Most likely this was a consequence of water buildup in the catalyst system,[16] as the simple replacement of the MS with fresh ones effectively restored the activity to the initial value (recycle 5, entry 8). The accumulation of water could also explain the presence in the reaction mixture of the free aldol **7** besides the silylated form **6**: this is probably a consequence of the hydrolysis of Me_3SiOTf involved in the catalytic cycle, which is known to effect the in situ conversion of **7** into **6**.[16] Indeed, the relative amount of **6** steadily decreased in the course of the runs, unless fresh MS were added in the fifth recycle (Figure 1).

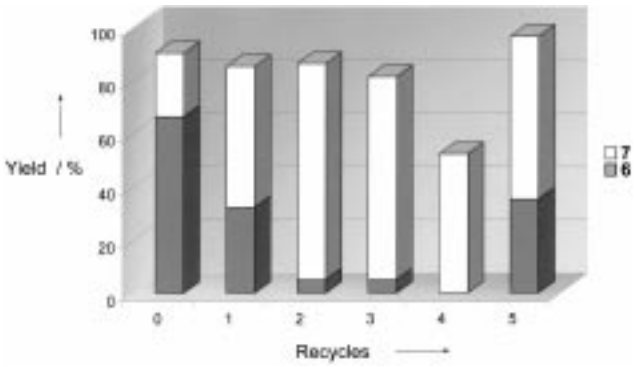

Figure 1. Catalytic activity and product distribution in recycle runs.

The finding that **3** that was recovered after the reactions was green suggested that some copper salt could be retained by the polymer-bound ligand. This prompted us to investigate the possibility of recycling the whole catalyst **3** · $Cu(OTf)_2$ by performing two further runs without the addition of any $Cu(OTf)_2$ (entries 9 and 10). Under these conditions the reaction progressively slowed down. Nevertheless, complete conversion of the substrates could be achieved, albeit at longer times, and a slight increase in the *ee* values was also observed.

Finally, preliminary experiments showed that **3** · $Cu(OTf)_2$ is also active in the catalysis of the Mukaiyama reaction between nucleophilic reagents (2-trimethylsilyloxyfuran) and electrophilic reagents (benzyloxyacetaldehyde) that differ from **4** and **5**. While low *ee* values (10–30 %) were generally obtained, both at 0 and −78 °C, the addition of (*Z*)-1-*tert*-butylthio-1-trimethylsilyloxypropene to methyl pyruvate at 0 °C[16] afforded **8** (*syn*:*anti* = 83:17, *syn* 79 % *ee*) with a stereoselectivity comparable with that obtained with the soluble ligand **1** (R = *t*Bu) under the same conditions (*syn*:*anti* = 85:15, *syn* 81 % *ee*).

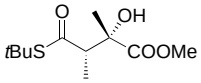

8

In summary, a convenient route for the preparation of the insoluble polystyrene-supported bis-oxazoline ligand **3** was developed. The use of **3** in the copper(II)-catalyzed aldol addition of silylthioketene acetals to methyl pyruvate led to the first example of a highly enantioselective Mukaiyama reaction involving a heterogeneous catalyst system.[18] Moreover, **3** could be easily recovered by simple filtration and reused several times without any loss of activity and stereoselectivity. Studies are currently underway to extend the scope of the reaction and to develop materials suitable for low-temperature applications.

Experimental Section

General procedure for the Mukaiyama aldol reaction with **3**: in a Schlenk tube provided with a glass frit, **3** (100 mg, 0.031 mmol of supported ligand) and $Cu(OTf)_2$ (0.019 mmol) in dry THF (1 mL) were stirred for 1 h at RT. Activated 3 Å MS (100 mg) were added, and stirring was continued for 1 h.

  1433-7851/01/4013-2520 $ 17.50+.50/0 *Angew. Chem. Int. Ed.* **2001**, *40*, No. 13

The mixture was then cooled to $-78\,^{\circ}C$ and sequentially treated with methyl pyruvate **5** (0.25 mmol) containing methyl-1-naphthoate (internal standard) and ketene thioacetal **4** (0.30 mmol). After transferring the Schlenk tube into an ice bath, samples were taken at time intervals and filtered through a short (2 cm) silica gel plug,[19] and the conversion and the **6**/**7** ratio were determined by GLC.[16] When conversion was complete, the reaction mixture was filtered under an inert atmosphere, and the filtrate containing **6** and **7** was hydrolyzed as described.[16] Yield and *ee* of **7** were determined by ^{1}H NMR spectroscopy and HPLC (Chiralcel OD-H, 0.5 mL min^{-1}, hexane/2-propanol 99:1), respectively.

The recovered complex **3** · $Cu(OTf)_2$ was washed with dry CH_2Cl_2 and dried under vacuum. The MS could be mechanically removed at this stage. Recycle runs were carried out according to the general procedure, beginning with the addition of the initial amount of $Cu(OTf)_2$ (entries 4–8) or skipping this step (entries 9–10).

Received: December 6, 2000 [Z16236]

[1] a) *Comprehensive Asymmetric Catalysis* (Eds.: E. N. Jacobsen, A. Pfaltz, H. Yamamoto), Springer, Berlin, **1999**; b) *Transition Metals for Organic Synthesis* (Eds.: M. Beller, C. Bolm), Wiley-VCH, Weinheim, **1998**.

[2] *Chiral Catalyst Immobilization and Recycling* (Eds.: D. E. De Vos, I. F. J. Vankelecom, P. A. Jacobs), Wiley-VCH, Weinheim, **2000**.

[3] a) S. J. Shuttleworth, S. M. Allin, P. K. Sharma, *Synthesis* **1997**, 1217–1239; b) P. Hodge, *Chem. Soc. Rev.* **1997**, *26*, 417–424.

[4] a) Q. H. Fan, C. Y. Ren, C. H. Yeung, W. H. Hu, A. S. C. Chen, *J. Am. Chem. Soc.* **1999**, *121*, 7407–7408; b) ref. [2], chap. 9.

[5] a) P. Salvadori, D. Pini, A. Petri, *Synlett* **1999**, 1181–1190; b) C. Bolm, G. Arne, *Eur. J. Org. Chem.* **1998**, *1*, 21–27; c) L. Canali, E. Cowan, H. Deleuze, C. L. Gibson, D. Sherrington, *J. Chem. Soc. Perkin Trans. 1* **2000**, 2055–2066; d) T. S. Reger, K. D. Janda, *J. Am. Chem. Soc.* **2000**, *122*, 6929–6934; e) ref. [2], chap. 10.

[6] a) B. Altava, M. I. Burguete, J. M. Fraile, J. I. García, S. V. Luis, J. A. Mayoral, M. J. Vincent, *Angew. Chem.* **2000**, *112*, 1563–1566; *Angew. Chem. Int. Ed.* **2000**, *39*, 1503–1506, and references therein; b) ref. [2], chap. 11.

[7] A. Mandoli, D. Pini, S. Orlandi, F. Mazzini, P. Salvadori, *Tetrahedron: Asymmetry* **1998**, *9*, 1479–1482.

[8] a) A. K. Ghosh, P. Mathivanan, J. Cappiello, *Tetrahedron: Asymmetry* **1998**, *9*, 1–45, and references therein; b) J. Johnson, D. A. Evans, *Acc. Chem. Res.* **2000**, *33*, 325–335 and references therein.

[9] For asymmetric cyclopropanation with structurally related aza-bis-oxazoline ligands linked to a soluble polymer, see M. Glos, O. Reiser, *Org. Lett.* **2000**, *14*, 2045–2048.

[10] J. M. Fraile, J. I. García, J. A. Mayoral, T. Tarnai, M. A. Harmer, *J. Catal.* **1999**, *186*, 214–221.

[11] C. Langham, S. Taylor, D. Bethell, P. McMorn, P. C. Bulman Page, D. J. Willock, C. Sly, F. E. Hancock, F. King, G. J. Hutchings, *J. Chem. Soc. Perkin Trans. 2* **1999**, *5*, 1043–1049.

[12] a) D. A. Evans, J. S. Johnson, E. J. Olhava, *J. Am. Chem. Soc.* **2000**, *122*, 1635–1649; b) D. A. Evans, E. J. Olhava, J. S. Johnson, J. M. Janey, *Angew. Chem.* **1998**, *110*, 3554–3557; *Angew. Chem. Int. Ed.* **1998**, *37*, 3372–3375.

[13] D. A. Evans, G. S. Peterson, G. S. Johnson, D. M. Barnes, K. R. Campos, K. A. Woerpel, *J. Org. Chem.* **1998**, *63*, 4541–4544.

[14] a) D. C. Sherrington, *Chem. Commun.* **1998**, 2275–2286; b) A. Guyot, M. Bartholin, *Prog. Polym. Sci.* **1982**, *8*, 277–332.

[15] R. P. Singh, *Bull. Soc. Chim. Fr.* **1997**, *134*, 765–768.

[16] D. A. Evans, C. S. Burgey, M. C. Kozlowski, S. W. Tregay, *J. Am. Chem. Soc.* **1999**, *121*, 686–699.

[17] Control experiments showed that the enantioselectivities for the formation of **6** and **7** were identical within the experimental uncertainty. Therefore the *ee* values were routinely determined after the conversion of **6** to **7** (see *Experimental Section*).

[18] The heterogeneous nature of the catalytic system was demonstrated by the fact that removing **3** · $Cu(OTf)_2$ by filtration at 30% conversion completely stopped the reaction.

[19] This treatment did not cause desilylation of **6**.

Self-Assembly of Pyramidal Tetrapalladium Complexes with a Halide at the Apex**

Camino Bartolomé, Raquel de Blas, Pablo Espinet,* José M. Martín-Álvarez, and Fernando Villafañe

Compared to the ubiquitous presence of μ_1-X and μ_2-X ligands (X = halide), and the frequent μ_3-X coordination (often involved in cubane-like structures), higher coordination numbers for halide ligands in discrete molecules are much less common.[1] A coordination number four (μ_4-X) is rare. Apart from a few scattered cases found in polynuclear V, Mn, Zn, or Sb compounds,[2] the examples known seem to concentrate on d^{10} Cu^I,[3] Ag^I, or Hg^{II} complexes.

The group of Hawthorne[4] has reported a number of such structures based on [12]mercuracarborand-4 macrocycles containing four Hg atoms defining a square plane. These electrophilic Hg atoms can bind one halide in an almost square-planar (for X = Cl) or square-pyramidal (for X = I) fashion, depending on the size of the halide. Removal of the halide guest regenerates the free host. On the other hand, the group of Puddephatt has reported the inclusion of halides in electrophilic bowl-shaped calix(4)arene complexes of Cu^I or Ag^I, where the geometry imposed by the calixarene host can stabilize either μ_3- or μ_4-binding modes of the halide, depending on the size of the latter.[5] The mercury macrocycles cited above, as well as other similar ones containing three or five mercury atoms, can even take a second halide to give bipyramidal structures with one halide at each apex.[6] In all these cases the hosting electrophilic metal centers are d^{10} ions which are involved in a macrocyclic structure which exists independently of the presence of the μ_4-binding halide. We present here a case of self-assembly of d^8 metal centers and halides around a pyramidal halide to give tetrapalladium complexes. Unlike the cases reported by Hawthorne and Puddephat, in our case the metallamacrocycle owes its formation to the halide acting as a template.

The reaction of precursors of "Pd(Fmes)" (Fmes = 2,4,6-tris(trifluoromethyl)phenyl) such as **1** or **2** (Scheme 1)[7] with halides QX (the overall ratio of Pd:X is 4:5) in CH_2Cl_2 affords high yields of the tetrametallic species $Q[Pd_4(Fmes)_4X_5]$ (**3**) (X = Cl, Br, I; Q = PPh_4 or PPN (bis(diphenylphosphane)-iminium)).[8] The formation of compounds **3** involves the displacement of MeCN and becomes easier in the order I > Br > Cl; thus, only for X = I is compound **3** readily formed starting from the MeCN-rich complex **2**.

Figure 1 shows the crystal structure of the anion in $(PPN)[Pd_4(Fmes)_4Cl_5]$. The four Pd atoms display a square-

[*] Prof. P. Espinet, C. Bartolomé, R. de Blas, J. M. Martín-Álvarez, F. Villafañe
Departamento de Química Inorgánica
Facultad de Ciencias
Universidad de Valladolid
47005 Valladolid (Spain)
Fax: (+349) 83-423013
E-mail: espinet@qi.uva.es

[**] This work was supported by the DGESIC (Project No. MAT99-0971) and the JCyL (Project No. VA17/00B). We thank Prof. Odile Eisenstein for very useful discussions during her stay as Iberdrola Visiting Professor.

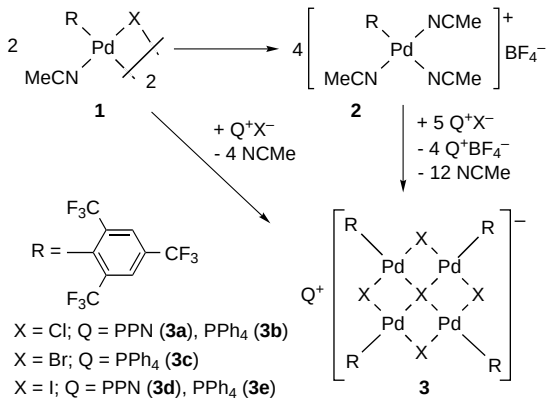

Scheme 1. Synthesis of **3** from **1** or **2**.

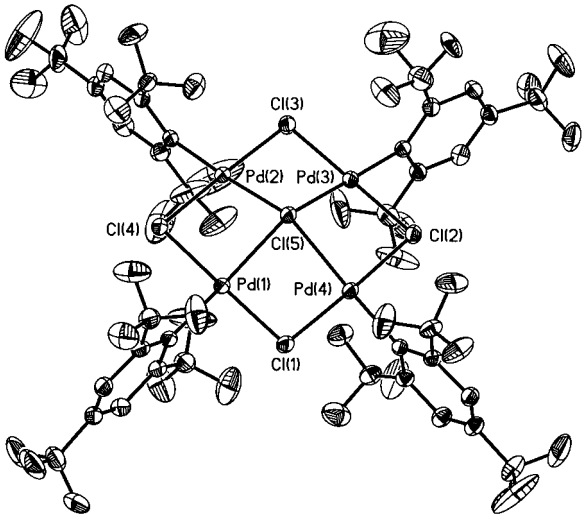

Figure 1. Structure of the anion in the complex (PPN)[$Pd_4(Fmes)_4Cl_5$] (ORTEP view; 30% probability ellipsoids).

planar coordination defined by the *ipso*-C of Fmes, two μ_2-Cl atoms, and the apical μ_4-Cl atom. The latter is located 1.01 Å above the plane defined by the four Pd and the four μ_2-Cl atoms. The μ_4-Cl–Pd distances are 2.56 Å (av), whereas the μ_2-Cl–Pd distances are 2.32 Å (av).[9]

In the systems reported by Hawthorne et al. and Puddephatt et al. (Scheme 2a) the size of the cavity in the metallamacrocycle is independent of the halide to be hosted

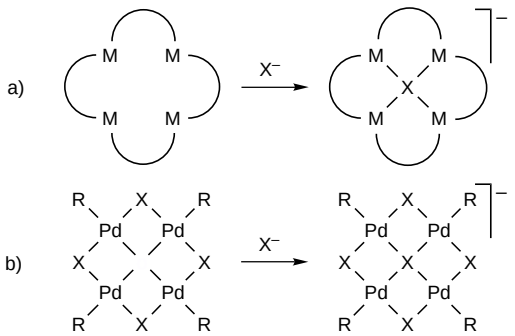

Scheme 2. Incorporation of a halide (X^-) into: a) a metalla-host with a cavity size fixed by the ancillary ligands; b) a hypothetical metalla-host with a cavity size varying with X^- (not implying a real formation pathway).

(although there is some flexibility), whereas in complexes **3** the halide determines both the size of the guest and the cavity (Scheme 2b), and a perfect μ_4-X square-planar coordination with perfectly square-planar-coordinated Pd atoms would require equal bond lengths for μ_2-X–Pd and μ_4-X–Pd. This is not expected since M–X bond lengths increase with an increasing degree of bridging for X.[3, 10] Consequently, the elongation of these bonds forces the central X to be out of the plane defined by the four Pd atoms, the molecule adopting a pyramidal geometry. The preference for pyramidal μ_4-X coordination compared to square-planar μ_4-X has been studied by extended Hückel calculations,[3, 5] and is mostly due to the transformation of a nonbonding orbital in the square-planar geometry (the p_z of X) into a bonding one upon pyramidalization. This leads, in simple terms, to the involvement of three electron pairs of X^- in the formation of four Pd–X bonds, whereas the other two electrons remain as a lone pair on X. Hence these bonds are electron-deficient and long. The less electronegative halogen atoms should, overall, be better donors and atenuate more the intrinsic electron deficiency of the μ_4 bridges. This explains the stability trend observed, I > Br > Cl.

The complexes display fluxional behavior in solution in noncoordinating solvents which renders equivalent the otherwise diastereotopic internal and external $(CF_3)_{ortho}$ groups. The process has been studied by ^{19}F NMR spectroscopy. The rate of the fluxional process increases in the order Cl > Br > I. Coalescence (at 282.4 MHz for ^{19}F) could be attained only for X = I, Br. Simulation using the gNMR program afforded the activation parameters given in footnote [11]. Although affected by large errors, overall they suggest that the differences in rate in CD_2Cl_2 or $CDCl_3$ for the different complexes are largely associated with entropy, whereas activation enthalpies show only small differences upon changing the halide or the cation, keeping $\Delta H^{\neq}$ at around a value of 38 kJ mol^{-1}.

Different processes that could explain the dynamic behavior observed were considered:

1) Rotation of the Fmes group around the Pd–C bond is excluded by severe steric hindrance.[12]
2) Mechanisms involving Pd–X bond fission (such as apical X^- dissociation – recoordination, or splitting and reforming of one μ_2-bridge, with change of conformation) should be discarded since the differences in Pd–X bond energies should produce noticeably different $\Delta H^{\neq}$ values for the different halides. Moreover, catalytic X^- or slightly coordinating solvents (acetone) should accelerate these processes opening an associative pathway for them, which is not observed. Also, if Pd–X bond fission mechanisms were fast, X exchange in mixtures of complexes **3** with different X ligands should also be fast, and in fact it takes hours in $CDCl_3$ before traces of apparent rearrangement are detected.
3) This leads to inversion of the pyramid as the most likely mechanism.

The inversion of the pyramidal C_{4v} anion implies a D_{4h} transition state with square-planar coordination for the central halide. Density functional thoery (DFT) calculations (B3LYP) of the difference in energy between these two

  1433-7851/01/4013-2522 $ 17.50+.50/0

species were made for the model compound $[Pd_4(H)_4Cl_5]^-$ (Figure 2).[13] A value of 44.1 kJ mol^{-1} was found, which is not in contradiction with the experimental values and suggests that the process is feasible. The transition state implies a

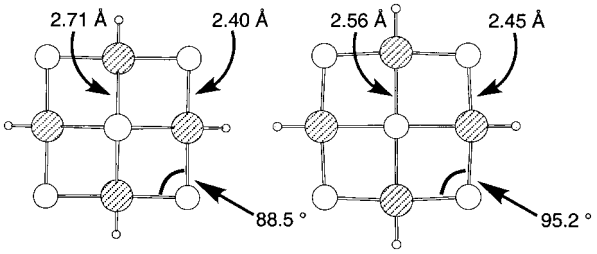

Figure 2. DFT(B3LYP)-optimized structure for the pyramidal fundamental state (left) and the planar transition state (right) of the model compound $[Pd_4(H)_4Cl_5]^-$.

considerable shrinkage of the Pd–X bonds to the central halide (from 2.71 to 2.56 Å) and a much smaller stretch of those to the bridging halides (from 2.40 to 2.45 Å). The latter is minimized by opening the Pd-X-Pd angle at μ_2-X (from 88.5 to 95.2°).

Received: February 9, 2001 [Z16592]

[1] A. J. Edwards, *Halogens as Ligands* in *Comprehensive Coordination Chemistry*, *Vol. 2*, Pergamon, Oxford, **1987**, pp. 675–688.

[2] a) D. D. Heinrich, K. Folting, W. E. Streib, J. C. Huffman, G. Christou, *J. Chem. Soc. Chem. Commun.* **1989**, 1411–1413; b) G. B. Karet, Z. Sun, D. D. Heinrich, J. K. McCusker, K. Folting, W. E. Streib, J. C. Huffman, D. N. Hendrickson, G. Christou, *Inorg. Chem.* **1996**, *35*, 6450–6460; c) S. Wang, J. C. Huffman, K. Folting, W. E. Streib, E. B. Lobkovsky, G. Christou, *Angew. Chem.* **1991**, *103*, 1681; *Angew. Chem. Int. Ed. Engl.* **1991**, *30*, 1672–1674; d) H.-L. Tsai, S. Wang, K. Folting, W. E. Streib, D. N. Hendrickson, G. Christou, *J. Am. Chem. Soc.* **1995**, *117*, 2503–2514; e) I. G. Dance, *J. Chem. Soc. Chem. Commun.* **1980**, 818–820; f) A. L. Rheingold, A. G. Landers, P. Dahlstrom, J. Zubieta, *J. Chem. Soc. Chem. Commun.* **1979**, 143–144.

[3] Particularly in halocuprates, see: L. Subrumanian, R. Hoffman, *Inorg. Chem*. **1992**, *31*, 1021–1029, and references therein.

[4] X. Yang, C. B. Knobler, M. F. Hawthorne, *Angew. Chem.* **1991**, *103*, 1519; *Angew. Chem. Int. Ed. Engl.* **1991**, *11*, 1507–1508; b) Z. Zheng, X. Yang, C. B. Knobler, M. F. Hawthorne, *J. Am. Chem. Soc.* **1993**, *115*, 5320–5321; c) X. Yang, C. B. Knobler, Z. Zheng, M. F. Hawthorne, *J. Am. Chem. Soc.* **1994**, *116*, 7142–7159; d) Z. Zheng, C. B. Knobler, M. F. Hawthorne, *J. Am. Chem. Soc.* **1995**, *117*, 5105–5113.

[5] a) W. Xu, J. J. Vittal, R. J. Puddephatt, *J. Am. Chem. Soc.* **1993**, *115*, 6456–6457; b) W. Xu, J. J. Vittal, R. J. Puddephatt, *J. Am. Chem. Soc.* **1995**, *117*, 8362–8371.

[6] a) Z. Zheng, C. B. Knobler, M. D. Mortimer, G. Kong, M. F. Hawthorne, *Inorg. Chem.* **1996**, *35*, 1235–1243; b) W. B. Shur, I. A. Tikhonova, F. M. Dolgushin, A. I. Yanovsky, Yu. Y. Struchkov, A. Yu. Volkonsky, E. V. Solodova, S. Yu. Panov, P. V. Petrovskii, M. E. Vol'pin, *J. Organomet. Chem.* **1993**, *443*, C19-C21; c) W. B. Shur, I. A. Tikhonova, A. I. Yanovsky, Yu. Y. Struchkov, P. V. Petrovskii, S. Yu. Panov, G. G. Furin, M. E. Vol'pin, *J. Organomet. Chem.* **1991**, *418*, C29-C32.

[7] The starting materials **1** and **2** were prepared from [Pd(Fmes)(μ-Cl)(NCMe)]$_2$, which was obtained by refluxing [PdCl(Fmes)(COD)] in MeCN. [PdCl(Fmes)(COD)] has been reported: C. Bartolomé, P. Espinet, F. Villafañe, S. Giesa, A. Martín, A. G. Orpen, *Organometallics* **1996**, *15*, 2019–2028.

[8] All new compounds were fully characterized by elemental analyses and spectroscopic methods. **3a**: Orange crystals; yield 68%; ^{1}H NMR (300 MHz, $CDCl_3$, 298 K): $\delta = 7.70$ (m, 6H; C_6H_5), 7.56 (s, 8H; $C_6H_2(CF_3)_3$), 7.52 (m, 24H; C_6H_5); ^{19}F NMR (282.4 MHz, $CDCl_3$, 298 K): $\delta = -57.51$ (s, 24F; *ortho*-CF_3), -63.34 (s, 12F; *para*-CF_3); ^{31}P{^{1}H} NMR (121.4 MHz, $CDCl_3$, 298 K): $\delta = 21.84$ (s); elemental analysis calcd (%) for $C_{73}H_{40}NCl_7F_{36}P_2Pd_4$: C 37.30, H 1.72, N 0.6; found: C 37.74, H 1.83, N 0.84. **3b**: Orange crystals; yield 68%; ^{1}H NMR (300 MHz, $CDCl_3$, 298 K): $\delta = 8.00$ (m, 4H; C_6H_5), 7.87 (m, 8H; C_6H_5), 7.73 (m, 8H; C_6H_5), 7.57 (s, 8H; $C_6H_2(CF_3)_3$); ^{19}F NMR (282.4 MHz, $CDCl_3$, 298 K): $\delta = -57.45$ (s, 24F; *ortho*-CF_3), -63.36 (s, 12F; *para*-CF_3); ^{31}P{^{1}H} NMR (121.4 MHz, $CDCl_3$, 298 K): $\delta = 24.15$ (s); elemental analysis calcd (%) for $C_{60}H_{28}F_{36}Cl_5PPd_4$: C 34.87, H 1.37; found: C 35.73, H 1.73. **3c**: Orange crystals; yield 61%; ^{1}H NMR (300 MHz, $CDCl_3$, 298 K): $\delta = 8.02$ (m, 4H; C_6H_5), 7.88 (m, 8H; C_6H_5), 7.73 (m, 8H; C_6H_5), 7.61 (s, 8H; $C_6H_2(CF_3)_3$); ^{19}F NMR (282.4 MHz, $CDCl_3$, 298 K): $\delta = -56.80$ (s, 24F; *ortho*-CF_3), -63.30 (s, 12F; *para*-CF_3); ^{31}P{^{1}H} NMR (121.4 MHz, $CDCl_3$, 298 K): $\delta = 24.15$ (s); ^{1}H NMR (300 MHz, CD_2Cl_2, 298 K): $\delta = 7.92$ (m, 4H; C_6H_5), 7.74 (m, 8H; C_6H_5), 7.64 (s, 8H; $C_6H_2(CF_3)_3$), 7.60 (m, 8H; C_6H_5); ^{19}F NMR (282.4 MHz, CD_2Cl_2, 298 K): $\delta = -56.56$ (s, 24F; *ortho*-CF_3), -63.11 (s, 12F; *para*-CF_3). ^{1}H NMR (300 MHz, CD_2Cl_2, 183 K): $\delta = 7.87$ (m, 4H; C_6H_5), 7.70 (m, 8H; C_6H_5), 7.60 (a, 8H; $C_6H_2(CF_3)_3$), 7.56 (m, 8H; C_6H_5); ^{19}F NMR (282.4 MHz, CD_2Cl_2, 183 K): $\delta = -56.05$ (s, 12F; *ortho*-CF_3), -57.10 (s, 12F; *ortho*-CF_3), -62.58 (s, 12F; *para*-CF_3); elemental analysis calcd (%) for $C_{60}H_{28}F_{36}Br_5PPd_4$: C 31.49, H 1.23; found: C 31.62, H 1.28. **3d**: Orange crystals; yield 51%; ^{1}H NMR (300 MHz, $CDCl_3$, 298 K): $\delta = 7.72$ (m, 6H; C_6H_5), 7.65 (s, 8H; $C_6H_2(CF_3)_3$), 7.53 (m, 24H; C_6H_5); ^{19}F NMR (282.4 MHz, $CDCl_3$, 298 K): $\delta = -56.47$ (s, 24F; *ortho*-CF_3), -63.21 (s, 12F; *para*-CF_3); ^{31}P{^{1}H} NMR (121.4 MHz, $CDCl_3$, 298 K): $\delta = 21.8$ (s); ^{1}H NMR (300 MHz, CD_2Cl_2, 298 K): $\delta = 7.65$ (m, 6H; C_6H_5), 7.52 (s, 8H; $C_6H_2(CF_3)_3$), 7.50 (m, 24H; C_6H_5); ^{19}F NMR (282.4 MHz, CD_2Cl_2, 298 K): $\delta = -56.17$ (s, 24F; *ortho*-CF_3), -63.05 (s, 12F; *para*-CF_3); ^{1}H NMR (300 MHz, CD_2Cl_2, 203 K): $\delta = 7.62$ (m, 6H; C_6H_5), 7.50 (m, 32H; $C_6H_2(CF_3)_3 + C_6H_5$); ^{19}F NMR (282.4 MHz, CD_2Cl_2, 203 K): $\delta = -55.67$ (s, 12F; *ortho*-CF_3), -56.90 (s, 12F; *ortho*-CF_3), -62.58 (s, 12F; *para*-CF_3); elemental analysis calcd (%) for $C_{72}H_{38}NF_{36}I_5P_2Pd_4$: C 31.76, H 1.41, N 0.51; found: C 31.62, H 1.45, N 0.81. **3e**: Orange crystals; yield 66%; ^{1}H NMR (300 MHz, $CDCl_3$, 298 K): $\delta = 8.01$ (m, 4H; C_6H_5), 7.88 (m, 8H; C_6H_5), 7.73 (m, 8H; C_6H_5), 7.66 (s, 8H; $C_6H_2(CF_3)_3$); ^{19}F NMR (282.4 MHz, $CDCl_3$, 298 K): $\delta = -56.43$ (s, 24F; *ortho*-CF_3), -63.23 (s, 12F; *para*-CF_3); ^{31}P{^{1}H} NMR (121.4 MHz, $CDCl_3$, 298 K): $\delta = 24.17$ (s); ^{1}H NMR (300 MHz, $CDCl_3$, 213 K): $\delta = 8.03$ (m, 4H; C_6H_5), 7.90 (m, 8H; C_6H_5), 7.70 (m, 16H; $C_6H_5 + C_6H_2(CF_3)_3$); ^{19}F NMR (300 MHz, $CDCl_3$, 213 K): $\delta = -56.03$ (s, 12F; *ortho*-CF_3), -56.98 (s, 12F; *ortho*-CF_3), -62.81 (s, 12F; *para*-CF_3); ^{1}H NMR (300 MHz, CD_2Cl_2, 298 K): $\delta = 7.90$ (m, 4H; C_6H_5), 7.75 (m, 8H; C_6H_5), 7.70 (s, 8H; $C_6H_2(CF_3)_3$), 7.60 (m, 8H; C_6H_5); ^{19}F NMR (282.4 MHz, CD_2Cl_2, 298 K): $\delta = -56.16$ (s, 24F; *ortho*-CF_3), -63.05 (s, 12F; *para*-CF_3); ^{1}H NMR (300 MHz, CD_2Cl_2, 193 K): $\delta = 7.88$ (m, 4H; C_6H_5), 7.65 (m, 24H; $C_6H_5 + C_6H_2(CF_3)_3$); ^{19}F NMR (282.4 MHz, CD_2Cl_2, 193 K): $\delta = -55.65$ (s, 12F; *ortho*-CF_3), -56.90 (s, 12F; *ortho*-CF_3), -62.57 (s, 12F; *para*-CF_3); elemental analysis calcd (%) for $C_{60}H_{28}F_{36}I_5PPd_4$: C 28.55, H 1.12; found: C 28.52, H 1.10.

[9] Crystallographic data (excluding structure factors) for the structure reported in this paper have been deposited with the Cambridge Crystallographic Data Centre as supplementary publication no. CCDC-157188 (**3a**). Copies of the data can be obtained free of charge on application to CCDC, 12 Union Road, Cambridge CB2 1EZ, UK (fax: (+44) 1223-336-033; e-mail: deposit@ccdc.cam.ac.uk).

[10] M. D. Janssen, A. L. Spek, D. M. Grove, G. van Koten, *Inorg. Chem.* **1996**, *35*, 4078–4081.

[11] gNMR version 3.6, P. H. M. Budzelaar, IvorySoft, **1996**. **3c** in CD_2Cl_2: $\Delta H^{\neq} = 37.5 \pm 1.9$ kJ mol^{-1}, $\Delta S^{\neq} = -7 \pm 9$ J mol^{-1} K^{-1}, $\Delta G^{\neq}_{coal} = 39 \pm 3$ kJ mol^{-1} at 207 K, $\Delta G^{\neq}_{273} = 39 \pm 3$ kJ mol^{-1}; **3e** in CD_2Cl_2: $\Delta H^{\neq} = 39 \pm 2$ kJ mol^{-1}, $\Delta S^{\neq} = -31 \pm 10$ J mol^{-1} K^{-1}, $\Delta G^{\neq}_{coal} = 47 \pm 3$ kJ mol^{-1} at 248 K, $\Delta G^{\neq}_{273} = 47 \pm 3$ kJ mol^{-1}; **3d** in CD_2Cl_2: same values as the previous; **3e** in $CDCl_3$: $\Delta H^{\neq} = 36 \pm 4$ kJ mol^{-1}, $\Delta S^{\neq} = -44 \pm 15$ J mol^{-1} K^{-1}, $\Delta G^{\neq}_{coal} = 47 \pm 5$ kJ mol^{-1} at 241 K, $\Delta G^{\neq}_{273} = 48 \pm 6$ kJ mol^{-1}.

[12] For restricted rotation in other hindered Pd systems see, for instance: J. A. Casares, P. Espinet, J. M. Martínez-Ilarduya, Y.-S. Lin, *Organometallics* **1997**, *16*, 770–779.

[13] The calculations were carried out with the Gaussian 98 suite of programs: Gaussian 98 (Revision A.7), M. J. Frisch, G. W. Trucks, H. B. Schlegel, G. E. Scuseria, M. A. Robb, J. R. Cheeseman, V. G. Zakrzewski, J. A. Montgomery, R. E. Stratmann, J. C. Burant, S. Dapprich, J. M. Millam, A. D. Daniels, K. N. Kudin, M. C. Strain, O. Farkas, J. Tomasi, V. Barone, M. Cossi, R. Cammi, B. Mennucci, C. Pomelli, C. Adamo, S. Clifford, J. Ochterski, G. A. Petersson, P. Y. Ayala, Q. Cui, K. Morokuma, D. K. Malick, A. D. Rabuck, K. Raghavachari, J. B. Foresman, J. Cioslowski, J. V. Ortiz, B. B. Stefanov, G. Liu, A. Liashenko, P. Piskorz, I. Komaromi, R. Gomperts, R. L. Martin, D. J. Fox, T. Keith, M. A. Al-Laham, C. Y. Peng, A. Nanayakkara, C. Gonzalez, M. Challacombe, P. M. W. Gill, B. G. Johnson, W. Chen, M. W. Wong, J. L. Andres, M. Head-Gordon, E. S. Replogle, J. A. Pople, Gaussian, Inc., Pittsburgh, PA, **1998**. Pd was represented with the Hay-Wadt relativistic core potential (ECP) for the 28 innermost electrons and its associated double-ζ basis set.[14] Cl was also described with the Los Alamos ECPs and their associated double-ζ basis set augmented by a d polarization function.[15, 16] A 6–31G(d,p) basis set was used for H atoms.[17] Full optimizations without symmetry constraints have been carried out at the B3LYP level.[18, 19]
[14] P. J. Hay, W. R. Wadt, *J. Chem. Phys.* **1985**, *82*, 299.
[15] W. R. Wadt, P. J. Hay, *J. Chem. Phys.* **1985**, *82*, 284.
[16] A. Hölwarth, M. Böhme, S. Dapprich, A. W. Ehlers, A. Gobbi, V. Jonas, K. Köhler, R. Stegmann, A. Veldkamp, G. Frenking, *Chem. Phys. Lett.* **1993**, *208*, 237.
[17] P. C. Hariharan, J. A. Pople, *Theor. Chim. Acta* **1973**, *28*, 213.
[18] A. D. Becke, *J. Chem. Phys.* **1993**, *98*, 5648.
[19] C. Lee, W. Yang, R. G. Parr, *Phys. Rev. B* **1988**, *37*, 785.

Tin-Free Radical Acylation Reactions with Methanesulfonyl Oxime Ether**

Sunggak Kim,* Hyun-Ji Song, Tae-Lim Choi, and Joo-Yong Yoon

Recent advances in radical reactions have greatly benefited from the efficiency of organotin reagents as mediators. However, organotin reagents are highly toxic, and it is difficult to remove their residues from the products. These disadvantages have proved to be a serious barrier to industrial applications. To solve the problems associated with toxic organotin reagents, several alternative approaches, including the use of polymer-supported organotin reagents and organosilanes, have been utilized with some success.[1] Recently, a few tin-free carbon–carbon bond-forming reactions were reported; they include organosulfone-mediated radical allylation, alkenylation, alkynylation, and azidation reactions.[2–4]

Recently, we reported highly efficient tin-mediated radical acylation reactions with sulfonyl oxime ethers [Eq. (1)].[5] We then studied the possibility of environmentally benign tin-free

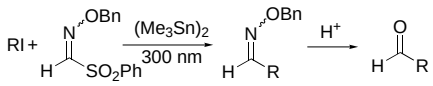

(1)

radical acylation reactions. Our approach is largely based on the tin-free radical allylation reaction of Zard et al. [Eq. (2)][2]

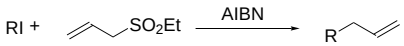

(2)

and involves thermal decomposition of an alkylsulfonyl radical (path a) and subsequent transfer of an iodine atom (path b),[6] as outlined in Scheme 1. The problem with tin-free

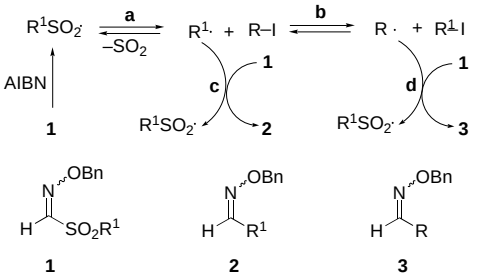

Scheme 1. Pathways for the radical reaction of an alkyl iodide with **1**.

radical acylation arises from the fast addition of an alkyl radical to sulfonyl oxime ether **1** to afford oxime ether **2**.[7] Since the direct addition of the alkyl radical to sulfonyl oxime ether **1** (path c) would compete with transfer of an iodine atom (path b) in the radical acylation approach, efficient iodine transfer is a key factor for the success of this approach.

We first studied the efficiency of iodine-atom transfer from a secondary alkyl iodide to an ethyl radical relative to the addition of the ethyl radical to ethanesulfonyl oxime ether **4** [Eq. (3)]. Treatment of cyclohexyl iodide with an equimolar

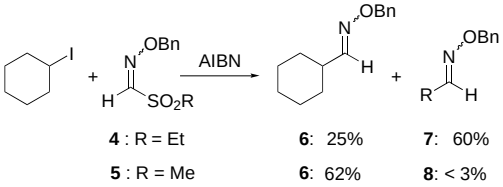

(3)

amount of **4** and azobisisobutyronitrile (AIBN; 0.1 equiv) in refluxing heptane for 24 h resulted in a 25:60 mixture of two oxime ethers **6** and **7**. Evidently, addition of the ethyl radical to **4** is more than two times faster than the transfer of the iodine atom from cyclohexyl iodide to the ethyl radical. Although the yield of **6** was increased to 48% along with 21% of **7** by using a large excess of cyclohexyl iodide (5 equiv), the serious problem of the formation of **7** could not be solved, and this indicates that **4** is not suitable for tin-free radical acylation with secondary alkyl iodides.

We next turned our attention to methanesulfonyl oxime ether **5**. Although it was reported that the methanesulfonyl

[*] Prof. Dr. S. Kim, H.-J. Song, T.-L. Choi, Dr. J.-Y. Yoon
Center for Molecular Design and Synthesis
and Department of Chemistry
School of Molecular Science
Korea Advanced Institute of Science and Technology
Taejon 305-701 (Korea)
Fax: (+82) 42-869-8370
E-mail: skim@mail.kaist.ac.kr

[**] We thank the CMDS and the BK21 project for financial support.

  1433-7851/01/4013-2524 $ 17.50+.50/0

radical hardly decomposes into SO_2 and a methyl radical,[8] we found that decomposition of the methanesulfonyl radical occurred at 120 °C. When cyclohexyl iodide was treated with **5** in refluxing heptane in the presence of AIBN for 40 h, cyclohexyl oxime ether **6** was isolated in 62 % yield along with a trace of methyl oxime ether **8**, that is, transfer of the iodine atom was much faster than the direct addition process. Thus, **5** solved the problem we faced with secondary alkyl iodides. Since the use of AIBN in heptane required 40 h at reflux, the reaction was carried out in octane at 120 °C with V-40 (azobis(cyclohexanecarbonitrile)) as initiator, and this shortened the reaction time to 6 h. As shown in Table 1, the results

Table 1. Synthesis of oxime ethers from alkyl iodides and tellurides by using **5** and **9**.

Substrate[a]	Product	Yield [%]	
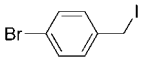	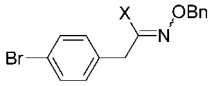	X = H	80
		X = CO_2Et	73
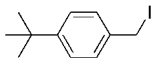	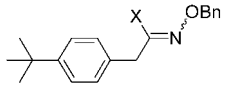	X = H	78
		X = CO_2Et	75
	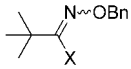	X = H	71
		X = CO_2Et	64
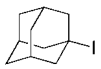	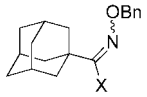	X = H	70
		X = CO_2Et	70
	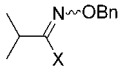	X = H	67
		X = CO_2Et	64
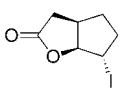	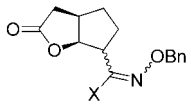	X = H	72[b]
		X = CO_2Et	63[c]
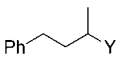	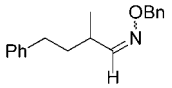	Y = I, X = H	67
		Y = TePh, X = H	77
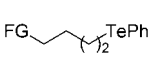	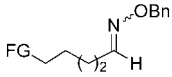	FG = OPh[d]	78
		FG = OTBS[d]	77
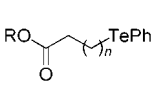	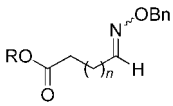	FG = OCOPh[d]	72
		R = Me, n = 1	71
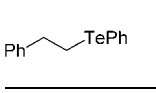	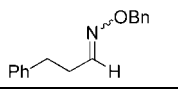	R = Et, n = 2	71
			76

[a] For iodides, in octane at 120 °C for 6 h. For tellurides, in $tBuC_6H_5$ at 140 °C for 24 h. [b] *exo*:*endo* = 4.5:1. [c] *exo*:*endo* = 1.8:1. [d] FG = functional group.

obtained with **5** were quite satisfactory; the corresponding oxime ethers were obtained in good yields (65–80 %). The present approach was further extended to the synthesis of α-oxime ester **10**, a synthetic equivalent of an α-keto ester, by using ethoxycarbonyl oxime ether **9** [Eq. (4)].[9]

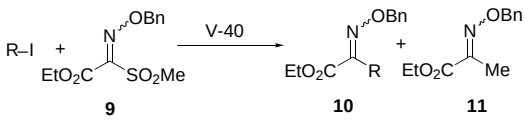

9 **10** **11** (4)

The reaction was carried out under the same conditions and afforded **10** in good yields (64 to 75 %) without formation of **11** (Table 1).

Primary alkyl iodides did not work well with **5** and **9**. Due to the small energy difference between the methyl radical and a primary alkyl radical, iodine-atom transfer competed with the direct addition of the methyl radical to **5** [Eq. (5)]. Treatment of 4-phenoxybutyl iodide (**12**) with an equimolar amount of **5** in *tert*-butylbenzene at 140 °C for 30 h, which gave a 45:25 mixture of the desired oxime ether **15** and **8**, demonstrates the inefficiency of **5** with primary alkyl iodides.

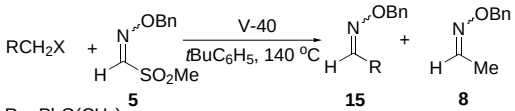

(5)

R = $PhO(CH_2)_3$	**5**	**15**	**8**
12 : X = I		45%	25%
13 : X = S(C=S)OEt		65%	20%
14 : X = TePh		78%	0%

To solve the problem of slow iodine-atom transfer associated with primary alkyl iodides, we searched for better radical-accepting systems than alkyl iodides, and xanthates were our initial choice.[10] The reaction of xanthate **13** with **5** and V-40 under the same conditions afforded a 65:20 mixture of **15** and **8** and indicated that transfer of the xanthate group is slightly faster than that of the iodine atom.

Since the xanthate could not solve the present problem associated with the direct addition of the methyl radical to **5**, we turned our attention to organic tellurides, which have been utilized to generate alkyl and acyl radicals.[11, 12] Gratifyingly, reaction of phenyl telluride **14** with **5** and V-40 in *tert*-butylbenzene at 140 °C for 24 h gave **15** in 78 % yield without any indication of the formation of **8**. This result is somewhat surprising, because tansfer of an iodine atom and of a phenyl telluride group are known to proceed approximately at the same rate,[13] although there was a previous report that vinyl radicals abstract a phenyl telluride group about ten times faster than an iodine atom.[14] Therefore, we performed a competition experiment [Eq. (6)]. Reaction of an equimolar

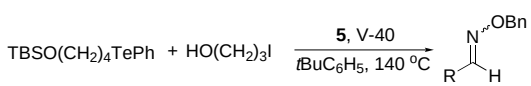

16 **17** **18** : R = $TBSO(CH_2)_4$ (65%)
19 : R = $HO(CH_2)_3$ (< 4%) (6)

mixture of phenyl telluride **16**, iodide **17**, and **5** with V-40 (0.2 equiv) in *tert*-butylbenzene at 140 °C for 20 h afforded **18** in 65 % yield along with a small amount of **19** (< 4 %), and this clearly indicates the higher efficiency of transfer of a phenyl

telluride group relative to that of an iodine atom.[15] Some experimental results are included in Table 1 and demonstrate the efficiency of the phenyl telluride approach. The reaction was successful with secondary and primary alkyl tellurides. We briefly examined a sequential radical reaction involving a cyclization and acylation sequence [Eq. (7)]. Reaction of **21**

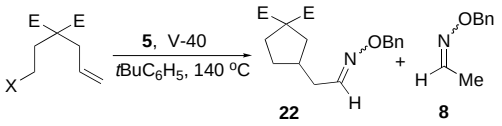

(7)

	22	**8**
20: X = I	31%	55%
21: X = TePh	67%	0%

with **5** under the same conditions afforded the desired oxime ether **22** in 67% yield, whereas the use of iodide **20** gave **22** in 31% yield along with **8** (55%); this demonstrates the efficiency of the phenyl telluride group as a radical precursor.

Experimental Section

Typical procedure: A degassed solution of 1-bromo-4-iodomethyl-benzene (118 mg, 0.40 mmol), *O*-benzyl-1-(methanesulfonyl)formaldoxime (**5**, 128 mg, 0.60 mmol) and V-40 (20 mg, 0.08 mmol) in freshly distilled octane (2 mL) was heated to reflux under N_2 for 8 h. The solvent was evaporated under reduced pressure, and the residue was purified by chromatography on a silica gel column (*n*-hexane: ethyl acetate 1:15) to yield *O*-benzyl-1-(4-bromobenzyl)formaldehyde (98 mg, 0.32 mmol, 80% yield, $E:Z = 1.1:1$). ^{1}H NMR ($CDCl_3$, 200 MHz): *E* isomer: $\delta = 3.45$ (d, $J = 6.4$ Hz, 2H), 5.08 (s, 2H), 7.06 (d, $J = 2.2$ Hz, 2H), 7.32–7.43 (m, 7H), 7.49 (t, $J = 6.4$ Hz, 1H); *Z* isomer: $\delta = 3.65$ (d, $J = 5.4$ Hz, 2H), 5.15 (s, 2H), 6.80 (t, $J = 5.4$ Hz, 1H), 7.02 (d, $J = 2.2$ Hz, 2H), 7.32–7.43 (m, 7H); ^{13}C NMR ($CDCl_3$, 100 MHz): $\delta = 31.9$, 35.3, 75.8, 76.1, 120.5, 120.8, 127.8, 127.9, 128.2, 128.4, 128.6, 128.8, 130.4, 130.5, 131.7, 131.8, 135.3, 135.8, 137.6, 137.7, 149.0, 149.3; IR (NaCl): $\tilde{\nu} = 3031$, 2928, 1656, 1586, 1488, 1454, 1367, 1276, 1072, 1012 cm^{-1}; HR-MS: [M^+] calcd for $C_{15}H_{14}BrNO$: 303.0259; found: 303.0257.

Received: February 5, 2001 [Z16557]

[1] P. A. Baguley, J. C. Walton, *Angew. Chem.* **1998**, *110*, 3272–3283; *Angew. Chem. Int. Ed.* **1998**, *37*, 3072–3082, and references therein.

[2] a) B. Quiclet-Sire, S. Z. Zard, *J. Am. Chem. Soc.* **1996**, *118*, 1209–1210; b) F. L. Guyader, B. Quiclet-Sire, S. Seguin, S. Z. Zard, *J. Am. Chem. Soc.* **1997**, *119*, 7410–7411; c) F. Bertrand, B. Quielet-Sire, S. Z. Zard, *Angew. Chem.* **1999**, *111*, 2135–2138; *Angew. Chem. Int. Ed.* **1999**, *38*, 1943–1946.

[3] a) J. Gong, P. L. Fuchs, *J. Am. Chem. Soc.* **1996**, *118*, 4486–4487; b) J. Gong, P. L. Fuchs, *Tetrahedron Lett.* **1997**, *38*, 787–790; c) J. Xiang, P. L. Fuchs, *J. Am. Chem. Soc.* **1996**, *118*, 11986–11987; d) J. Xiang, W. Jiang, J. Gong, P. L. Fuchs, *J. Am. Chem. Soc.* **1997**, *119*, 4123–4129.

[4] C. Ollivier, P. Renaud, *J. Am. Chem. Soc.* **2000**, *122*, 6496–6497.

[5] a) S. Kim, I. Y. Lee, J.-Y. Yoon, D. H. Oh, *J. Am. Chem. Soc.* **1996**, *118*, 5138–5139; b) S. Kim, J.-Y. Yoon, *J. Am. Chem. Soc.* **1997**, *119*, 5982–5983.

[6] a) D. P. Curran, M.-H. Chen, D. Kim, *J. Am. Chem. Soc.* **1986**, *108*, 2489–2490; b) D. P. Curran, D. Kim, *Tetrahedron Lett.* **1986**, *27*, 5821–5814; c) D. P. Curran, D. Kim, *Tetrahedron* **1991**, *47*, 6171–6188; d) D. P. Curran, D. Kim, C. Zigler, *Tetrahedron* **1991**, *47*, 6189–6196.

[7] S. Kim, I. Y. Lee, *Tetrahedron Lett.* **1998**, *39*, 1587–1590.

[8] a) A. Horowitz, L. A. Rajbenbach, *J. Am. Chem. Soc.* **1975**, *97*, 10–13; b) C. Chatgilialoglu in *The Chemistry of Sulfones and Sulfoxides* (Eds.: S. Patai, Z. Rappoport, C. J. M. Stirling), Wiley, Chichester, **1988**, pp. 1089–1113; c) M. Bertrand, *Org. Prep. Proced. Int.* **1994**, *26*, 257–290.

[9] S. Kim, J.-Y. Yoon, I. Y. Lee, *Synlett* **1997**, 475–476.

[10] a) D. Crich, L. Quintero, *Chem. Rev.* **1989**, *89*, 1413–1432; b) J. Boivin, J. Camara, S. Z. Zard, *J. Am. Chem. Soc.* **1992**, *114*, 7909–7910; c) B. Quiclet-Sire, S. Z. Zard, *J. Am. Chem. Soc.* **1996**, *118*, 9190–9191; d) S. Z. Zard, *Angew. Chem.* **1997**, *109*, 724–737; *Angew. Chem. Int. Ed. Engl.* **1997**, *36*, 672–685; e) B. Quiclet-Sire, S. Seguin, S. Z. Zard, *Angew. Chem.* **1998**, *110*, 3056–3058; *Angew. Chem. Int. Ed.* **1998**, *37*, 2864–2866.

[11] a) D. H. R. Barton, J. C. Jaszberenyi, E. A. Theodorakis, *J. Am. Chem. Soc.* **1992**, *114*, 5904–5905; b) M. A. Lucas, C. H. Schiesser, *J. Org. Chem.* **1996**, *61*, 5754–5761.

[12] a) C. Chen, D. Crich, A. Papadatos, *J. Am. Chem. Soc.* **1992**, *114*, 8313–8314; b) C. Chen, D. Crich, *Tetrahedron Lett.* **1993**, *34*, 1545–1548; c) D. Crich, C. Chen, J.-T. Hwang, H. Yuan, A. Papadatos, R. I. Walter, *J. Am. Chem. Soc.* **1994**, *116*, 8937–8951.

[13] D. P. Curran, A. A. Martin-Esker, S.-B. Ko, M. Newcomb, *J. Org. Chem.* **1993**, *58*, 4691–4695.

[14] L.-B. Han, K.-I. Ishihara, N. Kambe, A. Ogawa, I. Ryu, N. Sonoda, *J. Am. Chem. Soc.* **1992**, *114*, 7591–7592.

[15] We thank the referees for suggesting a competition experiment and for drawing our attention to ref. [13].

Cyclodextrin Cavities as Probes for Ligand-Exchange Processes

Eric Engeldinger, Dominique Armspach,* and Dominique Matt*

Cyclodextrins (CDs) have attracted a lot of attention as chiral building blocks for the construction of enzyme mimics because of their ability to bind a wide range of organic substrates in water.[1–4] Combining CDs with transition metals has proven a very attractive goal in terms of achieving highly selective and efficient catalysis.[5–11] One of the challenges, so far not met, is to force a metal that is covalently linked to a CD framework to be confined in the cavity where maximum interaction between the first coordination sphere of the metal and the CD walls is expected to take place so as to stabilize unusual coordination modes. In addition, cavities with introverted[12] functionalities could provide new catalysts where a metal center operates inside a spatially restricted environment.[13–15] We report here the first α-CD-based multitopic ligand (**2**) capable of hosting metal–organic fragments. As shown by NMR investigations, the complexes derived from this ligand display unique intra- and intermolecular ligand-exchange phenomena at the included metal center.

We anticipated that an easy way to ensure metal encapsulation in a cavity would be to use an α-CD derivative bearing

[*] Dr. D. Armspach, Dr. D. Matt, E. Engeldinger
Laboratoire de Chimie Inorganique Moléculaire, UMR 7513 CNRS
Université Louis Pasteur
1, rue Blaise Pascal, 67008 Strasbourg Cedex (France)
Fax: (+33) 3-90-240-722
E-mail: dmatt@chimie.u-strasbg.fr

Supporting information for this article is available on the WWW under http://www.angewandte.com or from the author.

  1433-7851/01/4013-2526 $ 17.50+.50/0

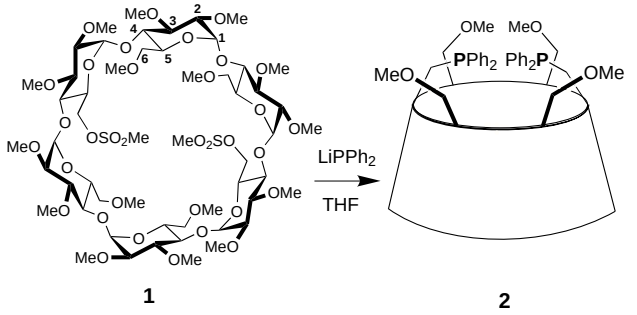

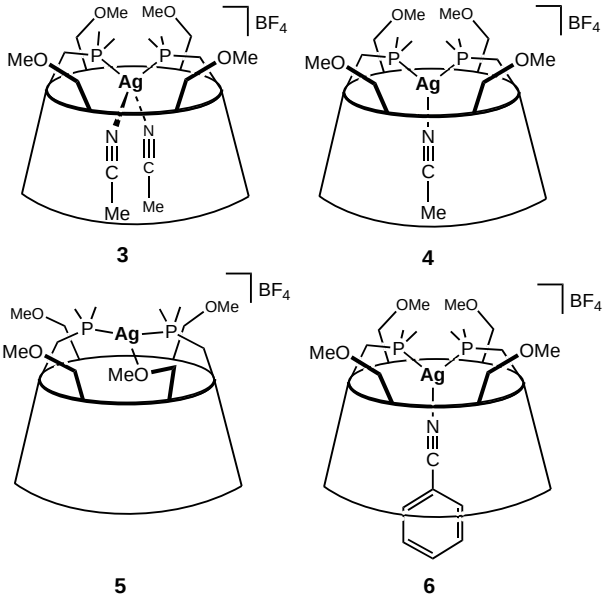

donor functions that preferentially point inside the CD. This feature is realized in diphosphane **2**, in which the orientation of the phosphorus lone pairs is controlled by steric interactions between the CD matrix and the closely appended phosphanyl groups. The presence of adjacent methoxy groups provides additional binding sites that may help metal stabilization. Two diphenylphosphanyl fragments were grafted onto the C-6 atoms of the A and D units of an α-CD platform by using a method developed by Brown et al. for the functionalization of trehalose units.[16] Thus, the reaction of the known dimesylate **1**[17] with lithium diphenyl phosphide in THF afforded compound **2** in high yield [Eq. (1)]. The ^{31}P NMR spectrum of the resulting chiral diphosphane consists of a singlet at $\delta = -17.9$ commensurate with its expected C_2 symmetry. The latter was confirmed by the presence of eight methyl signals as well as three doublets for the H-1 protons in the ^{1}H NMR spectrum. Interestingly, the proximity of the chiral cavity produces a strong differentiation between the two phenyl groups attached to each phosphorus atom as revealed by ^{13}C NMR spectroscopy. This effect is no longer observed when the coordinating atoms are separated from the C-6 atoms by longer spacers like phenylene.[18]

The reaction of ligand **2** with one equivalent of $AgBF_4$ in MeCN leads to the quantitative formation of the complex $[Ag(\mathbf{2})(CH_3CN)_2]BF_4$ (**3**), which is only stable in the presence of a large excess of MeCN (>15 equiv). The formulation of **3** was inferred from its ES-MS spectrum, which revealed the presence of a strong peak for the $[M+H_2O]^+$ ion[19] together with fragmentation peaks resulting from loss of one and two molecules of MeCN. The ^{1}H, ^{13}C, and ^{31}P NMR spectra are all consistent with a C_2-symmetrical complex. Furthermore, the 2D ROESY spectrum of **3** in a $CDCl_3$ solution containing 15 equivalents of MeCN clearly shows cross-peaks corresponding to NOEs between the coordinated MeCN molecules[20] and all the H-3 CD protons as well as two types of H-5 CD proton[21] but no through-space correlations between MeCN with protons outside the cavity.[22] These observations are fully consistent with coordinated MeCN molecules that are located inside the cavity.

Upon evaporation of MeCN, **3** loses coordinated MeCN to produce complexes **4** and **5** in a 80:20 mixture whose ratio does not decrease significantly after prolonged drying in vacuo at 90 °C. However, as confirmed by ^{31}P NMR spectroscopy and microanalysis, quantitative formation of **5** occurs when acetone is added to the mixture prior to evaporation. Coordination of one of the four MeO-6 groups to the silver atom in **5** was inferred from a temperature-dependent ^{1}H NMR study. Thus, at room temperature, the ^{1}H NMR spectrum of **5**, recorded in $C_2D_2Cl_4$, reveals the presence of two distinctive species (45:55 ratio) both of which have averaged C_2 symmetry. As the sample is heated, the signals first broaden, then coalesce near 70 °C, and finally sharpen to produce a spectrum with half the number of signals, consistent with a rapid equilibration of the (B,E)[23] and (C,F) glucose units (Scheme 1, equilibrium B). The calculated energy barrier for this process is about 67.8 kJ mol^{-1}. Upon cooling a CD_2Cl_2 solution of **5** to -20 °C, the room-temperature

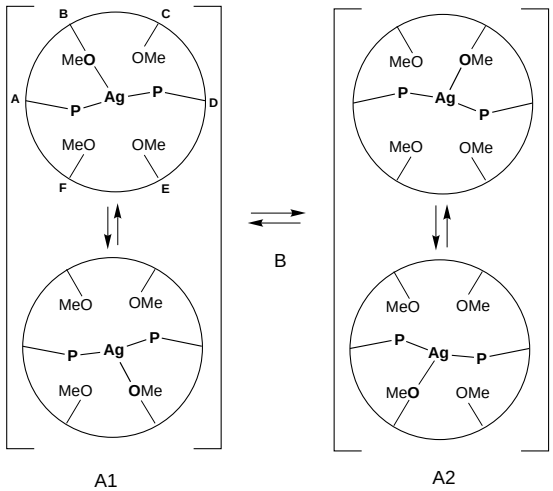

Scheme 1. Hemilabile behavior of ligand **2** in complex **5**. A1 and A2, low-energy dynamics; B, high-energy exchange processes.

spectrum no longer persists. Indeed, two new sets of signals emerge that correspond to two C_1-symmetrical species, reflecting a slow exchange on the ^{1}H NMR time scale between diametrically opposed MeO-6 groups (Scheme 1, equilibria A1 and A2).[24] Overall, our findings are best rationalized in terms of ligand fluxionality about a tricoordinate silver ion, the dynamics involving alternative binding of

all four ether groups. Unsurprisingly, the hemilabile[25] behavior of ligand **2** allows substitution of the coordinated oxygen atom by stronger donors.

The addition of 5–10 equivalents of MeCN to a solution of **5** in $CDCl_3$ led to a mixture of complexes **3** and **4**, both of which interconvert with **5**, as revealed by NMR experiments. A larger excess of MeCN causes **4** to bind an extra MeCN molecule to give **3** exclusively. Conversely, dilution of solutions containing **3** with $CDCl_3$ regenerated compounds **4** and **5**. The C_2 symmetry of the trigonal complex **4** was confirmed by NMR spectroscopy as well as by a single-crystal X-ray diffraction study (Figure 1). As anticipated, the two

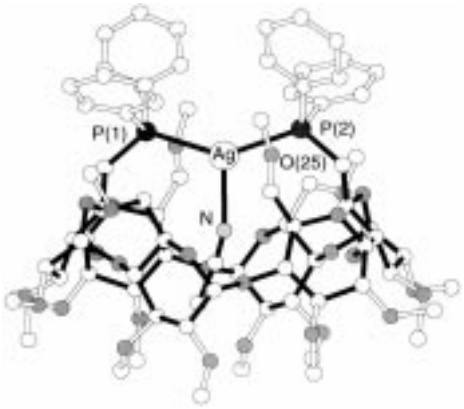

Figure 1. X-ray structure of **4** showing the encapsulated MeCN ligand. The BF_4^- ion and the solvent molecules are not shown. Selected bond lengths [Å] and angles [°]: Ag-P(1) 2.570(4), Ag-P(2) 2.558(4), Ag-N(1) 2.41 (1), P(1)-Ag-P(2) 142.9(1), P(1)-Ag-N(1) 108.9(4), P(2)-Ag-N(1) 108.2(4), Ag-N(1)-C(1) 158.3 (2), N(1)-C(1)-C(2) 173.2 (2). Shortest Ag···O separation: 3.86(1) Å (Ag-O(25)).

phosphorus atoms point towards the interior of the cavity. The trigonal-planar coordination mode forces the coordinated MeCN molecule to be included in the CD cavity which does not undergo significant deformation upon complexation. However, compared to the related complex $[Ag(PPh_3)_2(NCMe)]BF_4$,[26] the Ag–P bonds are unusually long (av 2.56 Å vs. 2.44 Å), reflecting the shortness of the two phosphane arms. Incidentally, the stereochemistry of the silver atom significantly deviates from an ideal trigonal geometry; the P-Ag-P angle (142.9(1)°) is considerably larger than 120°. This geometry is comparable to those observed in trigonal-planar silver complexes obtained with Venanzi's *trans*-spanning ligands.[27] Interestingly, the Ag–N bond is also longer than usual (2.41(1) Å vs. 2.321(2) Å in $[Ag(PPh_3)_2(NCMe)]BF_4$), consistent with a weakly bonded nitrile. Finally, we note that the nitrile rod is slightly bent with respect to the Ag–N axis (Ag-N(1)-C(1) 158.3(2)°).

The aforementioned experiments provide, for the first time, spectroscopic evidence for dinitrile complexes of the type $[Ag(phosphane)_2(MeCN)_2]^+$, although such species have already been proposed.[28] In contrast, related monoacetonitrile silver cations are well documented.[26] Subtle interactions between the cavity and the acetonitrile ligand may contribute to the unexpected stabilization of the "$Ag(MeCN)_2$" unit by cavitand **2**.

Finally, the addition of benzonitrile (ca. 8 equiv) to a solution of **3** in a $CHCl_3$/MeCN mixture (**3**/MeCN = 1:15) resulted in the quantitative formation of complex **6** in which a single benzonitrile molecule is coordinated to the silver ion, as revealed by the corresponding ES-MS spectrum. A range of correlations between some H-3 as well as MeO-3 protons[29] and aromatic protons belonging to the entrapped guest in the 2D ROESY spectrum of **6** confirmed the inclusion of benzonitrile in the CD cavity. Careful examination of the 2D spectra reveals that, upon complexation, the orientation of the benzonitrile plane must be close to that of the P-Ag-P plane. In addition, as a result of the magnetic field anisotropy created by the included phenyl ring, the MeO-3 and MeO-2 signals in the ^{1}H NMR spectrum ($CDCl_3$) are considerably more spread out in **6** than in **3** ($\Delta\delta = 0.65$ vs. 0.2). Clearly, the CD cavity does not allow the coordination of more than one benzonitrile molecule, but can easily accomodate two smaller nitrile ligands such as MeCN. Favorable van der Waals interactions between the inner walls of the CD torus and the cavity-matching phenyl residue, together with the better electron-donating ability of benzonitrile, are likely to account for the higher stability of **6** compared to **4**.

Experimental Section

2: Selected data: ^{1}H NMR (400.1 MHz, $CDCl_3$, 25 °C; assignment by COSY): $\delta = 2.18$, 3.29 (AB, $^2J_{AB} = 10.4$ Hz, 4H; H-6$^{C,F\ or\ B,E}$), 2.50, 2.67 (br AB, 4H; H-6^{A,D}), 2.76 (s, 6H; CH_3O-6), 2.99 (s, 6H; CH_3O-6), 3.10 (dd, 2H; H-2$^{C,F\,or\,B,E}$), 3.15 (dd, 2H; H-2$^{B,E\,or\,C,F}$), 3.22 (dd, 2H; H-2^{A,D}), 3.28, 4.05 (AB, $^2J_{AB} = 10.5$ Hz, 4H; H-6$^{B,E\ or\ C,F}$), 3.40 (t, 2H; H-4^{A,D}), 3.45 (s, 6H; OCH_3), 3.47 (s, 6H; OCH_3), 3.51 (s, 6H; OCH_3), 3.57 (t, 2H; H-3^{A,D}), 3.58 (t, 2H; H-3$^{C,F\ or\ B,E}$), 3.59 (t, 2H; H-3$^{B,E\ or\ C,F}$), 3.61 (s, 6H; OCH_3), 3.63 (s, 6H; OCH_3), 3.64 (t, 2H; H-4$^{C,F\,or\,B,E}$), 3.64 (t, 2H; H-5$^{C,F\ or\ B,E}$), 3.65 (s, 6H; OCH_3), 3.71 (t, $^3J = 8.9$ Hz, 2H; H-4$^{B,E\ or\ C,F}$), 3.79 (m, 2H, $^3J = 9.6$ Hz, 2H; H-5$^{B,E\ or\ C,F}$), 4.39 (m, $^3J = 8.8$ Hz, 2H; H-5^{A,D}), 4.93 (d, $^3J_{H\text{-}2,H\text{-}1} = 2.9$ Hz, 2H; H-1^{A,D}), 5.01 (d, $^3J_{H\text{-}2,H\text{-}1} = 3.2$ Hz, 2H; H-1$^{B,E\,or\,C,F}$), 5.03 (d, $^3J_{H\text{-}2,H\text{-}1} = 3.6$ Hz, 2H; H-1$^{C,F\,or\,B,E}$), 7.22–7.64 (m, 20H; arom. H); ^{31}P{^{1}H} NMR (121.5 MHz, $CDCl_3$, 25 °C): $\delta = -17.8$ (s). Elemental analysis (%): calcd for $C_{76}H_{110}O_{28}P_2$ (1533.62): C 59.52, H 7.23; found: C 59.80, H 7.48.

3: The ^{31}P NMR spectrum in $CDCl_3$ reveals the presence of a mixture of **3**, **4**, and **5** (^{31}P{^{1}H} NMR (121.5 MHz, $CDCl_3$, 25 °C): $\delta = 7.7$ (2d, $^{107}J_{Ag,P} = 458$, $^{109}J_{Ag,P} = 529$ Hz; **3**), 6.1 (2d, $^{107}J_{Ag,P} = 417$, $^{109}J_{Ag,P} = 480$ Hz; **4**), −3.5 (2d, $^{107}J_{Ag,P} = 503$, $^{109}J_{Ag,P} = 581$ Hz; **5**)). When the spectrum was recorded in pure CD_3CN, only **3** was detected. ^{1}H NMR (400.1 MHz, CD_3CN, 25 °C): $\delta = 2.52$ (d, 2H, $^2J = 10.6$ Hz; H-6b^{A,D}, tentative assignment), 2.78 (s, 6H; CH_3O-6), 2.83 (s, 6H; CH_3O-6), 3.43 (s, 6H; OCH_3), 3.44 (s, 6H; OCH_3), 3.49 (s, 6H; OCH_3), 3.56 (s, 6H; OCH_3), 3.57 (s, 6H; OCH_3), 3.60 (s, 6H; OCH_3), 2.84–3.69 (32H; H-2, H-3, H-4, H-5^{B,C,E,F}, H-6a, H-6b^{B,C,E,F}), 4.44 (m, 2H; H-5^{A,D}), 4.79 (d, $^3J_{H\text{-}2,H\text{-}1} = 2.6$ Hz, 2H; H-1), 4.95 (d, $^3J_{H\text{-}2,H\text{-}1} = 3.2$ Hz, 2H; H-1), 5.14 (d, $^3J_{H\text{-}2,H\text{-}1} = 3.2$ Hz, 2H; H-1), 7.35–7.80 (m, 20H; arom. H); ^{31}P{^{1}H} NMR (121.5 MHz, CD_3CN, 25 °C): $\delta = 7.6$ (2d, $^{107}J_{Ag,P} = 458$, $^{109}J_{Ag,P} = 529$ Hz); MS (ES): m/z (%): 1741.3 (13) [$M^+ - BF_4 + H_2O$]. As deduced from 2D NMR experiments, the Me signals of free and coordinated MeCN overlap ($\delta = 1.90$–2.10). All protons of **3** could be assigned by a COSY experiment ($CDCl_3$/CH_3CN). The latter experiment also allowed to unambiguously distinguish protons of **3** from those of **4**.

5: ^{1}H NMR (500.1 MHz, $C_2D_2Cl_4$, 27 °C): $\delta = 2.81$ (s, 3H; CH_3O-6), 2.90 (s, 3H; CH_3O-6), 3.07 (s, 3H; CH_3O-6), 3.24 (s, 3H; CH_3O-6), 3.36 (s, 3H; OCH_3), 3.42 (s, 3H; OCH_3), 3.47 (s, 6H; OCH_3), 3.49 (s, 6H; OCH_3), 3.51 (s, 3H; OCH_3), 3.59 (s, 3H; OCH_3), 3.63 (s, 6H; OCH_3), 3.64 (s, 3H; OCH_3), 3.74 (s, 3H; OCH_3), 2.80–4.30 (36H, H-2, H-3, H-4, H-5, H-6), 4.67 (d, $^3J_{H\text{-}1,H\text{-}2} = 2.0$ Hz, 2H; H-1), 4.79 (d, $^3J_{H\text{-}1,H\text{-}2} = 4.2$ Hz, 2H; H-1), 4.90 (d, $^3J_{H\text{-}1,H\text{-}2} = 2.6$ Hz, 2H; H-1), 5.09 (d, $^3J_{H\text{-}1,H\text{-}2} = 3.0$ Hz, 2H; H-1), 5.39 (d, $^3J_{H\text{-}1,H\text{-}2} = 3.0$ Hz, 2H; H-1), 5.45 (d, $^3J_{H\text{-}1,H\text{-}2} = 3.6$ Hz, 2H; H-1), 7.10–7.65 (20H; arom. H); ^{31}P{^{1}H} NMR (121.5 MHz, $C_2D_2Cl_4$, 25 °C): $\delta = 11.37$ (2d, $^{107}J_{Ag,P} = 488$, $^{109}J_{Ag,P} = 565$ Hz; **5a**), 11.60 (2d, $^{107}J_{Ag,P} = 483$, $^{109}J_{Ag,P} =$

  1433-7851/01/4013-2528 $ 17.50+.50/0

559 Hz; **5b**). Elemental analysis (%): calcd for $C_{76}H_{110}O_{28}P_2BF_4Ag$ (1728.30): C 52.82, H 6.41; found: C 53.08, H 6.45; MS (FAB): *m/z* (%): 1657.4 (60) $[M^+ - BF_4 + O]$, 1641.4 (100) $[M^+ - BF_4]$.

6: ^{1}H NMR (400.1 MHz, $CDCl_3/C_6H_5CN$, 25 °C; assignment by COSY): $\delta = 2.28$, 3.60 (AB, $^2J_{AB} = 10.2$ Hz, 4H; H-6$^{B,E \text{ or } C,F}$), 2.73 (s, 6H; OCH_3), 2.76, 3.30–3.35 (br AB (×2), 8H; H-6^{A,D} and H-6$^{C,F \text{ or } B,E}$), 2.93 (s, 6H; OCH_3), 2.95 (t, 2H; H-3$^{B,E \text{ or } C,F}$), 2.95 (t, 2H; H-3$^{C,F \text{ or } B,E}$), 3.00 (d, 2H; H-2$^{C,F \text{ or } B,E}$), 3.03 (s, 6H; OCH_3), 3.05 (d, 2H; H-5$^{C,F \text{ or } B,E}$), 3.05 (d, 2H; H-2$^{B,E \text{ or } C,F}$), 3.32 (s, 6H; OCH_3), 3.35 (d, 2H; H-2^{A,D}), 3.37 (s, 6H; OCH_3), 3.40 (d, 2H; H-5$^{B,E \text{ or } C,F}$), 3.50 (s, 6H; OCH_3), 3.50 (br, 2H; H-4^{A,D}), 3.52 (s, 6H; OCH_3), 3.55 (d, 2H; H-4$^{B,E \text{ or } C,F}$), 3.65 (d, 2H; H-4$^{C,F \text{ or } B,E}$) 3.70 (s, 6H; OCH_3), 3.75 (t, 2H; H-3^{A,D}), 4.70 (m, 2H; H-5^{A,D}), 4.84 (d, $^3J_{H\text{-}2,H\text{-}1} = 2.2$ Hz, 2H; H-1$^{C,F \text{ or } B,E}$), 4.88 (d, $^3J_{H\text{-}2,H\text{-}1} = 2.6$ Hz, 2H; H-1^{A,D}), 5.16 (d, $^3J_{H\text{-}2,H\text{-}1} = 3.3$ Hz, 2H; H-1$^{B,E \text{ or } C,F}$), 7.35–7.90 (m, 20H, arom. H); $^{31}P\{^1H\}$ NMR (121.5 MHz, $CDCl_3/C_6H_5CN$, 25 °C): $\delta = 8.7$ (2d, $^{107}J_{Ag,P} = 458$, $^{109}J_{Ag,P} = 529$ Hz); MS (ES): *m/z* (%): 1744.7 (22) $[M^+ - BF_4]$.

Crystal structure analysis of $\mathbf{4} \cdot H_2O \cdot 3CH_3CN$: crystals suitable for X-ray diffraction were obtained by slow diffusion of diisopropyl ether into a butanone–acetonitrile (100:1, v/v) solution of the complex; $M_r = 1910.56$, triclinic, space group $P\bar{1}$, $a = 13.7530(4)$, $b = 14.4944(6)$, $c = 15.0189(6)$ Å, $V = 2447.8(6)$ Å^3, $Z = 1$, $\rho = 1.30$ g cm^{-3}, $Mo_{K\alpha}$ radiation ($\lambda = 0.71073$ Å), $\mu = 0.321$ mm^{-1}. Data were collected on a Kappa CCD Enraf Nonius system at 173 K. The structure was solved by direct methods and refined on F_o^2 by full-matrix least-squares. All non-hydrogen atoms were refined anisotropically. The absolute structure was determined by refining Flack's *x* parameter. $R1 = 0.069$ and $\omega R2 = 0.089$ for 5753 data with $I > 3\sigma(I)$. Crystallographic data (excluding structure factors) for the structure reported in this paper have been deposited with the Cambridge Crystallographic Data Centre as supplementary publication no. CCDC-157445. Copies of the data can be obtained free of charge on application to CCDC, 12 Union Road, Cambridge CB21EZ, UK (fax: (+44) 1223-336-033; e-mail: deposit@ccdc.cam.ac.uk).

Received: February 5, 2001 [Z16553]

[1] I. Tabushi, *Acc. Chem. Res.* **1982**, *15*, 66–72.
[2] Y. Murakami, J.-i. Kikichi, Y. Hisaeda, O. Hayashida, *Chem. Rev.* **1996**, *96*, 721–758.
[3] Cyclodextrins: *Comprehensive Supramolecular Chemistry*, *Vol. 3* (Eds.: J. L. Atwood, J. E. D. Davies, D. D. Macnicol, F. Vögtle), Pergamon, Oxford, **1996**.
[4] R. Breslow, S. D. Dong, *Chem. Rev.* **1998**, *98*, 1997–2011.
[5] J. F. Stoddart, R. Zarzycki, *Recl. Trav. Chim. Pays-Bas* **1988**, *107–109*, 515–528.
[6] E. U. Akkaya, A. W. Czarnik, *J. Am. Chem. Soc.* **1988**, *110*, 8553–8554.
[7] R. Breslow, B. Zhang, *J. Am. Chem. Soc.* **1992**, *114*, 5882–5883.
[8] M. Sawamura, K. Kitayama, Y. Ito, *Tetrahedron: Asymmetry* **1993**, *4*, 1829–1832.
[9] R. Breslow, B. Zhang, *J. Am. Chem. Soc.* **1994**, *116*, 7893–7894.
[10] M. Reetz, S. R. Waldvogel, *Angew. Chem.* **1997**, *109*, 870–873; *Angew. Chem. Int. Ed. Engl.* **1997**, *36*, 865–867.
[11] M. T. Reetz, *Catal. Today* **1998**, *42*, 399–411.
[12] A. R. Renslo, J. Rebek, Jr., *Angew. Chem.* **2000**, *112*, 3419–3421; *Angew. Chem. Int. Ed.* **2000**, *39*, 3281–3283.
[13] H. K. A. C. Coolen, P. W. N. M. van Leeuwen, R. J. M. Nolte, *Angew. Chem.* **1992**, *104*, 906–909; *Angew. Chem. Int. Ed. Engl.* **1992**, *31*, 905–907.
[14] S. Blanchard, L. Le Clainche, M.-N. Rager, B. Chansou, J.-P. Tuchagues, A. F. Duprat, Y. Le Mest, O. Reinaud, *Angew. Chem.* **1998**, *110*, 2861–2864; *Angew. Chem. Int. Ed.* **1998**, *39*, 2732–2735.
[15] L. Le Clainche, Y. Rondelez, O. Sénèque, S. Blanchard, M. Campion, M. Giorgi, A. F. Duprat, Y. Le Mest, O. Reinaud, *C. R. Acad. Sci. Ser. IIc* **2000**, 811–819.
[16] J. M. Brown, S. J. Cook, A. G. Kent, *Tetrahedron* **1986**, *42*, 5097–5104.
[17] D. Armspach, D. Matt, N. Kyritsakas, *Polyhedron* **2001**, *20*, 663–668.
[18] D. A. Armspach, D. Matt, *Chem. Commun.* **1999**, 1073–1074.
[19] Complex **5** crystallized with a water molecule located outside the cavity. The latter is hydrogen-bonded to the BF_4^- ion and a MeO-3 oxygen atom. Similar noncovalent aggregates are known to withstand the conditions used for this ES-MS experiment.
[20] Coordinated MeCN molecules could not be differentiated from uncoordinated ones.
[21] H.-J. Schneider, F. Hacket, V. Rüdiger, *Chem. Rev.* **1998**, *98*, 1755–1785.
[22] This includes H-1, H-2, H-4, H-6, OMe-3, and OMe-6 protons. Molecular models show that coordination of MeCN molecules outside the cavity would result in strong steric interactions with some of the OMe-6 and H-6 protons.
[23] Owing to C_2 symmetry, the B and C glucose units are equivalent to the E and F units, respectively.
[24] The whole variable-temperature NMR study required the use of two distinct solvents, CD_2Cl_2 (−40–20 °C) and $C_2D_2Cl_4$ (20–100 °C). The coalescence temperature for the two low-energy processes is close to the boiling point of CD_2Cl_2 and hence the corresponding activation barriers could not be determined accurately.
[25] A. Bader, E. Lindner, *Coord. Chem. Rev.* **1991**, *108*, 27–110.
[26] R. E. Bachman, D. F. Andretta, *Inorg. Chem.* **1998**, *37*, 5657–5663.
[27] M. Camalli, F. Caruso, S. Chaloupka, P. N. Kapoor, P. S. Pregosin, L. M. Venanzi, *Helv. Chim. Acta* **1984**, *67*, 1603–1611.
[28] D. K. Johnson, P. S. Pregosin, L. M. Venanzi, *Helv. Chim. Acta* **1976**, *59*, 2691–2703.
[29] Unlike the MeO-2 groups, the MeO-3 protons are known to point towards the cavity interior. See ref. [21].

Ruthenium Nitrides: Redox Chemistry and Photolability of the Ru–Nitrido Group**

Lucia Bonomo, Euro Solari, Rosario Scopelliti, and Carlo Floriani*

The metal nitride[1] group plays a key role in nitrogen transfer to organic[2–4] and inorganic[5] substrates. Such reactivity exists when the nitrido group is associated with a labile metal, which generally displays catalytic properties. To this end we considered the ruthenium ion in *meso*-octamethylporphyrinogen,[6] which is related to porphyrin—the macrocycle par excellence in ruthenium chemistry. Ruthenium nitride chemistry[7] has received considerable attention in the recent past, and some major issues are considered here: 1) the formation of the Ru≡N group by cleavage of N–N bonds[7] which mimic the N_2 molecule; 2) the redox chemistry associated with the [Ru≡N] fragment, with the intent of tuning the nucleophilic–electrophilic properties of the nitrido group;[7a,b] 3) the relationship between the terminal [Ru≡N] and the bridging [Ru=N=Ru] groups; 4) the photolabilization of Ru–N bonds; and 5) the use of a tetrapyrrolic macrocycle related to porphyrin, a key ligand in Ru chemistry and one with which the Ru≡N group has so far not been associated.

[*] C. Floriani, L. Bonomo, E. Solari, R. Scopelliti
Institut de Chimie Minérale et Analytique
Université de Lausanne
BCH, 1015 Lausanne (Switzerland)
Fax: (+41) 21-692-3905
E-mail: carlo.floriani@icma.unil.ch

[**] This work was supported by the "Fonds National Suisse de la Recherche Scientifique" (Grant No. 20-61'246.00).

Supporting information for this article is available on the WWW under http://www.angewandte.com or from the author.

Ruthenium(II) *meso*-octamethylporphyrinogen (**1**)[8] (Scheme 1) was synthesized by the methodology that has been applied to a variety of metals.[6] The reaction of **1** with diphenyldiazomethane led to the terminal Ru^{VI} nitrido complex **3** via the intermediate **2**. The reaction first forms the Ru^{IV} diphenylhydrazone, which then spontaneously undergoes a reductive cleavage of the N–N single bond to give **3** and $Ph_2C{=}N^-$, both of which were identified.

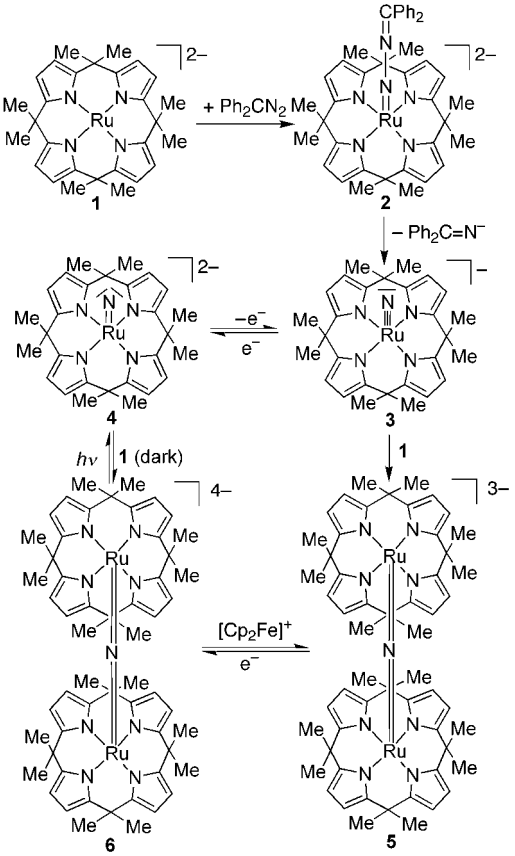

Scheme 1. Formation of Ru≡N and Ru=N=Ru groups and their redox chemistry.

The terminal nitrido complex **3** undergoes a reversible one-electron reduction to the dianion **4**,[8] which contains a Ru^V ion ($\mu = 1.84\,\mu_B$ at 293 K). The major structural difference between **3** and **4** is expected to be the Ru–N bond length[7] (1.569(6) Å in **3**).[9] The two structures are quite similar. Complex **3** occurs in an ion-separated form with a $[Na(dme)_3]^+$ countercation (dme = 1,2-dimethoxyethane). The anion shown in Figure 1[10] has C_{2v} symmetry, and it exhibits the usual saddle conformation, with the metal atom –0.482(3) Å out of the N_4 mean plane.

The moderate electrophilicity of the nitrido nitrogen atom in **3** allowed the formation of the dimer **5**[8] when it was treated with an equimolar amount of the electron-rich **1**. Complex **5** is a diamagnetic, dinuclear Ru^{IV} compound and is thermally and photochemically inert. It undergoes a reversible one-electron reduction to **6**, which contains an unpaired electron ($\mu = 1.60\,\mu_B$ at 293 K). The synthesis of **6** can be equally well performed by treating **4** with **1** in equimolar amounts in the dark. The two bridging nitrido complexes differ significantly, not only in their chemical behavior, but also in their structures. The Ru-N-Ru skeleton[7] is linear in both cases (**5**, 180°; **6**, 179.5(2)°), while the $Ru–N_{av}$ distance changes from 1.768(9) Å in **5**[8] to 1.826(3) Å in **6**. In **6**, the two Ru–porphyrinogen fragments sandwich two sodium ions and a nitrido group (Figure 2),[10] the two remaining $[Na(thf)_3]$ cations being weakly bonded to the periphery. The two Ru–porphyrinogen moieties display a structure similar to that of **3**, with a saddle conformation of the ligand and protrusion of Ru1 and Ru2 by 0.506(1) and –0.510(1) Å, respectively, from their N_4 planes. The sodium cations Na1 and Na2 are η^5 bonded to two pyrrolyl anions (Na1–η^5-Pyr 2.385(2) Å, 2.380(2) Å; Na2–η^5-Pyr 2.376(2) Å, 2.378(2) Å) and they experience a short contact with the nitrido anion (Na1 ··· N9 3.032(3) Å, Na2 ··· N9 3.102(3) Å).

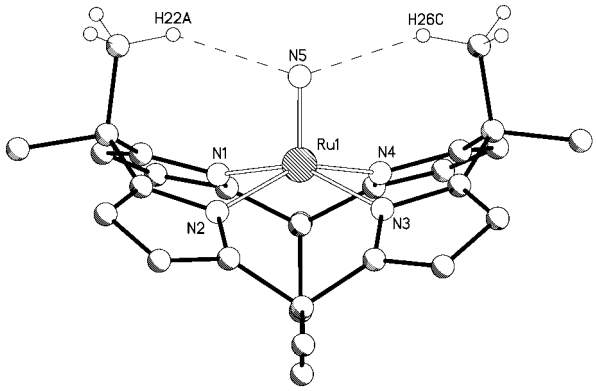

Figure 1. Ball-and-stick diagram for **3** ($[Na(dme)_3]^+$, free DME molecule, and hydrogen atoms omitted for clarity). Selected bond lengths [Å]: Ru1-N5 1.569(6), Ru1-N1 1.996(6), Ru1-N2 2.042(7), Ru1-N3 2.009(7), Ru1-N4 1.971(7).

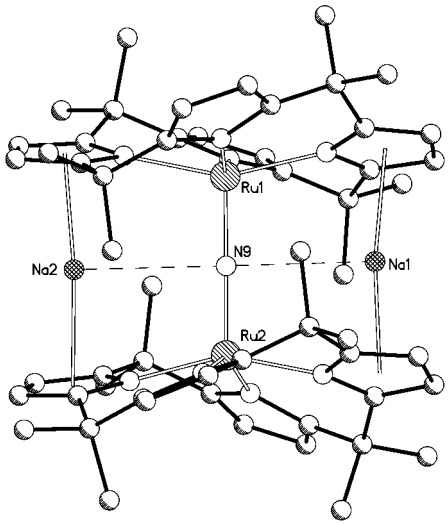

Figure 2. Ball-and-stick representation of **6** ($[Na(thf)_3]^+$, Na^+, and hydrogen atoms omitted for clarity). Selected bond lengths [Å]: Ru1-N_{av} 2.099(2), Ru1-N9 1.827(3), Ru2-N_{av} 2.097(2), Ru2-N9 1.825(3).

The above results suggest: 1) how a metal–nitrido functionality can be synthesized from dinitrogen or related organic groups; 2) how to tune the nature and hence the

  1433-7851/01/4013-2530 $ 17.50+.50/0 *Angew. Chem. Int. Ed.* **2001**, *40*, No. 13

reactivity of the Ru nitrido group; 3) how to make homo- or heterodinuclear nitrido complexes;[11] and 4) how to labilize the [Ru=N] group.

Experimental Section

1: $[RuCl_2(cod)]$ (cod = 1,5-cyclooctadiene; 6.19 g, 22.0 mmol) was added to a solution of $[Me_8N_4Na_4(thf)_4]$ (17.8 g, 22.0 mmol) in DME (300 mL). The reaction mixture was refluxed for 24 h, and the NaCl was filtered off. The resulting solution was allowed to stand at $-20\,^{\circ}C$, and the resulting orange crystalline product was collected and dried in vacuo (11 g, 45%). Crystals suitable for X-ray diffraction were grown from DME. ^1H NMR (400 MHz, [D$_6$]DMSO, 25 °C, TMS): $\delta = 5.74$ (s, 8H, C_4H_2N), 3.41 (s, 24H, DME), 3.23 (s, 36H, DME), 1.43 (s, 24H, CH_3); ^{13}C NMR (400 MHz, [D$_6$]DMSO, 25 °C): $\delta = 146.1$, 100.1, 71.0, 58.0, 39.1, 36.9; elemental analysis (%) calcd for $\mathbf{1}\cdot 6\,C_4H_{10}O_2$, $C_{52}H_{92}N_4Na_2O_{12}Ru$ ($M_r = 1112.4$): C 56.15, H 8.34, N 5.04; found: C 55.91, H 8.40, N 4.96.

3: Compound **1** (19.0 g, 17.1 mmol) was added to a solution of diphenyldiazomethane (3.32 g, 17.1 mmol) in THF (600 mL) at $-40\,^{\circ}C$. The reaction mixture was slowly warmed to room temperature and stirred overnight. The resultant dark amber solution was concentrated, and then Et_2O (200 mL) was added. An amber microcrystalline solid was isolated (10.6 g, 74.6%). Ph_2CNH was detected by gas-chromatography and characterized by mass spectroscopy from a hydrolyzed sample of the mother liquor. Crystals suitable for X-ray diffraction were grown from DME. ^1H NMR (400 MHz, [D$_6$]benzene/[D$_8$]THF, 298 K, TMS): $\delta = 6.33$ (s, 8H, C_4H_2N), 3.22 (s, 12H, DME), 3.05 (s, 18H, DME), 1.88 (s, 12H, CH_3), 1.54 (br s, 12H, CH_3); elemental analysis (%) calcd for **3**, $C_{40}H_{62}N_5NaO_6Ru$ (M_r = 833.01): C 57.67, H 7.50, N 8.41; found: C 57.41, H 7.45, N 8.22.

6: Method A: Sodium (38.0 mg, 1.64 mmol) and a catalytic amount of naphthalene were added to a suspension of **5** (1.38 g, 1.64 mmol) in THF (80 mL) at room temperature. The reaction mixture was stirred for 36 h, after which a green solid formed (0.98 g, 80%). Crystals suitable for X-ray diffraction were grown from THF/Et_2O. Elemental analysis (%) calcd for **6**, $C_{72}H_{96}N_9Na_4O_4Ru_2$ ($M_r = 1445.68$): C 59.82, H 6.69, N 8.72; found: C 59.98, H 6.75, N 8.52; $\mu_{eff} = 1.60\,\mu_B$ at 293 K; UV/Vis (THF/DME): λ_{max} [nm] (ε [mol^{-1} dm^3 cm^{-1}]) = 286 (35898), 338 (18114), 486 (2676), 582 (698), 674 (973).

6: Method B: An equimolar mixture of **1** (1.42 g, 1.28 mmol) and **4** (1.05 g, 1.28 mmol) in THF (100 mL) was allowed to stand in the dark for 2 h. The resulting green suspension was concentrated to 30 mL, and Et_2O (100 mL) was added. The bright green crystalline solid that precipitated was collected and then dried in vacuo (1.64 g, 89%). Crystals suitable for X-ray diffraction were grown from THF.

Photolysis of **6**: A green solution of **6** in THF/DME was irradiated with visible light. The resulting yellow solution reverted to the initial green one on allowing it to stand in the dark. When the yellow solution was cooled to $-40\,^{\circ}C$ under continuous irradiation, orange crystals of **1** were isolated. The presence of **1** in solution was further supported by the ^1H NMR spectrum.

Received: February 12, 2001 [Z16600]

[1] For a review of metal nitrido complexes, see a) K. Dehnicke, J. Strähle, *Angew. Chem.* **1992**, *104*, 978; *Angew. Chem. Int. Ed. Engl.* **1992**, *31*, 955; b) W. A. Nugent, B. L. Haymore, *Coord. Chem. Rev.* **1980**, *31*, 123; see also W. A. Nugent, J. M. Mayer, *Metal–Ligand Multiple Bonds*, Wiley-Interscience, New York, **1988**.

[2] For metal-catalyzed aziridination with PhI=NTs, see a) D. A. Evans, M. M. Faul, M. T. Bilodeau, *J. Am. Chem. Soc.* **1994**, *116*, 2742, and references therein; b) Z. Li, Z. R. Quan, E. N. Jacobsen, *J. Am. Chem. Soc.* **1995**, *117*, 5889; and references therein; c) K. Noda, N. Hosoya, R. Irie, Y. Ito, T. Katsuki, *Synlett* **1993**, 469; d) K. J. O'Connor, S.-J. Wey, C. J. Burrows, *Tetrahedron Lett.* **1992**, *33*, 1001.

[3] For a review on available aziridination and amination methods, see J. E. G. Kemp in *Comprehensive Organic Synthesis*, *Vol. 7* (Ed.: S. V. Ley), Pergamon, Oxford, **1991**, p. 469; see also: E. Vedejs, H. Sano, *Tetrahedron Lett.* **1992**, *33*, 3261.

[4] a) J. T. Groves, T. Takahashi, *J. Am. Chem. Soc.* **1983**, *105*, 2074; b) J. T. Groves, T. Takahashi, W. M. Butler, *Inorg. Chem.* **1983**, *22*, 884; c) J. Du Bois, J. Hong, E. M. Carreira, M. W. Day, *J. Am. Chem. Soc.* **1996**, *118*, 915.

[5] W. R. Murphy, Jr., K. Takeuchi, M. H. Barley, T. J. Meyer, *Inorg. Chem.* **1986**, *25*, 1041.

[6] C. Floriani, R. Floriani-Moro in *The Porphyrin Handbook*, *Vol. 3* (Eds.: K. M. Kadish, K. M. Smith, R. Guilard), Academic Press, Burlington, MA, **1999**, chap. 24, pp. 385–403 and chap. 25, pp. 405–420.

[7] a) C. M. Che, *Pure Appl. Chem.* **1995**, *67*, 225; b) W.-H. Chiu, C.-X. Guo, K.-K. Cheung, C.-M. Che, *Inorg. Chem.* **1996**, *35*, 540; c) P.-M. Chan, W.-Y. Yu, C.-M. Che, K.-K. Cheung, *J. Chem. Soc. Dalton Trans.* **1998**, 3183; d) D. Sellmann, M. W. Wemple, W. Donaubauer, F. W. Heinemann, *Inorg. Chem.* **1997**, *36*, 1397; e) H.-C. Liang, P. A. Shapley, *Organometallics* **1996**, *15*, 1331; f) T. Jüstel, J. Bendix, N. Metzler-Nolte, T. Weyhermüller, B. Nuber, K. Wieghardt, *Inorg. Chem.* **1998**, *37*, 35; g) M. Haukka, M. Ahlgrén, T. A. Pakkanen, *J. Chem. Soc. Dalton Trans.* **1996**, 1927.

[8] The synthesis of **1** is reported in the Supporting Information and in L. Bonomo, C. Stern, E. Solari, R. Scopelliti, C. Floriani, *Angew. Chem.* **2001**, *113*, 1497; *Angew. Chem. Int. Ed.* **2001**, *40*, 1449.

[9] The Ru=N group in **4** is affected by disorder. After solving this problem, 1.74(1) and 1.78(3) Å were obtained as the bond lengths for the two different sites A and B (occupancy factor for A: 0.51(1)).

[10] Crystal structure analysis of **3**: $[C_{28}H_{32}N_5Ru][Na(C_4H_{10}O_2)_3]\cdot(C_4H_{10}O_2)$, $M_r = 923.13$, orthorhombic, space group $Pca2_1$, $a = 31.587(6)$, $b = 11.802(2)$, $c = 12.986(3)$ Å, $V = 4841.0(17)$ Å^3, $Z = 4$, $\rho_{calcd} = 1.267$ g cm^{-3}, $F(000) = 1960$, $Mo_{K\alpha}$ radiation ($\lambda = 0.71070$ Å), $\mu(Mo_{K\alpha}) = 0.385$ mm^{-1}; $x = 0.06(5)$; crystal dimensions $0.24 \times 0.20 \times 0.14$ mm^3. Diffraction data were collected on a mar345 Imaging Plate at 143 K. For 4071 observed reflections ($I > 2\sigma(I)$) and 533 parameters, the conventional R factor was 0.0525 ($wR2 = 0.1390$ for 6730 independent reflections). Crystal structure analysis of **6**: $[C_{56}H_{64}N_9Ru_2][Na]_2[Na(C_4H_8O)_3]_2$, $M_r = 1589.89$, monoclinic, space group $P2_1$, $a = 13.8984(8)$, $b = 15.7887(8)$, $c = 17.5436(9)$ Å, $\beta = 95.929(5)^{\circ}$, $V = 3829.1(4)$ Å^3, $Z = 2$, $\rho_{calcd} = 1.379$ g cm^{-3}, $F(000) = 1670$, $Mo_{K\alpha}$ radiation ($\lambda = 0.71073$ Å), $\mu(Mo_{K\alpha}) = 0.476$ mm^{-1}; $x = 0.025(14)$; crystal dimensions $0.34 \times 0.30 \times 0.20$ mm. Diffraction data were collected on a Kuma diffractometer with a κ geometry and equipped with a CCD detector at 143 K. For 16324 observed reflections ($I > 2\sigma(I)$) and 910 parameters, the conventional R value was 0.0277 ($wR2 = 0.0665$ for 16674 independent reflections). Crystallographic data (excluding structure factors) for the structures reported in this paper have been deposited with the Cambridge Crystallographic Data Centre as supplementary publication nos. CCDC-158333 (**3**) and CCDC-158334 (**6**). Copies of the data can be obtained free of charge on application to CCDC, 12 Union Road, Cambridge CB2 1EZ, UK (fax: (+44) 1223-336-033; e-mail: deposit@ccdc.cam.ac.uk).

[11] The phthalocyanine (Pc) bis-ruthenium μ-nitrido species, [(Pc)Ru–N–Ru(Pc)] and the mixed-ligand heterobimetallic analogue [(tpp)Fe^{IV}–N–Ru^{III}(Pc)] (tpp = tetraphenylporphyrin) have been previously reported: a) G. Rossi, M. Gardini, G. Pennesi, C. Ercolani, V. L. Goedken, *J. Chem. Soc. Dalton Trans.* **1989**, 183; b) C. Ercolani, J. Jubb, G. Pennesi, U. Russo, G. Trigiante, *Inorg. Chem.* **1995**, *34*, 2535.

  1433-7851/01/4013-2531 $ 17.50+.50/0

DFT Calculation of Intermolecular Nuclear Spin–Spin Coupling in van der Waals Dimers**

Alessandro Bagno,* Giacomo Saielli, and Gianfranco Scorrano

Nuclear magnetic resonance is probably the most powerful technique for the determination of molecular structure and conformation in solution; a wide array of experimental methods is available, which exploit scalar (spin–spin) or dipolar (nuclear Overhauser effect) coupling. Spin–spin couplings are normally thought of as probes of connectivities through covalent bonds only. Lately, however, it has been demonstrated that spin–spin coupling can also be transmitted through various types of hydrogen bonds (HBs).[1–6] Most notably, the sensitivity of NMR experiments has made it possible to detect through-HB coupling constants as low as 0.14 Hz.[3] These findings have stimulated much theoretical work aimed at understanding the factors affecting such coupling constants.[1, 7–11]

An obvious extension is that spin–spin coupling might be detectable even in the case of dispersion-bound van der Waals complexes. In fact, Salsbury and Harris calculated a very small ($<10^{-3}$ Hz) coupling for Xe···Xe and Xe···H.[12] Apart from fundamental implications, exploitation of such couplings might become important in at least two areas, namely the use of optically pumped Xe as a spin probe[12] and structural investigations of host–guest complexes, which often owe their stability to favorable dispersive interactions.[13] Hence, we have carried out a computational investigation of intermolecular spin–spin couplings in methane–benzene and benzene–benzene dimers as models.

The stabilization energy for the two dimers has been calculated using Gaussian 98[14] at the MP2/cc-pVTZ level,[15–17] corrected for the basis-set superposition error.[18] The geometry of the individual monomers was kept fixed.

Spin–spin coupling constants were calculated with deMon-NMR,[19] which allows the calculation of the three major contributions to the nuclear spin–spin coupling: the Fermi contact (FC), the paramagnetic spin-orbit (PSO), and the diamagnetic spin-orbit (DSO) contributions. The spin–dipole term is often negligible, especially for simple hydrocarbons[20] and when the nuclei are separated by relatively large distances.[19e]

The local Vosko-Wilk-Nusair (VWN) exchange correlation functional[21] was used with the IGLO-III basis set.[22] A preliminary set of calculations on the methane–methane dimer (not reported here) showed that VWN gives essentially the same results as the gradient-corrected Perdew functional (PWP), which is preferred for couplings involving covalent bonds.[19e] Moreover, the VWN functional requires a much more coarse integration grid than the PWP while maintaining the same accuracy,[19] thus reducing the computational time by a factor of five. For these reasons, we have used the VWN functional for the calculations presented here. The perturbation ($\lambda = 0.001$)[19e] was placed on the lighter (hydrogen) atom of a methane or benzene molecule, as shown in Figure 1; this yields the couplings with all the essentially equivalent hydrogen and carbon atoms of the other molecule. The same computational scheme was adopted[7] for through-HB couplings in peptide models, in which a very good accuracy was obtained. Further validation is provided by the values of direct couplings ($^1J_{C,H}$) in the methane, ethylene, and benzene molecules at the PWP/IGLO-III level, which are less than 4% smaller than experimental values. All results are compiled in Table 1.

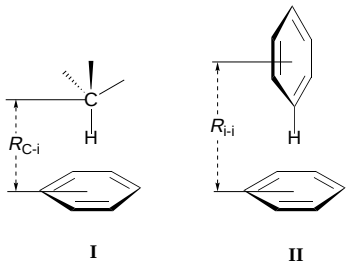

I **II**

Figure 1. Schematic representation of the two dimers.

Table 1. Main contributions to the intermolecular spin–spin couplings at some selected distances.

	R [Å]	J_{HH} [Hz]			$J_{C,H}$ [Hz]		
		FC	PSO	DSO	FC	PSO	DSO
CH_4–C_6H_6 (**I**)							
	4.485	0.00	−0.21	0.21	0.02	−0.19	0.26
	3.685	0.00	−0.13	0.12	0.11	−0.30	0.41
	3.285	0.01	−0.02	0.00	0.19	−0.42	0.53
C_6H_6–C_6H_6 (**II**)							
	5.100	0.00	−0.33	0.32	0.08	−0.36	0.46
	4.900	0.00	−0.30	0.28	0.11	−0.42	0.52
	4.400	0.04	−0.16	0.13	0.07	−0.64	0.73

As an example of an alkyl–aromatic interaction, we have considered the methane–benzene dimer in the configuration **I** (Figure 1). The geometry of both monomers has been optimized at the MP2/cc-pVTZ level. The interaction energy is reported in Figure 2 as a function of the intermolecular separation $R_{C\text{-}i}$ between the carbon atom of the methane and the center of symmetry of the benzene molecule. The MP2 interaction energy has a minimum at $R_{C\text{-}i} = 3.685$ Å with a stabilization energy of 1.40 kcal mol^{-1}. The $J_{H,H}$ coupling is essentially zero over the distances investigated. On the contrary, a weak but detectable coupling exists between the hydrogen of the methane and the carbon atoms of the benzene molecule, about 0.3 Hz at $R_{C\text{-}i} \approx 3.3$ Å. For $J_{H,H}$ we have a large compensation between the PSO and DSO terms (Table 1), as previously noted in covalent species,[23] whereas for $J_{C,H}$ the compensation is incomplete.

An arrangement of atoms similar to **I** has been found, for example, in the inclusion complex of *tert*-butylcalix[4]arene

[*] Dr. A. Bagno, Dr. G. Saielli, Prof. G. Scorrano
Centro CNR Meccanismi Reazioni Organiche
Dipartimento di Chimica Organica
Università degli Studi di Padova
Via Marzolo 1, 35131, Padova (Italy)
Fax: (+39) 0498275239
E-mail: alex@chor.unipd.it

[**] The authors wish to thank V. G. Malkin and O. L. Malkina for providing the *deMon-NMR* program and for helpful discussions.

  1433-7851/01/4013-2532 $ 17.50+.50/0

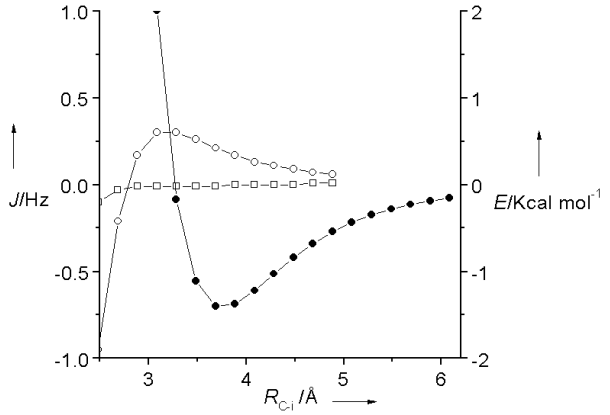

Figure 2. Interaction energies and coupling constants for the $CH_4-C_6H_6$ dimer **I** as a function of the $R_{C\text{-}i}$ distance (VWN/IGLO-III). MP2 interaction energy (●); $J_{H,H}$ couplings (□); $J_{C,H}$ couplings (○).

and acetonitrile.[24] In that case, the $R_{C\text{-}i}$ distance between the methyl carbon and the center of symmetry of one of the benzene rings was 3.71 Å, that is, almost exactly the distance corresponding to the energy minimum in Figure 2.

We have chosen the T-shaped configuration **II** of the benzene–benzene dimer in Figure 1 using the experimental geometries for the benzene monomers.[25] The interaction energies are reported in Figure 3 as a function of the

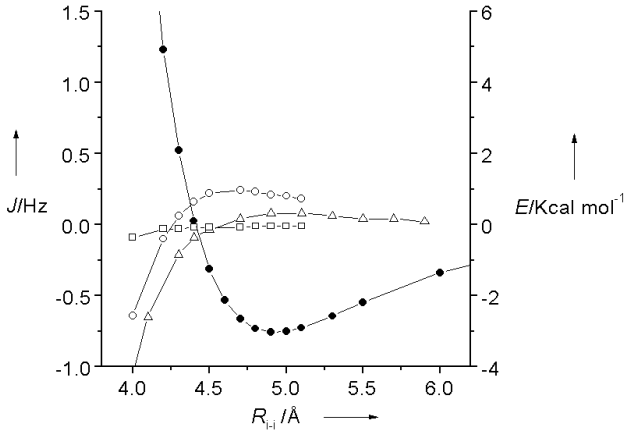

Figure 3. Interaction energies and coupling constants for the $C_6H_6-C_6H_6$ dimer **II** as a function of the $R_{i\text{-}i}$ distance (VWN/IGLO-III). MP2 interaction energy (●); $J_{H,H}$ couplings (□); $J_{C,H}$ couplings (○); FC contribution to $J_{C,H}$ couplings (MPWPW91/cc-pVTZ) (△).

intermolecular separation $R_{i\text{-}i}$ between the centers of symmetry of the benzene molecules. The MP2 energy has a deeper minimum (3.02 kcal mol^{-1} at $R_{i\text{-}i} = 4.90$ Å). As for **I**, $J_{H,H}$ couplings are again almost zero, whereas $J_{C,H}$ couplings are about 0.2 Hz at the equilibrium distance. In Figure 3 we also report the FC contribution to $J_{C,H}$ calculated with the MPWPW91 functional[26, 27] and the cc-pVTZ basis set. We observe the same qualitative behaviour of the spin–spin coupling as a function of the intermolecular separation despite the differences in the functional and basis set used.

In some rotaxane complexes,[28] the distance between the centroids of the aromatic rings, roughly arranged as in **II**, were in the range 4.8–5.2 Å, again very close to the distance for which we observe the minimum of the interaction energy.

We also note a nonmonotonic trend followed by $J_{C,H}$ in the stabilizing region, as previously noted for $F^- \cdots (HF)_n$ complexes.[5]

A qualitative picture of the mechanism responsible for the through-space spin–spin coupling in the dimers we have investigated is provided by Figure 4, which shows a molecular orbital of **II** at the equilibrium distance connecting the perturbed hydrogen with the hydrogen and carbon atoms of the other molecule.

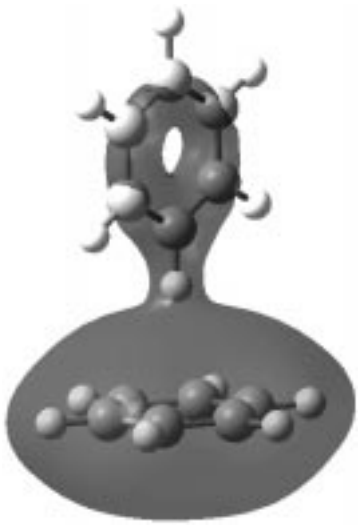

Figure 4. Isosurface at an electron density value of 0.005 for the occupied molecular orbital no. 13 (MP2/cc-pVTZ) for the benzene dimer **II** at the equilibrium distance.

In conclusion, intermolecular spin–spin coupling in these van der Waals dimers is not negligible (0.2–0.3 Hz) for spatial arrangements where the interaction is stabilizing. However, even though such values should lie within the scope of current experimental NMR methods, these model systems are not suitable for an experimental verification, due to their too-large exchange rate compared to the small couplings. On the other hand, some host–guest complexes with similar structural features may have sufficient stabilities and lifetimes. In this respect, our predictions indicate $J_{C,H}$ couplings as the most likely candidates for such experiments.

Received: February 22, 2001 [Z16669]

[1] See: G. Gemmecker, *Angew. Chem.* **2000**, *112*, 1276; *Angew. Chem. Int. Ed.* **2000**, *39*, 1224, and references therein for a concise summary on this field up to 1999.
[2] F. Löhr, S. G. Mayhew, H. Rüterjans, *J. Am. Chem. Soc.* **2000**, *122*, 9289.
[3] A. Liu, A. Majumdar, F. Jiang, N. Chernichenko, E. Skripkin, D. J. Patel, *J. Am. Chem. Soc.* **2000**, *122*, 11226.
[4] M. Mishima, M. Hatanaka, S. Yokoyama, T. Ikegami, M. Wälchli, Y. Ito, M. Shirakawa, *J. Am. Chem. Soc.* **2000**, *122*, 5883.
[5] I. G. Shenderovich, S. N. Smirnov, G. S. Denisov, V. A. Gindin, N. S. Golubev, A. Dunger, R. Reibke, S. Kirpekar, O. L. Malkina, H.-H. Limbach, *Ber. Bunsenges. Phys. Chem.* **1998**, *102*, 422.
[6] J. E. Del Bene, S. A. Perera, R. J. Bartlett, I. Alkorta, J. Elguero, *J. Phys. Chem. A* **2000**, *104*, 7165.
[7] C. Scheurer, R. Brüschweiler, *J. Am. Chem. Soc.* **1999**, *121*, 8661.
[8] J. E. Del Bene, S. A. Perera, R. J. Bartlett, *J. Phys. Chem. A* **2001**, *123*, 930, and previous papers by the same authors.

  1433-7851/01/4013-2533 $ 17.50+.50/0

[9] a) M. Pecul, J. Leszczynski, J. Sadlej, *J. Phys. Chem. A* **2000**, *104*, 8105; b) M. Pecul, J. Leszczynski, J. Sadlej, *J. Chem. Phys.* **2000**, *112*, 7930.
[10] W. D. Arnold, J. Mao, H. Sun, E. Oldfield, *J. Am. Chem. Soc.* **2000**, *122*, 12164.
[11] A. Bagno, *Chem. Eur. J.* **2000**, *6*, 2925.
[12] F. R. Salsbury, R. A. Harris, *Mol. Phys.* **1998**, *94*, 307.
[13] M. Nishio, M. Hirota, Y. Umezawa, *The CH/π Interaction, Evidence, Nature and Consequences*, Wiley-VCH, New York, NY, **1998**.
[14] Gaussian 98 (Revision A.7), M. J. Frisch, G. W. Trucks, H. B. Schlegel, G. E. Scuseria, M. A. Robb, J. R. Cheeseman, V. G. Zakrzewski, J. A. Montgomery, R. E. Stratmann, J. C. Burant, S. Dapprich, J. M. Millam, A. D. Daniels, K. N. Kudin, M. C. Strain, O. Farkas, J. Tomasi, V. Barone, M. Cossi, R. Cammi, B. Mennucci, C. Pomelli, C. Adamo, S. Clifford, J. Ochterski, G. A. Petersson, P. Y. Ayala, Q. Cui, K. Morokuma, D. K. Malick, A. D. Rabuck, K. Raghavachari, J. B. Foresman, J. Cioslowski, J. V. Ortiz, B. B. Stefanov, G. Liu, A. Liashenko, P. Piskorz, I. Komaromi, R. Gomperts, R. L. Martin, D. J. Fox, T. Keith, M. A. Al-Laham, C. Y. Peng, A. Nanayakkara, C. Gonzalez, M. Challacombe, P. M. W. Gill, B. G. Johnson, W. Chen, M. W. Wong, J. L. Andres, M. Head-Gordon, E. S. Replogle, J. A. Pople, Gaussian, Inc., Pittsburgh, PA, **1998**.
[15] T. H. Dunning, *J. Chem. Phys.* **1987**, *98*, 1007.
[16] S. Tsuzuki, T. Uchimaru, M. Mikami, K. Tanabe, *Chem. Phys. Lett.* **1996**, *252*, 206.
[17] S. Tsuzuki, K. Tanabe, *J. Phys. Chem.* **1991**, *95*, 2272.
[18] S. F. Boys, F. Bernardi, *Mol. Phys.* **1970**, *19*, 553.
[19] a) D. R. Salahub, R. Fournier, P. Mlynarski, I. Papai, A. St-Amant, J. Ushio in *Density Functional Methods in Chemistry* (Eds.: J. Labanowski, J. Andzelm), Springer, New York, NY, **1991**; b) A. St-Amant, D. R. Salahub, *Chem. Phys. Lett.* **1990**, *169*, 387; c) V. G. Malkin, O. L. Malkina, M. E. Casida, D. R. Salahub, *J. Am. Chem. Soc.* **1994**, *116*, 5898; d) V. G. Malkin, O. L. Malkina, L. A. Eriksson, D. R. Salahub, *Modern Density Functional Theory: A Tool For Chemistry*, *Vol. 2* (Eds.: J. M. Seminario, P. Politzer), Elsevier, Amsterdam, **1995**; e) V. G. Malkin, O. L. Malkina, D. R. Salahub, *Chem. Phys. Lett.* **1994**, *221*, 91; f) O. L. Malkina, D. R. Salahub, V. G. Malkin, *J. Chem. Phys.* **1996**, *105*, 8793.
[20] T. Helgaker, M. Watson, N. C. Handy, *J. Chem. Phys.* **2000**, *113*, 9402.
[21] S. H. Vosko, L. Wilk, M. Nusair, *Can. J. Phys.* **1980**, *58*, 1200.
[22] W. Kutzelnigg, U. Fleischer, M. Schindler, *NMR—Basic Principles and Progress*, *Vol. 23*, Springer, Berlin, **1990**.
[23] A. Bagno, *Chem. Eur. J.* **2001**, *7*, 1652–1661.
[24] W. Xu, R. J. Puddephatt, L. Manojlovic-Muir, K. W. Muir, C. S. Frampton, *J. Inclusion Phenom. Mol. Recognit. Chem.* **1994**, *19*, 277.
[25] *Handbook of Chemistry and Physics*, 69th ed., CRC, Boca Raton, FL, **1988–1989**.
[26] C. Adamo, V. Barone, *J. Chem. Phys.* **1998**, *108*, 664.
[27] K. Burke, J. P. Perdew, Y. Wang in *Electronic Density Functional Theory: Recent Progress and New Directions*, (Eds.: J. F. Dobson, G. Vignale, M. P. Das), Plenum Press, New York, NY, **1998**.
[28] P. L. Anelli, P. R. Ashton, R. Ballardini, V. Balzani, M. Delgado, M. T. Gandolfi, T. T. Goodnow, A. E. Kaifer, D. Philp, M. Pietraszkiewicz, L. Prodi, M. V. Reddington, A. M. Z. Slawin, N. Spencer, J. F. Stoddart, C. Vincent, D. J. Williams, *J. Am. Chem. Soc.* **1992**, *114*, 193.

A Three-Component Coupling Reaction of Aldehydes, Amines, and Alkynes

Satoshi Sakaguchi, Takashi Kubo, and Yasutaka Ishii*

Since the decisive breakthrough in 1993 by Murai et al., who achieved a highly efficient ruthenium-catalyzed addition of aromatic C–H bonds to olefins,[1] carbon–carbon bond formation through the activation of C–H bonds by transition metal complexes is recognized as a new category of chemistry.[2, 3] So far there have been a number of cases of C–C bond formation through activation of the C–H bond adjacent to the heteroatom.[3–5] Recently, it was shown that some iridium complexes cleave the C–H bond of nitriles[6] or 1-naphthols[7] to provide a new C–C bond. To the best of our knowledge, however, no reports have appeared on C–C bond formation by the activation of C–H bonds neighboring the nitrogen atom of imines. In continuation of our studies on iridium-catalyzed reactions of imines,[8] we have now found a new type of C–H bond activation adjacent to the nitrogen atom of imines by an iridium complex, leading to a three-component coupling reaction of aldehydes, amines, and alkynes.

The reaction of *n*-butyraldehyde (**1a**), *n*-butylamine (**2a**), and 1-octyne (**3a**) was selected as a model reaction and examined in the presence of a catalytic amount of [{Ir(cod)Cl}$_2$] (cod = cycloocta-1,5-diene) under various reaction conditions [Eq. (1), Table 1]. To a solution containing

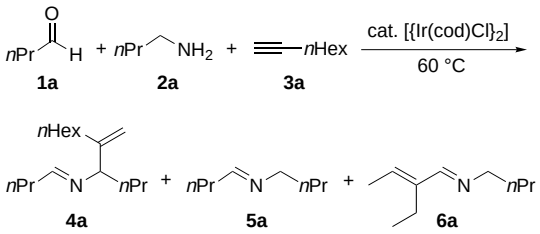

(1)

[{Ir(cod)Cl}$_2$] in THF was added a 1:1:1 mixture of **1a**, **2a**, and **3a**. The reaction was carried out with stirring at 60 °C for 15 h, giving the coupling products *N*-butyliden(2-hexylpropylallyl)amine (**4a**), imine **5a**, and α,β-unsaturated imine **6a** in 57%, 28% and 11% yields, respectively (Table 1, run 1). When two equivalents of **1a** and **3a** with respect to **2a** were employed, **4a** was formed in higher yield (72%, run 2). Interestingly, the reaction took place at 50 °C to give **4a** in moderate yield (56%, run 4), although the usual catalytic addition of C–H bonds to alkenes and alkynes calls for higher reaction temperatures (>100 °C).[1–5] When the reaction was terminated after 7 h, a considerable amount of imine **5a** remained unchanged (run 5). This shows that the reaction is

[*] Prof. Y. Ishii, S. Sakaguchi, T. Kubo
Department of Applied Chemistry
Faculty of Engineering & High Technology Research Center
Kansai University
Suita, Osaka 564-8680 (Japan)
Fax: (+81) 6-6339-4026
E-mail: ishii@ipcku.kansai-u.ac.jp

  1433-7851/01/4013-2534 $ 17.50+.50/0

Table 1. Results of the three-component coupling reaction of *n*-butyraldehyde (**1a**), *n*-butylamine (**2a**), and 1-octyne (**3a**) catalyzed by $[\{Ir(cod)Cl\}_2]$ under various conditions [Eq. (1)].[a]

Run	Solvent	Yield [%][b]		
		4a	**5a**	**6a**
1[c]	THF	57	28	11
2	THF	72	7	12
3[d]	THF	48	8	16
4[e]	THF	56	13	12
5[f]	THF	54	32	10
6[g]	THF	68	3	18
7[h]	THF	49	13	15
8[i]	THF	0	2	40
9	DME	64	7	8
10	toluene	53	11	13
11	EtOH	9	26	34

[a] Reaction conditions: **1a** (0.5 mmol), **2a** (0.25 mmol), **3a** (0.5 mmol), $[\{Ir(cod)Cl\}_2]$ (0.025 mmol), solvent (2 mL), 60 °C, 15 h. [b] Yield based on amount of **2a** used. [c] As in [a], except: **1a** (0.25 mmol), **3a** (0.25 mmol). [d] As in [a], except: THF (1 mL). [e] As in [a], except: 50 °C. [f] As in [a], except: 7 h. [g] Compound **5a** (0.25 mmol) was allowed to react with **3a** (0.5 mmol) under the same reaction conditions as run 2. [h] Catalyst: $[\{Ir(cyclooctene)_2Cl\}_2]$ (0.025 mmol). [i] Catalyst: $IrCl_3$ (0.025 mmol).

initiated by the reaction of **1a** with **2a**, leading to the imine **5a**. Indeed, the reaction of imine **5a** with **3a** under the influence of the Ir complex in THF gave **4a** in satisfactory yield (run 6). The catalytic activity of $[\{Ir(cyclooctene)_2Cl\}_2]$ was lower than that of $[\{Ir(cod)Cl\}_2]$, and $IrCl_3$ was inert (runs 7 and 8). Among the solvents examined, THF was found to be the best, followed by DME and toluene. A protic solvent like EtOH promoted an aldol-type reaction of imine **5a** to **6a** rather than the coupling reaction (runs 9–11).

The reaction shown in Equation (1) seems to proceed through the following reaction path (Scheme 1): First, the Ir^I complex **A** coordinates to **5a**, which is generated in situ from aldehyde **1a** and amine **2a**. Oxidative addition of the Ir^I center at the C–H bond adjacent to the nitrogen atom in **5a** affords Ir^{III} complex **C**. Coordination of alkyne **3a** followed by insertion in complex **D** gives iridium complex **E**, and subsequent reductive elimination forms the coupling product **4a**. To obtain further insight into the reaction pathway, the reaction of *N*-butyliden-1,1-dideuteriobutylamine ($[D_2]$**5a**), prepared independently, with **3a** under the influence of $[\{Ir(cod)Cl\}_2]$ was examined [Eq. (2)]. As expected the coupling product $[D_2]$**4a**, in which a deuterium atom is

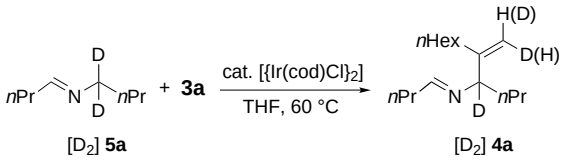

(2)

incorporated at the terminal triple bond of **3a**, was produced. It is noteworthy that $[D_2]$**4a** consisted of a single geometrical isomer. This shows that the present coupling reaction takes place with high stereoselectivity, although it is not clear where the stereochemistry comes from.

On the basis of these results, the three-component coupling reactions of several different aldehydes, amines and alkynes were examined (Table 2). In most cases the reactions produced the corresponding coupling products in fair to good yields (runs 1, 3–6). The reaction with the internal alkyne 4-octyne (**3c**) did not form a three-component coupling product, but instead **5a** and **6a** (run 2). Needless to say, no coupling reaction took place upon use of *tert*-butylamine, which has no α-hydrogen atom (run 7). The reaction of benzaldehyde or crotonaldehyde or 2-octanone with **2a** and **3a** is unfortunately difficult to carry out under these conditions. Finally, almost no reaction took place upon treatment of 2-aminoethanol or allyl amine with **1a** and **3a**.

Table 2. Results of the three-component coupling reaction of various aldehydes, amines, and alkynes catalyzed by $[\{Ir(cod)Cl\}_2]$.[a]

Run	Aldehyde	Amine	Alkyne	Yield [%] of **4**
1	**1a**	**2a**	*n*Bu **3b**	74
2	**1a**	**2a**	*n*Bu *n*Bu **3c**	0[b]
3	**1b**	**2a**	**3a**	73
4	**1c**	**2a**	**3a**	62
5	**1a**	**2b**	**3a**	60
6	**1a**	**2c**	**3a**	45
7	**1a**	**2d**	**3a**	0

[a] The aldehyde (0.5 mmol), amine (0.25 mmol), and alkyne (0.5 mmol) were allowed to react in THF (2 mL) in the presence of a catalytic amount of $[\{Ir(cod)Cl\}_2]$ (0.025 mmol) at 60 °C for 15 h. [b] Compounds **5a** (83%) and **6a** (4%) were obtained.

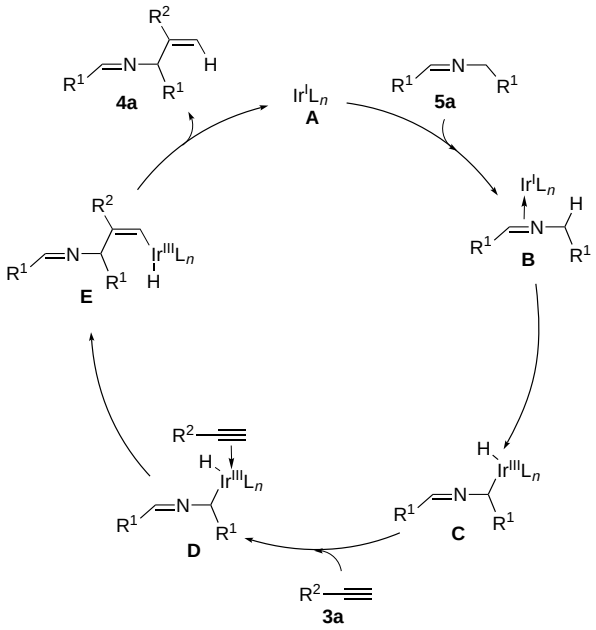

Scheme 1. A possible reaction path for the three-component reaction. $R^1 = n$Pr, $R^2 = n$Hex; L_n = ligand.

The reaction of **1a**, **2a**, and trimethylsilylacetylene (**3d**) under the influence of [{Ir(cod)Cl}$_2$] afforded an adduct, butyl(1-propyl-3-trimethylsily-2-propynyl)amine [**7**; Eq. (3)].

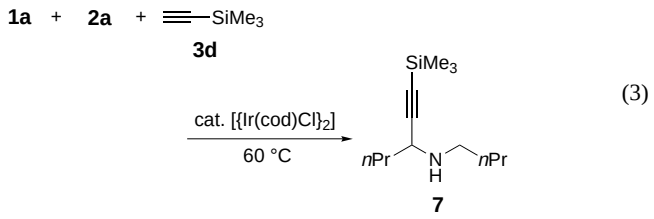

(3)

Here the the alkyne **3d** has added to the double bond of the imine **5a** initially formed, in contrast to the reaction of the aliphatic alkyne **3a**. It is probable that the reaction proceeds through the oxidative addition of the Ir^{I} complex to the terminal C–H bond of alkyne **3d**, followed by insertion of the imine to the resulting Ir–H complex. Recently, Miyaura et al. reported that the iridium-catalyzed dimerization of terminal alkynes involves the oxidative addition of a low-valent Ir complex to alkyne, followed by insertion of an alternative alkyne to give dimers.[9]

In summary, we have developed a new reaction of aldehydes, amines, and alkynes catalyzed by an Ir complex to produce three-component coupling products. These products are difficult to obtain by conventional organic synthetic methods.

Experimental Section

Representative procedure: The aldehyde (0.5 mmol), amine (0.25 mmol), and alkyne (0.5 mmol) were added under Ar to a solution of [{Ir(cod)Cl}$_2$] (0.025 mmol) in THF (2.0 mL). Then the reaction mixture was stirred at 60 °C for 15 h. The reaction was quenched with wet Et_2O, and the products were isolated by column chromatography (230–400 mesh Al_2O_3, hexane) and purified by distillation under reduced presure. After the reaction, GC and GC-MS analyses were performed. The yields of the products were estimated from the peak areas based on the internal standard technique using GC.

4a: ^{1}H NMR: $\delta = 7.59$ (t, $J = 4.9$ Hz, 1H), 4.91 (s, 1H), 4.76 (d, $J = 1.3$ Hz, 1H), 3.41 (t, $J = 6.9$ Hz, 1H), 2.25 (dt, $J = 5.3$, 7.3 Hz, 2H), 2.04 (t, $J =$ 7.3 Hz, 2H), 1.65–1.09 (m, 14H), 0.95 (t, $J = 7.6$ Hz, 3H), 0.88 (t, $J = 4.6$ Hz, 6H); ^{13}C NMR: $\delta = 163.8$, 151.7, 108.9, 76.0, 37.6, 36.7, 32.5, 31.7, 29.1, 27.7, 22.5, 19.6, 14.0, 13.8, 13.7; IR (neat) 2957, 1667, 1462, 897 cm^{-1}; MS (70 ev) m/z (%): 237 (0.3) [M^+], 194 (100), 180 (5), 166 (16).

7: ^{1}H NMR: $\delta = 3.35$ (dd, $J = 7.7$, 5.9 Hz, 1H), 2.84 (ddd, $J = 6.6$, 8.4, 11.4 Hz, 1H), 2.56 (ddd, $J = 5.9$, 8.0, 11.4 Hz, 1H), 1.61–1.33 (m, 8H), 0.94 (t, $J = 7.3$ Hz, 3H), 0.91 (t, $J = 7.3$ Hz, 3H), 0.16 (s, 9H); ^{13}C NMR: $\delta =$ 100.2, 87.3, 50.6, 47.0, 38.0, 32.1, 20.4, 19.2, 13.9, 13.8, 0.1; IR (neat) 3299, 2959, 2159, 1458, 1243, 842 cm^{-1}; MS (70 ev) m/z (%): 182 (100), 109 (4), 73 (12).

Received: February 26, 2001 [Z16687]

[1] S. Murai, F. Kakiuchi, S. Sekine, Y. Tanaka, A. Kamatani, M. Sonoda, N. Chatani, *Nature* **1993**, *366*, 529–531.

[2] S.-I. Murahashi, H. Takaya, *Acc. Chem. Res.* **2000**, *33*, 225–233; G. Dyker, *Angew. Chem.* **1999**, *111*, 1808–1822; *Angew. Chem. Int. Ed.* **1999**, *38*, 1698–1712; A. Sen, *Acc. Chem. Res.* **1998**, *31*, 550–557; A. E. Shilov, G. B. Shul'pin, *Chem. Rev.* **1997**, *97*, 2879–2932; B. A. Arndtsen, R. G. Bergman, T. A. Mobley, T. H. Peterson, *Acc. Chem. Res.* **1995**, *28*, 154–162; A. D. Ryabov, *Chem. Rev.* **1990**, *90*, 403–424.

[3] *Activation of Unreactive Bonds and Organic Synthesis* (Ed.: S. Murai), Springer, New York, **1999**; N. Chatani, T. Fukuyama, H. Tatamidani, F. Kakiuchi, S. Murai, *J. Org. Chem.* **2000**, *65*, 4039–4047; Y. Ie, N. Chatani, T. Ogo, D. R. Marshall, T. Fukuyama, F. Kakiuchi, S. Murai, *J. Org. Chem.* **2000**, *65*, 1475–1488, and references therein; K. Kokubo, K. Matsumasa, Y. Nishinaka, M. Miura, M. Nomura, *Bull. Chem. Soc. Jpn.* **1999**, *72*, 303–311, and references therein.

[4] *Activation and Functionalization of Alkanes* (Ed.: C. L. Hill), Wiley, New York, **1989**; C. Jia, W. Lu, J. Oyamada, T. Kitamura, K. Matsuda, M. Irie, Y. Fujiwara, *J. Am. Chem. Soc.* **2000**, *122*, 7252–7263; H. M. L. Davies, T. Hansen, M. R. Churchill, *J. Am. Chem. Soc.* **2000**, *122*, 3063–3070; H. Chen, S. Schlecht, T. C. Semple, J. F. Hartwig, *Science* **2000**, *287*, 1995–1997.

[5] D. M. Tellers, R. G. Bergman, *J. Am. Chem. Soc.* **2000**, *122*, 954–955; F. Torres, E. Sola, M. Martín, J. A. López, F. J. Lahoz, L. A. Oro, *J. Am. Chem. Soc.* **1999**, *121*, 10632–10633; S. Niu, M. B. Hall, *J. Am. Chem. Soc.* **1998**, *120*, 6169–6170; J. C. W. Lohrenz, H. Jacobsen, *Angew. Chem.* **1996**, *108*, 1403–1405; *Angew. Chem. Int. Ed. Engl.* **1996**, *35*, 1305–1307; B. A. Arndtsen, R. G. Bergman, *Science* **1995**, *270*, 1970–1973.

[6] H. Takaya, T. Naota, S.-I. Murahashi, *J. Am. Chem. Soc.* **1998**, *120*, 4244–4245.

[7] T. Satoh, Y. Nishinaka, M. Miura, M. Nomura, *Chem. Lett.* **1999**, 615–616.

[8] T. Kubo, S. Sakaguchi, Y. Ishii, *Chem. Commun.* **2000**, 625–626.

[9] T. Ohmura, S.-I. Yorozuya, Y. Yamamoto, N. Miyaura, *Organometallics* **2000**, *19*, 365–367.

Unprecedented Detection of Distinct Barriers Involving Formally Enantiotopic Substituents: Phenyl Rotation in Solid Diphenyl Sulfoxide**

Daniele Casarini,* Lodovico Lunazzi,* and Andrea Mazzanti

It has been pointed out that "the vast majority of molecules are chiral, not achiral; to realize it, one only needs a sufficiently fine spatial or temporal resolution of measurement".[2] To illustrate this point herein, we refer to the recent observation that dimesityl sulfoxide ($Mes_2S{=}O$; Mes = 2,4,6-trimethylphenyl), which by convention is an achiral molecule

[*] Prof. D. Casarini
Dipartimento di Chimica, Università della Basilicata
Via N. Sauro, 85, Potenza, 85100 (Italy)
Fax: (+39) 0971 202 223
E-mail: casarini@unibas.it
Prof. L. Lunazzi, Dr. A. Mazzanti
Dipartamento di Chimica Organica "A. Mangini"
Università di Bologna
Risorgimento, 4, Bologna, 40136 (Italy)
Fax: (+39) 051-209-3654
E-mail: lunazzi@ms.fci.unibo.it

[**] Conformational Studies by Dynamic NMR. Part 82. For Part 80 see ref. [1a], for Part 81 see ref. [1b]. We thank J. E. Anderson (University College, London, UK), S. E. Biali (Hebrew University, Jerusalem, Israel), R. K. Harris (University of Durham, UK), W. B. Jennings (University College, Cork, Ireland), A. Rassat (École Normale Superieure, Paris, France) for critical reading of the manuscript, and I.Co.C.E.A., CNR, Bologna for access to the 400-MHz and solid-state NMR spectroscopy facilities. Financial support was received from MURST (national project "Stereoselection in Organic Synthesis") and from the University of Bologna (Funds for selected research topics 1999–2001).

  1433-7851/01/4013-2536 $ 17.50+.50/0

(C_s point group by virtue of the symmetry plane created by the fast Mes–SO rotation), appears chiral in the crystalline state.[1a] This is a consequence of the two mesityl rings adopting a propellerlike conformation, which deprives the molecule of its symmetry plane: the "static" molecule thus belongs to the C_1 point group. For this reason the solid-state ^{13}C cross-polarization magic-angle-spinning (CP-MAS) NMR spectrum at ambient temperature displays anisochronous lines for the methyl substituents:[1a] the two rings, in fact, are not symmetry related and are therefore diastereotopic. The same situation is observed in solution,[1a] as shown by the NMR spectra taken at a temperature ($-177\,^{\circ}C$) low enough to "freeze" the Mes–SO rotation that makes the molecule apparently achiral.

Like dimesityl sulfoxide, diphenyl sulfoxide is achiral under conditions of fast rotation about the Ph–SO bond but, contrary to dimesityl sulfoxide, is achiral also in its ground state conformation, since the plane of symmetry is maintained even when the Ph–SO rotation is blocked. Molecular mechanics calculations[3] show (Figure 1) that both the Ph–SO dihedral angles have equal absolute values (28°), thus leading to a symmetric butterflylike shape (C_s point group), at variance with the propellerlike conformation (C_1 point group) of dimesityl sulfoxide.[4] Diphenyl sulfoxide also adopts a butterflylike conformation in the crystalline state, as shown by X-ray diffraction studies (see Experimental Section) of a single crystal in which the two Ph–SO dihedral angles appear to coincide (11.7° and 11.4°)[5] within experimental error (Figure 1); the difference with respect to the calculated values are a result of the flattening effect of the lattice. (Computation[6] and X-ray diffraction[7] studies indicate that benzophenone, in which the SO has been replaced by a CO group, maintains the same propellerlike structure as its more hindered analogue, dimesityl ketone, at variance with the behavior of diphenyl sulfoxide with respect to dimesityl sulfoxide.)

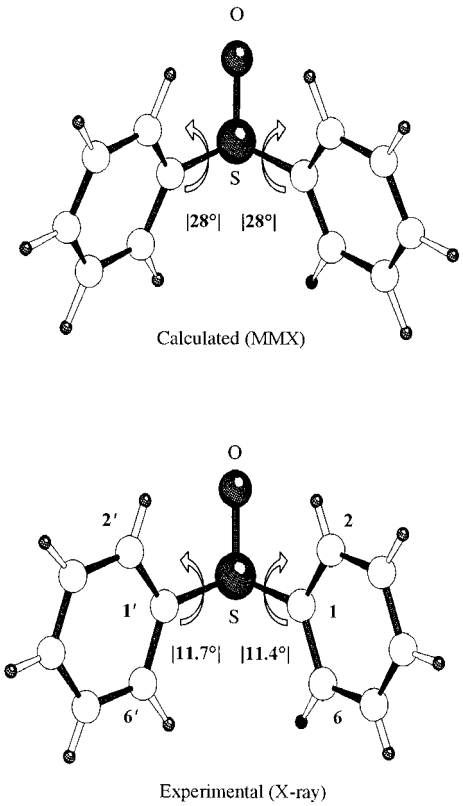

Figure 1. Computed structure (MMX force field[3]) of diphenyl sulfoxide (top). Underneath is reported the structure obtained by X-ray diffraction.

The crystal space group $P2_1/n$ of diphenyl sulfoxide has a center but does not have a plane of symmetry, whereas the molecule has a plane but not a center of symmetry (site symmetry different from molecular symmetry), so that the two phenyl rings reside in two different spatial environments and are therefore diastereotopic. Accordingly, the solid-state ^{13}C CP-MAS NMR spectrum at $-30\,^{\circ}C$ displays anisochronous signals for the carbon atoms of one ring with respect to those of the other.

As shown in Figure 2c two lines each are observed for the quaternary as well for the *para* carbon atoms, and three lines (1:1:2) were assigned to four *ortho* carbon atoms.[8] The four *meta* carbon atoms yield a single signal, owing to a fortuitous coincidence of the corresponding lines. The line-shape simulation (Figure 3, bottom right) indicates that the *ortho* line with double intensity actually comprises two different peaks with a separation (15 Hz) smaller than the line width

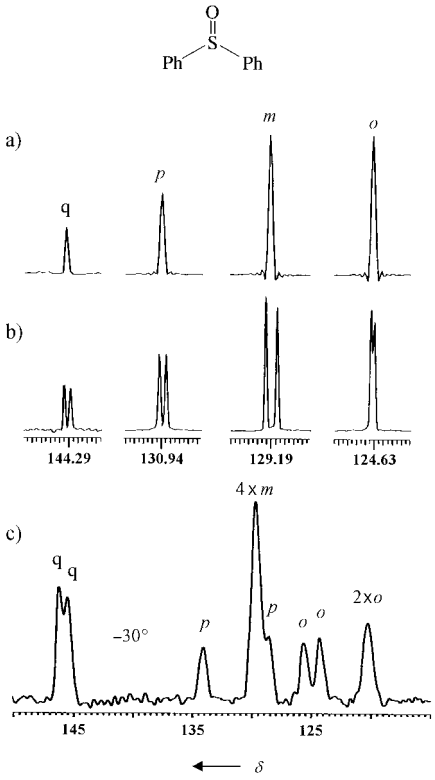

Figure 2. a) ^{13}C NMR (100.6 MHz) spectrum of diphenyl sulfoxide in a solution of $CDCl_3$ at ambient temperature: the quaternary, *para*, *meta*, and *ortho* carbon atoms are labeled as q, *p*, *m*, and *o*, respectively. b) The same spectrum (100.6 MHz) taken at ambient temperature in a chiral environment:[16] the splitting of the lines cover the range 0.8 Hz (*ortho* carbon atoms) – 2.7 Hz (*meta* carbon atoms). c) Static ^{13}C NMR (75.45 MHz) CP-MAS spectrum of solid diphenyl sulfoxide at $-30\,^{\circ}C$.

  1433-7851/01/4013-2537 $ 17.50+.50/0

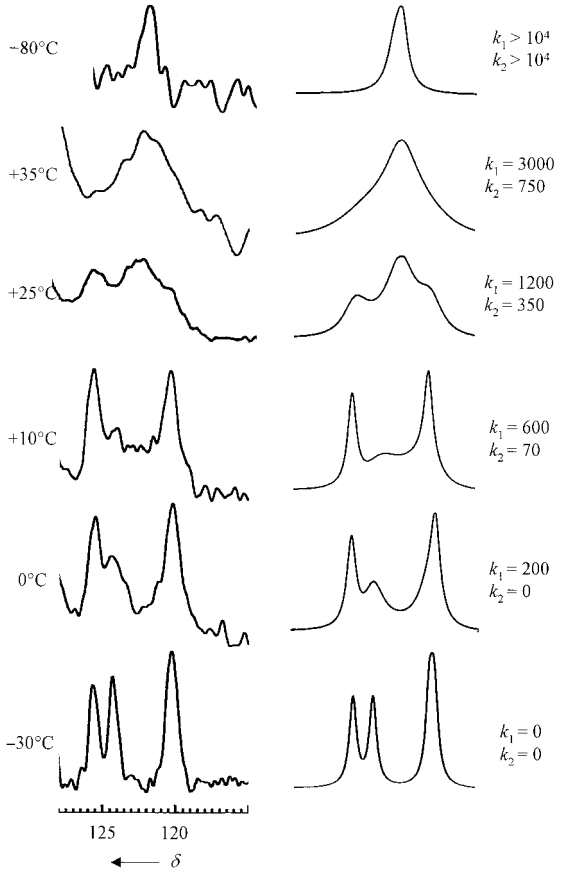

Figure 3. Dynamic solid-state ^{13}C NMR spectrum (75.45 MHz) of the *ortho* carbon atoms of diphenyl sulfoxide as a function of temperature (left). On the right is displayed the computer simulation obtained with the pairs of rate constants (k_1 and k_2 in s^{-1}) reported.

(27 Hz), thus explaining why its height is less than twice the height of the other two signals. There are therefore four anisochronous signals (two for each phenyl group) related to the four *ortho* carbon atoms of the static molecule,[9] as expected on the basis of a blocked rotation about the Ph–SO bonds[10] coexisting with different site and molecular symmetries.

The anisochronous signals observed at $-30\,^{\circ}C$ in the ^{13}C NMR spectrum of crystalline diphenyl sulfoxide are a consequence of the sulfur atom being a prochiral tetrahedral center[11] with two enantiotopic ligands in the isolated molecule.[11–14] For this reason the situation encountered in the crystal is similar (although not identical) to that occurring in a fluid chiral medium in that "enantiotopic groups exhibit their distinctiveness only in a chiral extramolecular environment".[12] Actually, the four ^{13}C NMR spectral lines (which correspond to four heterotopic ring carbon atoms) observed in an achiral solution (Figure 2a), split into pairs[15] (Figure 2b) when the spectrum is taken in a chiral environment:[16] here the two phenyl groups become diastereotopic and consequently give rise to anisochronous signals. The difference between the situation in the crystal and that in solution is because of the fact that to convert two enantiotopic into diastereotopic ligands, it is not strictly necessary to have a chiral extramolecular environment: a more general requirement should actually state that it is sufficient to have the element of symmetry of the external environment not coincident with that of the molecule. For instance the $P2_1/n$ space group, which has a center of symmetry, is not chiral (as is the Pirkle alcohol[16] employed to obtain the spectrum of Figure 2b), yet the solid-state spectral lines are anisochronous because, when such a situation occurs, the arrangement of the molecules embedded in the crystal packing gives rise, in practice, to a chiral object, thus rendering diastereotopic the ligands that are enantiotopic when the molecule is considered isolated from its environment. In the situation encountered here the two phenyl groups of diphenyl sulfoxide should thus display differences in all their observable features, and such a distinctiveness should include not only the static but also the dynamic properties. However, the chances of the latter differences becoming experimentally detectable are likely to be very low. This explains why, to the best of our knowledge, distinct dynamic effects have not been reported for any molecule that should have exhibited such features, that is, one with a structure and symmetry analogous to that of an achiral sulfoxide. A rare event, however, can occasionally be discovered in a serendipitous way and indeed it was by sheer chance that we found such evidence in the present case.

On raising the temperature of the diphenyl sulfoxide solid-state spectrum above $-30\,^{\circ}C$, the lines for the *ortho* carbon atoms broaden significantly and subsequently coalesce, ultimately displaying a single signal above ambient temperature (Figure 3). This feature is a result of the Ph–SO rotation process exchanging the *ortho* positions[17] (the occurrence of dynamic NMR spectroscopy effects in the crystalline state is well documented[18]). On the contrary, the signals of the quaternary and *para* carbon atoms remain sharp, because they lie in the local rotation axis and do not experience the effects of the exchange process.[19] Likewise, the signal for the *meta* carbon atoms remains sharp, owing to the coincidental overlap of the corresponding lines.

An interesting feature was however observed: when the inner pair of lines corresponding to the *ortho* carbon atoms begin to broaden, the outer lines remain sharp, and when the inner lines coalesce, the outer lines are broadened but still separated. Likewise when the outer lines reach their coalescence temperature, the inner lines have already merged into a single peak. These observations suggest that one of the two rings rotates faster than the other, which means that there are two free energies of activation for two distinguishable rotation processes.

This was proven in a quantitative way by the line-shape simulation[20] displayed in Figure 3, which allowed the values of the two rate constants to be determined at various temperatures.[21] Even if the absolute temperatures are in error of a few degrees, this does not affect the difference in the k values, since each pair of these rate constants was determined at exactly the same temperature. Thus, for example, at $0\,^{\circ}C$ (Figure 3) one ring makes 200 ± 40 rotations per second, whereas the other is essentially static, as it has a negligible rotation rate. The two free energies of activation ($\Delta G^{\ddagger}$) derived from the two sets of rate constants[22] differ by 1.0 ± 0.2 kcal mol^{-1}, and their absolute values are 14.0 and 13.0 kcal mol^{-1}. The temperatures where different rate constants (k_1 and k_2 values) could be identified encompass,

  1433-7851/01/4013-2538 $ 17.50+.50/0

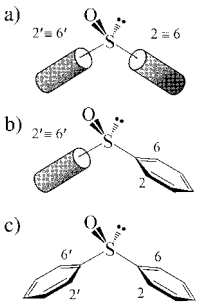

Scheme 1. Pictorial representation of the time averaged shape of crystalline Ph_2SO as function of the two distinct rotation rates about the Ph–SO bonds.

approximately, the -10° to $+35\,^\circ C$ range. At even higher temperatures, the two rotation rates are still expected to be different, but such a difference cannot be measured anymore by the NMR spectroscopy technique: for instance, the spectrum at $+80\,^\circ C$ in Figure 3 could be simulated with two essentially equal rate constants.

To give an approximate image of the effect illustrated here, the phenyl rings were drawn (Scheme 1a) as hexagons to indicate the static situation at low temperature. At the temperature when the rotation of one ring is slow and that of the other is fast in the NMR time-scale (about $0\,^\circ C$), the rotating ring was drawn as a cylinder (Scheme 1b) where the ortho positions $2'$ and $6'$ interchange rapidly, whereas the motionless ring is still drawn as a hexagon. Finally, both phenyl groups were drawn (Scheme 1c) as cylinders (where both the pairs 2,6 and $2'$,$6'$ are scrambled) to symbolize their fast rotation at higher temperatures.

In conclusion, distinctive stereodynamic processes that involve the two enantiotopic substituents of a formally achiral molecule (e.g. diphenyl sulfoxide) can be observed only in situations where the anisotropic environment (in this case the crystal packing) renders the two groups symmetry nonequivalent, thus making the whole supramolecular system chiral; on the contrary this effect cannot be detected in achiral isotropic media, unless the formally achiral molecule adopts a chiral conformation.[23]

Experimental Section

X-ray diffraction—Crystal Data of Diphenyl sulfoxide: $C_{12}H_{10}OS$ (202.26), monoclinic, space group $P2_1/n$, $Z=4$, $a=8.3490(3)$, $b=14.0970(5)$, $c=8.9170(3)$ Å, $\beta=101.1150(10)$, $V=1029.81(6)$ Å^3, $D_c=1.305$ g cm^{-3}, $F(000)=424$, $\mu M_o=0.275$ cm^{-1}, $T=293$ K. Data were collected using a graphite monochromated $Mo_{K\alpha}$ X-radiation ($\lambda=0.71073$ Å) range $2.74^\circ<\theta<35.00^\circ$. Of 18196 reflections measured, 4533 were found to be independent ($R_{int}=0.0324$), 2696 of which were considered as observed [$I>2\sigma(I)$], and were used in the refinement of 103 parameters leading to a final R_1 of 0.0496 and a R_{all} of 0.0764. The structure was solved by direct methods and refined by full-matrix least squares on F^2, using SHELXTL 97 program packages. In refinements were used weights according to the Scheme $w=[\sigma^2(F_o^2)+(0.1007P)^2+0.0000P]^{-1}$, where $P=(F_o^2)+2F_c^2)/3$. The phenyl rings were assumed to be regular hexagons, the hydrogen atoms were located by geometrical calculations and refined by using a "riding" method; $wR_2=0.1727$. The goodness-of-fit parameter S was 1.023. Largest difference between peak and hole was 0.283 and -0.283 e Å^{-3}. Crystallographic data (excluding structure factors) for the structures reported in this paper have been deposited with the Cambridge Crystallographic Data Centre as supplementary publication no. CCDC-156961. Copies of the data can be obtained free of charge on application to CCDC, 12 Union Road, Cambridge CB2 1EZ, UK (fax: (+44) 1223-336-033; e-mail: deposit@ccdc.cam.ac.uk).

NMR measurements: The ^{13}C NMR solution spectra were obtained at 100.6 MHz (Varian, Mercury) and the ^{13}C NMR solid-state CP-MAS spectra at 75.45 MHz (Bruker CXP spectrometer). For the latter measurements, solid diphenyl sulfoxide (the same batch from which the crystal for X-ray diffraction had been selected) was introduced into a tightly sealed 7-mm zirconia rotor, and spun at the magic angle with a speed of about 3.5 KHz. The chemical shifts were measured with respect to the lower frequency signal of the adamantane ($\delta=29.4$ ppm). The assignment of the CH carbon atoms was obtained by the "nonquaternary suppression" pulse sequence. The signals for the *ortho* and *meta* carbon atoms were assigned by comparison with those of the solution spectrum. In $CDCl_3$, the two lines assigned to four carbon atoms at $\delta=129.2$ and 124.6 correspond to the single line at $\delta=129.4$ and to the average position ($\delta=122.5$) of the four exchanging lines of the solid-state spectrum, respectively. When the ^{13}C solution spectrum is obtained in the undecoupled mode, the line at $\delta=129.2$ displays long-range coupling to a single hydrogen atom, and the signal at $\delta=124.6$ shows long-range coupling to two hydrogen atoms. Therefore, the former is unambiguously assigned to a *meta* and the latter to an *ortho* carbon atom.[24] Cooling was achieved by means of a flow of dry nitrogen, precooled in a heat exchanger immersed in liquid nitrogen. The temperatures of the solid-state spectra were calibrated by using the shift dependence of the ^{13}C lines of 2-chlorobutane absorbed on solid decalite,[25] assuming a dependence equal to that observed in neat liquid, which had been previously calibrated by using a Ni/Cu thermocouple.

Received: February 6, 2001 [Z16559]

[1] a) D. Casarini, S. Grilli, L. Lunazzi, A. Mazzanti, *J. Org. Chem.* **2001**, *66*, 2757–2763; b) S. Grilli, L. Lunazzi, A. Mazzanti, *J. Org. Chem.*, in press.

[2] H. Zabrodsky, D. Avnir, *J. Am. Chem. Soc.* **1995**, *117*, 462; see also: D. Avnir, O. Katzenelson, H. Zabrodsky Hel-Or, *Chem. Eur. J.* **1996**, *2*, 744.

[3] MMX force field as implemented in the computer package PC Model, Serena Software, Bloomington, IN, USA.

[4] The Ar–SO dihedral angles of dimesitylsulfoxide were calculated[1a] to be equal to $+107^\circ$ and -9° (MMX force field). In the analogous hindered 2,2′,6,6′-tetramethyldiphenyl sulfoxide, the experimental values for these angles were $+113^\circ$ and -9° (X-ray diffraction).[1a]

[5] These are the absolute values of the dihedral angles O-S-C1-C2 and O-S-C1′-C2′, respectively (Figure 1), and are in good agreement with those (11.8° and 10.9°) obtained from the X-ray data reported in: A. V. Yatsenko, S. V. Medvedev, A. I. Tursina, L. A. Aslanov, *Zh. Obs. Khim.* **1986**, *56*, 2330.

[6] R. J. Abraham, I. S. Haworth, *J. Chem. Soc. Perkin Trans. 2* **1988**, 1429.

[7] E. B. Fleischer, N. Sung, S. Hawkinson, *J. Phys. Chem.* **1968**, *72*, 4311.

[8] The chemical shifts of the 75.45-MHz CP-MAS ^{13}C NMR spectrum (Figure 2c) are: $\delta=146.1$ (q), $\delta=145.35$ (q), $\delta=134.0$ (*p*), $\delta=129.4$ ($4\times m$), $\delta=128.5$ (*p*), $\delta=125.6$ (*o*), $\delta=124.2$ (*o*), $\delta=120.2$ ($2\times o$). Line-shape simulation (Figure 2) shows that the latter signal is the combination of two lines at $\delta=120.3$ and 120.1.

[9] The assignment of the signals to the *meta* and *ortho* carbon atoms was performed as described in the Experimental Section. Such an assignment is, however, immaterial for what concerns the dynamic process; the conclusion would be the same even if signals for the *meta* and *ortho* carbon atoms were identified incorrectly.

[10] Such a restricted rotation was observed in solution, even at the lowest attained temperature (about $-175\,^\circ C$), in agreement with MM calculations,[3] which predict a barrier as low as 1.6 kcal mol^{-1} for the independent Ph–SO rotation in the isolated molecule. Clearly, the crystal lattice imposes additional restrictions on the motion that renders the transition-state energy higher than in solution, thereby allowing detection of the dynamic process by CP-MAS NMR spectroscopy. An increase in the barriers to internal motions in the solid state with respect to solution has been reported in a number of cases (see ref. [18]).

[11] K. R. Hanson, *J. Am. Chem.Soc.* **1966**, *88*, 2731.

[12] K. Mislow, M. Raban, *Top. Stereochem.* **1967**, *1*, 1; see also: K. Mislow, *Top. Stereochem.* **1999**, *22*, 1.

[13] W. B. Jennings, *Chem. Rev.* **1975**, *75*, 307.

[14] E. L. Eliel, *J. Chem. Educ.* **1980**, *57*, 52.

[15] The fast Ph–SO bond rotation that still occurs in the chiral solution makes the ortho carbon atoms (C-2 ≡ C-6 and C-2′ ≡ C-6′) give rise to two (Figure 2b) rather than four lines (Figure 2c). The Ph–SO rotation in the crystal at $-30\,^\circ C$ is frozen in the NMR time-scale, so that within each of the two phenyl groups, the *ortho* positions are *syn* or *anti* to the oxygen atom (C-2 ≠ C-6 and C-2′ ≠ C-6′).

[16] The chiral environment was obtained by the addition an appropriate amount of enantiopure (*R*)-(−)-1-(9-anthryl)-2,2,2,-trifluoroethanol to a $CDCl_3$ solution (see: W. H. Pirkle, *J. Am. Chem. Soc.* **1966**, *88*, 1837).
[17] Under conditions of fast exchange, two averaged lines should actually be observable, one for each pair of *ortho* carbon atoms of the two rapidly rotating phenyl groups. However, the separation of these two averaged lines ($\Delta\delta = 0.6$) is too small to be resolved, as also shown by the computer line-shape simulation (see Figure 3).
[18] F. G. Riddell, S. Arumagam, J. E. Anderson, *J. Chem. Soc. Chem. Commun.* **1991**, 1525; P. J. Barrie, J. E. Anderson, *J. Chem. Soc. Perkin Trans. 2* **1992**, 2031; F. G. Riddell, S. Arumagam, K. D. M. Harris, M. Rogerson, J. H. Strange, *J. Am. Chem. Soc.* **1993**, *115*, 1881; A. E. Aliev, K. D. M. Harris, D. C. Apperley, *J. Chem. Soc. Chem. Commun.* **1993**, 251; F. G. Riddell, G. Bernath, F. Fülöp, *J. Am. Chem. Soc.* **1995**, *117*, 2327; D. Casarini, L. Lunazzi, A. Mazzanti, *J. Org. Chem.* **1998**, *63*, 9125; L. Lunazzi, A. Mazzanti, D. Casarini, O. De Lucchi, F. Fabris, *J. Org. Chem.* **2000**, *65*, 883; J. E. Anderson, D. Casarini, L. Lunazzi, A. Mazzanti, *J. Org. Chem.* **2000**, *65*, 1729; D. Casarini, L. Lunazzi, A. Mazzanti, G. Simon, *J. Org. Chem.* **2000**, *65*, 3207.
[19] This feature guarantees that the observed dynamic process cannot be caused by a 180° rotation of the whole molecule within the crystal, leading to an exchange of the positions of the two phenyl groups. In this case, the signals of the quaternary and *para* carbon atoms should also have displayed line-broadening effects, as observed with the signals for the *ortho* carbon atoms.
[20] Use was made of a PC version of the DNMR6 computer program n° 633 of QCPE, Indiana University, Bloomington, IN, USA.
[21] The shift separation between the inner pair of lines ($\Delta\delta = 3.9$) is too close to that between the outer pair ($\Delta\delta = 5.5$)[8] to account for the observed line shape on the basis of a unique free energy of activation, as clearly demonstrated by the computer simulation. When the two rings were assumed to have identical rotation rates (i.e. coincident $\Delta G^{\neq}$ values), it was impossible to reproduce the experimental dynamic spectra of Figure 3.
[22] As is usually observed in rotation processes, in the present experiment the $\Delta G^{\neq}$ values were found also to be independent of temperature, which indicates a negligible value for the corresponding $\Delta S^{\neq}$; see: D. Casarini, L. Lunazzi, E. Foresti, D. Macciantelli, *J. Org. Chem.* **1994**, *59*, 4637.
[23] An example of this type is provided by the two different rotation barriers measured for the *tert*-butyl substituents in (tBu)$_2$CH(iPr), owing to the molecule adopting a chiral conformation when the CH−iPr bond rotation is frozen (J. E. Anderson, B. R. Bettels, H. M. R. Hoffman, P. Pauluth, S. Hellmann, H. D. Beckhaus, C. Ruchardt, *Tetrahedron* **1988**, *44*, 3701).
[24] F. W. Wehrli, A. P. Marchand, S. Wherli, *Interpretation of C-13 NMR Spectra*, 2nd ed., Wiley, Chichester, **1988**, pp. 74–75.
[25] D. Casarini, L. Lunazzi, A. Mazzanti, *J. Org. Chem.* **1998**, *63*, 9125; see also: A. E. Aliev, K. D. M. Harris, *Magn. Reson. Chem.* **1994**, *32*, 366.

Exceptionally Long (≥ 2.9 Å) C–C Bonds between $[TCNE]^-$ Ions: Two-Electron, Four-Center π* – π* C–C Bonding in π-$[TCNE]_2^{2-}$**

Juan J. Novoa,* Pilar Lafuente, Rico E. Del Sesto, and Joel S. Miller*

Dedicated to the memory of Linus Pauling on the occasion of the 100th anniversary of his birth

We present here an exceptionally long C–C bonding interaction that has spectroscopic (IR and UV/Vis), structural, and magnetic properties expected for a bond and that complies with Pauling's definition of a chemical bond.[1] Strong carbon–carbon bonding is the essence of organic chemistry. The length of a C–C single bond, that is, 1.54 Å found in the diamond allotrope of carbon, is among the essential information learned by all organic chemistry students. This is the length of a single bond between sp^3-hybridized carbon atoms and is the longest of all common C–C bonds, although elongated C–C bonds as long as 1.73 Å have been reported.[2] These bonds form whenever two carbon atoms possessing an unpaired electron are close to each other (e.g., as occurs for two $^{\bullet}CH_3$ radicals, which form ethane). When the carbon atoms are radical anions (or radical cations), due to their strong coulombic repulsion, bonds do not form. Thus, many electron transfer salts involving radicals are stable, and as a consequence exhibit interesting electrical and optical properties. Herein, however, we show that C–C interactions having all the properties of a chemical bond are present between pairs of $[TCNE]^-$ ions in some TCNE-based electron transfer salts, and that this type of bonding is present for many other reduced strong electron acceptors, for example, cyanil,[3] 7,7,8,8-tetracyano-*p*-quinodimethane (TCNQ),[4] perfluoro-7,7,8,8-tetracyano-*p*-quinodimethane ($TCNQF_4$),[5] and 2,3-dichloro-5,6-dicyanobenzoquinone (DDQ).[6]

Strong organic electron acceptors (**A**) such as TCNE and TCNQ form stable electron transfer salts that contain $[\mathbf{A}]^{\bullet-}$. These salts were crucial for the discovery and development of molecule-based metals,[7] which subsequently led to the discovery of molecule-based superconductors,[8] as well as molecule-based magnets.[9]

[*] Prof. J. J. Novoa, P. Lafuente
Department of Physical Chemistry
University of Barcelona
Av. Diagonal, 647, 08028 Barcelona (Spain)
Fax: (+34) 93-402-1231
Prof. J. S. Miller, R. E. Del Sesto
Department of Chemistry
University of Utah
Salt Lake City, UT, 84112 (USA)
Fax: (+1) 801-581-8433

[**] The authors gratefully acknowledge the support from the U.S. National Science Foundation (Grant No. CHE9320478) and the U.S. DOE (Grant No. DE FG 03-93ER45504). J.J.N. and P.L. also thank for support by CICYT (project PB98-1166-C02-02) and CIRIT (1999SGR-00046), and a grant of computer time provided by CESCA-CEPBA and the University of Barcelona. In addition, P.L. thanks the Ministerio de Educación y Cultura for her doctoral fellowship grant.

Supporting information for this article is available on the WWW under http://www.angewandte.com or from the author.

Open-shell $[\mathbf{A}]^{\bullet-}$ species can form numerous structures; examples are $[TCNE]^{\bullet-}$ (**1**),[10] its σ dimer octacyanobutanediide, $[C_4(CN)_8]^{2-}$ (**2**),[11] and its π dimer, $[TCNE]_2^{2-}$ (**3**).[12–19] $[M^{II}(NCMe)_2\{C_4(CN)_8\}]$ (M = Mn, Fe) are examples of **2** and possess the octacyanobutanediide dianion μ_4-$[C_4(CN)_8]^{2-}$[11, 20] with a long (1.6 Å) central C_{sp^3}–C_{sp^3} σ bond.[11] Structure **3**, as well as other π-$[\mathbf{A}]_2^{2-}$ dimers, represents an unusual class of organic compounds as they possess exceptionally long (≥2.83 Å) π-bonding interactions,[18] which are substantially less than the π-C van der Waals radius of 3.4 Å, and the cyano substituents deviate by 3.6 to 6.5° (one-half of the *trans*-NC···CN dihedral angle) from the formal TCNE plane. These are π dimers because the intradimer C–C bonding primarily occurs through overlap of the π* orbitals at the four central sp^2-like carbon atoms. The presence of bonding is experimentally supported by structural, spectroscopic (UV/Vis and IR), and magnetic data (vide infra).

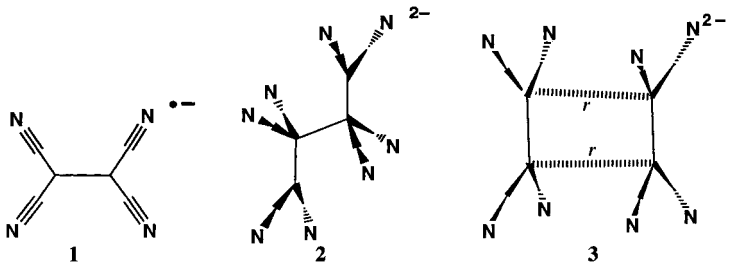

These dimers self-assemble to form supramolecular aggregates. The intradimer π*–π* C–C distances are twice that of a typical C–C bond and have properties that differ from those of van der Waals interactions, but are similar to those associated with normal covalent bonds. Hence, to understand the unusual nature of the long C–C bonding, the electronic structure, IR spectra, diamagnetic behavior, and stability of these π-$[\mathbf{A}]_2^{2-}$ dimers, we embarked upon a systematic computational and experimental study of π-$[TCNE]_2^{2-}$ dimers.[21, 22]

The properties of the $[TCNE]_2^{2-}$ dimers (Table 1) arise from the unpaired electron on each of the monomers and their anionic character. Consequently, two factors dominate the formation of these dimers: 1) the electrostatic repulsion (E_{coul}) between two anionic $[TCNE]^{\bullet-}$ fragments, and 2) the attractive forces arising from intradimer bonding (E_{bond}), either σ or π, that is, $E_{int} = E_{coul} + E_{bond}$. The energy E_{coul} for the anion–anion interaction is always repulsive, while E_{bond} is taken as being attractive, as it corresponds to the interaction of two singly occupied molecular orbitals (SOMOs). When $E_{coul} > E_{bond}$, the $[\mathbf{A}]^{\bullet-}$ units repel each other and there is no minimum-energy structure. If $E_{bond} > E_{coul}$ there will be a stable energy minimum on the potential energy surface (Figure 1). Additionally, when $E_{bond} \sim E_{coul}$ metastable dimers form, that is, the energy of such a minimum lies above the energy of two $[\mathbf{A}]^{\bullet-}$ monomers, but the dimer does not break into these fragments due to the presence of a barrier towards dissociation (Figure 1). Although metastable species cannot form in the gas phase at finite temperature, it can occur in a crystal if 1) the thermal energy is smaller than the barrier for the formation of the dimer from the fragments, or 2) the attractive electrostatic interactions with the cations are sufficient to overcome the coulombic energy barrier of $[TCNE]_2^{2-}$. Otherwise the dimers are repulsive. The existence of $[TCNE]_2^{2-}$ dimers in the solid state[11, 12] is consistent with either a stable or a metastable dimer being formed, although the latter is the situation (vide infra).

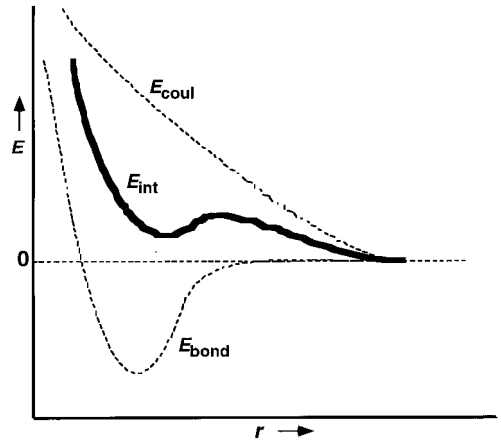

Figure 1. The total interaction energy curve (E_{int}) and its coulombic (E_{coul}) and bonding (E_{bond}) components.

The stability of the isolated π-$[TCNE]_2^{2-}$ dimer can be estimated by computing the shape of the $[TCNE]^{\bullet-}\cdots[TCNE]^{\bullet-}$ gas-phase potential energy surface as a function of the intradimer separation *r*.[23] The RB3LYP

Table 1. Intradimer C–C distances, deviation from planarity, vibrational frequencies for structurally characterized π-$[TCNE]_2^{2-}$ dimers (s, m, and w indicate a strong, medium, or weak band, respectively).

Compound	Form	Intradimer C–C distance [Å]	C–C distance [Å]	Deviation from plane[a] [deg]	ν_{CN} [cm^{-1}]
$[Cu(PPh_3)(TCNE)]_2$[12]	π-[σ-$TCNE]_2^{2-}$	2.92	1.397	5.1	2193 w, 2173 m, 2162 s
$[Cr(C_6H_6)_2]_2[TCNE]_2$[13]	π-$[TCNE]_2^{2-}$	2.904	1.436	6.0	2189 m, 2170 s, 2159 s
$[Cr(C_6Me_3H_3)_2]_2[TCNE]_2$[13]	π-$[TCNE]_2^{2-}$	3.09	1.45	5.2	[b]
$[Fe(C_5H_4)_2C_3H_6]_2[TCNE]_2$[14, 16]	π-$[TCNE]_2^{2-}$	2.90	1.35	5.5	2191 m, 2169 s, 2161 s
$[K(glyme)]_2[TCNE]_2$[15]	π-$[TCNE]_2^{2-}$	2.987	1.423	3.6	[b]
$[Fe(C_5H_5)(C_5Me_5)]_2[TCNE]_3(THF)$[16]	π-$[TCNE]_2^{2-}$	2.90	1.372	5.75	2190 m, 2173 s, 2159 s
$[Fe(C_5H_5)(C_5Me_5)]_2[TCNE]_3(CH_2Cl_2)$[16]	π-$[TCNE]_2^{2-}$	2.833	1.441	6.45	2190 m, 2173 s, 2160 s
$[(Me_2N)_2CC(NMe_2)_2][TCNE]_2$[18, 19]	π-$[TCNE]_2^{2-}$	2.922	1.406	4.0	2193 m, 2174 s, 2163 s
$Tl_2[TCNE]_2$[18]	μ_4-π-$[TCNE]_2^{2-}$	2.874	1.51	4.5	2190 s, 2173 sh, 2162 s

[a] Calculated from one-half of the average *trans*-NC···CN dihedral angle using CrystalMaker4. [b] Not reported.

curve (Figure 2) indicates that the $[TCNE]^{\bullet-}\cdots[TCNE]^{\bullet-}$ interaction is repulsive and has two metastable minima, located at short (ca. 1.8 Å) and long distance (ca. 3.1 Å), which when fully optimized were found to be minimum-energy structures.[24, 25] Their optimal geometry is close to the observed structures (see Supporting Information). However,

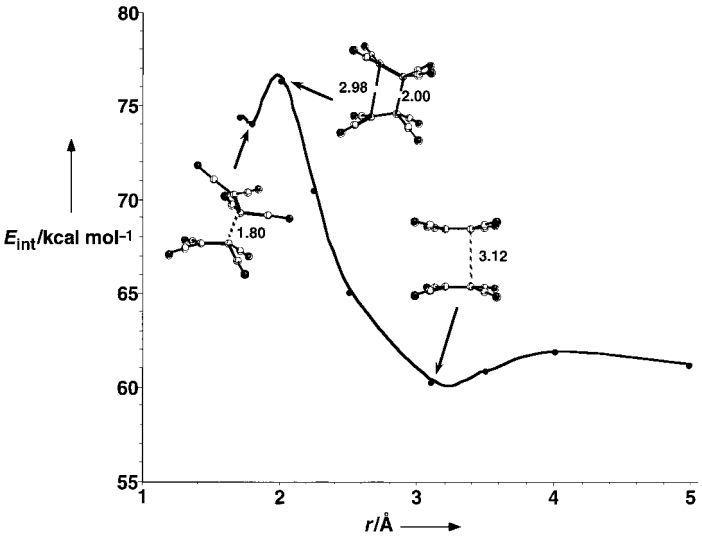

Figure 2. Computed adiabatic potential energy surface along r for the π-$[TCNE]_2^{2-}$ dimer at the RB3LYP level.

UB3LYP and MCSCF calculations using the same basis set indicated that there are no long-distance minima, that is, that the minima found at the RB3LYP level are a result of the double occupancy restriction imposed on the wavefunctions. As this double occupancy is not physically necessary, the dimers possess no real minima at long distances. The absence of a minimum is attributed to the electrostatic component (E_{coul}) between the anions, which exceeds the E_{bond} component. Therefore, the dimers in the crystalline state are a consequence of the attractive cation$\cdots[TCNE]^-$ interaction that exceeds the repulsive $[TCNE]^-\cdots[TCNE]^-$ interaction and gives rise to energetically stable neutral $(cation)_n[TCNE]_m$ supramolecular aggregates, for example, $n = m = 2$.[26]

This is computationally illustrated for $[K(glyme)]_2[TCNE]_2$[15, 27] (Figure 3). The energetic stability of the π-$[TCNE]_2^{2-}$ dimer is attributed to $K_2[TCNE]_2$, which possesses a π-$[TCNE]_2^{2-}$ dimer and two K^+ ions (2.91 ± 0.16) Å from the N atoms nominally midway between the two parallel $[TCNE]^-$ planes (Figure 3). The intradimer C–C separation is about 3.0 Å, which is significantly less than the sum of the van der Waals radii of 3.4 Å; the C–C interdimer separation is about 4.5 Å. At the UHF/6-31 + G(2d,2p) level the $[TCNE]_2^{2-}$ with the short intradimer distance has a repulsive interaction of 103.0 kcal mol^{-1} in its lowest triplet state. However, the $K^+\cdots[TCNE]^-$ interactions within the $K_2[TCNE]_2$ fragment are attractive by 75.0 kcal mol^{-1}. Thus, although the $[TCNE]_2^{2-}$ dimers are energetically unstable with respect to dissociation, neutral $K_2[TCNE]_2$ is stable with respect to dissociation by 158.4 kcal mol^{-1}.[28] This is typical of the interactions found in many ionic molecular crystals, whose energetics can be studied by ab initio methods and the proper

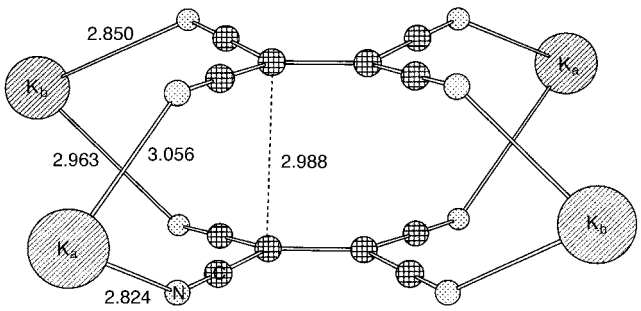

Figure 3. Geometry of the neutral $K_2[TCNE]_2$ unit used to calculate the energetics of the intermolecular interaction in the $[K(glyme)]_2[TCNE]_2$ crystal.[15] The key intermolecular distances between the fragments are given in Å. Note that there are two different crystallographic K^+ sites and thus two combinations for the $K_2[TCNE]_2$ aggregate. In our calculations each combination was used independently and the results were averaged. The unit has a net charge of zero.

model units.[29] Therefore, despite the repulsive nature of the interaction between the two $[TCNE]^{\bullet-}$ ions of the $K_2[TCNE]_2$ supramolecular fragment, these anions form a dimer with a short intradimer separation of 3 Å. As a consequence, the singly occupied π* orbitals of the $[TCNE]^{\bullet-}$ monomers overlap, leading to intermolecular bonding and antibonding dimer orbitals separated by a nonnegligible energy gap, Δ, that is similar to the one observed for energetically stable bonds. Due to this gap, the $[TCNE]_2^{2-}$ intradimer interactions exhibit all the structural, spectroscopic, and magnetic properties of a bond, as discussed below.

Ab initio UBLYP/6-31 + G(2d,2p) calculations[30] on an isolated $[TCNE]^{\bullet-}$ fragment show that it has a planar structure similar to that of $TCNE^0$[31] obtained with the same geometry and method, except that the central C–C distance increases from 1.367 Å in $TCNE^0$ to 1.437 Å in the $[TCNE]^{\bullet-}$, while the C≡N distance undergoes a minor increase from 1.158 to 1.167 Å. The extra electron resides in the b_{2g} SOMO of π* symmetry (Figure 4), which is primarily located in the central C–C bond and on the N atoms, with similar weights for those C and N atoms. Likewise, the Mulliken population analysis indicates that the extra electron is equally shared by these C and N atoms (ca. 0.18 e$^-$ per atom), in agreement with

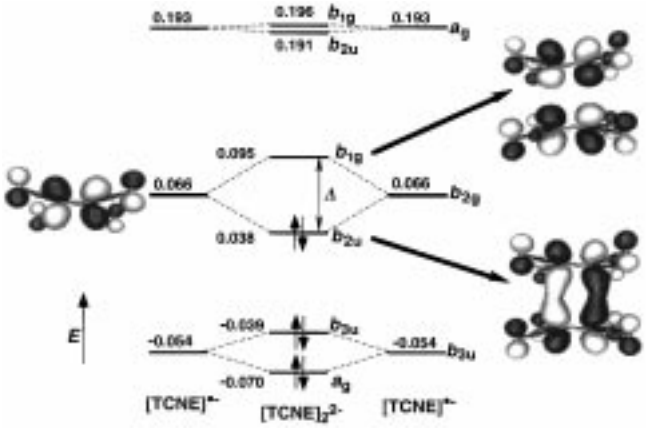

Figure 4. Shape of the π-$[TCNE]_2^{2-}$ dimer orbitals generated from the SOMO orbital of the $[TCNE]^{\bullet-}$ fragments.

  1433-7851/01/4013-2542 $ 17.50+.50/0 *Angew. Chem. Int. Ed.* **2001**, *40*, No. 13

the experimental data.[32–34] Similar results were obtained by using UHF and MCSCF methods.

When the b_{2g} SOMOs of two $[TCNE]^{\bullet-}$ fragments overlap in the π-$[TCNE]_2^{2-}$ dimer, bonding and antibonding orbitals of b_{2u} and b_{1g} symmetry, respectively, form (Figure 4). When the energy separation between these two orbitals, $\Delta(r)$ (Figure 4), is small, which occurs at large values of r, as those found in the $\pi^*-\pi^*$ C–C bonds, each orbital will be singly occupied and $b_{2u}{}^1b_{1g}{}^1$ is the most stable configuration.

The presence of $\Delta(r)$ greater than zero gives rise to two singlet states, namely 1^1A_{1g} and 2^1A_{1g}, whose energy difference is the source of a UV/Vis electronic transition, and a new absorption is observed at about 15300 cm^{-1} (654 nm, 1.90 eV) for $Tl_2[TCNE]_2$ ($r = 2.874$ Å)[19] (Figure 5a), $[(Me_2N)_2CC(NMe_2)_2][TCNE]_2$ ($r = 2.922$ Å),[18] and $[Cr^I(C_6H_6)]_2[TCNE]_2$ ($r = 2.904$ Å).[13] This absorption also explains the observed dark blue-purple color of these dimeric compounds. The disagreement between the experimental and calculated values is expected due to the approximate nature of the CIS method,[35] in particular, to the limitations that the method presents for the accurate description of excited states. Another possible source of error is the use of isolated π-$[TCNE]_2^{2-}$ dimers in the calculations, as such a model cannot properly account for variations induced by the cations in the electronic structure of the dimers.

It is also a manifestation of bond formation that the IR spectrum of the dimer differs from that of its fragments. $[TCNE]^{\bullet-}$ has two strong[36] $\nu_{C\equiv N}$ vibrations at around 2200 cm^{-1} (calcd), which correspond to the experimentally observed absorptions at 2183 and 2144 cm^{-1}.[31b] In contrast, for π-$[TCNE]_2^{2-}$ three $\nu_{C\equiv N}$ vibrations are obtained at the RB3LYP/6-31+G level indicative of bond formation between the two $[TCNE]^{\bullet-}$ fragments. This is in accord with the average observed $\nu_{C\equiv N}$ absorptions at 2191 m, 2172 s, and 2161 s cm^{-1} (Table 1). Furthermore, a characteristic high-intensity absorption at about 1400 cm^{-1}, not observed for $[TCNE]^{\bullet-}$, is predicted for the π-$[TCNE]_2^{2-}$ dimer. This new absorption is due to the antisymmetric combination of the intrafragment C–C stretches of each fragment's central C–C bond, which becomes allowed and gains intensity due to electron-vibrational coupling.[37] This absorption, which has been experimentally elusive as it is obscured by the Nujol matrix, occurs at 1361 cm^{-1} in a KBr matrix for both $Tl_2^I[TCNE]_2$[18] (Figure 5b) and $[Cr^I(C_6H_6)]_2[TCNE]_2$.[13] Thus, the π-$[TCNE]_2^{2-}$ dimer can be experimentally identified by 1) an additional strong $\nu_{C\equiv N}$ absorbance, 2) the shift of the three $\nu_{C\equiv N}$ absorbances towards higher frequencies, and 3) a new absorption at around 1360 cm^{-1}.

Another manifestation of the intradimer C–C bonding is the change in hybridization of the central carbon atoms as the intradimer distance decreases. This decrease is followed by changes in the *trans*-NC-C-C-CN angle, while the CN substituents move out of the $[TCNE]^-$ plane by 3.6–6.5° (av 5.1°), Table 1. This change is also observed in the optimized geometries in Figure 2, and is the expected when a C–C bond is formed with an sp^2 C atom. Intradimer bond formation also affects the magnetic properties. When doublet $[TCNE]^{\bullet-}$ fragments approach each other to form the π-$[TCNE]_2^{2-}$ dimer, $\Delta(r)$ and the singlet–triplet separation increase, such

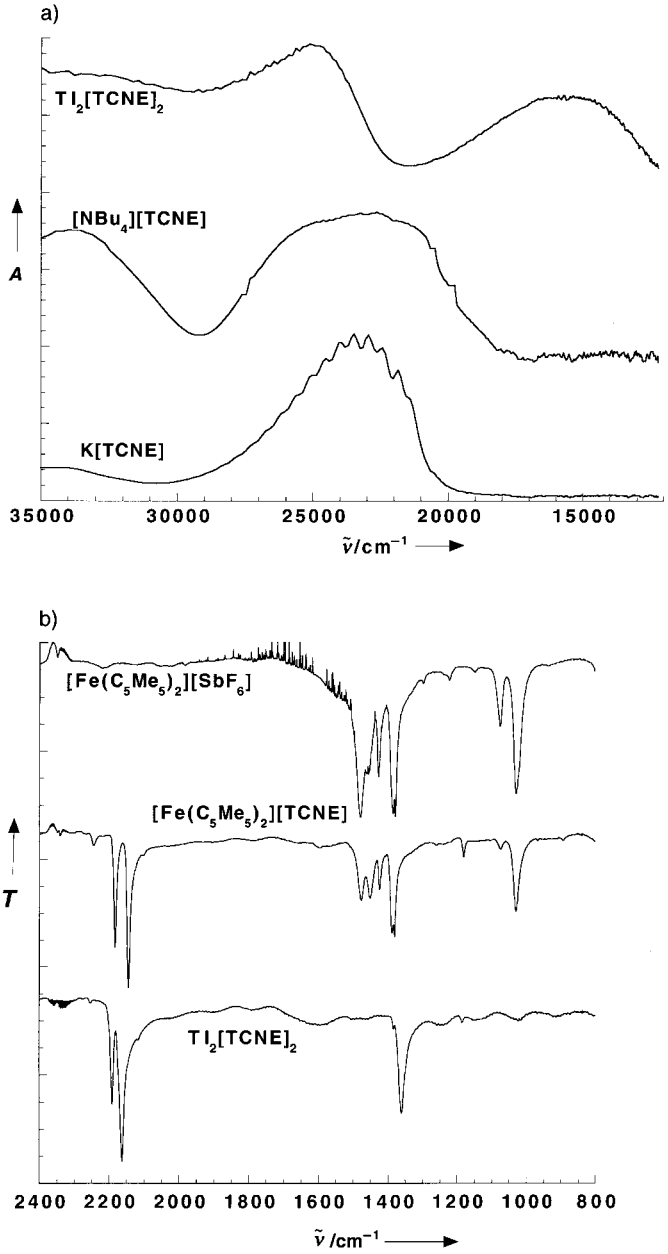

Figure 5. Experimental UV/Vis (a) and IR spectra (b) of some $[TCNE]^-$ salts. The absorption at 25000 cm^{-1} for solid $Tl_2[TCNE]_2$ (KBr pellet) is assigned to a transition in $[TCNE]^-$ similar to the one observed for K[TCNE] in solution (30 mM in MeCN). The UV/Vis spectrum of $[NBu_4][TCNE]$ was recorded as a KBr pellet. In addition to the IR spectrum of $[TCNE]^{\bullet-}$ as the $[Fe(C_5Me_5)_2]^+$ salt, the spectrum of a $[Fe(C_5Me_5)_2]^+$ salt whose anion does not absorb in this reagion is given to help elucidating the contribution of the cation to the spectrum of $[Fe(C_5Me_5)_2][TCNE]$.

that the antiferromagnetically coupled singlet state is the only state that is thermally populated.

The observed properties of the π-$[TCNE]_2^{2-}$ dimer are consistent with those expected from the formation of a covalent C–C bond between two $[TCNE]^{\bullet-}$ ions. However, due to the repulsive electrostatic interactions, the $[TCNE]^- \cdots [TCNE]^-$ interactions are energetically unstable unless stabilized by the presence of cations. In contrast, the neutral system $(cation)_2[TCNE]_2$ is energetically stable due to the

  1433-7851/01/4013-2543 $ 17.50+.50/0

attractive electrostatic cation$\cdots$[TCNE]$^-$ interactions, and enables the direct overlap of the SOMOs of the [TCNE]$^-$ monomers through four carbon atoms and thus is responsible for the existence of cation-mediated $\pi^*-\pi^*$ C–C covalent bonding that occurs in the $(\text{cation})_2[\text{TCNE}]_2$ aggregates. As this two-electron bond emerges from the overlap of the SOMO orbitals of the [TCNE]$^-$, it is not hypervalent.[38] Therefore, it cannot be present when the HOMO is doubly occupied. Hence, this cation-mediated $\pi^*-\pi^*$ C–C bond complies with Pauling's definition of a chemical bond,[1] a key tenet of chemistry, and exhibits all the physical properties expected from a classical C–C covalent bond.

In summary, the formation of π-$[\text{TCNE}]_2^{2-}$ dimers from the corresponding monomers is endothermic, due to repulsive electrostatic anion$\cdots$anion interactions, but they can be stabilized by energetically stronger attractive electrostatic anion$\cdots$cation interactions. When the [TCNE]$^-\cdots$[TCNE]$^-$ distance is sufficiently short, cation-mediated sub-van der Waals $\pi^*-\pi^*$ C–C bonding between the [TCNE]$^{\bullet-}$ ions' central C–C bonds occurs by self-assembly. This supramolecular $(K^+)_2[\text{TCNE}]_2^{2-}$ aggregate is stable by 158.4 kcal mol^{-1}, and the two-electron, four-center $\pi^*-\pi^*$ C–C bonding leads to structural, spectroscopic, and magnetic consequences that are observed. Structurally, in addition to the $\pi^*-\pi^*$ C–C bonds with sub-van der Waals distances of about 2.9 Å, the CN substituents deviate from the [TCNE]$^-$ plane by 3.6 to 6.5°. Spectroscopically, a new IR absorption occurs at around 1360 cm^{-1} ($\nu_{C=C}$), the two $\nu_{C\equiv N}$ absorptions observed for isolated [TCNE]$^{\bullet-}$ shift to higher energy, and a third $\nu_{C\equiv N}$ absorption appears; the characteristic $\nu_{C\equiv N}$ values are 2191 m, 2172 s, and 2161 s cm^{-1}. Also, a new electronic absorption assigned to the $S_0 \rightarrow S_1$ ($b_{2u}{}^2b_{1g}{}^0, {}^1A_{1g} \rightarrow b_{2u}{}^1b_{1g}{}^1, {}^1B_{1u}$) transition occurs at about 15300 cm^{-1} (1.90 eV) that gives these dimeric compounds the observed dark blue-purple color. Finally, the diamagnetic-like behavior of the π-$[\text{TCNE}]_2^{2-}$ dimers is due to population of only the singlet state for this coupled dimer.

Received: December 28, 2000
Revised: March 27, 2001 [Z16342]

[1] "*…there is a chemical bond between two atoms or groups of atoms in the case that the forces acting between them are such as to lead to an aggregate with sufficient stability to make it convenient for the chemist to consider it as an independent molecular species.*" L. Pauling, *The Nature of the Chemical Bond*, 3rd ed., Cornell University Press, Ithaca, **1960**, p. 6.

[2] G. Kaupp, J. Boy, *Angew. Chem.* **1997**, *109*, 48; *Angew. Chem. Int. Ed. Engl.* **1997**, *36*, 48; F. Toda, *Eur. J. Org. Chem.* **2000**, 1377.

[3] C. Vazquez, J. C. Calabrese, D. A. Dixon, J. S. Miller, *J. Org. Chem.* **1993**, *58*, 65.

[4] See for example: A. H. Reis, Jr., E. Gebert, J. S. Miller, *Inorg. Chem.* **1981**, *20*, 313; S. Z. Goldberg, B. Spivack, G. Stanley, R. Eisenberg, D. M. Braitsch, J. S. Miller, M. Abkowitz, *J. Am. Chem. Soc.* **1977**, *99*, 110; M. C. Grossel, F. A. Evans, J. A. Hriljac, K. Prout, S. C. Weston, *J. Chem. Soc. Chem. Commun.* **1990**, 1494; M. T. Axcondo, L. Ballester, S. Golhen, A. Gutierrez, L. Ouahab, S. Yartsev, P. Delhaes, *J. Mater. Chem.* **1999**, *9*, 1237; R. C. Hynes, J. R. Morton, K. F. Preston, A. J. Williams, F. Evans, M. C. Grossel, L. H. Sutcliffe, S. C. Weston, *J. Chem. Soc. Faraday Trans.* **1991**, *87*, 2229; J. S. Miller, J. H. Zhang, W. M. Reiff, L. D. Preston, A. H. Reis, Jr., E. Gerbert, M. Extine, J. Troup, M. D. Ward, *J. Phys. Chem.* **1987**, *91*, 4344.

[5] M. T. Johnson, A. M. Arif, J. S. Miller, *Eur. J. Inorg. Chem.* **2000**, 1781, and references therein.

[6] See for example: G. Zanotti, *Acta Crystallogr. Sect. B* **1982**, *38*, 1225; J. S. Miller, P. J. Krusic, D. A. Dixon, W. M. Reiff, J. H. Zhang, E. C. Anderson, A. J. Epstein, *J. Am. Chem. Soc.* **1986**, *108*, 4459; J. J. Mayerle, J. B. Torance, *Bull. Chem. Soc. Jpn.* **1981**, *54*, 3170; Y.-K. Yan, M. P. Mingos, T. E. Müller, D. J. Williams, *J. Chem. Soc. Dalton Trans.* **1995**, 2509; A. Marzotto, D. A. Clemente, L. Pasimeni, *J. Crystallogr. Spectrosc. Res.* **1988**, *18*, 545.

[7] *Handbook of Conducting Polymers* (Eds.: T. A. Skotheim, R. L. Elsenbaumer, J. R. Reynolds), 2nd ed., Marcel Dekker, New York, **1998**; J. R. Ferraro, J. M. Williams, *Introduction to Synthetic Electrical Conductors*, Academic Press, Orlando, **1987**.

[8] J. M. Williams, *Organic Superconductors (Including Fullerenes): Synthesis, Structure, Properties, and Theory*, Prentice Hall, Englewood Cliffs, **1992**; T. Ishiguro, K. Yamaji, G. Saito, *Organic Superconductors*, Springer, New York, **1998**.

[9] V. I. Ovcharenko, R. Z. Sagdeev, *Russ. Chem. Rev.* **1999**, *68*, 345; M. Kinoshita, *Phil. Trans. R. Soc. London A* **1999**, *357*, 2855; J. S. Miller, A. J. Epstein, *Chem. Commun.* **1998**, 1319; J. S. Miller, A. J. Epstein, *Chem. Eng. News* **1995**, *73*(40), 30; J. S. Miller, A. J. Epstein, *Angew. Chem.* **1994**, *106*, 399; *Angew. Chem. Int. Ed. Engl.* **1994**, *33*, 385; O. Kahn, *Adv. Inorg. Chem.* **1995**, *43*, 179.

[10] See for example: J. S. Miller, J. C. Calabrese, H. Rommelmann, S. Chittipeddi, A. J. Epstein, J. H. Zhang, W. M. Reiff, *J. Am. Chem. Soc.* **1987**, *109*, 769.

[11] J. Zhang, L. M. Liable-Sands, A. L. Rheingold, R. E. Del Sesto, D. C. Gordon, B. M. Burkhart, J. S. Miller, *Chem. Commun.* **1998**, 1385.

[12] M. M. Olmsted, G. Speier, L. Szabo, *J. Chem. Soc. Chem. Commun.* **1994**, 541.

[13] J. S. Miller, D. M. O'Hare, A. Charkraborty, A. J. Epstein, *J. Am. Chem. Soc.* **1989**, *111*, 7853.

[14] D. A. Lemervoskii, R. A. Stukan, B. N. Tarasevich, Tu. L. Slovokhotov, M. Yu. Antipin, A. E. Kalinin, Yu. T. Struchov, *Coord. Khim.* **1981**, *7*, 118.

[15] H. Bock, K. Ruppert, D. Fenske, H. Goesmann, *Z. Anorg. Allg. Chem.* **1995**, *595*, 275.

[16] J. S. Miller, J. C. Calabrese, C. Vazques, R. S. McLean, D. T. Glatzhofer, J. W. Raebiger, *Inorg. Chem.* **2001**, *40*, 2578.

[17] S. A. Clemente, A. Marzotto, *J. Mater. Chem.* **1996**, *6*, 941.

[18] M. T. Johnson, C. F. Campana, B. M. Foxman, W. Desmarais, M. J. Vela, J. S. Miller, *Eur. J. Chem.* **2000**, *6*, 1805.

[19] J. R. Fox, B. M. Foxman, D. Guerrer, J. S. Miller, A. H. Reis, Jr., *J. Mater. Chem.* **1996**, *6*, 1627.

[20] Similar π-$[\text{TCNQ}]_2^{2-}$ dimers have also been reported; see for example: H. Zhao, R. A. Heinz, K. R. Dunbar, R. D. Rogers, *J. Am. Chem. Soc.* **1996**, *118*, 12844.

[21] $[\text{TCNE}]_2^{2-}$ dimers were selected due to the relative simplicity of the acceptor compared to other π-$[\mathbf{A}]_2^{2-}$ dimers.

[22] All the computations were done using the Gaussian 98 suite of programs. Gaussian 98 (Revision A.7), M. J. Frisch, G. W. Trucks, H. B. Schlegel, G. E. Scuseria, M. A. Robb, J. R. Cheeseman, V. G. Zakrzewski, J. A. Montgomery, R. E. Stratmann, J. C. Burant, S. Dapprich, J. M. Millam, A. D. Daniels, K. N. Kudin, M. C. Strain, O. Farkas, J. Tomasi, V. Barone, M. Cossi, R. Cammi, B. Mennucci, C. Pomelli, C. Adamo, S. Clifford, J. Ochterski, G. A. Petersson, P. Y. Ayala, Q. Cui, K. Morokuma, D. K. Malick, A. D. Rabuck, K. Raghavachari, J. B. Foresman, J. Cioslowski, J. V. Ortiz, B. B. Stefanov, G. Liu, A. Liashenko, P. Piskorz, I. Komaromi, R. Gomperts, R. L. Martin, D. J. Fox, T. Keith, M. A. Al-Laham, C. Y. Peng, A. Nanayakkara, C. Gonzalez, M. Challacombe, P. M. W. Gill, B. G. Johnson, W. Chen, M. W. Wong, J. L. Andres, M. Head-Gordon, E. S. Replogle, J. A. Pople, Gaussian, Inc., Pittsburgh, PA, **1998**.

[23] First we explored this surface with RHF and RB3LYP calculations using the 6-31 + G and 6-31 + G(d) basis sets, which include diffuse functions for the proper description of the additional valence electron of the anion. All geometrical parameters except *r* were optimized for each point of this curve.

[24] The minimum-energy structures were verified by looking at the number of nonimaginary frequencies. In all of the optimized geometries the frequencies were positive. Therefore, well-characterized minimum-energy structures of the π-$[\text{TCNE}]_2^{2-}$ dimers were identified.

  1433-7851/01/4013-2544 $ 17.50+.50/0

[25] The presence of minima in a potential energy surface requires a transition state connecting these minima; this was observed for the π-$[TCNE]_2^{2-}$ dimer (Figure 2). It originates from the energy required to reduce the bond order of the central C–C bond enabling the change in hybridization of the central C atom from sp^2 in conformer **3** to sp^3 in conformer **2**. Near this maximum is the true transition state that separates **3** and **2**. More elaborate UB3LYP and MCSCF calculations—the UB3LYP calculations for the open-shell singlet (S_1) state were done within the broken symmetry approximation; the results of the broken symmetry calculations were tested by MCSCF(6,4) calculations on the potential energy curves of the π-$[TCNE]_2^{2-}$ dimer, using a complete active space of six electrons and four orbitals; for these calculations the 6-31 + G basis set employed in the B3LYP calculations was used; for any given geometry, the population of the b_{2u}, b_{1g}, and antibonding b_{2u} orbitals in these MCSCF calculations differs by $< 0.1\ e^-$ with respect to the B3LYP results for the same geometry, in agreement with the UB3LYP results; the shape of the S_0 and S_1 curves at the MCSCF level is also similar to that found at the UB3LYP level, and a full geometry optimization at the MCSCF level starting from the RB3LYP minimum goes towards dissociation into the fragments without a barrier—were run for each point in Figure 2, which confirmed the repulsive nature of the $[TCNE]^{\bullet-} \cdots [TCNE]^{\bullet-}$ interaction, and also indicated that the π-$[TCNE]_2^{2-}$ dimer **3** presents no barrier towards dissociation into two $[TCNE]^-$ monomers, being the only minimum at short distances (the π-$[TCNE]_2^{2-}$ dimer has $r =$ 1.61 Å and average dihedral angles that range from 36.5 to 45.9°, and has $E_{int} = 94.9\ kcal\,mol^{-1}$; see Supporting Information). Thus, the minimum nature of the π dimer in the RHF and RB3LYP calculations is an artifact of the double occupancy restriction imposed to the orbitals in these methods.

[26] π-$[TCNQ]_2^{2-}$ has been observed in solution: M. Itoh, *Bull. Chem. Soc. Jpn.* **1972**, *45*, 1947; Y. Oohashi, T. Sakat, *Bull. Chem. Soc. Jpn.* **1973**, *46*, 3330.

[27] Preliminary calculations indicate that the size or type of the cation does not play an important role in the electrostatic stabilization.

[28] This number is the result of adding $E(K_1^+ \cdots K_2^+) + E([TCNE]^- \cdots [TCNE]^-) + 2E([TCNE]^- \cdots K_1^+) + 2E([TCNE]^- \cdots K_2^+)$, which are, respectively, 30.5, 103.0, −70.9, and −75.0 $kcal\,mol^{-1}$; there are two different K^+ ions in the $K_2[TCNE]_2$ aggregate, placed in a nonsymmetrical form relative to the $[TCNE]^-$ ions (at 3.06 and 2.82 Å); this is the reason for the multiplication by two of the $[TCNE]^- \cdots K^+$ interaction energy terms.

[29] D. Braga, F. Grepioni, J. J. Novoa, *Chem. Commun*. **1998**, 1959; J. J. Novoa, I. Nobeli, F. Greppioni, D. Braga, *New J. Chem.* **2000**, 5; J. J. Novoa in *Implications of Molecular Materials Structure for New Technologies* (Eds.: J. A. K. Howard, F. H. Allen, G. P. Shields), Kluwer, Amsterdam, **1999**.

[30] The nonlocal B3LYP exchange and correlation DFT functional and the 6-31 + G(2d,2p) basis set with a determinant in which the orbitals are not restricted to be doubly occupied were used. The B3LYP is a combination of the nonlocal three-parameter exchange functional (A. D. Becke, *J. Chem. Phys.* **1993**, *98*, 5648) and the nonlocal LYP correlation functional (C. Lee, W. Yang, R. G. Parr, *Phys. Rev. B* **1998**, *37*, 785).

[31] a) P. Becker, P. Coppens, R. K. Ross, *J. Am. Chem. Soc.* **1973**, *95*, 7604; b) D. A. Dixon, J. S. Miller, *J. Am. Chem. Soc.* **1987**, *109*, 3656.

[32] A. Zheludev, A. Grand, E. Ressouche, J. Schweizer, B. Morin, A. J. Epstein, D. A. Dixon, J. S. Miller, *J. Am. Chem. Soc.* **1994**, *116*, 7243.

[33] The tendency to delocalize the charge on the peripheral atoms cannot be attributed to the electronegativity of the CN group, as it is not found for either $[C_2H_4]^{\bullet-}$ or $[C_2F_4]^{\bullet-}$ by UB3LYP/6-31 + G(2d,2p) calculations, although F is more electronegative than the CN group. Therefore, this behavior can only be explained as associated delocalization due to the presence of low-energy resonance forms in which the unpaired electron is delocalized over the CN groups.

[34] An "atoms-in-molecules" critical point analysis (R. F. Bader, *Atoms in Molecules*, Clarendon, Oxford, **1990**) on $K_2[TCNE]_2$ identifies the intradimer bonding as having (3, −1) bond critical points between the two $[TCNE]^-$ units at the RB3LYP level.

[35] J. B. Foresman, M. Head-Gordon, J. A. Pople, M. J. Frisch, *J. Phys. Chem.* **1992**, *96*, 135.

[36] There are also two weak peaks (ca. 10% of the intensity of the stronger peaks) at about 2200 cm^{-1}.

[37] Similar results were noted for π-$[TCNQ]_2^{2-}$: M. J. Rice, N. O. Lipari, S. Strassler, *Phys. Rev. Lett.* **1977**, *39*, 1359.

[38] It should be noted that in addition to the short C–C π bonding interactions, longer $[TCNE]^- \cdots [TCNE]^-$ interactions are frequently present, but at these long distances (> 3.5 Å) the bonding properties disappear, due to the exponential behavior of the orbital overlap integrals, responsible for Δ.

  1433-7851/01/4013-2545 $ 17.50+.50/0

ANGEWANDTE CHEMIE
A Journal of the Gesellschaft Deutscher Chemiker
INTERNATIONAL EDITION
2001
40/14
Pages 2557 – 2724

COVER PICTURE

The cover picture shows nanometer-thin elastomeric membranes made from polyisobutene star polymers with ionic head groups. Spreading of the polymers onto a water surface yields fluid monolayers. These can be transferred to cover openings in solid substrates. After transfer, the ionic head groups aggregate, cross-link the membrane, and thus give rise to elastomeric properties. For example applying a small overpressure from one side gives rise to comparatively large, reversible deformations. These elastomeric membranes could be used in micromechanical devices such as membrane pumps and valves. More details on these membranes are reported by F. Mallwitz and W. Goedel on pages 2645 ff.

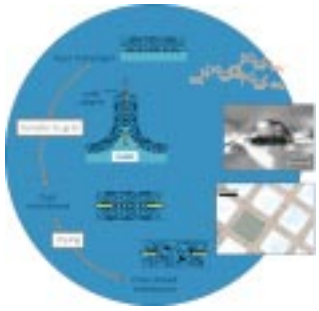

REVIEWS

Contents

The science of serendipity: the accidental use of a hypercatalytic amount of a Ziegler – Natta catalyst gave polyacetylene films, such as the one shown in the transmission electron micrograph. This "mishap" opened the way to new conducting polymers, (legal) doping, and the award of the Nobel prize for chemistry.

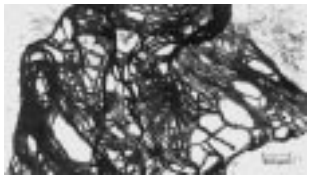

Angew. Chem. **2001**, *113*, 2642 – 2648

Keywords: chemical doping · conducting materials · Nobel lecture · polyacetylene · Ziegler – Natta

  1433-7851/01/4014-2559 $ 17.50+.50/0

Keywords: conducting materials · liquid crystals · nano-electronics · Nobel lecture · polymers

Keywords: chemical doping · conducting materials · Nobel lecture · polyacetylene · solid-state physics

VIPs

The following communications are "Very Important Papers" in the opinion of two referees. They will be published shortly (that marked with a diamond will be published in the next issue). Short summaries of these articles can be found on the *Angewandte Chemie* homepage at the address http://www.angewandte.com

  1433-7851/01/4014-2560 $ 17.50+.50/0

  1433-7851/01/4014-2561 $ 17.50+.50/0

  1433-7851/01/4014-2562 $ 17.50+.50/0

  1433-7851/01/4014-2563 $ 17.50+.50/0

  1433-7851/01/4014-2564 $ 17.50+.50/0

  1433-7851/01/4014-2565 $ 17.50+.50/0

  1433-7851/01/4014-2566 $ 17.50+.50/0

  1433-7851/01/4014-2567 $ 17.50+.50/0

  1433-7851/01/4014-2568 $ 17.50+.50/0

Supporting information on the WWW (see article for access details).

* Author to whom correspondence should be addressed

BOOKS

WEB SITES

SERVICE

Issue 13, 2001 was published online on June 28, 2001.

Don't forget all the Tables of Contents from 1995 onwards may be still found on the WWW under: http://www.angewandte.com

1433-7851/01/4014-2570 $ 17.50+.50/0

Nobel Prize in Chemistry 2000
Electrically Conductive Plastic

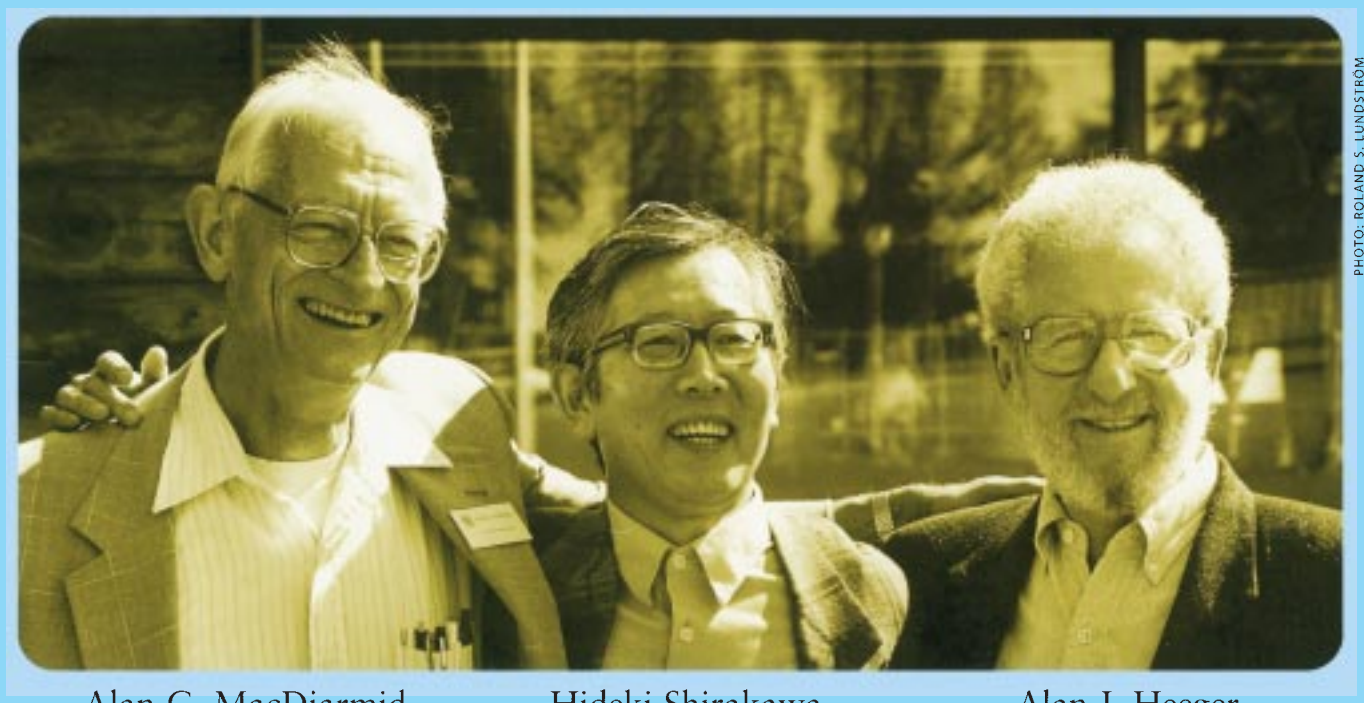

PHOTO: ROLAND S. LUNDSTRÖM

Alan G. MacDiarmid
University of Pennsylvania,
Philadelphia, USA

Hideki Shirakawa
Emeritus,
University of Tsukuba, Japan

Alan J. Heeger
University of California
at Santa Barbara, USA

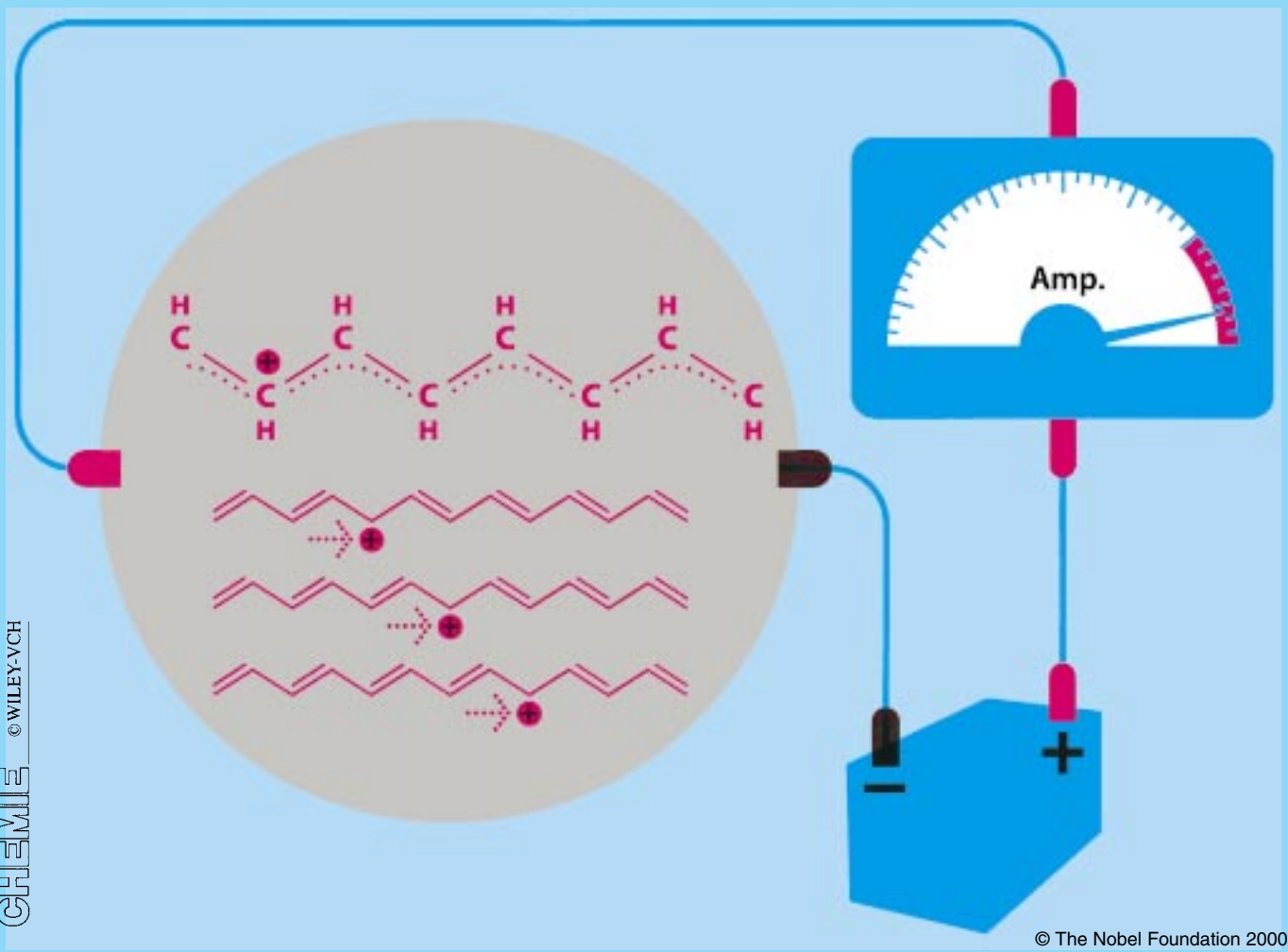

ANGEWANDTE CHEMIE © WILEY-VCH

The Discovery of Polyacetylene Film: The Dawning of an Era of Conducting Polymers (Nobel Lecture)**

Hideki Shirakawa*

This lecture is not directly related to our discovery and development of conducting polymers to which the Nobel Prize in Chemistry 2000 was awarded. However, I would like to present my previous work that I had carried out just before we reached the discovery of chemical doping. I hope that this will be of use and deepen your understandings by learning what had happened before and how we reached the idea of chemical doping.

Keywords: chemical doping · conducting materials · Nobel lecture · polyacetylene · Ziegler–Natta catalysts

1. Prologue

It has been recognized for many years that a very long linear-conjugated polyene might have various interesting properties, especially optical, electrical, and magnetic properties. The definition of the polyene is that an even number of methyne (=CH−) groups is covalently bonded to form a linear carbon chain bearing one π electron on each carbon atom. Therefore, the chemical structure of the polyene is best represented by a formula $H(CH{=}CH)_nH$, where *n* denotes the number of repeating units. Recently *polyacetylene* has become a more popular name than polyene because polyacetylene, synthesized by the polymerization of acetylene, has been used extensively as specimens for various studies.

Pople and Walmsley described in their article in 1962[1] that *"Although it is not possible to synthesize very long polyenes (polyacetylene) at present, general interest in conjugated polymers with related, but rather more complex, structures makes a full study of the electronic states of this simple polymer worthwhile"*. Although the first polymerization of acetylene was reported in no later than 1958 by Natta and co-workers,[2] who prepared polyacetylene that is structurally identical to the very long conjugated polyene, the work was not accepted widely in the field. Before that time interest in this compound was limited, for chemists, to theoretical approaches to explain a red-shift of absorption maximum (bathochromic effect) and an increase in absorption coefficient (hyperchromic effect) with increasing the number of repeating units in the conjugation, and to elucidate bond alternation in connection with an electron–phonon interaction for physicists. An accumulation of experimental observations on relatively short polyenes[3–8] coupled with theoretical considerations such as the free-electron model and simple Hückel molecular orbital treatments strongly suggested that the difference between the lengths of double and single bonds decreases with increasing the conjugation and that all the bonds tend to be of equal length in an infinitely long polyene. In other words, one would expect that the infinitely long, one-dimensional arrangement of π electrons forms a half-filled band, or that the highest occupied (HO) and the lowest unoccupied (LU) π-electron bands merge with each other, leading to metallic behavior.[9, 10] In the 1950s, however, it became theoretically clear that the polyene with bond alternation is energetically more stable than that with bonds of equal length.[1, 11–13] Since two geometrical isomers, *trans* and *cis*, are possible for each double bond, two isomeric forms, all-*trans* (**1**) and all-*cis* (**2**), are expected as the two extremes of polyacetylene isomers. Experimentally the carbon–carbon bond lengths in poly-

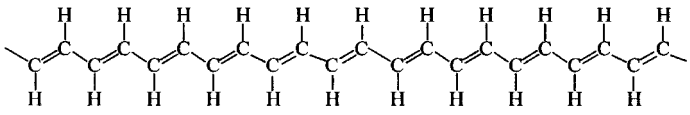

1

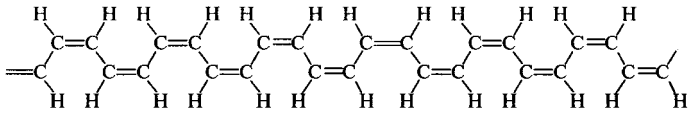

2

[*] Prof. H. Shirakawa
University of Tsukuba
Tsukuba, Ibaraki 305-8577 (Japan)
Fax: (+81) 45-971-1389
E-mail: hideki@ims.tsukuba.ac.jp

acetylene were directly measured by Yannoni and Clarke[14] with use of the nutation NMR spectroscopy, 1.36 and 1.44 Å for the double and single bonds, respectively, in the *trans* form and 1.37 Å for the double bond in the *cis* form.

Even after the first synthesis by Natta and co-workers,[2] polyacetylene remained for some time a material of interest to only a few organic [15, 16] and polymer chemists[17–19] because the product was obtained as insoluble and infusible powders.

2. *trans* or *cis*?

Among the few chemists working on polyacetylene, S. Ikeda and co-workers had been studying a mechanism of acetylene polymerization in connection with olefin polymerization by various Ziegler–Natta catalysts. They found that the polymerization yields not only highly polymerized polyacetylene but also benzene, that is, a cyclic trimer of acetylene, and that the ratio of these two products depends upon species of Ziegler–Natta catalyst used. They also found the formation of alkylbenzenes as a minor by-product of the acetylene polymerization with a catalyst system composed of titanium tetrachloride and trialkylaluminum. In a series of experiments using carbon-14 and deuterium, they noted that a labeled ethyl group is introduced in the ethylbenzene when triethylaluminum labeled with carbon-14 or deuterium is used as the co-catalyst.[20] In other experiments on the oxidation of polyacetylene by alkaline potassium permanganate, they observed the formation of propionic and acetic acids that are derived from the alkyl groups in the trialkylaluminum used as the co-catalyst.[20] From these results, they concluded that polyacetylene and benzene could be formed from the same active site of the catalyst system. Thus, the reaction proceeds by *cis*-opening of the triple bond in acetylene followed by a *cis* insertion into the titanium–alkyl bond of the catalyst. This mechanism fits the orbital interaction consideration by Fukui and Inagaki,[21] for the role of the catalyst according to which the initially formed configuration of the double bond is *cis* as a result of favored orbital interaction between the inserting acetylene and the active site of the catalyst. Whether cyclic trimerization occurs to give benzene or polymerization proceeds to give polyacetylene is determined by the conformation of the growing chain that takes either cisoid or transoid structure in the vicinity of the active site of the catalyst.[22] As no *cis* form had been known until then, an important question remained: why is the mechanism capable of yielding only a *trans* configuration of the double bonds in polyacetylene?[2, 19]

3. Discovery of Film Synthesis

The conventional method of polymerization in the laboratory is such that the catalyst solution is stirred thoroughly to carry out the reaction under homogeneous conditions. The acetylene polymerization has not been an exception: it was customary for polymer chemists who synthesized polyacetylene to bubble acetylene gas into a stirred catalyst solution. Unfortunately, the product was obtained as an intractable black powder that is very difficult to make into samples of a shape suitable for measurement of spectra and physical properties because of its insolubility and infusibility.

In 1967, soon after I joined Ikeda's group, we succeeded in synthesizing polyacetylene directly in the form of a thin film[23] by a fortuitous error. After a series of experiments to reproduce the error, we noticed that we had used a concentration of the Ziegler–Natta catalyst nearly a thousand times greater than that usually used. It is worth noting that the insolubility of polyacetylene contributes to the formation of the film. In addition, it was found that the film is composed of entangled micro-fibers (called fibrils), this discovery was made by transmission electron microscope observation of an extremely thin film and by scanning electron microscope observation of the surface of a thick film (Figure 1). The fibril diameter is in the range of 20–100 nm depending upon the

Hideki Shirakawa was born in Tokyo, Japan on August 20, 1936. He received his B.S., M.S., and Ph.D. from the Tokyo Institute of Technology. After completion of his Ph.D. in 1966, he joined Professor Sakuji Ikeda's group at the Research Laboratory for Resources Utilization, Tokyo Institute of Technology, where he investigated acetylene polymerization for the elucidation of the polymerization mechanism by Ziegler–Natta catalysts. In 1967, he noticed on formation of polyacetylene in a form of a film with metallic luster following an unforeseeable experimental error by one of his co-workers. By chance, this silvery film caught the eyes of Professor Alan G. MacDiarmid, he was invited to work in University of Pennsylvania for one year during 1976 and 1977 where they found the chemical doping of acetylene jointly with Professor Alan J. Heeger. In November 1979, he moved from the Tokyo Institute of Technology to the Institute of Materials Science, University of Tsukuba, where he was appointed Associate Professor. In October 1982, he was promoted to full professor and worked on polyacetylene and other conducting polymers. He retired from the University of Tsukuba at the end of March 2000. He is currently a member of Council for Science and Technology Policy, Cabinet Office. He received the Award of the Society of Polymer Science, Japan in 1983, Award for Distinguished Service in Advancement of Polymer Science, from the Society of Polymer Science, Japan in 2000, the Order of Culture in 2000 from Japanese Government, and the Nobel Prize for Chemistry in 2000.

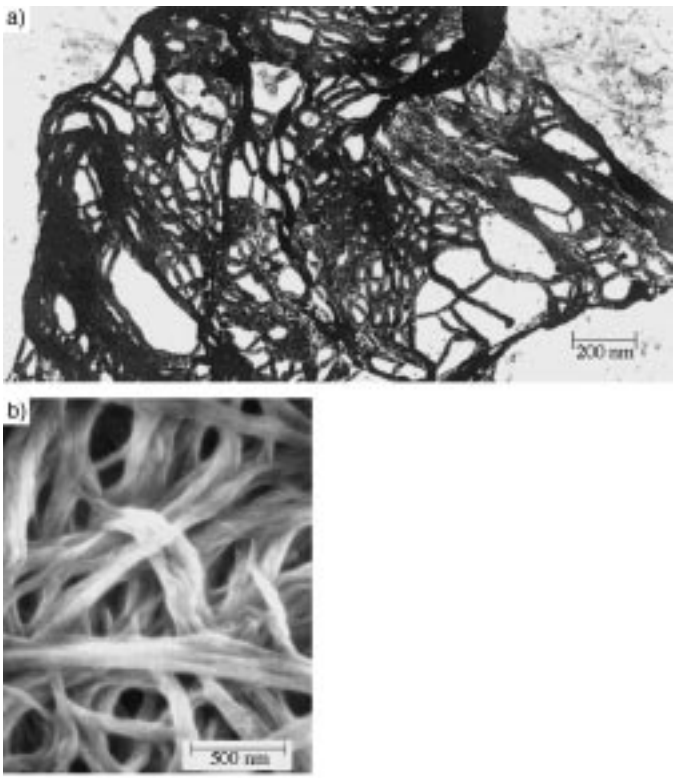

Figure 1. a) Transmission electron micrograph of an extremely thin film of polyacetylene. b) Scanning electron micrograph of the surface of a thick polyacetylene film.

polymerization conditions. These inherent properties of polyacetylene are absolutely necessary for the film formation even under the higher concentration of the catalyst. One more important factor that should be added is that the catalyst used at that time, $Ti(O\text{-}n\text{-}C_4H_9)_4/(C_2H_5)_3Al$, was quite unique from the viewpoint of its good solubility in organic solvents, such as hexane or toluene, to give a homogeneous solution, and its high activity to give exclusively high molecular weight and crystalline polymers. On the contrary, most Ziegler–Natta catalysts form precipitates to give inhomogeneous solutions when a titanium compound is mixed with alkylaluminum.

The use of the films enabled us to obtain clear infrared spectra, as shown in Figure 2,[24] and analysis of these spectra indicated that the configuration of the double bonds strongly depends on the temperature of polymerization. The *trans* contents of polyacetylene prepared by the Ziegler–Natta catalysts decreases with decreasing polymerization temperature (Table 1). Thermal study[25] indicated that the irreversible isomerization of the *cis* form occurs at temperatures higher than 145 °C to give the *trans* form. Thus

Table 1. The *trans* contents of polyacetylene prepared at different temperatures *T*.[a]

T [°C]	*trans* Content [%]	T [°C]	*trans* Content [%]
150	100.0	0	21.4
100	92.5	−18	4.6
50	67.6	−78	1.9
18	40.7		

[a] Catalyst: $Ti(O\text{-}n\text{-}C_4H_9)_4/(C_2H_5)_3A1$, Ti/Al = 4, [Ti] = 10 mmol L^{-1}.

the *cis* form is thermodynamically less stable than the *trans* one. The observed *cis*-rich polyacetylene synthesized at lower temperatures suggested the *cis*-opening of the triple bond of the acetylene monomer consistent with the *cis*-opening mechanism proposed by Ikeda.[22] In case of the polymerization being carried out at higher temperatures, spontaneous isomerization of the growing chain of *cis* double bonds occurs to give *trans* ones, also consistent with the *cis*-opening mechanism proposed by Ikeda.[22] The *cis*-opening mechanism has been supported by the nutation NMR study[14] and by the infrared study of copolymers of acetylene and $[D_2]$acetylene.[24] In conclusion, the open problem why only *trans* polyacetylene had been known was solved by the use of films.

4. Electrical Properties of "As-Prepared" Polyacetylene Films

The electrical resistivity of "as-prepared" (untreated) films with various *cis*/*trans* contents was measured by the conventional two-probe method under vacuum in a temperature

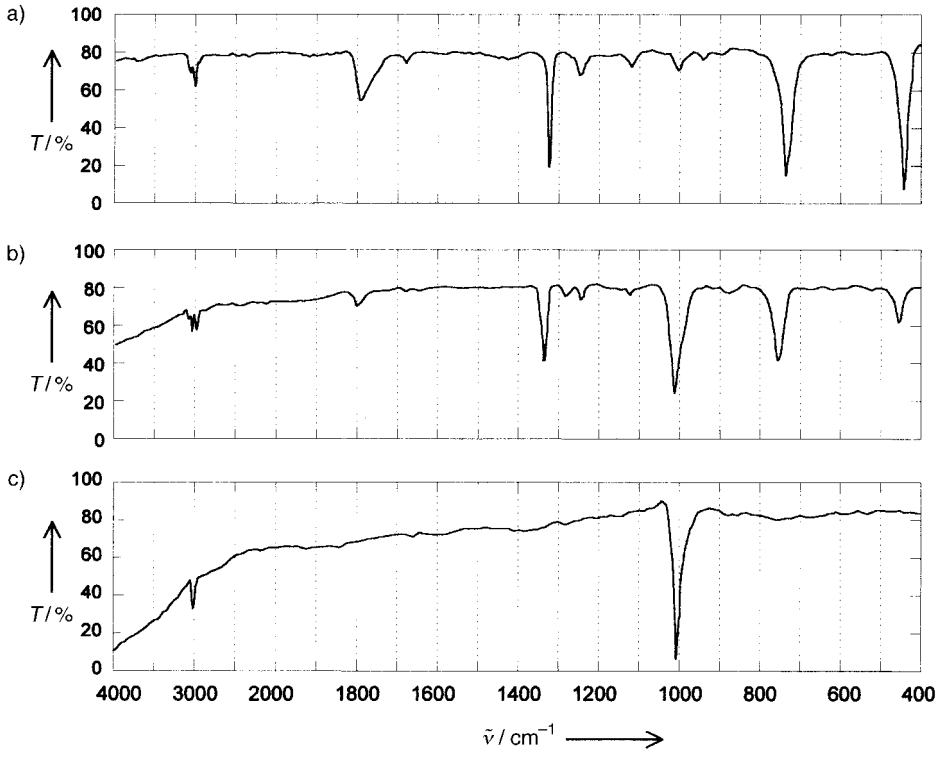

Figure 2. Infrared spectra of polyacetylene synthesized at a) −78 °C, b) 20 °C, and c) 150 °C. Cf. ref. [24], Figure 4.

range of $-120-+20\,^{\circ}C$.[26] The resistivity and energy gap of *trans*-rich polyacetylenes were $1.0\times10^{4}\,\Omega cm$ and 0.56 eV, respectively, whereas the values of a *cis*-rich (80%) one were $2.4\times10^{8}\,\Omega cm$ and 0.93 eV, respectively. Hatano et al.[17] reported that the resistivity and energy gap measured on compressed pellets of powder polyacetylene synthesized by the same catalyst system are in the range of 1.4×10^{4} and $4.2\times10^{5}\,\Omega cm$, and 0.46 eV, respectively, in good agreement with those for *trans*-rich polyacetylene film. In conclusion, it became apparent that the intrinsic electrical properties do not change very much between powder and film.

5. Halogenation of the Polyacetylene Films

Since no improvement in electrical conductivity was observed in film form, we tried to use the polyacetylene films as a source of graphite films as the carbon content of the polymer is as high as 92.3%. Thermograms from differential thermal analysis of *cis*-rich polymer revealed the existence of two exothermic peaks at 145 and 325 °C and one endothermic peak at 420 °C which were assigned to *cis*–*trans* isomerization, hydrogen migration accompanied with cross-linking reaction, and thermal decomposition, respectively[25] (Scheme 1). Thermogravimetric analysis showed that weight loss reached 63% at 420 °C. Therefore, pyrolysis of as-prepared polyacetylene films is not suitable for the preparation of graphite films.

Electrophilic addition of halogens such as chlorine and bromine to a carbon–carbon double bond is a well-known reaction and proceeds with good yield and few side reactions. Elimination of hydrogen halide from adjacent carbon atoms in a halogenated hydrocarbon is also a well-known reaction to introduce a carbon–carbon double or triple bond. Since polyacetylene reacts with chlorine and bromine under mild conditions, we thought carbonization might be possible by combining the both reactions. Thus, a polyacetylene film was treated with chlorine at room temperature to give a chlorinated polyacetylene film, which was subsequently treated with a basic reagent to eliminate hydrogen chloride to give a carbon film in satisfactory yield. However, we found that the carbon film was hardly graphitized even when heated at 2000 °C for several hours.

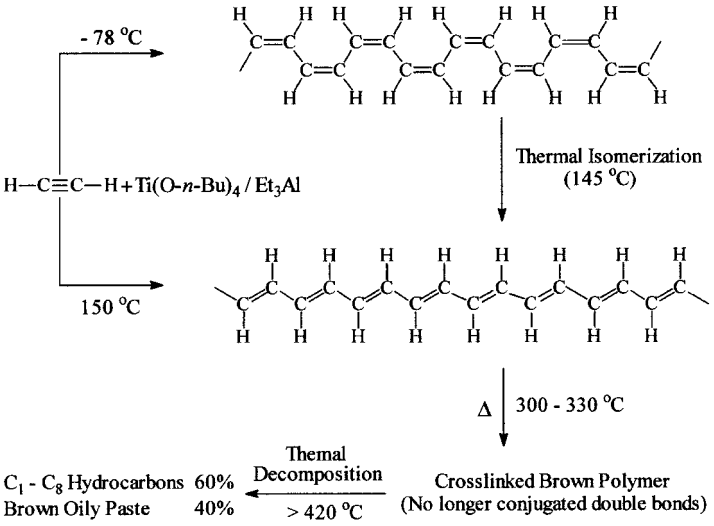

Scheme 1. Thermal characteristics of polyacetylene.

Fully chlorinated polyacetylene has a chemical structure of $-(CHCl\text{-}CHCl)_n-$, corresponding to a polymer of 1,2-dichloroethylene. It is known, however, that 1,2-disubstituted ethylenes hardly ever polymerize. Therefore, the chlorination of polyacetylene is the sole method to synthesize poly(1,2-dichloroethylene). To investigate the chlorination process of the polyacetylene film, in situ measurements were planned to obtain infrared spectra during the chlorination of the polyacetylene film.

It is well known that chlorination of the simplest conjugated polyene, 1,3-butadiene, gives two isomeric products, the 1,2-addition product (3,4-dichloro-1-butene) and the 1,4-addition product (1,4-dichloro-2-butene). Likewise, 1,3,5-hexatriene gives three isomers, 1,2-, 1,4-, and 1,6-addition products. The reason why the reaction gives various products is explained by the existence of different resonance structures in the intermediate (Scheme 2). The third isomer is thermodynamically the most stable because the molecule has an inner conjugated diene structure with the largest energy of resonance stabilization.

The motivation for the study was to confirm that the 1,2*n*-addition of chlorine might occur as the initial step of the reaction as shown in Scheme 3. Since the longer inner polyene structure has the larger energy of resonance stabilization, it is anticipated that products of 1,2*n*-addition with larger *n* predominate, rather than a 1,2-addition product at the initial step of the reaction or in the partially chlorinated polyacetylene. If such structures could be detected by infrared spectroscopy, one might expect that the positive charge on the intermediate carbocation is able to migrate far away from the reaction site through the conjugated polyene structure.

Contrary to this expectation, the infrared spectrophotometer recorded no spectrum but only a 100% absorption line in the full range of 4000 to 400 cm^{-1} immediately after addition of a trace amount of chlorine to the film. The polyacetylene film changed into an opaque material because

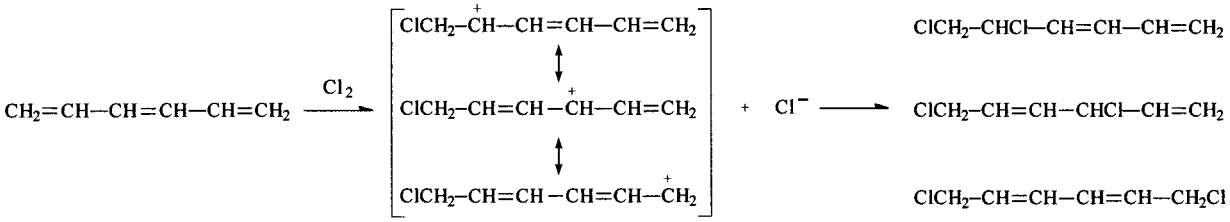

Scheme 2. Possible resonance structures for the intermediate during the chlorination of 1,3,5-hexatriene to give three chlorinated products.

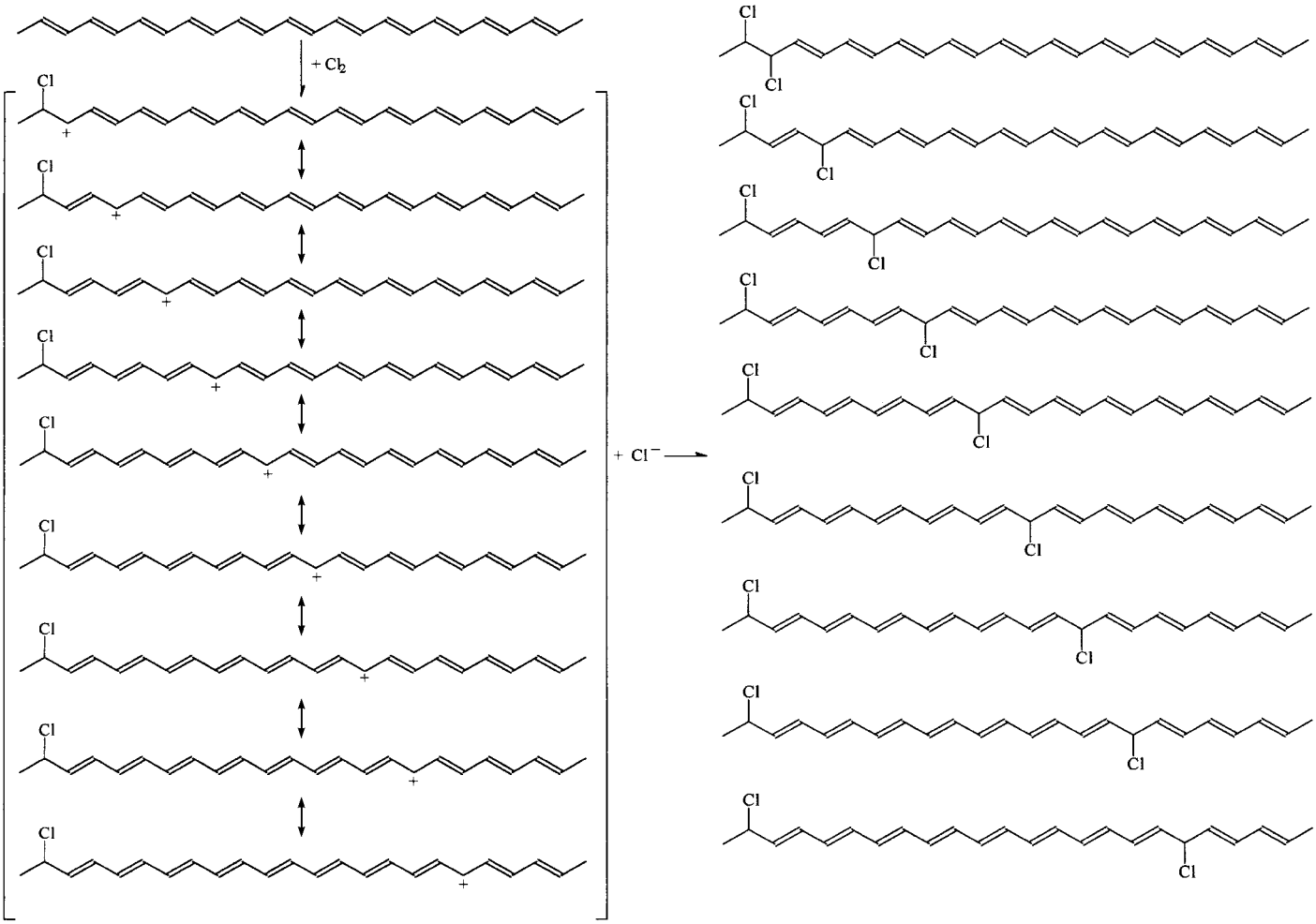

Scheme 3. Possible resonance structures for the intermediate in the chlorination of polyacetylene, the expected chemical structures of partially chlorinated polyacetylene are also shown.

of some very strong absorptions. Upon continued reaction with additional chlorine, the spectrum became clearer to give that corresponding to a chlorinated polyacetylene.

6. Epilogue

Later, we know that the very strong absorption is the so-called "doping induced infrared band" composed of three bands at 1397, 1288, and 888 cm^{-1},[27–29] which have extremely strong absorption coefficients compared with those of the as-prepared polymer. The observed isotope shifts of these bands in the spectra of poly([$^{13}C_2$]acetylene) and poly([D_2]acetylene) demonstrated that these bands are of vibrational origin[27] in the vicinity of the carbocation or positively charged carbon atom in the conjugated polyene. At present, the carbocation formed in long conjugated polyenes is widely known as a positively charged soliton[30] that acts as a charge carrier for the electrical conduction. At that time, to my regret, I did not recognize that this carbocation could be a charge carrier and thus polyacetylene could be the first conducting polymer. To open an era of conducting polymers, we had to wait until we intentionally carried out the doping experiment with bromine at the University of Pennsylvania, on Tuesday 23rd, of November 1976, and then later also successively with iodine.[31, 32]

At the end of my lecture I want to express my heartfelt thanks to the late Professor Sakuji Ikeda who gave me a chance to work on the acetylene polymerization, to Professor Masahiro Hatano who contributed to the semiconducting polymers and encouraged me on my work, to the late Professor Shu Kambara who organized our polymer research group and supported us in our work even after his retirement, and to Dr. Hyung Chick Pyun with whom I encountered the discovery of polyacetylene film by the fortuitous error. Dr. Takeo Ito was the first graduate student to work for me and who made a great contribution at the initial stage of this work. My special thanks are to Professors Shiro Maeda, Takehiko Shimanouchi, and Mitsuo Tasumi for helpful discussion on the vibration analyses study. I am indebted to Mr. Shigeru Ando for measurements of solid-state properties and to Professor Yoshio Sakai for electrical conductivity measurements. Throughout this period, our research was partly supported by Grant-in-Aids for Scientific Research from Ministry of Education, Culture and Science of Japan.

Received: January 22, 2001 [A 445]

[1] J. A. Pople, S. H. Walmsley, *Mol. Phys.* **1962**, *5*, 15.
[2] G. Natta, G. Mazzanti, P. Corradini, *Atti Accad. Naz. Lincei Cl. Sci. Fis. Mat. Nat. Rend.* **1958**, *25*, 3.
[3] R. Kuhn, *Angew. Chem.* **1937**, *50*, 703.
[4] J. H. C. Nayler, M. C. Whiting, *J. Chem. Soc.* **1965**, 3037.
[5] F. Bohlmann, H. Manhardt, *Chem. Ber.* **1956**, *89*, 1307.
[6] F. Sondheimer, D. A. Ben-Efraim, R. Wolovsky, *J. Am. Chem. Soc.* **1961**, *83*, 1675.
[7] Y. Takeuchi, A. Yasuhara, S. Akiyama, M. Nakagawa, *Bull. Chem. Soc. Jpn.* **1973**, *46*, 2822.
[8] K. Knoll, R. R. Schrock, *J. Am. Chem. Soc.* **1989**, *111*, 7989.
[9] N. S. Bayliss, *J. Chem. Phys.* **1948**, *16*, 287; N. S. Bayliss, *Quart. Rev.* **1952**, *6*, 319.
[10] H. Kuhn, *Helv. Chim. Acta* **1948**, *31*, 1441.
[11] Y. Ooshika, *J. Phys. Soc. Jpn.* **1957**, *12*, 1238; Y. Ooshika, *J. Phys. Soc. Jpn.* **1957**, *12*, 1246.
[12] H. C. Longuet-Higgins, L. Salem, *Proc. R. Soc. A* **1959**, 172.
[13] M. Tsuji, S. Fuzinaga, T. Hashino, *Rev. Mod. Phys.* **1960**, *32*, 425.
[14] C. S. Yannoni, T. C. Clarke, *Phys. Rev. Lett.* **1983**, *51*, 1191.
[15] L. B. Luttinger, J. *Org. Chem.* **1962**, *27*, 1591.
[16] W. E. Daniels, *J. Org. Chem.* **1964**, *29*, 2936.
[17] M. Hatano, S. Kambara, S. Okamoto, *J. Polym. Sci.* **1961**, *51*, 26.
[18] W. H. Watson, Jr., W. C. MeMordie, Jr., L. G. Lands, *J. Polym. Sci.* **1961**, *55*, 137.
[19] D. J. Berets, D. S. Smith, *Trans. Faraday Soc.* **1968**, 823.
[20] S. Ikeda, A. Tamaki, *J. Polym. Sci. Polym. Lett. Ed.* **1966**, *4*, *605*.
[21] K. Fukui, S. Inagaki, *J. Am. Chem. Soc.* **1975**, *96*, 4445.
[22] S. Ikeda, *Kogyo Kagaku Zasshi* **1967**, *70*, 1880.
[23] T. Ito, H. Shirakawa, S. Ikeda, *J. Polym. Sci. Polym. Chem. Ed.* **1974**, *12*, 11.
[24] H. Shirakawa, S. Ikeda, *Polym. J.* **1971**, *2*, 231.
[25] T. Ito, H. Shirakawa, S. Ikeda, *J. Polym. Sci. Polym. Chem. Ed.* **1975**, *13*, 1943.
[26] H. Shirakawa, T. Ito, S. Ikeda, *Makromol. Chem.* **1978**, *179*, 1565.
[27] I. Harada, Y. Furukawa, M. Tasumi, H. Shirakawa, S. Ikeda, *J. Chem. Phys.* **1980**, *73*, 4746.
[28] J. F. Rabolt, T. C. Clarke, G. B. Street, *J. Chem. Phys.* **1979**, *71*, 4614.
[29] C. R. Fincher, Jr., M. Ozaki, A. J. Heeger, A. G. MacDiarmid, *Phys. Rev. B* **1979**, *19*, 4140.
[30] W. P. Su, J. R. Sebrieffer, A. J. Heeger, *Phys. Rev. Lett.* **1979**, *42*, 1698.
[31] H. Shirakawa, F. J. Louis, A. G. MacDiarmid, C. K. Chiang, A. J. Heeger, *J. Chem. Soc. Chem. Commun.* **1977**, 578.
[32] C. K. Chiang, C. R. Fincher, Jr., Y. W. Park, A. J. Heeger, H. Shirakawa, B. J. Louis, S. C. Gau, A. G. MacDiarmid, *Phys. Rev. Lett.* **1977**, *39*, 1098.

"Synthetic Metals": A Novel Role for Organic Polymers (Nobel Lecture)**

Alan G. MacDiarmid*

Since the initial discovery in 1977, that polyacetylene $(CH)_x$, now commonly known as the prototype conducting polymer, could be p- or n-doped either chemically or electrochemically to the metallic state, the development of the field of conducting polymers has continued to accelerate at an unexpectedly rapid rate and a variety of other conducting polymers and their derivatives have been discovered. Other types of doping are also possible, such as "photo-doping" and "charge-injection doping" in which no counter dopant ion is involved. One exciting challenge is the development of low-cost disposable plastic/paper electronic devices. Conventional inorganic conductors, such as metals, and semiconductors, such as silicon, commonly require multiple etching and lithographic steps in fabricating them for use in electronic devices. The number of processing and etching steps involved limits the minimum price. On the other hand, conducting polymers combine many advantages of plastics, for example, flexibility and processing from solution, with the additional advantage of conductivity in the metallic or semiconducting regimes; however, the lack of simple methods to obtain inexpensive conductive polymer shapes/patterns limit many applications. Herein is described a novel, simple, and cheap method to prepare patterns of conducting polymers by a process which we term, "Line Patterning".

Keywords: conducting materials · liquid crystals · nano-electronics · Nobel lecture · polymers

Introduction

An organic polymer that possesses the electrical, electronic, magnetic, and optical properties of a metal while retaining the mechanical properties, processibility, etc. commonly associated with a conventional polymer, is termed an "intrinsically conducting polymer" (ICP) more commonly known as a "synthetic metal". Its properties are intrinsic to a "doped" form of the polymer. This class of polymer is completely different from "conducting polymers" which are merely a physical mixture of a nonconductive polymer with a conducting material such as a metal or carbon powder distributed throughout the material.

The Concept of Doping

Conjugated organic polymers are either electrical insulators or semiconductors. Those that can have their conductivity increased by several orders of magnitude from the semiconductor regime are generally referred to as "electronic polymers" and have become of very great scientific and technological importance since 1990 because of their use in light emitting diodes.[1] The emeraldine base form of polyaniline and *trans*-$(CH)_x$ are shown in Figure 1 to illustrate the increases in electrical conductivity of many orders of magni-

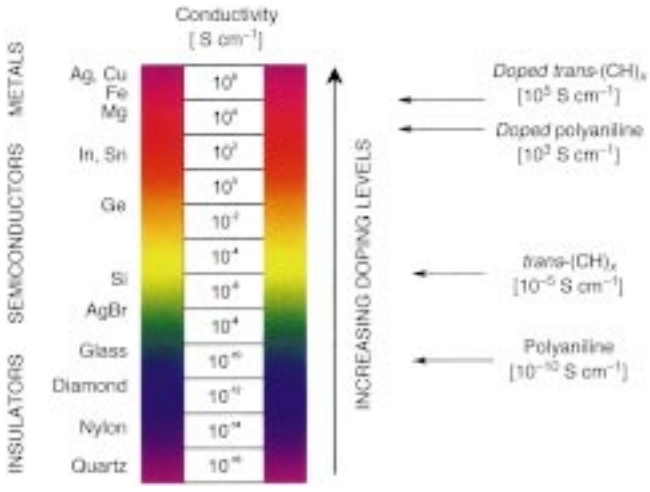

Figure 1. Conductivity of electronic polymers. Conductivity increases with increased doping.

[*] Prof. A. G. MacDiarmid
Department of Chemistry
University of Pennsylvania
Philadelphia, PA 19104-6323 (USA)
Fax: (+1) 215-898-8378
E-mail: macdiarm@sas.upenn.edu

tude which can be obtained by doping. The conductivity attainable by an electronic polymer has very recently been increased an infinite number of times by the discovery of superconductivity in regioregular poly(3-hexylthiophene).[2] Although this phenomenon was present only in a very thin layer of the polymer in a Field Effect (FET) configuration at a very low temperature (ca. 2 K) it represents an historical quantum leap—superconductivity in an organic polymer!

Prior to the discovery of the novel protonic acid doping of polyaniline, during which the number of electrons associated with the polymer chain remain unchanged,[3] the doping of all conducting polymers had previously been accomplished by redox doping. This involves the partial addition (reduction) or removal (oxidation) of electrons to or from the π system of the polymer backbone.[4–6]

The concept of doping is the unique, central, underlying, and unifying theme which distinguishes conducting polymers from all other types of polymers.[7] During the doping process, an organic polymer, either an insulator or semiconductor having a small conductivity, typically in the range 10^{-10} to $10^{-5}\,S\,cm^{-1}$, is converted into a polymer which is in the "metallic" conducting regime (ca. 1 to $10^{4}\,S\,cm^{-1}$). The controlled addition of known, usually small ($\leq 10\%$) non-stoichiometric quantities of chemical species results in *dramatic* changes in the electronic, electrical, magnetic, optical, and structural properties of the polymer. Doping is reversible to produce the original polymer with little or no degradation of the polymer backbone. Both doping and undoping processes, involving dopant counterions which stabilize the doped state, may be carried out chemically or electrochemically.[6] Transitory doping by methods which introduce no dopant ions are also known.[8]

By controllably adjusting the doping level, a conductivity anywhere between that of the non-doped (insulating or semiconducting) and that of the fully doped (highly conducting) form of the polymer can be easily obtained. Conducting blends of a (doped) conducting polymer with a conventional polymer (insulator), whose conductivity can be adjusted by varying the relative proportions of each polymer, can be made.[9] This permits the optimization of the best properties of each type of polymer.

Since the initial discovery in 1977, that polyacetylene $(CH)_x$, now commonly known as the prototype conducting polymer, could be p- or n-doped either chemically or electrochemically to the metallic state,[7, 10, 11] the development of the field of conducting polymers has continued to accelerate at an unexpectedly rapid rate and a variety of other conducting polymers and their derivatives have been discovered.[5, 6] This rapid growth rate has been stimulated by the field's fundamental synthetic novelty and importance to a cross-disciplinary section of investigators—chemists, electrochemists, biochemists, experimental and theoretical physicists, and electronic and electrical engineers—and to important technological emerging applications of these materials.

In the "doped" state, the backbone of a conducting polymer consists of a delocalized π system. In the undoped state, the polymer may have a conjugated backbone such as in *trans*-$(CH)_x$ which is retained in a modified form after doping, or it may have a nonconjugated backbone, as in polyaniline (leucoemeraldine base form), which becomes truly conjugated only after p-doping, or a nonconjugated structure as in the emeraldine base form of polyaniline which becomes conjugated only after protonic acid doping.

Redox Doping

All conducting polymers (and most of their derivatives), for example, poly-(*para*-phenylene) (**1**), poly(phenylenevinylene) (**2**), polypyrrole (**3**), polythiophene (**4**), polyfuran (**5**),

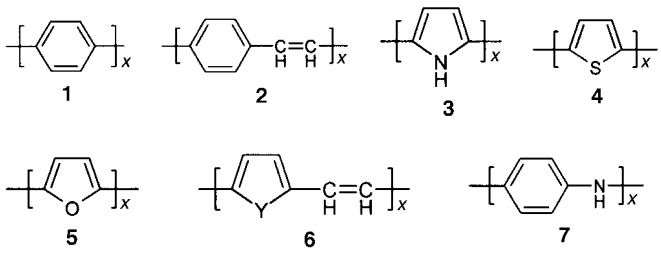

poly(heteroaromatic vinylenes) (**6**; where Y = NH, NR, S, O); polyaniline (**7**), etc., undergo either p- and/or n-redox doping

Alan MacDiarmid was born in New Zealand 74 years ago and after obtaining his higher education at the University of New Zealand (M.Sc. 1950), University of Wisconsin (Ph.D. 1953), and Cambridge University (Ph.D. 1955), he joined the faculty of the University of Pennsylvania in 1955, where he is currently Blanchard Professor of Chemistry. During the past 24 years he has been involved exclusively with conducting polymers, particularly the synthesis, chemistry, doping, electrochemistry, conductivity, magnetic and optical properties, and processing of polyacetylene and polyaniline. He is the author/co-author of approximately 600 research papers and 20 patents. He is the recipient of numerous awards and honorary degrees both nationally and internationally. In 1973, he began research on $(SN)_x$, an unusual polymeric material with metallic conductivity. His interest in organic conducting polymers began in 1975 when he was introduced to a new form of polyacetylene by Dr. Hideki Shirakawa at the Tokyo Institute of Technology. The ensuing collaboration between MacDiarmid, Shirakawa, and Alan Heeger (then at the Department of Physics at the University of Pennsylvania) led to the historic discovery of metallic conductivity in an organic polymer, and the award of the Nobel Prize for Chemisty, 2000.

by chemical and/or electrochemical processes during which the number of electrons associated with the polymer backbone changes.[5, 6] Selected examples of the different types of doping are presented below.

Chemical and Electrochemical p-Doping

p-Doping, that is, partial oxidation of the π backbone of an organic polymer, was first discovered by treating *trans*-$(CH)_x$ with an oxidizing agent such as iodine,[7] [Eq. (1)]

$$\textit{trans}\text{-}(CH)_x + 1.5xy\,I_2 \longrightarrow [CH^{+y}(I_3)_y^-]_x \ (y \le 0.07) \quad (1)$$

This process was accompanied by an increase in conductivity from ca. $10^{-5}\,S\,cm^{-1}$ to ca. $10^3\,S\,cm^{-1}$. If the polymer is stretch-oriented five- to six-fold before doping, conductivities parallel to the direction of stretching up to around $10^5\,S\,cm^{-1}$ can be obtained.[5, 6]

Approximately 85% of the positive charge is delocalized over 15 CH units (depicted in Scheme 1 for simplicity over only five units) to give a positive soliton.

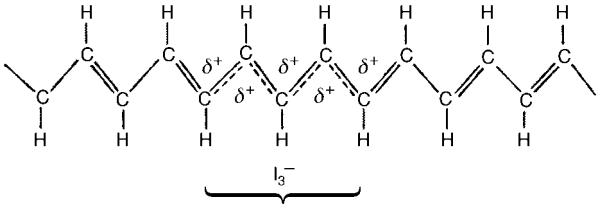

Scheme 1.

p-Doping can also be accomplished by electrochemical anodic oxidation by immersing a *trans*-$(CH)_x$ film in, for example, a solution of $LiClO_4$ dissolved in propylene carbonate and attaching it to the positive terminal of a DC (direct current) power source, the negative terminal being attached to an electrode also immersed in the solution,[10] [Eq. (2)].

$$\textit{trans}\text{-}(CH)_x + (xy)\,(ClO_4)^- \longrightarrow [(CH^{+y}(ClO_4)^{y-}]_x + (xy)e^- \ (y \le 0.1) \quad (2)$$

Chemical and Electrochemical n-Doping

n-Doping, that is, partial reduction of the backbone π system of an organic polymer, was also discovered using *trans*-$(CH)_x$ by treating it with a reducing agent such as liquid sodium amalgam or preferably sodium naphthaline[7] [Eq. (3) (Nphth = naphthaline)].

$$\textit{trans}\text{-}(CH)_x + (xy)Na^+(Nphth)^- \longrightarrow [Na_y^+(CH)^{-y}]_x + Nphth \ (y \le 0.1) \quad (3)$$

The antibonding π system is partially populated by this process which is accompanied by an increase in conductivity of about $10^3\,S\,cm^{-1}$.

n-Doping can also be carried out by electrochemical cathodic reduction[11] by immersing a *trans*-$(CH)_x$ film in, for example, a solution of LiClO, dissolved in tetrahydrofuran and attaching it to the negative terminal of a DC power source, the positive terminal being attached to an electrode also immersed in the solution [Eq. (4)].

$$\textit{trans}\text{-}(CH)_x + (xy)Li^+ + (xy)e^- \longrightarrow [Li_y^+(CH)^{-y}]_x \ (y \le 0.1) \quad (4)$$

In all chemical and electrochemical p- and n-doping processes discovered for $(CH)_x$ and for the analogous processes in other conducting polymers, counter "dopant" ions are introduced which stabilize the charge on the polymer backbone. In each case, spectroscopic signatures, for example, those of solitons, polarons, bipolarons, etc., are obtained characteristic of the given charged polymer. However, the doping phenomena concept extends considerably beyond that given above to "doping" processes where no counter dopant ion is involved, that is, to doping processes in which transitory "doped" species are produced, which have similar spectroscopic signatures to polymers containing dopant ions. This type of doping can provide information not obtainable by chemical or electrochemical doping. Examples of such types of redox doping which can be termed "photo-doping" and "charge-injection doping" are given below.

Doping Involving no Dopant Ions

Photo-Doping

When *trans*-$(CH)_x$ for example, is exposed to radiation of energy greater than its band gap, electrons are promoted across the gap and the polymer undergoes "photo-doping". Under appropriate experimental conditions, spectroscopic signatures characteristic of, for example, solitons can be observed[12] (Scheme 2). The positive and negative solitons

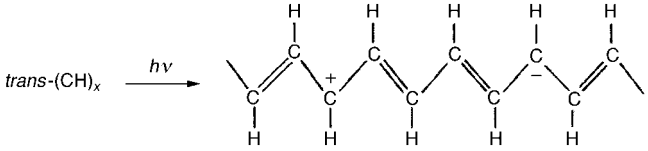

Scheme 2.

are here illustrated diagrammatically for simplicity as residing only on one CH unit; they are actually delocalized over ca. 15 CH units. They disappear rapidly because of the recombination of electrons and holes when irradiation is discontinued. If a potential is applied during irradiation, then the electrons and holes separate and photoconductivity is observed.

Charge-Injection Doping

Charge-injection doping is most conveniently carried out using a metal/insulator/semiconductor (MIS) configuration involving a metal and a conducting polymer separated by a thin layer of a high dielectric strength insulator. It was this approach, which resulted in the observance of superconductivity in a polythiophene derivative, as described previously. Application of an appropriate potential across the structure

can give rise, for example, to a surface charge layer, the "accumulation" layer which has been extensively investigated for conducting polymers.[8, 13] The resulting charges in the polymer, for example, $(CH)_x$ or poly(3-hexylthiophene), are present without any associated dopant ion. The spectroscopic properties of the charged species so formed can therefore be examined in the absence of dopant ion. Using this approach, spectroscopic studies of $(CH)_x$ show the signatures characteristic of solitons and the mid-gap absorption band observed in the chemically and electrochemically doped polymer. However, coulombic interaction between charge on the chain and dopant ion is a very strong interaction and one that can totally alter the energetics of the system.

Non-Redox Doping

This type of doping differs from redox doping described above in that the number of electrons associated with the polymer backbone does not change during the doping process. The energy levels are rearranged during doping. The emeraldine base form of polyaniline was the first example of the doping of an organic polymer to a highly conducting regime by a process of this type to produce an environmentally stable polysemiquinone radical cation. This was accomplished by treating emeraldine base with aqueous protonic acids (Scheme 3) and is accompanied by a nine to ten order of magnitude increase in conductivity (up to around 3 $S\,cm^{-1}$) to produce the protonated emeraldine base.[14–16] Protonic acid doping has subsequently been extended to systems such as poly(heteroaromatic vinylenes).[17]

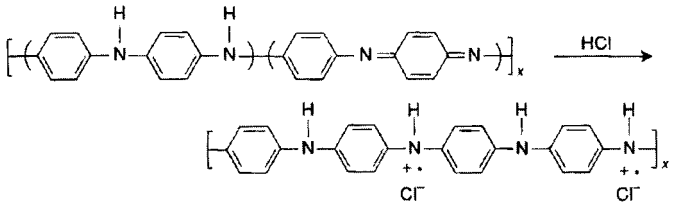

Scheme 3.

The Polyanilines

The polyanilines refer to a very important class of electronic/conducting polymers. They can be considered as being derived from a polymer, the base form of which has the generalized composition given in Scheme 4a, and which consists of alternating reduced, and oxidized, repeat units (Scheme 4a).[3, 14, 15] The *average* oxidation state can be varied continuously from $y = 1$ to give the completely reduced polymer, to $y = 0.5$ to give the "half-oxidized" polymer, to $y = 0$ to give the completely oxidized polymer (Scheme 4b–d). The terms "leucoemeraldine", "emeraldine", and "pernigraniline" refer to the different oxidation states of the polymer where $y = 1$, 0.5, and 0, respectively, either in the base form, for example, emeraldine base, or in the protonated salt form, for example, emeraldine hydrochloride.[3, 14, 15] In principle, the imine nitrogen atoms can be protonated in

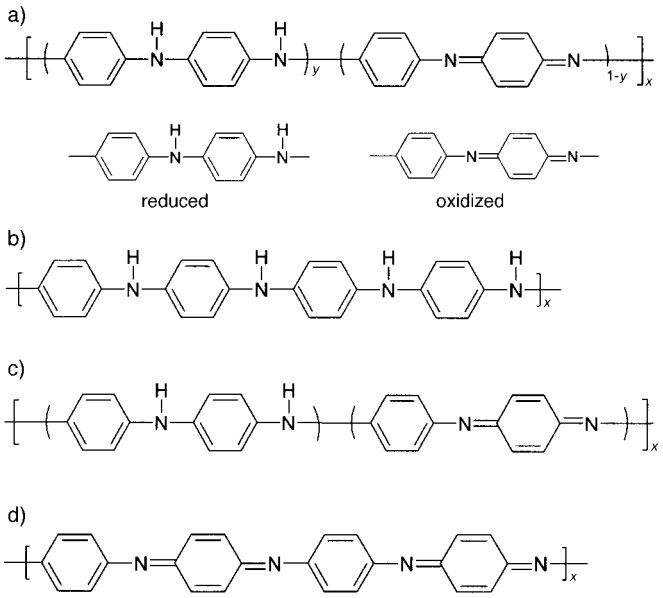

Scheme 4. a) Generalized composition of polyanilines indicating the reduced and oxidized repeat units, b) completely reduced polymer, c) half-oxidized polymer, d) fully oxidized polymer.

whole or in part to give the corresponding salts, the degree of protonation of the polymeric base depending on its oxidation state and on the pH of the aqueous acid. Complete protonation of the imine nitrogen atoms in emeraldine base by aqueous HCl, for example, results in the formation of a delocalized polysemiquinone radical cation[3, 15, 18] and is accompanied by an increase in conductivity of about 10^{10}.

The partly protonated emeraldine hydrochloride salt can be synthesized easily either by the chemical or electrochemical oxidative polymerization of aniline.[3, 14, 15] It can be deprotonated by aqueous ammonium hydroxide to give emeraldine base powder (a semiconductor).

Allowed Oxidation States

As can be seen from the generalized formula of polyaniline base (Scheme 4a), the polymer could, *in principle*, exist in a continuum of oxidation states ranging from the completely reduced material in the leucoemeraldine oxidation state, $y = 1$ to the completely oxidized material in the pernigraniline oxidation state, $y = 0$. However, we have shown[16] that at least in *N*-methyl-2-pyrrolidinone (NMP) solution in the range $y = 1$ to $y = 0.5$ (emeraldine oxidation state) only two chromophores are present, characteristic of $y = 1$, and $y = 0.5$ species and that all intermediate oxidation states consist, at the molecular level, only of *mixtures* of the chromophores characteristic of these two states.

Since most of the properties of polyaniline of interest are concerned with the solid state, we have carried out a series of studies in the solid state which show that the same phenomenon is true in the $y = 1$ to $y = 0.5$ oxidation-state range and in the $y = 0.5$ to $y = 0$ oxidation-state range. Within each of these ranges all intermediate oxidation states consist, at the

molecular level, only of mixtures of the chromophores characteristic of the two states defining the beginning and end of each range.[19, 20]

Doping

Polyaniline holds a special position amongst conducting polymers in that its most highly conducting doped form can be reached by two completely different processes—protonic acid doping and oxidative doping. Protonic acid doping of emeraldine base units with, for example 1M aqueous HCl results in complete protonation of the imime nitrogen atoms to give the fully protonated emeraldine hydrochloride salt.[14, 15]

As shown in Figure 2, protonation is accompanied by a 9 to 10 order of magnitude increase in conductivity reaching saturation in ca. 1M aqueous HCl.

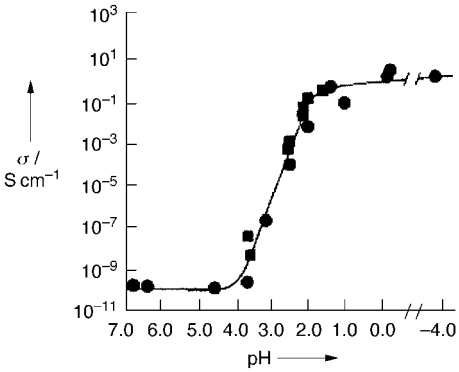

Figure 2. Conductivity of emeraldine base as a function of the pH of the HCl dopant solution as it undergoes protonic acid doping (● and ■ represent two independent series of experiments).[14, 15]

The same doped polymer can be obtained by chemical oxidation (p-doping) of leucoemeraldine base.[3] This actually involves the oxidation of the σ/π system rather than just the π system of the polymer as is usually the case in p-type doping. Its reaction with a solution of chlorine in carbon tetrachloride proceeds to give emeraldine hydrochloride (Scheme 5).

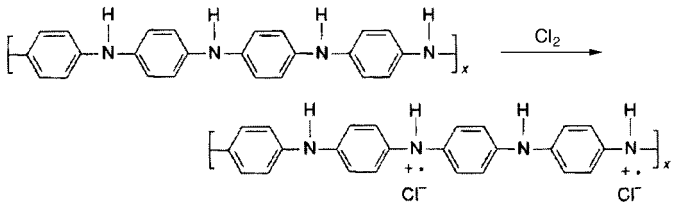

Scheme 5.

Nanoelectronics

The basic purpose of this research is to blend the now well-established field of electronic/conducting polymers with the new, emerging field of nanoscience, by electrostatic fabrication ("electrospinning") to produce "nanoelectronics"—electronic junctions and devices significantly smaller than the diameter of a human hair (ca. 50000 nm). It is commonly accepted that a nanomaterial is defined as one consisting of a substance or structure which exhibits at least one dimension of less than 100 nm (0.1 μm).[21]

Our objectives were: 1) to develop a method by which nanofibers (diameter < 100 nm) of organic polymers could be controllably and reproducibly fabricated such that in one given preparation, all fibers would have a diameter < 100 nm *and* 2) to reproducibly and controllably fabricate, for the first time, nanofibers of electronic polymers (in their semiconducting and metallic regimes) *and/or* their blends in conventional organic polymers for the purpose of ascertaining their applicability in the fabrication of nanoelectronic devices.

We have made substantial progress in achieving these objectives by using a relatively little known, simple, convenient, and inexpensive "electrospinning" method.[22–27] We have previously reported[23] fabrication of the first conducting polymer fibers (diameter ≈ 950 nm to 2100 nm) of polyaniline doped with *rac*-camphorsulfonic acid (PAn·HCSA) as a blend in poly(ethylene oxide) (PEO). We were surprised to find that an electronic polymer, such as polyaniline, which might have been expected to be more susceptible to degradation than most conventional organic polymers, survived, without observable chemical or physical change, following the 25000 V electrospinning fabrication process in air at room temperature.

Electrospinning

The electrospinning technique involves a simple, rapid, inexpensive, electrostatic, nonmechanical method in which a polymer solution in a variety of different possible common solvents, including water, is placed in a hypodermic syringe or in a glass pipette, at a fixed distance (5 – 30 cm) from a metal cathode.[24] The positive (anode) terminal of a variable high voltage transformer is attached to the metal tip of the hypodermic syringe or to a wire inserted into the polymer solution in the glass pipette, the negative terminal being attached to the metal cathode. The tip of the syringe can be placed vertically over the cathode or at any other convenient angle to it. When the voltage applied between the anode and cathode reaches a critical value, ca. 14000 V at a ca. 20 cm separation, the charge overcomes the surface tension of the deformed drop of the polymer solution on the tip of the syringe and a jet is produced. Since the polymer molecules all bear the same (positive) charge, they repel each other while traveling in air during a few milliseconds from the anode to cathode and become separated.[25] At the same time, evaporation of the solvent molecules occurs rapidly. Evaporation of solvent is also enhanced because the similarly charged (positive) solvent molecules repel each other. Under appropriate conditions, dry, meters-long fibers accumulate on the surface of the cathode resulting in a nonwoven mesh of nano- to micron-diameter fibers depending on experimental parameters (Figure 3).

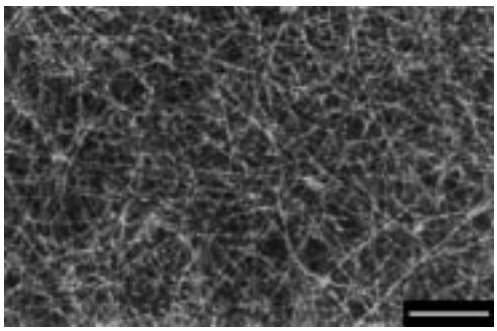

Figure 3. 50 wt % Nanofiber blend of PAn · HCSA fabricated from 2 wt % PAn · HCSA and 2 wt % PEO from chloroform solution at 25000 V (anode/cathode separation, 25 cm). Scale bar: 100000 nm.

Nanofiber Fabrication

Since the submicron fibers (500 – 1600 nm) obtained in our initial work[23] were not classifiable as true "nanofibers", our immediate objective was to break the "nanotechnology barrier" and to consistently and reproducibly fabricate true nanofibers (diameter < 100 nm) of an organic polymer. This was accomplished (see Figure 4) using an 8 wt % solution of

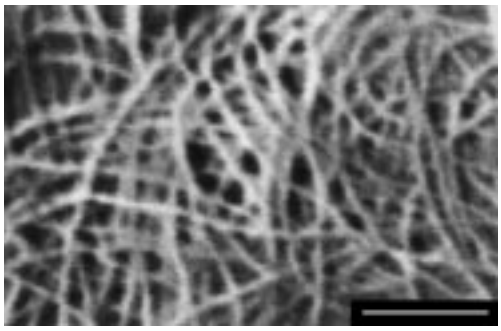

Figure 4. Electrospun fibers of polystyrene (see text). Scale bar: 1000 nm. The extended length of the fibers is clearly visible.

polystyrene (M_w 212400) in tetrahydrofuran at a potential of 20000 V between the anode and cathode which were separated by 30 cm. The fibers were collected as a mat on an aluminum target and were found to have diameter characteristics: average: 43.1 nm, maximum: 55.0 nm, minimum: 26.9 nm. Other studies involving polystyrene gave fibers whose diameters were consistently < 100 nm; average: 30.5 nm (maximum: 44.8 nm, minimum: 16.0 nm). It might also be noted that the 16 nm fiber is only around 30 polystyrene molecules wide. It is also of interest to note that a 16 nm fiber, such as the one mentioned above, lies well within the ca. 4 – 30 nm diameter range of multiwalled carbon nanotubes.[26]

Electronic Polymer Fibers

By using a previously applied method for producing polyaniline fibers[27] we have prepared highly conducting sulfuric acid doped polyaniline fibers (diameters, average: 139 nm, maximum: 275 nm, minimum: 96 nm) by placing a ca. 20 wt % solution of polyaniline in 98 % sulfuric acid in a glass pipette with the tip ca. 3 cm above the surface of a copper cathode immersed in pure water at 5000 V potential difference. The fibers collect in or on the surface of the water. The conductivity of a single fiber was ca. 0.1 $S\,cm^{-1}$, as expected since partial fiber de-doping occurred in the water cathode. The diameter and length of the fibers appear (Figure 5) to be sensitive to the nature of the polyaniline used. No great difficulty is foreseen in producing fibers < 100 nm diameter.

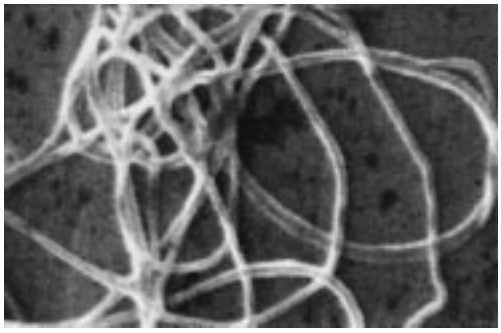

Figure 5. 100 % polyaniline fiber with an average diameter of 139 nm.

It is relatively easy to prepare conducting blends of PAn.HCSA in a variety of different conventional polymers such as polyethylene oxide, polystyrene, polyacrylonitrile, etc. For example, ca. 20 wt % blends of PAn · HCSA in polystyrene (M_w 114200) are obtained by electrospinning a chloroform solution; fiber diameter characteristics: average: 85.8 nm, maximum: 100.0 nm, minimum: 72.0 nm. These fibers are sufficiently electrically conductive that their scanning electron micrographs (SEMs) may be recorded without the necessity of applying a gold coating.

Separate, individual nanofibers can be collected and examined if so desired. An appropriate substrate—glass slide, silicon wafer, or loop of copper wire, etc.—is held between the anode and cathode at a position close to the cathode for a few seconds to collect individual fibers (see Figure 6).

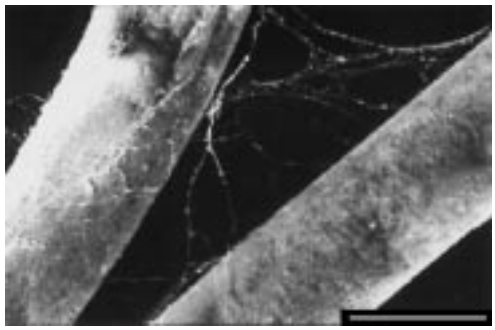

Figure 6. Polystyrene fibers collected on a bent copper wire (magnification 33 ×) and subsequently coated with a thin layer of polypyrrole by in situ deposition from aqueous solution. Scale bar: 1 mm.

Current/voltage (I/V) curves are given in Figure 7 for a single 419 nm diameter fiber (Fiber 1) and for a ca. 600 nm diameter fiber (Fiber 2) of a blend of 50 wt % PAn · HCSA and poly(ethylene oxide) collected on a silicon wafer coated with a thin layer of SiO_2. Two gold electrodes separated by 60.3 μm are deposited on the fiber after its deposition on the substrate.

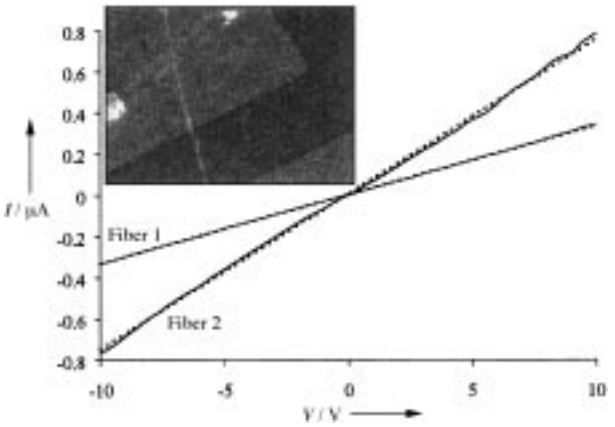

Figure 7. Current/voltage curves of 50 wt % PAn·HCSA/PEO blend nanofiber (see text).

Nanofibers as Substrates

The large surface to volume ratio offered by nanofibers makes them excellent, potentially useful substrates for the fabrication of coaxial nanofibers consisting of superimposed layers of different materials. Catalysts and electronically active materials can be deposited on them by chemical, electrochemical, solvent, chemical vapor, or other means, for use in nanoelectronic junctions and devices.

We have found, for example, that polyacrylonitrile nanofibers can be easily and evenly coated with a 20–25 nm layer of conducting polypyrrole (Figure 8) by immersion in an aqueous solution of polymerizing polypyrrole.[28] Analogously, we have found that electroless deposition of metals can also be performed. Polyacrylonitrile fibers, for example, can be evenly coated with gold by electroless deposition.[29]

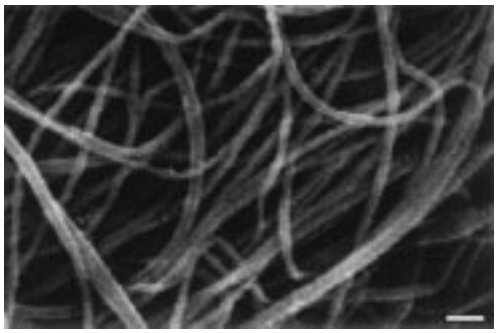

Figure 8. Scanning electron micrograph of conducting polypyrrole-coated polyacrylonitrile nanofibers. Scale bar: 1000 nm.

Carbon Nanofibers

As reported polyacrylonitrile fibers may be thermally converted into carbon nanofibers with some shrinkage.[30] We have similarly converted polyacrylonitrile nanofibers into carbon nanofibers.

In summary, electronic polymers have been used for the past 20 years to produce rectifying diodes by Schottky and p/n junctions, transistors, light-emitting devices, photovoltaic cells, rechargeable batteries, etc.[1] Now, the ability to fabricate nanofibers of electronic polymers which are only a few molecules thick suggests the emergence of a field of nanoelectronics whereby the electronic properties of such nanofibers can be exploited for technological purposes.

Line Patterning of Conducting Polymers[30]

One of the exciting challenges of the first part of this century will be the development of low-cost disposable plastic/paper electronic devices.[31–33] Conventional inorganic conductors, such as metals, and semiconductors, such as silicon, commonly require multiple etching and lithographic steps in fabricating them for use in electronic devices. The number of processing steps and chemical etching steps involved limit the minimum price and therefore their applicability in disposable electronics. On the other hand, conducting polymers combine many advantages of plastics, for example, flexibility and processing from solution, with the additional advantage of conductivity either in the metallic or semiconducting regimes; however, the lack of simple methods to obtain inexpensive conductive polymer shapes/patterns limit many applications. We here describe a novel, simple, and cheap method to prepare patterns of conducting polymers by a process which we term, "Line Patterning".

Line Patterning uses the difference in selected physical and/or chemical properties between a substrate and insulating lines which have been printed on it by a conventional copying or printing process towards a fluid (or vapor) to which they are both simultaneously exposed. The substrate and printed lines react differently or at different rates with the fluid (or vapor) to which they have been exposed. This results in a nonuniform deposition on the substrate as compared to the printed lines. If the fluid contains a conducting polymer, which remains as a film after evaporation of the solvent, a pattern of conducting polymer results. A pattern is first designed on a computer and is then printed on, for example, an overhead transparency using a standard, non-modified office laser printer.

The printed (insulating) lines can be easily removed, if necessary, in a few seconds by ultrasonic treatment in toluene, dissolving the printed lines and leaving a clean pattern of deposited material on the substrate whose shape was originally defined by the now nonexistent printed lines. Line Patterning has the following advantages: no photolithography is involved; no printing of conducting polymer is involved; it uses only, for example, a standard office laser printer, which is not modified in any way; commercially available flexible, transparent plastic or paper substrates can be used; solutions of commercially available conducting or nonconducting polymers can be used from which the polymers may be deposited on substrates, it is inexpensive; rapid development of customized patterns (within hours) from a computer designed pattern to product is routine.

We have exploited, for example, the observation that a commercial dispersion of poly-3,4-ethylenedioxythiophene (PEDOT, "Baytron P", Bayer Corp.) wets commercial plastic overhead transparency, but not the lines printed on it by a standard office laser printer. A coating of PEDOT can be

applied by a roller and after evaporation of the solvent; the printed lines can be easily and cleanly removed by sonication, leaving only the conducting polymer on the transparency.

Two electrodes were prepared in this way, each containing 25 lines inch^{-1}. A drop of a standard commercial polymer dispersed liquid crystal (PDLC) display[34] mixture containing an optical adhesive and 15 μm spacer spheres was placed on the center of each electrode. The second electrode was placed on top at an angle of 90° to the first. This resulted in a (25 × 25), that is, 625 pixels (square-inch matrix)$^{-1}$ (Figure 9). Exposure to UV light for a few minutes resulted in polymerization of the mixture to bind the two electrodes together and to produce a free-standing working PDLC display device. When an electrode pattern of 100 lines inch^{-1} was used a working 10000 pixel square-inch^{-1} display was produced.

Figure 9. Fabrication of a 625 pixel PDLC display (see text).

We have devised a novel way of separating conducting polymer circuits from each other by making use of the height (ca. 4–5 μm) of the printed toner lines, made by using a standard office printer, above the substrate, for example, on an overhead transparency. This is illustrated (Figures 10 and 11) by a "push button" switch to open and close a simple electrical circuit. A combination of two patterned transparencies where the two adjacent conductive areas are electrically separated from each other by two ca. 4–5 μm nonconductive printed toner lines is obtained by placing the printed lines on top of each other as shown in Figures 11 and 12. Depression of the areas labeled "PRESS" causes the upper transparency to bend. This electrically connects the conducting PEDOT surfaces. When released, the transparency film returns back to its original position, thus breaking the electrical circuit.

The two-dimensional conducting polymer circuits may be readily converted into three-dimensional circuits by two different methods as shown in Figure 12 simply by 1) stapling two two-dimensional circuits together using a common office stapler. The metal staple joins together electrically the conducting polymer areas on two different substrates *or* 2) making a pinhole through the sheets, as shown, before applying the PEDOT solution. Some of the solution enters the pinhole and joins together electrically the conducting surfaces on the two different circuits.

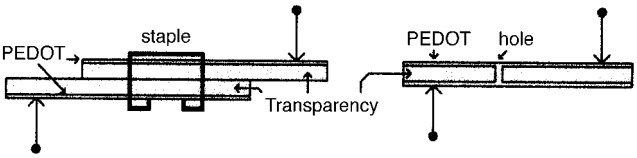

Figure 12. Three-dimensional connections; a) connected with staple, b) connected by a coated hole; ● = connection to power supply.

We have recently observed a curious field effect which thin films of PEDOT exhibit when exposed to a positive gate potential in an FET configuration as shown in Figure 13. A source/drain electrode and a gate electrode are prepared by Line Patterning and are covered by a thin layer of PEDOT as described above. A drop of the optical adhesive containing spacer spheres described above is placed on the source/drain

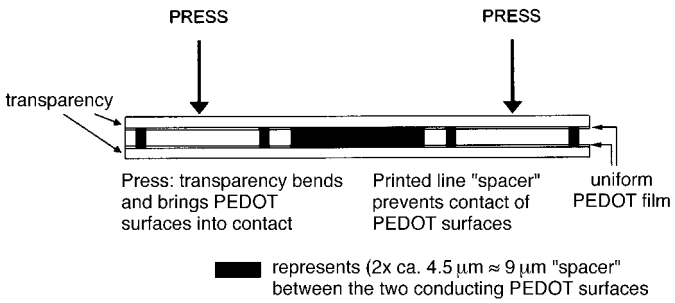

Figure 10. A simple electronic circuit ("push button" switch).

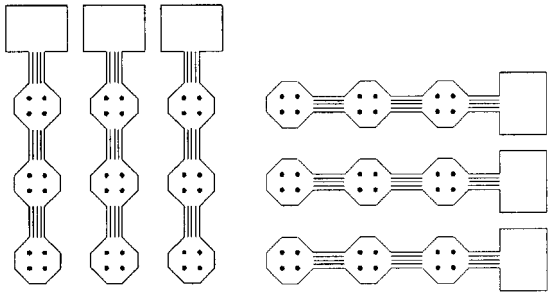

Figure 11. "Push button" switch.

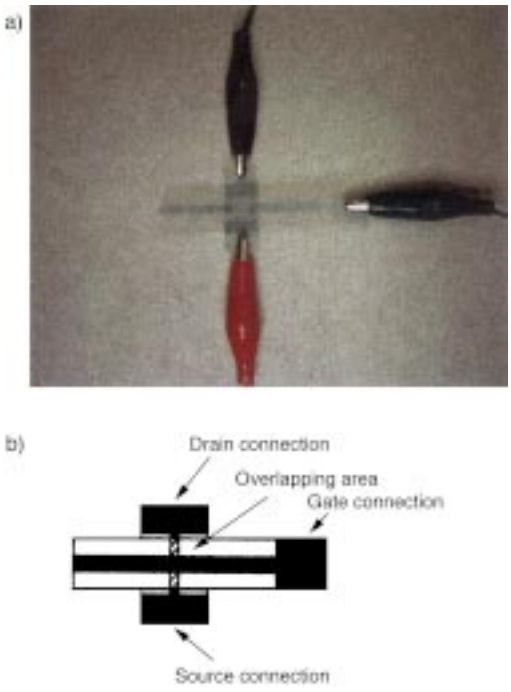

Figure 13. Field-effect doped "PEDOT". a) FET-type device, b) field-effect configuration.

electrode upon which the gate electrode is then placed at 90°. The two electrodes are manually squeezed together and the optical adhesive is polymerized by exposure to UV light as was done for the PDLC display described above. Several thousand of these interconnected transistor-type devices could be readily fabricated per square inch by the Line Patterning process, if it were considered desirable. The free-standing, flexible device shown in Figures 13 and 14 is produced.

Figure 14. FET-type device.

The device exhibits the same general reversible features commonly associated with a field effect transistor (FET) as shown in Figure 15. The doped "metallic" PEDOT film ($\sigma \approx 2\ S\,cm^{-1}$ at room temperature) would not be expected to show a change in conductivity by exposure to a field of this type

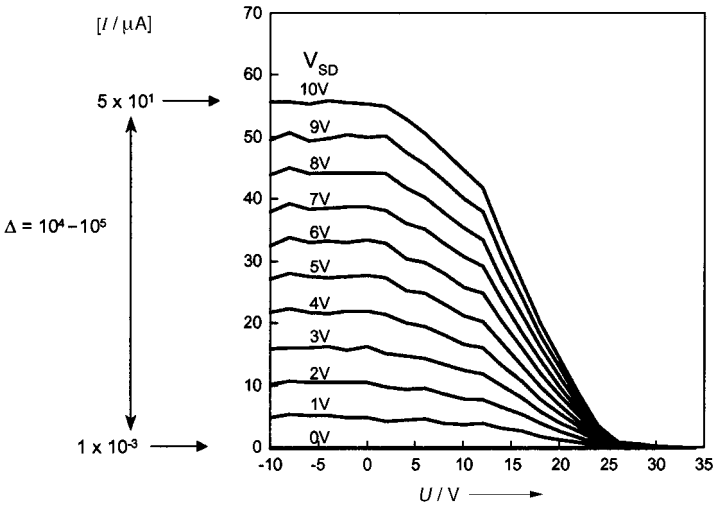

Figure 15. Field effect transistor characteristics. I = source – drain current; U = gate voltage.

under the configuration used. We believe this effect presents an entirely new method for ascertaining the nature of highly doped "metallic" conducting polymers. It has frequently been postulated that a doped conducting polymer consists of metallic "islands" surrounded by lowly conducting "beaches" as shown in Figure 16. We postulate that in the effect we have observed only the lowly conducting "beaches" and not the metallic "islands" respond to the applied field. The application of an electric field changes the conductivity of the

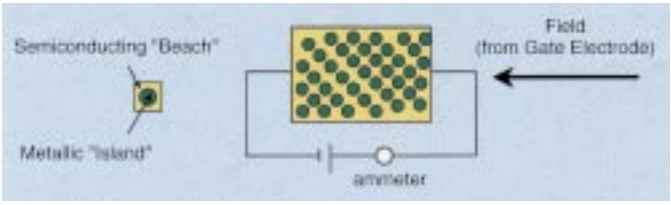

Figure 16. Percolation field effect in doped conducting polymers. Metallic "islands" separated by "beaches" of non- or lowly conducting (semiconducting) polymer. The field changes the conductivity of the semiconducting "beaches" but not that of the metallic "islands"—hence the field changes the extent of electrical percolation between the metallic "islands"—and therefore changes the bulk conductivity of the material.

"beaches" and hence the extent of electrical percolation in the source/drain PEDOT electrode between the metallic "islands", hence changing the bulk conductivity of the material. The response time for our device is much slower than for a conventional field effect transistor. We therefore conjecture that the chief changes in conductivity are probably caused by slow diffusion of the dopant anions under influence of the applied field. On removal of the field the system reverts to its original state.

Preliminary studies show that the effect is also present in polyaniline; it may therefore possibly be found in many other conducting polymers and would thus represent a general phenomenon characteristic of all conducting polymers, at least within certain ranges of doping.

Summary

- Polyacetylene, $(CH)_x$, the simplest organic polymer, can be reversibly doped to the metallic regime by partial oxidation or reduction either chemically or electrochemically.
- Polyaniline can be doped to the metallic regime by a simple acid/base protonation.
- A large number of electronic conductive polymers are now known.
- A variety of technological applications of electronic conductive polymers, present and projected, are apparent.

This Nobel Prize has world-wide implications since it shows the ever-increasing importance of interdisciplinary research—in this case collaborative research between a polymer chemist, Hideki Shirakawa,[35] Alan Heeger,[36] a physicist, and myself, an organometallic chemist. Each of us had the task of learning the specialized scientific language of the other in order to collectively focus on one specific scientific challenge, an example of where 1 + 1 + 1 is more than 3!

The prize is also recognition of the good fortune that Alan, Hideki, and I had in having each other as such excellent colleagues and also in having such creative colleagues in each of our respective individual research groups—the work stemming from a research group cannot be better than the persons carrying it out. The prize is a recognition of them and their work and also the work of countless others world-wide during the past 23 years who put the "flesh on the skeleton work" carried out by us in the 1970's at Penn (University of

Pennsylvania). If it were not for them there would be no prize today in the field.

Research in an experimental science (and also in many other fields) cannot be accomplished without financial support for stipends, apparatus, supplies and the like. A funding organization and project officers within such an organization have tremendous control over the future of science and technology in any given country. In this respect Dr. Kenneth J. Wynne, my contracting officer at the US Office of Naval Research for many years, before his recent retirement, had the scientific intuition and foresight to fund our first work on conducting polymers—the first funding of work of this type anywhere in the world. He funded it because of its scientific interest. The fact that it now has great technological potential was not a consideration at that time.

"Of what use is a beautiful poem"? It gives intellectual stimulation and enjoyment. Similarly with research. If it has some practical use, that is merely "icing on the cake!"

Early studies: Polyacetylene, $(CH)_x$: Alan J. Heeger[36] (formerly, Physics Department, University of Pennsylvania), Hideki Shirakawa[35] (Tsukuba University), and many undergraduate, graduate students, and post doctoral fellows. Financial support: Principally, US Office of Naval Research (Dr. K. J. Wynne, Program Manager); University of Pennsylvania Materials Science Laboratory.

Polyaniline: Arthur J. Epstein (Physics Dept., Ohio State University) and many undergraduate, graduate students, and post doctoral fellows. Financial support: Principally, US Office of Naval Research (Dr. K. J. Wynne, Program Manager); University of Pennsylvania Materials Science Laboratory.

Recent Studies: Nanofibers ("Electrospinning"): I. D. Norris, J. Gao, F. K. Ko, W. E. Jones, Jr., A. T. Johnson, Jr. Financial support: US Office of Naval Research (Dr. K. J. Wynne, Program Manager); Army Research Office—MURI.

Line Patterning: D. Hohnholz, H. Okuzaki. Financial support: Subcontract, Kent Displays, Inc. (ONR-SBIR Program); US Office of Naval Research (Dr. K. J. Wynne, Program Manager); Fellowship from Ministry of Education, Science, Culture and Sports, Japan.

Received: May 2, 2001 [A 470]

[1] *Handbook of Organic Conductive Materials and Polymers* (Ed.: H. S. Nalwa), Wiley, New York, **1997**; *Handbook of Conducting Polymers* (Eds.: T. A. Skotheim, R. L. Elsenbaumer, J. F. Reynolds), 2nd ed., Marcel Dekker, New York, **1998**.

[2] J. H. Schon, A. Dodabalapur, Z. Bao, C. Kloc, O. Schenker, B. Batlogg, *Nature* **2001**, *410*, 189.

[3] A. G. MacDiarmid, A. J. Epstein, *Faraday Discuss. Chem. Soc.* **1989**, *88*, 317, and refs therein.

[4] A. G. MacDiarmid, A. J. Heeger, *Synth. Met.* **1979/80**, *1*, 101, and refs therein.

[5] *Handbook of Conducting Polymers*, *Vol 1&2* (Ed.: T. A. Skotheim), Marcel Dekker, New York, **1986**.

[6] M. G. Kanatzidis, *Chem. Eng. News* **1990**, *68*(49), 36.

[7] C. K. Chiang, C. R. Fincher, Jr., Y. W. Park, A. J. Heeger, H. Shirakawa, E. J. Louis, A. G. MacDiarmid, *Phys. Rev. Lett.* **1977**, *39*, 1098; C. K. Chiang, M. A. Druy, S. C. Gau, A. J. Heeger, E. J. Louis, A. G. MacDiarmid, *J. Am. Chem. Soc.* **1978**, *100*, 1013.

[8] K. E. Ziemelis, A. T. Hussain, D. D. C. Bradley, R. H. Friend, J. Rilhe, G. Wegner, *Phys. Rev. Lett.* **1991**, *66*, 2231.

[9] V. G. Kulkarni, W. R. Mathew, J. C. Campbell, C. J. Dinkins, P. J. Durbin, *49th ANTEC Conference Proceedings* (Montreal, Canada 5–9 May), Society of Plastic Engineers and Plastic Engineering, **1991**, p. 663; L. W. Shacklette, N. F. Colaneri, V. G. Kulkarni, B. Wessling, in *49th ANTEC Conference Proceedings* (Montreal, Canada, 5–9 May), Society of Plastic Engineers and Plastic Engineering, **1991**, p. 665.

[10] P. J. Nigrey, A. G. MacDiarmid, A. J. Heeger, *J. Chem. Soc. Chem. Commun.* **1979**, 594.

[11] D. MacInnes, Jr., M. A. Druy, P. J. Nigrey, D. P. Nairns, A. G. MacDiarmid, A. J. Heeger, *J. Chem. Soc. Chem. Commun.* **1981**, 317.

[12] A. J. Heeger, S. Kivelson, J. R. Schrieffer, W.-P. Su, *Rev. Mod. Phys.* **1988**, *60*, 781, and refs therein.

[13] J. H. Burroughes, C. A. Jones, R. H. Friend, *Nature* **1988**, *335*, 137; J. H. Burroughes, D. D. C. Bradley, A. R. Brown, R. N. Marks, K. Mackay, R. H. Friend, P. L. Burns, A. B. Holmes, *Nature* **1990**, *347*, 539.

[14] J. C. Chiang, A. G. MacDiarmid, *Synth. Met.* **1986**, *13*, 193.

[15] A. G. MacDiarmid, J.-C. Chiang, A. F. Richter, A. J. Epstein, *Synth. Met.* **1987**, *18*, 285.

[16] A. G. MacDiarmid, A. J. Epstein, *Faraday Discuss. Chem. Soc.* **1989**, *88*, 317, and refs therein; A. G. MacDiarmid, A. J. Epstein in *Science and Applications* of *Conducting Polymers* (Eds.: W. R. Salaneck, D. T. Clark, E. J. Samuelsen), Adam Hilger, Bristol, **1990**, p. 117.

[17] C. C. Han, R. L. Elsenbaumer, *Synth. Met.* **1989**, *30*, 123.

[18] A. G. MacDiarmid, J.-C. Chiang, A. F. Richter, N. L. D. Somasiri, A. J. Epstein in *Conducting Polymers* (Ed.: L. Alcacér), Reidel, Dordrecht, **1987**, p. 105.

[19] F. L. Lu, F. Wudl, M. Nowak, A. J. Heeger, *J. Am. Chem. Soc.* **1986**, *108*, 8311.

[20] Y. Sun, A. G. MacDiarmid, A. J. Epstein, *J. Chem. Soc. Chem. Commun.* **1990**, 529.

[21] "Nanotechnology: A Revolution in the Making—Vision for R&D in the Next Decade": Report of the Interagency Working Group on Nanoscience, Engineering, and Technology, March 10, **1999**.

[22] A. Formhals, US-A 1 975 504, **1934**.

[23] I. D. Norris, M. M. Shaker, F. K. Ko, A. G. MacDiarmid, *Synth. Met.* **2000**, *114*, 109; A. G. MacDiarmid, W. E. Jones, Jr., I. D. Norris, J. Gao, A. T. Johnson, Jr., N. J. Pinto, J. Hone, B. Han, F. K. Ko, H. Okuzaki, M. Llagune, *Synth. Met.* **2001**, *119*, 27.

[24] J. Doshi, D. H. Reneker, *J. Electrost.* **1995**, *35*, 151; P. W. Gibson, H. L. Schreuder-Gibson, D. Riven, *AIChE J.* **1999**, *45*, 190.

[25] D. H. Reneker, A. L. Yarin, H. Fong, S. Koombhongse, *J. Appl. Phys.* **2000**, *87*, 4531.

[26] S. Iijima, *Nature* **1991**, *354*, 56.

[27] D. H. Reneker, I. Chun, *Nanotechnology* **1996**, *7*, 216.

[28] Z. Huang, P.-C. Wang, A. G. MacDiarmid, Y. Xia, G. M. Whitesides, *Langmuir* **1997**, *13*, 6480; R. V. Gregory, W. C. Kimbrell, H. H. Kuhn, *Synth. Met.* **1989**, *28*, C823.

[29] A. M. Sullivan, P. A. Kohl, *J. Electrochem. Soc.* **1995**, *142*, 2250.

[30] I. Chun, D. H. Reneker, H. Fong, X. Fang, J. Deitzel, N. B. Tan, K. Kearns, *J. Adv. Mater.* **1999**, *31*, 36; D. Hohnholz, A. G. MacDiarmid, *Synth. Met.* **2001**, *121*, 1327.

[31] A. Dodabalapur, Z. Bao, A. Makhija, J. G. Laquindanum, V. R. Raju, Y. Feng, H. E. Katz, J. Rogers, *Appl. Phys. Lett.* **1998**, *73*, 142, and refs therein.

[32] C. J. Drury, C. M. J. Mutsaers, C. M. Hart, M. Matters, D. M. de Leeuw, *Appl. Phys. Lett.* **1998**, *73*, 108, and refs therein.

[33] H. Okusaki, Y. Osada, *J. Intell. Mater. Syst. Struct.* **1993**, *4*, 50.

[34] "Licristal E7" (Merck Corp., Germany), "NOA-65 Optical Adhesive" (Norland Products, NH).

[35] H. Shirakawa, *Angew. Chem.* **2001**, *113*, 2642; *Angew. Chem. Int. Ed.* **2001**, *40*, 2574.

[36] A. J. Heeger, *Angew. Chem.* **2001**, *113*, 2660; *Angew. Chem. Int. Ed.* **2001**, *40*, 2591.

Semiconducting and Metallic Polymers: The Fourth Generation of Polymeric Materials (Nobel Lecture)**

Alan J. Heeger*

When asked to explain the importance of the discovery of conducting polymers, I offer two basic answers: first they did not (could not?) exist, and second, that they offer a unique combination of properties not available from any other known materials. The first expresses an intellectual challenge; the second expresses a promise for utility in a wide variety of applications.

Keywords: conducting materials · doping · Nobel lecture · polyacetylene · solid-state physics

1. Introduction

In 1976, Alan MacDiarmid, Hideki Shirakawa, and I, together with a talented group of graduate students and postdoctoral researchers discovered conducting polymers and the ability to dope these polymers over the full range from insulator to metal.[1, 2] This was particularly exciting because it created a new field of research on the boundary between chemistry and condensed-matter physics, and because it created a number of opportunities:

- Conducting polymers opened the way to progress in understanding the fundamental chemistry and physics of π-bonded macromolecules
- Conducting polymers provided an opportunity to address questions that had been of fundamental interest to quantum chemistry for decades:
  Is there bond alternation in long-chain polyenes?
  What is the relative importance of the electron–electron and the electron–lattice interactions in π-bonded macromolecules?
- Conducting polymers provided an opportunity to address fundamental issues of importance to condensed-matter physics as well, including, for example, the metal–insulator transition as envisioned by Neville Mott and Philip Anderson and the instability of one-dimensional metals discovered by Rudolph Peierls (the "Peierls Instability")
- Finally—and perhaps most important—conducting polymers offered the promise of achieving a new generation of polymers: materials which exhibit the electrical and optical properties of metals or semiconductors *and* which retain the attractive mechanical properties and processing advantages of polymers.

Conducting polymers are the most recent generation of polymers.[3] Polymeric materials in the form of wood, bone, skin, and fibers have been used by man since prehistoric time. Although organic chemistry as a science dates back to the eighteenth century, polymer science on a molecular basis is a development of the twentieth century. Hermann Staudinger developed the concept of macromolecules during the 1920s. Staudinger's proposal was openly opposed by leading scientists, but the data eventually confirmed the existence of macromolecules. Staudinger was awarded the Nobel Prize in Chemistry in 1953 "for his discoveries in the field of macromolecular chemistry". While carrying out basic research on polymerization reactions at the DuPont company, Wallace Carothers invented nylon in 1935. Carothers research showed the great industrial potential of synthetic polymers; a potential which became reality in a remarkably short time. Today, synthetic polymers are used in larger quantities than any other class of materials (larger by volume and larger by weight, even though such polymers have densities close to unity). Polymer synthesis in the 1950s was dominated by Karl Ziegler and Giulio Natta whose discoveries of polymerization catalysts were of great importance for the development of the modern "plastics" industry. Ziegler and Natta were awarded the Nobel Prize in Chemistry in 1963 "for their discoveries in the field of the chemistry and technology of high polymers". Paul Flory was the next "giant" of polymer chemistry; he created modern polymer science through his experimental and theoretical studies of macromolecules.

[*] A. J. Heeger
Department of Physics, Materials Department
Institute for Polymers and Organic Solids
University of California, Santa Barbara
Santa Barbara, CA, 93106 (USA)
Fax: (+1) 805-893-4755
E-mail: AHeeger@Uniax.com

Biography, Reminiscence, and Thanks

Alan J. Heeger: I was born on a bitter cold morning (−20°F below zero) in Sioux City (Iowa) on January 22, 1936. I was told that when my father went out in the cold that morning to go to the hospital to visit his wife and newborn first son, his car would not start. Despite advice to the contrary, he walked to the hospital; his ears were frostbitten on the way.

The Heeger family came to Sioux City (Iowa) from Russia as Jewish immigrants in 1904 when my father was a small boy (age four). My mother was born in Omaha (Nebraska); she was a first generation child of Jewish immigrants. My mother and father were married in the midst of the Great Depression. My early years were spent in Akron (Iowa), a small midwestern town of 1000 people, approximately 35 miles from Sioux City. I went to elementary school in Akron and my brother, Gerald, was born in Akron. My father died when I was nine years old, it was his 45th birthday. After my father's death, we moved to Omaha, so my mother could be closer to her family. She raised us as a single parent in a house that we shared with her sister and her sister's children.

One of my earliest memories, is of my mother telling me of the importance of obtaining a university education. When she graduated from high school, she received a scholarship to go on to university but went to work instead; she was needed by her parents to help support the family. It was always clear to me that it was my responsibility to go to university; prior to my generation no one on either side of my family had an education that went beyond high school. I and my brother were the first in our family to receive the PhD degree.

My high school years were fun and frustrating, typical of the teen years. The most important accomplishment was meeting my wife, Ruth. I have loved her for nearly fifty years, and she remains my best friend.

I was always a good student, but I do not remember science being especially easy. On the contrary, I recall that in high school, physics was somewhat mysterious. I was impatient to get on with my education, to get on with "more important" things, and therefore completed high school one year early.

My undergraduate years at the University of Nebraska were a special time in my life; the combination of partying and intellectual awakening that is what the undergraduate years are supposed to be. I went to the University with the goal of becoming an engineer; I had no concept that one could pursue science as a career. After one semester, I was convinced that engineering was not for me, and I completed my undergraduate studies with a dual major in Physics and Mathematics. The highlight was a course (in my senior year) in Modern Physics taught by Theodore Jorgensen. Professor Jorgensen introduced me to quantum physics and twentieth century science. I was honored by the University of Nebraska in 1998 with a Doctor of Science (h.c.) and had the pleasure of giving a Physics colloquium at that time. Ted Jorgensen came to the lecture; he was 92 and working hard on revising his book on the Physics of Golf.

Again, I was impatient to get on with "real physics". I started the path toward my PhD in Physics at University of California, Berkeley while working part time for Lockheed Space and Missle Division in Palo Alto, CA. When I started at Berkeley, my goal was to do a theoretical thesis under Charles Kittel. Thus, when the decision was made to go for my degree on a full-time basis, I went first to Kittel and asked if I could work for him. Kittel had just returned from a trip to Moscow where he met Landau, and he told me that Landau required that a prospective student had to pass a rigorous examination before he would agree to take the student into his research group. Kittel indicated that I should take the PhD qualifier and come back to him after I had done so. When I came back to discuss my future with him, Kittel told me that he would take me on. He said, however, that although I could do a thesis under his direction in solid-state theory, he did not think I would be a first-rate theorist. He recommended instead that I consider working with someone who does experimental work in close interaction with theory. This was perhaps the best advice that anyone ever gave me—and I followed his advice. I joined the research group of Alan Portis.

I remember with clarity my first day in the laboratory. I was doing "original research"; at last I was involved with real physics. After only one day of carrying out magnetic measurements on an insulating antiferromagnet, $KMnF_3$, I wrote a theory of antiferroelectric antiferromagnets and presented it to Portis with great pride. He was patient with me then and again a few days later when I apologized and told him my theory was nonsense. Through my interactions with Portis (I recall spending many hours talking with him in his office), I learned how to think about physics; more important, I began to learn about good taste in the choice of problems.

After completing my degree, I went directly to join the Physics Department at the University of Pennsylvania (PENN) where I remained for over twenty years. It was an exciting period for condensed-matter physics at PENN. Eli Burstein had made major progress in building the solid-state group; he convinced Robert Schrieffer to come to PENN, and he and Schrieffer attracted an outstanding group of young people. Beginning with my experimental studies of magnetic impurities in metals and the Kondo Effect, I learned many-body physics from Schrieffer.

Anthony Garito introduced me to tetracyanoquinodimethane (TCNQ); I brought him into my research group for post-doctoral research. We worked together from 1970 through 1975 on the metal physics of TTF-TCNQ and on the discovery of

the Peierls instability in quasi-one-dimensional π-stacked molecular crystals. Although the direct observation (with both X-ray diffraction and neutron scattering) of the incommensurate Peierls distortion with wave number $q = 2k_F$ proved that we were on the right track, this was a time of controversy and stress.

In 1975, the first papers on the novel metallic polymer, poly(sulfur-nitride), $(SN)_x$ appeared in the literature. I was intrigued by this unusual quasi-1D metal and wanted to get into the game. I learned that Alan MacDiarmid, a professor in the Chemistry Department at PENN, had a background in sulfur-nitride chemistry, and I made an appointment to see him with the goal of convincing him to collaborate with me and to synthesize $(SN)_x$. I recall that we met late in the afternoon of an autumn day. After quite a long discussion during which I made little progress toward my goal, I realized that while I was saying "$(SN)_x$", he was hearing "$(Sn)_x$". Needless to say, he was not impressed with my enthusiasm for $(Sn)_x$ being a metal; any chemist knew that tin was a metal!

Once MacDiarmid and I got past this initial language problem, a true collaboration began. We realized that it was a long reach across the Chemistry–Physics boundary, and we were determined to learn from one another. Although we collaborated during the week, we typically met on Saturday mornings with no agenda; just to try to learn from one another. At that time, I was fascinated with the metal–insulator transition as envisioned by Mott. I recall that I tried to convey my interest in this problem to MacDiarmid by asking him to consider a linear chain of hydrogen atoms as a model system. He balked right away; a linear chain of hydrogen atoms did not exist. After discussion, we focused in on the abstraction of a chain of π-bonded −CH− units as an example of a system that would have one unpaired electron per repeat unit. Shortly thereafter, MacDiarmid went to Japan for a visit. MacDiarmid is a very visual person. He loved the golden color of films and crystals of $(SN)_x$, and he showed samples and photos of this golden material during his lectures. After one such lecture, a Japanese scientist came up to him during the coffee break and told MacDiarmid that he, too, had some shiny films. Thus, MacDiarmid was introduced to Hidekei Shirakawa and to polyacteylene.

When MacDiarmid returned from Japan, he told me with great excitement about $(CH)_x$. With the help of a small addition to an ONR grant from the Program Officer, Kenneth Wynne, we were able to bring Hideki Shirakawa to PENN as a Visiting Scientist. The initial discovery of the remarkable increase in electrical conductivity of $(CH)_x$ and the identification of that increase as resulting from a transition from insulator (semiconductor) to metal followed in a very short time.

The soliton in polyacetylene was born with the observation of an electron spin resonance (ESR) signal in the pure material where there should not have been one. Building on the earlier work by Michael Rice on phase-solitons, I realized that if one drew a domain wall between the two identical forms with opposite bond alternation, one would have an unpaired spin and postulated that the origin of the ESR signal might be a bond-alternation domain wall. Curt Fincher, then a graduate student in my research group, had recently discovered the doping-enhanced infrared vibrational modes which became a signature of the doping. In a luncheon seminar before the solid-state group at PENN, I argued that these doping-induced IR modes might arise from the enhanced electric field at IR frequencies that would result if a charged bond-alternation domain wall were to move back and forth driven by the external field of the incident IR radiation. Schrieffer listened closely and made some comments about "kinks" at the end of my talk. A few days later he showed me how the mid-gap state would arise from the formation of such a bond-alternation domain wall and how that mid-gap state would have a reversed spin/charge relation relative to that of fermions. Wu-Pei Su then worked this out in detail, and the SSH papers were written.

I was drawn to Santa Barbara by the promise of a singular opportunity to build a special Physics Department, by the promise of continuing my close collaboration with Bob Schrieffer, by the opportunity to work with Fred Wudl, and—frankly—by the lure of this beautiful place. Wudl, then a synthetic chemist at Bell Laboratories, and I were recruited to the University of California, Santa Barbara (UCSB) together and enjoyed a close and productive collaboration over a period of 15 years. Daniel Moses and I have worked together for 20 years, initially at PENN and then at UCSB. Dan dragged me into ultra-fast pulsed-laser spectroscopy and into fast-transient photoconductivity as probes of the excited states of semiconducting polymers. Dan continues in his efforts to resolve the remaining fundamental scientific issues in the field of semiconducting polymers with creativity and with determination.

In 1986, in the process of building the Macromolecular division of our newly formed Materials Department, we convinced Paul Smith to leave DuPont Central Research and come to UCSB. Whereas I and Alan MacDiarmid and most of the early players in the conducting polymer field were amateurs in the field of polymer science, Paul was a professional. He quickly hammered into my head the importance of making conducting polymers processible, and he had the annoying habit of asking me embarrassing questions such as "What is the intrinsic electrical conductivity of a conducting polymer?". Anything I know about the processing and mechanical properties of polymers, I learned from Paul.

In 1990, Paul Smith and I decided that conducting polymers as materials had developed to a level of maturity that commercial products were possible. With this as a goal, we founded UNIAX Corporation. Fortunately, on a trip to China in 1986, I met Yong Cao and immediately realized that he was a remarkable scientist. I was able to bring him to Santa Barbara in 1987. Initially, he worked with Paul and with me at UCSB. When we founded UNIAX, Yong Cao was the first employee. His creativity, determination and scientific strength were critical to our scientific progress and to the success of UNIAX. During the 1990s, UNIAX played a leading role in developing the science and technology of conducting polymers with many important contributions.

The twenty-five years since the discovery of conducting polymers have taken me on a great ride; always on the frontier and always with the challenge of exciting discoveries. In 1990, the discovery of polymer LEDs by Richard Friend and colleagues at Cambridge gave the field a boost with the promise of important technology and with the excitement of an entirely new set of phenomena to study. In 1992, while doing post-doctoral research in my group at UCSB, Serdar Saricifici discovered ultrafast photo-induced electron transfer from semiconducting polymers to acceptors such as C_{60}. This discovery resulted in the development of polymer photodetectors and photovoltaic cells that offer promise for use in a variety of applications. In 1996, the discovery of amplified spontaneous emission and lasing (simultaneously by our group, by Richard Friend's group at Cambridge and by Valy Vardeny's group at Utah) opened yet another potentially important direction. And it goes on. None of this could have been accomplished without the hard work, dedication and creativity of the students and post-docs with whom I have had the pleasure of working over the past forty years. I thank them all.

I have enjoyed the life of a scientist while sharing both the exciting days and the disappointments with Ruth. She has filled my life with love and surrounded me with beauty. She has also gallantly put up with my eccentricities for more than forty years. We have succeeded in starting an academic dynasty; our two sons, Peter and David are both academics. Peter is a professor and medical doctor who is doing research on immunology at Case Western Reserve University. David is a professor and neuroscientist at Stanford University where he studies human vision. I have had the great pleasure of collaborating and publishing articles (as co-author) with both of my sons. Now I am looking forward to the emergence of my four grandchildren, Brett, Jordan, Julia, and Alice, as the next generation of the Heeger family. Of all the congratulations that I have received as a result of the Nobel Prize, I took greatest pleasure from their pride in their grandfather.

Flory's insights and deep understanding of macromolecular phenomena are summarized in his book, *Principles of Polymer Chemistry*, published in 1953, and still useful (and used) today. Flory was awarded the Nobel Prize in Chemistry in 1974 "for his fundamental achievements, both theoretical and experimental, in the physical chemistry of macromolecules".

Because the saturated polymers studied by Staudinger, Flory, Ziegler, and Natta are insulators, they were viewed as uninteresting from the point of view of electronic materials. Although this is true for saturated polymers (in which all of the four valence electrons of carbon are used up in covalent bonds), in conjugated polymers the electronic configuration is fundamentally different. In conjugated polymers, the chemical bonding leads to one unpaired electron (the π elecron) per carbon atom. Moreover, π bonding, in which the carbon orbitals are in the sp^2p_z configuration and in which the orbitals of successive carbon atoms along the backbone overlap, leads to electron delocalization along the backbone of the polymer. This electronic delocalization provides the "highway" for charge mobility along the backbone of the polymer chain.

As a result, therefore, the electronic structure in conducting polymers is determined by the chain symmetry (i.e. the number and kind of atoms within the repeat unit), with the result that such polymers can exhibit semiconducting or even metallic properties. In his lecture at the Nobel Symposium (NS-81) in 1991, Professor Bengt Rånby designated electrically conducting polymers as the "*fourth generation of polymeric materials*".[3]

The classic example is polyacetylene, $(-CH)_n$, in which each carbon is σ bonded to only two neighboring carbons and one hydrogen atom with one π electron on each carbon. If the carbon–carbon bond lengths were equal, the chemical formula, $(-CH)_n$ with one unpaired electron per formula unit would imply a metallic state. Alternatively, if the electron–electron interactions were too strong, $(-CH)_n$ would be an antiferromagnetic Mott insulator. The easy conversion into the metallic state on doping[1, 2] together with a variety of studies of the neutral polymer have eliminated the antiferromagnetic Mott insulator as a possibility.

In real polyacetylene, the structure is dimerized as a result of the Peierls Instability with two carbon atoms in the repeat unit, $(-CH{=}CH)_n$. Thus, the π band is divided into π and π^* bands. Since each band can hold two electrons per atom (spin up and spin down), the π band is filled and the π^* band is empty. The energy difference between the highest occupied state in the π band and the lowest unoccupied state in the π^* band is the $\pi-\pi^*$ energy gap, E_g. The bond-alternated structure of polyacetylene is characteristic of conjugated polymers (Scheme 1). Consequently, since there are no partially filled bands conjugated polymers are typically semiconductors. Because E_g depends upon the molecular structure of the repeat unit, synthetic chemists are provided with the opportunity and the challenge to control the energy gap by design at the molecular level.

Although initially built upon the foundations of quantum chemistry and condensed-matter physics, it soon became clear that entirely new concepts were involved in the science of conducting polymers. The discovery of nonlinear excitations in this class of polymers, solitons in systems in which the ground state is degenerate, and confined soliton pairs (polarons and bipolarons) in systems in which the ground state degeneracy has been lifted by the molecular structure, opened entirely new directions for the study of the interconnection of chemical and electronic structure. The spin–charge separation characteristic of solitons and the reversal of the spin–charge relationship (relative to that expected for electrons as fermions) in polyacetylene challenged the foundations of quantum physics. The study of solitons in polyacetylene,[4] stimulated by the Su–Schrieffer–Heeger (SSH) papers[5, 6] dominated the first half of the 1980s.

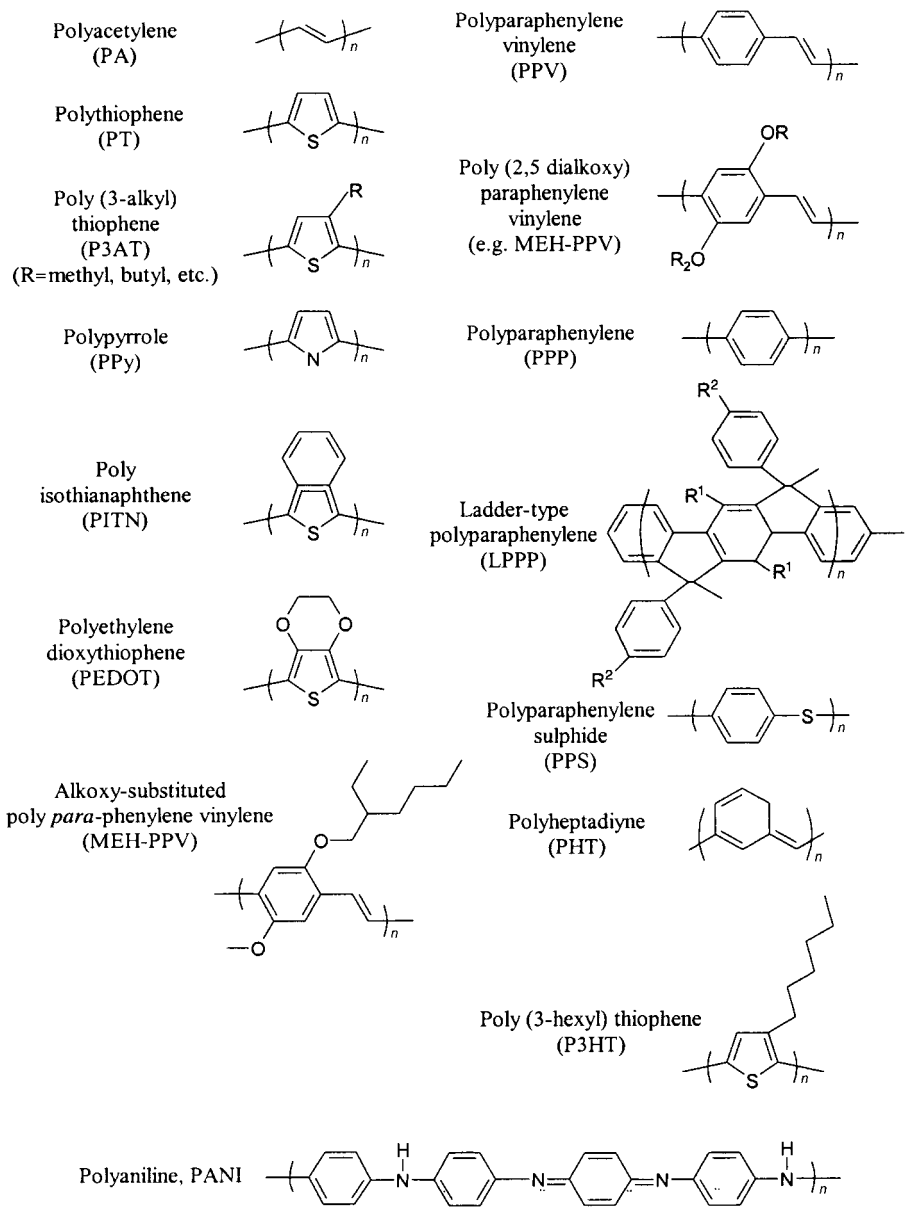

Scheme 1. Examples of a few conjugated polymers, note the bond-alternated structures.

The opportunity to synthesize new conducting polymers with improved/desired properties began to attract the attention of synthetic chemists in the 1980s. Although it would be an overstatement to claim that chemists can now control the energy gap of semiconducting polymers through molecular design, we certainly have come a long way toward that goal.

Reversible "doping" of conducting polymers, with associated control of the electrical conductivity over the full range from insulator to metal, can be accomplished either by chemical doping or by electrochemical doping. Concurrent with the doping, the electrochemical potential (the Fermi level) is moved either by a redox reaction or an acid–base reaction into a region of energy where there is a high density of electronic states; charge neutrality is maintained by the introduction of counter ions. Metallic polymers are, therefore, salts. The electrical conductivity results from the existence of charge carriers (through doping) and from the ability of those charge carriers to move along the π-bonded "highway". Consequently, doped conjugated polymers are good conductors for two reasons:

a) Doping introduces carriers into the electronic structure. Since every repeat unit is a potential redox site, conjugated polymers can be doped n-type (reduced) or p-type (oxidized) to a relatively high density of charge carriers[7]
b) The attraction of an electron in one repeat unit to the nuclei in the neighboring units leads to carrier delocalization along the polymer chain and to charge-carrier mobility, which is extended into three dimensions through interchain electron transfer.

Disorder, however, limits the carrier mobility and, in the metallic state, limits the electrical conductivity. Indeed, research directed toward conjugated polymers with improved structural order and hence higher mobility is a focus of current activity in the field.

Figure 1 shows the early results on the conductivity of polyacetylene as a function of the doping level; even in these early studies the conductivity increased by more than a factor of 10^7 to a level approaching that of a metal.[2]

The electrochemical doping of conducting polymers was discovered by the MacDiarmid–Heeger collaboration in 1980 and opened yet another scientific direction.[8] The electrochemistry of conducting polymers has developed into a field of its own with applications that range from polymer batteries and electrochromic windows to light-emitting electrochemical cells.[9]

Although I have emphasized the processing advantages of polymers, even as late as 1990, there were no known examples of stable metallic polymers which could be processed *in the metallic form* (a requirement for broad use in industrial products). This major outstanding problem was first solved with polyaniline (PANI). PANI has been investigated extensively for over 100 years and attracted interest as a conducting material for several important reasons; the monomer is inexpensive, the polymerization reaction is straightforward and proceeds with high yield, and PANI has excellent stability. As shown by Alan MacDiarmid and his collaborators in the mid-80s, polyaniline can be rendered conducting through two independent routes; oxidation (either chemically or electro-

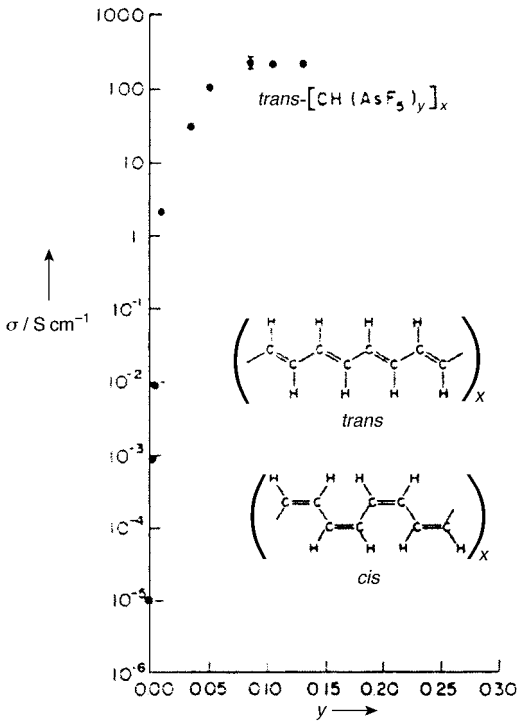

Figure 1. Electrical conductivity of *trans*-$(CH)_x$ as a function of (AsF_5) dopant concentration. The *trans* and *cis* polymer structures are shown in the inset.

chemically) of the leuco-emeraldine base or protonation of the emeraldine base through acid–base chemistry.[10] Because the insertion of counter ions is involved in both routes; conducting polyaniline is a salt (a polycation with one anion per repeat unit).

Processing high molecular weight polyaniline into useful objects and devices proved to be a difficult problem. Yong Cao, Paul Smith, and I made important progress in 1991 by using functionalized protonic acids to both convert PANI into the metallic form and, simultaneously, render the resulting PANI complex soluble in common organic solvents.[11] The functionalized counter ion acts like a "surfactant" in that the charged head group is ionically bound to the oppositely charged protonated PANI chain, and the "tail" is chosen to be compatible with nonpolar or weakly polar organic liquids (in the case of solutions) or the host polymer (in the case of blends). The processibility of PANI induced by the "surfactant" counter ions has enabled the fabrication of conducting polymer blends with a variety of host polymers.[12] Since the blends are melt-processible as well, the counter ion induced processibility of polyaniline provides a route to conducting polymer blends for use in industrial products. The "surfactant" counter ions offer an unexpected advantage; they lead to the formation of a self-assembled network morphology in the PANI polyblends.[13] Because of these interpenetrating networks, the threshold for the onset of electrical conductivity in blends with traditional insulating host polymers is reduced to volume fractions well below 1 %.[14] The PANI network is sufficiently robust that it remains connected and conducting even after the removal of the host polymer, thus opening another new direction; the fabrication of novel electrodes for use in electronic devices. The use of "surfactant" counter ions was introduced with the goal of making PANI processible in the conducting form. The self-assembly of phase-separated networks was an unexpected—but very welcome—bonus.

Conducting polymers were initially attractive because of the fundamental interest in the doping and the doping-induced metal–insulator transition. However, the chemistry and physics of these polymers in their non-doped semiconducting state are of great interest because they provide a route to "plastic electronic" devices. Although polymer diodes were fabricated and characterized in the 1980s,[15] the discovery of light-emitting diodes (LEDs) by Richard Friend and colleagues at Cambridge in 1990[16] provided the stimulus for a major push in this direction. The polymer light-emitting diode is, however, only one of a larger class of devices in the emerging class of "plastic" opto-electronic devices, including lasers, high sensitivity plastic photodiodes (and photodiode arrays) and photovoltaic cells, ultrafast image processors (optical computers), thin-film transistors, and all-polymer integrated circuits; in each case these sophisticated electronic components are fabricated from semiconducting and metallic polymers. All of these have a common structure: they are thin-film devices in which the active layers are fabricated by casting the semiconducting and/or metallic polymers from solution (e.g. spin-casting or ink-jet printing).

2. Doping

Charge injection onto conjugated, semiconducting macromolecular chains, "doping", leads to the wide variety of interesting and important phenomena which define the field. As summarized in Figure 2, reversible charge injection by "doping" can be accomplished in a number of ways.

2.1. Chemical Doping by Charge Transfer

The initial discovery of the ability to dope conjugated polymers involved charge-transfer redox chemistry; oxidation (p-type doping), or reduction (n-type doping),[1, 2, 7] as illustrated with the following examples:

a) p-type doping [Eq. (1)]

$$(\pi\text{-polymer})_n + 3/2\,n\,y(I_2) \longrightarrow [(\pi\text{-polymer})^{+y}(I_3^-)_y]_n \quad (1)$$

b) n-type doping [Eq. (2)]

$$(\pi\text{-polymer})_n + [Na^+(C_{10}H_8)^{-\bullet}]_y \longrightarrow [(Na^+)_y(\pi\text{-polymer})^{-y}]_n + (C_{10}H_8)^0 \quad (2)$$

When the doping level is sufficiently high, the electronic structure evolves to that of a metal.

2.2. Electrochemical Doping

Although chemical (charge transfer) doping is an efficient and straightforward process, it is typically difficult to control.

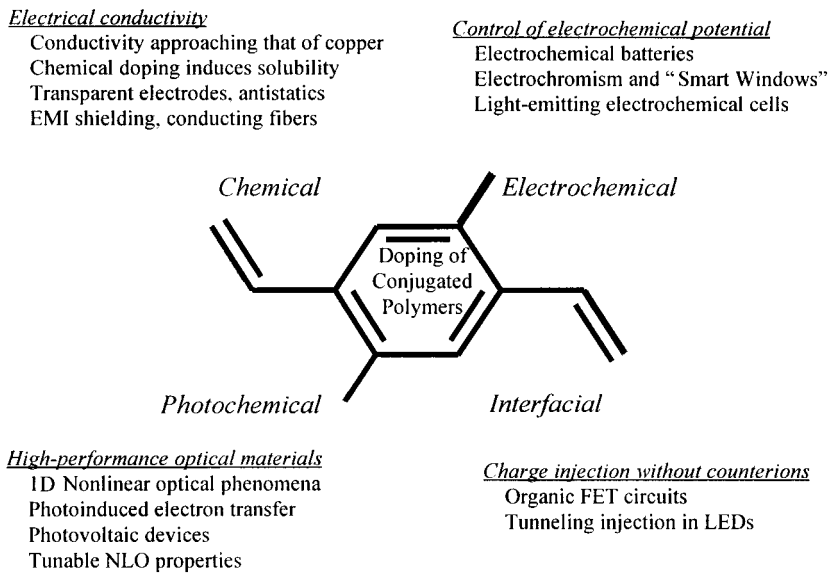

Figure 2. Doping mechanisms and related applications.

Complete doping to the highest concentrations yields reasonably high-quality materials. However, attempts to obtain intermediate doping levels often result in inhomogeneous doping. Electrochemical doping was invented to solve this problem.[8] In electrochemical doping, the electrode supplies the redox charge to the conducting polymer, while ions diffuse into (or out of) the polymer structure from the nearby electrolyte to compensate the electronic charge. The doping level is determined by the voltage between the conducting polymer and the counter electrode; at electrochemical equilibrium the doping level is precisely defined by that voltage. Thus, doping at any level can be achieved by setting the electrochemical cell at a fixed applied voltage and simply waiting as long as necessary for the system to come to electrochemical equilibrium (as indicated by the current through the cell going to zero). Electrochemical doping is illustrated by the following examples:

a) p-type doping [Eq. (3)]

$$(\pi\text{-polymer})_n + [Li^+(BF_4^-)]_{soln} \longrightarrow [(\pi\text{-polymer})^{+y}(BF_4^-)_y]_n + Li_{electrode} \quad (3)$$

b) n-type doping [Eq. (4)]

$$(\pi\text{-polymer})_n + Li_{electrode} \longrightarrow [(Li^+)_y(\pi\text{-polymer})^{-y}]_n + [Li^+(BF_4^-)]_{soln} \quad (4)$$

2.3. Doping of Polyaniline by Acid–Base Chemistry

Polyaniline provides the prototypical example of a chemically distinct doping mechanism.[10] Protonation by acid–base chemistry leads to an internal redox reaction and the conversion from semiconductor (the emeraldine base) into metal (the emeraldine salt). The doping mechanism is shown in Scheme 2. The chemical structure of the semiconducting emeraldine-base form of polyaniline is that of an alternating copolymer. Upon protonation of the emeraldine base to the emeraldine salt, the proton induced spin-unpairing mechanism leads to a structural change with one unpaired spin per repeat unit, *but with no change in the number of electrons*.[17, 18] The result is a half-filled band and, potentially, a metallic state where there is a positive charge in each repeat unit (from protonation) and an associated counter ion (e.g. Cl^-, HSO_4^-, dodecylbenzenesulfonate ($DBSA^-$) etc., the counter ion is not shown in Scheme 2). This remarkable conversion from semiconductor into metal has been well-described, but it is not well understood from the view of basic theory. There are no calculations which show that the metallic (emeraldine salt) final state is lower in energy than the semiconductor and no detailed understanding of the rearrangement reactions sketched in Scheme 2.

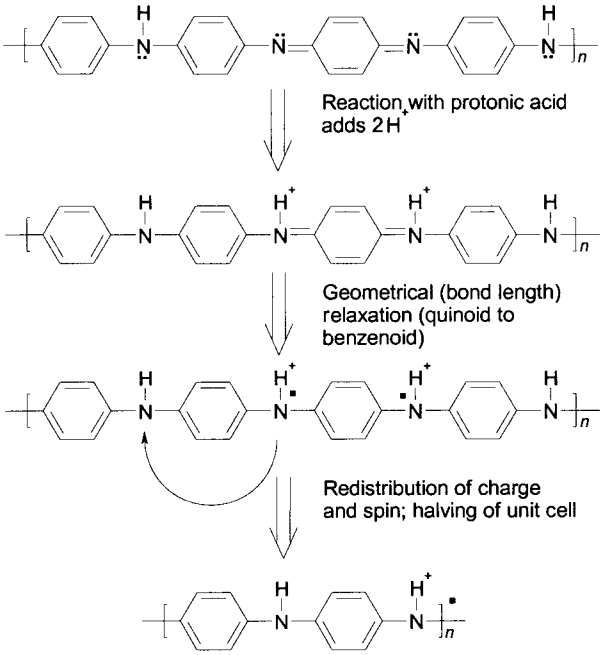

Scheme 2. Protonation induced spin unpairing in polyaniline, conversion from insulator into metal with no change in the number of electrons. The counter ion is not shown.

2.4. Photo-doping

The semiconducting polymer is locally oxidized and (nearby) reduced by photo-absorption and charge separation (electron–hole pair creation and separation into "free" carriers), Equation (5), where y is the number of electron–hole pairs (dependent upon the pump rate in competition with the recombination rate).

$$(\pi\text{-polymer})_n + h\nu \longrightarrow [\{\pi\text{-polymer}\}^{+y} + \{\pi\text{-polymer}\}^{-y}]_n \quad (5)$$

The branching ratio between free carriers and bound excitons (and the closely related issue of the magnitude of the exciton binding energy) is a subject of continuing discussion.[19]

Following photoexcitation from the ground state (^1A_g in the notation of molecular spectroscopy) to the lowest energy state with proper symmetry (^1B_u), recombination to the ground state can be either radiative (luminescence) or nonradiative. Some families of conjugated polymers exhibit high luminescence quantum efficiencies (for example, poly(phenylene vinylene) (PPV), and poly(paraphenylene) (PPP) and their soluble derivatives); others do not (for example, polyacetylene and the polythiophenes). A number of mechanisms have been identified that lead to low quantum efficiencies for photoluminescence. Rapid bond relaxation in the excited state and the formation of solitons with states at mid gap prevent radiative recombination in polyacetlyene.[4] The existence of an A_g state or a triplet excited state below the ^1B_u state will favor nonradiative recombination (in both cases, direct radiative transitions to the ground state are forbidden). Interchain interactions in the excited state ("excimers") also lead to nonradiative channels for decay.[20–22]

2.5. Charge Injection at a Metal–Semiconducting Polymer Interface

Electrons and holes can be injected from metallic contacts into the π^* and π bands, respectively:

a) Hole injection into an otherwise filled π band [Eq. (6)]

$$(\pi\text{-polymer})_n - y(e^-) \longrightarrow [(\pi\text{-polymer})^{+y}]_n \quad (6)$$

b) Electron injection into an empty π^* band [Eq. (7)]

$$(\pi\text{-polymer})_n + y(e^-) \longrightarrow [(\pi\text{-polymer})^{-y}]_n \quad (7)$$

In the case of charge injection at a metal–semiconducting (MS) polymer interface, the polymer is oxidized or reduced (electrons are added to the π^* band or removed from the π band). However, the polymer is not doped in the sense of chemical or electrochemical doping, for there are no counter ions. This distinction becomes particularly clear when comparing charge injection in the polymer light-emitting diode[16, 23] (where there are no ions) with that in the polymer light-emitting electrochemical cell where electrochemical doping with associated redistribution of ions provides the mechanism for charge injection.[9]

As indicated in Figure 2, each of the methods of charge-injection doping leads to unique and important phenomena. In the case of chemical and/or electrochemical doping, the induced electrical conductivity is permanent, until the carriers are chemically compensated or until the carriers are purposely removed by "undoping". In the case of photo-excitation, the photoconductivity is transient and lasts only until the excitations are either trapped or decay back to the ground state. In the case of charge injection at an MS interface, electrons reside in the π^* band and/or holes reside in the π band only as long as the biasing voltage is applied.

Because of the self-localization associated with the formation of solitons, polarons, and bipolarons, charge injection leads to the formation of localized structural distortions and electronic states in the energy gap.[4] In the case of "photodoping", the redistribution of oscillator strength associated with the sub-gap infrared absorption and the corresponding bleaching of the interband ($\pi-\pi^*$) transition provide a route to nonlinear optical (NLO) response. Real occupation of low energy excited states[4, 24] and virtual occupation of higher-energy excited states (in the context of perturbation theory)[25] lead to, respectively, resonant and nonresonant NLO response.

By charge-injection doping at an MS interface, the polymer semiconductor can be used as the active element in thin-film diodes[15] and field-effect transistors (FETs).[26–28] Tomozawa et al.[15] demonstrated the first example of an electronic-device component fabricated by casting the active polymer directly from solution; even these early diodes exhibited excellent current–voltage characteristics. Dual-carrier injection in metal/polymer/metal structures provides the basis for polymer light-emitting diodes (LEDs).[23] In polymer LEDs, electrons and holes are injected from the cathode and anode, respectively, into the undoped semiconducting polymer; light is emitted when the injected electrons and holes meet in the bulk of the polymer and recombine with the emission of radiation.[16] Thus, as summarized in Figure 2, doping is a common feature of conducting polymers; doping leads to a remarkably wide-range of electronic phenomena.

3. Novel Properties Generate New Technology

As emphasized in the Introduction, conducting polymers exhibit novel properties; properties not typically available in other materials. I focus on a few of these as illustrative examples:

a) Semiconducting and metallic polymers which are soluble in and processible from common solvents
b) Transparent conductors
c) Semiconductors in which the Fermi energy can be controlled and shifted over a relatively wide range.

In each case, the property is related to a fundamental feature of the chemistry and/or physics of the class of conducting polymers. These novel properties enable a number of applications including polymer LEDs, conducting polymers as electrochromic materials, polymer photodetectors, and polymer photovoltaic cells.

3.1. Semiconducting and Metallic Polymers which are Soluble in, and Processible from, Common Solvents

Because the interchain electron-transfer interactions of conjugated polymers are relatively strong compared with the van der Waals and hydrogen-bonding interchain interactions typical of saturated polymers, conducting polymers tend to be insoluble and infusible. Thus, there was serious doubt in the early years following the discovery that π-conjugated polymers could be doped to the metallic state as to whether or not

processing methods could be developed. Significant progress has been made using four basic approaches:

1. Side-chain functionalization; principally used for processing semiconducting polymers from solution in organic solvents or from water
2. Precursor-route chemistry, principally used for processing polyacetylene and PPV into thin films
3. Counter-ion induced processing, principally used for processing polyaniline in the metallic form from organic solvents
4. Aqueous colloidal dispersions created by template synthesis, principally used for processing polyaniline and poly(ethylenedioxythiophene) (PEDOT).

The addition of moderately long side chains onto the monomer units resulted in derivatives of polythiophene, the poly(3-alkylthiophenes), or P3ATs; see Scheme 1. Since the side chains decrease the interchain coupling and increase the entropy, these derivatives can be processed either from solution or from the melt. Similarly, side-chain functionalization of PPV (see Scheme 1) has progressed to the point where a variety of semiconducting polymers and copolymers are available with energy gaps that span the visible spectrum.[29] Water solubility was achieved by incorporating polar groups such as $(CH_2)_nSO_3^-M^+$ (M = metal) into the side chains (so-called "self-doped" polymers).[30, 31]

The ability to fabricate optical-quality thin films by spin-casting from solution has proven to be an enabling step in the development of plastic electronic devices such as diodes, photodiodes, LEDs, LECs, optocouplers, and thin-film transistors.[32]

The counter-ion induced processibility of "metallic" polyaniline utilizes bifunctional counter ions such as DBSA to render the polymer soluble.[11] The charge on the SO_3^- ion head group forms an ionic bond with the positive charge (proton) on the PANI chain; the hydrocarbon tail "likes" organic solvents. Processing PANI in the conducting form resulted in materials with improved homogeneity and crystallinity, and with correspondingly improved electrical conductivities;[33] the solubility of "metallic" PANI in organic solvents has also enabled the fabrication of conducting blends of PANI with a variety of insulating host polymers.[11, 12] These polymer blends exhibit a remarkably low percolation threshold as a result of the spontaneous formation of an interpenetrating-network morphology.[13]

Template-guided synthesis of conducting polymers was first reported by S. C. Yang and colleagues.[34] The molecular template, in most cases, polyacids such as polystyrene sulfonic acid, binds the monomer, for example aniline, to form molecular complexes which are dispersed in water as colloidal particles. Upon polymerization, the aniline monomers form polyaniline and remain attached to the template to form the template–polyaniline complex. By judicious choice of the template molecule and the polymerization conditions, stable submicron-size colloidal particles of polyaniline–template aggregate can be formed during polymerization. The stabilization against coagulation arises from the Coulomb repulsion between particles, which is a result of the surface charge provided by the extra sulfonic acid groups in polystyrene sulfonic acid. Very stable dispersions of polyaniline–polystyrene sulfonic acid complexes can be made with particle sizes less than 1 μm.[34] Transparent films with a specific resistivity of 1–10 Ω cm can be cast from such dispersions.

Poly(ethylenedioxythiophene)–polystyrene sulfonate (PEDOT–PSS) can be prepared as a stable dispersion in water.[34, 35] Films of PEDOT–PSS are semi-transparent and can be spin-cast with a surface resistance of approximately 500 Ω cm^{-2} and with 75 % transmission.

3.2. Transparent Metallic Polymers

Metals reflect light at frequencies below the plasma frequency, ω_p, defined in Equation 8 where N is the number of electrons per unit volume, e is the electron charge, and m^* is the effective mass (the "optical mass") of the electrons in the solid.

$$\omega_p^2 = 4\pi N e^2/m^* \quad (8)$$

At frequencies above the plasma frequency, metals are transparent.[36] For conventional metals (Na, Cu, Ag, etc.), N is of order 10^{23} per unit volume. As a result, the plasma frequency is in the ultraviolet; therefore, conventional metals appear shiny and "metallic-looking" in the spectral range over which the human eye is sensitive.

Metallic polymers have a lower density of electrons; both the length of the repeat unit along the chain and the interchain spacing are relatively large compared to the interatomic distances in conventional metals. Typically, therefore, for metallic polymers N is of order $2-5\times10^{21}$ cm^{-3}. Thus, for metallic polymers, the plasma frequency is at approximately 1 eV.[37, 38] The reflectance of high quality, metallic polypyrrole (PPy; doped with PF_6) is shown in Figure 3. Metallic polymers

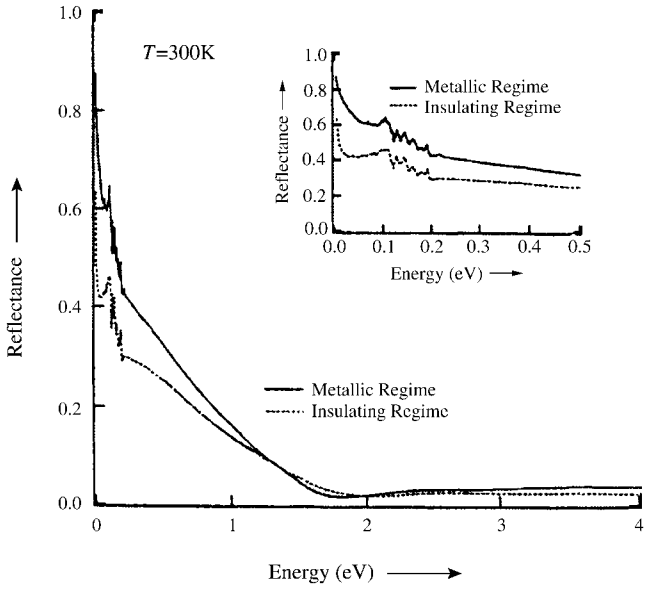

Figure 3. Reflectance spectra of PPy-PF_6 near the metal–insulator transition; inset shows the low-energy spectra with expanded scale.

exhibit high reflectance (and thus look "shiny") in the infrared, but they are semitransparent in the visible part of the spectrum. The residual absorption above the plasma frequency arises from interband ($\pi-\pi^*$) transitions between the partially filled π band and the lowest energy π^* band.

Optical-quality thin films of metallic polymers are useful, therefore, as transparent electrodes.[39] For example, polyaniline,[40] polypyrrole,[41] and PEDOT[42] (Scheme 1) have been used as transparent hole-injecting electrodes in polymer LEDs (the initial demonstration of mechanically flexible polymer LEDs utilized PANI as the anode[40]). Transparent conducting films can be used for a variety of purposes; for example, as antistatic coatings, as electrodes in liquid-crystal display cells or in polymer LEDs, or for fabricating electrochromic windows.

3.3. Semiconductors in which the Fermi Energy can be Shifted across the Energy Gap

In comparison with traditional inorganic semiconductors, semiconducting polymers cannot be considered materials with ultra-high purity. As a result, although many device concepts have been demonstrated using semiconducting polymers as the active materials,[32] there was early skepticism that these novel semiconductors could be used in commercial applications.

In some ways, however, semiconducting polymers are more robust than their inorganic counterparts. In particular, whereas pinning of the Fermi energy by surface states is a major problem in conventional semiconductors, the Fermi energy can be controlled and shifted all the way across the energy gap in conjugated polymers. The absence of Fermi-level pinning and the ability to shift the chemical potential all the way across the energy gap are fundamentally important; these novel features of semiconducting polymers underlie the operation of polymer LEDs, polymer LECs, and polymer photodiodes.

One might have expected chemical reactions between the metal electrode and the polymer to lead to interface states that pin the Fermi level, as in inorganic semiconductors. Experiments have shown, however, that these interfacial interactions do not lead to pinning of the Fermi level. For example, electroabsorption measurements were used to determine the built-in electric field in metal–semiconductor–metal (MSM) structures of the kind used for polymer LEDs.[43] The results indicated that the maximum internal field is nearly equal to the single-particle energy gap; the built-in field directly tracked the difference in work functions of the two metal electrodes, as originally proposed by Parker.[23] Thus, the Fermi level is not pinned by surface states. The absence of Fermi-level pinning in semiconducting polymers is a major advantage: conceptually, it greatly simplifies the device physics, and technologically, it greatly simplifies the device fabrication.

4. Semiconducting Polymers: Electronic Structure and Bond Relaxation in Excited States

4.1. Band Structure, Electron–Lattice Interaction, Electron–Electron Interaction, and Disorder

Although the linear and nonlinear optical properties of conducting polymers have been investigated for over a decade, there is still controversy over the description of the elementary excitations. Are the lowest-energy elementary excitations mobile charge carriers (charged polarons) either injected at the contacts or created directly via inter-band photoexcitation, or are the lowest-energy excitations bound neutral excitons?[19] The answer is of obvious importance from the perspective of our basic understanding of the physics of conducting polymers. The answer is also important for applications based on these materials.

The central issue relates to the strength of the electron–electron interactions relative to the bandwidth, relative to the electron–phonon interaction and relative to the strength of the mean disorder potential. Strong electron–electron interactions (electron–hole attraction) lead to the creation of localized and strongly correlated negative and positive polaron pairs: neutral polaron excitons. Well screened electrons and holes with associated lattice distortions (charged polarons) on the other hand, are more appropriately described using a band picture supplemented by the electron–phonon interaction. Molecular solids such as anthracene[44] are examples of the former, where the absorption is dominated by excitonic features; whereas inorganic semiconductors such as Si and GaAs are examples of the latter (where rigid band theory is a good approximation).

The electronic structure of conjugated polymers was described by SSH[5, 6] in terms of a quasi-one-dimensional tight-binding model in which the π electrons are coupled to distortions in the polymer backbone by the electron–phonon interaction. In the SSH model, photoexcitation across the $\pi-\pi^*$ band gap creates the self-localized, nonlinear excitations of conducting polymers; solitons (in degenerate ground state systems), polarons, and bipolarons.[4] Direct photogeneration of solitons and polarons is enabled by the Franck–Condon overlap between the uniform chain in the ground state and the distorted chain in the excited state.[45, 46] When the ground state is nondegenerate, as in the PPVs, charged polaron pairs can either separate as mobile charged polarons or form bound polaron–excitons; that is, neutral bipolarons bound by a combination their Coulomb attraction and their shared distortion. Photoluminescence can be described in terms of the radiative decay of polaron-excitons.

Conjugated polymers are π-bonded *macromolecules*, molecules in which the fundamental monomer unit is repeated many, many times. Thus, N, the Staudinger index as in $(CH)_N$, is large. Since the end-points are not important when N is large, the π-electron transfer integral (denoted as "β" in molecular orbital theory,[47] and "t" in tight-binding theory) tends to delocalize the electronic wavefunctions over the entire macromolecular chain. This tendency toward delocalization is limited by disorder (which tends to localize the wavefunctions) and by the Coulomb interaction, which binds

electrons when transferred to a nearby repeat unit to the positive charge left behind; that is, to the "hole".

In principle, disorder can be controlled. Chain extended and chain aligned samples can be prepared. Indeed, by utilizing the method of gel-processing of blends of conjugated polymers in polyethylene,[48] a high degree of structural order has been attained.[45, 46] Thus, as a starting point, it is useful to consider idealized samples in which the macromolecular chains are chain extended and chain aligned.

The relative importance of the Coulomb interaction versus the band structure is a classic problem of the field. In tight-binding theory, the π-electron band structure extends over a band width, $W = 2zt$ where z is the number of nearest neighbors. Thus, for linear polymers with $z = 2$ and $t \approx 2.5$ eV, $W \approx 10$ eV.[4] Since the size of the monomer, typically 5 – 10 Å along the chain axis, is the smallest length in the problem, the monomer length is the effective "Bohr radius". Thus, on general grounds, one expects the electron – hole binding energy to be reduced from 13.5 eV (the electron – proton Coulomb binding energy in the H atom where the Bohr radius is 0.53 Å) by a factor of 10 – 20 simply because of the change in length scale. Dielectric screening provides an additional reduction factor of ε, where $\varepsilon \approx 3$ (typical of conjugated polymers) is the dielectric constant for an electric field along the chain. Thus, the binding energy is expected to be no more than a few tenths of an eV. Since the typical band widths and band gaps are all in the eV range, one can start with a one-electron band approach and treat the Coulomb energy as a perturbation. In this description, the electron – hole bound states are Wannier excitons which are delocalized over a number of repeat units. There are obvious cases where this argument breaks down. For example, one finds that in structures containing benzene rings, specific sub-bands have bandwidth near zero (nodes in the wavefunction reduce the effective transfer integral to zero). When electrons and holes occupy such narrow bands, the corresponding excitons are easily localized by the Coulomb interaction onto a single monomer. Thus, in general, one can expect both "Wannier-like" excitons and "Frenkel-like" excitons for electrons and holes originating from different bands in the same polymer.

4.2. Electronic Structure of Polyacetylene

Trans-polyacetylene (*trans*-$(CH)_x$) was the first highly conducting organic polymer.[1, 2] The simple chemical structure, −CH− units repeated (see Scheme 3 a), implies that each carbon contributes a single p_z electron to the π band. As a result, the π band would be half-filled. Thus, based upon this structure, an individual chain of neutral polyacetylene would be a metal; since the electrons in this idealized metal could move only along the chain, polyacetylene would be a one-dimensional (1D) metal. However, experimental studies show clearly that neutral polyacetylene is a semiconductor with an energy gap of approximately 1.5 eV. Rudolf Peierls showed many years ago[49] that 1D metals are unstable with respect to a structural distortion which opens an energy gap at the Fermi level, thus rendering them semiconductors. In the Peierls instability, the periodicity ($\Lambda = \pi/k_F$) of the distortion is

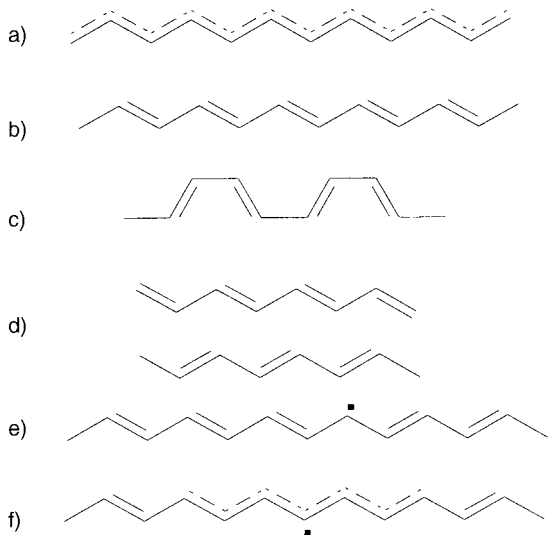

Scheme 3. Polyacetylene: a) undimerized structure, b) dimerized structure resulting from Peierls instability, c) *cis*-polyacatylene, d) degenerate A and B phases in *trans*-polyacetylene, e) soliton in *trans*-polyacetylene, f) the soliton domain wall extending over a number of carbon atoms.

determined by the magnitude of the Fermi wave-vector (k_F). Since $k_F = \pi/2a$ for the half-filled band of *trans*-$(CH)_x$, the Peierls distortion doubles the unit cell, converting *trans*-$(CH)_x$ into *trans*-$(-HC{=}CH-)_x$, see Scheme 3 b where, schematically, the dimerization is drawn as alternating single bonds and double bonds (in reality, shorter and longer bonds). The π band of $(CH)_x$ is split into two sub-bands, a fully occupied π band (the valence band in semiconductor terminology) and an empty π* band (the conduction band), each with a wide bandwidth (~5 eV) and significant dispersion. The resulting band structure and associated density of states, shown in Figure 4, results from the opening of the band gap that originates from the doubling of the unit cell as a result of the bond alternation caused by the Peierls instability of the 1D metal.

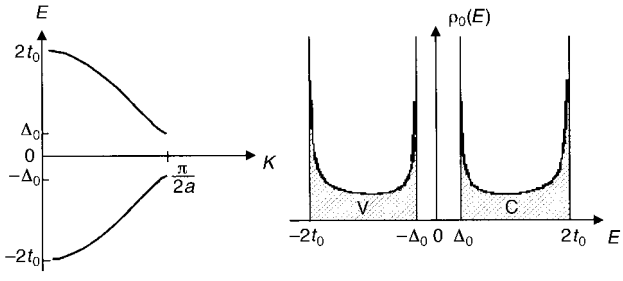

Figure 4. Electronic structure of semiconducting polyacetylene; left: band structure, right: density of states. The energy opens at $k = \pi/2a$ as a result of Peierls distortion.

Shortly after the initial discovery of doping and the metal – insulator transition in polyacetylene, the SSH description of the electronic structure was proposed.[5, 6] The construction of the remarkably successful SSH Hamiltonian was based on two assumptions:

1. the π-electronic structure can be treated in the tight-binding approximation with a transfer integral $t \approx 2.5$ eV

2. the chain of carbon atoms is coupled to the local electron density through the length of the chemical bonds [Eq. (9)] where $t_{n,n+1}$ is the bond-length dependent hopping integral from site n to $n+1$, and u_n is the displacement from equilibrium of the n^{th} carbon atom.

$$t_{n,n+1} = t_o + \alpha(u_{n+1} - u_n) \tag{9}$$

The first assumption defines the lowest order hopping integral, t_o, in the tight-binding term that forms the basis of the Hamiltonian. The second assumption provides the first-order correction to the hopping integral. This term couples the electronic states to the molecular geometry, giving the electron–phonon (el–ph) interaction where α is the el–ph coupling constant. The bond-length dependent hopping integral is physically correct, as indicated by bond alternation observed in polyacetylene.[50, 51] The precise form of Equation (9), in which the dependence of the hopping integral on the C–C distance is linearized for small deviations about t_o, is the first term in a Taylor expansion. The resulting SSH Hamiltonian is then written as the sum of three terms[5, 6] [Eq. (10)] where p_n are the nuclear momenta, u_n are the displacements from equilibrium, m is the carbon mass, and K is an effective spring constant. The $c^+_{n,\sigma}$ and $c_{n,\sigma}$ are the fermion creation and annihilation operators for site n and spin σ.

$$H_{SSH} = \sum_{n,\sigma}[-t_0 + \alpha(u_{n+1} - u_n)](c^+_{n+1,\sigma}c_{n,\sigma} + c^+_{n,\sigma}c_{n+1,\sigma}) + \sum_n \frac{p_n^2}{2m} + \frac{1}{2}K\sum_n (u_{n+1} - u_n)^2 \tag{10}$$

The last two terms are, respectively, a harmonic "spring constant" term which represents the increase in potential energy that results from displacement from the uniform bond lengths in $(CH)_x$ and a kinetic-energy term for the nuclear motion.

The spontaneous symmetry breaking that results from the Peierls instability implies that for the ground state of a pristine chain, the total energy is minimized for $|u_n| > 0$. Thus, to describe the bond alternation in the ground state [Eq. (11)].

$$u_n \rightarrow \langle u_n \rangle = (-1)^n u_o \tag{11}$$

With this mean-field approximation, the value u_o which minimizes the energy of the system can be calculated as a function of the other parameters in the Hamiltonian.[4–6] Qualitatively, however, one sees that u_o and $-u_o$ both minimize the energy for *trans*-polyacetylene since the bonds all make the same angle with respect to the chain axis. Hence, the energy as a function of u has a double minimum at $\pm u_o$, as shown in Figure 5. The corresponding structures of the two degenerate ground states are shown in Scheme 3d. The double minimum of Figure 5 implies that nonlinear excitations, solitons, will be important. In polymers with a nondegenerate ground state, the degeneracy indicated in Figure 5 is lifted; for a nondegenerate ground state polymer, the absolute minimum energy occurs at a single value of u.

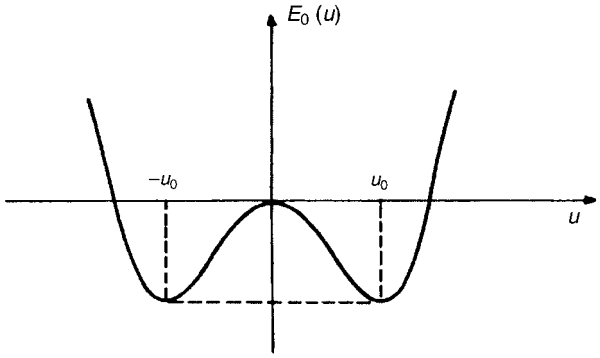

Figure 5. Total energy of the dimerized polyacetylene chain; note the double minimum associated with the spontaneous symmetry breaking and the two-fold degenerate ground state.

4.3. The Electronic Structure of Poly(phenylene vinylene)

Poly(phenylene vinylene) (PPV) and its soluble derivatives have emerged as the prototypical luminescent semiconducting polymers. Since PPV has a nondegenerate ground state, structural relaxation in the excited state leads to the formation of polarons, bipolarons, and neutral excitons. Prior to treating the structural relaxation in the excited state, however, one needs to develop a satisfactory description of the electronic excited states.

In PPV, with eight carbons in the main-chain repeat unit, the π band is split into eight sub-bands. Since each band can hold precisely two electrons per repeat unit, the four π sub-bands with the lowest energy are filled and the four π* sub-bands are empty. Thus, I begin with a description at the one-electron level, that is, from the point of view of band theory.

Brazovskii, Kirova, and Bishop[52, 53] treated the band structure of PPV with a tight-binding Hamiltonian, using standard values for the hopping integrals. The el–ph coupling [Eq. (9)], can be included after defining the basic band structure of the semiconductor. From this simple ansatz, basis states which reflect the intrinsic symmetry of the phenyl ring and the dimer were calculated and used to expand the wavefunction. The basis states hybridize as a result of ring-to-dimer hopping, thus yielding the $6+2=8$ sub-bands in the π system of PPV.

The resulting band structure (Figure 6) has a number of important features. Six of the sub-bands (three occupied and three unoccupied), labeled D and D* in Figure 6, are broad,

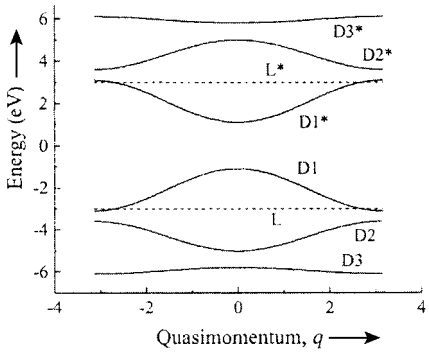

Figure 6. Electronic band structure of PPV.

and the corresponding wavefunctions are delocalized along the chain. The other two bands labeled L and L* (one occupied and one unoccupied), are narrow and the corresponding wavefunctions have amplitudes which are localized on the ring. The L and L* sub-bands derive from the two ring states whose wavefunctions have nodes at the *para* linkage sites; as a result, these states do not participate in hopping and the sub-bands do not acquire the resulting dispersion. On the contrary, the delocalized D and D* sub-bands have relatively high dispersion ($\sim$1.7 eV), indicating good delocalization over both ring and dimer states.

Starting from this simple yet physically robust model of the band structure, the discussion of the electronic structure can be extended to include the effect of the Coulomb interaction. The delocalized nature of D1 and D1* implies that, for electron correlation effects involving these sub-bands, it is appropriate to compute an effective mass from the dispersion curves and then compute the corresponding 1D hydrogenic levels. From the k^2-dependence of the dispersion near the zone center, the effective masses in D1 and D1* are $m^* = 0.067\,m_e$.

Using the well-known result for the binding energy of a hydrogenic-like state in 1D, the exciton associated with the lowest energy electronic transition (D1 $\rightarrow$D1*) has a binding energy and effective radii given by Equations (12a):

$$E_b = E_b^* \ln^2(a_b/a_\perp) \qquad a_b = a_b^* [\ln(a_b/a_\perp)]^{-1} \tag{12a}$$

where the terms are defined as in Equations (12b) and ε is the dielectric susceptibility, $\hbar$ is Planck's constant, m^* is the electron effective mass at the zone center in k-space (for PPV, $m^* \approx 0.067\,m_e$), e is the electron charge and $a_\perp \sim 2$ Å (the "width" of the chain).

$$E_b^* = \frac{m* e^4}{\varepsilon^2 \hbar^2} \qquad a_b^* = \frac{\hbar^2 \varepsilon}{m* e^2} \tag{12b}$$

From Equation (12a), $E_b \approx 0.1$ – -0.2 eV (depending on the value assumed for $a_\perp$) and a radius of approximately 30 Å.

In addition to this weakly bound Wannier–Mott exciton, there are two other excitons in this model. The degenerate D1–L1* and L1–D1* transitions are treated by assuming an immobile (massive) carrier in the L or L* sub-band and a mobile carrier in the D or D* sub-band. The resulting bound state has a binding energy of $\sim$0.8 eV, and is a more tightly bound (but still somewhat delocalized) exciton. Finally, the L–L* transition forms a very tightly bound Frenkel exciton, localized on the phenyl ring.

With the electronic excitations established, they can be compared to the data obtained from optical absorption measurements. An unambiguous test of the agreement between the proposed electronic structure (Figure 6) and experiment requires data from chain-extended and chain-oriented samples of macromolecular PPVs. With macromolecular samples, chain-end boundary conditions are not important; with oriented polymers, the polarization of the various absorptions with respect to the chain axis can be determined. Recent polarized absorption studies of highly oriented PPV and PPP indicate that the one-electron model is a good starting point.[54, 55]

4.4. Solitons, Polarons, and Polaron Excitons: The Elementary Excitations of Conducting Polymers

Although bond relaxation in the excited state is implicitly allowed through the bond-length dependent hopping integral in the SSH model, the effect of bond relaxation, and the formation of solitons, polarons, and bipolarons, has not been explicit in Section 4.3. These important concepts are summarized in the following paragraphs. In the related experimental studies, *trans*-polyacetylene and polythipohene were used as the model systems for the degenerate ground-state polymer and the nondegenerate ground-state polymer, respectively.[4]

4.4.1. Solitons

Charge storage on the polymer chain leads to structural relaxation, which in turn localizes the charge. The simplest example of the dramatic effect of this structural relaxation is the soliton in *trans*-polyacetylene. The soliton is a domain boundary between the two possible degenerate ground-state configurations of *trans*-(−CH=CH−)$_N$, the "A" Phase and the "B" Phase. For simplicity, we often draw the chemical structure of the soliton as an abrupt change from A Phase to B Phase, as shown in Scheme 3e. In agreement with the predictions of the SSH model,[4] however, the experimental evidence indicates that the structural relaxation in the vicinity of the domain boundary extends over approximately seven carbon atoms, as illustrated in Scheme 3f. The corresponding spin and charge distributions are similarly delocalized.

The value of a picture like Scheme 3e quickly becomes evident when one tries to understand the quantum numbers of the soliton and the reversed charge–spin relationship that characterizes the solitons of polyacetylene (see Figure 7c). Since the nonbonding, or mid-gap, state formed by the chain relaxation can then be mapped to a specific atomic site, the resulting distribution of charge and spin can be easily addressed; if the state is unoccupied (doubly occupied), the carbon atom at the boundary is left with a positive (negative) charge, but there are no unpaired spins; the charged soliton is positively (negatively) charged and spinless. Single occupation of the soliton state neutralizes the electronic charge of the carbon nucleus, while introducing an unpaired spin onto the chain. The localized electronic state associated with the soliton is a nonbonding state at an energy which lies at the middle of the π–π^* gap, between the bonding and antibonding levels of the perfect chain. On the other hand, the defect is both topological and mobile because of the translational symmetry of the chain. Such a topological and mobile defect is historically referred to as a soliton.[4–6] The term "soliton" (S) refers simultaneously to all three types of solitons; the quantum numbers for spin and charge enter only when referring to a specific type (for example, neutral solitons found as defects from the synthesis of undoped material or charged solitons created by photoexcitation), and even then, the spin is only implicit. Another feature of the soliton terminology is the natural definition of an "anti-soliton" (AS) as a reverse boundary from B Phase back to A Phase in Scheme 3e and 3f. The anti-soliton allows for conservation of soliton number upon doping or upon photoexcitation.

4.4.2. Polarons and Bipolarons

In cases such as poly(thiophene), PPV, PPP, and *cis*-polyacetylene where the two possible bond-alternation patterns are not energetically degenerate, confined soliton–antisoliton pairs, polarons, and bipolarons, are the stable nonlinear excitation and the stable charge-storage states.[56, 57] A polaron can be thought of as a bound state of a charged soliton and a neutral soliton whose mid-gap energy states hybridize to form bonding and antibonding levels. The neutral soliton contributes no charge and a single spin, as noted above, and the charged soliton carries charge of $\pm e$ and no spin; the resulting polaron then has the usual charge–spin relationship of fermions; $q = \pm e$ and $s = 1/2$. The polaron is illustrated schematically for PPP in Figure 7a and b. The positive

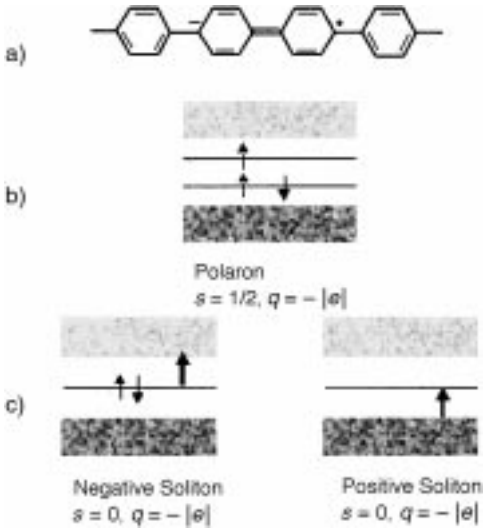

Figure 7. a) Schematic picture of a polaron in PPP, b) band diagram of an electron polaron ; for a hole polaron the lower gap state is single occupied and the upper gap state is empty, c) band diagrams for positive and negative solitons with associated electronic transitions.

(negative) polaron is a radical cation (anion), a quasiparticle consisting of a single electronic charge dressed with a local geometrical relaxation of the bond lengths. Similarly, a bipolaron is a bound state of two charged solitons of like charge (or two polarons whose neutral solitons annihilate each other) with two corresponding mid-gap levels, as illustrated in Figure 8a and b. Since each charged soliton carries a single electronic charge and no spin, the bipolaron has charge $\pm 2e$ and zero spin. The positive (negative) bipolaron is a spinless dication (dianion); a doubly charged bound state of two polarons bound together by the overlap of a common lattice distortion (enhanced geometrical relaxation of the bond lengths).

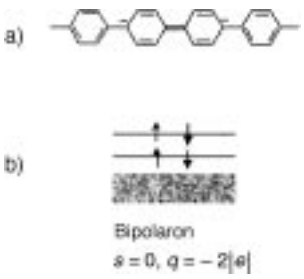

Figure 8. Bipolarons in polymer with nondegenerate ground state, a) schematic picture of a negative bipolaron, b) bond diagram for a negative bipolaron, for a positive bipolaron, both gap states are unoccupied.

4.4.3. Solitons and Polarons in Conjugated Polymers: Experimental Results

The models outlined above for solitons, polarons, and bipolarons make concrete predictions of experimentally observable phenomena, and indeed theoretical progress would not have been possible without concurrent experimental investigation. Optical probes of the mid-gap electronic states (see Figure 7c) and magnetic measurements of spin concentrations and spin distributions contributed greatly to the refinement and verification of theoretical predictions. For a detailed review of the experimental results, the reader is referred to the *Review of Modern Physics* article on this subject.[4]

5. Photoinduced Electron Transfer

The discovery of photoinduced electron transfer in composites of conducting polymers (as donors, D) and buckminsterfullerene, C_{60}, and its derivatives (as acceptors, A) opened a number of new opportunities for semiconducting polymers.[58, 59] A schematic description of the photoinduced electron transfer process is displayed in Scheme 4.

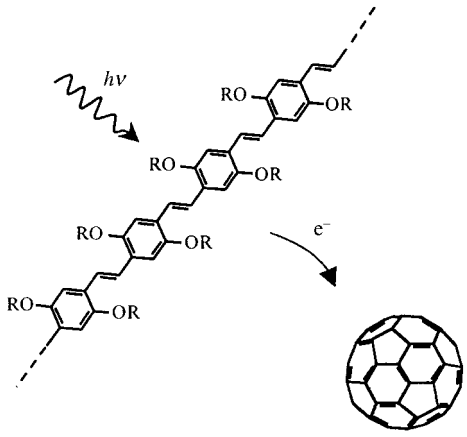

Scheme 4. Photoinduced electron transfer from a conjugated semiconducting polymer to C_{60}.

A broad range of studies has been carried out to fully characterize this photoinduced charge transfer, culminating with a study of the dynamics of photoinduced electron transfer from semiconducting polymers to C_{60} using femtosecond time-resolved measurements.[60, 61] These studies demonstrated that the charge transfer occurs within 50 femtoseconds after photo-excitation. Since the charge-transfer rate is more than 1000 times faster than any competing process (the luminescence lifetime is greater than 300 picoseconds), the quantum efficiency for charge separation approaches UNITY! Moreover, the charge-transferred state is metastable.[62, 63]

Semiconducting polymers are electron donors upon photoexcitation (electrons promoted to the antibonding π^* band). The idea of using this property in conjunction with a molecular electron acceptor to achieve long-lived charge separation is based on the stability of the photoinduced

nonlinear excitations (such as polarons) on the conjugated polymer backbone. Buckminsterfullerene (C_{60}) is an excellent electron acceptor capable of taking on as many as six electrons;[64] C_{60}, therefore, forms charge-transfer salts with a variety of strong donors. It is reasonable, therefore to consider electron transfer from photo-excited semiconducting polymers to C_{60}. Figure 9 shows a schematic energy-level

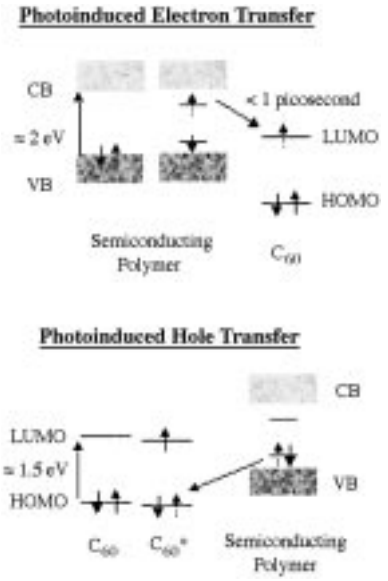

Figure 9. Energy-band diagram for photoinduced electron transfer and photoinduced hole transfer between semiconducting polymers and C_{60}.

diagram of the photoinduced electron (or hole) transfer process, which can be described in terms of the following steps:

Step 1: $D + A \rightarrow {}^{1,3}D^* + A$ (excitation on D)

Step 2: ${}^{1,3}D^* + A \rightarrow {}^{1,3}(D-A)^*$ (excitation delocalized on D – A complex)

Step 3: ${}^{1,3}(D-A)^* \rightarrow {}^{1,3}(D^{\delta+}-A^{\delta-})^*$ (charge transfer initiated)

Step 4: ${}^{1,3}(D^{\delta+}-A^{\delta-})^* \rightarrow {}^{1,3}(D^{+\bullet}-A^{-\bullet})$ (ion radical pair formed)

Step 5: ${}^{1,3}(D^{+\bullet}-A^{-\bullet}) \rightarrow D^{+\bullet} + A^{-\bullet}$ (charge separation)

where the donor (D) and acceptor (A) units are either covalently bound (intramolecular), or spatially close but not covalently bonded (intermolecular); steps 1 and 3 denote singlet or triplet excited states, respectively.

Since the partial charge transfer at step 3 is strongly dependent on the surrounding medium there is a continuous range for the transfer rate, $0 < \delta < 1$. At step 4, $\delta = 1$, that is, a whole electron is transferred. At each step, the D – A system can relax back to the ground state either by releasing energy to the "lattice" (in the form of heat) or through light emission (provided the radiative transition is allowed). The electron-transfer step (step 4) describes the formation of an ion radical pair; this does not occur unless $I_{D^*} - A_A - U_C < 0$, where I_{D^*} is the ionization potential of the excited state (D*) of the donor, A_A is the electron affinity of the acceptor, and U_C is the Coulomb energy of the separated radicals (including polarization effects). Stabilization of the charge separation (step 5) can be enabled by carrier delocalization on the D^+ (and/or A^-) species and by structural relaxation. The symmetrical process of hole transfer from the photoexcited acceptor to the donor is described in an analogous way, and can be driven by photoabsorption in spectral regions where the acceptor can be photoexcited but not the donor.

Even though the photoinduced electron-transfer reaction is energetically favorable, energy must be conserved in the process. In semiconducting polymers, the excess energy is readily taken up by promoting the hole to a higher energy state in the π^* band. Ultimately, therefore, the ultrafast nature of the photoinduced electron-transfer process results from the delocalized nature of the π electrons. Once the photoexcited electron is transferred to an acceptor unit, the resulting cation radical (positive polaron) species on the conjugated polymer backbone is relatively stable. Thus, photoinduced electron transfer from the conjugated-polymer donor onto an acceptor moiety can be viewed as "*photo-doping*" (see Figure 2). The forward to reverse asymmetry of the photoinduced charge separation in the conducting polymer/C_{60} system is nevertheless remarkable; the asymmetry is orders of magnitude greater than that observed in the photosynthesis of green plants.

Definitive evidence of charge transfer and charge separation was obtained from light-induced ESR (LESR) experiments.[58, 63, 65] Upon illuminating the conjugated polymer/C_{60} composites with light with $h\nu > E_{\pi\text{-}\pi^*}$ where $E_{\pi\text{-}\pi^*}$ is the energy gap of the conjugated polymer (donor), two photoinduced ESR signals can be resolved; one at $g = 2.00$ and the other at $g = 1.99$.[58, 63] The higher g-value line is assigned to the conjugated polymer cation (polaron) and the lower g-value line to the C_{60}^- ion. The assignment of the lower g-value line to C_{60}^- ion is unambiguous, for this low g-value was measured earlier;[64] the higher g-value is typical of conjugated polymers. The LESR signal vanishes above 200 K; this rules out permanent photochemical changes as the origin of the ESR signal and demonstrates the reversibility of the photoinduced electron transfer. The integrated LESR intensity shows two peaks with equivalent intensities. The temperature dependence of the LESR signal intensity shows Arrhenius behavior with activation energy of approximately 15 meV. This result suggests a phonon assisted back-relaxation mechanism of the photoinduced charge-separated state.[63]

In MEH – PPV/C_{60} composites, the strong photoluminescence of MEH – PPV is quenched by a factor in excess of 10^3, and the luminescence decay time is reduced from $\tau_o = 550$ ps to $\tau_{rad} \ll 60$ ps (the instrumental resolution) indicating that charge transfer has cut-off the radiative decay.[58, 62, 63] An estimate of the transfer rate, $1/\tau_{ct}$, can be obtained from the quenching of the photoluminescence [Eq. (13)] where $1/\tau_o$ and $1/\tau_{rad}$ are the radiative decay rates, I_o and I_{comp} are the integrated photoluminescence intensities of MEH – PPV and the MEH – PPV/C_{60} composite, respectively.

$$1/\tau_{ct} \approx (1/\tau_{rad})I_o/I_{comp} \qquad (13)$$

The data imply, therefore, that $1/\tau_{ct} > 10^{12}$; that is, electron transfer occurs on the sub-picosecond time scale. The ultrafast charge-transfer process was subsequently time resolved;[60, 61] the data directly confirm that charge transfer occurs within a few hundred femtoseconds.

The photoinduced electron-transfer process serves to sensitize the photoconductivity of the semiconducting polymer.[66] Time-resolved transient photocurrent measurements indicate that the addition of as little as 1% of C_{60} into the semiconducting polymer results in an increase of initial photocurrent by an order of magnitude. This increase of the photocarrier generation efficiency is accompanied by an increase in lifetime of the photocarriers upon adding C_{60}. Thus, the ultrafast photoinduced electron transfer from the semiconducting polymer onto C_{60} not only enhances the charge-carrier generation in the host polymer but also serves to prevent recombination by separating the charges and stabilizing the charge separation.

Conjugated polymers with higher electron affinities (e.g. cyano-substituted PPV) function as the acceptor component with MEH–PPV as the donor.[67, 68] Through control of the morphology of the phase separation into an interpenetrating bicontinuous network of D and A phases, high interfacial area was achieved within a bulk material: a "bulk D/A heterojunction" that yields efficient photoinduced charge separation.[67–70] These all-polymer phase-separated blends were successfully used in fabricating solar cells with efficiencies that approach those fabricated from amorphous silicon.[69]

6. Metallic Polymers and the Metal–Insulator Transition

6.1. Metallic Polymers with High Performance Electrical and Mechanical Properties

An early (and continuing) goal of the field of conducting polymers was the creation of materials with high electrical conductivity *and* with the excellent mechanical properties of polymers. This goal has been achieved; more importantly the conditions for realizing this combination of properties are understood and can be applied to new materials.

Electrical conductivity results from the existence of charge carriers and the ability of those carriers to move. In principle, broad π-electron bandwidths (often several eV) can lead to relatively high carrier mobilities.[4] As a result of the same intrachain π bonding and the relatively strong interchain electron-transfer interaction, the mechanical properties (Young's modulus and tensile strength) of conjugated polymers are potentially superior to those of saturated polymers. Thus, metallic polymers offer the promise of truly high performance; high conductivity plus superior mechanical properties.

This combination of high electrical conductivity and outstanding mechanical properties has been demonstrated for doped polyacetylene.[70–75]

6.2. Metal–Insulator Transition in Doped Conducting Polymers

6.2.1. The Role of Disorder

Ioffe and Regel[76] argued that as the extent of disorder increased in a metallic system, there was a limit to metallic behavior; when the mean free path becomes equal to the interatomic spacing, coherent metallic transport would not be possible. Thus, the Ioffe–Regel criterion is defined in Equation (14) where k_F is the Fermi wave number and l is the mean free path. The metallic regime corresponds to $k_F l \gg 1$.

$$k_F l \approx 1 \tag{14}$$

Based on the Ioffe–Regel criterion, Mott proposed[77, 78] that a metal–insulator (M–I) transition must occur when the disorder is sufficiently large that $k_F l < 1$. In recognition of Anderson's early work on disorder induced localization, Mott called this M–I transition the "Anderson transition".[79] In the limit where $k_F l \ll 1$ (i.e. where the strength of the random disorder potential is large compared to the bandwidth), all states become localized and the system is called a "Fermi glass".[80] A Fermi glass is an insulator with a continuous density of localized states occupied according to Fermi statistics. Although there is no energy gap, the behavior is that of an insulator because the states at the Fermi energy are spatially localized.

The scaling theory of localization demonstrated that the disorder-induced M–I transition was a true phase transition with a well-defined critical point.[81] MacMillan[82] and Larkin and Khmelnitskii,[83] showed that near the critical regime of Anderson localization a power-law temperature dependence is to be expected for the conductivity.

The M–I transition in conducting polymers is particularly interesting; critical behavior has been observed over a relatively wide temperature range in a number of systems, including polyacetylene, polypyrrole, poly(*p*-phenylenevinylene), and polyaniline.[33] In each case, the metallic, critical, and insulating regimes near the M–I transition have been identified. The critical regime is tunable in conducting polymers by varying the extent of disorder (i.e. by studying samples with different $\rho_r \equiv \rho(1.4\ \mathrm{K})/\rho(300\ \mathrm{K})$), or by applying external pressure and/or magnetic fields. The transitions from metallic to critical behavior and from critical to insulating behavior have been induced with a magnetic field, and from insulating to critical and then to metallic behavior with increasing external pressure.[33]

In the metallic regime, the zero temperature conductivity remains finite with magnitude that depends on the extent of the disorder. Metallic behavior has been demonstrated for conducting polymers with $\sigma(T)$ remaining constant as T approaches zero.[33] Well into the metallic regime where the mean free path extends over many repeat units, the residual resistivity will become small, as in a typical metal. However, this truly metallic regime, with $k_F l \gg 1$ has not yet been achieved.

6.2.2. Infrared Reflectance Studies of the Metallic State and the Metal–Insulator Transition

Infrared (IR) reflectance measurements have played an important role in clarifying the metal physics of conducting polymers. To clarify the nature of the metallic state, high precision reflectance measurements were carried out over a

wide spectral range on a series of PPy – PF_6 samples in the insulating, critical, and metallic regimes near the M – I transition.[84] Since the reflectance in the infrared (IR) is sensitive to the charge dynamics of carriers near the Fermi energy (E_F), such a systematic reflectance study can provide information on the electronic states near E_F and how those states evolve as the system passes through the M – I transition. The data demonstrate that metallic PPy – PF_6 is a "disordered metal" and that the M – I transition is driven by disorder; similar results were obtained for polyaniline.[37, 85]

Figure 10 shows $\sigma(\omega)$ for a series of PPy – PF_6 samples (A – F) as obtained from Kramers – Kronig transformation of $R(\omega)$ at room temperature. For the most metallic samples, $R(\omega)$ exhibits metal-like features; a free-carrier plasma resonance

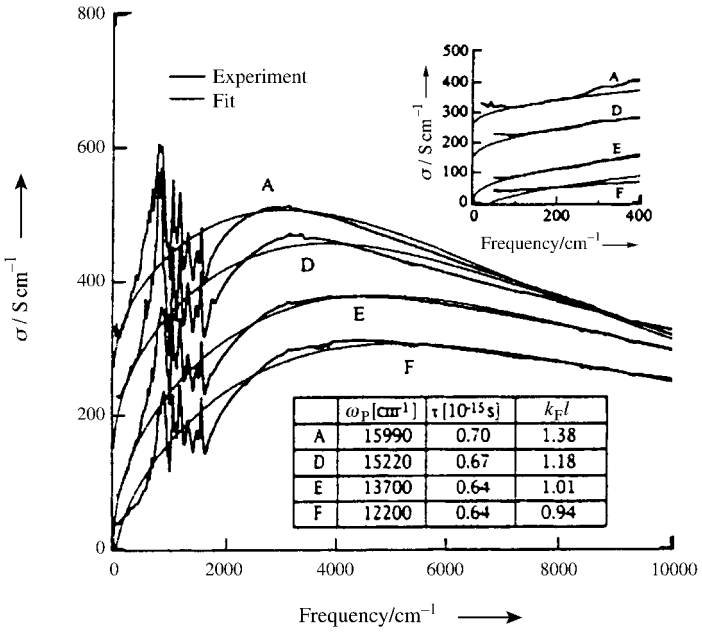

	ω_P [cm^{-1}]	τ [10^{-15} s]	$k_F l$
A	15990	0.70	1.38
D	15220	0.67	1.18
E	13700	0.64	1.01
F	12200	0.64	0.94

Figure 10. Frequency dependent conductivity $\sigma(\omega)$ for Ppy-PF_6. The inset shows the far-IR data in greater detail.

as indicated by a minimum in $R(\omega)$ near 1 eV and high $R(\omega)$ in the far IR. As PPy – PF_6 goes from the metallic to the insulating regime via the critical regime (samples A through F), $\sigma(\omega)$ is gradually suppressed in the IR. In the insulating regime (F), $\sigma(\omega)$ remains well below that of the metallic sample (A) throughout the IR range. The $\sigma(\omega)$ spectra are in excellent correspondence with the transport results (this is especially clear at low frequencies in Figure 10); the better the quality of the sample, as defined by the higher σ_{DC}(300 K), the higher $R(\omega)$ in the IR.[84]

In the far-IR (below 100 cm^{-1}), the Hagen – Rubens (H – R) approximation provides an excellent fit to $R(\omega)$ [Eq. (15)],[36] where σ_{H-R} is the ω-independent conductivity.

$$R_{H-R}(\omega) = 1 - (2\omega/\pi\sigma_{H-R})^{1/2} \quad (15)$$

The σ_{H-R} values obtained from the Hagen – Rubens fits are in remarkably good agreement with the measured values of σ_{DC}(300 K). The excellent fits and the agreement between σ_{H-R} and σ_{DC}(300 K) imply a weak ω dependence in the corresponding optical conductivity, $\sigma(\omega)$, for $\omega < 100$ cm^{-1}. The $\sigma(\omega)$ data are fully consistent with the "localization-modified Drude model" (LMD) [Eq. (16)][86] where k_F is the Fermi wave-number and l is the mean free path.

$$\sigma_{LD}(\omega) = \sigma_{Drude}\{1 - C[1 - (3\tau\omega)^{1/2}]/(k_F l)^2\} \quad (16)$$

In this model, the zero-frequency limit determines the constant C (precisely at the M – I Transition, $C = 1$) while a fit to $\sigma(\omega)$ determines $k_F l$. The suppressed $\sigma(\omega)$ as ω approaches zero arises from weak localization induced by disorder.[84] The $\sigma(\omega)$ data from the various regimes were fit with the functional dependence predicted by the LMD model; Figure 10 illustrates the excellent agreement of the fits to the data with the parameters summarized in the inset. The phonon features around 400 – 2000 cm^{-1} are, of course, not included in the LMD model. There are small deviations for $\omega < 100$ cm^{-1} (more important in the less metallic samples), below which phonon-assisted hopping makes a measurable contribution to $\sigma(\omega)$ and to the DC (direct current) conductivity.

The parameters obtained from the fits are reasonable. The screened plasma frequency, $\Omega_p = \omega_p/(\varepsilon_\infty)^{1/2} = 1.5 \times 10^4$ cm^{-1}, is in good agreement with the frequency of the minimum in $R(\omega)$, and τ is typical of disordered metals ($\tau \approx 10^{-14} - 10^{-15}$ s). The quantity $k_F l$ is of particular interest for it characterizes the extent of disorder and is often considered as an order parameter in localization theory.[87, 88] For all four samples represented in Figure 10, $k_F l \approx 1$, implying that all are close to the M – I transition. As the disorder increases and the system moves from the metallic regime (sample A with $k_F l = 1.38$) to the critical regime (sample E with $k_F l = 1.01$), $k_F l$ approaches the Ioffe – Regel limit,[76] precisely as would be expected. In the insulating regime (sample F) $k_F l = 0.94 < 1$, consistent with localization of the electronic states at E_F. Thus, the IR reflectance data obtained for metallic polymers indicate that they are disordered metals near the disorder-induced M – I transition. There is remarkable consistency between the conclusion obtained from transport studies and from IR reflectance measurements.

6.3. Striving Toward More Perfect Materials—Chain Extension, Chain Alignment, and Interchain Order

Experimental studies have established that for conducting polymers, the electrical properties and the mechanical properties improve together, in a correlated manner, as the degree of chain extension and chain alignment are improved. Polyacetylene remains the prototype example.

Figure 11 shows the correlation between the electrical conductivity (σ) and the draw ratio (λ) for iodine-doped polyacetylene films; the conductivity increases approximately linearly with the draw ratio.[73] The slope of σ versus λ is approximately a factor of two larger for the thinner films (evidently the details of polymerization and/or doping result in more homogeneous, higher quality material for the thinner films). X-ray diffraction studies of these drawn films exhibited

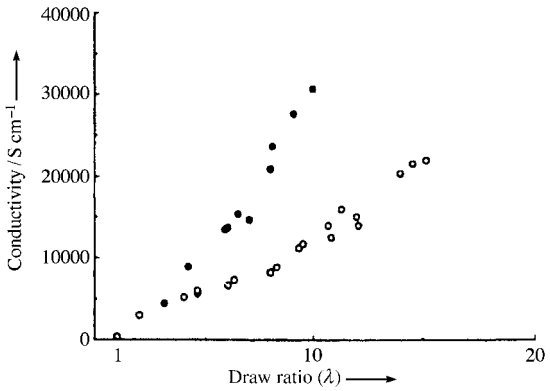

Figure 11. Electrical conductivity of iodine-doped polyacetylene (parallel to the draw axis) versus draw ratio; ● thin films of thickness 3–5 μm, ○ films of thickness 25–30 μm.

a high degree of structural order that improves with the draw ratio; the structural-coherence length perpendicular to the draw direction increases by about a factor of two as the films are drawn, from 10 nm at $\lambda = 4$ to 20 nm at $\lambda = 15$.[73] Consistent with the chain orientation and the improved structural order, the anisotropy ($\sigma_{\parallel}/\sigma_{\perp}$) in the electrical conductivity increased with the draw ratio, approaching 250 as $\lambda \rightarrow 15$ (although $\sigma_{\parallel}$ increased dramatically as a function of λ, $\sigma_{\perp}$ remains essentially constant). These data set a lower limit on the intrinsic anisotropy and demonstrate that heavily doped polyacetylene is a highly anisotropic metal with relatively weak interchain coupling.

Does the weak interchain coupling imply poor mechanical properties? The answer is "No"; for films with $\lambda = 15$, Young's modulus reaches 50 GPa and the tensile strength approaches 1 GPa, mechanical properties which are characteristic of high-performance materials. More importantly, the data demonstrate a direct correlation between the electrical conductivity and the mechanical properties. The linear relationship implies that the increase in both the conductivity and the modulus (or tensile strength) with draw ratio result from increased uniaxial orientation, improved lateral packing, and enhanced interchain interaction. The correlations between the electrical conductivity and the mechanical properties observed for polyacetylene are general. This correlation has been demonstrated in every case studied,[31] and can be understood as a general feature of conducting polymers.

Although the electrical conductivity is enhanced by the relatively high mobility associated with intrachain transport, one must have the possibility of interchain charge transfer to avoid the localization inherent to systems with a 1D electronic structure.[77] The electrical conductivity becomes three-dimensional (3D; and thereby truly metallic) only if there is high probability that an electron will have diffused to a neighboring chain prior to traveling between defects on a single chain. For well-ordered crystalline material in which the chains have precise phase order, the interchain diffusion is a coherent process. In this limit, the condition for extended anisotropic transport is given in Equation (17)[89] where L is the coherence length, a is the length of the chain repeat unit, t_o is the intrachain π-electron transfer integral, and t_{3d} is the interchain π-electron transfer integral.

$$L/a \gg (t_o/t_{3d}) \quad (17)$$

A precisely analogous argument can be constructed for achieving the intrinsic strength of a polymer material; that is, the strength of the main-chain covalent bonds. If E_o is the energy required to break the covalent main-chain bond and E_{3d} is the weaker interchain bonding energy (from van der Waals forces and hydrogen bonding), then the requirement is coherence over a length L such that Equation (18) holds.[90]

$$L/a \gg E_o/E_{3d} \quad (18)$$

In this limit, the large number, L/a, of weak interchain bonds add coherently such that the polymer fails by breaking of the covalent bond. The direct analogy between Equations (17) and (18) is evident. When the interchain structural order is "nematic" (i.e. without precise phase order), the conditions become $L/a \gg (t_o/t_{3d})^2$ and $L/a \gg (E_o/E_{3d})^2$, respectively.[89] Thus, the achievement of high-performance materials with nematic order requires even greater longer-range intrachain coherence.

In fact, for conjugated polymers, E_o results from a combination of σ and π bonds (the latter being equal to t_o) and E_{3d} is dominated by the interchain transfer integral, t_{3d}. Thus, the inequalities imply that, quite generally, the conductivity and the mechanical properties will improve in a correlated manner as the degree of chain alignment is increased. This prediction is in excellent agreement with data obtained from studies of the poly(3-alkylthiophenes), the poly(phenylene vinylenes), poly(thienylene vinylene), and polyacetylene.[31]

Assuming that the linear correlation persists to even higher draw ratios, the extrapolated modulus of 300 GPa for polyacetylene would imply that the electrical conductivity of perfectly oriented polyacetylene would be approximately 2×10^5 S cm^{-1}.[91] However, this extrapolated value might still be limited by structural defects (e.g. sp^3 defects, etc.) rather than by intrinsic phonon scattering.

A theoretical estimate of the intrinsic conductivity, limited by phonon scattering, yields the Equation (19)[89] where $\sigma_{\parallel}$ is the conductivity parallel to the chain, h is Plancks's constant, α is the strength of the electron–phonon interaction, M is the mass of the repeat unit of length a, and t_o is the transfer integral (2–3 eV).

$$\sigma_{\parallel} = (e^2/2ha)na^3(2\pi M\omega_0 t_0^2/\alpha^2 h)\exp[h\partial_{ph}/k_B T] \quad (19)$$

Using parameters obtained by experiment, Equation (19) predicts $\sigma_{\parallel} = 2 \times 10^6$ S cm^{-1} at room temperature,[89] more than an order of magnitude greater than that achieved to date. The exponential dependence upon T arises from the fact that backscattering must involve a high-energy phonon with wave number near the zone boundary. The high conductivity values and the exponential increase in conductivity on lowering the temperature predicted by Equation (19) indicates that the achievement of metallic polymers in which the macromolecules are chain extended and chain aligned is a major opportunity.

6.4. The Possibility of Superconductivity in Metallic Polymers

Superconductivity has not yet been observed in doped conjugated polymers. Might one expect superconductivity? If so what are the materials requirements? There is every reason to be optimistic that superconductivity will be discovered in doped conjugated polymers:

a) They are metals
b) The coupling of the electronic structure to the molecular structure is well known. Upon doping, the bond lengths change such that charge is stored in solitons, polarons, and bipolarons. Thus, the electron–phonon interaction that is responsible for superconductivity in conventional metals, leads to important effects in metallic polymers. In this context, doubly charged bipolarons can be thought of as analogous to real-space Cooper pairs.

As shown above, however, currently available metallic polymers are barely metallic; their electronic properties are dominated by disorder with mean free paths close to the Ioffe–Regel criterion for disorder induced localization.

It is interesting to compare the transport properties of available metallic polymers with those of the underdoped high-T_c (critical temperature) superconductors at doping levels where $k_F l \sim 1$. For example, when $YBa_2Cu_3O_{7-\delta}$ is underdoped to values of δ such that the resistivity *increases* as the temperature is lowered with $\rho_r \equiv \rho(1.4\ K)/\rho(300\ K) \approx 2$ (i.e. with temperature dependence similar to that found in the best metallic polymers), the disorder associated with the random occupation of the oxygen sites quenches the superconductivity.

The phase diagrams of $MBa_2Cu_3O_{7-\delta}$ (where M = Y, Dy, etc.) have been thoroughly studied.[92] For large δ, $MBa_2Cu_3O_{7-\delta}$ are antiferromagnetic insulators; increasing the oxygen concentration introduces carriers into the CuO_2 planes and results in a transition from the antiferromagnetic insulating phase to the metallic and superconducting phase. The changes in resistivity which occur during this evolution from insulator to metal (and superconductor) have been followed in detail in a continuous set of resistivity measurements carried out on ultra-thin films.[93, 94] Thus, the prototypical high-T_c "superconductors" show behavior characteristic of the disorder-induced metal–insulator transition. Near the metal–insulator transition, the ρ versus T curves look remarkably similar to those obtained from "metallic" polyaniline, polypyrrole, and PPV. At doping levels near the metal–insulator transition there is no sign whatever of the fact that these copper-oxide systems exhibit superconductivity with the highest known transition temperatures.

The point is quite clear. One cannot expect to make any progress toward superconductivity in metallic polymers until there is a major improvement in the quality of materials to the point where the mean free path is much longer than the characteristic monomer repeat units. When this has been achieved, $k_F l \gg 1$ and the resistivity will be truly metal-like, decreasing as the temperature decreases. The unresolved question is how to realize the required improvements in structural order? This remains as a major challenge to the field.

Although the required structural order is lacking in materials that are currently available, there is evidence that in metallic polyaniline, the electronic states near the Fermi energy interact strongly and selectively with a specific optical phonon mode.[95] The 1598 cm^{-1} Raman-active vibrational mode (A_g symmetry) exhibits a distinct resonance enhancement associated with the mid-IR absorption in metallic polyaniline. Since the mid-IR oscillator strength results from the intraband free-carrier Drude absorption, the resonant enhancement suggests that the symmetry of the electronic wavefunctions near E_F matches the vibrational pattern of the 1598 cm^{-1} normal mode. Quantum-chemical calculations of the electronic wavefunctions and analysis of the normal modes verified that this is in fact true.[95] Since the coupling of the electronic states near E_F to lattice vibrations is known to lead to superconductivity in metals, the demonstration of resonant coupling to a specific vibrational mode provides some optimism; at least this is the kind of feature that one would like to see.

The story of superconductivity in metallic polymers has not yet begun. If and when superconductivity is discovered in this class of materials, that discovery will create a new research opportunity that will be exciting and potentially important.

7. Applications

Solid-state photonic devices are a class of devices in which the quantum of light, the photon, plays a role. They function by utilizing the electro-optical and/or opto-electronic effects in solid-state materials. Because the interband optical transition (absorption and/or emission) is involved in photonic phenomena and because photon energies from near infrared (IR) to near ultraviolet (UV) are of interest, the relevant materials are semiconductors with band gaps in the range from 1 to 3 eV. Typical inorganic semiconductors used for photonic devices are Si, Ge, GaAs, GaP, GaN, and SiC. Photonic devices are often classified into three categories: light sources (light-emitting diodes, diode lasers etc.), photodetectors (photoconductors, photodiodes etc.), and energy-conversion devices (photovoltaic cells). All three are important. Because photonic devices are utilized in a wide-range of applications, they continue to provide a focus for research laboratories all over the world.

Most of the photonic phenomena known in conventional inorganic semiconductors have been observed in these semiconducting polymers.[32] The dream of using such materials in high performance "plastic" photonic devices is rapidly becoming reality: high-performance photonic devices fabricated from conjugated polymers have been demonstrated, including light-emitting diodes, light-emitting electrochemical cells, photovoltaic cells, photodetectors, and optocouplers; that is, all the categories which characterize the field of photonic devices. These polymer-based devices have reached performance levels comparable to or even better than their inorganic counterparts.

This Nobel Lecture is, perhaps, not the proper place to discuss in detail the many current and anticipated applications of semiconducting and metallic polymers; there is simply

neither time in the presentation nor space in the written document to do justice to the subject. Suffice it to say here that I am convinced that we are on the verge of a revolution in "Plastic Electronics". I refer those interested to recent reviews that focus on these important developments.[97] The advances in printing technology, for example, high resolution ink-jet printing, to fabricate semiconductor devices by processing the conducting polymer from solution has proven to be an enabling step in the development of plastic electronic devices such as diodes, photodiodes, LEDs, LECs, optocouplers, and thin-film transistors.[32]

8. Concluding Comments

I am greatly honored to receive the Nobel Prize in Chemistry for "the discovery and development of conducting polymers". The science of semiconducting and metallic polymers is inherently interdisciplinary; it falls at the intersection of Chemistry and Physics. In creating and expanding this "fourth generation" of polymers, we attempted to understand nature with sufficient depth that we could achieve materials with novel and unique properties; properties that are not otherwise available. This was (and is) an elegant and somewhat dangerous exercise; elegant because it required the synthesis of knowledge from the two disciplines, and dangerous because one is always pushing beyond the knowledge and experience of his background. I started out as a physicist, however, I am what I have become. I have evolved, with the help of many colleagues in the international scientific community, into an interdisciplnary scientist. That my work and that of my colleagues Alan MacDiarmid and Hideki Shirakawa has had sufficient impact on Chemistry to be recognized by the Nobel Prize gives me, therefore, particular satisfaction.

Received: February 13 , 2001 [A 451]

[1] H. Shirakawa, E. J. Louis, A. G. MacDiarmid, C. K. Chiang, A. J. Heeger, *Chem. Commun*. **1977**, 578.
[2] C. K. Chiang, C. R. Fincher, Jr., Y. W. Park, A. J. Heeger, H. Shirakawa, E. J. Louis, *Phys. Rev. Lett.* **1977**, *39*, 1098.
[3] B. Rånby in *Conjugated Polymers and Related Materials: The Interconnectionof Chemical and Electronic Structures* (Eds.: W. R. Salaneck, I. Lundström, B. Rånby), Oxford University Press, Oxford, **1993**, chap. 3.
[4] A. J. Heeger, S. Kivelson, J. R. Schrieffer, W. P. Su, *Rev. Mod. Phys.* **1988**, *60*, 781.
[5] W. P. Su, J. R. Schrieffer, A. J. Heeger, *Phys. Rev. Lett.* **1979**, *42*, 1698.
[6] W. P. Su, J. R. Schrieffer, A. J. Heeger, *Phys. Rev. B* **1980**, *22*, 2099.
[7] C. K. Chiang, S. C. Gau, C. R. Fincher, Jr., Y. W. Park, A. G. MacDiarmid, *Appl. Phys. Lett.* **1978**, *33*, 18.
[8] P. J.Nigrey, A. G. MacDiarmid, A. J. Heeger, *J. Chem. Soc. Chem. Commun*. **1979**, 594; C. Jones, P. M. Jordan, A. G. Chaudhry, M. Akhtar, *J. Chem. Soc. Chem. Commun*. **1979**, 96; R. D. Bach, D. H. Lucast, *J. Chem. Soc. Chem. Commun*. **1979**, 593.
[9] Q. Pei, G. Yu, C. Zhang, Y. Yang, A. J. Heeger, *Science* **1995**, *269*, 1086.
[10] W. R. Salaneck, I. Lundstrom, W. S. Haung, A. G. MacDiarmid, *Synth. Met.* **1986**, *13*, 291.
[11] Y. Cao, P. Smith, A. J. Heeger, *Synth. Met*. **1992**, *48*, 91.
[12] Y. Cao, P. Smith, A. J. Heeger, US-A 5 232 631.
[13] C. Y. Yang, Y. Cao, P. Smith, A. J. Heeger, *Synth. Met*. **1992**, *53*, 293.
[14] M. Reghu, Y. Cao, D. Moses, A. J. Heeger, *Phys. Rev. B* **1993**, *497*, 1758.
[15] H. Tomozawa, D. Braun, S. Philips, A. J. Heeger, H. Kroemer, *Synth. Met*. **1987**, *22*, 63; H. Tomozawa, D. Braun, S. D. Philips, R. Worland, A. J. Heeger, *Synth. Met*. **1989**, *28*, C687.
[16] J. H. Burroughes, D. D. C. Bradley, A. R. Brown, R. N. Marks, R. H. Friend, P. L. Burns, A. B. Holmes, *Nature* **1990**, *347*, 539.
[17] A. G. MacDiarmid, A. J.Epstein in *Conjugated Polymeric Materials: Opportunities in Electronics, Optical Electronics, Molecular Electronics* (Eds.: J. L. Bredas, R. R. Chance), Kluwer Academic, Dordrecht, **1990**, p. 53.
[18] F. Wudl, R. O. Angus, F. L. Lu, P. M. Allemand, D. J. Vachon, M. Nowak, Z. X. Liu, A. J. Heeger, *J. Am. Chem. Soc.* **1987**, *109*, 3677.
[19] N. S. Sariciftci, *Primary Photoexcitations in Conjugated Polymers*, World Scientific, Singapore, **1998**.
[20] S. A. Jenekhe, J. A. Osaheni, *Science* **1994**, *265*, 765.
[21] J. Cornil, D. A. do Santos, X. Crispin, R. Silbey, J. L. Bredas, *J. Am. Chem. Soc.* **1998**, *120*, 1289.
[22] L. J. Rothberg, M. Yan, F. Papadimitrakopoulos, M. E. Galvin, E. W. Kwock, T. M. Miller, *Synth. Met.* **1996**, *80*, 41.
[23] I. D. Parker, *J. Appl. Phys.* **1994**, *75*, 1656.
[24] E. S. Maniloff, D. Vacar, D. W. McBranch, H. Wang, B. R. Mattes, J. Gao, A. J. Heeger, *Opt. Commun.* **1997**, *141*, 243.
[25] L. Y. Chiang, A. F. Garito, D. J. Sandman, *Proceedings of the Materials Research Society*, *Vol. 247*, Materials Research Society, Pittsburgh, **1992**.
[26] F. Garnier, R. Hajlaoui, A. Yasser, P. Svrivastava, *Science* **1994**, *265*, 1684.
[27] J. H. Burroughes, C. A. Jones, R. H. Friend, *Nature* **1988**, *335*, 137.
[28] C. J. Drury, C. M. J. Mutsaers, C. M. Hart, M. Matters, D. M. de Leeuw, *Appl. Phys. Lett*. **1998**, *73*, 108.
[29] F. Hide, M. Diaz-Garcia. B. Schwartz, M. Andersson, Q.Pei, A. J. Heeger, *Science* **1996**, *73*, 1833.
[30] M. Kobayashi, N. Colaneri, M. Boysel, F. Wudl, A. J. Heeger, *J. Chem. Phys.* **1985**, *83*, 5717.
[31] A. J. Heeger, P. Smith in *Conjugated Polymers* (Eds.: J. L. Bredas, R. Silbey), Kluwer Academic, Dordrecht, **1991**.
[32] G. Yu, A. J. Heeger in *The Physics of Semiconductors*, *Vol. 1* (Eds.: M. Schleffer, R. Zimmerman), World Scientific, Singapore, **1996**.
[33] R. Menon, C. O. Yoon, D. Moses, A. J. Heeger in *Handbook of Conducting Polymers* (Eds.: T. A. Skotheim, R. L. Elsenbaumer, J. R. Reynolds), 2nd ed., Marcel Dekker, New York, **1998**, p. 85.
[34] L. Sun, S. C. Yang, *Polym. Prepr. Am. Chem. Soc. Div. Polym. Chem.* **1992**, *33*, 379; G. Heywang, F. Jonas, *Adv. Mater*. **1992**, *4*, 116.
[35] J. Friedrich, K. Werner, US-A 5 300 575.
[36] C. Kittel, *Introduction to Solid State Physics*, Wiley, New York, **1986**.
[37] K. Lee, A. J. Heeger, Y. Cao, *Phys. Rev. B* **1993**, *48*, 14 884.
[38] K. Lee, R. Menon, C. O. Yoon, A. J. Heeger, *Phys. Rev. B* **1995**, *52*, 4779.
[39] Y. Cao, G. M. Treacy, P. Smith, A. J. Heeger, *Appl. Phys. Lett.* **1992**, *60*, 2711.
[40] G. Gustafsson, Y. Cao, G. M. Treacy, F. Klavetter, N. Colaneri, A. J. Heeger, *Nature* **1992**, *357*, 477.
[41] J. Gao, A. J. Heeger, J. Y. Lee, C. Y. Kim, *Synth. Met.* **1996**, *82*, 221.
[42] Y. Cao, G. Yu, C. Zhang, R. Menon, A. J. Heeger, *Synth. Met*. **1997**, *87*, 171.
[43] I. H. Campbell, T. W. Hagler, D. L. Smith, J. P. Ferraris, *Phys. Rev. Lett.* **1996**, *76*, 1900.
[44] M. Pope, C. E. Swenberg, *Electronic Processes in Organic Crystals*, Clarendon Press, Oxford, **1982**.
[45] T. W. Hagler, A. J. Heeger, *Chem. Phys. Lett.* **1992**, *189*, 333.
[46] T. W. Hagler, K. Pakbaz, K. Voss, A. J. Heeger, *Phys. Rev. B* **1991**, *44*, 8652.
[47] A. Streitweiser, *Molecular Orbital Theory for Organic Chemists*, Wiley, New York, **1961**.
[48] P. Smith, P. J. Lemstra, J. P. L. Pijpers, A. M. Kile, Colloid, *Polym. Sci*. **1981**, *259*, 1070.
[49] R. E. Peierls, *Quantum Theory of Solids*, Clarendon Press, Oxford, **1955**.
[50] C. R. Fincher, C. E. Chen, A. J. Heeger, A. G. MacDiarmid, J. B. Hastings, *Phys. Rev. Lett.* **1982**, *48*, 100.

[51] C. S. Yannoni, T. C. Clarke, *Phys. Rev. Lett*. **1983**, *52* 1191.
[52] S. Brazovskii, N. Kirova, A. R. Bishop, *Opt. Mater*. **1998**, *9*, 465.
[53] N. Kirova, S. Brazovskii, A. R. Bishop, *Synth. Met.* **1999**, *100*, 29.
[54] E. K. Miller, D. Yoshida, C. Y. Yang, A. J. Heeger, *Phys. Rev. B* **1999**, *59*, 4661.
[55] E. K. Miller, C. Y. Yang, A. J. Heeger, *Phys. Rev. B* **2000**, *62*, 6889.
[56] K. Fesser, A. R. Bishop, D. Campbell, *Phys. Rev. B* **1983**, *27*, 4804.
[57] S. A. Brazovski, N. Kirova, *Sov. Phys. JETP (Engl. Transl.)* **1981**, *33*, 4.
[58] N. S. Sariciftci, L. Smilowitz, A. J. Heeger, F. Wudl, *Science* **1992**, *258*, 1474.
[59] S. Morita, A. A. Zakhidov, Y. Yoshino, *Solid State Commun*. **1992**, *82*, 249.
[60] B. Kraabel, D. McBranch, N. S. Sariciftci, D. Moses, A. J. Heeger, *Mol. Cryst. Liq. Cryst.* **1994**, *256*, 733; B. Kraabel, J. C. Hummelen, D. Vacar, D. Moses, N. S. Sariciftci, A. J. Heeger, *J. Chem. Phys.* **1996**, *104*, 4267.
[61] G. Lanzani, C. Zenz, G. Cerullo, W. Graupner, G. Leising, U. Scherf, S. De Silvestri, *Synth. Met*. **2000**, *111 – 112*, 493.
[62] L. Smilowitz, N. S. Sariciftci, R. Wu, C. Gettinger, A. J. Heeger, F. Wudl, *Phys. Rev. B* **1993**, *47*, 13835.
[63] N. S. Sariciftci, A. J. Heeger, *Int. J. Mod. Phys. B* **1994**, *8*, 237.
[64] P. M. Allemand, G. Srdanov, A. Koch, F. Wudl, *J. Am. Chem. Soc.* **1991**, *113*, 1050.
[65] K. Lee, R. Jansson, N. S. Sariciftci, A. J. Heeger, *Phys. Rev. B* **1994**, *49*, 5781.
[66] C. H. Lee, G. Yu, D. Moses, K. Pakbaz, C. Zhang, N. S. Sariciftci, A. J. Heeger, F. Wudl, *Phys. Rev. B* **1993**, *48*, 15425.
[67] G. Yu, A. J. Heeger, *J. Appl. Phys.* **1995**, *78*, 4510.
[68] J. J. M. Halls, C. M. Walsh, N. C. Greenham, E. A. Marseglia, R. H. Friend, S. C. Moratti, A. B. Holmes, *Nature* **1995**, *376*, 498.
[69] G. Yu, J. Gao, J. C. Hummelen, F. Wudl, A. J. Heeger, *Science* **1995**, *270*, 1789.
[70] C. Y. Yang, A. J. Heeger, *Synth. Met*. **1996**, *83*, 85.
[71] K. Akagi, M. Suezaki, H. Shirakawa, H. Kyotani, M. Shimamura, Y. Tanabe, *Synth. Met.* **1989**, *28*, D1.
[72] J. Tsukomoto, *Jpn. J. Appl. Phys.* **1990**, *29*, 1.
[73] Y. Cao, P. Smith, A. J. Heeger, *Polymer* **1991**, *32*, 1210.
[74] T. Schimmel, W. Reiss, J. Gmeiner, M. Schworer, H. Naarmann, N. Theophilou, *Solid State Commun*. **1998**, *65*, 1311.
[75] S. Tokito, P. Smith, A. J. Heeger, *Polymer* **1991**, *32*, 464.
[76] A. F. Ioffe, A. R. Regel, *Prog. Semicond.* **1960**, *4*, 237.
[77] N. F. Mott, E. A. Davis, *Electronic Processes in Noncrystalline Matrials*, Oxford University Press, Oxford, **1979**.
[78] N. F. Mott, *Metal-Insulator Transition*, Taylor & Francis, London, **1990**.
[79] P. W. Anderson, *Phys. Rev. B* **1958**, *109*, 1492.
[80] P. W. Anderson, *Comments Solid State Phys.* **1970**, *2*, 193.
[81] E. Abrahams, P. W. Anderson, D. C. Licciardello, T. V. Ramakrishnan, *Phys. Rev. Lett.* **1979**, *42*, 695.
[82] W. L. McMillan, *Phys. Rev. B* **1981**, *24*, 2739.
[83] A. I. Larkin, D. E. khmelnitskii, *Sov. Phys. JETP (Engl. Transl.)* **1982**, *56*, 647.
[84] K. Lee, E. K. Miller, A. N. Aleshin, R. Menon, A. J. Heeger, J. H. Kim, C. O. Yoon, H. Lee, *Adv. Mater*. **1998**, *10*, 456.
[85] K. Lee, A. J. Heeger, Y. Cao, *Synth. Met*. **1995**, *69*, 261.
[86] N. F. Mott, M. Kaveh, *Adv. Phys.* **1985**, *34*, 329.
[87] T. G. Castner in *Hopping Transport in Solids* (Eds.: M. Pollak, B. I. Shlovskii), Elsevier Science, Amsterdam, **1991**.
[88] P. A. Lee, T. V. Ramakrishnan, *Rev. Mod. Phys.* **1985**, *57*, 287.
[89] S. Kivelson, A. J. Heeger, *Synth. Met*. **1987**, *22*, 371.
[90] A. J. Heeger, *Faraday Discuss. Chem. Soc*. **1989**, *88*, 1.
[91] S. Tokito, P. Smith, A. J. Heeger, *Polymer* **1991**, *32*, 464.
[92] J. M. Tranquada in *Earlier and Recent Aspects of Superconductivity* (Eds.: J. G. Bednorz, K. A. Müller), Springer, Berlin, **1990**.
[93] T. Wang, K. M. Beauchamp, D. D. Berkley, B. R. Johnson, J. X. Liu, J. Zhang, A. M. Goldman, *Phys. Rev. B* **1991**, *43*, 8623.
[94] G. Yu, C. H. Lee, A. J. Heeger, N. Herron, E. M. McCarron, L. Cong, G. C. Spalding, C. A. Nordman, A. M. Goldman, *Phys. Rev. B* **1992**, *45*, 4964.
[95] N. S. Sariciftci, A. J. Heeger, V. Krasevec, P. Venturini, D. Mihailovic, Y. Cao, J. Libert, J. L. Bredas, *Synth. Met*. **1994**, *62*, 107.
[96] M. D. McGehee, E. K. Miller, D. Moses, A. J. Heeger in *Advances in Synthetic Metals: Twenty Years of Progress in Science and Technology* (Eds.: P. Bernier, S. Lefrant, G. Bidan, Elsevier Science, Lausanne, **1999**.
[97] M. D. McGehee, A. J. Heeger, *Adv. Mater.*, in press.

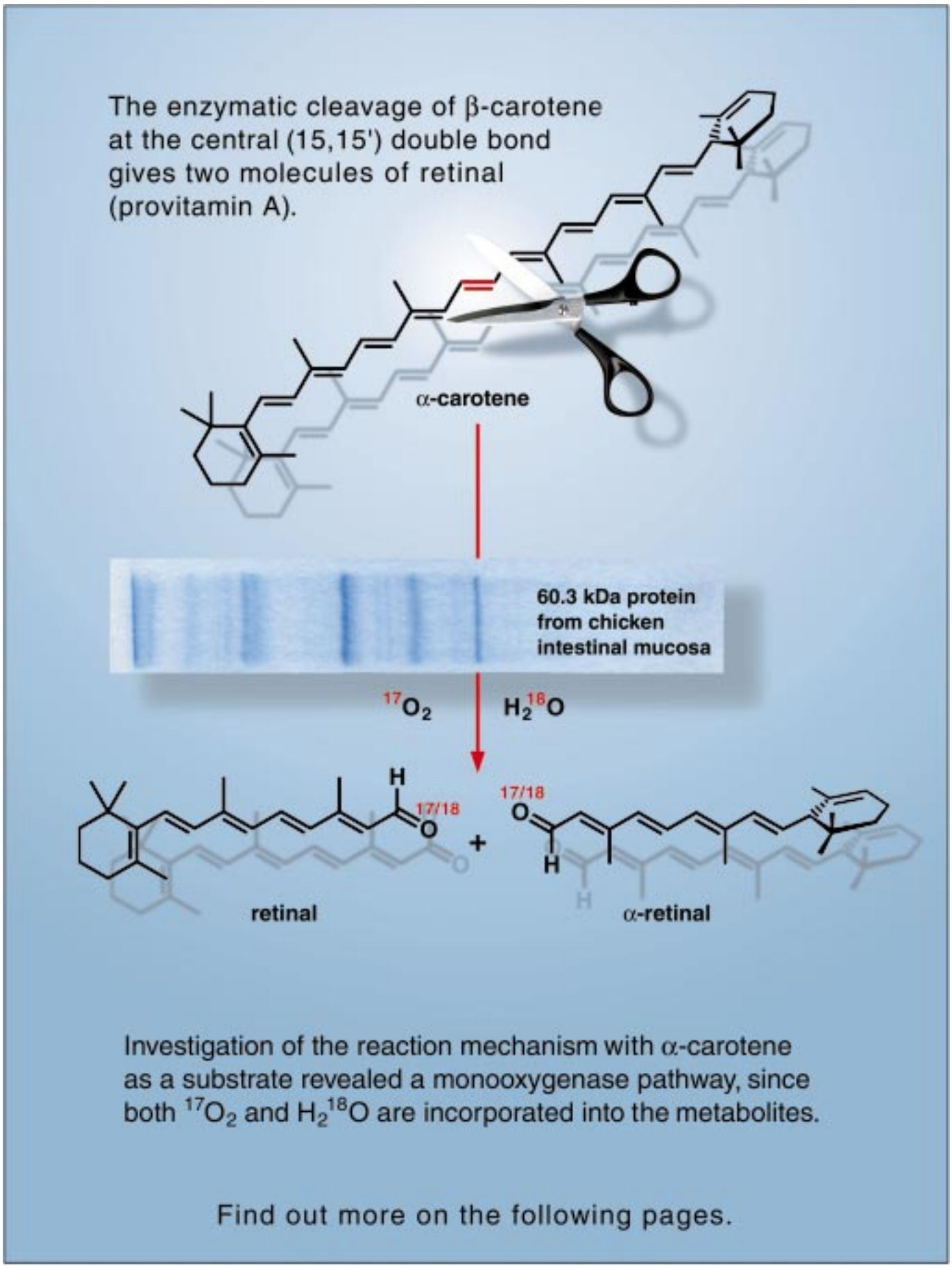

  1433-7851/01/4014-2613 $ 17.50+.50/0

The Reaction Mechanism of the Enzyme-Catalyzed Central Cleavage of β-Carotene to Retinal**

Michele G. Leuenberger, Caroline Engeloch-Jarret, and Wolf-D. Woggon*

Dedicated to Professor Synnøve Liaaen-Jensen

Although it has been known since 1930 that vitamin A or retinol (**1**) derives in vivo from β-carotene (**2**),[1] the enzymatic origin of β-carotene cleavage was only shown in 1965 when Olson and Hayaishi reported the identification of in vitro activity of an enzyme from rat liver and rat intestine. This enzyme catalyzes the central cleavage of **2** to retinal (β-retinal, **3**; Scheme 1).[2] Later an alternative, probably less significant, pathway was discovered involving excentric cleavage of **2** to yield apo-carotenals such as **4**, which are subsequently degraded to **3**.[3]

During the last 35 years many groups have tried unsuccessfully to purify the enzyme catalyzing the central cleavage of β-carotene **2**,[4] and quite a number of mechanistic investigations have been published which involved crude enzyme preparations or in vivo experiments.[2, 5, 6] Solid information, however, could only be obtained for two aspects of the problem: The enzyme requires molecular oxygen, and the central cleavage proceeds stoichiometrically to yield approximately two moles of retinal from one mole of β-carotene.[7] Most of the other experiments regarding the incorporation of oxygen from water and concerning the metal involved in catalysis can be valued as inadequate.[8] Nevertheless the enzyme that catalyzes the central cleavage of **2** was termed β-carotene 15,15′-dioxygenase (EC1.13.11.21) and often the enzyme was believed to be an iron dioxygenase.[2, 9]

Recently we[10a] and others[10b] have been able for the first time to identify the protein which catalyzes the central cleavage. We have developed a purification protocol for the enzyme from chicken intestinal mucosa and it has become possible to overexpress the functional 60.3 kDa protein in BHK (baby hamster kidney) cells.[10a,c] We have also investigated the substrate specificity of the enzyme with the aim of identifying a nonsymmetrical carotenoid that could be utilized for investigation of the mechanism.[11] This aspect was mainly overlooked in earlier work, we believe. However, only the use of a nonsymmetrical carotenoid as a substrate to yield different aldehydes can provide exact information on the incorporation of oxygen from water and/or air into cleavage products and, hence, distinguish a monooxygenase from a dioxygenase mechanism.

Substrate specificity studies revealed three nonsymmetrical carotenoids, **5**–**7**, that are readily cleaved by the enzyme (40–50% of the yield obtained for **2** under standard conditions) to furnish the corresponding aldehydes, for example, **5** →**3** and **8** (Scheme 2). α-Carotene **5** was chosen as the best candidate because it was available in isomerically pure form, and it was expected that aldehydes **3** and **8** would behave similarly in the subsequent reactions that would be required for mass spectrometry (MS) analysis of the distribution of the labeled oxygen in both cleavage products. In this context it is important to note that aldehydes such as **3** and **8** are not directly suitable for isotopic analysis of an oxygen label in the carbonyl group[12] because this label easily exchanges with the medium at the pH value of incubation (pH 7.8).[13] Thus, we decided for a combined enzyme assay with addition of horse liver alcohol dehydrogenase (HLADH) to reduce **3** and **8** in situ to the corresponding alcohols retinol (**1**) and α-retinol (**9**). Alcohols **1** and **9** are also unsuitable for tandem gas chromatography/mass spectrometry (GC-MS) analysis because both eliminate water. Thus, after quenching of the incubation and high-pressure liquid chromatography (HPLC) purification of alcohols **1** and **9** (Figure 1a), derivatization to the silyl ethers **10** and **11** was required (Figure 1b).

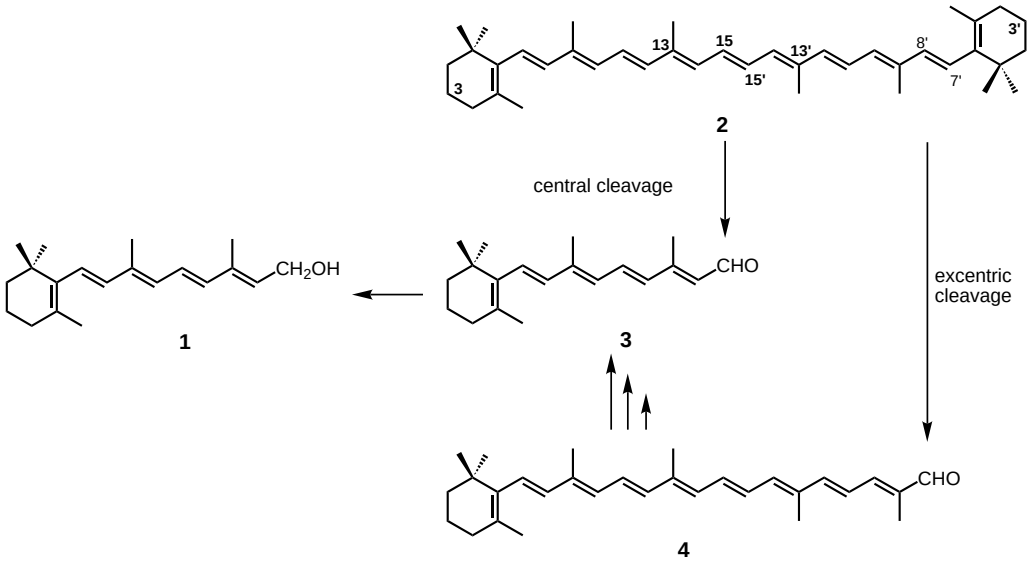

Scheme 1. Enzymatic cleavage of β-carotene **2**. Routes to the formation of retinol **1**.

Control experiments revealed that the rates of reduction of **3** and **8** are the same. Exchange of the carbonyl oxygen of **3** with the buffer medium was investigated under conditions similar to the incubation conditions, that is, **3** was added to a

[*] Prof. W.-D. Woggon, Dipl.-Chem. M. G. Leuenberger, Dr. C. Engeloch-Jarret
Institute of Organic Chemistry
University of Basel
St. Johanns-Ring 19, 4056 Basel (Switzerland)
Fax: (+41) 61-267-1102
E-mail: wolf-d.woggon@unibas.ch

[**] This research was supported by F. Hoffmann–La Roche AG and the Swiss National Science Foundation. We are grateful to F. Hoffmann–La Roche AG for a generous gift of carotenoids and Dr. Claus Bornemann for preliminary experiments.

  1433-7851/01/4014-2614 $ 17.50+.50/0

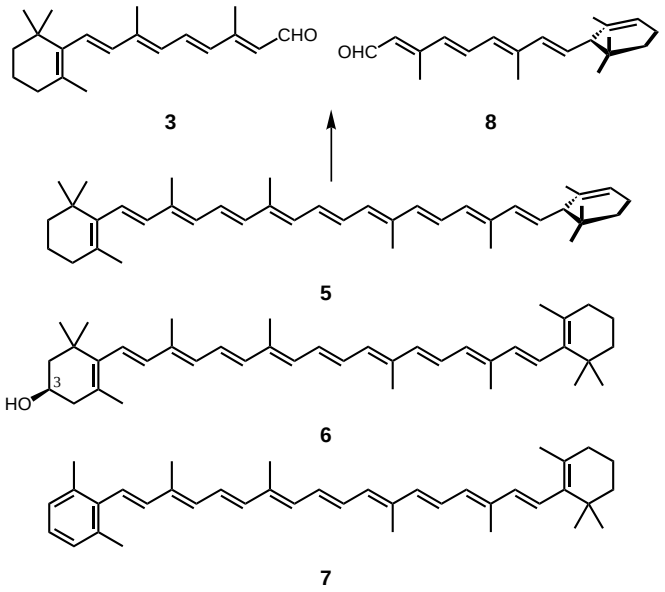

Scheme 2. Nonsymmetrical substrate analogues of the enzyme that catalyzes the central cleavage of **2**. Cleavage of α-carotene **5** to form the aldehydes **3** and **8**.

solution of HLADH in $H_2{}^{18}O$ as slowly as it would be produced by enzymatic cleavage of **5** (3.5 nmol h^{-1}). According to MS analysis of the retinyl silylether **10**, exchange of the ^{18}O label between **3** and $H_2{}^{18}O$ is $<5\,\%$.

For the decisive incubation experiment with **5** the native enzyme was employed due to its favorable turnover, which is $\approx$2.5 times higher than the hexahistidine-tailed protein overexpressed in BHK cells. Highly enriched oxygen sources, such as 85 % $^{17}O_2$ and 95 % $H_2{}^{18}O$, were used. GC-MS analysis of the silylethers **10** and **11** with the focus on the molecular ion

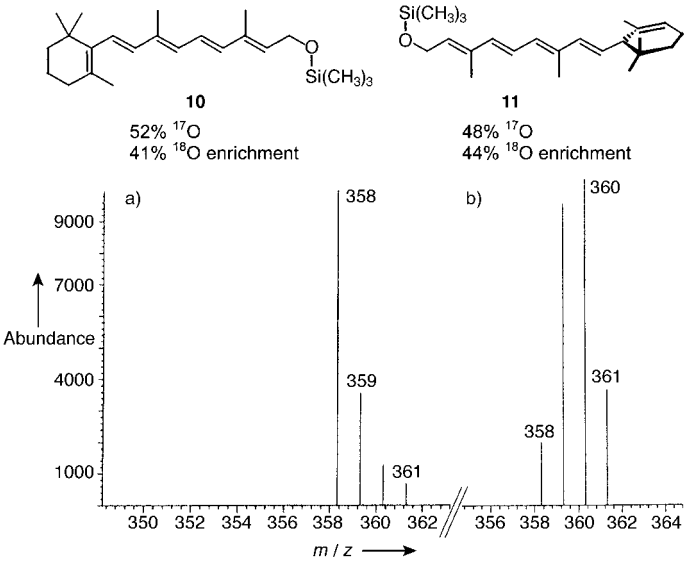

Figure 2. Mass spectra: a) silylether **10** with natural abundance of oxygen isotopes; b) $^{17}O/^{18}O$-enriched **10** from incubation of **5** in the presence of $^{17}O_2$ and $H_2{}^{18}O$.

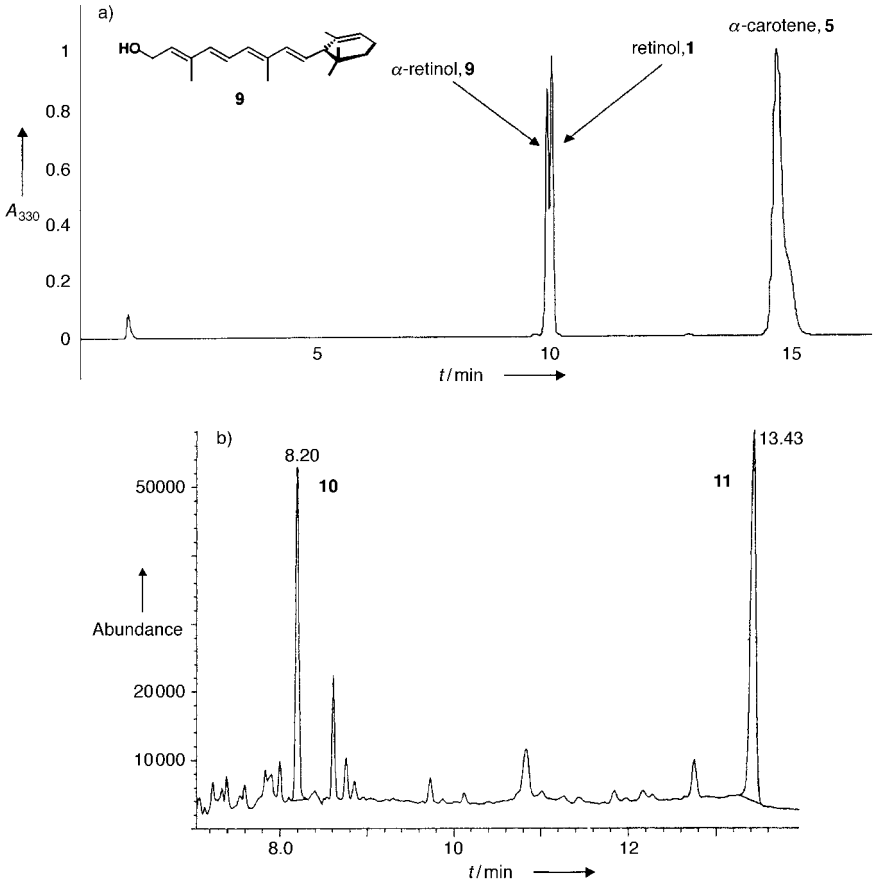

Figure 1. a) HPLC trace recorded after incubation of α-carotene **5**; b) GC trace for **10** and **11**, the silylethers of the metabolites of **5**.

area revealed, within experimental error, equal enrichment of the ^{17}O and ^{18}O label in both derivatives of metabolites **3** and **8** (Figure 2). This result proves for the first time the incorporation of one ^{17}O atom of molecular oxygen and the concomitant incorporation of one ^{18}O atom from labeled water.

Accordingly, and in contrast to earlier beliefs, the reaction mechanism of enzymatic central β-carotene cleavage is not in agreement with a dioxygenase-catalyzed procedure. A dioxygenase mechanism ([2+2] cycloaddition to the central C15–C15′ double bond, followed by fragmentation of the intermediate dioxetane) would require the incorporation of one complete oxygen molecule into the product aldehydes and the absence of any ^{18}O label originating from the labeled water.

Experimental evidence provided here accounts for a monooxygenase-type mechanism, as shown in Scheme 3, in which the first step is an epoxidation of the central double bond of **5**. This is followed by unselective ring opening with water and final diol cleavage to yield the aldehydes **3** and **8**.

Another small experimental detail agrees with the monooxygenase mechanism. Given the enrichment of the labels in both oxygen

  1433-7851/01/4014-2615 $ 17.50+.50/0

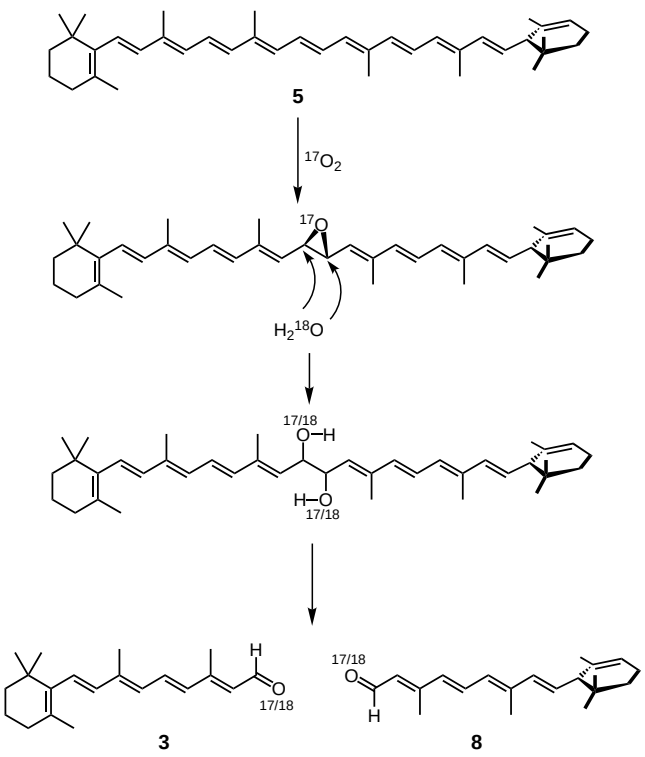

Scheme 3. The reaction mechanism of the central cleavage of α-carotene **5** catalyzed by the 60.3 kDa cytosolic monooxygenase purified from chicken's intestinal mucosa. The mechanism for β-carotene **2** is thought to be analogous.

sources, one would expect, in case of quantitative O-incorporation, the following isotopic enrichments for **10** and **11**: 10 % ^{16}O, 42.5 % ^{17}O, and 47.5 % ^{18}O. Experimentally, however, one finds 5 – 8 % higher ^{17}O enrichment than calculated along with the correspondingly lower ^{18}O enrichment (systematic deviation $\leq \pm 2$ %). This difference can be explained by assuming that ^{17}O-labeled water originating from $^{17}O_2$ cleavage in the active site "dilutes" the $H_2{}^{18}O$ oxygen source in situ.

The nature of the metal complex involved in O_2 cleavage and epoxidation still has to be elucidated. At present it is only certain that this first step of carotene metabolism is not a P450-catalyzed reaction because the heme-thiolate chromophore ($\lambda_{max} \sim 415$nm) is absent in the purified protein (broad absorption without fine structure between 200 – 280 nm) as well as in the overexpressed enzyme. Interestingly the monooxygenase mechanism resembles, at least in part (the epoxidation), the mechanism we previously proposed for a supramolecular enzyme model catalyzing the regioselective cleavage of **2** and **7**.[14]

Experimental Section

Enzymatic reaction conditions: α-carotene **5** ((6′*R*)-β,ε-carotene) was obtained from F. Hoffmann-La Roche (Basel) and stored at $-18\,^{\circ}C$. A stock solution of **5** in benzene (10 mM) was freshly prepared. In a glass vial the stock solution of **5** (40 μL), α-tocopherol solution (50 μL, 43 mg mL^{-1} in hexane), and tween 40 solution (200 μL, 400 μL in 10 mL acetone) were evaporated with a gentle stream of N_2 in a heated block (45 °C). Tricine buffer ($H_2{}^{18}O > 95$ %; 1 mL, 150 mM; pH 7.8, 45 °C) was added and the solution was gently mixed until almost complete solubilization. The substrate solution was added to a 25-mL flask containing tricine buffer ($H_2{}^{18}O > 95$ %; 3.5 mL, 150 mM; pH 7.8), glutathione (12 mg), sodium cholate (1 mg), and nicotinamide adenine dinucleotide, reduced form (NADH; 50 mg). The mixture was cooled to $-180\,^{\circ}C$ while connected to a high-vacuum line (3×10^{-2} mbar) and then degassed three times. Finally labeled molecular oxygen (> 85 % $^{17}O_2$; 20 mL; 2.15 bar) was condensed on the surface of the frozen solution ($-180\,^{\circ}C$). The mixture was allowed to warm up, and after reaching 25 °C the system was allowed to equilibrate over 30 min. In a separate flask the enzyme purified by hydrophobic interaction chromatography (HIC)[15] (from ≈10 g mucosa of one chicken's duodenum) was dissolved in tricine buffer ($H_2{}^{18}O > 95$ %; 500 μL, 150 mM; pH 7.8). HLADH (80 μL, 11.1 mg mL^{-1}, 2.9 U mg^{-1} protein; Fluka AG, Buchs) was added. Argon was passed through the solution for 30 min/25 °C to remove $^{16}O_2$. The enzymatic reaction was started by adding this solution to the substrate solution (final concentration of **5**: 80 μM). After incubation for 7.5 h at 37 °C in the dark, the reaction was quenched by addition of acetonitrile (4 mL). The mixture was extracted three times with chloroform (4 mL) and the collected organic phases were evaporated to dryness.

Purification by HPLC: The residue obtained as described above was separated by analytical HPLC (LiChrospher 100 RP-18 5 μm, dimensions: 125 × 4.6 mm, 25 °C, flow rate: 1 mL min^{-1}, eluents and gradients: 100 % solution of acetonitrile/1 % NH_4OAc_{aq} (1:1) →100 % solution of acetonitrile/*i*PrOH (1:1) over 10 min, the eluent remained the same for 5 min, then →100 % solution of acetonitrile/1 % NH_4OAc_{aq} (1:1) over 2 min; diode array detector at 330 nm for **1** (R_t=10.0 min) and **9** (R_t = 9.9 min), and 455 nm for **5** (R_t = 14.9 min). The mixture of retinoids was collected, evaporated, and concentrated in a 100-μL vial.

Silylation and GC-MS analysis: The mixture of the two products **1** and **9** was dissolved in hexane (5 μL). A syringe was purged several times with *N*,*O*-bis(trimethylsilyl)acetamide and then directly used to take an aliquot (1 μL) of the solution of **1** and **9**. Thus, silylation occurred in the syringe followed by immediate splitless injection (285 °C) into the GC column (cross-linked 5 % phenylmethyl silicone, dimensions: 25 m × 0.2 mm, film thickness: 0.33 μm, 30 s purge delay; temperature program: 150 °C →250 °C at 25 °C min^{-1} and then constant at 250 °C).[16] Selected ion monitoring analysis (electron ionization, 70 eV) was pursued for the [M^+] regions of the spectra for **10** (R_t = 8.2 min) and **11** (R_t = 13.4 min). The retention times of the retinoids **1** and **9** on HPLC and of the silyl derivatives **10** and **11** on GC were confirmed by injection of authentic material.

Received: April 6, 2001 [Z16919]

[1] T. Moore, *Biochem. J.* **1930**, *24*, 696 – 702.
[2] J. A. Olson, O. Hayaishi, *Proc. Natl. Acad. Sci. USA* **1965**, *54*, 1365 – 1370.
[3] a) S. Hansen, W. Maret, *Biochemistry* **1988**, *27*, 200 – 206; b) A. A. Dmitrovskii in *New Trends in Biological Chemistry* (Ed.: T. Ozawa), Japan Scientific Societies, Tokyo, **1991**, pp. 297 – 308; c) X.-D. Wang, G. Tang, J. G. Fox, N. I. Krinsky, R. M. Russell, *Arch. Biochem. Biophys.* **1991**, *258*, 8 – 16; d) K.-J. Yeum, A. L. Dos Anjos Ferreira, D. Smith, N. I. Krinsky, R. M. Russell, *Free Radical Biol. Med.* **2000**, *29*, 105 – 114.
[4] a) G. Britton, S. Liaaen-Jensen, H. Pfander in *Carotenoids*, *Vol. 3* (Eds.: G. Britton, S. Liaaen-Jensen, H. Pfander), Birkhäuser, Basel, **1998**, p. 10; b) D. Sklan, *Br. J. Nutr.* **1983**, *50*, 417 – 425; c) M. R. Lakshman, H. Chansang, J. A. Olson, *J. Lipid Res.* **1972**, *13*, 477 – 482; d) N. H. Fidge, F. R. Smith, D. S. Goodman, *Biochem. J.* **1969**, *114*, 689 – 694.
[5] a) D. S. Goodman, H. S. Huang, *Science* **1965**, *149*, 879 – 880; b) for an overview, see: J. A. Olson in *Modern Nutrition in Health and Disease* (Eds.: M. E. Shils, J. A. Olson, M. Shike, A. C. Ross), 9th ed., Williams and Wilkins, Baltimore, **1999**, pp. 525 – 542.
[6] K. Harashima, *Biochim. Biophys. Acta* **1964**, *90*, 211.
[7] A. Nagao, A. During, C. Hoshino, J. Terao, J. A. Olson, *Arch. Biochem. Biophys.* **1996**, *328*, 57 – 63.
[8] B. B. Vartapetyan, A. A. Dmitrovskii, D. G. Alkhazov, I. Kh. Lemberg, A. B. Girshin, G. M. Gusinskii, N. A. Starikova, N. N. Erofeeva, I. P. Bogdanova, *Biokhimiya (Moskow) Engl. Transl.* **1966**, *31*, 759 – 763.
[9] J. A. Olson, *Am. J. Clin. Nutr.* **1969**, *22*, 953 – 962.
[10] a) A. Wyss, G. Wirtz, W.-D. Woggon, R. Brugger, M. Wyss, A. Friedlein, H. Bachmann, W. Hunziker, *Biochem. Biophys. Res.*

  1433-7851/01/4014-2616 $ 17.50+.50/0

Commun. **2000**, *271*, 334 – 336; b) J. von Lintig, K. Vogt, *J. Biol. Chem.* **2000**, *275*, 11915 – 11920; c) A. Wyss, G. Wirtz, W.-D. Woggon, R. Brugger, M. Wyss, A. Friedlein, H. Bachmann, W. Hunziker, *Biochem. J.* **2001**, *354*, 521 – 529.

[11] G. M. Wirtz, C. Bornemann, A. Giger, R. K. Müller, H. Schneider, G. Schlotterbeck, G. Schiefer, W.-D. Woggon, *Helv. Chim. Acta* **2001**, in press.

[12] J. Rétey, A. Umani-Ronchi, J. Seibel, D. Arigoni, *Experientia* **1966**, *22*, 502 – 503.

[13] J. Devery, B. V. Milborrow, *Br. J. Nutr.* **1994**, *72*, 397 – 414.

[14] a) R. R. French, P. Holzer, M. G. Leuenberger, W.-D. Woggon, *Angew. Chem.* **2000**, *112*, 1321 – 1323; *Angew. Chem. Int. Ed.* **2000**, *39*, 1267 – 1269; b) W.-D. Woggon, *Chimia* **2000**, 57; c) R. R. French, J. Wirz, W.-D. Woggon, *Helv. Chim. Acta* **1998**, *81*, 1521 – 1527.

[15] C. Engeloch-Jarret, M. G. Leuenberger, W.-D. Woggon, unpublished results.

[16] G. J. Handelman, M. J. Haskell, A. D. Jones, A. J. Clifford, *Anal. Chem.* **1993**, *65*, 2024 – 2028.

Saddle-Shaped Six-Coordinate Iron(III) Porphyrin Complexes Showing a Novel Spin Crossover between $S = 1/2$ and $S = 3/2$ Spin States**

Takahisa Ikeue, Yoshiki Ohgo, Tatsuya Yamaguchi, Masashi Takahashi,* Masuo Takeda, and Mikio Nakamura*

Spin states of iron(III) porphyrins are controlled by the number and nature of axial ligands.[1] The coordination of nitrogen bases such as imidazole (HIm) and pyridine results in the formation of low-spin ($S = 1/2$) six-coordinate complexes. In contrast, anionic ligands such as Cl^- and F^- lead to the formation of five-coordinate high-spin ($S = 5/2$) complexes. Maltempo discussed a spin-admixed $S = 3/2$, 5/2 state on the basis of quantum mechanical calculations, and suggested that the $S = 3/2$ state is an important contributor to the spin state of certain bacterial heme proteins known as cytochromes c′.[2]

[*] Prof. Dr. M. Nakamura, Dr. T. Ikeue, Dr. Y. Ohgo, T. Yamaguchi
Department of Chemistry
Toho University School of Medicine
Tokyo 143-8540 (Japan)
Fax: (+81) 3-5493-5430
E-mail: mnakamu@med.toho-u.ac.jp
Prof. Dr. M. Takahashi, Prof. Dr. M. Takeda
Department of Chemistry
Faculty of Science, Toho University
Funabashi, 274-8510 (Japan)
Fax: (+81) 47-475-1855
E-mail: takahasi@chem.sci.toho-u.ac.jp

[**] This work was supported by a Grant in Aid for Scientific Research on Priority Areas (A; no. 12020257 to M.N.) from the Ministry of Education, Culture, Sports, Science, and Technology, Japan. T.I. is grateful to the JSPS for a Research Fellowship for young scientists. We thank the Research Center for Molecular Materials, the Institute for Molecular Science (IMS), for support. The authors are grateful to Mr. Masahiro Sakai of the IMS for the assistance with the SQUID measurements.

Supporting information for this article is available on the WWW under http://www.angewandte.com or from the author.

We and others recently reported that highly nonplanar (porphyrinato)iron(III) complexes with weak axial ligands show a quite pure intermediate spin state.[3, 4] The results were ascribed to the short $Fe{-}N_{por}$ bonds of the nonplanar porphyrin rings and the weak coordination ability of the axial ligands.[5] We therefore expected that the spin state of nonplanar $[Fe^{III}(oetpp)L_2]ClO_4$ (**1**–**5**) could change from

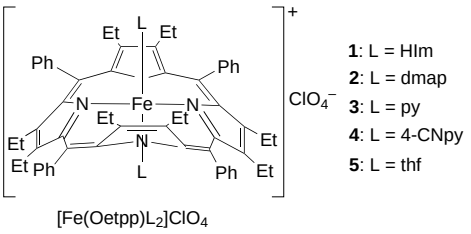

$[Fe(Oetpp)L_2]ClO_4$

the pure $S = 1/2$ to the pure $S = 3/2$ state as the axial ligand changes from strong HIm to weak THF; the order of the coordination ability is HIm > dmap > py > 4-CNpy > thf.[6] Of particular interest are the spin states of **2**–**4** because the axial ligands of these complexes are ranked between HIm and THF.

Table 1 lists the Mössbauer parameters, isomer shift (IS; relative to α-iron foil at 290 K), and quadrupole splitting (QS) measured at ambient and liquid nitrogen temperatures. The QS values for **1** and **2** at ambient temperature were within the range of low-spin complexes.[7] The IS and QS values for **4** (0.37 and 3.26 mm s^{-1}, respectively) were close to those for **5** (0.41 and 3.65 mm s^{-1}); **5** has been fully characterized as the quite pure intermediate-spin complex.[4] Thus, from the viewpoint of Mössbauer spectroscopy, **1** and **2** are the low-spin complexes, while **4** is the intermediate-spin complex at ambient temperature. Figure 1 shows the Mössbauer spectra of **3** and **4** taken at ambient temperature and 80 K. The features change as the temperature is lowered. Complex **4** exhibited a new doublet (site B) below 230 K, and the relative intensities for this site increased on decreasing the temperature. The values for sites A and B are in the range of intermediate-spin and low-spin complexes, respectively, and both spin states co-exist at low temperature. This observation implies the occurrence of a novel spin-crossover process [Eq. (1)].[8, 9]

Table 1. Mössbauer parameters and spin state (S) of **1**–**5**.

		T [K]	IS [mm s^{-1}]	QS [mm s^{-1}]	Γ_1 [mm s^{-1}]	Γ_2 [mm s^{-1}]	S
1		297	0.18	1.82	0.24	0.25	1/2
		78	0.26	1.86	0.40	0.62	1/2
2		290	0.19	2.21	0.27	0.32	1/2
		80	0.26	2.31	0.55	0.89	1/2
3		290	0.32	2.76	0.27	0.29	3/2 – 1/2
		80	0.25	2.29	0.47	0.64	1/2
4	site A	295	0.37	3.26	0.32	0.33	3/2
	site A	80	0.57	3.03	0.47	0.47	3/2
	site B	80	0.20	2.70	0.64	0.64	1/2
5		290	0.41	3.65	0.32	0.26	3/2
		80	0.50	3.50	0.77	0.49	3/2

low spin ($S = 1/2$) $\rightleftharpoons$ intermediate spin ($S = 3/2$) (1)

  1433-7851/01/4014-2617 $ 17.50+.50/0

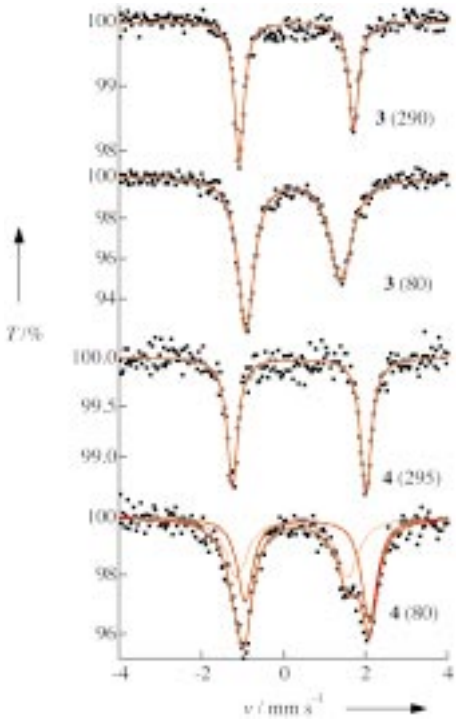

Figure 1. ^{57}Fe Mössbauer spectra of **3** and **4** measured on microcrystalline samples at ambient temperature and 80 K (as indicated in the parentheses).

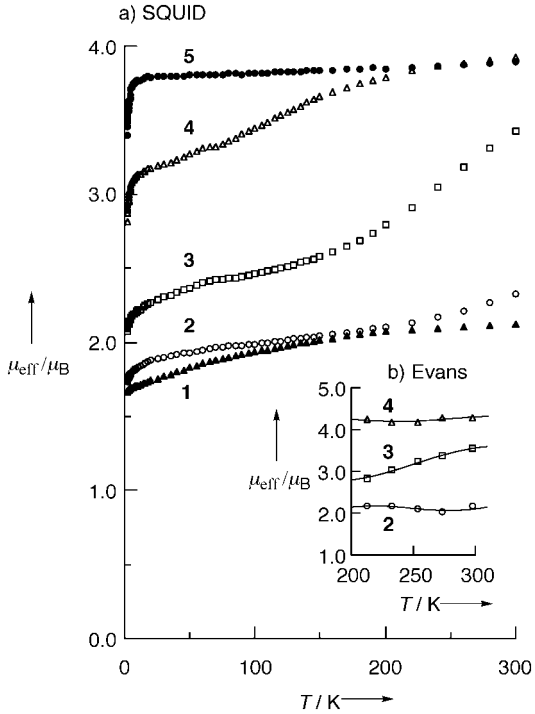

Figure 2. Temperature dependence of the effective magnetic moments of **1**–**5** taken for microcrystalline samples by SQUID magnetometry. Inset: Effective magnetic moments determined in CH_2Cl_2 by the Evans method.

While **4** exhibited a new doublet at low temperature, **3** maintained a set of doublets throughout the temperature range measured. The IS and QS values of **3**, however, showed an unexpected decrease on lowering the temperature and were almost the same as those of **2** below 150 K. This result suggests that **3** exists as the low-spin state below 150 K. Since, however, the IS and QS values of **3** at ambient temperature were close to those of intermediate-spin complexes, it is also considered to be a spin-crossover complex. The observation of only one set of doublets in **3** could be explained in terms of the fast spin transition on the Mössbauer time scale (10^7 s^{-1}) over 150–290 K when two iron sites are present.

Figure 2 shows the effective magnetic moments (μ_{eff}) of microcrystalline samples measured with a SQUID magnetometer over 2–300 K. The results confirm that **1** and **2** are in the $S = 1/2$ state. A major part of **3** is in the $S = 1/2$ state below 150 K, but the population of the $S = 3/2$ state considerably increases above this temperature. Similarly, **4** is a mixture of the $S = 1/2$ and $S = 3/2$ states below 200 K, although it exists almost exclusively as the $S = 3/2$ complex above 200 K. These results support the occurrence of the spin-crossover process [Eq. (1)] in **3** and **4**, as suggested by the Mössbauer spectroscopy results. As mentioned, **5** is a quite pure intermediate-spin complex as shown by the μ_{eff} value being maintained at 3.80 ± 0.09 μ_B in the range 5–300 K.[4] The EPR spectra taken for the solid samples at 4.2 K are consistent with the conclusions obtained from the Mössbauer spectroscopy and SQUID magnetometry measurements.[10]

The spin states of these complexes in solution have been studied. The solution magnetic moments (inset, Figure 2) were determined by the Evans method over the temperature range 193–298 K. The μ_{eff} values of **2** and **4** were almost constant, 2.1 ± 0.1 and 4.2 ± 0.1 μ_B, respectively, which are close to the spin-only values expected for the $S = 1/2$ and $S = 3/2$ complexes, respectively. As in the case of the solid sample, the μ_{eff} value of **3** in solution decreased from 3.5 μ_B (298 K) to 2.6 μ_B (193 K), which suggests the spin-crossover process also occurs in solution. Table 2 shows the ^{1}H NMR chemical shifts

Table 2. ^{1}H NMR chemical shifts recorded in CD_2Cl_2 at 223 K.

	L	*meso* Phenyl			Pyrrole		Axial ligand
		o	*m*	*p*	CH_2	CH_3	ring protons
1	HIm	2.8	4.7	6.0	3.2, 11.8	1.3	
2	dmap	3.2	4.8	6.0	3.4, 12.5	1.3	15.8, −2.7
3	py	8.5	5.1	8.5	8.2, 27.9	0.3	35.9, 29.6
4	4-CNpy	14.4	4.2	13.7	19.3, 55.5	−1.7	113.7, 72.5

at 223 K. The large downfield shifts of the CH_2 and ligand (L) signals on going from **2** to **4** suggest that the spin densities at the β-pyrrole and the ligand carbon atoms increase from **2** → **4**. The result can be explained in terms of the increase in population of the $S = 3/2$ state relative to that of the $S = 1/2$ state.[4] Table 3 shows the ^{13}C NMR chemical shifts at 223 K.[11] The most characteristic feature is the large upfield shift of the *meso* carbon atom (C–Ph) on going from **2** ($\delta = -28$) to **4** ($\delta = -451$); the chemical shift of the *meso* carbon atom at $\delta = -451$ ($\delta = -235$ at 298 K) is unprecedented in ^{13}C NMR spectroscopy of iron(III) porphyrins, and suggests that the major part of **4** is in the $S = 3/2$ state.[12–14] Thus, the observation of the extremely upfield-shifted signal of the *meso* carbon atom by ^{13}C NMR spectroscopy could be a good proof for the intermediate-spin complex.[15] In fact, the pure intermediate-spin complex **5** also showed the signal corre-

  1433-7851/01/4014-2618 $ 17.50+.50/0

Table 3. ^{13}C NMR chemical shifts recorded in CD_2Cl_2 at 223 K.

	L	*meso*	*ipso*	*o*	*m*	*p*	Pyrrole (α)	Pyrrole (β)	CH_2	CH_3
1	HIm	−37	166	97	122	123	143	156	−38	105
2	dmap	−28	159	102	122	123	132	164	−40	102
3	py	−135	249	31	124	119	284	223	−53	162
4	4-CNpy	−451	458	−160	130	105	590	304	−80	264

sponding to the *meso* carbon atom to be fairly upfield shifted ($\delta = -265$ at 223 K).[16]

Figure 3 shows the temperature dependence of the ^{13}C chemical shifts of the *meso* carbon atoms. While the chemical

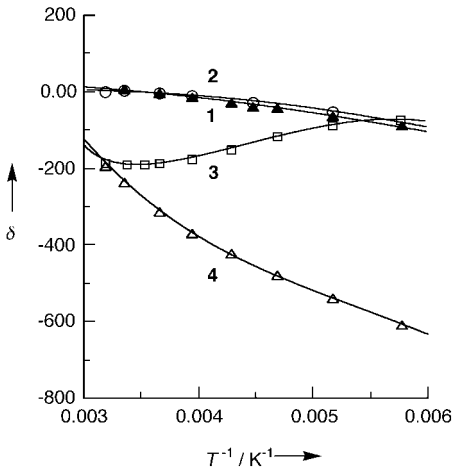

Figure 3. Temperature dependence of the chemical shifts of the *meso* ^{13}C atoms of **1**–**4** taken in CD_2Cl_2.

shift of the meso carbon atom of **3** was quite similar to that of **4** at 298 K, the value approached that of **2** at 200 K. Since **2** and **4** are considered to be the pure $S = 1/2$ and $S = 3/2$ complexes, respectively, in this temperature range, the spin-crossover constant K_{sc} of **3** is calculated according to Equation (2).

$$K_{sc} = (\delta_{dmap} - \delta_{py})/(\delta_{py} - \delta_{4\text{-}CNpy}) \quad (2)$$

The plots of $\log(K_{sc})$ versus $1/T$ showed a good linear relationship, from which the thermodynamic parameters were obtained as $\Delta H = 16.9\ kJ\,mol^{-1}$ and $\Delta S = 66.6\ J\,mol^{-1}\,K^{-1}$. Although the spin-crossover process between the $S = 1/2$ and $S = 3/2$ states is not unprecedented in iron(III) complexes,[8, 9] this is, to the best of our knowledge, the first example in iron(III) porphyrin complexes.

It is interesting to compare the spin state of saddle-shaped **4** with that of ruffled $[Fe^{III}(TiPrP)(4\text{-}CNPy)_2]ClO_4$.[6] Although both complexes are supposed to have short $Fe{-}N_{por}$ bonds as a result of the deformation of the porphyrin ring, $[Fe^{III}(TiPrP)(4\text{-}CNPy)_2]ClO_4$ is in the low-spin state with a $(d_{xz}, d_{yz})^4(d_{xy})^1$ electron configuration.[14] The result is ascribed to the difference in the energy gap between the d_{z^2} and d_π orbitals; the energy gap is larger in $[Fe^{III}(TiPrP)(4\text{-}CNPy)_2]ClO_4$ than in **4** since the d_π orbitals of the former complex is located below the d_{xy} orbital. In addition, the coordination of 4-CNPy is much stronger in the ruffled complex than in saddle-shaped **4** for steric reasons, which further increases the energy gap.[17] Consequently, $[Fe^{III}(TiPrP)(4\text{-}CNPy)_2]ClO_4$ maintains the low-spin state. If 4-CNpy is replaced by thf, both saddle-shaped **5** and ruffled $[Fe^{III}(TiPrP)(thf)_2]ClO_4$ show quite pure intermediate-spin characteristics.[4]

In conclusion, we have shown that the saddle-shaped complexes $[Fe^{III}(oetpp)L_2]ClO_4$ exhibit a novel spin-crossover process between the $S = 1/2$ and $S = 3/2$ states, and that the $S = 3/2$ population increases as the coordination ability of the axial ligand is weakened. It should be emphasized here that the novel spin-crossover process in six-coordinate iron(III) porphyrins is realized by the tremendous deformation of the porphyrin rings. The large destabilization of the $d_{x^2-y^2}$ orbital caused by the short $Fe{-}N_{por}$ bonds insulates the $S = 5/2$ state from the other electronic ground states. The spin state of the iron(III) ions can hence be finely tuned by the field strength of the axial ligands, thus leading to the formation of the complex with the pure $S = 1/2$ state (**1**), complexes showing the novel $S = 1/2 \rightleftharpoons S = 3/2$ process (**2**–**4**), and the complex with the pure $S = 3/2$ state (**5**).

Experimental Section

$[Fe^{III}(oetpp)Cl]$ and *meso*-^{13}C-enriched $[Fe^{III}(oetpp)Cl]$ were prepared according to the literature.[18, 19]

5: A solution (15 mL) of $AgClO_4$ (6.1 mg, 2.9×10^{-5} mol) in THF was added to a dry solution of $[Fe^{III}(oetpp)Cl]$ (26.1 mg, 2.8×10^{-5} mol) in THF (20 mL). After the removal of AgCl by filtration, heptane (20 mL) was added, and the solution was allowed to stand overnight. The purple crystals were collected by filtration, washed with hexane, and dried in vacuo for 10 min at 25 °C to give 25 mg (87 %) of **5**, which was characterized as the quite pure intermediate-spin complex.[4] **1**–**4** were prepared by the addition of an excess amount of ligand to a solution of **5** in CH_2Cl_2 followed by recrystallization from CH_2Cl_2/heptane. The ^1H and ^{13}C NMR data are shown in Tables 1 and 2, respectively.

The ^1H and ^{13}C NMR spectra were recorded on a JEOL LA300 spectrometer operating at 300.4 MHz for proton spectroscopy. EPR spectra were recorded on a Bruker E500 spectrometer operating at the X band and equipped with an Oxford helium cryostat. The solid-state magnetic susceptibilities were measured between 2 and 300 K under a magnetic field of 0.5 T with a SQUID magnetometer (Quantum Design MPMS-7). The measured data were corrected for diamagnetic contributions. Iron-57 Mössbauer spectra were measured on a Wissel Mössbauer spectrometer system. The samples were kept in a gas-flow cryostat and the $^{57}Co(Rh)$ source was kept at room temperature. Isomer shifts (δ) are given relative to α-iron foil at room temperature.

Received: February 5, 2001
Revised: May 7, 2001 [Z16551]

[1] W. R. Scheidt in *The Porphyrin Handbook*, *Vol. 3* (Eds.: K. M. Kadishi, K. M. Smith, R. Guilard), Academic Press, San Diego, **2000**, pp. 49–112.
[2] M. M. Maltempo, *J. Chem. Phys.* **1974**, *61*, 2540–2547.

[3] J.-P. Simonato, J. Pecaut, L. L. Pape, J.-L. Oddou, C. Jeandey, M. Shang, W. R. Scheidt, J. Wojacynski, S. Wolowiec, L. Latos-Grazynski, J.-C. Marchon, *Inorg. Chem*. **2000**, *39*, 3978 – 3987.

[4] T. Ikeue, T. Saitoh, T. Yamaguchi, Y. Ohgo, M. Nakamura, M. Takahashi, M. Takeda, *Chem. Commun*. **2000**, 1989 – 1990.

[5] D. R. Evans, C. A. Reed, *J. Am. Chem. Soc.* **2000**, *122*, 4660 – 4667.

[6] Abbreviations: oetpp, T*i*PrP, and TEtP are dianions of 2,3,7,8,12,13,17,18-octaethyl-5,10,15,20-tetraphenylporphyrin, *meso*-tetraisopropylporphyrin, and *meso*-tetraethylporphyrin, respectively. dmap: 4-dimethylaminopyridine; py: pyridine; 4-CNpy: 4-cyanopyridine; HIm: imidazole; 2-MeIm: 2-methylimidazole.

[7] J. Sams, T. B. Tsin in *The Porphyrins*, *Vol. IV* (Ed.: D. Dolphin), Academic Press, New York, **1979**, pp. 425 – 478.

[8] K. D. Hodges, R. G. Wollmann, S. L. Kessel, D. N. Hendrickson, D. G. Van Derveer, E. K. Barefield, *J. Am. Chem. Soc.* **1979**, *101*, 906 – 917.

[9] W. O. Koch, V. Schünemann, M. Gerdan, A. X. Trautwein, H.-J. Krüger, *Chem. Eur. J.* **1998**, *4*, 686 – 691.

[10] EPR measurements: **1:** $g = 2.79, 2.35, 1.63$ ($S = 1/2$); $g = 3.25$ ($S = 1/2$). **2:** $g = 3.06, 2.14, 1.42$ ($S = 1/2$). **3:** $g = 3.39, 2.08$ ($S = 1/2$). **4**: $g = 4.28, 3.80, 2.08$ ($S = 3/2$).

[11] The signals corresponding to the *meso* carbon atoms were assigned unambiguously by the use of *meso*-^{13}C-enriched complexes. The α-pyrrole and *ipso*-phenyl signals were assigned on the basis of their coupling with the *meso* carbon atom of the labeled complexes.

[12] High-spin and low-spin complexes show *meso* signals at $\delta = 500 – 600$ and 50 – 100, respectively, at room temperature.[13] Some low-spin complexes with the less common $(d_{xz}, d_{yz})^4(d_{xy})^1$ electronic configuration exhibit the signals further downfield ($\delta = 700 – 800$).[14]

[13] "Physical Bioinorganic Chemistry Series 1": H. Goff in *Iron Porphyrin*, *Part I* (Eds.: A. B. P. Lever, H. B. Gray), Addison-Wesley, Reading, **1983**, pp. 237 – 281.

[14] T. Ikeue, Y. Ohgo, T. Saitoh, M. Nakamura, H. Fujii, M. Yokoyama, *J. Am. Chem. Soc.* **2000**, *122*, 4068 – 4076.

[15] The large downfield shifts of the α- and β-pyrrole signals are consistent with the occupancy of unpaired electrons in both the d_{xz} and d_{yz} orbitals; the unpaired electrons in these orbitals are transferred to the pyrrole carbon atoms by a d_π-$3e_g$ interaction. Since the $3e_g$ orbital has zero electron density at the *meso* carbon atom, the large upfield shift of the *meso* signal is ascribed to the spin polarization from the neighboring α-pyrrole carbon atom.[14]

[16] The extent of the upfield shift of the *meso* carbon atom is not necessarily proportional to the $S = 3/2$ contribution. The large difference in the shifts of the *meso* carbon atoms between **4** and **5** ($\Delta\delta = 186$ at 223 K) could be the indication that the d_π-$3e_g$ interaction in **4** is much stronger than that in **5** as a result of the difference in the nature of the axial ligands.

[17] Although the X-ray crystal structures of **4** and $[Fe^{III}(T\mathit{i}PrP)(4\text{-}CNpy)_2]ClO_4$ are not available at present, a preliminary result has shown that saddled **3** has much longer Fe–N(axial ligand) bonds than ruffled $[Fe^{III}(TEtP)(2\text{-}MeIm)_2]Cl$; the average bond lengths are 2.203(3) and 2.02(1) Å, respectively. Y. Ohgo, T. Ikeue, M. Nakamura, unpublished results.

[18] K. M. Barigia, M. D. Berber, J. Fajer, C. J. Medforth, M. W. Renner, K. M. Smith, *J. Am. Chem. Soc.* **1990**, *112*, 8851 – 8857.

[19] R.-J. Cheng, P.-Y. Chen, P.-R. Gau, C.-C. Chen, S.-M. Peng, *J. Am. Chem. Soc*. **1997**, *119*, 2563 – 2569.

Molecular Paneling by Coordination: An $M_{15}L_6$ Hexahedral Molecular Capsule having Clefts for Reversible Guest Inclusion

Kazuhiko Umemoto, Hitoshi Tsukui, Takahiro Kusukawa, Kumar Biradha, and Makoto Fujita*

The construction of three-dimensional (3D) molecular structures by linking two-dimensional (2D), planar organic components through metal coordination provides a new concept that is termed molecular paneling.[1] A family of 2D components are coordinated by transition metals to give rise to various hollow 3D polyhedral structures.[2–8] The triangular *exo*-hexadentate ligand **2** has been recently shown to give $M_{18}L_6$ hexahedral coordination capsule **4** by linking together with Pd^{II} building block **1**.[4b] This coordination capsule has a

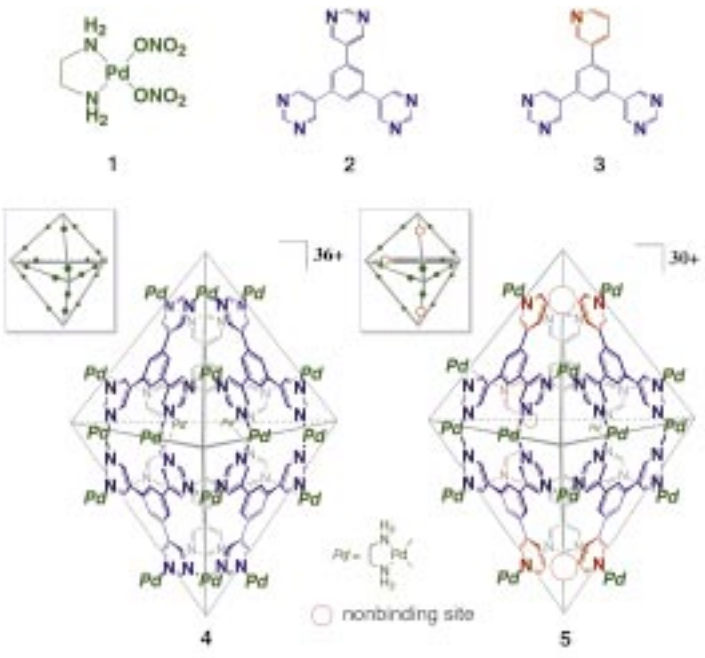

very stable closed-shell structure which makes it difficult to encapsulate guest molecules. We have designed another molecular panel **3**, which is similar to **2** but misses one binding site, to prepare a hexahedral capsule with more

[*] Prof. Dr. M. Fujita,[+] H. Tsukui, Dr. T. Kusukawa, Dr. K. Biradha
Department of Applied Chemistry
Graduate School of Engineering, Nagoya University
Chikusaku, Nagoya 464-8603 (Japan)
Fax: (+81) 52-789-3199
E-mail: mfujita@apchem.nagoya-u.ac.jp

Dr. K. Umemoto
The Graduate University for Advanced Studies
Myodaiji, Okazaki 444-8585 (Japan)

[+] Prof. Fujita is responsible for the Core Research for Evolutional Science and Technology (CREST) project of the Japan Science and Technology Corporation (JST).

Supporting information for this article is available on the WWW under http://www.angewandte.com or from the author.

  1433-7851/01/4014-2620 $ 17.50+.50/0

flexibility that would allow guest encapsulation and release. We show that, despite the lack of one binding site, ligand **3** is assembled into a unique $M_{15}L_6$ hexahedral structure **5** without the formation of any other positional isomers. An important finding is that capsule **5** can encapsulate/exchange guest molecules reversibly through the clefts at the nonbinding sites of the capsule.[9]

When ligand **3**[10] was treated with Pd^{II} complex **1** in D_2O at room temperature for 24 h we obtained a complex NMR spectrum (Figure 1), from which the presence of 39 proton signals was confirmed in the aromatic region. The observed 39 protons correspond to the total number of protons of three ligands, which suggested the assembly of a $(3L)_n$-type entity. Since the only possible $(3L)_n$ structure is a hexahedron, we proposed an $M_{15}L_6$ composition with a hexahedral framework. All the protons were fully assigned for three symmetrically ligands by H–H relay COSY and NOESY experiments.[11] Furthermore, through-space correlation by NOESY experiments made the connectivity of the six ligands clear. As a consequence, the structure was assigned as **5**. It is remarkable that, of the many possible structures, only a single isomer of a hexahedral structure was assembled from 21 small components (15 metals and 6 ligands) and fully assigned by NMR techniques alone.

The complex **5** was isolated as a colorless precipitate in 83% yield by adding a large amount of EtOH to the reaction mixture. The elemental analysis of **5** was consistent with a formula of $C_{144}H_{198}N_{90}O_{90}Pd_{15}\cdot 25\,H_2O$.

The hexahedral structure of **5** was unambiguously determined by an X-ray crystallographic analysis of a single crystal of **5** (Figure 2). As expected, the crystal structure of **5** displayed the hexahedral $M_{15}L_6$ assembly with two nonbinding sites located around the apical corners and another one situated on the equatorial corner (Figure 2a–c). As a result, ligand **3** is placed in three different environments. In the X-ray structure 28 out of the 30 nitrate anions of **5** were found: five existed inside the capsule and the remaining were outside.

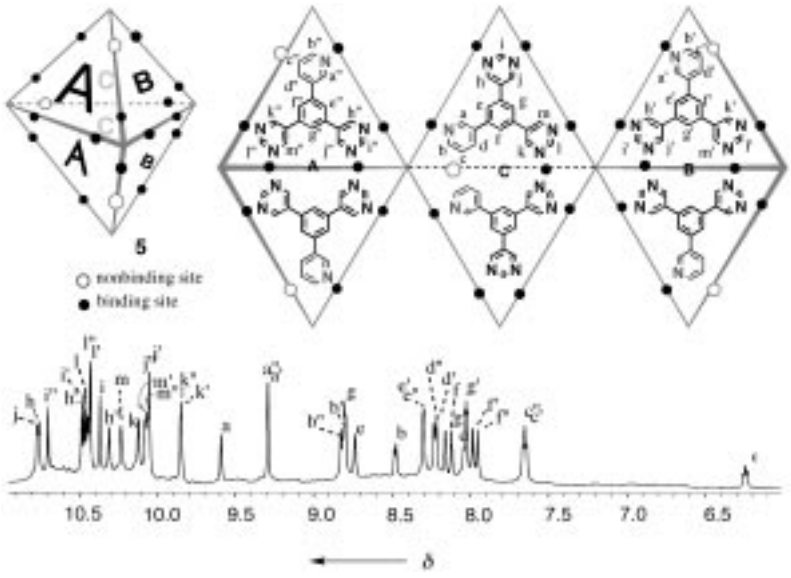

Figure 1. ^1H NMR spectra showing the formation of hexahedral capsule **5** (500 MHz, D_2O, TMS as external standard).

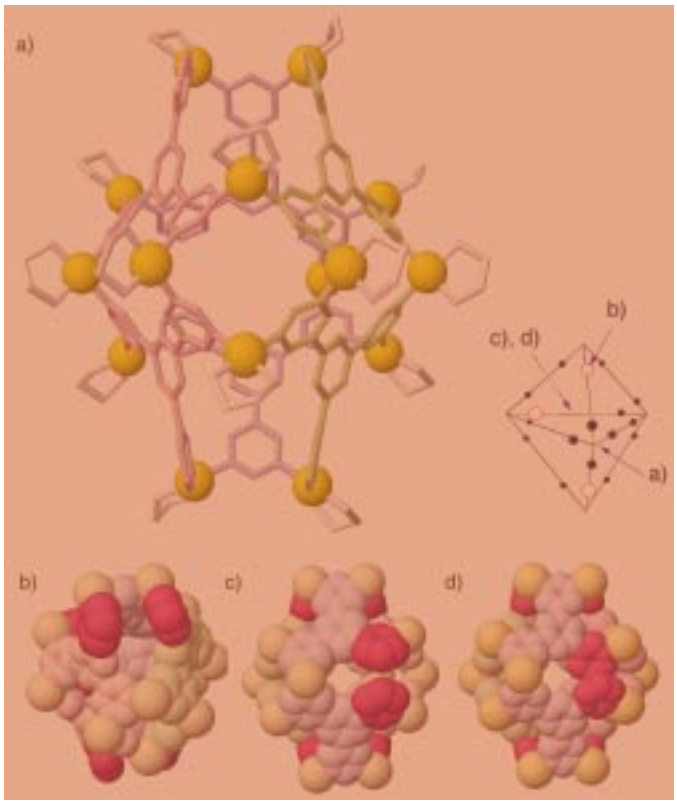

Figure 2. The crystal structure of **5**. Although two crystallographically independent structures **5a** and **5b** are found in the solid state, only structure **5a** is represented, except in (d). In (b)–(d), the ancillary ethylenediamine ligands on the Pd ions are omitted for clarity. The nonbinding sites are emphasized with red-colored 3-pyridyl groups. a) The ball and cylindrical representation of the front view; b) a view from an apical direction; c) a view from the back side; d) the same view of structure **5b**.

Interestingly, the X-ray analysis of capsule **5** showed the presence of two crystallographically independent structures (**5a** and **5b**) for capsule **5**. The difference between **5a** and **5b** is that a 3-pyridyl group at the equatorial site flips outward in **5a** but inward in **5b** (Figure 2c, d). The large upfield shift of H_c at $\delta = 6.3$ is most probably the result of the inward flipping of the 3-pyridyl group bearing H_c and suggests that structure **5b** is dominant in solution.

The size and the shape of complex **5** are almost the same as those of **4**. However, the striking feature of capsule **5** is the presence of three clefts at nonbinding sites. The clefts at the two apical sites are relatively large (3.5–5.0 Å) but the cleft at the equatorial site is almost closed. Thus, the capsule may encapsulate small molecules through the apical clefts (Figure 2b).[9j] In fact, the encapsulation of CBr_4 was observed when this guest was suspended in a solution of **5** in D_2O at room temperature. The facile complexation was completed within 10 min, as monitored by ^1H and ^{13}C NMR spectroscopy (Figure 3). The chemical shifts of the host were significantly changed and, moreover, the entrapped CBr_4 was observed at $\delta = -26.9$ in the ^{13}C NMR spectrum. The host–guest ratio was estimated to be 1:2 by inverse-gated ^1H-decoupling ^{13}C NMR spectroscopy.[12] Guest encapsulation was also observed

  1433-7851/01/4014-2621 $ 17.50+.50/0

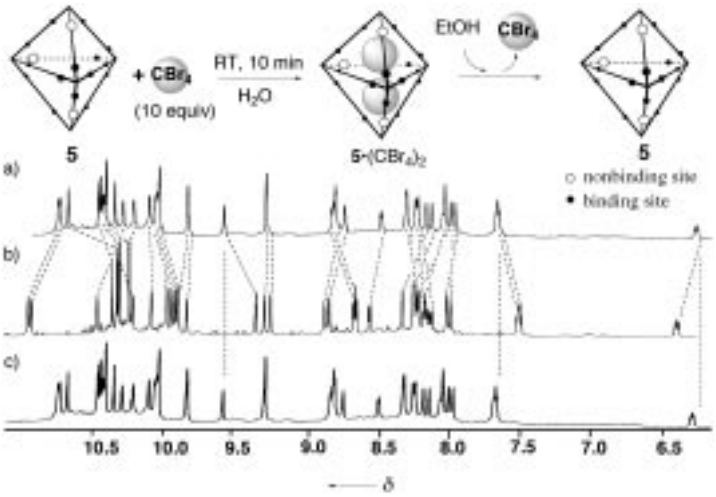

Figure 3. ^{1}H NMR spectra showing the reversible encapsulation of guests by **5** (500 MHz, D_2O, TMS as an external standard); a) complex **5**; b) complex **5**·$(CBr_4)_2$ formed upon the addition of 10 equivalents CBr_4 (suspended); c) the spectrum after the addition of excess EtOH.

with similar small molecules such as CH_2Br_2 and $CHCl_3$. The formation of hydrophobic interactions in the capsule should be the driving force for encapsulation. Thus, the addition of ethanol to the aqueous solution of **5**·$(CBr_4)_2$ induced the decapsulation of CBr_4, as monitored by NMR spectroscopy (Figure 3c).[13]

Experimental Section

5: Ligand **3** (7.9 mg, 0.025 mmol) was suspended in an aqueous solution (0.7 mL) of **1** (20.3 mg, 0.07 mmol) and left to stand for 24 h at room temperature. The addition of a large amount of EtOH to the mixture precipitated **5** as a colorless powder (22.1 mg, 83 %). M.p. 240 °C (decomp); ^{1}H NMR (500 MHz, D_2O, 25 °C): $\delta = 2.90-3.15$ (m, 30H), 6.24 (dd, $J = 5.3$, 6.1 Hz, 1H), 7.65 (dd, $J = 5.3$, 6.1 Hz, 2H), 7.95 (s, 1H), 7.98 (s, 1H), 8.02 (s, 1H), 8.03 (d, $J = 6.1$ Hz, 1H), 8.12 (s, 1H), 8.16 (s, 1H), 8.22 (d, $J = 6.1$ Hz, 2H), 8.30 (s, 2H), 8.48 (d, $J = 5.3$ Hz, 1H), 8.73 (s, 1H), 8.80 (s, 1H), 8.81 (d, $J = 5.3$ Hz, 2H), 9.29 (s, 2H), 9.59 (s, 1H), 9.85 (s, 2H), 10.05 (s, 2H), 10.06 (s, 1H), 10.07 (s, 1H), 10.12 (s, 1H), 10.23 (s, 1H), 10.31 (s, 1H), 10.37 (s, 1H), 10.43 (s, 2H), 10.45 (s, 1H), 10.46 (s, 1H), 10.48 (s, 1H), 10.69 (s, 1H), 10.75 (s, 1H), 10.76 (s, 1H); ^{13}C NMR (125 MHz, D_2O, 25 °C): $\delta = 47.4$ (CH), 47.6 (CH), 47.7 (CH), 124.6 (CH), 125.0 (CH), 125.5 (CH), 126.3 (CH), 126.6 (CH), 127.0 (CH), 127.1 (CH), 127.9 (CH), 128.0 (CH), 128.4 (CH), 128.8 (CH), 129.2 (CH), 130.5 (Cq), 131.1 (Cq), 131.6 (Cq), 131.7 (Cq), 131.9 (Cq), 132.3 (Cq), 134.8 (Cq), 135.0 (Cq), 135.2 (Cq), 135.3 (Cq), 136.0 (Cq), 136.8 (Cq), 136.9 (Cq), 137.3 (Cq), 137.4 (Cq), 137.6 (Cq), 137.7 (Cq), 137.9 (Cq), 138.5 (CH), 138.6 (CH), 139.0 (CH), 149.4 (CH × 2), 149.6 (CH), 150.7 (CH), 150.8 (CH × 2), 158.5 (CH), 158.7 (CH), 158.8 (CH), 158.9–159.0 (CH × 4), 159.8–160.3 (CH × 9), 160.6 (CH), 160.9 (CH); IR (KBr) 3480, 3210, 3100, 1610, 1431, 1380, 1080, 840, 725 cm^{-1}. Elemental analysis calcd for $C_{144}H_{198}N_{90}O_{90}Pd_{15}\cdot 25H_2O$: C 25.91, H 3.74, N 18.88; found: C 25.93, H 3.81, N 18.94.

X-ray structural analysis of **5**: The single crystal was obtained by the slow diffusion of methanol into an aqueous solution of **5** at 20 °C for 7 days. A single crystal of **5** ($0.20 \times 0.15 \times 0.15$ mm^3) was mounted onto a glass fiber. All measurements were made on a charge-coupled device (CCD) plate area detector with graphite monochromated $Mo_{K\alpha}$ radiation. The data were collected at 173(2) K. Crystal data for **5**: $C_{144}H_{198}N_{90}O_{90}Pd_{15}\cdot 57.5H_2O\cdot 1.5MeOH$, $M_r = 7309.91$, triclinic, space group $P\bar{1}$, $a = 26.503(3)$, $b = 30.887(3)$, $c = 35.743(4)$ Å, $\alpha = 85.468(2)$, $\beta = 85.735(2)$, $\gamma = 89.850(2)°$, $V = 29086(6)$ Å^3, $\rho_{calcd} = 1.669$ mg m^{-3}, $Z = 4$, $F(000) = 14816$, $\mu(Mo_{K\alpha}) = 1.016$ mm^{-1}, $\lambda(Mo_{K\alpha}) = 0.71073$ Å, 189592 reflections measured, 131409 observed ($I > 2\sigma(I)$), number of variables 6859, $R_1 = 0.0867$, $wR_2 = 0.2189$. Crystallographic data (excluding structure factors) for the structure reported in this paper have been deposited with the Cambridge Crystallographic Data Centre as supplementary publication no. CCDC-159454. Copies of the data can be obtained free of charge on application to CCDC, 12 Union Road, Cambridge CB21EZ, UK (fax: (+44) 1223-336-033; e-mail: deposit@ccdc.cam.ac.uk).

Received: March 26, 2001 [Z16848]

[1] For a review, see M. Fujita, K. Umemoto, M. Yoshizawa, N. Fujita, T. Kusukawa, K. Biradha, *Chem. Commun*. **2001**, 509–518.

[2] a) R. W. Saalfrank, A. Stark, K. Peters, H. G. von Schnering, *Angew. Chem*. **1988**, *100*, 878–880; *Angew. Chem. Int. Ed. Engl.* **1988**, *27*, 851–853; b) R. W. Saalfrank in *Molecular Self-Assembly: Organic Versus Inorganic Approaches*, *Vol. 96* (Ed.: M. Fujita), Springer, Berlin, **2000**, chap. 2, pp. 149–176.

[3] a) P. Baxter, J.-M. Lehn, A. DeCian, J. Fischer, *Angew. Chem*. **1993**, *105*, 92–95; *Angew. Chem. Int. Ed. Engl.* **1993**, *32*, 69–72; b) P. N. W. Baxter, J.-M. Lehn, G. Baum, D. Fenske, *Chem. Eur. J.* **1999**, *5*, 102–112; c) P. N. W. Baxter, J.-M. Lehn, B. O. Kneisel, G. Baum, D. Fenske, *Chem. Eur. J.* **1999**, *5*, 113–120.

[4] a) M. Fujita, D. Oguro, M. Miyazawa, H. Oka, K. Yamaguchi, K. Ogura, *Nature* **1995**, *378*, 469–471; b) N. Takeda, K. Umemoto, K. Yamaguchi, M. Fujita, *Nature* **1999**, *398*, 794–796; c) K. Umemoto, K. Yamaguchi, M. Fujita, *J. Am. Chem. Soc*. **2000**, *122*, 7150–7151.

[5] a) C. Brückner, R. E. Powers, K. N. Raymond, *Angew. Chem*. **1998**, *110*, 1937–1940; *Angew. Chem. Int. Ed*. **1998**, *37*, 1837–1840; b) D. L. Caulder, K. N. Raymond, *Acc. Chem. Res.* **1999**, *32*, 975–982.

[6] a) P. J. Stang, B. Olenyuk, D. C. Muddiman, R. D. Smith, *Organometallics* **1997**, *16*, 3094–3096; b) B. Olenyuk, J. A. Whiteford, A. Fechtenkötter, P. J. Stang, *Nature* **1999**, *398*, 796–799; c) S. Leininger, B. Olenyuk, P. J. Stang, *Chem. Rev*. **2000**, *100*, 853–908.

[7] C. M. Hartshorn, P. J. Steel, *Chem. Commun*. **1997**, 541–542.

[8] B. F. Abrahams, S. J. Egan, R. Robson, *J. Am. Chem. Soc*. **1999**, *121*, 3535–3536.

[9] Molecular capsules: a) D. J. Cram, J. M. Cram, *Container Molecules and Their Guests*, Royal Society of Chemistry, Cambridge, **1994**; b) P. Timmerman, W. Verboom, F. C. J. M. van Veggel, J. P. M. van Duynhoven, D. N. Reinhoudt, *Angew. Chem*. **1994**, *106*, 2437–2440; *Angew. Chem. Int. Ed. Engl.* **1994**, *33*, 2345–2348; c) L. R. MacGillivray, J. L. Atwood, *Nature* **1997**, *389*, 469–472; d) M. M. Conn, J. Rebek, Jr., *Chem. Rev.* **1997**, *97*, 1647–1668; e) T. Heinz, D. M. Rudkevich, J. Rebek, Jr., *Nature* **1998**, *394*, 764–766; f) J. J. Gonzalez, P. Prados, J. de Mendoza, *Angew. Chem*. **1999**, *111*, 546–549; *Angew. Chem. Int. Ed.* **1999**, *38*, 525–528; g) A. Ikeda, M. Yoshimura, H. Udzu, C. Fukuhara, S. Shinkai, *J. Am. Chem. Soc*. **1999**, *121*, 4296–4297; h) M. Ziegler, J. L. Brumaghim, K. N. Raymond, *Angew. Chem*. **2000**, *112*, 4285–4287; *Angew. Chem. Int. Ed*. **2000**, *39*, 4119–4121; i) N. Cuminetti, M. H. K. Ebbing, P. Prados, J. de Mendoza, E. Dalcanale, *Tetrahedron Lett*. **2001**, *42*, 527–530; j) R. Warmuth, J. Yoon, *Acc. Chem. Res.* **2001**, *34*, 95–105.

[10] Ligand **3** was prepared by the Suzuki–Miyaura coupling of 3,5-pyrimidylboronic acid pinacol ester and 3,5-dibromo-1-(3-pyridyl)-benzene. Satisfactory spectral and analytical data were obtained. For the details, see the Supporting Information.

[11] For example, 13 protons H_a-H_m should exist on the same ligand because of the following observations: 1) protons of each ring are correlated by relay COSY experiments; 2) the core C_6H_3 ring is correlated with other heteroaromatic rings of the same ligand by NOESY experiments.

[12] a) M. L. Martin, G. J. Martin, J. J. Delpuech, *Practical NMR Spectroscopy*, Heyden, London, **1984**, chap. 9, pp. 350–376; b) E. D. Becker, *High Resolution NMR*, Academic Press, New York, **1980**, chap. 12; c) C. H. Sotak, C. L. Dumoulin, G. C. Levy, *Top. Carbon-13 NMR Spectrosc.* **1984**, 91–121; d) L. D. Field, S. Sternhell, *Analytical NMR*, Wiley, Chichester, **1989**, chap. 3, pp. 41–63.

[13] For the synthesis and physical properties of **5**·$(CBr_4)_2$, see the Supporting Information.

  1433-7851/01/4014-2622 $ 17.50+.50/0

A Chiral Metal Surface**

Michael Schunack, Erik Lægsgaard, Ivan Stensgaard, Ib Johannsen, and Flemming Besenbacher*

Chirality is a property commonly associated with organic molecules, biological materials, or inorganic salts. A metal (and its associated surfaces) is normally achiral as a result of the mirror symmetry of its close-packed structures. Chirality can, however, be added to the surface by adsorbing chiral auxiliary molecules onto the substrate surface—a phenomenon often referred to as "chiral modification". A number of recent studies have reported on the nucleation and growth of such chiral structures within the adsorbed molecular monolayer by the deposition of chiral/prochiral molecules onto the surface of an achiral substrate.[1] Chiral surfaces are generally of great interest in fields such as heterogeneous, asymmetric catalysis and chemical sensors, and for studying the separation of chiral compounds and nonlinear optical materials.[2]

Earlier attempts to create a chiral metal surface tried to exploit the chirality of a homochiral substrate material such as quartz to transfer the chirality to a deposited metal film.[3] Single-crystal metal surfaces with a low Miller index, for example, {100}, {110}, or {111} surfaces, consist of atomically flat terraces that are separated by step edges where one atomic plane meets the next. These step edges contain a certain fraction of so-called kink sites, and it was recently pointed out that such kink sites possess an intrinsic chirality.[4, 5] Surfaces that exclusively contain kink sites of a specific chirality can be formed by cutting single crystals along certain high Miller index directions (see below).[4–6] A recent study indicated that adsorption of L-lysine onto an achiral Cu(100) surface may lead to the partial formation of chiral kink sites at step edges during a step-facetting process.[7]

Herein we report how the adsorption of molecules can bestow chirality onto the extended flat terraces of a single-crystal surface. The chirality is caused by a pronounced surface-restructuring that is induced chemically by the adsorption of chiral molecules. This is revealed directly on the atomic scale by intentionally pushing the molecules aside by means of scanning tunneling microscopy (STM): we find that at full coverage every molecule is associated with a chiral hole in the underlying surface. The observed molecule–hole complexes extend homogeneously over the entire surface and segregate spontaneously into enantiomorphic domains upon gentle annealing, thereby creating a perfectly ordered chiral metal surface.

The molecule–surface system under investigation is 2,5,8,11,14,17-hexa-(*tert*-butyl)decacyclene molecules (HtBDC, $C_{60}H_{66}$) adsorbed on a Cu(110) surface (Figure 1 A). The overall conformation of the molecule in the gas phase is

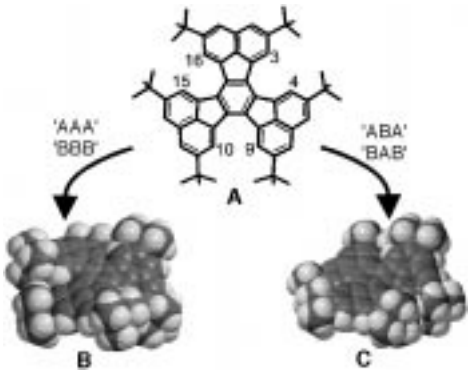

Figure 1. A) Molecular structure of 2,5,8,11,14,17-hexa(*tert*-butyl)decacyclene (HtBDC). Space-filling model of the two low-energy conformations: B) propeller shape of the AAA/BBB conformation, and C) boat shape of the ABA/BAB conformation.[19] The numbers label the positions of the interacting hydrogen atoms that lead to the local A and B conformations (see text for details).

determined by the steric repulsion of the 3/4, 9/10, and 15/16 hydrogen atoms at the peripheral naphthalene groups which leads to a distortion of the molecule. This process results in local conformations, where, for example, the 3-hydrogen atom is located above or below the adjacent 4-hydrogen atom, and is referred to as local A or B conformation, respectively. The three pairs of interacting hydrogen atoms result in the existence of four stereoisomers: AAA, BBB, ABA, and BAB.[8] The two sets AAA/BBB and ABA/BAB are both enantiomers. The first conformation leads to a chiral propeller-shaped molecule with D_3 symmetry (Figure 1 B),[9] whereas the second conformation leads to a boat-shaped molecule that is slightly distorted from the achiral C_s symmetry (Figure 1 C). Simple force-field calculations indicate that the second conformation has a 0.13 eV higher energy than the D_3-symmetric molecule.[10]

At room temperature (RT) individual HtBDC molecules are highly mobile on the planar Cu(110) surface and diffuse rapidly at the timescale of STM imaging (seconds). The molecules primarily decorate the steps at low coverages, but linear islands of molecules nucleate randomly on the terraces above a certain coverage (Figure 2 A). The islands consist of double rows of molecules aligned along the symmetry-equivalent $[\bar{1}1\bar{2}]$ and $[\bar{1}12]$ directions of the Cu(110) surface and fluctuate in size, as seen from STM movies.[11] The diffusion of the molecules is frozen out at low sample temperatures (<150 K), and individual molecules are imaged as six lobes arranged in a distorted hexagon with threefold rotational symmetry. Each lobe corresponds to a tunnel-current contribution of the *tert*-butyl groups, as confirmed by elastic-scattering quantum chemistry calculations (Figure 2 A).[12]

[*] Prof. Dr. F. Besenbacher, M. Schunack, Dr. E. Lægsgaard, Prof. Dr. I. Stensgaard
CAMP and Institute of Physics and Astronomy
University of Aarhus
Ny Munkegade, 8000 Aarhus C (Denmark)
Fax: (+45) 86120740
E-mail: fbe@ifa.au.dk
Dr. I. Johannsen
The Danish Polymer Centre
Risø National Laboratory, 4000 Roskilde (Denmark)

[**] We would like to acknowledge fruitful discussions with Trolle Linderoth as well as the financial support from the Danish National Research Foundation through the Center for Atomic-scale Materials Physics (CAMP), from the VELUX Foundation, and from the EU networks "Manipulation of individual atoms and molecules" and "Bottom up Nanomachines".

  1433-7851/01/4014-2623 $ 17.50+.50/0

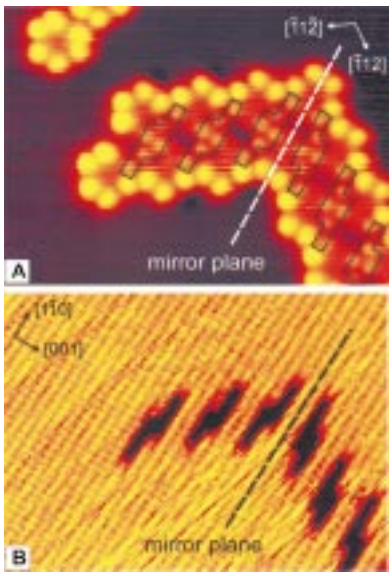

Figure 2. A) Constant current images (110 × 82 Å^2) of the HtBDC double-row structure and immobilized single molecules at 25 K ($V = 1250$ mV, $I = 0.42$ nA). Holes in the restructured surface are framed black. B) Holes underneath the molecules after pushing the molecules aside. The holes consist of approximately 14 Cu atoms expelled from the surface in two adjacent [1$\bar{1}$0] rows ($V = 10$ mV, $I = 1.78$ nA).

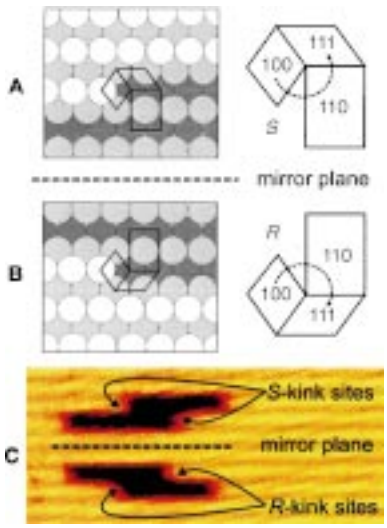

Figure 3. Illustration of chirality and nomenclature of kink sites on an fcc{110} surface.[5] The black frames in the ball models mark the unit cells of the three surface orientations—(100), (110), and (111)—involved in the kink formation, as labeled in the enlarged drawings (see text for details). A) *S* configuration; B) *R* configuration; C) STM image of the two hole types which demonstrates the positions of the kink sites.

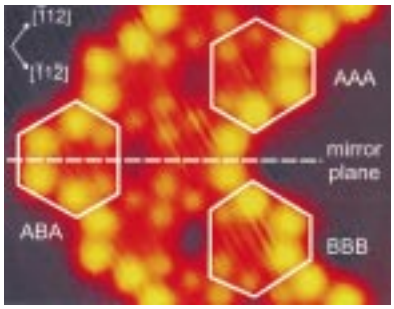

Figure 4. STM images of the double-row structure. Chiral AAA and BBB conformations along the rows and achiral ABA conformation in the elbows are indicated.

We have recently shown that molecules can be pushed away by operating the STM tip in manipulation mode.[13] This enabled us to directly examine the underlying Cu(110) surface, which revealed a pronounced restructuring into a characteristic trench-base structure: 14 Cu atoms are dug out of the surface to which the molecules are anchored (Figure 2B). These holes explain the variation in the intensity of the six lobes of the molecules within the molecular double rows: the dimmer lobes correspond to *tert*-butyl groups located on top of a hole.[13]

The holes formed in the surface contain kink sites and are therefore chiral, as explained in the following. The chirality of kink sites and the nomenclature according to Ahmadi et al. are shown in Figure 3A and B.[5] When the surface is viewed from above, a kink site is of *R* configuration if the sequence of the surface orientations meeting at the kink site runs clockwise in the order {111}-{100}-{110} (corresponding to a decreasing density of atoms in the topmost layer) and of *S* configuration if the orientation runs counter-clockwise.[14] As shown in Figure 3C the holes contain either two *R* or two *S* kinks, which in the following are referred to as *RR* and *SS* holes, and are consequently chiral, that is, nonsuperimposable by simple translation or rotation.

The imaging of the double-row structures seems to reflect the molecules' different conformations (Figure 4). All molecules along the [$\bar{1}1\bar{2}$] rows are imaged identically and reflect a certain conformation, whereas the molecules along the [$\bar{1}12$] rows have the enantiomorphic conformation—the molecules within a given double row are superimposable by a 180° rotation. Hence, the two molecule conformations are chiral and nonsuperimposable. If we tentatively assume that the STM images of the molecules can be interpreted as simple geometric height corrugations, then the molecules along the rows correspond to the AAA and BBB conformations: three bright and three dim lobes of the molecules reflect the two sets of three *tert*-butyl groups lying in two parallel planes, as seen in the propeller conformation model in Figure 1B. Within this interpretation the molecules at the elbows interconnecting the rows thus correspond to the (achiral) ABA conformations: The four bright and two dim lobes (or two bright and four dim lobes) reflect the two sets of four and two *tert*-butyl groups lying in two parallel planes (see the model of the boat conformation in Figure 1C). We must, however, keep in mind that, in principle, STM images do not simply reveal geometrical height contours.[15]

We speculate that the chirality of the Cu surface is imprinted into the surface by the chiral molecules: the adsorption of chiral molecules on top of chiral holes leads to diastereomeric complexes with different interaction energies. The AAA (BBB) conformation may, for example, have a lower interaction energy with an *RR* (*SS*) hole than with an *SS* (*RR*) hole. Accordingly, one type of enantiomeric hole will be decorated with one and only one enantiomeric conformation of the molecule. It would therefore be very interesting to perform theoretical STM simulations of the different conformations and compare them with the experimental findings.

  1433-7851/01/4014-2624 $ 17.50+.50/0

Figure 5 depicts the growth of HtBDC molecules on the Cu(110) surface at increasing coverage (measured in monolayers (ML), where 1 ML is defined as the number of atoms per unit area in the unreconstructed Cu surface layer). Since the HtBDC molecules are fairly large (diameter $\approx$15 Å), a saturated molecular overlayer only corresponds to a coverage of approximately 0.03 ML (see below).

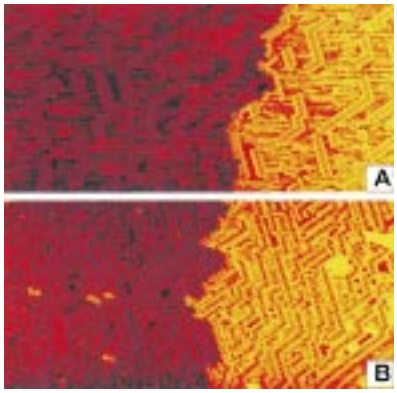

Figure 5. Constant current STM images at RT with increasing coverages of zigzagged HtBDC rows (1000×500 Å^2, $V = 1250$ mV, $I = 0.55$ nA): A) approximately 0.01 ML; B) approximately 0.03 ML.

The molecular rows grow in length and density with increasing coverage, and the zigzag rows, which alternate irregularly along the $[\bar{1}1\bar{2}]$ and $[\bar{1}12]$ direction, eventually cover the entire surface (Figure 5). If this unordered saturated overlayer is annealed at 410 K for around 10 min, uniform domains with diameters in the range of 100 – 1000 Å build up. Each of these domains consists of densely packed rows along the $[\bar{1}1\bar{2}]$ or $[\bar{1}12]$ direction exclusively (Figure 6 A), which demonstrates that the straight double-row structure is indeed thermodynamically stable and energetically preferred over the zigzagged rows.

A model of the ordered, saturated structure is sketched in Figure 6 B, and shows the commensurable superstructure of the molecules. A unit cell contains two HtBDC molecules and 64 Cu atoms, that is, the saturated coverage is $2/64 \approx 0.031$ ML. We conclude from the unequivocal correlation between the row direction and the hole type underneath,[16] that the holes within a given domain are all alike and hence the domains are homochiral. Moreover, *every* molecule is connected with a chiral kink site. This occurrence demonstrates how the molecules induce chirality to the extended terraces of the metal crystal surface.

Since a domain contains molecules of one enantiomeric conformation exclusively, an explanation of how the two conformations separate into domains, namely, how the adsorbate layer rearranges from unordered zigzag rows (= racemic conglomerate) into large chiral domains (= racemic compounds), is necessary. Separation by diffusion seems rather unlikely because of the dense packing. A local rearrangement seems, however, possible as a result of the low inversion energy between the HtBDC conformations AAA and BBB.[17] At the same time the holes underneath the molecular layer in the Cu surface can easily be converted from *RR* into *SS* by diffusion of Cu atoms. The overall surface is

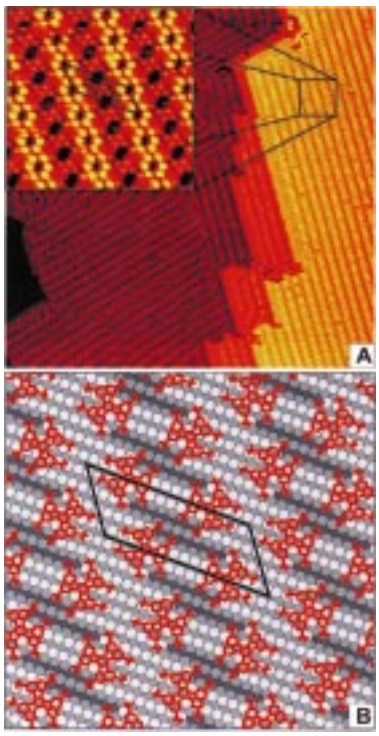

Figure 6. Constant-current STM image at RT after annealing the fully covered surface (see Figure 5 B) at 410 K. A) Domains of densely packed molecules along the $[\bar{1}1\bar{2}]$ and $[\bar{1}12]$ directions (1000×1000 Å^2, $V =$ 1250 mV, $I = 0.51$ nA). The inset shows a close-up of a domain (100×100 Å^2, $V = 1768$ mV, $I = 0.30$ nA): the $\left(\begin{smallmatrix} 4 & 4 \\ 16 & 0 \end{smallmatrix}\right)$ unit cell and the hole contour are framed black. B) Ball model of the double-row structure—the substrate atoms are shaded darker whenever the layers lie deeper. The molecules are shown in red and the unit cell is framed black.

racemic, because of the conformational flexibility of the HtBDC molecules, and consists of equal amounts of both domains. We propose that an overall homochirally restructured surface may be obtained by using slightly modified HtBDC molecules where, for example, surrounding groups larger than *tert*-butyl groups force the molecule to be conformationally fixed in the AAA or BBB form.

In conclusion, we have shown that the adsorption of chiral molecules can bestow chirality onto the extended, flat metal terraces. Previously, chiral surfaces have mainly been formed by adsorbing chiral molecules onto an (unreconstructed) achiral surface, thus forming molecular overlayer domains which are chiral. Our finding of chirality in a metal surface itself may shed new light on the mechanistic understanding of the catalytic behavior of chirally modified surfaces. Catalytic surfaces are generally considered as a static checkerboard providing adsorption sites for the chiral auxiliary and the reactants, while we have shown that a chiral restructuring of the substrate surface may have to be taken into account.

Experimental Section

The experiments were performed in an ultrahigh vacuum (UHV, base pressure $< 10^{-10}$ mbar) chamber equipped with a home-built low- and variable-temperature STM capable of operating at 25 – 400 K.[18] The Cu(110) surface was cleaned by cycles of 2.0 keV Ne ion bombardment followed by annealing at 820 K.

The HtBDC powder was degassed in UHV at 400 K for several hours prior to use. The molecules were dosed in UHV onto the clean Cu(110) surface

  1433-7851/01/4014-2625 $ 17.50+.50/0

by organic molecular beam deposition out of a resistively heated glass crucible at 450 K with a deposition rate of around 0.0001 ML s^{-1}. The substrate was kept at RT. The amount of dosed HtBDC molecules on the surface was controlled by keeping the crucible temperature constant and varying the exposure time (5 – 600 s). The STM images at low temperatures were obtained by cooling the sample down to the desired temperature after the deposition of the molecules at RT.

Received: February 13, 2001
Revised: April 20, 2001 [Z16608]

[1] a) F. Stevens, D. J. Dyer, D. M. Walba, *Angew. Chem.* **1996**, *108*, 955; *Angew. Chem. Int. Ed. Engl.* **1996**, *35*, 900; b) G. P. Lopinski, D. J. Moffatt, D. D. M. Wayner, R. A. Wolkow, *Nature* **1998**, *392*, 909; c) M. O. Lorenzo, C. J. Baddeley, C. Muryn, R. Raval, *Nature* **2000**, *404*, 376; d) F. C. De Feyter, P. C. M. Grim, M. Rücker, P. Vanoppen, C. Meiners, M. Sieffert, S. Valiyaveettil, K. Müllen, F. C. De Schryver, *Angew. Chem.* **1998**, *110*, 1281; *Angew. Chem. Int. Ed.* **1998**, *37*, 1223; e) M. Böhringer, K. Morgenstern, W.-D. Schneider, R. Berndt, *Angew. Chem.* **1999**, *111*, 832; *Angew. Chem. Int. Ed.* **1999**, *38*, 821; f) J. V. Barth, J. Weckesser, C. Cai, P. Günther, L. Bürgi, O. Jeandupeux, K. Kern, *Angew. Chem.* **2000**, *112*, 1285; *Angew. Chem. Int. Ed.* **2000**, *39*, 1230.
[2] a) *Chiral Reactions in Heterogeneous Catalysis* (Eds.: G. Jannes, V. Dubois), Plenum, New York, **1995**; b) H. U. Blaser, *Tetrahedron: Asymmetry* **1991**, *2*, 843; c) A. Baiker, H. U. Blaser in *Handbook of Heterogeneous Catalysis*, *Vol. 5* (Eds.: G. Ertl, H. Knözinger, J. Weitkamp), Wiley-VCH, Weinheim, **1997**, p. 2422; d) L. Hecht, L. Barron, *Chem. Phys. Lett.* **1994**, *225*, 525.
[3] a) G. M. Schwab, L. Rudolph, *Naturwissenschaften* **1932**, *20*, 363; b) G. M. Schwab, F. Rost, L. Rudolph, *Kolloid Z.* **1934**, *68*, 157; c) K.-H. Ernst, M. Böhringer, C. F. McFadden, P. Hug, U. Müller, U. Ellerbeck, *Nanotechnology* **1999**, *10*, 355.
[4] C. F. McFadden, P. S. Cremer, A. J. Gellman, *Langmuir* **1996**, *12*, 2483.
[5] A. Ahmadi, G. Attard, J. Feliu, A. Rodes, *Langmuir* **1999**, *15*, 2420.
[6] a) D. S. Sholl, *Langmuir* **1998**, *14*, 862; b) T. D. Power, D. S. Sholl, *J. Vac. Sci. Technol. A* **1999**, *17*, 1700; c) G. Attard, A. Ahmadi, J. Feliu, A. Rodes, E. Herrero, S. Blais, G. Jerkiewicz, *Phys. Chem. B* **1999**, *103*, 1381.
[7] X. Zhao, *J. Am. Chem. Soc.* **2000**, *122*, 12584.
[8] Permutations of ABA and BAB reproduce the same molecule rotated by $\pm 120^\circ$.
[9] D. M. Ho, R. A. Pascal, Jr., *Chem. Mater.* **1993**, *5*, 1358.
[10] K. Zimmermann, R. Goddard, C. Krüger, M. W. Haenel, *Tetrahedron Lett.* **1996**, *37*, 8371.
[11] See movie at http://www.ifa.au.dk/camp/movies/htbdc.mpg. General remarks about STM movies can be found in F. Besenbacher, *Rep. Prog. Phys.* **1996**, *59*, 1737.
[12] J. K. Gimzewski, C. Joachim, R. R. Schlittler, V. Langlais, H. Tang, I. Johannsen, *Science* **1998**, *281*, 531.
[13] M. Schunack, L. Petersen, A. Kühnle, E. Lægsgaard, I. Stensgaard, I. Johannsen, F. Besenbacher, *Phys. Rev. Lett.* **2001**, *86*, 456.
[14] This terminology is in analogy with the Cahn – Ingold – Prelog sequence rule for chiral substances, see, for example, F. A. Carey, R. J. Sundberg, *Advanced Organic Chemistry*, *Part A*, 3rd ed., Plenum, New York, **1990**, chap. 2.
[15] a) P. S. Weiss, D. M. Eigler, *Phys. Rev. Lett.* **1993**, *71*, 3139; b) P. Sautet, M.-L. Bocquet, *Phys. Rev. B* **1996**, *53*, 4910; b) P. Sautet, *Chem. Rev.* **1997**, *97*, 1097.
[16] The correlation was confirmed by manipulating several molecular double-row structures and checking the restructuring underneath. Attempts to push molecules away from densely packed domains did not succeed in resolving the underlying restructured surface directly.
[17] The activation energy for the inversion of the closely related decacyclene molecule was calculated to be only 0.13 eV; see ref. [9].
[18] L. Petersen, M. Schunack, B. Schaefer, T. R. Linderoth, P. B. Rasmussen, P. T. Sprunger, E. Lægsgaard, I. Stensgaard, F. Besenbacher, *Rev. Sci. Instrum.* **2001**, *72*, 1438.
[19] The conformations in Figure 1B and C are derived from molecular-mechanics force-field calculations using the Titan software from Wavefunction, Inc.

Organophosphorus Dendrimers as New Gelators for Hydrogels

Christelle Marmillon, Fabienne Gauffre, Tadek Gulik-Krzywicki, Christophe Loup, Anne-Marie Caminade,* Jean-Pierre Majoral,* Jean-Pierre Vors, and Elmar Rump

Owing to their numerous applications in different fields (cosmetics, health care, textile, paper, packaging, oil field, photographic industry, etc) gels continue to attract considerable attention.[1] They can be considered as composite materials made of a three-dimensional (3D) supramolecular network imprisoning a large quantity of liquid. The driving force for the formation of gels can be van der Waals, hydrophobic, fluorophobic, $\pi-\pi$ stacking, dipole – dipole, weak coordination interactions, or hydrogen bonds. A number of small molecules are able to form gels such as steroids, fatty acids, copper chelates, fluorinated alkanes, peptides, cyclic dipsipeptides, anthracene derivatives, amino pyridines, calixarenes. More sophisticated macromolecules such as bisarborols (bidirectional molecules with a lipophilic central chain substituted on the end with polyalcohol groups) were found to act also as gelators in water[2] or in hot solvent mixtures such as ethanol/water or dimethylformamide/water.[3] Very recently Aida et al.[4] described the formation of physical gels in acetonitrile with peptide core dendrimers.

Herein we report the first examples of the use of hydrosoluble dendrimers as new gelators in water that allow the confinement of a variety of organic and organometallic substances under very mild conditions.

Polycationic dendrimers **3-[G$_0$]** – **3-[G$_4$]** (P(S) core, generation 0 to 4, pyridinium chloride as terminal groups), **4-[G$_0$]** – **4-[G$_4$]** (P(S) core, ammonium chloride as terminal groups), **6-[G$_2$]** (P_3N_3 core, pyridinium chloride as terminal groups) are prepared in quantitative yield by reacting the corresponding dendrimers **1-[G$_0$]** – **1-[G$_4$]** or **2-[G$_2$]**[5] (terminal aldehyde groups) with either Girard-P reagent or Girard-T reagent in methanol (Scheme 1). The polycationic dendrimer **5-[G$_1$]** (P(S) core, pyridinium acetate as terminal groups) is obtained by anion exchange from **3-[G$_1$]** and sodium acetate. All dendrimers are characterized as a mixture of isomers around the terminal CH=N–NH–C(O)–CH_2 linkage as shown by ^{13}C NMR spectroscopy. Indeed two signals are detected at $\delta =$ 61.8 – 63.0 for the terminal CH_2 groups and at $\delta = 162.3 - 168.1$ for the carbonyl groups. ^{1}H NMR spectra confirm the

[*] Dr. A.-M. Caminade, Dr. J.-P. Majoral, Dr. C. Marmillon, Dr. F. Gauffre, C. Loup
Laboratoire de Chimie de Coordination, CNRS
205 route de Narbonne, 31077 Toulouse cedex 04 (France)
Fax: (+33) 5-61-55-30-03
E-mail: caminade@lcc-toulouse.fr, majoral@lcc-toulouse.fr
Dr. T. Gulik-Krzywicki
Centre de Génétique Moléculaire, CNRS
91198 Gif-sur-Yvette (France)
Dr. J.-P. Vors, Dr. E. Rump
Aventis Crop Science
14-20 rue Pierre Baizet, BP 9163, 69263 Lyon cedex 09 (France)

Supporting information for this article is available on the WWW under http://www.angewandte.com or from the author.

  1433-7851/01/4014-2626 $ 17.50+.50/0

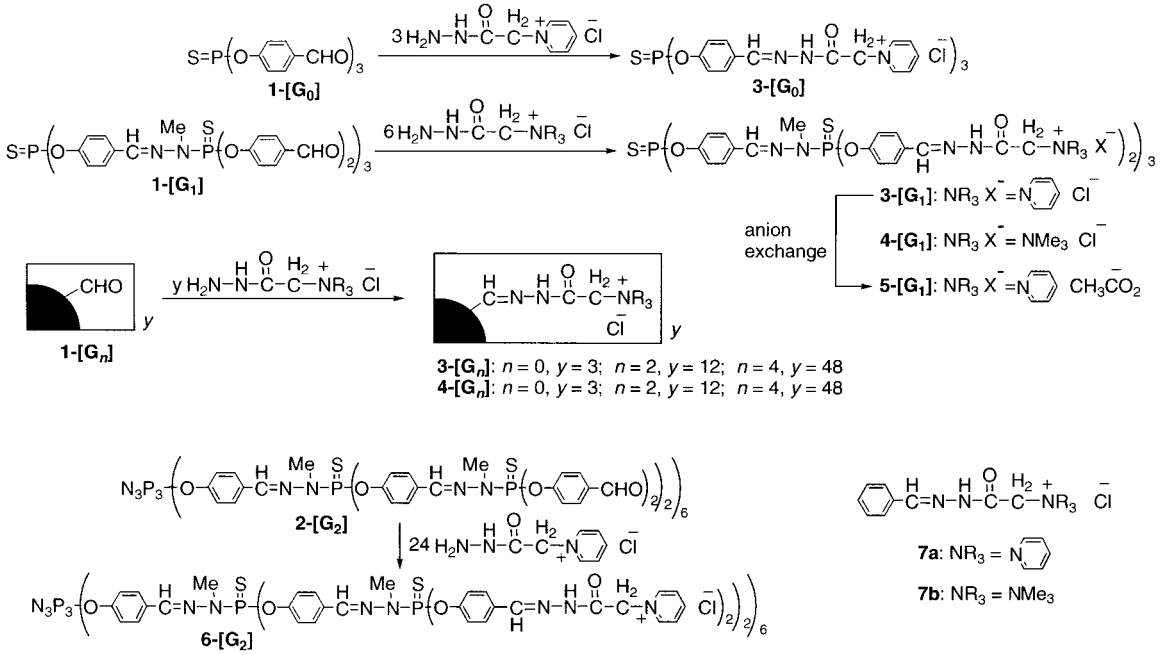

Scheme 1. Preparation of dendrimers **3-[G$_0$]** – **3-[G$_4$]**, **4-[G$_0$]** – **4-[G$_4$]**, **5-[G$_1$]**, and **6-[G$_2$]**.

presence of such inseparable isomers as already noted for other Girard derivatives.[6] Dendrimers of generation 1 to 4 form reversible rigid gels when dissolved in water. In general, gelation is observed at concentrations of 1.5 – 1.8 % in weight. At lower concentrations, a gel phase separates and leaves a layer of free water. Around 7500 water molecules are estimated to be gelled by a molecule of dendrimer of generation 1 (**3-[G$_1$]**, **4-[G$_1$]**, **5-[G$_1$]**) and around 70000 by a molecule of dendrimer of generation 4 (**3-[G$_4$]**, **4-[G$_4$]**), that is gelation of about 1200 – 1400 molecules of water per terminal ammonium or pyridinium unit, regardless of the generation considered. The gelation time is strongly dependent on the experimental conditions and on the nature of terminal groups. The best results are obtained when an aqueous solution of dendrimer is heated at 60 – 65 °C for 11 – 13 days. Dendrimers **3-[G$_n$]** ($n = 1-4$) form gels more quickly than dendrimers **4-[G$_n$]** ($n = 1-4$) and only slight changes were observed when moving from the lowest generation ($n = 1$) to the highest dendrimer ($n = 4$) or when moving from a trifunctionalized core (**3-[G$_1$]** – **3-[G$_4$]** or **4-[G$_1$]** – **4-[G$_4$]**) to a hexafunctionalized one (**6-[G$_2$]**) (Table 1). Introduction of defects at the surface of dendrimers through incomplete Schiff reactions between starting dendrimers **1-[G$_n$]** and Girard-P or Girard-T reagents does not hinder the formation of gels. $Cl^-/CH_3CO_2^-$ ion exchange leads to an acceleration of the gelation process: gelation with **5-[G$_1$]** (acetate as counteranion), for example, is achieved in four days at 60 – 65 °C, whereas gelation with **3-[G$_1$]** (chlorine as counteranion) requires twenty days. Interestingly, no gelation is detected with the monomers **7a**, **b** resulting from the condensation reaction between benzaldehyde and Girard-P or -T reagents.

Remarkably gelation time is also dramatically shortened in the presence of hydrosoluble components (by 10 to 30 %) such as buffer (TRIS (tris(hydroxymethyl)aminomethane), etc), metal salts (Ni, Y, Er acetates), acids (citric, ascorbic, lactic, L-tartric, etc), dithioerythritol (DTE), sodium salt of ethylenediaminetetraacetate (EDTA) (Table 2, Figure 1). In-

Table 1. Gelation of polycationic dendrimers (1.8 %) in aqueous solutions at 60 – 65 °C (Cl^- as counterion).

Dendrimers	Gelation time[a] [days]	Dendrimers	Gelation time[a] [days]
3-[G$_0$]	partial gelation	**4-[G$_0$]**	no gelation
3-[G$_1$]	20	**4-[G$_1$]**	75
3-[G$_2$]	20	**4-[G$_2$]**	75
3-[G$_4$]	13	**4-[G$_4$]**	60
5-[G$_1$][b]	4	**6-[G$_2$]**	11

[a] Gelation was regarded as finished when all the solution is geled. [b] Acetate as counteranion.

Table 2. Gelation of dendrimers **3-[G$_4$]** and **4-[G$_4$]** (1.8 %) in water at 60 – 65 °C with confinement of various components.

Components	pH	Gelation time [h][a]
	3-[G$_4$]	
$Ni(Ac)_2 \cdot 4H_2O$ 10 %	6.6	12
$Ni(Ac)_2 \cdot 4H_2O$ 30 %	6.0	7
$Y(Ac)_3 \cdot 4H_2O$ 20 %	6.0	12
$Er(Ac)_3 \cdot 4H_2O$ 10 %	5.8	4
TRIS buffer	9.3	3
D,L-lactic acid		8
ascorbic acid 10 %	2.0	12
L-tartric acid 10 %		12
citric acid 10 %	1.4	5[b]
DTE 2.3 %		96
EDTA, 4Na 10 %		3
$Er(Ac)_3 \cdot 4H_2O$ 10 %	5.8	240[c]
	4-[G$_4$]	
$Ni(Ac)_2 \cdot 4H_2O$ 10 %	6.6	48
TRIS buffer	9.3	48
EDTA, 4Na 10 %		20

[a] Gelation was regarded as finished when all the solution is geled. [b] Bad cohesion of the gel. [c] Room temperature.

  1433-7851/01/4014-2627 $ 17.50+.50/0

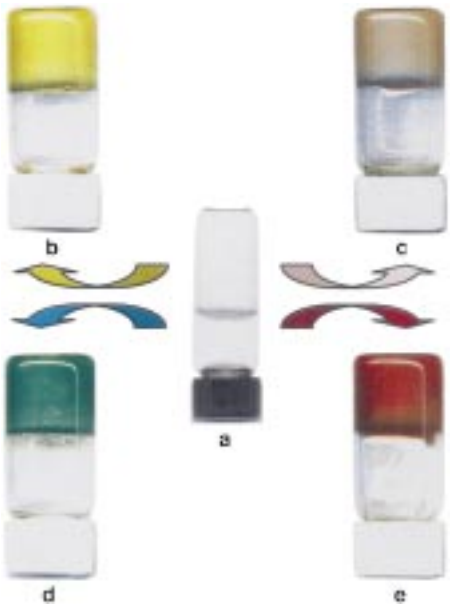

Figure 1. Rigid gels shown in upturned flasks. a) Hydrogel formed with **3-[G_4]** (1.8% in water). b) Hydrogel formed with **3-[G_4]** (1.8% in water) and TRIS buffer (10%). c) Hydrogel formed with **3-[G_4]** (1.8% in water) and $Er(OAc)_3 \cdot 4H_2O$, 10%. d) Hydrogel formed with **3-[G_4]** (1.8% in water) and $Ni(OAc)_3 \cdot 4H_2O$ (10%). e) Hydrogel formed with **3-[G_4]** (1.8% in water) and ascorbic acid (10%).

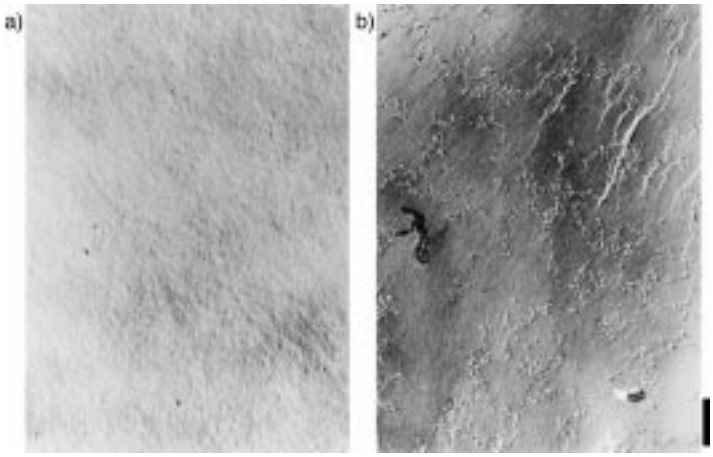

Figure 2. Freeze-fracture electron micrographs of a sample of dendrimer **3-[G_4]** (2%) in water/glycerol (70/30); bar: 500 nm for both figures. a) Solution prior to gelation. b) Gel. Aggregates appear as black dots (the white streaks are shadows due to the freeze-fracture technique).

deed gelation and confinement take place at room temperature in a few hours for dendrimers of generations 1–4. Remarkably too, a rigid gel is formed with dendrimer **3-[G_0]** in the presence of erbium acetate after heating at 60–65 °C for 12 h.

Confinement and gelation are not pH-dependent: both dendrimers form gels in the pH range of 2–9 in aqueous solutions containing the above-mentioned components. The resulting translucent gels are stable for several months, they do not flow, and can even be crushed into pieces. The internal structure of the gels was examined by freeze-fracture electron microscopy. The samples were prepared with a water/glycerol (70/30) mixture as solvent in order to prevent the formation of ice crystals during the freezing stage. Electron micrographs of a **3-[G_4]** sample prior to and after gelation are displayed in Figures 2a and b, respectively. The size of the dendrimer (the diameter is approximately 7–8 nm for a dendrimer of generation 4) is of the order of the limit of resolution by this technique. Prior to gelation (Figure 2a) the texture is homogeneous and the isolated dendrimers can only be seen as small dots on very careful examination of the micrograph, while after gelation the images (Figure 2b) reveal a network of aggregated dendrimers that contrasts clearly with the smooth areas of solvents. The geometry of the network resembles that found in gels from other types of particles (milk proteins, clay), which is not surprising since dendrimers can be considered as nanoscale particles. In addition, observation of Figure 2b and other freeze-fracture electron micrographs suggests that the dendrimers are not covalently bonded in the gel state. Indeed, the dendrimer network does not seem continuous, which means that some molecules of dendrimers are left on the other side of the fracture when they are pulled apart. This is usually not the case when elements are linked by covalent bonds. The assumption of noncovalent bonds between dendrimers in the gel (i.e. the gel is a so-called "physical" gel) is supported by several observations of reversibility. For instance, addition of acetonitrile to the surface of gels allows the progressive dissolution of gels,[7] which can be formed again through slow removal of acetonitrile at room temperature. Gel formation is, however, not thermoreversible.

Most types of weak interactions known to favor the formation of gels can occur for dendrimers **3**–**6**: intermolecular hydrogen bonding, face-to-face $\pi-\pi$ aromatic stacking, and hydrophobic effects due to the internal backbone of dendrimers. Figure 3 illustrates these supramolecular interactions for dendrimers **3-[G_n]**. Moreover acceleration of the rate of gelation of dendrimers in the presence of acetates could be explained by the bridging of anions which probably participate to the formation of the networks.

The relative ease with which hydrogels with polycationic phosphorus-containing dendrimers are obtained is in marked contrast with what is reported for the formation of hydrogels from water-soluble linear phosphorus polymers, that is polyphosphazenes. For instance, ^{60}Co gamma irradiation of a poly[bis(methoxyethoxyethoxy)]phosphazene is necessary to promote cross-linking, through formation of intermolecular carbon–carbon bonds, which converts this water-soluble polymer to a material that imbibes water to form a pH-sensitive hydrogel.[8] Moreover, the possibility to incorporate ligands or metals within the cascade structure of dendrimers or at the core various functional groups[9] renders the hydrogels made from dendrimers much more attractive for new applications in different fields such as drug delivery, enzyme or antigen immobilization, and catalysis.

Remarkably, freeze-drying of gels **3-[G_2]**–**3-[G_4]** at low temperature gave rise to opaque aerogels which retained the size and form of the hydrogels. Aerogels were characterized by scanning electron microscopy, which showed some ramified fiberlike constructions (Figure 4).

  1433-7851/01/4014-2628 $ 17.50+.50/0

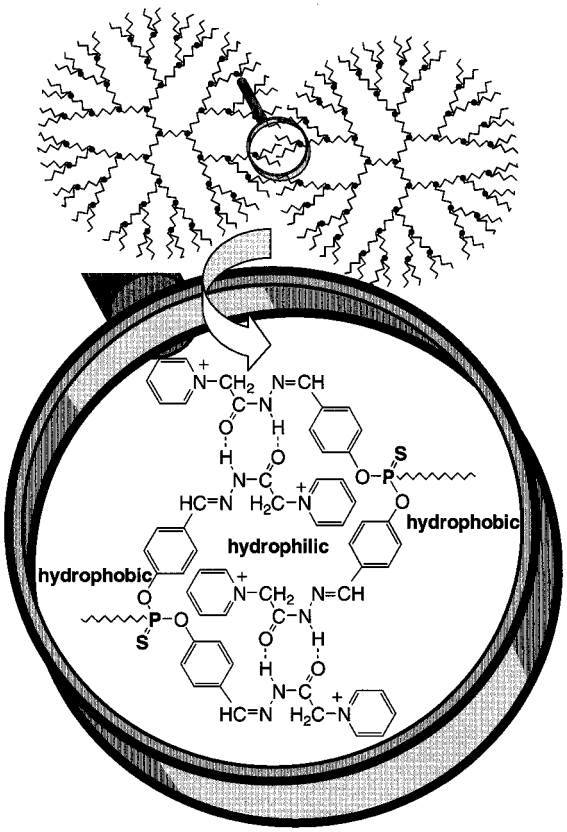

Figure 3. Supramolecular interactions (hydrogen bonds, $\pi-\pi$ aromatic stacking, hydrophobic effects) as driving forces for the formation of gels.

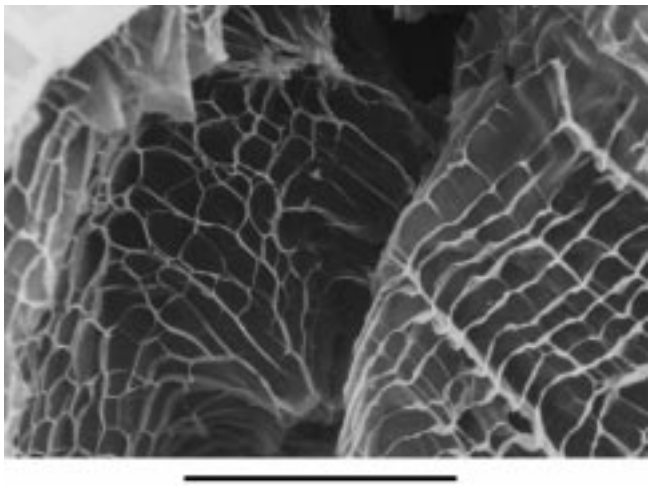

Figure 4. SEM image of a freeze-dried gel (**3-[G_4]**) (20 kV); bar: 200 μm.

In conclusion we have described a new type of gel based on phosphorus-containing dendrimers. These gels can be obtained under very mild conditions and allow the confinement of a number of active substances.

Received: December 14, 2000
Revised: April 17, 2001 [Z16273]

[1] a) For a recent review, see: P. Terech, R. G. Weiss, *Chem. Rev.* **1997**, *97*, 3133, and references therein; b) for recent papers see for example J. H. van Hesch, B. L. Feringa, *Angew. Chem.* **2000**, *112*, 2351; *Angew. Chem. Int. Ed.* **2000**, *39*, 2263; L. A. Estroff, A. D. Hamilton, *Angew. Chem.* **2000**, *112*, 3589; *Angew. Chem. Int. Ed.* **2000**, *39*, 3447; L. A. Cuccia, J. M. Lehn, J. C. Homo, M. Schmutz, *Angew. Chem.* **2000**, *112*, 239; *Angew. Chem. Int. Ed.* **2000**, *39*, 233; R. Oda, I. Huc, S. J. Candau, *Angew. Chem.* **1998**, *110*, 2835; *Angew. Chem. Int. Ed.* **1998**, *37*, 2689; c) P. Terech, I. Furman, R. G. Weiss, H. Bois-Laurent, J. P. Desvergnes, R. Ramasseul, *Faraday Discuss.* **1995**, *101*, 345.

[2] a) G. R. Newkome, G. R. Baker, S. Arai, M. J. Saunders, P. S. Russo, K. J. Theriot, C. N. Moorefield, L. E. Rogers, J. E. Miller, T. R. Lieux, M. E. Murray, B. Phillips, L. Pascal, *J. Am. Chem. Soc.* **1990**, *112*, 8458; b) G. R. Newkome, C. N. Moorefield, G. R. Baker, R. K. Behera, G. H. Escamilla, M. J. Sanders, *Angew. Chem.* **1992**, *104*, 901; *Angew. Chem. Int. Ed. Engl.* **1992**, *31*, 917.

[3] M. Jorgensen, K. Bechgaard, *J. Org. Chem.* **1994**, *59*, 5877.

[4] W. D. Jang, D. L. Jiang, T. Aida, *J. Am. Chem. Soc.* **2000**, *122*, 3232.

[5] N. Launay, A. M. Caminade, R. Lahana, J. P. Majoral, *Angew. Chem.* **1994**, *106*, 1682; *Angew. Chem. Int. Ed. Engl.* **1994**, *33*, 1589. For a review, see: J. P. Majoral, A. M. Caminade, *Chem. Rev.* **1999**, *99*, 845.

[6] J. T. Beckvermit, D. J. Anziano, C. K. Murray, *J. Org. Chem.* **1996**, *61*, 9038.

[7] ^{31}P and ^{1}H NMR spectra of the product obtained after redissolution of the gel in acetonitrile and removal of the solvents showed no difference to the ^{1}P and ^{1}H NMR spectra of the former dendrimer. This is in agreement with the formation of a physical gel.

[8] a) H. R. Allcock, *Polym. Mater. Sci. Eng.* **1993**, *69*, 98; b) H. R. Allcock, A. M. A. Ambrosio, *Biomaterials* **1996**, *17*, 2295.

[9] a) C. Galliot, C. Larré, A. M. Caminade, J. P. Majoral, *Science* **1997**, *277*, 1981; b) C. Larré, D. Bressolles, C. Turrin, B. Donnadieu, A. M. Caminade, J. P. Majoral, *J. Am. Chem. Soc.* **1998**, *120*, 13070.

trans-$[Fe(CN)_4(CO)_2]^{2-}$, a 21st Century [Fe(CN)(CO)] Compound**

Jianfeng Jiang and Stephen A. Koch*

$[Fe^{II}(CN)_5(CO)]^{3-}$ was reported in the 19th century,[1] and $[Fe(CN)(CO)_4]^{1-}$ was characterized in the 20th century.[2] Here we report the synthesis and characterization of the third monomeric iron complex with exclusively CO and CN^- ligands.[3] The discovery of the [Fe(CN)(CO)] moieties at the catalytic centers of NiFe and Fe-only hydrogenases[4] dramatically increased interest in Fe compounds with CN^- and CO ligands.[5] These enzymes provided the first examples of either CO or CN^- as native ligands in a metalloprotein. Simple [Fe(CN)(CO)] complexes are possible intermediates in the biosynthesis of the $[Fe(CN)_y(CO)_x]$ centers in hydrogenases and are possible complexes in prebiotic chemistry.[6]

trans-$[Fe(CN)_4(CO)_2]^{2-}$ (**1**) is generated in solution by the simple addition of 4 equiv of NaCN to an aqueous solution of $FeCl_2 \cdot 4H_2O$ under an atmosphere of CO. The anion was isolated as the colorless crystalline solid $Na_2(dmf)_4$-**1**, which is

[*] Prof. S. A. Koch, J. Jiang
Department of Chemistry
State University of New York at Stony Brook
Stony Brook, NY 11794-3400 (USA)
Fax: (+1) 631-632-7960
E-mail: Stephen.Koch@sunysb.edu

[**] This work was supported by a National Institutes of Health Grant (GM 58000). We thank Professors Michelle Millar and Albert Haim for discussion.

stable in air for at least several months. As far as we can determine, this compound has never been described in the literature. This is surprising considering the simplicity of the synthesis and the nearly three centuries of interest in Fe – CN chemistry.[7]

The X-ray crystal structure of $Na_2(dmf)_4$-**1** (Figure 1) established the *trans* octahedral arrangement of the CO and CN ligands in the centrosymmetric $[Fe(CN)_4(CO)_2]^{2-}$ anion.[8] The Fe–CO distance (1.800(5) Å) and Fe–CN distances

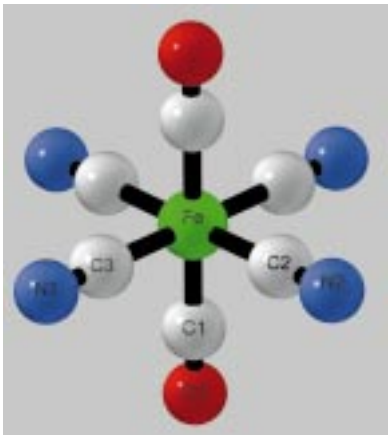

Figure 1. Structural diagram of $[Fe^{II}(CN)_4(CO)_2]^{2-}$. Selected bond lengths [Å] and angles [°]: Fe1-C1 1.800(5), Fe1-C3 1.923(3), Fe1-C2 1.929(4), C1-O1 1.122(5), C3-N3 1.150(4); C2-Fe1-C3 90.05(12), Fe1-C1-O1 178.8(4).

(1.926(4) Å) are consistent with those in other recently solved structures of [Fe(CN)(CO)] compounds.[5] *cis*-$[L_2Fe(CN)_4]$ complexes have been structurally characterized, where L_2 is a bidentate ligand such as ethylenediamine, bipyridine, or 1,10-phenanthroline,[9] but **1** is the first example of a *cis*- or *trans*-$[L_2Fe(CN)_4]$ complex in which L are monodentate ligands. Such $[L_2M(CN)_4]$ compounds in which L is monodentate are rare for the entire transition metal series. The Na cations and the DMF molecules combine with the $[Fe(CN)_4(CO)_2]^{2-}$ anions to create a two-dimensional array (Figure 2). The Na cations occur in pairs linked by two DMF molecules, and each Na cation is also coordinated by a terminal DMF molecule and to two NC groups of the anion. As a result, each cyano group bridges Fe and Na atoms.

The IR spectrum of $Na_2(dmf)_4$-**1** indicates that the *trans* stereochemistry is preserved in solution. As expected for a compound with D_{4h} symmetry, there are single CO and CN stretching bands at 1992 and 2104 cm^{-1} in DMF. There is no evidence for the *cis* isomer in a solution of the isolated product or in the original synthesis solution. These observations contrast with our investigations on a possible alternative synthetic route to **1**. The reaction of 4 equiv of NaCN with $[FeI_2(CO)_4]$ gives solutions that exhibit two equally intense CO stretching bands in Me_2SO at 2016 and 1960 cm^{-1}, consistent with a *cis* arrangement of CO ligands. Simple bonding considerations would suggest that the *cis* isomer of $[Fe(CN)_4(CO)_2]^{2-}$ would be more stable than the *trans* isomer.

The CO and CN stretching frequencies show a pronounced solvent dependence. In water, the CO band (2048 cm^{-1}) is shifted by 56 cm^{-1} to higher energy relative to that in DMF,

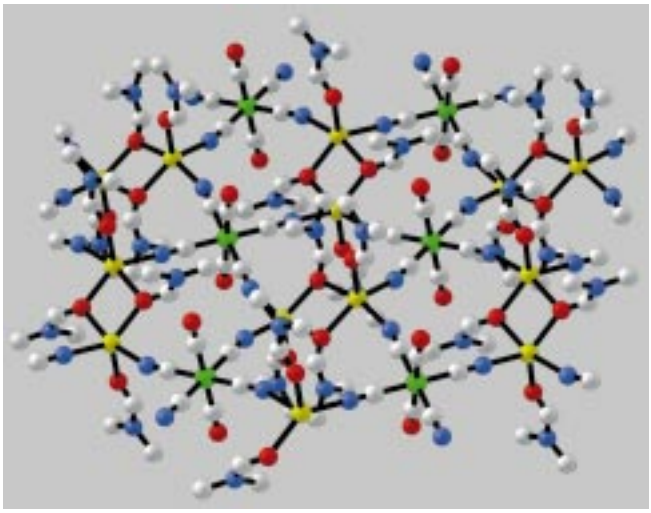

Figure 2. Structural diagram of the two-dimensional lattice showing the interaction of the Na cations with the $[Fe(CN)_4(CO)_2]^{2-}$ anions and DMF. Selected bond lengths [Å]: N3-Na1 2.410(3), N2-Na1 2.385(4), O3-Na1 2.339(3).

while the CN band (2104 cm^{-1}) remains virtually unchanged. The CO stretching band occurs at 2029 cm^{-1} in MeOH, and at 2005 cm^{-1} in CH_2Cl_2. Hydrogen bonding to the CN^- ligands decreases the σ-donor ability of these ligands with a resultant decrease in the electron density available for back-donation to the CO ligands.[10] The solid-state IR spectrum of $Na_2(dmf)_4$-**1**, which has CN and CO stretching bands at 2115 and 2025 cm^{-1}, suggests that the interaction of the Na cation with the $[Fe(CN)_4(CO)_2]^{2-}$ anion has an effect comparable to the hydrogen bonding in MeOH solution. The ^{13}C NMR spectrum of **1** in D_2O shows signals at $\delta = 206$ and 150, which are assigned to the CO and the CN^- ligands. Compound **1** undergoes quasireversible oxidation at +1.38 V (vs SCE) in DMF solution.

$[Fe(CN)_6]^{4-}$, $[Fe(CN)_5(CO)]^{3-}$, and **1** create a series of octahedral low-spin d^6 Fe^{II} complexes which enables comparisons of spectroscopic properties and redox potentials as CN^- is substituted by CO (Table 1). The trends are those expected for the substitution of a good σ-donor/weak π-acceptor CN^- ligand by a poor σ-donor/strong π-acceptor CO ligand. The $Fe^{3+/2+}$ couples shift by 1.155 and 1.125 V as CN^- ligands are stepwise replaced by CO ligands. This gives an experimental measurement of the stabilizing effect of CO versus CN^- for lower oxidation states. The oxidation states of the various redox states of iron-only hydrogenases remain unresolved.[11]

Table 1. Effect of CO/CN^- ligand substitution on spectroscopic and redox properties of $[Fe(CN)_{(6-x)}(CO)_x]^{n-}$ complexes.

	$\tilde{\nu}_{CN}$ [cm^{-1}] (H_2O)	$\delta_{^{13}C}$ of CN (D_2O)	Fe^{III}/Fe^{II} redox potential [V] (Me_2SO, vs SCE[a])
$K_4[Fe^{II}(CN)_6]$	2044[12]	177[13]	−0.90[10]
$Na_3[Fe^{II}(CN)_5(CO)]$	2075 (*cis*)[14]	162.5 (*cis*) 163.4 (*trans*)[15]	0.255[14]
$[Fe^{II}(CN)_4(CO)_2]^{2-}$	2104	150	1.38

[a] SCE = saturated calomel electrode.

  1433-7851/01/4014-2630 $ 17.50+.50/0

The reactivity of $[Fe^{II}(CN)_4(CO)_2]^{2-}$ and its use as a building block for solid-state materials are under active investigation.

Experimental Section

$Na_2(dmf)_4$-**1**: An aqueous solution (50 mL) of NaCN (0.417g, 8.51 mmol) was added dropwise to an aqueous solution (50 mL) of $FeCl_2 \cdot 4H_2O$ (0.422 g, 2.12 mmol) under a CO atmosphere. The reaction mixture was stirred under a CO atmosphere for 18 h. The water was removed under vacuum, and the residue was extracted with 30 mL of DMF. The product (0.520 g, 44% yield) was obtained by the addition of diethyl ether, filtration, and washing with cold ethanol.

Received: February 23, 2001 [Z16671]

[1] J. A. Muller, *C. R. Hebd. Seances Acad. Sci.* **1887**, *104*, 992; *Gmelin*, *Vol. 36B*, **1976**, p. 24.

[2] S. A. Goldfield, K. N. Raymond, *Inorg. Chem.* **1974**, *13*, 770.

[3] The $[Fe(CN)(CO)_4Fe(CO)_4]^-$ dimer has also been synthesized: J. K. Ruff, *Inorg. Chem.* **1969**, *8*, 86.

[4] a) J. C. Fontecilla-Camps, S. W. Ragsdale, *Adv. Inorg. Chem.* **1999**, *47*, 283; b) M. W. W. Adams, E. I. Stiefel, *Curr. Opin. Chem. Biol.* **2000**, *4*, 214; c) J. W. Peters, *Curr. Opin. Struct. Biol.* **1999**, *9*, 670; d) A. J. Pierik, W. Roseboom, R. P. Happe, K. A. Bagley, S. P. J. Albracht, *J. Biol. Chem.* **1999**, *274*, 3331; e) A. Volbeda, E. Garcin, C. Piras, A. L. deLacey, V. M. Fernandez, E. C. Hatchikian, M. Frey, J. C. Fontecilla-Camps, *J. Am. Chem. Soc.* **1996**, *118*, 12989; f) J. W. Peters, W. N. Lanzilotta, B. J. Lemon, L. C. Seefeldt, *Science* **1998**, *282*, 1853; g) Y. Nicolet, C. Piras, P. Legrand, C. E. Hatchikian, J. C. Fontecilla-Camps, *Structure* **1999**, *7*, 13.

[5] a) H.-F. Hsu, S. A. Koch, C. V. Popescu, E. Münck, *J. Am. Chem. Soc.* **1997**, *119*, 8371; b) C. H. Lai, W. Z. Lee, M. L. Miller, J. H. Reibenspies, D. J. Darensbourg, M. Y. Darensbourg, *J. Am. Chem. Soc.* **1998**, *120*, 10103; c) W. F. Liaw, N. H. Lee, C. H. Chen, C. M. Lee, G. H. Lee, S. M. Peng, *J. Am. Chem. Soc.* **2000**, *122*, 488; d) M. Y. Darensbourg, E. J. Lyon, J. J. Smee, *Coord. Chem. Rev.* **2000**, *206*, 533; e) M. Schmidt, S. M. Contakes, T. B. Rauchfuss, *J. Am. Chem. Soc.* **1999**, *121*, 9736; f) E. J. Lyon, I. P. Georgakaki, J. H. Reibenspies, M. Y. Darensbourg, *Angew. Chem.* **1999**, *111*, 3373; *Angew. Chem. Int. Ed.* **1999**, *38*, 3178; g) A. L. Cloirec, S. P. Best, S. Borg, S. C. Davies, D. J. Evans, D. L. Hughes, C. J. Pickett, *Chem. Commun.* **1999**, 2285.

[6] A. D. Keefe, S. L. Miller, *Orig. Life Evol. Biosph.* **1996**, *26*, 111.

[7] a) A. G. Sharpe, *The Chemistry of Cyano Complexes of the Transition Metals*, Academic Press, New York, **1976**; b) K. R. Dunbar, R. A. Heintz, *Prog. Inorg. Chem.* **1997**, *45*, 283.

[8] Crystal data for $Na_2(dmf)_4$-**1** ($C_{18}H_{28}FeN_8Na_2O_6$): Monoclinic, space group $I2/a$, $a = 12.7422(12)$ Å, $b = 13.0333(13)$ Å, $c = 17.708(2)$ Å, $\beta = 97.891(2)^\circ$, $V = 2913.0(5)$ Å^3, $Z = 4$. A total of 2112 unique reflections with $I > 2\sigma(I)$ were refined to $R_1 = 0.0471$, $wR_2 = 0.1209$. Crystallographic data (excluding structure factors) for the structure reported in this paper have been deposited with the Cambridge Crystallographic Data Centre as supplementary publication no. CCDC-158180. Copies of the data can be obtained free of charge on application to CCDC, 12 Union Road, Cambridge CB21EZ, UK (fax: (+44) 1223-336-033; e-mail: deposit@ccdc.cam.ac.uk).

[9] a) A. A. Schilt, *J. Am. Chem. Soc.* **1960**, *82*, 3000; b) G. G. Christoph, V. L. Goedken, *J. Am. Chem. Soc.* **1973**, *95*, 3869; c) M. Nieuwenhuyzen, B. Bertram, J. F. Gallagher, J. G. Vos, *Acta Crystallogr. Sect. C* **1998**, *54*, 603.

[10] R. E. Noftle, D. Petcher, *J. Electroanal. Chem.* **1990**, *293*, 273, and references therein.

[11] a) C. V. Popescu, E. Münck, *J. Am. Chem. Soc.* **1999**, *121*, 7877; b) A. L. de Lacey, C. Stadler, C. Cavazza, E. C. Hatchikian, V. M. Fernandez, *J. Am. Chem. Soc.* **2000**, *122*, 11232, and references therein; c) A. S. Pereira, P. Tavares, I. Moura, J. J. G. Moura, B. H. Huynh, *J. Am. Chem. Soc.* **2001**, *123*, 2771.

[12] L. H. Jones, *Inorg. Chem.* **1963**, *2*, 777.

[13] J. J. Pesek, W. R. Mason, *Inorg. Chem.* **1979**, *18*, 924.

[14] J. F. Jiang, S. A. Koch, submitted.

[15] H. E. Toma, J. A. Vanin, J. M. Malin, *Inorg. Chim. Acta* **1979**, *33*, L157.

Synthesis, Biological, and Immunological Properties of Cyclic Peptides from *Plasmodium Falciparum* Merozoite Surface Protein-1**

Eduardo Lioy,* Jorge Suarez, Fanny Guzmàn, Sibylle Siegrist, Gerd Pluschke, and Manuel E. Patarroyo*

Malaria is the most important parasitic disease in humans, and in 1997 a malaria risk of varying degrees existed in 100 countries. In 92 of these, transmission included the malignant (*Plasmodium falciparum*) form of the disease, which causes 1.5 to 2.7 million deaths each year.

In spite of intensive efforts, not a single vaccine against a human parasitic disease is currently commercially available, and only one vaccine candidate, namely Spf66,[1] reached phase III clinical trials. Most efforts to develop synthetic peptide vaccines have focused on the use of short, linear B-cell epitopes to elicit the desired immune response. However, linear peptides are inherently flexible molecules and are proteolytically unstable in serum.[2] Conformationally restricted cyclic peptides have the potential to preserve the original secondary structure of the native proteins and in many cases this has been shown to constitute an important feature for a peptide to behave as a good immunogen.[3] Furthermore, it has long been known that the cyclization of a peptide may induce higher binding affinities and a greater degree of specificity in peptide–receptor interactions.[4]

The invasion process of malaria merozoites into human red blood cells (RBCs) is a crucial step in the life cycle of the parasite in the vertebrate host and gives rise to the blood stage part of the parasite cycle, which is responsible for the clinical manifestations of malaria.[5] The rationale of our approach was the identification of small, structurally defined peptide structures that mimic the interaction of the parasitic Merozoite Surface Protein 1 (MSP-1) from *P. falciparum* with the human RBC. Induction of antibodies to such mimics may be useful for studying and blocking these interactions.

To better characterize ligand–receptor interactions that are involved in the invasion process of RBCs, we studied the effect of the introduction of conformational constraints into a linear lead peptide. In parallel, we also studied the effect of peptide cyclization on epitope immunogenicity.

For this purpose, the central part of the 42-61 N-Terminal MSP-1 fragment (Peptide 1513: GYSLFQKEKMVL-NEGTSGTA) was cyclized by using a modified version of the backbone cyclization method.[6] The peptide 1513 plays a decisive role in the recognition of RBC receptors by malaria

[*] Dr. E. Lioy, Prof. Dr. M. E. Patarroyo, Dr. J. Suarez, Dr. F. Guzmàn
Fundaciòn Instituto de Inmunologia de Colombia (FIDIC)
Diag. 53 No. 34-53, AA 33086 Bogotà (Colombia)
Fax: (+57) 1-280-3999
E-mail: elioy@inwind.it, mepatarr@mail.com
Dr. E. Lioy, S. Siegrist, Dr. G. Pluschke
Swiss Tropical Institute (Switzerland)

[**] This work was supported by a long-term fellowship of the Human Frontier Science Program Organization (HFSPO-LT 25/97) and by a Research Grant from the Roche Research Foundation.

parasites, and previous studies[7] showed that this linear peptide binds to RBCs with a 200 nM affinity.

To determine which amino acid (AA) residues are essential for ligand–receptor interactions within the linear lead peptide, we substituted each AA by alanine (Alan scan) and determined the RBC binding affinity of the resulting peptides by measuring their ability to inhibit the binding of the original peptide (binding inhibition assay). The alanine analogues were synthesized by Boc-SPPS (SPPS = solid-phase peptide synthesis, Boc = *tert*-butoxycarbonyl) by using 4-methylbenzhydrylamine (4-MBHA) resin and *N*,*N*′-dicyclohexylcarbodiimide/1-hydroxy-1*H*-benzotriazole activation. Free peptides were obtained by cleavage with HF, purified by dialysis and analyzed by RP-HPLC and MALDI-TOF MS (matrix-assisted laser-desorption/ionization time-of-flight mass spectrometry). The lead peptide 1513 was radiolabeled with $Na^{125}I$ by using the methodology of Yamamura et al.[8] Human RBCs (2×10^7) were incubated for one hour at room temperature with ^{125}I-radiolabeled peptide 1513 (10 nM) in the absence or presence of each Ala analogue (at 10, 100, and 800 nM) as described earlier.[9] Results obtained by using 100-nM unlabeled peptide 1513 are shown in Figure 1. Analogues with substitutions in the central part (…Q**K**E**KM**VL…), especially of the AAs highlighted in bold, were not able to inhibit the binding of the original peptide, demonstrating the importance of these residues for the binding process.

Based on these results, we designed a set of cyclic peptides that contain the essential AAs involved in the ligand–receptor interaction of MSP-1 with the RBC. To introduce

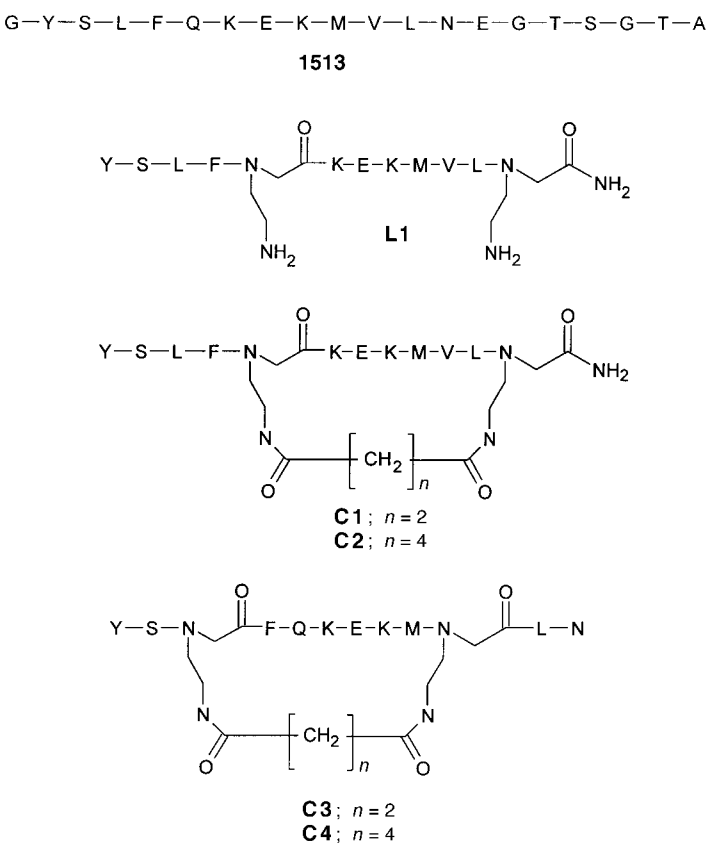

Scheme 1. Linear and cyclic peptide analogues of the AA 42-61 N-terminal MSP-1 fragment.

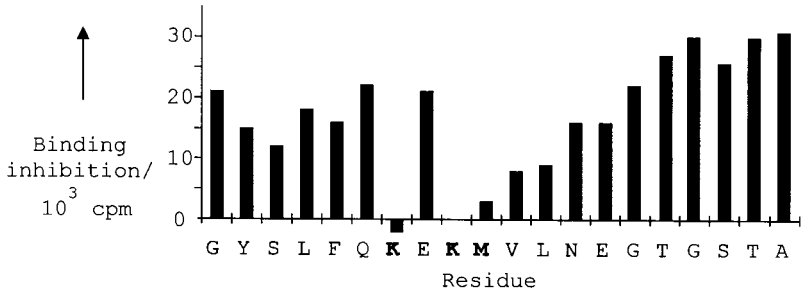

Figure 1. Inhibition of RBC binding of peptide 1513 by its Ala analogues (Ala-Scan).

conformational restraints, peptide cyclization was accomplished by the introduction of two aminoethylglycine subunits, which in all cases are separated by seven AAs. These two subunits were linked by diacid bridges of varying length, resulting in cyclic analogues **C1**–**C4** and the linear control peptide **L1** (Scheme 1).

Fmoc-*N*-(2-aminoethyl)-Boc-glycine (**1**; Fmoc = 9-fluorenylmethoxycarbonyl), which is necessary for the cyclization of resin-supported peptides, was obtained from the previously described[10] Fmoc-*N*-(2-aminoethyl)glycine-*tert*-butylester (**5**) in two steps (Scheme 2). First, the carboxy group was deprotected with 100% TFA, and then a Boc group was introduced at the secondary amine functionality by the reaction of **6** with Boc anhydride in an acetone/water mixture. The bridging monomer **2** was obtained by the reaction of succinic anhydride and 9-fluorenylmethanol (FmOH). Monoesterification of excess DCC/DMAP-activated adipic acid with 9-FmOH yielded bridging monomer **3** (Scheme 2).

All cyclic peptides were obtained by using a solid-phase variation of the backbone-to-backbone cyclization strategy developed by Bitain et al.[6] The peptides were synthesized on a 4-MBHA resin by using a combined Boc/Fmoc strategy (Scheme 3). The peptide chains were elongated by a Boc strategy with HATU activation, whereas the introduction of the bridging elements as well as peptide cyclization was performed by a Fmoc cycle and HATU activation. The peptides were cleaved from the solid support by liquid HF following a low/high protocol. Crude peptides were purified by RP-HPLC and analyzed by RP-HPLC and MALDI-TOF MS. All peptides were obtained in >80% yield and high purity (>95%).

Peptide polymers for immunization studies were obtained from monomeric peptides carrying additional N- and C-terminal CG or GC residues, respectively. The polymerization was accomplished by cysteine oxidation with oxygen at pH 7.4. Peptides for RBC binding studies were radiolabeled with $Na^{125}I$ by using the chloramine T method.[8] To determine binding dissociation constants (K_D), 2×10^7 human RBCs were incubated with increasing concentrations of radiolabeled peptide, as previously described.[9] The affinity constants (K_D) and Hill coefficients were calculated by using Scatchard

  1433-7851/01/4014-2632 $ 17.50+.50/0 *Angew. Chem. Int. Ed.* **2001**, *40*, No. 14

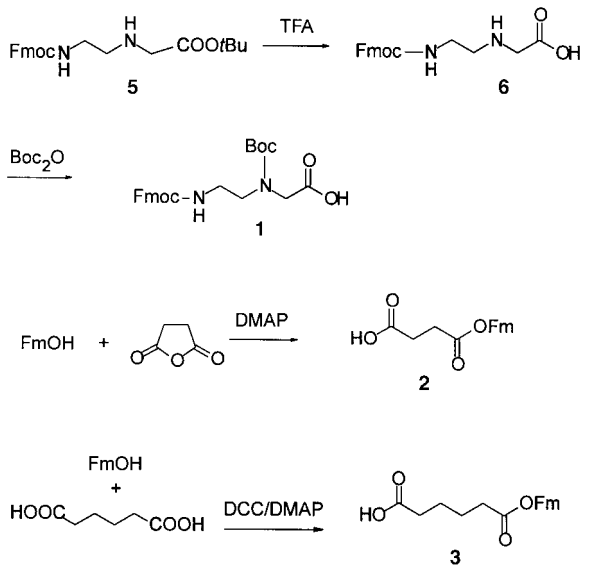

Scheme 2. Synthesis of the modified AA **1**, and of bridging alkyldiacid derivatives **2** and **3** for the SPPS of N-backbone cyclic peptides.

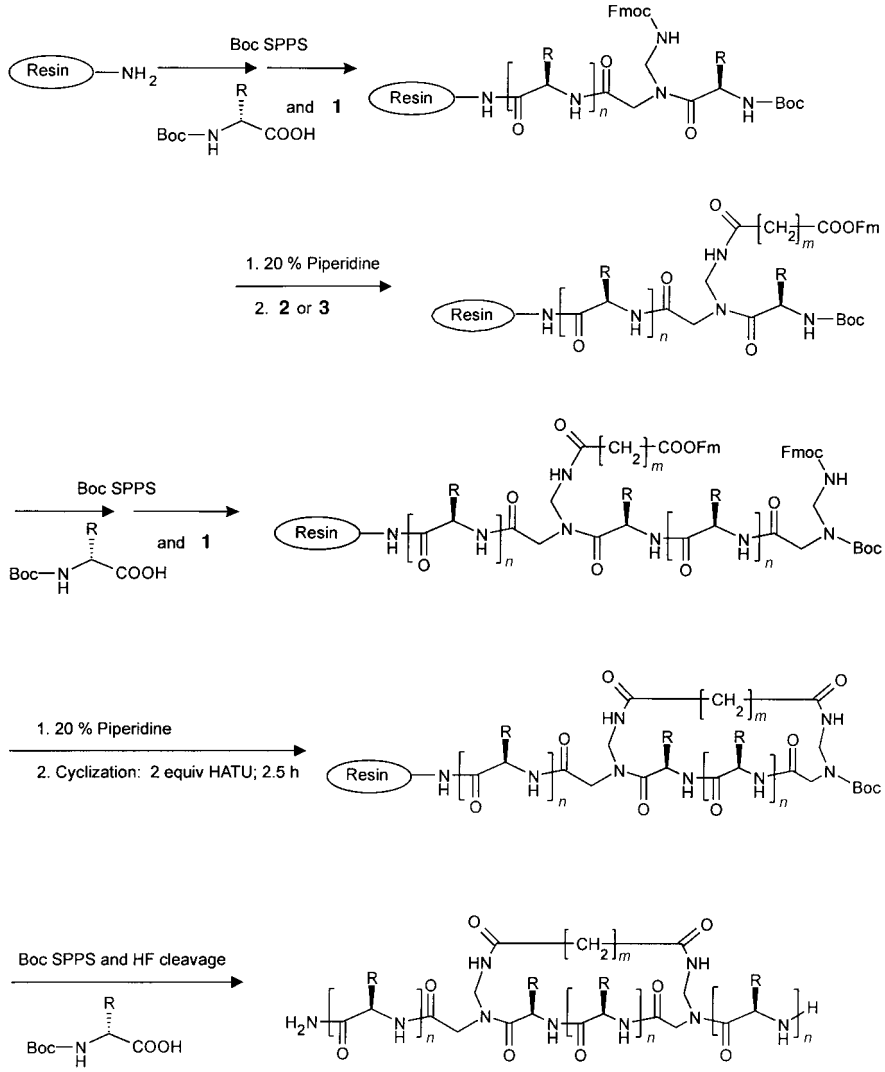

Scheme 3. General strategy for the synthesis of N-backbone cyclic peptide analogues of the AA 42-61 N-terminal MSP-1 fragment. HATU = *N*-[(dimethylamino)-1*H*-1,2,3-triazole[4,5-*b*]-pyridin-1-yl-methylene]-*N*-methylmethanaminium hexafluorophosphate.

analysis.[9] All cyclic peptides showed high binding affinities to RBCs. Cyclic peptide **C1** ($K_D = 470$ nM) had the highest affinity, and its corresponding linear control **L1** had the lowest ($K_D = 2.75$ μM) (Figure 2).

The interaction of the linear peptide 1513 and its cyclic analogues with receptors on the RBC surface was further analyzed by gel autoradiography. For this purpose, RBC membrane preparations from the binding assay were used. Radiolabeled peptides were cross-linked with receptors on the RBC by using bis(sulfosuccinimidylsuberate) (10 μM) as described earlier.[11]

Membrane proteins were separated by using SDS PAGE (SDS PAGE = sodium sulfate dodecyl polyacrylamide gel electrophoresis) and the resulting gel was used to expose a Kodak X-OMAT film, which was developed autoradiographically. Figure 3 shows that RBC membrane preparations with cyclic peptides displayed only one sharp radioactive band with an approximate molecular weight of 19 kDa. In contrast, the linear peptide 1513 preparation showed a diffuse band at the same molecular weight, indicating that cyclic peptides interact with higher specificity with the RBC membrane.

For the characterization of the immunogenicity of the cyclic peptides, *Aotus* monkeys were immunized with each of the polymeric peptide 1513 analogues as well as with the polymeric parent peptide and the linear control **L1**. Four monkeys per group were immunized by subcutaneous inoculation of three 125-μg peptide doses at 20-day intervals. Antibody titres determined in sera of the immunized monkeys by ELISA (ELISA = enzyme-linked immunosorbent assay) showed that none of the linear peptides induced a humoral immune response, whereas all cyclic analogues induced high antibody titres (ranging from 1:16 000 to 1:256 000). Immune sera from all four *Aotus* monkeys immunized with the cyclic peptide **C2** were able to recognize in Western blots with blood stage parasite lysates MSP-1 processing products of a molecular weight of 42 and 83 kDa (Figure 4), which contain the peptide 1513 sequence and are displayed on the surface of the parasites in the late schizont stage.[12]

To further substantiate that the cyclic peptide **C2** can induce parasite-binding antibodies, spleen cells of **C2**-immunized mice were used to generate B cell hybridomas by the polyethylene glycol fusion method.[13] Of the eight **C2**-specific monoclonal antibodies identified by ELISA, two (designated S1.2 and S1.7) exhibited binding to the N-terminal portion of MSP-1 (AA 34-595 from *P. falciparum* strain MAD-20 recombi-

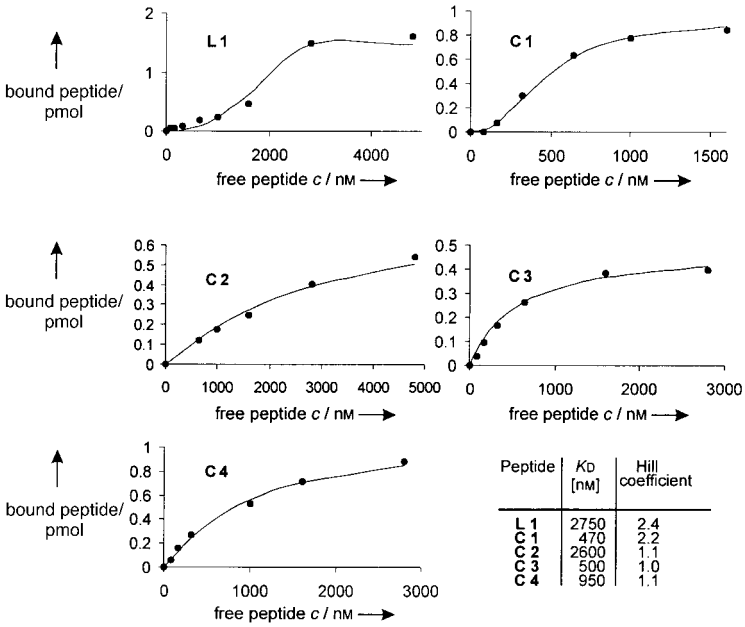

Figure 2. RBC binding of cyclic peptides C1 – C4 and of the linear peptide L1. Saturation curves, K_D values, and Hill coefficients shown in the table were calculated by using Scatchard analysis.

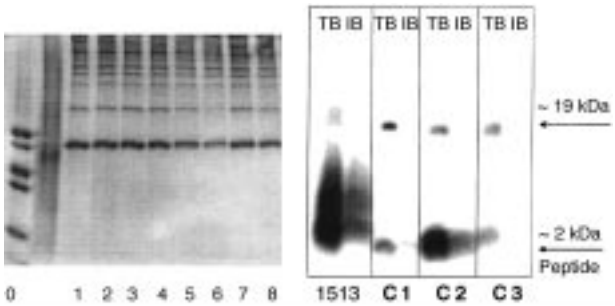

Figure 3. Analysis of peptide binding to RBC cell-surface proteins by SDS PAGE and autoradiography. RBCs were incubated with radiolabeled peptides 1513, **C1**, **C2**, and **C3**. After cross-linking with bis(sulfosuccinimidylsuberate) (10 μM), membrane proteins were separated by SDS PAGE (left side). The corresponding gel autoradiography is shown on the right side. 0 = MWM (molecular weight marker), 1 = 1513 TB (total binding), 2 = 1513 IB (inhibited binding, with 100-fold excess of unlabeled peptide), 3 = **C1** TB, 4 = **C1** IB, 4 = **C2** TB, 5 = **C2** TB, 6 = **C2** IB, 7 = **C3** TB, 8 = **C3** IB.

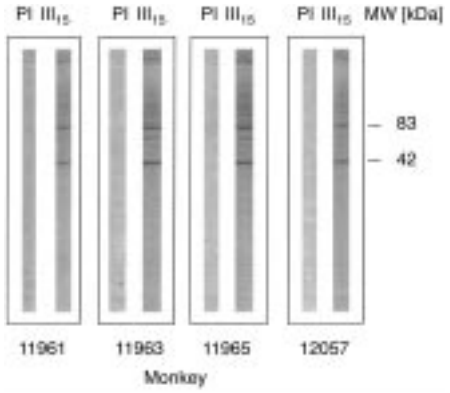

Figure 4. Western blot analysis of solubilized antigens obtained from late stage *P. falciparum* schizonts by using sera from *Aotus* monkeys immunized with cyclic peptide **C2**. PI = pre-immune sera; III_{15} = sera taken 15 days after third dose.

nantly expressed in *E. coli*) in ELISA (data not shown). The same two monoclonal antibodies also exhibited binding to malaria blood stage parasites in an indirect immunofluorescence assay (Figure 5C), whereas the other six **C2**-specific monoclonal antibodies did not bind (Figure 5A).

In summary, the small cyclic peptides presented in this work are able to effectively mimic an important structural element of MSP-1. The 12-mer cyclic peptides **C1** – **C3** showed an increased specificity in ligand – receptor interactions with a 19 kDa receptor on the RBC membrane, when compared with the larger 20-mer parent peptide. The ability of antibodies induced against cyclic peptides to recognize *P. falciparum* MSP-1 on the cell surface of blood stage parasites indicates that they are an effective structural mimic of a functionally important MSP-1 epitope. Cyclic peptides may thus be useful in the design of epitope-focussed synthetic peptide vaccines.

Received: April 9, 2001 [Z16927]

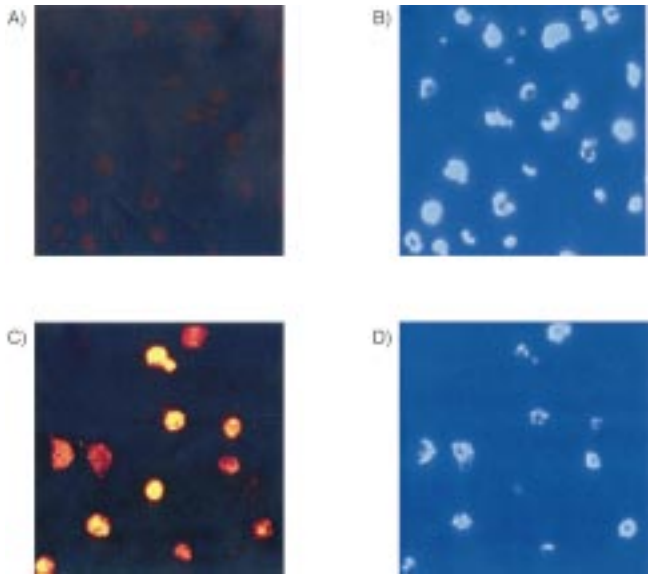

Figure 5. Indirect immunofluorescence staining of *P. falciparum* blood stage parasites by using Cy-3 conjugated goat anti-mouse IgM-specific antibodies for detection of bound antibody. As a control, parasite DNA was counter-stained with Hoechst 33285 (B and D) as described.[13] C) Shows staining of parasites by the anti-**C2** monoclonal antibody S1.2. In contrast, monoclonal antibody S1.8 did not bind to MSP-1 (A).

[1] M. E. Patarroyo, R. Amador, P. Clavijo, A. Moreno, F. Guzman, P. Romero, R. Tascon, A. Franco, L. A. Murillo, G. Ponton, G. Trujillo, *Nature* **1988**, *332*, 158 – 161.
[2] F. Al-Obeidi, A. M. Castrucci, M. E. Hadley, V. J. Hruby, *J. Med. Chem.* **1989**, *32*, 2555 – 2561.
[3] R. Jemmerson, *Proc. Natl. Acad. Sci USA* **1987**, *84*, 9180 – 9184.
[4] H. Kessler, *Angew. Chem.* **1982**, *94*, 509 – 520; *Angew. Chem. Int. Ed. Engl.* **1982**, *21*, 512 – 523.
[5] T. J. Hadley, F. Klotz, L. H. Miller, *Annu. Rev. Microbiol.* **1986**, *40*, 451 – 477.

  1433-7851/01/4014-2634 $ 17.50+.50/0

[6] G. Bitan, I. Sukhotinsky, Y. Mashriki, M. Hanani, Z. Selinger, C. Gilon, *J. Pept. Res.* **1997**, *49*, 421 – 426.
[7] M. Urquiza, L. E. Rodriguez, J. E. Suarez, F. Guzmán, M. Ocampo, H. Curtidor, C. Segura, E. Trujillo, M. E. Patarroyo, *Parasite Immunol.* **1996**, *18*, 515 – 526.
[8] H. L. Yamamura, S. J. Enna, M. J. Kuhar, *Neurotransmitter Receptor Binding*, Raven, New York, **1985**.
[9] M. Ocampo, M. Urquiza, F. Guzmán, L. E. Rodriguez, J. Suarez, H. Curtidor, J. Rosas, M. Diaz, M. E. Patarroyo, *J. Pept. Res.* **2000**, *55*, 216 – 223.
[10] S. A. Thomson, J. A. Josey, R. Cadilla, M. D. Gaul, C. F. Hassman, M. J. Luzzio, A. J. Pipe, K. L. Reed, D. J. Ricca, R. W. Wiethe, S. A. Noble, *Tetrahedron* **1995**, *51*, 6179 – 6194.
[11] A. Puentes, J. Garcia, R. Vera, Q. R. Lopez, M. Urquiza, M. Vanegas, L. M. Salazar, M. E. Patarroyo, *Parasitology* **2000**, *49*, 105 – 117.
[12] A. A. Holder, R. R. Freeman, *J. Exp. Med.* **1984**, *156*, 1528 – 1538.
[13] F. Pöltl-Frank, R. Zurbriggen, A. Helg, F. Stuart, J. Robinson, R. Glück, G. Pluschke, *Clin. Exp. Immunol.* **1999**, *117*, 496 – 503.

  1433-7851/01/4014-2635 $ 17.50+.50/0

Zeosil Nanoslabs: Building Blocks in *n*Pr_4N^+-Mediated Synthesis of MFI Zeolite**

Christine E. A. Kirschhock, Véronique Buschmann, Sebastien Kremer, Raman Ravishankar, Christophe J. Y. Houssin, Barbara L. Mojet, Rutger A. van Santen, Piet J. Grobet, Pierre A. Jacobs, and Johan A. Martens*

The tetrapropylammonium (TPA)-ion-mediated formation of MFI-type zeolite from monomeric and polymeric silica sources has been studied. A similar mechanism involving self-organization of identical nanoscopic zeolite particles was observed independent of silicon source. Transmission electron microscopy (TEM) and small-angle X-ray scattering (SAXS) studies revealed the quantitative formation of rectangular, nanometer-sized slabs from silica sources by the reaction with an aqueous solution of TPA hydroxide. Zeosil nanoslabs with dimensions of $2.7 \times 1.0 \times 1.3$, $4 \times 2 \times 1.3$, $4 \times 4 \times 1.3$, and $8 \times 8 \times 1.3$ nm^3 result from the self-assembly of 2, 6, 12, and 48 TPA-containing precursors, respectively. Zeosil nanoslab surfaces are provided with alkyl pins and silicate framework holes. These nanoslabs combine to form tablets and MFI-type zeolite crystals.

Application of the hydrothermal gel method for zeolite synthesis has led to the large diversity of synthetic zeolite materials known today.[1] Structure specificity is obtained by using organic structure-directing agents. Whereas it was recognized early that silicate-based crystals nucleate and grow from silicate oligomers,[2] progress in identification of precursors and their polycondensation processes was hindered by the presence of gel. The possibility of growing zeolites from "clear solution" rendered the processes experimentally more accessible,[3] and led to the present discovery of zeosil nanoslabs, which we identified as building blocks in the TPA-ion-mediated synthesis of zeolite MFI.

The zeosil silicalite-1 with a silicon dioxide framework and MFI framework topology,[4] crystallizes by heating a "clear solution" prepared from tetraethylorthosilicate (TEOS), tetrapropylammonium hydroxide (TPAOH), and water.[5] In the "clear solutions" studied in this work, all silicon was incorporated in nanosized particles.[6] Clear solution obtained from the hydrolysis of TEOS at 20 °C in aqueous TPAOH solution[7] was spread on a grid for TEM studies. By taking all necessary precautions,[8] we managed to observe a large number of nanosized particles (Figure 1 a). They were conglomerated and embedded in an organic matrix, which stemmed from TPA. The particles survived only a few seconds

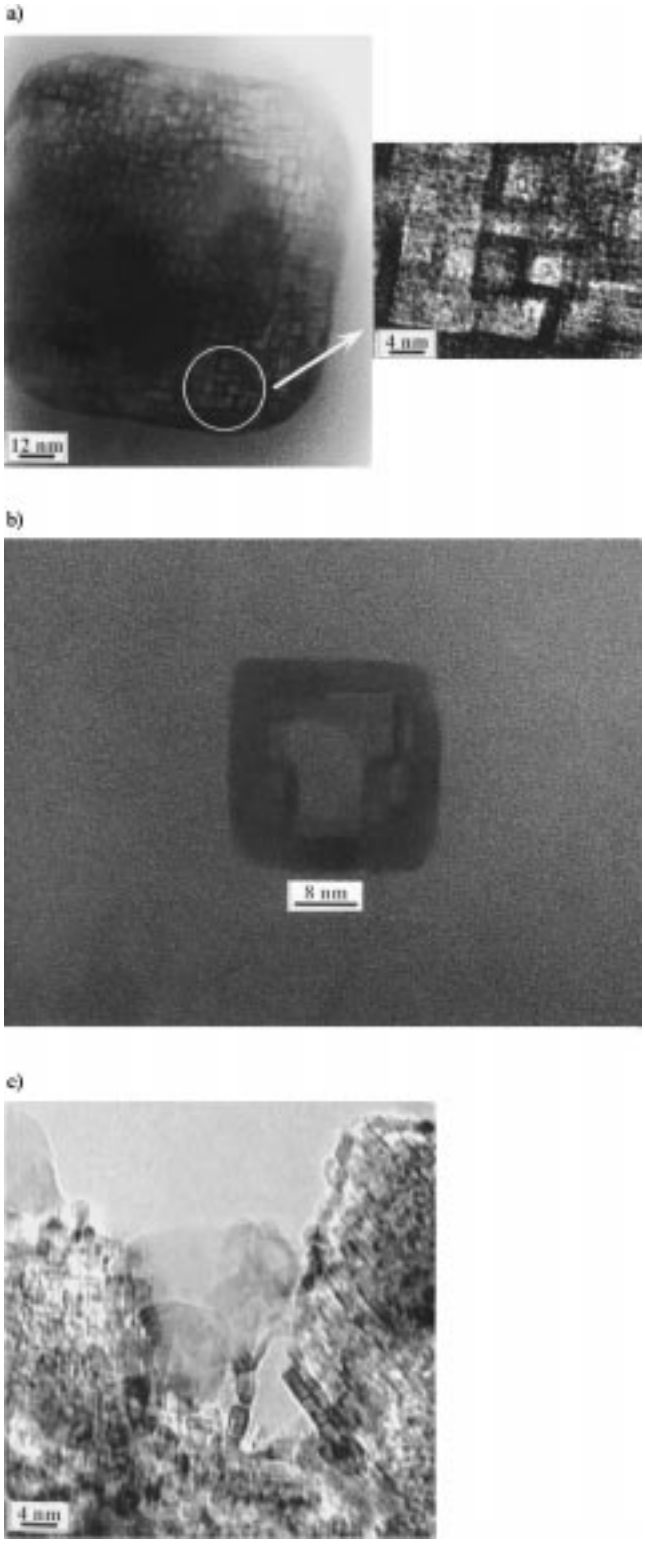

Figure 1. a) TEM images of nanoslabs **1**, prepared from the TEOS/TPAOH/water system;[7] b) occasionally observed larger block in nanoslab **1** sample; c) nanoslabs **3**, prepared from silicic acid, TPAOH, and NaOH.[11] Observations made with Philips CM200 TEM (200 kV, point resolution 0.19 nm) and a JEOL JEM3010 (300 kV, point resolution 0.17 nm) instruments equipped with a Gatan GIF200 electron energy loss spectrometer.

[*] Prof. J. A. Martens, Dr. C. E. A. Kirschhock, S. Kremer, Dr. R. Ravishankar, Prof. P. J. Grobet, Prof. P. A. Jacobs
Department of Interface Chemistry, K.U. Leuven
Kasteelpark Arenberg 23, 3001 Leuven (Belgium)
Fax: (+32) 16-321998
E-mail: johan.martens@agr.kuleuven.ac.be
Dr. V. Buschmann
Materials Science Department
Technische Universität Darmstadt
Darmstadt (Germany)
C. J. Y. Houssin, Dr. B. L. Mojet, Prof. R. A. van Santen
Schuit Institute of Catalysis
Eindhoven University of Technology, Eindhoven (The Netherlands)

[**] C.E.A.K., J.A.M., and P.A.J. acknowledge the Belgian Government for sponsoring in the frame of IUAP-PAI program. J.A.M. and P.A.J. acknowledge FWO Vlaanderen for a research grant.

  1433-7851/01/4014-2637 $ 17.50+.50/0

in the electron beam. This and their movements hindered the recording of diffraction patterns. The average in-plane dimensions of individual particles (nanoslabs **1**) were about 4×4 nm^2, with a thickness of about 1 nm as revealed by the dimensions of standing particles. Occasionally, larger blocks (Figure 1 b) were observed which had in-plane dimensions corresponding to multiples of 4 nm, suggesting they were formed through sidewise coalescence of elementary nanoslabs **1** of dimensions 4×4 nm^2.

The SAXS pattern of a suspension of nanoslab **1** is shown in Figure 2 a. The asymmetric line shape reveals deviation from spherical particle morphology. For slabs measuring 4×4 nm^2,

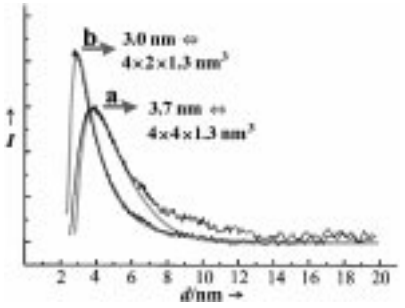

Figure 2. SAXS curves of suspensions of **1** (curve a) and **3** (curve b). Position and shape of measured intensities agree with simulated patterns (gray lines),[9] assuming uniform slablike bodies of dimensions $4 \times 4 \times 1.3$ (curve a) and $4 \times 2 \times 1.3$ nm^3 (curve b). Measurements performed at the DUBBLE beamline (European Synchrotron Radiation Facility, Grenoble, France) by using a 2D gas-filled detector and a wavelength of 0.099 nm.

the observed characteristic length d of 3.7 nm corresponds to a thickness of 1.3 nm.[9] Thus the shape and position of the experimental scattering curve match with the theoretical scattering function for slabs measuring $4 \times 4 \times 1.3$ nm^3 (Figure 2 a).[9] The SAXS study reveals the almost exclusive presence of a large number of unique and identical particles. The scattering intensity at d values larger than 6 nm, which is not accounted for by the theoretical curve, stems from the small amount of larger blocks also revealed by TEM (Figure 1 b) and formed from nanoslab **1** by fusion. The thickness of 1.3 nm, derived from analysis of SAXS patterns, coincides with the range of characteristic step heights of 1.2 ± 0.3 nm determined on evaporated suspensions by using atomic force microscopy.[10] The distribution of edge (Q^2), surface (Q^3), and bulk (Q^4) silicon atoms, determined with ^{29}Si MAS NMR spectroscopy, is also in agreement with dimensions of 1.3, 4, and 4 nm in the a, b, and c crystallographic directions of silicalite-1, respectively.[10]

A suspension of nanoslab **1** was heated for 2 h at 100 °C. The SAXS Porod plot (Figure 3) shows a region with negative slope of -2 characteristic of flat surfaces having a characteristic length d of about 7.3 nm. This d value corresponds to bodies of $8 \times 8 \times 1.3$ nm^3,[9] designated as nanoplates **2**, obtained by systematic two-by-two sidewise joining of four nanoslabs **1**.

Industrial MFI-type zeolite crystallization processes start with silica rather than TEOS, and sodium hydroxide provides the necessary alkaline conditions. TEM studies of the product from room temperature digestion of silicic acid in an aqueous

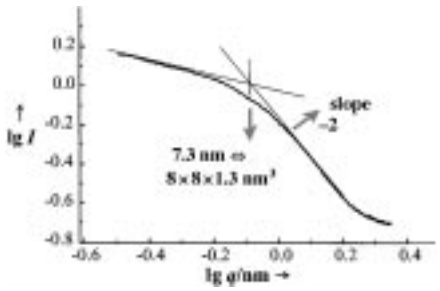

Figure 3. SAXS Porod plot of nanoplates **2**. Measurement conditions see legend to Figure 2.

solution of TPA and sodium hydroxide[11] revealed the occurrence of rectangular particles designated nanoslab **3** with in-plane dimensions of 4×2 nm^2 (Figure 1 c). The SAXS pattern of this sample (Figure 2 b) was again in excellent agreement with the theoretical scattering curve of uniform slab-shaped bodies. Introduction of the 4×2 nm^2 dimensions of nanoslab **3** derived from the TEM studies in the theoretical scattering expression revealed a thickness of 1.3 nm,[9] similar to those for **1** and **2** prepared from TEOS.

The polymerization of silica from TEOS proceeds over a bicyclic pentamer, a pentacyclic octamer, a tetracyclic undecamer, and finally the precursor **4**.[12] This precursor is unique to the MFI framework connectivity, occludes a TPA molecule, and measures $1.3 \times 1.0 \times 1.3$ nm^3.[6, 12] This silica polymerization process is driven by creation of hydrophobic silica surfaces, which shield the propyl groups of the TPA ion from the aqueous solution.

An ^{29}Si NMR spectrum recorded at an early stage of silicic acid digestion by TPAOH provided evidence for the occurrence of a bicyclic pentamer, a tetracyclic undecamer, and the precursor **4** (Figure 4 a),[13] and the same silica polymerization sequence as with TEOS. The ^{29}Si NMR signals were very weak and substantially broadened compared to those in the spectrum of precursor **4** in the TEOS system (Figure 4 b) because the silicate species were not solution-borne but still adsorbed on remaining solid silica. ^{29}Si NMR signals were absent after removal of the solids by filtration over a filter

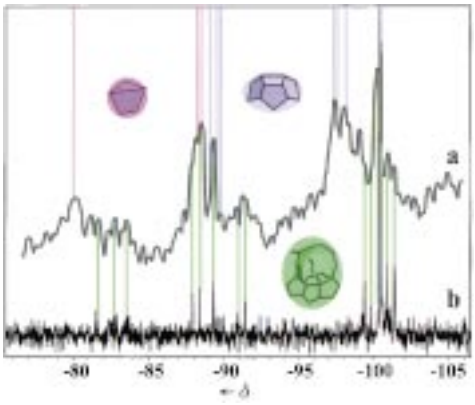

Figure 4. ^{29}Si NMR spectrum at an early stage of silicic acid digestion (a). Chemical shifts of the bicyclic pentamer, the tetracyclic undecamer, and the precursor **4** taken from ref. [12] are indicated. For comparison, the ^{29}Si NMR spectrum of precursor **4** in the TEOS system (b).[12] Spectra recorded on a Bruker AMX 300 MHz at 0 °C using a pulse length of 4 μs (45° pulse), repeating time of 20 s,[12] and 2000 accumulations.

  1433-7851/01/4014-2638 $ 17.50+.50/0 *Angew. Chem. Int. Ed.* **2001**, *40*, No. 14

with a pore size of 100 nm. The presence of amorphous colloidal silica together with the oligomers was manifested in the broad underlying signals in the ^{29}Si NMR spectrum (Figure 4a).

Additional evidence for formation of nanoslabs by self-assembly of precursor **4** irrespective of the silica source came from experiments with higher concentrations of TPAOH.[14] The products derived from TEOS and silicic acid exhibited a very similar scattering curve that can be simulated by the scattering of double precursor **5** with measurements of $2.7 \times 1.0 \times 1.3$ nm^3 (Figure 5).

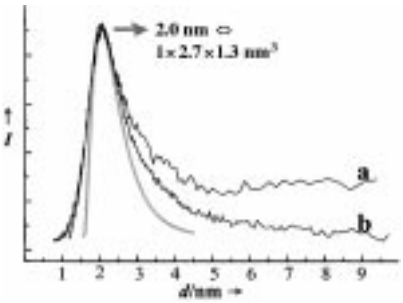

Figure 5. SAXS curves of clear solutions prepared from TEOS (a) and silicic acid (b) with an excess of TPAOH. The gray curve shows the simulation using the shape factor of a slab corresponding to two sidewise-linked precursors **4**. a) Data obtained on a Stoe Stadi P instrument, $Cu_{K\alpha 1}$ radiation, and a position sensitive detector (5°); b) measured as described in legend to Figure 2.

The self-assembly of precursor **4** into specific nanoslabs depending on TPA and sodium concentration (Figure 6) reflects the peculiar colloidal properties of these organic–inorganic hybrid materials. At 100 °C, suspended nanoplates **2** gradually form stacks which finally join sidewise to give the bulk MFI-type zeosil.[15] The stacked nanoplates are evident in the crystal morphology.[16]

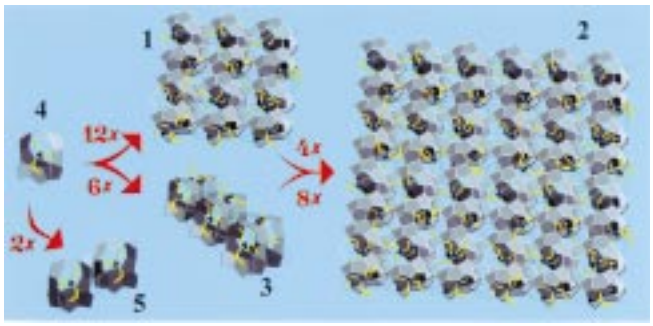

Figure 6. Schematic representation of the atomic structure of MFI-type zeosil nanoslabs **1**, nanoplate **2**, nanoslab **3**, their precursor **4**, and the double precursor **5**. The alkyl chains of TPA molecules are in yellow, nitrogen atoms in blue. The gray areas depict the silicate framework, at the corners of which are found silicon atoms, which are linked along the edges by oxygen atoms.

The present observation of nanoslabs in differently prepared suspensions suggests that the particles with equivalent diameters of 2.8–4.3 nm, which have been detected in MFI-type zeolite syntheses with dynamic light scattering, SAXS, and neutron scattering,[17] also belong to the nanoslab family. This further supports the view that the formation and self-organization of nanoslabs are key steps in TPA-ion-mediated MFI synthesis. The observation and identification of zeosil nanoslabs can be exploited to modify the properties of zeolite-like products by manipulation of the aggregation conditions.

The surfaces of the nanoslabs are covered with pins and holes (Figure 6). Propyl groups of trapped TPA ions protruding out of the three faces of each nanoslab provide the pins, while the micropore openings on the opposite sides form the holes. At room temperature, a steric barrier caused by the propyl groups prevents the fusion of nanoslabs.[15] Even here there is already a strong tendency for self-organization, as revealed by the TEM photograph of the film formed by evaporation of the clear solution (Figure 1a). This self-organization can be directed to prepare organized physical bodies, monoliths, and liquid crystals. A concentrated suspension of nanoslabs exhibits schlieren patterns after ultrasonification. Transparent zeosil films with homogeneous thickness were prepared by spreading a suspension of nanoslab **1** onto a glass support and adding methanol after partial drying. Zeosil nanoslabs are versatile building blocks. By substituting TPAOH with TBAOH (tetrabutylammonium hydroxide), nanoslabs with MEL zeolite framework topology can be obtained.[6] Incorporation of titanium and aluminum atoms in MFI zeosil nanoslabs is possible as well.[18]

Received: November 17, 2000
Revised: April 3, 2001 [Z16125]

[1] R. M. Barrer, *Hydrothermal Chemistry of Zeolites*, Academic Press, London, **1982**.
[2] "Zeolite Microporous Solids: Synthesis, Structure and Reactivity": J.-P. Gilson, *NATO ASI Ser. Ser. C* **1992**, *352*, 511–529.
[3] a) S. Ueda, N. Kageyama, H. Murata, M. Koizumi, S. Kobayashi, Y. Fujiwara, Y. Kyoguku, *J. Phys. Chem.* **1984**, *88*, 2128–2131; b) "Zeolite Synthesis": J. J. Keijsper, M. F. M. Post, *ACS Symp. Ser.* **1989**, *398*, 28–48; c) C. C. J. Den Ouden, R. W. Thompson, *J. Colloid Interface Sci.* **1991**, *143*, 77–84.
[4] a) H. Gies, *Stud. Surf. Sci. Catal.* **1994**, *85*, 295–325; b) E. M. Flanigen, J. M. Bennet, R. W. Grose, J. P. Cohen, R. L. Patton, R. M. Kirchner, J. V. Smith, *Nature* **1978**, *271*, 512–516.
[5] a) A. E. Persson, B. J. Schoeman, J. Sterte, J.-E. Otterstedt, *Zeolites* **1994**, *14*, 557–567; b) P. P. E. A. De Moor, T. P. M. Beelen, R. A. van Santen, *J. Phys. Chem. B* **1999**, *103*, 1639–1650; c) J. N. Watson, L. E. Iton, R. I. Keir, J. C. Thomas, T. L. Dowling, J. W. White, *J. Phys. Chem. B* **1997**, *101*, 10094–10104.
[6] C. E. A. Kirschhock, R. Ravishankar, L. Van Looveren, P. A. Jacobs, J. A. Martens, *J. Phys. Chem. B* **1999**, *103*, 4972–4978.
[7] The molar composition expressed in oxide ratios: $(TPA_2O)(SiO_2)_5$-$(H_2O)_{60}(EtOH)_{20}$.
[8] Precautions: a defocused electron beam, rather low magnifications, and a video camera connected to the TEM-camera to monitor any possible change in time.
[9] The mathematical expression for the scattering function of uniform isolated slabs is given in ref. [6]. The shape of the scattering function mirrors the distribution of possible trajectories through the body. The relation between the characteristic length d with maximum scattering intensity and the diagonal in space D of the slab is $d = 0.64\,D$.[6] The observed SAXS patterns agree much less with other particle shapes, like spheres.
[10] R. Ravishankar, C. E. A. Kirschhock, P. P. Knops-Gerrits, E. J. P. Feijen, P. J. Grobet, P. Vanoppen, F. C. De Schryver, G. Miehe, H. Fuess, B. J. Schoeman, P. A. Jacobs, J. A. Martens, *J. Phys. Chem. B*, **1999**, *103*, 4960–4964.

  1433-7851/01/4014-2639 $ 17.50+.50/0

[11] The molar composition of this mixture prepared from silicic acid, TPAOH, and NaOH: $(TPA_2O)(SiO_2)_4(Na_2O)_{0.33}(H_2O)_{47}$.
[12] C. E. A. Kirschhock, R. Ravishankar, P. J. Grobet, P. A. Jacobs, J. A. Martens, *J. Phys. Chem. B* **1999**, *103*, 4965 – 4971.
[13] The molar composition of this mixture prepared from silicic acid and TPAOH: $(TPA_2O)(SiO_2)_4(H_2O)_{47}$; the suspension was gently heated to 50 °C to initiate reaction.
[14] The molar composition of the TEOS system: $(TPA_2O)(SiO_2)_{3.75}$-$(H_2O)_{30}(EtOH)_{15}$; in the silicic acid system, the sample was the final product from the preparation of ref. [11].
[15] C. E. A. Kirschhock, R. Ravishankar, P. A. Jacobs, J. A. Martens, *J. Phys. Chem. B* **1999**, *103*, 11021 – 11027.
[16] R. Ravishankar, C. E. A. Kirschhock, B. J. Schoeman, P. Vanoppen, P. J. Grobet, S. Storck, W. F. Maier, J. A. Martens, F. C. De Schryver, P. A. Jacobs, *J. Phys. Chem. B* **1998**, *102*, 4588 – 4597.
[17] a) J. N. Watson, A. S. Brown, L. E. Iton, J. W. White, *J. Chem. Soc. Faraday Trans.* ***1998***, *94*, 2181 – 2186; b) S. L. Burkett, M. E. Davis, *J. Phys. Chem.* **1994**, *98*, 4647 – 4653; c) P. P. E. A. De Moor, T. P. M. Beelen, R. A. Van Santen, *Microporous Mater.* **1997**, *9*, 117 – 130; d) T. A. M. Twomey, M. Mackay, H. P. C. E. Kuipers, R. W. Thompson, *Zeolites* **1994**, *14*, 162 – 168; e) B. J. Schoeman, *Stud. Surf. Sci. Catal.* **1997**, *105*, 647 – 654.
[18] R. Ravishankar, C. E. A. Kirschhock, B. J. Schoeman, D. De Vos, P. J. Grobet, P. A. Jacobs, J. A. Martens in *Proc. 12th Int. Zeolite Conf.*, *Vol. III* (Eds.: M. M. J. Treacy, B. K. Marcus, M. E. Bisher, J. B. Higgins), Materials Research Society, Warrendale, **1999**, pp. 1825 – 1832.

A Colorimetric ATP Sensor Based on 1,3,5-Triarylpent-2-en-1,5-diones**

Félix Sancenón, Ana B. Descalzo, Ramón Martínez-Máñez,* Miguel A. Miranda, and Juan Soto

The development of systems that are capable of sensing or recognizing and are based on supramolecular concepts is an area of current interest.[1] One of the most appealing approaches involves the construction of chromoionophores. Although such systems have been widely used for the analysis of metal cations,[2] chromogenic sensors for the "naked-eye" sensing of anions are not common;[3] this is especially the case in aqueous environments.[4]

We report here the synthesis of 1,3,5-triarylpent-2-en-1,5-dione derivatives and demonstrate their ability to act as colorimetric anion sensors. The new family of chromogenic reagents is easily obtained by condensation of the 2,6-diphenylpyrylium cation with N-functionalized anilines. For instance, the reaction of *N*-phenyl-1-aza-7,10-dioxa-4,13-dithiacyclopentadecane with 2,6-diphenylpyrylium gave the 1,3,5-triaryl-1,5-pentanedione derivative **1** after column chromatography (Scheme 1). The NMR (^1H, ^{13}C) and mass spectra of **1** are consistent with the proposed formulation. The UV/Vis spectrum of **1** shows bands in the range of 200 – 300 nm along with a band centered at 380 nm, which is responsible for the pale yellow color of the receptor.

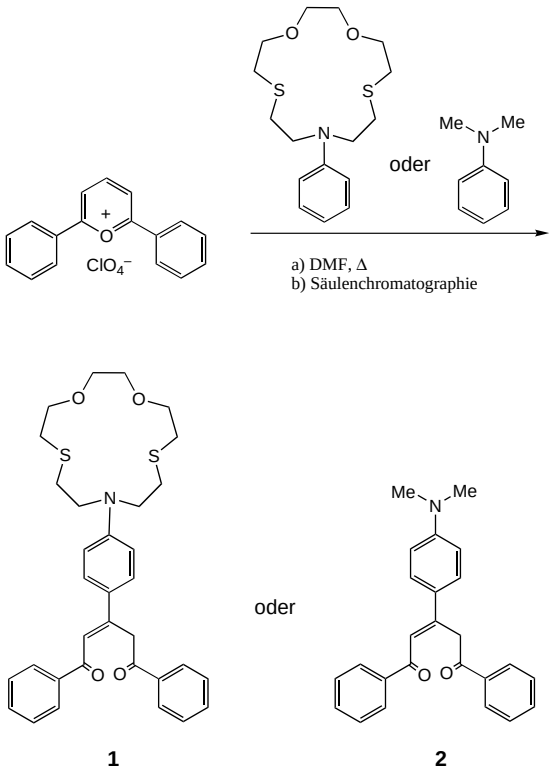

Scheme 1. Synthesis of the 1,3,5-triaryl-1,5-pentanedione derivatives **1** and **2**. The reaction is carried out in refluxing dimethylformamide (DMF) for 3 h, and subsequent column chromatography on alumina with CH_2Cl_2/MeOH (50/1 v/v) as eluent provides **1** (35 % yield) or **2** (50 % yield).

The 1,5-pentanedione system of **1** can be readily transformed into the corresponding pyrylium ion (Scheme 2):[5] Addition of nitric acid to solutions of **1** in 1,4-dioxane/water (70/30 v/v) caused a dramatic change in color from yellow to magenta. This change was accompanied by a new intense

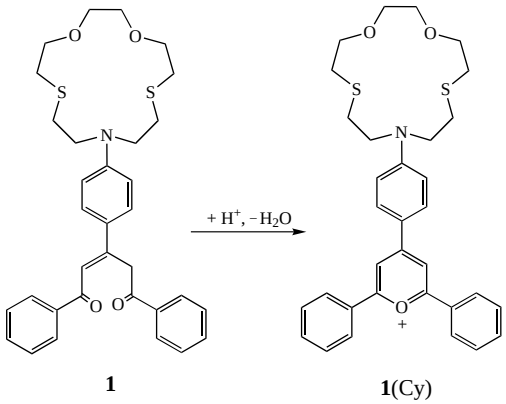

Scheme 2. Transformation of the 1,5-pentanedione **1** into the pyrylium cation **1**(Cy).

[*] Dr. R. Martínez-Máñez, F. Sancenón, A. B. Descalzo, Prof. M. A. Miranda, Dr. J. Soto
Departamento de Química
Universidad Politécnica de Valencia
Camino de Vera s/n, 46071 Valencia (Spain)
Fax: (+34) 9-6-387-7349
E-mail: rmaez@qim.upv.es

[**] This research was supported by the Ministerio de Ciencia y Tecnología (proyecto PB98-1430-C02-02, 1FD97-0508-C03-01, and AMB99-0504-C02-01). F.S. also thanks the Ministerio de Educación y Cultura for a Doctoral Fellowship.

  1433-7851/01/4014-2640 $ 17.50+.50/0

band centered at 550 nm in the UV/Vis spectrum. We ascribe this new band to the highly delocalized pyrylium cation formed upon cyclization. This cation was isolated as the perchlorate salt, and the spectroscopic characterization fully supported the proposed formulation.

The changes in the absorption spectrum of **1** at neutral pH values upon addition of anions such as chloride, bromide, sulfate, and phosphate (as tetrabutylammonium salts) as well as ATP, ADP, and GMP (as sodium salts) have also been studied. The photograph in Figure 1 shows the color changes

Figure 1. Color changes induced on **1** (1.0×10^{-4} M) at pH 6 in the presence of the following anions in dioxane/water (70/30 v/v): from left to right: no anion, bromide, chloride, phosphate, sulfate, GMP, ADP, and ATP.

after addition of equimolar amounts of these anions to **1** in dioxane/water at pH 6. At this pH value, **1** forms a yellow solution, either alone or in the presence of bromide, chloride, phosphate, GMP, or ADP. Upon addition of sulfate, the solution turns pale red. However, the most remarkable effect is observed in the presence of ATP, whereby a bright magenta color is fully developed.

The analytical determination of anions, for instance in water or in biological systems, is commonly carried out in the presence of alkali and alkali earth cations. Therefore, we also studied the effect that the metal ions Li^+, Na^+, K^+, Ca^{2+}, and Mg^{2+} (as their nitrate or perchlorate salts) have on solutions of **1** at pH 6. We found that there is no analytical interference, as the presence of these cations does not induce any significant color change.

A more detailed study has been carried out using basic solutions of **1** containing equimolar amounts of the corresponding anions, which were placed in dioxane/water (70/30 v/v) and subsequently acidified. The absorbance at 550 nm was then monitored at different pH values; the results are shown in Figure 2a. The pH values where the transformation of the diketonic form (yellow) to the pyrylium form (magenta) takes place are in the range 2–5. Cyclization and color development are thus a function of the pH value of the medium. Enhancement of the absorbance at 550 nm is ascribed to ring closure, as stated above. In general there is no remarkable effect in the presence of the anions, except for ATP, which is able to shift selectively the pH at which the magenta color is observed towards higher values. At acidic pH the situation is more complex, and in general all the anions studied modify the pH value at which the solution changes

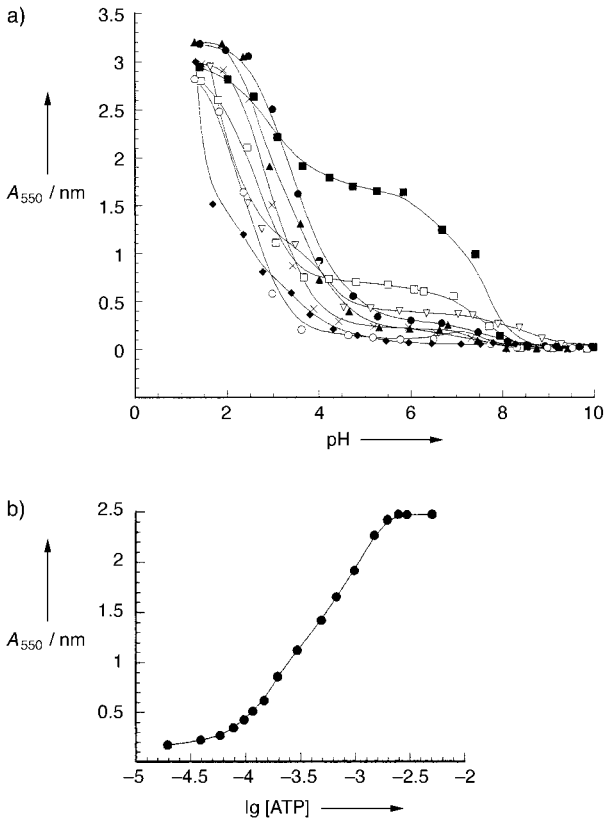

Figure 2. a) Plot of the absorbance at 550 nm (A_{550}) as a function of the pH value for **1** (●) and **1** in the presence of the anions chloride (×), bromide (▲), sulfate (□), phosphate (○), ATP (■), ADP (▽), and GMP (◆) in dioxane/water (70/30 v/v). b) Absorbance at 550 nm of **1** (1.0×10^{-4} M) versus the logarithm of the ATP concentration at pH 6 in dioxane/water (70/30 v/v).

from yellow to magenta. However, in the range pH 2–4 there is no selective pattern.

It can be concluded that there is a remarkable selective ATP colorimetric detection. Hence, **1** is a selective chromogenic reagent for the sensing of ATP.[6] It is important to note that the color change in **1** from yellow to magenta observed upon addition of ATP is a very simple and easy "naked-eye" method. Additionally the pyrylium cation formed from **1**, responsible for the color change, has a molar absorptivity as high as 30600 L mol^{-1} cm^{-1}; this allows sensitive spectrophotometric detection of the anion ATP. Figure 2b shows the color response as a function of the ATP concentration at pH 6 ($[\mathbf{1}] = 9.5 \times 10^{-5}$ M). Under these conditions, a linear response range from 40 to 1100 ppm of ATP was found (higher ATP concentrations result in the formation of a precipitate).

For the sake of comparison compound **2** was also synthesized by reaction of *N*,*N*-dimethylaniline and 2,6-diphenylpyrylium (Scheme 1). Figure 3 shows a photograph of the color changes observed for **2** in dioxane/water (70/30 v/v) at pH 6 in the presence of certain anions. There is a remarkable switch from yellow to magenta in the presence of sulfate, ADP, and ATP, whereas bromide, chloride, phosphate, and GMP do not change the color of the **2** solution. The addition of Li^+, Na^+, K^+, Ca^{2+}, or Mg^{2+} had no effect. In the absence of ATP and ADP, **2** can be considered as a selective chromogenic reagent for sulfate.

  1433-7851/01/4014-2641 $ 17.50+.50/0

Figure 3. Color changes induced on **2** (1.0×10^{-4} M) at pH 6 in the presence of the following anions in dioxane/water (70/30 v/v): from left to right: no anion, bromide, chloride, phosphate, sulfate, GMP, ADP, and ATP.

Although further studies need to be carried out to correlate selectivity and molecular architecture, some preliminary considerations concerning the origin of the color change can be advanced. First of all, the occurrence of ring closure as a function of the pH value can be ascribed to the well-known chemistry of the pyrylium cation. It has been reported that nucleophilic attack of hydroxide anions or related nucleophiles over C2 results in ring opening, with the formation of 1,5-diketones (see form **1** in Scheme 2).[7] In a similar manner, under certain circumstances, **1** is able to undergo intramolecular cyclization to restore structure **1**(Cy). As stated above, for **1** and **2** the color change is observed in the pH range of about 2–5. In this pH range protonation of the aniline nitrogen atom is expected to take place. Consequently, there is an apparent correspondence between protonation of the amine and transformation of the diketone to the pyrylium. To explain this observation, it should be considered that cyclization must result from nucleophilic attack of the hydroxyl group of the enol tautomer at C1 of the carbonyl group (see structure **I** in Scheme 3). When the amine is not protonated the electron density at C1 is too high; in other words, the resonance structure **II** makes a significant contribution and, hence, nucleophilic attack is disfavored. Upon protonation, the nitrogen lone pair is engaged, and structure **II** does not play a role. As a consequence, one would expect C1 to be more electrophilic and thus subject to attack by the enol.

To explain the color change observed in the presence of certain anions, one should consider that structure **I** contains functional groups such as amine, enol, and carbonyl that are capable of coordinating anions through electrostatic forces or hydrogen bonding. By such coordination it could be possible to modulate the nucleophilic character of the hydroxyl oxygen atom of the enol tautomer or the electrophilic character of the C1 carbonyl carbon atom. A possible explanation might involve coordination between the receptor **1** and ATP in such a way that the pK_a value of the amine increases, therefore favoring cyclization at higher pH values.

In conclusion we have synthesized a new family of easy-to-prepare chromogenic reagents and have found a highly selective color response against ATP in an aqueous–organic environment. Remarkably, ATP is capable of changing the absorption spectrum of **1** in the pH range 4–8, whereas inorganic anions (with the exception of sulfate), other anions of biological importance, and cations do not induce any color change. In this sense, **1** is a chromogenic reagent for ATP sensing. In the absence of biological anions, **2** can be considered a selective chromogenic reagent for sulfate.

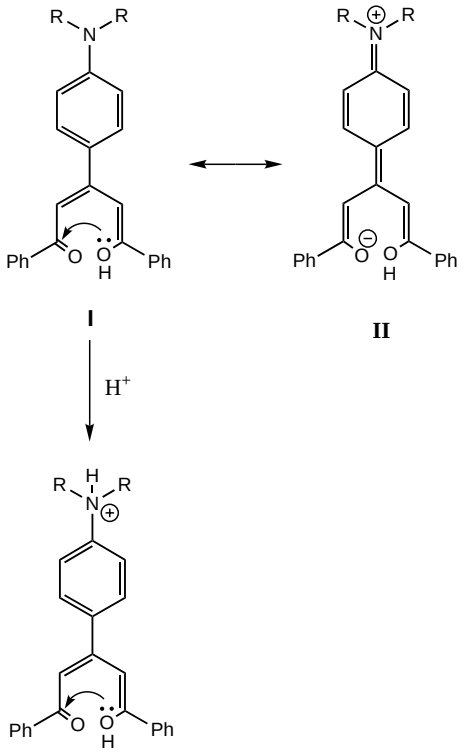

Scheme 3. Proposed resonance structures involved in the ring closure of 1,5-pentanediones **1** and **2** to the corresponding pyrylium cations.

Received: January 26, 2001 [Z16516]

[1] A. P. de Silva, H. Q. N. Gunaratne, T. Gunnlaugsson, J. M. A. Huxley, C. P. McCoy, J. T. Rademacher, T. E. Rice, *Chem. Rev.* **1997**, *97*, 1515–1566; F. P. Schmidtchen, M. Berger, *Chem. Rev.* **1997**, *97*, 1609–1646; M. M. G. Antonisse, D. N. Reinhoudt, *Chem. Commun.* **1998**, 443–448; N. E. Izatt, R. L. Bruening, K. E. Krakowiak, S. R. Izatt, *Ind. Eng. Chem. Res.* **2000**, *39*, 3405–3411; P. D. Beer, P. A. Gale, *Angew. Chem.* **2001**, *113*, 502–532; *Angew. Chem. Int. Ed.* **2001**, *40*, 486–516.

[2] See, for example, T. Hayashita, K. Kunogi, H. Yamamoto, S. Shinkai, *Anal. Sci.* **1997**, *13*, 161–166; T. Hayashita, N. Teramae, T. Kuboyama, S. Nakamura, H. Yamamoto, H. Nakamura, *J. Inclusion Phenom. Mol. Recognit. Chem.* **1998**, *32*, 251–265; S. Kolusheva, T. Shahal, R. Jelinek, *J. Am. Chem. Soc.* **2000**, *122*, 776–780; M. Micheloni, M. Formica, V. Fusi, P. Romani, R. Pontellini, P. Dapporto, P. Paoli, P. Rossi, B. Valtancoli, *Eur. J. Inorg. Chem.* **2000**, 51–57.

[3] J. L. Sessler, A. Andrievsky, V. Král, V. Lynch, *J. Am. Chem. Soc.* **1997**, *119*, 9385–9392; A. Metzger, E. V. Anslyn, *Angew. Chem.* **1998**, *110*, 682–684; *Angew. Chem. Int. Ed.* **1998**, *37*, 649–652; S. Watanabe, O. Onogawa, Y. Komatsu, K. Yoshida, *J. Am. Chem. Soc.* **1998**, *120*, 229–230; K. Niikura, A. Metzger, E. V. Anslyn, *J. Am. Chem. Soc.* **1998**, *120*, 8533–8534; J. J. Lavigne, E. V. Anslyn, *Angew. Chem.* **1999**, *111*, 3903–3906; *Angew. Chem. Int. Ed.* **1999**, *38*, 3666–3669; C. B. Black, B. Andrioletti, A. C. Try, C. Ruiperez, J. L. Sessler, *J. Am. Chem. Soc.* **1999**, *121*, 10438–10439; P. A. Gale, L. J. Twyman, C. I. Handlin, J. L. Sessler, *Chem. Commun.* **1999**, 1851–1852; H. Miyaji, W. Sato, J. L. Sessler, *Angew. Chem.* **2000**, *112*, 1847–1850; *Angew. Chem. Int. Ed.* **2000**, *39*, 1777–1780; P. Anzenbacher, Jr., A. C. Try, H. Miyaji, K. Jursikova, V. M. Lynch, M. Marquez, J. L. Sessler, *J. Am. Chem. Soc.* **2000**, *122*, 10268–10272; H. Miyaji, J. L. Sessler, *Angew. Chem.* **2001**, *113*, 158–161; *Angew. Chem. Int. Ed.* **2001**, *40*, 154–157.

  1433-7851/01/4014-2642 $ 17.50+.50/0

[4] V. Král, H. Furuta, K. Shreder, V. Lynch, J. L. Sessler, *J. Am. Chem. Soc.* **1996**, *118*, 1595 – 1607; H. Hisamoto, H. Tohma, T. Yamada, K. Yamauchi, D. Siswanta, N. Yoshioka, K. Suzuki, *Anal. Chim. Acta* **1998**, *373*, 271 – 289; V. Amendola, E. Bastianello, L. Fabbrizzi, C. Mangano, P. Pallavicini, A. Perotti, A. Manotti-Lanfredi, F. Ugozzoli, *Angew. Chem.* **2000**, *112*, 3039 – 3042; *Angew. Chem. Int. Ed.* **2000**, *39*, 2917 – 2920.

[5] For a related transformation, see F. Pina, M. J. Melo, M. Maestri, P. Passaniti, V. Balzani, *J. Am. Chem. Soc.* **2000**, *122*, 4496 – 4498.

[6] For recently reported ATP fluorescent sensors, see M. T. Albelda, M. A. Bernardo, E. García-España, M. L. Godino-Salido, S. V. Luis, M. J. Melo, F. Pina, C. Soriano, *J. Chem. Soc. Perkin Trans. 2* **1999**, 2545 – 2549; S. E. Schneider, S. N. O'Neil, E. V. Anslyn, *J. Am. Chem. Soc.* **2000**, *122*, 542 – 543; M. E. Padilla-Tosta, J. M. Lloris, R. Martínez-Máñez, T. Pardo, F. Sancenón, J. Soto, M. D. Marcos, *Eur. J. Inorg. Chem.* **2001**, 1221 – 1226.

[7] G. Schwarzenbach, K. Lutz, *Helv. Chim. Acta* **1940**, *23*, 1147; E. N. Marvell, G. Caple, T. A. Gosink, G. Zimmer, *J. Am. Chem. Soc.* **1966**, *88*, 619 – 620.

High-Pressure Synthesis of γ-P_3N_5 at 11 GPa and 1500 °C in a Multianvil Assembly: A Binary Phosphorus(V) Nitride with a Three-Dimensional Network Structure from PN_4 Tetrahedra and Tetragonal PN_5 Pyramids**

Kai Landskron, Hubert Huppertz, Jürgen Senker, and Wolfgang Schnick*

Phosphorus(V) nitride, P_3N_5, has structural similarities to the polymeric nonmetal nitrides α- and β-Si_3N_4 as well as to cubic boron nitride (*c*-BN). These compounds are built up from three-dimensional networks of linked TN_4 tetrahedra (T = B, Si, P). In cubic boron nitride as well as in α- and β-silicon nitride corner-sharing tetrahedra exclusively occur, whereas in α-P_3N_5 corner- and edge-sharing PN_4 units exist.[1, 2] Recently the synthesis of cubic γ-Si_3N_4 was reported. This high-pressure modification, which crystallizes in the spinel structure type, consists of SiN_4 tetrahedra and SiN_6 octahedra.[3]

With respect to its material properties phosphorus(V) nitride differs significantly from BN and Si_3N_4: P_3N_5 is thermally stable only up to 850 °C, whereas boron nitride and silicon nitride decompose at much higher temperatures.[1] The thermal lability of phosphorus(V) nitrides is an important reason why the synthesis of highly condensed crystalline nitridophosphates (molar ratio P:N > 1:2) is difficult. The irreversible elimination of N_2, which is the main process during the thermal decomposition of phosphorus(V) nitrides, can be suppressed by using high-pressure conditions. Recently, the synthesis of highly condensed nitridophosphates by reaction of the respective metal azides with P_3N_5 was successfully carried out at about 4 GPa and 1300 °C. We obtained the alkali and alkaline earth nitridophosphates (e.g. M^IPN_2, $M^IP_4N_7$, $M^I_3P_6N_{11}$, $M^{II}P_2N_4$)[4] without thermal decomposition of P_3N_5 or the reaction products.

By increasing the pressure further we have now been able to synthesize the high-pressure phase γ-P_3N_5. The reaction was carried out at 1500 °C and 11 GPa with partially crystalline P_3N_5 as starting material. The reaction was performed by using a boron nitride capsule in a multianvil assembly, which allowed the synthesis of about 50 mg γ-P_3N_5 (see Experimental Section).

The crystal structure of γ-P_3N_5 (Table 1) was determined by direct methods from powder X-ray diffraction data and refined using the Rietveld method (Figure 1).[5] The novel high-pressure modification consists of a polymeric three-dimensional network structure of linked PN_4 tetrahedra and tetragonal-pyramidal PN_5 units. In accord with the nomen-

Table 1. Atomic parameters and isotropic thermal displacement factors [pm²] of γ-P_3N_5.[a]

Atom	Wyckoff position	*x*	*y*	*z*	U_{iso}
P1	2*a*	0	0	0.3114(10)	274(14)
P2	4*c*	0.8191(2)	1/2	−0.0420(9)	360(10)
N1	2*b*	0	1/2	0.5159(15)	62(29)
N2	4*c*	0.8953(4)	0	0.0768(9)	214(19)
N3	4*c*	0.7265(6)	1/2	0.2196(12)	263(25)

[a] The temperature factor is defined by $\exp(-8\pi^2 U_{iso}\sin^2\theta/\lambda^2)$, space group *Imm*2, $a = 1287.20(5)$, $b = 261.312(6)$, $c = 440.04(2)$ pm, $Z = 2$.

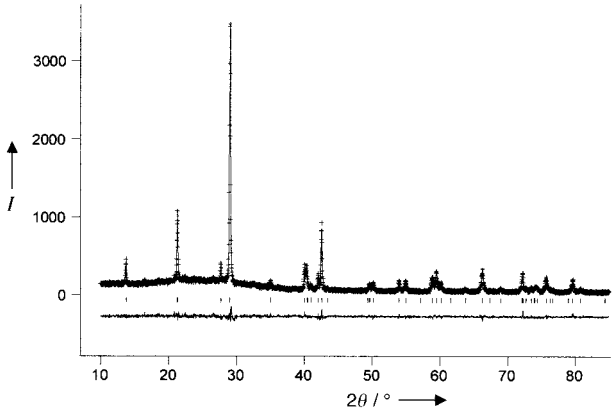

Figure 1. Observed (crosses) and calculated (line) X-ray powder diffraction pattern as well as difference profile (bottom line) of the Rietveld refinement of γ-P_3N_5. Positions of Bragg reflections are marked by vertical lines. The diffraction pattern was obtained with a conventional STOE-Stadi-P powder diffractometer ($Cu_{K\alpha1}$, $\lambda = 154.05$ pm).

[*] Prof. Dr. W. Schnick, Dipl.-Chem. K. Landskron, Dr. H. Huppertz, Dr. J. Senker
Department Chemie der Ludwig-Maximilians-Universität
81377 München (Germany)
Fax: (+49) 89-2180-7440
E-mail: wsc@cup.uni-muenchen.de

[**] This work was supported by the Fonds der Chemischen Industrie and the Deutsche Forschungsgemeinschaft (Gottfried-Wilhelm-Leibniz-Programm). The authors thank Dr. D. Frost and Prof. Dr. D. C. Rubie, Bayerisches Geoinstitut, Universität Bayreuth, as well as Dr. P. Ulmer, ETH Zürich, for help in adapting the multianvil-technique. Also many thanks to W. Wünschheim, Department Chemie, LMU München for the development and programming of software for the high-pressure experiments.

  1433-7851/01/4014-2643 $ 17.50+.50/0

clature for silicates introduced by Liebau, γ-phosphorus(v) nitride can be described as a phosphorus nitridophosphate nitride $P^{[5]}_2[P^{[4]}N_3]N_2$ (the superscripted number in square brackets after the element symbol denotes the coordination number).[6] Rods from *trans*-edge-sharing PN_5 units running along [010] are linked by vertices, leading to the formation of layers perpendicular to [100] (Figure 2). These layers are

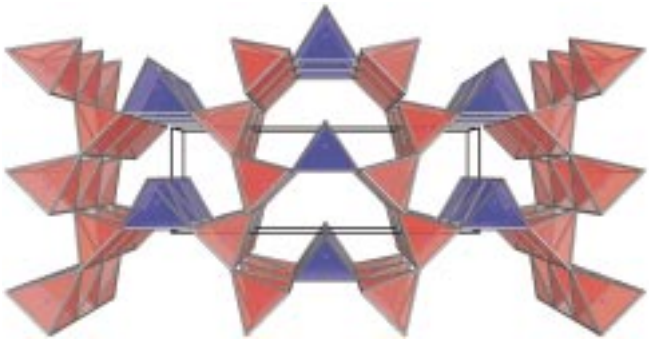

Figure 2. Crystal structure of γ-P_3N_5, view along [010]. Layers of edge-sharing and corner-sharing PN_5 pyramids (red) are linked by rods of corner-sharing PN_4 tetrahedra (blue) to give a three-dimensional network structure.

reminiscent of fragments of the rutile structure type, in which the octahedra have been cut off at one vertex to give tetragonal pyramids (Figure 3). Rods of corner-sharing PN_4 tetrahedra running along [010] link the layers built up from

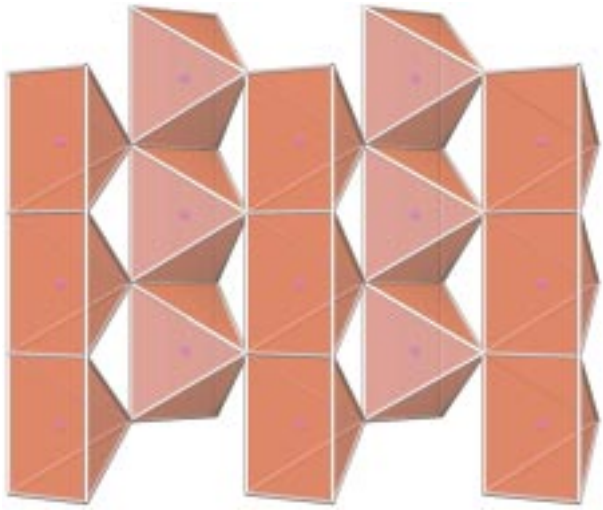

Figure 3. Layers of rods of *trans*-edge-sharing tetragonal PN_5 pyramids linked through vertices are reminiscent of fragments of the crystal strucure of rutile; view along [100].

PN_5 units (Figure 2). In accordance with the pressure–coordination rule[7] a partial increase of the coordination number of the phosphorus atoms from four in α-P_3N_5 to five in γ-P_3N_5 is observed. The bond lengths P–N in the PN_5 pyramids (166(1), 171(1), and 177(1) pm) are significantly longer than in the PN_4 tetrahedra (159(1) and 170(1) pm) (Figures 4 and 5), which corresponds to the pressure–distance paradox.[8] A quite similar observation is made in the spinel structure of cubic γ-Si_3N_4, in which the coordination numbers of silicon

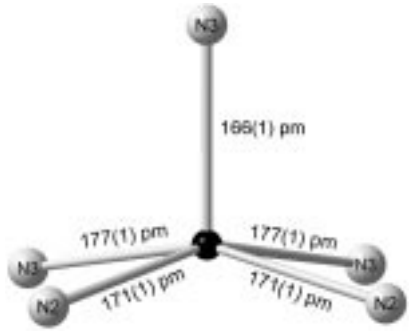

Figure 4. Tetragonal PN_5 pyramids in γ-P_3N_5 (∢(N-P-N) $2\times100(1)^\circ$, $2\times101(1)^\circ$, $2\times79(1)^\circ$, $95(1)^\circ$, $99(1)^\circ$, $2\times158(1)^\circ$).

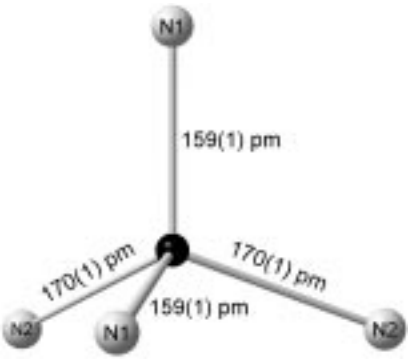

Figure 5. PN_4 tetrahedra in γ-P_3N_5, the P atoms show nearly regular tetrahedral coordination by N atoms (∢(N-P-N) $105(1)^\circ$, $4\times110(1)^\circ$, $111(1)^\circ$).

are partially increased from four to six compared to those in α- and β-Si_3N_4, which are the stable phases at normal pressure.[3]

All nitridophosphates investigated to date are built up by PN_4 tetrahedra.[1, 4] PN_5 units are known from molecular spirocyclic compounds, but exact structural data exists for a few cases only.[9] In accordance with the VSEPR concept, which favors the trigonal-bipyramidal conformation over the square-pyramidal one, distorted PN_5 bipyramids are observed in all studied compounds. The P–N bond lengths in the trigonal bipyramids of aminodiazadiphosphetospirobis(triazaphosphole) are similar to those in the PN_5 pyramids of γ-P_3N_5.[9a] In contrast, P–N compounds with square- or tetragonal-pyramidal PN_5 units are unknown yet.

In γ-P_3N_5 the bond lengths of the PN_4 and PN_5 units vary far less than in α-P_3N_5 (151–174 pm), which is exclusively built up from PN_4 tetrahedra. This and the fact that phosphorus(v) nitride synthesized at normal pressure is often obtained as β-P_3N_5, a stacking variant derived from α-P_3N_5, or as a stacking fault variant indicates steric stress in α-P_3N_5.[2, 10]

One fifth of the N atoms in γ-P_3N_5 is neighbored by two P atoms ($N^{[2]}$). All residual N atoms are bound to three P atoms ($N^{[3]}$). The P–$N^{[2]}$ bonds (159 pm) are significantly shorter than the P–$N^{[3]}$ bonds (166–177 pm). Compared to α-P_3N_5 (two fifth $N^{[3]}$, three-fifths $N^{[2]}$) the average coordination number of the N atoms is increased. The sum of the bond angles at $N^{[3]}$ is nearly 360° for each atom. The angles P-$N^{[2]}$-P (111°) are significantly smaller than in α-P_3N_5 (142, 143, and 171°, respectively).[2] They are similar to the corresponding angles in the P–N sodalites $M_{(7-x)}H_{2x}[P_{12}N_{24}]Y_y$ (125–126°)

  1433-7851/01/4014-2644 $ 17.50+.50/0

built exclusively from $N^{[2]}$ bridges,[1] $LiPN_2$ (124°),[1] and HPN_2 (130°).[11]

The density of γ-P_3N_5 is 32% higher than the density of α-P_3N_5 (values from the X-ray structure determination: 2.77 (α-P_3N_5),[2] 3.65 $g\,cm^{-3}$ (γ-P_3N_5)). Therefore the high-pressure phase could show interesting materials properties (e.g. great hardness or low compressibility) similar to those predicted for cubic γ-Si_3N_4 obtained under comparable conditions (1700 °C, 15 GPa).[3]

Experimental Section

The high-pressure synthesis of γ-P_3N_5 was carried out using the multianvil-technique and a hydraulic 1000 t press.[12, 13] Cr_2O_3-doped MgO octahedra (Ceramic Substrates & Components Ltd., Isle of Wight) with an edge length of 18 mm were used. Eight truncated tungsten carbide cubes (Toshiba Grade F, edge length: 32 mm, truncation edge length: 11 mm) separated by pyrophyllite gaskets served as anvils for the compression of the octahedra ("18/11 assembly" in conventional terminology). Partially crystalline P_3N_5, synthesized in accordance with reference [14], was loaded in a cylindrical capsule from hexagonal boron nitride (Henze, Kempten), (volume: ca. 35 mm^3) and sealed with a BN cap. The capsule was centered within two nested graphite tubes of different length, which acted as an electrical resistance heater. The remaining volume at both ends of the sample capsule was filled with two cylindrical pieces from MgO. This arrangement was placed into a ZrO_2 tube and then transferred into a pierced MgO octahedron. The electrical contact of the graphite tubes was arranged by two plates from molybdenum.

The assembly was compressed up to 11 GPa at room temperature over five hours and then heated up to 1500 °C within 30 min. The sample was held for five minutes at this temperature and then quenched to room temperature. Then the pressure was released over 15 h. The temperature was measured by using a $W_{97}Re_3-W_{75}Re_{25}$ thermocouple, which was attached coaxially to the resistance heater. Further details about pressure calibration and temperature measurement are described in reference [15].

After the removal of the BN capsule γ-P_3N_5 was obtained as a crystalline, sinterted, white product. Elemental analysis (%): calcd: P 57.02, N 42.98; found: P 54.8, N 41.6, O 2.3. The absence of hydrogen (N–H) was checked by IR spectroscopy. Owing to the weaker bonds the signals of the vibrations in the P–N network of γ-P_3N_5 are shifted to significantly lower wavenumbers than in α-P_3N_5. Moreover γ-P_3N_5 was characterized by ^{31}P-MAS-NMR spectroscopy ($\nu_0 = 202.473$ MHz). The investigation using a rotation frequency ν_{rot} of 30 kHz revealed two very sharp signals at $\delta = -12$ and -101 (reference: 85% H_3PO_4). The integration of the completely relaxed signals (recycle delay: 5000 s) showed an intensity ratio of 1:1.98, which is in good accordance with the results obtained from the X-ray investigations. This issue and the comparison with the ^{31}P-MAS-NMR data of α-P_3N_5[10] allow the assignment of signals at $\delta = -12$ to the tetrahedral site and the one at $\delta = -101$ to the PN_5 pyramids.

Received: March 5, 2001 [Z16712]

[1] W. Schnick, *Angew. Chem.* **1993**, *105*, 846; *Angew. Chem. Int. Ed. Engl.* **1993**, *32*, 806.

[2] a) S. Horstmann, E. Irran, W. Schnick, *Angew. Chem.* **1997**, *109*, 1938; *Angew. Chem. Int. Ed. Engl.* **1997**, *36*, 1873; b) S. Horstmann, E. Irran, W. Schnick, *Z. Anorg. Allg. Chem.* **1998**, *624*, 620.

[3] a) A. Zerr, G. Miehe, G. Serghiou, M. Schwarz, E. Kroke, R. Riedel, H. Fueß, P. Kroll, R. Boehler, *Nature* **1999**, *400*, 340; b) M. Schwarz, G. Miehe, A. Zerr, E. Kroke, B. Poe, H. Fuess, R. Riedel, *Adv. Mater.* **2000**, *12*, 883.

[4] a) K. Landskron, E. Irran, W. Schnick, *Chem. Eur. J.* **1999**, *5*, 2548; b) K. Landskron, W. Schnick, *J. Solid State Chem.* **2001**, *156*, 390; c) K. Landskron, S. Schmid, W. Schnick, unpublished results.

[5] The X-ray investigations of γ-P_3N_5 were performed with a conventional powder diffractometer STOE Stadi P in Debye–Scherrer geometry using $Cu_{K\alpha1}$ radiation. The powder diffraction pattern was indexed unambiguously in orthorhombic symmetry by using the program WERNER. From systematic absences the space groups $I222$, $I2_12_12_1$, $Imm2$, and $Immm$ were considered. The integration and extraction of the intensities as well as the structure solution by direct methods was carried out by using the program EXPO. The position of all atoms in chemically plausible locations was only achievable in the space group $Imm2$. The Rietveld refinement of the crystal structure data was performed with the program GSAS. The scaling factor, the lattice constants, the zero point, and the background were refined initially. The profile was fitted by a pseudo-Voigt function corrected for asymmetry. All atom positions and thermal displacement factors were refined. $Imm2$, $a = 1287.20(5)$, $b = 261.312(6)$, $c = 440.04(2)$ pm, $V = 148.0 \times 10^6$ pm^3, $Z = 2$, $\rho_{calcd} = 3.657$ $g\,cm^{-3}$, $\lambda = 154.05$ pm, measured range $10° < 2\theta < 85°$, 7500 data points, 41 reflections, $R_p = 0.073$, $wR_p = 0.094$, $R_F = 0.048$. Further details on the crystal structure investigation may be obtained from the Fachinformationszentrum Karlsruhe, 76344 Eggenstein-Leopoldshafen, Germany (fax: (+49) 7247-808-666; e-mail: crysdata@fiz-karlsruhe.de), on quoting the depository number CSD-411847.

[6] F. Liebau, *Structural Chemistry of Silicates*, Springer, Berlin, **1985**.

[7] A. Neuhaus, *Chimia* **1964**, *18*, 93.

[8] W. Kleber, K.-T. Wilke, *Krist. Tech.* **1969**, *4*, 165.

[9] a) R. Day, A. Schmidpeter, R. Holmes, *Inorg. Chem.* **1983**, *22*, 3696; b) D. Schomburg, U. Wermuth, R. Schmutzler, *Phosphorus Sulfur Silicon* **1986**, *26*, 193; c) D. Schomburg, U. Wermuth, R. Schmutzler, *Chem. Ber.* **1987**, *120*, 1713; d) P. G. Jones, A. Meyer, R. Schmutzler, *Z. Naturforsch. B* **1990**, *45*, 175; e) J. Breker, P. G. Jones, R. Schmutzler, *Phosphorus Sulfur Silicon* **1990**, *53*, 193.

[10] W. Schnick, J. Lücke, F. Krumeich, *Chem. Mater.* **1996**, *8*, 281.

[11] a) W. Schnick, J. Lücke, *Z. Anorg. Allg. Chem.* **1992**, *610*, 121; b) H. Jacobs, R. Nymwegen, S. Doyle, T. Wroblewski, W. Kockelmann, *Z. Anorg. Allg. Chem.* **1997**, *623*, 1467.

[12] D. Walker, M. A. Carpenter, C. M. Hitch, *Am. Mineral.* **1990**, *75*, 1020.

[13] D. Walker, *Am. Mineral.* **1991**, *76*, 1092.

[14] V. Schultz-Coulon, W. Schnick, *Z. Anorg. Allg. Chem.* **1997**, *623*, 69.

[15] D. C. Rubie, *Phase Transitions* **1999**, *68*, 431.

Physically Cross-Linked Ultrathin Elastomeric Membranes**

Frank Mallwitz and Werner A. Goedel*

Thin, freely suspended membranes are of great interest for use in micromechanical devices, sensors, and actuators that require repeated elastic deformation, such as accelerometers or membrane valves. The ongoing miniaturization of these devices creates a demand for progressively thin membranes with a broad range of mechanical properties, especially with

[*] Dr. W. A. Goedel
Universität Ulm
Organische und Makromolekulare Chemie OC3
89069 Ulm (Germany)
Fax: (+49) 731-502-2883
E-mail: werner.goedel@chemie.uni-ulm.de

Dr. F. Mallwitz
Humboldt-Universität zu Berlin
Fachbereich Physik
Berlin (Germany)

[**] This work was supported by the Max-Planck Gesellschaft, the Deutsche Forschungsgemeinschaft (project Gö 693/2), and the Kalhof-Rose Stiftung. The experiments were conducted at the Max-Planck-Institut für Kolloid- & Grenzflächenforschung, Berlin. We thank H. Möhwald (MPI-KGF), M. Antonietti (MPI-KGF), M. Möller (Universität Ulm), and J. Rabe (Humboldt Universität Berlin) for support and fruitful discussions.

high stress resistance and elasticity. One way of making extremely thin, usually rigid, membranes is to assemble monolayers of non-water-soluble amphiphiles at the air–water interface, and then transfer them by Langmuir–Blodgett (LB) transfer to cover holes in solid substrates.[1–4] In previous publications we reported that monolayers of liquid polymers with ionic head groups can be covalently cross-linked by irradiation on the water surface[5] and then transferred to solid substrates to form nanometer-thin elastomeric membranes.[6] Unfortunately, using these procedures, one generates a solid monolayer already on the water surface. Thus, the monolayer is unable to undergo the two-dimensional flow neccessary for LB transfer.[7] It is therefore desirable to have substances that form fluid monolayers at the air–water interface, that can be transferred to form freely suspended membranes, and that can be stabilized by cross-linking shortly after transfer.

Herein, we report for the first time that this goal can be achieved by using physical instead of covalent cross-linking: In bulk or in nonpolar solvents, ionic groups attached to nonpolar polymers have a tendency to form aggregates that are composed of several ionic groups and the corresponding counterions. These aggregates act as cross-linking sites and give rise to elastic behavior provided that each polymer chain has at least two ionic groups.[8–10] In contrast to covalent cross-linking, however, these aggregates can be broken up upon addition of polar solvents. In the polymer monolayers considered here, the ionic head groups bind to the water surface (see Figure 1top). In this polar environment, aggregation of the ionic groups is unlikely. Thus the monolayers behave as viscous liquids and can be transferred to a substrate with holes to form initially a fluid membrane with a water core. Once the residual water drains or evaporates, however, the ionic groups of the polymer chain aggregate and thus effectively cross-link the membrane (Figure 1).

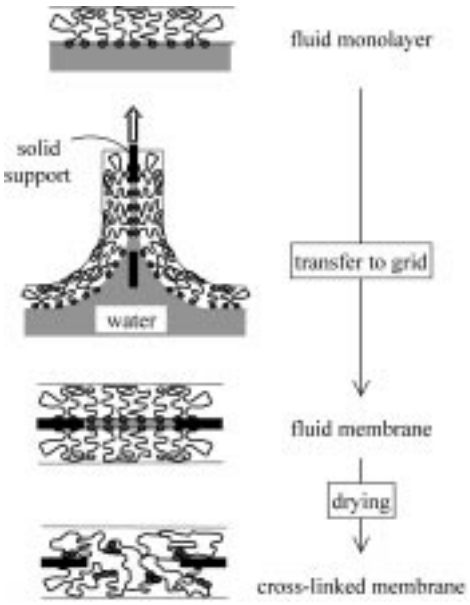

Figure 1. Scheme of the formation of a freely suspended membrane made from monolayers of polymers with ionic head groups. Langmuir–Blodgett transfer of the monolayer generates a freely suspended membrane, which is physically cross-linked by aggregation of ionic head groups after drying.

Linear polyisobutenes with a single sulfonate head group, and three-armed star polyisobutenes with an ionic head group on each arm have been prepared by "living" carbocationic polymerization.[11–13] The structures of the molecules and the associated chain lengths are depicted in the inset of Figure 2. The polymers, which have a glass transition temperature well below room temperature,[14] were spread at 15 °C from 4×10^{-4} wt % solutions in ethanol/pentane mixtures (1/50 by weight) and transferred at 20 °C to copper electron microscopy grids under conditions similar those used previously.[6]

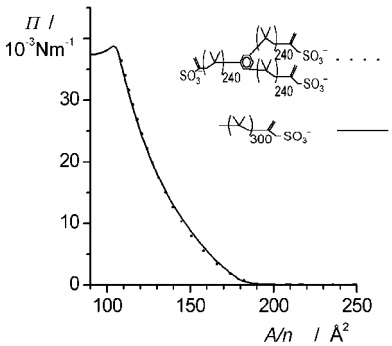

Figure 2. Plot of lateral pressure *(Π)* versus area per head group *(A/n)* of polyisobutenes with ionic head groups. ——: linear polymers with one sulfonate group at one end; ••••: three-armed star polymers with three sulfonate groups (one at the end of each arm).

The lateral pressure/area isotherms on the water surface (Figure 2) show that the area per head group occupied by a three-armed star polymer is very similar to the area occupied by a linear polymer with a single head group. Thus, the star architecture and the presence of several head groups does not hinder spreading of the anchored polymers.

If monolayers of polymers with only one head group are transferred to copper grids with 70 μm holes, they initially cover the holes, as a 40 nm[15] thin bilayer formed during the transfer. However, these membranes rupture within minutes after transfer. As an example a membrane made by LB transfer of polyisobutene with a single head group and a chain length of 300 repeat units is shown in Figure 3 top). Within 30 min, all membrane-covered holes in the grid rupture (see Figure 3 bottom). Presumably these membranes are stabilized only by a temporary network formed by entanglements of the polymer chains. These entanglements, however, cannot stabilize the membrane on a longer time scale and thus rupture occurs. This assumption is supported by rhelogical investigations of monolayers at the water–air inter-

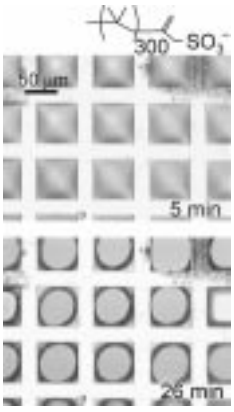

Figure 3. A freely suspended membrane generated by LB transfer of a monolayer of polyisobutene with a single ionic head group per polymer chain (300 repeat units per chain). The membranes rupture within 30 min (light microscopy image with top and bottom illumination.)

  1433-7851/01/4014-2646 $ 17.50+.50/0 *Angew. Chem. Int. Ed.* **2001**, *40*, No. 14

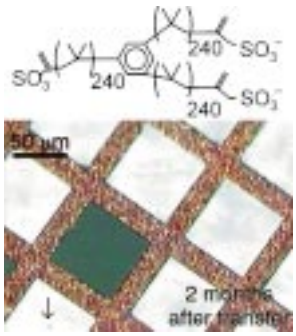

Figure 4. A freely suspended membrane generated by LB transfer of a monolayer of a three-armed polyisobutene star polymer with an ionic head group at each arm (240 repeat units per arm). The membrane is stable for months (light microscopy images with top illumination).

face before transfer[16] and by the fact that the stability of these membranes decreases with decreasing chain length.

Monolayers of three-armed star polymers with an ionic head group at each arm can be transferred to copper grids to generate freely suspended membranes as in the previous case. However, these membranes are stable for months. For example, Figure 4 depicts a light microscopy image of a freely suspended membrane of a three-armed star polymer two months after its generation by LB transfer. Immediately after transfer approximately 80% of the holes were covered with a freely suspended membrane. (The dark window in the middle left of Figure 4 was not covered by a membrane.) Two months later these membranes still cover the holes of the grid. In the lower left of Figure 4, an approximately 5 μm wide hole is visible as a dark spot (arrow). Even though the membrane in this part of the image is punctured, it does not rupture. Similar membranes transferred to grids with 250 μm holes are still intact 12 months after preparation.

This behavior is only observed in the case of polymers with more than one ionic group per chain and the stability increases with the number of ionic groups per chain. In addition, the membranes rupture when exposed to vapor of polar solvents such as dimethyl sulfoxide (within 3 min if exposed 1 h after transfer, within 30 min if exposed to DMSO 11 months after transfer). Therefore, it is likely that in the freely suspended membranes the ionic head groups form aggregates and thus give rise to physical cross-linking. We note, however, that the monolayers on the water surface before LB transfer do not appear to be cross-linked permanently but can undergo a two-dimensional flow towards the substrate during the transfer process.[17] Evidently, the cross-linking takes place by aggregation of the ionic groups only after the transfer—as schematically depicted in Figure 1. In this respect the monolayer investigated here offers an advantage compared to photochemically cross-linked monolayers[6] which are unable to undergo two-dimensional flow on the water surface.

As indicated schematically in Figure 5 the freely suspended membranes can be deformed reversibly by applying an asymmetric overpressure. In Figure 6a–c a continuously increasing overpressure of approximately 100–1000 Pa is applied to an initially flat freely suspended membrane from below. As a result of the overpressure, the membrane bulges upward. Upon release of the overpressure this deformation is completely reversible and can be repeated multiple times.

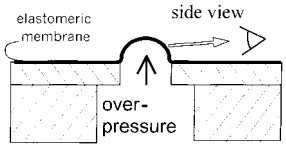

Figure 5. Test of the elastic properties of freely suspended membranes by applying an overpressure from below.

In summary, Langmuir–Blodgett transfer of monolayers of hydrophobic polymers with low glass transition can generate elastomeric freely suspended membranes, provided that the polymer chains bear more than one ionic group per polymer molecule. Most likely these membranes are stabilized by physical cross-linking due to the aggregation of the ionic head groups *after* draining and drying of the transferred monolayers.

Received: October 25, 2000
Revised: April 4, 2001 [Z15990]

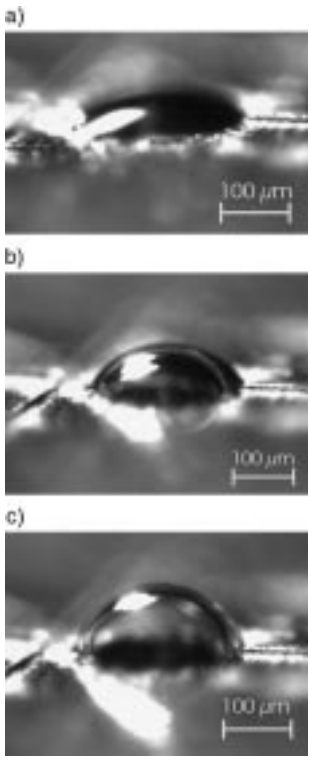

Figure 6. Light microscopy images (side view, side illumination) of a freely suspended membrane of a three-armed star polymer with ionic head groups on each arm, which spans a 300 μm hole. A small overpressure (approximately 100–1000 Pa) is applied from below and the membrane bulges upwards (a→c). This deformation is reversible upon release of the overpressure and can be repeated multiple times.

[1] O. Albrecht, A. Laschewsky, H. Ringsdorf, *J. Membr. Sci.* **1985**, *22*, 187.
[2] M. Seufert, C. Fakirov, G. Wegner, *Adv. Mater.* **1995**, *7*, 52.
[3] M. Kunitake, T. Nishi, H. Yamamoto, K. Nasu, O. Manabr, N. Nakashima, *Langmuir* **1994**, *10*, 3207.
[4] W. A. Goedel, C. Peyratout, L. Ouali, V. Schädler *Adv. Mater.* **1999**, *11*, 213.
[5] R. Heger, W. A. Goedel, *Prog. Colloid Polym. Sci.* **1997**, *105*, 167.
[6] W. A. Goedel, R. Heger, *Langmuir* **1998**, *14*, 3470.
[7] F. W. Embs, G. Wegner, D. Neher, P. Albouy, R. D. Miller, C. G. Willson, W. Schrepp, *Macromolecules* **1991**, *24*, 5068.
[8] G. Bronze, R. Jerome, P. Teyssie, C. Marco, *Polym. Bull.* **1981**, *4*, 241.
[9] M. Möller, E. Mühleisen, J. Omeis in *Physical Networks—Polymers and Gels* (Eds.: W. Burchard, S. B. Ross-Murphy), Elsevier, London, **1990**, pp. 45–64.
[10] a) S. Bagrodia, Y. Mohajer, G. L. Wilkes, R. F. Storey, J. P. Kennedey, *Polym. Bull.* **1983**, *9*, 174; b) M. R. Tant, G. L. Wilkes, R. Storey, J. P. Kennedey, *Polym. Bull.* **1985**, *13*, 541.
[11] R. Santos, J. P. Kennedy, M. Walters, *Polym. Bull.* **1984**, *11*, 261.
[12] a) J. P. Kennedy, L. R. Ross, J. E. Lackey, O. Nuyken, *Polym. Bull.* **1981**, *4*, 67; b) J. P. Kennedy, L. R. Ross, O. Nuyken, *Polym. Bull.* **1981**, *5*, 5.
[13] R. F. Storey, Y. Lee, *J. Polym. Sci. Polym. Chem.* **1991**, *29*, 317.
[14] The glass transition temperature of the polymer ($T_g = -63\,^{\circ}C$) was determined by differential scanning calorimetry (DSC).
[15] The thickness of a monolayer is equal to the surface concentration divided by the density of the polymer. The surface concentration is given by the molar mass of polymer divided by (Avogadro's constant × area per molecule).
[16] C. Luap, W. A. Goedel, *Macromolecules* **2001**, *34*, 1343.
[17] The fluidity of the monolayer can be checked by applying dust particles to the surface and by monitoring their displacement during transfer.

  1433-7851/01/4014-2647 $ 17.50+.50/0

A Cyclic Hexapeptide Containing L-Proline and 6-Aminopicolinic Acid Subunits Binds Anions in Water**

Stefan Kubik,* Richard Goddard, Ralf Kirchner, Dirk Nolting, and Jürgen Seidel

The biological importance of many anions explains why the development of artificial anion receptors is an important area of supramolecular chemistry.[1, 2] Artificial receptors in which the substrate is bound by hydrogen bonds as in natural systems are, however, often only active in nonpolar solvents.[2b] For complexation in water, stronger interactions, such as electrostatic or coordinative interactions, are normally necessary because of the high solvation energy of many anions.[2a] In this article we show that the cyclic hexapeptide **1** is able to bind anions such as halides and sulfates through hydrogen bonds even in aqueous solutions.[3] The anions are held in a cavity that results from the aggregation of two cyclopeptide molecules. This type of complex formation is similar to the guest-induced self-association of a resorcarene derivative recently described by Böhmer and co-workers,[4] and the structure of the complex resembles a molecular capsule.[5] In contrast to real capsules, however, the anion complexes of **1** are not stabilized by additional intermolecular interactions between the two cyclopeptide moieties.

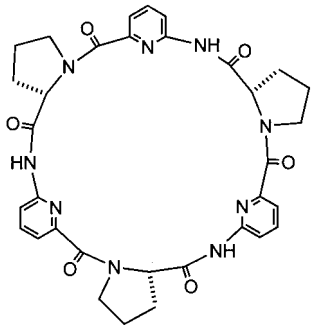

1

Compound **1** was synthesized from the two amino acid building blocks Boc-L-proline and 6-aminopicolinic acid benzyl ester, in analogy to the method previously described by us.[6] The picolinic acid derivative was prepared from 6-amino-2-picoline in a four-step synthesis according to known methods.[7]

The X-ray crystal structure analysis of the trihydrate of **1** shows that the conformation of the peptide in the crystal has exact C_3 symmetry. All the protons of the NH groups are arranged on the same side as the nitrogen atoms of the pyridine rings, the tertiary amides adopt the *cis* conformation, and the planes of the aromatic units lie approximately parallel to the C_3 axis of the macrocycle (Figure 1).[8] A water molecule of crystallization is bound to each NH group. In addition to the trihydrate of **1**, we have also obtained, under different conditions, crystals containing nine water molecules per cyclopeptide subunit, as well as crystals containing one acetone and three water molecules.[9] Since the conformation of **1** is practically identical in all these crystals in spite of differing environments (average deviations of the non-hydrogen atoms: 0.31 and 0.49 Å), it is probably the thermodynamically preferred conformation.

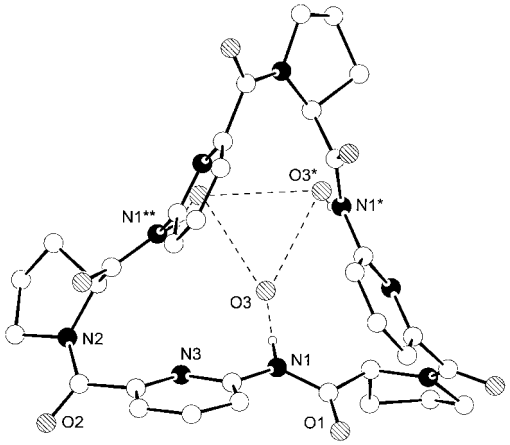

Figure 1. Crystal structure of $\mathbf{1}\cdot 3H_2O$. Selected distances [Å]: N1-O3 2.907(2), O3-O3* 2.930(2), N1-N1* 4.463(2).

NMR spectroscopic investigations show that in polar media, such as [D_6]DMSO or D_2O/CD_3OD mixtures, **1** adopts a conformation which corresponds to that observed in the crystal structure shown in Figure 1. On addition of one equivalent of *n*-butyltrimethylammonium tosylate to a 2 mM solution of **1** in [D_6]DMSO, downfield shifts of 0.77 ppm and 0.47 ppm are observed for the NMR signals of the NH protons and the H(α) protons, respectively. In the case of the corresponding iodide, the shifts of these signals are, respectively, 0.04 and 0.14 ppm. A shift of the cation signals is not observed in either spectrum ($\Delta\delta < 0.001$ ppm). Thus, in contrast to other, structurally similar cyclopeptides, interaction between **1** and ammonium cations cannot be demonstrated.[6] The downfield shift of the NH signals is, however, a typical indication of the involvement of these protons in hydrogen bonds to the anions.[2, 3] We were able to confirm this type of interaction by FT-IR spectroscopy with the tosylate complex of **1** in 1% [D_6]DMSO/$CDCl_3$. Furthermore, NOESY NMR spectroscopic studies showed that the conformation of **1** in the tosylate complex corresponds to that observed for the crystal in the X-ray analysis shown. The shift of the H(α) protons that results from the complexation of the anions

[*] Dr. S. Kubik
Institut für Organische Chemie und Makromolekulare Chemie, Heinrich-Heine-Universität
Universitätsstrasse 1, 40225 Düsseldorf (Germany)
Fax: (+49) 211-81-14788
E-mail: kubik@uni-duesseldorf.de
Dr. R. Goddard
Max-Planck-Institut für Kohlenforschung
Kaiser-Wilhelm-Platz 1
45470 Mülheim an der Ruhr (Germany)
Dipl.-Chem. R. Kirchner, Dr. J. Seidel
Institut für Physikalische Chemie
Technische Universität Bergakademie Freiberg
Leipziger Strasse 29, 09596 Freiberg (Germany)
Dipl.-Chem. D. Nolting
Institut für Physikalische Chemie und Elektrochemie, Heinrich-Heine-Universität
Universitätsstrasse 1, 40225 Düsseldorf (Germany)

[**] This work was sponsored by the Deutsche Forschungsgemeinschaft. S.K. thanks D. Kubik for her committed help with the synthetic work and Prof. G. Wulff for his support.

Supporting information for this article is available on the WWW under http://www.angewandte.com or from the author.

  1433-7851/01/4014-2648 $ 17.50+.50/0

thus stems from the spatial proximity of these protons to the negative charge density of the anions bound to the NH groups of **1**. This shift can be considered as an additional indication of the interaction of the peptide with anions. It allows one to demonstrate anion complexation in protic and, hence, more strongly competitive solvents than DMSO. Thus, even in 80% D_2O/CD_3OD the H(α) signal of the peptide is shifted downfield after addition of, for example, sodium iodide (Figure 2). Investigations of **1** in pure water were not possible because its solubility in water was too low.

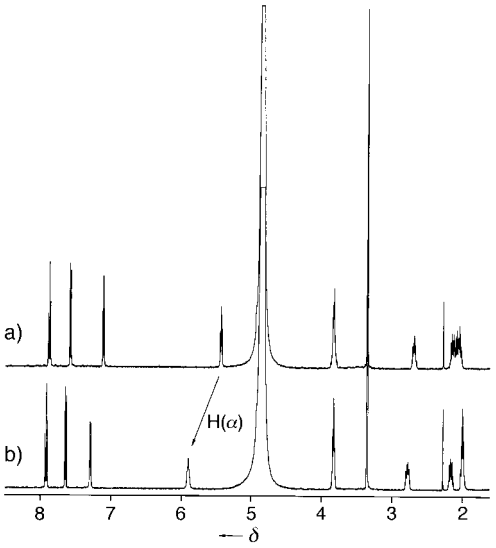

Figure 2. Part of the ^{1}H NMR spectrum of **1** in 80% D_2O/CD_3OD (2 mM) before (a) and after (b) addition of 10 equivalents of NaI.

Apart from iodide, interaction of **1** with chloride, bromide, sulfate, benzenesulfonate, and carbonate in the solvent mixture 80% D_2O/CD_3OD could also be clearly detected by ^{1}H NMR spectroscopy. A weaker interaction was found for the anions HCO_3^-, HPO_4^{2-}, $H_2PO_4^-$, NO_3^-, and OAc^-. Since the complexation of the halides, of sulfate, and sulfonate can be followed in aqueous solutions at pH 7 without addition of buffer, we have initially concentrated our investigations on these anions.

With a Job plot, a 1:1 stoichiometry was determined for the complex between **1** and the sodium salt of benzenesulfonic acid in 80% D_2O/CD_3OD. An NMR titration, in which the position of the signal for the H(α) protons of **1** was followed, gave a stability constant of $44 \pm 5\ M^{-1}$ ($\Delta\delta_{max} = 0.38$ ppm, 298 K) for this complex.[10] In contrast, for the halides and sulfate, it was unexpectedly found that each of these anions is bound by two cyclopeptide molecules. The existence of such 2:1 complexes in solution was confirmed by electrospray ionization mass spectrometry (ESI-MS). All the possible 1:1 and 2:1 halide complexes are, for example, visible next to one another in the ESI-MS spectrum when 0.33 equivalents of each NaCl, NaBr, and NaI are added to a solution of **1** in 80% H_2O/CH_3OH (Figure 3). Since ESI-MS allows the relative complex stability of supramolecular aggregates to be approximately estimated,[11] one can infer from the intensity of the peaks that the stability of the three halide complexes increases

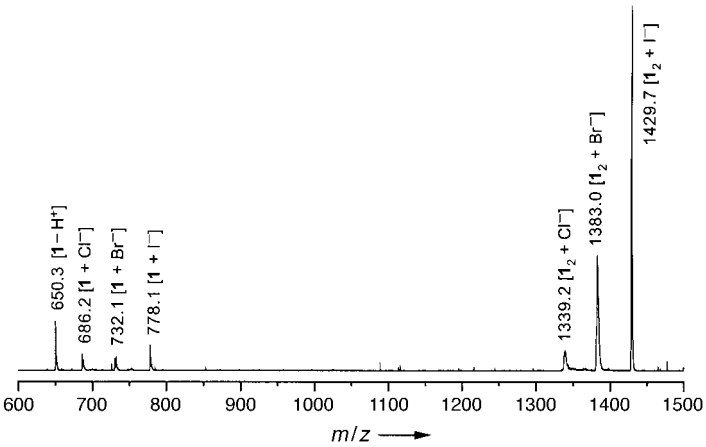

Figure 3. ESI mass spectrum of **1** in 80% H_2O/CH_3OH (100 μM) after addition of 0.33 equivalents of each NaI, NaBr, and NaCl.

in the order $Cl^- < Br^- < I^-$.[12] In the case of the sulfate complex of **1**, the 2:1 complex $\mathbf{1}_2 \cdot SO_4^{2-}$ can also be identified next to the 1:1 complex in the ESI mass spectrum.

Important information about the structure of these 2:1 complexes was provided by an X-ray crystal structure analysis of the iodide complex (Figure 4).[13] Since suitable crystals of this complex could only be obtained from acetone/hexane/H_2O solution, the observed structure does not necessarily correspond to that of the complex structure in aqueous solution. The fact that 17 water molecules are bound for every four $\mathbf{1}_2 \cdot I^-$ units indicates, however, that water is necessary for the formation of the crystals.[14] Moreover, the two independent iodide complexes in the unit cell have almost identical geometries in spite of differing environments. The iodide anion is located in a cavity between two cyclopeptide molecules,[14] which interlock perfectly like gears, with corresponding planes of two pyridyl–carbonyl–proline units coming together in close contact. The conformation of both peptide subunits corresponds to that of free **1**. Six NH groups point into the cavity and bind the enclosed anion with hydrogen bonds. The coordination geometry of the iodide anion is approximately trigonal prismatic, constrained by the arrangement of the two cyclopeptide moieties to each other. The sodium ions are coordinated to the carbonyl groups of **1**; however, they connect different 2:1 complexes in the crystal, not the two peptide units of a single complex. Intermolecular interactions between both peptide units that cause additional stabilization of the aggregate are not evident, besides those resulting from the binding of the anion.

Molecular modeling studies[15] revealed that sulfate and the smaller halides can also be enclosed in the cavity between the two cyclopeptide units. In the case of the sulfate anion, the calculations showed that hydrogen bonds between the NH groups of both peptides and the oxygen atoms of the sulfate are possible. For partially protonated anions the number of possible hydrogen bonds is reduced, which explains the poorer binding of, for example, HCO_3^-, HPO_4^{2-}, and $H_2PO_4^-$. The steric bulk of the phenyl ring in the benzenesulfonate anion prevents complexation of the anion by a second cyclopeptide so that in this case only a 1:1 complex is possible.

  1433-7851/01/4014-2649 $ 17.50+.50/0

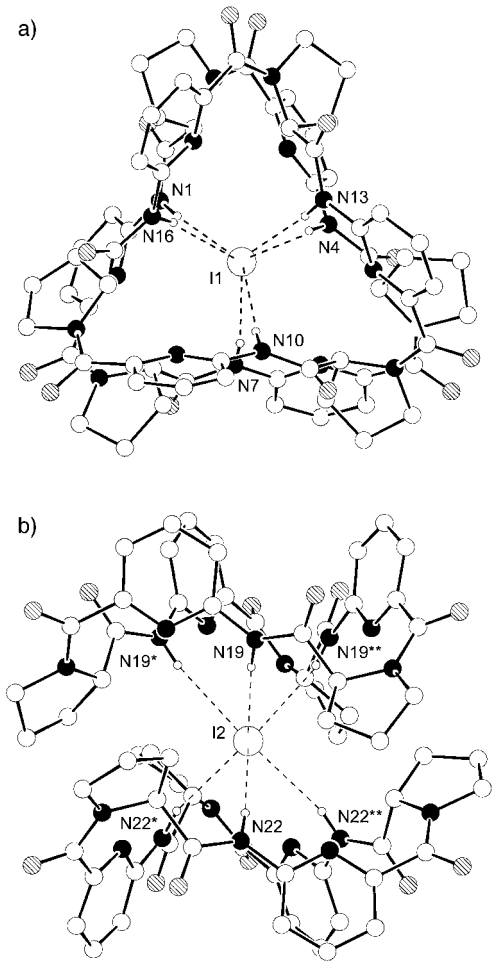

Figure 4. Cross-sections of the crystal structure of $4(\mathbf{1}_2 \cdot I^-) \cdot 4Na^+ \cdot 9C_3H_6O \cdot 17H_2O$: a) view from above, b) view from the side. Selected distances [Å]: I1-N1 3.784(3), I1-N4 3.724(3), I1-N7 3.922(3), I1-N10 3.736(4), I1-N13 3.935(4), I1-N16 3.886(3), N1-N4 4.485(5), N1-N16 5.514(5), I2-N19 3.662(3), I2-N22 3.650(4), N19-N19* 4.564(5), N19-N22 5.196(4).

In microcalorimetric investigations a small endothermic effect was found for the complex formation between **1** and NaI.[12] The formation of hydrogen bonds between the peptide and the iodide anion is apparently not able to compensate for the energy necessary for the desolvation of host and guest. Thus, entropic reasons must be mainly responsible for the anion complexation by **1**, that is, the release of solvent molecules from the solvation shells of the anion and the cyclopeptide. Similar effects have already been described for other anion receptors in polar solvents.[16]

Our investigations show that the peptide **1** can be used to complex anions in aqueous solution. As a result of the particular binding mechanism of **1**, the anion loses its solvent shell during formation of the complex and is shielded from the surrounding solvent in the complex. The interactions between the receptor and substrate are thereby strengthened. Peptide **1** is thus able to imitate principles that play an important role during the recognition of anions by natural receptors.

Received: January 31, 2001
Revised: April 23, 2001 [Z16538]

[1] J.-M. Lehn, *Supramolecular Chemistry*, VCH, Weinheim, **1995**.
[2] For relevant reviews, see: a) F. P. Schmidtchen, M. Berger, *Chem. Rev.* **1997**, *97*, 1609 – 1646; b) M. M. G. Antonisse, D. N. Reinhoudt, *Chem. Commun.* **1998**, 443 – 448.
[3] For further examples of neutral anion receptors that are effective in polar solvents, see: H. Ishida, M. Suga, K. Donowaki, K. Ohkubo, *J. Org. Chem.* **1995**, *60*, 5374 – 5375; K. Worm, F. P. Schmidtchen, *Angew. Chem.* **1995**, *107*, 71 – 73; *Angew. Chem. Int. Ed. Engl.* **1995**, *34*, 65 – 66; C. Raposo, N. Pérez, M. Almaraz, L. Mussons, C. Caballero, J. R. Morán, *Tetrahedron Lett.* **1995**, *36*, 3255 – 3258; R. C. Jagessar, M. Shang, W. R. Scheidt, D. H. Burns, *J. Am. Chem. Soc.* **1998**, *120*, 11684 – 11692; P. Anzenbacher, Jr., K. Jursíková, J. L. Sessler, *J. Am. Chem. Soc.* **2000**, *122*, 9350 – 9351; B. H. M. Snellink-Ruël, M. M. G. Antonisse, J. F. J. Engbersen, P. Timmerman, D. N. Reinhoudt, *Eur. J. Org. Chem.* **2000**, 165 – 170; F. Werner, H.-J. Schneider, *Helv. Chim. Acta* **2000**, *83*, 465 – 478.
[4] A. Shivanyuk, E. F. Paulus, V. Böhmer, *Angew. Chem.* **1999**, *111*, 3091 – 3094; *Angew. Chem. Int. Ed.* **1999**, *38*, 2906 – 2909.
[5] R. Wyler, J. de Mendoza, J. Rebek, Jr., *Angew. Chem.* **1993**, *105*, 1820 – 1821; *Angew. Chem. Int. Ed. Engl.* **1993**, *32*, 1699 – 1701; M. M. Conn, J. Rebek, Jr., *Chem. Rev.* **1997**, *97*, 1647 – 1668; J. Rebek, Jr., *Chem. Commun.* **2000**, 637 – 643.
[6] S. Kubik, R. Goddard, *J. Org. Chem.* **1999**, *64*, 9475 – 9486; S. Kubik, R. Goddard, *Eur. J. Org. Chem.* **2001**, 311 – 322.
[7] A. Janecka, T. Janecki, S. Shan, C. Bowers, K. Folkers, *J. Med. Chem.* **1994**, *37*, 2238 – 2241.
[8] Crystal data for $\mathbf{1} \cdot 3H_2O$:[9] Colorless crystals from MeOH/H_2O, $C_{33}H_{33}N_9O_6 \cdot 3H_2O$, $M_r = 705.73$, trigonal, space group $R3$ (No. 146), $a = 14.2352(9)$, $c = 15.1711(9)$ Å, $V = 2662.4(3)$ Å^3, $T = 100$ K, $Z = 3$, $\rho_{calcd} = 1.32$ g cm^{-3}, $\mu = 0.098$ mm^{-1}, crystal size $0.34 \times 0.23 \times 0.15$ mm, Siemens SMART diffractometer, $Mo_{K\alpha}$ radiation, $2.13 < \theta < 33.15^\circ$, 9588 measured reflections, 4209 independent and 3493 with $I > 2\sigma(I)$, programs SHELXS-97 and SHELXL-97; both programs are from G. M. Sheldrick, University of Göttingen, **1997**; 162 parameters, $R1 = 0.042$, $wR2$ (all data) $= 0.095$, $(\Delta/\sigma)_{max} = 0.0$, hydrogen atoms on H_2O refined isotropically, otherwise calculated, max./min. residual density 0.852/ – 0.373 e Å^{-3}.
[9] Crystallographic data (excluding structure factors) for the structures reported in this paper have been deposited with the Cambridge Crystallographic Data Centre as supplementary publication nos. CCDC-156896 – 156899 ($\mathbf{1} \cdot 3H_2O$, $\mathbf{1} \cdot C_3H_6O \cdot 3H_2O$, $\mathbf{1} \cdot 9H_2O$, and $4(\mathbf{1}_2 \cdot I^-) \cdot 4Na^+ \cdot 9C_3H_6O \cdot 17H_2O$). Copies of the data can be obtained free of charge on application to CCDC, 12 Union Road, Cambridge CB2 1EZ, UK (fax: (+44) 1223-336-033; e-mail: deposit@ccdc.cam.ac.uk).
[10] K. A. Connors, *Binding Constants*, Wiley, New York, **1987**.
[11] X. Cheng, R. Chen, J. E. Bruce, B. L. Schwartz, G. A. Anderson, S. A. Hofstadler, D. C. Gale, R. D. Smith, J. Gao, G. B. Sigal, M. Mammen, G. M. Whitesides, *J. Am. Chem. Soc.* **1995**, *117*, 8859 – 8860; P. A. Brady, J. K. M. Sanders, *New J. Chem.* **1998**, 411 – 417.
[12] Attempts to determine the stability constants K_1 and K_2 of the 2:1 complexes of **1** using NMR titrations were unsuccessful since the nonlinear regressions of the saturation curves gave no unique solutions. For a quantitative determination of the complex stability using microcalorimetry the observed effects were too small. Recently, however, we have structurally modified peptide **1** so that the formation of 2:1 complexes is prevented. Using this modified peptide it is possible to estimate relatively accurately the magnitude of the stability constants K_1 for anion complexes of **1** and to calculate K_1 and K_2 with this information. These results will be reported elsewhere shortly.
[13] Crystal data for $4(\mathbf{1}_2 \cdot I^-) \cdot 4Na^+ \cdot 9C_3H_6O \cdot 17H_2O$:[9] Colorless crystals from acetone/hexane/H_2O, $4((C_{33}H_{33}N_9O_6)_2 \cdot I^-) \cdot 4Na^+ \cdot 9C_3H_6O \cdot 17H_2O$, $M_r = 6642.01$, trigonal, space group $P3$ (No. 143), $a = 27.4212(1)$, $c = 12.7273(1)$ Å, $V = 8287.81(8)$ Å^3, $T = 100$ K, $Z = 1$, $\rho_{calcd} = 1.33$ g cm^{-3}, $\mu = 0.468$ mm^{-1}, crystal size $0.315 \times 0.30 \times 0.13$ mm, Nonius KappaCCD diffractometer, $Mo_{K\alpha}$ radiation, $1.05 < \theta < 32.59^\circ$, 51733 measured reflections, 36424 independent and 31610 with $I > 2\sigma(I)$, programs SHELXS-97 and SHELXL-97; both programs from G. M. Sheldrick, University of Göttingen, **1997**; 1308 parameters, $R1 = 0.057$, $wR2$ (all data) $= 0.157$, $(\Delta/\sigma)_{max} = 0.002$, hydrogen atoms on water molecules not calculated, max./min. residual electron density 1.307/ – 1.303 e Å^{-3}.

  1433-7851/01/4014-2650 $ 17.50+.50/0

[14] The complete structure of $4(\mathbf{1}_2\cdot I^-)\cdot 4Na^+\cdot 9C_3H_6O\cdot 17H_2O$ is a catemer. The main motif is the $\mathbf{1}_2\cdot I^-$ unit. There are two independent $\mathbf{1}_2\cdot I^-$ units in the unit cell and both have very similar conformations. Sodium ions and solvent molecules surround these groups, but in contrast to the anions, there are two types of sodium ions in the structure. One is pentacoordinated. Three coordination sites are occupied by carbonyl groups of neighboring cyclopeptides, one by the oxygen atom of a bound acetone molecule, and the remaining coordination site is occupied by a water molecule. This cation has a trigonal bipyramidal coordination geometry. The other sodium ion is merely tetrahedrally coordinated. Again three coordination sites are occupied by carbonyl groups of neighboring cyclopeptides and on the remaining coordination site sits a water molecule. In addition, there are two independent uncoordinated acetone molecules and five independent water molecules in the asymmetric unit.

[15] The calculations were performed on a Silicon Graphics Workstation using the program Cerius^2 (Molecular Simulations Inc.) and the Dreiding 2.21 force field: S. L. Mayo, B. D. Olafson, W. A. Goddard III, *J. Phys. Chem.* **1990**, *94*, 8897 – 8909.

[16] B. Linton, A. D. Hamilton, *Tetrahedron* **1999**, *55*, 6027 – 6038; M. Berger, F. P. Schmidtchen, *J. Am. Chem. Soc.* **1999**, *121*, 9986 – 9993; for another example of an artificial receptor for which hydrophobic effects are important for guest complexation, see: T. Haino, D. M. Rudkevich, J. Rebek, Jr., *J. Am. Chem. Soc.* **1999**, *121*, 11253 – 11254; T. Haino, D. M. Rudkevich, A. Shivanyuk, K. Rissanen, J. Rebek, Jr., *Chem. Eur. J.* **2000**, *6*, 3797 – 3805.

First O–H–N Hydrogen Bond with a Centered Proton Obtained by Thermally Induced Proton Migration**

Thomas Steiner,* Irena Majerz,* and Chick C. Wilson*

There is great current interest in the strongest types of hydrogen bonds, both in the chemical and the biological fields.[1] In contrast to "normal" and weak hydrogen bonds, which are primarily electrostatic $X^{\delta-}$–$H^{\delta+}\cdots Y^{\delta-}$ interactions,[2, 3] very strong hydrogen bonds have a quasi-covalent character.[4] In such a three-center four-electron bond X–H–Y, the H atom is involved in two partial covalent bonds of comparable bond orders. Very strong hydrogen bonds are stable in solution and in crystals, but have also been proposed to occur in intermediates of chemical[5] and enzymatic[6] reactions. In particular the latter proposal has led to heated and controversial discussions.[7] Very strong homonuclear hydrogen bonds (X–H–X) are experimentally well accessible, and numerous examples of centered or almost centered geometries have been reliably found by neutron diffraction experiments.[8] For heteronuclear hydrogen bonds, the structural information is much poorer. There are a few examples of X-ray crystal structures with O–H–N bonds in which the H atom has at least similar distances to O and N,[9, 10] but accuracies are poor, and not a single case was found as yet in neutron diffraction studies.[11] We now have been able to produce for the first time an exactly centered O–H–N hydrogen bond and characterize it by neutron diffraction. To achieve this goal, we used the effect of thermally induced proton migration, which we monitored by variable-temperature time-of-flight Laue neutron diffraction.

A good model system to study very short O–H–N hydrogen bonds are adducts of pentachlorophenol (PCP) with pyridine bases.[12, 13] The pK_a values of PCP and pyridine are similar, and suitable substitutions at the pyridine ring allow fine tuning of its pK_a value to match the one of PCP in an optimal way.[14] In a series of X-ray crystal structures, substituted pyridine · PCP complexes were found to crystallize as formally molecular or ionic adducts linked by hydrogen bonds $O–H\cdots N$ or $O^-\cdots H–N^+$, respectively, depending on the base selected.[15] The shortest hydrogen bond was found in crystalline 4-MePy · PCP (4-MePy = 4-methylpyridine), in which the $O\cdots N$ distance is 2.515(4) Å at 80 K,[10] and the H atom is situated approximately midway between the O and N atoms (Table 1). However, X-ray diffraction does not allow to determine the position of the H atom with an accuracy that is sufficient for a quantitative discussion.

To characterize the hydrogen bond in 4-MePy · PCP reliably, we determined the crystal structure by means of neutron diffraction (ND) at 20 K. The extremely short hydrogen bond ($O\cdots N$ 2.506(2) Å) has the center of gravity of the vibrating proton slightly off-center in the direction of the N atom (N–H 1.206(6), O–H 1.309(7) Å, N–H–O 170.4(6)°, Table 1). This represents by far the shortest O–H–N hydrogen bond for which ND data has been obtained. The most interesting observation, however, came as a complete surprise to us, and emerges from comparison with the X-ray crystal structures at room temperature[16] and at 80 K.[10] The overall crystal

Table 1. Geometrical parameters of the hydrogen bond in 4-MePy · PCP.

T [K]	O–H [Å]	H–N [Å]	Δ(X–H) [Å]	$O\cdots N$ [Å]	O–H–N [°]
RT, X-ray[16]	1.09(6)	1.47(6)	–	2.552(4)	170(5)
200	1.228(11)	1.306(11)	– 0.078(11)	2.525(4)	170.5(10)
150	1.229(11)	1.300(11)	– 0.071(11)	2.519(4)	169.6(10)
125	1.241(10)	1.288(10)	– 0.047(10)	2.519(4)	169.6(10)
100	1.258(8)	1.265(8)	– 0.007(8)	2.513(3)	170.1(8)
80	1.266(8)	1.255(8)	0.011(8)	2.513(3)	170.9(8)
80, X-ray[10]	1.22(4)	1.29(4)	–	2.515(4)	176(5)
60	1.275(10)	1.249(10)	0.026(10)	2.515(4)	170.9(10)
45	1.279(8)	1.242(8)	0.037(8)	2.513(3)	170.8(8)
20[a]	1.309(7)	1.206(6)	0.103(7)	2.506(2)	170.4(6)

[a] Measured on a different crystal than that at the other temperatures.

[*] Dr. T. Steiner
Institut für Chemie-Kristallographie
Freie Universität Berlin
Takustrasse 6, 14195 Berlin (Germany)
Fax: (+49) 30-838-56702
E-mail: steiner@chemie.fu-berlin.de
Dr. I. Majerz
Faculty of Chemistry
University of Wroclaw
50-383 Wroclaw (Poland)
Fax: (+48) 71-328-2348
E-mail: maj@wchuwr.chem.uni.wroc.pl
Dr. C. C. Wilson
ISIS Facility, CLRC Rutherford Appleton Laboratory
Didcot, Oxon, OX11 0QX (UK)
Fax: (+44) 1235-445720
E-mail: c.c.wilson@rl.ac.uk

[**] Parts of this work were supported through EPSRC grant GR/L7102 (to C.C.W.)

packing is always the same, but at room temperature the H atom of the hydrogen bond is (on time average) closer to the O atom, at 80 K it is roughly in the center, and at 20 K it is slightly closer to the N atom. Several factors can lead to such an effect,[17] and to gain further insight into this potentially important matter, we performed a variable-temperature ND study on the substance.

Variable-temperature single-crystal ND is an exceptionally powerful experimental technique. In conventional ND on steady-state sources, the collection of a data set for a substance such as 4-MePy · PCP takes several days. The recently developed time-of-flight Laue diffraction method[18] and suitable large area detectors allow routine data acquisition in substantially shorter times. Using a crystal of about 22 mm^3 volume, we were able to collect ND data at seven temperatures in the range 45 – 200 K at a rate of one data set per day (by using the time-of-flight Laue diffractometer SXD of the ISIS facility, see Experimental Section). The structure is ordered at all temperatures, and no sign of a phase transition is observed. The center of gravity of the proton alters with temperature, gradually migrating from being closer to the O atom (at high temperature) to being closer to the N atom (at low temperature; Table 1). Such a phenomenon has not, to our knowledge, been observed before. The proton migration amounts to about 5×10^{-4} Å K^{-1}, and the equidistant position is passed through at around 90 K. In Figure 1, the structure is

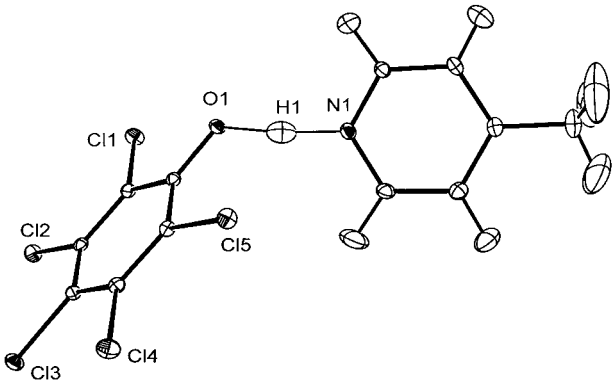

Figure 1. Neutron diffraction crystal structure of 4-MePy · PCP at 100 K. Displacement ellipsoids are drawn at the 30% probability level. The displacement amplitude of H1 is larger along the hydrogen bond than perpendicular to it, but is in no way exceedingly large when compared with those of the other H atoms in the structure.

drawn with the H atom closest to the center (100 K); the O–H and H–N distances differ by less than one standard uncertainty. In Figure 2, only the hydrogen-bonded atoms are drawn for all temperatures, showing how the H atom migrates over a distance of almost 0.1 Å in the temperature range 20 – 200 K (see the figure legend for details).

The structural data in Table 1 must be put in the context of all other published ND data of hydrogen bonds between O and N centers. This is best done by using the crystal correlation method.[19] Figure 3a shows a scatterplot of N–H against O–H distances; the small dots indicate data from published ND crystal structures, and represent exclusively strongly asymmetric hydrogen bonds either of the type O–H···N or N–H···O. The central part of the plot, which has been empty until now,[11] is populated by our data on pyridine · PCP complexes.[20] The line of dots at roughly equal N–H and O–H distances shows the thermally induced proton migration in 4-MePy · PCP. It is seen that O–H and N–H distances are well correlated over the whole range, without any sudden changes in slope or other discontinuities (Figure 3a). This parallels earlier observations in homonuclear O–H–O hydrogen bonds,[19, 21] and is in line with solution NMR spectroscopic data of other O–H–N-bonded systems.[22] The scatterplot of the O–H (or H–O) distance against the O···N separation, Figure 3b, shows a smooth correlation with two branches, one representing O–H···N and the other N–H···O hydrogen bonds. The two branches join at an O···N distance of about 2.51 Å.

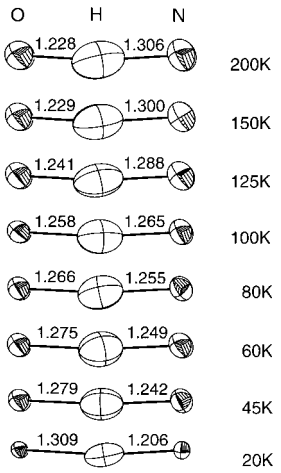

Figure 2. The hydrogen bond in 4-MePy · PCP as observed by neutron diffraction at eight different temperatures; displacement ellipsoids are drawn at the 50% probability level. The equidistant H atom position occurs at around 90 K.

Conclusions concerning proton-transfer phenomena can be drawn from the data in Figure 3a and b. A hypothetical proton transfer process along the line of the data points in Figure 3a or 3b requires a mechanism that is associated with concomitant shortening (to 2.51 Å) and subsequent widening of the O···N separation. In that case, no tunneling event is necessary. If changes in the environment of a hydrogen bond lead to suitable changes in the proton affinities of the atoms, such a mechanism should be possible, but seems quite speculative at this point. A proton-transfer event by tunneling, on the other hand, may be interpreted as a vertical jump from one branch to the other in Figure 3b. It does not require critical positioning of the O and N atoms, but since a potential well has to be penetrated, transfer rates will fall sharply with increasing O···N distances. Since the positions of the O and N atoms and their surroundings are not static, a hybrid mechanism can be envisaged that exploits initial hydrogen-bond shortening as a result of environmental fluctuations, be it stochastic or targeted as in enzymatic processes, followed by proton-tunneling through a temporarily lowered barrier.

The novel experimental finding of this work is that crystalline 4-MePy · PCP contains an O–H–N hydrogen bond with a (time-averaged) H atom position that migrates upon cooling, from a position closer to the O atom to one closer to the N atom. This effect allows the H atom position to be tuned within a 0.1 Å range merely by adjusting the temperature. The range includes the elusive geometrically centered O–H–N hydrogen bond, which has been observed experimentally for the first time (see also ref. [23]). We cannot decide herein if this is a result of a change in the thermal population of a constant but unsymmetrical hydrogen-bond potential, or of subtle changes in the hydrogen-bond potential itself. The new

  1433-7851/01/4014-2652 $ 17.50+.50/0

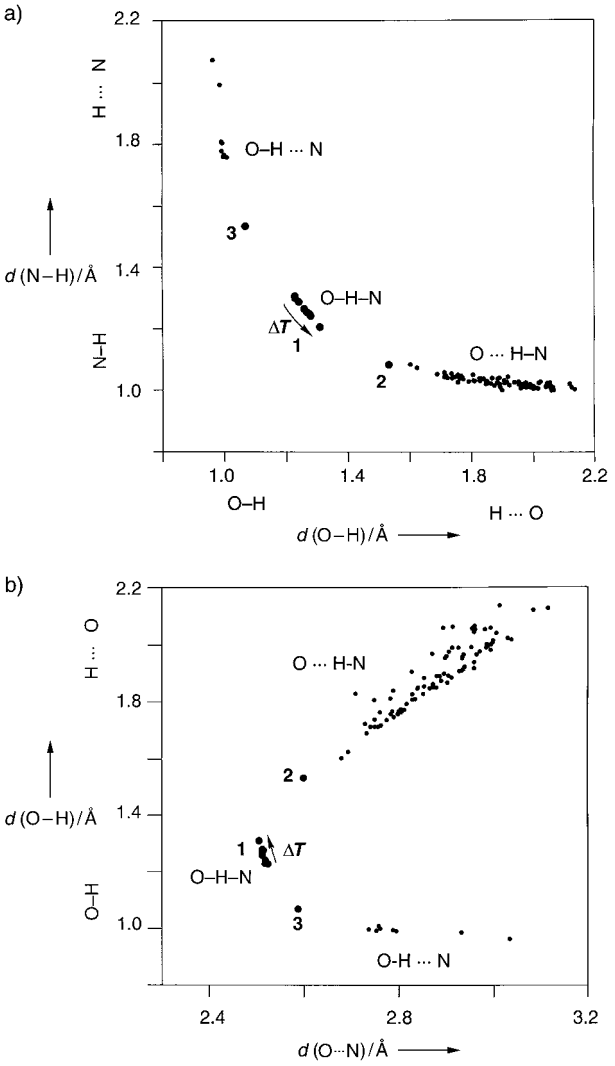

Figure 3. Crystal correlation results for O–H···N and N–H···O bonds based on neutron diffraction data. a) Scatterplot of N–H versus O–H distances in O–H–N hydrogen bonds. b) Scatterplot of O–H versus O···N distances in O–H–N hydrogen bonds. Large symbols: 1: 4-MePy·PCP at eight temperatures; 2: 2,4-Me_2Py·PCP; and 3: 2-MePy·PCP.[20] Small symbols show previously published data.[11]

data allow us to draw essentially complete pictures of distance correlations in O–H–N hydrogen bonds. Finally, we add that we see here only a relatively small degree of enhanced vibration of the H atom along the hydrogen bond, indicating a potential with a well-defined single minimum.

Experimental Section

After purification of the starting materials (4-MePy (Merck) was distilled, whereas PCP (Fluka) was sublimed), the complex 4-MePy·PCP was prepared in CCl_4 in the presence of excess base. Activated charcoal was added, the mixture was heated to reflux, and then filtered. Large single crystals of the 4-MePy·PCP complex with volumes of up to 50 mm^3 were then obtained by slow evaporation (room temperature) of the solvent.

All ND experiments were performed on the SXD instrument at the ISIS pulsed-spallation neutron source, with the time-of-flight Laue diffraction method.[18] This method uses a pulsed wavelength-sorted white neutron beam, along with large area position-sensitive detectors, to allow a large volume of reciprocal space to be measured in a single crystal setting (a "frame"). Collection of a data set comprises a series of such frames, each accumulated with a stationary crystal-detector arrangement. First, ND data were collected for 4-MePy·PCP at 20 K on a single crystal of approximate dimensions $4.5 \times 3 \times 2$ mm^3 (triclinic, space group $P\bar{1}$ (no. 2), $a = 7.236(2)$, $b = 8.929(3)$, $c = 13.058(4)$ Å, $\alpha = 99.84(3)$, $\beta = 118.04(2)$, $\gamma = 103.30(2)^\circ$, $V = 685.4(4)$ Å^3, $Z = 2$). Over two days, 42 frames were collected, yielding 5612 unique reflection intensities, with acceptable data extending to about 0.45-Å resolution. The second experiment was initiated only after the 20 K structure analysis has been finished. By then, the original crystal was lost, and a new crystal had to be used (dimensions $5 \times 3 \times 1.5$ mm^3). ND data were collected at eight temperatures in the order 100, 60, 80, 150, 200, 125, 45, and 300 K (temperature stabilities better than ± 1 K) within seven days. The final 300-K data set was unusable owing to fast sublimation of the crystal. Because of the need for fast data collection, only 20 frames were collected at each temperature, leading to crystallographically slightly incomplete data sets with around 2600 reflection intensities at each of the lower temperatures (realistic crystallographic resolution about 0.65 Å) and around 1850 reflections for the three highest temperatures.

The structures were refined anisotropically (SHELXL) starting from the known X-ray crystal structure. The data/parameter ratios (for unique data $I > 2\sigma(I)$): 23.0 (20 K), 11.1 (45 K), 7.9 (60 K), 10.8 (80 K), 10.0 (100 K), 7.6 (125 K), 7.8 (150 K), 7.4 (200 K). The final crystallographic R values are 0.076 at 20 K, and between 0.082 and 0.090 at the other temperatures. These values are in the usual range for Laue-diffraction data.[18] Crystallographic data (excluding structure factors) for the structures reported in this paper have been deposited with the Cambridge Crystallographic Data Centre as supplementary publication nos. CCDC-156061 – CCDC-156068. Copies of the data can be obtained free of charge on application to CCDC, 12 Union Road, Cambridge CB2 1EZ, UK (fax: (+44) 1223-336-033; e-mail: deposit@ccdc.cam.ac.uk).

Received: January 22, 2001 [Z16474]

[1] G. A. Jeffrey, *An Introduction to Hydrogen Bonding*, Oxford University Press, Oxford, **1997**.

[2] G. A. Jeffrey, W. Saenger, *Hydrogen Bonding in Biological Structures*, Springer, Berlin, **1991**.

[3] G. R. Desiraju, T. Steiner, *The Weak Hydrogen Bond in Structural Chemistry and Biology*, Oxford University Press, Oxford, **1999**.

[4] a) P. Gilli, V. Ferretti, V. Bertolasi, G. Gilli, *J. Am. Chem. Soc.* **1994**, *116*, 909 – 915; b) P. Gilli, V. Bertolasi, V. Ferretti, G. Gilli, *J. Am. Chem. Soc.* **2000**, *122*, 10405 – 10417.

[5] F. Hibbert, J. Emsley, *Adv. Phys. Org. Chem.* **1990**, *26*, 255 – 379.

[6] W. W. Cleland, M. M. Kreevoy, *Science* **1994**, *264*, 1887 – 1890.

[7] a) J. Lin, W. M. Westler, W. W. Cleland, J. L. Markley, P. A. Frey, *Proc. Natl. Acad. Sci. USA* **1998**, *95*, 14664 – 14668; b) S. Scheiner, T. Kar, *J. Am. Chem. Soc.* **1995**, *117*, 6970 – 6975; c) A. Warshel, A. Papazyan, *Proc. Natl. Acad. Sci. USA* **1996**, *93*, 13665 – 13670; d) B. Schiott, B. B. Iversen, G. K. H. Madsen, F. K. Larsen, T. C. Bruice, *Proc. Natl. Acad. Sci. USA* **1998**, *95*, 12799 – 12802; e) A. J. Mulholland, P. D. Lyne, M. Karplus, *J. Am. Chem. Soc.* **2000**, *122*, 534 – 535.

[8] a) H. Küppers, F. Takusagawa, T. F. Koetzle, *J. Chem. Phys.* **1985**, *82*, 5636 – 5647; b) F. Fillaux, N. Leygue, J. Tomkinson, A. Cousson, W. Paulus, *Chem. Phys.* **1999**, *244*, 387 – 403; c) G. K. H. Madsen, C. Wilson, T. M. Nymand, G. J. McIntyre, F. K. Larsen, *J. Phys. Chem. A* **1999**, *103*, 8684 – 8690; d) C. C. Wilson, *Single Crystal Neutron Diffraction from Molecular Materials*, World Scientific, Singapore, **2000**, pp. 225 – 228.

[9] F. Takusagawa, K. Hirotsu, A. Shimada, *Bull. Chem. Soc. Jpn.* **1973**, *46*, 2292 – 2299.

[10] Z. Malarski, I. Majerz, T. Lis, *J. Mol. Struct.* **1996**, *380*, 249 – 256.

[11] T. Steiner, *J. Phys. Chem. A* **1998**, *102*, 7041 – 7052.

[12] a) Z. Malarski, M. Rospenk, L. Sobczyk, E. Grech, *J. Phys. Chem.* **1982**, *86*, 401 – 406; b) L. Sobczyk, *Ber. Bunsenges. Phys. Chem.* **1998**, *102*, 377 – 383.

[13] a) G. Albrecht, G. Zundel, *J. Chem. Soc. Faraday Trans. 1* **1984**, *80*, 535 – 561; b) G. Zundel, *Adv. Chem. Phys.* **2000**, *111*, 1 – 218.

[14] A necessary (but not sufficient) condition for the formation of very short hydrogen bonds is the matching of the pK_a values of the atoms. The numerical value of $\Delta pK_a = pK_a(\text{base}) - pK_a(\text{acid})$ for "50% proton transfer" depends on the system selected,[13b] and also on the environment. In amine·PCP adducts, very strong O–H–N hydrogen

  1433-7851/01/4014-2653 $ 17.50+.50/0

bonds are formed in a "critical range" of ΔpK_a values scattered roughly around 1.0.[12, 13] For substituted pyridine · PCP adducts in CCl_4 solution, an ideal ΔpK_a for "50% proton transfer" is reported as 1.6.[13a] Since a more polar environment generally favors more ionic forms, it must be expected that in crystals, a pyridine · PCP adduct with $\Delta pK_a = 1.6$ is formally ionic (N^+–H···O^-) and adducts with really 50% proton transfer are characterized by $\Delta pK_a < 1.6$. Because the influence of the crystalline environment cannot be predicted quantitatively, one cannot predict the exact hydrogen-bond geometry from a known ΔpK_a value and molecular geometry. In any case, the ΔpK_a of 0.77[12] makes 4-MePy · PCP an interesting candidate in the search for an O–H–N bond with a centered H atom ($pK_a = 5.22$ (Py), 6.03 (4-MePy), 5.26 (PCP)).[12a]

[15] I. Majerz, Z. Malarski, L. Sobczyk, *Chem. Phys. Lett.* **1997**, *274*, 361 – 364.

[16] Z. Malarski, I. Majerz, T. Lis, *J. Mol. Struct.* **1987**, *158*, 369 – 377.

[17] The observation that the H atom is on time-average closer to the O atom at room temperature, and closer to the N atom at 20 K could have a number of reasons: 1) The substance might be dimorphic, with one crystal form having a different kind of hydrogen bond than the other. 2) There might be gradual proton migration upon cooling; this is the effect that was actually found in the second experiment. 3) The H atom might be disordered over two positions, one closer to the O atom and the other closer to the N atom, and relative occupancies change with temperature; similar effects are known, for example, with the O–H···O hydrogen bond in benzoic acid: C. C. Wilson, N. Shankland, A. J. Florence, *J. Chem. Soc. Faraday Trans.* **1996**, *92*, 5051 – 5057. 4) The difference between the structures at room temperature and at 20 K might be nothing more than an artifact caused by experimental inaccuracies.

[18] a) C. C. Wilson in *Neutron Scattering Data Analysis* (Ed.: M. W. Johnson), Adam Hilger, Bristol, **1990**, chap. 2; b) C. C. Wilson, *J. Mol. Struct.* **1997**, *405*, 207 – 217.

[19] H.-B. Bürgi, J. D. Dunitz, *Acc. Chem. Res.* **1983**, *16*, 153 – 161.

[20] Data point 2 is from 2,4-Me_2Py · PCP at 20 K; crystal structure to be published elsewhere. Data point 3 is from 2-MePy · PCP at 30 K: T. Steiner, C. C. Wilson, I. Majerz, *Chem. Commun.* **2000**, 1231 – 1232.

[21] T. Steiner, W. Saenger, *Acta Crystallogr. Sect. B* **1994**, *50*, 348 – 357.

[22] S. N. Smirnov, N. S. Golubev, G. S. Denisov, H. Benedict, P. Schah-Mohammedi, H.-H. Limbach, *J. Am. Chem. Soc.* **1996**, *118*, 4094 – 4101.

[23] In 4-MePy · PCP, the hydrogen bond is geometrically centered at about 90 K. This H position is singular in geometric terms, but not the one where the O–H and H–N bonds have equal "bond orders" $s = ½$. Free O–H and N–H covalent bonds have different lengths (e.g. 0.957 and 1.012 Å in H_2O and H_3N vapor, respectively), and also O–H and N–H bonds with $s = ½$ should have different X–H distances. Even the most recent parametrization of distance/valence relations is very inaccurate for strong O–H–N bonds, because no experimental data from that region could be used,[11] but suggests that an O–H bond with $s = ½$ is 0.060 Å shorter than an N–H bond with $s = ½$. According to Table 1, this situation occurs in 4-MePy · PCP between 125 and 150 K.

Nitroglycal Concatenation: A Broadly Applicable and Efficient Approach to the Synthesis of Complex O-Glycans**

Gottfried A. Winterfeld and Richard R. Schmidt*

The mucin class of glycopeptides has attracted much attention in recent years, because it subsumes numerous structures of fundamental importance in biological processes such as fertilization, parasitic infection, inflammation, immune defense, cell-growth, and cell – cell adhesion.[1] Synthesis of the characteristic α-glycosidic linkage between 2-acetamido-2-deoxy-D-galactopyranose and the hydroxy groups of L-serine and L-threonine, however, proved difficult. Most syntheses of α-O-linked glycopeptides rely essentially on the methodology introduced by Paulsen in 1978: The glycosylations are carried out with glycosyl donors that have a non-participating azido group at position 2 as latent amino function as well as a leaving group at the anomeric center.[2, 3] Enzymatic syntheses have also been reported, for example the synthesis of Core 1 and the corresponding sialylated Core 1 structure.[4] Core structures are defined as the binding region of the saccharides directly bound to the protein.[19] Recently, we have shown that for the synthesis of the simplest mucin structure, the T_N antigen, Michael addition to 2-nitrogalactal may serve as an efficient alternative approach.[5] This fundamentally new approach has now been developed to a comprehensive and powerful methodology that provides highly stereoselective access to 3-O- and 6-O-branched mucin structures.

All mucin core structures contain at the reducing end a *N*-acetylgalactosamine α-glycosidically linked to L-serine or L-threonine. Eight core structures of mucin-type glycopeptides have been identified to date; they bear additional glycosyl residues at either position 6 or position 3 or at both positions to form complex O-glycans (Scheme 1). To demonstrate that nitroglycal concatenation is a well-suited tool for the synthesis of all members of the mucin family we strategically chose two target molecules from the 6-O-branched structures (ST_N antigen and Core 7) and one target molecule from the 3-O-branched structures (Core 1). These structures are generated by reaction sequences I – III (Scheme 2 and 3).

For reaction sequences I and II as well as for the synthesis of T_N building blocks, nitroglycal **2** is the key intermediate of our synthesis. Nitroglycal **2** can be obtained in 84% yield from protected galactal **1**[6] by using a two-step, one-pot procedure involving addition of acetyl nitrate to the glycal functionality and subsequent elimination of acetic acid (Scheme 2).[5]

[*] Prof. Dr. R. R. Schmidt, Dr. G. A. Winterfeld
Fachbereich Chemie, Universität Konstanz, Fach M 725
78457 Konstanz (Germany)
Fax: (+49) 7531-883135
E-mail: Richard.Schmidt@uni-konstanz.de

[**] This work was supported by the Deutsche Forschungsgemeinschaft and the European Community (grant no. FAIR-CT 97-3142). G.A.W. gratefully acknowledges a RIKEN/Studienstiftung des Deutschen Volkes fellowship. We are grateful to Dr. A. Geyer for his help in the structural assignments by NMR experiments and to Dr. K.-H. Jung for his help in the preparation of the manuscript.

  1433-7851/01/4014-2654 $ 17.50+.50/0

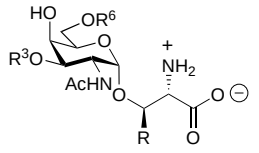

	R^6
Core 6:	GlcNAc β (1-6) →
Core 7:	GalNAc α (1-6) →
ST_N-Antigen:	Neu5Ac α (2-6) →

	R^3
Core 1:	Gal β (1-3) →
Core 3:	GlcNAc β (1-3) →
Core 5:	GalNAc α (1-3) →
Core 8:	Gal α (1-3) →

	R^3, R^6
Core 2:	GlcNAc β (1-6) → Gal β (1-3) →
Core 4:	GlcNAc β (1-6) → GlcNAc β (1-3) →

Scheme 1. Core structures of mucin-type O-glycans.

Protected serine **3a** and threonine **3b** add to this glycosyl donor **2** in virtually quantitative yield and under complete stereocontrol to form the desired α-linked 2-nitroglycosides **4a** and **4b**, respectively. The base-catalyzed glycosylation, which requires 0.1 equivalents of potassium *tert*-butoxide, is performed at room temperature and reaches completion within 10 min in the serine case and within 120 min in the threonine case. Compared to our previous observations with a perbenzylated nitrogalactal,[5] glycosyl donor **2** bearing a sterically demanding protective group at position 6 shows significantly enhanced reactivity and stereocontrol.

The peracetylated T_N antigens **10a** and **10b** are accessible from glycosides **4a** and **4b** in 81% yield after removal of silyl protective groups, reduction of the nitro group with Raney

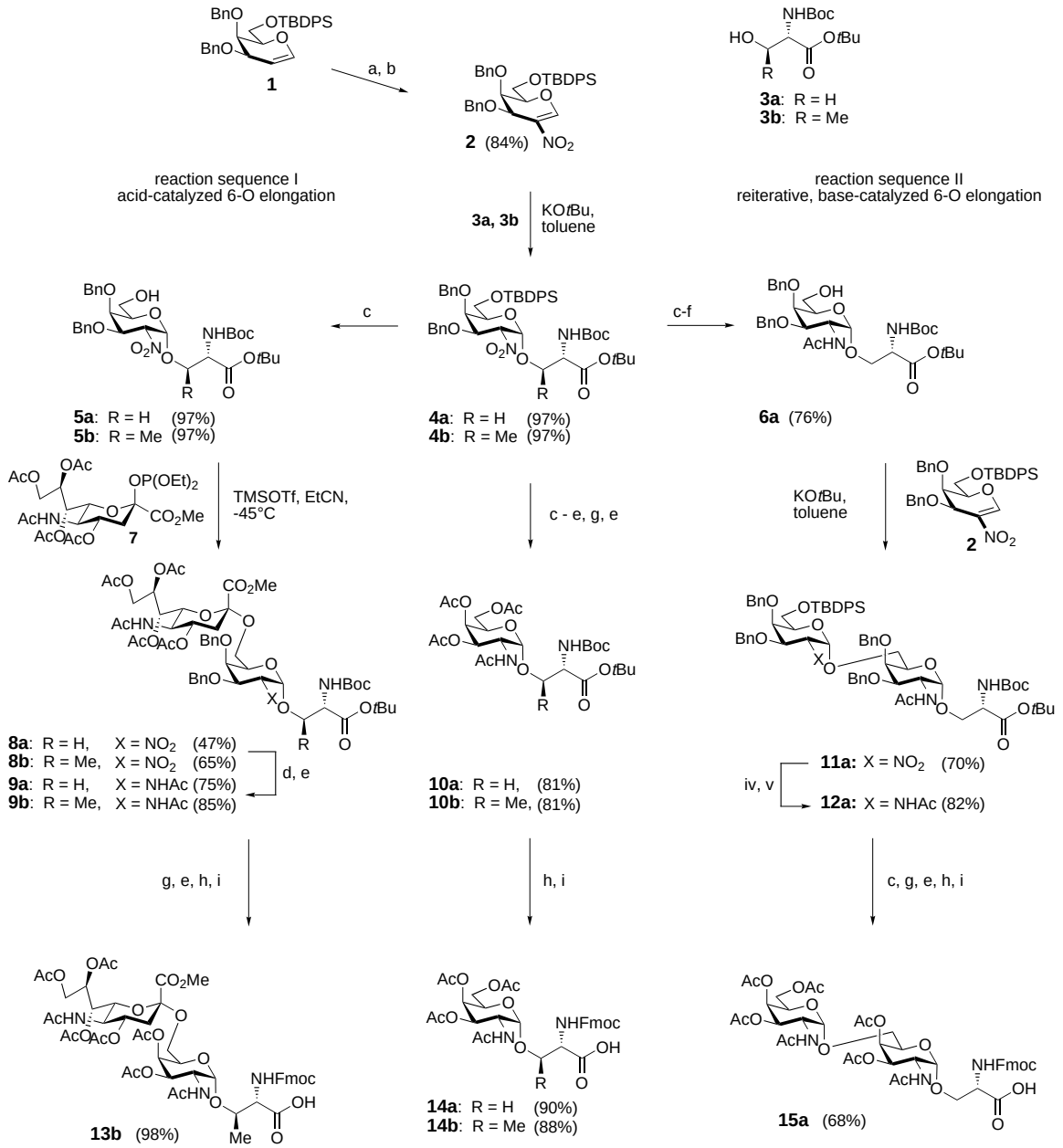

Scheme 2. Synthesis of T_N antigen, ST_N antigen, and Core 7 building blocks for glycopeptide synthesis; a) HNO_3, Ac_2O; b) Et_3N, CH_2Cl_2; c) TBAF, AcOH, THF; d) Raney-Ni T4 (Pt), H_2, EtOH; e) Ac_2O, pyridine; f) NaOMe, MeOH; g) Pd/C, H_2, AcOH, MeOH; h) TFA, CH_2Cl_2; i) Fmoc-ONSu, $NaHCO_3$, MeCN, H_2O. Ac = acetyl, Bn = benzyl, Boc = *tert*-butoxycarbonyl, Fmoc = fluoren-9-ylmethoxycarbonyl, Su = succinimidyl, TBDPS = *tert*-butyldiphenylsilyl, TFA = trifluoroacetic acid.

  1433-7851/01/4014-2655 $ 17.50+.50/0

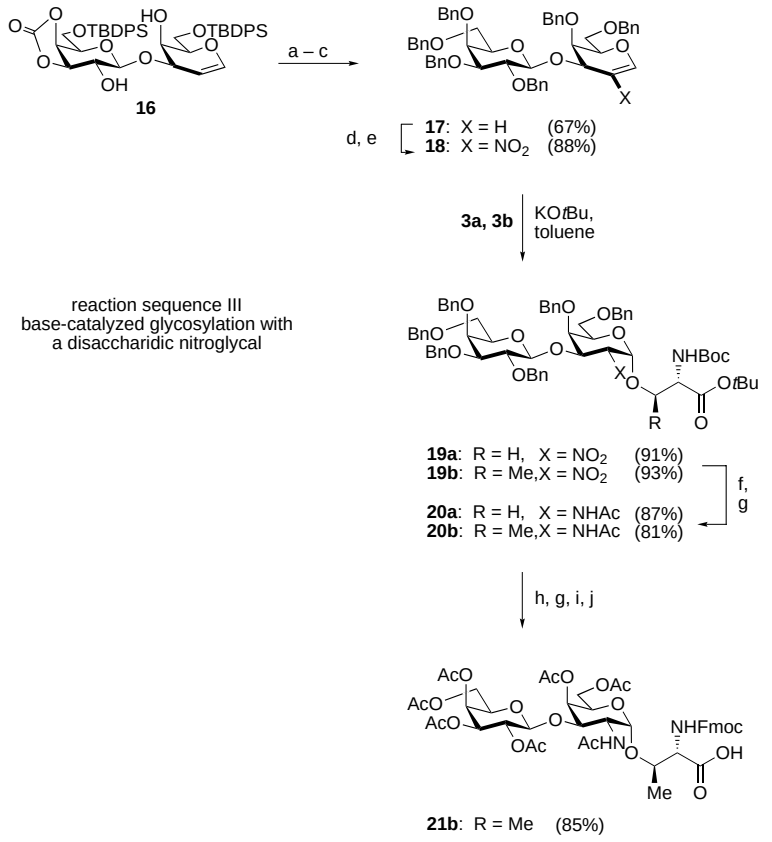

Scheme 3. Synthesis of a Core 1 building block for glycopeptide synthesis; a) NaOMe, MeOH; b) TBAF, THF; c) BnBr, NaH, DMF; d) Ac_2O, HNO_3; e) Et_3N, CH_2Cl_2; f) Raney-Ni T4 (Pt), H_2, EtOH; g) Ac_2O, pyridine; h) Pd/C, H_2, AcOH, MeOH; i) TFA, CH_2Cl_2; j) Fmoc-ONSu, $NaHCO_3$, MeCN, H_2O.

nickel T4/H_2,[5] N-acetylation, and protective group manipulations (Scheme 2). Known[7] building blocks for glycopeptide synthesis **14a** and **14b**[8] are obtained after cleavage of Boc and *tert*-butyl protective groups on the amino acid moiety and installation of the Fmoc protective group.

The ST_N antigen **13b** displays an α-linked *N*-acetylneuraminic acid unit at the 6-O position of the T_N structure. To arrive at a suitable glycosyl acceptor for the acid-catalyzed sialylation reaction, silyl protection at position 6 was removed by using a buffered tetrabutylammonium fluoride (TBAF) solution in THF (Scheme 2, reaction sequence I).[9] Nitroglycosides **5a** and **5b** can be applied to a sialylation reaction with neuraminic acid phosphite **7**[10] under Lewis acid catalysis. At $-45\,^{\circ}C$ in propionitrile the reaction affords α-linked sialosides **8a** and **8b**. The nitro group of these disaccharides can then be reduced to the amine and N-acetylated to afford derivatives **9a** and **9b**. Removal of the benzyl protective groups, peracetylation, removal of the *tert*-butyl protective group and exchange of the Boc for the Fmoc protective group affords the known ST_N building block **13b**[11, 12] suitable for glycopeptide synthesis.

Core 7 bears a second α-linked galactosamine moiety at position 6 of the T_N structure. This second unit may be installed by using a reiterative Michael-addition approach (Scheme 2, reaction sequence II). The 6-position of nitroglycoside **4a** is unmasked as mentioned before and the nitro group reduced to the amine and N-acetylated. Glycosyl acceptor **6a** is glycosylated making repeated use of nitrogalactal **2**. Again the glycosylation affords stereoselectively the α-glycoside **11a**. The second glycosylation cycle is completed by reduction of the nitro group and N-acetylation of the resulting amine to afford **12a**. The synthesis of building block **15a**[13] is achieved after exchange of all protective groups on the carbohydrate moiety of **12a** for acetyl groups, removal of both Boc and *tert*-butyl groups, and installation of the Fmoc protective group.

Having demonstrated the efficiency of nitroglycal concatenation for the synthesis of unsubtituted and 6-O-substituted O-glycans by elongation of a preformed T_N structure, we devised a Core 1 synthesis to open the methodology towards 3-O-branched structures and to the use of disaccharidic glycals in the nitration/Michael addition protocol. We started from known disaccharide glycal **16**,[14] which was converted to the per-O-benzylated derivative **17** (Scheme 3, reaction sequence III). Glycal **17** undergoes addition of acetyl nitrate and elimination of acetic acid as described for **1**[5] to afford the corresponding nitroglycal **18**. This Michael acceptor was glycosylated under standard conditions with **3a** and **3b** to give the corresponding α-glycosides **19a** and **19b**. Reduction of the nitro groups proceeded similarly to all previous examples and afforded the acetamido glycosides **20a** and **20b** after N-acetylation. Benzyl protective groups were exchanged for acetyl protective groups, the protective groups on the amino acid moiety were removed, and finally the Fmoc protective group was introduced to give the known[7b,g, 15] target building block **21b**.[16]

In conclusion, the syntheses of T_N and ST_N antigens as well as Core 7 and Core 1 structures have been achieved by using Michael addition reactions to nitroglycals as the key reaction. Nitroglycal concatenation has been applied reiteratively and combined with either anomeric leaving-group-based glycosylations[17] or the glycal assembly method,[18] demonstrating its versatility. The readily available starting nitroglycals as well as the stereochemically defined outcome of all base-catalyzed glycosylations shown here highlight this new methodology.

Experimental Section

2: Concentrated nitric acid (24 mL, 0.38 mol) was added dropwise to acetic anhydride (240 mL) at $10\,^{\circ}C$ under constant stirring. The external temperature was further lowered to $-10\,^{\circ}C$ to keep the internal temperature in the range of $10-20\,^{\circ}C$ during the addition. Once the addition was complete, the solution was cooled further to $-50\,^{\circ}C$ upon which a precipitate formed. Then a solution of galactal **1** (30 g, 0.053 mol) in acetic anhydride (120 mL) was added over a period of 10–15 min, and the mixture stirred at this temperature for 30 min. After the reaction mixture had been allowed to warm to $-22\,^{\circ}C$, it became clear. The reaction mixture was poured into iced water (500 mL), brine (250 mL) was added, and the aqueous layer extracted with diethyl ether (3×300 mL). The combined organic extracts were dried over sodium sulfate and the solvents removed by coevaporation with toluene. The crude intermediate 2-nitrogalactopyranose was dissolved in dichloromethane (50 mL) and slowly added to an ice-cold, stirred solution of triethylamine (22 mL, 0.159 mol) in dichloromethane (50 mL). After complete addition the cooling bath was removed and stirring

  1433-7851/01/4014-2656 $ 17.50+.50/0 *Angew. Chem. Int. Ed.* **2001**, *40*, No. 14

continued for 20 min. The organic phase was washed with 2 N HCl solution and dried over sodium sulfate. Removal of the volatiles and column chromatographic purification (toluene/ethyl acetate 98:2) of the residue furnished **2** as a light yellow oil (27 g, 84 %). $[\alpha]_D^{25} = -7.5$ ($c = 12$, $CHCl_3$). ^{1}H NMR (600 MHz, $CDCl_3$, 25 °C, TMS): $\delta = 7.77$ (s, 1H; 1-H), 7.61 – 7.60 (m, 3H; arom. H), 7.41 – 7.40 (m, 2H; arom. H), 7.34 – 7.14 (m, 15H; arom. H), 4.78 (d, $^3J_{3,4} = 3.5$ Hz, 1H; 3-H), 4.75 (d, $^2J = 10.9$ Hz, 1H; benzyl. H), 4.68 (d, $^2J = 10.9$ Hz, 1H; benzyl. H), 4.59 – 4.57 (m, 2H; 5-H, benzyl. H), 4.51 (d, $^2J = 12.0$ Hz, benzyl. H), 4.22 – 4.14 (m, 2H; 6-H, H6′), 3.81 (t, $^3J_{4,3} = 4.6$, $^3J_{4,5} = 4.6$ Hz, 1H; 4-H), 1.05 (s, 9H; C_4H_9); MS (FAB): *m*/*z*: 610 $[M+H]^+$, 632 $[M+Na]^+$.

4b: Nitrogalactal **2** (13 g, 21.3 mmol) and **3b** (7.1 g, 25.6 mmol) were dried under high vacuum and dissolved in dry toluene (250 mL) under argon. Then potassium *tert*-butoxide solution (2.1 mL of a 1 M solution in THF) was added and stirring continued for 120 min. Acetic acid (2 mL) was used to acidify the reaction mixture and all solvents were removed under reduced pressure. The residue was purified by column chromatography (toluene/ethyl acetate 20:1) to furnish **4b** as a colorless oil (18.3 g, 97 %). $[\alpha]_D^{25} = +53.3$ ($c = 5$, $CHCl_3$); ^{1}H NMR (600 MHz, $CDCl_3$, 25 °C, TMS): $\delta = 7.61 - 7.60$ (m, 4H; arom. H), 7.39 – 7.18 (m, 16H; arom. H), 5.32 (d, $^3J_{1,2} = 4.4$ Hz, 1H; 1-H), 4.96 (d, $^3J_{NH,\alpha} = 9.7$ Hz, 1H; NH), 4.93 (dd, $^3J_{2,1} = 4.1$, $^3J_{2,3} = 10.6$ Hz, 1H; 2-H), 4.83 (d, $^2J = 11.0$ Hz, 1H; benzyl. H), 4.77 (d, $^2J = 11.0$ Hz, 1H; benzyl. H), 4.50 (d, $^2J = 11.1$ Hz, 1H; benzyl. H), 4.43 (dd, $^3J_{3,2} = 10.6$, $^3J_{3,4} = 2.9$ Hz, 1H; 3-H), 4.24 – 4.23 (br d, 1H; β-H), 4.06 – 4.05 (m, 2H; α-H, 4-H), 3.88 (br t, $^3J_{5,6} = 6.8$, $^3J_{5,6'} = 6.8$ Hz, 1H; 5-H), 3.74 (dd, $^3J_{6,5} = 7.6$, $^2J_{6,6'} = 10.3$ Hz, 1H; 6-H), 3.68 (dd, $^3J_{6',5} = 5.9$, $^2J_{6',6} = 10.0$ Hz, 1H; 6′-H), 1.49, 1.45 (2s, 18H; $2\,C_4H_9$), 1.04 (s, 9H; C_4H_9). MS (FAB): *m*/*z*: 907 $[M+Na]^+$.

Received: January 8, 2001 [Z16382]

[1] a) A. Varki, *Glycobiology* **1993**, *3*, 97 – 130; b) I. Brockhausen, *Biochem. Biophys. Acta* **1999**, *1473*, 67 – 95.

[2] H. Paulsen, W. Stenzel, *Chem. Ber.* **1978**, *111*, 2334 – 2347; H. Paulsen, W. Stenzel, *Chem. Ber.* **1978**, *111*, 2348 – 2357; H. Paulsen, C. Kolar, W. Stenzel, *Chem. Ber.* **1978**, *111*, 2358 – 2369; H. Paulsen, C. Kolar, *Chem. Ber.* **1979**, *112*, 3190 – 3202.

[3] a) B. Ferrari, A. A. Pavia, *Carbohydr. Res.* **1980**, *79*, C1 – C7; b) H. Paulsen, J.-P. Hölck, *Carbohydr. Res.* **1982**, *109*, 89 – 107; c) G. Grundler, R. R. Schmidt, *Liebigs Ann.* **1984**, 1826 – 1847; d) W. Kinzy, R. R. Schmidt, *Carbohydr. Res.* **1987**, *164*, 265 – 276; e) H. Paulsen, W. Rauwald, U. Weichert, *Liebigs Ann.* **1988**, 75 – 86; f) W. Kinzy, R. R. Schmidt, *Carbohydr. Res.* **1989**, *193*, 33 – 47; g) Y. Nakahara, H. Iijima, S. Sibayama, T. Ogawa, *Tetrahedron Lett.* **1990**, *31*, 6897 – 6900; h) X.-T. Chen, D. Sames, S. J. Danishefsky, *J. Am. Chem. Soc.* **1998**, *120*, 7760 – 7769; i) M. Elofsson, L. A. Salvador, I. Kihlberg, *Tetrahedron* **1997**, *53*, 369 – 390; j) O. Seitz, *ChemBioChem* **2000**, *1*, 214 – 246; k) H. Herzner, T. Reipen, M. Schultz, H. Kunz, *Chem. Ber.* **2000**, *100*, 4495 – 4537.

[4] a) S. Bay, O. Berthie-Vergnes, V. Biberovic, D. Cantacuzène, *Carbohydr. Res.* **1997**, *303*, 25 – 31; b) G. Dudziak, N. Bézay, T. Schwientek, H. Clausen, H. Kunz, A. Liese, *Tetrahedron*, **2000**, *56*, 5865 – 5869.

[5] G. A. Winterfeld, Y. Ito, T. Ogawa, R. R. Schmidt, *Eur. J. Org. Chem.* **1999**, 1167 – 1171.

[6] C. M. Timmers, S. C. M. Wigchert, M. A. Leeuwenburgh, G. A. van der Marel, J. H. van Boom, *Eur. J. Org. Chem.* **1998**, 91 – 97.

[7] a) H. Paulsen, K. Adermann, *Liebigs Ann. Chem.* **1989**, 739 – 750; b) B. Lüning, T. Norberg, I. Tejbrant, *Glycoconjugate J.* **1989**, *6*, 5 – 19; c) L. Biondi, F. Filira, M. Gobbo, B. Scolaro, R. Rocchi, F. Cavaggion, *Int. J. Pept. Protein Res.* **1991**, *37*, 112 – 121; d) M. Gommer, H. Kunz, *Synlett* **1991**, 593 – 595; e) L. Szabó, I. Ramza, C. Langdon, R. Polt, *Carbohydr. Res.* **1995**, *6*, 5 – 19; f) T. Vuljanic, K.-E. Bergquist, H. Clausen, S. Roy, J. Kihlberg, *Tetrahedron* **1996**, *52*, 7983 – 8000; g) M. Lenck, H. Kunz, *J. Prakt. Chem.* **1997**, 322 – 334; h) S. D. Kuduk, J. B. Schwarz, X.-T. Chen, P. W. Glunz, D. Sames, G. Ragupathi, P. O. Livingston, S. I. Danishefsky, *J. Am. Chem. Soc.* **1998**, *120*, 12474 – 12845.

[8] The NMR data of **14a**, **b** are in excellent agreement with the reported data in ref. [7]. However, varying optical rotation values were reported: **14a**: $[\alpha]_D^{25} = +88.0$ ($c = 0.3$, $CHCl_3$), ref. [7a]: $[\alpha]_D^{20} = +89.9$ ($c = 1$, $CHCl_3$), ref. [7d]: $[\alpha]_D^{22} = +82.3$ ($c = 1$, $CHCl_3$), ref. [7e]: $[\alpha]_D = +87.5$ ($c = 2$, $CHCl_3$), ref. [7f]: $[\alpha]_D^{23} = +74.4$ ($c = 1$, $CHCl_3$); **14b**: $[\alpha]_D^{25} = +61.5$ ($c = 0.2$, $CHCl_3$), ref. [7a]: $[\alpha]_D^{20} = +65.0$ ($c = 1.45$, $CHCl_3$), ref. [7b]: $[\alpha]_D^{20} = +90$ ($c = 0.4 - 0.7$, $CHCl_3$), ref. [7c]: $[\alpha]_D^{25} = +64$ ($c = 1.5$, $CHCl_3$), ref. [7d]: $[\alpha]_D^{22} = +75.8$ ($c = 1$, $CHCl_3$), Ref. [7e]: $[\alpha]_D = +59$ ($c = 0.5$, $CHCl_3$), ref. [7f]: $[\alpha]_D^{23} = +72$ ($c = 0.72$, $CHCl_3$), ref. [7g]: $[\alpha]_D^{23} = +63.7$ ($c = 1.0$, $CHCl_3$), ref. [7 h]: $[\alpha]_D^{23} = +90.6$ ($c = 1.55$, $CHCl_3$).

[9] S. Hanessian, P. Lavallee, *Can. J. Chem.* **1975**, *53*, 2975 – 2979; S. Hanessian, P. Lavallee, *Can. J. Chem.* **1977**, *55*, 562 – 565.

[10] T. J. Martin, R. R. Schmidt, *Tetrahedron Lett.* **1992**, *33*, 6123 – 6126; T. J. Martin, R. Brescello, A. Toepfer, R. R. Schmidt, *Glycoconjugate J.* **1993**, *10*, 16 – 25.

[11] a) B. Liebe, H. Kunz, *Angew. Chem.* **1997**, *109*, 629 – 631; *Angew. Chem. Int. Ed. Engl.* **1997**, *36*, 618 – 621; b) B. Liebe, H. Kunz, *Helv. Chim. Acta* **1997**, *80*, 1473 – 1482; c) J. B. Schwarz, S. D. Kuduk, X.-T. Chen, D. Sames, P. W. Glunz, S. J. Danishefsky, *J. Am. Chem. Soc.* **1999**, *121*, 2662 – 2673.

[12] **13b**: $[\alpha]_D^{25} = +35.5$ ($c = 2.5$, $CHCl_3$), ref. [11b]: $[\alpha]_D^{22} = +28.9$ ($c = 1.0$, MeOH), ref. [11c]: $[\alpha]_D^{23} = +36.7$ ($c = 1.04$, $CHCl_3$).

[13] **15a**: $[\alpha]_D^{25} = +88.8$ ($c = 1$, $CHCl_3$); ^{1}H NMR (600 MHz, $CDCl_3$): $\delta =$ 7.89 (d, $J = 7.5$ Hz, 2H; arom. H), 7.71 (t, $J = 7.7$ Hz, 2H; arom. H) 7.40 – 7.30 (m, 4H; arom. H), 5.45 (d, $^3J_{4,3} = 3.2$ Hz, 1H; 4a-H), 5.33 (d, $^3J_{4,3} = 2.6$ Hz, 1H; 4b-H), 5.21 – 5.17 (m, 2H; 3a-H, 3b-H) 4.88 (d, $^3J_{1,2} = 3.3$ Hz, 1H; 1a-H), 4.77 (d, $^3J_{1,2} = 3.5$ Hz, 1H; 1b-H), 4.55 – 4.42 (m, 4H; β-H, β'-H, 2a-H), 4.35 (t, $^3J_{5,6} = 6.6$, $^3J_{5,6'} = 5.6$ Hz, 1H; 5a-H), 4.28 – 4.23 (m, 3H; 5b-H, α-H, Fmoc-CH), 4.02 (dd, $^3J_{6,5} = 6.0$, $^2J_{6,6'} =$ 11.2 Hz, 1H; 6b-H), 3.95(s, 2H; Fmoc-CH_2), 3.83 (dd, $^3J_{6',5} = 7.0$, $^2J_{6',6} = 11.1$ Hz, 1H; 6b′-H), 3.77 (t, $^3J_{6,6'} = 9.6$ Hz, 1H; 6a-H), 3.34 (dd, $^3J_{6',5} = 5.0$, $^2J_{6',6} = 9.9$ Hz, 1H; 6a′-H), 2.14 – 1.86 (7s, 21H; 5 OAc, 2 NHAc); ^{13}C NMR (150.8 MHz, $CDCl_3$): $\delta = 174.0 - 172.0$ (8C), 145.3 – 121.0 (12C), 100.0 (1a-C), 99.1 (1b-C), 71.5 (Fmoc-CH_2), 70.1 (3a-C), 69.8 (3b-C), 69.3 (4a-C), 68.8 (2-C, 5a-C, 4b-C), 68.0 (5b-C), 67.4 (6a-C), 63.0 (6b-C), 57.7 (Fmoc-CH), 49.0 (2a-C), 48.7 (2b-C), 48.4 (α-C), 22.8, 22.7, 20.7 (2C), 20.5; MS (FAB): *m*/*z*: 966 $[M+Na]^+$, 988 $[M+2Na-H]^+$.

[14] M. T. Bilodeau, T. K. Park, S. Hu, J. T. Randolph, S. J. Danishefsky, P. O. Livingston, S. Zhang, *J. Am. Chem. Soc.* **1995**, *117*, 7840 – 7841.

[15] N. Mathieux, H. Paulsen, M. Meldal, K. Bock, *J. Chem. Soc. Perkin Trans. 1* **1997**, 2359 – 2368.

[16] **21b**: The ^{1}H NMR data are in excellent agreement with reported data in ref. [7b]. Again differences in the optical rotation values were found: $[\alpha]_D^{25} = +25.7$ ($c = 2$, $CHCl_3$), ref. [7b]: $[\alpha]_D^{21} = +67$ ($c = 0.4 - 0.7$, $CHCl_3$), ref. [7g]: $[\alpha]_D^{23} = +69.2$ ($c = 1$, $CHCl_3$).

[17] R. R. Schmidt, *Angew. Chem.* **1986**, *98*, 213 – 236; *Angew. Chem. Int. Ed. Engl.* **1986**, *25*, 212 – 235; R. R. Schmidt, W. Kinzy, *Adv. Carbohydr. Chem. Biochem.* **1994**, *50*, 21 – 213.

[18] S. J. Danishefsky, M. T. Bilodeau, *Angew. Chem.* **1996**, *108*, 1482 – 1522; *Angew. Chem. Int. Ed. Engl.* **1996**, *35*, 1380 – 1419.

[19] H. Paulsen, *Angew. Chem.* **1990**, *102*, 851 – 867; *Angew. Chem. Int. Ed. Engl.* **1990**, *29*, 823 – 839.

Barium Triphenylmethanide: An Examination of Anion Basicity**

Jacob S. Alexander and Karin Ruhlandt-Senge*

Interest in the organometallic compounds of calcium, strontium, and barium has focused mainly on those complexes with π-type ligands such as cyclopentadienyl, fluorenyl, and indenyl.[1a] In contrast, organometallic compounds of these metals with metal–C σ bonds have been relatively unexplored owing largely to their high reactivity.[2] The recently discovered utility of these compounds as polymerization initiators,[3] in the synthesis of functionalized polymers,[4] and in organic synthesis outlines the need for intensified investigation.[5] Examples of structurally characterized organometallic compounds with metal–C σ bonds are mainly focused on calcium, whereas strontium and barium compounds of this type are less well known.[1b] Structurally authenticated examples include the acetylides $[M(CCSiPh_3)_2([18]crown-6)]$ (M = Ca, Sr, Ba) published by our group.[6] Other examples include a barium derivative exhibiting a barium–alkenyl bond, and a barium compound bearing phosphonium dibenzylide anions.[7, 8]

Recent research in our laboratory has focused on the use of triphenylmethane as a hydrocarbon source. Previous work using the triphenylmethanide anion concentrated on alkali metals, and resulted in an array of monomeric species displaying contact ion pairs, in which the geometry around the anion is slightly removed from planarity.[9–13] Structurally authenticated examples of alkaline earth metal triphenylmethanides are limited to $[Mg(CPh_3)Br(OEt_2)_2]$.[14]

Our initial reaction scheme involved transamination in the presence of a crown ether, a synthetic method well proven for the above-mentioned acetylides [Eq. (1)].[6]

$$[Ba\{N(SiMe_3)_2\}_2(thf)_2] + 2\,HCPh_3 \xrightarrow{[18]crown\text{-}6,\ THF} [Ba(CPh_3)_2([18]crown\text{-}6)] + 2\,HN(SiMe_3)_2 \quad (1)$$

However, this reaction did not afford the target compound. Rather, the product of an ether-cleavage reaction was obtained, the novel heteroleptic vinyl ether amide **1** [Eq. (2)].

$$2\,[Ba\{N(SiMe_3)_2\}_2(thf)_2] + 4\,HCPh_3 \xrightarrow{[18]crown\text{-}6,\ THF} \underset{\mathbf{1}}{[\{Ba(C_{12}H_{23}O_6)N(SiMe_3)_2\}_2]} + 2\,HN(SiMe_3)_2 + 4\,HCPh_3 \quad (2)$$

Ring opening of the crown ether by a strongly basic anion is an undesirable but common side reaction. Compound **1** is a rare example of structural verification of the event and allows rationalization of the mechanism of its formation (see Figure 1).

Considering the species involved in this reaction, it was proposed that after the deprotonation of the triphenylmethane by the bis(bis-silylamide) a transient metal–carbon bond is formed with the barium center, thus preventing the planarization of the ligand at the central carbon atom. From this favorable position, the very reactive quasi-pyramidal anion readily deprotonates the crown ether, which leads to the regeneration of the triphenylmethane and to the formation of the observed product.

The pK_a values of the amide $^-N(SiMe_3)_2$ and of the Ph_3C^- ions are very similar and indicate that either anion could be responsible for the deprotonation of the crown ether, but the reproducible isolation of $HCPh_3$ indicates the involvement of Ph_3C^- in this deprotonation reaction. This argument is further supported by the vivid red color of the solution, which indicates the intermittent formation of the Ph_3C^- ion. This result supports previous work by Bradley et al. who, on the basis of ^1H NMR spectroscopic results, propose cleavage of the crown ether in its reaction with the barium amide $[Ba\{N(SiMe_3)_2\}_2(thf)_2]$ in THF under release of the amine $HN(SiMe_3)_2$.[23]

Previous work by Power et al. has shown that coordinatively saturating the cation to form a charge-separated species would induce the formation of a resonance-stabilized planar triphenylmethanide ion.[15] It can be assumed that such stabilization reduces the basic character of the anion, thus preventing ether scission. These grounds prompted the use of hexamethylphosphoramide (HMPA) in addition to the crown ether to afford such a complex. Utilization of this route, however, also gave the cleaved ether product **1**. It was not until the recently available dibenzylbarium was used as a starting material that the reaction afforded the desired product, the monomeric barium triphenylmethanide compound **2** [Eq. (3)].[18]

$$Ba(C_7H_7)_2 + 2\,HCPh_3 \xrightarrow[HMPA]{[18]crown\text{-}6,\ THF} \underset{\mathbf{2}}{[Ba(CPh_3)_2([18]crown\text{-}6)(HMPA)_2]} + 2\,C_7H_8 \quad (3)$$

It is probable that the larger difference in the pK_a value of the benzyl anion and the amide allows a larger thermodynamic drive toward an irreversible reaction with triphenylmethane, while the small difference in the pK_a values between the amide and triphenylmethane allows possible frequent proton exchanges and consequently leads to the cleavage of the crown ether.[22]

The barium centers in **1** are seven-coordinate (Figure 1); the coordination sphere of each Ba atom is filled by two μ_2-oxo bridges, four oxygen atoms from the ether, and the amide ligand. The bridging oxygen atoms are slightly asymmetric with metal–oxo distances of 2.611 Å and 2.573 Å, a Ba1-O1-Ba1A bridging angle of 105.32°, and a O1-Ba1-O1A angle of 74.68°. The distances between the metal center and the ether oxygen atoms increase slightly moving along the chain (2.860–2.954 Å). These slightly elongated distances are reasonable when compared with those of known compounds with less ring strain. The Ba–N distance of 2.714 Å, and the

[*] Prof. Dr. K. Ruhlandt-Senge, J. S. Alexander
Department of Chemistry
1-014 Center for Science and Technology
Syracuse University
Syracuse, NY 13244-4100 (USA)
Fax (+1) 315-443-4070
E-mail: kruhland@syr.edu

[**] This work was supported by the National Science Foundation (CHE-9702246). Purchase of the X-ray Diffractometer was made possible with grants from the NSF (CHE-95-27898), the W. M. Keck Foundation, and Syracuse University.

  1433-7851/01/4014-2658 $ 17.50+.50/0

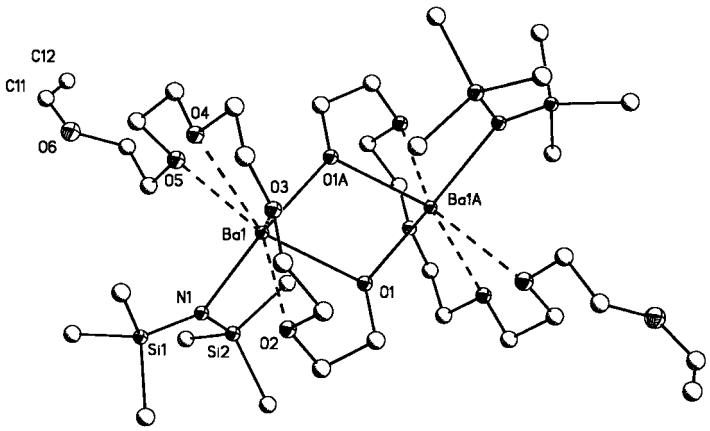

Figure 1. Structure of **1** (anisotropic displacement parameters of non-carbon atoms depict 30% probability; hydrogen atoms are omitted for clarity).

C11–C12 double-bond length of 1.294 Å are unexceptional. The Ba–Ba distance of 4.122 Å belies any metal–metal interaction.

The structure analysis of **2** reveals a charge-separated barium triphenylmethanide (Figure 2). The dication is surrounded by [18]crown-6 and two HMPA molecules. The barium atom resides on a crystallographic center of symmetry,

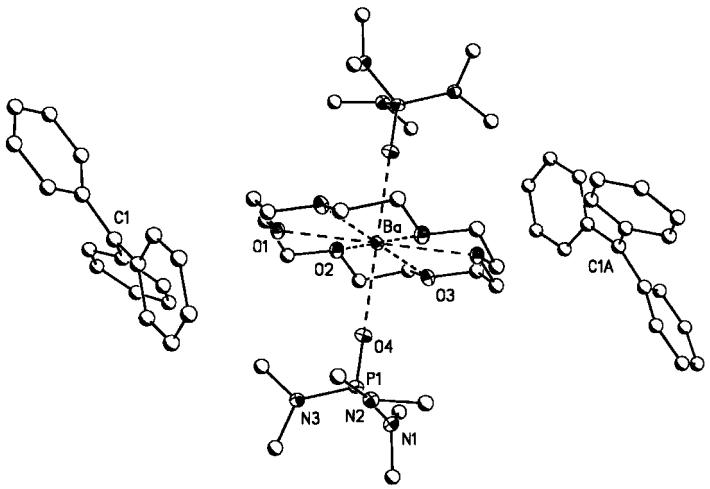

Figure 2. Structure of **2** (anisotropic displacement parameters of non-carbon atoms depict 30% probability; hydrogen atoms are omitted for clarity).

and lies in the center of the ether ring with an average Ba–O distance of 2.785 Å. The O donors of the HMPA molecules are 2.587 Å from the metal. Of particular interest is the environment around the anionic center. The planar conformation of the anion resembles that of the anion in separated structure of $[Li([12]crown\text{-}4)_2][CPh_3]$, while the central atoms of the contact ion pairs exhibit slight (0.05–0.1 Å) deviations from planarity, lending credence to resonance stability in **2**.[15] The phenyl rings in **2** adopt the familiar propeller geometry with angles of 35.6°, 32.7°, and 24.9°, as well as an average torsion angle of 31.1°. These values agree well with those reported earlier as well as that predicted by calculations (35 ± 2°).[16] The bond lengths from the central carbon are noteworthy; the C1–C2 distance of 1.445 is slightly shorter than the C1–C8 and C1–C14 distances of 1.464, but is not unexpected considering this phenyl group is oriented closest to planarity to give maximum orbital overlap. The sp^2 character of the anionic center is clearly indicated with little deviation from 120°.

In summary, we present two novel barium organometallic compounds with distinct structural characteristics. While the exact mechanistic rationale for the formation of these interesting compounds is still under intense scrutiny, we are certain that a combination of anion basicity as well as the choice of appropriate starting material is critical. Recent results for the calcium and strontium congeners have confirmed this to be the case.[24]

Experimental Section

All reactions were performed under vigorous exclusion of water and oxygen. The compounds $[Ba\{N(SiMe_3)_2\}_2(thf)_2]$ and $Ba(C_7H_7)_2$ were prepared by literature methods.[17, 18] All reagents and solvents were purified by standard procedures.

1: Solutions were prepared of $[Ba\{N(SiMe_3)_2\}_2(thf)_2]$ (0.8 g, 1.4 mmol), Ph_3CH (0.72 g, 3.0 mmol), and [18]crown-6 (0.4 g, 1.54 mmol) each in THF (25 mL). The amide solution was subsequently cooled to −80 °C and triphenylmethane added dropwise. After the mixture had been cooled, the crown ether was added dropwise and the solution was stirred at −80 °C for two hours. The pale yellow solution was allowed to warm slowly to room temperature, turning ruby red at about 0 °C. The red solution, resulting from some contamination by the vibrant trityl anion, was filtered, concentrated, and layered with hexane. This solution was stored at −20 °C and colorless crystals formed overnight. M.p. 88–89 °C; yield: 0.32 g, (57.0%); ^{1}H NMR (300 MHz, 25 °C, [D$_6$]benzene): $\delta = 0.45$ (s, 36H; $SiMe_3$), 3.00, 3.10, 3.19, 3.34, 3.52, 3.59, 3.82, 3.93, 4.19 (t, cleaved crown), 3.97 (d; OCHCH_2), 6.41 (dd; OCHCH$_2$); ^{13}C NMR (300 MHz, 25 °C, [D$_6$]benzene): $\delta = 6.97$ ($SiMe_3$), 63.30, 67.05, 68.10, 69.58, 70.01, 70.17, 70.61, 70.90, 77.22, 87.04 (cleaved [18]crown-6), 87.40 (OCHCH_2), 152.24 (OCHCH$_2$).

2: Three 100 mL Schlenk flasks were charged with dibenzylbarium (0.43 g, 1.0 mmol), PH_3CH (0.48 g, 2.0 mmol), and [18]crown-6 (0.27 g, 1.0 mmol) and cooled to −80 °C. Subsequently, THF (15 mL) was added to each flask. The triphenylmethane solution was added slowly to the dibenzylbarium solution followed by HMPA (0.4 mL, 2.1 mmol), affording a bright red solution. The crown ether was added and the solution was stirred at −80 °C for three hours, the volume was reduced, and the solution stored at −20 °C. Dark red crystals formed within 12 h. M.p. 158–160 °C; yield: 0.54 g, (35.9%); ^{1}H NMR (300 MHz, 25 °C, [D$_8$]THF): $\delta = 3.42$ (m, 32H; [18]crown-6, THF), 1.58 (8H; THF), 2.42 (d, 36H; HMPA), 7.06–7.11 (m, 30H; Ph_3C); ^{13}C NMR (300 MHz, 25 °C, [D$_8$]THF): $\delta = 37.27$ (HMPA), 71.82 ([18]crown-6), 127.12 (*p*-C), 129.14 (*m*-C), 130.42 (*o*-C), 132.0 (CC_6H_5), 145.24 (CC_6H_5).

Crystal structure analyses: **1**: $BaC_{18}H_{41}NO_6Si_2$, $M_r = 561.04$, triclinic, space group $P\bar{1}$, $a = 10.2359(9)$, $b = 11.1793(10)$, $c = 12.5402(11)$ Å, $\alpha = 83.299(2)$, $\beta = 69.827(2)$, $\gamma = 87.176(1)°$, $V = 1337.7(2)$ Å^3, $T = 94(2)$ K, $Z = 2$, $\mu = 1.602$ mm^{-1} ($Mo_{K\alpha}$ radiation); colorless blocks $0.40 \times 0.30 \times 0.20$ mm^3; 6047 independent reflections ($3.5 \le 2\theta \le 56.58°$); $R_1 = 0.0338$ ($I > 2\sigma(I)$), w$R_2 = 0.0909$ (all data). **2**: $BaC_{70}H_{106}N_6O_{10}P_2$, $M_r = 1390.89$, monoclinic, space group $P2_1/n$, $a = 12.8699(9)$, $b = 21.1572(14)$, $c = 13.3671(9)$ Å, $\beta = 100.855(1)°$, $V = 3574.6(4)$ Å^3, $T = 94(2)$ K, $Z = 2$, $\mu = 0.659$ mm^{-1}($Mo_{K\alpha}$ radiation); red blocks $0.40 \times 0.20 \times 0.10$ mm^3; 6288 independent reflections ($3.6 \le 2\theta \le 50.00°$); $R_1 = 0.0447$ ($I > 2\sigma(I)$), w$R_2 = 0.1208$ (all data). The crystals were mounted on the diffractometer as described previously,[19] and the data were collected using a Bruker SMART system (CCD detector).[20] Both crystal structures were solved by using direct methods and were refined by full-matrix least-squares refinement on F^2.[21] All non-hydrogen atoms were refined anisotropically. Crystallographic data (excluding structure factors) for the structures reported in this paper have been deposited with the Cambridge Crystallographic Data Centre as supple-

mentary publication no. CCDC-157686 and CCDC-157687. Copies of the data can be obtained free of charge on application to CCDC, 12 Union Road, Cambridge CB2 1EZ, UK (fax: (+44) 1223-336-033; e-mail: deposit @ccdc.cam.ac.uk).

Received: February 14, 2001 [Z16613]

[1] a) T. P. Hanusa, *Acc. Chem. Res.* **1993**, *93*, 1023; b) T. P. Hanusa, *Coord. Chem. Rev.* **2000**, *210*, 329, and references therein.
[2] For example: a) G. E. Coates, M. L. H. Green, K. Wade, *Organometallic Compounds*, *Vol. 1*, Methuen, London, **1969**; b) S. T. Ioffe, A. N. Nesmeyanov, *The Organo Compounds of Magnesium, Beryllium, Calcium, Strontium, and Barium*, North Holland, Amsterdam, **1967**.
[3] a) L. C. Tang, C. Mathis, B. Francois, *J. Organomet. Chem.* **1983**, *243*, 359; b) B. De Groof, M. Van Beulen, M. Szwarc, *Macromolecules* **1975**, *8*, 396; c) B. De Groof, W. Morteier, M. Van Beulen, M. Szwarc, *Macromolecules* **1977**, *10*, 598.
[4] R. A. O'Brien, T. Chen, R. D. Rieke, *J. Org. Chem.* **1992**, *57*, 2667.
[5] a) A. Yanagisawa, S. Habaue, K. Ysaue, H. Yamamoto, *J. Am. Chem. Soc.* **1994**, *116*, 6130; b) A. Yanagisawa, K. Ogasawara, K. Ysaue, H. Yamamoto, *Chem. Commun.* **1996**, 367, and references therein.
[6] D. C. Green, U. Englich, K. Ruhlandt-Senge, *Angew. Chem.* **1999**, *111*, 365; *Angew. Chem. Int. Ed.* **1999**, *38*, 354.
[7] M. Westerhausen, M. H. Diesger, H. Nöth, T. Seifert, A. Pfitzner, *J. Am. Chem. Soc.* **1998**, *120*, 6722.
[8] S. Harder, M. Lutz, *Organometallics* **1997**, *16*, 225.
[9] J. J. Brooks, G. D. Stucky, *J. Am. Chem. Soc.* **1972**, *94*, 7333.
[10] R. A. Bartlett, H. V. R. Dias, P. P. Power, *J. Organomet. Chem.* **1988**, *341*, 1.
[11] H. Koster, E. Weiss, *J. Organomet. Chem.* **1979**, *168*, 273.
[12] D. Hoffman, W. Bauer, P. von R. Schleyer, U. Pieper, D. Stalke, *Organometallics* **1993**, *12*, 1193.
[13] H. Viebrock, T. Panther, U. Behrens, E. Weiss, *J. Organomet. Chem.* **1995**, *491*, 19.
[14] L. M. Engelhardt, S. Harvey, C. L. Raston, A. H. White, *J. Organomet. Chem.* **1988**, *341*, 39.
[15] M. M. Olmstead, P. P. Power, *J. Am. Chem. Soc.* **1985**, *107*, 2174.
[16] R. Hoffmann, R. Bissell, D. Farnum, *J. Phys. Chem.* **1969**, *73*, 1789.
[17] B. A. Vaartstra, J. C. Huffman, W. E. Streib, K. G. Caulton, *Inorg. Chem.* **1991**, *30*, 121.
[18] A. Weeber, S. Harder, H. H. Brintzinger, K. Knoll, *Organometallics* **2000**, *19*, 1325.
[19] H. Hope, *Progr. Inorg. Chem.* **1994**, *41*, 1.
[20] S. Chadwick, K. Ruhlandt-Senge, *Chem. Eur. J.* **1998**, *4*, 1768.
[21] G. M. Sheldrick, SHELXTL Version 5, Siemens Analytical X-ray Instruments, Madison, WI, **1994**.
[22] A reviewer noted that utilization of hydrocarbons as solvent should suppress the cleavage reaction, considering the sparing solubility of the dibenzylbarium. However, this advantage is offset by the difficulties introduced by a heterogenous reaction system.
[23] D. C. Bradley, M. B. Hursthouse, A. A. Ibrahim, K. M. Abdul Malik, M. Motevalli, R. Moseler, H. Powell, J. D. Runnacles, A. C. Sullivan, *Polyhedron* **1990**, *9*, 2959.
[24] J. S. Alexander, K. Ruhlandt-Senge, unpublished results.

Dicyclopenta[*a*,*d*]cyclooctene: A [14]Annulene Containing Two Zero-Atom Cross-Links**

Mitsunori Oda,* Yukinari Sakamoto, Takanori Kajioka, Takuya Uchiyama, Ryuta Miyatake, and Shigeyasu Kuroda*

The insertion of two zero-atom cross-links between the carbon atoms of the hypothetical all-*cis*-[14]annulene (**1**) provides many types of (benzenoid and non-benzenoid) tricyclic hydrocarbons of the formula $C_{14}H_{10}$, depending on the site of the linkages. With constitutional restriction limited

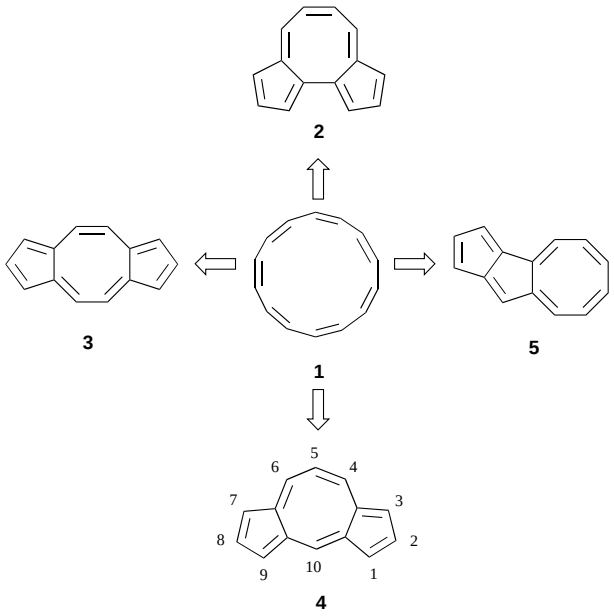

to the production of five- and eight-membered rings, four nonalternant hydrocarbons are formed: dicyclopentacyclooctenes **2**–**4** and cyclooctapentalene (**5**).[1] Compared to alternant benzenoid isomers, such as anthracene and phenanthrene, very little is known about these relatively small parent nonalternant hydrocarbons. Prinzbach and co-workers reported on attempts to synthesize the [*a*,*c*]isomer **2**,[2] and Hafner et al. published the synthesis of the 2,7-di(*tert*-butyl) derivative (**6**) of the [*a*,*e*]isomer **3**.[3] Hydrocarbon **6** has a planar structure and diamagnetic character and, most notably, exhibits the

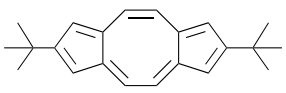

6

[*] Dr. M. Oda, Prof. Dr. S. Kuroda, Y. Sakamoto, Dr. T. Kajioka, T. Uchiyama, Dr. R. Miyatake
Department of Applied Chemistry, Faculty of Engineering
Toyama University
Gofuku 3190, Toyama 930-8555 (Japan)
Fax: (+81) 76-445-6819
E-mail: oda@eng.toyama-u.ac.jp
kuro@eng.toyama-u.ac.jp

[**] This work was financially supported by a Grant-in-Aid for Scientific Research (no. 09640631 to M.O. and no. 10640513 to S.K.) from the Ministry of Education, Science, Culture and Sports, Japan

  1433-7851/01/4014-2660 $ 17.50+.50/0

longest wavelength absorption maximum ($\lambda_{max} = 1375$ nm) observed for hydrocarbons with a 14π conjugated system. Here we present the synthesis and spectroscopic properties of the [*a*,*d*]isomer **4**, the first parent of this class of nonalternant hydrocarbons.

Our synthetic strategy for **4** is based on 14π-electrocyclization[4, 5] across the two pentafulvenoid moieties of the precursor 6-dimethylamino-1-{2-(pentafulven-6-yl)ethenyl}-pentafulvene (**8**), with formation of the central eight-membered ring, and subsequent deamination (Scheme 1). This approach is analogous to the azulene synthesis developed by Hafner and Ziegler.[6]

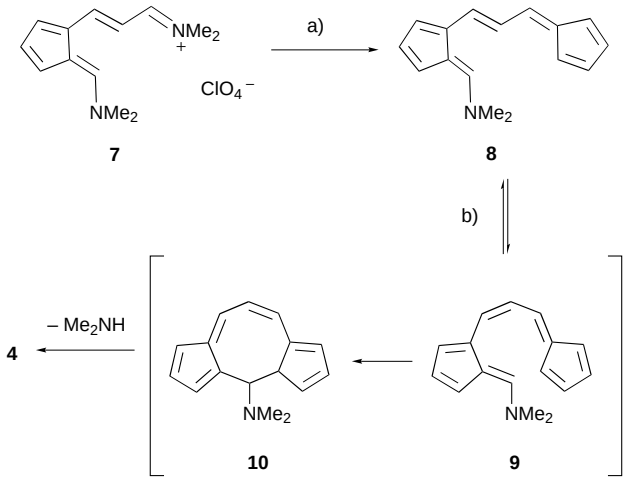

Scheme 1. Synthesis of **4**. a) Sodium cyclopentadienide, THF, 0 °C, 15 min, 63 %; b) reflux in 2,6-lutidine, 90 min, 2 %.

The precursor **8** was prepared by reaction of sodium cyclopentadienide and 6-dimethylamino-1-(3-dimethylimino-1-propenyl)pentafulvene perchlorate (**7**)[7] in 63 % yield. The pentafulvene **8**, isolated as green plates, is stable in the solid state and in solution below 100 °C; decomposition is observed over 150 °C. Thermal electrocyclization of **8** to **4** under reflux in hydrocarbon, alcohol, and ether solvents in a range of 150 – 250 °C was unsuccessful and gave only gummy dark-colored material, independent of the concentration of **8**.[8] Reactions in DMF or in basic solvents such as pyridine, picoline, and quinoline gave **4** in yields of less than 1 %. The best yield of 2 % was obtained upon reaction in 2,6-lutidine at reflux temperature. Product **4** was isolated as red-purple leaflets after chromatography on silica gel and recrystallization from methanol/water.

The ^{1}H and ^{13}C NMR spectra of **4** (see the Experimental Section) document the double-bond delocalization in the periphery of the ring system and, thus, the diamagnetic property of the compound. Six distinct ^{1}H NMR signals and eight ^{13}C NMR signals indicate the molecular symmetry of **4**, which bears a C_2 axis through C-5 and C-10. The $^3J_{HH}$ coupling constants also confirm the 14π electron delocalization. For example, two triplets for H-2 (or H-8) and H-5 in the ^{1}H NMR spectrum directly evidence two sets of equal coupling constants between ^3J(H-1,H-2)/^3J(H-8,H-9) and ^3J(H-2,H-3)/^3J(H-7,H-8) and between ^3J(H-4,H-5) and ^3J(H-5,H-6). The average ^{1}H chemical shift ($\delta = 7.64$) of **4** is comparable to that of azulene ($\delta = 7.64$)[9] and is larger than that of naphthalene ($\delta = 7.48$),[10] indicating the appreciable diamagnetic nature of **4**.

The UV/Vis spectrum of **4** shows the longest wavelength maximum at 767 nm, which is about 600 nm less than that of **6**. Figure 1 shows correlations of frontier molecular orbitals

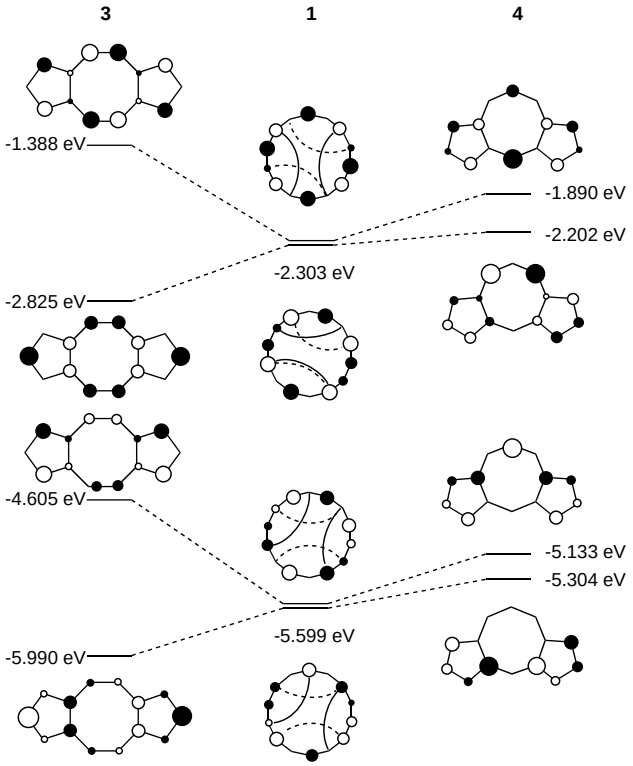

Figure 1. Correlations of frontier molecular orbitals between [14]annulene (**1**) and dicyclopentacyclooctenes **3** and **4** based on calculations at the MB3LYP/6-31G* level of theory. The broken and solid curves in **1** are the cross-links required to form **3** and **4**, respectively.

between [14]annulene (**1**) and dicyclopentacyclooctenes **3** and **4** based on calculations at the MB3LYP/6-31G* level of theory.[11] The annulene **1** has a doubly degenerate HOMO and LUMO; the pair of orbitals forming the HOMO correlate to the HOMO and the HOMO−1 of **3** and **4**, and those forming the LUMO correlate to the LUMO and the LUMO+1 of **3** and **4**. As indicated in Figure 1, **3** has a destabilized HOMO and a stabilized LUMO, whereas **4** has a destabilized HOMO and a slightly destabilized LUMO relative to **1**. Thus **4** should absorb longer wavelength light upon excitation than **1** and much shorter wavelength light than **3**. Although all-*cis*-[14]annulene (**1**) is unknown, its geometrical isomer, dehydro[14]annulenes, and bridged [14]annulenes have been synthesized. Among them, those with a planar structure and without transannular interaction across the bridge[12–16] show the longest wavelength maxima at 558 – 633 nm in their UV/Vis spectra; these values are indeed lower than that observed for **4**. Since the crystals of **4** obtained so far were not suitable for X-ray crystallographic analysis, we are currently focusing on synthesizing simple derivatives for this purpose.

  1433-7851/01/4014-2661 $ 17.50+.50/0

Experimental Section

8: Compound **7** (30.3 g, 0.1 mol) was added to a stirred solution of sodium cyclopentadienide (0.1 mol) in THF (600 mL) at 0 °C under nitrogen atmosphere. After the mixture was stirred at 0 °C for 15 min, solids were formed and removed by suction filtration through a celite pad. The solids and celite were washed with ethyl acetate/hexane (1/4), and the filtrate was concentrated under vacuum. The residual solids were purified by recrystallization from CH_2Cl_2/hexane (1/2) to give **8** as green plates (14.0 g, 63 % yield). M.p. 145 – 147 °C; ^{1}H NMR (400 MHz, $CDCl_3$): $\delta = 3.29$ (s, 6H; NCH_3), 6.26 (dt, $J = 5.0$, 1.7, 1H), 6.45 (ddm, $J = 5.0$, 3.1 Hz, 1H), 6.54 (ddm, $J = 5.0$, 3.1 Hz, 1H), 6.58 (ddm, $J = 4.6$, 2.9 Hz, 1H), 6.67 (dm, $J =$ 5.0 Hz, 1H), 6.73 (dm, $J = 4.6$ Hz, 1H), 6.89 (dm, $J = 2.9$ Hz, 1H), 6.99 (d, $J = 12.4$ Hz, 1H), 7.00 (d, $J = 14.4$ Hz, 1H), 7.19 (dd, $J = 14.4$, 12.4 Hz, 1H), 7.41 (s, 1H); ^{13}C NMR (100 MHz, $CDCl_3$, −30 °C): $\delta = 40.7$, 48.0, 114.0, 117.7, 118.9, 119.7, 121.4, 124.5, 129.2, 130.9, 131.4, 134.5, 141.2, 142.3, 147.6; IR (KBr): $\tilde{\nu} = 1623$, 1580, 1359, 1055 cm^{-1}; elemental analysis calcd for $C_{16}H_{17}N$: C 86.06, H 7.69, N 6.27; found: C 85.97, H 7.72, N 5.99.

4: A solution of **8** (1.00 g, 4.48 mmol) in 2,6-lutidine (200 mL) was refluxed under nitrogen atmosphere for 90 min. The solvent was removed under vacuum. The dark-colored solids were suspended in hexane (50 mL), and insoluble black solids were removed by filtration. The filtrate was concentrated with an evaporator, and the residue was purified by chromatography on silica gel with hexane as eluent to provide **4** as a dark red solid (16.5 mg, 2 % yield). An analytical sample of **4** as red-purple leaflets was obtained by recrystallization from methanol/water (7/1). M.p. 139 – 140 °C; ^{1}H NMR (400 MHz, $CDCl_3$): $\delta = 6.58$ (d, $J = 11.6$ Hz, 2H; H-4,6), 7.37 (t, $J = 4.0$ Hz, 2H; H-2, 8), 7.59 (dd, $J = 4.0$, 1.6 Hz, 2H; H-3,7), 7.71 (dd, $J = 4.0$, 1.6 Hz, 2H; H-1,9), 7.94 (t, $J = 11.6$ Hz, 1H; H-5), 8.64 (s, 1H; H-10); ^{13}C NMR (100 MHz, $CDCl_3$): $\delta = 113.7$ (C-5), 128.9 (C-2,8), 129.5 (C-8a, 9a), 133.3 (C-3a, 6a), 138.4 (C-3, 7), 139.4 (C-1, 9), 140.0 (C-4, 6), 141.2 (C-10); IR (KBr): $\tilde{\nu} = 1589$, 1413, 1396, 1192, 774, 749 cm^{-1}; MS (70 eV): m/z (%): 179 ($M^+ + 1$, 15), 178 (M^+, 100), 177 (26), 152 (31), 76 (21); UV/Vis (*n*-hexane): λ_{max} (ε) = 213 (15100), 218 (15000), 222 (15200), 238 sh (11000), 248 sh (7840), 273 sh (7760), 283 (9770), 290 sh (8320), 329 sh (38900), 344 (112000), 446 (1070), 468 sh (933), 498 sh (812), 531 (851), 608 (186), 631 (186), 649 (194), 663 (224), 677 (257), 692 sh (355), 701 (407), 718 (427), 737 (437), 750 (746), 767 (1290), 800 sh (36), 818 sh nm (12); elemental analysis calcd for $C_{14}H_{10}$: C 94.35, H 5.65; found: C 94.19, H 5.80.

Received: February 5, 2001 [Z16554]

[1] For theoretical studies on **3**, see M. E. Vol'pin, *Russ. Chem. Rev.* **1960**, *29*, 129 – 160; A. Toyota, *Bull. Chem. Soc. Jpn.* **1975**, *48*, 1152 – 1156; M. Randic, *J. Am. Chem. Soc.* **1977**, *99*, 444 – 450.

[2] O. Schweikert, T. Netscher, G. L. McMullen, L. Knothe, H. Prinzbach, *Chem. Ber.* **1984**, *117*, 2006 – 2026.

[3] K. Hafner, G. F. Thiele, C. Mink, *Angew. Chem.* **1988**, *100*, 1213 – 1215; *Angew. Chem. Int. Ed. Engl.* **1988**, *27*, 1191 – 1192.

[4] Examples of 14π-electrocyclization to construct conjugated medium-to-large sized ring systems are reported in ref. [2] and the following: E. Vogel, H. M. Deger, P. Helbel, P. Lex, *Angew. Chem.* **1980**, *92*, 943 – 944; *Angew. Chem. Int. Ed. Engl.* **1980**, *19*, 919 – 921; H. Prinzbach, H. Babsh, D. Hunkler, *Tetrahedron Lett.* **1978**, 649 – 652.

[5] For analogous 12π electrocyclization across two pentafulvenoid moieties, see K. Hafner, B. Stowasser, H.-P. Krimmer, S. Fischer, M. C. Böhm, H. J. Lindner, *Angew. Chem.* **1986**, *98*, 646 – 648; *Angew. Chem. Int. Ed. Engl.* **1986**, *25*, 630 – 632; K. Hafner, *Pure Appl. Chem.* **1990**, *62*, 531 – 540; T. S. Balaban, S. Schardt, V. Sturm, K. Hafner, *Angew. Chem.* **1995**, *107*, 360 – 363; *Angew. Chem. Int. Ed. Engl.* **1995**, *34*, 330 – 332.

[6] K. Ziegler, K. Hafner, *Angew. Chem.* **1955**, *67*, 301; K. Hafner, *Liebigs Ann. Chem.* **1957**, *606*, 79 – 89; K. Hafner, K.-P. Meinhardt, *Org. Synth.* **1984**, *62*, 134 – 139.

[7] "Carbocyclische p-Elektronen-Systeme": K.-P. Zeller, *Methoden Org. Chem.* (*Houben-Weyl*), *4th ed. 1952* –, Vol. 5, 2c, **1985**, p. 612.

[8] In the case of **8**, vapor-phase pyrolysis, photolysis, and radical cation cyclization with *N,N,N*-tris(4-bromophenyl)aminium hexachloroantimonate were unsuccessful.

[9] This value was obtained by measurements in $CDCl_3$ with a 400-MHz spectrometer. For previous NMR studies of azulenes, see ref. [7], p. 130; R. J. Llinas, D. Roard, M. Derbesy, E. J. Vincent, *Can. J. Chem.* **1967**, *53*, 2911 – 2916.

[10] M. Hesse, H. Meier, B. Zeeh, *Spectroscopic Methods in Organic Chemistry*, Thieme, Stuttgart, **1997**.

[11] The density functional calculations were carried out on an IBM RS/6000-397 computer using the MULLIKEN program (ver. 2.0.0, 1995, IBM Co.). The MB3LYP (MBecke3LYP) functional in MULLIKEN uses the local correlation function of Perdew and Wang instead of the Vosko, Wilk, and Nusair functional, and is very similar to Becke3LPY density by Stephens et al. For these functionals, see J. P. Perdew, Y. Wang, *Phys. Rev. B* **1992**, *45*, 13244 – 13249; S. H. Vosko, L. Wilk, M. Nusair, *Can. J. Phys.* **1980**, *58*, 1200 – 1211; P. J. Stephens, F. J. Devlin, C. F. Chabolowski, M. J. Frisch, *J. Phys. Chem.* **1994**, *98*, 11623 – 11627.

[12] J. Mayer, F. Sondheimer, *J. Am. Chem. Soc.* **1966**, *88*, 602 – 603.

[13] F. Sondheimer, Y. Gaoni, L. M. Jackman, N. A. Bailey, R. Mason, *J. Am. Chem. Soc.* **1962**, *84*, 4595 – 4596.

[14] R. H. Mitchell, V. Boekelheide, *J. Am. Chem. Soc.* **1974**, *96*, 1547 – 1557.

[15] V. Boekelheide, J. B. Phillips, *J. Am. Chem. Soc.* **1967**, *89*, 1695 – 1704.

[16] W. Huber, J. Lex, T. Meul, K. Müllen, *Angew. Chem.* **1981**, *93*, 401 – 402; *Angew. Chem. Int. Ed. Engl.* **1981**, *20*, 391 – 392.

Nonorthogonal Dilithium-1,3-biborataallenes Containing Planar-Tetracoordinate Carbon Atoms**

Yüksel Sahin, Michael Hartmann, Gertraud Geiseler, Dieter Schweikart, Christian Balzereit, Gernot Frenking, Werner Massa, and Armin Berndt*

Orthogonality ($\Theta = 90°$) of the planes of the terminal atoms of the allene skeleton and their neighbors, here referred to as "terminal planes", is a characteristic feature of allenes. Strong deviation from this orthogonality has been observed up to now only for an allene skeleton as part of a highly strained six-membered ring.[1] Almost orthogonal ($\Theta = 92°$)[2] terminal planes have also been found for the heteroallene **1** of the ion pair $\mathbf{1} \cdot Li \cdot 3Et_2O$ (Scheme 1),[2] where **1** contains four sterically demanding aryl substituents. Here we present contact-ion triples of **2a**, which is isoelectronic with **1**, and of related tetraaryl-1,3-diboratallenes **2b** – **d** and show their planes

[*] Prof. Dr. A. Berndt, Dr. Y. Sahin, Dr. M. Hartmann, G. Geiseler, Dr. D. Schweikart, Dr. C. Balzereit, Prof. Dr. G. Frenking, Prof. Dr. W. Massa
Fachbereich Chemie der Universität Marburg
35032 Marburg
Fax: (+49) 6421-2828917
E-mail: berndt@chemie.uni-marburg.de

[**] This work was supported by Deutsche Forschungsgemeinschaft and the Fonds der Chemischen Industrie.

  1433-7851/01/4014-2662 $ 17.50+.50/0

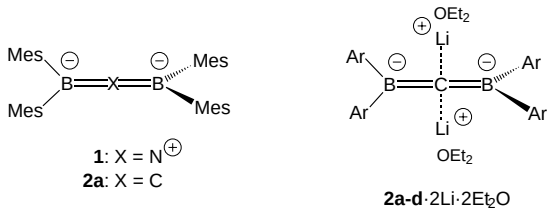

Scheme 1. Isoelectronic heteroallenes **1** and **2a** as well as contact-ion triples of the 1,3-diborataallenes **2a**–**d** (substituent key see Scheme 2).

deviate by up to 36° from orthogonality. The central carbon atoms in **2a**–**d**·2 Li·2 Et_2O are planar-tetracoordinate.[3–7]

The 1,3-diborataallenes **2a**–**d** were prepared analogously to **2e**[8] from anions **3a**–**c** and two equivalents of aryllithium compounds (Scheme 2). The NMR chemical shifts of the

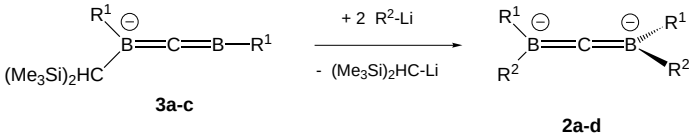

Scheme 2. Syntheses of 1,3-diborataallenes **2a**–**d** from 1-bora-3-borataallenes **3a**–**c** and aryllithium compounds LiR^2. Substituent key: **a**: $R^1 = R^2 = 2,4,6$-trimethylphenyl (mesityl, Mes); **b**: $R^1 = R^2 = 2,3,5,6$-tetramethylphenyl (duryl, Dur); **c**: $R^1 = R^2 = 2,6$-dimethyl-4-*tert*-butylphenyl; **d**: R^1 = Dur, $R^2 = 2,4,5$-trimethylphenyl; **e**: R^1 = Mes, R^2 = *tert*-butyl.

carbon atoms of their skeletons (Table 1) lie in the range characteristic for allenes. Figure 1 shows the crystal structures of **2b**·2 Li·2 Et_2O and **2d**·2 Li·2 Et_2O.[9] In Table 1 relevant experimental structure data of **2a**–**d** are compared to those calculated at the B3LYP level[10] for tetraphenyl- and tetra(*o*-methylphenyl)-1,3-diborataallenes, **2f** and **2g**, as well as for the unsubstituted 1,3-diborataallene **2h**.

The 1,3-diborataallenes **2a**–**d** form contact-ion triples each with two lithium cations which, in addition, are coordinated to one molecule of Et_2O. The atoms of the skeleton B=C=B are

Table 1. Selected NMR and structural data of contact-ion triples of **2a**–**e** (exp) and **2f**–**h** (calcd).

	$\delta(^{13}C)$ (CB_2)	$\delta^{11}B$	Θ [°]	Li-C-Li [°]	B-C-B [°]	$H_3C\cdots CH_3$[a] [pm]
2a·2 Li·2 Et_2O	205	26	124.9	174.9	179.4	346 346
2b·2 Li·2 Et_2O	206	28	119.0	176.2	177.2	334.1 337.2
2c·2 Li·2 Et_2O	205	27	125.8	177.1	179.2	347.3 342.4
2d·2 Li·2 Et_2O	215	27	96.7	174.5	176.3	373.7[b] 383.5[b]
2e·2 Li·2 Et_2O	180	32	97	120.1	168.4	585.1 401.9[c]
2f·2 Li·2 Me_2O	–	–	95.5	177.5	180.0	–
2f·2 Li	–	–	114.4	179.8	180.0	–
2g·2 Li	–	–	133.9	180.0	180.0	381.3
2h·2 Li	–	–	89.7	150.4	180.0	–

[a] Distance between *o*-methyl carbon atoms (see Figure 1 top). [b] Distance $H_3C\cdots C_o$-H between *o*-methyl carbon atoms and *o*-carbon atoms (see Figure 1 bottom). [c] Distance between methyl carbon atoms of *tert*-butyl groups at different boron atoms.

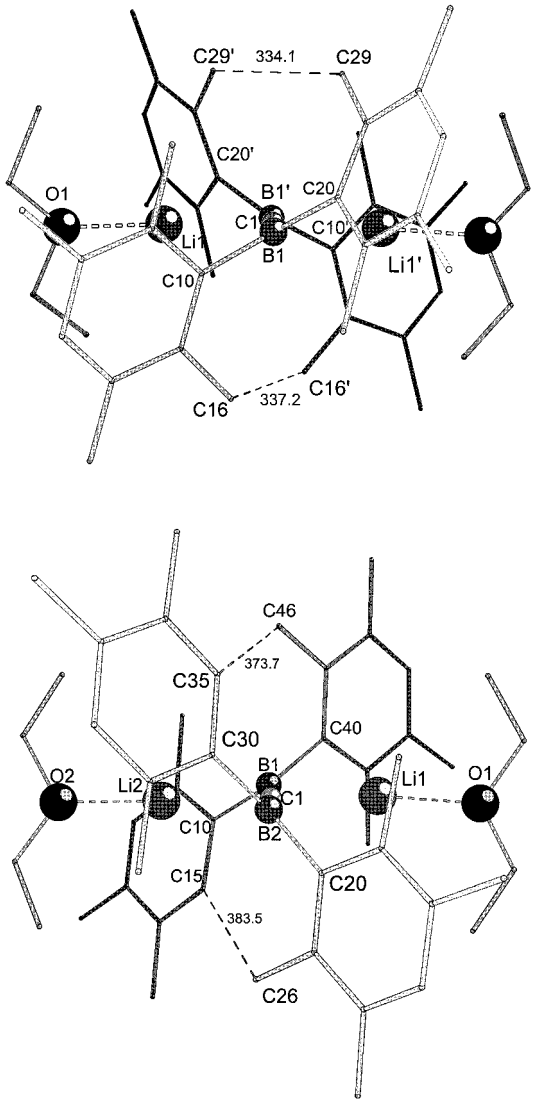

Figure 1. Crystal structures of **2b**·2 Li·2 Et_2O (top) and **2d**·2 Li·2 Et_2O (bottom). Selected bond lengths [pm] and angles [°] (completing Table 1). **2b**·2 Li·2 Et_2O: C1-B1 146.5(1), B1-C10 164.9(2), B1-C20 166.6(2), C1-Li1 206.1(2), B1-Li1 253.0(3), B1-Li1′ 252.5(3), O-Li1 193.9(2), C10-Li1 248.1(3), C20-Li1 276.3(3); C1-B1-C10 119.3(1), C1-B1-C20 127.1 (1), C10-B1-C20 113.4(1); **2d**·2 Li·2 Et_2O: C1-B1 145.8(7), C1-B2 146.8(7), B1-C10 162.0(8), B1-C40 162.9(7), B2-C20 162.9(7), B2-C30 161.7(6), C1-Li1 199.8(11), C1-Li2 205.2(11), B1-Li1 244.0(13), B1-Li2 243.8(10), B2-Li1 257.7(12), B2-Li2 253.6(14), O1-Li1 189.9(11), O2-Li2 190.3(10), C20-Li1 294(1), C40-Li1 256(2), C10-Li2 249(1), C30-Li2 275(1); C1-B1-C10 121.6(4), C1-B1-C40 122.8(4), C10-B1-C40 115.6(4), C1-B2-C20 124.6(4), C1-B2-C30 118.4(4), C20-B2-C30 117.0(4).

arranged almost linear (176–179°). The terminal planes C_i-B1-C_i and C_i-B3-C_i in **2a**–**d**·2 Li·2 Et_2O form angles of Θ = 125, 119, 126, and 97°, respectively, with each other, and thus, deviate considerably from orthogonality in **2a**–**c**·2 Li·2 Et_2O. The central carbon atoms of all four contact-ion triples **2a**–**d**·2 Li·2 Et_2O are surrounded by two boron atoms and two lithium ions in a planar arrangement. With Li-C-B angles close to 90°, they are—like Al_4C anions[11]—rare examples of species in which planar-tetracoordinate carbon atoms form angles of comparable size with all their neighbors.

The heteroallenes **2a**–**c** that deviate strongly from orthogonality have short nonbonding distances (334–347 pm, see

Table 1) between carbon atoms of *ortho*-methyl groups of aryl substituents, which are bound to different boron atoms and coordinated to different lithium ions (**2b**: C29 ··· C29′ and C16 ··· C16′). These distances are considerably shorter than the sum of the van der Waals radii of two methyl groups (400 pm).[12] Figure 1 reveals that these nonbonding distances would become even shorter, if the angle between the terminal planes decreased to approach 90°. The terminal planes of **2d** · 2 Li · 2 Et_2O deviate only by 7° from orthogonality. This can be explained by the lack of steric hindrance because two of the aryl groups of **2d** · 2 Li · 2 Et_2O bear only a hydrogen atom at an *ortho*-carbon atom. The distances of these *ortho*-carbon atoms to the carbon atoms of *ortho*-methyl groups of duryl substituents are considerably longer (374 and 384 pm) than those between *ortho*-methyl groups in **2a**–**c** · 2 Li · 2 Et_2O. Thus, steric hindrance plays an important role in the deviation from orthogonality in **2a**–**c** · 2 Li · 2 Et_2O. However, four aryl substituents each with two *ortho*-methyl groups *alone* are not sufficient to create strong distortions, as seen by the angle of $\Theta = 92°$ for **1**.[2] Evidently, interactions of the aryl rings with the lithium cations, which are absent in the solvent-separated ion pair **1** · Li · 3 Et_2O, play a decisive role in contact-ion triples **2a**–**c** · 2 Li_2 · 2 Et_2O.

This argumentation is supported by calculations at the B3LYP/6-31G(d) level for contact-ion triples of tetraphenyl-1,3-diborataallene **2f** with and without ether ligands at the lithium cations. A torsion angle of 95.5° is obtained for **2f** · 2 Li · 2 Me_2O, but a considerably larger angle of 114.4° for **2f** · 2 Li (Scheme 3). There are four short Li ··· C_i distances (250.0 ± 0.6 pm) in **2f** · 2 Li, but two significantly longer ones (260.1 pm) and two very long distances (271.3 pm) in **2f** · 2 Li_2 · 2 Me_2O. These differences can be explained by the well-known[13] decrease of the coordination ability of lithium cations versus π ligands by ether ligands. Since **2f** · 2 Li · 2 Me_2O without *ortho*-methyl substituents shows almost no deviation from orthogonality ($\Theta = 95.5°$), the strong deviations in contact-ion triples **2a**–**c** · 2 Li · 2 Et_2O must be due to steric hindrance; **2f** · Li_2 *without* coordinated ether molecules deviates considerably from orthogonality inspite of lacking steric hindrance. Adding steric hindrance to ether-free contact-ion triples of dilithium tetraaryl-1,3-diborataallenes leads to even stronger deviations from orthogonality: a torsion angle of 133.9° is calculated for **2g** · 2 Li (Scheme 3).

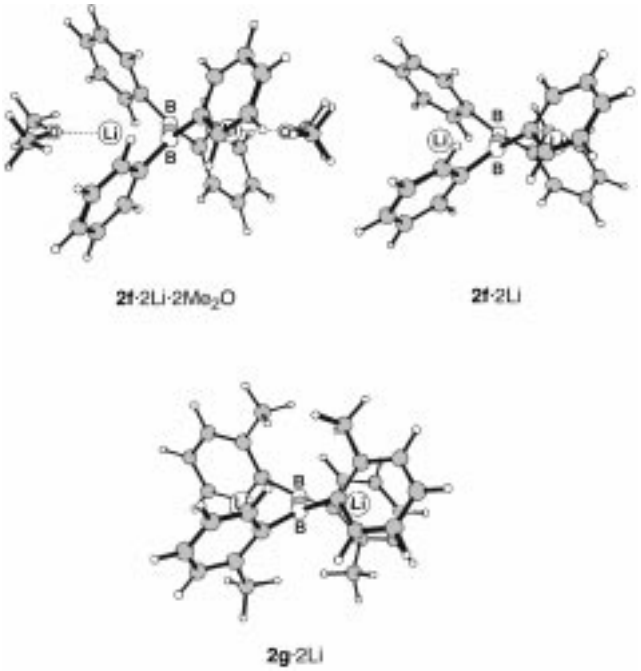

Scheme 3. Calculated structures for contact-ion triples from tetraphenyl- and tetra-(*o*-methylphenyl)-1,3-diborataallenes **2f** and **2g** and two lithium ions *without* (top right and bottom) and *with* dimethyl ether ligands (top left).

Calculations[10] also show that 1,3-diborataallenes are considerably easier to distort than isoelectronic allenes.[14] According to our calculations, planarization requires 43.6 kcal mol^{-1} for unsubstituted allene but only 24.7 kcal mol^{-1} for unsubstituted 1,3-diborataallene **2h**. Even smaller energies are calculated for the contact-ion triples **2h** · 2 Li · 2 Me_2O and **2h** · 2 Li: 20.4 and 15.3 kcal mol^{-1}, respectively (Scheme 4).[15]

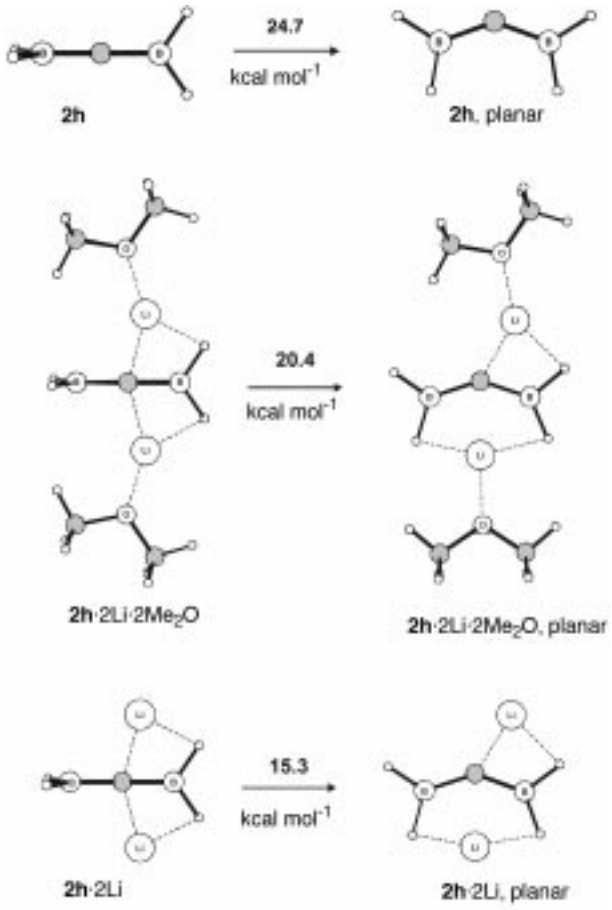

Scheme 4. Energies for the planarization of unsubstituted 1,3-diborataallene **2h** (top) and its contact-ion triples with two lithium ions *without* (bottom) and *with* (center) dimethyl ether ligands.

In conclusion, the strong deviations from orthogonality in dilithium-1,3-diborataallenes **2a**–**c** · 2 Li · 2 Et_2O are due to the following effects: distortion towards planarity requires less energy in 1,3-diborataallene than in allene, and interaction of the lithium cations with the π electrons of the

  1433-7851/01/4014-2664 $ 17.50+.50/0

arylsubstituents leads to steric hindrance between *ortho*-methyl groups of aryl substituents bound to different boron atoms.

Received: January 22, 2001
Revised: April 5, 2001 [Z16476]

[1] T. Shimizu, F. Hojo, W. Ando, *J. Am. Chem. Soc.* **1993**, *115*, 3111. For detection of six-membered allenes as reactive intermediates see: M. Christl, S. Groetsch, *Eur. J. Org. Chem.* **2000**, 1871, and references therein.

[2] R. A. Bartlett, H. Chen, H. V. R. Dias, M. M. Olmstead, P. P. Power, *J. Am. Chem. Soc.* **1988**, *110*, 446; IR characterization of tBu$_2$B=N=BtBu$_2\cdot$Li$\cdot$2TMEDA: H. Nöth, H. Prigge, *Chem. Ber.* **1987**, *120*, 907.

[3] The allene skeleton of a ditungsten complex of unsubstituted allene containing a planar tetracoordinate central carbon atom is strongly bent (141°), the "terminal planes" H-C-H are orthogonal with respect to the C-C-C plane. However, these planes do not lie in the *same* plane: R. H. Cayton, S. T. Chacon, M. H. Chisholm, M. J. Hampden-Smith, J. C. Huffman, K. Folting, P. D. Ellis, B. A. Huggins, *Angew. Chem.* **1989**, *101*, 1547; *Angew. Chem. Int. Ed. Engl.* **1989**, *28*, 1523; S. T. Chacon, M. H. Chisholm, K. Folting, J. C. Huffman, M. J. Hampden-Smith, *Organometallics* **1991**, *10*, 3722.

[4] The central carbon atom of the contact-ion triple **2e**$\cdot$2Li$\cdot$2Et$_2$O of 1,3-dimesityl-1,3-di-*tert*-butyl-1,3-diborataallene **2e**,[8] in contrast, is surrounded in a distorted tetrahedral manner.

[5] For molecules containing planar-tetracoordinate carbon atoms surrounded by two lithium cations and two carbon atoms, see ref. [6], for those with transition metals as neighbors, see ref. [7].

[6] K. Ruhlandt-Senge, J. J. Ellison, R. J. Wehmschulte, F. Pauer, P. P. Power, *J. Am. Chem. Soc.* **1993**, *115*, 11353.

[7] D. Röttger, G. Erker, *Angew. Chem.* **1997**, *109*, 840; *Angew. Chem. Int. Ed. Engl.* **1997**, *36*, 812; G. Erker, *Chem. Soc. Rev.* **1999**, *28*, 307; R. Choukroun, P. Cassoux, *Acc. Chem. Res.* **1999**, *32*, 494.

[8] M. Pilz, J. Allwohn, R. Hunold, W. Massa, A. Berndt, *Angew. Chem.* **1988**, *100*, 1421; *Angew. Chem. Int. Ed. Engl.* **1988**, *27*, 1370.

[9] Crystal structure determinations: **2a**$\cdot$2Li$\cdot$2Et$_2$O: Owing to bad crystal quality and severe disorder of ether molecules the actual results of X-ray structure analyses are not yet satisfactory ($R = 0.12$). Thus, only a few preliminary geometrical data are included here. **2b**$\cdot$2Li$\cdot$2Et$_2$O: A colorless crystal ($0.60 \times 0.45 \times 0.25$ mm) was investigated at 193 K on an IPDS area-detector system (Stoe) using Mo$_{K\alpha}$ radiation. $C_{49}H_{72}B_2Li_2O_2$, monoclinic, space group $C2/c$, $Z = 4$, $a =$ 2179.8(1), $b = 935.03(4)$, $c = 2199.4(1)$ pm, $\beta = 97.750(7)°$, $V =$ 4441.7×10^{-30} m^3, $\rho_{calcd} = 1.090$ Mg m^{-3}. A total of 16991 reflections were collected up to $\theta = 26°$, 4324 unique ($R_{int} = 0.031$), 2972 with $I > 2\sigma(I)$. The structure was solved by direct methods and refined against all F^2 data by full-matrix least-squares methods with H atoms "riding" on calculated positions; $wR_2 = 0.1013$ for all reflections, $R = 0.0374$ for the observed ones. **2c**$\cdot$2Li$\cdot$2Et$_2$O$\cdot$3toluene: A light-yellow crystal ($0.55 \times 0.30 \times 0.12$ mm) was investigated at 193 K on an IPDS area-detector system (Stoe) using Mo$_{K\alpha}$ radiation. $C_{78}H_{112}B_2Li_2O_2$, monoclinic, space group $P2_1/c$, $Z = 4$, $a = 1819.4(7)$, $b = 2645.7(4)$, $c =$ 1695.0(4) pm, $\beta = 117.4(4)°$, $V = 7242 \times 10^{-30}$ m^3, $\rho_{calcd} = 1.025$ Mg m^{-3}. A total of 40229 reflections were collected up to $\theta = 24.1°$, 11144 unique ($R_{int} = 0.114$), 3365 with $I > 2\sigma(I)$. The structure was solved by direct methods and refined against all F^2 data by full-matrix least-squares methods with H atoms "riding" on calculated positions; $wR_2 = 0.247$ for all reflections, $R = 0.0795$ for the observed ones. The modest quality may be attributed to the weak scattering power of the crystal and strong disorder of the three toluene molecules, which were refined using split-atom positions. **2d**$\cdot$2Li$\cdot$2Et$_2$O: A light-yellow crystal ($0.30 \times 0.30 \times 0.20$ mm) was investigated at 193 K on an IPDS area-detector system (Stoe) using Mo$_{K\alpha}$ radiation. $C_{47}H_{68}B_2Li_2O_2$, orthorhombic, space group $Pca2_1$, $Z = 4$, $a = 1585.6(1)$, $b = 1553.2(1)$, $c = 1829.6(1)$ pm, $V = 4505.3 \times 10^{-30}$ m^3, $\rho_{calcd} = 1.033$ Mg m^{-3}. A total of 24410 reflections were collected up to $\theta = 24.15°$, 7088 unique ($R_{int} = 0.121$), 2893 with $I > 2\sigma(I)$. The structure was solved by direct methods and refined against all F^2 data by full-matrix least-squares methods with H atoms "riding" on calculated positions; $wR_2 = 0.1760$ for all reflections, $R = 0.0605$ für the observed ones. Crystallographic data (excluding structure factors) for the structures reported in this paper have been deposited with the Cambridge Crystallographic Data Centre as supplementary publication no. CCDC-156101 (**2b**$\cdot$2Li$\cdot$2Et$_2$O), CCDC-156102 (**2c**$\cdot$2Li$\cdot$2Et$_2$O), and CCDC-156103 (**2d**$\cdot$2Li$\cdot$2Et$_2$O). Copies of the data can be obtained free of charge on application to CCDC, 12 Union Road, Cambridge CB2 1EZ, UK (fax: (+44) 1223-336-033; e-mail: deposit@ccdc.cam.ac.uk).

[10] a) All geometries were optimized by using the B3LYP hybrid functional with a 6-31G(d) basis set. For the calculation of the structures and rotational barriers of the 1,3-diborataallenes **2h**, **2h**$\cdot$2Li, and **2h**$\cdot$2Li$\cdot$2OMe$_2$ it was necessary to augment the basis set with diffuse functions at the havier atoms 6-31+G(d). All structures were characterized to be local minima or transition states by calculating the vibrational frequencies. b) Gaussian 98 (Revision A.7), M. J. Frisch, G. W. Trucks, H. B. Schlegel, G. E. Scuseria, M. A. Robb, J. R. Cheeseman, V. G. Zakrzewski, J. A. Montgomery, R. E. Stratmann, J. C. Burant, S. Dapprich, J. M. Millam, A. D. Daniels, K. N. Kudin, M. C. Strain, O. Farkas, J. Tomasi, V. Barone, M. Cossi, R. Cammi, B. Mennucci, C. Pomelli, C. Adamo, S. Clifford, J. Ochterski, G. A. Petersson, P. Y. Ayala, Q. Cui, K. Morokuma, D. K. Malick, A. D. Rabuck, K. Raghavachari, J. B. Foresman, J. Cioslowski, J. V. Ortiz, B. B. Stefanov, G. Liu, A. Liashenko, P. Piskorz, I. Komaromi, R. Gomperts, R. L. Martin, D. J. Fox, T. Keith, M. A. Al-Laham, C. Y. Peng, A. Nanayakkara, C. Gonzalez, M. Challacombe, P. M. W. Gill, B. G. Johnson, W. Chen, M. W. Wong, J. L. Andres, M. Head-Gordon, E. S. Replogle, J. A. Pople, Gaussian, Inc., Pittsburgh, PA, **1998**; c) A. D. Becke, *J. Chem. Phys.* **1993**, *98*, 1372; A. D. Becke, *J. Chem. Phys.* **1993**, *98*, 5648; d) C. Lee, W. Yang, R. G. Parr, *Phys. Rev. B* **1988**, *37*, 785.

[11] X. Li, H.-F. Zhang, L.-S. Wang, G. D. Geske, A. I. Boldyrev, *Angew. Chem.* **2000**, *112*, 3776; *Angew. Chem. Int. Ed.* **2000**, *39*, 3630, and references therein.

[12] L. Pauling, *The Nature of the Chemical Bond*, 3rd ed., Cornell University Press, Ithaca, NY, **1973**.

[13] For the effect of n-ligands on the strength of interactions between lithium cations and π ligands, see: D. Scheschkewitz, M. Menzel, M. Hofmann, P. von R. Schleyer, G. Geiseler, W. Massa, K. Harms, A. Berndt, *Angew. Chem.* **1999**, *111*, 3116; *Angew. Chem. Int. Ed.* **1999**, *38*, 2936, and references therein.

[14] H. F. Bettinger, P. R. Schreiner, P. von R. Schleyer, H. F. Schaefer III, *J. Phys. Chem.* **1996**, *100*, 16147. The rotational barrier of the unsubstituted allene was calculated to be 44.6 or 45.5 kcal mol^{-1} depending on the level of calculation used.

[15] Exact handling of the biradical singlet character of this species requires a multideterminant procedure. The rotational barriers of this work are based on open-shell B3LYP calculations which, according to reference [14], are sufficient to determine such barriers.

  1433-7851/01/4014-2665 $ 17.50+.50/0

Synthesis and Structure of a Dimeric Alkyldibariumtriszincate with a Tetraanionic Triszincate Ligand and a Unique Central $Ba_4Zn_2C_6$ Moiety**

Matthias Westerhausen,* Christian Gückel, and Peter Mayer

The interest in molecules with Ba–C σ bonds has risen over the years,[1] although the structural proof of a dialkylbarium compound is still lacking.[2] Already many years ago, it was expected[3] that the alkyl compounds of the heavy alkaline earth metals would represent a valuable expansion of the series of organometallic reagents. The application of dibenzylbarium as a polymerization initiator serves as an example,[4] however, here as in other benzyl compounds,[5] side-on-bonded benzyl anions should be present. Even though barocenes are a well-documented substance class,[6] there are only very few examples of σ-bonded organyl groups.[2] Bis(triphenylsilylethynyl)barium was structurally characterized after complexation of the metal atoms with crown ethers.[7] A dimeric alkenylbarium phospholide[8] contains a central planar Ba_2C_2 cycle. Furthermore, the coordination of carbenes at barocenes leads to molecules with Ba–C bonds,[9] on the other hand the carbene adducts of barium bis[bis(trimethylsilyl)amide] dissociate in solution.[10] Barium zincates were investigated many years ago[11] because they are useful polymerization catalysts for isoprene.[12] Through the activation of barium metal, we have recently transmetalated bis(trimethylsilylmethyl)zinc and thereby isolated barium bis[tris(trimethylsilylmethyl)zincate] (**1**).[13] In toluene or THF the corresponding solvate adducts of barium bis[tris(trimethylsilylmethyl)zincate] were isolated, whereas from aliphatic hydrocarbons the coligand-free derivative was obtained.[13] Even by using ultrasound no further transmetalation was observed. But if this zincate suspension in heptane reacts with additional distilled barium metal under application of ultrasound of high energy, the color of the solution turns red and the precipitation of elemental zinc is observed. Cooling of this solution yields colorless crystals of compound **2** and tetramethylsilane can be detected in the reaction solution by NMR spectroscopy (Scheme 1).

These drastic reaction conditions lead to a further transmetalation of the tris(trimethylsilylmethyl)zincate anions and to the formation of bis(trimethylsilylmethyl)barium **A**. This reactive compound, which is not detectable in solution, immediately metalates a methylene group of zincate anions still present in solution. The resulting dianion again metalates a methylene group of the zincate anion. Finally, the triszincate tetraanion forms, which precipitates from heptane in the form of the dimeric barium salt shown in Scheme 2. Tetramethylsilane was detected in the solution; however, there were no indications of the development of hydrogen gas.

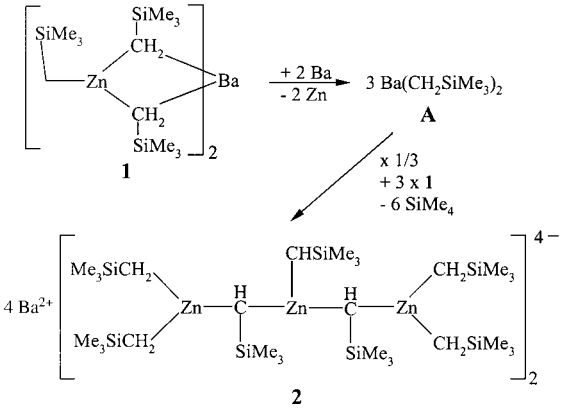

Scheme 1. Synthesis of **2** by transmetalation of barium bis[tris(trimethylsilylmethyl)zincate] with barium.

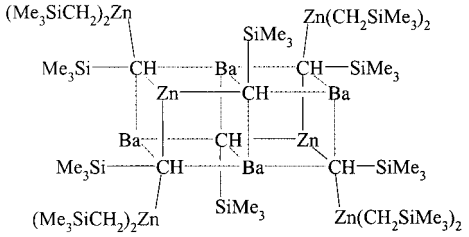

Scheme 2. Constitution of compound **2**.

The molecular structure[14] of compound **2** is easily understood starting from the central $Ba_4Zn_2C_6$ cage, which can be regarded as a distorted double cube with a common Ba_2C_2 face. This structure is depicted in Figure 1; the central structural moiety is highlighted. On the one hand distortions

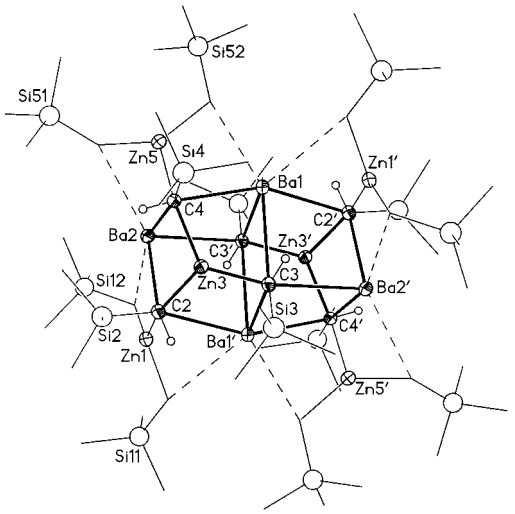

Figure 1. Molecular structure of **2**. The ellipsoids represent a probability of 60%, the Si atoms were drawn with arbitrary radii. The atoms generated by inversion symmetry are marked with primes. Selected bond lengths [pm]: Ba1-C2′ 299.4(4), Ba1-C3 320.0(4), Ba1-C3′ 286.2(4), Ba1-C4 289.8(3), Ba2-C2 283.6(3), Ba2-C3′ 302.8(3), Ba2-C4 299.0(4), Zn3-C2 213.0(4), Zn3-C3 207.0(3), Zn3-C4 211.2(4).

[*] Prof. Dr. M. Westerhausen, C. Gückel, Dr. P. Mayer
Department Chemie der Ludwig-Maximilians-Universität München
Butenandtstrasse 9 (Haus D), 81377 München (Germany)
Fax: (+49) 89-2180-7867
E-mail: maw@cup.uni-muenchen.de

[**] This research was supported by the Deutsche Forschungsgemeinschaft and the Fonds der Chemischen Industrie. We are also grateful to Prof. Dr. P. Klüfers and Dr. H. Piotrowski for their kind assistance.

  1433-7851/01/4014-2666 $ 17.50+.50/0

are induced by the nearly trigonal-planar environment of Zn3 (angle sum $\Sigma(CZnC) = 357.6^\circ$), on the other hand the Ba–C bonds are clearly longer than the Zn–C bonds.

This dimeric alkyldibarium triszincate is also remarkable in that this compound represents only the second structurally characterized example of a geminal biszincated alkane.[15] In this molecule several carbon atoms show an unusual high coordination number; the coordination spheres of C2 (Ba1′, Ba2, Si2, Zn1, Zn3, and H2), C3 (Ba1, Ba1′, Ba2′, Si3, Zn3, and H3), and C4 (Ba1, Ba2, Si4, Zn3, Zn5, and H4) are distorted octahedra. The hydrogen atoms at these carbon centers were refined isotropically without restraints. These large coordination numbers as well as the anionic charges partly located on neighboring atoms lead to very large Zn–C bond lengths of up to 215 pm (Zn5–C4), an elongation of approximately 20 pm in comparison to the Zn–C bond in dialkylzinc.[16] Figure 2 shows the tetraanionic tris(zincate) ligand of **2**; to clarify the distorted octahedral coordination of the carbanionic centers, the bonds to the barium atoms are shown as thin lines. In contrast to the Zn–C bonds the Si–C distances show no dependency on the coordination number of the corresponding carbon atoms. An expected elongation of the Si–C bonds of the hypervalent C atoms is compensated by the electrostatic attraction between the carbanions and the silicon atoms.

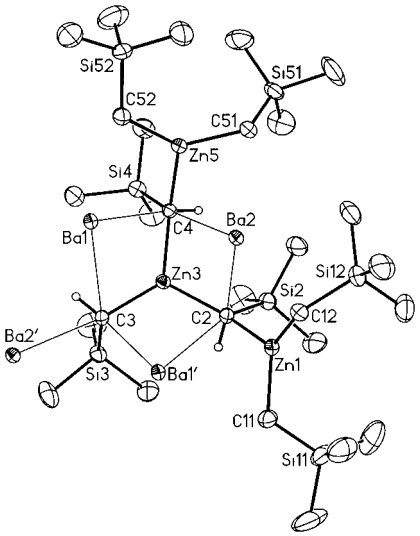

Figure 2. Structure and coordination behavior of the tetraanionic tris(zincate) ligand of **2**. The ellipsoids represent a probability of 50%, the H atoms at C2, C3, and C4 are shown with arbitrary radii and were refined isotropically. Selected bond lengths [pm] and angles [°]: Zn1-C11 202.6(4), Zn1-C12 206.3(4), Zn1-C2 214.0(4), C2-Si2 185.5(4), C2-H2 103(4), Zn3-C2 213.0(4), Zn3-C3 207.0(3), Zn3-C4 211.2(4), C3-Si3 184.3(3), C3-H3 100(5), C4-Si4 185.2(4), C4-H4 95(4), Zn5-C4 215.2(3), Zn5-C51 203.3(4), Zn5-C52 203.6(4); C11-Zn1-C12 122.1(2), C11-Zn1-C2 110.6(2), C12-Zn1-C2 124.2(2), C2-Zn3-C3 118.4(2), C2-Zn3-C4 113.2(1), C3-Zn3-C4 126.0(2), C4-Zn5-C51 112.2(2), C4-Zn5-C52 117.8(2), C51-Zn5-C52 127.9(2).

The Ba–C bond lengths within the $Ba_4Zn_2C_6$ cage vary between 283.6 (Ba2–C2) and 320.0 pm (Ba1–C3). The coordination spheres of the barium atoms are completed by agostic bonds to methylene groups (symbolized as broken lines in Figure 1). The shortest Ba–C bonds lie in the range of σ bonds, for example, in the crown ether complex of barium bis(triphenylsilylacetylide) (285 pm)[7] and in the dimeric alkenylbarium phospholide (288 and 307 pm).[8] Significantly longer Ba–C bonds are found in the barium bis[tris(trimethylsilylmethyl)zincates].[13]

The preparation of **2** proves that the transmetalation of zincates offers a strategy for the synthesis of alkylbarium compounds. Owing to the high reactivity of dialkylbarium, zincate anions that are still present in solution are metalated immediately, which leads finally to the above-mentioned tetraanion. The structure contains a centrosymmetric $Ba_4Zn_2C_6$ double cage as the central moiety, in which carbon atoms with unusual coordination numbers of 6 are present. Long Zn–C distances occur owing to the high negative charges.

Experimental Section

All experiments were carried out under an argon atmosphere. The solvents were dried according to common procedures and distilled under argon, deuterated solvents were degassed and saturated with argon. The distillation of barium was performed according to a literature procedure.[17] The NMR spectra were recorded on Jeol GSX-270 and EX-400 spectrometers, positive signs describe low field shifts. Melting points were determined from compounds which were sealed under argon in capillaries.

Barium bis[tris(trimethylsilylmethyl)]zincate (**1**) (1.04 g, 1.31 mmol), prepared from bis(trimethylsilylmethyl)zinc (0.94 g, 3.92 mmol) and distilled barium (0.28 g, 2.03 mmol), was dissolved in heptane (20 mL). Distilled barium (0.30 g, 2.18 mmol) was added to this solution under the argon atmosphere. The solution was stirred continually for seven days under simultanous treatment with ultrasound (Branson Sonifier W-450 with a titanium resonator), during which time the solution turned red. The excess barium and precipitated zinc metal were then removed. The solution was reduced to half of the original volume. Cooling to $+4\,^\circ C$ yielded colorless crystals of **2** (0.64 g, 0.60 mmol; 76%) within a few days. M.p. 195 °C (decomp; carbonization). ^1H NMR (C_6D_6): $\delta = -0.65$ (brs; CH_2), 0.20–0.37 (m; $SiMe_3$), an unambiguous assignment of the CH groups was not possible; $^{13}C\{^1H\}$ NMR (C_6D_6): $\delta = 3.50$ (brs; $SiMe_3$), 7.68 (brs; CH_2), further signals were neither detectable at high nor at low temperatures; IR: $\tilde{\nu} = 1582$ m, 1473 w, 1437 w, 1384 sh, 1373 w, 1353 sh, 1287 sh, 1245 vs, 1165 vw, 1132 vw, 1096 vw, 1051 w, 1023 w, 930 s, 856 vs, 838 sh, 829 sh, 745 s, 718 sh, 697 sh, 685 sh, 513 w, 480 w, 465 sh, 424 sh, 363 w, 347 w, 319 sh; elemental analysis (%) calcd ($C_{28}H_{74}Ba_2Si_7Zn_3$, 1078.32): C 31.18, H 6.92; found: C 30.87, H 6.91.

Received: February 8, 2001 [Z16578]

[1] a) B. G. Gowenlock, W. E. Lindsell, *J. Organomet. Chem. Libr.* **1977**, *3*, 1; b) W. A. Wojtczak, P. F. Fleig, M. J. Hampden-Smith, *Adv. Organomet. Chem.* **1996**, *40*, 215.
[2] T. P. Hanusa, *Coord. Chem. Rev.* **2000**, *210*, 329.
[3] J. J. Eisch, R. B. King, *Organometallic Synthesis*, *Vol. 2*, Academic Press, New York, **1981**, p. 101.
[4] A. Weeber, S. Harder, H. H. Brintzinger, K. Knoll, *Organometallics* **2000**, *19*, 1325.
[5] a) M. G. Gardiner, C. L. Raston, H. Viebrock, *Chem. Commun.* **1996**, 1795; b) S. Harder, M. Lutz, *Organometallics* **1997**, *16*, 225.
[6] a) P. Jutzi, *J. Organomet. Chem.* **1990**, *400*, 1; b) T. P. Hanusa, *Polyhedron* **1990**, *9*, 1345; c) T. P. Hanusa, *Chem. Rev.* **1993**, *93*, 1023; d) D. J. Burkey, T. P. Hanusa, *Comments Inorg. Chem.* **1995**, *17*, 41; e) M. L. Hays, T. P. Hanusa, *Adv. Organomet. Chem.* **1996**, *40*, 117; f) A. J. Bridgeman, *J. Chem. Soc. Dalton Trans.* **1997**, 2887; g) P. Jutzi, *Chem. Unserer Zeit* **1999**, *33*, 342; h) P. Jutzi, *Chem. Rev.* **1999**, *99*, 969.
[7] D. C. Green, U. Englich, K. Ruhlandt-Senge, *Angew. Chem.* **1999**, *111*, 365; *Angew. Chem. Int. Ed.* **1999**, *38*, 354.

  1433-7851/01/4014-2667 $ 17.50+.50/0

[8] M. Westerhausen, M. H. Digeser, H. Nöth, T. Seifert, A. Pfitzner, *J. Am. Chem. Soc.* **1998**, *120*, 6722.
[9] A. J. Arduengo, F. Davidson, R. Krafczyk, W. J. Marshall, M. Tamm, *Organometallics* **1998**, *17*, 3375.
[10] W. A. Herrmann, C. Köcher, *Angew. Chem.* **1997**, *109*, 2257; *Angew. Chem. Int. Ed. Engl.* **1997**, *36*, 2162.
[11] a) H. Gilman, L. A. Woods, *J. Am. Chem. Soc.* **1945**, *67*, 520; b) H. Gilman, A. H. Haubein, G. O'Donnell, L. A. Woods, *J. Am. Chem. Soc.* **1945**, *67*, 922; c) F. Kaufmann, A. Geraudelle, B. Kaempf, F. Schué, A. Deluzarche, A. Maillard, *J. Organomet. Chem.* **1970**, *24*, 13; d) Y. Kawakami, Y. Yasuda, T. Tsuruta, *Bull. Chem. Soc. Jpn.* **1971**, *44*, 1164.
[12] F. Kaufmann, S. Alev, A. Collet, F. Schué, B. Kaempf, A. Deluzarche, *Eur. Polym. J.* **1976**, *12*, 209.
[13] M. Westerhausen, C. Gückel, T. Habereder, M. Vogt, M. Warchhold, H. Nöth, *Organometallics* **2001** *20*, 893.
[14] Crystal structure determination of **2**: $C_{56}H_{148}Ba_4Si_{14}Zn_6$, 2156.62 g mol^{-1}, triclinic, space group $P\bar{1}$, $a = 1397.7(1)$, $b = 1421.9(2)$, $c = 1445.6(1)$ pm, $\alpha = 98.85(1)$, $\beta = 110.37(1)$, $\gamma = 108.89(1)^\circ$, $V = 2.4304(4)$ nm^3, $Z = 1$, $T = 200(2)$ K, $3.6 < 2\theta < 51.8^\circ$, colorless platelet, $0.25 \times 0.15 \times 0.07$ mm, $\rho = 1.474$ g cm^{-3}, $\mu = 3.244$ mm^{-1}, numerical absorption correction ($T_{min}/T_{max} = 0.579/0.814$), 17137 reflections, 8753 independent reflections ($R_{int} = 0.0271$), 6775 observed reflections ($I > 2\sigma(I)$), 373 parameters, w$R_2 = 0.0589$ (all reflections, on F^2), $R_1 = 0.0355$ (all reflexes, on F^2), $R_1 = 0.0216$ (observed reflections), goodness-of-fit $s = 0.923$. Residual electron density: 597/ − 700 e nm^{-3}. Crystallographic data (excluding structure factors) for the structure reported in this paper have been deposited with the Cambridge Crystallographic Data Centre as supplementary publication no. CCDC-157452. Copies of the data can be obtained free of charge on application to CCDC, 12 Union Road, Cambridge CB2 1EZ, UK (fax: (+44) 1223-336-033; e-mail: deposit@ccdc.cam.ac.uk).
[15] The first structural proof of a geminal biszincated alkane was described by Andrews and co-workers: P. C. Andrews, C. L. Raston, B. W. Skelton, A. H. White, *Organometallics* **1998**, *17*, 779.
[16] a) M. Melnik, J. Skoršepa, K. Györyová, C. E. Holloway, *J. Organomet. Chem.* **1995**, *503*, 1; b) C. Eaborn, J. D. Smith, *Coord. Chem. Rev.* **1996**, *154*, 125; c) A. Almenningen, T. U. Helgaker, A. Haaland, S. Samdal, *Acta Chem. Scand. Ser. A* **1982**, *36*, 159; d) M. Westerhausen, B. Rademacher, *J. Organomet. Chem.* **1993**, *443*, 25.
[17] a) J. Evers, A. Weiss, E. Kaldis, J. Muheim, *J. Less-Common Met.* **1973**, *30*, 83; b) E. Kaldis, J. Muheim, J. Evers, A. Weiss, *J. Less-Common Met.* **1973**, *31*, 169; c) P. Ehrlich, H. J. Seifert in *Handbuch der Präparativen Anorganischen Chemie*, *Vol. 2* (Ed.: G. Brauer), 3rd ed., Enke, Stuttgart, **1978**, p. 917.

  1433-7851/01/4014-2668 $ 17.50+.50/0

Synthesis of a Nanoporous Polymer with Hexagonal Channels from Supramolecular Discotic Liquid Crystals**

Hyung-Kun Lee, Hyoyoung Lee, Young Ho Ko, Young Joo Chang, Nam-Keun Oh, Wang-Cheol Zin, and Kimoon Kim*

The design and synthesis of new materials with controlled nanostructures is a subject of intense research.[1, 2] Organic materials with ordered nanometer-sized pores have useful applications in such areas as separation and catalysis.[3] Recently, Gin and co-workers reported an elegant method for preparing nanoporous organic materials with regular channels that involved cross-linking amphiphilic monomers in lyotropic liquid crystalline phases.[4] They have also demonstrated that such materials are not only useful in preparing nanocomposites,[4d,e] but can also function as efficient heterogeneous catalysts.[4f,g]

Our interests in discotic liquid crystals[5] led us to synthesize supramolecular liquid crystalline materials with hexagonal columnar mesophases that were self-assembled from long-chain alkoxybenzoic acids and a benzotri(imidazole) core through formation of intermolecular hydrogen bonds.[6] Based on this work, we now report a simple and novel way to prepare nanoporous organic materials with hexagonal channels. In this method, a large, flat organic core of a polymerizable supramolecular discotic liquid crystal serves as a template and the ordered channels are easily created by removing the template core after formation of a cross-linked polymer matrix. To the best of our knowledge, the synthesis of nanoporous materials by this route has not been investigated.

The benzotri(imidazole) core **1**[7] and polymerizable alkoxybenzoic acid **2**[4c] form a 1:3 supramolecular complex (**3**; Scheme 1) through hydrogen-bonding interactions. The complex **3** shows a thermotropic liquid crystalline phase from 23.0 to 74.7 °C on heating,[8] which has been confirmed by differential scanning calorimetry, polarized optical microscopy, and

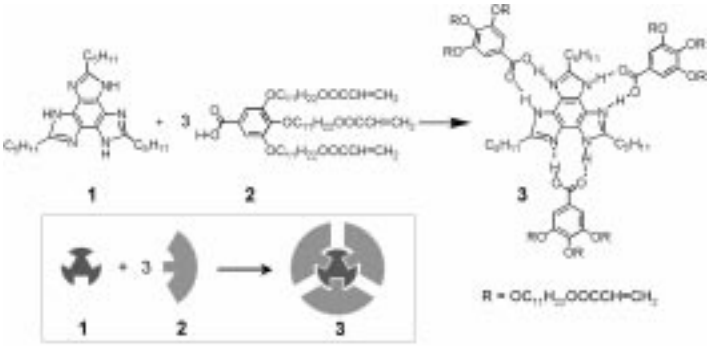

Scheme 1. Supramolecular discotic liquid crystal **3** formed from **1** and **2**.

X-ray diffraction studies. The X-ray diffraction study of **3** by using synchrotron radiation reveals first and second diffraction peaks at 33.5 and 19.4 Å, respectively, with a reciprocal spacing ratio of $1:\sqrt{3}$. This ratio is consistent with a hexagonal columnar (Col_h) mesophase with a lattice constant (or an intercolumnar distance) of 38.7 Å. A diffuse halo is observed in the wide-angle region at $2\theta = 20^\circ$ as a result of the liquidlike properties of the molten aliphatic chains.

Irradiation of **3** in a liquid crystalline phase with UV light induces polymerization of the acrylate moieties at the termini of the alkoxy chains to give **4** (Scheme 2). About 70 % of the acrylate moieties in **4** are estimated to be polymerized, as judged by FT-IR spectroscopic analysis.[9] The cross-linked polymer **4** maintains the hexagonal columnar structure with essentially the same lattice constants (Table 1).

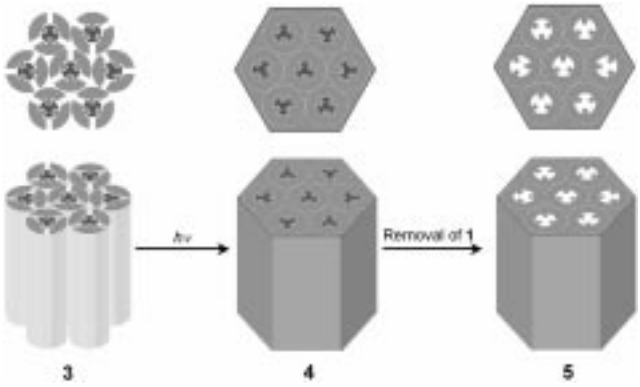

Scheme 2. Synthesis of nanoporous polymer **5** with hexagonal columnar channels from supramolecular discotic liquid crystal **3**.

Table 1. X-ray diffraction data of **3**, **4**, and **5**.

Compound	Temp.	*hkl*	d_{obs} [Å]	Mesophase parameter [Å]
3	60 °C	(100)	33.5	$a = 38.7$
		(110)	19.4	
		halo	4.4	
4	RT	(100)	33.4	$a = 38.6$
		(110)	19.3	
		halo	4.4	
5	RT	(100)	32.8	$a = 37.8$
		(110)	18.9	
		halo	4.3	

[*] Prof. K. Kim, Dr. H.-K. Lee, Dr. H. Lee, Dr. Y. H. Ko, Y. J. Chang
National Creative Research Initiative Center
for Smart Supramolecules
and
Department of Chemistry
Division of Molecular and Life Sciences
Pohang University of Science and Technology
San 31 Hyojadong, Pohang 790-784 (Republic of Korea)
Fax: (+82) 54-279-8129
E-mail: kkim@postech.ac.kr
N.-K. Oh, Prof. W.-C. Zin
Department of Materials Science and Engineering
Pohang University of Science and Technology
San 31 Hyojadong, Pohang 790-784 (Republic of Korea)

[**] We gratefully acknowledge the Korean Ministry of Science and Technology (Creative Research Initiative Program) for support of this work, and the Korean Ministry of Education (Brain Korea 21 program) for graduate studentships (H.-K.L. and Y.J.C). We also thank Dr. Y. S. Kang and Mr. J. H. Kim for gas permeability experiments and Prof. B. H. Sohn and Prof. P. K. Bharadwaj for helpful discussions. The X-ray diffraction measurements were performed at the Pohang Accelerator Laboratory (Beamline 3C2).

Supporting information for this article is available on the WWW under http://www.angewandte.com or from the author.

  1433-7851/01/4014-2669 $ 17.50+.50/0

Sonication of **4** in a mixture of methanol and 3 N HCl results in the removal of the benzotri(imidazole) core **1** from **4** to produce the porous polymer **5**. The removal of the benzotri(imidazole) core has been confirmed by ^{13}C cross-polarization magic-angle spinning (CP/MAS) NMR spectroscopy (Figure 1 a, b): the peak at $\delta = 118$ almost disappears and the

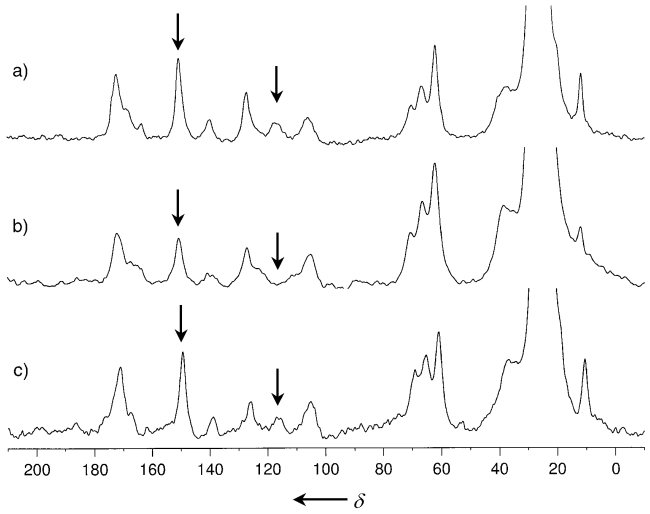

Figure 1. ^{13}C CP/MAS NMR spectra of a) **4**, b) **5**, and c) **4** reconstituted from **5** and **1**.

intensity of the signal at $\delta = 150$ decreases substantially. The former peak corresponds to the central benzene core of **1** and the latter corresponds to the imidazole carbon atom, the chemical shift of which overlaps with that of the carbonyl carbon atoms of the benzoate group in **5**. The amount of extracted benzotri(imidazole) core **1**, as determined by UV/Vis spectroscopy, indicates that approximately 90% of the core is removed from **4**.

Most importantly, the de-cored polymer **5** shows an X-ray diffraction pattern nearly identical to those of **3** and **4** (Table 1), which indicates that **5** maintains the same hexagonal columnar structure. Each of the columns in **5** has a channel with an effective diameter of about 10 Å. The reconstitution of the core is achieved by incubating **5** in a solution of **1** for 24 h. The ^{13}C CP/MAS NMR spectrum of the reconstituted sample shows that intensities of the signals at $\delta = 118$ and 150 are almost identical to those in **4**. The amount of reincorporated **1** is estimated to be 70–80% of that in **4**. On the other hand, the tri-N-methylated derivative of **1** is only slightly incorporated into the channels of **5** under similar conditions.[10] These results suggest that the porous polymer **5** effectively recognizes the original template **1**.

We have performed preliminary gas permeability measurements to demonstrate the porous nature of **5**. The N_2 gas permeability constant measured for a membrane of **5** is approximately $2 \times 10^{-9}\ cm^2\,s^{-1}\,cm^{-1}\,Pa^{-1}$, which is about four orders of magnitude higher than that for low-density polyethylene.[11] The high gas permeability confirms the porous nature of the film of **5**.[12] Further characterization of the pores in **5** by imaging techniques, such as transmission electron microscopy and atomic force microscopy, and by sorption experiments are in progress.

In summary, nanoporous cross-linked polymers with hexagonal columnar channels have been prepared by a new method that uses thermotropic supramolecular liquid crystals as templates. The size and shape of the channels as well as the functional groups lining the channels are expected to be controlled with carefully designed template cores. Helical channels with one-handedness may also be introduced.[13] Such nanoporous polymers with highly ordered channel structures may find useful applications in many areas including recognition, separation, catalysis, and synthesis of nanocomposites.

Experimental Section

3: Compounds **1** and **2** were synthesized according to the literature.[4c, 7] A mixture of **1** (80.9 mg, 0.198 mmol) in methanol and **2** (499 mg, 0.593 mmol) in $CHCl_3$ was stirred for 30 min. The solvent was then removed under reduced pressure. The residue was redissolved in $CHCl_3$ and the solution was stirred for 30 min. Evaporation of the solvent produced **3** in a quantitative yield. ^1H NMR (500 MHz, $CDCl_3$): $\delta = 0.91$ (d, 7H), 1.21–1.46 (m, 194H), 3.21 (d, 4H), 4.01 (d, 20H), 4.10 (t, 18H), 5.77 (d, 8H), 6.08 (m, 8H), 6.36 (d, 8H), 7.37 (s, 6H); ^{13}C NMR (125 MHz, $CDCl_3$): $\delta = 14.41, 22.78, 26.49, 29.02, 29.68, 29.79, 29.95, 30.02, 30.76, 38.01, 39.48, 65.12, 69.51, 73.87, 108.83, 120.98, 126.93, 129.03, 130.87, 142.59, 153.12, 166.76, 170.81, 171.80$; IR (KBr): $\tilde{\nu} = 1729$ (C=O), 1636 cm^{-1} (C=C); MS (matrix-assisted laser desorption/ionization time-of-flight (MALDI-TOF)): m/z: 2939.1 $[M^+]$.

4: Compound **3** was placed between two glass plates at 30 °C. This sample showed the characteristic texture of a columnar liquid crystalline phase. The sample was irradiated with UV light (365 nm) for 3 h to give a polymer film which was detached from the glass plates and washed with $CHCl_3$ and methanol to produce **4**. ^{13}C CP/MAS NMR (125 MHz) $\delta = 4.87, 11.90, 24.23, 27.44, 38.05, 62.12, 66.75, 70.56, 105.92, 118.22, 127.49, 139.97, 150.33, 168.26, 171.95$; IR (KBr): $\tilde{\nu} = 1728$ (C=O), 1637 cm^{-1} (C=C); elemental analysis (%) calcd for $C_{171}H_{270}N_6O_{33} \cdot H_2O$: C 69.51, H 9.36, N 2.83; found: C 69.11, H 9.32, N 2.65.

5: Compound **4** was soaked in a mixture of aqueous 3 N HCl (12.5 mL) and methanol (12.5 mL) and then sonicated for 9 h before washing with $CHCl_3$, methanol, and water to produce **5**. ^{13}C CP/MAS NMR (125 MHz): $\delta = 12.26, 27.28, 38.18, 62.12, 66.43, 105.45, 127.16, 140.53, 150.40, 171.60$. The amount of **1** removed from **4** was determined by UV/Vis spectroscopy.

Reconstitution of the core in **5**: The porous polymer **5** after soaking in a 0.010 M solution of **1** in $CHCl_3$/MeOH (9/1) was shaken for 24 h at room temperature and finally washed with $CHCl_3$ and methanol. Reconstitution of the core was confirmed by ^{13}C CP/MAS NMR spectroscopy (see Figure 1 c). The core was removed from the reconstituted sample and quantified using the same procedure described above in order to estimate the amount of **1** incorporated into **5**.

Received: October 24, 2000
Revised: April 26, 2001 [Z15985]

[1] a) P. Calvert, P. Rieke, *Chem. Mater.* **1996**, *8*, 1715; b) J. Wen, G. L. Wilkes, *Chem. Mater.* **1996**, *8*, 1667; c) E. P. Giannelis, *Chem. Mater.* **1996**, *8*, 1728; d) H. L. Frisch, J. E. Mark, *Chem. Mater.* **1996**, *8*, 1735; e) C. R. Martin, *Chem. Mater.* **1996**, *8*, 1739.

[2] a) M. Muthukumar, C. K. Ober, E. L. Thomas, *Science* **1997**, *277*, 1225; b) G. Decher, *Science* **1997**, *277*, 1232; c) S. I. Stupp, P. V. Braun, *Science* **1997**, *277*, 1242; d) Z.-R. Chen, J. A. Kornfield, S. S. Smith, J. T. Grothaus, M. M. Satkowski, *Science* **1997**, *277*, 1248.

[3] a) P. J. Langley, J. Hulliger, *Chem. Soc. Rev.* **1999**, *28*, 279; b) K. D. M. Harris, *Chem. Soc. Rev.* **1997**, *26*, 279; c) R. Arad-Yellin, B. S. Green, M. Knossow, G. Tsoucaris in *Inclusion Compounds*, *Vol. 3* (Eds.: J. L. Atwood, J. E. D. Davies, D. D. MacNicol), Academic Press, London, **1984**, p. 263; d) J.-S. Seo, D. Whang, H. Lee, S.-I. Jun, J. Oh, Y.-J. Jeon, K. Kim, *Nature* **2000**, *404*, 982; e) K. Endo, T. Koike, T. Sawaki, O.

  1433-7851/01/4014-2670 $ 17.50+.50/0

Hayashida, H. Masuda, Y. Aoyama, *J. Am. Chem. Soc.* **1997**, *119*, 4117; f) W. E. Moerner, L. Kador, *Phys. Rev. Lett.* **1989**, *62*, 2535; g) S. Tomaru, S. Zembutsu, M. Kawachi, M. Kobayashi, *J. Chem. Soc. Chem. Commun.* **1984**, 1207; h) D. F. Eaton, A. G. Anderson, W. Tam, Y. Wang, *J. Am. Chem. Soc.* **1987**, *109*, 1886.

[4] a) D. L. Gin, D. H. Gray, R. C. Smith, *Synlett* **1999**, 1509; b) D. H. Gray, S. Hu, E. Juang, D. L. Gin, *Adv. Mater.* **1997**, *9*, 731; c) R. C. Smith, W. M. Fischer, D. L. Gin, *J. Am. Chem. Soc.* **1997**, *119*, 4092; d) D. H. Gray, D. L. Gin, *Chem. Mater.* **1998**, *10*, 1827; e) H. Deng, D. L. Gin, R. C. Smith, *J. Am. Chem. Soc.* **1998**, *120*, 3522; f) E. Kim, D. L. Gin, *Polym. Mater. Sci. Eng.* **1998**, *79*, 64; g) A. Miller, E. Kim, D. H. Gray, D. L. Gin, *Angew. Chem.* **1999**, *111*, 3205; *Angew. Chem. Int. Ed.* **1999**, *38*, 3022.

[5] a) S. J. Kim, S. H. Kang, K.-M. Park, H. Kim, W.-C. Jin, M.-G. Choi, K. Kim, *Chem. Mater.* **1998**, *10*, 1889; b) S. H. Kang, M. O. Kim, H.-K. Lee, Y.-S. Kang, W.-C. Zin, K. Kim, *Chem. Commun.* **1999**, 93; c) S. H. Kang, Y.-S. Kang, W.-C. Zin, G. Olbrechts, K. Wostyn, K. Clays, A. Persoons, K. Kim, *Chem. Commun.* **1999**, 1661.

[6] a) Benzotri(imidazole) **1** and 3,4-didodecyloxybenzoic acid form a 1:3 supramolecular complex through formation of intermolecular hydrogen bonds which exhibits a hexagonal columnar mesophase from 97.3 to 112.0 °C on heating. An X-ray diffraction study confirms the presence of a hexagonal columnar mesophase with a lattice constant of 33.3 Å. H.-K. Lee, M.Sc. Thesis, Pohang Univerisity of Science and Technology, December 8, **1999**; b) similar supramolecular liquid crystals with a columnar mesophase formed with a tribasic core and long chain alkoxybenzoic acids were recently reported: A. Kraft, A. Reichert, R. Kleppinger, *Chem. Commun.* **2000**, 1015.

[7] B. Kohne, K. Praefcke, T. Derz, T. Gondro, F. Frolow, *Angew. Chem.* **1986**, *98*, 627; *Angew. Chem. Int. Ed. Engl.* **1986**, *25*, 650.

[8] No immediate formation of a mesophase is observed upon cooling **3** from the isotropic state to room temperature. However, a mesophase slowly appears in 2–3 days upon standing at room temperature.

[9] a) D. J. Broer, G. N. Mol, G. Challa, *Macromol. Chem.* **1989**, *190*, 19; b) D. J. Broer, J. Boven, G. N. Mol, G. Challa, *Macromol. Chem.* **1989**, *190*, 2255.

[10] Incorporation of **1** and its tri-N-methylated derivative (**1′**) into **5** was studied by soaking **5** in $CDCl_3/CD_3OD$ containing either one equivalent of **1** or **1′** in a sealed NMR tube. The amount of **1** or **1′** remaining in solution was monitored by ^1H NMR spectroscopy by using bromoform as an internal standard. About 40% of **1** was found to be incorporated into **5** after 40 h, whereas almost no **1′** was incorporated. Similarly, 1,3,5-benzenetricarboxylic acid, which is the right size to fit into the channels, is only slightly incorporated into **5**.

[11] J. Brandrup, E. H. Immergut, *Polymer Handbook*, 3rd ed., Wiley, New York, **1989**.

[12] Nanoporous triblock copolymer membranes, which have much larger pores than **5** does, are reported to have gas permeability constants six orders of magnitude higher than that for low-density polyethylene: G. Liu, J. Ding, S. Stewart, *Angew. Chem.* **1999**, *111*, 884; *Angew. Chem. Int. Ed.* **1999**, *38*, 835.

[13] Helical discotic mesophases have been reported recently: a) H. Engelkamp, S. Middelbeek, R. J. M. Nolte, *Science* **1999**, *284*, 785; b) S. T. Trzaska, H.-F. Hsu, T. M. Swager, *J. Am. Chem. Soc.* **1999**, *121*, 4518; c) A. R. A. Palmans, J. A. J. M. Vekemans, E. E. Havinga, E. W. Meijer, *Angew. Chem.* **1997**, *109*, 2763; *Angew. Chem. Int. Ed. Engl.* **1997**, *36*, 2648; d) L. Brunsveld, H. Zhang, M. Glasbeek, J. A. J. M. Vekemans, E. W. Meijer, *J. Am. Chem. Soc.* **2000**, *122*, 6175.

Enantioselective Incorporation of Azobenzenes into Oligodeoxyribonucleotide for Effective Photoregulation of Duplex Formation**

Hiroyuki Asanuma,* Tohru Takarada, Takayuki Yoshida, Daisuke Tamaru, Xingguo Liang, and Makoto Komiyama*

Various organic molecules have been introduced into oligodeoxyribonucleotides (ODNs) by means of linkers to provide new functionalities.[1] We already reported that the *cis* → *trans* isomerization of an azobenzene moiety in the side chain of ODNs could reversibly photoregulate the formation and dissociation of its duplex: a *trans*-azobenzene moiety in the ODN stabilizes the duplex, whereas the *cis* form destabilizes it.[2] By using this modified ODN as a modulator, a T7 DNA polymerase reaction could also be photoregulated.[3] For even more effective photoregulation, the change in melting temperature ΔT_m induced by the *trans* → *cis* isomerization should be enhanced. A promising strategy for this purpose is to introduce multiple azobenzene groups into the ODN. However, the modified ODN was previously synthesized from the corresponding racemic mixture of phosphoramidite monomers, which were obtained from a prochiral diol as starting material (Scheme 1 A). Thus, two diastereomers were inevitably produced.[4] Since their photoregulation capabilities are significantly different,[2a] the azobenzene moieties should be enantioselectively incorporated into the ODN for more effective photoregulation. With these racemic phosphoramidite monomers, it is practically impossible to synthesize diastereochemically pure ODNs containing multiple azobenzene groups, and hence the optically pure phosphoramidite monomer is essential.

We chose threoninol as the linker (Scheme 1 B) for two reasons: 1) optically pure diols can be synthesized from the corresponding D- or L-threonine, and 2) perturbation of the framework of our previous prochiral linker (Scheme 1 A) is minimized.[5] Both L- and D-threoninol were used as optically pure linkers, and two azobenzene moieties were enantioselectively introduced. It was shown that a D-threoninol-tethered azobenzene moiety induces much larger ΔT_m on photoisomerization than does an L-threoninol-tethered one.

[*] Prof. Dr. H. Asanuma, Prof. Dr. M. Komiyama, Dr. T. Takarada,[+] T. Yoshida, D. Tamaru, X. Liang
Research Center for Advanced Science and Technology
The University of Tokyo
Komaba, Meguro-ku, Tokyo 153-8904 (Japan)
Fax: (+81) 3-5452-5209
E-mail: asanuma@mkomi.rcast.u-tokyo.ac.jp
komiyama@mkomi.rcast.u-tokyo.ac.jp

[+] Current address:
Department of Applied Chemistry, Graduate School of Engineering
Kyushu University, Hakozaki, Higashi-ku, Fukuoka 812-8581 (Japan)

[**] This work was partially supported by a Grant-in-Aid for Scientific Research from the Ministry of Education, Culture, Sports, Science and Technology, Japan (Molecular Synchronization for Design of New Materials System). The support by the Grant from "Research for the Future" Program of the Japan Society for the Promotion of Science (JSPS-RFTF97I00301) is also acknowledged.

Supporting information for this article is available on the WWW under http://www.angewandte.com or from the author.

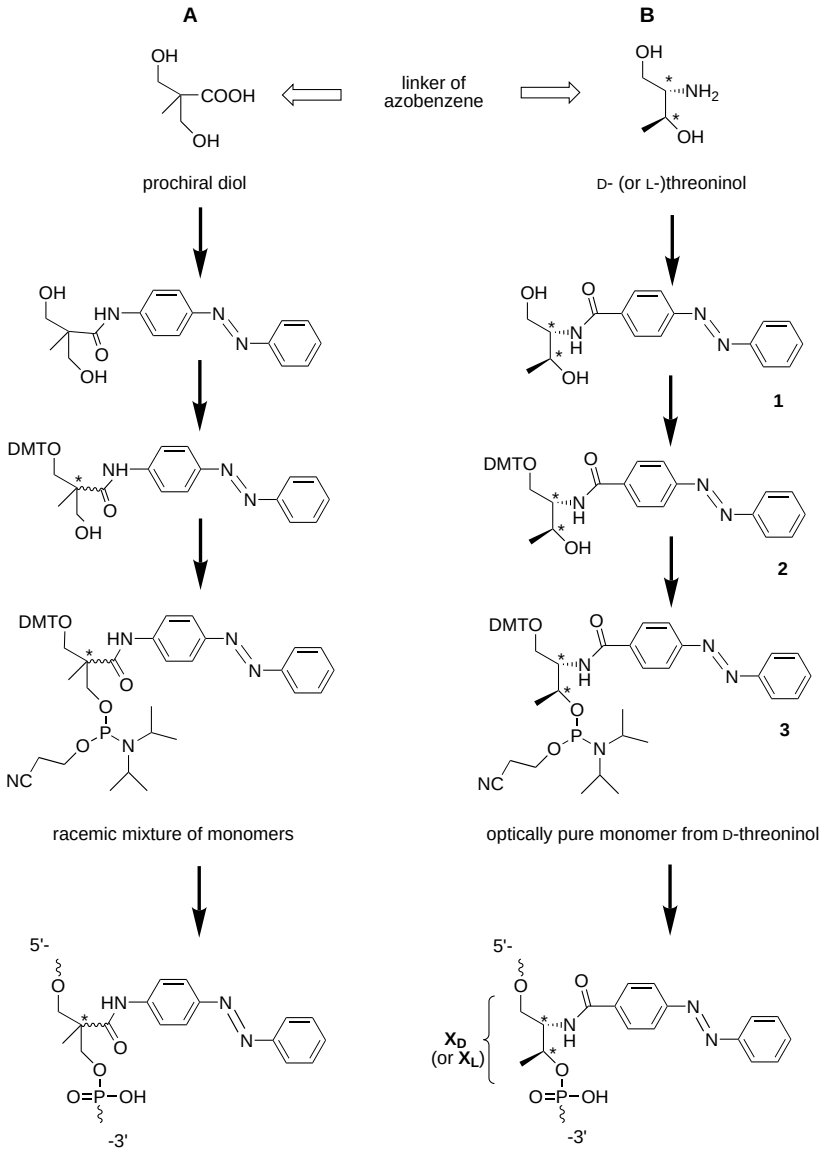

Scheme 1. Modified ODN carrying an azobenzene moiety attached by a prochiral diol linker (A) and by a chiral diol linker (B). DMT = 4,4-dimethoxytrityl.

Furthermore, an even larger ΔT_m is obtained by introducing two D-threoninol-tethered azobenzene groups.

The azobenzene moieties of all the modified ODNs (Table 1) overwhelmingly adopted the *trans* form before UV irradiation. On UV irradiation ($300 < \lambda < 400$ nm), they promptly isomerized to the *cis* form. The isomerization was reversible: the *cis*-azobenzene moiety was isomerized to the *trans* form by irradiation with visible light ($\lambda > 420$ nm).[6] The melting temperatures of the duplexes formed by the modified DNAs and their complementary counterpart in the *trans* or *cis* form are summarized in Table 1.[7] The ΔT_m significantly depended on the chirality of the linker. The melting temperature of the duplex formed by **L1**, containing one azobenzene moiety linked through L-threoninol, and its complementary counterpart **C** decreased from 45.1 (*trans*-azobenzene) to 40.8 °C on *trans* → *cis* isomerization.[8] The ΔT_m induced by the photoisomerization was 4.3 °C. In contrast, a much larger ΔT_m was induced when the azobenzene moiety was tethered by D-threoninol: the T_m of the *trans*- and *cis*-**D1**/**C** duplexes were 50.9 and 36.6 °C, respectively ($\Delta T_m = 14.3$ °C). The duplex was more strongly stabilized by *trans*-azobenzene that was tethered by D-threoninol as opposed to the L-form, whereas it was strongly destabilized by D-threoninol-tethered *cis*-azobenzene. As a result, a larger ΔT_m was accomplished by the D-threoninol linker.

By using the present optically pure linkers, two azobenzene moieties can be enantioselectively incorporated into ODNs, and it was found that the chirality of the linker then affects ΔT_m to an even greater extent. When two azobenzene moieties were introduced into the ODN through two L-threoninol residues (**LL2**), the melting curve of the *trans*-**LL2**/**C** duplex was almost superimposed on that of *cis*-**LL2**/**C** (Figure 1a; $\Delta T_m \approx 0$ °C).[9] With two azobenzene moieties on two D-threoninol residues (**DD2**), however, the two curves are widely separated from each other (Figure 1b). The ΔT_m of **DD2**/**C** was as large as 21.5 °C, which fairly exceeded the ΔT_m of **D1**/**C** duplex (14.3 °C) involving one azobenzene moiety. The order of the ΔT_m for all the possible diastereomers was as follows: **DD2** > **LD2** > **DL2** >

Table 1. Melting temperature T_m of the duplexes between the modified ODN and its complementary counterpart.[a]

ODN[b]	Sequence	T_m [°C]		ΔT_m [°C][c]
		trans	*cis*	
L1	5′-GCGA$\mathbf{X_L}$GTCG-3′	45.1	40.8	4.3
D1	5′-GCGA$\mathbf{X_D}$GTCG-3′	50.9	36.6	14.3
LL2	5′-GC$\mathbf{X_L}$GAGT$\mathbf{X_L}$CG-3′	25.4	25.5	−0.1
DL2	5′-GC$\mathbf{X_D}$GAGT$\mathbf{X_L}$CG-3′	31.9	22.2	9.7
LD2	5′-GC$\mathbf{X_L}$GAGT$\mathbf{X_D}$CG-3′	38.7	22.9	15.8
DD2	5′-GC$\mathbf{X_D}$GAGT$\mathbf{X_D}$CG-3′	43.9	22.4	21.5

[a] The complementary counterpart is ODN **C** (3′-CGCTCAGC-5′) for all the ODNs. [b] $\mathbf{X_L}$ and $\mathbf{X_D}$ denote the azobenzene moieties (see Scheme 1B) tethered on L- and D-threoninol, respectively. T_m of 5′-GCGAGTCG-3′/3′-CGCTCAGC-5′ duplex without $\mathbf{X_D}$ or $\mathbf{X_L}$ is 46.6 °C. [c] Change in T_m induced by *cis* → *trans* isomerization.

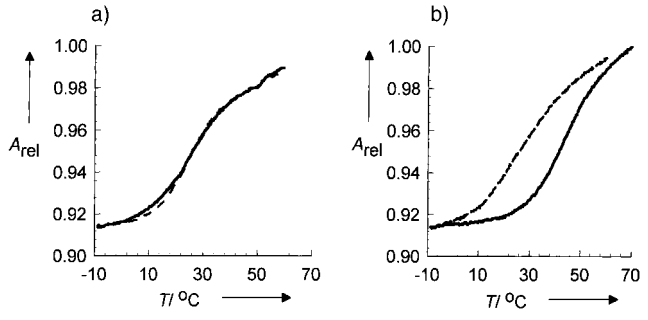

Figure 1. Melting curves for the duplex formation of **LL2**/**C** (a) and **DD2**/**C** (b) in the *trans* (solid lines) and *cis* forms (dashed line). The T_m values obtained from these curves are listed in Table 1. A_{rel} = relative absorbance.

  1433-7851/01/4014-2672 $ 17.50+.50/0 *Angew. Chem. Int. Ed.* **2001**, *40*, No. 14

LL2 $\approx 0\,^{\circ}C$, that is, D-threoninol is advantageous as a linker for azobenzene moieties.

According to a molecular model, the azobenzene moiety on a D-threoninol residue protrudes towards the minor groove, and that on an L-threoninol residue towards the major groove (see Supporting Information). In the narrow, minor groove, a structural change of azobenzene would significantly affect the stability of the duplex, whereas the effect should be smaller in the wide, major groove.[10] Therefore, the D-threoninol-tethered azobenzene induces larger ΔT_m values.

In conclusion, azobenzene moieties were enantioselectively introduced into ODNs by using optically pure linkers. D-Threoninol is an excellent linker of azobenzene for the effective photoregulation of duplex formation.[11]

Experimental Section

Synthesis of the azobenzene-containing phosphoramidite monomer:[12] D- or L-threoninol was obtained by the reduction of the corresponding D- or L-threonine methyl ester with $LiAlH_4$ in dry THF.[13] Then the D-threoninol was coupled with 4-phenylazobenzoic acid in the presence of dicyclohexylcarbodiimide and 1-hydroxybenzotriazole in DMF (yield 80%). **1**: ^{1}H NMR: (500 MHz, $CDCl_3$): $\delta = 7.96-7.38$ (m, 9H, ArH of azobenzene), 7.12 (d, $^3J(H,H) = 8.0$ Hz, 1H, N*H*CO), 4.33 (m, 1H, C*H*(OH)CH_3), 4.09 (m, 1H, HOCH_2C*H*(NHCO)), 3.98 (d, $^3J(H,H) = 4.5$ Hz, 2H, CH_2OH), 1.29 (d, $^3J(H,H) = 6.5$ Hz, 3H, CH(OH)CH_3); ESI-MS: *m*/*z*: 313.7; calcd for [**1**+H$^+$]: 314.1.

Tritylation of **1**: 4,4-dimethoxytrityl chloride (DMT-Cl) in CH_2Cl_2 was added to a dry pyridine solution containing **1** and dimethylaminopyridine (yield of **2**: 63%). **2**: ^{1}H NMR for **2** (500 MHz, $CDCl_3$): $\delta = 8.00-6.78$ (m, 23H, ArH of DMT, azobenzene; N*H*CO), 4.25 (m, 1H, C*H*(OH)CH_3), 4.17 (m, 1H, OCH_2C*H*(NHCO)), 3.77, 3.76 (s, 6H, $C_6H_4OCH_3$), 3.60, 3.42 (dd, $^2J(H,H) = 10.0$, $^3J(H,H) = 4.0$ Hz, 2H, CH_2ODMT), 1.23 (d, $^3J(H,H) = 6.5$, 3H, CH(OH)CH_3). ESI-MS for **2**: *m*/*z*: 638.1; calcd for [**2**+Na$^+$]: 638.3.

3: In dry acetonitrile under nitrogen, **2** and 2-cyanoethyl *N*,*N*,*N*′,*N*′-tetraisopropylphosphorodiamidite were treated with 1*H*-tetrazole according to the recommended procedure.[2b] ^{1}H NMR (500 MHz, $CDCl_3$): $\delta = 8.00-6.79$ (m, 22H, ArH of DMT, azobenzene), 6.62 (d, $^3J(H,H) = 8.5$ Hz, 1H, N*H*CO), 4.48 (m, 1H, C*H*(CH_3)OP), 4.39 (m, 1H, OCH_2C*H*(NHCO)), 4.21–4.10 (m, 2H, CH_2OP), 3.77 and 3.76 (s, 6H, $C_6H_4OCH_3$), 3.57–3.34 (m, 4H, C*H*(CH_3)$_2$, CH_2ODMT), 2.76–2.72 (m, 2H, CH_2CN), 1.30–1.25 (m, 15H, CH(CH_3)$_2$, CH(OP)CH_3). ESI-MS: *m*/*z*: 838.1; calcd for [**3**+Na$^+$]: 838.4.

The phosphoramidite monomer of the L-isomer was synthesized from L-threoninol by the same procedure as the D-isomer.

Synthesis of azobenzene-containing modified ODNs: All the modified oligonucleotides in Table 1 were synthesized on an automated DNA synthesizer by using the phosphoramidite monomer **3** and conventional monomer. The coupling efficiency of the monomer **3** was as high as those of conventional monomers, as judged from the coloration of released trityl cation. After the recommended workup, they were purified by reversed-phase HPLC.

MALDI-TOF MS: *m*/*z*: **L1**: 2824, **D1**: 2824 (calcd for [**L1** – H$^+$]: 2823); **LL2**: 3198, **DD2**: 3195, **LD2**: 3198, **DL2**: 3197 (calcd for [**LL2** – H$^+$]: 3197).

Received: March 12, 2001 [Z16756]

[1] a) E. T. Kool, *Chem. Rev.* **1997**, *97*, 1473–1488; b) K. Yamana, A. Yoshikawa, R. Noda, H. Nakao, *Nucleosides Nucleotides* **1998**, *17*, 233–242; c) F.-X. Barre, C. Giovannangeli, C. Hélène, A. Harel-Bellan, *Nucleic Acids Res.* **1999**, *27*, 743–749; d) A. K. Ogawa, Y. Wu, D. L. McMinn, J. Liu, P. G. Schultz, F. E. Romesberg, *J. Am. Chem. Soc.* **2000**, *122*, 3274–3287; f) T. A. Taton, C. A. Mirkin, R. L. Letsinger, *Science* **2000**, *289*, 1757–1760.

[2] a) H. Asanuma, T. Ito, T. Yoshida, X. Liang, M. Komiyama, *Angew. Chem.* **1999**, *111*, 2547–2549; *Angew. Chem. Int. Ed.* **1999**, *38*, 2393–2395; b) H. Asanuma, T. Yoshida, T. Ito, M. Komiyama, *Tetrahedron Lett.* **1999**, *40*, 7995–7998; c) H. Asanuma, T. Yoshida, X. Liang, M. Komiyama, *Chem. Lett.* **2000**, 108–109; d) H. Asanuma, X. Liang, T. Yoshida, A. Yamazawa, M. Komiyama, *Angew. Chem.* **2000**, *112*, 1372–1374; *Angew. Chem. Int. Ed.* **2000**, *39*, 1316–1318.

[3] Whether the DNA elongation is terminated at the desired site or proceeds to the end of the template DNA is clearly dictated by photoinduced *cis*–*trans* isomerization of azobenzene: A. Yamazawa, X. Liang, H. Asanuma, M. Komiyama, *Angew. Chem.* **2000**, *112*, 2446–2447; *Angew. Chem. Int. Ed.* **2000**, *39*, 2356–2357.

[4] They could be separated by reversed-phase HPLC in a certain sequence, but their configurations remain unknown.

[5] Fukui and Reynolds introduced functional moieties into ODNs using a L-threoninol linker. However, the D enantiomer has not yet been used: a) K. Fukui, M. Morimoto, H. Segawa, K. Tanaka, T. Shimidzu, *Bioconjugate Chem.* **1996**, *7*, 349–355; b) M. A. Reynolds, T. A. Beck, R. I. Hogrefe, A. McCaffrey, L. J. Arnold, Jr., M. M. Vaghefi, *Bioconjugate Chem.* **1992**, *3*, 366–374.

[6] The azobenzene moiety was isomerized by irradiation with the light from a 150-W Xenon lamp 10 min through an appropriate filter (UV-D36C from Asahi Technoglass Corporation for the *trans* →*cis* isomerization, and L-42 for the *cis* →*trans* isomerization).

[7] The concentration of each ODN was 5 μM in pH 7.0 phosphate buffer (10 mM) in the presence of 0.1M NaCl. The T_m value was determined from the maximum in the first derivative of the melting curve, which was obtained by measuring the absorbance at 260 nm as a function of temperature. The heating rate was $1.0\,^{\circ}C\,min^{-1}$.[2a] Throughout the T_m measurement, the fractions of *cis* and *trans* isomers remained almost constant, as monitored by UV/Vis spectroscopy.

[8] For **L1** and **D1**, the azobenzene moiety adopted the *trans* form to an extent of greater than 98% in the dark, and the *cis* form amounted to 76% after UV irradiation, as determined by reversed-phase HPLC and UV spectroscopy.

[9] In the dark, greater than 98% of the azobenzene moieties adopted the *trans* form in all four diastereomers. Both of the *trans*-azobenzene moieties were promptly isomerized to *cis* form on UV irradiation (*cis* fraction 62%).

[10] The photoregulation of duplex formation is based on the stabilization of the duplex by the planar *trans*-azobenzene and destabilization by the nonplanar *cis*-azobenzene.[2a, d] Intercalation of *trans*-azobenzene into the base pairs was revealed in both diastereomers (**D1**/**C** and **L1**/**C**) by the bathochromic shift of the peak maximum of azobenzene resulting from the duplex formation (see Supporting Information). Weak but explicit circular dichroism was also negatively induced for both *trans*-**D1**/**C** and *trans*-**L1**/**C** at 330 nm, where the peak maximum of azobenzene exists (see Supporting Information). This fact also supports the intercalation of *trans*-azobenzene (R. Lyng, A. Rodger, B. Nordén, *Biopolymers* **1992**, *32*, 1201–1214).

[11] The present results are applicable, for example, to the photoregulation of the RNA polymerase reaction or gene expression by antisense strategy, since these processes involve the dissociation of DNA duplexes into single strands prior to chemical reaction.

[12] More detailed synthetic procedures are described in the Supporting Information.

[13] C. F. Stanfield, J. E. Parker, P. Kanellis, *J. Org. Chem.* **1981**, *46*, 4799–4800.

Cleavage of Tellurium–Carbon Bonds of Hexavalent Organotellurium Compounds by Potassium Graphite**

Masataka Miyasato, Mao Minoura, and Kin-ya Akiba*

Recently, we reported on the synthesis of the hexaaryltellurium compounds Ar_6Te (**1**: Ar = 4-$CF_3C_6H_4$) and Ph_6Te,[1] the first neutral hexaarylated compounds.[2] These hexaaryl compounds are stable to atmospheric moisture and are inert to nucleophiles such as alkyllithium reagents. Here we report that one of the Te–C bonds of **1** is readily cleaved by potassium graphite (KC_8)[3] to afford $Ar_5Te^-K^+C_8$ (**2**·K^+C_8) (Scheme 1). The reaction of **2**·K^+C_8 with CH_3I gave quantitatively Ar_5TeCH_3 (**3**), which could not be obtained from $Ar_5Te^-Li^+$.[4]

We tried to reduce **1** with lithium or sodium–naphthalenide, lithium 4,4′-di-*tert*-butylbiphenylide, Na amalgam, NaK alloy, and K under various conditions, but **1** was recovered quantitatively in all cases. However, in the reaction of **1** with KC_8[3] the expected **2**·K^+C_8 was generated even at −78 °C in THF. By ^{125}Te NMR spectroscopy, a singlet ($\delta = 600$ at −45 °C) was observed. The ^{125}Te NMR chemical shift in THF was comparable to that of $Ar_5Te^-Li^+$ (**2**·Li^+, $\delta = 588$), which was prepared from Ar_4Te ($\delta = 505$)[5] and ArLi. A remarkable difference between **2**·Li^+ and **2**·K^+C_8 was noted, however, when **2**·Li^+ or **2**·K^+C_8 was treated with CH_3I. Although Ar_5TeCH_3 (**3**) was not obtained at all from **2**·Li^+ under various conditions, **3** was obtained quantitatively from **2**·K^+C_8 up to −20 °C (Scheme 1 and Table 1). The remarkable reactivity of **2**·K^+C_8 is presumably attributable to the intercalation of the potassium cation in graphite. Since $Ph_5Te^-Li^+$[4a] was reported to be in an equilibrium with Ph_4Te and PhLi, the failure of **2**·Li^+ to react with CH_3I could be due to a much higher rate of the reaction of ArLi (in the equilibrium) with CH_3I than with **2**·Li^+ (Curtin–Hammett situation[6]). Therefore, the quantitative formation of **3** from **2**·K^+C_8 strongly indicated that **2**·K^+C_8 should be the exclusive species, if any, in the equilibrium with Ar_4Te and $ArKC_8$. Since the potassium cation is intercalated by graphite,[3] the resulting K^+C_8 is a weakly coordinating cation and would not tend to aggregate. That is, typical ion pairing is suppressed by intercalation of K^+ in graphite. Since $ArKC_8$ should be unstable because of the lack of aggregation, the equilibrium between **2**·K^+C_8, Ar_4Te, and $ArKC_8$ shifts toward **2**·K^+C_8, which becomes the exclusive anion. To our knowledge such a unique effect of graphite has not been noted so far, although the importance of graphite has been reported for some reactions.[3a,c] In fact, no **3** was obtained by the reaction of CH_3I with $Ar_5Te^-K^+$ (**2**·K^+), which was prepared from Ar_5TeX (X = Cl, Br)[7] and potassium without graphite. Although weakly coordinating anions have recently attracted extensive interest,[8] weakly coordinating cations have not been reported, apart from complexation of metal cations by crown ethers or cryptands. The present K^+C_8 system can be regarded as a new weakly coordinating cation.

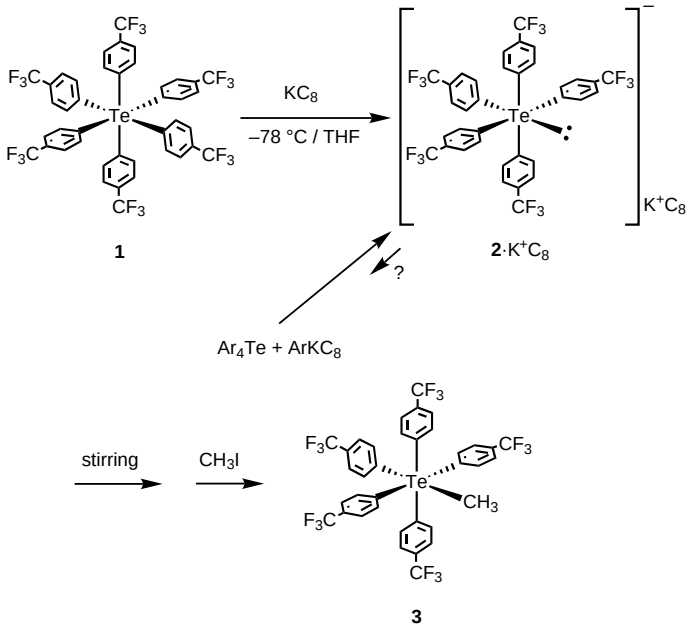

Scheme 1. Reaction of Ar_6Te (**1**) to give **3** via **2**·K^+C_8.

Table 1. Yield of **3** in the reaction of Ar_6Te with KC_8, followed by reaction with CH_3I.

T [°C]	t [h]	Yield of **3** [%]
−78	1	98
−45	1	98
	12	35
−20	1	98
0	0.5	15
20	0.5	0[a]

[a] Products were Ar_2Te, Ar_2, and ArI.

With pentaarylmonomethyltellurium **3** in hand, the selective cleavage of the two different tellurium–carbon bonds, namely, Te–Ar and Te–CH_3, was of interest. The reaction of **3** with excess KC_8 at −78 °C, followed by addition of CH_3I, gave $Ar_4Te(CH_3)_2$ (*trans*-**4**) in 14% yield, and 75% of **3** was recovered (Scheme 2). X-ray analysis of *trans*-**4**[9] confirmed the *trans* arrangement of the two methyl groups (Figure 1).

[*] Prof. K.-y. Akiba,[+] M. Miyasato
Department of Chemistry, Graduate School of Science
Hiroshima University
1-3-1 Kagamiyama, Higashi-Hiroshima 739-8526 (Japan)
Fax: (+81) 824-24-0723
E-mail: akiba@sci.hiroshima-u.ac.jp, akibaky@mn.waseda.ac.jp
Dr. M. Minoura
Department of Chemistry, School of Science
Kitasato University
1-15-1 Kitasato, Sagamihara 228-8555 (Japan)
[+] Present address:
Advanced Research Center for Science and Engineering
Waseda University
3-4-1 Ohkubo, Shinjuku-ku, Tokyo 169-8555 (Japan)
Fax: (+81) 3-5286-3165

[**] This work was supported by a Grant-in-Aid for Scientific Research (No. 11304044 and 12740352) from the Ministry of Education, Science, Sports, and Culture of the Japanese Government. The support of the Nishida Research Fund for Fundamental Organic Chemistry (to M. Minoura) is also acknowledged.

  1433-7851/01/4014-2674 $ 17.50+.50/0

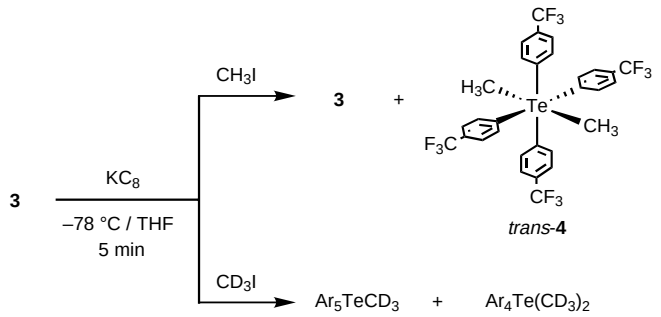

Scheme 2. Reaction of Ar_5TeCH_3 (**3**) with KC_8, followed by reaction with CH_3I or CD_3I.

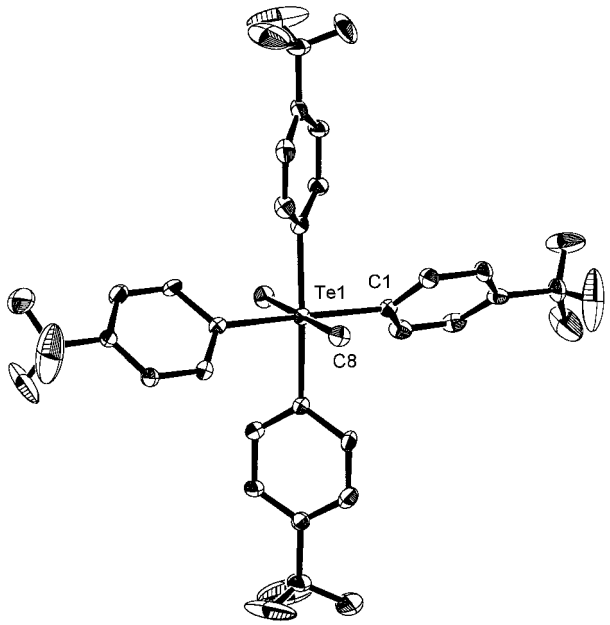

Figure 1. Crystal structure (30% thermal ellipsoids) of *trans*-**4**. Selected bond lengths [Å]: Te-C1 2.205(5), Te-C8 2.182(8).

When CD_3I was used instead of CH_3I, Ar_5TeCD_3 (68% yield) and $Ar_4Te(CD_3)_2$ (12% yield) were obtained. These results showed that cleavage of the Te–C bonds took place almost quantitatively and the Te–CH_3 bond was cleaved in preference to the five Te–Ar bonds. This unexpected selectivity can be explained as shown in Scheme 3. As a first step one-electron reduction took place, followed by formation of Ar_5Te^- ($\mathbf{2}\cdot K^+C_8$) and $CH_3^\bullet$ rather than $Ar_4TeCH_3^-$ ($\mathbf{5}\cdot K^+C_8$) and $Ar^\bullet$. The selectivity could be related to the higher stability of $\mathbf{2}\cdot K^+C_8$ relative to that of $\mathbf{5}\cdot K^+C_8$. Formation of $Ar_4Te(CD_3)_2$ suggested the presence of the novel hypervalent dianion Ar_4Te^{2-} [$\mathbf{6}\cdot 2(K^+C_8)$]. In the ^{125}Te NMR of the supernatant of the reaction mixture from **3** with KC_8 in THF at $-78\,^\circ C$ before addition of CH_3I, two signals were observed at $\delta = 591$ ($\mathbf{2}\cdot K^+C_8$: $\delta = 600$ at $-45\,^\circ C$) and $\delta = 385$. The latter high-field signal could be assigned to $\mathbf{6}\cdot 2(K^+C_8)$, since **3** and **4** were obtained quantitatively after addition of CH_3I to the solution. Note that conversion of $\mathbf{2}\cdot K^+C_8$ to $\mathbf{6}\cdot 2(K^+C_8)$ did not take place, because only one of the six tellurium–aryl bonds in **1** was cleaved even with an excess of KC_8 (Scheme 1).

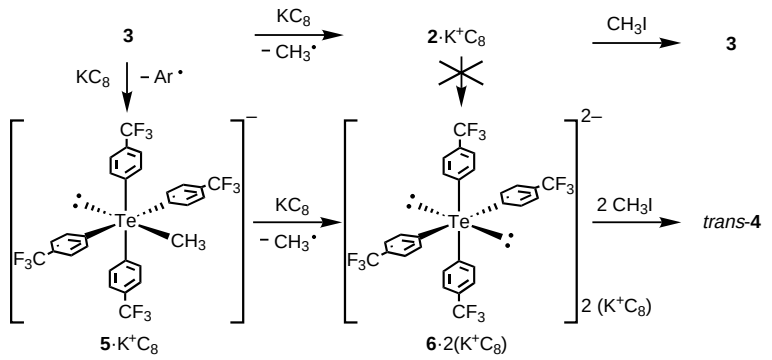

Scheme 3. Possible mechanism for formation of **3** and *trans*-**4**.

Experimental Section

$\mathbf{2}\cdot K^+C_8$ and **3**: A solution of **1** in THF (30 mL) (1.55 g, 1.55 mmol) was added to freshly prepared potassium graphite (KC_8: K 0.187 g, 4.76 mmol; C 0.361 g, 30.1 mmol) at $-78\,^\circ C$. After 1 h of stirring, CH_3I (1.00 mL, 16.1 mmol) was added at the same temperature, and the reaction mixture was allowed to warm to room temperature. Graphite powder was filtered off and the solvent and excess CH_3I were removed in vacuo. Recycling HPLC gave 1.32 g (97.9%) of **3**: colorless needles, m.p. 258–259 °C (decomp); ^{1}H NMR (400 MHz, $CDCl_3$, 25 °C, $CHCl_3$): $\delta = 2.35$ (s, 3H; CH_3), 7.45 (d, $^3J(H,H) = 8$ Hz, 8H; *cis*-2-H), 7.52 (d, $^3J(H,H) = 8$ Hz, 8H; *cis*-3-H), 7.54 (d, $^3J(H,H) = 8$ Hz, 2H; *trans*-2-H), 7.67 (d, $^3J(H,H) = 8$ Hz, 2H; *trans*-3-H); ^{19}F NMR (376 MHz, $CDCl_3$, 25 °C, $CFCl_3$): $\delta = -63.1$ (12F; *cis*-CF_3), -63.3 (3F; *trans*-CF_3); ^{13}C NMR (100 MHz, $CDCl_3$, 25 °C, $CDCl_3$): $\delta = 33.8$ (q, $^1J(C,Te) = 12$ Hz; CH_3), 123.8 (q, $^1J(C,F) = 273$ Hz; *cis*- and *trans*-CF_3), 124.9 (d; *cis*-3-C), 125.2 (d; *trans*-3-C), 131.1 (q, $^2J(C,F) = 33$ Hz; *cis*-4-C), 131.2 (q, $^2J(C,F) = 33$ Hz; *trans*-4-C), 133.1 (d; *trans*-2-C), 133.7 (d; *cis*-2-C), 153.9 (s, $^1J(C,Te) = 21$ Hz; *trans*-1-C), 157.2 (s, $^1J(C,Te) = 64$ Hz; *cis*-1-C); ^{125}Te NMR (126 MHz, $CDCl_3$, 25 °C, $(CH_3)_2Te$): $\delta = 345$; elemental analysis (%) calcd for $C_{36}H_{23}F_{15}Te$: C 49.81, H 2.67; found: C 49.62, H 2.41.

trans-**4**: A solution of **3** (0.712 g, 0.820 mmol) in THF (20 mL) was added to freshly prepared potassium graphite (KC_8: K 0.239 g, 6.11 mmol; C 0.364 g, 30.3 mmol) at $-78\,^\circ C$. After 5 min of stirring, CH_3I (0.75 mL, 12.0 mmol) was added at the same temperature, and the reaction mixture was allowed to warm to room temperature. Graphite powder was filtered off, and the solvent and excess CH_3I were removed in vacuo. Recycling HPLC gave 530 mg (74.5%) of **3** and 82.8 mg (13.7%) of *trans*-**4**: colorless cubes, m.p. 275–276 °C (decomp); ^{1}H NMR (400 MHz, $CDCl_3$, 25 °C, $CHCl_3$): $\delta = 2.25$ (s, 6H; CH_3), 7.40 (d, $^3J(H,H) = 8$ Hz, 8H; 2-H), 7.52 (d, $^3J(H,H) = 8$ Hz, 8H; 3-H); ^{19}F NMR (376 MHz, $CDCl_3$, 25 °C, $CFCl_3$): $\delta = -63.1$; ^{13}C NMR (100 MHz, $CDCl_3$, 25 °C, $CDCl_3$): $\delta = 30.9$ (q, $^1J(C,Te) = 13$ Hz; CH_3), 124.0 (q, $^1J(C,F) = 273$ Hz; CF_3), 124.7 (d; 3-C), 130.6 (q, $^1J(C,F) = 33$ Hz; 4-C), 132.7 (d; 2-C), 160.3 (s, $^1J(C,Te) = 105$ Hz; 1-C); ^{125}Te NMR (126 MHz, $CDCl_3$, 25 °C, $(CH_3)_2Te$): $\delta = 272$; elemental analysis (%) calcd for $C_{30}H_{22}F_{12}Te$: C 48.82, H 3.00; found: C 48.71, H 2.91.

Received: March 14, 2001 [Z 16774]

[1] M. Minoura, T. Sagami, K.-y. Akiba, C. Modrakowski, A. Sudau, K. Seppelt, S. Wallenhauer, *Angew. Chem.* **1996**, *108*, 2827–2829; *Angew. Chem. Int. Ed. Engl.* **1996**, *35*, 2660–2662; M. Minoura, T. Sagami, M. Miyasato, K.-y. Akiba, *Tetrahedron* **1997**, *53*, 12195–12202.

[2] Neutral hexamethylated element compounds: Me_6Te: a) L. Ahmed, J. A. Morrison, *J. Am. Chem. Soc.* **1990**, *112*, 7411–7413; b) A. Haaland, H. P. Verne, H. V. Volden, J. A. Morrison, *J. Am. Chem. Soc.* **1995**, *117*, 7554–7555; c) J. E. Fowler, T. P. Hamilton, H. F. Schaefer III, *J. Am. Chem. Soc.* **1993**, *115*, 4155–4158; d) J. E. Fowler, H. F. Schaefer III, K. N. Raymond, *Inorg. Chem.* **1996**, *35*, 279–

281; Me_6W: e) A. J. Shortland, G. Wilkinson, *J. Chem. Soc. Dalton Trans.* **1973**, 872–876; f) A. L. Galyer, G. Wilkinson, *J. Chem. Soc. Dalton Trans.* **1976**, 2235–2238; g) A. Haaland, A. Hammel, K. Rypdal, H. V. Volden, *J. Am. Chem. Soc.* **1990**, *112*, 4547–4549; h) V. Pfennig, K. Seppelt, *Science* **1996**, *271*, 626–628; Me_6Re: i) K. Mertis, G. Wilkinson, *J. Chem. Soc. Dalton Trans.* **1976**, 1488–1492.

[3] For example, see: a) A. Fürstner, *Angew. Chem.* **1993**, *105*, 171–198; *Angew. Chem. Int. Ed. Engl.* **1993**, *32*, 164–189; b) R. Csuk, B. I. Glanzer, A. Fürstner, *Adv. Organomet. Chem.* **1988**, *28*, 85–137; c) D. Savoia, C. Trombini, A. Umani-Ronchi, *Pure Appl. Chem.* **1985**, *57*, 1887–1896; d) H. Selig, L. B. Ebert, *Adv. Inorg. Chem. Radiochem.* **1980**, *23*, 281–327; e) J.-M. Lalancette, G. Rollin, P. Dumas, *Can. J. Chem.* **1972**, *50*, 3058–3062.

[4] For preparation of $Ph_5Te^-Li^+$ by reaction of Ph_4Te with PhLi, see: a) H. J. Reich, D. P. Green, N. H. Phillips, J. P. Borst, I. L. Reich, *Phosphorus Sulfur Silicon Relat. Elem.* **1992**, *67*, 83–97; b) G. Wittig, H. Fritz, *Justus Liebigs Ann. Chem.* **1952**, *577*, 39–46; for $R_5Te^-Li^+$, see c) D. Hellwinkel, G. Fahrbach, *Chem. Ber.* **1968**, *101*, 574–584; d) D. Hellwinkel, *Ann. NY Acad. Sci.* **1972**, *192*, 158–166; R_3Te^-: e) H. J. Reich, D. P. Green, N. H. Phillips, *J. Am. Chem. Soc.* **1991**, *113*, 1414–1416; f) S. Ogawa, S. Sato, Y. Masutomi, N. Furukawa, *Phosphorus Sulfur Silicon Relat. Elem.* **1992**, *67*, 99–102; g) S. Ogawa, Y. Masutomi, N. Furukawa, T. Erata, *Heteroat. Chem.* **1992**, *3*, 423–429; h) S. Ogawa, Y. Masutomi, T. Erata, N. Furukawa, *Chem. Lett.* **1992**, 2471–2474; i) Y. Masutomi, N. Furukawa, T. Erata, *Heteroat. Chem.* **1995**, *6*, 19–27.

[5] Spectral data of Ar_4Te: ^1H NMR (400 MHz, C_6D_6, 25 °C, C_6D_5H): $\delta =$ 7.12 (d, $^3J(H,H) = 8$ Hz, 8H; 2-H), 7.26 (d, $^3J(H,H) = 8$ Hz, 8H; 3-H); ^{19}F NMR (376 MHz, C_6D_6, 25 °C, $CFCl_3$): $\delta = -62.7$; ^{13}C NMR (100 MHz, C_6D_6, 25 °C, C_6D_6): $\delta = 124.6$ (q, $^1J(C,F) = 273$ Hz; CF_3), 125.8 (d; 3-C), 130.9 (q, $^1J(C,F) = 33$ Hz; 4-C), 133.5 (d; 2-C), 152.3 (s, $^1J(C,Te) = 230$ Hz; 1-C); ^{125}Te NMR (126 MHz, C_6D_6, 25 °C, $(CH_3)_2Te$): $\delta = 490$; M. Minoura, M. Miyasato, K.-y. Akiba, unpublished results.

[6] N. S. Isaacs, *Physical Organic Chemistry*, Longman Scientific and Technical, Essex, **1987**, p. 315.

[7] M. Minoura, T. Sagami, K.-y. Akiba, unpublished results. For Ph_5TeCl, see: M. Minoura, T. Mukuda, T. Sagami, K.-y. Akiba, *J. Am. Chem. Soc.* **1999**, *121*, 10852–10853.

[8] For recent reviews and reports, see: a) C. A. Reed, *Acc. Chem. Res.* **1998**, *31*, 133–139; b) E. Y.-X. Chen, T. J. Marks, *Chem. Rev.* **2000**, *100*, 1391–1434.

[9] Crystal data for *trans*-**4**: cubic, space group $P\bar{4}3n$ (no. 218), $a =$ 16.9860(2) Å, $V = 4900.87(9)$ Å^3, $Z = 6$, $\rho_{calcd} = 1.50$ g cm^{-3}; $R = 0.0599$ ($Rw = 0.1041$) for 973 observed reflections (99 parameters) with $I > 3\sigma(I)$; GOF = 1.417. Crystallographic data (excluding structure factors) for the structure reported in this paper have been deposited with the Cambridge Crystallographic Data Centre as supplementary publication no. CCDC-159924. Copies of the data can be obtained free of charge on application to CCDC, 12 Union Road, Cambridge CB2 1EZ, UK (fax: (+44) 1223-336-033; e-mail: deposit@ccdc.cam.ac.uk). Data were collected at 200 K on a Mac Science DIP2030 imaging plate with graphite-monochromated $Mo_{K\alpha}$ radiation ($\lambda = 0.71073$ Å). Unit cell parameters were determined by autoindexing several images in each data set separately with the program DENZO (Mac Science). For each data set, rotation images were collected in 3° increments with a total rotation of 180° about ϕ. Data were processed by using SCALEPACK. The structure was solved by using the teXsan (Rigaku) system and refined by full-matrix least-squares methods.

Highly Sensitive Novel Biosensor Based on an Immobilized *lac* Repressor**

Ibolya Bontidean, Ashok Kumar, Elisabeth Csöregi, Igor Yu. Galaev, and Bo Mattiasson*

Sequence-specific interactions of proteins with DNA are central to all aspects of the utilization of genetic information in any organism. The lactose repressor of *E. coli* served as a paradigm for such interactions even before the chemical structure of the interacting partners was elucidated.[1] The *lac* repressor protein recognizes the *lac* operator, a particular region of base pairs in the chromosome of *E. coli* and binds to it tightly with a dissociation constant of 10^{-11}–10^{-13} M.[2] Site-specific recognition of DNA by the *lac* repressor is interrupted by an inducer, such as lactose, to allow the production of the enzymes necessary for the utilization of this carbon source.[3] A major conformational change in the *lac* repressor structure takes place as the result of inducer binding.[4, 5] The majority of inducers that bind to the *lac* repressor are galactose derivatives, such as isopropyl-D-thiogalactoside (IPTG), *o*-nitrophenyl-D-galactoside (ONPG), and 1,6-allolactose.[6] Other sugars like *o*-nitrophenylfucoside (ONPF) also bind strongly to the *lac* repressor.[7]

Capacitance measurements have been successfully used as a basis for the construction of biosensors for sensitive detection of the human chorionic gonadotropin (HCG) hormone, by immobilization of antibodies on the electrode surface.[8] Heavy metals can also be detected, with heavy metal binding proteins as recognition elements.[9, 10] The capacitive transduction principle has now been used for the development of a biosensor to monitor inducer molecules or DNA, through the use of a repressor protein as the biological recognition element.

Biosensors prepared by immobilizing the *lac* repressor protein on a gold surface modified with thioctic acid have been used in the experimental set-up presented schematically, along with the detection principle in Figure 1. The specificity of *lac* repressor based biosensors for operator DNA was tested by injections of plasmid p310 DNA, two linearized plasmid DNAs, and genomic DNA. Plasmid p310 DNA (2455 base pairs (bp) in length) was constructed by cloning a 24 bp fragment that contains the *lac* ideal operator into the *Nhe*I site of plasmid pEE4. One linearized plasmid DNA was obtained by digestion of the plasmid p310 DNA with *Eco*RI, and the target *lac* operator (the second linearized plasmid DNA) was excised as an 84 bp fragment by cutting with *Eco*RI and *Hind*III.

[*] Prof. Dr. B. Mattiasson, I. Bontidean, Dr. A. Kumar, Dr. E. Csöregi, Dr. I. Yu. Galaev
Department of Biotechnology
Center for Chemistry and Chemical Engineering
Lund University
22100, Lund (Sweden)
Fax: (+46) 46-222-4713
E-mail: Bo.Mattiasson@biotek.lu.se

[**] This work was supported with grants given by the Swedish Engineering Research Council (TFR). Prof. Muller Hill and Dr. Andrew Barker are acknowledged for providing plasmids and the *Escherichia coli* BMH 8117 strain.

  1433-7851/01/4014-2676 $ 17.50+.50/0

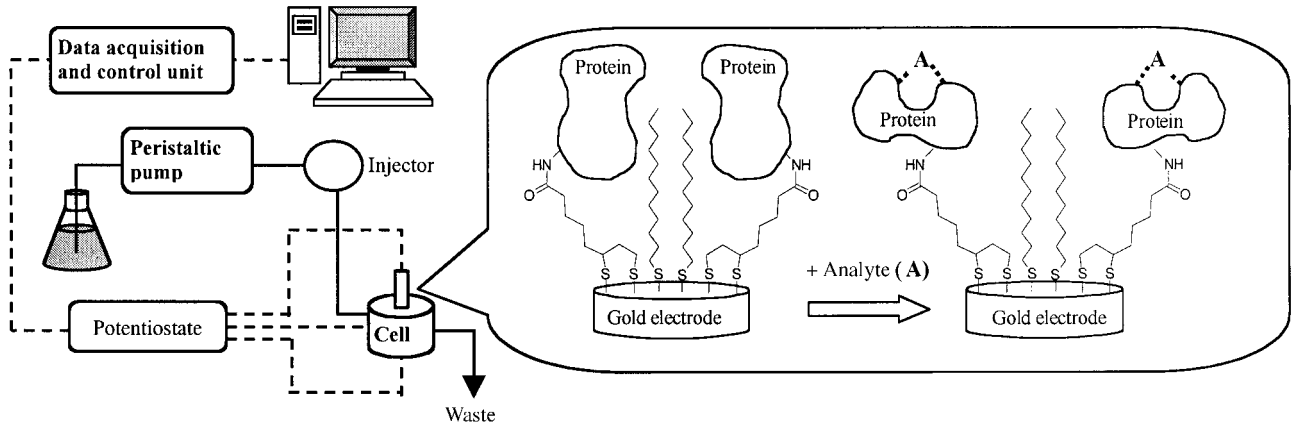

Figure 1. Experimental set-up and detection principle.

The signals obtained (Figure 2) with linearized plasmid DNAs were higher than those obtained for circular plasmid DNA, probably due to the steric constraints that diminish the ability of the *lac* repressor to bind to the operator when the operator is included in the circular plasmid. Nonspecific genomic DNA gave low signals; these results show the ability of the sensor modified with the *lac* repressor to distinguish the operator DNA from the nonoperator genomic DNA or from nonlinearized circular plasmid DNA.

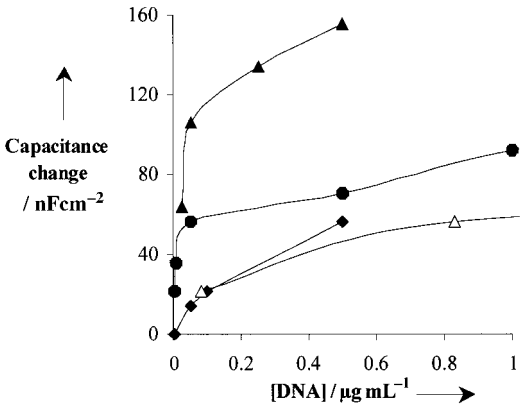

Figure 2. Specificity of the biosensor for different DNA sequences: Plasmid DNA linearized with *Eco*RI (▲); plasmid DNA linearized with *Eco*RI and *Hind*III (●); plasmid DNA (◆); genomic DNA (△). Measurements were carried out in 10 mM potassium phosphate buffer (pH 7.2) containing 1 mM dithiothreitol (DTT) with a flow rate of 0.25 mL min^{-1} and a sample injection volume of 250 μL.

The linearized DNA sequences of different size that contained the *lac* operator produced different capacitance signals (Figure 2). When the linearized plasmid with the complete base sequence (2455 bp) was used, the observed capacitance signal was about threefold higher than the one obtained with the target *lac* operator (84 bp fragment with the mixture of nontarget larger fragment). In the latter case, lower capacitance changes were obtained due to the smaller size of the specific operator fragment. The different sensitivities observed indicate clearly that the electrode modified with the *lac* repressor protein specifically recognizes the operator DNA fragment.

The sensitivity of the modified electrodes towards the inducer molecules decreased in the order: $S_{ONPG} > S_{IPTG} > S_{\alpha\text{-D-lactose}}$ (Figure 3). The sugar derivative with the highest

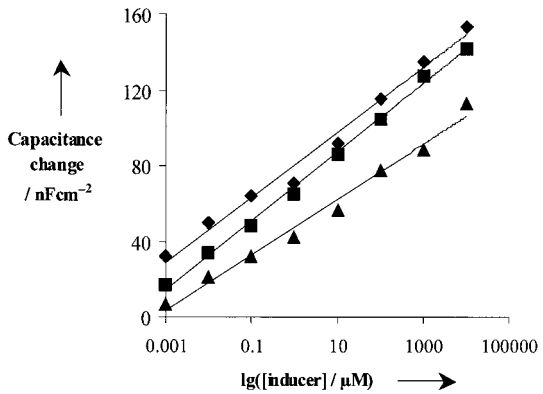

Figure 3. Calibration curves for different inducer molecules: ONPG (◆); IPTG (■); lactose (▲). Experimental conditions were as given in Figure 2.

molecular weight ($M_w = 310$), α-D-lactose, gave the lowest signal, while IPTG ($M_w = 230$) and ONPG ($M_w = 301$) yielded similar higher responses. All three inducers were detected in the 1 nM – 10 mM concentration range. When saturating amounts of IPTG were injected in the system, the sequential injection of the plasmid DNA linearized with *Eco*RI did not cause any further change in capacitance, which suggests that the operator binding did not occur. The binding of the inducer to the immobilized *lac* repressor protein prevents the repressor binding to the operator.

The obtained results clearly demonstrate the possibility of utilizing capacitance biosensors based on the *lac* repressor protein for the assay of specific DNA sequences and inducers in a highly sensitive manner (nanomolar range). The use of repressor proteins in biosensors represents a new general approach in bioanalysis, which is comparable in selectivity and affinity to methods involving monoclonal antibodies (mAbs). However, mAbs are normally not so specific for small molecules like the inducers, and mAbs against specific DNA sequences may be rather difficult to obtain. There are many repressor proteins both in the human proteome and in various bacteria, hence, one could expect numerous repressor pro-

  1433-7851/01/4014-2677 $ 17.50+.50/0

teins to exist which exhibit high selectivity and affinity towards both specific DNA sequences and different inducers.

Experimental Section

Biosensors were prepared by immobilizing the *lac* repressor protein through carbodiimide covalent coupling onto a gold surface modified with thioctic acid.[8] The *lac* repressor was purified as described previously from *Escherichia coli* BMH 8117 (genotype: F^-, Δ(*lac-pro*AB) *thi*, *gyr*A (Nal^R), *supE*, λ).[11] The Ap^R plasmid pWB1000, which constitutively overexpresses wild-type *lac* repressor, and plasmid p310, which contains the *lac* ideal operator, were cloned into the *NheI* site of plasmid pEE4.[12] Competent *E. coli* BMH 8117 cells were transformed with the plasmids according to standard procedures.[13] The cells were grown in double YT medium in 1 L culture flasks at 37 °C with shaking, harvested after 16–20 h of incubation, washed twice with buffer (0.2 M tris(hydroxymethyl)aminomethane–HCl (Tris-HCl; pH 7.2) containing 0.2 M KCl, 10 mM $MgCl_2$, 5% (v/v) glycerol, 1 mM NaN_3, 0.3 mM DTT, and 1 mM phenylmethanesulfonyl fluoride (PMSF)), and stored frozen.

The plasmid DNA containing the *lac* operator was isolated from the cells harboring plasmid p310 with the miniprep Qiagen kit method according to the manufacturer's instructions. When performing measurements with linearized plasmid DNA, the plasmid DNA was digested with *Eco*RI (for the complete 2455 bp sequence) or *Eco*RI and *Hind*III (for the 84 bp sequence). The plasmids were linearized by digestion with the respective enzymes at 37 °C for 1 h.

Gold electrodes were polished, treated with ultrasound, plasma cleaned, and then pretreated with thioctic acid, as described earlier.[8] Next, the thioctic acid self-assembled electrodes were thoroughly washed with pure ethanol, dried, and activated in a 1% solution of 1-(-3-dimethylaminopropyl)-3-ethyl-carbodiimide hydrochloride in dried acetonitrile for 5 h. After washing with 100 mM potassium phosphate buffer (pH 8), the electrodes were dipped into a protein solution (approximately 0.05 mg mL^{-1}) at 4 °C for 24 h. The electrodes were washed again with phosphate buffer and immersed for 20 minutes in a 10 mM solution of 1-dodecanethiol in ethanol. A final washing of the protein-modified electrode with phosphate buffer completed the electrode preparation.

The electrode modified with the *lac* repressor was inserted as the working electrode in a three-electrode flow cell with a dead volume of approximately 10 μL. A platinum foil and a platinum wire served as the auxiliary and reference electrodes, respectively. An extra Ag/AgCl reference electrode was placed in the outlet stream to compare the potential with the platinum reference electrode just before measurements were made. In order to apply 50 mV on the working electrode, a computer was used to compare the potential of the Pt with the potential of the Ag/AgCl before applying the pulse on the working electrode. The carrier buffer (10 mM potassium phosphate buffer, pH 7.2) containing 1 mM DTT was degassed before use and pumped at a flow rate of 0.25 mL min^{-1}. Samples of 250 μL volume were injected in the carrier flow.

Measurements were made as described earlier by applying a 50 mV potential pulse and recording the current transient.[8] The current values were collected with a frequency of 50 kHz, and the first 10 values were used for the evaluation of capacitance.

Received: February 9, 2001 [Z16590]

[1] K. S. Mattews, J. C. Nichols, *Prog. Nucleic Acid Res. Mol. Biol.* **1998**, *58*, 127–164.
[2] B. Müller-Hill, *Prog. Biophys. Mol. Biol.* **1975**, *30*, 227–252.
[3] A. Jobe, S. Bourgeois, *J. Mol. Biol.* **1973**, *75*, 303–313.
[4] M. Matsuura, Y. Ohshima, T. Horiuchi, *Biochem. Biophys. Res. Commun.* **1972**, *47*, 1438–1443.
[5] Y. Oshima, M. Matsuura, T. Horiuchi, *Biochem. Biophys. Res. Commun.* **1972**, *47*, 1444–1450.
[6] M. D. Barkley, A. D. Riggs, S. Bourgeois, *Biochemistry* **1975**, *14*, 1700–1712.
[7] A. D. Riggs, R. F. Newby, S. Bourgeois, *J. Mol. Biol.* **1970**, *51*, 303–314.
[8] C. Berggren, G. Johansson, *Anal. Chem.* **1997**, *69*, 3651–3657.
[9] I. Bontidean, C. Berggren, G. Johansson, E. Csöregi, B. Mattiasson, J. R. Lloyd, K. Jakerman, N. L. Brown, *Anal. Chem.* **1998**, *70*, 4162–4169.
[10] I. Bontidean, J. R. Lloyd, J. L. Hobman, J. R. Wilson, E. Csöregi, B. Mattiasson, N. L. Brown, *J. Inorg. Biochem.* **2000**, *79*, 225–229.
[11] A. Kumar, I. Yu. Galaev, B. Mattiasson, *Bioseparation* **1999**, *8*, 307–316.
[12] A. Barker, R. Fickert, S. Oehler, *J. Mol. Biol.* **1998**, *278*, 549–558.
[13] J. Sambrook, E. F. Fritsch, T. Maniatis, *Molecular Cloning: A Laboratory Manual*, 2nd ed., Cold Spring Harbor Laboratory Press, Cold Spring Harbor, **1989**.

Noncovalent Assembly of [2]Rotaxane Architectures**

Christopher A. Hunter,* Caroline M. R. Low, Martin J. Packer, Sharon E. Spey, Jeremy G. Vinter, Myroslav O. Vysotsky, and Cristiano Zonta

Self-organization is an attractive approach to the construction of complex molecular architectures such as grids, cages, and topological objects.[1–3] The synthesis of catenanes and rotaxanes employs noncovalent binding interactions to template the formation of the covalently interlocked structures.[4] The key noncovalent intermediate is the [2]pseudorotaxane, where a guest molecule is threaded through the plane of a macrocycle.[5, 6] The latent topological properties of this intermediate are kinetically trapped by macrocylization to give [2]catenanes or by the introduction of bulky stopper groups to give [2]rotaxanes. Recently, there have been reports of catenane structures composed of interpenetrating self-assembled macrocycles: metal–ligand interactions have been used to construct [2]catenanes from as many as eight separate molecular components (Figure 1a).[7, 8] To date, only covalent [2]rotaxanes have been constructed using two interlocked molecules.[4, 9] Here we describe a three-molecule approach to noncovalent [2]rotaxane architectures, where the macrocycle self-assembles around a complementary guest (Figure 1b).

[*] Prof. C. A. Hunter, Dr. M. J. Packer, S. E. Spey, Dr. M. O. Vysotsky, C. Zonta
Centre for Chemical Biology
Krebs Institute for Biomolecular Science
Department of Chemistry
University of Sheffield
Sheffield S3 7HF (UK)
Fax: (+44) 114-273-8673
E-mail: C.Hunter@Sheffield.ac.uk
Dr. C. M. R. Low, Dr. J. G. Vinter
James Black Foundation
68 Half Moon Lane, Dulwich
London SE24 9JE (UK)

[**] We thank Dr. C. J. Craven and Dr. J. P. Waltho for the 600 MHz NMR spectra. We also thank the Royal Society/NATO & FCO Chevening (M.O.V.), the Lister Institute (C.A.H.), the EPSRC (M.J.P.), and the James Black Foundation (C.Z.) for funding.

  1433-7851/01/4014-2678 $ 17.50+.50/0

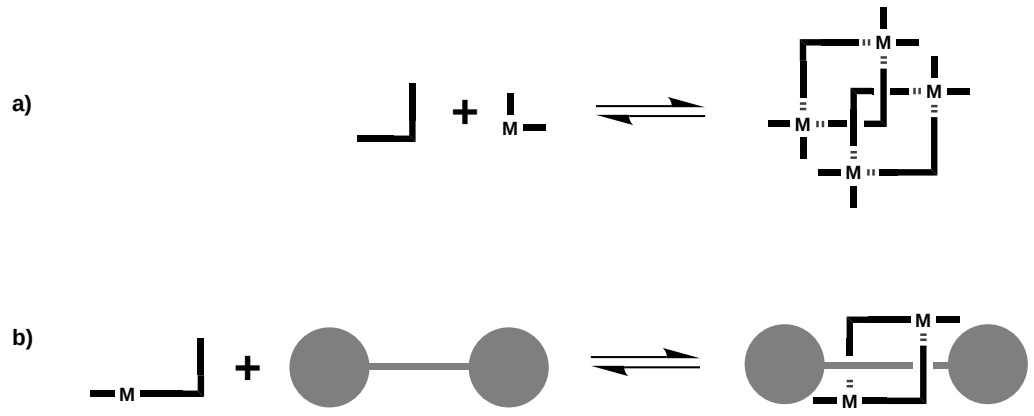

Figure 1. Self-assembly of a) [2]catenanes and b) [2]rotaxanes by using coordination chemistry.

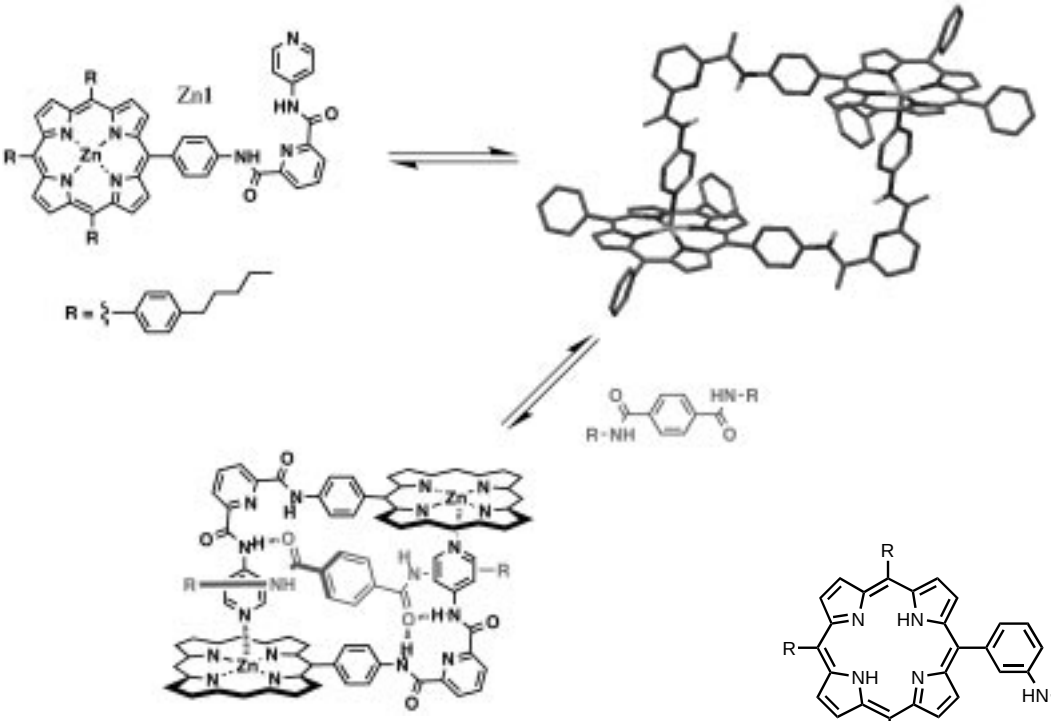

Figure 2. Zn**1** self-assembles to form a dimeric macrocyle. The X-ray crystal structure of the resulting dimer $(Zn\mathbf{1})_2$ is shown, along with a schematic diagram of the complexes formed with terephthalic acid derivatives (solubilizing groups R are omitted for clarity).

We have been studying the self-assembly of macrocyclic porphyrin oligomers through the use of coordination interactions between zinc porphyrin and pyridine.[10] Figure 2 shows the X-ray crystal structure of a macrocyclic porphyrin dimer ($(Zn\mathbf{1})_2$) that we had previously characterized by solution spectroscopy and vapor pressure osmometry and have now confirmed by crystallography.[11] Cooperativity in the macrocyclization process means that this system is exceptionally stable (the dimerization constant is $2 \times 10^8\,M^{-1}$), hence Zn**1** behaves as a macrocycle across a wide range of concentrations in noncompetitive solvents. However, the kinetic lability of the zinc–pyridine interaction means that the dimer is in dynamic equilibrium with the monomer, and here we show how this can be exploited in the construction of [2]rotaxanes.

$(Zn\mathbf{1})_2$ forms 1:1 complexes with terephthalic acid derivatives in chloroform (for diamides $K_a \approx 10^3\,M^{-1}$),[10a] and modeling studies suggest that the geometry of the complex corresponds to a pseudorotaxane architecture (Figure 2). To test this hypothesis we investigated the influence of bulky stopper groups on the dynamic properties of these complexes. Modeling studies suggested that porphyrin end-groups should be sufficiently large to function as stoppers.[12, 13] $H_4\mathbf{2}$ and a model compound **3**, which lacks the stopper groups, were therefore prepared from terephthaloyl dichloride and the corresponding amines.[14]

The ^1H NMR spectrum of mixtures of Zn**1** and $H_4\mathbf{2}$ showed signals corresponding to the pure compounds as well as a set of new resonances. Integration of these signals indicated the formation of a 2:1 complex (namely,

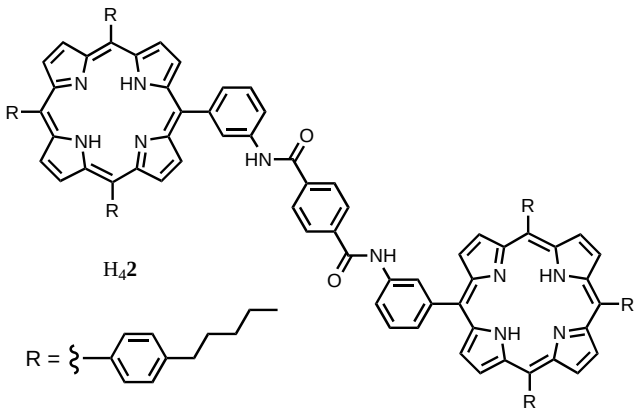

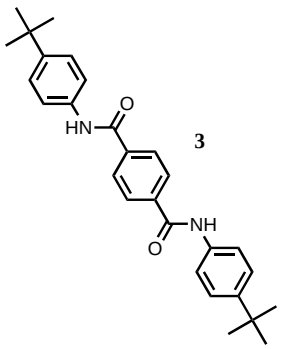

  1433-7851/01/4014-2679 $ 17.50+.50/0

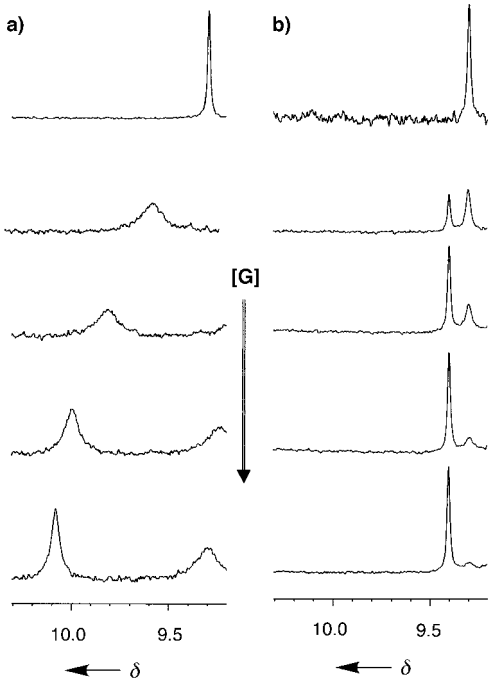

Figure 3. The amide region of the ^{1}H NMR spectra of Zn**1** (0.5 mM) in the presence of increasing amounts of guest (G; 0.2–1.2 mM). a) When the guest is **3**, the free and bound species are in fast exchange, which results in a single averaged signal (the new signal that appears at $\delta = 9.5$ towards the end of the titration is from a different amide). b) When the guest is H_4**2**, distinct slow-exchange signals are observed for the free and bound species.

$(Zn\mathbf{1})_2 \cdot H_4\mathbf{2}$) which is in slow exchange with the free species on the ^{1}H NMR timescale (Figure 3b). A titration experiment yielded an association constant of $1.8 \pm 0.4 \times 10^4\,M^{-1}$. The ^{1}H NMR spectra of mixtures of Zn**1** and **3** showed large changes in the chemical shifts of several signals relative to the corresponding spectra of the pure compounds. However, in contrast to the H_4**2** case, the free and bound species are in fast exchange in this system (Figure 3a). Titration data for the formation of the $(Zn\mathbf{1})_2 \cdot \mathbf{3}$ complex fitted to a 2:1 stoichiometry and gave an association constant of $3.3 \pm 0.9 \times 10^4\,M^{-1}$. The amide protons of $(Zn\mathbf{1})_2$ show upfield complexation-induced changes in their chemical shifts in both complexes (Figure 3), which suggests that the mode of binding for both systems is the formation of the H-bonded complex shown in Figure 2.

The ^{1}H NMR spectra of the $(Zn\mathbf{1})_2 \cdot H_4\mathbf{2}$ complex was extremely complicated, which indicates that the symmetry of both components is broken. However, COSY and ROESY spectra allowed the assignment of all the signals; the complexation-induced changes in chemical shift (CIS) relative to $(Zn\mathbf{1})_2$ and H_4**2** are shown in Figure 4a. The downfield shifts for the signals corresponding to the amide protons of $(Zn\mathbf{1})_2$ are indicative of the presence of hydrogen-bonding interactions. The upfield shift of the NH signal of the H_4**2** pyrrole group and the very large upfield shifts of the signals corresponding to the 2,6-dicarbonylpyridine groups of $(Zn\mathbf{1})_2$ suggest that there are face-to-face aromatic stacking interactions between these subunits in the complex. All of the porphyrin *meso*-phenyl groups lose their symmetry in the complex as a result of a combination of slow rotation around the porphyrin–phenyl bond and the asymmetry of the environments on the two faces of the porphyrin subunits.

Excluding the pentyl side-chains, there are a total of 59 different signals, and this system is therefore ideally suited to NMR structure determination using the CIS values.[15] In

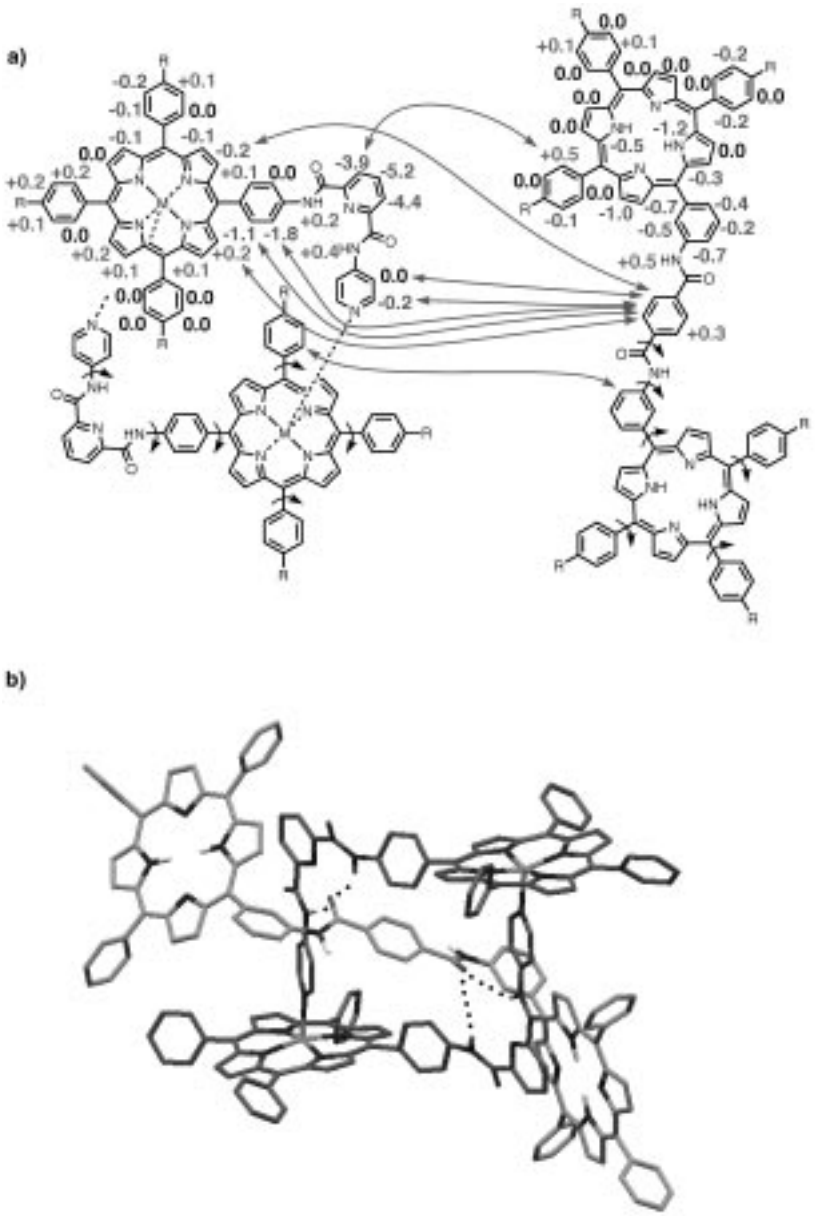

Figure 4. a) Intermolecular NOEs and CIS values obtained from the 400 MHz ROESY spectrum of $(Zn\mathbf{1})_2 \cdot H_4\mathbf{2}$ at 274 K in $CDCl_3$. The two pyrrole NH signals cannot be unambiguously assigned, but the assignment shown matches the calculated CIS values. The bonds that were allowed to rotate in the course of the conformational search are also indicated. Since both molecules have twofold symmetry, only one set of rotatable bonds is marked in each case, but all symmetry-related bonds were allowed to rotate. b) Three-dimensional structure of the $(Zn\mathbf{1})_2 \cdot H_4\mathbf{2}$ rotaxane determined from the NMR data in shown in (a).

  1433-7851/01/4014-2680 $ 17.50+.50/0 *Angew. Chem. Int. Ed.* **2001**, *40*, No. 14

addition, eight intermolecular NOEs were observed in the ROESY experiment (Figure 4a), and these are important for constraining the search space in the structure determination. The two components of the complex, $(Zn\mathbf{1})_2$ and $H_4\mathbf{2}$, were allowed to move and rotate freely relative to one another, and all of the flexible torsions (the phenyl–porphyrin and phenyl/pyridyl–amide bonds indicated in Figure 4a) were varied in the course of the conformational search. The structure for which the 59 calculated CIS values best match the experimental values is illustrated in Figure 4b (rms difference = 0.01 ppm). This structure clearly shows that the complex has the [2]rotaxane architecture illustrated in Figure 1a.

$(Zn\mathbf{1})_2 \cdot H_4\mathbf{2}$ and $(Zn\mathbf{1})_2 \cdot \mathbf{3}$ form complexes with similar structure and stability, but the kinetic properties are quite different. On heating the $(Zn\mathbf{1})_2 \cdot H_4\mathbf{2}$ complex, coalescence of some signals is observed in the ^{1}H NMR spectrum as the system moves into fast exchange, but the complexity of the spectrum and temperature-dependent changes in the populations of the free and bound species makes it difficult to reliably assign all coalescence temperatures. However, coalescence of the signals corresponding to the free and bound amide protons of $(Zn\mathbf{1})_2$ gives an activation energy of 71 ± 3 kJ mol^{-1} at 320 K.[16] On cooling the $(Zn\mathbf{1})_2 \cdot \mathbf{3}$ complex, some signals in the ^{1}H NMR spectrum broaden and split. Coalescence of the signals arising from the free and bound pyridine protons of $(Zn\mathbf{1})_2$ gives an activation energy of 60 ± 2 kJ mol^{-1} at 255 K. Thus the barrier to exchange between free and bound species is significantly larger for $(Zn\mathbf{1})_2 \cdot H_4\mathbf{2}$ than for $(Zn\mathbf{1})_2 \cdot \mathbf{3}$. We interpret this as evidence for the two different exchange pathways illustrated in Figure 5: $(Zn\mathbf{1})_2 \cdot \mathbf{3}$ forms a [2]pseudorotaxane where there is no significant barrier to exit and entry of **3** in the macrocycle, while $(Zn\mathbf{1})_2 \cdot H_4\mathbf{2}$ forms a [2]rotaxane where exit or entry of $H_4\mathbf{2}$ requires opening of the macrocycle by breaking one of the coordination bonds.

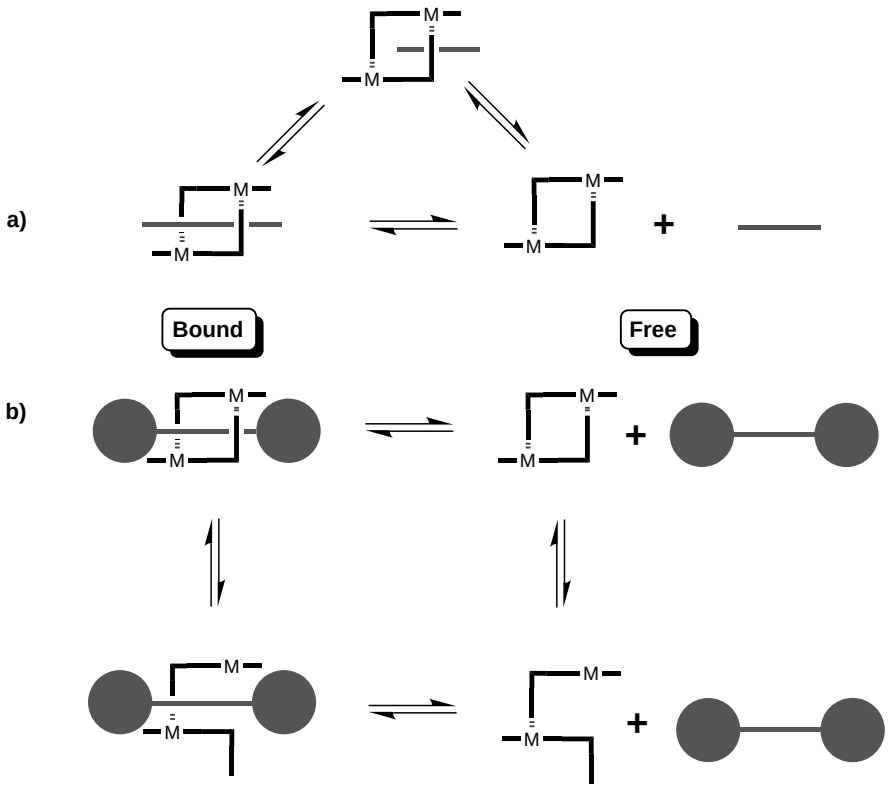

Figure 5. Pathways involved in exchange between free and bound species. a) In a pseudorotaxane, the guest slips directly out of the macrocycle. b) In a rotaxane, the macrocycle must be opened before the guest can depart.

In conclusion, we have demonstrated that self-assembled macrocycles can be used in the construction of stable [2]rotaxane architectures. The photochemical properties of the porphyrin subunits should confer this system with interesting photophysical properties: for example, singlet energy transfer between the macrocycle and axle components.[17]

Experimental Section

$H_4\mathbf{2}$: A solution of 5,10,15-tris(4-*n*-pentylphenyl)-20-(3-aminophenyl)-21*H*,23*H*-porphin[14] (0.2856 g, 0.34 mmol) and triethylamine (0.07 mL, 0.51 mmol) in dry dichloromethane (10 mL) was added to a solution of terephthaloyl dichloride (0.0172 g, 85 mmol) in dry dichloromethane (20 mL), and the reaction mixture was left stirring overnight at room temperature. After evaporation of the solvent under reduced pressure, the products were separated by column chromatography on silica gel using a mixture of dichloromethane/triethylamine (2500/1) as eluant. After recrystallization from $CHCl_3/CH_3OH$ (1/2), 0.0573 g (37%) of $H_4\mathbf{2}$ were obtained. M.p. 204–206 °C; ^{1}H NMR (400 MHz, $CDCl_3$, 20 °C, $c = 1.105 \times 10^{-3}$ M, TMS): $\delta = 8.84$ (s, 16H, CH), 8.26 (s, 2H, NH), 8.19 (d, $^3J(H,H) = 8$ Hz, 2H, CH), 8.07 (m, 12H, CH), 8.00 (br s, 4H, CH), 7.86 (s, 4H, CH), 7.68 (t, $^3J(H,H) = 8$ Hz, 2H, CH), 7.51 (m, 12H, CH), 2.91 (t, $^3J(H,H) = 7.2$ Hz, 4H, CH_2), 2.89 (t, $^3J(H,H) = 7.6$ Hz, 8H, CH_2), 1.88 (m, 12H, CH_2), 1.49 (m, 24H, CH_2), 1.01 (t, $^3J(H,H) = 7.2$ Hz, 6H, CH_3), 0.99 (t, $^3J(H,H) = 7.2$ Hz, 12H, CH_3), −2.80 (s, 4H, NH); UV/Vis (dichloromethane): λ_{max} (ε) = 648 (6900), 592 (7560), 552 (11700), 515 (20500), 419 nm (401000); FAB-MS: *m*/*z* (%): 1811 (100) $[M+H]^+$; calcd for $C_{126}H_{124}N_{10}O_2$: $[M]^+$: 1810.

3: 4-*tert*-Butylaniline (2.40 g, 16.1 mmol) was added to a solution of terephthaloyl dichloride (0.5448 g, 2.68 mmol) in dry dichloromethane (50 mL), and the reaction mixture was left at room temperature overnight with stirring. After cooling the reaction mixture to room temperature, it was evaporated to dryness under reduced pressure, then THF (50 mL) was added. The ammonium salt crystallized out of solution, and after filtration, the solution was evaporated under reduced pressure, and the white crystalline compound was recrystallized from a mixture of ethanol (63 mL) and water (13 mL). The solid was filtered and dried under vacuum for 4 h to yield 0.658 g (57%) of desired product **3**. M.p. > 270 °C; ^{1}H NMR (400 MHz, [D$_6$]DMSO, 20 °C, TMS): $\delta = 10.31$ (s, 2H, NH), 8.09 (s, 4H, CH), 7.71 (d, 4H, $^3J(H,H) = 8.9$ Hz, CH), 7.38 (d, 4H, $^3J(H,H) = 8.9$ Hz, CH), 1.29 (s, 18H, CH_3); FAB-MS: *m*/*z* (%): 429 (100) $[M+H]^+$. Elemental analysis calcd (%) for $C_{28}H_{32}N_2O_2$: C 78.47, H 7.53, N 6.53; found: C 78.63, H 7.49, N 6.42.

NMR structure determination: The method used to determine the three-dimensional structures from CIS values has been described in detail elsewhere.[15] The structure of the $(Zn\mathbf{1})_2$ dimer was taken from the X-ray crystal structure and the $H_4\mathbf{2}$ moiety was built in XED 2.8 using standard bond lengths and angles.[18] A genetic algorithm was used to optimize the conformation of the complex so that the calculated CIS values matched the experimental values as closely as possible. We allowed intermolecular

translation (±5 Å) and rotation (±180°) as well as intramolecular torsional changes (±180°) for the 24 bonds highlighted in Figure 4a. The pentyl side-chains were ignored since their conformation is not defined by the experimental data. van der Waals clashes were penalized at distances of less than 2 Å for intermolecular clashes and 1 Å for intramolecular clashes for non-hydrogen atoms. The eight NOE constraints illustrated in Figure 4a were imposed by applying a penalty if the inter-proton separation exceeded 6 Å. The search converged to a value of $R_{expt}/R_{\Delta\delta}$ of 11 in about 6000 generations for a population of 1000 (R_{expt} is the root mean square (rms) of the experimentally observed CIS values, and $R_{\Delta\delta}$ is the rms difference between the calculated and experimental values).

Received: February 12, 2001 [Z16598]

[1] J.-M. Lehn, *Supramolecular Chemistry—Concepts and Perspectives*, VCH, Weinheim, **1995**.

[2] a) N. Branda, P. Wyler, J. Rebek, Jr., *Science* **1994**, *263*, 1267–1268; b) K. D. Shimizu, J. Rebek, Jr., *Proc. Natl. Acad. Sci. USA* **1995**, *92*, 12403–12407; c) B. Olenyuk, A. Fechtenkotter, P. J. Stang, *J. Chem. Soc. Dalton Trans.* **1998**, 1707–1728; d) M. Fujita, S.-Y. Yu, T. Kusukawa, H. Funaki, K. Ogura, K. Yamaguchi, *Angew. Chem.* **1998**, *110*, 2192–2196; *Angew. Chem. Int. Ed.* **1998**, *37*, 2082–2085.

[3] a) D. B. Amabilino, J. F. Stoddart, *Chem. Rev.* **1995**, *95*, 2725–2828; b) S.-G. Roh, K.-M. Park, G.-J. Park, S. Sakamoto, K. Yamaguchi, K. Kim, *Angew. Chem.* **1999**, *111*, 672–675; *Angew. Chem. Int. Ed.* **1999**, *38*, 638–640.

[4] a) P. R. Ashton, E. J. T. Chrystal, P. T. Glink, S. Menzer, C. Schiavo, N. Spencer, J. F. Stoddart, P. A. Tasker, A. J. P. White, D. J. Williams, *Chem. Eur. J.* **1996**, *2*, 709–728; b) P. N. W. Baxter, H. Sleiman, J.-M. Lehn, K. Rissanen, *Angew. Chem.* **1997**, *109*, 1350–1352; *Angew. Chem. Int. Ed. Engl.* **1997**, *36*, 1294–1296; c) C. Gong, H. W. Gibson, *Angew. Chem.* **1998**, *110*, 323–327; *Angew. Chem. Int. Ed.* **1998**, *37*, 310–314; d) R. E. Gillard, F. M. Raymo, J. F. Stoddart, *Chem. Eur. J.* **1997**, *3*, 1933–1940; e) M. Gomez-Lopez, J. F. Stoddart, *Bull. Soc. Chim. Belg.* **1997**, *106*, 491–500; f) D. A. Leigh, A. Murphy, J. P. Smart, A. M. Z. Slawin, *Angew. Chem.* **1997**, *109*, 736–756; *Angew. Chem. Int. Ed. Engl.* **1997**, *36*, 728–732; g) S. Anderson, H. L. Anderson, *Angew. Chem.* **1996**, *108*, 2075–2078; *Angew. Chem. Int. Ed. Engl.* **1996**, *35*, 1956–1959; h) H. L. Anderson, M. R. Craig, T. D. W. Claridge, M. G. Hutchings, *Chem. Commun.* **1999**, 1537–1538; i) A. Lütringhaus, F. Cramer, H. Prinzbach, F. M. Henglein, *Justus Liebigs Ann. Chem.* **1958**, *185*, 183; j) R. S. Wylie, D. H. Macartney, *J. Am. Chem. Soc.* **1992**, *114*, 3136–3138; k) G. Wenz, E. von der Bey, L. Schmidt, *Angew. Chem.* **1992**, *104*, 758–710; *Angew. Chem. Int. Ed. Engl.* **1992**, *31*, 783–785.

[5] P. R. Ashton, D. Philp, N. Spencer, J. F. Stoddart, *J. Chem. Soc. Chem. Commun.* **1991**, 1677–1679.

[6] G. A. Breault, C. A. Hunter, P. C. Mayers, *Tetrahedron* **1999**, *55*, 5265–5293.

[7] a) M. Fujita, F. Ibukuro, H. Hagihara, K. Ogura, *Nature* **1994**, *367*, 720–723; b) M. Fujita, M. Ayoagi, F. Ibukuro, K. Ogura, K. Yamaguchi, *J. Am. Chem. Soc.* **1998**, *120*, 611; c) M. Fujita, *Acc. Chem. Res.* **1999**, *32*, 53–61.

[8] A. C. Try, M. M. Harding, D. G. Hamilton, J. K. M. Sanders, *Chem. Commun.* **1998**, 723–724.

[9] During the course of this work, a related rotaxane structure was reported in which the cyclic component was closed by coordination interactions; see K.-S. Jeong, J. S. Choi, S.-Y. Chang, H.-Y. Chang, *Angew. Chem.* **2000**, *112*, 1758–1761; *Angew. Chem. Int. Ed.* **2000**, *39*, 1692–1695.

[10] a) C. A. Hunter, L. D. Sarson, *Angew. Chem.* **1994**, *106*, 2424–2427; *Angew. Chem. Int. Ed. Engl.* **1994**, *33*, 2313–2316; b) X. Chi, A. J. Guerin, R. A. Haycock, C. A. Hunter, L. D. Sarson, *J. Chem. Soc. Chem. Commun.* **1995**, 2567–2569; X. Chi, A. J. Guerin, R. A. Haycock, C. A. Hunter, L. D. Sarson, *J. Chem. Soc. Chem. Commun.* **1995**, 2563–2565.

[11] Crystal data for $C_{142}H_{132}N_{16}O_4Zn_2$, $M_r = 2257.38$, crystallizes from chloroform as purple blocks, crystal dimensions $0.18 \times 0.16 \times 0.07$ mm. Triclinic, space group $P\bar{1}$ (C_i^1, no. 2), $a = 11.676(7)$, $b = 16.849(10)$, $c = 17.478(11)$ Å, $\alpha = 116.307(12)$, $\beta = 100.205(14)$, $\gamma = 95.904(13)°$, $U = 2969(3)$ Å^3, $Z = 1$, $\rho_{calcd} = 1.263$ Mg m^3, $Mo_{K\alpha}$ radiation ($\lambda = 0.71073$ Å), $\mu(Mo_{K\alpha}) = 0.468$ mm^{-1}, $F(000) = 1188$. Data collected were measured on a Bruker Smart CCD area detector with Oxford Cryosystems low-temperature system. Cell parameters were refined from the setting angles of 78 reflections (range $1.34 < \theta < 28.47°$). Crystallographic data (excluding structure factors) for the structure reported in this paper have been deposited with the Cambridge Crystallographic Data Centre as supplementary publication no. CCDC-157703. Copies of the data can be obtained free of charge on application to CCDC, 12 Union Road, Cambridge CB2 1EZ, UK (fax: (+44) 1223-336-033; e-mail: deposit@ccdc.cam.ac.uk

[12] P. R. Ashton, I. Baxter, M. C. T. Fyfe, F. M. Raymo, N. Spencer, J. F. Stoddart, A. J. P. White, D. J. Williams, *J. Am. Chem. Soc.* **1998**, *120*, 2297–2307.

[13] a) J.-C. Chambron, S. Chardon-Noblat, A. Harriman, V. Heitz, J.-P. Sauvage, *Pure Appl. Chem.* **1993**, *11*, 2343–2349; b) J.-C. Chambron, J.-P. Sauvage, *Chem. Eur. J.* **1998**, *4*, 1362–1366.

[14] M. Gardner, A. J. Guerin, C. A. Hunter, U. Michelsen, C. Rotger, *New J. Chem.* **1999**, 309–316.

[15] C. A. Hunter, M. J. Packer, *Chem. Eur. J.* **1999**, 5, 1891–1897.

[16] J. Sandström, *Dynamic NMR Spectroscopy*, Academic Press, London, **1982**, p. 77–123.

[17] R. A. Haycock, A. Yartsev, U. Michelsen, V. Sundstrom, C. A. Hunter, *Angew. Chem.* **2000**, *112*, 3616–3619; *Angew. Chem. Int. Ed.* **2000**, *39*, 3762–3765.

[18] J. G. Vinter, *J. Comput. Aided Mol. Des.* **1994**, *8*, 653–668.

Synthetic seco Forms of (−)-Diazonamide A**

Jing Li, Xin Chen, Anthony W. G. Burgett, and Patrick G. Harran*

Diazonamide A (**1**, Scheme 1) is a uniquely structured peptide metabolite whose potential pharmacological value and low natural abundance[1] have fueled an interest in its preparation—a pursuit that continues to gain momentum.[2] Our studies[3] in this area have centered upon a ring-contracting glycol rearrangement that stereoselectively assembles a central diazonamide C10 triarylacetaldehyde. Elaborations on this core provide intermediate **2**, wherein D/E biaryl synthesis was to occur through oxidation; the event timed late to obviate consideration of fixed axial chirality maintained in the eastern region of **1**.[2c,h] Notably, both aerobic and anaerobic oxidations of **2** generate biaryl ether **3** rather than the target D/E biaryl compound.[4] This fact was not directly recognized and experiments attempting to transform **3** into **1** would come to highlight additional limitations of the design; particularly in its provisions for oxidation state adjustment at C11 and peripheral halogenations. These

[*] Prof. P. G. Harran, J. Li, X. Chen, A. W. G. Burgett
Department of Biochemistry
University of Texas, Southwestern Medical Center at Dallas
Dallas, TX 75390-9038 (USA)
Fax: (+1) 214-648-6455
E-mail: pharra@biochem.swmed.edu

[**] We thank Prof. Michael Roth for advice and insight and Ms. Susan Jeong for invaluable experimental assistance. Funding was provided by the NIH (RO1-GM60591), the NSF (CAREER 9984282), the Howard Hughes Medical Institute (junior faculty support), and the Robert A. Welch Foundation.

  1433-7851/01/4014-2682 $ 17.50+.50/0

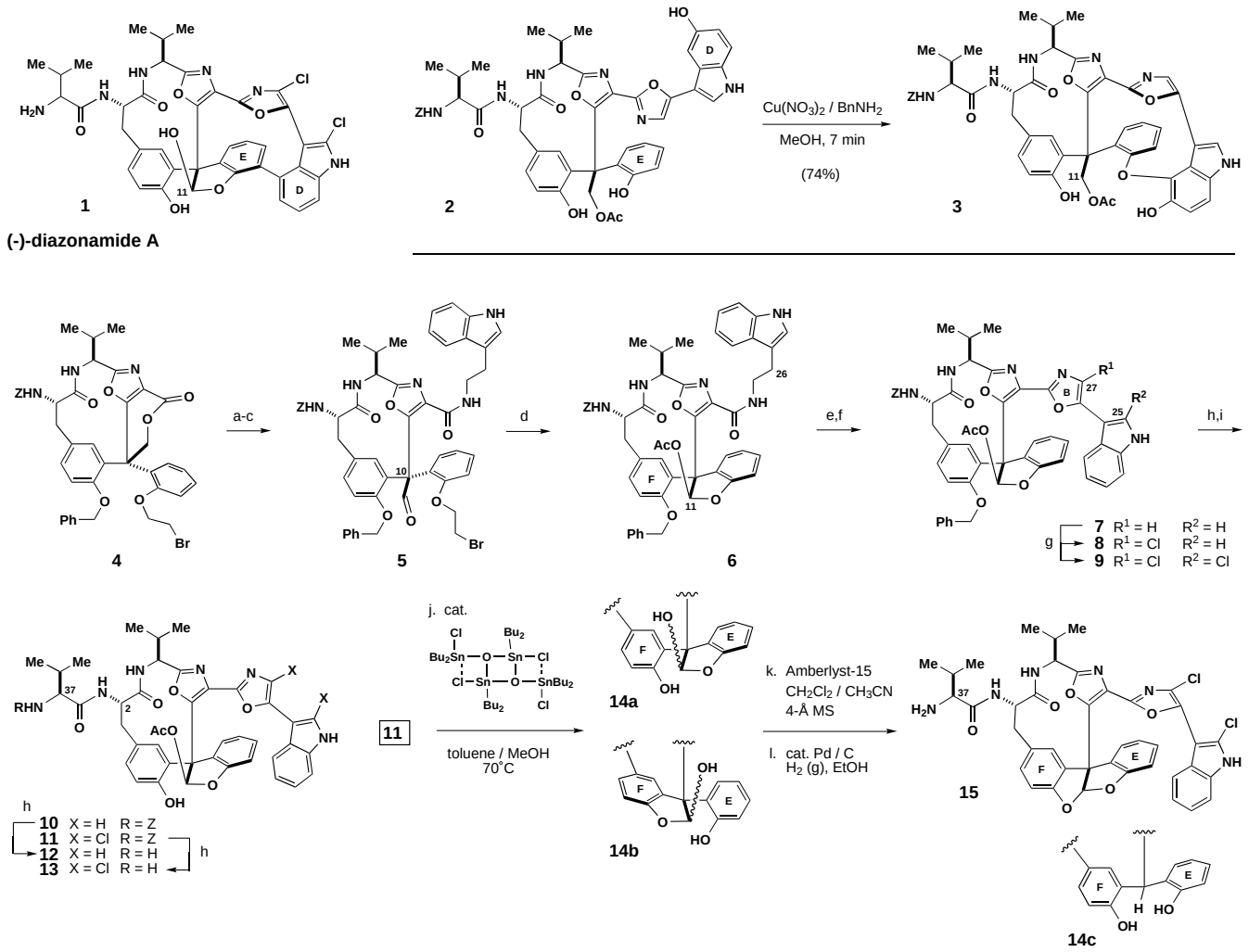

Scheme 1. Reaction conditions: a) LiOH, THF/H_2O; b) Dess–Martin periodinane, CH_2Cl_2; c) tryptamine hydrochloride, HATU, $(i\text{Pr})_2\text{NEt}$, DMF, $-30\,^\circ\text{C}$ (60% from **4**); d) Rieke zinc (excess), THF, $0\,^\circ\text{C}$; Ac_2O quench (74%); e) DDQ, THF/H_2O (82%); f) $(Cl_3C)_2$, Ph_3P, Et_3N, THF (77%); g) NCS (2.1 equiv), CCl_4/THF, $35\,^\circ\text{C}$, 14 h (85%); h) Pd black, 1 atm H_2(g), MeOH; i) Z-L-Val-OH, TBTU, $(i\text{Pr})_2\text{NEt}$, DMF. HATU = *O*-(7-azabenzotriazol-1-yl)-*N*,*N*,*N*′,*N*′-tetramethyluronium hexafluorophosphate, DDQ = 2,3-dichloro-5,6-dicyano-1,4-benzoquinone, TBTU = 2-(1*H*-benzotriazol-1-yl)-1,1,3,3-tetramethyluronium tetrafluoroborate.

aspects of the problem prompted a model study that culminates in the synthesis of structure **15**. Polycycle **15** is a desiccated, two-electron reduction product of **1** which is biologically active and luminescent upon photoexcitation.

Valerolactone **4** (Scheme 1) is a common precursor of advanced synthetic intermediates. The central features of the sequence used to prepare this compound have been published.[3a] Hydrolysis of its lactone ring, periodinane oxidation of the resultant neopentyl carbinol, and incorporation of tryptamine by amidation affords triarylacetaldehyde **5**. Aldehydes of this type are susceptible to deformylation (generating a corresponding C10 triarylmethane) under various conditions, and progress requires a tailored protection/deprotection scheme. Protection is achieved by subjecting **5** to active-zinc reduction[5] to initiate ethylene extrusion, and the metallohemiacetal putatively formed in situ is intercepted with Ac_2O. α-Acetoxybenzofuran **6** is thus conveniently generated as a single diastereomer (likely *S*-configured at C11)[6] in 74% yield. Four-electron oxidation at the indole benzylic position (C26) of **6**, and dehydration of the resultant β-keto amide,[2k] closes the B-ring to afford **7**. Halogenation of the 3-oxazoylindole segment in this context is controlled and facile. *N*-chlorosuccinimide (NCS) halogenates **7** at positions C27 and C25, in that order. Monochloride **8** can be isolated or **7** can be converted directly into bischloride **9**.[7] Re-exposing **8** to NCS provides **9** although, beginning with **7** or **8**, reagent stoichiometry must be metered to avoid production of a trichlorinated indolenine contaminant.[8]

Chlorine substituents do not interfere with the hydrogenolytic removal of protecting groups. For example, **11** is efficiently produced from **9** by heterogeneous hydrogenolysis followed by condensing the amine liberated at C2 with Z-L-Val-OH (Z = benzyloxycarbonyl). Bis(des-chloro) congener **10** is similarly prepared. Difficulty arises only when attempting to unmask the hemiacetal at C11. Alkaline hydrolysis induces deformylative degradation, the 2-chloroindole ring is intolerant of aqueous acid, and anhydrous acid treatment leads (inefficiently) to a C11 diphenyl acetal (see below). In our hands, transesterification with methanol catalyzed by an Otera stannoxane is uniquely successful.[9] Under these

  1433-7851/01/4014-2683 $ 17.50+.50/0

conditions **11** converts into a free hemiacetal in near quantitative yield. The ^{1}H NMR spectra of the product show the signals are broadened and temperature-dependent in hydroxylic solvents, but sharp at RT in [D_8]THF. However, the precise structure and configuration of this species (for example, **14a** versus **14b**) has not been assigned; a task complicated by increasing contamination on handling.[10] Fortunately, dehydrating the molecule with acidic resin gives a stable diphenyl acetal whose hydrogenolysis provides structure **15**.

The pathway to **15** represents an intact model for late-stage diazonamide functional group manipulations. In addition, this compound and its phenolic hemiacetal congeners have provided an initial look into diazonamide structure/activity relationships. Compounds **13** and **15** inhibit the growth of cultured human malignant melanoma SK-MEL-5 in a time and dose-dependent manner ($GI_{50} = 7$ and 9 μM, respectively).[11] However, while data indicates that **1** may target the mitotic machinery in mammalian cells,[1d,e] we find no evidence for **12**–**15** acting similarly. For example, flow cytometry studies show that cultures of human colorectal carcinoma HCT-116 incubated with **13** ($GI_{50} = 22$ μM) do not accumulate as a tetraploid population. Moreover, immunofluorescence microscopy fails to detect any effects on cytosolic tubulin architecture or an impairment of mitotic cell division (data not shown). This last experiment images a fluorescent antibody that recognizes an epitope on α-tubulin. Notably, compounds **12**–**15** themselves emit a blue luminescence upon ultraviolet photoexcitation (Figure 1B).[12] We have been able to directly visualize the uptake and localization of **13** in living cultures of human ovarian adenocarcinoma OVCAR-3. In comparison to an over-exposed negative control (Figure 1C), OVCAR-3 cells incubated with **13** (100 μM, 37 °C), washed, and imaged[13] show a bright perinuclear fluorescence which concentrates in vesicular patterns over several hours (Figure 1D). Luminescent **13** is clearly membrane permeant and appears not to associate with cytoskeletal elements. Interpretation of the results would be premature, since we lack a positive control (namely, **1**) and **13** is about 10^3-fold less toxic towards OVCAR-3 than is **1**.[1d] However, in all likelihood, the cellular toxicity manifested by these topographically altered forms of diazonamide is through mechanisms unrelated to that of the natural product. To address the latter, we are using experience gained in preparing **13**–**15** to re-approach synthetic diazonamides along new pathways. For example, in an effort to shift reliance away from one-electron oxidation methods to a reversible, heterolytic process for synthesis of the D/E biaryl bond, we have recently prepared 7-hydroxytryptamine conjugate **16** (Scheme 2).

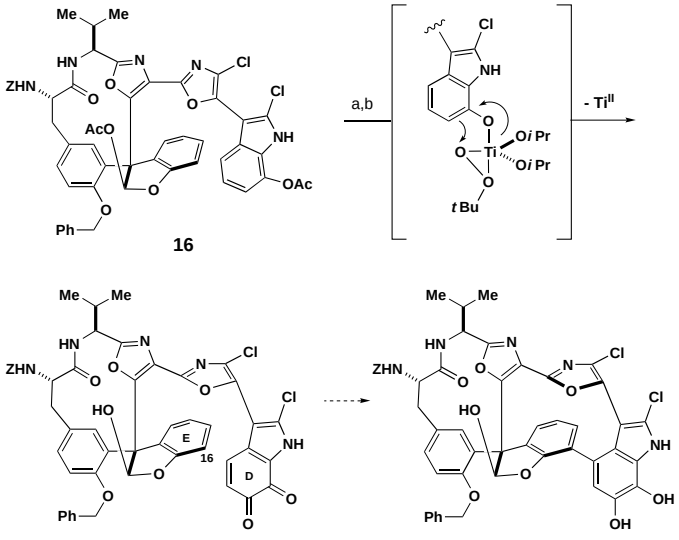

Scheme 2. Reaction conditions: a) 20 mol% $[Bu_2Sn(O)Cl]_2$, toluene/MeOH 70 °C (91%); b) $(i\text{PrO})_4\text{Ti}$ (2 equiv), 3-Å molecular sieve, CH_2Cl_2, −10 °C; tBuOOH (5 equiv), −10° → 0 °C; aq $(COOH)_2$ (65% at ≈70% conversion).

Catalyzed deacetylation of this material followed by a novel, regioselective α-hydroxylation of the resultant 7-hydroxyindole[14] provides the blood-red indoloquinone **17**. One might envision that acid activation of **17** will engage the indoloquinone with the E-ring phenol in a reversible Michael addition—a C–C-bonded product of which is a prototropic form of indolocatechol **18**. This idea is laden with challenge,[15] yet it finds compelling analogy in the putative biogenesis of the tryptophan tryptophylquinone prosthetic cofactor of methylamine dehydrogenase.[16]

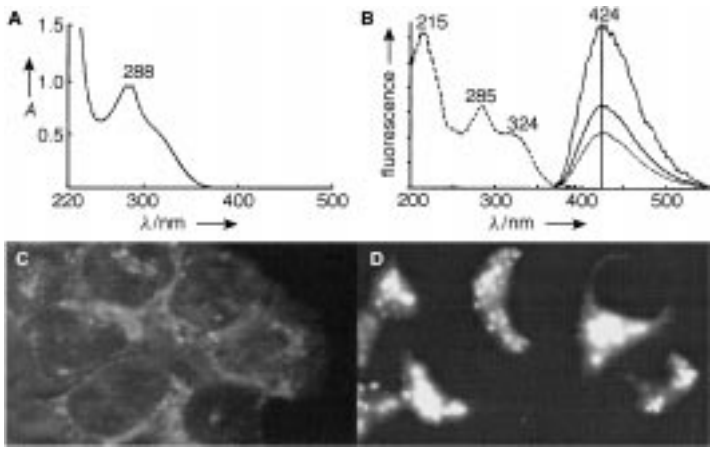

Figure 1. A) UV/Vis spectrum of **13** (64 μM in MeOH), $\varepsilon =$ 1790 L mol^{-1} cm^{-1} at 324 nm. B) Normalized fluorescence excitation (dashed) and emission (solid) spectra of **13** (2.8 μM in MeOH). C) Digital fluorescence micrograph (63×) of untreated OVCAR-3 cells (5.8 s exposure). D) Digital fluorescence micrograph (100×) of OVCAR-3 cells (1.7 s exposure) pre-incubated with **13** (100 μM, 12 h, 37 °C).

Experimental Section

15: Amberlyst-15 resin (ca. 85 mg) and 4-Å molecular sieves (ca. 75 mg) were added to a solution of crude **14** (7.6 mg, 8.2 μmol) in anhydrous CH_3CN (200 μL) and CH_2Cl_2 (1.5 mL). The mixture was warmed to 32 °C and stirred for 14 h. Filtration (EtOAc transfer), concentration, and purification by flash chromatography (SiO_2, EtOAc/benzene 3/7) afforded a cream film (7.1 mg, 84%; $R_f = 0.42$ (EtOAc/benzene 4/6); electrospray-MS (ES-MS): calcd for $C_{48}H_{42}Cl_2N_6O_8$ $[M+H]^+$: 901.25, found: 901.20; calcd for $C_{48}H_{42}Cl_2N_6O_8$ $[M-H]^-$: 899.23, found: 899.16). This residue (7.8 μmol) was dissolved in absolute ethanol (0.9 mL) and 10% Pd/C (2 mg) added. The mixture was placed under balloon-pressure H_2 and stirred vigorously for 1 h. Filtration through celite and concentration provided material which was purified by preparative thin-layer chroma-

  1433-7851/01/4014-2684 $ 17.50+.50/0 *Angew. Chem. Int. Ed.* **2001**, *40*, No. 14

tography (SiO_2, MeOH/CH_2Cl_2 1/9) to afford **15** (3.7 mg, 62%). $R_f = 0.14$ (MeOH/CH_2Cl_2 1/9); $[\alpha]_D^{25} = -219.1^\circ$ ($c = 0.14$, MeOH); IR (film): $\tilde{\nu} =$ 3278, 3062, 2962, 2928, 2873, 1652, 1492, 1462, 1342, 1248, 1066, 954, 904, 746 cm^{-1}; ^1H NMR (400 MHz, [D$_8$]THF, 25 °C): $\delta = 7.88-7.84$ (m, 2H), 7.49–7.46 (m, 1H), 7.40 (d, $J = 1.8$ Hz, 1H), 7.35–7.32 (m, 2H), 7.27–7.00 (m, 6H), 6.85 (d, $J = 8.2$ Hz, 1H), 6.79 (td, $J = 7.5$, 0.9 Hz, 1H), 6.71 (d, $J =$ 8.1 Hz, 1H), 4.95 (dd, $J = 7.3$, 1.3 Hz, 1H), 4.37–4.31 (m, 1H), 3.25 (t, $J =$ 12.0 Hz, 1H), 3.03 (d, $J = 4.4$ Hz, 1H), 2.69 (dd, $J = 12.4$, 3.4 Hz, 1H), 2.21–2.16 (m, 2H), 2.02–2.00 (m, 2H), 1.09 (d, $J = 6.8$ Hz, 3H), 0.98 (d, $J =$ 6.8 Hz, 3H), 0.94 (d, $J = 6.8$ Hz, 3H), 0.86 (d, $J = 7.0$ Hz, 3H); ES-MS: calcd for $C_{40}H_{36}Cl_2N_6O_6$ $[M+H]^+$: 767.22, found: 767.34; calcd for $C_{40}H_{36}Cl_2N_6O_6$ $[M-H]^-$: 765.20, found: 765.30; HR-MS (FAB) calcd for $C_{40}H_{36}Cl_2N_6O_6$ $[M+Li]$: 773.2233, found: 773.2248.

Received: April 23, 2001 [Z16981]

[1] a) N. Lindquist, W. Fenical, G. D. Van Duyne, J. Clardy, *J. Am. Chem. Soc*. **1991**, *113*, 2303–2304; b) N. Lindquist, PhD thesis, University of California, San Diego, CA, **1989**; c) C. Petit, *San Francisco Chronicle*, January 31, **1997**, p. A4; d) COMPARE analysis of **1** was completed at the National Cancer Institute (Developmental Therapeutics Program) on December 1, 1997; NSC: D-700089-Y/1. Exp. ID:9712SR87-64; e) W. Fenical, personal communication.

[2] a) J. D. Kreisberg, P. Magnus, E. G. McIver, *Tetrahedron Lett.* **2001**, *42*, 627–629; b) P. Wipf, J. L. Methot, *Org. Lett.* **2001**, *3*, 1261–1264; c) K. C. Nicolaou, S. A. Snyder, K. B. Simonsen, A. E. Koumbis, *Angew. Chem.* **2000**, *112*, 3615–3620; *Angew. Chem. Int. Ed.* **2000**, *39*, 3473–3478; d) D. E. Fuerst, B. M. Stoltz, J. L. Wood, *Org. Lett*. **2000**, *2*, 3521–3523; e) M. C. Bagley, C. J. Moody, A. G. Pepper, *Tetrahedron Lett*. **2000**, *41*, 6901–6904; f) M. C. Bagley, S. L. Hind, C. J. Moody, *Tetrahedron Lett*. **2000**, *41*, 6897–6900; g) F. Lach, C. J. Moody, *Tetrahedron Lett*. **2000**, *41*, 6893–6896; h) E. Vedejs, D. A. Barda, *Org. Lett.* **2000**, *2*, 1033–1035; i) E. Vedejs, J. Wang, *Org. Lett.* **2000**, *2*, 1031–1032; j) P. Magnus, E. G. McIver, *Tetrahedron Lett*. **2000**, *41*, 831–834; k) F. Chan, P. Magnus, E. G. McIver, *Tetrahedron Lett*. **2000**, *41*, 835–838; l) H. C. Hang, E. Drotleff, G. I. Elliott, T. A. Ritsema, J. P. Konopelski, *Synthesis* **1999**, 398–400; m) P. Magnus, J. D. Kreisberg, *Tetrahedron Lett*. **1999**, *40*, 451–454; n) A. Boto, M. Ling, G. Meek, G. Pattenden, *Tetrahedron Lett*. **1998**, *39*, 8167–8170; o) P. Wipf, F. Yokokawa, *Tetrahedron Lett*. **1998**, *39*, 2223–2226; p) T. F. Jamison, PhD thesis, Harvard University, Cambridge, MA, **1997**; q) C. J. Moody, K. J. Doyle, M. C. Elliott, T. J. Mowlem, *J. Chem. Soc. Perkin Trans. 1* **1997**, *16*, 2413–2419; r) J. P. Konopelski, J. M. Hottenroth, H. M. Oltra, E. A. Véliz, Z. C. Yang, *Synlett* **1996**, 609–611; s) C. J. Moody, K. J. Doyle, M. C. Elliott, T. J. Mowlem, *Pure Appl. Chem*. **1994**, *66*, 2107–2110.

[3] a) X. Chen, L. Esser, P. G. Harran, *Angew. Chem.* **2000**, *112*, 967–970; *Angew. Chem. Int. Ed.* **2000**, *39*, 937–940; b) S. Jeong, X. Chen, P. G. Harran, *J. Org. Chem*. **1998**, *63*, 8640–8641.

[4] The phenolic oxidation of **2** shown in Scheme 1 is the most efficient identified. Ether **3** is also produced on treatment with di-μ-hydroxo-bis[(*N*,*N*,*N*′,*N*′-tetramethyl-ethylenediamine)copper(II)] chloride (TCI America) under an O_2 atmosphere and with various peroxidase isoforms in buffered media. Other oxidants examined (for example, Fe^{III}, V^{V}, Pb^{IV}, Tl^{III}) provide dimers and/or intractibles. Among the possible two-electron oxidation products of **2**, two are regioisomeric (single atropisomers) D/E biaryls (namely, *ortho*–*ortho* and/or *ortho*–*para* coupling). Neither has been convincingly detected in an oxidation of **2**.

[5] L. Zhu, R. M. Wehmeyer, R. D. Rieke, *J. Org. Chem.* **1991**, *56*, 1445–1453.

[6] Models of a macrolactam conformer paralleling that observed in the X-ray structure of a relative (ref. [3a]) indicate destabilizing non-bonded interactions between the benzyl ether of the F-ring and the C11 acetoxy substituent in (11*R*)-**6**.

[7] Chlorination of **7** causes a downfield shift of C25-H which, in the ^1H NMR spectrum (400 MHz, $CDCl_3$) of **8**, remains coupled ($\delta = 7.66$, $J = 2.8$ Hz) to an exchangeable (D_2O) signal at $\delta = 8.41$ (indole NH). The chlorine content of **8** and **9** was ascertained by mass spectrometry.

[8] Similar observations have been made in a model study by Magnus and McIver (ref. [2j]).

[9] For an early synthetic application of related methodology, see: S. L. Schreiber, H. V. Meyers, *J. Am. Chem. Soc.* **1988**, *110*, 5198–5200.

[10] Passage of **14** through silica generates trace (5–10%) by-products tentatively assigned as C10 epimers of **14c** (by mass spectrometry). This problem is magnified with hydrogenolyzed samples of crude **14**. By reducing the benzyl carbamate of **14** net deformylation is avoided only under conditions of transfer hydrogenation in neutral phosphate buffer containing excess Mg^{2+} ions. The crude product cannot be purified or adequately characterized.

[11] Crude samples of **14** also perform in this assay ($GI_{50} \approx 5$ μM). No significant difference in potency is observed in the *epi*-C37 series (derived from D-valine).

[12] Compound **13** has a fluorescence quantum yield (QY) of 0.45, as estimated by emission at 350–550 nm relative to an equal optical density of 1-aminoanthracene (QY = 0.61) in MeOH. Nonchlorinated congener **12** is more intensely luminescent (λ_{max}^{ex} 348 nm, λ_{max}^{em} 438 nm, $\varepsilon = 7960\ L\,mol^{-1}\,cm^{-1}$ at 348 nm, QY = 0.62) but less active against OVCAR-3.

[13] Fluorescence micrographs were obtained on a Zeiss Axiovert 100M microscope using the OpenLab Imaging System and a Chroma Tech filter set optimized for 4′,6-diamidino-2-phenylindole, dihydrochloride (DAPI) imaging (λ_{max}^{ex} 359 nm, λ_{max}^{em} 461 nm).

[14] For a seminal demonstration of ML_n (M = Ti, Zr, V)/alkyl hydroperoxide oxidations of phenols and naphthols, see: K. Krohn, H. Rieger, K. Khanbabaee, *Chem. Ber.* **1989**, *122*, 2323–2330.

[15] Preliminary results for treatment of **17** with lanthanide triflates are encouraging. We are now working through issues of product autooxidation, handling, and stability of both **17** and "**18**", as well as conclusive structural assignments. Details will be provided in a forthcoming full article.

[16] W. S. McIntire, D. E. Wemmer, A. Chistoserdov, M. E. Lidstrom, *Science* **1991**, *252*, 817–823.

Ring-Opening Polymerization of 1-Methylene-2-phenylcyclopropane Catalyzed by a Pd Complex To Afford Regioregulated Polymers**

Daisuke Takeuchi, Sunwook Kim, and Kohtaro Osakada*

Palladium(II) complexes with N-donor ligands have recently attracted significant interest as a result of their utility as alkene polymerization catalysis.[1] Strained cyclic olefins such as cyclopropenes and norbornadiene also undergo addition polymerization catalyzed by palladium(II) complexes.[2] On the other hand, much less effort has been devoted to applying Pd catalysis to polymer synthesis that involves ring opening of the monomer. Herein we report a ring-opening polymerization of 1-methylene-2-phenylcyclopropane that is catalyzed by a Pd complex to give a polymer with a highly

[*] Prof. Dr. K. Osakada, Dr. D. Takeuchi, S. Kim
Chemical Resources Laboratory
Tokyo Institute of Technology
4259 Nagatsuta, Midori-ku, Yokohama 226-8503 (Japan)
Fax: (+81) 45-924-5224
E-mail: kosakada@res.titech.ac.jp

[**] This work was supported by a Grant-in-Aid for Scientific Research from the Ministry of Education, Science, Sports, and Culture, Japan.

Supporting information for this article is available on the WWW under http://www.angewandte.com or from the author.

regulated structure. We also propose a unique mechanism for the polymer chain growth on the basis of detailed studies on the polymerization.[3]

$[Pd(\eta^3\text{-}CH_2CHCH_2)(ArN{=}CH{-}CH{=}NAr)]BF_4$ (**1**: Ar = 4-MeC_6H_4) and $[Pd(\eta^3\text{-}PhCHCHCH_2)(ArN{=}CH{-}CH{=}NAr)]BF_4$ (**2**: Ar = 4-MeC_6H_4) catalyze the ring-opening polymerization of 1-methylene-2-phenylcyclopropane (**I**) at 80 °C in acetonitrile to give polymer **II** with the *exo*-methylene group in the repeating unit [Eq. (1)].[4] The polymer was characterized by means of the ^1H and $^{13}C\{^1H\}$ NMR spectra shown in Figure 1 a and b. The ^1H NMR signals at $\delta = 4.3-5.0$ and the $^{13}C\{^1H\}$ NMR signals at $\delta = 110.6$ and 111.2 correspond to the hydrogen and the carbon atoms of the $=CH_2$ group, respectively; the other signals were assigned to the other hydrogen and carbon atoms in the structure.[5] Signals corresponding to $-CH{=}CR-$ (R = H, Ph) and the cyclopropyl group, which should exhibit the corresponding signals at $\delta = 5.5-6.5$ and $\delta = 1.5-0.0$, respectively, are entirely absent in the ^1H NMR spectrum. The $^{13}C\{^1H\}$ NMR signal of the *ipso* carbon atom of the phenyl group appears as four resonances in the range $\delta =$ 148.3 – 150.0. They are assigned to four possible triads (*rr*, *rm*, *mr*, and *mm*) with regard to the chiral benzyl carbon atom in the repeating unit.[6] A similar poly(styrene-*co*-CO) with a regulated head-to-tail linkage of the monomer units also exhibits four distinct $^{13}C\{^1H\}$ NMR peaks at $\delta = 134.8-136.5$ for the *ipso* phenyl carbon atom, whereas the polymer with a disordered linkage shows a significantly broadened peak in the same region.[7] All these NMR data indicate that the produced polymer **II** has a well-regulated head-to-tail sequence of the single repeating unit $-CH_2-C(=CH_2)-CH(Ph)-$.

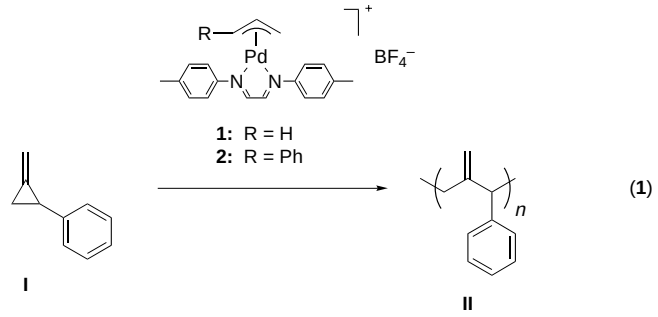

(1)

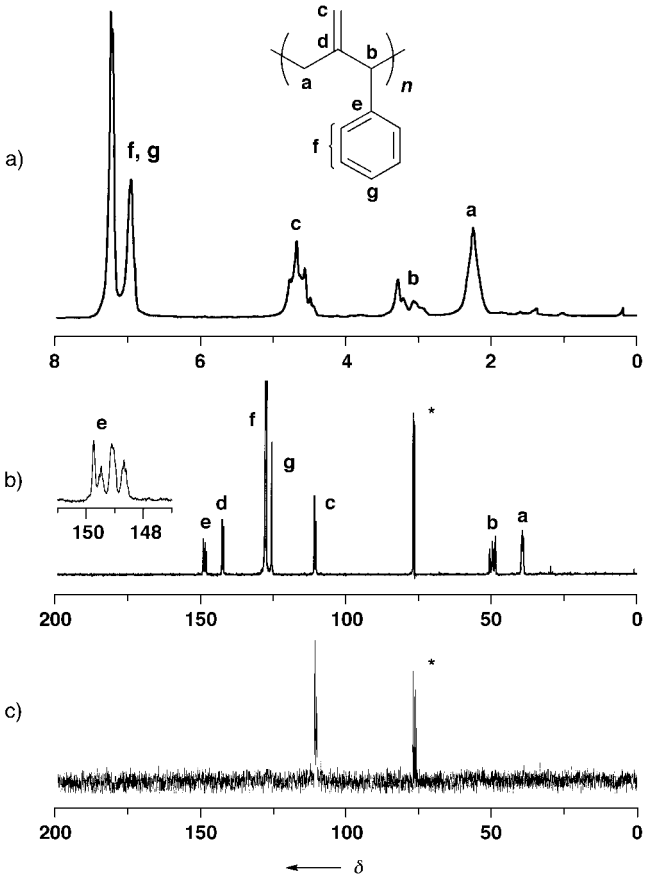

Figure 1. a) ^1H and b) $^{13}C\{^1H\}$ NMR spectra of **II** in $CDCl_3$ at 25 °C. The polymerization of 1-methylene-2-phenylcyclopropane (**I**) was carried out in the presence of **1** ([**1**] = 25 mM, [**I**]/[**1**] = 70/1) in CH_3CN at 80 °C (entry 1 in Table 1). c) $^{13}C\{^1H\}$ NMR spectrum of **II**-^{13}C in $CDCl_3$ at 25 °C. The polymerization conditions are the same as above. Peaks with asterisks in (b) and (c) correspond to the solvent.

The ring-opening polymerization of **I** is also promoted by [PdCl(Me)(ArN=CH−CH=NAr)] (**3**: Ar = 4-$MeOC_6H_4$, **4**: Ar = 4-MeC_6H_4, **5**: Ar = 2,6-(iPr)$_2C_6H_3$) and by a mixture of

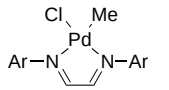

3: Ar = 4-MeC_6H_4
4: Ar = 4-$MeOC_6H_4$
5: Ar = 2,6-iPr$_2C_6H_3$

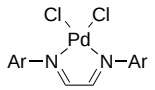

6: Ar = 4-MeC_6H_4

$[PdCl_2(ArN{=}CH{-}CH{=}NAr)]$ (**6**: Ar = 4-MeC_6H_4) and $AgBF_4$, whereas $[(\eta^3\text{-}CH_2CHCH_2)Pd(PPh_3)_2]BF_4$ does not bring about the polymerization. Table 1 summarizes the results of the polymerization of **I**. The produced polymers have molecular weights M_n of approximately 5000 with an M_w/M_n ratio of 1.44 – 1.54 (gel-permeation chromatography (GPC), polystyrene standards). The polymerization of **I** when catalyzed by a mixture of **6** and $AgPF_6$ with a [**I**]/[**6**] ratio of 200/1 gives a product having an M_n value as high as 11 000 ($M_w/M_n = 1.59$). The polymerization of **I** by **3** displays first-order kinetics with respect to the monomer, and has an activation energy E_a of 67.6 kJ mol^{-1}.

Table 1. Polymerization of 1-methylene-2-phenylcyclopropane when catalyzed by Pd complexes.[a]

Entry	Catalyst	Time [h]	Conv [%][b]	M_n[c]	M_w/M_n[c]
1	**1**	3	82	4000	1.47
2	**2**	10	95	5900	1.48
3[d]	**3**	21	75	4800	1.48
4	**4**	24	93	5700	1.44
5	**5**	24	85	4000	1.54
6[e]	**6** + $AgBF_4$	6	94	5700	1.46
7[e,f]	**6** + $AgPF_6$	15	89	11000	1.59
8[e]	[g]	48	trace	–	–

[a] Reaction conditions: [Pd] = 25 mM, [**I**] = 1.8 M, at 80 °C in MeCN unless otherwise stated. [b] Ratio of the consumed monomer to the originally charged monomer. [c] Determined by GPC in THF with polystyrene standards. [d] In *N*-methylpyrrolidinone. [e] [Pd]/[Ag] = 1/3. [f] [Pd] = 25 mM, [**I**] = 5.0 M. [g] $[(\eta^3\text{-}CH_2CHCH_2)Pd(PPh_3)_2]BF_4$.

  1433-7851/01/4014-2686 $ 17.50+.50/0 *Angew. Chem. Int. Ed.* **2001**, *40*, No. 14

The polymerization of **I** by **1** and **2** in a low monomer-to-catalyst molar ratio ([**I**]/[**Pd**] = 20/1) produces polymers with low molecular weights (**II′** and **II″**, respectively) in quantitative yield. The $^{13}C\{^1H\}$ NMR spectra of **II′** and **II″** contain the

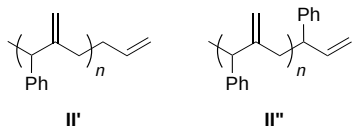

II' **II"**

signals of the respective terminal groups, $CH_2{=}CH{-}CH_2{-}$ and $CH_2{=}CH{-}CH(Ph){-}$.[8] On the basis of these results, the polymerization is initiated by formation of a C–C bond between the monomer and the allyl group bonded to the Pd ion. The existence of the $CH_2{=}CH{-}CH(Ph){-}$ terminal group of **II″** and its well-regulated head-to-tail sequence of the repeating unit indicate that insertion of the monomer occurs preferentially into the Pd–CHPh bond of the η^3-1-phenylallylpalladium species both in the initiation step and in the propagation step of the polymerization.[9, 10]

The polymerization of 1-methylene-2-phenyl-3[^{13}C]-cyclopropane (**I**-^{13}C) produces polymer **II**-^{13}C whose NMR spectra provided the essential information to explain the mechanism of polymer growth [Eq. (2)]. The $^{13}C\{^1H\}$ NMR spectrum of

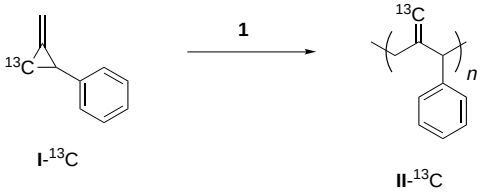

I-^{13}C **II**-^{13}C (**2**)

II-^{13}C (Figure 1c) shows signals at $\delta = 110.4$ and 110.9. These signals arise from the ^{13}C-enriched carbon atom and correspond to the $=CH_2$ carbon atom of the polymer. This result indicates selective cleavage of the distal C–C bond of the monomer during the polymerization. Scheme 1a illustrates a plausible mechanism of the polymerization initiated by **2**. The 2,1-insertion of the monomer into the Pd–CHPh bond of **2** leads to the formation of a cyclopropylpalladium intermediate which undergoes rapid β-alkyl activation,[11] which leads to regeneration of a π-allylpalladium complex. Repetition of the above procedure accounts for the smooth polymerization that gives the product in a regulated head-to-tail sequence of monomer units. This polymerization mechanism contrasts that proposed for the metallocene-catalyzed polymerization of methylenecyclopropane (Scheme 1b), in which polymer growth takes place by repetition of the 1,2-insertion of the monomer into the metal–alkyl bond and subsequent β-alkyl elimination.

In conclusion, we have demonstrated the ring-opening polymerization of 1-methylene-2-phenylcyclopropane catalyzed by a Pd complex to give structurally regulated polymers, and a new mechanism for polymer growth accompanied by ring opening of the monomer. The stable growing polymer end containing a π-allyl–Pd bond is suitable for smooth and selective insertion of the monomers at temperatures as high as 80 °C.

Received: March 8, 2001 [Z16735]

[1] a) S. D. Ittel, L. K. Johnson, M. Brookhart, *Chem. Rev.* **2000**, *100*, 1169–1203; b) G. J. P. Britovsek, V. C. Gibson, D. F. Wass, *Angew. Chem.* **1999**, *111*, 448–468; *Angew. Chem. Int. Ed.* **1999**, *38*, 428–447; c) S. Mecking, *Coord. Chem. Rev.* **2000**, *203*, 325–351; d) A. C. Gottfried, M. Brookhart, *Macromolecules* **2001**, *34*, 1140–1142; e) D. J. Tempel, L. K. Johnson, R. L. Huff, P. S. White, M. Brookhart, *J. Am. Chem. Soc.* **2000**, *122*, 6686–6700.

[2] a) S. Rush, A. Reinmuth, W. Risse, J. O'Brien, D. R. Ferro, I. Tritto, *J. Am. Chem. Soc.* **1996**, *118*, 12230–12231; b) C. Mehler, W. Risse, *Macromolecules* **1992**, *25*, 4226–4228.

[3] Electrophilic metallocene cations of Zr and Lu were found to promote the ring-opening polymerization of unsubstituted methylenecyclopropane, where the produced polymer was furnished with vinylidene groups or polyspiropyrane depending on the catalyst: a) X. Yang, A. L. Jia, T. J. Marks, *J. Am. Chem. Soc.* **1993**, *115*, 3392–3393; b) L. Jia, X. Yang, A. M. Seyam, I. D. L. Albert, P.-F. Fu, S. Yang, T. J. Marks, *J. Am. Chem. Soc.* **1996**, *118*, 7900–7913.

[4] Details of synthesis and physical data of the polymers are available in the Supporting Information.

[5] Selected NMR data of the structurally related compound $PhCH_2C(=CH_2)CH_2CH_3$: ^{1}H NMR ($CDCl_3$): $\delta = 1.99$ (q, 2H, CH_2Me), 3.36 (s, 2H, $PhCH_2$), 4.78 (dd, 2H, $C{=}CH_2$), 7.18–7.29 (m, 5H, Ph); $^{13}C\{^1H\}$ NMR ($CDCl_3$): $\delta = 28.1$ (CH_2Me), 43.2 ($PhCH_2$), 109.8 ($C{=}CH_2$), 125.3(*p*-Ph), 128.2–128.9 (*o*, *m*-Ph), 139.9 ($C{=}CH_2$), 150.6 (*ipso*-Ph).

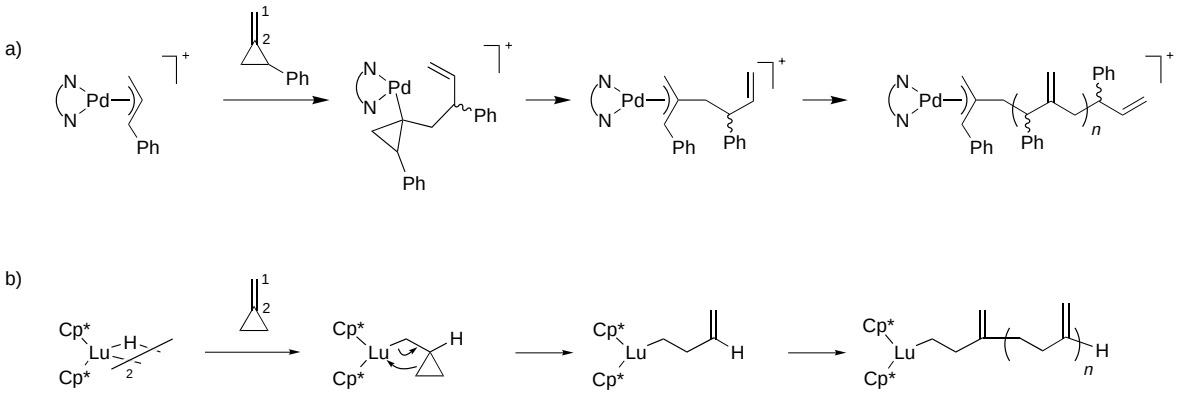

Scheme 1. Plausible mechanism of the polymerization of methylenecyclopropanes by a) palladium complexes and b) lutenocene complexes.

  1433-7851/01/4014-2687 $ 17.50+.50/0

[6] The four $^{13}C\{^1H\}$ NMR signals corresponding to the triads did not show any significant difference in their relative peak intensity, which suggests that the polymerization is not stereoselective.
[7] A. Aeby, A. Gsponer, G. Consiglio, *J. Am. Chem. Soc.* **1998**, *120*, 11000 – 11001.
[8] $^{13}C\{^1H\}$ NMR data ($CDCl_3$) of the terminal groups: **II′**: $\delta = 138.4$ (CH_2=), 114.4 (=CH−), 34.1 (CH_2); **II″**: $\delta = 141.7$ (CH_2=), 114.3 (=CH−), 47.8 (CHPh). The signals were assigned by comparison of the positions with those of CH_2=CHCHPhCH_3 and *trans*-PhCH=CHCH_2CH_3.
[9] The formation of π-allyl−Pd species by the insertion of methylenecyclopropanes into H−Pd bonds has been proposed to account for results of coupling reactions of methylenecyclopropanes with malonates or amines when catalyzed by a Pd complex; see N. Tsukada, A. Shibuya, I. Nakamura, Y. Yamamoto, *J. Am. Chem. Soc.* **1997**, *119*, 8123 – 8124.
[10] The reaction of a 1,3-diene with π-allyl−Pd complexes was also reported to cause formation of a C−C bond between a vinyl carbon atom of the diene and a sterically hindered π-allyl carbon atom of the complex; see R. P. Hughes, J. Powell, *J. Am. Chem. Soc.* **1972**, *94*, 7723 – 7732. Their results may be accounted for by assuming a 2,1-insertion of a double bond of butadiene into the more sterically hindered Pd−C bond of the π-allylpalladium complex, although they suggested another kind of mechanism at that time.
[11] a) L. Resconi, F. Piemontesi, G. Franciscono, L. Abis, T. Fiorani, *J. Am. Chem. Soc.* **1992**, *114*, 1025 – 1032; b) Z. Guo, D. C. Swenson, R. F. Jordan, *Organometallics* **1994**, *13*, 1424 – 1432; c) B. C. Ankianiec, V. Christou, D. T. Hardy, S. K. Thomson, G. B. Young, *J. Am. Chem. Soc.* **1994**, *116*, 9963 – 9978; d) T. C. Flood, J. A. Statler, *Organometallics* **1984**, *3*, 1795 – 1803.

Nematic Dendrimers Based on Carbosilazane Cores**

Ralf Elsäßer, Georg H. Mehl,* John W. Goodby, and Michael Veith

Research on dendritic liquid crystal systems has focused mainly on the investigation of materials that exhibit layered, columnar, cubic-phase structures.[1, 2] The emphasis has been associated with the chemical structure of these systems, in which a dendritic core and a periphery consisting of functional groups of different chemical composition, which are responsible for self-assembly processes, leads to nanoscopic phase segregation between core and periphery.[3, 4]

Thus, well-defined dendritic systems that exhibit nematic phase behavior and that are characterized only by orientational ordering and contain functional groups promoting nanophase separation have attracted considerable interest. The opposing forces of the nematic director field, which are attributed to the peripheral mesogens, and the tendency of the dendritic cores to undergo phase separation should lead to a new class of compounds with interesting properties in the liquid-crystalline (LC) state.[5]

This structural concept should allow the decoupling of the transition behavior and the ordering of the LC phase from the size of the molecules, which is a long-standing aim of LC polymer research. The materials should additionally be characterized by comparatively low viscosities.

The use of carbosilazane cores **1** – **5**, which display an overall threefold symmetry and possess a planar central core, allows the synthesis of microphase-separated systems.[6] The

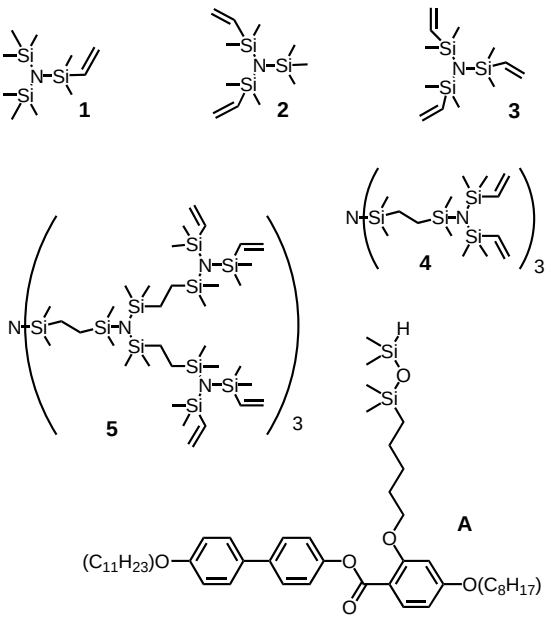

absence of nucleophilicity in the nitrogen atoms prevents complexation of ionic species in the dendritic core, which is detrimental for most electrooptic applications. Furthermore the use of these comparatively novel compounds, which are closer in structure to synthons applied in nonaqueous sol – gel synthesis of ceramic precursors than to conventional organic materials, is an attractive preparative challenge.

The synthesis of the dendritic and multipodal cores **3** to **5** has been reported earlier and is based on the reaction of the potassium salt of divinyltetramethyldisilazane (K[N{$SiMe_2$vinyl}$_2$]) with chlorodimethylvinylsilane, which leads to the center of the dendritic system **3** (G_0).[6] Hydrosilylation of **3** with dimethylchlorosilane and the subsequent reaction with K[N{$SiMe_2$vinyl}$_2$] leads to compound **4** (G_1). Repetition of this divergent synthesis allows the preparation of compound **5** (G_2) and higher generation carbosilazane dendrimers, which bear functional vinyl groups at the periphery of the molecules. Compound **2**, which provides access to a dimeric system, was obtained by the reaction K[N{$SiMe_2$vinyl}$_2$] with trimethylchlorsilane. The carbosilazane **1**, which was synthesized to complete the homologous series, was obtained by the reaction

[*] Dr. G. H. Mehl, Dr. R. Elsäßer, Prof. J. W. Goodby
Department of Chemistry
Hull University
Hull HU6 7RX (UK)
Fax: (+44) 1482-466411
E-mail: g.h.mehl@chem.hull.ac.uk
Prof. M. Veith
Institut für Anorganische Chemie
Universität des Saarlandes
Postfach 151150, 66041 Saarbrücken (Germany)

[**] We acknowledge the EU for funding in the framework of the TMR network "Molecular Design of Functional Liquid Crystals" and thank the members of the network for the many helpful discussions.

  1433-7851/01/4014-2688 $ 17.50+.50/0

of dimethylvinylchlorosilane with $K[N\{SiMe_3\}_2]$; thus the transition from monomeric to multipodal to dendritic systems can be investigated with this series of compounds.

The desired nematic phase behavior was achieved by using the mesogenic group **A**, whose synthesis has been reported previously.[7] The design of a mesogen such as **A** consisting of three aromatic rings connected by an ester group, flanked by terminal octyl and undecyl groups linked to the dendritic core through a short lateral spacer of five methylene groups and a 1,1,3,3-tetramethyldisiloxane group was judged to give the appropriate balance between coupling and flexibility and to be suitable to achieve nematic phase behavior close to ambient temperature and to avoid the occurrence of higher ordered LC phases.

A hydrosilylation reaction using Karstedt's catalyst in toluene was employed for the coupling of mesogens and dendritic cores.[8] To achieve complete reaction of the functional vinyl groups, the reaction mixture was kept between 40–45 °C; higher reaction temperatures led to the formation of by-products and the degradation of the catalyst, and lower reaction temperatures to incomplete conversion. The formation of the products was monitored by the disappearance of peaks at $\delta = 5.7$, 5.9, and 6.3 in the ^{1}H NMR spectrum (and at $\delta = 130.7$ and 143.6 in the ^{13}C NMR spectrum), which are associated with the vinyl groups, and the appearance of signals at $\delta = 0.4$ and 0.5 in ^{1}H NMR spectrum (and at $\delta = 10.1$ and 12.7 in the ^{13}C NMR spectrum), which are indicative of the formation of CH_2–Si bonds. The final products were purified by column chromatography by using alumina (Brockmann II) as the stationary phase (the use of silica led to the cleavage of the Si–N bonds) and dichloromethane/hexane as eluent.[9] GPC analysis of the compounds **3A**, **4A**, and **5A** yielded values for the polydispersity ($\langle M_w\rangle/\langle M_n\rangle$) of 1.03 and smaller.

All of the final products show enantiotropic nematic phase behavior. Figure 1 shows a schematic representation of a dendritic molecule in the nematic phase. Polarized light transmission microscopy of these compounds is characterized by the immediate formation of typical nematic defect textures of low viscosity (a schlieren texture) with two and four brush defects ($s \pm ½$ and 1), as each material is cooled from the isotropic to the liquid crystalline state. The values for the transition temperatures, and the associated enthalpies and entropies for the second heating cycles obtained from differential scanning calorimetry (DSC) studies of each compound are listed in Table 1.

Figure 1. Schematic representation of a dendritic structure in the nematic phase.

The addition of the bulky carbosilazane group **1** to **A**, which results in **1A**, leads to the anticipated decrease of the stability range of the nematic phase from 38.5 °C for **A** to 18.7 °C for **1A** (Table 1). Increasing the number of side chains from one for **1A** to three for **3A** (G_0) leads to an expected increase in the isotropization temperature to 41.6 °C for **3A**; higher than that of the monomeric material **A** by 3.1 °C. The isotropization temperatures of the compounds **1A** (18.7 °C) and **2A** (36.5 °C), which are lower than that of **A** (38.5 °C), highlight that the formation of the nematic state is not favored in microphase-separated systems, when compared with smectic LC systems.[1, 2, 4]

Table 1. Transition temperatures as determined by DSC.[a]

Compound	Transitions [°C], {ΔH [J g^{-1}]}	$(\Delta S_{mol}/R)n^{-1}$
A	cr 17.0 N 38.5 {0.70} Iso	0.21
1A	cr −30.3 N 18.7 {0.31} Iso	0.13
2A	cr −12.6 N 36.5 {0.66} Iso	0.23
3A	T_g −26.0 N 41.6 {0.66} Iso	0.22
4A	T_g −23.0 N 40.1 {0.58} Iso	0.21
5A	T_g −22.3 N 40.9 {0.53 } Iso	0.20

[a] cr = crystalline, N = nematic, Iso = isotropic liquid, T_g = glass transition temperature [$(\Delta S_{mol}/R)n^{-1}$] normalized reduced transition entropy (n = number of mesogens).

A further increase of the size of the molecules from the generation G_0 compound **3A** to the dendritic generation G_1 compound **4A** and to the generation G_2 compound **5A** does not have a great influence on the isotropization temperature: 41.6 (**3A**), 40.1 (**4A**), and 40.9 °C (**5A**).

The low values for the transition enthalpies (ΔH) ranging from 0.31 to 0.71 J g^{-1} of this series, when compared to many other nematic systems, suggest the presence of low ordered systems. The values of 0.20–0.23 (exception **1A**) for the normalized isotropization entropy $(\Delta S/R)n^{-1}$ at the nematic to isotropic transition, are lower than those for smectic systems and are in line with the expected results for a less ordered LC phase. Interestingly, this change in entropy, which is related to the nematic ordering at the isotropization temperature, is almost independent of the size of the molecule whether it is a low molar mass material or a dendritic polymer. The lower value for entropic data of **1A** is attributed to the bulky carbosilazane group which impairs the nematic ordering.

These results indicate that the synthesis of these nanophase-structured nematic dendrimers leads to macromolecules with LC properties similar to those of comparable low molar mass compounds.

Received: December 11, 2000
Revised: February 28, 2001 [Z16254]

[1] a) M. W. P. L. Baars, S. H. M. Söntjens, H. M. Fischer, H. W. J. Peerlings, E. W. Meijer, *Chem. Eur. J.* **1998**, *4*, 2456; b) K. Lorenz, D. Hölter, B. Stühn, R. Mühlhaupt, H. Frey, *Adv. Mater.* **1996**, *8*, 414; c) S. A. Ponomarenko, E. A. Rebrov, A. Y. Bobrovsky, N. I. Boiko, A. M. Muzafarov, V. P. Shibaev, *Liq. Cryst.* **1996**, *21*, 1.

[2] a) R. M. Richardson, S. A. Ponomarenko, N. I. Boiko, V. P. Shibaev, *Liq. Cryst.* **1999**, *26*, 1; b) V. Percec, P. W. Chu, M. Kawasumi, *Macromolecules* **1994**, *27*, 4441; c) J. H. Cameron, A. Facher, G. Lattermann, S. Diele, *Adv. Mater.* **1997**, *9*, 398.

[3] a) M. Ibn-Elhaj, H. J. Coles, D. Gouillon, A. Skoulios, *J. Phys. II* **1993**, *3*, 1807; b) R. W. Date, C. T. Imrie, G. R. Luckhurst, J. M. Seddon, *Liq. Cryst.* **1992**, *12*, 203; c) M.-H. Li, L. Detre, P. Cluzeau, N. Isaert, H.-T. Nguyen, *Liq. Cryst.* **1998**, *24*, 347.

[4] C. Tschierske, *J. Mater. Chem.* **1998**, *8*, 1485; b) G. H. Mehl, J. W. Goodby, *Chem. Ber.* **1996**, *129*, 521; c) G. H. Mehl, J. W. Goodby, *Chem. Commun.* **1999**, 13; d) V. Percec, P. J. Turkaly, A. D. Asandai, *Macromolecules* **1997**, *30*, 943.

[5] a) F. Hessel, H. Finkelmann, *Polym. Bull.* **1985**, *14*, 3751; b) G. W. Gray, J. S. Hill, D. Lacey, *Mol. Cryst. Liq. Cryst.* **1991**, *197*, 43; c) S.

  1433-7851/01/4014-2689 $ 17.50+.50/0

Lecommandoux, M. F. Archard, F. Hardouin, *Liq. Cryst.* **1998**, *25*, 85; d) A. Sunder, M.-F. Quincy, R. Mühlhaupt, H. Frey, *Angew. Chem.* **1999**, *111*, 3107; *Angew. Chem. Int. Ed*. **1999**, *38*, 2928; e) J.-L. Serrano, J. Barbera, personal communication.

[6] M. Veith, R. Elsäßer, R.-P. Krüger, *Organometallics* **1999**, *18*, 656.

[7] R. Elsäßer, G. H. Mehl, J. W. Goodby, D. J. Photinos, *Chem. Commun*. **2000**, 851.

[8] B. D. Karstedt, General Electrics, US-Patent 3.814.730, **1974**; [*Chem. Abstr*. **1974**, *80*, 16134j].

[9] Compound **5** (150 mg, 6.1×10^{-5} mol) and compound **A** (1.3 g, 1.64×10^{-3} mol) were dissolved in dry toluene (10 mL). Fifteen drops of a solution of Karstedt's catalyst in xylenes (3.5%; Fluorochem) were added and the reaction mixture was stirred overnight at 45 °C. Volatiles were evaporated and the residue was purified by column chromatography on alumina (Brockmann II). The polarity of the eluent was varied from hexane/dichloromethane ratios of 3/1 to 1/3. Yield of isolated product: 60 mg (8%). ^{1}H NMR (399.7 MHz, CD_2Cl_2, 25 °C): $\delta = 0.01$ (s, 144H; -OSi(CH_3)$_2$-), 0.16–0.17 (5s (not resolved), 180H; NSi(CH_3)$_2$-), 0.35–0.60 (m, 108H; SiCH_2-), 0.88 (2t (not resolved), 72H; -CH_3), 1.2–1.6 (m, -CH_2-, 360H), 1.75–1.84 (m, 72H; CH_2CH$_2$O), 4.00 (3t (not resolved), -CH_2O), 6.51 (m, 24H; CH, (carbonyl)), 6.95, 7.20, 7.50, 7.56 (4d, 4×24H; CH, biphenyl unit), 7.98 (d, 12H; CH, (carbonyl)); ^{13}C NMR (100.4 MHz, CD_2Cl_2, 25 °C): $\delta = -0.18$, 0.53 (-Si(CH_3)$_2$O-Si(CH_3)$_2$-), 3.43, 3.50 (-N{Si(CH_3)$_2$-}$_2$), 11.1, 12.7 (NSi(Me)$_2$CH_2CH_2-Si(Me)$_2$O-), 14.0 (NSi(Me)$_2$CH_2CH_2Si(Me)$_2$N-), 14.3 (CH_3), 18.7 (CH_2Si(Me)$_2$O), 23.1–32.3 (-CH_2-), 68.5, 68.7, 69.3 (-CH_2O), 100.5, 105.5, 111.6, 115.1, 122.6, 127.7, 128.3, 133.0, 134.5, 138.5, 150.6, 159.2, 161.9, 164.8 (C aromatic), 164.3 (-*C*(O)O); GPC (THF, toluene standard) ($\langle M_w \rangle / \langle M_n \rangle$) = 1.024.

Spin-Labeled Dendrimers in EPR Imaging with Low Molecular Weight Nitroxides

Alexander T. Yordanov, Ken-ichi Yamada, Murali C. Krishna, James B. Mitchell, Eric Woller, Mary Cloninger, and Martin W. Brechbiel*

Electron paramagnetic resonance (EPR) imaging is an emerging technology that shows great promise in medical research applications for measuring free radical distribution, metabolism, and extent of oxygenation in tumors, organs and tissues.[1] However, the stable nitroxyl radicals (nitroxides) which these applications utilize, such as 4-hydroxy-2,2,6,6-tetramethylpiperidine-1-oxyl (TEMPOL), are prone to bioreduction to the analogous diamagnetic, EPR-silent hydroxylamines (i.e., TEMPOL-H; Scheme 1). The nitroxide and the hydroxylamine species rapidly establish an equilibrium that strongly favors the hydroxylamine in vivo.[2] Thus, the short half-life of nitroxides in vivo ($t_{1/2} \approx 3$ min) has limited further development and wide application of EPR imaging in the biomedical field.

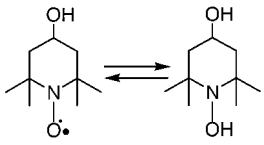

TEMPOL TEMPOL-H

Scheme 1. The equilibrium established between TEMPOL and TEMPOL-H. The latter is favored in vivo.

Recently it was reported that intravenous injection of polynitroxyl-albumin (PNA) caused reoxidation of free hydroxylamine (shown to remain in the body for a relatively long period of time) back to the paramagnetic nitroxide.[3] This reagent has enabled high-resolution EPR imaging of rat heart and may also permit various therapeutic applications of nitroxides. Alternatively, polyamidoamine (PAMAM) Starburst™ dendrimers are spherical macromolecules which can be produced in successive generations, each with a specified and defined size and molecular weight as well as a high number of terminal primary amino groups.[4] Because of these characteristics and the low immunogenicity, PAMAMs are finding utility in a variety of applications, many of which are biomedical.[5] Due to their macromolecular nature, dendrimers are impermeable and when injected intravenously distribute primarily in the vascular space. This is in contrast to TEMPOL and TEMPOL-H, which are membrane permeable and move readily between the extra- and intracellular spaces, the latter being the major sites of nitroxide reduction.[6] Recently dendrimers labeled with 2,2,6,6-tetramethylpiperidine-1-oxyl (TEMPO) were used to evaluate the heterogenicity of their carbohydrate-substituted surfaces.[7a] Previous EPR studies of lower generation dendrimers with 2,2,5,5-tetramethylpyrrolidin-1-oxyl (PROXYL) conjugates have shown that the large spin–spin interaction encountered by dendrimer-labeled nitroxides causes extensive broadening of the EPR spectra, effectively making the latter indistinguishable from the base line.[7b] In contrast, the low molecular weight nitroxides exhibit sharp EPR spectra, and the intensities of the bands can be easily measured. Here we report the preparation and characterization of two novel spin-labeled dendrimers, a polynitroxyl G-6 PAMAM™ dendrimer with 198 (G-6-TEMPO-198) or with 80 (G-6-TEMPO-80) free TEMPO radicals on the surface of the macromolecule. We show that both dendrimers reoxidize TEMPOL-H back to its EPR-active form, TEMPOL, and therefore are potential TEMPO free radical, life-supporting agents for EPR imaging.

The commercially available G-6 PAMAM™ dendrimers are synthetic oblate spheroidal macromolecules composed of an ethylenediamine initiator core and repeating polyamidoamino units resulting in 256 amines on the surface. To attach TEMPO free radicals to the parent G-6 dendrimer, 4-amino-2,2,6,6-tetramethylpiperidine-1-oxyl (**1**, 4-amino-TEMPO) was first converted into 2,2,6,6-tetramethylpiperidine-1-oxyl-4-succinamic acid (**2**), which subsequently reacted to form the *N*-hydroxysuccinimidyl ester **3** (Scheme 2). Compounds **2** and **3** were characterized by their exact fast atom bombardment (FAB) mass spectra. No satisfactory elemental analyses could

[*] Dr. M. W. Brechbiel, Dr. A. T. Yordanov
Radioimmune & Inorganic Chemistry Section
Bldg. 10, Room B3B69
Radiation Oncology Branch
NCI, National Institutes of Health
Bethesda, MD 20892 (USA)
Fax: (+1) 301-402-1923
E-mail: martinwb@box-m.nih.gov

Dr. K.-i. Yamada, Dr. M. C. Krishna, Dr. J. B. Mitchell
Radiation Biology Branch
NCI, National Institutes of Health
Bethesda, MD 20892 (USA)

E. Woller, Dr. M. Cloninger
Department of Chemistry and Biochemistry
Montana State University
Bozeman, MT 59717 (USA)

  1433-7851/01/4014-2690 $ 17.50+.50/0

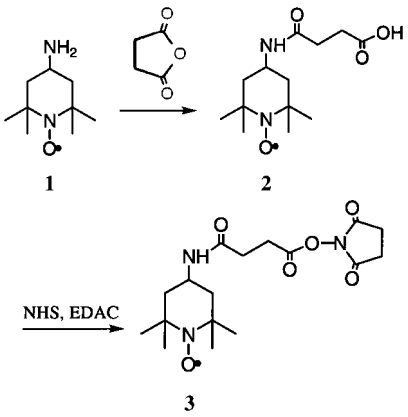

Scheme 2. Synthesis of *N*-hydroxysuccinimidyl-TEMPO active ester **3**. EDAC = 1-ethyl-3-(3-dimethyl-aminopropyl)carbodiimide, NHS = *N*-hydroxysuccinimide.

be obtained for these compounds due to their extremely hygroscopic nature.

Treatment of the parent G-6 PAMAM™ dendrimer with either an excess or a stoichiometric amount of **3** resulted in G-6-TEMPO-198 and G-6-TEMPO-80, in which either 198 or 80 TEMPO radicals are attached to the dendrimer (Scheme 3). The degree of substitution was confirmed by matrix-assisted laser desorption ionization time-of-flight (MALDI-TOF) mass spectroscopy[8] (*m*/*z*: 102 000 and 72 000, compared to 50 900 for the nonlabeled G-6 dendrimer). When mixed with TEMPOL-H, both dendrimer nitroxyl conjugates reoxidized the hydroxylamine back to TEMPOL, the EPR-active analogue, as clearly seen from the sharp increase in the intensity of the TEMPOL-produced EPR signal within minutes (Figure 1). There was no reoxidation when TEMPOL-H was mixed with the G-6 dendrimer lacking conjugation to TEMPO. Increasing the degree of labeling of the dendrimer with **3** resulted in increasing the reoxidation rate, with equilibrium being reached after 30 min with G-6-TEMPO-80 and after 20 min with G-6-198.

Since aggregation can often create particles with undesirable characteristics for in vivo applications, due to both size and high immunogenicity, a multi-angle light scattering (MALS) analysis of the two spin-labeled dendrimers was also performed. This analysis revealed that in aqueous solution the highly substituted G-6-TEMPO-198 aggregates to form particles with an average molecular weight of 549 000 (degree of aggregation ≈ 5.4) and a radius of 18.8 nm. This high degree of aggregation is attributed to the highly lipophilic nature of the G-6-TEMPO-198 surface. An aggregate of this size would most likely obstruct narrow blood capillaries in some tissues, cause precipitable masses in vivo, and thus be a source of toxicity. The MALS analysis of the less highly substituted G-6-TEMPO-80, on the other hand, revealed particles with an average molecular weight of 113 100 (degree of aggregation ≈ 1.6) and a radius of less than 10 nm. Thus, the lower degree of substitution in G-6-TEMPO-80 decreases the lipophilic nature of the surface and thus the potential for aggregation in aqueous media.

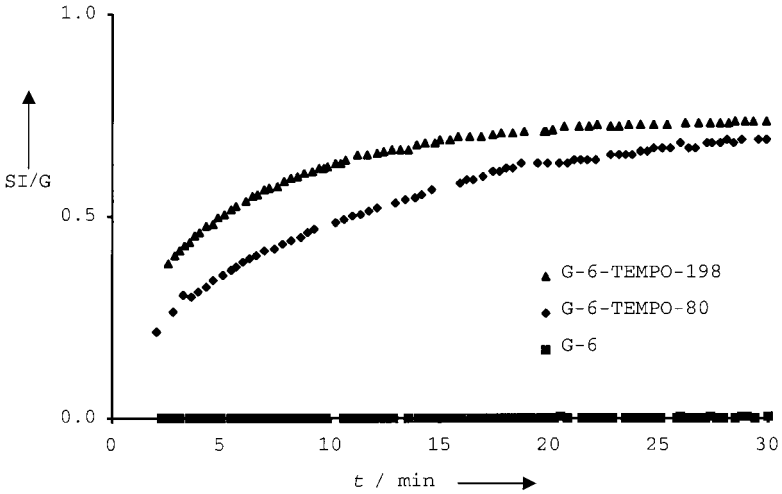

Figure 1. Plot of the intensity of the EPR signal of TEMPOL, formed by reoxidation of TEMPOL-H with spin-labeled PAMAM™ dendrimers, as a function of time *t* after addition of the dendrimer. SI = signal intensity, G = gain.

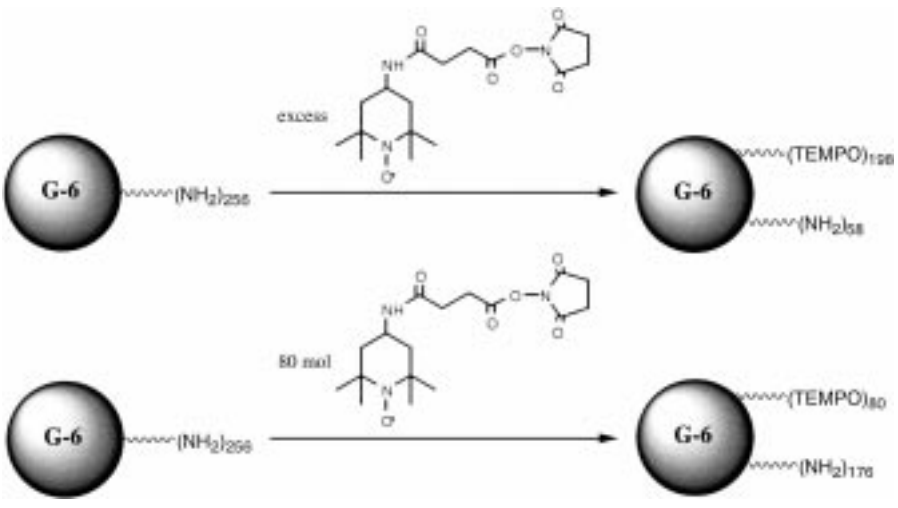

Scheme 3. Synthesis of G-6-TEMPO-198 and G-6-TEMPO-80.

Our study has shown that spin-labeled G-6 dendrimers are potential candidates for TEMPO free radical life supporters in EPR imaging. Currently, murine model studies are under way to determine the prolonging effect of G-6-TEMPO-80 on the half-life of TEMPOL in vivo and possible applications of this dendrimer in EPR imaging technics.

Experimental Section

General: All reactions were carried out under argon. Anhydrous THF, 4-amino-TEMPO, succinic anhydride, EDAC, and NHS were purchased from Aldrich Chemical Co., Milwaukee, WI. The PAMAM™ dendrimer, generation 6, ethylenediamine core, was generously provided by Dendritech Inc.,

  1433-7851/01/4014-2691 $ 17.50+.50/0

Midland, MI. DMSO was dried over 4-Å molecular sieves. Exact FAB mass spectra were obtained on an Extrel 4000 instrument in the positive-ion detection mode. Elemental analyses were performed by Galbraith Laboratories, Inc., Knoxville, TN. The MALDI mass spectra were acquired using a PerSeptive Biosystems Voyager RP time-of-flight mass spectrometer. Positive-ion mass spectra were acquired in the linear mode, and the ions were generated by using a nitrogen laser (337 nm) pulsed at 3 Hz with a pulse width of 3 ns. Ions were accelerated at 30000 V and amplified using a multichannel plate. Spectra (70 to 180) were summed into a 500-MHz Techtronix digital storage oscilloscope and downloaded to a computer for data processing. All data processing was performed using GRAMS (Gallactic Industries, Salem, NH). Spectra of TEMPO-labeled dendrimers were obtained using a *trans*-3-indoleacrylic acid matrix with a matrix:-analyte ratio of 8000:1. Bovine serum albumin (BSA, MW = 66431 g mol^{-1}) was used as an external standard. An aliquot corresponding to 12 pmol of the analyte was deposited on the laser target.[9] The MALS analyses were performed by Wyatt Technology Corporation, Santa Barbara, CA, using a DAWN EOS detector with a solid-state laser operating at 690 nm. Nanopure water (G-6-TEMPO-80) or 17 mM acetic acid (G-6-TEMPO-198) were used as solvents. The EPR spectra were recorded on a Varian E9 X-band spectrometer with a field of 3368 G, a modulation frequency of 100 kHz, a modulation amplitude of 1 G, and a microwave power of 10 mW.

2: 4-Amino-TEMPO (**1**) was first purified by gradient elution flash chromatography ($CH_2Cl_2 \rightarrow CH_2Cl_2$/MeOH 4/1). Succinic anhydride (1.6 g) was added to the purified 4-amino-TEMPO (2.8 g) in THF (150 mL), and the reaction mixture was stirred at ambient temperature for 18 h. The solvent was evaporated to near dryness, and the residue subjected to gradient elution flash chromatography ($CH_2Cl_2 \rightarrow CH_2Cl_2$/MeOH 9/1). The hygroscopic solid was immediately used in the next step. Yield 2.1 g (47%). Exact FAB mass spectrum: 273.1797 [M^+], calcd: 273.1814.

3: Compound **2** (8.0 g) was dissolved in THF (300 mL), after which first NHS (3.45 g) and then EDAC (5.8 g) were added. The mixture was stirred at ambient temperature for 18 h. The solvent was evaporated, the residue redissolved in $CHCl_3$ (300 mL), and the mixture extracted with water (2 × 100 mL). The organic phase was then separated and dried over $MgSO_4$, and its volume reduced to about 10 mL. The product was isolated by gradient elution flash chromatography ($CH_2Cl_2 \rightarrow CH_2Cl_2$/MeOH 9/1). Yield 8.5 g (78%). Exact FAB mass spectrum: 370.1972 [M^+], calcd: 370.1978.

General procedure for the preparation of G-6-TEMPO-198 and G-6-TEMPO-80: A 10% stock solution of G-6 PAMAM™ dendrimer (15 mL) was lyophilized and the resultant solid heated to 80 °C in DMSO (200 mL) to affect complete dissolution. A solution of active ester **3** (6.0 g or 0.98 g, respectively) in DMSO (100 mL) was then added, followed by triethylamine (100 mL). The reaction mixture was then stirred at 90 °C for 72 h. After cooling, the triethylamine was removed by evaporation and the solution diluted with 10% aqueous acetic acid (300 mL) and methanol (200 mL). Unchanged active ester and *N*-hydroxysuccinimide were removed by ultrafiltration with deionized water by using a stirred cell (Amicon, MA) fitted with a 30-K membrane (Filtron, MA). Occasional precipitation of a solid material in the cell occurred. In such cases, the precipitate was brought back into solution by the addition of small portions of methanol and 10% aqueous acetic acid, after which the diafiltration was continued until no low molecular weight species were detected inside the cell (size-exclusion HPLC). The resulting solute was lyophilized to obtain the products as light orange powders. G-6-TEMPO-198: C 53.72, H 8.56, N 16.10. MALDI-TOF mass spectra: number average MW 101000; weight average MW 102000. G-6-TEMPO-80: C 49.56, H 8.13, N 16.75. MALDI-TOF mass spectra: number average MW 71000; weight average MW 72000.

Reoxidation of TEMPOL-H by spin-labeled dendrimers: The oxidation of TEMPOL-H (1 mM) to TEMPOL by TEMPO-conjugated dendrimer in the presence of 50 μM dendrimer was performed in Ar-saturated water (G-6-TEMPO-198) or Ar-saturated PBS (G-6-TEMPO-80 and G-6), and measured as a function of time. The plotted signal intensity due to the reoxidized TEMPOL-H (divided by gain, see Figure 1) was adjusted by subtracting the signal intensities of blank solutions of G-6-TEMPO-198 or G-6-TEMPO-80.

Received: December 13, 2000 [Z16270]

[1] a) L. J. Berliner in *Magnetic Resonance Microscopy* (Eds.: B. Blumich, W. Kuhn), VCH, Weinheim, **1992**, pp. 151–163; b) L. J. Berliner, H. Fujii, X. Wan, S. J. Lukiewicz, *Magn. Reson. Med.* **1987**, *4*, 380–384.

[2] S. M. Hahn, F. J. Sullivan, A. M. DeLuca, M. C. Krishna, N. Wersto, D. Venzon, A. Russo, J. B. Mitchell, *Free Radical Biol. Med.* **1997**, *22*, 1211–1216.

[3] a) P. Kuppusamy, P. Wang, J. L. Zweier, M. C. Krishna, J. B. Mitchell, L. Ma, C. E. Trimble, C. J. C. Hsia, *Biochemistry* **1996**, *35*, 7051–7057. b) P. Kuppusamy, P. Wang, R. A. Shankar, L. Ma, C. E. Trimble, C. J. C. Hsia, J. L. Zweier, *Magn. Reson. Med.* **1998**, *40*, 806–811.

[4] D. A. Tomalia, A. M. Naylor, W. A. Goddard III, *Angew. Chem.* **1990**, *102*, 119–157; *Angew. Chem. Int. Ed. Engl.* **1990**, *29*, 138–175.

[5] a) J. C. Roberts, M. K. Bhalgat, R. T. Zera, *J. Biomed. Mater. Res.* **1996**, *30*, 53–65; b) C. Wu, M. W. Brechbiel, R. W. Kozak, O. A. Gansow, *Bioorg. Med. Chem. Lett.* **1994**, *4*, 449–454; c) L. H. Bryant, Jr., J. W. M. Bulte in *Focus on Biotechnology*, *Vol. X: Physics and Chemistry Basis for Biotechnology* (Eds.: M. de Cuyper, J. W. M. Bulte), Kluwer, Dordrecht, in press; d) L. H. Bryant, M. W. Brechbiel, C. C. Wu, J. W. M. Bulte, V. Herynek, J. A. Frank, *JMRI J. Magn. Reson. Imaging* **1999**, *9*, 348–352; e) E. C. Wiener, M. W. Brechbiel, H. Brothers, R. L. Magin, O. A. Gansow, D. A. Tomalia, P. C. Lauterbur, *Magn. Reson. Med.* **1994**, *31*, 1–8.

[6] a) K. Chen, P. D. Morse II, H. M. Swartz, *Biochim. Biophys. Acta* **1988**, *943*, 477–484; b) K. Chen, H. M. Swartz, *Biochim. Biophys. Acta* **1988**, *970*, 270–277; c) H. M. Swartz, M. Sentjurc, P. D. Morse II, *Biochim. Biophys. Acta* **1986**, *888*, 82–90.

[7] a) E. Walter, E. K. Woller, K. Sebby, D. Singel, M. J. Cloninger, presented at the 49th Natural Products Gordon Conference, Plymouth, New Hampshire, August 2000; b) A. W. Bosman, R. A. J. Janssen, E. W. Meijer, *Macromolecules* **1997**, *30*, 3606–3611.

[8] P. R. Ashton, S. E. Boyd, C. L. Brown, N. Jayaraman, J. F. Stoddart, *Angew. Chem.* **1997**, *109*, 756–759; *Angew. Chem. Int. Ed. Engl.* **1997**, *36*, 732–735.

[9] E. K. Woller, M. J. Cloninger, unpublished results.

Photochemical Carbonylation of Ethane under Supercritical Conditions**

Thomas E. Bitterwolf,* Dinara Lukmanova Kline, John C. Linehan, Clement R. Yonker, and R. Shane Addleman

The photochemical carbonylation of hydrocarbons and aromatic compounds [Eq. (1)] by rhodium catalysts of the general formula [Rh(CO)L_2Cl] (where L = PMe_3, PPh_3) is

(1)

[*] Prof. T. E. Bitterwolf, D. Lukmanova Kline
Department of Chemistry, University of Idaho
Moscow, ID 83844-2343 (USA)
Fax: (+1) 208-885-6173
E-mail: bitterte@uidaho.edu

J. C. Linehan, C. R. Yonker, R. S. Addleman
Chemical Sciences Department
Pacific Northwest National Laboratory
PO Box 999, Richland, WA 99352 (USA)

[**] This work is supported by the Research Corporation and the Director, Office of Science, Office of Basic Energy Sciences, Chemical Sciences Division of the US Department of Energy under contract DE-ACO6-76RLO 1830.

well known,[1] and the mechanism of these reactions has been examined by several groups.[2] This reaction has been extended to liquid propane[3] and recently the carbonylation of benzene to benzaldehyde and benzyl alcohol in supercritical CO_2 ($scCO_2$), has been reported in the patent literature.[4]

Methane and ethane are the major constituents of natural gas and are attractive C_1 and C_2 synthons for organic synthesis. Direct conversion to their alcohols would be particularly attractive, but carbonylation to the $n+1$ aldehydes would also open up a significant hydrocarbon reservoir to nonfuel applications. A wide range of catalytic reactions have been examined in supercritical media[5, 6] although to the best of our knowledge only the patent noted above has utilized the $[Rh(CO)(PMe_3)_2Cl]$ photochemical catalyst. The research presented herein was undertaken to establish whether photocatalytic carbonylation could be extended to methane and ethane, and to provide a preliminary understanding of the behavior of the catalyst under supercritical conditions.

Supercritical ethane, sc-ethane, ($T_c = 32.1\,^\circ C$, $P_c = 48.8$ atm) is an excellent solvent for organometallic catalysts. As the introduction of solutes and gases such as CO alters the phase behavior of supercritical fluids, photochemical studies in these single-phase mixtures were carried out at ethane pressures and temperatures well above the critical point.

Single-phase mixtures of ethane (100 atm), CO (13.6 atm), and $[Rh(CO)(PMe_3)_2Cl]$ (5.0 mg) were photolyzed at 60 °C with a high-pressure mercury lamp for 12 h. A quartz-windowed water filter was used to remove IR radiation from the source beam, but otherwise the light was unfiltered. During this time bands of the catalyst (1969 cm^{-1}) were found to decrease slightly, while a new band grew in at 1734 cm^{-1}. After photolysis the reaction mixture was vented into a cooled Schlenk flask and the recovered product was analyzed by mass spectrometry, which confirmed the presence of propionaldehyde. No effort has been made to optimize the yields from these photolyses.

Poliakoff and co-workers have photolyzed $[Cp^*Ir(CO)_2]$ ($Cp^* = C_5Me_5$) in single-phase mixtures of methane (270 atm, 295 K) and observed the oxidative addition product, $[Cp^*Ir(CO)(H)(CH_3)]$ by IR spectroscopy.[6h] Under similar conditions (300 atm methane, 10 atm CO, 308 K) we detected no bands attributable to $[Rh(CO)(PMe_3)_2Cl]$ in the supercritical phase. The lack of solubility of the catalyst under these conditions made it impossible to proceed with the photochemical studies.

Our inability to carry out the photolyses in sc-methane prompted us to examine the possibility of using a mixed-solvent system with $scCO_2$ ($T_c = 31.1\,^\circ C$, $P_c = 73$ atm) as the primary medium. The solubility of the rhodium compound in single-phase mixtures of CO_2 (40 °C, 75 – 90 atm) was established by using the Chrastil relationship.[7] Under the conditions used in our studies the solubility of the rhodium catalyst was found to be on the order of 8×10^{-5} M, and the rhodium catalyst displayed strong bands in the metal carbonyl region of the IR spectrum. Full details of this methodology for determining the solubilities in $scCO_2$ will be published separately.[8]

Photolysis of a mixture of single-phase mixtures of CO_2 (110 atm), CO (10 atm), and ethane (34 atm) with 3.4 mg of catalyst at 40 °C for 12 h resulted in the decrease in the band for the catalyst (1966 cm^{-1}) and the appearance of a new band at 1743 cm^{-1}. After photolysis the reaction mixture was vented into $CDCl_3$, and an NMR spectrum confirmed the presence of propionaldehyde. Yields are less than 5% based on initial loading of ethane under these conditions.

Attempts to carry out analogous reactions with methane in single-phase CO_2 mixtures were unsuccessful in that no new bands were observed in the region where one might expect the carbonyl stretching band of acetaldehyde, nor was any aldehyde detected by NMR spectroscopy of the vented reaction mixtures. Neither increasing the photolysis times nor the pressure of methane altered these results.

To our surprise we have found that the rhodium catalyst reacts slowly thermally and more rapidly photochemically with CO (10 atm) in single-phase CO_2 mixtures to give a product with IR bands at 2102 and 2006 cm^{-1}. In contrast, high-pressure IR studies established that $[Rh(CO)(PMe_3)_2Cl]$ did not thermally react with CO (34 atm) in petroleum ether over two days. $[Rh(CO)_2(PMe_3)Cl]$ has been found to display IR bands at 2093 and 2001 cm^{-1} in petroleum ether,[9] and we tentatively assign the new bands in the CO_2 mixtures to this species.

When the rhodium catalyst was photolyzed in single-phase CO_2 mixtures without other reactants a band at 1984 cm^{-1} was found to grow in as the catalyst band diminished. This mixture was vented into a Schlenk flask in a dry box, and the nonvolatile products were taken up into air-free $CDCl_3$. ^{13}P NMR spectroscopy established the presence of $OPMe_3$ in the photolyzed sample, as well at a new doublet at $\delta = 27.0$ ($J_{Rh,P} = 116$ Hz). Bands at 1983 cm^{-1} have been observed in petroleum ether solutions of $[Rh_2(CO)_4(\mu\text{-}Cl)]$ and PMe_3 (1:2) and are attributed to the formation of *cis*- and *trans*-$[Rh_2(CO)_2(PMe_3)_2(\mu\text{-}Cl)_2]$. The reactions of the rhodium catalyst in CO_2 with and without excess CO are presented in Scheme 1.

It is known that $[Rh(CO_2)(PBu_3)_2Cl]$ undergoes slow thermal decomposition at room temperature to $[Rh(CO)(OPBu_3)(PBu_3)Cl]$,[10] and that $[Rh(PR_3)_3Cl]$ and excess

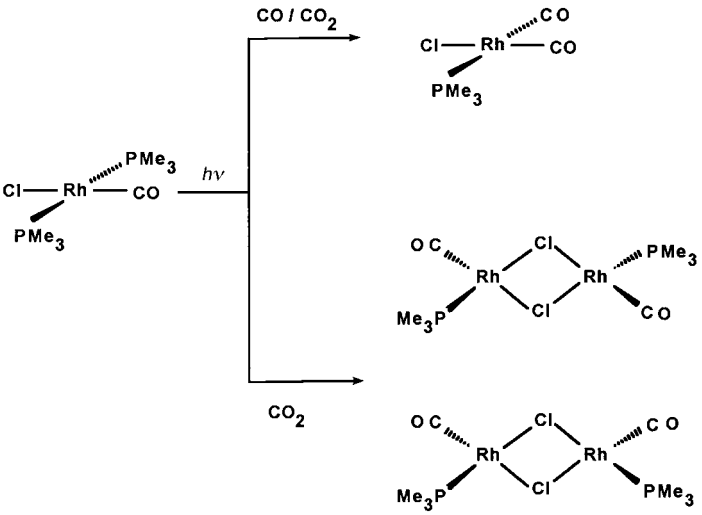

Scheme 1. Photochemical reaction of $[Rh(CO)(PMe_3)_2Cl]$ in $scCO_2$ with and without excess CO.

  1433-7851/01/4014-2693 $ 17.50+.50/0

phosphane react catalytically with CO_2 in refluxing decalin (ca. 185 °C) to give OPR_3 in the rate order $PPh_3 < PBuPh_2 < PEt_3$.[11] The rate for the PPh_3 derivative is about 20 turnovers per day. In the current studies, it appears that CO_2 undergoes reaction with the catalyst to give $OPMe_3$. In the presence of an excess of CO $[Rh(CO)_2(PMe_3)Cl]$ is formed, while in the absence of CO $[Rh_2(CO)_2(PMe_3)_2(\mu\text{-}Cl)_2]$ is formed. We are presently investigating the mechanism of this reaction.

These studies have established the feasibility of carrying out photocatalysis of ethane to propionaldehyde in either single-phase ethane or CO_2 mixtures. A competing side reaction probably involving CO_2 cleavage and phosphine oxide formation may preclude the use of CO_2 as a medium for these rhodium catalysts.

Experimental Section

A thermostated, stainless steel, high-pressure photolysis cell fitted with CaF_2 IR windows and a sapphire photolysis window was used in all high-pressure studies. The cell volume is about 12 mL and the IR pathlength is 0.1 mm. A small spin bar inside the cell was used for mixing. The cell was designed with a maximum pressure rating of 700 atm. IR spectra were recorded on a Perkin Elmer Spectrum 1000 FT IR Spectrometer. $[Rh(CO)(PMe_3)_2Cl]$ was prepared by standard literature methods.[12]

In a typical reaction, the rhodium catalyst was added to the cell as a solid, then the sealed cell was charged with reactant gases using a high-pressure line equipped with a syringe pump. Gases such as CO_2 and ethane were condensed into the syringe pump by chilling the pump with ice packs and then charged into the heated cell.

Reaction mixtures were photolyzed by using a 350-W high-pressure Hg lamp. A 30-mm quartz-windowed, water filter was used to remove IR wavelengths from the incident beam. Photolysis times of 6 – 12 h were used, and IR spectra were recorded at the beginning of each photolysis reaction and at regular intervals during the photolysis. Samples for mass spectrometric and NMR analysis were recovered by venting the sample through a restrictor tube directly into $DCCl_3$ in a N_2-flushed Schlenk flask immersed in an ice water bath.

Received: November 6, 2000
Revised: April 30, 2001 [Z16046]

[1] a) W. T. Bowse, A. S. Goldman, *J. Am. Chem. Soc.* **1992**, *114*, 350 – 351; b) T. Sakakura, T. Sodeyama, K. Sasaki, K. Wada, K. M. Tanaka, *J. Am. Chem. Soc.* **1990**, *112*, 7221 – 7229; c) M. Tanaka, T. Sakakura, *Pure Appl. Chem.* **1990**, *62*, 1147 – 1150; A. J. Kinin, R. Eisenberg, *Organometallics* **1988**, *7*, 2124 – 2129; d) T. Sakakura, K. Sasaki, Y. Tokunaga, K. Wada, M. Tanaka, *Chem. Lett.* **1888**, 155 – 158; e) T. Sakakura, M. Tanaka, *J. Chem. Soc. Chem. Commun.* **1987**, 758 – 759; f) T. Sakakura, M. Tanaka, *Chem. Lett.* **1987**, 1113 – 1116; g) T. Sakakura, M. Tanaka, *Chem. Lett.* **1987**, 249 – 252; A. J. Kunin, R. Eisenberg, *J. Am. Chem. Soc.* **1986**, *108*, 535 – 536.

[2] a) J. S. Bridgewater, B. Lee, S. Bernhard, J. R. Schoonover, P. C. Ford, *Organometallics* **1997**, *16*, 5592 – 5594; b) G. P. Rosini, W. T. Boese, A. S. Goldman, *J. Am. Chem. Soc.* **1994**, *116*, 9498 – 9505; c) C. T. Spillett, P. C. Ford, *J. Am. Chem. Soc.* **1989**, *111*, 1932 – 1933; d) D. A. Wink, P. C. Ford, *J. Am. Chem. Soc.* **1987**, *109*, 436 – 442; e) D. Wink, P. C. Ford, *J. Am. Chem. Soc.* **1985**, *107*, 1794 – 1796.

[3] T Sakakura, K. Ishiguro, M. Okano, T. Sako, *Chem. Lett.* **1997**, 1089 – 1090.

[4] T Sakakura, T. Sako (Jpn. Kokai Tokkyo Koho), JP 1105763 [9905763], **1999** [*Chem. Abstr.* **1999**, *130*, 110052d].

[5] "Metal-Complex-Catalyzed Reactions": P. G. Jessop, W. Leitner in *Chemical Synthesis Using Supercritical Fluids* (Eds.: P. G. Jessop, W. Leitner), Wiley-VCH, New York, **1999**, and references therein.

[6] a) D. R. Palo, C. Erkey, *Ind. Eng. Chem. Res.* **1998**, *37*, 4203 – 4206; b) P. G. Jessop, Y. Hsiao, T. Ikariya, R. Noyori, *J. Am. Chem. Soc.* **1996**, *118*, 344 – 355; c) P. G. Jessop, T. Ikariya, R. Noyori, *Nature* **1994**, *368*, 231 – 233; d) P. G. Jessop, T. Ikariya, R. Noyori, *Science* **1995**, *269*, 1065 – 1069; e) J. A. Banister, P. D. Lee, M. Poliakoff, *Organometallics* **1995**, *14*, 3876 – 3885; M. A. Banister, S. M. Howdle, M. Poliakoff, *J. Chem. Soc. Chem. Commun.* **1993**, 1814 – 1815; f) M. Poliakoff, S. M. Howdle, S. G. Kazarian, *Angew. Chem.* **1995**, *107*, 1409 – 1432; *Angew. Chem. Int. Ed. Engl.* **1995**, *34*, 1275 – 1295; g) M. J. Banks, S. Feng, M. F. Gross, W. Tumas, *J. Am. Chem. Soc.* **1995**, *117*, 8277 – 8278; h) J. A. Banister, A. I. Cooper, S. M. Howdle, M. Jobling, M. Poliakoff, *Organometallics* **1996**, *15*, 1804 – 1812.

[7] a) J. Chrastil, *J. Phys. Chem.* **1982**, *86*, 3016; b) R. S. Addleman, M. J. Carrott, C. M. Wai, *Anal. Chem.* **2000**, *72*, 4015 – 4022.

[8] R. S. Addleman, C. R. Yonker, J. C. Linehan, T. E. Bitterwolf, D. L. Klein, unpublished results.

[9] a) T. E. Bitterwolf, unpublished results, **1999**; b) for $L = PPh_3$ and PMe_2Ph see: A. R. Sanger, *Can. J. Chem.* **1985**, *63*, 571 – 575.

[10] M. Aresta, C. F. Nobile, *Inorg. Chim. Acta* **1977**, *24*, L49 – L50.

[11] K. M. Nicholas, *J. Organomet. Chem.* **1980**, *188*, C10 – C12.

[12] A. J. Deeming, B. L. Shaw, *J. Chem. Soc. A* **1969**, 597 – 602.

Rearrangement of a Tricyclic 2,5-Cyclohexadienone: Towards a General Synthetic Route to the Daphnanes and (+)-Resiniferatoxin**

Stona R. Jackson, Michael G. Johnson, Masafumi Mikami, Sojiro Shiokawa, and Erick M. Carreira*

The daphnane resiniferatoxin[1] (RTX) and structurally related tiglianes possess complex, densely functionalized architectures, along with important biological activity, that have inspired much innovative research in chemistry and biology. The recent isolation and cloning of the principal receptor targeted by resiniferatoxin holds great promise for the development of RTX-related therapeutics.[2, 3] In this regard, parallel advances in the design and synthesis of analogues is imperative because these may serve as cellular probes and useful pharmacologically important compounds.

[*] Prof. Dr. E. M. Carreira, S. R. Jackson, M. G. Johnson, M. Mikami, S. Shiokawa
Laboratorium für Organische Chemie
ETH-Zentrum, Universitätsstrasse 16
8092, Zürich (Switzerland)
Fax: (+41) 1-632-1328
E-mail: Carreira@org.chem.ethz.ch

[**] We wish to gratefully acknowledge the support of Daiso Ltd., Japan (M.M.), and Meiji Seika Kaisha Ltd., Japan (S.S.). M.J. thanks Pharmacia-UpJohn for a graduate fellowship during his third year at Caltech. Financial support was provided by the Packard Foundation, the National Science Foundation (USA), the National Institutes of Health (USA), and by generous funds from Eli Lilly, Merck, Novartis, Pfizer, Pharmacia-Upjohn, Zeneca, the Eidgenössische Technische Hochschule (ETH), the Kontaktgruppe für Forschungsfragen (KGF), and Hoffmann La Roche.

Supporting information for this article is available on the WWW under http://www.angewandte.com or from the author.

  1433-7851/01/4014-2694 $ 17.50+.50/0

Progress in the synthesis of related bioactive tiglianes (such as phorbol) has generated methods for the construction of daphnanes,[4] and has culminated in the synthesis of resiniferatoxin by Wender et al.[5] We have been engaged in a program focussed on the synthesis of resiniferatoxin with an aim of developing an efficient, distinct approach to this daphnane skeleton. In this communication, we document a high yielding photorearrangement of **1** to a 5,7,6-tricyclic structure **2** (82% yield; Scheme 1). Utilization of this key transformation provides ready access to the conveniently functionalized, versatile template **2**, which can be elaborated as the daphnane skeleton to form **3**.

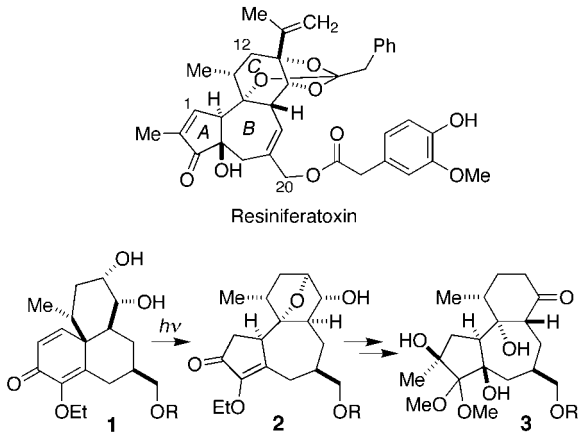

Scheme 1. The structure of resiniferatoxin, and the strategy of forming highly functionalized skeleton **3** through a key photorearrangement reaction.

In approaching the synthesis challenge, we were aware of the classic α-santonin to isophotosantonic lactone photorearrangement, which typically proceeds in 30–40% yield and which has inspired numerous studies and applications in the synthesis of bicyclic compounds.[6] At the outset of our synthetic analysis aimed at applying this photorearrangement reaction to **1** two critical issues were of concern: 1) the additional torsional strain associated with the tricyclic substrate may disfavor formation of the necessary cyclopropenyl intermediate [see **4**, Eq. (1)]; and 2) if this intermediate was

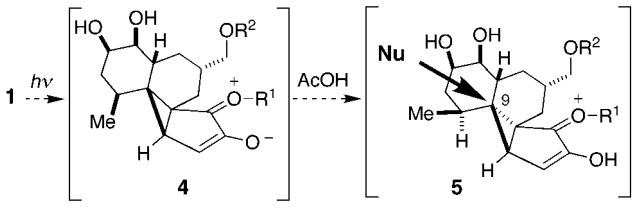

formed, the sterics associated at the C-9 electrophilic site might preclude stereoselective opening in the desired sense [see **5**, Eq. (1)]. In this regard, the failure of certain polycyclic dienones to undergo photorearrangement because of steric encumbrance has been documented.[7] Accordingly, precedence was lacking for the rearrangement of spirofused tricyclic systems.

The synthesis of the requisite tricyclic photosubstrate commences with **6** (Scheme 2).[8] Through a short sequence

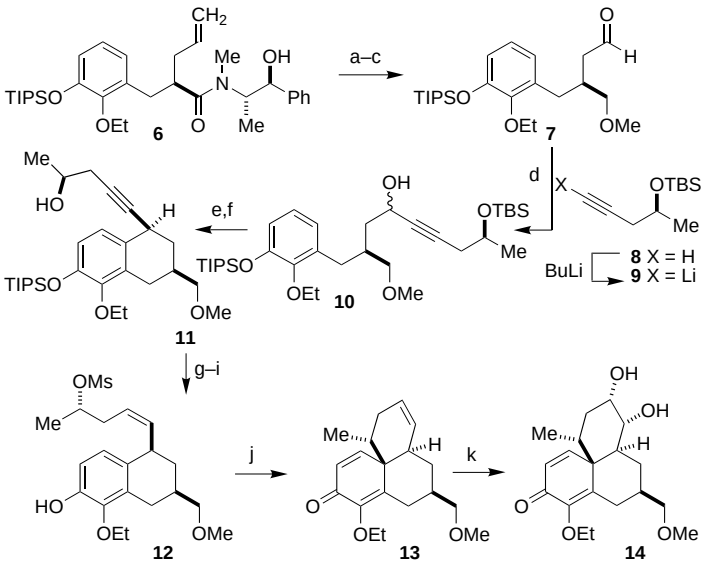

Scheme 2. a) $LiNH_2BH_3$, THF, 0 °C, 86%; b) MeI, NaH, THF, RT, 96%; c) 1. O_3, CH_2Cl_2, −78 °C; 2. PPh_3, 91%; d) THF, −78 °C, 81%; e) 1. $Co_2(CO)_8$, CH_2Cl_2, −78 °C; 2. $BF_3 \cdot OEt_2$, −78 °C, 76%; f) I_2, benzene, RT, 79%; g) H_2, Pd/C, pyridine, 92%; h) $MeSO_2Cl$, NEt_3, CH_2Cl_2, −78 °C, 98%; i) TBAF, THF, 0 °C, 97%; j) KO*t*amyl, HO*t*amyl, 102 °C, 74%; k) 0.1 equiv OsO_4, NMO, acetone, H_2O, 72%. Ms = mesyl = methanesulfonyl, NMO = 4-methylmorpholine *N*-oxide, TBAF = tetrabutylammonium fluoride, TBS = *tert*-butyldimethylsilyl, THF = tetrahydrofuran, TIPS = triisopropylsilyl.

of reactions amide **6** was transformed into aldehyde **7**. Addition of acetylide **9**[9] to **7** afforded alcohols **10** in 81% yield as an inconsequential mixture of diastereomers. These served as substrates for a cobalt-mediated ring annulation,[10] to furnish **11** in 60% yield as a single diastereomer.[11, 12] Semihydrogenation of **11** afforded a *cis* olefin which was elaborated to **12** in 90% overall yield. Cyclohexadienone **13** was formed from **12** (74% yield) through intramolecular *para-C*-alkylation.[13] Chemo- and stereoselective dihydroxylation of **13** afforded **14** in 72% yield and 90:10 diastereomeric ratio (d.r.).[11]

Dienones **13** and **14** can both serve as substrates for the strategic photorearrangement to furnish the daphnane skeleton. Photorearrangement of **13** with the conditions reported for α-santonin,[6a] afforded product **15** in 20–40% yield [Eq. (2)]. However, in TFA/HOAc **14** underwent the photo-

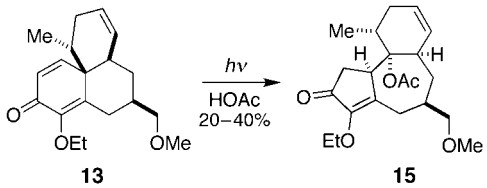

rearrangement cleanly (72%); moreover, in TFA/dioxane or TFA/pentane **16** was isolated in 78 and 82% yields, respectively [Eq. (3)]. Having established a route to the daphnane 5,7,6-tricyclic system, we proceeded to establish that **16** could be a useful template for further elaboration.[14]

  1433-7851/01/4014-2695 $ 17.50+.50/0

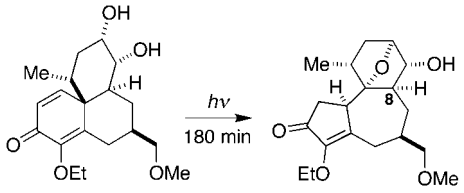

14 16

Conditions	Yield
33% TFA in HOAc	72%
33% TFA in pentane	82%
33% TFA in 1,4-dioxane	78%

The elaboration of **16** commenced with stereoselective addition of $MeLi/CeCl_3$ to the five-membered A ring (Scheme 3); the well-defined concave and convex domains of **16** furnish **17** as a single diastereomer.[11] This reaction

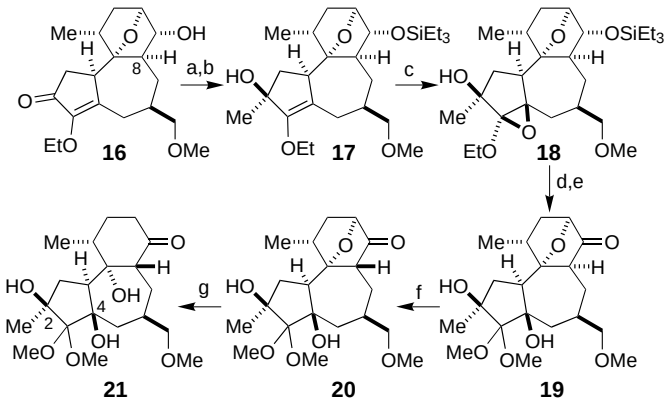

Scheme 3. a) Et_3SiCl, imidazole, CH_2Cl_2, 0 °C, 90 %; b) MeLi, $CeCl_3$, THF, −78 °C, 88 %; c) $VO(acac)_2$, TBHP, benzene, RT, 84 %; d) CSA, MeOH, RT, 95 %; e) TPAP, NMO, CH_2Cl_2, RT, 88 %; f) NaOMe, MeOH, 65 °C, 61 %; g) SmI_2, THF/H_2O, 0 °C, 80 %. acac = acetylacetone, CSA = (+)-camphorsulfonic acid, TBHP = *tert*-butylhydroperoxide, TPAP = tetrapropylammonium perruthenate.

provides an allylic alcohol suitably disposed to serve in subsequent stereoselective functionalization of the enol ether and, thus, installation of the requisite C-4 alcohol with the desired stereochemistry. Directed epoxidation of allylic alcohol **17** afforded exclusively the stable epoxy acetal **18** (84 %). Simultaneous transketalization and deprotection of the TES ether at the C-13 position generated intermediate dimethyl ketal **19**, after oxidation to the corresponding ketone. Through this short reaction sequence, the compatibility of the strategy with the appropriate functionalization reactions of the A ring is established.

We subsequently set out to determine the viability of the strategy in connection with functionalization of the six-membered C ring. Elaboration of this subunit commenced from ketone **19**. This ketone undergoes epimerization cleanly (10 mol % NaOMe) to yield a separable mixture of epimers **19** and **20** (1.6:1). Little material is lost through this transformation, and iterative application of the alkaline conditions to recovered ketone **19** yields > 90 % of the desired epimer **20** after three cycles. Treatment of **20** with SmI_2 in THF/H_2O resulted in C–O bond cleavage to furnish hydroxy ketone **21** (80 %).[15] It is noteworthy that the conversion of ring C proceeds smoothly without the observation of potentially complicating retroaldol or elimination reactions.

We have demonstrated the utility of a 2,5-cyclohexadienone photorearrangement within a complex tricyclic system for the formation of a highly functionalized template structure for the daphnanes. The five-membered A ring of the advanced intermediate can be functionalized in a series of stereoselective reactions to incorporate the C-2 methyl group and the C-4 tertiary hydroxy group with the latter in the stereochemical configuration found in many daphnanes. The C ring is similarly amenable to synthetic elaboration. The chemistry we have described should not only find use in the ongoing approaches to the synthesis of resiniferatoxin and related daphnanes, but also, importantly, be useful in the preparation of potentially useful analogues for pharmacological studies. It is worth noting with respect to the latter that, commencing from **6**, the tricyclic core **16** is accessed in only 12 steps with an overall yield of 9 %.

Received: March 26, 2001 [Z 16853]

[1] Isolation: M. Hergenhahn, W. Adolf, E. Hecker, *Tetrahedron Lett.* **1975**, *16*, 1595.

[2] See, for example: M. B. Chancellor, W. C. De Groat, *J. Urology* **1999**, *162*, 3.

[3] "Resiniferatoxin—An Ultrapotent Capsaicin Analogue": P. M. Blumberg, A. Szállási, G. Acs in *Capsaicin in the Study of Pain*, Academic Press, New York, **1993**, chap. 3, pp. 45–62.

[4] Synthesis of phorbol and approaches to tiglianes: a) P. A. Wender, K. D. Rice, M. E. Schnute, *J. Am. Chem. Soc.* **1997**, *119*, 7897; b) J. H. Rigby, P. C. Kierkus, *J. Am. Chem. Soc.* **1989**, *111*, 4125; c) R. Tokunoh, H. Tomiyama, M. Sodeoka, M. Shibasaki, *Tetrahedron Lett.* **1996**, *37*, 2449; d) W. G. Dauben, J. Dinges, T. C. Smith, *J. Org. Chem.* **1993**, *58*, 7635; e) L. A. Paquette, D. R. Sauer, S. D. Edmondson, D. Friedrich, *Tetrahedron* **1994**, *50*, 4071; reviews of synthetic approaches to tiglianes and daphnanes: f) J. H. Rigby, *Stud. Nat. Prod. Chem.* **1993**, *12*, 233; g) L. Paquette, F. Gallou, Z. Zhao, D. G. Young, J. Liu, J. Yang, D. Friedrich, *J. Am. Chem. Soc.* **2000**, *122*, 9610.

[5] P. A. Wender, C. D. Jesudason, H. Nakahira, N. Tamura, A. L. Tebbe, Y. Ueno, *J. Am. Chem. Soc.* **1997**, *119*, 12976.

[6] a) D. H. R. Barton, P. DeMayo, M. Shafiq, *J. Chem. Soc.* **1957**, 929; D. H. R. Barton, P. DeMayo, M. Shafiq, *J. Chem. Soc.* **1958**, 141; D. H. R. Barton, P. DeMayo, M. Shafiq, *J. Chem. Soc.* **1958**, 3314; D. H. R. Barton, P. DeMayo, M. Shafiq, *Proc. Chem. Soc.* **1957**, 205; b) D. Arigoni, H. Bosshard, H. Bruderer, G. Büchi, O. Jäger, L. J. Krebaum, *Helv. Chim. Acta* **1957**, *40*, 1732; c) E. Piers, K. F. Cheng, *Can. J. Chem.* **1970**, *48*, 2234; d) A. E. Greene, N. Kann, P. Delair, *J. Chem. Soc. Perkin Trans. 1* **1994**, 1651; e) P. Metz, S. Bertels, R. Fröhlich, *J. Am. Chem. Soc.* **1993**, *115*, 12595; f) A. F. Greene, M. T. Edgar, *J. Org. Chem.* **1989**, *54*, 1468; f) D. Caine, F. N. Tuller, *J. Org. Chem.* **1973**, *38*, 3663; g) D. Caine, J. T. Gupton, *J. Org. Chem.* **1975**, *40*, 809.

[7] H. E. Zimmerman, G. Jones, *J. Am. Chem. Soc.* **1970**, *92*, 2753.

[8] Compound **6** is conveniently prepared in preparatively useful quantities (> 75 g, 85–90 % yield, 94:6 d.r.) through the asymmetric enolate alkylation reaction of Myers et al.: A. G. Myers, B. H. Yang, H. Chen, L. McKinstry, D. J. Kopecky, J. L. Gleason, *J. Am. Chem. Soc.* **1997**, *119*, 6496. Details for the synthesis of **6** can be found in the Supporting Information.

[9] The alkyne **9** was synthesized as described previously: R. M. Rzasa, D. Romo, D. J. Stirling, J. W. Blunt, M. H. G. Munro, *Tetrahedron Lett.* **1995**, *36*, 5307.

[10] K. M. Nicholas, *Acc. Chem. Res.* **1987**, *20*, 207.

[11] The diastereomeric ratio was determined with ^1H NMR spectroscopic methods.

  1433-7851/01/4014-2696 $ 17.50+.50/0

[12] The stereochemical outcome of the reaction was established through analysis with ^{1}H NMR spectroscopy. In addition, compound **11** was identical in all respects to the same compound prepared through an independent route which afforded a crystalline derivative.
[13] S. Winstein, R. Baird, *J. Am. Chem. Soc.* **1962**, *84*, 788.
[14] It is important to take note of the fact that the stereochemical outcome of the photorearrangement reaction is such that epimerization of the C-8 ring fusion in **16** is necessary; nonetheless, a number of different intermediates could be envisioned to provide the required inversion at this stereocenter.
[15] a) S. Hanessian, C. Girard, *Synlett* **1994**, 861; b) G. A. Molander, G. Hahn, *J. Org. Chem.* **1986**, *51*, 1135.

Activation, Tuning, and Immobilization of Homogeneous Catalysts in an Ionic Liquid/ Compressed CO_2 Continuous-Flow System**

Andreas Bösmann, Giancarlo Franciò, Edo Janssen, Maurizio Solinas, Walter Leitner,* and Peter Wasserscheid*

Dedicated to Professor Ernst-Gottfried Jäger on the occasion of his 65th birthday

The quest for new strategies to immobilize organometallic catalysts is one of the major challenges in homogeneous catalysis. Ionic liquids (ILs) are emerging as excellent solvents for transition metal catalysts. In many applications they are used for multiphasic reaction systems because of their miscibility gap with the reaction products.[1] Supercritical carbon dioxide ($scCO_2$) is also of increasing interest because it combines an environmentally benign character with favorable physico-chemical properties for chemical synthesis.[2, 3] Catalyst separation schemes have been devised on the basis of the tuneable phase behavior of $scCO_2$ (CESS process).[4] We report here a new continuous-flow catalytic system based on the combination of these two solvents systems, which are at the extreme ends of the volatility and polarity scale. We provide convincing evidence that the interplay of their complementary properties offers new intriguing possibilities for catalytic synthesis.

[*] Dr. P. Wasserscheid, Dipl.-Chem. A. Bösmann
Institut für Technische Chemie und
Makromolekulare Chemie der RWTH Aachen
Worringer Weg 1, 52074 Aachen (Germany)
Fax: (+49) 241-8888-177
E-mail: wasserscheidp@itmc.rwth-aachen.de
Priv.-Doz. Dr. W. Leitner, Dr. G. Franciò, E. Janssen, M. Solinas
Max-Planck-Institut für Kohlenforschung
Kaiser-Wilhelm-Platz 1, 45470 Mülheim an der Ruhr (Germany)
Fax: (+49) 208-306-2993
E-mail: leitner@mpi-muelheim.mpg.de

[**] This work was supported by the Max Planck Society, the DFG (Gerhard-Hess-Award to W.L.), and the Fonds der Chemischen Industrie. The fruitful input of Dipl.-Chem. Heike Stemmer and Dr. Andreas Wegner (both Mülheim) during the early phase of the project is gratefully acknowledged.

Recently, the research groups of Brennecke and Beckman described the phase behavior of biphasic systems consisting of an IL and supercritical CO_2.[5] They demonstrated that $scCO_2$ is highly soluble in some ILs, while the same ILs show no detectable solubility in the $scCO_2$ phase. Moreover, it was found that $scCO_2$ can be used to extract high-boiling organic substances from ILs without any cross-contamination of the extract with the IL. Intrigued by these pioneering studies, we and others[6, 7] started to explore this unique phase behavior for homogeneous catalysis. While our investigations were in progress, Jessop et al. used $scCO_2$ to isolate the products of a catalytic hydrogenation that was carried out in an IL.[6a] Baker, Tumas, and co-workers conducted catalytic hydrogenations of, for example, 1-decene directly in a biphasic reaction mixture consisting of the IL 1-*n*-butyl-3-methylimidazolium (BMIM) hexafluorophosphate and $scCO_2$. The ionic catalyst solution could be re-used in up to four consecutive batch experiments.[6b]

We demonstrate here that the combination of a suitable IL and compressed CO_2 can offer much more potential for process optimization than just a simple protocol for batchwise catalyst recycling. By using this unusual biphasic system we were able to activate, tune, and immobilize Ni-catalyst **1** in a continuous flow system for the hydrovinylation of styrene (Scheme 1).

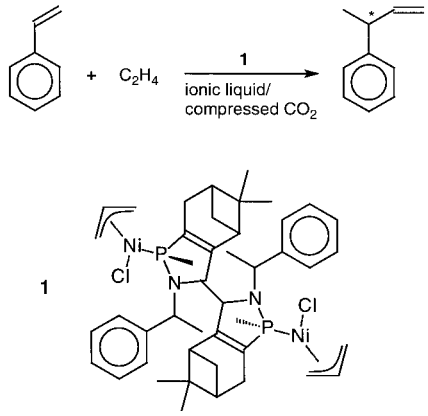

Scheme 1. The hydrovinylation reaction and the Wilke's catalyst **1**.

Hydrovinylation is the transition metal catalyzed codimerization of alkenes with ethene to yield 3-substituted 1-butenes.[8] This powerful carbon–carbon bond forming reaction can be achieved with high enantioselectivity using Wilke's complex **1** as a catalyst precursor.[9] In conventional solvents pre-catalyst **1** needs to be activated with a chloride-abstracting agent, for example, the highly flammable $Et_3Al_2Cl_3$.[8, 9] Some of us reported the use of complex **1** in liquid and supercritical CO_2 after activation with alkali salts of weakly coordinating anions such as Na[BARF] (BARF = tetrakis[3,5-bis(trifluoromethyl)phenyl]borate).[10] In a first set of experiments we aimed to identify suitable ILs that would allow the activation of **1** for the enantioselective hydrovinylation of styrene in the presence of compressed CO_2 (Table 1).[11]

The synthesis of the ILs comprising the bistriflic amide anion ($(CF_3SO_2)_2N$, Tf_2N) and the cations 1-ethyl-3-methyl-

  1433-7851/01/4014-2697 $ 17.50+.50/0

Table 1. Hydrovinylation of styrene in a IL/compressed CO_2 reaction system.[11]

Entry	Ionic liquid	Conversion [%]	3-Phenyl-1-butene [%]	Isomers [%]	Oligomers [%]	*ee* (*R*) [%]
1	[EMIM][Tf_2N]	69.9	65.3	0.8	3.8	53.4
2	[EMIM][BF_4]	39.6	38.9	0.7	–	34.2
3	[EMIM][Al{$OC(CF_3)_2Ph$}$_4$]	90.5	87.5	0.7	2.3	78.2
4[a]	[EMIM][BARF]	100	63.8	26.2	10.0	89.4
5	[4-MBP][Tf_2N]	70.5	69.7	0.8	–	58.4
6	[4-MBP][BF_4]	35.5	34.8	0.7	–	44.2
7	Li[Tf_2N][b]	24.4	23.8	0.6	–	65.9
8	Na[BF_4][b]	5.0	5.0	–	–	n.d.

[a] $T = 25\,^{\circ}C$. [b] Solid salts; anion/Ni = 100/1.

imidazolium (EMIM) and 1-*n*-butyl-4-methylpyridinium (4-MBP) was carried out following a general procedure described by Bônhote et al.[12] [EMIM][BF_4], [4-MBP][BF_4], [EMIM][Al{$OC(CF_3)_2Ph$}$_4$], and [EMIM][BARF] were synthesized by treating [EMIM]Cl and [4-MBP]Cl (both purchased from Solvent Innovation GmbH, Cologne[13]) in dry acetone with Na[BF_4], Na[Al{$OC(CF_3)_2Ph$}$_4$], and Na[BARF], respectively.[14]

Catalyst **1** was activated in all IL/CO_2 systems under investigation, but the effectiveness of the activation is clearly very dependent on the nature of the IL's anion. A comparison of the results in different ILs with EMIM as the common cation reveals that the level of conversion drops in the order BARF > Al[$OC(CF_3)_2Ph$]$_4$ > Tf_2N > BF_4 (entries 1–4). This trend is consistent with the estimated nucleophilicity/coordination strength of the anions. The high activity of catalyst **1** in [EMIM][BARF] leads to a significant amount of consecutive isomerization and oligomerization, even at room temperature (entry 4).

The specific environment of the ionic solvent system appears to activate catalyst **1** beyond a simple anion-exchange reaction. This is emphasized by the observation that even the addition of a 100-fold excess of Li[Tf_2N] or Na[BF_4] in pure CO_2 lead at best to a moderate activation of **1** relative to any of the ILs with the corresponding counterions (entries 7, 8).

There is also a significant intrinsic influence of the anion on the enantioselectivity of the reaction, as revealed by comparing experiments with negligible consecutive reactions (entries 1–3; 5/6).[15] The cation of the IL also exhibits a significant influence on the performance of **1**. At comparable conversions, higher *ee* values were found with [4-MBP][BF_4] and [4-MBP][Tf_2N] than the corresponding [EMIM] salts (entries 1/5, 2/6). This first observation of a cation effect on enantioselective catalysis in ILs may open up new avenues for catalyst tuning.

The influence of the reaction conditions was assessed briefly for the system [EMIM][Tf_2N]/CO_2. Increasing the partial pressure of ethylene and decreasing the temperature was found to suppress the consecutive side reaction. A 58% conversion of styrene (styrene/Ni = 1000/1) was achieved after 1 h under 40 bar of ethylene at 0 °C, with 3-phenyl-1-butene being detected as the only product (71% *ee* of the *R* isomer).

Encouraged by these results, we evaluated the batchwise recycling of catalyst **1** in ionic liquids. The products could be readily isolated from the IL/CO_2 system by extraction with scCO_2. However, similar to what had been seen for the hydrovinylation in compressed CO_2 alone,[10] the active nickel species deactivated rapidly within three to four batchwise cycles. We speculated that this disappointing result was related mainly to the instability of the active species in the absence of substrate and that this could be avoided by continuous operation in a flow reactor.

Our continuous flow apparatus for homogeneous catalysis in IL/CO_2 systems is depicted schematically in Figure 1. The ionic catalyst solution is placed into the reactor R where it is in intimate contact with the continuous reaction phase entering from the bottom. The reaction phase is made up in the mixer from a pulsed flow of ethylene and a continuous flow of styrene and compressed CO_2.[16] Figure 2 shows the results of a lifetime study for catalyst **1** dissolved, activated, and immobilized in the system [EMIM][Tf_2N]/CO_2 by this straightforward technique. Catalyst **1** shows a remarkably stable activity over 61 h, and enantioselectivity drops only slightly over the long reaction period. The results clearly indicate—at least for the hydrovinylation of styrene with

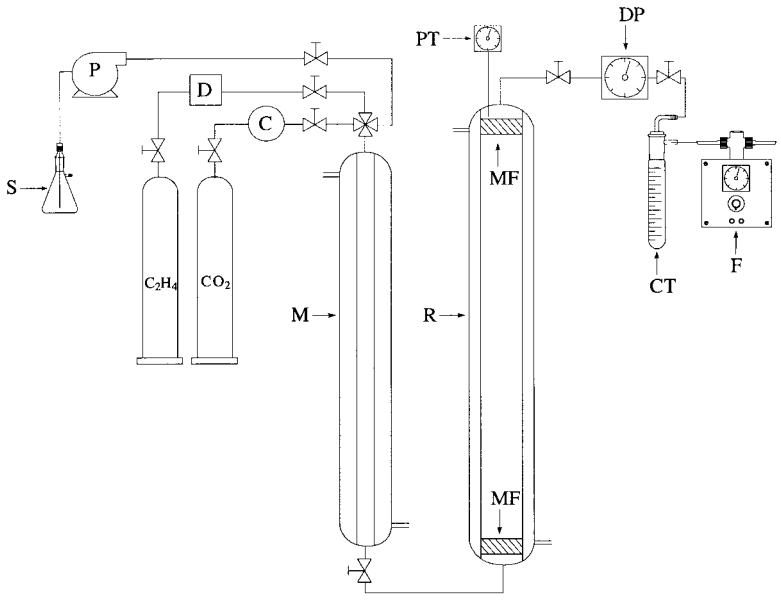

Figure 1. Schematic view of the continuous-flow reaction apparatus. The parts are labeled as follows: C: compressor, CT: cold trap, D: dosimeter, DP: depressurizer, F: flowmeter, M: mixer, MF: metal filter, P: HPLC pump, PT: pressure transducer and thermocouple, R: reactor, S: styrene.

  1433-7851/01/4014-2698 $ 17.50+.50/0

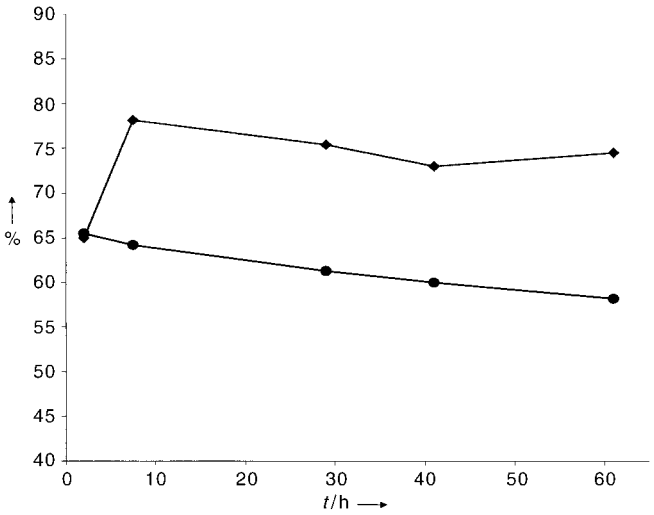

Figure 2. Lifetime study for catalyst **1** activated and immobilized in the system [EMIM][$(CF_3SO_2)_2$N]/compressed CO_2 during the hydrovinylation of styrene,(●: *ee* value; ◆: conversion).

1—that an IL catalyst solution can show excellent catalytic performance during continuous product extraction with compressed CO_2.

As a general conclusion, continuous flow systems consisting of an ionic catalyst solution and compressed CO_2 offer a new intriguing immobilization technique for homogeneous catalysis. The combination of nonvolatile ILs with nonhazardous CO_2 represents a particularly attractive approach to environmentally benign processes. The IL in combination with CO_2 provides the potential to activate and tune the organometallic catalyst. Furthermore, product separation from the catalyst is now possible without exposing the catalyst to a variation of temperature, pressure, or substrate concentration. In contrast to the use of pure IL, the compressed CO_2 greatly decreases the viscosity of the ionic catalyst solution, thus facilitating mass transfer during the catalytic reaction. Moreover, the use of CO_2 as the mobile phase enables a reactor design that is very similar to a classical fixed-bed reactor.[17] Thus, our new immobilization technique provides an attractive approach to combine the molecular design of homogeneous catalysts with the advanced process design of heterogeneous catalysis.

Received: March 26, 2001 [Z16854]

[1] Reviews: a) P. Wasserscheid, W. Keim, *Angew. Chem.* **2000**, *112*, 3926 – 3945; *Angew. Chem. Int. Ed.* **2000**, *39*, 3772 – 3789; b) T. Welton, *Chem. Rev.* **1999**, *99*, 2071 – 2083; c) J. D. Holbrey, K. R. Seddon, *Clean Prod. Process.* **1999**, *1*, 223 – 236.

[2] *Chemical Synthesis Using Supercritical Fluids* (Eds.: P. G. Jessop, W. Leitner), Wiley-VCH, Weinheim, **1999**.

[3] For selected reviews, see a) P. G. Jessop, T. Ikariya, R. Noyori, *Science* **1995**, *269*, 1065 – 1067; b) D. A. Morgenstern, R. M. LeLacheur, D. K. Morita, S. L. Borkowsky, S. Feng, G. H. Brown, L. Luan, M. F. Gross, M. J. Burk, W. Tumas, *ACS Symp. Ser.* **1996**, *626*, 132 – 151; c) P. G. Jessop, T. Ikariya, R. Noyori, *Chem. Rev.* **1999**, *99*, 475 – 493; d) W. Leitner, *Top. Curr. Chem.* **1999**, *206*, 107 – 132.

[4] a) G. Franciò, K. Wittmann, W. Leitner, *J. Organomet. Chem.* **2001**, *621*, 130 – 142; b) S. Kainz, A. Brinkmann, W. Leitner, A. Pfaltz, *J. Am. Chem. Soc.* **1999**, *121*, 6421 – 6429; c) D. Koch, W. Leitner, *J. Am. Chem. Soc.* **1998**, *120*, 13398 – 13404.

[5] L. A. Blanchard, D. Hancu, E. J. Beckman, J. F. Brennecke, *Nature* **1999**, *399*, 28 – 29.

[6] a) R. A. Brown, P. Pollett, E. McKoon, C. A. Eckert, C. L. Liotta, P. G. Jessop, *J. Am. Chem. Soc.* **2001**, *123*, 1254 – 1255; b) F. Liu, M. B. Abrams, R. T. Baker, W. Tumas, *Chem. Commun.* **2001**, 433 – 434.

[7] Hydroformylation in an IL/scCO_2 continuous-flow system was published while this manuscript was under review, see M. F. Sellin, P. B. Webb, D. J. Cole-Hamilton, *Chem. Commun.* **2001**, 781 – 782.

[8] For reviews, see a) P. W. Jolly, G. Wilke in *Applied Homogenous Catalysis with Organic Compounds 2* (Eds.: B. Cornils, W. A. Herrman), Wiley-VCH, **1996**, pp. 1024 – 1048; b) T. V. RajanBabu, N. Nomura, J. Jin, B. Radetich, H. Park, M. Nandi, *Chem. Eur. J.* **1999**, *5*, 1963 – 1968.

[9] G. Wilke, J. Monkiewicz, DOS 3618169, Priority 30.05.86 [*Chem. Abstr.* **1988**, *109*, P6735].

[10] A. Wegner, W. Leitner, *Chem. Commun.* **1999**, 1583 – 1584.

[11] In a typical experiment, a stainless-steel high-pressure reactor (V = 10 mL) equipped with thick-wall glass windows, a PTFE stirring bar, and a thermocouple was charged with ionic liquid (2 mL) and ethene (0.3 g, 10 mmol) under an argon atmosphere. A dosing unit containing a styrene solution of **1** (0.3 mL, styrene/Ni = 350/1) was connected to the reactor through a ball valve and pressurized with CO_2 (7 g). The reactor was filled through another valve with CO_2 (9 g). The reaction mixture was then warmed to 40 °C, while the dosing unit was heated to 60 °C. Opening the ball valve started the reaction which was allowed to proceed for 1 h. After venting the volatiles through a cold trap, the IL was extracted with pentane, and the combined extract and trap contents were analyzed by GC-MS.

[12] P. Bonhôte, A.-P. Dias, N. Papageorgiou, K. Kalyanasundaram, M. Grätzel, *Inorg. Chem.* **1996**, *35*, 1168 – 1178.

[13] http://www.solvent-innovation.com.

[14] P. A. Z. Suarez, J. E. L. Dullius, S. Einloft, R. F. de Souza, J. Dupont, *Polyhedron* **1996**, *15*, 1217 – 1219.

[15] For the influence of consecutive isomerization on the *ee* value, see R. Bayersdörfer, B. Ganter, U. Englert, W. Keim, D. Vogt, *J. Organomet. Chem.* **1998**, *552*, 187 – 194.

[16] The reactor (R, Figure 1) was filled, in an argon atmosphere, with a solution of **1** (0.1659 g, 0.19 mmol) in [EMIM][Tf_2N] (39 mL) and cooled to 0 °C. The reactor pressure was maintained constant at 80 bar by the continuous flow of compressed CO_2 (the exit flow was adjusted to about 30 L min^{-1}). The reaction was then allowed to proceed with a constant styrene flow of 0.01 mL min^{-1} and pulses of C_2H_4 (1 mL, 90 bar) every 0.5 min.

[17] For the use of CO_2 as a mobile phase in classical heterogeneous catalysis, see W. K. Gray, F. R. Smail, M. G. Hitzler, S. K. Ross, M. Poliakoff, *J. Am. Chem. Soc.* **1999**, *121*, 10711 – 10718.

  1433-7851/01/4014-2699 $ 17.50+.50/0

Polymetallic Cobalt and Manganese Cages with Phosphinate and Phosphonate Ligands**

Euan K. Brechin, Robert A. Coxall, Andrew Parkin, Simon Parsons, Peter A. Tasker,* and Richard E. P. Winpenny*

Paramagnetic metal cage complexes have become a focus for a great deal of research since the discovery that certain cages could retain magnetic orientation in the absence of a magnetic field.[1] These "single-molecule magnets" therefore act as molecular magnetic storage devices, and accompanying physical phenomena, such as quantum-tunneling of the magnetization,[2] make them objects of both technological and fundamental scientific interest. Ligands used in synthesizing such cage complexes are however comparatively restricted, with the majority of examples involving carboxylates and alkoxides.[1, 3]

Cage complexes featuring phosphonate ligands are rare. Several cages involving vanadium have been reported, chiefly by Zubieta and co-workers,[4] some cages featuring aluminum have appeared recently,[5] and a fascinating dodecanuclear copper(II) cage was reported in 2000 by Chandrasekhar and Kingsley.[6] Perhaps most exciting are the redox-active $\{Mn_4\}$ cages described by the Dismukes group.[7] Other than the $\{Cu_{12}\}$ example complexes of the later 3d metals with phosphonate ligands tend to be restricted to layered structures.[8] This observation is intriguing, for it suggests that if phosphonate ligands could be induced to form cage complexes, the propensity to support two-dimensional (2D) structures might lead to preferential formation of disclike cages. The structural anisotropy might in turn lead to anisotropy in magnetic behavior, which could be of interest in the formation of new single-molecule magnets.[1] Here we report studies of the reactions of these ligands with middle and late 3d metals, which demonstrate that phosphonates can be incorporated in such cages, but only in the presence of coligands.

The chief difficulty in the use of phosphonates for cage formation is the insolubility of the products of reactions between 3d metal salts and the ligands. For example, reaction of cobalt hydroxide with phenylphosphonate leads to intractable powders that do not dissolve in any common solvent. However, if a second ligand is added to the mixture, and the phosphonate concentration kept low, intensely colored solutions can be produced. Thus cobalt hydroxide and $PhPO_3H_2$ were added to 6-chloro-2-hydroxypyridine (Hchp) in molar ratios of 1:1/3:2, and the mixture heated to above the melting point of Hchp. The purple paste that results could be dissolved in a range of solvents. Crystals of **1** form in moderate yield from EtOAc, while crystals of **2** form in poor yield from $MeCN/Et_2O$. In both cases X-ray analysis[9] reveal formation of $\{Co_{13}\}$ cages. The crystallization of two very similar cages from different solvents suggests that the cages are formed during the initial reaction, rather than forming during crystallization.

$[Co_{13}(OH)_3(chp)_{19}(O_3PPh)_2(H_2O)_2(EtOAc)_2]$ **1**

$[Co_{13}(OH)_3(chp)_{19}(O_3PPh)_2(H_2O)_2(Hchp)_2]$ **2**

The structures are highly irregular and essentially identical, differing in the replacement of the two terminal EtOAc ligands in **1** by Hchp ligands in **2**. The following description and figure use the atom numbering for **1**. At the core of both cages are two phosphonate ligands, which each bind to five cobalt centers; adopting a [5.221] mode (as described using Harris notation,[10] see Scheme 1). Four cobalt centers (Co1, Co2, Co4, and Co11) are bound to both of these ligands, with a further two Co atoms (Co3 and Co5) bound to a single $PhPO_3^{2-}$ ligand (Figure 1a). Each of these six cobalt centers is six-coordinate, and shares two O atoms with neighboring cobalt centers of the core (Figure 1b). This creates a helical array of cobalt centers, beginning with Co5 and moving in an anticlockwise direction to Co3. The remaining seven cobalt sites are arranged around three sides of this central core (Figure 1b). Three of these sites share two O atom bridges with Co sites of the core (Co6, Co8, and Co12), while two sites share a single oxygen with a Co atom of the core (Co7 and Co13). Co9 shares three O atoms with two different central cobalt centers (Co1 and Co5), while the final site (Co10) shares two bridging oxygen atoms with two different cobalt centers (Co2 and Co11).

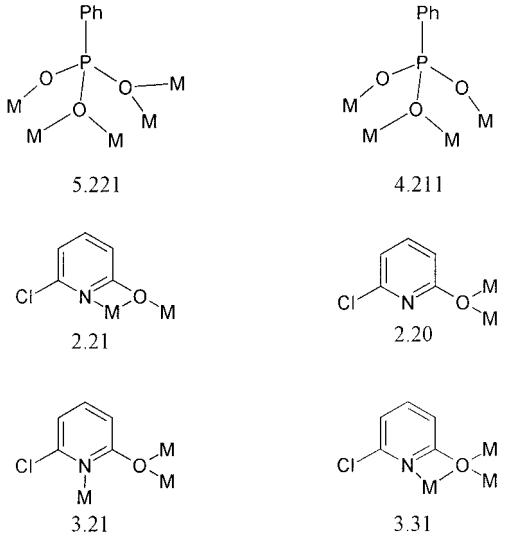

Scheme 1. The bonding modes displayed by phosphonate and pyridonate ligands, with the Harris notation for each mode.

The cage also contains three μ_3-hydroxide ligands: O1 is bound exclusively to Co atoms of the core (Co3, Co4, and

[*] Prof. R. E. P. Winpenny
Department of Chemistry
The University of Manchester
Oxford Road, Manchester M13 9PL (UK)
Fax: (+44) 161-275-4616
E-mail: richard.winpenny@man.ac.uk
Prof. P. A. Tasker, Dr. E. K. Brechin, Dr. R. A. Coxall, A. Parkin, Dr. S. Parsons
Department of Chemistry
The University of Edinburgh (UK)
Fax: (+44) 131-650-4743

[**] This work was supported by the EPSRC (UK).

  1433-7851/01/4014-2700 $ 17.50+.50/0

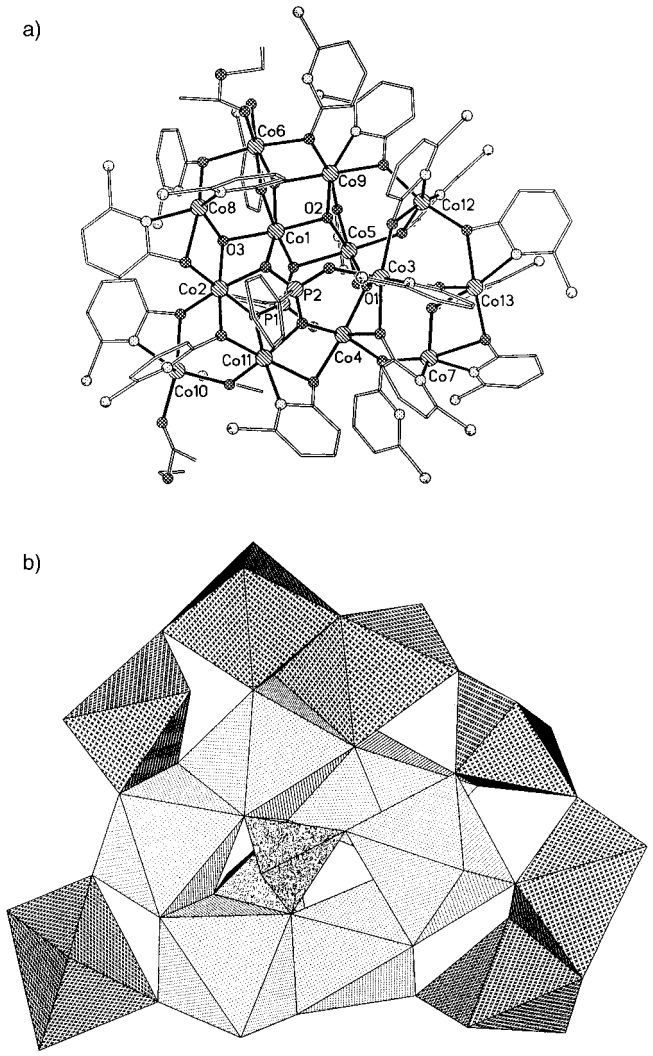

Figure 1. a) The structure of **1** in the crystal. Bond length ranges [Å]: Co-O(O_3PPh) 1.988 – 2.259, Co-O(chp) 1.994 – 2.348, Co-O(hydroxide) 1.998 – 2.109, Co-O(H_2O) 2.049 – 2.094, Co-O(EtOAc) 2.120 – 2.175, Co-N(chp) 2.050 – 2.241 (av esd 0.013). b) A polyhedral representation of the Co and P sites in **1** and **2**, viewed from the same position as Figure 1a. Shading: P sites, random heavy dots; core Co sites, regular dots; external Co sites, regular crosses.

Co5), while O2 and O3 each bind to two cobalt centers from the core and one of the exterior cobalt sites. The nineteen chp ligands in the cage adopt four bonding modes. Using Harris notation[10] these can be described as a [2.21] mode, adopted by eleven pyridonates, a [2.20] mode, adopted by three ligands, a [3.21] mode, adopted by two ligands, and the [3.31] mode, adopted by one pyridonate (see Scheme 1). In the homoleptic complex $[Co_9(chp)_{18}]$, which is prepared from a similar reaction in the absence of the phosphonate, all pyridonates adopt the [2.21] mode.[11] Two water and two ethylacetate molecules are found bound as terminal ligands. The cobalt sites can all be considered six-coordinate, however in some cases the sixth bond is markedly longer. Five cobalt centers (Co1, Co2, Co4, Co5, and Co6) are each bound to six O donors, three (Co3, Co9, and Co11) are bound to five O and one N donors, three (Co8, Co12, and Co13) to four O and two N atoms, and two (Co7 and Co10) to three O and three N donors.

High-nuclearity Co^{II} cages remain comparatively rare. Two nonanuclear cages are known, with pyridonate[11] and di-2-pyridylketone[12] as ligands. A series of deca- and dodecanuclear cages based on trigonal prisms have been reported featuring pyridonates and carboxylates.[13] Another tridecanuclear cage has been described,[14] and one larger cage which contains twenty-four metal centers.[15] There are also many larger clusters known with cobalt in lower oxidation states.[16]

A second method for introducing a phosphonate or phosphinate ligand without causing an immediate precipitate is to react the ligand with a preformed cage. Reaction of the mixed-valence cage $[Mn_3O(O_2CPh)_6(py)_2(H_2O)]$ (py = pyridine)[17] with an equimolar quantity of phenylphosphinic acid in MeCN gives crystals of **3**. Structural analysis[9] shows that the triangular oxo-centered array of manganese centers found in the precursor cage is retained, but two such triangles have been linked through two phosphinate and two phosphonate ligands (Figure 2). The formation of the phosphonate in **3** is presumably through aerial oxidation in presence of the manganese centers.

$[Mn_6O_2(O_3PPh)_2(O_2PHPh)_2(O_2CPh)_8(py)_2]$ **3**

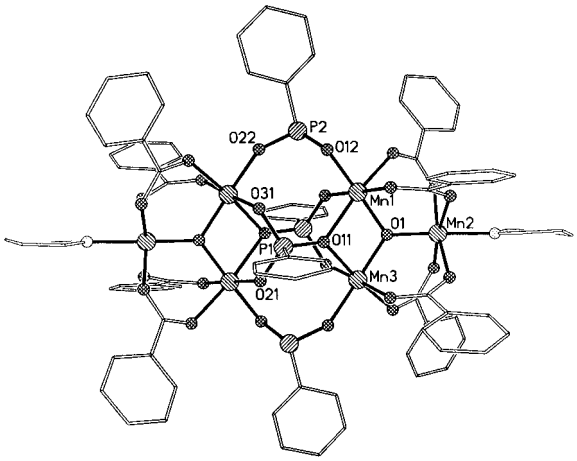

Figure 2. The structure of **3** in the crystal. Bond length ranges [Å]: Mn-O(equatorial sites) 1.844 – 2.042, Mn-O(Jahn – Teller elongated sites) 2.105 – 2.257 (av esd 0.008). Bond angle ranges [°]: *cis* at Mn 78.6 – 99.1, *trans* at Mn 169.5 – 178.7 (av. esd 0.3).

Complex **3** is centrosymmetric. The unique phosphonate ligand bridges four manganese centers, using a [4.211] binding mode (see Scheme 1).[10] Therefore one edge of the manganese triangle in one cage is bridged by the phosphonate in a 1,3-manner akin to a carboxylate, while a single μ_2-oxygen from the symmetry-equivalent phosphonate bridges the same edge. The two phosphinate ligands form a bridge between the two triangles in a 1,3-fashion. The remainder of the triangles are unchanged from those in the precursor cages, with four bridging benzoate groups and a terminal pyridine completing the coordination spheres of the manganese centers, which are all six-coordinate. Charge balance requires that the metals are present as Mn^{III}, and the Jahn – Teller elongation typical of this oxidation state is observed for all three crystallographically independent sites. Complex **3** can also be made from the homovalent triangle $[Mn_3O(O_2CPh)_6(py)_3](ClO_4)$.

The formation of **3** suggests many further reactions, which may prove exciting. It appears that phosphonate ligands can displace carboxylate ligands from one cage and simultaneously act as a bridge to a related cage. This implies a method for synthesizing larger metal arrays from reaction of metal carboxylate cages with phosphonates. Hexanuclear manganese cages are far from rare.[3] A series of such cages exist in which the metal polyhedron is based on an edge-sharing bitetrahedron,[18] and several $\{Mn_6\}$ cages have very high magnetic spin ground states, for example, a radical-bridged Mn^{II} wheel[19] and Mn^{III} octahedron featuring dibenzoylmethane ligands.[20]

Magnetic studies of **1** and **3** in both cases show a decline in $\chi_m T$ as the temperature is lowered (χ_m = molar magnetic susceptibility). For **1** this decline, from a room temperature value of about 42.2 emu K mol^{-1} to a value of 10.1 emu K mol^{-1} at 1.8 K, is presumably due to a combination of antiferromagnetic exchange between Co^{II} centers and the usual crystal field effects of Co^{II}. For **3** the decline, from a room temperature value of 21.5 emu K mol^{-1} to zero at 1.8 K, is due to antiferromagnetic exchange. Isolated oxo-centered triangles display spin frustration, and tend to have nondiamagnetic ground states.[17, 21] Therefore the low-temperature value suggests there is significant exchange between the Mn^{III} triangles, presumably mediated by the phosphinate and phosphonate ligands.

Experimental Section

1: Freshly prepared cobalt hydroxide (5.4 mmol) was mixed with Hchp (11 mmol) and $PhPO_3H_2$ (1.8 mmol), and the mixture heated to 130 °C for 10 min. The resulting purple paste was extracted repeatedly with aliquots of EtOAc (5 mL), and the solutions allowed to stand at room temperature. Yield: 34 %. Elemental analysis calcd (%) for $C_{119}H_{98}Cl_{19}Co_{13}N_{19}O_{36}P_2$: C 36.89, H 2.53, N 6.87; found: C 36.89, H 2.35, N 6.77.

2: This was prepared by an analogous procedure to **1** but crystallized by extracting the sample with aliquots of MeCN (5 mL) and allowing diethyl ether to diffuse into the solutions. Yield: < 5 %. No elemental analysis obtained.

3: $[Mn_3O(O_2CPh)_6(py)_2(H_2O)]$[17] (0.23 mmol) was dissolved in MeCN (10 mL) and HO_2PHPh (0.21 mmol) in MeCN (5 mL) added. The solution was filtered and allowed to evaporate slowly at room temperature. Yield: 26 %. Elemental analysis calcd (%) for $C_{90}H_{72}Mn_6N_2O_{28}P_4$: C 51.89, H 3.48, N 1.34; found: C 50.42, H 3.52, N 1.05.

Received: February 22, 2001 [Z16665]

[1] a) R. Sessoli, H.-L. Tsai, A. R. Schake, S. Wang, J. B. Vincent, K. Folting, D. Gatteschi, G. Christou, D. N. Hendrickson, *J. Am. Chem. Soc.* **1993**, *115*, 1804 – 1816; b) Z. M. Sun, D. Ruiz, E. Rumberger, C. D. Incarvito, K. Folting, A. L. Rheingold, G. Christou, D. N. Hendrickson, *Inorg. Chem.* **1998**, *37*, 4758 – 4759; c) C. Sangregorio, T. Ohm, C. Paulsen, R. Sessoli, D. Gatteschi, *Phys. Rev. Lett.* **1997**, *78*, 4645 – 4648; d) Z. Sun, C. M. Grant, S. L. Castro, D. N. Hendrickson, G. Christou, *Chem. Commun.* **1998**, 721 – 722; e) M. W. Wemple, D. M. Adams, K. S. Hagen, K. Folting, D. N. Hendrickson, G. Christou, *J. Chem. Soc. Chem. Commun.* **1995**, 1591 – 1593; f) E. K. Brechin, J. Yoo, M. Nakano, J. C. Huffman, D. N. Hendrickson, G. Christou, *Chem. Commun.* **1999**, 783 – 784; g) A. L. Barra, A. Caneschi, D. Gatteschi, D. P. Goldberg, R. Sessoli, *J. Solid State Chem.* **1999**, *145*, 484 – 487; h) A. L. Barra, A. Caneschi, A. Cornia, F. F. deBiani, D. Gatteschi, C. Sangregorio, R. Sessoli, L. Sorace, *J. Am. Chem. Soc.* **1999**, *121*, 5302 – 5310.

[2] a) J. R. Friedman, M. P. Sarachik, J. Tejada, R. Ziolo, *Phys. Rev. Lett.* **1996**, *76*, 3830 – 3832; b) L. Thomas, F. Lionti, R. Ballou, D. Gatteschi, R. Sessoli, B. Barbara, *Nature* **1996**, *383*, 145 – 147.

[3] R. E. P. Winpenny, *Adv. Inorg. Chem.*, in press, and references therein.

[4] M. I. Khan, J. Zubieta, *Prog. Inorg. Chem.* **1995**, *43*, 1 – 149, and references therein.

[5] M. G. Walawalker, H. W. Roesky, R. Murugavel, *Acc. Chem. Res.* **1999**, *32*, 117 – 126, and references therein.

[6] V. Chandrasekhar, S. Kingsley, *Angew. Chem.* **2000**, *112*, 2410 – 2412; *Angew. Chem. Int. Ed.* **2000**, *39*, 2320 – 2322.

[7] a) W. F. Ruettinger, D. M. Ho, G. C. Dismukes, *Inorg. Chem.* **1999**, *38*, 1036 – 1037; b) W. F. Ruettinger, G. C. Dismukes, *Inorg. Chem.* **2000**, *39*, 1021 – 1027.

[8] A. Clearfield, *Prog. Inorg. Chem.* **1998**, *47*, 371 – 510.

[9] Crystal data for **1**: $C_{119}H_{98}Cl_{19}Co_{13}N_{19}O_{36}P_2$, $M_r = 3872$, triclinic, $P\bar{1}$, $a = 16.880(5)$, $b = 17.978(5)$, $c = 29.874(10)$ Å, $\alpha = 104.47(2)$, $\beta = 102.391(15)$, $\gamma = 94.077(18)^\circ$, $V = 8499(4)$ Å^3, $Z = 2$, $T = 220.0(2)$ K, crystal size $0.39 \times 0.35 \times 0.19$ mm, $\mu(Mo_{K\alpha}) = 1.619$ mm^{-1}. Crystal data for **2**: $C_{139.5}H_{135}Cl_{21.5}Co_{13}N_{23.5}O_{37.5}P_2$, $M_r = 4331$, triclinic, $P\bar{1}$, $a = 16.964(7)$, $b = 21.564(9)$, $c = 25.142(10)$ Å, $\alpha = 98.556(7)$, $\beta = 98.280(7)$, $\gamma = 101.171(7)^\circ$, $V = 8780(6)$ Å^3, $Z = 2$, $T = 150.0(2)$ K, crystal size $0.15 \times 0.13 \times 0.08$ mm, $\mu(Mo_{K\alpha}) = 1.615$ mm^{-1}. Crystal data for **3**: $C_{95}H_{79.5}Mn_6N_{4.5}O_{28}P_4$, $M_r = 2186$, triclinic, $P\bar{1}$, $a = 12.440(3)$, $b = 13.640(3)$, $c = 17.010(4)$ Å, $\alpha = 96.511(4)$, $\beta = 109.479(3)$, $\gamma = 112.445(4)^\circ$, $V = 2417.2(9)$ Å^3, $Z = 1$ (the molecule lies on an inversion center), $T = 150.0(2)$ K, crystal size $0.20 \times 0.05 \times 0.02$ mm, $\mu(Mo_{K\alpha}) = 0.906$ mm^{-1}. Data for **1** were collected with a Stoe Stadi-4 diffractometer; data for **2** and **3** were collected on a Bruker Smart APEX CCD area detector. Both diffractometers were equipped with an Oxford Cryosystems low-temperature device. Absorption corrections were applied to all data by face-indexing for **1** (min./max. transmission: 0.624/0.829), by using ψ scan data for **2** (min./max. transmission: 0.658/0.928), and by using Sadabs (area-detector absorption correction; Siemens Industrial Automation Inc., Madison, WI, **1996**) for **3** (min./max. transmission: 0.806/0.928). The structures were solved by direct methods using SHELXS-97 for **1** and **2** (G. M. Sheldrick, SHELX97, Programs for Crystal Structure Analysis, University of Göttingen, **1998**), and SIR92 for **3** (A. Altomare, G. Cascarano, C. Giacovazzo, A. Guagliardi, *J. Appl. Crystallogr.* **1993**, *26*, 343), and completed by iterative cycles of ΔF syntheses and full-matrix least-squares refinement against F^2 (G. M. Sheldrick, SHELX97, Programs for Crystal Structure Analysis, University of Göttingen, **1998**). In **2** there is one chp ligand disordered over two orientations, with a common oxygen position, while in **3** the crystallographically unique $PhPHO_2$ ligand is disordered over two orientations with common O sites. In **1** and **2** there were diffuse regions of solvent of crystallization, which was treated by the method of van der Sluis and Speck (P. van der Sluis, A. L. Spek, *Acta Crystallogr. Sect. A* **1990**, *46*, 194 – 201). A half-occupancy molecule of Hchp was also found in the lattice of **2**. Hydrogen atoms were included in calculated positions, riding on parent carbon atoms, with $U(H) = 1.2\,U_{eq}(C)$ for aromatic H atoms and $U(H) = 1.5\,U_{eq}(C)$ for methyl hydrogen atoms. All full-weight non-hydrogen atoms were refined with anisotropic displacement parameters to give: for **1**, for 995 parameters, $wR2 = 0.1959$ for 15739 unique data ($2\theta \le 40^\circ$), $R1 = 0.0854$ for 6002 data with $F_o > 4\sigma(F)$, max./min. residual electron density 0.724/ – 0.540 e Å^3; for **2**, for 1955 parameters, $wR2 = 0.2456$ for 30480 unique data ($2\theta \le 50^\circ$), $R1 = 0.0868$ for 13202 data with $F_o > 4\sigma(F)$, max./min. residual electron density 1.327/ – 1.233 e Å^3; for **3**, for 622 parameters, $wR2 = 0.1597$ for 4510 unique data ($2\theta \le 40^\circ$), $R1 = 0.0673$ for 2297 data with $F_o > 4\sigma(F)$, max./min. residual electron density 0.401/ – 0.419 e Å^3. Crystallographic data (excluding structure factors) for the structures reported in this paper have been deposited with the Cambridge Crystallographic Data Centre as supplementary publication no. CCDC-158429, CCDC-158430, and CCDC-158431. Copies of the data can be obtained free of charge on application to CCDC, 12 Union Road, Cambridge CB2 1EZ, UK (fax: (+44) 1223-336-033; e-mail: deposit@ccdc.cam.ac.uk).

[10] Harris notation describes the binding mode as $[X.Y_1Y_2Y_3\ldots Y_n]$, where X is the overall number of metals bound by the whole ligand, and each value of Y refers to the number of metal atoms attached to

  1433-7851/01/4014-2702 $ 17.50+.50/0

the different donor atoms. Therefore for chp, there will be two values for Y, while for $PhPO_3^{2-}$ there will be three values of Y. The ordering of Y is listed by the Cahn–Ingold–Prelog priority rules, hence O before N. See: R. A. Coxall, S. G. Harris, D. K. Henderson, S. Parsons, P. A. Tasker, R. E. P. Winpenny, *Dalton Trans.* **2000**, 2349–2356.

[11] E. K. Brechin, S. G. Harris, S. Parsons, R. E. P. Winpenny, *Angew. Chem.* **1997**, *109*, 2055–2057; *Angew. Chem. Int. Ed. Engl.* **1997**, *36*, 1967–1969.

[12] A. Tsohos, S. Dionyssopoloulou, C. P. Raptopoulou, A. Terzis, E. G. Bakalbassis, S. P. Perlepes, *Angew. Chem.* **1999**, *111*, 1036–1038; *Angew. Chem. Int. Ed.* **1999**, *38*, 983–985.

[13] a) C. Benelli, A. J. Blake, E. K. Brechin, S. J. Coles, A. Graham, S. G. Harris, S. Meier, A. Parkin, S. Parsons, A. M. Seddon, R. E. P. Winpenny, *Chem. Eur. J.* **2000**, *6*, 883–896; b) A. Graham, S. Meier, S. Parsons, R. E. P. Winpenny, *Chem. Commun.* **2000**, 811–812.

[14] E. K. Brechin, A. Graham, A. Parkin, S. Parsons, A. M. Seddon, R. E. P. Winpenny, *Dalton Trans.* **2000**, 3242–3252.

[15] E. K. Brechin, S. G. Harris, A. Harrison, S. Parsons, A. G. Whittaker, R. E. P. Winpenny, *Chem. Commun.* **1997**, 653–654.

[16] V. Calvo-Perez, M. Shang, G. P. A. Yap, A. L. Rheingold, T. P. Fehlner, *Polyhedron* **1999**, *18*, 1869–1880.

[17] J. B. Vincent, H.-R. Chang, K. Folting, J. C. Huffman, G. Christou, D. N. Hendrickson, *J. Am. Chem. Soc.* **1987**, *109*, 5703–5711.

[18] a) A. R. E. Baikie, A. J. Howes, M. B. Hursthouse, A. B. Quick, P. Thornton, *J. Chem. Soc. Chem. Commun.* **1986**, 1587–1588; b) A. S. Batsanov, Yu. T. Struchkov, G. A. Timco, N. V. Gérbéléu, O. S. Manole, S. V. Grebenko, *Koord. Khim.* **1994**, *20*, 604–606; c) A. R. Schake, J. B. Vincent, Q. Li, P. D. W Boyd, K. Folting, J. C. Huffman, D. N. Hendrickson, G. Christou, *Inorg. Chem.* **1989**, *28*, 1915–1923.

[19] A. Caneschi, D. Gatteschi, J. Laugier, P. Rey, R. Sessoli, C. Zanchini, *J. Am. Chem. Soc.* **1988**, *110*, 2795–2799.

[20] G. Aromi, M. J. Knapp, J.-P. Claude, J. C. Huffman, D. N. Hendrickson, G. Christou, *J. Am. Chem. Soc.* **1999**, *121*, 5489–5499.

[21] E. Libby, J. K. McCusker, E. A. Schmitt, K. Folting, D. N. Hendrickson, G. Christou, *Inorg. Chem.* **1991**, *30*, 3486–3495.

Remote Communication between Charge Centers and Hydrogen-Bonding Sites: Possibility for a Signal Transducer?**

Ito Chao* and Tsong-Song Hwang

Hydrogen bonding and charge interactions are both essential for molecular recognition and the self-assembly of biological macromolecules. They are also employed heavily in the design of new systems for fundamental, biological, and materials research. The influence of a charge-bearing functional group on pK_a values[1] and chemical reactivity[2] has been well documented in the form of Hammett-type substituent constants in physical organic studies. Changes in the hydrogen-bonding behavior of ligands upon complexation with cationic transition metal centers have been indicated by theoretical calculations.[3] Such calculations also indicated that anions could induce a large cooperative effect in the hydrogen-bonding network of peptides.[4] Enhancement was observed experimentally in urea·carboxylate binding when the carbonyl group of the urea molecule was coordinated to a Lewis acid.[5] The optical property of $[Ru(bpy)_3]^{2+}$ (bpy = bipyridine) in a phosphodiester sensor was changed when the hydrogen-bonding sites were bound.[6] Although both hydrogen-bonding and charge-bearing sites are important in molecular recognition, interestingly, it is not common to find examples in supramolecular chemistry in which hydrogen-bonding sites are designed to be controlled by a covalently bound charge-bearing substituent. Charge-assisted C–H···X hydrogen bonds have been recognized in recent years[7] and metallocene complexes have been used to achieve redox-switched binding.[8] Nevertheless, the binding sites are basically adjacent to the charged centers, and we felt that charge centers can have a more far-reaching influence on a binding site.

If a charged group and a binding site can communicate with each other, one can use a three-component system (a charged group, a linker, and a binding site) as a signal transducer. The charge-bearing group can be viewed as a reaction site, whose charge state can be altered by reactions such as protonation, metalation, oxidation, reduction, or chemical transformation of a functional group. On the basis of this concept we designed test compounds **1a**–**d** and **2a**–**d**, and calculated the energies

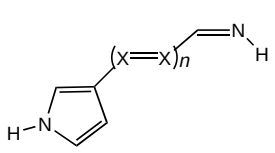

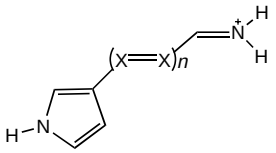

1a: X = CH, *n* = 1
1b: X = CH, *n* = 2
1c: X = CH, *n* = 3
1d: X = CH, *n* = 4

2a: X = CH, *n* = 1
2b: X = CH, *n* = 2
2c: X = CH, *n* = 3
2d: X = CH, *n* = 4

3a: X = N, *n* = 1
3b: X = N, *n* = 2
3c: X = N, *n* = 3
3d: X = N, *n* = 4

4a: X = N, *n* = 1
4b: X = N, *n* = 2
4c: X = N, *n* = 3
4d: X = N, *n* = 4

of formation of a hydrogen bond (binding energies) to find out how efficiently the reaction and binding centers can communicate with each other. In these compounds the reaction center is an imine group and the binding center is pyrrole; compounds **1a**–**d** are neutral imines and **2a**–**d** are cationic iminium compounds. Ammonia was chosen as the hydrogen-bonding partner of the N–H group of pyrrole for the sake of geometric simplicity, since it only has one lone pair of electrons. The ammonia binding energy of **2a** (-13.17 kcal mol^{-1}) at the HF/6-31G* level is double that of cationic **1a** (-6.84 kcal mol^{-1}) (Table 1).[9] While the binding energies of neutral systems (**1a**–**d**) remain fairly constant as the linker gets longer, the binding energies of cationic systems

[*] Prof. I. Chao, Dr. T.-S. Hwang
Institute of Chemistry
Academia Sinica
Taipei 115 (Taiwan)
Fax: (+886) 2-2783-1237
E-mail: ichao@chem.sinica.edu.tw

[**] This work was supported by the National Science Council and Academia Sinica of Taiwan (ROC). The granting of computer time by the National Center for High-Performance Computing and the Computing Center of Academia Sinica is acknowledged. We also thank Ning Juan for her assistance in preparing the manuscript.

Supporting information for this article is available on the WWW under http://www.angewandte.com or from the author.

  1433-7851/01/4014-2703 $ 17.50+.50/0

Table 1. Binding energies (kcal mol^{-1}) of the three-component systems (**1**–**4**) with NH_3 calculated at the HF/6-31G* level.

	1	2	3	4
a	– 6.84	– 13.17	– 7.39	– 15.50
b	– 6.73	– 12.04	– 7.66	– 16.45
c	– 6.64	– 11.18	– 7.84	– 17.99
d	– 6.57	– 10.47	– 7.95	– 19.07

(**2a**–**d**) decrease gradually, as one would expect. Nevertheless, even when the N···N distance is as far as 14 Å in **2d**, the binding energy is – 10.47 kcal mol^{-1}, which is still significantly stronger than the neutral systems.

In our search for new types of linkers we replaced the carbon linkers with nitrogen linkers (**3a**–**d**, **4a**–**d**). The binding energy of cationic **4a** (– 15.50 kcal mol^{-1}) with ammonia was also roughly double that of **3a** (– 7.39 kcal mol^{-1}). To our surprise, the binding energies of **4a**–**d** got larger as the linker got longer (Table 1). If we think of our molecules as signal transducers, the increase in binding energy means that the signal sent by the reaction center dose not die out as the wire becomes longer, instead, the wire acts as an amplifier to enhance the signal. Results at higher levels of theory for the cationic N=N series **4a**–**d** (Table 2) are in line with the HF/6-31G* results, even though the extent of energy increase varies. These results are in direct contrast with the concept that through-bond or through-space effects of a functional group should diminish with increasing distance.

Table 2. Binding energies (kcal mol^{-1}) of **4a**–**d** with NH_3 calculated with ab initio and DFT methods.

	4a	4b	4c	4d
HF/6-31G*	– 15.50	– 16.45	– 17.99	– 19.07
HF/6-31 + G**	– 13.41	– 14.29	– 15.77	– 16.78
HF/6-31 + G(2d,2p)	– 12.94	– 13.90	– 15.36	– 16.33
B3LYP/6-31G*	– 19.19	– 19.37	– 19.57	– 19.79
B3LYP/6-31 + G**	– 16.06	– 16.26	–	–
MP2/6-31G*	– 18.72	– 19.27	– 20.08	– 21.43
MP4(SDQ)/6-31G*	– 17.75	– 19.04	–	–
MP4(SDQ)/6-31G*//B3LYP/6-31G*	– 17.42	– 18.30	–	–

Examination of calculated structures of uncomplexed **2a**–**d** and **4a**–**d** reveals that the importance of resonance form **B** in Scheme 1 increases in **4a**–**d** as the linker gets longer, but decreases in **2a**–**d**. For example, the C–N bond (labeled *r* in Scheme 1) in the pyrrole ring was shorter in **4d** (1.281 Å) than in **4a** (1.305 Å). In series **2**, *r* is shorter in **2a** (1.325 Å) than in **2d** (1.340 Å).[10] The Mulliken charge of H_A (Scheme 1) in **4a**–**d** increases from 0.448 to 0.467 at the HF/6-31G* level of theory as the importance of resonance form **B** increases.[11] This observation is in good agreement with the increase in binding ability as the length of the N linker increases. The shift in the N=N ↔ N–N resonance is not without precedence. The importance of the N–N resonance form was invoked in a recent study of negative solvatochromism of azo dyes to rationalize a polar ground state.[12] The larger driving force for favoring form **B** in **4a**–**d** than in **2a**–**d** can be understood by the weaker bond strength of N=N relative to the C=N and C=C bonds;[13] some of the weaker N=N bonds in form **A** become C=N bonds in form **B** (Scheme 1). The increasing binding ability of pyrrole in series **4** probably reflects the larger electron-withdrawing power of longer N linkers. From a more practical standpoint, it is difficult to synthesize consecutive N=N bonds. We have, therefore, tested the same type of cationic compounds with $-((CH{=}CH)_n{-}N{=}N)_x-$ linkers. Their binding energies are shown in Table 3. It is found that the signal-amplifying phenomenon persists as *x* varies from 1 to 2. The ability of the linkers in Table 3 to maintain the influence of a charge center is significantly better than the pure C linkers (**2a**–**d**), although the degree of increase in the binding energy is smaller than that of pure N linkers (**4a**–**d**).

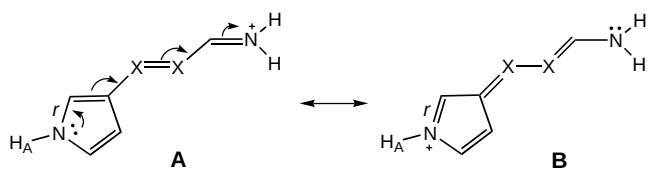

Scheme 1. Charge delocalization of the protonated system.

Table 3. Ammonia binding energies (kcal mol^{-1}) of the protonated three-component system with different linkers at the HF/6-31G* level.

	x = 1	*x* = 2
$-(CH{=}CH{-}N{=}N)_x-$	– 14.63	– 15.62
$-((CH{=}CH)_2{-}N{=}N)_x-$	– 13.90	– 14.49
$-((CH{=}CH)_3{-}N{=}N)_x-$	– 13.19	– 13.64
$-((CH{=}CH)_4{-}N{=}N)_x-$	– 12.61	– 12.98

It is known that the medium has a profound influence on the binding geometry of DNA base pairs[14] and on the structure and electronic properties of organic materials with conjugated π systems.[15] Therefore, we are currently examining the effects of counterions and solvent molecules on our three-component system. Preliminary studies showed that the existence of a counterion indeed reduces the binding energy of a cationic system, but the binding energy is still significantly higher than that of the neutral system. Whether the effect of a counterion could be reduced by using different types of counterions or by using anion-binding hosts is under investigation.

In conclusion, we have explored the possibility of using a reaction center to modulate the binding behavior of a remote hydrogen-bonding site. This concept of "remote control" mechanism can be incorporated into the design of new types of chemical sensors and be used to tune the structure and properties of supramolecular assemblies. The contrasting behavior of pure C and pure N linkers demonstrates that linkers with different chemical compositions may have a very different effect on the communication between reaction and binding centers.

Received: January 11, 2001
Revised: April 23, 2001 [Z16407]

[1] a) R. Luo, M. S. Head, J. Moult, M. K. Gilson, *J. Am. Chem. Soc.* **1998**, *120*, 6138–6146; b) C. F. Bernasconi, J. A. Moreira, L. L. Huang, K. W. Kittredge, *J. Am. Chem. Soc.* **1999**, *121*, 1674–1680; c) J. B. Tobin, P. A. Frey, *J. Am. Chem. Soc.* **1996**, *118*, 12253–12260.

  1433-7851/01/4014-2704 $ 17.50+.50/0

[2] R. D. Bach, C. Canepa, M. N. Glukhovtsev, *J. Am. Chem. Soc.* **1999**, *121*, 6542 – 6555.
[3] a) I. L. Zilberberg, V. I. Avdeev, G. M. Zhidomirov, *THEOCHEM* **1997**, *418*, 73 – 81; b) J. E. McGrady, D. M. P. Mingos, *J. Chem. Soc. Perkin Trans. 2* **1996**, 355 – 358.
[4] H. Guo, D. R. Salahub, *Angew. Chem.* **1998**, *110*, 3155 – 3160; *Angew. Chem. Int. Ed.* **1998**, *37*, 2985 – 2990.
[5] M. P. Hughes, B. D. Smith, *J. Org. Chem.* **1997**, *62*, 4492 – 4499.
[6] S. Watanabe, O. Onogawa, Y. Komatsu, K. Yoshida, *J. Am. Chem. Soc.* **1998**, *120*, 229 – 230.
[7] a) S. V. Lindeman, D. Kosynkin, J. K. Kochi, *J. Am. Chem. Soc.* **1998**, *120*, 13268 – 13269; b) K. N. Houk, S. Menzer, S. P. Newton, F. M. Raymo, J. F. Stoddart, D. J. Williams, *J. Am. Chem. Soc.* **1999**, *121*, 1479 – 1487; c) P. R. Ashton, M. C. T. Fyfe, P. T. Glink, S. Menzer, J. F. Stoddart, A. J. P. White, D. J. Williams, *J. Am. Chem. Soc.* **1997**, *119*, 12514 – 12524; d) D. Braga, F. Grepioni, *J. Chem. Soc. Dalton Trans.* **1999**, 1 – 8, and references therein.
[8] J. D. Carr, S. J. Coles, M. B. Hursthouse, M. E. Light, J. H. R. Tucker, J. Westwood, *Angew. Chem.* **2000**, *112*, 3434 – 3437; *Angew. Chem. Int. Ed.* **2000**, *39*, 3296 – 3299.
[9] All calculations were carried out with Gaussian 98 and the binding energies listed have counterpoise correction for basis-set superposition errors.
[10] The structures were calculated at the HF/6-31G* level. See the Supporting Information for more structural details.
[11] The charge of H_A in **2a** – **d** decreased from 0.435 to 0.418.
[12] J. J. Kim, K. Funabiki, H. Muramatsu, K. Shibata, S. H. Kim, H. Shiozaki, H. Hartmann, M. Matsui, *Chem. Commun.* **2000**, 753 – 754.
[13] The bond energies of HN=NH, CH_2=NH, and CH_2=CH_2 are ca. 109, ca. 154, and 163 kcal mol^{-1}, respectively: S. W. Benson, *J. Chem. Educ.* **1965**, *42*, 502 – 518. The differences in the bond energies of single bonds (N–N, C–N, and C–C) are smaller, so they are not as important as double bonds in determining the relative importance of forms **A** and **B**.
[14] C. F. Guerra, F. M. Bickelhaupt, J. G. Snijders, E. J. Baerends, *J. Am. Chem. Soc.* **2000**, *122*, 4117 – 4128, and reference [4] therein.
[15] For example, see J. Gao, C. Alhambra, *J. Am. Chem. Soc.* **1997**, *119*, 2962 – 2963, and references therein.

nido ↔ *closo* Interconversion of Six-Vertex Metallacarboranes: Access to CoC_2B_3 and CoC_2B_4 Clusters with Nonadjacent Carbon Atoms**

Hans-Jörg Schanz, Michal Sabat, and Russell N. Grimes*

Metallacarborane chemistry has been well developed for 12-vertex (icosahedral) and 7-vertex (pentagonal bipyramidal) clusters and, to a lesser extent, for other systems having 8 to 14 vertices.[1] In contrast, little is known of the smallest members of the metallacarborane family, for example, 6-vertex *closo*-MC_2B_3 polyhedra. The first such species were prepared in the 1970s[2, 3] by thermal insertion of metal reagents into *closo*-1,5-$C_2B_3H_5$, a relatively inaccessible small carborane. To date, fewer than half a dozen 6-vertex *closo*-metallacarboranes have been reported,[2–4] and just one crystal structure of a *closo*-MC_2B_3 system is available.[3] In principle, such clusters should be accessible by the oxidation of *nido*-$LMC_2B_3H_5^{2-}$ open-cage dianions having 16 skeletal electrons, generating neutral 14-electron *closo*-$LMC_2B_3H_5$ species as predicted from simple electron-counting arguments (Wade's rules).[5] However, no such conversion has been reported experimentally, and earlier attempts to do this in our laboratory were unsuccessful; our experience has been that oxidants sufficiently strong to remove two electrons tend to degrade the cage structure.

It seemed possible that this problem might be circumvented by modifying the cluster to make it easier to oxidize. Here we report an application of this approach, in which a tribrominated *nido*-1,2,3-MC_2B_3 cage with adjacent carbon atoms undergoes oxidative closure to form the desired *closo* system. This product in turn can be converted into 7-vertex *closo*- and 6-vertex *nido*-metallacarboranes having nonadjacent carbon atoms, families that have heretofore been difficult to access.

Deprotonation of the 4,6-dichloro- or dibromo-*nido*-cobaltacarboranes[6] **2a** or **2b** (Scheme 1) with sodium hydride in THF, followed by addition of 2-bromo-2-nitropropane and

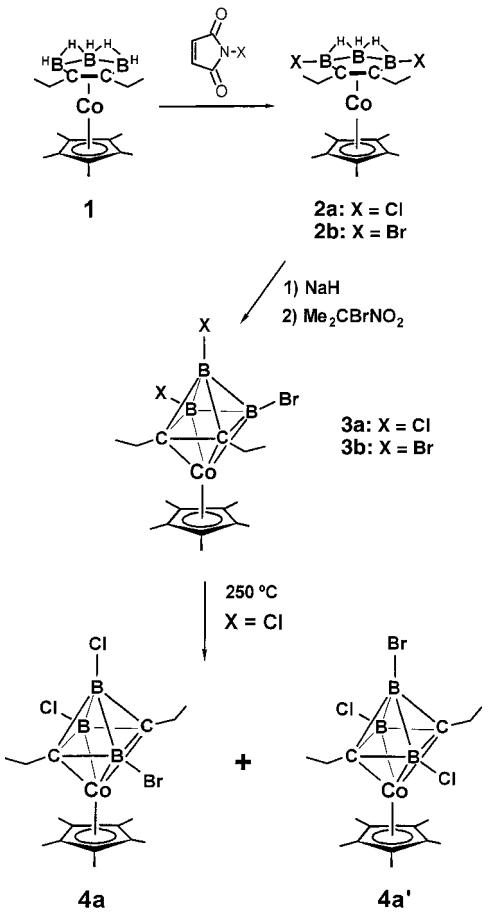

Scheme 1. Synthesis of **3a** and **3b** as well as the thermal rearrangement of **3a** to form a mixture of isomers **4a** and **4a′**.

[*] Prof. Dr. R. N. Grimes, Dr. H.-J. Schanz, Dr. M. Sabat
Department of Chemistry
University of Virginia
Charlottesville, VA 22901 (USA)
Fax: (+1) 804-924-3710
E-mail: rng@virginia.edu

[**] Organotransition-Metal Metallacarboranes, part 57. This work was supported in part by the National Science Foundation (grant CHE 9980708) and the Alexander von Humboldt Foundation (Feodor Lynen postdoctoral fellowship to H.-J. Schanz). Part 56: M. Bluhm, H. Pritzkow, W. Siebert, R. N. Grimes, *Angew. Chem.* **2000**, *112*, 4736; *Angew. Chem. Int. Ed.* **2000**, *39*, 4562.

purification of the product by column chromatography on silica in air, afforded orange crystals of **3a** or **3b** (Cp* = C_5Me_5). Characterization of these two products by ^1H, ^{11}B, and ^{13}C NMR spectroscopy and mass spectrometry, and an X-ray crystal structure determination on **3b**,[7] established the octahedral cluster geometry shown in Figure 1. The

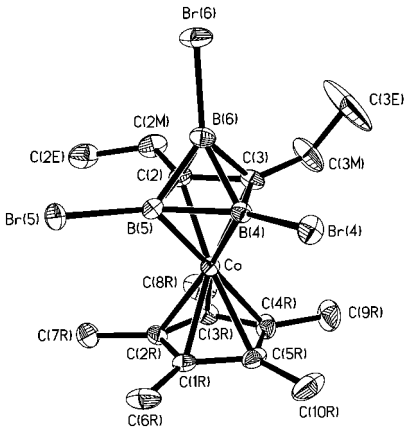

Figure 1. Molecular structure of **3b**. Selected distances [Å] and angles [°]: C(2)–C(3) 1.502(6), Co–C_5 ring 1.660(2), Co–C_2B_2 ring 1.605(2); B(5)-C(2)-C(3) 94.0(3), C(2)-C(3)-B(4) 94.9(3), C(3)-B(4)-B(5) 86.4(3), C(2)-B(5)-B(4) 84.7(3).

C(2)–C(3) interaction is significantly longer than the skeletal C–C bonds in 7-vertex MC_2B_4 and $M_2C_2B_3$ *closo* clusters,[1] but is comparable to the corresponding distance in the 6-vertex carborane 1,2-$C_2B_4H_6$ (1.535 Å) as determined from gas-phase electron diffraction.[8] In 1,2-$(Me_3Si)_2C_2B_4H_4$ the C–C bond is somewhat longer (1.59(4) Å from X-ray crystallography), with the lengthening attributed to the $SiMe_3$ groups.[9]

closo-[1,2,3-Cp*Co($Et_2C_2B_3$-4,6-Cl_2-5-Br)] **3a**

closo-[1,2,3-Cp*Co($Et_2C_2B_3Br_3$)] **3b**

Thermal rearrangement of cluster **3a** in vacuo at 250 °C effected separation of the skeletal carbon atoms, yielding a mixture of isomers **4a** and **4a′** (50 % yield, Scheme 1). In the case of **3b**, a single product **4b** was formed in 94 % yield (Scheme 2). The isomers **4a** and **4a′** were not separated, but the nonadjacent-carbon *closo*-[1,2,4-Cp*CoC_2B_3] cage structure shown is supported by spectroscopic data and by analogy with **4b**. These cluster interconversions—the first to be demonstrated in 6-vertex metallacarborane systems—are reminiscent of the thermal rearrangement of 1,2-$C_2B_4H_6$ to 1,6-$C_2B_4H_6$ at 250 °C.[10]

closo-1,2,4-[Cp*Co($Et_2C_2B_3Br_3$)] **4b**

Cage opening of the *closo* cluster **3b** with lithium–naphthalene in THF gave a presumed *nido*-cobaltacarborane dianion (not isolated), which underwent boron insertion with phenyldichloroborane to form bright yellow crystalline **5**, which was isolated in 35 % yield (Scheme 2); the same compound was also generated in lower yield from the

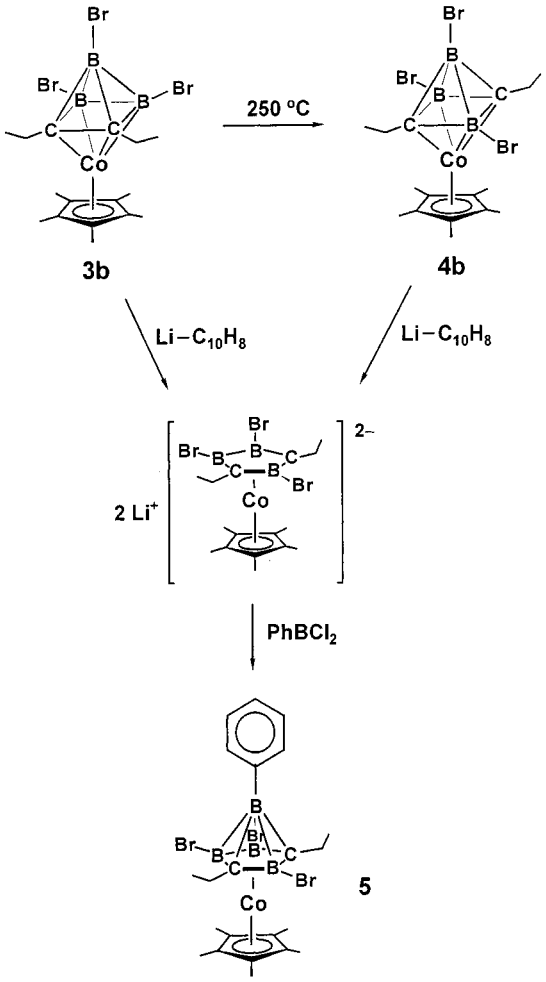

Scheme 2. Reactivity of cluster **3b**.

nonadjacent-carbon isomer **4b** by an analogous procedure. The structure of **5** (Figure 2), was confirmed from multinuclear NMR spectroscopy, mass spectrometry, and X-ray crystallography.[7]

closo-[1,2,4-Cp*Co($Et_2C_2B_4$-3,5,6-Br_3-7-Ph)] **5**

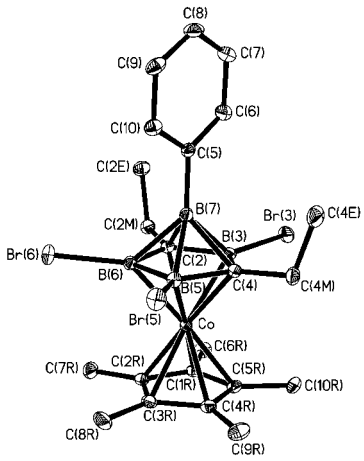

Figure 2. Molecular structure of **5**. Selected distances [Å]: C(2)–B(3) 1.551(3), B(3)–C(4) 1.556(3), C(4)–B(5) 1.542(3), B(5)–B(6) 1.658(4), B(6)–C(2) 1.548(3), Co–C_5 ring 1.641(1), Co–C_2B_3 ring 1.581(1).

  1433-7851/01/4014-2706 $ 17.50+.50/0 *Angew. Chem. Int. Ed.* **2001**, *40*, No. 14

Three processes that are fundamental to the synthesis of large carboranes[1]—oxidative cage closure, reductive cage opening, and thermal rearrangement—have been applied here for the first time to 6-vertex metallacarboranes, allowing rational syntheses of new clusters. The results demonstrate the practical synthetic applicability of skeletal electron-counting considerations to these smallest members of the metallacarborane family.

Experimental Section

3a: NaH (30 mg, 1.3 mmol) was added to a solution of **2a**[6] (96 mg, 0.25 mmol) in absolute THF (15 mL), and the mixture was stirred at RT for 15 min. Addition of 2-bromo-2-nitropropane (400 mg, 2.50 mmol) produced an instant color change from orange to green. After 2–3 h the color returned to orange-red. The reaction mixture was stirred for another 10 h and then opened to the air, and water (0.2 mL) was added to remove residual NaH. Volatile material was removed under reduced pressure, and the residue was suspended in CH_2Cl_2 (3 mL) and filtered through 5 cm of silica gel. An orange-red band was eluted with hexanes/CH_2Cl_2 (1/1) to yield 68 mg of crude material after removal all volatile components. Pure **3a** was obtained by thin-layer chromatography (TLC) on silica gel (20 cm) with hexanes to give an intense yellow band ($R_f = 0.40$) that was eluted with CH_2Cl_2. Volatile components were then removed to afford 35 mg (33 %) of **3a**. ^{1}H NMR (300 MHz, $CDCl_3$): $\delta = 1.88$ (m, 4H, CH_2 (Et)), 1.84 (s, 15H, C_5Me_5), 1.14 (t), 1.13 (t, 6H, CH_3 (Et)); ^{11}B NMR (96.4 MHz, 25 °C, $CDCl_3$): $\delta = 15.0$, 9.1 (B4, B5), 6.3 (B6); ^{13}C NMR (75.5 MHz, 25 °C, $CDCl_3$): $\delta = 92.4$ (C_5Me_5), 19.7, 19.3 (CH_2 (Et)), 12.0, 11.8 (CH_3 (Et)), 9.1 (C_5Me_5) (cage C not observed); CI^+-MS: *m*/*z* (%): 461.3 (100) [M^+].

3b: The procedure for the synthesis of **3a** was followed using **2b** (142 mg, 0.30 mmol) in absolute THF (20 mL) and 2-bromo-2-nitropropane (470 mg, 2.93 mmol), yielding 96 mg of crude material, which on TLC purification gave 81 mg (49 %)of air-stable **3b** (m.p. 215–220 °C). Cooling of a saturated solution in hexanes at −20 °C gave suitable crystals for X-ray diffraction. ^{1}H NMR (300 MHz, 25 °C, $CDCl_3$): $\delta = 1.90$ (m, 4H, CH_2 (Et)), 1.83 (s, 15H, C_5Me_5), 1.15 (t, 6H, CH_3 (Et)); ^{11}B NMR (96.4 MHz, 25 °C, $CDCl_3$): $\delta = 10.8$ (2B), 2.6 (1B); ^{13}C NMR (75.5 MHz, 25 °C, $CDCl_3$): $\delta =$ 92.6 (C_5Me_5), 63.7 (br s, cage C), 20.2 (CH_2 (Et)), 11.8 (CH_3 (Et)), 9.1 (C_5Me_5); CI^+-MS: *m*/*z* (%): 549.6 (65) [M^+], 275.3 (100) [M^+ − Cp*Co − Br].

4a and **4a′**: Compound **3a** (20 mg, 0.044 mmol) was heated to 250 °C in vacuo in a Pyrex tube for 18 h and then opened to the air at RT. The product was dissolved in CH_2Cl_2 (2 mL) and filtered through 5 cm of silica gel in hexanes/CH_2Cl_2 (1/1), eluting a strong yellow band. Removal of volatile components gave a 3:2 orange-red solid mixture of air-stable **4a** and **4a′**, which was further purified by TLC (silica gel, hexanes, intense orange-yellow band $R_f = 0.40$) to give 10 mg (50 %) of product. ^{1}H NMR (300 MHz, 25 °C, $CDCl_3$): $\delta = 1.80$ (s, 2 equiv), 1.79 (s, 3 equiv, 15H, C_5Me_5), 1.58 (m, 4H, CH_2 (Et)), 1.00 (m, 6H, CH_3 (Et)); ^{13}C NMR (75.5 MHz, 25 °C, $CDCl_3$): $\delta = 92.1$ (C_5Me_5), 65.1 (cage C), 19.5 (CH_2 (Et)), 13.0 (CH_3 (Et)), 9.0 (C_5Me_5); CI^+-MS: *m*/*z* (%): 461.3 (100) [M^+].

4b: Treatment of **3b** (78 mg, 0.14 mmol) as in the synthesis of **4a** and **4a′**, with elution of the product with hexanes/CH_2Cl_2 (1/1), gave an intense yellow band from which volatile components were removed to afford pure orange-red solid **4b** (73 mg, 94 %; m.p. 215–220 °C). While solid **4b** is air-stable, solutions in chlorinated solvents turn dark green after several days, indicating decomposition. ^{1}H NMR (300 MHz, 25 °C, $CDCl_3$): $\delta = 1.78$ (s, 15H, C_5Me_5), 1.60 (q, 4H, CH_2 (Et)), 1.01 (t, 6H, CH_3 (Et)); ^{11}B NMR (96.4 MHz, 25 °C, $CDCl_3$): $\delta = 7.6$ (B6), 2.6 (B3, B5); ^{13}C NMR (75.5 MHz, 25 °C, $CDCl_3$): $\delta = 92.2$ (C_5Me_5), 83.7 (br s, cage-C), 19.9 (CH_2 (Et)), 12.9 (CH_3 (Et)), 9.0 (C_5Me_5); CI^+-MS: *m*/*z* (%): 549.3 (30) [M^+], 275.1 (100) [M^+ − Cp*Co − Br].

5: Lithium–naphthalene in THF (0.1 mL, 1 M) was added dropwise to **4b** (20 mg, 0.036 mmol) in diethyl ether (10 mL) at RT until no instant decolorization of the intensely colored solution of $LiC_{10}H_8$ occurred. The solvent was removed in vacuo and the residue was dissolved in toluene (10 mL). Phenyldichloroborane (10 mg, 0.063 mmol) was added and the reaction mixture was stirred for 12 h at RT. Following removal of solvent, the residue was taken up in CH_2Cl_2 (2 mL) and the suspension was filtered through 5 cm of silica gel, eluting the crude product with hexanes/CH_2Cl_2 (1/1). Elution of **5** in hexanes followed by CH_2Cl_2 through 20 cm of silica gel afforded a bright yellow band ($R_f = 0.35$), which upon removal of solvent gave yellow solid air-stable **5** (8 mg, 35 %; m.p. 199–202 °C). The identical procedure using **3b** as starting material (20 mg, 0.036 mmol) afforded 4 mg (17 %) of pure **5**. Slow evaporation of a saturated solution in hexanes at RT gave suitable crystals for X-ray diffraction. ^{1}H NMR (300 MHz, 25 °C, $CDCl_3$): $\delta = 7.28$ (d, 2H), 7.15 (t, 1H), 7.06 (t, 2H, C_6H_5), 2.38 (m, 2H), 2.09 (m, 2H, CH_2 (Et)), 1.78 (s, 15H, C_5Me_5), 0.68 (t, 6H, CH_3 (Et)); ^{11}B NMR (96.4 MHz, 50 °C, [D_6]acetone): $\delta = 9.6$ (br s, B5, B6), 7.1, 6.8 (br s, B3, B7); ^{13}C NMR (75.5 MHz, 25 °C, $CDCl_3$): $\delta = 133.6$, 128.3, 126.9 (C_6H_5, *ipso*-C not found), 93.1 (C_5Me_5), 22.6 (CH_2 (Et)), 13.2 (CH_3 (Et)), 8.5 (C_5Me_5) (cage C not found); CI^+-MS: *m*/*z* (%): 637.1 (80), 638.9 (70) [M^+], 560.0 (80), 559.1 (100), 558.1 (70), 557.1 (50) [$M^+ - C_6H_5$] and [M^+ − Br].

Received: March 9, 2001 [Z16739]

[1] a) M. F. Hawthorne, G. B. Dunks, *Science* **1972**, *178*, 462; b) R. N. Grimes in *Comprehensive Organometallic Chemistry II*, *Vol. 1* (Eds.: E. W. Abel, F. G. A. Stone, G. Wilkinson), Pergamon, Oxford, **1995**, p. 373, and references therein; c) N. S. Hosmane in *Contemporary Boron Chemistry* (Eds.: M. Davidson, A. K. Hughes, T. B. Marder, K. Wade), Royal Society of Chemistry, Cambridge, **2000**, p. 299, and references therein.

[2] [1,2,4-$(CO)_3FeC_2B_3H_5$] and [1,2,4-$CpCoC_2B_3H_5$]: V. R. Miller, L. G. Sneddon, D. C. Beer, R. N. Grimes, *J. Am. Chem. Soc.* **1974**, *96*, 3090.

[3] [1,2,4-$(Et_3P)_2CoC_2B_3H_5$] and [1,2,4-$(Et_3P)_2HCoC_2B_3H_5$]: G. K. Barker, M. Green, M. P. Garcia, F. G. A. Stone, J.-M. Bassett, A. J. Welch, *J. Chem. Soc. Chem. Commun.* **1980**, 1266.

[4] [$(CO)_9Fe_3C_2BH$]: X. Meng, T. P. Fehlner, A. Rheingold, *Organometallics* **1990**, *9*, 5. Six-vertex *closo*-metallaboranes are known: see L. Barton, D. K. Srivastava in *Comprehensive Organometallic Chemistry II*, *Vol. 1* (Eds.: E. W. Abel, F. G. A. Stone, G. Wilkinson), Pergamon, Oxford, **1995**, p. 275, and references therein.

[5] a) K. Wade, *Adv. Inorg. Chem. Radiochem.* **1976**, *18*, 1; b) D. M. P. Mingos, *Acc. Chem. Res.* **1984**, *17*, 311.

[6] K. E. Stockman, D. L. Garrett, R. N. Grimes, *Organometallics* **1995**, *14*, 4661.

[7] Crystal structure determinations: Data were collected on a Bruker SMART APEX CCD diffractometer ($Mo_{K\alpha}$ radiation, $\lambda = 0.71073$ Å, ω scans) at 153 K. For each structure, a total of 1321 frames were collected with a scan width of 0.3° in ω and an exposure time of 30 s per frame. The frames were integrated with the Bruker SAINT software package using a narrow-frame integration algorithm, and the structures were solved and refined using the Bruker SHEXTL software package. **3b** ($C_{16}H_{25}B_3Br_3Co$): $M_r = 548.45$, monoclinic, space group $P2_1/c$, $a = 8.5481(4)$, $b = 14.1576(6)$, $c = 17.6004(8)$ Å, $\beta = 102.659(1)°$, $V = 2078.23(16)$ Å^3, $Z = 4$, $\rho_{calcd} = 1.753$ g cm^{-3}. Of 16311 measured reflections, 5723 were independent ($R_{int} = 0.031$), 214 parameters, $R1 = 0.041$ (for reflections with $I > 2\sigma(I)$), $wR2 = 0.116$ (for all reflections), max./min. residual electron density 1.413/ − 1.142 e Å^{-3}. Hydrogen atoms, except for those of the C(3M)−C(3E) ethyl group, were fixed in the calculated positions. **5** ($C_{22}H_{30}B_4Br_3Co$): $M_r = 636.36$, monoclinic, space group $P2_1/c$, $a = 9.2268$ (5), $b = 31.709$ (2), $c = 9.3033$ (5) Å, $\beta = 113.963(1)°$, $V = 2487.3(2)$ Å^3, $Z = 4$, $\rho_{calcd} =$ 1.699 g cm^{-3}. Of 18623 measured reflections, 6165 were independent ($R_{int} = 0.027$), 391 parameters, $R1 = 0.025$ (for reflections with $I > 2\sigma(I)$), $wR2 = 0.061$ (for all reflections), max./min. residual electron density 0.485/ − 0.738 e Å^{-3}. All hydrogen atoms were found in the difference Fourier maps and were refined with isotropic displacement parameters. Crystallographic data (excluding structure factors) for the structures reported in this paper have been deposited with the Cambridge Crystallographic Data Centre as supplementary publication no. CCDC-159114 (**3b**) and -159115 (**5**). Copies of the data can be obtained free of charge on application to CCDC, 12 Union Road, Cambridge CB2 1EZ, UK (fax: (+44) 1223-336-033; e-mail: deposit@ccdc.cam.ac.uk).

[8] E. A. McNeill, F. R. Scholer, *Inorg. Chem.* **1975**, *14*, 1081.

[9] J. A. Maguire, K.-J. Lu, C. J. Thomas, T. G. Gray, Y. Wang, J. F. Eintracht, N. S. Hosmane, H. Binder, M. Wanitschek, H. Borrmann, A. Simon, H. Oberhammer, *Chem. Eur. J.* **1997**, *3*, 1059.

[10] T. P. Onak, R. P. Drake, G. B. Dunks, *Inorg. Chem.* **1964**, *3*, 1686.

Inherent Asymmetry of Constitutionally Equivalent Methyl Groups in the H/D Equilibration of *n*- and *i*-$C_3H_7Fe(OH)^+$ Complexes**

Claudia Trage, Waltraud Zummack, Detlef Schröder, and Helmut Schwarz*

Dedicated to Graham Cooks on the occasion of his 60th birthday

Reversible β-hydrogen transfer, a key reaction in organometallic chemistry, often relies on an alignment of the alkyl residue in terms of an agostic interaction (Scheme 1). Here,

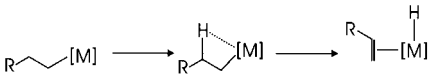

Scheme 1. Reversible β-hydrogen transfer with an agostic interaction.

we report that in the course of an *n*-propyl $\rightleftarrows$ isopropyl isomerization, operative in Fe^+-mediated dehydration of propanols, the transiently formed constitutionally identical methyl groups remain inequivalent. In general, water loss is believed to commence with complexation of the metal cation at oxygen, followed by oxidative insertion into the C–O bond (Scheme 2: **1** $\rightarrow$ **2** or **1′** $\rightarrow$ **2′**).[1, 2] Next, β-hydrogen transfers lead to either a hydrido hydroxy complex **3** or directly[3] to the bisligated complex **4**; the latter decomposes preferentially by loss of water, because H_2O is less strongly bound to Fe^+ than propene.[4] In fact, the metastable ions **1** and **1′** show almost exclusive elimination of water (> 99 %) on the microsecond time scale.[6] The key question concerns the reversibility of the β-hydrogen transfer steps **2** $\rightleftarrows$ **2′**, which is addressed by examination of the H/D equilibration in unimolecular reactions of metastable complexes of Fe^+ with a set of selectively deuterated propanols[7] by using tandem mass spectrometry.[8, 9]

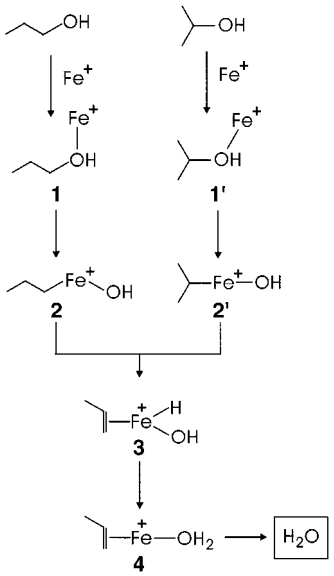

Scheme 2. Schematic reaction pathway for the loss of water from [Fe/propanol]$^+$.

Inspection of the experimental data in Tables 1 and 2 leads to three immediate conclusions: 1) extensive H/D equilibration is observed, 2) the complexes of labeled *n*- and isopropanol show distinctly different H_2O/HDO ratios, and 3) the hydroxy groups of **1** and **1′** do not participate in the H/D scrambling. While metal-mediated H/D equilibrations have been observed frequently, such cases are often described only phenomenologically, rather than analyzed rigorously.[10]

Table 1. H_2O/HDO losses from metastable complexes of Fe^+ with labeled isopropanols.

Substrate	Experiment[a]		Model A[b]		Model B[c]		Statistical[d]	
	H_2O	HDO	H_2O	HDO	H_2O	HDO	H_2O	HDO
$CH_3CH(OD)CH_3$	< 1[e]	> 99	0.0	100.0	0.0	100.0	0.0	100.0
$CH_3CD(OH)CH_3$	94.9	5.1	95.4	4.6	94.9	5.1	85.7	14.3
$CH_3CH(OH)CD_3$	73.4	26.6	70.7	29.3	73.0	27.0	57.1	42.9
$CH_2DCD(OH)CH_2D$	77.1	22.9	75.8	24.2	77.3	22.7	57.1	42.9
$CHD_2CH(OH)CHD_2$	58.6	41.4	56.6	43.4	59.0	41.0	42.9	57.1
$CD_3CH(OH)CD_3$	14.9	85.1	16.4	83.6	14.9	85.1	14.3	85.7
$CD_3CD(OH)CD_3$	< 0.7	> 99.3[f]	0.0	100.0	0.0	100.0	0.0	100.0

[a] Averaged intensities obtained in three independent experiments normalized to $\Sigma = 100$. The experimental error is less than ± 0.8. [b] Parameters: $k_{sel} = 0.381$ and KIE = 2.02. [c] Parameters: $k_{sel} = 0.515$, $KIE_{sel} = 2.33$, and $KIE_{ex} = 2.24$. [d] Calculated by assuming statistical distribution of all seven H/D atoms of the $C_3H_{7-n}D_n$ units. [e] Upper limit of H_2O loss derived from analysis of the MI spectra of $CH_3CH(OD)CH_3/Fe^+$ at various degrees of O-deuteration (due to H/D exchange in the inlet system). [f] Lower limit of HDO loss derived from analysis of the noise level in the MI spectra of $CD_3CD(OH)CD_3/Fe^+$.

Table 2. H_2O/HDO losses from metastable complexes of Fe^+ with labeled *n*-propanols.

Substrate	Experiment[a]		Model B[b]		Model C[c]		Statistical[d]	
	H_2O	HDO	H_2O	HDO	H_2O	HDO	H_2O	HDO
$CH_3CH_2CH_2OD$	< 2[e]	> 98	0.0	100.0	0.0	100.0	0.0	100.0
$CH_3CH_2CD_2OH$	82.6	17.4	86.4	13.6	83.0	17.0	71.4	28.6
$CH_3CD_2CH_2OH$	79.5	20.5	81.3	18.7	80.3	19.7	71.4	28.6
$CH_2DCHDCH_2OH$	85.4	14.6	83.7	16.3	84.8	15.2	71.4	28.6
$CHD_2CH_2CH_2OH$	89.1	10.9	86.4	13.6	88.8	11.2	71.4	28.6
$CH_2DCHDCHDOH$	75.0	25.0	74.6	25.4	73.7	26.3	57.1	42.9
$CD_3CH_2CH_2OH$	81.2	18.8	77.0	23.0	82.0	18.0	57.1	42.9
$CD_3CD_2CH_2OH$	50.3	49.7	46.8	53.2	50.3	49.7	28.6	71.4
$CD_3CD_2CD_2OH$	< 0.4	> 99.6[f]	0.0	100.0	0.0	100.0	0.0	100.0

[a] Averaged intensities obtained in three independent experiments normalized to $\Sigma = 100$. The experimental error is less than ± 0.8. [b] Parameters: $k_{sel} = -0.033$, $KIE_{sel} = -0.250$, and $KIE_{ex} = 2.24$. [c] Parameters: $k_{sel} = 0.068$, $KIE_{sel} = 2.72$, and $KIE_{ex} = 2.25$, $f_{as} = 0.7$. [d] Calculated by assuming statistical distribution of all seven H/D atoms of the $C_3H_{7-n}D_n$ units. [e] Upper limit of H_2O loss derived from analysis of the MI spectra of $CH_3CH_2CH_2OD/Fe^+$ at various degrees of O-deuteration (due to H/D exchange in the inlet system). [f] Lower limit of HDO loss derived from analysis of the noise level in the MI spectra of $CD_3CD_2CD_2OH/Fe^+$.

Herein we present such a quantitative analysis.[11] We begin with isopropanol **1′** as the analysis is more simple due to the constitutional equivalence of the methyl groups. At first, we assume that β-H and β-D transfers are associated with a kinetic isotope effect (KIE). Irrespective of the chosen KIEs, however, the experimental data systematically deviate from statistical H/D equilibration, such that a certain degree of a specific 1,2-elimination (k_{sel}) needs to be included. Thus, for the description of the H_2O/HDO ratios for isopropanol/Fe^+,

[*] Prof. Dr. H. Schwarz, Dipl.-Chem. C. Trage, W. Zummack, Dr. D. Schröder
Institut für Chemie der Technischen Universität Berlin
Strasse des 17. Juni 135, 10623 Berlin (Germany)
Fax: (+49) 30-314-21102
E-mail: Helmut.Schwarz@www.chem.tu-berlin.de

[**] We thank the Volkswagen-Stiftung, the Deutsche Forschungsgemeinschaft, and the Fonds der Chemischen Industrie for generous funding.

  1433-7851/01/4014-2708 $ 17.50+.50/0

we end up in a system of kinetic equations with KIE and k_{sel} as parameters (model **A**). While this two-parameter model, in which the same KIE is employed for the specific and unspecific paths, yields a reasonable fit of the experimental ratios, some discrepancies remain. Significant improvement is obtained, if one differentiates between the KIEs of the selective 1,2-elimination and of the exchange reaction, that is, using k_{sel}, KIE_{sel}, and KIE_{ex} as variables (model **B**). With these three parameters, the experimental data can be modeled within the experimental error.[12] In summary, the data suggest that the sequence **2** ⇄ **2′** is partially reversible with an irreversible outlet via **4** to the products; the latter conclusion is based on the lack of participation of the OH group in H/D exchange.[13] We note in passing that H/D exchange is also absent for the bisligated complex $[(C_3D_6)Fe(H_2O)]^+$ generated independently by chemical ionization (CI) of $[Fe(CO)_5]$, H_2O, and $[D_6]$propene.

Application of model **B** to the *n*-propanol/Fe^+ system results in poor agreement between experimental and modeled data and, more importantly, unrealistic parameters, for example, $k_{sel} < 0$, emerge. Prior to any discussion of the appropriateness of the models (numerical inaccuracies etc.), the experimental data clearly indicate that *another* variable is required. The comparison of the $[D_2]$isotopomers is most instructive in this respect. Thus, the H_2O/HDO ratios for the [1,1-D_2] and [2,2-D_2] compounds are very similar, though not identical, indicating almost complete scrambling of the H/D atoms of the methylene groups. However, the [2,3-D_2]- and [3,3-D_2]isotopologues show significantly lower amounts of HDO losses; in fact, it takes the [3,3,3-D_3] sample to reach the H_2O/HDO ratios of the [1,1-D_2] and [2,2-D_2] compounds. Accordingly, while the H/D atoms at C1 and C2 undergo almost complete scrambling, the terminal methyl group participates to a lower extent. This conclusion is, however, in obvious contradiction to an H/D equilibration in alkyl metal compounds by reversible β-hydrogen transfer (see Scheme 2), because it would imply a *n*-propyl to isopropyl isomerization without an isopropyl intermediate! In other words, the classical view of an involvement of an isopropyl moiety with two constitutionally equivalent methyl groups contradicts the experimental findings. Therefore, an asymmetry factor f_{as} is introduced as an additional parameter (model **C**). This parameter describes the nonequivalency of the C1 and C3 positions in the conversion **2** ⇄ **2′**. Model **C** provides a reasonable fit of the experimental data which is not as perfect as in the isopropanol/Fe^+ system, but is inside the error margins of the experiment. A key point to be made is that the asymmetry of the C1 and C3 positions is still visible in the product formation, even though the KIEs > 2 indicate that β-H(D) transfer contributes to the rate-determining step.

Kinetic modeling of elementary reactions, however, only provides numbers and no chemical insight. What kinds of structural effects could cause asymmetry between the existing and the emerging methyl groups as in the isomerization of a propyl unit? A clue is provided by the hypothesis that metal cation binding to alkyl fragments bearing β-hydrogen atoms is inherently associated with an agostic interaction; in fact, structures without agostic interactions are no minima, but saddle points.[15] Accordingly, the central part of Scheme 2 is extended in Scheme 3, where C1 of *n*-propanol is deliberately marked by a dot. For *n*-propanol/Fe^+, equilibration of the H/D atoms at C1 and C2 could occur through the reversible

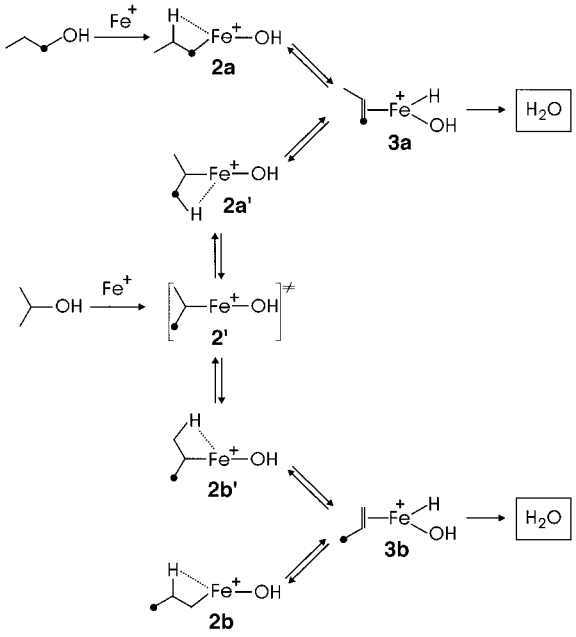

Scheme 3. Extended model for the loss of water from [Fe/propanol]$^+$ considering the nonequivalency of the two methyl groups.

sequence **2a** ⇄ **2a′**. Participation of the original C3 position is, however, only achieved through the classical structure **2′**, which is assumed to be a transition structure for the degenerate interconversion **2a′** ⇄ **2b′**. The experimentally shown nonequivalence of the C1 and C3 positions in the H/D equilibration of *n*-propanol/Fe^+ further suggests that the related barrier is sufficiently high to compete with the irreversible hydrogen transfer to the hydroxy group (**3** → **4** → products).

The inherent asymmetry of alkyl metal compounds assumed is, perhaps, of more general relevance as it may also help to understand some of the puzzling results obtained in olefin hydrogenation, for example, isotopically scrambled products having a uniform stereochemistry,[16] as well as the diastereoselectivity of transition metal and metallocene-catalyzed olefin polymerization.[17] Further mechanistic studies as well as a theoretical examination of this challenging problem are in progress.

Received: April 25, 2001 [Z16994]

[1] J. Allison, D. P. Ridge, *J. Am. Chem. Soc.* **1979**, *101*, 4998.
[2] K. Eller, *Coord. Chem. Rev.* **1993**, *126*, 93.
[3] a) M. C. Holthausen, A. Fiedler, H. Schwarz, W. Koch, *J. Phys. Chem.* **1996**, *100*, 6236; b) M. C. Holthausen, W. Koch, *Helv. Chim. Acta* **1996**, *79*, 1939.
[4] $D(Fe^+–H_2O) = 30.6 \pm 1.8$ kcal mol^{-1} versus $D(Fe^+–C_3H_6) = 37 \pm 2$ kcal mol^{-1},[5]
[5] *Organometallic Ion Chemistry* (Ed.: B. S. Freiser), Kluwer, Dordrecht, **1996**, p. 283.

  1433-7851/01/4014-2709 $ 17.50+.50/0

[6] For a previous experimental study of some labeled *n*-propanol/Fe^+ complexes, see: S. Karrass, T. Prüsse, K. Eller, H. Schwarz, *J. Am. Chem. Soc.* **1989**, *111*, 9018.
[7] The synthesis of the labeled propanols followed well-established preparative procedures. In brief, the [O-D]propanols were prepared by treatment of the corresponding sodium propanolates with D_2O. The [1,1-D_2]-, [2,2-D_3]-, [2,2,3,3,3-D_5]-, and [1,1,2,2,3,3,3-D_7]-*n*-propanols were made by reduction of the corresponding acids with $LiAlH_4$ or $LiAlD_4$, respectively. Catalytic reduction of unlabeled and [1-D_1]-prop-2-en-1-ol with deuterium afforded [2,3-D_2]- and [1,2,3-D_3]-*n*-propanols, respectively; the labeled allyl alcohol was made by reduction of acrolein with $LiAlD_4$. [3,3-D_2]- and [3,3,3-D_3]-*n*-propanols were prepared by Cu^I-catalyzed addition of the corresponding methyl Grignard reagents to ethylene oxide. Except the preparation of [1,1,1-D_3]isopropanol by addition of CD_3MgI to acetaldehyde, all labeled isopropanols were made by reduction of acetone, [D_6]acetone, 1,3-dichloroacetone, and [1,1,3,3-D_4]-1,3-dichloroacetone with $LiAlH_4$ or $LiAlD_4$, respectively.
[8] The experiments were performed with a modified VG ZAB/HF/AMD four-sector mass spectrometer of BEBE configuration (B stands for magnetic and E for electric sectors) which has been described previously.[9] Briefly, propanol/Fe^+ complexes were generated by chemical ionization of a mixture of [$Fe(CO)_5$] and the corresponding propanol. The ions were accelerated to 8 keV kinetic energy and mass-selected by means of B(1)/E(1) at a resolution of $m/\Delta m \approx 3000$. Unimolecular fragmentations of metastable ions occurring in the field-free region preceding B(2) were recorded by scanning this sector. A total of 10 to 30 scans were averaged to improve the signal-to-noise-ratio, and the data are the averages of at least three independent measurements.
[9] C. A. Schalley, D. Schröder, H. Schwarz, *Int. J. Mass Spectrom. Ion Processes* **1996**, *153*, 173.
[10] This criticism includes our own work, for example: a) S. Karrass, T. Prüsse, K. Eller, H. Schwarz, *J. Am. Chem. Soc.* **1989**, *111*, 9018; b) D. Schröder, W. Zummack, H. Schwarz, *J. Am. Chem. Soc.* **1994**, *116*, 5857; c) R. Wesendrup, C. A. Schalley, D. Schröder, H. Schwarz, *Organometallics* **1996**, *15*, 1435.
[11] The details of the algebraic formalisms used as well as a sensitivity analysis will be reported in a full article; they are available from Claudia.Trage@www.chem.tu-berlin.de.
[12] Note that secondary kinetic isotope effects need not be considered explicitly, because they are either inherently included in the analysis or cancel out in the H_2O/HDO ratios.
[13] Additional information, which will be presented in a full article, suggests that the C–O bond insertion **1** → **2** is also quasi-irreversible for the metastable ions. This conclusion is further supported by the substantial barrier predicted for the insertion of Fe^+ into the C–O bond of methanol.[14]
[14] Y. Shiota, K. Yoshizawa, *J. Am. Chem. Soc.* **2000**, *122*, 12317, and references therein.
[15] See also: D. Schröder, C. Trage, H. Schwarz, D. Danovich, D. Shaik, *Int. J. Mass Spectrom.* **2000**, *200*, 163.
[16] Review: J. M. Brown, *Angew. Chem.* **1987**, *99*, 169; *Angew. Chem. Int. Ed. Engl.* **1987**, *26*, 190.
[17] a) Review: H.-H. Brintzinger, D. Fischer, R. Mühlhaupt, B. Rieger, R. Waymouth, *Angew. Chem.* **1995**, *107*, 1255; *Angew. Chem. Int. Ed. Engl.* **1995**, *34*, 1143; b) D. J. Tempel, L. K. Johnson, R. L. Huff, P. S. White, M. Brookhart, *J. Am. Chem. Soc.* **2000**, *122*, 6686.

A Novel Hemiporphyrazine Comprising Three Isoindolediimine and Three Thiadiazole Units**

Nagao Kobayashi,* Sayaka Inagaki,
Victor N. Nemykin, and Taro Nonomura

Large aromatic macrocyclic compounds such as porphyrins and phthalocyanines have attracted the interest of many chemists.[1, 2] In the phthalocyanine family, naphthalocyanines are important analogues and have been used in commercial fields such as read/write compact discs. Although not often used in practice, perhaps the next best known phthalocyanine analogues are hemiporphyrazines, which can be obtained by the condensation reaction of equimolar amounts of 1*H*-isoindole-1,3(2*H*)-diimines and 2,6-diaminopyridines.[3] Around a decade ago, a new member, synthesized from 1*H*-isoindole-1,3(2*H*)-diimines and 2,5-diamino-1,3,4-triazoles, was introduced into this family, and now such hemiporphyrazines are conventionally known as triazole hemiporphyrazine **3** (Scheme 1).[4] These compounds are cyclic tetramers

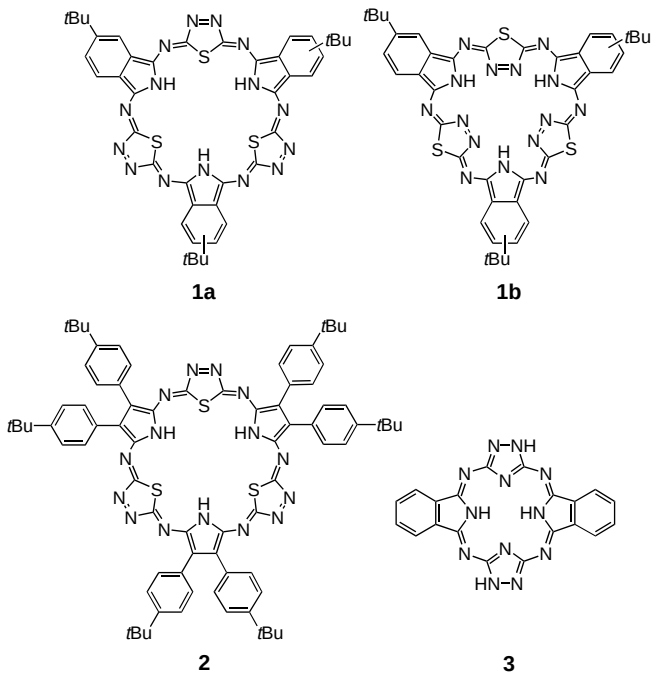

Scheme 1. Two possible structures **1a** and **1b** for the condensation products of 2,5-diamino-1,3,4-thiadiazole and 5-*tert*-butylisoindolediimine, and a possible structure for compound **2**. The triazole hemiporphyrazine structure is shown at the bottom right.

[*] Prof. Dr. Dr. N. Kobayashi, S. Inagaki, Dr. V. N. Nemykin, Dr. T. Nonomura
Department of Chemistry
Graduate School of Science, Tohoku University
Sendai 980-8578 (Japan)
Fax: (+81) 22-217-7719
E-mail: nagaok@mail.cc.tohoku.ac.jp

[**] This work was supported partly by a Grant-in-Aid for Scientific Research (B) No. 11440192 and the Shorai Foundation for Science & Technology.

Supporting information for this article is available on the WWW under http://www.angewandte.com or from the author.

  1433-7851/01/4014-2710 $ 17.50+.50/0

consisting of two units each ("2+2"), and it has long been common knowledge that 2+2 type compounds are obtained from the above type of reaction. In contrast, here we report that the use of 2,5-diamino-1,3,4-thiadiazole (TDA) produces, as the exclusive cyclic products, the unusual cyclic hexamers **1a** and **1b**, each consisting of three isoindolediimine and three thiadiazole units (3+3) (Scheme 1). These may be termed thiadiazole superhemiporphyrazines, in keeping with the relationship between phthalocyanine and superphthalocyanine.

By analogy with the 2+2 synthesis of 1,2,4-triazole-containing hemiporphyrazines,[4] a mixture of equimolar amounts of TDA[5] and 5-*tert*-butyl-1*H*-isoindole-1,3(2*H*)-diimine was heated to reflux in butanol for 48 h to produce a deep red material, which was collected by filtration and washed with methanol. It was then extracted with hot chloroform, and the extract subjected to chromatography on a silica gel column, first with chloroform, then chloroform/methanol (8/2). The first, yellow-orange and the second, red fraction were collected and analyzed, together with an unresolved residue, by several spectroscopic methods. The second red fraction was an open-chain 2+2 oligomer containing terminal amino groups, while the residue consisted of open-chain *n*+*n* polymers. Surprisingly, the first fraction gave satisfactory data to substantiate the formation of 3+3 cyclic hexamers (26%; the final purification was carried out by gel-permeation chromatography (Bio-beads SX-2, Bio-rad)),[6] while no cyclic tetramer was detected. In a similar manner, the use of 3,4-bis(4-*tert*-butylphenyl)-3-pyrroline-2,5-diimine[7] in place of isoindolediimine produced a similar cyclic hexamer, namely, **2**.[6, 8] As a plausible explanation for the formation of the hexamer, we can consider the different covalent radii of sulfur (1.82 Å) and nitrogen (1.48 Å).[9] Sulfur atoms are larger than nitrogen atoms, and as a result, the estimated angle (calculation at the PM3 level[10]) between the two C–N_{amino} bonds in TDA becomes 164°, as opposed to 140° in 2,5-diamino-1,3,4-triazole. Thus, if TDA is used as one of the two starting materials, it becomes more difficult to form a macrocycle from a smaller number of constituent units.

Figure 1 shows the electronic absorption and magnetic circular dichroism (MCD) spectra of **1**. In addition to two small absorption peaks at 499 and 471 nm, two intense main peaks appeared at 412 and 391 nm, and two bands of medium intensity were observed in the UV region. Compared with the spectrum of metal-free triazolehemiporphyrazine,[11] the two main peaks are shifted slightly to the red, while the intensity of the UV bands relative to that of the main bands is smaller, and the shape of the spectrum somewhat resembles those of [18]annulene derivatives.[12] The MCD spectrum gave many dispersion type curves (plausibly mostly Faraday *A* terms) corresponding to the absorption peaks. It is difficult to determine which of the two structures of **1** (i.e., **1a** and **1b** in Scheme 1) contributes more to the spectra, since semiempirical calculations at the ZINDO/1[9] and AM1[13] levels produced both **1a** and **1b** as stable structures, although those using the PM3 Hamiltonian preferred the structure **1b**. In addition, ZINDO/S calculations at the ZINDO/1 level predicted similar spectra for structures **1a** and **1b**, which reproduced the experimental spectra.[8] Furthermore, the

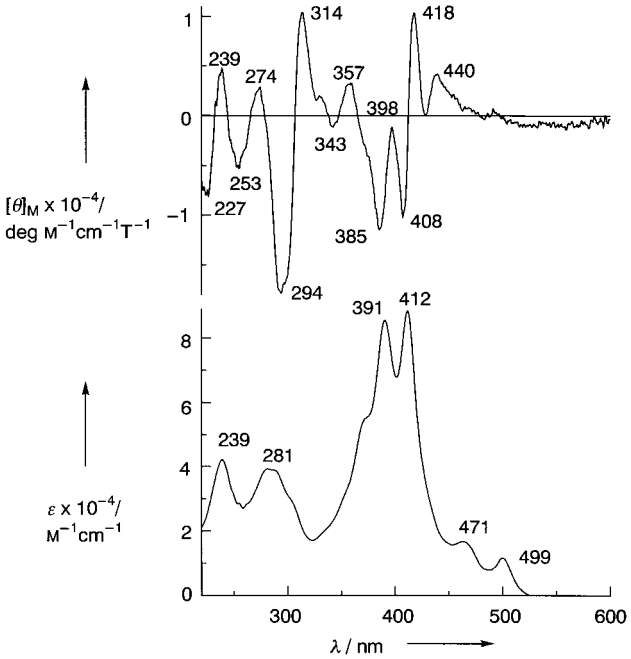

Figure 1. Electronic absorption (bottom) and MCD (top) spectra of **1** in THF.

large Stokes shift of **1** (70 nm, 2465 cm^{-1}, not shown) indicates that **1** is a very flexible molecule. Accordingly, both **1a** and **1b** can be considered as structures of **1**.

Figure 2 shows the ESI-TOF mass and absorption spectra of the nickel complex of **1**, which was obtained by a nickel-insertion reaction in butanol.[6] The experimental distribution pattern of the mass spectrum agrees almost perfectly with that calculated for [**1** – 3H+3Ni], and indicates that three nickel ions were incorporated into the skeleton of **1**. This is a phenomenon not seen in any porphyrinic compounds, including phthalocyanines and porphyrazines. The shape of the absorption spectrum differs greatly from that of **1** in Figure 1. The two very sharp, intense absorption peaks of **1** at 391 and 412 nm changed into two broad peaks of medium intensity, while the two medium-intensity peaks at 239 and 281 nm appear to have merged into a peak at 257 nm in $Ni_3 \cdot$ **1**.

In conclusion, we have described the synthesis and some properties of unusual and relatively flexible 3+3 macrocycles obtained from condensation reactions between an isoindolediimine or 3,4-bis(4-*tert*-butylphenyl)-3-pyrroline-2,5-diimine and 2,5-diamino-1,3,4-thiadiazole as a new member of the phthalocyanine family. Superphthalocyanines have been prepared exclusively with uranium as a template,[14] and its size led to a superphthalocyanine structure composed of five isoindolediimine rings. Here, the wide angle between the two C–N_{amino} bonds in diaminothiadiazole controls the size of the condensation product. Most interestingly, metal-insertion reactions led to the incorporation of three nickel or copper[8] atoms, and the resulting complexes exhibit totally different spectra from **1**. The details of the results of calculations, MCD and fluorescence spectroscopy, and electrochemistry will be reported in a full paper.

Received: March 12, 2001 [Z16759]

  1433-7851/01/4014-2711 $ 17.50+.50/0

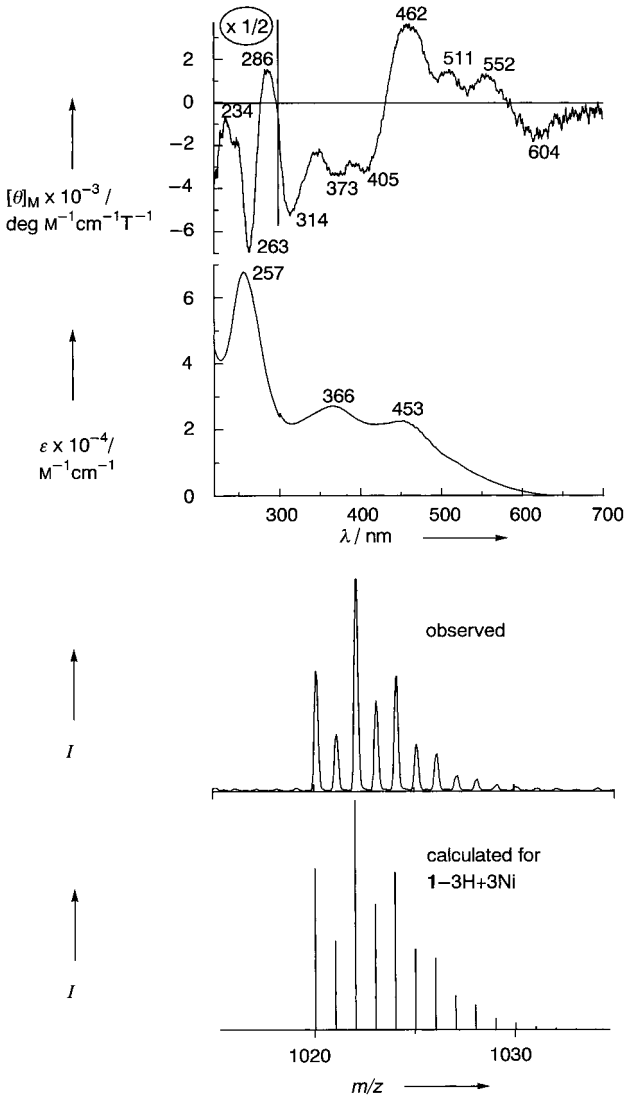

Figure 2. MCD (top) and electronic absorption (2nd from the top) spectra in THF and experimental (2nd from the bottom) and theoretical (bottom) ESI-MS spectra of $Ni_3 \cdot \mathbf{1}$.

[1] a) *Phthalocyanines: Properties and Applications*, *Vol. 1–4* (Eds.: C. C. Leznoff, A. B. P. Lever), VCH, New York, **1989**, **1992**, **1993**, **1996**; b) *Phthalocyanines: Chemistry and Functions* (Eds.: H. Shirai, N. Kobayashi), IPC, Tokyo, **1997**.

[2] *Handbook of Porphyrins and Phthalocyanines*, *Vol. 1–10* (Eds.: K. M. Kadish, K. M. Smith, R. Guilard), Academic Press, New York, **1999**.

[3] J. A. Elvidge, R. P. Linstead, *J. Chem. Soc.* **1952**, 5008.

[4] a) F. Fernandez-Lazaro, T. Torres, B. Hauschhel, M. Hanack, *Chem. Rev.* **1998**, *98*, 563; b) F. Fernandez-Lazaro, M. A. Diaz-Garcia, A. Sastre, P. Delhaes, C. Mingotaudo, F. Agullo-Lopez, T. Torres, *Synth. Met.* **1998**, *93*, 213.

[5] E. Fromm, *Liebigs Ann. Chem*. **1923**, *433*, 1.

[6] Selected data for new macrocycles: **1**: elemental analysis (%) calcd for $C_{42}H_{39}N_{15}S_3$: C 59.36, H 4.59, N 24.73, S 11.31; found: C 59.07, H 4.83, N 24.60, S 11.07; FAB-MS (*m*-nitrobenzyl alcohol): *m*/*z*: 850 [M^++H]; ^{1}H NMR (400 MHz, $CDCl_3$): $\delta = 12.47$ (s, 3H, NH), 8.01 (m, 3H, ArH), 7.84 (m, 3H, arom), 7.67 (m, 3H, ArH), 1.45–1.47 (m, 27H, *t*Bu); IR (KBr): $\tilde{\nu} = 3225$ (NH), 2961 (CH, *t*Bu), 1645, 1616, 1489, 1406, 1366, 1317, 1223, 1132, 1089, 1032, 837 cm^{-1}; UV/Vis (THF): λ_{max} ($\varepsilon \times 10^{-4}$) = 499 (1.2), 471 (1.7), 412 (8.7), 391 (8.5), 281 (3.1), 239 nm (3.7). $Ni_3 \cdot \mathbf{1}$: elemental analysis (%) calcd for $C_{42}H_{36}N_{15}Ni_3S_3 \cdot 3H_2O$: C 46.83, H 3.93, N 19.51; found: C 46.00, H 4.04, N 17.20; ESI-TOF MS: *m*/*z*: 1020 [M^+]; ^{1}H NMR (400 MHz, $CDCl_3$): $\delta = 7.81–7.24$ (m, 9H, ArH), 1.45–1.42 (m, 27H, *t*Bu); UV/Vis (THF): λ_{max} ($\varepsilon \times 10^{-4}$) = 453 (2.3), 366 (2.7), 257 nm (6.8). **2**: Elemental analysis (%) calcd for $C_{78}H_{81}N_{15}S_3$: C 70.72, H 6.16, N 15.86, S 7.26; found: C 71.05, H 6.93, N 15.04, S 7.03; ESI-TOF MS: *m*/*z*: 1324.5 [M^++H]; ^{1}H NMR (400 MHz, $CDCl_3$): $\delta = 12.32$ (s, 3H, NH), 7.51 (d, $J = 8.4$ Hz, 12H, ArH), 7.41 (d, $J = 8.4$ Hz, 12H, ArH), 1.37 (s, 54H, *t*Bu); UV/Vis (THF): λ_{max} ($\varepsilon \times 10^{-4}$) = 551 (1.2), 510 (1.9), 449 (8.1), 426 (8.0), 328 (2.9), 265 nm (4.2).

[7] T. F. Baumann, A. G. M. Barrett, B. M. Hoffman, *Inorg. Chem.* **1997**, *36*, 5661.

[8] See Supporting Information.

[9] A. J. Gorden, R. A. Ford, *The Chemists Companion*, Wiley, New York, **1972**.

[10] J. I. P. Stewart, *J. Comput. Aided Mol. Des.* **1990**, *4*, 1.

[11] T. Torre, M. V. Martinez-Diaz, P. R. Ashton, T. Torres, *J. Org. Chem.* **1998**, *63*, 8888.

[12] B. Briat, D. A. Schooley, R. Records, E. Bunnenberg, C. Djerassi, *J. Am. Chem. Soc.* **1967**, *89*, 7062.

[13] M. J. S. Dewar, E. G. Zoebisch, E. F. Healey, J. P. Stewart, *J. Am. Chem. Soc.* **1985**, *107*, 3902.

[14] T. J. Marks, D. R. Stojakovic, *J. Am. Chem. Soc.* **1978**, *100*, 1695.

New Paradigms for Organic Catalysts: The First Organocatalytic Living Polymerization**

Fredrik Nederberg, Eric F. Connor, Michael Möller, Thierry Glauser, and James L. Hedrick*

In the last three decades, a significant effort has gone into the development of biodegradable polymers with the object of designing resorbable biomaterials and, more recently, for designing commodity thermoplastics from renewable resources. Aliphatic polyesters, particularly poly(lactide), combine biocompatibility and biodegradability with remarkable physical properties and possess the requisite thermal stability at the processing temperatures. Advances in organometallic chemistry in the design and synthesis of single-site metal catalysts for olefin,[1] ring opening metathesis,[2] and ring opening polymerization techniques[3] have enabled the preparation of well-defined functional polymeric materials with predictable molecular weights and narrow polydispersities. The ring-opening polymerization (ROP) of lactide has been accomplished with a variety of metal catalysts including aluminum, tin, zinc, and yttrium through a coordination–insertion mechanism.[4] Currently, considerable research is directed towards the preparation of organometallic compounds with tailored ligands that produced poly(lactides) with controlled stereochemistry and microstructure.[3, 5] However, there are few reports on the ROPs of lactides which do not use organometallic promoters.[6] Alternative strategies using only

[*] J. L. Hedrick, F. Nederberg, E. F. Connor, M. Möller, T. Glauser
IBM Almaden Research Center
San Jose, CA 95120 (USA)
Fax: (+1) 408-927-3310
E-mail: hedrick@almaden.ibm.com

[**] The authors would like to thank the NSF Center on Polymer Interfaces and Macromolecular Assemblies (CPIMA). T.G. expresses his thanks to the Swiss Academy of Engineering Sciences (SATW) and the Swiss National Science Foundation.

  1433-7851/01/4014-2712 $ 17.50+.50/0

organic compounds as reaction catalysts have led to new and versatile organocatalysts amenable to a number of asymmetric transformations.[7] The extension of organic catalysis to controlled polymerizations would be a highly desirable alternative to traditional organometallic approaches.

Here we detail the first organocatalytic approach to the living ROP of lactide using strongly basic amines as transesterification catalysts. 4-(Dimethylamino)pyridine (DMAP) and related bases such as 4-pyrrolidinopyridine (PPY) are widely used and prove to be extremely efficient reagents for acylation, alkylation, silation, phosphorylation, condensation, and transesterification reactions.[8] Taber and co-workers[9] discovered the effectiveness of DMAP as a transesterification catalyst for β-keto esters. Others[10] showed that the removal of the alcohol coproduct in the transesterification reaction biased the equilibrium towards product. In another example, Menger and McCann[11] demonstrated quantitative transesterification of methyl *p*-nitrobenzoate to methyl acetate using DMAP immobilized on cross-linked polystyrene. Morken and Taylor[12a] combined solid-phase synthesis and combinatorial chemistry to rapidly produce a large number of organic transesterification catalysts to survey acylation reactions. A variety of other transesterification procedures using DMAP have been reported.[12, 13] The strategy employed for the ROP of lactide using an organic transesterification catalyst is as follows: First, a nucleophile such as an alcohol must be used to initiate the polymerization of lactide in the presence of the organic catalyst, providing a means of contolling molecular weight and end group functionality. Polymerization proceeds when a terminal ω-hydroxyl group acts as the nucleophile and reacts with additional lactide/DMAP. Second, the ring-opening reaction does not evolve a coproduct and since the ring opening is enthalpically driven, the equilibrium is prejudiced towards polymerization. When this general approach is considered, it is apparent that a proliferation of variables must be well thought-out. For example, the type and concentration of amine, solution or bulk-reaction conditions, polymerization temperature, undesirable transesterification side reactions, and the general classes of initiators all influence the polymerization. To survey these variables, a parallel approach to polymer synthesis, designed to enable rapid screening of optimal catalyst/initiator systems and associated polymerization conditions, was employed. The Quest 210 robotic reactor proved to be an excellent platform for performing up to 20 polymerizations in parallel, providing the necessary environment, temperature control, and agitation to accomplish the ROP.[14]

The catalytic behavior of DMAP and PPY in the polymerization of lactide was studied in dichloromethane at 35 °C using ethanol as the initiator with 0.1 to 4.0 equivalents of amine relative to initiating alcohol (see Table 1). Although a number of polymerization media were evaluated, most of the polymerizations were conducted in dichloromethane, since it is a good solvent for both the lactide and poly(lactide). Under anhydrous conditions, no detectable polymerization of lactide was observed in this solvent in the presence of these amines without the addition of a nucleophile. Amine concentrations of 0.1 equiv relative to initiator (ethanol) produced only modest conversions after prolonged reaction times. Conversely, higher amine concentrations proved to be active and highly selective for the ROP of lactide in 100 % yields with no adverse side reactions, as evidenced by the retention of the narrow polydispersities. A targeted degree of polymerization (DP) of 30 was calculated from the monomer-to-initiator ratio, and a value of 29 was obtained by ^{1}H NMR analysis of the end groups (36 h).[15] The polydispersity was 1.13. A plot of molecular weight versus monomer conversion for the ROP of lactide initiated from ethanol in the presence of DMAP is shown in Figure 1. The correlation between molecular weight

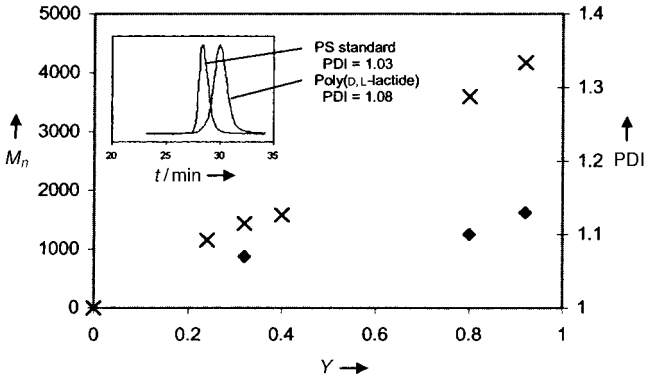

Figure 1. Plot of molecular weight (M_n, ×) versus monomer conversion (Y) for the ROP of lactide initiated from ethanol in the presence of DMAP. The polydispersities (PDI, ◆) are also shown. Inset: The GPC traces for a polystyrene calibration standard together with poly(D,L-lactide) are also shown to facilitate comparison and demonstrate the narrow polydispersity.

and conversion is consistent with a living polymerization. The polydispersities are extremely low and, unlike for most organometallic-promoted polymerizations,[16] remained invariant to high monomer conversions (100 % conversion, 36 h). To investigate possible undesirable transesterification reactions, the polymerization was allowed to continue; the polydispersity after 72 and 96 h reaction time was 1.08 and 1.10, respectively, without a detectable change in molecular weight. In another experiment, two polylactides having different molecular weights were stirred in dichloromethane for 24 h (35 °C) in the presence of DMAP and closely followed by gel permeation chromatography (GPC).[17] No transesterification reactions were detected by GPC, as each of the polymers retained their initial elution volumes. Importantly, once quantitative monomer conversion is achieved no undesirable transesterification side reactions were evident, and these combined data point to a living polymerization process.

The versatility of the organocatalyzed ROP of lactide is demonstrated by the data in Table 1, which contains selected results of the poly(lactide) polymerization initiated from assorted alcohols in the presence of several amines for different targeted molecular weights in either dichloromethane or in bulk. The amines DMAP and PPY showed comparable catalytic activity, producing polymers with molecular weights that closely tracked the monomer-to-initiator ratio (M/I) with extremely narrow polydispersities (entries 5 – 16). Moreover, ^{13}C NMR spectroscopy and calorimetry studies on the polymerization of the enantiomerically pure L-lactide (entry 19) clearly show that racemization does

  1433-7851/01/4014-2713 $ 17.50+.50/0

Table 1. Characteristics of poly(lactides) prepared by reactions catalyzed by organic compounds.

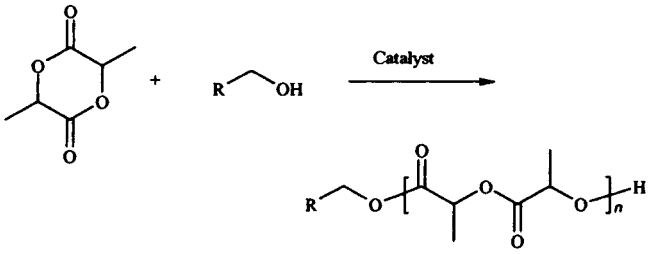

Entry	Catalyst[a]	Initiator	T [°C]	t	M/I[b]	DP[c]	PDI[d]
1	DMAP (0.1 equiv)	EtOH	35	96 h	30	5	/
2	DMAP (1 equiv)	EtOH	35	60 h	30	29	1.13
3	DMAP (2 equiv)	EtOH	35	36 h	30	29	1.13
4	DMAP (4 equiv)	EtOH	35	24 h	30	29	1.08
5	DMAP (2 equiv)	EtOH	35	24 h	15	17	1.12
6	DMAP (2 equiv)	EtOH	35	36 h	30	29	1.13
7	DMAP (2 equiv)	EtOH	35	50 h	60	62	1.10
8	DMAP (4 equiv)	EtOH	35	64 h	100	78	1.10
9	DMAP (2 equiv)	$PhCH_2OH$	35	30 h	30	43	1.08
10	DMAP (2 equiv)	$PhCH_2OH$	135	5 min	30	29	1.10
11	DMAP (2 equiv)	$PhCH_2OH$	135	10 min	60	42	1.09
12	DMAP (4 equiv)	$PhCH_2OH$	135	20 min	100	77	1.19
13	DMAP (2 equiv)	$PhCH_2OH$	135	20 min	140	120	1.14
14	PPY (2 equiv)	EtOH	35	20 h	30	31	1.10
15	PPY (2 equiv)	$PhCH_2OH$	35	20 h	30	27	1.08
16	PPY (2 equiv)	$PhCH_2OH$	135	10 min	30	32	1.16
17	DMAP (2 equiv)	$(CH_3)_2CHOH$	35	48 h	30	35	1.12
18	DMAP on PS	EtOH	35	70 h	30	25	1.08
19	DMAP (2 equiv)/L-lactide	EtOH	35	30	30	29	1.06
20	DMAP (2 equiv)/L-lactide	$PhCH_2OH$	185	6 min	30	30	1.18
21	DMAP (2 equiv)/L-lactide	$PhCH_2OH$	185	8 min	60	50	1.14

[a] The equivalents of amine relative to initiating alcohol are given in parentheses. [b] Monomer-to-initiator ratio. [c] Degree of polymerization. [d] Polydispersity index.

not occur.[18] In addition, secondary alcohols effectively initiated the polymerization, which proceeded in quantitative yields (entry 17). Bulk polymerizations of D,L- and L-lactide were also investigated at 135 and 185 °C, respectively, using benzyl alcohol as the initiator. Narrowly dispersed poly(lactides) were obtained in about 5 to 20 minutes, depending on the targeted molecular weight (entries 10–13, 15, 20, 21). Poly(L-lactide) required a higher polymerization temperature since it is semicrystalline with a melting point around 180 °C. The molecular weights correlate closely to the monomer-to-initiator ratio, and even at these polymerization temperatures, the polydispersities remained narrow. In each case, the organic catalyst could be recovered in excess of 85 % yield. DMAP immobilized onto polystyrene particles also proved to be an effective media for catalyzing the ROP of lactide (entry 18). The molecular weights, polydispersities, and polymerization kinetics achieved from the solid-supported catalyst were comparable to those from previous experiments. In these experiments using the solid supported catalyst, the base was easily removed by filtration.

One plausible polymerization pathway is through a monomer-activated mechanism. Initiation occurs when a nucleophile such as an alcohol reacts with a lactide–DMAP complex to form the mono adduct, and the α-chain end of the poly(lactide) bears an ester functionality derived from the alcohol, as in related acylation reactions (Scheme 1).[12a]

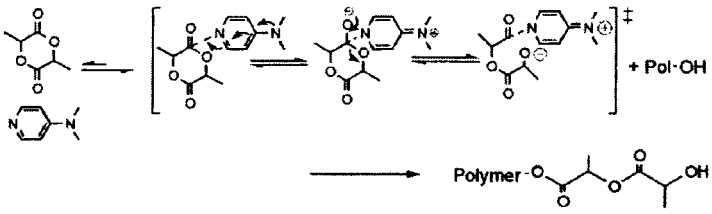

Scheme 1. A plausible polymerization pathway.

Polymerization proceeds when the terminal ω-hydroxyl group acts as a nucleophile to facilitate further chain growth. Consistent with this mechanism, the ^{1}H NMR spectrum of poly(lactide) initiated with ethanol using DMAP as the catalyst shows resonances associated with the ethoxy ester and the hydroxyl chain ends (Figure 2). To further substantiate the initiation step, the reaction of excess benzyl alcohol with one equivalent of DMAP (based on lactide) was investigated. The lactide was ring opened with formation of the benzyl ester; however, due to the large excess of the benzyl alcohol and DMAP catalyst, transesterification with the diester product afforded the monoester.[19] This product was isolated, characterized, and subsequently used to initiate the controlled polymerization of lactide using the same polymerization techniques as for the reactions in Table 1 (DP target 30, measured 29, PDI 1.09). These data support an initiation and polymerization mechanism which proceeds

  1433-7851/01/4014-2714 $ 17.50+.50/0

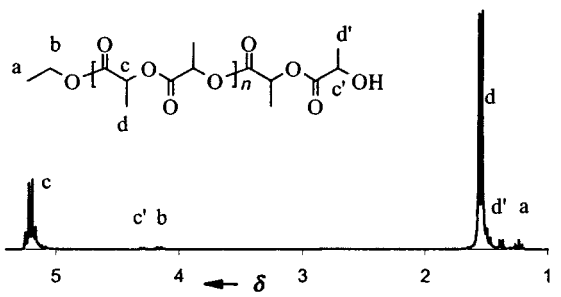

Figure 2. ^{1}H NMR spectrum of polylactide initiated from ethanol in the presence of DMAP.

through a monomer-activation intermediate. This polymerization mechanism is similar, in many aspects, to that of modern controlled radical polymerization techniques, where the predominate species are dormant polymer chains with minimally active radical species. In this way, termination and side reactions are minimized, producing narrow polydispersities. By analogy, the narrow polydispersities realized in the amine-catalyzed lactide polymerization is a manifestation of the presence of predominately dormant chains with minimal active species.

The synthetic utility of selected amines as transesterification catalysts for "living" ring-opening polymerization of lactide was demonstrated. Mild and highly selective polymerization conditions produced poly(lactides) with predictable molecular weights and extremely narrow polydispersities (ca. 1.1), characteristic of a living polymerization with a specific reaction site. New strategies for organocatalysis that enable the formation of highly enantioselective polylactide from racemic mixtures will be forthcoming.

Received: March 19, 2001 [Z16789]

[1] For example, a) G. W. Coates, R. M. Waymouth, *Science* **1995**, *267*, 217–219; b) H. Brintzinger, D. Fischer, R. Mülhaupt, B. Rieger, R. M. Waymouth, *Angew. Chem.* **1995**, *107*, 1255–1283; *Angew. Chem. Int. Ed. Engl.* **1995**, *34*, 1143–1170; erratum: H. Brintzinger, D. Fischer, R. Mülhaupt, B. Rieger, R. M. Waymouth, *Angew. Chem.* **1995**, *107*, 1652; *Angew. Chem. Int. Ed. Engl.* **1995**, *34*, 1368; c) B. Small, M. Brookhart, *Macromolecules* **1999**, *32*, 2120–2130.

[2] For example, a) R. R. Schrock, *Acc. Chem. Res.* **1990**, *23*, 158–165; b) R. H. Grubbs, *Pure Appl. Chem.* **1996**, *31*, 1829–1833; c) G. W. Coates, *Chem. Rev.* **2000**, *100*, 1223–1252.

[3] For example, a) T. M. Ovitt, G. W. Coates, *J. Am. Chem. Soc.* **1999**, *121*, 4072–4074; b) B. M. Chamberlain, Y. Sun, J. R. Hagadorn, E. W. Hemmesch, V. G. Young, Jr., M. Pink, M. A. Hillmyer, W. B. Tolman, *Macromolecules* **1999**, *32*, 2400–2402; c) M. Cheng, A. B. Attygalle, E. Lobkovsky, G. W. Coates, *J. Am. Chem. Soc.* **1999**, *121*, 11583–11585; d) M. H. Chisholm, N. Eilerts, J. Huffman, S. Iyre, M. Pacold, K. Phomphrai, *J. Am. Chem. Soc.* **2001**, published on the web.

[4] For example, a) A. Kowalski, A. Duda, S. Penczek, *Macromolecules* **2000**, *33*, 7359–7370; b) P. Dubois, C. Jacobs, R. Jerome, P. Tessie, *Macromolecules* **1991**, *24*, 2266–2270; c) H. R. Kricheldorf, S. Lee, S. Bush, *Macromolecules* **1996**, *29*, 1375–1381; d) W. M. Stevels, P. Dijkstra, J. Feijen, *Trends Polym. Sci.* **1997**, *5*, 300–305; e) B. O'Keef, S. Monnier, M. A. Hillmyer, W. B. Tolman, *J. Am. Chem. Soc.* **2001**, *123*, 339–340.

[5] For example, A. Dove, V. C. Gibson, E. L. Marshall, A. J. P. White, D. Williams, *Chem. Commun.* **2001**, 283–284.

[6] For example, a) A. Kumar, R. A. Gross, *J. Am. Chem. Soc.* **2000**, *122*, 11767–11770; b) A. Kumar, R. A. Gross, *Biomacromolecules* **2000**, *1*, 133–138; c) S. Kobayashi, H. Uyama, S. Namekawa, H. Hayakawa, *Macromolecules* **1998**, *31*, 5655–5659.

[7] For example, a) K. A. Ahrendt, C. J. Borths, D. W. C. MacMillan, *J. Am. Chem. Soc.* **2000**, *122*, 4243–4244; b) W. S. Jen, J. J. M. Wiener, D. W. C. MacMillan, *J. Am. Chem. Soc.* **2000**, *122*, 9874–9875; c) V. M. Dong, D. W. C. MacMillan, *J. Am. Chem. Soc.* **2001**, *123*, 2448–2449; d) G. C. Fu, *Acc. Chem. Res.* **2000**, *33*, 412–420; e) S. Arai, S. Bellemin-Laponnaz, G. C. Fu, *Angew. Chem.* **2001**, *113*, 240; *Angew. Chem. Int. Ed.* **2001**, *40*, 234; f) B. Tao, M. C. Lo, G. C. Fu, *J. Am. Chem. Soc.* **2001**, *123*, 353–354. See also the recent Highlight article: H. Gröger, J. Wilken, *Angew. Chem.* **2001**, *113*, 545–548; *Angew. Chem. Int. Ed.* **2001**, *40*, 529–532.

[8] For example, a) G. Höfle, W. Steglich, H. Vorbrüggen, *Angew. Chem.* **1978**, *90*, 602–615; *Angew. Chem. Int. Ed. Engl.* **1978**, *17*, 569–583; b) N. Spassky, M. Wisniewski, C. Pluta, A. LeBorgne, *Macromol. Chem. Phys.* **1996**, *197*, 2627–2637.

[9] D. F. Taber, J. Amedio, Y. K. Patel, *J. Org. Chem.* **1985**, *50*, 3618–3619; b) D. F. Taber, B. Deker, M. D. Gaul, *J. Am. Chem. Soc.* **1987**, *109*, 7488–7494.

[10] a) J. C. Gelbert, T. A. Kelley, *J. Org. Chem.* **1988**, *53*, 449–450; b) J. Christoffers, N. Onal, *Eur. J. Org. Chem.* **2000**, *8*, 1633–1635.

[11] F. M. Menger, D. J. McCann, *J. Org. Chem.* **1985**, *50*, 3928–3930.

[12] a) S. J. Taylor, J. P. Morken, *Science* **1998**, *280*, 267; b) D.-W. Su, Y.-C. Wang, T.-H. Yan, *Tetrahedron Lett.* **1999**, *40*, 4197–4198; c) Y. Basel, A. Hassner, *J. Org. Chem.* **2000**, *65*, 6368–6380; d) C. P. Decicco, R. N. Buckle, *J. Org. Chem.* **1992**, *57*, 1005–1008; e) J. S. Witzeman, W. D. Nottingham, *J. Org. Chem.* **1991**, *56*, 1713–1718; f) S. Hatakeyama, K. Satoh, K. Sakurai, S. Takano, *Tetrahedron Lett.* **1987**, 2713–2716.

[13] a) Y. Kishimoto, P. Eckerie, T. Miyatake, M. Kainosho, A. Ono, T. Ikariya, R. Noyori, *J. Am. Chem. Soc.* **1999**, *121*, 12035–12044; b) K. B. Wagener, J. Linert, J. E. O'Gara, *Pure Appl. Chem.* **1994**, *31*, 775–782.

[14] Initial screening of different organic catalysts, solvents, and a variety of polymerization conditions was performed on a Quest 210 reactor (Argonaut Technologies). This robotic reactor allowed up to 20 polymerizations to be performed in parallel under the appropriate environment. Polymers with targeted DPs of 30 were prepared and assayed by size-exclusion chromatography (SEC) and ^{1}H NMR spectroscopy to optimize the polydispersity and the molecular weight control. For a general discription of ROP in Quest, see *Argonaut Application Note* **33**.

[15] General procedure for D,L-lactide polymerization: A round-bottom flask equipped with a stirbar and sealed with a septum was flame-dried under vacuum and purged with nitrogen. The D,L-lactide (1.0 g, 6.94 mmol) and DMAP (0.56 g, 0.46 mmol, for DP = 30) was added in a glove box. Dichloromethane (≈5 mL) and ethanol (14 μL, 0.23 mmol) were added, and the flask was heated to 35 °C. The polymer was isolated in cold methanol and dried to a constant weight, 100% yield. ^{1}H NMR ([D$_6$]acetone): δ = 1.46–1.56 (d, 3H, CH$_3$), 5.05–5.25 (q, H, CH); ^{13}C NMR ([D$_6$]acetone): δ = 17.0 (CH$_3$), 69.8 (CH), 169.8 (CO).

[16] M. Möller, R. Kånge, J. L. Hedrick, *J. Polym. Sci. Part A* **2000**, *28*, 2067–2073.

[17] Poly(D,L-lactide) (0.5 g) with a molecular weight of about 11000 was dissolved in CH_2Cl_2 (5 mL) together with a poly(D,L-lactide) with a molecular weight of about 4000. DMAP (0.056 g, 0.46 mmol) was heated at 35 °C for 24 h; the reaction was followed by GPC.

[18] Catalyzed with DMAP: ^{1}H NMR ([D$_6$]acetone): δ = 1.46–1.56 (d, 3H, CH$_3$), 5.05–5.25 (q, H, CH); ^{13}C-NMR: δ = 17.0 (CH$_3$), 69.8 (CH), 169.8 (CO). Catalyzed with Sn(OTf)$_2$: ^{1}H NMR ([D$_6$]acetone): δ = 1.46–1.56 (d, 3H, CH$_3$), 5.05–5.25 (q, H, CH); ^{13}C NMR ([D$_6$]acetone): δ = 17.0 (CH$_3$), 69.8 (CH), 169.8 (CO).

[19] In a glove box, D,L-lactide (1.0 g, 6.94 mmol) and DMAP (1 equiv based on D,L-lactide, 0.848 g, 6.94 mmol) was added to a round-bottom flask. An excess of benzyl alcohol (10 equiv based on D,L-lactide (7.18 mL, 0.069 mmol) was charged together with CH_2Cl_2, and the reaction flask was slowly heated to 35 °C (5 h). The product was isolated by flash chromatography (CH_2Cl_2/ethyl acetate 90/10). ^{1}H NMR ([D$_6$]acetone): δ = 1.34 (d, 3H, CH$_3$), 2.05 (s, H, OH), 4.30 (q, H, CH), 5.16 (s, 2H, CH$_2$), 7.40–7.30 (m, 5H, C$_6$H$_5$); ^{13}C NMR ([D$_6$]acetone): δ = 175.4, 137.3, 129.3, 128.9, 128.8, 67.6, 66.8, 20.8.

ANGEWANDTE CHEMIE
INTERNATIONAL EDITION
A Journal of the Gesellschaft Deutscher Chemiker
2001
40/15
Pages 2725–2934

COVER PICTURE

The cover picture shows in the background the whole cell of a methanotrophic bacterium on which are superimposed components of methane monooxygenase (the structure of the hydroxylase component (top), one of the two four-helix bundles that house the catalytic diiron centers (left)) and a schematic diagram of the catalytic cycle by which the enzyme converts dioxygen and methane into methanol and water. More about this unusual enzyme system is reported by Lippard et al. on p. 2782 ff.

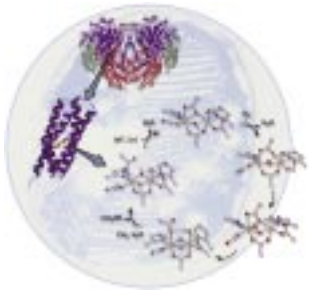

REVIEWS

Contents

Theoretical considerations and chemical reasoning lead us to claim that Ag–F bonding in Ag^{III} and Ag^{II} fluorides is substantially covalent, and in this way will resemble Cu–O bonding in Cu^{II} and Cu^{III} oxides. The prospect is that if appropriately modified, such high oxidation-state silver fluorides (for example, $CsAgF_3$ (shown here), made by Hoppe and co-workers) might be superconducting.

Angew. Chem. **2001**, *113*, 2816–2859

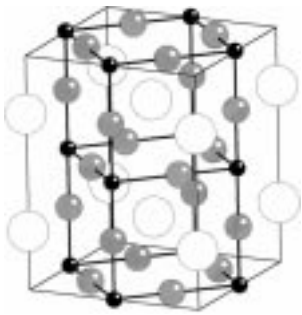

Keywords: conducting materials · electronic structure · fluorides · silver · superconductors

  1433-7851/01/4015-2727 $ 17.50+.50/0

HIGHLIGHTS

VIPs

The following communications are "Very Important Papers" in the opinion of two referees. They will be published shortly. Short summaries of these articles can be found on the *Angewandte Chemie* homepage at the address http://www.angewandte.com

  1433-7851/01/4015-2728 $ 17.50+.50/0

COMMUNICATIONS

  1433-7851/01/4015-2729 $ 17.50+.50/0

  1433-7851/01/4015-2730 $ 17.50+.50/0

  1433-7851/01/4015-2731 $ 17.50+.50/0

  1433-7851/01/4015-2732 $ 17.50+.50/0

  1433-7851/01/4015-2734 $ 17.50+.50/0

  1433-7851/01/4015-2735 $ 17.50+.50/0

  1433-7851/01/4015-2736 $ 17.50+.50/0

Supporting information on the WWW (see article for access details).

* Author to whom correspondence should be addressed

BOOKS

  1433-7851/01/4015-2737 $ 17.50+.50/0

WEB SITES

SERVICE

Issue 14, 2001 was published online on July 10, 2001.

Don't forget all the Tables of Contents from 1995 onwards may be still found on the WWW under: http://www.angewandte.com

  1433-7851/01/4015-2738 $ 17.50+.50/0

	1	2		3	4	5	6	7	8	9	10	11	12	13	14	15	16	17	18
1	1 H																		2 He
2	3 Li	4 Be												5 B	6 C	7 N	8 O	9 F	10 Ne
3	11 Na	12 Mg												13 Al	14 Si	15 P	16 S	17 Cl	18 Ar
4	19 K	20 Ca		21 Sc	22 Ti	23 V	24 Cr	25 Mn	26 Fe	27 Co	28 Ni	29 Cu	30 Zn	31 Ga	32 Ge	33 As	34 Se	35 Br	36 Kr
5	37 Rb	38 Sr		39 Y	40 Zr	41 Nb	42 Mo	43 Tc	44 Ru	45 Rh	46 Pd	47 Ag	48 Cd	49 In	50 Sn	51 Sb	52 Te	53 I	54 Xe
6	55 Cs	56 Ba	*	71 Lu	72 Hf	73 Ta	74 W	75 Re	76 Os	77 Ir	78 Pt	79 Au	80 Hg	81 Tl	82 Pb	83 Bi	84 Po	85 At	86 Rn
7	87 Fr	88 Ra	**	103 Lr	104 Rf	105 Db	106 Sg	107 Bh	108 Hs	109 Mt	110 Uun	111 Uuu	112 Uub	113 Uut	114 Uuq	115 Uup	116 Uuh	117 Uus	118 Uuo

*	57 La	58 Ce	59 Pr	60 Nd	61 Pm	62 Sm	63 Eu	64 Gd	65 Tb	66 Dy	67 Ho	68 Er	69 Tm	70 Yb	
**	89 Ac	90 Th	91 Pa	92 U	93 Np	94 Pu	95 Am	96 Cm	97 Bk	98 Cf	99 Es	100 Fm	101 Md	102 No	

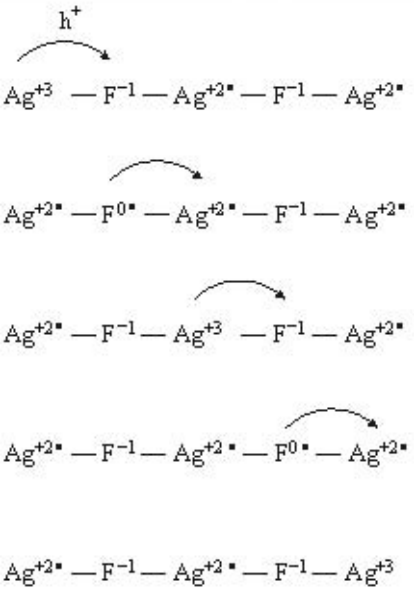

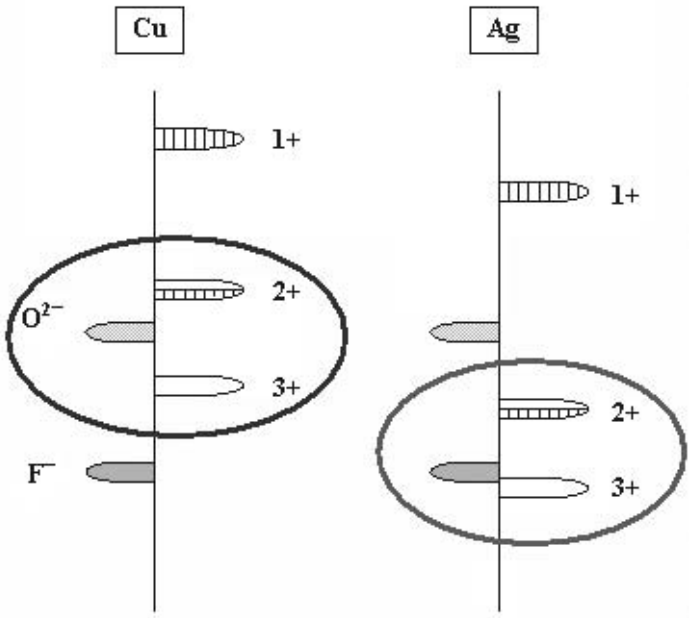

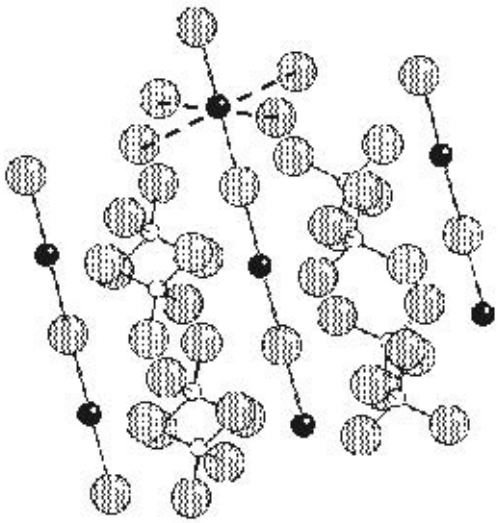

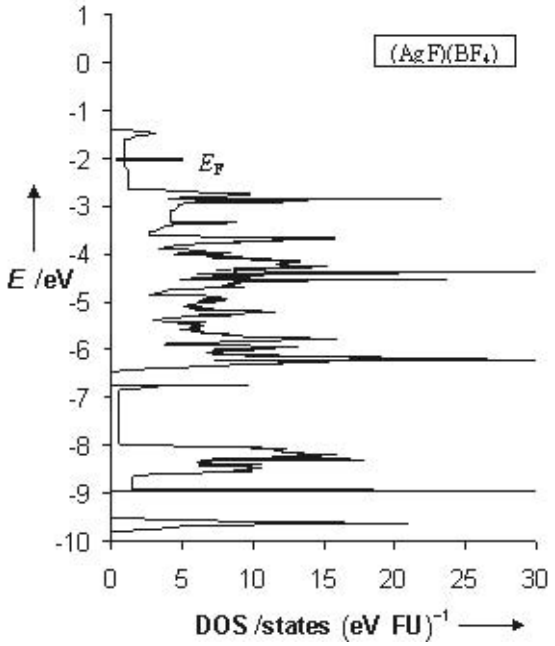

Real and Hypothetical Intermediate-Valence Ag^{II}/Ag^{III} and Ag^{II}/Ag^{I} Fluoride Systems as Potential Superconductors

Wojciech Grochala and Roald Hoffmann*

Dedicated to Professor Neil Bartlett,
with our deep admiration for his chemistry—he made molecules which were unimaginable

With the aim of gauging their potential as conducting or superconducting materials, we examine the crystal structures and magnetic properties of the roughly one hundred binary, ternary, and quaternary Ag^{II} and Ag^{III} fluorides in the solid state reported up to date. The Ag^{II} cation appears in these species usually in a distorted octahedral environment, either in an $[AgF]^+$ infinite chain or as $[AgF_2]$ sheets. Sometimes one finds discrete square-planar $[AgF_4]^{2-}$ ions. The Ag^{III} cation occurs usually in the form of isolated square-planar $[AgF_4]^-$ ions. Systems containing $Ag^{III}(d^8)$ centers are typically diamagnetic. On the other hand, the rich spectrum of $Ag^{II}(d^9)$ environments in binary and ternary fluorides leads to most diverse magnetic properties, ranging from paramagnetism, through temperature-independent paramagnetism (characteristic for half-filled band and metallic behavior) and antiferromagnetism, to weak ferromagnetism. Ag^{II} and Ag^{III} have the same d-electron count as $Cu^{II}(d^9)$ and $Cu^{III}(d^8)$, respectively. F^- and O^{2-} ions are isoelectronic, closed-shell (s^2p^6) species; both are weak-field ligands. Led by these similarities, and by some experimental evidence, we examine analogies between the superconducting cuprates ($Cu^{II}/Cu^{III}-O^{2-}$ and $Cu^{II}/Cu^{I}-O^{2-}$ systems) and the formally mixed-valence $Ag^{II}/Ag^{III}-F^-$ and $Ag^{II}/Ag^{I}-F^-$ phases. For this purpose we perform electronic-structure computations for a number of structurally characterized binary and ternary Ag^{I}, Ag^{II}, and Ag^{III} fluorides and compare the results with similar calculations for oxocuprate superconductors. Electronic levels in the vicinity of the Fermi level (x^2-y^2 or z^2) have usually strongly mixed Ag(d)/F(p) character and are Ag–F antibonding, thus providing the potential of efficient vibronic coupling (typical for d^9 systems with substantially covalent bonds). According to our computations this is the result not only of a coincidence in orbital energies; surprisingly the Ag–F bonding is substantially covalent in Ag^{II} and Ag^{III} fluorides. The electron density of state at the Fermi level (DOS_F) for silver fluoride materials and frequencies of the metal–ligand stretching modes have values close to those for copper oxides. The above features suggest that properly hole- or electron-doped Ag^{II} fluorides might be good BCS-type superconductors. We analyze a comproportionation/disproportionation equilibrium in the hole-doped Ag^{II} fluorides, and the possible appearance of holes in the F(p) band. It seems that there is a chance of generating an $Ag^{III}-F^-/Ag^{II}-F^0$ "ionic/covalent" curve crossing in the hole-doped $Ag^{II}-F^-$ fluorides, significantly increasing vibronic coupling.

Keywords: conducting materials · electronic structure · fluorides · silver · superconductors

1. Introduction

This paper builds to a claim and a prospect. Both are based on theoretical considerations and chemical reasoning. The claim is that the Ag–F bonding in Ag^{III} and (to lesser extent) Ag^{II} fluorides is substantially covalent. The prospect is that such high oxidation-state silver fluorides might be superconducting, if modified in certain ways. But before we get to the evidence and argument, some beautiful synthetic and structural work on the known binary and ternary Ag^{II} and Ag^{III} fluorides has to be reviewed.[1]

About a hundred binary, ternary, and quaternary silver fluorides are known, among them six binary species: Ag_2F, AgF, AgF_2, Ag_2F_5, Ag_3F_8, and AgF_3. The reasons for interest in silver fluorides in various oxidation states vary. For Ag_2F (silver subfluoride) its metallic conductivity[2, 3] and super-

[*] Prof. Dr. R. Hoffmann, Dr. W. Grochala
Department of Chemistry and Chemical Biology
and Cornell Center for Materials Research
Cornell University, Ithaca NY, 18453-1301 (USA)
Fax: (+1) 607-255-5707
E-mail: rh34@cornell.edu

  1433-7851/01/4015-2743 $ 17.50+.50/0

conductivity[4] have been the focus, while AgF has been studied in context of Ag^+ ion diffusion,[5] phase transitions under elevated pressure,[6–10] and with relevance to photographic development.[11] On the other hand, Ag^{II} compounds are of interest because of the enormous oxidizing properties of Ag^{II} centers,[12, 13] as well for the disproportionation of Ag^{II} to Ag^{I} and Ag^{III}. For example, AgF_2 is known in both the disproportionated (high-temperature) $Ag^{I}[Ag^{III}F_4]$[14] and nondisproportionated (low-temperature) $Ag^{II}F_2$ form.[15] The higher silver fluorides (Ag_2F_5, Ag_3F_8, and AgF_3) were first prepared in 1991;[16] all of them have been structurally characterized.[17–19]

Ag^{II} is a unique species. It is peculiar to fluorine systems,[20] and disproportionates to Ag^{I} and Ag^{III} in oxides.[21–23] The Ag^{II} ion is also an extremely strong oxidizing agent, one of the most powerful known. For example, cationic Ag^{II} in anhydrous HF solutions oxidizes Xe^0 to Xe^{II}.[24, 25] The Ag^{III} ion is common to fluoride systems, as well, in agreement with the rule that fluorine stabilizes high oxidation states of most elements. Cationic Ag^{III} in anhydrous HF solutions is an even stronger oxidizing agent than Ag^{II}; it oxidizes $[MF_6]^-$ (M = Pt, Ru) to MF_6.[26] Solvated Ag^{III} is an oxidizer of unsurpassed power, better than Kr^{II},[27] and (together with solvated Ni^{IV}) probably the best oxidizing agent available in inorganic chemistry.

In the last two decades, the chemistry of Ag^{II} and Ag^{III} fluoride systems has developed significantly. New, previously unknown systems such as $Ag^{I}[Ag^{III}F_4]$,[14] $[Ag^{II}F]^+[SbF_6]^-$,[28] and $[Ag^{II}F]^+[BF_4]^-$[29] (the latter is probably metallic) have been synthesized. The chemistry of Ag^{II} and Ag^{III} has recently inspired the first successful efforts to stabilize the rare Au^{II} center in fluoride complexes.[30] The chemistry of another powerful oxidizer, Ni^{IV}, has also developed.[31]

Ag^{II} is isoelectronic with Cu^{II} (d^9 configuration). F^- and O^{2-} are isoelectronic ions, closed-shell species; both F^- and O^{2-} are weak-field ligands. These similarities inspired our theoretical investigations. Given the existence of the superconducting cuprates ($Cu^{II}/Cu^{III}-O^{2-}$ systems), one might be naturally interested in the analogous $Ag^{II}/Ag^{III}-F^-$ solids. As we will show, Ag^{II}–F^- bonds are substantially covalent (similar to Cu^{II}–O^{2-} bonds), thus providing potentially large values of a vibronic coupling constant in a crystal.[32]

To investigate theoretically the possible occurrence of superconductivity in one-dimensional (1D) and two-dimensional (2D) Ag–F nets, we compute density of states (DOS) and the composition of states near the Fermi level for some selected Ag–F systems and compare these with corresponding calculations for the cuprate superconductors. Subsequently we look at Ag^{I}, Ag^{II}, and Ag^{III} fluoride systems analogous to the isoelectronic fluorides, chlorides, and oxides of Cu and Au. We also consider hypothetical intermediate-valence (comproportionated) Ag^{II}/Ag^{I} or Ag^{II}/Ag^{III} systems and the mixed-valence (disproportionated, Peierls-distorted) ones. The design of class III[33] or class II[33] Ag^{II}/Ag^{I} or Ag^{II}/Ag^{III} fluoride systems might eventually provide us with an understanding of the conditions for strong dynamic band-gap opening at the Fermi level, possibly leading to superconductivity. We show, however, that such intermediate-valence Ag^{II}/Ag^{I} and Ag^{II}/Ag^{III} systems will not be easy to reach in practice. In a separate contribution we will propose a number of so-far unknown quaternary, possibly intermediate-valence Ag^{II}/Ag^{III} and Ag^{II}/Ag^{I} fluorides.

2. Contents

The Review is organized as follows: in Sections 3.1 and 3.2 we review the experimental data on the known binary and ternary Ag^{II} and Ag^{III} fluorides. In Section 3.3 we present

Roald Hoffmann was born in 1937 in Złoczów, Poland. He came to the USA in 1949 and studied chemistry at Columbia University and Harvard University (Ph.D. 1962). Since 1965 he has been at Cornell University, now as the Frank H. T. Rhodes Professor of Humane Letters. He has received many of the honors of his profession, including the 1981 Nobel Prize in Chemistry (shared with Kenichi Fukui). He also has a career as a writer, that profession sometimes overlapping his chemistry, sometimes not. He writes poems, essays, nonfiction, and plays. His interest in chemistry was stimulated by the life of Maria Skłodowska Curie, and he has learned nearly all he knows about silver fluorides from another Pole, his coauthor.


R. Hoffmann


W. Grochala

Wojciech Grochala was born in Warsaw (Poland), in 1972. He received his Ph.D. degree from the University of Warsaw in 1998, and came to Cornell University (US) as a postdoctoral fellow in 1999. His studies on resonance Raman spectroscopy with Prof. Jolanta Bukowska initiated his interest in vibronic coupling. He studied chemical aspects of this phenomenon with Prof. Roald Hoffmann, with support from The Kosciuszko Foundation. His research then focused on prediction of new superconducting materials in the solid state. He is currently working with Prof. Peter P. Edwards as a Royal Society Fellow at the University of Birmingham (UK), searching for experimental evidence of superconductivity in doped Ag^{II} fluorides.

results of density functional theory (DFT) band-structure calculations for a selection of the experimental structures. In Section 3.4 we examine analogies and differences in geometric and electronic structure between well-known superconducting oxocuprates and Ag–F systems. We also look here at Ag^{I}, Ag^{II}, and Ag^{III} fluorides from the perspective of analogous fluorides, chlorides, and oxides of Cu and Au. In Section 3.5 we analyze our DFT electronic-structure calculations for several structurally characterized binary and ternary Ag^{II} and Ag^{III} fluorides in the context of potential superconductivity in these systems. We also discuss the comproportionation–disproportionation equilibrium in the hole- and electron-doped Ag^{II} fluorides. Finally, in Section 3.6 we briefly discuss a general "chemical" strategy to obtain intermediate-valence Ag^{II}/Ag^{III} and Ag^{II}/Ag^{I} silver fluoride compounds.

3. Results and Analysis

3.1. Review of Structural Data for Binary and Ternary Ag^{II} and Ag^{III} Fluorides

We begin by looking at the structure and magnetic properties of all experimentally known binary and ternary Ag^{II} and Ag^{III} fluorides. This is not just a review, but a reasoned preparation for an exploration of the suitability of Ag–F chemistry for expanding the known repertoire of inorganic superconductors.

3.1.1. Structures Containing Magnetically Isolated Ag^{II} Centers

There are known over twenty ternary and quaternary fluorides containing magnetically isolated Ag^{II} centers.[34] They belong to five principal types:

a) $Ag^{II}[MF_4^-]_2$, M = Ag,[16] Au;[19, 35]
b) $Ag^{II}[MF_6^-]_2$, M = Bi,[28] Sb,[36, 37] Ru/Bi,[28] Nb,[38] Ta;[38]
c) $Ag^{II}[MF_6^{2-}]$, M = Ge,[39] Sn,[18, 39, 40] Pb,[39, 40] Ti,[18, 39] Zr,[39, 40] Hf,[39] Rh,[39] Pd,[18, 39, 41] Pt,[18, 39, 41] Mn[42] Cr[43]
d) $Ag_3M_2F_{14}$, M = Hf,[44] Zr[44]
e) $K_3Ag_2M_4F_{23}$, M = Hf,[45] Zr.[45]

In addition, isolated Ag^{II} centers occurs in $NaAgZr_2F_{11}$, the only known member of a $M^{I}Ag^{II}Zr_2F_{11}$ series.[46, 47] Properties and structural data for these solids are listed in Table 1.

Although $AgMF_6$, M = Zr, Hf, are claimed in refs. [39, 40], in fact they have not been synthesized so far. Prof. B. G. Müller writes about these compounds in a personal communication to us:

"Trying to synthesize $AgMF_6$ (M = Zr, Hf) similar to other compounds of the same formular type by reaction of a mixture of, for example, $Ag_2SO_4 + 2\,ZrOCl_2 \cdot 8\,H_2O + F_2/Ar$ at higher temperature one obtains deep blue–violet powder samples of $Ag_3Zr_2F_{14} + ZrF_4$ (*together* giving the analytical value of "$AgZrF_6$"). At that time all powder patterns were very complex, so it was not possible to identify for example ZrF_4 or other compounds. Later I found out by single-crystal structure determination that obviously $Ag_3Zr_2F_{14}$ was the only product." [*]

Those substances which contain nonmagnetic dopants (such as Ti^{4+} or Sb^{5+} ions) are typical dilute one-electron paramagnets (the Ag^{II} centers are magnetically isolated) and obey the Curie–Weiss law with $\mu_{eff} = 1.8–2.1\ \mu_B$. The largest deviation from Curie-law behavior is observed for $AgTiF_6$ (Curie constant $\Theta = -70$ K).[48] The magnetic behavior of compounds with magnetic dopants (such as Ru^{5+} or Mn^{4+} ions) is more complex. The Ag^{II} cation is found in these substances usually in the elongated octahedral (4+2) environment.[49, 50] A typical Ag^{II}–F^- bond length is 2.00–2.15 Å. Two additional, more weakly bound, fluoride anions typically coordinate the Ag^{II} centers at 2.35–2.44 Å. Such coordination of Ag^{II} most often results in a deep blue color of these compounds.

$AgSb_2F_{12}$ is a very interesting substance. It occurs in both paramagnetic α-$AgSb_2F_{12}$[36] and diamagnetic β-$AgSb_2F_{12}$ form.[37, 51] The structure of the α form is shown in Figure 1. The formula $Ag^{I}Ag^{III}[SbF_6^-]_2$ has been suggested[37] for the β form. Mixed-valence (and not intermediate-valence) character of the β form might be confirmed, for example, by the (2+4) and (4+2) local environments for the Ag^{I} and Ag^{III} centers, respectively.[52] Unfortunately, there is still no structural data for the β-$AgSb_2F_{12}$ form. Valence isomerism in $AgSb_2F_{12}$ is not improbable. A similar phenomenon has been observed for AgF_2 (see Sections 3.1.4 and 3.6.1)[15, 16] and for $Ag[Ag(CF_3)_4]$.[53] Existence of a mixed-valence $AgSb_2F_{12}$ form then would be the third interesting example of this subtle redox equilibrium in Ag^{II}–F^- systems.

Compounds in the $Ag_3M^{IV}_2F_{14}$ family (M = Zr, Hf) contain two types of nonequivalent Ag atoms (Figure 2). The isolated Ag(1) atom has a typical elongated octahedral coordination. The Ag(2) atom occurs in distorted tetragonal (1+1+2) coordination, with two shorter (1.997–2.092 Å) and two longer (2.147 Å) Ag–F bonds (we neglect here four very long distances of 2.6–2.8 Å; their inclusion leads to an unusual hexagonal bipyramidal coordination of the Ag center by F atoms). Two Ag(2) atoms are linked together in a linear $[Ag_2F_3]^+$ ion (we neglect here all the Ag–F contacts of 2.147 Å). The formula of this compound might be tentatively written as $[Ag_2F_3]^+Ag^{II}[Hf_2F_{11}]^{3-}$. The presence of the $[Ag_2F_3]^+$ unit links the $Ag_3M^{IV}_2F_{14}$ family of compounds to those containing $[Ag^{II}–F^-]$ infinite chains (see next Section).[54]

Quaternary compounds $K_3Ag_2M_4F_{23}$, M = Zr, Hf (Figure 3) provide still another example of an "unusual" coordination at Ag^{II} centers: a pentagonal bipyramid. Isolated bipyramids are strongly distorted, with equatorial distances of 2×2.04 Å, 2.29 Å, and 2×2.64–2.67 Å, and axial ones of 2.20–2.25 Å. Neglecting two very long contacts of 2.64–2.67 Å gives us an

[*] Here, and elsewhere in the paper, we show in boxes the comments of Neil Bartlett and Berndt G. Müller (private communication, August–September 2000) on the material presented. We feel that these remarks are extremely valuable, not just as historical commentary, but also in revealing much interesting and unpublished chemistry.

Table 1. Comparison of structural information and properties for solids which contain magnetically isolated Ag^{2+} ions in an elongated octahedral environment.

Compound	Crystal data[a]	$R(Ag^{II}–F^-)$ [Å]	$R(Ag^{II}\cdots F^-)$ [Å]	Color	Magnetic behavior (temperature range [K])	μ_{eff} [μ_B]	Θ[b] [K]
$Ag^{II}[AuF_4]_2$	monoclinic $P2_1/n$, $a=5.229$, $b=11.066$, $c=5.516$, $\beta=94.6$, $Z=2$	2.072 – 2.162	2.484 – 3.028	light green	Curie-Weiss (6 – 280)	1.82	− 2
$Ag^{II}[AgF_4]_2$	monoclinic $P2_1/n$, $a=5.047$, $b=11.054$, $c=5.449$, $\beta=97.2$, $Z=2$	2.056 – 2.200	2.558 – 2.900	red-brown	Curie-Weiss (4 – 280)	1.92	− 4
$Ag^{II}[BiF_6]_2$	triclinic $P\bar{1}$, $a=5.218$ $b=5.579$ $c=8.934$, $\alpha=76.1$, $\beta=88.9$, $\gamma=65.1$	2.096, 2.122	2.440	turquoise	Curie-Weiss (35 – 280)	2.1	–
$Ag^{II}[BiF_6][RuF_6]$	isostructural with $Ag^{II}[BiF_6]_2$	–	–	olive green	Curie-Weiss (13 – 251), $T_C=37$ K	–	–
$Ag^{II}[SbF_6]_2$	triclinic $P\bar{1}$, $a=5.224$ $b=5.467$ $c=8.779$, $\alpha=75.8$, $\beta=89.0$, $\gamma=65.3$	2.095, 2.132	2.431	blue	param.	1.95	+ 3
$Ag^{II}[NbF_6]_2$	triclinic $P\bar{1}$, $a=9.061$, $b=5.670$, $c=5.207$, $\alpha=118.7$, $\beta=91.6$, $\gamma=102.3$	–	–	blue	–	–	–
$Ag^{II}[TaF_6]_2$	triclinic $P\bar{1}$, $a=9.044$, $b=5.596$, $c=5.198$, $\alpha=118.8$, $\beta=91.5$, $\gamma=102.4$	2.030, 2.067	2.367	blue	param.	1.95	–
$Ag_3Hf_2F_{14}$	monoclinic $C2/m$, $a=9.249$, $b=6.686$, $c=9.073$, $\beta=90.30$	1) 2.066, 2) 1.997 – 2.147	1) 2.354, 2) 2.608 – 2.788	blue violet	antiferrom.	1.1	–
$Ag_3Zr_2F_{14}$	monoclinic $C2/m$, $a=9.225$, $b=6.676$, $c=9.063$, $\beta=91.30$	–	–	blue violet	antiferrom.	1.1	–
$M^{II}Ag_2Zr_2F_{14}$, $M^{II}Ag_2Hf_2F_{14}$ (M = Mg, Ni, Zn, Cu)	M = Cu: monoclinic $C2/m$, $a=9.123$, $b=6.612$, $c=8.994$, $\beta=90.7$			blue or red violet			
$AgM^{II}_2Zr_2F_{14}$, $AgM^{II}_2Hf_2F_{14}$ (M = Ca, Cd, Hg)	–			emerald or bright green			
$K_3Ag_2Zr_4F_{23}$	monoclinic $P2_1/c$, $a=7.838$, $b=11.174$, $c=10.156$, $\beta=97.45$	2.041 – 2.042	2.197 – 2.294	blue	param.		
$K_3Ag_2Hf_4F_{23}$	monoclinic $P2_1/c$, $a=7.821$, $b=11.154$, $c=10.131$, $\beta=97.51$	–	–	blue	param.	1.99	+ 2.8
$NaAgZr_2F_{11}$	triclinic $P\bar{1}$, $a=7.809$, $b=5.700$, $c=5.832$ $\alpha=106.1$, $\beta=111.5$, $\gamma=96.6$	2.048	2.181 – 2.339	blue	param.	1.87	–
$Ag^{II}[GeF_6]$	–	–	–	light blue	param.	–	–
$Ag^{II}[SnF_6]$	triclinic $P\bar{1}$, $a=5.204$, $b=5.253$, $c=5.632$, $\alpha=115.7$, $\beta=89.3$, $\gamma=118.8$	2.100 – 2.102	2.411	light blue	param.	1.99	− 6
$Ag^{II}[PbF_6]$	–	–	–	light blue	param.	1.92	− 24
$Ag^{II}[TiF_6]$	triclinic $P\bar{1}$, $a=5.160$, $b=5.161$, $c=5.675$, $\alpha=117.0$, $\beta=91.3$, $\gamma=118.5$	2.124 – 2.174	2.326	light blue	param.	2.21	− 70
$Ag^{II}[MnF_6]$	–	–	–	black brown	param.	4.43	− 66
$Ag^{II}[CrF_6]$	–	–	–	brown	–	–	–
$Ag^{II}[RhF_6]$	–	–	–	black	param.	–	–
$Ag^{II}[PdF_6]$	triclinic $P\bar{1}$, $a=5.023$, $b=5.085$, $c=9.976$, $\alpha=89.6$, $\beta=103.1$, $\gamma=120.9$	1) 2.083 – 2.116, 2) 2.065 – 2.158	1) 2.421, 2) 2.404	deep brown or dark green	param.	1.97 or 1.80	4.4
$Ag^{II}[PtF_6]$	triclinic $a=5.04$, $b=5.10$, $c=10.04$, $\alpha=90.1$, $\beta=103.0$, $\gamma=120.5$	–	–	brown violet, brown or dark violet	param.	–	–

[a] Crystal symmetry, space group, cell dimensions [Å], angles [°], number of formula units per unit cell. [b] Θ is defined by equation: $\chi = C/(T-\Theta)$, where χ is magnetic susceptibility, C is Curie constant, T is temperature, and Θ a measure of deviation (positive or negative) from the Curie – Weiss law.

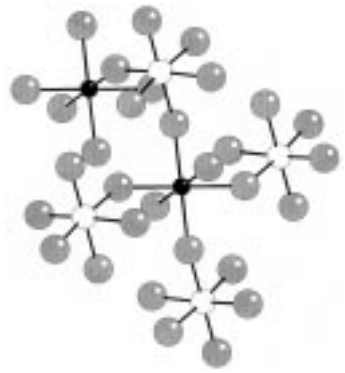

Figure 1. Crystal structure of $Ag^{II}[SbF_6]_2$; Ag: black spheres, Sb: white spheres, F: light gray spheres. The octahedral coordination of the Ag^{II} center is elongated.

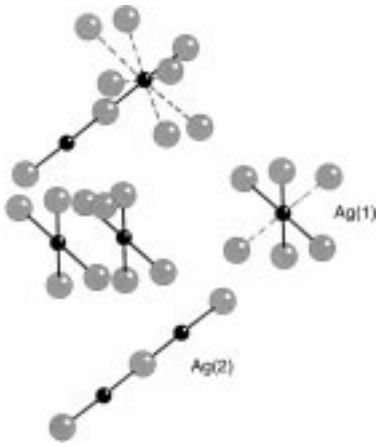

Figure 2. Crystal structure of $Ag_3Hf_2F_{14}$. Ag(1) in elongated octahedral coordination (longer axial bonds are indicated by broken lines) and Ag(2) with distorted hexagonal bipyramidal coordination (black spheres), F: light gray spheres, Hf atoms have been omitted. Notice the linear $[Ag(2)_2F_3]^+$ ions in the structure of this compound.

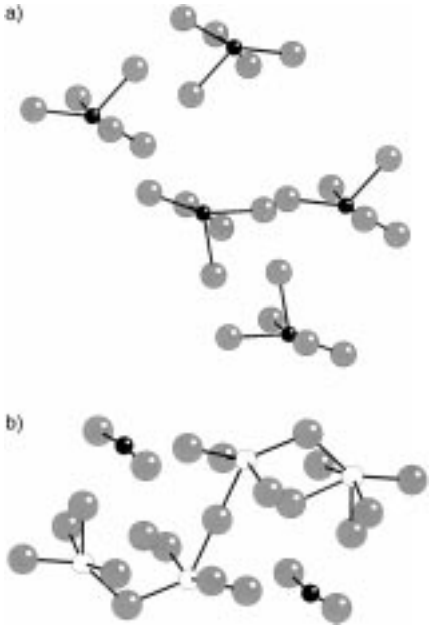

Figure 3. Two views of the crystal structure of $K_3Ag_2Zr_4F_{23}$; a) Zr and K atoms have been omitted. Note the pentagonal pyramid of F atoms around the Ag centers in this compound; Ag: black spheres, F: light gray spheres; b) K atoms have been omitted. Note the isolated $[AgF_2]^0$ units and the $[Zr_4F_{19}]^{3-}$ ions; Ag: black spheres, Zr: white spheres, F: light gray spheres.

alternative coordination of the Ag center: a distorted tetragonal pyramid (Figure 3a). Two very short Ag–F bonds of 2.04 Å (Ag–F(2) and Ag–F(6) in Müller's original notation) with an F-Ag-F angle of 173.9° point to the presence of isolated $[AgF_2^0]$ units in the structure (Figure 3b). The formula of this compound might be written as: $[K^+]_3[AgF_2]_2[Zr_4F_{19}]^{3-}$.

The Zr- and Hf-containing ternary and quaternary Ag^{II} fluorides which contain isolated $[AgF_2^0]$ and $[Ag_2F_3]^+$ units thus provide insight into the first stages of infinite $[Ag^{II}-F^-]_\infty$ chain formation, according to the process in Equation (1). A hypothetical $[Ag_3F_4]^{2+}$ ion and higher members of this homologous series have not yet been made.[55]

$$[AgF_2^0] \xrightarrow{+[AgF^+]} [Ag_2F_3]^+ \xrightarrow{+[AgF^+]} [Ag_3F_4]^{2+} \xrightarrow{+[AgF^+]} \cdots \xrightarrow{+[AgF^+]} \{[AgF]^+\}_\infty \quad (1)$$

The structure of $NaAgZr_2F_{11}$ contains isolated Ag^{II} centers with an interesting 2+2+2 distorted octahedral coordination (2×2.048 Å, 2×2.181 Å, 2×2.339 Å). A similar distortion of the octahedron is also found in $CsAgF_3$ (see Section 3.1.3) and in $[AgF]^+[RuF_6]^-$ (Section 3.1.2).

3.1.2. Structures Containing $[Ag^{II}-F^-]^+$ Infinite Chains

There are many ternary fluorides known containing infinite $[Ag^{II}-F^-]$ chains.[56, 57] They belong to three principal types:

a) $[AgF]^+[MF_4]^-$, M = Au,[29] B[29]

b) $[AgF]^+[MF_6]^-$, M = Bi,[28] Sb,[28] As,[29, 58, 59] Au,[29] Ir,[28] Ru[28]

c) $\{[AgF]^+\}_2[AgF_4]^-[MF_6]^-$, where M = Au,[14] Pt,[14] Ru,[14] As,[14] Sb.[14]

Infinite $[Ag^{II}-F^-]$ chains are also found in quaternary fluorides of the formula:

d) $[AgF]^+[M_3(M')_3^{IV}F_{19}]^-$, M = Cd, Ca, Hg; M′ = Zr, Hf[60]

e) $M^IAg^{II}(M')^{III}F_6$, M = Cs, Rb, K; M′ = Al, Ga, In, Tl, Sc, Fe, Co.[61, 62]

Properties and structural data for these solids are listed in Table 2. Most of these substances are temperature-independent paramagnets. This feature is anticipated for a partially filled band, obeying Fermi–Dirac statistics. Many of these compounds indeed exhibit high reflectance (bronze-luster), typical for metals. The magnetic interaction between paramagnetic Ag^{II} centers might formally lead to antiferromagnetic properties, as for the isostructural pseudo-1D $[CuF]^+[AuF_4]^-$ below 85 K. However, this is not the case for most Ag^{II} compounds. A Peierls distortion has been suggested for $[AgF]^+[AsF_6]^-$, $[AgF]^+[SbF_6]^-$, and $[AgF]^+[AuF_6]^-$.[63] Further investigations show, however, that a sudden drop in magnetic susceptibility (for all three of the above substances at 63 K) occurs on washing them with anhydrous HF and should be probably attributed to an impurity. Neil Bartlett writes:

"In our first paper on the AgF^+ salts [ref. [29] herein] we were not at the time aware that the "dips" in susceptibility that we were observing in the $[AgF]^+[MF_6]^-$ were a consequence of the washing of them with anhydrous HF. At the same time I was puzzled (and still am) by the absence of a Peierls distortion in the $[AgF][BF_4]$ structure—we even did that

Table 2. Comparison of structural information and properties for solids containing infinite $[Ag^{II}–F]^+$ chains.

Copmound	Crystal data[a]	$R(Ag^{II}–F^-)$ [Å]	$R(Ag^{II}\cdots F^-)$ [Å]	∢(F-Ag-F) [°]	∢(Ag-F-Ag) [°]	Magnetic behavior (temperature range [K])	Color
$[AgF][BF_4]$	tetragonal, $P4/n$, $a=6.700$, $b=4.011$	2.002 – 2.010	2.327 – 2.330	180.0	180.0	temp.-indep. param. (6 – 280)	violet or bronze
$[AgF][AuF_4]$	triclinic, $P\bar{1}$, $a=5.906$, $b=4.769$, $c=3.933$, $\alpha=107.0$, $\beta=99.5$, $\gamma=90.8$	2.072 – 2.162 or 1.967[b]	2.484	180.0[b]	180.0[b]		
$[AgF][AgF_4]$	triclinic, $P\bar{1}$, $a=5.00$, $b=11.09$, $c=7.36$, $\alpha=90.1$, $\beta=106.5$, $\gamma=90.2$	2.008 – 2.036	2.370 – 2.619				chestnut brown
$[AgF][BiF_6]$	–					temp.-indep. param. (50 – 280)	
$[AgF][SbF_6]$	–					temp.-indep. param. (63 – 280)	
$[AgF][AsF_6]$	orthorhombic, $Pnma$, $a=7.585$, $b=6.997$, $c=9.85$	1.995, 2.004	2.394 – 2.439	175.5	143.3	temp.-indep. param.[c] (63 – 280)	
$[AgF][AuF_6]$	orthorhombic, $Pnma$, $a=7.600$, $b=7.156$, $c=10.137$					temp.-indep. param.[c] (63 – 280)	
$[AgF][IrF_6]$	orthorhombic, $Pnma$, $a=7.628$, $b=7.067$, $c=10.253$	1.977, 2.014	2.311 – 2.467	176.1	146.0		
$[AgF][RuF_6]$	monoclinic, $P2_1/n$, $a=8.343$, $b=5.493$, $c=11.929$, $\beta=108.4$	2.007 – 2.018, 2.140 – 2.158[d]	2.548 – 2.659	155.9	176.2	temp.-indep. param. (40 – 280)	
$[AgF]_2[AsF_6][AgF_4]$	monoclinic, $P2/c$, $a=5.605$, $b=5.257$, $c=7.806$, $\beta=96.6$	2.003	2.32 – 2.34	180.0	153.9	temp.-indep. param. (50 – 280), Curie-like dependence below 50 K	black
$[AgF]_2[SbF_6][AgF_4]$	monoclinic, $P2/c$, $a=5.70$, $b=5.27$, $c=7.83$, $\beta=97.2$	–	–	–	–	–	–
$[AgF]_2[AuF_6][AgF_4]$	monoclinic, $P2/c$, $a=5.66$, $b=5.24$, $c=7.79$, $\beta=97.5$	–	–	–	–	–	–
$[AgF]_2[PtF_6][AgF_4]$	monoclinic, $P2/c$, $a=5.69$, $b=5.25$, $c=7.81$, $\beta=97.7$	–	–	–	–	–	–
$[AgF]_2[RuF_6][AgF_4]$	monoclinic, $P2/c$, $a=5.67$, $b=5.23$, $c=7.80$, $\beta=97.2$	–	–	–	–	–	–
$AgM'_3M_3F_{20}$ ($M'=$ Cd, Ca, Hg; M = Zr, Hf)	hexagonal, $P6_3/m$, $a=10.48–10.59$, $c=8.286–8.330$	2.072 – 2.103	2.28 – 2.31	180.0	180.0	param., $\Theta=0–20$ K, M = Zr: antiferrom., $T_N=3$ K	green
$CsAgAlF_6$	orthorhombic, $Pnma$, $a=7.38$, $b=7.24$, $c=10.35$	2.06 – 2.08	2.29	177.1	125.9	antiferrom., $\mu=1.30\,\mu_B$	ultramarine blue
$CsAgFeF_6$	orthorhombic, $Pnma$, $a=7.33$, $b=7.56$, $c=10.55$	2.047 – 2.054	2.27 – 2.30	175.5	126.9	–	dark green
$CsAgM'F_6$ ($M'=$ Sc, In, Tl)	cubic, $a=10.79–10.88$	$6\times 2.03–2.07$[e]	–			antiferrom., $\mu=1.16–1.30\,\mu_B$	green, gray green
$RbAg(Al,Fe)F_6$	orthorhombic, $Pnma$, $a=7.19$, $b=7.39$, $c=10.32$						dark green

[a] Crystal symmetry, space group, cell dimensions [Å], angles [°]. [b] Computed with the assumption that the compound has the $[CuF]^+[AuF_4]^-$ structure. [c] On possible Peierls distortion at 63 K, see text. [d] Complex structure; see text. [e] In this structure ("$RbNiCrF_6$"-type) the Ag^{II} and M^{III} (Sc, In, Tl) centers are statistically distributed on the same position, so it is not possible (by powder data) to locate the Ag^{II} center or describe its coordination (B. G. Müller).

structure twice (first on a blue crystal, second on a bronze one—the structures were the same). I conjectured (incorrectly) that the "dips" in susceptibility in the $[AgF]^+[MF_6]^-$ salts might be due to a Peierls distortion. They are a consequence of solvolysis of the $[AgF]^+[MF_6]^-$ salts by the anhydrous HF. X-ray powder patterns of the washed materials are indistinguishable from those of the salts, which do not show the "dips". Figure 6 of our later paper [ref. [28] herein] gives the susceptibility data for high purity $[AgF]^+[MF_6]^-$ (M = As, Bi) but the $[AgF][IrF_6]$ data, showing a "dip" near 63 K probably contains the mystery material. Incidentally, we made many attempts (but only at ~293 K) to detect metallic conductivity in $[AgF][BF_4]$ and the $[AgF]^+[MF_6]^-$ salts (even in single crystals) but without success."

The structure of $[AgF]^+[BF_4]^-$ is shown in Figure 4. Usually the Ag^{II} cation is found in these substances in a compressed octahedral (2+4) environment. A typical Ag^{II}–F^- bond length is 1.98 – 2.18 Å. Four additional more weakly bound fluoride anions coordinate the Ag^{II} center at 2.31 – 2.47 Å.[64] The $Ag^{II}–F^-$ units are joined into $\{[AgF]^+\}_\infty$ chains, presumably responsible for the temperature-independent paramagnetism

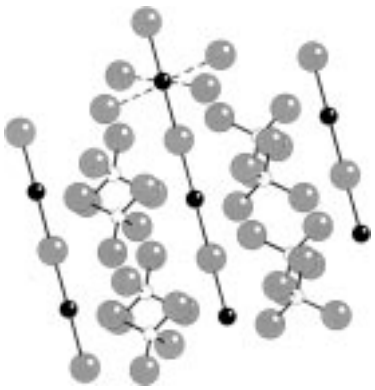

Figure 4. Crystal structure of $[AgF]^+[BF_4]^-$ showing the infinite linear $[AgF]^+$ chains. The octahedral coordination of the Ag^{II} center is compressed. Longer bonds are indicated by broken lines; Ag: black spheres, B: small white spheres, F: light gray spheres.

of these substances. The $\{[AgF]^+\}_\infty$ chain may be linear ($\sphericalangle$(Ag-F-Ag) = 180°, $\sphericalangle$(F-Ag-F) = 180°), as in $[AgF]^+[BF_4]^-$, bent only at the F atoms ($\sphericalangle$(Ag-F-Ag) = 154°, $\sphericalangle$(F-Ag-F) = 180°), as in $\{[AgF]^+\}_2[AsF_6]^-[AgF_4]^-$, or bent at the Ag atoms ($\sphericalangle$(Ag-F-Ag) = 176°, $\sphericalangle$(F-Ag-F) = 143°), as in $[AgF]^+[AsF_6]^-$. $\{[AgF]^+\}_\infty$ zigzag chains occur also in the quaternary $CsAgAlF_6$ (Figure 5). Kinked $\{[AgF]^+\}_\infty$ chains run at right angles to the $\{[AlF_5]^{2-}\}_\infty$ chains in this interesting compound.

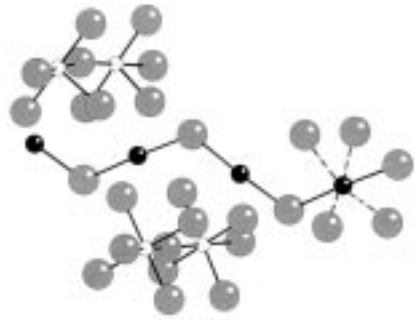

Figure 5. Crystal structure of $Cs^+[AgF]^+[AlF_5]^{2-}$ showing the infinite kinked $[AgF]^+$ chains. Note the Ag^{II} centers in a compressed octahedral coordination, longer bonds indicated by broken lines; Ag: black spheres, Al: white spheres, F: light gray spheres (Cs atoms have been omitted).

There are also kinked $\{[AgF]^+\}_\infty$ chains in Ag_2F_5 (= $[AgF]^+[AgF_4]^-$; structure illustrated in Figure 17 and described in Section 3.1.6); the local coordination of the Ag^{II} center is approximately of the 2+4 type. The structure of $[AgF]^+[AuF_4]^-$ is unknown. Most probably it has a structure similar to that of $[AgF]^+[AgF_4]^-$, with kinked $\{[AgF]^+\}_\infty$ chains. But if $[AgF]^+[AuF_4]^-$ is instead isostructural with $[CuF]^+[AuF_4]^-$, then it would have linear $\{[AgF]^+\}_\infty$ chains, and the Ag^{II}–F^- bond length would be unusually short, 1.967 Å.

Surprisingly the structure of $[AgF]^+[RuF_6]^-$ (shown in ref. 28[65]) differs from the structures of the other members of the $[AgF]^+[MF_6]^-$ series. $[AgF]^+[RuF_6]^-$ contains a ribbonlike structure, similar to the polymeric puckered sheets in the structure of AgF_2 (see Section 3.1.4). The local environment of the Ag^{II} center is of the (2+2+2) type, with two short Ag^{II}–F^- bonds of 2.007 – 2.018 Å, two longer bonds of 2.140 – 2.158 Å, and two very long separations of 2.548 – 2.659 Å. The structure of the $[AgF_2]_\infty$ ribbon in $[AgF]^+[RuF_6]^-$ may be considered intermediate between the $\{[AgF]^+\}_\infty$ chain and the $[AgF_2]_\infty$ puckered sheet.

The recently discovered $[AgF]^+[M'_3M_3F_{19}]^-$ family (where M′ = Cd, Ca, Hg; M = Zr, Hf) is an interesting exception.[60] These compounds crystallize in a hexagonal system and the local coordination of F atoms around the Ag centers is regular trigonal bipyramidal (Figure 6). Such coordination is not found in any other silver fluoride, except for the $K_3Ag_2M_4F_{23}$ (M = Zr, Hf) series. It is remarkable that in spite of the significant dilution of the Ag centers in this material, $[AgF]^+$ infinite chains are formed.

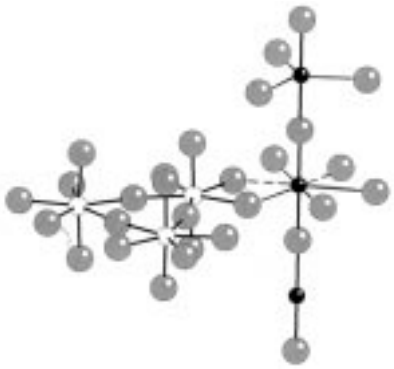

Figure 6. Crystal structure of $[AgF]^+[Cd^{2+}]_3[Zr_3F_{18}]^{6-}[F^-]$, showing the infinite linear $[AgF]^+$ chains and the isolated $[Zr_3F_{18}]^{6-}$ ions. Note the trigonal bipyramidal (or alternatively distorted hexagonal bipyramidal) coordination of the Ag^{II} centers; Ag: black spheres, Zr: white spheres, F: light gray spheres (Cd atoms are omitted).

3.1.3. Structures Containing Infinite $[Ag^{II}(F^-)_2]$ Planes or Isolated $[Ag^{II}(F^-)_4]^{2-}$ Squares

There are several ternary fluorides known containing infinite $[AgF_2]_\infty$ planes or isolated $[Ag^{II}(F^-)_4]^{2-}$ squares. They belong to four principal types:

a) $[MF][AgF_2]$, M = Cs,[66–68] Rb,[66, 68] K,[66–68] Na[68]
b) $[MF]_2[AgF_2]$, M = Cs,[69] Rb,[69] K,[66, 69] Na[68]
c) $M[AgF_4]$, M = Ba,[67, 70, 71] Sr,[67, 70, 71] Ca,[70, 71] Cd,[70, 71] Hg[70, 71]
d) $[MF_2]_2[AgF_2]$, M = Ba.[67]

In addition, a puckered $[AgF_2]_\infty$ sheet is found in AgF_2 (described in Section 3.1.4). Properties and structural data for ternary fluorides containing infinite $[AgF_2]_\infty$ planes or isolated $[Ag^{II}(F^-)_4]^{2-}$ squares are listed in Table 3.

Compounds in the $M[AgF_4]$ series are paramagnets and obey the Curie – Weiss law with $\mu_{eff} = 1.6 - 1.9\ \mu_B$. On the other hand, substances in the $[MF][AgF_2]$ and $[MF]_2[AgF_2]$ series exhibit strong collective magnetic behavior and metallic luster, as exemplified by the antiferromagnets $[RbF]_2[AgF_2]$, $[CsF]_2[AgF_2]$, and $[KF]_2[AgF_2]$.[72]

The structures of $[CsF][AgF_2]$ and $[CsF]_2[AgF_2]$ are shown in Figures 7 and 8, respectively. The Ag^{II} cation is found in

Table 3. Comparison of structural information and magnetic properties for solids containing an Ag^{2+} ion in square AgF_2 sheets and isolated $[AgF_4]^{2-}$ squares. Data for AgF_2 (puckered sheets) and AgF_3 (helical chains) are also included.

Compoud	Structure data[a]	$R(Ag^{II}–F^-)$ [Å]	$R(Ag^{II}\cdots F^-)$ [Å]	Magnetic behavior (temperature range [K])	μ_{eff} [μ_B]	Θ [K]	Notes
$[CsF][AgF_2]$	tetragonal, $a=6.48$, $c=8.52$	2.07, 2.13	2.51	$T_N=50$ K, above temp.indep. param.			forms dimorphs
$[RbF][AgF_2]$	tetragonal, $a=6.33$, $c=8.44$	2.06, 2.10	2.42	antiferrom., over T_N temp.indep. param.			T_N = ?
$[KF][AgF_2]$	orthorhombic, $a=6.18$, $b=6.27$, $c=8.30$	2.08	2.20	$T_N=80$ K, above temp.indep. param.			
$[CsF]_2[AgF_2]$	tetragonal, $a=4.58$, $c=14.19$	2.128	2.29	antiferrom., $T_N=20$ K		+45	metallic luster
$[RbF]_2[AgF_2]$	–			Curie-Weiss (60–300) antiferrom., $T_N=25$ K	1.6	+44	metallic luster
$[KF]_2[AgF_2]$	–			antiferrom., $T_N=60$ K	1.9, 1.6	+6	metallic luster
$[BaF_2][AgF_2]$	$a=6.03$, $c=11.46$	ca. 2.05		Curie-Weiss (6–280)	1.9	−4	$KBrF_4$-type
$[SrF_2][AgF_2]$	$a=5.73$, $c=11.12$	ca. 2.05		Curie-Weiss (6–280)	1.9	−6	$KBrF_4$-type
$[HgF_2][AgF_2]$	$a=5.52$, $c=10.92$	ca. 2.05		Curie-Weiss (6–280)	1.9	−6	$KBrF_4$-type
$[CaF_2][AgF_2]$	$a=5.49$, $c=10.86$	ca. 2.05		Curie-Weiss (6–280)	1.9		$KBrF_4$-type
$[CdF_2][AgF_2]$	$a=5.42$, $c=10.80$	ca. 2.05		Curie-Weiss (6–280)	1.9		$KBrF_4$-type
$[BaF_2]_2[AgF_2]$	$a=4.32$, $c=17.6$, $Z=2$			Curie-Weiss	1.8	+4	$[BaF_2]_2[CuF_2]$-Typ?
α-AgF_2	orthorhombic, *Pbca*, $a=5.073$, $b=5.529$, $c=5.813$	2.068–2.074	2.584	complex behavior (see text), $T_C=163$ K			cf. $T_C(CuF_2)=69$ K
AgF_3	hexagonal, $a=5.078$,$c=15.452$, $V_0=345.1$	1.863–1.990	2.540	diamagnetic			

[a] Crystal symmetry, space group, cell dimensions [Å], angles [°], number of formula units per unit cell.

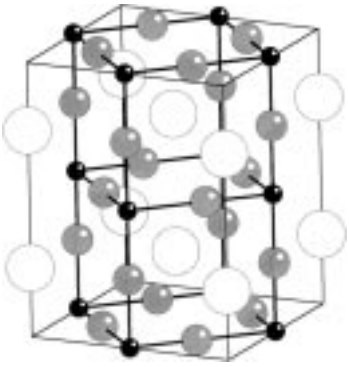

Figure 7. Unit cell of $[CsF][AgF_2]$. Note the elongated octahedral coordination of the Ag^{II} centers; Ag: black spheres, Cs: white spheres, F: gray spheres.

Figure 8. Unit cell of $[CsF]_2[AgF_2]$. Note the elongated octahedral coordination of the Ag^{II} centers; Ag: black spheres, Cs: white spheres, F: gray spheres.

these substances in an elongated (2+2+2; for $CsAgF_3$) or compressed (2+4; for Cs_2AgF_4) octahedral environment. In the first case, the Ag^{II}–F^- bond length is in the range 2.06–2.13 Å and two additional fluoride anions coordinate to the Ag^{II} center at 2.42–2.51 Å. In the latter case, a typical Ag^{II}–F^- bond length is 2.13 Å and four additional fluoride anions coordinate the Ag^{II} center at 2.29 Å. In both cases, $[AgF_2]_\infty$ planes are found.

The strongly elongated octahedral coordination of the Ag centers in Cs_2AgF_4 (and Rb_2AgF_4) deduced from ESR spectra[73] does not agree with structural data for Cs_2AgF_4.[69] Herein we have preferred the crystallographic structure of Cs_2AgF_4 over the ESR data. Prof. B. G. Müller writes:

"All structural data of compounds M_2AgF_4 (M = K, Rb, Cs) as well as Ba_2AgF_6 are based on powder data, spacegroup and especially *f*-parameters [i.e. parameters determining position of atoms in [MF] layers along the crystallographic *c* axis; note by W.G. and R.H.] therefore could not determined exactly at that time, but the violet color is typical for planar $[AgF_4]$ groups."

$[KF][AgF_2]$ is an interesting exception. It adopts the $CsAgF_3$ structure, but exhibits an orthorhombic distortion, the only one in its series. This distortion leads to slight deviations of the four F-Ag-F angles from 90°. Here the $[AgF_6]$ units appear as compressed octahedra, with two short Ag^{II}–F^- bonds of 2.08 Å and four longer Ag^{II}–F^- separations of 2.20 Å.[74]

Compounds in the series $M[AgF_4]$, where M = Ba, Sr, Ca, Cd, Hg, crystallize in a $KBrF_4$ structure, as do the $MAgF_4$ compounds (M = K, Rb, Cs—see Section 3.1.5). The coordi-

Figure 9. Hypothetical unit cell of $[BaF_2]_2$-$[AgF_2]$; Ag: black spheres, Ba: white spheres, F: gray spheres.

nation of the Ag^{II} centers in these compounds is very different from that found in the $[MF][AgF_2]$ series: Ag is found here as isolated AgF_4^{2-} ion squares.[75] The $M^{II}AgF_4$ compounds are typical dilute paramagnets.[76] Unfortunately, refinements of the structures of $M^{II}AgF_4$ compounds have not been published.

The only known compound in the $[MF_2]_2[AgF_2]$ series, Ba_2AgF_6, is paramagnetic, and probably crystallizes in a tetragonal system with the Ba_2ZnF_6 structure (Figure 9) or in the related Ba_2CuF_6 structure.[77] Although its structure has not been determined, we may assume that it contains $[AgF_2]$ planes with Ag^{II} centers in a distorted octahedral or almost square-planar coordination (similar to the $[MF][AgF_2]$ and $[MF]_2[AgF_2]$ series) and an average in-plane Ag–F bond length of about 2.16 Å ($=a/2 = 4.32$ Å/2).

3.1.4. The Structures of α-AgF_2 and AgF_3

Because of the confusion in the literature regarding two simple binary silver fluorides, AgF_2 and AgF_3, with unique structures, they are treated separately here.

AgF_2 occurs in two forms: a disproportionated (high-temperature) $Ag^I[Ag^{III}F_4]$ and a nondisproportionated (low-temperature) $Ag^{II}F_2$ form. Hereafter we call these β- and α-AgF_2, respectively. α-AgF_2 is blue and changes color to brown on contact with air.[66] There has been a long debate on the crystal structure of α-AgF_2. Ruff and Giese[78] proposed in 1934 an orthorhombic $HgCl_2$-like structure for α-AgF_2 with lattice constants $a = 6.24$, $b = 5.48$, $c = 4.86$ Å and with four formula units per cell. In 1966, Charpin et al.[79] also found an orthorhombic unit cell with $a = 5.813$, $b = 5.529$, $c = 5.073$ Å. In the same year, however, Baturina et al.[80] proposed a distorted rutile structure for α-AgF_2 similar to the monoclinic CuF_2 structure. Then, in 1971 the measurements of Fischer et al.[15] confirmed the orthorhombic structure derived previously by Charpin et al., and the structure of α-AgF_2 was refined. Still, in 1988 a new structure (pseudohexagonal with unit cell dimensions of $a = 5.870$, $b = 5.572$, $c = 5.112$ Å) was proposed by Kiselev et al.[81] for a solid with formal composition AgF_2. The latest data by Jesih et al.[82] agreed again with the assignment made by Charpin et al.

The structural data for α-AgF_2 by Fischer et al. are included in Table 3. The structure of α-AgF_2 is presented in Figure 10. α-AgF_2 contains a puckered AgF_2 sheet with four short (2.068 – 2.074 Å) Ag–F bonds. Each Ag atom is coordinated by two additional F atoms at 2.584 Å, originating from neighboring AgF_2 sheets. The distance between two closest Ag atoms is only 3.78 Å. Indeed, α-AgF_2 is a weak ferromagnet with a Curie temperature T_c of 163 K.[83] The magnetic structure of this compound is very complex:[84] "The spin configuration consists of ferromagnetic planes parallel to

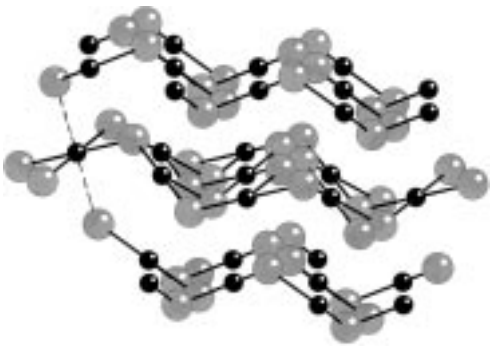

Figure 10. Crystal structure of AgF_2, view showing the puckered AgF_2 sheets. Note (at left) the elongated octahedral coordination of the Ag^{II} centers; Ag: black spheres, F: gray spheres.

(100). The main components of the magnetic moments are parallel to *a* and form an antiferromagnetic structure where silver atoms occupying centers of AgF_4 squares with a common fluorine have opposite spin directions. In addition, small ferromagnetic components point along *c*, i.e. perpendicular to the puckered AgF_2 layers […]. The resultant magnetic structure is slightly canted with spins parallel to the pseudohexagonal close-packed nets formed by the fluorines perpendicular to *b*."[85]

The long-range antiferromagnetic order in α-AgF_2 below the Curie temperature is also emphasized by the largest deviation from Curie – Weiss law among compounds containing Ag^{II} centers ($\Theta = -715$ K).

There has also been much controversy about AgF_3. AgF_3 was synthesized by Žemva et al.[16] as late as in 1991. It seems that previous claims of AgF_3 by Bougon et al.[86] and by Kiselev et al.[13] were not sufficiently documented. The structure of AgF_3 was finally refined in the hexagonal system. (Figure 11). The structure contains unique helical $[Ag(F_{2/2})(F_{2/1})]$ chains of 6_1 (or 6_5) symmetry, with four short (1.863 – 1.990 Å) and two long (2.540 Å) Ag–F bonds. The F-Ag-F angle between the two shortest Ag–F bonds is 140.2°, while the Ag-F-Ag angle between the two shortest Ag–F bonds is 176.6°. The distance from the Ag center to the

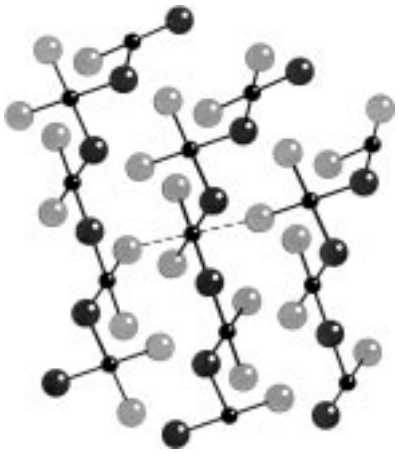

Figure 11. Crystal structure of AgF_3, view showing the helical AgF_3 chains. Note the elongated octahedral coordination of the Ag^{III} centers; Ag: small black spheres, F: Large gray spheres and black spheres (two slightly different kinds of F atoms).

bridging F atom is untypically large for silver(III) fluorides (1.99 Å) close to the shortest Ag^{II}–F^- bond seen in quasi-1D silver(II) fluorides (2.00 Å). The structure of AgF_3 has no counterpart in other solid Ag^{II} or Ag^{III} fluorides, and is analogous only to the structure of AuF_3.[16, 87, 88] AgF_3 is thermodynamically unstable and releases F_2 at $+25\,^\circ C$ on contact with anhydrous hydrogen fluoride.[89] It might be used for energy and fluorine storage.

We thought that adducts of AgF_3 and the strongest F-abstracting agents such as SbF_5 and BiF_5 might exist (at low temperatures) Prof. Bartlett confirms (private communication, 2000) that this was attempted in the 90's.

"We tried very hard to get $[Ag^{III}F_2]^+[AsF_6]^-$, by adding AsF_5 to anhydrous HF over AgF_3 at dry-ice temperatures. The anhydrous HF and AsF_5 were removed at low temperature, but […] the product was $[AgF]^+[AsF_6]^-$. George Lucier did, I believe, try BiF_5 with AgF_3. All of the efforts to make $[AgF_2]^+$ indicated that it must be a very fragile species. Because of these failures I suggested to George that we carry out experiments to detect the $[AgF_2]^+$ as a powerfully oxidizing transient. I guessed that the cation would be a strong enough one-electron oxidizer to take the electron from $[PtF_6]^-$ (we knew that Ag^{II} would not oxidize it). George was able to obtain a better than 70% yield of PtF_6 with BiF_5 as the F-acceptor. This certainly implies a long life for the $[AgF_2]^+$ at room temperatures (at which the MF_6, M = Pt, Ru, Rh, are generated). My guess is that an appropriate stoichiometric quantity of SbF_5 in anhydrous HF, at $-80\,^\circ C$, added (slowly) to a similarly cooled suspension of AgF_3 in anhydrous HF, could give $[AgF_2]^+[Sb_2F_{11}]^-$. Certainly one must avoid excess acid at any point in the synthesis, and the AgF_3 be given adequate time to react and dissolve as the $[AgF_2]^+$ salt."

3.1.5. Structures Containing Isolated $[Ag^{III}(F^-)_4]^-$ Squares or Isolated $[Ag^{III}(F^-)_6]^{3-}$ Octahedra

Ag^{III} is "isoelectronic" with Au^{III} and Pd^{II} (d^8 configuration). Square-planar coordination for $[AgF_4]^-$ is expected,[90] and indeed is typical both for Ag^{III} (and for Au^{III} and Pd^{II}) containing species. It is found in many ternary Ag^{III} fluorides in the series $M^I[AgF_4]^-$ (M = Cs,[68, 91, 92] Rb,[68, 91, 92] K,[68, 91–93] Na,[68, 92] Li,[94] O_2,[13] XeF_5.[95, 96]). Compounds isostructural to the $Ln[AuF_4]_3$, $LnF[AuF_4]_2$, $Ln_2F[AuF_4]_5$, or $Ln_2F_7[AuF_4]$ series (Ln = lanthanide)[97] have not yet been synthesized.

The structures of $MAgF_5$ (M = Ba[91]) and M_2AgF_5 (M = Rb[68]) are unknown.

Table 4 presents structural data for solids containing square $[AgF_4]^-$ units. Figure 12 shows the structure of $KAgF_4$.

The crystal structures of ternary fluorides containing the Ag^{III} cation are similar to structures containing the Au^{III} cation[98, 99] (crystallized in the $KBrF_4$ structural type). These

Table 4. Comparison of structural information and magnetic properties for solids containing an Ag^{3+} ion in isolated $[AgF_4]^-$ squares and in isolated $[AgF_6]^{3-}$ octahedra.

Compound	Crystal data[a]	$R(Ag^{III}–F^-)$ [Å]	$R(Ag^{III}\cdots F^-)$ [Å]	Magnetic behavior (temperature range [K])	Notes
$Cs[AgF_4]$	tetragonal, $a = 4.308$, $c = 7.048$			diamagnetic	$NaAlF_4$-Structure?
$Rb[AgF_4]$	tetragonal, $a = 6.043$, $c = 12.318$			diamagnetic	
$K[AgF_4]$	tetragonal, $a = 5.902$, $c = 11.806$ oder $a = 5.847$, $c = 11.553$	4×1.889	8×3.086	diamagnetic	
$Na[AgF_4]$	tetragonal, $a = 5.551$, $c = 10.649$			diamagnetic	
$Li[AgF_4]$	monoclinic, probably $C2/c$, $a = 4.87$, $b = 5.93$, $c = 10.08$, $\beta = 93.0$, $Z = 4$			diamagnetic	
$[XeF_5]^+[AgF_4]^-$	tetragonal, $I4/m$, $a = 5.593$, $c = 20.379$	1.902		diamagnetic	
$[O_2]^+[AgF_4]$	hexagonal, $a = 8.186$, $c = 9.904$				
$Ba[AgF_4]_2$	$KAgF_4$ defect structure?				
$Ag[AgF_4]_2$	monoclinic, $P2_1/n$, $a = 5.047$, $b = 11.054$, $c = 5.449$, $\beta = 97.2$, $Z = 2$	1.846 – 1.909	2.786 – 3.313	Curie-Weiss (4 – 280)	red brown
Rb_2AgF_5	tetragonal, $a = 6.094$, $c = 12.414$				
$[BaF_2][AgF_3]$				diamagnetic	yellow, decompostion
Rb_3AgF_6	tetragonal, $a = 6.190$, $c = 12.034$			?	high-spin?
Cs_2KAgF_6	cubic, $a = 9.175$	6×2.13	(octahedral coordination)	param.	high-spin?

[a] Crystal symmetry, space group, cell dimensions [Å], angles [°], number of formula units per unit cell.

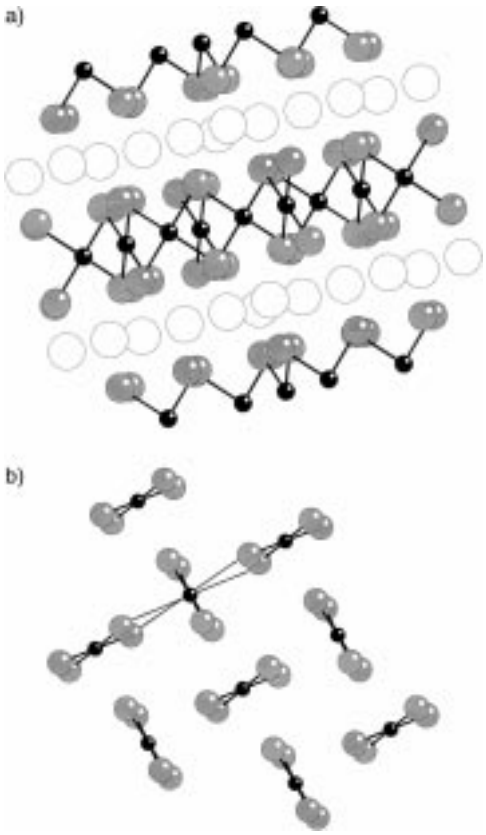

Figure 12. Crystal structure of $KAgF_4$; a) view showing the layers of isolated square $[AgF_4]^-$ ions; Ag: black spheres, K: white spheres, F: gray spheres; b) view showing the relative orientation of the square $[AgF_4]^-$ ions. Note the 4+4 coordination of the Ag^{III} centers; Ag: black spheres, F: gray spheres (K atoms have been omitted).

contains the isolated square-planar $[AgF_4]^-$ unit, with four equivalent short (1.89–1.91 Å) Ag–F bonds. There are also four additional secondary Ag···F interactions at 2.9–3.0 Å. The d^8 metal configuration is expected to be diamagnetic in this conformation. Interestingly, another high-symmetry structure of composition ABX_4 (in which AgF_2 planes might occur, Figure 13), the $NaAlF_4$ structure, is not preferred by the majority of compounds containing $[AgF_4]^-$ or $[AgF_4]^{2-}$ ions.

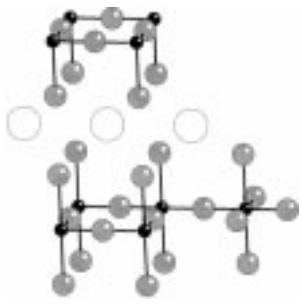

Figure 13. Hypothetical crystal structure of $CsAgF_4$ in the $NaAlF_4$ structure, view showing AgF_2 and CsF_2 layers. Note the elongated octahedral coordination of the Ag^{III} centers; Ag: black spheres, Cs: white spheres, F: gray spheres.

The structure of $CsAgF_4$, ($Z = 1$) is claimed to be simpler than that of $KAgF_4$ ($Z = 4$); a reduction of unit-cell dimensions by $\sqrt{2}$ (a, b) and by 2 (c) has been discussed.[68, 92] Under these conditions, $CsAgF_4$ might be the only $MAgF_4$ compound which adopts the $NaAlF_4$ structure. The $NaAlF_4$ structure indeed might be preferred over the $KBrF_4$ structure because of the large dimensions of the Cs^+ ion (ca. 167 pm) which stabilizes puckered CsF_2 sheets.[100]

It is worth mentioning that the presence of high spin (HS) Ag^{III} centers in the deep purple red Cs_2KAgF_6[68, 101] and in Rb_3AgF_6,[68] in which the Ag^{III} centers are in an undistorted octahedral environment (Figure 14) has been discussed. It was initially uncertain whether the paramagnetism of the samples might be attributed to the products of reactor corrosion. The synthesis of Cs_2KAgF_6 has been repeated in an Al_2O_3 reactor, to exclude paramagnetic pollutants.[102]

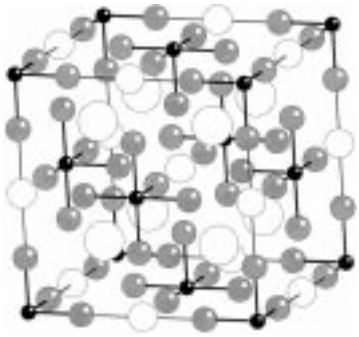

Figure 14. Unit cell of Cs_2KAgF_6. The structure contains isolated $[AgF_6]^{3-}$ octahedra; Ag: black spheres, F: light gray spheres, Cs: large white spheres, K: medium white spheres.

Could it be that the fluoride crystal field is so low that the typical square-planar environment low spin (LS) d^8 configuration might not necessarily be preferred for Ag^{III} centers (similar to paramagnetic Cu^{III} centers in $M^I_3CuF_6$ compounds)? The crystal structure of Cs_2KAgF_6 seems to confirm the presence of HS Ag^{III} centers. There are six equivalent long (2.13 Å) Ag–F bonds; dramatic elongation of the Ag–F bonds in Cs_2KAgF_6 compared to compounds containing LS Ag^{III} (1.90 Å) might be attributed to the occupation of both strongly antibonding Ag(d) orbitals ($x^2 - y^2$ and z^2) by one electron each. Bonding in HS Ag^{III} fluorides is thus probably more ionic than in LS Ag^{III} compounds.

3.1.6. *Mixed-Valence Ag^{II}/Ag^{I} and Ag^{II}/Ag^{III} Systems*

Several formally mixed-valence Ag^{II}/Ag^{III} systems have been introduced in previous sections. These are: Ag_2F_5, Ag_3F_8 (that is, $Ag^{II}\{[AgF_4]^-\}_2$), and Ag_3MF_{12}, (that is, $\{[AgF]^+\}_2[AgF_4]^-[MF_6]^-$ where M = Au, Pt, Ru, As, Sb). These compounds are typical disproportionated (mixed-valence) compounds. For example, $\{[AgF]^+\}_2[AgF_4]^-[AsF_6]^-$ contains kinked $[Ag^{II}F]^+$ chains and isolated $[Ag^{III}F_4]^-$ squares (Figure 15). The local coordinations of the Ag^{II} and Ag^{III} centers also differ greatly in Ag_3F_8 and Ag_2F_5 (see Figure 16 and 17, and Tables 1 and 2, respectively).

Ag_3F_8 has a very interesting structure (Figure 16). One may distinguish in it ribbons of the formula $Ag^{II}[Ag^{III}F_4]_2$. Local 2+2+2+2 coordination of the Ag^{II} center is not found in any other silver fluoride (there are four short 2.06–2.20 Å and four long 2.59–2.90 Å Ag-F distances), and may be considered as a distorted square-planar coordination. The Ag^{III} cation also occurs in a square-planar environment with four

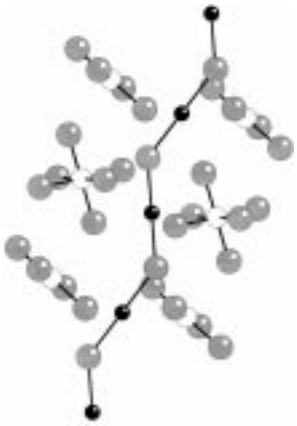

Figure 15. Crystal structure of $[AgF]_2[AgF_4][AsF_6]$. The structure contains an infinite kinked $[AgF]^+$ chain, isolated $[AgF_4]^-$ square planes, and isolated $[AsF_6]^-$ octahedra; Ag^{II}: black spheres, Ag^{III} and As^{VI}: white spheres, F: light gray spheres.

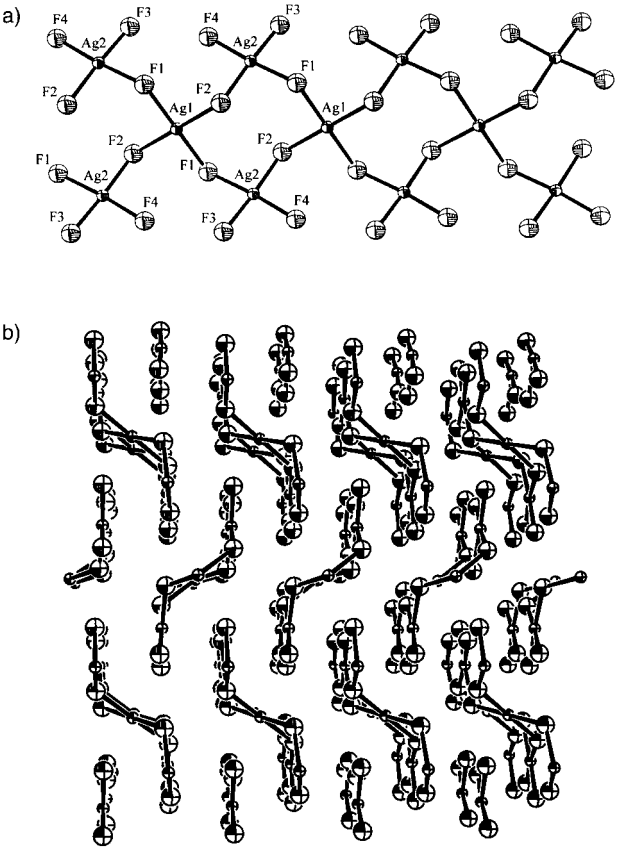

Figure 16. Crystal structure of $Ag[AgF_4]_2$. There are infinite "ribbons" in the structure, stacked in the *c* direction. Local coordination of the Ag^{II} and Ag^{III} centers is elongated octahedral; a) view of a ribbon; b) stacking of the $Ag[AgF_4]_2$ ribbons. Illustration courtesy of N. Bartlett.

Ag–F bonds of 1.85 – 1.91 Å and four secondary interactions at 2.79 – 3.31 Å. The unique $Ag[AgF_4]_2$ ribbons are stacked along one of the crystallographic axes.

The structure of Ag_2F_5, another binary mixed-valence silver fluoride, is very complex (Figure 17). There are three different kinds of Ag^{II} and three different kinds of Ag^{III} atoms. All the Ag^{II} cations have a similar coordination sphere, a compressed octahedron with two short Ag–F bonds (2.006 – 2.033 Å) and four long Ag–F bonds (2.14 – 2.58 Å). The Ag^{II} cations are joined in a kinked $[AgF]^+$ infinite chain ($\measuredangle$(Ag-F-Ag) = 144 – 145°, $\measuredangle$(F-Ag-F) = 176 – 180°). An approximate formula of this compound may be written as $[AgF][AgF_4]$. On the other hand, all the Ag^{III} cations are in a typical square-planar coordination with four F atoms at 1.89 – 1.92 Å and two F atoms much further away. It would be interesting to trace the magnetic interaction of the paramagnetic Ag^{II} centers; unfortunately, no magnetic measurements have been carried out for Ag_2F_5.

Figure 17. Crystal structure of $[AgF][AgF_4]$, view showing an infinite $[AgF]^+$ zigzag chain surrounded by $[AgF_4]^-$ ions. The local coordination of the Ag^{II} and Ag^{III} centers is elongated octahedral and square planar, respectively; Ag^{II} and Ag^{III}: black spheres, F: gray spheres.

We will now introduce two more mixed-valence compounds: a nonstoichiometric $AgF_{2+\delta}$ and $CsAgF_{3+\delta}$ ($0 < \delta < 1$). In this Section we will not include the genuine intermediate-valence fluoride of Ag^{III} and Ag^{V}, paramagnetic $Cs_2Ag^{IV}F_6$, crystallizing in the K_2PtCl_6 structure.[103]

Phases with formula $CsAgF_{3+\delta}$ are created upon thermal decomposition of $CsAgF_4$ at about 370 – 500 °C.[68, 92] $CsAgF_{3.53}$, obtained at 500 °C, crystallizes in a body-centered tetragonal system with $a = 6.339$ Å and $c = 9.150$ Å. It is a red-brown, formally mixed-valence compound, possibly a solid solution of $CsAgF_3$ and $CsAgF_4$, or—more probably—a compound with a defect $CsAgF_3$ structure (having CsF/AgF_2/CsF_2/AgF_2 layer order?). Strikingly, no similar $MAgF_{3+\delta}$ phases are obtained with this method for M = Rb, K, Na. Structural, spectroscopic, magnetic, and electric conductivity data is missing for the $CsAgF_{3+\delta}$ phases, these phases have not been investigated so far by other groups; most probably it is a disproportionated compound, as suggested by infrared (IR) spectra (the IR spectrum of $CsAgF_{3.53}$ may be obtained by overlapping the spectra for $CsAgF_3$ and $CsAgF_4$). It would be of interest to examine closer the coexistence of the Ag^{II} and Ag^{III} centers in this compound by varying the external pressure.

The same group claims $AgF_{2+\delta}$ is another nonstoichiometric compound containing silver in an oxidation state close to II.[81, 104] However, they find that the $AgF_{2+\delta}$ which they investigate is a single phase only in the range $-0.09 < \delta < 0.01$. No further data are given for this compound. The presence of $AgF_{1.91}$ does not seem improbable to us. For example, it is known that $AgF_{2.00}$ crystals are usually nonstoichiometric on the surface, and they are evidently F deficient.[105] $AgF_{2.00}$ might decompose slowly, releasing F_2. Neil

Bartlett (private communication) comments on this subject are as follows:

"Your comments on off-stoichiometry AgF_2 reminded me of work done in my lab in Vancouver in the mid-60's. My postdoctoral associate D. Stewart found that the action of F_2 on Ag^+ in anhydrous HF precipitated material of composition Ag_9F_{16} (i.e. $AgF_{1.78}$), whereas fluorination of silver nitrate in a bomb gave stoichiometric AgF_2. Both materials gave the same powder pattern, as far as line position was concerned, but some relative line intensities were different. I do still have X-ray photographs in my immediate possession. These show the orthorhombic cell of Ag_9F_{16} to be indistinguishable in size from that of AgF_2! I should add that the magnetic properties of Ag_9F_{16} are very similar to those of AgF_2 and the molar susceptibilities of Ag_9F_{16} and Ag_8F_{16} are essentially the same! I spoke on these findings at a "Fluorine Meeting" sometime in the later 60's (2nd European Symposium on Fluorine Chemistry, Göttingen 1968). From time to time over the past 35 years I have had various people look at this problem. My co-worker R. Hagiwara, in the early 90's, repeated D. Stewart's preparations and confirmed them, but we did not solve the structural problem posed by Ag_9F_{16}. That Ag^+ could be incorporated into the AgF_2 stucture and not change the unit cell size defies common sense. Clearly this merits careful re-examination, and should not be given serious weight in one's thinking until the findings are beyond all doubt."

To the best of our knowledge, $AgF_{1.91}$ would be the only example of a formally mixed-valence[106] Ag^{II}/Ag^{I} compound to date.

It is difficult to predict whether hypothetical quaternary Ag^{II}/Ag^{III} and Ag^{II}/Ag^{I} fluorides might have a decisively comproportionated (intermediate-valence) or rather a disproportionated (mixed-valence) character. We will examine this prospect closer in Section 3.6.2.

As we conclude our tour through known Ag^{II} and Ag^{III} compounds, we want to pay tribute to the groups who did this incredibly difficult work. In Germany, the pioneering effort was that of R. Hoppe and B. G. Müller, who synthesized the first Ag^{II} fluorides and determined their structures. More than half of the known compounds originate from this group. We have already mentioned the important contributions of N. Bartlett;[107] we also want to cite specifically the work of B. Žemva, the first to apply successfully acid–base reactions in anhydrous HF for synthesis of binary metal fluorides in high oxidation states.

3.2. Summary Analysis of Structural and Magnetic Data for Binary and Ternary Ag^{II} and Ag^{III} Fluorides

3.2.1. Coordination Preferences of Ag^{I}, Ag^{II}, and Ag^{III} in a Fluoride Environment

Let us summarize the coordination preferences of Ag^{II} and Ag^{III} in a fluoride environment, based on the extensive experimental data presented in Sections 3.1.1–3.1.6. The diverse ways of coordination of Ag atoms by F^- ions may be understood by thinking of them as distortions from octahedral coordination. Such a unified view provides a comparative, qualitative background for linear, compressed octahedral, elongated octahedral, and finally, the square-planar geometry (rare trigonal bipyramid, pentagonal bipyramid, and tetragonal pyramid coordinations are not included here). A quantitative comparison may be obtained through the dimensionless distortion parameter D which is defined as the ratio of the axial bond length R_{ax} to the equatorial bond length R_{eq} in a distorted octahedron [Eq. (2)].

$$D = R_{ax}/R_{eq} \quad (2)$$

In Table 5 we give several structural parameters, for selected Ag^{II} and Ag^{III} fluorides, such as the axial and equatorial bond lengths, R_{ax} and R_{eq},[108] the distortion

Table 5. List of axial R_{ax} and equatorial R_{eq} bond lengths in distorted octahedral Ag^{II} and Ag^{III} fluoride complexes, together with distortion parameter $D = R_{ax}/R_{eq}$ and the shortest Ag–Ag distance R(Ag–Ag). The structures optimized in the DFT computations are also included.

Verbindung	R_{ax} [Å]	R_{eq} [Å]	D	R(Ag–Ag) [Å]
Ag^{II} compounds:				
experimental				
$[AgF]AgF_4$	2.006–2.033	2.14–2.58	0.78–0.94	3.825
$[AgF]AsF_6$	1.995–2.004	2.394–2.439	0.83	3.795
$[AgF]IrF_6$	1.977–2.014	2.311–2.467	0.84	3.817
$[AgF]AuF_6$	2.072–2.162	2.484	0.85	3.800
$[AgF]AuF_4$	1.967[a]			3.933[a]
$[AgF]_2[AgF_4][AsF_6]$	2.003	2.32–2.34	0.86	3.903
$[AgF]BF_4$	2.002–2.009	2.327–2.330	0.86	4.011
$CsAgFeF_6$	2.04–2.05	2.27–2.30	0.89	3.67
$CsAgAlF_6$	2.06–2.08	2.29	0.90	3.69
$Ag(M')^{II}_3M^{IV}_3F_{20}$	2.072–2.103	2.28–2.31	0.91	4.175
Cs_2AgF_4	2.128	2.29	0.93	4.580
$KAgF_3$	2.075	2.201	0.94	4.402
ideal octahedra			*1.00*	
$NaAgZr_2F_{11}$	2.048–2.182	2.339	1.07–1.14	5.701
$Ag_3Zr_2F_{14}$	1.981–2.076			3.963
$Ag_3Hf_2F_{14}$	1) 2.354, 2) 1.997–2.147	1) 2.066, 2) 2.608–2.788	1) 1.14, 2) 0.74–0.79	3.972
α-$Ag^{II}[SbF_6]_2$	2.431	2.095–2.132	1.15	5.224
$Ag^{II}[BiF_6]_2$	2.440	2.096–2.122	1.16	5.218
$Ag^{II}[NbF_6]_2$				5.207
$Ag^{II}[TaF_6]_2$	2.367	2.030–2.067	1.16	5.198
$RbAgF_3$	2.42	2.06–2.10	1.16	4.220
$CsAgF_3$	2.51	2.07–2.13	1.20	4.260
$[AgF]RuF_6$	2.548–2.659	2.007–2.018, 2.140–2.158	1.21–1.29	3.940
AgF_2	2.584	2.068–2.074	1.25	3.776
$CdAgF_4$ ($KBrF_4$-type)		ca. 2.05		3.833
$BaAgF_4$ ($KBrF_4$-type)		ca. 2.05		4.264
Ag^{III} compounds:				
experimental				
AgF_3	2.540	1.863–1.990	1.28–1.36	3.500
$[AgF]AgF_4$	1.890–1.927	2.635–3.320	1.38–1.74	3.726
$[AgF]_2[AgF_4][AsF_6]$	2.61	1.80–1.81	1.45	7.806
XeF_5AgF_4	2.921	1.902	1.54	3.955
$KAgF_4$	ca.3.08	1.889	1.63	4.134
calculated				
$KAgF_4$ ($NaAlF_4$-type)	1.989	2.012	0.99	4.024
$RbAgF_4$ ($NaAlF_4$-type)	1.983	2.024	0.98	4.048
$CsAgF_4$ ($NaAlF_4$-type)	1.972	2.047	0.96	4.098

[a] Computed with the assumption of the $[CuF][AuF_4]$ structural type.

parameter D, and the closest distance between two Ag^{II} centers or between two Ag^{III} centers R(Ag–Ag). Data for structures optimized in the DFT computations (see Section 3.3) is also included.

Clearly, the Ag^{II} center exhibits a fascinating flexibility toward Jahn–Teller distortion from the ideal octahedral geometry in different fluoride-dopant environments. The distortion parameter D ranges from 0.78 (linear coordination), through 0.94 (compressed octahedron), and 1.07 (elongated octahedron), to 1.25 (square planar). The transition between the compressed and elongated octahedron is thus rather smooth (Figure 18). For Ag^{III} compounds with typical square-planar coordination, D usually takes on very large values (1.45–1.63).

The affinity of Ag centers towards F^- ions apparently increases with the increasing formal oxidation state of Ag. Ag^{III} is a very strong Lewis acid, which is found practically only in anionic form, as $[AgF_4]^-$ or $[AgF_6]^{3-}$. On the other hand, Ag^I is a very weak Lewis acid, found typically as an isolated cation.

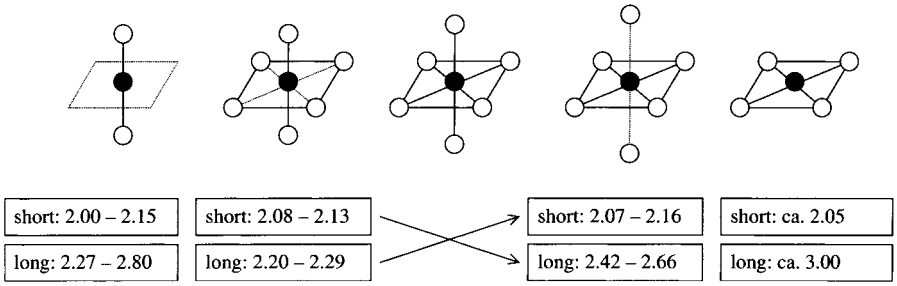

Figure 18. The Ag^{II}–F^- bond lengths [Å] in different geometric environments.

The diversity of crystal structures of binary and ternary Ag^{II} fluorides is very interesting. Ag^{II} may act as a cation, as a neutral species, and as an anion, as exemplified by:

1) isolated Ag^{II} cations, as in $Ag[BiF_6]_2$
2) $[AgF]^+$ ions in linear chains (two strong Ag–F bonds)
3) isolated $[Ag_2F_3]^+$ ions
4) $[AgF_2]^0$ in AgF_2 planes with elongated octahedral coordination (four strong bonds, but the F atoms are shared with other Ag atoms) or in isolated $[AgF_2]^0$ units
5) $[AgF_4]^{2-}$ ions in the form of isolated squares (four strong bonds) or in AgF_2 planes with compressed octahedral coordination (two strong bonds and four weak bonds, but F atoms are shared with other Ag atoms).

It is very important to understand this chameleonlike, amphoteric behavior of Ag^{II} centers in different fluoride complexes, so as to be able to manipulate it in a desired manner. We hope to reach this goal by analyzing the electronic structure of several structurally well-characterized compounds of Ag^{II} and Ag^{III} (Section 3.3).

3.2.2. Summary of Magnetic Behavior of Silver Fluorides

The magnetic behavior of the Ag^{II} fluorides is very diverse. Undoubtedly, exchange and superexchange are strongly dependent on the distance between the Ag^{II} centers, and the way in which they are joined by F^- ions. Figure 19 shows a graph of the Ag–Ag separation in different Ag^I, Ag^{II}, and Ag^{III} fluorides.

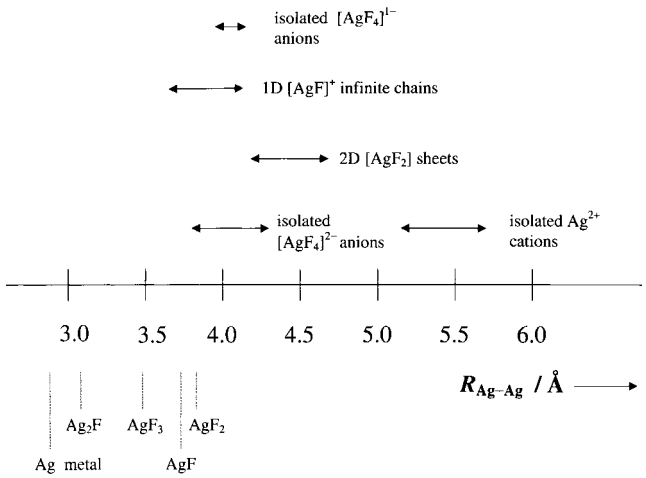

Figure 19. The shortest Ag–Ag distances in different Ag fluorides.

The closest Ag–Ag separation in magnetically dilute $Ag^{II}(d^9)$ fluorides is in the range 5.1–5.5 Å. These compounds are paramagnets. The Ag–Ag separation drops to 4.2–4.6 Å in compounds containing $[AgF_2]_\infty$ sheets. Most of these are weak antiferromagnets; Neél temperatures T_N do not exceed 80 K. AgF_2 is an exception; it is a weak ferromagnet with an Ag–Ag separation of 3.78 Å and Ag-F-Ag angles of 118–130°. But there is also antiferromagnetic order in this compound below the Curie temperature T_c (note that both the Curie temperature for ferromagnetic AgF_2 and the Neél temperatures for antiferromagnetic fluorides correlate with the closest Ag–Ag separation; see Figure 29 and Section 3.6.1.). Compounds containing isolated $[AgF_4]^{2-}$ ions have Ag–Ag separations in the range 3.8–4.3 Å. Still they are paramagnetic, probably a result of the mutually perpendicular orientation of half-filled x^2-y^2 orbitals on different Ag centers. Solids with $\{[AgF]^+\}_\infty$ chains have Ag–Ag separations of 3.7–4.2 Å. Most of them (with both linear or kinked $\{[AgF]^+\}_\infty$ chains and "short" Ag–Ag separations of 4.0–4.2 Å) are temperature-independent paramagnets. There might be a tendency to undergo Peierls distortion (resulting in a diamagnetic phase) in some of them at low temperatures. Compounds of $Ag^{III}(d^8)$ containing isolated $[AgF_4]^-$ ions have the closest Ag–Ag approach of about 4.0 Å (still too far for any significant overlap) and they are diamagnetic. AgF and ternary $Ag^I(d^{10})$ fluorides have the closest Ag–Ag separation of around 2.9–3.5 Å, and are diamagnetic.

3.3. DFT Band-Structure Calculations for Selected Binary and Ternary Ag^{II}, Ag^{III}, and Ag^I Fluorides

To determine the electronic structure of binary and ternary Ag^{II}, Ag^{III}, and Ag^I fluorides in geometrically different environments, we performed DFT band-structure calculations

for a selection of structurally well-characterized binary and ternary fluorides. Our main interest is in extended 1D and 2D structures containing Ag^{II} centers. Such compounds might in principle have a half-filled band, and possibly be metallic. Hence, for the DFT calculations we have chosen: 1) [AgF][BF_4], representative of compounds with a linear $[AgF]^+$ chain, 2) $CsAgF_3$, as an example of compounds with AgF_2 planes and elongated octahedral coordination of the Ag center, 3) Cs_2AgF_4, with an undistorted K_2NiF_4 structure, and 4) AgF_2, with a puckered-sheet structure. Since we would like also to look at Ag^{II} compounds from a broader perspective, we have added computations for Ag^{III} and Ag^{I} compounds: 5) $KAgF_4$, an example of isolated Ag^{III} centers as $[AgF_4]^-$ ions, and 6) AgF, an Ag^{I} fluoride. We also include computational data for 7) a hypothetical form of $KAgF_4$, as optimized in the $NaAlF_4$ structure ($Z=1$).

In the literature we could not find any electronic-structure calculations for Ag^{II} and Ag^{III} fluorides in the solid state.

3.3.1. Methods of Calculations

The density-functional theory (DFT) computations have been performed with the Vienna Ab Initio Simulation Package (VASP)[109, 110] version 4.4. This code performs ionic and electronic optimizations using soft and ultrasoft Vanderbilt potentials to describe the electron–ion interactions. VASP uses very effective matrix diagonalization schemes and Pulay mixing to evaluate the electronic ground state. This allows reduction in the number of plane waves in the basis set and saves much computational time.

The electronic wavefunctions were expanded into plane-waves with a typical cutoff of 500 ± 100 eV for electronic minimizations (density of states, DOS calculations). The energy difference of 1×10^{-3} eV per unit cell between two cycles has been used as a termination criterion for both electronic and ionic minimizations. We have used a conjugate gradient algorithm for ionic minimizations. Final DOS computations have been done with the highest precision (cutoff is set to 130 % of the typical value) and largest number of k-points. We have used automatic Monkhorst-Pack k-points generation schemes. Standard pseudopotentials included in VASP 4.0 have been used for all atoms without further modifications. Our computations are not spin polarized.

In our analysis, we need to see the contribution of various atomic orbitals to the total DOS, so as to gauge the extent of ionicity or covalence of the Ag–F bond.[111] All the atomic contributions to the DOS are shown *per one atom* of given type, if not otherwise indicated. The total DOS is always given per one formula unit ($Z=1$).

The results of our calculations are presented in Figure 21–27. In each Figure we show the DOS, and various contributions to them. There is a vast amount of information in our calculations; we have attempted to summarize the salient features in numerical form in Table 6. To support the interpretation of the results, we show first in Figure 20 the well-known diagram of the way the metal orbitals split in the various distorted octahedral ligand fields. We have assumed a weakly π-electron-donating ligand, such as F^- ions, involved in *both* σ and π bonding with the metal. The axial (z) distance *increases*, and the equatorial distances (x, y) *decrease* from left to right in Figure 20. In the O_h symmetry octahedron the distances are, of course, equal. Clearly, the e_{2g} level splits along such a distortion coordinate, its important z^2 component moves systematically down (from left to right), and x^2-y^2 moves up in energy. The t_{2g} set in O_h transforms as e + a in D_{4h}. It is the extent of π bonding which controls the magnitude of the splitting of the e and a sets. The diagram is only schematic, deviations from this general picture may occur. For example (depending on the relative strength of the σ and π bonding), the xy level might lie above the z^2 level in a square-planar coordination, and the xz, yz levels might lie above the x^2-y^2 level in a linear coordination.

Table 6. Comparison of important parameters for several binary and ternary Ag^{I}, Ag^{II}, and Ag^{III} fluorides in the solid state (results of DFT plane-wave pseudopotential computations). Chemical formula, formal oxidation state of Ag (OS), number of formula units in the elementary cell Z, total energy per formula unit (E [eV FU^{-1}]), energy of the Fermi level (E_F [eV]), total density of states at the Fermi level (DOS_F [states (eV FU)$^{-1}$], density of states corresponding to d^9 occupation ($DOS_{1/2}$), composition (%) of $DOS_{1/2}$ ($Ag_{1/2}$, $F_{1/2}$, $Dop_{1/2}$; Dop = dopant), the $Ag_{1/2}$:$F_{1/2}$ ratio, maximum splitting of the F(p) and Ag(d) levels (ΔE_{split} [eV]), and dispersion of d^9-d^{10} band (ΔE_{disp} [eV]). For compounds with two kinds of F atoms (F(1), F(2)) the contributions (%) of F(1) and F(2) to $DOS_{1/2}$ have been separated.

Chemical formula	AgF	AgF_2	$CsAgF_3$	Cs_2AgF_4	[AgF]BF_4	$KAgF_4$	$KAgF_4$[a]
OS	+1	+2	+2	+2	+2	+3	+3
Z	4	4	4	2	2	4	1
E [eV FE^{-1}]	−7.73	−11.60	−21.29	−30.20	−37.56	−24.40	−23.89
E_F [eV]	−0.28	−0.72	−2.63	−2.96	−2.21	−2.02[b]	−1.23
DOS_F [states (eV FE)$^{-1}$]	0.000	1.114	0.997	2.596	1.070	0.000	n.d.[c]
$DOS_{1/2}$ [states (eV FE)$^{-1}$]	3.210[d]	1.114	0.997	2.596	1.070	5.710[e]	n.d.
$Ag_{1/2}$ [%]	81	65	71	61	71	34	n.d.
F(1) [%]	–	–	15	19	16	–	n.d.
F(2) [%]	–	–	8	10	13	–	n.d.
$F_{1/2}$ [%]	19	35	23	29	29	64	n.d.
$Dop_{1/2}$ [%]	–	–	6 (Cs)	10 (Cs)	0 (B)	–	n.d.
$Ag_{1/2}$:$F_{1/2}$	4.26	1.86	3.09	2.10	2.45	0.53	n.d.
ΔE_{split} [eV]	5.6	7.5	6.2	5.4	8.4	8.0	n.d.
ΔE_{disp} [eV]	0.7	1.5	1.5	1.0	1.4	0.3	n.d.

[a] Optimized in the $NaAlF_4$ structure. [b] Midway between highest filled (−2.94) and lowest unfilled (−1.09) band. [c] n.d. = not determined. [d] At −0.607 eV. [e] At −3.157 eV.

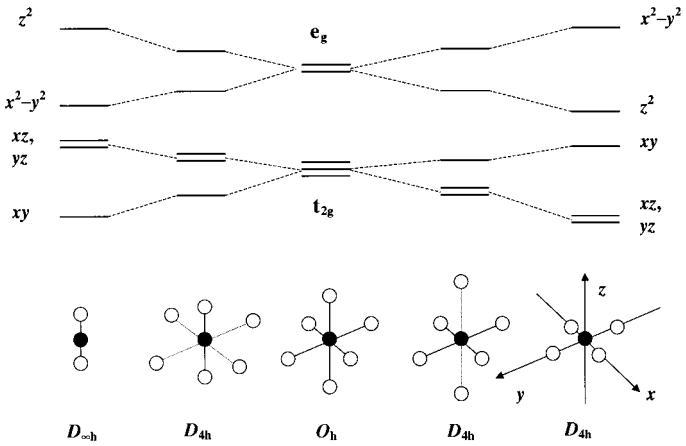

Figure 20. Energy diagram of the d-block levels of a transition metal in an undistorted and a distorted octahedral ligand field, a weakly electron-donating ligand creating both σ and π bonds with the metal center has been assumed. The apical (z) distance increases and the equatorial distances (x, y) decrease from left to right.

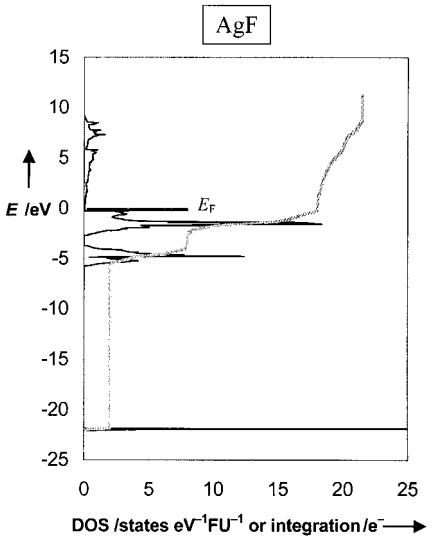

Figure 21. Total DOS of AgF (black curve) and its integration (gray curve).

What is important is that the z^2 levels will form the uppermost band (empty for Ag^{III} (d^8), half filled for Ag^{II} (d^9)) for compounds with a compressed octahedral (or almost linear) coordination of the Ag centers, while for compounds with elongated octahedral (or even square-planar) coordination of the Ag centers, the uppermost band will be built of x^2-y^2 levels.

3.3.2. *Electronic Structure of AgF: An Ag^I Compound*

We begin with a simple cubic Ag^I halide, as a calibration. AgF crystallizes in the NaCl structure ($Z = 4$). Each Ag^+ ion is surrounded by six F^- ions at a distance of 2.467 Å. The electronic structure of AgF has been subject of several previous theoretical studies.[11, 112–115]

Our results (Figure 21) resemble in their essential features the literature results.[11] In AgF one sees several sets of states centered approximately at 1) −22, 2) −5, 3) −2 (valence band), 4) +5 (conduction band), and 5) +7.5 eV. Analysis of the different atomic contributions to DOS and the DOS integration allows us to classify the very narrow (in energy) group of states at −22 eV (1) as mainly F(2s), and the rather broad bands at +5 to +7.5 eV (4 and 5) as mainly being Ag(5s) and Ag(5p).[116] Two remaining sets of states extend over the energy range −5.8 to −0.2 eV. The first set (2) is at −3.7 to −5.8 eV and is dominated by F(p); the second set (3) at −0.2 to −2.6 eV (valence band), is mainly Ag(d).

Our computational results, similar to those of Onwuagba,[11] do not give a significant gap between the valence and conduction bands. This is because of the large width of the Ag(s) band, which almost penetrates the uppermost Ag(d) bands. This is actually a problem (perhaps a deficiency of the DFT calculations), for AgF is clearly a semiconductor with a substantial indirect band gap of 2.7–2.8 eV.[117] The DOS near the top of the valence band (0.1 eV below the Fermi level) is composed of 76% Ag(d) and 23% F(p) states.

Figures 22a–c show a smaller energy window, omitting the low lying F(s) levels and the conduction band, the total DOS of AgF, but now in a smaller −10 eV to +1 eV energy range, and its breakdown into the most important contributions: Ag(d) and F(p). To facilitate comparison with other silver fluorides, we will consequently show in the following Figures the total DOS and Ag(d) and F(p) contributions within exactly the same energy window.

We imagine that AgF is ionic; what evidence is there in the calculations for or against such an assignment? There is a gap between the uppermost F(p) and the lowermost Ag(d) states of about 1.1 eV (Figure 22a). Only 10% of the all Ag(s,p,d) states enter the F(p) band, while 76% of the all Ag(s,p,d) states are in the Ag(d) band. The remaining Ag(s,p,d) states are found in the conduction band (14%); their contribution to the F(s) bands is negligible. Overall, mixing of F and Ag states is relatively weak: the contribution of the Ag(d) states to the

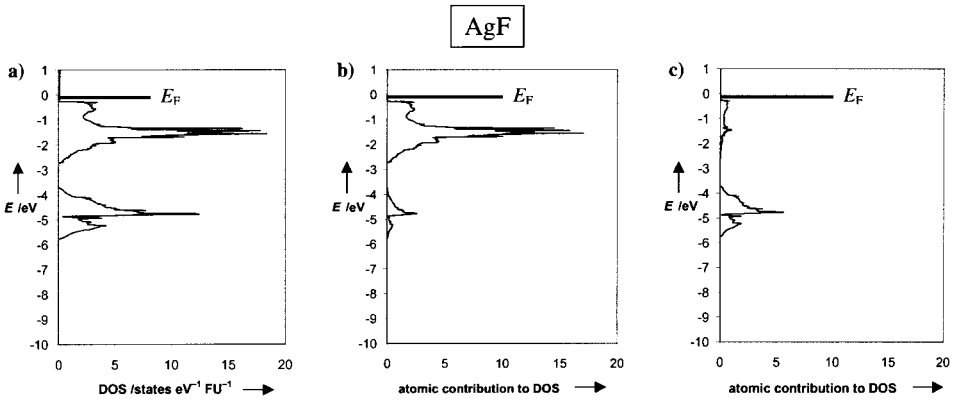

Figure 22. a) Total DOS of AgF in the −10 to +1 eV range and the contributions to it by b) Ag(d) and c) F(p) states.

F(p) band is rather small, as is the contribution of the F(p) states to the Ag(d) band. Based on these observations, we would argue that bonding in AgF indeed has predominantly ionic character, and the formulation of this compound is close to $[Ag^+F^-]$.

But even AgF shows some covalency; recall the composition 76% Ag(d) and 23% F(p) (cited above) of the states at the top of the valence band. We note here that, as much as the simplistic human mind would like to have it, there is no absolute division of ionic and covalent bonding, a situation we know from H_2. There are just extremes, more or less ionic or covalent—AgF is closer to the ionic limit.

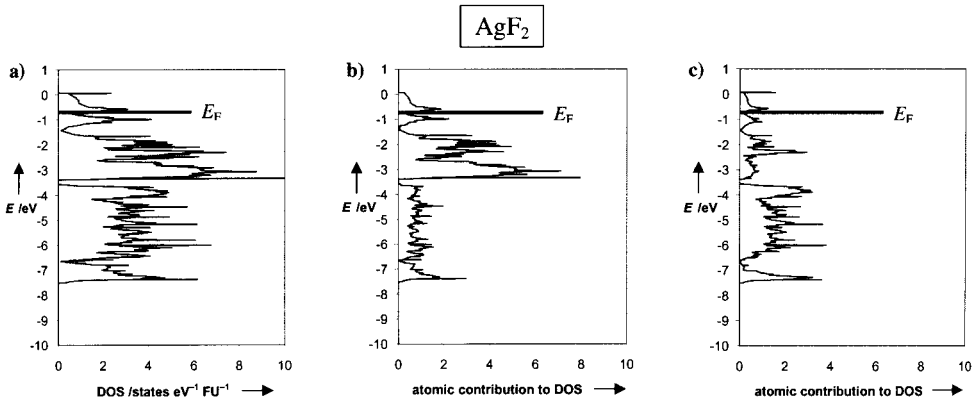

Figure 23. a) Total DOS of AgF_2 in the -10 to $+1$ eV range and its partitioning to b) Ag(d) and c) F(p) states.

3.3.3. Electronic Structure of AgF_2: An Ag^{II} Compound

The crystal structure of AgF_2 is composed of puckered sheets of AgF_2 stoichiometry (see Figure 10). The DOS of this interesting compound (shown in Figure 23a–c) in the -7.5 to $+0.1$ eV range is composed of states with mixed Ag(d)/F(p) character. In the region from -7.5 to -3.5 eV one finds states that are thoroughly mixed Ag(d)/F(p) but are dominated by F(p). The reverse is true in the upper band, from -3.4 to $+0.1$ eV, mainly Ag(d) with strong F(p) mixture. In a normal picture of metal–ligand bonding the Ag(d)/F(p) wavefunctions in the lowermost states of the former band are Ag–F bonding,[118] and the corresponding orbitals in the uppermost states of the latter band are Ag–F antibonding. Much experience and the workings of perturbation theory would argue for such a characterization.[119] In the discussion that follows, we will make a corresponding assignment of bonding character to various groups of states.

There is an indication of a substantial covalent contribution to the bonding in AgF_2. The overall contribution of the Ag(s,p,d) states to the "F(p)" band is larger than in AgF, as is the contribution of the F states to the "Ag(d)" band. For example, 30% of the total Ag(s,p,d) states are in the "F(p)" band, and 57% of the Ag(s,p,d) states are in the "Ag(d)" band. The remaining Ag(s,p,d) states are to be found in the conduction band (12%) and in the "F(s)" band (1%). Clearly, there is increased mixing of the F(p) and Ag(d) states in AgF_2, as compared to AgF.

The uppermost σ^* (x^2-y^2) band is nicely split off from the rest of the Ag(d) block, half-filled and split in two, which gives DOS peaks at -1.0 and -0.6 eV. Certainly, this is not a consequence of the two slightly different Ag–F bond lengths (2.068 and 2.074 Å); the puckering of the $[AgF_2]$ sheets is likely to be the reason for the x^2-y^2 band split. The Fermi level E_F is in a region of a substantial DOS, pointing to metallic character. A spin-polarized computation would be needed to confirm this.[120] Experimentally, AgF_2 is a spin-canted ferromagnet.

3.3.4. Electronic Structure of $KAgF_4$: An Ag^{III} Compound

$KAgF_4$ and $BaAgF_4$ are isotypic examples of $KBrF_4$-type structures (see Figure 12) containing isolated Ag^{III}/Ag^{II} centers in the form of square planar $[AgF_4]^-$ and $[AgF_4]^{2-}$ ions, respectively. $BaAgF_4$ contains magnetically isolated Ag^{II} centers, and is paramagnetic. $KAgF_4$ is diamagnetic. Unfortunately, the structure of $BaAgF_4$ has not been refined; we have computed only the DOS of $KAgF_4$. The DOS of $KAgF_4$ (Figure 24a–c) is composed of sharp peaks in the -9.0 to -0.7 eV range (in the energy range shown; there are other F states below). The sharp band profile is, of course, characteristic of a molecular compound—it shows bands at specific (molecular) levels, with little dispersion. There is also a set of unfilled Ag(s) and Ag(p) states of at $+3.0$ to $+7.5$ eV (above the energy window shown). As for the Ag^{II}-containing compounds, the Ag(d) and F(p) states are strongly mixed with each other, within many of the sharp molecular bands.

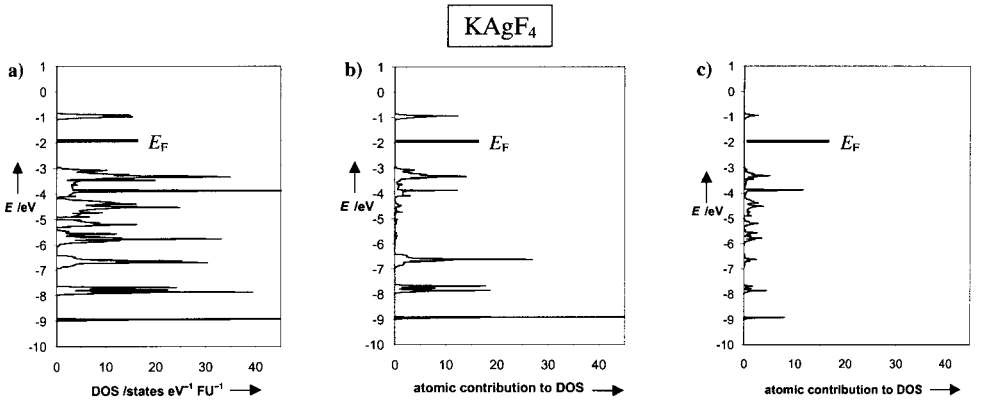

Figure 24. a) Total DOS of $KAgF_4$ in the -10 to $+1$ eV range and its partitioning to b) Ag(d) and c) F(p) states. The contribution of F(p) states is per *one* F atom.

Probably the most interesting feature of $KAgF_4$ is that the "quite molecular" DOS in the region of the Ag–F bonding states (-6.5 to -9.0 eV) is dominated by Ag(d) states, while in the uppermost Ag–F antibonding states (sharp DOS peak at -0.7 eV, unfilled) there is a slight excess of F(2p) orbitals (a contribution per *one* F atom is shown in Figure 24c, there are four F atoms). The classical picture used for ionic inorganic compounds (states originating from main group ligand orbitals below the d-block metal), that is, an ionic formulation of $KAgF_4$ as $K^{I}Ag^{III}(F^{-})_4$, must be modified in this case.

The Ag–F bonding is substantially covalent in $KAgF_4$. AgF_3 (at $+20\,^{\circ}C$) and $KAgF_4$ (at about $+370\,^{\circ}C$) both evolve molecular F_2. We see theoretically (as we did in a survey of the chemistry) that Ag^{III} is able to generate holes in the F(p) band.[121] This is rather rare in transition metal chemistry, to put it mildly.[122]

The uppermost σ^* x^2-y^2 group of states (the sharp DOS peak at about -0.9 eV) is not filled, as expected for a square-planar molecular compound. The computed band gap between the occupied z^2 and the unoccupied x^2-y^2 levels is about 2.0 eV. It is thus smaller than the experimental optical band gap of about 3 eV (the compound is yellow, it absorbs in the violet). According to our computations, $KAgF_4$ should be an insulating material, in agreement with experimental results.

The energy penalty to be paid upon transformation of $KAgF_4$ from the $KBrF_4$ to the $NaAlF_4$ structure was of interest to us. $KAgF_4$ in the $NaAlF_4$ structure would be a 2D compound, containing AgF_2 and KF_2 layers (Figure 13).[123] We have optimized $KAgF_4$ in the $NaAlF_4$ structure to evaluate the energy of transformation. The computed value is quite large, about 0.5 eV per formula unit. Clearly, $[AgF_4]^-$ is an exceptionally weak F^- donor, unable to donate F^- ions to a weak F^- acceptor (K^+). This means that attempts to obtain quasi-2D structures containing Ag^{III} units may be unsuccessful.

3.3.5. Electronic Structure of [AgF][BF$_4$]: An Ag^{II} Compound with Linear [AgF]$^+$ Chains

The electronic structure of $[AgF][BF_4]$ is shown in Figure 25a–d. This phase contains linear $[AgF]^+$ chains (from here on the AgF fluorine atom will be called F(1)) and isolated $[BF_4]^-$ ions (the BF_4^- fluorine is F(2)). The σ states of the closed-shell molecular tetrahedral $[BF_4]^-$ unit are at about -9.8 to -8.0 eV, forming quite narrow bands.[124] They have mixed B/F(2) character with a dominant F(2) component. There are also broad, bonding[118] bands of σ levels of the $[AgF]^+$ chain, lying in the -6.8 to -8.0 eV range. These bands are presumably composed of Ag(z^2) and F(p) orbitals, since the coordination of the Ag center is compressed octahedral (see Figures 5 and 24). Our analysis here depends in part on a partitioning of the total DOS into $[BF_4]^-$ and $[AgF]^+$ sublattice contributions, which we have studied, but do not present here.

There is another set of bands in the -6.5 to -1.4 eV region. These bands originate mainly from the nonbonding[125] F(p) and antibonding[118] Ag(d)/F(p) levels (the nonbonding levels of the F(2) atoms contribute mainly in the lower energy range

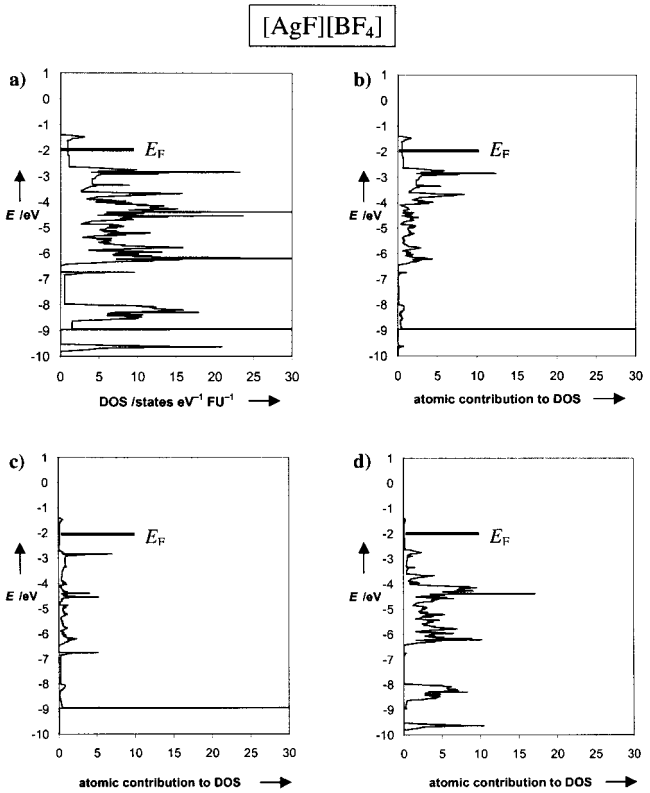

Figure 25. a) Total DOS of $[AgF(1)][BF(2)_4]$ ($\equiv [AgF][BF_4]$) in the -10 to $+1$ eV range and the contributions to it by b) Ag(d), c) F(1)(p) and d) F(2)(p) states.

from -6.5 to -4.0 eV). There is no gap between the nonbonding (F) and antibonding (Ag/F) levels, but the integration of the DOS (not shown here) allows us divide this region between the "π-type lone pairs of F atoms" (-6.5 to -4.0 eV, 20p electrons from 5F atoms) and "Ag(d) levels" (-4.0 to -1.4 eV, room for 10 Ag(d) electrons). The latter bands, however, have in fact mixed F/Ag character; the DOS at the Fermi level has contributions from both Ag (71%) and F states (29%).

The interaction between the $[AgF]^+$ and $[BF_4]^-$ sublattices is weak, but noticeable. In the important Fermi level region, the contribution from four F(2) atoms is roughly as large as the contribution from one F(1) atom. According to our computations, $[AgF][BF_4]$ is a quasi-1D metal, the unpaired electrons being delocalized in the uppermost σ^* z^2 band. This is in agreement with its experimentally derived Pauli temperature-independent paramagnetism, and the metallic luster of the compound.

3.3.6. Electronic Structure of CsAgF$_3$

The complete DOS of perovskite $[CsF][AgF_2]$ and its decomposition into different atomic contributions are shown in Figure 26a–d. The structure (see Figure 7) contains AgF_2 planes (the F atoms in these planes will be called F(1)) and CsF planes (the CsF fluorine is F(2)); the coordination of the Ag unit is elongated octahedral. The DOS in the -9.0 to

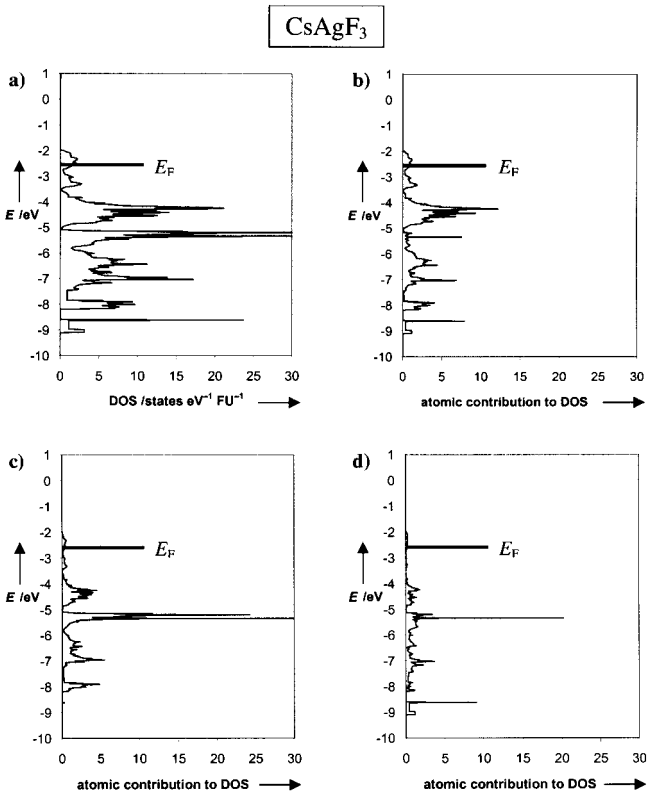

Figure 26. a) Total DOS of $[AgF(1)_2][CsF(2)]$ ($\equiv CsAgF_3$) in the -10 to $+1$ eV range and its partitioning into b) Ag(d), c) F(1)(p) and d) F(2)(p) states.

-2.0 eV region is composed of mixed Ag(d) and F(p) states (Cs does not contribute significantly in this energy window). Integration of DOS and analysis of atomic contributions allow us to divide these states into ones with dominant F character (-9.0 to -5.0 eV) and those with dominant Ag contribution (-5.0 to -2.0 eV). The uppermost σ* Ag–F antibonding (x^2-y^2) band is split into two bands, centered around -2.7 eV. The reason for this split may be in the geometric structure of the $AgF(1)_2$ planes: there are two different AgF(1) bond lengths of 2.06 Å and 2.13 Å in this sheet.

There is an indication of a covalent contribution to the bonding in $CsAgF_3$. As much as 43% of the Ag(s,p,d) states goes to the "F(p)" band, and 49% of the Ag(s,p,d) states remains in the $10e^-$ "Ag(d)" band. The rest of the Ag(s,p,d) states may be found in the conduction band (7%) and the "F(s)" band (1%). Compare these numbers to the respective ones for AgF_2. Apparently, about 14% of the Ag states are transferred from the "Ag(d)" and "Ag(s,p)" bands to the "F(p)" and "F(s)" bands in $[CsF][AgF_2]$. Making the puckered $[AgF_2]$ sheets present in AgF_2 planar, and sandwiching them between the [CsF] layers, probably introduces some positive charge into the $[AgF_2]$ planes, and increases the covalency of Ag–F bonding.

$[CsF][AgF_2]$, which exhibits metallic luster and is a Pauli paramagnet above T_N, should indeed be metallic, according to our computations; the unpaired electrons are delocalized in the uppermost σ* x^2-y^2 band of the $[AgF_2]$ sheets.

3.3.7. Electronic Structure of Cs_2AgF_4

Cs_2AgF_4 is an example of a compound with alternating AgF_2 planes (the F atoms here will be called F(1)) and two CsF planes (with F(2) atoms; see Figure 8). This compound has a structure similar to perovskite-related K_2NiF_4; the only difference is in the compressed (and not elongated) octahedral environment around the metal center.[73] There are two equal Ag–F(1) bonds in the structure of Cs_2AgF_4 (compare to $CsAgF_3$ with two different Ag–F(1) bonds). The DOS of this compound (shown in Figure 27a–d) in the -8.1 to -2.8 eV range is composed of states having mixed Ag(d) and F(p) character, as in $CsAgF_3$. Analyzing the integration curve and contributions of different sites, we may divide these states roughly into Ag–F bonding ones (-8.1 to -6.3 eV, with dominant F(p) contribution), Ag–F nonbonding ones (-6.3 to -5.3 eV), and Ag–F antibonding ones (-5.3 to -2.8 eV, with dominant metal contribution; "Ag(d)" bands).

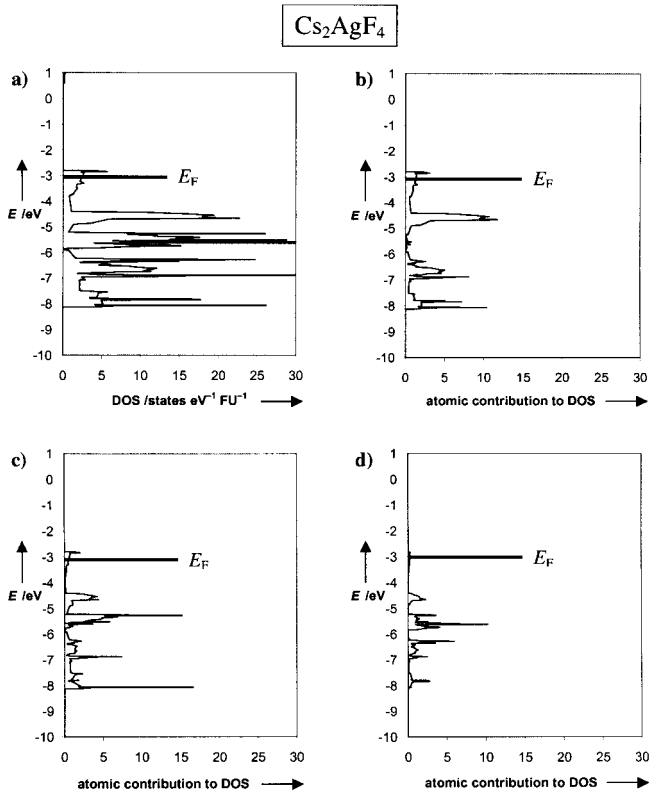

Figure 27. a) Total DOS of $[AgF(1)_2][CsF(2)]_2$ ($\equiv Cs_2AgF_4$) in the -10 to $+1$ eV range and its partitioning to b) Ag(d), c) F(1)(p) and d) F(2)(p) states.

The covalency of the Ag–F bonding in Cs_2AgF_4 is quite similar to that in $CsAgF_3$. For example 43% of the all Ag(s,p,d) states are in the "F(p)" band, and 50% of the Ag(s,p,d) states are in the $10e^-$ "Ag(d)" band. The remaining Ag(s,p,d) states are in the conduction band (6%) and in the "F(s)" band (1%).

The uppermost group of states is half-filled and is not split. States at the Fermi level are composed of Ag orbitals (61%), F(1) orbitals (19%), and F(2) orbitals (10%). The atomic contributions of F(1) and F(2) (per *one* F atom) to the states at

the Fermi level are very similar, 9.5 % and 10 %, respectively. It is interesting that the substantial difference in the Ag–F(1) and Ag–F(2) bond lengths (2.29 Å and 2.19 Å, respectively) is not reflected in different contributions from F(1) and F(2) to the states at the Fermi level, as one might expect from Figure 20. Most probably the states at the Fermi level originate from both σ* z^2 and σ* x^2-y^2 bands. There is substantial DOS at the Fermi level; Cs_2AgF_4 is metallic, according to our computations.

3.3.8. *Summary of Electronic Structure Computations for Ag^{II}, Ag^{III}, and Ag^{I} Fluorides*

Analysis of the data from Table 6 allows a semi-quantitative comparison of the bonding situation in $[AgF]^+$ infinite chains, $[AgF_2]^0$ planes, and in systems containing isolated Ag^I and Ag^{III} species.

In the Ag^{II}-containing compounds, the states at the Fermi level are composed of mixed F(p) and Ag(d) levels (the states at the Fermi level are presumably Ag–F antibonding). It is very instructive to compare contributions from the Ag and F orbitals to the DOS for different compounds of Ag^I, Ag^{II}, and Ag^{III}. For this purpose we have computed the composition of the total DOS corresponding to the d^9 configuration ($DOS_{1/2}$ in Table 6, the index ½ refers to the half-filling of this band for the d^9 configuration; $DOS_{1/2} = DOS_F$ for compounds of Ag^{II}) in all compounds of Ag^I, Ag^{II}, and Ag^{III} investigated. The position of $DOS_{1/2}$ shifts predictably to lower energy with the oxidation state of silver: about −0.6 eV for Ag^I, about −2.0 to −3.0 eV for Ag^{II}, and −3.2 eV for Ag^{III}. These levels are composed predominantly of Ag orbitals (80 % Ag) for Ag^I, show slight domination of silver (60–70 % Ag) for Ag^{II}, and are dominated by F orbitals (35 % Ag) for Ag^{III}. The relative contribution of Ag and F orbitals to the bands corresponding to the d^9 occupation in $KAgF_4$ is such that the Ag atom contributes roughly the same to these states as one F atom. Clearly, an increase in the Ag oxidation state (introducing holes into the band structure of the Ag^I and Ag^{II} compounds) leads to increased covalency of the Ag–F bond.

The Ag^{II}–F^- bonding is substantially covalent in character.[126] The Ag–F bonding in $KAgF_4$ (Ag^{III}) is more, and in AgF (Ag^I) is less covalent than that in Ag^{II} fluorides. The lowest occupied Ag(d)/F(p) bonding states are dominated by F(s,p) contributions in AgF and by Ag(s,p,d) contributions in $KAgF_4$. Apparently, Ag(d) states "sink" into the F(p) ones, as we move from Ag^I through Ag^{II} to Ag^{III} compounds.

The most pronounced covalent character of the Ag^{II}–F^- bond is obtained for $[AgF][BF_4]$ (the ratio of the total Ag:F contributions is 2.45:2[127] = 1.23). This is in agreement with our intuition on quasi-1D and quasi-2D structures. The affinity of Ag^{II} towards F^- ions is such that it creates either two very strong, short ("more covalent") bonds (as in $[AgF][BF_4]$) or four longer ("more ionic"), but still appreciably strong bonds (as in $BaAgF_4$). The coordination found in compounds with AgF_2 planes appears to be intermediate between the two limiting cases described above.

The energies of the Fermi level (E_F) of course vary in a wide range (−3.0 to −0.7 eV) for the Ag^{II} compounds, for example, $E_F = -0.3$ eV for AgF, and $E_F = -2.0$ eV for $KAgF_4$. Cs_2AgF_4 and $CsAgF_3$ are predicted[128] to be the strongest oxidizing agents among the systems studied, stronger even than $KAgF_4$ (Ag^{III}-containing compound). This is also revealed in the contribution of Ag(s,p,d) states to the occupied Ag–F bonding states, which increases in the direction: AgF_2 (31 %) < $CsAgF_3 \approx Cs_2AgF_4$ (44 %). This effect might be connected with introducing a partial positive charge into the $[AgF_2]$ sheets when they are gradually separated upon intercalation of the [CsF] layers. A choice between Na, K, Rb, and Cs, and between $MAgF_3$ and M_2AgF_4 structures should leave some space for manipulation of this charge.

The magnitude of the DOS_F found in Ag^{II}–F^- compounds ranges from about 1 to about 2.6 states (eV FU)$^{-1}$, where FU = formula unit. The largest value, of 2.6 states (eV FU)$^{-1}$, is computed for Cs_2AgF_4. Very large local DOS (sharp peaks in DOS) are found, as expected, for $KAgF_4$ ($DOS_{1/2} \approx$ 10 states (eV FU)$^{-1}$, a compound containing molecular $[AgF_4]^-$ centers.

The difference in energy between the F(p) (bottom of the Ag–F bonding levels) and the Ag(d) bands (top of the Ag–F antibonding levels) is 5.4–8.4 eV in all silver fluorides investigated. The d^8-d^{10} uppermost two-electron band is spread over 1.0–1.5 eV in Ag^{II} fluorides, and over only 0.3–0.7 eV in compounds of Ag^I and Ag^{III} containing fairly well separated Ag centers.

$KAgF_4$ crystallizes in a $KBrF_4$ structure (with isolated $[AgF_4]^-$ units; Figure 12). We wanted to see how much this structure is favored over the simple $NaAlF_4$ structure (having $[AgF_2]^+$ planes; Figure 13). The calculated preference is 0.5 eV FU^{-1}. This value suggests that introducing Ag^{III} centers into the AgF_2^0 sheets in $KAgF_3$ should be very difficult, if it is to happen without decomposition of this structure into isolated $[AgF_4]^-$ ions. Ag^{III} usually needs four "unshared" F^- ligands, while Ag^{II} (a weaker Lewis acid) is typically saturated having between two and four "shared" F^- ions. $CsAgF_4$ is probably the only $MAgF_4$ compound which crystallizes in the $NaAlF_4$ structure. The $NaAlF_4$ structure might be preferred for this compound, because of the large dimensions of the Cs^+ ion.[100]

Why did we not pursue the theoretical analysis in this paper with the extended Hückel method but instead used the VASP density-functional code? With the extended Hückel procedure we would have been able to apply a host of interpretational tools analyzing orbital contributions in detail, and looking at bonding through overlap or Hamilton populations. The reason we did not do so is that the problem at hand (a comparison of bonding in Ag^I, Ag^{II}, and Ag^{III} fluorides) is singularly unsuited to the extended Hückel method, despite our substantial experience with it. The extended Hückel method, in its usual implementation, does not allow the energies of Ag orbitals (or their extent in space) to vary as the oxidation state of silver varies. And yet that variation is at the heart of what we wish to understand—the real and important differences among Ag^I, Ag^{II}, and Ag^{III} centers. For this reason we were willing to give up interpretability for greater accuracy.

3.4. Analogies and Differences among the Ag^{II}-, Cu^{II}-, and Au^{II}-Containing Systems

Ag^{II} is isoelectronic with Cu^{II} and with ephemeral Au^{II}. Hence, it is instructive to analyze the behavior of Ag^{II}-containing systems from the perspective of analogous Cu^{II} and Au^{II} compounds.

3.4.1. General Comparison of the Properties of Ag, Cu, and Au in Different Oxidation States

"Like copper, silver and gold have a single s electron outside a completed d shell, but in spite of the similarity in electronic structures and ionization potentials there are few resemblances between Ag, Au, and Cu. And there are no simple explanations for many of the differences although some of the differences between Ag and Au may be traced to relativistic effects on the 6s electrons of the latter." [129]

We begin a discussion of this topic with several arguments of a chemical nature, based on electronegativities, oxidation states, and some structural aspects. Numerical data relevant to the discussion are collected in Table 7. An analogous comparison for F and O is shown in Table 11 in the Appendix.

Table 7. Comparison of several important properties of Cu, Ag, and Au and their compounds.[a]

	Cu	Ag	Au
1st E_i [kJ mol^{-1}]	745.5	731.0	890.1
2nd E_i [kJ mol^{-1}]	1957.9	2070	1980
3rd E_i [kJ mol^{-1}]	3555	3361	no data
1st E_{ea} [kJ mol^{-1}]	118.4	125.6	222.8
Pauling EN	1.90	1.93	2.54
Mulliken-Jaffe EN	1.49 (4s)	1.47 (5s)	1.87 (6s)
redox potential E^0 [V] (acidic solution):			
	? (Cu^{III}/Cu^{II})	1.980 (Ag^{II}/Ag^{I})	1.83 (Au^{I}/Au^{0})
	0.520 (Cu^{I}/Cu^{0})	1.67 (Ag_2O_3/Ag^{I})	1.52 (Au^{III}/Au^{0})
	0.159 (Cu^{II}/Cu^{I})	1.36 (Ag_2O_3/Ag^{II})	1.36 (Au^{III}/Au^{I})
		0.799 (Ag^{I}/Ag^{0})	
redox potential E^0 [V] (basic solution):			
	–	1.757 (Ag_2O_3/Ag^{I})	–
		1.711 (Ag_2O_3/Ag_2O_2)	
		0.604 (AgO/Ag_2O)	
		0.342 (Ag_2O/Ag)	
$R(M^{I})$ [Å]	0.91 (cn = 6, O_h)	1.42 (cn = 8, cubic)	1.51 (cn = 6, O_h)
	0.74 (cn = 4, T_d)	1.29 (cn = 6, O_h)	
		1.14 (cn = 4, T_d)	
$R(M^{II})$ [Å]	0.87 (cn = 6, O_h)	1.08 (cn = 6, O_h)	1.09 (cn = 6, O_h)
	0.71 (cn = 4, T_d)	0.93 (cn = 4, D_{4h})	
	0.71 (cn = 4, D_{4h})		
$R(M^{III})$ [Å]	0.68 (cn = 6, O_h)	0.89 cn = 6, O_h)	0.99 (cn = 6, O_h)
		0.81 cn = 4, D_{4h})	0.82 (cn = 4, D_{4h})
$R(M^{V})$ [Å] (calcd)	0.38 (cn = 6, O_h)	0.53 cn = 6, O_h)	0.56 (cn = 6, O_h)
R(vdW) [Å]	1.40	1.72	1.66
bond enthalpy [kJ mol^{-1}] of diatomic molecules MX:			
X = O	269.0 ± 20.9	220.1 ± 20.9	221.8 ± 20.9
X = Cl	382.8 ± 4.6	341.4	343 ± 9.6
X = F	413.4 ± 13	354.4 ± 16.3	–
melting (T_m), boiling (T_b) sublimation (T_s) and/or decomposition (T_d) [°C]:			
M^{I} oxide	T_m = 1235, T_d = 1800	T_d = 230	–
M^{I} chloride	T_m = 430	T_m = 455, T_b = 1550	T_d = 170 (→Au+$AuCl_3$)
M^{I} fluoride	T_d = 908	T_m = 435, T_b = 1159	–
M^{II} oxide	T_m = 1326	–	–
M^{II} chloride	T_m = 620, T_d = 993	–	–
M^{II} fluoride	T_d = 950	T_m = 690, T_d = 700	–
M^{III} oxide	–	–	T_d = 160 (−O), T_d = 250 (−3O)
M^{III} chloride	–	–	T_d = 256
M^{III} fluoride	T_d = −40	T_d = 20	T_s = 300

[a] E_i = ionization energy; E_{ea} = electron affinity; EN = electronegativity (in Pauling units); cn = coordination number; vdW = van der Waals.

The Pauling electronegativities (PENs) for Cu, Ag, and Au are 1.90, 1.93, and 2.54, respectively.[130] Such diversity of PENs within a given transition metal group is otherwise observed only in Group 6. Absolute values of PEN allow one to classify Cu and Ag midway between the most electropositive ("most metallic"[131]) element in the d-block, Hf (PEN(Hf) = 1.30), and the most electronegative ("most nonmetallic") one, Au itself. The PEN(Au) = 2.54 is appreciable; chemists call Au a noble metal. The PEN(Au) compares with PEN of several nonmetallic or semimetallic elements, such as C (2.55), Se (2.55), and I (2.66). However, the Mulliken – Jaffe electronegativity of Au is 1.87, much below values for I (2.74, for 14.3 % s orbital[132]), Se (2.60, for 16.7 % s orbital[132]), and C (2.48, sp^3 orbital[132]), weakening our PEN-based classification of Au as a nonmetal.[133]

"Typical" oxidation states are II (and I) for Cu, I (and II) for Ag, and III (and I) for Au.[134] Cu^{III} occurs less frequently than Cu^{II}.[135] Au^{I} has a strong tendency towards disproportionation to metallic Au^0 and Au^{III}. Au^{II} was first reported in solution,[136] is stable in the gas phase,[137] and immensely rare in the solid state.[138–140] Oxidation state V has been obtained for several Au compounds;[88, 95, 141–144] it has been claimed in one case for Ag,[145] and has never been reached for Cu.[146] Apparently, the relative availability of two $d(z^2)$ electrons for removal from the square planar $M^{III}(d^8)$ species is related to the contraction of the $d(z^2)$ lone pair, in the order: Cu (the most contracted, most difficult to oxidize) > Ag > Au (the least contracted).

A fluoride environment stabilizes the "untypical" oxidation state II of Au and Ag. A number of fluoride complexes of Ag^{II} have been prepared and structurally characterized (see Section 3.1). Also, the first "purely inorganic" Au^{II} complexes in the solid state have been obtained in fluoride systems.[19, 30, 147]

The relative stability of different oxidation states of Cu, Ag, and Au in different ligand environments is very interesting. It is known that Cu^{II} exhibits strong "chemical affinity"[148] to O^{2-}; for Cu^{I} and Ag^{I} this is true for S^{2-} and Cl^{-}; and for Au^{III} and Au^{I} to Cl^{-} (compare, for example, melting, boiling, sublimation, and decomposition temperatures of different compounds of Group 11 metals, given in Table 1). Usually a

large chemical affinity is indicative of *covalent* bonding between the elements. In this context, the large affinity of Ag^{II} to F^- ions is of great interest.[149] It hints at efficient mixing of the Ag(d) and F(p,s) orbitals, which we have already noticed in the band calculations, and is provided by the energetic proximity and similar spatial extent of these orbitals. Surprisingly strong mixing of the fluorine and silver orbitals has been noted even for Ag^I (a relatively weak Lewis acid) in an fcc phase of AgF.[150, 151]

Ag^{II} is an incredible species. When solvated in anhydrous hydrogen fluoride, it is one of the best oxidizing agents known. It oxidizes Xe to Xe^{II}, generates $C_6F_6^+$ salts from C_6F_6, liberates IrF_6 from its anion and $S_2O_6F_2$ from SO_3F^- ions, and oxidizes $CF_3CF{=}CF_2$ quantitatively to $CF_3CF_2CF_3$. It has been stated in the literature that the electronegativity (in context of orbital electronegativity or configuration energy) of Ag^{II} (and even more likely of Ag^{III}) is close to that of the F^- ion itself.[152] These experimental observations, together with the fact that many Ag^{II} and Ag^{III} compounds easily liberate F_2, indeed point to an energetic proximity of the Ag(d) and F(p,s) orbitals.

Valuable information about the character of the M–F (M = Cu, Ag, Au) bond is provided by theoretical studies for MF, MF_2, and MF_3 molecules in the gas phase, M = Cu,[153–158] Ag,[153, 156, 159, 160] Au.[153, 156, 161, 162] These studies clearly indicate, that:

a) The largest relativistic contraction of bond lengths occurs for Au^I (0.36 Å), followed by Ag^I, Au^{II}, and Au^{III} (ca. 0.16–0.18 Å)[163]
b) Relativistic effects are responsible for weakening of Au^I bonding to electronegative ligands, as compared to a hypothetical nonrelativistic case[164]
c) The decomposition of $[MF_4]^-$ species according to equation: $[MF_4]^- + E_{dec} \rightarrow [MF_2]^- + F_2$, is least favored for M = Ag, thus indicating great stability of Ag^{III}–F^- bonds
d) A very strong coupling of the neutral $Ag(4d^{10}5s^1)F(2s^22p^5)$ and ionic $Ag^+(4d^{10}5s^0)F^-(2s^22p^6)$ configurations ("valence tautomerism"[165]) is observed at relatively short interatomic separation in the $^{3,1}\Sigma^+$ states of the AgF molecule (for CuF only the ionic configuration contributes appreciably). Again, a leading motive is strong covalent Ag–F bonding.

Large covalency is seen also in relativistic computations for Au^{III} and Au^V molecular fluorides,[166] and is also deduced from electronic absorption[167] and ESR[168] spectra of the corresponding solids.

3.4.2. Comparison of Geometric Structures of Fluorides, Oxides, and Chlorides of Ag, Cu, and Au in the Solid State

The diversity of the chemistry of the three Group 11 members is impressive. Despite of it, interestingly, there is still much structural similarity between Ag-, Cu-, and Au-containing solids:

a) The very stable M^I complexes often show a linear geometry with two ligands. This is exemplified by Cu_2O, $[AgCl_2]^-$, the $[AgO_2]$ unit,[169] and $[AuCl_2]^-$.
b) M^{II} complexes typically have an elongated octahedral coordination geometry, as seen in $Cu^{II}(OH_2)_6$, α-$CuZrF_6$, $CsAgF_3$, and $Au[SbF_6]_2$. This is consistent with a strong Jahn–Teller distortion in the d^9 configuration.
c) Sometimes M^{II} complexes have a compressed octahedral geometry, as in $KCuF_3$[170, 171] and K_2CuF_4,[172] $KAgF_3$ and Cs_2AgF_4. This is the opposite phase of the Jahn–Teller deformation mentioned in (b).[173]
d) More seldom, the M^{II} complexes are two-coordinate linear species (with four additional weak interactions), as seen for $[CuF][AuF_4]$[174] and $[AgF][BF_4]$. This could be seen as the limiting case of an compressed octahedron.
e) The M^{III} complexes usually have a local square-planar geometry, as in the case of $[CuF_4]^-$,[175] $[AgF_4]^-$,[176] $[AuF_4]^-$, $[AuCl_4]^-$, and the $[AuO_4]$ unit.[177] This is of course what would be expected of a d^8 transition metal complex.
f) Cu^{III} (and much more seldom high-spin Ag^{III}) complexes are also found as octahedral species (elongated in K_3CuF_6, undistorted in Cs_2KAgF_6).

Given the similarity of the covalent radii of Ag and Au (especially in oxidation states II and III), the occurrence of isotypic compounds for these two metals is not surprising. Also, as may be seen from the above comparison, compounds of Cu and Ag are often isotypic, although there are some deviations from this rule. An interesting example of similarity of Ag and Cu is provided by a fluoride complex, $Ag^{II}_3[ZrF_7]_2$.[178] Two kinds of Ag^{II} center appear in this compound. It is known that one of these centers, Ag(1), may be easily substituted by Cu^{II}, thus giving $Cu^{II}Ag^{II}_2[ZrF_7]_2$, a mixed Ag/Cu compound. $Ag^I_2Cu^{II}_2O_3$, isotypic with $Cu^I_2Cu^{II}_2O_3$, is another example.[179]

Many structural features are shared between the Ag^{II} fluorides and the famous cuprate superconductors.[180]

The $[AgF_2]_\infty$ planes occurring in some $MAgF_3$ and M_2AgF_4 compounds are typical of the analogous $MCuF_3$ and M_2CuF_4 compounds, and they also bring to mind $[CuO_2]_\infty$ planes, an essential structural element for superconductivity in cuprates.[181] For example, $CsAgF_3$ adopts a slightly distorted perovskite structure (Figure 7), typical for some oxobismuthate superconductors. Cs_2AgF_4 crystallizes in the perovskite-related K_2NiF_4 structure (Figure 8), which occurs in superconducting $La_{2-x}Sr_xCuO_4$ and Sr_2RuO_4. The Ag center has elongated octahedral hexa-coordination in $CsAgF_3$ and Cs_2AgF_4. On the other hand, $[MX]_\infty$ chains[182] are observed in both Ag and Cu fluorides (Figure 5, 8, 10) and in some cuprate superconductors for example YBCO. Also Ag centers in a distorted tetragonal pyramidal penta-coordination, similar to pentacoordinate Cu in some oxocuprates (Figure 3), are known. Strong $[CuO_2]_\infty$ interlayer coupling, which leads to record critical temperatures, is found in the oxocuprate superconductors with tetragonal tetra coordination of Cu. Analogous AgF_2 planes with Ag centers in a tetragonal tetra coordination are still not known.

3.4.3. Comparison of Ag–F Systems, Superconducting Cu–O Systems and Members of Other Superconducting Families

The computational results for the Ag–F systems presented in Section 3.3, together with computational and experimental

results for different Ag–O,[183–188] Ag–Cl,[189] Cu–F,[190, 191] Cu–O,[183, 191–195] Cu–Cl,[183, 196, 197] Au–F,[30, 1a] Au–O,[183, 198] and Au–Cl[199, 200] systems in the literature, allow us examine Ag–F compounds from a broader perspective.

In Figure 28 we show a schematic energy level or DOS diagram (similar to some extent to the Zaanen–Sawatzky–Allen diagram[201]) for sulphide, chloride, oxide, and fluoride systems of Cu, Ag, and Au and summarize the essential

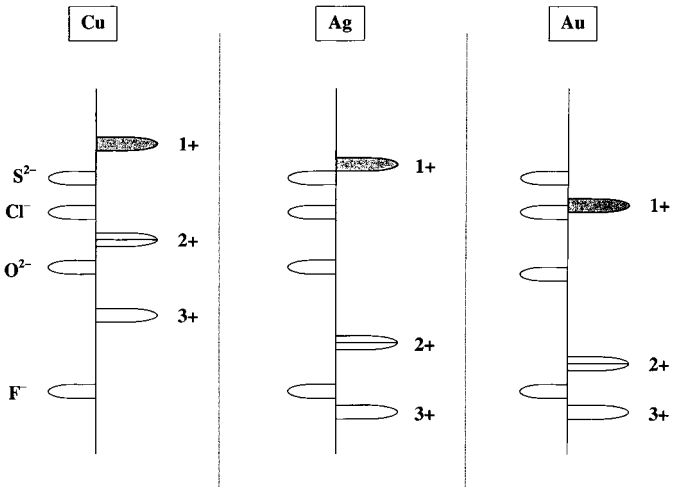

Figure 28. A schematic energy level diagram for sulphide, chloride, oxide, and fluoride systems of Cu, Ag, and Au in different oxidation states. The levels of the anion are on the left side, the levels of cations are on the right side.

features of the solid-state chemistry of different oxidation states of Cu, Ag and Au.[202] For example, Figure 28 shows that Cu_2S_3 (also $CuCl_3$, and Cu_2O_3) does not exist, because Cu^{III} would oxidize sulfide anions to disulfide, or even to elementary sulfur. Analogous depopulation of the nonmetal states (holes in nonmetal levels) would be certainly observed for Cl and O, as well. Of course, the position of p nonmetal states and d metal states is flexible to some extent, and not rigidly set on the energy scale (this is especially true for larger, more polarizable anions and cations; the counter-ions also have some influence). This explains several known deviations from our simple picture, for example, why $AuCl_3$ or $Ag[W_6Br_{14}]$[203] exist.

A tendency of M^{II} to disproportionate into M^{I} and M^{III} is more difficult to deduce, depending as it does on many factors. In a simplistic picture these are: 1) the degree to which the electrons of the M^{III} cations are in orbitals that are more contracted than those of the M^{II} centers (this decreases the energy of the M–L bonding orbitals), 2) the degree to which M^{I} expands compared to M^{II} (this increases the energy of the M–L antibonding orbitals), 3) the separation of hypothetical M^{II} cations in a given solid, and 4) the spatial extent of the half-filled atomic orbital of the M^{II} atoms. Criteria (3) and (4) are most important for "ionic" substances, where half-filled orbitals are localized on a metal center.

There are further analogies between Ag–F systems and superconducting oxocuprates. Cu^{II} oxide complexes are very stable towards disproportionation, as are Ag^{II} fluoride complexes. Cu^{III} oxide complexes are relatively thermodynamically unstable, similar to Ag^{III} fluoride complexes. The former complexes are obtained by prolonged oxidation in a stream of O_2; they spontaneously release oxygen. Ag^{III} fluorides may be obtained only by fluorination with powerful oxidizers such as O_2F,[204] F_2,[13] O_2F_2, XeF_2, and KrF_2, and they easily evolve F_2.[205]

3.5. Hypothetical Intermediate-Valence Quaternary Fluoride Ag^{II}/Ag^{III} and Ag^{II}/Ag^{I} Systems as Potential Superconductors?

3.5.1. BCS Contribution to Superconductivity

We proceed to compare quantitatively the Ag–F systems with several well-known families of superconductors. In the spirit of the theory developed by Bardeen, Cooper, and Schrieffer (BCS theory)[206] one needs to consider three important parameters: a density of states at the Fermi level (DOS_F), an electron–phonon coupling constant, and a cut-off frequency of the phonon spectrum.[207]

Frequencies of the stretching vibrations in Ag^{III}–F^- compounds reach 600 cm^{-1}, (similar to those of oxocuprate superconductors), thus providing reasonably large Debye temperatures; the corresponding values for Ag^{II}–F^- compounds are lower by around 20–30 %.[208]

Here we concentrate on the DOS_F and the degree to which states near the Fermi level in 1D and 2D nets originate from metal and ligand; covalency of the M–L bond directly influences the strength of the electron–phonon coupling.[209] Numerical data supporting the following discussion are listed in Table 8.[210]

We must preface our remarks with a caveat. It is a daunting task, beyond our (or anyone's) powers, to compare critically computational results for Ag–F and Cu–O compounds. These results are obtained by several researchers using very different computational methods. We go ahead, but *the* reader is cautioned that the comparison that follows is somewhat shaky.

Consider first the DOS_F. It may be seen that the Ag^{II}–F^- compounds have DOS_F ($\approx$1.0 to 2.6 states (eV FU)$^{-1}$) smaller by a factor of about 2–4 than those for metallic YNi_2B_2C or HfN_2 systems, similar to oxocuprates and Sr_2RuO_4, and larger by a factor of 4–8 than oxobismuthates, oxoantimonates, and fullerides. In addition, there are attractive DOS peaks close to E_F for AgF_2 (Figure 23a), with DOS values exceeding DOS_F by about three times.[211] They might be accessible by hole- or electron-doping in the AgF_2 planes.

In silver fluorides the states at the Fermi level are usually dominated by the contribution of metal states (60–70 %), which exceed that of the nonmetal (anion) states (30–40 %). This agrees roughly with the charge distributions in the $3b_{1g}$ half-filled orbital of the $[AgF_6]^{4-}$ ion (73–77 % Ag, 27–23 % F, multiple scattering Xα (MS-Xα), and self consistent charge extended Hückel (SCCEH) results.[212] A more rigorous approach should, of course, take into account the ratio of Ag and F atoms participating in the bonding in a given compound.

Oxocuprates are definitely the most widely investigated superconducting family. Much attention has been paid to bismuthates and ruthenates as well. Let us compare the

Table 8. Comparison of important features of Ag–F compounds (obtained from our DFT computations) and several cuprate and non-cuprate superconductors (literature data).

Compound	T_c [K]	DOS_F[a] [states (eV FE)$^{-1}$]	M_{tot} [%]	X_{tot} [%]	Dop_{tot} [%]	M_{tot}:X_{tot}	R(M–X) [Å]	Ref.
silverfluorides:								
AgF_2	–	1.114	65	35	–	1.71	4×2.07, 2×2.58 (Ag-F)	
$[AgF][BF_4]$	–	1.070	71	29	0 (B)	1.15[b]	4×2.33, 2×2.01 (Ag-F)	
$CsAgF_3$	–	0.997	71	23	7 (Cs)	1.68	$4\times2.07-2.13$, 2×2.51 (Ag-F)	
Cs_2AgF_4	–	2.596	61	29	10 (Cs)	2.63	4×2.29, 2×2.13 (Ag-F)	
oxocuprates:								
$HgBa_2Ca_2Cu_3O_{8+x}$	134							[213, 214]
$Tl_2Ba_2Ca_2Cu_3O_{10}$	128–125	1.268	55	39	5 (Tl), 0.5 (Ba), 0.5 (Ca)	1.41	4×1.925, 1×2.66 (Cu-O)	[215]
$(Sr_{1-x}Ca_x)_{1-y}CuO_{2+x}$[c]	110	0.50[r]	30[r]	45[r]	25[r] (Sr)	0.67[r]	4×1.93, 2×2.50 (Cu-O)	[216]
$HgBa_2CuO_{4+x}$	96	1.5[r]					4×1.94, 2×2.81 (Cu-O)	[217]
$Tl_2Ba_2CuO_{6+x}$	90	4.23	12	65	20 (Tl), 3 (Ba)	0.19		[218]
$YBa_2Cu_3O_7$ (YBCO)	93	1.10	33	66	1 (Y, Ba)	0.50	4×1.93, 1×2.26 (Cu-O)	[219]
$YBa_2Cu_2PbO_x$	80							[220]
$CaCuO_{2+x}$	80	0.42[r]	29[r]	48[r]	24[r] (Ca)	0.60[r]		[221]
Sr_2CuO_{3+x}	70						4×1.882, 2×1.932 (Cu-O)	[222]
$PbCdSr_3BaCaYCu_4O_{14}$	47							[223]
$La_{2-x}Sr_xCuO_4$	35[d]	1.935	49	47	4 (La)	1.05	4×1.90, 2×2.40 (Cu-O)	[224]
$Pb_2La_{2-x}Sr_xCu_2O_{6+\delta}$	33[e]	1.762	55	41	4 (Pb)	1.34		[225]
$Ba_2YRu_{0.85}Cu_{0.15}O_{6-x}$	30							[210]
$Nd_{2-x}Ce_xSr_2Cu_2NbO_{10}$	28	3.75[r]	38[r]	60[r]				[226, 227]
$Nd_{2-x}Ce_xCuO_4$	21							[228]
$Bi_2Sr_2CuO_6$	12	1.06	36	43	19 (Bi), 3 (Sr)	0.84		[218]
other oxides:								
$Ba_{1-x}K_xBiO_3$	30–26[f]	0.26[r]	54[r]	46[r]	0 (Ba)		6×2.128 (Bi-O)	[229]
$Li_{1+x}Ti_{2-x}O_3$	13.7							[210]
$Ba(Pb,Bi)O_3$	12						6×2.128 (Bi-O)	[230]
$M'_xKCa_2Nb_3O_{10}$ (M' = Li, Na)	6–3							[231]
$Li_{0.8}NbO_2$	5.5							[210]
M'_xWO_3 (M' = Li–Cs)	5.4–1.1							[210]
$Ba(Pb,Sb)O_3$[g]	3.5–2.8	0.378	34	66	0 (Ba)	0.52		[232]
$Li_{0.9}Mo_6O_{17}$	2							[210]
$(Ag_7O_8)(NO_3)$	1.4							[233]
Sr_2RuO_4	1.35[234]	1.8[r]	53[r]	47[r]	0 (Sr)		4×1.930, 2×2.061 (Ru-O)	[235]
NbO, TiO[h]	1.0–0.8							[210]
$SrTiO_3$	0.2–0.3							[210]
non-oxide materials:								
Rb_2CsC_{60}	35							[236, 237]
$Li_{0.16}Hf(NCl)$	25.5	2.3[238]					2.108 (Hf-N)[i]	[239]
Nb_3Ge[j]	23.2	1.83						[240]
V_3Si[j]	23	1.84						[241]
K_3C_{60}	18.5	0.28,[242] 0.16[243]						[236]
S	17.0[k]							[244, 245]
$LuNi_2B_2C$	16.6	2.4						[246]
YNi_2B_2C	15.6	4.03	54 (Ni)	30 (Y)	9 (B), 7 (C)			[247]
$PbMo_6S_8$[l]	15.2							[210]
$Li_{0.16}Zr(NCl)$	12.5	0.92[238]					2.099, 2.339 (Zr-N)	[248]
[κ-(BEDT-TTF)Cu{N(CN)$_2$}]Br[s]	12[249]							[210]
Na_2CsC_{60}	11.7	0.665						[250]
$CaTaN_2$	10	0.7						[251]
Nb	9.3	1.43						[252]
HfV_2[m]	8.9	2.95						[253]
Ba_8Si_{46}	8.0							[254]
$BaHfN_2$	8						2.186, 2.05 (Hf-N)	[255]
$La_2C_2Br_2$	7							[256]
$SrSn_3$	5.4							[257]
Hg[n]	4.2							[258]
anthracene[o]	4							[259]
SmS	3	2.2[r]						[260]
UPd_2Al_2[p]	2.0							[210]
CsI	2[q]							[261]
UPt_3[p]	0.43							[210]
KC_8	0.4–0.1	0.3						[262]

[a] DOS is presented per one metal atom for oxocuprates and oxobismuthates, per one carbon atom for fullerides, and per one nickel atom for nickel borocarbides. [b] Original value for this 1D compound has been multiplied by 2, to provide comparison with 2D structures. [c] DOS data for $x = 0$ and $y = 0$, T_c for $x = 0.3$ and $y = 0.1$. [d] For $x = 0.15$. [e] For $x = 1$ and $\delta = 0.1$. [f] For $x = 0.4$. [g] Computational data are for $BaSbO_3$. [h] Both are nonstoichiometric, defect compounds. [i] For undoped HfNCl. [j] A15 phase. [k] Under high pressure. It is the highest T_c value among elements. [l] Chevrel phase. [m] C15 Laves phases. [n] The first superconductor known. [o] It is the highest T_c value in charge-injected molecular crystals. [p] A heavy fermion superconductor. [q] Above 180 GPa. [r] Data estimated from figures presented in a given references. [s] BEDT-TTF = bis(ethylenedithio)tetrathiafulvalen.

constitution of the states at the Fermi level for these families of compounds and for silver fluorides. First, the contribution of the metal to DOS_F never surpasses 55% in oxide superconductors. If we compare the partitioning of the DOS_F into metal and nonmetal contributions for compounds with similar metal-to-anion atom ratios, we find for $CsAgF_3$ 71:23, the 2223 compound $Tl_2Ba_2Ca_2Cu_3O_{10}$ 55:39, and $(Ba,K)BiO_3$ 54:46, Cs_2AgF_4 61:29 and La_2CuO_4 49:47, or $AgBF_5$ 71:29 and $(Nd,Ce)_2Sr_2NbCu_2O_{10}$ 38:60. Apparently, the Ag–F systems are slightly more ionic than the Cu, Bi, and Ru oxides. Since large vibronic coupling is likely to be associated with strongly bonding or strongly antibonding orbitals (the latter is the case for d^9 systems), the lower covalency for Ag–F systems in comparison with the CuO ones would result in some decrease in the electron–phonon coupling constant.

We retreat a little from the calculations to an ionicity index, the useful concept of optical electronegativity (OEN) introduced by Jørgensen in late '50s.[263] Some experimental data suggest that OEN $(F^-) = 3.9$ and OEN $(O^{2-}) = 3.5$,[264] others that OEN $(F^-) = 3.6-3.7$ and OEN $(O^{2-}) = 3.2-3.5$.[265] Values of OEN for Cu^{II} and Ag^{II} are 2.4 and 2.8, respectively.[212] Given that the differences of OEN between Cu^{II} and O^{2-} and between Ag^{II} and F^- ions are similar (0.8–1.1), the ionicity/covalency of the Cu^{II}–O^{2-} and Ag^{II}–F^- bonds should then be comparable.[266] The same conclusion may be obtained for the Cu^{III}–O^{2-} and Ag^{III}–F^- bonds.

The contribution of dopant levels to the states at the Fermi level, which increases the DOS_F and thus potentially increases the superconductivity critical temperature T_C, is the last topic of this section. It has to be admitted that compared to Tl, Bi, or Ca in oxocuprates dopants contribute relatively weakly to DOS_F in Ag–F systems. This situation might change if Sb, As, Ge, Si, Ti, Al, Be (and other elements forming strong bonds with F) were used as cationic or anionic dopants in the Ag–F systems.

There is much geometric instability of the CuO_2 nets in cuprate superconductors, most importantly a tetragonal-to-orthorhombic distortion. This distortion has a dramatic influence on the superconducting properties of these substances. Similarly, a tetragonal-to-orthorhombic distortion is observed when the Rb center in $RbAgF_3$ is substituted for K. Phase separation is often observed in oxocuprates,[267] and it occurs also for $BaAgF_5$, which easily separates into BaF_2 and $Ba[AgF_4]_2$. The frequencies of the Ag–F stretching vibrations in Ag^{III}–F compounds reach 600 cm^{-1}, similar to the frequencies of the Cu–O stretching modes of the oxocuprates, which are most important for superconductivity. Finally, many of the Ag^{II}–F compounds are often ground-state antiferromagnets, as are some Cu^{II}–O^{2-} systems that are parent compounds for electron- or hole-doped Cu^{II}/Cu^{III} and Cu^{II}/Cu^{I} superconductors.

Note that silver is one of very few elements, which—in such a low oxidation state (+II)—creates substantially covalent extended nets in combination with the most electronegative element, fluorine. It also introduces holes into the F(p) band, at oxidation state +III.[268]

Interesting superconducting solids containing $[Ag_7O_8]^+$ clusters, for example, $[Ag_7O_8]^+[HF_2]^-$,[269] $[Ag_7O_8]^+[NO_3]^-$,[233] $[Ag_7O_8]^+[F]^-$,[270, 271] $[Ag_7O_8]^+[ClO_4]^-$,[271] $[Ag_7O_8]^+[BF_4]^-$,[272] $[Ag_7O_8]^+[HSO_4]^-$,[271, 273] and $[Ag_7O_8]^+[HCO_3]^-$[274] are known. The highest superconducting critical temperature (T_c) reported for these compounds is only 1.4 K ($[Ag_7O_8]^+[NO_3]^-$).[272] These are II/III mixed-valence (probably class II) compounds, with an average +2.43 oxidation state of silver.[275] The proximity of Ag(d) and F(p) levels, appreciably Ag/F-mixed character of the strongly Ag–F antibonding levels in proximity of the Fermi level, and relatively large values of DOS_F in Ag^{II} fluoride systems temptingly suggest that Ag^{II} fluoride systems might be much better "BCS superconductors" than the known Ag^{II} oxide clusters.[276]

3.5.2. *Non-BCS Contribution to Superconductivity: A "Magic Electronic State"*

Burdett has suggested that a "magic electronic state" occurs in superconducting oxocuprates.[277] This concept is very simple. Burdett argues that high-temperature superconductivity is likely to occur when there are enormously large variations in the wavefunction, which changes its character from one dominated by copper to another dominated by oxygen contributions [Eq. (3a), (3b)].

$$Cu^{III} + O^{2-} \longrightarrow Cu^{II\bullet} + O^{-\bullet} \quad (3a)$$

$$Cu^{II\bullet} + O^{2-} \longrightarrow Cu^{I} + O^{-\bullet} \quad (3b)$$

The equations [Eq. (3a), (3b)] describe the introduction of holes into the "oxygen band" by Cu^{III} and even Cu^{II} centers. If there is a precarious balance of this type small changes in the Cu–O distance might lead to effective transfer of charge (electrons) between copper centers through the oxygen p orbitals, thus inducing free flow of electric current.

Burdett draws an analogy between this phenomenon and another one, that of ionic and covalent curves crossing in alkali halides ("harpooning", Mulliken's sudden electron transfer[278]) [for example: Eq (4)]

$$Na^{I} + Cl^- \longrightarrow Na^{0\bullet} + Cl^{\bullet} \quad (4)$$

The major difference is that harpooning happens at large distances of several Å's in alkali halides, but electron transfer at relatively short distances of about 1.9 Å in cuprates. The covalent/ionic curve crossing in cuprates is avoided and leads to "repulsion" of the diabatic potential energy surfaces. This results in adiabatic curves, separated by an energy gap. It has been proposed independently that the position of the LUMOs of the bridging anion with respect to the metal levels plays a crucial role for disproportionation of mixed-valence *molecular* compounds.[279]

According to Burdett's concept, the magic electronic state might occur the Robin and Day class III [33] mixed-valence solids (fully comproportionated, intermediate-valence ones). We think, however, that Burdett's idea might also be extended to class II [33] mixed-valence compounds (systems with partial comproportionation), if higher frequency vibrational modes are considered ("dynamical comproportionation", "fluctuating valence").[280]

Indeed, computations of layered oxocuprates with CuO_2 planes (Table 8) suggest that the Fermi level has strongly mixed Cu/O character. For example, the computed ratio of atomic Cu to O contributions to the DOS_F is 1.41 for $Tl_2Ba_2Ca_2Cu_3O_{10}$, 1.34 for $Pb_2La_{2-x}Sr_xCu_2O_{6+\delta}$, 1.05 for $La_{2-x}Cu_xO_4$, 0.84 for $Bi_2Sr_2CuO_6$, 0.67 for $(Sr_{1-x}Ca_x)_{1-y}CuO_{2+x}$, 0.50 for $YBa_2Cu_3O_7$, and 0.19 for $TlBa_2CuO_6$. A similar situation also occurs in non-cuprate superconducting oxides (0.52 for $Ba(Pb,Bi)O_3$). These numbers suggest that the ground state of different Cu^{II} or Bi^{IV} oxides might be dominated by O or Cu/Bi contributions, and that proper hole- or electron-doping in the system might shift this situation towards the desired one in which crossing of the ionic and covalent curves is avoided.

Introduction of holes into the fluorine band by Ag^{III} or Ag^{II} centers [Eq (5a), (5b)] is probably more difficult than introducing holes into the oxygen band by Cu^{III} [see Equation (3a)].[281]

$$Ag^{III} + F^- \longrightarrow Ag^{II\bullet} + F^{0\bullet}, \quad (5a)$$

$$Ag^{II\bullet} + F^- \longrightarrow Ag^{I} + F^{0\bullet}, \quad (5b)$$

Ag^{III} and even Ag^{II} centers easily generate holes in the oxygen band (these two species decompose water, and are relatively unstable in oxides; AgO is in fact $Ag^IAg^{III}O_2$). But would they manage to generate holes in the fluorine band? Are the processes described by Equations (5a) and (5b) realistic?

There is some experimental and theoretical evidence that process (5a) and even (5b) might occur. As we have pointed out in Section 3.5.1 our computations (Table 2) document that the contributions of Ag and F to the DOS_F in several Ag^{II} fluorides are quite similar to the respective Cu and O contributions in oxocuprates with similar metal:anion ratios in the chemical formula. Since Ag^{II} fluorides seem, however, a little more ionic than oxides of Cu^{II}, Burdett's "magic electronic state" might be reached only in some hole-doped Ag^{II} fluorides. This seems less probable in the electron-doped systems, [Equation (5b)], and such a conclusion is supported by experimental observations. After hypothetical recombination of fluorine radicals according to the Equation (6a) gaseous fluorine is released upon heating from many Ag^{III} fluorides (usually at 300–400 °C) and even from Ag^{II} fluorides (usually at 500–700 °C). An analogous reaction in copper oxides might involve $O^{-\bullet}$ (isoelectronic to $F^{0\bullet}$) [Eq. (6b)], as has been discussed by many workers in the field.[281]

$$2F^{0\bullet} \longrightarrow F_2 \quad (6a)$$

$$2O^{-\bullet} \longrightarrow O_2^{2-} \quad (6b)$$

In our analysis of potential superconductivity in silver fluorides we have used one "physical" model (BCS) and one "chemical" one (Burdett's ideas). There are other models, intuitively attractive—Goddard's exchange coupling, Simon's flat-band scenario, etc. We cannot do everything, especially in the current situation of lack of consensus on the way to explain high-T_C materials—the reader we hope will forgive us for moving ahead with these two models.

In the next Section we will analyze approaches which are commonly used to generate superconductivity in oxocuprates, and we will try to adapt them in theory for silver fluorides.

3.6. How to Obtain Superconductivity in Intermediate-Valence Ag^{II}/Ag^{III} and Ag^{II}/Ag^{I} Fluorides?

3.6.1. Impediments to Superconductivity and Overcoming These

In the previous Section we have pointed out many striking similarities between Cu^{II}–O^{2-} and Ag^{II}–F^- compounds. We will try now to explore for the Ag–F systems the same strategies that are used to generate superconductivity in doped Cu^{II}–O^{2-} systems. Let us first give a brief description of the general approach used in oxocuprates.

At least five interesting phenomena may occur in mixed-valence systems, including three electron "*pairings*" (cases (a), (b), and (d) below). Some of them are connected with breaking the symmetry of the wavefunction (its spatial and/or spin part) describing a system.[282] Solid-state systems formally containing radicals $M^{n+\bullet}$ (for example $Ag^{2+\bullet}$), usually exhibit tendencies toward the following four processes:

a) covalent M–M bond creation [Eq. (7)]

$$M^{n+\bullet} + M^{n+\bullet} \longrightarrow (M{:}M)^{2n+} \quad (7)$$

b) disproportionation (taking on various guises, described as a "charge-density wave", "charge localization via Peierls distortion", "freezing of oxidation states", "lone pair creation") [Eq. (8)]

$$M^{n+\bullet} + M^{n+\bullet} \longrightarrow {:}M^{(n-1)+} + M^{(n+1)+} \quad (8)$$

c) ferromagnetism ($\uparrow\uparrow$) or antiferromagnetism ($\uparrow\downarrow$) (connected often to a "spin-density wave")

d) superconductivity ("creation of boson Cooper pairs", "resonating valence bond", "strong coupling of electrons at the Fermi level with optical phonon", "gap opening at the Fermi level")

e) one may get "normal" metallic behavior instead of superconductivity in such systems.

Process (d) is of greatest interest to us, so we have to learn how the first three effects might be avoided or quenched. We also try to avoid behavior (e) in silver fluorides by providing a sufficiently large value of the vibronic (electron–phonon) coupling constant. Let us think now of competing/coexisting[283] possibilities (a)–(d) in the context of Ag^{II}–F systems.

Covalent M–M bond creation (a) is empirically unlikely for Group 11 M^{II} (d^9) systems. It occurs more often for isoelectronic Group 18 M^I systems such as Ni^I,[284] Pd^I,[285] and Pt^I[286] and is quite common for Group 17 M^0 systems, that is, Co^0,[287] Rh^0,[288] and Ir^0.[289] In principle, the pairing of electrons into bonds and the low bond strength that would follow is prevented in M^{II} (d^9) systems by the low bond strength that would follow and by coulombic repulsion of the metal centers. Nevertheless, spin pairing (some would call it "a very weak

Cu–Cu bond") occurs, for example, in some Cu^{II} compounds, such as the acetates.[290, 291]

The disproportionation tendencies (b) of Cu, Ag, and Au[292] in different environments are collected in Table 9. Generally speaking, Ag^{II} fluorides crystallizing in extended nets do *not* have a tendency toward disproportionation to Ag^{I} and Ag^{III}. But several interesting exceptions exist. A binary fluoride, AgF_2, is one of them. It is known that AgF_2 occurs in two forms, a disproportionated one (high-temperature) and a nondisproportionated one (low-temperature). A formula $Ag[AgF_4]$ may be assigned to the first (diamagnetic) form. $Ag[SbF_6]_2$ is another example of "valence tautomerism" of Ag–F compounds. This compound contains isolated Ag^{II} centers; it would be very interesting to examine whether indeed and why it exhibits a tendency to disproportionation. "Valence tautomerism" has been also suggested for $[AgF][AsF_6]$, $[AgF][SbF_6]$, and $[AgF][AuF_6]$, since Peierls transitions had been anticipated—probably erroneously—for these compounds.[293]

Table 9. Summary of the disproportionation tendency in M^{II}/A systems ($M = Cu, Ag, Au$; $A = Cl^-, O^{2-}, F^-$).

	Cu^{II}	Ag^{II}	Au^{II}
Cl^-	NO	YES	YES
O^{2-}	NO	YES	YES
F^-	NO	NO[a]	YES[b]

[a] Three examples of disproportionated systems are known to date. [b] Five examples of comproportionated systems are known to date.

It is interesting that a more pronounced tendency towards charge separation may be obtained in Ag^{II}–F systems upon hole doping. Several examples of mixed-valence Ag^{II}/Ag^{III} fluorides are known ($[AgF][AgF_4]$, $Ag[AgF_4]_2$, and $[AgF]_2[AgF_4][AsF_6]$). As far as we know, intermediate valence Ag^{II}/Ag^{III} fluorides have not been obtained so far. There is evidence for an Ag^{II}/Ag^{I} fluoride as a nonstoichiometric AgF_{2-x} species. It is not known whether it is a mixed-valence or an intermediate valence compound.

Let us examine next possibility (c), the occurrence of collective magnetic phenomena in Ag^{II} fluorides. Relevant numeric data are collected in Table 10 and illustrated in Figure 29.

The magnetic behavior of silver fluorides is very diverse (see Section 3.2.2). We find among these phases Curie-law obeying paramagnets, paramagnets with strong deviation from the Curie law (such as silver titanate), temperature-independent paramagnets, and antiferromagnets.[294] Also a weak ferromagnetic component has been suggested for AgF_2. The strength of the antiferromagnetic coupling of Ag^{II} fluorides (measured by their Neél temperature T_N) proves its strong dependence on the distance between interacting paramagnetic centers (Figure 29). The data available are limited, so we can plot only five points in our T_N versus R(Ag–Ag) dependence graph (including the Curie temperature for AgF_2, a weak ferromagnet with a strong antiferromagnetic component). The dependence is nearly linear for four quasi-2D fluorides with half-filled $x^2 - y^2$ bands.[295] The only point breaking linearity is that for a 1D antiferromagnet, with a half-filled z^2 band. Using Figure 29, we may predict that

Table 10. Magnetic behavior of the selected Ag^{II}–F systems; antiferromagnets are listed in the order of increasing Neél T_N temperature.

Compound	$R(Ag^{II}–F)$ [Å]	$R(Ag^{II}–Ag^{II})$ [Å]	Magnetic behavior (temperature range [K])	T_N, T_C, or Θ [K]
$[BaF_2]_2[AgF_2]$	ca. 2.16[a]	ca. 4.32[a]	param.	$\Theta = +4$
$Ag^{II}[SbF_6]_2$	2.095 – 2.132	5.224	temp.-indep. param. (50 – 280)	$\Theta = +3$
$BaAgF_4$	2.05	4.264	param., Curie-Weiss (6 – 280)	$\Theta = -4$
$Ag^{II}[BiF_6]_2$	2.096 – 2.122	5.218	temp.-indep. param. (35 – 280)	$\Theta \approx -40$
$Ag^{II}[TiF_4]$	2.122 – 2.181	–	param. with strong spin coupling	$\Theta = -70$[b]
$[AgF]^+[Cd^{2+}]_3[Zr_3F_{19}]^{7-}$	2.102	4.205	antiferrom., above T_N temp.-indep. param.	$T_N = 3$
$[CsF]_2[AgF_2]$	2.29	4.580	antiferrom.	$T_N = 20$
$[RbF]_2[AgF_2]$	–	–	Curie-Weiss (60 – 300), antiferrom.	$T_N = 25$
$[AgF]_2[AsF_6][AgF_4]$	2.003	3.903	temp.-indep. param. (50 – 280) below 50 K Curie-like behavior	
$[CsF][AgF_2]$	2.07 – 2.13	4.260	above T_N temp.-indep. param.	$T_N = 50$
$[RbF][AgF_2]$	2.06 – 2.10	4.220	antiferrom., above T_N temp.-indep. param.	$T_N = ?$
$[KF]_2[AgF_2]$	–	–	antiferrom.	$T_N = 60$
$[AgF]^+[AuF_6]^-$	–	3.800	temp.-indep. param. (63 – 280)	
$[AgF]^+[AsF_6]^-$	1.995 – 2.004	3.795	temp.-indep. param. (63 – 280)	
$[AgF]^+[BF_4]^-$	2.002 – 2.009	4.011	temp.-indep. param. (6 – 280)	
$[KF][AgF_2]$	2.08	4.16	antiferrom., above T_N temp.-indep. param.	$T_N = 80$
α-AgF_2	2.068 – 2.074	3.776	weak spin-canted ferromagnet, strong antiferrom. coupling	$T_C = 163$, $\Theta = -715$

[a] The Ba_2ZnF_6 structure was assumed. [b] AgF_2 impurity may be source of large negative Θ value.

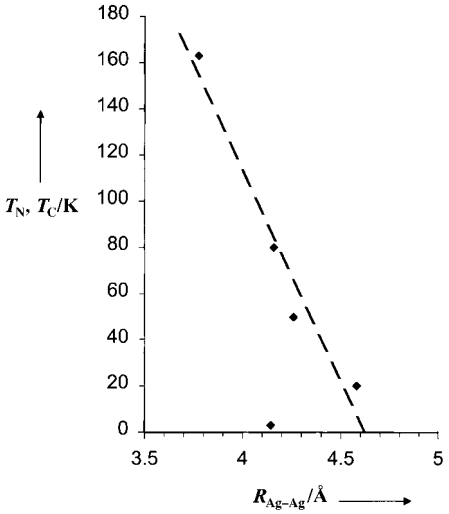

Figure 29. Correlation between the Neél temperature T_N (in the antiferromagnetic Ag^{II} fluorides) or the Curie temperature T_c (in ferromagnetic AgF_2) and the closest Ag–Ag distance. The point off the linear dependence is from $[AgF]^+[Cd^{2+}]_3[Zr_3F_{19}]^{7-}$.

antiferromagnetic behavior would not be observed for quasi-2D Ag^{II} fluorides with the closest Ag – Ag separation larger than 4.7 Å. It may be also seen from Table 10 that antiferromagnetism is usually weak or not observed in substances containing a kinked $[AgF]^+$ infinite chain. Antiferromagnetic superexchange occurs preferably in the 180° or 90° M-X-M conformation, and the above observation is in accordance with this rule (yet $AgFBF_4$ is an exception from it).

What about the possibility of decreasing the energy of a system by electron condensation into spin-less boson[296] pairs (possibility (d)?). In principle, people have elaborated numerous approaches to this unusual phenomenon. A brief summary of a vast literature is that we have a lot of clever people not reading each other's papers. There is little consensus. We tend to think of superconductivity in the spirit of a simple BCS theory, supported by Burdett's "magic state" approach. It is known that although the original BCS theory does not explain quantitatively high-temperature superconductivity, still a vibronic component is very important in ceramic materials.[297–299] Its importance is also apparent in Burdett's approach. In our view (we are voicing an opinion), superconductivity might be understood as a "dynamic" Peierls distortion,[300] to some degree similar to the "static" one which occurs in the "intermediate" class II of mixed-valence compounds. In other words, sometimes a large tendency to antisymmetrization might be hidden in geometrically symmetric or almost symmetric systems. Such a tendency may reveal itself only in a dynamic way, but does not lead to a definite, "static" band- gap opening, such as occurs during strong "frozen" Peierls distortion in a system with a half-filled band.[301]

In our recent studies of molecular systems, we have shown that large values of off-diagonal dynamic linear vibronic coupling constant may be obtained in triatomic molecules built of hard Lewis acids and bases of large electronegativity, with bonds as short and as strongly covalent as possible.[302–305] The same numerical and qualitative conclusions were reached for the diagonal vibronic coupling constant in T_1 states of diatomic AB molecules (A, B = halogen, alkali metal, or H). Ag^{II} is a very hard Lewis acid, and the F^- ion is a very hard Lewis base. We also showed how one could apply these conclusions to extended materials.[306] Our interest in covalent, strongly oxidizing ("very electronegative") Ag–F systems originates in large part from our theoretical findings for molecules.[307]

What approaches are used to generate superconductivity in different solids? Hole or electron doping in an antiferromagnetic insulator[308] (or semiconductor) is the most common one. It is illustrated schematically in Figure 30. The left part of the graph shows doping of the half-filled band with electrons.

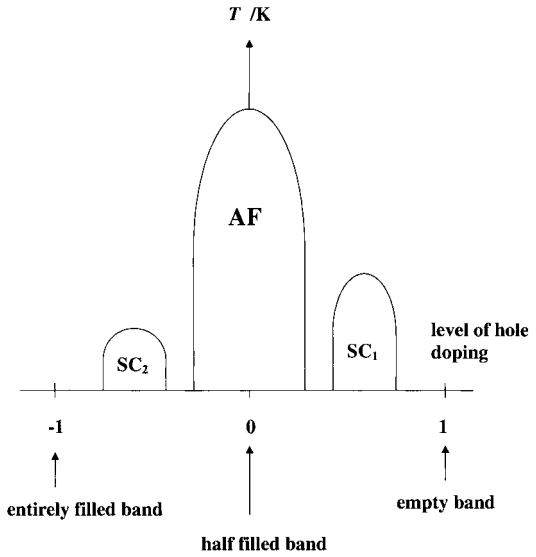

Figure 30. Scheme showing the appearance of two superconducting phases, SC_1 and SC_2, in the course of hole- (right side) or electron-doping (left side) of the antiferromagnetic (AF) parent compound with a half-filled band.

The right part illustrates doping with holes. The antiferromagnetism weakens and even disappears with increase of the doping level, both with electrons and holes. Diluting paramagnetic centers with electrons leads in case of the M–X antibonding band (as in cuprates) to elongation of the M–X bonds, and doping with holes leads to their compression. Quenching of antiferromagnetism should be thus a steeper function of doping level when electrons are doped into the half-filled band. Two superconducting phases (SC_1 and SC_2 in Figure 30) may appear on either side of the "antiferromagnetic" region, at certain levels of doping. Although critical superconducting temperatures obtained in electron-doped oxocuprates are an order of magnitude smaller than those for hole-doped systems, there is a belief that there are essential similarities in the appearance of superconductivity in both these families.[309]

The precise control of the distance between Cu centers proves to be one of the most important factors governing superconductivity in cuprate layered materials, this is because of the enormous sensitivity of T_C to the Cu–O bond length.[310]

This control may be accomplished, for example, with use of a proper dopant. We think, a cationic dopant, which directly adjoins the formally negatively charged $[CuO_2]^{(2-\delta)-}$ planes[311] plays the role of a "clip", inducing "internal stress" in CuO_2 planes and preventing a "frozen" Peierls distortion (but allowing a dynamic one). We call such a dopant a "primary dopant", in contrast to other ("secondary") dopants present in the unit cell. An "improper" primary dopant may be sometimes successfully replaced by external pressure, according to a simple rule: the larger the dopant—the larger the external pressure necessary to prevent static Peierls distortion.[312] Following the same rule, systems with too small dopants will exhibit an "inverse" dependence of T_C versus pressure, that is, their critical temperatures should *decrease* with external pressure.[313–316]

Ca^{II} ($R_{ion} = 1.00$ Å), Hg^{II} ($R_{ion} = 0.96$ Å), Bi^{III} ($R_{ion} = 1.03$ Å), La^{III} ($R_{ion} = 1.03$ Å), Y^{III} ($R_{ion} = 0.90$ Å), Sr^{II} ($R_{ion} = 1.18$ Å), and Pb^{II} ($R_{ion} = 1.19$ Å), are the best dopants found so far for "clipping" CuO_2 planes (the average Cu–O distance is 1.88–1.95 Å, and the best dopants, the first three in the list, have $R_{ion} \approx 1.00$ Å[317]). A "primary" role for some of these dopants is exemplified by the large critical temperatures of 85 K reached in recently prepared $CaCuO_{3-\delta}$ monocrystals[318] (the oxygen content was not optimized), 96 K for $HgBa_2CuO_{4-\delta}$,[217] and 100 K for $Sr_3Cu_2O_{5+\delta}$.[319]

3.6.2. How to Obtain Intermediate-Valence Ag^{II}/Ag^{III} and Ag^{II}/Ag^{I} Fluoride Systems? Which Dopants Should One Use?

Neil Bartlett wrote in a description of his research:[152]

> "The aim of this work is the synthesis and characterization of new two and three dimensional solids that may be useful in electrical energy storage. Fluorides are emphasized because fluorine is small, lightweight, and highly electronegative. Thus high oxidation-state fluorides such as those of cobalt, nickel, copper or silver have high oxidizing potential and low formula weights. Emphasis is placed on the thermodynamically unstable fluorides, which have sufficient kinetic stability to be easily stored. Such fluorides are not only powerful oxidizers, but the metal center in each is comparable in electronegativity to fluorine. It is probable therefore, that some of the thermodynamically unstable fluorides will be metallic or even superconducting (like some copper oxide systems)."

In the gas phase, both Ag^{II}[320] and Au^{II}[321] are relatively stable. This situation may change dramatically in the solid state, where metal centers may communicate with one another; the first fluoride complexes of Au^{II} in the solid state have been synthesized only in the last decade.

Importantly, strongly hole-doped binary and ternary Ag^{II} fluorides, such as $Ag[AgF_4]_2$, $[AgF][AgF_4]$, and $[AgF]_2[AgF_4][AsF_6]$ (the formal oxidation state of Ag in these substances is +2.67, +2.5, and +2.33, respectively) are *not* stable toward disproportionation to Ag^{II} and Ag^{III} (see Figure 16, 17, and 15, respectively). Interesting attempts to melt the first two substances with alkali fluorides led to decomposition of the samples. On the other hand, very little is known about a nonstoichiometric AgF_{2-x} ($x \approx 0.1$), formally a mixed-valence Ag^{II}/Ag^{I} compound, an electron-doped silver fluoride of Ag^{II}. Given the dramatically different affinity of Ag^{I}, Ag^{II}, and Ag^{III} towards F, strategies to obtain intermediate-valence Ag^{II}/Ag^{I} and Ag^{II}/Ag^{III} compounds will undoubtedly differ significantly. Let us remind ourselves of the preferences of Ag^{I}, Ag^{II}, and Ag^{III} for bonding with F^- ions:

a) Ag^{I} interacts quite weakly with the F^- ion, and its Lewis acidity is saturated already at one F atom per Ag atom.
b) Ag^{II} exhibits stronger, but diverse affinity towards F^-. Ag^{II} appears as the cation in $[AgF]^+$ infinite chains (creating two very strong bonds and four much weaker ones), as an isolated neutral $[AgF_2]$ species, and as an anion in isolated $[AgF_4]^{2-}$ units. The intermediate stages known (2+4, 2+2+2, and 4+2 coordination) emphasize the "amphoteric" behavior of Ag^{II} in fluoride systems.
c) Ag^{III} is the strongest F^--abstracting agent known among these three oxidation states of silver. It occurs in isolated $[AgF_4]^-$ units (low-spin form) or even in isolated $[AgF_6]^{3-}$ units (high-spin form). Only in thermodynamically unstable AgF_3 do the Ag^{III} assemble into quasi-1D helical chains.

Given the very different coordination preferences of Ag^{I}, Ag^{II}, and Ag^{III} towards F, and very different Ag^{n+}–F^- bond lengths (2.46 Å,[322], 2.00–2.07 Å, and 1.88 Å for $n = 1$, 2, 3, respectively), the comproportionation–disproportionation equilibrium in the hole- and electron-doped Ag^{II} fluorides should be definitely shifted towards disproportionation. In other words, Ag^{I} or Ag^{III} will appear in Ag^{II} compounds as local defects of the crystal structure. It also means that construction of intermediate valence hole- and electron-doped Ag^{II} fluorides will be a difficult goal to reach in practice. How might one do it?

The broad spectrum of coordination environments seen in the Ag^{I}, Ag^{II}, and Ag^{III} fluorides poses very specific requirements for construction of an intermediate-valence system. The tactics for constructing Ag^{I}/Ag^{II} and Ag^{II}/Ag^{III} systems will differ substantially. Our intuition is that the Ag^{II}/Ag^{III} systems might be obtained only in fluorine-deficient systems, involving very "hard", strongly F-abstracting dopants. These dopants play a primary role in net-arrangement by covalent-bond creation, and prevent the affinity of Ag^{III} to F^- ions from being spontaneously fulfilled. On the other hand, the Ag^{I}/Ag^{II} systems might be obtained in moderately fluorine-deficient systems, using moderately potent F-abstracting dopants. Such dopants will not liberate the Ag^+ ion[323] and thus will not destroy the 1D or 2D structure of the Ag–F net.

Covalent bonding between dopant and O centers in cuprates, as well as its interaction with z^2 lone pairs on Cu atoms also seems essential for 1) regulation of charge residing on CuO_2 planes, 2) for tuning the relative position of Cu(d) and O(p) levels, and 3) for introducing desired stress into the CuO_2 planes. Addition of dopant levels to the DOS_F is another important role played by the dopant in different classes of superconducting materials.[324] This premise suggests that it makes sense to use Be, B, Al, C, Si, Ge, P, As, Sb, Bi, Se,

Te, I (as well as Ti, Zr, Hf, V, Nb, Ta, W, Mo, Ru, Os, Rh, Ir, Ni, Pd, Pt), as potential dopants for Ag–F systems. thus creating strong bonds with F centers at certain—usually the highest accessible—oxidation states.

When we showed him a draft of this paper, Prof. Bartlett described further his experimental search for superconductivity in Ag/F compounds in a private communication to us (August 2000):

"You may be surprised to learn that I have been looking for a superconductor in the Ag/F system for the past 8 years because of observations that we made in 1992. Briefly, we noted that whenever we prepared a $[AgF]^+[MF_6]^-$ salt and washed it with anhydrous HF, the magnetic susceptibility exhibited a sharp drop at 63 K, suggestive of a superconducting transition caused by an impurity. Since this anomaly (it looks like a Meissner effect) was independent of M = Sb, As, Au (ref. [29] herein), I assumed that the impurity was a mixed oxidation-state Ag^{II}/Ag^{III} fluoride. The material that exhibits the 63 K anomally, does not produce identifying lines in the X-ray diffraction pattern (the parent materials give sharp strong patterns). My surmise has therefore been that the quantity present is small (< 5%). This surmise is obviously not valid if the material is non-crystalline. This set in train a set of investigations […]. My first and still favoured guess was that the 63 K diamagnetic phenomenon was caused by an electron-oxidized AgF_2 sheet-structure [i.e. $[AgF_2]^{n+}$, $n < 1$] intercalated (perhaps non-stoichiometrically) by $[AgF_4]^-$ species. I also allowed that $[MF_6]^-$ could be an intercalating species. It is my belief that some disorder in the placement of the anionic charges is necessary, if hole localization is to be avoided. […] I do not believe that a one dimensional $\{[AgF]^+\}_\infty$ chain would give rise to superconduction! […] It was this set of thoughts that caused me to look at the oxidation of AgF_2 with $[O_2]^+$ salts, unfortunately we only obtained the linearly coordinated $[AgF]_2[MF_6][AgF_4]$ salts. The $[AgF]_2[MF_6][AgF_4]$ salts do not show the anomaly until they are washed with anhydrous HF (i.e. solvolysed). We never obtained an intercalated sheet structure, like that of $Au[AuF_4]_2Au[SbF_6]_2$. It could be that an off-stoichiometry silver relative of the latter is the desired material."

4. Summary and Outlook

In this paper we have gathered all experimental data known to us to date for binary and ternary Ag^{II} and Ag^{III} fluoride systems in the solid state, with an emphasis on structures and magnetic properties.

Although about 100 Ag^{II} and Ag^{III} fluorides are known, much experimental and theoretical data for these interesting materials is missing. Crystal structures are known for about 40% of these compounds, we estimate, and have been refined only for about 15% of them. On the other hand, magnetic measurements have been carried out for almost all of them. Spectroscopic (IR,[325] Raman, UV/Vis,[326] NMR,[327] ESR[326, 328]) and thermodynamic data is often lacking. Electric conductivity measurements have not been performed as a function of temperature, external pressure, and magnetic field for many of these substances.[329] There is also no basic experimental data on the electronic structure of Ag^{II} fluorides (X-ray and UV photoelectron spectroscopy (XPS, UPS), EXAFS (extended X-ray absorpsion fine structure), XANES (X-ray absorption near edge structure) etc.). The majority of these compounds has been synthesized in only two groups: one previously led by Hoppe and now by Müller (Gießen), another one directed by Bartlett (Berkeley).

"Whatever causes superconductivity above 40 K, it seems to involve the layers containing copper and oxygen atoms, which are common to all compounds exhibiting a high critical temperature T_C."[330] Chemistry is a living science. For example, only 10 years ago the existence of nondisproportionated Au^{II} in the solid state would be questioned. Today we know from experiment that fluoride complexes of Au^{II} are relatively stable in solid state.[30]

It is our opinion that both 2D and 1D Ag–F structures may, under certain conditions, give rise to superconductivity (also when doped with electrons, and not only with holes). And a special design is required to provide similar environments for Ag^{I} and Ag^{II}, or Ag^{II} and Ag^{III} species (some stress has to be introduced into the structures) in potential superconducting materials. This is very difficult to do for Ag^{II}/Ag^{III} compounds (and also for Au^{II}/Au^{III} ones; note that $Au[AuF_4]_2Au[SbF_6]_2$ is a *mixed-valence* species, with average Au^{II}–F and Au^{III}–F bond lengths of 2.12 Å and 1.92 Å, respectively, see Figure 5 in ref. [30]). We think that Ag^{III} is most likely to enter AgF_2 planes as a local defect. Synthesis of intermediate-valence Ag^{II}/Ag^{I} compounds seems easier to us. The stretching force constant for the approximately 2.46 Å long Ag^{I}–F bond is rather small, and one may compress it so that the Ag^{I}–F bond resembles an Ag^{II}–F bond. However, following the same line of reasoning, the prospect for superconductivity in the Ag^{I}/Ag^{II} systems appears to be less than that for Ag^{II}/Ag^{III} ones.

Led by the isoelectronic character of Ag^{II} and Cu^{II} (d^9), and F^- and O^{2-} (s^2p^6) species, by the similarity of the ligand-field of F^- and O^{2-} ions, a strong covalent contribution in both Cu^{II}–O^{2-} and Ag^{II}–F^- bonding, apparent crystal structure analogies, as well as by our previous theoretical considerations on molecular systems,[302–305] we have analyzed the hypothetical occurrence of superconductivity in hole- or electron-doped Ag^{II} fluorides. In particular, we have studied 1D (infinite chains)[331] and 2D (AgF_2 sheets) Ag–F nets, having formally mixed-valence Ag^{II}/Ag^{I} and Ag^{II}/Ag^{III} character. For this purpose we have examined analogies between the well-known superconducting cuprates (Cu^{II}/Cu^{III}–O^{2-} and Cu^{II}/Cu^{I}–O^{2-} systems) and the Ag^{II}/Cu^{III}–F^- and Ag^{II}/Ag^{I}–F^- solids.

To explain the connection between geometrical features and the electronic properties of these systems, we performed density functional theory (DFT) electronic-structure computations for some selected compounds. The DOS of Ag^{II} and Ag^{III} compounds in the -10.0 eV to 0.0 eV energy range contains sets of Ag–F bonding, Ag–F nonbonding, and Ag–F antibonding states. The relative position of the predominantly Ag(d) orbitals shifts predictably down as one goes from Ag^{I} to Ag^{II} to Ag^{III}, crossing the F(p) band near Ag^{III}.

In the calculations the Ag^{II}–F^- bonds appear to be substantially covalent (similar to Cu^{II}–O^{2-} bonds). States in the vicinity of the Fermi level in Ag^{II} fluorides usually have strongly mixed Ag(d)/F(p) character and are Ag–F antibonding, thus providing the potential for efficient vibronic coupling. The values of DOS_F and metal–ligand stretching frequencies for Ag–F materials are also close to those for oxocuprates. In addition, an "ionic/covalent" curve crossing is expected in some hole-doped Ag^{II} fluorides, which might lead to the "magic electronic state" suggested by Burdett for oxocuprates.

In a separate paper we will show how to apply in practice the idea of using a dopant which "clips" the Ag-F-Ag fragments in 1D and 2D structures. We will analyze the possible structural and electronic changes in Ag^{II}–F systems upon hole- and electron-doping, and we will discuss strategies for preserving an intermediate-valence character of these systems, while repressing a tendency toward their disproportionation through dynamic band-gap opening. We intend to propose a concrete crystal-engineering based experimental strategy to 1) increase the density of states at the Fermi level, 2) augment the electron–phonon coupling constant, 3) dilute paramagnetic Ag^{II} centers (quenching antiferromagnetism), 4) prevent Peierls distortion (preserving the intermediate-valence character of a system), and 5) generate the "ionic/covalent" curve crossing. We expect that under such conditions superconductivity might be induced in the Ag–F nets.

Intermediate-valence quaternary Ag–F compounds are not going to be easy to make, and possibly might be supported by applying external pressure. This factor may shift the comproportionation equilibrium and allow metallization of the mixed-valence compound.[332]

5. Acknowledgements

This research was conducted using the resources of the Cornell Theory Center, which receives funding from Cornell University, New York State, the National Center for Research Resources at the National Institute of Health, the National Science Foundation, the Defense Department Modernization Program, the United States Department of Agriculture, and corporate partners. This work was also supported by the Cornell Center for Materials Research (CCMR), a Materials Research Science and Engineering Center of the National Science Foundation (DMR-9632275) and by NSF Research Grant (CHE 99-70089). The authors gratefully acknowledge Neil Bartlett, Bernd G. Müller, and Miguel Moreno for their valuable comments, and Prof. Bartlett's permission for reproducing here Figure 16 as well as for allowing us to quote him. Bernd G. Müller also allowed us to quote him and kindly sent us unpublished crystal structure data for Ag_2F_5 and $AgMF_6$ ($M = Sn, Ti, Pd$). We also thank Stephen Lee for making the VASP code available to us, to Robert Konecny and Peter Kroll for technical help, and to Gion Calzaferri for his comments on AgF. Stimulating discussions with Bill Wedemeyer are greatly appreciated.

Received: September 25, 2000 [A 431]

6. Appendix

Table 11. Comparison of several important properties of oxygen and fluorine and their compounds.

	O	F
1st E_i [kJ mol^{-1}]	1313.9	6050.4
1st E_{ea} [kJ mol^{-1}]	141	328
Pauling EN	3.44	3.98
Mulliken-Jaffe EN	3.41 (16.7 % s)	3.91 (14.3 % s)
redox potential E^0 [V] (acidic solution):		
	1.76 (H_2O_2/H_2O)	3.05 (F_2/HF)
	1.23 (O_2/H_2O)	2.98 (F_2/HF_2^-)
	0.695 (O_2/H_2O_2)	
	−0.13 (O_2/HO_2)	
Redox potential E^0 [V] (basic solution):		
	0.87 (HO_2^-/OH^-)	2.87 (F_2/F^-)
	0.40 (O_2/OH^-)	
	0.20 (O_2^-/HO_2^-)	
	−0.06 (O_2/HO_2^-)	
$R(X^0)$ [Å]	1.21	1.42
$R(X^{-1})$ [Å]	1.76 (Pauling)	1.36 (Pauling), 1.19 (cn = 6, O_h), 1.17 (cn = 4, T_d)
$R(X^{-2})$ [Å]	1.40 (Pauling), 1.28 (cn = 8), 1.24 (cn = 4, T_d)	–
R(vdW) [Å]	1.52	1.47
bond enthalpy [kJ mol^{-1}] of diatomic BX molecules:		
B = F	222 ± 17	158.8
B = O	498.4 ± 0.2	222 ± 17
B = H	427.6	570 ± 0.1
B = Li	333.5 ± 8.4	577 ± 21
B = Cs	295.8 ± 62.8	519 ± 8

[a] E_i = ionisation energy; E_{ea} = electron affinity; EN = electronegativity (in Pauling units); cn = coordination number; vdW = van der Waals.

[1] a) There is an important review paper on the Ag^{II} and Ag^{III} fluorides known up to 1987: B. G. Müller, *Angew. Chem.* **1987**, *99*, 120; *Angew. Chem. Int. Ed. Engl.* **1987**, *26*, 1081. The author has concentrated on the comparison of Ag, Cu, Au, and Pd, fluorides and on synthetic and structural aspects. Another review on transition metal derivatives of strong protonic acids and superacids mentions selected Ag^{II} compounds b) F. Aubke, M. S. R. Cader, F. Mistry in *Synthetic Fluorine Chemistry* (Eds.: G. A. Olah, R. D. Chambers, G. K. S. Prakash), Wiley, New York, **1992**, chap. 3, p. 43). See also two other excellent reviews c) on crystal structure and bonding in transition metal fluoro compounds: W. Massa, D. Babel, *Chem. Rev.* **1988**, *88*, 275; and d) on classification of heavy metal fluorides with a body-centered cubic cationic sublattice: S. V. Borisov, N. A. Bliznyuk, E. S. Kuklina, *J. Struct. Chem.* **1994**, *35*, 279. However, silver fluorides are not covered by these last two reviews.

[2] S. Ido, S. Uchida, K. Kitazawa, S. Tanaka, *J. Phys. Soc. Jpn.* **1988**, *57*, 997.

[3] H. Kawamura, I. Shirotani, T. Hirooka, M. Fujihira, Y. Maruyama, H. Inokuchi, *Chem. Phys. Lett.* **1972**, *15*, 594.

[4] Ag_2F, which adopts the $Cd[OH]_2$ structure, is superconducting at 0.06 K: a) M. B. Robin, K. Andres, T. H. Geballe, N. A. Kuebler, D. B. McWhan, *Phys. Rev. Lett.* **1966**, *17*, 917; b) K. Andres, N. A. Kuebler, M. B. Robin, *J. Phys. Chem. Solids* **1966**, *27*, 1747.

[5] A. M. Raaen, I. Svare, T. A. Fjeldly, *Phys. Rev. B* **1980**, *21*, 4895.

[6] S. Hull, P. Berastegui, *J. Phys. Condens. Matter* **1998**, *10*, 7945.

[7] P. M. Halleck, J. C. Jamieson, C. W. T. T. Pistorius, *J. Phys. Chem. Solids* **1972**, *33*, 769.

[8] J. C. Jamieson, P. M. Halleck, R. B. Roof, C. W. T. T. Pistorius, *J. Phys. Chem. Solids* **1975**, *36*, 939.

[9] E. V. Gevorkyan, *Izv. Vyssh. Uchebn. Zaved. Fiz.* **1976**, *9*, 119.

[10] a) J. C. Jamieson, P. M. Halleck, R. B. Roof, C. W. Pistorius, *J. Phys. Chem. Solids* **1975**, *36*, 939; b) P. M. Halleck, J. C. Jamieson, C. W. Pistorius, *J. Phys. Chem. Solids* **1972**, *33*, 769.

[11] B. N. Onwuagba, *Solid State Commun*. **1996**, *97*, 267.

[12] N. Bartlett, G. M. Lucier, C. Shen, W. J. Casteel, Jr., L. Chacon, J. Münzenberg, B. Žemva, *J. Fluorine Chem*. **1995**, *71*, 163.

[13] Yu. M. Kiselev, A. I. Popov, K. V. Bukharin, A. A. Timakov, M. V. Korobov, *Russ. J. Inorg. Chem.* (*Engl. Transl.*) **1988**, *33*, 1852.

[14] C. Shen, B. Žemva, G. M. Lucier, O. Graudejus, J. A. Allman, N. Bartlett, *Inorg. Chem*. **1999**, *38*, 4570.

[15] a) P. Fisher, D. Schwarzenbach, H. M. Rietveld, *J. Phys. Chem. Solids* **1971**, *32*, 543; b) P. Fisher, G. Roult, D. Schwarzenbach, *J. Phys. Chem. Solids* **1971**, *32*, 1641.

[16] B. Žemva, K. Lutar, A. Jesih, W. J. Casteel, Jr., A. P. Wilkinson, D. E. Cox, R. B. Von Dreele, H. Borrmann, N. Bartlett, *J. Am. Chem. Soc*. **1991**, *113*, 4192.

[17] It seems that previous claims of obtaining AgF_3 (a) R. Bougon, M. Lance, *C. R. Acad. Sci. Ser. 2* **1983**, *297*, 117; b) R. Bougon, T. Bui Huy, M. Lance, H. Abazli, *Inorg. Chem*. **1984**, 23, 3667; c) ref. [13]) were premature.

[18] M. Kraus, M. Müller, R. Fischer, R. Schmidt, D. Koller, B. G. Müller, *J. Fluorine Chem.* **2000**, *101*, 165.

[19] O. Graudejus, A. P. Wilkinson, N. Bartlett, *Inorg. Chem.* **2000**, *39*, 1545.

[20] Very few examples of the Ag^{2+} ion in Cl^- and Br^- systems are known. For $[Pd(dddt)_2]Ag_{1.5}Br_{3.5}$ (dddt = 5,6-dihydro-1,4-dithiin-2,3-dithiolate) see: a) E. B. Yagubskii, L. A. Kushch, V. V. Gritsenko, O. A. Dyachenko, L. I. Buravov, A. G. Khomenko, *Synth. Met.* **1995**, *70*, 1039; b) L. A. Kushch, S. V. Konovalikhin, L. I. Buravov, A. G. Khomenko, G. V. Shilov, K. Van, O. A. Dyachenko, E. B. Yagubskii, C. Rovira, E. Canadell, *J. Phys. I* **1996**, *6*, 1555; c) S. V. Kapelnitskii, L. A. Kushch, *Phys. Solid State Engl. Transl.* **2000**, *42*, 350. For Ag^{II} in Cl^- and Br^- host lattices see: d) T. Miyanaga, *J. Phys. Soc. Jpn.* **1979**, *46*, 167; e) M. Moreno, *J. Phys. Soc. Jpn.* **1975**, *53*, 1545; f) J. A. Aramburu, M. Moreno, *Solid State Commun.* **1986**, *58*, 305; g) J. A. Aramburu, M. Moreno, *Solid State Commun.* **1987**, *62*, 513.

[21] M. Jansen, P. Fischer, *J. Less-Common Met.* **1988**, *137*, 123.

[22] B. Standke, M. Jansen, *Z. Anorg. Allg. Chem*. **1986**, *535*, 39.

[23] However, Ag^{II} centers may be stabilized as an impurity in some oxide hosts, see for example: a) J. L. Pascual, L. Seijo, Z. Barandiaran, *J. Chem. Phys.* **1993**, *98*, 9715. Ag^{II} also oxidizes water, but an $[Ag(OH)_4]^-$ ion has been observed in highly basic solutions b) R. J. Lancashire in *Comprehensive Coordination Chemistry*, *Vol. 5* (Eds.: G. Wilkinson, R. D. Gillard, J. A. McCleverty), Pergamon Press, Oxford, **1987**, chap. 54. A theoretical study of a hypothetical $[Ag(OH_2)_6]^{2+}$ ion has been performed c) R. Åkeson, L. G. M. Pettersson, M. Sandström, U. Wahlgren, *J. Am. Chem. Soc.* **1994**, *116*, 8691.

[24] B. Žemva, R. Hagiwara, W. J. Casteel, Jr., K. Lutar, A. Jesih, N. Bartlett, *J. Am. Chem. Soc*. **1990**, *112*, 4846.

[25] R. Hagiwara, F. Hollander, C. Maines, N. Bartlett, *Eur. J. Solid State Inorg. Chem.* **1991**, *28*, 855.

[26] G. M. Lucier, C. Shen, W. J. Casteel, Jr., L. Chacon, N. Bartlett, *J. Fluorine Chem*. **1995**, *72*, 157.

[27] B. Žemva, *C. R. Acad. Sci. Ser. II C* **1998**, *1*, 151.

[28] G. M. Lucier, J. Münzenberg, W. J. Casteel, Jr., N. Bartlett, *Inorg. Chem*. **1995**, *34*, 2692.

[29] W. J. Casteel, Jr., G. M. Lucier, R. Hagiwara, H. Borrmann, N. Bartlett, *J. Solid State Chem*. **1992**, *96*, 84.

[30] S. H. Elder, G. M. Lucier, F. J. Hollander, N. Bartlett, *J. Am. Chem. Soc*. **1997**, *119*, 1020.

[31] J. M. Whalen, G. M. Lucier, L. Chacón, N. Bartlett, *J. Fluorine Chem*. **1998**, *88*, 107.

[32] It is known that large vibronic coupling is connected with orbital mixing involving strongly bonding or strongly antibonding levels. For details, see the excellent review: T. Bally, W. T. Borden in *Reviews in Computational Chemistry*, *Vol. 13* (Eds.: K. B. Lipkowitz, D. B. Boyd), Wiley, New York, **1999**, p. 1.

[33] Mixed-valence compounds have been divided by Robin and Day into three classes: class I (disproportionated compounds, with completely localized electrons), class III (comproportionated compounds, completely delocalized electrons) and class II (an intermediate between I and III; dynamic comproportionation at vibrational frequencies may exist in this interesting class). See: M. B. Robin, P. Day, *Adv. Inorg. Chem. Radiochem.* **1967**, *10*, 247.

[34] $CsAgMnF_7$ exists, being presumably the first member of the quaternary $M^IAg^{II}(M')^{IV}F_7$ series (see short mention in B. G. Müller, R. Hoppe, *Z. Anorg. Allg. Chem*. **1973**, *395*, 239).

[35] R. Fischer, B. G. Müller, *Z. Anorg. Allg. Chem*. **1997**, *623*, 1729.

[36] D. Gantar, I. Leban, B. Frlec, J. H. Holloway, *J. Chem. Soc. Dalton Trans*. **1987**, 2379.

[37] M. S. R. Cader, F. Aubke, *Can. J. Chem*. **1989**, *67*, 1700.

[38] "$Ag[MF_6]_2$ (M = Nb, Ta), Ternary Fluorides of Divalent Silver": B. G. Müller, *Angew. Chem*. **1987**, *99*, 685; *Angew. Chem. Int. Ed. Engl.* **1987**, *26*, 689.

[39] B. G. Müller, R. Hoppe, *Z. Anorg. Allg. Chem*. **1972**, *392*, 37. Note added in proof (July 20, 2001): in the meantime a study of $AgM^{IV}F_6$ (M = Sn, Ti, Pb, Pd, Pt, Rh) was published. R. Fischer, B. G. Müller, *Z. Anorg. Allg. Chem.* **2001**, *627*, 445.

[40] R. Hoppe, B. G. Müller, *Naturwissenschaften* **1969**, *56*, 35.

[41] O. Graudejus, S. H. Elder, G. M. Lucier, C. Shen, N. Bartlett, *Inorg. Chem.* **1999**, *38*, 2503.

[42] R. Hoppe, G. Siebert, *Z. Anorg. Allg. Chem*. **1970**, *376*, 261.

[43] G. Siebert, R. Hoppe, R. Homann, *Naturwissenschaften* **1971**, *58*, 95.

[44] B. G. Müller, *Z. Anorg. Allg. Chem*. **1987**, *553*, 196. It is noteworthy that Cu, Ni, Zn, or Mg may substitute one Ag(1) atom, while Ca, Cd, or Hg may substitute two Ag(2) atoms.

[45] D. Koller, B. G. Müller, *Z. Anorg. Allg. Chem*. **2000**, *626*, 1429.

[46] B. G. Müller, *Z. Anorg. Allg. Chem*. **1987**, *553*, 205.

[47] Many other families of ternary and quaternary Cu^{II} fluorides, for example $M^I_3Cu_3M^{IV}F_{12}$ (M^I = Cs, M^{IV} = Zr, Hf), are known (M. Müller, B. G. Müller, *Z. Anorg. Allg. Chem.* **1995**, *621*, 993); however, Ag^{II} analogues have not been prepared so far.

[48] The large negative value of Θ for $AgTiF_6$ probably comes from impurities, i.e. AgF_2, because the former compound can only be synthesized with difficulties by high-pressure fluorination (B. G. Müller, personal communication, **2000**).

[49] The only exception occurs for $Ag_3Hf_2F_{14}$, where Ag(2) is found in 4+4 coordination.

[50] G. C. Allen, R. F. McMeeking, R. Hoppe, B. G. Müller, *J. Chem. Soc. Chem. Commun.* **1972**, 291.

[51] One should not exclude that the postulated diamagnetic form of "$Ag[SbF_6]_2$" is in fact $Ag[Sb_2F_{11}]$, an Ag^I compound (N. Bartlett, personal communication, **2000**).

[52] Details of the crystal structure might also reveal the order of the F-abstracting strength of two very hard Lewis acids, Ag^{III} and Sb^V.

[53] W. Dukat, D. Naumann, *Rev. Chim. Miner.* **1986**, *23*, 589.

[54] The $[Ag_2F_3]^+$ unit also may be expected in the $2\,AgF_2 \cdot AsF_5$ adduct, similar to analogous Sn^{II} and Xe^{II} compounds. For details, see: B. Frlec, D. Gantar, J. H. Holloway, *J. Fluorine Chem.* **1982**, *20*, 385.

[55] $[Ag_3F_9]^{3-}$ ions, analogous to the $[Cu_3F_9]^{3-}$ triangular ions with F bridges between Cu centers,[47] are not known; neither are Ag^{II} analogues of the $KCu^{II}MF_7$ family (M = Zr, Hf), see: M. Kraus, B. G. Müller, *Z. Anorg. Allg. Chem.* **2000**, *626*, 1929.

[56] $[AgF]^+[W_2O_2F_9]^-$ is probably the only oxofluoride material containing infinite $[AgF]^+$ chains (Y. Katayama, R. Hagiwara, Y. Ito, *J. Fluorine Chem.* **1995**, *74*, 89). It is a very strong oxidizer, similar to other compounds in this class. Its structure is not known. Although it oxidizes Xe to Xe^{II} in HF at room temperature, this compound does not liberate a peroxide anion from its structure. Most probably, oxygen atoms are not directly neighboring the Ag center in this compound.

[57] See also a review on bonding in crystals containing 1D bridged and unbridged Group 11 and 12 (d^{10}) linear, zigzag, and helical chains: C. X. Cui, M. Kertesz, *Inorg. Chem.* **1990**, *29*, 2568. Silver fluorides are not covered by this review.

[58] D. Gantar, B. Frlec, D. R. Russell, J. H. Holloway, *Acta Crystallogr. Sect. C* **1987**, *43*, 618.

[59] a) B. Frlec, D. Gantar, J. H. Holloway, *J. Fluorine Chem.* **1982**, *20*, 217; b) B. Frlec, D. Gantar, J. H. Holloway, *J. Fluorine Chem.* **1982**, *20*, 385. $[AgF_2]_2[AsF_5]$ has also been claimed, but no reliably pure samples of this compound were available for detailed investigation of its physical properties.

[60] O. Graudejus, B. G. Müller, *Z. Anorg. Allg. Chem*. **1996**, *622*, 1549.

[61] B. G. Müller, *J. Fluorine Chem*. **1981**, *17*, 317.
[62] B. G. Müller, R. Hoppe, *Z. Anorg. Allg. Chem*. **1973**, *395*, 239.
[63] Note that diamagnetic behavior might also imply superconducting properties of some impurity present in all samples.
[64] There are also some transition metal fluorides with infinite [MF] chains, but with an elongated octahedral coordination of the M atom, $Tl_2MnF_5 \cdot H_2O$ is a good example (P. Nuñez, A. Tressaud, J. Darriet, P. Hagenmuller, G. Hahn, G. Frenzen, W. Massa, D. Babel, A. Boireau, J. L. Soubeyroux, *Inorg. Chem.* **1991**, *31*, 770).
[65] We could not recreate the crystal structure of $[AgF]^+[RuF_6]^-$ as given in ref. [28] from the unit cell coordinates, probably because of an error in the crystal coordinates of the Ag or F(1) atom.
[66] R. H. Odenthal, R. Hoppe, *Monatsh. Chem*. **1971**, *102*, 1340.
[67] R. H. Odenthal, D. Paus, R. Hoppe, *Z. Anorg. Allg. Chem*. **1974**, *407*, 151.
[68] A. I. Popov, Yu. M. Kiselev, *Russ. J. Inorg. Chem. Engl. Transl.* **1988**, *33*, 965. It cannot be excluded that Na_2AgF_4 contains $[AgF_3]^-$ 1D chains rather than 2D $[AgF_2]$ planes, by analogy to Na_2CuF_4.
[69] R. H. Odenthal, D. Paus, R. Hoppe, *Z. Anorg. Allg. Chem*. **1974**, *407*, 144.
[70] R. H. Odenthal, R. Hoppe, *Z. Anorg. Allg. Chem*. **1971**, *385*, 92.
[71] R. H. Odenthal, R. Hoppe, *Naturwissenschaften* **1970**, *57*, 305.
[72] An interesting pressure-induced transition from a ferromagnetic to an antiferromagnetic state has been studied for analogous Cu^{II} compounds (T. Kawamoto, N. Suzuki, *J. Phys. Soc. Jpn.* **1997**, *66*, 2487). There are no such studies for Ag^{II} compounds.
[73] C. Friebel, D. Reinen, *Z. Anorg. Allg. Chem.* **1975**, *413*, 51.
[74] Similar tetragonally compressed octahedra occur for several Cu^{II} fluorides, such as $KCuF_3$: a) A. Okazaki, *J. Phys. Soc. Jpn.* **1969**, *26*, 870; b) A. J. Edwards, R. D. Peacock, *J. Chem. Soc.* **1959**, 4126; K_2CuF_4: c) K. Knox, *J. Chem. Phys.* **1959**, *30*, 991; d) M. Kaneko, G. Kubawara, A. Misu, *Solid State Commun.* **1976**, *18*, 1085; and for isolated Cu^{2+} ions in one of crystallographic positions in a Ba_2ZnF_6 host lattice: e) G. Steffen, D. Reinen, H. Stratemeler, M. J. Riley, M. A. Hitchman, H. E. Matthies, K. Recker, F. Wallrafen, J. R. Niklas, *Inorg. Chem.* **1990**, *29*, 2123. This relatively rare environment of d^9 systems has been predicted to occur in an ionic environment: f) A. D. Liehr, C. J. Ballhausen, *Ann. Phys. NY* **1958**, *3*, 304.
[75] Square-planar coordination of the Ag^{II} center is also found in the $[Ag^{II}(py)_4]$ cation (py = pyridine). Similar square-planar coordination of Cu^{II} centers is rare in fluoride systems. $SrCuF_4$ and $CaCuF_4$ with a Cu–F bond length of 1.88 Å are probably the only two examples known (H. G. von Schnering, B. Kolloch, A. Kolodziejczyk, *Angew. Chem.* **1971**, *83*, 440; *Angew. Chem. Int. Ed. Engl.* **1971**, *10*, 413). Isolated Cu^{2+} ions also adopt a square-planar F_4 coordination in a Ba_2ZnF_6 host lattice in one crystallographic position.[38]
[76] G. C. Allen, R. F. McMeeking, *J. Chem. Soc. Dalton Trans.* **1976**, 1063.
[77] H. G. von Schnering, *Z. Anorg. Allg. Chem*. **1973**, *400*, 201.
[78] O. Ruff, M. Giese, *Z. Anorg. Allg. Chem*. **1934**, *219*, 143.
[79] P. Charpin, A.-J. Dianoux, H. Marquet-Ellis, C. Nguyen-Nghi, *C. R. Seances Acad. Sci. Ser. B* **1966**, *263*, 1359.
[80] E. A. Baturina, Yu. A. Lukyanychev, L. N. Rastorguev, *Zh. Strukt. Khim*. **1966**, *7*, 627.
[81] Yu. M. Kiselev, A. I. Popov, A. A. Timakov, K. V. Bukharin, V. F. Sukhoverkhov, *Russ. J. Inorg. Chem. Engl. Transl.* **1988**, *33*, 708.
[82] A. Jesih, K. Lutar, B. Žemva, B. Bachmann, S. Becker, B. G. Müller, R. Hoppe, *Z. Anorg. Allg. Chem*. **1990**, *588*, 77.
[83] The high-pressure black form of AgF_2 (B. G. Müller, *Naturwissenschaften* **1979**, *66*, 519) has a Curie temperature of 160 K.
[84] There has been much controversy over the magnetic behavior of α-AgF_2. The oldest contributions (a) E. Gruner, W. Klemm, *Naturwissenschaften* **1937**, *25*, 59, and ref. [78]), suggest strong paramagnetism of AgF_2 or emphasize ferromagnetic properties of AgF_2 (with a Curie temperature of 163 K). More recent studies (ref. [79] and b) D. Paus, R. Hoppe, *Z. Anorg. Allg. Chem.* **1977**, *431*, 207) suggest ferrimagnetism of AgF_2. Müller discusses ferromagnetism.[83] Fischer et al. have noted a small ferromagnetic component perpendicular to the AgF_2 sheets and a long-range antiferromagnetic ordering below the Curie temperature of 163 K.[15] Finally, Bastow et al. assigned antiferromagnetic properties to AgF_2 and give a Neél temperature $T_N = 163$ K; c) T. J. Bastow, H. J. Whitfield, R. W. Cockman, *Solid State Commun.* **1981**, *39*, 325. Perhaps the uncertain magnetic properties of AgF_2 are caused by the nonstoichiometry of this compound. In our paper we follow the results of Fischer's et al. careful study.
[85] Citation taken from ref. [15b)].
[86] R. Bougon, T. Bui Huy, M. Lance, H. Abazli, *Inorg. Chem*. **1984**, *23*, 3667.
[87] F. W. Einstein, P. R. Rao, J. Trotter, N. Bartlett, *J. Chem. Soc. A* **1967**, 478.
[88] N. Bartlett, *Gold Bull.* **1998**, *31*, 22.
[89] Compare the decomposition temperature of AgF_3 to the value for CuF_3 (−40 °C) and the sublimation temperature of AuF_3 (+300 °C). Compounds of Ag^{III} and also AgF_2 have been used as fluorinating agents in organic and inorganic synthesis, see for example: a) T. Nakajima, Y. Matsuo, B. Žemva, A. Jesih, *Carbon* **1996**, *34*, 1595; b) T. Nakajima, M. Koh, V. Gupta, B. Žemva, K. Lutar, *Electrochim. Acta* **2000**, *45*, 1655; c) P. R. Slater, J. P. Hodges, M. G. Francesconi, P. P. Edwards, C. Greaves, I. Gameson, M. Slaski, *Physica C* **1995**, *253*, 16; d) G. B. Peacock, I. Gameson, M. Slaski, J. J. Capponi, P. P. Edwards, *Physica C* **1997**, *289*, 153; e) Z. Bugarceic, S. Novokmet, Z. Senic, Z. Bugarceic, *Monatsh. Chem.* **2000**, *131*, 799; f) S. Takubo, A. Sekiya, *J. Fluorine Chem.* **1998**, *87*, 105. Compounds of Mn^{IV}, Cu^{IV}, Ni^{IV}, Pt^{VI}, Tb^{IV}, and M^{VI} (M = U, Mo, W) are other popular solid pure fluorine gas generators, see: g) K. O. Christe, R. D. Wilson, *Inorg. Chem.* **1987**, *26*, 2554; h) N. S. Chilingarov, J. V. Rau, L. N. Sidorov, L. Bencze, A. Popovic, V. F. Sukhovernikov, *J. Fluorine Chem.* **2000**, *104*, 291.
[90] Isoelectronic Cu^{III} ion sometimes adopts an octahedral coordination in fluoride complexes, for example in cryolite NaK_2CuF_6 (C. S. Gopinath, *J. Chem. Soc. Faraday Trans.* **1996**, *92*, 3605). Octahedral coordination is also found in many Pd^{II} fluorides, such as $PdMF_6$ (M = Ti, Sn, Pt), although square-planar Pd^{II} is also known in fluoride environments (e.g. in K_2PdF_4, or $CaPdF_4$). Octahedral coordination has been suggested for Ag^{III} only in Cs_2KAgF_6.
[91] R. Hoppe, *Z. Anorg. Allg. Chem.* **1957**, *292*, 29.
[92] A. I. Popov, Yu. M. Kiselev, V. F. Sukhoverkhov, V. I. Spitsyn, *Dokl. Akad. Nauk SSSR* **1987**, *296*, 424.
[93] K. Lutar, S. Milicev, B. Žemva, B. G. Müller, B. Bachmann, R. Hoppe, *Eur. J. Solid State Inorg. Chem*. **1991**, *28*, 1335.
[94] G. M. Lucier, J. M. Whalen, N. Bartlett, *J. Fluorine Chem.* **1998**, *89*, 101.
[95] K. Lutar, A. Jesih, B. Žemva, *Rev. Chem. Miner.* **1986**, *23*, 565.
[96] K. Lutar, A. Jesih, I. Leban, B. Žemva, N. Bartlett, *Inorg. Chem.* **1989**, *28*, 3467.
[97] a) U. Engelmann, B. G. Müller, *Z. Anorg. Allg. Chem*. **1990**, *589*, 51; b) U. Engelmann, B. G. Müller, *Z. Anorg. Allg. Chem*. **1992**, *618*, 43; c) U. Engelmann, B. G. Müller, *Z. Anorg. Allg. Chem*. **1993**, *619*, 1661; d) R. Schmidt, B. G. Müller, *Z. Anorg. Allg. Chem*. **1999**, *625*, 602; e) O. Graudejus, B. G. Müller, *Z. Anorg. Allg. Chem*. **1996**, *622*, 187.
[98] B. G. Müller, *Z. Anorg. Allg. Chem*. **1987**, *555*, 57.
[99] U. Engelmann, B. G. Müller, *Z. Anorg. Allg. Chem*. **1991**, *598/599*, 103.
[100] The stability of $CsAgF_4$ in the $NaAlF_4$ structure should be significant, because R(Cs–F) (ca. 3.0 – 3.2 Å) > $\sqrt{2}\,R$(Ag–F) (R(Ag–F) ≈ 1.9 Å).
[101] R. Hoppe, R. Homann, *Naturwissenschaften* **1966**, *53*, 501.
[102] B. G. Müller, personal communication, **2000**.
[103] $Cs_2Ag^{III}_{0.5}Ag^{V}_{0.5}F_6$ and related $Cs_2Ga_{0.5}Ag^{V}_{0.5}F_6$ seem to be the only claims of Ag^{V} compounds: P. Sorbe, J. Grannec, J. Portier, P. Hagenmuller, *J. Fluorine Chem*. **1978**, *11*, 243.
[104] Attempts to synthesize another mixed-valence fluoride, Ag^{I}-$Ag^{II}Zr_2F_{11}$, did not succeed: D. Koller, B. G. Müller, *Z. Anorg. Allg. Chem*. **2000**, *626*, 1426.
[105] J. T. Wolan, G. B. Hoflund, *Appl. Surf. Sci*. **1998**, *125*, 251.
[106] Hypothethical mixed-valence Ag^{II}/Ag^{I} fluorides are interesting in the context of isoelectronic Cu^{II}/Cu^{I} oxides. The latter are often mixed- and not intermediate-valence compounds. See for example: a) S. J. Hibble, J. Köhler, A. Simon, S. Paider, *J. Solid State Chem.* **1990**, *88*, 534; b) G. Tams, H. Müller-Buschbaum, *J. Alloys Compd.* **1992**, *189*, 241.
[107] A fascinating description of Prof. Bartlett's adventure with fluorine chemistry may be found in N. Bartlett in *Fluorine Chemistry at the*

Millennium - Fascinated by Fluorine (Ed.: E. Banks), Elsevier, Oxford **2000**, chap. 3, p. 29.
[108] Note that despite Jahn–Teller distortion, "an average Ag^{II}–F^- distance" of 2.22–2.30 Å is preserved in pseudooctahedral complexes of Ag^{II}. For similar properties of Cu^{II} compounds see: a) J. Gažo, I. B. Bersuker, J. Garaj, M. Kabešova, J. Kohout, H. Langfelderova, M. Melník, M. Serator, F. Valach, *Coord. Chem. Rev.* **1976**, *19*, 253; b) I. B. Bersuker, *J. Coord. Chem.* **1995**, *34*, 289.
[109] G. Kresse, J. Farthmuller, *Phys. Rev. B* **1993**, *47*, 558.
[110] G. Kresse, J. Farthmuller, *Comput. Mater. Sci.* **1996**, *6*, 15.
[111] Unfortunately, this is not as easy a matter to evaluate as one might imagine. The VASP program requires that one choose certain Wigner–Seitz radii for the atoms in the lattice; the electrons within a certain radius sphere are then integrated. There are two problems that arise: 1) the choice of the radius of the sphere (should it be the same for Ag^I, Ag^{II}, Ag^{III}, or for F and F^-?), and 2) what about the electrons in the interstices between the spheres? We would like to emphasize that the raw computed atomic contributions do not quite add up to the total DOS. To divide the total DOS into atomic (on-site) contributions we have used the following Wigner–Seitz radii [Å]: Ag (1.503), F (0.714), K (2.275), Rb (2.418), Cs (2.831), B (0.905). Such a choice leaves no more than 15% of total electron density located in interstices between atomic spheres. The % atomic contributions to the electron density have been rescaled for each compound to add up to 100% (proportionally to the atomic contributions computed by VASP). Assumption of too large a radius for Ag and/or too small a radius of F may lead to overestimation of the covalency of the Ag–F bonds.
[112] M. R. Hayns, J.-L. Calais, *J. Phys. C* **1973**, *6*, 2625.
[113] R. C. Birtcher, P. W. Deutsch, J. F. Wendelken, A. B. Kunz, *J. Phys. C* **1972**, *5*, 562.
[114] N. J. M. Geipel, B. A. Hess, *Chem. Phys. Lett.* **1997**, *273*, 62.
[115] V. C. Jain, J. Shanker, *Pramana* **1979**, *13*, 31.
[116] From here on we will drop the principal quantum number in describing F, Ag, and Cu states.
[117] a) A. P. Marchetti, G. L. Bottger, *Phys. Rev. B* **1971**, *3*, 2604; b) M. G. Mason, *J. Electron Spectrosc. Relat. Phenom.* **1972**, *52*, 591; c) W. B. Fowler, *Phys. Status Solidi* **1972**, *52*, 591. Interestingly, both direct and indirect band gaps do not appear to scale properly in going from AgCl to AgF; that is, gaps increase and then decrease in the order AgBr → AgCl → AgF.
[118] Since the ligand s, p levels lie lower than the metal d levels, bands originating essentially from the ligand levels should be metal–ligand bonding, and bands originating from the latter should be metal–ligand antibonding.
[119] Unfortunately, the bonding index in the computational code available to us, the Crystal Orbital Overlap Population (T. Hughbanks, R. Hoffmann, *J. Am. Chem. Soc.* **1983**, *105*, 3528), is too sensitive to the choice of Wigner–Seitz radii to allow a reliable bonding assesement.
[120] In principle we should carry out spin-polarized calculations on AgF_2, but we have chosen not to do so, because our primary aim is to compare AgF_2 with other silver fluorides so as to determine the approximate position of Ag(d) and F(p) states. The Curie temperature of AgF_2 is rather low, and results of a precise spin-polarized calculation should not be substantially different from the ones obtained by us. Similar reasoning is valid for antiferromagnets with low Neél temperatures, such as $CsAgF_3$ and Cs_2AgF_4.
[121] Discussions of the degree of covalency, and on generating holes in the F(p) band by tetravalent lanthanide cations (strong oxidizers, similarly to trivalent Ag centers) may be found in: a) Z. Hu, E. J. Cho, G. Kaindl, B. G. Müller, *Phys. Rev. B* **1995**, *51*, 7514; b) Z. Hu, G. Kaindl, B. G. Müller, *J. Alloys Compd.* **1997**, *246*, 177.
[122] In the context of superconductivity, it is of great interest whether holes might be generated in the F(p) band in the hole-doped Ag^{II} fluorides which create extended 1D and 2D nets. We will consider this problem further on in this paper, and in separate work.
[123] The distorted MF_2 layers occur also in pseudo-3D antiferromagnetic $TlMnF_4$ (P. Nuñez, A. Tressaud, J. Grannec, P. Hagenmuller, W. Massa, D. Babel, A. Boireau, J. L. Soubeyroux, *Z. Anorg. Allg. Chem.* **1992**, *609*, 71).
[124] The very narrow F(s) bands at about −25 eV and rather broad Ag(s,p) bands at +5 to +8 eV are not shown in the Figures. The very sharp DOS peak at about −9 eV (so narrow that it almost does not contribute to DOS integration) is puzzling. It is probably an artifact of the calculation.
[125] The Ag–F nonbonding states may be recognized both by their dominant F(p) character, and by kinks in the integration of the total DOS.
[126] Indication of energetic proximity of Ag(d) (in Ag^{II}) and F(p) orbitals is provided also by electronic and ESR spectra,[326, 328] and by electrochemistry. The reduction potential of Ag^{II}/Ag^I in *liquid* HF is +2.27 V, rather close to the F_2/F^- potential (+2.71 V). The Ag^I/Ag^0 redox pair is left far behind, at +0.88 V (see: *Comprehensive Inorganic Chemistry* (Eds.: J. C. Bailar, H. J. Emeleus, R. Nyholm, A. F. Trotman-Dickenson), Pergamon, Oxford, **1973**, p. 1053, and refs therein). Values of redox potentials in *aqueous* solutions are lower, but still very positive: +2.0 V for $[AgO]^+/Ag^I$, +2.1 V for $[AgO]^+/Ag^{II}$, +1.98 V for Ag^{II}/Ag^I, and +0.80 V for Ag^I/Ag^0 (see: J. W. Laist, *Comprehensive Inorganic Chemistry*, *Vol. 2* (Eds.: M. C. Sneed, J. L. Maynard, R. C. Brasted), D. Van Nostrand, Toronto, **1954**, p. 144).
[127] There are two strong Ag–F bonds in 1D compounds, in contrast to four strong bonds in 2D compounds with an elongated octahedral configuration of F atoms around Ag atoms. Hence, one needs to divide the value of Ag_{tot}/F_{tot} obtained for a linear chain in 1D $[AgF][BF_4]$ by a factor of 2, to compare it with respective values for AgF_2 sheets in 2D substances.
[128] Based on E_F criterion only.
[129] F. A. Cotton, G. Wilkinson, *Advanced Inorganic Chemistry*, *5th ed.*, Wiley, New York, **1988**.
[130] Data obtained from http://www.webelements.com/.
[131] We use the term "metallic" here focusing on electronegativity values, rather than the electric conductivity in elementary Ag, Cu, and Au. Metals in this classical definition have small electronegativity values and easily form cations; nonmetals have large electronegativity and act mostly as anions in compounds.
[132] The Mulliken–Jaffe EN here is calculated using a weighted average over valence s and p orbitals.
[133] "The elements Cu, Ag, and Au lie on the border between transition metals and Main Group metals ("meta-metals"), but are "true" transition metals in the narrower sense insofar as, in contrast to the elements Zn, Cd, and Hg, d electrons can still be involved in their bonding. […] The fluorides are of particular importance insofar as they are the only compounds in which certain oxidation states can exist." Citation from ref. [1a].
[134] Au^{III} is found in several complexes of Au containing organic ligands, such as $[(C_2H_5)_2AuBr]_2$. Also, $Au(OTeF_5)_3$, an oxyfluoride of Au^{III}, exists (P. Huppmann, H. Hartl, K. Seppelt, *Z. Anorg. Allg. Chem.* **1985**, *524*, 26).
[135] Exotic paramagnetic Cu^{IV} occurs in orange-red compounds with formula M_2CuF_6 (M = Cs, Rb), which crystallize in the K_2PtCl_6 structure. For details, see: a) W. Harnischmacher, R. Hoppe, *Angew. Chem.* **1973**, *85*, 590; *Angew. Chem. Int. Ed. Engl.* **1973**, *12*, 582; b) P. Sorbe, J. Grannec, J. Portier, P. Hagenmuller, *C. R. Hebd. Seances Acad. Sci. Ser. C* **1976**, *282*, 663; c) D. Kissel, R. Hoppe, *Z. Anorg. Allg. Chem.* **1988**, *559*, 40; d) W. Carl, D. Kissel, R. Hoppe, *Eur. J. Solid State Inorg. Chem.* **1990**, *27*, 5. The presence of Au^{IV} in $Sn_{1-x}Au_xF_4$ (e) M. Bork, R. Hoppe, A. Hofstaetter, A. Scharmann, F. E. Wagner, *Z. Anorg. Allg. Chem.* **1996**, *622*, 1721) has not been confirmed by others.
[136] F. G. Herring, G. Hwang, K. C. Lee, F. Mistry, P. S. Phillips, H. Willner, F. Aubke, *J. Am. Chem. Soc.* **1992**, *114*, 1271.
[137] N. R. Walker, R. R. Wright, P. E. Barran, A. J. Stace, *Organometallics* **1999**, *18*, 3569.
[138] a) T. J. Bergendahl, J. W. Waters, *Inorg. Chem.* **1975**, *14*, 2556; b) T. Mori, H. Inokuchi, *Solid State Commun.* **1987**, *62*, 525; and ref. [97d].
[139] Plenty of "pseudo-Au^{II}" compounds exist, $Cs_2[Au^ICl_2][Au^{III}Cl_4]$ is a classical example.
[140] Very recently, $[AuXe_4]^{2+}\{[Sb_2F_{11}]^-\}_2$, a so-far unique Au–Xe compound, has been obtained (S. Seidel, K. Seppelt, *16th International*

Symposium on Fluorine Chemistry, Durham, UK, **2000**). Also $[F_3AsAu]^+[SbF_6]^-$, another compound containing a rare Au^I–As^{III} bond, exists (R. Küster, K. Seppelt, *Z. Anorg. Allg. Chem.* **2000**, *626*, 236).
[141] K. Leary, N. Bartlett, *J. Chem. Soc. Chem. Commun.* **1972**, 903.
[142] A. J. Edwards, W. E. Falconer, J. E. Griffiths, W. A. Sunder, M. J. Vasile, *J. Chem. Soc. Dalton Trans.* **1974**, 1129.
[143] G. Kaindl, K. Leary, N. Bartlett, *J. Chem. Phys.* **1973**, *59*, 5050.
[144] M. J. Vasile, T. J. Richardson, F. A. Stevie, W. E. Falconer, *J. Chem. Soc. Dalton Trans.* **1976**, 351.
[145] P. Sorbe, J. Grannec, J. Portier, P. Hagenmuller, *J. Fluorine Chem.* **1978**, *11*, 243.
[146] For ionic radii of M^V and hypothetical M^{IV} see: A. I. Popov, N. S. Kopelev, Yu. M. Kiselev, *Dokl. Akad. Nauk. SSSR* **1988**, *301*, 623.
[147] R. Schmidt, B. G. Müller, *Z. Anorg. Allg. Chem.* **1999**, *625*, 605.
[148] Chemistry has adopted, at least in colloquial usage, a traditional term of alchemy, "affinity" or "chemical affinity". A strong affinity of certain elements for each other (such as Hg or Ag for S) has been known for millennia. A relationship may be drawn between an "affinity" of two elements and the strength of bonding between them. Extended systems with a net of strong, covalent bonds (such as diamond) are usually less volatile than systems having weaker bonds (such as metallic sodium); the latter melt, sublime, or decompose easier than the former.
[149] Fluorine adsorbs easily on the surface of metallic Ag (in contrast to metallic Au). However, this is because of a redox reaction, and AgF is formed (M. A. Loudiana, J. T. Dickinson, A. Schmid, E. J. Ashley, *Appl. Surf. Sci.* **1987**, *28*, 311).
[150] A. B. Kunz, *Phys. Rev. B* **1982**, *26*, 26.
[151] B. N. Onwuagba, *Solid State Commun.* **1996**, *97*, 267.
[152] http://www.lbl.gov/LBL-Programs/CSD/HTMLFiles/Chem-Eng_htmls/Bartlett_HighEngOx.html.
[153] M. Ilias, P. Furdik, M. Urban, *J. Phys. Chem. A* **1998**, *102*, 5263.
[154] M. Seth, F. Cooke, P. Schwerdtfeger, J.-L. Heully, M. Pelissier, *J. Chem. Phys.* **1998**, *109*, 3935.
[155] V. G. Solomonik, J. E. Boggs, J. F. Stanton, *J. Mol. Struct. (THEOCHEM)* **2000**, *496*, 213.
[156] J. K. Laerdahl, T. Saue, K. Faegri, Jr., *Theor. Chem. Acc.* **1997**, *97*, 177.
[157] J. K. Laerdahl, T. Saue, K. Faegri, *Theor. Chem. Acc.* **1997**, *97*, 177.
[158] H. Wang, J. L. Gole, *J. Chem. Phys.* **1993**, *98*, 9311.
[159] A. Ramirez-Solis, J. Schamps, *J. Chem. Phys.* **1995**, *102*, 4482.
[160] A. Ramirez-Solis, J. P. Daudey, *J. Chem. Phys.* **2000**, *113*, 8580.
[161] The existence of the AuF molecule has been controversial for years. Only very recently has it been confirmed. See: a) C. J. Evans, M. C. L. Gerry, *J. Am. Chem. Soc.* **2000**, *122*, 1560; b) S. Andreev, J. Belbruno, *Chem. Phys. Lett.* **2000**, *329*, 490.
[162] B. Reffy, M. Kolonits, A. Schulz, T. M. Klapotke, M. Hargittai, *J. Am. Chem. Soc.* **2000**, *122*, 3127.
[163] Relativistic bond length contraction is even more pronounced for Au^0 than for Au^I. For example, it is about 0.35 Å for the Au–Au bond in the Au_2 molecule a) P. Pyykkö, J.-P. Desclaux, *Acc. Chem. Res.* **1979**, *12*, 276); and "only" 0.28 Å for the Au–H bond in the AuH molecule (b) K. S. Pitzer, *Acc. Chem. Res.* **1979**, *12*, 271).
[164] a) P. Schwerdtfeger, M. Dolg, W. H. E. Schwarz, G. A. Bowmaker, P. D. W. Boyd, *J. Chem. Phys.* **1989**, *91*, 1762; b) P. Schwerdtfeger, P. D. W. Boyd, A. K. Burrell, W. T. Robinson, *Inorg. Chem.* **1990**, *29*, 3593.
[165] The term "valence tautomerism" is often used for quinone complexes of Fe, Co, or Mn in the solid state, with respect to the transfer of electrons between metal center and quinone moiety. See for example: a) C. G. Pierpont, C. W. Lange, *Prog. Inorg. Chem.* **1994**, *41*, 331; b) D. Ruiz-Molina, J. Veciana, K. Wurst, D. N. Hendrickson, C. Rovira, *Inorg. Chem.* **2000**, *39*, 617. The term also has a long history in the organic chemistry of olefins, and molecular rearrangements.
[166] P. Schwerdtfeger, P. D. W. Boyd, S. Brienne, A. K. Burrell, *Inorg. Chem.* **1992**, *31*, 3411.
[167] A. L. Hector, W. Levason, M. T. Weller, E. G. Hope, *J. Fluorine Chem.* **1997**, *86*, 105.
[168] C. Friebel, *Solid State Commun.* **1974**, *15*, 639.
[169] S. Deibele, J. Curda, E.-M. Peters, M. Jansen, *Chem. Commun*. **2000**, 679.
[170] M. Hidaka, T. Eguchi, I. Yamada, *J. Phys. Soc. Jpn.* **1998**, *67*, 2488.
[171] A. I. Popov, Yu. M. Kiselev, *Russ. J. Inorg. Chem. Engl. Transl.* **1988**, *33*, 1307.
[172] M. Kaneko, G. Kubawara, A. Misu, *Solid State Commun.* **1976**, *18*, 1085.
[173] A compressed octahedral geometry is often adopted by Cu^{II} and Ag^{II} in host fluoride lattices (lattice strain often dominates over Jahn–Teller effect).
[174] "FCu[AuF_4], an Unusual Copper(II) Fluoroaurate(III)": B. G. Müller, *Angew. Chem*. **1987**, *99*, 685; *Angew. Chem. Int. Ed. Engl.* **1987**, *26*, 688.
[175] T. Fleischer, R. Hoppe, *Z. Anorg. Allg. Chem.* **1982**, *492*, 76.
[176] Several compounds of Ag^{III} with organic ligands are known: Ag^{III} octaethylporphyrin perchlorate a) D. Karweik, N. Winograd, D. G. Davis, K. M. Kadish, *J. Am. Chem. Soc.* **1974**, *96*, 591; [Ag(ttp)], ttp = tetratolylporphyrin; b) J.-L. Du, G. R. Eaton, S. S. Eaton, *J. Magn. Reson. A* **1996**, *119*, 240; $[Ag(py)_4(NCMe)](MoF_6)_3$ and $[Ag(py)_2(NCMe)_3](UF_6)_3$ c) J. Iqbal, D. W. A. Sharp, J. M. Winfield, *J. Chem. Soc. Dalton Trans.* **1989**, 461; and $Ag(CF_3)_3 \cdot CH_3CN$ d) D. Naumann, W. Tyrra, F. Trinius, W. Wessel, T. Roy, *J. Fluorine Chem.* **2000**, *101*, 131. Unfortunately, the structures of these compounds have not been determined. There are also many compounds of Au^{III} with organic ligands; see for example: e) S. Komiya, S. Meguro, A. Shibue, S. Ozaki, *J. Organomet. Chem.* **1987**, *328*, C40.
[177] An oxoaurate [AuO_4] unit occurs for example in $M^{II}Au^{III}[Au^{III}O_4]$, M = Ca, Sr, Ba, see: a) G. Krämer, M. Jansen, *J. Solid State Chem.* **1995**, *118*, 247; b) J.-H. Park, J. B. Parise, *Chem. Mater.* **1995**, *7*, 1055; in Bi_2AuO_5 and Bi_4AuO_9: c) J. Geb, M. Jansen, *J. Solid State Chem.* **1996**, *122*, 364; in $LnAu_2O_9$ (Ln = Nd, Gd): d) C. Steiner, M. Andratschke, K.-J. Range, *Z. Naturforsch. B* **1996**, *51*, 811; and in interesting La_4LiAuO_8, which crystallizes in the Nd_2CuO_4 structure: e) W. Pietzuch, S. A. Warda, W. Massa, D. Reinen, *Z. Anorg. Allg. Chem*. **2000**, *626*, 113.
[178] B. G. Müller, *Z. Anorg. Allg. Chem*. **1987**, *553*, 196.
[179] a) P. Gómez-Romero, E. M. Tejada-Rosales, M. Rosa Palacín, *Angew. Chem.* **1999**, *111*, 544; *Angew. Chem. Int. Ed.* **1999**, *38*, 524; b) J. Köhler, *Nachr. Chem.* **2000**, *48*, 254.
[180] See three excellent papers on crystal and electronic structure of oxocuprates: a) H. Müller-Buschbaum, *Angew. Chem.* **1989**, *101*, 1503; *Angew. Chem. Int. Ed. Engl.* **1989**, *28*, 1472; b) B. Raveau, M. Hervieu, C. Michel, D. Groult, J. Provost, *Eur. J. Solid State Inorg. Chem.* **1990**, *27*, 25; c) J. K. Burdett, G. V. Kulkarni, *Phys. Rev. B* **1989**, *40*, 8908.
[181] As a referee correctly reminds us, there are some differences between O^{2-} and F^- ions with respect to their capability to transport charges. Linear bridges, a probable prerequisite for the electron delocalization required for superconductivity, are much more frequent in oxides than in fluorides.
[182] See also the excellent review on bonding in crystals containing 1D bridged and unbridged Group 11 and 12 linear, zigzag, and helical chains: C. X. Cui, M. Kertesz, *Inorg. Chem.* **1990**, *29*, 2568.
[183] J. K. Burdett, S. Serov, *J. Am. Chem. Soc.* **1995**, *117*, 12788.
[184] K.-T. Park, D. L. Novikov, V. A. Gubanov, A. J. Freeman, *Phys. Rev. B* **1994**, *49*, 4425.
[185] L. H. Tjeng, M. B. J. Meinders, J. van Elp, J. Ghijsen, G. A. Savatzky, R. L. Johnson, *Phys. Rev. B* **1990**, *41*, 3190.
[186] M. T. Czyzyk, R. A. de Groot, G. Dalba, P. Fornasini, A. Kiesiel, F. Rocca, E. Burattini, *Phys. Rev. B* **1989**, *39*, 9831.
[187] A. Deb, A. K. Chatterjee, *J. Phys. Condens. Matter* **1998**, *10*, 11719.
[188] K. Heidebrecht, M. Jansen, S. Krause, A. M. Bradshaw, *J. Solid State Chem.* **1990**, *89*, 60.
[189] D. Vogel, P. Krüger, J. Pollmann, *Phys. Rev. B* **1998**, *58*, 3865.
[190] T. Kawamoto, N. Suzuki, *J. Phys. Soc. Jpn.* **1997**, *66*, 2487.
[191] Z. Hu, G. Kaindl, S. A. Warda, D. Reinen, F. M. F. de Groot, B. G. Müller, *Chem. Phys.* **1998**, *232*, 63.
[192] R. Zimmermann, P. Steiner, R. Claessen, F. Reinert, S. Hufner, P. Dufek, *J. Phys. Condens. Matter* **1999**, *11*, 1657.
[193] R. Zimmermann, P. Steiner, R. Claessen, F. Reinert, S. Hufner, *J. Electron Spectrosc. Relat. Phenom.* **1998**, *96*, 179.

[194] J. C. Parlebas, M. A. Khan, T. Uozumi, K. Okada, A. Kotani, *J. Electron Spectrosc. Relat. Phenom.* **1995**, *71*, 117.
[195] a) G. Keindl, O. Strebel, O. Kolodziejczyk, A. Schäfers, W. Kiems, R. Lösch, S. Kemmler-Sack, R. Hoppe, H. P. Müller, D. Kissel, *Physica B* **1989**, *158*, 446; b) T. Mizokawa, H. Nataname, K. Fujimori, H. Akeyama, H. Kondoh, H. Hurada, N. Kosugi, *Phys. Rev. Lett.* **1991**, *67*, 1638.
[196] S. Kim, R. S. Williams, *Phys. Rev. B* **1987**, *35*, 2823.
[197] H.-C. Hsueh, J. R. Maclean, G. Y. Guo, M.-H. Lee, S. J. Clark, G. J. Ackland, J. Crain, *Phys. Rev. B* **1995**, *51*, 12216.
[198] C. R. Aita, N. C. Tran, *J. Vac. Sci. Technol. A* **1991**, *9*, 1498.
[199] T. Ishii, R. Sekine, T. Enoki, E. Miyazaki, T. Miyamae, T. Miyazaki, *J. Phys. Soc. Jpn.* **1997**, *66*, 3424.
[200] A. P. Wilkinson, L. K. Templeton, D. H. Templeton, *J. Solid State Chem.* **1995**, *118*, 383.
[201] J. Zaanen, G. A. Sawatzky, J. W. Allen, *Phys. Rev. Lett.* **1985**, *55*, 418.
[202] The energy of Au(d) levels is very strongly influenced by relativistic effects; it may even happen that the d orbitals of Au are *above* the d orbitals of Ag (in a certain oxidation state).
[203] Y.-Q. Zheng, H. Borrmann, Y. Grin, K. Peters, H. G. von Schnering, *Z. Anorg. Allg. Chem*. **1999**, *625*, 2115.
[204] G. M. Lucier, C. Shen, S. H. Elder, N. Bartlett, *Inorg. Chem.* **1998**, *37*, 3829.
[205] For details of thermal decomposition, see Table 3 in ref. [92].
[206] J. Bardeen, L. N. Cooper, J. R. Schrieffer, *Phys. Rev.* **1957**, *108*, 175.
[207] In principle, "BCS theory lacks material aspect".[207b] There has been much effort to translate BCS predictions to chemical language. We note here the work of three groups with a chemical and physical orientation: a) K. A. Müller in *Phase Separation in Cuprate Superconductors, Proceedings* (Eds.: E. Sigmund, K. A. Müller), Springer, Berlin, **1993**, p. 1; b) A. Simon, *Angew. Chem.* **1997**, *109*, 1879; *Angew. Chem. Int. Ed. Engl.* **1997**, *36*, 1788; c) A. W. Sleight, *Acc. Chem. Res.* **1995**, *28*, 103.
[208] The largest values of the Ag–F stretching frequencies are about 650 cm^{-1} for Ag^{V}, 600 cm^{-1} for Ag^{III}, 450 cm^{-1} for Ag^{II}, and about 170–320 cm^{-1} for Ag^{I} compounds, thus uniformly dropping with decrease of formal oxidation state of silver. See a) R. A. Nyquist, R. O. Kagel, *Infrared Spectra of Inorganic Compounds*, Academic Press, New York, **1971**, p. 362; b) S. Milicev, *Croat. Chim. Acta* **1992**, *65*, 125; c) G. L. Bottger, A. L. Geddes, *J. Chem. Phys.* **1972**, *56*, 3725; and refs. [13] and [205]. The stretching frequency for the AgF molecule (515 cm^{-1}) is significantly larger than in Ag^{I} fluorides in the solid state: d) J. Hoeft, F. J. Lovas, E. Tiemann, T. Törring, *Z. Naturforsch. A* **1970**, *25*, 35. The largest Cu–O stretching frequencies for oxocuprate superconductors ("oxygen modes") are typically about 580–630 cm^{-1} see, for example e) F. Gervais, R. Lobo, *Z. Phys. B* **1997**, *104*, 681; f) N. Watanabe, N. Koshizuka, *Eur. Phys. J. B* **2000**, *15*, 29; g) B. Roughani, L. C. Sengupta, S. Sundaram, W. C. H. Joiner, *Z. Phys. B* **1992**, *86*, 3.
[209] Usually, an increase in covalency induces an increase of the vibronic coupling constant. However, examples are known when a decrease of covalency is connected with increase of vibronic coupling: a) J. A. Aramburu, M. Moreno, K. Doclo, C. Daul, M. T. Barriuso, *J. Chem. Phys.* **1999**, *110*, 1497; b) J. A. Aramburu, M. T. Barriuso, M. Moreno, *J. Phys. Condens. Matter* **1996**, *8*, 6901. This fact is rationalized in a simple model: c) K. Wissing, M. T. Barriuso, J. A. Aramburu, M. Moreno, *J. Chem. Phys.* **1999**, *111*, 10217. We have not computed the electron–phonon coupling constant for Ag–F systems; for that exact calculations of the phonon spectrum would be required, and this is beyond our capabilities.
[210] The T_C values are taken in part from the Beilstein inorganic compounds database: a) Beilstein Information, vers. 4.0 (Build 11), Copyright© 1995–1998 Beilstein Informationssystems GmbH. We also used b) C. N. R. Rao, B. Raveau, *Transition Metal Oxides*, *2nd ed.*, Wiley, New York, **1998**.
[211] The metallic character of AgF_2 computed here might be erroneous because of the nonpolarized spin-character of our calculations (AgF_2 is a spin-canted ferromagnet). For example, metallic character is obtained for $CaCuO_2$ in nonpolarized spin calculations, contrary to experiment (R. V. Kasowski, S.-I. Hatta, W. Y. Hsu, *Solid State Commun.* **1993**, *85*, 837).
[212] a) J. A. Aramburu, M. Moreno, M. T. Barriuso, *J. Phys. Condens. Matter* **1992**, *4*, 9089; b) R. Valiente, J. A. Aramburu, M. T. Barriuso, M. Moreno, *J. Phys. Condens. Matter* **1994**, *6*, 4515; c) R. Valiente, J. A. Aramburu, M. T. Barriuso, M. Moreno, *Internat. J. Quant. Chem.* **1994**, *52*, 1051.
[213] $T_C = 166$ K (−111 °C) at elevated pressure (L. Gao, Y. Y. Xue, F. Chen, Q. Ziong, R. L. Meng, D. Ramirez, C. W. Chu, J. H. Eggert, H. K. Mao, *Phys. Rev. B* **1994**, *50*, 4260). Since 1994 this 1223 compound holds the world record of critical superconducting temperature.
[214] a) A. Schilling, O. Jeandupeux, J. D. Guo, H. R. Ott, *Physica C* **1993**, *216*, 6; b) C. W. Chu, L. Gao, F. Chen, Z. J. Huang, R. L. Meng, Y. Y. Xue, *Nature* **1993**, *365*, 323; c) C. W. Chu, *IEEE Trans. Appl. Supercond.* **1997**, *7*, 80.
[215] J. Yu, S. Massidda, A. J. Freeman, *Physica C* **1988**, *152*, 273.
[216] D. L. Novikov, V. A. Gubanov, A. J. Freeman, *Physica C* **1993**, *210*, 301.
[217] S. N. Putilin, E. V. Antipov, O. Chmaissen, M. Marezio, *Nature* **1993**, *326*, 226.
[218] P. Strange, J. M. F. Gunn, *J. Phys. Condens. Matter* **1989**, *1*, 6843.
[219] T. Jarlborg, *Solid State Commun.* **1988**, *67*, 297; Compare also: B. Szpunar, V. H. Smith, Jr., *Phys. Rev. B* **1988**, *37*, 7525.
[220] D. Bhattacharya, D. K. Pandya, S. C. Kashyap, L. C. Pathak, S. Mishra, D. Sen, K. L. Chopra, *Physica C* **1990**, *170*, 245.
[221] D. L. Novikov, V. A. Gubanov, A. J. Freeman, *Physica C* **1993**, *210*, 301. Also compare to: H. Wu, Q. Zheng, X. Gong, H. Q. Lin, *J. Phys. Condens. Matter* **1999**, *11*, 4637.
[222] Y. Shimakawa, J. D. Jorgensen, J. F. Mitchell, B. A. Hunter, H. Shaked, D. G. Hinks, R. L. Hitterman, *Physica C* **1994**, *228*, 73.
[223] W. J. Yu, Z. Q. Mao, X. M. Liu, M. L. Tian, G. E. Zhou, Y. H. Zhang, *Physica C* **1996**, *261*, 27.
[224] K. Takegahara, H. Harima, A. Yanase, *Jpn. J. Appl. Phys.* **1987**, *26*, L352.
[225] D. Reefman, F. J. M. Benschop, H. B. Brom, R. A. de Groot, J. M. van Ruitenbeek, *Physica C* **1992**, *201*, 119.
[226] A Ta analogue of this Nb compound, $Nd_{2-x}Ce_xSr_2Cu_2TaO_{10}$, is also superconducting for $x = 0.5$ with $T_C = 28$ K.
[227] L. F. Mattheiss, *Phys. Rev. B* **1992**, *46*, 11171.
[228] Y. Tokura, H. Tagaki, S. Uchida, *Nature* **1989**, *337*, 345.
[229] a) L. F. Mattheiß, D. R. Hamann, *Phys. Rev. Lett.* **1988**, *60*, 2681; b) R. J. Cava, B. Batlogg, J. J. Krajewski, R. Farrow, L. W. Rupp, A. E. White, K. Short, W. F. Peck, T. Kometani, *Nature* **1988**, *332*, 814. Numerical data taken from ref. [80a].
[230] G. K. Wertheim, J. P. Remeika, D. N. E. Buchanan, *Phys. Rev. B* **1982**, *26*, 2120.
[231] H. Fukuoka, T. Isami, S. Yamanaka, *Chem. Lett.* **1997**, *8*, 703.
[232] J. P. Julien, D. A. Papaconstantopoulos, F. Cyrot-Lackmann, A. Pasturel, *Phys. Rev. B* **1991**, *43*, 2903.
[233] M. Robin, K. Andres, T. H. Geballe, N. A. Kuebler, D. B. McWhan, *Phys. Rev. Lett.* **1966**, *17*, 917.
[234] There is evidence for unique triplet Cooper pairs in this compound.
[235] T. Oguchi, *Phys. Rev. B* **1995**, *51*, 1385.
[236] Rb_2CsC_{60} with $T_C = 33–35$ K holds the T_C record among fullerides. Values of $T_C = 40$ K for Cs_3C_{60} (a) T. T. M. Palstra, O. Zhou, Y. Iwasa, P. E. Sulewski, R. M. Fleming, B. R. Zegarski, *Solid State Commun.* **1995**, *93*, 327) and $T_C = 45$ K for $Tl_{2.2}Rb_{2.7}C_{60}$ (b) Z. Iqbal, R. H. Baughman, B. L. Ramakrishna, S. Khare, N. S. Murthy, H. J. Bornemann, D. E. Morris, *Science* **1991**, *254*, 826) have not been confirmed.
[237] a) R. C. Haddon, *Acc. Chem. Res.* **1992**, *25*, 127; b) O. Zhou, D. Cox, *J. Phys. Chem. Solids* **1992**, *53*, 11.
[238] S. Yamanaka, H. Kawaji, K. Hotehama, M. Ohashi, *Adv. Mater.* **1996**, *8*, 771.
[239] a) S. Yamanaka, K.-I. Hotehama, H. Kawaji, *Nature* **1998**, *392*, 580; b) S. Yamanaka, *Annu. Rev. Mater. Sci.* **2000**, *30*, 53.
[240] L. F. Mattheiß, L. R. Testardi, W. W. Yao, *Phys. Rev. B* **1978**, *17*, 4640.
[241] B. M. Klein, L. L. Boyer, D. A. Papaconstantopoulos, L. F. Mattheiß, *Phys. Rev. B* **1978**, *18*, 6411.
[242] M.-Z. Huang, Y.-N. Xu, W. Y. Ching, *J. Chem. Phys.* **1992**, *96*, 1648.
[243] D. L. Novikov, V. A. Gubanov, A. J. Freeman, *Physica C* **1992**, *191*, 399.
[244] Value under high pressure. This is the largest T_c value among the pure elements.
[245] S. P. Rudin, A. Y. Liu, *Phys. Rev. Lett.* **1999**, *83*, 3049, and refs therein.

[246] L. F. Mattheiß, *Phys. Rev. B* **1994**, *49*, 13279.
[247] J. I. Lee, T. S. Zhao, I. G. Kim, B. I. Min, S. J. Youn, *Phys. Rev. B* **1994**, *50*, 4030.
[248] a) H. Kawaji, K. Hotehama, S. Yamanaka, *Chem. Mater.* **1997**, *9*, 2127; b) S. Ya. Istomin, J. Köhler, A. Simon, *Physica C* **1999**, *319*, 219; c) I. Hase, Y. Nishihara, *Phys. Rev. B* **1999**, *60*, 1573.
[249] The largest T_C among organic charge-transfer complexes.
[250] J. Lu, L. Zhang, *Solid State Commun.* **1998**, *105*, 99, and refs therein.
[251] a) V. Balbarin, R. B. Van Dover, F. J. Disalvo, *J. Phys. Chem. Solids* **1996**, *57*, 1919; b) H. Smolinski, W. Weber, *Z. Phys. B* **1997**, *104*, 741.
[252] D. A. Papaconstantopoulos, L. L. Boyer, B. M. Klein, A. R. Williams, V. L. Moruzzi, J. F. Janak, *Phys. Rev. B* **1977**, *15*, 4221.
[253] T. Jarlborg, A. J. Freeman, *Phys. Rev. B* **1980**, *22*, 2332.
[254] S. Yamanaka, E. Enishi, H. Fukuoka, M. Yasukawa, *Inorg. Chem.* **2000**, *39*, 56.
[255] D. H. Gregory, M. G. Baker, P. P. Edwards, M. Slaski, D. J. Siddons, *J. Solid State Chem.* **1998**, *137*, 62.
[256] K. Ahn, B. J. Gibson, R. K. Kremer, H. Mattausch, A. Stolovits, A. Simon, *J. Phys. Chem. B* **1999**, *103*, 5446.
[257] T. F. Fässler, S. Hoffmann, *Z. Anorg. Allg. Chem.* **2000**, *626*, 106.
[258] H. Kamerlingh-Onnes, *Commun. Phys. Lab. Univ. Leiden Suppl.* **1913**, *34*.
[259] a) J. H. Schön, Ch. Kloc, B. Batlogg, *Nature* **2000**, *406*, 702; b) P. Phillips, *Nature* **2000**, *406*, 687.
[260] R. Schumann, M. Richter, L. Steinbeck, H. Eschrig, *Phys. Rev. B* **1995**, *52*, 8801.
[261] M. I. Eremets, K. Shimizu, T. C. Kobayashi, K. Amaya, *J. Phys. Condens. Matter* **1998**, *10*, 11519.
[262] T. Inoshita, Y. Nishihara, *Phys. Rev. B* **1998**, *58*, R1707.
[263] C. K. Jørgensen, *Mol. Phys.* **1959**, *2*, 309.
[264] H. So, M. T. Pope, *Inorg. Chem.* **1972**, *11*, 1441.
[265] A. K. Bridson, J. H. Holloway, E. G. Hope, P. J. Townson, W. Levason, J. S. Ogden, *J. Chem. Soc. Dalton Trans.* **1991**, 3127.
[266] The electronegativity of Ag^{II} is so large that an unpaired electron resides more on the ligands than on the metal in $[AgCl_6]^{4-}$ (M:L = 45:58) and $[AgBr_6]^{4-}$ ions (30:70). See SCCEH results in ref. [212c].
[267] a) *Phase Separation in Cuprate Superconductors* (Eds.: E. Sigmund, K. A. Müller), Springer, Berlin, **1993**; b) R. S. Markiewicz, *Physica C* **1989**, *162–164*, 215.
[268] In looking at the literature we have found that Tl^{II} (very rare because of its tendency to disproportionation) introduces holes into a Cl^- band, just like Ag^{II} centers do (see: a) U. Rogulis, J.-M. Spaeth, I. Cabria, J. A. Aramburu, M. T. Barriuso, *J. Phys. Condens. Matter* **1998**, *10*, 6473; b) I. Cabria, M. Moreno, J. A. Aramburu, M. T. Barriuso, U. Rogulis, J.-M. Spaeth, *J. Phys. Condens. Matter* **1998**, *10*, 6481). It should not be then excluded that Tl^{III} would be able to oxidize F^- ions, just like Ag^{III}. However, OEN of Tl^{II} (2.1) is much smaller than that of Ag^{II} (2.8); and the redox potential of the Tl^{III}/Tl^{I} redox pair is less positive by about 0.8 V from that of the Ag^{II}/Ag^{I}: c) A. F. Clifford, W. D. Pardieck, M. W. Wadley, *J. Phys. Chem.* **1966**, *70*, 3241.
[269] A. C. Gossard, D. K. Hindermann, M. B. Robin, N. A. Kuebler, T. H. Geballe, *J. Am. Chem. Soc.* **1967**, *89*, 7121.
[270] W. S. Graaf, H. H. Stadelmeier, *J. Electrochem. Soc.* **1958**, *105*, 446.
[271] J. A. McMillan, *Chem. Rev.* **1962**, *62*, 65.
[272] a) M. B. Robin, K. Andres, T. H. Geballe, N. A. Kuebler, D. B. McWhan, *Phys. Rev. Lett.* **1966**, *17*, 917; b) K. Andres, N. A. Kuebler, M. B. Robin, *J. Phys. Chem. Solids* **1966**, *27*, 1747.
[273] A. B. Neiding, I. A. Kazarnovskii, *Dokl. Akad. Nauk. SSSR* **1951**, *78*, 713.
[274] M. Jansen, S. Vensky, *Z. Naturforsch. B* **2000**, *55*, 882.
[275] There are also other conducting Ag–O cluster compounds, such as $Ag[Ag_3O_4]_2[NO_3]$. See for example: B. E. Breyfogle, R. J. Phillips, J. A. Switzer, *Chem. Mater.* **1992**, *4*, 1356.
[276] Several other Ag-containing superconductors are known, for example: LaAg alloy with $T_C = 1.1$ K a) J. S. Schilling, S. Methfessel, R. N. Shelton, *Solid State Commun.* **1977**, *24*, 659; b) organic $[et]_2Ag[CF_3]_4[tce]$ (et = bis(ethylenedithio)tetrathiafulvalene, tce = 1,1,2-trichloroethane) with $T_C = 11.1$ K, J. A. Schlueter, K. D. Carlson, U. Geiser, H. H. Wang, J. M. Williams, W. K. Kwok, J. A. Fendrich, U. Welp, P. M. Keane, J. D. Dudek, A. S. Komosa, D. Naumann, T. Roy, J. E. Schirber, W. R. Bayles, B. Dodrill, *Physica C* **1994**, *233*, 379; and many Ag-doped oxocuprates, e.g. $Bi_{1.6}Pb_{0.4}Sr_2Ca_3(Cu_{1-x}Ag_x)_4O_{12+x}$: c) J. E. Rodriguez, A. Marino, *Phys. Rev. B* **1999**, *60*, 9845. There is also a large family of halogen- (including fluorine-) doped cuprates, e.g. d) M. Al-Mamouri, P. P. Edwards, C. Greaves, M. Slaski, *Nature* **1994**, *369*, 382; e) I.-G. Chen, S. Sen, D. M. Stefanescu, *Appl. Phys. Lett.* **1988**, *52*, 1355; f) S. D'Arco, M. S. Islam, *Phys. Rev. B* **1997**, *55*, 3141; g) S. Adachi, T. Tatsuki, T. Kamura, K. Tanabe, *Chem. Mater.* **1998**, *10*, 2860).
[277] a) J. K. Burdett, *Inorg. Chem.* **1993**, *32*, 3915. It is significant that avoided crossing seems to be important for such different superconducting materials as oxocuprates and samarium sulphide SmS: b) C. M. Varma, *Rev. Mod. Phys.* **1976**, *48*, 218. Independent calculations confirm the hypothesis of dual character of the wavefunction for oxobismuthates, as well: c) N. C. Pyper, P. P. Edwards in *Polarons and Bipolarons in High-T_C Superconductors and Related Materials* (Eds.: E. K. H. Salje, A. S. Alexandrov, W. Y. Liang), Cambridge University Press, Cambridge, **1995**.
[278] The phenomenon of multiple charge-transfer excitation is a source of "valence tautomerism",[165] and of the "mnemon effect". For the latter see: a) L. Z. Stolarczyk, L. Piela, *Chem. Phys.* **1984**, *85*, 451; b) N. Guihery, G. Durand, M.-B. Lepetit, J.-P. Malrieu, *Chem. Phys.* **1994**, *183*, 61; c) Y. Toyozawa in *Relaxations of Excited States and Photo-Induced Structural Phase Transitions* (Ed.: K. Nasu), Springer, Berlin, **1997**, p. 17.
[279] S. Ernst, V. Kasack, W. Kaim, *Inorg. Chem.* **1988**, *27*, 1146.
[280] Note here some similarity of Burdett's approach to a "resonance" formalism, used by the "resonating valence bond" theory of superconductivity in the solid state: a) P. W. Anderson, *Science* **1987**, *235*, 1196; b) P. W. Anderson, G. Baskaran, Z. Zou, T. Hsu, *Phys. Rev. Lett.* **1987**, *58*, 2790; c) G. Baskaran, Z. Zou, P. W. Anderson, *Solid State Commun.* **1987**, *63*, 2790.
[281] Much attention has been paid to the role of peroxide anions (generated presumably in the process: $2O^{-\bullet} \rightarrow O_2^{2-}$) for superconductivity. See e.g. a) G. Tavčar, B. Ogorevč, V. Hudnik, S. Pejovnik, *Physica C* **1991**, *175*, 607; b) J.-H. Choy, D.-Y. Jung, S.-J. Kim, Q. W. Choi, G. Damazeau, *Physica C* **1991**, *185–189*, 763; and a recent discussion: c) A. R. Anderson, Murakami, G. J. Russell, *Physica C* **2000**, *334*, 229.
[282] See also an interesting article on symmetry breaking: H. Genz, *Interdiscip. Sci. Rev.* **1999**, *24*, 129.
[283] H. Tajima, M. Inokuchi, S. Ikeda, M. Arifuku, T. Naito, M. Tamura, T. Ohta, A. Kobayashi, R. Kato, H. Kobayashi, H. Kuroda, *Synth. Met.* **1995**, *70*, 1035.
[284] D. L. DeLaet, D. R. Powell, C. P. Kubiak, *Organometallics* **1985**, *4*, 954.
[285] R. D. Feltham, G. Elbaze, R. Ortega, C. Eck, J. Dubrawski, *Inorg. Chem.* **1985**, *24*, 1503.
[286] A. M. Bradford, E. Kristof, M. Rashidi, D.-S. Yang, N. C. Payne, R. J. Puddephatt, *Inorg. Chem.* **1994**, *33*, 2355.
[287] M. Ganesan, S. S. Krishnamurthy, M. Nethaji, *J. Organomet. Chem.* **1988**, *570*, 247.
[288] J. A. Jenkins, M. Cowie, *Organometallics* **1992**, *11*, 2767.
[289] B. R. Sutherland, M. Cowie, *Organometallics* **1985**, *4*, 1637.
[290] P. Sharrock, M. Melnik, *Can. J. Chem.* **1985**, *63*, 52.
[291] F. Valach, M. Tokarcik, T. Maris, D. J. Watkin, C. K. Prout, *Z. Kristallogr.* **2000**, *215*, 56.
[292] For example $CsAuCl_3$ is disproportionated to Au^{I} and Au^{III} a) N. Elliott, L. Pauling, *J. Am. Chem. Soc.* **1938**, *60*, 1846, and may be metallized at an external pressure of 60 kB b) R. Keller, J. Fenner, W. B. Holzapfek, *Mater. Res. Bull.* **1974**, *9*, 1664; c) P. Day, C. Vettier, G. Parisot, *Inorg. Chem.* **1978**, *17*, 2319.
[293] On coexistence of CDW (charge density wave), SDW (spin density wave), and superconductivity, see, for example: a) H. Tajima, M. Inokuchi, S. Ikeda, M. Arifuku, T. Naito, M. Tamura, T. Ohta, A. Kobayashi, R. Kato, H. Kobayashi, H. Kuroda, *Synth. Met.* **1995**, *70*, 1035; b) C.-H. Du, W. J. Lin, Y. Su, B. K. Tanner, P. D. Hatton, D. Casa, B. Keimer, J. P. Hill, C. S. Oglesby, H. Hohl, *J. Phys. Condens. Matter* **2000**, *12*, 5361. On CDW for underdoped cuprates see: c) A. Mourachkine, *Supercond. Sci. Technol.* **2000**, *13*, 1378.
[294] AgF_2, a ferromagnet with Curie temperature of 163 K, also exhibits the strongest antiferromagnetic coupling among Ag^{II} compounds. Isoelectronic and isostructural CuF_2 has a Curie temperature of 69 K.

[295] Interestingly, the order of the T_N versus size of cationic dopant M is reversed for $MAgF_3$ and M_2AgF_4 compounds, M = K, Rb, Cs.

[296] In fact, the statistics of Cooper pairs differ from those of bosons.

[297] Bednorz and Müller refer to the Jahn–Teller effect as a possible mechanism responsible for the enhancement of the critical superconducting temperature a) J. G. Bednorz, K. A. Müller, *Z. Phys. B* **1986**, *64*, 189. Considerations based on Jahn–Teller and pseudo Jahn–Teller effect have been applied to many charge-transfer processes in condensed media, see e.g.: b) J. Ulstrup in *Lecture Notes in Chemistry, Vol. 10* (Eds.: G. Berthier, M. J. S. Dewar, H. Fisher, K. Fukui, H. Hartmann, H. H. Jaffe, J. Jortner, W. Kutzelnigg, K. Ruedenberg, E. Scrocco, W. Zeil), Springer, Berlin, **1979**; c) H. E. M. Christensen, L. S. Conrad, J. M. Hammerstadt-Pedersen, J. Ulstrup in *Condensed Matter Physics Aspects of Electrochemistry (*Eds.: M. P. Tosi, A. A. Kornyshev), World Scientific, Singapore, **1991**; d) H. A. Jahn, E. Teller, *Proc. R. Soc. London Ser. A* **1937**, *161*, 220; e) I. B. Bersuker, *The Jahn-Teller Effect and Vibronic Interactions in Modern Chemistry*, Plenum, New York, **1984**; f) R. Englman, *The Jahn-Teller Effect*, Wiley, New York, **1972**; g) M. K. Grover, R. Silbey, *J. Chem. Phys.* **1970**, *52*, 2099). Similar thinking is widespread nowadays in the literature on superconductivity, too; see e.g.: h) A. Calles, J. R. Soto, J. J. Castro, E. Yépez, *Physica C* **1997**, *282–287*, 1623; i) L. R. Falvello, *J. Chem. Soc. Dalton Trans.* **1997**, 4463; j) D. Reinen, H. O. Wellern, J. Wegwerth, *Z. Phys. B* **1997**, *104*, 595.

[298] On the actual importance of vibronic (and generally lattice–electron coupling) effects for superconductivity see: 1) oxocuprates: a) A. S. Alexandrov, P. Edwards, *Physica C* **2000**, *33*, 97 and refs therein; b) J. K. Burdett, G. V. Kulkarni, *Phys. Rev. B* **1989**, *40*, 8908; c) T. Jarlborg, *Solid State Commun.* **1988**, *67*, 297; 2) oxobismuthates: d) V. Meregalli, S. Y. Savrasov, *Phys. Rev. B* **1998**, *57*, 14453; e) O. Navarro, E. Chavira, *Physica C* **1997**, *282–287*, 1825; f) M. Shirai, N. Suzuki, K. Motizuki, *J. Phys. Condens. Matter* **1990**, *2*, 3553; 3) fullerides: g) M. Schluter, M. Lanoo, M. Needels, G. A. Baraff, D. Tomanek, *Phys. Rev. Lett.* **1992**, *68*, 526; h) R. A. Jishi, M. S. Dresselhaus, *Phys. Rev. B* **1992**, *45*, 2579; i) D. L. Novikov, V. A. Gubanov, A. J. Freeman, *Physica C* **1992**, *191*, 399; j) V. Z. Kresin, *Phys. Rev. B* **1992**, *46*, 14883; k) Y. Asai, Y. Kawaguchi, *Phys. Rev. B* **1992**, *46*, 1265; l) R. Rai, *Z. Phys. B* **1996**, *99*, 327; 4) silicide clathrates: m) K. Yoshizawa, T. Kato, T. Yamabe, *J. Chem. Phys.* **1998**, *108*, 7637; n) K. Yoshizawa, T. Kato, M. Tachibana, T. Yamabe, *J. Phys. Chem. A* **1998**, *102*, 10113; 5) borocarbides: o) F. Gompf, W. Reichardt, H. Schober, B, Renker, M. Buchgeister, *Phys. Rev. B* **1997**, *55*, 9058; 6) mercury fluoroarsenates: p) J. J. M. Slot, M. Boon, M. Weger, *Solid State Commun.* **1985**, *56*, 645. On the accuracy of BCS predictions in different classes of superconductors see: r) B. Chakraverty, T. Ramakrishnan, *Physica C* **1997**, *282–287*, 290.

[299] On the theory of vibronic coupling see: a) G. Herzberg, E. Teller, *Z. Phys. Chem. B* **1933**, *21*, 410; b) G. Herzberg, H. C. Longuet-Higgins, *Discuss. Faraday Soc.* **1963**, *35*, 77; c) H. C. Longuet-Higgins, *Proc. R. Soc. London Ser. A* **1975**, *344*, 147; d) W. Siebrand, M. Zgierski in *Excited States*, *Vol. 4* (Ed.: E. C. Lim), **1979**; e) G. Herzberg, *Molecular Spectra and Molecular Structure*, *Vol. 3*, Van Nostrand Reinhold, New York, **1966**; f) G. Fischer, *Vibronic Coupling*, Academic Press, London, **1984**; g) H. Köppel, L. S. Cederbaum, W. Domcke, *J. Chem. Phys.* **1988**, *89*, 2023; h) I. B. Bersuker, V. Z. Polinger, *Vibronic Interactions in Molecules and Crystals* (Ed.: V. I. Goldanskii), Springer, Berlin, **1983**.

[300] Relationship between the dynamic Jahn–Teller effect and superconductivity has been described in: a) D. P. Clougherty, K. H. Johnson, M. E. McHenry, *Physica C* **1989**, *162–164*, 1475. A simple theoretical approach to dynamic band-gap opening in typical low-dimensional metals may be found in: b) M. T. Green, V. Robert, J. K. Burdett, *J. Phys. Chem. B* **1997**, *101*, 10290.

[301] As the reader may note, thinking of superconductivity in connection to a stress introduced into 1D or 2D structures, we are interested mainly in *linear* chains and *nonpuckered* sheets. The obvious reason for that is that kinked chains or puckered sheets are likely to be much less resistant to strain upon introduction of stress, and are of the interest to us only if they return to higher symmetry upon doping. For relationship between T_C and buckling of CuO_2 planes in oxocuprates, see: O. Chmaissem, J. D. Jorgensen, S. Short, A. Knizhnik, Y. Eckstein, H. Shaked, *Nature* **1999**, *397*, 45.

[302] Part 1, W. Grochala, R. Konecny, R. Hoffmann, *Chem. Phys.*, submitted.

[303] Part 2, W. Grochala, R. Hoffmann, *New J. Chem.* **2001**, *25*, 108.

[304] Part 3, W. Grochala, R. Hoffmann, *J. Phys. Chem. A* **2000**, *104*, 9740.

[305] Part 4, W. Grochala, R. Hoffmann, *Pol. J. Chem.*, in press.

[306] Part 5, W. Grochala, R. Hoffmann, P. P. Edwards, unpublished results.

[307] Similar language, of a "covalency" approach to superconductivity has been widely used by A. Sleight ref. [207c]. Also Phillips discussed covalence/ionic instabilities as an important factor in superconductivity (J. C. Phillips, *Phys. Rev. Lett.* **1972**, *29*, 1551).

[308] On correlation of antiferromagnetic and superconducting properties, see, for example: a) K. Prassides, A. Lappas, *Chem. Br.* **1994**, 725; b) T. Otsuka, A. Kobayashi, Y. Miyamoto, J. Kiuchi, N. Wada, E. Ojima, H. Fujiwara, H. Kobayashi, *Chem. Lett.* **2000**, 732; c) S. Alam, *Phys. Lett. A* **2000**, *272*, 107. On interpretation of oxobismuthates as doped Peierls insulators see: d) M. J. Rice, Y. R. Wang, *Physica C* **1989**, *157*, 192. On the relationship between ferromagnetism and superconductivity see: e) S. S. Saxena, P. Agarwal, K. Ahilan, F. M. Grosche, R. K. W. Haselwimmer, M. J. Steiner, E. Pugh, I. R. Walker, S. R. Julian, P. Monthoux, G. G. Lonzarich, A. Huxley, I. Sheikin, D. Braithwaite, J. Flouquet, *Nature* **2000**, *406*, 587; f) P. Coleman, *Nature* **2000**, *406*, 580.

[309] L. Jansen, R. Block, *Phys. A* **1999**, *271*, 169.

[310] For the necessity of subtle control of a distance between two metal centers, see the predictions of a simple model we used in ref. [302].

[311] Sometimes a "clipping" dopant may occur in a layer, which does not neighbor directly a CuO_2 plane; Hg^{II} in $HgBa_2CuO_{4-\delta}$ is a good example.

[312] The real situation in oxocuprates is, in fact, much more complicated. Both external pressure and chemical substitutions *have* great impact on the T_C of cuprate materials. But "chemical pressure" is *equivalent* to external pressure only for $La_{2-x}(Ba_{1-y}Sr_y)_xCuO_4$, see: M. Marezio, F. Licci, A. Gauzzi, *Physica C* **2000**, *337*, 195.

[313] Instead of introducing anisotropic stress in oxocuprates, see e.g.: a) Kh. A. Ziq, N. M. Hamdan, J. Schirokoff, *Physica C* **1994**, *235–240*, 1217; a method of epitaxial strain may be used to increase T_C: b) J.-P. Locquet, J. Perret, J. Fompeyrine, E. Mächler, J. W. Seo, G. van Tendeloo, *Nature* **1998**, *394*, 453. Both methods have their limitations for increasing T_C; see: c) L. Jansen, R. Block, *Nature* **1999**, *399*, 114; d) I. K. Schuller, *Nature* **1998**, *394*, 419. Stress may be also applied to increase T_C or to induce superconductivity in initially nonsuperconducting non-oxocuprate materials (see for example: e) D. Agassi, T. K. Chu, *Phys. Status Solidi B* **1990**, *160*, 601; f) W. D. Gill, R. L. Greene, G. B. Street, W. A. Little, *Phys. Rev. Lett.* **1975**, *35*, 1732; g) J. E. Schirber, L. J. Azvedo, J. F. Kwak, E. L. Venturni, P. C. W. Leung, M. A. Beno, H. H. Wang, J. M. Williams, *Phys. Rev. B* **1986**, *33*, 1987; h) C. E. Campos, J. S. Brooks, P. J. M. Van Bentum, J. A. A. J. Perenboom, S. J. Klepper, P. S. Sandhu, S. Valfells, Y. Tanaka, T. Kinoshita, N. Kinoshita, M. Tokumoto, H. Anzai, *Phys. Rev. B* **1995**, *52*, R7014; i) R. Brand, W. W. Webb, *Solid State Commun.* **1969**, *7*, 19.

[314] Indeed, there are *optimal* values of T_C which may be obtained when applying external pressure. For elegant experimental evidence see: a) J. Gopalakrishnan in *Thallium-Based High-Temperature Superconductors* (Eds.: A. M. Herman, J. V. Jakhmi), Marcel Dekker, New York, **1995**, p. 7; b) N. E.Moulton, E.Skeleton in *Thallium-Based High-Temperature Superconductors* (Eds.: A. M. Herman, J. V. Jakhmi), Marcel Dekker, New York, **1995**, p. 437. See also: c) "High-T_C Superconductivity 1996: Ten Years After the Discovery": P. P. Edwards, G. B. Peacock, J. P. Hodges, A. Asab, I. Gameson, *NATO ASI Ser.* **1997**, *343*, 135.

[315] Disproportionated systems most often have larger molar volume than the comproportionated ones. The same feature is expected for disproportionated Ag^I/Ag^{III} fluorides. Note that the average of the Ag^I–F and Ag^{III}–F bond lengths ($[2.46 + 1.88]/2 = 2.17$ Å) is *larger* than the typical Ag^{II}–F bond length (2.07–2.13 Å). Apparently, depopulation of the Ag–F antibonding orbitals ($d^9 \rightarrow d^8$) results in smaller shortening of the Ag–F bond length than elongation of the Ag–F bond length upon population of the Ag–F antibonding orbitals ($d^9 \rightarrow d^{10}$).

[316] A simple approach to lattice effects in conducting perovskite-type oxides may be found in: J. P. Attfiled, *Chem. Mater.* **1998**, *10*, 3239.

[317] Thus, we may easily compute that the best dopants clipping the AgF_2 planes (with Ag–F distances of 2.07 – 2.13 Å) should have ionic radii of 1.10 – 1.17 Å. These might be Ac^{III} ($R_{ion} = 1.12$ Å), Sr^{II} ($R_{ion} =$ 1.18 Å), and Pb^{II} ($R_{ion} = 1.19$ Å, if not oxidized to Pb^{IV}). Na^{I} ($R_{ion} =$ 1.02 Å), K^{I} and Ba^{II} ($R_{ion} = 1.39$ Å) seem less appropriate. The radii of hypothetically good dopants found in this semiempirical way are much smaller than those satisfying the corresponding condition in the perovskite structure ($R_{ion}^{opt} = 1.74 – 1.82$ Å if we assume R_{ion} (F^-) = 1.19 Å, and $R_{ion}^{opt} = 1.57 – 1.65$ Å if we assume R_{ion} (F^-) = 1.36 Å see Table 11 in Appendix).

[318] J. Karpinski, H. Schwer, X. Mangelschots, K. Conder, A. Morawski, T. Lada, A. Paszewin, *Physica C* **1994**, *234*, 10. We are not aware of any attempts to synthesize a I/III mixed-valence $Ca_{1-\delta}Na_{\delta}CuO_2$.

[319] Z. Hiroi, M. Takano, M. Azuma, Y. Takeda, *Nature* **1993**, *364*, 315.

[320] N. R. Walker, R. R. Wright, A. J. Stace, *J. Am. Chem. Soc.* **1999**, *121*, 4837.

[321] N. R. Walker, R. R. Wright, P. E. Barran, A. J. Stace, *Organometallics* **1999**, *18*, 3569.

[322] A small force constant for Ag^{I}–F stretching is indicated by the relatively broad range of Ag^{I}–F separations found in different compounds. For example, Ag^{I}–F bond lengths of 2.196 – 2.571 Å are found in $[Ag_2C_2 \cdot 8AgF]$ (G. C. Guo, G. D. Zhou, Q. G. Wang, T. C. W. Mak, *Angew. Chem.* **1998**, *110*, 652; *Angew. Chem. Int. Ed.* **1998**, *37*, 630). The shortest of these distances (2.20 Å) is still longer than a typical Ag^{II}–F bond length (2.07 – 2.13 Å).

[323] For example, there are no Ag–F nets in $Ag[SbF_6]$, instead there are isolated Ag^+ ions. Sb^{V} is a too strong a F abstracting agent for Ag^{I} to create a 1D $[AgF][SbF_5]$ net. On the other hand, Ag^{II} is also too weak a F abstracting agent to create 1D $[AgF]^+[SnF_5]^-$ or 2D $[AgF_2][SnF_4]$ nets in $Ag^{II}[SnF_6]^{2-}$. Redox potentials and magnetic properties of dopants also have to be taken into account. For example, doping of Ag^{II} compounds with U^{V} usually results in the reaction: $U^{V} + Ag^{II} \rightarrow U^{VI} + Ag^{I}$ (for details, see: P. A. G. O'Hare, J. G. Malm, *J. Chem. Thermodyn.* **1984**, *16*, 753).

[324] For example, Ba levels add to DOS_F in Ba_6Si_{46}, a clathrate Si compound, effectively increasing T_C compared to Na compounds. For details, see: S. Saito, A. Oshiyama, *Phys. Rev. B* **1995**, *51*, 2628.

[325] Some IR absorption spectra have been published. See ref. [208] for details.

[326] Four older contributions should be noted here: a) C. Friebel, *Solid State Commun.* **1974**, *15*, 639, b) C. Friebel, D. Reinen, *Z. Anorg. Allg. Chem.* **1975**, *413*, 51; c) G. C. Allen, K. D. Warren, *Inorg. Chem.* **1969**, *8*, 1895; d) G. C. Allen, R. F. McMeeking, *J. Chem. Soc. Dalton Trans.* **1976**, 1063. There are also more recent data on optical spectra of Ag^{III} fluoride complexes: e) A. L. Hector, W. Levason, M. T. Weller, E. G. Hope, *J. Fluorine Chem.* **1997**, *86*, 105.

[327] As far as we know, ^{19}F and ^{109}Ag NMR spectra have been published so far only for $KAgF_4$ (R. Eujen, B. Žemva, *J. Fluorine Chem.* **1999**, *99*, 139), and for AgF_2 (ref. [84c]).

[328] Much information has been collected on ESR and optical spectra of Ag^{2+} ions isolated in fluoride hosts, see for example: a) H. Bill, D. Lovy, H. Hagemann, *Solid State Commun.* **1989**, *70*, 511; b) A. Monnier, A. Gerber, H. Bill, *J. Chem. Phys.* **1991**, *94*, 5891; c) E. Minner, D. Lovy, H. Bill, *J. Chem. Phys.* **1993**, *99*, 6378; d) D. C. Von Hoene, Dissertation, University of Cincinnati (USA), **1968**; e) M. V. Eremin, V. A. Ulanov, M. M. Zaripov, *Appl. Magn. Reson.* **1998**, *14*, 435; f) P. Bautinaud, A. Monnier, D. Lovy, H. Bill, *J. Phys. Chem. Solids* **2000**, *61*, 1663, and ref. [212]. There is also data for Ag^{2+} ions in other hosts, e.g. KNO_3: g) K. Chandrasekharan, V. S. Murty, *Physica B* **1995**, *205*, 349; $CdCl_2$ and $CdBr_2$: h) T. Miyanaga, *J. Phys. Soc. Jpn.* **1979**, *46*, 167.

[329] Electric resistance measurements in these substances may be very difficult, because even the surface of solid Au rods might be oxidized by the sample measured, as pointed out in ref. [14].

[330] B. G. Levi, *Phys. Today* **1996**, *49*, 17.

[331] There has been much discussion on one-dimensionality in oxocuprates. It appears that there are 1D "charge stripes" in the electronic structure of the CuO_2 planes a) J. Zaanen, *Science* **1999**, *286*, 251). There are also 1D (in geometric and electronic sense) "ladder oxocuprates", for which the largest $T_C = 12$ K b) M. Uehara, T. Nagata, J. Akimitsu, H. Takahashi, N. Ori, K. Kinoshita, *J. Phys. Soc. Jpn.* **1996**, *65*, 2764; c) ref. [330]). For an effective exciton mechanism of superconductivity in 1D structures see: d) J. E. Hirsch, D. J. Scalapino, *Phys. Rev. B* **1985**, *32*, 117; e) Z. Tesanovic, A. R. Bishop, R. L. Martin, *Solid State Commun.* **1988**, *68*, 337. Nanoscale one-dimensionality has also been discussed. There are many advantages, but also many technical problems with the synthesis of pseudo 1D metallic wires f) P. P. Edwards, P. A. Anderson, L. J. Woodall, A. Porch, A. R. Armstrong, *Mater. Sci. Eng.* **1996**, *217*, 198; g) A. Kelly, *Sci. Am.* **1965**, *212*(*2*), 28.

[332] Our preliminary DFT computations for $[AgF][AgF_4]$ in the $[CuF]$-$[AuF_4]$ structure indicate that pressure-induced metallization might occur at several GPa.

ANGEWANDTE CHEMIE

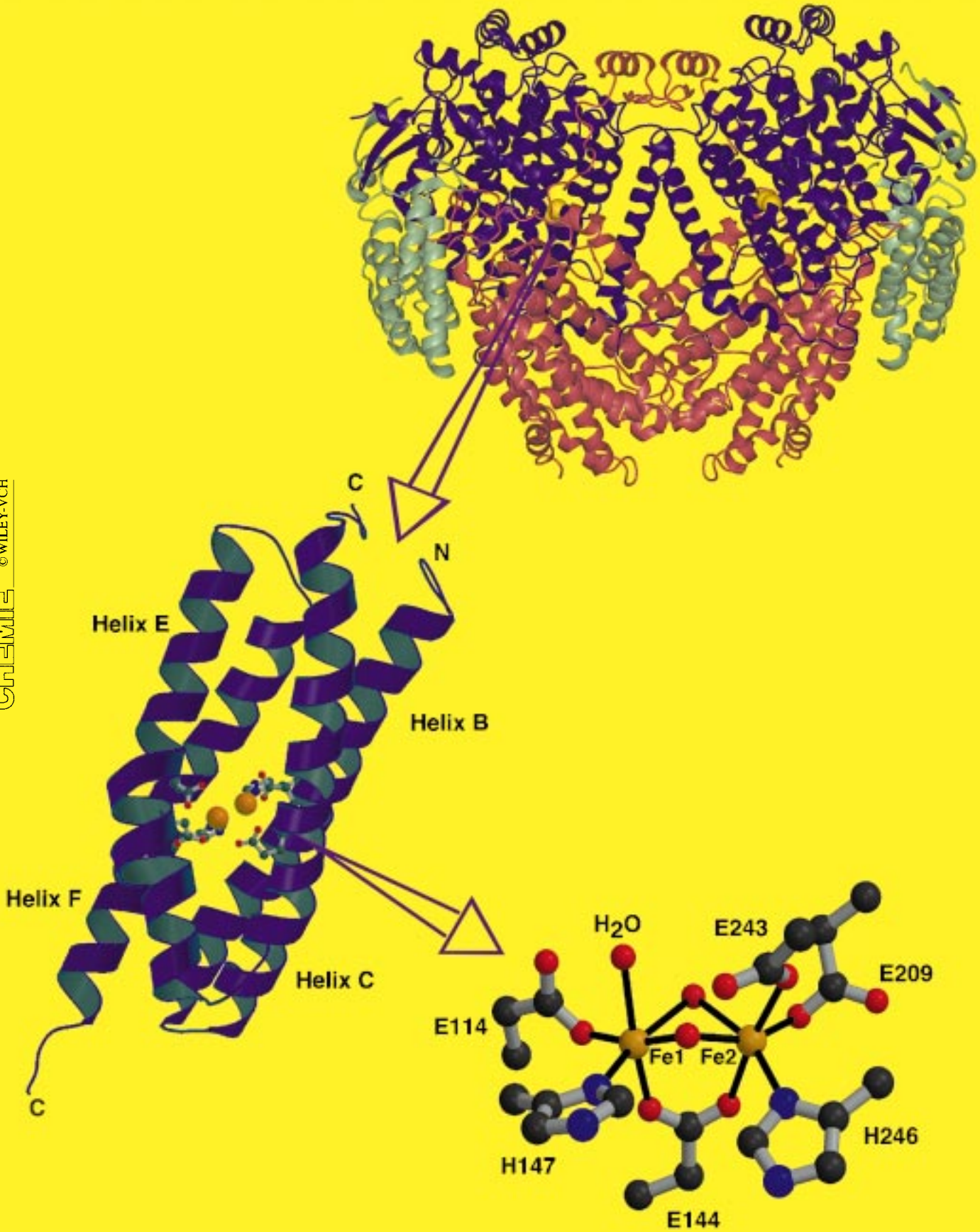

Dioxygen Activation and Methane Hydroxylation by Soluble Methane Monooxygenase: A Tale of Two Irons and Three Proteins**

Maarten Merkx, Daniel A. Kopp, Matthew H. Sazinsky, Jessica L. Blazyk, Jens Müller, and Stephen J. Lippard*

Methanotrophic bacteria are capable of using methane as their sole source of carbon and energy. The first step in methane metabolism, the oxidation of methane to methanol, is catalyzed by a fascinating enzyme system called methane monooxygenase (MMO). The selective oxidation of the very stable C–H bond in methane under ambient conditions is a remarkable feat that has not yet been repeated by synthetic catalysts and has attracted considerable scientific and commercial interest. The best studied MMO is a complex enzyme system that consists of three soluble protein components, all of which are required for efficient catalysis. Dioxygen activation and subsequent methane hydroxylation are catalyzed by a hydroxylase enzyme that contains a non-heme diiron site. A reductase protein accepts electrons from NADH and transfers them to the hydroxylase where they are used for the reductive activation of O_2. The third protein component couples electron and dioxygen consumption with methane oxidation. In this review we examine different aspects of catalysis by the MMO proteins, including the mechanisms of dioxygen activation at the diiron site and substrate hydroxylation by the activated oxygen species. We also discuss the role of complex formation between the different protein components in regulating various aspects of catalysis.

Keywords: bioinorganic chemistry · C–H activation · oxidoreductases · O–O activation · oxygenation

1. Introduction

Methane monooxygenases (MMOs) catalyze the selective oxidation of methane to methanol [Eq. (1)].[1–6]

$$CH_4 + NADH + H^+ + O_2 \longrightarrow CH_3OH + NAD^+ + H_2O \quad (1)$$

This reaction is the essential first step in a metabolic pathway used by methanotrophic bacteria to consume methane as their sole source of carbon and energy (Scheme 1).[7] Methanotrophs reside at the boundary of aerobic and anaerobic environments, where both methane and dioxygen exist. Methane is produced by methanogenic bacteria, which reduce CO_2 to CH_4 in various anaerobic surroundings such as oceans, lakes, and wetlands.[8] Methanotrophs play an essential role in the global carbon cycle by limiting the amount of methane, a more potent greenhouse gas than carbon dioxide, that reaches the atmosphere.[9]

Virtually all methanotrophs express a membrane-bound, particulate form of MMO (pMMO).[10, 11] This 94-kDa enzyme contains about 12–15 copper atoms distributed between two distinct kinds of sites. It has been hypothesized that one of the copper clusters serves as the active site for methane hydroxylation and the other as an electron carrier.[12–16] Detailed characterization of pMMO has been hampered by its instability and by difficulties in purification. Some methanotrophs can also express a second, soluble type of MMO (sMMO) under conditions of low copper availability. sMMO is much more stable and easier to purify, and has therefore attracted considerable attention. The active site of sMMO contains a non-heme diiron center and, in contrast to pMMO, can accommodate a wide variety of hydrocarbon substrates besides methane. Included are saturated and unsaturated, linear, branched, and cyclic hydrocarbons up to about C_8, as well as aromatic, heterocyclic, and chlorinated compounds.[9, 17–22] Because of this broad spectrum of oxidizable substrates, methanotrophic bacteria can assist in bioremediation of the environment, such as in the removal of petroleum products from beaches contaminated by oil tanker spillage.[23] The efficient conversion of methane into methanol, the signature reaction of MMOs, is also of commercial interest.

[*] Prof. Dr. S. J. Lippard, Dr. M. Merkx, D. A. Kopp, M. H. Sazinsky, J. L. Blazyk, Dr. J. Müller
Department of Chemistry
Massachusetts Institute of Technology
77 Massachusetts Avenue 18-590
Cambridge, MA 02139 (USA)
Fax: (+1) 617-258-8150
E-mail: lippard@lippard.mit.edu

[**] A list of abbreviations can be found in Section 7.

  1433-7851/01/4015-2783 $ 17.50+.50/0

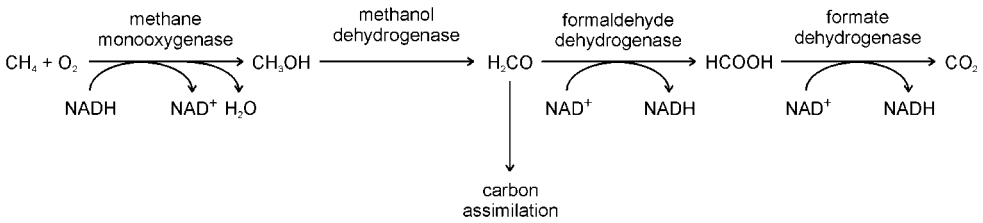

Scheme 1. Metabolic pathway for methane oxidation in *Methylococcus capsulatus* (Bath).

A liquid derivative of natural gas would be more economical to transport, an important consideration for the exploitation of natural gas resources in remote areas. Whereas the successful application of the MMO enzyme on an industrial scale is doubtful, chemical insights gathered from enzymological studies could guide the development of better synthetic catalysts.

Soluble MMO is a complex three-component system (Figure 1).[24–27] sMMO systems isolated from *Methylococcus capsulatus* (Bath) and *Methylosinus trichosporium* OB3b have been investigated extensively and two of their three component proteins have been structurally characterized.[28–33] Oxidation of methane by dioxygen occurs at a carboxylate-bridged diiron center located in the α subunit of the hydroxylase protein MMOH, a 251-kDa $\alpha_2\beta_2\gamma_2$ heterodimer. Electrons

M. Merkx S. J. Lippard J. Müller

D. A. Kopp J. L. Blazyk M. H. Sazinsky

Maarten Merkx (Drs in Chemistry, 1995, University of Nijmegen, The Netherlands; PhD in Chemistry, 1999, University of Amsterdam, The Netherlands) did his graduate research with Professor Bruce A. Averill studying the mechanistic role of the diiron center in purple acid phosphatase. He is presently a Human Frontier of Science Program postdoctoral fellow in Professor Lippard's group, working on the mechanism of methane monooxygenase. His research interest is in the field of metalloenzyme catalysis.

Daniel A. Kopp received a BS degree in Chemistry and Biology from the College of William and Mary, Williamsburg, Virginia, in 1997. While there he researched solvent effects on conformational equilibria in small amides under the supervision of Professor Kathleen M. Morgan. When he is not in the lab, Dan enjoys hiking, playing guitar, and spending time with his wife Karen.

Matthew H. Sazinsky received a BS degree in Chemistry from Haverford College, Haverford, Pennsylvania, in 1999. While there he investigated the functional role of zinc in porphobilinogen synthase under the supervision of Professor Robert C. Scarrow and Dr. Eileen K. Jaffe (Fox Chase Cancer Center, Philadelphia, Pennsylvania). He is currently studying component interactions in sMMO. His research interests are in structural biology and metalloenzymology.

Jessica L. Blazyk received a BS degree in chemistry from the Honors Tutorial College at Ohio University (Athens, Ohio) in 1996. As an undergraduate, she performed research on the mechanism of manganese catalase in the laboratory of Professor James E. Penner-Hahn at the University of Michigan in Ann Arbor, Michigan. She is currently a Howard Hughes Medical Institute predoctoral fellow in Professor Lippard's group, studying electron transfer reactions in the sMMO system.

Jens Müller studied chemistry at the University of Dortmund and at University College, London. He received his PhD in 1999 under the supervision of Professor Bernhard Lippert for studies of platinum-stabilized, parallel-stranded DNA and stabilization of rare tautomers of nucleobases. Currently, he is working in the groups of Professor Lippard (MIT) and Professor Gerhard Wagner (Harvard Medical School) as a Feodor-Lynen postdoctoral fellow. His present research interests include the determination of solution structures of proteins.

Stephen J. Lippard is the Arthur Amos Noyes Professor of Chemistry at the Massachusetts Institute of Technology and is Head of the Chemistry Department. A member of the National Academy of Sciences, the National Institute of Medicine, and the American Academy of Arts and Sciences, his research activities span the fields of inorganic and biological chemistry. Working to unravel the mysteries of soluble methane monooxygenase has been one of his scientific passions for more than a decade.

Overall reaction: $CH_4 + O_2 + 2H^+ + 2e^- \longrightarrow CH_3OH + H_2O$

Figure 1. Schematic view of the three protein components that form the soluble methane monooxygenase enzyme and their roles in catalysis. Only one of two non-heme diiron centers in the MMOH dimer is depicted.

for this reaction are provided by a reductase protein, MMOR, which oxidizes NADH and transfers its electrons to MMOH. Efficient catalysis requires the presence of a third protein, MMOB, which serves several regulatory roles.

An important reason for the scientific interest in sMMO is its unique ability to oxidize the very stable C–H bond in methane. This feat distinguishes sMMO from other monooxygenase enzymes such as cytochrome P450.[34] Cytochrome P450 and sMMO represent two different solutions to the problem of dioxygen activation for hydrocarbon oxidation.[35] Cytochrome P450 enzymes activate dioxygen at a cysteine-ligated Fe–porphyrin unit, whereas non-heme diiron centers are employed by sMMO and related multicomponent monooxygenases. Similar carboxylate-bridged dinuclear iron centers occur in other proteins, where they perform a wide variety of functions. Included are the reversible binding of O_2 in hemerythrin, formation of a stable radical in class I ribonucleotide reductase, desaturation of fatty acid chains by stearoyl-ACP Δ^9 desaturase, oxidation and storage of iron in ferritin, and possibly dioxygen sensing in the bacterial chemotaxis protein DcrH.[3, 36–40] The diversity of chemical reactivity displayed by non-heme diiron centers rivals that of heme groups, and both often serve similar functions in metalloproteins.[35] Understanding the factors that tune these iron centers to perform a specific function is of fundamental importance.[41]

Another aspect of sMMO catalysis that has attracted much attention is the mechanism by which catalysis is regulated. The activation of unreactive C–H bonds requires the generation of a potent activated oxygen intermediate, which necessitates the tight regulation of electron, proton, and substrate delivery. An important method of regulation employed by multicomponent enzyme systems such as sMMO is to separate physically the site of electron entry from the site where molecular oxygen is reductively activated. In addition, several more subtle types of regulation have been identified.

Soluble MMO thus represents a wonderful system for studying the fundamental chemistry of dioxygen activation and of methane hydroxylation at the diiron site, as well as the regulatory mechanisms employed by a multicomponent oxygenase, including long-range electron transfer. Both aspects of MMO catalysis are discussed in this review. In Section 2, we take a closer look at the three components of sMMO with emphasis on their structures. Section 3 presents key information obtained by time-resolved spectroscopic techniques on the nature of several catalytic intermediates, both for the reductive activation of dioxygen and for electron transfer from NADH through MMOR to MMOH. The mechanism of substrate hydroxylation has been evaluated both with the use of molecular reporter probes and by calculations at the density functional theory (DFT) level (Section 4). Section 5 describes the role of component interactions in the regulation of various aspects of catalysis. As we shall see, biological methane oxidation is very much a tale of two irons and three proteins.

2. Protein Components of Soluble Methane Monooxygenase

The three protein components that form the soluble MMO enzyme system, MMOH, MMOR, and MMOB, have been characterized by a variety of kinetic, spectroscopic, and structural techniques. Before we describe structures of these components in more detail, some general features of sMMO and related multicomponent oxygenases warrant discussion.

The hydroxylase enzyme MMOH is a 251-kDa dimer of three subunits in an $\alpha_2\beta_2\gamma_2$ configuration (α, 60.6 kDa; β, 45.0 kDa; γ, 19.8 kDa).[24, 26] Each α subunit contains a carboxylate- and hydroxo-bridged dinuclear iron center, where dioxygen activation and methane hydroxylation occur. MMOR is a 38.5-kDa iron–sulfur flavoprotein that shuttles electrons from NADH through its flavin adenine dinucleotide (FAD) and [2Fe–2S] cofactors to the hydroxylase active site.[27, 42, 43] MMOB (15.9 kDa) contains no prosthetic groups and modulates MMO reactivity by forming specific complexes with the hydroxylase that indirectly affect the structure and reactivity of the diiron site.[24, 27, 44–50] In *M. trichosporium* OB3b, MMOH, MMOB, and MMOR represent 12, 0.5, and 0.1–0.3 wt%, respectively, of soluble protein in a cell-free extract prepared under low copper concentrations. Therefore, on a molar basis, approximately equivalent concentrations of MMOH and MMOB are present in the cell, whereas the reductase concentration is only 10% that of the other components.[24] Similar results have been reported for soluble cell extracts from *Methylocystis* sp. strain WI14.[51]

The genes encoding the sMMO proteins of *M. capsulatus* (Bath),[52–54] *M. trichosporium* OB3b,[30, 55, 56] *Methylocystis* sp. strain M,[57] *Methylocystis* sp. strain WI14,[51] and *Methylomonas* sp. strains KSPIII and KSWIII have been identified and sequenced.[58] These genes are clustered on a 5.5-kb operon, comprising *mmoX*, *mmoY*, *mmoB*, *mmoZ*, *orfY*, and *mmoC*, which code, respectively, for $MMOH_\alpha$, $MMOH_\beta$, MMOB, $MMOH_\gamma$, a protein of unidentified function (OrfY, 12 kDa), and MMOR (Figure 2). Expression in *M. capsulatus* (Bath) is controlled by a single σ^{70}-dependent, copper-regulated pro-

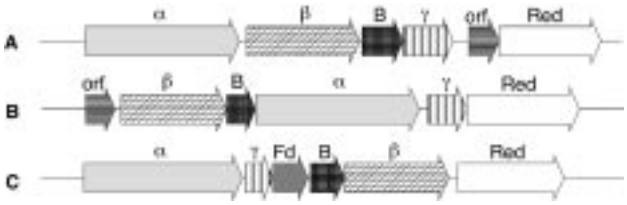

Figure 2. Organization of the sMMO operon (**A**) and operons of related multicomponent monooxygenases (**B**,**C**). Arrangement **B** occurs for phenol hydroxylase and benzene/toluene-2-monooxygenase, whereas arrangement **C** is found for toluene-3-monooxygenase, toluene-4-monooxygenase, and *Xanthobacter* alkene monooxygenase. The components are encoded as follows: α, β, and γ: hydroxylase (or epoxidase) subunits; B: coupling protein; Red: reductase; Fd: ferredoxin; orf: open reading frame (DmpK protein in phenol hydroxylase). Reprinted with permission from ref. [54]. Copyright (2000) Blackwell Science.

moter located upstream of the *mmoX* gene, such that in the native bacterium the sMMO system is produced only under conditions of low copper concentration.[59] Transcription of the *M. trichosporium* OB3b sMMO genes is directed from a σ^{54}-like promoter upstream of *mmoX* and a σ^{70}-like promoter located in the intercistronic region between *mmoX* and *mmoY*.[59, 60]

Amino acid sequences of these six sets of sMMO proteins are universally conserved as follows: $MMOH_{\alpha}$, 73.6%; $MMOH_{\beta}$, 46.8%; MMOB, 55.6%; $MMOH_{\gamma}$, 35.7%; OrfY, 19.4%; and MMOR, 37.4%. The function of OrfY has remained unclear; the protein has not been isolated from any of the native organisms and exhibits no significant homology with other known proteins.[54, 61] Although the overall percent identity for the putative OrfY products is fairly low (19.4%), there is a central region with a significantly greater number of conserved residues (44.4%). Very recently we have expressed OrfY from *M. capsulatus* (Bath) in *E. coli*. In contrast to an earlier report,[11] Western blot analysis of *M. capsulatus* (Bath) soluble cell extracts with an antibody to OrfY clearly showed the presence of the OrfY protein, albeit at much lower levels than that of MMOH (1–2%). Recombinant OrfY inhibits the MMO-catalyzed epoxidation of propene, probably by binding directly to MMOH.[62] These results clearly suggest that OrfY plays a functional role in the sMMO system. One possibility is that the protein participates in the assembly of the hydroxylase diiron centers, a function assigned to a protein of similar size but no apparent sequence homology, DmpK, in the related phenol hydroxylase from *Pseudomonas* sp. CF600.[63] Despite our new evidence for a fourth component, the title of this review is still appropriate, for we have no reason at present to suspect that OrfY functions in sMMO catalysis.

Several monooxygenases, including benzene/toluene-2-monooxygenase,[64] toluene-3-monooxygenase,[65, 66] toluene-4-monooxygenase,[67–70] phenol hydroxylase,[71–74] and alkene monooxygenase,[75–80] are quite similar to sMMO. All of these protein systems contain a hydroxylase with two or three subunits housing a non-heme carboxylate-bridged diiron center, a reductase, and a coupling protein. In addition, dioxygen is the oxidant in each of the hydroxylation or epoxidation reactions they catalyze. Sequence alignments demonstrate that many amino acid residues are highly conserved across this set of proteins, especially at the diiron active site of the hydroxylase α subunit.[54, 66, 68, 80–82] sMMO is thus far the best studied member of these oxygenases.

High-yield recombinant expression systems have been developed for both MMOB and, more recently, MMOR in *E. coli*.[31, 54, 61, 83, 84] The ability to express MMOR in high yield is particularly important for structural studies because only small amounts of this protein can be isolated from the native organism. Recombinant expression of MMOH has proved to be more challenging. MMOH expressed in *E. coli* does not fold properly, which results in the formation of inclusion bodies.[11, 85] Plasmids carrying the *M. trichosporium* OB3b MMOH genes yield active enzyme when expressed in certain strains of *Pseudomonas* or in native *M. trichosporium* OB3b cells in which the chromosomal copy of the *mmoX* gene has been disrupted.[86–89] Purification and characterization of recombinant MMOH and mutant MMOH proteins from these expression systems have not been reported, however.

2.1. MMOH

Although all three components of sMMO are necessary for efficient catalysis, MMOH alone can activate dioxygen and hydroxylate various hydrocarbons in the absence of the other components when it is chemically reduced to the diferrous state.[24, 50] Therefore, the chemistry of dioxygen activation and substrate hydroxylation takes place at the diiron centers in the α subunits of MMOH. Much effort has been devoted to the characterization of the structural features of the diiron site in its various oxidation states and in the transient intermediates of the dioxygen activation reaction. In this section we first present the most important structural insights gained from spectroscopic studies. This discussion is followed by an examination of X-ray crystal structure determinations of MMOH in a variety of crystal forms, oxidation states, and substrate analogue and product complexes, which together provide insight into the dynamics of the MMOH active site.

2.1.1. Spectroscopic Characterization of MMOH

The diiron center of MMOH has been thoroughly characterized by a variety of spectroscopic techniques including EXAFS,[90–95] EPR,[44, 46, 47, 92, 96–100] ENDOR/ESEEM,[47, 99, 101–107] optical,[24, 92] MCD,[108–110] and Mössbauer techniques.[24, 47, 50, 92, 111] The spectroscopic properties of non-heme iron sites in enzymes, including those of MMOH, have recently been reviewed.[39] Here we focus on studies most relevant to enzyme catalysis (see Table 1).

The diiron site of MMOH can exist in three stable oxidation states, $Fe^{III}Fe^{III}$ ($MMOH_{ox}$), $Fe^{III}Fe^{II}$ ($MMOH_{mv}$), and $Fe^{II}Fe^{II}$ ($MMOH_{red}$). In $MMOH_{ox}$, the high-spin ferric irons are antiferromagnetically coupled to form a diamagnetic ground state that is EPR silent.[92, 96, 111, 112] Unlike hemerythrin, ribonucleotide reductase, and stearoyl-ACP Δ^9 desaturase, proteins that have a bridging oxo group in the diferric oxidation state,[39, 81, 113–116] antiferromagnetic spin exchange in $MMOH_{ox}$ is mediated by more weakly coupling bridging ligands. EXAFS studies of $MMOH_{ox}$ showed no evidence for

Table 1. Spectroscopic properties of MMO hydroxylase (H) in the presence and absence of MMOB (B).

	Source[a]	EPR/ENDOR		Mössbauer					EXAFS	
		EPR g values	Hyperfine coupling	J [cm^{-1}][l]	δ(Fe 1) [$mm\,s^{-1}$]	ΔE_Q(Fe 1) [$mm\,s^{-1}$]	δ(Fe 2) [$mm\,s^{-1}$]	ΔE_Q(Fe 2) [$mm\,s^{-1}$]	Fe–Fe distance	Other distances
H_{ox}	MCB	1.94, 1.87, 1.72 1.82, 1.77, 1.68[b,c]			0.51 0.72[n,o]	1.12 1.46[n,o]	0.50 0.47[n,o]	0.79 1.33[n,o]	3.42 Å[h]	1st O/N shell at 2.06 – 2.09 Å
H_{ox}	MTO	1.94, 1.86, 1.79 1.85, 1.75, 1.7[b,d]		-7 ± 3[f]	0.51[f]	1.16[f]	0.50[f]	0.87[f]	60 % 3.01 Å 40 % 3.36 Å[q]	2 O/N at 1.96 Å 3 O/N at 2.09 Å
$H_{ox}+B$	MCB	1.94, 1.86, 1.79 1.82, 1.77, 1.68[b,c]							3.39 Å[r]	same as $MMOH_{ox}$
$H_{ox}+B$	MTO	1.97, 1.86, 1.75 1.90, 1.79, 1.59[b,d]							same as $MMOH_{ox}$[q]	
H_{mv}	MCB	1.94, 1.87, 1.72[c]	14 – 30 MHz (μ-OH) 8 MHz ($FeOH_{(2)}$)[j]	-32[h]					3.42 Å[h,r,s]	
H_{mv}	MTO	1.94, 1.86, 1.75[d,e,f]	13 – 23 MHz (μ-OH) 8 MHz ($FeOH_{(2)}$)[k]	-30[g]	0.48[p,f]	-1.3[p,f]	1.19[p,f]	2.4[p,f]		
$H_{mv}+B$	MCB	1.88, 1.77, 1.63[c]								
$H_{mv}+B$	MTO	1.86, 1.77, 1.62[f,g]		-5[g]						
H_{red}	MCB	15[h]			1.3[n,o]	2.8[n,o]	1.3[n,o]	2.8[n,o]	no Fe–Fe scattering[r,s]	
H_{red}	MTO	16[e,f,g]		0.35[m]	1.3[f,n]	3.0[f,n]	1.3[f,n]	2.7[f,n]		
$H_{red}+B$	MTO	16 (sharper than H_{red})[g,h]								

[a] MCB: *Methylococcus capsulatus* (Bath); MTO: *Methylosinus trichosporium* OB3b. [b] EPR parameters for cryogenically reduced $MMOH_{ox}$ species. [c] Ref. [100]. [d] Ref. [98]. [e] Ref. [111]. [f] Ref. [47]. [g] Ref. [44]. [h] Ref. [92]. [i] Ref. [46]. [j] Ref. [102]. [k] Ref. [103]. [l] Values are reported using the convention $H=-2JS_1S_2$. [m] Ref. [97]. [n] Measured at 4 K. [o] Ref. [50]. [p] Measured at 150 K. [q] Ref. [94]. [r] Ref. [93]. [s] Ref. [91].

short 1.75 – 1.80 Å Fe–O bonds characteristic of $\{Fe_2(\mu\text{-oxo})\}^{4+}$ units, and optical spectra similarly lacked absorbances at 350 and 500 – 600 nm that are typical of oxo-bridged diferric complexes.[24, 39, 91, 94] Analysis of one-electron reduced analogues of $MMOH_{ox}$, obtained after cryoreduction of frozen $MMOH_{ox}$ samples by γ-irradiation, has allowed characterization of small molecule-bound and protein component-bound forms of $MMOH_{ox}$ by EPR spectroscopy.[98, 100, 117, 118] These studies demonstrate that the diiron site of $MMOH_{ox}$ is affected by binding of MMOB but not of MMOR. Product alcohols such as methanol and phenol bind to the dimetallic center, whereas glycerol and DMSO, an inhibitor, bind only in the presence of MMOB. Binding of phenol to $MMOH_{ox}$ has also been observed by resonance Raman spectroscopy.[119]

Structural studies of the mixed-valent oxidation state are of limited direct relevance to the catalytic mechanism, because $MMOH_{mv}$ does not react with dioxygen. Moreover, two-electron transfer to $MMOH_{ox}$ is favored in the ternary MMOH – MMOB – MMOR complex.[2, 45, 96, 120] Antiferromagnetic coupling between high-spin Fe^{III} and high-spin Fe^{II} results in an $S=1/2$ ground state, which gives rise to a rhombic EPR spectrum with $g<2$.[47, 96, 112] Advanced pulsed EPR techniques have been used to study the binding of substrate/product-like small molecules to the diiron center in $MMOH_{mv}$ and to monitor the effects of component interactions on its structure. Signals corresponding to a bridging hydroxo group and water or hydroxide ion bound at a terminal position have been identified with ENDOR/ESEEM spectroscopy.[101–103] Hyperfine couplings between the diiron center and ^2H- and ^{13}C-labeled DMSO, ^{13}C-labeled MeOH, and acetate reveal that all three molecules bind directly to the diiron center.[99, 101, 106]

Mössbauer spectroscopy demonstrates that both iron atoms are high-spin ferrous and weakly ferromagnetically coupled in the reduced diiron(II) oxidation state.[47, 92, 111] The resulting integer spin system has a low-lying doublet that is split in zero applied field by an energy with an average value in the microwave range, giving rise to a very characteristic EPR absorption around $g=16$.[97, 105, 108] The $g=16$ signal of $MMOH_{red}$ has proved to be very useful for monitoring the reaction of $MMOH_{red}$ with O_2 (see Section 3). MCD spectra are consistent with the presence of two five-coordinate, square-pyramidal ferrous centers.[108–110] MMOB binding affects primarily the coordination geometry of one of the two Fe atoms. In contrast to $MMOH_{ox}$, substrate/product-like molecules such as MeOH, DMSO, and MeCN do not seem to bind to $MMOH_{red}$. Products such as MeOH and phenol that bind to $MMOH_{ox}$ are thus released when $MMOH_{ox}$ is reduced to $MMOH_{red}$, which facilitates substrate binding in the next catalytic cycle.

2.1.2. Crystal Structures of MMOH

The crystal structure of $MMOH_{ox}$ from *M. capsulatus* (Bath), reported in 1993, provided the first high-resolution view of the MMOH protein structure and the details of its diiron site.[28, 121] The elucidation of the MMOH structure laid the foundation for much of our current knowledge about transient intermediates in the activation of dioxygen, allowed for the calibration of theoretical calculations on MMOH, and suggested modes for substrate access and component interactions. Since then, crystal structures of MMOH have been reported for $MMOH_{ox}$ from *M. trichosporium* OB3b,[30] and for MMOH from *M. capsulatus* (Bath) in different crystal forms, oxidation states, and in the presence of various

substrates and products.[28, 29, 33, 121–123] Table 2 lists 19 MMOH samples for which structures have been crystallographically determined. Since the two αβγ protomers from the *M. capsulatus* (Bath) crystals are not related by crystallographic symmetry, the 17 *M. capsulatus* (Bath) structures represent a collection of 34 independent active site geometries. Such a collection of structures of the same protein provides important information about the flexibility of amino acid side chains at the active site. These structures reveal conformational changes that may occur during catalysis and its regulation. Rather than describing all of these structures in detail, we focus here on their common features and discuss differences that may be relevant to MMOH function. In general, the global conformation of the protein remains unperturbed among the various forms of MMOH, with changes concentrated at the diiron center and a few residues at or near the active site. We restrict our discussion to structures obtained for MMOH from *M. capsulatus* (Bath), but the *M. trichosporium* OB3b active site geometry and overall protein structure are quite similar.

The architecture of MMOH is that of a heart-shaped $\alpha_2\beta_2\gamma_2$ dimer (Figure 3) and consists almost entirely of α-helical secondary structure. The subunits are arranged as two αβγ protomers that are related by a noncrystallographic, twofold symmetry axis. Extensive helical contacts between the α and β subunits of each protomer are responsible for dimer formation. At the interface between each of the monomers, a canyon region with dimensions of approximately 80 Å × 40 Å × 20 Å is formed. The γ subunits flank the two sides of the hydroxylase and are not involved in dimer formation.

The diiron centers reside in four-helix bundles that are formed by helices B, C, E, and F in the core of the α subunit (Figure 3). Helices B and E each contribute a glutamate residue (Glu114, Glu209) to the diiron center, whereas helices C and F each donate two iron-coordinating residues in the form of a Glu-Xxx-Xxx-His motif. The remainder of the coordination sphere is occupied by solvent-derived ligands.

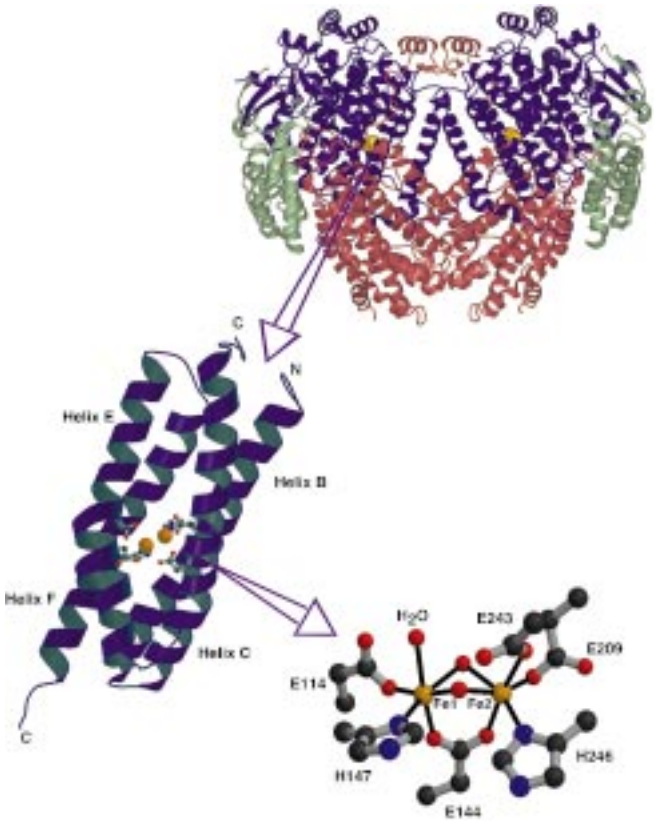

Figure 3. Three structural levels in MMOH from *M. capsulatus* (Bath). Top: Overall fold of MMOH with the twofold symmetry axis running vertically. α: purple; β: red; γ: green. Middle: ribbon diagram of four-helix bundle with Glu (E) and His (H) ligands depicted in ball-and-stick form. Bottom: ball-and-stick model of the diiron center in $MMOH_{ox}$. This figure was produced with the programs Molmol,[231] Molscript,[232] and Raster3d.[233]

Very similar structures occur in other enzymes that use a carboxylate-bridged diiron center to activate dioxygen, including the R2 subunit of class I ribonucleotide reductase and stearoyl-ACP Δ^9 desaturase.[113, 124, 125]

Table 2. Crystal structures of MMOH.

Species[a]	Redox state[b]	Experimental conditions	Crystal form	Resolution [Å]	PDB reference
MCB	ox	277 K	Form I	2.20	1MMO[28]
MCB	ox	113 K	Form I	1.70	pending[29]
MCB	ox	100 K	Form II	1.96	1FZ1[33]
MCB	red	100 K	Form I	1.70	1MTY[122]
MCB	red	reduced in crystal, 100 K	Form II	2.15	1FYZ[33]
MCB	red	grown from $MMOH_{red}$, 100 K	Form II	2.40	1FZ5[33]
MCB	mv	reduced in crystal, 100 K	Form II	2.15	1FZ2[33]
MCB	mv	grown from $MMOH_{mv}$, 100 K	Form II	2.07	1FZ0[33]
MCB	ox	methanol soaked, 100 K	Form II	2.05	1FZ6[123]
MCB	ox	ethanol soaked, 100 K	Form II	1.96	1FZ7[123]
MCB	ox	DMSO soaked, 100 K	Form I	1.70	pending[224]
MCB	ox	100 K, xenon pressurized	Form I	3.30	1FZI[129]
MCB	ox	100 K, xenon pressurized	Form II	2.60	1FZH[129]
MCB	ox	dibromomethane grown, 100 K	Form II	2.10	1FZ8[129]
MCB	ox	iodoethane grown, 100 K	Form II	2.30	1FZ9[129]
MCB	ox	pH 8.5 soaked, 100 K	Form II	2.38	1FZ4[33]
MCB	ox	pH 6.2 soaked, 100 K	Form II	2.03	1FZ3[33]
MTO	ox	291 K	Form I	2.00	1MHY[30]
MTO	ox	291 K	Form II	2.70	1MHZ[30]

[a] MCB: *Methylococcus capsulatus* (Bath); MTO: *Methylosinus trichosporium* OB3b. [b] Oxidation states: ox, $Fe^{III}Fe^{III}$; red, $Fe^{II}Fe^{II}$; mv, $Fe^{III}Fe^{II}$.

Figure 4 illustrates the diiron center geometries as they appear in crystallographically characterized forms of MMOH. In all $MMOH_{ox}$ structures (Figure 4A–D), both iron atoms have distorted octahedral environments. Fe1 is invariably coordinated by His147, monodentate Glu114, and a terminal water molecule, while Fe2 is coordinated by His246 and monodentate Glu209 and Glu243. Flexibility occurs in the positioning of Glu243, which can form hydrogen bonds to the bridging hydroxide ion or to the terminal water coordinated to Fe1. The iron atoms are bridged by Glu144 (unsymmetrically), a hydroxide ion, and a third ligand. The identity of the third bridging ligand, and with it the Fe–Fe distance, is variable. Bridging water,[29] hydroxide,[30] $H_3O_2^-$,[33] acetate,[28] and formate[33] groups have all been reported in this third position, depending on crystal form, protomer, species, and temperature of data collection. Different ligands can even occupy this bridging position for two protomers in the same molecule of MMOH, indicating that subtle conformational differences between the two protomers can affect the binding affinity of this site. Such flexibility is consistent with this site being the locus of dioxygen activation and methane hydroxylation,[29] a hypothesis supported recently by the finding that both MeOH and EtOH bind at this position (Figure 4I–J).[123]

Significant changes occur at the diiron center upon reduction to the diferrous state.[28, 29, 33] The most notable change is in Glu243, which undergoes a carboxylate shift that displaces the bridging hydroxide ion and forms a bidentate chelating interaction with Fe2 and a single bond to Fe1 (Figure 4E, F). A similar carboxylate bridging mode has recently been observed for the corresponding diferrous centers of D84E and azide-soaked F208A/Y122F mutants of the R2 protein of ribonucleotide reductase.[126, 127] Some variability is observed for the water/hydroxide ligand that occupies the bridging site distal to the two histidine residues, the coordination of which can change from symmetric to weak, asymmetric binding. The distance between the Glu144 oxygen atom and Fe2 decreases from 2.6 Å to 2.3 Å, thereby shifting the carboxylate coordination mode of this ligand from semi-bridging in $MMOH_{ox}$ to bridging in $MMOH_{red}$.

Based on these structures, dioxygen binding most likely occurs by substitution of the weakly coordinating bridging water molecule distal to the histidines. This site directly faces a hydrophobic cavity adjacent to the diiron center. It should be remembered, however, that $MMOH_{red}$ is not very reactive in the absence of MMOB,[49] and that the geometry of the $MMOH_{red}$ active site that reacts with O_2 may differ from that seen in any of the crystal structures.

The diiron centers in $MMOH_{mv}$ and $MMOH_{DMSO}$, formed by soaking $MMOH_{ox}$ crystals with the inhibitor DMSO (10 Vol.%), are similar and severely distorted compared to those of $MMOH_{ox}$ and $MMOH_{red}$ (Figure 4G, H).[29, 33] Although neither structure is directly relevant to MMO catalysis, they provide additional insight into the geometric variability that is possible for the carboxylate-bridged diiron centers in MMOH. In both structures the coordination at Fe1 remains unperturbed, whereas that of Fe2 differs markedly, with Fe2 moving 1 Å perpendicular to the Fe–Fe vector. In the $MMOH_{mv}$ structure, Fe2 is four coordinate, with Glu209, Glu243, His246, and μ-OH serving as monodentate ligands. Bidentate coordination of Glu243 and the coordination of a terminal water molecule afford octahedral geometry at Fe2 in $MMOH_{DMSO}$.

A recurring observation is that the coordination environment at Fe2 is much more flexible than that at Fe1. Comparison of individual B factors reveals considerably more thermal motion at Fe2, and recent work indicates that, under certain conditions, Fe2 is bound less tightly than Fe1.[33] We therefore conclude that Fe2 is most likely the iron atom that is more affected by MMOB binding. As argued previously from CD/MCD data,[108–110] only one of the two iron atoms is significantly affected when the coupling protein interacts with the hydroxylase. MMOB may affect the conformation of Fe2 by altering the conformation of the surface-exposed helices E and F, which contain all of the amino acids (Glu243, His246, and Glu209) that coordinate to Fe2.

The MMOH protein serves not only to supply ligands for the two iron atoms. In order for chemistry to occur at the diiron center, electrons, dioxygen, and hydrocarbon substrates all need to be provided through processes that are tightly regulated. A sequence alignment analysis of sMMOs, toluene monooxygenases, alkene monooxygenases, and phenol hydroxylases reveals a universally conserved hydrogen-bonding network extending outward from the diiron site to the hydroxylase surface.[54] This network includes the iron-coordinating histidine residues as well as Tyr67 and Lys74 at the protein exterior on helix A in the MMOH canyon and located $\sim$10 Å from the diiron site (Figure 5). A similar hydrogen bonding network is present in the R2 protein of ribonucleotide reductase, where it is proposed to be involved in electron transfer.[128] It is possible that electron injection into MMOH from MMOR occurs along this pathway.

The MMO active site contains a hydrophobic substrate-binding pocket at a site distal to the histidines with a volume of approximately 185 $Å^3$. This pocket favors the binding of hydrophobic guests, such as methane and dioxygen. Several possibilities have been considered for substrate entry into and product egress from the active site cavity.[122, 129] The shortest and most direct route for substrate entry into the cavity is through a gap between helices E and F. Conformational changes in these helices, altered side-chain rotamer conformations due to normal protein breathing, or MMOB binding may potentially allow substrate to "wiggle" its way into the active site. A comparison of the structures of $MMOH_{ox}$ and $MMOH_{red}$ does reveal slight conformational differences for these helices.[33]

A different mode of entry for substrates into the active site would involve a series of movements through some of the five hydrophobic cavities identified in the α subunit (Figure 6). A potential route would traverse cavities 3 and 2 running from the surface of the protein through the hydrophobic core of the α subunit to active site cavity 1.[33, 122] Crystallographic studies with xenon-pressurized form I and form II $MMOH_{ox}$ crystals revealed localization of ordered Xe in cavity 2.[129] Because the van der Waals radius of Xe is almost identical to that of methane ($\sim$2.15 Å), its binding in cavity 2 indicates that the buried hydrophobic pockets of the α subunit should be accessible to the natural substrate. Leu110, which acts as a

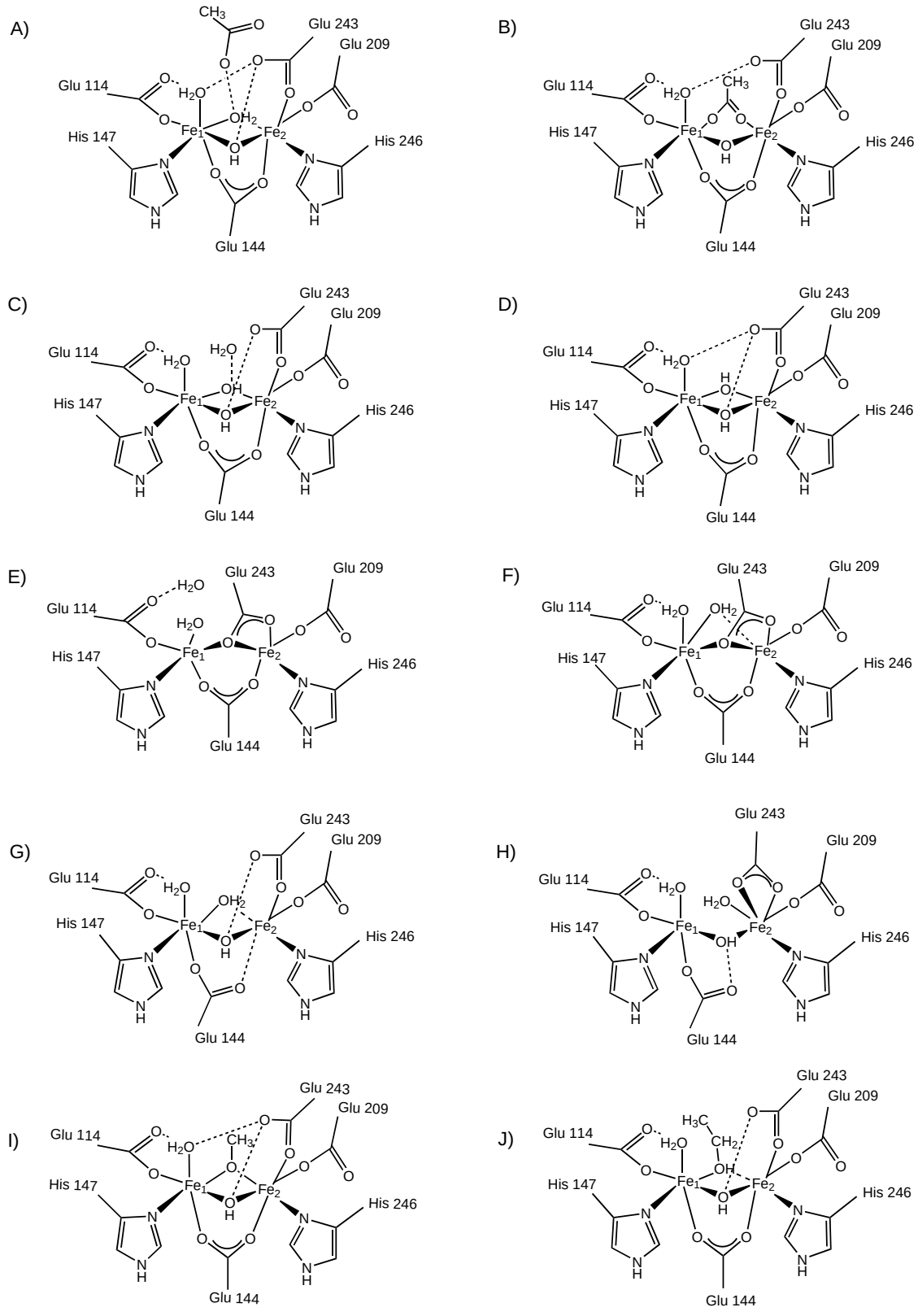

Figure 4. Coordination geometries for the diiron center of MMOH in various states: A) $MMOH_{ox}$, form I at 160 K; B) $MMOH_{ox}$, form I at 277 K; C) $MMOH_{ox}$, form II; D) $MMOH_{ox}$ from *M. trichosporium* OB3b, form I; E) $MMOH_{red}$, form I; F) $MMOH_{red}$, form II; G) $MMOH_{mv}$; H) $MMOH_{ox}$ soaked in 10% DMSO; I) $MMOH_{ox}$ soaked in 1M MeOH; J) $MMOH_{ox}$ soaked in 1M EtOH. All structures are for the enzyme from *M. capsulatus* (Bath), except (D) which is from *M. trichosporium* OB3b. The amino acid numbering for all structures is that of the enzyme from *M. capsulatus* (Bath). Dashed lines represent hydrogen bonds or very weak Fe–O interactions.

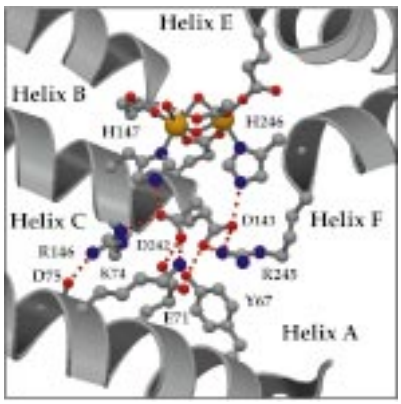

Figure 5. Structure of MMOH showing the hydrogen-bonding network of conserved residues that are proposed to be involved in electron transfer. The network extends from the two iron-coordinating histidines to the surface residues Tyr67 (Y67) and Lys74 (K74). This figure was produced with the programs Molscript and Raster3d.[232, 233] Reprinted with permission from ref. [234]. Copyright (2001) Wiley.

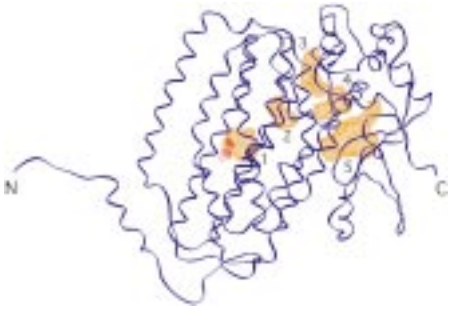

Figure 6. Ribbon diagram of MMOH α subunit showing five hydrophobic pockets that may be involved in substrate binding and transport to the active site. The figure was generated with the program O.[235] Reprinted with permission from ref. [122]. Copyright (1997) Wiley-Liss.

barrier between cavities 1 and 2, shifts from a "closed" to an "open" position upon reduction of MMOH in crystal form I (Figure 7). Only the opened rotamer is observed in the reduced and oxidized structures of form II MMOH from *M. capsulatus* (Bath), however.[33, 122] Another conserved residue that adopts different conformations is Asn214. The side chain of Asn214 points outward to the solvent in $MMOH_{ox}$, but is oriented inward toward the diiron site in all $MMOH_{red}$ structures.[33] This residue may therefore help to mediate the effects of MMOB on the redox properties of MMOH. Events such as reduction of the diiron center or binding of the other MMO components may control the conformation of Leu110 and other residues in order to "gate" the entry of substrate or solvent into the active site. Such a "leucine gate" was originally proposed to regulate access of O_2 to the diiron center in hemerythrin,[130, 131] but recent studies are more consistent with a role for Leu98 in gating access of solvent and not O_2.[132, 133]

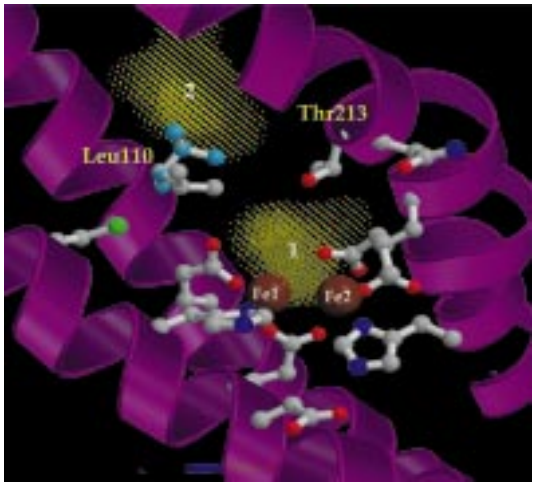

Figure 7. A closer look at the MMOH active site. Two conformations ("closed" in blue, "open" in gray) are depicted for Leu110, which may act as a gate that separates the hydrophobic cavities 1 and 2 (shown in yellow). This figure was produced with the programs Molscript and Raster3d.[232, 233]

2.2. MMOB

Addition of MMOB to the other sMMO components affects both the rate and the regioselectivity of hydroxylase-catalyzed reactions as well as the redox potentials of the MMOH diiron center (see Section 5 for additional discussion).[2, 24, 44–46, 48–50, 134] Similar effector proteins occur in other multicomponent monooxygenases such as toluene, phenol, and alkene monooxygenase.[54, 135] A variety of spectroscopic techniques suggest that MMOB exerts its effects on MMOH by binding in the vicinity of the diiron site and slightly altering its structure.[44, 46, 93, 98, 100, 108–110] Details of how the small, cofactorless MMOB protein regulates various aspects of MMO catalysis remain enigmatic. The recent elucidation of the three-dimensional structure of MMOB by NMR spectroscopy has yielded important geometric insights into the possible nature of the MMOH–MMOB interaction, however, and provides a good starting point for further studies of the mechanism of regulation by MMOB.

The structures of MMOB from both *M. capsulatus* (Bath) and *M. trichosporium* OB3b (Figure 8) have been solved by NMR spectroscopy, with average backbone root-mean square deviation (RMSD) values for the protein core of 0.46 Å and 1.1 Å, respectively.[31, 32] The core of MMOB, residues 35–127 in *M. capsulatus* (Bath), consists of seven β strands arranged into two antiparallel β sheets oriented almost perpendicular to each other (Figure 8A). Three α helices bridge the cleft

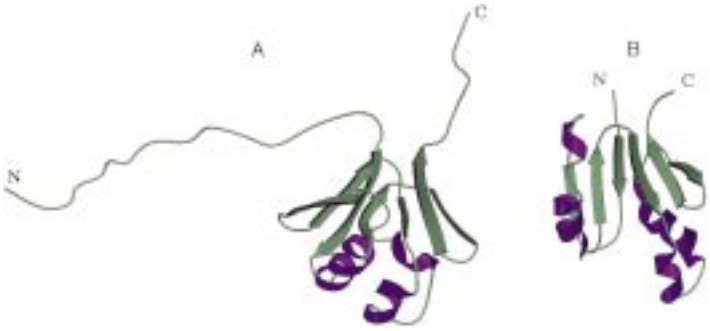

Figure 8. Ribbon diagrams of MMOB structures from A) *M. capsulatus* (Bath) (File in the protein data bank (PDB): 1CKV) and B) *M. trichosporium* OB3b (File in the PDB: 2MOB). This figure was produced with the programs Molscript and Raster3d.[232, 233]

between the two β sheets to create the globular core of the protein. The first 35 and the last 12 amino acids of MMOB are not well defined in the NMR structure, but NMR and CD experiments suggest that a part of the N terminus may form a helical structure.[31, 32, 83] Proteolytic cleavage in the N-terminal region completely inactivates MMOB.[83, 134, 136]

Structures have been determined by NMR spectroscopy for effector proteins of two other multicomponent hydroxylases, P2 in phenol hydroxylase from *Pseudomonas* sp. CF600 and T4moD in toluene-4-monooxygenase from *Pseudomonas mendocina*.[135, 137] The secondary structures of both effector proteins are similar to those found in MMOB, and the tertiary structure of T4moD is similar to that of MMOB from *M. capsulatus* (Bath) as well. Differences between MMOB and P2, which has a flatter structure with a "doughnut hole" in the center of the protein, may be explained by a lack of constraints in the latter structure, as indicated by a backbone RMSD of 2.48 Å. In addition, whereas NMR spectroscopy indicates that P2 interacts with substrate, such interactions have not been observed for MMOB.[31, 137]

NMR experiments with MMOB in the presence of the hydroxylase have identified several conserved surface residues that may be involved in binding to the larger hydroxylase protein.[32] Mapping those residues that show line-broadened NMR signals in the presence of MMOH onto the three-dimensional structure of MMOB indicates that most are located on the side of the protein that also contains the conserved residues E53, E94, L96, G97, F100, and D108 (Figure 9). Both the N and C termini extend from the other side of MMOB. In addition, NMR signals of a highly conserved region at the N terminus, residues 22 – 26, also experience line broadening at 25 °C. These results suggest that the lower half of MMOB is buried in some region of the hydroxylase, presumably the "canyon", whereas the upper half remains exposed to solvent. Interaction of the N terminus with surface residues of MMOH may explain the line broadening observed for residues 22 – 26.[28, 32, 33] This model is consistent with results from chemical cross-linking experiments that show MMOB interacting with the α subunit of MMOH.[44]

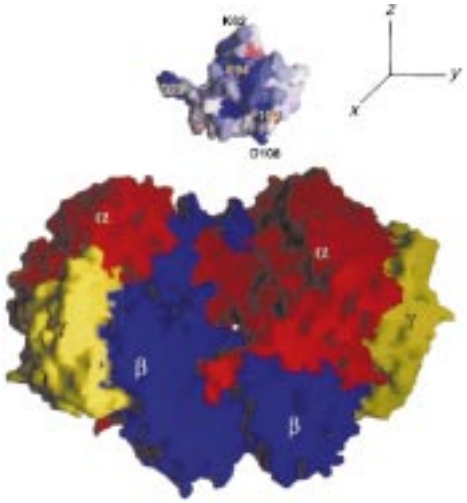

Figure 9. A surface diagram model for docking of MMOB (top) into the canyon of MMOH (bottom). Residues on MMOB that are most affected by binding to MMOH are colored blue and those least affected are colored red. For clarity, MMOB has been translated away from its proposed docking site on the surface of the hydroxylase and rotated clockwise about the y-axis by 90° to expose the residues on the "lower" half of MMOB most affected by MMOH binding. This figure was produced with the program Grasp.[236] Reprinted with permission from ref. [32]. Copyright (1999) National Academy of Sciences.

2.3. MMOR

MMOR is the one MMO component for which no three-dimensional structure has yet been determined. MMOR contains one [2Fe–2S] cluster and one FAD cofactor, which both facilitate electron transfer from NADH to MMOH.[24, 25, 27, 42, 43, 138, 139] In the absence of MMOH, the protein can transfer electrons from NADH to a variety of electron acceptors, including $K_3[Fe(CN)_6]$ and 2,6-dichloroindophenol (2,6-dichloro-*N*-(4-hydroxyphenyl)-1,4-benzoquinonimine), or it can reduce O_2 to hydrogen peroxide.[27, 138]

The [2Fe–2S] cluster is located in the N-terminal portion of MMOR and exhibits significant sequence homology with ferredoxins of plants, cyanobacteria, and archaebacteria.[53] Its optical,[27, 43] EPR,[43, 47, 138, 140] and Mössbauer[47] spectra are typical of those found for other [2Fe–2S]-type ferredoxins. The FAD cofactor is located in the C-terminal domain of MMOR, as is the NADH binding region. Upon one-electron reduction of the FAD cofactor, optical bands at 590 and 650 nm appear that are characteristic of a neutral semiquinone radical intermediate.[25, 27, 43, 84] The redox potentials of the MMOR cofactors are such that electron transfer in the physiological direction is favored: NADH ($E^{\circ\prime} = -320$ mV) → FAD ($E^{\circ\prime} = -266/-176$ mV) →[2Fe–2S] ($E^{\circ\prime} = -209$ mV) →MMOH ($E^{\circ\prime} \sim +100$ mV for ternary MMOH – MMOB – MMOR complex).[*][2, 42, 45, 84, 120, 140] The MMOR redox potentials are not significantly affected by the presence of MMOH or MMOB.[84]

In the absence of a high-resolution structure for MMOR, some structural insights may be gleaned from the X-ray diffraction results for related proteins, phthalate dioxygenase reductase (PDR) (Figure 10) and a complex between maize leaf [2Fe–2S] ferredoxin (Fd) and Fd–$NADP^+$ oxidoreductase (FNR).[141–143] Like MMOR, PDR shuttles electrons from NADH through flavin and [2Fe–2S] cofactors to an iron-containing oxygenase. The organization of the flavin and [2Fe–2S] domains is reversed, however, and PDR uses a flavin mononucleotide (FMN) instead of FAD.[141] In PDR, the [2Fe–2S]- and NADH-binding domains adopt the shape of a kidney bean, with the isoalloxazine group of FMN optimally positioned in the central cleft to mediate electron transfer from NADH to the [2Fe–2S] center. The distance between the closest Fe of the [2Fe–2S] center and the 8-methyl group of FMN is only 7.2 Å.

[*] The MMOR potentials listed are the ones most recently determined in our laboratory for the recombinant protein.[84] Similar values have been reported previously for native MMOR.[42, 140] All potentials are relative to the normal hydrogen electrode.

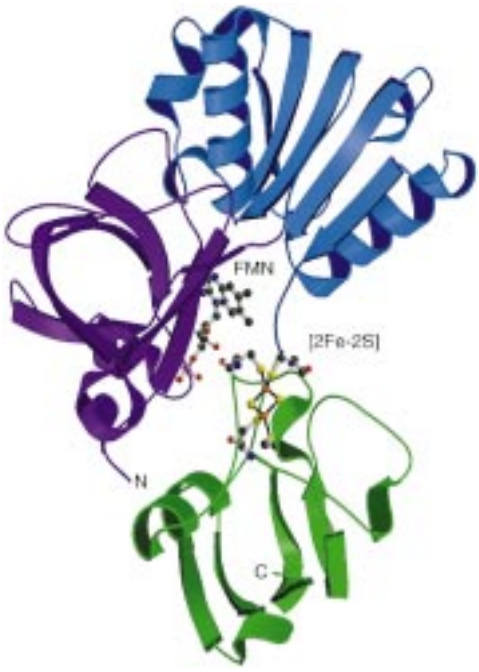

Figure 10. Ribbon diagram representation of the crystal structure of phthalate dioxygenase reductase showing the [2Fe–2S] and FMN cofactors in ball-and-stick representation (File in the PDB: 2PIA). The [2Fe–2S], FMN, and NADH-binding domains are colored in green, purple, and blue, respectively.[141] This figure was produced with the programs Molscript and Raster3d.[232, 233]

The complex between maize leaf [2Fe–2S] ferredoxin and Fd–NADP$^+$ oxidoreductase functions like MMOR and PDR, but the ferredoxin and flavin/NADP$^+$ binding parts are separate proteins instead of domains of the same protein. The overall folds of both proteins in this complex are similar to those of the corresponding domains in PDR, which indicates a common electron transfer pathway that is likely to exist in MMOR as well. One difference between the Fd–FNR complex and PDR is the orientation of the ferredoxin domain, which is rotated by about 180° around the axis from the closest Fe of the [2Fe–2S] center and the 8-methyl group of the flavin cofactor. It remains to be established which orientation is present in MMOR, but both result in approximately the same distance between the [2Fe–2S] center and the flavin cofactor.

3. Snapshots of the Catalytic Cycle

Knowing the three-dimensional structure of every intermediate on the enzymatic pathway is an enzymologist's ultimate dream, because it would allow a molecular movie to be compiled that illustrates how the enzyme works. The multicomponent nature of the MMO system makes the application of time-resolved crystallography difficult,[144] but time-resolved spectroscopic techniques have been remarkably successful in identifying and characterizing several intermediates in the catalytic cycle of MMO.[27, 50, 145–148] Two aspects of MMO catalysis have been studied by using time-resolved spectroscopy, the MMOR-promoted reduction of the diiron center by NADH and the dioxygen-activation and methane-hydroxylation steps at the MMOH diiron center.

3.1. Electron Transfer from NADH through MMOR to the Diiron Center in MMOH

Soluble methane monooxygenases employ a sophisticated electron transfer system with NADH-oxidizing and methane-hydroxylating sites on two separate proteins. This physical separation limits futile cycles whereby only NADH rather than NADH and methane are oxidized. Related systems can be found in bacterial monooxygenases, dioxygenases, and photosynthetic and respiratory electron transport chains.[3, 54, 149–151] Understanding all aspects of electron transfer within the MMO system and its regulation by component interactions may prove to be complex. Nonetheless, some intermediates of both the intramolecular (reduction of MMOR by NADH) and intermolecular (reduction of MMOH by MMOR) electron transfer steps have been identified by using stopped-flow optical spectroscopy.[27, 139]

Scheme 2 depicts intermediates that form during the reaction of MMOR$_{ox}$ with NADH.[27, 84] The first observable intermediate, termed CT1, is assigned as a charge-transfer complex between the nicotinamide moiety of NADH and the isoalloxazine ring of FAD. The rate of formation of CT1 becomes saturated as the concentration of NADH is increased, which indicates that NADH binding occurs in two steps. The initial Michaelis complex (MC1) is spectroscopically silent. A second charge-transfer intermediate, CT2, forms upon hydride transfer from NADH to FAD. CT2 has a more intense and lower energy absorbance band than CT1, because the π-stacking interaction now occurs between the NAD$^+$ cation and the FADH$^-$ anion. Release of NAD$^+$ and partial electron transfer from FADH$^-$ to [2Fe–2S]$_{ox}$ are observed to occur simultaneously. This single-electron transfer step yields a flavin semiquinone and [2Fe–2S]$_{red}$.

When NADH is mixed with a 1:1 complex of MMOH$_{ox}$ and MMOR$_{ox}$, the early steps of NADH binding to MMOR and hydride transfer are largely unchanged.[27] NAD$^+$ release and electron transfer from FADH$^-$ proceed at rates similar to those seen for MMOR alone, although this state comprises a mixture of complexes with two electrons in MMOR and complexes with one electron in MMOR and the other

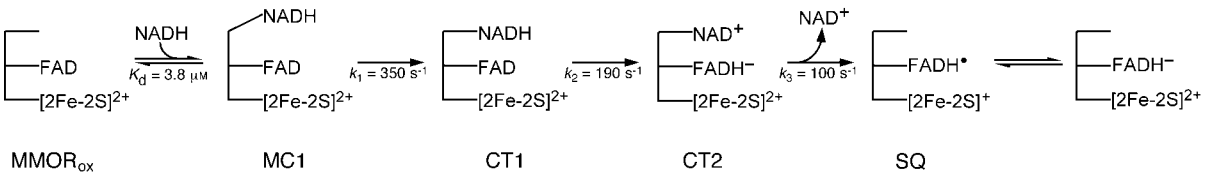

Scheme 2. Intermediates formed upon reaction of MMOR$_{ox}$ with NADH.

electron in MMOH. Further electron-transfer steps to MMOH, ultimately to afford $MMOH_{red}$, proceed at slower rates. Addition of MMOB increases the rate of these intermolecular electron-transfer reactions, with maximum rates observed when one equivalent of MMOB is present per MMOH. Methanol retards intermolecular electron transfer, whereas methane has no effect.

The presence of additional electron-transfer steps occurring among cofactors of MMOR complicates the spectral analysis for the intermolecular electron-transfer reaction. Studies using prereduced MMOR or studies using just the N-terminal ferredoxin-like domain of MMOR should resolve this problem and allow a better understanding of intermolecular electron transfer from MMOR to MMOH.[152]

3.2. Transient Intermediates in the Activation of O_2

Methane monooxygenase has proved to be a rewarding system for studying the molecular details of dioxygen activation at a non-heme diiron center. Two critical properties of sMMO are responsible for this success. First, chemically reduced MMOH can react with O_2 and substrate to afford hydroxylated products and $MMOH_{ox}$ in the absence of the other MMO components.[24] Although the yields for this single-turnover reaction are variable and below 40%, this result nonetheless proves that activation of dioxygen and the actual hydroxylation reaction both take place at the MMOH protein.[24, 50] Even more important is that, in the presence of MMOB, the energetics of the reaction pathway are such that several intermediates build up in significant amounts before they decay.

Figure 11 displays species in the catalytic cycle that have been detected during the single-turnover reaction of $MMOH_{red}$ with O_2 in the absence and presence of substrate.[50, 145, 147, 148] The reaction can be monitored continuously by using stopped-flow optical spectroscopy to detect colored intermediates or discontinuously by using the freeze–quench method in combination with EPR, Mössbauer, and EXAFS spectroscopy. The decay of $MMOH_{red}$ has been followed by EPR (decay of the $g = 16$ signal) and Mössbauer spectroscopy.[49, 50, 120, 145] In the presence of MMOB, the $g = 16$ signal of $MMOH_{red}$ from *M. trichosporium* OB3b decays at a rate of $22 \pm 5\ s^{-1}$ at 4 °C. No new EPR signals appear on this time scale.[145] The decay of $MMOH_{red}$ is independent of the dioxygen concentration between 0.3 and 0.7 mM, which indicates the formation of a transient Michaelis complex between $MMOH_{red}$ and O_2 prior to the decay of the $g = 16$ signal. No such complex forms between $MMOH_{ox}$ and O_2, however.[153] A fact that is not often mentioned in reviews and discussions on the mechanism of dioxygen activation by MMOH is that a substantial portion of $MMOH_{red}$ seems to be inactive and is converted into $MMOH_{ox}$ on a timescale that is too slow to be catalytically relevant.[50, 95, 146, 147, 154, 155] The presence of these two populations of $MMOH_{red}$ is a complicating factor in the spectroscopic characterization of intermediates.

The first intermediate that is observed spectroscopically following the decay of $MMOH_{red}$ is $MMOH_{peroxo}$. First

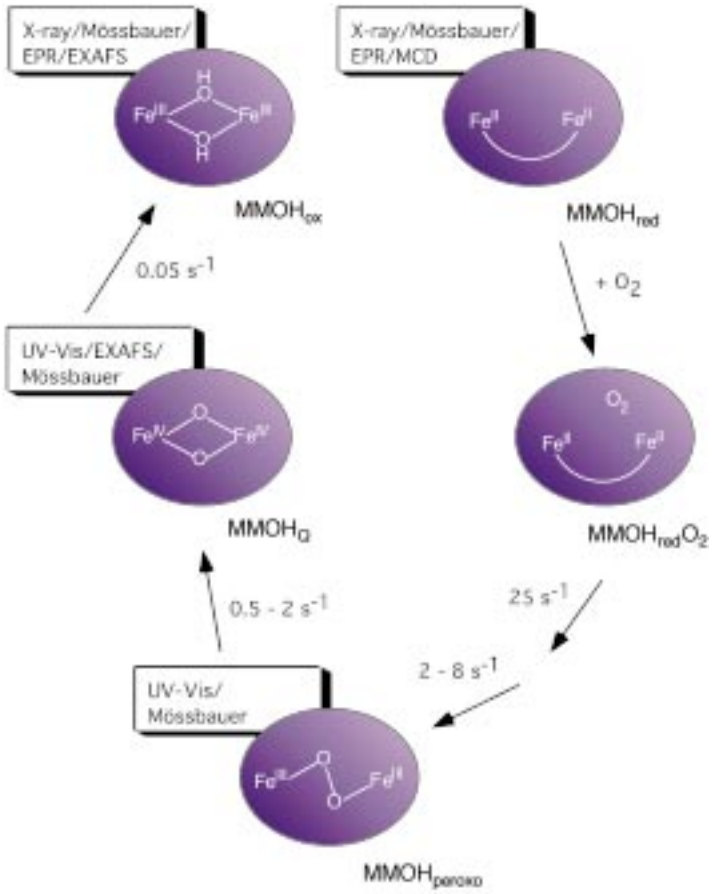

Figure 11. Schematic overview of the catalytic intermediates observed for the single turnover reaction of $MMOH_{red}$ with O_2. Techniques used to characterize the various intermediates are indicated. Structures other than those shown here have been proposed for the $MMOH_{peroxo}$ and $MMOH_Q$ intermediates. The rate constants are from studies of both the *M. capsulatus* (Bath) and the *M. trichosporium* OB3b enzymes and were determined in MOPS buffer (MOPS = 3-(*N*-morpholino)propanesulfonic acid; pH 7.0) at 4 °C.

detected for *M. capsulatus* (Bath), $MMOH_{peroxo}$ has optical bands at 420 ($\varepsilon = 4000\ M^{-1}cm^{-1}$) and 725 nm ($\varepsilon = 1800\ M^{-1}cm^{-1}$).[50, 147, 154, 155] A similar intermediate has recently been reported for the enzyme from *M. trichosporium* OB3b with $\lambda_{max} = 700$ nm ($\varepsilon = 2500\ M^{-1}cm^{-1}$),[156] although the intensity of the absorption band at 420 nm may be lower.[157] The Mössbauer spectrum of $MMOH_{peroxo}$ consists of a sharp quadrupole doublet with $\delta = 0.66\ mm\,s^{-1}$ and $\Delta E_Q = 1.51\ mm\,s^{-1}$, which is consistent with two high-spin iron(III) centers having a similar coordination geometry.[50, 154] $MMOH_{peroxo}$ is diamagnetic at 4 K as a result of antiferromagnetic coupling between the two Fe^{III} ions. Intermediates with similar optical and Mössbauer properties have been detected in a number of other diiron proteins that activate O_2, including stearoyl-ACP Δ^9 desaturase, the D84E mutant of the R2 protein of class I ribonucleotide reductase, and frog ferritin. No reliable resonance Raman data have yet been obtained for $MMOH_{peroxo}$,[155, 158] although resonance Raman spectroscopy has identified all of the other peroxo intermediates as μ-1,2-peroxo diiron(III) complexes. Table 3 compares the spectroscopic properties of these species with those of a structurally characterized μ-peroxo diiron(III) model complex.

Table 3. Spectroscopic properties of peroxo-bridged diiron(III) centers in proteins and a model complex.

	Vis		Resonance Raman		Mössbauer (4.2 K)	
	λ_{max} [nm]	ε [$M^{-1}cm^{-1}$]	O–O [cm^{-1}]	Fe–O [cm^{-1}]	δ [$mm\,s^{-1}$]	ΔE_Q [$mm\,s^{-1}$]
MMO (*M. caps.*)	700	1800[147]	–	–	0.66	1.51[50, 154]
MMO (*M. trich.*)	725	2500[156]	–	–	0.67	1.51[95]
R2-D84E	700	1500[225]	890[39]	–	0.63	1.58[225]
R2-D84E/W48F[226]	700	–	870	458	–	–
Δ^9 desaturase	700	1200[227, 228]	898	442[227]	0.68	1.90
					0.64	1.06[228]
frog M ferritin	650[229]	–	851	485(s) 499(as)[230]	0.62	1.08[229]
cis-μ-1,2-peroxo Fe_2^{III}	694	2650[159]	888[159]	–	0.66	1.40[159]

This diiron(III) synthetic model with optical and Mössbauer properties that are very similar to those of $MMOH_{peroxo}$ was structurally characterized and shown to contain a *cis*-μ-1,2 peroxo group.[159] The peroxo intermediate found for frog M ferritin is the only one thus far characterized by EXAFS spectroscopy.[160] A surprisingly short Fe–Fe distance of 2.53 Å, compared to the value of 4.004 Å in the synthetic model complex,[159] implies the presence of two single-atom bridges in addition to the μ-1,2 peroxo bridge. The structure of the ferritin peroxo intermediate is not necessarily similar to peroxo intermediates in other diiron proteins, however. Ferritin is the only protein listed in Table 3 that is not involved in the oxidation of organic substrates. Its peroxo intermediate also has somewhat lower values for λ_{max} (650 nm), ΔE_Q (1.06 $mm\,s^{-1}$), and the O–O stretching frequency (851 cm^{-1}) than those of the other diiron proteins.

Although time-resolved optical and Mössbauer studies were initially interpreted with a model in which a single peroxo intermediate forms directly from $MMOH_{red}$ and O_2, more recent stopped-flow optical studies on enzymes from both *M. capsulatus* (Bath) and *M. trichosporium* OB3b have provided evidence for the formation of one or more species preceding $MMOH_{peroxo}$. The rates for formation and decay of $MMOH_{peroxo}$ from the latter organism are pH dependent, both being faster at low pH values.[156] A single pK_a value of 7.6 was reported for both reactions. The formation rate of $MMOH_{peroxo}$ is significantly lower than the decay rate of the $g = 16$ EPR signal of $MMOH_{red}$, and the decay of the $g = 16$ signal is pH independent. Both observations can be explained by the presence of an intermediate that lacks both the $g = 16$ EPR signal and the optical characteristics of $MMOH_{peroxo}$. Recently, it was shown that a model incorporating a species between $MMOH_{red}$ and $MMOH_{peroxo}$ (named P*) better describes the absorbance changes, especially at early time points.[157] The formation rate of P* is equal to the decay rate of $MMOH_{red}$ as determined by EPR spectroscopy, whereas its decay rate corresponds to the formation rate of $MMOH_{peroxo}$. Recent stopped-flow optical studies on *M. capsulatus* (Bath) MMOH found a formation rate constant for $MMOH_{peroxo}$ of only 1–2 s^{-1} at 4 °C, which is lower than that of 25 s^{-1} which was originally reported.[147] This result was also interpreted as indicative of the presence of an intermediate preceding $MMOH_{peroxo}$, which could be a different peroxo species or a superoxo complex. In contrast to the *M. trichosporium* OB3b enzyme, formation and decay of $MMOH_{peroxo}$ is pH independent for the enzyme from *M. capsulatus* (Bath).[50]

A different approach to probe the nature of early steps in the activation of dioxygen is to measure the oxygen kinetic isotope effect (KIE) for MMO catalysis. A KIE of 1.016 ($v/K(^{16}O^{16}O)/v/K(^{18}O^{16}O)$, v = velocity, K = Michaelis constant) was obtained for the enzyme from *M. capsulatus* (Bath), both in the presence and absence of acetonitrile as the substrate.[153] A KIE of 1.016 indicates a significant decrease in O–O bond order up to the first irreversible step in the activation of dioxygen and argues against the formation of a tight, irreversible $MMOH_{red}$–O_2 complex. The magnitude of the KIE is consistent with one-electron reduction of O_2 to superoxide as the first irreversible step in dioxygen activation. Other possibilities cannot be ruled out, however. Formation of a superoxide species has also been proposed to be the first irreversible step in the reductive activation of dioxygen in a number of other oxygen-activating metalloenzymes.[161, 162]

Most peroxo complexes prepared as synthetic models are stable only at low temperature and tend to decay directly to form diferric species.[1, 163–165] In contrast, the protein matrix surrounding the diiron center in MMOH allows $MMOH_{peroxo}$ to be converted into a high-valent oxo intermediate, termed $MMOH_Q$. Formation and decay of $MMOH_Q$ can be monitored conveniently by stopped-flow spectroscopy due to its bright yellow color ($\varepsilon_{350nm} = 3600\,M^{-1}cm^{-1}$; $\varepsilon_{420nm} = 7200\,M^{-1}cm^{-1}$).[50, 145–147, 154, 157] In the absence of substrate, $MMOH_Q$ decays slowly (approximately 0.05 s^{-1}) to form $MMOH_{ox}$. Unlike the decay of $MMOH_{peroxo}$, which is not affected by the presence of most substrates (see Section 4 for an important exception), the decay rate of $MMOH_Q$ increases in the presence of hydrocarbon substrates.[50, 145, 147, 157] This observation identifies $MMOH_Q$ as the active oxygen intermediate that reacts with methane and other substrates. For methane and most other substrates, the decay rate of $MMOH_Q$ depends linearly on the substrate concentration, which suggests that substrates are not tightly bound in the active site.[50, 145, 147, 157] The Eyring plot for $MMOH_Q$ decay in the presence of methane is linear for *M. capsulatus* (Bath), but nonlinear behavior has been reported recently for the enzyme from *M. trichosporium* OB3b. Curiously, the latter result was interpreted by a two-step model for $MMOH_Q$ decay in which the rate-limiting step changes from C–H bond scission at low temperatures to substrate binding at high temperatures.[157] No intermediates have been identified in the reaction of $MMOH_Q$ with methane and other hydrocarbon substrates. Only for nitrobenzene has formation of a distinct product

complex been spectroscopically observed.[50, 145] For this substrate, product release from the hydrophobic active site can be observed because of the distinct color difference between the protonated *p*-nitrophenol in the hydrophobic active site and the deprotonated *p*-nitrophenolate ion in the bulk solution. In this particular case, the rate of product release is similar to the turnover rate from steady-state measurements, consistent with product release being the rate-limiting step in the oxygenation of nitrobenzene.

Characterization of $MMOH_Q$ by rapid freeze–quench (RFQ) Mössbauer spectroscopy revealed that both iron atoms have isomer shifts that are significantly smaller than those typical of diiron(III) complexes and more consistent with a diiron(IV) assignment.[50, 146] The sharp quadrupole doublet observed for the *M. trichosporium* OB3b enzyme ($\delta = 0.17\ mm\,s^{-1}$ and $\Delta E_Q = 0.53\ mm\,s$) suggests similar ligand environments for both iron atoms, whereas two slightly different iron environments were detected for the *M. capsulatus* (Bath) enzyme (Fe 1: $\delta = 0.21\ mm\,s^{-1}$, $\Delta E_Q = 0.68\ mm\,s^{-1}$; Fe 2: $\delta = 0.14\ mm\,s^{-1}$, $\Delta E_Q = 0.55\ mm\,s^{-1}$). The absence of splitting in these quadrupole doublets at high applied magnetic field strongly supports the formulation of $MMOH_Q$ as a diiron(IV) cluster having a diamagnetic ground state due to antiferromagnetic coupling between the iron atoms.

Important structural information has also been obtained from analysis of the EXAFS spectra of RFQ samples containing high amounts (40–60%) of $MMOH_Q$.[95] A very short Fe–Fe distance of 2.46 Å was reported, together with one short (1.77 Å) and one long (2.0 Å) Fe–O bond. The short Fe–Fe distance strongly indicates the presence of at least two single oxygen bridges. An additional carboxylate bridge was proposed to explain the short Fe–Fe distance in $MMOH_Q$ compared to model complexes with similar structures. An EXAFS analysis of the enzyme from *M. capsulatus* (Bath) supports the presence of a short Fe–Fe distance in $MMOH_Q$.[166]

An important mechanistic question is whether the O–O bond in $MMOH_{peroxo}$ is cleaved homolytically or heterolytically to form $MMOH_Q$. Figure 12 depicts two possibilities for the conversion of $MMOH_{peroxo}$ into $MMOH_Q$. In the heterolytic mechanism, a monodentate peroxo complex may form in

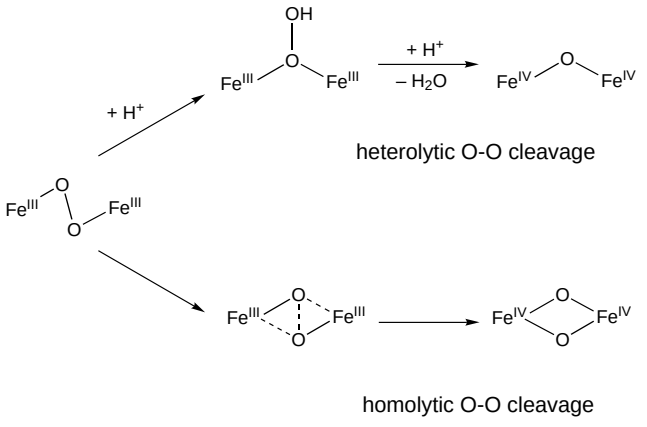

Figure 12. Comparison of the heterolytic and homolytic cleavage mechanisms for the conversion of $MMOH_{peroxo}$ into $MMOH_Q$.

which one of the oxygen atoms is protonated. Addition of a second proton to this oxygen facilitates heterolytic cleavage of the O–O bond and formation of a high-valent diiron complex in which one of the dioxygen-derived oxygen atoms forms an oxo bridge, while the other is released as water. This mechanism resembles those proposed for the P450 monooxygenases and heme-containing peroxidases, in which protonation of a ferric hydroperoxo complex also results in heterolytic O–O bond cleavage and the release of water. The oxidation state in the $Fe^{IV}{=}O(P^{\bullet+})$ intermediate (compound I, where P = porphyrin) that is believed to be formed in this step is equivalent to that in $MMOH_Q$. In the heme-containing enzymes, oxidizing equivalents are stored on both the iron and the porphyrin ring, whereas the same oxidation state is reached in MMO by oxidizing two iron atoms to the +4 level. The pH dependence observed for the formation and the decay of $MMOH_{peroxo}$ for the M. *trichosporium* OB3b enzyme is consistent with such a mechanism.[156] The linear proton inventory plots reported in the same study imply transfer of a single proton in the transition states of both reactions. Finally, the formation of $MMOH_Q$ shows a positive entropy change, which could be due to release of water.[50, 147]

A fundamentally different mechanism is one in which the O–O bond is cleaved homolytically resulting in a bis(μ-oxo)diiron(IV) species. Oxygen–oxygen bond cleavage by dicopper centers is believed to proceed by such a mechanism.[167–169] In this case, both dioxygen-derived oxygen atoms become bridging oxide ligands of the diiron center, and water is released in some step following the decay of $MMOH_Q$.

Distinguishing between these mechanistic possibilities would benefit from more detailed knowledge of the $MMOH_Q$ structure. Although EXAFS spectroscopy indicates the presence of at least two single-atom bridges, it cannot distinguish between two oxo bridges, a structure that is most easily explained by homolytic cleavage of the O–O bond in $MMOH_{peroxo}$, and a structure with one oxo and one or more single-oxygen glutamate bridges. The latter structure would support heterolytic cleavage of the O–O bond. The EXAFS spectrum of $MMOH_Q$ is remarkably similar to that of intermediate X, a high-valent intermediate that is formed transiently during the reaction of the diferrous R2 protein of ribonucleotide reductase with O_2.[170] Like $MMOH_Q$, intermediate X has a short Fe–Fe distance of 2.5 Å, and thus a structure with at least two single-atom bridges. In contrast to $MMOH_Q$, intermediate X is best described as a mixed-valent $Fe^{III}Fe^{IV}$ species.[171] Antiferromagnetic coupling between Fe^{III} and Fe^{IV} gives rise to an $S = 1/2$ ground state, which has allowed its structure to be characterized thoroughly by using EPR and ENDOR spectroscopy.[172] Labeling studies using $^{17}O_2$ and $H_2{}^{17}O$ show that one of the oxygen atoms of the O_2 molecule forms an oxo bridge, while the other oxygen atom forms a terminal aqua ligand to Fe^{III}.[172, 173] This result in turn implies that one of the single-atom bridges in intermediate X is provided by a carboxylate ligand.

To probe further the relationship between the structures of intermediate X and $MMOH_Q$, we recently employed radiolytic reduction at 77 K to produce a one-electron reduced form of $MMOH_Q$ (called $MMOH_{Q_X}$). $MMOH_{Q_X}$ is expected to

retain the structure of $MMOH_Q$, because of the low temperature at which it is generated.[174] The Mössbauer parameters of $MMOH_{Qx}$ are remarkably similar to those reported for intermediate X: Fe1: $\delta = 0.48\ mm\,s^{-1}$, $\Delta E_Q = -0.9\ mm\,s^{-1}$; Fe2: $\delta = 0.14\ mm\,s^{-1}$, $\Delta E_Q = -0.6\ mm\,s^{-1}$.[171] EPR/ENDOR studies on $MMOH_{Qx}$ similar to the ones done on intermediate X with $^{17}O_2$ and $H_2{}^{17}O$ could help to distinguish between the homolytic and heterolytic O–O bond cleavage mechanisms. Such studies are difficult because of the presence of intense EPR signals from free radicals that are generated by the high-energy γ-rays used for radiolytic reduction.

Recently several groups have applied DFT to calculate the MMO catalytic pathway.[175–184] DFT calculations can afford insights into reasonable structures for the spectroscopically detected oxygen intermediates and suggest species that have remained undetected so far. In addition, they provide a powerful tool to probe the nature of the reaction between $MMOH_Q$ and substrates (see Section 4). MMO is especially amenable to the DFT approach because most of the important chemistry involving dioxygen activation and substrate oxygenation occurs at the diiron center. Models with a relatively small number of atoms may therefore describe the active site satisfactorily.

The most extensive DFT study reported thus far uses a model based on approximately 100 atoms.[182] Such a relatively large model was required for these calculations to reproduce faithfully the structures of $MMOH_{ox}$ and $MMOH_{red}$, both known from X-ray crystallography. Figure 13 provides a "DFT view" of the catalytic cycle of MMO from this work, and shows those structures for $MMOH_{superoxo}$, $MMOH_{peroxo}$, and $MMOH_Q$ intermediates having the lowest energy. A remarkable finding of these calculations is the suggestion that a coordinated water remains ligated to Fe1 in a terminal position throughout the catalytic cycle. The energies of the superoxo and peroxo complexes are comparable. The asymmetric nature of $MMOH_{peroxo}$ is somewhat surprising in view of the sharp quadrupole doublet observed in the Mössbauer spectrum of this intermediate. A recent DFT study that used a smaller model of 40 atoms suggests a slightly more stable, symmetric μ-η^2:η^2 nonplanar (butterfly) peroxo structure as an alternative for the $MMOH_{peroxo}$ structure depicted in Figure 13 (see also below).[184]

The DFT structure of $MMOH_Q$ is reasonably consistent with spectroscopic data, including the presence of a short Fe–Fe distance of 2.67 Å and an antiferromagnetically coupled spin state. In contrast to the EXAFS study that

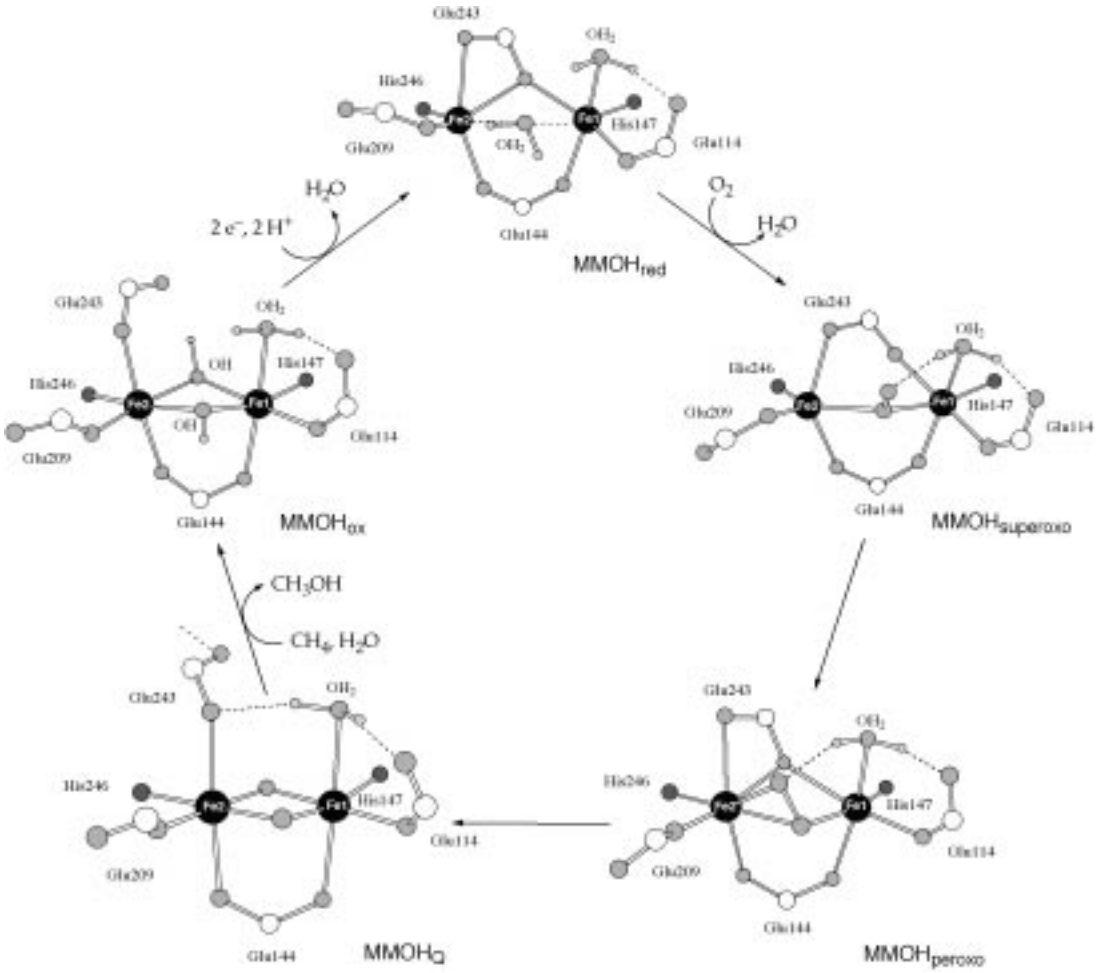

Figure 13. A "DFT view" of the catalytic cycle of MMO. Note that the positions of Fe1 and Fe2 are reversed compared to other figures in this paper, to allow a better view of the dioxygen activation reaction. Adapted with permission from ref. [182]. Copyright (2000) American Chemical Society.

reported the presence of one short (1.77 Å) and one long (2.0 Å) Fe–O bond, however, the DFT structure of $MMOH_Q$ shows more symmetrically bridging oxo groups, as reflected in Fe–O bond distances of 1.76 and 1.81 Å. The recent DFT study that used a smaller set of 40 atoms confirmed that this $MMOH_Q$ structure, with one bridging carboxylate and one water directly coordinated to one of the iron atoms, is significantly more stable than the structures with two bridging carboxylates found in earlier DFT calculations.[184] The same study also investigated the mechanism of O–O bond cleavage in the conversion of $MMOH_{peroxo}$ into $MMOH_Q$. A homolytic mechanism was proposed starting from a μ-η^2:η^2 nonplanar (butterfly) $MMOH_{peroxo}$ structure. Only one of the iron atoms was invoked as being actively involved in the cleavage reaction. DFT calculations using the 100-atom model confirm the existence of this μ-η^2:η^2 peroxo structure in the transition from $MMOH_{peroxo}$ into $MMOH_Q$.[185] Additional DFT calculations are required to clarify further the nature of this and other steps in the dioxygen activation reaction.

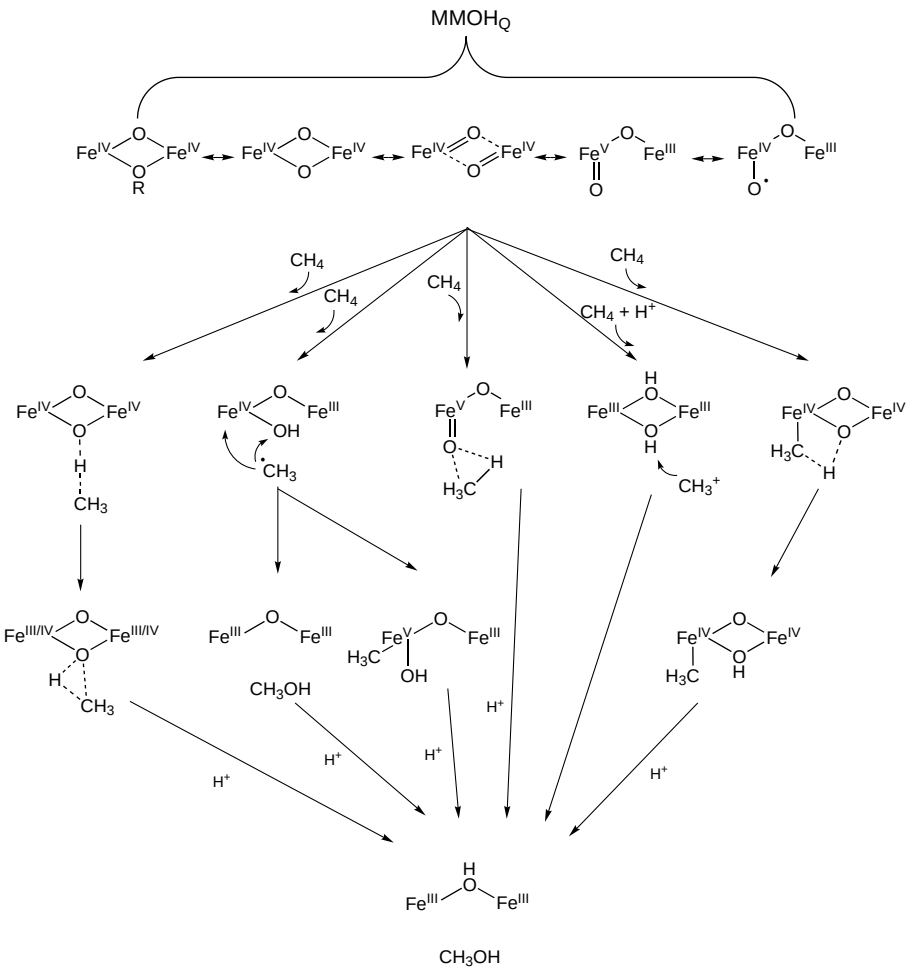

Figure 14. Some of the mechanisms proposed for hydroxylation of methane by $MMOH_Q$.

4. Mechanism of Hydrocarbon Hydroxylation

The spectroscopic studies of transient species described in the preceding section have yielded key insights into the nature of intermediates involved in dioxygen activation and have identified $MMOH_Q$ as the intermediate that reacts with methane and other hydrocarbons. The next question is to understand how $MMOH_Q$ hydroxylates substrate molecules. Since no intermediates have been observed for this step by using rapid-mixing spectroscopic methods, more indirect methods have been applied. Substrate probes have helped to delineate the chemical characteristics of the hydroxylation steps, and theoretical studies have been employed to probe the mechanistic details.

Mechanistic proposals for the hydroxylation of the C–H bond have been thoroughly reviewed.[1, 3, 5, 186–192] The possibilities depicted in Figure 14 illustrate some of the important issues: What is the structure of $MMOH_Q$ that reacts with methane? Is the reactive species best formulated as a bis(μ-oxo)diiron(IV) moiety, as proposed by EXAFS studies, or as an Fe^{III}–O–Fe^{V}=O species? Are the iron atoms coordinatively saturated, or are they five-coordinate, to allow the formation of Fe–C bonds? Are (short-lived) substrate radicals involved, in a mechanism that is similar to the widely cited oxygen-rebound mechanism proposed for cytochrome P450 monooxygenases? Or is hydroxylation better described by a concerted mechanism in which an activated oxygen atom inserts directly into a C–H bond?

Most of the experimental approaches that can distinguish between these mechanistic proposals rely on the use of reporter substrates, molecules that yield different products depending on the type of reaction they undergo. MMO has a broad substrate selectivity, and many different compounds have been used in such studies. One method is to investigate alkane substrates made chiral by isotopic substitution. Concerted mechanisms would predict either complete retention or complete inversion of stereochemistry at the hydroxylated carbon atom, whereas the formation of radical or carbocation intermediates should result in full racemization. Hydroxylation of (*R*)- or (*S*)-[1-^{2}H,1-^{3}H]ethane occurs predominantly (64–74%) with retention of configuration for both *M. capsulatus* (Bath) and *M. trichosporium* OB3b,[186, 193] and with approximately 90% retention for [2-^{3}H]butane.[193] Initially, the observation of a measurable amount of racemization was taken as evidence for a radical-based intermediate species.[186] Others pointed out, however, that 70% retention corresponds to a rebound rate for the putative ethyl radical of

1×10^{13} s^{-1}.[193] Such a large rate constant is inconsistent with the formation solely of a discrete radical intermediate.

A substantial amount of work has been devoted to the use of radical-clock substrate probes.[194–196] These compounds undergo rearrangement of their carbon skeletons following hydrogen-atom abstraction. Because rate constants for such rearrangements have been experimentally determined, analysis of product ratios from MMO-catalyzed hydroxylation allows calculation of lifetimes for any substrate radical species. The vast majority of the radical-clock substrates tested with the *M. capsulatus* (Bath) enzyme yield only unrearranged products; this finding argues against discrete radical species occurring during MMO catalysis.[197, 198] From a series of cyclopropane-based radical-clock substrates that were studied for the *M. trichosporium* OB3b enzyme, most again showed no rearranged products.[199] Such results place an upper limit of 150 fs on the lifetime for a radical species, too short to account for the formation of a discrete radical intermediate.

Rearranged products have been reported for four specific substrates, however, all of which can discriminate between radical- and carbocation-type rearrangements.[199–203] The three best-studied cases are depicted in Figure 15. Oxidation of 1,1-dimethylcyclopropane gives mostly the unrearranged product (1-methylcyclopropyl)methanol, but also small amounts of the radical-type rearrangement product (3-methyl-3-buten-1-ol, 6%) and the carbocation-type product (1-methylcyclobutanol, 13%).[200] Similar results were obtained by using (*trans,trans*-2-methoxy-3-phenylcyclopropyl)-methane as the substrate,[202] and the carbocation-type product 1-homocubanol was obtained as the major product from the oxygenation of methylcubane.[201–203]

An alternative method to test for the involvement of radical intermediates is applying spin traps. Steady-state oxidation of methane, methanol, and acetonitrile in the presence of such spin traps and subsequent analysis by EPR spectroscopy showed the formation of adducts with substrate radicals.[204, 205] It is difficult to assess whether these species are due to some minor formation of radicals or represent true catalytic intermediates, however.

Studies of the $^1H/^2H$ kinetic isotope effect can provide information about the nature of a transition state in which the C–H bond is broken. Large kinetic isotope effects have been correlated with a linear O–H–C geometry and substantial C–H bond cleavage in the transition state.[206, 207] The series CH_4, CH_3D, CH_2D_2, CHD_3, and CD_4 was investigated to probe kinetic isotope effects for the MMO enzyme from *M. trichosporium* OB3b. Both the rate of $MMOH_Q$ decay and product ratios were analyzed.[208] A surprisingly large isotope effect of 50–100 was found for $MMOH_Q$ decay for CH_4 versus CD_4, whereas a significantly smaller but still large value of 28 was reported for *M. capsulatus* (Bath).[147] For *M. trichosporium* OB3b no kinetic isotope effects were observed for $MMOH_Q$ decay using larger substrates (C_2H_6 versus C_2D_6 and C_3H_8 versus C_3D_8), however, which was rationalized by assuming that a substrate-binding step determines the rate of $MMOH_Q$ decay for these substrates rather than C–H bond breakage.[157] A similar lack of kinetic isotope effect for ethane has been observed for *M. capsulatus* (Bath).[209]

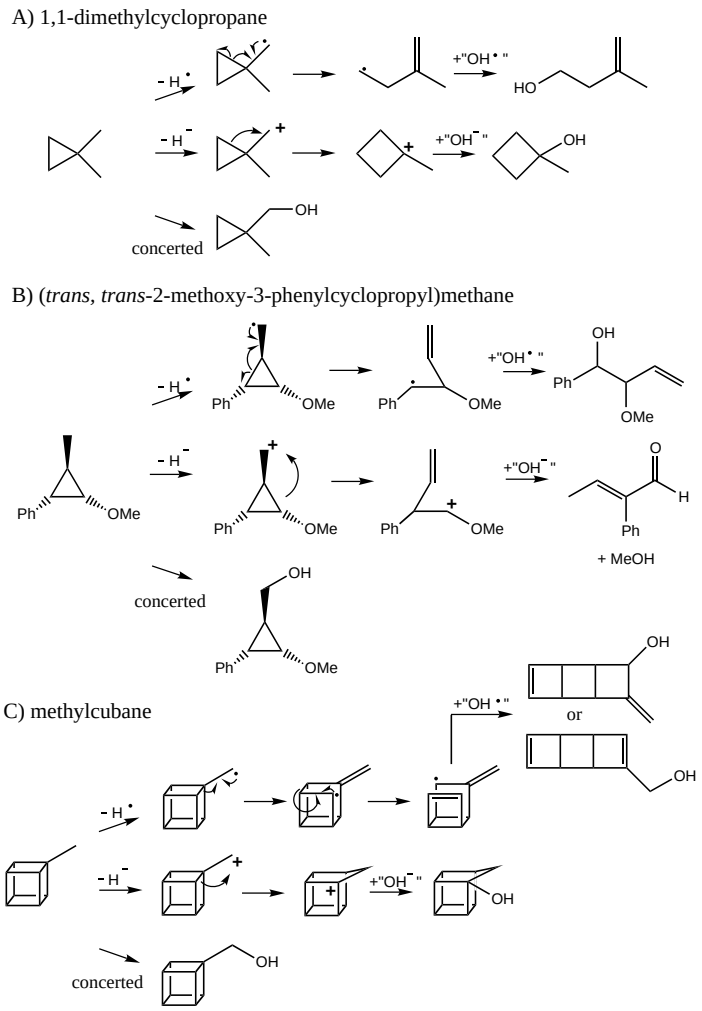

Figure 15. Three substrates that react differently depending on the type of hydroxylation reaction (radical intermediate, carbocation intermediate, or concerted). Products from more than one type of reaction have been observed with all three substrates.

Intramolecular kinetic isotope effects for methane obtained by studying product ratios yield smaller values, which also depend on the specific methane isotopomer (19.3 for CH_4 versus CD_4, but only 3.9 for the intramolecular effect in CD_3H). Experiments using chiral ethane gave intramolecular isotope effects in the range of 3–4.[186, 193] For comparison, typical k_H/k_D values of 7–10 were reported for P450 hydroxylation.[34] The reaction of CD_4 with $^{18}O_2$ results in 100% $CD_3{}^{18}OH$, and shows no exchange of oxygen or methyl hydrogen atoms with the solvent.[208] Hydrogen tunneling was proposed as the most likely reason for the large isotope effect on $MMOH_Q$ decay. The discrepancies between the different KIEs indicate the presence of a complex mechanism of $MMOH_Q$ decay, and/or substrate oxidation by pathways other than $MMOH_Q$ decay.

Several theoretical studies have been employed to probe the mechanism of the hydroxylation reaction, most of them using DFT methods (see also Section 3). Initially a simple model was investigated for $MMOH_Q$ involving a bis(μ-oxo)-diiron(IV) core with a bridging formate and terminal hydroxo and water ligands.[210] In this model, which has an all-oxygen

atom donor set, the most stable configuration has five-coordinate iron atoms. $MMOH_Q$ abstracts a hydrogen atom from methane to give an $Fe^{III}(\mu\text{-}O)(\mu\text{-}OH)Fe^{IV}$ species with an iron-bound methyl group, although the precise outcome of the reaction depends on the spin state assigned to the starting iron complex. Later work using a larger model, a bis(μ-oxo)diiron(IV) with two bridging formates, two terminal formates, and two imidazole ligands, also favors hydrogen-atom abstraction as the pathway for methane activation.[177] Attempts to find a transition state corresponding to another mechanism failed. By using a similar model for $MMOH_Q$, evidence was again presented for hydrogen-atom abstraction by a diiron(IV) species.[176] The resulting methyl radical interacts weakly with the iron atoms, which could explain the apparent short lifetime of radical intermediates calculated from radical-clock and chiral-ethane studies. It should be noted that, in the latter model, methane approaches the diiron core from a position that is not accessible in the protein active site.

A two-step concerted mechanism was proposed on the basis of a simple model for $MMOH_Q$ that is coordinatively unsaturated, a bis(μ-oxo)diiron(IV) core supported by a bridging formate with a hydroxide ligand on one iron and two hydroxides on the other iron atom.[179, 181, 211, 212] This diiron complex first forms a complex with methane, which is followed by hydrogen-atom abstraction via a four-center transition state to give an intermediate with a bridging hydroxide and an iron-bound methyl group. The methyl group then migrates to form a C–O bond with the bridging hydroxide and afford a methanol complex.

Most recently, DFT calculations were performed with the intention of trying to understand the mechanisms of both dioxygen and methane activation in sMMO.[182–184] By using a much larger model of the active site than previous studies, structures were predicted for the $MMOH_{peroxo}$, $MMOH_Q$, and putative $MMOH_{superoxo}$ intermediates (see Section 3). The model of $MMOH_Q$ used in this study has a bis(μ-oxo)diiron(IV) core, but it differs from other models in that the water molecule bound to Fe1 is not displaced by Glu243 (see Figure 13). The site distal to the two histidine ligands, which faces the hydrophobic substrate binding site, was the only position that was acceptable for methane approach to the diiron center. The only energetically reasonable reaction pathway for methane was a straight-on approach to the bridging oxygen atom (Figure 16). The calculated activation energy for this reaction is 13.2 kcal mol^{-1}, which is in reasonable agreement with the 9–12 kcal mol^{-1} obtained experimentally.[50, 147, 157, 209] In this transition state, the hydrogen atom facing the bridging oxide is partially bound to both oxygen and carbon (Figure 16). Interestingly, two different reaction pathways were identified that emerge from this starting point.

One pathway involves methyl radical recoil and formation of the O–H bond yielding a (μ-hydroxo)diiron center (①, Figure 16). In order for the methyl radical to rebound, the OH group must rotate and make a 93° angle with the C–O bond axis, a process calculated to take 5–10 ps. This time is sufficient for an ethyl radical in solution to racemize completely, but DFT calculations indicate that a steric clash between the CH_2 fragment and the newly formed O–H bond in the active site can significantly retard rotation around the C–C bond.[213]

A second, nonsynchronous concerted pathway was also identified that affords methanol from the transition state with a negligible energy barrier (②, Figure 16). In this mechanism, the O–H bond first shortens to 0.97 Å without breaking the partial bond to the methane carbon atom. Next the hydrogen atom rotates to make a 80–90° angle with the C–O axis while the carbon rotates in the opposite direction towards the oxygen atom. This entire process has a reaction barrier of only 1 kcal mol^{-1}.

The presence of two reaction channels with comparable activation energies can explain the partial retention of configuration observed with chiral ethane.[213] Products derived from the radical rebound channel undergo partial racemization, while those deriving from the concerted channel retain their configuration. The partitioning between these two reaction channels quantitatively accounts for the chiral ethane results and should be substrate dependent. Larger radical-clock substrates will favor the concerted mechanism because they have more difficulty reversing their trajectory to form a separate radical once the transition state is reached. A second study using a smaller set of 40 atoms also suggested the presence of two different pathways after initial hydrogen-atom abstraction, depending on the substrate.[184] Methylcyclopropane and ethane were computed to be immediately ionized after hydrogen atom abstraction to form a carbocation. The activation energy for final recombination of this carbocation to form a hydroxylated product is small. The reaction may even be described as nonsynchronous concerted. How important the radical recoil/rebound pathway is for methane remains to be established, but the finding that methyl radicals can be detected by using spin traps suggests that at least some methane oxidation may occur by this pathway.

Comparing the different calculational studies reveals that the predicted mechanism of methane activation is strongly dependent on the model selected for $MMOH_Q$ and the number of atoms used to describe it. Critical in the evaluation of these models is how well they relate to experimental results. In addition to reproducing the crystal structures for $MMOH_{ox}$ and $MMOH_{red}$, the largest DFT model does well in predicting reasonable values for the activation energy and in providing a rationale for seemingly contradictory results with mechanistic probe substrates.

Not only may substrates react with $MMOH_Q$ in different ways, but it is also possible that different substrates react with different oxygen intermediates, or that a single substrate reacts with different oxygen intermediates by different mechanisms. A linear relationship between the decay rate of $MMOH_{peroxo}$ and propene concentration has been observed for *M. capsulatus* (Bath), indicating that propene reacts directly with $MMOH_{peroxo}$.[147] No evidence for reaction of $MMOH_{peroxo}$ with propene was found in a study using the *M. trichosporium* OB3b enzyme, but the propene concentration used in this study may have been too low to observe its effect on the $MMOH_{peroxo}$ decay rate.[157] Additional support for propene oxidation by $MMOH_{peroxo}$ comes from the finding

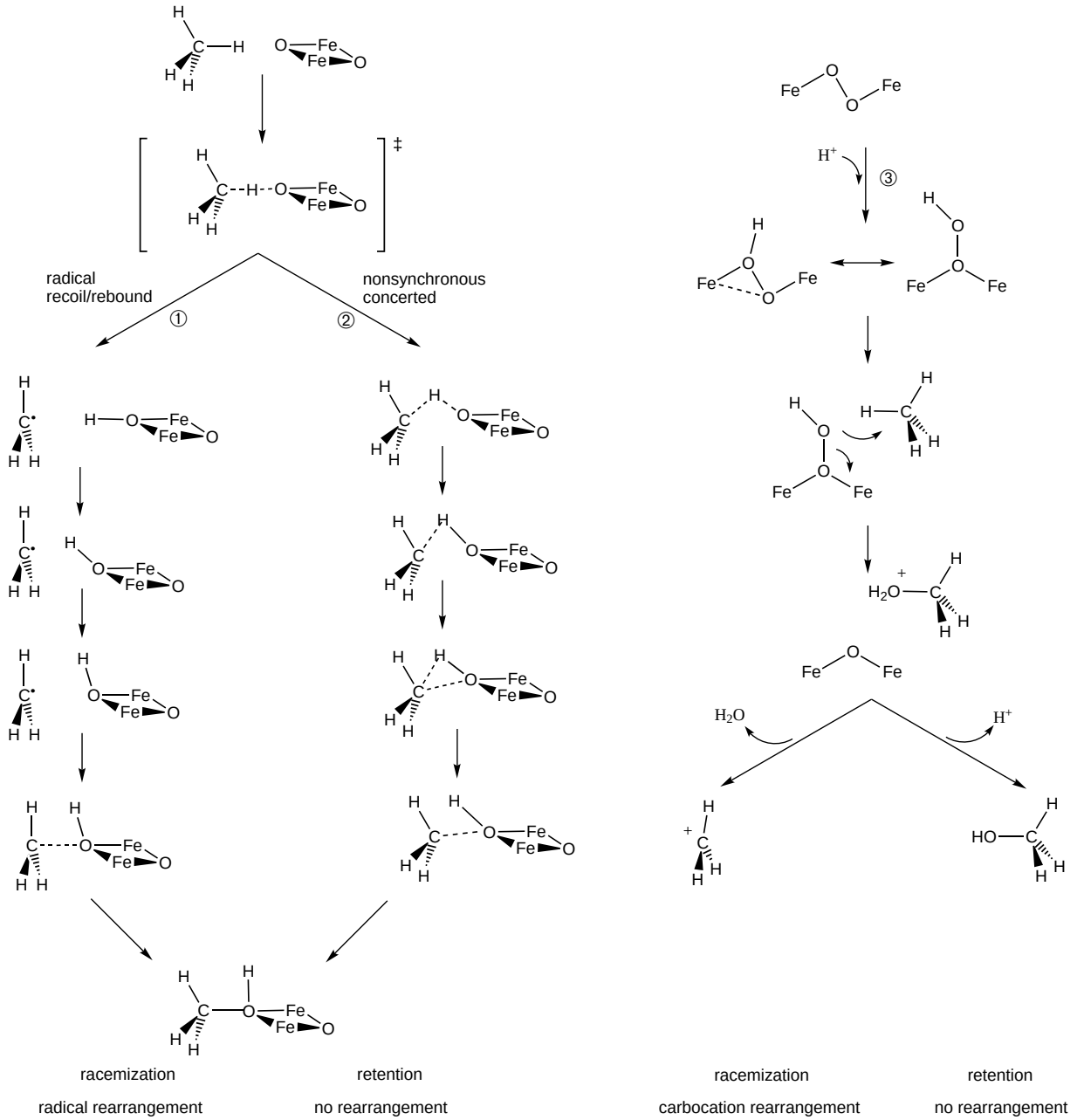

Figure 16. Model for the hydroxylation mechanism of MMO. The recoil/rebound and (nonsynchronous) concerted mechanisms (① and ②, respectively) are those suggested by recent DFT calculations.[183, 213] In addition, a mechanism for the involvement of $MMOH_{peroxo}$ in epoxidation and hydroxylation is suggested (③) based on related cytochrome P450 chemistry. The outcome of experiments with mechanistic probe substrates as predicted for each pathway is also depicted (First row: expected stereochemistry; second row: mechanistic probes).

that epoxidation of propene remains tightly coupled to NADH consumption, even at high MMOR:MMOH ratios, whereas uncoupling is observed with methane at MMOR:MMOH > 0.2.[27] Uncoupling probably occurs when MMOR provides additional electrons to either $MMOH_Q$ or $MMOH_{peroxo}$ to form H_2O and $MMOH_{ox}$. Propene reacts with $MMOH_{peroxo}$ and can thus compete with the oxidase reaction, whereas methane, which reacts only with $MMOH_Q$,[147] cannot.

Recent studies on cytochrome P450 have also provided evidence for the presence of more than one active oxygen intermediate.[214–218] Epoxidation of cyclohexene and 2-butene is enhanced at the expense of hydroxylation in site-directed mutants in which the proton transfer pathway responsible for the formation of the high-valent Fe^{IV}=O species is disrupted. The ferric hydroperoxide intermediate, which is still formed in these mutants, can epoxidize alkenes but is less active in hydroxylation reactions, which proceed primarily via the high-valent intermediate. It has been argued that the ferric hydroperoxide inserts OH^+ into substrates.[217, 219] Insertion of OH^+ into a C–H bond results in formation of a C–OH_2^+ unit, which can deprotonate to form an alcohol product or solvolyze to yield the carbocation product that has been detected with various substrate probes. Consistent with this

hypothesis is the finding that P450 mutants defective in forming compound I yield more carbocation-derived rearrangement products. Therefore, one explanation for the carbocation-derived products sometimes observed for MMO is that they react with a protonated peroxide intermediate prior to the formation of $MMOH_Q$ (③, Figure 16).[50, 145, 147]

5. Regulation of Catalysis by Component Interactions

The three protein components that comprise the soluble methane monooxygenase system orchestrate a series of electron-transfer and oxygen-activation reactions that result in the efficient and sustainable conversion of methane and dioxygen into methanol and water. The dynamic interactions between MMOH, MMOB, and MMOR are complex, and a detailed understanding of them is still incomplete. In this section we examine the various roles of component interactions in MMO catalysis and discuss what is known about the spatial and temporal relationships between the individual components.

An early and important illustration of the complexity of component interactions was the finding that steady-state hydroxylation rates increase with increasing MMOB concentration to a maximum at MMOB:MMOH = 2:1, but decrease at higher MMOB:MMOH ratios.[27, 44, 50] Recently several aspects of component interactions for the *M. capsulatus* (Bath) enzyme were investigated by using a combination of steady-state kinetic, calorimetric, and spectroscopic methods.[27] MMOR catalyzes the reduction of O_2 by NADH to H_2O_2 at relatively low rates in the absence of other MMO components. Addition of either MMOH, or MMOH and MMOB, increases the rate of oxidase activity but abolishes H_2O_2 formation, and O_2 is probably reduced completely to water. In the presence of methane, NADH oxidation and O_2 consumption are completely coupled to substrate hydroxylation at MMOR:MMOH < 0.2, whereas higher MMOR concentrations result in leakage of reducing equivalents in the form of oxidase activity. The steady-state hydroxylase and oxidase activities at various MMOB:MMOH and MMOR:MMOH ratios are best described by a model in which MMOB and MMOR bind noncompetitively at distinct sites on MMOH, both with a 2:1 stoichiometry.[27] This model yields K_d values for MMOB and MMOR binding in the 0.1 – 1 μM range, in good agreement with K_d values obtained by isothermal titration calorimetry. Kinetic information on MMOB and MMOR binding to MMOH has been obtained by stopped-flow fluorescence spectroscopy. Binding of MMOB and MMOR occurs in two steps, a rapid preequilibrium followed by a much slower isomerization equilibrium. Dissociation rate constants for the preequilibria of MMOH with MMOR (60 s^{-1} at 45 °C) and MMOB (26 s^{-1} at 45 °C) are significantly faster than the steady-state turnover rate for MMO.

Several important differences with regard to component interactions seem to exist between the enzymes from *M. capsulatus* (Bath) and *M. trichosporium* OB3b. Fluorescence titration studies on the enzyme from *M. trichosporium* OB3b showed the formation of a tight MMOB – MMOR complex ($K_d = 0.4$ μM),[44] whereas neither fluorescence spectroscopy nor isothermal titration calorimetry showed any evidence for complex formation between MMOB and MMOR for *M. capsulatus* (Bath).[27] Steady-state kinetic data for the *M. trichosporium* OB3b enzyme were interpreted by using a model in which MMOB and MMOR compete for binding sites on MMOH at high MMOB:MMOH ratios,[44] but a noncompetitive model was favored for *M. capsulatus* (Bath).[27] It is important to remember that *M. trichosporium* OB3b and *M. capsulatus* (Bath), although both methanotrophs, belong to evolutionarily distinct classes of bacteria. Differences between the two sMMO systems may be most prominent in component interactions.

MMOB and MMOR not only affect the rate and efficiency of catalysis by MMOH, but they also determine the regioselectivity of hydroxylation reactions.[46, 50] A study on the *M. trichosporium* OB3b enzyme found distinct product distributions for the oxygenation of isopentane by three different systems capable of oxygenation: I: MMOH, MMOR, NADH, and O_2; II: MMOH and H_2O_2; III: $MMOH_{red}$ and O_2 (single turnover).[46] Addition of as little as 0.1 mol equiv of MMOB changed the product distributions of systems I and III to one common outcome. Maximal rates for systems I and III were reached only at 1.5 – 2.0 MMOB per MMOH, however. In contrast, the hydrogen peroxide catalyzed system II was fully inhibited by MMOB at a 1:1 MMOB:MMOH ratio. Similar results have been reported for the hydrogen peroxide sustained hydroxylation by MMOH from *M. capsulatus* (Bath).[220]

There are several examples of the effect of component interactions on specific catalytic steps. MMOB enhances electron transfer rates between MMOR and MMOH.[27] As mentioned before, MMOB affects the kinetics of the dioxygen-activation reaction in such a way that several intermediates can be observed in its presence, whereas none are seen for the reaction of $MMOH_{red}$ alone with O_2. Reaction of $MMOH_{red}$ with O_2 is 1000-fold faster in the presence of MMOB.[49] The effect of different MMOB:MMOH ratios on the kinetics of $MMOH_Q$ formation and decay were interpreted to indicate that the presence of MMOB increases the formation rates of both $MMOH_{peroxo}$ and $MMOH_Q$, while decay of $MMOH_Q$ is relatively unaffected.[49] Various kinetic steps are also influenced by mutation of several amino acids in MMOB. Substitution of the conserved His 33 by alanine decreases the formation rate of $MMOH_{peroxo}$ by more than 50-fold. The quadruple mutant (N107G/S109A/S110A/T111A) has no effect on the formation rates for $MMOH_{peroxo}$ and $MMOH_Q$, but instead leads to a threefold increase in $MMOH_Q$ decay in the presence of larger substrates such as furan.[221] Studies on the enzyme from *M. trichosporium* OB3b also indicated that the presence of either 1.0 or 0.1 equivalents of MMOR decreases the O_2-induced decay rate of $MMOH_{red}$ in the MMOH:MMOB complex from 22 to 1.2 s^{-1}.[120] The rate of $MMOH_Q$ formation increases in the presence of 0.1 mole equivalents of MMOR, however, which means that, even in the presence of small quantities of reductase, formation of $MMOH_{peroxo}$ is no longer observed.[120]

The profound effects of MMOB and MMOR observed in both single-turnover reactions and in steady-state catalysis imply that component interactions affect the diiron active site. Both components affect the redox potentials $E_1^{o'}$ and $E_2^{o'}$ of MMOH.[2, 45, 48, 96, 120, 222] Binding of MMOB decreases the potential for both equilibria equally and substantially, which means that MMOB binds more tightly to $MMOH_{ox}$ than to $MMOH_{red}$. Binding of both MMOB and MMOR increases both potentials sharply in such a way that two-electron transfer becomes favored (*M. capsulatus* (Bath): $E_2^{o'} > E_1^{o'} \approx 100$ mV; *M. trichosporium* OB3b: $E_1^{o'} = 76$ mV $E_2^{o'} = 125$ mV, all potentials are relative to the normal hydrogen electrode).

Spectroscopic evidence for structural changes in the diiron site has been obtained only for MMOB binding. MMOR binding does not affect the spectroscopic properties of the diiron site. MMOB binding has only a subtle effect on EXAFS spectra.[93] MCD studies on $MMOH_{red}$ showed that MMOB disturbs the coordination geometry of one iron, probably that corresponding to Fe2 in the crystal structure of MMOH (see Section 2).[108–110] Binding of MMOB has been detected by EPR spectroscopy for all three oxidation states of MMOH.[44, 46, 98, 100] Titration of MMOB to $MMOH_{mv}$ showed full conversion into the spectrum of the MMOH:MMOB complex after addition of 1.7 MMOB per MMOH, which indicates a 1:2 binding stoichiometry. Surprisingly, only 0.6 mol equivalents of MMOB are needed to reach the same point for $MMOH_{red}$,[46] providing yet another example of a component effect that is maximal at substoichiometric ratios. Other illustrations of the same phenomenon include the effect of MMOB on substrate hydroxylation regioselectivity and the effects of MMOR on both the MMOH redox potential and the rate of $MMOH_{red}$ oxidation by O_2.[46, 120] All of these effects are indicative of hysteresis, which could occur when binding and dissociation of, for example, MMOR to $MMOH_{red}$ are faster than relaxation within MMOH from a complexed structure to its free conformational state. Therefore, a single molecule of MMOB or MMOR can service several molecules of MMOH. The 1:1:0.1 molar ratio of MMOH:MMOB:MMOR found in methanotrophic bacteria indicates that such hysteresis may be functionally important in vivo as well.[24, 51]

A detailed structural picture of the component complexes is currently unavailable, because no X-ray structure has yet been obtained. Chemical cross-linking experiments revealed that MMOB and MMOR bind to the α and β subunits of MMOH, respectively.[44] Small angle X-ray scattering experiments have been performed on *M. capsulatus* (Bath) sMMO to address whether or not significant conformational changes occur upon MMOB or MMOR binding to MMOH.[223] A major distortion of the MMOH structure was observed only when a 1:10:10 stoichiometry of MMOH:MMOB:MMOR was employed, ratios that are physiologically and functionally unreasonable. Addition of MMOB or MMOR, alone in a 1:2 ratio or together in a 1:2:2 stoichiometry, did not lead to structural distortions large enough to be detected by this technique. The model for the MMOH – MMOB complex that was discussed in Section 2.2 on the basis of NMR experiments is consistent with the X-ray scattering experiments, because binding of MMOB in the canyon region of MMOH is not expected to distort the overall ellipsoid form of MMOH. X-ray structure determinations of component complexes will be necessary to reveal the structural basis for component effects, however.

6. Summary and Outlook

A wide variety of methodologies derived from the disciplines of microbiology, enzymology, structural biology, and inorganic, physical, organic, and quantum chemistry have contributed to our current understanding of catalysis by the soluble methane monooxygenase system. High-resolution structures are available for two of the three protein components, MMOH and MMOB. Structural information about the diiron center in a variety of redox and complex states has provided important insights into the geometric flexibility that allows it to accommodate readily oxidation states ranging from $Fe^{II}Fe^{II}$ to $Fe^{IV}Fe^{IV}$. A unique feature of sMMO is that several intermediates in the dioxygen activation reaction build up sequentially before they decay, even in the absence of substrate, which has enabled a still incomplete molecular movie of dioxygen activation to be compiled. DFT calculations have begun to contribute new suggestions for the structures of oxygen intermediates and to provide insights into the reactions of these intermediates with substrates.

Although the basic sequence of events in dioxygen activation and substrate hydroxylation is now known, especially with regard to the role of the diiron center, other aspects of catalysis are less clear. One of these is the role of protein residues in formation of oxygen intermediates, electron and proton transfer, and substrate binding/access to the diiron active site. A high-yield recombinant expression system for MMOH would help to answer these questions by the application of site-directed mutagenesis. The recent finding that a fourth protein component (OrfY) exists in *M. capsulatus* (Bath) cells and interacts with MMOH raises the important question of its function in vivo.

Component interactions tightly control various reactions in the sMMO system. High-resolution structural information on MMOR and component complexes is required, however, to understand how component interactions regulate catalysis. For example, what structural changes in the vicinity of the $MMOH_{red}$ active site make it much more reactive toward dioxygen, and how does binding of MMOB at the surface of MMOH lead to those structural changes? More sophisticated programs and faster computers will allow the application of DFT and quantum mechanical molecular dynamics calculations using larger active site models and probing different aspects of MMO catalysis. More detailed structural information on $MMOH_{peroxo}$, $MMOH_Q$, and perhaps still undiscovered intermediates is crucial for providing well-defined starting structures for these calculations, however. An ultimate test for our understanding of MMO catalysis would be the successful design of a synthetic MMO model that catalyzes the hydroxylation of methane with an efficiency and specificity similar to that of the native enzyme.

This work was supported by a grant from the National Institute of General Medical Sciences. M.M. is a Human

Frontier of Science Program postdoctoral fellow. D.A.K. is supported by a National Institutes of Health Biotechnology Training Grant. J.L.B. is a Howard Hughes Medical Institute predoctoral fellow, and J.M. is a Feodor-Lynen postdoctoral fellow.

7. Appendix: Abbreviations

CD:	circular dichroism
CT1:	charge-transfer complex 1
CT2:	charge-transfer complex 2
DFT:	density functional theory
DMSO:	dimethyl sulfoxide
$E^{\circ\prime}$:	formal redox potential at pH 7.0
ENDOR:	electron-nuclear double resonance
EPR:	electron paramagnetic resonance
ESEEM:	electron-spin echo envelope modulation
EXAFS:	extended X-ray absorption fine structure
FAD:	flavin adenine dinucleotide
Fd:	ferredoxin
FMN:	flavin mononucleotide
FNR:	Fd – $NADP^+$ oxidoreductase
KIE:	kinetic isotope effect
MC1:	Michaelis complex 1
MCD:	magnetic circular dichroism
MMO:	methane monooxygenase
MMOB:	regulatory protein of sMMO
MMOH:	hydroxylase protein of sMMO
$MMOH_{DMSO}$:	complex of MMOH with DMSO
$MMOH_{mv}$:	MMOH in the mixed-valent $Fe^{III}Fe^{II}$ oxidation state
$MMOH_{ox}$:	MMOH in the $Fe^{III}Fe^{III}$ oxidation state
$MMOH_{peroxo}$:	peroxo intermediate in dioxygen activation, also named H_{peroxo} or compound P
$MMOH_Q$:	high-valent intermediate in dioxygen activation, also named compound Q
$MMOH_{Q_x}$:	one-electron reduced, $Fe^{III}Fe^{IV}$ form of $MMOH_Q$, formed by radiolytic reduction at 77 K
$MMOH_{red}$:	MMOH in the $Fe^{II}Fe^{II}$ oxidation state
$MMOH_{superoxo}$:	superoxo intermediate in dioxygen activation
MMOR:	reductase protein of sMMO
NAD^+:	nicotinamide adenine dinucleotide, oxidized form
NADH:	nicotinamide adenine dinucleotide, reduced form
$NADP^+$:	nicotinamide adenine dinucleotide phosphate, oxidized form
P2:	regulatory protein in phenol hydroxylase from *Pseudomonas* sp. CF600
PDR:	phthalate dioxygenase reductase
pMMO:	particulate methane monooxygenase
RFQ:	rapid freeze – quench
sMMO:	soluble methane monooxygenase
SQ:	semiquinone

Received: January 10, 2001
Revised: May 3, 2001 [A 442]

[1] A. L. Feig, S. J. Lippard, *Chem. Rev.* **1994**, *94*, 759 – 805.
[2] K. E. Liu, S. J. Lippard, *Adv. Inorg. Chem.* **1995**, *42*, 263 – 289.
[3] B. J. Wallar, J. D. Lipscomb, *Chem. Rev.* **1996**, *96*, 2625 – 2657.
[4] A. M. Valentine, S. J. Lippard, *J. Chem. Soc. Dalton Trans.* **1997**, 3925 – 3931.
[5] R. J. Deeth, H. Dalton, *J. Biol. Inorg. Chem.* **1998**, *3*, 302 – 306.
[6] L. Westerheide, M. Pascaly, B. Krebs, *Curr. Opin. Chem. Biol.* **2000**, *4*, 235 – 241.
[7] R. S. Hanson, T. E. Hanson, *Microbiol. Rev.* **1996**, *60*, 439 – 471.
[8] C. Anthony, *The Biochemistry of Methylotrophs*, Academic Press, London, **1982**.
[9] I. J. Higgins, D. J. Best, R. C. Hammond, *Nature* **1980**, *286*, 561 – 564.
[10] J. C. Murrell, *Biodegradation* **1994**, *5*, 145 – 159.
[11] J. C. Murrell, B. Gilbert, I. R. McDonald, *Arch. Microbiol.* **2000**, *173*, 325 – 332.
[12] H.-H. T. Nguyen, M. Zhu, S. J. Elliot, K. H. Nakagawa, B. Hedman, A. M. Costello, T. L. Peeples, B. Wilkinson, H. Morimoto, P. G. Williams, H. G. Floss, M. E. Lidstrom, K. O. Hodgson, S. I. Chan in *Microbial Growth on C_1 Compounds* (Eds.: M. E. Lidstrom, F. R. Tabita), Kluwer Academic, Dordrecht, **1996**, pp. 150 – 158.
[13] H.-H. T. Nguyen, K. H. Nakagawa, B. Hedman, S. J. Elliott, M. E. Lidstrom, K. O. Hodgson, S. I. Chan, *J. Am. Chem. Soc.* **1996**, *118*, 12766 – 12776.
[14] H.-H. T. Nguyen, S. J. Eliott, J. H.-K. Yip, S. I. Chan, *J. Biol. Chem.* **1998**, *273*, 7957 – 7966.
[15] M. Takeguchi, K. Miyakawa, I. Okura, *J. Mol. Catal. A* **1998**, *132*, 145 – 153.
[16] J. A. Zahn, A. A. DiSpirito, *J. Bacteriol.* **1996**, *178*, 1018 – 1029.
[17] J. Colby, D. I. Stirling, H. Dalton, *Biochem. J.* **1977**, *165*, 395 – 402.
[18] H. Dalton, *Adv. Appl. Microbiol.* **1980**, *26*, 71 – 87.
[19] J. Green, H. Dalton, *J. Biol. Chem.* **1989**, *264*, 17698 – 17703.
[20] B. G. Fox, J. G. Borneman, L. P. Wackett, J. D. Lipscomb, *Biochemistry* **1990**, *29*, 6419 – 6427.
[21] M. J. Rataj, J. E. Kauth, M. I. Donnelly, *J. Biol. Chem.* **1991**, *266*, 18684 – 18690.
[22] K. K. Andersson, W. A. Froland, S.-K. Lee, J. D. Lipscomb, *New J. Chem.* **1991**, *15*, 411 – 415.
[23] J. R. Bragg, R. C. Prince, E. J. Harner, R. M. Atlas, *Nature* **1994**, *368*, 413 – 418.
[24] B. G. Fox, W. A. Froland, J. E. Dege, J. D. Lipscomb, *J. Biol. Chem.* **1989**, *264*, 10023 – 10033.
[25] J. Colby, H. Dalton, *Biochem. J.* **1978**, *171*, 461 – 468.
[26] M. P. Woodland, H. Dalton, *J. Biol. Chem.* **1984**, *259*, 53 – 59.
[27] G. T. Gassner, S. J. Lippard, *Biochemistry* **1999**, *38*, 12768 – 12785.
[28] A. C. Rosenzweig, C. A. Frederick, S. J. Lippard, P. Nordlund, *Nature* **1993**, *366*, 537 – 543.
[29] A. C. Rosenzweig, P. Nordlund, P. M. Takahara, C. A. Frederick, S. J. Lippard, *Chem. Biol.* **1995**, *2*, 409 – 418.
[30] N. Elango, R. Radhakrishnan, W. A. Froland, B. J. Wallar, C. A. Earhart, J. D. Lipscomb, D. H. Ohlendorf, *Protein Sci.* **1997**, *6*, 556 – 568.
[31] S.-L. Chang, B. J. Wallar, J. D. Lipscomb, K. H. Mayo, *Biochemistry* **1999**, *38*, 5799 – 5812.
[32] K. J. Walters, G. T. Gassner, S. J. Lippard, G. Wagner, *Proc. Natl. Acad. Sci. USA* **1999**, *96*, 7877 – 7882.
[33] D. A. Whittington, S. J. Lippard, *J. Am. Chem. Soc.* **2001**, *123*, 827 – 838.
[34] P. R. Ortiz de Montellano in *Cytochrome P450: Structure, Mechanism, and Biochemistry* (Eds.: P. R. Ortiz de Montellano), Plenum, New York, **1995**, pp. 245 – 303.
[35] S. S. Stahl, S. J. Lippard in *Iron Metabolism: Inorganic Biochemistry and Regulatory Mechanims* (Eds.: G. C. Ferreira, J. J. G. Moura, R. Franco), Wiley-VCH, Weinheim, **1999**, pp. 303 – 321.
[36] J. B. Vincent, G. L. Olivier-Lilley, B. A. Averill, *Chem. Rev.* **1990**, *90*, 1447 – 1467.
[37] D. E. Edmondson, B. H. Huynh, *Inorg. Chim. Acta* **1996**, *252*, 399 – 404.
[38] D. M. Kurtz, Jr., *J. Biol. Inorg. Chem.* **1997**, *2*, 159 – 167.
[39] E. I. Solomon, T. C. Brunold, M. I. Davis, J. N. Kemsley, S.-K. Lee, N. Lehnert, F. Neese, A. J. Skulan, Y.-S. Yang, J. Zhou, *Chem. Rev.* **2000**, *100*, 235 – 349.

[40] J. Xiong, D. M. Kurtz, Jr., J. Ai, J. Sanders-Loehr, *Biochemistry* **2000**, *39*, 5117 – 5125.
[41] S. J. Lippard, J. M. Berg, Principles of Bioinorganic Chemistry, University Science Books, Mill Valley, CA, **1994**.
[42] J. Lund, M. P. Woodland, H. Dalton, *Eur. J. Biochem.* **1985**, *147*, 297 – 305.
[43] J. Lund, H. Dalton, *Eur. J. Biochem.* **1985**, *147*, 291 – 296.
[44] B. G. Fox, Y. Liu, J. E. Dege, J. D. Lipscomb, *J. Biol. Chem.* **1991**, *266*, 540 – 550.
[45] K. E. Liu, S. J. Lippard, *J. Biol. Chem.* **1991**, *266*, 12836 – 12839.
[46] W. A. Froland, K. K. Andersson, S.-K. Lee, Y. Liu, J. D. Lipscomb, *J. Biol. Chem.* **1992**, *267*, 17588 – 17597.
[47] B. G. Fox, M. P. Hendrich, K. K. Surerus, K. K. Andersson, W. A. Froland, J. D. Lipscomb, E. Münck, *J. Am. Chem. Soc.* **1993**, *115*, 3688 – 3701.
[48] K. E. Paulsen, Y. Liu, B. G. Fox, J. D. Lipscomb, E. Münck, M. T. Stankovich, *Biochemistry* **1994**, *33*, 713 – 722.
[49] Y. Liu, J. C. Nesheim, S.-K. Lee, J. D. Lipscomb, *J. Biol. Chem.* **1995**, *270*, 24662 – 24665.
[50] K. E. Liu, A. M. Valentine, D. Wang, B. H. Huynh, D. E. Edmondson, A. Salifoglou, S. J. Lippard, *J. Am. Chem. Soc.* **1995**, *117*, 10174 – 10185.
[51] S. Grosse, L. Laramee, K.-D. Wendlandt, I. R. McDonald, C. B. Miguez, H.-P. Kleber, *Appl. Environ. Microbiol.* **1999**, *65*, 3929 – 3935.
[52] A. C. Stainthorpe, J. C. Murrell, G. P. C. Salmond, H. Dalton, V. Lees, *Arch. Microbiol.* **1989**, *152*, 154 – 159.
[53] A. C. Stainthorpe, V. Lees, G. P. C. Salmond, H. Dalton, J. C. Murrell, *Gene* **1990**, *91*, 27 – 34.
[54] D. E. Coufal, J. L. Blazyk, D. A. Whittington, W. W. Wu, A. C. Rosenzweig, S. J. Lippard, *Eur. J. Biochem.* **2000**, *267*, 2174 – 2185.
[55] D. L. N. Cardy, V. Laidler, G. P. C. Salmond, J. C. Murrell, *Arch. Microbiol.* **1991**, *156*, 477 – 483.
[56] D. L. N. Cardy, V. Laidler, G. P. C. Salmond, J. C. Murrell, *Mol. Microbiol.* **1991**, *5*, 335 – 342.
[57] I. R. McDonald, H. Uchiyama, S. Kambe, O. Yagi, J. C. Murrell, *Appl. Environ. Microbiol.* **1997**, *63*, 1898 – 1904.
[58] T. Shigematsu, S. Hanada, M. Eguchi, Y. Kamagata, T. Kanagawa, R. Kurane, *Appl. Environ. Microbiol.* **1999**, *65*, 5198 – 5206.
[59] A. K. Nielsen, K. Gerdes, H. Degn, J. C. Murrell, *Microbiology* **1996**, *142*, 1289 – 1296.
[60] A. K. Nielsen, K. Gerdes, J. C. Murrell, *Mol. Microbiol.* **1997**, *25*, 399 – 409.
[61] C. A. West, G. P. C. Salmond, H. Dalton, J. C. Murrell, *J. Gen. Microbiol.* **1992**, *138*, 1301 – 1307.
[62] M. Merkx, S. J. Lippard, **2001**, unpublished results.
[63] J. Powlowski, J. Sealy, V. Shingler, E. Cadieux, *J. Biol. Chem.* **1997**, *272*, 945 – 951.
[64] G. R. Johnson, R. H. Olsen, *Appl. Environ. Microbiol.* **1995**, *61*, 3336 – 3346.
[65] R. H. Olsen, J. J. Kukor, B. Kaphammer, *J. Bacteriol.* **1994**, *176*, 3749 – 3756.
[66] A. M. Byrne, J. J. Kukor, R. H. Olsen, *Gene* **1995**, *154*, 65 – 70.
[67] G. M. Whited, D. T. Gibson, *J. Bacteriol.* **1991**, *173*, 3010 – 3016.
[68] K.-M. Yen, M. R. Karl, L. M. Blatt, M. J. Simon, R. B. Winter, P. R. Fausset, H. S. Lu, A. A. Harcourt, K. K. Chen, *J. Bacteriol.* **1991**, *173*, 5315 – 5327.
[69] K.-M. Yen, M. R. Karl, *J. Bacteriol.* **1992**, *174*, 7253 – 7261.
[70] J. D. Pikus, J. M. Studts, C. Achim, K. E. Kauffmann, E. Münck, R. J. Steffan, K. McClay, B. G. Fox, *Biochemistry* **1996**, *35*, 9106 – 9119.
[71] V. Shingler, F. C. H. Franklin, M. Tsuda, D. Holroyd, M. Bagdasarian, *J. Gen. Microbiol.* **1989**, *135*, 1083 – 1092.
[72] I. Nordlund, J. Powlowski, V. Shingler, *J. Bacteriol.* **1990**, *172*, 6826 – 6833.
[73] J. Powlowski, V. Shingler, *J. Bacteriol.* **1990**, *172*, 6834 – 6840.
[74] I. Nordlund, J. Powlowski, Å. Hagström, V. Shingler, *J. Gen. Microbiol.* **1993**, *139*, 2695 – 2703.
[75] H. Saeki, K. Furuhashi, *J. Ferment. Bioeng.* **1994**, *78*, 399 – 406.
[76] A. Miura, H. Dalton, *Biosci. Biotechnol. Biochem.* **1995**, *59*, 853 – 859.
[77] F. J. Small, S. A. Ensign, *J. Biol. Chem.* **1997**, *272*, 24913 – 24920.
[78] S. C. Gallagher, R. Cammack, H. Dalton, *Eur. J. Biochem.* **1997**, *247*, 635 – 641.
[79] N.-Y. Zhou, A. Jenkins, C. K. N. C. K. Chion, D. J. Leak, *FEBS Lett.* **1998**, *430*, 181 – 185.
[80] N.-Y. Zhou, A. Jenkins, C. K. N. C. K. Chion, D. J. Leak, *Appl. Environ. Microbiol.* **1999**, *65*, 1589 – 1595.
[81] B. G. Fox, J. Shanklin, J. Ai, T. M. Loehr, J. Sanders-Loehr, *Biochemistry* **1994**, *33*, 12776 – 12786.
[82] S. C. Gallagher, A. George, H. Dalton, *Eur. J. Biochem.* **1998**, *254*, 480 – 489.
[83] H. Brandstetter, D. A. Whittington, S. J. Lippard, C. A. Frederick, *Chem. Biol.* **1999**, *6*, 441 – 449.
[84] D. A. Kopp, G. T. Gassner, J. L. Blazyk, S. J. Lippard, **2001**, unpublished results.
[85] D. E. Coufal, J. L. Blazyk, M. Merkx, S. J. Lippard, **2001**, unpublished results.
[86] D. Jahng, T. K. Wood, *Appl. Environ. Microbiol.* **1994**, *60*, 2473 – 2482.
[87] D. Jahng, C. S. Kim, R. S. Hanson, T. K. Wood, *Biotechnol. Bioeng.* **1996**, *51*, 349 – 359.
[88] J. S. Lloyd, P. De Marco, H. Dalton, J. C. Murrell, *Arch. Microbiol.* **1999**, *171*, 364 – 370.
[89] J. S. Lloyd, R. Finch, H. Dalton, J. C. Murrell, *Microbiol.* **1999**, *145*, 461 – 470.
[90] A. Ericson, B. Hedman, K. O. Hodgson, J. Green, H. Dalton, J. G. Bentsen, R. H. Beer, S. J. Lippard, *J. Am. Chem. Soc.* **1988**, *110*, 2330 – 2332.
[91] J. DeWitt, B. Hedman, A. Ericson, K. O. Hodgson, J. Bentsen, R. Beer, S. J. Lippard, J. Green, H. Dalton, *Physica B* **1989**, *158*, 97 – 98.
[92] J. G. DeWitt, J. G. Bentsen, A. C. Rosenzweig, B. Hedman, J. Green, S. Pilkington, G. C. Papaefthymiou, H. Dalton, K. O. Hodgson, S. J. Lippard, *J. Am. Chem. Soc.* **1991**, *113*, 9219 – 9235.
[93] J. G. DeWitt, A. C. Rosenzweig, A. Salifoglou, B. Hedman, S. J. Lippard, K. O. Hodgson, *Inorg. Chem.* **1995**, *34*, 2505 – 2515.
[94] L. Shu, Y. Liu, J. D. Lipscomb, L. Que, Jr., *J. Biol. Inorg. Chem.* **1996**, *1*, 297 – 304.
[95] L. Shu, J. C. Nesheim, K. Kauffmann, E. Münck, J. D. Lipscomb, L. Que, Jr., *Science* **1997**, *275*, 515 – 518.
[96] M. P. Woodland, D. S. Patil, R. Cammack, H. Dalton, *Biochim. Biophys. Acta* **1986**, *873*, 237 – 242.
[97] M. P. Hendrich, E. Münck, B. G. Fox, J. D. Lipscomb, *J. Am. Chem. Soc.* **1990**, *112*, 5861 – 5865.
[98] A. Davydov, R. Davydov, A. Gräslund, J. D. Lipscomb, K. K. Andersson, *J. Biol. Chem.* **1997**, *272*, 7022 – 7026.
[99] J.-P. Willems, A. M. Valentine, R. Gurbiel, S. J. Lippard, B. M. Hoffman, *J. Am. Chem. Soc.* **1998**, *120*, 9410 – 9416.
[100] R. Davydov, A. M. Valentine, S. Komar-Panicucci, B. M. Hoffman, S. J. Lippard, *Biochemistry* **1999**, *38*, 4188 – 4197.
[101] M. P. Hendrich, B. G. Fox, K. K. Andersson, P. G. Debrunner, J. D. Lipscomb, *J. Biol. Chem.* **1992**, *267*, 261 – 269.
[102] V. J. DeRose, K. E. Liu, D. M. Kurtz, Jr., B. M. Hoffman, S. J. Lippard, *J. Am. Chem. Soc.* **1993**, *115*, 6440 – 6441.
[103] H. Thomann, M. Bernardo, J. M. McCormick, S. Pulver, K. K. Andersson, J. D. Lipscomb, E. I. Solomon, *J. Am. Chem. Soc.* **1993**, *115*, 8881 – 8882.
[104] C. J. Bender, A. C. Rosenzweig, S. J. Lippard, J. Peisach, *J. Biol. Chem.* **1994**, *269*, 15993 – 15998.
[105] B. M. Hoffman, B. E. Sturgeon, P. E. Doan, V. J. DeRose, K. E. Liu, S. J. Lippard, *J. Am. Chem. Soc.* **1994**, *116*, 6023 – 6024.
[106] V. J. DeRose, K. E. Liu, S. J. Lippard, B. M. Hoffman, *J. Am. Chem. Soc.* **1996**, *118*, 121 – 134.
[107] B. E. Sturgeon, P. E. Doan, K. E. Liu, D. Burdi, W. H. Tong, J. M. Nocek, N. Gupta, J. Stubbe, D. M. Kurtz, Jr., S. J. Lippard, B. M. Hoffman, *J. Am. Chem. Soc.* **1997**, *119*, 375 – 386.
[108] S. Pulver, W. A. Froland, B. G. Fox, J. D. Lipscomb, E. I. Solomon, *J. Am. Chem. Soc.* **1993**, *115*, 12409 – 12422.
[109] S. Pulver, W. A. Froland, B. G. Fox, J. D. Lipscomb, E. I. Solomon, *J. Am. Chem. Soc.* **1994**, *116*, 4529.
[110] S. C. Pulver, W. A. Froland, J. D. Lipscomb, E. I. Solomon, *J. Am. Chem. Soc.* **1997**, *119*, 387 – 395.
[111] B. G. Fox, K. K. Surerus, E. Münck, J. D. Lipscomb, *J. Biol. Chem.* **1988**, *263*, 10553 – 10556.

[112] B. G. Fox, J. D. Lipscomb, *Biochem. Biophys. Res. Commun.* **1988**, *154*, 165 – 170.
[113] P. Nordlund, B.-M. Sjöberg, H. Eklund, *Nature* **1990**, *345*, 593 – 598.
[114] M. A. Holmes, I. Le Trong, S. Turley, L. C. Sieker, R. E. Stenkamp, *J. Mol. Biol.* **1991**, *220*, 583 – 593.
[115] P. Nordlund, H. Eklund, *J. Mol. Biol.* **1993**, *232*, 123 – 164.
[116] R. E. Stenkamp, *Chem. Rev.* **1994**, *94*, 715 – 726.
[117] R. M. Davydov, S. Ménage, M. Fontecave, A. Gräslund, A. Ehrenberg, *J. Biol. Inorg. Chem.* **1997**, *2*, 242 – 255.
[118] R. M. Davydov, J. Smieja, S. A. Dikanov, Y. Zang, L. Que, Jr., M. K. Bowman, *J. Biol. Inorg. Chem.* **1999**, *4*, 292 – 301.
[119] K. K. Andersson, T. E. Elgren, L. Que, Jr., J. D. Lipscomb, *J. Am. Chem. Soc.* **1992**, *114*, 8711 – 8713.
[120] Y. Liu, J. C. Nesheim, K. E. Paulsen, M. T. Stankovich, J. D. Lipscomb, *Biochemistry* **1997**, *36*, 5223 – 5233.
[121] A. C. Rosenzweig, S. J. Lippard, *Acc. Chem. Res.* **1994**, *27*, 229 – 236.
[122] A. C. Rosenzweig, H. Brandstetter, D. A. Whittington, P. Nordlund, S. J. Lippard, C. A. Frederick, *Proteins* **1997**, *29*, 141 – 152.
[123] D. A. Whittington, M. H. Sazinsky, S. J. Lippard, *J. Am. Chem. Soc.* **2001**, *123*, 1794 – 1795.
[124] Y. Lindqvist, W. Huang, G. Schneider, J. Shanklin, *EMBO J.* **1996**, *15*, 4081 – 4092.
[125] A. Lombardi, C. M. Summa, S. Geremia, L. Randaccio, V. Pavone, W. F. DeGrado, *Proc. Natl. Acad. Sci. USA* **2000**, *97*, 6298 – 6305.
[126] M. E. Andersson, M. Högbom, A. Rinaldo-Matthis, K. K. Andersson, B.-M. Sjöberg, P. Nordlund, *J. Am. Chem. Soc.* **1999**, *121*, 2346 – 2352.
[127] W. C. Voegtli, N. Khidekel, J. Baldwin, B. A. Ley, J. M. Bollinger, Jr., A. C. Rosenzweig, *J. Am. Chem. Soc.* **2000**, *122*, 3255 – 3261.
[128] J. Stubbe, W. A. van der Donk, *Chem. Rev.* **1998**, *98*, 705 – 762.
[129] D. A. Whittington, A. C. Rosenzweig, C. A. Frederick, S. J. Lippard, *Biochemistry* **2001**, *40*, 3476 – 3482.
[130] G. M. Raner, L. J. Martins, W. R. Ellis, Jr., *Biochemistry* **1997**, *36*, 7037 – 7043.
[131] L. J. Martins, C. P. Hill, W. R. Ellis, Jr., *Biochemistry* **1997**, *36*, 7044 – 7048.
[132] J. Xiong, R. S. Phillips, D. M. Kurtz, Jr., S. Jin, J. Ai, J. Sanders-Loehr, *Biochemistry* **2000**, *39*, 8526 – 8536.
[133] C. S. Farmer, D. M. Kurtz, Jr., R. S. Phillips, J. Ai, J. Sanders-Loehr, *J. Biol. Chem.* **2000**, *275*, 17043 – 17050.
[134] Y. Shinohara, H. Uchiyama, O. Yagi, I. Kusakabe, *J. Ferment. Bioeng.* **1998**, *85*, 37 – 42.
[135] H. Hemmi, J. M. Studts, Y. K. Chae, J. Song, J. L. Markley, B. G. Fox, *Biochemistry* **2001**, *40*, 3512 – 3524.
[136] J. S. Lloyd, A. Bhambra, J. C. Murrell, H. Dalton, *Eur. J. Biochem.* **1997**, *248*, 72 – 79.
[137] H. Qian, U. Edlund, J. Powlowski, V. Shingler, I. Sethson, *Biochemistry* **1997**, *36*, 495 – 504.
[138] J. Colby, H. Dalton, *Biochem. J.* **1979**, *177*, 903 – 908.
[139] J. Green, H. Dalton, *Biochem. J.* **1989**, *259*, 167 – 172.
[140] R. C. Prince, R. N. Patel, *FEBS Lett.* **1986**, *203*, 127 – 130.
[141] C. C. Correll, C. J. Batie, D. P. Ballou, M. L. Ludwig, *Science* **1992**, *258*, 1604 – 1610.
[142] C. C. Correll, M. L. Ludwig, C. M. Bruns, P. A. Karplus, *Protein Sci.* **1993**, *2*, 2112 – 2133.
[143] G. Kurisu, M. Kusunoki, E. Katoh, T. Yamazaki, K. Teshima, Y. Onda, Y. Kimata-Ariga, T. Hase, *Nat. Struct. Biol.* **2001**, *8*, 117 – 121.
[144] K. Moffat, *Nat. Struct. Biol.* **1998**, *5*, 641 – 645.
[145] S.-K. Lee, J. C. Nesheim, J. D. Lipscomb, *J. Biol. Chem.* **1993**, *268*, 21569 – 21577.
[146] S.-K. Lee, B. G. Fox, W. A. Froland, J. D. Lipscomb, E. Münck, *J. Am. Chem. Soc.* **1993**, *115*, 6450 – 6451.
[147] A. M. Valentine, S. S. Stahl, S. J. Lippard, *J. Am. Chem. Soc.* **1999**, *121*, 3876 – 3887.
[148] J. D. Lipscomb, S.-K. Lee, J. C. Nesheim, Y. Jin, B. J. Wallar, X.-Y. Zhang in *Iron Metabolism: Inorganic Biochemistry and Regulatory Mechanisms* (Eds.: G. C. Ferreira, J. J. G. Moura, R. Franco), Wiley-VCH, Weinheim, **1999**, pp. 323 – 339.
[149] R. E. Blankenship, W. W. Parson, *Annu. Rev. Biochem.* **1978**, *47*, 635 – 653.
[150] J. E. Walker, *Q. Rev. Biophys.* **1992**, *25*, 253 – 324.
[151] G. T. Gassner, M. L. Ludwig, D. L. Gatti, C. C. Correll, D. P. Ballou, *FASEB J.* **1995**, *9*, 1411 – 1418.
[152] J. L. Blazyk, G. T. Gassner, S. J. Lippard, **2001**, unpublished results.
[153] S. S. Stahl, W. A. Francisco, M. Merkx, J. P. Klinman, S. J. Lippard, *J. Biol. Chem.* **2001**, *276*, 4549 – 4553.
[154] K. E. Liu, D. Wang, B. H. Huynh, D. E. Edmondson, A. Salifoglou, S. J. Lippard, *J. Am. Chem. Soc.* **1994**, *116*, 7465 – 7466.
[155] K. E. Liu, A. M. Valentine, D. Qiu, D. E. Edmondson, E. H. Appelman, T. G. Spiro, S. J. Lippard, *J. Am. Chem. Soc.* **1995**, *117*, 4997 – 4998.
[156] S.-K. Lee, J. D. Lipscomb, *Biochemistry* **1999**, *38*, 4423 – 4432.
[157] B. J. Brazeau, J. D. Lipscomb, *Biochemistry* **2000**, *39*, 13503 – 13515.
[158] K. E. Liu, A. M. Valentine, D. Qiu, D. E. Edmondson, E. H. Appelman, T. G. Spiro, S. J. Lippard, *J. Am. Chem. Soc.* **1997**, *119*, 11134.
[159] K. Kim, S. J. Lippard, *J. Am. Chem. Soc.* **1996**, *118*, 4914 – 4915.
[160] J. Hwang, C. Krebs, B. H. Huynh, D. E. Edmondson, E. C. Theil, J. E. Penner-Hahn, *Science* **2000**, *287*, 122 – 125.
[161] Q. Su, J. P. Klinman, *Biochemistry* **1998**, *37*, 12513 – 12525.
[162] W. A. Francisco, G. Tian, P. F. Fitzpatrick, J. P. Klinman, *J. Am. Chem. Soc.* **1998**, *120*, 4057 – 4062.
[163] A. L. Feig, A. Masschelein, A. Bakac, S. J. Lippard, *J. Am. Chem. Soc.* **1997**, *119*, 334 – 342.
[164] L. Que, Jr., *J. Chem. Soc. Dalton Trans.* **1997**, 3933 – 3940.
[165] J. Du Bois, T. J. Mizoguchi, S. J. Lippard, *Coord. Chem. Rev.* **2000**, *200*, 443 – 485.
[166] J. L. DuBois, M. J. Latimer, A. M. Valentine, S. S. Stahl, B. Hedman, S. J. Lippard, K. O. Hodgson, **2001**, unpublished results.
[167] E. I. Solomon, U. M. Sundaram, T. E. Machonkin, *Chem. Rev.* **1996**, *96*, 2563 – 2605.
[168] J. Cahoy, P. L. Holland, W. B. Tolman, *Inorg. Chem.* **1999**, *38*, 2161 – 2168.
[169] V. Mahadevan, R. J. M. Klein Gebbink, T. D. P. Stack, *Curr. Opin. Chem. Biol.* **2000**, *4*, 228 – 234.
[170] P. J. Riggs-Gelasco, L. Shu, S. Chen, D. Burdi, B. H. Huynh, L. Que, Jr., J. Stubbe, *J. Am. Chem. Soc.* **1998**, *120*, 849 – 860.
[171] B. E. Sturgeon, D. Burdi, S. Chen, B.-H. Huynh, D. E. Edmondson, J. Stubbe, B. M. Hoffman, *J. Am. Chem. Soc.* **1996**, *118*, 7551 – 7557.
[172] N. Ravi, J. M. Bollinger, Jr., B. H. Huynh, D. E. Edmondson, J. Stubbe, *J. Am. Chem. Soc.* **1994**, *116*, 8007 – 8014.
[173] D. Burdi, J.-P. Willems, P. Riggs-Gelasco, W. E. Antholine, J. Stubbe, B. M. Hoffman, *J. Am. Chem. Soc.* **1998**, *120*, 12910 – 12919.
[174] A. M. Valentine, P. Tavares, A. S. Pereira, R. Davydov, C. Krebs, B. M. Hoffman, D. E. Edmondson, B. H. Huynh, S. J. Lippard, *J. Am. Chem. Soc.* **1998**, *120*, 2190 – 2191.
[175] P. E. M. Siegbahn, M. R. A. Blomberg, *Annu. Rev. Phys. Chem.* **1999**, *50*, 221 – 249.
[176] H. Basch, K. Mogi, D. G. Musaev, K. Morokuma, *J. Am. Chem. Soc.* **1999**, *121*, 7249 – 7256.
[177] P. E. M. Siegbahn, *Inorg. Chem.* **1999**, *38*, 2880 – 2889.
[178] K. Yoshizawa, Y. Yokomichi, Y. Shiota, T. Ohta, T. Yamabe, *Chem. Lett.* **1997**, 587 – 588.
[179] K. Yoshizawa, T. Ohta, T. Yamabe, *Bull. Chem. Soc. Jpn.* **1998**, *71*, 1899 – 1909.
[180] K. Yoshizawa, T. Ohta, T. Yamabe, *Nippon Kagaku Kaishi* **1998**, 451 – 459.
[181] K. Yoshizawa, *J. Inorg. Biochem.* **2000**, *78*, 23 – 34.
[182] B. D. Dunietz, M. D. Beachy, Y. Cao, D. A. Whittington, S. J. Lippard, R. A. Friesner, *J. Am. Chem. Soc.* **2000**, *122*, 2828 – 2839.
[183] B. F. Gherman, B. D. Dunietz, D. A. Whittington, S. J. Lippard, R. A. Friesner, *J. Am. Chem. Soc.* **2001**, *123*, 3836 – 3837.
[184] P. E. M. Siegbahn, *J. Biol. Inorg. Chem.* **2001**, *6*, 27 – 45.
[185] B. F. Gherman, S. J. Lippard, R. A. Friesner, **2001**, unpublished results.
[186] N. D. Priestley, H. G. Floss, W. A. Froland, J. D. Lipscomb, P. G. Williams, H. Morimoto, *J. Am. Chem. Soc.* **1992**, *114*, 7561 – 7562.
[187] A. A. Shteinman, *J. Biol. Inorg. Chem.* **1998**, *3*, 325 – 330.
[188] E. Nordlander, K. K. Andersson, *J. Biol. Inorg. Chem.* **1998**, *3*, 300 – 301.
[189] P. E. M. Siegbahn, R. H. Crabtree, P. Nordlund, *J. Biol. Inorg. Chem.* **1998**, *3*, 314 – 317.
[190] D. A. Whittington, A. M. Valentine, S. J. Lippard, *J. Biol. Inorg. Chem.* **1998**, *3*, 307 – 313.

[191] K. Yoshizawa, *J. Biol. Inorg. Chem.* **1998**, *3*, 318 – 324.
[192] J. D. Lipscomb, L. Que, Jr., *J. Biol. Inorg. Chem.* **1998**, *3*, 331 – 336.
[193] A. M. Valentine, B. Wilkinson, K. E. Liu, S. Komar-Panicucci, N. D. Priestley, P. G. Williams, H. Morimoto, H. G. Floss, S. J. Lippard, *J. Am. Chem. Soc.* **1997**, *119*, 1818 – 1827.
[194] D. Griller, K. U. Ingold, *Acc. Chem. Res.* **1980**, *13*, 317 – 323.
[195] P. R. Ortiz de Montellano, R. A. Stearns, *J. Am. Chem. Soc.* **1987**, *109*, 3415 – 3420.
[196] M. Newcomb, *Tetrahedron* **1993**, *49*, 1151 – 1176.
[197] K. E. Liu, C. C. Johnson, M. Newcomb, S. J. Lippard, *J. Am. Chem. Soc.* **1993**, *115*, 939 – 947.
[198] A. M. Valentine, M.-H. Le Tadic-Biadatti, P. H. Toy, M. Newcomb, S. J. Lippard, *J. Biol. Chem.* **1999**, *274*, 10771 – 10776.
[199] Y. Jin, J. D. Lipscomb, *Biochim. Biophys. Acta* **2000**, *1543*, 47 – 59.
[200] F. Ruzicka, D.-S. Huang, M. I. Donnelly, P. A. Frey, *Biochemistry* **1990**, *29*, 1696 – 1700.
[201] S.-Y. Choi, P. E. Eaton, P. F. Hollenberg, K. E. Liu, S. J. Lippard, M. Newcomb, D. A. Putt, S. P. Upadhyaya, Y. Xiong, *J. Am. Chem. Soc.* **1996**, *118*, 6547 – 6555.
[202] S.-Y. Choi, P. E. Eaton, D. A. Kopp, S. J. Lippard, M. Newcomb, R. Shen, *J. Am. Chem. Soc.* **1999**, *121*, 12198 – 12199.
[203] Y. Jin, J. D. Lipscomb, *Biochemistry* **1999**, *38*, 6178 – 6186.
[204] N. Deighton, I. D. Podmore, M. C. R. Symons, P. C. Wilkins, H. Dalton, *J. Chem. Soc. Chem. Commun.* **1991**, 1086 – 1087.
[205] P. C. Wilkins, H. Dalton, I. D. Podmore, N. Deighton, M. C. R. Symons, *Eur. J. Biochem.* **1992**, *210*, 67 – 72.
[206] C. D. Ritchie, *Physical Organic Chemistry: The Fundamental Concepts*, Marcel Dekker, New York, **1990**, pp. 289 – 307.
[207] R. A. More O'Ferrall, *J. Chem. Soc. B* **1970**, 785 – 790.
[208] J. C. Nesheim, J. D. Lipscomb, *Biochemistry* **1996**, *35*, 10240 – 10247.
[209] E. A. Ambundo, S. J. Lippard, **2001**, unpublished results.
[210] P. E. M. Siegbahn, R. H. Crabtree, *J. Am. Chem. Soc.* **1997**, *119*, 3103 – 3113.
[211] K. Yoshizawa, T. Ohta, T. Yamabe, R. Hoffmann, *J. Am. Chem. Soc.* **1997**, *119*, 12311 – 12321.
[212] K. Yoshizawa, T. Ohta, Y. Shiota, T. Yamabe, *Chem. Lett.* **1997**, 1213 – 1214.
[213] V. Guallar, B. F. Gherman, S. J. Lippard, W. H. Miller, R. A. Friesner, **2001**, unpublished reults.
[214] A. D. N. Vaz, S. J. Pernecky, G. M. Raner, M. J. Coon, *Proc. Natl. Acad. Sci. USA* **1996**, *93*, 4644 – 4648.
[215] P. H. Toy, M. Newcomb, M. J. Coon, A. D. N. Vaz, *J. Am. Chem. Soc.* **1998**, *120*, 9718 – 9719.
[216] A. D. N. Vaz, D. F. McGinnity, M. J. Coon, *Proc. Natl. Acad. Sci. USA* **1998**, *95*, 3555 – 3560.
[217] M. Newcomb, P. H. Toy, *Acc. Chem. Res.* **2000**, *33*, 449 – 455.
[218] M. Newcomb, R. Shen, S.-Y. Choi, P. H. Toy, P. F. Hollenberg, A. D. N. Vaz, M. J. Coon, *J. Am. Chem. Soc.* **2000**, *122*, 2677 – 2686.
[219] M. Newcomb, M.-H. Le Tadic-Biadatti, D. L. Chestney, E. S. Roberts, P. F. Hollenberg, *J. Am. Chem. Soc.* **1995**, *117*, 12085 – 12091.
[220] Y. Jiang, P. C. Wilkins, H. Dalton, *Biochim. Biophys. Acta* **1993**, *1163*, 105 – 112.
[221] B. J. Wallar, J. D. Lipscomb, *Biochemistry* **2001**, *40*, 2220 – 2233.
[222] J. Kazlauskaite, H. A. O. Hill, P. C. Wilkins, H. Dalton, *Eur. J. Biochem.* **1996**, *241*, 552 – 556.
[223] S. C. Gallagher, A. J. Callaghan, J. Zhao, H. Dalton, J. Trewhella, *Biochemistry* **1999**, *38*, 6752 – 6760.
[224] A. C. Rosenzweig, C. A. Frederick, S. J. Lippard in *Microbial Growth on C_1 Compounds* (Eds.: M. E. Lidstrom, F. R. Tabita), Kluwer, Dordrecht, **1996**, pp. 141 – 149.
[225] J. M. Bollinger, Jr., C. Krebs, A. Vicol, S. Chen, B. A. Ley, D. E. Edmondson, B. H. Huynh, *J. Am. Chem. Soc.* **1998**, *120*, 1094 – 1095.
[226] P. Moënne-Loccoz, J. Baldwin, B. A. Ley, T. M. Loehr, J. M. Bollinger, Jr., *Biochemistry* **1998**, *37*, 14659 – 14663.
[227] J. A. Broadwater, J. Ai, T. M. Loehr, J. Sanders-Loehr, B. G. Fox, *Biochemistry* **1998**, *37*, 14664 – 14671.
[228] J. A. Broadwater, C. Achim, E. Münck, B. G. Fox, *Biochemistry* **1999**, *38*, 12197 – 12204.
[229] A. S. Pereira, W. Small, C. Krebs, P. Tavares, D. E. Edmondson, E. C. Theil, B. H. Huynh, *Biochemistry* **1998**, *37*, 9871 – 9876.
[230] P. Moënne-Loccoz, C. Krebs, K. Herlihy, D. E. Edmondson, E. C. Theil, B. H. Huynh, T. M. Loehr, *Biochemistry* **1999**, *38*, 5290 – 5295.
[231] R. Koradi, M. Billeter, K. Wüthrich, *J. Mol. Graphics* **1996**, *14*, 51 – 55.
[232] P. J. Kraulis, *J. Appl. Crystallogr.* **1991**, *24*, 946 – 950.
[233] E. A. Merritt, M. E. P. Murphy, *Acta Crystallogr. Sect. D* **1994**, *50*, 869 – 873.
[234] D. A. Whittington, S. J. Lippard in *Handbook of Metalloproteins* (Eds.: A. Messerschmidt, R. Huber, T. Poulos, K. Wieghardt), Wiley, Chichester, **2001**, pp. 712 – 724.
[235] T. A. Jones, J.-Y. Zou, S. W. Cowan, M. Kjeldgaard, *Acta Crystallogr. Sect. A* **1991**, *47*, 110 – 119.
[236] A. J. Nicholls, *GRASP Manual*, Columbia University, New York, **1993**.

The Structure of $[Fe(CO)_4]$—An Important New Chapter in a Long-Running Story

Martyn Poliakoff* and James J. Turner*

In memory of Ernst A. Koerner von Gustorf (1932–1975) and Jeremy K. Burdett (1947–1997)

"It is of the highest importance in the art of detection to be able to recognize out of a number of facts which are incidental and which are vital."
from "The Memoirs of Sherlock Holmes"

$[Fe(CO)_4]$ is a coordinatively unsaturated intermediate usually generated from the stable compound $[Fe(CO)_5]$. Its study has spanned more than 30 years. The recently published paper by Zewail and colleagues[1] in *Angewandte Chemie* represents a major step in the field. Taken together with two recent publications by Fuss and co-workers[2] and Harris and co-workers[3] this paper provides a significant advance in our understanding of $[Fe(CO)_4]$. However, as explained in this Highlight, several questions remain to be answered. For convenience, the discussion is divided into three parts: what was known prior to 1990; what has been discovered since;[4] what happens next.

$[Fe(CO)_4]$ before 1990

The structure and reactions of $[Fe(CO)_4]$ were first established by IR spectroscopy and matrix isolation experiments in 1973/1974.[5] We showed that UV photolysis of $[Fe(CO)_5]$ (^{1}**5**) in low-temperature matrices (ca. 10 K) generates $[Fe(CO)_4]$ with a triplet ground state (^{3}**4**) (Scheme 1; the angles shown for ^{3}**4** are the averages for several matrices with individual errors of $\pm 3^\circ$).

Burdett[6] was the first to show, by rather simple molecular orbital theory, that the expected ground state of $[Fe(CO)_4]$ is indeed a triplet (actually $^3B_2$) with a C_{2v} structure and C-Fe-C bond angles of 135° and 110°, close to the experimental values; the singlet state (^{1}**4**) is somewhat higher in energy. In Ne and Ar matrices, the only further reaction is reversal of the primary photochemical act (i.e. ^{3}**4** $\rightarrow$ ^{1}**5**) by either near-IR irradiation or annealing (i.e. warming) of the matrices. On the other hand, with CH_4 and Xe matrices, ^{3}**4** could be converted by a single photon of near-IR or IR (2000 cm^{-1}) radiation into singlet species ^{1}**4**$\cdot CH_4$ and ^{1}**4**$\cdot$Xe (Scheme 1; the errors in the bond angles for ^{1}**4**$\cdot CH_4$ are $\pm 2^\circ$). There was no evidence for any "uncomplexed" singlet $[Fe(CO)_4]$ (^{1}**4**). It is important to stress that the conversions ^{3}**4** $\rightarrow$ ^{1}**4**$\cdot CH_4$ and ^{3}**4** $\rightarrow$ ^{1}**4**$\cdot$Xe involve very little energy, implying low activation energies. By contrast, the reverse reactions (^{1}**4**$\cdot CH_4 \rightarrow$ ^{3}**4**, and ^{1}**4**$\cdot$Xe $\rightarrow$ ^{3}**4**) could only be brought about by UV radiation ($\lambda >$ 375 nm). With hindsight, one can now see that the interaction of CH_4 and Xe (but not Ne or Ar) with the singlet $[Fe(CO)_4]$ (^{1}**4**) must cause the energies of ^{1}**4**$\cdot CH_4$ and ^{1}**4**$\cdot$Xe to be *below* that of ^{3}**4**. Presumably the interaction energy of ^{3}**4** with CH_4 and Xe is insignificant. (In their recent paper, Harris and co-workers[3] point out that there are good theoretical reasons for supposing that interaction of alkanes with triplet metal carbonyl species is negligible, but that interaction with singlet metal species can be significant). It is also noteworthy that in a hydrocarbon glass at 77 K (presumably the nearest low-temperature equivalent to an alkane solvent), only the species ^{1}**4**$\cdot$alkane was produced,[5] that is there was no evidence for ^{3}**4**. Later matrix isolation experiments, using continuous IR lasers, showed that ^{3}**4** could be isomerized by a rather unusual non-Berry pseudorotation mechanism, explained on the basis of a unique example of the Jahn–Teller effect.[7] This low-energy (<2000 cm^{-1}) process is illustrated in Scheme 2, in which X represents a CO group, isotopically enriched with ^{13}C.

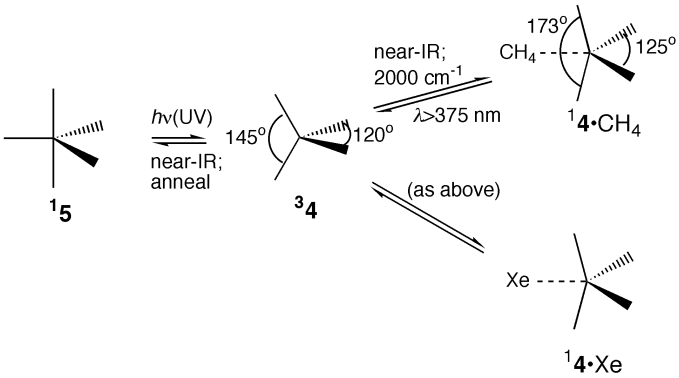

Scheme 1. Photochemistry of $[Fe(CO)_5]$ in low-temperature matrices.[5] See text for details.

[*] Prof. M. Poliakoff, Prof. J. J. Turner
School of Chemistry
University of Nottingham
Nottingham, NG7 2RD (UK)
Fax: (+44) 115-951-3058
E-mail: Martyn.poliakoff@nottingham.ac.uk

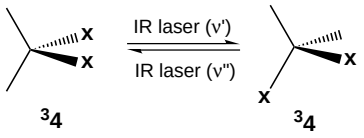

Scheme 2. Wavelength-selective IR laser photoisomerization of $[Fe(CO)_4]$ in low-temperature matrices.[7]

In the mid 1980s, experiments moved into the gas phase where solvent interactions should be absent. Weitz and co-workers[8] carried out experiments with $[Fe(CO)_5]$ in the gas phase, by employing laser UV flash photolysis with fast time-resolved IR detection (TR-IR). The first important point is that, in the gas phase, loss of more than one CO group can occur depending on the photolysis wavelength, whereas in condensed phases the primary photochemical act involves the loss of only a single CO group. The reason for this phase-dependent behavior is well understood in terms of energy transfer from vibrationally excited carbonyl molecules to the solvent or matrix. For the present purposes, the most important observation was that $[Fe(CO)_4]$ could be detected with ν(C–O) frequencies close to those observed for ^{3}**4** in a Ne matrix. This confirmed that the structure of triplet $[Fe(CO)_4]$ (^{3}**4**), which had been deduced from IR matrix frequencies, was not an artefact arising from interactions with matrix. Moreover the gas-phase work showed that ^{3}**4** reacted relatively slowly with either CO or $[Fe(CO)_5]$, a result expected from the spin-forbidden nature of these reactions.

It is also interesting to summarize what was *not* known before 1990:

1) Gas-phase IR studies had revealed no evidence for ^{1}**4**, nor species equivalent to ^{1}**4**·Xe or ^{1}**4**·CH_4.
2) The photochemical route from ground state $[Fe(CO)_5]$ (^{1}**5**) to ground state $[Fe(CO)_4]$ (^{3}**4**) was unclear, that is did it proceed by a singlet pathway (^{1}**5** → [^{1}**5**]* → ^{1}**4** → ^{3}**4**) or a triplet pathway (^{1}**5** → [^{1}**5**]* → [^{3}**5**]* → ^{3}**4**)?
3) Preliminary flash photolysis/IR detection studies on $[Fe(CO)_5]$ in solution had failed to identify any intermediates.[9a]
4) The triplet – singlet energy gap (^{3}**4**/^{1}**4**) was an experimental unknown.
5) There were no really accurate calculations on the structures of ^{3}**4** and ^{1}**4**, including the energy gap, nor were there any estimates of the interaction energies between ^{1}**4** and species such as Xe and CH_4.

[Fe(CO)$_4$] since 1990

In a lecture published in 1992, Grevels reported[9b] preliminary results on the ν(CO) TR-IR spectrum obtained after flash photolysis (309 nm) of $[Fe(CO)_5]$ in CO-saturated cyclohexane. A transient, with an IR spectrum which was very similar to that of ^{1}**4**·CH_4 in a matrix, was identified and assigned to ^{1}**4**·cyclohexane. This intermediate decayed in about 10 μs. There was no evidence for precursor ^{3}**4**, but this is hardly unexpected given the time-resolution of the experiment (ca. 1 μs).

In 1991/92 Weitz[10] returned to a TR-IR study of $[Fe(CO)_5]$ in the gas phase but using continuously tunable IR diode lasers rather than a line-tunable CO laser. These experiments yielded some fascinating new data about $[Fe(CO)_5]$, its fragments and their kinetics. Interestingly a great deal of the interpretation of the bimolecular reactions, such as $[Fe(CO)_3] + [Fe(CO)_5] \rightarrow [Fe_2(CO)_8]$, was based on earlier matrix isolation experiments[11] on the photochemistry of $[Fe_2(CO)_9]$. However, in the context of this Highlight, the most important observation was detection of a band at 1975 cm^{-1}, assigned to the singlet state of $[Fe(CO)_4]$ (i.e. ^{1}**4**). Although the authors did not comment on the fact, allowing for "matrix shifts", this band is close to the most intense band of ^{1}**4**·CH_4, detected in solid CH_4 at 20 K. The chemistry of ^{1}**4** was shown to involve both intersystem crossing (ISC) to ^{3}**4** and reaction with $[Fe(CO)_5]$ to give $[Fe_2(CO)_9]$ in an excited state. The rate of ISC, through collisions with the argon buffer gas, was slower than expected for gas kinetic by a factor of 40, but the reaction with $[Fe(CO)_5]$ was faster, approximately gas kinetic, thereby confirming the spin state of singlet $[Fe(CO)_4]$ (^{1}**4**). In comparison, the corresponding reactions of triplet $[Fe(CO)_4]$ (^{3}**4**) are very slow.[8] Not surprisingly, ^{1}**4** could only be detected when the pressure of buffer gas was low; at higher pressures, ISC to ^{3}**4** was too fast for it to be detected with the time resolution of the experiments (many ns). Thus, these experiments confirm that ^{3}**4** is the ground state with a low-lying singlet state, ^{1}**4**, above it.

In some extremely sophisticated gas-phase experiments, Fuss and co-workers[2] combined femtosecond UV laser excitation with time-of-flight mass spectrometry. They proposed that photolysis of $[Fe(CO)_5]$ at 267 nm proceeds via an excited singlet state ([^{1}**5**]*) to yield (in ca. 30 fs) $[Fe(CO)_4]$ in an excited singlet state ($^1B_2$), which then rapidly decays (ca. 50 fs), via the $^1T_2$ state, to the lowest singlet state ($^1A_1$, ^{1}**4**). This is the singlet pathway mentioned above. The Jahn – Teller distortion of the $^1T_2$ state was modeled on the earlier non-Berry pseudorotation proposed for ^{3}**4** (Scheme 2).[7] One might have expected to observe the $^1A_1$ state decaying to the ground triplet state (^{1}**4** → ^{3}**4**) but the time resolution was too short (< 500 ps) to follow ISC in the gas phase; in practice, what was seen was the very rapid ejection (3.3 ps) of a further CO group from ^{1}**4** to yield $[Fe(CO)_3]$, probably in an excited singlet state (the ground state of C_{3v} $[Fe(CO)_3]$ is almost certainly a triplet, $^3A_2$).

This Highlight has been prompted by the latest results on $[Fe(CO)_4]$, in which Zewail and colleagues[1] have used a new apparatus for ultrafast electron diffraction, which combines femtosecond lasers with electron diffraction imaging, to determine absolutely the structure of $[Fe(CO)_4]$. By using 620 nm irradiation, $[Fe(CO)_5]$ is photolyzed by a two-photon process which is of sufficiently low energy to limit the fragmentation pattern (see below for comment about energetics) to only ^{3}**4** and ^{1}**4**, and $[Fe(CO)_3]$ in its ground state ($^3A_2$). In an experimental tour de force, they were able to determine the structure of the primary photolysis product and to assign this structure to the $^1A_1$ state of $[Fe(CO)_4]$, (^{1}**4**) (Figure 1).

This confirms the singlet pathway proposed by Fuss and coworkers[2] Once more, it would be expected that ^{1}**4** should decay by ISC to ^{3}**4**, but again the time scale (< 200 ps) of these experiments does not permit the detection of the triplet. What

  1433-7851/01/4015;-2810 $ 17.50+.50/0 *Angew. Chem. Int. Ed.* **2001**, *40*, No. 15;

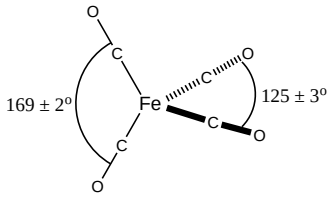

Figure 1. Structure of singlet $[Fe(CO)_4]$, ($^1A_1$, ^{1}**4**), determined by electron diffraction.[1] The bond lengths [Å] are: CO groups at 169°: Fe-C 1.81 ± 0.03, C-O 1.14 ± 0.05; CO groups at 125°: Fe-C 1.77 ± 0.03, C-O 1.15 ± 0.06. The C-Fe-C angles (169° and 125°) should be compared with those of ^{1}**4**·CH_4 in the matrix (Scheme 1; 173° and 125°).

is very striking about the structure of ^{1}**4** is that the C-Fe-C bond angles are uncannily close to those determined[5] more than 25 years ago for ^{1}**4**·CH_4, where angles were calculated from relative IR intensities by using scissors to cut the bands out from the paper trace of the IR spectrum and weighing the paper! Zewail's experiment suggests that, although the interaction of ^{1}**4** with (matrix)CH_4 is sufficient to lower the energy of ^{1}**4**·CH_4 below that of ^{3}**4**, the interaction produces almost no change in the geometry of the singlet $[Fe(CO)_4]$ fragment. Thus, these latest gas-phase experiments are entirely consistent with predictions made on the basis of early matrix experiments.

We now turn to the latest experiments in solution. For some time, Harris and colleagues have been highly successful in applying pico- and femtosecond TR-IR to the study of the primary processes in organometallic photochemistry. Their latest paper[3] examines the behavior of several compounds including $[Fe(CO)_5]$. Their TR-IR data revealed an intermediate formed from $[Fe(CO)_5]$ within 26 ps and stable for more than 660 ps. The same intermediate was detected in $HSiEt_3$ solution but it reacted within about 1.2 ns to form $[HFe(CO)_4(SiEt_3)]$. The IR bands of this intermediate in heptane, 1965 and 1987 cm^{-1}, correspond closely to those observed for ^{3}**4** in a CH_4 matrix (1966, 1992/1985 cm^{-1}) (note: *not* ^{1}**4**·CH_4) and, as the authors claim, it is extremely likely that the intermediate is indeed $[Fe(CO)_4]$ in the $^3B_2$ ground state. The intriguing question is: "where is the expected ^{1}**4**·solvent?"

If Fuss's and Zewail's gas-phase results apply to the primary steps in solution, then there seems to be only one explanation, namely that ^{1}**4** is indeed produced initially, but that ISC in solution is so fast that only ^{3}**4** is detected. It is worth pointing out that "hot" molecules display "smeared out" IR spectra until relaxation to the equilibrated solution intermediate occurs, a process which takes many ps for metal carbonyls in hydrocarbon solution.[12] Thus, it is just possible that ^{1}**4** is produced initially but it is too "hot" to distinguish spectroscopically, and it converts to ^{3}**4** before detection. Presumably one would have to argue that, on the very fast time scales, ^{1}**4** is just too hot to be stabilized by interaction with the solvent (i.e. there is no "hot" ^{1}**4**·solvent). An alternative explanation is that the pathway in solution follows a triplet pathway rather than the singlet pathway observed in the gas phase. Given the matrix behavior of ^{1}**4**·Xe and ^{1}**4**·CH_4, and the fact that only ^{1}**4**·alkane can be detected in hydrocarbon glasses,[5] and that ^{1}**4**·cyclohexane is detected on the microsecond time scale in room temperature solution,[9b] one would expect that ^{3}**4** should convert to ^{1}**4**·heptane over a long time scale. However, this clearly does not happen, at least within about 1 ns, the approximate long time limit of Harris's apparatus. It would be intriguing to look for ^{1}**4**·heptane on time scales between 1 ns and 1 μs.[13]

Harris's evidence for ^{3}**4** in solution is consistent with elegant, but perfectly conventional, quantum yield measurements of the photoreaction of $[Fe(CO)_5]$ with phosphites[9b] and phosphines, L. [14] At high ratios of L:$[Fe(CO)_5]$, which suppress mechanisms involving reaction of $[Fe(CO)_4]$ with $[Fe(CO)_5]$, photolysis leads to the formation of both $[^1Fe(CO)_4L]$ and $[^1Fe(CO)_3L_2]$ as primary photoproducts. This is rather surprising since formation of $[Fe(CO)_3L_2]$ must proceed in solution by a single-photon mechanism; in other words the photochemistry does not involve sequential photolysis of $[Fe(CO)_5]$ and $[Fe(CO)_4L]$. The proposed mechanisms[2, 9b, 14] all involve ^{3}**4**, but they differ in what other intermediates are implicated; these include: $[^1Fe(CO)_4]$ (i.e. ^{1}**4**), $[^1Fe(CO)_4]$·solvent (i.e. ^{1}**4**·solvent), $[^1Fe(CO)_3L]$·solvent, $[^3Fe(CO)_4L]$, $[^3Fe(CO)_3L]$ and $[^3Fe(CO)_3L_2]$. Very recent picosecond TR-IR results[13] in neat triethylphosphine indicate the presence of $[^3Fe(CO)_3L]$, but not $[^3Fe(CO)_4L]$. Clearly we are some way off pinning down the exact mechanism.

[Fe(CO)$_4$]—The Next Step?

Where does all this leave us? First of all, we have almost entirely ignored recent high-level computational work as well as gas-phase experiments designed to measure the various dissociation energies principally because the results are not always in agreement![15] Thus, although everyone agrees that both ^{3}**4** and ^{1}**4** have C_{2v} structures, the range of bond lengths and bond angles is wide and depends on the details of the calculation. Moreover, although all agree that ^{1}**4** lies above ^{3}**4**, the predicted energy gap varies from about 0.7 to 20 kcal mol^{-1}. Therefore, what would we, as experimentalists, really like to see next? There are three outstanding challenges. It would be marvellous if the structure of gas-phase ^{3}**4** could be unequivocally determined by a "nonsporting" method such as Zewail's diffraction technique; it would be equally enthralling if ^{1}**4** could be unequivocally identified in a "noncomplexing" solvent; finally the ^{1}**4**/^{3}**4** energy gap needs to be measured somehow. We look forward to seeing such results in print!

[1] H. Ihee, J. Cao, A. H. Zewail, *Angew. Chem.* **2001**, *113*, 1580; *Angew. Chem. Int. Ed.* **2001**, *40*, 1532.
[2] S. A. Trushin, W. Fuss, K. L. Kompa, W. E. Schmid, *J. Phys. Chem. A* **2000**, *104*, 1997.
[3] P. T. Snee, C. K. Payne, K. T. Kotz, H. Yang, C. B. Harris, *J. Am. Chem. Soc.* **2001**, *123*, 2255.
[4] A useful review of all but the latest work: N. Leadbeater, *Coord. Chem. Rev.* **1999**, *188*, 35.
[5] M. Poliakoff, J. J. Turner, *J. Chem. Soc. Dalton Trans.* **1973**, 1351; M. Poliakoff, J. J. Turner, *J. Chem. Soc. Dalton Trans.* **1974**, 2276; T. J. Barton, R. Grinter, A. J. Thomson, B. Davies, M. Poliakoff, *J. Chem. Soc. Chem. Commun.* **1977**, 841; see also the review: M. Poliakoff, E. Weitz, *Acc. Chem. Res.* **1987**, *20*, 408.
[6] J. K. Burdett, *J. Chem. Soc. Faraday Trans. 2* **1974**, *70*, 1599; for other work prior to 1990, see: M. Elian, R. Hoffmann, *Inorg. Chem.* **1975**,

  1433-7851/01/4015;-2811 $ 17.50+.50/0

14, 1058; C. Daniel, M. Bernard, A. Dedieu, R. Wiest, A. Veillard, *J. Phys. Chem.* **1984**, *88*, 4805.
[7] B. Davies, A. McNeish, M. Poliakoff, J. J. Turner, *J. Am. Chem. Soc.* **1977**, *99*, 7573; M. Poliakoff, A. Ceulemans, *J. Am. Chem. Soc.* **1984**, *106*, 50.
[8] A. J. Ouderkirk, P. Werner, N. L. Schultz, E. Weitz, *J. Am. Chem. Soc.* **1983**, *105*, 3354; T. A. Seder, A. J. Ouderkirk, E. Weitz, *J. Chem. Phys.* **1986**, *85*, 1977.
[9] a) Although the short-lived species $[Fe(CO)_4]\cdot C_6D_6$ was identified: S. P. Church, F.-W. Grevels, H. Hermann, J. M. Kelly, W. E. Klotzbücher, K. Schaffner, *J. Chem. Soc. Chem. Commun.* **1985**, 594; b) F.-W. Grevels in *Photoprocesses in Transition Metal Complexes, Biosystems and Other Molecules. Experiment and Theory* (Ed.: E. Kochanski), Kluwer, Dordrecht, **1992**, p. 141.
[10] R. J. Ryther, E. Weitz, *J. Phys. Chem.* **1991**, *95*, 9841; R. J. Ryther, E. Weitz, *J. Phys. Chem.* **1992**, *96*, 2561.
[11] M. Poliakoff, J. J. Turner, *J. Chem. Soc. A* **1971**, 2403; S. C. Fletcher, M. Poliakoff, J. J. Turner, *Inorg. Chem.* **1986**, *25*, 3597.
[12] S. M. Arrivo, T. P. Dougherty, W. Tandy Grubbs, E. J. Heilweil, *Chem. Phys. Lett.* **1995**, *235*, 247; E. J. Heilweil, R. R. Cavanagh, J. C. Stephenson, *Chem. Phys. Lett.* **1987**, *134*, 181.
[13] P. T. Snee, C. B. Harris, private communication.
[14] S. K. Nayak, T. J. Burkey, *J. Am. Chem. Soc.* **1993**, *115*, 6391; S. K. Nayak, G. J. Farrell, T. J. Burkey, *Inorg. Chem.* **1994**, *33*, 2236.
[15] See ref. [1–3] for discussion of values; see also: O. Gonzalez-Blanco, U. Branchadell, *J. Chem. Phys.* **1999**, *110*, 778. It is interesting that calculations in ref. [3] suggest an energy of interaction between ^{1}**4** and C_2H_6 of about 7 kcal mol^{-1}, and a ^{1}**4**/^{3}**4** gap of about 6 kcal mol^{-1}. On this basis, the solvent-stabilized singlet $[Fe(CO)_4]$ (i.e. ^{1}**4**·solvent), has approximately the same energy as ground-state triplet $[Fe(CO)_4]$ (i.e. ^{3}**4**).

IBX—New Reactions with an Old Reagent

Thomas Wirth*

Hypervalent iodine reagents have attracted increasing interest during the last decade because of their selective, mild, and environmentally friendly properties as oxidizing agents in organic synthesis.[1] 2-Iodoxybenzoic acid (IBX, 1-hydroxy-1,2-benziodoxol-3(1*H*)-one 1-oxide **1**) was first reported in 1893[2] but has been rarely used in reactions, probably due to its insolubility in most organic solvents.[3] Dess and Martin transformed IBX (**1**) into the much more soluble Dess–Martin periodinane (DMP, 1,1,1-triacetoxy-1,1-dihydro-1,2-benziodoxol-3(1*H*)-one **2**),[3, 4] which has received much attention. Improved procedures for the synthesis of reagents **1** and **2** have been disclosed recently.[5–7]

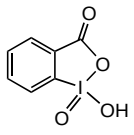

1 (IBX)

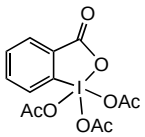

2 (DMP)

The broad functional group tolerance of these reagents and high-yielding reactions without over-oxidation have made DMP (**2**) very prominent for the oxidation of alcohols to the corresponding carbonyl compounds. But IBX (**1**) in DMSO was also found to be a highly efficient reagent for the clean oxidation of alcohols **3** to carbonyl compounds **4** even in the presence of thioethers or amines[8, 9] (the number of reported examples are given below the arrows here and in the following). It is also possible to selectively oxidize 1,2-diols to 1,2-diketo derivatives without oxidative cleavage of the glycol C–C bond.[8, 10] The selective oxidation of 1,4-diols **5** to the corresponding γ-lactols **6** can also be realized.[11, 12]

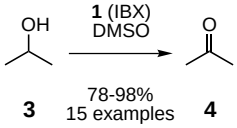

3 **4**

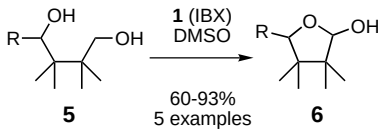

5 **6**

The first step in these oxidation reactions is a fast pre-equilibrium, which can be formally considered as ligand exchange (hydroxy–alkyloxy) on the iodine atom. The product **7** then disproportionates to the carbonyl derivative **4** and the iodosoarene **8** (IBA).[10]

The known paths for the oxidation of alcohols have been extended by recent reports utilizing IBX (**1**) and DMP (**2**)[13] in other transformations. The introduction of an α,β-double bond into carbonyl compounds is sometimes a challenging transformation, which is predominantly performed by using selenium or palladium reagents. A ligand exchange on IBX with the ketone-enolate might be involved in the key step in the mechanism of this new and general procedure. Although the reaction proceeds only at elevated temperatures (65–85 °C), even acid-labile carbonyl compounds can be employed in the process, from which derivatives **9** are obtained in good

[*] Prof. T. Wirth
Department of Chemistry
Cardiff University
PO Box 912, Cardiff CF10 3TB (UK)
Fax: (+44) 29-2087-6968
E-mail: wirth@cf.ac.uk

  1433-7851/01/4015;-2812 $ 17.50+.50/0

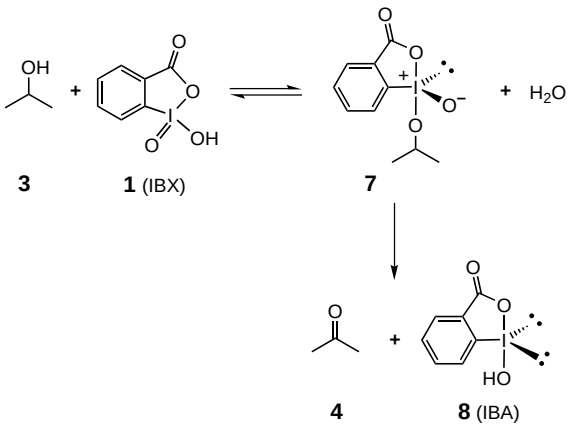

yields.[14] Even alcohols can be converted to α,β-unsaturated carbonyl compounds directly by using an excess of IBX (**1**), as shown in the oxidation of the phenylalanine derivative **10** to **11**.

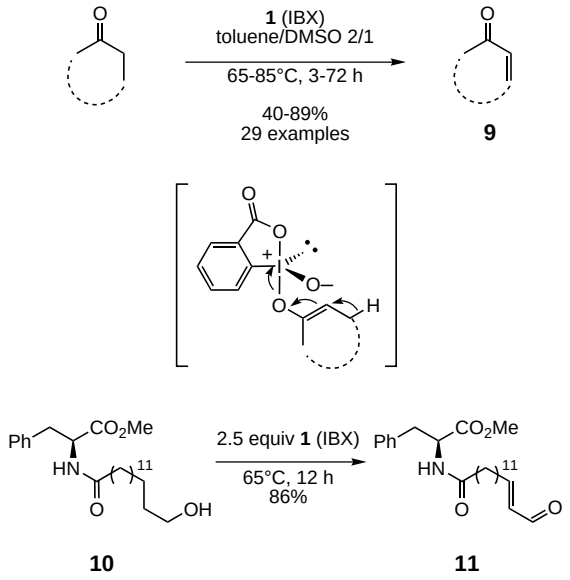

Although hypervalent iodine compounds are often used as oxidants and sometimes as electrophilic reagents, the cyclization of aryl-substituted unsaturated amines to heterocycles **13** is started by a single-electron transfer (SET) reaction. Either **1** or an IBX · THF adduct serves as the oxidant to initiate the heterocyclization by a SET process. The subsequently generated N-centered radical will then cyclize in a 5-*exo*-*trig* manner to yield, after hydrogen abstraction from the solvent, heterocycles of type **13**. The cyclization of amides to γ-lactams offers the possibility to synthesize even a variety of annelated heterocyclic compounds. The IBX-mediated cyclization of (thio)carbamates and ureas to (thio)oxazolidinones and cyclic ureas can be followed by hydrolysis to synthesize, for example, 1,2-amino alcohols of type **14**.[15] The fast access to the carbamate starting materials by adding allylic alcohols to isocyanates allows the rapid generation of compound libraries.[16]

The mechanism of this transformation has been investigated in detail. Although amide radicals have already been employed in cyclization reactions,[17] their involvement in the IBX-mediated reaction has been proven by a detailed analysis.[15b] It was concluded that the irreversible SET from the aryl moiety to the IBX · THF adduct is the rate-determining step of the reaction and can only proceed with a free *ortho*-position in the substrate as shown in the mesomeric structures **A** and **B**.

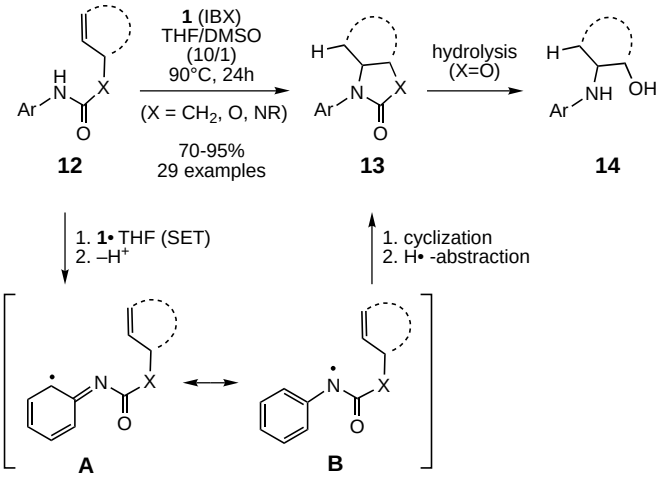

On the basis of this reaction mechanism, a process for the oxidation of the benzylic position has been developed recently. This reaction is quite general and proceeds with an excess of **1** at higher temperatures. Over-oxidation of compounds **15** with R′ = H to the corresponding carboxylic acids was not observed, and the yields of ketones or aldehydes **16** even with labile substrates were generally quite high.[18]

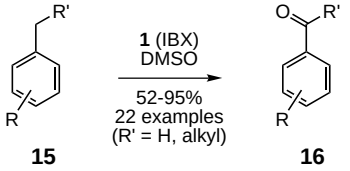

To show the selectivity and controllability of these IBX-mediated reactions, substrate **17** was synthesized and converted in a series of steps to compound **21**. The cyclization reaction **20** → **21** must not necessarily be the last step in the sequence.

As shown recently in the hydrolysis of phosphonofluoridates, **1** can also be used as a catalyst with oxone being the stoichiometric oxidant.[19] IBX (**1**) is able to oxidize thiols selectively to the corresponding disulfides.[20] It can also be used as a versatile reagent for the cleavage of oximes and tosylhydrazones to the corresponding carbonyl compounds.[21] The first attempts to synthesize chiral reagents derived from IBX have appeared, although the selectivities obtained in the sulfide oxidation are low (up to 16 % *ee*).[22] The development of electronically modified IBX reagents[23] to tune electron

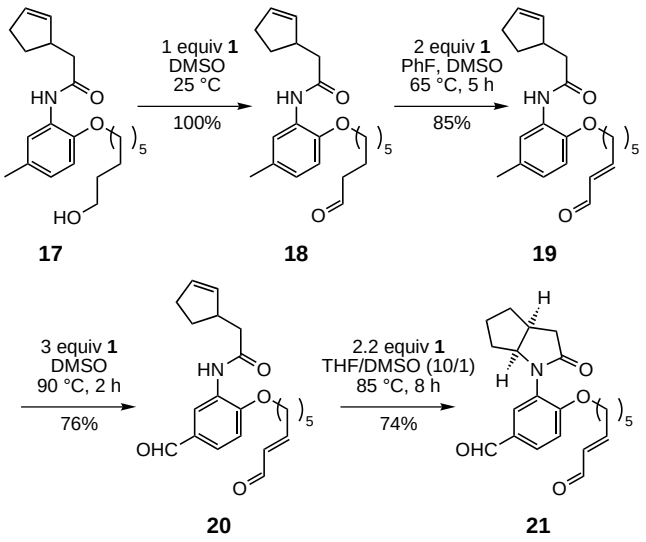

transfer processes, their application to new reactions, and the synthesis of polymer-bound IBX[24] for rapid combinatorial chemistry will undoubtedly be reported in literature in the near future.

[1] a) A. Varvoglis, *Hypervalent Iodine in Organic Synthesis*, Academic Press, London, **1997**; b) T. Wirth, U. H. Hirt, *Synthesis* **1999**, 1271 – 1287.

[2] C. Hartmann, V. Meyer, *Chem. Ber.* **1893**, *26*, 1727 – 1732.

[3] D. B. Dess, J. C. Martin, *J. Am. Chem. Soc.* **1991**, *113*, 7277 – 7278.

[4] D. B. Dess, J. C. Martin, *J. Org. Chem.* **1983**, *48*, 4155 – 4156.

[5] IBX: M. Frigerio, M. Santagostino, S. Sputore, *J. Org. Chem.* **1999**, *64*, 4537 – 4538.

[6] DMP: a) R. E. Ireland, L. J. Liu, *J. Org. Chem.* **1993**, *58*, 2899; b) S. D. Meyer, S. L. Schreiber, *J. Org. Chem.* **1994**, *59*, 7549 – 7552; c) R. K. Boeckman, P. Shao, J. J. Mullins, *Org. Synth*. **1999**, *76*, 194 – 198.

[7] **Caution!** IBX and DMP are explosive under impact or heating $>200\,^{\circ}C$: J. B. Plumb, D. J. Harper, *Chem. Eng. News* **1990**, *68*(29), 3.

[8] M. Frigerio, M. Santagostino, *Tetrahedron Lett.* **1994**, *35*, 8019 – 8022.

[9] M. Frigerio, M. Santagostino, S. Sputore, G. Palmisano, *J. Org. Chem.* **1995**, *60*, 7272 – 7276.

[10] With DMP 1,2-diols are cleaved at the C–C bond: S. De Munari, M. Frigerio, M. Santagostino, *J. Org. Chem.* **1996**, *61*, 9272 – 9279.

[11] a) E. J. Corey, A. Palani, *Tetrahedron Lett.* **1995**, *36*, 3485 – 3488; b) E. J. Corey, A. Palani, *Tetrahedron Lett.* **1995**, *36*, 7945 – 7948.

[12] 1,5-Diols can also be converted to lactols: a) J. M. Bueno, J. M. Coterón, J. L. Chiara, A. Fernández-Mayoralas, J. M. Fiandor, N. Valle, *Tetrahedron Lett.* **2000**, *41*, 4379 – 4382; b) J. Roels, P. Metz, *Synlett* **2001**, 789 – 790.

[13] a) K. C. Nicolaou, Y.-L. Zhong, P. S. Baran, *Angew. Chem.* **2000**, *112*, 636 – 639; *Angew. Chem. Int. Ed.* **2000**, *39*, 622 – 625; b) K. C. Nicolaou, K. Sugita, P. S. Baran, Y.-L. Zhong, *Angew. Chem.* **2001**, *113*, 213 – 216; *Angew. Chem. Int. Ed.* **2001**, *40*, 207 – 210; c) K. C. Nicolaou, Y.-L. Zhong, P. S. Baran, K. Sugita, *Angew. Chem.* **2001**, *113*, 2203 – 2207; *Angew. Chem. Int. Ed.* **2001**, *40*, 2145 – 2149.

[14] K. C. Nicolaou, Y.-L. Zhong, P. S. Baran, *J. Am. Chem. Soc.* **2000**, *122*, 7596 – 7597.

[15] a) K. C. Nicolaou, Y.-L. Zhong, P. S. Baran, *Angew. Chem.* **2000**, *112*, 639 – 642; *Angew. Chem. Int. Ed.* **2000**, *39*, 625 – 628; b) K. C. Nicolaou, P. S. Baran, R. Kranich, Y.-L. Zhong, K. Sugita, N. Zou, *Angew. Chem.* **2001**, *113*, 208 – 212; *Angew. Chem. Int. Ed.* **2001**, *40*, 202 – 206.

[16] K. C. Nicolaou, P. S. Baran, Y.-L. Zhong, J. A. Vega, *Angew. Chem.* **2000**, *112*, 2625 – 2629; *Angew. Chem. Int. Ed.* **2000**, *39*, 2525 – 2529.

[17] a) J. L. Esker, M. Newcomb, *Tetrahedron Lett.* **1993**, *34*, 6877 – 6880; b) B. Giese, B. Kopping, T. Göbel, J. Dickhaut, G. Thoma, K. J. Kulicke, F. Trach, *Org. React.* **1996**, *48*, 301 – 856.

[18] K. C. Nicolaou, P. S. Baran, Y.-L. Zhong, *J. Am. Chem. Soc.* **2001**, *123*, 3183 – 3185.

[19] C. A. Bunton, H. J. Foroudian, N. D. Gillitt, *J. Phys. Org. Chem.* **1999**, *12*, 758 – 764.

[20] R. A. Moss, H. Morales-Rojas, H. Zhang, B. Park, *Langmuir* **1999**, *15*, 2738 – 2744.

[21] D. S. Bose, P. Srinivas, *Synlett* **1998**, 977 – 978.

[22] V. V. Zhdankin, J. T. Smart, P. Zhao, P. Kiprof, *Tetrahedron Lett.* **2000**, *41*, 5299 – 5302.

[23] a) A. R. Katritzky, B. L. Duell, H. D. Durst, B. L. Knier, *J. Org. Chem.* **1988**, *53*, 3972 – 3978; b) V. V. Zhdankin, R. M. Arbit, B. J. Lynch, P. Kiprof, *J. Org. Chem.* **1998**, *63*, 6590 – 6596.

[24] For the reduction and quantitative removal of iodine species after IBX oxidations by a thiosulfate resin, see: J. J. Parlow, B. L. Case, M. S. South, *Tetrahedron* **1999**, *55*, 6785 – 6796.

  1433-7851/01/4015;-2814 $ 17.50+.50/0

Diastereoselective aldol reactions via boron enolates have been successfully performed in water by using a catalytic amount of a boron source.

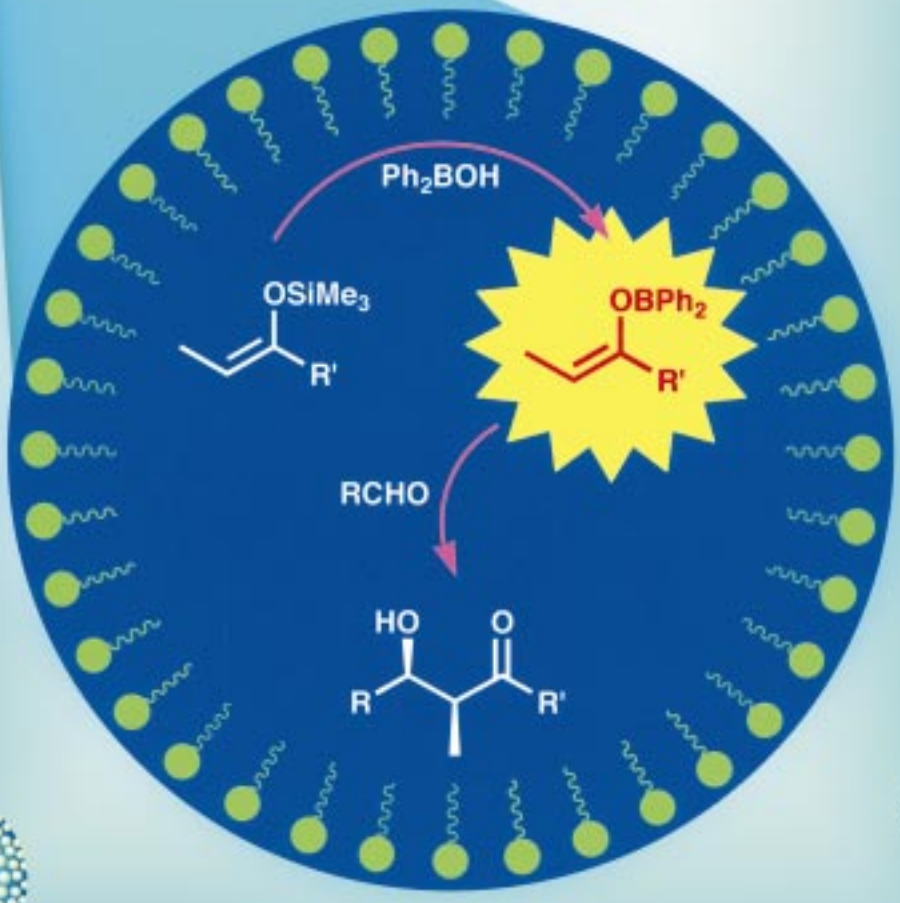

These reactions take place in colloidal particles formed from substrates and a surfactant and protect the boron enolates from hydrolysis. For more information see the following pages.

  1433-7851/01/4015-2815 $ 17.50+.50/0

Catalytic Use of a Boron Source for Boron Enolate Mediated Stereoselective Aldol Reactions in Water**

Yuichiro Mori, Kei Manabe, and Shū Kobayashi*

Boron enolate chemistry has been well-established and several useful reactions using boron enolates have been developed. However, stoichiometric amounts of boron sources such as dialkylboron triflates have been required in all cases so far reported. Herein, we disclose the first example of the catalytic use of a boron source in boron enolate mediated stereoselective aldol reactions.[1] Interestingly, the reactions proceed in water without using any organic solvents.

Recently, we reported the use of Lewis acid surfactant combined catalysts (LASCs) in organic synthesis in water.[2] LASCs create colloidal particles of approximately 1 μm diameter with organic materials in water, and useful synthetic reactions such as aldol, allylation, Mannich, and Michael reactions were shown to proceed smoothly in the presence of a LASC. In the course of our investigations to improve the reaction system, we tested various compounds which might act as better catalysts in water. We chose the Mukaiyama aldol reaction as a model reaction. After screening various catalysts, we found diphenylborinic acid (Ph_2BOH, **1**),[3, 4] which is stable in water, was an effective catalyst in the presence of sodium dodecyl sulfate (SDS) as a surfactant.[5] We then examined a reaction of benzaldehyde with the silyl enolate **2** in water (Table 1). While the reaction proceeded very slowly in the presence of 0.1 equivalents of **1** and SDS (Table 1, entry 1), a dramatic improvement of the yield was observed when benzoic acid was added to this system (entry 2). To our surprise, the diastereoselectivity (*syn*/*anti*) of the product was much higher than that of the previously reported LASC system.[6] In the presence of SDS only (entry 3), or in the presence of benzoic acid and SDS (without **1**, entry 4), the desired adducts were obtained in low yields with low diastereoselectivities. In the presence of **1** and benzoic acid (without SDS), high *syn* selectivity was obtained, albeit the yield was low (entry 5). The best yield and selectivity were obtained when **1** (0.1 equiv), SDS (0.1 equiv), and benzoic acid (0.01 equiv) were used at 0 °C (entry 6). Note that the use of water as a solvent is essential in this reaction. The reaction proceeded sluggishly in organic solvents such as dichloromethane and diethyl ether (entries 7, 8). Much lower yield than that in water was obtained under neat conditions (entry 9).

Table 1. Mukaiyama aldol reaction using **1** in water.

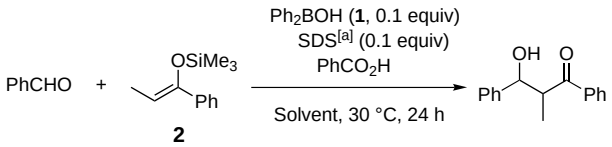

Entry	Solvent	$PhCO_2H$ [equiv]	Yield [%]	*syn*/*anti*
1	H_2O	–	trace	–
2	H_2O	0.01	90	92/8
3[b]	H_2O	–	2	53/47
4[b]	H_2O	0.01	27	58/42
5[c]	H_2O	0.01	4	91/9
6[d]	H_2O	0.01	93	94/6
7	Et_2O	0.01	trace	–
8	CH_2Cl_2	0.01	trace	–
9	–	0.01	24	90/10

[a] Sodium dodecyl sulfate. [b] Without **1**. [c] Without SDS. [d] 0 °C.

Several examples of the aldol reactions are shown in Table 2. In all cases, the reactions proceeded smoothly in the presence of **1** (0.1 equiv), SDS (0.1 equiv), and benzoic acid (0.01 equiv) to afford the corresponding adducts in good yields. When (*Z*)-3-trimethylsiloxy-2-pentene was used, the highest diastereoselectivity (*syn*/*anti* = 96/4 and 97/3) was obtained (entries 1 and 8). In all cases, high *syn* selectivity was observed when *Z*-enolates were used (*syn*/*anti* = 90/10 – 97/3). Not only aromatic aldehydes but also α,β-unsaturated and aliphatic aldehydes gave high *syn* selectivity. Although lower diastereoselectivity was observed when *E*-enolates were used (entries 2 and 10), reverse diastereoselectivity was observed when both stereoisomers of the silyl enolate derived from *tert*-butyl thiopropionate were used (entries 4 and 5).

The high *syn* selectivity observed in these reactions is remarkable because lower diastereoselectivities are obtained in the Lewis acid catalyzed Mukaiyama aldol reactions in water. For the metal-catalyzed aldol reactions of aldehydes with silyl enolates only two reaction mechanisms are known. One is the Lewis acid mechanism,[7] and the other involves a metal enolate as a reaction intermediate generated by silicon – metal exchange.[8] In the present reaction system, the latter mechanism can explain the results more clearly. That the diastereoselection was reversed by using the stereoisomers of the silyl enolate derived from *tert*-butyl thioester (Table 2, entries 4 and 5) supports the hypothesis because this type of reversal was also observed in the traditional boron enolate mechanism which involves a chairlike six-membered transition state. Furthermore, the trend that *anti* selectivity is poorer than *syn* selectivity in our reactions is also found in the traditional boron enolate mediated aldol reactions.[9] Thus, we proposed a mechanism which involved a boron enolate as a reaction intermediate (the boron enolate mechanism, Scheme 1). The mechanism is based on the hypothesis that **1** can react with a silyl enolate to form the corresponding boron enolate under the reaction conditions.[10] When a *Z*-enolate was used, an aldehyde and the boron enolate would react via a chairlike six-membered transition state to give the *syn* aldol product. The B–O bond of the initial aldol product **5** is presumed to be easily cleaved by hydrolysis, and **1** can be

[*] Prof. Dr. S. Kobayashi, Dr. Y. Mori, Dr. K. Manabe
Graduate School of Pharmaceutical Sciences
The University of Tokyo, CREST
Japan Science and Technology Corporation (JST)
Hongo, Bunkyo-ku, Tokyo 113-0033 (Japan)
Fax: (+81) 3-5684-0634
E-mail: skobayas@mol.f.u-tokyo.ac.jp

[**] This work was partially supported by a Grant-in-Aid for Scientific Research from the Ministry of Education, Science, Sports, and Culture, Japan. Y. M. thanks the JSPS fellowship for Japanese Junior Scientists.

Supporting information for this article is available on the WWW under http://www.angewandte.com or from the author.

  1433-7851/01/4015-2816 $ 17.50+.50/0

Table 2. Mukaiyama aldol reactions using **1** in water.[a]

Entry	Substrate		Yield [%]	*syn*/*anti*
1[b]	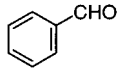	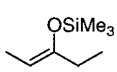 [e]	60	96/4
2[b]		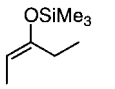 [f]	72	53/47
3[b]		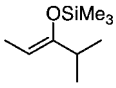 [g]	72	95/5
4[b,c]		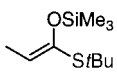 [h]	62	96/4
5[b,c]		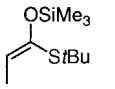 [i]	84[k]	39/61
6[b]	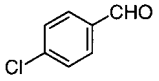	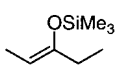	51	95/5
7		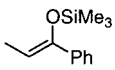 [j]	92	90/10
8[b]	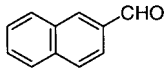	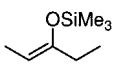	74	97/3
9	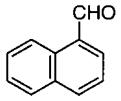	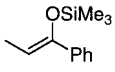	80	92/8
10		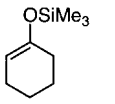	79	47/53
11[d]	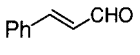	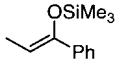	76	91/9
12	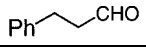		61	92/8

[a] Conditions: silyl enolate (1.5 equiv), **1** (0.1 equiv), $PhCO_2H$ (0.01 equiv), SDS (0.1 equiv), H_2O (aldehyde: 167 mM), 30 °C, 4–24 h. [b] Silyl enolate (3.0 equiv). [c] 0 °C. [d] $PhCO_2H$ (0.1 equiv). [e] $Z/E = > 99/< 1$. [f] $Z/E = 19/81$. [g] $Z/E = 96/4$. [h] $Z/E = 2/98$. [i] $Z/E = 97/3$. [j] $Z/E = > 99/< 1$. [k] 72 h.

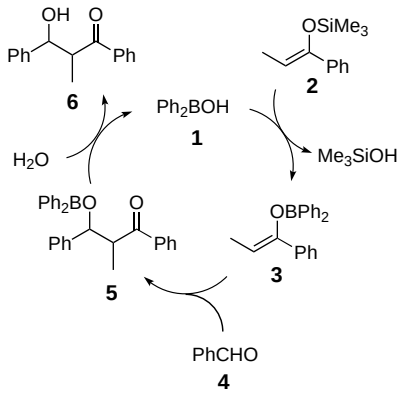

Scheme 1. Proposed boron enolate mechanism.

regenerated. In this mechanism, benzoic acid[11] may accelerate the Si–B exchange step, which is thought to be a rate-determining step.

To obtain information about the mechanism, kinetic studies were undertaken. The rate of disappearance of silyl enolate **2** was examined (Figure 1a). It was found that the rate was

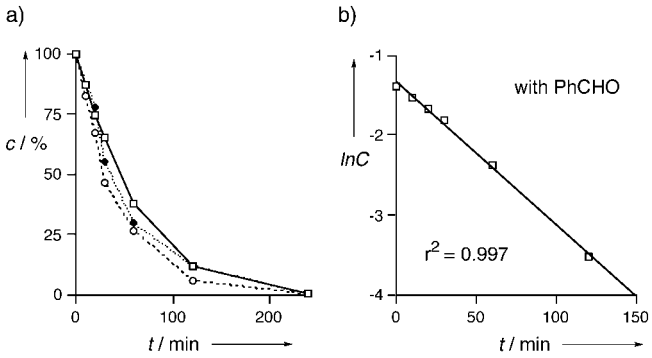

Figure 1. Changes of the amount of **2** during the reactions using **1** as a catalyst in water with □: benzaldehyde, ◆: cyclohexanecarboxaldehyde, ○: no aldehyde, *C*: Concentration of **2** in water (mol L^{-1}). Conditions: **2** (1.5 equiv), **1** (0.1 equiv), $PhCO_2H$ (0.1 equiv), SDS (0.1 equiv), H_2O (aldehyde: 167 mM), 30 °C. The amount of **2** was determined by HPLC (acetophenone was used as an internal standard). See text for further details

independent of the reactivity of the aldehydes. The reactivity of the aldehydes (benzaldehyde (more reactive), cyclohexanecarboxaldehyde (less reactive, 34% yield under the conditions of Figure 1)) has no significant effect on the disappearance rate of **2**. Furthermore, the amount of **2** also decreased at the same rate when no aldehyde was added to the reaction system. In addition, the rate was found to be dependent only on the amount of **2**, following first-order kinetics ($k = 3.0 \times 10^{-4}$ s^{-1}, Figure 1b). These facts support the boron enolate mechanism rather than the Lewis acid mechanism, because the reactivity and the absence of the aldehyde are presumed to affect the rate of disappearance of the silyl enolate in the Lewis acid mechanism. In our mechanism, the aldol-addition step should be very fast because of the instability of the boron enolate in water. The results of the kinetic studies suggest the Si–B exchange step, not the aldol-addition step, is the rate-determining step because the rate depends only on the amount of the remaining silyl enolate.[12] The formed boron enolate would react rapidly with an aldehyde or be hydrolyzed to form the corresponding ketone. The cleavage of the B–O bond of the initial aldol product **5** should be fast because of the acidity of the reaction media (pH ≈ 4). Thus, the boron enolate mechanism is much more likely than the Lewis acid mechanism. As far as we know, this is the first example of the formation of boron enolate using a catalytic amount of a boron source.

In summary, we have found that highly diastereoselective aldol reactions via boron enolates have been successfully performed in water using a catalytic amount of a boron source. The reactions proceed smoothly in water at ambient temperature while traditional boron aldol reactions need lower temperature and strictly anhydrous conditions. Water is used as the sole solvent, and thus should lead to environmentally friendly systems. Further investigations to improve the yield and selectivity and to clarify the detailed mechanism of these reactions are now in progress.

  1433-7851/01/4015-2817 $ 17.50+.50/0

Experimental Section

A typical experimental procedure: aldehyde (0.25 mmol) and silyl enolate (0.375 mmol) were added successively at 30 °C to a stirred white suspension of diphenylborinic acid (0.025 mmol), benzoic acid (0.0025 mmol), and SDS (0.025 mmol) in water (1.5 mL). After 24 h, saturated aq. $NaHCO_3$ (5 mL) and brine (5 mL) were added, and the mixture was extracted with ethyl acetate, dried over Na_2SO_4, and concentrated. The aldol product was purified by preparative thin layer chromatography (TLC; SiO_2, ethyl acetate/hexane = 1/3).

Received: March 27, 2001 [Z16861]

[1] For boron-mediated aldol reactions, see: a) B.-M. Kim, S. F. Williams, S. Masamune in *Comprehensive Organic Synthesis*, *Vol. 2* (Eds.: B. M. Trost, I. Fleming, C. H. Heathcock), Pergamon, Oxford, **1991**, pp. 239–268; b) W. Fenzl, R. Köster, *Liebigs Ann. Chem.* **1975**, 1322–1338; c) T. Inoue, T. Mukaiyama, *Bull. Chem. Soc. Jpn.* **1980**, *53*, 174–178; d) D. A. Evans, J. V. Nelson, E. Vogel, T. R. Taber, *J. Am. Chem. Soc.* **1981**, *103*, 3099–3111; e) S. Masamune, S. Mori, D. Van Horn, D. W. Brooks, *Tetrahedron Lett.* **1979**, *19*, 1665–1668.

[2] For LASC-mediated carbon–carbon bond forming reactions in water, see: a) S. Kobayashi, T. Wakabayashi, *Tetrahedron Lett.* **1998**, *39*, 5389–5392; b) S. Otto, J. B. F. N. Engberts, J. C. T. Kwak, *J. Am. Chem. Soc.* **1998**, *120*, 9517–9525; c) K. Manabe, S. Kobayashi, *Synlett* **1999**, 547–548; d) K. Manabe, S. Kobayashi, *Tetrahedron Lett.* **1999**, *40*, 3773–3776; e) S. Kobayashi, Y. Mori, S. Nagayama, K. Manabe, *Green Chem.* **1999**, 175–177; f) K. Manabe, Y. Mori, S. Nagayama, K. Odashima, S. Kobayashi, *Inorg. Chim. Acta* **1999**, *296*, 158–163; g) K. Manabe, Y. Mori, S. Kobayashi, *Tetrahedron* **1999**, *55*, 11203–11208; h) Y. Mori, K. Kakumoto, K. Manabe, S. Kobayashi, *Tetrahedron Lett.* **2000**, *41*, 3107–3111; i) K. Manabe, Y. Mori, T. Wakabayashi, S. Nagayama, S. Kobayashi, *J. Am. Chem. Soc.* **2000**, *122*, 7202–7207.

[3] Ph_2BOH can be easily prepared from its ethanolamine ester, see: G. E. Coates, J. G. Livingstone, *J. Chem. Soc.* **1961**, 4909–4911.

[4] Ph_2BOH was used for the generation of a boron enolate from ethoxyacetylene, see: M. Murakami, T. Mukaiyama, *Chem. Lett.* **1982**, 241–244.

[5] Anionic surfactants are effective, see the Supporting Information.

[6] When a Lewis acid (for example, $Sc(O_3SOC_{12}H_{25})_3$) was used in water, the diastereoselectivity was *syn*/*anti* = 49/51 (substrates: aldehyde **4** and silyl enolate **2**), see: refs. [2a,i].

[7] Diarylborinic acids with electron-withdrawing substituents at their aryl groups are known to function as Lewis acids for Mukaiyama aldol reactions in dichloromethane, see: K. Ishihara, H. Kurihara, H. Yamamoto, *Synlett* **1997**, 597–599.

[8] The examples of catalytic use of metals for generating metal enolates from silyl enolates in stereoselective aldol reactions have been reported, see: a) G. A. Slough, R. G. Bergman, C. H. Heathcock, *J. Am. Chem. Soc.* **1989**, *111*, 938–949; b) M. Sodeoka, K. Ohrai, M. Shibasaki, *J. Org. Chem.* **1995**, *60*, 2648–2649; c) J. Krüger, E. M. Carreira, *J. Am. Chem. Soc.* **1998**, *120*, 837–838; d) O. Fujimura, *J. Am. Chem. Soc.* **1998**, *120*, 10032–10039.

[9] Y. Li, M. N. Paddon-Row, K. N. Houk, *J. Org. Chem.* **1990**, *55*, 481–493.

[10] The examples of the generation of boron enolates from silyl enolates using stoichiometric amounts of boron sources in organic solvents have been reported, see: a) I. Kuwajima, M. Kato, A. Mori, *Tetrahedron Lett.* **1980**, *21*, 4291–4294; b) M. Wada, *Chem. Lett.* **1981**, 153–156.

[11] Various Brønsted acids are effective, see the Supporting Information.

[12] The reaction also showed first-order dependence with respect to the catalyst combination (**1**-SDS-$PhCO_2H$ (1:1:0.1)), see the Supporting Information.

CH/π Attraction: The Origin of Enantioselectivity in Transfer Hydrogenation of Aromatic Carbonyl Compounds Catalyzed by Chiral η^6-Arene-Ruthenium(II) Complexes**

Masashi Yamakawa, Issaku Yamada, and Ryoji Noyori*

In asymmetric catalysis using chiral transition metal complexes, metal ligands generally affect the stability of stereodetermining transition states (TSs) by exerting electronic influences on metallic centers and also by through-space interactions with the assembled substrates. In our enantioselective asymmetric transfer hydrogenation of aryl alkyl ketones[1–3] or [1-^{2}H]benzaldehydes[4] by using 2-propanol or formic acid, we intuitively selected $Ru^{II}(\eta^6$-arene) catalysts that possess a chiral 2-amino alcohol or related auxiliary. A theoretical study has now revealed that the enantioselectivity originates not only from the chiral geometry of the five-membered chelate ring but also from the CH/π attractive interaction[5] between the η^6-arene ligand and the carbonyl aryl substituent, instead of conventional nonbonded repulsion. This TS stabilization is reminiscent of the origin of *endo* selectivity in the Diels–Alder reaction that is based on an attractive secondary interaction between nonreacting sites.[6]

A combined system of [RuCl{(*R*,*R*)-YCH(C_6H_5)CH(C_6H_5)NH_2}(η^6-arene)] (Y = O or NTs) and an alkaline base in 2-propanol catalyzes transfer hydrogenation of aromatic ketones or aldehydes to give the corresponding *R* alcohols with fair to excellent enantiomeric purity.[1–4] The real reducing complex is [RuH{(*R*,*R*)-YCH(C_6H_5)CH(C_6H_5)NH_2}(η^6-arene)].[2c, 7, 8] The general stereochemical outcome[1–4] prompted us to study the TS structures by hybrid density functional theory-based (DFT) calculations.[9, 10]

Transfer hydrogenation of carbonyl substrates with **1** occurs by a novel metal–ligand bifunctional catalysis[1, 2c, 7, 8] (Scheme 1). The hydridic Ru–H and protic N–H_{ax} in the 18e complex **1** are transferred simultaneously to the C=O bond in **2** to form the 16e complex **3** and alcohol **4**. The process is reversible. The chiral complex (*R*,*R*)-**1** reacts with **2** preferentially via "proximal" TS *Si*-**5** instead of "distal" *Re*-**5**, giving *R*-enriched **4**. The calculation for the reaction of (*R*,*R*)-**1** (η^6-arene = C_6H_6) and benzaldehyde at the RMP2/BS-II//B3LYP/LANL2DZ level[10] indicated that 1) the hydrogen

[*] Prof. Dr. R. Noyori, Dr. I. Yamada
Department of Chemistry and Research Center for Materials Science
Nagoya University, Chikusa, Nagoya 464-8602 (Japan)
Fax: (+81) 52-783-4177
E-mail: noyori@chem3.chem.nagoya-u.ac.jp
Prof. M. Yamakawa
Kinjo Gakuin University
Omori, Moriyama, Nagoya 463-8521 (Japan)
Fax: (+81) 52-798-0370

[**] This work was financially supported by a Grant-in-Aid for Scientific Research (No. 07CE2004) from the Ministry of Education, Culture, Sports, Science, and Technology, Japan.

Supporting information for this article is available on the WWW under http://www.angewandte.com or from the author.

  1433-7851/01/4015-2818 $ 17.50+.50/0

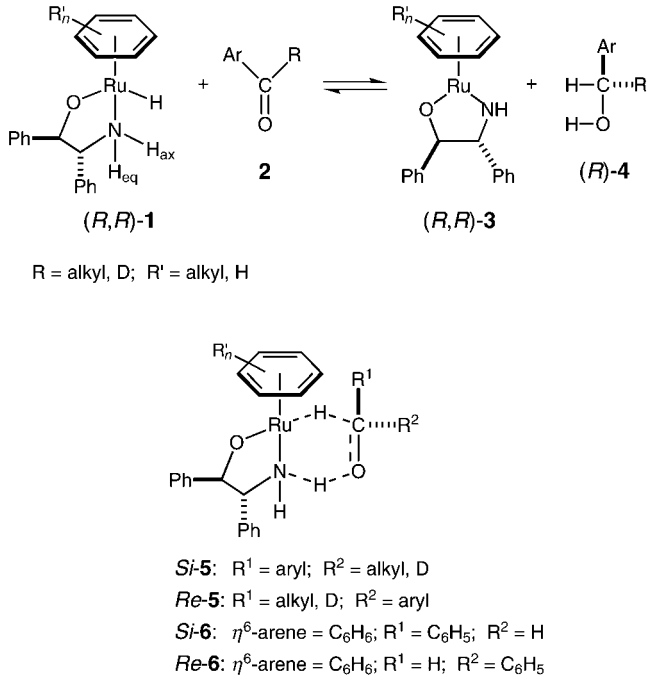

Scheme 1. Asymmetric hydrogen transfer via a metal–ligand bifunctional mechanism.

transfer, which gives (*R*,*R*)-**3** and benzyl alcohol, occurs via a hydrogen-bonded intermediate[7] with an endothermicity of 14.5 kJ mol^{-1}, while dehydrogenation of 2-propanol with (*R*,*R*)-**3** is exothermic by 9.1 kJ mol^{-1}; 2) the spatially congested TS, *Si*-**6**, is more stable than the uncrowded TS, *Re*-**6**, by 8.6 kJ mol^{-1} (E_a = 47.8 versus 56.4 kJ mol^{-1}); 3) the 5/6-fused bicyclic core structures of *Si*-**6** and *Re*-**6** are geometrically very similar; 4) in both TSs, no aggravating steric effects arise from the two phenyl rings in the N,O-chelate ligand, the shortest H···H distance in the less stable *Re*-**6** being 2.620 Å (much longer than the sum of the van der Waals radii, 2.4 Å); and 5) the more stable *Si*-**6** contains a short interatomic distance (2.993 Å) between a η^6-benzene C*H* and a phenyl C(sp^2) atom (Figure 1).

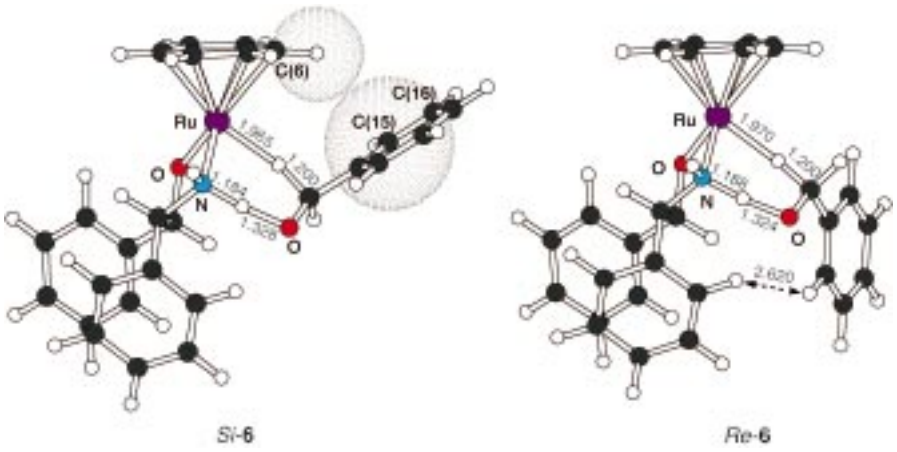

Figure 1. Diastereomeric transition structures, *Si*-**6** (favored) and *Re*-**6** (less favored). The geometries were optimized at the B3LYP/LANL2DZ level. *Si*-**6**: C(6)H···C(15) 2.993 Å, C(6)H···C(16) 3.372 Å; Ru-H-C 152.0°, N-H-O 167.4°, RuH-C-O 109.8°, H-Ru-N-HO 12.0°. *Re*-**6**: Ru-H-C 148.7°, N-H-O 167.6°, RuH-C-O 110.0°, H-Ru-N-HO 15.0°. The bond lengths are given in Å. The dotted surfaces indicate the van der Waals radii of the atoms.

To fully elucidate the origin of the preference for the more crowded TS, we performed the more reliable calculation by using [RuH(OCH$_2$CH$_2$NH$_2$)(η^6-C$_6$H$_6$)] (**7**) and the higher

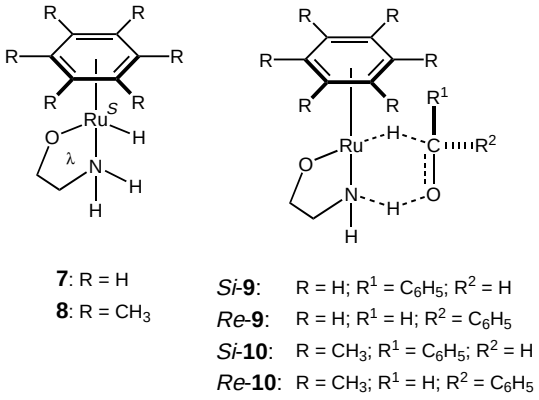

quality basis sets (RMP2/BS-III//B3LYP/BS-I). This model, like the real system (*R*,*R*)-**1** (η^6-arene = C$_6$H$_6$), possesses a λ conformation for the chiral N,O-chelate ring and an *S* configuration at the Ru stereogenic center. This result is consistent with the above energy profile. The reaction of **7** and benzaldehyde to give the 16e Ru amide complex and benzyl alcohol takes place with an endothermicity of 20.8 kJ mol^{-1}, whereas regeneration of **7** by 2-propanol is exothermic by 18.3 kJ mol^{-1}. In the aldehyde reduction, the proximal TS, *Si*-**9**, is favored over the distal isomer, *Re*-**9**, by 12.3 kJ mol^{-1} (E_a = 40.1 versus 52.4 kJ mol^{-1}) (see Supporting Information for details). Most significantly, *Si*-**9** is more stabilized by the CH/π attraction between the η^6-benzene and the phenyl substituent (Figure 2a). The C(6)H···C(15) distance in *Si*-**9**, 2.860 Å, is close to the sum of the van der Waals radii, 2.9 Å. In fact, C(6)H with a significant positive natural population analysis (NPA) charge interacts with highly negative C(15) and C(16) by means of largely electrostatic and slight covalent attractions, with Mulliken bond populations of +0.0080 and +0.0040, respectively. The C(sp^2)H/π attraction between the two aromatic rings becomes conspicuous with the through-bond linkage of the Ru···H···C moiety, and this feature is distinct from the conventional T-shaped interaction.[5] The C*H* donating property of benzene is greatly enhanced upon metal complexation;[11] in going from free benzene to *Si*-**9**, the positive charge of C(sp^2)H increases from +0.235 au to +0.267–0.278 au, or even to +0.286 au at C(6)H. In contrast, the hydride approach to the carbonyl carbon atom in benzaldehyde reverses the relative charge distribution at the *ortho*/*para* versus *meta* positions, resulting in an increase in the C*H*-accepting ability at the *ortho* and *para* carbon atoms. In particular, the negative charges at the interacting C(15) (−0.245 au) is much larger than in free

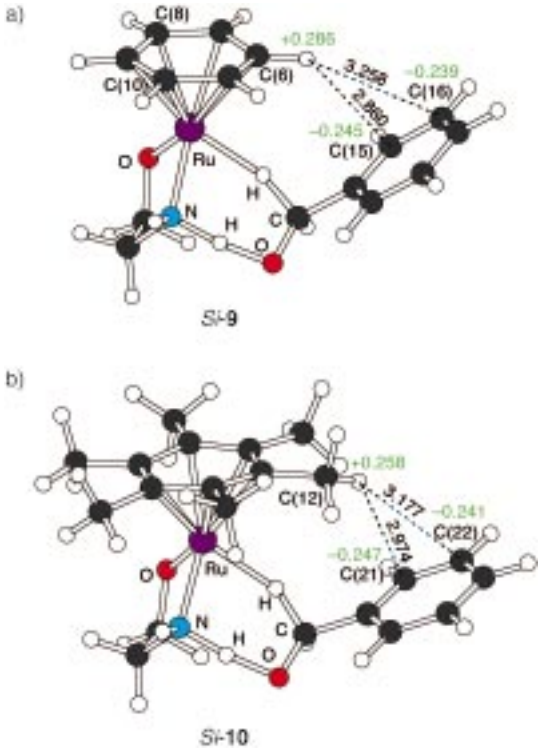

Figure 2. CH/π attractive interaction between the η^6-arene ligand and phenyl group in a) *Si*-**9** and b) *Si*-**10**. The geometries were optimized at the B3LYP/BS-I level. *Si*-**9**: Ru-H 1.990 Å, RuH-C 1.204 Å, O-H 1.269 Å, N-HO 1.217 Å, N-Ru 2.090 Å; Ru-H-C 152.5°, N-H-O 168.0°, RuH-C-O 110.4°, H-Ru-N-HO 13.9°. *Si*-**10**: Ru-H 2.010 Å, RuH-C 1.200 Å, O-H 1.289 Å, N-HO 1.204 Å, N-Ru 2.095 Å; Ru-H-C 153.4°, N-H-O 168.0°, RuH-C-O 110.8°, H-Ru-N-HO 11.0°. The interatomic distances are shown by dashed lines (Å) and the NPA charges (au) are given in green.

benzaldehyde (−0.195), whereas C(16) is inherently electron-rich (−0.239 in *Si*-**9** versus −0.236 in benzaldehyde). The RMP2/BS-I optimizations have led to the same conclusion, suggesting a greater CH/π interaction with a very short C(6)H···C(15) distance, 2.609 Å (see Supporting Information).

This mechanism uniformly explains the role of aryl substituents in asymmetric reactions of aromatic aldehydes and ketones[1–4] catalyzed by **1** and its analogues. The reaction of aliphatic aldehydes in 2-propanol is much less enantioselective.[4] Electron-donating substituents in [1-^{2}H]benzaldehyde tend to increase the enantioselectivity owing to the greater secondary interaction caused by the higher CH-accepting ability of the π-electron-rich aromatic ring, whereas electron-withdrawing groups lower the enantioselectivity.[4] The *ee* value of the *R* product in the reaction of substituted [1-^{2}H]benzaldehydes with (*R*,*R*)-**1** (arene = C_6H_6) decreases from 61% for the *p*-CH_3O derivative to 45% for the parent benzaldehyde and to 20% for the *p*-CF_3 compound.[4, 12] The reaction of 4-cyano-4′-methoxybenzophenone, a skeletally symmetrical but electronically unsymmetrical diaryl ketone, in the presence of (*R*,*R*)-**1** (arene = C_6H_6; 0.025 M 2-propanol solution, ketone/RuCl precursor/*t*BuOK 50:1:2, 20 °C, 12 h) gives *p*-cyano-*p*′-methoxybenzhydrol in an *R*/*S* ratio of 67:33 (100% conversion) as a result of the greater η^6-benzene/*p*-methoxyphenyl CH/π interaction.

The rate and stereoselectivity are influenced by the electronic and steric properties of alkyl groups in the η^6-arene ligand. Because both *Si*-**9** and *Re*-**9** possess smaller negative NPA charges at C(6), C(8), and C(10) (−0.218, −0.196, and −0.227 au, respectively, for *Si*-**9** (Figure 2a)) in comparison to other carbon atoms (−0.258 to −0.278 au), electron-donating alkyl groups at such positions stabilize the TSs. Despite the presence of six methyl groups, the Ru complex **8** is predicted to reduce benzaldehyde with a lower activation energy (28.5 versus 40.1 kJ mol^{-1}) than and with a similar endothermicity (17.6 versus 20.8 kJ mol^{-1}) to **7**. The TS for dehydrogenation of 2-propanol is also more stabilized with the hexamethylbenzene complex (28.6 versus 33.6 kJ mol^{-1}). Furthermore, the aldehyde reduction with **8** proceeds preferentially via TS *Si*-**10** (Figure 2b), giving the same sense of asymmetric induction as with **7**. The C(sp^3)H/π attractions[13] stabilize the sterically congested *Si*-TS more than the uncrowded isomer by 7.0 kJ mol^{-1} (E_a = 28.5 versus 35.5 kJ mol^{-1}), although the presence of methyl groups distorts the core six-membered geometry considerably from that of nonmethylated *Si*-**9**.[13] In *Si*-**10**, the atomic distances between C(12)H and C(21) and C(22) in the aldehyde phenyl are 2.974 and 3.177 Å, respectively. The attraction reflects the distinct positive NPA charge at C(12)H (+0.258 au; free hexamethylbenzene +0.237 to +0.239 au) and the large negative charges at C(21) (−0.247 au) and C(22) (−0.241 au). In agreement with such calculations, the catalytic reduction of [1-^{2}H]benzaldehyde with (*R*,*R*)-**1** (arene = $C_6(CH_3)_6$) in 2-propanol takes place 3.4 times faster than the reaction with (*R*,*R*)-**1** (arene = C_6H_6) and gives (*R*)-[1-^{2}H]-benzyl alcohol with somewhat lower *ee* (32% versus 45%).[12]

Organometallic chemistry often utilizes arene ligands. The two- to six-electron donors affect the electronic properties of the metallic center and also exert steric influences on neighboring ligands.[14] Here we show previously unrecognized effects of arene ligands. Thus in some cases[1–3] (though not always), ring alkylation can facilitate reactions and also generate a larger asymmetric bias through enhanced electron donation and/or attractive secondary interaction, only if other perturbations remain similar. This possibility is in contrast to the long-held view that ring alkylation decelerates reactions but increases stereoselectivity through the enhanced nonbonded repulsion. In fact, the η^6-*p*-cymene, -mesitylene, or -hexamethylbenzene ligands are superior to η^6-benzene in asymmetric reactions of certain aromatic ketones.[1–3] This study not only explains a range of experimental findings with Ru^{II}-catalyzed asymmetric transfer hydrogenation but also encourages a reconsideration of the origin of selectivity and reactivity observed in many other reactions promoted by transition metal–arene/cyclopentadienyl complexes.[15, 16]

Calculation Method

The Gaussian 98 program[9] was used for all calculations. All geometries of **1**, **3** (η^6-arene = C_6H_6), and TSs **6** were fully optimized by the Becke's three-parameter hybrid density functional method[10] using the LANL2DZ basis set (B3LYP/LANL2DZ). The structures of TSs **9** and **10** as well as the equilibrium structures **7** and **8** were optimized by the B3LYP level using the decontracted LANL2DZ basis set for Ru and the 6-31G(d) basis sets for other atoms (B3LYP/BS-I). The vibrational frequencies and zero-point

  1433-7851/01/4015-2820 $ 17.50+.50/0 *Angew. Chem. Int. Ed.* **2001**, *40*, No. 15

energy (ZPE) were also calculated. The ground states and TSs were determined by the number of imaginary frequencies. The energies of **1**, **3** (η^6-arene = C_6H_6), and TSs **6** were obtained by the single-point calculations of the second-order Møller-Plesset method using the decontracted LANL2DZ basis set with an f-polarization function ($\alpha = 1.235$)[17] for Ru, 6-311 + G(d) for the phenyl groups, and 6-311 + + G(d,p) for other atoms (RMP2/BS-II). Energies of the other compounds were obtained by single-point calculations of the RMP2 method using the same basis set as BS-II for Ru and 6-311 + + G(d,p) for remaining atoms (RMP2/BS-III). Relative energies were corrected with unscaled ZPE. NPA[18] was carried out at the B3LYP/BS-I level. The Mulliken bond population was calculated by the restricted Hartree–Fock (RHF/BS-I) procedure using the geometries obtained by B3LYP/BS-I.

Received: August 9, 2000
Revised: May 29, 2001 [Z15610]

[1] a) R. Noyori, S. Hashiguchi, *Acc. Chem. Res.* **1997**, *30*, 97–102; b) M. J. Palmer, M. Wills, *Tetrahedron: Asymmetry* **1999**, *10*, 2045–2061.

[2] a) S. Hashiguchi, A. Fujii, T. Takehara, T. Ikariya, R. Noyori, *J. Am. Chem. Soc.* **1995**, *117*, 7562–7563; b) A. Fujii, S. Hashiguchi, N. Uematsu, T. Ikariya, R. Noyori, *J. Am. Chem. Soc.* **1996**, *118*, 2521–2522; c) K.-J. Haack, S. Hashiguchi, A. Fujii, T. Ikariya, R. Noyori, *Angew. Chem.* **1997**, *109*, 297–300; *Angew. Chem. Int. Ed. Engl.* **1997**, *36*, 285–288; d) S. Hashiguchi, A. Fujii, K.-J. Haack, K. Matsumura, T. Ikariya, R. Noyori, *Angew. Chem.* **1997**, *109*, 300–303; *Angew. Chem. Int. Ed. Engl.* **1997**, *36*, 288–290; e) K. Matsumura, S. Hashiguchi, T. Ikariya, R. Noyori, *J. Am. Chem. Soc.* **1997**, *119*, 8738–8739.

[3] J. Takehara, S. Hashiguchi, A. Fujii, S. Inoue, T. Ikariya, R. Noyori, *Chem. Commun.* **1996**, 233–234.

[4] I. Yamada, R. Noyori, *Org. Lett.* **2000**, *2*, 3425–3427.

[5] a) M. Nishio, M. Hirota, Y. Umezawa in *The CH/π Interaction: Evidence, Nature, and Consequences* (Ed.: A. P. Marchand), Wiley-VCH, Weinheim, **1998**, chap. 2, pp. 11–45; b) Y. Umezawa, S. Tsuboyama, H. Takahashi, J. Uzawa, M. Nishio, *Tetrahedron* **1999**, *55*, 10047–10056; c) J. H. Williams, *Acc. Chem. Res.* **1993**, *26*, 593–598; d) P. Hobza, H. L. Selzle, E. W. Schlag, *J. Am. Chem. Soc.* **1994**, *116*, 3500–3506; e) S. V. Lindeman, D. Kosynkin, J. K. Kochi, *J. Am. Chem. Soc.* **1998**, *120*, 13268–13269, and references therein.

[6] R. B. Woodward, R. Hoffmann, *Angew. Chem.* **1969**, *81*, 797–869; *Angew. Chem. Int. Ed. Engl.* **1969**, *8*, 781–853.

[7] M. Yamakawa, H. Ito, R. Noyori, *J. Am. Chem. Soc.* **2000**, *122*, 1466–1478.

[8] D. A. Alonso, P. Brandt, S. J. M. Nordin, P. G. Andersson, *J. Am. Chem. Soc.* **1999**, *121*, 9580–9588.

[9] Gaussian 98 (Revision A.6), M. J. Frisch, G. W. Trucks, H. B. Schlegel, G. E. Scuseria, M. A. Robb, J. R. Cheeseman, V. G. Zakrzewski, J. A. Montgomery, Jr., R. E. Stratmann, J. C. Burant, S. Dapprich, J. M. Millam, A. D. Daniels, K. N. Kudin, M. C. Strain, O. Farkas, J. Tomasi, V. Barone, M. Cossi, R. Cammi, B. Mennucci, C. Pomelli, C. Adamo, S. Clifford, J. Ochterski, G. A. Petersson, P. Y. Ayala, Q. Cui, K. Morokuma, D. K. Malick, A. D. Rabuck, K. Raghavachari, J. B. Foresman, J. Cioslowski, J. V. Ortiz, B. B. Stefanov, G. Liu, A. Liashenko, P. Piskorz, I. Komaromi, R. Gomperts, R. L. Martin, D. J. Fox, T. Keith, M. A. Al-Laham, C. Y. Peng, A. Nanayakkara, C. Gonzalez, M. Challacombe, P. M. W. Gill, B. G. Johnson, W. Chen, M. W. Wong, J. L. Andres, C. Gonzalez M. Head-Gordon, E. S. Replogle, J. A. Pople, Gaussian, Inc., Pittsburgh, PA, **1998**..

[10] a) C. Lee, W. Yang, R. G. Parr, *Phys. Rev. B* **1988**, *37*, 785–789; b) A. D. Becke, *J. Chem. Phys.* **1993**, *98*, 5648–5652.

[11] M. F. Semmelhack, *Ann. N.Y. Acad. Sci.* **1977**, *295*, 36–51.

[12] The reaction of these substrates catalyzed by [RuH{(*R*,*R*)-NTsCH(C_6H_5)CH(C_6H_5)NH_2}(η^6-C_6H_6)] affords the *R* alcohols with 99, 97, and 96% *ee*, respectively.[4] The enhanced enantioselectivity is a result of an additional *N*-Ts/η^6-arene nonbonded interaction that destabilizes the *Re*-TS to some extent. Unlike in the reaction catalyzed by **1**, replacement of the C_6H_6 ligand by $C_6(CH_3)_6$ lowers the reaction rate.

[13] a) Y. Kodama, K. Nishihata, M. Nishio, N. Nakagawa, *Tetrahedron Lett.* **1977**, *24*, 2105–2108; b) P. J. Breen, J. A. Warren, E. R. Bernstein, J. I. Seeman, *J. Am. Chem. Soc.* **1987**, *109*, 3453–3455; c) Y. Nakai, K. Inoue, G. Yamamoto, M. Oki, *Bull. Chem. Soc. Jpn.* **1989**, *62*, 2923–2931; d) J. E. Anderson, V. Bru-Capdeville, P. A. Kirsch, J. S. Lomas, *J. Chem. Soc. Chem. Commun.* **1994**, 1077–1078.

[14] a) W. E. Silverhorn, *Adv. Organomet. Chem.*, **1975**, *13*, 47–137; b) E. L. Muetterties, J. R. Bleeke, E. J. Wucherer, T. A. Albright, *Chem. Rev.* **1982**, *82*, 499–525.

[15] a) K. Mashima, T. Abe, K. Tani, *Chem. Lett.* **1998**, 1199–1200; b) K. Murata, T. Ikariya, R. Noyori, *J. Org. Chem.* **1999**, *64*, 2186–2187; c) J. Mao, D. C. Baker, *Org. Lett.* **1999**, *1*, 841–843.

[16] Related phenomena: a) H. Brunner, *Angew. Chem.* **1983**, *95*, 921–931; *Angew. Chem. Int. Ed. Engl.* **1983**, *22*, 897–907; b) R. W. Quan, Z. Li, E. N. Jacobsen, *J. Am. Chem. Soc.* **1996**, *118*, 8156–8157; c) J. A. Gladysz, B. J. Boone, *Angew. Chem.* **1997**, *109*, 566–602; *Angew. Chem. Int. Ed. Engl.* **1997**, *36*, 550–583; d) E. P. Kündig, C. M. Saudan, G. Bernardinelli, *Angew. Chem.* **1999**, *111*, 1298–1301; *Angew. Chem. Int. Ed.* **1999**, *38*, 1220–1223.

[17] A. W. Ehlers, M. Böhme, S. Dapprich, A. Gobbi, A. Höllwarth, V. Jonas, K. F. Köhler, R. Stegmann, A. Veldkamp, G. Frenking, *Chem. Phys. Lett.* **1993**, *208*, 111–114.

[18] a) E. D. Glendening, A. E. Reed, J. E. Carpenter, F. Weinhold, NBO, version 3.1, Gaussian, Inc., Pittsburgh, PA, **1998**.

Architecture of Polymeric Superstructures: Self-Color Tone Films Constructed by Mesoscopically Ordered Cubic Lattices

Koji Ishizu,* Susumu Shiratori,* and Takafumi Hosokawa*

It is well known that submicron-sized colloidal spheres form a body-centered cubic (BCC) or face-centered cubic (FCC) lattice in aqueous solution.[1] Ascher et al.[2] have developed an approach to permanently lock the ordering of a crystalline colloidal array in a hydrogel matrix. We have also constructed polymeric superstructures by the free-radical polymerization of *N*-vinylpyrrolidone (VP) monomer after polypyrrole microspheres had become arranged into a BCC lattice in a solution of the VP monomer.[3] More recently, we demonstrated that core–shell polymer microspheres[4] and highly branched star polymers[5] led to a hierarchical structural transformation of the cubic lattices. That is, these radially branched polymers formed a lattice with a BCC structure near the overlap threshold (*C**, concentration where the coils begin to become densely packed). This structure changed to a FCC lattice in the bulk region of the films. After these branched polymers had formed a cubic lattice in polymerizable vinyl monomer, the polymeric superstructures were locked permanently into an ordered lattice in a solid matrix by means of free-radical polymerization.[6] This technique is one of the best methods for creating nanoscopic polymeric superstructures composed of two or three phase-separated

[*] Prof. Dr. K. Ishizu, S. Shiratori, T. Hosokawa
Department of Organic Materials and Macromolecules
Tokyo Institute of Technology
2-12-1, Ookayama, Meguro-ku, Tokyo 152-8552 (Japan)
Fax: (+81) 3-5734-2888
E-mail: kishizu@polymer.titech.ac.jp

  1433-7851/01/4015-2821 $ 17.50+.50/0

microdomains. However, the microspheres, which had relatively large particle diameters, were packed in an irregular arrangement as a result of polymerization-induced phase separation. Herein we report the architecture of films of polymeric superstructures, especially of self-color tone films (developed color films without some kinds of color formers), formed by the locking of a polymer matrix through graft polymerization of photofunctional core–shell polymer microspheres.

The construction of the polymeric superstructures (three phase-separated microdomains) is illustrated in Scheme 1. The well-defined polystyrene-block-poly(4-vinylpyridine) (PS-block-P4VP) diblock copolymers (SV1: $\bar{M}_n = 18.6 \times 10^4$, P4VP block 30 mol% and SV2: $\bar{M}_n = 8.5 \times 10^4$, P4VP block 43 mol%) were prepared by a sequential anionic polymerization technique. The details concerning the synthesis and characterization of diblock copolymers have been given elsewhere.[7] Figure 1a and 1b show the transmission electron microscopy (TEM) photographs of SV1 cast from chloroform/toluene (1/3, v/v) and SV2 cast from chloroform/dioxane (6/4, v/v), respectively. The dark portions are the P4VP phases selectively stained with OsO_4. The morphological structures of the SV1 and SV2 specimens showed dispersed P4VP spheres in a PS matrix and alternating P4VP/PS lamellae, respectively. The periodic distance of the lamellae for SV2 was 92 nm (PS lamella: 41 nm; P4VP lamella: 51 nm).

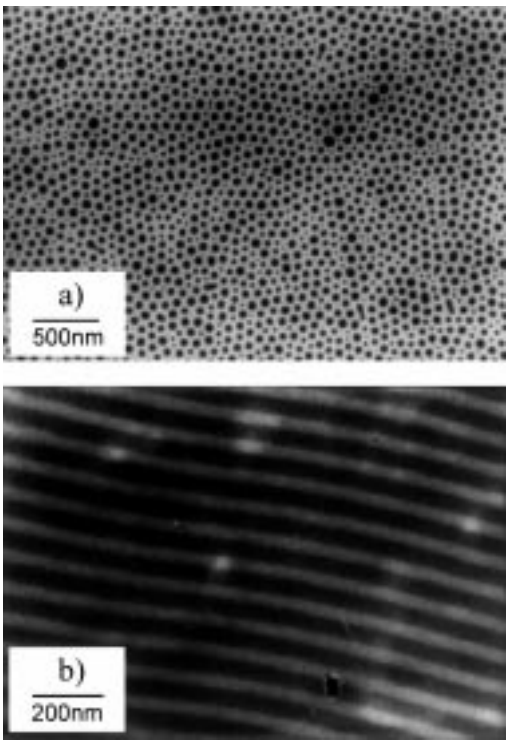

Figure 1. TEM photographs of PS-block-P4VP diblock copolymer films: a) SV1 cast from chloroform/toluene (1/3, v/v); b) SV2 cast from chloroform/dioxane (6/4, v/v).

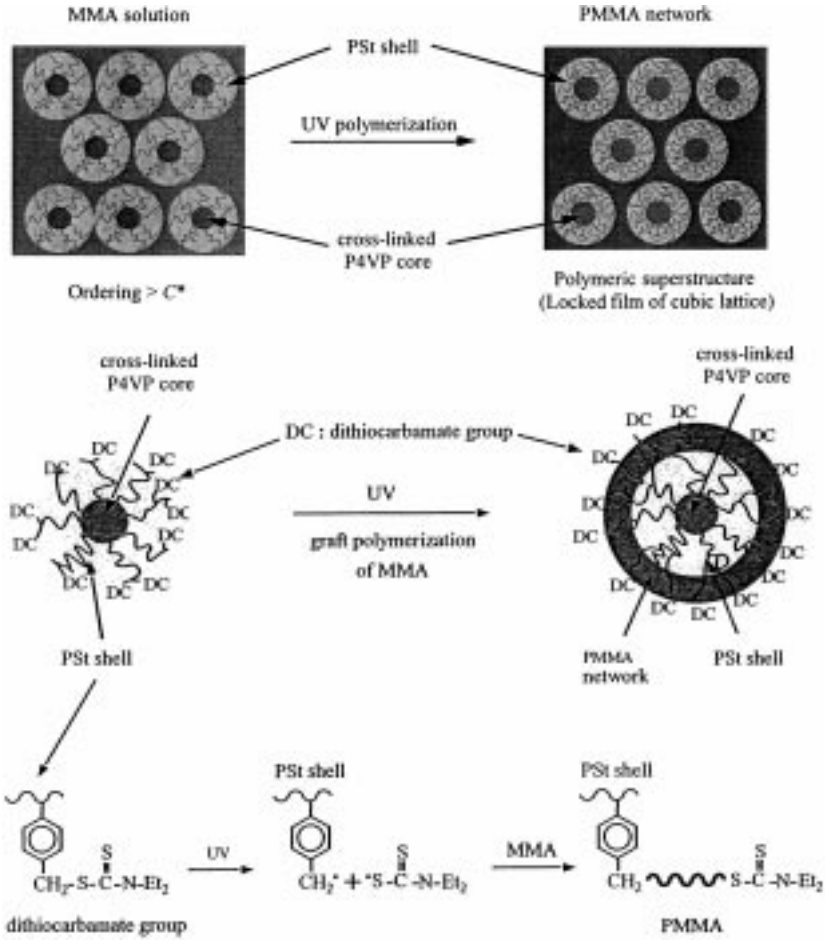

Scheme 1. Illustration of the polymeric superstructures and the reaction scheme locking the nanoscopic cubic lattices.

The core–shell polymer microspheres (SV-M) were synthesized by cross-linking the segregated chains in the spherical microdomains of P4VP with 1,4-dibromobutane (DBB) vapor at room temperature. The details concerning the synthesis and characterization of such microspheres have been given previously.[8] Characteristics of the SV1-M microsphere are listed in Table 1. The cross-link density of the P4VP cores was 19.4 mol%. A TEM photograph of SV1-M microspheres cast from benzene showed the same texture as the SV1 diblock copolymer. The average diameter (D_c) of the cross-linked P4VP cores, which had a narrow size distribution, was estimated to be 60.4 nm from a survey of 300 samples picked from the photographs obtained. It was shown previously by small-angle X-ray scattering (SAXS) measurements that the P4VP cores were packed in a FCC arrangement in a bulk film.[4] The hydrodynamic diameter ($D_H = 190$ nm) of the microspheres was determined by means of dynamic light scattering (DLS) measurements. The C^*[9] value of SV1-M in benzene was calculated from the D_H value and total molecular weight of the microsphere to be 6.52 wt%.

Photofunctional core–shell microspheres (SV1-MP) were prepared as follows. The PS shell of the parent microspheres was chloro-

  1433-7851/01/4015-2822 $ 17.50+.50/0

Table 1. Characteristics of core–shell microsphere SV1-M.

Code	$\bar{D}_c$ [nm][a]	$10^{-7}M_r$[b]	CD [mol %][c]	f[d]	$\bar{D}_H$ [nm][e]	C^* [wt %][f]
SV1-M 6.52	60.4	26.9	19.4	14	48	190

[a] Diameter of the P4VP cores as determined from the TEM photographs. [b] Total molecular weight of the microspheres were determined by static light scattering (SLS) measurements. [c] Cross-link density of the P4VP domains as determined by Volhard titration. [d] Branch number (aggregation number of diblock copolymers) as estimated from the M_r value of the microsphere and the M_n value of the branched block. [e] Hydrodynamic diameter of the microsphere as determined by dynamic light scattering (DLS) measurements in benzene. [f] Overlap threshold in benzene solution calculated from the D_H value.

methylated with chloromethyl methyl ether in the presence of a stannic chloride catalyst.[10] It is well known that the reaction of a chloromethyl group with diethyldithiocarbamic acid sodium salt quantitatively forms a dithiocarbamate (DC) group.[11] These microspheres (6 g) were treated with diethyldithiocarbamic acid sodium salt (1 g) in *N*,*N*-dimethylformamide/water (3/4, v/v) at room temperature for 8 h in a brown flask. The density of chloromethyl groups on the PS shell was determined to be 15 mol % by ^{1}H NMR spectroscopy ($CDCl_3$) from the integrated peak ratios at $\delta = 4.5$ (methylene protons of the *p*-chloromethyl groups) and $\delta = 6.5-7.4$ (aromatic protons of the PS shell). ^{1}H NMR spectroscopic analysis of the characteristic peak of the *N*-substituted methyl protons of DC groups at $\delta = 3.5$ showed that the photofunctional DC groups were introduced quantitatively to the PS shell portion under the reaction conditions used. Figure 2a shows a TEM photograph of SV1-MP cast from a 1.0 wt % benzene solution. This specimen corresponds to the restructured film from the core–shell microspheres. This photograph shows that dark cross-linked P4VP cores with a narrow size distribution are dispersed in a PS matrix.

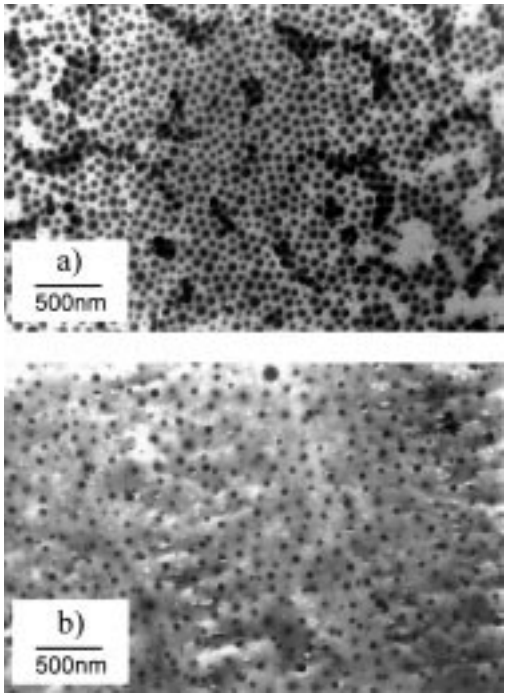

Figure 2. TEM photographs of a photofunctional core–shell polymer microsphere SV1-MP cast from 1.0 wt % benzene solution (a), and locking film MP-L (b).

The locking of the cubic lattice was performed as follows: a solution of SV1-MP microspheres (7 wt %) in methyl methacrylate (MMA; addition of ethylene glycol dimethacrylate as a cross-linker; 50 vol % for monomer) was sandwiched between two glass plates. Graft copolymerization of the photofunctional microspheres was carried out by UV irradiation (250-W high-pressure mercury lamp) in a nitrogen atmosphere at 20 °C for 5 h. SAXS measurements showed that the microspheres formed a lattice with a BCC structure near the C^* value of the MMA solution.[4] We obtained not only a transparent film but also a blue film (MP-L) by this procedure. An ultrathin film (80-nm thick) was prepared by cutting with a microtome (Reinhert–Nissei, Ultracut N) and stained with OsO_4 to obtain a two-dimensional picture of the packing structure of the microsphere in the composite films. Figure 2b shows a TEM photograph of the film specimen of MP-L after locking treatment. The dark portions correspond to cross-linked cores of P4VP stained with OsO_4. The white portions correspond to the PS and poly(methyl methacrylate) (PMMA) network. This texture indicates that cross-linked cores of P4VP are locked in a state of molecular dispersion in a PMMA network, but that the two-dimensional long-range order is not perfectly maintained. The photofunctional microspheres in this system undergo graft polymerization radially to form three-component copolymers. Therefore, it seems that the microspheres are hard to move during network formation. The polymeric superstructure prepared by locking is composed of three phase-separated microdomains, namely, a cross-linked P4VP core, a PS shell, and the PMMA network. Each step of the preparation of polymeric superstructures is shown in Figure 3. Figures 3a and 3b show the photographs of a solution of microspheres in MMA (before locking treatment) and the locking transparent film MP-L, respectively. The solution of microspheres in MMA shows an emulsion tinged with blue. After locking treatment, polymeric superstructure MP-L exhibits a self-blue color tone.

Similar optical behavior was also observed in the diblock copolymer film SV2 which exhibits a lamellar morphology.[12] We cross-linked the segregated chains in the P4VP lamellar layers of the SV2 film with DBB vapor ($CD = 18$ mol %) and obtained a transparent film tinged with yellow. This cross-linked film was insoluble in organic solvents such as benzene and chloroform. We have discovered also that the swollen film exhibits various interference colors (the periodic distance of the lamellae is more than 100 nm; Figure 3c in benzene). It was mentioned earlier that the periodic distance of the lamellae was 92 nm in the solid state. The cross-linked P4VP phases were converted into hydrophilic phases by quaternization, which resulted in the PS lamellar layers swelling in benzene.

Polymeric superstructure films such as an ordered alloy diffract light and closely follows the Bragg diffraction equation [Eq. (1)]:

$$m\lambda = 2nd\sin\theta \quad (1)$$

where m is the order of diffraction, λ is the wavelength of incident light, n is the refractive index of the alloy, d is the

  1433-7851/01/4015-2823 $ 17.50+.50/0

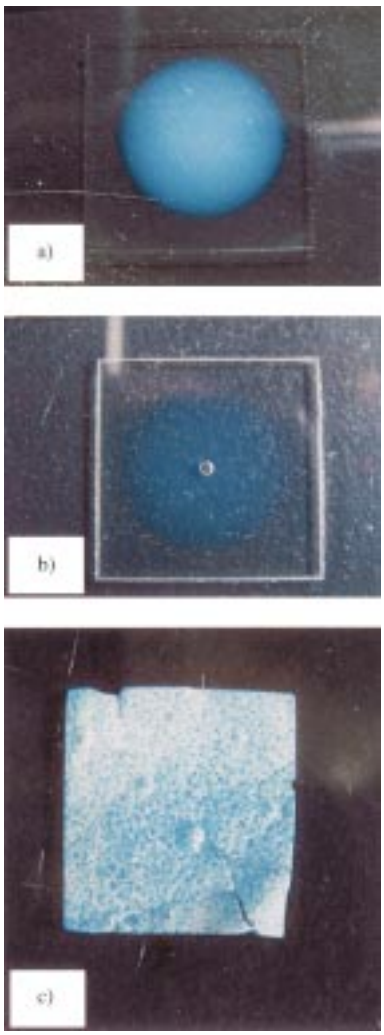

Figure 3. TEM photographs of a) a solution of the microspheres in MMA; b) locking film MP-L; c) a swollen film of cross-linked SV2 which exhibits a lamellar morphology in benzene.

interplanar spacing, and θ is the glancing angle between the incident light and the diffracting crystal planes. n is defined by Equation (2):

$$n = n_A\phi_A + n_B\phi_B + n_C\phi_C \quad (2)$$

where ϕ is the volume fraction of each component and subscripts A, B, and C indicate the three phase-separated components, namely, the P4VP core, PS shell, and PMMA matrix, respectively. The Bragg spacing d_1 is related to the cell edge a_c of the cubic lattice and the nearest neighbor distance (D_S) of the spheres [Eqs. (3), (4)]:

$$D_S = (\sqrt{3}/2)a_c = \left(\sqrt{3/2}\right)d_1 \quad \text{for BCC} \quad (3)$$

$$D_S = (1/\sqrt{2})a_c = \left(\sqrt{3/2}\right)d_1 \quad \text{for FCC} \quad (4)$$

The interplanar spacings of superstructures can be controlled by changing the monomer concentration and the type of cubic lattices. The work here demonstrates a method for preparing polymeric superstructures composed of nanoscopic cubic lattices. These materials can be used for light modulation in tunable diffracting and transmitting optical devices. We are investigating the diffraction behavior of the polymeric superstructure films with a near-IR spectrophotometer.

Received: March 8, 2001 [Z16732]

[1] R. Kesavamoothy, S. Tandon, S. Xu, S. Lagannathan, S. A. Asher, *J. Colloid Interface Sci.* **1992**, *153*, 188–198; D. J. W. Aastuen, N. A. Clark, L. K. Cotter, B. Ackerson, *Phys. Rev. Lett.* **1986**, *57*, 1733–1736; P. A. Hitner, Y. S. Papir, M. Krieger, *J. Phys. Chem.* **1971**, *75*, 1881–1886; Y. Monovoukas, A. P. Gast, *J. Colloid Interface Sci.* **1989**, *128*, 533–548; A. Kose, T. Osaki, Y. Kobayashi, K. Tokano, S. Hachisu, *J. Colloid Interface Sci.* **1973**, *44*, 330–338

[2] S. A. Asher, J. Holtz, L. Liu, Z. Wu, *J. Am. Chem. Soc.* **1994**, *116*, 4997–4998.

[3] K. Ishizu, K. Honda, *Polymer* **1997**, *38*, 689–693.

[4] K. Ishizu, *Prog. Polym. Sci.* **1998**, *23*, 1383–1408.

[5] K. Ishizu, T. Ono, S. Uchida, *J. Colloid Interface Sci.* **1997**, *192*, 189–193.

[6] K. Ishizu, T. Ikemoto, A. Ichimura, *Polymer* **1998**, *39*, 449–454; K. Ishizu, A. Ichimura, T. Ono, *Polymer* **1998**, *39*, 2579–2582.

[7] K. Ishizu, T. Fukutomi, *J. Polym. Sci. Polym. Chem. Ed.* **1988**, *26*, 281–286.

[8] K. Ishizu, *J. Colloid Interface Sci.* **1993**, *156*, 299–304.

[9] W. W. Glassley, *Adv. Polym. Sci.* **1974**, *16*, 1–179.

[10] G. D. Jones, *Ind. Eng. Chem.* **1952**, *44*, 2686–2692.

[11] M. Ookawara, T. Yamashina, K. Ishiyama, E. Imoto, *Kogyo Kagaku Zasshi* **1963**, *66*, 1383–1389.

[12] K. Ishizu, T. Hosokawa, K. Tsubaki, *Eur. Polym. J.* **2000**, *36*, 1333–1338.

Incorporation of Peptide Isosteres into Enantioselective Peptide-Based Catalysts as Mechanistic Probes**

Melissa M. Vasbinder, Elizabeth R. Jarvo, and Scott J. Miller*

The discovery of small-molecule mimics of enzymes has been a longstanding objective at the interface of bioorganic chemistry and organic synthesis.[1] We have been studying small peptide catalysts within this context because they offer great opportunities for structural variation (i.e., diversity).[2, 3] Furthermore, they offer a direct analogy to enzymes because such catalysts are composed entirely of the same fundamental building blocks, amino acid subunits. As such, we have been interested in determining the mechanistic basis for the enantioselectivities that such catalysts afford.[4, 5]

[*] Prof. S. J. Miller, M. M. Vasbinder, E. R. Jarvo
Department of Chemistry, Boston College
Chestnut Hill, MA 02467-3860 (USA)
Fax: (+1) 617-552-3620
E-mail: scott.miller.1@bc.edu

[**] This research is supported by the U.S. National Science Foundation (CHE-9874963). We are also grateful to the U.S. NIH (GM-57595), DuPont, Eli Lilly, Glaxo–Wellcome, and Merck for research support. S.J.M. is a Fellow of the Alfred P. Sloan Foundation, a Cottrell Scholar of Research Corporation, and a Camille Dreyfus Teacher-Scholar.

Supporting information for this article is available on the WWW under http://www.angewandte.com or from the author.

  1433-7851/01/4015-2824 $ 17.50+.50/0

In particular, we have found that substantial selectivity factors (k_{rel} values) can be obtained for the kinetic resolution of substrates such as **1** (Scheme 1).[6, 7] Tetrapeptide **2** catalyzes the kinetic resolution with a k_{rel} value of 28; octapeptide catalyst **3** accomplishes this resolution with $k_{rel} > 50$. The resolutions are more effective with substrates like **1**, which contain an acetamide functional group, than with unfunctionalized substrates.[2] Furthermore, previously reported kinetic studies have revealed (for catalyst **3**) that the reaction appears to be first order in both substrate **1** and catalyst **3**. Given the role of the substrate amide, and the stereochemical identity of the fast and slow reacting enantiomers, we sought to develop a structural model that would account for the sense and degree of enantiospecificity observed with each catalyst.

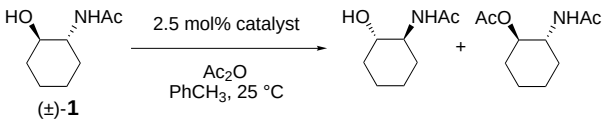

Scheme 1. Kinetic resolution of **1**.

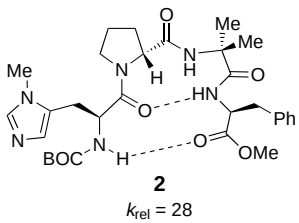

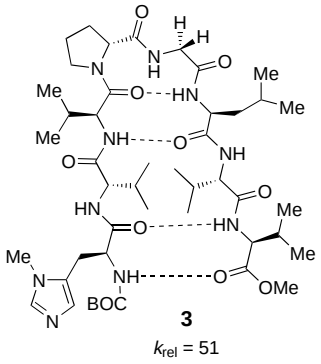

The development of our mechanistic model began with a determination of the solution conformation of catalyst **2**. Two-dimensional NMR spectroscopic techniques (COSY, ROESY), in combination with solvent titrations of the peptide hydrogen bonding network,[8] revealed that peptide **2** possesses the two intramolecular hydrogen bonds illustrated in Figure 1. Furthermore, the Aib N–H (Aib = α-amino isobutyric acid) and the prolyl C_α-H atoms exhibit a significant NOE (Figure 1).[9] The kinetic resolution of **1** with catalyst **2** leads to a situation where (*R*,*R*)-**1** is the fast reacting enantiomer.[10] Such enantiospecificity is consistent with a transition state that could involve the two-point contact shown in structure **TS2-(*R*,*R*)**. It is plausible that the first contact involves the hydroxy group of **1** attacking the acyl imidazolium ion;[11] the second could involve a hydrogen bond between the substrate and the D-Pro-Aib amide group that serves as the hydrogen bond donor. Consistent with transition state stabilization, reactions of the functionalized substrates (e.g. **1**) are substantially faster than those that lack secondary amides. Furthermore, (*S*,*S*)-**1** cannot readily achieve an analogous two-point contact without a conformational change in either the substrate, catalyst, or both species (cf. **TS2-(*S*,*S*)**).

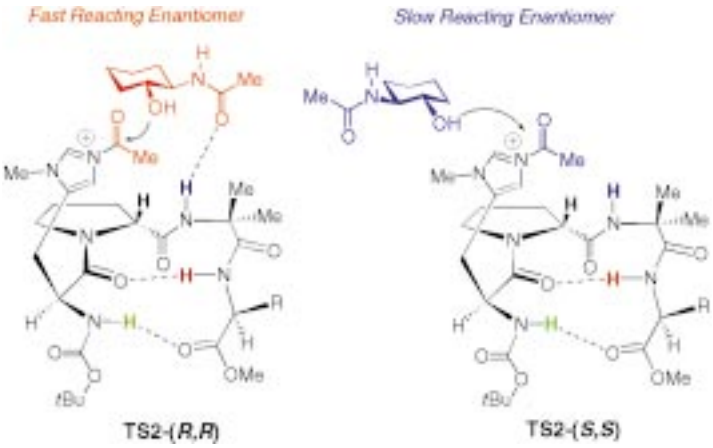

We required an experiment to test this hypothesis. One possibility that seemed to offer an unambiguous interpretation involved the synthesis and evaluation of so-called olefin isosteres.[12] Such compounds are important in the peptidomimetic arena owing to their propensity to adopt conformations that can be nearly superimposable on their parent peptide. The key advantages of olefin isosteres as mechanistic probes are the potentially identical conformations, but total absence of the polar amide functional group that could participate in a key intermolecular interaction with substrate. Compound **4**[13] thus emerged as a potential mechanistic probe for the behavior of **2**.

With catalyst **4** in hand, we set out to establish that its conformation is similar to peptide **2**. The same NMR spectroscopic experiments that had been applied to **2** were carried out with **4**, and indeed the ground-state solution conformations appear similar (Figure 2). The D-Pro C_α-H exhibits a substantial NOE interaction with the alkene proton of **4** that is analogous to the Aib-NH of **2**. Furthermore, titrations of the hydrogen bonding network suggest that both the BOC-NH (BOC = *tert*-butoxycarbonyl) and the Phe-NH (Phe = phenylalanine) hydrogen atoms are involved in intramolecular hydrogen bonds.[14]

Most notable is the performance of isostere **4** in kinetic resolutions in comparison with peptide **2**. Whereas peptide **2** effects kinetic resolution with a k_{rel} value of 28, isostere **4** provides no enantioselectivity

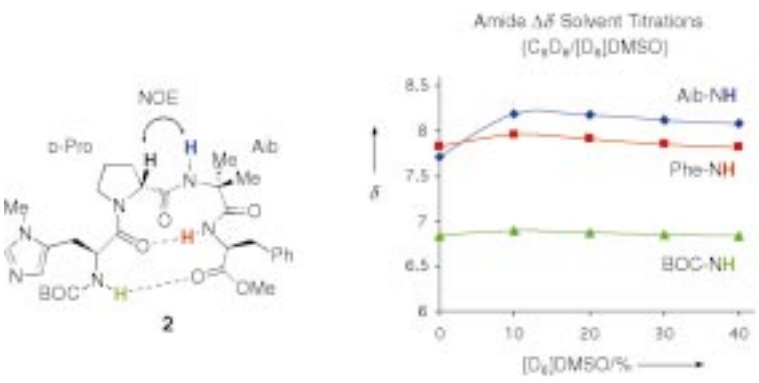

Figure 1. ^{1}H NMR data for peptide **2**.

  1433-7851/01/4015-2825 $ 17.50+.50/0

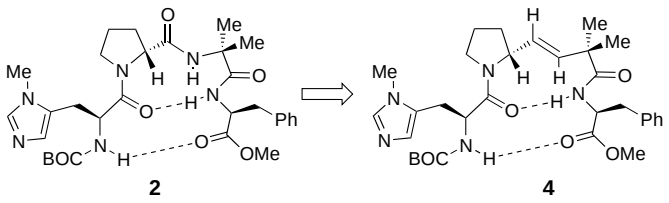

Scheme 2. Compound **4**, a potential mechanistic probe for the behavior of **2**.

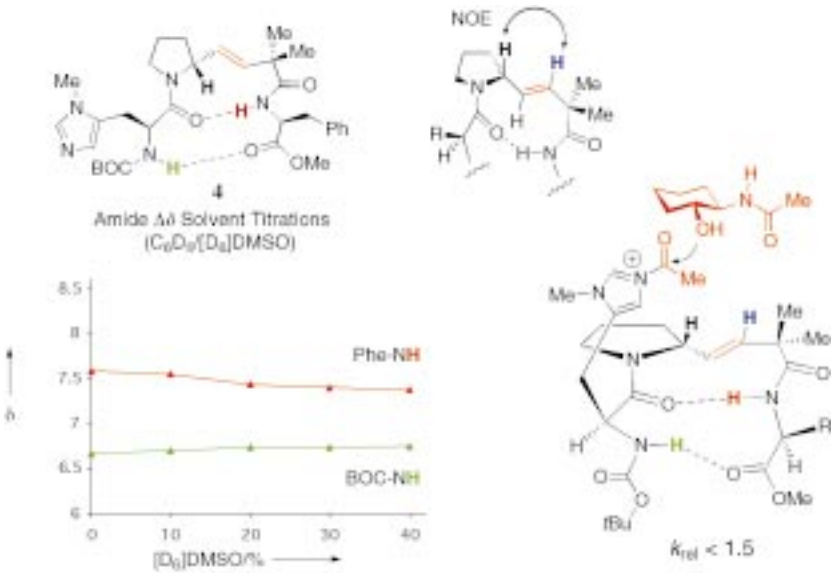

Figure 2. ^{1}H NMR data for peptide **4**.

($k_{rel} < 1.5$), despite possessing a very similar conformation. Catalyst **4** also mediates a much slower reaction relative to that catalyzed by **2**. This observation is consistent with a critical role for the D-Pro-Aib amide of peptide **2**.

We wished to show that these results were not specific to substrate **1** (Table 1). Peptide **2** provides a k_{rel} value of 17 and 6 for the seven- (**10**) and five-membered (**11**) homologs of **1**, respectively. Isostere **4** is completely ineffective in terms of asymmetric induction with these other substrates ($k_{rel} < 1.5$), demonstrating that the D-Pro-Aib amide is critical for these substrates as well.

With some evidence supporting the pivotal role of the prolyl amide for the asymmetric catalysis achieved with tetrapeptide **2**, we then turned our attention to the octapeptide **3**. Octapeptides are substantially more complicated than tetrapeptides; the derivation of a structural hypothesis for enantioselectivity is therefore more difficult. Nevertheless, as shown in Scheme 3, we were once again intrigued by the potential role of the prolyl (D-Pro-Aib) amide in orchestrating the observed enantiospecificity. Although this site is more remote from the nucleophilic histidine residue at the N-terminus, it appeared from molecular models that the distance between the two functional groups could actually be optimal. Isostere **12** is thus an appropriate catalyst to test this hypothesis.

The synthesis of octapeptide isostere **12** is analogous to that of tetrapeptide **4** (see Supporting Information). Preliminary ^{1}H NMR spectroscopic experiments were conducted with catalysts **3** and **12**, and the results point to similar conformations. Both catalysts afford well-defined ^{1}H NMR spectra in homogeneous $CDCl_3$ solution. Peptides **3** and **12** also afford NOE signals and amide NH titration data that are consistent with a Type II′ conformation at the turn of the corresponding β-hairpins.[15–17]

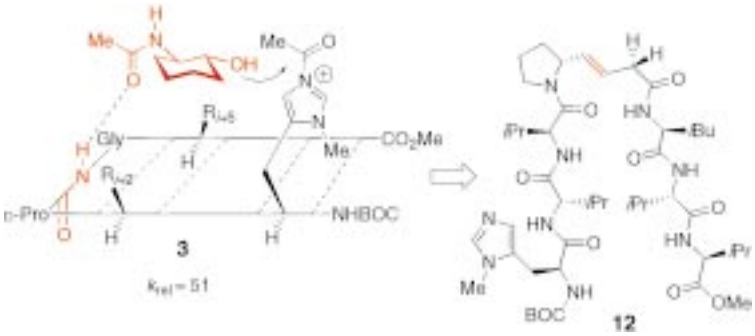

Scheme 3. Potential interaction of **1** with octapeptide **3**. Isostere **12** is an appropriate model to study the role of the prolyl amide.

Table 1. Selectivities for various substrates in kinetic resolutions with peptide catalysts.[a]

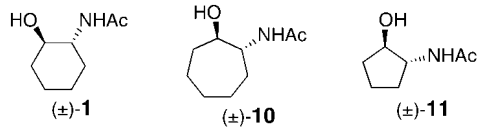

Entry	Catalyst	Racemic substrate	Conversion	$k(R,R)/k(S,S)$
1	**2**	**1**	49%	28
2	**2**	**10**	51%	17
3	**2**	**11**	56%	6
4	**4**	**1**	50%	< 1.5
5	**4**	**10**	52%	< 1.5
6	**4**	**11**	50%	< 1.5

[a] The reactions were conducted with 1–2 mol% catalyst (5.9 mM in substrate, toluene solvent) at 25 °C. Conversions and enantioselectivities were measured by chiral GLC (Chiraldex GTA).

The comparison of peptide **3** and isostere **12** in a catalytic setting provides a striking result. Whereas replacement of the prolyl amide with an apolar alkene in the tetrapeptide series (**2** → **4**) eradicates enantioselectivity, suggesting the site of a key catalyst–substrate contact, in the octapeptide series (**3** → **12**) the two catalysts afford nearly identical selectivity (Table 2). For the six-membered ring **1**, octapeptide **3** affords a k_{rel} value of 51 (Table 2, entry 1). With isostere **12**, the resolution proceeds with $k_{rel} = 50$ (Table 2, entry 4). These nearly identical results suggest that the two catalysts may share substantial mechanistic similarity with respect to the enantioselectivity-determining steps. Furthermore, these data strongly refute the proposition that the D-Pro-Gly amide group of **3** is a key transition state contact for the reaction of substrate **1**.

  1433-7851/01/4015-2826 $ 17.50+.50/0 *Angew. Chem. Int. Ed.* **2001**, *40*, No. 15

Table 2. Selectivities for various substrates in kinetic resolutions with peptide catalysts.[a]

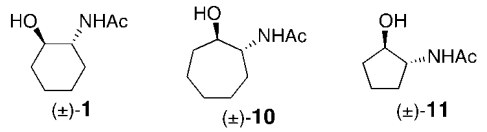

Entry	Catalyst	Racemic substrate	Conversion	$k(R,R)/k(S,S)$
1	**3**	**1**	50%	51
2	**3**	**10**	45%	15
3	**3**	**11**	49%	27
4	**12**	**1**	53%	50
5	**12**	**10**	47%	31
6	**12**	**11**	53%	26

[a] The reactions were conducted with 1–2 mol% catalyst (5.9 mM in substrate, toluene solvent) at 25 °C. Conversions and enantioselectivities were measured by chiral GLC (Chiraldex GTA).

Once again, we found that these observations are mirrored with other substrates in this class (Table 2). Whereas catalyst **3** affords a $k_{rel} = 27$ for five-membered ring **11**, isostere **12** affords a nearly identical k_{rel} of 26 (Table 2, entries 3 and 6). For seven-membered ring **10**, catalyst **3** affords $k_{rel} = 15$; isostere **12** is actually more selective for this substrate, affording $k_{rel} = 31$ (Table 2, entries 2 and 5). These results underscore both the functional similarity of octapeptide **3** and isostere **12**, and the greater complexity in analyzing the octapeptide system. If there is a unique contact between the amides of substrates such as **1** and peptide **3**, it appears not to be at the D-Pro-Gly linkage.

In summary, we report an approach to probing the mechanisms by which peptide-based enantioselective catalysts function. Relying on conformational analogies between such catalysts and their derived alkene isosteres, we have uncovered a specific, kinetically significant amide in a tetrapeptide system. Applying the same approach to a highly selective octapeptide system, we have excluded the central amide of a β-hairpin as the kinetically significant binding site. Additional studies along these lines should provide further mechanistic insight into the inner workings of peptide-based catalysts and, potentially, their more complex enzymatic counterparts.

Received: March 21, 2001 [Z16818]

[1] a) R. Breslow, *Acc. Chem. Res.* **1995**, *28*, 146; b) Y. Murakami, J. Kikuchi, Y. Hiseada, O. Hayashida, *Chem. Rev.* **1996**, *96*, 721.

[2] a) E. R. Jarvo, G. T. Copeland, N. Papaioannou, P. J. Bonitatebus, S. J. Miller, *J. Am. Chem. Soc.* **1999**, *121*, 11638; b) G. T. Copeland, S. J. Miller, *J. Am. Chem. Soc.* **1999**, *121*, 4306.

[3] For other enantioselective catalysts that rely exclusively on peptide, or peptide-like functionality, see: a) M. S. Sigman, E. N. Jacobsen, *J. Am. Chem. Soc.* **1998**, *120*, 4901, and references therein; b) for a representative approach that involves a de novo designed protein, see: K. S. Broo, L. Brive, P. Ahlberg, L. Baltzer, *J. Am. Chem. Soc.* **1997**, *119*, 11362.

[4] C.-H. Wong, G. M. Whitesides, *Enzymes in Synthetic Organic Chemistry*, Elsevier, Oxford, **1994**, chap. 2.

[5] a) S. H. Gellman, *Curr. Opin. Chem. Biol.* **1998**, *2*, 717; b) W. F. DeGrado, C. M. Summa, V. Pavone, F. Nastri, A. Lombardi, *Annu. Rev. Biochem.* **1999**, *68*, 779.

[6] For reviews of catalytic kinetic resolution, see: a) J. M. Keith, J. F. Larrow, E. N. Jacobsen, *Adv. Synth. Catal.* **2001**, *343*, 5; b) A. H. Hoveyda, M. T. Didiuk, *Curr. Org. Chem.* **1998**, *2*, 537.

[7] For other representative nonenzymatic catalysts that effect kinetic resolution of racemic alcohols, see: a) G. C. Fu, *Acc. Chem. Res.* **2000**, *33*, 412; b) E. Vedejs, O. Daugulis, *J. Am. Chem. Soc.* **1999**, *121*, 5813; c) A. C. Spivey, T. Fekner, S. E. Spey, *J. Org. Chem.* **2000**, *65*, 3154; d) T. Kawabata, M. Nagato, K. Takasu, K. Fuji, *J. Am. Chem. Soc.* **1997**, *119*, 3169.

[8] Chemical shifts of solvent-exposed amide protons migrate significantly downfield with increasing concentrations of DMSO, while those involved in intramolecular hydrogen bonds do not. See: a) Y. V. Venkatachalapathi, B. V. Venkataram Prasad, P. Balaram, *Biochemistry* **1982**, *21*, 5502; b) Y. V. Venkatachalapathi, P. Balaram, *Biopolymers* **1981**, *20*, 625.

[9] G. T. Copeland, E. R. Jarvo, S. J. Miller, *J. Org. Chem.* **1998**, *63*, 6784.

[10] Assigned according to the method of Jacobsen: S. E. Schaus, J. F. Larrow, E. N. Jacobsen, *J. Org. Chem.* **1997**, *62*, 4197.

[11] Nucleophilic versus general base catalysis with alkylimidazoles has been a subject of debate. We have adopted the nucleophilic paradigm for this analysis. a) E. Guibe-Jampel, G. Bram, M. Vilkas, *Bull. Soc. Chim. Fr.* **1973**, 1021; b) G. Höfle, W. Steglich, H. Vorbrüggen, *Angew. Chem.* **1978**, *90*, 602; *Angew. Chem. Int. Ed. Engl.* **1978**, *17*, 569; c) N. K. Pandit, K. A. Connors, *J. Pharm. Sci.* **1982**, *71*, 485.

[12] a) J. Gante, *Angew. Chem.* **1994**, *106*, 1780; *Angew. Chem. Int. Ed. Engl.* **1994**, *33*, 1699; b) R. R. Gardner, G.-B. Liang, S. H. Gellman, *J. Am. Chem. Soc.* **1995**, *117*, 3280; c) P. Wipf, T. C. Henninger, S. J. Geib, *J. Org. Chem.* **1998**, *63*, 6088.

[13] The synthesis of **4** is described in the Supporting Information.

[14] With increasing DMSO concentration, a minor amount of a second species appears in solution. As DMSO is removed in vacuo, the species disappears.

[15] For several examples of the conformational influence of L-Pro versus D-Pro residues that favor the adoption of β-hairpins, see: a) T. S. Haque, J. C. Little, S. H. Gellman, *J. Am. Chem. Soc.* **1996**, *118*, 6975; b) I. L. Karle, S. K. Awasthi, P. Balaram, *Proc. Natl. Acad. Sci. USA* **1996**, *93*, 8189; c) M. D. Struthers, R. P. Cheng, B. Imperiali, *Science* **1996**, *271*, 342.

[16] S. R. Raghothama, S. K. Awasti, P. Balaram, *J. Chem. Soc. Perkin Trans. 2* **1998**, 137.

[17] Details may be found in the Supporting Information.

Ion-Pair Recognition by Nucleoside Self-Assembly: Guanosine Hexadecamers Bind Cations and Anions**

Xiaodong Shi, James C. Fettinger, and Jeffery T. Davis*

Ion-pair recognition calls for receptors with separate cation and anion binding sites. Ditopic hosts typically have these discrete binding sites built into their covalent frameworks.[1, 2] A more efficient approach might be to use noncovalent interactions to build the ion-pair receptor from multiple components.[3] Below, we describe a prime example of how

[*] Prof. J. T. Davis, X. Shi, Dr. J. C. Fettinger
Department of Chemistry and Biochemistry
University of Maryland
College Park, MD 20742 (USA)
Fax: (+1) 301-314-9121
E-mail: jd140@umail.umd.edu.

[**] This research is sponsored by the Separations and Analysis program of the U.S. Department of Energy. J.D. thanks the Dreyfus Foundation for a Teacher-Scholar Award. We thank LaTarsha Riddick for help with experiments.

Supporting information for this article is available on the WWW under http://www.angewandte.com or from the author.

self-assembly provides a supramolecular complex with Lewis basic and Lewis acidic sites for the simultaneous binding of cations and anions. Hydrogen-bonding, ion-dipole, and base-stacking interactions provide a tubular complex with a cation-loaded interior. Meanwhile, an array of hydrogen-bond donors on the receptor's surface enables anion coordination. The ligands, cations, and anions all cooperate to control assembly of a 22-component complex.

The G-quartet is a macrocycle formed by hydrogen-bonded guanosine units (Scheme 1).[4, 5] Alkali metal cations template G-quartet formation from guanosine nucleotides in water,[6] and these cation-filled G-quartets stack to give octamers, dodecamers, hexadecamers, and higher aggregates.[7, 8] Gottarelli's group and our group have shown that lipophilic nucleosides also self-associate in nonpolar solvents.[9–11] While G-quartet formation is undoubtedly cation-dependent, Gottarelli and co-workers made the striking discovery that lipophilic guanosine analogues could coextract chiral anions from water into organic solvents with enantioselectivity.[12] This result implies that G-quartet aggregates (G-quadruplexes) might be able to recognize ion pairs in solution. In this paper, we use X-ray crystallography and NMR spectroscopy to obtain a clearer picture of how the nucleosides, cations, and anions are organized in a lipophilic G-quadruplex.[13] While the structure and dynamics of this model system are interesting, our main point is that self-assembly can provide selective ion-pair receptors.

We previously determined that the K^+, Pb^{2+}, and Ba^{2+} G-quadruplexes formed from G**1** and metal picrate salts are D_4-symmetric hexadecamers in the solid state.[11b, 9d,e] As illustrated for Ba^{2+} in Scheme 1, the Pb^{2+} and Ba^{2+} G-quadruplexes consist of two C_4-symmetric $(G\mathbf{1})_8 \cdot M^{2+}$ octamers. The G-quartets within each octamer are stacked head-to-tail,[14] with a 30° rotation between layers. The divalent cations, each interacting with eight nucleosides, are well separated from their picrate counterions (> 8.5 Å). These anions are not, however, uninvolved spectators. In the solid-state, the four picrate groups join the $G_8 \cdot M^{2+}$ octamers together by hydrogen bonding with the NH_B amino protons that project from the two "inner" G-quartets (bonding of one picrate anion is shown in Scheme 1). Overall, 16 nucleosides, 2 cations, and 4 anions form a complex that has dimensions of $25 \times 25 \times 30$ Å and a molecular weight greater than 7600 Da.

This study's major goal was to determine whether the lipophilic G-quadruplex maintains its coordination to the picrate anions in solution. Does this complex exist as a picrate-bound hexadecamer, $(G\mathbf{1})_{16} \cdot 2M^{2+} \cdot 4Pic^-$, in solution, or does it dissociate to give $(G\mathbf{1})_8 \cdot M^{2+} \cdot 2Pic^-$ octamers? It is a challenge to distinguish an octamer $(G\mathbf{1})_8 \cdot M^{2+}$ from a hexadecamer $(G\mathbf{1})_{16} \cdot 2M^{2+}$ by NMR spectroscopy. Both species have the same G**1** to picrate anion ratio, making determination of stoichiometry ambiguous. Also, the ^1H NMR spectra for a C_4-symmetric $(G\mathbf{1})_8 \cdot M^{2+}$ octamer and a D_4-symmetric $(G\mathbf{1})_{16} \cdot 2M^{2+}$ hexadecamer would be indistinguishable based on symmetry considerations.

Below, we demonstrate that the picrate-bound G-quadruplex is a hexadecamer in CD_2Cl_2 solution. Strong evidence for this structure comes from NMR cross-over experiments wherein G**1** and a 1:1 mixture of Sr^{2+} and Ba^{2+} picrate salts give a 1:1:2 statistical combination of three complexes: $(G\mathbf{1})_{16} \cdot 2Ba^{2+} \cdot 4Pic^-$, $(G\mathbf{1})_{16} \cdot 2Sr^{2+} \cdot 4Pic^-$, and the "mixed" hexadecamer $(G\mathbf{1})_8 \cdot Ba^{2+} \cdot (G\mathbf{1})_8 \cdot Sr^{2+} \cdot 4Pic^-$. Other NMR spectroscopy and circular dichroism (CD) data indicate that the picrate anions bind to the G-quadruplex in solution.

Before carrying out solution experiments, we first determined that the solid-state structure of $(G\mathbf{1})_{16} \cdot 2Sr^{2+} \cdot 4Pic^-$ is isomorphous with its Ba^{2+} analogue (see the Supporting Information).[15] The octacoordinate Sr^{2+} cations are located between G-quartet layers, and two $(G\mathbf{1})_8 \cdot Sr^{2+}$ octamers stack head-to-head to give the D_4-symmetric hexadecamer, $(G\mathbf{1})_{16} \cdot 2Sr^{2+} \cdot 4Pic^-$. The four picrate anions are hydrogen bonded to the exocyclic amines of the two "inner" G_4-quartets (in the same way as illustrated for Ba^{2+} in Scheme 1).

The picrate anions that clamp together the two "inner" G-quartets in the hexadecamer's crystal structure also associate with the G-quadruplex in solution. The CD spectrum obtained after dissolving $(G\mathbf{1})_{16} \cdot 2Ba^{2+} \cdot 4Pic^-$ in CD_2Cl_2 has a prominent Cotton band at 380 nm which corresponds to the absorbance signal of the picrate anion (Figure 1 A). This induced CD band indicates that the achiral picrate anions remain stereoselectively bound to the chiral G-quadruplex in CD_2Cl_2.[12, 16]

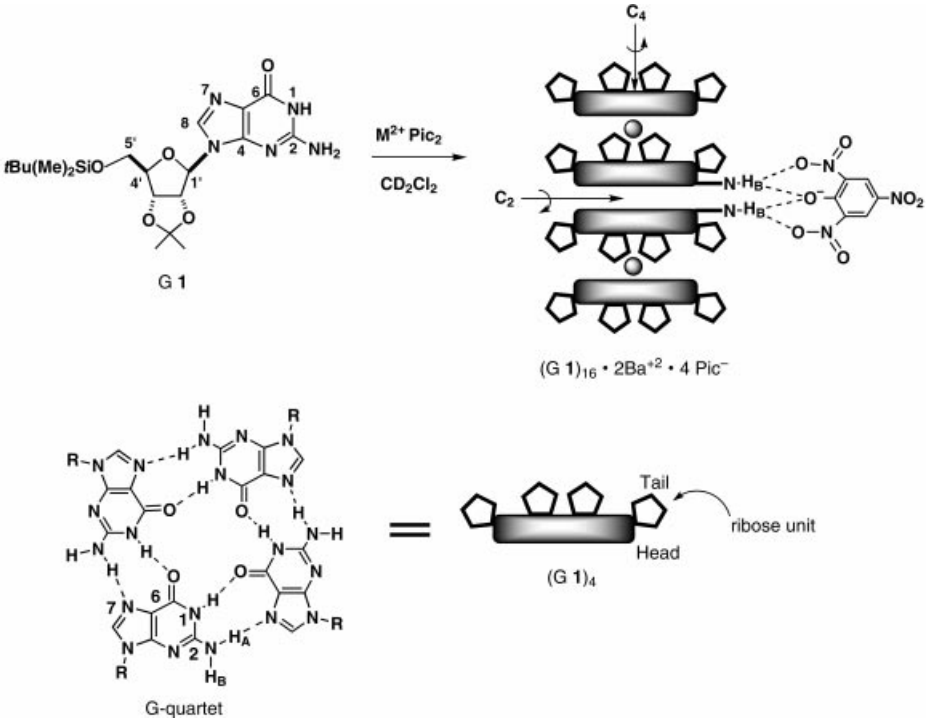

Scheme 1. A lipophilic G-quadruplex that binds ion pairs. Pic = picrate, R = 5′-silyl-2′,3′-isopropylidene-D-ribose.

  1433-7851/01/4015-2828 $ 17.50+.50/0 *Angew. Chem. Int. Ed.* **2001**, *40*, No. 15

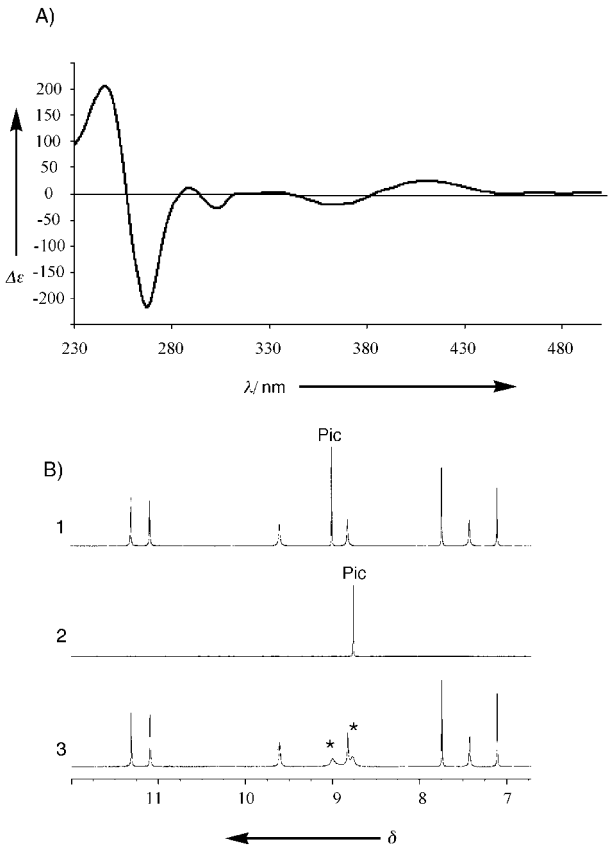

Figure 1. A) Circular dichroism spectra for $(G\mathbf{1})_{16}\cdot 2Ba^{2+}\cdot 4Pic^{-}$ (5.0×10^{-3} mM) in CH_2Cl_2 at 25 °C. The band at 256 nm corresponds to the G**1** chromophore while the induced band near 380 nm corresponds to the picrate anion. B) A region of the ^{1}H NMR spectra in CD_2Cl_2 at 25 °C and with a complex concentration of 0.6 mM for: 1) $(G\mathbf{1})_{16}\cdot 2Ba^{2+}\cdot 4Pic^{-}$, 2) [2.2.2]-cryptand$\cdot Ba^{2+}\cdot 2Pic^{-}$, and 3) a 1:1 mixture of $(G\mathbf{1})_{16}\cdot 2Ba^{2+}\cdot 4Pic^{-}$ and [2.2.2]-cryptand$\cdot Ba^{2+}\cdot 2Pic^{-}$. The asterisks identify the NMR signals which correspond to the two slowly exchanging picrate anions.

More evidence for G-quadruplex–picrate interactions in solution was obtained from ^{1}H NMR experiments. A mixture of the Ba^{2+} picrate G-quadruplex complex and [2.2.2]-cryptand/$BaPic_2$ in CD_2Cl_2 showed separate NMR signals for the picrate protons (Figure 1B). Since [2.2.2]-cryptand sequesters Ba^{2+},[17] the picrate anion should only be loosely coordinated, if at all, to the cryptate. The two different picrate proton NMR signals, marked with asterisks in spectrum 3 (Figure 1B), indicate that anion exchange between the Ba^{2+} G-quadruplex and the Ba^{2+} cryptate is slow on the chemical shift timescale, with millisecond lifetimes for the bound anion. The slow NMR exchange and the induced CD band confirm that the picrate anions remain intimately associated with the G-quadruplex in CD_2Cl_2 solution.[18]

The ^{1}H NMR data in Figure 2 show that the lipophilic G-quadruplexes are hexadecamers in solution. A water solution containing a 1:1 ratio of Ba^{2+} and Sr^{2+} picrates was stirred with a CD_2Cl_2 solution of G**1** (9.6 mM) for 24 hours. Lipophilic G**1** extracted picrate salts into CD_2Cl_2 to give a 1:1:2 ratio of three species: $(G\mathbf{1})_{16}\cdot 2Ba^{2+}\cdot 4Pic^{-}$, $(G\mathbf{1})_{16}\cdot 2Sr^{2+}\cdot 4Pic^{-}$, and a new complex with four sets of ^{1}H NMR spectroscopic signals. A D_4-symmetric hexadecamer, such as $(G\mathbf{1})_{16}\cdot 2Ba^{2+}\cdot 4Pic^{-}$ or $(G\mathbf{1})_{16}\cdot 2Sr^{2+}\cdot 4Pic^{-}$, has only two sets of NMR signals, one set for the two degenerate "inner" G_4-quartets and one set for the degenerate "outer" G_4-quartets. A lower-symmetry hexadecamer, such as $(G\mathbf{1})_8\cdot Ba^{2+}\cdot(G\mathbf{1})_8\cdot Sr^{2+}\cdot 4Pic^{-}$, should have four sets of NMR signals for its nonequivalent G-quartets. After the salt extraction (Figure 2C), signals are present for "inner" and "outer" H8 protons of $(G\mathbf{1})_{16}\cdot 2Ba^{2+}\cdot 4Pic^{-}$ and $(G\mathbf{1})_{16}\cdot 2Sr^{2+}\cdot 4Pic^{-}$. Importantly, signals of the appropriate intensity for two new "inner" and two new "outer" H8 protons are also present. These four new signals must arise from the mixed hexadecamer, $(G\mathbf{1})_8\cdot Ba^{2+}\cdot(G\mathbf{1})_8\cdot Sr^{2+}\cdot 4Pic^{-}$. Two of the new H8 proton signals belong to the Ba^{2+}-bound G-quartets, while the other new H8 proton resonances are due to the G-quartets that sandwich Sr^{2+}. Scheme 2 illustrates this process. This experiment, done under thermodynamic conditions,[19] indicates that these complexes are hexadecamers in CD_2Cl_2. If the aggregates were $G_8\cdot M^{2+}$ octamers, we would not observe diagnostic NMR spectroscopic signals for a mixed complex upon extraction of Ba^{2+} and Sr^{2+} picrates.

A different cross-over experiment in CD_2Cl_2 highlights the impressive kinetic stability of these guanosine hexadecamers. Crystalline $(G\mathbf{1})_{16}\cdot 2Sr^{2+}\cdot 4Pic^{-}$ and $(G\mathbf{1})_{16}\cdot 2Ba^{2+}\cdot 4Pic^{-}$ were combined to give a 1:1 mixture of the G-quadruplexes (0.6 mM) in CD_2Cl_2. An NMR spectroscopy stack plot shows slow formation ($t_{1/2}=42$ h) of the mixed hexadecamer $(G\mathbf{1})_8\cdot Ba^{2+}\cdot(G\mathbf{1})_8\cdot Sr^{2+}\cdot 4Pic^{-}$ (Figure 3). Again, a 1:1:2 statistical ratio of the three complexes was obtained at equilibrium.

While there are many possible mechanisms for ligand and cation exchange between $(G\mathbf{1})_{16}\cdot 2Ba^{2+}\cdot 4Pic^{-}$ and $(G\mathbf{1})_{16}\cdot 2Sr^{2+}\cdot 4Pic^{-}$, the slow equilibration illustrated in Figure 3 implies that the four picrate anions hold the G-quadruplex together tightly in solution. If bridging interactions between bound anions and the "inner" G-quartets are significant in

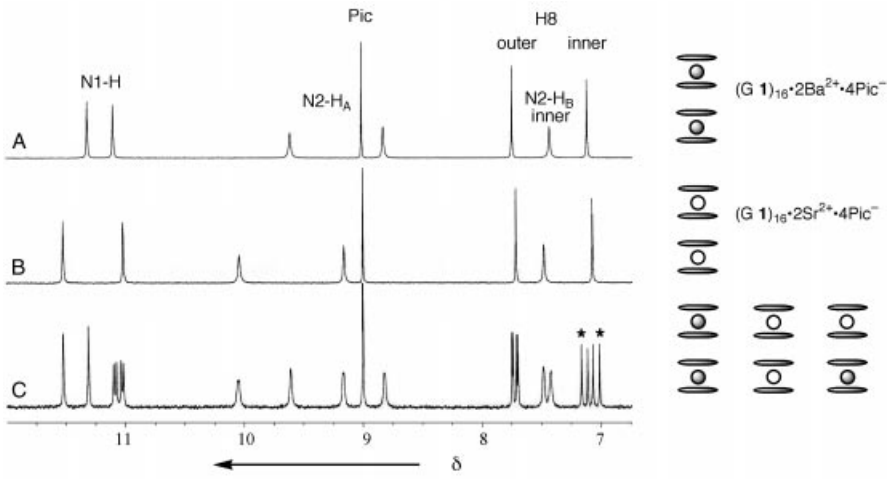

Figure 2. The "H8 region" of the ^{1}H NMR spectra: A) $(G\mathbf{1})_{16}\cdot 2Ba^{2+}\cdot 4Pic^{-}$, B) $(G\mathbf{1})_{16}\cdot 2Sr^{2+}\cdot 4Pic^{-}$, C) after stirring a CD_2Cl_2 solution of G**1** with an aqueous solution of a 1:1 mixture of Ba^{2+} and Sr^{2+} picrates for 24 h. Spectra were recorded for samples (0.6 mM) in CD_2Cl_2 at 25 °C. The "inner" H8 proton resonances for the mixed hexadecamer $(G\mathbf{1})_8\cdot Ba^{2+}\cdot(G\mathbf{1})_8\cdot Sr^{2+}\cdot 4Pic^{-}$ are identified by asterisks.

  1433-7851/01/4015-2829 $ 17.50+.50/0

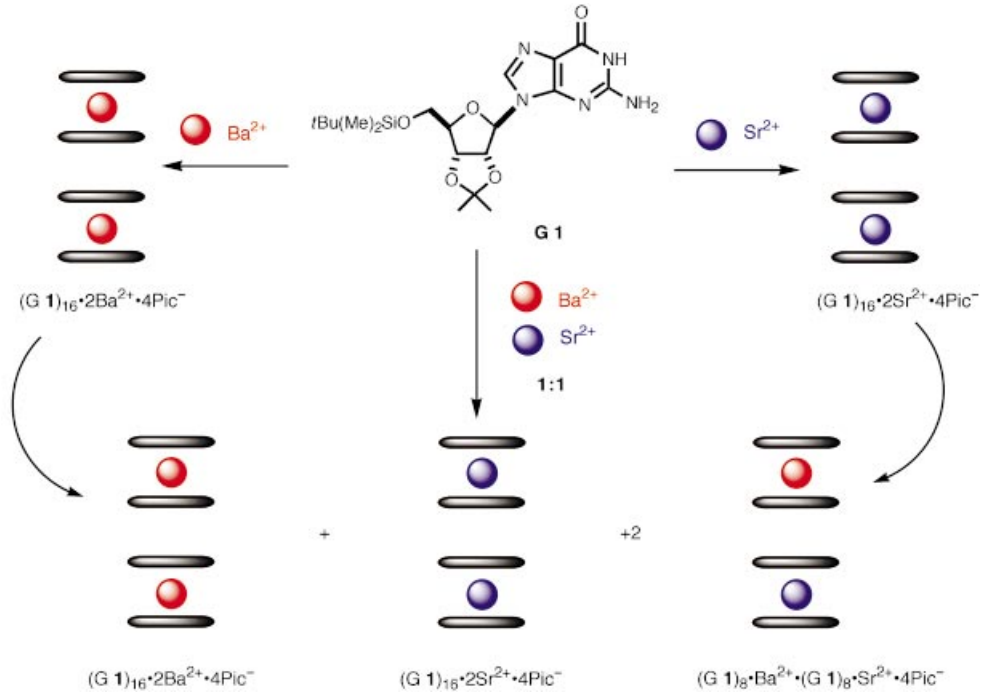

Scheme 2. Self-assembly of G**1** with Ba^{2+} and Sr^{2+} picrates gives a statistical mixture of hexadecameric G-quadruplexes.

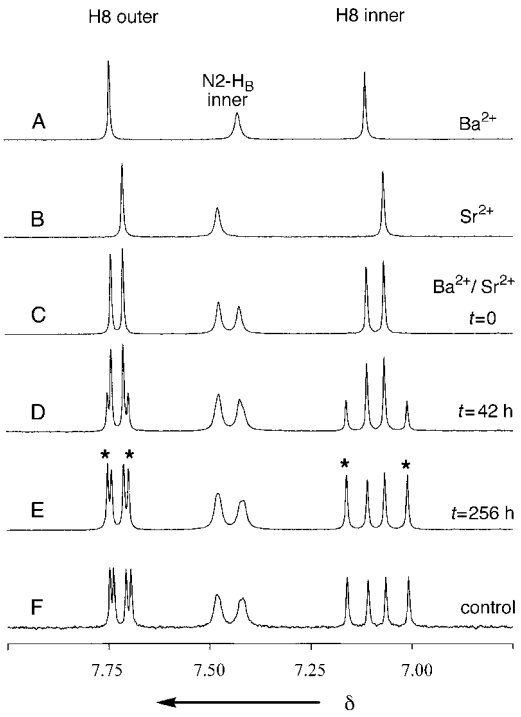

Figure 3. The "H8 region" of the ^{1}H NMR spectra for: A) $(G\mathbf{1})_{16}\cdot 2Ba^{2+}\cdot 4Pic^-$, B) $(G\mathbf{1})_{16}\cdot 2Sr^{2+}\cdot 4Pic^-$, C) a 1:1 mixture of $(G\mathbf{1})_{16}\cdot 2Ba^{2+}\cdot 4Pic^-$ and $(G\mathbf{1})_{16}\cdot 2Sr^{2+}\cdot 4Pic^-$ immediately after mixing, D) 42 h after mixing, E) 6 days after mixing, F) after stirring a CD_2Cl_2 solution of G**1** with an aqueous solution of a 1:1 mixture of Ba^{2+} and Sr^{2+} picrates for 24 h. Spectra were recorded for samples (0.6 mM) in CD_2Cl_2 at 25 °C. The H8 proton resonances for the mixed hexadecamer $(G\mathbf{1})_8\cdot Ba^{2+}\cdot(G\mathbf{1})_8\cdot Sr^{2+}\cdot 4Pic^-$ are identified by asterisks.

solution, then the anion's identity should modulate the hexadecamer's kinetic stability. Any change in the kinetic stability of the G-quadruplex due to the identity of the bound anion should be reflected in an altered formation rate for the mixed hexadecamer. Using thiocyanate, an anion that should not bridge $(G\mathbf{1})_8\cdot M^{2+}$ octamers as effectively as the picrate anion, we found that the anion can significantly affect the hexadecamer's kinetic stability. Thus, 1:1 mixtures of crystalline $(G\mathbf{1})_{16}\cdot 2Ba^{2+}\cdot 4(SCN^-)$ and $(G\mathbf{1})_{16}\cdot 2Sr^{2+}\cdot 4(SCN^-)$ also equilibrated to a statistical 1:1:2 ratio of complexes, but with a half-life of only $t_{1/2}=0.5$ h at room temperature in CD_2Cl_2. This equilibration rate for the thiocyanate complexes was approximately two orders of magnitude faster than that for the picrate complexes, $(G\mathbf{1})_{16}\cdot 2Ba^{2+}\cdot 4Pic^-$ and $(G\mathbf{1})_{16}\cdot 2Sr^{2+}\cdot 4Pic$. This result is consistent with the G-quadruplex having a stronger affinity for the picrate anion, as compared to the thiocyanate. Finally, the lipophilic G-quadruplex appears to be cooperative in its ion-pair binding. Extraction of a water solution containing 100 equivalents of KSCN and 1 equivalent of $Ba(Pic)_2$ with a CD_2Cl_2 solution of G**1** (10 mM) showed that only $(G\mathbf{1})_{16}\cdot 2Ba^{2+}\cdot 4Pic^-$ was formed in the organic phase. This self-assembled ion-pair receptor prefers to bind the divalent Ba^{2+} over the monovalent K^+ and the picrate anion over the thiocyanate.

While G-quartets are well-known cation receptors, our most significant finding in this paper is that the anion can also help control G-quadruplex structure and stability in solution. The lipophilic G**1** and divalent picrate salts form a guanosine hexadecamer in both the crystalline state and in CD_2Cl_2 solution. Self-assembly of monomeric ligands to give ditopic receptors with discrete cation and anion binding sites promises to be a fundamentally powerful approach for selective ion-pair recognition.

Received: March 26, 2001 [Z16845]

[1] Reviews: a) M. M. G. Antonisse, D. N. Reinhoudt, *Chem. Commun.* **1998**, 443–448; b) P. A. Gale, *Coord. Chem. Rev.* **1998**, *199*, 181–233.
[2] Recent ditopic receptors: a) N. Pelizzi, A. Casnati, A. Friggeri, R. Ungaro, *J. Chem. Soc. Perkin Trans. 2* **1998**, 1307–1311; b) S. Kubik, *J. Am. Chem. Soc.* **1999**, *121*, 5846–5855; c) M. J. Deetz, M. Shang, B. D. Smith, *J. Am. Chem. Soc.* **2000**, *122*, 6201–6207; d) L. A. J. Chrisstoffels, F. de Jong, D. N. Reinhoudt, S. Sivelli, L. Gazzola, A. Casnati, R. Ungaro, *J. Am. Chem. Soc.* **1999**, *121*, 10142–10151; e) J. B. Cooper, M. G. B. Drew, P. D. P. Beer, *J. Chem. Soc. Dalton Trans.* **2000**, 2721–2728.
[3] Supramolecular complexes that contain cations and anions: a) B. Hasenknopf, J.-M. Lehn, B. O. Kneisel, G. Baum, D. Fenske, *Angew. Chem.* **1996**, *108*, 1987–1990; *Angew. Chem. Int. Ed. Engl.* **1996**, *35*, 1838–1840; b) R. Vilar, D. M. P. Mingos, A. J. P. White, D. J. Williams, *Angew. Chem.* **1998**, *110*, 1323–1326; *Angew. Chem. Int. Ed.* **1998**, *37*,

  1433-7851/01/4015-2830 $ 17.50+.50/0

1258 – 1261; c) D. A. McMorran, P. J. Steel, *Angew. Chem.* **1998**, *110*, 3495 – 3497; *Angew. Chem. Int. Ed.* **1998**, *37*, 3295 – 3297; d) P. R. Ashton, S. J. Cantrill, J. A. Preece, J. F. Stoddart, Z. H. Wang, A. J. P. White, D. J. Williams, *Org. Lett*. **1999**, *1*, 1917 – 1920.

[4] M. Gellert, M. N. Lipsett, D. R. Davies, *Proc. Natl. Acad. Sci. USA* **1962**, *48*, 2013.

[5] W. Guschlbauer, J. F. Chantot, D. J. Thiele, *J. Biomol. Struct. Dyn.* **1990**, *8*, 491 – 511.

[6] T. J. Pinnavaia, C. L. Marshall, C. M. Mettler, E. D. Becker, *J. Am. Chem. Soc.* **1978**, *100*, 3625 – 3627.

[7] M. Borzo, C. Detellier, P. Laszlo, A. Paris, *J. Am. Chem. Soc.* **1980**, *102*, 1124 – 1134.

[8] E. Bouhoutsos-Brown, C. L. Marshall, T. J. Pinnavaia, *J. Am. Chem. Soc.* **1982**, *104*, 6576 – 6584.

[9] a) J. T. Davis, S. Tirumala, J. R. Jenssen, E. Radler, D. Fabris, *J. Org. Chem*. **1995**, *60*, 4167 – 4176; b) M. Cai, A. L. Marlow, J. C. Fettinger, D. Fabris, T. J. Haverlock, B. A. Moyer, J. T. Davis, *Angew. Chem.* **2000**, *112*, 1339 – 1341; *Angew. Chem. Int. Ed.* **2000**, *39*, 1283 – 1285; c) X. Shi, J. C. Fettinger, M. Cai, J. T. Davis, *Angew. Chem.* **2000**, *112*, 3254 – 3257; *Angew. Chem. Int. Ed.* **2000**, *39*, 3124 – 3127; d) F. W. Kotch, J. C. Fettinger, J. T. Davis, *Org. Lett.* **2000**, *2*, 3277 – 3280; e) X. Shi, J. C. Fettinger, J. T. Davis, *J. Am. Chem. Soc*. **2001**, in press.

[10] G. Gottarelli, S. Masiero, G. P. Spada, *J. Chem. Soc. Chem. Commun*. **1995**, 2555 – 2557.

[11] a) A. L. Marlow, E. Mezzina, G. P. Spada, S. Masiero, J. T. Davis, G. Gottarelli, *J. Org. Chem*. **1999**, *64*, 5116 – 5123; b) S. L. Forman, J. C. Fettinger, S. Pieraccini, G. Gottarelli, J. T. Davis, *J. Am. Chem. Soc.* **2000**, *122*, 4060 – 4067.

[12] V. Andrisano, G. Gottarelli, S. Masiero, E. H. Heijne, S. Pieraccini, G. P. Spada, *Angew. Chem.* **1999**, *111*, 2543 – 2544; *Angew. Chem. Int. Ed*. **1999**, *38*, 2386 – 2388.

[13] A cation is not always required for G-quartet formation: J. L. Sessler, M. Sathiosatham, K. Doerr, V. Lynch, K. A. Abboud, *Angew. Chem.* **2000**, *112*, 1356 – 1359; *Angew. Chem. Int. Ed.* **2000**, *39*, 1300 – 1303.

[14] The G-quartet's diastereotopic faces are defined so that the "head" has a clockwise rotation of the N–H $\cdots$ O=C hydrogen bonds. As depicted in Scheme 1, the four D-ribose sugars are located on the G-quartet's "tail".

[15] Crystal data for $(G\mathbf{1})_{16}\cdot 2Sr^{2+}\cdot 4Pic^{-}\cdot (H_2O)_{23.25}\cdot (CH_3CN)_{3.5}$: $C_{335}H_{561}Sr_2N_{95.5}O_{131.25}Si_{16}$; $M_r = 8651.47$, crystal dimensions $0.636\times 0.455\times 0.127$ mm^3, tetragonal, space group $I4$, $a = 30.5043$, $b = 30.5043$, $c = 25.802(3)$ Å, $V = 24{,}009(3)$ Å^3, $Z = 2$, $D_x = 1.197$ mg m^{-3}, $\mu Mo_{K\alpha} = 0.347$ mm^{-1}. Data were collected on a Bruker SMART 1000 CCD diffractometer at 193(2) K. Structure determination was done by direct methods using the program XS.[20] Refinement, using the XL program,[21] was done to convergence on F^2 with $R(F) = 11.12\,\%$ and $wR(F^2) = 23.43\,\%$ for all 15685 independent reflections [$R(F) = 8.84\,\%$, $wR(F^2) = 22.09\,\%$ for those 12150 data with $F_o > 4\sigma(F_o)$]. Crystallographic data (excluding structure factors) for the structure reported in this paper have been deposited with the Cambridge Crystallographic Data Centre as supplementary publication no. CCDC-160231. Copies of the data can be obtained free of charge on application to CCDC, 12 Union Road, Cambridge CB2 1EZ, UK (fax: (+44) 1223-336-033; e-mail: deposit@ccdc.cam.ac.uk).

[16] G. Gottarelli, S. Masiero, G. P. Spada, *Enantiomer* **1998**, *3*, 429 – 438.

[17] [2.2.2]-cryptand binds Ba^{2+} strongly ($K_A > 10^{11}$ M^{-1}): J.-M. Lehn, J. P. Sauvage, *J. Am. Chem. Soc.* **1975**, *97*, 6700 – 6707.

[18] Monitoring picrate coordination by NMR: a) V. Böhmer, A. Dalla Cort, L. Mandolini, *J. Org. Chem.* **2001**, *66*, 1900 – 1902; b) G. G. Talanova, N. S. A. Elkarim, V. S. Talanov, R. E. Hanes, H.-S. Hwang, R. A. Bartsch, R. D. Rogers, *J. Am. Chem. Soc.* **1999**, *121*, 11281 – 11290.

[19] Fortunately, $(G\mathbf{1})_{16}\cdot 2Sr^{2+}\cdot 4Pic^{-}$, $(G\mathbf{1})_{16}\cdot 2Ba^{2+}\cdot 4Pic^{-}$, and $(G\mathbf{1})_8\cdot Ba^{2+}\cdot (G\mathbf{1})_8\cdot Sr^{2+}\cdot 4Pic^{-}$ have similar stabilities so that a statistical distribution of complexes was obtained.

[20] G. M. Sheldrick, *Acta Crystallogr. Sect. A* **1990**, *46*, 467 – 473.

[21] G. M. Sheldrick, Shelxl-93, Program for the Refinement of Crystal Structures, **1993**, University of Göttingen, Germany.

Nickel(II) Phosphate VSB-5: A Magnetic Nanoporous Hydrogenation Catalyst with 24-Ring Tunnels**

Nathalie Guillou, Qiuming Gao, Paul M. Forster, Jong-San Chang, Marc Noguès, Sang-Eon Park,* Gérard Férey,* and Anthony K. Cheetham*

Aluminosilicate zeolites and related nanoporous materials are used widely in the domains of separation, ion-exchange, and shape-selective catalysis.[1–3] The majority of catalytic processes that use zeolites involve acid-catalyzed reactions, for example hydrocarbon isomerization, cracking, alkylation, and dehydration,[1, 3] though recently there has been a surge in interest in partial oxidation reactions based upon titanosilicate materials and transition metal substituted aluminophosphates.[4] It would be of great interest to create nanoporous materials that catalyze other types of reactions, such as shape-selective hydrogenations, but it has not so far proved possible to achieve this in a zeolite catalyst without introduction of extra-framework Ni and noble metal clusters. The underlying challenge here is to design a nanoporous system based on, say, nickel, that is both functional and thermally stable with respect to chemical or structural degradation.[5, 6] We recently showed that the open-framework nickel(II) phosphate, VSB-1 (Versailles – Santa Barbara-1), is sufficiently stable to be rendered nanoporous and exhibits typical zeolitic properties.[7] Furthermore, this large-pore material has interesting catalytic properties suitable for reactions that require only weak acidity.[8] Herein, we describe a second nanoporous nickel phosphate, VSB-5, which exhibits redox properties that

[*] Prof. G. Férey, Prof. A. K. Cheetham, Dr. N. Guillou, Dr. Q. Gao
Dr. M. Noguès
Institut Lavoisier, UMR CNRS C 8637
Université de Versailles Saint-Quentin-en-Yvelines
45 avenue des Etats-Unis, 78035 Versailles Cedex (France)
Fax: (+33) 1-39-25-43-58
E-mail: ferey@chimie.uvsq.fr
cheetham@mrl.ucsb.edu

Prof. A. K. Cheetham, Dr. Q. Gao, P. M. Forster, Dr. J.-S. Chang
Materials Research Laboratory
University of California
Santa Barbara, CA 93106 (USA)
Fax: (+1) 805-893-8797

Dr. S.-E. Park, Dr. J.-S. Chang
Catalysis Center for Molecular Engineering
Korea Research Institute of Chemical Technology (KRICT)
P. O. Box 107, Yusung, Taejon 305-606 (Korea)
Fax: (+82) 42-860-7676
E-mail: separk@pado.krict.re.kr

[**] A.K.C. thanks the Fondation de l'Ecole Normale Supérieure and the Région de l'Ile de France for a Chaire Internationale de Recherche, Blaise Pascal. We also thank the CNRS for financial support and for providing a Poste Rouge for Q.G. and a PICS to the two groups for cooperation. The authors are indebted to D. S. Kim for his support with pore size analysis. We thank the Korean Ministry of Science and Technology (Key Research Program, KK-0005-F0) for supporting this work, and the Korea Science and Engineering Foundation (KOSEF) Fellowship for J.S.C. is gratefully acknowledged. J.S.C. was partially supported by the U.S. Department of Energy under grant DE-FG03-96ER14672. P.M.F. was supported by the National Science Foundation under the MRSEC Program (NSF-DMR-96-32716).

enable it to catalyze partial hydrogenation reactions with high selectivity.

$Ni_{20}[(OH)_{12}(H_2O)_6][(HPO_4)_8(PO_4)_4]\cdot 12H_2O$ VSB-5

VSB-5 can be synthesized between pH 7.3 and 11.0, and over a wide range of Ni/P ratios and concentrations, with little apparent change in the product. Although VSB-5 has not been prepared without an amine present, the particular amine does not seem to be important. For example, we have used a range of diamines from 1,2-ethylenediamine through to 1,8-octanediamine. In a typical synthesis, $NiCl_2\cdot 6H_2O$ (6.0 g; Aldrich) was dissolved in H_2O (60 mL), followed by the addition of H_3PO_4 (6.2 g, 85 %, Fisher) and 1,3-diaminopropane (9.8 g, Aldrich). A green precipitate formed during the addition of the amine, but dissolved with stirring. The final solution was deep purple with a pH of 9.0. After heating in a 120 mL Teflon-lined Parr autoclave at 180 °C for five days, phase-pure VSB-5 was present as a brown solution at pH 10.1. Elemental analysis gave the following results: Ni 40.66 wt %, and P 12.84 wt %. IR spectroscopy revealed that neither amine nor ammonium were introduced into the structure.

X-ray thermodiffractometry[9] shows that the structure of the parent phase is clearly sustained up to about 723 K (Figure 1). It then collapses to form an amorphous phase and recrystallizes to yield condensed $Ni_3(PO_4)_2$ at higher temperatures. Thermogravimetric analysis (TGA)[10] (see insert in Figure 1) of the VSB-5 revealed distinct weight losses of 7.3 (up to 130 °C), 5.7 (200 to 400 °C), 5.7 (450 °C), and 1.1 % (500 to 850 °C). Taken together with the chemical analysis and the structure (see below), these results suggest the chemical composition given above.

Brunauer–Emmet–Teller (BET)[11] surface area and pore structure analysis gives a typical Type-1 isotherm and a surface area of 500(10) m^2g^{-1}. The surface area per gram is comparable to that of a large-pore zeolite, considering that VSB-5 ($\sim$2.6 $g cm^{-3}$) is approximately two times more dense than a typical zeolite. To our knowledge, this surface area is the highest value reported to date for open-framework metal phosphate materials. The pore size distribution, which was monodisperse, gave a pore radius of about 6.4 Å by using the method of Horvath–Kawazoe.

The structure of VSB-5 was solved by ab initio structure solution from laboratory data.[12] Pattern indexing, which was performed by using the computer program DICVOL91,[13] yielded a hexagonal unit cell ($a = 18.209(1)$, $c = 6.3898(7)$ Å; $V = 1834.8(3)$ Å^3). Systematic absences ($0k0$, $k = 2n+1$) were consistent with the space groups $P6_3$ and $P6_3/m$. Structure solution from the X-ray powder diffraction data was performed with the EXPO package, integrating EXTRA,[14] a full pattern decomposition program, and SIR97.[15] The centrosymmetric space group $P6_3/m$ was chosen to solve the structure, and the atomic coordinates obtained by direct methods were used as the starting model in the Rietveld refinement using FULLPROF.[16] Figure 2 shows the final fit obtained between calculated and observed patterns. It corresponds to satisfactory crystal model indicators ($R_B = 0.068$ and $R_F = 0.054$) and profile factors ($R_P = 0.100$ and $R_{wP} = 0.129$).[17]

The view of the structure given in Figure 3 shows that VSB-5 presents a one-dimensional system of pores running in the [001] direction. These tunnels are delineated by 24 NiO_6 octahedra, which are connected by sharing faces, edges, and corners. The pore diameter, based on the distance across the pore of the activated solid (10.2 Å), is in reasonable agreement with the value from the porosimetry data (12.8 Å) when the radii of coordinated oxygen atoms are considered.

Magnetic susceptibility and magnetization measurements[18] reveal antiferromagnetic ordering at 14 K with a Curie–Weiss θ value of -49.5 K. There is evidence of a second magnetic transition at about 6 K, which possibly involves spin canting. The low value of T_N in relation to θ is similar to that found in VSB-1,[7] suggesting that the structure may be magnetically frustrated.

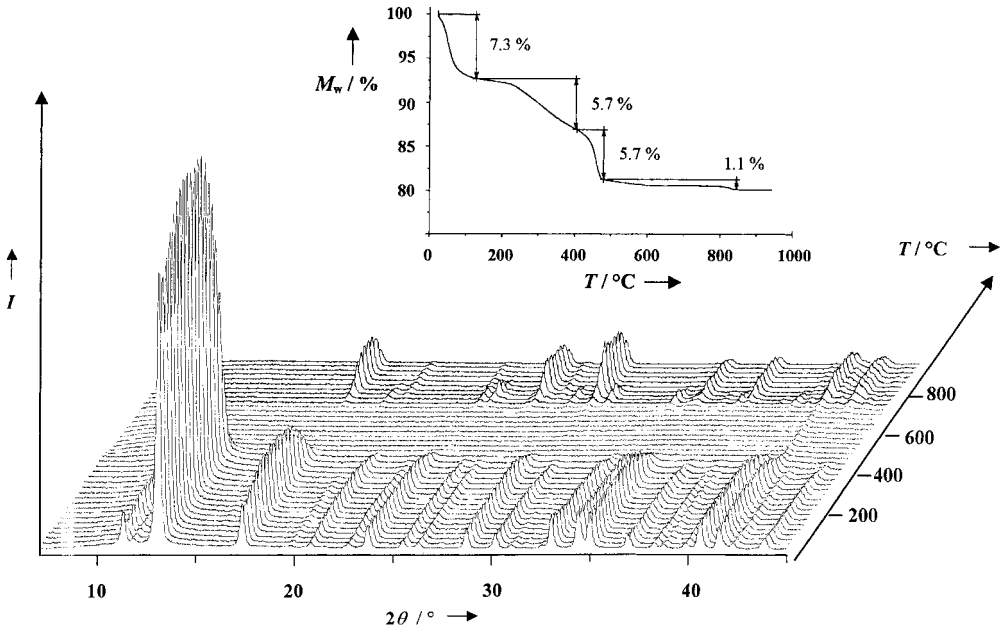

Figure 1. Thermal evolution of the diffractograms during the heating of VSB-5 in air (the line at 41.7° (2θ) in the amorphous zone corresponds to pollution of Pt strip). The TGA curve under oxygen is shown as an insert. I = intensity in arbitrary units.

In view of the possible accessibility of framework Ni atoms for catalytic reactions, we explored the hydrogenation activity of VSB-5.[19] The reduction of 1,3-butadiene to butenes, which requires mild hydrogenation ability, was chosen for this purpose. Selective hydrogenation of 1,3-butadiene to 1-butene in the C4 fraction plays an important role for the production of high-purity alkene streams on an industrial scale.[20] VSB-1 and $Ni_3(PO_4)_2$ were run for comparison. The results show the remarkable perform-

  1433-7851/01/4015-2832 $ 17.50+.50/0

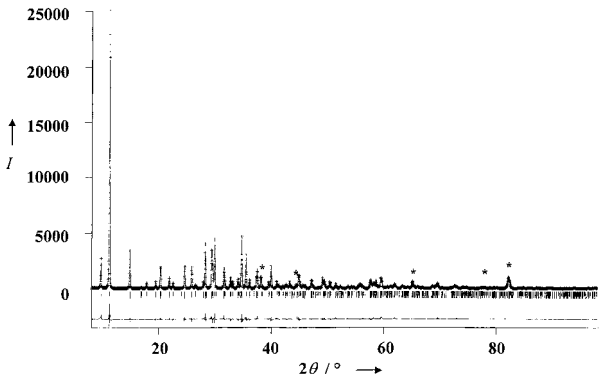

Figure 2. Final Rietveld plot for VSB-5. Observed (crosses) and calculated (line) powder X-ray data, the lower line is the difference curve. Asterisks (*) indicate spurious lines of the sample holder. I = X-ray intensity in arbitrary units.

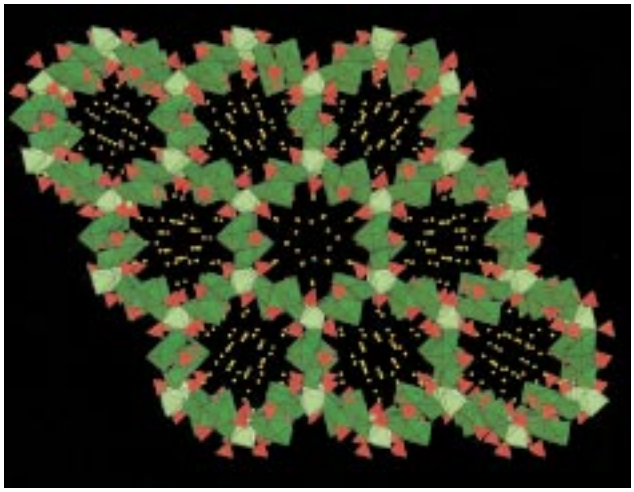

Figure 3. A view of the structure of VSB-5 down [001]. NiO_6 octahedra are shown in light green (disordered Ni3) and dark green (Ni1 and Ni2) and PO_4 tetrahedra are shown in red.

ance of VSB-5 in this reaction (Table 1). VSB-1, by comparison, was only mildly active, while condensed $Ni_3(PO_4)_2$ shows strong hydrogenation activity leading to a high selectivity for butane. The different selectivities of VSB-5 and condensed $Ni_3(PO_4)_2$ for butenes (see Table 1 for the main butenes formed) suggest the availability of framework Ni atoms in the nanoporous structure for selective hydrogenation. Further studies on shape-selective hydrogenation of di-olefins with different molecular dimensions are currently underway.

In the light of the basic synthetic conditions and the abundant hydroxide present in the framework, we investigated whether VSB-5 is capable of supporting base-catalyzed reactions. Using the decomposition of 2-methyl-3-butyn-2-ol (MBOH) as a test reaction,[22] we also examined the acid, base, and even amphoteric properties of VSB-5.[21] The conversion of MBOH gives acetone and acetylene over base sites, or 3-methyl-3-buten-1-yne (Mbyne) with 3-methyl-2-buten-1-al over acid sites. Table 2 shows the catalytic results for the conversion of MBOH over VSB-5 and VSB-1. To our surprise, VSB-5 exhibits very high MBOH conversion (99% at 573 K) as well as high selectivity (>99%) for the formation of acetone and acetylene, unambiguously confirming its base character. In contrast, VSB-1 gives only poor conversion (10%) of MBOH and a mixture of several products at 573 K, indicating that it possesses only poor acidity and basicity.

Table 2. Catalytic conversion of 2-methyl-3-butyn-2-ol over VSB-1 and VSB-5 materials.[a]

Catalyst	S_{BET} [$m^2 g^{-1}$]	T [°C]	MBOH conversion[b] [%]	Selectivity [%] acetone	acetylene	Mbyne[c]
VSB-1	183	250	2.7	38.1	38.9	23.0
		300	10.0	37.9	39.8	22.3
VSB-5	500	250	22.6	49.1	49.0	1.9
		300	99.0	50.2	49.0	0.8

[a] Reaction conditions: p(MBOH) = 2 kPa, W/F = 125 g h mol^{-1}, time on stream = 10 min. [b] MBOH: 2-methyl-3-butyn-2-ol. [c] Mbyne: 3-methyl-3-buten-1-yne.

In summary, VSB-5, a nanoporous nickel phosphate, has been synthesized by hydrothermal methods. This new material is found to have four important properties: nanoporosity, good thermal stability, antiferromagnetic ordering, and hydrogenation and basic catalytic character. The basic character presumably stems from the presence of OH anions in the framework. The efficacy of VSB-5 for partial hydrogenation reactions suggests the availability of active sites associated with framework Ni atoms.

Received: February 26, 2001 [Z16683]

[1] A. Corma, *Chem. Rev.* **1997**, *97*, 2373–2419.
[2] M. E. Davis, *Chem. Eur. J.* **1997**, *3*, 1745–1750.
[3] a) J. M. Thomas, *Sci. Am.* **1992**, *266*, 112–118; b) J. M. Thomas, *Angew. Chem.* **1994**, *106*, 963–989; *Angew. Chem. Int. Ed. Engl.* **1994**, *33*, 913–937.
[4] a) T. Taramasso, G. Perego, B. Notari (Eniriceche), US Patent US-A 4410501, **1983**; b) R. J. Saxton, *Top. Catal.* **1999**, *9*, 43–57; c) B. Notari, *Adv. Catal.* **1996**, *41*, 253–334; d) R. Raja, G. Sankar, J. M. Thomas, *Angew. Chem.* **2000**, *112*, 2403–2406; *Angew. Chem. Int. Ed.* **2000**, *39*, 2313–2316; e) J. Chen, R. H. Jones, S Natarajan, M. B. Hursthouse,

Table 1. Selective hydrogenation of 1,3-butadiene (BD) over VSB-1 and VSB-5.[a]

Catalyst	H Act.[d] [h]	T [°C]	BD conversion [%]	S_{butene}[e] [%]	Selectivity [%] *n*-butane	1-butene	*trans*-2-butene	*cis*-2-butene
VSB-1[b]	16	200	1.0	99.9	0.1	34.0	36.7	29.2
VSB-5[b]	4	200	10.3	97.9	2.1	48.4	30.5	19.0
VSB-5[b]	16	200	68.4	97.6	2.4	52.4	28.5	16.7
VSB-5[b]	24	100	81.1	95.8	4.2	50.9	32.0	12.9
VSB-5[c]	16	100	99.6	21.4	78.6	14.0	1.3	6.1
$Ni_3(PO_4)_2$	4	100	99.5	47.7	52.3	27.4	7.3	13.0

[a] Reaction conditions: p(BD) = 10.1 kPa, W/F = 0.3 g s mL^{-1}, H_2/BD = 3, time on stream = 2 h. [b] Calcination at 350 °C for 4 h. [c] Calcination at 550 °C for 4 h. [d] Activation time under 5% H_2 in He at 350 °C. [e] Selectivity to give butene products.

  1433-7851/01/4015-2833 $ 17.50+.50/0

J. M. Thomas, *Angew. Chem.* **1994**, *106*, 667–668; *Angew. Chem. Int. Ed. Engl.* **1994**, *33*, 639–641.
[5] M. A. Drezdzon, *Inorg. Chem.* **1988**, *27*, 4628–4632.
[6] A. K. Cheetham, G. Férey, T. Loiseau, *Angew. Chem.* **1999**, *111*, 3466–3492; *Angew. Chem. Int. Ed.* **1999**, *38*, 3268–3292.
[7] N. Guillou, Q. Gao, M. Nogues, R. E. Morris, M. Hervieu, G. Férey, A. K. Cheetham, *C. R. Acad. Sci. Paris* **1999**, *2*, 387–392.
[8] J.-S. Chang, S.-E. Park, Q. Gao, G. Férey, A. K. Cheetham, *Chem. Commun.* **2001**, *9*, 859–860.
[9] Thermodiffractometry was performed under air in an Anton Paar HTK16 high-temperature device of a Siemens D5000 X-ray powder diffractometer ($\theta-\theta$ mode; $Co_{K\alpha}$ radiation $\lambda = 1.7903$ Å), equipped with a M Braun linear position sensitive detector (PSD). Patterns were scanned with a resolution of 0.0147° and a divergence slit of 0.1° over an angular range of 5–50° (2θ), at 25 °C intervals up to 1000 °C; rate of increase of temperature: 0.1 °C s^{-1}; see Figure 1.
[10] TGA data were obtained on a TGA 2050 thermogravimetric analyser thermobalance using a sample synthesized by using 1,3-diaminopropane.
[11] BET analysis was performed by using a Micromeritics ASAP2400 porosimeter on a sample activated at 350 °C for four days.
[12] The X-ray powder diffraction data for VSB-5 were collected on a Siemens D5000 diffractometer by using $Cu_{K\alpha}$ radiation ($\lambda = 1.5418$ Å). To avoid preferred orientation effects, the synthesis was carried out under stirring conditions, keeping the same experimental conditions with the same molar ratio and filling rate. The resulting powder was then loaded in the sample holder. The powder diffraction pattern was scanned over an angular range of 4–120° (2θ). The counting times were 27 s per step to 59.98° (2θ) and 54 s per step from 60.00° (2θ) to the end of the scan (to improve the counting statistics of the high-angle region). The full pattern was then scaled to the lower counting time. An accurate determination of the peak positions and relative intensities was carried out by using the software package DIFFRACT-AT.
[13] A. Boultif, D. Louër, *J. Appl. Crystallogr.* **1991**, *24*, 987–993.
[14] A. Altomare, M. C. Burla, G. Cascarano, C. Giacovazzo, A. Guagliardi, A. G. G. Moliterni, G. Polidori, *J. Appl. Crystallogr.* **1995**, *28*, 842–846.
[15] A. Altomare, M. C. Burla, M. Camalli, G. L. Cascarano, C. Giacovazzo, A. Guargliardi, A. G. G. Moliterni, G. Polidori, R. Spagna. *J. Appl. Crystallogr.* **1999**, *32*, 115–119.
[16] J. Rodriguez-Carvajal, *Collected Abstracts of Powder Diffraction Meeting* (Toulouse, France) **1990**, p. 127.
[17] Further details on the crystal structure investigation may be obtained from the Fachinformationszentrum Karlsruhe, 76344 Eggenstein-Leopoldshafen, Germany (fax: (+49) 7247-808-666; e-mail: crysdata@fiz-karlsruhe.de), on quoting the depository number CSD-411917.
[18] Magnetization measurements were performed in the temperature range 4–295 K at 5 kG and 100 G on a Quantum Design Squid magnetometer (MPMS-5).
[19] The selective hydrogenation of 1,3-butadiene to butenes was carried out in a continuous fixed-bed reactor made of quartz at atmospheric pressure. Before catalytic measurement, the catalyst was reduced with 5% hydrogen in helium at 350 °C for 4–24 h. The reaction was carried out while introducing mixture of 1,3-butadiene (99.0%) and pure hydrogen under helium. The effluent stream from the reactor was analyzed by an on-line gas chromatograph (HP 5890 Series II) fitted with a capillary column (J&W Alumina) and a flame-ionization detector.
[20] H. Arnold, F. Doebert, J. Gaube in *Handbook of Heterogeneous Catalysis*, *Vol. 5* (Eds.: G. Ertl, H. Knoezinger, J. Weitkamp), VCH, Weinheim, **1997**, pp. 2165–2186.
[21] E. Iglesia, D. G. Barton, J. A. Biscardi, M. J. L. Gines, S. L. Soled, *Catal. Today* **1997**, *38*, 339–360.
[22] Decomposition of MBOH (>99%, Aldrich) was carried out in a plug-flow glass reactor with an internal diameter of 10 mm. The MBOH was placed in a vaporizer in which a helium flow was saturated with the alcohol vapor at 298 K and then the MBOH/helium mixture was fed into the reactor. The catalytic activity of VSB-5 was examined after the calcination of the fresh sample at 623 K for 4 h in air. Reaction products were analyzed by an on-line gas chromatograph (Hewlett-Packard model 5890II) fitted with a capillary column (J&W DB-WAX) and a flame-ionization detector.

Spherical Aromaticity of Inorganic Cage Molecules**

Andreas Hirsch,* Zhongfang Chen, and Haijun Jiao

We have shown recently that the icosahedral fullerenes C_{20}, C_{60}, and C_{80} reach maximum spherical aromaticity if their π shells are completely filled.[1] This is nicely demonstrated, for example, by the very pronounced diatropic character of the $2(N+1)^2$ π systems of the C_{20}^{2+} ($N=2$), C_{60}^{10+} ($N=4$), and C_{80}^{8+} ($N=5$) ions with perfect I_h symmetry. Here we extend this treatment of spherical aromaticity to a set of well-known inorganic cage compounds and demonstrate that they are highly aromatic because of the closed-shell nature of both their σ and π systems.

Tetrahedral clusters P_4 and As_4 form metastable solid allotropes, whereas Sb_4 and Bi_4 are high-temperature modifications existing only in liquid or in the gas phase. Tetrahedral N_4 (T_d), being the most stable singlet N_4 isomer,[2] was recently generated in a plasma as the first neutral polynitrogen species.[3] The calculated nucleus-independent chemical shifts (NICS)[4, 5] at the cage centers of these T_d-symmetrical clusters with optimized bond lengths (Figure 1)

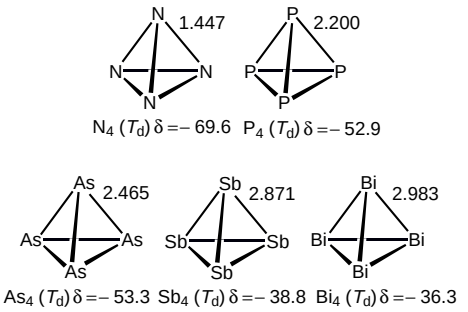

Figure 1. Optimized bond lengths [Å] and NICS values [δ] for E_4 (T_d) clusters (E = N, P, As, Sb, Bi).

are given in Table 1. The highly negative NICS values of all clusters are a result of pronounced diamagnetic ring currents. The pronounced diatropic character of these clusters is not a result of the addition of four individual increments consisting of three-membered rings, but a new quality of the entire cages. This is clearly reflected by the fact that: 1) the NICS and the NICS per valence electron (NICS/e) values in the center of the cages are considerably more negative than those in the

[*] Prof. Dr. A. Hirsch, Dr. Z. Chen, Dr. H. Jiao[+]
Institut für Organische Chemie der Universität Erlangen-Nürnberg
Henkestrasse 42
91054 Erlangen (Germany)
Fax: (+49) 9131-85-26864
E-mail: hirsch@organik.uni-erlangen.de
[+] Laboratoire de Chimie du Solide et Inorganique Moléculaire
UMR 6511 CNRS, Université de Rennes 1, Institut de Chimie de Rennes, 35042 Rennes Cedex (France)
[**] This work was supported by the Alexander von Humboldt Stiftung (Z. Chen), the Centre National de la Recherche Scientifique (H. Jiao), and the Fonds der Chemischen Industrie. We thank Prof. Dr. T. F. Fässler for his helpful discussion and reprints.

  1433-7851/01/4015-2834 $ 17.50+.50/0

Table 1. Calculated NICS values [δ] for E_4 (T_d), E_3H_3 (C_{3v}), and HE_4^+ (C_{3v}).

Type	NICS	Compound				
E_4[a]		N_4	P_4	As_4	Sb_4	Bi_4
	NICS[b]	−69.6	−52.9	−53.3	−38.8	−36.3
	NICS/e[c]	−3.5	−2.6	−2.7	−1.9	−1.8
	NICS[d]	−69.4	−52.3	−52.4	−38.7	−36.2
E_3H_3[a]		N_3H_3	P_3H_3	As_3H_3	Sb_3H_3	Bi_3H_3
	NICS[d]	−51.5	−33.5	−33.8	−26.6	−25.0
	NICS/e[c,d]	−2.9	−1.9	−1.9	−1.5	−1.4
HE_4^+[a]		HN_4^+	HP_4^+	HAs_4^+	HSb_4^+	HBi_4^+
	NICS[b]	−64.0	−40.4	−35.8	−22.1	−10.0

[a] All are energy minima. [b] At the cage center. [c] NICS per valence electron (NICS/e). [d] At the center (E_3) of the trigons.

center of the three-membered E_3H_3-rings (C_{3v}) (Table 1); 2) the NICS values in the center of the three-membered E_3H_3-rings (C_{3v}) are less negative than those in the center of the trigonal faces of E_4 (Table 1), and 3) the NICS/e values of four E_3H_3 increments at a location corresponding to the cage center of E_4 are considerably lower than those of the E_4 cage centers. For example the sum of the NICS/e values of four P_3H_3 units 0.45 Å away from the center of each plane which corresponds to the middle of the P_4 cage is $\delta = -1.3$ whereas that of P_4 itself is $\delta = -2.6$.

The calculated MO schemes of E_4 are in line with earlier calculations[6] and clearly reflect the closed-shell nature of both the σ and π subsystems (Figure 2). The σ system contains

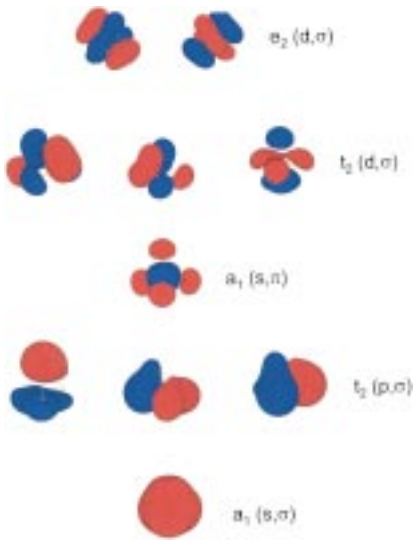

Figure 2. Representation of the MOs of P_4 (HyperChem 5.1). The a_1 (s,π) orbital is a cluster π orbital.[1, 7] As a result of the pyramidalization of the cluster atoms the endohedral overlap of atomic p orbitals is much more pronounced than the exohedral overlap.

$2(N_\sigma+1)^2$ σ electrons ($N_\sigma = 2$) and consists of a cluster s orbital, three degenerate cluster p orbitals, and two sets of cluster d orbitals (e and t_2), while the π system contains $2(N_\pi+1)^2$ π electrons ($N_\pi = 0$).[7] With respect to the model of the spherical electron gas,[1, 8] the splitting of the cluster d orbitals of σ systems is a consequence of symmetry lowering from K_h to T_d. With the complete filling of all σ and π shells the angular momenta are symmetrically distributed[1, 8] and the clusters are double spherically aromatic.[9] The HOMOs are the e (d,σ) orbitals (Figure 2). Electrons within the frontier region are the most mobile and contribute predominantly to the ring-current effect. Therefore, the diatropic character of these clusters is mainly determined by the σ electrons. Incomplete filling of the shells, accompanied by asymmetrical distribution of the angular momenta, causes reduction of aromatic character or even establishment of antiaromaticity. This is shown, for example, with the system P_4^{2-} where one of the three originally degenerate LUMOs of P_4 is occupied causing a symmetry lowering to C_{2v} (P–P = 2.159, 2.280, and 3.222 Å) and a NICS value of only $\delta = -23.0$; while the system P_4^{2+} has also lower symmetry (D_2, P–P = 2.168 and 2.670 Å) and a NICS value of $\delta = -15.6$.

The cluster ions Si_4^{4-}, Ge_4^{4-}, Sn_4^{4-}, and Pb_4^{4-}[10, 11] are isoelectronic with P_4, As_4, Sb_4, and Bi_4, have the same MO structure, and exhibit a comparable pronounced diatropic character and double spherical $2(N+1)^2$ aromaticity (Figure 3).

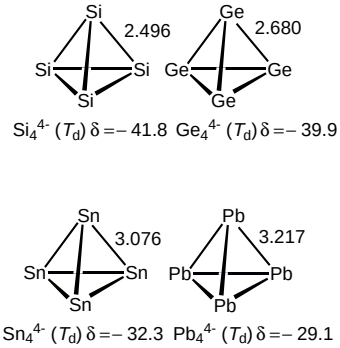

Figure 3. Optimized bond lengths [Å] and NICS values [δ] for E_4^{4-} (T_d) clusters (E = Si, Ge, Sn, Pb).

A set of less symmetrical clusters containing nine atoms is represented by the Zintl[12] ions shown in Figures 4–6 and Table 2. The D_{3h} symmetrical *closo*-cages E_9^{4-} (E = Si,[13] Ge,[14] Sn,[14c, 15] Pb[15e, 16]) and Bi_9^{5+}[17] (Figure 4) represent energy minima and do not obey the Wade rules.[18] A reason for their stability could be the double spherically $2(N+1)^2$ aromatic configuration of their valence-electron system containing 32 σ ($N_\sigma = 3$) and 8 π electrons ($N_\pi = 1$). In contrast to the T_d clusters (Figure 1 and 3) their MO schemes are characterized by a variety of crossovers between the subshells and a considerable decrease in orbital degeneracy of the completely filled σ (s, p, d, f) and π (s, p) levels. However, they still exhibit very high NICS values approaching those of some highly aromatic fullerenes with closed π shells.[1] The HOMO of these clusters is the a_2''(f,σ) orbital which corroborates earlier calculations.[19]

The corresponding *nido* structures with C_{4v} symmetry are slightly less stable (Figure 5, Table 2).[19] They are also double spherically $2(N+1)^2$ aromatic. Their HOMOs (f,σ), however, are two-fold degenerate.[19] E_9^{4-} clusters are known to be fluxional on the NMR time scale.[20] The D_{3h} cages can smoothly rearrange into the corresponding C_{4v} cages. Most of the corresponding Wade rule obeying *closo* cages E_9^{2-} (E = Sn, Pb)[21] and Bi_9^{7+} are unknown (Figure 6, Table 2), while

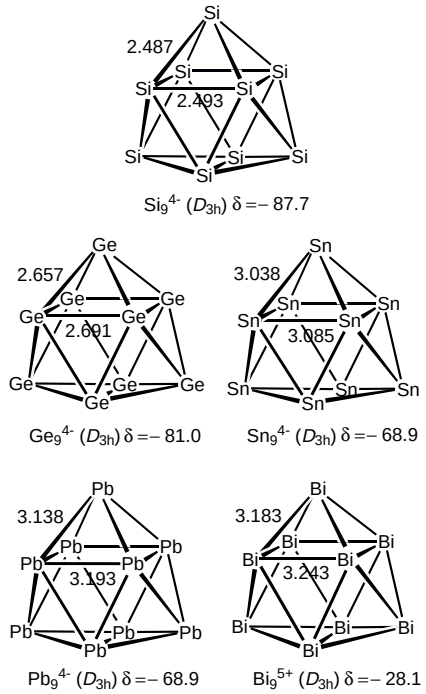

Figure 4. Optimized bond lengths [Å] and NICS values [δ] for E_9^{4-} (D_{3h}) clusters (E = Si, Ge, Sn, Pb) and Bi_9^{5+} (D_{3h}).

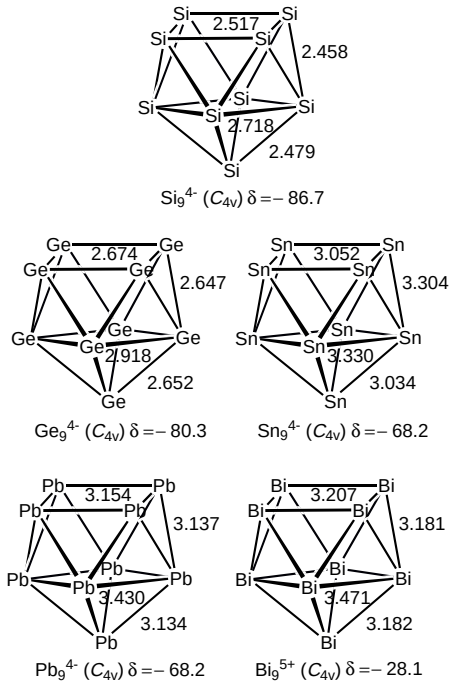

Figure 5. Optimized bond lengths [Å] and NICS values [δ] for E_9^{4-} (C_{4v}) clusters (E = Si, Ge, Sn, Pb) and Bi_9^{5+} (C_{4v}).

Ge_9^{2-} was reported.[14b] Noteworthy is that their σ shells are not completely filled, since the a_2''(f,σ) orbital is now empty leaving the a_2' (f,σ) as the HOMO.[19] As a consequence, the NICS values are considerably lower than those of the corresponding double $2(N+1)^2$ aromatic systems (Figure 4, Table 2). In all cases the HOMOs are σ orbitals and the π levels are inner-shell states.[19]

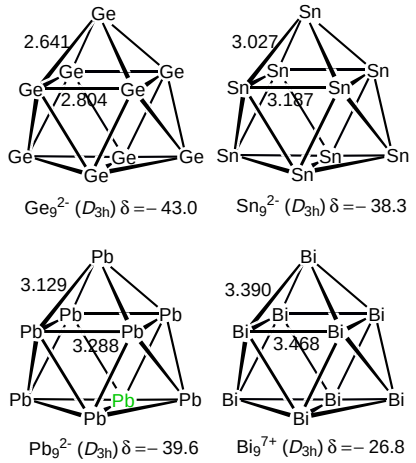

Figure 6. Optimized bond lengths [Å] and NICS values [δ] for E_9^{2-} clusters (D_{3h}) (E = Ge, Sn, Pb) and Bi_9^{7+} (D_{3h}).

Table 2. Calculated NICS values [δ] and relative energies E_{rel} [kcal mol^{-1}] for E_9^{4-}, E_9^{2-}, Bi_9^{5+}, and Bi_9^{7+}.

Species	symmetry	NICS	E_{rel}	Reference
Si_9^{4-}	*closo* (D_{3h})	– 87.7	0.0	[13]
	nido (C_{4v})	– 86.7	1.1	[13]
Ge_9^{4-}				
	closo (D_{3h})	– 81.0	0.0	[a]
	nido (C_{4v})	– 80.3	0.8	[14]
Sn_9^{4-}	*closo* (D_{3h})	– 68.9	0.0	[a]
	nido (C_{4v})	– 68.2	0.8	[14c, 15]
Pb_9^{4-}	*closo* (D_{3h})	– 68.9	0.0	[16]
	nido (C_{4v})	– 68.3	1.0	[15e, 16]
Bi_9^{5+}	*closo* (D_{3h})	– 28.1	0.0	[17]
	nido (C_{4v})	– 28.1	0.4	[a]
Ge_9^{2-}	*closo* (D_{3h})	– 43.0	–	[14b]
Sn_9^{2-}	*closo* (D_{3h})	– 38.3	–	[a]
Pb_9^{2-}	*closo* (D_{3h})	– 39.6	–	[a]
Bi_9^{7+}	*closo* (D_{3h})	– 26.8	–	[a]

[a] Unknown experimentally.

Protonation of E_4 (E = N, P, As, Sb, Bi) leading to the isoelectronic C_{3v}-symmetrical cages HE_4^+ causes a reduction of the NICS values (i.e. becomes less negative) because of a reduction of electron mobility (Table 1). However, especially the clusters HE_4^+ (E = N, P, As) are still highly aromatic. The corresponding cluster σ and π orbitals[7] are closely related to those of the parent E_4 cages. The only difference is the presence of the exohedral protons, making the H–E fragments *pseudo* cluster atoms.[7] The complete protonation of all cluster atoms is realized in the *closo*-boranes $B_nH_n^{2-}$ (n = 5–12). As reported by Schleyer and Najafian,[22] the *closo*-boranes $B_nH_n^{2-}$ are highly diatropic with NICS values of the cluster centers ranging from $\delta = -24.5$ to -34.4. The closed-shell nature of O_h $B_6H_6^{2-}$, for example, is realized with $2(N_\pi+1)^2$ π electrons ($N_\pi = 1$) and $2(N_\sigma+1)^2$ σ electrons ($N_\sigma = 2$; Figure 7). The I_h-symmetrical $B_{12}H_{12}^{2-}$ ion contains $(N_\pi+1)^2$ π electrons ($N_\pi = 2$) and $2(N_\sigma+1)^2$ σ electrons ($N_\sigma = 3$). Note that these two highly symmetrical systems are double spherical aromatic and exhibit the highest NICS values in this series.[22]

In contrast to the carbon-based fullerene clusters the HOMOs within the highly symmetrical inorganic cage com-

  1433-7851/01/4015-2836 $ 17.50+.50/0 *Angew. Chem. Int. Ed.* **2001**, *40*, No. 15

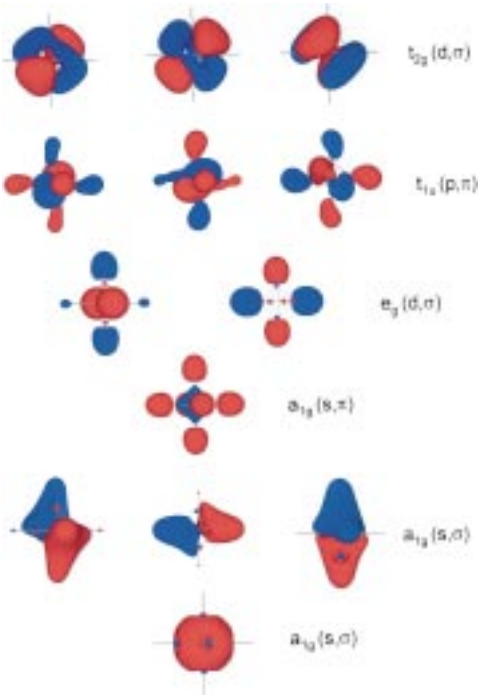

Figure 7. Representation of the MOs of $B_6H_6^{2-}$ (HyperChem 5.1).

pounds investigated here are σ orbitals. Like the spherical $2(N_\pi+1)^2$ aromaticity of the fullerenes the double spherical aromaticity of inorganic cage compounds involving both the whole π and σ system is a consequence of complete filling of the corresponding shells that can be deduced with group theory from molecular s, p, d, ⋯ shells of a spherical electron gas by reduction of the K_h symmetry to the cluster symmetry under consideration. As we will show in an forthcoming publication small and less symmetrical clusters such as Bi_5^{3+} do not obey the $2(N+1)^2$ rule and their aromaticity is reduced compared to systems with completely filled shells. However, we will also demonstrate that the spherical electron gas model[1, 8] that we used to deduce the $2(N+1)^2$ count rule forms the basis to treat any cluster type with a closed-cage structure. It can even be used by symmetry lowering to deduce the Hückel count rule for the cyclic annulenes. This leads to a unified picture of aromaticity and understanding of the special stability and reactivity of nonorganic molecules.[23]

Received: January 5, 2001
Revised: May 10, 2001 [Z16375]

[1] A. Hirsch, Z. Chen, H. Jiao, *Angew. Chem.* **2000**, *112*, 4079 – 4081; *Angew. Chem. Int. Ed.* **2000**, *39*, 3915 – 3917.

[2] a) M. N. Glukhovtsev, H. Jiao, P. von R. Schleyer, *Inorg. Chem.* **1996**, *35*, 7124 – 7133; b) K. Kobayashi, H. Miura, S. Nagase, *J. Mol. Struct. (THEOCHEM)* **1994**, *117*, 69 – 77.

[3] J. P. Zheng, J. Waluk, J. Spanget-Larsen, D. M. Blake, J. George Radziszewski, *Chem. Phys. Lett.* **2000**, *328*, 227 – 233.

[4] NICS-*N*ucleus *I*ndependent *C*hemical *S*hifts: P. von R. Schleyer, C. Maerker, A. Dransfeld, H. Jiao, N. J. R. van Eikema Hommes, *J. Am. Chem. Soc.* **1996**, *118*, 6317 – 6318.

[5] Geometry optimizations and frequency calculations were carried out at the B3LYP density functional level of theory with the 6 – 311 + G** basis set for E = N, P, As, Si, Ge; and LANL2DZp basis set for E = Sb, Bi, Sn, Pb; a) P. J. Hay, W. R. Wadt, *J. Chem. Phys.* **1985**, *82*, 299; b) T. H. Dunning, Jr., P. J. Hay, *Modern Theoretical Chemistry*, (Ed.: H. F. Schaefer III), Plenum, New York, **1976**, p. 1. For polarization functions see: S. Huzinaga, J. Anzelm, M. Klobukowski, E. Radzio-Andzelm, Y. Sakai, H. Tatewaki, *Gaussian Basis Sets for Molecular Calculations*, Elsevier, Amsterdam, **1984**. NICS were calculated at the same level with the same corresponding basis sets and optimized geometries. All calculations were done with the Gaussian 98 (Revision A.7), M. J. Frisch, G. W. Trucks, H. B. Schlegel, G. E. Scuseria, M. A. Robb, J. R. Cheeseman, V. G. Zakrzewski, J. A. Montgomery, R. E. Stratmann, J. C. Burant, S. Dapprich, J. M. Millam, A. D. Daniels, K. N. Kudin, M. C. Strain, O. Farkas, J. Tomasi, V. Barone, M. Cossi, R. Cammi, B. Mennucci, C. Pomelli, C. Adamo, S. Clifford, J. Ochterski, G. A. Petersson, P. Y. Ayala, Q. Cui, K. Morokuma, D. K. Malick, A. D. Rabuck, K. Raghavachari, J. B. Foresman, J. Cioslowski, J. V. Ortiz, B. B. Stefanov, G. Liu, A. Liashenko, P. Piskorz, I. Komaromi, R. Gomperts, R. L. Martin, D. J. Fox, T. Keith, M. A. Al-Laham, C. Y. Peng, A. Nanayakkara, C. Gonzalez, M. Challacombe, P. M. W. Gill, B. G. Johnson, W. Chen, M. W. Wong, J. L. Andres, M. Head-Gordon, E. S. Replogle, J. A. Pople, Gaussian, Inc., Pittsburgh, PA, **1998**..

[6] H. Zhang, K. Balasubramanian, *J. Chem. Phys.* **1992**, *97*, 3437 – 3444.

[7] In analogy to the nonplanar fullerenes (see ref. [1] and P. C. Haddon, *Science* **1993**, *261*, 1545 – 1550) a cluster π orbital is defined as an orbital containing a nodal plane spanned by all cluster heavy atoms. A similar definition which also allows the presence of protons within the mobile electron system (*closo*-boranes, CH^+ fragments) is given in T. A. Albright, J. K. Burdett, M.-H. Whangbo, *Orbital Interactions in Chemistry*, Wiley, New York, **1985**.

[8] A. Hirsch, *Top. Curr. Chem.* **1999**, *199*, 1 – 65. In addition to our inert-gas model and electron-counting rule for fullerene chemistry, there are highly related electron-counting rules for understanding the structures and bonding of transition metal clusters and various boron hydrides. For example, the tensor surface harmonic (TSH) theory which considers a molecule (or a cluster of atoms) as a central atom surround by a sphere of electron density, which is representative of the ligand co-ordination sphere. This leads to an approximate classification of the cluster orbitals in terms of angular momentum quantum numbers (we thank one referee for pointing out the spherical shell model which has the magic number of electrons (2, 8, 20, 40, 70, …, and the possibilities in-between e.g., 10, 18, 26, 34, …). For theoretical background and applications, see: A. J. Stone, *Mol. Phys.* **1980**, *41*, 1339 – 1354; A. J. Stone, *Inorg. Chem.* **1981**, *20*, 563 – 571; A. J. Stone, *Polyhedron* **1984**, *3*, 1299 – 1306; A. J. Stone, M. J. Alderton, *Inorg. Chem.* **1982**, *21*, 2297 – 2302). This theory has been generalized and extended (*Complementary Spherical Electron Density Model*) by D. M. Mingos, J. C. Hawes in *Structure and Bonding*, Springer, Berlin, **1985**, p. 1 – 63, and references therein. For further applications, see: P. W. Fowler, *Polyhedron* **1985**, *4*, 2051 – 2057; D. B. Redmond, *J. Chem. Soc. Faraday Trans.* **1983**, *79*, 1791 – 1809.

[9] Double aromaticity for planar systems, see: P. von R. Schleyer, H. Jiao, M. N. Glukhovtsev, J. Chandrasekhar, E. Kraka, **1994**, *116*, 10129 – 10134.

[10] I. F. Hewaidy, E. Busmann, W. Klemm, *Z. Anorg. Allg. Chem.* **1964**, *328*, 283 – 293.

[11] a) H. Schäfer, *Annu. Rev. Mater. Sci.* **1985**, *15*, 1 – 41; b) G. Kliche, M. Schwarz, H. G. von Schnering, *Angew. Chem.* **1987**, *99*, 350 – 352; *Angew. Chem. Int. Ed. Engl.* **1987**, *26*, 349 – 351.

[12] For some recent reviews, see: a) J. D. Corbett, *Angew. Chem.* **2000**, *112*, 682 – 704; *Angew. Chem. Int. Ed.* **2000**, *39*, 670 – 690; b) J. D. Corbett, *Struct. Bonding (Berlin)* **1997**, *87*, 157 – 193; c) J. D. Corbett, *Chemistry, Structures and Bonding of Zintl Phases and Ions* (Ed.: S. Kauzlarich), VCH, New York, **1996**, chap. 3. d) J. D. Corbett, *Chem. Rev.* **1985**, *85*, 383 – 397.

[13] a) H. G. von Schnering, M. Somer, M. Kaupp, W. Carrillo-Cabrera, M. Baitinger, A. Schmeding, Y. Grin, *Angew. Chem.* **1998**, *100*, 1507 – 2509; *Angew. Chem. Int. Ed.* **1998**, *37*, 2359 – 2361; b) V. Queneau, E. Todorov, S. C. Sevov, *J. Am. Chem. Soc.* **1998**, *120*, 3263 – 3264.

[14] a) V. Queneau, S. C. Sevov, *Angew. Chem.* **1997**, *109*, 1818 – 1820; *Angew. Chem. Int. Ed. Engl.* **1997**, *36*, 1754 – 1756; b) C. H. E. Belin, J. D. Corbett, A. Cisar, *J. Am. Chem. Soc.* **1977**, *99*, 7163 – 7169; c) H. G. von Schnering, M. Baitinger, U. Bolle, W. Carrillo-Cabrera, J. Curda, Y. Grin, F. Heinemann, J. Llanos, K. Peters, A. Schmeding, M.

  1433-7851/01/4015-2837 $ 17.50+.50/0

Somer, *Z. Anorg. Allg. Chem.* **1997**, *623*, 1037 – 1039. For some discussions on the paramagnetic E_9^{3-} and $[E_9E_9]^{6-}$ ions (E = Ge, Sn, Pb), see: d) T. F. Fässler, M. Hunziker, *Inorg. Chem.* **1994**, *33*, 5380 – 5381; e) T. F. Fässler, U. Schütz, *Inorg. Chem.* **1999**, *38*, 1866 – 1870; f) T. F. Fässler, M. Hunziker, *Z. Anorg. Allg. Chem.* **1996**, *622*, 837 – 844; g) T. F. Fässler, H.-J. Muhr, M. Hunziker, *Eur. J. Inorg. Chem.* **1998**, 1433 – 1438; h) T. F. Fässler, M. Hunziker, M. E. Spahr, *Z. Anorg. Allg. Chem.* **2000**, *626*, 692 – 700, and references therein.

[15] a) J. D. Corbett, P. A. Edwards, *J. Am. Chem. Soc.* **1977**, *99*, 3313 – 3317; b) D. Kummer, L. Diehl, *Angew. Chem.* **1970**, *82*, 881 – 882; *Angew. Chem. Int. Ed. Engl.* **1970**, *9*, 895; c) B. W. Eichhorn, R. Haushalter, W. T. Pennington, *J. Am. Chem. Soc.* **1988**, *110*, 8704 – 8706; d) R. Burns, J. D. Corbett, *Inorg. Chem.* **1985**, *24*, 1489 – 1492; e) N. Korber, A. Fleischmann, *J. Chem. Soc. Dalton Trans.* **2001**, 383 – 385.

[16] a) V. Queneau, S. C. Sevov, *Inorg. Chem.* **1998**, *37*, 1358 – 1360; b) E. Todorov, S. C. Sevov, *Inorg. Chem.* **1998**, *37*, 3889 – 3891; c) J. Campbell, D. A. Dixon, H. P. A. Mercier, G. J. Schrobilgen, *Inorg. Chem.* **1995**, *34*, 5798 – 5809.

[17] R. M. Friedman, J. D. Corbett, *Inorg. Chem.* **1973**, *12*, 1134 – 1139.

[18] M. E. O'Neill, K. Wade, *J. Mol. Struct.* **1983**, *103*, 259 – 268.

[19] L. L. Lohr, Jr., *Inorg. Chem.* **1981**, *20*, 4229 – 4235.

[20] a) R. W. Rudolph, W. L. Wilson, F. Parker, R. C. Taylor, D. C. Young, *J. Am. Chem. Soc.* **1978**, *100*, 4629 – 4630; b) R. W. Rudolph, W. L. Wilson, R. C. Taylon, *J. Am. Chem. Soc.* **1981**, *103*, 2480 – 2481.

[21] One referee asked about the sources of the disagreement between theory and experiment: the major problems are 1) the quality of the crystals, the role of the counter ions, and packing in the solid states; 2) the choice of model system, the effect of electron correlation, and the size of the employed basis set including relativistic correction.

[22] P. von R. Schleyer, K. Najafian, *Inorg. Chem.* **1998**, *37*, 3454 – 3470.

[23] X. Li, A. E. Kuznetsiv, H.-F. Zhang, A. I. Bodyrev, L.-S. Wang, *Science* **2001**, *291*, 859 – 861; b) D.-K. Seo, J. D. Corbett, *Science* **2001**, *291*, 841 – 842.

  1433-7851/01/4015-2838 $ 17.50+.50/0

Time- and Space-Resolved Luminescence of a Photonic Dye–Zeolite Antenna**

Marc Pauchard, Stefan Huber, Rachel Méallet-Renault, Huub Maas, Robert Pansu, and Gion Calzaferri*

Organic dye molecules tend to form aggregates which are known to cause fast thermal relaxation of the electronically excited states. They are often unstable on irradiation under many conditions. Encapsulation in an appropriate host not only prevents the dyes from dimerization and protects them against unwanted bimolecular reactions and isomerization, but it can also lead to supramolecular organization. We found that zeolite L is a very suitable host material for the development of organic/inorganic composites with photonic antenna properties for light harvesting and transport.[1, 2] Zeolite L is a crystalline aluminosilicate in which connected SiO_4 and AlO_4 tetrahedra give rise to one-dimensional channels arranged in a hexagonal structure.[3–5] Other host materials with linear channels, such as AlPO-5, ZSM-5, and mesostructured systems, have been studied for obtaining new optical materials.[6–11] Control of the shape and size of the crystals is a necessary prerequisite for particular applications. Large crystals of a few hundred to a few thousand nanometers are very useful for studying the optical and photophysical properties of dye–zeolite composites on single crystals by means of optical microscopy methods.[12, 13] Crystals in the range of a few tens to a few hundred nanometers are needed for high-efficiency photonic antenna materials, useful as fluorescent microprobes in cell biology and analytical chemistry,[14] for developing a new generation of dye-sensitized solid-state solar cells,[15] or for preparing a new generation of light-emitting diodes. A synthesis which allows fine tuning of zeolite L materials in the size range from 30 nm to 3000 nm is available.[16] We recently reported the preparation of sophisticated bipolar optical antennae for light harvesting and transport.[17] The principle is based on the use of a zeolite L crystal as the host for organizing several thousand dyes as monomers into well-defined zones (Figure 1 A). After selective excitation of dye1, located in the middle part, the light energy is carried spectrally from the blue to green (dye2) to red (dye3) and spatially from the crystal center to its left and right surface.

The general synthesis concept of this kind of sandwich materials is based on the specific geometrical constraints imposed by the parallel arrangement of one-dimensional channels of the host. Zeolite L crystals usually have cylinder morphology. The number of parallel channels which coincide with the *c* axis of the hexagonal framework is equal to $1.07r_{cyl}^2$, where r_{cyl} is the radius of the crystal in nm. The length of a unit cell along the *c* axis is 0.75 nm. This means that a crystal of, for example, 900 nm diameter and 1500 nm length gives rise to about 217 000 parallel channels, each consisting of 2000 unit cells (u.c.). Under appropriate conditions, molecules enter the channels from both sides with the same probability. For the preparation of the material depicted in Figure 1 A, we first inserted a neutral dye1 from the gas phase, filling the channels to the desired degree (see Scheme 3 in reference [17]). Although neutral dyes are usually displaced by water molecules, conditions could be found under which a cationic dye2 could be added from an aqueous suspension. The process could be sufficiently well controlled so that a specifically desired space was left for the third dye3 to be inserted. This principle can be extended to more than three different dyes.

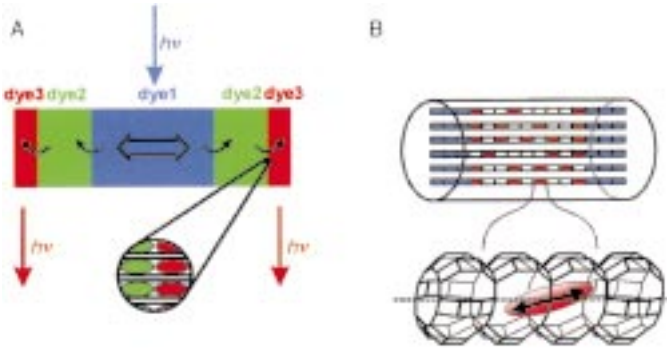

Figure 1. A) Principle of a bipolar three-dye photonic antenna. The enlarged section shows the organization of individual dye molecules at the domain boundary between dye2 and dye3. B) Schematic representation of a cylindrical zeolite L crystal consisting of organized dyes with donor molecules at both ends and acceptor molecules in the middle part. The enlargement shows a detailed view of a channel with a dye and its electronic transition moment (arrow) which is parallel for long molecules and bent for shorter ones with respect to the channel axis. The diameter of the channel windows is 0.71 nm and the largest free diameter is 1.26 nm. The center-to-center distance between two channels is 1.84 nm.

We were interested in reversing the scheme in Figure 1 A and in having a red dye in the center, followed by a green and then a blue one because such systems could become useful for analytical purposes or for developing a new generation of LEDs. It turned out that it is indeed possible to prepare such materials with, for example, Ox^+ (red) in the middle followed by Py^+ (green) and POPOP (blue) (Scheme 1).

The Ox^+ and Py^+ dye molecules are incorporated into the zeolite by ion exchange from an aqueous solution. After drying the loaded zeolite together with the neutral dye at 70 °C/4×10^{-3} mbar in a glass ampoule for 6 h, the ampoule is sealed and the neutral dye is incorporated into the Ox^+/Py^+-loaded zeolite in a rotating oven at 150 °C for 60 h. The ampoule is broken and the zeolite is immediately suspended in dry *n*-butanol. The final product is obtained after washing the zeolite with dry *n*-butanol.

The characterization is simplified when working with relatively large crystals. It is unambiguous when dealing with only two different dyes and we therefore report data on such a

[*] Prof. Dr. G. Calzaferri, Dr. M. Pauchard, Dipl.-Chem. S. Huber, Dipl.-Chem. H. Maas
Department of Chemistry and Biochemistry
University of Berne
3012 Berne (Switzerland)
Fax: (+41) 31-6313994
E-mail: Gion.Calzaferri@iac.unibe.ch
Dr. R. Méallet-Renault, Dr. R. Pansu
PPSM, Ecole Normale Supérieure de Cachan
94235 Cachan Cedex (France)

[**] This work is part of the Swiss National Science Foundation Project NFP 47 (4047-057481).

  1433-7851/01/4015-2839 $ 17.50+.50/0

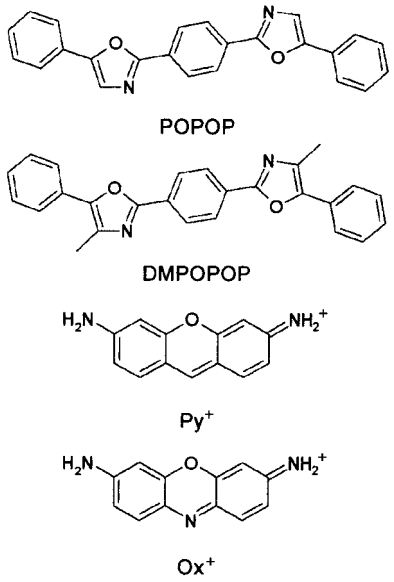

Scheme 1. Dyes used for the introduction into zeolite L.

system (Figure 1B). The rectangles symbolize adsorption sites, consisting of one, two, or more unit cells, depending on the size of the dyes. Red marked rectangles are filled with red-emitting dyes and blue marked ones with blue-emitting dyes. We have realized this by first inserting Ox^+ and then DMPOPOP into zeolite L. This material represents the first dye–zeolite composite with the ability to transport electronic excitation energy from the border of the cylindrical crystal to its center. The dyes were chosen because of their favorable structural and spectroscopic properties. Their absorption and fluorescence spectra (Figure 2A) are well separated in energy so that the individual components can be clearly distinguished. Nevertheless, the spectral overlap $J_{DMPOPOP,Ox^+}$ between the emission of DMPOPOP and the absorption of Ox^+ is sufficient to allow energy transfer from DMPOPOP to Ox^+ ($J_{DMPOPOP,Ox^+} = 6 \times 10^{-14}\ cm^3\,M^{-1}$).

Stationary energy migration experiments were carried out on an ensemble, and space- and time-resolved measurements were made on single crystals containing 0.0475 Ox^+ per u.c. located in the middle and 0.043 DMPOPOP per u.c. at both ends. An Ox^+ molecule occupies two unit cells and a DMPOPOP molecule three of them, due to their size. This means that the occupation probability per site was 0.095 and 0.13, respectively. The energy transfer from excited DMPOPOP molecules to an Ox^+ molecule can be observed upon specific excitation of the DMPOPOP molecule at 325 nm (Figure 2B). We show, as a reference (dashed line in Figure 2B), the luminescence observed for a sample containing the same amount of Ox^+, but no DMPOPOP. From this it is evident that the appearance of the emission above 600 nm is due to energy transfer from excited DMPOPOP to Ox^+.

Important results were obtained in single-crystal experiments. We know that the $S_1 \leftrightarrow S_0$ π,π^* electronic transition moment of Ox^+ shows a cone-shaped distribution with a half-cone angle of 72° with respect to the channel axis, while it is parallel for DMPOPOP.[12] Observing crystals in a microscope equipped with polarizers, an appropriate set of filters, and using an immersion lens, one can see the pictures shown in Figure 3B. The blue emission on the left is observed through a polarizer parallel to the cylinder axis when specifically exciting DMPOPOP at $\lambda = 330-385$ nm, while the red emission in the middle is seen when the polarizer is turned into the vertical position. The picture on the right-hand side is observed without polarizer upon excitation of Ox^+ at $\lambda = 545-580$ nm. The shape of the crystal as determined by electron microscopy is shown in Figure 3C.

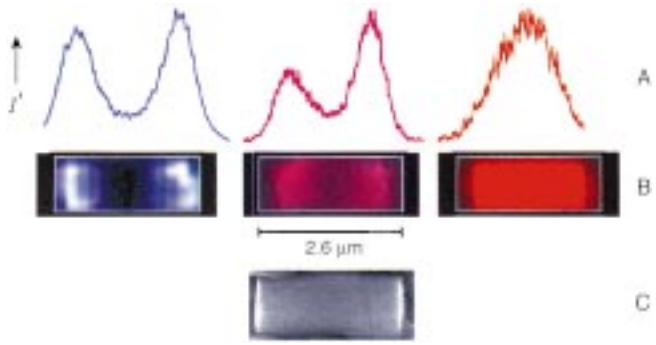

Figure 3. A) Scanning confocal optical microscopy results of a DMPOPOP,Ox^+–zeolite L crystal. B) Immersion microscopy images. C) Side view of a zeolite crystal observed by means of electron microscopy. For details see text.

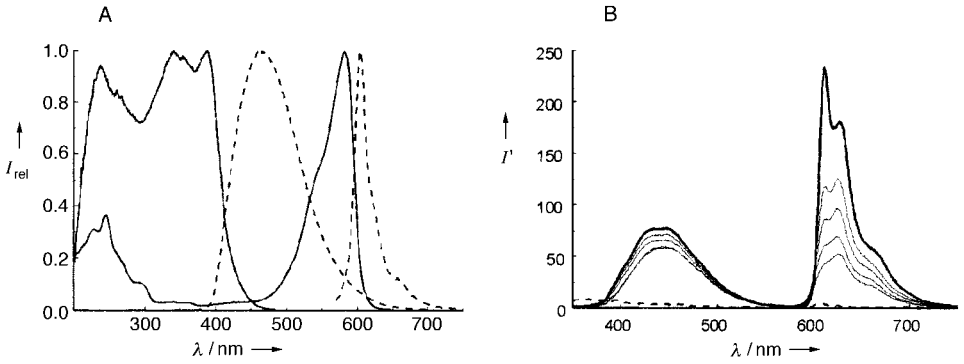

Figure 2. A) Excitation (solid) and emission (dashed) spectra of DMPOPOP–zeolite L in 1-butanol (388 nm, 464 nm) and of Ox^+–zeolite L in water (595 nm, 605 nm); ($\varepsilon_{DMPOPOP}$ (λ_{max}) ~ 50000 $L\,mol^{-1}\,cm^{-1}$, ε_{Ox^+} (λ_{max}) ~ 84000 $L\,mol^{-1}\,cm^{-1}$). The spectra are scaled to the same height (I_{rel}). In the confocal microscopy experiments DMPOPOP was excited at 320 nm and the emission detected at 470 nm, whereas Ox^+ was excited at 490 nm and the emission detected at 660 nm. B) Temperature dependence of the luminescence of DMPOPOP,Ox^+–zeolite L samples upon excitation at 325 nm (bold spectrum is at 80 K, the others at higher temperatures up to room temperature). The dashed line is the luminescence of Ox^+–zeolite L upon excitation at 330 nm at 80 K (as a reference). I' = photon count in Hz.

Confocal microscopy data were measured by means of instrumentation which has been reported in reference [18]. The intensity profile on the left of Figure 3A was observed when scanning the emission at 470 nm along the crystal axis, upon excitation at 320 nm. The profile in the middle was observed when monitoring the emission at $\lambda >$ 610 nm after excitation at

  1433-7851/01/4015-2840 $ 17.50+.50/0

320 nm, while the profile on the right was seen when the sample was excited at 490 nm. These data show that the organization of the dyes inside the crystal corresponds to the scheme in Figure 1B. They also beautifully illustrate the energy transfer from the DMPOPOP to the Ox^+ and that the energy migration length of excited Ox^+ is not sufficient to fill such large crystals homogeneously, as expected from theoretical considerations.[1] Energy transfer and migration in this system is governed by the dipole–dipole mechanism, which is also known as Förster energy transfer.[19–21]

The fluorescence decay of DMPOPOP observed on a single DMPOPOP–zeolite L crystal excited at 320 nm can be roughly described by a biexponential (31%, 3.35 ns; 69%, 1.0 ns) with an average fluorescence lifetime of 1.78 ns (Figure 4A, blue). The decay of Ox^+ observed on a single DMPOPOP,Ox^+–zeolite L crystal excited at 495 nm is also biexponential (57%, 2.6 ns; 43%, 0.5 ns) with an average fluorescence lifetime of 1.71 ns (Figure 4A, green). The decay of DMPOPOP in such a crystal excited at 320 nm and observed at 470 nm is more complex and has an average fluorescence lifetime of 300 ps (Figure 4A, red). The reason for this is that energy transfer takes place from excited DMPOPOP to Ox^+. The reduction of the excited donor lifetime expectancy by a factor of 6 means that 83% of the absorbed photons are transferred from excited DMPOPOP to Ox^+ by Förster energy transfer.

After excitation of a DMPOPOP,Ox^+–zeolite L crystal at 320 nm, the Ox^+ emission was measured at different positions in the crystal. The emission wavelength was chosen above 660 nm to make sure that no DMPOPOP emission was mixed in. Four regions indicated by the colors yellow, red, green, and blue can be distinguished (Figure 4B and C). The yellow signal outside the crystal is due to noise and scattered photons. The red signal, observed at the border of the crystal, originates from excited Ox^+ molecules that are very close to the DMPOPOP molecules. They have a fast rise time and decay. The rise time is somewhat slower if we move further into the crystal (green) and it is substantially delayed in the middle part of the crystal (blue). The presence of a slow rise time and of a delayed decay shows that Ox^+ fluorescence is excited indirectly through DMPOPOP. The spatial dependence of this effect beautifully demonstrates the dynamics of the energy transfer and energy migration from the border of the crystal to the center, which means that our dream of an "inverted photonic antenna" as illustrated in Figure 1B has become reality. This is a sound basis for detailed experimental and theoretical studies of the challenging opportunities of supramolecularly organized dyes in the channels of appropriate microporous host materials for light harvesting, transport, and trapping.

Received: February 21, 2001 [Z16656]

[1] N. Gfeller, G. Calzaferri, *J. Phys. Chem.* **1997**, *101*, 1396.
[2] G. Calzaferri, D. Brühwiler, S. Megelski, M. Pfenniger, M. Pauchard, B. Hennessy, H. Maas, A. Devaux, U. Graf, *Solid State Sci.* **2000**, *2*, 421.
[3] D. W. Breck, *Zeolite Molecular Sieves*, Wiley, New York, **1974**.
[4] W. M. Meier, D. H. Olsen, C. Bärlocher, *Atlas of Zeolite Structure Types*, Elsevier, London, **1996**.
[5] T. Ohsuna, Y. Horikawa, K. Hiraga, *Chem. Mater.* **1998**, *10*, 688.

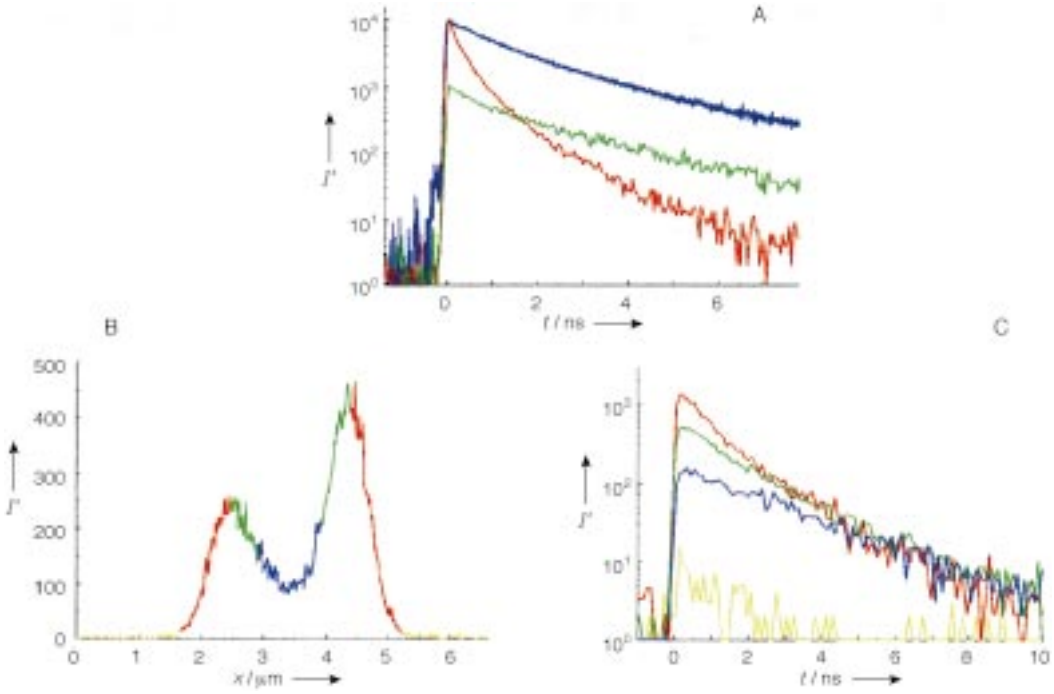

Figure 4. Luminescence decay on single dye-loaded zeolite L crystals in a confocal microscope. A) Decay observed as an average over the whole crystal. Blue: Decay of DMPOPOP fluorescence at 470 nm when a DMPOPOP-zeolite L crystal is excited at 320 nm with 1.2-ps pulses. Green: Decay of Ox^+ luninescence at (600 ± 4) nm when a DMPOPOP,Ox^+–zeolite L crystal is excited at 495 nm. Red: Decay of DMPOPOP luminescence at 470 nm when a DMPOPOP,Ox^+–zeolite L crystal is excited at 320 nm. B and C) Time- and space-resolved confocal microscopy results for a DMPOPOP,Ox^+–zeolite L crystal. B) Decay of the Ox^+ emission similar to that in Figure 3A (middle) but with the different regions indicated by different colors (yellow, red, green, and blue). C) Decay of the luminescence of Ox^+ above 660 nm when a DMPOPOP,Ox^+–zeolite L crystal is excited at 320 nm at the different positions indicated in B).

  1433-7851/01/4015-2841 $ 17.50+.50/0

[6] G. Schulz-Ekloff, D. Wöhrle, B. van Duffel, R. A. Schoonheydt, *Microporous Mesoporous Mater.*, in press.
[7] U. Vietze, O. Krauss, F. Laeri, G. Ihlein, F. Schüth, B. Limburg, M. Abraham, *Phys. Rev. Lett.* **1998**, *81*, 4628.
[8] T. Bein, *Chem. Mater.* **1996**, *8*, 1636.
[9] L. Werner, J. Caro, G. Finger, J. Kornatowski, *Zeolites* **1992**, *12*, 658.
[10] V. Ramamurthy in *Photochemistry in Organized and Constraint Media* (Ed.: V. Ramamurthy), VCH, New York, **1991**, chap. 10.
[11] G. Wirnsberger, G. D. Stucky, *ChemPhysChem* **2000**, *1*, 90.
[12] S. Megelski, A. Lieb, M. Pauchard, A. Drechsler, S. Glaus, C. Debus, A. J. Meixner, G. Calzaferri, *J. Phys. Chem. B* **2001**, *105*, 25.
[13] M. Pfenniger, G. Calzaferri, *ChemPhysChem* **2000**, *4*, 211.
[14] J. R. Lacowicz, *Principles of Fluorescence Spectroscopy*, 3rd ed., Kluwer/Plenum, New York, **1999**.
[15] D. L. Dexter, *J. Lumin.* **1979**, *18/19*, 779.
[16] S. Megelski, G. Calzaferri, *Adv. Funct. Mater.* **2001**, in press.
[17] M. Pauchard, A. Devaux, G. Calzaferri, *Chem. Eur. J.* **2000**, *6*, 3456.
[18] L. Schoutteten, P. Denjean, R. B. Pansu, *J. Fluoresc.* **1997**, *7*, 155.
[19] T. Förster, *Ann. Phys. Leipzig* **1948**, *2*, 55; T. Förster, *Fluoreszenz Organischer Verbindungen*, Vandenhoeck & Ruprecht, Göttingen, **1951**.
[20] D. L. Dexter, *J. Phys. Chem.* **1952**, *21*, 836.
[21] H. Kuhn, *J. Chem. Phys.* **1964**, *41*, 652.

A Fully Characterized Complex Ion with Unreduced TCNQ as Fourfold Bridging Ligand: $[(\mu_4\text{-TCNQ})\{fac\text{-Re(CO)}_3\text{(bpy)}\}_4]^{4+}$**

Heiko Hartmann, Wolfgang Kaim,* Ingo Hartenbach, Thomas Schleid, Matthias Wanner, and Jan Fiedler

Coordination compounds of 7,7,8,8-tetracyano-*p*-quinodimethane (TCNQ) and of the related tetracyanoethene (TCNE)[1] have found wide interest in materials science as potential organic conductors[2] and molecular magnets.[3] As universal π-acceptor components and archetypical "non-innocent" ligands, these TCNX molecules can exist in several readily accessible oxidation states ($TCNX^0$, paramagnetic $TCNX^{\bullet-}$ or $TCNX^{2-}$), they may form stacks with mixed valency, they can be coordinated through the carbon π system, or act as σ donors through the nitrile-N atoms and thus bind (bridge) up to four metal centers. All these features have led to a wide variety of unusual geometrical and electronic structures.[1] Although discrete complexes with tetranucleating TCNQ or TCNE ligands have been reported with manganese,[4] ruthenium,[5] osmium,[6] iron,[7] rhenium,[8] and copper,[9] no structural information has been obtained yet for such species. Based on spectroscopic data, some of these systems were described as tetrametalla π systems with extensive metal/ligand electron delocalization.[4–6] On the other hand, there has been a number of structurally characterized coordination polymers involving silver,[10, 11] dimolybdenum,[12] diruthenium,[13] and dirhodium units;[13] however, these extended systems could not be studied as individual entities in solution, for example, by electrochemical methods.

Using the nitrile-binding and potentially π back-donating organometallic complex fragment $[Re(CO)_3(bpy)]^+$ (bpy = 2,2′-bipyridine),[14] we have now obtained the tetranuclear complex cation $[(\mu_4\text{-TCNQ})\{fac\text{-Re(CO)}_3\text{(bpy)}\}_4]^{4+}$ (**1**),[15] which has unprecedented electronic characteristics and which could be structurally studied as the tetrakis(hexafluorophosphate) salt.[16]

There are no unusual interionic contacts in the crystal, especially no indications for coordination polymer formation. Figure 1 illustrates that the TCNQ molecule acts as an

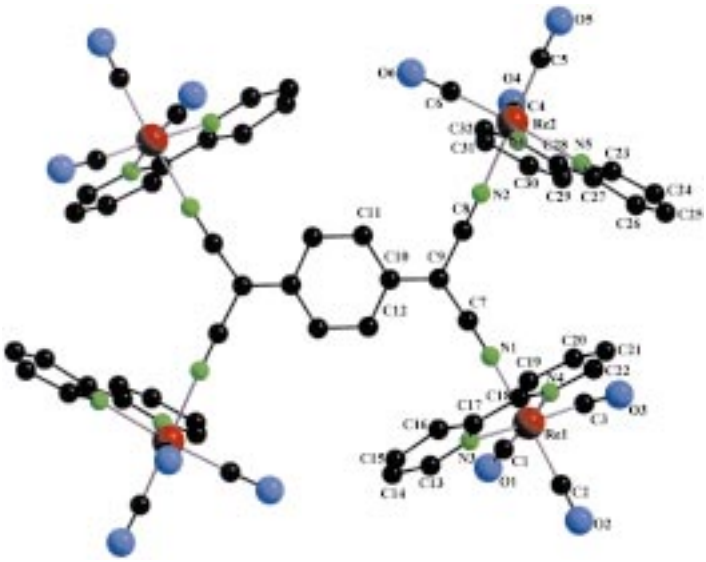

Figure 1. Molecular structure of the tetracation **1** in the crystal of $[(\mu_4\text{-TCNQ})\{fac\text{-Re(CO)}_3\text{(bpy)}\}_4](PF_6)_4$ (**1**-$(PF_6)_4$). Selected bond lengths [Å] and angles [°]: Re1-N1 2.098(7), Re1-N3 2.175(8), Re1-N4 2.137(10), Re2-N2 2.121(8), Re2-N5 2.216(10), Re2-N6 2.161(10), C7-C9 1.390(14), C8-C9 1.487(13), C9-C10 1.377(14), C10-C11 1.423(14), C11-C12 1.372(16), C10-C12 1.453(15), Re1-Re2 8.18, Re1-Re2A 10.02, Re1-Re1A 12.97, Re2-Re2A 12.89; C9-C7-N1 176.0(10), C9-C8-N2 178.2(11), C7-N1-Re1 170.9(8), C8-N2-Re2 174.2(9).

esentially planar $\mu_4,\eta^1{:}\eta^1{:}\eta^1{:}\eta^1$-bridging ligand towards four cations $[fac\text{-Re(CO)}_3\text{(bpy)}]^+$. In comparison to TCNQ, $TCNQ^{\bullet-}$ and the coordination polymers referred to above,[13] the bond parameters of the bridging molecule in the cation **1** point to relatively little metal-to-ligand π-electron delocalization, as illustrated by the bond length of 1.377(14) Å for the exocyclic bond (C9–C10). This bond should lengthen towards a C–C single bond value on significant electron acquisition by TCNQ.[1] The binding of $[fac\text{-Re(CO)}_3\text{(bpy)}]^+$ by the nitrile groups of TCNQ occurs in two different conformations, either

[*] Prof. Dr. W. Kaim, Dipl.-Chem. H. Hartmann, Dipl.-Chem. I. Hartenbach, Prof. Dr. T. Schleid, Dipl.-Chem. M. Wanner
Institut für Anorganische Chemie
Universität Stuttgart
Pfaffenwaldring 55, 70550 Stuttgart (Germany)
Fax: (+49) 711-685-4165
E-mail: kaim@iac.uni-stuttgart.de
Dr. J. Fiedler
J. Heyrovsky Institute of Physical Chemistry
Academy of Sciences of the Czech Republic
Dolejškova 3, 18223 Prague (Czech Republic)

[**] This work was supported by the Deutsche Forschungsgemeinschaft and the Fonds der Chemischen Industrie. TCNQ = 7,7,8,8-tetracyano-*p*-quinodimethane, bpy = 2,2′-bipyridine.

  1433-7851/01/4015-2842 $ 17.50+.50/0

with the bpy coligand inversion-symmetrically situated above or below the C-N-Re axis (at Re1) or with the bpy molecule twisted away from the center of the tetracation (at Re2). While the structural data already suggest a relatively small extent of π back-donation from the organorhenium centers towards highly π-accepting TCNQ, the electrochemical results are even more striking (Table 1).

Table 1. Reduction potentials E[a] of TCNQ and its tetranuclear complexes $[(\mu_4\text{-TCNQ})\{ML_n\}_4]^k$.

$\{ML_n\}$	k	E_{red1}	E_{red2}	K_c[b]	Medium[c]	Ref.
$\{Re(CO)_3(bpy)\}$	4+	+0.45[d]	+0.09[d]	$10^{6.1}$	CH_2Cl_2	this work
$\{Os(PiPr_3)_2(CO)(H)Cl\}$	0	−0.20	−0.94	$10^{12.5}$	CH_2Cl_2	[6b]
– (free TCNQ)	0	−0.29	−0.88	$10^{10.0}$	CH_2Cl_2	[6b]
– (free TCNQ)	0	−0.25	−0.97	$10^{12.2}$	CH_3CN	[5b]
– (free TCNQ)	0	−0.19[e]	−0.78[e]	$10^{10.0}$	DMF	[4]
$\{Ru(NH_3)_5\}$	8+	−0.59	−0.84	$10^{4.2}$	CH_3CN	[5b]
$\{Mn(CO)_2(C_5Me_5)\}$	0	−0.58[e]	−0.80[e,f]	$\approx 10^{3.2}$	DMF	[4]
$\{Fe(dppe)(C_5H_5)\}$[g]	4+	−1.15[e]	−1.30[e]	$10^{2.5}$	CH_2Cl_2	[7]

[a] Potentials in V versus Fc^+/Fc^0. [b] Comproportionation constant for the one-electron-reduced intermediate: $K_c = 10^{(E_{red1}-E_{red2})/59\ mV}$. [c] 0.1M Bu_4NPF_6 as electrolyte. [d] Converted from measurements vs. cobaltocenium/cobaltocene (−1.35 V vs. Fc^+/Fc^0). [e] Converted from measurements vs. SCE (−0.50 V vs. Fc^+/Fc^0). [f] Peak potential for irreversible reduction. [g] dppe = 1,2-bis(diphenylphosphanyl)ethane.

In contrast to the other discrete complexes $[(\mu_4\text{-TCNQ})\{ML_n\}_4]^k$ studied so far,[4–7] the cation **1** is much easier to reduce (by 0.74 V!) than the free TCNQ ligand (Table 1). Such behavior would be expected for metal complexes of conventional π-acceptor ligands such as bipyridines and related molecules.[14, 17] However, the extremely strong π-accepting capacity of TCNQ usually results in a situation with negative shifts of the reduction potentials (Table 1) where metal-to-ligand electron transfer through π back-donation overcompensates the effect from the σ polarization exerted by the Lewis acidic metal centers, leading to an anionic TCNQ ligand.[1, 4–7] In other words, the "normal" effect[17] of a large positive shift of the ligand reduction potential upon metal coordination would be the exception for ligands such as TCNQ[4, 18] and it has been observed here for the first time.

Table 1 illustrates the variability of the comproportionation constant K_c of the paramagnetic intermediate in the typical two-step reduction sequence for TCNQ and its tetranuclear complexes. In this respect, the tetrarhenium compound adopts an intermediate position between strongly metal–ligand π-coupled systems (small K_c) and free TCNQ (large K_c). Oxidation of the complex cation occurs irreversibly at a very high potential of +1.45 V versus ferrocenium/ferrocene (Fc^+/Fc^0).

Vibrational spectroscopic data are in agreement with the interpretation of the structural and the electrochemical results: At 2241 cm^{-1} in nujol, the single nitrile stretching band of **1**-$(PF_6)_4$ is shifted to *higher* energies than in free TCNQ (2228 cm^{-1}), in contrast to what is usually observed.[1, 4–9] The δ(CH) bending mode of coordinated TCNQ is found at 840 cm^{-1}, which has usually been interpreted as an indication of "partial reduction" of the TCNQ ligand.[13]

The absorption spectrum of **1**-$(PF_6)_4$ in CH_2Cl_2 shows an intense metal-to-ligand charge transfer (MLCT) band at 680 nm. This value is distinctly lower than the charge transfer (MLCT or LMCT)[18] maxima observed for tetranuclear TCNQ complexes of manganese (1418 nm in toluene),[4b] ruthenium (935 nm in acetonitrile),[5b] osmium (1170 nm in 1,2-dichloroethane),[6b] or iron (1008 nm in CH_2Cl_2).[7] Even poorly soluble $[(\mu_4\text{-TCNQ})\{Re(CO)_4Cl\}_4]$ has an absorption maximum at 990 nm in toluene.[8] The intra-ligand $\pi \rightarrow \pi^*$ transition is shifted from 395 nm in free TCNQ to 382 nm in **1**.

One-electron reduction to $[(\mu_4\text{-TCNQ})\{fac\text{-}Re(CO)_3(bpy)\}_4]^{3+}$ produces new absorption bands at 1020, 905, 425(sh), and 405 nm (Figure 2). The first three bands signify a slightly perturbed $TCNQ^{\bullet-}$ chromophore (free $TCNQ^{\bullet-}$ has 842, 761, and 420 nm[19]); the band at 405 nm is tentatively attributed to a hypsochromically shifted MLCT transition.[5b] The ESR signal of the paramagnetic trication in glassy frozen CH_2Cl_2 at 3.4 K or 110 K exhibits two g components at $g_1 = 2.014$ and $g_{2,3} = 2.006$. This small g anisotropy despite the presence of four rhenium atoms with their large spin–orbit coupling contributions supports the notion of TCNQ-localized spin.[5b, 6b]

This assignment is further supported by results from IR spectroelectrochemistry in dichloromethane.[15] Whereas the metal carbonyl stretching bands move only by about 10 cm^{-1} or less on successive electron acquisition by **1**, the nitrile stretching bands are shifted from 2235 cm^{-1} via 2223 and 2182 cm^{-1} for the trication to 2210 and 2149 cm^{-1} for the doubly reduced species.

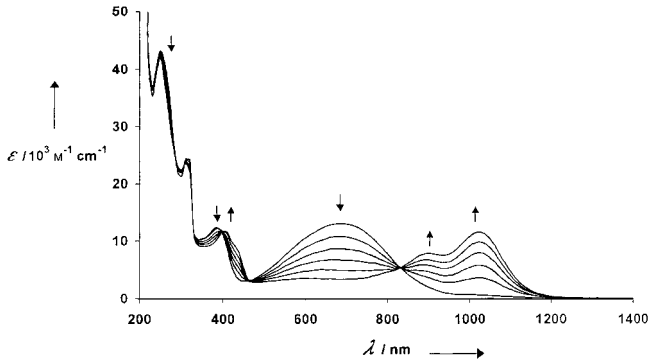

Figure 2. Spectral response of **1**-$(PF_6)_4$ on one-electron reduction in CH_2Cl_2/0.1M Bu_4NPF_6.

In summary, we have not only obtained the first structure analysis of a discrete tetranuclear complex of TCNQ, **1** is also the first such well-characterized TCNQ species which exhibits the "normal" response of metal coordination to a π-acceptor ligand. As a consequence, the fourfold coordination of rhenium(I) causes a shift of +0.74 V for the potential of a clearly TCNQ-based reduction—a remarkable result considering the already very facile reduction of free TCNQ and the capacity of rhenium(I) species for π back-donation. Further study of the stabilized reduced states will be our next objective. Since bis-chelating α-diimines of the bpy type are available[20] and the *fac*-$Re(CO)_3$ group is well suited to act as innocent anchoring corner in molecular rectangles[20] or inorganic clusters,[21] the discrete ion presented here can serve as a starting point for more extended systems.

Received: March 16, 2001 [Z16780]

[1] W. Kaim, M. Moscherosch, *Coord. Chem. Rev.* **1994**, *129*, 157.
[2] a) T. Seto, M. Inoue, M. M. Inoue, D. Nakmaura, *Bull. Chem. Soc. Jpn.* **1983**, *56*, 1903; b) G. Long, R. D. Willett, *Inorg. Chim. Acta* **2001**, *313*, 1.
[3] a) J. S. Miller, A. J. Epstein, *Angew. Chem.* **1994**, *106*, 399; *Angew. Chem. Int. Ed. Engl.* **1994**, *33*, 385; b) J. S. Miller, A. J. Epstein, *Chem. Eng. News* **1995**, *73*(40), 30; c) D. C. Gordon, L. Deakin, A. M. Arif, J. S. Miller, *J. Am. Chem. Soc.* **2000**, *122*, 290; d) K. I. Pokhodnya, A. J. Epstein, J. S. Miller, *Adv. Mater.* **2000**, *12*, 410.
[4] a) R. Gross, W. Kaim, *Angew. Chem.* **1987**, *99*, 257; *Angew. Chem. Int. Ed. Engl.* **1987**, *26*, 251; b) R. Gross-Lannert, W. Kaim, B. Olbrich-Deussner, *Inorg. Chem.* **1990**, *29*, 5046.
[5] a) M. Moscherosch, W. Kaim, *Inorg. Chim. Acta* **1993**, *206*, 229; b) M. Moscherosch, E. Waldhör, H. Binder, W. Kaim, J. Fiedler, *Inorg. Chem.* **1995**, *34*, 4326.
[6] a) F. Baumann, M. Heilmann, W. Matheis, A. Schulz, W. Kaim, J. Jordanov, *Inorg. Chim. Acta* **1996**, *251*, 239; b) F. Baumann, W. Kaim, J. A. Olabe, A. Parisse, J. Jordanov, *J. Chem. Soc. Dalton Trans.* **1997**, 4455.
[7] C. Diaz, A. Arancibia, *Polyhedron* **2000**, *19*, 137.
[8] M. Leirer, G. Knör, A. Vogler, *Inorg. Chem. Commun.* **1999**, *2*, 110. For a trinuclear complex $[(\mu_3\text{-TCNQ})\{Re(CO)_5\}_3](BF_4)_3$ see: W. Sacher U. Nagel, W. Beck, *Chem. Ber.* **1987**, *120*, 895.
[9] S. Berger, H. Hartmann, M. Wanner, J. Fiedler, W. Kaim, *Inorg. Chim. Acta* **2001**, *314*, 22.
[10] L. Shields, *J. Chem. Soc. Faraday Trans. 2* **1985**, *81*, 1.
[11] S. A. O'Kane, R. Clérac, H. Zhao, X. Ouyang, J. R. Galán-Mascarós, R. Heintz, K. R. Dunbar, *J. Solid State Chem.* **2000**, *152*, 159.
[12] C. Campana, K. R. Dunbar, X. Ouyang, *Chem. Commun.* **1996**, 2427.
[13] H. Miyasaka, C. S. Campos-Fernández, R. Clérac, K. R. Dunbar, *Angew. Chem.* **2000**, *112*, 3989; *Angew. Chem. Int. Ed.* **2000**, *39*, 3831.
[14] a) A. Klein, C. Vogler, W. Kaim, *Organometallics* **1996**, *15*, 236; b) S. Berger, A. Klein, W. Kaim, J. Fiedler, *Inorg. Chem.* **1998**, *37*, 5664.
[15] A mixture containing $[Re(CO)_3(bpy)Cl]$ (300 mg, 0.650 mmol) and $AgPF_6$ (176 mg, 0.696 mmol) in dichloromethane (20 mL) and methanol (5 mL) was stirred for 18 h at room temperature. After filtration over celite and removal of the solvents the yellow residue was redissolved in CH_2Cl_2 (20 mL) and treated with a solution of TCNQ (33 mg, 0.163 mmol) in CH_2Cl_2 (10 mL). To the blue solution formed after 8 h (IR monitoring) *n*-pentane was added (10 mL). Cooling to $-30\,^{\circ}C$ produced a dark blue precipitate which was collected, redissolved in dichloromethane, and reprecipitated with *n*-pentane. Drying under vacuum yielded **1**-$(PF_6)_4$ (150 mg; 37 %). Elemental analysis calcd (%) for $C_{64}H_{36}F_{24}N_{12}O_{12}P_4Re_4$: C 30.87, H 1.46, N 6.75; found: C 30.65, H 1.46, N 6.40; ^{1}H NMR (CD_2Cl_2): $\delta = 7.32$ (s, 4H; TCNQ-H), 7.71 (dd, 8H; $H^{5,5'}$(bpy)), 8.26 (dd, 8H; $H^{4,4'}$(bpy)), 8.43 (d, 8H; $H^{3,3'}$(bpy)), 8.99 (d, 8H; $H^{6,6'}$(bpy)); IR (nujol): $\tilde{\nu} = 2241$ (ν(CN)), 2031, 1967, 1950 (ν(CO)), 840 cm^{-1} (δ(CH)); IR spectroelectrochemistry (CH_2Cl_2/0.1 M Bu_4NPF_6): tetracation: $\tilde{\nu} = 2235$ (ν(CN)), 2039, 1956, 1945 cm^{-1} (ν(CO)); trication: $\tilde{\nu} = 2223$, 2182 (ν(CN)), 2038, 1945, 1940sh cm^{-1} (ν(CO)); dication: 2210(br), 2149 (ν(CN)), 2036, 1934(br) cm^{-1} (ν(CO)); UV/Vis (CH_2Cl_2): λ_{max} (ε) = 680 (13100), 382 (12400), 321 (26700) nm ($M^{-1}cm^{-1}$); UV/Vis spectroelectrochemistry (CH_2Cl_2/0.1 M Bu_4NPF_6): trication: $\lambda_{max}(\varepsilon) = 1020$ (12100), 905 (9000), 425(sh), 405 (11800), 305 (23600) nm ($M^{-1}cm^{-1}$).
[16] Single crystals were obtained from a saturated solution in CD_2Cl_2. $C_{64}H_{36}F_{24}N_{12}O_{12}P_4Re_4$: Dark blue rods, $0.8 \times 0.1 \times 0.05$ mm, monoclinic, space group $P2_1/n$, $a = 10.3137(4)$, $b = 22.0360(5)$, $c = 20.6476(6)$ Å, $\beta = 97.2520(1)^{\circ}$, $V = 4655.1(2)$ Å^3, $T = 293$ K, $Z = 2$, $\rho_{calcd} = 1.776$ g cm^{-3}, $\mu(Mo_{K\alpha}) = 5.356$ cm^{-1}, 17485 reflections measured, 6048 observed with $I > 2\sigma(I)$. $R_1 = 0.0603$, $wR_2 = 0.1564$, GOF = 1.026, min/max electron density $-0.938/0.949$ e Å^{-3}. Crystallographic data (excluding structure factors) for the structure reported in this paper have been deposited with the Cambridge Crystallographic Data Centre as supplementary publication no. CCDC-160093. Copies of the data can be obtained free of charge on application to CCDC, 12 Union Road, Cambridge CB2 1EZ, UK (fax: (+44) 1223-336-033; e-mail: deposit@ccdc.cam.ac.uk).
[17] a) W. Kaim, B. Olbrich-Deussner, R. Gross, S. Ernst, S. Kohlmann, C. Bessenbacher in *Importance of Paramagnetic Organometallic Species in Activation, Selectivity and Catalysis* (Ed.: M. Chanon), Kluwer, Dordrecht, **1989**, p. 283; b) R. Gross, W. Kaim, *J. Organomet. Chem.* **1987**, *333*, 347.
[18] a) B. Olbrich-Deussner, R. Gross, W. Kaim, *J. Organomet. Chem.* **1989**, *366*, 155; b) B. Olbrich-Deussner, W. Kaim, R. Gross-Lannert, *Inorg. Chem.* **1989**, *28*, 3113.
[19] L. R. Melby, R. J. Harder, W. R. Hertler, W. Mahler, R. E. Benson, W. E. Mochel, *J. Am. Chem. Soc.* **1962**, *84*, 3374.
[20] H. Hartmann, S. Berger, R. Winter, J. Fiedler, W. Kaim, *Inorg. Chem.* **2000**, *39*, 4977.
[21] F. M. Hornung, K. W. Klinkhammer, W. Kaim, *Chem. Commun.* **1998**, 2055.

Targeting Molecular Recognition: Exploring the Dual Role of Functional Pseudoprolines in the Design of SH3 Ligands**

Gabriele Tuchscherer,* Daniel Grell, Yoshiro Tatsu, Patricia Durieux, Jimena Fernandez-Carneado, Beatrice Hengst, Christian Kardinal, and Stephan Feller*

Protein–protein interactions that are mediated by the binding of proline-rich sequences are involved in a large variety of cellular processes, for example, signal transduction, motility, membrane trafficking, and cell division.[1–5] Such proline-rich ligands adopt a left-handed polyproline II (PPII) helical conformation and bind to a highly conserved patch of aromatic amino acids. These residues are positioned to accommodate the unique geometric properties of a PPII helix on the recognition surface of, for example, SH3 domains, and to participate in van der Waals contacts and specific hydrogen bonds between carbonyl oxygen atoms of the ligand backbone and functionalities on the aromatic residues of the protein.[6] SH3 domains are enticing conceptual targets for pharmacological intervention in a number of pathologies, for example, AIDS, cancer, and inflammatory diseases, since they occur in several critical, intracellular signaling proteins.[5b, 7] The essential feature of most SH3 binding ligands is the consensus sequence Pro-Xaa-Xaa-Pro (where Xaa represents various amino acids).[8] Synthetic[5, 9] and phage-displayed[7, 10] combinatorial peptide libraries have been generated to understand the ligand properties in more detail, and these studies have yielded compounds that in general bind to SH3 domains with equal or slightly lower affinity than natural Pro-

[*] Priv.-Doz. Dr. G. Tuchscherer, Dr. D. Grell, Dr. Y. Tatsu, Dipl.-Chem. P. Durieux, Dipl.-Chem. J. Fernandez-Carneado, Dr. B. Hengst
Institut für Organische Chemie
Universität Lausanne
BCH-Dorigny, 1015 Lausanne (Switzerland)
Fax: (+41) 21-692-3955
E-mail: gabriele.tuchscherer@ico.unil.ch
Priv.-Doz. Dr. S. Feller, Dr. C. Kardinal
Labor für Molekulare Onkologie, MSZ
Universität Würzburg
97078 Würzburg (Germany)
Fax: (+49) 931-201-3835
E-mail: stephan.feller@mail.uni-wuerzburg.de

[**] This work was supported by the Swiss National Science Foundation.

Xaa-Xaa-Pro peptides. A step further in the design of SH3 inhibitors with improved affinity and selectivity was taken by introducing non-natural, N-substituted residues at key positions in a mSoS-derived ("son of sevenless", a guanine nucleotide exchange factor, m = mouse) dodecapeptide. It was argued that N-substituted peptoids with various side chains can be used for optimizing complementarity, and hence affinity, by increasing the number of contacts between the ligand and the domain.[5c,d]

However, a left-handed PPII conformation of the peptide remains a structural requirement for the effective binding of proline-rich ligands to SH3 domains. On the basis of these considerations the recently introduced concept of pseudoprolines (ΨPro), that is, Ser-, Thr-, or Cys-derived proline-like structures (Figure 1) with enhanced inherent properties of natural L-Pro,[11] offers a new path for further design strategies.[12] In particular, the nature of the substituents (R^1 and R^2) at the C2 position of ΨPro permits the *cis*/*trans* isomerization equilibrium to occur and thus the polyproline helix transitions (PPI/PPII) to be tailored.[11a,b]

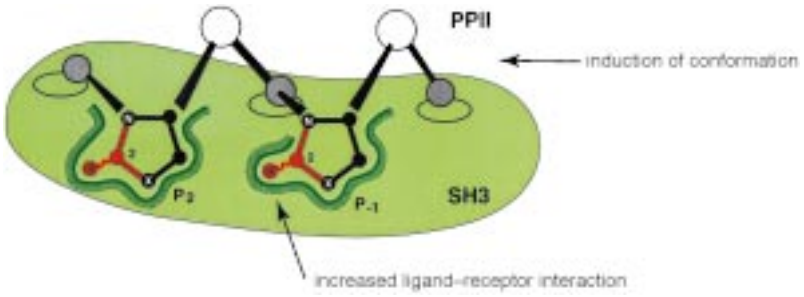

Figure 1. The dual role of functional pseudoprolines (ΨPro) in ligand recognition by the SH3 domain (gray and white spheres resemble amino acids): The formation of the schematically represented PPII helical conformation is a prerequisite for the binding of Pro-rich regions to SH3 domains. Favorable contributions for high affinity binding—complementarity in shape and thus close packing of the side chains—are not provided because of the lack of functional groups in the proline ring structure. The dual functionality of ΨPro, that is, induction of the PPII helical conformation and optimization of van der Waals contacts through the C2 substituents R^1 and R^2, leads to optimized packing and thus to higher affinity and potential specificity.

Besides its potential for adopting a PPII helical conformation, the incorporation of substituents of variable size and polarity at the C2 position of ΨPro offers a powerful tool to modulate the ligand–receptor interactions. As depicted in Figure 1, ΨPro building blocks exert a dual functionality in 1) inducing and stabilizing the relevant PPII conformation and 2) increasing and optimizing the van der Waals contacts and the formation of hydrogen bonds to the receptor. Most notably, the generation of a library of different substituents at C2 allows the factors contributing to affinity and specificity in protein–protein interactions to be explored, and to further elucidate ligand recognition by SH3 domains at a molecular level.

To exploit this principle for the design of novel SH3 ligands, the two proline residues at positions P_{-1} and P_2 in the SoS-derived peptide Val-Pro-Xaa-Pro-Val-Ser-Xaa-Pro-Lys-Lys-Lys (**1**) were replaced by ΨPro moieties (Xaa = Ser($\Psi pro^{Ph,H}$)).[13] Molecular modeling studies based on existing crystal structures revealed that C2-monosubstituted ΨPro systems with an *S* configuration results in energetically more favorable receptor interactions relative to the corresponding *R* epimers. The slightly tilted phenyl group at the *S*-configured center can be readily accommodated at sites P_{-1} and P_2 (Figure 2) with only minor structural changes in the SH3 binding pocket (for example, torsions around side chains χ_1 of Tyr 7 in P_2). The hydrogen bond between Tyr 52 and the backbone of the ligand is retained. Substituents with an *R* configuration at C2 point directly towards the SH3 domain, and result in steric clashes, particularly with the intimately packed Tyr 52 residue at P_2 or the Trp 36 residue at P_{-1}. These

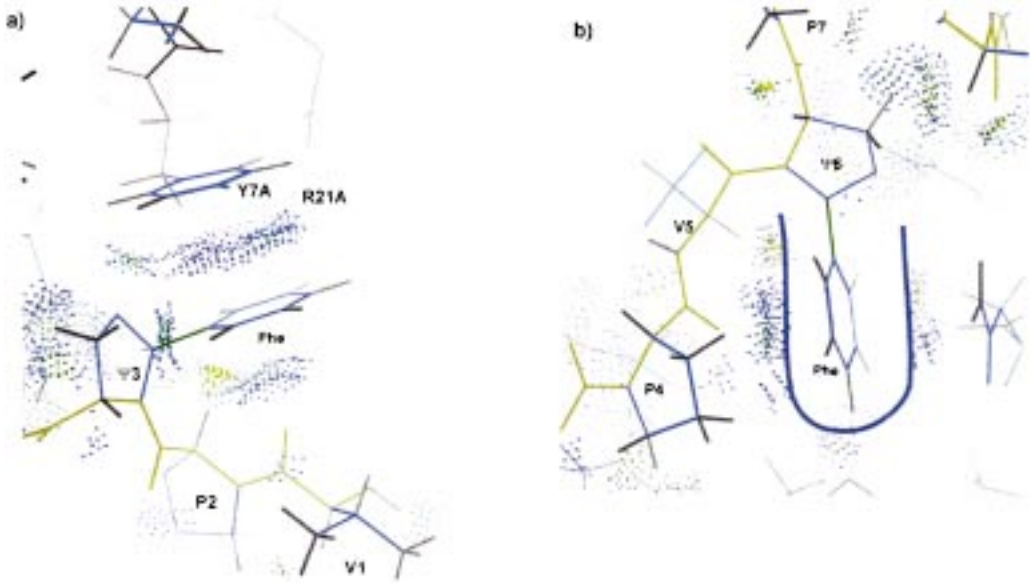

Figure 2. Close-up view of the SH3 binding pockets P_2 and P_{-1} depicting the contact surface dots[19] of the MD-averaged structure of peptide **1**: a) one possible binding mode at P_2 characterized by dominant van der Waals interactions between Tyr 7 and the phenyl substituent at C2; b) close packing in the P_{-1} binding pocket.

  1433-7851/01/4015-2845 $ 17.50+.50/0

steric clashes can be compensated for only by major conformational shifts in the protein or the ligand.

The resulting structures obtained from molecular dynamics (MD) simulations[14] are very similar (Figure 3), but have a slightly increased overall mobility than the native proline-rich ligand sequence (average root mean square deviation (rmsd) from the X-ray structure < 0.7 Å). This increased mobility is possibly the result of two different binding modes for the phenyl ring in position P_2.

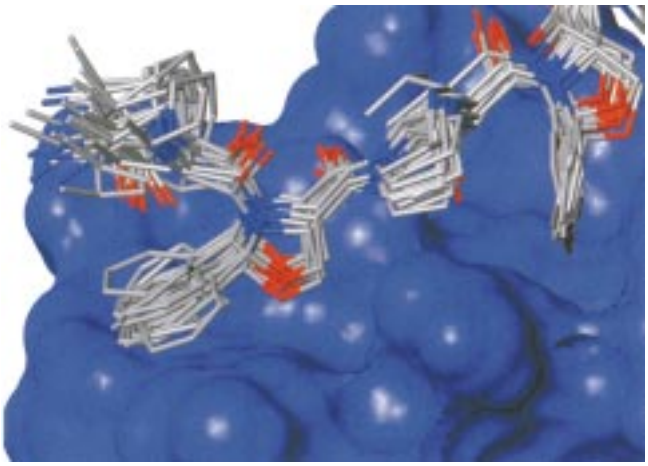

Figure 3. Superposition of 40 snapshots resulting from MD simulations of **1** (stick representation, hydrogen atoms are omitted for clarity) in a complex with the N-terminal Grb2-SH3 domain (Connolly surface).

The *S* configuration at the C2 position of the ring enables ligands to be designed with an optimized complementarity to the topography of the SH3 domain. Starting from an initial PPII helix conformation of about 40% of the investigated Pro- or ΨPro model peptides, ΨPro-containing ligands preferentially adopt a PPII conformation as a result of a markedly increased rate of isomerization about the tertiary Xaa-ΨPro–amide bond compared to oligo-L-Pro peptides.[11b]

The *S* conformers of the oxazolidine derivative Pro-Ser($\Psi^{Ph,H}$pro) and Val-Ser(Ψpro^{Ph,H}) were stereoselectively synthesized by using the post-insertion strategy.[11] The corresponding dipeptides Fmoc-Xaa-Ser-OH (Xaa = Pro, Val; Fmoc = 9-fluorenylmethoxycarbonyl) were treated with benzaldehyde dimethylacetal to yield the kinetically preferred *S*-configurated pseudoprolines.[15] These building blocks were used for the stepwise synthesis of the model peptide **1** on a solid support by Fmoc strategies.[16] The HPLC chromatogram of the peptides after cleavage from the resin shows a relatively broad peak of molecules of identical mass which indicates the existence of different, but distinct, conformations arising from the presence of the ΨPro moieties. Treatment of the peptide with trifluoroacetic acid (TFA) resulted in a sharpening of the peak shape as a consequence of the opening of the ΨPro ring restoring the parent Ser residue (Figure 4).

Circular dichroism (CD) studies of the model peptide Pro-Pro-Pro-Ser(ΨPro^{Ph,H})-Pro-Val-Ser(ΨPro^{Ph,H})-Pro-Pro-Pro-Pro (**2**) in H_2O shows the characteristic bands of a PPII conformation, that is, a strong negative Cotton effect at

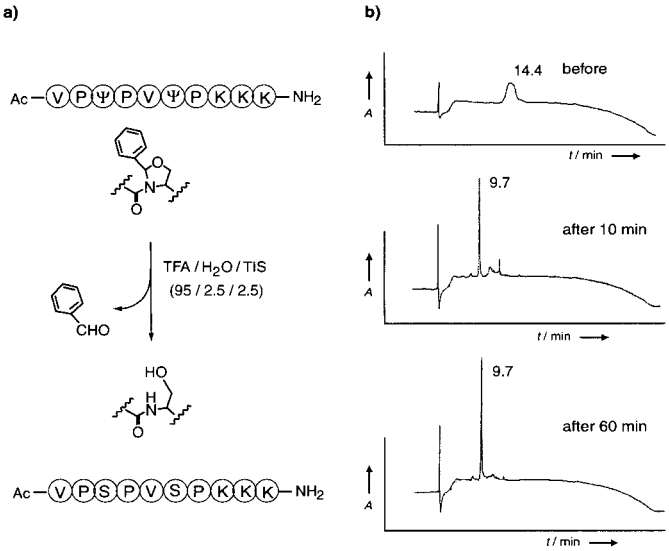

Figure 4. a) Acid treatment of peptides containing pseudoproline (Ψpro) leads to ring opening and thus to restoration of the parent amino acid (Ser); b) opening of the Ψpro-ring structure as monitored by HPLC (see text). TIS = triisopropylsilane.

$\lambda = 206$ nm and a slightly positive value at $\lambda = 228$ nm (Figure 5a). Interestingly, peptide **2** displays a transition to an unordered conformation rather than to a PPI helix in

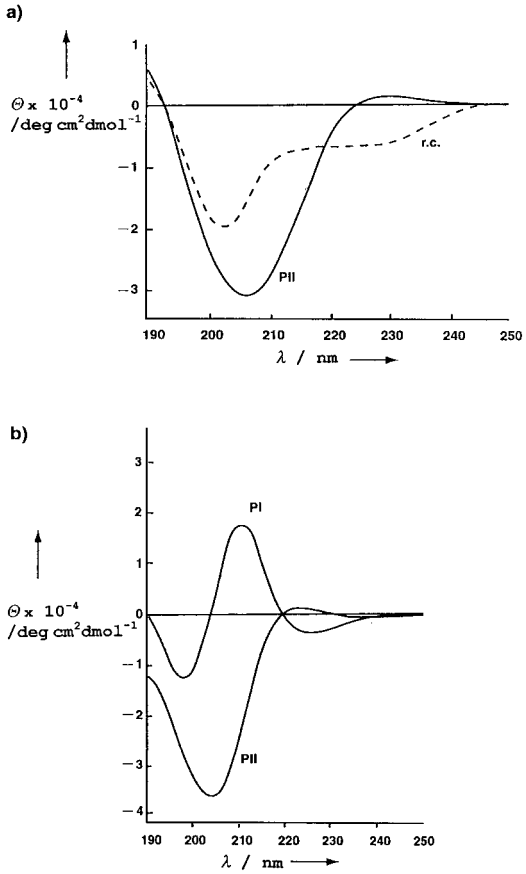

Figure 5. a) CD spectra of the ΨPro-containing peptide **2**: the spectrum measured in water shows the characteristics of a PPII helix (——) while that in propanol shows a random coil (r.c.) conformation (- - - -); $c = 1$ mg mL^{-1}. b) CD spectra of the solvent-induced PPI (propanol)/PPII (water) interconversion of poly-L-proline.

  1433-7851/01/4015-2846 $ 17.50+.50/0 *Angew. Chem. Int. Ed.* **2001**, *40*, No. 15

n-propanol/water (99.5/0.5, v/v), as observed in homooligo-Pro peptides (Figure 5b). These results are in harmony with previous results which show that two ΨPro units that have a slight preference for forming *cis* amide bonds are not sufficient to induce and stabilize a PPI helix.[11, 15]

Initial in vitro assessments of the binding activity of the model monoarylated pseudoproline-containing peptide **1** to the Crk, Crkl, and Grb-2 SH3 domains by measurement of the fluorescence of Trp residues revealed dissociation constants in the lower micromolecular range, which is typical for protein–protein interactions mediated by SH3 domains. Most notably, relative to the native L-Pro-rich sequence, the ΨPro peptides exhibit an enhanced binding specificity without loss of affinity to Crk- and Crkl-SH3 domains. In competition assays using whole cell lysates[17] from the human chronic myelogenous leukemia (CML) K562 cell line,[18] ΨPro peptides have been shown to inhibit formation of the Grb2-SH3(N)/SoS complex (Figure 6). This observation indicates that C2-substituted ΨPro moieties indeed exert the postulated dual functionality in enhancing the proline effect in the recognition process.

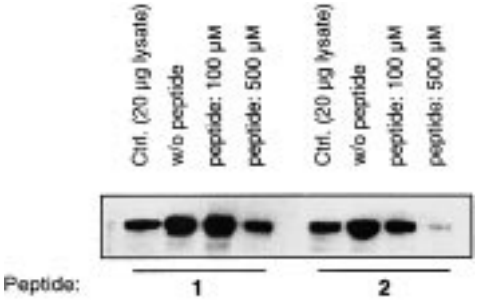

Figure 6. Western blot of the inhibition of the Grb2-SH3(N)/SoS complex formation by the native SoS sequence and a peptide containing a Cys-derived monoarylated pseudoproline. Peptides: **1** = Ac-VPPPVPPKKK-NH_2; **2** = Ac-VPPPVC($\Psi Pro^{Ph,H}$)PKKK-NH_2.

In conclusion, pseudoprolines have proven to be highly versatile for studying ligand recognition that is mediated by SH3 domains—an essential facet of cellular regulation, and thus for protein–protein interactions, in general. The results support the concept that functional pseudoprolines have a dual role, as exemplified by the successful design of novel SH3 ligands of remarkable bioactivity. A unique feature of ΨPro building blocks is that the C2 substituents facilitate optimal complementarity of the SH3 topography upon ligand recognition, and thus modulate the binding affinity and specificity, as well as promote the induction of the required helical PPII conformation in accelerating *cis*–*trans* isomerizations. Further optimizations of the ligand–receptor interactions by generating C2-substituted ΨPro libraries through applying post-insertion strategies are currently in progress.

Experimental Section

The peptides were synthesized according to standard procedures for solid-phase peptide synthesis (SPPS)[16] by applying the Fmoc strategy on Sieber amide resin.[20] The pseudoproline residue, a serine-derived 2-phenyl-2*H*-1,3-oxazolidine-4-carboxylic acid (Ser($\Psi pro^{Ph,H}$) was introduced during SPPS as a preformed dipeptide building block.[11] Briefly, the corresponding dipeptide, Fmoc-Pro-Ser-OH or Fmoc-Val-Ser-OH, was dissolved in THF and refluxed with 10 equivalents of benzaldehyde dimethylacetal and 0.2 equivalents of pyridinium *p*-toluenesulfonate (PTTS) for 1.5 h. After work-up, the two epimers were separated by flash chromatography on silica gel with CH_2Cl_2/MeOH (100/5, v/v), and characterized by electrospray-ionization mass spectrometry (ESI-MS) and ^1H NMR spectroscopy (Finnigan APCI/ESI and a Brucker DPX-400 spectrometer, respectively).

After the synthesis of the sequences using a twofold excess of amino acids or the ΨPro-dipeptides, the peptides were cleaved from the resin with TFA (1% in dichloromethane), purified by reversed-phase HPLC, and characterized by ESI-MS (**1**: *m*/*z* 1189; **2**: *m*/*z* 1287). Removal of the (4,4-dimethyl-2,6-dioxocyclohexylidene)ethyl (Dde) protecting groups on the lysine residues in **1** was achieved with 2% H_2NNH_2 in DMF prior to cleavage of the peptide from the resin.

The CD spectra were recorded on a Jobin Yvon Mark VI circular dichrometer in quartz cells (path length 0.1 cm) with a peptide concentration of 0.1 mg mL^{-1} in H_2O and *n*-propanol/water (99.5/0.5, v/v).

Inhibition of the formation of the Grb2-SH3(N)/SoS complex by the peptides was tested with the human chronic myelogenous leukemia (CML) cell line K562 cultured in RPMI 1640 with 5% fetal bovine serum (FBS; GibcoBRL) and penicillin/streptomycin (GibcoBRL). Cell lysis was performed as described in ref. [17] and the in vitro inhibition carried out with the total cell lysate. 20 µg of the GST-tagged Grb2-SH3(N) fusion protein was preincubated for 2 h at 4 °C in 250 µL of IP buffer (20 mM TrisHCl pH 7.5, 1 mM Na_2EDTA, 100 mM NaCl, 5 vol. % glycerol, 0.1% Tween 20 (Roth) containing protease inhibitors (0.2 mg mL^{-1} phenylmethylsulfonyl fluoride (Sigma), 10 µg mL^{-1} aprotinin (Roth), 0.5 µg mL^{-1} leupeptin (Serva), 5 µg mL^{-1} antipain · HCl (Sigma), 0.7 µg mL^{-1} pepstatin (Roche)), and glutathione-sepharose beads. The K562 protein (250 µg) and the peptides (at the concentrations indicated in Figure 6) were pre-mixed in 250 µL of IP buffer, added to the SH3 domain, and incubated overnight. Precipitates were washed three times in 0.5% TX buffer (20 mM TrisHCl (Tris = tris(hydroxmethyl)aminoethane) pH 7.5, 100 mM NaCl, 5% (v/v) glycerol, 1 mM Na_2EDTA (EDTA = ethylenediaminetetraacetate), 0.5% Triton X-100 (Sigma)). After sodium dodecyl sulfate–polyacrylamide gel electrophoresis (SDS-PAGE) and semi-dryblotting, the SoS bound to GST-Grb2 SH3(N) was detected with anti-SoS antiserum (Upstate Biotechnology Inc.).

Received: January 22, 2001 [Z 16480]

[1] J. Kuriyan, D. Cowburn, *Annu. Rev. Biophys. Biomol. Struct.* **1997**, *26*, 259–288.
[2] M. J. Macias, M. Hyvonen, E. Baraldi, J. Schultz, M. Sudol, M. Saraste, H. Oschkinat, *Nature* **1996**, *382*, 646–649.
[3] a) A. A. Federov, E. Federov, F. Gertler, S. C. Almo, *Nat. Struct. Biol.* **1999**, *6*, 661–665; b) F. B. Gertler, K. Niebuhr, M. Reinhard, J. Wehland, P. Soriano, *Cell* **1996**, *87*, 227–239; c) S. M. Ahern-Djamali, A. R. Comer, C. Bachmann, A. S. Kastenmeier, S. K. Reddy, M. C. Beckerle, U. Walte, F. M. Hoffmann, *Mol. Biol. Cell* **1998**, *9*, 2157–2171.
[4] N. M. Mahoney, D. A. Rozwarski, E. Federov, A. A. Federov, S. C. Almo, *Nat. Struct. Biol.* **1999**, *6*, 666–671.
[5] a) W. A. Lim, F. M. Richards, R. O. Fox, *Nature* **1994**, *372*, 375–379; b) S. Feng, J. K. Chen, H. Yu, J. A. Simon, S. L. Schreiber, *Science* **1994**, *266*, 1241–1247; c) J. T. Nguyen, C. W. Turck, F. E. Cohen, R. N. Zuckermann, W. A. Lim, *Science* **1998**, *282*, 2088–2092; d) B. Aghazadeh, M. K. Rosen, *Chem. Biol.* **1999**, *6*, R241–R246.
[6] a) G. Siligardi, A. F. Drake, *Biopolymers* **1995**, *37*, 281–292; b) B. J. Stapley, T. P. Creamer, *Prot. Sci.* **1999**, *8*, 587–595.
[7] a) D. C. Dalgarno, M. C. Botfield, R. J. Rickles, *Biopolymers* **1997**, *43*, 383–400; b) J. E. Ladbury, S. Arold, *Chem. Biol.* **2000**, *7*, R3–R8.
[8] M. Lewitzky, C. Kardinal, N. H. Gehring, E. K. Schmidt, B. Konkol, M. Eulitz, W. Birchmeier, U. Schaeper, S. Feller, *Oncogene* **2001**, in press.
[9] a) A. P. Combs, T. M. Kapoor, S. Feng, J. K. Chen, L. F. Daude-Snow, S. L. Schreiber, *J. Am. Chem. Soc.* **1996**, *118*, 287–288; b) T. M. Kapoor, A. Hamilton Andreotti, S. L. Schreiber, *J. Am. Chem. Soc.* **1998**, *120*, 23–29; c) J. P. Morken, T. M. Kapoor, S. Feng, F. Shirai, S. L. Schreiber, *J. Am. Chem. Soc.* **1998**, *120*, 30–36.

[10] a) C. Cheadle, Y. Ivashchenko, V. South, G. H. Searfoss, S. French, R. Howk, G. A. Ricca, M. Jaye, *J. Biol. Chem.* **1994**, *269*, 24034 – 24039; b) A. B. Sparks, L. A. Quilliam, J. M. Thorn, C. J. Der, B. K. Kay, *J. Biol. Chem*. **1994**, *269*, 23853 – 23856; c) R. J. Rickles, M. C. Botfield, X. M. Zhou, P. A. Henry, J. S. Brugge, M. J. Zoller, *Proc. Natl. Acad. Sci. USA* **1995**, *92*, 10909 – 10913.

[11] a) T. Wöhr, F. Wahl, A. Nefzi, B. Rohwedder, T. Sato, X. Sun, M. Mutter, *J. Am. Chem. Soc.* **1996**, *118*, 9218 – 9227; b) M. Mutter, T. Wöhr, S. Gioria, M. Keller, *Biopolymers* **1999**, *51*, 121 – 128; c) A. Wittelsberger, M. Keller, L. Scarpellino, L. Patiny, H. Acha-Orbea, M. Mutter, *Angew. Chem*. **2000**, *112*, 1153 – 1156; *Angew. Chem. Int. Ed*. **2000**, *39*, 1111 – 1115.

[12] X. Wu, B. Knudsen, S. M. Feller, J. Zheng, A. Sali, D. Cowburn, H. Hanafusa, J. Kuriyan, *Structure* **1995**, *3*, 215.

[13] D. Bowtell, P. Fu, M. Simon, P. Senior, *Proc. Natl. Acad. Sci. USA* **1992**, *89*, 6511 – 6515; P. Chardin, J. H. Camonis, N. W. Gale, L. Van Aelst, M. H. Wigler, D. Bar-Sagi, *Science* **1993**, *60*, 1338 – 1343; M. Rozakis-Adcock, R. Fernley, J. Wade, T. Pawson, D. Bowtell, *Nature* **1993**, *363*, 83 – 85.

[14] The molecular graphics package INSIGHT II (version 97, Molecular Simulations, **1997**) was used. Energy minimizations and MD simulations were performed on a Silicon Graphics OCTANE by using the program CVFF/FDISCOVER (version 97, Molecular Simulations, **1997**). The simulations were performed with a cut-off distance of 12 Å, a time step of 1 fs, and a distance-dependent dielectricity constant ε of $4.00\,r$ (r = distance) The backbone coordinates of the N-terminal SH3 domain were restrained to their initial positions. Implicit treatment of solvation and conformational restraints permitted long run times of MD simulations within an appropriate time scale. After 5000 steps of steepest descent minimization, the system was heated to 298 K by applying the standard FDISCOVER protocol. After an initialization time of 10 ps, the simulation run was continued for 1 ns. Averaged structures were generated for the last 50 ps of the simulation and further minimized for 500 steps of steepest descent, followed by a conjugate gradient minimization until the rms gradient was < 0.01 kcal mol^{-1} Å^{-1}. After this procedure, the peptide ligand Val-Pro-Ser(Ψpro^{Ph,H})-Pro-Val-Ser(Ψpro^{Ph,H})-Pro-Arg-Arg-Arg was compared with Val-Pro-Pro-Pro-Val-Pro-Pro-Arg-Arg-Arg, the decameric native SoS peptide sequence 3gbq.[21] The fluctuation was analyzed for the last 500 ps of the simulation.

[15] M. Keller, M. Mutter, C. Lehmann, *Synlett* **1999**, *S1*, 935 – 939; M. Keller, C. Lehmann, M. Mutter, *Tetrahedron* **1999**, *55*, 413 – 422.

[16] J. M. Stewart, J. D. Young, *Solid Phase Peptide Synthesis*, 2nd ed., Pierce Chemical, Rockford, IL, **1984**.

[17] E. Klein, H. Ben-Bassat, H. Neumann, P. Ralph, J. Zeuthen, A. Polliack, F. Vanky, *Int. J. Cancer* **1976**, *18*, 421 – 431.

[18] G. Posern, J. Zheng, B. S. Knudsen, C. Kardinal, K. B. Muller, J. Voss, T. Shishido, D. Cowburn, G. Cheng, B. Wang, G. D. Kruh, S. K. Burell, C. A. Jacobson, D. M. Lenz, T. J. Zamborelli, K. Adermann, H. Hanafusa, S. M. Feller, *Oncogene* **1998**, *16*, 1903 – 1912.

[19] J. M. Word, S. C. Lovell, T. H. LaBean, H. C. Taylor, M. E. Zalis, B. K. Presley, J. S. Richardson, D. C. Richardson, *J. Mol. Biol.* **1999**, *285*, 1711 – 1733.

[20] P. Sieber, *Tetrahedron Lett*. **1987**, *28*, 2107.

[21] M. Wittekind, C. Mapelli, V. Lee, V. Goldfarb, M. S. Friedrichs, C. A. Meyers, L. Müller, *J. Mol. Biol*. **1997**, *267*, 933 – 952.

Designed Molecules for Self-Assembly: The Controlled Formation of Two Chiral Self-Assembled Polynuclear Species with Predetermined Configuration**

Thomas Bark, Mathias Düggeli, Helen Stoeckli-Evans, and Alex von Zelewsky*

Self-assembly reactions are not yet as predictable to the same degree as classical reaction sequences. Often, highly interesting structures are obtained through a combination of intuition, conjecture, and serendipity.[1] Herein, we report the formation of two closely related supramolecular structures that were obtained in a programmed way. Our intention is to fabricate supramolecular complexes of the type **A** from octahedrally coordinating metal ions.

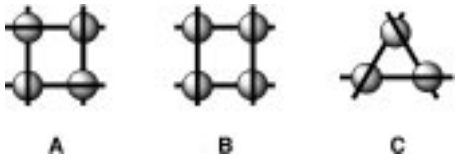

Complexes of this type are chiral (D_4 symmetry) as a consequence of the special way the ligand strands enfold the cations. Chirality is the main feature that distinguishes them from the related grid-type complexes **B** investigated by J.-M. Lehn and co-workers,[2a,b] and other recently reported molecular squares.[2c,d]

To achieve such structures we had to design a ligand that fulfils the following demands: 1) it must offer two terpyridine-type binding sites to cover each half of the coordination sphere of an OC-6 cation in a *mer* configuration; 2) it must be geometrically rigid, and define the side of a square in a tetranuclear self-assembled species; and 3) the orientation of the binding vectors of the two terpyridine (terpy) units must be antiparallel, in order to make the ligand coordinate to the metal ions once from "above" and once from "below" the plane defined by the four metal ions. These requirements, and especially the relative orientation of the binding sites, are fulfilled in ligand L^1, in which two 2,2′-bipyridin-6-yl groups are attached to a central pyrazine ring at positions 2 and 5.[3]

[*] Prof. Dr. A. von Zelewsky, T. Bark, M. Düggeli
Department of Chemistry
University of Fribourg
Pérolles, 1700 Fribourg (Switzerland)
Fax: (+41) 26-300-97-38
E-mail: alexander.vonzelewsky@unifr.ch

Prof. Dr. H. Stoeckli-Evans[+]
Institute of Chemistry
University of Neuchâtel
Avenue de Bellevaux 51, 2000 Neuchâtel (Switzerland)

[+] Crystal structure analysis.

[**] This work was financially supported by the Swiss National Science Foundation. We thank F. Nydegger for ESI-MS measurements and F. Fehr for conducting NOE experiments. Prof. C. W. Schläpfer and Prof. C. A. Daul are thanked for fruitful discussions.

Supporting information for this article is available on the WWW under http://www.angewandte.com or from the author.

  1433-7851/01/4015-2848 $ 17.50+.50/0

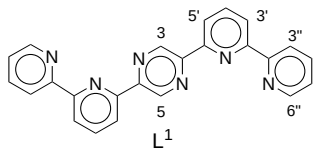

L^1

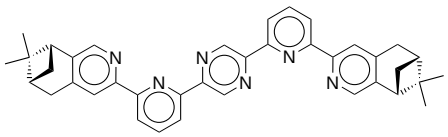

L^2

This ligand yields the desired tetrameric assembly with Zn^{2+} ions. The solution behavior of $[Zn_4(L^1)_4](PF_6)_8$ (**1**) in MeCN was investigated by electrospray-ionization mass spectrometry (ESI-MS) as well as by ^1H and ^{13}C NMR spectroscopy. The mass spectrum (Figure 1 a) reveals the tetrameric structure of **1** and displays peaks that are attributed unambiguously (from their isotopic distribution pattern) to fragments of the type $[Zn_4(L^1)_4](PF_6)_n$ ($n = 3-6$).

The ^1H NMR spectrum of the complex in CD_3CN displays one half-set of hydrogen atoms that originate from L^1; the symmetry of the ligand is thus not broken upon complexation. All resonances have been identified by 2D experiments ($^1H^1H$-COSY, NOE). The spectrum of **1** is always accompanied by a minor species with the same number of signals and the same coupling patterns. The relative amount of this minor species *increases* at lower overall concentrations of **1** and *decreases* at higher temperatures. Detailed studies revealed the existence of an equilibrium between a trimer[4] of type **C** and a tetramer, with the tetramer being the major species in the concentration range investigated. The thermodynamic parameters of this equilibrium are given in Figure 2.

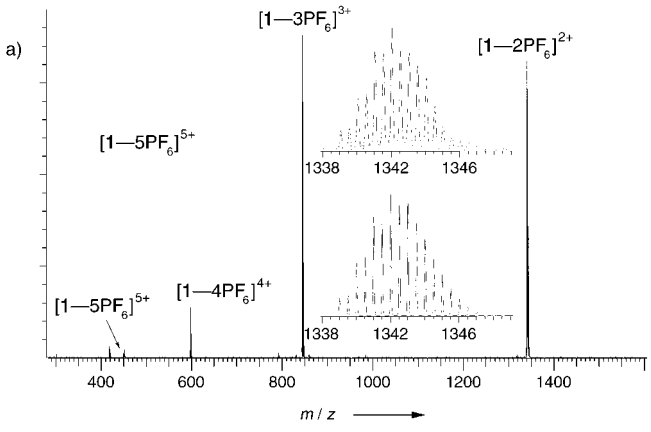

Figure 1. a) ESI mass spectrum of $[Zn_4(L^1)_4](PF_6)_8$ (a) and $[Zn_4(L^2)_4](PF_6)_8$ (b) in MeCN. Inset: found (top in both) and calculated (bottom in both) isotopic distribution for $\{[Zn_4(L^1)_4](PF_6)_6\}^{2+}$ and $\{[Zn_4(L^2)_4](PF_6)_5\}^{3+}$, respectively.

$$3\ [Zn_4(L^1)_4](PF_6)_8 \underset{MeCN}{\overset{K}{\rightleftharpoons}} 4\ [Zn_3(L^1)_3](PF_6)_6$$

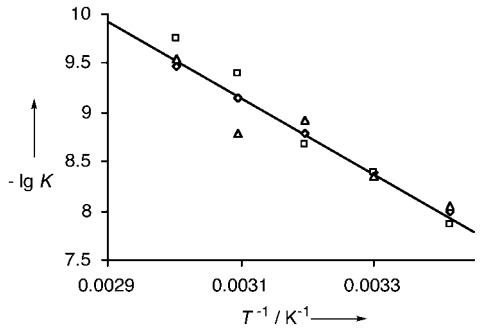

Figure 2. Temperature dependence of the tetramer/trimer equilibrium. The thermodynamic data were obtained by ^1H NMR spectroscopy. The equlibrium constants have been calculated from the integrals over three different protons (◇: H–C(3′); △: H–C(5′); □: H–C(3‴)). The resulting thermodynamic constants are: $\lg K^\circ(303\ K) = -(8.43 \pm 0.02)$; $\Delta H^\circ = -(74.5 \pm 10.0)\ kJ\,mol^{-1}$; $\Delta S^\circ = -(406 \pm 12)\ J\,mol^{-1}\,K^{-1}$.

The formation of the trimeric form from the tetramer is hence exothermic but endotropic. The negative ΔH° value must be the result of a better solvation of the trimeric complexes. The higher "ring strain" in the trimer resulting from a strong deviation from the ideal octahedral coordination geometry at the Zn^{2+} ions can probably be neglected because of the absence of ligand-field stabilization in Zn^{2+} ions. Thus the reduction of "void space" on going from the tetramer to the trimer dominates the reaction enthalpy. The negative reaction entropy is not easily understood, as both the number of complex ions and the configurational diversity increase upon the formation of the trimer. The same counter-intuitive behavior has been reported very recently for the equilibrium between the hexameric and tetrameric form of a silver-containing circular helicate.[5]

Complex **1** crystallizes[6] from $MeNO_2/Et_2O$ as a racemic compound in the centrosymmetrical space group *C*2/*c* (Figure 3). The symmetry of the complex in the crystal is C_2, and the zinc ions define a symmetrical trapezoid which is close to a square ($\alpha = 89.49(0.01)^\circ$, $\beta = 90.51(0.01)^\circ$). The lengths of the coordinative bonds are not unusual: Zn–N(pyridine) varies from 2.050 to 2.126 Å, while the bonds to the pyrazine nitrogen atoms are considerably longer (2.244–2.311 Å), probably as a result of electronic communication through the pyrazine ring. Two of the eight PF_6^- counterions are in close contact with the complex ion and occupy positions

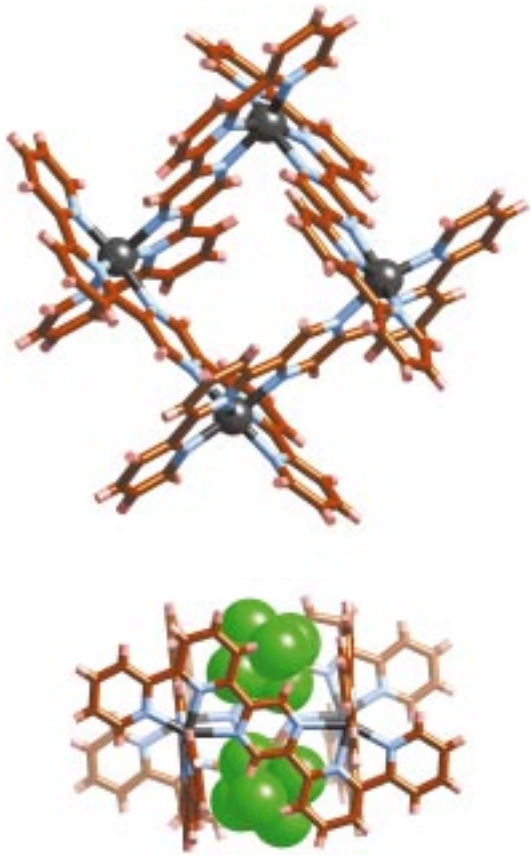

Figure 3. Crystal structure of the racemic compound $[Zn_4(L^1)_4](PF_6)_8$. Only the all-$\vec{\Delta}$ enantiomer is shown.

above and below the center of the square (Figure 3). Large numbers of disordered solvent molecules complicated the refinement of the structure. Related structures have been reported with the commercial ligand bispyridyltetrazine.[7]

After having obtained the racemic complex **1**, we envisaged the *stereoselective synthesis* of similar molecular assemblies. For this purpose we developed L^2, a chiral derivative of L^1. By rendering the ligand chiral, the all-$\vec{\Delta}$ and all-$\vec{\Lambda}$ isomers of the complex, which are enantiomers in the case of achiral L^1, will become diastereomers with L^2 (**D** and **E** in Scheme 1).

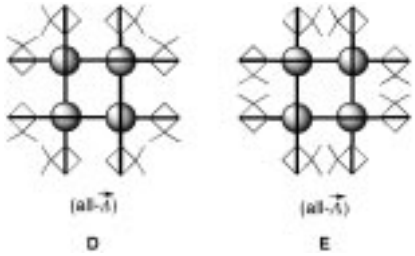

Scheme 1. Schematic representation of the two diastereomers of tetranuclear complexes with L^2. The methyl groups of the pinene moieties in **D** point to each other at the "corners" of the square, while in **E** their orientation is along the sides of the quadrangle.

The "chiralization" (that is, chiral derivatization) of the ligand was achieved quite straightforwardly by introducing pinene moieties, a technique used many times before for pyridine-type ligands.[8] The auto-assembly process delivers the tetranuclear Zn^{2+} complex (all-$\vec{\Delta}$)-$[Zn_4((R,R)\text{-}L^2)_4](PF_6)_8$ (**2**) as the major product with a high diastereomeric excess and in high yield.

The ^1H NMR spectrum shows that three minor species are also present; these species are presumably the other diastereomer of the tetramer and the two diastereomers of the trimer. Although further quantitative analysis of the NMR data is difficult because the signals are insufficiently separated, we can confirm that for a concentration suitable for NMR measurement (here 11.7 mmol L^{-1}), over 95% of the mass of complex **2** is present as the dominant diastereomer of the tetrameric complex, which is the same as that found in the solid state.

The crystal[9] contains only one diastereomer of **2** (type **D**, Scheme 1). The asymmetric unit comprises one complex molecule (Figure 4), and all the Zn^{2+} ions are thus crystallographically inequivalent. The parameters of the coordinative

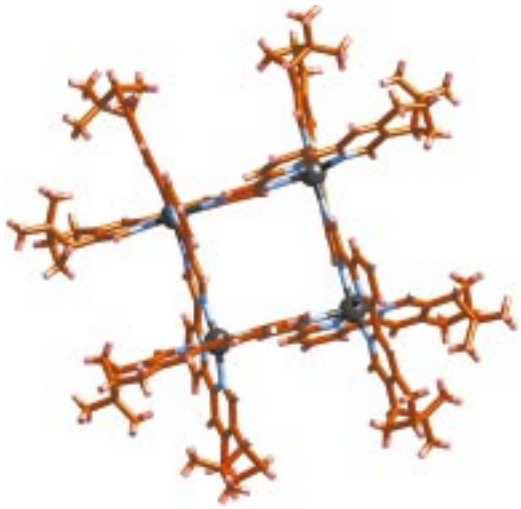

Figure 4. Crystal structure of $[Zn_4(L^2)_4](PF_6)_8$.

bonds are in the usual range (Zn–N(pyridine) 2.077 – 2.171 Å, Zn–N(pyrazine) 2.234 – 2.359 Å). Again, two PF_6^- ions are in close contact with the complex ion (not displayed). The X-ray structure analysis does not only establish the *relative* configuration of the complex (configuration of the ligand ↔ configuration at the metal centers), but it also confirms the *absolute configuration*; the Flack parameter[10] converged to 0.016(13) for the absolute structure containing the $(R,R)/\vec{\Delta}$ isomer of the complex.

In conclusion, we have reported a new type of chiral square complex and presented for the first time the configurational predetermination of the metal centers in such a tetramer by the use of a chiral ligand.

Experimental Section

The syntheses of L^1 and L^2 will be reported, together with isomeric and related pyrazine containing ligands, in a forthcoming publication.

rac-$[Zn_4(L^1)_4](PF_6)_8$ (**1**) was obtained by treating L^1 with a stoichiometric amount of $Zn(ClO_4)_2 \cdot 6H_2O$ in a small volume of MeCN. The ligand dissolved within a few minutes, and after one day at RT, the complex was isolated by precipitation from an aqueous NH_4PF_6 solution.

  1433-7851/01/4015-2850 $ 17.50+.50/0

$[Zn_4(L^2)_4](PF_6)_8$ (**2**) was prepared similarly, but the reaction mixture needed to be refluxed and the subsequent PF_6^- salt recrystallized from $MeCN/Et_2O$. The yields in both cases exceeded 95%. **ATTENTION**: The intermediate perchlorate salts of the complexes are explosive.

Received: March 19, 2001 [Z16796]

[1] a) B. Hasenknopf, J.-M. Lehn, B. O. Kneisel, G. Baum, D. Fenske, *Angew. Chem.* **1996**, *108*, 1987–1990; *Angew. Chem. Int. Ed. Engl.* **1996**, *35*, 1838–1840; b) O. Mamula, A. von Zelewsky, G. Bernadinelli, *Angew. Chem.* **1998**, *110*, 302–305; *Angew. Chem. Int. Ed.* **1998**, *37*, 289–293; c) O. Mamula, A. von Zelewsky, T. Bark, G. Bernadinelli, *Angew. Chem.* **1999**, *111*, 3129–3133; *Angew. Chem. Int. Ed.* **1999**, *38*, 2945–2948.

[2] a) M. Ruben, E. Breuning, J.-P. Gisselbrecht, J.-M. Lehn, *Angew. Chem.* **2000**, *112*, 4312–4315; *Angew. Chem. Int. Ed.* **2000**, *39*, 4139–4142; b) A. M. Garcia, F. J. Romero-Salguero, D. M. Bassani, J.-M. Lehn, G. Baum, D. Fenske, *Chem. Eur. J.* **1999**, *5*, 1803–1808, and references therein; c) S. Toyota, C. R. Woods, M. Benaglia, R. Haldimann, K. Wärnmark, K. Hardcastle, J. S. Siegel, *Angew. Chem.* **2001**, *113*, 773–776; *Angew. Chem. Int. Ed.* **2001**, *40*, 751–754; d) J. R. Galán-Mascarós, K. R. Dunbar, *Chem. Commun.* **2001**, 217–218.

[3] In contrast, the isomeric ligand 2,3-bis(2,2′-bipyridin-6-yl)pyrazine with Co^{2+} ions yields a dinuclear "metallocyclophane". F. Heirtzler, T. Weyhermüller, *J. Chem. Soc. Dalton Trans.* **1997**, 3653–3654.

[4] The solid-state structure of a related trimeric complex obtained from $ZnCl_2$ and 2,5-bis(2-pyridyl)pyrazine has been reported: A. Neels, H. Stoeckli-Evans, *Inorg. Chem.* **1999**, *38*, 6164–6170.

[5] O. Mamula, F. J. Monlien, A. Porquet, G. Hopfgartner, A. E. Merbach, A. von Zelewsky, *Chem. Eur. J.* **2001**, *7*, 533–539.

[6] Crystal data for **1**: $C_{109}H_{100}F_{48}N_{26}O_8P_8Zn_4$, $M_r = 3323.39$; pale yellow block, $0.40 \times 0.40 \times 0.30\ mm^3$, obtained from $MeNO_2$/EtOH/MeOH by the diffusion of Et_2O. $\mu = 0.947\ mm^{-1}$, $F(000) = 6688$. Monoclinic, space group $C2/c$, $a = 19.8633(12)$, $b = 31.1631(17)$, $c = 22.8036(12)$ Å, $\alpha = 90$, $\beta = 110.562(6)$, $\gamma = 90°$, $V = 13216.2(13)$ Å^3, $Z = 4$, $\rho_{calcd} = 1670\ kg\,m^{-3}$. Data collection at 153 K on a Stoe Image Plate Diffraction system, by using graphite-monochromated $Mo_{K\alpha}$ radiation ($\lambda = 0.71073$ Å). Image plate distance: 70 mm, ϕ oscillation scans 0–190°, step $\Delta\phi = 1°$, $2\theta = 3.27–52.1°$, $d_{max}/d_{min} = 12.45/0.81$ Å. A total of 49250 reflections of which 12828 were independent and used to refine 857 parameters. 6968 observed reflections with $I > 2\sigma(I)$. $R = 0.0748$, $wR_2 = 0.2002$ (observed); $R = 0.1216$, $wR_2 = 0.2214$ (all data). The structure was solved by direct methods (SHELXS-97) and refined anisotropically on F^2 (SHELXL-97). Hydrogen atoms were included in calculated positions and treated as riding atoms. Max./min. residual electron density $+1.274/-1.056$ e A^{-3}. One molecule of CH_3NO_2 was located in the asymmetric unit together with a considerable amount of highly disordered, and difficult to identify, solvent. The SQUEEZE routine in PLATON (A. L. Spek, *Acta Crystallogr. Sect. A* **1990**, *46*, C43) was used to modify the HKL data and indicated the presence of the equivalent of 515 electrons per unit cell. This value was equated to one MeOH, one EtOH, and two Et_2O molecules per molecule of complex. b) Crystallographic data (excluding structure factors) for the structures reported in this paper have been deposited with the Cambridge Crystallographic Data Centre as supplementary publication nos. CCDC-159770 (**1**) and -159771 (**2**). Copies of the data can be obtained free of charge on application to CCDC, 12 Union Road, Cambridge CB2 1EZ, UK (fax: (+44) 1223-336-033; e-mail: deposit@ccdc.cam.ac.uk).

[7] K. R. Dunbar and co-workers have reported the tetrameric complex $[Ni_4(bptz)_4(MeCN)_8](BF_4)_8$ (bptz = 3,6-bis(pyridyl)-1,2,4,5-tetrazine): C. S. Campos-Fernandez, R. Clérac, K. R. Dunbar, *Angew. Chem.* **1999**, *111*, 3685–3688; *Angew. Chem. Int. Ed.* **1999**, *38*, 3477–3479. The group of X.-H. Bu and M. Mitsuhiko obtained the tetrameric Zn^{2+} complex from the same ligand, and this complex resolved spontaneously into enantiomers upon crystallization: X.-H. Bu, M. Hiromasa, K. Tanaka, K. Biradha, S. Furusho, M. Shionoya, *Chem. Commun.* **2000**, 971–972.

[8] a) U. Knof, A. von Zelewsky, *Angew. Chem.* **1999**, *111*, 312–333; *Angew. Chem. Int. Ed.* **1999**, *38*, 302–322; b) A. von Zelewsky, O. Mamula, *J. Chem. Soc. Dalton Trans.* **2000**, 219–231.

[9] Crystal data for **2**: $C_{169}H_{199}F_{48}N_{31}O_{12}P_8Zn_4$, $M_r = 4277.83$; pale yellow rod, $0.30 \times 0.20 \times 0.15\ mm^3$, from $MeCN/MeOH/Et_2O$. $\mu = 0.605\ mm^{-1}$, $F(000) = 2198$. Triclinic, space group $P1$, $a = 13.7635(10)$, $b = 18.9612(11)$, $c = 21.8334(16)$ Å, $\alpha = 102.476(8)$, $\beta = 106.002(9)$, $\gamma = 90.240(8)°$, $V = 5335.5(6)$ Å^3, $Z = 1$, $\rho_{calcd} = 1331\ kg\,m^{-3}$, data collection (at 153 K) and refinement as for **1**. $2\theta = 3.72–51.82°$, $\phi = 0–200°$, $\Delta\phi = 1°$. In total 42111 reflections were collected of which 34862 were independent and used to refine 1622 parameters. $R = 0.0717$ and $wR_2 = 0.1604$ for 13535 observed reflections ($I > 2\sigma(I)$); $R = 0.1711$ and $wR_2 = 0.1871$ for all data. Disordered solvent was equated to 7 MeCN, 3 MeOH, and 11 H_2O molecules. The PF_6^- ions are disordered and suffer from thermal motion. Flack parameter[10] $x = 0.016(13)$. Max./min. residual electron density $+0.811/-0.441$ e Å^{-3}.[6b]

[10] H. D. Flack, *Acta Crystallogr. Sect. A* **1983**, *39*, 876–881.

By Overexpression in the Yeast *Pichia pastoris* to Enhanced Enantioselectivity: New Aspects in the Application of Pig Liver Esterase**

Anna Musidlowska, Stefan Lange, and Uwe T. Bornscheuer*

Dedicated to Professor Günter Schmidt-Kastner on the occasion of his 75th birthday

Lipases and esterases can be used as efficient biocatalysts for the preparation of a wide variety of optically pure compounds.[1] Whereas a range of lipases—especially of microbial origin—are commercially available, only a few esterases can be obtained for the kinetic resolution of racemates or desymmetrization. In the majority of publications, pig liver esterase[2] (PLE) is used, which is isolated from pig liver by extraction. Although it has been demonstrated that this preparation can convert a broad range of compounds at partially very high stereoselectivity, its application is connected with a number of disadvantages. Besides a variation of the esterase content between different batches, the presence of other hydrolases particularly has to be considered as problematic with respect to stereoselectivity.[3] Furthermore, it has been shown that PLE consists of several isoenzymes,[4] which in part differ considerably in their substrate specificity. Thus, electrophoretic separation by isoelectric focusing enabled access to PLE fractions that,

[*] Prof. Dr. U. T. Bornscheuer, A. Musidlowska
Institute of Chemistry and Biochemistry
Department of Technical Chemistry and Biotechnology
Greifswald University
Soldmannstrasse 16, 17487 Greifswald (Germany)
Fax: (+49) 3834-86-4373
E-mail: bornsche@mail.uni-greifswald.de
S. Lange
Institute of Technical Biochemistry
Stuttgart University (Germany)

[**] We thank the Konrad-Adenauer foundation (St. Augustin, Germany) for a stipend to A.M., Prof. R. D. Schmid (Institute of Technical Biochemistry, Stuttgart University) for his support and discussions, and A. Gollin for the synthesis of the acetates.

besides other substances, preferentially converted butyrylcholine (an action comparable to butryrylcholine esterase), proline-β-naphthylamide, and methylbutyrate.[5a,b] Öhrner and co-workers[5c] not only found an influence by the chainlength of *p*-nitrophenyl esters on the activity of different PLE fractions, but also a significant change in enantioselectivity in the hydrolysis of prostereogenic substrates. In contrast, Jones and co-workers reported that different isoenzymes show almost no differences in the stereoselective hydrolysis of several monocyclic and acyclic diesters. Only differences in activity were reported.[6]

The production of enzymes at stable and defined composition can be achieved by overexpression of the encoding genes in suitable host organisms such as *Escherichia coli*, *Pichia pastoris*, or *Aspergillus oryzae*. Indeed, several esterases[7] and lipases[8] are thus produced. The cloning of putative pig liver esterase genes has already been described: Takahashi and co-workers[9a,b] cloned a gene, isolated from pig liver, which encoded for a proline-β-naphthylamidase. Later, the same group[10] and Heymann's group[11] demonstrated that, with high probability, it was actually PLE that was cloned. The same holds true for a glycerolester hydrolase,[12] which is distinguished only by 16 amino acids from the protein sequence published by Takahashi and co-workers. However, the functional expression of active enzymes was not reported by any of the research groups.

We have now succeeded for the first time in the overexpression of active PLE in the yeast *Pichia pastoris*.[13] Thus, we can now produce recombinant PLE (rPLE) at stable product quality without interfering influences of other isoenzymes and hydrolases. The rPLE shows almost identical pH and temperature profiles[13] and a similar substrate spectrum in the hydrolysis of simple (achiral) esters and triacylglycerides compared to nonrecombinant PLE (Figure 1). It has to be emphasized that only rPLE does not cleave triolein, which is a typical lipase substrate. This exemplifies the impurity of commercial preparations containing other hydrolases. Beside a biochemical characterization, we were especially interested in the stereoselectivity of rPLE in the conversion of chiral substrates in comparison to commercial preparations,[14] as this represents by far the most important area of application for PLE.

Whereas in the PLE-catalyzed kinetic resolution of (*R*,*S*)-(1-phenylethyl)acetate (**1**) similar enantioselectivities[15] between $E = 5.7$ and 7.9 were determined in all cases (Table 1), significantly higher enantioselectivities were found in the hydrolysis of (*R*,*S*)-1-phenyl-2-propyl acetate (**2**; Table 2) or (*R*,*S*)-1-phenyl-2-butyl acetate (**3**; Table 3) with the recombinant PLE in comparison to reactions with PLE preparations from Fluka, Sigma, or Roche Diagnostics (Chirazyme E1 or E2). In the hydrolysis of **3**, these preparations showed only very low enantioselectivities ($E = 1.4 - 4.0$), whereas *E* values much greater than 100 were determined with recombinant PLE (Table 3). For **2**, this increase of enantioselectivitiy was less pronounced, but here we observed an inversion of enantiopreference (Table 2). With commercial esterases the *R* alcohol was preferentially formed, whereas with rPLE the *S* alcohol was produced. These results can be explained by the fact that we cloned the γ subunit of PLE,[13] but commercial

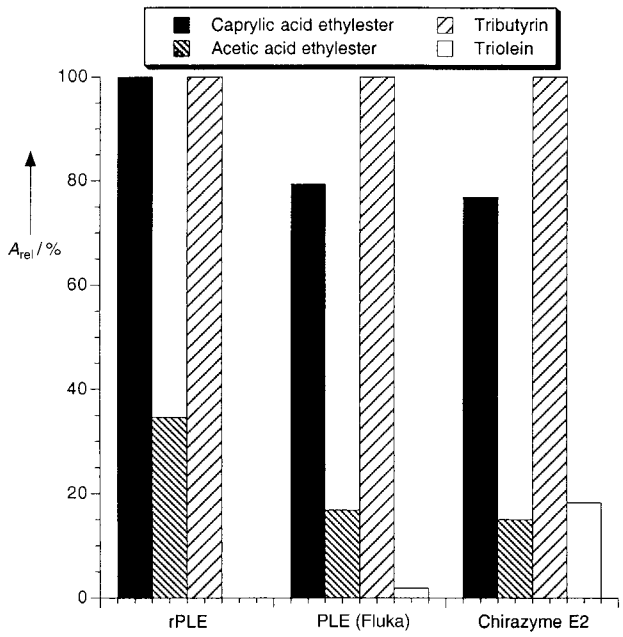

Figure 1. Comparison of the hydrolytic activity (A_{rel}) of recombinant PLE (rPLE) with commercial preparations from Fluka and Roche Diagnostics (Chirazyme E2) towards different achiral esters.

Table 1. Enantioselectivity of different pig liver esterases in the kinetic resolution of **1**.

PLE[a]	*t* [h]	Enantiomeric excess (*ee*)		Conversion [%]	*E*[b]
		ee_S [%][c]	ee_P [%][c]		
recombinant	1	58	53	53	5.7
Fluka	1.5	65	56	54	6.8
Sigma	1	72	58	55	7.8
Chirazyme E1	5	73	58	56	7.9

[a] In all reactions 0.5 U of esterase (based on pNPA-assay) were used. [b] The enantioselectivity *E* was calculated according to the method of Chen et al. (1982).[15] [c] ee_S = enantiomeric excess of the nonconverted substrate, ee_P = enantiomeric excess of the product. In all cases the product alcohol **1a** had *R* configuration and the nonconverted acetate **1** had *S* configuration.

Table 2. Enantioselectivity of different pig liver esterases in the kinetic resolution of **2**.

PLE[a]	*t* [h]	Enantiomeric excess		Conversion [%]	*E*[b]
		ee_S [%]	ee_P [%]		
recombinant	2	75 (*R*)	70 (*S*)	52	12.6
Fluka	1.5	35 (*S*)	44 (*R*)	44	3.6
Sigma	1.5	24 (*S*)	32 (*R*)	43	2.4
Chirazyme E1	1.5	22 (*S*)	43 (*R*)	34	3.1
Chirazyme E2	1	9 (*S*)	9 (*R*)	50	1.3

[a], [b] See Table 1.

Table 3. Enantioselectivity of different pig liver esterases in the kinetic resolution of **3**.

PLE[a]	t [h]	Enantiomeric excess		Conversion [%]	*E*[b]
		ee_S [%][c]	ee_P [%][c]		
Recombinant	2	57	> 99	36	≫ 100
Fluka	2	12	12	49	1.4
Sigma	1	17	11	59	1.5
Chirazyme E-1	2	19	18	52	1.7
Chirazyme E-2	1	58	40	59	4.0

[a], [b] See Table 1. [c] In all cases the product alcohol **3a** had *S* configuration and the nonconverted acetate **3** had *R* configuration.

  1433-7851/01/4015-2852 $ 17.50+.50/0 *Angew. Chem. Int. Ed.* **2001**, *40*, No. 15

preparations are a mixture of subunits, which differ considerably in sequence and molecular weight.[5] This, of course, can also effect substrate selectivity and enantioselectivity.

Thus, the application of recombinant PLE now also allows the synthesis, in high optical purity, of compounds which have so far not been accessible by PLE-catalyzed reactions. Furthermore, the successful functional expression now makes the manipulation of enzyme properties by site-directed mutagenesis or directed evolution[16] feasible.

Experimental Section

Production of recombinant pig liver esterase (rPLE): For expression of rPLE, the yeast *Pichia pastoris*—bearing the genomic-integrated gene that encodes the esterase under the control of the methanol-inducible alcohol oxidase 1 promotor (AOX1)—was grown according to the protocol given by the manufacturer (Invitrogen, Carlsbad, CA, USA), first in BMGY media containing glycerol (1% (v/v)) and then in BMMY media that contained methanol (0.5% (v/v)) as the carbon source and inducer. Induction of rPLE expression was maintained by daily addition of methanol (0.5% (v/v)). After 96 h, the cells were removed by centrifugation and the supernatant was concentrated for 15 min at 4000 g with 20 mL Centricons (NMWL 30000, Ultracel-PL membrane, Millipore). The activity thus obtained was 10 U mL^{-1} (pNPA-assay), which corresponds to $\sim$500 U mg^{-1} protein.

Determination of esterase activity: Photometric determination of esterase activity was performed by hydrolysis of *p*-nitrophenyl acetate (pNPA).[7d] One unit (U) of esterase corresponds to the amount of enzyme that releases 1 μmol of *p*-nitrophenol per min.

The substrate spectrum of PLE was measured with a pH-Stat (Schott, Mainz, Germany) by hydrolysis of different esters (caprylic acid ethylester, acetic acid ethylester, tributyrin, or triolein) at 37 °C and pH 7.5.[7d] One unit (U) of esterase corresponds to the amount of enzyme that releases 1 μmol of acid per min. The thus-determined highest activity was set as the 100% value.

Esterase-catalyzed kinetic resolution of the acetates: Acetates **1**–**3** (10 mM) were dissolved in sodium phosphate buffer (pH 7.5, 50 mM) in 1-mL reaction vials and the kinetic resolution was started by addition of esterase (0.5 U, based on the pNPA assay). To stop the reaction, the mixture was extracted with dichloromethane and the organic phase was dried over anhydrous sodium sulfate. The determination of enantiomeric purity and conversion was performed by gas chromatography (column: heptakis(2,6-*O*-methyl-3-*O*-pentyl)-β-cyclodextrin; carrier gas: H_2; flame ionization detector).

Retention times [min]: **1** (100 °C isothermal): (*S*)-**1** 3.7 min, (*R*)-**1** 5.8 min, (*R*)-**1a** 6.7 min, (*S*)-**1a** 7.6 min; **2** (75 °C isothermal): (*S*)-**2** 26.5 min, (*R*)-**2** 42.3 min, (*S*)-**2a** 32.6 min, (*R*)-**2a** 34.2 min; **3** (90 °C isothermal): (*S*)-**3** 17.6 min, (*R*)-**3** 20.2 min, (*S*)-**3a** 24.8 min, (*R*)-**3a** 27.4 min. The absolute configurations given for **1** are based on comparison with commercial (*R*)-**1a**. In case of **2** and **3** the *R* preference of the lipase Amano PS, as recorded in the literature,[17] served as the reference.

Received: December 13, 2000 [Z16264]
Publication delayed at author's request

[1] a) U. T. Bornscheuer, R. J. Kazlauskas, *Hydrolases in Organic Synthesis—Regio- and Stereoselective Biotransformations*, Wiley-VCH, Weinheim, **1999**; b) R. D. Schmid, R. Verger, *Angew. Chem.* **1998**, *110*, 1694–1720; *Angew. Chem. Int. Ed.* **1998**, *37*, 1608–1633; c) K. Faber, *Biotransformations in Organic Chemistry*, Springer, Berlin, **2000**.
[2] a) L.-M. Zhu, M. C. Tedford, *Tetrahedron* **1990**, *46*, 6587–6611; b) J. B. Jones, *Pure Appl. Chem.* **1990**, *62*, 1445–1448; c) C. Tamm, *Indian J. Chem. Sect. B* **1993**, *32*, 190–194; d) S. J. Phythian in *Biotechnology*, *Vol. 8a* (Eds.: H.-J. Rehm, G. Reed, A. Pühler, P. J. W. Stadler, D. R. Kelly), Wiley-VCH, Weinheim, **1998**, pp. 193–241.
[3] D. Seebach, M. Eberle, *Chimia* **1986**, *40*, 315–318.
[4] D. Farb, W. D. Jencks, *Arch. Biochem. Biophys.* **1980**, *203*, 214–226.
[5] a) E. Heymann, W. Junge, *Eur. J. Biochem.* **1979**, *95*, 509–518; b) W. Junge, E. Heymann, *Eur. J. Biochem.* **1979**, *95*, 519–525; c) N. Öhrner, A. Mattson, T. Norin, K. Hult, *Biocatalysis* **1990**, *4*, 81–88.
[6] L. K. P. Lam, C. M. Brown, B. deJeso, L. Lym, E. J. Toone, J. B. Jones, *J. Am. Chem. Soc.* **1988**, *110*, 4409–4411.
[7] a) V. Khalameyzer, U. T. Bornscheuer, *Biotechnol. Lett.* **1999**, *21*, 101–104; b) N. Krebsfänger, F. Zocher, J. Altenbuchner, U. T. Bornscheuer, *Enzyme Microb. Technol.* **1998**, *21*, 641–646; c) M. Nishizawa, M. Shimizu, H. Ohkawa, M. Kanaoka, *Appl. Environ. Microbiol.* **1995**, *61*, 3208–3215; d) V. Khalameyzer, I. Fischer, U. T. Bornscheuer, J. Altenbuchner, *Appl. Environ. Microbiol.* **1999**, *65*, 477–482.
[8] a) D. T. Quyen, C. Schmidt-Dannert, R. D. Schmid, *Appl. Environ. Microbiol.* **1999**, *65*, 787–794; b) E. Catoni, C. Schmidt-Dannert, S. Brocca, R. D. Schmid, *Biotechnol. Tech.* **1997**, *11*, 689–695; c) B. Huge-Jensen, F. Andreasen, T. Christensen, M. Christensen, L. Thim, E. Boel, *Lipids* **1989**, *24*, 781–785.
[9] a) T. Takahashi, A. Ikai, K. Takahashi, *J. Biol. Chem.* **1989**, *264*, 11565–11571; b) T. Takahashi, M. Nishigai, A. Ikai, K. Takahashi, *FEBS Lett.* **1991**, *280*, 297–300.
[10] M. Matsushima, H. Inoue, M. Ichinose, S. Tsukada, K. Miki, K. Kurokawa, T. Takahashi, K. Takahashi, *FEBS Lett.* **1991**, *293*, 37–41.
[11] E. Heymann, K. Peter, *Biol. Chem. Hoppe-Seyler* **1993**, *374*, 1033–1036.
[12] L. David, X. J. Guo, C. Villard, A. Moulin, A. Puigserver, *Eur. J. Biochem.* **1998**, *257*, 142–148.
[13] For the strategy used in the cloning and expression of rPLE, see: S. Lange, A. Musidlowska, C. Schmidt-Dannert, J. Schmitt, U. T. Bornscheuer, *ChemBioChem*, **2001**, *2*, 576–582.
[14] For comparison, PLE preparations from Fluka, Sigma, and Roche Diagnostics (Chirazyme E1, E2) were used.
[15] C. S. Chen, Y. Fujimoto, G. Girdaukas, C. J. Sih, *J. Am. Chem. Soc.* **1982**, *104*, 7294–7299.
[16] a) U. T. Bornscheuer, *Biocatal. Biotransform.* **2001**, *19*, 84–96; b) U. T. Bornscheuer, *Angew. Chem.* **1998**, *110*, 3285–3288; *Angew. Chem. Int. Ed.* **1998**, *37*, 3105–3108; c) F. H. Arnold, *Acc. Chem. Res.* **1998**, *31*, 125–131.
[17] A. L. Gutman, D. Brenner, A. Boltanski, *Tetrahedron: Asymmetry* **1993**, *4*, 839–844.

Hydrolysis/Polycondensation in the Solid State: Access to Crystalline Silica-Based Hybrid Materials**

Bruno Boury,* Frédéric Ben, and Robert J. P. Corriu

Silicon-based hybrid materials allow the association at the molecular level of the properties of an organic group with the specific properties of a Si–O–Si network (transparency, chemical and thermal stability).[1–6] They are generally prepared by hydrolytic polycondensation from organic units covalently bound to trialkoxysilyl groups ($Si(OR')_3$, R′ = Me

[*] Dr. B. Boury, F. Ben, Prof. R. J. P. Corriu
Laboratoire de Chimie Moléculaire et Organisation du Solide
UMR 5637, Université de Montpellier II
Place E. Bataillon, 34095 Montpellier Cedex 5 (France)
Fax: (+33) 467-143-852
E-mail: boury@crit.univ-montp2.fr

[**] The authors are grateful to Dr. C. Dumas from the LBS laboratory at the Université de Montpellier I for the two-dimensional X-ray analysis.

  1433-7851/01/4015-2853 $ 17.50+.50/0

or Et). This sol–gel process is performed under mild conditions in solution and, in most cases, the process leads to formation of amorphous material.[7] In the case of R-[Si(OR′)$_3$]$_n$ ($n \geq 2$) precursors, the corresponding hybrid materials prepared are organopolysilsesquioxanes (OPS) of the general formula R-[SiO$_{1.5}$]$_n$ [Eq. (1)]. Moreover, when R is a rigid organic group, a birefringent phenomenon indicates short-range organization at the mesoscopic level.[8–10]

$$\text{R-[Si(OR')}_3]_n \xrightarrow[\text{solvent + catalyst}]{H_2O} \text{R-[SiO}_{1.5}]_n + 3n\ \text{R'OH} \qquad (1)$$

Nevertheless, a truly precise control of the organization of such materials would certainly represent an additional advantage in cases where the organic group R could provide chemical or physical properties to the material (optical, magnetic, etc…). Here we report an alternative way to achieve the formation of Si–O–Si three-dimensional networks using crystallized alkylchlorosilanes as precursors. Chlorine atoms as leaving groups allow a chemical transformation and we found that their hydolysis/polycondensation can be performed in the solid state, according to the ideal situation shown in Equation (2), by direct contact of the insoluble compound in an excess of water (gaseous or liquid).

$$\underset{\text{(solid)}}{\text{R-[SiCl}_3]_n} \xrightarrow[\text{(vapor or liquid)}]{H_2O} \underset{\text{(solid)}}{\text{R-[SiO}_{1.5}]_n} + 3n\ \text{HCl} \qquad (2)$$

To demonstrate the potential of this approach we have used bis(trichlorosilyl)dibenzyl **1** as a precursor and obtained the corresponding hybrid material **2**, according to the ideal situation represented in Equation (3). Compound **2** was

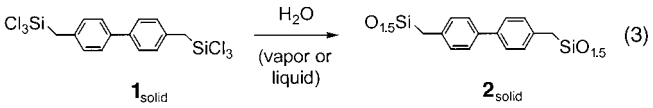

$\mathbf{1}_{solid}$ $\mathbf{2}_{solid}$ (3)

prepared by a Benkeser reaction;[11, 12] it is crystalline, with a high melting point, and the bulky and hydrophobic aryl group prevents any solubility in water. The precursor **1** is melted and cast as a film with a thickness of 0.5 mm. When cooled back to room temperature, the white pieces of precursor are directly put into water ($8 < pH < 9$) where they remain insoluble and white. The chemical transformation occurs in the solid by a solid/liquid reaction and a slightly exothermicity is evidenced by the temperature increase (up to 30–32 °C). After 8 days, a white solid is filtered off, washed with solvents (diethyl ether and acetone), and dried. Chemical transformation is readily evident from elemental analysis, which reveals a level of chlorine of 47.5 % in **1** and of less than 0.6 % in **2**. (The lower value of the actual carbon content, compared to the theoretical one, may be ascribed to noncondensed Si–OH groups.)

The ^{29}Si CP MAS NMR spectroscopic experiment agrees with complete hydrolysis of Si–Cl bonds and partial polycondensation of the Si–OH bonds (Figure 1). Compound **1** presents a signal at $\delta = 8.06$, while three signals are observed

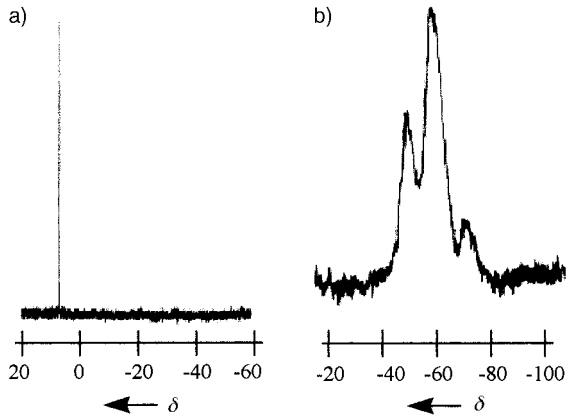

Figure 1. ^{29}Si NMR spectra of **1** (in $CDCl_3$) and **2** (by solid-state CP MAS NMR analysis).

for **2** and are attributed, respectively, to T^1 ($\delta = 50.8$, C*Si*(OH)$_2$(OSi)), T^2 ($\delta = 59.5$, C*Si*(OH)(OSi)$_2$), and T^3 signals ($\delta = 68.8$, C*Si*(OSi)$_3$) where T^y is the level of condensation at a particular center. Although the level of polycondensation achieved is not the highest possible, no signal from T^0 ($\delta = 41.5$, C*Si*(OH)$_3$) is observable; this indicates that each silicon atom is linked by at least one Si–O–Si bond to the rest of the solid. The relative intensity of the $T^1/T^2/T^3$ signals is 34/56/10 and corresponds to an overall level of polycondensation of 59 %. Apparently a fully condensed system is difficult to achieve in this case, either because of the increasing difficulty in the diffusion of water through the cross-linked solid or because, with consideration of the relative position of the Si–Cl bond in the molecular packing, increasing the Si–O–Si units would require a too great distortion of the initial crystal sructure. Both elemental and NMR spectroscopic analyses demonstrate the formation of the Si–O–Si network without the cleavage of Si–C bonds and the elimination of the organic groups that would result.

We have looked at the X-ray powder diffraction of the precursor **1** and the hybrid material **2** to investigate the presence of a well-defined organization. For **1**, a set of Bragg's rings is observed in a two-dimensional (2D) experiment, which reveal the microcrystallized structure of the starting chlorosilane **1** (Figure 2). Such signals are not preserved by the hydrolysis step; analysis of **2** indicates totally different Bragg's rings and suggests an important transformation of the initial organization. However, although the initial structure is lost, Bragg's rings are present for **2** and they evidence a high level of organization. The difference between the X-ray powder diffraction results for **1** and **2** shows that the linking of **1** by Si–O–Si bonds results in an important modification of distances, orientation, and general organization of the molecular units.

The anisotropy of the solid has also been investigated at the mesoscopic range by examining the birefringence of the material before and after hydrolysis/polycondensation. This is performed by filling a glass cell of 30 mm thickness with pure melted precursor **1** by capillarity. When cooled to room temperature, compound **1** solidifies as white, shiny, long needles (Figure 3 a). The hydrolysis/polycondensation of **1** is promoted by placing the cell in a dessicator with a 70 %

  1433-7851/01/4015-2854 $ 17.50+.50/0 *Angew. Chem. Int. Ed.* **2001**, *40*, No. 15

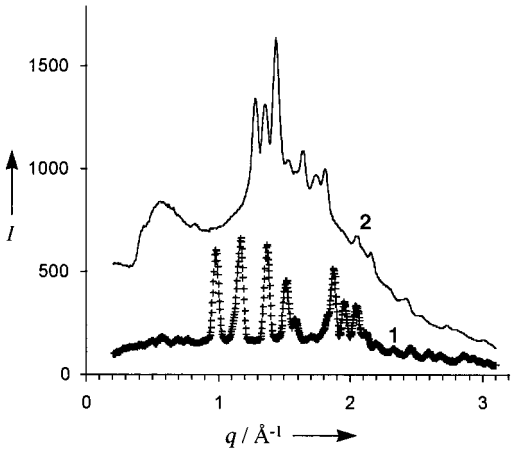

Figure 2. X-ray powder diffraction patterns of solids **1** and **2**. I = intensity.

relative humidity (at 20–22 °C) so that diffusion of water vapor occurs through the cell.[8] At this stage the reaction is a solid/gas reaction occurring between the vapor of water and the solid chlorosilane **1**. After 8 days, the chemical transformation is evidenced by the lack of melting when the solid is heated up to 200 °C. Pictures of the same region of the cell were taken before and after hydrolysis/polycondensation (Figure 3 a and b).

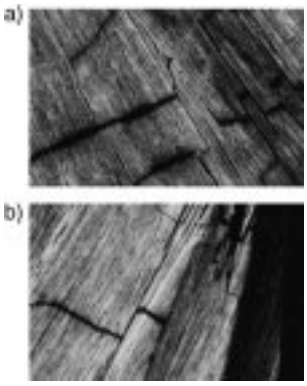

Figure 3. Microscopy pictures of a) **1** and b) **2**. (Pictures taken in polarized light.)

Firstly, it appears that the transformation occurs without dramatic destruction of the solid as the shape of the initial crystalline needles remains after the chemical transformation. Secondly, as for the starting compound **1**, a very high birefringence is measured in the resulting hybrid material: 25×10^{-3} for **1**, 20×10^{-3} for **2**. The preservation of the anisotropy confirms the X-ray diffraction analysis. As an example, a gel of **1** prepared by the classical sol–gel process with THF as the solvent exhibits a birefringence of 2.5×10^{-3}, that is ten times lower than **2**, and this demonstrates the higher degree of anisotropy achievable with the solid-state hydrolysis/polycondensation process. Therefore a high level of organization is present at the microscopic level (as demonstrated by X-ray analysis) and also at the mesoscopic level (as demonstrated by the high birefringence). In addition, organization is also present at the macroscopic level, as evidenced by the conservation of the needle shapes of the material in the micron range.

From a general point of view, some solid-state reactions in molecular compounds are known,[13, 14] but they generally correspond to a transformation of the molecular compound or to intermolecular reactions. Very few concern polymerization—the most well-known examples are topological polymerization of diacetylene compounds[15–17] or polymerization of aromatic compounds like distyrylpyrazine and phenylenediacrylic acid.[18] To our knowledge, this is the first example involving chlorosilane, and here we have observed a solid-state chemical process that combines the hydrolysis of a molecular compound and the subsequent intermolecular polycondensation reaction.

The process relies on the reactivity of the Si–Cl bond toward water. This reactivity is high and well-established in previous organosilicon chemistry,[19] and it allows transformation by a solid/liquid or a solid/gas reaction. The chemical pathway certainly relies on the diffusion of water through the solid and the hydrolysis of the Si–Cl bonds. Thus, the Si–OH bond that forms can quickly react by polycondensation with the Si–Cl group of neighboring molecules to form the Si–O–Si network. In turn, elimination of HCl occurs by diffusion through the solid to the water phase, as evidenced by a decrease in the pH value of the water. This process does not need any catalyst, however it requires a molecular packing where the Si–Cl bonds are close enough to react. Formation of the Si–O–Si network may also occur by polycondensation of neighboring Si–OH groups; such a process is facilitated by the acidity of the medium, which permits the formation of $Si[OH_2]^+$ intermediate species.

From a structural point of view, a Riedvelt procedure cannot be expected for **2** due to the low quality of the X-ray diffraction pattern. For compound **1**, a packing of the molecular units based on $\pi-\pi$ interaction can be proposed from the crystal structure of similar bis(trichlorosily)benzyl compounds.[12] However, halogen–halogen interaction may also play an important role, as pointed out for supramolecular crystal engineering.[20]

Those results show the possibility of hydrolyzing and polycondensing a chlorosilane with the architecture of the molecular solid as a scaffold, to form a highly organized covalent solid. We note that the polycondensation level is high and of a similar level to those generally obtained for this type of material prepared by sol–gel processes.[21] Indeed, the high level of Si–O–Si bonds is achieved without an "amorphisation". The formation of the solid is not related to the formation of aggregates and colloids, which are generally described as intermediates in the sol–gel process.[7] By this approach, a "crystallized" silica-based hybrid material can be prepared from a molecular solid directly, by hydrolysis/polycondensation in the solid state without any solvent or catalyst.

Experimental Section

Preparation of the cell has been reported previously although, in this case, cells were not coated with any polymer.[10] Preparation of precursor **1** was carried out as described in the literature.[12] Optical properties of the materials were observed with a Laborlux 12POLS polarizing microscope. Photographs were taken with a Leica MPS28 camera. The birefringence was obtained from the expression $\Delta l = \Delta n\, d$, where Δl is the optical path difference and d is the cell thickness. Δl is measured by a Berek compensator. ^{29}Si NMR spectra were recorded on a Bruker AM300 spectrometer at 59.620 MHz (acquisition time: 10 s, contact time: 2 ms, scans: 7400, rotating speed: 5000 Hz, internal standard: tetramethylsilane). Elemental analyses were performed by the "Service Central de Microanalyse du CNRS" in Vernaison (France). The X-ray experiments were performed on a 2D detector with a rotating anode apparatus (radiation: $Cu_{K\alpha}$, $\lambda = 1.542$ Å). The samples were ground in an agate mortar under nitrogen and put in a 1-mm diameter, 8-mm length glass Lindeman

capillary. For the imaging-plate apparatus the acquisition time was 3600–7200 seconds (distance between source and detector: 150 mm, diameter of plate: 300 mm).

Precursor **1**: m.p.:151.5 °C; ^{29}Si NMR (CP MAS): $\delta = 8.06$.

Hybrid material **2**: ^{29}Si NMR (CP MAS): $\delta = -50.8(T^1)$, $-59.5(T^2)$, $-68.8(T^3)$; CP MAS NMR spectroscopy is not always quantitative, however, single-pulse experiments did not reveal any significant variation in relative peak intensity from the CP MAS NMR spectra in the case of alkylene-bridged polysilsesquioxanes with structure similar to **2**.[21, 22] Elemental analysis calcd for $O_{1.5}SiCH_2(C_6H_4)_2CH_2SiO_{1.5}$: C 59.1, H 4.2, Cl 0 %; found: C 55.2, H 4.9, Cl 0.66 %.

Received: February 19, 2001 [Z16637]

[1] R. J. P. Corriu, D. Leclercq, *Angew. Chem.* **1996**, *108*, 1524; *Angew. Chem. Int. Ed. Engl.* **1996**, *35*, 1420.
[2] D. A. Loy, K. J. Shea, *Chem. Rev.* **1995**, *95*, 1431.
[3] J. Livage, C. Sanchez, F. Babonneau in *Chemistry of Advanced Materials: An Overview* (Eds.: L. V. Interrante, M. J. Hampden-Smith), VCH, New York, **1998**.
[4] P. Judenstein, C. Sanchez, *J. Mater. Chem.* **1996**, *6*, 511.
[5] R. J. P. Corriu, *Angew. Chem.* **2000**, *112*, 1432; *Angew. Chem. Int. Ed.* **2000**, *39*, 1376.
[6] R. J. P. Corriu, *Polyhedron* **1998**, *17*, 925.
[7] C. J. Brinker, G. W. Scherer, *Sol–Gel Science*, Academic Press, Boston, **1990**.
[8] B. Boury, R. J. P. Corriu, P. Delord, M. Nobili, V. Le Strat, *Angew. Chem.* **1999**, *111*, 3366; *Angew. Chem. Int. Ed.* **1999**, *38*, 3172.
[9] B. Boury, R. J. P. Corriu, P. Delord, V. Le Strat, *J. Non-Cryst. Solids* **2000**, *265*, 41.
[10] F. Ben, B. Boury, R. J. P. Corriu, *Chem. Mater.* **2000**, *12*, 3249.
[11] R. A. Benkeser, *Acc. Chem. Res.* **1971**, *4*, 94.
[12] M. Motevalli, D. Li Ou, A. C. Sullivan, *J. Organomet. Chem.* **1993**, *445*, 35.
[13] K. Tanaka, F. Toda, *Chem. Rev.* **2000**, *100*, 1025.
[14] V. Ramamurthy, K. Venikatesan, *Chem. Rev.* **1987**, *87*, 433.
[15] J. Kato, K. Nakamura, S. Yamasaki, K. Tokushige, T. Amano, *J. Polym. Sci. Part A* **1989**, *27*, 1853.
[16] G. Adler, *Cryst. Liq. Cryst.* **1983**, *93*, 1.
[17] G. Wegner, *Pure Appl. Chem.* **1977**, *49*, 443.
[18] M. Nakanishi, M. Hasegawa, Y. Sasada, *J. Polym. Sci. Part A* **1972**, *10*, 1537.
[19] C. Eaborn, *Organosilicon Compounds*, Butterworths, London, **1960**.
[20] G. R. Desiraju, *Angew. Chem.* **1995**, *107*, 2541; *Angew. Chem. Int. Ed. Engl.* **1995**, *34*, 2311.
[21] G. Cerveau, R. J. P. Corriu, C. Lepeytre, H. P. Mutin, *J. Mater. Chem.* **1998**, *8*, 2707.
[22] H. W. Oviatt, K. J. Shea, J. H. Small, *Chem. Mater.* **1993**, *5*, 943.

A More Efficient Catalyst for the Carbonylation of Chloroarenes**

Wolfgang Mägerlein, Adriano F. Indolese, and Matthias Beller*

Dedicated to Professor K. Barry Sharpless on the occasion of his 60th birthday

Palladium-catalyzed C–C bond formation with aryl halides is, at the moment, one of the most important organometallic reactions used in synthetic organic chemistry.[1] However, the palladium-catalyzed carbonylation[2] has been investigated far less intensively than the well known Heck, Suzuki, or Stille reactions, although it offers the practical preparation of a broad spectrum of aromatic carboxylic acid derivatives from simple, commercially available building blocks (Scheme 1).[3]

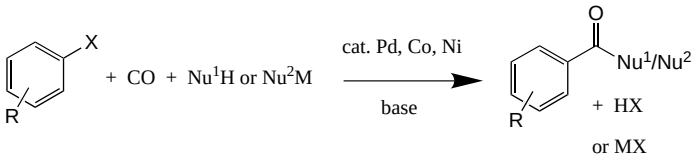

X = I, Br, Cl, N_2^+, OSO_2R', ArI^+, IO_2, SO_2Cl

M = Na, K, BR'_2, AlR'_2, SnR'_3, SiR'_3

Nu^1 = OH, OR', NR'_2, F, Cl, SR'; Nu^2 = H, alkyl, aryl, CN, alkenyl, alkinyl, $R'CO_2$

Scheme 1. Carbonylation of aryl–X compounds.

Of the aryl halides aryl chlorides, because of their ready availability and low cost, are particularly interesting starting materials for "refinement". These substrates are, however, comparatively inert towards conventional palladium–aryl phosphane catalysts because the dissociation energy of the C(sp^2)–Cl bond is relatively large (402, 339, and 272 kJ mol^{-1} for PhCl, PhBr, and PhI, respectively, at 298 K). Whereas significant progress has been made in recent years in the activation of chloroarenes for Suzuki, Heck, and other similar reactions,[4, 5] the efficient carbonylation of chloroarenes remains a problem without a general solution. The crux of the problem is the coordination of CO to the metal center, the π-acceptor character of this ligand reduces the activity of the

[*] Prof. Dr. M. Beller, Dr. W. Mägerlein
Institut für Organische Katalyseforschung (IfOK) an der Universität Rostock e.V.
Buchbinderstrasse 5–6, 18055 Rostock (Germany)
Fax: (+49) 381-46693-24
E-mail: matthias.beller@ifok.uni-rostock.de
Dr. A. F. Indolese
Solvias AG, WRO-1055.622
Klybeckstrasse 191, 4002 Basel (Switzerland)

[**] Palladium-Catalyzed Reactions for Fine Chemical Synthesis, Part 19. This project was suported by the Solvias AG, Basel (Switzerland), and from the Bildungsministerium des Landes Mecklenburg-Vorpommern. We thank Dres. H.-U. Blaser, M. Studer, A. Schnyder, and F. Spindler (Solvias AG) for helpful contributions, M. Heyken (IfOK) for technical support, and Dr. C. Fischer, K. Kortus, and S. Buchholz (IfOK) for analytical work. Part 18: ref. [10].

  1433-7851/01/4015-2856 $ 17.50+.50/0

palladium complex towards oxidative insertion into the C–Cl bond. An additional difficulty is that the agglomeration of Pd atoms and the formation of clusters, which deactivates the catalyst, proceeds particularly readily in the presence of CO.[6] This problem *cannot* be solved through the use of sterically demanding monodentate ligands, so successfully employed in the reactions named above.

To date, the only successful palladium-catalyzed carbonylation, in good yield, of unactivated chloroarenes was with the 1,3-bis(diisopropylphosphanyl)propane (dippp) ligand used by Milstein and co-workers[7]. The drawbacks with this ligand are its difficult synthesis and the high sensitivity of the pyrophoric phosphane. In addition, no catalyst productivities (TON = turnover number) > 100 are reported for this system. Other catalyst systems give less than satisfying yields (< 40 %) and/or catalytic productivities (TON < 40) in the carbonylation of unactivated chloroarenes.[8]

Herein we describe a new palladium catalyst system that allows an efficient carbonylation of electron poor, neutral, and electron rich aryl chlorides in good to very good yields. With regard to catalytic productivity, all the results reported so far for the carbonylation of aryl chlorides are surpassed by at least an order of magnitude. Advantageously the ligands used are relatively air stable and commercially available.

To develop a generally applicable catalyst system for the carbonylation of unactivated aryl chlorides we have chosen the alkoxycarbonylation of chlorobenzene as a model reaction system. Our previous catalyst system ([$PdCl_2(PhCN)_2$]/dppb; P:Pd = 8:1; dppb = 1,4-bis(diphenylphosphanyl)butane), optimized for 4-bromoacetophenone[9] and diverse activated chloroheteroarenes,[10] served as the starting point for these investigations. Preliminary experiments with 0.5 mol % Pd catalyst showed that at reaction temperatures from 145 to 160 °C and CO pressures of 3 to 20 bar, the alkoxycarbonylation of chlorobenzene did not proceed with any significant level of conversion. Also, palladium-complex catalysts with sterically demanding, basic, monodentate phosphane ligands, such as tricyclohexylphosphane, tri-*tert*-butylphosphane, *n*-butyldiadamantylphosphane, gave unsatisfying yields of product (< 20 %).

To impede the formation of less-active palladium carbonyl complexes we decided to study the effects of chelating phosphane ligands. With this aim in mind ferrocenylphosphanes[11] struck us as being particularly interesting in that this class of ligand can be prepared from simple precursors allowing modular modification of the final, comparatively stable ligands. The best known example of the basic ferrocenylphosphanes is Josiphos (**1**) which is used in the elegant Novartis process for the large-scale industrial preparation of the agrochemical Metolachlor.[12]

The alkoxycarbonylation of chlorobenzene with CO and *n*-butanol in the presence of 0.5 mol % [$PdCl_2(PhCN)_2$]/**1** at just 145 °C indeed gave a yield of 49 %. With the Pd–Josiphos catalyst the catalyst productivity (TON = 98) and the catalytic activity (turnover frequency (TOF) = 6.5 h^{-1}) are already comparable with the best result reported for the alkoxycarbonylation of chlorobenzene.[7] On the basis of this promising start further 1,2- and 1,1′-disubstituted ferrocenylphosphanes **2**–**6** were tested in the model reaction (Scheme 2).

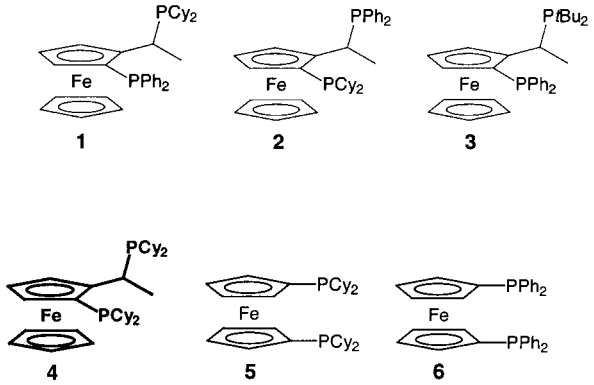

Scheme 2. The ferrocenylphosphanes used. Cy = cyclohexyl.

The best results were delivered by a catalyst based on the ligand 1-[2-(dicyclohexylphosphanyl)ferrocenyl]ethyldicyclohexylphosphane (**4**). Under the reaction conditions given above this ligand gave a conversion of 78 % and a yield of 67 % of the target product *n*-butyl benzoate. To further improve the selectivity and catalytic productivity of the carbonylation reaction the [$PdCl_2(PhCN)_2$]/**4** system was studied more closely (Table 1).

Table 1. Investigation of the alkoxycarbonylation of chlorobenzene in the presence of [$PdCl_2(PhCN)_2$]/**4**.[a]

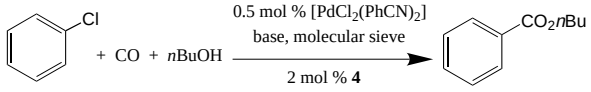

Entry	*T* [°C]	*p* [bar]	mol % Pd	P:Pd	Equiv. base	Conversion [%][b]	Ester yield [%][b]	Selectivity [%][c]
1	145	3	0.5	8	3 NaOAc	78	67	86
2	145	1	0.5	8	3 NaOAc	97	73	75
3	145	1	0.5	16	3 NaOAc	100	72	72
4	145	1	0.5	8	1 NaOAc	97	81	84
5[d]	145	3	0.5	8	3 Na_2CO_3	100	99	99
6[d]	145	1	0.5	8	3 Na_2CO_3	100	97	97
7[d]	130	1	0.5	8	3 Na_2CO_3	85	79	93
8[d]	145	1	0.05	80[14]	3 Na_2CO_3	100	78	78

[a] 7 mmol chlorobenzene, 14 mL *n*-butanol, molecular sieves 4 Å, 18 h. [b] Determined by GC with diethylene glycol di-*n*-butylether as the internal standard. [c] Selectivity = yield of ester/conversion. [d] 16 h.

  1433-7851/01/4015-2857 $ 17.50+.50/0

In the presence of NaOAc (OAc = acetate) as base and reducing the CO pressure from 3 to 1 bar lead to almost quantitative conversion (Table 1, entries 2 and 3), and *n*-butyl benzoate was obtained in 72–73% yield. The only by-product detected was benzoic acid, generated from hydrolysis of the product ester. This by-product is formed by attack of the acetate on the palladium–acyl complex and subsequent hydrolysis, and through transesterification of the acetic acid formed (from HCl and NaOAc). Consequently reducing the amount of NaOAc (Table 1, entry 4) gives a significantly higher yield of the desired ester. By employing Na_2CO_3 as the base (Table 1, entries 5–8) the carbonylation proceeded with quantitative conversion and excellent selectivity (>99%) under 1 as well as 3 bar of CO. Although we chose a general reaction time of 16 h for the conversion, concentration–time profiles of the model reaction show that under the optimized conditions the conversion is complete in 5 to 6 h (under 1 bar CO). When the reaction temperature is reduced to 130 °C then the conversion is reduced to 85%, however, the yield of the desired product is still almost 80%.

To the best of our knowledge these reactions represent the first alkoxycarbonylation of unactivated chloroarenes that give good yields under 150 °C.[13] The catalyst productivities of the $[PdCl_2(PhCN)_2]$/**4** system significantly surpass all the literature values. In the presence of only 0.05 mol% $[PdCl_2(PhCN)_2]$[14] 78% *n*-butyl benzoate is still formed, which corresponds to a TON of 1560 and a catalytic activity (TOF) of around 100 h^{-1}.

After developing an efficient catalyst system for the model reaction we were interested in the reaction of chlorobenzene and CO with other nucleophliles, as well as the alkoxycarboxylation of different chloroarenes. In all the reactions the standard conditions were as described above (0.5 mol% Pd, P:Pd = 8:1, 3 equivalents of Na_2CO_3, molecular sieves (4 Å), 145 °C, 1 bar CO, 16 h). The results are summarized in Tables 2 and 3.

Table 2. Carbonylation of chlorobenzene with various nucleophiles.[a]

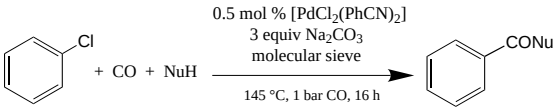

Entry	Nucleophile	Conversion	Product	Yield [%][b]	Selectivity [%][c]
1[d]	*n*BuOH	100	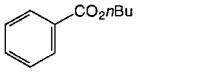	97 (85)	100
2[e]	2-pentanol	85	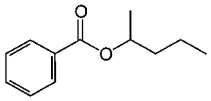	58 (40)	81
3[f]	H_2O	95	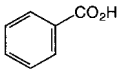	84 (84)	100
4[g]	nPr_2NH	100	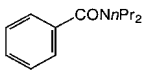	94 (65)	75

[a] 7 mmol chlorobenzene. [b] Yield (GC) of all carbonylation products (ester or amide + acid). GC yield of the product was determined with with diethylene glycol di-*n*-butylether as the internal standard. Yield of the isolated products in parentheses. [c] Chemoselectivity = GC yield of the product/total yield of carbonylation products. [d] 14 mL *n*-butanol. [e] 17 mL 2-pentanol. [f] 2.7 mL water, 11.3 mL dioxane. [g] 3 mL di-*n*-propylamine, 9 mL *N*,*N*-dimethylformamide.

Table 3. Butoxycarbonylation of various chloroarenes.[a]

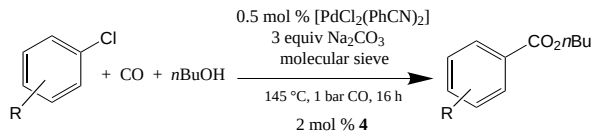

Entry	Chloroarene	Conversion [%]	Product	Yield [%][b]	Selectivity [%][c]
1	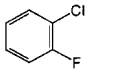	100	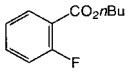	100 (76)	95
2	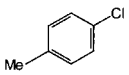	100	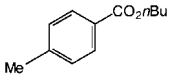	98 (80)	92
3	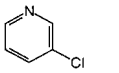	100	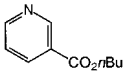	> 72 (67)	100
4	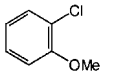	100	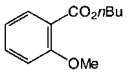	95 (91)	100
5	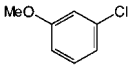	100	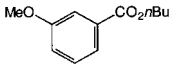	95 (68)	84
6	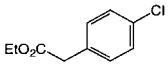	> 99	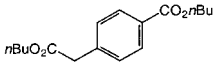	93 (68)	86

[a] 7 mmol chloroarene, 14 mL *n*-butanol. [b] Total yield (GC) of carbonylation products (ester + acid). GC yield of the product was determined with diethylene glycol di-*n*-butylether as the internal standard. Yield of the isolated product in parentheses. [c] Chemoselectivity = GC yield of the ester/total yield of carbonylation products.

Whereas with secondary alcohols noticeably lower yields (58%) of carbonylation products and selectivities (81%) were obtained, with water the reaction proceeded smoothly and carboxylic acids were obtained directly in 84% yield. This observation is of particular interest for the fine chemicals industry where free acids are the most interesting products. In addition the carbonylation of chlorobenzene with di-*n*-propylamine proceeds in good yield to the corresponding benzamide (70%). In this case the isolated by-products were benzoic acid (16%) and dimethylbenzamide (7%).

All the reactions of the various aryl chlorides with CO and *n*-butanol (Table 3) gave quantitative conversions. 2-Chlorofluorobenzene and 4-chlorotoluene give the corresponding carbonylation products in excellent yield (98–100%; Table 3, entries 1 and 2). Also deactivated N-heteroaryl chlorides react in good yield, for example, 3-chloropyridine in 72% yield to nicotinate. The electron rich and sterically demanding 2-chloroanisol gave the desired product in near to quantitative yield (95%; Table 3, entry 4). Surprisingly the reaction of 3-chloroanisol is noticeably less selective and the corresponding ester is only obtained in 80% together with 15% *m*-methoxybenzoic acid. Use of 4-chlorophenyl ethyl acetate delivers 4-(butoxycarbonyl)phenyl butyl acetate also in 80% yield. These results show that even the labile phenyl ethyl acetate unit is easily tolerated under the reaction conditions however, it does undergo transesterification.

  1433-7851/01/4015-2858 $ 17.50+.50/0 *Angew. Chem. Int. Ed.* **2001**, *40*, No. 15

Experimental Section

General procedure for the alkoxycarbonylation of chloroarenes: the corresponding chloroarene (7 mmol), *n*-butanol (14 mL), $[PdCl_2(PhCN)_2]$ (13.4 mg, 0.035 mmol, 0.5 mol%), and ligand **4** (84.9 mg, 0.140 mmol, 2 mol%) were added to a Schlenk flask under argon (orange solution). Sodium carbonate (2.226 g, 21 mmol, 3 equiv) and molecular sieves (4 Å, ca. 3 g) were added to the reaction autoclave. Following evacuation and replacement with argon (three cycles) the reaction mixture was transferred with a PVC hose ($\varnothing \approx 2$ mm) under a slight excess pressure of argon from the Schlenk flask into the autoclave. The autoclave was closed and heated to the reaction temperature (145 °C). The reaction pressure (1 bar CO) was held constant by means of a CO reservoir, connected to the autoclave by a pressure regulator. After 16 h reaction time the autoclave was cooled to room temperature and the yellow orange mixture diluted with dichloromethane (70 mL). After washing with water (70 mL) the aqueous phase was extracted with dichloromethane (2×20 mL), and the combined organic phases were dried over magnesium sulfate, filtered, and concentrated under reduced pressure. The crude product was then purified by column chromatography (silica gel, EtOAc/hexane).

Received: March 20, 2001 [Z16812]

[1] a) J. Tsuji, *Palladium Reagents and Catalysts: Innovations in Organic Synthesis*, Wiley, Chichester, **1995**; b) F. Diederich, P. J. Stang, *Metal-Catalyzed Cross-Coupling Reactions*, Wiley-VCH, Weinheim, **1998**; c) M. Beller, C. Bolm, *Transition Metals for Organic Synthesis*, Wiley-VCH, Weinheim, **1998**.

[2] a) A. Schoenberg, I. Bartoletti, R. F. Heck, *J. Org. Chem.* **1974**, *39*, 3318 – 3326; b) S. A. Vinogradov, D. F. Wilson, *Tetrahedron Lett.* **1998**, *39*, 8935 – 8938.

[3] a) H. M. Colquhoun, D. J. Thompson, M. V. Twigg, *Carbonylation, Direct Synthesis of Carbonyl Compounds*, Plenum, New York, **1991**; b) M. Beller in *Applied Homogeneous Catalysis with Organometallic Compounds*, *Vol. 2* (Eds.: B. Cornils, W. A. Herrmann), VCH, Weinheim, **1996**, pp. 148 – 159; c) M. Beller, B. Cornils, C. D. Frohning, C. W. Kohlpaintner, *J. Mol. Catal.* **1995**, *104*, 17 – 85.

[4] Review: a) I. P. Beletskaya, *Chem. Rev.* **2000**, *100*, 3009 – 3066; b) V. V. Grushin, H. Alper, *Top. Organomet. Chem.* **1999**, *3*, 193 – 226; c) T. H. Riermeier, A. Zapf, M. Beller, *Top. Catal.* **1997**, *4*, 301 – 309.

[5] Selected recent articles on chloroarene activation with regard to Heck and Suzuki reactions: a) A. Ehrentraut, A. Zapf, M. Beller, *Synlett* **2000**, 1589 – 1592; b) A. Ehrentraut, A. Zapf, M. Beller, *Angew. Chem.* **2000**, *112*, 4315 – 4317; *Angew. Chem. Int. Ed.* **2000**, *39*, 4153 – 4155; c) M. Gómez Andreu, A. Zapf, M. Beller, *Chem. Commun.* **2000**, 2475 – 2476; d) A. Zapf, M. Beller, *Chem. Eur. J.* **2000**, *6*, 1830 – 1833; e) V. P. W. Böhm, C. W. K. Gstöttmayr, T. Weskamp, W. A. Herrmann, *J. Organomet. Chem.* **2000**, *595*, 186 – 190; f) C. Zhang, M. L. Trudell, S. P. Nolan, *Tetrahedron Lett.* **2000**, *41*, 595 – 598; g) A. F. Littke, G. C. Fu, *J. Org. Chem.* **1999**, *64*, 10 – 11; h) K. H. Shaughnessy, P. Kim, J. F. Hartwig, *J. Am. Chem. Soc.* **1999**, *121*, 2123 – 2132; i) A. F. Littke, G. C. Fu, *Angew. Chem.* **1998**, *110*, 3586 – 3587; *Angew. Chem. Int. Ed.* **1998**, *37*, 3387 – 3388; j) J. P. Wolfe, R. A. Singer, B. H. Yang, S. L. Buchwald, *J. Am. Chem. Soc.* **1999**, *121*, 9550 – 9561; k) J. P. Wolfe, S. L. Buchwald, *Angew. Chem.* **1999**, *111*, 2570 – 2573; *Angew. Chem. Int. Ed.* **1999**, *38*, 2413 – 2416; l) X. Bei, T. Crevier, A. S. Guram, B. Jandeleit, T. S. Powers, H. W. Turner, T. Uno, W. H. Weinberg, *Tetrahedron Lett.* **1999**, *40*, 3855 – 3858; m) M. Beller, A. Zapf, *Synlett* **1998**, 792 – 794.

[6] a) T. A. Stromnova, I. I. Moiseev, *Russ. Chem. Rev.* **1998**, *67*, 485 – 514; b) K. Kudo, M. Hidai, Y. Uchida, *J. Organomet. Chem.* **1971**, *33*, 393 – 398; c) M. Hidai, M. Kokura, Y. Uchida, *J. Organomet. Chem.* **1973**, *52*, 431 – 435.

[7] a) Y. Ben-David, M. Portnoy, D. Milstein, *J. Am. Chem. Soc.* **1989**, *111*, 8742 – 8744; b) Y. Ben-David, M. Portnoy, D. Milstein, *J. Chem. Soc. Chem. Commun.* **1989**, 1816 – 1817; c) M. Portnoy, D. Milstein, *Organometallics* **1993**, *12*, 1655 – 1664.

[8] a) M. Huser, M.-T. Youinou, J. A. Osborn, *Angew. Chem.* **1989**, *101*, 1427 – 1430; *Angew. Chem. Int. Ed. Engl.* **1989**, *28*, 1386 – 1389; b) V. V. Grushin, H. Alper, *J. Chem. Soc. Chem. Commun.* **1992**, 611 – 612; c) T. Miyawaki, K. Nomura, M. Hazama, G. Suzukamo, *J. Mol. Catal.* **1997**, *120*, L9 – L11; d) V. Dufaud, J. Thivolle-Cazat, J.-M. Basset, *J. Chem. Soc. Chem. Commun.* **1990**, 426 – 427; e) R. J. Perry, B. D. J. Wilson, *J. Org. Chem.* **1996**, *61*, 7482 – 7485.

[9] a) W. Mägerlein, M. Beller, A. F. Indolese, *J. Mol. Catal.* **2000**, *156*, 213.

[10] M. Beller, W. Mägerlein, A. Indolese, C. Fischer, *Synthesis* **2001**, 1098 – 1109.

[11] a) A. Togni, C. Breutel, A. Schnyder, F. Spindler, H. Landert, A. Tijani, *J. Am. Chem. Soc.* **1994**, *116*, 4062 – 4066; b) T. Hayashi in *Ferrocenes* (Eds.: A. Togni, T. Hayashi), VCH, Weinheim, **1995**, pp. 105 – 142; c) A. Togni, *Chimia* **1996**, *50*, 86 – 93.

[12] a) F. Spindler, H.-U. Blaser, *Enantiomer* **1999**, *4*, 557 – 568; b) H.-U. Blaser, H. P. Buser, K. Coers, R. Hanreich, H.-P. Jalett, E. Jelsch, B. Pugin, H.-D. Schneider, F. Spindler A. Wegmann, *Chimia* **1999**, *53*, 275 – 280.

[13] In a long reaction time experiment on the alkoxycarbonylation of chlorobenzene with 5 mol% Pd catalyst a conversion of 48% (selectivity 91%) was reached after 5 days even at a reaction temperature of 90 °C.

[14] A P:Pd ratio of 80:1 was chosen for these experiments to maintain a ligand concentration 2 mol%. In earlier work on carbonylation reactions we showed that for the stabilization of the Pd catalyst the ligand concentration and not the ligand:palladium ratio is important.[9]

Synthesis, Structure, and Reactivity of a Diphosphadiferratetrahedrane with a Fe–Fe Double Bond**

Christine Eichhorn, Otto J. Scherer,* Thorsten Sögding, and Gotthelf Wolmershäuser

Dedicated to Professor Marianne Baudler on the occasion of her 80th birthday

Whereas in the chemistry of acetylene complexes of iron, compound **1** containing a C_2Fe_2 tetrahedrane framework and a Fe–Fe double bond was prepared and crystallographically characterized already in 1976,[1] for the iso(valence)electronic and isolobal ($HC \leftrightarrow P$, $HC{\equiv}CH \mathrel{\hat{=}} {:}P{\equiv}P{:}$) diphosphadiferratetrahedranes only the complex **2** with a Fe–Fe single bond and additional P-coordination is known.[2]

Diphosphadimetallatetrahedranes of the type $[\{L_nM\}_2(\mu\text{-}\eta^2{:}\eta^2\text{-}P_2)]$ ($L_nM = 15$ valence-electron(VE) fragment)[3] synthesized to date all display M–M single bonds, and with six skeleton electron pairs (SEPs) for the tetrahedral M_2P_2 framework are considered as *nido* clusters. According to theoretical investigations a decrease (5 SEPs) as well as an increase (7 SEPs) in the number of electrons in the skeleton lead to changes of the M_2P_2 framework.[4]

[*] Prof. Dr. O. J. Scherer, Dipl.-Chem. C. Eichhorn, Dipl.-Chem. T. Sögding, Dr. G. Wolmershäuser[+]
Fachbereich Chemie der Universität
Erwin-Schrödinger-Strasse, 67663 Kaiserslautern (Germany)
Fax: (+49) 631-205-4676
E-mail: oscherer@rhrk.uni-kl.de

[+] Crystal structure analysis.

[**] This work was supported by the Fonds der Chemischen Industrie and by the Graduiertenkolleg „Phosphorchemie als Bindeglied verschiedener chemischer Disziplinen“.

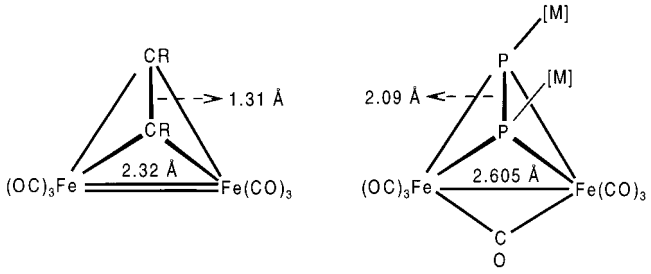

1: R = *t*Bu **2**: [M] = $Cr(CO)_5$

If the thermolysis time for the reaction with butterfly molecule **3** is reduced from about 3 h to about 45 min, the diphosphadiferratetrahedrane **4** with a Fe–Fe double bond (formally a diphosphadimetallatetrahedrene) is obtained in 18 % yield together with the known complexes [Cp‴Fe-(η^5-P_5)] (**5**) and [{Cp‴Fe}$_2$(μ-η^4:η^4-P_4)] (**6**) (Scheme 1).[5]

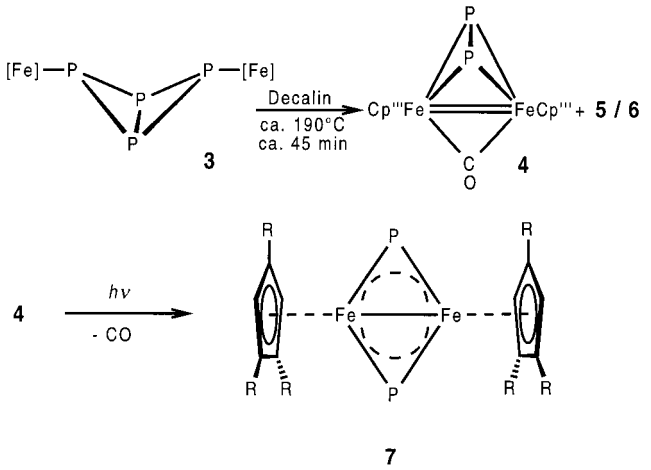

Scheme 1. Preparation of complexes **4** and **7** from the butterfly molecule **3**. [Fe] = $Fe(CO)_2Cp'''$, Cp‴ = 1,2,4-$tBu_3C_5H_2$, R = *t*Bu.

Complex **4** forms air- and light-sensitive green crystals,[6] which are soluble to very soluble in *n*-hexane, toluene, and dichloromethane. The μ-CO band occurs at 1761 cm^{-1} in the IR spectrum and a singlet appears at $\delta = 776.3$ in the $^{31}P\{^1H\}$ NMR spectrum. Compound **4** has 5 SEPs; thus, one less than **2**.[4a]

The crystal structure analysis[7] for the tetrahedral Fe_2P_2 framwork (Figure 1) of **4** revealed a P–P bond length of 2.064(2) Å (see also ref. [3]), which is therefore slightly shorter than that in **2** (2.09 Å).[2] The Fe–Fe bond length of 2.3944(10) Å lies in the range for Fe–Fe double bonds and is slightly longer than that in **1** (2.32 Å), but considerably shorter than that in **2** (2.605 Å). The iron atoms are almost symmetrically bridged (Fe1–C1 1.9236(6), Fe2–C1 1.914(6) Å) by the CO ligand; their distances to the phosphorus atoms (2.2867(16) – 2.2948(17) Å) are on average 2.29 Å (2.28 Å for **2**).[2] The planar Cp‴ five-membered rings deviate by 16.7° from a parallel arrangement and the Fe1-Fe2-$Cp'''_{centroid}$ as well as Fe2-Fe1-$Cp'''_{centroid}$ angles by 7.3 and 7.2°, respectively, from linearity.

The P_2 building block of **4** is split photochemically under elimination of CO to a complex with two bent μ-P ligands

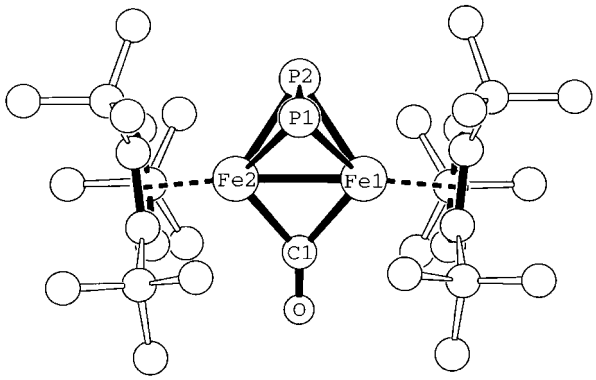

Figure 1. Structure of **4** in the crystal. Bond lengths [Å] and angles [°]: Fe1-Fe2 2.3944(10), Fe1-P1 2.2915(18), Fe1-P2 2.2867(16), Fe2-P1 2.2890(19), Fe2-P2 2.2948(17), P1-P2 2.064(2), Fe1-C1 1.923(6), Fe2-C1 1.914(6), Fe1-$Cp'''_{centroid}$ 1.75, Fe2-$Cp'''_{centroid}$ 1.74; Fe1-P1-Fe2 63.03(5), Fe1-P2-Fe2 63.02(5), P1-Fe1-P2 53.60(6), P1-Fe2-P2 53.53(6), Fe1-C1-Fe2 77.2(2), Fe1-Fe2-$Cp'''_{centroid}$ 172.70, Fe2-Fe1-$Cp'''_{centroid}$ 172.80.

(→**7**, Scheme 1; the question still remains unanswered as to whether this formally involves the formation of a P_2Fe_2 tetrahedrane with a Fe–Fe triple bond). Although there are a few complexes with μ_3-P ligands,[3, 8, 10] the only comparable example with such a μ-P bridging ligand is [{$(ArO)_2W$}$_2$-(μ-P){P*t*BuP$(OAr)_2$}] (**8**), which was prepared from *t*BuC≡P and [{$(ArO)_3W$}$_2$]($W \equiv W$).[9]

The dark green crystals of **7** show solubility behavior similar to that of **4**.[6] The $^{31}P\{^1H\}$ NMR signal of **7** at δ=1406.9 is shifted to extremely low field (see also ref. [10]), and compared to the signal of the starting material **4** it is shifted by 630.6 ppm. The crystal structure analysis of **7** (Figure 2) reveals a rhombic Fe_2P_2 four-membered ring,[7] in which the

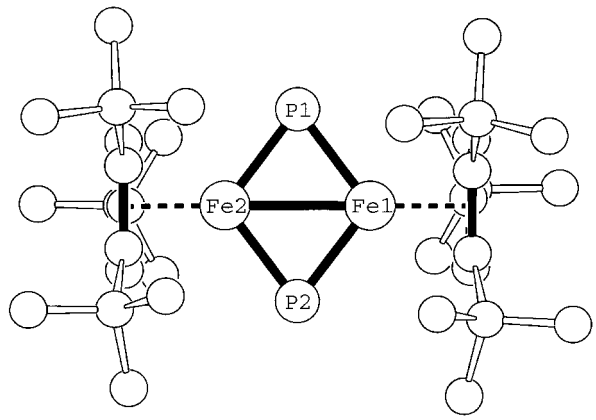

Figure 2. Structure of **7** in the crystal. Bond lengths [Å] and angles [°]: Fe1-Fe2 2.5004(4), Fe1-P1 2.1069(7), Fe1-P2 2.0994(7), Fe2-P1 2.1068(7), Fe2-P2 2.1015(8), Fe1-$Cp'''_{centroid}$ 1.73, Fe2-$Cp'''_{centroid}$ 1.73; Fe1-P1-Fe2 72.80(2), Fe1-P2-Fe2 73.06(2), P1-Fe1-P2 107.06(3), P1-Fe2-P2 106.99(3).

atoms deviate from the least squares plane by at most 0.0211 Å. The normals of the Fe1-Fe2-P1 plane and that of the Fe1-Fe2-P2 plane form an angle of 2.8°. The Fe1–Fe2 bond length of 2.5004(4) Å corresponds almost exactly to the average value from that in **2** (single bond) and that in **4** (double bond). If the bent μ-P ligands are each considered as 3e$^-$ donors, then for the diamagnetic complex **7** the two Fe

  1433-7851/01/4015-2860 $ 17.50+.50/0

atoms achieve 18 VE when one formally postulates a Fe–Fe double bond. As expected, in the transition from **4** to **7** a considerable shortening occurs of the Fe–P distances (Fe–P 2.29 and 2.10 Å (av), respectively; multiple bond contributions). In **7** the angles at the P atoms (Fe-P-Fe 72.80(2), 73.06(2)°) are considerably smaller than those at the Fe atoms (P-Fe-P 107.06(3), 106.99(3)°). The almost ideally eclipsed Cp‴ five-membered rings (Figure 2) deviate only slightly (2.3°) from a parallel orientation and are arranged almost orthogonal (91.5, 89.2°) to the four-membered ring.

Experimental Section

4: Compound **3** (970 mg, 1.19 mmol) was dissolved in decalin (ca. 150 mL) and heated under stirring to 190 °C (reflux). After about 45 min the CO bands of the starting material **3** were no longer visible by IR spectroscopy.[5] The solvent was removed under vacuum. The red-brown residue was dissolved in dichloromethane (ca. 10 mL) and the solution was treated with silylated silica gel (ca. 2 g). The mixture was transferred to a column (20 × 2 cm) filled with silica gel and petroleum ether. At −20 °C (cryostat) a pale green fraction, which contained **5** (60 mg, 12 %), was eluted with petroleum ether. Compound **6** (370 mg, 44 %) was obtained as the second, dark red fraction with petroleum ether/toluene (20/1). Compound **4** (150 mg, 18 %) was eluted as a dark green solution with petroleum ether/toluene (10/1), and was recrystallized from hexane.

7: A dark green solution of **4** (150 mg, 0.22 mmol) in toluene (ca. 120 mL) was photolyzed at room temperature (150-W mercury high-pressure lamp). After 4.5 h the band for the bridging CO ligand of the starting material was no longer detected in the IR spectrum of the reaction mixture. The solvent was removed under vacuum, and the residue was taken up in heptane. A pale brown insoluble solid was separated on a frit; owing to its poor solubility this could not be characterized further. Compound **7** (90 mg, 63 %) was obtained as a yellow-brown powder from the eluate, and was recrystallized from hexane.

Received: April 11, 2001 [Z16932]

[1] F. A. Cotton, J. D. Jammerson, B. R. Stults, *J. Am. Chem. Soc.* **1976**, *98*, 1774 – 1779.

[2] H. Lang, G. Huttner, L. Zsolnai, G. Mohr, B. Sigwarth, U. Weber, O. Orama, I. Jibril, *J. Organomet. Chem.* **1986**, *304*, 157 – 179.

[3] Recent reviews: O. J. Scherer, *Acc. Chem. Res.* **1999**, *32*, 751 – 762; K. H. Whitmire, *Adv. Organomet. Chem.* **1998**, *42*, 1 – 145; M. Peruzzini, I. de los Rios, A. Romerosa, F. Vizza, *Eur. J. Inorg. Chem.* **2001**, 593 – 608.

[4] a) J.-F. Halet, J.-Y. Saillard, *J. Organomet. Chem.* **1987**, *327*, 365 – 377; b) D. M. Hoffman, R. Hoffmann, R. Fisel, *J. Am. Chem. Soc.* **1982**, *104*, 3858 – 3875.

[5] O. J. Scherer, T. Hilt, G. Wolmershäuser, *Organometallics* **1998**, *17*, 4110 – 4112.

[6] Spectroscopic data of compounds **4** and **7**: ^{31}P NMR (167.97 MHz, C_6D_6, 85 % H_3PO_4 external; $T = 298$ K): **4**: $\delta = 776.3$ (s, 2P); **7**: $\delta = 1406.9$ (s, 2P); ^{1}H NMR (200.13 and 400.14 MHz, C_6D_6, C_6D_5H internal; $T = 298$ K): **4**: $\delta = 4.61$ (s, 2H), 1.34 (s, 18H), 1.13 (s, 9H); **7**: $\delta = 6.59$ (s, 2H), 1.37 (s,18H), 1.29 (s, 9H); IR (toluene): **4**: $\tilde{\nu}$(CO) = 1761 cm^{-1} (vs).

[7] Crystal structure data of **4** [**7**]: $C_{35}H_{58}Fe_2OP_2$ [$C_{34}H_{58}Fe_2P_2$], $M_r = 668.5$ [640.4], monoclinic [monoclinic], space group $P2_1/n$ [$P2_1/n$], $a = 14.15624(13)$ [11.7825(8)], $b = 14.1991(10)$ [10.4476(4)], $c = 18.171(2)$ Å [28.5310(17)], $\beta = 99.277(12)°$ [91.156(8)], $V = 3604.7(6)$ Å^3 [3511.4(3)], $Z = 4$ [4], $\rho_{calcd} = 1.232$ g cm^{-3} [1.211], $T = 293(2)$ K, $\theta = 2.04 – 26.08°$ [2.95 – 25.68], 25078 [46082] measured reflections, 7016 [6644] independent reflections ($R_{int} = 0.1449$ [0.0504]), $R1 = 0.0465$ [0.0373], $wR2 = 0.0687$ [0.0996] ($I > 2\sigma(I)$); $R1 = 0.1500$ [0.0451], $wR2 = 0.0889$ [0.1043] (all data); diffractometer: Siemens P4 [Stoe IPDS]; structure solution: direct methods; program: SHELXS-97 [SIR 92 (A. Altomare, G. Cascarano, G. Giacovazzo, A. Gualiardi, M. C. Burla, G. Polidori, M. Camalli, *J. Appl. Crystallogr.* **1994**, *27*, 435)]; structure refinement: full-matrix least-squares methods against F^2; program: SHELXL-97 (G. M. Sheldrick, Universität Göttingen, **1997**); data/parameters: 7016/379 [6644/361]. Crystallographic data (excluding structure factors) for the structures reported in this paper have been deposited with the Cambridge Crystallographic Data Center as supplementary publication nos. CCDC-163506 (**4**) and CCDC-163507 (**7**). Copies of the data can be obtained free of charge on application to CCDC, 12 Union Road, Cambridge CB2 1EZ, UK (fax: (+44) 1223-336-033; e-mail: deposit@ccdc.cam.ac.uk).

[8] O. J. Scherer, M. Ehses, G. Wolmershäuser, *Angew. Chem.* **1998**, *110*, 530 – 533; *Angew. Chem. Int. Ed.* **1998**, *37*, 507 – 510; P. Kramkowski, G. Baum, U. Radius, M. Kaupp, M. Scheer, *Chem. Eur. J.* **1999**, *5*, 2890 – 2898.

[9] P. Kramkowski, M. Scheer, *Angew. Chem.* **2000**, *112*, 959 – 962; *Angew. Chem. Int. Ed.* **2000**, *39*, 928 – 931.

[10] G. Huttner, H. Lang in *Multiple Bonds and Low Coordination in Phosphorus Chemistry* (Eds.: M. Regitz, O. J. Scherer), Thieme, Stuttgart, **1990**, p. 48.

Evidence for σ Dimerization During Anodic Redox Switching of 1,3,5-Tripyrrolidinobenzene: A New Molecular Switch**

Jürgen Heinze,* Christian Willmann, and Peter Bäuerle

The dimerization of radical ions of conjugated aromatic systems has been discussed in the literature for more than 20 years.[1–10] In the case of radical cations, experimental data have led many authors to postulate the formation of weakly reacting π dimers. This assumption, however, is not able to fully explain the experimental results. In the case of radical anions, by contrast, the formation of covalently bonded σ dimers is generally accepted.[2, 11–18] This controversy over the σ or π dimerization of radical ions is unresolved primarily as a consequence of the widely held view that because of coulombic repulsion between charged molecules only weak reactions are possible. This argument overlooked and overlooks first the presence of the counterions, which drastically diminish repulsion, and second that even in moderately polar solutions the level of coulombic interactions is low compared to the gas phase.

Interpretations of the measurements of radical cations in connection with the π-dimer hypothesis are based almost exclusively on the results for UV/Vis spectra obtained at different temperatures. Contrary to expectations, in UV spectra dimerization is usually detected in the short-wave

[*] Prof. Dr. J. Heinze, C. Willmann
Institut für Physikalische Chemie der Universität Freiburg und Freiburger Materialforschungszentrum
Albertstrasse 21, 79104 Freiburg (Germany)
Fax: (+49) 761-2036237
E-mail: heinze@uni-freiburg.de
Prof. Dr. P. Bäuerle
Abteilung Organische Chemie II, Universität Ulm,
Albert-Einstein-Allee 11, 891018 Ulm (Germany)

[**] This work was supported by the DFG, the VW Foundation, and the Fonds der Chemischen Industrie.

dimer bands. Thus, normal charge-transfer interactions cannot be used to interpret such "π dimerizations"; instead, typical solid-state phenomena, such as the Davydov shift, are used.[19, 20] Further support for the π-dimer hypothesis came from electrochemical studies using cyclic voltammetry, which apparently indicated reversible redox processes without follow-up reactions. However, in none of these examples were fast-scan experiments conducted for different concentrations or at different low temperatures.

In the meantime, more recent electrochemical investigations on oligomeric thiophenes, polyenes, and other aromatic compounds provide conclusive proof that the dimerization of their radical cations leads to the formation of covalent σ bonds,[21–26] as has been shown for radical anions.[11–18] These reactions are obviously driven by the strong tendency for unpaired electrons to couple, forming a σ bond.

In the past, the π-dimer hypothesis was particularly popular in connection with the coupling of radical cations of aromatic amines.[27–29] The publications of Effenberger et al. prove that this is not necessarily compelling. Indeed, by oxidizing 1,3,5-tripyrrolidinobenzene (**1**), they succeeded in isolating a dimeric σ complex **2**[30–34] [Eq. (1)] and, by using X-ray structure analysis, were able to unequivocally prove the existence of the σ bond in the solid state.

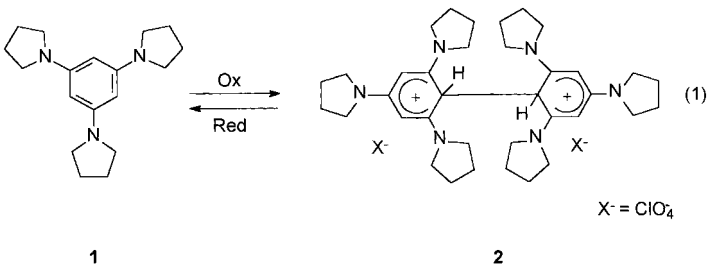

(1)

1 **2**

For compound **1**, there are no electrochemical data on the formation of σ dimers during redox switching. As structural data unequivocally prove the formation of dicationic σ dimers after the oxidation of **1**, electrochemical measurements should also provide incontrovertible evidence for the dimerization mechanism in solution.

Herein we shall report cyclic voltammetric and spectroscopic investigations into the oxidation of **1** and the reduction of the dimeric σ complex **2**. We shall demonstrate that, after the formation of radical cations, **1** spontaneously reacts to form the dimeric σ complex **2**, which after reduction "reversibly" dissociates to generate **1** again.

In normal voltammetric experiments, the oxidation of **1** at about $E^{a}_{p1} = +0.3$ V versus Ag/AgCl at room temperature is an irreversible process (Figure 1a). The resulting follow-up product is reduced only at about $E^{c}_{p1} = -1.0$ V, which indicates the high stability of this product. Another oxidation step takes place at about $E^{a}_{p2} = +0.8$ V, and the corresponding reduction at about $E^{c}_{p2} = -0.15$ V (Figure 1b). The peak current value of the second oxidation step is exactly half of the current value of the first oxidation step. The conclusion to be drawn from the cyclic voltammogram data, which are in perfect agreement

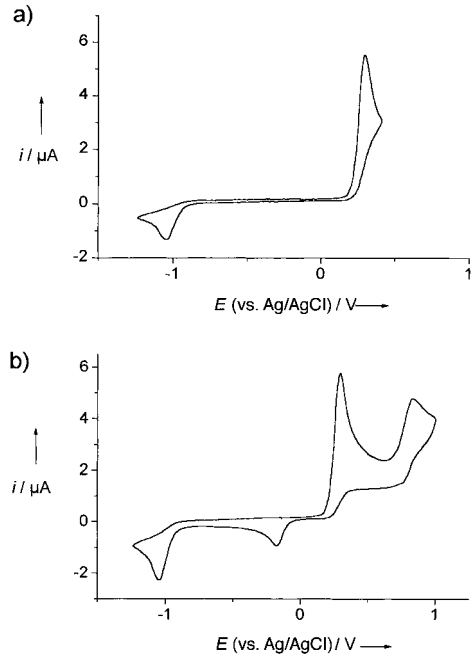

Figure 1. Cyclic voltammograms of **1** in CH_3CN/0.1 M $TBAPF_6$; $v = 0.2$ V s^{-1}; $T = 293$ K; $c = 1.2 \times 10^{-3}$ M: a) to 0.5 V, b) to 1.0 V.

with the chemical findings, is the formation of a dimer at the radical cation level. Nothing is known about the nature of the follow-up reaction after the second redox step. But it does include an oxidation step involving the transfer of one electron, followed by another chemical reaction. At present, this second redox step serves only as further evidence for the formation of the σ dimer **2**, however, it will be the focus of future research. The large difference between the redox potential of the monomer **1** and that of the dicationic dimer **2** is characteristic of both carbocations and carbanions and the corresponding radical ions. Even simple molecular orbital considerations[35] but also AM1 and PM3 calculations show that the dimer in its charged state is considerably more stable than the monomeric radical cation.

To provide further evidence for dimerization, we carried out voltammetric experiments on the σ complex **2**, present as a salt, under the same conditions as for **1** (Figure 2a, b). As can be seen in Figure 2a, the characteristic oxidation peak at 0.3 V appears only in a second cycle, that is, only after the cathodic wave has been passed at −1.0 V, and the reduction of **2** and the associated cleavage into the starting monomer **1**. Repeating the experiment at a higher potential, it is possible to observe the above-mentioned oxidation peak at about +0.8 V for the oxidation of the dicationic dimer of **2**. Similarly, in a second cycle the peak for the oxidation of the monomer **1** at +0.3 V appears (Figure 2b). Finally, Figure 2c shows the result of the simultaneous voltammetric measurement of **1** and **2** in acetonitrile. That the only peaks to appear are the oxidation peaks previously established at +0.3 V and +0.8 V and the corresponding reduction peaks at +0.15 V and −1.0 V is clear evidence that after the formation of the radical cations, **1** is irreversibly dimerized to the σ complex **2**, after which **2** is reduced again at about −1.0 V and then dissociates into **1** (Scheme 1).

  1433-7851/01/4015-2862 $ 17.50+.50/0 *Angew. Chem. Int. Ed.* **2001**, *40*, No. 15

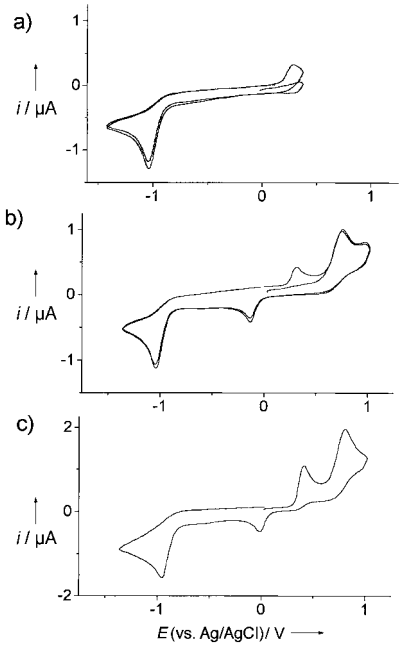

Figure 2. Cyclic voltammograms in $CH_3CN/0.1\,M\,TBAPF_6$; $v = 0.2\,V\,s^{-1}$, $T = 293$ K; a), b) cyclic voltammograms of **2**, $c(\mathbf{2}) = 2.75 \times 10^{-4}$ M; c) cyclic voltammogram of **1** and **2**, $c(\mathbf{1}) = 2.23 \times 10^{-4}$ M; $c(\mathbf{2}) = 2.275 \times 10^{-4}$ M.

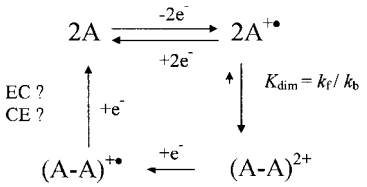

Scheme 1. Mechanism of the oxidation and reduction of **1**; E = electrochemical step, C = chemical step.

As further proof of this scheme, UV absorption spectra of both **1** and **2** were measured in a spectro-electrochemical cell.[36] Figure 3a shows a spectrum for **1** with an unpolarized electrode, with maximum absorption at 244 nm, this agrees with the spectrum of **1** in the literature.[37–39] If a potential of +0.4 V is applied, monomer **1** is oxidized, and the resulting spectrum shows main absorption maxima at 261 nm, 346 nm, and 430 nm, which agrees with the spectra for the dimeric σ complex **2**.[31] If the potential is changed to −1.1 V, the σ dimer **2** is reduced and one obtains, as expected, the spectrum of the starting species **1**. Figure 3b compares the spectra of **2** (open circuit conditions) and **1** after the oxidation at +0.4 V. The identical spectra are further evidence for the assumption that the radical cations formed on the oxidation of **1** react to form the dimeric σ complex **2**. The spectra of **2** after reduction at −1.0 V and of **1** (open circuit conditions) are also identical, which clearly demonstrates that the dicationic σ dimer **2** is reduced again to **1** at −1.0 V (Figure 3a, b).

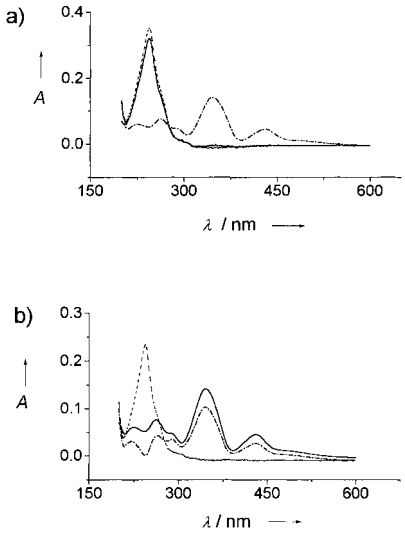

Figure 3. UV measurements of **1** and **2** in a spectro-electrochemical cell,[36] in $CH_3CN/0.1\,M\,TBAPF_6$, $c(\mathbf{1}) = 1.1 \times 10^{-3}$ M, $c(\mathbf{2}) = 5.1 \times 10^{-4}$ M; a) **1** at 0 V (——), **1** at 0.4 V (–·–·), **1** at −1.1 V (----); b) **1** at 0.4 V(——), **2** at 0 V (–·–·), **2** at −1.0 V (----).

As the results presented here show, the oxidation of **1** at room temperature and medium concentrations ($c = 1.3 \times 10^{-3}$ M) is irreversible. The resulting radical cations dimerize to form the σ complex **2**. However, reversible processes are very frequently observed in other dimerization reactions of radical ions,[20–25] that is, the dimer is formed and dissociates within the time scale of the experiment. Consistent with this finding, in voltammetric experiments at room temperature, with slow scan rates, and at low concentrations only the monomeric radical ion is found. Normally, the equilibrium constants for these dimerizations range from 10^2 to $10^7\,M^{-1}$, and the rate constants reach values of up to $10^5\,M^{-1}\,s^{-1}$.

As we can also assume a dynamic dimerization equilibrium in the presence of the radical cation of **1**, we carried out experiments at low concentrations (1.9×10^{-4} M), increased temperatures, and higher scan rates. Clearly, at 50 °C in acetonitrile and a scan rate of $10\,V\,s^{-1}$, the reduction of the radical cation formed from **1** can already be observed in the reverse scan. At $200\,V\,s^{-1}$, the dimerization proceeds only slowly (Figure 4). The conclusion is that the equilibrium constant of the dimerization falls as the temperature rises, while the rate constant for the dissociation of the dimers rises significantly faster than the rate constant for the dimerization.

A quantitative analysis of the data for the scan rates in the range from $0.2\,V\,s^{-1}$ to $10\,V\,s^{-1}$ at room temperature was carried out with the help of digital simulation (Digisim, Bioanalytical Systems). Figure 5 presents the results of these simulations for reaction Scheme 1 with two very different scan rates. In the oxidation range the agreement between the experimental and simulated data is excellent. The values were as follows: equilibrium con-

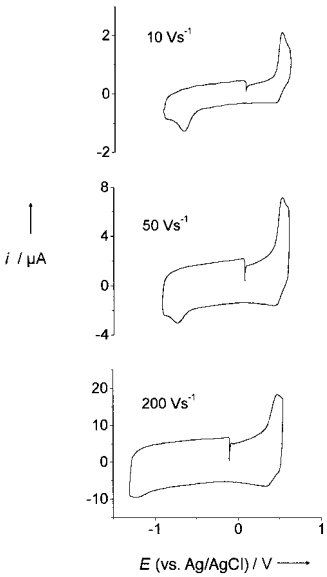

Figure 4. Cyclic voltammograms of **1** in $CH_3CN/0.1\,M$ $TBAPF_6$, $T = 323$ K, $c = 1.9 \times 10^{-4}$ M.

  1433-7851/01/4015-2863 $ 17.50+.50/0

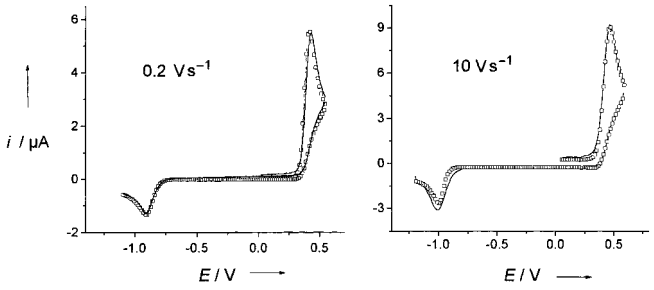

Figure 5. Experimental (——) and simulated (Digisim; □) cyclic voltammograms for the oxidation of **1** at scan rates of $v = 0.2$ (left) and $10\,V\,s^{-1}$ (right). The simulated data were approximated to the experimental results for the oxidation of **1** in $CH_3CN/0.1\,M\,TBAPF_6$, $c = 1.2\ 10^{-3}\,M$, $T = 298$ K. Disc elelctrode: $d = 1$ mm (left), $d = 0.5$ mm (right).

stant $K_{eq} = 3.3 \times 10^{11}\,M^{-1}$, rate constants for formation $k_f = 4.3 \times 10^{6}\,M^{-1}\,s^{-1}$, and breakdown $k_b = 1.3 \times 10^{-5}\,s^{-1}$ of the dimer. Measurements and simulations at various temperatures provided a rough estimate for the activation energy of $E_A = 29\,kJ\,mol^{-1}$. This, in turn, indicates a diffusion-controlled reaction, as in other radical-ion coupling processes.[21–23]

The quantitative analysis shows that the dimerization takes place, as assumed, between the radical cations (RR coupling) and not, as often postulated for irreversible processes, between the neutral species and radical cations (RS coupling). It is also noteworthy that the dimerization step is, in principle, chemically reversible. After reduction of the dimer the starting species is regenerated. The switching between the monomeric and dimeric system can be repeated many times without any decomposition of the system.[40] This is a new example of a redox-controlled molecular switch.[26]

Regarding the elimination of protons in the formation of conducting polymers, it is of note that under the given experimental conditions no protons were eliminated from **2**. Owing to the electron-donating amino nitrogens, the acidity of the dimer is so weak that rearomatization from the dicationic σ dimer to the neutral biphenyl cannot take place and can be achieved only after the addition of strong bases. A similar tendency can be observed in the formation of conducting oligomers and polymers, for example, polythiophene, where the stability of σ intermediates formed during coupling increases with the length of the growing chain.

Experimental Section

Compounds **1**[41] and **2**[32] were synthesized according to the literature. The cyclic voltammetric experiments were performed under an argon atmosphere with a three-electrode arrangement: a platinum disc electrode $d =$ 1 mm (or 0.5 mm) as working electrode, platinum wire as the counter electrode, and a silver wire as pseudo reference electrode. The potentials were determined relative to the cobaltocinium/cobaltocene redox pair and are given in relation to Ag/AgCl. Solutions of $0.1\,M$ $TBAPF_6$ ($TBA = Bu_4N^+$) in acetonitrile were used as electrolytes. The UV/Vis spectra were recorded in a spectro-electrochemical cell that we built ourselves which combines cyclic voltammetry and UV/Vis spectroscopy.[36]

Received: January 18, 2001 [Z16453]

[1] J. B. Torrance, B. A. Scott, B. Welber, F. B. Kaufman, P. E. Seiden, *Phys. Rev. B* **1979**, *19*, 730–741.
[2] J. M. Savéant, *Acta Chem. Scand. Sect. B* **1983**, *37*, 365–378.
[3] V. D. Parker, M. Tilset, *J. Am. Chem. Soc.* **1986**, *108*, 6371–6377.
[4] A. Sakamoto, Y. Furukawa, M. Tasumi, *J. Phys. Chem.* **1987**, *101*, 1726–1732.
[5] a) J. R. Lenhard, R. L. Parton, *J. Am. Chem. Soc.* **1987**, *109*, 5808–5813; b) R. L. Parben, J. R. Lenhard, *J. Org Chem.* **1990**, *55*, 49–57.
[6] M. G. Hill, K. R. Mann, L. L. Miller, J.-F. Peeneau, *J. Am. Chem. Soc.* **1992**, *114*, 2728–2730.
[7] P. Hapiot, P. Audebert, K. Monnier, J.-M. Pernaut, P. Garcia, *Chem. Mater.* **1994**, 1549–1555.
[8] Y. Hong, Y. Yu, L. L. Miller, *Synth. Met.* **1995**, *74*, 133–135.
[9] J. A. E. H. van Haare, L. Groenendaal, E. E. Havinga, R. A. J. Jansen, E. W. Meijer, *Angew. Chem.* **1996**, *108*, 696–699; *Angew. Chem. Int. Ed. Engl.* **1996**, *35*, 638–640.
[10] D. D. Graf, R. G. Duan, J. P. Campbell, L. L. Miller, K. R. Mann, *J. Am. Chem. Soc.* **1997**, *119*, 5888–5899.
[11] I. B. Goldberg, D. Bogd, R. Hirasawa, A. J. Bard, *J. Phys. Chem.* **1974**, *78*, 295–299.
[12] C. Z. Smith, J. H. P. Utley, *J. Chem. Res. Synop.* **1982**, 18–1.
[13] V. D. Parker, *Acta Chem. Scand. Sect. B* **1981**, *35*, 595–599.
[14] V. D. Parker, D. Bethell, *Acta Chem. Scand. Sect. B* **1981**, *35*, 691–699.
[15] O. Hammerich, V. D. Parker, *Acta Chem. Scand. Sect. B* **1983**, *37*, 379.
[16] M. Svaan, V. D. Parker, *Acta Chem. Scand. Sect. B.* **1985**, *39*, 445–451.
[17] R. M. Crooks, A. J. Bard, *J. Electroanal. Chem.* **1988**, *240*, 253–280.
[18] W. Freund, S. Hünig, *J. Org. Chem.* **1987**, *52*, 2154–2161.
[19] A. S. Davydov, *Theory of Molecular Excitons*, Plenum Press, New York, **1971**.
[20] J. J. Aperloo, R. A. J. Janssen, P. R. L. Malenfant, L. Groenendaal, J. N. J. Fedet, *J. Am. Chem. Soc.* **2000**, *122*, 7042–7051.
[21] A. Smie, J. Heinze, *Angew. Chem.* **1997**, *109*, 375–379; *Angew. Chem. Int. Ed. Engl.* **1997**, *36*, 363–367.
[22] P. Tschuncky, J. Heinze, A. Smie, G. Engelmann, G. Koßmehl, *J. Elelectroanal. Chem.* **1997**, *433*, 223–226.
[23] J. Heinze, P. Tschuncky, A. Smie, *J. Solid State Electrochem.* **1998**, *2*, 102–109.
[24] P. Hübler, J. Heinze, *Ber. Bunsenges. Phys. Chem.* **1998**, *102*, 1506–1509.
[25] J. Heinze, H. John, M. Dietrich, P. Tschuncky, *Synth. Met.* **2001**, in press.
[26] R. Rathore, P. Le Magueres, S. V. Lindeman, J. K. Kochi, *Angew. Chem.* **2000**, *112*, 818–820; *Angew. Chem. Int. Ed.* **2000**, *39*, 809–812.
[27] K. Kimura, H. Yamada, H. Tsubomura, *J. Chem. Phys.* **1968**, *48*, 440–444.
[28] K. Uemura, S. Nakayama, Y. Seo, K. Suzuki, Y. Ooshika, *Bull. Chem. Soc. Jpn.* **1966**, *39*, 1348.
[29] H. Awano, O. Ichikana, K. Sawada, H. Okigashi *Ber. Bunsenges. Phys. Chem.* **1996**, *100*, 1700–1705.
[30] F. Effenberger, K.-E. Mack, R. Niess, F. Reisinger, A. Steinbach, W.-D. Stohrer, J. J. Srezowski, I. Rommel, A. Maier, *J. Org. Chem.* **1988**, *53*, 4379–4386.
[31] F. Effenberger, F. Reisinger, K. H. Schönwälder, P. Bäuerle, J. J. Stezowski, K. H. Jogun, K. Schöllkopf, W.-D. Stohrer, *J. Am. Chem. Soc.* **1987**, *109*, 882–892.
[32] F. Effenberger, W.-D. Stohrer, K.-E. Mack, F. Reisinger, W. Seufert, H. E. A. Kramer, R. Föll, E. Vogelmann, *J. Am. Chem. Soc.* **1990**, *112*, 4849–4857.
[33] F. Effenberger, P. Bäuerle, W. Seufert, W.-D. Stohrer, *Chem. Ber.* **1990**, *123*, 193–200.
[34] F. Effenberger, *Acc. Chem. Res.* **1989**, *22*, 27–35.
[35] E. Heilbronner, H.Bock, *Das HMO-Model und seine Anwendung*, Verlag Chemie, Weinheim, **1968**.
[36] C. Geskes, J. Heinze, *J. Electroanal. Chem.* **1996**, *418*, 167–173.
[37] W. Knoche, W. Sachs, S. Vogel, *Bull. Soc. Chim. Fr.* **1988**, 377–382.
[38] W. Knoche, S. Vogel, *J. Chem. Soc. Perkin Trans. 2* **1988**, 1937–1988.
[39] W. Sachs, W. Knoche, C. Herrmann, *J. Chem. Soc. Perkin Trans. 2* **1991**, 701–710.
[40] Multisweep cyclic voltammograms were measured at a scan rate of $3\,V\,s^{-1}$ for 1 h without any changes in the response. This corresponds to a switching number of 7000.
[41] F. Effenberger, R. Niess, *Chem. Ber.* **1968**, *101*, 3787–3793.

  1433-7851/01/4015-2864 $ 17.50+.50/0

$[(\mu_4\text{-H})Rh_4(PNNP)_2(CO)_4]^+$: A Novel Hydride Bridging Mode**

Shukichi Tanaka and Munetaka Akita*

Bridging hydride is a key structural feature of transition metal cluster compounds[1] and a number of cluster compounds containing doubly (μ) and triply (μ_3) bridging hydrido ligands are known. Compounds with a hydrido ligand bridging more than three metal atoms, however, are still rare (Figure 1). To the best of our knowledge, only one example each

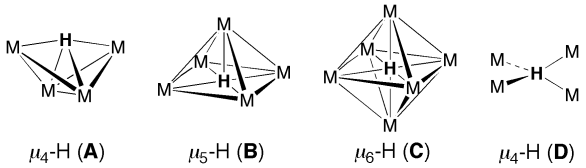

Figure 1. Structural types for compounds containing hydrido ligands bridging more than three metal centers.

for a μ_4- and μ_5-hydride complex has been reported and only the structural types **A**–**C** have been characterized for μ_n-H complexes ($n \geq 4$).[2] In addition, the multiply bridging hydrido ligands in all the previous examples are associated with cluster frameworks as in **A**–**C**. During the course of our study on the interaction of dinuclear species with hydrosilanes,[3] we have encountered a novel **D**-type μ_4-hydrido ligand, which holds four isolated metal centers together through M–H interactions. This work reveals that a cluster framework supported by metal–metal bonds is not essential for a multiply bridging hydride.

When a THF solution of $[Rh_2(PNNP)(CO)_2]BF_4$ (**1**BF_4; PNNP = 3,5-bis(diphenylphosphinomethyl)pyrazolate)[4] was treated with a hydrosilane, such as $HSiEt_3$, $HSiMe_2Ph$, and H_2SiPh_2 (Scheme 1), the purple product **2**BF_4 precipitated

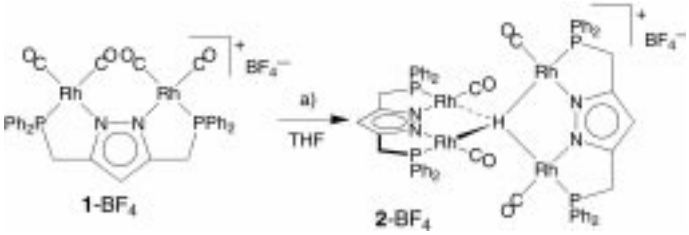

Scheme 1. a) $HSiEt_3$, $HSiMe_2Ph$, or H_2SiPh_2.

from the mixture; the ^{1}H NMR spectrum of **2**BF_4 shows a complicated hydride resonance signal (Figure 2a). The intensity of this hydride signal and an electrospray ionization mass spectrometry (ESI-MS) spectrum suggest the formation of a

[*] Prof. Dr. M. Akita, S. Tanaka
Chemical Resources Laboratory
Tokyo Institute of Technology
4259 Nagatsuta, Midori-ku, Yokohama 226-8503 (Japan)
Fax: (+81) 45-924-5230
E-mail: makita@res.titech.ac.jp

[**] PNNP = 3,5-bis(diphenylphosphanylmethyl)pyrazolate.

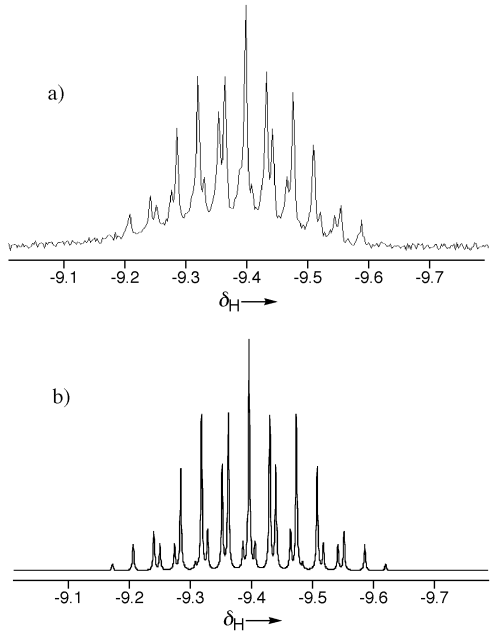

Figure 2. 400 MHz ^{1}H NMR spectra of **2**BF_4 (hydride region). a) Observed spectrum (in CD_2Cl_2); b) simulated spectrum, $\delta_H = -9.39$ (J(Rh,H) = 31.2, J(P,H) = 13.6 Hz).

dimeric species (m/z: 1451, the molecular ion peak for **2**) formulated as $[(H)Rh_4(PNNP)_2(CO)_4]BF_4$ (**2**BF_4). The same product was obtained irrespective of the hydrosilane used, which suggests that the hydrosilane serves as a hydride donor; the reaction of **1**BF_4 with $[D_2]SiPh_2$ resulted in selective deuteration of the bridging hydride in $[D_1]$**2**BF_4 as confirmed by ^{1}H NMR spectroscopy and ESI-MS. For the $[Rh_2(PNNP)(CO)_2]$ moiety of **2**, only a single set of signals arising from the CH_2PPh_2 (^{1}H, ^{13}C, and ^{31}P NMR spectroscopy), pyrazolyl (^{1}H and ^{13}C NMR spectroscopy), and CO moieties (infrared (IR) and ^{13}C NMR spectroscopy) was observed suggesting a four-fold symmetrical structure. In addition, the complicated hydride signal was successfully analyzed and found to result from coupling with four equivalent Rh–P units (^1J(Rh,H) = 31.2 Hz, ^2J(P,H) = 13.6 Hz; Figure 2b). The spectral data are consistent with a tetrarhodium complex with a tetrahedral or square planar Rh_4 array linked by a symmetrically bridging μ_4-hydrido ligand, $[(\mu_4\text{-H})Rh_4(PNNP)_2(CO)_4]BF_4$ (**2**BF_4).

Despite many attempts a single crystal of **2**BF_4 could not be obtained, but anion exchange with $NaBPh_4$ afforded $[(\mu_4\text{-H})Rh_4(PNNP)_2(CO)_4]BPh_4$ (**2**BPh_4) as deep purple plates, suitable for X-ray crystallography (Figure 3).[5] The two $[Rh_2(PNNP)(CO)_2]$ subunits are arranged almost perpendicular to each other to form a Rh_4 tetrahedron, and the hydride atom (H1) refined isotropically can be located in the middle of the Rh_4 tetrahedron as is consistent with the spectral data. Thus **2**BPh_4 is found to be the second example of a structurally characterized $(\mu_4\text{-H})M_4$ complex, after the $[(\mu_4\text{-H})W_4(OCH_2tBu)_{12}]^-$ ion[2a,b] in which the μ_4-hydrido ligand is supported on a butterfly M_4 cluster framework (type **A**; Figure 1).

The Rh_4 tetrahedron in **2** is distorted to a small extent; the Rh···Rh separations between the two subunits are in the

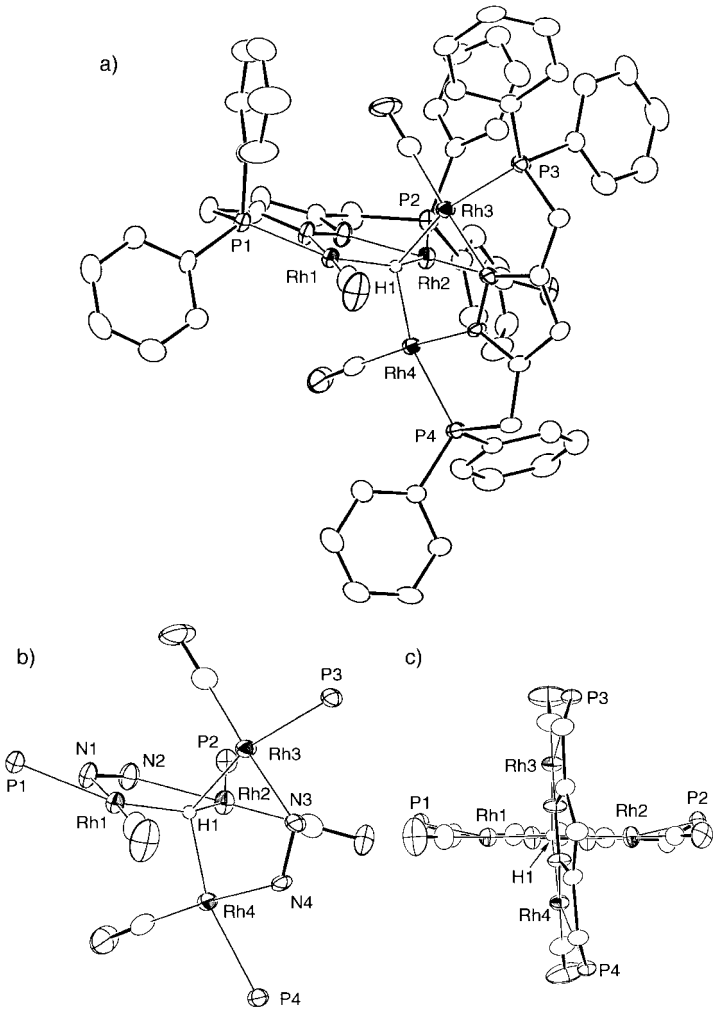

Figure 3. a) Molecular structure of the cation of $\mathbf{2}BPh_4$ thermal ellipsoids set at the 30% probability level. b) An expanded view of the core. c) A side view of the core.

range of 2.89–3.10 Å (Rh1···Rh3 2.9083(9), Rh1···Rh4 2.8890(7), Rh2···Rh3 3.1022(6), Rh2···Rh4 2.8969(8); Rh1···Rh2 3.4730(8), Rh3···Rh4 3.4153(6) Å) and the H1 atom is not equidistant from the four Rh centers (Rh–H 1.70–2.05 Å). The side view (Figure3c) shows that, in both of the $[Rh_2(PNNP)(CO)_2]$ subunits, the two five-membered $RhPC_2N$ chelate rings fused to the central pyrazolyl ring are slightly folded in the same direction leading to envelope-type conformations. This folding causes distortion in the solid state but fast flipping of the chelate rings in solution should account for the apparently symmetrical configuration suggested by the spectral features. No change in the ^1H (Rh–H) and ^{31}P NMR spectroscopy signals was detected upon cooling to $-80\,^\circ C$. The Rh···Rh separations are slightly longer than the sum of the atomic radii of Rh (2.68 Å). If some Rh–Rh bonding interaction is present, it should induce distortion of the square-planar coordination geometry of the d^8 metal center Rh^I. However, the four Rh coordination planes are virtually planar (sum of the inter-ligand angles: 360(3)°), thus the Rh–Rh bonding interaction is negligible and the close Rh–Rh contacts result from the very small hydrogen atom linking the four rhodium atoms. Thus the hydrido ligand in complex **2** is characterized as the first example of a **D**-type μ_4-hydride in a discrete molecule (cation). The bridging hydrido ligand encapsulated in the Rh_4 tetrahedron is shielded from the outside and, accordingly, $\mathbf{2}BF_4$ is stable in CH_2Cl_2.

The μ_4-hydride complex $\mathbf{2}BF_4$ should be formed by a sequence of 1) initial hydride transfer from $HSiR_3$ to $\mathbf{1}BF_4$ to form the neutral dinuclear μ-hydride intermediate, $[(\mu\text{-H})\text{-}Rh_2(PNNP)(CO)_2]$, and 2) further interaction with another molecule of $\mathbf{1}BF_4$. The dissociation of the labile CO ligands *trans* to P centers in rhodium complexes has already been noted by Bosnich and co-workers,[4] thus, $\mathbf{1}BF_4$ forms a coordinatively unsaturated species, which is trapped by the hydrido ligand in $[(\mu\text{-H})Rh_2(PNNP)(CO)_2]$ to give $\mathbf{2}BF_4$. Note that reaction of $\mathbf{1}BF_4$ with $LiHBEt_3$ or $NaBH_4$ did not afford $\mathbf{2}BF_4$ but a mixture of unidentified products.

Although the metal part of **2** is electron deficient (with 58 valence electrons: 64 valence electrons expected ($16\,e^- \times 4$)), such an unsaturated electronic structure must be kinetically stabilized by the bulky PNNP ligands surrounding the Rh_4 tetrahedron. Preliminary extended-Hückel molecular orbital (EHMO) analysis reveals that the tetranuclear structure is formed by interaction of the hydride orbital with the LUMO of the tetranuclear $[Rh_4(PNNP)_2(CO)_4]^{2+}$ fragment, where the four σ-type rhodium d orbitals of the in-phase combination are projected toward the center of the Rh_4 tetrahedron, that is, towards the position occupied by the μ_4-hydrido ligand. A similar MO feature was noted for the μ_4-H tetratungsten cluster compound mentioned above.[2a,b]

In conclusion, the present study reveals that support by a metal–metal bonded cluster framework is not essential for a multiply bridging hydride (μ_n-H: $n \geq 4$). In all the previous examples (**A**–**C**; Figure 1) the multiply bridging hydrido ligand appears to be protected by the cluster framework, whereas, in the present system, the hydride is not accommodated in a cavity formed by the cluster framework but binds the four isolated rhodium centers (which are not connected by metal–metal bonds) together. The binding force is strong enough to bring the Rh centers close enough together so that the distances between them are comparable to the sum of the atomic radii. The unique feature of the $[Rh_2(PNNP)(CO)_2]^+$ fragment with the two vacant *cis*-oriented coordination sites is now under further study.

Experimental Section

$\mathbf{2}BF_4$: $\mathbf{1}BF_4$ (258 mg, 0.272 mmol) was added to a THF solution (20 mL) of $HSiEt_3$ (40 μL, 0.25 mmol) and the resultant mixture was stirred at ambient temperature until gas evolution ceased (ca. 1.5 h). The supernatant solution was removed by cannula and the remaining purple precipitate was washed with a minimum amount of THF and dried under reduced pressure. $\mathbf{2}BF_4$ (119 mg, 0.078 mmol, 57% yield) was obtained as deep purple powder. Crystallization from CH_2Cl_2/hexane afforded deep purple plates. ^1H NMR (400 MHz, CD_2Cl_2, 25 °C): $\delta = -9.39$ (quintet of quintets, $^1J(Rh,H) = 31.2$ Hz, $^2J(P,H) = 13.6$ Hz, 1H; μ_4-H), 3.68 (d, $^2J(P,H) = 10$ Hz, 8H; CH_2P), 6.24 (s, 2H; 4-pyrazolyl ring proton), 7.4–7.7 (m, 40H; Ph); $^{31}P\{^1H\}$ NMR (81 MHz, $CDCl_3$, 25 °C): $\delta = 57.41$ (d, $J(Rh,P) = 200$ Hz); $^{13}C\{^1H\}$ NMR (100 MHz, CD_2Cl_2, 25 °C): $\delta = 31.8$ (d, $^1J(P,C) = 29$ Hz; CH_2P), 100.3 (t, $J = 12$ Hz; 4-pz), 129.5 (d, $^3J(P,C) = 13$ Hz; *m*-Ph), 131.7 (s; *p*-Ph), 132.9 (d, $^2J(P,C) = 13$ Hz; *o*-Ph), 133.0 (d, $^1J(P,C) = 50$ Hz; *ipso*-Ph), 155.4 (dd, $J = 9$, 4 Hz; 3,5-pz), 192.4 (dd, $^1J(Rh,C) = 62$, $^2J(P,C) = 11$ Hz; RhCO); IR (KBr): $\tilde{\nu} = 1983\ cm^{-1}$ (CO); ESI-MS: *m*/*z*: 1451 [M^+] for the cation (**2**).

  1433-7851/01/4015-2866 $ 17.50+.50/0 *Angew. Chem. Int. Ed.* **2001**, *40*, No. 15

2BPh_4: A THF/CH_2Cl_2 solution (1/1; 3 mL) of $NaBPh_4$ (42 mg, 0.12 mmol) was added to a THF/CH_2Cl_2 solution (1/1; 10 mL) of **2**BF_4 (100 mg, 0.06 mmol) and the mixture was stirred for 20 min. After concentration to ca. 6 mL hexane (8 mL) was added to form precipitates, which were collected by filtration. The solid was dissolved in CH_2Cl_2 (1.5 mL). Hexane (1 mL) was added and purple **2**BPh_4 (80 mg, 0.045 mmol, 75% yield) was obtained by crystallization at $-20\,^{\circ}C$.

Received: March 20, 2001 [Z16810]

[1] a) *Comprehensive Organometallic Chemistry II* (Eds.: E. W. Abel, F. G. A. Stone, G. Wilkinson), Pergamon, Oxford, **1995**; b) D. F. Shriver, H. Kaesz, R. D. Adams, *The Chemistry of Metal Cluster Complexes*, VCH, New York, **1990**; c) *Metal Clusters in Chemistry*, *Vols. 1–3* (Eds.: P. Braunstein, L. A. Oro, P. R. Raithby), Wiley-VCH, Weinheim, Germany, **1999**.

[2] μ_4-H: $[(\mu_4\text{-H})W_4(OCH_2tBu)_{12}]^-$: a) T. A. Budzichowski, M. H. Chisholm, J. C. Huffman, O. Eisenstein, *Angew. Chem.* **1994**, *106*, 203; *Angew. Chem. Int. Ed. Engl.* **1994**, *33*, 191; b) T. A. Budzichowski, M. H. Chisholm, J. C. Huffman, K. S. Kramer, O. Eisenstein, *J. Chem. Soc. Dalton Trans.* **1998**, 2563; μ_5-H: $[(\mu_5\text{-H})_2Rh_{13}(CO)_{24}]^{3-}$: c) R. Bau, M. H. Drabnis, L. Garlaschelli, W. T. Klooster, Z. Xie, T. F. Koetzle, S. Martinengo, *Science* **1997**, *275*, 1099, and references therein; μ_6-H: $[(\mu_6\text{-H})Ni_{12}(CO)_{21}]^{3-}$: d) R. W. Broach, L. F. Dahl, G. Longoni, P. Chini, A. J. Schultz, J. M. Williams, *Adv. Chem. Ser.* **1978**, *167*, 93; $[(\mu_6\text{-H})Ru_6(CO)_{18}]^-$: e) C. R. Eady, B. F. G. Johnson, J. Lewis, M. C. Malatesta, P. Machin, M. McPartlin, *J. Chem. Soc. Chem. Commun.* **1976**, 945; f) P. F. Jackson, B. F. G. Johnson, J. Lewis, P. R. Raithby, M. McPartlin, W. J. H. Nelson, K. D. Rouse, J. Allibon, S. A. Mason, *J. Chem. Soc. Chem. Commun.* **1980**, 295; g) W. P. Mul, C. J. Elsevier, M. A. Vuurman, W. J. J. Smeets, A. L. Spek, J. L. de Boer, *J. Organomet. Chem.* **1997**, *532*, 89; $[(\mu_6\text{-H})Co_6(CO)_{15}]^-$: h) D. W. Hart, R. G. Teller, C.-Y. Wei, R. Bau, G. Longoni, S. Campanella, P. Chini, T. F. Koetzle, *Angew. Chem.* **1979**, *91*, 86; *Angew. Chem. Int. Ed. Engl.* **1979**, *18*, 80; i) D. W. Hart, R. G. Teller, C.-Y. Wei, R. Bau, G. Longoni, S. Campanella, P. Chini, T. F. Koetzle, *J. Am. Chem. Soc.* **1981**, *103*, 1458; $[(\mu_6\text{-H})Ru_7(CO)_{19}(\mu\text{-}CNMe_2)]$: j) R. D. Adams, J. E. Babin, J. T. Tanner, *Organometallics* **1988**, *7*, 2027.

[3] M. Akita, *Appl. Catal.* **2000**, *200*, 153, and references therein.

[4] T. G. Schenk, J. M. Downs, C. R. C. Milne, P. B. Mackenzie, H. Boucher, J. Whelan, B. Bosnich, *Inorg. Chem.* **1985**, *24*, 2334; T. G. Schenk, C. R. C. Milne, J. F. Sawyer, B. Bosnich, *Inorg. Chem.* **1985**, *24*, 2338; see also: B. Bosnich, *Inorg. Chem.* **1999**, *38*, 2554.

[5] Crystal data for **2**$BPh_4 \cdot 2\,CH_2Cl_2 \cdot 0.5$ hexane: $C_{91}H_{82}BN_4O_4P_4Cl_4Rh_4$, $M_W = 1983.74$, triclinic, space group $P\bar{1}$, $a = 17.8753(14)$, $b = 18.8768(13)$, $c = 13.7743(10)$ Å, $\alpha = 103.703(3)$, $\beta = 97.179(5)$, $\gamma = 105.748(5)^{\circ}$, $V = 4256.1(6)$ Å^3, $Z = 2$, $\rho_{calcd} = 1.548$ g cm^{-3}, $\mu = 1.016$ cm^{-1}, $R_1 = 0.0664$ (on F^2) for the 11879 unique data ($wR_2 = 0.1792$ for all 16104 data) with $F > 4\sigma(F)$ and 968 parameters. X-ray diffraction measurements were made on a Rigaku RAXIS IV imaging plate area detector with graphite-monochromated $Mo_{K\alpha}$ radiation at $-60\,^{\circ}C$. The structure was solved by a combination of the direct methods (SHELXS86) and DIRDIF. Least-squares refinements were carried out using SHELXL97 linked to teXsan (Single Crystal Structure Analysis Package, ver. 1.11, Rigaku Corporation, Tokyo **2000**). Crystallographic data (excluding structure factors) for the structure reported in this paper have been deposited with the Cambridge Crystallographic Data Centre as supplementary publication no. CCDC-159668. Copies of the data can be obtained free of charge on application to CCDC, 12 Union Road, Cambridge CB21EZ, UK (fax: (+44) 1223-336-033; e-mail: deposit@ccdc.cam.ac.uk).

Double Photoionization of Dimethylaminobenzonitrile in Solution: A Three-Quantum Process with Intervening Chemical Step**

Martin Goez* and Valentin Zubarev

Photoionization in solution is a compelling subject of investigation because of the vast importance of the hydrated electron e^-_{aq} for chemical and biological processes.[1] At wavelengths greater than about 300 nm, more than one photon is usually needed to eject an electron from a stable molecule. This is normally realized by an absorption–absorption sequence (two consecutive absorption steps), where the second photon ionizes an electronically excited state of the substrate.

As we recently demonstrated, the insertion of an electron-transfer step between the two absorption processes can greatly facilitate two-photon ionization.[2] With this variant, the second photon ionizes the radical anion resulting from electron-transfer quenching of the excited substrate. Experimental evidence obtained so far seems to indicate that at least for aromatic ketones and quinones the actual photoionization step is intrinsically more efficient by an order of magnitude or more for the radical anion than for the excited $n\pi^*$ triplet state.[2d, 3]

Up to now, this mechanistic variant has only been explored with intermolecular quenching. When both absorption steps are to occur during the same laser flash, that is, typically within a few nanoseconds, this puts considerable constraints on the chemical system: even in the case of a diffusion-controlled electron transfer disproportionately high quencher concentrations must still be employed.[2d] The use of *intra*molecular charge transfer (ICT) is an obvious approach to overcome this difficulty. On the basis of the above experimental observation, one would expect photoionization of an excited state to be the more facile the greater its charge transfer (CT) character is.

Dimethylaminobenzonitrile (DMABN) is a classical ICT compound as far as its first excited singlet state is concerned. However, with regard to the lowest triplet state T_1 the situation is less clear. From an analysis of its deactivation pathways[4] and from the absence of an appreciable volume change in laser-induced optoacoustic spectroscopy[5] it was inferred that T_1 does not possess a pronounced CT character. In contrast, the results of time-resolved infrared measurements indicate that in T_1 a substantial negative charge is located on the cyano group, and it was proposed that there might be two closely lying triplet states, a CT and a non-CT one, with an equilibrium between them.[6]

DMABN can be photoionized in liquid solution at 266 and 308 nm; from a quadratic intensity dependence of the yield of

[*] Prof. Dr. M. Goez, Dr. V. Zubarev
Fachbereich Chemie
Martin-Luther-Universität Halle-Wittenberg
Kurt-Mothes-Strasse 2, 06120 Halle/Saale (Germany)
Fax: (+49) 345-55-27-657
E-mail: goez@chemie.uni-halle.de

[**] This work was supported by the Volkswagenstiftung.

$e^{\bullet}_{aq}$ at low light levels this was concluded to occur by a consecutive two-photon process.[4, 7] The starting point of the present work was our observation, made when we attempted to determine the absolute quantum yields of this photoionization to obtain some evidence as to the CT character of T_1, that this photoreaction must be considerably more complex than previously thought.

Because DMABN is hardly soluble in water, most of the measurements were carried out in micellar solutions (sodium dodecyl sulfate, SDS) with a neutral pH in the aqueous phase. As a positive side effect, this microheterogeneous environment also slows down charge recombination considerably; compared to homogeneous phase (water/methanol), we typically observed an increase of the life of $e^{\bullet}_{aq}$ by an order of magnitude. The solutions were degassed, and oxygen was excluded. Nanosecond laser-flash photolysis (excimer laser and/or Nd:YAG laser) with UV/Vis detection was used. Our setup[2b] allows one- and two-pulse (i.e., two-color) experiments.

By scavenging experiments with N_2O it was ascertained that in our system no other species besides $e^{\bullet}_{aq}$ absorbs at 830 nm. The experimentally observed optical density at that wavelength thus directly yields the electron concentration.[8] Figure 1 a shows the dependence of this concentration, relative to the starting concentration c_0 of DMABN, on the laser intensity in a single-pulse experiment using 308 nm light.

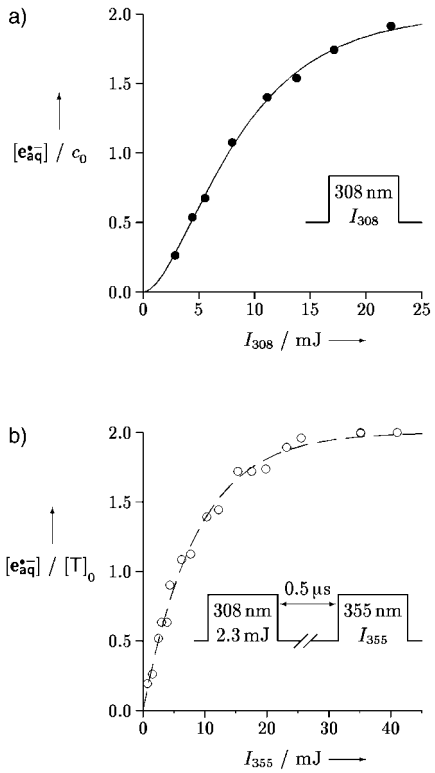

Figure 1. Photoionization of 2.7×10^{-5} M DMABN in aqueous SDS solution (0.031 M). The laser pulse sequences used are displayed as insets. Pulse widths are about 20 ns for 308 nm and about 5 ns for 355 nm. Shown are the concentrations of the hydrated electron $[e^{\bullet}_{aq}]$ relative to the starting concentration of DMABN c_0 in the single-pulse experiment (a), and relative to the starting concentration of the triplet $[T]_0$ in the two-pulse experiment (b) as functions of the laser intensity I_{308} and I_{355}, respectively. The fit curves are explained in the text.

The surprising result is that, quite obviously, *two electrons* are produced from *one substrate molecule*.

At low light levels, where photoionization is negligible, a transient spectrum is obtained under our experimental conditions that is identical to that reported[9] for the lowest triplet state T_1 of DMABN apart from a red-shift by about 30 nm, which we attribute to the different polarity in our case (aqueous micellar environment versus ethanol). The triplet has a half life of 90 µs under these conditions. With increasing laser power, its signal (absorption maximum at 390 nm, which is not obscured by peaks of other species) first increases and then decreases again, indicating that the excited state preceding photoionization in our experiments is T_1 of DMABN.

To gain more information about the photoionization, we carried out two-pulse experiments. The first pulse, at 308 nm, was attenuated so as to produce only a very small amount of electrons (about 1 % of c_0) but a substantial amount of the triplet. The known extinction coefficient[9] of the triplet at its absorption maximum allowed calculation of its absolute concentration $[T]_0$, which was found to be about 12 % of c_0. After a delay of 500 ns, a second pulse was applied, this time at 355 nm. The absorbance of DMABN at this wavelength is about 40 times lower than at 308 nm, and by control experiments it was ensured that even at the highest available laser power only an insignificant amount of $e^{\bullet}_{aq}$ is obtained by the single-pulse scheme at 355 nm. However, in the two-pulse experiment, complete conversion of the triplet into $e^{\bullet}_{aq}$ can be achieved. Figure 1 b depicts the dependence of the electron yield, relative to $[T]_0$, on the intensity of the second pulse. It is clearly seen that, in line with the result of the single-pulse experiment of Figure 1 a, one molecule of the triplet ultimately yields two electrons.

A direct ejection of two electrons from triplet DMABN is very improbable at the wavelengths used because it would lead to a chemical species of rather high energy (a dication). It is much more reasonable to assume two successive ionizations with an intervening chemical step, where the first electron stems from the triplet and the second from another intermediate that is produced by a secondary chemical transformation of the radical cation resulting from ionization of the triplet. The chemical transformation of the radical cation to give an ionizable species must be fast on the timescale of the laser pulses, otherwise complete ionization, as is found in both the single- and the two-pulse experiments, could not occur; for this reason, one would not expect the radical cation to be observable in our experiments but only the subsequent species. Spectra taken at moderate light intensity in N_2O saturated solution (to scavenge the electron) indeed revealed the presence of two other transients, besides the triplet, with absorbance maxima at 370 nm and 495 nm. From the intensity dependences, the former must correspond to an ionizable intermediate and the latter to the final photoproduct. The overall reaction thus proceeds according to Scheme 1, where G, T, C, X, and P are ground state, triplet, (unobservable) radical cation, secondary ionizable species, and final product, respectively.

The three photoreactions can be described as first-order processes with rate constants k_1, k_2, and k_3, because the

  1433-7851/01/4015-2868 $ 17.50+.50/0

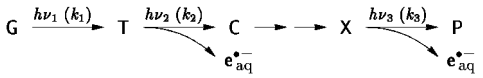

Scheme 1. Overall reaction scheme for the photoionization. For explanation of the symbols, see text.

solutions in our experiments are optically thin. Since C can be ignored in the kinetic equations, the actual shape of the ionizing pulse does not play any role, and the electron yield is completely determined by the total intensity I, with k_1 to k_3 possessing the dimension of a reciprocal energy.[2d] The result for the two-pulse experiment, that is, electron concentration $[e^{\bullet}_{aq}]$ relative to concentration $[T]_0$ of the triplet after the first pulse, is given by Equation (1).

$$\frac{e^{\bullet}_{aq}}{[T]_0} = 2 - \frac{(2k_3 - k_2)\exp(-k_2 I) - k_2 \exp(-k_3 I)}{k_2 - k_3} \quad (1)$$

A fit of Equation (1) to the data is shown in Figure 1b. The fit is very well-conditioned, with the initial slope of the curve being determined by k_2 alone. From each of the constants k_i, the quantum yield of the respective photoionization ϕ_{ion} can be calculated if the absolute extinction coefficient at the excitation wavelength λ_{exc} is known.[2d] For triplet DMABN, ε at λ_{exc} was obtained from the spectrum taken at sufficiently low light levels, where the amount of photoionization is negligible, and ε_{max} given in the literature.[9] The extinction coefficient of X at λ_{exc} followed from its observed absorbance and its concentration, which was measured by converting it completely into $e^{\bullet}_{aq}$. With these data, we arrive at a value of ϕ_{ion} for triplet DMABN of 0.48 at 355 nm. The very high efficiency of this ionization seems to indicate considerable charge-transfer character of the DMABN triplet, which would corroborate the conclusions drawn from transient infrared experiments.[6] For the ionization of X, a quantum yield of 0.13 is obtained.

On the basis of Scheme 1, a closed form expression can also be derived for the intensity dependence in the one-pulse experiment [Eq. (2)].

$$\frac{[e^{\bullet}_{aq}]}{c_0} = 2 + \frac{k_2(k_1 - 2k_3)}{(k_1 - k_2)(k_1 - k_3)}\exp(-k_1 I) - \frac{k_1(k_2 - 2k_3)}{(k_1 - k_2)(k_2 - k_3)} \cdot \exp(-k_2 I) - \frac{k_1 k_2}{(k_1 - k_3)(k_2 - k_3)}\exp(-k_3 I) \quad (2)$$

A fit of Equation (2) to the data (compare Figure 1a) was found to be less well-conditioned owing to a pronounced cross correlation between the parameters but gave quantum yields ϕ_{ion} similar to those in the two-pulse experiment. When only low light levels are being used, as in the earlier experiments reported,[4, 7] the mechanism in Scheme 1 is indistinguishable from a usual two-photon ionization: under these conditions, a quadratic intensity dependence of the electron yield is found in both cases because $(k_1 k_2)I^2/2$ is the first nonvanishing term of the respective series expansion (of Equation (2), and of Equation (7) of ref. [2d]). The identical coefficient of I^2 reflects the chemically obvious fact that at low light levels photoionization of X, which is a late intermediate in the reaction sequence of Scheme 1, is negligible, whereas at high levels it contributes as much to the electron yield as does photoionization of the triplet, an early intermediate.

Lastly, we turn to the intriguing question: what species X is ionized in the final step of the reaction? From the findings presented here, and by comparison with related *inter*-molecular photoionizations involving alphatic amines,[2b] we conclude that the reaction C→X proceeds as shown in Scheme 2. The primary result of photoionization of the ICT triplet must be the nitrogen-centered radical cation of

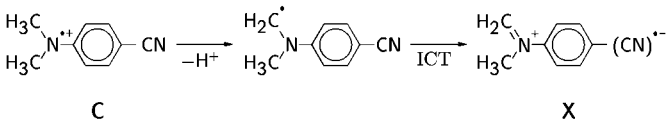

Scheme 2. Intervening chemical reactions in DMABN photoionization.

DMABN.[10] It is known that such aminium radical cations are easily deprotonated at an α carbon to give α-amino alkyl radicals,[11] and that the latter are strongly reducing species.[12] The benzonitrile radical anion moiety that was already contained in the charge-separated triplet is thus regenerated by another ICT process, and is then available for a second photoionization. This mechanism is corroborated by two experimental observations. First, in water/alcohol mixtures, rather than a micellar environment, a slight pH dependence is found: at pH 12 two electrons per molecule of DMABN are formed but at pH 6, where deprotonation of C would be expected to be slower, this limiting value is not quite reached, which would indicate that the deprotonation becomes rate-limiting. Second, with *para*-aminobenzonitrile, where this particular deprotonation is no longer possible, only one electron per substrate molecule is indeed obtained (see also ref. [10]).

Received: February 20, 2001 [Z16649]

[1] See, for instance, a) G. Steinberg-Yfrach, P. A. Liddell, C.-C. Hung, A. L. Moore, D. Gust, T. A. Moore, *Nature* **1997**, *385*, 239–240; b) H. Schindelin, C. Kisker, J. L. Schlessman, J. B. Howard, D. C. Rees, *Nature* **1997**, *387*, 370–376; c) M. H. B. Stowell, T. M. McPhillips, D. C. Rees, S. M. Soltis, E. Abresch, G. Feher, *Science* **1997**, *276*, 812–816.

[2] a) V. Zubarev, M. Goez, *Angew. Chem.* **1997**, *109*, 2779–2781; *Angew. Chem. Int. Ed. Engl.* **1997**, *36*, 2664–2666; b) M. Goez, V. Zubarev, G. Eckert, *J. Am. Chem. Soc.* **1998**, *120*, 5347–5348; c) M. Goez, V. Zubarev, *J. Phys. Chem. A* **1999**, *103*, 9605–9613; d) M. Goez, V. Zubarev, *Chem. Phys.* **2000**, *256*, 107–116.

[3] M. Goez, D. Leine, unpublished results.

[4] G. Köhler, G. Grabner, K. Rotkiewicz, *Chem. Phys.* **1993**, *173*, 275–290.

[5] N. Chattopadhyay, M. van der Auweraer, F. C. De Schryver, *Chem. Phys. Lett.* **1997**, *279*, 303–308.

[6] M. Hashimoto, H. Hamaguchi, *J. Phys. Chem.* **1995**, *99*, 7875–7877.

[7] R. J. Visser, P. C. M. Weisenborn, J. Konijnenberg, B. H. Huizer, C. A. G. O. Varma, *J. Photochem.* **1986**, *32*, 217–233.

[8] ε_{830} was determined relative to the absorption maximum, for which the extinction coefficient was taken from J. W. T. Spinks, R. J. Wood, *An Introduction to Radiation Chemistry*, 2nd ed., Wiley, New York, **1976**.

[9] T. Okada, M. Uesugi, G. Köhler, K. Rechthaler, K. Rotkiewicz, W. Rettig, G. Grabner, *Chem. Phys.* **1999**, *241*, 327–337.

[10] F. Saito, F. Tobita, H. Shizuka, *J. Photochem. Photobiol. A* **1997**, *106*, 119–126.

[11] G. P. Gardini, J. Bargon, *J. Chem. Soc. Chem. Commun.* **1980**, 757–758.

[12] K.-O. Hiller, K.-D. Asmus, *J. Phys. Chem.* **1983**, *87*, 3682–3688.

  1433-7851/01/4015-2869 $ 17.50+.50/0

How Does Ethene Inactivate Cytochrome P450 En Route to Its Epoxidation? A Density Functional Study**

Sam P. de Visser, François Ogliaro, and Sason Shaik*

Cytochrome P450 is one of the principal enzymes in the "oxygen machinery" of biosystems. The enzyme functions as a mono-oxygenase in the biosynthesis of steroids, and in the transformation of hydrophobic molecules such as alkanes into alcohols, which are water soluble and thus secreted from the body.[1–3] A large turnover number of the enzyme is essential, and is limited inter alia by side reactions, which form dead-end compounds, so called suicidal complexes. Therefore, the enzyme itself is inactivated in the course of the vital processes. Identification of the mechanisms that "poison" the enzyme is an important task and constitutes the focus herein.

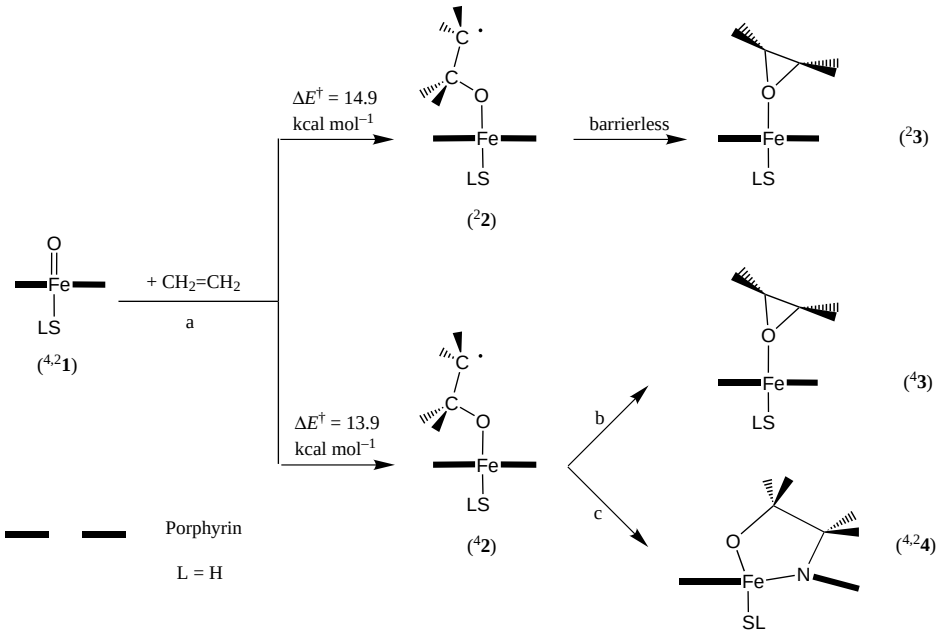

Scheme 1. Schematic description of the mechanisms of ethylene epoxidation (ref. [14]) and suicidal complex formation.

Olefin epoxidation is one of the processes that have been implicated to generate suicidal complexes as dead-end products.[1, 3] Indeed, heme-type enzymes were shown to produce suicidal products in reactions with pharmaceutical and environmental agents.[4] In particular, terminal olefins and acetylenes react by N-alkylation of the heme-group. The *N*-alkyl hemes have been shown to result in hepatic porphyrias accompanied by the formation of the so-called "green pigment". The formation of these suicidal complexes was observed in catalytic reactions of cytochrome P450[4–10] as well as chloroperoxidases (CPO).[11–13] Such a suicidal complex is schematically depicted as **4** in Scheme 1. The mechanism and energetics of its formation in relation to those for the epoxidation process itself are addressed in the present paper by means of density functional theoretical calculations (DFT).

The epoxidation mechanism was recently[14] investigated using the simplified iron–oxo species (**1**, L = H) and ethene (Scheme 1). Starting from either the quartet (high spin) ^{4}**1** or the doublet (low spin) ^{2}**1** species, the bond-activation step a, with barriers ($\Delta E^{\ddagger}$) of approximately 14–15 kcal mol^{-1}, leads to radical complex intermediates **2**, which upon ring closure lead to the epoxide complex **3**. The high-spin intermediate ^{4}**2** was shown[1, 14] to be responsible for stereochemical scrambling and formation of *cis*/*trans* mixtures of the epoxides. Depending on the lifetime of ^{4}**2**, the suicidal reaction c (Scheme 1) may be competitive with the ring-closure step b (Scheme 1). Other side reactions of ^{4}**2** are possible, but the present study focuses on the suicidal reaction.

The following calculations were performed by using the Jaguar 4.0 program package[15] with the unrestricted hybrid density functional (UB3LYP) in combination with an LACVP basis set on iron and a 6-31G basis set on the rest of the atoms. Previous calculations with larger basis sets have shown that these types of basis sets are sufficient to give good qualitative results.[14, 16]

Since the previous study[14] revealed that the low-spin intermediates ^{2}**2** form the epoxide complex ^{2}**3** in a barrierless fashion (Scheme 1), we focus herein on the suicidal reaction nascent from ^{4}**2**. The intermediate ^{4}**2** has two electromeric forms, which differ in the oxidation state of the iron. The two forms are depicted in Figure 1 along with the orbital diagram of the key valence orbitals. These are the $\delta(d_{x^2-y^2})$ orbital and the $\pi^*(d_{xz}, d_{yz})$ orbitals on iron, the porphyrin a_{2u}-type orbital, the hybrid orbital of the radical of the intermediate ($\phi_{C^{\cdot}}$), and two vacant d orbitals on the iron. The ^{4}**2**-IV and ^{4}**2**-III intermediates differ in the occupation of the π^* and a_{2u} orbitals as indicated in Figure 1.

The electronic structure of the suicidal complex ^{4}**4** is quite different from that of the radical complexes ^{4}**2**-III and ^{4}**2**-IV. It involves $\delta(d_{x^2-y^2})^2\ \pi^*(d_{xz})^1\ \pi^*(d_{yz})^1\ \sigma^*(d_{xy})^1\ a_{2u}{}^2$ occupation (Figure 1). Thus, the transformation of **2** into **4** is attended by population of the high-lying $\sigma^*(d_{xy})$ orbital that involves antibonding interactions in the four Fe–N linkages in the iron–porphyrin plane. As shall be seen later it is this reorganization that is responsible for the formation of the suicidal complex and for gauging the corresponding suicidal barrier.

[*] Prof. S. Shaik, Dr. S. P. de Visser, Dr. F. Ogliaro
Department of Organic Chemistry and
The Lise Meitner-Minerva Center
for Computational Quantum Chemistry
The Hebrew University of Jerusalem
91904 Jerusalem (Israel)
Fax: (+972) 2-658-4680
E-mail: sason@yfaat.ch.huji.ac.il

[**] The research is supported in part by the ISF and in part by the Ministry of Science, Culture, and Sport. F.O. acknowledges the European Union for a Marie Curie Fellowship.

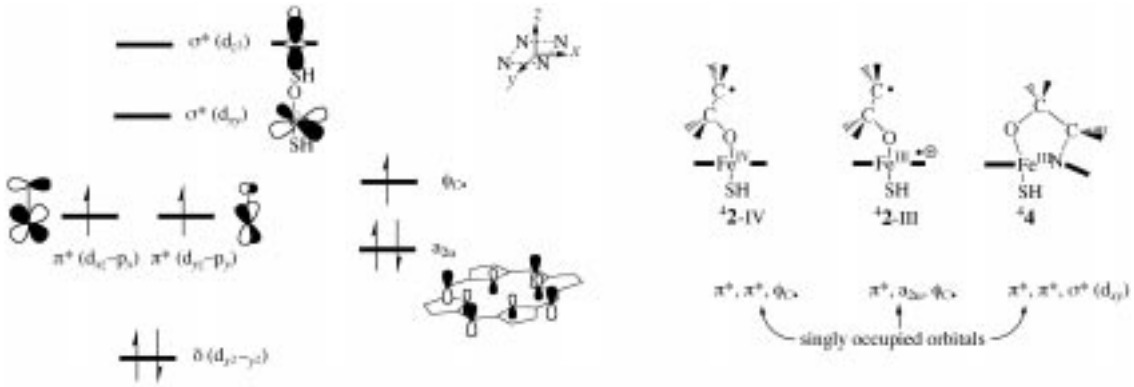

Figure 1. The highest occupied and lowest virtual orbitals with occupations for ^{4}**2**-IV (left). The coordinate axes are drawn vis-à-vis the nitrogen atoms of the porphyrin ring. The singly occupied orbitals for the various complexes (^{4}**2** and ^{4}**4**) are written on the right hand side.

Figure 2 depicts the optimized geometries of the suicidal complex (^{2,4}**4**), the Fe^{III} (^{4}**2**-III) and Fe^{IV} (^{4}**2**-IV) radical complexes in the most stable *anti* conformations, and the corresponding *gauche* conformations, ^{4}**2**-III′ and ^{4}**2**-IV′, which are local minima on the rotational surface. Formation of the suicidal complex disrupts the planarity in the porphyrin ring. The nitrogen atom involved in the ring closure is lifted out of the plane of the remaining nitrogen atoms by 6.9°, leading to puckering of the corresponding pyrrole ring. This ring in turn loses its π-bonding as indicated by the C–N bond of 1.439 (1.474) Å compared with the other pyrrole rings in which these bond lengths are approximately 1.37 Å. Additionally, the Fe–O distance is augmented to 1.866 Å with respect to the radical complexes **2**-III and **2**-IV.

The most significant change in ^{4}**4** relative to its precursors is the Fe–N distance in the suicidal ring; 2.438 Å compared with 2.016 Å or 2.019 Å (on average) for ^{4}**2**-IV and ^{4}**2**-III, respectively. This long Fe–N bond is a result of the $\sigma^*(d_{xy})$ occupancy and therefore the formation of ^{4}**4** is attended by C–N bond formation at the expense of Fe–N displacement and some rupture of the π-bonding in the pyrrole ring that involves the nitrogen site of attack. The data for the low-spin form of the suicidal complex ^{2}**4** are shown alongside the high-spin form in Figure 2. In ^{2}**4**, the $\sigma^*(d_{xy})$ orbital is vacant, while the complex still is in the Fe^{III} oxidation state with a $\delta^2\,\pi^*(d_{yz})^2\,\pi^*(d_{xz})^1$ configuration. In accord, the Fe–N distance is now close to normal (2.195 Å), albeit somewhat elongated by the nitrogen pyramidality. The low-spin ^{2}**4** is

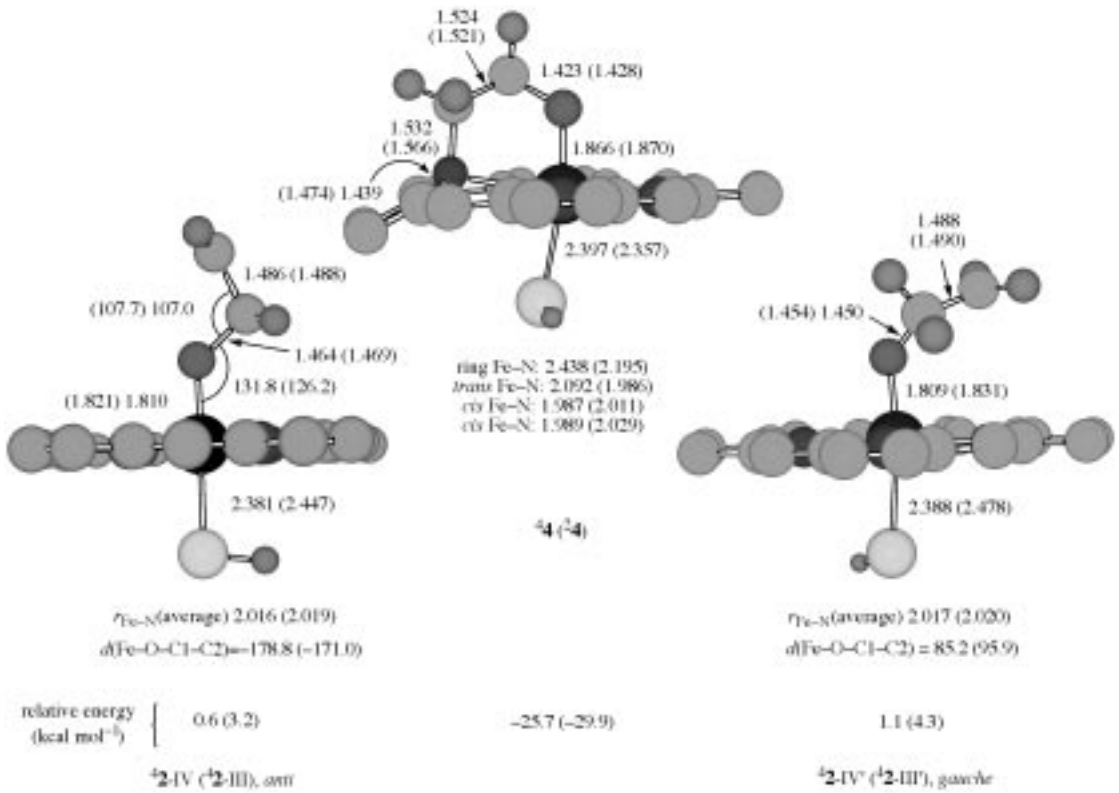

Figure 2. Optimized geometries of ^{4}**2**-IV (^{4}**2**-III), ^{2,4}**4** (middle) and ^{4}**2**-IV′ (^{4}**2**-III′) (right). Bond lengths are reported in angstroms and bond angles in degrees. The relative energies of the clusters are given with respect to the sum of the reactants (^{4}**1**+CH_2=CH_2) and are summarized at the bottom of the figure.

  1433-7851/01/4015-2872 $ 17.50+.50/0 *Angew. Chem. Int. Ed.* **2001**, *40*, No. 15

4.2 kcal mol^{-1} more stable than the high-spin suicidal complex, ^{4}**4**.

Figure 3 is an energy profile for a geometry scan from the radical complex toward the suicidal complex. Each point represents a full optimization with one fixed coordinate representing the C–N bond distance. The optimized radical

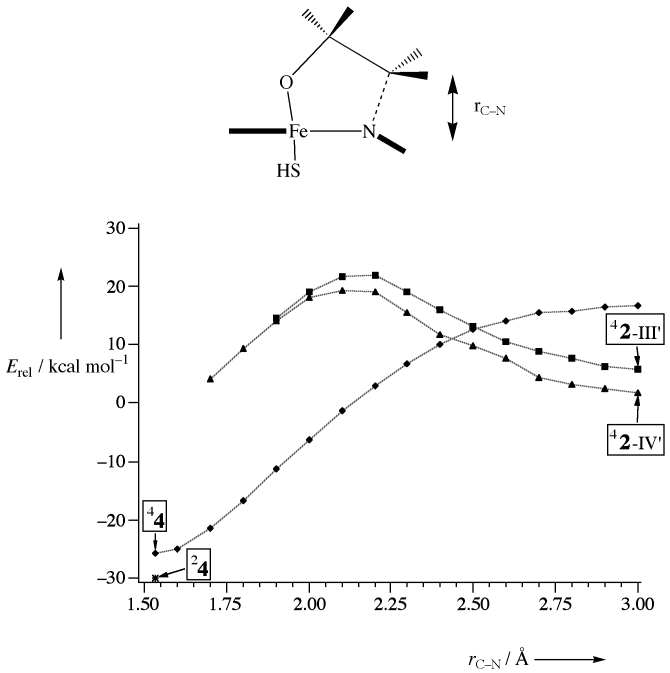

Figure 3. Energy profile for the reaction of ^{4}**4** leading to ^{4}**2**-IV′ and ^{4}**2**-III′. Each point represents a full geometry optimization with a fixed Fe–N bond distance. The energies are given relative to the sum of the reactants (kcal mol^{-1}). The relative energy of the ^{2}**4** complex has been marked with an asterisk.

complexes in the *gauche* orientation have a C–N interatomic distance of 3.306 Å (^{4}**2**-III′) and 3.245 Å (^{4}**2**-IV′), as shown in Figure 2. The *gauche* conformers are local minima and are 1.1 (Fe^{III}) and 0.5 kcal mol^{-1} (Fe^{IV}) higher in energy than their *anti* conformers. Adiabatic excitation from the lowest state (^{4}**2**-IV′) by 11.0 kcal mol^{-1} leads to the excited state that has a singly occupied $\sigma^*(d_{xy})$ orbital. This state has the correct electronic configuration and therefore falls in a barrierless fashion into the suicidal complex (^{4}**4**).

In contrast, the ^{4}**2**-IV′ and ^{4}**2**-III′ states rise up in energy along the same coordinate. An approximate real crossing point[17] between the suicidal energy profile and the profiles of the two radical states, was estimated to occur at $r_{C-N} \approx 2.7-2.8$ Å. Relative to the onset energies of the *anti* conformers ^{4}**2**-III and ^{4}**2**-IV, the height of the crossing point is approximately 10 – 12 kcal mol^{-1}. The suicidal barrier will be smaller as a result of avoided crossing.[17] While a multireference configuration interaction treatment will be required eventually to calculate the barrier for the suicidal process, this is still beyond reach. Therefore, the value determined here can be taken as an upper bound estimate of the barrier for the formation of the suicidal complex on the high-spin surface.[17]

In order to pinpoint the intermediate-radical state responsible for the suicidal process, we must consider the barriers of the various processes experienced by ^{4}**2**-III and ^{4}**2**-IV vis-à-vis the suicidal barrier as summarized in Table 1. It is clear that the ^{4}**2**-IV intermediate will participate mostly in epoxide formation. In contrast, for ^{4}**2**-III the suicidal barrier and the epoxidation barrier are approximately equal and therefore

Table 1. Barriers for individual processes starting at the radical complexes ^{4}**2**.[a]

Reactant	Product	ΔE^{+} [kcal mol^{-1}]	Reaction
^{4}**2**-III	^{4}**2**-III′	1.1	internal C–O rotation
^{4}**2**-III	^{4}**2**-III	1.4	internal CH_2 rotation
^{4}**2**-III	^{4}**3**	7.2	epoxidation
^{4}**2**-III	^{4}**4**	≤ 10[17]	suicidal complex
^{4}**2**-IV	^{4}**2**-IV′	0.5	internal C–O rotation
^{4}**2**-IV	^{4}**2**-IV	1.4	internal CH_2 rotation
^{4}**2**-IV	^{4}**3**	2.3	epoxidation
^{4}**2**-IV	^{4}**4**	≤ 10[17]	suicidal complex

[a] The barrier leading from ^{4}**1** to ^{4}**2**-IV is 13.9 kcal mol^{-1} (Scheme 1). Equilibration of ^{4}**2**-IV and ^{4}**2**-III is expected to be fast.[14]

the ^{4}**2**-III intermediate will participate in two competing ring-closure processes; one leads to epoxide ^{4}**3** and the other to the suicidal complex ^{4}**4**. Furthermore, it is seen that the C–C rotational barrier of ^{4}**2**-III, responsible for stereochemical scrambling of the epoxide is lower than either ring-closure or suicidal-complex formation. Therefore, ^{4}**2**-III will participate in at least three competing reactions. Another event that may result in the low-spin suicidal complex ^{2}**4** must involve spin-state crossover from the quartet surfaces in Figure 3 to the doublet surface, and end in the ^{2}**4** complex. A spin crossover that leads to ^{2}**4** is likely to take place near the ^{4}**4**/^{4}**2**-III and ^{4}**4**/^{4}**2**-IV crossover points.[18]

In conclusion, theoretical studies on a model P450 system with ethene have shown that competing reactions can take place, leading to either epoxide or suicidal products.[19] Both these products are nascent from the same initial intermediate radical complex **2**. The ^{4}**2**-III complex has a substantial barrier for epoxide formation and a roughly equal barrier for crossing to the suicidal complex. This implies that competing epoxidation and suicidal-complex formation reactions can take place from the ^{4}**2**-III isomer. In the polar environment of the protein pocket and polar solvents such as water, this particular state is favored relative to the ^{4}**2**-IV isomer,[20] thus enhancing the suicidal-complex formation in polar solvents. Moreover, the same intermediate ^{4}**2**-III, which is responsible for *cis*/*trans* scrambling in epoxidation processes[1, 14, 21] is implicated in this study as a source of destruction of the enzyme cytochrome P450.[22] This specificity could hopefully be probed by experimental means.

Received: November 15, 2000 [Z16115]

[1] J. T. Groves, Y.-Z. Hang in *Cytochrome P450: Structure, Mechanisms and Biochemistry* (Ed.: P. R. Ortiz de Montellano), 2nd ed., Plenum Press, New York, **1995**, chap. 1, p. 3.

[2] I. Schlichting, J. Berendzen, K. Chu, R. M. Stock, S. A. Maves, D. E. Benson, R. M. Sweet, D. Ringe, G. A. Petsko, S. G. Sligar, *Science* **2000**, *287*, 1615.

[3] *The Porphyrin Handbook*, *Vol. 4* (Eds.: K. M. Kadish, K. M. Smith, R. Guilard), Academic Press, San Diego, **2000**; in particular the following chapters: a) D. Mansuy, P. Battioni, chap. 26; b) J. T. Groves, K.

  1433-7851/01/4015-2873 $ 17.50+.50/0

Shalyaev, J. Lee, chap. 27; c) K. S. Suslick, chap. 28; d) Y. Watanabe, chap. 30; e) B. Meunier, A. Robert, G. Pratviel, J. Bernadou, chap. 31.
[4] P. R. Ortiz de Montellano, H. S. Beilan, K. L. Kunze, B. A. Mico, *J. Biol. Chem.* **1981**, *256*, 4395.
[5] K. L. Kunze, B. L. K. Mangold, C. Wheeler, H. S. Beilan, P. R. Ortiz de Montellano, *J. Biol. Chem.* **1983**, *258*, 4202.
[6] P. R. Ortiz de Montellano, B. L. K. Mangold, C. Wheeler, K. L. Kunze, N. O. Reich, *J. Biol. Chem.* **1983**, *258*, 4208.
[7] T. Mashiko, D. Dolphin, T. Nakano, T. G. Traylor, *J. Am. Chem. Soc.* **1985**, *107*, 3735.
[8] J. P. Collman, P. D. Hampton, J. I. Brauman, *J. Am. Chem. Soc.* **1990**, *112*, 2977; J. P. Collman, P. D. Hampton, J. I. Brauman, *J. Am. Chem. Soc.* **1990**, *112*, 2987.
[9] B. T. Luke, J. R. Collins, G. H. Loew, A. D. McLean, *J. Am. Chem. Soc.* **1990**, *112*, 8686.
[10] Z.-Q. Tian, J. Richards, T. G. Traylor, *J. Am. Chem. Soc.* **1995**, *117*, 21.
[11] A. F. Dexter, L. P. Hager, *J. Am. Chem. Soc.* **1995**, *117*, 817.
[12] P. G. Debrunner, A. F. Dexter, C. E. Schulz, Y.-M. Xia, L. P. Hager, *Proc. Natl. Acad. Sci. USA* **1996**, *93*, 12791.
[13] H.-I. Lee, A. F. Dexter, Y.-C. Fann, F. J. Lakner, L. P. Hager, B. M. Hoffman, *J. Am. Chem. Soc.* **1997**, *119*, 4059.
[14] S. P. de Visser, F. Ogliaro, N. Harris, S. Shaik, *J. Am. Chem. Soc.*, **2001**, *123*, 3037.
[15] Jaguar 4.0, Schrödinger Inc., Portland, OR, **1998**.
[16] F. Ogliaro, N. Harris, S. Cohen, M. Filatov, S. P. de Visser, S. Shaik, *J. Am. Chem. Soc.* **2000**, *122*, 8977.
[17] Since the two states have the same overall symmetry, they should have avoided the crossing and produced a normal saddle point. However, since the Kohn–Sham method uses a single determinant, the DFT calculation results in a surface crossing. Our attempts to evade the crossing by starting with a guess that had mixed orbitals (of the two species) were not successful. The "real" crossing point was estimated by a series of calculations of the ^{4}**2**-III and ^{4}**4** structures which have the same geometric parameters.
[18] A spin crossover near the minima of ^{4}**2** and ^{2}**2** will simply lead to low-spin epoxidation through the low-energy path available to ^{2}**2** (see Scheme 1).
[19] It is likely that the fate of ^{4}**2**-III is more complex in view of the fact that propylene undergoes an unusual hydrogen/deuterium exchange during its epoxidation. See: J. T. Groves, G. E. Avaria-Neisser, K. M. Fish, M. Imachi, R. L. Kuczkowski, *J. Am. Chem. Soc.* **1986**, *108*, 3837.
[20] a) J. T. Groves, Z. Gross, M. K. Stern, *Inorg. Chem.* **1994**, *33*, 5065; b) M. Filatov, N. Harris, S. Shaik, *Angew. Chem.* **1999**, *111*, 3730; *Angew. Chem. Int. Ed.* **1999**, *38*, 3512.
[21] Z. Gross, S. Nimri, C. M. Barzilay, L. Simkhovich, *J. Biol. Inorg. Chem.* **1997**, *2*, 492.
[22] The ^{2}**2** intermediates have very small barriers for ring closure to epoxide formation (^{2}**3**). If these barriers grant them finite lifetimes, we cannot rule out some bifurcation of ^{2}**2** to the corresponding suicidal complex ^{2}**4**. However, most of the suicidal process is likely to occur from the high-spin intermediate.

Chameleon States: High-Valent Metal–Oxo Species of Cytochrome P450 and Its Ruthenium Analogue**

François Ogliaro, Samüel P. de Visser, John T. Groves,* and Sason Shaik*

There is a continuing search for efficient and robust catalysts that can perform monooxygenation of organic compounds.[1] High-valent metal–oxo porphyrin species **1** (Figure 1) constitute such an important family.[2] The members of this family are analogous to the principal oxidant of

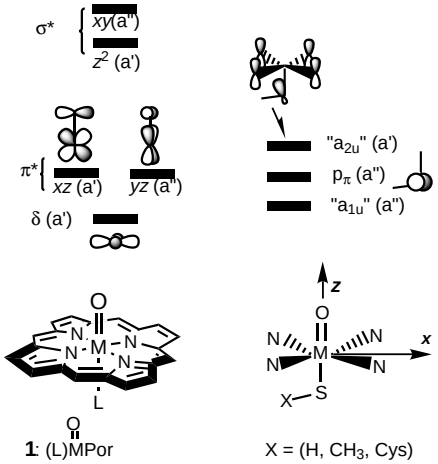

Figure 1. Key orbitals for **1** with thiolate ligands.

enzymes such as cytochrome P450 (CP450) or chloroperoxidase (CPO), and this analogy endows the (L)PorM^{z}O species with an added allure. While iron and manganese are the most ubiquitous metal centers in biological systems, ruthenium is present in artificially designed systems which are attractive potent catalysts.[2c] A fundamental question concerns the nature of the ground state of these catalysts, and the relationship between their electronic structure and monooxygenation capability. This is the focus of the present paper which uses density functional (DFT) calculations to compare the electromeric states for [(L)PorM^{z}O] (M = Fe, Ru; z = III–V; L = SH and SCH_3). As shall be seen, the Fe and Ru

[*] Prof. S. Shaik, Dr. F. Ogliaro, Dr. S. P. de Visser
Department of Organic Chemistry and
The Lise Meitner-Minerva Center for
Computational Quantum Chemistry
The Hebrew University of Jerusalem
91904 Jerusalem (Israel)
Fax: (+972) 2-658-4680
E-mail: sason@yfaat.ch.huji.ac.il
Prof. J. T. Groves
Department of Chemistry, Princeton University
Princeton, NJ 08544-1009 (USA)
Fax: (+1) 60-9-258-0348
E-mail: jtgroves@pop.princeton.edu

[**] The research in HU was sponsored by the Binational German Israeli Foundation (GIF) and by the Israeli Ministry of Science, Culture and Sport. Partial support by the US National Science Foundation (CHE-9814301) to J.T.G. is acknowledged. F.O. thanks the EU for a Marie Curie Fellowship.

  1433-7851/01/4015-2874 $ 17.50+.50/0

states are very different in both spin and metal oxidation states. Furthermore, medium polarity exerts a strong influence on most of the low-lying states of both iron and ruthenium complexes which behave like chameleon states, changing nature in response to the environment.

We briefly review the rich chemical patterns that are associated with the ground states of these oxidants, by reference to the key orbitals of **1** (L = thiolate) in Figure 1. The orbital set on the left-hand side involves the five d-type orbitals of the metal, labeled as δ, π*, and σ* according to the bonding between the iron center and the oxygen atom.[3] The set on the right-hand side shows relevant porphyrin and ligand orbitals. The "a_{2u}" orbital is delocalized primarily over the porphyrin ring and the axial thiolate ligand, and hence this orbital depends on the nature of the axial ligand.[3] The second orbital is a p_π-type orbital of the ligand, while the third is "a_{1u}".[4] The latter two orbitals are antisymmetric to the *xz* plane and in principle can mix, albeit weakly due to a very small overlap. In the high-valent catalysts, there are nine electrons, which have to be distributed among the entire set of orbitals. The occupation mode in these orbitals determines the oxidation state of the metal and the porphyrin, as well as the spin situation of the complex.

The ground state of the principal oxidant of CP450 is considered to be the triradicaloid species $[(L)Por^{+\cdot}Fe^{IV}O]$ (called also compound I (Cpd I)).[5] It involves triplet electrons in the π* orbitals of the $Fe^{IV}O$ moiety weakly coupled to a third electron in the "a_{2u}" orbital.[3, 6] The one-electron reduced species ($[(L)PorFe^{IV}O]$, Compound II (Cpd II)) is a less reactive oxidant.[2b,c] Derivatives of $[PorRu^{IV}O]$ are also inactive as catalysts and behave by analogy to Cpd II.[2c, 7, 8] It was thought initially that the active monooxygenating species in ruthenium catalysts was the dioxo compound $[PorRu^{VI}O_2]$[9] (singlet δ^2 state). It has become evident that the more active form of the ruthenium catalyst is in fact the $[(L)PorRu^{V}O]$.[2c, 10] While few $[L_5Ru^{V}O]$ catalysts are known with a variety of macrocyclic ligands,[11] the putative active species of $[(L)PorRu^{V}O]$ has not been isolated nor has it ever been characterized by any physical means. In the iron chemistry, an Fe^{V} species used to be implicated in the Gif reagent,[12] but not anymore. The highly sought $[PorFe^{V}O]$ species was reported in a recent experimental study[2b, 13] of iron porphyrin chemistry, in a chemical equilibrium between Cpd I and the iron(v) species, $[(L)PorFe^{V}O]$. The equilibrium between the species was found to be sensitive to the environment and to substituents on porphyrin. However, unlike $[(L)PorRu^{V}O]$, which is expected to be a low-spin ($S = ½$) $\delta^2\,\pi^{*1}$ state,[11a] the Fe^{V} electromer was reported to possess a high-spin ($S = 3/2$) $\delta^1\,\pi^{*2}$ ground state and to be less reactive than its Cpd I electromer.[2b, 13] The paucity of data on the natures and structures of the Ru^{V} and Fe^{V} species, along with their puzzling reactivity patterns pose a fundamental research agenda which is addressed here by means of hybrid (B3LYP) DFT calculations.

Calculations were done with the JAGUAR 4.0 package,[14] using wherever possible both restricted (RODFT) and unrestricted (UDFT) hybrid functional, B3LYP[15] with full geometry optimization and frequency characterization. The effect of the medium was studied with JAGUAR's implementation of the polarized continuum model, using a dielectric constant of 5.7, which mimics a nonpolar environment. The LACVP/6-31G basis set was used in all calculations.[16] Two metal centers, M = Fe, Ru, and two ligands, L = HS^-, CH_3S^-, were compared.

Table 1 collects the relative data for the various electromeric states. The orbital occupation (see Figure 1) of all the states is given along with the commonly used state designation and its C_s symmetry. For example, the first two states are designated as $^{2,4}A_{2u}(M^{IV})$ to emphasize the single occupancy of the "a_{2u}" orbital, and the formal oxidation state IV of the metal determined by the d^4 occupation. The quartet and doublet spin situations characterize the ferromagnetic and antiferromagnetic coupling between the "a_{2u}" electron and those occupying the two π* orbitals. Designations of other states follow similar logic.[3] Among them are the $^{2,4}\Pi_S(M^{IV})$ and $^{2,4}A_{1u}(M^{IV})$ states where, in addition to the singly occupied π* orbitals, a third one is either the sulfur p_π or porphyrin "a_{1u}" orbitals, respectively. Among the possible M^{V} states, entry 10 in Table 1 lists the state discussed by Watanabe et al.[2b, 13] with the $\delta^1\,\pi^{*1}\,\pi^{*1}$ open shell. Table 1, entries 8 and 9 show the corresponding low-spin doublet states $^2\Pi_{xz,yz}(M^{V})$ with $\delta^2\,\pi^{*1}$ occupation. Also shown is either the $^2\Pi_{yz}(M^{III})$ state, which corresponds to $[(L)Por^{++}M^{III}O]$ with a single electron in π^*_{yz}.

It is apparent that for iron, the ground state is the antiferromagnetic state $^2A_{2u}(Fe^{IV})$ (Table 1, entry 2), for both

Table 1. States, orbital occupancies (refer to Figure 1), and relatives energies for the isolated molecule and for the molecule in a polarizing medium.

Entry	State	C_S symmetry	Orbital occupancy	E_{rel} [kcal mol^{-1}]			
				Fe, L = SH (SCH_3)		Ru	
				$\varepsilon = 1$	$\varepsilon = 5.7$	$\varepsilon = 1$	$\varepsilon = 5.7$
1	$^4A_{2u}(M^{IV})$	$^4A''$	$a_{1u}^2\,p_\pi^2\,\delta^2\,\pi_{xz}^{*1}\,\pi_{yz}^{*1}\,a_{2u}^1$	0.0 (0.00)	0.0	0.0	0.0
2	$^2A_{2u}(M^{IV})$	$^2A''$	$a_{1u}^2\,p_\pi^2\,\delta^2\,\pi_{xz}^{*1}\,\pi_{yz}^{*1}\,a_{2u}^1$	−0.07 (+0.03)	−0.12	−0.56	−0.35
3	$^4\Pi_S(M^{IV})$	$^4A'$	$a_{1u}^2\,p_\pi^1\,\delta^2\,\pi_{xz}^{*1}\,\pi_{yz}^{*1}\,a_{2u}^2$	+5.66 (+0.47)	+8.85	+3.89	+9.34
4	$^2\Pi_S(M^{IV})$	$^2A'$	$a_{1u}^2\,p_\pi^1\,\delta^2\,\pi_{xz}^{*1}\,\pi_{yz}^{*1}\,a_{2u}^2$	+5.63 (+0.31)	+8.69	[a]	[a]
5	$^6\Delta_{xy}(M^{IV})$	$^6A'$	$a_{1u}^2\,p_\pi^2\,\delta^1\,\pi_{xz}^{*1}\,\pi_{yz}^{*1}\,a_{2u}^1\,\sigma_{xy}^{*1}$	+14.27	+15.05	[a]	[a]
6	$^4A_{1u}(M^{IV})$	$^4A'$	$a_{1u}^1\,p_\pi^2\,\delta^2\,\pi_{xz}^{*1}\,\pi_{yz}^{*1}\,a_{2u}^2$	+21.27[b]	[a]	+17.31[b]	[a]
7	$^2\Pi_{xz}(M^{V})$	$^2A'$	$a_{1u}^2\,p_\pi^2\,\delta^2\,\pi_{xz}^{*1}\,\pi_{yz}^{*0}\,a_{2u}^2$	+21.66 (+21.25)	[a]	−5.14	+0.25
8	$^2\Pi_{yz}(M^{V})$	$^2A''$	$a_{1u}^2\,p_\pi^2\,\delta^2\,\pi_{xz}^{*0}\,\pi_{yz}^{*1}\,a_{2u}^2$	+16.34 (+20.45)	[a]	−3.57	+1.38
9	$^2\Pi_{yz}(M^{III})$	$^2A''$	$a_{1u}^2\,p_\pi^2\,\delta^2\,\pi_{xz}^{*2}\,\pi_{yz}^{*1}\,a_{2u}^0$	+26.43[c]	[a]	[a]	[a]
10	$^4\Delta(M^{V})$	$^4A''$	$a_{1u}^2\,p_\pi^2\,\delta^1\,\pi_{xz}^{*1}\,\pi_{yz}^{*1}\,a_{2u}^2$	+26.55[b]	[a]	+20.58[b]	[a]

[a] Converged on the lower energy state with the same symmetry. [b] Single point calculation using the $^4A_{2u}$ geometry. [c] Single point calculation using the $^2\Pi_{yz}(M^{V})$ geometry.

  1433-7851/01/4015-2875 $ 17.50+.50/0

the isolated molecule as well as when it is under the influence of medium polarization. The iron(v) states (Table 1, entries 7 and 8) are much higher lying. Changing the ligand to CH_3S^-, which is a better π- and σ-donor than $L = HS^-$, does not change this conclusion. Here, the axial ligand does not affect the $^2A_{2u}(Fe^{IV}) - {}^2\Pi_{xz,yz}(Fe^{V})$ energy gap. Likewise, the $^4\Delta(Fe^{V})$ state of Cpd I (Table 1, entry 10) is significantly higher lying than the $^2A_{2u}(Fe^{IV})$ ground state. The $^4A_{1u}(Fe^{IV})$ state (Table 1, entry 6), which was assigned as the ground state in a few Cpd I species of iron porphyrin complexes with substituted porphyrin,[4] is found here to lie 21.27 kcal mol^{-1} higher than $^2A_{2u}(Fe^{IV})$.

In contrast to the situation for iron, the ground state for ruthenium is the $^2\Pi_{xz}(M^{V})$, followed by $^2\Pi_{yz}(M^{V})$ (Table 1, entries 7 and 8). In both states an electron from the d-manifold (π*) is shifted to fill the "a_{2u}" hole, leaving behind a d^3 configuration with a single unpaired electron in either one of the π orbitals (Figure 1). By analogy with the iron system, the $^4A_{1u}(Ru^{IV})$ and $^4\Delta(Ru^{V})$ states are calculated to lie considerably higher than the ground state. Medium polarization packs the states $^{4,2}A_{2u}(Ru^{IV})$ and $^2\Pi_{xz,yz}(M^{V})$ within 1.73 kcal mol^{-1}, and endows the ruthenium complex with a ground state that is likely to be an equilibrating $Ru^{IV} - Ru^{V}$ mixture. Another difference with respect to iron, is that ruthenium complexes have a stronger preference for antiferromagnetic coupling.

Figure 2 shows the key geometric details of the low-energy states for the iron and ruthenium complexes in the isolated and "solvated" states. The C_1 and C_s geometries[3, 17] of the ground state for the iron complex are almost identical, and

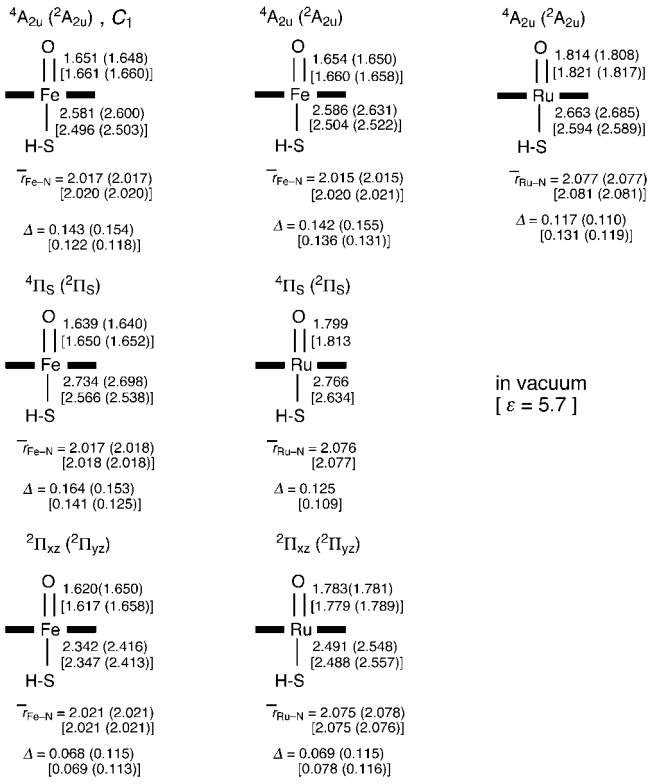

Figure 2. Key geometric parameters for states of **1** (L = SH) in the isolated molecule and for the molecule in a polarized medium (in square brackets).

therefore all other species were investigated at the C_s point group. The Fe–O bond length is almost constant for all the states in the isolated molecule and when under the influence of medium polarity. The r_{Fe-O} value of 1.62 – 1.66 Å is in accord with experimentally determined values in a variety of Cpd I and Cpd II species.[2, 5] The Ru–O bond length varies between 1.78 – 1.82 Å, where generally $r_{Ru^{IV}-O} > r_{Ru^{V}-O}$. Experimental Ru–O distances for $Ru^{VI, VIII}$ or for pentacoordinated Ru^{V} complexes with macrocyclic ligands other than porphyrin cluster lie between 1.70 – 1.77 Å, and exhibit the same shortening with an increase in the oxidation state of the metal.[2, 8, 10, 11] X-ray data obtained for a closely related *trans*-dioxo-Ru^{VI}-porphyrin complex $[Ru^{VI}(tdcpp)O_2]$ (tdcpp = $C_9H_{15}Cl_6O_4P$) revealed two long Ru=O bonds of 1.729 Å.[2c]

The M–S bond length is more variable and exhibits a significant response to the state identity and the polarity of the medium. With the exception of $^2\Pi_{xz,yz}(M^{V})$ states, which show hardly any response to medium polarity, in all other states increasing polarity causes a significant shortening of this bond. This is in accord with previous studies[3, 17] of the Fe–S bond, which revealed a very flexible bond (the stretch frequency is $\omega_{FeS} = 160$ cm^{-1} compared with 320 cm^{-1} calculated for the resting state), which undergoes shortening and strengthening due to hydrogen bonding and medium polarity. This effect in $^{4,2}A_{2u}(Fe^{IV})$ was shown to persist up to triple-ζ polarized basis sets.[17]

Figure 3 shows the spin density distribution for the various states. The $^{4,2}A_{2u}(M^{IV})$ and $^{2,4}\Pi_S(M^{IV})$ states are seen to undergo a dramatic change in their electronic structure with medium polarization effect. Both states contain two triplet electrons on the M=O moiety, and this feature is fixed whether the molecule is isolated or "solvated". But the third unpaired electron "shifts its location" upon "solvation". Thus, the $^{4,2}A_{2u}(Fe^{IV})$ states change from a thiolate-centered radical to a porphyrin-centered radical (see C_1 structure).[18] The $^{4,2}A_{2u}(Ru^{IV})$ states already have a dominant porphyrin-radical character in vacuum, and polarity further accentuates this character. The $^{2,4}\Pi_S(M^{IV})$ states undergo an even more dramatic change from almost a pure thiolate radical state to a mixed porphyrin – thiolate radical state. Thus, $^{4,2}A_{2u}(M^{IV})$ and $^{2,4}\Pi_S(M^{IV})$ are chameleon states with a hybrid nature that adjusts to the change in the environment.

In contrast, the $^2\Pi_{xz,yz}(M^{V})$ states exhibit a less significant change since the electronic structure does not allow any sulfur → porphyrin electron shift. In UDFT there is some change which is larger in Ru than in Fe, but in RODFT the spin distribution is fixed. These less mutable electronic structures are in harmony with the unchanged geometries of these states. At present we are unable to tell whether the UDFT spin density is an artifact of spin contamination ($\langle S^2 \rangle = 1.12 - 1.14$ in Ru) or is a real electronic effect. We therefore focus on the RODFT results, which are free of the spin contamination. According to these results, the $^2\Pi_{xz,yz}(M^{V})$ states are localized $\pi^*_{xz,yz}(M=O)$ radicals.

Two questions arise at this point: 1) what are the roots of M–S bond shortening and its characteristic electronic reorganization in the chameleon states? 2) What causes the preference of ruthenium for Ru^{V} and iron for Fe^{IV}? These questions are addressed in Figures 4 and 5.

  1433-7851/01/4015-2876 $ 17.50+.50/0 *Angew. Chem. Int. Ed.* **2001**, *40*, No. 15

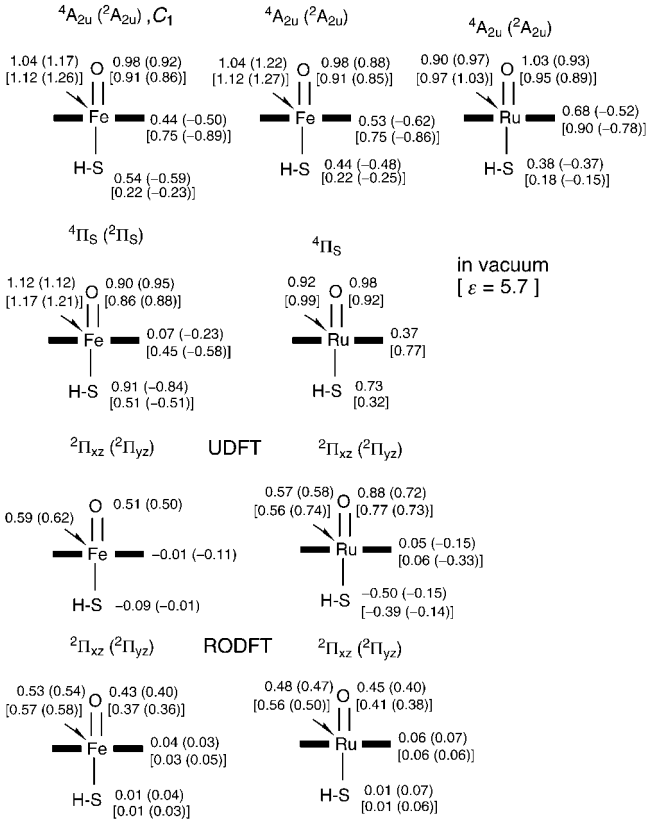

Figure 3. Group spin-densities in states of **1** (L = SH) for isolated states and for the molecule in a polarized medium (in square brackets).

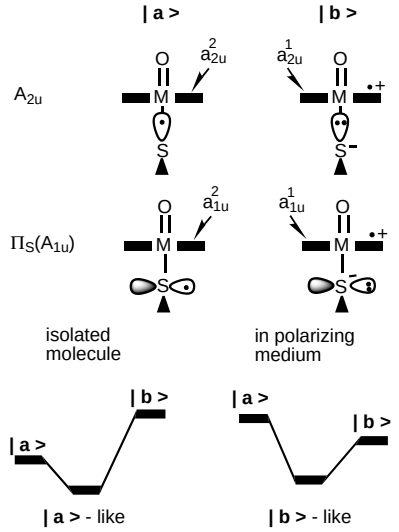

Figure 4. Resonance structures ($|\mathbf{a}\rangle$ and $|\mathbf{b}\rangle$), which contribute to the "redox mesomerism" in the A_{2u} and Π_s states of **1**; L = HS, and their mixing in the isolated molecule and in a polarizing medium.

Following our recent study[17] of hydrogen bonding and polarity effect on the $^{4,2}A_{2u}(Fe^{IV})$ states, Figure 4 shows the resonance structure hybrids, $|\mathbf{a}\rangle$ and $|\mathbf{b}\rangle$, which contribute to the $^{4,2}A_{2u}(M^{IV})$ and $^{2,4}\Pi_S(M^{IV})$ states. In the A_{2u} states, these hybrids involve shifting one electron from the p_σ hybrid of the thiolate to the pure porphyrin a_{2u} orbital, while for the Π_S states the shift is between the p_π and a_{1u} orbitals.[19] The resonance mixing diagrams show that the mixing of the

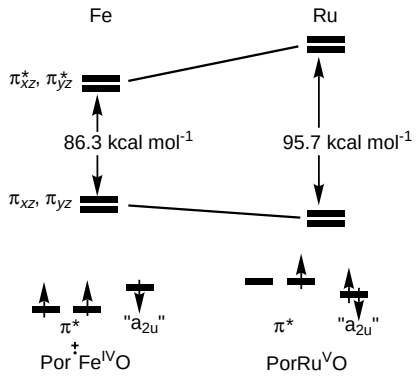

Figure 5. π – π* orbital energy gaps for **1**; L = HS with M = Fe and Ru, and corresponding π* – "a_{2u}" relative orbital ordering.

structures to form hybrid states, as recognized before[2, 20] and termed "redox mesomerism".[2a, 20c] In the isolated molecular state, the thiolate radical structures, $|\mathbf{a}\rangle$, are lower in energy and the resulting state has a predominant thiolate radical nature of the σ- or π-types, in accord with the state identity. On the other hand, in a polarizing medium (or by mere hydrogen bonding to the thiolate[17]) structures $|\mathbf{b}\rangle$, which are polarizable due to the internal charge separation, are stabilized and become the lower ones. The resulting state now has a predominant porphyrin radical character. In the solvated $^{4,2}A_{2u}(M^{IV})$ states, the radical is located in the a_{2u} orbital and predominantly on porphyrin, while in the solvated $^{2,4}\Pi_S(M^{IV})$ states the radical is localized in the a_{1u} orbital and a more appropriate designation of these latter states is $^{4,2}A_{1u}(M^{IV})$-like. What determines the chameleon character of the states is the closeness of the resonance structures. The donor property of the axial ligand is crucial; ligands which are both good σ- and π-donors will give rise to chameleon states. In contrast, poor donor ligands do not lead to such chameleon behavior, and will generate states with fixed porphyrin-radical natures.

The different oxidation state preference of iron and ruthenium can be understood by consideration of the mixing of the metal and oxygen orbitals to form the π and π* orbitals (Figure 5). Thus, the 3d orbitals of iron are spatially smaller than the ruthenium 4d orbitals, and therefore the corresponding 3d(Fe) – 2p(O) overlap is significantly smaller than the 4d(Ru) – 2p(O) overlap.[21] This causes a stronger interaction for the ruthenium, which can be seen from the calculated π and π* orbital energy gaps. The weak interaction in iron leaves the π* orbitals below "a_{2u}" and leads to a [Por$^{+\cdot}$Fe^{IV}O] ground state. In contrast, due to the strong interactions in ruthenium, the π* orbitals rise above "a_{2u}" and the ground state becomes [PorRu^{V}O]. It is apparent that a corresponding [PorFe^{V}O] state can be stabilized, as concluded by Watanabe et al.,[2b, 13] when the "a_{2u}" orbital of the porphyrin is sufficiently lowered by electron-withdrawing substituents on the porphyrin. However, the [PorFe^{V}O] and [PorRu^{V}O] states will still be different in their spin state preferences due to the fact that the 3d – 3d exchange is significantly larger than the 4d – 4d exchange.[21] Thus, to enjoy the stabilizing 3d – 3d exchange, [PorFe^{V}O] will have a propensity for a $\delta^1\pi^{*1}_{xz}\,\pi^{*1}_{yz}$ orbital occupancy in a $^4\Delta(Fe^V)$ state. In contrast, the smaller

4d–4d exchange in ruthenium will prefer the low-spin $^2\Pi_{xz,yz}(Ru^V)$ states, as observed in this study.

In conclusion, the Ru^VO complex is shown to be distinctly different in its electronic structure than the iron. The vacant π^* orbital in the Ru^VO catalyst will endow this reagent with a heightened electrophilic nature, which will be more pronounced with substrates which are better electron donors. Preliminary experimental results by one of us[22] reveal indeed such a heightened electrophilic nature in the oxidation reactions of substituted toluene by a ruthenium porphyrin catalyst. The electrophilicity of the ruthenium catalyst is found to be larger than the corresponding Cpd I of iron, and even larger than that of an electronegative hydrogen abstractor, a bromine atom. Another interesting aspect of the ruthenium catalyst is the equilibrium of the closely lying $^2\Pi_{xz,yz}(Ru^V)$ and Cpd I states $^{4,2}A_{2u}(Ru^{IV})$. Moreover, for an axial ligand which is a good π-donor the $^{4,2}\Pi_S(Ru^{IV})$/$^{4,2}A_{1u}(Ru^{IV})$ states equilibrium will also be important. Within this dense manifold of ground states, a multistate reactivity may develop with mixed electrophilic and Cpd I–radical characters. Finally, sensitivity to the polarity of the environment is expected in view of the chameleon nature of the $^{4,2}A_{2u}(Ru^{IV})$ states.

Received: February 26, 2001 [Z16689]

[1] *Biomimetic Oxidations Catalyzed by Transition Metal Complexes* (Ed.: B. Meunier), Imperial College Press, London, **1999**.

[2] a) B. Meunier, J. Bernadou, *Struct. Bonding* **2000**, *97*, 1; b) Y. Watanabe in *The Porphyrin Handbook*, *Vol. 4* (Eds.: K. M. Kadish, K. M. Smith, R. Guilard), Academic Press, San Diego, **2000**, pp. 97–117; c) J. T. Groves, K. Shalyaev, J. Lee in *The Porphyrin Handbook*, *Vol. 4* (Eds.: K. M. Kadish, K. M. Smith, R. Guilard), Academic Press, San Diego, **2000**, pp. 17–40.

[3] F. Ogliaro, S. Cohen, M. Filatov, N. Harris, S. Shaik, *Angew. Chem.* **2000**, *112*, 4009; *Angew. Chem. Int. Ed.* **2000**, *39*, 3851.

[4] R. Weiss, D. Mandon, T. Wolter, A. X. Trautwein, M. Muther, B. Eckhard, E. Bill, A. Gold, K. Jayaray, J. Terner, *J. Biol. Inorg. Chem.* **1996**, *1*, 377.

[5] I. Schlichting, J. Berendzen, K. Chu, A. M. Stock, S. A. Maves, D. A. Benson, R. M. Sweet, D. Ringe, G. A. Petsko, S. G. Sligar, *Science* **2000**, *287*, 1615.

[6] a) D. L. Harris, G. H. Loew, *Chem. Rev.* **2000**, *100*, 407; b) for a sulfur radical description, see: M. T. Green, *J. Am. Chem. Soc.* **1999**, *121*, 7939; J. Antony, M. Grodzicki, A. X. Trautwein, *J. Phys. Chem. A* **1997**, *101*, 2692.

[7] Z. Gross, S. Ini, *Inorg. Chem.* **1999**, *38*, 1446.

[8] J. T. Groves, J. S. Roman, *J. Am. Chem. Soc.* **1995**, *117*, 5594.

[9] J. T. Groves, R. Quinn, *J. Am. Chem. Soc.* **1985**, *107*, 5790.

[10] J. T. Groves, M. Bonchio, T. Carafiglio, K. Shalyaev, *J. Am. Chem. Soc.* **1996**, *118*, 8961.

[11] a) N. L. P. Fackler, S. Zhang, T. V. O'Halloran, *J. Am. Chem. Soc.* **1996**, *118*, 481; b) C.-M. Che, K.-Y. Wong, T. C. W. Mak, *J. Chem. Soc. Chem. Commun.* **1985**, 988; c) A. C. Dengel, W. P. Griffin, C. A. O'Mahoney, D. J. Williams, *J. Chem. Soc. Chem. Commun.* **1989**, 1720; d) C.-M. Che, K.-Y. Wong, T. C. W. Mak, *J. Am. Chem. Soc.* **1990**, *112*, 2284; e) C.-M. Che, K.-Y. Wong, T. C. W. Mak, *Inorg. Chem.* **1987**, *26*, 2289; f) A. C. Dengel, W. P. Griffith, *Inorg. Chem.* **1991**, *30*, 869.

[12] D. H. R. Barton, D. Doller, *Acc. Chem. Res.* **1992**, *25*, 504.

[13] T. Murakami, K. Yamaguchi, Y. Watanabe, I. Morishima, *Bull. Chem. Soc. Jpn.* **1998**, *71*, 1343.

[14] JAGUAR 4.0, Schrödinger, Inc., Portland OR, **1998**. All isolated molecule calculations were double checked for consistency using GAUSSIAN 98 (Gaussian 98, Revision A.7, M. J. Frisch, G. W. Trucks, H. B. Schlegel, G. E. Scuseria, M. A. Robb, J. R. Cheeseman, V. G. Zakrzewski, J. A. Montgomery, Jr., R. E. Stratmann, J. C. Burant, S. Dapprich, J. M. Millam, A. D. Daniels, K. N. Kudin, M. C. Strain, O. Farkas, J. Tomasi, V. Barone, M. Cossi, R. Cammi, B. Mennucci, C. Pomelli, C. Adamo, S. Clifford, J. Ochterski, G. A. Petersson, P. Y. Ayala, Q. Cui, K. Morokuma, D. K. Malick, A. D. Rabuck, K. Raghavachari, J. B. Foresman, J. Cioslowski, J. V. Ortiz, A. G. Baboul, B. B. Stefanov, G. Lui, A. Liashenko, P. Piskorz, I. Komaromi, R. Gomperts, R. L. Martin, D. J. Fox, T. Keith, M. A. Al-Laham, C. Y. Peng, A. Nanayakkara, C. Gonzalez, M. Challacombe, P. M. W. Gill, B. G. Johnson, W. Chen, M. W. Wong, J. L. Andres, M. Head-Gordon, E. S. Replogle, J. A. Pople, Gaussian, Inc., Pittsburgh, PA, **1998**). All solvent calculations were carried out by using chlorobenzene as the polarizing medium. JAGUAR uses a polarized continuum solvent model with good performance. See: B. Marten, K. Kim, C. Cortis, R. A. Friesner, R. B. Murphy, M. N. Ringnalda, D. Sitkoff, B. Honig, *J. Phys. Chem.* **1996**, *100*, 11775; J. Crystal, R. A. Friesner, *J. Phys. Chem. A* **2000**, *104*, 2362.

[15] P. J. Stevens, F. J. Devlin, C. F. Chablowski, M. J. Frisch, *J. Phys. Chem.* **1994**, *98*, 11623.

[16] LACVP is derived from LAN2DZ: J. P. Hay, W. R. Wadt, *J. Chem. Phys.* **1985**, *82*, 299.

[17] F. Ogliaro, S. Cohen, S. P. de Visser, S. Shaik, *J. Am. Chem. Soc.* **2000**, *122*, 12892.

[18] The same results were obtained for $L = CysS^-$ as a ligand,[3] where the spin density on the ligand in the isolated molecule is 0.67 with LACVP/6-31G. Note that for all the thiolate ligands, the "a_{2u}" natural orbital reveals a second-order mixing with the in-plane π^*_{xz} orbital due to the tilting of the ligand off the nodal plane of the π^*_{xz} orbital.

[19] The $a_{1u}-p_\pi$ mixing is evident from the natural orbitals of the Π_S states. Available from the authors.

[20] a) J. H. Dawson, M. Sono, *Chem. Rev.* **1987**, *87*, 1255; b) P. M. Champion, *J. Am. Chem. Soc.* **1989**, *111*, 3433; c) J. Bernadou, A.-S. Fabiano, A. Robert, B. Meunier, *J. Am. Chem. Soc.* **1994**, *116*, 9375; d) W.-D. Woggon, *Top. Curr. Chem.* **1996**, *184*, 40.

[21] G. Ohanessian, W. A. Goddard III, *Acc. Chem. Res.* **1990**, *23*, 386.

[22] a) J. T. Groves, preliminary data presented at the ICPP-1 symposium, Dijon, July 2000; b) the electronic features of the catalytic hydroxylations that pass through the putative $[(L)PorRu^VO]$ species have been probed through studies of the relative reactivity of *para*-substituted toluenes. A typical Hammett treatment of data for the Ru(TPFPP)/2,6-dichloropyridine *N*-oxide system[10] produced a highly negative $\rho^+ = -2.0$ at 40 °C indicating an unusually large charge separation in the transition state of hydroxylation. The absolute value of this correlation coefficient is much greater than that for the relative rates of the competitive oxidation of toluenes by electrophilic $oxoFe^{IV}$ porphyrin radical cation, $[Fe^{IV}(TPP^{+\cdot})(O)]$, the active oxidant in the Fe^{III} (TPP)Cl/PhIO system ($\rho^+ = -0.83$) (P. Inchley, J. R. Lindsey Smith, R. J. Lower, *New J. Chem.* **1989**, *13*, 669). For comparison, a typical radical reaction like the $H^\cdot$ abstraction from $XC_6H_4CH_3$ by *tert*-butoxy radicals, $\rho^+ = -0.4$ has been reported and a $\rho^+ = -1.4$ was measured for bromination with $Br^\cdot$ radicals (G. A. Russel, *Free Radicals*, Wiley-Interscience, New York, **1973**).

  1433-7851/01/4015-2878 $ 17.50+.50/0

The First Organically Templated Open-Framework Niobium Silicate and Germanate Phases: Low-Temperature Hydrothermal Syntheses of $[(C_4N_2H_{11})Nb_3SiO_{10}]$ (NSH-1) and $[(C_4N_2H_{11})Nb_3GeO_{10}]$ (NGH-1)**

Robin J. Francis* and Allan J. Jacobson

Stable, crystalline, microporous materials are of immense practical importance for commercial applications such as catalysis, absorption, ion-exchange, and separation.[1, 2] The continuing need for microporous materials that display new framework topologies and novel catalytic properties has spurred increasing interest in extending the range of known structure types and compositions. To date, the vast majority of microporous materials are constructed from tetrahedral building units.[3, 4] A much smaller class of materials are those constructed from mixed octahedral–tetrahedral frameworks. Such materials are likely to display framework topologies and properties that are substantially different from those observed in purely tetrahedral materials.[5] However, a limited number of such mixed frameworks have been reported to date.

The synthesis of microporous niobium silicates and germanates is a particularly unexplored area. The only structurally characterized examples are niobium-containing nenadkevichite analogues,[6] and an open-framework potassium niobium germanate, $[K_3Nb_5GeO_{16}]\cdot 2H_2O$, synthesized hydrothermally at very high temperatures and pressures.[7] The hydrothermal synthesis of a microporous sodium niobium silicate, AM-11, has been reported, but its structure is currently unknown.[8] We are not aware of any reported syntheses of organically templated niobium silicate or germanate materials performed under mild ($<200\,^{\circ}C$, $P<25$ atm) hydrothermal conditions.

We report here the synthesis of the first organically templated open-framework niobium silicate and germanate phases, namely $[(C_4N_2H_{11})Nb_3SiO_{10}]$ (NSH-1) and $[(C_4N_2H_{11})Nb_3GeO_{10}]$ (NGH-1).

$[(C_4N_2H_{11})Nb_3SiO_{10}]$ (NSH-1) and $[(C_4N_2H_{11})Nb_3GeO_{10}]$ (NGH-1) were synthesized in high yield (>70% based on Nb) under hydrothermal conditions. The structures of NSH-1 and NGH-1 were solved from powder diffraction data, and refined by using the Rietveld method.[9] NSH-1 and NGH-1 are isostructural. The framework asymmetric unit of NSH-1 is shown in Figure 1a. The open-framework structure of NSH-1 and NGH-1 can be viewed as being formed from two

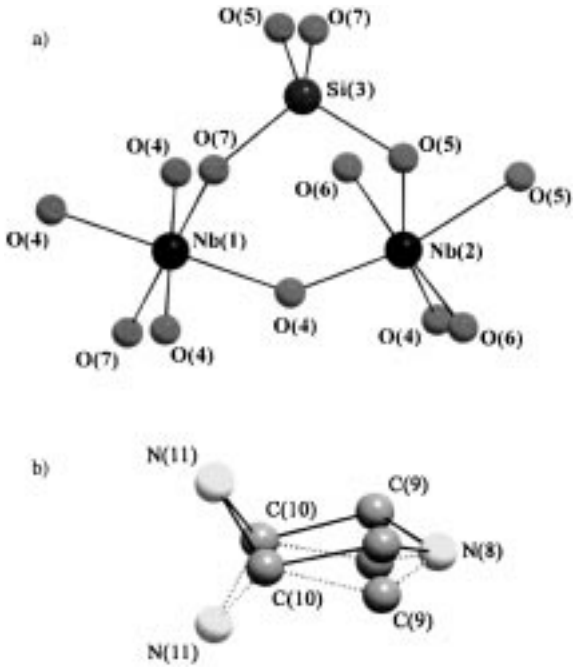

Figure 1. a) The framework asymmetric unit of $[(C_4N_2H_{11})Nb_3SiO_{10}]$ (NSH-1) showing the local coordination and the atomic-labeling scheme. b) The two possible orientations of the piperazine template due to statistical disorder of the C(9) and N(11) atoms.

interconnected chainlike structural motifs. The first consists of two edge-shared $Nb(2)O_6$ octahedra that are further connected by corner-shared O(6) atoms to form infinite double columns running along the [010] direction. A second chain of $[NbO_6\text{-}Si(Ge)O_4\text{-}NbO_6]_n$ polyhedra is formed from corner-sharing $Nb(1)O_6$ octahedra and $Si(Ge)O_4$ tetrahedra and runs along the [100] direction. The two chains are cross-linked through O(4) atoms to form the open-framework structure.

The Nb(1) atoms reside at the center of an almost regular octahedron with an average Nb–O distance of 2.050(7) Å for NSH-1 and 1.977(8) Å for NGH-1. The Nb(2) atom resides in a somewhat more distorted coordination with a d_{av}(Nb–O) of 2.011(6) Å for NSH-1 and 2.032(9) Å for NGH-1. The Si or Ge atoms reside at the center of an almost perfectly regular tetrahedron with a d_{av}(Si–O) of 1.6156(5) Å for NSH-1 and a d_{av}(Ge–O) of 1.775(13) Å for NGH-1. The results of bond valence sum calculations[10] for the Nb, Si, and Ge atoms were in good agreement with the expected values.

The three-dimensional framework structure of NSH-1 and NGH-1 (shown in Figure 2) consists of a network of three interconnecting one-dimensional channels, two consisting of six-membered rings (6-MR) of polyhedra and the other an eight-membered ring (8-MR). The two 6-MR channels are formed from six NbO_6 corner-linked units. The first runs along the [100] direction; the second along the [111] direction. The 8-MR channels are constructed from six NbO_6 and two GeO_4 units and run along the [010] direction perpendicular to one of the 6-MR channels and at an angle of 55° to the other. The

[*] Dr. R. J. Francis, Prof. A. J. Jacobson
Department of Chemistry
University of Houston
Houston, TX 77204-5641 (USA)
Fax: (+1) 713-743-2787
E-mail: robin@xray.phys.uh.edu

[**] We thank the National Science Foundation (DMR-9805881) and the Robert A. Welch Foundation for support. This work made use of MRSEC/TCSUH Shared Experimental Facilities supported by the National Science Foundation under Award Number DMR-9632667 and the Texas Center for Superconductivity at the University of Houston. Work at the National Synchrotron Light Source at Brookhaven National Laboratory was partially supported by the Division of Materials Sciences, U.S. Departmentof Energy under contract DE-AC02-98CH10886. We thank Dr. Kent Ross for collecting the energy-dispersive X-ray analysis (EDAX) data and scanning electron microscopy (SEM) data, and Dr. Tom Vogt for assistance in collecting the X7A powder data.

  1433-7851/01/4015-2879 $ 17.50+.50/0

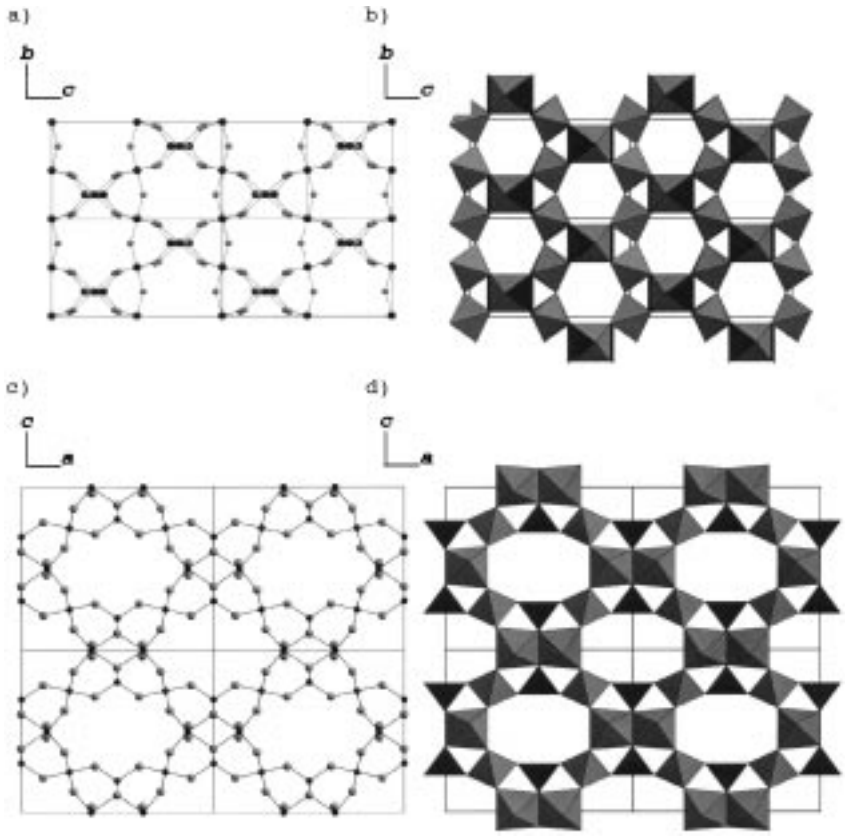

Figure 2. a, b) Representations of the framework structure of $[(C_4N_2H_{11})Nb_3SiO_{10}]$ (NSH-1) and $[(C_4N_2H_{11})Nb_3GeO_{10}]$ (NGH-1) viewed along the *a* axis, showing the 6-MR channels. c, d) Representations of the framework viewed along the *b* axis, showing the larger 8-MR channels. The niobium, silicon (germanium), and oxygen atoms atoms are represented as black, medium gray, and light gray spheres, respectively. In b) and d) NbO_6 octahedra are shown in gray, $Si(Ge)O_4$ tetrahedra in black. The template molecules are omitted for clarity.

three channels intersect at approximately (0, 0.25, 0.125) forming an irregular, roughly triangular shaped cavity centered at that position (see Figure 3). The 6-MR channels are almost circular in cross-section with a shortest oxygen – oxygen distance across the channel of 5.6 Å, giving a "free-pore diameter" (using the atomic radii of Shannon[11]) of about 2.8 Å. The large 8-MR channels are elliptical in shape with an approximate free-pore diameter of 3.4 × 5.0 Å. The maximum free-diameter across the cavity is approximately 5.7 Å. The piperazinium cations reside in the center of the cavities. One of each of the two carbon and nitrogen atoms are statistically disordered over two sites giving rise to two possible orientations of the piperazinium cations as shown in Figure 1b. On the basis of charge-balance considerations the piperazine molecules are assumed to be monoprotonated. This is consistent with the pH value of the reaction (ca. 9) and the pK_a values for piperazine in aqueous solution.[12] Very strong hydrogen bonds are observed between the N(8) atom, two O(5) atoms, and two O(6) atoms (N–O distances 2.7 – 2.9 Å). Somewhat weaker hydrogen bonds are formed between the N(11) atoms and two O(7) atoms (N–O distance 3.1 Å). As can be seen from Figure 3 the piperazinium cation is a very good "fit" for the cavity of NSH-1 and NGH-1.

The structure of NSH-1 and NGH-1 shows some similarities to the structure of $[K_3Nb_5GeO_{16}] \cdot 2H_2O$. In particular infinite double columns of NbO_6 octahedra and $[NbO_6\text{-}Si(Ge)O_4\text{-}NbO_6]_n$ chain motifs are observed in both structure types. However, in $[K_3Nb_5GeO_{16}] \cdot 2H_2O$ single vertex-sharing columns of NbO_6 octahedra are found, whereas NSH-1 and NGH-1 contain only double columns. As a result while in NSH-1 and NGH-1 cavities are only formed at the intersection of the larger 8-MR channels and the 6-MR channels, in $[K_3Nb_5GeO_{16}] \cdot 2H_2O$ smaller cavities are also formed at the intersection of two 6-MR channels. The structural differences are undoubtedly caused by the difference in sizes of the K^+ and piperazinium cations.

Elemental analyses of NSH-1 and NGH-1 consistently gave a Nb:Si/Ge ratio of less than the 3:1 suggested by the X-ray diffraction data. Niobium vacancies within the structures of NSH-1 and NGH-1, either distributed statistically throughout the structure or present as extended layer-like defects, are the most likely cause of the difference from the ideal stoichiometry. Close inspection of the powder diffraction patterns reveals that the widths of each of the reflections are not exactly equal. In particular, the 101 reflection is significantly broadened relative to the 011 reflection, indicating disorder in the [101] lattice direction. Inspection of the structure suggests a

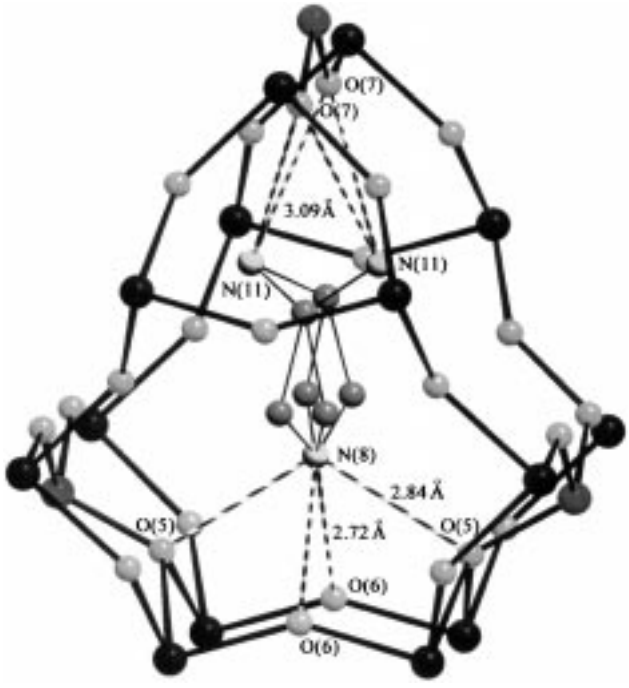

Figure 3. The location of the piperazinium cations in the cavities formed at the intersection of the 6-MR and 8-MR channels. The niobium, silicon (germanium), and oxygen atoms atoms are represented as black, medium gray, and light gray spheres, respectively. The two possible orientations of the template are shown. Hydrogen bonding interactions are shown by dashed lines.

  1433-7851/01/4015-2880 $ 17.50+.50/0 *Angew. Chem. Int. Ed.* **2001**, *40*, No. 15

mechanism by which disorder can be introduced in this direction that also accounts for the observed niobium deficiency. If all of the Nb(1) atoms in a (101) "layer" are removed, the remaining structural motifs can be connected through corner-shared Nb(2) and Si(Ge) polyhedra to form structures containing six-membered channels along the [010] direction. Modeling studies suggest that if such layers of Nb(1) atoms are removed at random, order is lost along the [101] direction but maintained in the [011] direction.

Thermal analysis of NSH-1 and NGH-1 revealed that loss of the template occurs between about 200 and 520 °C. Powder X-ray diffraction patterns of samples of NSH-1 and NGH-1 heated for 1–2 h at 350 and 440 °C, respectively, indicated that the frameworks remain intact following loss of the template, although a substantial loss of crystallinity was evident. IR spectroscopy confirmed complete loss of the template from the calcined materials. Heating at substantially higher temperatures produced amorphous materials.

Ion-exchange experiments revealed that the piperazinium cations in NSH-1 and NGH-1 could be successfully exchanged for Na^+ and K^+ ions, as demonstrated by small changes in the powder X-ray diffraction patterns and the diminution in the intensity of the carbon–carbon and carbon–nitrogen stretches in the IR spectra. The materials largely retained their crystallinity following the exchange procedure, although some line broadening was observed.

In summary, we have described the low-temperature hydrothermal synthesis and structure of the first examples of organically templated open-framework niobium silicates and germanates. The materials display thermal stability and ion-exchange capability. Given the large variety of organic templates that could be used in this synthetic regime, and the range of compositions seen in condensed niobium silicates and germanates, the scope for the synthesis of further novel materials in this class appears to be very large.

Experimental Section

Syntheses were conducted hydrothermally in a Teflon-lined autoclave (23 mL).

NSH-1: Nb_2O_5 (0.089 g,99.5 %, Aldrich) was dissolved in aqueous HF (0.167 g 48 wt %, Aldrich) and heated to 110 °C for 4 h. After cooling, this solution was combined with SiO_2 (0.120 g, fumed, 99.8 %, Aldrich), piperazine (0.459 g, 99 %, Aldrich), H_2O (2.88 g), and ethylene glycol (5 g) and heated at 160 °C for 25 days. A fine white powder (particle size ca. 0.2 μm) of NSH-1 was recovered. NGH-1 was synthesized following the same procedure, by using 0.209 g of GeO_2 (99.99 %, Aldrich) instead of the SiO_2. A fine white powder of NGH-1 (ca. 0.4 μm) was obtained after heating at 160 °C for six days.

Ion-exchange reactions were performed by stirring 100 mg samples in 2 M aqueous solutions (10 mL) of either NaCl or KCl at 60 °C for 12 h. Thermogravimetric analyses were performed in flowing dry air on a Thermal Instruments TGA 2950 instrument at a ramp rate of 5 K min^{-1}. IR spectra were collected on a Mattson FTIR 5000 spectrometer (KBr method).

Received: March 12, 2001 [Z16758]

[1] P. B. Venuto, *Microporous Mater.* **1994**, *2*, 297.
[2] T. J. Barton, L. M. Bull, W. G. Klemperer, D. A. Loy, B. McEnaney, M. Misono, P. A. Monson, G. Pez, G. W. Scherer, J. C. Vartuli, O. M. Yaghi, *Chem. Mater.* **1999**, *11*, 2633.
[3] W. M. Meier, D. H. Olson, C. Baerlocher, *Atlas of Zeolite Structure Types*, Elsevier, Boston, **1996**.
[4] R. J. Francis, D. O'Hare, *J. Chem. Soc. Dalton Trans.* **1998**, 3133.
[5] J. Rocha, M. W. Anderson, *Eur. J. Inorg. Chem.* **2000**, 801.
[6] J. Rocha, P. Brandao, Z. Lin, A. P. Esculcas, A. Ferreira, M. W. Anderson, *J. Phys. Chem.* **1996**, *101*, 14978.
[7] W. T. A. Harrison, T. E. Gier, G. D. Stucky, *J. Solid State Chem.* **1995**, *115*, 373.
[8] J. Rocha, P. Brandao, A. Phillippou, M. W. Anderson, *Chem. Commun.* **1998**, 2687.
[9] Powder diffraction data on NGH-1 were collected on beamline X7A of the NSLS, Brookhaven National Laboratory, $\lambda = 0.70117$ Å, over the range $2-47°$ 2θ. The pattern was indexed by using the orthorhombic cell $a = 13.0861(2)$, $b = 7.4937(2)$, $c = 11.4967(4)$ Å, space group *Imma* (no. 74). The structure was solved by using the direct methods package EXPO.[13] This solution was then used in the Rietveld analysis of the structure using the software package GSAS.[14] The template atom positions were determined from difference Fourier syntheses. Soft constraints were applied to the C–C and C–N bond lengths in the refinement. The final refinement consisted of 70 structural and profile parameters and proceeded smoothly to convergence, with $R_p = 0.0605$, $R_{wp} = 0.0716$, $R_F = 0.0552$, $R_F2 = 0.0778$, $\chi^2 = 7.732$. Powder diffraction data on NSH-1 were collected on a Scintag 2000 diffractometer using Cu radiation over the range $8-100°$ 2θ. Unit cell refinement gave $a = 12.9041(4)$, $b = 7.4967(3)$, $c = 11.4471(5)$ Å, space group *Imma*. The structure solution of NGH-1 was used as the starting model in the Rietveld analysis. The refinement proceeded smoothly to convergence, with $R_p = 0.0590$, $R_{wp} = 0.0459$, $R_F = 0.0609$, $R_F2 = 0.0722$, $\chi^2 = 0.9493$. Soft constraints were applied to the C–C and C–N bond lengths. Crystallographic data (excluding structure factors) for the structures reported in this paper have been deposited with the Cambridge Crystallographic Data Centre as supplementary publication no." CCDC-163346 (NSH-1) and CCDC-163347 (NGH-1). Copies of the data can be obtained free of charge on application to CCDC, 12 Union Road, Cambridge CB2 1EZ, UK (fax: (+44) 1223-336-033; e-mail: deposit@ccdc.cam.ac.uk).
[10] N. E. Brese, M. O'Keeffe, *Acta Crystallogr. Sect. B* **1991**, *47*, 192.
[11] R. D. Shannon, *Acta Crystallogr. Sect. A* **1976**, *32*, 751.
[12] R. C. Weast, *Handbook of Chemistry and Physics*, Chemical Rubber Company, Cleveland, **1972**.
[13] A. Altomare, M. C. Burla, M. Camalli, B. Carrozzini, G. L. Cascarano, C. Giacovazzo, A. Guagliardi, A. G. Giuseppina-Moliterni, G. Polidori, R. Rizzi, *J. Appl. Crystallogr.* **1999**, *32*, 339.
[14] A. C. Larson, R. B. V. Dreele, *Los Alamos Natl. Lab. Rep.* **1987**, La-UR-86-748.

A Lewis Acid Catalyst Anchored on Silica Grafted with Quaternary Alkylammonium Chloride Moieties**

Thundi M. Jyothi, Mark L. Kaliya, and Miron V. Landau*

The development of novel catalytic materials based on mesoporous supports by chemically binding the active species on their surfaces has become of profound importance in recent years owing to the benefits of catalyst heterogeniza-

[*] Prof. M. V. Landau, Dr. T. M. Jyothi, Dr. M. L. Kaliya
Blechner Center for Industrial Catalysis and Process Development
Department of Chemical Engineering
Ben Gurion University of the Negev
Beer Sheva-84105 (Israel)
Fax: (+972) 8-6472902
E-mail: mlandau@bgumail.bgu.ac.il

[**] T.M.J. is grateful to the Blechner fund for a postdoctoral fellowship.

  1433-7851/01/4015-2881 $ 17.50+.50/0

tion.[1] This can potentially lead to enhanced activity and/or product selectivity while avoiding the drawbacks of catalyst instability and limited reusability. Although polymer-supported catalysts have been widely used in synthesis, catalysts based on high-surface-area inorganic supports are preferred due to their higher thermal stability and better rates of molecular diffusion.[2] The corrosivity and potential environmental hazards associated with common Lewis acid catalysts such as $AlCl_3$, BF_3, and $SnCl_4$, as well as difficulties in catalyst recycling, have aroused great interest in finding alternatives. Direct immobilization of such catalysts on inorganic supports appears to be easy, but their application is rather limited due to possible leaching of the supported species during the reaction.[2b,3] Also, the mineral acid evolved in the reaction of surface hydroxy groups with the Lewis acid is sometimes retained on the catalyst and can even change the nature of the support.[4]

In connection with our ongoing research on the Prins condensation of alkenes and formaldehyde to give valuable unsaturated alcohols (Scheme 1), we developed a new catalyst

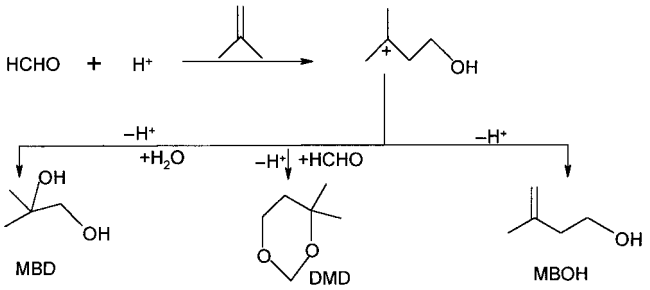

Scheme 1. Prins condensation of isobutene with formaldehyde. MBD = 3-methylbutane-1,3-diol, DMD = 4,4-dimethyl-1,3-dioxane, MBOH = 3-methyl-3-buten-1-ol.

by anchoring the active $SnCl_4$ catalyst on silica functionalized with organic quaternary ammonium chloride moieties. Our methodology is based on the fact that the nucleophilic addition of tetraalkylammonium halides to $SnCl_4$ leads to the formation of pentacoordinate anionic tin species.[5] Such complexes of general formula $[NR_4]^+[SnCl_5]^-$ resemble ionic liquids or molten salts.[6] Ionic liquids, which can be prepared by the reaction of a tetraalkylammonium halide $NR_4^+X^-$ with a Lewis acid MX, are effective Friedel–Crafts catalysts. Holderich et al. immobilized such ionic liquids directly on various inorganic supports and used them in alkylation reactions.[7]

A recent patent described the use of $SnCl_4$ anchored to an ion-exchange resin containing tetraalkylammonium chloride substituents in the Prins condensation of isobutene and formaldehyde for the selective synthesis of 3-methyl-3-buten-1-ol (MBOH), which is an important synthesis block for industrially valuable terpenes.[8] Zeolite catalysts such as ZSM-5 and FeMCM-22 were used in the selective synthesis of MBOH, but the yield was unsatisfactory.[9] Also, MBOH was prepared from isobutene and formaldehyde by using metal chlorides such as $SnCl_4$ and $ZnCl_2$ under mild conditions, but the yield was low due to the formation of many side products.[10]

Preliminary experiments on the Prins condensation of isobutene with formaldehyde indicated that complexation of $SnCl_4$ with a tetraalkylammonium chloride leads to improved selectivity for the unsaturated alcohol MBOH. Such complexes were grafted onto silica by two methods (Scheme 2).

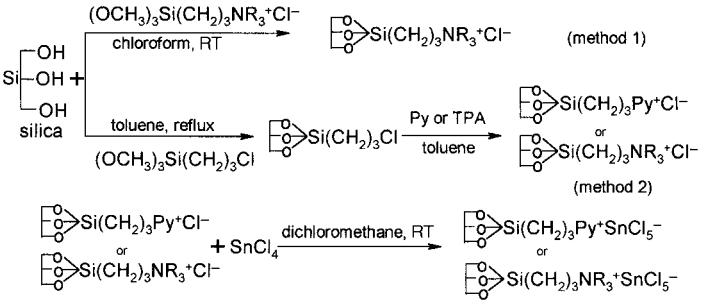

Scheme 2. Preparation of $SnCl_4$ anchored on tetraalkylammonium chloride functionalized silica. Py = pyridine, TPA = tetrapropylammonium chloride, R = alkyl.

Formation of a complex between $SnCl_4$ and the tetraalkylammonium chloride moiety was confirmed by ^{119}Sn NMR spectroscopy. A shift in the NMR signal from $\delta = -665.0$ to -725.2 after the reaction with tetraalkylammonium chloride reflects the change in the coordination number of tin. Moreover, the tin/chlorine atomic ratio, determined by elemental analysis, was in accordance with formation of such a complex.

The results of the Prins condensation of isobutene and formaldehyde on various complexes are summarized in Table 1. Clearly, complexation of $SnCl_4$ with tetraalkylammonium chloride improves the selectivity for the unsaturated alcohol. Tin(IV) chloride alone under anhydrous conditions displayed high activity, but the selectivity for MBOH was poor. The solvent (acetonitrile, chloroform, or dichloromethane) had little influence on formaldehyde conversion and MBOH selectivity. However, the use of an aqueous formaldehyde solution instead of paraformaldehyde adversely

Table 1. Prins condensation of isobutene and formaldehyde over NR_4Cl–$SnCl_4$ complexes.[a]

Entry	Catalyst	Solvent/ HCHO	Conversion of formaldehyde [%]	MBOH selectivity [%][g]	MBOH yield [%][h]
1	$SnCl_4$	$CHCl_3$/pf[b]	97.4	54.6	53.0
2	$SnCl_4$-TPAC[c]	$CHCl_3$/pf	77.1	89.0	68.7
3	$SnCl_4$-TPAC	CH_2Cl_2/pf	77.3	88.5	68.4
4	SnCl4-TPAC	CH_3CN/pf	75.9	87.7	66.7
5	$SnCl_4$-TPAC	CH_3CN/aq[d]	59.7	40.0	22.0
6	$SnCl_4$-BTEAC[e]	$CHCl_3$/pf	76.6	87.1	66.7
7	$SnCl_4$-TMSPAC[f]	$CHCl_3$/pf	70.3	89.4	62.8
8	No catalyst	$CHCl_3$/pf	–	–	–

[a] 56 g isobutene, 3 g paraformaldehyde, catalyst containing 4 mmol of $SnCl_4$, and 40 g of chloroform solvent were introduced into the reactor and stirred for 2 h at 60 °C. [b] Paraformaldehyde. [c] Tetrapropylammonium chloride–$SnCl_4$ complex. [d] 30% aqueous solution of formaldehyde. [e] Benzyltriethylammonium chloride–$SnCl_4$ complex. [f] Complex prepared from [3-(trimethoxysilyl)propyl]octadecyldimethylammonium chloride and $SnCl_4$. [g] Other products included 4,4-dimethyl-1,3-dioxane and traces of polycondensation products. [h] Yield was determined by using 2-butanol as an internal standard.

  1433-7851/01/4015-2882 $ 17.50+.50/0 *Angew. Chem. Int. Ed.* **2001**, *40*, No. 15

affected the conversion and MBOH selectivity. Under these conditions, larger amounts of side products such as 4,4-dimethyl-1,3-dioxane (DMD) and 3-methylbutane-1,3-diol (MBD) were formed. Hence, to maximize the yield of MBOH, anhydrous conditions were maintained in all other experiments.

Various silica-based catalysts were tested in the selective synthesis of MBOH (Table 2). For comparison, the $NR_4^+SnCl_5^-$ complex immobilized directly on silica and silica-supported $SnCl_4$ were also tested. The catalysts immobilized on silica that was functionalized with organic quaternary ammonium moieties showed the highest selectivity for MBOH (88–93%). X-ray fluorescence (XRF) analysis of the filtrate after the reaction (detection limit: >0.5 ppm of Sn) indicated no leaching of tin from the catalyst. Furthermore, when a subsequent reaction was performed with the filtrate after separating the catalyst no formaldehyde conversion occurred. Recycling of the catalyst led to no appreciable loss in activity. Increasing the reaction time to 3.5 h increased the MBOH yield to 76% (entry 7) and 81% (entry 9). The catalyst prepared by treating a solution of $SnCl_4$ in chloroform with silica (silica/$SnCl_4$) is prone to leaching during the reaction. Analysis of the filtrate after the reaction showed that around 39% of the tin chloride had been leached out. Moreover, the performance of this catalyst in the selective synthesis of MBOH is poor (entry 3) compared to immobilized complexes. Direct immobilization of the complex on silica (SIL/TPA^+-$SnCl_5^-$) also resulted in lower catalytic activity and MBOH yield relative to the pure complex $SnCl_4$–TPAC and the SIL-$TPA^+SnCl_5^-$ catalyst. The turnover number (TON), that is, the number of moles of formaldehyde converted per mole of catalyst per unit time, for the SIL-$TPA^+SnCl_5^-$ catalyst (TON = 8.0) was 83% of that obtained in a homogeneously catalyzed reaction (TON = 9.6, Table 1, entry 2) at similar MBOH selectivities. Direct immobilization of the complex reduced the relative TON to 74% (TON = 7.3).

Table 2. Condensation of isobutene and formaldehyde to give 3-methyl-3-buten-1-ol (MBOH) over silica-based catalysts and with catalyst recycling.[a]

Entry	Catalyst	$SnCl_4$ loading [mmol g^{-1} support]	Conversion of formaldehyde [%]	MBOH selectivity [%]	MBOH yield [%]
1	SIL-$TPA^+SnCl_5^-$[b]	0.32	64.1	88.1	56.4
2	SIL/$TPA^+SnCl_5^-$[c]	0.32	57.0	79.8	45.5
3	Silica/$SnCl_4$	0.95	77.9	63.2	49.2
4	SIL-$NR_4^+SnCl_5^-$[d]	0.78	64.6	92.8	59.9
5	recycle 1[e]	0.78	63.3	91.1	57.6
6	recycle 2	–	61.9	91.0	56.3
7	SIL-$NR_4^+SnCl_5^-$[f]	0.78	100	76.1	76.1
8	SIL-$Py^+/SnCl_5^-$[g]	0.48	66.3	91.9	60.9
9	SIL-$Py^+/SnCl_5^-$[f]	0.48	97.8	82.6	80.7

[a] Reaction conditions were as in Table 1, and in all cases the amount of catalyst containing 4 mmol of $SnCl_4$ was used. [b] Tetrapropylammonium chloride functionalized silica complex. [c] Direct immobilization of complex on silica. [d] Catalyst prepared by method 1. [e] Recycling of SIL-$NR_4^+SnCl_5^-$ after exhaustive washing with dichloromethane. [f] Reaction continued for 3.5 h. [g] Pyridinium chloride functionalized silica complex.

The present methodology of immobilizing a Lewis acid is of wide practical utility due to the possibility of anchoring various metal halides to give novel supported catalysts for different organic reactions. This type of anchoring could be advantageous for obtaining catalysts with high stability and longer lifetime. Unlike catalysts with a directly attached Lewis acid, prepared by the reaction of surface hydroxy groups of the support with hydrolyzable groups in the Lewis acid, the present catalyst is stable under the experimental conditions due to the formation of strong Si–O–Si bonds on the catalyst surface. Moreover, we believe that the the active sites will be more readily accessible to the reactants, since they are further from the silica surface.

In conclusion, we have demonstrated a new supported Lewis acid catalyst which is resistant to leaching and shows high selectivity in the synthesis of 3-methyl-3-butene-1-ol by the Prins condensation of isobutene and formaldehyde. Further work is underway to exploit these supported Lewis acid catalysts for developing clean technology in fine-chemical synthesis.

Experimental Section

All manipulations were performed under dry and inert conditions in a glove box, and all solvents were dried by standard procedures. $SnCl_4$–TPAC complex was prepared by the dropwise addition of anhydrous $SnCl_4$ (4 mmol) to a solution of tetrapropylammonium chloride (4 mmol) in dichloromethane (40 g) with constant stirring. The mixture was stirred overnight at ambient temperature, and the solution was concentrated in vacuum to give a white crystalline material, which was recrystallized from dichloromethane/hexane and stored under moisture-free conditions. Elemental analysis (%): calcd: Sn 24.61, Cl 36.74; found: Sn 24.78, Cl 36.40.

Silica gel (surface area: 500 $m^2 g^{-1}$) with an average pore diameter of 6 nm and particle size between 0.063 and 0.20 mm (Aldrich), preheated at 473 K for 6 h, was used as support. In method 1, silica (5 g) was treated with a solution of [3-(trimethoxysilyl)propyl]octadecyldimethylammonium chloride (4.82 g, 7 mmol, Aldrich) in chloroform to give tetraalkylammonium chloride functionalized silica. The excess of the reagent was removed by exhaustive Soxhlet extraction with dichloromethane and finally dried in vacuum. In method 2, silica support (5 g) was first treated with a solution of trimethoxysilylpropyl chloride (3 g, 14.64 mmol, Aldrich) in toluene under reflux for 5 h. The excess of the reagent was removed as explained above, and the propylated silica was treated with an excess of pyridine or tripropylamine (6–7 g) in toluene for 24 h under reflux to give pyridinium chloride functionalized and tetrapropylammonium chloride functionalized silica, respectively.

The amount of chloride ions present on the functionalized silica was determined by treating the solid with 0.1N nitric acid, followed by titration with a standard $AgNO_3$ solution and potassium chromate indicator.

The tin chloride was anchored on functionalized silica by treating a suspension of the amount of modified silica containing 4 mmol of chloride anion in dicholoromethane with a solution of anhydrous $SnCl_4$ (1.04 g, 4 mmol) with stirring for 12 h (Scheme 2). After the reaction, the catalyst was collected by filtration and subjected to Soxhlet extraction to remove loosely bound species.

Silica/TPA-$SnCl_4$ catalyst was prepared by adding a chloroform solution of the complex prepared as mentioned above to 4 g of predried silica support suspended in chloroform with constant stirring. The excess solvent was removed after stirring overnight, and the material was extracted with chloroform for 12 h in a Soxhlet apparatus. The material was finally dried and kept under moisture-free conditions before use.

The Prins condensation of isobutene and formaldehyde was carried out at 60 °C under autogenous pressure by introducing isobutene (56.1 g, 1.0 mol), paraformaldehyde (3 g, 0.1 mol), the solvent (40 g), and the amount of catalyst containing 4 mmol of $SnCl_4$ into a 250-mL Büchi autoclave. After stirring the mixture for 2 h, isobutene was released, the solid catalyst was separated, and the filtrate was analyzed on a gas chromatograph equipped with a capillary column (DB WAX) and thermal conductivity detector.

Received: February 23, 2001 [Z16673]

[1] a) J. H. Clark, D. J. Macquarrie, *Chem. Commun*. **1998**, 853; b) A. Cauvel, G. Renard, D. Brunel, *J. Org. Chem*. **1997**, *62*, 1325; c) Y. V. S. Rao, D. E. De Vos, P. A. Jacobs, *Angew. Chem.* **1997**, *109*, 2776; *Angew. Chem. Int. Ed. Engl*. **1997**, *36*, 2661; d) I. Rodriguez, S. Iborra, A. Corma, F. Rey, J. L. Jorda, *Chem. Commun*. **1999**, 593.
[2] *Chemistry of Waste Minimization* (Ed.: J. H. Clark), Chapman and Hall, London, **1995**, p. 141; b) T. W. Bastock, J. H. Clark in *Speciality Chemicals* (Ed.: B. Pearson), Elsevier, London, **1992**.
[3] a) A. Krzywicki, M. Marczewski, *J. Chem. Soc. Faraday Trans. 1* **1980**, 1311; b) R. S. Drago, S. C. Petrosius, P. B. Kaufman, *J. Mol. Catal*. **1984**, *89*, 317.
[4] J. B. Butrille, T. J. Pinnavaia, *Catal. Today* **1992**, *14*, 141.
[5] S. E. Johnson, C. B. Knobler, *Organometallics* **1992**, *11*, 3684.
[6] G. A. Parshall, *J. Am. Chem. Soc*. **1972**, *94*, 8716.
[7] a) P. Wasserscheid, W. Keim, *Angew. Chem.* **2000**, *112*, 3926; *Angew. Chem. Int. Ed*. **2000**, *39*, 3772; b) C. DeCastro, E. Sauvage, M. H. Valkenberg, W. F. Holderich, *J. Catal*. **2000**, *196*, 86.
[8] Kuraray Co. Ltd., Jpn. Pat. H09-262478, **1997**.
[9] a) T. Yashima, Y. Katoh, T. Komatsu, *Stud. Surf. Sci. Catal*. **1999**, *125*, 507; b) C. D. Chang, N. J. Mogan, Jpn. Pat. 55-113732, **1980**; c) H. Fujiwara, H. Shinohara, T. Yoshida, Jpn. Pat. 58-164534, **1983**.
[10] L. A. Mikeska, E. Arundale, US Pat. 2308192 [*Chem. Abstr.* **1943**, *37*, 3450]; Canadian Pat. 417, 600; British Pat. 545, 191 [*Chem. Abstr.* **1942**, *36*, 7030].

Molecular Models of Titania–Silica Systems and a Late Transition Metal Complex Grafted Thereon**

Rosa Fandos,* Antonio Otero,* Ana Rodríguez, María José Ruiz, and Pilar Terreros

Titania–silica materials are the focus of much attention on account of their unique properties:[1, 2] 1) they can act as catalysts for a wide variety of processes; 2) they are suitable supports for late transition metal catalysts because they improve the mechanical strength, thermal stability, and surface area relative to TiO_2 supports.[3] Although titania–silica materials have been extensively used as catalysts and supports for a great variety of reactions, and several well-defined soluble metallasiloxanes[4, 5] have been used to mimic and facilitate the understanding of the situation in solid materials, until now no molecular models have been reported for late transition metal catalysts supported on titania–silica. We previously reported[6] the synthesis of the complex $[Cp^*Ti(\mu_3\text{-}O)_3\{Rh(cod)\}_3]$ (cod = 1,5-cyclooctadiene, $Cp^* = \eta^5\text{-}C_5Me_5$), which can be regarded as a model of rhodium supported on titania. We have now extended our studies to modeling a rhodium complex supported on titania–silica. Here we report on the synthesis of the dimetallic titanium alkyl siloxide complexes $[\{Cp^*TiMe(O_2SiPh_2)\}_2]$ (**1**) and $[Cp^*Ti(O_2SiPh_2)_3TiCp^*]$ (**2**), which can be regarded as models for the above-mentioned titania–silica systems. The reaction of **1** with $[\{Rh(\mu\text{-}OH)(cod)\}_2]$ leads to the formation of $[\{Cp^*Ti(O_2SiPh_2)(\mu_3\text{-}O)Rh(cod)\}_2]$ (**3**), which can be regarded as an unprecedented molecular model of a late transition metal supported on titania–silica.

The titanium complex $[Cp^*TiMe_3]$ reacts with diphenylsilanediol to afford the yellow solid **1** (Scheme 1), which was isolated in good yield (76%) as a mixture of two isomers. By comparison with the previously reported analogous titanium

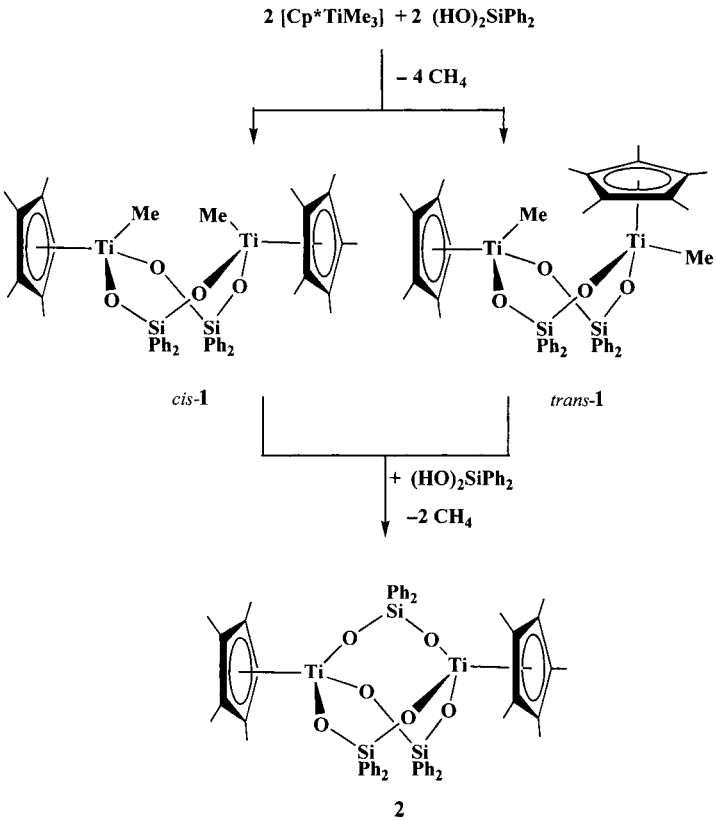

Scheme 1. Synthesis of **1** and **2**.

complexes,[7] we propose that **1** is a dimer in which the siloxide ligands act as bridges between two titanium atoms, and the two isomers are the *cis* and *trans* forms.[8] According to variable-temperature (VT) NMR experiments in $[D_8]$toluene, the ratio of the two isomers does not change up to 353 K. It is also independent of the concentration of the sample and the solvent ($[D_8]$toluene, C_6D_6, $CDCl_3$, $[D_8]$THF). According to

[*] Dr. R. Fandos, Dr. M. J. Ruiz
Departamento de Química Inorgánica, Orgánica y Bioquímica
Facultad de Ciencias del Medio Ambiente
Universidad de Castilla-La Mancha
Avda. Carlos III, s/n 45071 Toledo (Spain)
Fax: (+34) 926-25-53-18
Prof. Dr. A. Otero
Departamento de Química Inorgánica, Orgánica y Bioquímica
Facultad de Químicas, Universidad de Castilla-La Mancha
Campus de Ciudad Real, 13071 Ciudad Real (Spain)
Fax: (+34) 926-29-53-18
E-mail: aotero@qino-cr.uclm.es
Dr. A. Rodríguez
ETS Ingenieros Industriales, Universidad de Castilla-La Mancha
Avda. Camilo José Cela, 3, 13071 Ciudad Real (Spain)
Dr. P. Terreros
Instituto de Catálisis y Petroleoquímica, CSIC
Cantoblanco, 28049 Madrid (Spain)

[**] Financial support from the Dirección General de Enseñanza Superior e Investigación, Spain (Grant. No. D.G.E.S. PB98-0159-C02-01) is gratefully acknowledged. We thank Prof. Dr. J. L. G. Fierro, Instituto de Catálisis y Petroleoquímica, for XPS measurements.

  1433-7851/01/4015-2884 $ 17.50+.50/0

the ^{13}C NMR spectrum, the phenyl groups in the *trans* isomer are in the same chemical environment, while those in the *cis* isomer are not; this was to be expected in the case of conformationally flexible molecules. Reaction of *cis*-/*trans*-**1** with one equivalent of diphenylsilanediol in chloroform at 60 °C affords exclusively **2**, which was isolated as a yellow solid in 69 % yield (Scheme 1). Reaction of **1** with $[\{Rh(\mu\text{-}OH)(cod)\}_2]$[9] gave the heterometallic complex $[\{Cp^*Ti(O_2SiPh_2)(\mu_3\text{-}O)Rh(cod)\}_2]$ (**3**) [Eq. (1)]. It was isolated as a crystalline orange solid. The molecular structure of

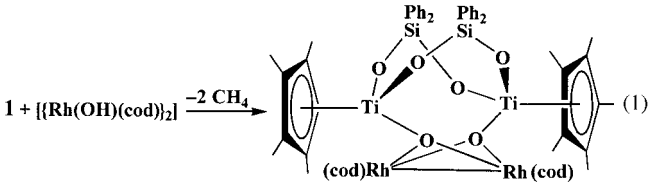

(1)

3

3 was determined by an X-ray diffraction study[10] and shows an eight-membered titanium-containing siloxane ring to which the two rhodium atoms are anchored by μ_3-oxo ligands (Figure 1). The geometry around the titanium atom is that of a

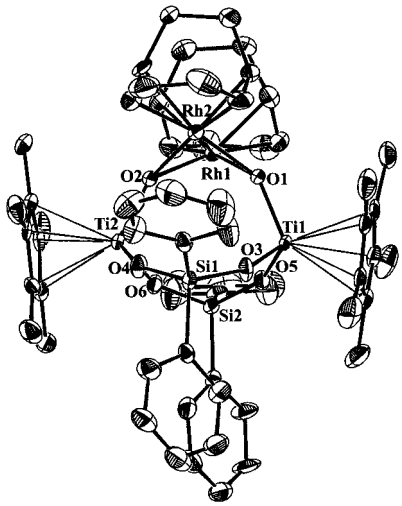

Figure 1. Structure of complex **2**. Selected bond lengths [Å] and angles [°]: Ti1-O1 1.796(6), Ti1-O3 1.847(6), Ti1-O5 1.860(6), Ti2-O2 1.784(6), Ti2-O4 1.846(6), Ti2-O6 1.863(6), Rh1-O1 2.135(6), Rh1-O2 2.145(6), Rh1-Rh2 2.746(1), Si1-O3 1.612(6), Si1-O4 1.625(6); O1-Rh1-O2 78.8(2), O1-Ti1-O3 104.5(3), Ti1-O1-Rh2 134.0(3), Ti1-O1-Rh1 125.1(3), Ti2-O2-Rh2 131.9(3), Ti2-O2-Rh1 130.7(3), Rh2-O1-Rh1 80.3(2).

distorted tetrahedron, and the rhodium atoms are in approximately square-planar environments. Distances from the titanium atom to the oxygen atoms bonded to the silicon are somewhat longer than those in $[\{Cp^*TiCl(O_2SiPh_2)\}_2]$,[7] while angles around the oxygen atoms are smaller, probably due to the more constrained geometry. The Rh1−Rh2 distance (2.746(1) Å) is short enough to propose a metal–metal bonding interaction,[11] while the Ti−Rh distances, which range between 3.491(2) and 3.608(3) Å, are so large that metal–metal interactions can be ruled out.[6]

The room-temperature ^{13}C and ^1H NMR spectra of complex **3** show that the two siloxane groups are in the same chemical environment, while the phenyl groups bonded to each silicon atom are different, in agreement with the structural data. On the other hand, both cod ligands are also equivalent. A ^1H VT-NMR experiment showed that these ligands are fluxional. At 291 K the spectrum contains two broad signals corresponding to the two different chemical environments for the olefinic protons of the cod ligand. At 297 K they coalesce, and the broad signal at higher temperatures points to rapid interchange. According to the spectra, no other ligand is involved in the interchange process. In agreement with these ^1H NMR data, both *cis*- and *trans*-**1** react with $Ph_2Si(OH)_2$ and $[\{Rh(\mu\text{-}OH)(cod)\}_2]$ at approximately the same rate to yield **2** and **3**, respectively. Hence, under the reaction conditions the *trans* isomer must undergo rearrangement to form these complexes. To explain this process we propose that the first step in the reaction of *trans*-**1** with diphenylsilanediol (Scheme 2) could be the protonolysis

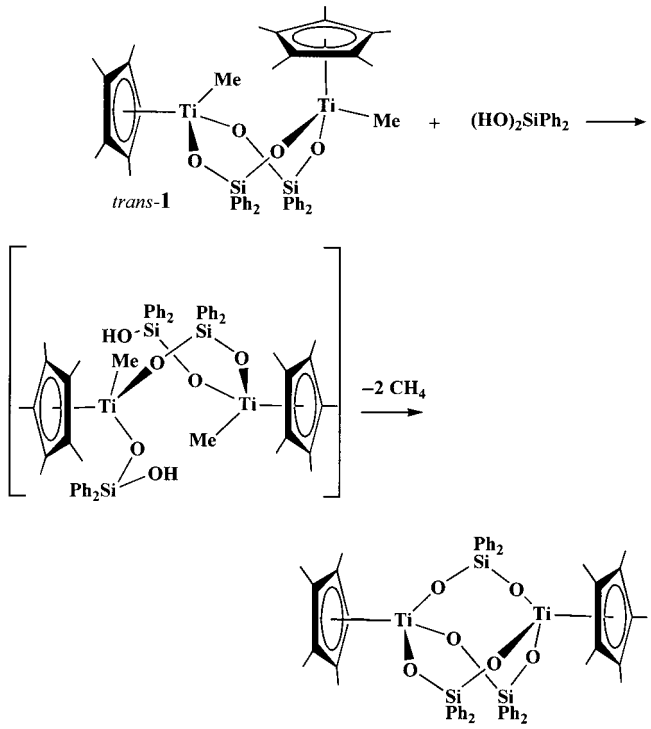

2

Scheme 2. Proposed steps in the synthesis of **2** from *trans*-**1**.

of a Ti−O bond to yield a $Ti(OSiPh_2OH)$ moiety that subsequently induces protonolysis of the Ti−Me bonds to give **2**. This implies the unusual preferential breaking of a Ti−O bond rather than a Ti−Me bond. However, it agrees with the proposal that the reactivity of Ti−O−Ti bonds toward H_2O or MeOH (or protonolysis in general) is responsible for the deactivation of titania–silica catalysts in oxidation reactions[12] and for the formation of inhomogeneous materials in sol–gel processes.[13] The formation of **3** by reaction of **1** with $[\{Rh(\mu\text{-}OH)(cod)\}_2]$ could be explained by the same reaction path. To prove that protonolysis of the

  1433-7851/01/4015-2885 $ 17.50+.50/0

Ti–O bond is a feasible step in the mechanism of formation of **2** and **3** from **1**, we treated **2** with an excess of [{Rh(μ-OH)(cod)}$_2$] in a NMR tube in C_6D_6 at 70 °C, and **3** was formed as the main product.

The FT-IR spectra show strong absorptions at 979 and 941 cm^{-1} for **1**, 994 and 935 cm^{-1} for **2**, and 974, 967, 941, and 923 cm^{-1} for **3**, which can be tentatively assigned to the Si-O-Ti stretching/bending modes. The features of the Ti-O-Si ring-breathing mode cannot be assigned unambiguously, because they overlap with characteristic absorptions of the phenyl groups between 750 and 700 cm^{-1}.[14] In **3**, the bands at 675 and 614 cm^{-1} can be ascribed to Ti-O-Rh. The Raman spectra show very weak bands for the Si-O-Ti groups in **1** and **2**, while in the spectrum of **3** this vibration mode is located at 953 cm^{-1}. The binding energy of the Ti $2p_{3/2}$ core level for **3** is 458.0 eV, which is 1.1 eV higher than that of [Cp*Ti(μ_3-O)$_3${Rh(cod)}$_3$]. This is consistent with the presence of Si-O-Ti moieties in which Si can withdraw electron density from Ti^{IV}.[1] The Rh $3d_{5/2}$ binding energy is 308.9 eV, in agreement with expected values for Rh^{I} complexes.[15]

In conclusion, we have described new dimetallic titanium alkyl siloxide complexes which can be considered as molecular models for titania–silica species, and a novel molecular model for a late transition metal supported on titania–silica. We are extending our work to prepare other late transition metal molecular models and to study their potential catalytic activity in epoxidation and oxidation processes.

Experimental Section

1: Diphenylsilanediol (0.257 g, 1.19 mmol) was added to a solution of [Cp*TiMe$_3$] (0.273 g, 1.19 mmol) in toluene (5 mL). After 1 h, the solvent was removed under vacuum and the residue extracted with pentane. The solvent was partially evaporated, and the solution was cooled to −30 °C overnight to yield **1** as a crystalline yellow solid. Yield: 0.373 g (76 %); IR (KBr): $\tilde{\nu}$ = 1428 (m), 1377 (w), 1120 (s), 1110 (s) 1030 (s), 998 (s), 979 (vs), 941 (vs), 887 (w), 740 (m), 713 (s), 700 (s), 516 cm^{-1} (s); ^{1}H NMR (200 MHz, $CDCl_3$): mixture of isomers (42 % *cis*, 58 % *trans*): δ = 0.48 (s, TiMe, *cis* isomer), 0.53 (s, TiMe, *trans* isomer), 1.70 (s, Cp*, *cis* isomer), 1.73 (s, Cp*, *trans* isomer), 7.29 (m, Ph, *cis* and *trans*), 7.49 (m, Ph, *cis* and *trans*); ^{13}C{^{1}H} NMR: *trans* isomer: δ = 12.2 (s, Cp*), 49.4 (s, TiMe), 123.4 (Cp*), 127.5 (s, Ph), 129.5 (s, Ph), 134.9 (s, Ph), 138.1 (s, *ipso*-C of Ph); *cis* isomer:δ = 12.2 (s, Cp*), 49.6 (s, TiMe), 123.2 (Cp*), 128.0 (s, Ph), 128.1 (s, Ph), 129.9 (s, Ph), 130.0 (s, Ph), 135.1 (s, Ph), 135.4 (s, Ph), 136.7 (s, *ipso*-C of Ph), 139.7 (s, *ipso*-C of Ph); elemental analysis (%) calcd for $C_{46}H_{56}O_4Si_2Ti_2$: C 66.98, H 6.84; found: C 66.34, H 6.80.

2: Diphenylsilanediol (0.084 g, 0.39 mmol) was added to a solution of **1** (0.320 g, 0.39 mmol) in chloroform (5 mL), and the solution was heated to 60 °C for 6 h. Then the solvent was removed under vacuum and the residue washed twice with pentane (3 mL) to yield **2** as a yellow solid. Yield: 0.273 g (69 %); IR (KBr): $\tilde{\nu}$ = 1428 (m), 1377 (w), 1123 (s), 1113 (s) 1027 (s), 1015 (s), 999 (s), 994 (vs), 935 (s), 907 (vs), 876 (s), 860 (m), 740 (m), 713 (m), 799 (s), 507 cm^{-1} (s); ^{1}H NMR (200 MHz, $CDCl_3$): δ = 1.93 (s, 30 H, Cp*), 7.08 (m, 12 H, Ph), 7.25 (m, 6 H, Ph), 7.42 (m, 12 H, Ph); ^{13}C{^{1}H} NMR: δ = 12.5 (s, Cp*), 126.6 (Cp*), 127.8 (s, Ph), 129.6 (s, Ph), 135.5 (s, Ph), 137.9 (s, *ipso*-C of Ph); elemental analysis (%) calcd for $C_{56}H_{60}O_6Si_3Ti_2$: C 66.65, H 5.99; found: C 66.42, H 6.15.

3 · 0.5 C_7H_8 · 0.25 C_5H_{12}: [{Rh(OH)(cod)}$_2$] (0.081 g, 0.18 mmol) was added to a solution of **1** (0.143 g, 0.18 mmol) in THF. The suspension was allowed to stand at room temperature for 24 h. The solvent was removed under vacuum and the residue extracted with toluene. Slow diffusion of pentane into the toluene solution yielded **3** as yellow crystals. Yield: 0.130 g (54 %); IR (KBr): $\tilde{\nu}$ = 1475 (w), 1448 (w), 1428 (w), 1374 (w), 1110 (s), 1030 (w), 998 (sh), 994 (s), 974 (vs), 967 (s), 957 (vs), 941 (s), 923 (vs), 891 (w), 868 (m), 775 (w), 744 (s), 737 (s), 700 (s), 682 (m), 675 (m), 614 (w), 515 (s), 504 cm^{-1} (m); ^{1}H NMR (200 MHz, C_6D_6): δ = 1.20 (br, 4 H, cod), 1.42 (br, 8 H, cod), 2.06 (s, 30 H, Cp*), 2.38 (br, 4 H, cod), 4.10 (br, 4 H, cod), 4.19 (br, 4 H, cod), 6.82 (m, 3 H, Ph), 7.43 (m, 5 H, Ph), 8.38 (m, 2 H, Ph); ^{13}C{^{1}H} NMR: δ = 12.51 (Cp*), 30.1 (br, cod) 31.2 (br, cod), 72, 3 (br, cod), 75.5 (br, cod), 122.1 (s, Cp*), 126.7 (s, Ph), 128.2 (s, Ph), 128.9 (s, Ph), 129.2 (s, Ph), 135.5 (s, Ph), 135.7 (s, Ph), 139.8 (s, Ph), 142. 21 (s, Ph); elemental analysis (%) calcd for $C_{64.75}H_{81}O_6Rh_2Si_2Ti_2$: C 59.24, H 6.21; found C 59.16, H 6.39.

Received: February 8, 2001 [Z 16581]

[1] X. Gao, I. E. Wach, *Catal. Today* **1999**, *51*, 233, and references therein.

[2] a) A. Voigt, R. Murugavel, M. L. Montero, H. Wessel, F.-Q. Liu, H. W. Roesky, I. Usón, T. Albers, E. Parisini, *Angew. Chem.* **1997**, *109*, 1020; *Angew. Chem. Int. Ed. Engl.* **1997**, *36*, 1001; b) B. Notari, *Catal. Today* **1993**, *48*, 163; c) G. Bellusi, M. S. Rigutto, *Stud. Surf. Sci. Catal.* **1994**, *85*, 177; d) R. Murugavel, H. W. Roesky, *Angew. Chem.* **1997**, *109*, 491; *Angew. Chem. Int. Ed. Engl.* **1997**, *36*, 477; e) M. C. Kunduk, T. Maschmeyer, J. M. Thomas, B. F. G. Johnson, *Chem. Eur. J.* **1999**, *5*, 1481; f) J. M. Thomas, *Chem. Eur. J.* **1997**, *3*, 1557; g) J. M. Thomas, *Angew. Chem.* **1999**, *111*, 3800; *Angew. Chem. Int. Ed.* **1999**, *38*, 3588; h) R. J. Saxton, *Top. Catal.* **1999**, *9*, 43.

[3] M. A. Cauqui, J. J. Calvino, G. Cifredo, L. Esquivias, J. M. Rodríguez-Izquierdo, *J. Non-Cryst. Solids* **1992**, *147/148*, 758.

[4] a) J. L. Bennet, P. T. Wolczanski, *J. Am. Chem. Soc.* **1997**, *119*, 10696; b) R. Murugavel, V. Chandrasekhar, H. W. Roesky, *Acc. Chem. Res.* **1996**, *29*, 183; c) R. Murugavel, A. Voigt, M. G. Walawalkar, H. W. Roesky, *Chem. Rev.* **1996**, *96*, 2205; d) J. M. Thomas, G. Sankar, M. C. Klunduk, M. P. Attfield, T. Maschmeyer, B. F. G. Johnson, R. G. Bell, *J. Phys. Chem. B* **1999**, *103*, 8809; e) A. I. Gouzyr, H. Wessel, C. E. Barnes, H. W. Roesky, M. Teichert, I. Usón, *Inorg. Chem.* **1997**, *36*, 3392.

[5] a) R. Duchateau, H. C. L. Abbenhuis, R. A. van Santen, A. Meetsma, S. K.-H. Thiele, M. F. H. van Tol, *Organometallics* **1998**, *17*, 5663; b) R. Duchateau, U. Cremer, R. J. Harmsen, S. I. Mohamud, H. C. L. Abbenhuis, R. A. van Santen, A. Meetsma, S. K.-H. Thiele, M. F. H. van Tol, M. Kranenburg, *Organometallics* **1999**, *18*, 5447; c) R. Duchateau, H. C. L. Abbenhuis, R. A. van Santen, S. K.-H. Thiele, M. F. H. van Tol, *Organometallics* **1998**, *17*, 5222; d) R. Duchateau, R. A. van Santen, G. P. A. Yap, *Organometallics* **2000**, *19*, 809; e) F. J. Feher, T. A. Budzichowski, *Polyhedron* **1995**, *14*, 3239.

[6] R. Fandos, J. L. G. Fierro, M. M. Kubicki, A. Otero, P. Terreros, M. A. Vivar-Cerrato, *Organometallics* **1995**, *14*, 2162.

[7] a) F. Q. Liu, H.-G. Schmidt, M. Noltemeyer, C. Freire-Erdbrügger, G. M. Sheldrick, H. W. Roesky, *Z. Naturforsch. B* **1992**, *47*, 1085; b) L. King, A. C. Sullivan, *Coord. Chem. Rev.* **1999**, *189*, 19.

[8] F.-Q. Liu, I. Usón, H. W. Roesky, *J. Chem. Soc. Dalton Trans.* **1995**, 2453.

[9] R. Usón, L. A. Oro, J. A. Cabeza, *Inorg. Synth.* **1985**, *23*, 126.

[10] X-ray crystal structure determination of **3**: Suitable crystals of **3** · 0.5 C_7H_8 · 0.25 C_5H_{12} were grown from toluene/pentane. A orange crystal of approximate dimensions 0.5 × 0.3 × 0.2 mm was mounted in a glass capillary. Intensity data were collected at 298 K on a NONIUS-MACH3 diffractometer with graphite-monochromated $Mo_{K\alpha}$ radiation (λ = 0.71073 Å) by using $\omega/2\theta$ scans up to a maximum value of 56°. The intensities of two representative reflections measured every hour did not change significantly during the course of data collection. The asymmetric unit contains one molecule of **3** · 0.5 C_7H_8 · 0.25 C_5H_{12}. Data were corrected for Lorentzian and polarization effects, and empirical absorption correction was not necessary (μ = 8.68 cm^{-1}). The structure was solved by direct methods (SIR92).[16] Refinement on F^2 was carried out by full-matrix least-squares techniques (SHELXL97).[17] All non-hydrogen atoms were refined with anisotropic thermal parameters. The hydrogen atoms were included in calculated position and were refined isotropically. Crystal data: $C_{60}H_{78}O_6Rh_2Si_2Ti_2$ · 0.5 C_7H_8 · 0.25 C_5H_{12}, M_r = 1313.10; monoclinic, space group *C*2, *a* = 22.054(5), *b* = 11.954(7), *c* = 23.265(4) Å, β = 91.67(2)°, *V* = 6131(4) Å^3, *Z* = 4, ρ_{calcd} = 1.423 g cm^{-3}; data/restraints/parameters: 14 784/5/678, final *R* indices: R_1 = 0.0557, wR_2 = 0.1648 for reflections with $I > 2\sigma(I)$, GOF: 1.183; max./min. residual electron density: 1.354/−1.120 e Å^{-3}. Crystallographic data (excluding structure factors) for the structure reported in this paper have been

  1433-7851/01/4015-2886 $ 17.50+.50/0

deposited with the Cambridge Crystallographic Data Centre as supplementary publication no. CCDC-156951. Copies of the data can be obtained free of charge on application to CCDC, 12 Union Road, Cambridge CB2 1EZ, UK (fax: (+44) 1223-336-033; e-mail: deposit@ccdc.cam.ac.uk).

[11] D. Selent, P. Pickardt, J. Claus, *J. Organomet. Chem.* **1994**, *468*, 131.

[12] a) G. Deo, A. M. Turek, I. E. Wachs, D. R. C. Huybrechts, P. A. Jacobs, *Zeolites* **1993**, *13*, 365; b) X. Gao, S. R. Bare, J. L. G. Fierro, M. A. Banares, I. E. Wachs, *J. Phys. Chem.* **1998**, *102*, 5653.

[13] a) D. Hoebbel, M. Nacken, H. Schmidt, V. Huch, M. Veith, *J. Mater. Chem.* **1998**, *8*, 171; b) F.-Q. Liu, H. W. Roesky, H. G. Schmidt, M. Noltemeyer, *Organometallics* **1992**, *11*, 2965.

[14] A. Haouidi-Mazzah, P. Dhamelincourt, J. Gnado, A. Mazzah, *J. Raman Spectrosc.* **1995**, *26*, 1027.

[15] a) C. Furlani, G. Mattogno, G. Polzonetti, G. Sbrana, G. Valentini, *J. Catal.* **1985**, *94*, 335; b) C. Furlani, G. Mattogno, G. Polzonetti, G. Braca, G. Valentini, *Inorg. Chim. Acta* **1983**, *69*, 199. c) S. L. T. Anderson, M. S. Scurrell, *J. Catal.* **1981**, *71*, 233.

[16] A. Altomare, G. Cascarano, C. Giacovazzo, A. Guagliardi, M. C. Burla, G. Polidori, M. Camalli, *J. Appl. Crystallogr.* **1994**, 435.

[17] G. M. Sheldrick, SHELXL97, Program for the Refinement of Crystal Structures from Diffraction Data, University of Göttingen, Göttingen, Germany, **1997**.

Methylenation of Aldehydes: Transition Metal Catalyzed Formation of Salt-Free Phosphorus Ylides**

Hélène Lebel,* Valérie Paquet, and Caroline Proulx

Among the olefination processes,[1] the methylenation of carbonyl derivatives is a very important transformation in synthesis.[2] Recently even more attention has been devoted to this reaction since terminal alkenes are ideal precursors for ring-closing metathesis reactions.[3] Although the Wittig reaction has been quite reliable for performing this transformation, several drawbacks are still associated with it. The most important problems include the low reactivity of the reagent with sterically hindered carbonyl derivatives as well as the possible epimerization of base-sensitive substrates.[4] Several systems employing stoichiometric amounts of organometallic reagents have been developed to overcome these problems. For example, organometallic compounds based on titanium (Tebbe/Petasis) and zinc (Oshima/Lombardo) provide efficient methylenation of numerous carbonyl substrates.[5] However, the use of stoichiometric amounts of expensive and in some cases pyrophoric compounds, as well as the competitive reductive coupling of aldehydes observed with these reagents,[6] are undesired factors and indicate that there is still a significant need to develop new reagents to carry out this transformation. Few approaches to transition metal catalyzed olefinations have been disclosed, but they are all limited to the synthesis of α,β-unsaturated esters.[7, 8]

Numerous methods for the preparation of phosphorus ylides by deprotonation of phosphonium salts with a base have been reported.[9] Conversely, sulfur, oxonium, nitrogen, carbonyl, and thiocarbonyl ylides have been successfully prepared from diazo compounds with the use of transition metal catalysts.[10] However, with the exception of one report by Fujimura and Honma on the use of diazoacetate precursors,[11] such a strategy has never been applied to the preparation of phosphorus ylides. Here we disclose the first transition metal catalyzed methylenation of aldehydes, based on the synthesis of salt-free phosphorus ylides from diazo reagents.

In principle, the generation of $Ph_3P{=}CH_2$ (**1**) requires the use of CH_2N_2 as the diazo precursor (Scheme 1). Our first attempts at the methylenation of cinnamaldehyde (**3**) with

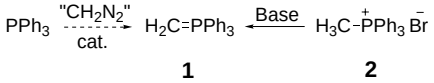

Scheme 1. Generation of **1**.

CH_2N_2 using $[RuCl(NO)(PPh_3)_2]$ as the catalyst were very disappointing (Table 1, entries 1, 2). No alkene product was observed, although $[RuCl(NO)(PPh_3)_2]$ is known to produce stable carbene species in the presence of CH_2N_2.[12] We also investigated $TMSCHN_2$ (TMS = trimethylsilyl) as a safer alternative to CH_2N_2, since $Ph_3P{=}CHTMS$ can be rapidly desilylated in the presence of an alcohol to generate the corresponding salt-free phosphorus methylide.[13, 14] The methylenation of **3** proceeded smoothly with $TMSCHN_2$ in the presence of PPh_3 and $[RuCl(NO)(PPh_3)_2]$. In the absence of an alcohol, diene **4** was produced quantitatively in 16 h (entry 3). In contrast, conversion was quantitative after 2 h when one equivalent of 2-propanol was added (entry 4). For comparison, only 45% conversion was observed for the formation of α,β-unsaturated ester **5** under similar conditions with ethyl diazoacetate (EDA, entry 5). We then surveyed various catalysts for the methylenation of **3** with $TMSCHN_2$, PPh_3, and 2-propanol. Many ruthenium and rhodium complexes effectively catalyzed the methylenation with $TMSCHN_2$ and 2-propanol, whereas low activity was often observed with EDA. The best catalytic activity was observed with Wilkinson's catalyst, $[RhCl(PPh_3)_3]$, which allowed the quantitative conversion of **3** into diene **4** within 30 min at 25 °C with $TMSCHN_2$ (entry 14). Again, the combination of $TMSCHN_2$ and 2-propanol proved to be superior to CH_2N_2 and EDA (entries 12, 13). Under similar conditions, $[\{Rh(OAc)_2\}_2]$ was inefficient at catalyzing the olefination of **3** (entries 23, 24).

The catalyst loading could be lowered to 2.5 mol% with no detrimental effect on the activity when $[RhCl(PPh_3)_3]$ was

[*] Prof. H. Lebel, V. Paquet, C. Proulx
Département de chimie
Université de Montréal
P.O. Box 6128, Station Downtown
Montréal, Québec, H3C 3J7 (Canada)
Fax: (+1) 514-343-2177
E-mail: lebelhe@chimie.umontreal.ca

[**] We thank the Charette group (Université de Montréal) for generously sharing their chemicals and equipment. This research was supported by NSERC (Canada), F.C.A.R (Québec), the Foundation for Innovation, and the Université de Montréal.

Supporting information for this article is available on the WWW under http://www.angewandte.com or from the author.

  1433-7851/01/4015-2887 $ 17.50+.50/0

Table 1. The effect of the catalyst on the olefination of **3**.

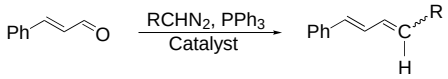

3 R = H (**4**), CO_2Et (**5**)

Entry	Catalyst[a]	Diazo compound	Conditions	Conv. [%][b] (product)
1	$[RuCl(NO)(PPh_3)_2]$	CH_2N_2	THF, 50 °C, 16 h	≤ 5
2	$[RuCl(NO)(PPh_3)_2]$	CH_2N_2	benzene, 50 °C, 16 h	≤ 5
3	$[RuCl(NO)(PPh_3)_2]$	$TMSCHN_2$	THF, 50 °C, 16 h	≥ 98 (**4**)
4	$[RuCl(NO)(PPh_3)_2]$	$TMSCHN_2$	THF/*i*PrOH, 50 °C, 2 h	≥ 98 (**4**)
5	$[RuCl(NO)(PPh_3)_2]$	EDA	THF, 50 °C, 16 h	45 (**5**)
6	$[RuCl_2(PPh_3)_3]$	$TMSCHN_2$	THF/*i*PrOH, 50 °C, 16 h	≥ 98 (**4**)
7	$[RuCl_2(PPh_3)_3]$	EDA	THF, 50 °C, 8 h	92 (**5**)[c]
8	$[Ru(NO)_2(PPh_3)_2]$	$TMSCHN_2$	THF/*i*PrOH, 50 °C, 16 h	90 (**4**)
9	$[Ru(NO)_2(PPh_3)_2]$	EDA	THF, 50 °C, 16 h	≤ 5
10	$[RuClCp(PPh_3)_2]$	$TMSCHN_2$	THF/*i*PrOH, 50 °C, 16 h	90 (**4**)
11	$[RuClCp(PPh_3)_2]$	EDA	THF, 50 °C, 16 h	40 (**5**)
12	$[RhCl(PPh_3)_3]$	CH_2N_2	THF, 25 °C, 16 h	60 (**4**)
13	$[RhCl(PPh_3)_3]$	EDA	THF, 25 °C, 16 h	60 (**5**)
14	$[RhCl(PPh_3)_3]$	$TMSCHN_2$	THF/*i*PrOH, 25 °C, 0.5 h	≥ 98 (**4**)
15	$[RhCl(PPh_3)_3]$[d]	$TMSCHN_2$	THF/*i*PrOH, 25 °C, 0.5 h	≥ 98 (**4**)
16	$[RhCl(PPh_3)_3]$	$TMSCHN_2$	THF/*i*PrOH, 0 °C, 16 h	31 (**4**)
17	$[RhCl(PPh_3)_3]$	$TMSCHN_2$	THF/MeOH, 25 °C, 0.5 h	78 (**4**)
18	$[RhCl(PPh_3)_3]$	$TMSCHN_2$	THF/EtOH, 25 °C, 0.5 h	87 (**4**)
19	$[RhCl(PPh_3)_3]$	$TMSCHN_2$	THF/*t*BuOH, 25 °C, 0.5 h	16 (**4**)
20	$[RhCl(PPh_3)_3]$	$TMSCHN_2$	CH_2Cl_2/*i*PrOH, 25 °C, 1 h	≥ 98 (**4**)
21	$[RhCl(PPh_3)_3]$	$TMSCHN_2$	Et_2O/*i*PrOH, 25 °C, 5 h	≥ 98 (**4**)
22	$[RhCl(PPh_3)_3]$	$TMSCHN_2$	toluene/*i*PrOH, 25 °C, 16 h	≥ 98 (**4**)
23	$[\{Rh(OAc)_2\}_2]$	EDA	THF, 25 °C, 16 h	≤ 5
24	$[\{Rh(OAc)_2\}_2]$	$TMSCHN_2$	THF/*i*PrOH, 25 °C, 16 h	≤ 5

[a] Catalyst: 5 mol %. [b] Determined by gas chromatography (GC). [c] Yield of isolated product, see reference [11]. [d] Catalyst: 2.5 mol %. EDA = ethyl

used with $TMSCHN_2$ and 2-propanol (Table 1, entry 15). Below this concentration, the reaction did not go to completion. Only 31 % conversion was observed when the reaction was carried out at 0 °C, (entry 16). 2-Propanol was the best alcohol surveyed (entries 14 vs 17 – 19). Although THF was the most effective solvent, equally high conversions were obtained in dichloromethane, diethyl ether, and toluene, but longer reaction times were required (entries 20 – 22).

The reaction conditions used were quite general (Table 2). In all cases, terminal alkenes were isolated in excellent yields. Methylenation of the aromatic aldehyde **12** produced the styrene derivative **13** in 60 % yield (entry 5). This result is impressive since the highest yield reported so far for the synthesis of **13** was only 33 % using Lombardo's reagent.[4f] The sterically hindered aldehyde **14** reacted smoothly to produce alkene **15** in 79 % yield (entry 6). In contrast, **15** was isolated in only 40 % and 50 % yield when **1** was generated from **2** upon reaction with PhLi or sodium 1,1,1,3,3,3-hexamethyldisilazane (NaHMDS), respectively (see Scheme 1).[15]

The reaction can be performed in the presence of secondary amides (Table 2, entry 5), enolizable ketones (entry 7), or epoxides (entry 8), and a wide variety of protecting groups are compatible (silyl and benzyl ethers, acetonides, carbamates). The reaction with aldehyde **16** was highly chemoselective and resulted in the exclusive formation of **17** in 87 % yield (entry 7). For comparison, alkene **17** was isolated in only 59 % yield, along with product **28** in 15 – 20 % yield, when **16** was treated with **1** generated by deprotonation of **2** with

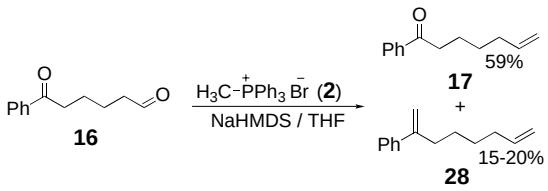

(1)

NaHMDS [Eq. (1)]. The new reaction conditions are mild and nonbasic, thus chiral nonracemic α-substituted aldehydes react without epimerization. The Garner's aldehyde **24** (93 % *ee*) was converted into **25** in 86 % yield and with 93 % *ee* (entry 11). Finally, aldehyde **26** afforded the terminal alkene **27** in 89 % yield while maintaining the stereochemical integrity of the adjacent chiral center (entry 12). These observations are in sharp contrast to the results obtained with non-lithium-free phosphorus ylides.[4]

In contrast to the reported methods of olefination based on decomposition of transition metal diazo compounds, it seems unlikely that the current reaction proceeds through a metal carbene intermediate. No reaction was observed when **3** was treated with the preformed metal carbene $[CH_2{=}RuCl(NO)(PPh_3)_2]$ obtained from CH_2N_2 and $[RuCl(NO)(PPh_3)_2]$.[12] In addition, no carbene was detected by spectroscopic methods when $TMSCHN_2$ and 2-propanol were added to $[RuCl(NO)(PPh_3)_2]$. Rhodium(II) acetate, known for producing metal carbenes with diazo compounds, was inefficient at catalyzing the olefination reaction at room temperature. Finally, it is known that diazo compounds react with Rh^I

  1433-7851/01/4015-2888 $ 17.50+.50/0

Table 2. The Rh-catalyzed methylenation of aldehydes.

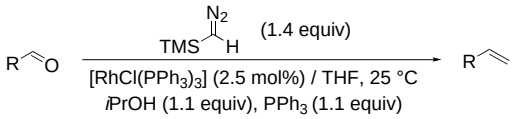

Entry	Substrate	Product	t [h]	Yield [%][a]
1	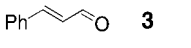 **3**	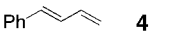 **4**	0.5	88
2	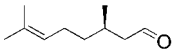 **6**	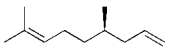 **7**	7	84
3	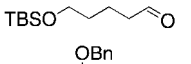 **8**	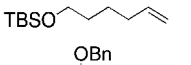 **9**	8	91
4	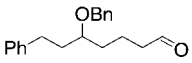 **10**	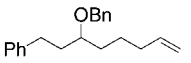 **11**	1	98
5	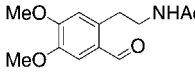 **12**	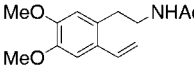 **13**	0.5	60
6	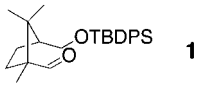 **14**	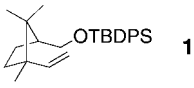 **15**	7	79
7	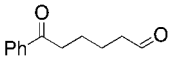 **16**	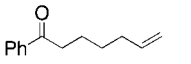 **17**	0.5	87
8	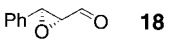 **18**	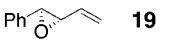 **19**	1	86
9	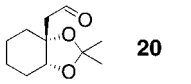 **20**	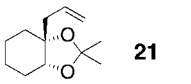 **21**	1.5	79
10	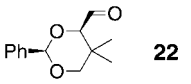 **22**	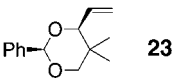 **23**	5	74
11	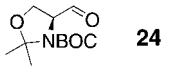 **24**	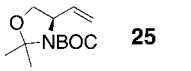 **25**	4	86
12	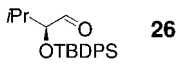 **26**	 **27**	3	89

[a] Yield of isolated product.

through nitrogen complexation and the adduct does not produce carbene species.[16] The proposed catalytic cycle involves the activation of the $TMSCHN_2$ by $[RhCl(PPh_3)_3]$ through nitrogen complexation. Nucleophilic attack by PPh_3 followed by desilylation (mediated by 2-propanol) and nitrogen extrusion leads to the formation of $Ph_3P{=}CH_2$ (**1**) and regeneration of the catalyst. The formation of **1** was confirmed by ^{31}P NMR spectroscopy when $TMSCHN_2$ (1.0 equiv) was mixed with PPh_3 (1.0 equiv), 2-propanol (1.0 equiv), and $[RhCl(PPh_3)_3]$ (2.5 mol%).

In conclusion, we have developed the first Rh^I-catalyzed methylenation of aldehydes using readily available reagents. The conditions are mild enough to be compatible with sensitive and enolizable substrates, thus highlighting the nonbasic character of phosphorus ylides in the absence of an inorganic component.

Experimental Section

Representative procedure: To a solution of $[RhCl(PPh_3)_3]$ (0.023 g, 0.025 mmol) and PPh_3 (0.577 g, 2.20 mmol) in THF (10 mL) was added 2-propanol (0.15 mL, 2.00 mmol) followed by the substrate (2.00 mmol). $TMSCHN_2$ (1.75 mL, 2.80 mmol) was added to the resulting red mixture. Immediate gas evolution was observed, and the mixture was stirred at room temperature. Extraction and subsequent purification by flash chromatography provide the desired alkene.

Received: February 21, 2001
Revised: May 7, 2001 [Z16654]

[1] a) J. M. J. Williams, *Preparation of Alkenes: A Practical Approach*, Oxford University Press, Oxford, UK, **1996**; b) B. E. Maryanoff, A. B. Reitz, *Chem. Rev.* **1989**, *89*, 863–927; c) E. Vedejs, M. J. Peterson in *Topics in Stereochemistry*, *Vol. 21*, **1994**, pp. 1–157; d) K. C. Nicolaou, M. W. Harter, J. L. Gunzner, A. Nadin, *Liebigs Ann.* **1997**, 1283–1301.

[2] S. E. Kelly in *Comprehensive Organic Synthesis*, *Vol. 1* (Eds.: B. M. Trost, I. Fleming, S. L. Schreiber), Pergamon, Oxford, **1991**, p. 729.

[3] a) L. Ackermann, D. El Tom, A. Furstner, *Tetrahedron* **2000**, *56*, 2195–2202; b) T. M. Trnka, R. H. Grubbs, *Acc. Chem. Res.* **2001**, *34*, 18–29; c) A. Fürstner, *Angew. Chem.* **2000**, *112*, 3140–3172; *Angew. Chem. Int. Ed.* **2000**, *39*, 3013–3043.

[4] For selected examples of methylenations of aldehydes, see a) M. Ito, C. Kibayashi, *Synthesis* **1993**, 137–140; b) E. Van der Eycken, D. De Keukeleire, A. De Bruyn, *Tetrahedron Lett.* **1995**, *36*, 3573–3576; c) R. M. Moriarty, H. Brumer, *Tetrahedron Lett.* **1995**, *36*, 9265–9268; d) H. Ina, M. Ito, C. Kibayashi, *J. Org. Chem.* **1996**, *61*, 1023–1029; e) J. M. Devaux, J. Gore, J. M. Vatele, *Tetrahedron: Asymmetry* **1998**, *9*, 1619–1626; f) T. Wirth, G. Fragale, *Synthesis* **1998**, *2*, 162–166; g) M. Sasaki, M. Inoue, K. Takamatsu, K. Tachibana, *J. Org. Chem.* **1999**, *64*, 9399–9415.

[5] a) S. H. Pine, *Org. React.* **1993**, *43*, 1–91; b) J. R. Stille in *Comprehensive Organometallic Chemistry II: A Review of the Literature*

  1433-7851/01/4015-2889 $ 17.50+.50/0

1982–1994, *Vol. 12* (Eds.: E. W. Abel, F. G. A. Stone, G. Wilkinson), Pergamon, Oxford, UK, **1995**, pp. 577–600.
[6] J. McMurry, *Chem. Rev.* **1989**, *89*, 1513–1524.
[7] a) W. A. Herrmann, P. W. Roesky, M. Wang, W. Scherer, *Organometallics* **1994**, *13*, 4531–4535; b) W. A. Herrmann, M. Wang, *Angew. Chem.* **1991**, *103*, 1709–1711; W. A. Herrmann, M. Wang, *Angew. Chem. Int. Ed. Engl.* **1991**, *30*, 1641–1643.
[8] a) B. E. Ledford, E. M. Carreira, *Tetrahedron Lett.* **1997**, *38*, 8125–8128; b) X. Y. Lu, H. Fang, Z. J. Ni, *J. Organomet. Chem.* **1989**, *373*, 77–84; c) Y. Liao, Y. Z. Huang, *Tetrahedron Lett.* **1990**, *31*, 5897–5900; d) Z. L. Zhou, Y. Z. Huang, L. L. Shi, *Tetrahedron* **1993**, *49*, 6821–6830.
[9] A. W. Johnson, *Ylides and Imines of Phosphorus*, Wiley, New York, **1993**.
[10] a) V. K. Aggarwal, H. Abdelrahman, R. V. H. Jones, H. Y. Lee, B. D. Reid, *J. Am. Chem. Soc.* **1994**, *116*, 5973–5974; b) V. K. Aggarwal, *Synlett* **1998**, 329–336, and references therein; c) V. K. Aggarwal, J. G. Ford, S. Fonquerna, H. Adams, R. V. H. Jones, R. Fieldhouse, *J. Am. Chem. Soc.* **1998**, *120*, 8328–8339; d) M. P. Doyle, D. C. Forbes, *Chem. Rev.* **1998**, *98*, 911–935; e) M. P. Doyle, M. A. McKervey, T. Ye, *Modern Catalytic Methods for Organic Synthesis with Diazo Compounds: From Cyclopropanes to Ylides*, Wiley, New York, **1998**.
[11] O. Fujimura, T. Honma, *Tetrahedron Lett.* **1998**, *39*, 625–626.
[12] A. K. Burrell, G. R. Clark, C. E. F. Rickard, W. R. Roper, A. H. Wright, *J. Chem. Soc. Dalton Trans.* **1991**, 609–614.
[13] a) H. Schmidbaur, *Acc. Chem. Res.* **1975**, *8*, 62–70, and references therein; b) E. Vedejs, G. R. Martinez, *J. Am. Chem. Soc.* **1979**, *101*, 6452–6454; c) E. Vedejs, F. G. West, *Chem. Rev.* **1986**, *86*, 941–955.
[14] The reaction of $TMSCHN_2$ with an alcohol does not produce CH_2N_2: a) N. Hashimoto, T. Aoyama, T. Shioiri, *Chem. Pharm. Bull.* **1981**, *29*, 1475–1478; b) T. Shioiri, T. Aoyama, S. Mori, *Org. Synth.* **1990**, *68*, 1–7.
[15] H. Lébèl, V. Paquet, unpublished results.
[16] a) P. Schwab, N. Mahr, J. Wolf, H. Werner, *Angew. Chem.* **1993**, *105*, 1498–1500; *Angew. Chem. Int. Ed. Engl.* **1993**, *32*, 1480–1482; b) H. Werner, P. Schwab, E. Bleuel, N. Mahr, P. Steinert, J. Wolf, *Chem. Eur. J.* **1997**, *3*, 1375–1384.

Carbanions Substituted by Transition Metals: Synthesis, Structure, and Configurational Restrictions of a Lithium Titanium Phosphonate

Jürgen F. K. Müller,* Klaus J. Kulicke, Markus Neuburger, and Martin Spichty

Lithium "carbanions" that are stabilized by transition metals represent a new class of organodimetallic reagents in which an acceptor-substituted anionic C atom is directly connected to a transition metal.[1] Such compounds are expected to possess properties that differ from those of ordinary acceptor-stabilized lithium compounds. In principle, multiple C–C bond-forming reactions are possible by the subsequent addition of various electrophiles, while the reactivity of the anionic C atom and its configurational stability could be directed by the steric and electronic impact of the transition metal.[2] Our main goal is the design and development of chirally modified organodimetallic reagents that facilitate highly stereoselective asymmetric transformations. Recently, we reported on the structure determination of a lithiated titanium sulfone, an intermediate that occurs in the *E*-selective olefination of aldehydes.[1, 3] As part of our program for the exploration and structure determination of new chiral organodimetallic compounds, we have synthesized a lithiated titanium phosphonate, determined its solid-state structure by X-ray analysis, and compared the experimental data with the results of density functional theory (DFT) calculations on a model system.[4, 5]

Dilithiation of dimethyl (trimethylsilylmethyl)phosphonate **1** with 2.2 equivalents of *n*BuLi in diethyl ether in the presence of a trace of water, followed by addition of $[TiCl(OiPr)_3]$ and removal of LiCl by filtration gave the lithium titanium phosphonate **3** as green crystals in 48% yield.[6] Figure 1 depicts a C3D plot of the aggregate **3**.

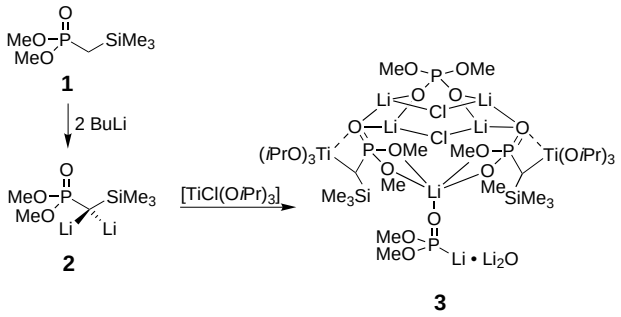

Compound **3** contains two monolithiated titanium phosphonate units together with two LiCl, Li_2O, lithiated

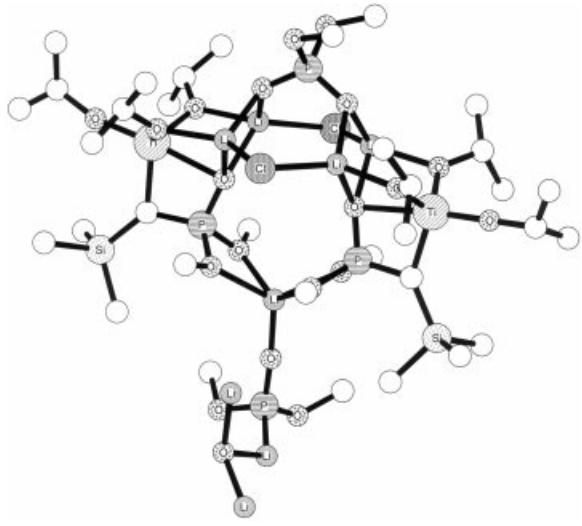

Figure 1. Molecular structure of **3**. Hydrogen atoms are omitted for clarity.

[*] Priv.-Doz. Dr. J. F. K. Müller, M. Neuburger
University of Basel
Institute of Inorganic Chemistry
Spitalstrasse 51, 4056 Basel (Switzerland)
Fax: (+41) 61-267-10-18
E-mail: juergen.mueller@unibas.ch
Dr. K. J. Kulicke, M. Spichty
University of Basel
Institute of Organic Chemistry
St.-Johanns-Ring 19, 4056 Basel (Switzerland)

  1433-7851/01/4015-2890 $ 17.50+.50/0

dimethylphosphonate, and lithiated dimethylphosphate as additional bridging ligands. The center of the aggregate is an eight-membered (Li-O-Li-Cl)$_2$ ring that serves as an aggregation nucleus for crystallization.[1] Each terminal phosphonate oxygen atom bridges two lithium atoms of this ring. The two methoxyl oxygen atoms of the phosphonate ester units coordinate to an external Li cation, and together with an additional oxygen atom of a dimethylphosphonate ligand, they result in a distorted square-pyramidal coordination sphere. The phosphonate unit itself is characterized by a P–Li bond and the complexation of a Li_2O molecule. The presence of Li_2O is crucial for the crystallization of **3**. We were unable to grow suitable crystals of **3** in the absence of H_2O; however, the strong disorder of the Li_2O molecules caused a moderate quality of the crystal structure analysis.[4] The eight-membered (Li-O-Li-Cl)$_2$ ring is capped by a bridging dimethylphosphate ligand—a decomposition product of a dilithiation–titanation sequence—to give a cage-type structure.[7] The titanated phosphonate moieties form a characteristic four-membered Ti-C-P-O chelate ring, a structural feature very similar to that in a lithium titanium sulfone.[1] The titanated anionic C_α atom has an essentially planar coordination sphere (sum of angles at C_α: 359.9°) and is devoid of C–Li contacts, as is typical for monolithiated phosphonates.[7] Accordingly, the electron lone pairs occupy a p orbital perpendicular to the P-C-Ti plane, an ideal orientation for stabilizing hyperconjugative interaction of the lone-pair orbital with the σ* orbitals of the P–O(phosphate ester) bonds [$n_C - \sigma^*(PO)$]. The Ti atoms are pentacoordinate with a distorted trigonal-bipyramidal geometry. The pseudoequatorial positions are occupied by two 2-propanolate O atoms and the C_α atom. The oxygen atom of the remaining 2-propanolate group and the phosphonate oxygen atom occupy the axial positions (O(*i*Pr)-Ti-O(phosphonate) 175.5(4)°). The Ti–C_α bond length in **3** of 2.01 Å is intermediate between normal Ti–C single bonds, as in a related titanated sulfone (2.174(4) Å), and those in titanium alkylidene complexes (2.008(4) Å).[8, 9] The P–C bond length of 1.64(1) Å is also significantly shortened after anionization and transmetalation relative to unmetalated phosphonates.[7] The additional complexation of the titanium atom by the terminal phosphonate oxygen atom results in a rather long Ti–O bond length of 2.302(8) Å, which compares to 1.883(8)–1.758(9) Å for the Ti–O bonds involving the alkoxyl O atoms and implies a relatively weakly bound Ti atom.

^{1}H, ^{13}C, ^{7}Li, and ^{31}P NMR spectra were recorded in [D_8]THF to gain some information on the solution structure of **3**. Whereas the ^{1}H NMR spectrum showed only very broad signals, the ^{13}C NMR spectrum revealed significant changes in chemical shift on metalation. The most dramatic effect was observed for the C_α signal, which shifted downfield to $\delta =$ 148.8 ($\Delta\delta = 135$). For comparison, the ^{13}C chemical shift of the C_α carbon of a monotitanated sulfone is $\delta = 52.4$, in contrast to a titanium carbene complex with $\delta = 191$.[3b, 9] The increase of 23 Hz in the J(C,P) coupling constant is a strong indication for a C_α atom with sp^2 character. We therefore conclude that a carbene-like Ti–C_α double bond is not present in solution and that the sp^2 character of the C_α atom in the Ti–C_α bond is responsible for the large downfield shift. The ^{31}P NMR spectrum exhibits two sharp signals at $\delta = 52.6$ and 38.6, as well as two broad signals at $\delta = 29.1$ and 25.9 that suggest a dynamic exchange phenomenon. Therefore, we cannot draw conclusions about the state of aggregation in solution, but it is reasonable to assume that the LiCl formed in situ may act as a template for aggregation.

To obtain deeper insight into the structure of **3**, we carried out DFT calculations (B3LYP) on the titanated carbanionic model system **4**, devoid of Li cations.[5] The calculated

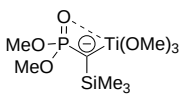

4

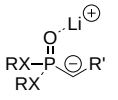

5, X = O, N

structure agrees very well with the X-ray crystal structure of **3**: the typical planar four-membered Ti-C-P-O(phosphonate) ring represents a minimum on the potential energy surface. The dihedral Ti-C-P-O angle of 3.9° resembles that of about 1° in the crystal. The Ti–C (2.065 Å vs 2.00(1) Å and 2.01(1) Å) and P–C bond lengths (1.667 Å vs 1.65(1) Å and 1.64(1) Å) are marginally longer than in the solid state. Especially the short Ti–C bond suggests significant hyperconjugative stabilization of the anionic charge by the titanium atom. The angles around the titanium atom are also similar to those in the solid state. Our special focus lies on the configurational stability of these titanium-substituted "carbanions", which might be a serious concern for stereoselective transformations. In phosphoryl-stabilized anions of type **5**, the interaction of the C_α lone-pair orbital with the σ* orbitals of the P–X bonds is crucial for the configurational stability: it increases the energy barrier for rotation about the C_α–P bond.[7] However, the barrier is only 6–8 kcal mol^{-1}, which is insufficient to prevent rotation, even at low temperature. Hence, the question arises to what extent the additional chelation of the titanium atom by the phosphonate oxygen atom in **3** enhances the configurational stability. Therefore, we calculated the energy profile of the rotation around the C_α–P bond in **4** (Figure 2), starting at the calculated minimum-energy conformation described above (**4A**). Rotation around the C_α–P bond by 60° leads to the maximum **4B**, about 6.5 kcal mol^{-1} higher in energy than **4A**. Further rotation yields the two minima **4C** and **4D**, both about 4 kcal mol^{-1} less stable than **4A**. According to this profile, a substantial increase of the configurational stability of **3** relative to phosphoryl-stabilized lithium carbanions cannot be expected. A reason for this might be the competing interaction of the empty titanium valence shell orbitals with the C_α lone-pair orbital, which is also consistent with the short Ti–C bond.[10]

We have described a new general route to heterodimetallic compounds by means of a dilithiation–transmetalation sequence. The resulting intermediate **3** can be regarded as a titanium-stabilized lithium compound, with potential application as a chemo- and stereoselective bis-electrophile in C–C bond-forming reactions. We are investigating soft transition metals such as zinc or copper to induce higher configurational stability.

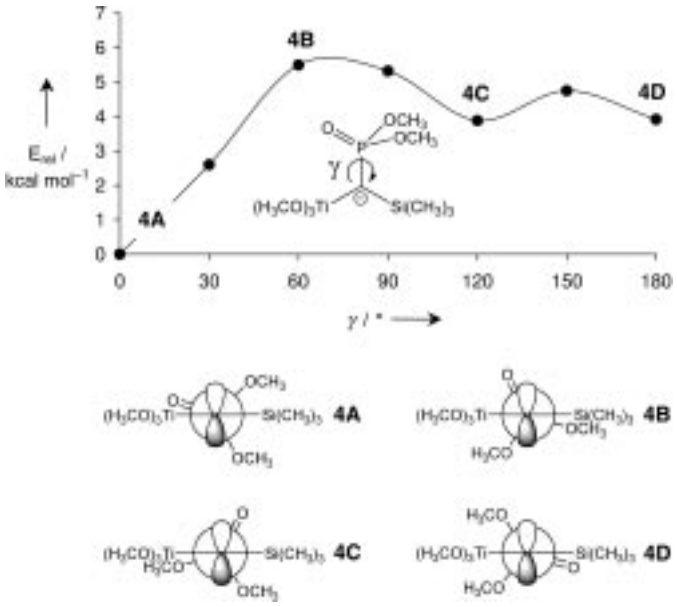

Figure 2. Energy profile for rotation about the C_α–P bond in **4**.

Experimental Section

3: A solution of **1** (100 mg, 0.51 mmol) in diethyl ether (2 mL) and H_2O in diethyl ether (0.45 mL, 0.11 M, 0.05 mmol) was treated with *n*BuLi in hexane (0.79 mL, 1.58 M, 1.25 mmol) at $-78\,^\circ$C. Stirring for 2 h at $0\,^\circ$C was followed by addition of a solution of [TiCl(O*i*Pr)$_3$] (132 mg, 0.51 mmol) in diethyl ether (2 mL). After filtration of the turbid solution, the remaining liquid was concentrated in vacuo and stored for 24 h at $-20\,^\circ$C until green crystals of **3**, suitable for X-ray analysis, had formed (112 mg, 48 %).

^{1}H NMR (500 MHz, [D$_8$]THF, 25 °C): $\delta = -0.02 - 0.29$ (br s, 9H, SiMe$_3$), 0.74 – 1.62 (m, 18H, O*i*Pr), 3.45 – 3.56 (m, 2H, O*i*Pr), 3.65 – 3.81 (m, 1H, O*i*Pr), 4.60 – 4.78 (m, 3H); ^{13}C NMR (125 MHz, [D$_8$]THF, 25 °C): $\delta = -3.01, -2.65, -2.45, -2.13, -2.02, 8.59, 11.45, 13.96, 14.08, 14.35, 24.28, 24.44, 24.59, 24.75, 26.54, 26.86, 32.16, 51.38, 51.71, 63.90, 69.69, 72.40, 72.84, 73.29, 73.64, 73.78, 74.11, 75.98, 77.43, 148.8$ (d, J(C,P) = 154 Hz); ^{31}P NMR (202 MHz, [D$_8$]THF, 25 °C, (PhO)$_3$PO): $\delta = 52.64, 37.12, 29.13, 25.96$; ^{7}Li NMR (194 MHz, [D$_8$]THF, 25 °C, LiCl): $\delta = 1.65$.

Received: January 24, 2001
Revised: May 14, 2001 [Z16496]

[1] J. F. K. Müller, M. Neuburger, H.-P. Weber, *J. Am. Chem. Soc.* **1999**, *121*, 12212 – 12213.

[2] a) I. Marek, J.-F. Normant, *Chem. Rev.* **1996**, *96*, 3241 – 3267; b) C. M. Thomson in *Dianion Chemistry in Organic Synthesis*, CRC, Boca Raton, FL, **1994**, pp. 1 – 250.

[3] a) For a review, see J. F. K. Müller, *Eur. J. Inorg. Chem.* **2000**, 789 – 799; b) H.-J. Gais, R. Hainz, H. Müller, P. R. Bruns, N. Giesen, G. Raabe, J. Runsink, S. Nienstedt, J. Decker, M. Schleusner, J. Hachtel, R. Loo, C.-W. Woo, P. Das, *Eur. J. Org. Chem.* **2000**, 3973 – 4009; c) J. Vollhardt, H.-J. Gais, K. L. Lukas, *Angew. Chem.* **1985**, *97*, 695 – 697; *Angew. Chem. Int. Ed. Engl.* **1985**, *24*, 696 – 697.

[4] X-ray crystal data for **3**: $C_{34}H_{84}Cl_2Li_{12}O_{22}P_4Si_2Ti_2$, $M_r = 1275.09$, triclinic, space group $P\bar{1}$, $a = 15.2286(9)$, $b = 16.6356(8)$, $c = 17.532(1)$ Å, $\alpha = 92.129(4)$, $\beta = 103.501(3)$, $\gamma = 115.368(3)^\circ$, $V = 3854.39$ Å^3, $Z = 2$, $F(000) = 1332$, $\rho = 1.099$ Mg m^{-3}, $\mu = 0.44$ mm^{-1}, crystal dimensions $0.08 \times 0.10 \times 0.22$ mm, $T = 193$ K, Mo$_{K\alpha}$ radiation ($\lambda = 0.71073$ Å), $\omega/2\theta$ scans, $\theta_{max} = 23.26^\circ$, 40810 measured reflections, 19311 independent reflections, 8312 reflections used in the refinement ($I > 3\sigma(I)$), 703 parameters, $R = 0.1136$, $R_w = 0.1294$, weighting scheme $\omega[1 - (\delta F/6\sigma F)^2]^2$, $\Delta\rho = 1.60/-0.96$ e Å^{-3}, $R = \Sigma(||F_o| - |F_c||)/\Sigma|F_o|$, $R_w = [\Sigma(|F_o| - |F_c|)^2\omega)/\Sigma F_o^2\omega)]^{1/2}$. Crystals of **3** were attached to a glass fiber with perfluoropolyether, mounted on the diffractometer, and cooled with an Oxford Cryostream to 193 K. Data were collected with a Nonius Kappa CCD area detector equipped with a graphite monochromator. The usual corrections were applied. The structure was solved by direct methods with the program SIR92.[11] Anisotropic least-squares full-matrix refinement was carried out on all non-hydrogen atoms by using the program CRYSTALS.[12] The positions of the hydrogen atoms were determined geometrically. The disordered Li_2O molecules in **3** were refined with appropriate restraints. Chebychev polynomial weights were used to complete the refinement.[13] Scattering factors were taken from the International Tables, Vol. IV, Table 2.2 B. Crystallographic data (excluding structure factors) for the structure reported in this paper have been deposited with the Cambridge Crystallographic Data Centre as supplementary publication no. CCDC-156555. Copies of the data can be obtained free of charge on application to CCDC, 12 Union Road, Cambridge CB2 1EZ, UK (fax: (+44) 1223-336-033; e-mail: deposit@ccdc.cam.ac.uk).

[5] All calculations were performed at the DFT level by using Becke's three-parameter hybrid functional with the correlation functional of Lee, Yang, and Parr.[14, 15] The following basis set was used for titanium: Wachters – Hay all-electron basis set[16, 17] with the scaling factors of Raghavachari and Trucks for first-row transition metals[18] and with additional diffuse (s,p,d) and polarization (f) functions specified in Gaussian 98 with 6-311 + G* basis set. For all other atoms the standard basis set 6-31G(d) was used. Initial coordinates for the geometry optimization of **4** were obtained by extracting the coordinates of **3** (without Li^+ ions) from the crystal structure and replacing the isopropyl groups by methyl groups. The optimized geometry of **4** was then used as a starting point for the calculation of the rotation profile. The dihedral angle γ(Ti-C-P-O(phosphonate)) was increased in 30° steps from 0 to 180°. For each value of γ, the geometry was reoptimized while keeping γ constrained. The electronic energies of these optimized rotamers revealed the rotation profile. All calculations were carried out with the program package Gaussian 98.[19]

[6] J. F. K. Müller, M. Neuburger, B. Spingler, *Angew. Chem.* **1999**, *111*, 97 – 99; *Angew. Chem. Int. Ed.* **1999**, *38*, 92 – 94.

[7] a) S. E. Denmark, K. A. Swiss, P. C. Miller, S. R. Wilson, *Heteroat. Chem.* **1998**, *9*, 209 – 218; b) M. Kranz, S. E. Denmark, K. A. Swiss, S. R. Wilson, *J. Org. Chem.* **1996**, *61*, 8551 – 8563; c) M. Kranz, S. E. Denmark, *J. Org. Chem.* **1995**, *60*, 5867 – 5878; d) C. J. Cramer, S. E. Denmark, P. C. Miller, R. L. Dorow, K. A. Swiss, S. R. Wilson, *J. Am. Chem. Soc.* **1994**, *116*, 2437 – 2447; e) W. Zarges, M. Marsch, K. Harms, F. Haller, G. Frenking, G. Boche, *Chem. Ber.* **1991**, *124*, 861 – 866.

[8] H.-J. Gais, J. Vollhardt, H. J. Lindner, H. Paulus, *Angew. Chem.* **1988**, *100*, 1562 – 1564; *Angew. Chem. Int. Ed. Engl.* **1988**, *27*, 1540 – 1542.

[9] R. G. Cavell, R. P. Kamalesh Babu, A. Kasani, R. McDonald, *J. Am. Chem. Soc.* **1999**, *121*, 5805 – 5806.

[10] a) O. G. Kulinkovich, A. de Meijere, *Chem. Rev.* **2000**, *100*, 2789 – 2834; b) M. T. Reetz, *Organotitanium Reagents in Organic Synthesis*, Springer, Berlin, **1986**, pp. 195 – 282; c) M. T. Reetz, *Top. Curr. Chem.* **1982**, *106*, 1 – 54; d) M. Brookhart, M. L. H. Green, *J. Organomet. Chem.* **1982**, *250*, 395 – 408.

[11] A. Altomare, G. Cascarano, G. Giacovazzo, A. Guagliardi, M. C. Burla, G. Polidori, M. Camalli, *J. Appl. Crystallogr.* **1994**, *27*, 435 – 435.

[12] D. J. Watkin, R. J. Carruthers, P. Betteridge, *Crystals*, Chemical Crystallography Laboratory, Oxford, **1985**.

[13] J. R. Carruthers, D. J. Watkin, *Acta Crystallogr. Sect. A* **1979**, *35*, 698 – 699.

[14] A. D. Becke, *J. Chem. Phys.* **1993**, *98*, 1372 – 1377.

[15] C. Lee, W. Yang, R. G. Parr, *Phys. Rev. B* **1988**, *37*, 785 – 789.

[16] A. J. H. Wachters, *J. Chem. Phys.* **1970**, *52*, 1033 – 1036.

[17] P. J. Hay, *J. Chem. Phys.* **1977**, *66*, 4377 – 4384.

[18] K. Raghavachari, G. W. Trucks, *J. Chem. Phys.* **1989**, *91*, 1062 – 1065.

[19] Gaussian 98 (Revision A.7), M. J. Frisch, G. W. Trucks, H. B. Schlegel, G. E. Scuseria, M. A. Robb, J. R. Cheeseman, V. G. Zakrzewski, J. A. Montgomery, R. E. Stratmann, J. C. Burant, S. Dapprich, J. M. Millam, A. D. Daniels, K. N. Kudin, M. C. Strain, O. Farkas, J. Tomasi, V. Barone, M. Cossi, R. Cammi, B. Mennucci, C. Pomelli, C. Adamo, S. Clifford, J. Ochterski, G. A. Petersson, P. Y. Ayala, Q. Cui, K.

  1433-7851/01/4015-2892 $ 17.50+.50/0

Morokuma, D. K. Malick, A. D. Rabuck, K. Raghavachari, J. B. Foresman, J. Cioslowski, J. V. Ortiz, B. B. Stefanov, G. Liu, A. Liashenko, P. Piskorz, I. Komaromi, R. Gomperts, R. L. Martin, D. J. Fox, T. Keith, M. A. Al-Laham, C. Y. Peng, A. Nanayakkara, C. Gonzalez, M. Challacombe, P. M. W. Gill, B. G. Johnson, W. Chen, M. W. Wong, J. L. Andres, M. Head-Gordon, E. S. Replogle, J. A. Pople, Gaussian, Inc., Pittsburgh, PA, **1998**.

Chemical Involvement of Solvent Water Molecules in Elementary Steps of the Fenton Oxidation Reaction**

Bernd Ensing, Francesco Buda, Peter Blöchl, and Evert J. Baerends*

The proposed reaction mechanisms for the oxidation of organic substrates with the Fenton reagents (a mixture of ferrous ions and hydrogen peroxide) can roughly be divided into two groups. The first group regards Fenton chemistry as the production of free hydroxyl radicals by the metal-catalyzed decomposition of the peroxide,[1] whereas the second group involves the formation of a highly reactive iron–oxo complex, such as the ferryl ion ($[Fe^{IV}O]^{2+}$), as the oxidative intermediate.[2] The issue is clearly of interest for both biooxidation research, in view of the prominent role of Fe ions, and for oxidation catalysis in general. However, despite the numerous studies over more than 60 years,[3–10] the controversy remains, since the extremely short lifetimes of the intermediates make definitive experiments very difficult. The major complication with quantum chemical calculations is that the water solvent has to be included in the study. Not only are the Fe^{2+} ions coordinated by six water molecules, but conceivable reaction products such as OH^-, H^+, and $OH^\bullet$ will also be solvated and/or propagate through the solution by chain reactions. It is therefore impossible to treat the solvent by just model potentials that describe interactions between intact H_2O molecules with other H_2O molecules and Fe^{2+} ions (let alone by a continuum model).

The explicit incorporation of the water solvent in the computational study is no longer an elusive goal. Indeed, the ab initio molecular dynamics (AIMD) method[11] allows for a parameter free, finite temperature simulation in which, at each time step, the forces are computed directly from the electronic structure determined by density functional theory (DFT). Therefore, within this approach there are no restrictions on reactive processes at the Fe center or in the solution.

Recently, we performed DFT calculations on the isolated (gas-phase) Fenton reactants,[12] and found that dissociation of the O–O bond of hydrogen peroxide molecule coordinated to pentaaqua Fe^{II} ions to form $[Fe(OH)(H_2O)_5]^{2+}$ and a $OH^\bullet$ cannot readily occur since this reaction is endothermic by 27 kcal mol^{-1}. This value is in fact already smaller than the approximate 60 kcal mol^{-1} required to break the O–O bond in isolated hydrogen peroxide. The reduction of the dissociation energy occurs because the $OH^\bullet$ that remains coordinated to the iron center leads to an Fe^{II}–$OH^\bullet$ bond (formally Fe^{III}–OH^-), which is stronger by about 30 kcal mol^{-1} than the original Fe^{II}–H_2O_2 bond. Nevertheless, there is still an endothermicity of 27 kcal mol^{-1}, and homolytic dissociation of the coordinated H_2O_2 molecule can only become exothermic through the energy gain associated with a second Fe–OH bond replacing a much weaker Fe–H_2O bond. This process occurs in the gas phase by the leaving $OH^\bullet$ abstracting a hydrogen atom from an adjacent coordinated H_2O molecule. A water molecule and a second strong Fe–OH bond is formed, and this process provides enough energy to make the reaction exothermic [Eq. (1)]. Hence, no $OH^\bullet$ results.

$$[Fe^{II}(H_2O)_5(H_2O_2)]^{2+} \rightarrow [Fe^{IV}(OH)_2(H_2O)_4]^{2+} + H_2O \quad (1)$$

We now turn to the study of this reaction in solution. We had already observed in the gas phase that a single water molecule, when added in a "second solvation shell" position, reacts with the $[Fe(OH)_2(H_2O)_4]^{2+}$ complex to form the presumably reactive iron–oxo (ferryl) ion $[FeO(H_2O)_5]^{2+}$ and an H_2O molecule. The energy barrier for this transformation would be too high without the chemical involvement of the "solvent" water molecule. Hence, solvent simulation is necessary since solvent molecules may be chemically involved in the formation of the ferryl ion. Moreover, they may be involved in the alternative pathway of $OH^\bullet$ formation, since solvent molecules may react with the $OH^\bullet$ and propagate it through the solution by a chain reaction. We have, therefore, performed spin-polarized AIMD simulations of (high spin, $S=2$) Fe^{2+}/H_2O_2 in water using the CP-PAW code[13] with the BP[14, 15] exchange-correlation functional. We applied periodic boundary conditions, as usually done in MD simulations,[16] to a relatively small cubic unit cell containing an Fe^{2+} ion, a H_2O_2 molecule, and 31 water molecules to emulate the infinite bulk environment but keep the computation feasible. The formal concentration of the reactants is therefore high but not unrealistic (technical details of AIMD simulations of solvation and (radical) reactions in water may be found in ref. [17–21]). The same parameters for the basis set and dynamics were used as in our previous study of the S_N2 reaction in water,[17] namely, a constant temperature[22] of $T=300$ K, a fictitious electron mass of $\mu_e=1000$ a.u.; a MD time step of $\Delta t=8$ a.u.; and a plane-wave cut-off of $k^2_{max}=30$ Ry. The box size was $L=$

[*] Prof. Dr. E. J. Baerends, Ir. B. Ensing, Dr. F. Buda
Theoretical Chemistry, Faculty of Exact Sciences
Vrije Universiteit Amsterdam
De Boelelaan 1083, 1081 HV Amsterdam (The Netherlands)
Fax: (+31) 20-44-47-629
E-mail: baerends@chem.vu.nl
Prof. Dr. P. Blöchl
Clausthal University of Technology
Clausthal-Zellerfeld (Germany)

[**] We gratefully acknowledge the helpful discussions with Michiel Gribnau (Unilever-Vlaardingen) and we thank the Netherlands Organization for Scientific Research (NWO) for support through the PPM-CMS program and the NCF for providing computer time.

9.900 Å. The accuracy of the BP functional to describe reactions in water has previously been discussed.[17]

After a 1.16-ps equilibration run (using bond constraints to avoid any reaction occuring beforehand), the MD simulation was started (without any bond constraints) and the evolution of the coordinated Fenton reagents in water was followed for 10.2 ps. Almost immediately, the peroxide dissociates into an OH group coordinated to the iron center and an OH$^{\bullet}$, which now does not attack an adjacent coordinated H_2O molecule (as in the gas-phase study) but instead attacks a solvent water molecule that was hydrogen bonded to the β-oxygen atom of hydrogen peroxide (see snapshots 1 and 2 in Figure 1). Snapshots 2 and 3 show that in a fast chain reaction the reactive radical is passed on via two solvent water molecules and the reaction is terminated by abstraction of a hydrogen atom from a water ligand of the aqua–iron complex in the neighboring cell, which, as a consequence of the periodic repetition, is identical to the complex from which the OH$^{\bullet}$ originated. The process may be looked upon as a concerted reaction rather than a chain reaction since the abstraction of a hydrogen atom from a coordinated H_2O molecule occurs virtually simultaneously with the breaking of the O–O bond. This mechanism agrees with the energy cost being too high for just an OH$^{\bullet}$ splitting off from a coordinated H_2O_2 molecule. A second OH ligand has to be formed simultaneously, either at the same Fe center, as happens in the gas phase, or at an adjacent Fe center, as observed in the present simulation in solution. As a matter of fact, since there is only one Fe complex in the unit cell, the net effect is still formation of a dihydroxide species, a result which is similar to abstraction of an H atom from an H_2O molecule coordinated at the same Fe center [Eq. (1)]. Of course, if more Fe complexes were present in a unit cell, abstraction of an H atom from a H_2O ligand in a nearby complex at which the hydrogen peroxide had not yet dissociated, or which did not have a hydrogen peroxide molecule coordinated at all, would lead to two monohydroxide complexes. The important point is that the formation of a free OH$^{\bullet}$ is not thermodynamically favorable, and the hydrogen peroxide only dissociates if an OH$^{\bullet}$ "shunt" through the solution to a coordinated H_2O molecule, either at the same center or an adjacent Fe center, quenches the radical.

Although, in principle, monohydroxide complexes may result if the OH$^{\bullet}$ shunt ends at a different Fe center to where it started, the more likely reaction path, in particular with a low concentration of Fe complexes, will be a chain involving a few solvent water molecules and ending at the same Fe center as where the hydrogen peroxide was coordinated, a process which leads to a dihydroxide complex. The high concentration of Fe^{2+} ions in our simulation, which leads to dihydroxides since the OH$^{\bullet}$ abstracts a H atom from an Fe center in a neighboring cell which already had an OH group present from the dissociation of H_2O_2, yields the same product. In establishing the high probability of formation of iron(IV) dihydroxide rather than free OH$^{\bullet}$ radicals, we also note that it remains to be seen whether the OH$^{\bullet}$ shunt, possibly through a chain of solvent molecules, could terminate at an organic substrate if that were in the neighborhood. This requires further investigation. If this were to occur, similar reaction products should arise, as in the case of the production of free OH$^{\bullet}$ radicals from, for example, radiation. The probability of such a mechanism occurring with a high concentration of an organic substrate might be sufficient to explain some of the experimental findings.

We observed in the simulations that the formed iron(IV) dihydroxide complex is in equilibrium with its conjugate base through proton donation from a water ligand to the solvent [Eq. (2)].

$$[Fe^{IV}(OH)_2(H_2O)_4]^{2+} + H_2O \rightleftharpoons [Fe^{IV}(OH)_3(H_2O)_3]^{+} + H_3O^{+} \quad (2)$$

Formation of the Fe(IV) dihydroxide complex also occurred in our gas-phase study, but of course the apparent acidity of the Fe^{IV} complex according to Equation (2) could not be observed in the gas phase. The dihydroxide complex is transformed in our simulation 1.7 ps after step 1 (during which time reaction (2) is going back and forth) into an iron–oxo complex by donation of a proton from a coordinated OH group to the solvent [Eq. (3)].

$$[Fe^{IV}(OH)_2(H_2O)_4]^{2+} + H_2O \rightarrow [Fe^{IV}O(OH)(H_2O)_4]^{+} + H_3O^{+} \quad (3)$$

We note that again the presence of solvent is crucial for this pathway to form the ferryl species, and enable an H^+ ion to

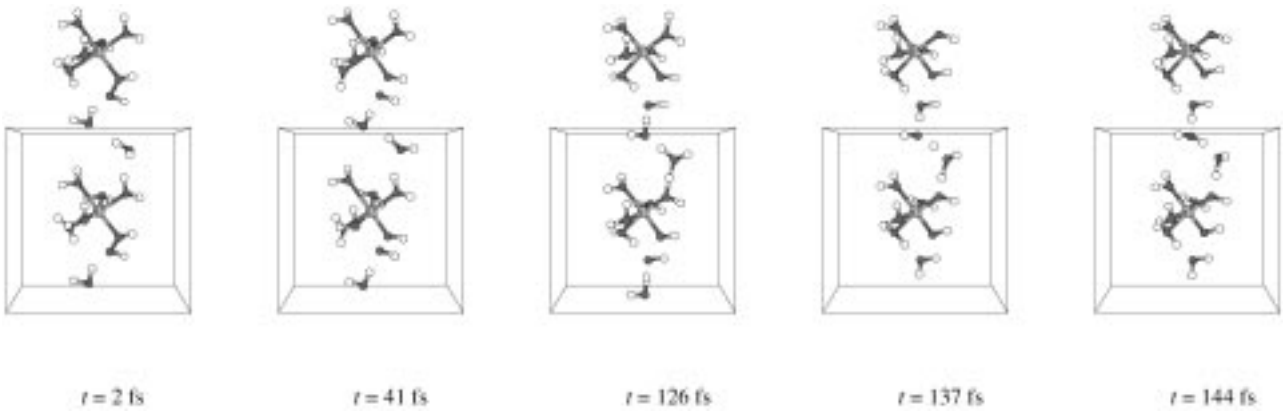

Figure 1. Five snapshots of step 1 of the reaction, starting at the moment that the R(OO) and R(FeO) constraints of H_2O_2 coordinated to $[Fe(H_2O)_5]^{2+}$ were released ($t = 0$). The hydrogen peroxide coordinated to the pentaaquairon complex is drawn in the center of the unit cell. One periodic image of the unit cell is drawn above it. The two solvent water molecules that are involved in the reaction are also shown but, for simplicity, the other solvent water molecules are left out. See text for further information.

  1433-7851/01/4015-2894 $ 17.50+.50/0

diffuse into the solvent. The ferryl species is also formed in the gas-phase simulation (being the thermodynamically favored end product), but in this case by migration of an H^+ ion to the second OH^- ligand. As mentioned before, the solvent involvement was already indicated by the introduction of a single water molecule into the second coordination sphere in the gas-phase study. This water molecule aided migration of the H^+ ion to form $[Fe^{IV}O(H_2O)_5]^{2+}$, but the present complete picture could only be obtained by the explicit introduction of the solvent at finite temperature.

In conclusion, the simulations in water solution confirm our gas-phase calculations of the formation of the iron(IV)–oxo complex from the Fenton reagents. We have assumed the formation of the pentaaquairon–hydrogen peroxide complex as the initial necessary step. Our results demonstrate the importance of full incorporation of the water as both a solvent and reagent in the initial reaction steps. The oxo complex is found to be the important oxidative intermediate in the Fenton reaction. How it acts as the reactive species in, for example, hydroxylation of aliphatic and aromatic substrates,[23–25] oxidation of alcohols, and in other reactions will be the subject of further study.

Received: March 22, 2001 [Z16828]

[1] F. Haber, J. Weiss, *Proc. R. Soc. London* **1934**, *147*, 332.
[2] W. C. Bray, M. H. Gorin, *J. Am. Chem. Soc.* **1932**, *54*, 2124.
[3] P. Wardman, L. P. Candeias, *Radiat. Res.* **1996**, *145*, 523.
[4] C. Walling, *Acc. Chem. Res.* **1998**, *31*, 155.
[5] D. T. Sawyer, A. Sobkowiak, T. Matsushita, *Acc. Chem. Res.* **1996**, *29*, 409.
[6] M. L. Kremer, *Phys. Chem. Chem. Phys.* **1999**, *1*, 3595.
[7] J. D. Rush, W. H. Koppenol, *J. Inorg. Biochem.* **1987**, *29*, 199.
[8] D. A. Wink, R. W. Nims, J. E. Saavedra, W. E. J. Utermahlen, P. C. Ford, *Proc. Natl. Acad. Sci. USA* **1994**, *91*, 6604.
[9] J. P. Hage, A. Llobet, D. T. Sawyer, *Bioorg. Med. Chem.* **1995**, *3*, 1383.
[10] C. Kim, K. Chen, J. Kim, L. Que, Jr., *J. Am. Chem. Soc.* **1997**, *119*, 5964.
[11] R. Car, M. Parrinello, *Phys. Rev. Lett.* **1985**, *55*, 2471.
[12] F. Buda, B. Ensing, M. C. M. Gribnau, E. J. Baerends, *Chem. Eur. J.* **2001**, in press.
[13] P. Blöchl, *Phys. Rev. B* **1994**, *24*, 17953.
[14] A. D. Becke, *J. Chem. Phys.* **1992**, *96*, 2155.
[15] J. P. Perdew, *Phys. Rev. B* **1986**, *33*, 8822, erratum: *Phys. Rev. B* **1986**, *34*, 7406.
[16] See, for example, D. Frenkel, B. Smit, *Understanding Molecular Simulation*, Academic Press, San Diego, **1996**.
[17] B. Ensing, E. J. Meijer, P. E. Blöchl, E. J. Baerends, *J. Phys. Chem. A* **2001**, *105*, 3300.
[18] M. Mohr, D. Marx, M. Parrinello, H. Zipse, *Chem. Eur. J.* **2000**, *6*, 4009.
[19] E. J. Meijer, E. J. Sprik, *J. Am. Chem. Soc.* **1998**, *120*, 6345.
[20] E. J. Meijer, M. Sprik, *J. Phys. Chem. A* **1998**, *102*, 2893.
[21] M. Tuckerman, K. Laasonen, M. Sprik, M. Parrinello, *J. Chem. Phys.* **1995**, *103*, 150.
[22] S. J. Nosé, *J. Chem. Phys.* **1984**, *81*, 511.
[23] D. Schröder, H. Schwarz, *Angew. Chem.* **1995**, *107*, 2126; *Angew. Chem. Int. Ed. Engl.* **1995**, *34*, 1973.
[24] K. Yoshizawa, Y. Shiota, T. Yamabe, *J. Am. Chem. Soc.* **1998**, *120*, 564.
[25] K. Yoshizawa, Y. Shiota, Y. Kagawa, T. Yamabe, *J. Phys. Chem. A* **2000**, *104*, 2552.

Insights into the Aryl–Aryl Exchange between Palladium and Phosphane Ligands in Pd^{II} Complexes: Preparation of Phthalocyanine-Containing Phosphonium Salts**

Gema de la Torre, Andreas Gouloumis, Purificación Vázquez, and Tomás Torres*

The employment of modern synthetic methods in the phthalocyanines (Pc) field[1] can provide a large variety of functionalized derivatives and complex structures based on these macrocycles which may have interesting applications in materials science. In the last few years many scientists, ourselves included, have concentrated on the preparation of unsymmetrically functionalized phthalocyanines[2, 3] and binuclear Pc derivatives in which the macrocyclic units are fused to each other[4, 5] or bridged through different kinds of spacers.[6–8] Our interest in noncentrosymmetric and octupolar[9] systems for nonlinear optical (NLO) applications[10] as well as in the preparation of molecular materials with multiple functions led us to the synthesis of phosphonium salts containing one phthalocyanine unit (Figure 1). Pc-containing phosphonium cations are targets of choice for the preparation of hybrid materials that combine magnetism with NLO properties.[11]

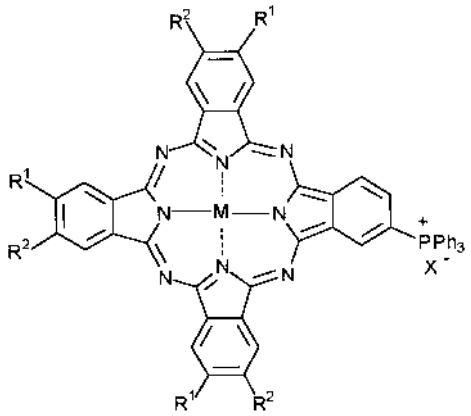

Figure 1. Phthalocyanine-phosphonium salts.

Tetraarylphosphonium salts can be formed by a palladium-catalyzed reaction between triphenylphosphane and an aryl bromide or iodide.[12] The mechanism of the quaternization reaction seems to involve oxidative addition of the aryl halide (ArI) to a palladium(0)–phosphane complex, followed by the reductive elimination of the phosphonium ion and a loss of the halide ion from the metal center (Scheme 1).

[*] Prof. T. Torres, Prof. P. Vázquez, Dr. G. de la Torre, A. Gouloumis
Departamento de Química Orgánica
Universidad Autónoma de Madrid
Cantoblanco, 28049-Madrid (Spain)
Fax: (+34) 91-397-3966
E-mail: tomas.torres@uam.es

[**] This work was supported by CICYT (Spain) through grant MAT-99-0180. We are indebted to Mr. G. Martin Fuchs, Laboratoire de Photonique Quantique et Moléculaire, Ecole Normale Supérieure de Cachan, France, for the NLO measurements.

  1433-7851/01/4015-2895 $ 17.50+.50/0

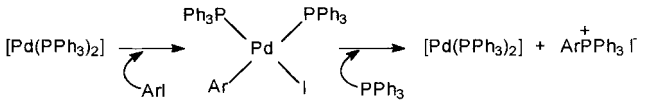

Scheme 1. Mechanism of formation of tetraarylphosphonium salts.

Considering this mechanism and that iodophthalocyanines give rise to oxidative-addition complexes,[6] we undertook the synthesis of these phosphonium derivatives by treating tri(*tert*-butyl)iodophthalocyaninate zinc(II) (**1**; ZnPcI)[6a] with PPh_3 in the presence of catalytic amounts of $[PdCl_2(PPh_3)_2]$ in DMF as solvent at 100 °C. Under these conditions, we observed the formation of the desired product $[(ZnPc)PPh_3]^+I^-$ (**2**) in 15% yield, in addition to another compound which was identified as a phosphonium salt containing two Pc-based units $[(ZnPc)_2PPh_2]^+I^-$ (**3**), isolated in 50% yield (Scheme 2).

The presence of **3** in the reaction mixture suggests that an exchange occurs between the phenyl groups on the phosphane ligand and the phthalocyanine-based unit in the oxidative-addition intermediate. Scrambling of aryl groups in Pd^{II} complexes with the triphenylposphane ligand has been observed by other authors.[13, 14] The nature of this interchange is explained[14–16] by the formation of an aryltriphenylphosphonium salt (e.g. **2**), followed by an oxidative addition to the palladium center as shown by the formation of **4** and **5** in Scheme 3.

Following these precedents, a phosphonium salt such as **2**, easily formed under these conditions, can undergo oxidative addition to give a mixture of compounds analogous to **4** and **5** (Scheme 3). Many $[(PPh_3)_2Pd(R)X]$ complexes can exchange phosphane ligands rapidly,[17] and such a process can generate

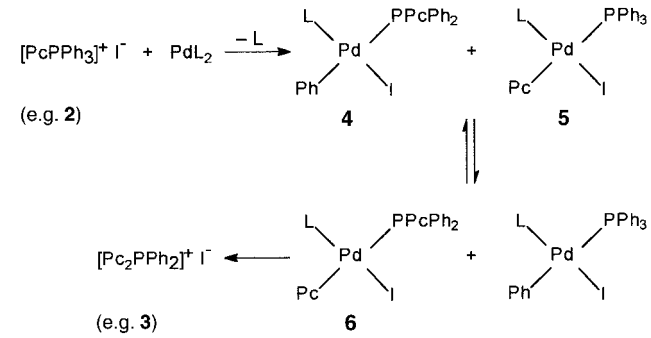

Scheme 3. Proposed mechanism for the formation of phthalocyanine-phosphonium salts **2** and **3**.

complex **6**, which in turn gives rise to a new phosphonium salt, such as **3**, by reductive elimination. The treatment of the isolated phosphonium salt **2** with a palladium complex without phosphane ligands furnishes a mixture of **2** and **3**, supporting the proposed mechanism.

The binuclear Pc-based system **3** is also of interest because of potential interactions between the two macrocyclic units. We have tested different palladium complexes and reaction conditions to obtain either **2** or **3** as the major product. First, the ratio of PPh_3 was increased in the hope of to obtaining exclusively the monophthalocyanine-based **2**.[16] Even on adding 5 equivalents of PPh_3, a mixture of **2** and **3** was isolated when using a catalytic amount of $[PdCl_2(PPh_3)_2]$. However, the reaction of **1** with equimolar amounts of $[PdCl_2(PPh_3)_2]$ either in the presence or absence of PPh_3 afforded **2** in 35% yield without traces of **3**. Longer reaction times do not result in an increase of the yield but to the

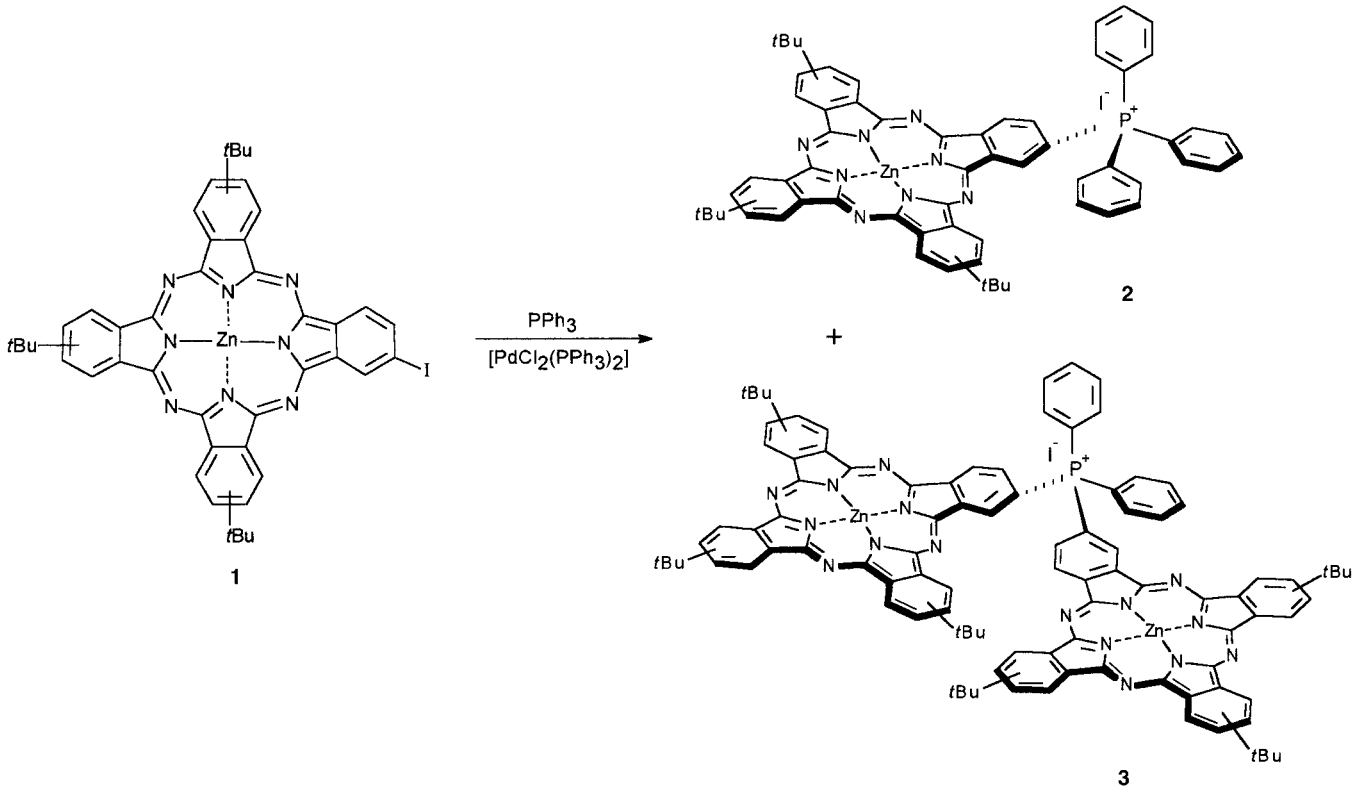

Scheme 2. Synthesis of phosphonium salts **2** and **3**.

  1433-7851/01/4015-2896 $ 17.50+.50/0

deposition of black palladium metal. A great amount of iodophthalocyanine **1** remains, but can be recovered after column chromatography of the crude reaction mixture.

When the reaction was carried out with $[Pd_2(dba)_3]$ (dba = *trans*, *trans*-dibenzylideneacetone) in a 1:1 ratio with **1** and in the presence of two equivalents of PPh_3, the only phosphonium salt isolated after 24 h was compound **3**, even though a mixture of **2** and **3** was detected by thin layer chromatography (TLC) early in the reaction. Under these conditions, oxidative addition of the phosphonium salt **2** to the Pd center seems to take place easily. The main difficulty is that undesired coupling reactions between **1** and dba also take place, so that the yield of **3** is around 40% lower than that obtained with the initial conditions employing a catalytic amount of $[PdCl_2(PPh_3)_2]$. Note that some of the trinuclear compound $[(ZnPc)_3PPh]^+I^-$ (**7**, Figure 2) is also detected in the crude mixture. The use of other palladium complexes, such as $[Pd(OAc)_2]$ (OAc = acetate) or $[PdCl_2(CH_3CN)_2]$, without phosphane ligands does not give an improvement in the yield of compound **3**.

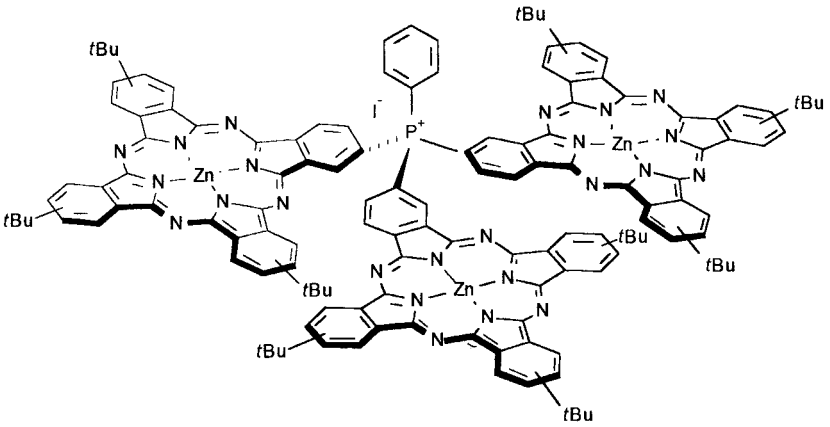

Figure 2. Aryltrisphthalocyanine-phosphonium salt $[(ZnPc)_3PPh]^+I^-$.

To obtain the derivative with three Pc-based units, we have also treated phosphonium salt **3** with $[Pd(OAc)_2]$ in a 1:1 ratio without adding **1**, thus affording **7** in a 3% yield. When phthalocyanine **1** is added to the mixture, the yield of **7** increases to around 10%.

We have confirmed that tetraarylphosphonium salts can undergo oxidative addition to palladium centers and may be responsible for the scrambling phenomenon. The relatively easy formation of these phthalocyanine-containing phosphonium salts may be related to the electron richness of the Pc core,[16] which stabilizes the developing positive charge as the phosphonium salt is generated. Trisphthalocyanine-based phosphonium salt **7** seems to be more hindered and difficult to form. Nevertheless, efforts will be made to improve the yield of this derivative and even to obtain the tetraphthalocyanine-phosphonium salt, already detected in trace amounts in the mass spectra of some reaction mixtures.

The second-order NLO responses at the molecular level for the dipolar compound **2** and octupolar phthalocyanine **7** have been determined through HyperRayleigh Light Scattering (HRS). The measured β_{HRS} values at $\lambda = 1.06$ μm in THF solution were 20.5×10^{-30} esu and 189×10^{-30} esu, respectively, for **2** and **7**. No multiphoton-induced luminescence has been detected at this wavelength. The high first-order hyperpolarizability value measured for compound **7** is comparable to those reported for subphthalocyanines, core-modified Pcs with octupolar character,[9a] and clearly superior to those available for related unsymmetrically substituted phthalocyanines with dipolar characteristics.[9b] This fact points out the role of "central acceptor" played by the positively charged phosphorus atom in tailoring the multipolar character of the hyperpolarizability.[10] A more detailed study on the NLO properties of this new family of compounds has been undertaken.

Experimental Section

All reactions were performed under an argon atmosphere. DMF was dried over CaH_2, distilled, and degassed before use. Mass spectra were obtained from a Bruker Reflex III matrix-assisted laser desorption/ionization time of flight (MALDI-TOF) spectrometer. UV/Vis spectra were recorded on a Hewlett Packard 8453 spectrometer. Analytical data were performed on the corresponding hexafluorophosphate (PF_6^-) salts prepared by standard ion exchange.

2: A mixture of iodophthalocyanine **1** (100 mg, 0.115 mmol) and $[PdCl_2(PPh_3)_2]$ (81 mg, 0.115 mmol) was heated at 100 °C for 24 h in DMF. After removal of the solvent under reduced pressure, column chromatography of the crude product(eluting with CH_2Cl_2/2-propanol 15/1) afforded compound **2** (20 mg, 15%); elemental analysis calcd (%) for $C_{62}H_{54}N_8F_6P_2Zn \cdot 2H_2O$ (1188.50): C 62.66, H 4.92, N 9.43; found C 61.93, H 4.85, N 9.17; MALDI-TOF (dithranol): *m*/*z*: 1005–1010 $[M-I^-]^+$; UV/Vis ($CHCl_3$): λ_{max} (ε) = 707 (375000), 665 (235000), 642 (135000), 602 (61000), 358 nm (152000).

3: Following the same procedure as for **2**, treatment of **1** (100 mg, 0.115 mmol) with $[PdCl_2(PPh_3)_2]$ (8 mg, 0.011 mmol) afforded compound **3** (52 mg, 50%) after column chromatography (THF/hexane 1/1; THF); elemental analysis calcd (%) for $C_{100}H_{88}N_{16}F_6P_2Zn_2 \cdot 2H_2O$ (1856.62): C 64.69, H 4.99, N 12.07; found C 63.80, H 5.27, N 11.75; MALDI-TOF (dithranol): *m*/*z*: 1671–1678 $[M-I^-]^+$; UV/Vis (THF): λ_{max} (ε) = 678 (172000), 666 (83000), 643 (51000), 603 (13000), 358 nm (63000).

7: A mixture of **3** (50 mg, 0.028 mmol), phthalocyanine **1** (24 mg, 0.028 mmol), and $Pd(OAc)_2$ was heated at 100 °C for 24 h. The green solution was evaporated under reduced pressure, the solid was purified by chromatography on silica gel (THF/hexane 1/1; THF; THF/MeOH 2/1), and washed with methanol, furnishing **7** (6 mg, 9%); elemental analysis calcd (%) for $C_{138}H_{122}N_{24}F_6P_2Zn_3 \cdot H_2O$ (2488.62): C 66.60, H 5.02, N 13.51; found C 66.10, H 5.36, N 13.18; MALDI-TOF (dithranol): *m*/*z*: 2338–2346 $[M-I^-]^+$; UV/Vis (THF): λ_{max} (ε) = 678 (229000), 348 nm (178000).

Received: December 22, 2000
Revised: May 14, 2001 [Z16324]

[1] N. B. McKeown, *Phthalocyanine Materials: Synthesis, Structure and Function*, Cambridge University Press, Cambridge, **1998**.
[2] E. M. Maya, C. García, E. M. García-Frutos, P. Vázquez, T. Torres, *J. Org. Chem.* **2000**, *65*, 2733–2739.
[3] N. Kobayashi, T. Ishizaki, K. Ishii, H. Konami, *J. Am. Chem. Soc.* **1999**, *121*, 9096–9110.
[4] G. de la Torre, M. V. Martínez-Díaz, P. R. Ashton, T. Torres, *J. Org. Chem.* **1998**, *63*, 8888–8893.
[5] K. Ishii, N. Kobayashi, Y. Higashi, T. Osa, D. Lelièvre, J. Simon, S. Yamauchi, *Chem. Commun.* **1999**, 969–970.

  1433-7851/01/4015-2897 $ 17.50+.50/0

[6] a) E. M. Maya, P. Vázquez, T. Torres, *Chem. Eur. J.* **1999**, *5*, 2004 – 2013; b) E. M. Maya, P. Vázquez, T. Torres, L. Gobi, F. Diederich, S. Pyo, L. Echegoyen, *J. Org. Chem.* **2000**, *65*, 823 – 830.
[7] a) E. M. García-Frutos, F. Fernández-Lázaro, E. M. Maya, P. Vázquez, T. Torres, *J. Org. Chem.* **2000**, *65*, 6841 – 6846; b) A. Gouloumis, S.-G. Liu, P. Vázquez, L. Echegoyen, T. Torres, *Chem. Commun*. **2001**, 399 – 400.
[8] a) R. Jung, K.-H. Schweikart, M. Hanack, *Eur. J. Org. Chem.* **1999**, 1687 – 1691; b) M. Hanack, P. Stihler, *Eur. J. Org. Chem.* **2000**, 303 – 311.
[9] a) B. del Rey, U. Keller, T. Torres, G. Rojo, F. Agulló-López, S. Nonell, C. Martí, S. Brasselet, I. Ledoux, J. Zyss, *J. Am. Chem. Soc.* **1998**, *120*, 12808 – 12817; b) G. de la Torre, P. Vázquez, F. Agulló-López, T. Torres, *J. Mater. Chem*. **1998**, *8*, 1671 – 1683.
[10] I. Ledoux, J. Zyss, *Chem. Rev.* **1994**, *94*, 77 – 105. The nonlinear optical properties of some three-dimensional phosphonium ion chromophores have been recently reported by C. Lambert, E. Schmälzlin, K. Meerholz, C. Bräuchle, *Chem. Eur. J.* **1998**, *4*, 512 – 521.
[11] It has been published recently that the combination of alternating single layers of a bimetallic ferromagnet and organic conductor cations gives rise to a hybrid material exhibiting both magnetic and NLO properties: E. Coronado, J. R. Galán-Mascarós, C. J. Gómez-García, V. Laukhin, *Nature* **2000**, *408*, 447 – 449.
[12] a) C. B. Ziegler, Jr., R. F. Heck, *J. Org. Chem.* **1978**, *43*, 2941 – 2946; b) T. Migita, T. Nagai, K. Kiuchi, M. Kosugi, *Bull. Chem. Soc. Jpn.* **1983**, *56*, 2869 – 2870.
[13] K.-C. Kong, C.-H. Cheng, *J. Am. Chem. Soc.* **1991**, *113*, 6313 – 6315.
[14] M. Sakamoto, I. Shimizu, A. Yamamoto, *Chem. Lett.* **1995**, 1101 – 1103.
[15] B. E. Segelstein, T. W. Butler, B. L. Chenard, *J. Org. Chem.* **1995**, *60*, 12 – 13.
[16] F. E. Goodson, T. I. Wallow, B. M. Novak, *J. Am. Chem. Soc.* **1997**, *119*, 12441 – 12453.
[17] J. R. Norton, E. G. Samsel, *J. Am. Chem. Soc.* **1984**, *106*, 5505 – 5512.

Synthesis of Tri- and Tetracoordinate Phosphorus Compounds Containing a PCF_3 Group by Nucleophilic Trifluoromethylation of the Corresponding PF Compounds

Izabela Tworowska, Wojciech Dąbkowski, and Jan Michalski*

Dedicated to Professor Marianne Baudler on the occasion of her 80th birthday

The introduction of a trifluoromethyl group into an organic compound can bring about remarkable changes in physical, chemical, and biological properties.[1] Therefore, the importance of fluorinated compounds in life sciences is rapidly increasing. Modification of the backbone of biophosphates by replacement of the anionic phosphodiester group with the neutral trifluoromethylphosphonato group should have steric, polar, and electronic effects similar to those of a hydroxyl group. Additionally, the lipophilicity should be enhanced.[2]

[*] Prof. Dr. J. Michalski, I. Tworowska, W. Dąbkowski
Centre of Molecular and Macromolecular Studies
Polish Academy of Sciences
90-363 Łódź, Sienkiewicza 112 (Poland)
Fax: (+48) 42 684-71-26
E-mail: jmich@bilbo.cbmm.lodz.pl

Tricoordinate P^{III}–CF_3 compounds may act as useful ligands in organometallic chemistry.[3] Among the variety of methods for introducing a CF_3 group into organic compounds, the application of (trifluoromethyl)trimethylsilane CF_3SiMe_3 (**1**) as nucleophilic trifluoromethylating reagent is rapidly becoming the method of choice. CF_3SiMe_3 was first synthesized by Ruppert et al. in 1984[4] and is commercially available. In contrast to organic compounds containing a CF_3 group, little is known about P^{III}–CF_3 compounds. P^{V}–F compounds, which are apparent candidates for nucleophilic trifluoromethylation by **1**, have been used for this purpose in only two cases.[5] So far no reaction of this kind has been described for P^{III}–F compounds.

Our interest in P–CF_3 compounds is related to our recent studies on phosphorus – fluorine compounds derived from alcohols of biological interest. The method of choice for preparing P^{III}–F groups is based on nucleophilic displacement of OAr^- from a P^{III}–OAr group by a fluoride ion [Eq. (1)].[6] Both types of P^{III} compounds, **2** and **3**, are available in excellent yield and exhibit a high degree of chemical and stereochemical stability.[7]

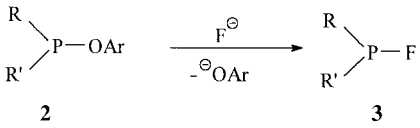

2 **3** (1)

We found that P^{III}–F compounds react with the Ruppert reagent **1** at 20 °C in THF or acetonitrile in almost quantitative yield [Eq. (2)].[8] The reaction is catalyzed by fluoride ions.

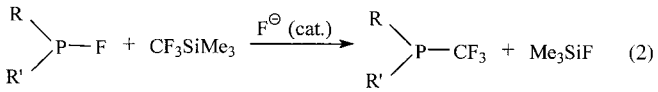

3 **4** (2)

Cesium fluoride is a convenient fluoride donor, but other donors such as tetrabutylammonium fluoride (TBAF) can also be used. As the fluoride ion is used in catalytic amounts, the catalytic cycle shown in Scheme 1 is proposed.

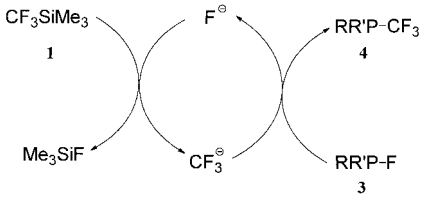

Scheme 1. Proposed cycle for the nucleophilic trifluoromethylation of P^{III}–F compounds by **1**.

The strength of the P–F bond is compensated by the high affinity of fluorine for the silicon center. An analogous mechanism should operate in the case of tetracoordinate phosphorus – fluorine compounds RR′P(X)F (X = O, S). The optimized protocol for this reaction was applied to a variety of

  1433-7851/01/4015-2898 $ 17.50+.50/0

P^{III}–F structures **3** containing alkoxy, alkylsulfanyl, amino, and aryl ligands and led to the corresponding P^{III}–CF_3 compounds **4** in good yield (Table 1). Compounds **4** derived from nucleosides can also be prepared efficiently by this method. Note that the high toxicity of some P^{III}–F and P^{III}–CF_3 compounds calls for special precautions.

Table 1. ^{31}P NMR and FAB-MS data of selected compounds.

Compound	$\delta(^{31}P)$[a]	J_{PCF} [Hz]	FAB-MS [M+H]	Yield [%][b]
4 (R, R′: $-SCH_2CH_2S-$)	40.82 (q)	63.515	193.2	65
4a[c]	111.91 (q)	76.987	1143.1	82
	112.02 (q)	77.012		
5[c]	−2.42 (q)	129.431	1159.1	90
	−2.50 (q)	127.963		
8	31.41 (sept)	87.901	270.2	75

[a] 81.014 MHz, $CDCl_3$, H_3PO_4 external standard. [b] Yields of isolated product after purification. [c] Mixture of two diastereoisomers (1:1).

The trifluoromethylphosphonate analogues of nucleotides were prepared from CF_3PBr_2 and nucleosides.[9] Dinucleoside trimethylsilylphosphonates were prepared by Ugi et al. from $CF_3P(NEt_2)_2$ in a multistep synthesis with low yield.[2] Our synthesis of dinucleoside trifluoromethylphosphonate **4a** derived from thymidine starts either from the dinucleotide phosphorofluoridite **3a** or from the corresponding phosphorofluoridate **6** (Scheme 2). Compounds **4a** and **5** were clearly

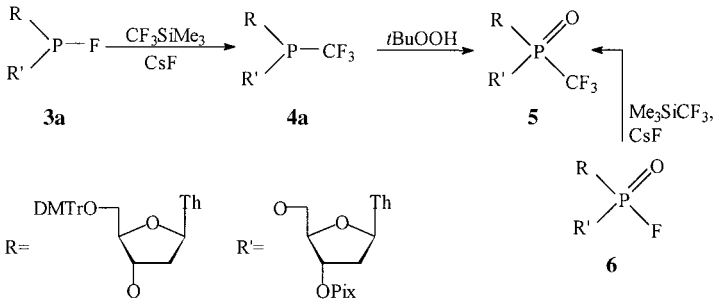

Scheme 2. Synthesis of **4a** and **5**. DMTr = 4,4′-dimethoxytrityl, Pix = 9-(9-phenyl)xanthenyl, Th = thymine residue.

revealed by ^{31}P NMR spectroscopy to be 1:1 mixtures of diastereoisomers (Table 1). The spectroscopic properties of the CF_3 phosphonate **5** are identical with those described by Ugi et al. The intermediate phosphonite **4a** undergoes slow ligand exchange in solution. Therefore its oxidation to the CF_3 phosphonate **5** should be performed without delay. Oxidation of **3a** to **6** and of **4a** to **5** was performed with *tert*-butyl hydroperoxide. The reactions shown in Scheme 2 proceed in high yield.

An important part of these studies was to develop a sequential procedure that combines formation of RR′P–F (**3**) with their transformation into the corresponding $RR'PCF_3$ [**4**; Eq. (3)]. We assume that in this case the intermediate **3** is formed and reacts at once with **1** to give **4**. The combined procedure takes place at 20 °C in high yield. An illustrative example of the sequential procedure is the synthesis of

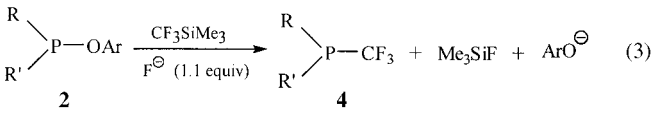

(3)

(diisopropylamino)bis(trifluoromethyl)phosphine **8** [Eq. (4), Table 1].[10]

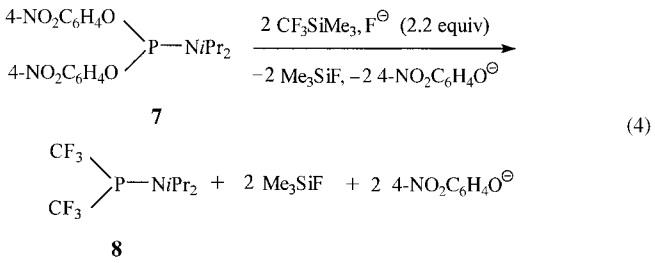

(4)

In conclusion, we have developed a general and highly efficient procedure for the conversion of P^{III}–F compounds into the corresponding P^{III}–CF_3 compounds by reaction with CF_3SiMe_3. The tricoordinate compounds are readily oxidized by *tert*-butylhydroperoxide to $P(O)CF_3$ compounds. The method is particularly useful as it is compatible with a sequential procedure combining formation of phosphorus–fluorine compounds from P^{III}-aryloxy precursors with the reaction leading to P^{III}–CF_3 groups. Both reactions require the presence of fluoride ions as substrate or catalyst. Our procedure is superior to those described previously.[2, 9]

Received: February 5, 2001
Revised: April 20, 2001 [Z16552]

[1] R. E. Banks, B. E. Smart, J. C. Tatlow, *Organofluorine Chemistry: Principles and Commercial Applications*, Plenum, New York, **1994**.
[2] a) M. Mayer, I. Ugi, W. Richter, *Tetrahedron Lett.* **1995**, *36*, 2047–2050; b) R. M. Karl, W. Richter, R. Klösel, M. Mayer, I. Ugi, *Nucleosides Nucleotides* **1996**, *15*, 379–386.
[3] a) R. P. Singh, J. M. Shreeve, *Tetrahedron* **2000**, *56*, 7613–7632, and references therein; b) R. Schmutzler, L. Heuer, D. Schomburg, *Phosphorus Sulfur Silicon Relat. Elem.* **1993**, *83*, 149–156; c) W. Volbach, I Ruppert, *Tetrahedron Lett.* **1983**, *24*, 5509–5512; d) D. J. Burton, R. M. Flynn, *Synthesis* **1979**, 615; e) K. Gosling, A. B. Burg, *J. Am. Chem. Soc.* **1968**, *90*, 2011–2014; f) R. G. Cavell, R. D. Leary, A. R. Sanger, A. J. Tomlinson, *Inorg. Chem.* **1973**, *12*, 1374–1380; g) R. G. Cavell, A. A. Pinkerton, W. Sim, A. J. Tomlinson, *Inorg. Chem.* **1979**, *18*, 2901–2908; h) F. W. Bennett, H. J. Emelens, R. N. Haszeldine, *J. Chem. Soc.* **1953**, 1565–1571.
[4] I. Ruppert, K. Schlich, W. Volbach, *Tetrahedron Lett.* **1984**, *25*, 2195–2198.
[5] a) F. M. Semchenko, O. G. Eremin, B. I. Martynov, *Zh. Obshch. Khim.* **1992**, *62*, 473–474; *J. Gen. Chem. USSR Engl. Transl.* **1992**, *62*, 385; b) R. P. Singh, A. Vij, R. L. Kirchmeier, J. M. Shreeve, *Inorg. Chem.* **2000**, *39*, 375–377.
[6] W. Dabkowski, I. Tworowska, *Tetrahedron Lett.* **1995**, *36*, 1095–1098.
[7] W. Dabkowski, I. Tworowska, J. Michalski, F. Cramer, *J. Chem. Soc. Chem. Commun.* **1995**, 1435–1436.
[8] Typical procedure for **4**: A solution of CF_3SiMe_3 (10 mmol) in dry THF (20 mL) was added dropwise at room temperature under nitrogen to a stirred mixture of **3** (10 mmol) and CsF (0.1 mmol) in dry THF (20 mL). After 4 h the solvent was evaporated in vacuo. The residue was purified by column chromatography (250–400 mesh silica gel, Merck 9385) or distilled under reduced pressure.

  1433-7851/01/4015-2899 $ 17.50+.50/0

[9] G. M. Blackburn, M.-J. Guo, *Tetrahedron Lett.* **1993**, *34*, 149 – 152.
[10] Typical procedure for **8**. A solution of CF_3SiMe_3 (10 mmol) in dry THF (20 mL) was added dropwise at room temperature under nitrogen to a stirred mixture of bis(4-nitrophenyl) *N*,*N*-diisopropylphosphoramidite **7** (5 mmol) and cesium fluoride (11 mmol) in dry THF (20 mL). After 4 h the cesium 4-nitrophenoxide salt was removed by filtration. The filtrate was concentrated in vacuo, and the residue was purified by distillation under reduced pressure.

The Thioglycoside and Glycosyl Phosphite of 5-Azido Sialic Acid: Excellent Donors for the α-Glycosylation of Primary Hydroxy Groups**

Chung-Shan Yu, Kenichi Niikura, Chun-Cheng Lin,* and Chi-Huey Wong*

N-Acetylneuraminic acid (sialic acid, NeuAc) is often found at the nonreducing end of glycoconjugates associated with important biological recognition events.[1] Although many glycosylation reagents are available for the synthesis of sialosides, addition of sialic acid with absolute α-glycosidic linkage remains a significant challenge.[2] Because of the sterically hindered tertiary anomeric center, the presence of an electron-withdrawing carboxyl group, and the lack of a participating auxiliary substituent adjacent to the anomeric center, most of the existing sialyl donors often have relatively low anomeric reactivities, and the sialylation reaction often proceeds with low yield, low α-stereoselectivity and significant undesirable elimination.

In order to tackle these problems, various new sialyl donors, including sialyl phosphites,[3] thioglycosides,[4] and xanthates,[5] have been developed. These donors give high α-selectivity in reactions with secondary hydroxyl groups, but they exhibit low α-selectivity, when primary hydroxyl groups are used as acceptors.[2a] In most cases, the content of undesirable β isomer ranged from 10 to 50% when secondary hydroxyl groups were used as acceptors and was more than 50% with primary hydroxy groups like the 9-OH group of sialic acid as acceptors. Anchimeric assistance by an auxiliary group at C-3[2d, 6] has been demonstrated to improve α-selectivity.

[*] Prof. Dr. C.-C. Lin, Dr. C.-S. Yu
Institute of Chemistry, Academia Sinica
Nankang, Taipei (Taiwan)
Fax: (+886) 2-2783-1237
E-mail: cclin@chem.sinica.edu.tw
Prof. Dr. C.-H. Wong, Dr. K. Niikura
Department of Chemistry
The Scripps Research Institute
10550 North Torrey Pines Road
La Jolla, CA 92037 (USA)
Fax: (+1) 858-784-2409
E-mail: wong@scripps.edu

[**] This research was supported by Academia Sinica (Taipei) and the NIH (USA).

Supporting information for this article is available on the WWW under http://www.angewandte.com or from the author.

Recently, the di-*N*-acetyl sialyl donor **1** has been shown to exhibit increased reactivity and yield in reaction with the 9- or 8-OH group of an appropriate acceptor,[7] and in certain cases

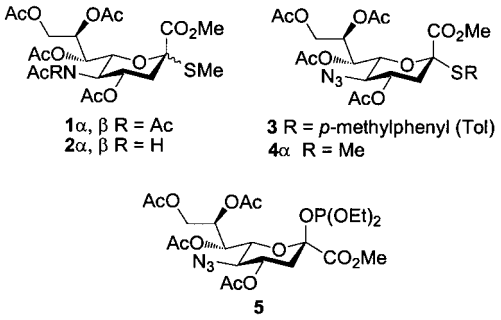

with higher α-selectivity.[8] The sialic acid 8-OH group was thought to engage in an intramolecular hydrogen bonding interaction with the O atom of the C-1 carbonyl or the 2-OR group, or to interact with the 5-NHAc group of **2**, thus weakening the nucleophilic activity.[7]

This undesirable interaction was circumvented by further acetylation of the NHAc group, and the NAc_2 derivative **1** gave an increased glycosylation yield;[7a] however, the α-selectivity was not improved, and a significant amount of β isomer was present in the product (ca. 30%). We report here the use of the thiosialosides **3** and **4** and the corresponding phosphite **5**, in which the 5-NHAc of **2** is replaced with the azido group, as α-selective glycosylation reagents for primary and secondary hydroxyl groups as acceptors. Sialylation reagents with a 5-azido group have been described in the literature,[9] but their effect on reactivity or stereoselectivity has not been studied, except that a low-yield (ca. 26%) sialylation was reported.[9b]

To prepare the glycosyl donors, the sialyl chloride **6**[10a] was treated with *p*-thiocresol in the presence of Hünig's base to give the α-thioglycoside **7**[10b] in crystalline form (Scheme 1). Subsequent N acetylation of **7** to give **8** could be easily achieved in high yield by treatment with isopropenyl acetate and a catalytic amount of TsOH.[7a] Complete deacetylation[11] of **7** followed by a catalytic diazo transfer[12] and acetylation of the hydroxyl groups gave **3**. The methylsulfanyl-substituted

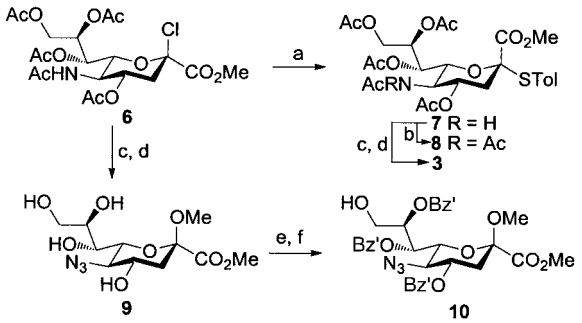

Scheme 1. a) Thiocresol, $NEtiPr_2$, CH_2Cl_2, RT, 18 h, 85%. b) Isopropenyl acetate, cat. TsOH, 60 °C, 15 h, 95%. c) MsOH, MeOH, 60 °C, 24 h, 55%. d) 1) TfN_3, $CuSO_4 \cdot 5H_2O$, MeOH, RT, 18 h; 2) Ac_2O, py, RT, 4 h (66% for two steps). e) *t*$BuMe_2SiCl$, py, DMAP, CH_2Cl_2, RT, 24 h, then *p*-ClC_6H_4COCl (Bz′Cl), RT, 18 h, 86%. f) HF/py, AcOH, THF, RT, 1 h, 94%.

  1433-7851/01/4015-2900 $ 17.50+.50/0

donors **1**[7a] and **2**[13] were synthesized as α/β mixtures according to the reported procedures. The α- and β-5-N_3 methylsulfanyl-substituted donors **4** were obtained from **2** by using similar methods as described in the synthesis of **3**. Under the acidic N,O deacetylation conditions, the Cl substituent of **6** was replaced by OMe; afterwards, the free amine was converted to azide to give **9**, which was further transformed to acceptor **10** as shown in Scheme 1.

We then turned our efforts to investigate the sialylation reactions, which were proceeded under standard reaction conditions. Acceptor **10** (1 equiv) was reacted with donor **3** (2 equiv) in the presence of NIS (3 equiv to donor), TfOH (3–10 mol% to NIS), and molecular sieves (3 Å) in MeCN at $-40\,^{\circ}C$ to give disaccharide **11** with exclusive formation of the hydroxy groups as acceptors (data not shown). The higher α-selectivity may be attributed to the formation of a more stable acetonitrile intermediate, **18**, and the less steric hindrance in the α face caused by the linear azido group.

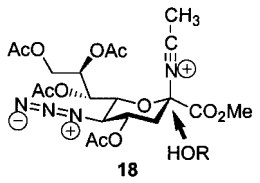

18

When the reaction solvent was changed to CH_2Cl_2, significant amounts of elimination (from donor) and acyl migration (from acceptor) products were found.

To further understand the azido group effect, we compared the relative reactivity values (measured by HPLC using methanol as acceptor and NIS as activator according to the procedure described previously[14]) of some sialylation reagents (Scheme 2). It is clear that the azido group has a

Table 1. Sialylation reactions leading to products **11**–**17**.

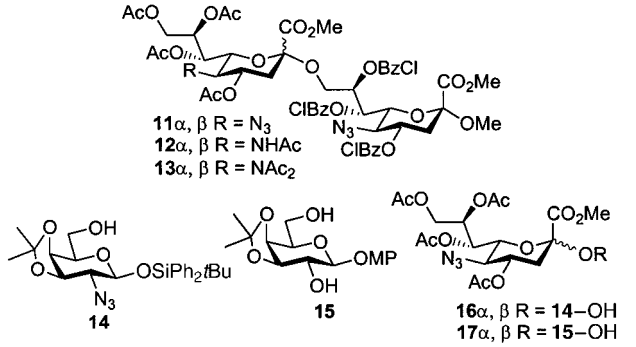

Entry	Donor	Acceptor	Product	Yield [%]	α:β
1	**3**	**10**	**11**α	65	α only
2	**4**α	**10**	**11**α	63	α only
3	**4**β	**10**	**11**α	60	α only
4	**7**	**10**	**12**α,β	75	3:1
5	**2**α,β	**10**	**12**α,β	60	2:1
6	**8**	**10**	**13**α,β	30	4:5
7	**1**α,β	**10**	**13**α,β	40	4:5
8	**3**	**14**	**16**α,β	53	10:1
9	**3**	**15**	**17**α,β	35	3:1

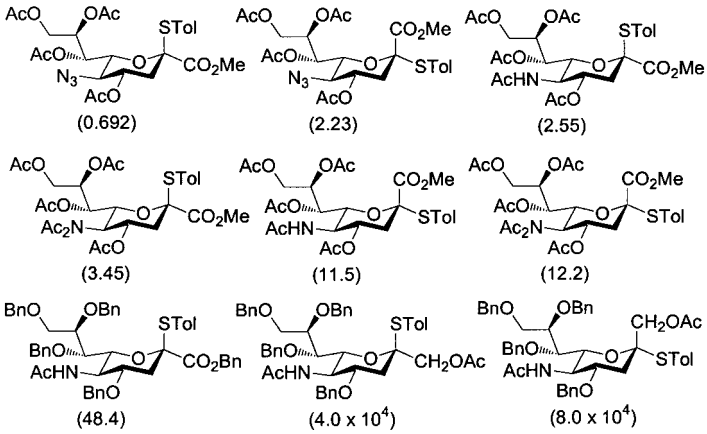

Scheme 2. The relative reactivity values (in parentheses) of sialic acid thioglycosides. The values are based on the corresponding α-thioglycoside of peracetylated mannose.

α isomer in 65% yield (Table 1). To our knowledge, this is the best α-selective sialylation reported so far for the synthesis of the disaccharide Neu5Acα(2→9)Neu5Ac.[2, 4, 7] Both donors **3** and **4** showed similar results (Table 1, entries 1–3), and the anomeric chirality of **4** did not influence α-selectivity and yield (entries 2 and 3). When the same acceptor was reacted with the thioglycoside donors **2** or **7** to give **12**, the α-selectivity decreased (entries 4 and 5). Notably, when acceptor **10** was treated with the di-*N*-acetyl donors **1** or **8** to give **13**, the yield and α-selectivity dramatically decreased (entries 6 and 7).

In order to further demonstrate that the azido donor **3** is a better α-selective donor for primary hydroxyl groups as acceptors, syntheses of the terminal disaccharides sialyl Tn antigen and GM_4 using acceptors **14** and **15** (MP = *p*-methoxyphenyl) were undertaken, and again the α-selectivity was better than with the corresponding 5-NHAc sialyl donors. In addition, the small amount of contaminating 5-azido β isomer can be easily separated by silica gel column chromatography. A similar result was obtained with secondary significant deactivation effect, and both *N*-acetyl and di-*N*-acetyl groups exhibit little difference. Reduction of the anomeric carboxyl group to a hydroxymethyl group remarkably enhances the anomeric reactivity; however, these glycosyl donors gave predominantly the β isomer in glycosidation.[15] Taken together, the azido group effect is apparently both electronic and steric: the linear and electron-withdrawing nature of N_3 stabilizes the reactive axial acetonitrile adduct[2a, 3b, 4] to allow the incoming nucleophile to approach the α face in an SN_2-like reaction.

In order to use the new azido sialyl donors in the synthesis of NeuAcα(2→9)NeuAc containing saccharides, the chemoselective glycosylation strategy[16] was applied. It has been reported that glycosyl phosphites and thioglycosides can be activated by TMSOTf and NIS/TfOH, respectively.[3, 4] The azido phosphite **5** and the azido thiocresol **20** were thus chosen as donor and acceptor, respectively, for the chemoselective glycosylation (Scheme 3). Thioglycoside **3** was treated with NBS followed by diethyl phosphochloridite[17] to give **5**. Compound **20** was obtained from **19** by using a similar method as described in the synthesis of **9**. The glycosylation of **20** by **5** was proceeded in CH_3CN at $-40\,^{\circ}C$ in the presence of TMSOTf to give **21** exclusively in the α

  1433-7851/01/4015-2901 $ 17.50+.50/0

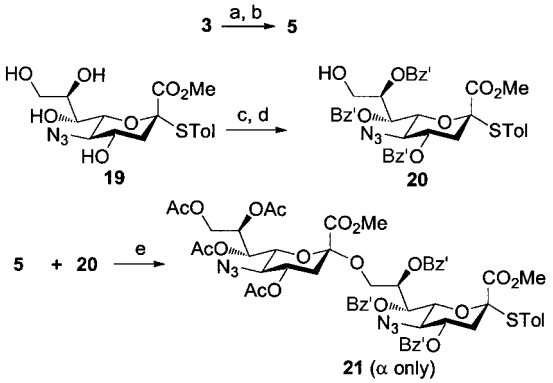

Scheme 3. a) NBS, acetone/H_2O, RT, 1 h, 91%. b) NEt_iPr_2, $ClP(OEt)_2$, CH_3CN, RT, 30 min, 65%. c) tBuMe$_2$SiCl, py, DMAP, CH_2Cl_2, RT, 1 h, then Bz′Cl, 0 °C to RT, 1 h, 88%. d) HF/py, AcOH, THF, 1 h, 89%. e) TMSOTf, 3 Å MS, CH_3CN, −40 °C, 30 min, 51%.

form (51%). Having the thiocresol leaving group, **21** is ready for the next glycosylation. The anomeric configurations of these sialodisaccharides were determined by NMR spectroscopy[7a, 13] based on the chemical shifts of H′-3e (α-glycosides are more downfield than β-glycosides), H′-4 (α-glycosides: $\delta < 5$, β-glycosides: $\delta > 5$), and the value of $\Delta\delta$\{H′9a, H′9b\} (α-glycosides: $\Delta\delta \sim 0.2$ ppm, β-glycosides: $\Delta\delta > 0.3$ ppm) as shown in Table 2.

Table 2. Partial ^{1}H NMR assignments of sialyl products.

	$\delta(H'_{3e})$	$\delta(H'_4$	$\lvert\delta(H'_{9a}) - \delta(H'_{9b})\rvert$
11α	2.59	4.72	0.16
21α	2.61	4.74	0.18
12α	2.46	4.75	0.07
23α	2.68	4.94	–
12β	2.31	5.08	0.68
23β	2.49	5.22	–
13α	2.64	5.41	0.20
25	2.57	5.22	–
13β	2.52	5.75	0.55
27α	2.52	4.76	0.39
16α	2.62	4.83	0.10
27β	2.45	5.12	0.51
16β	2.86	5.33	1.54
28α	2.53	4.77	–
17α	2.74	4.86	0.18
28β	2.49	5.14	–
17β	2.56	5.25	0.35
30	2.60	4.72	–

In order to investigate the effect of other protecting groups on the glycosylation stereoselectivity of the 5-azido sialyl donors, compound **22** was prepared from **19** and reacted with acceptor **10** under the standard conditions (Scheme 4). The product **23** obtained, however, contained a significant amount of the β isomer. Surprisingly, coupling of the α-linked disaccharide donor **21** with **24** (obtained from **23** by selective deprotection of the primary hydroxy group) gave only the β product **25**. Using the less hindered donor **26** with OAc at C-4 did not improve the α-selectivity (Scheme 5, for **27** and **28**). Coupling of **3** and **24**, however, gave mainly

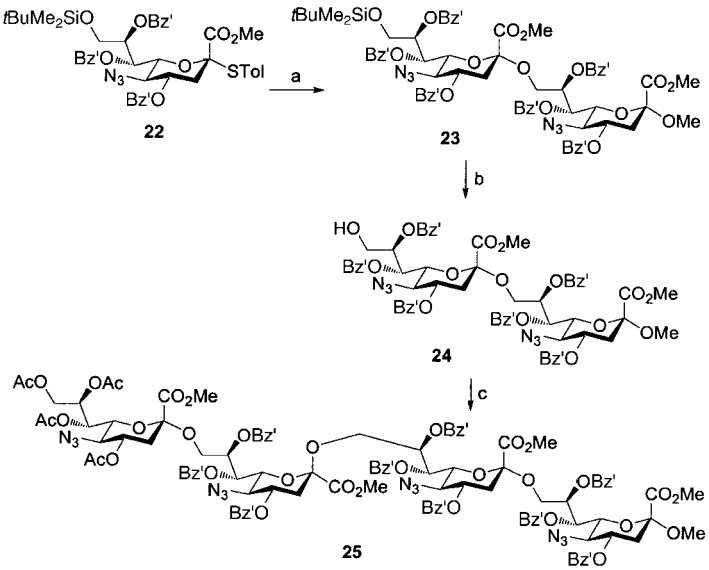

Scheme 4. a) **10**, NIS, TfOH, CH_3CN, 3 Å MS, −40 °C, 1 h, 51%, $\alpha:\beta =$ 1.1:1. b) HF/py, AcOH, THF, 1 h, 90%. c) **21**, NIS, TfOH, CH_3CN, 3 Å MS, −40 °C, 1 h, 32%, β.

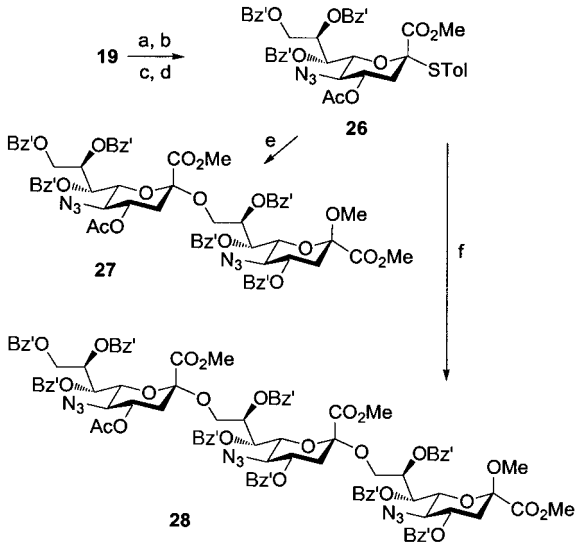

Scheme 5. a) 2,2-Dimethoxypropane, PTSA, 1 h, 90%. b) Ac_2O, py, −78 °C, 70%. c) 90% AcOH, 50 °C, 1 h. d) Bz′Cl (75%, for c and d). e) **10**, NIS, TfOH, CH_3CN, 3 Å MS, −40 °C, 2 h, 50%, $\alpha:\beta = 5:4$. f) **24**, NIS, TfOH, CH_3CN, 3 Å MS, −40 °C, 40%, $\alpha:\beta = 1:2$.

the α product ($\alpha/\beta = 6/1$) in 60% yield (not shown). In another experiment, compound **21** was converted to the peracetylated donor **29**, which was coupled with **10** to give the trisaccharide **30** in 45% yield with exclusive α-glycosidic linkage (Scheme 6). It appears that bulky substituents could override the azido group effect on the glycosylation stereoselectivity. The optimal sialyl donors for selective α-sialylation of the NeuAc 9-OH group are the 5-azido derivatives with *O*-acetyl protecting groups, including **3**–**5** and **29**.

In conclusion, it has been demonstrated that 5-azido sialyl donors with *O*-acetyl protecting groups are useful α-selective glycosylation reagents, especially for primary hydroxy groups as acceptors. In addition, a chemoselective glycosylation

  1433-7851/01/4015-2902 $ 17.50+.50/0

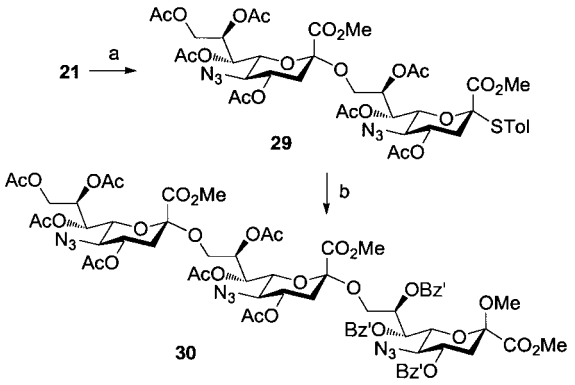

Scheme 6. a) 1) NaOMe, MeOH; 2) Ac_2O, py, RT, 85% for both steps. b) **10**, NIS, TfOH, CH_3CN, 3 Å MS, $-40\,^{\circ}C$, 1 h, 45%, α.

method has been developed for the synthesis of NeuAcα-(2→9)NeuAc as thioglycoside donor for use in subsequent glycosylations. The azido group can be reduced to the NH_2 group for acetylation or incorporation of other substituents. The method described for the synthesis of α-2,9-linked oligomers of sialic acid may find use in the preparation of carbohydrate-based vaccines.[1, 2]

Received: February 23, 2001 [Z16674]

[1] a) *Sialobiology and Other Novel Forms of Glycosylation* (Eds.: Y. Inoue, Y. C. Lee, F. A. Troy II), Gakushin, Osaka, **1999**; b) *Biology of the Sialic Acids* (Ed.: A. Rosenberg), Plenum, New York, **1995**.

[2] a) G.-J. Boons, A. V. Demchenko, *Chem. Rev.* **2000**, *100*, 4539; b) C.-H. Lin, C.-C. Lin in *The Molecular Immunology of Complex Carbohydrates 2* (Ed.: A. M. Wu), Kluwer/Plenum, New York, **2001**; c) M. P. DeNinno, *Synthesis* **1991**, 583; d) K. Okamoto, T. Goto, *Tetrahedron* **1990**, *46*, 5835; e) B. G. Davis, *J. Chem. Soc. Perkin Trans. 1* **2000**, 2137.

[3] a) H. Kondo, Y. Ichikawa, C.-H. Wong, *J. Am. Chem. Soc.* **1992**, *114*, 8748; b) T. J. Martin, R. R. Schmidt, *Tetrahedron Lett.* **1992**, *33*, 6123.

[4] A. Hasegawa in *Modern Methods in Carbohydrate Synthesis* (Eds.: S. H. Khan, R. A. O'Neil), Harwood, The Netherlands, **1996**.

[5] a) K. M. Halkes, P. M. St. Hilaire, A. M. Jansson, C. H. Gotfredsen, M. Meldal, B. G. Davis, *J. Chem. Soc. Perkin Trans. 1* **2000**, 2127; b) A. Marra, P. Sinaÿ, *Carbohydr. Res.* **1990**, *195*, 303; c) V. Martichonok, G. M. Whitesides, *J. Org. Chem.* **1996**, *61*, 1702; d) H. Lönn, K. Stenvall, *Tetrahedron Lett.* **1992**, *33*, 115.

[6] a) J. C. Castro-Palomino, Y. E. Tsvetkov, R. R. Schmidt, *J. Am. Chem. Soc.* **1998**, *120*, 8508; b) V. Martichonok, G. M. Whitesides, *J. Am. Chem. Soc.* **1996**, *118*, 8187; c) T. Ercégovic, G. Magnusson, *J. Org. Chem.* **1995**, *60*, 3378; d) Y. Ito, T. Ogawa, *Tetrahedron Lett.* **1988**, *29*, 3987; e) Y. Ito, S. Nunomura, S. Shibayama, T. Ogawa, *J. Org. Chem.* **1992**, *57*, 1821.

[7] a) A. V. Demchenko, G.-J. Boons, *Chem. Eur. J.* **1999**, *5*, 1278; b) A. V. Demchenko, G.-J. Boons, *Tetrahedron Lett.* **1998**, *39*, 3065.

[8] N. Hossain, G. Magnusson, *Tetrahedron Lett.* **1999**, *40*, 2217.

[9] a) M. A. Sparks, K. W. Williams, C. Lukacs, A. Schrell, C. Priebe, A. Spaltenstein, G. M. Whitesides, *Tetrahedron* **1993**, *49*, 1; b) G. Kuznik, B. Horsch, G. Kretzchmar, C. Unverzagt, *Bioorg. Med. Chem. Lett.* **1997**, *7*, 577.

[10] a) A. Marra, P. Sinaÿ, *Carbohydr. Res.* **1989**, *190*, 317; b) A. Marra, P. Sinaÿ, *Carbohydr. Res.* **1989**, *187*, 35.

[11] T. Sugata, Y. Kan, Y. Nagaregawa, T. Miyamoto, R. J. Higuchi, *J. Carbohydr. Chem.* **1997**, *16*, 917.

[12] P. B. Alper, S.-C. Hung, C.-H. Wong, *Tetrahedron Lett.* **1996**, *37*, 6029.

[13] a) A. Hasegawa, H. Ohki, T. Nagahama, H. Ishida, M. Kiso, *Carbohydr. Res.* **1991**, *212*, 277; b) O. Kanie, M. Kiso, A. Hasegawa, *J. Carbohydr. Chem.* **1988**, *7*, 501; c) K. Okamoto, T. Kondo, T. Goto, *Bull. Chem. Soc. Jpn.* **1987**, *60*, 637; d) H. Paulsen, H. Teitz, *Carbohydr. Res.* **1984**, *125*, 47; e) D. J. M. Van der Vleugel, W. A. R. Van Heeswijk, J. F. G. Vliegenthart-Hart, *Carbohydr. Res.* **1982**, *102*, 121; f) U. Dabrowski, H. Friebolin, R. Brossmer, M. Supp, *Tetrahedron Lett.* **1979**, *48*, 4637.

[14] Z. Zhang, I. R. Ollmann, S.-S. Ye, R. Wischnat, T. Baasov, C.-H. Wong, *J. Am. Chem. Soc.* **1999**, *121*, 734.

[15] X.-S. Ye, X. Huang, C.-H. Wong, *Chem. Commun.*, in press.

[16] a) Y. Ito, O. Kanie, T. Ogawa, *Angew. Chem.* **1996**, *108*, 2691; *Angew. Chem. Int. Ed. Engl.* **1996**, *35*, 2510; b) T. Zhu, G.-J. Boons, *Angew. Chem.* **1998**, *110*, 2000; *Angew. Chem. Int. Ed.* **1998**, *37*, 1898.

[17] T. M. Martin, R. Brescello, A. Toepfer, R. R. Schmidt, *Glycoconjugate J.* **1993**, *10*, 16.

Enzyme-Activated Gd^{3+} Magnetic Resonance Imaging Contrast Agents with a Prominent Receptor-Induced Magnetization Enhancement**

Alexander L. Nivorozhkin, Andrew F. Kolodziej, Peter Caravan, Matthew T. Greenfield, Randall B. Lauffer, and Thomas J. McMurry*

Gadolinium-based contrast agents for magnetic resonance imaging (MRI) enhance tissue contrast by increasing the relaxation rate ($1/T_1$) of water protons and are widely used in clinical diagnostics.[1] These compounds are mainly extracellular agents with nonspecific biodistribution. A new generation of contrast agents, currently under development, targets macromolecules associated with specific tissues or disease states, and thereby localizes the agent to the site of interest.[1, 2] Moreover, the binding of the agents to a macromolecule substantially slows molecular rotation of the Gd^{3+} complex resulting in an additional increase in the relaxivity and tissue contrast, a phenomenon known as RIME (receptor-induced magnetization enhancement).[3] The blood pool RIME agent MS-325, currently in Phase III clinical trials for noninvasive angiography, binds noncovalently to human serum albumin (HSA). It greatly reduces extravasation of the agent to surrounding tissue and increases the relaxivity five- to tenfold relative to the relaxivity in the absence of HSA binding.

The scope of targeted MRI agents is potentially limited in that many useful targets associated with disease states are present at nanomolar concentrations, which is too low to be accessible to MRI by the RIME approach alone. One method for localizing a high concentration of an agent at these targets is to exploit an enzymatic activity specific to the tissue or disease state to convert an MRI-silent agent into an activated MRI agent. In a model of this approach, β-galactosidase was used to change the ligand environment around a Gd^{3+} center

[*] Dr. T. J. McMurry, Dr. A. L. Nivorozhkin, Dr. A. F. Kolodziej, Dr. P. Caravan, M. T. Greenfield, Dr. R. B. Lauffer
EPIX Medical, Inc.
71 Rogers Street
Cambridge, MA 02142 (USA)
Fax: (+1) 617-250-6128
E-mail: tmcmurry@epixmed.com

[**] We thank Dr. Shrikumar Nair for helpful discussions.

  1433-7851/01/4015-2903 $ 17.50+.50/0

and the hydration number of an agent, and resulted in signal enhancement.[4]

We report here a new strategy in which a specific bioactivity can be coupled to the RIME mechanism to generate enhancement of the MRI signal (Scheme 1). The approach relies upon enzymatic transformation of a prodrug Gd^{3+} complex with poor HSA affinity and concomitant low relaxivity (a pro-RIME agent) to a species with improved HSA affinity and enhanced relaxivity. The conversion involved enzymatic removal from the Gd^{3+} complex of a masking group that inhibits HSA binding to expose a binding group with high HSA affinity.

Pro-RIME contrast agents **1** and **5** (Scheme 1) were designed to be cleaved by a human carboxypeptidase B, thrombin-activatable fibrinolysis inhibitor (TAFI). TAFI inhibits clot degradation by cleaving C-terminal lysine residues exposed on fibrin binding sites that are recognized by fibrinolytic proteases such as tPA and plasminogen.[5a,b] This enzyme functions at the crossroads of coagulation and fibrinolysis and has been implicated in thrombotic disease.[5c] The pro-RIME agents are composed of four moieties: 1) a masking group consisting of three lysine residues; 2) an HSA binding group; 3) a glycine linker; and 4) a signal generation group, Gd-DTPA. The trilysine masking group was selected because charged groups have generally poor HSA affinity[6, 7] and the C-terminal lysine residues were expected to be good substrates for cleavage by TAFI. Aryl groups are known to confer high HSA binding affinity,[1, 8, 9] and therefore the diphenylalanine and 3,5-diiodotyrosine residues in complexes **1** and **5**, respectively, were expected to bind well to HSA and enhance the agent's relaxivity when unmasked by TAFI turnover.

The relaxivity and HSA binding data of the trilysine pro-RIME agents at 24 and 37 °C as well as their final products from the enzymatic reaction are given in Table 1. In the absence of HSA, the relaxivities of **1** and the lysine-free product **4** are nearly identical. However, in the presence of 4.5 % (w/v) HSA at 24 °C, the relaxivity of **4** is enhanced by a factor of 30 % over **1** as a consequence of a significantly higher HSA binding affinity; at 37 °C, where the exchange of gadolinium-bound water molecules is more facile, the increase in relaxivity is over 100 %.

Table 1. Relaxivity (20 MHz) and HSA binding data.

Compound	r_1 [$mM^{-1}s^{-1}$] PBS[a]	(24 °C) HSA[b]	r_1 [$mM^{-1}s^{-1}$] PBS[a]	(37 °C) HSA[b]	[%] HSA bound
1	8.4	15.2	7.8	11.1	21.7
4	8.3	19.2	7.7	24.5	69.8
5	9.7	12.5	7.7	9.8	3.9
8	8.1	25.2	7.7	26.5	72.1

[a] Phosphate buffered saline (10 mM sodium phosphate, 150 mM sodium chloride, pH 7.4). [b] Human serum albumin (4.5 % w/v).

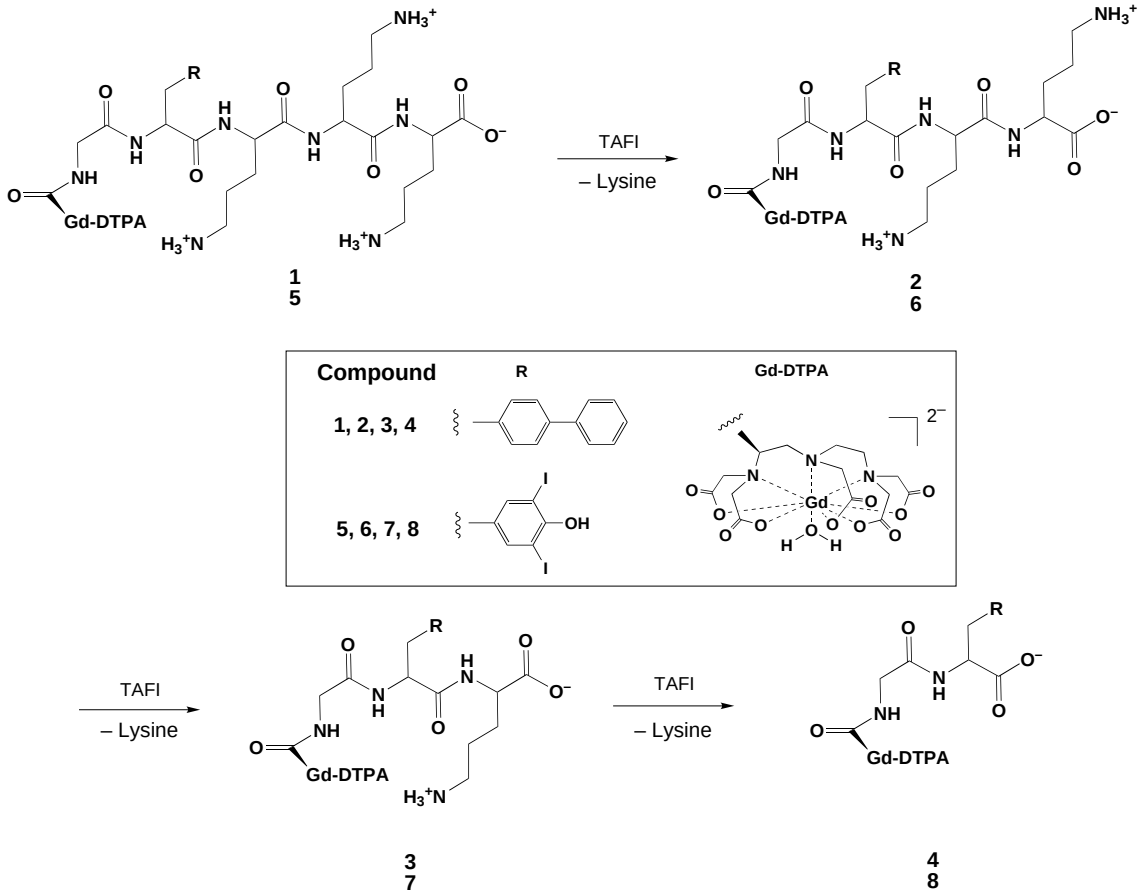

Scheme 1. Bioactivated Gd^{3+} contrast agents: a Gd^{3+} chelate (signaling domain) is coupled to an HSA binding moiety that is masked by an HSA shielding group. Enzyme activation releases the shielding group and promotes HSA binding.

  1433-7851/01/4015-2904 $ 17.50+.50/0

Complex **1** is rapidly converted into **4** at physiological concentrations of TAFI (75 nM). The kinetic parameters for the disappearance of **1** ($K_m = 340$ μM, $k_{cat} = 5.3\ s^{-1}$) are comparable to other substrates of TAFI such as hippurylarginine[10] ($K_m = 140$ μM, $k_{cat} = 21\ s^{-1}$). A reaction profile of the turnover of **1** (230 μM) by TAFI (75 nM) in the presence of 4.5% HSA (Figure 1A) was complete within one hour.

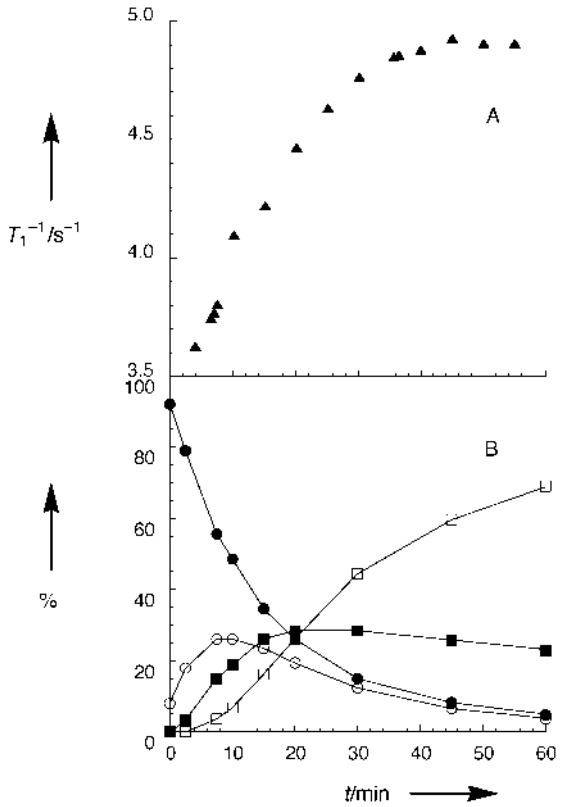

Figure 1. A) Time course of the TAFI-induced change in the relaxation rate of 0.2 mM **1** at 20 MHz in the presence of 4.5% (w/v) HSA. B) Time course of the conversion of **1** into **4**; the distribution of reaction species was quantified by HPLC: **1**: ●, **2**: ○, **3**: ■, **4**: □.

Analysis of the reaction mixture by high-pressure liquid chromatography (HPLC) after quenching at various times confirmed the production of the dilysine and monolysine intermediates **2** and **3**, respectively, as well as **4**. The increases in the $1/T_1$ values most closely paralleled the disappearance of **1** (Figure 1B). The value of $1/T_1$ increased from 3.6 to 4.8 s^{-1} between 0 and 30 min, while 85% of **1** was converted into **4** or intermediates. The value of $1/T_1$ changed only slightly (from 4.8 to 5.0 s^{-1}) between 30 and 60 min, while the concentration of **4** increased by 55% from 100 to 160 μM. Removal of the two C-terminal lysine residues resulted in the majority of the $1/T_1$ increase, whereas removal of the third lysine residue appeared to be less critical for achieving a significant RIME effect.

A second compound, **5**, exhibited a greater TAFI-induced RIME effect than **1**. The relaxivities of **5** and the non-lysine compound **8** in the presence of 4.5% HSA at 24 °C were 12.5 and 25.2 $mM^{-1}s^{-1}$, respectively. Complete conversion of **5** into **8** by TAFI was achieved at a micromolar enzyme concentration and generated an expected 100% relaxivity enhancement as a result of the observed 18-fold increase in the HSA binding activity. A reaction profile of TAFI reaction at nanomolar level (200 μM **5**, 75 nM TAFI, 4.5% w/v HSA), as monitored by the change in $1/T_1$, yielded a smaller effect because of the slower cleavage of the third lysine residue which competed with autoinactivation of TAFI. The monolysine intermediate **7** represented 83% of all the species at 30 min, whereas **8** accounted for 5% of the total. In contrast to **1**, removal of the third lysine residue was essential for attaining the maximal increase in the value of $1/T_1$. At the endpoint of the turnover by TAFI, **7** and **8** represented 44 and 51% of the reaction mixture, respectively, but the $1/T_1$ value had only increased by 26% to 3.8 s^{-1}. Although an approximately threefold relaxivity enhancement can ultimately be reached at 37 °C (Table 1), extended exposures of **5** to TAFI will be required to achieve a beneficial signal enhancement profile in vivo.

In summary, the feasibility of using MRI to detect an enzyme associated with a disease state was illustrated with an efficient pro-RIME contrast agent/TAFI/HSA system that resulted in clinically relevant relaxivity enhancement of the contrast agent. The bioactivation of the MRI agents we have described extends the RIME strategy to the detection of targets present at submicromolar concentrations. Work is in progress to apply this strategy to detecting other protease activities associated with disease states, such as matrix metalloproteinases (MMPs), which have been identified with certain types of cancer, or elastase, an enzyme associated with inflammation sites.

Experimental Section

The DTPA–peptide conjugates **1**, **4**, **5**, and **8** were prepared using 9-fluorenylmethoxycarbonyl (Fmoc) chemistry on a PAC-PEG-PS support with coupling methods based on *N*-[(dimethylamino)-1*H*-1,2,3-triazole[4,5-*b*]-pyridin-1-ylmethylene]-*N*-methylmethanaminium hexafluorophosphate/*N*,*N*-diisopropylethylamine (HATU/DIPEA). The resin was cleaved in trifluoroacetic acid/triisopropylsilane/water (TFA/TIS/H_2O; 45/1/1) for 2 h and the products purified by reversed-phase HPLC on a C_{18} column using a linear gradient of 0.1% TFA in acetonitrile and 0.1% aqueous TFA. The Gd^{3+} complexes were prepared in aqueous solution by treating the ligands with $GdCl_3$ at pH 5.5–7.5. The final Gd^{3+} concentrations were measured by inductively coupled plasma mass spectrometry (ICP-MS). The identity and purity of the ligands and Gd^{3+} complexes was confirmed by electrospray mass spectroscopy (ES-MS) and LC-MS methods.

The progress of enzymatic turnover of **1** and **5** was followed by measuring $1/T_1$ values. TAFI was activated prior to the reaction for 10 min at room temperature as a mixture of TAFI (250 nM) in thrombin (10 nM), thrombomodulin (25 nM) in 2-[4-(2-hydroxyethyl)-1-piperazinyl]ethanesulfonic acid (HEPES, 10 mM), NaCl (150 mM), and $CaCl_2$ (5 mM) at pH 7.5. All enzymes were purchased from Haematologic Technologies, Inc. (Essex Junction, VT). Upon addition of TAFI to the substrate, the reaction contained 75 nM TAFI, 200 μM **1** or **5**, 4.5% HSA, 3 mM HEPES, 7 mM sodium phosphate, 100 mM NaCl, and 1.5 mM $CaCl_2$ in a volume of 1 mL at pH 7.5. Aliquots for HPLC analysis (50 μL) were removed at various time points and quenched by the addition of TFA to a concentration of 1%. Reaction products were identified by HPLC and LC-MS and quantified by peak integration (absorbance at 220 nm). The activity of TAFI rapidly decreases at elevated temperatures[5c] which limited data collection conditions to 2 h at 24 °C.

The percentage of HSA binding was determined by ultrafiltration. The complex (100 μM) was incubated with 4.5% HSA in a solution containing 10 mM sodium phosphate and 100 mM NaCl at pH 7.5 (PBS; 15 min at

  1433-7851/01/4015-2905 $ 17.50+.50/0

37 °C) and the mixture was filtered in a UltraFree MC 30000 MWCO centrifugal filtration unit (Millipore) at 3500 g for 7 min at 37 °C. The concentration of free substrate in the filtrate was quantified by ICP-MS and the bound fraction was calculated as % bound = ([total]-[free])/[total].

The proton T_1 (longitudinal NMR relaxation time) value of water was measured at 20 MHz at 24 and 37 °C by inversion recovery on a Brucker Minispec; the data were obtained in PBS or with 4.5 % HSA by using 0–40 μM of the Gd^{3+} complex. The relaxivity (r_1) was determined from the slope of the plot of $1/T_1$ versus the sample concentration.

Received: March 19, 2001 [Z16799]

[1] P. Caravan, J. J. Ellison, T. J. McMurry, R. B. Lauffer, *Chem. Rev.* **1999**, *99*, 2293.

[2] R. B. Lauffer, D. J. Parmelee, S. Dunham, H. S. Ouellet, R. P. Dolan, S. Witte, T. J. McMurry, R. C. Walovich, *Radiology* **1998**, *207*, 529.

[3] Another strategy to improve the rotational correlation times and the relaxivity of the contrast agent consists of using polymer and dendrimer conjugates, although no such drugs have been reported to be at an advanced development stage.

[4] a) A. Y. Louiem, M. M. Huber, E. T. Ahrens, U. Rothbacher, R. Moats, R. E. Jacobs, S. Fraser, T. J. Meade, *Nat. Biotechnol.* **2000**, *18*, 321; b) R. A. Moats, S. E. Frazer, T. J. Meade, *Angew. Chem.* **1997**, *109*, 750; *Angew. Chem. Int. Ed. Engl.* **1997**, *36*, 726. Other recent examples of the Gd^{3+}-based MRI-targeted contrast agents and sensors are: c) W.-h. Li, S. E. Fraser, T. J. Meade, *J. Am. Chem. Soc.* **1999**, *121*, 1413; d) G. Lemieux, K. J. Yarema, C. L. Jacobs, C. R. Bertozzi, *J. Am. Chem. Soc.* **1999**, *121*, 4278; e) R. Bhorade, R. Weissleder, T. Nakakoshi, A. Moore, C.-H. Tung, *Bioconjugate Chem.* **2000**, *11*, 301; f) M. P. Lowe, D. Parker, *Chem. Commun.* **2000**, 707.

[5] a) D. L. Eaton, B. E. Malloy, S. P. Tsai, W. Henzel, D. Drayna, *J. Biol. Chem.* **1991**, *266*, 21833; b) L. Bajzar, R. Manuel, M. E. Nesheim, *J. Biol. Chem*. **1995**, *270*, 14477; c) M. E. Nesheim, *Fibrinolysis Proteolysis* **1999**, *13*, 72.

[6] T. Peters, Jr., *All About Albumin: Biochemistry, Genetics and, Medical Applications*, Academic Press, San Diego, **1996**.

[7] R. B. Lauffer, T. J. McMurry, S. Dunham, D. Scott, D. J. Parmelee, S. Dumas, WO-A 97/36619 [*Chem. Abstr*. **1997**, *127*, 316334.

[8] S. Aime, M. Chiaussa, G. Digilio, E. Gianolio, E. Terreno, *J. Biol. Inorg. Chem*. **1999**, *4*, 66.

[9] R. B. Lauffer, T. J. Brady, EP-A 222,886 B1 [*Chem. Abstr*. **1990**, *113*, 94083.

[10] L. Bajzar, J. Morser, M. E. Nesheim, *J. Biol. Chem.* **1996**, *271*, 16603.

Butane-2,3-Diacetal-Desymmetrized Glycolic Acid—A New Building Block for the Stereoselective Synthesis of Enantiopure α-Hydroxy Acids**

Elena Díez, Darren J. Dixon, and Steven V. Ley*

Of the many classes of functional groups and motifs present in biologically and pharmacologically important compounds, mono- or dialkylated α-hydroxy acids occur commonly.[1–3] As a result of this feature, a range of synthesis methods has appeared over the years.[4–11] A commonly adopted strategy is the α-alkylation of chiral glycolic acid equivalents.[12, 13] Following our earlier reports using dispiroketal desymmetrization for this purpose, we here report the design, preparation, and alkylation reactions of a new chiral glycolic acid equivalent—the butane-2,3-diacetal-desymmetrized glycolate **1**.[14]

Our synthetic plan relied on a chiral memory procedure[15] whereby the chirality of a readily available 3-halopropane-1,2-diol **2** would be used to fix the chirality of the butane diacetal group in the stereoselective protection step.[16] It was envisaged that the alkyl halide product **3** would undergo ready elimination of hydrogen halide to form the *exo*-methylene enol ether,[17] which, after oxidative cleavage, would yield the facially desymmetrized glycolate **1** (Scheme 1).

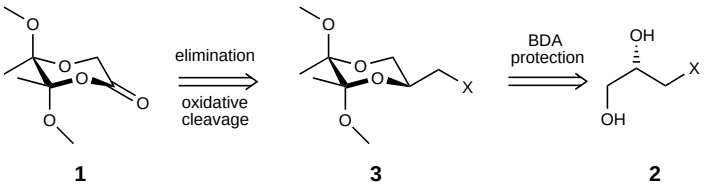

1 **3** **2**

Scheme 1. Synthetic strategy for the development of a BDA-desymmetrized glycolate equivalent (BDA = butane diacetal).

The initial route employed (*S*)-3-bromopropane-1,2-diol **4** (available by the Jacobsen dynamic hydrolytic resolution of epibromohydrin[18]) as starting material. Treatment with butane-2,3-dione (1.1 equiv) in methanol in the presence of trimethyl orthoformate (2.1 equiv) and camphorsulfonic acid (CSA; 0.1 equiv) at reflux for two hours lead to the BDA-protected alkyl bromide **5** as a single diastereomer in 84 % yield (Scheme 2). To a solution of this material in THF at 0 °C was added an excess (1.2 equiv) of potassium hexamethyldisilazide (KHMDS), which on warming to room temperature overnight, effected a smooth elimination to the desired *exo*-methylene enol ether **6** in 85 % yield. Ozonolysis under standard conditions, followed by triphenyl phosphaine workup, gave the desired building block **1** in 69 % yield as a colorless solid. Recrystallization of this material from diethyl ether/hexanes afforded **1** in > 99 % *ee* as determined by chiral GC.

This route was readily modified to allow synthesis on a multigram scale. Thus, the commercially available and relatively cheap (*S*)-3-chloropropane-1,2-diol[19] **7** was used as the starting material. Standard BDA protection of this compound under the identical conditions described for **5** gave the crude BDA adduct **8** which was treated with an excess of potassium *tert*-butoxide in THF at reflux for 30 minutes. Ozonolysis with a dimethyl sulfide (DMS) workup afforded the crude glycolate product as a colorless solid, which on recrystallization from diethyl ether/hexanes gave enantiomerically pure **1** in 56 % yield over the three steps (Scheme 2).

With multigram quantities of enantiopure **1** available, alkylation reactions were investigated. Initial methylation studies with lithium hexamethyldisilazide (LHMDS) and methyl iodide revealed a strong dependence of the crude

[*] Prof. Dr. S. V. Ley, Dr. E. Díez, Dr. D. J. Dixon
Department of Chemistry, University of Cambridge
Lensfield Road, Cambridge CB2 1EW (UK)
Fax: (+44) 1223-336-442
E-mail: svl1000@cam.ac.uk

[**] We thank the EU (Marie Curie Fellowship to E.D.), the EPSRC (to D.J.D.), the Novartis Research Fellowship (to S.V.L.), and Pfizer Gobal Research and Development, Groton, USA, for financial support.

  1433-7851/01/4015-2906 $ 17.50+.50/0

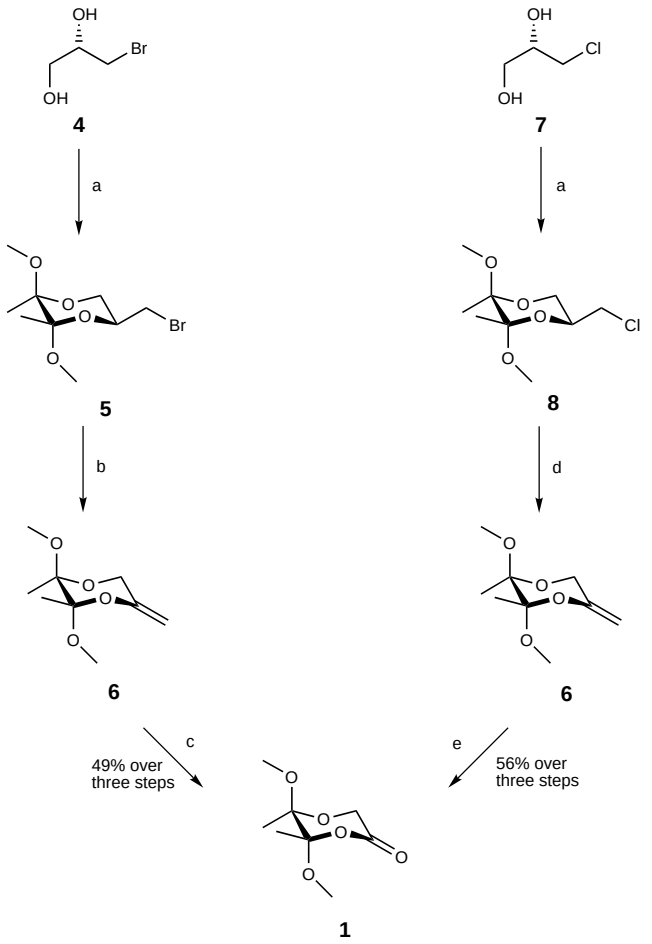

Scheme 2. Synthesis of BDA-desymmetrized glycolic acid from 1-halopropane-2,3-diols. a) MeCOCOMe (1.1 equiv), CSA (0.1 equiv), $CH(OMe)_3$ (2.1 equiv), MeOH, reflux, 2 h; b) KHMDS (1.2 equiv), THF, 0 °C→RT; c) O_3, CH_2Cl_2, −78 °C, then PPh_3 (1.1 equiv), −78 °C→RT; d) *t*BuOK (2.0 equiv), THF, reflux, 2 h; e) O_3, CH_2Cl_2/MeOH (1:1), −78 °C, then DMS (2.0 equiv), −78 °C→RT.

diastereomeric ratio (d.r.) on the equivalents of base used. Thus, with 1.05 equivalents of LHMDS, **9** and **10** were afforded in an excellent 70:1 ratio, alongside a small amount (≤10%) of dimethylated material. However, with 0.90 equivalents of LHMDS, the same products **9** and **10** were formed in the ratio of 9:1 with a yield of 84% at 93% conversion (Scheme 3).

Encouraged by these initial results we examined the alkylation reactions of **1** further. However, care was taken to ensure that the observed selectivity in the reactions was due

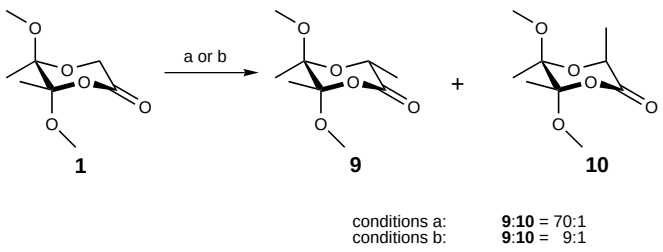

Scheme 3. Lithium enolate methylations of **1**. a) LHMDS (1.05 equiv), THF, −78 °C, 10 min, then MeI (3.0 equiv), −78 → −30 °C over 2 h, then AcOH (2.0 equiv); b) LHMDS (0.9 equiv), THF, −78 °C, 10 min, then MeI (3.0 equiv), −78 → −30 °C over 2 h, then AcOH (2.0 equiv).

to the principle attack of the lithium enolate of **1** on the alkyl halide and not through any secondary enhancement effect. This was implemented by using substoichiometric quantities of base. Table 1 shows the results for the alkylation of **1** with a range of alkyl halides using 0.95 equivalents of LHMDS and excess electrophile in THF at −78 to −30 °C.

Table 1. Monoalkylations of glycolate **1**.

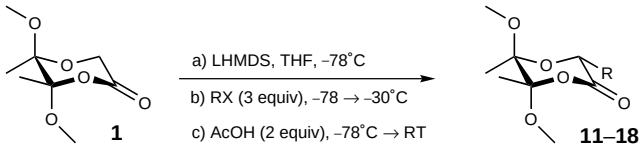

Entry	RX	d.r.	Product	Yield (conv.)
1	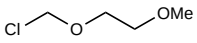	10:1[a]	**11**	64%
2		10:1[b]	**12**[c]	85% (97%)
3		15:1	**13**[d]	61% (87%)
4	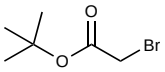	18:1[a]	**14**[d,e]	92%
5	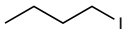	21:1	**15**	57%
6		60:1	**16**[c,d]	89% (96%)
7	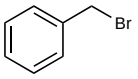	>99:1	**17**[e]	96%
8	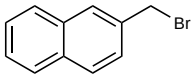	>99:1	**18**[d]	84% (91%)

[a] >99:1 after column chromatography. [b] >99:1 after recrystallization. [c] Configuration determined by single-crystal X-ray determination. [d] Configuration determined by NOE experiments. [e] Configuration determined by specific rotation comparison after deprotection.

In general, the selectivity of the alkylation improved with increasing size of the electrophile and the reactions gave good to excellent chemical yields of the alkylated products even with less reactive alkyl halides such as ethyl and butyl iodide. With bulky halides such as benzyl bromide and 2-(bromomethyl)naphthalene, no minor diastereomer could be detected within the crude reaction mixture. NOE experiments on the major diastereomeric products suggested the newly introduced alkyl group was located in an equatorial position and therefore the newly formed stereogenic center was of the (*R*)-configuration. Single-crystal X-ray determination of nitrile **12** and the allylated product **16** confirmed the stereochemical outcome. This suggested attack of the alkyl halide on the enolate carbon atom was occurring from the side opposing the 1,3-related axial methoxy group.

Further alkylation reactions of the monoalkylated products leading to the dialkylated products were also very effective. In the first case, successive treatment of the benzylated product **17** in THF at −78 °C with LHMDS (1.1 equiv) and methyl iodide (3.0 equiv) afforded the two diastereomers **19** and **20** in the ratio of 3:1 and in combined yield of 82% after separation

  1433-7851/01/4015-2907 $ 17.50+.50/0

by column chromatography. In a complimentary study the methylated glycolate product **9** was treated with LHMDS and then benzyl bromide. These conditions afforded **20** as the only observable diastereomeric product by ^{1}H NMR spectroscopy. The diastereoselectivities in the dialkylation studies clearly depend on the relative sizes of the attached alkyl group and the attacking electrophile (Scheme 4).[20]

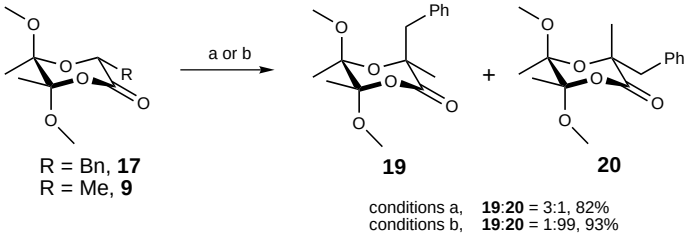

Scheme 4. Dialkylations of monoalkylated BDA-glycolates. a) R = Bn, LHMDS (1.1 equiv), THF, −78 °C, 10 min, then MeI (3.0 equiv), −78 → 0 °C over 2 h, then AcOH (2.0 equiv); b) R = Me, LHMDS (1.1 equiv), THF, −78 °C, 10 min, then BnBr (3.0 equiv), −78 → 0 °C over 2 h, then AcOH (2.0 equiv).

Removal of the BDA protecting group was easily accomplished for both the mono- and dialkylated products through acid-mediated hydrolysis or transesterification (Table 2). For entries 1, 2, and 5, the absolute configuration of the products was confirmed as (*R*) through comparison of the specific rotations of compounds **21**, **22**, and **25**, respectively, with those reported in the literature.[21]

Derivatization of **23** as the (*R*)- and (*S*)-Mosher's esters confirmed the enantiopurity as > 98 % *ee*, suggesting that no racemization was occurring in either the alkylation or the deprotection steps. In addition, this derivatization confirmed the stereochemistry as (*R*).[22]

Received: April 2, 2001 [Z16888]

Table 2. Deprotection of mono- and dialkylated BDA-glycolates.

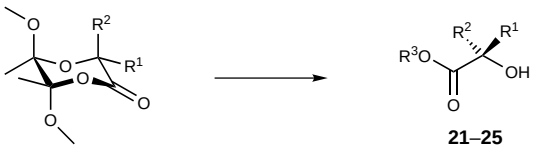

Entry	BDA glycolate	Conditions[a]	Product		Yield
1	**14**	A	**21**[b]	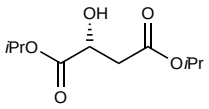	77 %
2	**17**	B	**22**[c]	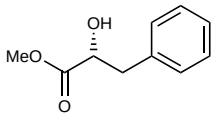	quant.
3	**18**	B	**23**	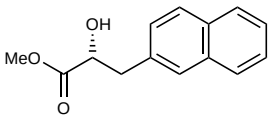	95 %
4	**20**	C	**24**	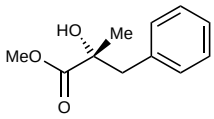	87 %
5	**20**	D	**25**[d]	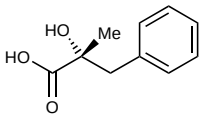	85 %

[a] Conditions: A) TMSCl in *i*PrOH (0.5 M), reflux; B) TMSCl in MeOH (0.5 M), 15 min, RT; C) TMSCl in MeOH (0.5 M), reflux; D) TFA/H_20 (9:1), 10 min, RT. [b] **21**: $[\alpha]_D^{32} = +10.0$ ($c = 3.12$, $CHCl_3$) (ref. [21]: $[\alpha]_D^{20} = +11.0$, ($c = 3.21$, $CHCl_3$)). [c] **22**: $[\alpha]_D^{32} = +6.4$ ($c = 1.82$, $CHCl_3$) (ref. [21] for *S*-isomer: $[\alpha]_D^{20} = -7.6$, ($c = 2.0$, $CHCl_3$)). [d] **25**: $[\alpha]_D^{32} = +12.8$ ($c = 1.66$, dioxane) (ref. [21]: $[\alpha]_D^{20} = +13.2$ ($c = 1.51$, dioxane)).

[1] G. M. Coppola, H. F. Schuster, *α-Hydroxy Acids in Enantioselective Synthesis*, VCH, Weinheim, **1997**.

[2] Y. Murakami, Y. Oshima, Y. Yasumoto, *Bull. Jpn. Soc. Sci. Fish*. **1982**, *48*, 69.

[3] a) J. Liang, E. D. Moher, R. E. Moore, D. W. Hoard, *J. Org. Chem*. **2000**, *65*, 3143; b) N. Sitachitta, R. T. Williamson, W. H. Gerwick, *J. Nat. Prod*. **2000**, *63*, 197; c) F. D. Horgen, W. Y. Yoshida, P. J. Scheuer, *J. Nat. Prod*. **2000**, *63*, 461.

[4] S. Hanessian, *Total Synthesis of Natural Products: The Chiron Approach*, Pergamon, Oxford, **1983**.

[5] a) F. A. Davis, B.-C. Chen, *Chem. Rev*. **1992**, *92*, 919; b) D. A. Evans, M. M. Morrissey, R. L. Dorow, *J. Am. Chem. Soc*. **1985**, *107*, 4346.

[6] a) S. V. Pansare, R. G. Ravi, R. P. Jain, *J. Org. Chem*. **1998**, *63*, 4120; b) S. V. Pansare, R. G. Ravi, *Tetrahedron* **1998**, *54*, 14549.

[7] a) I. S. Byun, Y. H. Kim, *Synth. Commun*. **1995**, *25*, 1963; b) M. J. Burk, C. S. Kalberg, A. Pizzano, *J. Am. Chem. Soc*. **1998**, *120*, 4345; c) H. C. Brown, B. T. Cho, W. S. Park, *J. Org. Chem*. **1986**, *51*, 3396; d) Z. Wang, B. La, J. M. Fortunak, X. J. Meng, G. W. Kabalka, *Tetrahedron Lett*. **1998**, *39*, 5501.

[8] See: T. Ooi, T. Miura, K. Takaya, H. Ichikawa, K. Maruoka, *Tetrahedron* **2001**, *57*, 867, and references therein.

[9] For examples, see: a) Y. N. Belokon, B. Green, N. S. Ikonnikov, M. North, T. Parsons, V. I. Tararov, *Tetrahedron* **2001**, *57*, 771; b) U. Hanefeld, Y. X. Li, R. A. Sheldon, T. Maschmeyer, *Synlett* **2000**, 1775, and references therein.

[10] F. F. Huerta, Y. R. S. Laxmi, J.-E. Bäckvall, *Org. Lett*. **2000**, *2*, 1037.

[11] a) M.-J. Kim, G. M. Whitesides, *J. Am. Chem. Soc*. **1988**, *110*, 2959; b) W. Adam, M. Lazarus, B. Boss, C. R. Saha-Moller, H.-U. Humpf, P. Schreier, *J. Org. Chem*. **1997**, *62*, 7841.

[12] a) H. Yu, C. E. Ballard, B. Wang, *Tetrahedron Lett*. **2001**, *42*, 1835; b) M. B. Andrus, B. B. V. Soma Sekhar, E. L. Meredith, N. Kent Dalley, *Org. Lett*. **2000**, *2*, 3035; c) M. T. Crimmins, K. A. Emmitte, J. D. Katz, *Org. Lett*. **2000**, *2*, 2165; d) J.-W. Chang, D.-P. Jang, B.-J. Uang, F.-L. Liao, S.-L. Wang, *Org. Lett*. **1999**, *1*, 2061; e) W. H. Pearson, M.-C. Cheng, *J. Org. Chem*. **1987**, *52*, 3176; f) D. Seebach, R. Naef, *Helv. Chim. Acta* **1981**, *64*, 2704; g) D. Seebach, *Modern Synthetic Methods* (Ed.: R. Scheffold), Springer, Berlin, **1986**, pp. 125–257; h) J. E. Jung, H. Ho, H.-D. Kim, *Tetrahedron Lett.* **2000**, *41*, 1793; i) P. Renauld, S. Abazi, *Helv. Chim. Acta* **1996**, *79*, 1696; j) M. Enomoto, Y. Ito, T. Katsuki, M. Yamaguchi, *Tetrahedron Lett.* **1985**, *25*, 1343; k) G. Helmchen, R. Wierzchowski, *Angew. Chem.* **1984**, *96*, 59; *Angew. Chem. Int. Ed. Engl.* **1984**, *23*, 60; l) T. R. Kelly, A. Arvanitis, *Tetrahedron Lett.* **1984**; *25*, 39; m) J. D'Angelo, O. Pagès, J. Maddaluno, F. Dumas, G. Revial, *Tetrahedron Lett.* **1983**, *24*, 5869.

[13] a) B. C. B. Bezuidenhoudt, G. H. Castle, S. V. Ley, *Tetrahedron Lett*. **1994**, *35*, 7447; b) B. C. B. Bezuidenhoudt, G. H. Castle, J. V. Geden, S. V. Ley, *Tetrahedron Lett*. **1994**, *35*, 7451; c) G. H. Castle, S. V. Ley, *Tetrahedron Lett*. **1994**, *35*, 7455; d) G.-J. Boons, R. Downham, K. S. Kim, S. V. Ley, M. Woods, *Tetrahedron* **1994**, *50*, 7157; e) R. Downham, K. S. Kim, S. V. Ley, M. Woods, *Tetrahedron Lett*. **1994**, *35*, 769.

[14] J. S. Barlow, D. J. Dixon, A. C. Foster, S. V. Ley, D. J. Reynolds, *J. Chem. Soc. Perkin Trans. 1* **1999**, 1627.

[15] a) D. J. Dixon, A. C. Foster, S. V. Ley, D. J. Reynolds, *J. Chem. Soc. Perkin Trans. 1* **1999**, 1635; b) D. J. Dixon, A. C. Foster, S. V. Ley, D. J. Reynolds, *J. Chem. Soc. Perkin Trans. 1* **1999**, 1631.

  1433-7851/01/4015-2908 $ 17.50+.50/0

[16] S. V. Ley, D. K. Baeschlin, D. J. Dixon, A. C. Foster, S. J. Ince, H. W. M. Priepke, D. J. Reynolds, *Chem. Rev.* **2001**, *101*, 53, and references therein.
[17] H. Orth, *Angew. Chem.* **1952**, *64*, 544.
[18] M. E. Furrow, S. E. Schaus, E. N. Jacobsen, *J. Org. Chem.* **1998**, *63*, 6776.
[19] Available from Aldrich in either enantiomeric form.
[20] For similar observations in reactions using dispiroketal-desymmetrized glycolic acid, see; a) G.-J. Boons, R. Downham, K. S. Kim, S. V. Ley, M. Woods, *Tetrahedron* **1994**, *50*, 7157; b) R. Downham, K. S. Kim, S. V. Ley, M. Woods, *Tetrahedron Lett.* **1994**, *35*, 769.
[21] Specific rotations: **21**: $[\alpha]_D^{32} = +10.0$ ($c = 3.12$, $CHCl_3$) (available from Aldrich, $[\alpha]_D^{20} = +11.0$, ($c = 3.21$, $CHCl_3$)); **22**: $[\alpha]_D^{32} = +6.4$ ($c = 1.82$, $CHCl_3$) (*S* isomer: $[\alpha]_D^{20} = -7.6$, ($c = 2.0$, $CHCl_3$), F. A. Davis, M. S. Haque, T. G. Ulatowski, J. C. Towson, *J. Org. Chem.* **1986**, *51*, 2402); **25**: $[\alpha]_D^{32} = +12.8$ ($c = 1.66$, dioxane) (*R*-isomer: $[\alpha]_D^{20} = +13.2$ ($c =$ 1.51, dioxane), S.-S. Jew, H.-A. Kim, J.-H. Kim, H.-G. Park, *Heterocycles* **1997**, *46*, 65).
[22] J. A. Dale, H. S. Mosher, *J. Am. Chem. Soc.* **1973**, *95*, 512.

Directed Assembly of Periodic Materials from Protein and Oligonucleotide-Modified Nanoparticle Building Blocks**

So-Jung Park, Anne A. Lazarides, Chad A. Mirkin,* and Robert L. Letsinger*

In 1996 we reported a method for utilizing DNA and its synthetically programmable sequence recognition properties to assemble nanoparticles functionalized with oligonucleotides into preconceived architectures (Figure 1 B).[1] Since that initial report, our research group and many others have shown that this strategy[2–8] and off-shoots of it that rely on protein–receptor and antibody–antigen interactions[9–12] can be used to generate a wide range of architectures with many unusual and, in some cases, useful chemical and physical properties.

Since proteins and certain protein receptors can be functionalized with oligonucleotides, one, in principle, could immobilize such molecules onto oligonucleotide-modified nanoparticles and generate a new class of hybrid particles that exhibit the high stability of the oligonucleotide-modified particles but with molecular recognition properties that are dictated by the surface-immobilized protein or receptor rather than the DNA. Alternatively, one could functionalize a protein that has multiple receptor binding sites with receptor-modified oligonucleotides so that the protein receptor complex could be used as one of the building blocks, in place of one of the inorganic nanoparticles, in our original materials assembly scheme. Herein, we use 13-nm gold particles, streptavidin, and biotinylated DNA to explore these hypotheses (Figure 1 A) and some of the physical and chemical properties of the resulting new bioinorganic materials.

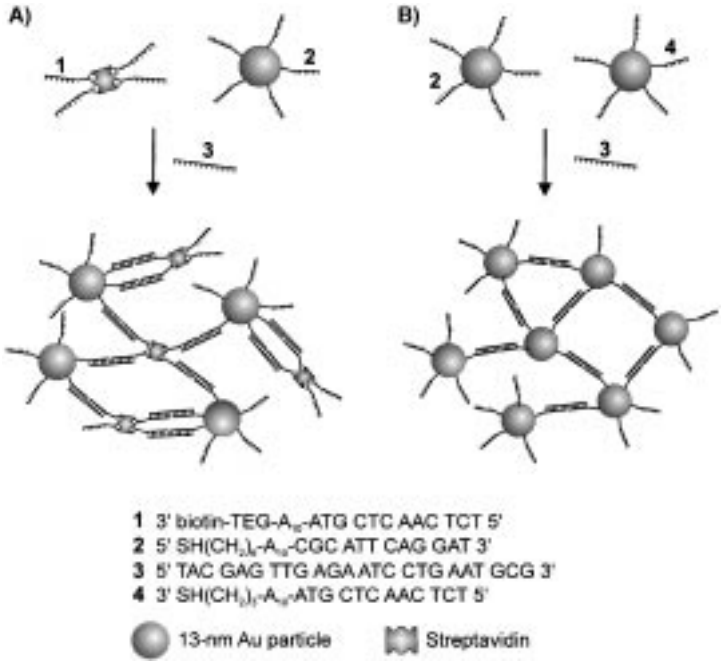

Figure 1. Schematic representation of DNA-directed assembly of Au nanoparticles and streptavidin. A) Assembly of oligonucleotide-functionalized streptavidin and Au nanoparticles (Au–STV assembly). B) Assembly of oligonucleotide-functionalized Au nanoparticles (Au–Au assembly). Note that **1** and **4** have the same DNA sequence.

The nanoparticle/protein assembly (Figure 1 A) reported herein relies on three building blocks: streptavidin complexed to four biotinylated oligonucleotides (**1**–STV), oligonucleotide-modified gold nanoparticles (**2**–Au), and a linker oligonucleotide (**3**) that has one half of its sequence complementary to **1** and the other half complementary to **2** (Figure 1). In a typical experiment, linker DNA (**3**; 10 μM, 21 μL) was introduced to a mixture of **2**–Au (9.7 nM, 260 μL) and **1**–STV (1.8 μM, 27 μL), or linker DNA **3** (10 μM, 21 μL) was premixed with **1**–STV (1.8 μM, 27 μL) and then the mixture was added to **2**–Au (9.7 nM, 260 μL) in 0.3 M phosphate-buffered saline (PBS) solution. Aggregates with similar properties could be formed by both methods, but premixing **3** and **1**–STV facilitates aggregate formation. Since a 13-nm gold particle is substantially larger than streptavidin ($4 \times 4 \times 5$ nm),[13, 14] a 1:20 molar ratio of Au nanoparticle to streptavidin was used to favor the formation of an extended polymeric structure rather than small aggregates comprised

[*] Prof. C. A. Mirkin, S.-J. Park, Prof. A. A. Lazarides
Department of Chemistry
and
Center for Nanofabrication and Molecular Self Assembly
Northwestern University
2145 Sheridan Road, Evanston, IL 60208-3113 (USA)
Fax: (+1) 847-467-5123
E-mail: camirkin@chem.nwu.edu
Prof. R. L. Letsinger
Department of Chemistry
Northwestern University
2145 Sheridan Road, Evanston, IL 60208-3113 (USA)
Fax: (+1) 847-491-2081
E-mail: rletsinger@chem.nwu.edu

[**] C.A.M. acknowledges DARPA, NSF, ARO, and NIH for support of this research. R.L.L. acknowledges the NIH. The DND-CAT Synchrotron Research Center is supported by E.I. Dupont de Nemours & Co., The Dow Chemical Company, the U.S. National Science Foundation through Grant DMR-9304725, and the State of Illinois through the Department of Commerce and the Board of Higher Education Grant IBHE HECA NWU 96. Use of the Advanced Photon Source was supported by the U.S. Department of Energy, Basic Energy Sciences, Office of Energy Research under Contract No. W-31-102-Eng-38.

Supporting information for this article is available on the WWW under http://www.angewandte.com or from the author.

of a few nanoparticles or a structure consisting of a single gold nanoparticle functionalized with a hybridized layer of streptavidin.

Interestingly, when **1**–STV, **2**–Au, and **3** were mixed at room temperature, no significant particle aggregation took place, even after three days, as evidenced by an unperturbed UV/Vis spectrum of the solution containing **1**–STV, **2**–Au, and **3**. However, raising the temperature of the solution (53 °C) to a few degrees below the melting temperature (T_m) of the DNA interconnects resulted in the growth of micrometer-sized aggregates (Figure 2A) and the characteristic red-shift and dampening of the Au plasmon resonance associated with particle assembly.[1] The transmission electron microscopy (TEM) image (Figure 2B) shows that the particles within the aggregates retain their physical shape prior to and after annealing, and shows that no particle fusion occurs. This result further demonstrates the stabilizing influence of the surface oligonucleotide layer. This requirement of thermal activation for initiating particle assembly is in contrast to the previously studied system involving two gold nanoparticle conjugates (Figure 1B) where, under very similar conditions, the oligonucleotide-modified gold particles assemble into aggregates within a few minutes upon adding linker DNA at room temperature.[1] This feature could be the result of: 1) the low collision probability in the Au–STV assembly system because of the lower DNA coverage on streptavidin (DNA:streptavidin = 4:1) relative to that on Au nanoparticles (DNA:particle ≈ 110:1),[15] or 2) initial formation of kinetic structures in which most or all of the DNA on a single streptavidin molecule binds to the DNA on a single particle. Aggregate formation could be facilitated by freezing the solution as well as heating it.[16] Finally, no aggregate formation was observed in a control experiment when a mixture of **1**–STV and **2**–Au (without **3**) was heated at 53 °C for 1 h. This observation demonstrates that aggregation in the three-component system (**1**–STV, **2**–Au, and **3**) is a DNA-driven process rather than one that results from nonspecific interactions.

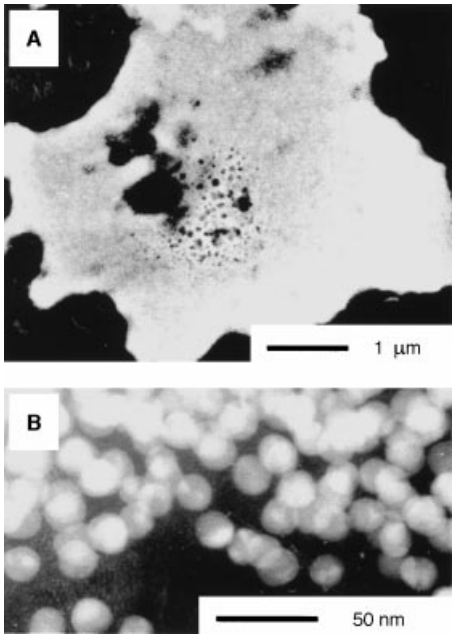

Figure 2. TEM images of 24-mer DNA linked aggregates of Au nanoparticles and streptavidin. A) Low magnification image showing an entire aggregate. B) High magnification image of a portion of the aggregate.

Melting experiments, based on UV/Vis spectroscopy, were performed on the streptavidin/nanoparticle aggregates (Figure 3A). Upon heating the aggregates, the extinction coefficient at 520 nm initially decreases, which results in a dip in the melting curve, and then abruptly increases when DNA melting takes place and the particles are dispersed. This dipping behavior has been observed in the pure gold nanoparticle system and has been attributed to aggregate growth prior to melting, that is, a type of aggregate "ripening".[5] After DNA melting has occurred, the Au plasmon resonance is centered at 520 nm, which is characteristic of dispersed 13-nm particles. These experiments further demonstrate that sequence-specific hybridization events, rather than nonspecific interactions, are effecting the particle/protein assembly and that the aggregation process is completely reversible.

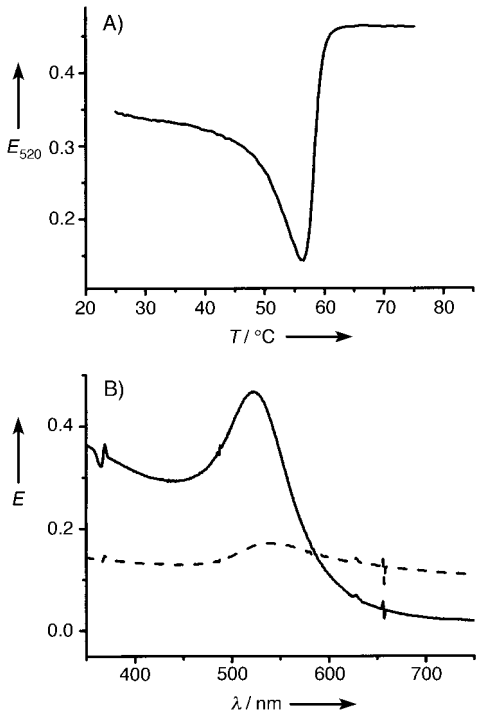

Figure 3. A) Thermal dissociation curve of the 24-mer DNA linked aggregates consisting of Au nanoparticles and streptavidin. The extinction coefficient at 520 nm was monitored as a function of temperature while stirring the solution. B) UV/Vis spectra of the solution measured before (– – – 56 °C) and after melting of the DNA (—— 65 °C).

An Au nanoparticle/protein assembly could also be formed through streptavidin/biotin interactions instead of hybridization-induced assembly. For example, in a typical experiment **1** (0.24 mM, 1.3 μL), **3** (10 μM, 32 μL), and **2**-modified nanoparticles (Au nanoparticle concentration: 9.7 nM, 260 μL) were mixed in 0.3 M PBS solution to generate biotin-modified Au particles. The mixture was heated at 60 °C for 10 min and then cooled to room temperature to facilitate hybridization. The solution containing **1**, **3**, and **2**-modified Au nanoparticles

  1433-7851/01/4015-2910 $ 17.50+.50/0

was added after 24 h to streptavidin (10 μM, 4.2 μL) in 0.3 M PBS, and heated to 50 °C to form the nanoparticle aggregates. The color of the solution turned purple indicating aggregate formation had occurred, and the aggregates could be disassembled to **2**-modified Au particles, **1**-modified streptavidin, and **3** by raising the temperature of the solution above the melting temperature (65 °C).

Small-angle X-ray scattering (SAXS)[7, 17, 18] data were collected for aggregates formed from the Au nanoparticle and streptavidin building blocks (**1** – STV, **2** – Au) and two different lengths of DNA linker (24-mer (**3**) and 48-mer), and they were compared to those for aggregates based on an Au – Au assembly with the same linking oligonucleotides (**2** – Au, **4** – Au, 24-mer linker (**3**), 48-mer linker; Figure 4). The 48-mer

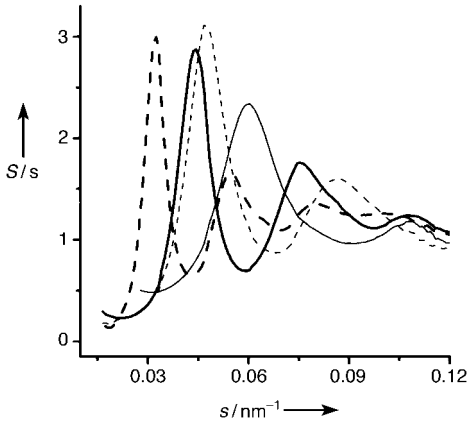

Figure 4. Structure factors of the DNA linked Au – STV (—— 24-mer-linked, – – – 48-mer-linked) and Au – Au assemblies (—— 24-mer-linked, – – – 48-mer-linked) from SAXS patterns. The aggregate solutions were heated at 47 °C for 30 min to obtain thermodynamic structures. The SAXS experiments were performed at the Dupont – Northwestern – Dow Collaborative Access Team (DND-CAT) Sector 5 of the Advanced Photon Source, Argonne National Laboratory with X-rays of wavelength 1.24 Å. Samples were placed in 1.2-mm flat cells between Kapton windows. The magnitude, $s(=q/2\pi)$, of the scattering vector is $2\sin(\theta)/\lambda$, where 2θ is the scattering angle and λ is the wavelength of the incident radiation. The scattered intensity $I(s)$ is approximately proportional to the structure factor $S(s)$ as follows: $I(s) \approx F^2(s)S(s)$, where $F^2(s)$ is the scattered intensity associated with the dispersed DNA-modified Au nanoparticles without linker. The scattering from streptavidin and DNA is negligible relative to the scattering from the Au nanoparticles.

linker was a duplex consisting of 5′TACGAGTTGAGACCGTTAAGACGAGGCAATCATGCAATCCTGAATGCG and 3′GGCAATTCTGCTCCGTTAGTACGT (the duplex region is underlined) with 12-mer sticky ends that are complementary to **1** and **2**. For design of the SAXS experiments, A_{10} spacers in **1**, **2**, and **4**, which were used in the above experiments to enhance the possibility of DNA hybridization,[15] were removed to create a more rigid system for use in the SAXS experiments. The aggregates linked by DNA showed relatively well-defined diffraction peaks, and the Au – STV aggregates exhibited diffraction peaks at smaller s values than the Au – Au aggregates formed from the same linker. This observation suggests a larger interparticle distance between the Au centers in the Au – STV system. Furthermore, the diffraction peaks shifted to smaller angles when 48-mer DNA was used as a linker instead of the 24-mer for both the Au – Au and Au – STV assemblies (Figure 4).

The pair distance distribution function (PDDF) $g(r)$ has been calculated from the SAXS patterns using Equation (1), where $q = (4\pi/\lambda)\sin(\theta)$ and ρ is the particle number density.[17, 18]

$$g(r) = 1 + (1/2\pi^2\rho r)\int q(S(q) - 1)\sin(qr)\mathrm{d}q \quad (1)$$

$g(r)$ gives the probability of finding a second particle as a function of distance r from a chosen particle. The nearest neighbor interparticle Au – Au distances (center to center distance) obtained from the PDDFs are 19.3, 25.4, 28.7, and 40.0 nm for the 24-mer-linked Au – Au, 48-mer-linked Au – Au, 24-mer-linked Au – STV, and 48-mer-linked Au – STV assemblies, respectively. A comparison of the interparticle distances for the Au – STV system and the Au – Au system clearly shows that the Au – STV assembly has the anticipated Au nanoparticle/streptavidin periodicity and that the two components (Au nanoparticle and streptavidin) are well separated by rigid DNA duplex linkers.

This study is important for the following reasons. 1) It demonstrates that the DNA-directed nanoparticle assembly method is extendable to protein-based structures, in addition to the inorganic nanoparticles studied thus far. Indeed, this is the first report demonstrating the reversible DNA-directed assembly of Au nanoparticles and a protein-based structure functionalized with DNA into macroscopic, periodic architectures. Other research groups have used a different strategy for preparing linear structures from 1.4-nm particles, DNA, and streptavidin.[9, 19, 20] 2) It is well known that many proteins, including streptavidin, will adsorb onto the surface of colloidal gold to form strongly bound complexes. Our experiments demonstrate the stabilizing influence of the high-density DNA layers on the nanoparticle surfaces and their resistance to streptavidin adsorption in the absence of hybridization. Therefore, they point towards a method for specifically immobilizing protein structures on nanoparticle surfaces through very specific interactions in a way that will not substantially perturb the activity of the protein. Particles with surface-adsorbed proteins have played an important role in immunochemistry,[21] and the development of stable protein/particle conjugates where the protein does not directly interact with the nanoparticle surface could lead to improved nanoparticle probes for histochemical studies and immunoassays.

Experimental Section

The methods for preparing oligonucleotide-modified 13-nm Au particles (**2** – Au) and linker DNA (**3**) are reported elsewhere.[2] **2** – Au and **3** were stored in a mixture of 0.3 M NaCl and 10 mM phosphate (pH 7) buffer (0.3 M PBS) prior to use. Biotin-modified DNA (**2**) was synthesized from Biotin TEG CPG support (Glen Research) and purified by literature methods.[2, 22] Streptavidin was purchased from Sigma and dissolved in 20 mM tris(hydroxymethyl)aminomethane (Tris) buffer (30 μM, pH 7.2). To make the streptavidin/DNA conjugate (**1** – STV), streptavidin was treated with **1** (8 equiv) in a mixture of 20 mM Tris (pH 7.2) and 0.2 mM ethylenediaminetetraacetate (EDTA) buffer solution at room temperature for 2 h on a shaker. Mixtures with different ratios of streptavidin to DNA (1:0.4, 1:1, 1:4) were also prepared for HPLC analysis. The streptavidin/DNA

  1433-7851/01/4015-2911 $ 17.50+.50/0

conjugates were separated from excess DNA by ion-exchange HPLC starting with 20 mM Tris (pH 7.2) and then using a 0.5 % min^{-1} gradient of a solution of 20 mM Tris and 1M NaCl at a flow rate of 1 mL min^{-1}, while monitoring the UV signal at 260 and 280 nm. The 1:0.4 streptavidin:DNA mixture showed two peaks at 45 and 56 min, while the 1:1 mixture showed four peaks at 45, 56, 67, and 71 min, which correspond to the 1:1, 2:1, 3:1, and 4:1 oligonucleotide:streptavidin complexes, respectively. The 1:4 mixture showed four peaks at the same positions but with increased intensity of the third (67 min) and fourth (71 min) peaks. The HPLC chromatogram of the 1:8 streptavidin:DNA mixture showed two main peaks, one at 59 min for recovered DNA and the other at 71 min for the 4:1 oligonucleotide:streptavidin complex. In addition, a shoulder at 67 min, assigned to the 3:1 complex, was also present. Purified streptavidin–biotinylated-DNA conjugates were concentrated and dispersed in 0.3 M PBS by ultrafiltration (centricon 30). Aggregates for TEM, thermal denaturation experiments, and SAXS measurements were prepared by freezing the solution containing **1**–STV, **2**–Au, and **3** in dry ice for 10 min, and thawing to facilitate hybridization prior to the measurement.

Received: February 26, 2001
Revised: May 22, 2001 [Z16692]

[1] C. A. Mirkin, R. L. Letsinger, R. C. Mucic, J. J. Storhoff, *Nature* **1996**, *382*, 607.
[2] J. J. Storhoff, R. Elghanian, R. C. Mucic, C. A. Mirkin, R. L. Letsinger, *J. Am. Chem. Soc.* **1998**, *120*, 1959.
[3] R. C. Mucic, J. J. Storhoff, C. A. Mirkin, R. L. Letsinger, *J. Am. Chem. Soc.* **1998**, *120*, 12674.
[4] G. P. Mitchell, C. A. Mirkin, R. L. Letsinger, *J. Am. Chem. Soc.* **1999**, *121*, 8122.
[5] J. J. Storhoff, A. A. Lazarides, C. A. Mirkin, R. L. Letsinger, R. C. Mucic, G. C. Schatz, *J. Am. Chem. Soc.* **2000**, *122*, 4640.
[6] T. A. Taton, R. C. Mucic, C. A. Mirkin, R. L. Letsinger, *J. Am. Chem. Soc.* **2000**, *122*, 6305.
[7] S.-J. Park, A. A. Lazarides, C. A. Mirkin, P. W. Brazis, C. R. Kannewurf, R. L. Letsinger, *Angew. Chem.* **2000**, *112*, 4003; *Angew. Chem. Int. Ed.* **2000**, *39*, 3845.
[8] T. A. Taton, C. A. Mirkin, R. L. Letsinger, *Science* **2000**, *289*, 1757.
[9] C. M. Niemeyer, W. Burger, J. Peplies, *Angew. Chem.* **1998**, *110*, 2391; *Angew. Chem. Int. Ed.* **1998**, *37*, 2265.
[10] W. Shenton, S. A. Davis, S. Mann, *Adv. Mater.* **1999**, *11*, 449.
[11] S. Connolly, D. Fitzmaurice, *Adv. Mater.* **1999**, *11*, 1202.
[12] M. Li, K. W. Wong, S. Mann, *Chem. Mater.* **1999**, *11*, 23.
[13] P. C. Weber, D. H. Ohlendorf, J. J. Wendoloski, F. R. Salemme, *Science* **1989**, *243*, 85.
[14] N. M. Green, *Methods Enzymol.* **1990**, *184*, 51.
[15] L. M. Demers, C. A. Mirkin, R. C. Mucic, R. A. Reynolds, R. L. Letsinger, R. Elghanian, G. Viswanadham, *Anal. Chem.* **2000**, *72*, 5535.
[16] R. Elghanian, J. J. Storhoff, R. C. Mucic, R. L. Letsinger, C. A. Mirkin, *Science* **1997**, *277*, 1078.
[17] A. Guinier, A. Fournet, *Small Angle Scattering of X-rays*, Wiley, New York, **1955**.
[18] B. A. Korgel, D. Fitzmaurice, *Phys. Rev. B* **1999**, *59*, 14191.
[19] C. M. Niemeyer, T. Sano, C. L. Smith, C. R. Cantor, *Nucleic Acids Res.* **1994**, *22*, 5530.
[20] C. M. Niemeyer, L. Boldt, B. Ceyhan, D. Blohm, *Anal. Biochem.* **1999**, *268*, 54.
[21] M. A. Hayat, *Colloidal Gold: Principles, Methods, and Applications*, Academic Press, San Diego, **1991**.
[22] T. Brown, D. J. S. Brown in *Oligonuclieotides and Analogues* (Ed.: F. Eckstein), Oxford University Press, New York, **1991**.

Ruthenium-Catalyzed One-Step Transformation of Propargylic Alcohols into Alkylidene Cyclobutenes: X-ray Characterization of an Ru(η^3-cyclobutenyl) Intermediate**

Jacques Le Paih, Sylvie Dérien, Christian Bruneau, Bernard Demerseman, Loïc Toupet, and Pierre H. Dixneuf*

Among unsaturated small cycles, cyclobutenes are especially useful as building-block precursors. They allow the general in situ generation of reactive functional 1,3-diene skeletons,[1] a key process for the synthesis of phytotoxic natural products[2] or polycyclic derivatives.[3] Cyclobutenes were also shown to be precursors of 1,5-dienes for access to pheromones by ring-opening catalysis.[4] The most general methods to produce simple cyclobutenes are based on the [2+2] cycloaddition of C≡C and C=C bonds, either photochemically[5] or with Lewis acids[6] and metal-based[7] catalysts, and on the zirconocene-catalyzed reaction of alkynyl halides with Grignard reagents.[8] In contrast, the access to alkylidenecyclobutenes is not straightforward and occurs by intramolecular thermal coupling of 1,5-diynes[9] or copper-mediated cyclization from 1,4-enynes.[10]

We have recently shown that the catalyst precursor [Cp*RuCl(cod)] (Cp* = C_5Me_5, cod = 1,5-cyclooctadiene) promotes the head-to-head coupling of two terminal alkynes, via a chelating biscarbene–ruthenium intermediate, which, upon addition of a carboxylic acid produces 1-acyloxybuta-1,3-dienes [Eq. (1)].[11] We now report that the same electron-rich precatalyst [Cp*RuCl(cod)] activates propargylic alcohols in a novel manner in the presence of a carboxylic acid. It leads to the one-step catalytic head-to-head cyclodimerization

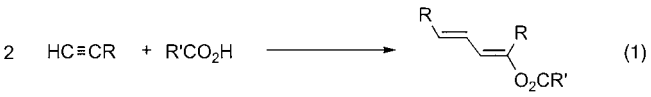

(1)

[*] Prof. P. H. Dixneuf, Dr. J. Le Paih, Dr. S. Dérien, Dr. C. Bruneau, Dr. B. Demerseman
Institut de Chimie de Rennes
UMR 6509 CNRS-Université de Rennes
Organométalliques et Catalyse
Campus de Beaulieu, 35042 Rennes (France)
Fax: (+33) 2-99286939
E-mail: pierre.dixneuf@univ-rennes1.fr
Dr. L. Toupet
Groupe Matière Condensée et Matériaux
UMR 6626 CNRS-Université de Rennes
Campus de Beaulieu, 35042 Rennes (France)

[**] This work was supported by the CNRS and the Ministère de la Recherche. The authors are grateful to the latter for a PhD grant to J. LP. The authors wish to thank the European Cost Program D17/003/00 and the Région Bretagne for financial support. They are also grateful to A. Bondon for helpful assistance in NMR analysis.

Supporting information for this article is available on the WWW under http://www.angewandte.com or from the author.

  1433-7851/01/4015-2912 $ 17.50+.50/0

of propargyl alcohols and to the formation of alkylidenecyclobutene derivatives [Eq. (2)] via cyclobutadiene– and cyclobutenyl–ruthenium intermediates, dehydration, and carboxylate addition.

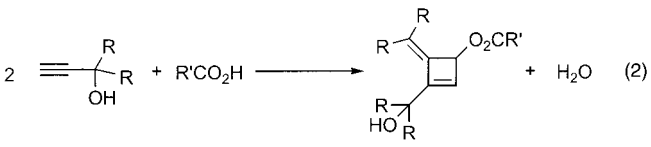

(2)

The reaction of 1,1-dimethylprop-2-ynol (**1**) with acetic acid in the presence of 5 mol% of [Cp*RuCl(cod)],[12] in isoprene as solvent at 40 °C for 20 h, affords the alkylidenecyclobutene derivative **4** in 57% yield [Eq. (3)]. Similarly, the prop-2-yn-1-ols **2** and **3** are catalytically converted into alkylidenecyclobutenes **5** (51%) and **6** (66%), respectively. The structures of compounds **4**–**6** were established by ^{1}H and ^{13}C NMR spectroscopy. A conclusive 2D NMR (NOESY) experiment showed that the alkene and methyne protons within the four-membered cycle are in the 1,2 positions.

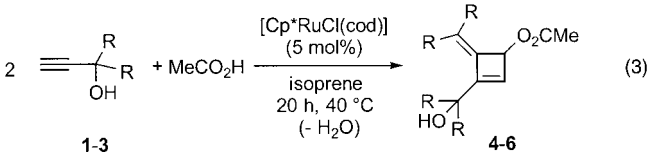

(3)

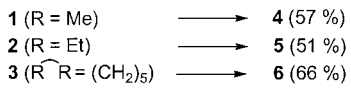

It is noteworthy that the reaction was restricted to propargylic alcohols bearing a terminal triple bond. However, the scope of the reaction was investigated in the cyclodimerization of propargyl alcohol **3** with a variety of carboxylic acids. The addition of acetic, benzoic, methoxyacetic, or pent-4-enoic acid to compound **3** in the presence of 5 mol% of catalyst [Cp*RuCl(cod)] selectively leads, under the previous conditions, to the catalytic formation of alkylidenecyclobutenes **6**–**9** isolated in 50–66% yield [Eq. (4)]. However, the reaction appears inhibited with stronger acids ($pK_a < 3.5$) such as cyanoacetic acid for which no conversion was observed.

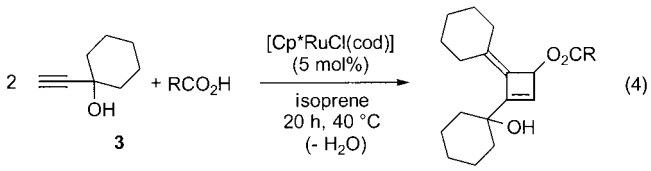

(4)

This novel catalytic reaction formally corresponds to a regioselective head-to-head carbon–carbon coupling of the alkynes with addition of carboxylic acid and elimination of water. This reaction drastically depends on the nature of the solvent. The conversion of **3** into **6** at 40 °C for 20 h in 2 mL of the two-electron coordinating solvents tetrahydrofuran or acetonitrile was always under 5%, and only 20% in dioxane. However, this conversion significantly increased when the reaction was performed in a diene as solvent. Thus, the conversion of **3** into **6** after 20 h at 40 °C in 2 mL of 1,3-cyclohexadiene, 1,5-cyclooctadiene, or isoprene, reached 60, 65, or 80%, respectively. The use of an excess of diene shows that the cyclodimerization of the alkyne is the favored process, as no codimerization of alkyne and diene takes place, whereas it does with allyl alcohol in the absence of acid.[13]

The nature of the products **4**–**9** suggested that one key intermediate was a cyclobutadiene–ruthenium complex rather than a chelating biscarbene complex as found for other terminal alkynes.[11] To investigate the mechanism, a set of stoichiometric reactions were successively performed. The reaction of [Cp*RuCl(cod)] with 5 equivalents of ethynylcyclohexanol (**3**), but in THF, for 2 h at room temperature afforded 90% of the cyclobutadiene complex **11**[14] (Scheme 1). As no X-ray structure of **11** could be determined,

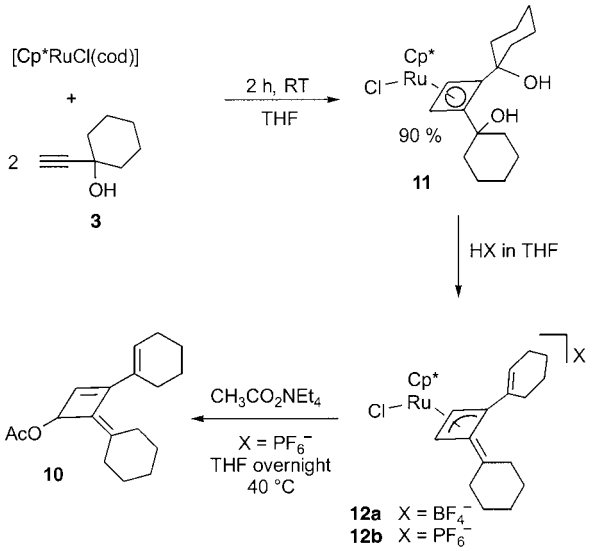

Scheme 1.

complex **11** was treated in THF at −60 °C with 1.1 equivalents of HBF_4 or HPF_6, which gave complexes **12a** and **12b**, respectively, in 90% yield (Scheme 1). The X-ray diffraction structure of single crystals of **12b** is shown in Figure 1.[15] It confirms the four-membered ring formation with the head-to-head alkyne coupling. However, it shows an unprecedented alkylidenecyclobutenyl ligand coordinated by an η^3-allyl C12-C13-C14 group (C12–C13 1.426(9), C13–C14 1.428(7), C11–C12 1.499(7), C11–C14 1.506(7) Å) and η^2-C11=C21 bond. This C11=C21 bond (1.364(8) Å) is bent 28.7° towards the metal with a strong Ru–C11 (2.194(4) Å) and a weak Ru–C21 (2.674(4) Å) interaction. The structure of complex **12b** dramatically contrasts with that of the (η^3-methylidenecyclobutenyl)Pd complex [(CH_2=C–C(*t*Bu)–C(*t*Bu)–CMe)-Pd(acac)][16] (acac = 2,4-pentanedione) for which the non-

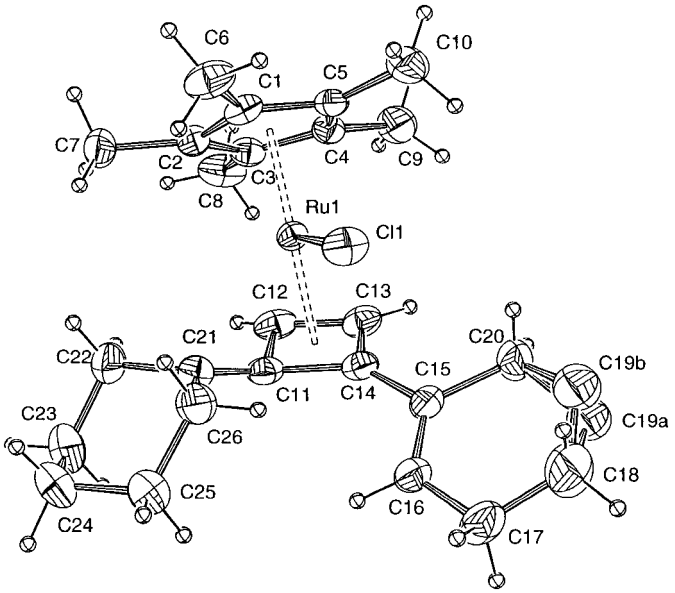

Figure 1. ORTEP drawing of the molecular structure of **12b** (thermal ellipsoids set at the 50% probability level): the PF_6 anion is omitted for clarity. Selected interatomic distances [Å] and angles [°]: Ru-Cl 2.3845(12), Ru-C11 2.194(4), Ru-C12 2.114(4), Ru-C13 2.237(5), Ru-C14 2.315(4), C11-C12 1.499(7), C12-C13 1.426(9), C13-C14 1.428(7), C14-C11 1.506(7), C14-C15 1.448(7), C15-C16 1.330(7), C21-C11 1.364(8); C11-C12-C13 90.7(4), C12-C13-C14 92.4(5), C13-C14-C11 90.3(4), C14-C11-C12 86.6(4).

coordinated C=CH_2 bond is bent away from the palladium atom and makes an angle of 20.4° with the allyl plane.

Addition of an excess of acetic acid to complex **11** in THF at 40 °C leads to the quantitative formation of derivative **6**. Complex **11** also catalyses the formation of derivative **6** under the conditions in Equation (3). Complex **12b** was also treated with 1.1 equivalents of $CH_3CO_2^-Et_4N^+$ in THF at 40 °C and 41% of derivative **10** was isolated (Scheme 1). The latter corresponds to the addition of the acetate to the nonsubstituted terminal carbon atom of the allyl group of **12b**, for example, to the dehydrated derivative of **6**.

On the basis of the nature of the isolated intermediates **11** and **12b** and on their reactivity, the realistic catalytic cycle described in Scheme 2 can be proposed. Protonation of **11′** is expected to give the cationic alkenylidenecyclobutenyl–metal intermediate **A** to which the carboxylate group adds at the unsubstituted allyl carbon giving intermediate **B**. The complexes **12a** and **12b** correspond to the dehydrated intermediate **A**.

This novel catalytic reaction constitutes a remarkable example of the combination of three molecules to afford only one high-value, multifunctional substrate with atom economy.

Experimental Section

General procedure for the catalytic synthesis of **4**–**9**: the propargylic alcohol (2.5 mmol) and the carboxylic acid (1.25 mmol) were added successively to a stirred solution of [Cp*RuCl(cod)] (0.125 mmol, 47 mg) in isoprene (2 mL) under a nitrogen atmosphere. The reaction mixture was then heated at 40 °C for 20 h. The solvent was removed under vacuum and the crude product was purified by column chromatography on silica gel with a diethyl ether/pentane mixture as eluent. The isolated yields are based on the propargylic alcohol. All compounds were fully characterized by spectroscopic methods (see Supporting Information). Selected data for

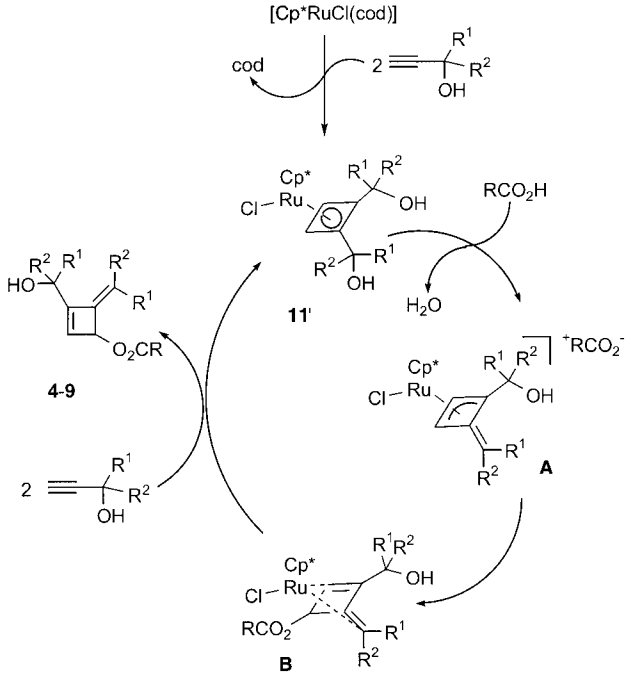

Scheme 2. Catalytic cycle.

6: ^{1}H NMR (200 MHz, $CDCl_3$): $\delta = 1.4-1.75$ (m, 17H, cyclohexyl CH_2 + OH), 2.01 (s, 3H, Me), 1.96–2.08 (m, 2H, cyclohexyl CH_2), 2.37–2.47 (m, 2H, cyclohexyl CH_2), 5.59 (d, 1H, $J = 0.5$ Hz, CH), 6.27 (s, 1H, =CH); ^{13}C NMR (50 MHz, $CDCl_3$): $\delta = 21.2$ (Me), 21.6, 21.7, 25.5, 26.4, 27.7, 27.9, 30.8, 31.4, 35.6, 35.8 (CH_2), 69.4 (C–OH), 72.4 (CH–O), 127.8 (=C), 129.3 (=C), 130.7 (=CH), 162.0 (=C), 171.3 (C=O); high resolution MS *m*/*z* calcd for [M^+] ($C_{18}H_{26}O_3$): 290.1882; found 290.1879.

11: 5 equivalents of 1-ethynylcyclohexanol (**3**; 3.7 mmol, 460 mg) were added to a solution of [Cp*RuCl(cod)] (0.74 mmol, 282 mg) in THF (10 mL) under a nitrogen atmosphere. After stirring at room temperature for 2 h the solvent was removed under vacuum, the solid residue was washed with anhydrous diethyl ether (3 × 15 mL), and dried under vacuum. The complex **11** was obtained as a brown powder (350 mg, 90%). ^{1}H NMR (200 MHz, CD_2Cl_2): $\delta = 0.94-1.09$ (m, 4H, cyclohexyl CH_2), 1.30–1.65 (m, 14H, cyclohexyl CH_2), 1.68 (s, 15H, C_5Me_5), 2.08–2.14 (m, 2H, cyclohexyl CH_2), 3.42 (s, 2H, =CH), 3.93 (s, 2H, OH); ^{13}C NMR (50 MHz, CD_2Cl_2): $\delta = 10.5$ (C_5Me_5), 21.7, 21.9, 25.8, 36.0, 42.2 (cyclohexyl CH_2), 69.4(C–OH), 69.8 (=CH), 92.5 (=C), 99.6 (C_5Me_5); IR (nujol): $\tilde{\nu} = 1654$, 3403, 3443 cm^{-1}; high resolution MS *m*/*z* calcd for [M^+] ($C_{26}H_{39}O_2ClRu$): 520.1686; found 520.1660.

12a and **12b**: 1.1 equivalents of acid HX (HBF_4 or HPF_6) were added to a solution of complex **11** (1 mmol, 520 mg) in THF (20 mL) under nitrogen atmosphere at −60 °C. The stirred reaction mixture was allowed to warm to room temperature and kept at this temperature for 3 h. The solvent was removed under vacuum, the solid washed with diethyl ether (3 × 15 mL) and dried under vacuum. For **12a** a solution of HBF_4 (155 μL; 60% w/w in diethyl ether) was used and **12a** was obtained as a dark red powder (510 mg, 90%). ^{1}H NMR (200 MHz, CD_2Cl_2): $\delta = 1.46-1.58$ (m, 14H, cyclohexyl CH_2), 1.83–1.90 (m, 2H, cyclohexyl CH_2), 1.83 (s, 15H, C_5Me_5), 2.23–2.29 (m, 2H, cyclohexyl CH_2), 5.06 (s, 1H, =CH), 5.56 (s, 1H, =CH), 6.05 (t, 1H, $J = 4$ Hz, cyclohexenyl =CH); ^{13}C NMR (50 MHz, CD_2Cl_2): $\delta =$ 10.6 (C_5Me_5), 21.5, 21.8, 24.2, 25.6, 26.3, 28.8, 31.4, 33.9, 35.9 (CH_2), 77.6, 86.8 (=CH), 93.5, 103.8, 128.9, 134.7 (=CH), 140.2 (=CH), 149.1 (=C); IR (nujol): $\tilde{\nu} = 1041$, 1559, 1632, 3095 cm^{-1}; elemental analysis calcd (%) for $C_{26}H_{36}RuClBF_4$: C 54.60, H 6.34, Cl 6.19; found: C 54.25, H 6.77, Cl 6.32.

For **12b** a solution of HPF_6 (175 μL, 60% w/w in water) was used and **12b** was obtained as a dark red powder (570 mg, 90%). ^{1}H NMR (200 MHz, CD_2Cl_2): $\delta = 1.46-1.59$ (m, 14H, cyclohexyl CH_2), 1.83–1.90 (m, 2H, cyclohexyl CH_2), 1.82 (s, 15H, C_5Me_5), 2.24–2.30 (m, 2H, cyclohexyl CH_2), 4.89 (s, 1H, =CH), 5.48 (s, 1H, =CH), 6.06 (t, 1H, $J = 4$ Hz, cyclohexenyl =CH); ^{13}C NMR (50 MHz, CD_2Cl_2): $\delta = 10.6$ (C_5Me_5), 21.4, 21.7, 24.2, 25.6,

  1433-7851/01/4015-2914 $ 17.50+.50/0 *Angew. Chem. Int. Ed.* **2001**, *40*, No. 15

26.3, 28.9, 31.5, 34.0, 35.4 (CH_2), 77.3, 86.3 (=CH), 93.4, 103.8, 128.8, 135.3 (=C), 140.7 (=CH), 149.3 (=C); IR (nujol): $\tilde{\nu} = 844$, 1561, 1630, 3103 cm^{-1}; elemental analysis calcd (%) for $C_{26}H_{36}RuClPF_6$: C 49.57, H 5.76, Cl 5.63; found: C 49.23, H 5.50, Cl 6.27. Microcrystals of complex **12b** were obtained in a dichloromethane/diethyl ether biphasic system.

Received: March 15, 2001 [Z16777]

[1] a) R. W. Aben, H. W. Scheeren, *J. Chem. Soc. Perkin Trans. 1* **1979**, 3132 – 3138; b) W. J. Leigh, J. A. Postigo, P. C. Vennerie, *J. Am. Chem. Soc.* **1995**, *117*, 7826 – 7827.

[2] a) A. Ichihara, R. Kimura, S. Yamada, S. Sakamura, *J. Am. Chem. Soc.* **1980**, *102*, 6353 – 6355; b) M. E. Jung, K. M. Halweg, *Tetrahedron Lett.* **1981**, *22*, 2735 – 2738.

[3] K. P. C. Vollhardt, *Angew. Chem.* **1984**, *96*, 539 – 541; *Angew. Chem. Int. Ed. Engl.* **1984**, *23*, 539 – 556.

[4] a) M. L. Randall, J. A. Tallarico, M. L. Snapper, *J. Am. Chem. Soc.* **1995**, *117*, 9610 – 9611; b) J. A. Tallarico, M. L. Randall, M. L. Snapper, *Tetrahedron* **1997**, *53*, 16511 – 16520; c) B. R. Maughon, M. Weck, B. Mohr, R. H. Grubbs, *Macromolecules* **1997**, *30*, 257 – 265.

[5] a) J. H. Kwon, S. J. Lee, S. C. Shim, *Tetrahedron Lett.* **1991**, *32*, 6719 – 6722; b) S. Aurrichio, A. Selva, A. M. Truscello, *Tetrahedron* **1997**, *53*, 17407 – 17416.

[6] a) B. B. Snider, D. J. Rodini, R. S. E. Conn, S. Sealfon, *J. Am. Chem. Soc.* **1979**, *101*, 5283 – 5293; b) B. B. Snider, D. M. Roush, D. J. Rodini, D. Gonzalez, D. Spindell, *J. Org. Chem.* **1980**, *45*, 2773 – 2785; c) L. Birkofer, D. Eichstädt, *J. Organomet. Chem.* **1986**, *307*, 279 – 284.

[7] a) K. Narasaka, Y. Hayashi, H. Shimadzu, S. Niihata, *J. Am. Chem. Soc.* **1992**, *114*, 8869 – 8885; Ru: b) A. Mitsudo, K. Kokuryo, Y. Takegami, *J. Chem. Soc. Chem. Commun.* **1976**, 722 – 723; c) T.-a. Mitsudo, K. Kokuryo, T. Shinsugi, Y. Nakagawa, Y. Watanabe, Y. Takegami, *J. Org. Chem.* **1979**, *44*, 4492 – 4496; d) T.-a. Mitsudo, H. Naruse, T. Kondo, Y. Ozaki, Y. Watanabe, *Angew. Chem.* **1994**, *106*, 595 – 597; *Angew. Chem. Int. Ed. Engl.* **1994**, *33*, 580 – 581; e) B. N. Warrener, G. Abbenante, C. H. L. Kennard, *J. Am. Chem. Soc.* **1994**, *116*, 3645 – 3646.

[8] K. Kasai, Y. Liu, R. Hara, T. Takahashi, *Chem. Commun.* **1998**, 1989 – 1990.

[9] L. Trabert, H. Hopf, *Liebigs Ann. Chem.* **1980**, 1786 – 1800.

[10] E. Piers, E. M. Boehringer, J. G. K. Yee, *J. Org. Chem.* **1998**, *63*, 8642 – 8643.

[11] J. Le Paih, S. Dérien, P. H. Dixneuf, *Chem. Commun.* **1999**, 1437 – 1438.

[12] P. J. Fagan, W. S. Mahoney, J. C. Calabrese, I. D. Williams, *Organometallics* **1990**, *9*, 1843 – 1852.

[13] S. Dérien, L. Ropartz, J. Le Paih, P. H. Dixneuf, *J. Org. Chem.* **1999**, *64*, 3524 – 3531.

[14] The NMR spectra with a single resonance (^1H) at $\delta = 3.42$ and a single resonance (^{13}C) at $\delta = 69.8$ for the alkenyl unit of the cycle show the symmetry of the complex **11**.

[15] Crystal structure analysis: $RuClC_{26}H_{36} \cdot PF_6$, $M_r = 630.04$, monoclinic, *I2/a*, $a = 22.704(1)$, $b = 11.221(1)$, $c = 23.530(2)$ Å, $\beta = 114.57(1)$, $V = 5451.8(7)$ Å^{-3}, $Z = 8$, $\rho = 1.535$ Mg m^{-3}, $\lambda(Mo_{K\alpha}) = 0.71073$ Å, $\mu = 7.86$ cm^{-1}, $F(000) = 2576$, $T = 293$ K. The crystal, dimensions $0.37 \times 0.27 \times 0.23$ mm was studied on a NONIUS Kappa CCD diffractometer with graphite monochromatized $Mo_{K\alpha}$ radiation. The cell parameters are obtained with 10 frames (psi rotation: 1° per frame). The data collection (Nonius, 1999) ($2\theta_{max} = 60°$, 176 frames (117 via 1.6° phi rotation and 16 s per frame, 52 via 1.6° omega rotation) range *hkl*: *h* −25.29, *k* 0.14, *l* −25.30) gives 22884 reflections. The data reduction leads to 6103 independent reflections from which 4681 with $I > 2.0\sigma(I)$. The absorption correction is made with a faces indexed crystal. The structure was solved with SIR-97 which reveals the non-hydrogen atoms of the cation and the anion. One atom (C19) of the cyclohexene ring appears disordered between two positions. After anisotropic refinement, many hydrogen atoms may be found with a Fourier Difference. The whole structure was refined with SHELXL 97 by the full-matrix least-square techniques (use of F^2 magnitude; *x*, *y*, *z*, β_{ij} for Ru, Cl, P, C, and F atoms, *x*, *y*, *z* in riding mode for H atoms ; 316 variables and 4681 observations with $I > 2.0\sigma(I)$; calcd $w = 1/[\sigma^2(F_o^2) + (0.122P)^2 + 10.23P]$ where $P = (F_o^2 + 2F_c^2)/3$ with the resulting $R = 0.058$, $R_w = 0.169$ and $S_w = 1.024$ (residual $\Delta\rho < 1.37$ e Å^{-3}). Crystallographic data (excluding structure factors) for the structure reported in this paper have been deposited with the Cambridge Crystallographic Data Centre as supplementary publication no. CCDC-160045. Copies of the data can be obtained free of charge on application to CCDC, 12 Union Road, Cambridge CB2 1EZ, UK (fax: (+44) 1223-336-033; e-mail: deposit@ccdc.cam.ac.uk).

[16] P. J. Ridgwell, P. M. Bailey, S. N. Wetherell, E. A. Kelley, P. M. Maitlis, *J. Chem. Soc. Dalton Trans.* **1982**, 999 – 1004.

Tandem Intramolecular Alkyne Silylformylation – Allylsilylation: A Case of Remote 1,5-Asymmetric Induction**

Steven J. O'Malley and James L. Leighton*

Dedicated to Professor David A. Evans on the occasion of his 60th birthday

As part of a program dedicated to the development of stereoselective catalytic methods for the synthesis of polyols, we have recently reported the tandem intramolecular silylformylation – allylsilylation of alkenes (Scheme 1a).[1, 2] Alkynes are well-known substrates for silylformylation,[3] and it seemed plausible that tandem allylsilylation of the resultant unsaturated aldehydes might occur as well (Scheme 1b). Interestingly, in this system the silicon-substituted carbon atom is no longer stereogenic. Thus, any diastereoselectivity

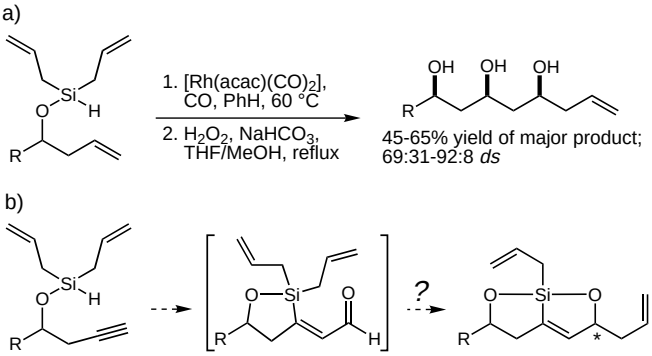

Scheme 1. a) Tandem alkene silylformylation – allylsilylation and b) proposed tandem alkyne silylformylation – allylsilylation. Hacac = acetylacetone.

[*] Prof. J. L. Leighton, S. J. O'Malley
Department of Chemistry, Columbia University
New York, NY 10027 (USA)
Fax: (+1) 212-932-1289
E-mail: leighton@chem.columbia.edu

[**] Financial support was provided by the National Institutes of Health (National Institute of General Medical Sciences, GM58133). We are grateful to Bristol-Myers Squibb for generous financial support in the form of an Unrestricted Grant in Synthetic Organic Chemistry to J.L.L. We thank Merck Research Laboratories and DuPont Pharmaceuticals for generous financial support.

Supporting information for this article is available on the WWW under http://www.angewandte.com or from the author.

  1433-7851/01/4015-2915 $ 17.50+.50/0

in the allylsilylation would have to derive from the original homopropargylic stereocenter, and would constitute an example of remote 1,5-stereoinduction.[4]

Our study commenced with diallylsilyl ether **1** [Eq. (1)]. Treatment of this silane with 1.0 mol% of $[Rh(acac)(CO)_2]$ and 6.9 MPa (1000 psi) of CO in benzene at 60 °C in a

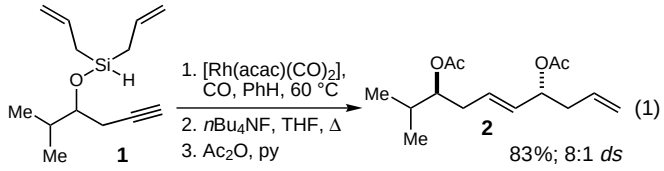

(1)

high-pressure reactor produced a yellow oil upon concentration. The unpurified material was subjected to protodesilylation (nBu$_4$NF, THF, reflux) and peracetylation (Ac_2O, pyridine (py)) to provide an 8:1 mixture of diacetate **2** and its *syn* diastereomer in 83% overall yield.[5, 6] Thus, the allylsilylation proceeded with good 1,5-diastereoselectivity, providing the 1,5-*anti* product as the major diastereomer, a result which is opposite to that observed with alkene substrates.

Optimization of the reaction conditions revealed that the catalyst loading could be reduced to 0.1 mol% with no decrease in efficiency. At significantly lower CO pressures, and/or at significantly lower temperatures there was a small improvement in the diastereoselectivity, accompanied, however, by a significant drop in reaction rate. We therefore settled on 6.9 MPa of CO in benzene at 60 °C as the standard reaction conditions.

With optimal reaction conditions identified, we set out to investigate the scope of the reaction with regard to homopropargylic and propargylic substituents (Table 1). Entries 1–6 clearly establish a direct correlation between the steric size of the homopropargylic substituent and the diastereoselectivity of the reaction, as well as a tolerance for alkyne and silyloxy functional groups. The superior diastereoselectivity shown in entry 7 indicates the stereochemically reinforcing

Table 1. Tandem alkyne silylformylation–allylsilylation.

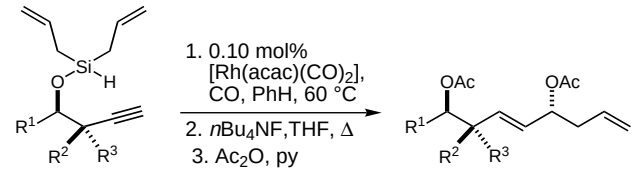

Entry	R^1	R^2	R^3	*ds*[a]	Yield [%][b]
1	*n*Pr	H	H	4:1	68
2	$HC{\equiv}CCH_2$	H	H	4:1	63
3[c]	$TBSOCH_2CH_2$	H	H	5:1	63
4	*i*Pr	H	H	8:1	83
5	Ph	H	H	7:1	83
6	*t*Bu	H	H	10:1	66
7	*i*Pr	Me	H	23:1	70
8	*i*Pr	H	Me	7:1	70

[a] 1,5-*anti*:1,5-*syn*; measured by gas chromatography. [b] Yield of the isolated purified mixture of diastereomers. [c] The *tert*-butyldimethylsilyl (TBS) group is cleaved during the protodesilylation step and the triacetate is isolated.

nature of a *syn* propargylic methyl group, whereas with an *anti* propargylic methyl group (entry 8) useful diastereoselectivity is still observed.

As an alternative to the protodesilylative workup of Table 1, we have also investigated an oxidative workup to provide β,β'-dihydroxyketone products. Subjection of silanes **1** and **4** to the standard tandem silylformylation–allylsilylation conditions, followed by evaporation of the solvent and subjection of the residue to the conditions of the Tamao oxidation[7] (H_2O_2, $NaHCO_3$, THF/MeOH, reflux) led to oxodiols **3** and **5** in 71 and 65% yields, respectively, and with identical diastereoselectivities to entries 4 and 7 in Table 1 [Eq. (2)]. The oxidative workup is noteworthy in the context of polyol synthesis in that diastereoselective ketone reductions would allow access to stereochemically diverse triol arrays.

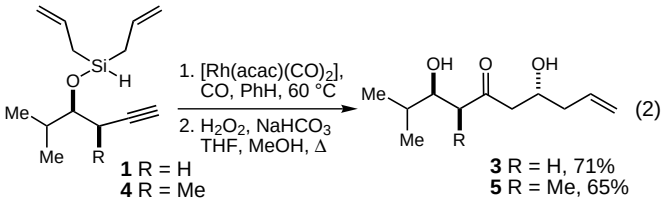

(2)

Based on arguments previously advanced,[1] and in analogy to the corresponding reactions of alkenes, we propose an uncatalyzed allylsilylation of the presumed aldehyde intermediates.[8] Binding of the aldehyde by the Lewis acidic silicon atom[9] is followed by intramolecular allylsilylation as depicted for aldehyde **6** (Scheme 2). In this model, the diastereoselectivity is determined by the relative rates at which the

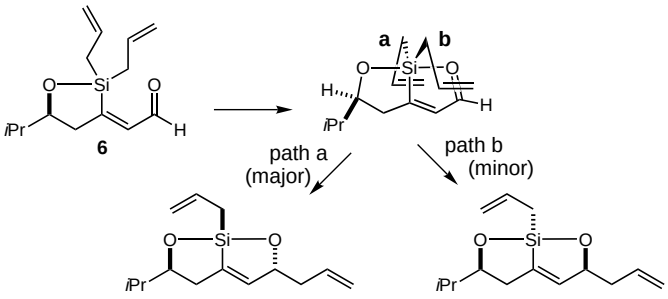

Scheme 2. Proposed model for remote 1,5-stereoinduction.

diastereotopic allyl groups transfer (path a vs. path b). A simple working hypothesis for the observed preference for path a would invoke a destabilizing steric interaction between the 2-propyl group and the allyl group **b**. The correlation between steric size of the homopropargylic substituent and the selectivity observed in entries 1–6 of Table 1 is consistent with this hypothesis as is the high selectivity observed in entry 7. The nearly identical selectivity observed in entries 4 and 8 is less well rationalized by this model and is suggestive of more subtle stereoelectronic effects.

A key feature of this model is that both of the diastereotopic allyl groups can transfer and each leads to a different product diastereomer. It could therefore be surmised that selective replacement of either allyl group with a nontrans-

  1433-7851/01/4015-2916 $ 17.50+.50/0

ferable group would lead to a stereospecific reaction. To gain support for this hypothesis we prepared silane **7** as a 1:1 mixture of diastereomers. Subjection of this mixture to the standard reaction conditions led, presumably by way of the illustrated 1:1 mixture of aldehydes, to a 1:1 mixture of diol diastereomers **8** and **9** (Scheme 3). The clear implication of this experiment is that either product diastereomer could be selected for, based only on the availability of the starting chiral silanes in diastereomerically pure form.

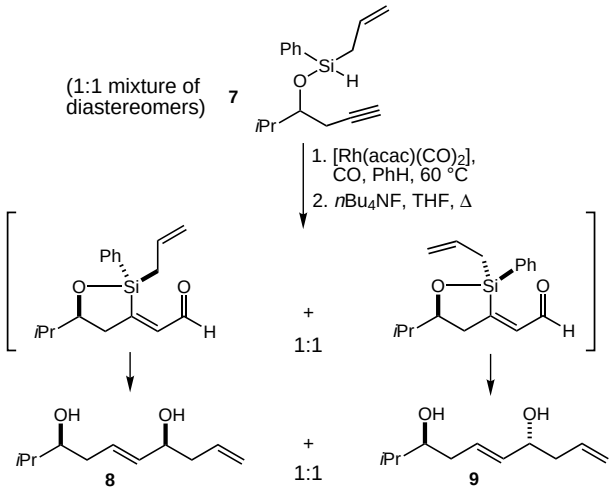

Scheme 3. Evidence for the stereochemical model.

The reactions reported here should find broad application in organic synthesis. The entire sequence (homopropargylic alcohol to 1,5-diol or oxodiol) can be carried out in a day and requires only readily available reagents ($HSiCl_3$, AllylMgBr, CO, nBu$_4$NF or H_2O_2). In the tandem silylformylation – allylsilylation reaction two new C–C bonds are formed as well as a remote stereocenter. Further studies to extend the synthetic utility of this process are in progress.

Experimental Section

Preparation of the diallylsilyl ethers: To a solution of the homopropargylic alcohol (10.0 mmol) in Et_2O (20 mL) is added trichlorosilane (20.0 mmol). The solution is heated at reflux for 2 h, and then concentrated (**Caution!** HCl evolution). The residue is redissolved in Et_2O (20 mL) and the solution is cooled to 0 °C. Allylmagnesium bromide (20.0 mL, 20.0 mmol, 1.0 M in Et_2O) is then added with vigorous stirring. The reaction mixture is warmed to room temperature and diluted with pentane. The mixture is filtered through a pad of Celite and the filtrate is concentrated. The residue is treated with pentane, and the mixture is filtered through a pad of Celite. The filtrate is concentrated and the residue is typically purified by distillation under vacuum (< 1.0 Torr).

Tandem Silylformylation – Allylsilylation: A glass liner for a stainless steel 45 mL Parr high-pressure reactor equipped with a stir bar and septum is charged with a solution of the diallylsilyl ether substrate (2.0 mmol) in benzene (6.0 mL). The solution is cooled to −78 °C and [Rh(acac)(CO)$_2$] (0.5 mg, 0.002 mmol) is added. The liner is inserted into the Parr reactor, and the pressure gauge and gas inlet assembly is attached. The reactor is charged to 3.4 MPa (500 psi) with CO, and vented. The reactor is then charged to 6.9 MPa (1000 psi) with CO and immersed (~2.5 cm) in an oil bath at 60 °C. After 2 – 3 h, the reactor is cooled to 0 °C and then vented. The solution is concentrated and the residue is immediately subjected to either workup procedure without further purification.

Protodesilylation: To a solution of the residue from the tandem silylformylation – allylsilylation in THF (10.0 mL) is added tetra-*n*-butylammonium fluoride (6.0 mL, 6.0 mmol, 1.0 M in THF). The solution is heated at reflux for 2 h, and then cooled. Saturated aqueous NH_4Cl is added, and the mixture is extracted with Et_2O. The combined organic layers are dried ($MgSO_4$), filtered and concentrated. The resulting diols may be purified by chromatography on silica gel.

Tamao oxidation: To a solution of the residue from the tandem silylformylation – allylsilylation in THF (3.0 mL) and MeOH (3.0 mL) is added $NaHCO_3$ (0.15 g, 1.8 mmol) and H_2O_2 (1.5 mL, 35 % in H_2O). The solution is heated at reflux for 3 h, and then cooled. Saturated aqueous NaCl is added, followed by saturated aqueous $Na_2S_2O_3$, and the mixture is extracted with Et_2O. The combined organic layers are dried ($MgSO_4$), filtered and concentrated. The resulting oxodiols may be purified by chromatography on silica gel.

Received: April 5, 2001 [Z16904]

[1] M. J. Zacuto, J. L. Leighton, *J. Am. Chem. Soc.* **2000**, *122*, 8587 – 8588.

[2] A conceptually similar tandem hydroformylation – allylboration reaction was earlier reported by Hoffmann et al., see: a) R. W. Hoffmann, D. Brückner, V. J. Gerusz, *Heterocycles* **2000**, *52*, 121 – 124; b) R. W. Hoffmann, J. Krüger, D. Brückner, *New J. Chem.* **2001**, *25*, 102 – 107; c) R. W. Hoffmann, D. Brückner, *New J. Chem.* **2001**, *25*, 369 – 373.

[3] a) I. Matsuda, A. Ogiso, S. Sato, Y. Izumi, *J. Am. Chem. Soc.* **1989**, *111*, 2332 – 2333; b) I. Ojima, P. Ingallina, R. J. Donovan, N. Clos, *Organometallics* **1991**, *10*, 38 – 41; c) I. Ojima, R. J. Donovan, W. R. Shay, *J. Am. Chem. Soc.* **1992**, *114*, 6580 – 6582; d) I. Ojima, M. Tzamarioudaki, C.-Y. Tsai, *J. Am. Chem. Soc.* **1994**, *116*, 3643 – 3644; e) F. Monteil, I. Matsuda, H. Alper, *J. Am. Chem. Soc.* **1995**, *117*, 4419 – 4420; f) I. Ojima, E. Vidal, M. Tzamarioudaki, I. Matsuda, *J. Am. Chem. Soc.* **1995**, *117*, 6797 – 6798; g) I. Ojima, J. V. McCullagh, W. R. Shay, *J. Organomet. Chem.* **1996**, *521*, 421 – 423.

[4] For examples of 1,5-stereoiduction in C–C bond forming reactions, see: a) J. Fujiwara, Y. Fukutani, M. Hasegawa, K. Maruoka, H. Yamamoto, *J. Am. Chem. Soc.* **1984**, *106*, 5004 – 5005; b) T. Harada, T. Hayashi, I. Wada, N. Iwaake, A. Oku, *J. Am. Chem. Soc.* **1987**, *109*, 527 – 532; c) K. Tomooka, T. Okinaga, K. Suzuki, G.-I. Tsuchihashi, *Tetrahedron Lett.* **1987**, *28*, 6335 – 6338; d) A. H. McNeill, E. J. Thomas, *Tetrahedron Lett.* **1990**, *31*, 6239 – 6242; e) G. Erker, F. Sosna, P. Betz, S. Werner, C. Krüger, *J. Am. Chem. Soc.* **1991**, *113*, 564 – 573; f) M. Nishida, E. Ueyama, H. Hayashi, Y. Ohtake, Y. Yamaura, E. Yanaginuma, O. Yonemitsu, A. Nishida, N. Kawahara, *J. Am. Chem. Soc.* **1994**, *116*, 6455 – 6456; g) M. P. Sibi, J. Ji, J. B. Sausker, C. P. Jasperse, *J. Am. Chem. Soc.* **1999**, *121*, 7517 – 7526; h) L. F. Tietze, C. Schünke, *Eur. J. Org. Chem.* **1998**, 2089 – 2099; i) D. Badone, J.-M. Bernassau, R. Cardamone, U. Guzzi, *Angew. Chem.* **1996**, *108*, 575 – 578; *Angew. Chem. Int. Ed. Engl.* **1996**, *35*, 535 – 538. j) I. Paterson, K. R. Gibson, R. M. Oballa, *Tetrahedron Lett.* **1996**, *37*, 8585 – 8588; k) D. A. Evans, P. J. Coleman, B. Côté, *J. Org. Chem.* **1997**, *62*, 788 – 789; l) L. N. Pridgen, K. Huang, S. Shilcrat, A. Tickner-Eldridge, C. DeBrosse, R. C. Haltiwanger, *Synlett* **1999**, 1612 – 1614; m) E. Nicolás, K. C. Russell, V. J. Hruby, *J. Org. Chem.* **1993**, *58*, 766 – 770 .

[5] Although the diols can be cleanly isolated, a quantitative assay of the diastereoselectivity (by gas chromatography) was best performed with the derived diacetates.

[6] See the Supporting Information for a description of the stereochemical proofs.

[7] For a review on the Tamao and Fleming oxidations, see: G. R. Jones, Y. Landais, *Tetrahedron* **1996**, *52*, 7599 – 7662.

[8] We are aware of only one other example of an uncatalyzed/unpromoted allylsilylation of aldehydes using a tetracoordinate allylsilane, see: K. Matsumoto, K. Oshima, K. Utimoto, *J. Org. Chem.* **1994**, *59*, 7152 – 7155.

[9] This is believed to be an example of ring strain-induced Lewis acidity. See ref. [1] and: a) E. F. Perozzi, R. S. Michalak, G. D. Figuly, W. H. Stevenson III, D. B. Dess, M. R. Ross, J. C. Martin, *J. Org. Chem.* **1981**, *46*, 1049 – 1053; b) S. E. Denmark, R. T. Jacobs, G. Dai-Ho, S. Wilson, *Organometallics* **1990**, *9*, 3015 – 3019; c) A. G. Myers, S. E. Kephart, H. Chen, *J. Am. Chem. Soc.* **1992**, *114*, 7922 – 7923; d) S. E. Denmark, B. D. Griedel, D. M. Coe, M. E. Schnute, *J. Am. Chem. Soc.* **1994**, *116*, 7026 – 7043; e) K. Omoto, Y. Sawada, H. Fujimoto, *J. Am. Chem. Soc.* **1996**, *118*, 1750 – 1755.

  1433-7851/01/4015-2917 $ 17.50+.50/0

Living Polymerization of Ethylene with a Titanium Complex Containing Two Phenoxy-Imine Chelate Ligands

Junji Saito, Makoto Mitani, Jun-ichi Mohri, Yasunori Yoshida, Shigekazu Matsui, Sei-ichi Ishii, Shin-ichi Kojoh, Norio Kashiwa, and Terunori Fujita*

Dedicated to Dr. Kenji Saeki on the occasion of his 60th birthday

Living polymerization of olefins is of great importance in the preparation of precisely controlled polymers such as monodisperse polymers, terminally functionalized polymers, and block copolymers, all of which are expected to display novel physical properties. Recent advances in the design and synthesis of well-defined transition metal complexes for olefin polymerization[1] have enabled the realization of living polymerization of various olefins.[2] On paper, living polymerization of an olefin providing high activity with high molecular weight value at high temperatures is feasible by controlling chain termination or transfer steps (e.g., β-hydride elimination, β-alkyl elimination, and chain transfer to a cocatalyst). However, the living polymerization of olefins is performed at low temperatures, normally below room temperature, to suppress these processes. Thus, it generally exhibits low activity with insufficient molecular weight value, highly restricting application to the preparation of the desired polymers.

We have acquired Group 4 transition metal complexes bearing two phenoxy-imine chelate ligands, named FI catalysts, which display high catalytic performance for the polymerization of ethylene, ethylene-propylene, or 1-hexene.[3] In the course of our studies on FI catalysts having one or more heteroatoms and/or heteroatom-containing substituents in the ligands, we found a fluorine-containing titanium FI catalyst that exhibits unprecedented catalytic performance for the polymerization of ethylene. Here we describe the highly active living polymerization of ethylene catalyzed by a titanium FI catalyst, creating high molecular weight polyethylene with a narrow polydispersity at high polymerization temperatures.

The fluorine-containing phenoxy-imine ligand employed in this study is *N*-(3-*tert*-butylsalicylidene)-2,3,4,5,6-pentafluoroaniline. The ligand was prepared in 98% yield by the Schiff base condensation of 2,3,4,5,6-pentafluoroaniline with 3-*tert*-butylsalicylaldehyde in toluene using *p*-toluenesulfonic acid (PTSA) as a catalyst. Complex **1** was obtained as a brown powder in 67% yield by treatment of $TiCl_4$ with two equivalents of the lithium salt of *N*-(3-*tert*-butylsalicylidene)-2,3,4,5,6-pentafluoroaniline in diethyl ether according to Scheme 1.

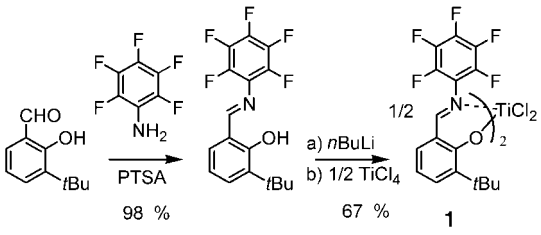

Scheme 1. Synthetic route to compound **1**. PTSA = *p*-toluenesulfonic acid.

Single crystals of complex **1** suitable for an X-ray structure determination were grown from a saturated solution in pentane/CH_2Cl_2. The structure features a distorted octahedral complex in which the titanium atom is bound to two *cis*-coordinated phenoxy-imine [O,N] chelating ligands (the oxygen atoms are situated in *trans* position, O-Ti-O 163.6°) and the two chlorine atoms (in *cis* position, Cl-Ti-Cl 96.4°; Figure 1).[4] Under the assumption that two chlorine-bound sites are transformed into olefin polymerization sites while retaining their *cis* relationship, an active species originating from complex **1** would have two *cis* sites for efficient olefin polymerization.

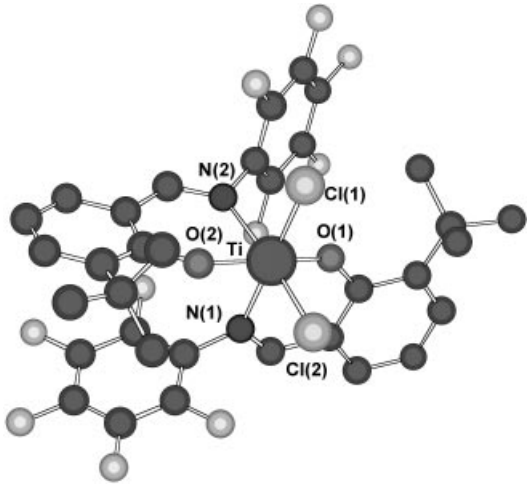

Figure 1. X-ray structure of **1**. Hydrogen atoms and a CH_2Cl_2 molecule have been omitted for clarity. Selected bond lengths [Å] and angles [°]: Ti–O(1) 1.841(3), Ti–O(2) 1.841(3), Ti–N(1) 2.240(4), Ti–N(2) 2.219(4), Ti–Cl(1) 2.289(2), Ti–Cl(2) 2.261(2); O(1)-Ti-O(2) 163.6(1), N(1)-Ti-N(2) 87.2(1) Cl(1)-Ti-Cl(2) 96.42(6).

Ethylene polymerizations were performed at 25 °C under atmospheric pressure for one minute with complex **1** and, for comparison, $[Cp_2ZrCl_2]$ and $[Cp_2TiCl_2]$ using methylalumoxane (MAO) as a cocatalyst. The results are presented in Table 1. Complex **1** proved to be competitive with the metallocenes in terms of catalytic activity. Thus, complex **1** displayed a very high turnover frequency (TOF) of 20000 $min^{-1}atm^{-1}$ (entry 1), which was comparable to those exhibited by $[Cp_2ZrCl_2]$ (18600 $min^{-1}atm^{-1}$, entry 2) and $[Cp_2TiCl_2]$ (30500 $min^{-1}atm^{-1}$, entry 3) under the same polymerization conditions. The melting temperature (T_m) of the produced polyethylene (entry 1) was 135.2 °C. The ^{13}C NMR analysis of the polymer indicates that the polyethylene has a linear structure with virtually no branching. The polyethylene produced with complex **1** possesses a narrow polydispersity

[*] Dr. T. Fujita, J. Saito, Dr. M. Mitani, J. Mohri, Y. Yoshida, S. Matsui, S. Ishii, Dr. S. Kojoh, Dr. N. Kashiwa
R&D Center, Mitsui Chemicals, Inc.
580-32 Nagaura, Sodegaura-City
Chiba 299-0265 (Japan)
Fax: (+81) 438-64-2375
E-mail: terunori.fujita@mitsui-chem.co.jp

  1433-7851/01/4015-2918 $ 17.50+.50/0

Table 1. Results of ethylene polymerization using complex **1**, $[Cp_2ZrCl_2]$, or $[Cp_2TiCl_2]$.[a]

Entry	Complex	Yield [g]	TOF [$min^{-1}atm^{-1}$]	M_n [$\times 10^3$]	M_w/M_n	T_m [°C]
1	**1**	0.28	20000	412	1.13	135.2
2	$[Cp_2ZrCl_2]$	0.26	18600	157	1.73	133.4
3	$[Cp_2TiCl_2]$	0.43	30500	309	1.97	134.9

[a] Conditions: ethylene, atmospheric pressure (1667 mL min^{-1}), toluene (250 mL), 25 °C, 1.0 min, catalyst (0.5 μmol), cocatalyst MAO (1.25 mmol, purchased from Albemarle).

($M_w/M_n = 1.13$), which suggests a living polymerization. The molecular weight ($M_n = 412000$) represents one of the highest values and the TOF of 20000 $min^{-1}atm^{-1}$ is one of the highest activities reported to date with regard to living ethylene polymerizations.

To further confirm the living polymerization, the M_n and M_w/M_n values of the polymerizations using diluted ethylene with nitrogen under atmospheric pressure at 25 °C were monitored as a function of polymerization time. A linear relationship between M_n and polymerization time as well as a narrow range of M_w/M_n values (1.05 – 1.13) were found for all runs, indicating a living polymerization (Figure 2a).[5] To the best of our knowledge, this is the first example of an exceptionally high speed, room-temperature living ethylene polymerization which produces very high molecular weight polyethylene with a narrow polydispersity ($M_w/M_n < 1.20$).[6]

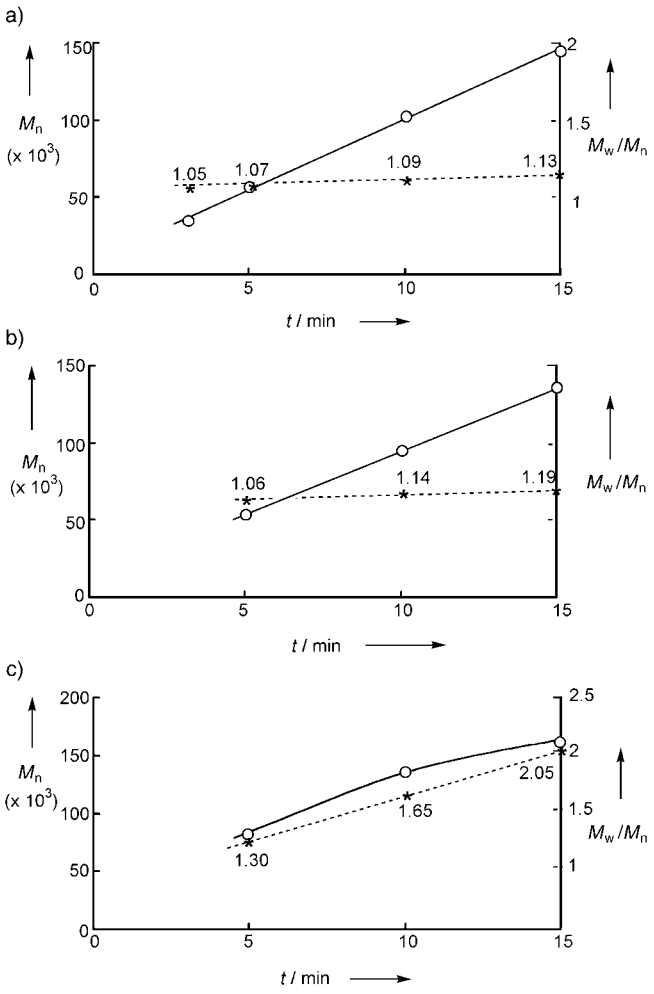

Figure 2. Plots of M_n and M_w/M_n as a function of polymerization time t for ethylene polymerization at a) 25 °C, b) 50 °C, and c) 75 °C using diluted ethylene (33 mL h^{-1} for a, b; 83 mL h^{-1} for c) with nitrogen (833 mL h^{-1}; **1**: 1 μmol, MAO: 1.25 mmol). ○: M_n, ∗: M_w/M_n.

Surprisingly, there is practically no chain termination or transfer step in the complex **1**/MAO system for at least 30 min, even in the absence of ethylene, indicating the high potential of the system for living ethylene polymerizations (Table 2). Thus, treatment of the complex **1**/MAO with ethylene-saturated toluene at room temperature under a nitrogen atmosphere for 35 min—the ethylene was substantially consumed within 5 min as indicated by entries 1 and 2—and subsequent ethylene gas feed (333 mL min^{-1}, 2 min) to the resulting mixture resulted in the formation of polyethylene having a narrow polydispersity ($M_w/M_n = 1.17$).

Table 2. Results of ethylene polymerization with complex **1** using ethylene-saturated toluene under N_2 or N_2 followed by ethylene feed.[a]

Entry	Conditions	Yield [g]	M_n [$\times 10^3$]	M_w/M_n
1	5 min under N_2	0.800	65.8	1.10
2	35 min under N_2	0.775	73.0	1.12
3	1. 35 min under N_2			
	2. 2 min with ethylene[b]	1.317	98.6	1.17

[a] Conditions: toluene (250 mL, saturated with ethylene), complex (10 μmol), cocatalyst MAO (2.5 mmol). [b] Ethylene (333 mL min^{-1}).

To investigate the living nature of the complex **1**/MAO catalyst system, ethylene polymerizations were carried out at higher temperatures (50, 75, and 90 °C). As summarized in Table 3, complex **1** was capable of producing polyethylenes having narrow polydispersities (M_w/M_n 1.08 – 1.15) at 50 and 75 °C.

Table 3. Results of ethylene polymerization with complex **1** at various temperatures.[a]

Entry	**1** [μmol]	T [°C]	t [min]	Yield [g]	TOF [$min^{-1}atm^{-1}$]	M_n [$\times 10^3$]	M_w/M_n
1	0.5	50	0.5	0.17	24300	257	1.08
2	0.5	50	1.0	0.30	21400	424	1.13
3	1.0	75	0.5	0.25	17900	214	1.09
4	1.0	75	1.0	0.45	16100	329	1.15
5	2.0	90	0.5	0.20	7140	102	1.22
6	2.0	90	1.0	0.46	8210	167	1.30

[a] Conditions: ethylene, atmospheric pressure (1667 mL min^{-1}), toluene (250 mL), cocatalyst MAO (1.25 mmol, purchased from Albemarle).

The M_n and M_w/M_n values of the polymerizations at 50 and 75 °C using diluted ethylene with nitrogen under atmospheric pressure were monitored as a function of polymerization time. At 50 °C a linear relationship between M_n and polymerization time as well as narrow M_w/M_n values were found for all runs ($M_w/M_n = 1.06 – 1.19$, Figure 2b). Moreover, at 75 °C, though chain termination or transfer and/or catalyst deactivation occurred, complex **1** still possessed some characteristics of living polymerization (Figure 2c). These results demonstrate that complex **1** has a great potential for living polymerization.

As an application of the living polymerization, we successfully synthesized polyethylene-*b*-poly(ethylene-*co*-propyl-

  1433-7851/01/4015-2919 $ 17.50+.50/0

ene) diblock copolymer and polyethylene-*b*-poly(ethylene-*co*-propylene)-*b*-polypropylene triblock copolymer by sequential addition of the monomers for the first time,[7] showing the usefulness of the titanium FI catalyst containing fluorine atoms in the ligands.

In summary, a new catalyst system for living ethylene polymerization at high temperatures has been introduced. The catalyst system promotes living ethylene polymerization at high temperatures and furnishes high molecular weight monodisperse polyethylene, displaying very high activity. With the catalyst system, a PE-*b*-(PE-*co*-PP) diblock copolymer and a PE-*b*-(PE-*co*-PP)-*b*-PP triblock copolymer have been prepared. The results described herein together with our previous reports[3] indicate that FI catalysts possess high potential for creating novel polymers. The results of polymerization using other olefins as well as mechanistic studies will be reported shortly.[8]

Experimental Section

Polyethylene synthesis: Ethylene polymerization was performed in a glass reactor (500 mL) equipped with a mechanical stirrer and a temperature probe. Toluene (250 mL) was introduced to the nitrogen-purged reactor and stirred (600 rpm). The toluene was thermostated to the prescribed polymerization temperature, and then the ethylene gas feed was started. After 10 min polymerization was initiated by the additions of 1.25 M MAO in toluene (1.0 mL, 1.25 mmol) and then 0.001M **1** in toluene (0.5 mL, 0.5 μmol) to the reactor, unless otherwise noted. The polymerization was quenched after the prescribed time by the addition of isobutyl alcohol (10 mL). The resulting mixture was added to acidic methanol (1000 mL including 2 mL of conc. HCl). The polyethylene was collected by filtration, washed with methanol (2×200 mL), and then dried to constant weight (80 °C, vacuum oven).

The polydispersity (M_w/M_n) and number average molecular weight (M_n) of polyethylene were measured by gel permeation chromatography at 145 °C using polyethylene calibration.

1: ^{1}H NMR (270 MHz, $CDCl_3$, 25 °C, TMS): $\delta = 1.35$ (s, 18H; *t*Bu), 7.02 (t, $^3J(H,H) = 7.6$ Hz, 2H), 7.29 (dd, $^3J(H,H) = 7.6$, 1.6 Hz, 2H), 7.64 (dd, $^3J(H,H) = 7.6$, 1.6 Hz, 2H), 8.22 (s, 2H; CH=N), 1.21 (t, $J =$ 7.0 Hz,(CH_3CH_2)O), 3.48 (q, $J = 7.0$ Hz,(CH_3CH_2)O); MS: *m*/*z* (%): 802 (100) [M^+]; elemental analysis calcd for $C_{34}H_{26}F_{10}Cl_2N_2O_2Ti + 1/3(C_2H_5)_2O$: C 51.25, H 3.57, N 3.38, F 22.95, Cl 8.52, Ti 5.78; found: C 51.71, H 4.04 N 3.79, F 21.68, Cl 8.92, Ti 5.40.

Received: March 14, 2001 [Z16775]

[1] Recent reviews: a) G. J. P. Britovsek, V. C. Gibson, D. F. Wass, *Angew. Chem.* **1999**, *111*, 448 – 468; *Angew. Chem. Int. Ed.* **1999**, *38*, 428 – 447; b) S. D. Ittel, L. K. Johnson, M. Brookhart, *Chem. Rev.* **2000**, *100*, 1169 – 1203.

[2] a) Y. Doi, S. Ueki, T. Keii, *Macromolecules*, **1979**, *12*, 814 – 819; b) G. Jeske, H. Lauke, H. Mauermann, P. N. Swepston, H. Schumann, T. J. Marks, *J. Am. Chem. Soc.* **1985**, *107*, 8091 – 8103; c) V. M. Mohring, G. Fink, *Angew. Chem.* **1985**, *97*, 982; *Angew. Chem. Int. Ed. Engl.* **1985**, *24*, 1001 – 1003; d) H. Yasuda, M. Furo, H. Yamamoto, A. Nakamura, S. Miyake, N. Kibino, *Macromolecules* **1992**, *25*, 5115 – 5116; e) K. Mashima, S. Fujikawa, A. Nakamura, *J. Am. Chem. Soc.* **1993**, *115*, 10990 – 10991; f) K. Mashima, S. Fujikawa, H. Urata, E. Tanaka, A. Nakamura, *J. Chem. Soc. Chem. Commum.* **1994**, 1623 – 1624; g) K. Mashima, S. Fujikawa, Y. Tanaka, H. Urata, T. Oshiki, E. Tanaka, A. Nakamura, *Organometallics*, **1995**, *14*, 2633 – 2640; h) M. Brookhart, J. M. DeSimone, B. E. Grant, M. J. Tanner, *Macromolecules* **1995**, *28*, 5378 – 5380; i) J. D. Scollard, D. H. McConville, *J. Am. Chem. Soc.*, **1996**, *118*, 10008 – 10009; j) C. M. Killian, D. J. Tempel, L. K. Johnson, M. Brookhart, *J. Am. Chem. Soc.* **1996**, *118*, 11664 – 11665; k) R. Baumann, W. M. Davis, R. R. Schrock, *J. Am. Chem. Soc.* **1997**, *119*, 3830 – 3831; l) H. Hagihara, T. Shiono, T. Ikeda, *Macromolecules* **1998**, *31*, 3184 – 3188; m) Y.-M. Jeon, S. J. Park, J. Heo, K. Kim, *Organometallics* **1998**, *17*, 3161 – 3163; n) Y. Fukui, M. Murata, K. Soga, *Macromol. Rapid Commun.* **1998**, *20*, 637 – 640; o) K. C. Jayaratne, L. R. Sita, *J. Am. Chem. Soc.* **2000**, *122*, 958 – 959; p) E. Y. Tshuva, I. Goldberg, M. Kol, *J. Am. Chem. Soc.* **2000**, *122*, 10706 – 10707; q) A. C. Gottfried, M. Brookhart, *Macromolecules* **2001**, *34*, 1140 – 1142; r) T. Matsugi, S. Matsui, S. Kojoh, Y. Takagi, Y. Inoue, T. Fujita, N. Kashiwa, *Chem. Lett*. **2001**, 566 – 567.

[3] a) T. Fujita, Y. Tohi, M. Mitani, S. Matsui, J. Saito, M. Nitabaru, K. Sugi, H. Makio, T. Tsutsui, (Mitsui Chemicals Inc.), EP 0874005, **1998**, [*Chem. Abstr*. **1998**, *129*, 331166]; b) S. Matsui, Y. Tohi, M. Mitani, J. Saito, H. Makio, H. Tanaka, M. Nitabaru, T. Nakano, T. Fujita, *Chem. Lett.* **1999**, 1065 – 1066; c) S. Matsui, M. Mitani, J. Saito, Y. Tohi, H. Makio, H. Tanaka, T. Fujita, *Chem. Lett.* **1999**, 1263 – 1264; d) S. Matsui, M. Mitani, J. Saito, N. Matsukawa, H. Tanaka, T. Nakano, T. Fujita, *Chem. Lett.* **2000**, 554 – 555; e) J. Saito, M. Mitani, S. Matsui, N. Kashiwa, T. Fujita, *Macromol. Rapid Commun.* **2000**, *21*, 1333 – 1336; f) S. Matsui, T. Fujita, *Catal. Today* **2001**, *169*, 99 – 104; g) N. Matsukawa, S. Matsui, M. Mitani, J. Saito, K. Tsuru, N. Kashiwa, T. Fujita, *J. Mol. Catal. A*, **2001**, *66*, 63 – 73; h) S. Matsui, M. Mitani, J. Saito, Y. Tohi, H. Makio, N. Matsukawa, Y. Takagi, K. Tsuru, M. Nitabaru, T. Nakano, H. Tanaka, N. Kashiwa, T. Fujita, *J. Am. Chem. Soc.*, in press; i) J. Saito, M. Mitani, S. Matsui, Y. Tohi, H. Makio, T. Nakano, H. Tanaka, N. Kashiwa, T. Fujita, *Macromol. Chem. Phys.*, in press; j) S. Ishii, J. Saito, M. Mitani, J. Mohri, N. Matsukawa, N. Kashiwa, T. Fujita, *J. Mol. Catal. A*, in press.

[4] Crystal data for complex **1** ($C_{34}H_{26}F_{10}Cl_2N_2O_2Ti+CH_2Cl_2$): $M_w =$ 888.31; crystal dimensions $0.40 \times 0.35 \times 0.07$ nm, monoclinic, $P2_1/n$, $a = 11.6786(2)$, $b = 25.6347(9)$, $c = 12.3467(1)$ Å, $\beta = 92.254(4)°$, $V =$ 3693.5(1) Å^3, $Z = 4$, $\rho_{calcd} = 1.597$ g cm^{-3}, $2\theta_{max} = 59.9°$, $F(000) = 1792$, $\mu(Mo_{K\alpha}) = 6.07$ cm^{-1}, Rigaku RAXIS-RAPID Imaging Plate, $Mo_{K\alpha}$ (λmax = 0.71069 Å), graphite monochromated, $T = -160$ °C, 32621 measured reflections, 9925 independent reflections, 9917 observed reflections($I > -3\sigma(I)$), The data were corrected for Lorentz and polarization effects, full-matrix least-squares refinement based on $|F^2|$, 487 parameters, hydrogen atom were included but not refined, $R1 =$ 0.048 (for 5207 data with $I > 2\sigma(I)$), R(Rw) = 0.084 (0.073), max./min. residual electron density 0.02/ – 0.02 e$^-$ Å^{-3}. Crystallographic data (excluding structure factors) for the structure reported in this paper have been deposited with the Cambridge Crystallographic Data Centre as supplementary publication no. CCDC-159669. Copies of the data can be obtained free of charge on application to CCDC, 12 Union Road, Cambridge CB21EZ, UK (fax: (+44) 1223-336-033; e-mail: deposit@ccdc.cam.ac.uk).

[5] [Cp_2TiCl_2] produced polyethylenes having an M_w/M_n value of 3.31 – 3.45 under the conditions described in Figure 2, indicating that Cp_2TiCl_2 did not promote living polymerization under these conditions.

[6] Because the corresponding titanium complex without any fluorine atoms in the ligand produced polyethylene having an M_w/M_n value of about 2.0,[3b] it is obvious that the presence of the fluorine atoms is required for living polymerization. Density functional theory (DFT) calculations suggest that a fluorine atom adjacent to the imine nitrogen atom of an active species for polymerization interacts with a β-hydrogen atom of a polymer chain (β-H···F 2.28 Å), probably preventing β-hydrogen transfer. Thus, this interaction may be responsible for the realization of living polymerization.

[7] Polyethylene-*b*-poly(ethylene-*co*-propylene) diblock copolymer: PE M_n 115000, M_w/M_n 1.10, PE-*b*-(PE-*co*-PP), M_n 211000 M_w/M_n 1.16 polyethylene-*b*-poly(ethylene-*co*-propylene)-*b*-polypropylene triblock copolymer: PE M_n 115000, M_w/M_n 1.10, PE-*b*-(PE-*co*-PP) M_n 211000 M_w/M_n 1.16, PE-*b*-(PE-*co*-PP)-*b*-sPP ([rr] = 87%): M_n 235000, M_w/M_n 1.15.

[8] a) J. Saito, M. Mitani, J. Mohri, S. Ishii, Y. Yoshida, T. Matsugi, S. Kojoh, N. Kashiwa, T. Fujita, *Chem. Lett.* **2001**, 576 – 577; b) S. Kojoh, T. Matsugi, J. Saito, M. Mitani, T. Fujita, N. Kashiwa, *Chem. Lett.*, in press; c) J. Saito, M. Mitani, M. Onda, J. Mohri, S. Ishii, Y. Yoshida, T. Nakano, H. Tanaka, T. Matsugi, S. Kojoh, N. Kashiwa, T. Fujita, *Macromol. Rapid Commun.*, in press.

  1433-7851/01/4015-2920 $ 17.50+.50/0

The First $In(OTf)_3$-Catalyzed Conversion of Kinetically Formed Homoallylic Alcohols into the Thermodynamically Preferred Regioisomers: Application to the Synthesis of 22α-Sterols**

Teck-Peng Loh,* Kui-Thong Tan, and Qi-Ying Hu

Processes which convert readily available kinetic products to their less readily accessible thermodynamic isomers are of synthetic value and mechanistic interest in organic synthesis.[1] In this respect, homoallylic alcohols are versatile building blocks for the synthesis of many biologically active molecules, and the allylation of carbonyl compounds and the carbonyl ene reaction offer ready access to this class of compounds.[2] Nevertheless, almost all current methods produce predominantly γ adducts, except in a few special cases, and hence access to the α adducts is restricted.[3] Coincidentally, our recent studies on the synthesis of various steroids with 22-oxygenated side chains required an efficient access to linear homoallylic 22-sterols,[4] for which the thermodynamically controlled conversion of the γ adduct to the corresponding α adduct appeared to be an appealing approach.[5] Here we describe the first $In(OTf)_3$-catalyzed conversion of branched homoallylic alcohols to the thermodynamically preferred linear regioisomers.

Given our interest in indium chemistry,[6] we explored this thermodynamic conversion on the basis of indium reagents.[7] In our initial study, 1-cyclohexyl-2-methylbut-3-en-1-ol (**1a**) was subjected to a series of experiments to evaluate the merits of various indium reagents [Eq. (1), Table 1]. Among them, $In(OTf)_3$ exhibited excellent efficiency in the conversion of **1a** to its linear isomer **2a** (Table 1, entry 4).[8]

Table 1. Evaluation of various indium reagents for the thermodynamic conversion (1).

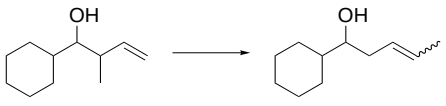

(1)

1a **2a**

Entry	Indium reagent	Yield [%]
1	In, allyl bromide, HMPA[a]	no reaction
2	InF_3[b]	no reaction
3	$InCl_3$[b]	no reaction
4	$In(OTf)_3$[b]	78%

[a] The reaction was performed with the branched isomer (0.5 mmol), In (1.0 mmol), bromide (1.5 mmol) and hexamethylphosphoramide (HMPA, 7.5 mmol) in THF (5 mL). [b] Reactions were performed with the branched isomer (0.5 mmol) and the Lewis acid (0.05 mmol) in CH_2Cl_2 (4 mL).

[*] Prof. Dr. T.-P. Loh, K.-T. Tan, Q.-Y. Hu
Department of Chemistry
National University of Singapore
3 Science Drive 3, Singapore 117543 (Singapore)
Fax: (+65) 779-1691
E-mail: chmlohtp@nus.edu.sg

[**] This research was supported by the National University of Singapore.
Supporting information for this article is available on the WWW under http://www.angewandte.com or from the author.

We then extended this method to a variety of substrates [Eq. (2), Table 2]. In most cases, the reactions afforded the linear isomers in moderate to good yields (except for entries 4 and 6). In addition, there appears to be a correlation between the relative stereochemistry of the substrate and the geometry at the double bond of the product (*syn* $\rightarrow Z$ and *anti* $\rightarrow E$; entries 7 and 8).

Table 2. $In(OTf)_3$-catalyzed thermodynamic conversion of homoallylic alcohols **1** [Eq. (2)].[a]

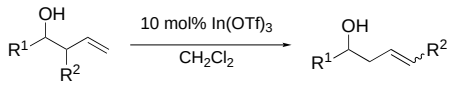

(2)

1 **2**

Entry	**1**	R^1	R^2	*anti*/*syn* of **1**[c]	*T* [°C]	Yield of **2** [%][b] (*E*/*Z*)
1	**1a**	*c*-C_6H_{11}	Me	80/20	25	78 (68/32)
2	**1b**	*c*-C_6H_{11}	Ph	98/2	25	81 (*E*)[d]
3	**1c**	*c*-C_6H_{11}	CO_2Et	85/15	40	69 (85/15)[e]
4	**1d**	Ph	CO_2Et	86/14	40	19 (*E*)
5	**1e**	$PhCH_2CH_2$	Me	50/50	25	72 (55/45)
6	**1f**	$PhCH_2CH_2$	Ph	70/30	25	36 (>99/1)[f]
7	**1g**	$PhCH_2CH_2$	CO_2Et	80/20	40	74 (84/16)[e]
8	**1g**	$PhCH_2CH_2$	CO_2Et	>99/1	40	78 (*E*)
9	**1h**	$CH_3(CH_2)_4$	Me	55/45	25	53 (65/35)
10	**1i**	$CH_3(CH_2)_4$	Ph	90/10	25	76 (97/3)[g]
11	**1j**	$CH_3(CH_2)_4$	CO_2Et	70/30	40	73 (80/20)[e]

[a] All reactions were performed with the branched isomer (0.5 mmol) and $In(OTf)_3$ (0.05 mmol) in CH_2Cl_2 (4 mL). [b] Yields of isolated products. [c] Determined by ^1H NMR (300 MHz). [d] 9% of **1b** was recovered (*syn* only). [e] *Z* isomer was obtained as lactenone. [f] 36% of **1f** was recovered (*anti*/*syn* 1/3). [g] 13% of **1i** was recovered (*syn* only).

A weak signal for an aldehydic proton at $\delta = 9.61$ was observed in the ^1H NMR spectrum of the crude reaction mixture when **1a** was treated with $In(OTf)_3$, which suggested the involvement of a retro-process that generates the free aldehyde in situ. To verify this, a crossover experiment was conducted (Scheme 1). A mixture of **1a** and **1g** was subjected to the reaction conditions, and the reaction was quenched after 12 h. Column chromatography gave **2a** (67%) and recovered **1g** (62%), together with 5% **2e** and **2c**. This proved that the conversion involves a retro-process that generate the parent aldehyde in situ.

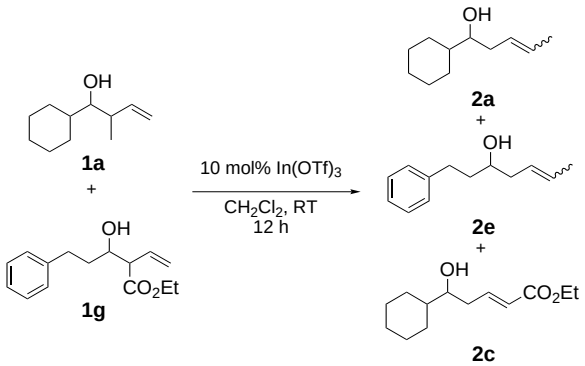

Scheme 1. Crossover exchange experiment.

  1433-7851/01/4015-2921 $ 17.50+.50/0

Afterwards the $In(OTf)_3$-catalyzed thermodynamic conversion was applied to the construction of steroidal side chains. The optically pure branched homoallylic sterols **1l** and **1k**[4] were subjected to the conversion procedure. A solution of **1l** or **1k** (1.0 equiv) in CH_2Cl_2 was added dropwise to a suspension of $In(OTf)_3$ (0.1 equiv) in CH_2Cl_2, and the mixture was heated to reflux for 48 h. The optically pure isomers **2l** and **2k** were obtained in good yield (71 and 73%, respectively) [Eq. (3)]. Interestingly, the stereochemistry at C-22

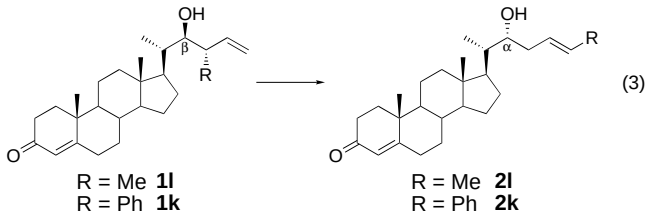

(3)

was assigned as 22α. In other words, the allyl fragment attaches to the steroid in an anti-Cram manner,[9] which excludes the possibility of re-addition of the allyl anion to the aldehyde. Therefore, a pericyclic pathway was invoked to account for this stereochemical outcome, for which the 2-oxonia [3,3]-sigmatropic rearrangement proposed by Nokami et al.[10] was adopted. The overall postulated reaction pathway for the $In(OTf)_3$-catalyzed thermodynamic conversion is shown in Scheme 2. Lewis acid catalyzed retro-ene[11] cleavage of the carbon–carbon bond releases the parent aldehyde, which subsequently promotes a 2-oxonia [3,3]-sigmatropic rearrangement to afford the stereochemically inverted homoallylic alcohol.

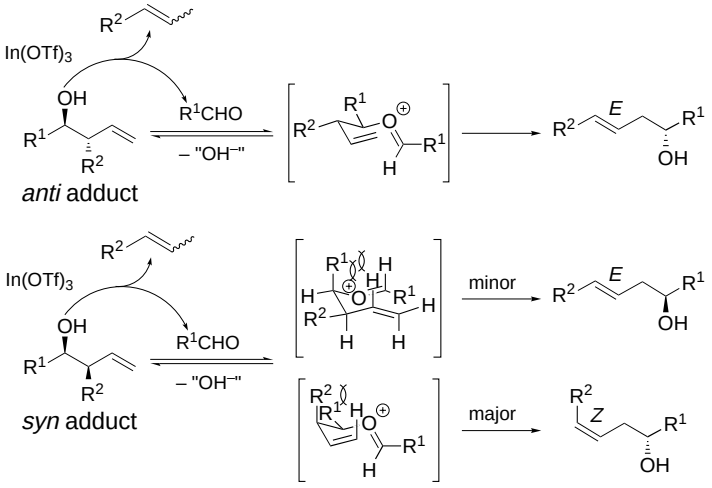

Scheme 2. Postulated reaction pathway for the conversion of branched to linear homoallylic alcohols.

In conclusion, an $In(OTf)_3$-catalyzed conversion of branched homoallylic alcohols to the thermodynamically preferred linear regioisomers has been developed. This method can be utilized for the construction of steroidal side chains with anti-Cram stereoselectivity. Hence, efficient access to 22α-oxygenated steroidal side chains, such as those in ecdysone derivatives,[9] is facilitated. As opposed to the previously proposed mechanisms involving transfer of allyl anions or concerted rearrangement for the equilibration of branched and linear homoallylic alcohols, our study of this thermodynamic conversion suggests that both retro-cleavage to generate the parent aldehyde in situ and a concerted rearrangement are involved, plausibly a retro-ene reaction followed by a 2-oxonia [3,3]-sigmatropic rearrangement in this case. This indicates the possibility of the concurrent involvement of both mechanisms for the generation of the thermodynamically preferred linear adducts in other allylation reactions. Further studies to verify this postulate are in progress.

Received: February 19, 2001
Revised: April 30, 2001 [Z16642]

[1] For some examples, see F. Barbot, P. Miginiac, *Tetrahedron Lett.* **1975**, 3829; R. N. Gedye, P. Arora, A. H. Khalil, *Can. J. Chem.* **1975**, *53*, 1943; L. E. Rice, M. C. Boston, H. O. Finklea, B. J. Suder, J. O. Frazier, T. Hudlicky, *J. Org. Chem.* **1984**, *49*, 1845; K. Tatsuta, T. Tamura, T. Mase, *Tetrahedron Lett.* **1999**, *40*, 1925.

[2] For reviews, see Y. Yamamoto, N. Asao, *Chem. Rev.* **1993**, *93*, 2207; W. R. Roush in *Comprehensive Organic Synthesis*, *Vol. 2* (Eds.: B. M. Trost, I. Fleming, C. H. Heathcock), Pergamon, Oxford, **1991**, pp. 1–53; K. Mikami, M. Shimizu, *Chem. Rev.* **1992**, *92*, 1021.

[3] For α-selective allylation, see A. Yanagisawa, S. Habaue, H. Yamamoto, *J. Am. Chem. Soc.* **1991**, *113*, 8955, and references therein.

[4] T.-P. Loh, Q.-Y. Hu, J. J. Vittal, *Synlett* **2000**, 523; T.-P. Loh, J. Xu, Q.-Y. Hu, J. J. Vittal, *Tetrahedron: Asymmetry* **2000**, *11*, 1565.

[5] A recent example: B.-C. Hong, J.-H. Hong, Y.-C. Tsai, *Angew. Chem.* **1998**, *110*, 482; *Angew. Chem. Int. Ed.* **1998**, *37*, 468.

[6] For some examples of our previous work on indium chemistry, see R.-B. Wang, C.-M. Lim, C.-H. Tan, B.-K. Lim, K.-Y. Sim, T.-P. Loh, *Tetrahedron: Asymmetry* **1995**, *6*, 1825; X.-R. Li, T.-P. Loh, *Tetrahedron: Asymmetry* **1996**, *7*, 1535; T.-P. Loh, J. Pei, G.-Q. Cao, *Chem. Commun.* **1996**, 1819; T.-P. Loh, G.-L. Chua, J. J. Vittal, M.-W. Wong, *Chem. Commun.* **1998**, 861.

[7] For some examples of obtaining α adducts from indium reagents, see S. Araki, H. Ito, N. Katsumura, Y. Butsugan, *J. Organomet. Chem.* **1989**, *369*, 291; S. Araki, N. Katsumura, Y. Butsugan, *J. Organomet. Chem.* **1991**, *415*, 7; M. B. Isaac, T.-H. Chan, *Tetrahedron Lett.* **1995**, *36*, 8957.

[8] Various Lewis acids were compared with $In(OTf)_3$ for their effectiveness in this thermodynamic conversion: $AlCl_3$ (no reaction), $La(OTf)_3$ (<5%), $Sn(OTf)_2$ (70%), $Yb(OTf)_3$ (<5%), $Cu(OTf)_2$ (66%), $Sc(OTf)_3$ (56%).

[9] Y. Yamamoto, S. Nishii, J.-I. Yamada, *J. Am. Chem. Soc.* **1986**, *108*, 7116.

[10] S. I. Sumida, M. Ohga, J. Mitani, J. Nokami, *J. Am. Chem. Soc*. **2000**, *122*, 1310; J. Nokami, L. Anthony, S. Sumida, *Chem. Eur. J.* **2000**, *6*, 2903.

[11] Review: J.-L. Ripoll, Y. Vallée, *Synthesis* **1993**, 659.

  1433-7851/01/4015-2922 $ 17.50+.50/0

Synthesis, Structure, and Properties of a Novel Heterooctametallic Complex Containing a Cyclic Ru_4Ni_4 Core**

Indrani Pal, Falguni Basuli, Thomas C. W. Mak, and Samaresh Bhattacharya*

There is considerable current interest in the chemistry of polynuclear complexes, largely because of their fascinating properties.[1] Mononuclear transition metal complexes of multidentate ligands in which some of the donor sites are unoccupied often serve as efficient building blocks for the construction of polynuclear assemblies.[2] In our attempts to generate new heteropolynuclear systems, we planned a stepwise synthetic strategy, and salicylaldehyde thiosemicarbazone (H_3saltsc, **1**) was chosen as the multidentate ligand for this study. This ligand has five potential donor sites: three N, one O, and one S atom. However, in its reaction with ruthenium and osmium, we observed an apparently unusual coordination mode in which the H_2saltsc ligand utilizes only one N and one S donor site and forms a four-membered chelate ring (**2**).[3] Further studies showed that this type of

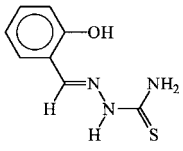

1

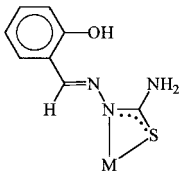

2

coordination mode is in fact quite normal not only for H_2saltsc but also for benzaldehyde thiosemicarbazones.[4] The three unused donor sites in **2** and their relative dispositions in space suggested that complexes containing this moiety should be able to bind to a second metal ion as a tridentate N,N,O donor ligand, and such a possibility is explored in the present study.

The mononuclear mixed-ligand ruthenium(II) complex $[Ru(bpy)_2(H_2saltsc)]^+$ (bpy = 2,2′-bipyridine) was prepared first. 2,2′-Bipyridine was chosen as the coligand because it is a recognized stabilizer of bivalent ruthenium, and complexes containing the $Ru(bpy)_2$ chromophore exhibit interesting luminescence properties,[5] so that a polynuclear complex constructed from $[Ru(bpy)_2(H_2saltsc)]^+$ building blocks may also be expected to display such behavior. $[Ru(bpy)_2(H_2saltsc)]ClO_4$ was obtained from the reaction of H_3saltsc with $[Ru(bpy)_2(EtOH)_2]^{2+}$, formed in situ from $[Ru(bpy)_2Cl_2]$ and $AgNO_3$ in warm ethanol in the presence of a base [Eq. (1)]. The crystal structure of $[Ru(bpy)_2(H_2saltsc)]ClO_4$ is

$$[Ru(bpy)_2Cl_2] \xrightarrow[EtOH]{AgNO_3} [Ru(bpy)_2(EtOH)_2]^{2+} \xrightarrow[NEt_3]{H_3saltsc} [Ru(bpy)_2(H_2saltsc)]^+ \xrightarrow{NaClO_4} [Ru(bpy)_2(H_2saltsc)]ClO_4 \quad (1)$$

displayed in Figure 1.[6] The H_2saltsc ligand is coordinated to ruthenium as a bidentate N,S donor in a four-membered chelate ring. The N_5S coordination sphere around ruthenium

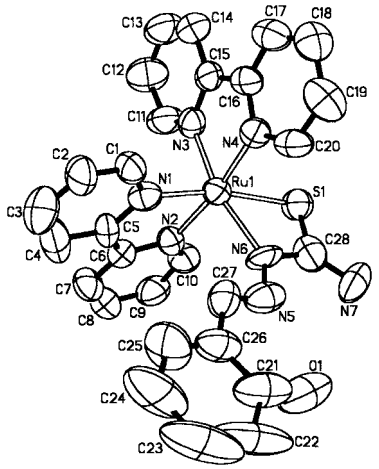

Figure 1. ORTEP plot of the structure of $[Ru(bpy)_2(H_2saltsc)]^+$. Selected bond lengths [Å] and angles [°]: Ru1-S1 2.430(5), Ru1-N6 2.068(12), S1-C28 1.70(2), C28-N7 1.33(2), C28-N6 1.41(2), N6-N5 1.41(2), N5-C27 1.24(2), C27-C26 1.47(3), C26-C21 1.40(4), C21-O1 1.28(4); N6-Ru1-S1 66.7(5), Ru1-S1-C28 82.6(7), N6-C28-S1 107.1(15), N7-C28-S1 125.6(17), C28-N6-N5 118.5(17), N6-N5-C27 119.3(19), N5-C27-C26 123(2), C27-C26-C21 121(3), O1-C21-C26 123(3).

is distorted from ideal octahedral geometry. The phenolic oxygen atom O1, the imine nitrogen atom N5, and the amine nitrogen atom N7 of the H_2saltsc ligand remained uncoordinated, and the $Ru(H_2saltsc)$ fragment is almost planar. The $[Ru(bpy)_2(H_2saltsc)]^+$ complex cation thus appears to be a suitable building block for the construction of polynuclear complexes, and to test this hypothesis, $[Ru(bpy)_2(H_2saltsc)]ClO_4$ was treated with one equivalent of $Ni(ClO_4)_2 \cdot 6H_2O$ in warm acetonitrile/ethanol. This reaction indeed afforded a polynuclear complex, namely $[\{Ru(bpy)_2(saltsc)\}_4Ni_4](ClO_4)_4$ [Eq. (2)].

$$4[Ru(bpy)_2(H_2saltsc)]ClO_4 + 4Ni(ClO_4)_2 \cdot 6H_2O \longrightarrow [\{Ru(bpy)_2(saltsc)\}_4Ni_4](ClO_4)_4 \quad (2)$$

Formation of the centrosymmetric, octametallic complex cation was confirmed by X-ray crystallography (Figure 2).[7] The coordinated H_2saltsc ligand of $[Ru(bpy)_2(H_2saltsc)]ClO_4$ has lost two further protons, one from the phenolic OH and the other from the NH_2 group, and the resulting saltsc ligand exhibits N,N,O coordination to the nickel(II) ion. The fourth coordination site of the nickel ion is occupied by the sulfur

[*] Dr. S. Bhattacharya, I. Pal, F. Basuli
Department of Chemistry
Inorganic Chemistry Section
Jadavpur University
Kolkata 700032 (India)
Fax: (+91) 33-473-4266
E-mail: samaresh_b@hotmail.com
Prof. Dr. T. C. W. Mak
Department of Chemistry
The Chinese University of Hong Kong
Shatin, New Territories (Hong Kong)

[**] This work was supported by a grant (Grant No. SP/S1/F33/98) from the Department of Science and Technology, New Delhi, India and Hong Kong Research Grants Council Earmarked Grant CUHK 4022/98P.

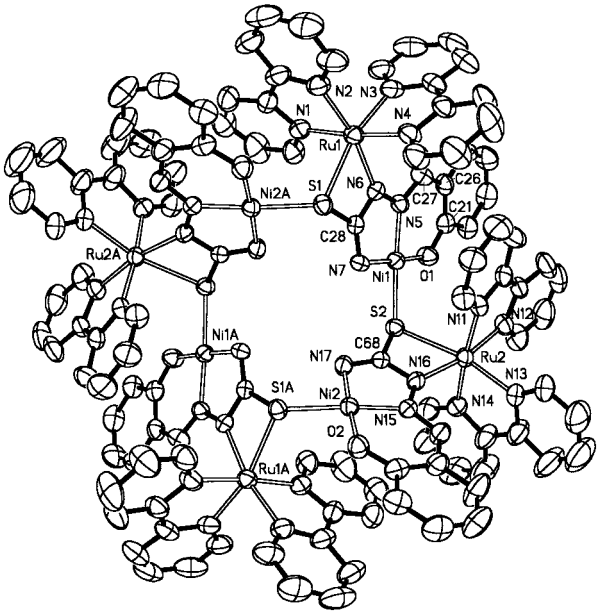

Figure 2. ORTEP plot of the structure of $[\{Ru(bpy)_2(saltsc)\}_4Ni_4]^{4+}$. Selected bond lengths [Å] and angles [°]: Ru1-S1 2.450(2), Ru1-N6 2.0936, S1-C28 1.789(8), C28-N7 1.303(9), C28-N6 1.319(10), N6-N5 1.390(9), N5-C27 1.301(10), C27-C26 1.406(12), C26-C21 1.402(12), C21-O1 1.321(10), Ni1-O1 1.831(6), Ni1-N7 1.868(7), Ni1-N5 1.853(6), Ni1-S2 2.213(2); N6-Ru1-S1 66.55(19), Ru1-S1-C28 80.0(3), N6-C28-S1 106.8(5), N7-C28-S1 132.2(6), C28-N6-N5 110.4(6), N6-N5-C27 119.5(7), N5-C27-C26 125.0(8), C27-C26-C21 122.3(8), O1-C21-C26 123.2(7), Ni1-O1-C21 128.3(5), O1-Ni1-N5 94.3(3), N5-Ni1-N7 83.6(3), Ni1-N7-C28 111.2(5), O1-Ni1-S2 83.53(18).

atom of another $Ru(bpy)_2(saltsc)Ni$ fragment, and the bridging sulfur atoms result in the formation of the cyclic octametallic $[\{Ru(bpy)_2(saltsc)\}_4Ni_4]^{4+}$ complex cation. It is noteworthy that in this complex all five available donor sites of the thiosemicarbazone ligand are involved in coordination, and this is unprecedented in the literature. The N_2OS coordination sphere around nickel is distorted from ideal square-planar geometry. While bond lengths within the NiN_2OS core are quite normal,[8] those in the Ru(saltsc) fragment of $[\{Ru(bpy)_2(saltsc)\}_4Ni_4](ClO_4)_4$ are slightly different to the corresponding bond lengths in the $Ru(H_2saltsc)$ fragment of $[Ru(bpy)_2(H_2saltsc)]ClO_4$ owing to coordination to nickel. The significant elongation of the C28–S1 bond is attributable to the bridging nature of the sulfur atom.

Both the mononuclear and octametallic complexes are diamagnetic; this indicates the presence of Ru^{II} (low-spin d^6, $S=0$) in both of them, and of Ni^{II} (square-planar d^8, $S=0$) in the octametallic complex. The ^1H NMR, conductance, and analytical data of the two complexes support their formulations. The cyclic voltammograms of $[Ru(bpy)_2(H_2saltsc)]ClO_4$ and $[Ru\{(bpy)_2(saltsc)\}_4Ni_4](ClO_4)_4$ recorded in $(Et_4N)ClO_4$/MeCN are shown in Figure 3. For $[Ru(bpy)_2(H_2saltsc)]ClO_4$ two oxidation waves are observed on the positive side of the saturated calomel electrode (SCE), and four successive reduction waves on the negative side. The first oxidation is reversible ($E_{1/2}=0.62$ V, $\Delta E_p=60$ mV, $i_{pa}=i_{pc}$) and is assigned to $Ru^{II}\rightarrow Ru^{III}$ oxidation. The second oxidation is irreversible ($E_{pa}=1.38$ V) and is probably ligand-centered. The reduction waves ($E_{pc}=-1.50$, -1.70, -1.87, and -2.39 V) are due to

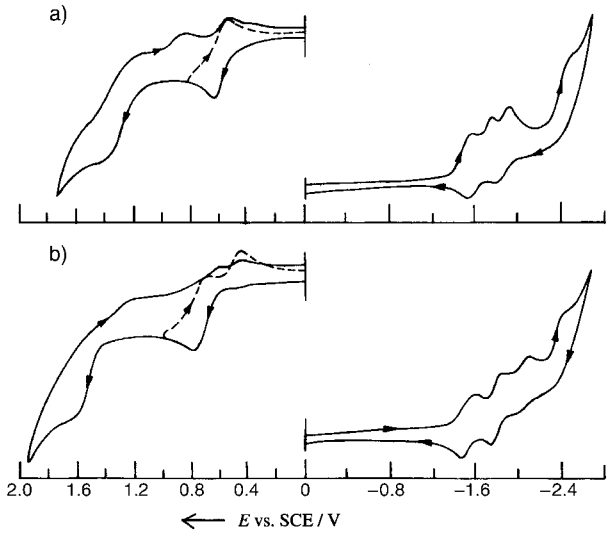

Figure 3. Cyclic voltammograms of a) $[Ru(bpy)_2(H_2saltsc)]ClO_4$ and b) $[\{Ru(bpy)_2(saltsc)\}_4Ni_4](ClO_4)_4$ in acetonitrile solution (0.1 M $(Et_4N)ClO_4$) at a scan rate of 50 mV s^{-1}.

reductions of the two coordinated bpy ligands. Each bpy ligand is known to undergo two one-electron reductions.[9] Hence, four successive one-electron reductions are expected for $[Ru(bpy)_2(H_2saltsc)]^+$, and all of them were observed experimentally. Cyclic voltammetric behavior of $[Ru\{(bpy)_2(saltsc)\}_4Ni_4](ClO_4)_4$ is qualitatively similar to that of $[Ru(bpy)_2(H_2saltsc)]ClO_4$. However, both oxidations are shifted to more positive values. The first oxidation is now irreversible ($E_{1/2}=0.75$ V, $i_{pa}>i_{pc}$), and the second remained irreversible ($E_{pa}=1.56$ V). All four reductions of the two bpy ligands in the $Ru(bpy)_2$ fragments were also observed ($E_{pc}=-1.55$, -1.81, -2.06, and -2.37 V) in this complex. The cyclic voltammetric results clearly indicate that there are no detectable metal–metal interactions in the octametallic complex.

Experimental Section

$[Ru(bpy)_2(H_2saltsc)]ClO_4$: $AgNO_3$ (65 mg, 0.38 mmol) was added to a solution of $[Ru(bpy)_2Cl_2]\cdot 2H_2O$ (100 mg, 0.19 mmol) in ethanol (30 mL). The mixture was warmed and stirred for 30 min. The deposited AgCl was separated by filtration, and $H_3saltsc$ (40 mg, 0.21 mmol) and NEt_3 (21 mg, 0.21 mmol) were added to the filtrate. The solution was heated to reflux for 2 h. It was then concentrated to ca. 10 mL, and a saturated aqueous solution of $NaClO_4$ (0.5 mL) was added. $[Ru(bpy)_2(H_2saltsc)]ClO_4$ separated as a dark precipitate, which was collected by filtration, washed with water, and dried in vacuo over P_4O_{10}. Recrystallization from acetonitrile/benzene gave 125 mg of $[Ru(bpy)_2(H_2saltsc)]ClO_4$ (92%) as a brownish red crystalline solid. Elemental analysis (%) calcd for $C_{28}H_{24}N_7O_5SClRu$: C 47.56, H 3.40, N 13.87; found: C 47.69, H 3.49, N 13.65.

$[\{Ru(bpy)_2(saltsc)\}_4Ni_4](ClO_4)_4$: $[Ru(bpy)_2(H_2saltsc)]ClO_4$ (100 mg, 0.14 mmol) was dissolved in warm ethanol (30 mL), and NEt_3 (14 mg, 0.14 mmol) and a solution of $Ni(ClO_4)_2\cdot 6H_2O$ (52 mg, 0.14 mmol) in acetonitrile (10 mL) were added to the stirred solution. The mixture was warmed and stirred for 5 h to afford 75 mg of $[\{Ru(bpy)_2(saltsc)\}_4Ni_4](ClO_4)_4$ (66%), which separated as a brown microcrystalline solid and was collected by filtration, washed with ethanol, and dried in air. Elemental analysis (%) calcd for $C_{28}H_{22}N_7O_5SClRuNi\cdot 2H_2O$: C 42.04, H 3.25, N 12.26; found: C 41.51, H 3.35, N 11.70.

Received: March 9, 2001
Revised: May 22, 2001 [Z16749]

  1433-7851/01/4015-2924 $ 17.50+.50/0

[1] a) V. Balzani, A. Juris, M. Venturi, S. Campagna, S. S. Wilcox, *Chem. Rev.* **1996**, *96*, 759 – 833; b) F. C. Anson, C. Shi, B. Steiger, *Acc. Chem. Res.* **1997**, *30*, 437 – 444; c) V. Balzani, S. Campagna, G. Denti, A. Juris, S. Serroni, M. Venturi, *Acc. Chem. Res.* **1998**, *31*, 26 – 34; d) J. A. McCleverty, M. D. Ward, *Acc. Chem. Res.* **1998**, *31*, 842 – 851; e) P. C. Ford, E. Cariati, J. Bourassa, *Chem. Rev.* **1999**, *99*, 3625 – 3647; f) Y. Xiong, L. N. Ji, *Coord. Chem. Rev.* **1999**, *185/186*, 711 – 733; g) H. E. Toma, K. Araki, *Coord. Chem. Rev.* **2000**, *196*, 307 – 329; h) D. T. McQuade, A. E. Pullen, T. M. Swager, *Chem. Rev.* **2000**, *100*, 2537 – 2574; i) A. D. Cutland, R. G. Makkani, J. W. Kampf, V. L. Pecoraro, *Angew. Chem.* **2000**, *112*, 2801 – 2803; *Angew. Chem. Int. Ed.* **2000**, *39*, 2689 – 2691; j) J. J. Bodwin, V. L. Pecoraro, *Inorg. Chem.* **2000**, *39*, 3434 – 3435; k) T. Konno, Y. Chikamoto, K. I. Okamoto, T. Yamaguchi, T. Ito, M. Hirotsu, *Angew. Chem.* **2000**, *112*, 4264 – 4267; *Angew. Chem. Int. Ed.* **2000**, *39*, 4098 – 4101; l) M. M. Ali, F. M. MacDonnell, *J. Am. Chem. Soc.* **2000**, *122*, 11527 – 11528; m) R. W. Saalfrank, S. Trummer, U. Reimann, M. M. Chowdhury, F. Hampel, O. Waldmann, *Angew. Chem.* **2000**, *112*, 3634 – 3636; *Angew. Chem. Int. Ed.* **2000**, *39*, 3492 – 3494; Erratum: R. W. Saalfrank, S. Trummer, U. Reimann, M. M. Chowdhury, F. Hampel, O. Waldmann, *Angew. Chem.* **2000**, *112*, 3885; *Angew. Chem. Int. Ed.* **2000**, *39*, 3736; n) E. Uller, B. Demleitner, I. Berndt, R. W. Saalfrank, *Struct. Bonding (Berlin)* **2000**, *96*, 149 – 175.

[2] a) M. D. Ward, *Inorg. Chem.* **1996**, *35*, 1712 – 1714; b) F. Birkelbach, T. Weyhemüller, M. Lengen, M. Gardan, A. X. Trautwein, K. Wieghardt, P. Chaudhuri, *J. Chem. Soc. Dalton Trans.* **1997**, 4529 – 4537; c) W. Paw, R. Eisenberg, *Inorg. Chem.* **1997**, *36*, 2287 – 2293; d) P. Majumdar, S. M. Peng, S. Goswami, *J. Chem. Soc. Dalton Trans.* **1998**, 1569 – 1574; e) G. A. Abakumov, V. K. Cherkasov, V. I. Nevodchikov, V. A. Kuropatov, B. C. Noll, C. G. Pierpont, *Inorg. Chem.* **1998**, *37*, 6117 – 6119; f) A. K. Das, A. Rueda, L. R. Falvello, S. M. Peng, S. Bhattacharya, *Inorg. Chem.* **1999**, *38*, 4365 – 4368; g) N. C. Fletcher, T. C. Robinson, A. Behrendt, J. C. Jeffery, Z. R. Reeves, M. D. Ward, *J. Chem. Soc. Dalton Trans.* **1999**, 2999 – 3006.

[3] F. Basuli, S. M. Peng, S. Bhattacharya, *Inorg. Chem.* **1997**, *36*, 5645 – 5647.

[4] a) F. Basuli, M. Ruf, C. G. Pierpont, S. Bhattacharya, *Inorg. Chem.* **1998**, *37*, 6113 – 6116; b) F. Basuli, S. M. Peng, S. Bhattacharya, *Inorg. Chem.* **2000**, *39*, 1120 – 1127.

[5] A. Juris, S. B. S. Campagna, V. Balzani, P. Belser, A. V. Zelewsky, *Coord. Chem. Rev.* **1988**, *84*, 85 – 227.

[6] a) X-ray structure analysis of $[Ru(bpy)_2(H_2saltsc)]ClO_4 \cdot 1/2\,C_6H_6 \cdot 1/2\,CH_2Cl_2$: $C_{31.50}H_{27}Cl_2N_7O_5RuS$, $M_r = 787.63$, monoclinic, space group $P2_1/c$, $a = 9.169(1)$, $b = 16.396(2)$, $c = 24.634(3)$ Å, $\beta = 99.075(8)^\circ$, $V = 3657.0(7)$ Å^3, $Z = 4$, $\rho_{calcd} = 1.431$ Mg m^{-3}; crystal dimensions $0.50 \times 0.30 \times 0.02$ mm. Data ($2\theta_{max} = 51.1^\circ$) were collected at 293(2) K on a Rigaku RAXIS-IIC imaging plate with graphite-monochromatized $Mo_{K\alpha}$ radiation ($\lambda = 0.71073$ Å), $\mu = 0.597$ mm^{-1}, transmission factors 0.755 – 1.148. The structure was solved by direct methods and refined by full-matrix least-squares methods on F^2. Hydrogen atoms were included but not refined. $R1 = 0.1267$ for 3296 observed reflections ($I > 2\sigma(I)$) and 418 parameters; $wR2 = 0.3507$ for 4634 unique reflections. Programs used: SHELXS-97 (structure solution) and SHELXL-97 (structure refinement). b) Crystallographic data (excluding structure factors) for the structures reported in this paper have been deposited with the Cambridge Crystallographic Data Centre as supplementary publication no. CCDC-156075 and -156076. Copies of the data can be obtained free of charge on application to CCDC, 12 Union Road, Cambridge CB2 1EZ, UK (fax: (+44) 1223-336-033; e-mail: deposit@ccdc.cam.ac.uk).

[7] X-ray structure analysis of $[\{Ru(bpy)_2(saltsc)\}_4Ni_4](ClO_4)_4 \cdot 4\,C_6H_6 \cdot 2\,MeCN$: $C_{140}H_{118}Cl_4N_{30}Ni_4O_{20}Ru_4S_4$, $M_r = 3449.80$, monoclinic, space group $P2/n$, $a = 18.386(3)$, $b = 12.268(2)$, $c = 36.398(6)$ Å, $\beta = 104.219(3)^\circ$, $V = 7959(2)$ Å^3, $Z = 2$; crystal dimensions $0.60 \times 0.47 \times 0.28$ mm, intensities ($2\theta_{max} = 56.2^\circ$) were collected at 293(2) K on a Bruker SMART 1000 CCD diffractometer with $Mo_{K\alpha}$ radiation ($\lambda = 0.71073$ Å), $\mu = 1.020$ mm^{-1}; absorption corrections with the SADABS program yielded relative transmission factors of 0.8075 – 1. $R1 = 0.0795$ for 10301 observed reflections ($I > 2\sigma(I)$) and 932 parameters; $wR2 = 0.2672$ for 19288 reflections.[6b]

[8] a) S. Padhye, *Coord. Chem. Rev.* **1985**, *63*, 127 – 160; b) M. Mathew, G. J. Palenik, G. R. Clark, *Inorg. Chem.* **1973**, *12*, 446 – 451.

[9] a) A. A. Vlcek, *Coord. Chem. Rev.* **1982**, *43*, 39 – 62; b) J. L. Kahl, K. W. Hanck, K. DeArmond, *J. Phys. Chem.* **1978**, *82*, 540 – 545.

Selective Photoproduction of O_2 from the Mn_4O_4 Cubane Core: A Structural and Functional Model for the Photosynthetic Water-Oxidizing Complex**

Masayuki Yagi, Kurt V. Wolf, Patrick J. Baesjou, Steven L. Bernasek, and G. Charles Dismukes*

Dedicated to Dr. Peter Gabriel

Both the announcement last year by the German Federal Government to eliminate the use of nuclear power generators by 2021[1] and the recent shortage of electric power in California USA place renewed emphasis on development of socially acceptable energy sources such as solar[2] and fuel cells.[3] The latter cells rely on energy generated by the combination of H_2 (or hydrocarbons) with O_2. Both of these molecules are expected to be produced by solar-based water-splitting catalysts ($H_2O \rightarrow \frac{1}{2}O_2 + H_2$), hence, the efforts to understand Nature's photosynthetic process of O_2 generation by water oxidation in plants,[4] and to functionally mimic the catalytic center,[5, 6] take on a pressing schedule. Key advances have occurred recently on both fronts with the first X-ray crystal structure at 3.8 Å resolution of the water-oxidizing complex (WOC) and its associated photochemical reaction center (photosystem II) from a cyanobacterium[7] and the first report of intramolecular O_2 photoproduction from the bridging oxygen atoms of a manganese – oxo cluster of cubane-type geometry, $L_6Mn_4O_4$ (**1**; L = diphenylphosphinate; $Ph_2PO_2^-$)

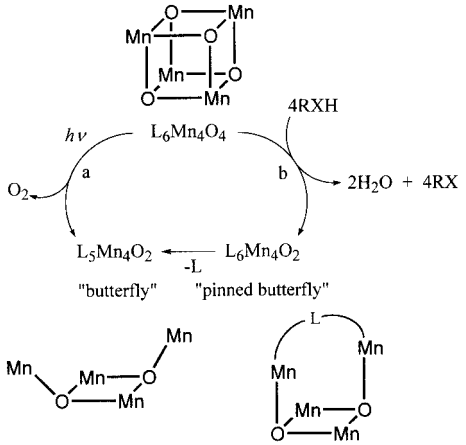

Scheme 1. Reactions of $L_6Mn_4O_4$ cubane complexes **1** and **1′**: a) UV photochemical reaction in the gas phase and b) reductive dehydration reaction in solution. RXH = organoammine, phenol, etc. Bridging phosphinates omitted for clarity.

[*] Prof. Dr. G. C. Dismukes, Prof. Dr. M. Yagi, K. V. Wolf
Dr. P. J. Baesjou Prof. Dr. S. L. Bernasek
Department of Chemistry
Princeton University
Princeton, NJ, 08544-1009, NJ (USA)
Fax: (+1) 609-258-1980
E-mail: dismukes@princeton.edu

[**] This research was supported by grants from the US National Institutes of Health (GM39932) and the National Science Foundation (CHE96-19190). Fellowship support was provided by the Japan Society for the Promotion of Science (M.Y.) and the Netherlands NOW Scholarship (P.B.).

(Scheme 1 path a).[8] O_2 release may proceed via a bridging peroxo transition state. This core type appears to be structurally similar to the WOC in its highest oxidation state.[9, 10] Complex **1** can also be reduced by weak reductants (including organoamines and phenols) that transfer hydrogen atoms to form $L_6Mn_4O_2$ and two water molecules derived from the core oxygen atoms (Scheme 1 path b).[11] Taken together these two reactions indicate a pathway for oxidizing water to O_2 that has the potential to be catalytic if the cycle can be closed.[5, 6]

Only two other manganese complexes have provided evidence for O_2 production from water. A covalently linked perfluorinated dimangano–porphyrin complex was reported to electrochemically oxidize water via O–O bond coupling within an unobserved $(Mn^{V}{=}O)_2$ intermediate, prior to oxidative destruction.[12] Also, $[(terpy)(H_2O)Mn(\mu\text{-}O)_2Mn(terpy)(H_2O)]^{3+}$ (terpy = 2,2′:6′,2″-terpyridine) was reported to produce O_2 from oxidized precursors, such as hydrogen persulfate (H_2SO_5) or hypochlorite (ClO^-), by nucleophillic addition to an unobserved $Mn^{V}{=}O$ intermediate, prior to catalyst destruction.[13, 14] However, in neither of these examples has the mechanism of O–O bond formation been conclusively established, nor are they likely to be a close model for the WOC.

Herein, we compare the photochemistry of manganese–oxo complexes having Mn_2O, Mn_2O_2, and Mn_3O_4 core types to that of the Mn_4O_4 cubane core. We find that the cubane core is unique in its ability to form O_2, and does so by selective rearrangement (without decomposition) to a complex with an Mn_4O_2 butterfly core.

For this study we have synthesized a new derivative of the cubane complex, $L'_6Mn_4O_4$ (**1′**), containing the facially bridging bis(tolyl)phosphinate ligand, $(MePh)_2PO_2^-$.[15] Importantly, **1′** is 100 times more soluble than **1** in nonpolar solvents, which permits concentrations up to ~40 mM in CH_2Cl_2. For mass spectrometric studies all the complexes were dissolved in a volatile organic solvent (CH_2Cl_2, CH_3OH) and deposited on a gold substrate prior to evaporation to dryness. Laser desorption/ionization mass spectrometry (LDI-MS) (excitation at 337 nm, 1 ns duration, power = 1.2–7.9 μJ) and quadrupole mass spectrometry (Q-MS) (excitation at 355 nm, 14 ns duration, power = 500 μJ; excitation at 532 nm, power = 3.3 mJ) were performed as previously described for mass detection of ions (*m*/*z* 150–2000 amu) and neutrals (< 40 amu), respectively.[8]

The positive-ion LDI-MS spectrum of **1′** produces only two peaks above *m*/*z* 150 (Figure 1 a) at *m*/*z* 1754.6 and 1477.4. The first peak corresponds to the parent cation $\mathbf{1'}^{+}$ (exact *m*/*z* 1755.2), while the latter peak is assigned to $L'_5Mn_4O_2^+$ (*m*/*z* 1477.9) arising from loss of one $(MePh)_2PO_2^-$ ligand (mass 245.2) and two O atoms from **1′**. These assignments are corroborated by the LDI-MS spectrum of the $L'_6Mn_4(^{18}O)_4$ isotopomer (Figure 1 b), in which the Mn_4O_4 core oxo units were replaced by ^{18}O atoms.[16] Only these two peaks were detected at all laser energies available (< 4 μJ pulse^{-1}). The peak height of the fragment peak (*m*/*z* 1447.9) increases, while the parent ion peak (*m*/*z* 1755.2) decreases with laser pulse energy. Data supporting this correlation were previously published for the diphenyl derivative **1**.[8] This trend was

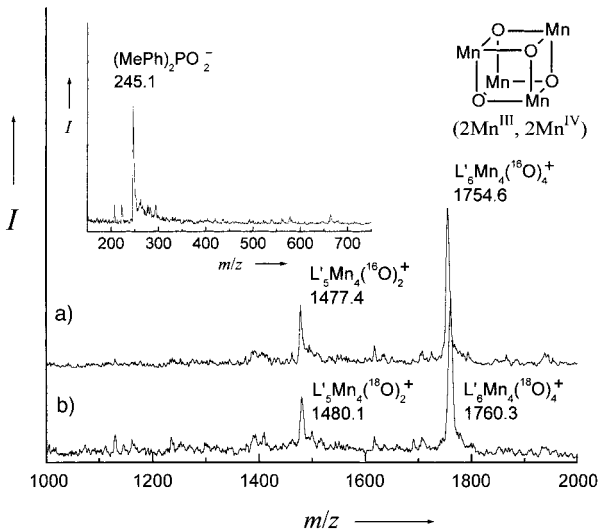

Figure 1. LDI-MS (positive ions) of a) $L'_6Mn_4O_4$ and b) $L'_6Mn_4(^{18}O)_4$ with 75% labeling of core oxo groups by ^{18}O. Excitation by N_2 laser at 337 nm; power = 2.9 μJ and 4.3 μJ for (a) and (b), respectively). Inset shows LDI-MS (negative-ions) of $L'_6Mn_4O_4$. The ordinate axis is intensity (*I*: arbitrary units).

attributed to the competition between decay of the excited state **1*** to the ground state **1** and the photochemical reaction given in [Eq. (1)].

$$L_6Mn_4O_4 \leftarrow L_6Mn_4O_4^{*} \rightarrow L_5Mn_4O_2^{+} + L^{-} + O_2 \quad (1)$$

Consistent with the fragmentation pattern in Figure 1, the negative-ion LDI-MS of **1′** revealed only a single major peak at *m*/*z* 245.1 in the range *m*/*z* 150–750, corresponding to the $(MePh)_2PO_2^-$ ligand (inset Figure 1). This photofragmentation pattern is identical to that observed for **1** prepared using $Ph_2PO_2^-$ as bridging ligand.[8] The Q-MS of **1′** (Figure 2 a) reveals that the photoreaction releases an O_2 molecule[17] and there is no evidence for any other oxygen-derived products (O, OH, OH_2).[18] Thermodynamic estimates indicate that the O–O bond enthalpy should contribute greatly

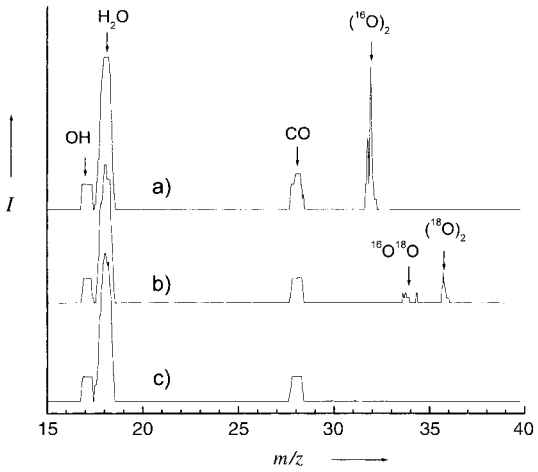

Figure 2. Q-MS of a) $L'_6Mn_4O_4$, b) $L'_6Mn_4(^{18}O)_4$ with 75% labeling of the core oxo groups by ^{18}O, and c) background (no complex). Internal standard peaks at *m*/*z* 17, 18, and 28 are from OH, H_2O, and CO. Excitation by Nd-YAG laser at 355 nm. The ordinate axis is intensity (*I*: arbitrary units).

  1433-7851/01/4015-2926 $ 17.50+.50/0 *Angew. Chem. Int. Ed.* **2001**, *40*, No. 15

(119 kcal mol^{-1}) to lowering the barrier to O_2 release.[8, 11] The data for the $L'_6Mn_4(^{18}O)_4$ isotopomer (Figure 2b) reveals that the product O_2 is derived exclusively from the intramolecular combination of core oxo units; none of the oxygen atoms of $(MePh)_2PO_2^-$ appear in the product O_2. These results explicitly show that laser UV excitation initiates a photochemical reaction in the gas phase (Scheme 1 path a). The relative quantum yield for O_2 production from **1′** increases with laser pulse energy and reaches 60% (not shown) at the maximum laser energy (7.9 μJ) available in our spectrometer (Table 1). These results extend the generality of the photochemistry previously observed with the first cubane complex **1** and summarized in Scheme 1 path a.

To determine if analogous photochemistry is observed with other manganese–oxo clusters the same experiments were carried out using the series of di- and trimanganese–oxo complexes[19] listed in Table 1. This includes complexes having different bridging groups: di(μ-oxo), di(μ-oxo)-mono(μ-carboxylato), and mono(μ-oxo)-di(μ-carboxylato) and different formal oxidation states of the Mn ions: (III, III), (III, IV) and (IV, IV, IV). Although all complexes absorb intensely at both UV excitation wavelengths (355 nm, and 337 nm), none of them produce molecular O_2 in significant yield when compared to the cubanes **1** and **1′**. LDI-MS reveals that these complexes do undergo laser-induced desorption and photoreactions at these wavelengths, leading to multiple fragments in the gas phase which vary with the laser power (not shown). However, the photo-products correspond to nonselective destruction of the complexes into multiple fragments. This is illustrated by the positive-ion LDI-MS spectrum of $[(bpy)_2Mn(\mu\text{-}O)_2Mn(bpy)_2](C1O_4)_3$ (**2;** bpy = 2,2′-bipyridine) shown in Figure 3. One observes five photo-induced intense peaks in the rage of m/z 100–2000. These correlate with the fragments derived from the decomposition of the core and ligands (Table 2). Neither a peak for the parent ion peak (m/z 255.5), nor for the intact core Mn_2O_2 fragment is detected. Rather, the preferred fragmentation leads to oxygen atoms which are detected exclusively in the two peaks assigned to $[(bpy)_nMnO_2]^+$

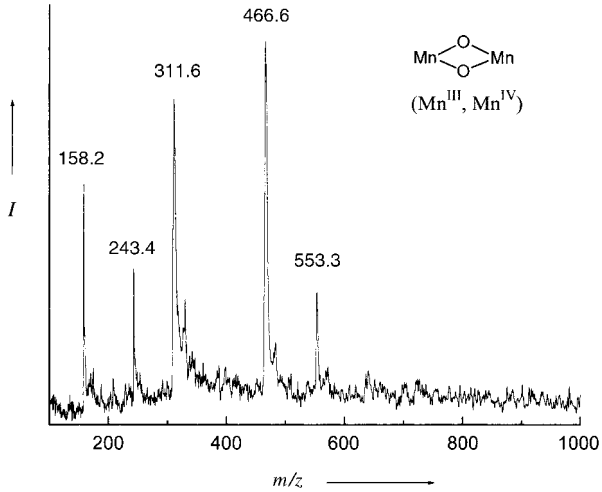

Figure 3. LDS-MS (positive-ions) of $[(bpy)_2Mn(\mu\text{-}O)_2Mn(bpy)_2](C1O_4)_3$. The ordinate axis is intensity (I: arbitrary units).

Table 2. Proposed assignments of LDI mass fragment peaks for $[(bpy)_2Mn(\mu\text{-}O)_2Mn(bpy)_2](ClO_4)_3$.

m/z[a]	Fragment	predicted m/z
158.2 ± 2.0	$bpyH^+$	157.2
243.4 ± 1.3	$[MnO_2(bpy)]^+$	243.1
311.6 ± 12.7	$[2bpy - H]^+$	311.4
466.6 ± 10.7	$[3bpy - 2H]^+$	466.5
553.3 ± 2.5	$[MnO_2(3bpy - 2H)]^+$	552.5

[a] m/z range denotes the full width at half height.

($n = 1, 3$). Thus, the dimeric $[Mn_2O_2]^{3+}$ core complex does not photorearrange to release O_2 despite having the same Mn oxidation state (Mn^{III}, Mn^{IV}) as **1′**; nor do any of the other core topologies shown in Table 1 containing the $[Mn(\mu\text{-}O)Mn]^{4+}$, $[Mn\ (\mu\text{-}O)_2Mn]^{3+}$, or $[Mn(\mu\text{-}O)_2Mn(\mu\text{-}O)_2Mn]^{4+}$ cores.

Laser excitation in the visible absorption band at 532 nm (14 ns duration, power = 3.3 mJ) failed to produce O_2 from any of the complexes given in Table 1, including **1** and **1′**, even at a six-fold higher pulse energy than at 355 nm (no Q-MS

Table 1. Structures of Mn complexes used, photochemical O_2 yield and asymmetric vibration energies of the Mn-O-Mn core.

Complex[a]		Oxidation state	Core geometry	Excitation wavelength [nm]	O_2 quantum relative yield[%][b]	Mn-O-Mn ν_{as} [cm^{-1}]
1	$L_6Mn_4O_4$	($2Mn^{III}$, $2Mn^{IV}$)	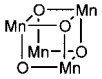	355 532	60[c] 0	633
1′	$L'_6Mn_4O_4$	($2Mn^{III}$, $2Mn^{IV}$)	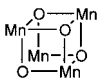	355 532	60[c] 0	633
2	$[(bpy)_2Mn(\mu\text{-}O)_2Mn(bpy)_2](ClO_4)_3$	(Mn^{III}, Mn^{IV})	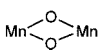	355 532	0 0	690
3	$[(HBPz_3)Mn(\mu\text{-}O)(\mu\text{-}RCO_2)_2Mn(HBPz_3)]$	($2Mn^{III}$)		355[d] 532[d] 355[e] 532[e]	0 0 0 0	716[d] 717[e]
4	$[(HBPz_3)Mn(\mu\text{-}O)_2(\mu\text{-}RCO_2)Mn\text{-}(\mu\text{-}O)_2(\mu\text{-}RCO_2)Mn(HBPz_3)]$	($3Mn^{IV}$)	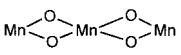	355[d] 532[d]	0 0	702[d]

L = $Ph_2PO_2^-$, L′ = $(MePh)_2PO_2^-$, bpy = 2,2′-bipyridine, $HBPz_3^-$ = hydrotris(1-pyrazolyl)borate; [a] The number of moles the complex used in each experiment is constant. [b] The zero quantum yield indicates values less than the detection limit for O_2 based on the sensitivity for O_2 detection from **1′** (< 3.7%). [c] The yield was taken as the ratio of LDI-MS peak heights ($L'_5Mn_4O_2/L'_6Mn_4O_4$). [d] R = CH_3, [e] R = C_2H_5.

  1433-7851/01/4015-2927 $ 17.50+.50/0

peaks at all!). Hence, the UV photoproduction of O_2 occurs exclusively for the Mn_4O_4 cubane core type upon excitation of the O→Mn charge-transfer absorption at 300 nm ($\varepsilon = 2.1 \times 10^4\,M^{-1}cm^{-1}$), but not the visible band at 498 nm ($\varepsilon = 1.4 \times 10^3\,M^{-1}cm^{-1}$).[8]. We may conclude that of the complexes listed in Table 1 only the Mn_4O_4 cubane core topology provides a favorable geometry for efficient and selective photorearrangement to produce O_2 by charge-transfer excitation. The $L'_5Mn_4O_2$ photoproduct of **1**′ (see below) is presumed to have a "butterfly" core geometry (Scheme 1). The gas-phase structure is unknown, and is only suggested based on comparison to the deoxygenated product, $L'_6Mn_4O_2$, produced in solution by chemical reduction.[11]

Importantly, no mass spectral evidence is found for the photochemical O_2 release from excited **1**′ without the loss of one $(MePh)_2PO_2^-$ ligand, nor of ligand release without the loss of O_2. The release of O_2 to form the pinned butterfly structure $L'_6Mn_4O_2$ is thermodynamically favored by $-6.2\,kcal\,mol^{-1}$ in the ground state, but is not observed because of a kinetic barrier that the present data show to be imposed by the phosphinate bridges.[8] The origin of the selective O_2 release observed for the photo-excited Mn_4O_4 cubane core appears to correlate with the considerably weaker Mn–O (core) bonds, as found by both X-ray diffraction (mean bond length 1.95 Å for **1** versus 1.8 Å for the Mn_2(III, IV) complex **2**, both in their ground states) and by their much lower-energy Mn-O-Mn core vibrations ($\tilde{\nu}_s = 516\,cm^{-1}$, $\tilde{\nu}_{as} = 633\,cm^{-1}$ for the symmetric and asymmetric modes stretches in the ground state) versus the model complexes in Table 1. The inter-oxygen separation in the core of **1** and **1**′ is 2.53–2.60 Å which is much longer than the O–O bond in hydrogen peroxide (1.50 Å) and O_2 (1.21 Å). Thus, it is clear that an O–O bond of appreciable stability can not be formed in the ground-state cubanes without large-scale distortion. The experimental data points to the release of a phosphinate bridge and further weakening of the O–Mn bonds in the photo-excited state as the trigger that enables the distortion of the core bonds to occur. The resulting distortion might then permit the oxygen atoms to move sufficiently close together to allow the large intermolecular O–O bond enthalpy ($-36\,kcal\,mol^{-1}$ in HO–OH) to contribute to lowering the activation barrier for O_2 formation. By contrast, the much stronger and shorter Mn–O bonds within the planar Mn_2O_2 rhombohedra of the dimer and trimer complexes in Table 1 may be why these core types photodecompose to MnO_2X fragments without Mn–O bond cleavage or O_2 formation.

EPR spectroscopy indicates that cubanes **1** and **1**′ have the same oxidation state as the so-called S_3 state of the WOC, or one-electron below the S_4 state that is the precursor to thermal O_2 release.[9, 10] This assignment is debatable particularly in light of data from X-ray absorption near-edge spectroscopy.[10] It will be interesting to see if the one-electron oxidized cubanes $\mathbf{1}^+$ and $\mathbf{1}'^+$, which have been isolated,[20] will also prove to be selective precursors to photolytic and/or thermal evolution of O_2. Based on EPR and X-ray absorption spectroscopic evidence distorted Mn_4O_4 cubane or $Mn_4O_2X_2$ pseudo-cubane cores have been implicated as possible core types for the S_3 and S_4 states of the WOC.[10] The present study indicates a molecular basis for why the cubane core topology appears to be uniquely suited for O_2 evolution.

Received: February 26, 2001 [Z16775]

[1] *Nucleonics Week*, McGraw-Hill, New York, (June 15, **2000**); *New York Times* (June 15, **2000**).
[2] A. J. Bard, M. A. Fox, *Acc. Chem. Res.* **1995**, *28*, 141–145.
[3] S. D. Park, J. M. Vohs, R. J. Gorte, *Nature* **2000**, *404*, 265–267.
[4] "Photosynthetic Water Oxidation": *Biochim. Biophys. Acta Bioenerg.* **2001**, *1503* (special issue).
[5] W. Ruettinger, G. C. Dismukes, *Chem. Rev.* **1997**, *97*, 1–24.
[6] M. Yagi, M. Kaneko, *Chem. Rev.* **2001**, *101*, 21–35.
[7] A. Zouni, H. T. Witt, J. Kern, P. Fromme, N. Krauss, W. Saenger, P. Orth, *Nature* **2001**, *409*, 739–743.
[8] W. Ruettinger, M. Yagi, K. Wolf, S. Bernasek, G. C. Dismukes, *J. Am. Chem. Soc.* **2000**, *122*, 10353–10357.
[9] G. C. Dismukes, W. Ruettinger, A. E. M. Boelrijk, D. Ho in *Proceedings XIth International Photosynthesis Congress, Vol. II* (Ed.: G. Garab), Kluwer Academic, Dordrecht, **1998**, pp. 1259–1264.
[10] T. G. Carrell, A. M. Tyryshkin, G. C. Dismukes, *J. Bioinorg. Chem.*, submitted.
[11] W. Ruettinger, G. C. Dismukes, *Inorg. Chem.* **2000**, *39*, 1021–1027; W. Ruettinger, G. C. Dismukes, *Inorg. Chem.* **2000**, *39*, 4186.
[12] Y. Naruta, M. Sasayama, T. Sasaki, *Angew. Chem.* **1994**, *106*, 1964–1965; *Angew. Chem. Int. Ed. Engl.* **1994**, *33*, 1839–1841.
[13] J. Limburg, J. S. Vrettos, L. M. Liable-Sands, A. L. Rheingold, R. H. Crabtree, G. W. Brudvig, *Science* **1999**, *283*, 1524–1527.
[14] J. Limburg, J. S. Vrettos, H. Y. Chen, J. C. de Paula, R. H. Crabtree, G. W. Brudvig, *J. Am. Chem. Soc.* **2001**, *123*, 423–430.
[15] **1**′ was synthesized according to the earlier reported synthesis of **1**[21] by replacing Ph_2PO_2H with $(MePh)_2PO_2H$ (65% yield). $(MePh)_2PO_2H$ was prepared by the Grignard reaction of MePhMgBr with Et_2N-$POCl_2$ according to the literature.[22] The ^1H NMR, MS, FT-IR, and electronic spectra indicate a symmetrical cubane core very similar to **1**.[21]
[16] Synthesis of $L'_6Mn_4(^{18}O)_4$ was performed starting from $[Mn_2(^{18}O)_2(bpy)_4](ClO_4)_3$ achieved by acid catalyzed exchange against 99% ^{18}O-enriched water. The incorporation of av. 75% ^{18}O was confirmed by FT-IR and LDI-MS analysis.
[17] Upon photoexcitation of **1**′ only a single peak was observed at *m*/*z* 32 corresponding to $(^{16}O)_2$. For $L'_6Mn_4(^{18}O)_4$ (av. 75% isotopic enrichment) two peaks at m/z 34 and 36 were observed, corresponding to $^{16}O^{18}O$ and $(^{18}O)_2$, respectively.
[18] Atmospheric H_2O and CO_2 in the mass spectrometer produce a constant background signal (Figure 2c), while photoproduced species can be distinguished by a "spike" appearance in the mass scan. The spikes arise as a result of the short laser pulse, which produces transient mass changes on a much shorter time scale than the slower sweep rates of the mass analyzer.
[19] These complexes were prepared and characterized according to refs. [23,24].
[20] W. F. Ruettinger, D. M. Ho, G. C. Dismukes, *Inorg. Chem.* **1999**, *38*, 1036–1037.
[21] W. F. Ruettinger, C. Campana, G. C. Dismukes, *J. Am. Chem. Soc.* **1997**, *119*, 6670–6671.
[22] P. C. Crofts in *Organic Phosphorous Compounds*, *Vol. 6* (Eds.: G. M. Kosolapoff, L. Maier), Wiley, New York, **1973**, pp. 1–209.
[23] J. E. Sheats, R. S. Czernuszewicz, G. C. Dismukes, A. L. Rheingold, V. Petrouleas, J. Stubbe, W. H. Armstrong, R. H. Beer, S. J. Lippard, *J. Am. Chem. Soc.* **1987**, *109*, 1435–1444.
[24] S. R. Cooper, M. Calvin, *J. Am. Chem. Soc.* **1977**, *99*, 6623–6630.

  1433-7851/01/4015-2928 $ 17.50+.50/0